Virchows Arch (2006) 448: 1–6
DOI 10.1007/s00428-005-0082-4

REVIEW ARTICLE

Susanne van Eeden · G. Johan A. Offerhaus

Historical, current and future perspectives on gastrointestinal and pancreatic endocrine tumors

Received: 21 June 2005 / Accepted: 25 August 2005 / Published online: 12 October 2005

Abstract Gastrointestinal and pancreatic endocrine tumors are neoplasms of which the pathogenesis is not completely understood and of which the clinical behavior is difficult to predict. Originally, Masson suggested that the cell of origin was an endocrine cell derived from the gastrointestinal epithelium. However, Pearse showed that the endocrine cells throughout the body shared various features, among others the amine precursor uptake and decarboxylation (APUD) capacity, and postulated the neural crest as the common origin for all APUD cells, a hypothesis that received support from the scientific community for many years. Now, biologists start to elucidate the various transcription factors that drive gastrointestinal development, and it has become evident that Masson was presumably right. Transcription factors relevant for development may also operate during tumorigenesis, and their expression may determine tumor biology. With other genetic factors, they may play a role in the pathogenesis of gastrointestinal and pancreatic endocrine tumors, and perhaps, their expression will turn out to be of prognostic or therapeutic value. In this review, current knowledge on the development of endocrine cells, hypotheses on the origin of endocrine tumors, genetic alterations, and prognostic factors are discussed. It is suggested that the increasing understanding of the normal development of gastrointestinal and pancreatic endocrine cells, the accumulating data on genetic alterations in endocrine tumors and the reappraisal of the hypotheses on their pathogenesis formulated in the past may help in elucidating their pathogenesis and in more accurately predicting prognosis.

Keywords Endocrine tumors · Gastrointestinal tract · Pancreas

S. van Eeden (✉) · G. J. A. Offerhaus
Department of Pathology, Academic Medical Center,
Meibergdreef 9,
1105 Amsterdam, The Netherlands
e-mail: s.vaneeden@amc.uva.nl
Tel.: +31-20-5665635
Fax: +31-20-6960389

History

When the French-born Canadian pathologist Pierre Masson retired 50 years ago, he left an impressive oeuvre containing interesting concepts on the origin of gastrointestinal endocrine cells and the pathogenesis of gastrointestinal and especially appendiceal carcinoids.

The term carcinoid had been introduced by Oberndorfer ('Karzinoide' meaning 'carcinoma-like'), who recognized this neoplasm as a separate entity, behaving less aggressively than conventional adenocarcinomas [45]. Masson demonstrated the argentaffin-staining properties of these tumors using a silver impregnation technique and proposed an origin from gastrointestinal endocrine cells. He was convinced that the gastrointestinal endocrine cells derive from the gastrointestinal epithelium itself and do not, as proposed by others, migrate from a neural plexus towards the mucosa. Moreover, he thought that appendiceal carcinoids originate from undifferentiated cells at the base of the crypts, which bud off the epithelium, form complexes with the subepithelial neural plexus, and subsequently acquire their endocrine granules, which, in a way, might be regarded as a sort of stem cell concept. Concerning carcinoids elsewhere in the gastrointestinal tract, he also described a subepithelial intraneural argentaffin cell as the cell of origin [42–44].

In the same period, Feyrter [20, 21] recognized that the endocrine cells scattered in the epithelium of various organs, including the gastrointestinal tract, might be regarded as part of a diffuse endocrine/paracrine system, and Masson's ideas were forgotten when Pearse showed that these cells share important ultrastructural and biochemical characteristics, especially the amine precursor uptake and decarboxylation (APUD) capacity. These observations were consistent with a common origin of the APUD cells, for which the neural crest appeared the only possible candidate [52].

However, experiments by Fontaine and Le Douarin [22] in quail-chick chimeras provided strong evidence against a neural crest origin of most endocrine cells, except thyroid C cells, ganglia, and paraganglia. Although their results

could not completely rule out an ectodermal origin of gastrointestinal endocrine cells, they pointed more towards an endodermal origin, thereby supporting Masson's view and forming a base for the stem cell concept used today [13].

Developmental biology

Illustrative of this concept is the current knowledge on the development of the endocrine cells in the intestine and pancreas at both the cellular and molecular level, to which data from animal models have contributed significantly.

The intestinal epithelium, which is of endodermal origin, contains four main cell types: enterocytes, goblet cells, Paneth cells, and endocrine cells. These are thought to arise from omnipotent stem cells at the base of the crypts of Lieberkühn. Experimental mouse models suggest that the omnipotent stem cells give rise to enterocyte precursors and to (common) precursors of goblet cells, Paneth cells, and endocrine cells, sometimes designated as secretory stem cells [28, 72]. This happens under the influence of transcription factors. A transcription factor encoded by a caudal-related homeobox gene and involved in early intestinal development and differentiation is Cdx2. Cdx2 expression is maintained in the adult intestinal epithelium, although expression in Paneth cells is weak [6, 63]. Differentiation into a secretory stem cell and its descendants is thought to be directed by transcription factors encoded by genes of the basic helix–loop helix (bHLH) family, of which Math1 is (one of) the first in the pathway [72]. As shown in Fig. 1, subsequent differentiation towards an endocrine cell is regulated by the transcription factor neurogenin 3 (ngn3) [28]. Its downstream target NeuroD/BETA2 is especially required for the development of secretin and cholecystokinin producing intestinal endocrine cells [48]. Endocrine differentiation is repressed by Notch signaling. Notch is a transmembrane receptor that exerts its function via lateral inhibition. Hes1 is an important transcriptional repressor of this pathway [29, 64]. Although an obvious role for ngn3 in the differentiation of goblet cells and Paneth cells has not been established, recently published data suggest its transient expression in a subset of their precursors [59].

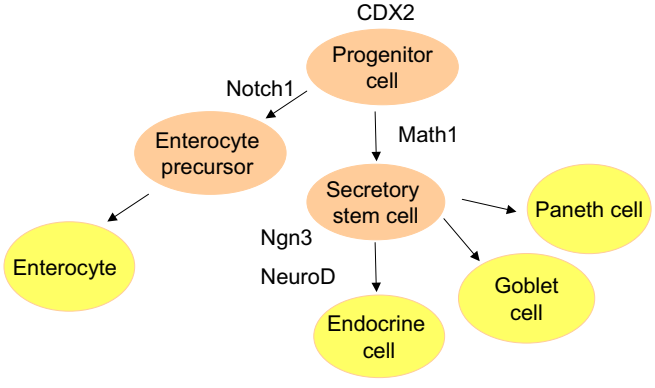

Fig. 1 This diagram shows transcription factors involved in the development of different intestinal epithelial cell types [28, 60, 72]

The development of the pancreatic endocrine cells, organized in the islets of Langerhans, shows differences from, but also striking similarities to, intestinal endocrine development. The pancreas arises from the duodenal region of the embryonic foregut, where expression of the pancreas duodenum homeodomain protein 1 (Pdx1) is required for the formation of the ventral and dorsal primordia, which, in a later stage, fuse to form the adult organ. At the cellular level, the pancreatic primordia contain Pdx1 positive epithelium, which forms primitive ducts from which the endocrine cells arise [1, 53]. As in the intestine, animal models indicate that ngn3 and neuroD/BETA2 play a role in this process [23, 48, 61], whereas Notch inhibits endocrine differentiation. For Notch, a role has been suggested in modulating the development of the exocrine pancreas [2] and, more recently, in keeping the undifferentiated state of pancreas precursor cells [24]. Math1, required in the intestine for differentiation towards a secretory stem cell phenotype, does not seem to play a role in pancreatic development [60]. Other transcription factors downstream of ngn3 and NeuroD/BETA2, involved in endocrine differentiation of the pancreas, are Pax4, Nkx2.2, Nkx6.1, Pax6, and Isl1 [62]. In the adult pancreas, Pdx1 is almost exclusively expressed in the insulin producing β cells, in which it plays a role in transcriptional activation of the insulin gene, together with NeuroD/BETA2 [41]. Although most endocrine cells are organized in the islets of Langerhans, scattered endocrine cells are found in the exocrine ducts. In a pancreatic duct ligation model in rats, expression of the putative stem cell markers c-kit and nestin and upregulation of the transcription factors Pdx1 and Nkx2.2 have been described, suggesting that in the pancreatic remodeling and neoformation process, similar mechanisms are involved as in embryonic development [54].

Developmental biology related to tumorigenesis

The increasing knowledge on embryonic development influences the ideas on tumor pathogenesis and may also be important in endocrine tumor pathology. A tumor is regarded as a clonal expansion that, in theory, originates from a genetically unstable and deregulated, terminally differentiated cell, from an unstable, deregulated precursor cell already committed to a certain line of differentiation, or from a deregulated, undifferentiated, omnipotent stem cell. Although an origin from a terminally differentiated cell cannot be ruled out, it has been suggested that pancreatic endocrine tumors have a precursor cell origin [30, 37, 69]. In part, this idea is based on the occurrence of mixed pancreatic tumors, consisting of an endocrine part combined with ductal or acinar features. The concept of derivation from a precursor cell or omnipotent stem cell is especially attractive for these mixed tumors, in which more than one cell type is present because it provides an overt explanation for their histological features. Another exam-

ple of a mixed tumor is a goblet cell carcinoid, in which the malignant counterparts of goblet cells, endocrine cells and Paneth cells can be found, which is suggestive of an origin from an intestinal secretory stem cell, which is thought to be the precursor of precisely these cell types. In contrast, scattered, supposedly nonneoplastic endocrine cells have been found in ductal adenocarcinomas of the pancreas that were not considered as an intrinsic part of the tumor [49].

In light of the presumed precursor cell origin of certain tumors, including tumors consisting of one cell type, an important consideration is that the transcription factors playing a role in embryonic development may drive tumorigenesis as well. The expression of Math1 in Merkel cell carcinoma (an endocrine tumor of the skin) [34] and its recently reported repression in colonic adenocarcinoma [36] are in support of this. Other examples of transcription factors expressed in tumors are CDX2 in intestinal tumors, including carcinoids, and thyroid transcription factor 1 (involved in thyroidal and pulmonary development) in tumors of the thyroid and lung [67, 71].

Knowledge on the role of transcription factors in (endocrine) tumors may help in elucidating their pathogenesis and may even, in the far future, provide a target for therapeutic options, such as specific intervention of the pathways governed by these molecules, and thereby inhibit or stimulate cellular activities of, for example, proliferation or differentiation. However, at this moment, data on the role of the transcription factors mentioned above in gastrointestinal and pancreatic endocrine tumors are limited to reports on the expression of CDX2 [3, 33].

Genetic alterations

More is known about generalized and also some specific molecular genetic abnormalities underlying gastrointestinal and pancreatic endocrine tumors. One of the genetic changes reported repeatedly in gastrointestinal endocrine tumors, especially in midgut carcinoids (carcinoids of jejunum, ileum, ascending colon, and appendix) and less frequently in pancreatic endocrine tumors, is loss on chromosomal arm 18q. Because, in most cases, no apparent alterations have been found in the tumor suppressor genes *DPC4* and *DCC*, which are located in the affected region, it has been suggested that a currently unknown gene on chromosome 18q is important in the pathogenesis of (especially midgut) endocrine tumors [7, 27, 32, 40, 55, 68, 73]. Because in some midgut carcinoids loss of chromosome 16q21 and gain of chromosome 4p14 have been found in metastases but not in the primary tumor, genes in this region may play a role in tumor progression [32]. Only in a minority of midgut carcinoids allelic loss on chromosomal arm 11q has been described [17, 32, 73], whereas deletions on chromosome 11q have been found more frequently in foregut carcinoids [17, 73]. The different genetic alterations found in foregut and midgut carcinoids suggest that these tumors develop and progress via different molecular pathways [17, 35, 56]. This may at least, in part, explain the clinical, histological, and immunohistochemical heterogeneity of these tumors, which is addressed in recent reviews on gastrointestinal endocrine tumors [46, 70].

Chromosome 11q13 harbors the tumor suppressor gene responsible for the hereditary syndrome multiple endocrine neoplasia type 1 (MEN1), which is associated with pancreatic endocrine tumors. Pancreatic, gastric, and duodenal endocrine tumors of MEN1 patients and a subset of their sporadic counterparts show loss of heterozygosity of the *MEN1* gene. Because allelic losses distal to this gene have been found, it has been suggested that chromosome 11q contains other tumor suppressor genes that may play a role in pathogenesis as well [11, 16–18, 27, 66]. Another hereditary syndrome associated with pancreatic endocrine tumors is Von Hippel–Lindau (VHL) disease, linked to a tumor suppressor gene on chromosome 3p25-26 [38]. Although pancreatic endocrine tumors frequently show loss in this region, mutations in the VHL gene have not been found in sporadic cases. It is likely that another tumor suppressor gene near the *VHL* gene plays a role in the pathogenesis of sporadic pancreatic endocrine tumors, and there are indications that allelic losses of chromosome 3p are involved in tumor progression [4, 15]. A role in tumor progression has also been suggested for putative tumor suppressor loci at chromosome 6q [5]. Moreover, allelic losses on the X chromosome were found in pancreatic endocrine tumors and correlated with aggressive tumor behavior [12, 56]. *C-myc* is an oncogene that may be involved in the pathogenesis of pancreatic endocrine tumors [37, 51], and genes with a tumor suppressor function on chromosome 9p, e.g., *Ink4A/Arf* encoding p16, may be of importance in both gastrointestinal and pancreatic endocrine tumors [37, 39, 47].

Alterations in tumor suppressor genes and oncogenes commonly involved in human cancer, like *TP53*, *Rb*, and *KRAS*, have been described in gastrointestinal and pancreatic endocrine tumors, especially in poorly differentiated endocrine carcinomas, but they do not seem to play a major role in pathogenesis [14, 50, 51, 57, 58].

Prognostic features

Some of the genetic alterations mentioned above, such as loss of heterozygosity on chromosome 3p, 6q, and X, may be involved in tumor progression and may turn out to be of prognostic value in the near future, but currently, there are no consistent genetic changes in endocrine tumors that can be used to predict tumor behavior in an individual patient. Also, based on histological criteria, it is difficult to predict prognosis. Generally, it is not a problem to recognize poorly differentiated endocrine carcinomas, which have histological features of small cell carcinoma. However, poorly differentiated endocrine carcinomas of large cell type are underdiagnosed because their endocrine nature is not always recognized and because the WHO classification does not provide clear diagnostic criteria.

In the group of better differentiated tumors, metastasis is the only reliable indicator of malignancy. Other prognostic

factors for pancreatic endocrine tumors have been described by Capella et al. [10], and assessment of malignancy in gastrointestinal endocrine tumors has also been comprehensively reviewed by Bordi et al. [8]. Despite the lack of unequivocal histological criteria for malignancy of a primary tumor, the WHO classification of endocrine tumors published in 2000 distinguishes benign tumors, tumors of uncertain behavior, and low-grade malignant and high-grade malignant carcinomas of the gastrointestinal tract [65] and pancreas [31], based on parameters for which prognostic value has been described [for gastrointestinal endocrine tumors, site, size, depth of invasion, and vasoinvasive growth, and for pancreatic endocrine tumors, also proliferative activity and functionality (i.e., causing a clinical syndrome by hormone secretion)]. In the WHO classification of tumors of the digestive system also published in 2000 [25], the same prognostic parameters are mentioned for gastrointestinal endocrine tumors, for some sites extended with proliferative activity, although a similar grading system is not explicitly presented. Also, the new WHO classification for pancreatic endocrine tumors (2004) [26] does not contain significant differences compared to the old version [31]. The classification system still contains the category of tumors of uncertain behavior, reflecting the lack of clear prognostic features in endocrine tumors.

A recent observation in pancreatic endocrine tumors is the correlation between immunohistochemical expression of cytokeratin 19 (Ck19) and aggressive behavior [19]. During embryonic development, Ck19 is transiently expressed in all pancreatic cells, including endocrine cells, but after 16 weeks of gestation, Ck19 gradually disappears from most cells in the islets of Langerhans, whereas its expression remains strong in the ducts [9]. In view of the presumed precursor cell origin of pancreatic endocrine tumors, it is tempting to speculate that more aggressive pancreatic endocrine tumors arise from an early precursor cell, which has not yet lost its Ck19 expression, or that they arise from a precursor cell that tends to differentiate towards a ductal phenotype not yet visible histologically, but already evident at the immunohistochemical level. The clinical value of Ck19 as a prognostic marker in pancreatic endocrine tumors remains to be evaluated.

Conclusion

The difficulties described above in accurately predicting prognosis of gastrointestinal and pancreatic endocrine tumors bring us back to the observations of Masson. He already described the unpredictable clinical behavior of gastrointestinal endocrine tumors and noticed the higher metastatic capability of ileal carcinoids compared to those of the appendix [43]. Although we probably would not agree with his explanation that this is due to the difference in intestinal motility between the ileum and appendix, it might be worthwhile to reconsider his ideas, in particular, on the origin of appendiceal carcinoids, and compare and test them with the knowledge and possibilities of today. Especially, evaluation of the role of transcription factors involved in differentiation and of genomic alterations in endocrine tumors may help in elucidating their pathogenesis and in establishing reliable prognostic parameters. It is predicted that especially Masson's concepts on origin and pathogenesis will appear much more valid than when these were considered over the past 50 years, once the molecular developmental biology of the endocrine cell population in the digestive tract has clarified their tumorigenesis 50 years from now. Would there then be better proof of Masson's vision than the century it took us to validate his concept?

Acknowledgements The authors are indebted to Professor G. Klöppel for critically reading the manuscript and for his suggestions.

References

1. Ahlgren U, Jonsson J, Edlund H (1996) The morphogenesis of the pancreatic mesenchyme is uncoupled from that of the pancreatic epithelium in IPF1/PDX1-deficient mice. Development 122:1409–1416
2. Apelqvist Å, Li H, Sommer L, Beatus P, Anderson DJ, Honjo T, Hrabe de Angelis M, Lendahl U, Edlund H (1999) Notch signalling controls pancreatic cell differentiation. Nature 400: 877–881
3. Barbareschi M, Roldo C, Zamboni G, Capelli P, Cavazza A, Macri E, Cangi MG, Chilosi M, Doglioni C (2004) *CDX-2* homeobox gene product expression in neuroendocrine tumors. Its role as a marker of intestinal neuroendocrine tumors. Am J Surg Pathol 28(9):1169–1176
4. Barghorn A, Komminoth P, Bachmann D, Rutimann K, Saremaslani P, Muletta-Feurer S, Perren A, Roth J, Heitz PU, Speel EJ (2001) Deletion at 3p25.3-p23 is frequently encountered in endocrine pancreatic tumours and is associated with metastatic progression. J Pathol 194:451–548
5. Barghorn A, Speel EJM, Farspour B, Saremaslani P, Schmid S, Perren A, Roth J, Heitz PU, Komminoth P (2001) Putative tumor suppressor loci at 6q22 and 6q23-q24 are involved in the malignant progression of sporadic endocrine pancreatic tumors. Am J Pathol 158:1903–1911
6. Beck F (2002) Homeobox genes in gut development. Gut 51:450–454
7. Beghelli S, Pelosi G, Zamboni G, Falconi M, Iacono C, Bordi C, Scarpa A (1998) Pancreatic endocrine tumours: evidence for a tumour suppressor pathogenesis and for a tumour suppressor gene on chromosome 17p. J Pathol 186:41–50
8. Bordi C, D'Adda T, Pizzi S, Crafa P, Rindi G (2002) The assessment of malignancy in endocrine tumours of the gastrointestinal tract. Curr Diagn Pathol 8:421–429
9. Bouwens L, Lu WG, de Krijger RR (1997) Proliferation and differentiation in the human fetal endocrine pancreas. Diabetologia 40:398–404
10. Capella C, La Rosa S, Solcia E (1997) Criteria for malignancy in pancreatic endocrine tumors. Endocr Pathol 8:87–90
11. Chakrabarti R, Srivatsan ES, Wood TF, Eubanks PJ, Ebrahimi SA, Gatti RA, Passaro E Jr, Sawicki MP (1998) Deletion mapping of endocrine tumors localizes a second tumor suppressor gene on chromosome band 11q13. Genes Chromosomes Cancer 22:130–137

12. Chen YJ, Vortmeyer A, Zhuang Z, Gibril F, Jensen RT (2004) X-chromosome loss of heterozygosity frequently occurs in gastrinomas and is correlated with aggressive tumor growth. Cancer 100:1379–1387
13. Cheng H, Leblond CP (1974) Origin, differentiation and renewal of the four main epithelial cell types in the mouse small intestine. V. Unitarian theory of the origin of the four epithelial cell types. Am J Anat 141:537–562
14. Chung DC, Smith AP, Louis DN, Graeme-Cook F, Warshaw AL, Arnold A (1997) Analysis of the retinoblastoma tumour suppressor gene in pancreatic endocrine tumours. Clin Endocrinol 47:523–528
15. Chung DC, Smith AP, Louis DN, Graeme-Cook F, Warshaw AL, Arnold A (1997) A novel pancreatic endocrine tumor suppressor gene locus on chromosome 3p with clinical prognostic implications. J Clin Invest 100(2):404–410
16. D'Adda T, Keller G, Bordi C, Höfler H (1999) Loss of heterozygosity in 11q13-14 regions in gastric neuroendocrine tumors not associated with multiple endocrine neoplasia type 1 syndrome. Lab Invest 79(6):671–677
17. D'Adda T, Pizzi S, Azzoni C, Bottarelli L, Crafa P, Pasquali C, Davoli C, Corletto VD, Delle Fave G, Bordi C (2002) Different patterns of 11q allelic losses in digestive endocrine tumors. Human Pathol 3:322–329
18. Debelenko LV, Emmert-Buck MR, Zhuang Z, Epshteyn E, Moskaluk CA, Jensen RT, Liotta LA, Lubensky IA (1997) The multiple endocrine neoplasia type I gene locus is involved in the pathogenesis of type II gastric carcinoids. Gastroenterology 113:773–781
19. Deshpande V, Fernandez-del Castillo C, Muzikansky A, Deshpande A, Zukerberg L, Warshaw AL, Lauwers GY (2004) Cytokeratin 19 is a powerful predictor of survival in pancreatic endocrine tumors. Am J Surg Pathol 28:1145–1153
20. Feyrter F (1938) Über diffuse endocrine epitheliale Organe. Leipzig Zentr Inn Med 29:545–571
21. Feyrter F (1956) Zur Lehre von den periferen endokrinen (parakrinen) Drüsen des Menschen. Neue Erkenntnisse. Wien Med Wochenschr 106(23):515–516
22. Fontaine J, Le Douarin NM (1977) Analysis of endoderm formation in the avian blastoderm by the use of quail-chick chimaeras. The problem of the neuroectodermal origin of the cells of the APUD series. J Embryol Exp Morphol 41:209–222
23. Graphin-Button A, Majithia AR, Melton DA (2001) Key events of pancreas formation are triggered in gut endoderm by ectopic expression of pancreatic regulatory genes. Genes Dev 15:444–454
24. Hald J, Hjort P, German MS, Madsen OD, Serup P, Jensen J (2003) Activated Notch1 prevents differentiation of pancreatic acinar cells and attenuate endocrine development. Dev Biol 260:426–437
25. Hamilton SR, Aaltonen LA (eds) (2000) World Health Organization international classification of tumours. Pathology and genetics of tumours of the digestive system. IARC Press, Lyon
26. Heitz PU, Komminoth P, Perren A, Klimstra DS, Dayal Y, Bordi C, Lechago J, Centeno BA, Klöppel G (2004) Pancreatic endocrine tumours: introduction. In: De Lellis RA, Lloyd RV, Heitz PU, Eng C (eds) World Health Organization international classification of tumours. Pathology and genetics of tumours of endocrine organs. IARC Press, Lyon, pp 177–182
27. Hessman O, Lindberg D, Einarsson A, Lillhager P, Carling T, Grimelius L, Eriksson B, Åkerström G, Westin G, Skogseid B (1999) Genetic alterations on 3p, 11q13, and 18q in nonfamilial and MEN I-associated pancreatic endocrine tumors. Genes Chromosomes Cancer 26:258–264
28. Jenny M, Uhl C, Roche C, Duluc I, Guillermin V, Guillemot F, Jensen J, Kedinger M, Gradwohl G (2002) Neurogenin3 is differentially required for endocrine cell fate specification in the intestinal and gastric epithelium. EMBO 21(23):6338–6347
29. Jensen J, Engholm Pedersen E, Galante P, Hald J, Heller RS, Ishibashi M, Kagayama R, Guillemot F, Serup P, Madsen OD (2000) Control of endodermal endocrine development by Hes-1. Nat Genet 24:36–44
30. Klimstra DS, Rosai J, Heffess CS (1994) Mixed acinar–endocrine carcinomas of the pancreas. Am J Surg Pathol 18 (8):765–778
31. Klöppel G, Heitz PU, Capella C, Solcia E (2000) Endocrine tumours of the pancreas. In: Solcia E, Klöppel G, Sobin LH (eds) World Health Organization international histological classification of tumours. Histological typing of endocrine tumours, 2nd edn. Springer, Berlin Heidelberg New York, pp 56–60
32. Kytölä S, Höög A, Nord B, Cedermark B, Frisk T, Larsson C, Kjellman M (2001) Comparative genomic hybridization identifies loss of 18q22-qter as an early and specific event in tumorigenesis of midgut carcinoids. Am J Pathol 158(5):1803–1808
33. La Rosa S, Rigoli E, Uccella S, Chiaravalli AM, Capella C (2004) CDX2 as a marker of intestinal EC-cells and related well-differentiated endocrine tumors. Virchows Arch 445(3): 248–254
34. Leonard JH, Cook AL, Van Gele M, Boyle GM, Inglis KJ, Speleman F, Sturm RA (2002) Proneural and proneuroendocrine transcription factor expression in cutaneous mechanoreceptor (Merkel) cells and Merkel cell carcinoma. Int J Cancer 101(2):103–110
35. Leotlela PD, Jauch A, Holtgreve-Grez H, Thakker RV (2003) Genetics of neuroendocrine and carcinoid tumors. Endocr-Relat Cancer 10:437–450
36. Leow CC, Romero MS, Ross S, Polakis P, Gao WQ (2004) Hath1, Down-regulated in colon adenocarcinomas, inhibits proliferation and tumorigenesis of colon cancer cells. Cancer Res 64:6050–6057
37. Lewis BC, Klimstra DS, Varmus HE (2003) The c-*myc* and PyMT oncogenes induce different tumor types in a somatic mouse model for pancreatic cancer. Genes Dev 17:3127–3138
38. Lubensky IA, Pack S, Ault D, Vortmeyer AO, Libutti SK, Choyke PL, Walther MM, Linehan WM, Zhuang Z (1998) Multiple neuroendocrine tumors of the pancreas in von Hippel–Lindau disease patients. Histopathological and molecular genetic analysis. Am J Pathol 153(1):223–231
39. Lubomierski N, Kersting M, Bert T, Muench K, Wulbrand U, Schuermann M, Bartsch D, Simon B (2001) Tumor suppressor genes in the *9p21* gene cluster are selective targets of inactivation in neuroendocrine gastroenteropancreatic tumors. Cancer Res 61:5905–5910
40. Löllgen RM, Hessman O, Szabo E, Westin G, Åkerström G (2001) Chromosome 18 deletions are common events in classical midgut carcinoid tumors. Int J Cancer 92:812–815
41. Madsen OD, Jensen J, Petersen HV, Pedersen EE, Oster A, Andersen FG, Jorgensen MC, Jensen PB, Larsson LI, Serup P (1997) Transcription factors contributing to the pancreatic beta-cell phenotype. Horm Metab Res 29(6):265–270
42. Masson P (1928) Carcinoids (argentaffin-cell tumors) and nerve hyperplasia of the appendicular mucosa. Am J Pathol IV(3): 181–211
43. Masson P (1951) La malignité des carcinoids du tube digestif. Mikroskopie 6:133–146
44. Masson P (1956) Tumeurs humaines. Histologie. Diagnostics Et Techniques, 2nd edn. Libraire Maloine, Paris, pp 530–539
45. Modlin IM, Shapiro MD, Kidd M (2004) Siegfried Oberndorfer: origins and perspectives of carcinoid tumors. Human Pathol 35 (12):1440–1451
46. Modlin IM, Kidd M, Latich I, Zikusoka MN, Shapiro MD (2005) Current status of gastrointestinal carcinoids. Gastroenterology 128(6):1717–1751
47. Muscarella P, Melvin WS, Fisher WE, Foor J, Ellison EC, Herman JC, Schirmer WJ, Hitchcock CL, DeYoung BR, Weghorst CM (1998) Genetic alterations in gastrinomas and non-functioning pancreatic neuroendocrine tumors: an analysis of p16/MTS1 tumor suppressor gene inactivation. Cancer Res 58:237–240
48. Naya FJ, Huang HP, Qiu Y, Mutoh H, DeMayo FJ, Leiter AB, Tsai MJ (1997) Diabetes, defective pancreatic morphogenesis, and abnormal enteroendocrine differentiation in BETA2/Neuro-D-deficient mice. Genes Dev 11:2323–2334

49. Ohike N, Jürgensen A, Pipeleers-Marichal M, Klöppel G (2003) Mixed ductal–endocrine carcinomas of the pancreas and ductal adenocarcinomas with scattered endocrine cells: characterization of the endocrine cells. Virchows Arch 442:258–265
50. Paraskevakou H, Saetta A, Skandalis K, Tseleni S, Athanassiadis A, Davaris PS (1999) Morphological–histochemical study of intestinal carcinoids and K-*ras* mutation analysis in appendiceal carcinoids. Pathol Oncol Res 5(3):205–210
51. Pavelić K, Hrašćan R, Kapitanovic S, Karapandza N, Vranes Z, Belicza M, Kruslin B, Cabrijan T (1995) Multiple genetic alterations in malignant metastatic insulinomas. J Pathol 177: 395–400
52. Pearse AGE (1969) The cytochemistry and ultrastructure of polypeptide hormone-producing cells of the APUD series and the embryologic, physiologic and pathologic implications of the concept. J Histochem Cytochem 17(5):303–313
53. Peters J, Jürgensen A, Klöppel G (2000) Ontogeny, differentiation and growth of the endocrine pancreas. Virchows Arch 436:527–538
54. Peters K, Panienka R, Li J, Klöppel G, Wang R (2005) Expression of stem cell markers and transcription factors during the remodeling of the rat pancreas after duct ligation. Virchows Arch 446:56–63
55. Perren A, Saremaslani P, Schmid S, Bonvin C, Locher T, Roth J, Heitz PU, Komminoth P (2003) *DPC4/Smad4*: no mutations, rare allelic imbalances, and retained protein expression in pancreatic endocrine tumors. Diagn Mol Pathol 12(4):181–186
56. Pizzi S, D'Adda T, Azzoni C, Rindi G, Grigolato P, Pasquali C, Corletto VD, Delle Fave G, Bordi C (2002) Malignancy-associated allelic losses on the X-chromosome in foregut but not in midgut endocrine tumours. J Pathol 196:401–407
57. Pizzi S, Azzoni C, Bassi D, Bottarelli L, Milione M, Bordi C (2003) Genetic alterations in poorly differentiated endocrine carcinomas of the gastrointestinal tract. Cancer 98:1273–1282
58. Ramnani DM, Wistuba II, Behrens C, Gazdar AF, Sobin LH, Albores-Saavedra J (1999) K-*ras* and p53 mutations in the pathogenesis of classical and goblet cell carcinoids of the appendix. Cancer 86:14–21
59. Schonhoff SE, Giel-Moloney M, Leiter AB (2004) *Neurogenin 3*-expressing progenitor cells in the gastrointestinal tract differentiate into both endocrine and non-endocrine cell types. Dev Biol 270:443–454
60. Schonhoff SE, Giel-Moloney M, Leiter AB (2004) Development and differentiation of gut endocrine cells. Endocrinology 145(6):2639–2644
61. Schwitzgebel VM, Scheel DW, Conners JR, Kalamaras J, Lee JE, Anderson DJ, Sussel L, Johnson JD, German MS (2000) Expression of neurogenin3 reveals an islet cell precursor population in the pancreas. Development 127:3533–3542
62. Schwitzgebel VM (2001) Programming of the pancreas. Mol Cell Endocrinol 185:99–108
63. Silberg DG, Swain GP, Suh ER, Traber PG (2000) Cdx1 and Cdx2 expression during intestinal development. Gastroenterology 119:961–971
64. Skipper M, Lewis J (2000) Getting to the guts of enteroendocrine differentiation. Nat Genet 24:3–4
65. Solcia E, Capella C, Klöppel G, Heitz PU, Sobin LH, Rosai J (2000) Endocrine tumours of the gastrointestinal tract. In: Solcia E, Klöppel G, Sobin LH (eds) World Health Organization international histological classification of tumours. Histological typing of endocrine tumours, 2nd edn. Springer, Berlin Heidelberg New York, pp 61–68
66. Speel EJM, Richter J, Moch H, Egenter C, Saremaslani P, Rutimann K, Zhao J, Barghorn A, Roth J, Heitz PU, Komminoth P (1999) Genetic differences in endocrine pancreatic tumor subtypes detected by comparative genomic hybridization. Am J Pathol 155(6):1787–1794
67. Stenhouse G, Fyfe N, King G, Chapman A, Kerr KM (2004) Thyroid transcription factor 1 in pulmonary adenocarcinoma. J Clin Pathol 57:383–387
68. Stumpf E, Aalto Y, Höög A, Kjellman M, Otonkoski T, Knuutila S, Andersson LC (2000) Chromosomal alterations in human pancreatic endocrine tumors. Genes Chromosomes Cancer 29:83–87
69. Vortmeyer AO, Huang S, Lubensky I, Zhuang Z (2004) Non-islet origin of pancreatic islet cell tumors. J Clin Endocrinol Metab 89(4):1934–1938
70. Warner RRP (2005) Enteroendocrine tumors other than carcinoid: a review of clinically significant advances. Gastroenterology 128:1668–1684
71. Werling RW, Yaziji H, Bacchi CE, Gown AM (2003) CDX2, a highly sensitive and specific marker of adenocarcinomas of intestinal origin: an immunohistochemical survey of 476 primary and metastatic carcinomas. Am J Surg Pathol 27(3): 303–310
72. Yang Q, Bermingham NA, Finegold MJ, Zoghbi HY (2001) Requirement of *Math1* for secretory cell lineage commitment in the mouse intestine. Science 294(5549):2155–2158
73. Zhao J, de Krijger RR, Meier D, Speel EJ, Saremaslani P, Muletta-Feurer S, Matter C, Roth J, Heitz PU, Komminoth P (2000) Genomic alterations in well-differentiated gastrointestinal and bronchial neuroendocrine tumors (carcinoids). Marked differences indicating diversity in molecular pathogenesis. Am J Pathol 157(5):1431–1438

Virchows Arch (2006) 448: 7–15
DOI 10.1007/s00428-005-0087-z

ORIGINAL ARTICLE

Giuseppe Pelosi · Elisabetta Schianchi · Patrizia Dell'Orto · Giulia Veronesi · Lorenzo Spaggiari · Felice Pasini · Gabriella Sozzi · Elisabeth Brambilla · Claudia Griso · Giuseppe Viale

Detecting cell-free circulating hTERT mRNA in the plasma may identify a subset of nonsmall cell lung cancer patients

Received: 29 June 2005 / Accepted: 31 August 2005 / Published online: 29 September 2005

Abstract Human telomerase reverse transcriptase (hTERT), the catalytic subunity of telomerase, a marker of cell immortalization, is upregulated in most tumors, including nonsmall cell lung cancer (NSCLC). However, little is known about the role of assessing cell-free plasma circulating hTERT mRNA for tracing these tumors. We investigated by RT–polymerase chain reaction (PCR) and real-time quantitative PCR the prevalence and functional implications of hTERT mRNA in both tumor tissue and paired plasma samples in 34 (27 males and 7 females) stages I–IIIB NSCLC patients (21 adenocarcinomas and 13 squamous-cell carcinomas) by using intron- and exon-spanning primers. Plasma samples of ten healthy volunteers and normal lung tissue were used as negative controls. We detected hTERT mRNA in the plasma of 4 out of 34 (12%) tumor patients, but none was detected in the ten plasma samples of healthy volunteers. Normal lung tissue was completely devoid of hTERT mRNA. No association was found between hTERT plasma mRNA and clinicopathologic variables of the patients' population. We conclude that cell-free circulating hTERT mRNA is detectable in a subset of patients, whereas it is consistently absent in healthy volunteers. It can be added to the panel of multiple genetic tracers to detect lung cancer in the plasma of patients, although, per se, it is not specific for this tumor.

Keywords Nonsmall cell lung cancer · Telomerase · hTERT · mRNA · Plasma · Detection · Real-time PCR · Diagnosis

G. Pelosi · E. Schianchi · P. Dell'Orto · G. Viale
Division of Pathology and Laboratory Medicine,
European Institute of Oncology
and University of Milan School of Medicine,
Milan, Italy

G. Pelosi (✉)
Divisione di Anatomia Patologica e Medicina di Laboratorio,
Istituto Europeo di Oncologia,
Via G. Ripamonti, 435,
20141 Milan, Italy
e-mail: giuseppe.pelosi@ieo.it
Tel.: +39-02-57489414
Fax: +39-02-57489417

E. Schianchi · G. Veronesi · L. Spaggiari
Division of Thoracic Surgery,
European Institute of Oncology,
Milan, Italy

F. Pasini · C. Griso
Institute of Medical Oncology,
University of Verona,
Verona, Italy

G. Sozzi
Department of Experimental Oncology,
National Cancer Institute,
Milan, Italy

E. Brambilla
Department of Pathology,
CHU Albert Michallon,
Grenoble, France

Introduction

Lung cancer is one of the leading causes of morbidity and death worldwide, with more than 1,200,000 new cases per year, accounting for about 12–15% of all cancers diagnosed in both genders [60]. Unfortunately, most lung carcinomas are discovered in an advanced stage, when the chances of definitive cure are dramatically reduced [13]. Only 10–20% of them are diagnosed when the disease is still limited to the lung without regional lymph node involvement (stage I, pT1–2 N0 M0). These patients may be successfully treated, and they have the highest likelihood of prolonged survival [8, 40]. The occurrence of local or systemic clinical symptoms is a late event that is usually associated with ominous prognosis [47]. Therefore, any effort is warranted to anticipate lung cancer diagnosis as much as possible, especially in high-risk populations of current or former heavy smokers [22, 48], to improve both the detection rate of lung cancer and patients' survival.

The use of molecular markers in body fluids, such as sputum, bronchial brush and lavage, and plasma or serum, has been proposed as a potentially useful diagnostic tool in both lung cancer patients and clinically negative high-risk

chronic smokers [23]. This approach is based on the detection of genetic/epigenetic changes shared by primary tumors [1, 2, 11, 37, 54, 59] or on the quantitative assays of cell-free total circulating DNA [57, 58]. More recent and exciting, however, is the discovery that many different types of cell-free circulating mRNA molecules may be detected in the bloodstream of patients with a variety of malignancies such as melanomas [10, 20, 29, 45], follicular lymphomas [9], and breast [3, 15, 28, 45, 55], large-bowel [9, 35, 56, 72], liver [38, 39, 44], esophagus [10], nasopharynx [36], thyroid [34, 45], prostate [5], and lung [12, 28] carcinomas, in hepatic cirrhosis and chronic hepatitis [38, 39], in patients with trauma [51] or diabetic retinopathy [18, 19], or in women during pregnancy for either fetal [43, 50, 62, 66, 67] or maternal [42] mRNA. The occurrence of detectable cell-free and stable RNA in the blood of such patients [63] challenges the long-lasting belief that extracellular mRNA is rapidly degraded by blood ribonuclease [52], opening novel options for non-invasive cancer diagnosis (reviewed in Wong and Lo [70]).

Human telomerase reverse transcriptase (hTERT), the catalytic subunit of telomerase, a marker of cell immortalization [6, 7, 25, 27, 64], is upregulated in up to 80–90% of all tumors, including most nonsmall cell lung cancer (NSCLC) [25, 31, 32, 46]. The hTERT subunit has been used as a plasma tracer in patients with malignant melanoma [45], follicular lymphoma [9], and breast [3, 45], large-bowel [9, 35], thyroid [45] and liver [38, 39] carcino-

Table 1 Clinicopathologic data of the 34 NSCLC patients under evaluation

Patient ID	Diagnosis	Age	Sex	Size (cm)	G	pT	pN	WHO stage	T-hTERT	P-hTERT	T-β-actin	P-β-actin
29	Adenocarcinoma	69	M	3.1	2	2	2	3A	+	−	+	+
34	Adenocarcinoma	57	M	4.5	3	3	0	2B	+	−	+	+
56	Adenocarcinoma	78	F	1.8	1	2	0	1B	+	−	+	−
60	Adenocarcinoma	63	M	4	2	2	1	2B	+	+	+	+
64	Adenocarcinoma	73	M	1.8	3	1	0	1A	+	−	+	−
84	Adenocarcinoma	65	M	2.5	2	1	0	1A	+	−	+	−
91	Adenocarcinoma	65	M	2.5	2	1	0	1A	−	−	+	+
92	Adenocarcinoma	82	F	3.1	3	2	0	1B	+	−	+	+
95	Adenocarcinoma	63	F	3.3	1	2	0	1B	+	+	+	+
102	Adenocarcinoma	48	M	2.8	2	1	2	3A	+	−	+	+
104	Adenocarcinoma	57	M	2.5	2	2	0	1B	+	−	+	+
115	Adenocarcinoma	72	F	4.8	2	2	1	2B	+	−	+	+
121	Adenocarcinoma	52	M	5.2	3	2	2	3A	+	−	+	+
148	Adenocarcinoma	61	M	1.3	2	2	2	3A	+	−	+	−
158	Adenocarcinoma	65	F	3.2	3	2	0	1B	+	−	+	−
186	Adenocarcinoma	51	F	6	3	1	0	1A	+	−	+	+
202	Adenocarcinoma	40	M	6 & 2	1	4 (m)[a]	0	3B	+	−	+	+
212	Adenocarcinoma	65	M	3.5	1	2	0	1B	+	−	+	+
248	Adenocarcinoma	63	M	3	2	1	2	3A	+	−	+	+
279	Adenocarcinoma	61	M	3.2	3	2	0	1B	+	−	+	+
302	Adenocarcinoma	83	M	4.5	2	2	0	1B	+	−	+	+
58	SCC	65	M	4	2	2	1	2B	+	+	+	+
98	SCC	63	M	8	3	2	1	2B	+	−	+	−
110	SCC	69	M	2.8	3	1	2	3A	+	−	+	−
125	SCC	82	M	6.5	2	2	1	2B	+	−	+	−
138	SCC	74	M	3.3	2	2	0	1B	+	−	+	+
157	SCC	79	M	8	2	2	0	1B	+	−	+	−
192	SCC	77	M	3.4	2	2	0	1B	+	+	+	+
197	SCC	72	M	9	3	3	1	3A	+	−	+	+
206	SCC	71	F	2.5	3	1	0	1A	+	−	+	−
232	SCC	71	M	4	2	3	0	2B	+	−	+	+
283	SCC	58	M	1.6	1	1	0	1A	+	−	+	+
304	SCC	77	M	3.2	3	2	0	1B	+	−	+	−
307	SCC	63	M	1.9	3	1	2	3A	+	−	+	+

T-hTERT tumoral tissue hTERT content, *P-hTERT* plasma hTERT content, *T-b-actin* tumoral tissue β-actin content, *P-b-actin* plasma b-actin content, *M* male, *F* female, *SCC* squamous-cell carcinoma

[a]pT4 for the presence of two neoplastic nodules in the same pulmonary lobe according to the WHO 2003 classification (6 and 2 cm in size, respectively)

ma, but little is currently known on the possible implications of cell-free plasma circulating hTERT mRNA in NSCLC patients.

Using real-time quantitative PCR, we document that cell-free circulating hTERT mRNA can be detected in a subset of NSCLC patients, independent of tumor clinicopathologic features, and may become a potentially useful diagnostic tool for these patients.

Materials and methods

Patients and controls

We evaluated plasma samples from 34 (27 men and 7 women) consecutive patients with newly diagnosed and previously untreated stages I–IIIB NSCLC at the European Institute of Oncology in 2004. Clinicopathologic characteristics of the patients are detailed in Table 1. All the patients had been studied preoperatively with clinical history, physical examination, respiratory function tests, total body CT and PET scans, and routine laboratory profile, and all underwent radical surgery inclusive of extended mediastinal lymph node dissection (median value 16.5 excised lymph nodes) to ensure a very accurate pathological staging.

Patients' ages ranged from 40 to 83 years for males (mean±SD 66±10; median 65) and from 51 to 82 years for females (mean±SD 69±10; median 71). According to the current World Health Organization (WHO) classification of lung tumors [61], there were 21 (62%) adenocarcinomas and 13 (38%) squamous-cell carcinomas. Tumor size ranged from 1.3 to 6 cm (mean±SD 3.4±1.3; median 3.2) in the former, and from 1.6 to 9 cm (mean±SD 4.5±2.5; median 3.4) in the latter. Among adenocarcinoma patients, four had *p*-stage IA, eight had *p*-stage IB, three had *p*-stage IIB, five had *p*-stage IIIA, and one had *p*-stage IIIB; among squamous-cell carcinoma patients, two had *p*-stage IA, four had *p*-stage IB, four had *p*-stage IIB, and three had *p*-stage IIIA (*p*=NS). Five (15%) carcinomas were well differentiated (four adenocarcinomas and one squamous-cell carcinoma), 16 (47%) were moderately differentiated (ten adenocarcinomas and six squamous-cell carcinomas), and 13 (38%) were poorly differentiated (seven adenocarcinomas and six squamous-cell carcinomas). All patients were smokers, and detailed smoking habit information was available for most of them.

Plasma samples of ten healthy health care, nonsmoker workers who volunteered to participate in the study were used as negative control. All patients and volunteers gave informed consent to be enrolled into the study that had been approved by the Institutional Review Board (IRB). Proliferative activity of primary tumors was assessed by Ki-67 immunostaining as previously reported [49]. Vascular invasion was considered as being absent or present, whereas tumor necrosis and lymphocytic infiltration were assessed as described elsewhere [57].

Plasma and tumor sample collection

Peripheral venous blood samples were collected from cancer patients before surgery and from healthy volunteers in two EDTA-treated, 7.5-ml blood collection tubes, processed within 30 min to avoid RNA degradation, by double centrifugation at 3,000×*g* for 10 min and then at 4,000×*g* for 20 min, at 4°C, to eliminate blood cell and fragments. One-milliliter plasma aliquots were then stored at −140°C and thawed only once before use. Tumor tissue and paired normal lung parenchyma specimens were immediately removed at the time of surgery and were partly snap-frozen in liquid nitrogen for RNA extraction or fixed in formalin and embedded in paraffin for routine histopathologic examination.

Ribonucleic acid extraction and reverse transcriptase–polymerase chain reaction

Plasma Two-phase experiments tested the effectiveness of different extraction procedures on the yield of detectable circulating mRNA in the plasma of NSCLC patients. First, five plasma samples of NSCLC patients were assayed for the presence of β-actin mRNA by using five commercially available extraction kits according to manufactures' instructions [QIAamp Viral RNA Mini Kit (Qiagen, Milan, Italy), RNeasy Mini Kit (Qiagen), RNeasy Micro Kit (Qiagen), a standard method based on Trizol LS Reagent (Invitrogen Corporation, Leek, The Netherlands), and a combination of Trizol LS Reagent with RNeasy Mini or Micro Kit]. As Trizol was the most flexible method and the most commonly used for RNA extraction from both tissues and body fluids [4, 65, 71, 72], we optimized the experimental procedure by testing different starting volumes of plasma (Fig. 1).

On the basis of these preliminary findings, in the second phase, the Trizol LS Reagent based method was used for the extraction of plasma mRNA in the whole series of 34 patients and ten controls with 3 ml of starting volume, which resulted in the highest yield of recovery. Briefly, 7.5 ml of Trizol LS Reagent was added to 3 ml of plasma in 15-ml tubes that were shaken for 15 min at room temperature, and then 2.4 ml of chloroform was added. Each sample was then incubated for 5 min at room temperature and centrifuged at 12,000×*g* for 15 min at 4°C to achieve separation into three phases. The upper aqueous phase containing RNA was transferred into new tubes and incubated with an equal volume of isopropyl alcohol and glycogen at −30°C for 2 h to ensure RNA precipitation. The mixture was centrifuged at 12,000×*g* for 10 min at 4°C, the supernatant was removed, and the pellet was washed by centrifugation (7,500×*g* for 5 min at 4°C) in cold 70% ethanol, allowed to dry for 5 min at room temperature, dissolved in 20 μl of RNase-free water, and stored at −140°C until use. DNase digestion and total RNA spectrophotometric quantitation were avoided to prevent RNA degradation or loss, and the specificity of the assay was ensured by the use of intron-spanning primers

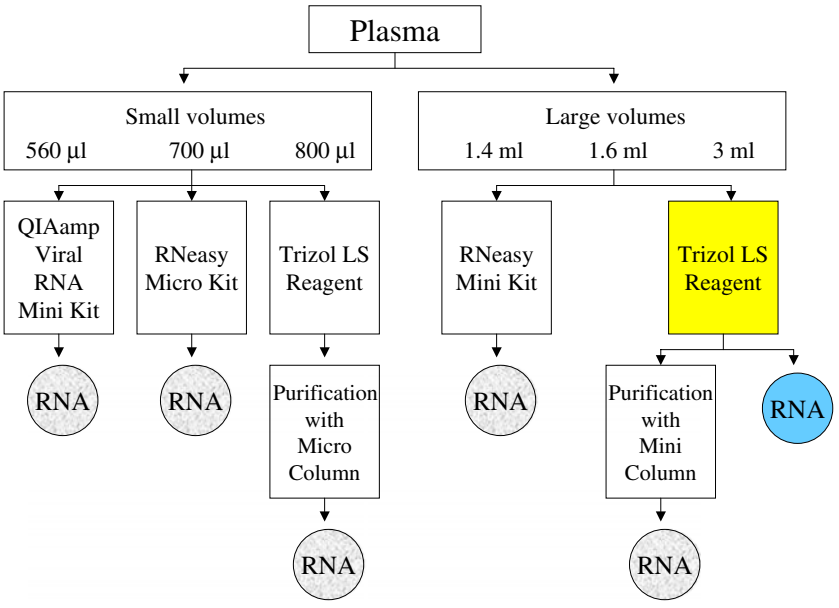

Fig. 1 Flowchart of the different extraction methods used in the study; the Trizol LS Reagent with 3 ml of plasma was then optimized for both patients and healthy controls

(see below). For RT-PCR analysis, 19 µl of the RNA solution was used.

Tissue Twenty 10-µm-thick frozen sections were cut from each tissue sample, either tumoral (containing at least 80% of neoplastic cells) or normal, added to 1 ml of Trizol Reagent, and processed according to manufacturer's instructions. The yield of extracted RNA was measured spectrophotometrically, and 3 µl of a solution containing 300 ng/µl RNA was used for RT-PCR analysis.

Reverse transcriptase–polymerase chain reaction Reverse transcription using Moloney Murine Leukemia Virus Reverse Transcriptase (M-MLV Reverse Transcriptase, Invitrogen) for tissue samples and GeneAmp RNA PCR Kit (Applied Biosystem, Foster City, CA) for plasma samples were used to generate cDNA for β-actin and hTERT analysis according to the manufacturers' instructions. RT conditions included a 10-min primer incubation step at 25°C, followed by a 42°C extension for 30 min, and a 99°C denaturation for 5 min (in case of tissue, the extension temperature was 37°C for 60 min).

β-actin and hTERT mRNA amplification was achieved using 2 µl of cDNA and AmpliTaq DNA polymerase (Applied Biosystem) for both plasma and tissue samples and specific intron-spanning primers (Table 2). In particular, pseudogene-free primers [30] were applied for β-actin mRNA amplification (annealing temperature 60°C, amplification product 172 bp) to minimize DNA contamination, and primers for an exon 3- to 4-spanning hTERT sequence [39] were chosen (annealing temperature 61°C, amplification product 145 bp). This sequence encodes for telomerase-specific T and 1 domains essential for the enzymatic function [68] that are not affected by alternative splicing in human cancers [14, 24, 41]. PCR conditions were an initial denaturation step at 94°C for 5 min, followed by 20 (plasma samples) or 35 (tissue samples) cycles of 94 (for 30 s), 60 (for 30 s), and 72°C (for 30 s), with a final elongation step at 72°C for 7 min (in case of hTERT, the melting temperature was 61°C for 40 s). The specificity of PCR reactions for both plasma and tissue analysis was checked by positive (A549 nonsmall cell lung cancer cell line) and negative (omitting cDNA and enzyme) controls.

Real-time polymerase chain reaction assay

Real-time PCR assay of plasma samples was performed for both β-actin and hTERT mRNAs in a final reaction volume of 20 µl using the TaqMan Universal PCR Master Mix (Applied Biosystem) containing 1 µl of preamplified cDNA according to the standard protocol of the ABI Prism 7700 Sequence Detector (Applied Biosystem). hTERT amplifi-

Table 2 PCR primers and fluorescently labeled probes

Primer/probe	Nucleotide sequence
RT-PCR	
β-actin F	5′-AGCCTCGCCTTTGCCGA-3′
β-actin R	5′-CTGGTGCCTGGGGCG-3′
h-TERT F Ext	5′-CGGAAGAGTGTCTGGAGCAA-3′
h-TERT R Ext	5′-GGATGAAGCGGAGTCTGGA-3′
Real-time PCR	
β-actin F	5′-AGCCTCGCCTTTGCCGA-3′
β-actin R	5′-CTGGTGCCTGGGGCG-3′
β-actin P	5′-CCGCCGCCCGTCCACACCCGCC-3′
h-TERT F Int	5′-GGAAGAGTGTCTGGAGCAAGTTG-3′
h-TERT R Int	5′-AGCTGCACCCTCTTCAAGTG-3′
h-TERT P	5′-AAAGCATTGGAATCAGACAG-3′

Internal primers and probe for hTERT real-time PCR were customer-designed and optimized by Applied Biosystem, Foster City, CA

F forward, *R* reverse, *Ext* external primers used for amplifying the hTERT gene in the first PCR reaction, *P* probe, *Int* internal primers used for real-time PCR

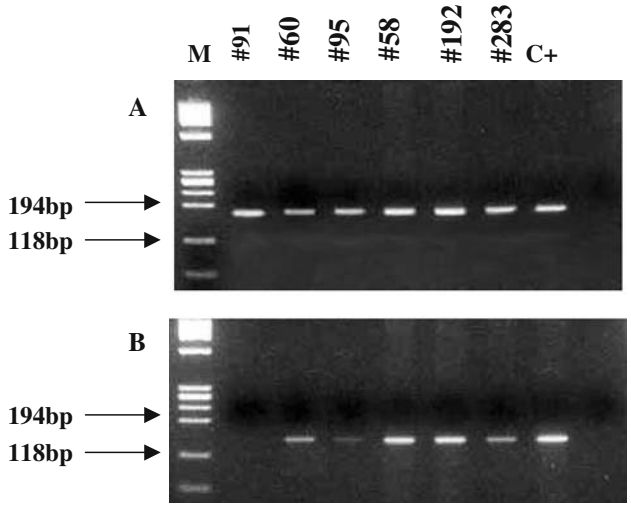

Fig. 2 Expression of hTERT mRNA in tissue samples of nonsmall cell lung cancer examined by RT-PCR for β-actin (**a**) and hTERT (**b**). *Lane 1*, marker (*M*) showing the positions for 118 and 194 bp. *Lanes 2–7*, tumor samples, including three adenocarcinoma (*#91*, *#60*, and *#95*) and three squamous-cell carcinoma (*#58*, *#192*, and *#283*) patients as detailed in Table 1. *Lane 8*, positive control (*C+*) consisting of A549 nonsmall cell lung cancer cell line

cation by nested PCR was performed using a mixture of customer-designed internal primers and probe specifically optimized, both purchased from Applied Biosystem, whereas primers for β-actin had been previously validated for quantitative assay [30]. Real-time PCR assay conditions were an initial denaturation step at 95°C for 10 min to activate the TaqMan followed by 40 cycles at 95 (for 15 s) and 60°C (for 1 min), and a final elongation step at 60°C for 1 min. Standard curves for both β-actin and hTERT mRNA quantification were prepared by amplifying serial dilutions of mRNA extracted from the A549 nonsmall cell lung cancer cell line from 625 to 19.5 pg/μl. The relative "input amount" values of each sample for the relevant transcripts were calculated plotting each Ct value on the corresponding standard curve. Each run of amplification included RNA of the same nonsmall cell lung cancer cell line used as a positive control and a negative control without cDNA. Duplicate tests were performed, and the mean value was calculated for each sample.

Statistics

Qualitative data were presented as frequencies and/or percentages and compared using the chi-square or Fisher exact test. All analyses were carried out using the SAS statistical software (SAS Institute, Inc., Cary, NC). All p values (significant if ≤0.05) were based on two-sided testing.

Results

Exon 3–4 hTERT mRNA was detected in 33 of 34 (97%) NSCLC samples, whereas normal lung tissue was completely devoid of any transcript. β-actin mRNA was found in 34 of 34 (100%) primary tumors and in all paired normal lung parenchyma samples (Fig. 2).

Exon 3–4 hTERT mRNA was detected in the plasma of 4 out of 33 (12%) hTERT-positive tumor patients, with normalized hTERT threshold ratios being 12.62 (case 60),

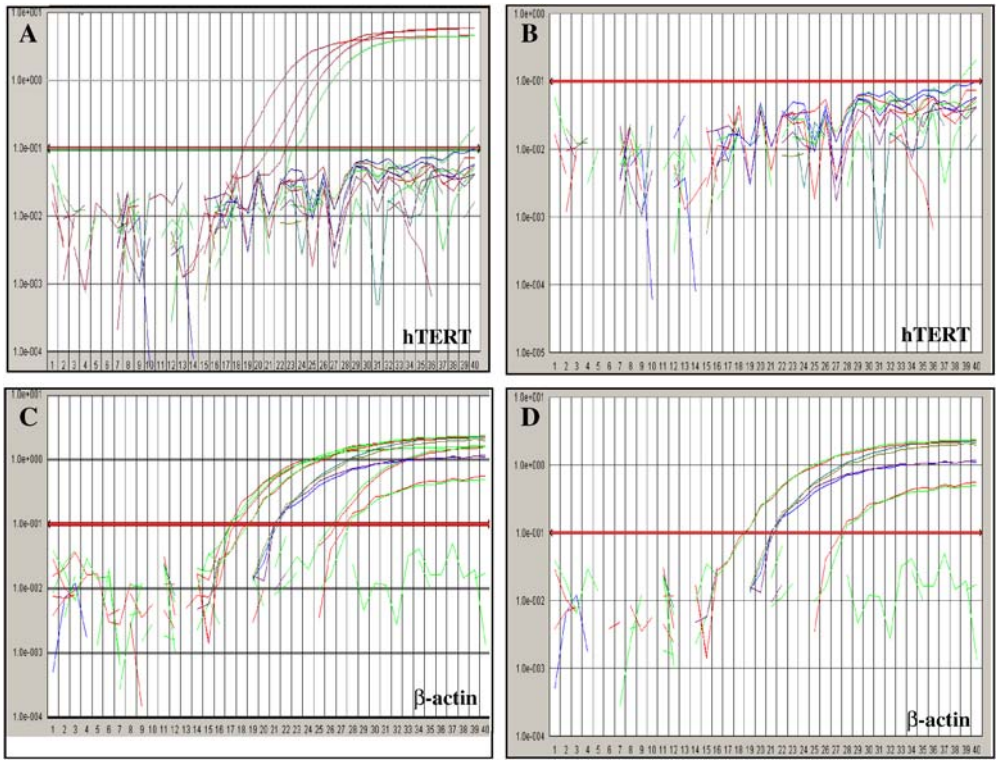

Fig. 3 Amplification plots of the real-time quantitative polymerase chain reaction for hTERT (**a**, **b**) and β-actin (**c**, **d**) in plasma mRNA from nonsmall cell lung cancer patients (**a**, **c**) and healthy volunteers (**b**, **d**). Plasma hTERT mRNA is detectable in a subset of patients only (**a**), but plasma hTERT mRNA is not detectable in the ten healthy volunteers (**b**), whereas plasma β-actin plasma mRNA is shared by both patients (**c**) and normal controls (**d**)

11.03 (case 95), 1.76 (case 58), and 6.92 (case 192), respectively. None of the ten plasma samples of nonsmoker healthy volunteers, as well as the single patient whose tumor was devoid of hTERT mRNA (Table 1, case 91), presented any detectable hTERT mRNA level in the plasma (Fig. 3a,b).

On the contrary, 23 of 34 (68%) NSCLC samples showed detectable levels of cell-free circulating β-actin mRNA, as did 6 of 10 (60%) nonsmoker healthy volunteers (Fig. 3c,d).

No significant relationship was found between the occurrence of hTERT mRNA in the plasma and clinicopathologic variables of the patients. In particular, the four patients (three males and one female) with detectable hTERT mRNA in the plasma harbored two adenocarcinomas (cases 60 and 95) and two squamous-cell carcinomas (cases 58 and 192), the ages ranged from 63 to 77 years, tumor size ranged from 3 to 4 cm, tumor grade ranged from G1 to G2, and tumor stage ranged from IB to IIB. Moreover, no relationship was found with the extent of tumor necrosis, the occurrence of vascular invasion, the lymphocytic infiltration, and the proliferative fraction.

Likewise, no significant correlation was found between the presence of β-actin mRNA in the plasma and any clinicopathologic variable of the NSCLC patients' population under evaluation.

Discussion

The main results of the current study are (a) cell-free circulating hTERT mRNA is detectable in a minority of NSCLC patients, but it is likely to be tumor-related because it is undetectable in healthy subjects and in patients with hTERT-negative tumors; (b) most patients and healthy individuals share cell-free circulating plasma mRNA of β-actin; and (c) plasma hTERT mRNA does not undergo complete degradation, and it remains detectable (although at very low levels).

A growing body of evidence supports that many different types of cell-free circulating mRNAs (housekeeping genes such as β-actin, 18S, β-GUS, or glyceraldehydephosphate dehydrogenase (GAPDH) [3, 9, 10, 35, 44, 45, 56, 72], various types of cytokeratins [10, 12, 55, 56], Her-2 [12], heterogeneous nuclear ribonucleicprotein (hnRNP) [12], thyroglobulin [34], tyrosinase [20, 29, 45], 5T4 [28], mammaglobin [15, 55], carcinoembryonic antigen (CEA) [56], protein gene product (PGP) 9.5 [12], prostate-specific membrane antigen [5], Epstein–Barr virus [36], and β-catenin [72]) may be detected in patients with a variety of malignancies, including breast [3, 15, 28, 45, 55], colon–rectum [9, 35, 56, 72], liver [39, 44], nasopharynx [36], esophagus [10], thyroid [34, 45], prostate [5] and lung [12, 28] carcinoma, malignant melanoma [10, 20, 29, 45], and follicular lymphoma [9]. Although hTERT mRNA has been already considered as a potential marker for malignant melanoma [45], follicular lymphoma [9], and breast [3, 45], colon–rectum [9, 35] and liver [38, 39] carcinoma, to the best of our knowledge, this is the first investigation on its detectability in the plasma of NSCLC patients. Highly sensitive real-time PCR assays have previously been used to identify hTERT mRNA in lymphoma, colorectal cancer, and hepatocellular carcinoma patients [9, 35, 38], β-catenin mRNA in colorectal cancer and adenoma patients [72], cytokeratins 19 and 20 mRNAs in esophageal carcinoma [10], thyroglobulin mRNA in thyroid carcinoma [34], prostate-specific membrane antigen mRNA in prostate carcinoma [5], and glyceraldehyde-3-phosphate dehydrogenase (GADPH) mRNA in hepatocellular carcinoma [44]. In NSCLC patients, however, this assay has not been used thus far.

We document that plasma β-actin plasma mRNA may be detected in most (67%) patients and healthy nonsmoker individuals (60%) in keeping with previous data reporting the detection of other plasma mRNAs such as GAPDH or 18S in both patients and controls [10, 44, 45]. Cell-free hTERT plasma mRNA was detectable in only 12% of NSCLC patients, at variance with a much higher prevalence (59%) in patients with malignant melanoma [45], follicular lymphoma (100%) [9], and breast (25–48%) [3, 45], thyroid (100%) [45], liver (90%) [38, 39], and colon–rectum carcinoma (82%) [35]. El-Hefnawy et al. [10], however, failed to reproducibly detect several types of cancer-related plasma mRNAs in patients with advanced malignant melanoma or esophageal carcinoma. The detection rate of hTERT mRNA in the plasma might depend on the tumor type, the methods used, or the levels of telomerase activity in tumor cells. In fact, a lower capacity of NSCLC cells to shed mRNA into the bloodstream or a selective degradation of hTERT mRNA to avoid telomerase reactivation by horizontal transfer to permissive cells—as suggested for DNA-containing apoptotic bodies [16, 26]—might be potential mechanisms accounting for these discrepancies. Assessing telomerase activity by Telomerase Repeat Amplification Protocol (TRAP) assay by means of the "*Telo*TAGGGG-Telomerase PCR Elisa^{PLUS} kit" (Roche Diagnostic, Mannheim, Germany) according to manufacturer's instructions, we found that only two (60 and 58) of the four patients with cell-free circulating hTERT mRNA were TRAP-positive, without any correlation between enzymatic activity in primary tumors and the corresponding normalized hTERT threshold ratio for circulating mRNA (data not shown). Moreover, there is no relationship between plasma levels of hTERT mRNA and tumor characteristics such as stage, grade, size, intratumoral necrosis, lympho-vascular invasion, lymphocytic infiltration, and proliferative faction in a similar manner as for cell-free circulating DNA [57] in the same type of tumor.

RNA protection in the blood may be provided by inclusion into lipoproteic complexes or phospholipids [10, 44, 63], either actively secreted by tumor cells in vivo, as the shedding of viral particles [53, 69], or released during programmed cell death possibly as apoptotic bodies [10, 17, 21]. The disappearance of mRNA in positive plasma samples after passing them through 0.2 μm-, but not 0.4-μm, filters (data not shown) supports that circulating RNA is likely to be particle-associated and partially protected in NSCLC as in other tumor types [10, 44].

Use of plasma instead of serum samples helps to avoid nucleic acid contamination by leukocytes [33] or platelets [10] during clotting. Moreover, to obtain reproducible results, we assayed 3 ml of plasma and set up a 20-cycle preamplification as previously advised by others [10] because either single-round RT-PCR or real-time PCR alone did not allow a consistent detection of plasma hTERT mRNA. Another critical point of PCR assay for circulating mRNA is the proper design of primers spanning exon junctions [10, 30] to improve specificity also in the phase of RT-PCR-based preamplification in keeping with others [10]. Conversely, other authors have chosen intraexon primers for plasma hTERT detection and added a DNase I treatment to assure specificity [9, 35]. This, however, does not eliminate completely the risk of cDNA amplification when considering the very high sensitivity of real-time PCR. Moreover, in keeping with other studies [3, 10], the spectrophotometric measurement of RNA was not feasible in our tumor series due to the low yield of extracted nucleic acids, raising some concerns on the findings obtained in other tumoral settings [9, 35].

We expressed our quantitative results of plasma hTERT mRNA by means of the normalized ratio between the input amount value of hTERT and that of β-actin within each case, although our final result could be in part affected by the inherent efficiency of the RT-PCR-based preamplification protocols (practically, lower than 100%). The numerical thresholds obtained in the four patients positive for plasma hTERT mRNA, however, documented the excess of this mRNA in tumor samples in comparison with a population of healthy volunteers.

Our results show that tumor-related hTERT mRNA can be detected in a subset of NSCLC patients, and it may be added to the panel of genetic plasma markers for lung cancer detection [1, 57–59], although it should be pointed out that this is only a tumor-related marker and not specific for lung cancer. Further studies addressing the entire profile of plasmatic mRNA molecules and case-control studies, including the analysis of high-risk heavy smokers, are clearly warranted to evaluate the potential of assaying cell-free circulating mRNA for early diagnosis or follow-up.

References

1. Andriani G, Conte D, Mastrrangelo T, Leon ME, Ratcliffe C, Roz L, Pelosi G, Goldstraw P, Sozzi G, Pastorino U (2004) Detecting lung cancer in plasma with the use of multiple genetic markers. Int J Cancer 108:91–96
2. Bruhn N, Beinert T, Oehm C, Jandrig B, Petersen I, Chen XQ, Possinger K, Fleischhacker M (2000) Detection of microsatellite alterations in the DNA isolated from tumor cells and from plasma DNA of patients with lung cancer. Ann N Y Acad Sci 906:72–82
3. Chen XQ, Bonnefoi H, Pelte MF, Lyautey J, Lederrey C, Movarekhi S, Schaeffer P, Mulcahy HE, Meyer P, Stroun M, Anker P (2000) Telomerase RNA as a detection marker in the serum of breast cancer patients. Clin Cancer Res 6:3823–3826
4. Chomczynski P, Sacchi N (1987) Single-step method of RNA isolation by acid guanidinium thiocyanate–phenol–chloroform extraction. Anal Biochem 162:156–159
5. Chu DC, Chuang CK, Liou YF, Tzou RD, Lee HC, Sun CF (2004) The use of real-time quantitative PCR to detect circulating prostate-specific membrane antigen mRNA in patients with prostate carcinoma. Ann N Y Acad Sci 1022:157–162
6. Counter CM, Avilion AA, Le Feuvre CE, Stewart NG, Greider CW, Harley CB, Bachetti S (1992) Telomere shortening associated with chromosome instability is arrested in immortal cells which express telomerase activity. EMBO J 11:1921–1929
7. Coursen JD, Bennett WP, Gollahon L, Shay JW, Harris CC (1997) Genomic instability and telomerase activity in human bronchial epithelial cells during immortalization by human papillomavirus-16 E6 and E7 genes. Exp Cell Res 235:245–253
8. D'Amico TA, Massey M, Herndon JE Jr, Moore MB, Harpole DH Jr (1999) A biologic risk model for stage I lung cancer: immunohistochemical analysis of 408 patients with the use of ten molecular markers. J Thorac Cardiovasc Surg 117:736–743
9. Dasi F, Lledo S, Garcia-Granero E, Ripoll R, Marugan M, Tormo M, Garcia-Conde J, Alino SF (2001) Real-time quantification in plasma of human telomerase reverse transcriptase (hTERT) mRNA: a simple blood test to monitor disease in cancer patients. Lab Invest 81:767–769
10. El-Hefnawy T, Raja S, Kelly L, Bigbee WL, Kirkwood JM, Luketich JD, Godfrey TE (2004) Characterization of amplifiable, circulating RNA in plasma and its potential as a tool for cancer diagnostics. Clin Chem 50:564–573
11. Esteller M, Sanchez-Cespedes M, Rosell R, Sidransky D, Baylin SB, Herman JG (1999) Detection of aberrant promoter hypermethylation of tumor suppressor genes in serum DNA from non-small cell lung cancer patients. Cancer Res 59:67–70
12. Fleischhacker M, Beinert T, Ermitsch M, Seferi D, Possinger K, Engelmann C, Jandrig B (2001) Detection of amplifiable messenger RNA in the serum of patients with lung cancer. Ann N Y Acad Sci 945:179–188
13. Fu JB, Kau TY, Severson RK, Kalemkerian GP (2005) Lung cancer in women: analysis of the national surveillance, epidemiology, and end results database. Chest 127:768–777
14. Fujiwara M, Kamma H, Wu W, Hamasaki M, Kaneko S, Horiguchi H, Matsui-Horiguchi M, Satoh H (2004) Expression and alternative splicing pattern of human telomerase reverse transcriptase in human lung cancer cells. Int J Oncol 24:925–930
15. Gal S, Fidler C, Lo YM, Chin K, Moore J, Harris AL, Wainscoat JS (2001) Detection of mammaglobin mRNA in the plasma of breast cancer patients. Ann N Y Acad Sci 945:192–194
16. Garcia-Olmo D, Garcia-Olmo DC, Ontanon J, Martinez E (2000) Horizontal transfer of DNA and the "genometastasis hypothesis". Blood 95:724–725
17. Halicka HD, Bedner E, Darzynkiewicz Z (2000) Segregation of RNA and separate packaging of DNA and RNA in apoptotic bodies during apoptosis. Exp Cell Res 260:248–256
18. Hamaoui K, Butt A, Powrie J, Swaminathan R (2004) Concentration of circulating rhodopsin mRNA in diabetic retinopathy. Clin Chem 50:2152–2155
19. Hamaoui K, Butt A, Powrie J, Swaminathan R (2004) Real-time quantitative PCR measurement of circulatory rhodopsin mRNA in healthy subjects and patients with diabetic retinopathy. Ann N Y Acad Sci 1022:152–156
20. Hasselmann DO, Rappl G, Rossler M, Ugurel S, Tilgen W, Reinhold U (2001) Detection of tumor-associated circulating mRNA in serum, plasma and blood cells from patients with disseminated malignant melanoma. Oncol Rep 8:115–118
21. Hasselmann DO, Rappl G, Tilgen W, Reinhold U (2001) Extracellular tyrosinase mRNA within apoptotic bodies is protected from degradation in human serum. Clin Chem 47:1488–1489
22. Henschke CI, McCauley DI, Yankelevitz DF, Naidich DP, McGuinness G, Miettinen OS, Libby DM, Pasmantier MW, Koizumi J, Altorki NK, Smith JP (1999) Early Lung Cancer Action Project: overall design and findings from baseline screening. Lancet 354:99–105

23. Hirsch FR, Franklin WA, Gazdar AF, Bunn PA (2001) Early detection of lung cancer: clinical perspectives of recent advances in biology and radiology. Clin Cancer Res 7:5–22
24. Hisatomi H, Ohyashiki K, Ohyashiki JH, Nagao K, Kanamaru T, Hirata H, Hibi N, Tsukada Y (2003) Expression profile of a gamma-deletion variant of the human telomerase reverse transcriptase gene. Neoplasia 5:193–197
25. Hiyama K, Hiyama E, Ishioka S, Yamakido M, Inai K, Gazdar AF, Piatyszek MA, Shay JW (1995) Telomerase activity in small-cell and non-small-cell lung cancers. J Natl Cancer Inst 87:895–902
26. Holmgren L, Szeles A, Rajnavölgy E, Folkman J, Klein G, Emberg I, Falk KJ (1999) Horizontal transfer of DNA by the uptake of apoptotic bodies. Blood 93:3956–3963
27. Holt SE, Shay JW (1999) Role of telomerase in cellular proliferation and cancer. J Cell Physiol 180:10–18
28. Kopreski MS, Benko FA, Gocke CD (2001) Circulating RNA as a tumor marker: detection of 5T4 mRNA in breast and lung cancer patient serum. Ann N Y Acad Sci 945:172–178
29. Kopreski MS, Benko FA, Kwak LW, Gocke CD (1999) Detection of tumor messenger RNA in the serum of patients with malignant melanoma. Clin Cancer Res 5:1961–1965
30. Kreuzer KA, Lass U, Landt O, Nitsche A, Laser J, Ellerbrok H, Pauli G, Huhn D, Schmidt CA (1999) Highly sensitive and specific fluorescence reverse transcription–PCR assay for the pseudogene-free detection of beta-actin transcripts as quantitative reference. Clin Chem 45:297–300
31. Lantuejoul S, Soria JC, Morat L, Lorimier P, Moro-Sibilot D, Sabatier L, Brambilla C, Brambilla E (2005) Telomere shortening and telomerase reverse transcriptase expression in preinvasive bronchial lesions. Clin Cancer Res 11:2074–2082
32. Lantuejoul S, Soria JC, Moro-Sibilot D, Morat L, Veyrenc S, Lorimier P, Brichon PY, Sabatier L, Brambilla C, Brambilla E (2004) Differential expression of telomerase reverse transcriptase (hTERT) in lung tumours. Br J Cancer 90:1222–1229
33. Lee TH, Montalvo L, Chrebtow V, Busch MP (2001) Quantitation of genomic DNA in plasma and serum samples: higher concentrations of genomic DNA found in serum than in plasma. Transfusion 41:276–282
34. Li D, Butt A, Clarke S, Swaminathana R (2004) Real-time quantitative PCR measurement of thyroglobulin mRNA in peripheral blood of thyroid cancer patients and healthy subjects. Ann N Y Acad Sci 1022:147–151
35. Lledo SM, Garcia-Granero E, Dasi F, Ripoli R, Garcia SA, Cervantes A, Alino SF (2004) Real time quantification in plasma of human telomerase reverse transcriptase (hTERT) mRNA in patients with colorectal cancer. Colorectal Dis 6:236–242
36. Lo KW, Lo YM, Leung SF, Tsang YS, Chan LY, Johnson PJ, Hjelm NM, Lee JC, Huang DP (1999) Analysis of cell-free Epstein–Barr virus associated RNA in the plasma of patients with nasopharyngeal carcinoma. Clin Chem 45:1292–1294
37. Miozzo M, Sozzi G, Musso K, Pilotti S, Incarbone M, Pastorino U, Pierotti MA (1996) Microsatellite alterations in bronchial and sputum specimens of lung cancer patients. Cancer Res 56:2258–2285
38. Miura N, Maeda Y, Kanbe T, Yazama H, Takeda Y, Sato R, Tsukamoto T, Sato E, Marumoto A, Harada T, Sano A, Kishimoto Y, Hirooka Y, Murawaki Y, Hasegawa J, Shiota G (2005) Serum human telomerase reverse transcriptase messenger RNA as a novel tumor marker for hepatocellular carcinoma. Clin Cancer Res 11:3205–3209
39. Miura N, Shiota G, Nakagawa T, Maeda Y, Sano A, Marumoto A, Kishimoto Y, Murawaki Y, Hasegawa J (2003) Sensitive detection of human telomerase reverse transcriptase mRNA in the serum of patients with hepatocellular carcinoma. Oncology 64:430–434
40. Mountain CF (2000) The international system for staging lung cancer. Semin Surg Oncol 18:106–115
41. Nagao K, Katsumata K, Aizawa Y, Saito N, Hirata H, Sasaki H, Yamamoto S, Hikiji K, Koiwa T, Hisatomi H (2004) Differential alternative splicing expressions of telomerase reverse transcriptase in gastrointestinal cell lines. Oncol Rep 11:127–131
42. Ng EK, Leung TN, Tsui NB, Lau TK, Panesar NS, Chiu RW, Lo YM (2003) The concentration of circulating corticotropin-releasing hormone mRNA in maternal plasma is increased in preeclampsia. Clin Chem 49:727–731
43. Ng EK, Tsui NB, Lau TK, Leung TN, Chiu RW, Panesar NS, Lit LC, Chan KW, Lo YM (2003) mRNA of placental origin is readily detectable in maternal plasma. Proc Natl Acad Sci USA 100:4748–4753
44. Ng EK, Tsui NBY, Lam NYL, Chiu RWK, Yu SCH, Wong SCC, Lo ESF, Rainer TH, Johnson PJ, Lo DYM (2002) Presence of filterable and nonfilterable mRNA in the plasma of cancer patients and healthy individuals. Clin Chem 48:1212–1217
45. Novakovic S, Hocevar M, Zgajnar J, Besic N, Stegel V (2004) Detection of telomerase RNA in the plasma of patients with breast cancer, malignant melanoma or thyroid cancer. Oncol Rep 11:245–252
46. Ohmura Y, Aoe M, Andou A, Shimizu N (2000) Telomerase activity and Bcl-2 expression in non-small cell lung cancer. Clin Cancer Res 6:2980–2987
47. Pasini F, Pelosi G, Valduga F, Durante E, de Manzoni G, Zaninelli M, Terzi A (2002) Late events and clinical prognostic factors in stage I non small cell lung cancer. Lung Cancer 171–177
48. Pastorino U, Bellomi M, Landoni C, De Fiori E, Arnaldi P, Picchio M, Pelosi G, Boyle P, Fazio F (2003) Early lung-cancer detection with spiral CT and positron emission tomography in heavy smokers: 2-year results. Lancet 362:593–597
49. Pelosi G, Fraggetta F, Pasini F, Maisonneuve P, Sonzogni A, Iannucci A, Terzi A, Bresaola E, Valduga F, Lupo C, Viale G (2001) Immunoreactivity for thyroid transcription factor-1 in stage I non-small cell lung carcinomas of the lung. Am J Surg Pathol 25:363–372
50. Poon LLM, Leung TN, Lau TK, Lo YMD (2000) Presence of fetal RNA in maternal plasma. Clin Chem 46:1832–1834
51. Rainer TH, Lam NY, Tsui NB, Ng EK, Chiu RW, Joynt GM, Lo YM (2004) Effects of filtration on glyceraldehyde-3-phosphate dehydrogenase mRNA in the plasma of trauma patients and healthy individuals. Clin Chem 50:206–208
52. Reddi KK, Holland JF (1976) Elevated serum ribonuclease in patients with pancreatic cancer. Proc Natl Acad Sci USA 73:2308–2310
53. Rosi A, Guidoni L, Luciani AM, Mariutti G, Viti V (1988) RNA-lipid complexes released from the plasma membrane of human colon carcinoma cells. Cancer Lett 39:153–160
54. Rykova EY, Skvortsova TE, Laktionov PP, Tamkovich SN, Bryzgunova OE, Starikov AV, Kuznetsova NP, Kolomiets SA, Sevostianova NV, Vlassov VV (2004) Investigation of tumor-derived extracellular DNA in blood of cancer patients by methylation-specific PCR. Nucleosides Nucleotides Nucleic Acids 23:855–859
55. Silva JM, Dominguez G, Silva J, Garcia JM, Sanchez A, Rodriguez O, Provencio M, Espana P, Bonilla F (2001) Detection of epithelial messenger RNA in the plasma of breast cancer patients is associated with poor prognosis tumor characteristics. Clin Cancer Res 7:2821–2825
56. Silva JM, Rodriguez R, Garcia JM, Munoz C, Silva J, Dominguez G, Provencio M, Espana P, Bonilla F (2002) Detection of epithelial tumour RNA in the plasma of colon cancer patients is associated with advanced stages and circulating tumour cells. Gut 50:530–534
57. Sozzi G, Conte D, Leon M, Ciricione R, Roz L, Ratcliffe C, Roz E, Cirenei N, Bellomi M, Pelosi G, Pierotti MA, Pastorino U (2003) Quantification of free circulating DNA as a diagnostic marker in lung cancer. J Clin Oncol 21:3902–3908

58. Sozzi G, Conte D, Mariani L, Lo Vullo S, Roz L, Lombardo C, Pierotti MA, Tavecchio L (2001) Analysis of circulating tumor DNA in plasma at diagnosis and during follow-up of lung cancer patients. Cancer Res 61:4675–4678
59. Sozzi G, Musso K, Ratcliffe C, Goldstraw P, Pierotti MA, Pastorino U (1999) Detection of microsatellite alterations in plasma DNA of non-small cell lung cancer patients: a prospect for early diagnosis. Clin Cancer Res 5:2689–2692
60. Stewart BW, Kleihues P (2003) World cancer report. IARC, Lyon
61. Travis WD, Brambilla E, Muller-Hermelink HK, Harris CC (2004) Tumours of the lung, pleura, thymus and heart. IARC, Lyon
62. Tsui NB, Chim SS, Chiu RW, Lau TK, Ng EK, Leung TN, Tong YK, Chan KC, Lo YM (2004) Systematic micro-array based identification of placental mRNA in maternal plasma: towards non-invasive prenatal gene expression profiling. J Med Genet 41:461–467
63. Tsui NBY, Ng EKO, Lo DYM (2002) Stability of endogenous and added RNA in blood specimens, serum, and plasma. Clin Chem 48:1647–1653
64. Vaziri H, Benchimol S (1999) Alternative pathways for the extension of cellular life span: inactivation of p53/pRb and expression of telomerase. Oncogene 18:7676–7680
65. Verhofstede C, Fransen K, Marissens D, Verhelst R, van der Groen G, Lauwers S, Zissis G, Plum J (1996) Isolation of HIV-1 RNA from plasma: evaluation of eight different extraction methods. J Virol Methods 60:155–159
66. Wataganara T, LeShane ES, Chen AY, Borgatta L, Peter I, Johnson KL, Bianchi DW (2004) Plasma gamma-globin gene expression suggests that fetal hematopoietic cells contribute to the pool of circulating cell-free fetal nucleic acids during pregnancy. Clin Chem 50:689–693
67. Wataganara T, Leshane ES, Chen AY, Sullivan LM, Peter I, Borgatta L, Johnson KL, Bianchi DW (2004) Circulating cell-free fetal nucleic acid analysis may be a novel marker of fetomaternal hemorrhage after elective first-trimester termination of pregnancy. Ann N Y Acad Sci 1022:129–134
68. Wick M, Zubov D, Hagen G (1999) Genomic organization and promoter characterization of the gene encoding the human telomerase reverse transcriptase (hTERT). Gene 232:97–106
69. Wieczorek AJ, Rhyner C, Block LH (1985) Isolation and characterization of an RNA-proteolipid complex associated with the malignant state in humans. Proc Natl Acad Sci USA 82:3455–3459
70. Wong BCK, Lo DYM (2003) Cell-free DNA and RNA in plasma as new tools for molecular diagnostics. Expert Rev Mol Diagn 3:785–797
71. Wong SC, Lo ES, Cheung MT (2004) An optimised protocol for the extraction of non-viral mRNA from human plasma frozen for three years. J Clin Pathol 57:766–768
72. Wong SC, Lo SF, Cheung MT, Ng KO, Tse CW, Lai BS, Lee KC, Lo YM (2004) Quantification of plasma beta-catenin mRNA in colorectal cancer and adenoma patients. Clin Cancer Res 10:1613–1617

Virchows Arch (2006) 448: 16–23
DOI 10.1007/s00428-005-0086-0

ORIGINAL ARTICLE

K. J. Schmitz · F. Grabellus · R. Callies · J. Wohlschlaeger · F. Otterbach · R. Kimmig · B. Levkau · K. W. Schmid · H. A. Baba

Relationship and prognostic significance of phospho-(serine 166)-murine double minute 2 and Akt activation in node-negative breast cancer with regard to p53 expression

Received: 10 May 2005 / Accepted: 1 September 2005 / Published online: 6 October 2005

Abstract The Akt signalling pathway plays a central role in tumourigenesis. Activation of Akt is related to a more aggressive phenotype in various human cancers, including breast cancer. Its activation contributes to cancer progression via pleiotropic effects, including suppression of apoptosis and modulation of cell cycle regulation. Murine double minute 2 (MDM2) is an oncoprotein that inhibits the function of p53 tumour suppressor protein. Cell culture studies show that Akt-related phosphorylation of MDM2 at serine 166 allows MDM2 to gain nuclear entry and fulfil its p53 regulating function. This study was designed to analyse the relationship of phospho-MDM2 (pMDM2) expression with Akt activation to determine a possible prognostic relevance of pMDM2 in node-negative breast cancer with respect to Akt activation and p53 status. pMDM2, phospho-Akt (pAkt) and p53 protein expression status were analysed immunohistochemically in 121 paraffin-embedded breast cancer cases. Expression of pMDM2 correlated with Akt activation ($P<0.001$). Univariate analysis identified pMDM2 as a prognostic factor ($P=0.0458$) in node-negative breast cancers. The unfavourable prognostic significance was even more pronounced in tumours with a $pMDM2^{+}/pAkt^{+}$ immunophenotype ($P=0.0205$). Stratification into a p53-negative subgroup further strengthened the adverse prognostic influence. These data confirm that MDM2 phosphorylation at serine 166 is mediated by Akt kinase. Besides the prognostic impact of pMDM2, our findings suggest that Akt-mediated modulation of the MDM2/p53 complex contributes to increased tumour aggressiveness especially in p53-negative breast cancers. However, due to the relatively small number of patients in this cohort, the results obtained need to be confirmed by larger cohorts.

Keywords Cancer · Mammary gland · Mol Oncol

K. J. Schmitz · F. Grabellus · J. Wohlschlaeger · F. Otterbach · K. W. Schmid · H. A. Baba (✉)
Institute of Pathology, Hufelandstr. 55,
45122 Essen, Germany
e-mail: hideo.baba@medizin.uni-essen.de
Tel.: +49-201-7233577
Fax: +49-201-7233378

K. J. Schmitz · F. Grabellus · R. Callies · J. Wohlschlaeger · F. Otterbach · R. Kimmig · K. W. Schmid · H. A. Baba
University Breast Cancer Centre Essen (UBZE),
Essen, Germany

R. Callies · R. Kimmig
Department of Obstetrics and Gynaecology,
University of Essen-Duisburg,
Essen, Germany

F. Otterbach · R. Kimmig · K. W. Schmid
West German Cancer Centre (WTZE),
Essen, Germany

B. Levkau
Institute of Pathophysiology, University of Essen-Duisburg,
Essen, Germany

Introduction

The murine double minute 2 (*MDM2*) gene was originally identified in a transformed tumourigenic 3T3 fibroblast cell line [3]. *MDM2* gene amplification and overexpression of its product have been described in several types of malignancies in humans [5, 16, 18]. P53 and MDM2 participate in a complex autoregulatory feedback loop, in which p53 stimulates *MDM2* expression, and MDM2 protein inhibits the activity of p53 by blocking p53 transcription [20]. Moreover, recent data show that the MDM2 oncoprotein forms a tight complex with wild-type p53 tumour suppressor gene protein, thereby conferring both its degradation and inactivation [11, 14]. Due to its inhibitory effect on p53, MDM2 protein overexpression was shown to be associated with uncontrolled cell proliferation [15].

Growth-factor-mediated activation of the PI3K/PKB (Akt) pathway is a key element of cellular survival and proliferation. Activation of Akt signalling is thought to stabilise MDM2 protein, thereby inhibiting p53-dependent apoptosis [9, 10, 19, 24, 30]. The Akt kinase and its significance in human malignomas, including breast can-

cer, has been the topic of recent research activities. A few studies have examined the potential prognostic value of the Akt kinase in breast cancer with varying results [22, 23]. We recently observed that activation of the Akt kinase is significantly associated with a reduced overall disease-specific survival [26]. Downstream signalling of activated Akt kinase contributes to tumour aggressiveness via several mechanisms, including regulation of apoptosis [4, 6], cell growth [2] and cell cycle control [27, 31]. Besides the well-known consequences of Akt activation, other effectors such as the oncoprotein MDM2 and the p53 tumour suppressor protein have been implicated in Akt-induced tumour survival [10].

Thus, the aim of the present study was to analyse a possible cross talk between pAkt, pMDM2 and p53 in node-negative breast cancer and to determine the prognostic value of phosphorylated MDM2 expression. In an immunohistochemical approach with phospho-specific antibodies, the MDM2 (serine 166) and Akt (serine 473) protein expressions were examined in 121 surgically resected node-negative breast cancer specimens. These results were compared with a broad range of clinicopathological parameters as well as the immunohistochemically determined p53 status of the present series with a mean follow up period of 7.7 years.

Material and methods

Patients

This study comprised 121 female breast cancer patients (mean age 61 years) operated at the Clinic of Gynaecology (University of Essen-Duisburg, Germany) between 1989 and 1996 who underwent surgery and further adjuvant therapy. Clinical records and follow-up information (overall survival) were available in all cases. Only patients without lymph node metastasis were included in the study. The negative lymph node status was confirmed histologically after standard axillary dissection. All surgical material was fixed in 4% formalin and routinely processed. The tumours were classified according to the pathological tumor-node-metastasis (pTNM) system (6th edition) and graded according to Elston and Ellis [8]. During follow-up, 21 out of 121 patients died. Eighteen patients died from breast cancer; the three remaining patients died from either benign (two patients) or concurrent cancer disease (one patient) and were thus excluded from survival analysis. Statistical analysis was based on a mean follow-up period of 7.7 years.

Immunohistochemistry

In the present study, polyclonal rabbit-anti-human phospho-MDM2 (serine 166) antibodies (Cell Signalling Technology, Beverly, MA, USA; 1:25), monoclonal anti-human-p53 antibodies (directed against both wild-type and mutated-type p53 protein, Biogenex, San Ramon, CA, USA; clone D07, ready-to-use antibody), monoclonal anti-human-p53 antibodies (directed against mutant-type p53 protein, DakoCytomation, Carpinteria, CA, USA; clone PAb240, 1:25) and polyclonal rabbit-anti-human phospho-Akt (serine 473) antibodies (Santa Cruz Biotechnology, CA, USA; 1:2,000) were used. The mutant-type p53 antibodies (clone PAb240) react with the PAb240 epitope, which is inaccessible to binding by PAb240 in its wild-type or native configuration but is exposed on mutant forms of p53 with altered protein conformation [28]. The alkaline phosphatase anti-alkaline phosphatase (APAAP) method was used for antibody demonstration on 5-µm-thick paraffin sections. Following a high-temperature antigen unmasking technique, pAkt and pMDM2 were incubated overnight in a humidified chamber at 4°C. Immunostaining of p53 (clone D07) was performed after high-temperature antigen retrieval. Slides were incubated with the primary antibody for 45 min at 37°C. The ready-to-use Powervision Kit (Immunologic, Duiven, The Netherlands) was used for antibody demonstration. Immunostaining of p53 (clone PAb240) was carried out with an automated staining device (DAKO Autostainer). After antigen retrieval the primary antibody was incubated for 30 min at 1:25 dilution; antibody demonstration was achieved using a commercially available anti-mouse immunoglobulin (Ig)G detection kit (EnVision, DakoCytomation). Positive controls were included in each staining series. Mouse Ig, replacing the primary antibody, was used as negative controls.

For the demonstration of a possible colocalization of pMDM2 and pAkt, immunofluorescence double labelling was performed. After antigen retrieval the slides were first incubated with the antibodies directed against pAkt (1:100). Antibody detection was performed with a fluorescein-isothiocyanate (FITC)-conjugated antibody [donkey-anti-rabbit (anti-Fab) antibody, Dianova, Hamburg, Germany; 1:50]. Due to the utilization of two primary rabbit-anti-human antibodies, the remaining epitopes of the host species of the primary polyclonal pAkt-antibody were covered by unconjugated anti-Fab antibodies. Afterwards, the slides were incubated with the pMDM2-antibody for 1 h at room temperature. Subsequently, a secondary biotinylated anti-F(ab′)2 antibody (donkey-anti-rabbit, Dianova; 1:4,000) was applied, and detection was achieved with the fluorescent streptavidin–indocarbocyanin(Cy3) complex. Finally, the sections were counterstained with 4c6-diamidino-2-phenylindole·2HCl (DAPI) solution (Sigma, Taufkirchen, Germany;1:50,000). Mouse Ig, replacing the primary antibody, was used as negative controls. Fluorescence microscopy was carried out with an Axioplan microscope (Zeiss, Germany) by using the appropriate filter system. Photographs were digitally processed with the AxioVision Software (Zeiss).

The oestrogen receptor (ER) status was determined using an anti-human ER alpha antibody (clone 1D5, DAKO, Glostrup, Denmark) as described earlier [26].

Mitotic count

Mitotic count (MC) was carried out taking into consideration the actual area of ten high-power fields (HPFs) of the Nikon Eclipse E600 microscope. MC results were grouped as 0–8, 9–17 and more than 17 mitotic figures per HPF (field diameter 0.55 mm) [7].

Statistical analysis

Phospho-MDM2 and phospho-Akt immunostainings were assessed by two of the authors (K.J.S. and F.G.) in a blind-trial fashion without knowledge of the clinical outcome. The mean percentage of both counts was used for statistical analysis. All data were converted to a PC and statistically analysed using SPSS version 12 for Windows (SPSS Inc., Chicago, IL, USA). Relationships between ordinal parameters were investigated using two-tailed χ^2 analysis. Differences between the mean values of pMDM2 and pAkt percentages of the various tumour types were compared with the one-way analysis of variance (ANOVA) test. Overall survival (OS) curves were estimated using the Kaplan–Meier method, and any differences in the survival curves were compared by the log-rank test. For multivariate analysis, the Cox regression model was used. Overall, 95% confidence intervals were used throughout.

Results

Immunohistochemical analysis of phospho-MDM2 (serine 166)

In tumour cells phospho-MDM2 immunostaining was exclusively located to nuclei without any detectable cytoplasmic staining. Normal breast tissue showed scattered, mostly weak to moderately positive nuclei. The percentage of pMDM2-positive tumour cell nuclei ranged from 4 to 88%, with a mean value of 62%. Tumours with percentage values lower than the mean value were classified as "low pMDM2 staining status", and the remainder were classified as "high pMDM2 staining status". χ^2 analysis revealed significant differences of pMDM2 staining status among the various tumour types investigated (P=0.019), with invasive ductal carcinomas showing significantly higher amounts of positive stained nuclei than invasive lobular (P=0.042) and mucinous carcinomas (P<0.001). In comparison to all other tumour types, mucinous carcinomas revealed lower amounts of positive stained tumour cells (P<0.005). Tumours with higher amounts of pMDM2-positive cells exhibited significantly higher mitotic rates (P=0.046). χ^2 analysis revealed no statistically significant differences among cases with different histological grading. The results are summarised in Table 1. Representative immunohistochemical stainings are shown in Fig. 1.

Table 1 Clinico-pathological data and phospho-MDM2 (serine 166) expression of 121 node-negative breast cancers

Phospho-MDM2 (serine 166) expression status (N=121)			
	Low, n (%)	High, n (%)	P value*
Total adenocarcinoma	50 (41.3)	71 (58.7)	
Tumour type			P=0.019
Invasive ductal	29 (33)	59 (67)	
Invasive lobular	14 (66.7)	7 (33.3)	
Mucinous	4 (80)	1 (20)	
Tubulo/tubulo-lobular	1 (50)	1 (50)	
Others	2 (40)	3 (60)	
Mitotic count			P=0.046
0–8	28 (53.8)	24 (46.2)	
9–16	15 (34.1)	29 (65.9)	
>16	7 (28)	18 (72)	
Histological grading			Not significant
Well differentiated	15 (55.6)	12 (44.4)	
Moderately differentiated	27 (42.2)	37 (57.8)	
Poorly differentiated	8 (26.7)	22 (73.3)	
Tumour size			Not significant
pT1(a, b, c)	30 (42.3)	41 (57.7)	
pT2	19 (39.6)	29 (60.4)	
pT3 and 4	1 (50)	1 (50)	

Low percentage of phospho-MDM2-positive cells <62% (mean value), *High* percentage of phospho-MDM2-positive cells ≥62% (mean value)
*P value of χ^2 analysis

Immunohistochemical analysis of phospho-Akt

Immunostaining for pAkt was predominantly localized to tumour nuclei. A faint cytoplasmic, but specific, pAkt staining was only occasionally noticed but was disregarded for the calculation of immunohistochemical scores. The number of positive immunoreactive tumour nuclei was counted within 300 cells in the invasive tumour front, as tumour aggressiveness is considered to be highest here. The result was expressed as percentage. The percentage of pAkt-positive tumour cell nuclei ranged from 5 to 83% (mean 61.8%). In accordance with our previous study [25], tumours were separated into two groups, with 45% as the cut-off value for pAkt overexpression. Phospho-pAkt-positive tumours showed a statistically very highly significant association with a high pMDM2 staining status (P=0.003; χ^2 analysis) but not with the MC, p53 or ER status. In comparison to all other tumour types, mucinous carcinomas revealed lower amounts of positive stained tumour cells (P<0.05).

Immunohistochemical analysis of p53 protein expression

p53 immunostaining for both antibodies was restricted to tumour nuclei. Tumour-adjacent normal breast tissue com-

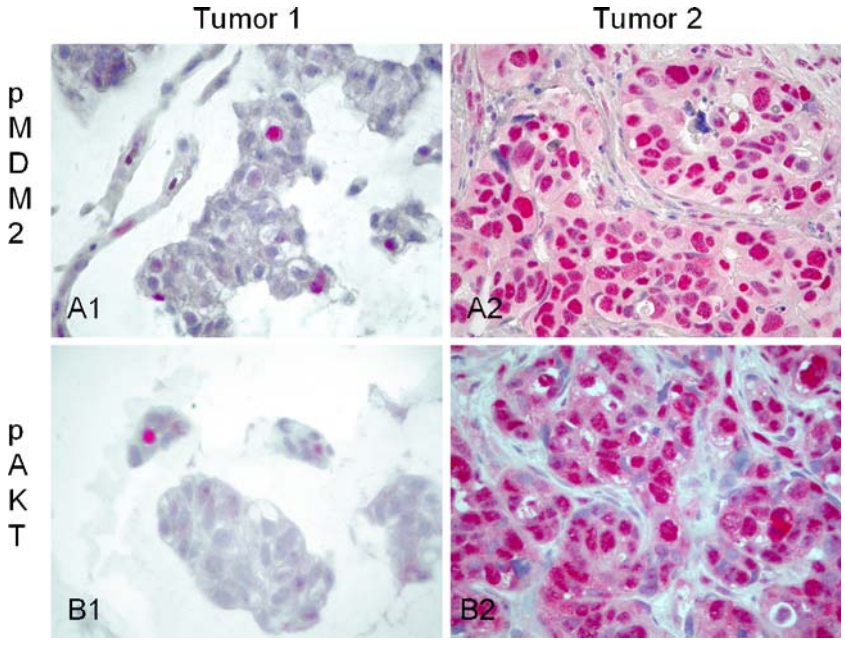

Fig. 1 Representative immunohistochemical stainings of serial sections of two tumours for phospho-Akt and phospho-MDM2. Tumours with few phospho-MDM2 stained tumour cells (*A1*) revealed more frequently a scattered nuclear phospho-Akt staining (*B1*), whereas tumours showing abundant phospho-Akt stained tumour cells exhibited in many cases a high percentage of strongly nuclear phospho-MDM2 stained tumour nuclei. Original magnification, ×400

pletely lacked p53 immunoreactivity. In invase carcinoma p53 staining was scored as follows: no immunoreactivity or positive staining in less than 10% of tumour cells (−) and positive staining in more than 10% of tumour cells (+). Of all the tumours, 18.2% were classified as p53-positive using the p53 clone D07 antibody, and 6.9% were classified using the clone PAb240 antibody.

Six out of seven cases classified as p53-positive with the mutated-type antibody (clone PAb240) have also been classified as positive with the p53 antibody D07. Tumours classified as p53-positive (clone D07) showed a statistically significant association, with a lower differentiation grade and higher MC ($P<0.001$). No further relationship

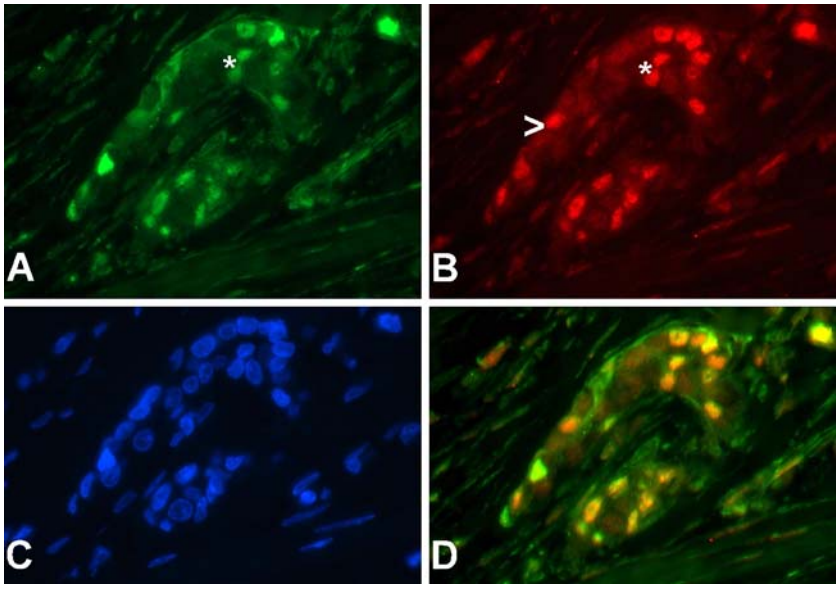

Fig. 2 Double immunofluorescence staining for phospho-Akt (serine 473) (*green signal*) and phospho-MDM2 (serine 166) (*red signal*) in a randomly chosen node-negative breast carcinoma. **A** Immunolabelling for phospho-Akt exhibits several stained tumour nuclei (*green signal*). **B** Immunolabelling for phospho-MDM2 (serine 166) shows scattered strongly stained tumour nuclei (*red signal*). Notice several tumour nuclei stained for both phospho-Akt and phospho-MDM2 (*asterisk*). **C** Counterstaining with DAPI solution marks all cell nuclei irrespective of immunolabelling. **D** The digital overlay of phospho-Akt and phospho-MDM2 fluorescence indicates colocalization in several yellow stained tumour nuclei. Other tumour nuclei lack both phospho-Akt and phospho-MDM2 immunostaining. The colocalization of phospho-MDM2 and phospho-Akt in the same tumour cell supports our hypothesis that activation of the Akt signalling pathway is associated with increased MDM2 phosphorylation (×1,000)

between p53 immunophenotype and pathological parameters was observed.

Correlations among pMDM2 expression, pAkt expression, p53 protein accumulation and ER status

Statistical analysis (regression analysis) revealed a significant direct correlation of the pMDM2 and pAkt staining scores ($P<0.001$). No correlation was observed between pMDM2 status, ER status or p53 immunophenotype—p53 protein expression lacked correlation with both pAkt and the ER status.

Double immunofluorescence

Double immunofluorescence staining of randomly selected tumour samples with markers for pAkt (green signal) and pMDM2 (red signal) showed a colocalization of both phosphorylated proteins in tumour-cell nuclei (Fig. 2).

Prognosis

Only four out of 50 (8%) patients with a tumour showing low pMDM2 staining status died from breast cancer. However, 14 out of 68 (20.6%) patients classified as high pMDM2 staining status died from breast cancer. Overall survival was inversely associated with a low pMDM2 staining. To explore in more detail the relative prognostic

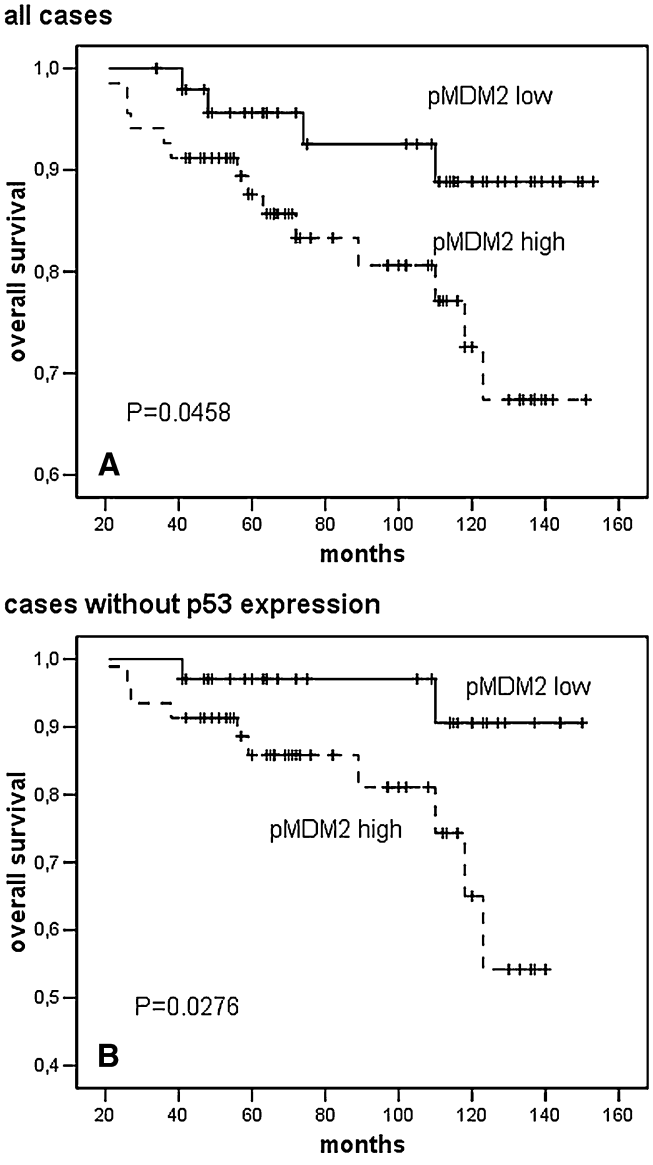

Fig. 3 Kaplan–Meier survival curves for disease-specific overall survival with respect to pMDM2 in the subgroups of **A** all cases and **B** cases without p53 expression of both p53 antibodies

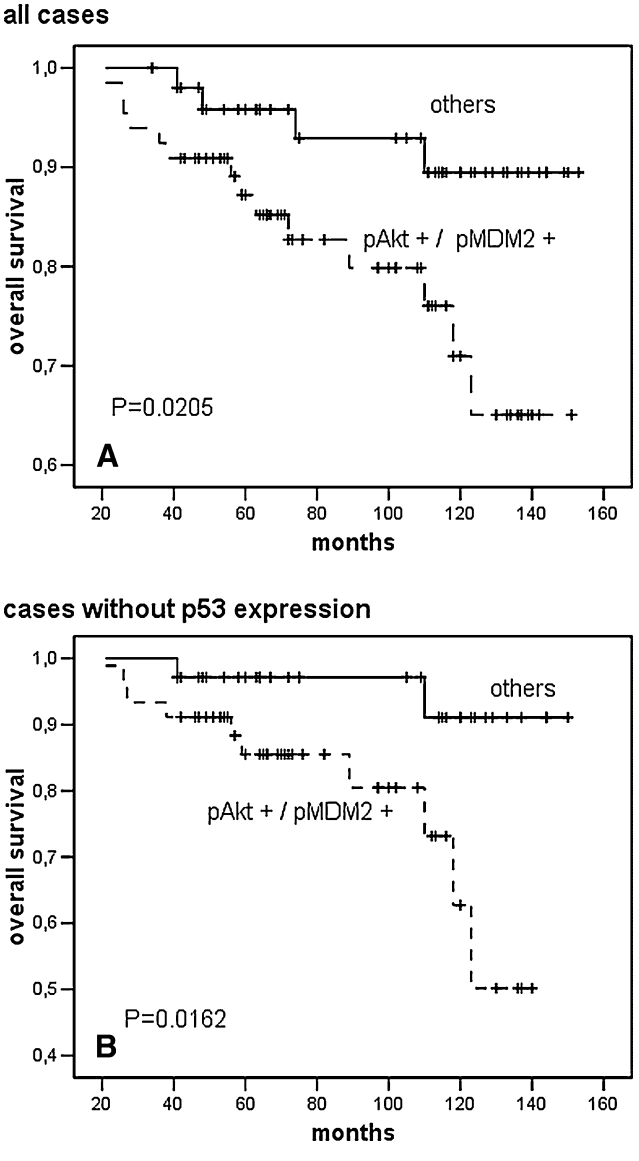

Fig. 4 Kaplan–Meier survival curves for disease-specific overall survival with respect to combined pMDM2/pAkt immunophenotype in the subgroups of **A** all cases and **B** cases without p53 expression of both p53 antibodies

Table 2 Results of multivariate analysis (Cox regression) to determine the independent prognostic value of different variables in relation to overall survival

Covariate	Relative risk (e^{β})	95% CI	*P* value
pAkt/pMDM2 (+/+ vs +/−, −/+, −/−)	2.362	0.758–7.359	0.138
Histological grade (1, 2, 3)	3.665	1.197–11.215	0.023[a]
Oestrogen receptor status, negative vs positive	0.572	0.187–1.751	0.328
Mitotic count, 0–8 vs 9–21 vs >16	0.676	0.286–1.601	0.374

[a]Statistically significant

contribution of pAkt, we divided the cases into the following categories: (1) pMDM2 low (−) vs high (+) staining and (2) combined pMDM2/pAkt immunophenotype. Using p53 negativity for both antibodies as stratification parameter in the Kaplan–Meier analysis, a high pMDM2 staining status (concerning the complete series) was statistically significantly associated with a reduced disease-specific OS (P=0.0458; Fig. 3A). The unfavourable prognostic effect of tumours with a high pMDM2 staining status increased in the p53-negative subgroup (P=0.0276; Fig. 3B).

The combined pMDM2/pAkt immunophenotype revealed an additional significant influence on disease-specific OS (P=0.0205; Fig. 4A) showing the worst clinical outcome for $pMDM2^{+}/pAkt^{+}$ tumours. The unfavourable prognostic effect of $pMDM2^{+}/pAkt^{+}$ tumours again increased in the p53-negative subgroup (P=0.0162; Fig. 4B).

Parallel analysis reveal that histological grading (P=0.0010), MC (P=0.0464) and a negative ER status (P=0.0179) were significantly related to a decreased OS, whereas p53 protein expression was not associated with prognosis. Disease-specific OS and the relevant clinicopathological parameters (histological grading, ER status, MC and pAkt/pMDM2 combined phenotype) were subject to multivariate analysis; only histological grading was statistically associated with disease-specific OS (Cox regression analysis, P=0.023) (Table 2).

Discussion

Particularly in patients with node-negative breast cancer, novel markers defining node-negative high-risk patients, who would benefit from adjuvant therapy, would be desirable. This study was designed to investigate the cross talk of phospho-MDM2, phospho-Akt and p53 in node-negative breast cancer. In addition the prognostic relevance of the post-translational modified MDM2 (phosphorylation at serine 166) as well as its combination with pAkt was assessed.

MDM2 is an oncoprotein inhibiting the function of p53 tumour suppressor protein. Its accumulation in neoplastic cells is due to gene amplification, enhanced transcription/translation or post-translational modification, but apparently, only the latter two mechanisms seem to be of relevance in breast cancer [21]. Recent in vitro data suggest that Akt-dependent phosphorylation of MDM2 at serine 166 leads to an increase in MDM2 stability by protecting it from proteosome-dependent degradation, with the consequence of p53 down-regulation [9, 10].

Our results indicate a significant direct correlation between pMDM2 expression and Akt activation, supporting the concept that activation of the Akt signalling pathway is associated with increased MDM2 phosphorylation. The demonstration of pAkt and pMDM2 colocalization in double immunofluorescence staining argues in favour for this hypothesis. Furthermore, our data are in accordance with recently published observations describing a coincidence of low MDM2 expression and decreased Akt activation in human non-small-cell lung cancers [29].

To the best of our knowledge there are only three MDM2 studies in breast cancer published in the literature; however, these studies arrived at contradictory data concerning the prognostic relevance of MDM2 protein expression [1, 12, 13]. These conflicting results could be due to the complex autoregulatory feedback loop between these two proteins that interact both on the protein level and on the level of gene transcription [21]. Interpretation of MDM2 protein expression in tumours is limited by several parameters, e.g. complexity of the underlying p53–MDM2 interaction, multiplicity of protein isoforms and modifications, the absence of a standard expression definition for overexpression and lack of distinction between cytoplasmic and nuclear staining.

The present study is the first to examine the prognostic value of the phosphorylated MDM2 protein in node-negative breast cancer. Since previous studies using antibodies against the non-phosphorylated MDM2 reveal contradictory results, the investigation of the phosphorylated MDM2 oncoprotein may help to clarify the role of MDM2. Additionally, the utilized phospho-specific antibody detects phosphorylation at serine 166 via Akt kinase and, thus, offers the chance to semi-quantify the modified MDM2 oncoprotein in its presumed p53 regulating status. In contrast to both cytoplasmic and nuclear staining of the non-phosphorylated MDM2 immunohistochemistry observed in other studies [21], the phospho-specific antibody used in our present study was shown to exclusively stain tumour cell nuclei, enabling a simple and reproducible interpretation of pMDM2 staining results. The finding of a constant nuclear pMDM2 staining is in accordance with recent data describing an Akt-promoted nuclear translocation of MDM2 from the cytoplasma to the nucleus [17].

Concerning survival, univariate analysis showed a significantly correlation of pMDM2 overexpression with an unfavourable prognosis. The adverse prognostic effect increased in tumours with a combined $pMDM2^{+}/pAkt^{+}$ immunophenotype. However, multivariate analysis failed to prove its independent prognostic value. Since Akt-mediated phosphorylation of MDM2 promotes degradation and inactivation of p53, particularly wild-type p53, an additional survival analysis with a restriction to cases

lacking p53 expression was performed. It is interesting to see that the level of significance in both the pMDM2-positive and the combined $pAkt^{+}/pMDM2^{+}$ subgroups increased, suggesting that the functional inactivation of p53 via Akt-related MDM2 phosphorylation might be more effective in breast cancer lacking a p53 overexpression or mutation. We are, of course, aware that an immunohistochemical approach is ultimately not the gold standard to identify tumours with wild-type p53, but the determination of the p53 genotype was beyond the scope of this study.

In conclusion, this study demonstrates that phosphorylation of MDM2 at serine 166 seems to be induced by the Akt(PKB) kinase not only (as recent data suggested) in vitro but also in vivo. The findings put additional emphasis on the role of Akt-mediated MDM2 phosphorylation as a negative regulator of p53-dependent growth control and illuminates the diversity of biological effects of activated Akt/PKB signalling in breast cancer. Besides the well-known relevance of this serine–threonine kinase in inhibiting cell death via modification of proapoptotic proteins such as Bad, Forkhead transcription factor and caspase 9 [4, 6], the Akt kinase may promote cell survival by influencing the p53–MDM2 loop. This could at least partly explain the poor clinical outcome of breast cancer patients with Akt activation as previously described in a paper [26]. Since Akt-induced MDM2 phosphorylation results in the functional inactivation of primarily wild-type p53, it is tempting to speculate that this mechanism represents one of the various signalling events leading to increased tumour aggressiveness in breast cancers lacking p53 mutations but exhibiting Akt activation. The statistical power of this study is, unfortunately, reduced due to the relatively small number of participating patients and heterogeneity of tumours. Therefore, it is necessary to confirm these promising results in larger cohorts.

Acknowledgements The technical assistance of Dorothe Möllmann and Caroline Stang is gratefully acknowledged. We thank Jack and Mave Brown for critical reading of the manuscript. This work was supported by the local research fund (IFORES) of the University of Essen.

References

1. Bankfalvi A, Tory K, Kemper M, Breukelmann D, Cubick C, Poremba C, Fuzesi L, Lelle RJ, Bocker W (2000) Clinical relevance of immunohistochemical expression of p53-targeted gene products mdm-2, p21 and bcl-2 in breast carcinoma. Pathol Res Pract 196:489–501
2. Blume-Jensen P, Hunter T (2001) Oncogenic kinase signalling. Nature 411:355–365
3. Cahilly-Snyder L, Yang-Feng T, Francke U, George DL (1987) Molecular analysis and chromosomal mapping of amplified genes isolated from a transformed mouse 3T3 cell line. Somat Cell Mol Genet 13:235–244
4. Cardone MH, Roy N, Stennicke HR, Salvesen GS, Franke TF, Stanbridge E, Frisch S, Reed JC (1998) Regulation of cell death protease caspase-9 by phosphorylation. Science 282:1318–1321
5. Courjal F, Cuny M, Rodriguez C, Louason G, Speiser P, Katsaros D, Tanner MM, Zeillinger R, Theillet C (1996) DNA amplifications at 20q13 and MDM2 define distinct subsets of evolved breast and ovarian tumours. Br J Cancer 74:1984–1989
6. Datta SR, Brunet A, Greenberg ME (1999) Cellular survival: a play in three Akts. Genes Dev 13:2905–2927
7. Ellis PS, Whitehead R (1981) Mitosis counting—a need for reappraisal. Hum Pathol 12:3–4
8. Elston CW, Ellis IO (1991) Pathological prognostic factors in breast cancer I. The value of histological grade in breast cancer: experience from a large study with long term follow up. Histopathology 19:403–410
9. Feng J, Tamaskovic R, Yang Z, Brazil DP, Merlo A, Hess D, Hemmings BA (2004) Stabilization of Mdm2 via decreased ubiquitination is mediated by protein kinase B/Akt-dependent phosphorylation. J Biol Chem 279:35510–35517
10. Gottlieb TM, Leal JF, Seger R, Taya Y, Oren M (2002) Cross-talk between Akt, p53 and Mdm2: possible implications for the regulation of apoptosis. Oncogene 21:1299–1303
11. Haupt Y, Maya R, Kazaz A, Oren M (1997) Mdm2 promotes the rapid degradation of p53. Nature 387:296–299
12. Hori M, Shimazaki J, Inagawa S, Itabashi M, Hori M (2002) Overexpression of MDM2 oncoprotein correlates with possession of oestrogen receptor alpha and lack of MDM2 mRNA splice variants in human breast cancer. Breast Cancer Res Treat 71:77–83
13. Jiang M, Shao ZM, Wu J, Lu JS, Yu LM, Yuan JD, Han QX, Shen ZZ, Fontana JA (1997) p21/waf1/cip1 and mdm-2 expression in breast carcinoma patients as related to prognosis. Int J Cancer 74:529–534
14. Kubbutat MH, Jones SN, Vousden KH (1997) Regulation of p53 stability by Mdm2. Nature 387:299–303
15. Lu W, Pochampally R, Chen L, Traidej M, Wang Y, Chen J (2000) Nuclear exclusion of p53 in a subset of tumours requires MDM2 function. Oncogene 19:232–240
16. Marchetti A, Buttitta F, Girlando S, Dalla PP, Pellegrini S, Fina P, Doglioni C, Bevilacqua G, Barbareschi M (1995) mdm2 gene alterations and mdm2 protein expression in breast carcinomas. J Pathol 175:31–38
17. Mayo LD, Donner DB (2001) A phosphatidylinositol 3-kinase/Akt pathway promotes translocation of Mdm2 from the cytoplasm to the nucleus. Proc Natl Acad Sci USA 98:11598–11603
18. Momand J, Jung D, Wilczynski S, Niland J (1998) The MDM2 gene amplification database. Nucleic Acids Res 26:3453–3459
19. Ogawara Y, Kishishita S, Obata T, Isazawa Y, Suzuki T, Tanaka K, Masuyama N, Gotoh Y (2002) Akt enhances Mdm2-mediated ubiquitination and degradation of p53. J Biol Chem 277:21843–21850
20. Oliner JD, Pietenpol JA, Thiagalingam S, Gyuris J, Kinzler KW, Vogelstein B (1993) Oncoprotein MDM2 conceals the activation domain of tumour suppressor p53. Nature 362:857–860
21. Onel K, Cordon-Cardo C (2004) MDM2 and prognosis. Mol Cancer Res 2:1–8
22. Panigrahi AR, Pinder SE, Chan SY, Paish EC, Robertson JF, Ellis IO (2004) The role of PTEN and its signalling pathways, including AKT, in breast cancer; an assessment of relationships with other prognostic factors and with outcome. J Pathol 204:93–100
23. Perez-Tenorio G, Stal O (2002) Activation of AKT/PKB in breast cancer predicts a worse outcome among endocrine treated patients. Br J Cancer 86:540–545

24. Sabbatini P, McCormick F (1999) Phosphoinositide 3-OH kinase (PI3K) and PKB/Akt delay the onset of p53-mediated, transcriptionally dependent apoptosis. J Biol Chem 274:24263–24269
25. Schmitz KJ, Grabellus F, Callies R, Otterbach F, Wohlschlaeger J, Levkau B, Kimmig R, Schmid KW, Baba HA (2005) High expression of focal adhesion kinase (p125FAK) in node-negative breast cancer is related to overexpression of HER-2/neu and activated Akt kinase but does not predict outcome. Breast Cancer Res 7:R194–R203
26. Schmitz KJ, Otterbach F, Callies R, Levkau B, Holscher M, Hoffmann O, Grabellus F, Kimmig R, Schmid KW, Baba HA (2004) Prognostic relevance of activated Akt kinase in node-negative breast cancer: a clinicopathological study of 99 cases. Mod Pathol 17:15–21
27. Shin I, Yakes FM, Rojo F, Shin NY, Bakin AV, Baselga J, Arteaga CL (2002) PKB/Akt mediates cell-cycle progression by phosphorylation of p27(Kip1) at threonine 157 and modulation of its cellular localization. Nat Med 8:1145–1152
28. Stephen CW, Lane DP (1992) Mutant conformation of p53. Precise epitope mapping using a filamentous phage epitope library. J Mol Biol 225:577–583
29. Wang YC, Lin RK, Tan YH, Chen JT, Chen CY, Wang YC (2005) Wild-type p53 overexpression and its correlation with MDM2 and p14ARF alterations: an alternative pathway to non-small-cell lung cancer. J Clin Oncol 23:154–164
30. Yamaguchi A, Tamatani M, Matsuzaki H, Namikawa K, Kiyama H, Vitek MP, Mitsuda N, Tohyama M (2001) Akt activation protects hippocampal neurons from apoptosis by inhibiting transcriptional activity of p53. J Biol Chem 276: 5256–5264
31. Zhou BP, Liao Y, Xia W, Spohn B, Lee MH, Hung MC (2001) Cytoplasmic localization of p21Cip1/WAF1 by Akt-induced phosphorylation in HER-2/neu-overexpressing cells. Nat Cell Biol 3:245–252

Virchows Arch (2006) 448: 24–28
DOI 10.1007/s00428-005-0090-4

ORIGINAL ARTICLE

K. Tomić · D. Tomas · I. Tomašković
M. Kos · M. Belicza · B. Krušlin

Renal artery changes in patients with primary renal cell carcinoma

Received: 26 February 2005 / Accepted: 1 September 2005 / Published online: 28 September 2005

Abstract Arterial fibromuscular dysplasia (FMD) is a noninflammatory, nonatherosclerotic, occlusive condition of the systemic arteries, most frequently affecting renal arteries. Renal cell carcinoma (RCC) might be associated with arterial hypertension; however, there are no data in the literature regarding the relationship between RCC and associated renal artery changes. We analyzed a consecutive series of 57 (35 male and 22 female) patients aging from 35 to 79 years (mean 58.9 years) who underwent nephrectomy due to RCC in the year 2003. The patients had RCC measuring from 2 to 16 cm (mean 7.1 cm). Specimens were routinely fixed, embedded in paraffin, cut, and stained with hematoxylin and eosin, Mallory trichrome method, and orcein. Renal arteries of 26 patients (20 male, 6 female) showed no changes. In these patients, RCC measured 2.5–11 cm in largest diameter (mean 6.6 cm). In 24 patients (10 male, 14 female), renal arteries showed FMD. RCCs in these patients measured between 2 and 16 cm (mean 8.0 cm). Seven patients had atherosclerotic changes in renal arteries. In this series, FMD was found in a significant proportion of patients with RCC, mainly in women. The cause of such changes and their relationship with RCC and systemic hypertension should be further analyzed.

Keywords Fibromuscular dysplasia · Renal cell carcinoma · Renal arteries

Presented in part at the XXV International Academy of Pathology Congress, Brisbane, Australia, October 10–15, 2004.

K. Tomić
General Hospital Josip Benčević,
Slavonski Brod, Croatia

D. Tomas · M. Kos · M. Belicza · B. Krušlin (✉)
Ljudevit Jurak University Department of Pathology,
Sestre milosrdnice University Hospital,
Vinogradska 29,
Zagreb, Croatia
e-mail: bkruslin@kbsm.hr
Tel.: +385-1-3787177
Fax: +385-1-3787244

I. Tomašković
Department of Urology,
Sestre milosrdnice University Hospital,
Zagreb, Croatia

Introduction

The renal arteries arise from the abdominal aorta at the level of L2, and the right renal artery is longer than the left one. Different lesions may involve main renal artery including atherosclerosis, fibromuscular dysplasia, and some other conditions, such as Takayasu arteritis, radiation injury, and congenital malformations [11].

Arterial fibromuscular dysplasia (FMD) is a noninflammatory, nonatherosclerotic, occlusive condition of systemic arteries, the renal arteries being most frequently affected. Major clinical conditions associated with FMD are hypertension, stroke, claudication, and intestinal ischemia [7]. FMD of renal arteries is bilateral in nearly half of patients, more commonly on the right side (3:1), is usually diagnosed in the fourth decade, with female predominance, and most frequently involving the distal two thirds of the renal artery and its branches [11, 12]. Incidence of the FMD found at autopsy study is about 1% [4, 8].

There are three principal pathologic types of FMD: intimal, medial, and adventitial fibromuscular dysplasia. Primary intimal fibroplasia (type I) is a rare condition that occurs in children and young adults, comprising about 2 to 5% of all FMD lesions [3, 9, 14, 15], and sometimes it can be difficult to distinguish this type of FMD from nonspecific fibrosis as seen in atherosclerosis [9]. This type can be connected with progressive renal artery obstruction and ischemic atrophy of the kidney [3]. Medial fibromuscular dysplasia (type II) can be further subdivided into three subtypes: medial "muscular" hyperplasia (type IIa), medial fibroplasia with aneurysms (type IIb), and perimedial fibroplasias (type IIc), of which medial fibroplasia is the most common type of FMD (about 70%). The lesion

usually affects women aging 25 to 50 years, with bilateral involvement in about 60% [3, 9]. Adventitial fibroplasia (type III) is very rare and represents less than 1% of all FMDs [3].

Atherosclerosis is a generalized progressive arterial disease associated with localized arterial occlusions and aneurysms [11]. It accounts for 90% of the cases of renal artery stenosis and usually involves the ostium and proximal third of the main renal artery and perirenal aorta [12].

Renal cell carcinoma (RCC) represents 2% of all human malignancies and over 90% of all malignancies of the kidney. It is two to three times more common in men than in women, and the average age at diagnosis is 55 to 60 years [2, 11]. History of blood hypertension, obesity, and tobacco smoking increases the risk of RCC [1, 11].

The aim of this study was to analyze renal artery changes in patients with renal cell carcinoma.

Materials and methods

A consecutive series of 74 patients aging from 35 to 79 years with RCC who underwent nephrectomy in the year 2003 (44 male and 30 female) was analyzed. Seventeen patients (nine male and eight female) were excluded from the study because five of them had only partial nephrectomy; two were sent for consultation from other hospitals (without renal arteries); in four cases, renal arteries were tangentially cut; and in six specimens, renal arteries were not sampled. Finally, the study group consisted of 57 patients. All relevant patients' data including age, sex, tumor grade and size, the extent of tumor necrosis, blood pressure, and vena cava status were analyzed. There were 35 male and 22 female patients with RCC ranging in age from 35 to 79 years (mean 58.9 years). The size of RCC was from 2 to 16 cm (mean 7.1 cm). Renal artery and vein as well as ureter margin were routinely analyzed. Specimens were routinely fixed in 10% buffered formaldehyde, embedded in paraffin, cut, and stained with hematoxylin and eosin, Mallory trichrome method, and orcein, and examined by light microscopy. Immunohistochemistry was performed by Microwave Streptavidine Immunoperoxidase protocol (MSIP) in DAKO TechMate Horizon automated immunostainer. We used primary antibodies to smooth muscle actin (SMA) that were purchased from DAKO, Copenhagen, Denmark. Dilution of the antibody was "ready to use." Nuclear grade of RCC was determined according to Fuhrmann et al. [4].

Statistical analysis used in this study included F test, T test/Cochran–Cox method, and χ^2 test. Level of significance was set at $p<0.05$.

The classification of FMD included pathologic processes of intimal, medial, and adventitial fibroplasia [3, 9, 15].

Results

Renal arteries of 26 patients (20 male and 6 female) ranging in age from 38 to 74 years (mean 58.6 years) showed no changes. RCC in these patients measured 2.5–11 cm in largest diameter (mean 6.6 cm). In 24 patients (10 male, 14 female) aging from 35 to 79 years (mean 60.0 years), renal

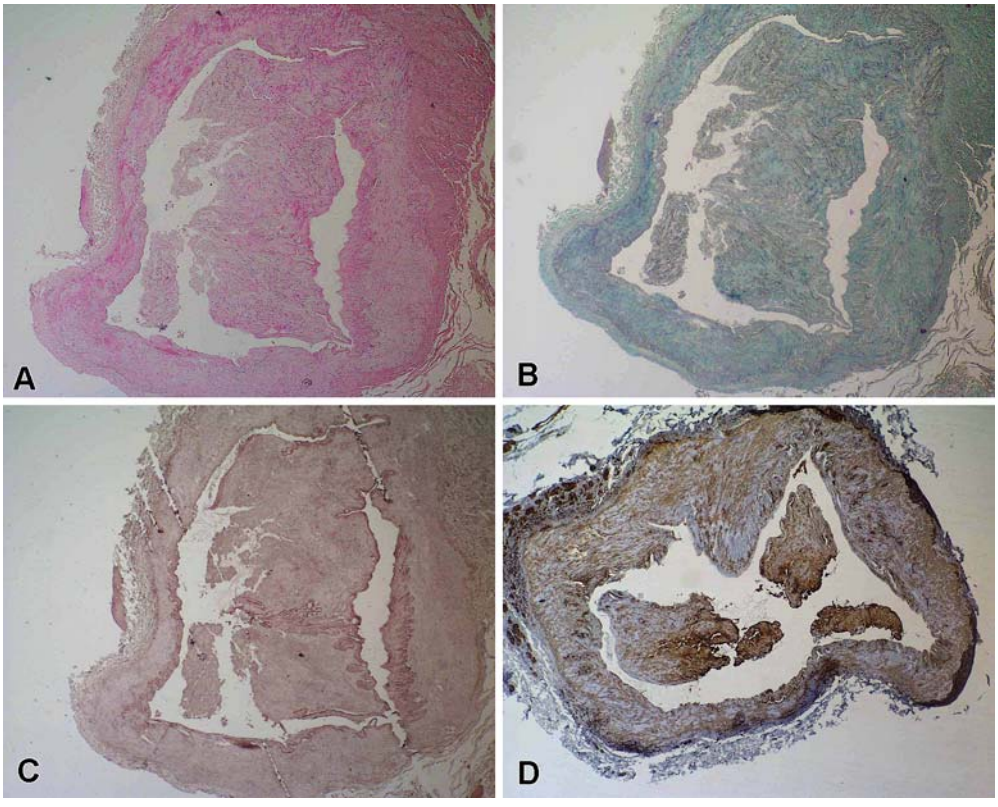

Fig. 1 Renal artery dysplasia of medial fibromuscular type IIb in a patient with renal cell carcinoma. **a** Hematoxylin and eosin-stained section showing protrusion of fibromuscular ridge into the arterial lumen, **b** Mallory-stained section showing proliferation of smooth muscle and connective tissue, **c** Orcein-stained section showing the internal lamina, **d** Smooth muscle actin (SMA) immunostaining showing architectural disarray of the smooth muscle cells. (All microphotographs were made under low magnification, 40×.)

Table 1 Clinicopathologic features of 57 patients with renal cell carcinoma with regard to renal artery status

	Group I	Group II	Group III
Male	20	10	5
Female	6	14	2
Age	38–74 years (mean 58.6)	35–79 years (mean 60.0)	60–69 years (mean 62.0)
Tumor size	2.5–11 cm (mean 6.6)	2–16 cm (mean 8)	2.5–14 cm (mean 6.4)
Tumor necrosis	Less than 50%, 21 More than 50%, 5	Less than 50%, 19 More than 50%, 5	Less than 50%, 6 More than 50%, 1
Blood pressure	110/70–160/100 mmHg (mean 125/84.5)	110/80–200/100 mmHg (mean 138.5/86)	115/70–145/85 mmHg (mean 134/79)
Cell type of RCC	Clear cell, 10; chromophilic eosinophilic, 5; mixed (clear and eosinophilic), 7; mixed with sarcomatoid component, 3; chromophobe, 1	Clear cell, 8; chromophilic eosinophilic, 3; mixed (clear and eosinophilic), 8; mixed with sarcomatoid component, 5	Clear cell, 5; chromophilic eosinophilic, 1; mixed with sarcomatoid component, 1
Nuclear grade	G1, 3 G2, 7 G3, 10 G4, 6	G1, 0 G2, 8 G3, 9 G4, 7	G1, 1 G2, 6 G3, 0 G4, 0

Group I, without artery changes; group II, FMD; Group III, atherosclerosis

arteries showed FMD (Fig. 1), and RCC in these patients were between 2 and 16 cm (mean 8 cm), while 7 patients (5 male and 2 female) aging 60–69 years (mean 62.0 years) had atherosclerotic changes in renal arteries. Tumor size in this group was 2.5–14 cm (mean 6.4 cm). In the first group (cases without renal artery changes), there were three patients with tumorous infiltration of the renal vein. The same number of cases with renal vein infiltration was found in the second group (fibromuscular changes of renal arteries), while only one patient from the third group who had atherosclerotic changes of renal arteries had tumorous infiltration of renal vein. Blood pressure in patients from the first group was from 100/70 to 160/100 mmHg (mean 125/84.5 mmHg), in the second group 110/80 to 200/100 mmHg (mean 138.5/86 mmHg), and in the third group 115/70 to 145/85 mmHg (mean 134/79 mmHg). There were no data about the blood pressure for 14 (24.6%) patients. Four patients with no renal artery changes and five patients from the second group (FMD) were receiving antihypertensive therapy. Necrosis was observed in 45 of 57 tumors (78.9%). There was no statistically significant correlation between the presence (p=0.750) and type (p=0.052) of FMD and the extent of the necrosis in RCCs. Tumors with type I of FMD 3/7 (42.9%) showed more than 50% necrosis, while only 1/15 (6.7%) tumors with FMD type IIb had the same extent of necrosis. One of two cases with FMD type IIa showed necrosis in more than 50% of tumor mass.

Clinicopathologic features of patients with renal cell carcinoma are shown in Tables 1 and 2.

Table 2 Clinicopathologic features of 57 patients with RCC regarding three different types of FMD

	Type I	Type IIa	Type IIb
Male	3	0	7
Female	4	2	8
Age	52–74 years (mean 62)	35–66 years (mean 50)	36–79 years (mean 60.5)
Tumor size	2–14 cm (mean 7.4)	6–12 cm (mean 9.0)	3–16 cm (mean 8.0)
Blood pressure	120/70–200/100 mmHg (mean 150/90)	120/80–140/95 mmHg (mean 130/87.5)	110/80–175/95 mmHg (mean 136.3/84.2)
Nuclear grade	Predominantly G3	Predominantly G2	Equally G2, 3, and 4
Cell type of RCC	Clear cell, 2; chromophilic eosinophilic, 1; mixed (clear and eosinophilic), 3; mixed with sarcomatoid component, 1	Chromophilic eosinophilic, 2	Clear cell, 6; chromophilic eosinophilic, 1; mixed (clear and eosinophilic, 3; mixed with sarcomatoid component, 5
Tumor necrosis	Less than 50%, 4 More than 50%, 3	Less than 50%, 1 More than 50%, 1	Less than 50%, 14 More than 50%, 1

Type I, intimal; type IIa, medial muscular; type IIb, medial fibromuscular

Statistical analysis showed no significant difference in the age (p=0.486), tumor size (p=0.112), and mean systolic (p=0.918) and diastolic (p=0.448) blood pressure between the first and the second group of patients. However, FMD was found significantly more often in female patients (p=0.009). Furthermore, there was no statistically significant difference in the age, tumor size, and blood pressure between the first and third group and second and third group of patients. In the group of patients with atherosclerosis and without significant pathomorphologic changes of renal arteries, men were more frequent (p=0.028).

Discussion

The incidence of RCC is significantly higher in people with a history of blood hypertension that is not dependent on obesity and tobacco smoking. One of the causes of hypertension is renal artery stenosis due to atherosclerosis in 90% of cases [12].

Fibromuscular dysplasia accounts for less than 10% of cases of renal artery stenosis, the medial type representing about 90% of cases [8, 14].

Atherosclerotic renal artery stenosis is a common and progressive disease; however, it is probable that many atherosclerotic stenoses are never detected because refractory hypertension or renal failure does not develop [12]. In the hypertensive population, high blood pressure may be attributed to renovascular FMD in less than 2% of patients [15]. In patients with renovascular hypertension, FMD is the underlying cause in 20–50% of cases [8]. The etiology of FMD is unknown, although many theories have been advanced, including those involving a genetic predisposition, smoking, hormonal factors, and disorders of vasa vasorum as risk factors [8, 14].

The patients with FMD may be asymptomatic, and the natural history of the disease is relatively benign with progression occurring in only the minority of patients [8].

In our previous study, fibromuscular dysplasia of renal arteries was found in a significant proportion of patients with RCC, mainly in females [7]. These changes might be primary, but also could be the result of some other factors or the effect of the tumor itself.

Hypertension has been implicated as a risk factor for the development of RCC, but quantitative data concerning the levels of blood pressure are limited [1]. A small case-control study based on medical records found that the risk of RCC was higher with higher blood pressure within 5 to 10 years before the diagnosis of RCC. In the study with long-term follow-up, Chow et al. [1] showed that blood pressure was positively related to the risk of RCC. The risk of RCC in men with diastolic pressure of 90 mmHg or more was more than double the risk in men with diastolic pressure below 70 mmHg. Similar data were reported on the relationship and risk for systolic pressure [1, 13].

In our study, renal artery changes were observed in 31 out of 57 patients with RCC. There was no correlation between blood pressure and the presence of FMD.

There are few studies on the relation between RCC and blood pressure that were based on relatively small number of subjects except for the study of Chow et al. [1] on 363,992 Swedish men in whom 759 RCC developed during the 25 years period of follow-up.

Grossly, RCC usually shows large areas of necrosis. Such changes are usually attributed to some abnormalities in tumor vascularization. The data in the literature pointed out to the relationship between the presence and extent of tumor necrosis in RCC and different features including tumor size, cell type, nuclear grade as well as microvessel density and the expression of different markers [6]. However, there are no data about the relationship between fibromuscular dysplasia-like changes and renal cell carcinoma. Onishi et al. [10] reported histological features of hypovascular and avascular RCC; however, the cause of vascular changes was not further analyzed. We observed tumor necrosis in 78.9% of tumors, but there was no statistically significant correlation between the presence and type of FMD and the extent of the necrosis of RCC. However, it seems that a larger study is needed to confirm the relationship between FMD type and tumor necrosis.

On the basis of our results, we may conclude that fibromuscular dysplasia of renal artery occurs in a significant proportion of female patients with renal cell carcinoma, while male patients more frequently had atherosclerosis or no pathomorphologic renal artery changes. However, further studies are needed to elucidate these changes and to determine whether these are primary or represent a consequence of the tumor.

References

1. Chow WH, Gridley G, Fraumeni JF, Järvholm B (2000) Obesity, hypertension, and the risk of kidney cancer in men. N Engl J Med 343:1305–1311
2. Eble JN, Sauter G, Epstein JI, Sesterhenn IA (eds) (2004) Tumors of the urinary system and male genital organs, World health organization classification of tumors. IARC Press, Lyon
3. Fenves AZ, Ram VS (1999) Fibromuscular dysplasia of the renal arteries. Curr Hypertens Rep 1:546–549
4. Fuhrman SA, Lasky LC, Limas C (1982) Prognostic significance of morphologic parameters in renal cell carcinoma. Am J Surg Pathol 6:655–663
5. Heffelinger MJ, Holley KE, Harrison Jr EG, Hunt JC (1970) Arterial fibromuscular dysplasia studied at autopsy. Am J Clin Pathol 54:274 (abstract)
6. Hemmerlein B, Kugler A, Olisik R, Ringert RH, Radzun HJ, Thelen P (2001) Vascular endothelial growth factor expression, angiogenesis, and necrosis in renal cell carcinomas. Virchows Arch 439:645–652
7. Krušlin B, Tomić K, Turčić M, Tomas D, Kos M, Belicza M (2005) Renal artery changes in patients with primary adenocarcinoma of the kidney. Pathol Int 55:40
8. Luscher TF, Lie JT, Stanson AW, Houser OW, Hollier LH, Sheps SG (1987) Arterial fibromuscular dysplasia. Mayo Clin Proc 62:931–952
9. Nickeleit V, Moll S, Cynke E, Brunner FP, Michatsch MJ (1999) A young woman with high blood pressure on haemodialysis: it is never too late to evaluate hypertension. Nephrol Dial Transplant 14:2734–2737

10. Onishi T, Oishi Y, Goto H, Yanada S, Abe K (2002) Histological features of hypovascular or avascular renal cell carcinoma: the experience at four university hospitals. Int J Clin Oncol 7:159–164
11. Rosai J (ed) (2004) Rosai and Ackerman's surgical pathology. Mosby, St. Louis
12. Safian RD, Textor SC (2001) Renal artery stenosis. N Engl J Med 344:431–442
13. Shapiro JA, Williams MA, Weiss NS, Stergachis A, LaCroix AZ, Barlow WE (1999) Hypertension, antihypertensive medication use and risk of renal cell carcinoma. Am J Epidemiol 149:521–530
14. Stanley JC, Gewertz BL, Bove EL, Sottiurai V, Fry WJ (1975) Arterial fibrodysplasia. Histopathologic character and current etiologic concepts. Arch Surg 110:561–566
15. Youngberg SP, Sheps SG, Strong CG (1977) Fibromuscular disease of the renal arteries. Med Clin North Am 61:623–641

Virchows Arch (2006) 448: 29–34
DOI 10.1007/s00428-005-0084-2

ORIGINAL ARTICLE

Sofia Asioli · Gianluca Marucci · Guido Ficarra · Mark Stephens · Maria P. Foschini · Ian O. Ellis · Vincenzo Eusebi

Polymorphous adenocarcinoma of the breast. Report of three cases

Received: 24 May 2005 / Accepted: 28 August 2005 / Published online: 12 October 2005

Abstract We report three cases of polymorphous adenocarcinoma (PLA) of the breast in 37-, 55- and 74-year-old women, respectively. The patients have no evidence of previous malignancy. The tumours consist of monotonous cells showing a wide spectrum of growth patterns: solid nests, trabeculae, tubules, cribriform structures, strands and fascicles reminiscent of polymorphous low-grade adenocarcinoma of salivary glands. To our knowledge, PLA has never been reported in the breast; therefore, this tumour should be added to the list of neoplastic lesions of the breasts that have the same features as those of the salivary glands.

Keywords Polymorphous carcinoma · Breast · Salivary glands

S. Asioli · G. Marucci · M. P. Foschini · V. Eusebi
Section of Pathology, Department of Oncology,
University of Bologna, Bellaria Hospital,
Bologna, Italy

G. Ficarra
Department of Pathology,
University of Modena and Reggio Emilia,
Modena, Italy

M. Stephens
Department of Histopathology,
University Hospital of North Staffordshire,
Stafford, UK

I. O. Ellis
Department of Histopathology,
Nottingham City Hospital, University of Nottingham,
Nottingham, UK

V. Eusebi (✉)
Anatomia Patologica, Ospedale Bellaria,
Università di Bologna,
Via Altura No. 3,
40139 Bologna, Italy
e-mail: vincenzo.eusebi@unibo.it
Tel.: +39-51-6225523
Fax: +39-51-6225759

Introduction

Polymorphous low-grade adenocarcinoma (PLGA) of minor salivary glands is a term given by Evans and Batsakis [8] to a clinicopathological entity of an intraoral malignant tumour, which is also named as terminal duct carcinoma of the oral cavity [13] or as lobular carcinoma of intraoral minor salivary gland origin [12]. These latter authors emphasized similarities between tumours they have described and invasive lobular carcinomas (ILCs) of the breast.

PLGA is virtually exclusive of minor salivary glands of the oral cavity [1, 3]; in rare occasions, it has been reported in the parotid [19] and, in even rarer occasions, in other sites such as the lung [17], skin [24], vulva and vagina [27] and lacrimal glands [22]. The purpose of the present paper is to describe three cases of tumours in the breast with morphology similar to that of PLGA of the salivary glands. To the best of our knowledge, tumours with these features and in such site have not been reported in the literature.

Case report

Patient 1

In 1994, a 37-year-old woman presented with a mass that measured 1.5 cm and was located in the left breast.

The patient had no evidence of previous oropharyngeal primary tumour. She underwent quadrantectomy with axillary lymph node dissection (13 lymph nodes) followed by radiotherapy. On gross examination, the nodule was surrounded by fibrofatty tissue, appeared tan and firm and displayed indistinct borders.

The patient developed liver metastases in early 1997 and died with widespread metastases later in the same year.

Patient 2

A 55-year-old woman presented with a 3.5-cm-diameter firm nodule located in the internal superior quadrant of the

Table 1 Antibodies used

Antibody	Clone	Source	Dilution, AnR
Keratin 7	OV-TL 12/30	Dako	1:100, AnR°
Keratin 14	LL002	Biogenex	1:100, AnR*
SMA	1A4	Dako	1:100, AnR not performed
P63	4A4	Neomarkers	1:200, AnR*
ER	1D5	Dako	1:50, AnR*
PR	PgR636	Dako	1:50, AnR*
AR	AR 441	Neomarkers	1:100, AnR*
E-cadherin	HECD-1	Zymed	1:1,000, AnR*
EMA	E 29	Dako	1:600, AnR not performed
c-Kit	Polyclonal	Dako	1:70, AnR*
Chromogranin	LK2H10	Biogenex	1:400, AnR*
GFAP	6F2	Dako	1:1,200, AnR*
Bcl-2	M0887	Dako	1:20, AnR*

SMA Smooth muscle actin, *AR* androgen receptor, *ER* estrogen receptor, *PR* progesterone receptor, *EMA* epithelial membrane antigen, *AnR°* antigen retrieval submitting sections at enzymatic digestion for 30 min in protease, *AnR** antigen retrieval (submitting sections at high pressure for 6 min at 100°C in citrate buffer)

right breast, which was found to be mammographically positive for carcinoma in November 2004. Fine-needle biopsy showed atypical epithelial cells without myoepithelial cell layers that were considered suspicious of carcinoma. The patient underwent quadrantectomy with axillary lymph node dissection (20 lymph nodes) followed by radiotherapy.

When last contacted, the patient was well 6 months after surgery.

Patient 3

In April 2005, a 74-year-old patient presented with a firm nodule in the upper internal quadrant of the left breast. Fine-needle aspiration led to a positive smear for carcinoma. The patient was treated with simple mastectomy together with axillary dissection (11 lymph nodes). The nodule measured 4 cm in its greatest axis, was hard and grey white and had infiltrative margins. There has been no significant follow-up to date.

Materials and methods

Two cases were retrieved from V.E.'s consult files. Case 3 was encountered among routine cases.

Tissues were fixed in buffered formalin and routinely processed with paraffin. Slides were stained with haematoxylin–eosin; for immunohistochemistry, the ABC method was employed. Source, dilution and antigen retrieval of the antibodies used are listed in Table 1.

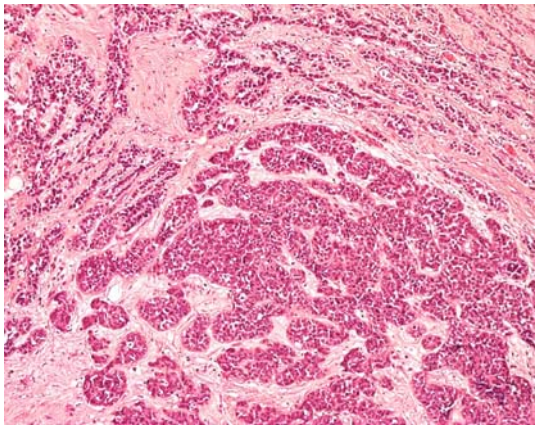

Fig. 1 *Case 1*: The tumour shows a central core composed of solid nests, while at the periphery, neoplastic cells invade in an Indian-file pattern

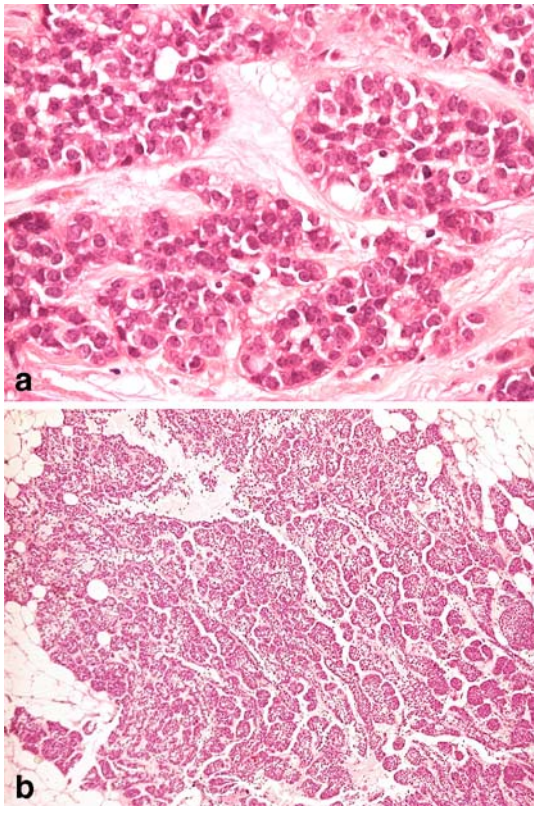

Fig. 2 **a** *Case 1*: Solid nests as observed in the centre of the tumour. Neoplastic cells show round, monotonous nuclei. **b** *Case 2*: Solid nests also characterize the tumour centre of this case

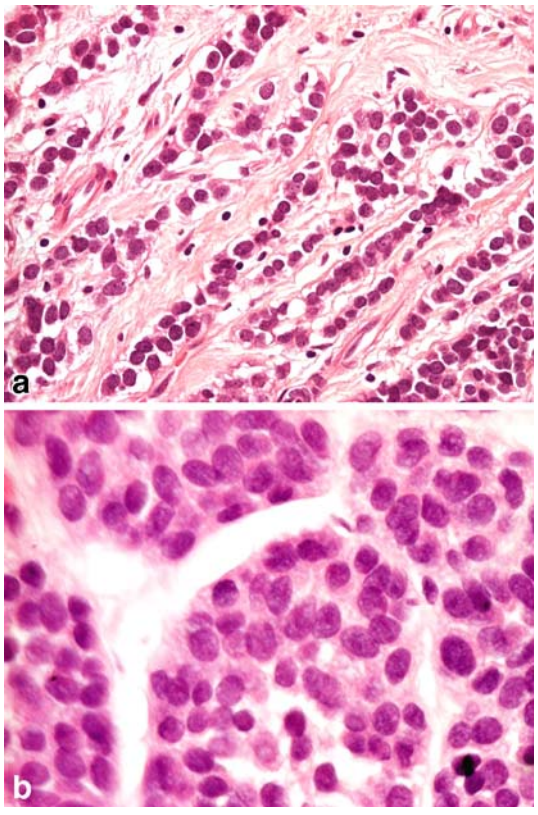

Fig. 3 *Case 1*: **a** Neoplastic cells showing typical "Indian-file" pattern. Round, monotonous nuclei are displayed by neoplastic cells. **b** Cells of a nest showing round, monotonous nuclei

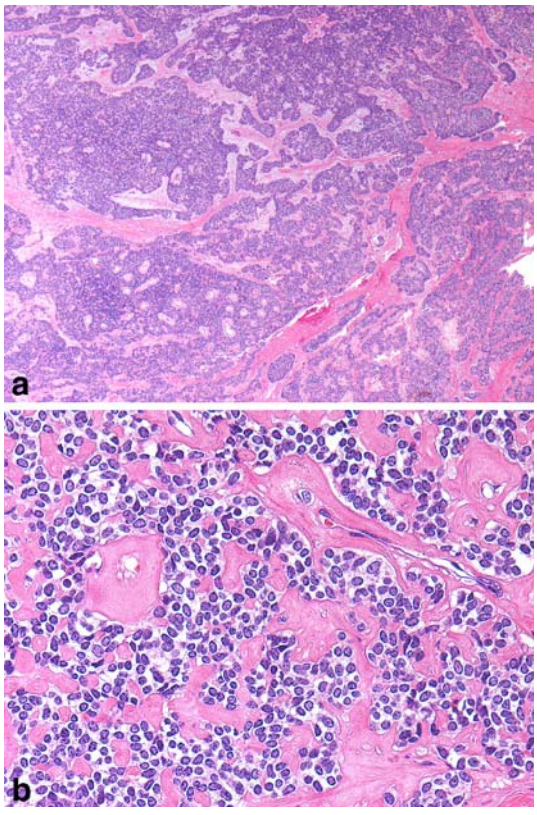

Fig. 4 *Case 3*: **a** Solid nests and sheets as seen at low power. **b** Basal lamina-like material is observed among neoplastic cells

Histology and immunohistochemistry

Patients are described together because their histology and immunohistochemistry are very similar. Microscopically, neoplasms are nonencapsulated and exhibit cells that invade surrounding breast tissues (Fig. 1).

Neoplastic cells show a wide spectrum of growth patterns consisting of solid nests and large areas that are mostly located in the centre of the tumours (Fig. 2a and b), while at periphery trabeculae, occasional tubules and alveolar structures are mostly represented. In some areas, the neoplastic cells show the single-file pattern typical of ILCs (Fig. 3a). Combinations and transitions among all these patterns are frequent. Occasionally entrapped pre-existing ducts, mostly located at the periphery of the tumour, are evident in case 2.

Tumour cells are composed of elements showing moderately variable round to ovoid nuclei with dispersed vesicular chromatin, inconspicuous to small nucleoli and prominent nuclear membrane (Fig. 3b). Mitoses average 10/10, 10/10 and 12/10 high-power fields (HPF; ×400). No tumour necrosis is seen. The stroma within the tumours is collagenous; in case 3, abundant basal lamina is present among the neoplastic cells (Fig. 4). Cytology (i.e. vesicular nuclei) shows the same features as those of the invasive counterpart. All cases are scored as grade 2 [5]. Neither vascular nor nerve invasion is present. No metastases are found in regional lymph nodes in all cases. In situ duct carcinoma of intermediate differentiation [15] is observed at the edge of the invasive lesion in case 3.

The three tumours show similar immunohistochemical features, with minor variations. Keratin 7 strongly and diffusely stains several areas of both lesions, while it appears absent mostly at the periphery of both neoplasms, where resemblance with ILC is more evident (Fig. 5). Keratin 14 is absent in cases 1 and 3, while it occasionally stains cells of case 2. Smooth muscle actin is consistently absent in all cases, as is P63 in cases 1 and 3. The same

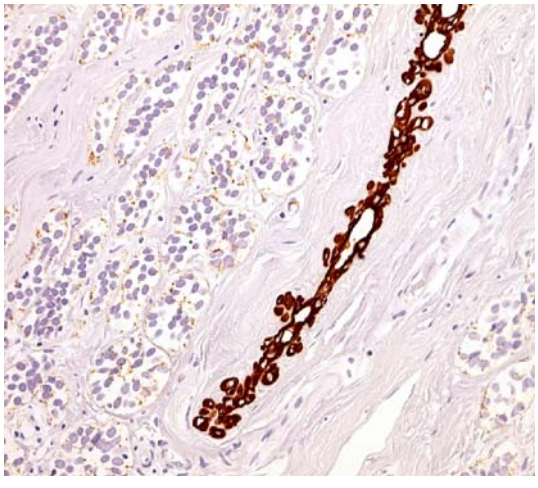

Fig. 5 *Case 1*: Keratin 7 stains residual mammary glands, but neoplastic cells are consistently negative

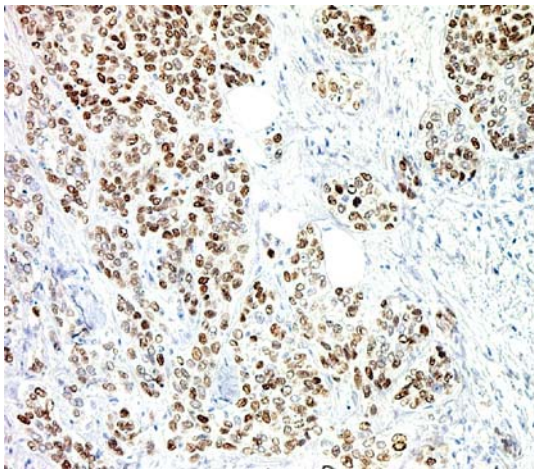

Fig. 6 *Case 2*: P63 stains several nuclei of this neoplastic area

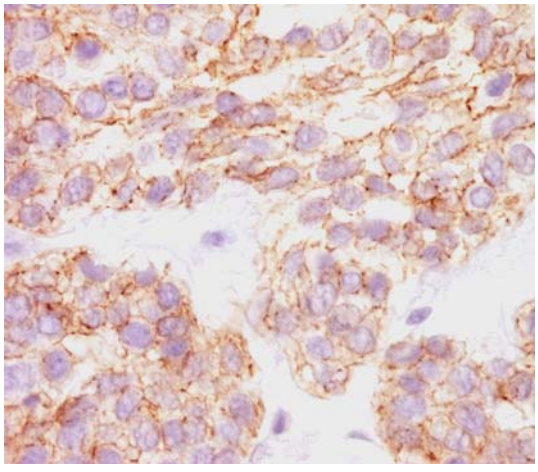

Fig. 7 *Case 2*: E-cadherin stains only segments of the cytoplasmic membrane (fragmented E-cadherin)

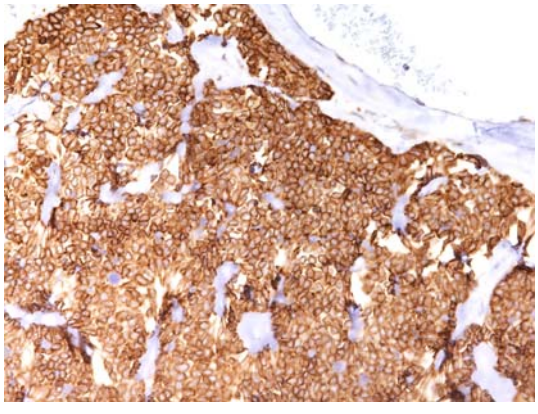

Fig. 8 *Case 3*: Most of the neoplastic elements are consistently positive for Bcl-2

Table 2 Immunohistochemical results

Antisera	Case 1	Case 2	Case 3
Keratin 7	±	±	±
Keratin 14	−	±	±
SMA	−	−	−
P63	−	±	−
ER	−	−	−
PR	−	−	−
AR	ND	−	−
E-cadherin	+	+Fragmented	+Fragmented
EMA	−	−	−
c-Kit	ND	−	−
Chromogranin	ND	−	−
GFAP	ND	−	±
Bcl-2	ND	+	+

SMA Smooth muscle actin, *AR* androgen receptor, *ER* estrogen receptor, *PR* progesterone receptor, *EMA* epithelial membrane antigen, *ND* not done

antibody stains the nuclei of several neoplastic cellular nests, while it is absent in other areas in case 2 (Fig. 6). E-cadherin stains most of the cells from all cases. The stain does not outline the cell membrane, as is usually seen in duct carcinoma, but shows interruption of staining, here named as "fragmented" E-cadherin stain (Fig. 7). Epithelial membrane antigen (EMA) is negative in the three tumours, as are estrogen receptor (ER) and progesterone receptor (PR). Androgen receptors, c-kit and chromogranin are consistently negative in the two cases stained (cases 2 and 3). On the contrary, Blc-2 strongly stains the two cases tested (cases 2 and 3) (Fig. 8). Glial fibrillary acidic protein (GFAP) stains only small areas in case 3 (Table 2).

Discussion

We describe three cases of breast carcinoma with features of polymorphous adenocarcinoma (PLA) similar to those referred to as PLGA of the salivary glands. In recent years, most of the tumours seen in salivary glands have also been reported in the breast [11]. These include, in addition to the well-delineated adenoid cystic carcinoma (ACC) [16], mucoepidermoid [4], acinic cell [2] and syringoid [11, 25] carcinomas. Lesions also shared by the two organs are duct carcinoma [11, 13], mixed salivary gland tumours [18] (including carcinoma ex-pleomorphic adenoma) [14] and adenomyoepithelioma [6] (not to mention pure myoepithelial cell carcinomas) [10]. All these tumours of the breast are morphologically similar to those of the salivary glands, although clinical behaviour can differ, being more aggressive in the salivary gland as a general rule [11].

The three present cases displayed a very polymorphous structure consisting of central areas showing solid nests, surrounded at the periphery by alveolar and cribriform structures as well as trabeculae and Indian-file-arranged cells. Neoplastic elements had moderate variability of nuclei that appeared round to ovoid, with sparse vesicular

chromatin. Mitoses ranged from 10 to 12 per 10 HPF, and necrotic areas were absent. Bcl-2 was strongly positive in the two cases tested, and GFAP showed areas of positive elements in one case. All these features were consistent with the features of PLGA as described in minor salivary glands [1, 8].

The present tumours in the salivary glands have to be distinguished from ACCs. The fact that they show only one type of cell and are devoid of actin-positive elements in both cases, as well as of c-kit in cases 2 and 3, renders these tumours different from ACC, which, on the contrary and by definition, shows two types of cells and actin-positive elements [16].

ILC was simulated in the present cases by the Indian-file pattern shown in some peripheral areas. The neoplastic cells from the three cases were E-cadherin-positive, and EMA, ER and PR were, on the contrary, distinctly negative, with all features being different from those seen in ILC [7, 26]. Androgen receptors were consistently negative in the two cases stained (cases 2 and 3)—a finding that was not common in ILCs, which were positive in nearly 90% of the cases [21].

No evidence of neuroendocrine differentiation was present both at structural and immunohistochemical levels [20].

Admittedly, cases 2 and 3 are recent patients, but case 1 had a very aggressive clinical course, with the patient dying of widespread disease 3 years after diagnosis. All three cases were scored as grade 2, were of large sizes and had invasive margins at the moment of diagnosis. No ER and PR were present. Therefore, it seems that, in view of the present data, the biological behaviour and morphological features of the three tumours are more in consonance with those of high-grade carcinomas. In this respect, it seems that the term *low grade*, as used for the PLGA of the salivary glands, is not appropriate for the present breast tumours.

In the salivary glands, no fewer than 13 of 40 PLGA cases reported by Evans and Luna [9] had local recurrences; six cases presented with lymph node metastases and three cases had distant metastases. These data are in consonance with other reports of PLGA [23] in which it appears that, even in salivary glands, it remains an aggressive lesion and, consequently, the term *low grade* does not seem appropriate anymore. In the skin, three of six cases of adenocarcinoma with features very similar to those of the PLGA of the salivary glands recurred (two cases) or metastasized (one case) [24]. Aggressive clinical behaviour led these same authors [24] to name their lesion as polymorphous carcinoma of the sweat glands—a name that can also be adopted in carcinoma of the breast for the same reason. At variance with the present cases, the PLGA of the salivary glands frequently shows neurotropism [1]. This might be due to the limited number of the present cases or due to different anatomic sites of origin, as the same phenomenon is seen in ACCs occurring in the breast [16].

In conclusion, the purpose of the present paper was to report on three cases of PLA of the breast, the last of salivary-gland-like tumours that has not yet been reported in this site. We propose that the three cases presented in this report fill this gap.

Acknowledgements The work was financed by grant no. 2002064975 (Cofin 2002) of the Ministry of University and Research and by the University of Bologna (60%). Dr. G. Collina is thanked for providing us access to case 3.

References

1. Castle JT, Thompson LD, Frommelt RA, Wenig BM, Kessler HP (1999) Polymorphous low grade adenocarcinoma: a clinicopathological study of 164 cases. Cancer 86:207–219
2. Damiani S, Pasquinelli G, Lamovec J, Peterse JL, Eusebi V (2000) Acinic cell carcinoma of the breast: an immunohistochemical and ultrastructural study. Virchows Arch 437:78–81
3. Darling MR, Schneider JW, Phillips VM (2002) Polymorphous low-grade adenocarcinoma and adenoid cystic carcinoma: a review and comparison of immunohistochemical markers. Oncology 38:641–645
4. Di Tommaso L, Foschini MP, Ragazzini T et al (2005) Mucoepidermoid carcinoma of the breast. Virchows Arch 444:13–19
5. Elston CW, Ellis IO (1998) Assessment of histological grade. In: Elston CW, Ellis IO (eds) The breast. Livingstone, Edinburgh, pp 365–384
6. Eusebi V, Casadei GP, Bussolati G, Azzopardi JG (1987) Adenomyoepithelioma of the breast with a distinctive type of apocrine adenosis. Histopathology 11:305–315
7. Eusebi V, Pich A, Macchiorlatti E, Bussolati G (1977) Morpho-functional differentiation in lobular carcinoma of the breast. Histopathology 1:301–314
8. Evans HL, Batsakis JG (1984) Polymorphous low-grade adenocarcinoma of minor salivary gland. Cancer 53:935–942
9. Evans HL, Luna MA (2000) Polymorphous low-grade adenocarcinoma. A study of 40 cases with long-term follow up and an evaluation of the importance of papillary areas. Am J Surg Pathol 24(10):1319–1328
10. Foschini MP, Eusebi V (1998) Carcinoma of the breast showing myoepithelial cell differentiation. Virchows Arch 432:303–310
11. Foschini MP, Reis-Filho JS, Eusebi V, Lakhani SR (2003) Salivary gland-like tumours of the breast: surgical and molecular pathology. J Clin Pathol 56:497–506
12. Freedman PD, Lumerman H (1983) Lobular carcinoma of intraoral minor salivary gland origin. Report of twelve cases. Oral Surg Oral Med Oral Pathol 56:157–166
13. Garland TA, Innes DJ, Fechner RE (1984) Salivary duct carcinoma. Am J Clin Pathol 81:436–441
14. Hayes MM, Lesack D, Girardet C, Del Vecchio M, Eusebi V (2005) Carcinoma ex-pleomorphic adenoma of the breast. Report of three cases suggesting a relationship to metaplastic carcinoma of matrix producing type. Virchows Arch 446:142–149
15. Holland R, Peterse JL, Millis RR et al (1994) Ductal carcinoma in situ: a proposal for a new classification. Semin Diagn Pathol 11(3):167–180
16. Lamovec J, Us-Krasovec M, Zidar A, Kljiun A (1989) Adenoid cystic carcinoma of the breast: a histologic, cytologic and immunohistochemical study. Semin Diagn Pathol 6:153–164
17. Lee VKM, Mccaughan BC, Scolyer RA (2004) Polymorphous low-grade adenocarcinoma in the lung: a case report. Int J Surg Pathol 12:287–292
18. Moran CA, Suster S, Carter D (1990) Benign mixed tumors (pleomorphic adenomas) of the breast. Am J Surg Pathol 14 (10):913–921
19. Nagao T, Gaffey TA, Kay PA, Minato H, Serizawa H, Lewis JE (2004) Polymorphous low-grade adenocarcinoma of the major salivary glands: report of three cases in an unusual location. Histopathology 44:164–171

20. Papotti M, Macrì L, Finzi G, Capella C, Eusebi V, Bussolati G (1989) Neuroendocrine differentiation in carcinomas of the breast: a study of 51 cases. Semin Diagn Pathol 6:174–188
21. Riva C, Dainese E, Caprara G et al (2005) Immunohistochemical study of androgen receptors in breast carcinoma. Evidence of their frequent expression in lobular carcinoma. Virchows Arch 1–6 (Epub ahead of print)
22. Selva D, Davis GJ, Dodd T, Rootman J (2004) Polymorphous low-grade adenocarcinoma of the lacrimal gland. Arch Ophthalmol 122:915–917
23. Simpson RHW, Reis-Filho JS, Pereira EM, Ribeiro AC, Abdulkadir A (2002) Polymorphous low-grade adenocarcinoma of the salivary glands with transformation to high-grade carcinoma. Histopathology 41:2509–2259
24. Suster S, Wong TY (1994) Polymorphous sweat gland carcinoma. Histopathology 25:31–39
25. Van Hoeven KH, Drudis T, Cranor ML, Erlandson RA, Rosen PP (1993) Low-grade adenosquamous carcinoma of the breast: a clinicopathologic study of 32 cases with ultrastructural analysis. Am J Surg Pathol 17(3):248–258
26. Vos CB, Cleton-Jansen AM, Berx G (1997) E-cadherin inactivation in lobular carcinoma in situ of the breast: an early event in tumorigenesis. Br J Cancer 76:1131–1133
27. Young S, Leon M, Talerman A, Teresi M, Emmadi R (2003) Polymorphous low-grade adenocarcinoma of the vulva and vagina: a tumor resembling adenoid cystic carcinoma. Int J Surg Pathol 11:43–49

Virchows Arch (2006) 448: 35–45
DOI 10.1007/s00428-005-0081-5

ORIGINAL ARTICLE

David Mondada · Fredrik T. Bosman · Charlotte Fontolliet · Walter K. F. Seelentag

Elevated hepatocyte paraffin 1 and neprilysin expression in hepatocellular carcinoma are correlated with longer survival

Received: 14 April 2005 / Accepted: 25 August 2005 / Published online: 12 October 2005

Abstract Hepatocyte paraffin 1 (Hep Par 1) and neprilysin (CD10) are well-known markers of hepatocellular carcinoma (HCC). To assess their potential prognostic role, we conducted a retrospective analysis of 97 formalin-fixed and paraffin-embedded HCC from patients treated by surgery with curative intent, using standard immunohistochemical procedures and semiquantitative analysis. Strong Hep Par 1 expression and canalicular CD10 staining pattern were significantly correlated with smaller tumor size (p=0.007 and 0.04, respectively). On univariate analysis, longer overall survival was observed in patients with strong Hep Par 1 expression (p=0.0005) and in patients with a CD10can staining pattern (p=0.02). On multivariate analysis, the combined immunohistochemical score (CIS) obtained by addition of Hep Par 1 and CD10can scores and subtraction of cytoplasmic CD10 score was retained as the single most important prognostic factor (p=0.001). Patients with a CIS <4 had a 3.5-fold increased risk of death, as compared to those with a CIS ≥4. In conclusion, strong Hep Par 1 expression, presence of CD10can labeling, and absence of CD10cyt staining are favorable prognostic factors in HCC, which can be easily combined into a single immunohistochemical score for routine clinical use.

Keywords Carcinoma · Hepatocellular · Immunohistochemistry · Antibodies · Monoclonal · Prognosis

D. Mondada · F. T. Bosman · C. Fontolliet · W. K. F. Seelentag (✉)
Institute of Pathology, University of Lausanne,
Bugnon 25,
1011 Lausanne, Switzerland
e-mail: Walter.Seelentag@hospvd.ch
Tel.: +41-21-3147208
Fax: +41-21-3147115

Introduction

Prognosis of hepatocellular carcinoma (HCC) after hepatic resection with curative intent remains very poor despite improved surgical techniques [17, 23, 26]. In addition, in low endemic areas like Switzerland, HCC is often discovered in elderly patients with a long-standing alcoholic cirrhosis and at high operative risk. Therefore, adequate prognostic stratification of the patients to guide the clinician in treatment choice is essential. The most important histopathologic prognostic factors are tumor size, vascular invasion, tumor multifocality, and tumor grade [1, 24, 29, 30]. Combined scores based on histological features or image analysis have also been proposed [23]. In addition, the prognostic significance of a variety of gene products related to the cell cycle or to cell adhesion has been described in the literature, such as the tumor-suppressor gene p53, the cell cycle inhibitors p21, p27, and cyclin D, and the cell adhesion molecule beta-catenin [18, 20, 31]. However, none of these markers have found their way into routine clinical use.

Hepatocyte paraffin 1 (Hep Par 1) [2, 21, 27, 38] and neprilysin (CD10 or CALLA) [5, 40] are well-established markers of HCC, and their use as diagnostic aid is well documented in the literature. Hep Par 1 has been obtained by immunizing mice with a crude antigen extracted from human liver tissue [38]. It reacts with a hepatocyte-specific epitope of the mitochondrial membrane [21, 22, 38], resulting in a granular cytoplasmic staining pattern. This marker has been shown to be highly specific for normal and neoplastic liver tissue. CD10 is a zinc-dependant cell membrane metallopeptidase, which participates in the postsecretory processing of neuropeptidases and peptide hormones [37]. In the past, it has been widely used as a marker of lymphoblasts in acute lymphoblastic leukemia [4]. More recently, it has also been shown that CD10 is expressed on the canalicular domain of the cell membrane in normal and neoplastic liver tissue [7, 11, 12].

Specificity of these two markers has been well established in the literature, allowing the distinction of HCC

from cholangiocarcinomas and carcinoma metastases to the liver [25, 27, 28]. Surprisingly, to our knowledge, despite several studies on the diagnostic value of these markers and their association with tumor grade and growth pattern, the possible association of their expression with survival has never been examined in detail. In reviewing our pilot series of HCC, the extent of Hep Par 1 and canalicular CD10 (CD10can) expression seemed to be related to the degree of differentiation. In contrast, cytoplasmic CD10 (CD10cyt) expression seemed to be restricted to cases with low Hep Par 1 and CD10can expression. We therefore decided to systematically evaluate the prognostic value of these three parameters. In the current retrospective study, we analyze the immunohistochemical expression of Hep Par 1 and CD10 in formalin-fixed and paraffin-embedded HCC tissue from patients who underwent either partial hepatectomy with curative intent or total hepatectomy followed by liver transplantation to assess their prognostic value.

Patients and methods

Patients and tissue samples

All patients (n=122) who underwent either partial hepatectomy with curative intent or total hepatectomy with liver transplantation because of primary HCC and who were diagnosed at the Institute of Pathology in Lausanne, Switzerland, between January 1992 and May 2001 were selected for this retrospective study. Excluded were patients with mixed hepato-choloangiocarcinoma (n=8), fibrolamellar carcinoma (n=1), inadequate follow-up (n=11), missing material for immunohistochemistry (n=2), and patients who died within 30 days after diagnosis (n=3). The ethics committee of our institution approved the study protocol.

The remaining 97 patients consisted of typical Western European patients whose clinical characteristics were similar to those of several other published series [9, 26, 32]. Treatment was partial liver resection in 72 patients (74%) and total hepatectomy followed by liver transplantation in 25 patients (26%). Most patients (78%) were men. The median age was 63 years (range 14 to 89 years) and was similar for male and female patients. Cirrhosis was found in 67 patients (69%). Serology was positive for hepatitis B virus surface antigen in 10 patients (10%) and hepatitis C virus antigen in 18 patients (19%). Preoperative aspartate aminotransferase, alanine aminotransferase, gamma glutamyl transferase, and alpha-fetoprotein (AFP) levels were also recorded. Overall survival time was calculated from date of diagnosis to date of death or date of last follow-up until closure of the study which was chosen at 30 August 2002. Intermediate outcomes were not considered. Median follow-up time computed according the Kaplan–Meier estimate of potential follow-up was 47 months. Overall median survival time was 28 months in the whole cohort and 23 months in the subgroup of patients treated with partial hepatectomy.

All specimens were fixed in 10% buffered formalin and embedded in paraffin according to standard histological practice. All available hematoxylin/eosin-stained sections (mean 3, range 1 to 12) were reviewed by two experienced pathologists (D.M. and C.F.), and a representative paraffin block containing both carcinoma and nontumorous tissue was selected for immunohistochemistry. Tumor stage was determined using the International Union against Cancer's tumor–nodes–metastasis (TNM) classification of malignant tumors [34]. Because of small sample size, stages pT1 and pT2 were grouped together. Tumors were divided into grades 1, 2, 3, and 4 according to Edmondson and Steiner [13]. In the case of a heterogeneous tumor, the highest grade was retained for the database. Classification of tumor architecture into trabecular, acinar, compact, and scirrhous growth pattern was performed according to the World Health Organization's criteria [16]. Because of relatively low numbers of tumors in the various non-trabecular categories, they were grouped together for statistical analysis. Tumor size, tumor multifocality (solitary nodules/multiple nodules), and microvascular invasion (MVI) were also recorded. Hepatocellular Prognostic Index (HPI) was computed according to Lauwers et al. [23], using the following formula: HPI = (MVI status × 0.459) + (nuclear grade × 0.287). Two prognostic groups were derived from this index: HPI-low (HPI≤0.746), corresponding to patients with rather good prognosis according to Lauwers et al. [23], and HPI-high (HPI>0.746), corresponding to patients with poor prognosis.

With regard to tumor stage, 33 patients (34%) had stages I and II disease, 29 (30%) had stage III, and 35 had (36%) stage IV. Most HCC were less than 5 cm in size (n=58, 60%), solitary (n=54, 56%), and with a trabecular architecture (n=75, 77%). The tumor differentiation was grade 1 in 15 HCC (15%), grade 2 in 47 (48%), grade 3 in 27 (28%), and grade 4 in 8 (8%). MVI was present in 35 HCC (36%). HPI was high in 51 tumors (53%).

Immunohistochemistry

Immunohistochemistry was performed with mouse monoclonal antibodies directed against Hep Par 1 (clone OCH1E5, DAKO) and CD10 (clone 56C6, Novocastra) using the streptavidin biotin complex (ABC) method. In brief, 3–4 μ tissue sections were mounted on aminopropylmethoxysilane-coated slides, deparaffinized in xylene, and rehydrated in a graded alcohol series. Endogenous peroxidase was blocked with 1% H_2O_2 in methanol for 30 min at room temperature. Antigen retrieval was performed by boiling the sections (microwave) in 10 mM citrate buffer pH 6.0 for 15 min (Hep Par 1) or 1 mM in EDTA pH 7.5 for 15 min (CD10). After conditioning with normal horse serum at a 1:30 dilution for 5 min, the sections were incubated either with anti-Hep Par 1 at a 1:10 dilution for 1 h or with anti-CD10 at a 1:20 dilution overnight. Detection was performed using biotinylated anti-mouse IgG at a 1:200 dilution and peroxidase-conjugated ABC complex (both from Vector Laboratories) according to the manufacturer's specifications. Between all steps, sections were washed in Tris-buffered saline. Peroxidase activity was revealed with

3,3-diaminobenzidine-tetrahydrochloride as chromogen, and sections were counterstained with Mayer's hematoxylin.

Primary antibodies were omitted as a negative control. Nontumorous liver tissue adjacent to HCC and present on the same slide was used as positive control.

The immunohistochemical Hep Par 1 and CD10 staining of all slides was evaluated independently by two observers (D.M. and W.K.F.S) in a blinded manner. Divergent scorings were discussed until a consensus was reached. To assess reproducibility, a subset of slides was analyzed by a third pathologist (F.T.B.), who had not done the initial evaluation based on the information contained in this manuscript without additional training. Individual tumor cells were considered to be positive for Hep Par 1 when their cytoplasmic staining intensity was similar or stronger than that of the adjacent nontumorous hepatocytes. CD10cyt staining was considered to be positive in tumor cells when the cytoplasm showed unambigous labeling in contrast to the preexisting hepatocytes which were negative. Positive CD10can staining was defined as crisp focal labeling of the canalicular aspects of the tumor cell membrane when its intensity was similar or stronger than that of the nontumorous canaliculi.

Based on the percentage of positive cells, Hep Par 1, CD10can, and CD10cyt immunolabelings were semiquantitatively classified into four groups, based on a priori determined cutoff points. In the first group, less than 5% of the tumor cells were positive (score 0); in the second group, 5 to 30% of the tumor was positive (score 1); in the third group, 30 to 90% of the tumor cells were positive (score 2); and in the last group, more than 90% of the tumor was positive (score 3).

A combined immunohistochemical score (CIS) was computed as follows: CIS = Hep Par 1 score + CD10can score − CD10cyt score.

Statistical analysis

Correlation tests between immunohistochemical and clinicopathological parameters were performed using either Kruskal–Wallis tests (for continuous or ordered variables such as age, HPI, or tumor grade) or Chi-squared tests (for categorical variables), unless there was concern regarding an inadequate number of observations, in which case, a Fisher's exact test was used [3].

Overall interobserver agreement was compared using kappa statistics. According to common usage, kappa values of ≤0.5 were considered "poor", 0.51–0.6 "moderate", 0.61–0.8 "good", and >0.8 "excellent".

For Fisher's exact tests and survival analysis, clinicopathological and immunohistochemical variables were dichotomized into groups of similar size as follows: age <65 vs. ≥65 years, tumor size ≤5 vs. >5 cm, HPI ≤0.746 (low) vs. >0.746 (high), Hep Par 1<3 vs. =3, CD10can <2 vs. ≥2, CD10cyt <1 vs. ≥1, and CIS <4 vs. ≥4.

Survival percentages over time were calculated by the Kaplan–Meier method [19], and their corresponding standard errors were determined using the formula of Greenwood [15]. Univariate associations between the potential prognostic factors and overall survival were tested using the log-rank test.

Prognostic variables which had been at least marginally significant in univariate analysis (log-rank test <0.1) were further analyzed in various Cox regression models using backward selection with $p<0.05$ as the exit criterion.

Given the relatively small number of outcome events, several distinct Cox regression models with a limited number of covariates had to be evaluated [6].

Estimated hazard ratios of death, with respect to the indicated reference group, their 95% confidence intervals (CI), and p values were calculated with appropriate binary variables to identify each group of interest [10]. Values of hazard ratios greater than unity indicated increased rates of death with respect to the chosen reference category.

To evaluate the impact of type of surgery, univariate and multivariate analysis were done on the whole study population as well as on the subgroup of patients with partial liver resection.

Statistical analyses were carried out by means of the software packages Stata, S-plus 2000, and SPSS.

All probability values were evaluated by two-sided tests, and differences were considered to be significant if the p value was less than 0.05.

Results

Correlation of Hep Par 1 and CD10 immunolabeling with clinicopathological features

Hep Par 1 resulted in a diffuse labeling of the cytoplasm of nontumorous hepatocytes, which served as internal positive control, with a distinctive granular pattern. It was independent of the underlying liver pathology, and there was no staining difference between cirrhotic and non-cirrhotic liver tissue. Most HCC showed a similar cytoplasmic labeling, albeit at a highly variable intensity (Fig. 1a–c). Hep Par 1 expression, evaluated semiquantitatively as outlined in "Patients and methods", was extensive (score 3) in 54 (55%) HCC, partial (score 2) in 31 (32%) HCC, and focal or absent (score 1 or 0) in 13 (13%) HCC.

CD10 labeled in nontumorous liver exclusively the luminal portion of bile canaliculi of the hepatocytes as well as the luminal surface of the bile duct epithelium. There was no staining difference between cirrhotic and non-cirrhotic liver. In HCC, a similar canalicular staining pattern was seen forming sharp branching lines which were typically located between cells and not within them (Fig. 1d–f). CD10can labeling was widespread (score 3) in 20 (21%) HCC, partial (score 2) in 38 (39%) HCC, focal (score 1) in 11 (11%) HCC, and completely absent in 28 (29%) HCC. In addition, some HCC displayed a CD10cyt labeling (Fig. 1g,h), and very few tumors exhibited a diffuse cell membrane staining. This type of staining was not seen in nontumorous hepatocytes. CD10cyt staining

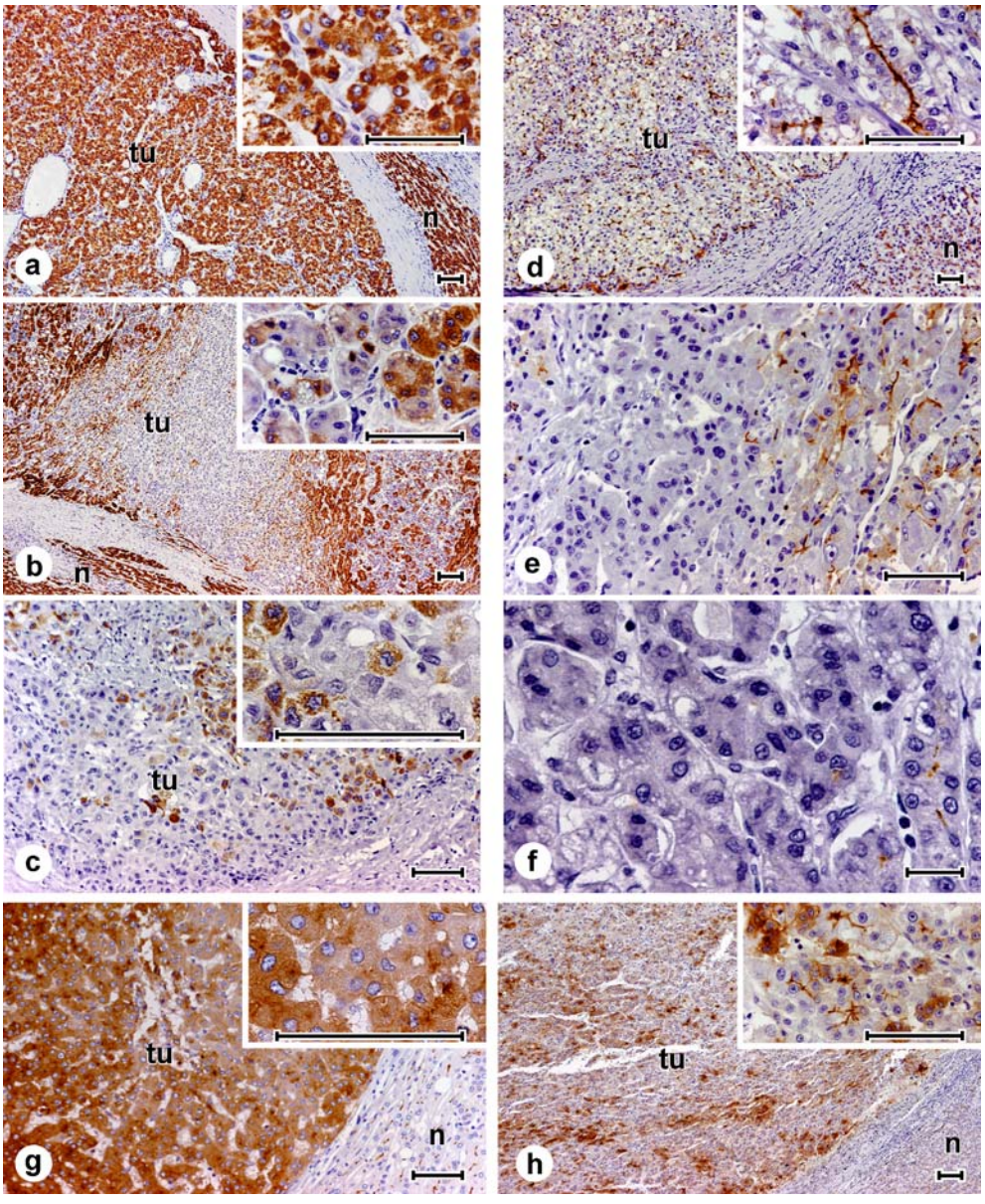

Fig. 1 Representative examples of immunohistochemical staining in HCC for Hep Par 1 (**a**–**c**) and CD10 (**d**–**h**): individual tumor cells (*tu*) are considered positive for Hep Par 1 when their cytoplasmic immunolabeling is similar to that of adjacent nontumorous hepatocytes (*n*). CD10 labeling is considered to be canalicular (**d**–**f**) when there is a crisp linear staining between adjacent tumor cells (*inset*, **d**). CD10cyt staining is considered significant if individual tumor cells show an unambigous cytoplasmic staining in contrast to surrounding nontumorous liver tissue which is negative (**g**–**h**). Scoring is based on the percentage of positive tumor cells: score 3, more than 90% labeled tumor cells (**a**, **d**, and **g**); score 2, between 30 and 90% (**b**, **e**, and **h**); and score 1, less than 30% positive tumor cells (**c** and **f**). *Scale bars* 100 μm

was extensive (score 3) in 5 (5%) HCC, partial (score 2) in 23 (24%) HCC, focal (score 1) in 18 (19%) HCC, and absent in 51 (52%) HCC.

Correlations between immunohistochemical features and histopathologic parameters are reported in detail in Table 1. High levels of Hep Par 1 expression (score=3) were significantly correlated with small tumor size (p=0.007), absence of MVI (p=0.03), and low HPI (p=0.04). In addition, Hep Par 1 expression decreased with increasing tumor grade in a significant manner (p=0.01; Fig. 2a). All other parameters, including International Union Against Cancer tumor stage and tumor pattern, lacked any significant correlation with Hep Par 1 score. Extensive CD10can labeling (score≥2) was more frequent in small HCC (p=0.04) and male patients (p=0.01). Like Hep Par 1, CD10can expression was reduced in poorly differentiated tumors (p=0.03; Fig. 2b). CD10cyt staining was not correlated with any clinicopathological feature. A high CIS (≥4) showed a highly significant correlation with reduced tumor size (p=0.05), and it was also more frequently observed in male patients (p=0.04). Furthermore, CIS decreased with decreasing tumor differentiation (p=0.05; Fig. 2c).

To assess reproducibility, a subset of immunolabelings was reviewed by another pathologist without particular training. The interobserver agreement was excellent for Hep Par 1 and CD10can labeling (κ=0.87) and moderate for CD10cyt labeling (κ=0.53).

Correlation of Hep Par 1 and CD10 expression with survival by univariate analysis

To determine the prognostic value of Hep Par 1 and CD10 labeling, the immunohistochemical scores were analyzed as categorical variables using cutoff points that were chosen in a manner to split the study population in two

Table 1 Relationship between expression of Hep Par 1 or CD10 and pathological factors

Factor	Total number of patients	Number of patients with Hep Par 1 score =3	*p* values[a]	CD10 canalicular score ≥2	*p* values	CD10 cytoplasmic score ≥1	*p* values	CIS[b] ≥4	*p* values
Tumor size (cm)									
≤5	58	39 (67%)[c]	0.007	40 (70%)	0.04	20 (51%)	NS	29 (50%)	0.005
>5	39	15 (39%)		18 (46%)		26 (45%)		8 (21%)	
MVI									
Absent	62	40 (65%)	0.03	37 (60%)	NS	29 (47%)	NS	26 (42%)	NS
Present	35	14 (40%)		21 (60%)		17 (49%)		11 (31%)	
HPI[d]									
Low	46	31 (67%)	0.04	30 (65%)	NS	23 (50%)	NS	21 (46%)	NS
High	51	23 (45%)		28 (55%)		23 (45%)		16 (31%)	

NS Statistically not significant
[a]Two-sided *p* values obtained by Fisher's exact test, which are considered to be significant if $p<0.05$, of marginal significance if $0.05\leq p<0.1$, and not significant if $p\geq 0.1$
[b]CIS (score Hep Par 1 staining+score CD10 canalicular staining−score CD10 cytoplasmic staining)
[c]Percentages are computed with regard to number of patients for a given factor category
[d]HPI according to Lauwers et al. [23]

groups of similar size. To detect a possible bias resulting from the type of surgery, univariate and multivariate survival analyses were done not only on the whole study population but also on the subgroup of patients with partial liver resection. On univariate analysis (Table 2) of the whole cohort, Hep Par 1 expression and CD10can labeling were significantly associated with overall survival (p=0.0005 and 0.02, respectively). Indeed, median survival time of patients with tumors showing a strong Hep Par 1 staining (score=3) was more than 100 months in contrast to patients with a score of <3 who survived only 15 months (Fig. 3a). Similarly, survival of patients with an at least moderate CD10can staining (score ≥2) was 54 months in contrast to 17 months for the other patients (Fig. 3b). Similar results were found in the subgroup of patients with partial liver resection, who showed also a significant association of strong Hep Par 1 staining with longer median overall survival (33 vs. 14 months, p=0.03). There was a trend toward better overall survival among patients with a CD10can score of ≥2 (28 vs. 16 months, p=0.09). In contrast,

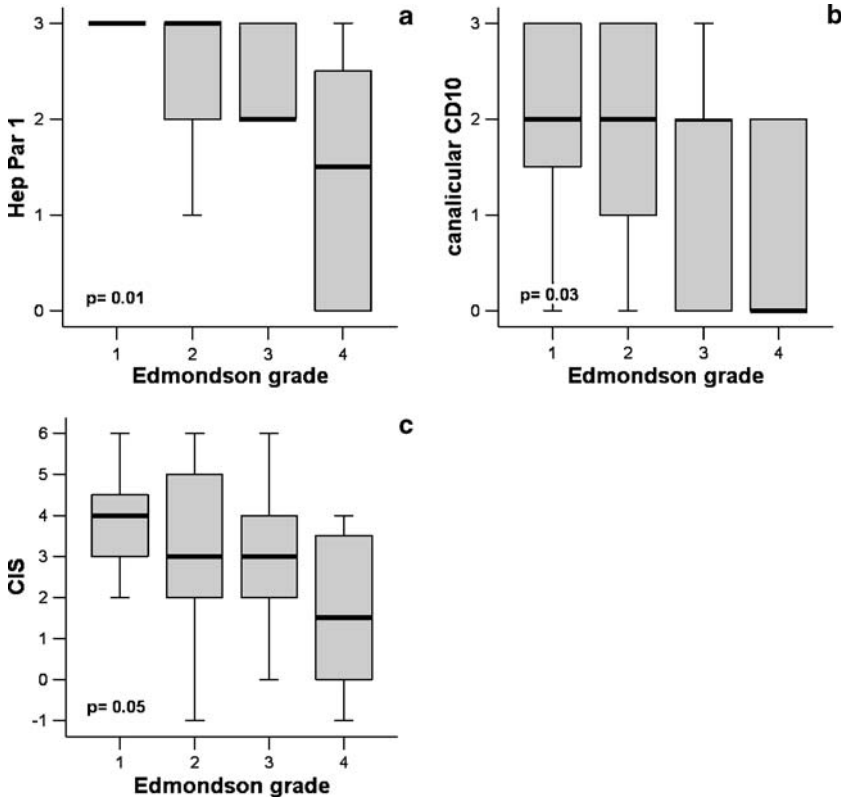

Fig. 2 Correlation between Edmondson and Steiner's tumor grade and immunohistochemical scores: Hep Par 1 expression is significantly decreased in grades 3 and 4 carcinomas (**a**). CD10can expression is highly decreased in grade 4 tumors (**b**). Combined immunohistochemical score (CIS=Hep Par 1 score + CD10can score − CD10cyt score) shows a progressive decrease with increasing tumor grade (**c**). *p* values were determined using Kruskal–Wallis tests

Table 2 Univariate analysis of the immunohistochemical factors

Immunohistochemical score	All patients				Only patients treated by partial resection			
	Number of patients (censored)	Median survival time (month)	95% CI (month)	*p* values[a]	Number of patients (censored)	Median survival time (month)	95% CI (month)	*p* values
Hep Par 1								
<3	43 (9)	15	9–21	0.0005	36 (6)	14	6–22	0.03
=3	54 (32)	>100	–		36 (18)	33	6–60	
CD10 canalicular staining								
<2	39 (11)	17	7–27	0.02	31 (7)	16	6–26	0.09
≥2	58 (30)	54	24–84		41 (17)	28	4–52	
CD10 cytoplasmic staining								
<1	51 (24)	31	17–45	NS	34 (13)	27	10–44	NS
≥1	46 (17)	27	11–43		38 (11)	16	0–33	
CIS[b]								
<4	60 (16)	17	9–25	0.0004	48 (9)	16	13–19	0.004
≥4	37 (25)	>80	–		24 (15)	>80		

NS Statistically not significant

[a]Two-sided *p* values obtained by log-rank test, which are considered to be significant if $p<0.05$, of marginal significance if $0.05\leq p<0.1$, and not significant if $p\geq 0.1$

[b]CIS (score Hep Par 1 staining + score CD10 canalicular staining − score CD10 cytoplasmic staining)

there was only a weak association between CD10cyt labeling and overall survival in the whole cohort (p=0.2) and in the subgroup of patients with partial resection (p=0.3). Patients with CD10cyt positive tumors tended to have a reduced overall survival as compared to patients with CD10cyt negative tumors.

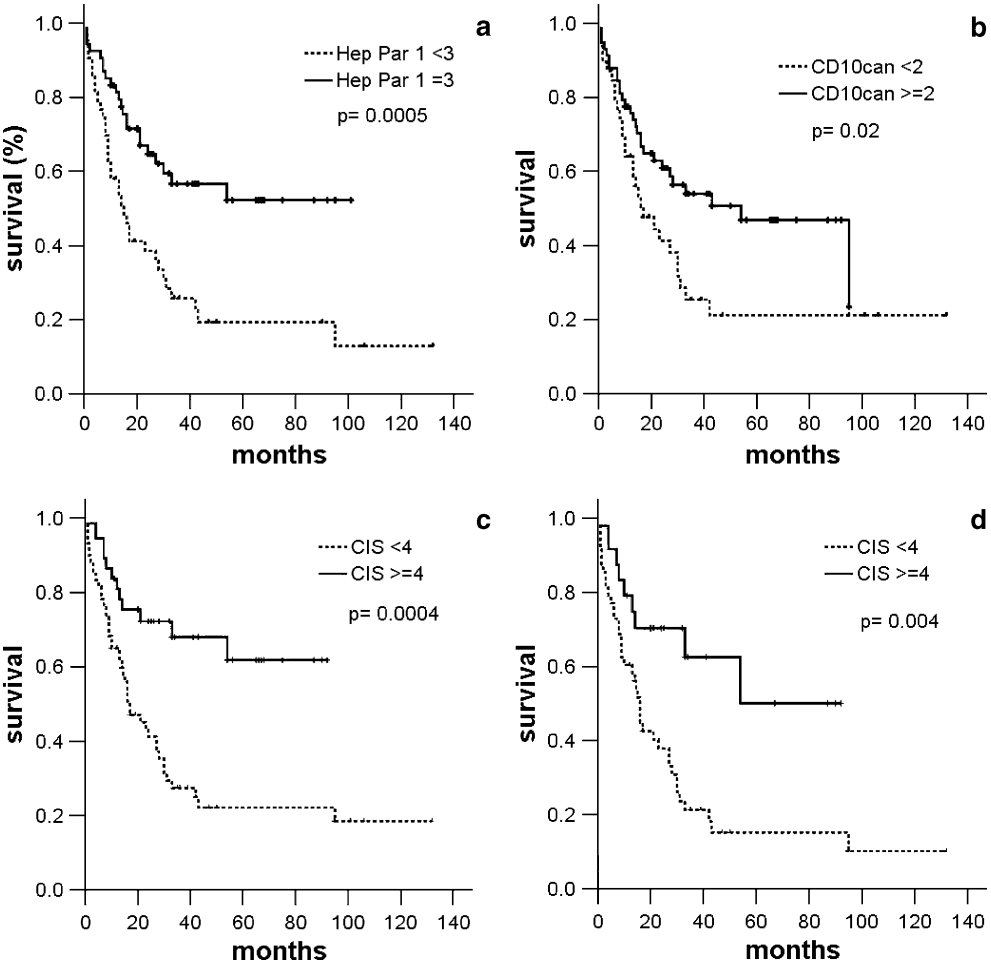

Fig. 3 Overall survival curves of all 97 patients who underwent either partial hepatectomy with curative intent or total hepatectomy with liver transplantation according to Hep Par 1 score (**a**), CD10can score (**b**), combined immunohistochemical score (CIS=Hep Par 1 score + CD10can score − CD10cyt score) (**c**). Overall survival curves of the subgroup of 72 patients who underwent partial hepatectomy with curative intent according to combined immunohistochemical score (**d**). *p* values were determined using the log-rank test

To be able to use these immunohistochemical parameters in a routine clinical setting, they were combined into a simple score according to the following formula: CIS = Hep Par 1 score + CD10can score − CD10cyt score. On univariate analysis, there was a highly significant correlation between CIS and overall survival in both the whole cohort (p=0.0004) and the patients with partial liver resection (p=0.01). In the whole study population, patients with a CIS ≥4 survived more than 80 months whereas the median overall survival of the others was only 17 months (Fig. 3c). Similar median overall survival times were found in the subgroup of partially resected patients (80 vs. 16 months; Fig. 3d).

Multivariate survival analysis

Multivariate analysis was performed using several Cox regression models with a limited number of covariates, because the number of outcome events did not allow the evaluation of all pertinent parameters at once. Prognostic variables which had been at least marginally significant (log-rank test <0.1) in univariate analysis (tumor size, stage, multifocality, and grade as well as MVI, HPI, and surgical margins; Table 3) were further analyzed in various Cox regression models using backward selection with p<0.05 as the exit criterion. Following clinicopathological parameters had no impact on survival in univariate analysis and were not further assessed in multivariate models: preoperative transaminase levels and cholestatic parameters, viral hepatitis B and C, alcohol-related liver disease, cigarette smoking, sex, age, and tumor growth pattern. Although not statistically significant on univariate analysis in our series, concomitant liver cirrhosis and preoperative AFP levels were included in a multivariate model because they are well-known prognostic markers.

In the models including only clinicopathological parameters, the retained prognostic factors were tumor multifocality and size in the whole cohort and tumor multifocality and grade in the subgroup of patients with liver resection (model 1 from Table 4).

In the model including Hep Par 1, CD10can, and CD10cyt, all three immunohistochemical parameters were retained, and the regression coefficients (whole cohort) were 0.72, 0.77, and 0.78 for Hep Par 1, CD10can, and CD10cyt, respectively (model 2 from Table 4). Taken

Table 3 Univariate analysis of the clinicopathological factors

Factor[a]	All patients				Only patients treated by partial resection			
	Number of patients (censored)	Median survival time (month)	95% CI (month)	p values[b]	Number of patients (censored)	Median survival time (month)	95% CI (month)	p values
Tumor size								
≤5 cm	58 (33)	54	6–102	0.0006	37 (17)	33	17–49	0.07
>5 cm	39 (8)	14	9–19		35 (7)	14	8–20	
Tumor stage (TNM)								
I+II	33 (21)	95	2–188	0.001	22 (12)	42	26–58	0.06
III	29 (11)	27	14–40		23 (7)	21	4–38	
IV	35 (9)	14	9–19		27 (5)	13	6–20	
Tumor multifocality								
solitary	43 (25)	95	5–185	0.001	31 (15)	33	21–45	0.007
multiple	54 (16)	14	9–19		41 (9)	13	7–19	
Edmondson and Steiner's grade								
1	20 (13)	43	–	0.04	16 (10)	43	20–66	0.07
2	44 (17)	27	12–42		31 (7)	15	5–25	
3+4	33 (11)	16	6–26		25 (7)	16	11–21	
MVI								
Absent	62 (31)	42	27–57	0.04	46 (18)	30	22–38	0.2
Present	35 (10)	15	8–21		26 (6)	10	5–15	
HPI[c]								
Low	46 (25)	54	8–100	0.03	34 (15)	42	18–66	0.1
High	51 (16)	16	13–19		38 (9)	15	11–18	
Surgical margins								
Negative	78 (37)	33	17–49	0.05	56 (22)	30	18–42	0.01
Positive	14 (4)	9	7–11		11 (2)	9	6–12	

[a]Following factors did not show a significant impact on survival (p>0.2) and are omitted from this table for simplicity: concomitant liver cirrhosis, etiology of underlying liver pathology (alcohol, hepatitis B, and hepatitis C), as well as preoperative AFP levels, cytolytic, and cholestatic parameters

[b]Two-sided p values obtained by log-rank test, which are considered to be significant if p<0.05, of marginal significance if 0.05≤ p<0.1 and NS if p≥0.1

[c]HPI was computed according to Lauwers et al. [23]

Table 4 Details of some Cox regression models

		All patients(total 97, censored 41)				Only patients treated by partial resection(total 72, censored 24)			
Model[a]	Variables included	Variables retained in the model	*p* values[b]	Relative risk [c]	95% CI	Variables retained in the model	*p* values	Relative risk[c]	95% CI
1	Stage, size, multifocality, grade, HPI[d]	Size >5 cm	0.009	2.1	1.2–3.5	Grade	0.05		
		Multifocality=multiple	0.01	2.1	1.2–3.8	=grade 2	0.01	3.1	1.3–7.8
						=grade 3+4	0.07	2.3	0.9–5.9
						Multifocality	0.005		
						=multiple		2.5	1.3–4.6
2	Hep Par 1 =3	Hep Par 1 =3	0.01	2.1[e]	1.2–3.6	CD10can ≥2	0.01	2.5[f]	1.2–4.8
	CD10can ≥2	CD10can ≥2	0.03	2.2[e]	1.1–4.3	CD10cyt ≥1	0.03	2.1[f]	1.1–4.2
	CD10cyt ≥1	CD10cyt ≥1	0.02	2.2[e]	1.1–4.1				
3	Size, multifocality, grade, surgical margins, Hep Par 1 =3	Hep Par 1 =3	0.01	2.7	1.5–4.7	Multifocality=multiple	0.008	2.5	1.3–4.9
		multifocality=multiple	0.04	2.4	1.3–4.4	Grade	0.06		
						=grade 2	0.02	3.0	1.2–7.5
						=grade 3+4	0.3	1.8	0.7–4.6
						Hep Par 1 =3	0.04	2.0	1.0–3.8
4	Size, multifocality, grade, surgical margins, CD10can ≥2	Multifocality=multiple	0.001	2.8	1.5–5.0	Multifocality=multiple	0.006	2.5	1.3–4.9
		CD10can ≥2	0.008	2.1	1.2–3.7	Grade	0.06	3.1	
						=grade 2	0.02	2.2	1.2–7.7
						=grade 3+4	0.1		0.9–5.7
5	Size, multifocality, grade, surgical margins, CIS[g]	CIS <4	0.001	3.5	1.7–7.3	CIS <4	0.004	3.7	1.5–8.9
		Multifocality=multiple	0.005	2.4	1.3–4.3	Multifocality=multiple	0.02	2.3	1.2–4.5
						Grade	0.04		
						=grade 2	0.01	3.2	1.3–8.2
						=grade 3+4	0.2	1.9	0.7–4.8
6	Size, multifocality, grade, cirrhosis, AFP[h], CIS	CIS <4	0.001	3.5	1.7–7.3	CIS <4	0.004	3.7	1.5–8.9
		Multifocality=multiple	0.005	2.4	1.3–4.3	Multifocality=multiple	0.02	2.3	1.2–4.5
						Grade	0.04		
						=grade 2	0.01	3.2	1.3–8.2
						=grade 3+4	0.2	1.9	0.7–4.8

[a]Model 1 includes only clinicopathological parameters. Model 2 includes only immunohistochemical parameters. Models 3 and 4 include clinicopathological parameters together with one immunohistochemical parameter. Models 5 and 6 include CIS in addition to clinicopathological parameters; both models retain the same final variables

[b]Significance of the Wald test, variables with $p>0.05$ were discarded from the model

[c]For dichotomous variables (size, multifocality and CIS), the relative risk is the predicted change of death hazard for a patient within the specified category as compared to the other one. For grade, the relative risk is such a change for a patient within the specified category as compared to the reference category (grade 1)

[d]HPI computed according to Lauwers et al. [23]

[e]Correlation coefficients for Hep Par 1 =3, CD10can ≥2, and CD10cyt ≥1 are 0.721, 0.772, and 0.775, respectively

[f]Correlation coefficients for CD10can ≥2 and CD10cyt ≥1 are 0.897 and 0.748, respectively

[g]CIS (score Hep Par 1 staining + score CD10 canalicular staining − score CD10 cytoplasmic staining)

[h]Preoperative AFP levels

together with the selected clinicopathological parameters, Hep Par 1 and CD10can were retained in the models (models 3 and 4 from Table 4, respectively). However, *p* values and relative risk were lower for Hep Par 1 and CD10can alone as compared to CIS (see below).

All models testing CIS in conjunction with different clinicopathological parameters resulted in the retention of the same final variables. Models 5 and 6 from Table 4 are representative examples. CIS was the most significant prognostic factor in both the complete cohort (p=0.001) and the subgroup of liver-resected patients (p=0,004). Patients with a CIS <4, as compared to those with a CIS ≥4, had a 3.5-fold (95% CI 1.7–7.3) and a 3.7-fold (95% CI 1.5–8.9) increased risk of death in the whole cohort and the subgroup of patients with liver resection, respectively. In the model of the whole cohort, tumor multifocality was the only additional prognostic factor (p=0.005): patients with multifocal HCC had a 2.4-fold (95% CI 1.3 to 4.3) increased risk of death as compared to those with solitary tumors. In the model of patients with liver resection only, tumor multifocality (p=0.02) and Edmondson and Steiner's grade (p=0.04) were retained in addition to CIS.

Discussion

Hepatocellular carcinoma is one of the most common malignant tumors worldwide that has typically poor prognosis regardless of the treatment, and its incidence and mortality are on the rise in Western nations [14]. Clinicians need prognostic indicators to inform their patients and to stratify them for eventual additional therapy. The present study of Hep Par 1 and CD10 expression in HCC by immunohistochemistry was undertaken to identify new prognostic markers for patients treated with curative intent by partial or total hepatectomy, the latter with liver transplantation.

In our study population, strong cytoplasmic Hep Par 1 and CD10can expression, as well as absent CD10cyt labeling, were correlated with longer overall survival. To obtain a practical algorithm for clinical use, these three immunohistochemical parameters were combined into a single immunohistochemical score, which showed a highly significant correlation with overall survival. Multivariate analysis proved CIS to be the most important independent prognostic factor, followed by tumor multifocality and Edmondson and Steiner's grade. Furthermore, CIS is superior to Hep Par 1 or CD10 scores alone with regard to risk assessment. To our knowledge, this is the first study to demonstrate the prognostic value of these markers, although their use is well documented in establishing the diagnosis of HCC [5, 7, 8, 38]. CIS was also the most significant prognostic indicator in the subgroup of patients treated by partial hepatectomy, which excludes the possibility of a bias due to the type of surgery. Unfortunately, the limited number of patients treated by total hepatectomy and the limited duration of follow-up precluded analysis of this subgroup. A future study is planned to examine in detail the prognostic value of Hep Par 1 and CD10 in this group of patients.

Prognostic indices are usually derived from the final Cox regression model by using the regression coefficients as weights for the corresponding scores [6]. However, we preferred a more simple prognostic index based on a weight of +1 for Hep Par 1 and CD10can and a weight of −1 for CD10cyt scores for two reasons. First, its determination is simple enough to be applicable in a routine setting. Second, as shown by the Cox model, including these three parameters, the absolute value of their regression coefficients is roughly the same (about 0.7), which justifies a posteriori such a score. Interestingly, several parameters, such as TNM stage, tumor size, MVI, HPI, and surgical resection margins, which are known in the literature to be of prognostic significance, were not retained in our Cox regression models. This can be explained by correlation of the immunohistochemical variables with these clinicopathological parameters, as shown in Table 1 for tumor size and grade, MVI and HPI. Second, tumor multifocality, which remains significant in our multivariate models, contains partly the same prognostic information as TNM stage, which is based on the former.

The precise biological mechanisms underlying the impact of Hep Par 1 and CD10 expression on prognosis have yet to be identified. It might be linked to the fact that Hep Par 1 and CD10can expressions are indicators of a high degree of differentiation. Indeed, in our series, there was a correlation between the expression of these markers and histological grade. These findings are in line with several reports in the literature [5, 8, 21, 39]. Another argument in favor of this hypothesis is the fact that poorly differentiated HCC are known to be devoid of bile canaliculi [5, 7]. Therefore, these tumors are frequently unreactive with antibodies directed against CD10 which is a neutral endopeptidase located at the luminal aspects of bile canaliculi. To explain the intriguing feature of CD10cyt labeling in the less differentiated and more aggressive tumors, one might also speculate that redistribution of CD10 from the cell surface to the cytoplasm is an indirect sign of lost cell polarity, which is one of the hallmarks of cancer [35]. This redistribution might be the consequence of aberrant glycosylation, alternative splicing, or a truncating mutation of the CD10 gene [33, 36].

In conclusion, our study identifies Hep Par 1 and CD10 expression as the most informative predictors of overall survival in HCC patients treated by partial liver resection with curative intent. Introduction of these parameters in clinical decision making, however, requires confirmation of these preliminary findings in another population of HCC patients. Whether these findings apply also to patients treated with total hepatectomy and liver transplantation as suggested by the present work will require further studies. Future prospective studies are also necessary to determine whether or not the CIS can be helpful for the choice of additional treatment and prediction of prognosis in patients who are beyond curative surgery.

Acknowledgements We thank M. Gillet (Department of Surgery, CHUV, Lausanne) for the patient data, S. Pampallona (Evolène, Switzerland) for advice on statistical analysis, and P. Chaubert and P. Shaw (Department of Pathology, CHUV, Lausanne) for help in immunohistochemistry and for critical review of the manuscript, respectively.

This study has been conducted in accordance with current Swiss law and been approved by the ethical committee of our institution.

References

1. Adachi E, Maeda T, Kajiyama K, Kinukawa N, Matsumata T, Sugimachi K, Tsuneyoshi M (1996) Factors correlated with portal venous invasion by hepatocellular carcinoma: univariate and multivariate analyses of 232 resected cases without preoperative treatments. Cancer 77:2022–2031
2. Anthony PP (2001) Hepatocellular carcinoma: an overview. Histopathology 39:109–118
3. Armitage P, Berry G, Matthews JNS (1987) Statistical methods in medical research, 2nd edn. Blackwell, Oxford
4. Bene MC, Faure GC (1997) CD10 in acute leukemias. GEIL (Groupe d'Etude Immunologique des Leucemies). Haematologica 82:205–210
5. Borscheri N, Roessner A, Rocken C (2001) Canalicular immunostaining of neprilysin (CD10) as a diagnostic marker for hepatocellular carcinomas. Am J Surg Pathol 25:1297–1303
6. Christensen E (1987) Multivariate survival analysis using Cox's regression model. Hepatology 7:1346–1358
7. Chu P, Arber DA (2000) Paraffin-section detection of CD10 in 505 nonhematopoietic neoplasms. Frequent expression in renal cell carcinoma and endometrial stromal sarcoma. Am J Clin Pathol 113:374–382
8. Chu PG, Ishizawa S, Wu E, Weiss LM (2002) Hepatocyte antigen as a marker of hepatocellular carcinoma: an immunohistochemical comparison to carcinoembryonic antigen, CD10, and alpha-fetoprotein. Am J Surg Pathol 26:978–988
9. Colombo M (1992) Hepatocellular carcinoma. J Hepatol 15:225–236
10. Cox D (1972) Regession models and life tables. J R Stat Soc B 34:187–220
11. Dragovic T, Deddish PA, Tan F, Weber G, Erdos EG (1994) Increased expression of neprilysin (neutral endopeptidase 24.11) in rat and human hepatocellular carcinomas. Lab Invest 70: 107–113
12. Dragovic T, Sekosan M, Becker RP, Erdos EG (1997) Detection of neutral endopeptidase 24.11 (neprilysin) in human hepatocellular carcinomas by immunocytochemistry. Anticancer Res 17: 3233–3238
13. Edmondson H, Steiner P (1954) Primary carcinoma of the liver: a study of 100 cases among 48,900 necropsies. Cancer 7:462–503
14. El-Serag HB, Mason AC (1999) Rising incidence of hepatocellular carcinoma in the United States. N Engl J Med 340:745–750
15. Greenwood M (1926) Reports on public health and medical subjects: the natural duration of cancer. HMSO 33:1–16
16. Hamilton SR, Aaltonen LA (eds) (2000) Pathology and genetics of tumors of the digestive system. IARC Press, Lyon
17. Hanazaki K, Kajikawa S, Koide N, Adachi W, Amano J (2001) Prognostic factors after hepatic resection for hepatocellular carcinoma with hepatitis C viral infection: univariate and multivariate analysis. Am J Gastroenterol 96:1243–1250
18. Inagawa S, Itabashi M, Adachi S, Kawamoto T, Hori M, Shimazaki J, Yoshimi F, Fukao K (2002) Expression and prognostic roles of beta-catenin in hepatocellular carcinoma: correlation with tumor progression and postoperative survival. Clin Cancer Res 8:450–456
19. Kaplan EL, Meier P (1958) Nonparametric estimation from incomplete observations. J Am Stat Assoc 53:457–481
20. Kobayashi T, Sugawara Y, Shi YZ, Makuuchi M (2002) Telomerase expression and p53 status in hepatocellular carcinoma. Am J Gastroenterol 97:3166–3171
21. Kumagai I, Masuda T, Sato S, Ishikawa K (2001) Immunoreactivity to monoclonal antibody, Hep Par 1, in human hepatocellular carcinomas according to histopathological grade and histological pattern. Hepatol Res 20:312–319
22. Lamps LW, Folpe AL (2003) The diagnostic value of hepatocyte paraffin antibody 1 in differentiating hepatocellular neoplasms from nonhepatic tumors: a review. Adv Anat Pathol 10:39–43
23. Lauwers GY, Terris B, Balis UJ, Batts KP, Regimbeau JM, Chang Y, Graeme-Cook F, Yamabe H, Ikai I, Cleary KR, Fujita S, Flejou JF, Zukerberg LR, Nagorney DM, Belghiti J, Yamaoka Y, Vauthey JN (2002) Prognostic histologic indicators of curatively resected hepatocellular carcinomas: a multi-institutional analysis of 425 patients with definition of a histologic prognostic index. Am J Surg Pathol 26:25–34
24. Lauwers GY, Vauthey JN (1998) Pathological aspects of hepatocellular carcinoma: a critical review of prognostic factors. Hepatogastroenterology 45:1197–1202
25. Leong AS, Sormunen RT, Tsui WM, Liew CT (1998) Hep Par 1 and selected antibodies in the immunohistological distinction of hepatocellular carcinoma from cholangiocarcinoma, combined tumours and metastatic carcinoma. Histopathology 33:318–324
26. Medina-Franco H, Sellers MT, Eckhoff DE, Bynon JS, Urist MM, Heslin MJ (2001) Multimodality treatment for patients with hepatocellular carcinoma: analysis of prognostic factors in a single Western institution series. J Gastrointest Surg 5:638–645
27. Minervini MI, Demetris AJ, Lee RG, Carr BI, Madariaga J, Nalesnik MA (1997) Utilization of hepatocyte-specific antibody in the immunocytochemical evaluation of liver tumors. Mod Pathol 10:686–692
28. Morrison C, Marsh W Jr, Frankel WL (2002) A comparison of CD10 to pCEA, MOC-31, and hepatocyte for the distinction of malignant tumors in the liver. Mod Pathol 15:1279–1287
29. Nzeako UC, Goodman ZD, Ishak KG (1996) Hepatocellular carcinoma in cirrhotic and noncirrhotic livers. A clinicohistopathologic study of 804 North American patients. Am J Clin Pathol 105:65–75
30. Okuda K (2002) Natural history of hepatocellular carcinoma including fibrolamellar and hepato-cholangiocarcinoma variants. J Gastroenterol Hepatol 17:401–405
31. Sato Y, Itoh F, Hareyama M, Satoh M, Hinoda Y, Seto M, Ueda R, Imai K (1999) Association of cyclin D1 expression with factors correlated with tumor progression in human hepatocellular carcinoma. J Gastroenterol 34:486–493
32. Schoniger-Hekele M, Muller C, Kutilek M, Oesterreicher C, Ferenci P, Gangl A (2001) Hepatocellular carcinoma in Central Europe: prognostic features and survival. Gut 48:103–109
33. Sezaki N, Ishimaru F, Tabayashi T, Kataoka I, Nakase K, Fujii K, Kozuka T, Nakayama H, Harada M, Tanimoto M (2003) The type 1 CD10/neutral endopeptidase 24.11 promoter: functional characterization of the 5′-untranslated region. Br J Haematol 123:177–183

34. Sobin LH, Wittekind C (eds) (2002) TNM classification of malignant tumors. Wiley, New York
35. Thiery JP, Humbert P, Russell S, Richardson H (2002) Epithelial-mesenchymal transitions in tumour progression Dlg, Scribble and Lgl in cell polarity, cell proliferation and cancer. Nat Rev Cancer 2:442–454
36. Turner AJ, Isaac RE, Coates D (2001) The neprilysin (NEP) family of zinc metalloendopeptidases: genomics and function. Bioessays 23:261–269
37. Turner AJ, Tanzawa K (1997) Mammalian membrane metallopeptidases: NEP, ECE, KELL, and PEX. Faseb J 11:355–364
38. Wennerberg AE, Nalesnik MA, Coleman WB (1993) Hepatocyte paraffin 1: a monoclonal antibody that reacts with hepatocytes and can be used for differential diagnosis of hepatic tumors. Am J Pathol 143:1050–1054
39. Wu PC, Fang JW, Lau VK, Lai CL, Lo CK, Lau JY (1996) Classification of hepatocellular carcinoma according to hepatocellular and biliary differentiation markers. Clinical and biological implications. Am J Pathol 149:1167–1175
40. Xiao SY, Wang HL, Hart J, Fleming D, Beard MR (2001) cDNA arrays and immunohistochemistry identification of CD10/CALLA expression in hepatocellular carcinoma. Am J Pathol 159:1415–1421

Virchows Arch (2006) 448: 46–51
DOI 10.1007/s00428-005-0078-0

ORIGINAL ARTICLE

Anne Rullier · Nathalie Senant · Walter Kisiel · Paulette Bioulac-Sage · Charles Balabaud · Brigitte Le Bail · Jean Rosenbaum

Expression of protease-activated receptors and tissue factor in human liver

Received: 12 May 2005 / Accepted: 22 August 2005 / Published online: 29 September 2005

Abstract Thrombin, acting via protease-activated receptors (PARs), and tissue factor (TF) are involved in inflammation, tissue repair and tumorigenesis. Hepatocellular carcinomas (HCCs) usually complicate chronic liver diseases characterised by inflammation and fibrosis. The aim of this study was to describe the expression of PARs and TF in normal liver, cirrhosis and HCCs. We performed an immunohistochemical detection of PAR-1, PAR-3, PAR-4 and human TF in human tissue samples from 19 subnormal livers, 33 cirrhosis and 30 HCCs. PAR-1 was found on endothelial cells of sinusoids and larger vessels. In cirrhosis, spindle-shaped cells within septa and T lymphocytes were PAR-1 positive. A few PAR-1-positive tumour cells were found in 10% of HCCs. PAR-4 expression was restricted to macrophages, B lymphocytes and nerves. PAR-3 expression was rare. Unexpectedly, TF was expressed in 95% of normal livers and in 94% of cirrhosis but only in 50% of HCCs ($p<0.001$). Staining was mostly hepatocellular. No association existed between TF labelling and clinicopathological characteristics of HCCs. In conclusion, the pattern of expression of PARs is compatible with its role in chronic liver disease by promoting inflammation via immune cells and neurogenic stimulation. However, our data do not support a role for PARs or TF in HCC progression.

Keywords Thrombin receptor · Tissue factor · Human liver · Immunohistochemistry · Liver neoplasm

A. Rullier (✉) · N. Senant · P. Bioulac-Sage · C. Balabaud · B. Le Bail · J. Rosenbaum
GREF/INSERM E362, Université Victor Segalen Bordeaux 2,
146, Rue Léo Saignat,
Bordeaux, 33076, France
e-mail: anne.rullier@chu-bordeaux.fr
Tel.: +33-55-7571771
Fax: +33-55-6514077

A. Rullier · N. Senant · P. Bioulac-Sage · C. Balabaud · B. Le Bail · J. Rosenbaum
IFR 66,
Bordeaux, 33076, France

A. Rullier · P. Bioulac-Sage · B. Le Bail
Department of Pathology, CHU de Bordeaux,
Hôpital Pellegrin,
Bordeaux, 33076, France

W. Kisiel
Department of Pathology,
University of New Mexico School of Medicine,
Albuquerque, NM, USA

Introduction

Thrombin is a multifunctional serine protease. Besides its key role in haemostasis, thrombin is also involved in inflammation and tissue repair processes. Indeed, it has long been known that thrombin is chemotactic for monocytes [2] and participates in lymphocyte activation [24]. More recently, thrombin was shown to stimulate the synthesis of connective tissue proteins by fibroblasts [7, 8]. Thrombin also increases the metastatic potential of tumour cells notably by promoting tumour cell adhesion to the endothelium and extracellular matrix [21, 41].

Thrombin is generated via a cascade of reactions whose physiological initiator is tissue factor (TF). TF is a 47-kDa transmembrane glycoprotein that is expressed physiologically in vascular endothelial cells, macrophages and blood monocytes [23]. TF does not normally come in contact with the circulation, but during tissue injury, it is locally expressed and binds to factor VII, thereby activating the extrinsic coagulation system. In inflammatory lesions, TF is expressed by endothelial cells and monocytes/macrophages [35]. TF is also expressed by most epithelial tumour cell types [6]. A correlation between elevated TF expression and advanced stages of malignancy has been confirmed in many human cancers, like colorectal carcinomas, gliomas, prostatic cancers, non-small-cell lung cancers, melanomas, and laryngeal and pancreatic carcinomas [1, 4, 19, 25, 34, 42, 43]. Whereas the extracellular domain of

TF is required as a coagulation activator, its cytoplasmic tail is also involved in cell signalisation events that could lead to inflammation, tumour cell survival, tumour angiogenesis, and cancer progression and metastasis [27].

Thrombin acts via activation of protease-activated receptors (PARs) that belong to a large family of G-protein-coupled seven transmembrane domain receptors. Thrombin cleaves the extracellular amino-terminal peptide of the receptor. The new N-terminal peptide, as a tethered ligand, binds to the body of the receptor itself, resulting in its activation. Three out of four PARs, PAR-1, PAR-3 and PAR-4, are activated by thrombin, whereas PAR-2 is activated by trypsin and mastocyte tryptase [9]. PAR-1, the first-described thrombin receptor, is expressed in smooth muscle and endothelial cells, fibroblasts and blood cells. In the liver, only one study reported in situ expression of PAR-1 in human samples from normal liver, chronic hepatitis, cirrhosis and fulminant hepatitis [22]. Recently, several publications strongly suggest that thrombin and PAR-1 are important for tumorigenesis and metastasis [3, 5, 15, 16, 33].

Hepatocellular carcinoma (HCC) is the main type of primary liver cancer. In Western countries, it occurs mainly as a complication of a pre-existing cirrhosis, most often secondary to chronic viral hepatitis C or B, or alcoholic liver disease. Whereas there is now accumulated evidence that thrombin and its receptors are involved in liver fibrogenesis [13, 17, 22], the role of the haemostatic cascade has been slightly addressed in HCC. Specifically, there are no published data on TF expression in HCC, while those on PAR expression are scarce [10].

Thus, the aim of this work was to study the distribution and localisation of thrombin receptors PAR-1, PAR-3 and PAR-4 and of TF in normal human liver, cirrhosis and HCC.

Materials and methods

Tissue samples

Eighty-two samples obtained during surgery were analysed. Sixteen histologically normal liver tissue samples were taken at a distance from benign liver tumours (focal nodular hyperplasia, n=2; hydatid cyst, n=1), and colorectal (n=12) and mammary (n=1) cancer metastasis. Six cirrhosis samples without associated HCC were also tested. Thirty HCC and surrounding liver tissue samples were studied in the same tissue section. Surrounding liver was cirrhotic in most cases, due to chronic hepatitis C or alcohol consumption (n=27), and was rarely subnormal (n=3). Twenty-six of the 30 HCCs were diagnosed in men with a mean age of 61 years. Half of the HCCs were multiple (16/30) with partial or complete tumour capsule (17/30). The mean tumour size was 4 cm (1–18.5 cm). HCCs were usually (26/30) classified as grade II or III according to Edmondson's grade. Features of vascular invasion were present in 15 out of 30 tumours and capsular invasion in only nine cases.

Methods

All samples were fixed in 10% formalin and embedded in paraffin. Serial tissue sections (4 μm thick) were cut, mounted on glass slides and dried at 56°C before dewaxing in xylene and rehydration in alcohols according to standard histological procedures. Antibodies against PARs were bought from Santa Cruz Biotechnology Inc. (Santa Cruz, CA): PAR-1 (monoclonal, clone ATAP2, dilution 1:1,000), PAR-3 (goat polyclonal, C-20, dilution 1:750), PAR-4 (goat polyclonal, C-20, dilution 1:3,500). All sections were subjected to heat-induced epitope retrieval using a vegetable steam cooker in citrate buffer pH 6 for 5 min, followed by inhibition of endogenous peroxidase (H_2O_2 0.3% in methanol, 30 min). Incubation of primary antibodies was done at room temperature for 45 min. After washing in phosphate-buffered saline, sections for PAR-3 and PAR-4 labelling were incubated with a rabbit anti-goat antibody (Dako, Glostrup, Denmark) at room temperature for 45 min before incubation with EnVision TM+ anti-rabbit polymer dextran (Dako). For PAR-1, sections were directly incubated with EnVision TM+ anti-mouse polymer dextran (Dako).

Tissue factor immunostaining was done in an automated immunostainer (Autostainer Plus, Dako) with a previously described anti-TF polyclonal antibody raised in rabbit [1]. After heat-induced antigenic retrieval in citrate buffer pH 6 for 10 min, endogenous peroxidase activity was inhibited. Non-specific binding was reduced by incubating the sections with 60% human serum with bovine serum albumin. Sections were incubated with anti-TF antibody (dilution 1:2,000) for 1 h. The staining was amplified by an EnVision TM+ anti-rabbit polymer dextran. TF immunostaining was also performed in frozen tissue from selected cases.

All stainings were revealed with a diaminobenzidine substrate source. Sections were counterstained with hemalum, dehydrated and mounted in Eukitt.

Tissue factor expression was evaluated semi-quantitatively as the percentage of positive cells [1] and was scored as 0 (no positive cells), 1 (≤10% positive cells), 2 (10 to 30% positive cells) or 3 (>30% positive cells).

Complementary immunohistochemical labelling using commercially antibodies to CD3 (Dako), CD20 (clone L26, Dako), alpha smooth muscle actin (clone 1A4, Dako) and CD68 (clone KP1, Dako) was also performed in selected cases on serial sections using an automated immunostainer (ES 320 Ventana, Tucson, AZ, USA) and an LSAB procedure (Ventana). Double immunostaining was also done using the DakoCytomation EnVision doublestain system (Dako), with PAR-1 (EnVision-Peroxidase, DAB substrate buffer) and alpha smooth muscle actin (EnVision-Alkalin phosphatase, Fast red substrate buffer), PAR-1 and CD31 (EnVision-Alkalin phosphatase, Fast red substrate buffer), and PAR-4 (EnVision-Peroxidase, DAB substrate buffer) and CD68 (EnVision-Alkalin phosphatase, Fast red substrate buffer).

Negative controls were systematically obtained by omitting the primary antibody. Lymphocytes were used as positive controls for PAR-1 and PAR-4, whereas prostatic carcinomas (n=3) were used for TF.

Statistical analysis

The chi-square test and Yates' derived Fisher's exact test were used for comparisons as appropriate. For patients with HCC, clinical data such as local and distant recurrences as well as follow-up were obtained from the Department of Liver Surgery and Transplantation. Five-year overall and disease-free survival data were determined by the actuarial Kaplan–Meier method. The impact of TF immunostaining on survival was evaluated by univariate analysis using the log-rank test. Statistical significance was set at $p<0.05$.

Results

Thrombin receptors

Protease-activated receptor-1

Endothelial cells from sinusoids and vessels were diffusely labelled in every sample whether normal or diseased without differences in intensity (Fig. 1a,e). In cirrhotic tissue, an immunostaining was observed in fibrous septa with an intensification around areas of ductular reaction; this staining appeared located to the cytoplasm of spindle-shaped cells resembling fibroblasts or myofibroblasts and co-expressing alpha smooth muscle actin (Fig. 1a,f). No staining of fibroblasts was observed in portal tracts of normal liver samples. Mononuclear inflammatory cells that look like lymphocytes were also labelled; they were located either in the lumen of sinusoids, in the mesenchyme of portal tracts or in fibrous septa. The lymphoid origin of these cells was confirmed in cases of viral hepatitis C with prominent lymphoid follicles. Indeed, PAR-1-positive cells were located at the periphery of the follicle and co-expressed the CD3 antigen, indicating that they were T lymphocytes (Fig. 1b,c). Normal hepatocytes and biliary epithelial cells were always negative.

In HCC, an immunostaining identical to that observed in cirrhotic septa was also observed in fibrotic bands inside the tumour and in the capsule, when present. In 3 out of 30 HCCs, clusters of tumour cells showed a delicate membranous staining (Fig. 1d).

Protease-activated receptor-3

PAR-3 immunolabelling was confined to scarce polymorphonuclear neutrophils within sinusoids in only one out of all specimens tested.

Protease-activated receptor-4

Whatever the type of tissue (normal, cirrhotic livers or HCC), three compartments of staining were noted: (1) B lymphocytes (CD20 positive) located at the centre of lymphoid follicles or dispersed in the lumen of sinusoids, portal tracts, fibrous septa and bands (Fig. 2b,c); (2) macrophagic cells (CD68 positive) such as Kupffer cells in sinusoids (Fig. 2a,e), histiocytes and giant cells found in portal tracts and occasionally in a few inflammatory HCCs; and (3) in nerves (Fig. 2d).

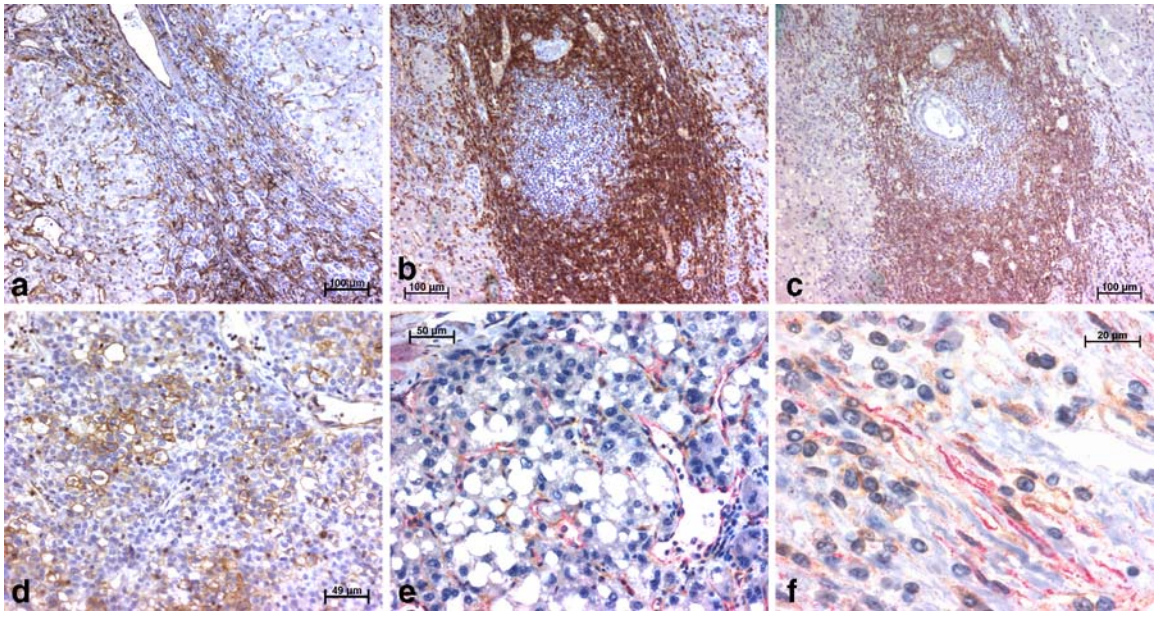

Fig. 1 Patterns of PAR-1 immunostaining: **a** endothelial cells from sinusoids and vessels as well as spindle-shaped cells in fibrous septa in cirrhotic tissue express PAR-1; **b** T lymphocytes express both PAR-1 and **c** CD3 antibody in follicles of post-hepatitis C cirrhosis in serial sections of the same case; **d** tumour cells in a grade III HCC showed a delicate membranous staining with PAR-1; **e** co-expression of CD31 (*red*) and PAR-1 (*brown*) in endothelial cells of sinusoids; **f** co-expression of alpha smooth muscle actin (*red*) and PAR-1 (*brown*) in spindle-shaped cells in fibrous septa

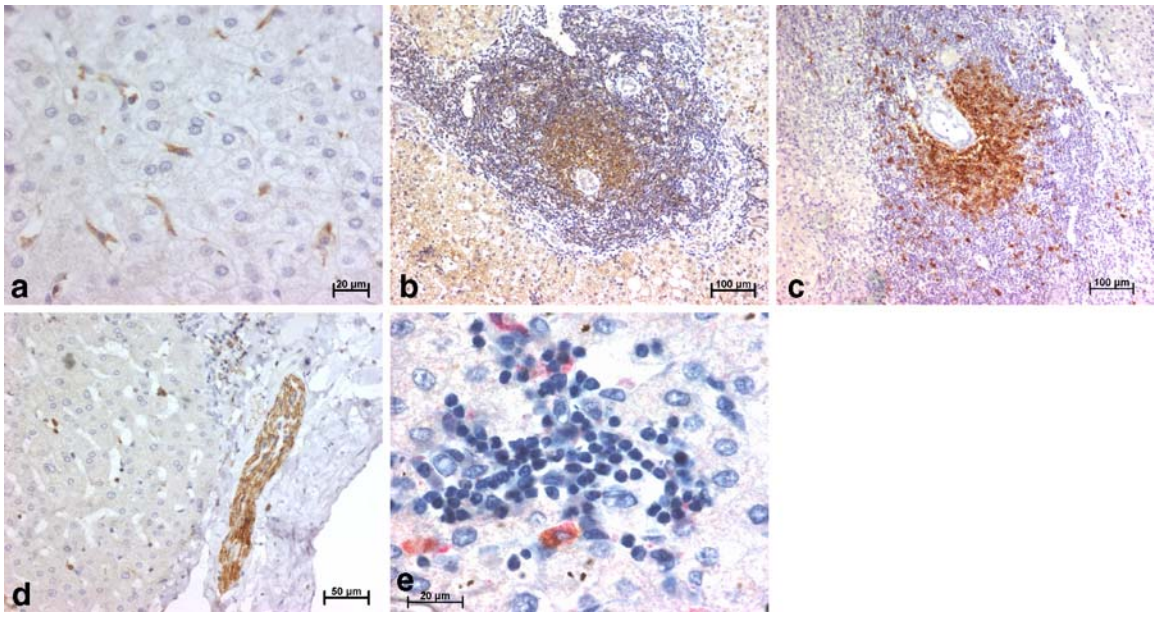

Fig. 2 Patterns of PAR-4 immunostaining: **a** Kupffer cells; **b** B lymphocytes in follicles in post-hepatitis C cirrhosis, which are also labelled with **c** CD20 antibody in serial sections of the same case; **d** nerve section; **e** co-expression of PAR-4 (*red*) and CD68 (*brown*) in Kupffer cells

Tissue factor

Tissue factor was expressed in 18/19 normal livers (95%) and 31/33 cirrhotic samples (94%; Table 1). The staining was mainly found in the cytoplasm of hepatocytes, sometimes with a polarised disposition at the sinusoidal pole (Fig. 3). In normal liver, the distribution of the hepatocellular staining was mainly centrolobular and enhanced in hepatocytes located under the Glisson's capsule. In cirrhosis, hepatocellular staining was diffuse in half of the cases, involving more than 30% of hepatocytes. Endothelial cells from neovessels and/or spindle-shaped cells within cirrhotic septa were sometimes stained.

On the other hand, TF labelling was observed in only 50% of the 30 HCCs tested. When present, the staining was found mainly in the cytoplasm of tumour cells and rarely in neovessels. Less than 10% of tumour cells were positive in 10 out of 15 cases and more than 30% in only a single case (Table 1). In each case, the percentage of positive cells in HCC was lower than in the surrounding tissue, either cirrhotic or not. In selected cases, a similar staining pattern for TF was found when using cryosections, indicating that the results were not secondary to a fixation artefact (data not shown). No staining was observed when omitting primary antibodies.

The percentage of TF-positive cells was significantly lower in HCC than in cirrhosis ($p<0.001$) (Table 1). There was no association between the positivity of TF immunostaining and known histoprognostic factors of HCC, i.e. tumour size, tumour number, Edmondson's grade, tumour capsule, capsular invasion and vascular invasion (data not shown). There was no association either between TF ex-

Table 1 Percentage of TF-positive cells in normal liver, cirrhosis and HCC

% Positive cells	0	≤10	10–30	>30	*p*
Normal liver (*n*=19)	1	7	3	8	<0.001*
Cirrhosis (*n*=33)	2	9	7	15	
HCC (*n*=30)	15	10	4	1	

*Yates' derived Fisher's exact test after regrouping 0/≤10 and 10–30/>30

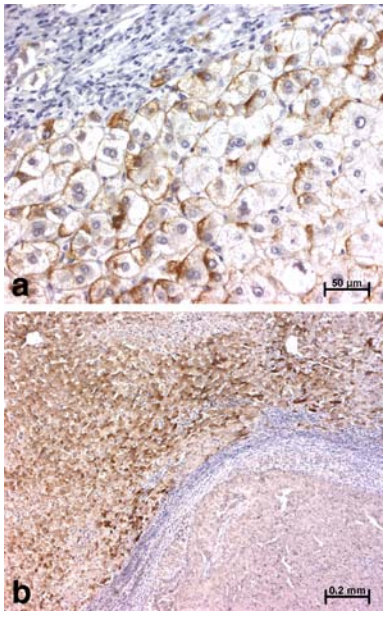

Fig. 3 TF immunostaining: **a** hepatocellular cytoplasmic staining exhibits a polarised disposition at the sinusoidal pole of the cells in cirrhotic tissue; **b** positive cirrhosis (*left*) beside negative encapsulated HCC (*right*)

pression in HCC and overall or disease-free survival with a median follow-up of patients of 11 months (range 1–41).

Discussion

In this report, we describe for the first time the distribution of the three thrombin receptors, PAR-1, PAR-3 and PAR-4, and of TF in a series of subnormal, cirrhotic and carcinomatous liver samples.

A single study previously reported in situ expression of PAR-1 in normal human liver, chronic hepatitis, cirrhosis and fulminant hepatitis [22]. Like in this publication, we found PAR-1 expression all along sinusoids, as well as in the endothelium of blood vessels and inflammatory cells in normal liver and chronic hepatitis. In cirrhosis, we also found PAR-1-positive cells in fibrous septa, within newly formed blood vessels and in spindle-shaped cells corresponding to fibroblasts or myofibroblasts (Fig. 1f). Many inflammatory cells also expressed PAR-1 as previously described [22]. In a few samples from HCV-infected patients with many lymphoid follicles, we were able to demonstrate that PAR-1-positive cells located at the periphery of the lymphoid nodules co-expressed the T-cell marker CD3 (Fig. 1). This finding is in keeping with other studies demonstrating that thrombin is a potent regulator of T lymphocytes in vitro and that thrombin receptors are available at the surface of human T and NK lymphocytes [12, 20, 30]. In contrast, PAR expression on B lymphocytes was reported as negative [18, 37]. However, these studies were performed before the description of PAR-4. When we labelled liver sections with a PAR-4 antibody, we found that lymphocytes in the centre of lymphoid follicles that expressed the B lineage marker CD20 also expressed PAR-4 (Fig. 2). Thus, within lymphoid follicles, PAR-1 labelling and PAR-4 labelling are mutually exclusive, resulting in a mirror image. This selectivity likely results in specific responses to various agonists. Firstly, it is known that thrombin action on PAR-1 or PAR-4 evokes distinct signalling pathways [32, 36, 40]. Secondly, besides being receptors for thrombin, both PAR-1 and PAR-4 also bind other molecules. This has been clearly shown for PAR-1 that is also stimulated by factor Xa [28] and activated protein C [29], while PAR-4 is also suggested to be a receptor for plasmin [26] and cathepsin G [31]. Finally, PAR-3 staining was an incidental finding since we found only a single case where a few polymorphonuclear cells were labelled. Altogether, our results in cirrhotic samples are in agreement with the proposed role for PARs in inflammatory processes. More specifically, they suggest that PARs could be involved in the regulation of the immune response, acting via T lymphocytes/PAR-1 for cellular immunity and B lymphocytes/PAR-4 for the humoral response. This is in agreement with one recent study that demonstrated the key role of PAR-1 in chronic inflammatory bowel disease [39]. Finally, as previously reported in other organs [11, 40], we found an expression of PAR-4 in nerve sections. This is in accordance with recent observations showing that several PARs are expressed in the nervous system and are likely involved in the regulation of neurogenic inflammation [38].

In HCC, thrombin receptors were essentially expressed within the same compartments as in the cirrhotic liver with no obvious differences in staining intensity. Only in three cases did we see a membrane staining of PAR-1 in a few clusters of tumour cells (Fig. 1). As observed by D'Andrea et al. [10], we showed that HCC-associated fibroblasts expressed PAR-1, whereas portal fibroblast from normal liver did not. However, in cirrhosis, which can be considered a preneoplastic step in the course of chronic liver disease, fibroblasts were also PAR-1 positive.

We also studied TF expression in the liver. To our knowledge, there are no previous data of such sort reported in human liver. TF expression was recently reported in a transgenic murine model of HCC where it was observed in endothelial cells and macrophages [14]. In contrast, in human liver, we found a predominant hepatocytic expression of TF. TF was expressed in the majority of non-tumour samples, either normal or cirrhotic. Normal livers sampled in the periphery of metastasis or of benign liver tumours were all positive, indicating that it is unlikely to have a bias due to the vicinity of a cancer. In light of the previous publications about other cancers [1, 34, 43], the lack of TF labelling in half of the HCCs was unexpected. This was unlikely a methodological problem due to the antibody used since prostatic carcinomas used as positive controls [25] were labelled as expected (data not shown). In addition, when positive for TF, HCCs were always less stained than the surrounding liver tissue. TF-positive HCCs were not different from TF-negative HCCs in terms of size, histological grade, local signs of invasiveness (vascular invasion, tumour capsule invasion) or outcome.

In conclusion, the pattern of expression of PARs in the course of chronic liver disease is compatible with the role proposed for these receptors in chronic inflammation. On the other hand and unlike in other organs, our data do not support a significant role for either PARs or TF in liver cancer progression.

Acknowledgements The authors are grateful to Maylis Capdepont who performed the statistical analyses.

This project was funded by the Comité de la Dordogne from the Ligue Nationale Contre le Cancer and by Région Aquitaine.

References

1. Abdulkadir SA, Carvalhal GF, Kaleem Z, Kisiel W, Humphrey PA, Catalona WJ, Milbrandt J (2000) Tissue factor expression and angiogenesis in human prostate carcinoma. Hum Pathol 31:443–447
2. Bar-Shavit R, Kahn A, Fenton JW II, Wilner GD (1983) Chemotactic response of monocytes to thrombin. J Cell Biol 96:282–285
3. Boire A, Covic L, Agarwal A, Jacques S, Sherifi S, Kuliopulos A (2005) PAR1 is a matrix metalloprotease-1 receptor that promotes invasion and tumorigenesis of breast cancer cells. Cell 120:303–313
4. Bromberg ME, Konigsberg WH, Madison JF, Pawashe A, Garen A (1995) Tissue factor promotes melanoma metastasis by a pathway independent of blood coagulation. Proc Natl Acad Sci U S A 92:8205–8209

5. Bromberg ME, Bailly MA, Konigsberg WH (2001) Role of protease-activated receptor 1 in tumor metastasis promoted by tissue factor. Thromb Haemost 86:1210–1214
6. Callander NS, Varki N, Rao LV (1992) Immunohistochemical identification of tissue factor in solid tumors. Cancer 70:1194–1201
7. Chambers RC, Dabbagh K, McAnulty RJ, Gray AJ, Blanc-Brude OP, Laurent GJ (1998) Thrombin stimulates fibroblast procollagen production via proteolytic activation of protease-activated receptor 1. Biochem J 333 (Pt 1):121–127
8. Chambers RC, Leoni P, Blanc-Brude OP, Wembridge DE, Laurent GJ (2000) Thrombin is a potent inducer of connective tissue growth factor production via proteolytic activation of protease-activated receptor-1. J Biol Chem 275:35584–35591
9. Coughlin SR (2000) Thrombin signalling and protease-activated receptors. Nature 407:258–264
10. D'Andrea MR, Derian CK, Santulli RJ, Andrade-Gordon P (2001) Differential expression of protease-activated receptors-1 and -2 in stromal fibroblasts of normal, benign, and malignant human tissues. Am J Pathol 158:2031–2041
11. D'Andrea MR, Saban MR, Nguyen NB, Andrade-Gordon P, Saban R (2003) Expression of protease-activated receptor-1, -2, -3, and -4 in control and experimentally inflamed mouse bladder. Am J Pathol 162:907–923
12. DiCuccio MN, Shami P, Hoffman M (1996) A functional tethered ligand thrombin receptor is present on human hematopoietic progenitor cells. Exp Hematol 24:914–918
13. Duplantier JG, Dubuisson L, Senant N, Freyburger G, Laurendeau I, Herbert JM, Desmouliere A, Rosenbaum J (2004) A role for thrombin in liver fibrosis. Gut 53:1682–1687
14. Dupuy E, Hainaud P, Villemain A, Bodevin-Phedre E, Brouland JP, Briand P, Tobelem G (2003) Tumoral angiogenesis and tissue factor expression during hepatocellular carcinoma progression in a transgenic mouse model. J Hepatol 38:793–802
15. Even-Ram S, Uziely B, Cohen P, Grisaru-Granovsky S, Maoz M, Ginzburg Y, Reich R, Vlodavsky I, Bar-Shavit R (1998) Thrombin receptor overexpression in malignant and physiological invasion processes. Nat Med 4:909–914
16. Even-Ram SC, Maoz M, Pokroy E, Reich R, Katz BZ, Gutwein P, Altevogt P, Bar-Shavit R (2001) Tumor cell invasion is promoted by activation of protease activated receptor-1 in cooperation with the alpha v beta 5 integrin. J Biol Chem 276:10952–10962
17. Fiorucci S, Antonelli E, Distrutti E, Severino B, Fiorentina R, Baldoni M, Caliendo G, Santagada V, Morelli A, Cirino G (2004) PAR1 antagonism protects against experimental liver fibrosis. Role of proteinase receptors in stellate cell activation. Hepatology 39:365–375
18. Howells GL, Macey M, Curtis MA, Stone SR (1993) Peripheral blood lymphocytes express the platelet-type thrombin receptor. Br J Haematol 84:156–160
19. Koomagi R, Volm M (1998) Tissue-factor expression in human non-small-cell lung carcinoma measured by immunohistochemistry: correlation between tissue factor and angiogenesis. Int J Cancer 79:19–22
20. Macey MG, Hou L, Milne T, Parameswaren V, Howe D, Cavenagh JD, Howells GL, Newland AC (1998) A CD4+ proliferation of large granular lymphocytes expresses the protease activated receptor-1. Br J Haematol 101:78–81
21. Maragoudakis ME, Kraniti N, Giannopoulou E, Alexopoulos K, Matsoukas J (2001) Modulation of angiogenesis and progelatinase a by thrombin receptor mimetics and antagonists. Endothelium 8:195–205
22. Marra F, DeFranco R, Grappone C, Milani S, Pinzani M, Pellegrini G, Laffi G, Gentilini P (1998) Expression of the thrombin receptor in human liver: up-regulation during acute and chronic injury. Hepatology 27:462–471
23. Nakasaki T, Wada H, Shigemori C, Miki C, Gabazza EC, Nobori T, Nakamura S, Shiku H (2002) Expression of tissue factor and vascular endothelial growth factor is associated with angiogenesis in colorectal cancer. Am J Hematol 69:247–254
24. Naldini A, Carney DH, Bocci V, Klimpel KD, Asuncion M, Soares LE, Klimpel GR (1993) Thrombin enhances T cell proliferative responses and cytokine production. Cell Immunol 147:367–377
25. Ohta S, Wada H, Nakazaki T, Maeda Y, Nobori T, Shiku H, Nakamura S, Nagakawa O, Furuya Y, Fuse H (2002) Expression of tissue factor is associated with clinical features and angiogenesis in prostate cancer. Anticancer Res 22:2991–2996
26. Quinton TM, Kim S, Derian CK, Jin J, Kunapuli SP (2004) Plasmin-mediated activation of platelets occurs by cleavage of protease-activated receptor 4. J Biol Chem 279:18434–18439
27. Rao LV, Pendurthi UR (2005) Tissue factor–factor VIIa signaling. Arterioscler Thromb Vasc Biol 25:47–56
28. Riewald M, Kravchenko VV, Petrovan RJ, O'Brien PJ, Brass LF, Ulevitch RJ, Ruf W (2001) Gene induction by coagulation factor Xa is mediated by activation of protease-activated receptor 1. Blood 97:3109–3116
29. Riewald M, Petrovan RJ, Donner A, Mueller BM, Ruf W (2002) Activation of endothelial cell protease activated receptor 1 by the protein C pathway. Science 296:1880–1882
30. Roche N, Stirling RG, Lim S, Oliver BG, Chung KF (2003) Regulation of protease-activated receptor-1 in mononuclear cells by neutrophil proteases. Respir Med 97:228–233
31. Sambrano GR, Huang W, Faruqi T, Mahrus S, Craik C, Coughlin SR (2000) Cathepsin G activates protease-activated receptor-4 in human platelets. J Biol Chem 275:6819–6823
32. Shapiro MJ, Weiss EJ, Faruqi TR, Coughlin SR (2000) Protease-activated receptors 1 and 4 are shut off with distinct kinetics after activation by thrombin. J Biol Chem 275:25216–25221
33. Shi X, Gangadharan B, Brass LF, Ruf W, Mueller BM (2004) Protease-activated receptors (PAR1 and PAR2) contribute to tumor cell motility and metastasis. Mol Cancer Res 2:395–402
34. Shigemori C, Wada H, Matsumoto K, Shiku H, Nakamura S, Suzuki H (1998) Tissue factor expression and metastatic potential of colorectal cancer. Thromb Haemost 80:894–898
35. Shoji M, Hancock WW, Abe K, Micko C, Casper KA, Baine RM, Wilcox JN, Danave I, Dillehay DL, Matthews E, Contrino J, Morrissey JH, Gordon S, Edgington TS, Kudryk B, Kreutzer DL, Rickles FR (1998) Activation of coagulation and angiogenesis in cancer: immunohistochemical localization in situ of clotting proteins and vascular endothelial growth factor in human cancer. Am J Pathol 152:399–411
36. Suo Z, Wu M, Citron BA, Gao C, Festoff BW (2003) Persistent protease-activated receptor 4 signaling mediates thrombin-induced microglial activation. J Biol Chem 278:31177–31183
37. Tordai A, Brass LF, Gelfand EW (1995) Tunicamycin inhibits the expression of functional thrombin receptors on human T-lymphoblastoid cells. Biochem Biophys Res Commun 206: 857–862
38. Vergnolle N, Ferazzini M, D'Andrea MR, Buddenkotte J, Steinhoff M (2003) Proteinase-activated receptors: novel signals for peripheral nerves. Trends Neurosci 26:496–500
39. Vergnolle N, Cellars L, Mencarelli A, Rizzo G, Swaminathan S, Beck P, Steinhoff M, Andrade-Gordon P, Bunnett NW, Hollenberg MD, Wallace JL, Cirino G, Fiorucci S (2004) A role for proteinase-activated receptor-1 in inflammatory bowel diseases. J Clin Invest 114:1444–1456
40. Wang H, Ubl JJ, Reiser G (2002) Four subtypes of protease-activated receptors, co-expressed in rat astrocytes, evoke different physiological signaling. Glia 37:53–63
41. Wojtukiewicz MZ, Tang DG, Ciarelli JJ, Nelson KK, Walz DA, Diglio CA, Mammen EF, Honn KV (1993) Thrombin increases the metastatic potential of tumor cells. Int J Cancer 54:793–806
42. Wojtukiewicz MZ, Zacharski LR, Rucinska M, Zimnoch L, Jaromin J, Rozanska-Kudelska M, Kisiel W, Kudryk BJ (1999) Expression of tissue factor and tissue factor pathway inhibitor in situ in laryngeal carcinoma. Thromb Haemost 82:1659–1662
43. Wojtukiewicz MZ, Rucinska M, Zacharski LR, Kozlowski L, Zimnoch L, Piotrowski Z, Kudryk BJ, Kisiel W (2001) Localization of blood coagulation factors in situ in pancreatic carcinoma. Thromb Haemost 86:1416–1420

Virchows Arch (2006) 448: 52–58
DOI 10.1007/s00428-005-0011-6

ORIGINAL ARTICLE

Y. Soini · S. Tommola · H. Helin · P. Martikainen

Claudins 1, 3, 4 and 5 in gastric carcinoma, loss of claudin expression associates with the diffuse subtype

Received: 31 March 2005 / Accepted: 17 May 2005 / Published online: 12 October 2005

Abstract In this study expression of claudins 1, 3, 4 and 5 were studied in 118 cases of gastric carcinoma and compared with proliferation, apoptosis and E-cadherin expression. Expression of all these claudins could be seen in gastric carcinoma, most prominently for claudin 4, and least expression was found for claudin 5. All claudins showed significantly more expression in gastric carcinomas of intestinal type. Their expression was significantly associated with each other. Expression of claudins 4 and 5 was associated with E-cadherin. Strong expression of claudin 5 was associated with higher cell proliferation and apoptosis. Claudin 3 expression had an association with a better prognosis of the patients, especially in the intestinal type. The results show that expression of claudins 1, 3, 4 and 5 is lower in diffuse-type gastric carcinomas. Possibly they play a role in determining the diffuse phenotype and loose cohesion of cells in diffuse type of gastric carcinoma in a similar manner as E-cadherin. The loss of their expression does not clearly associate with poorer prognosis of the patients, except for claudin 3, where strong expression was associated with a better outcome of the patients, a feature especially related to intestinal-type tumours.

Keywords Cancer · Gastric · Claudin · Adhesion · Metastasis

Y. Soini (✉)
Department of Pathology, University Hospital
of Oulu and Oulu University,
P.O. Box 5000, (Aapistie 5),
90014 Oulu, Finland
e-mail: msoini@cc.oulu.fi

S. Tommola · P. Martikainen
Department of Pathology, Tampere University Hospital,
P.O. Box 2000,
33521 Tampere, Finland

H. Helin
HUSLAB, Division of Pathology,
Helsinki University Central Hospital,
P.O. Box 400, 00029 HUS,
Helsinki, Finland

Introduction

Claudins are tight junctional proteins which are present at epithelial and endothelial cell membranes [22, 23]. Tight junctions are structures which regulate the flow of water, ions and various macromolecules through paracellular spaces, and claudins are crucial for this barrier function [22–24]. In addition to claudins, tight junctions contain occludin and tight junctional proteins zonula occludens ZO-1, ZO-2 and ZO-3, which show close association. ZO-2 associates with occludin and claudins at the cell membrane and also with ZO-1 and ZO-3 and the actin cytoskeleton [14]. At present, at least 23 different claudins are known in humans, and their expression may vary in different cells and tissues of the body [24]. Claudin 2, for example, is found in murine liver and kidney, but not in lung tissue [14]. On the other hand, claudin 4 is found in murine lung and kidney, but not in liver [14]. Claudin expression may also be different in some tissues like those in mouse and rabbit kidney, where variable expression is found in different tubular segments of the nephron [5, 16]. Claudin expression varies also in gastrointestinal tissues. In rat liver, claudin 4 was absent and claudin 5 was only present in endothelial cells, whereas claudin 3 was uniformly expressed and claudin 2 was more strongly expressed in periportal hepatocytes [15]. In rat pancreas, claudin 2 was expressed in junctional epithelia ductal cells, whereas claudin 5 was present in acinar cells and claudins 3 and 4 in both [15]. Site-specific differences in claudin expression can also be found in the gastrointestinal tract [15]. In rat gut, differences in claudin expression were also seen in mucosa between the surface and basal epithelia [15].

In human tissues and in tumours in general, expression of different claudins has not been extensively studied. Elevated claudin 3 expression compared to normal tissues has been shown in rat prostate carcinoma [9]. Similarly, overexpression of claudins 3 and 4 has been shown in breast and ovarian carcinoma [4, 6, 7]. On the other hand, loss of claudin 7 appears to be associated with a more aggressive behaviour of breast carcinoma [6]. In pancreatic adenocarcinoma and its precursor lesions, claudin 4 overexpression

has been found to be present [12, 20]. In soft tissue lesions, claudin 1 can be used as a marker for perineurinoma [1]. Interestingly also, claudins may have potential in treatment of cancer. In claudin-4-expressing pancreatic cancers, administration of clostridium perfringens enterotoxin results in tumour cell necrosis due to the fact that claudin 4 binds and serves as a receptor for this enterotoxin [13]. Similar results with claudins 3 and 4 have been obtained in breast carcinoma [7].

Distribution of claudin in gastric neoplastic or non-neoplastic tissues has not been studied so far. Our aim was to study the expression of claudins 1, 3, 4 and 5 in a set of gastric carcinomas. The results were associated with tumour proliferation and apoptosis as determined by Ki67 immunostaining and TUNEL assay. We also evaluated expression of claudins 1, 3, 4 and 5 as a prognostic marker by investigating their association with patient survival and tumour stage.

Materials and methods

Study material

There were 118 cases of gastric carcinoma collected from the files of the Central University Hospital of Tampere. Additionally, eight cases of non-neoplastic mucosa were included. All the materials had been fixed in 10% buffered formalin and embedded in paraffin. The array blocks were constructed with a custom-built instrument (Beecher Instruments, Silver Spring, MD, USA). The sample diameter of the tissue core in the array block was 600 μm. Because of the small size of the punch biopsy, at least three biopsies were obtained from the same case, and all samples were analysed. The histological diagnosis of the tumours was based on the criteria of Lauren et al. [3, 8]. The cases consisted of 50 intestinal-, 56 diffuse- and 12 mixed-type tumours. There were 24 stage-I, 26 stage-II, 43 stage-III and 25 stage-IV tumours [18]. In 50 cases, samples from local regional or distal lymph node or peritoneal metastases were available. Survival of patients and other relevant clinical data were obtained from patient journals.

Immunohistochemistry of claudins and E-cadherin

The primary antibodies used in the immunostaining were all purchased from Zymed Laboratories (South San Francisco, CA, USA) designed to be used in formalin-fixed, paraffin-embedded tissues. They were polyclonal rabbit anti-claudin 1 (clone JAY.8), polyclonal rabbit anti-claudin 3 (clone Z23.JM), monoclonal mouse anti-claudin 4 (clone 3E2C1), monoclonal mouse anti-claudin 5 (clone 4C3C2) and monoclonal mouse anti-E-cadherin (clone HECD-1) [17, 21]. Before application of the primary antibodies, the sections were heated in a microwave oven in 10 mmol/l citrate buffer, pH 6.0, for 10 min. For E-cadherin, pH 9.0 was used, and heating was done for 15 min. After 60 min incubation with the primary antibody (dilution 1:50 for anti-claudins 1, 3, 4, and 5, and 1:200 for E-cadherin), a biotinylated secondary antibody and Histostain-SP kit (Zymed Laboratories) was used. For all the immunostainings, the colour was developed by diaminobenzidine, after which, the sections were lightly counterstained with hematoxylin and mounted with Eukitt (Kindler, Freiburg, Germany).

Negative control stainings were carried out by substituting non-immune rabbit or mouse serum and PBS for the primary antibodies. As positive controls, non-neoplastic kidney, breast, skin and liver samples were used.

The immunostaining was assessed as follows:

−=no immunostaining present
+=less than 25% of cells positive
++=25–50% of cells positive
+++=50–75% of cells positive
++++=75–100% of cells positive

In the evaluation, membrane-bound positivity was considered significant. Inasmuch as several biopsies of same tumour were simultaneously present, all samples were evaluated separately, and the average value was used to represent the whole immunoreactivity in tumours.

Ki67 immunohistochemistry

The determination of cell proliferation activity in 5-μm tissue sections was based on the assessment of $Ki67^{MIB-1}$ immunoreactive cells. The antigen retrieval by microwave oven processing (in citrate buffer, twice at 850 W for 5 min) was followed by immunostaining with a mouse monoclonal antibody (IgG, Immunotech S.A. Marseilles, France) at 1:40 dilution. The bound antibodies were visualised with a streptavidin–biotin immunoperoxidase technique (Zymed Laboratories) using diaminobenzidine (0.5 mg/ml) as a chromogen. The sections were counterstained with ethyl green. The sections were analysed with a CAS image analyser giving the percentage of positively labelled tumour cell nuclei in 20 separate high-power fields for each tumour.

Assessment of apoptosis

Paraffin sections (3 μm) were cut on SuperFrost Plus objective slides (Menzel-Gläser, Germany). The sections were de-waxed in xylene and dehydrated through a graded series of ethanol to PBS. After proteinase K digestion (Sigma Chemical Co., St. Louis, MO, USA) for 15 min, apoptotic cells were demonstrated using an ApoTag in situ apoptosis detection kit (Oncor, Gaithersburg, MD, USA) according to the manufacturer's instructions. In the terminal deoxynucleotidyl transferase (TdT) nick end labelling method, the recommended TdT concentration was, however, reduced eightfold. Direct immunoperoxidase detection of digoxigenin-labelled dUTP was followed by counterstaining in 0.02% methyl green in 0.1 mol/l acetate buffer (pH 5.2) for 15 min.

Table 1 Claudins 1, 3, 4 and 5 expression in primary lesions of gastric carcinoma

	Claudin			
	1	3	4	5
–	19 (17.0%)	35 (30.7%)	14 (12.7%)	57 (50.4%)
+	8 (7.2%)	13 (11.4%)	5 (4.5%)	12 (10.6%)
++	25 (22.3%)	18 (15.8%)	22 (20%)	16 (14.1%)
+++	29 (25.9%)	11 (9.7%)	19 (17.2%)	15 (13.3%)
++++	31 (27.7%)	37 (32.4%)	50 (45.4%)	13 (11.5%)
Total	112	114	110	113

Statistical analysis

SPSS for Windows (Chicago, IL, USA) was used for statistical analysis. The significance of associations was determined using Fisher's exact probability test, correlation analysis and two-tailed *t* test. Survival was analysed with the Kaplan–Meier curve, and significance of associations was analysed with log rank, Breslow and Tarone–Ware tests. Cox regression multivariate model (stepwise forward) was used in multivariate analysis. Probability values ≤0.05 were considered significant.

Results

In non-neoplastic mucosa, strong claudin 1 expression was seen in corpus and antral epithelia and glands. Areas with intestinal metaplasia also showed expression. With claudin

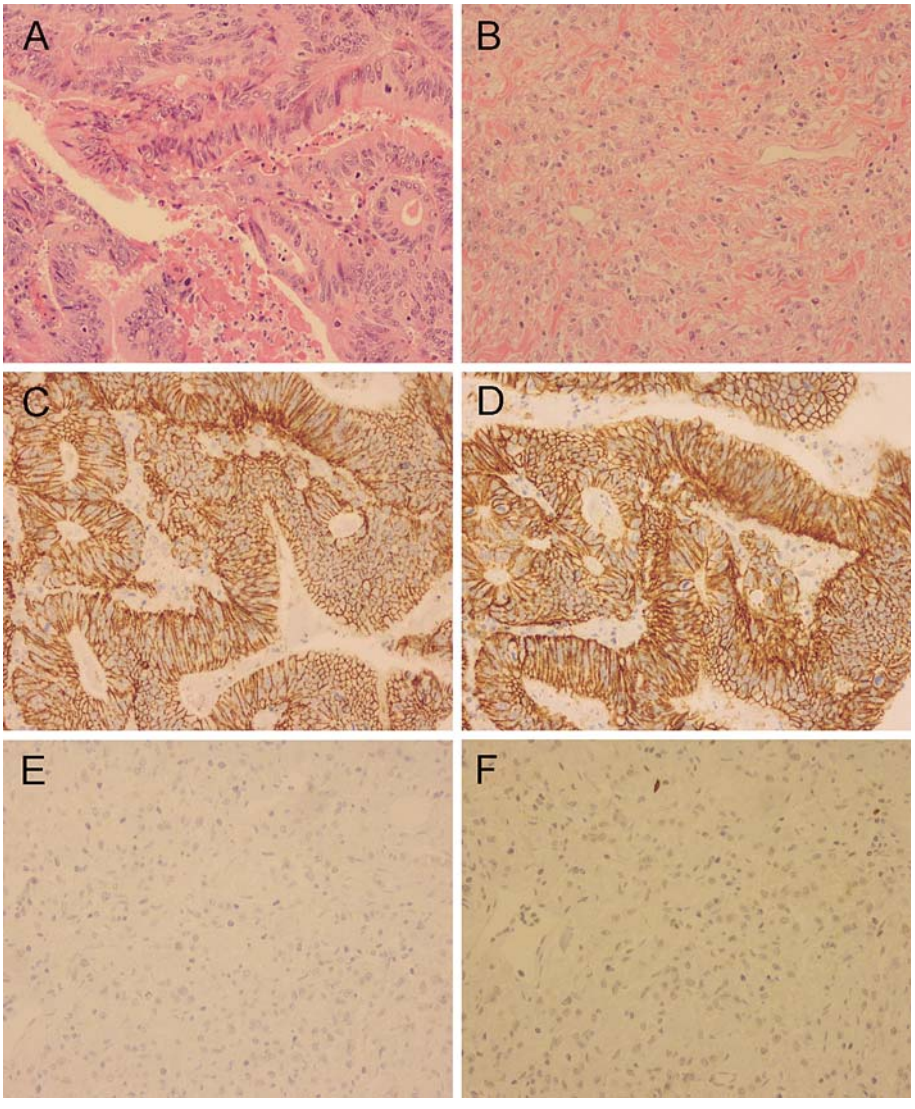

Fig. 1 Immunostaining of claudins 1 and 3 in gastric carcinoma. Histology of an example of an intestinal (**a**) and a diffuse (**b**) gastric carcinoma. Strong membranous expression for claudin 1 (**c**) and claudin 3 (**d**) is seen in an intestinal-type tumour, whereas the diffuse type is negative for claudin 1 (**e**) and claudin 3 (**f**)

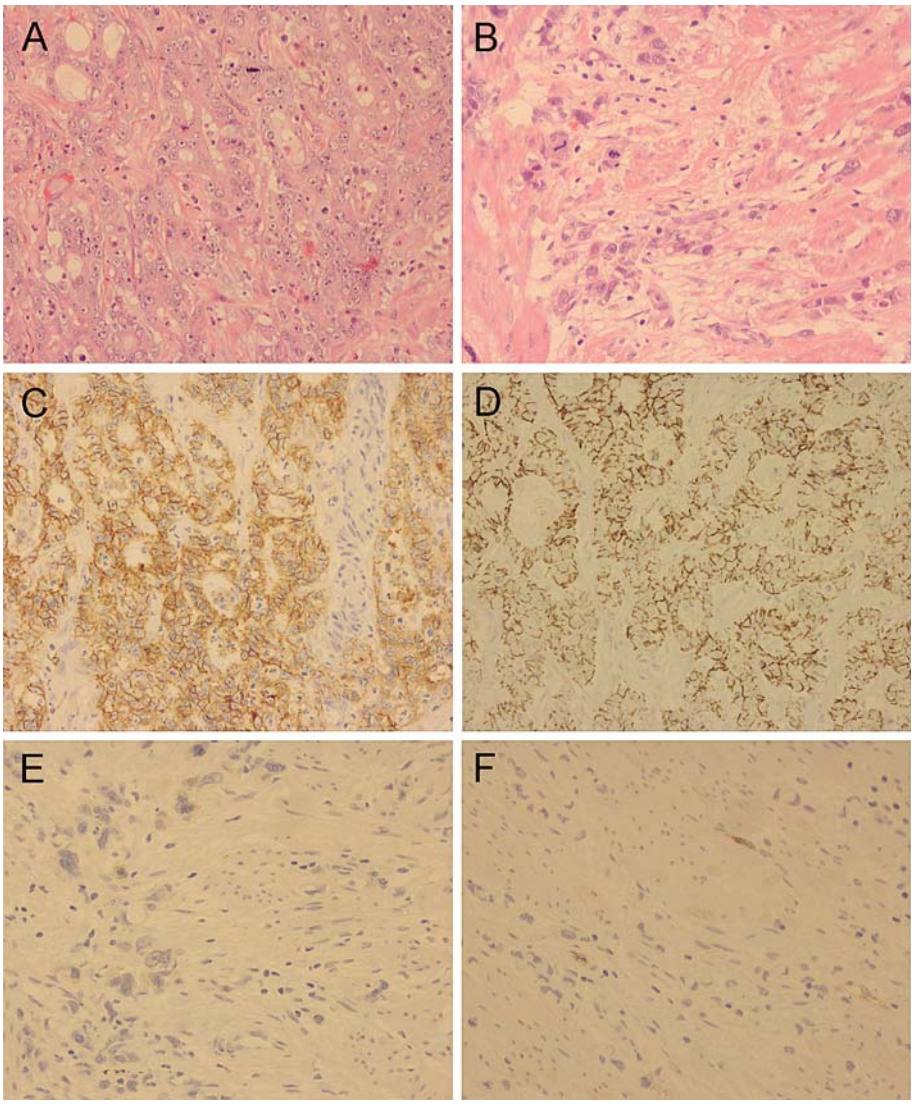

Fig. 2 Immunostaining of claudins 4 and 5 in gastric carcinoma. A histology of an example of another case of an intestinal (**a**) and a diffuse (**b**) gastric carcinoma. Strong membranous expression for claudin 4 (**c**) and claudin 5 (**d**) is seen in an intestinal-type tumour, whereas the diffuse type is negative for claudin 4 (**e**) and claudin 5 (**f**)

3, corpus-type mucosa showed strong expression, whereas expression was weaker in antral mucosa and in areas of intestinal metaplasia. Claudin 4 was weak in antral mucosa; only some basal glands showed staining. Staining in corpus mucosa was stronger, but weaker than with claudins 3 or 1. Areas with intestinal metaplasia, however, showed strong claudin 4 expression. Expression of claudin 5 was also seen in corpus-type mucosa and in intestinal metaplasia; antral mucosa again showed very weak expression.

The frequency of claudins 1, 3, 4 and 5 expression is shown in Table 1. As can be seen from the table, claudin 1 expression was observed in 83%, claudin 3 in 69%, claudin 4 in 87% and claudin 5 in 49% of the cases (Figs. 1 and 2). Strongest expression was seen for claudins 4 and 3, with

Table 2 Claudins 1, 3, 4 and 5 and E-cadherin expression in different histological types of gastric carcinomas (primary tumours)

		Diffuse	Mixed	Intestinal	Total	Apoptosis (%)	Proliferation (%)	Sum
Claudin 1	0	25	9	18	52	1.02±1.71	29.4±15.0	
	1	16	8	36	60	0.95±1.83	32.6±15.5	112
Claudin 3	0	30	13	23	66	1.17±1.91	28.4±14.8**	
	1	12	5	31	48	0.71±1.52	34.4±15.1	114
Claudin 4	0	20	10	13	43	0.67±1.40	28.5±15.7	
	1	18	8	41	67	1.18±1.98	32.3±14.9	110
Claudin 5	0	36	10	23	71	0.66±1.28*	28.8±16.4***	
	1	6	5	33	45	1.37±2.20	34.1±12.7	113
E-cadherin	0	22	8	15	45	1.33±0.22	27.9±15.3	
	1	18	5	39	62	1.59±0.21	29.2±13.6	107

For claudins 1, 3 and 4 and E-cadherin: *0* Negative or + or ++, *1* +++ or more
For claudin 5: *0* Negative or +, *1* ++ or more
*p=0.02
**p=0.01
***p=0.024

claudin 5 showing the least number of strongly positive cases. Inasmuch as the median point for expression of claudins 1, 3 and 4 was ++ and for claudin 5 about +, these were used as breaking points in analysing the data.

The frequency of claudin expression in gastric carcinomas of different histological types can be seen in Table 2. According to the histological diagnosis, diffuse-type tumours showed less claudin 1 (p=0.006), claudin 3 (p=0.004), claudin 4 (p=0.004) and claudin 5 (p=0.0001) positivity than intestinal types. No difference was observed between diffuse type and mixed type. There was, however, a significant difference in claudin expression between mixed and intestinal types in claudin 3 (p=0.03), claudin 4 (p=0.02) and claudin 5 (p=0.03) expression, with the latter tumours showing cases with more reactivity.

When compared to each other, significant associations were found between all claudins. There was a significant association between claudin 1 and claudin 3 (p<0.001), claudin 4 (p=0.002) and claudin 5 (p=0.002) expression. Claudin 3 associated with claudin 4 (p=0.001) and claudin 5 (p<0.001), and claudin 4 associated with claudin 5 (p<0.001) expression.

E-cadherin expression was also studied in the samples. Low expression was found in 42% and high expression in 57% of the cases. The distribution of immunoreactivity in different subtypes is shown in Table 2. In diffuse- and mixed-type carcinomas, 45 and 38%, respectively, showed strong positivity for E-cadherin, whereas 72% of intestinal-type carcinomas were strongly positive. There was a strong association between claudin 4 and claudin 5 and E-cadherin expression (p=0.002 and p=0.001, respectively) but not with claudin 1 (p=0.475) or claudin 3 (p=0.175). Diffuse carcinomas expressed claudin less frequently than the intestinal type (p=0.007). In addition, mixed-type tumours showed less reactivity than the intestinal types (p=0.03).

The mean apoptotic index in gastric carcinoma was 0.91±1.67%. No difference in apoptosis was found between different histological tumour types. There was no difference in the extent of apoptosis between claudins 1, 3 or 4 expression; tumours with stronger claudin 5 expression had, however, significantly more apoptosis (1.37±2.20 vs 0.66±1.28%, p=0.02). Apoptosis did not associate with survival of the patients (p=0.37), nor was it associated with tumour stage (p=0.35).

The mean proliferation index in gastric carcinomas was 31.16±15.36%. Diffuse gastric tumours had a significantly higher proliferation index (34.62±12.88%) than tumours of the intestinal type (25.37±18.13%, p=0.001). No difference was observed between stage-I–II and stage-III–IV tumours, and proliferation (p=0.72) (Table 3). Metastatic lesions had a slightly lower MIB index (25.64±14.21%) than primary lesions (30.32±15.04%), but the association did not reach statistical significance (p=0.058). As with apoptosis, tumours expressing stronger claudin 5 had a significantly higher proliferation index (34.1±12.7 vs 28.8±16.4%, p=0.024). Similar phenomenon was seen with claudin 3 (34.4±15.1 vs 28.4±14.8%, p=0.010).

There was no significant difference in survival between the different histological types of tumours (p=0.37, log

Table 3 Claudins 1, 3, 4 and 5 expression in relation to tumour stage and apoptosis and proliferation in tumours of different stages

		Stages I–II	Stages III–IV
Claudin 1	0	21	24
	1	23	29
Claudin 3	0	21	35
	1	23	19
Claudin 4	0	19	19
	1	24	34
Claudin 5	0	29	32
	1	16	23
Apoptosis		0.75±1.61%	0.83±1.12%
Proliferation		29.5±14.4%	30.4±16.1%

For claudins 1, 3 and 4: *0* Negative or + or ++, *1* +++ or more
For claudin 5: *0* Negative or +, *1* ++ or more

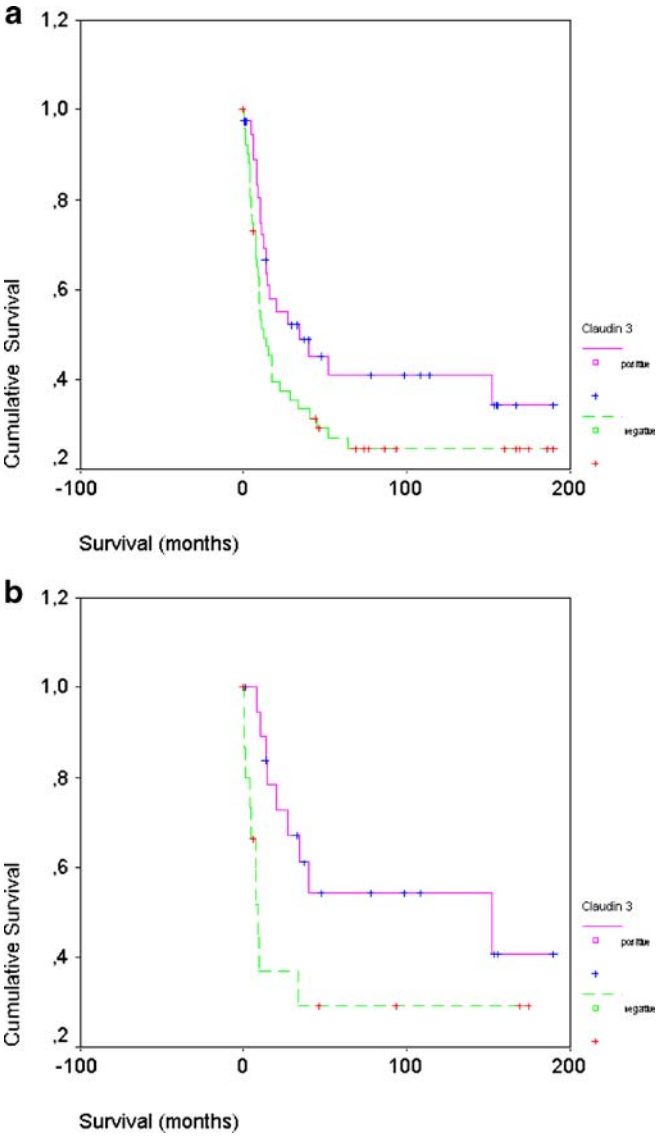

Fig. 3 Kaplar–Meyer curve for claudin 3 in the whole material (**a**) and separately in intestinal-type tumours (**b**). Patients with tumours expressing claudin 3 show a better survival than negative ones

rank). There was, however, a significant difference in survival between stage-I–II and stage-III–IV tumours ($p<0.0001$, log rank), but not between stage-I and stage-II tumours ($p=0.36$, log rank) or between stage-III and stage-IV tumours ($p=0.38$). In stage-I–II tumours, survival did not associate with proliferation ($p=0.90$). Similarly, in stage-III–IV tumours, survival did not associate with proliferation ($p=0.64$). Claudin expression was not associated with the stage of the tumours, nor was there any significant difference in claudin expression between primary and metastatic lesions. Expression of claudin 3 tended, however, to be stronger in lower stage tumours, but the association did not reach statistical significance ($p=0.067$). Claudin 1 ($p=0.40$), claudin 4 ($p=0.39$) or claudin 5 ($p=0.29$) did not associate with survival of the patients. With claudin 3, however, the association tested with log rank was near significant ($p=0.08$), and with Breslow ($p=0.035$) and Tarone–Ware ($p=0.049$), it was significant, with cases showing stronger claudin 3 having a better outcome (Fig. 3). If tumours of intestinal types were analysed separately, the association with claudin 3 expression was even stronger ($p=0.0113$, log rank; $p=0.0011$, Breslow; $p=0.0029$, Tarone–Ware), whereas no other claudin showed any significant association if diffuse and intestinal types were analysed separately. According to Cox's multivariate model, claudin 3 or any other claudins did not have independent prognostic value. In this respect, tumour stage was the only significant factor ($p=0.0094$).

Discussion

In this study, expression of claudins 1, 3, 4 and 5 was studied in 118 cases of gastric carcinoma. To evaluate changes of expression associated with tumour progression, samples from metastatic sites were also included. Some samples of non-neoplastic mucosa were also included.

The results show variable and heterogenous expression of claudins 1, 3, 4 and 5 in gastric carcinoma. The most prominent expression of claudins was seen for claudins 1 and 4, where about 80% of cases showed positivity, whereas expression was weaker for claudin 3, which showed 69% of cases positive, and for claudin 5, which showed 50% of cases positive.

Comparison of claudins in different epithelial types of tumours showed that diffuse-type carcinomas showed overall lower expression of claudins compared with intestinal types. Thus, loss of claudin expression may be one phenotypic feature distinguishing these two tumour types in analogy with E-cadherin, the expression of which is also lost in diffuse-type carcinoma [10, 11]. In accordance with this, we also observed lower E-cadherin expression in diffuse carcinomas. It might also be that loss of claudin and E-cadherin expression is somehow interrelated inasmuch as E-cadherin has been shown to influence the formation of tight junctions and desmosomes although it mainly mediates the assembly of adherens junctions [2, 25]. In line with this, there was an association between expression of claudins 4 and 5 and E-cadherin. At present, little data are, however, available on the functional association between E-cadherin and claudins.

E-cadherin expression has been associated with a poorer prognosis of the patients [10, 11]. In general, such an association could not be seen with claudins, except for claudin 3, where its lowered expression was associated with a marginally poorer prognosis. This feature appeared to be associated especially with intestinal types of tumours because when separately analysed, diffuse carcinomas did not show any significant association. According to Cox's multivariate model, the association with survival did not, however, have independent prognostic value. The only parameter showing independent prognostic value in this material was tumour stage. Stage was not, however, associated with claudin expression, neither did we find any differences in claudin expression between primary tumours and tumours from metastatic sites. Thus it appears that claudin expression has no significance during tumour progression. In intestinal metaplasia, which is a risk factor for gastric carcinoma [3], expression of claudins 1, 3, 4 and 5 seemed to differ at least from antral mucosa cells inasmuch as in the former, expression for claudin 1, 4 and 5 appeared to be more strongly present. It would be interesting in this respect to test their expression in early dysplastic lesions of gastric mucosa and other sites.

Claudin 5 has been associated with endothelial cells, and in some studies, it is suggested to be present only in endothelial cell junctions [22, 23]. In our previous studies, we, however, observed claudin 5 in carcinomas such as breast carcinoma [19]. In addition, in this study, claudin 5 expression was seen in a proportion of gastric carcinomas. Interestingly, claudin 5 expression seemed to be positively associated with biological markers associated with tumour growth, such as proliferation and apoptosis. The reason for this is obscure because there are no known mechanisms to link claudin 5 expression to them. Because claudin 5 is also present in endothelial cells, tumours showing claudin 5 expression could have some additional affinity for blood vessels. However, claudin 5 expression was not clearly different in metastatic lesions compared to primary tumours, indirectly speaking for the fact that its expression does not increase vascular invasion. On the other hand, some other claudins such as claudin 3 are also present on endothelial cells, and interactions based on claudin expression between endothelial and epithelial cells could thus be complex.

In conclusion, tight junctional proteins claudins 1, 3, 4 and 5 show variable expression in gastric carcinoma, and their expression seems to be lower in diffuse-type carcinomas. In this respect, they resemble E-cadherin and, together with this molecule, might contribute to the loose cohesion and histological appearance of diffuse carcinomas. Of the claudins studied here, claudin 3 expression appeared to be associated with a marginally better outcome for patients, a feature that was especially related to the intestinal type.

Acknowledgements The skillful technical assistance of Mrs. Eija Tomperi and Mirja Vahera is greatly appreciated.

References

1. Folpe AL, Billings SD, McKenney JK, Walsh SV, Nusrat A, Weiss SW (2002) Expression of claudin-1, a recently described tight junction-associated protein, distinguishes soft tissue perineurioma from potential mimics. Am J Surg Pathol 26:1620–1626
2. Gumbiner B, Stevenson B, Grimaldi A (1988) The role of the cell adhesion molecule uvomorulin in the formation and maintenance of the epithelial junctional complex. J Cell Biol 107: 1575–1587
3. Hamilton SR, Aaltonen LA (2000) Tumours of the digestive system. Pathology and genetics. World Health Organization classification of tumours. IARC Press, Lyon, France
4. Hough CD, Sherman-Baust CA, Pizer ES, Montz FJ, Im DD, Rosenshein NB, Cho KR, Riggins GJ, Morin PJ (2000) Large-scale serial analysis of gene expression reveals genes differentially expressed in ovarian cancer. Cancer Res 60:6281–6287
5. Kiuchi-Saishin Y, Gotoh S, Furuse M, Takasuga A, Tano Y, Tsukita S (2002) Differential expression patterns of claudins, tight junction membrane proteins, in mouse nephron segments. J Am Soc Nephrol 13:875–886
6. Kominsky SL, Argani P, Korz D, Evron E, Raman V, Garrett E, Rein A, Sauter G, Kallioniemi OP, Sukumar S (2003) Loss of the tight junction protein claudin-7 correlates with histological grade in both ductal carcinoma in situ and invasive ductal carcinoma of the breast. Oncogene 22:2021–2033
7. Kominsky SL, Vali M, Korz D, Gabig TG, Weitzman SA, Argani P, Sukumar S (2004) Clostridium perfringens enterotoxin elicits rapid and specific cytolysis of breast carcinoma cells mediated through tight junction proteins claudin 3 and 4. Am J Pathol 164:1627–1633
8. Lauren T (1965) The two histological main types of gastric carcinoma. Acta Pathol Microbiol Scand 64:34
9. Long H, Crean CD, Lee W-H, Cummings OW, Gabig TG (2001) Expression of clostridium perfringens enterotoxin receptors claudin-3 and claudin-4 in prostate cancer epithelium. Cancer Res 61:7878–7881
10. Machado JC, Carneiro F, Beck S, Rossi S, Lopes J, Taveira GA (1998) E-cadherin expression is correlated with the isolated cell/diffuse histotype and with the features of biological aggressiveness of gastric carcinoma. Int J Surg Pathol 6:135–144
11. Mayer B, Johnson JP, Leitl F, Jauch KW, Heiss MM, Schildberg FW, Birchmeier W, Funke I (1993) E-cadherin expression in primary and metastatic gastric cancer: down-regulation correlates with cellular dedifferentiation and glandular disintegration. Cancer Res 53:1690–1695
12. Michl P, Barth C, Buchholz M, Lerch MM, Rolke M, Holzmann KH, Menke A, Fensterer H, Giehl K, Lohr M, Leder G, Iwamura T, Adler G, Gress TM (2003) Claudin-4 expression decreases invasiveness and metastatic potential of pancreatic cancer. Cancer Res 63:6265–6271
13. Michl P, Buchholz M, Rolke M, Kunsch S, Lohr M, McClane B, Tsukita S, Leder G, Adler G, Gress TM (2001) Claudin 4: a new target for pancreatic cancer treatment using clostridium perfringens enterotoxin. Gastroenterology 121:678–684
14. Mitic LL, van Itallie CM, Anderson JM (2000) Molecular physiology and pathophysiology of tight junctions I. Tight junction structure and function: lesions from mutant animals and proteins. Am J Physiol Gastrointest Liver Physiol 279: G250–G254
15. Rahner C, Mitic LL, Anderson JM (2001) Heterogeneity in expression and subcellular localization of claudins 2, 3, 4, and 5 in the rat liver, pancreas, and gut. Gastroenterology 120:411–422
16. Reyes JL, Lamas M, Martin D, del Carmen Namorado M, Islas S, Luna J, Tauc M, Gonzalez-Mariscal L (2002) The renal segmental distribution of claudins changes with development. Kidney Int 62:476–487
17. Sanford JL, Edwards JD, Mays TA, Gong B, Merriam AP, Rafael-Fortney JA (2005) Claudin-5 localizes to the lateral membranes of cardiomyocytes and is altered in utrophin/dystrophin-deficient cardiomyopathic mice. J Mol Cell Cardiol 38: 323–332
18. Sobin LH, Wittekind CH (2002) TNM classification of malignant tumours. International Union Against Cancer (UICC), 6th edn. Wiley-Liss, New York
19. Soini Y (2004) Claudins 2, 3, 4 and 5 in Paget's disease and breast carcinoma. Hum Pathol 35:1531–1536
20. Terris B, Blaveri E, Crnogorac-Jurcevic T, Jones M, Missiaglia E, Ruszniewski P, Sauvanet A, Lemoine NR (2002) Characterization of gene expression profiles in intraductal papillary-mucinous tumors of the pancreas. Am J Pathol 160:1745–1754
21. Tokes AM, Kulka J, Paku S, Szik A, Paska C, Novak PK, Szilak L, Kiss A, Bögl K, Schaff Z (2005) Claudin 1, 3, and 4 proteins and mRNA expression in benign and malignant breast lesions: a research study. Breast Cancer Res 7:R295–R305
22. Tsukita S, Furuse M (2000) Pores in the wall: claudins constitute tight junction strands containing aqueous pores. J Cell Biol 149:13–16
23. Tsukita S, Furuse M (2002) Claudin-based barrier in simple and stratified cellular sheets. Curr Opin Cell Biol 14:531–536
24. Turksen K, Troy T-C (2004) Barriers built on claudins. J Cell Sci 117:2435–2447
25. Wheelock MJ, Jensen PJ (1992) Regulation of keratinocyte intercellular junction organization and epidermal morphogenesis by E-cadherin. J Cell Biol 117:415–425

Virchows Arch (2006) 448: 59–67
DOI 10.1007/s00428-005-0077-1

ORIGINAL ARTICLE

Zbigniew Rudzki · Rafał Kawa · Krzysztof Okoń · Ewa Szczygieł · Jerzy Stachura

Objective, planimetry-based assessment of megakaryocyte histological pictures in Philadelphia-chromosome-negative chronic myeloproliferative disorders: a perspective for a valuable adjunct diagnostic tool

Received: 14 June 2005 / Accepted: 19 August 2005 / Published online: 12 October 2005

Abstract Philadelphia-chromosome-negative chronic myeloproliferative disorders (Ph− CMPDs)—essential thrombocythemia (ET), chronic idiopathic myelofibrosis (CIMF), and polycythemia vera (PV)—may show clinical and morphological similarities, particularly at the early stages. The differential diagnosis of Ph− CMPDs is important due to their different treatment and prognosis. Cytological features of megakaryocytes are considered valuable in this differentiation. To establish an objective measure of megakaryocyte dysplasia in Ph− CMPDs, we performed computer-assisted morphometry of more than 4,000 cells from 20 cases of ET, 10 of CIMF, 10 of PV, and 10 controls. Megakaryocyte sets from three Ph− CMPDs differed significantly in respect to many planimetric parameters, but not a single shape or size parameter could have been used as a discriminative tool between the entities. However, the discriminant function analysis with the simultaneous assessment of 12 planimetric variables allowed for a proper classification of 20 of 20 ET, 10 of 10 PV, and 9 of 10 CIMF cases based solely on the morphometric features of megakaryocytes. Additionally, we identified certain new patterns of megakaryocytes specific for ET, PV, and CIMF, which, although not dominating in one Ph− CMPD, are unlikely to occur in two others. Objective measurements of megakaryocyte sizes and shapes may assist the diagnosis of Ph− CMPDs.

Z. Rudzki (✉) · K. Okoń · E. Szczygieł · J. Stachura
Department of Pathomorphology, Collegium Medicum,
Jagiellonian University,
Grzegórzecka 16,
31-531 Cracow, Poland
e-mail: mprudzki@cyf-kr.edu.pl
Tel.: +48-12-4215210
Fax: +48-12-4119725

R. Kawa
Institute of Computer Science, Jagiellonian University,
Cracow, Poland

Keywords Megakaryocytes · Chronic myeloproliferative disorders · Essential thrombocythemia · Polycythemia vera · Chronic idiopathic myelofibrosis

Introduction

Chronic myeloproliferative disorders (CMPDs) lacking the Philadelphia chromosome and/or its molecular equivalent —the BCR/ABL translocation (Ph−)—encompass a group of hematopoietic neoplasms usually characterized by an indolent but progressive course. Ph− CMPDs manifest with effective hemopoiesis, cellular bone marrow showing inconsistent tendency for fibrosis, and a variably increased risk of transformation into acute leukemia [10]. The most frequent Ph− CMPDs—essential thrombocythemia (ET), chronic idiopathic myelofibrosis (CIMF), and polycythemia vera (PV)—demonstrate both similarities and profound differences, with the worse prognosis attributed to CIMF, the intermediate to PV, and the most favorable to ET [2, 19]. The different biology of Ph− CMPD is reflected in the contemporary therapeutic approach. Some of the patients with CIMF are considered as candidates for an allogeneic bone marrow transplantation [4, 24], whereas many patients with ET require only a "watch and wait" approach or noncytotoxic medications [21]. A recent trend for the detection of Ph− CMPD at an earlier age, combined with the polarization of therapeutic strategies for the three basic entities, increased the demand for an accurate differential diagnosis particularly at the earlier stages, when the clinicopathological pictures of Ph− CMPD may markedly overlap.

The traditional diagnostic approach to Ph− CMPD was exemplified by the sets of criteria developed by the Polycythemia Vera Study Group (PVSG) for PV [1, 18], ET [17], and CIMF [11]. According to PVSG, the diagnostic "center of gravity" was placed within a clinical picture of a disease, whereas the histology of the neoplastic tissue was largely or even completely disregarded. An alternative approach stressing the utility of morphological assessment,

particularly the value of a trephine bone marrow biopsy, was proposed by the groups from Hanover [6, 7] and Cologne [28]. Of particular importance was the description of the very early ("prefibrotic") CIMF [26]. Most cases of prefibrotic CIMF, when diagnosed according to PVSG, are misclassified as ET or left unclassified [29]. Both approaches, the "clinical" and the "histological," were combined in the contemporary WHO classification criteria [10], although the impact of the PVSG on the WHO typology seems to be stronger. A recently published comprehensive set of diagnostic criteria based on both PVSG and WHO standards takes into account both the clinics and the pathology of Ph− CMPDs [15].

The issue of transition among individual Ph− CMPDs or the existence of borderline cases is highly controversial and not merely academic, taking into account the different consequences of specific diagnoses, particularly when the differentiation between ET and CIMF is considered. Another source of controversy is the very early stages of Ph− CMPD, when the diagnostic criteria usually cannot be fully met and the disease is frequently subclinical. Gradual lowering of the "diagnostic" platelet threshold for ET has gained wider acceptance [8, 13, 22], and the concept of an already mentioned prefibrotic CIMF was almost universally adopted. However, the notion that PV may present with the red blood cell values at the upper norm is still not accepted, although conceptually such a phase in the natural history of this disease has to exist. Both the "borderline" and the early cases of Ph− CMPD are not infrequently eliminated from the research series, but their stubborn existence in the clinical practice makes the differential diagnosis in the CIMF–ET–PV triangle sometimes very challenging and fascinating. The role of a surgical pathologist (hematopathologist) in this process should not be underestimated.

The histological assessment of bone marrow suspected for Ph− CMPD includes all aspects of hematopoietic, stromal, and osseous pathology in the context of complete clinical data, optimally accompanied also by peripheral blood and bone marrow smears. The most important single element of bone marrow histology in this context is the morphology of megakaryocytes, which was stressed by the seminal paper describing the Hanover classification [6] and which was also appreciated by the WHO [10]. According to both sources, the megakaryocytes in Ph− CMPD tend to cluster and show different and characteristic alterations in their morphology. In CIMF, they are pleomorphic, with balloon-shaped, not deeply lobulated nuclei; in PV, they show only minor shape deviations and are not really pleomorphic, whereas in ET, the typical megakaryocytes are described as enlarged and deeply lobulated [6].

We designed this study to provide a more objective measure of megakaryocyte shapes in Ph− CMPD. We tried to identify such numerical characteristics of their size and shape that could be potentially useful in the diagnostic practice. We stressed that our major goal was not in differentiating the normal megakaryocytes from their CMPD counterparts, as in the diagnostic practice, the histological differentiation between reactive conditions and Ph− CMPDs is usually relatively easy. Instead, we focused on the differences between otherwise typical cases of CIMF, PV, and ET to provide a starting point for classification of more challenging cases.

Materials and methods

The study material encompassed the representative trephine bone marrow biopsies from the files of the Department of Pathomorphology, Collegium Medicum, Jagiellonian University, from the consecutive patients diagnosed with ET, CIMF, and PV starting from the year 2000 and those not treated with cytostatics prior to the biopsy. We selected 10 cases of PV, 10 cases of CIMF, and 20 cases of ET fulfilling the WHO criteria for particular Ph− CMPDs [10]. The cases with suboptimal biopsy quality or those that raised any diagnostic controversies were avoided. Extremely advanced cases of PV (post polycythemic myelofibrosis) and CIMF (presenting with osteomyelosclerosis) were not considered. The basic clinical features of the study group are given in Table 1.

Since completely normal bone marrow tissue samples are practically unobtainable, we constructed a control group of 10 patients with no neoplastic bone marrow disease, mostly the negative pretreatment staging biopsies of patients with lymphoma demonstrating no significant pathology. All the trephines were routinely fixed in formaldehyde, decalcified in a commercial medium (Shandon TBD-1 Decalcifier, Thermo Electronic Corporation), embedded in paraffin, and cut into 3- to 4-μm sections. The dewaxed sections were stained with hematoxylin and eosin (H & E), periodic acid–Schiff, Giemsa, and Gomori silver. The latter three special stains were used for diagnostic purposes. The megakaryocytes were identified under

Table 1 Clinical features of 40 cases of Ph− CMPD whose megakaryocytes were evaluated in this study

Diagnosis	Age (range/mean), years	M/F	Splenomegaly	Hepatomegaly	WBC (mean±SD), $\times 10^9$/L	RBC (mean±SD), 10^{12}	Hemoglobin (mean±SD), g/dL	Hematocrit (mean±SD), %	Platelets (mean±SD), $\times 10^9$/L
CIMF	52–78/67.7	7/3	7/10	4/10	12.4±6.1	4.45±1.14	12.6±2.4	38.7±7.1	535±439
PV	34–76/61.4	5/5	7/10	2/10	11.9±4.9	7.13±0.75	17.2±2.4	57.3±5.2	496±315
ET	23–80/50.8	4/16	4/20	5/20	9.2±2.9	4.86±0.64	13.7±1.3	40.1±5.1	964±336
Control group	38–71/54.7	7/3	1/10	0/10	9.4±4.9	4.47±0.33	13.5±0.58	39.4±1.52	267±115

an Olympus BX41 microscope with an Olympus 60× UPlanApo lens. Electronic photographs of 20 consecutive nonoverlapping high-power fields along a serpentine way over the H & E slides were taken. The size of a single picture was 288.2×217 μm (0.062539 mm^2), represented by 4,080×3,072 (12,533,760) pixels. Only the areas containing well-preserved hematopoietic tissue were documented. This procedure was aimed at collecting a set of representative and nonbiased high-quality pictures of megakaryocytes for each case. Additionally, the H & E slides were screened with a ×20 lens to identify the most characteristic and diagnostic megakaryocytes for each case. These subjectively selected cells were then photographed using the ×60 lens (10 high-power fields/case) and constituted an accessory set of data.

Collected pictures were subjected to further processing using an application designed by one of us (KO) on the basis of the commercial image analysis system Analysis pro v. 3.2 (Soft Imaging System GmbH, Münster, Germany). This application allowed manual delineation of a selected cell and its nucleus and automatically converted the H & E picture of the cell into a two-color bitmap, performing also the measurements. Only the megakaryocytes with an identifiable nucleus were analyzed. The measurements included the standard parameters of the cell and its nucleus, such as the areas, maximal and minimal diameters, and the perimeters. The application recorded the number of nuclear lobes and allowed further calculation of secondary planimetric characteristics. These included the following:

- The nucleocytoplasmic (NC) ratio based on the quotient of respective areas
- The shape factor (SF), $SF=L^2/4\pi S$, where L represents the perimeter length and S the surface area
- The compactness factor (C), $C=D_{min}/D_{max}$, where D_{min} is the minimum diameter and D_{max} the maximum diameter

Fractal geometry may provide additional information on the shape complexity of biological structures [3]. To calculate the fractal dimensions of the megakaryocytes and their nuclei, the bitmaps were processed with a set of programs written by RK.

The differences between the groups (both diagnostic categories and individual cases) were explored using ANOVA, multiple ANOVA (MANOVA), and nested MANOVA, as well as nonparametric Kruskal–Wallis ANOVA methods with proper post hoc tests. Discriminant function analysis is used to predict membership in naturally occurring categories [9]. In this method, a variable is added to the model if it allows for a better discrimination of naturally existing groups. For each element (a megakaryocyte) the probabilities of belonging to a given class (like a disease entity) can be obtained [23]. This probability is based on the distance within a multidimensional space between a point representing the element (a megakaryocyte) and a central point ("centroid") for a whole diagnostic class, encompassing all its elements. Each dimension of the multidimensional space represents one selected planimetric parameter. Thus, all the megakaryocytes belonging to one diagnostic class (like CIMF or other Ph− CMPDs) form a "cloud" in a multidimensional space, and the location of each cell within this cloud can be specified. The average distance or average probability for all the megakaryocytes belonging to one case (one patient) may be considered as a candidate for a diagnostic parameter whose value takes into account all the relevant planimetric variables. The optimal combination of discriminative parameters included area, perimeter, shape factor, and fractal dimension of both the cytoplasm and the nucleus, and, additionally, the number of completely separated nuclear lobes, area-based NC ratio, maximal diameter of the cytoplasm, and elongation factor of the cytoplasm. All the "cytoplasmic" parameters referred in fact to the whole cellular cross sections, including the nuclear profile. These parameters were calculated for all 4,054 bitmaps (pictures of megakaryocytes). The results were normalized for each parameter, and for each case the means were counted. Mean results were submitted to the Discriminant Analysis module (one of the Multivariate Exploratory Techniques) of the STATISTICA v. 6.1 PL package (StatSoft Inc., Tulsa, OK, USA). The case was grouping variable and all 12 parameters were fixed as an independent variable list. Advanced options (stepwise analysis) were applied with the standard method, with 0.005 as the tolerance value. STATISTICA returned discriminant function analysis results, where a priori classification probabilities were established as the same for all groups, after which a posterior probability table was obtained.

All other statistical calculations were performed with the STATISTICA v. 6.1 PL. The statistical significance level was set at 0.05.

Results

The sets of the randomly selected megakaryocytes subjected to the image analysis encompassed 3,771 cells from Ph− CMPDs. This included 850 cells of CIMF (46–120/case, median 79.5), 1,140 of PV (51–225/case, median 96.5), and 1,781 of ET (36–162/case, median 78.5). As the cell sampling method reflected the differences in megakaryocyte density, these numbers may be easily converted to the density of megakaryocytes per square millimeter of bone marrow, yielding 68.0±17.6/mm^2 (mean±SD) for CIMF, 91.2±42.1/mm^2 for PV, and 71.2±29.7/mm^2 for ET. The control group contained 283 cells (18–51/case, median 27), with the average density of 22.6±8.1/mm^2. The much higher number of megakaryocytes in Ph− CMPDs compared to the normal or reactive marrow samples reflects their hyperproliferation in this group of diseases, and is a well-known phenomenon [6, 10, 15, 25]. The densities of megakaryocytes differed significantly between the study groups (Kruskal–Wallis ANOVA, $p<0.001$), but in the post hoc analysis, only the difference between control and each other group was significant. Tables 2 and 3 summarize the basic size and shape parameters for the cells and their nuclei, respectively.

Table 2 Cytoplasmic parameters of megakaryocytes in Ph− CMPD (mean±SD)

	Area (μm^2)	Maximal diameter (μm)	Shape factor	Compactness factor	Fractal dimension
CIMF	496±263	31.5±8.8	0.80±0.09	0.69±0.13	1.0464±0.0216
PV	477±248	28.7±7.8	0.85±0.08	0.75±0.11	1.0488±0.0256
ET	411±232	28.6±8.5	0.75±0.12	0.70±0.12	1.0570±0.0268
Control	392±139	27.3±5.5	0.82±0.8	0.73±0.11	1.0514±0.0237
p (ANOVA)	<0.01	<0.01	<0.01	<0.01	<0.01
Scheffé post hoc analysis					
ET vs PV	*p*<0.001	NS	*p*<0.001	*p*<0.001	*p*<0.001
CIMF vs PV	NS	*p*<0.001	*p*<0.001	*p*<0.001	*p*<0.05
ET vs CIMF	*p*<0.001	*p*<0.001	*p*<0.001	*p*<0.012	*p*<0.001
Control vs ET	NS	*p*<0.04	*p*<0.001	*p*<0.04	*p*<0.001
Control vs CIMF	*p*<0.001	*p*<0.001	*p*<0.002	*p*<0.001	*p*<0.01
Control vs PV	*p*<0.001	*p*<0.04	*p*<0.001	*p*<0.006	NS

NS Not significant

The most important results of the megakaryocyte morphometry in Ph− CMPDs may be summarized as follows: Megakaryocytes in Ph− CMPDs, particularly in PV and CIMF, are larger than the normal cells and show markedly greater size variability. The most irregular cell outlines, reflected by low values of the shape factor, characterize the cells in ET, whereas the PV megakaryocytes show very smooth cellular contours, even more regular than those of the normal megakaryocytes. The CIMF megakaryocytes are typically more elongated (low compactness factor) than those in other Ph− CMPDs and normal cells. Again, also in respect to the compactness factor, the PV megakaryocytes are even more regular than the normal cells.

The nuclear size roughly parallels the cytoplasmic size in all groups, but the relatively largest nuclei characterize the ET megakaryocytes. The NC ratio of PV cells is even smaller than that of the normal cells, in contrast to ET and CIMF. The shape and compactness factors of the nuclei of the PV cells are the highest, reflecting the relatively regular shapes of the megakaryocytic nuclei in this disease. Megakaryocytes in Ph− CMPDs show a marked tendency for the presence of completely separated nuclear lobes. The percentage of cells with two or more completely separated nuclear lobes is significantly higher in the ET megakaryocytes compared to other Ph− CMPDs. The analysis of the planimetric parameters of 2,959 megakaryocytes selected subjectively as the most characteristic for a given case demonstrated very similar tendencies, with a bias for larger cell sizes (data not shown).

Figure 1 illustrates the examples of megakaryocytes identified as specific for the particular Ph− CMPD by the discriminant function analysis. Of note are relatively large and slender megakaryocytes of CIMF and small, very regular cells with tiny nuclear cross sections found in PV. Several types of megakaryocytes were identified as unique for ET—these are long and slender cells smaller than those of CIMF; small, highly irregular firms with very strongly

Table 3 Nuclear parameters of megakaryocytes in Ph− CMPD (mean±SD)

	Area (μm^2)	NC (area ratio)	Shape factor	Compactness factor	Fractal dimension	≥2 Separated nuclear lobes
CIMF	137±86	0.28±0.11	0.62±0.17	0.66±0.12	1.0494±0.0459	22.8%
PV	117±76	0.25±0.09	0.66±0.17	0.69±0.11	1.0478±0.0468	22.5%
ET	128±91	0.32±0.14	0.63±0.17	0.69±0.12	1.0713±0.0548	35.6%
Control	112±55	0.29±0.10	0.64±0.16	0.67±0.12	1.0467±0.0444	11.3%
p	<0.01 (ANOVA)	<0.01 (ANOVA)	<0.01 (ANOVA)	<0.01 (ANOVA)	<0.01 (ANOVA)	$<1\times10^{-25}$ (χ^2)
Scheffé post hoc analysis						χ^2
ET vs PV	*p*<0.004	*p*<0.001	*p*<0.001	*p*<0.05	*p*<0.001	$p=7\times10^{-14}$
CIMF vs PV	*p*<0.001	*p*<0.001	*p*<0.001	*p*<0.001	NS	NS
ET vs CIMF	NS	*p*<0.001	NS	*p*<0.001	*p*<0.001	$p=4\times10^{-11}$
Control vs ET	*p*<0.03	*p*<0.002	NS	NS	*p*<0.001	$p<1\times10^{-15}$
Control vs CIMF	*p*<0.001	NS	NS	NS	NS	$p<1\times10^{-4}$
Control vs PV	NS	*p*<0.001	NS	*p*<0.04	NS	$p<1\times10^{-4}$

NS Not significant

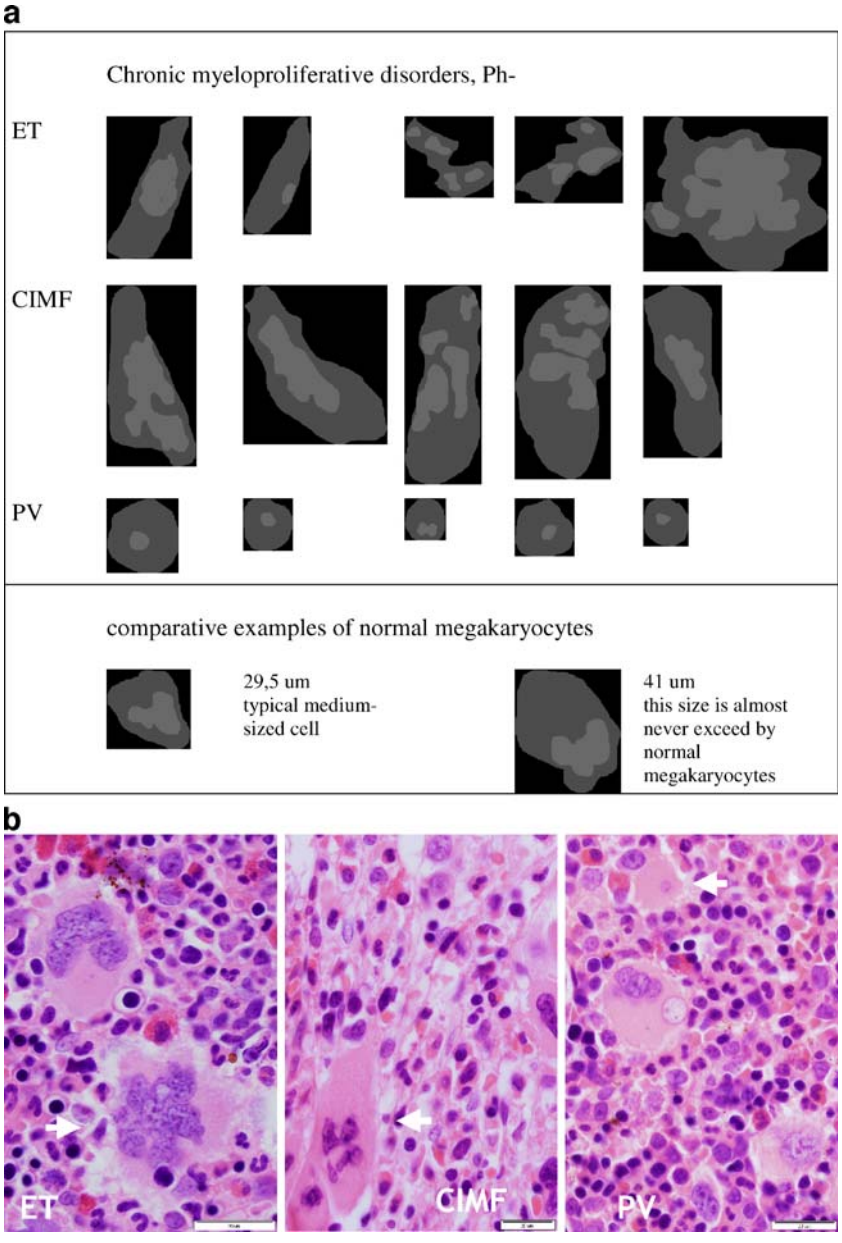

Fig. 1 Examples of characteristic megakaryocytes identified using discriminant function analysis. The cells of the illustrated types may be rare, but their presence is probably specific for given disorders. **a** Cellular profiles illustrating certain hallmark cells in ET (small slender cells with compact nuclei, highly irregular small cells, large cell with a medusa-like nucleus), PV (small round cells with tiny regular nuclear cross sections), and CIMF (very large slender cells). Two megakaryocytes from the control sets are given to illustrate the scale: an archetype medium-sized cell and a normal megakaryocyte with the maximal size achieved by the normal megakaryocytes. **b** Some hallmark megakaryocytes in their histological context. Scale bars correspond to 20 μm

segmented nuclei (usually clinging to other megakaryocytes); and relatively large cells with big, medusa-shaped nuclei (Fig. 1). The cells of all these types may be rare and may constitute a minority of megakaryocytes in a given case. However, they can be found in one Ph− CMPD (ET, PV, or CIMF), being unlikely to be found in the others. For instance, the cells specific for CIMF were selected on the basis of their belonging to the CIMF cloud, but outside the area of overlapping with the EP, PV, and normal clouds. The same principle was adopted for other Ph− CMPDs.

Despite the statistically significant differences at the level of sets composed of all the cells belonging to one disease category, the megakaryocyte populations in the individual cases of Ph− CMPDs showed a marked overlap in respect to the individual planimetric parameters. In other words, not a single numerical parameter can be used as a diagnostic "marker" for the differentiation within the CIMF–PV–ET triangle. The best single (but not perfect) discriminator is a cytoplasm shape factor, demonstrated in Fig. 2a. The PV cases show very characteristic profiles with high mean values and low standard deviation, but the differentiation between ET and CIMF on the basis of this sole parameter cannot be done. The same is true for another strong discriminator at the entity level: the degree of complete nuclear segmentation (Fig. 2b).

However, when numerous planimetric parameters are considered simultaneously using discriminant function analysis, the individual cases (represented by subsets of megakaryocytes) may be assigned to the diagnostic categories with the specified probabilities. The results of the discriminant function analysis are presented in Table 4. Using this approach, we were able to classify properly 9 of 10 cases of CIMF, 10 of 10 cases of PV, and 20 of 20 cases of ET.

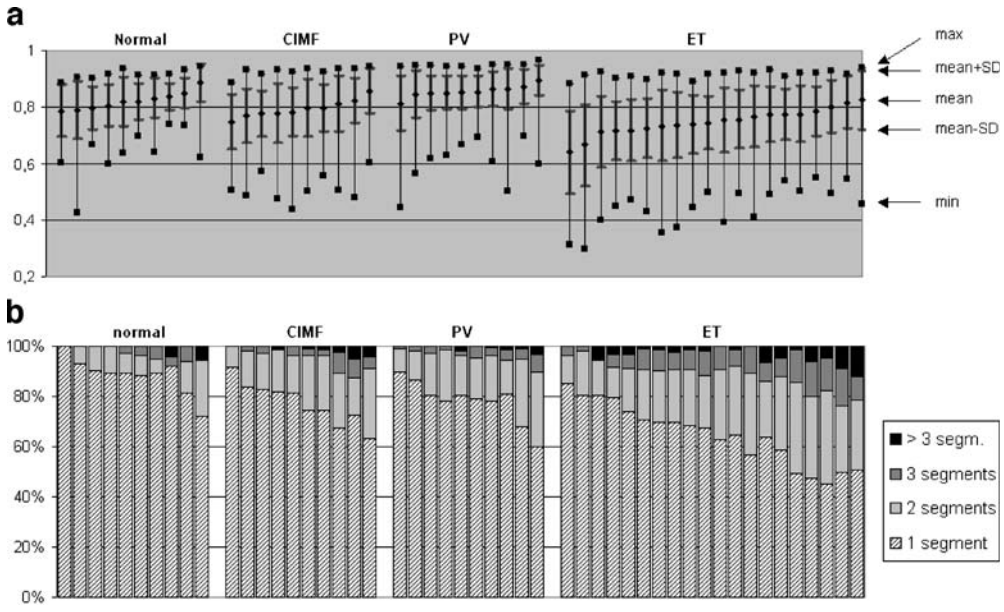

Fig. 2 Morphometric parameters constituting the strongest single disease discriminators among 40 cases of Ph− CMPD and 10 control cases. **a** The cytoplasm shape factor (measure of a shape roundness: *1* for a circle, *0* for a segment). **b** The degree of complete nuclear segmentation

Discussion

According to contemporary standards, the diagnostics of the Ph− CMPD is a multidisciplinary process including the meticulous analysis of the clinical picture, peripheral blood and bone marrow cytomorphology, bone marrow histology, and chromosomal or molecular exclusion of the BCR/ABL translocation. Despite this complex approach (or perhaps because of it?), the attempts of unequivocal classification fail for some cases, leading to an existence of a CMPD unclassifiable (CMPD-U) category or to long periods of uncertainty in respect to the exact nosological position of the disease in some patients. The CMPD-U group in a summary of 256 Ph− CMPD cases from our institution constitutes 13.4% [20] and, in most other series, 10–20% of all Ph− CMPDs [10]. The percentage of patients in whom a Ph− CMPD is suspected, but not explicitly diagnosed, is really unknown due to the elimination of these "limbo" cases from the research studies. Our knowledge on the pathology of Ph− CMPDs, particularly at the earlier stages, is still very limited, prompting the search for new diagnostic markers of these diseases. A recently published study based on a multidisciplinary, clinicopathological approach explored the heterogeneity within a group of cases fulfilling the PVSG criteria for ET [5]. Surprisingly, upon the reclassification of 142 cases based on the WHO criteria, only 21% fit the WHO ET category, the remaining cases being assigned to the WHO CIMF group or deemed to be unclassifiable (ET/CIMF). Florena et al. [5] also found that the new markers, like the proliferative activity, the percentage of CD34 blasts, and the parameters describing the megakaryocyte clustering, differentiated these Ph− CMPDs. Lundberg et al. found the quantitative and qualitative differences in bone marrow vascular pattern comparing nine cases of CML, seven cases of PV, and six cases of CIMF [14]. The presence of the numerous so-called "naked nuclei" of megakaryocytes may be a characteristic feature of CIMF [12]. Identification of new and possibly useful markers differentiating Ph− CMPDs in conjunction with the undeniable existence of still unclassifiable cases allows us to suspect that the classification system of Ph− CMPDs may undergo evolution in the nearest future.

Pathologists assessing the trephine bone marrow biopsies suspected for Ph− CMPD assign a great value to the features of megakaryocytes [6, 7, 15, 16, 27]. Increase in their number compared to the age norm, their clustering, and anomalies of the cytological features contribute markedly to the final diagnosis. Megakaryocytes are characterized by extremely complex shapes and significant inter- and intra-individual variability, making simple description of their anomalies very challenging. A planimetry-based approach adopted in this study was aimed at providing some objective data on megakaryocyte anomalies in Ph− CMPDs.

We decided to base our study on the histological material stained with H & E, the most widely used stain in a diagnostic histological practice. Our goal was to examine the megakaryocytes not "as they really are" (i.e., complex three-dimensional structures) but as we see them under the microscope in a situation of establishing an everyday diagnosis. That is why we relied upon routine staining instead of visualizing megakaryocytes with immunomarkers like CD42, CD61, or FVIIIR. Although these methods allow for an identification of the higher number of megakaryocytes, particularly the smaller forms [25], they are not necessarily routinely used for the evaluation of a trephine bone marrow biopsy suspected for Ph− CMPD. Besides, at least in our experience, the antigen unmasking procedures

Table 4 The discriminant function analysis of 40 cases of Ph− CMPD based on planimetric parameters of megakaryocytes (cytoplasmic and nuclear area, perimeter, shape factor and fractal dimension, the number of completely separated nuclear lobes, NC ratio, cytoplasmic maximal diameter, and elongation factor)

Case diagnosis based on WHO criteria	Discriminant function analysis-based probability of classifying as			
	CIMF	PV	ET	control
CIMF	**0.9906**	0.0014	0.0080	0.0000
CIMF	**0.9521**	0.0477	0.0001	0.0000
CIMF	0.0365	0.0003	0.9633	0.0000
CIMF	**0.9913**	0.0009	0.0076	0.0002
CIMF	**0.9970**	0.0003	0.0003	0.0024
CIMF	**0.9407**	0.0593	0.0001	0.0000
CIMF	**0.5702**	0.4298	0.0000	0.0000
CIMF	**0.5172**	0.4827	0.0000	0.0000
CIMF	**0.8707**	0.1290	0.0003	0.0000
CIMF	**0.9303**	0.0692	0.0005	0.0000
PV	0.0052	**0.9948**	0.0000	0.0000
PV	0.0147	**0.9853**	0.0000	0.0000
PV	0.0002	**0.9998**	0.0000	0.0000
PV	0.1898	**0.8102**	0.0000	0.0000
PV	0.0066	**0.9934**	0.0000	0.0000
PV	0.0097	**0.9903**	0.0000	0.0000
PV	0.0293	**0.9707**	0.0000	0.0000
PV	0.4919	**0.5024**	0.0056	0.0000
PV	0.0967	**0.9031**	0.0001	0.0001
PV	0.0922	**0.9077**	0.0000	0.0000
ET	0.0008	0.0000	**0.9992**	0.0000
ET	0.0000	0.0000	**1.0000**	0.0000
ET	0.0000	0.0000	**1.0000**	0.0000
ET	0.0169	0.0000	**0.9831**	0.0000
ET	0.1191	0.0001	**0.8808**	0.0000
ET	0.0000	0.0000	**1.0000**	0.0000
ET	0.0001	0.0000	**0.9999**	0.0000
ET	0.0000	0.0000	**1.0000**	0.0000
ET	0.0000	0.0000	**1.0000**	0.0000
ET	0.0000	0.0000	**1.0000**	0.0000
ET	0.0113	0.0000	**0.9887**	0.0000
ET	0.0000	0.0000	**1.0000**	0.0000
ET	0.0021	0.0003	**0.9976**	0.0000
ET	0.0785	0.0041	**0.9175**	0.0000
ET	0.0004	0.0000	**0.9996**	0.0000
ET	0.0000	0.0000	**1.0000**	0.0000
ET	0.0308	0.0055	**0.9637**	0.0000
ET	0.0002	0.0000	**0.9998**	0.0000
ET	0.0354	0.0000	**0.9646**	0.0000
ET	0.0000	0.0000	**1.0000**	0.0000
Control	0.0000	0.0000	0.0000	**1.0000**
Control	0.0000	0.0000	0.0000	**1.0000**
Control	0.0000	0.0000	0.0000	**1.0000**
Control	0.0000	0.0000	0.0000	**1.0000**
Control	0.0000	0.0000	0.0000	**1.0000**
Control	0.0000	0.0000	0.0000	**1.0000**
Control	0.0000	0.0000	0.0000	**1.0000**
Control	0.5503	0.0022	0.0001	0.4475
Control	0.0016	0.0000	0.0000	**0.9984**
Control	0.0000	0.0000	0.0000	**1.0000**

Boldfaced are the cases properly "classified," i.e., those with probability of the true diagnosis higher than that of the differential diagnoses. Underlined are misclassified cases

The values represent relative probabilities for a case to belong to a given diagnostic category (control, CIMF, PV, or ET), calculated as the average of the probabilities for all the megakaryocytes in this case

adopted to the trephines frequently cause some tissue loss and shape artifacts that could possibly influence the morphometric parameters. The histological slides contain cellular cross sections, whereas the smears visualize the whole cells and apparently could offer a better insight into the megakaryocyte cytomorphology. However, although the cells shown in the smears are not crosscut, they are neither reflecting the "true" picture of a megakaryocyte, as they are inevitably squeezed in the process of the smear preparation. In addition, the intensity of this distortion may be proportional to the object (cell) size. Also, smears are not particularly practical for megakaryocyte assessment in CMPD due to at least two additional factors: much lower number of cells visualized even in a good smear compared to a good trephine (two orders of magnitude more), and a strong influence of fibrosis on the smear contents. Particularly, the megakaryocytes from the areas of an intense local fibrosis could have been underrepresented in the smears in a systematic way. Microscopic examination of human tissue is inevitably based on the assessment of artifacts, and, in fact, histopathology is nothing more than a science of interpretation of the profoundly altered (fixed, cut, and stained) tissue pictures. Adopting this utilitarian perspective, it should not matter whether a characteristic and possibly diagnostic cellular cross section represents a plane corresponding to the maximal cellular diameter or a marginal section, as the valuable diagnostic information may be contained in fact in both pictures. We stress that in the present study we did not attempt to reconstruct the three-dimensional view of the megakaryocytes in CMPDs, but rather to identify some characteristic H & E pictures seen in everyday practice and to link them with the specific clinical context.

Our study, based on the objective analysis of a large set of megakaryocytes, allowed us to propose some more detailed description of "average" megakaryocytes in the three most frequent Ph− CMPDs. They may be summarized as follows:

CIMF: the largest megakaryocytes, but with the NC ratio resembling the normal cells; frequently elongated cellular shapes. The nuclei show irregular outlines but are lobulated to a lesser degree than in ET.

PV: the cells tend to be relatively large (comparable to CIMF) but show very regular and compact (most circle-like) shapes, even more regular than the normal cells. The presence of such megakaryocytes makes PV markedly different from two other Ph− CMPDs. The nuclei often are relatively small (NC ratio even smaller than in the normal cells and other Ph− CMPDs). The degree of nuclear lobulation is comparable to that in CIMF, but the nuclei show less irregular outlines and more compact shapes. Basing on many aspects of their morphology, the typical PV megakaryocytes may be described as large "hypernormal" cells.

ET: the mean cell size is comparable to that of normal cells and smaller than those in CIMF or PV, but the size variability in this group is most pronounced, and, notably, the giant cells not found in a normal marrow are present. The most elaborated cellular surfaces are reflected by the lowest shape factor. They have the highest NC ratio—nuclei are usually relatively large compared to cell sizes, although cells with very small nuclei are not infrequent (NC ratio is highly variable compared to other Ph− CMPDs and to the normal megakaryocytes). The nuclei show very prominent lobulation, with the highest fractal dimension and more than one third of the cells demonstrating more than two completely separated nuclear lobes. This is significantly higher than in other Ph− CMPDs (~20%) and in the normal cells (~11%).

Of course, the above descriptions pertain to the whole population of cells. The megakaryocytic populations in Ph− CMPDs are strongly diversified in practically all the aspects of their morphology to the extent of surpassing the variability of the normal cells. Occasionally, the presence of a few very atypical cells may provide a clue to the diagnosis, particularly in CIMF. Some rare but possibly "hallmark" types of the cells are illustrated in Fig. 1. They include extremely slender large cells (CIMF), almost perfectly round cells with disproportionally small and round nuclei (PV), and at least three types of atypical megakaryocytes in ET. We stress that these types of cells are not the most frequent for a given diagnostic category and in fact may constitute a small minority of megakaryocytes, being easily overlooked on screening inspection of a slide. For instance, in ET, the cells of this type correspond to approximately 2% of all megakaryocytes, whereas in the other two CMPDs, they may be slightly more numerous (up to 12%). Their presence is, however, very specific for a particular disease, as, for instance, the PV-specific almost-round megakaryocytes with tiny round nuclei are unlikely to be found in ET or CIMF.

The multiparameter planimetric analysis of megakaryocytes with our proposed algorithm based on the discriminant function-generated probabilities may be regarded as a basis for a future, potentially valuable adjunct in the diagnosis of Ph− CMPDs. Of course, we do not imply that this diagnosis could be made solely on the basis of sizes and shapes of the cells belonging to a single hematopoietic lineage, but our preliminary data suggest that the diagnostic strength of this approach may be surprisingly high, with sensitivities and specificities surpassing 90%. One wrongly assigned case (CIMF by WHO and ET by the discriminative planimetric analysis) assessed retrospectively did not pose diagnostic doubts pointing out at typical early CIMF, with anemia, low platelet counts (68,000/μL), and slight but clear bone marrow fibrosis (+2). The second misclassified case was a nonneoplastic control, clinically idiopathic thrombotic purpura with the presence of antiplatelet antibody. In the course of this study, this patient was splenectomized, and the histological examination of the spleen did not reveal any features of myeloid metaplasia typical of CIMF.

Our findings prove that the amount of diagnostic information hidden in the shapes and sizes of megakaryocytes may be really impressive and that most cases of otherwise typical Ph− CMPDs may be properly and objec-

tively classified solely basing on these data. We stress that no single planimetric parameter can be used as a categorization tool and that an efficient planimetry-based classification requires a multiparameter approach.

Several words of caution are mandatory. Our study is based on an analysis of a large number of cells but a limited number of cases (40 cases of Ph− CMPDs). The procedure in its current technical implementation is labor-intensive, with the bottleneck step being the manual delineation of megakaryocytes and their nuclei. The more advanced computerization of this procedure is a tempting solution, but as we already realized, it is not easy, mostly due to such factors such as clustering of megakaryocytes (problems in the automated cell delineation), emperipolesis, and very variable nuclear staining contributing to the difficulties in the automated nuclear contour finding. Our study at this step involved only the typical cases of ET, CIMF, and PV in order to establish a starting point for further research on more complicated cases, particularly the early stages and/or borderline pictures. Thus, our preliminary results definitely need validation based on the more extensive research. Nevertheless, we believe that the results are very promising, and the technique, particularly when more extensively semi-automated, may provide a valuable accessory diagnostic tool.

Acknowledgements This study was supported by the Committee for Scientific Research, grant no. 3 PO5B 084 24.

References

1. Berlin NI (1975) Diagnosis and classification of the polycythemias. Semin Hematol 12:339–351
2. Brodmann S, Passweg JR, Gratwohl A, Tichelli A, Skoda RC (2000) Myeloproliferative disorders: complications, survival and causes of death. Ann Hematol 79:312–318
3. Cross SS (1997) Fractals in pathology. J Pathol 182:1–8
4. Daly A, Song K, Nevill T, Nantel S, Toze C, Hogge D, Forrest D, Lavoie J, Sutherland H, Shepherd J, Hasegawa W, Lipton J, Messner H, Kiss T (2003) Stem cell transplantation for myelofibrosis: a report from two Canadian centers. Bone Marrow Transplant 32:35–40
5. Florena AM, Tripodo C, Iannitto E, Porcasi R, Ingrao S, Franco V (2004) Value of bone marrow biopsy in the diagnosis of essential thrombocythemia. Haematologica 89:911–919
6. Georgii A, Vykoupil KF, Buhr T, Choritz H, Dohler U, Kaloutsi V, Werner M (1990) Chronic myeloproliferative disorders in bone marrow biopsies. Pathol Res Pract 186:3–27
7. Georgii A, Buhr T, Buesche G, Kreft A, Choritz H (1996) Classification and staging of Ph-negative myeloproliferative disorders by histopathology from bone marrow biopsies. Leuk Lymphoma 22(Suppl 1):15–29
8. Harrison CN, Linch DC, Machin SJ (1998) Desirability and problems of early diagnosis of essential thrombocythaemia. Lancet 351:846–847
9. Huberty CJ (1994) Applied discriminant analysis. Wiley series in probability and statistics. Wiley-Interscience, New York
10. Jaffe ES, Harris NL, Stein H, Vardiman JW (eds) (2001) World Health Organization classification of tumours. Pathology and genetics of tumours of haematopoietic and lymphoid tissues. IARC, Lyon
11. Laszlo J (1975) Myeloproliferative disorders (MPD): myelofibrosis, myelosclerosis, extramedullary hematopoiesis, undifferentiated MPD, and hemorrhagic thrombocythemia. Semin Hematol 12:409–432
12. Lemancewicz D, Dzięcioł J, Kłoczko J, Litwiejko-Pietrynczak E, Bogusłowicz W (2003) Histomorphometric study of megakaryocytes in bone marrow in selected myeloproliferative and lymphoproliferative diseases. Folia Morphol (Warsz) 62:51–66
13. Lengfelder E, Hochhaus A, Kronawitter U, Hoche D, Queisser W, Jahn-Eder M, Burkhardt R, Reiter A, Ansari H, Hehlmann R (1998) Should a platelet limit of 600×10(9)/l be used as a diagnostic criterion in essential thrombocythaemia? An analysis of the natural course including early stages. Br J Haematol 100:15–23
14. Lundberg LG, Lerner R, Sundelin P, Rogers R, Folkman J, Palmblad J (2000) Bone marrow in polycythemia vera, chronic myelocytic leukemia, and myelofibrosis has an increased vascularity. Am J Pathol 157:15–19
15. Michiels JJ, Thiele J (2002) Clinical and pathological criteria for the diagnosis of essential thrombocythemia, polycythemia vera, and idiopathic myelofibrosis (agnogenic myeloid metaplasia). Int J Hematol 76:133–145
16. Michiels JJ (2004) Bone marrow histopathology and biological markers as specific clues to the differential diagnosis of essential thrombocythemia, polycythemia vera and prefibrotic or fibrotic agnogenic myeloid metaplasia. Hematol J 5:93–102
17. Murphy S, Peterson P, Iland H, Laszlo J (1997) Experience of the Polycythemia Vera Study Group with essential thrombocythemia: a final report on diagnostic criteria, survival, and leukemic transition by treatment. Semin Hematol 34:29–39
18. Pearson TC, Messinezy M (1996) The diagnostic criteria of polycythaemia rubra vera. Leuk Lymphoma 22(Suppl 1):87–93
19. Rozman C, Giralt M, Feliu E, Rubio D, Cortes MT (1991) Life expectancy of patients with chronic nonleukemic myeloproliferative disorders. Cancer 67:2658–2663
20. Rudzki Z, Papla B, Stachura J (2004) Chronic myeloproliferative diseases on a pathologist's desk—a dilemma of distinct entities versus a clinico-pathologic continuum. A descriptive study based on a material from the Polish population. Pol J Pathol 55:13–23
21. Ruggeri M, Finazzi G, Tosetto A, Riva S, Rodeghiero F, Barbui T (1998) No treatment for low-risk thrombocythaemia: results from a prospective study. Br J Haematol 103:772–777
22. Sacchi S, Vinci G, Gugliotta L, Rupoli S, Gargantini L, Martinelli V, Baravelli S, Lazzarino M, Finazzi G (2000) Diagnosis of essential thrombocythemia at platelet counts between 400 and 600×10(9)/L. Gruppo Italiano Malattie Mieloproliferative Croniche (GIMMC). Haematologica 85:492–495
23. StatSoft, Inc. (2004) Electronic statistics textbook. StatSoft, Tulsa. http://www.statsoft.com/textbook/stathome.html
24. Tefferi A, Deeg HJ (2004) Deciding on transplantation for myelofibrosis: setting the record straight. Mayo Clin Proc 79: 953–954
25. Thiele J, Wagner S, Degel C, Dienemann D, Wienhold S, Zankovich R, Fischer R, Stein H (1990) Megakaryocyte precursors (pro- and megakaryoblasts) in bone marrow tissue from patients with reactive thrombocytosis, polycythemia vera and primary (essential) thrombocythemia. An immunomorphometric study. Virchows Arch B Cell Pathol Incl Mol Pathol 58: 295–302
26. Thiele J, Kvasnicka HM, Boeltken B, Zankovich R, Diehl V, Fisher R (1999) Initial prefibrotic stages of idiopathic (primary) myelofibrosis (IMF)—a clinicopathological study. Leukemia 13:1741–1748
27. Thiele J, Kvasnicka HM, Diehl V, Fischer R, Michiels J (1999) Clinicopathological diagnosis and differential criteria of thrombocythemias in various myeloproliferative disorders by histopathology, histochemistry, and immunostaining from bone marrow biopsies. Leuk Lymphoma 33:207–218
28. Thiele J, Kvasnicka HM, Fischer R (1999) Histochemistry and morphometry on bone marrow biopsies in chronic myeloproliferative disorders—aids to diagnosis and classification. Ann Hematol 78:495–506
29. Thiele J, Kvasnicka HM (2003) Chronic myeloproliferative disorders with thrombocythemia: a comparative study of two classification systems (PVSG, WHO) on 839 patients. Ann Hematol 82:148–152

Virchows Arch (2006) 448: 68–74
DOI 10.1007/s00428-005-0075-3

ORIGINAL ARTICLE

Karsten Gravdal · Ole J. Halvorsen · Svein A. Haukaas · Lars A. Akslen

Expression of bFGF/FGFR-1 and vascular proliferation related to clinicopathologic features and tumor progress in localized prostate cancer

Received: 25 April 2005 / Accepted: 20 August 2005 / Published online: 12 October 2005

Abstract Microvessel density (MVD) has been associated with progression of prostate cancer. Although basic fibroblast growth factor (bFGF) is a known endothelial mitogen, the prognostic role of bFGF and its receptor FGFR-1 in prostate cancer has been controversial. The aim of our study was to examine the tissue distribution and prognostic significance of bFGF, FGFR-1, and microvascular proliferation. Sections from 104 radical prostatectomy specimens were examined by factor VIII/Ki-67 staining for proliferating capillary index (PCI) and MVD, and tissue microarray sections were immunostained for bFGF and FGFR-1. Increased PCI (median 0.49%) was related to strong stromal expression of bFGF (P=0.003) but was without prognostic impact. Strong bFGF staining was associated with well-differentiated tumors, no capsular penetration, low serum-prostate-specific antigen (s-PSA), low tumor cell proliferation, and increased time to biochemical failure (P=0.007), and was of independent prognostic importance in multivariate survival analysis. bFGF expression in vessels was associated with low MVD (P=0.0003). In contrast, strong tumor cell FGFR-1 expression was related to high preoperative s-PSA. Thus, increased stromal and vessel bFGF was associated with less aggressive tumors. Our findings indicate a complex relationship between bFGF/FGFR-1 expression and prognosis of prostate cancer. Vascular proliferation revealed no prognostic impact in this study.

Keywords Prostate cancer · Vessel proliferation · Ki-67 · bFGF · FGFR-1

K. Gravdal · O. J. Halvorsen · L. A. Akslen
Section for Pathology, The Gade Institute,
Haukeland University Hospital,
5021 Bergen, Norway
e-mail: Karsten.Gravdal@Haukeland.no
Tel.: +47-55-972587
Fax: +47-55-973158
e-mail: Ole.Halvorsen@gades.uib.no
Tel.: +47-55-973180
Fax: +47-55-973158

S. A. Haukaas
Department of Surgical Sciences,
Haukeland University Hospital,
Bergen, Norway

L. A. Akslen (✉)
Vascular Biology Program (Folkman Lab),
Karp Family Research Labs 12.125, Children's Hospital,
Harvard Medical School,
300 Longwood Avenue,
Boston, MA 02115-5737, USA
e-mail: Lars.Akslen@gades.uib.no
Tel.: +1-617-9192426
Fax: +1-617-7395891

Introduction

Angiogenesis is essential for the growth and metastatic spread of malignant tumors, and it has been applied as a marker for tumor aggressiveness in several cancers [3, 12, 23]. Microvessel density (MVD), as described by Weidner et al. [49] as an estimate of tumor-associated angiogenesis, is shown to provide strong and independent prognostic information in multiple tumors [23]. In prostate cancer, high MVD has been linked to aggressive behavior [1, 2, 15, 21, 42, 50] and thus correlated with histological grade [1, 42, 50], tumor stage [1, 2, 15, 42], preoperative serum-prostate-specific antigen (s-PSA) [21], and time to recurrence [21]. Also, presence of glomeruloid microvascular proliferation (GMP) has been associated with clinical recurrence in these tumors [41]. However, several limitations of MVD have been pointed out [23], and the identification of additional prognostic markers and regulators of the angiogenic process is of both scientific and clinical interest [23], especially due to the increased use of targeted anti-angiogenic therapy.

A few previous studies on other tumors have focused on vascular proliferation as a candidate angiogenic marker [10]. In prostate and breast cancer, studies on a low number of cases have suggested that vascular proliferation might have no prognostic value [13, 47, 48], but larger studies are needed to be conclusive.

Basic fibroblast growth factor (bFGF or FGF2) is a known mitogen for endothelial cells [6, 16]. The role of bFGF in prostate cancer has been controversial, both in terms of cellular localization and the relationship with clinicopathologic phenotype and prognosis. In some studies, bFGF expression has been found in stromal cells in both benign prostatic hyperplasia (BPH) [7, 19, 39] and prostate cancer [17], using immunohistochemical staining of human tissue. This is in line with findings that bFGF mRNA is localized to stromal cells in prostate tissue [25, 39, 44]. However, others have reported an expression of bFGF in tumor epithelium by immunohistochemistry [4, 9, 43, 44].

FGFR-1 is one of the four known FGF receptors with shared sequence homology, FGFR-1–4, and is known to be required for the development and maintenance of the vascular system [32]. These receptors are coded by four genes with alternative splicing of exons coding for Ig-loop III, which changes their affinity for the different FGF ligands [26, 34, 36]. FGFR-1 is expressed in prostate cancer mainly as the IIIc isoform [31], with affinity for aFGF, bFGF, FGF4, FGF6, FGF8, and FGF9 [34]. A shift from the FGFR-1 IIIb isoform to IIIc in prostate cancer increases its affinity to bFGF to about 50-fold [51]. FGFR-1 has been immunolocalized in benign prostatic basal and stromal cells, whereas luminal cells were negative [17]. In prostate cancer, increased immunoexpression of FGFR-1 in tumor cells was significantly associated with higher Gleason scores [17], but beyond this study, the immunohistochemical expression of FGFR-1 has received little attention in prostate cancer. In cell culture studies, activation of FGFR-1 [14] and transfection of nonfunctioning FGFR-1 [35] have linked the up-regulation of FGFR-1 to increased proliferation and tumor aggressiveness in prostate cancer. In a recent study, FGFR-4, but not FGFR-3, was up-regulated in prostate cancer, and its expression was associated with tumor grade and survival [20].

On this background, the aim of our present study was to examine the immunohistochemical expression and prognostic significance of bFGF and its receptor FGFR-1 in a well-characterized series of prostate cancer patients treated by radical prostatectomy and with long follow-up. We extended our analyses of bFGF/FGFR-1 by including vascular proliferation as estimated by Ki-67/factor VIII staining and MVD. Such angiogenic markers are important to obtain improved prognostication and as candidate markers of predictive value for adjuvant treatment [23].

Materials and methods

Patients

This radical prostatectomy material has been presented previously [21]. Briefly, a series of 104 consecutive hospital-based radical prostatectomy specimens occurring during 1988–1994 were included. None of the patients treated by radical prostatectomy received radiotherapy before biochemical failure or clinical recurrence.

Clinicopathologic variables

The following variables were studied retrospectively: patient age at operation, largest tumor dimension, WHO histological grade, capsular penetration, seminal vesicle invasion, involvement of surgical margins, presence of lymph node metastasis, s-PSA before and after surgical treatment, clinical stage, tumor cell proliferation (Ki-67), microvessel density (MVD) [3, 12, 23], and GMP [41].

Tissue sampling

The entire prostate was cut into 5-mm transverse serial sections and was totally embedded. The upper and lower sections were then cut into parallel sagittal sections. Based on hematoxylin–eosin (HE) stained whole mount slides, the area of highest WHO tumor grade was selected, and corresponding areas were cut out of the paraffin blocks, re-embedded in paraffin, and sectioned for immunohistochemistry.

Tissue microarrays (TMA)

The technique of TMA was introduced in 1998 [30] and validated by independent studies of several tumor markers [24, 33]. For TMA construction, representative tumor areas were identified on HE slides. Tissue cylinders with a diameter of 0.6 mm were punched from the donor block and mounted into a recipient paraffin block using a custom-made precision instrument (Beecher Instruments, Silver Spring, MD). Three parallel tissue cylinders were sampled from each case, as has been suggested [24]. Sections of the resulting TMA blocks (5 μm) were then made by standard technique and used for bFGF and FGFR-1 immunostaining.

Immunohistochemistry

The immunohistochemical staining was performed on formalin-fixed and paraffin-embedded archival tissue using regular slides (FVIII/Ki-67) and sections from TMA blocks (bFGF/FGFR-1).

Factor VIII/Ki-67 After de-paraffination, the tissue sections were subjected to heat-induced epitope retrieval in TRS, pH 9.9 (DakoCytomation, Copenhagen, Denmark, S3307), using a microwave oven at 500 W for 30 min. After pretreatment with proteinase K (Code S2032) in 10 min, the slides were incubated for 90 min with a monoclonal mouse Ki-67 antibody, clone MIB-1 (M7240, Dako, Copenhagen), diluted 1:50, and rabbit factor VIII (clone A0082, Dako) diluted 1:200, at room temperature. Secondary antibodies were HRP goat anti-rabbit Ig (P0448, Dako) diluted 1:50 and biotinylated goat anti-mouse Ig (E0433) diluted 1:100 with antibody diluent (S2022, Dako) and incubated for 60 min. For Ki-67, antigen localization was achieved by the 3-amino-9-ethylcarbazole-peroxidase (AEC-peroxidase) method, and for factor VIII by strep-

tavidin-biotinylated alcalic phosphatase method and fast blue.

Vessels located between benign glands at some distance from the tumor area served as positive internal controls. Slides in which the primary antibody was omitted served as negative controls.

bFGF and FGFR-1 After de-paraffination, TMA slides were subjected to heat-induced epitope retrieval in citrate buffer (pH=6.0) for 20 min, using a microwave oven at 500 W. The slides were then incubated overnight at room temperature with monoclonal anti-bFGF antibody (GF22, Oncogene, MA) diluted 1:200. For FGFR-1, a polyclonal FGFR-1 antibody (Flg, SC-121, Santa Cruz, CA) was used, diluted 1:150 and incubated for 1 h at room temperature. Staining for bFGF and FGFR-1 was performed on a Dako TechMate 500 slide processing equipment (Dako), using the standard avidin–biotin method. Finally, the antibody was localized by the AEC-peroxidase method with Harris hematoxylin as counterstain.

Evaluation of staining results

Microvessel density In order to quantitate microvessels, the sections were first examined at low and intermediate magnifications (×30, ×125) to identify the most vascular areas ("hot spots"), and counting was done within this area (entire tumor area), according to Weidner et al. [49], using 10 HPF (×250). The MVD counts were recorded as the average of all fields examined in each case, as described earlier [21].

Proliferating capillary index (PCI) The PCI was estimated as the fraction (%) of Ki-67 positive vessels, according to an earlier study [10]. Positive vessels were identified as vessels with staining of an endothelial cell nucleus in the vessel wall (Fig. 1a). Inflammatory cells in vessel lumens stained more weakly, and Ki-67 staining tumor cells close to the outside of vessel walls were excluded.

bFGF/FGFR-1 In our study, bFGF stained only stromal elements, including vessels (Fig. 1b), but not tumor cells, and expression in vessels and the stromal compartment was therefore recorded. FGFR-1 stained tumor cells (Fig. 1c) and not stromal elements, and expression in tumor cells was examined. For bFGF and FGFR-1, both staining intensity and positive area were recorded. A staining index (SI, values 0–9) was calculated as a product of staining intensity (0–3) and proportion of positive cells (0%=0, 1–10%=1, 11–50%=2, >50%=3). Strong staining (intensity 3) for bFGF was not found, and due to a great variation in proportion of positive cells in the 11–50% category, an additional cut point was used (11–25%, value 1.5). For vessel bFGF, staining in tumor-associated endothelial cells was recorded as absent or present. For statistical purposes, cut-off points for SI categories were based on the distribution of values.

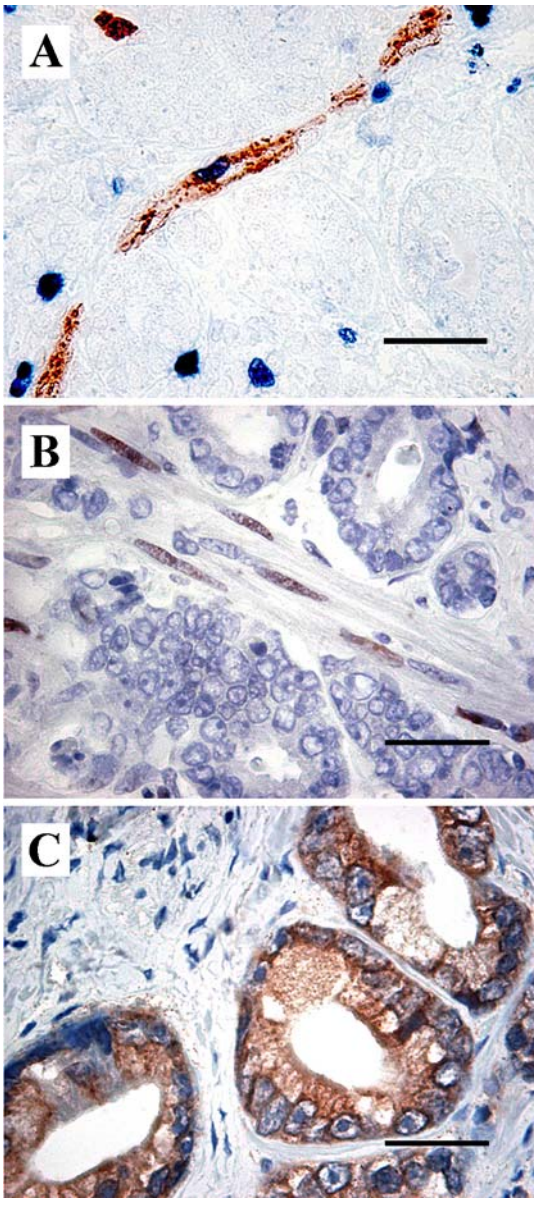

Fig. 1 Double immunostaining (factor VIII/Ki-67) for vascular proliferation, showing Ki-67 staining in a positive endothelial cell nucleus in prostate cancer (**a**). bFGF expression by immunohistochemistry is located in stromal cells, but negative in cancer cells (**b**). Positive FGFR-1 expression in tumor cells (**c**). Scale bar=25 μm

Follow-up

Data concerning s-PSA, loco-regional tumor recurrences, appearance of distant metastases, and patient survival were recorded [21]. Time from surgery until biochemical failure (defined as PSA elevation ≥0.5 ng/ml in two consecutive

Table 1 Median MVD, vascular proliferation (PCI), and expression of bFGF and FGFR-1 in 104 prostatic cancers

Variables	No. of patients	MVD[a]	P[b]	PCI (%)[a]	P[b]
Stromal bFGF			0.538		0.003
Weak	62	144		0.45	
Strong	42	134		0.66	
Vessel bFGF			0.0003		0.216
Negative	32	159		0.46	
Positive	72	123		0.56	
FGFR-1			0.270		0.660
Weak	57	133		0.49	
Strong	47	144		0.52	

[a]Median
[b]Mann–Whitney U test

blood samples) was noted, as well as the recurrence-free survival (time from surgery until the appearance of clinical loco-regional recurrences and/or distant spread). The last time of follow-up was December 2001. The median (mean) follow-up among patients without biochemical failure was 95 (94.6) months. During this period, 67 patients experienced biochemical failures, and 31 patients had clinical recurrences. No patients were lost to follow-up.

Statistics

Associations between variables were assessed by Mann–Whitney U test, and Pearson's chi-square test, when appropriate. Univariate survival analysis of time to biochemical failure and time to clinical recurrence was performed by the product-limit method (Kaplan–Meier method) and the log-rank test. The influence of covariates on failure-free survival was analyzed by the proportional hazard method and tested by the likelihood ratio (lratio) test. The level for inclusion of covariates in Cox's multivariate regression analysis was P=0.10. The analyses were performed by using the SPSS statistical package (ver 11.0, SPSS Inc., Chicago, IL, USA).

Results

Patient characteristics The median tumor dimension was 28 mm (range 10–45 mm). Of 104 cases, 10 tumors were well differentiated (WHO, histological grade), 66 moderately differentiated, and 28 poorly differentiated. Capsular penetration was demonstrated in 72 of 104 cases (69.2%). Seminal vesicle invasion was found in 35 of 104 cases (33.7%), and positive surgical margins were demonstrated in 55 of 104 cases (52.9%). Pelvic lymph node infiltration was found in 7 patients (6.7%) at the time of radical prostatectomy. Normal s-PSA value is for most practical purposes <4 ng/ml, but varies with age. The median preoperative s-PSA was 11.2 ng/ml (range 1.8–70.0). More details are available in a previous report [21].

Microvessel density The prognostic significance of MVD has previously been determined in this material [21]. Briefly, median MVD was 141 per millimeter squared (mean 151, range 55–324). The associations of MVD with actual parameters in this study are described below.

Proliferating capillary index Median PCI was 0.49% (mean 0.56%, range 0–1.79%). Increased PCI was significantly associated with high expression of stromal bFGF (P=0.003, Mann–Whitney U test, Table 1). PCI was not related to MVD, clinicopathologic parameters, time to biochemical failure or clinical recurrence. The median Ki-67 tumor cell proliferation index in our series was 6.7% [22].

Stromal expression of bFGF bFGF staining was mainly cytoplasmic, with a perinuclear concentration in stromal cells (Fig. 1b). Weak/absent staining (SI=0–1.5) was noted in 62 cases, and moderate staining (SI=2–8) in 42 cases. Strong stromal bFGF expression showed a significant association with well-differentiated tumors (WHO histological grade, Pearson's test, P=0.045), absence of capsular penetration (Pearson's test, P=0.028), low preoperative s-PSA (Pearson's test, P=0.01), and low tumor cell proliferation (Pearson's test, P=0.01).

Table 2 Univariate survival analysis (Kaplan–Meier method) by vascular proliferation (PCI), stromal bFGF expression, vascular bFGF expression, and FGFR-1 expression in tumor cells, using time to biochemical failure or clinical recurrence after radical prostatectomy in 104 prostatic cancers

Variables	Biochemical failure				Clinical recurrence		
	No.	Events	Estimated 5 years failure-free (%)	P[a]	Events	Estimated 5 years recurrence-free (%)	P[a]
PCI[b] (median)[c]				0.43			0.32
Low	52	35	47.2		18	76.2	
High	52	32	60.7		13	92.1	
Stromal bFGF				0.007			0.33
Weak	62	49	46.4		22	80.4	
Strong	42	18	65.5		9	89.9	
Vessel bFGF				0.09			0.12
Negative	32	25	43.8		14	78.1	
Positive	72	42	58.4		17	86.9	
FGFR-1				0.48			0.63
Weak	57	33	52.9		17	79.9	
Strong	47	34	55.1		14	89.2	

[a]Log-rank test
[b]*PCI* proliferating capillary index
[c]Survival analyses for PCI tertiles and quartiles; also nonsignificant

Vascular expression of bFGF Presence of vessel bFGF expression was associated with low MVD (P=0.0003, Mann–Whitney U test, Table 1).

Tumor cell expression of FGFR-1 Staining of FGFR-1 was mainly cytoplasmic in tumor cells, without nuclear staining (Fig. 1c). Weak or absent staining (SI=0–4) was noted in 57 cases, and strong staining (SI=6–9) was observed in 47 cases. Strong tumor cell FGFR-1 expression was associated with preoperative s-PSA above 11.1 ng/ml (median value, Pearson's test, P=0.04), but not with other variables.

Survival analysis In univariate survival analysis of time to biochemical failure, weak expression of stromal bFGF (SI=0–1.5) was associated with shorter time to biochemical failure (log-rank test, P=0.007, Table 2 and Fig. 2). Also, a nonsignificant trend between absent bFGF expression in tumor endothelial cells and shorter time to biochemical failure was present (log-rank test, P=0.09, Table 2). No significant survival differences were found for PCI and FGFR-1.

In multivariate survival analysis, including standard prognostic variables such as histological grade (by WHO), pathological stage and preoperative s-PSA as covariates, weak bFGF expression independently predicted biochemical failure (HR=1.8, P=0.03), along with pathological stage (HR=2.4, P<0.01), while histological grade (HR=1.7, P=0.06) was of borderline significance. When vessel bFGF was introduced separately into the Cox's multivariate analysis, with standard prognostic variables as covariates, negative vessel bFGF expression was also an independent predictor of time to biochemical failure (HR=2.8, P=0.001), as was pathological stage (HR=3.1, P<0.01), while histological grade (HR=1.7, P=0.07) and s-PSA (HR=1.7, P=0.07) were of borderline significance.

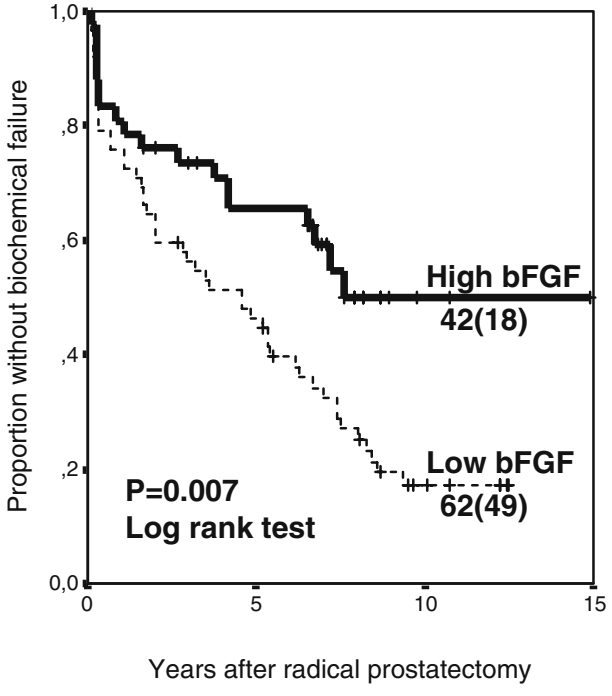

Fig. 2 Univariate survival analysis (Kaplan–Meier method): weak expression of stromal bFGF was significantly associated with decreased time to biochemical failure in localized prostate cancer. Number of patients in each group shown (events in *parenthesis*)

Discussion

We previously found that microvessel density (MVD) was a significant prognostic factor in this series of prostate cancer patients [21]. Since MVD has limitations as an angiogenic marker [23], it was of interest to focus on other aspects of the angiogenic phenotype. We found that the presence of proliferating vessels within the tumor tissue had no prognostic significance in this radical prostatectomy series. Vascular proliferation was not associated with MVD in accordance with data from a small study of prostate cancer [48]. In the latter study, no significant associations between vessel proliferation and MVD, Gleason score, or tumor proliferation (Ki-67) were found, but survival data were not presented. Our present series is the largest study of vascular proliferation in prostate cancer, and we are the first to report on patient prognosis and to use the method of double staining for Ki-67/factor VIII. This approach is assumed to be sensitive in detecting small and newly formed microvessels. Two studies on breast cancer reported no associations between vessel proliferation and MVD [13, 47], but these studies had no detailed survival data. In prostate cancer, the total amount of microvessels seems to be more important for clinical progress than the subgroup of newly formed vessels as detected by vascular proliferation. Still, increased vessel proliferation (PCI) was significantly associated with strong stromal expression of bFGF, and this finding is in accordance with bFGF as an endothelial cell mitogen [6, 16], thus validating PCI in this study.

Previous studies have differed regarding the anatomical localization of bFGF in prostate tissue. Our own study and four others have located bFGF mainly to stromal cells using immunohistochemistry [7, 17, 19, 39]. Some studies have also found bFGF expression in the tumor epithelium [4, 9, 43, 44], whereas three studies have located bFGF mRNA to stromal cells [25, 39, 44]. One of the latter studies still demonstrated bFGF positivity in the epithelial cells by immunohistochemistry [44]. Some of these differences might depend on the various antibodies used, as no single antibody localized bFGF to stroma and tumor cells simultaneously. bFGF has been shown to stimulate both stromal [19] and cultured epithelial cells [17] from the prostate. In one study, tumor cells were stimulated by autocrine bFGF production, although tumors did not show an increased malignancy in mice [38]. In our study, stromal bFGF expression was significantly associated with less aggressive tumors. The role of stromal bFGF in more aggressive prostate cancers might therefore be minor, and other angiogenic factors may be more important in this tumor subgroup.

Lack of bFGF expression in vessels tended to be associated with increased frequency of biochemical failure,

and vascular bFGF positivity was significantly associated with lower MVD. Expression of bFGF in vessels might indicate a more mature vasculature being associated with low-grade tumors. Similar observations have been reported for other tumors like melanoma [40], and bFGF has been suggested to promote vascular maturation [29].

In the prostate, other members of the FGF family have been reported, and some of these are locally stimulated by androgen, e.g., FGF-7, FGF-8, and FGF-10 [5]. FGF-9 is the predominant FGF in human prostate, but its role remains to be elucidated [37]. bFGF and FGF-7 might be induced by interleukin (IL)-1α and IL-8, and they may play a crucial role in the development of prostatic hyperplasia [18, 19]. Different FGF-8 isoforms have been reported to play a key role in prostate carcinogenesis [46], and stronger FGF-8 expression correlated with increasing Gleason score, tumor stage, and reduced survival [8]. Also, FGF-6 is increased in a subset of prostatic cancers [37]. It has been shown that especially aFGF, but also bFGF, FGF-8, and FGF-9, induces expression of metalloproteinases in prostate cancer, contributing to increased malignancy [28, 45].

Increased expression of FGFR-1 protein has been associated with poorly differentiated cancers [17], but immunohistochemical FGFR-1 expression has received little attention. Our finding that FGFR-1 expression in tumor cells was significantly associated with high preoperative s-PSA is in accordance with previous reports, linking up-regulation of this receptor to more aggressive tumor behavior [11, 14, 35]. In cell cultures from murine prostate cancer, activation of FGFR-1 in tumor cells was associated with increased proliferation [14]. Correspondingly, in cells cultured from human prostate cancer, transfection of nonfunctioning FGFR-1 resulted in 99% inhibition of tumor cell proliferation [35] given openings for new therapeutic alternatives targeting fibroblast growth factors. These studies indicate that up-regulation of FGFR-1 in prostate cancer cells is closely linked to increased proliferation and tumor aggressiveness. In contrast to FGFR-1, FGFR-4 has no IIIb splice variant, being expressed only as the IIIc isoform [27]. In a recent study, increased immunohistochemical expression of FGFR-4 was significantly linked to high Gleason scores and reduced disease-specific survival [20].

In summary, our study demonstrates that vascular proliferation does not appear to have any prognostic value in localized prostate cancer, although still significantly related to high expression of stromal bFGF, a known endothelial cell mitogen. Strong stromal expression of bFGF was significantly associated with increased time to recurrent disease, thus indicating a more low-grade tumor phenotype.

Acknowledgements The authors would like to thank Dr. med. Oddbjørn Straume, Mrs. Karen Bøhm-Nilsen, Mrs. Gerd Lillian Hallseth, Mr. Bendik Nordanger, and Mrs. Grethe Waaler for excellent technical assistance.

The experiments comply with the current laws of the country (Norway) in which they were performed.

References

1. Bono AV, Celato N, Cova V, Salvadore M, Chinetti S, Novario R (2002) Microvessel density in prostate carcinoma. Prostate Cancer Prostatic Dis 5:123–127
2. Brawer MK, Deering RE, Brown M, Preston SD, Bigler SA (1994) Predictors of pathologic stage in prostatic carcinoma. The role of neovascularity. Cancer 73:678–687
3. Carmeliet P (2003) Angiogenesis in health and disease. Nat Med 9:653–660
4. Cronauer MV, Hittmair A, Eder IE et al (1997) Basic fibroblast growth factor levels in cancer cells and in sera of patients suffering from proliferative disorders of the prostate. Prostate 31:223–233
5. Cronauer MV, Schulz WA, Seifert HH, Ackermann R, Burchardt M (2003) Fibroblast growth factors and their receptors in urological cancers: basic research and clinical implications. Eur Urol 43:309–319
6. Dell'era P, Nicoli S, Peri G, Nieddu M, Ennas MG, Presta M (2005) FGF2-induced upregulation of DNA polymerase-delta p12 subunit in endothelial cells. Oncogene 24:1117–1121
7. Deshmukh N, Scotson J, Dodson AR, Smith PH, Ke Y, Foster CS (1997) Differential expression of acidic and basic fibroblast growth factors in benign prostatic hyperplasia identified by immunohistochemistry. Br J Urol 80:869–874
8. Dorkin TJ, Robinson MC, Marsh C, Bjartell A, Neal DE, Leung HY (1999) FGF8 over-expression in prostate cancer is associated with decreased patient survival and persists in androgen independent disease. Oncogene 18:2755–2761
9. Dorkin TJ, Robinson MC, Marsh C, Neal DE, Leung HY (1999) aFGF immunoreactivity in prostate cancer and its co-localization with bFGF and FGF8. J Pathol 189:564–569
10. Eberhard A, Kahlert S, Goede V, Hemmerlein B, Plate KH, Augustin HG (2000) Heterogeneity of angiogenesis and blood vessel maturation in human tumors: implications for antiangiogenic tumor therapies. Cancer Res 60:1388–1393
11. Feng S, Wang F, Matsubara A, Kan M, McKeehan WL (1997) Fibroblast growth factor receptor 2 limits and receptor 1 accelerates tumorigenicity of prostate epithelial cells. Cancer Res 57:5369–5378
12. Folkman J (1971) Tumor angiogenesis: therapeutic implications. N Engl J Med 285:1182–1186
13. Fox SB, Gatter KC, Bicknell R, Going JJ, Stanton P, Cooke TG, Harris AL (1993) Relationship of endothelial cell proliferation to tumor vascularity in human breast cancer. Cancer Res 53:4161–4163
14. Freeman KW, Gangula RD, Welm BE, Ozen M, Foster BA, Rosen JM, Ittmann M, Greenberg NM, Spencer DM (2003) Conditional activation of fibroblast growth factor receptor (FGFR) 1, but not FGFR2, in prostate cancer cells leads to increased osteopontin induction, extracellular signal-regulated kinase activation, and in vivo proliferation. Cancer Res 63: 6237–6243
15. Fregene TA, Khanuja PS, Noto AC, Gehani SK, Van Egmont EM, Luz DA, Pienta KJ (1993) Tumor-associated angiogenesis in prostate cancer. Anticancer Res 13:2377–2381
16. Gaudric A, N'Guyen T, Moenner M, Glacet-Bernard A, Barritault D (1992) Quantification of angiogenesis due to basic fibroblast growth factor in a modified rabbit corneal model. Ophthalmic Res 24:181–188
17. Giri D, Ropiquet F, Ittmann M (1999) Alterations in expression of basic fibroblast growth factor (FGF) 2 and its receptor FGFR-1 in human prostate cancer. Clin Cancer Res 5:1063–1071
18. Giri D, Ittmann M (2000) Interleukin-1alpha is a paracrine inducer of FGF7, a key epithelial growth factor in benign prostatic hyperplasia. Am J Pathol 157:249–255
19. Giri D, Ittmann M (2001) Interleukin-8 is a paracrine inducer of fibroblast growth factor 2, a stromal and epithelial growth factor in benign prostatic hyperplasia. Am J Pathol 159:139–147

20. Gowardhan B, Douglas DA, Mathers ME, McKie AB, McCracken SR, Robson CN, Leung HY (2005) Evaluation of the fibroblast growth factor system as a potential target for therapy in human prostate cancer. Br J Cancer 92(2):320–327
21. Halvorsen OJ, Haukaas S, Hoisaeter PA, Akslen LA (2000) Independent prognostic importance of microvessel density in clinically localized prostate cancer. Anticancer Res 20:3791–3799
22. Halvorsen OJ, Haukaas S, Hoisaeter PA, Akslen LA (2001) Maximum Ki-67 staining in prostate cancer provides independent prognostic information after radical prostatectomy. Anticancer Res 21:4071–4076
23. Hlatky L, Hahnfeldt P, Folkman J (2002) Clinical application of antiangiogenic therapy: microvessel density, what it does and doesn't tell us. J Natl Cancer Inst 94:883–893
24. Hoos A, Urist MJ, Stojadinovic A et al (2001) Validation of tissue microarrays for immunohistochemical profiling of cancer specimens using the example of human fibroblastic tumors. Am J Pathol 158:1245–1251
25. Ittman M, Mansukhani A (1997) Expression of fibroblast growth factors (FGFs) and FGF receptors in human prostate. J Urol 157:351–356
26. Jaye M, Schlessinger J, Dionne CA (1992) Fibroblast growth factor receptor tyrosine kinases: molecular analysis and signal transduction. Biochim Biophys Acta 1135:185–199
27. Johnson DE, Lu J, Chen H, Werner S, Williams LT (1991) The human fibroblast growth factor receptor genes: a common structural arrangement underlies the mechanisms for generating receptor forms that differ in their third immunoglobulin domain. Mol Cell Biol 11:4627–4634
28. Klein RD, Maliner-Jongewaard MS, Udayakumar TS, Boyd JL, Nagle RB, Bowden GT (1999) Promatrilysin expression is induced by fibroblast growth factors in the prostatic carcinoma cell line LNCaP but not in normal primary prostate epithelial cells. Prostate 41:215–223
29. Kloth S, Gerdes J, Wanke C, Minuth WW (1998) Basic fibroblast growth factor is a morphogenic modulator in kidney vessel development. Kidney Int 53:970–978
30. Kononen J, Bubendorf L, Kallioniemi A et al (1998) Tissue microarrays for high-throughput molecular profiling of tumor specimens. Nat Med 4:844–847
31. Kwabi-Addo B, Ropiquet F, Giri D, Ittmann M (2001) Alternative splicing of fibroblast growth factor receptors in human prostate cancer. Prostate 46:163–172
32. Lee SH, Schloss DJ, Swain JL (2000) Maintenance of vascular integrity in the embryo requires signaling through the fibroblast growth factor receptor. J Biol Chem 275:33679–33687
33. Nocito A, Bubendorf L, Maria Tinner E et al (2001) Microarrays of bladder cancer tissue are highly representative of proliferation index and histological grade. J Pathol 194:349–357
34. Ornitz DM, Xu J, Colvin JS, McEwen DG, MacArthur CA, Coulier F, Gao G, Goldfarb M (1996) Receptor specificity of the fibroblast growth factor family. J Biol Chem 271:15292–15297
35. Ozen M, Giri D, Ropiquet F, Mansukhani A, Ittmann M (2001) Role of fibroblast growth factor receptor signaling in prostate cancer cell survival. J Natl Cancer Inst 93:1783–1790
36. Powers CJ, McLeskey SW, Wellstein A (2000) Fibroblast growth factors, their receptors and signaling. Endocr Relat Cancer 7:165–197
37. Ropiquet F, Giri D, Kwabi-Addo B, Mansukhani A, Ittmann M (2000) Increased expression of fibroblast growth factor 6 in human prostatic intraepithelial neoplasia and prostate cancer. Cancer Res 60:4245–4250
38. Russell PJ, Bennett S, Joshua A, Yu Y, Downing SR, Hill MA, Kingsley EA, Mason RS, Berry J (1999) Elevated expression of FGF-2 does not cause prostate cancer progression in LNCaP cells. Prostate 40:1–13
39. Sinowatz F, Schams D, Einspanier R, Arnold G, Pfeffer M, Temmim-Baker L, Amselgruber W, Plendl J (2000) Cellular localization of fibroblast growth factor 2 (FGF-2) in benign prostatic hyperplasia. Histol Histopathol 15:475–481
40. Straume O, Akslen LA (2002) Importance of vascular phenotype by basic fibroblast growth factor, and influence of the angiogenic factors basic fibroblast growth factor/fibroblast growth factor receptor-1 and ephrin-A1/EphA2 on melanoma progression. Am J Pathol 160:1009–1019
41. Straume O, Chappuis PO, Salvesen HB, Halvorsen OJ, Haukaas SA, Goffin JR, Begin LR, Foulkes WD, Akslen LA (2002) Prognostic importance of glomeruloid microvascular proliferation indicates an aggressive angiogenic phenotype in human cancers. Cancer Res 62:6808–6811
42. Strohmeyer D, Rossing C, Strauss F, Bauerfeind A, Kaufmann O, Loening S (2000) Tumor angiogenesis is associated with progression after radical prostatectomy in pT2/pT3 prostate cancer. Prostate 42:26–33
43. Strohmeyer D, Strauss F, Rossing C, Roberts C, Kaufmann O, Bartsch G, Effert P (2004) Expression of bFGF, VEGF and c-met and their correlation with microvessel density and progression in prostate carcinoma. Anticancer Res 24:1797–1804
44. Sugamoto T, Tanji N, Sato K, Fujita H, Nishio S, Sakanaka M, Yokoyama M (2001) The expression of basic fibroblast growth factor and vascular endothelial growth factor in prostatic adenocarcinoma: correlation with neovascularization. Anticancer Res 21:77–88
45. Udayakumar TS, Klein RD, Maliner MS, Nagle RB, Bowden GT (2001) Aberrant expression of fibroblast growth factor receptor-1 in prostate epithelial cells allows induction of promatrilysin expression by fibroblast growth factors. Int J Cancer 91:187–192
46. Valve EM, Nevalainen MT, Nurmi MJ, Laato MK, Martikainen PM, Harkonen PL (2001) Increased expression of FGF-8 isoforms and FGF receptors in human premalignant prostatic intraepithelial neoplasia lesions and prostate cancer. Lab Invest 81:815–826
47. Vartanian RK, Weidner N (1994) Correlation of intratumoral endothelial cell proliferation with microvessel density (tumor angiogenesis) and tumor cell proliferation in breast carcinoma. Am J Pathol 144:1188–1194
48. Vartanian RK, Weidner N (1995) Endothelial cell proliferation in prostatic carcinoma and prostatic hyperplasia: correlation with Gleason's score, microvessel density, and epithelial cell proliferation. Lab Invest 73:844–850
49. Weidner N, Semple JP, Welch WR, Folkman J (1991) Tumor angiogenesis and metastasis-correlation in invasive breast carcinoma. N Engl J Med 324:1–8
50. Weidner N, Carroll PR, Flax J, Blumenfeld W, Folkman J (1993) Tumor angiogenesis correlates with metastasis in invasive prostate carcinoma. Am J Pathol 143:401–409
51. Werner S, Duan DS, de Vries C, Peters KG, Johnson DE, Williams LT (1992) Differential splicing in the extracellular region of fibroblast growth factor receptor 1 generates receptor variants with different ligand-binding specificities. Mol Cell Biol 12:82–88

Virchows Arch (2006) 448: 75–79
DOI 10.1007/s00428-005-0073-5

ORIGINAL ARTICLE

Nina Zidar · Zvezdana Dolenc-Stražar · Jera Jeruc · Dušan Štajer

Immunohistochemical expression of activated caspase-3 in human myocardial infarction

Received: 23 May 2005 / Accepted: 19 August 2005 / Published online: 5 October 2005

Abstract There is mounting evidence that apoptosis is important in the pathogenesis of myocardial infarction (MI). One of the key events in the process of apoptosis is activation of caspase-3. Much attention has been recently paid to caspase inhibition as a potential treatment for ischemic cardiac disease. To predict the long-term effect of such treatment, it is essential to understand the significance of caspase-3 in the evolution of MI. Our aim was therefore to analyze immunohistochemical expression of activated caspase-3 in MI. Our study included autopsy samples of infarcted heart tissue from 50 patients with MI. Immunohistochemistry was performed by a sensitive peroxidase–streptavidin method on formalin-fixed, paraffin-embedded tissue, using monoclonal antibodies against activated (cleaved) caspase-3. We found caspase-3-positive myocytes in 18 MI less than 24 h old and in 3 MI that were presumably 48 h old. Their density (number of labeled myocytes/mm^2) was greater in patients who received reperfusion treatment (mean 0.160 ± 0.373 vs 0.025 ± 0.037, p=0.06). In MI older than 48 h, positive reaction was observed in neutrophil granulocytes in the interstitium and, in subacute MI, it was observed in mononuclear inflammatory cells, myofibroblasts, and vascular endothelial cells. Our results suggest that apoptosis of myocytes is an important mode of cell death in the early MI, being enhanced in patients who received reperfusion treatment. After 48 h, apoptosis is an important mechanism of the clearance of neutrophil granulocytes and other inflammatory cells and of scar formation. Treatment with caspase inhibitors therefore will not only affect myocyte loss but will also interfere with the clearance of neutrophils and with the transformation of granulation tissue into a scar.

Keywords Myocardial infarction · Evolution · Apoptosis · Detection · Caspase-3

The study complies with the current laws of the country in which they were performed.

N. Zidar (✉) · Z. Dolenc-Stražar · J. Jeruc
Institute of Pathology, Medical Faculty,
University of Ljubljana,
Korytkova 2,
1000 Ljubljana, Slovenia
e-mail: nina.zidar@mf.uni-lj.si
Tel.: +386-1-5437149
Fax: +386-1-5437101

D. Štajer
Centre for Intensive Internal Medicine,
University Medical Centre,
Zaloška 2,
1000 Ljubljana, Slovenia

Introduction

Studies in experimental animals and humans suggest that apoptosis is an important mechanism in the pathogenesis of various cardiac diseases, including myocardial infarction (MI). Despite extensive research, the etiopathogenesis, the distribution, and the significance of apoptosis in the initiation and evolution of MI in humans have not been entirely elucidated [3, 19, 25, 32].

An important controversial issue remains the identification of apoptotic cells. Apoptotic cells can be recognized by characteristic morphological features, such as chromatin condensation, cytoplasm shrinkage, nuclear fragmentation, sarcolemmal invaginations without loss of membrane integrity, and final engulfment of apoptotic bodies by macrophages [11, 18, 26]. However, these features are difficult to observe in the heart [17, 24]. Furthermore, morphology alone does not enable the recognition of cells early in the apoptotic pathway [30].

Several techniques for the detection of apoptotic cells have been developed, the most widely used being the terminal transferase-mediated DNA nick-end labeling (TUNEL) assay that recognizes cells containing DNA strand breaks. DNA strand breaks are not a unique feature of apoptosis, but occur also in necrosis, during repair of reversibly damaged DNA, and postmortem autolysis [13, 18, 32]. The validity of the TUNEL method to detect apoptosis is therefore controversial.

Recently, antibodies that recognize the activated (cleaved) caspase-3 have become commercially available.

Studies in various experimental models of apoptosis suggest that this is a reliable indicator of apoptotic rate, with a favorable comparison against the TUNEL assay [6, 8, 13, 30]. Only a few studies on caspase-3 expression in human MI have been reported, which were either based on a very limited number of patients [6] or were focused on the role of apoptosis in postinfarction remodeling [1, 2].

The aim of our study was to analyze the immunohistochemical expression of activated (cleaved) caspase-3 in human MI to evaluate its distribution in myocytes as well as in inflammatory cells and other interstitial cells that contribute to the healing process in MI. Finally, we tried to determine whether or not reperfusion treatment has any impact on caspase-3 expression in human MI.

Materials and methods

Our study included autopsy samples of infarcted heart tissue from 50 patients with MI. MI was diagnosed clinically by symptoms and/or ECG changes and was confirmed by elevated serum levels of markers of cardiac necrosis. In all cases, at least three samples from the infarcted region and border zone were available. Samples of heart tissue from five healthy persons who died in accidents were also included.

Tissue samples obtained at autopsies were fixed in 10% buffered formalin, embedded in paraffin, and cut at 4 μm for H&E slides. For immunohistochemistry, additional sections were cut. Antigen retrieval and staining with a cleaved caspase-3 (Asp175) antibody (Cell Signaling, Massachusetts, USA), diluted 1:40, was performed in an automatic immunostainer (Discovery, Ventana, Tucson, AZ, USA). Sections were treated with biotinylated secondary antibody, followed by incubation with peroxidase conjugated streptavidin. Visualization of the immunoreaction was carried out with 3.3′-diaminobenzidine. Finally, sections were counterstained with hematoxylin.

Tissue sections of colonic adenocarcinoma served as positive control. Sections treated without primary antibodies served as negative controls.

Morphometric analysis was performed by the image analysis system “Cell and Tissue Analysis” (Leica). The density of positive myocytes was expressed as the number of labeled myocytes/mm^2.

The duration of MI at the time of death was estimated from histologic changes, and all cases of MI were divided into three groups [35]:

- Group 1 (up to 24 h old): early signs of coagulation necrosis—myocyte hypereosinophilia, pyknosis of nuclei, waviness of fibers at the border, interstitial edema, no neutrophils, or occasional neutrophil in the interstitium.
- Group 2 (more than 1 day and less than 7 days old): signs of total coagulation necrosis—myocytes with shrunken eosinophilic cytoplasm, loss of nuclei, and cross striation, accompanied by edema and neutrophil infiltration of the interstitium.
- Group 3 (more than 7 days and less than 4 weeks old): formation of granulation and fibrous tissue, phagocytosis of dead myocytes.

Statistical analysis

Numerical variables are expressed as mean ± standard deviation. Differences between groups were tested by the Mann–Whitney *U* test.

Results

Among 50 patients, there were 30 males and 20 females, aged 57–89 years. There were 30 cases of MI less than 24 h old (group 1), 10 cases of MI that were more than 1 day and less than 7 days old (group 2), and 10 cases of MI that were more than 7 days and less than 4 weeks old (group 3). Eighteen patients had received reperfusion treatment (11 patients underwent thrombolysis, and 7 patients underwent percutaneous coronary intervention).

Antibodies against activated caspase-3 stained the cytoplasm of myocytes, which appeared morphologically normal (Figs. 1, 2). No nuclear staining was observed.

In MI less than 24 h old (group 1), caspase-3-positive myocytes were found in 18 of 30 cases. They were located at the border zone and never in the central zone of the MI. In very early MI, in which histologic changes were barely present, the determination of positive myocyte location was speculative. The density of positive myocytes ranged from 0.0111 to 1.2727/mm^2. It was greater in patients who received reperfusion treatment than in those who did not

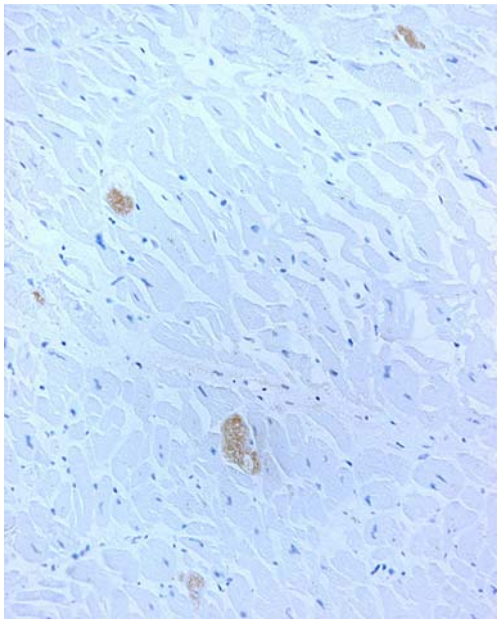

Fig. 1 Immunohistochemical staining for activated caspase-3 in early myocardial infarction: positive reaction in four myocytes. Original magnification ×200

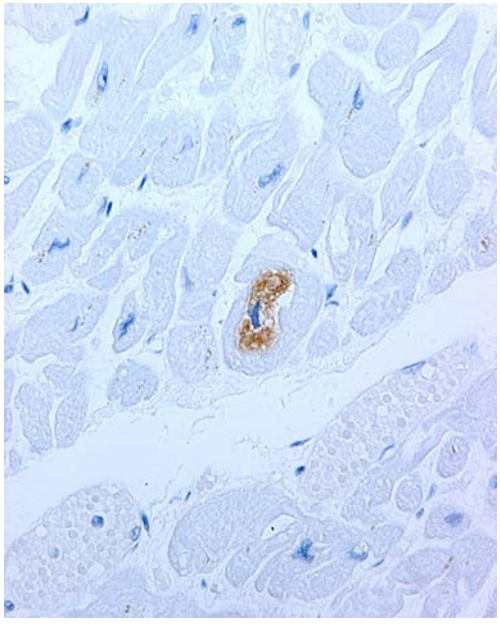

Fig. 2 Immunohistochemical staining for activated caspase-3 in early myocardial infarction: positive cytoplasmic reaction in a myocyte, which appears morphologically normal. Original magnification ×400

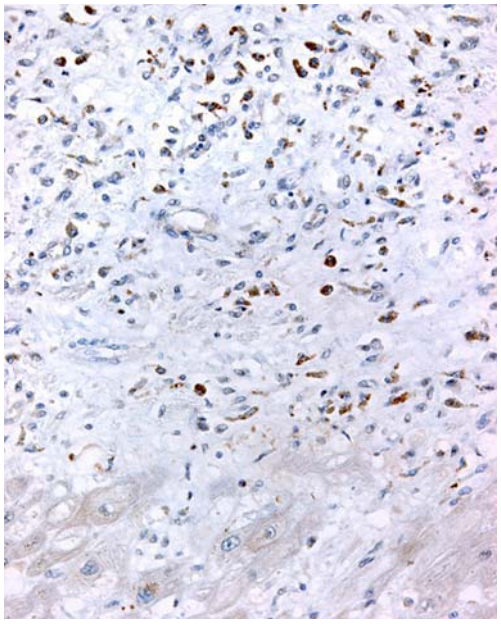

Fig. 4 Immunohistochemical staining for activated caspase-3 in subacute myocardial infarction: positive cytoplasmic reaction in mononuclear inflammatory cells, myofibroblasts, and vascular endothelial cells. Original magnification ×200

(mean 0.160±0.373 vs 0.025±0.037, p=0.06, Mann–Whitney U test). No difference was observed between patients with different modes of reperfusion treatment, but the number of patients was too small to draw any conclusions.

In MI more than 1 day and less than 7 days old (group 2), positive reaction for caspase-3 in myocytes was observed in three cases of MI that were presumably 48 h old. In this group, positive reaction was also observed in neutrophil granulocytes, which infiltrated the interstitium. The reaction was mostly cytoplasmic. Positive reaction was observed in neutrophils that appeared morphologically healthy as well as in apoptotic bodies. In some cases, necrotic myocytes were surrounded by a rim of caspase-3-positive neutrophils, and these were surrounded by caspase-3-negative neutrophils (Fig. 3). In some cases, positive and negative neutrophils were admixed haphazardly.

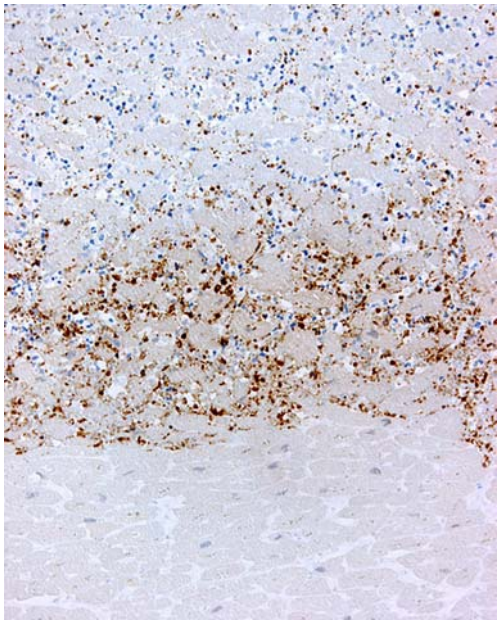

Fig. 3 Immunohistochemical staining for activated caspase-3 in acute myocardial infarction: positive reaction in numerous neutrophil granulocytes surrounding the necrotic myocytes. Apoptotic bodies are also positive. Original magnification ×200

In MI more than 7 days and less than 4 weeks old (group 3), positive reaction was observed in the cytoplasm of mononuclear inflammatory cells, myofibroblasts, and vascular endothelial cells (Fig. 4). The number of positive cells slowly decreased as granulation tissue was transforming into a fibrous scar.

In heart samples from five healthy persons, who died in accidents, no caspase-3-positive cells were found.

Discussion

One of the key events in the process of apoptosis is the activation of caspases (cleavage of procaspase to active caspase). Among them, caspase-3 is a central effector caspase in many cells, leading to DNase activation, followed by DNA fragmentation [10, 14]. Once cleaved through the activation of the apoptotic cascade, the peptide end of this active caspase represents a novel epitope not present in normal cells. The detection of this novel epitope is believed to be a unique and sensitive indicator of apoptosis. Antibodies to activated (cleaved) caspase-3 have recently become commercially available. Studies in various human tissues and cells have shown that they represent a useful tool to identify apoptotic cells in archival

material expanding the range of disease settings in which apoptosis can be accurately evaluated [13].

We studied the immunohistochemical expression of activated caspase-3 in human MI and found positive myocytes in acute MI during the first 2 days. Similar findings have been demonstrated in experimental MI and human MI [17, 23, 24, 27, 29] using other techniques for detecting apoptotic myocytes, most frequently the TUNEL method. The main difference between most of the previous studies and ours is a lower density of positive myocytes observed in our study. This can be easily explained as it has been shown that TUNEL is not entirely specific for apoptosis but labels also necrotic and autolytic cells, as well as cells during repair of reversibly damaged DNA [13, 32].

The density of caspase-3-positive myocytes was greater in patients who received reperfusion treatment than in those who did not. No difference was observed between patients with different mode of reperfusion treatment, but their number is too small to draw conclusions. Occasionally, positive reaction was observed in myocytes with contraction band necrosis, which is believed to be the hallmark of reperfusion injury [5]. Our findings are consistent with experimental studies that have shown that apoptosis is triggered by ischemia, but it is enhanced after reperfusion [9, 21, 33, 34]. Some experimental studies, on the contrary, have suggested that apoptosis is triggered only by reperfusion and not by ischemia [12, 33].

In contrast to myocytes, little attention has been given to the significance of apoptosis of other cells in the evolution of MI [15, 28]. Takemura et al. [27] have described TUNEL positivity, and Hayakawa et al. [15] have described caspase-3 positivity in infiltrated and proliferated interstitial cells in an experimental model of MI, suggesting that apoptosis might play an important role in the disappearance of these cells after MI. Consistent with these studies, we found positive reaction for caspase-3 in neutrophil granulocytes in the interstitium in acute MI. In subacute MI, characterized histologically by the proliferation of granulation and fibrous tissue, positive reaction was observed in mononuclear inflammatory cells, myofibroblasts, and vascular endothelial cells. The number of positive cells decreased as granulation tissue was transforming into a fibrous scar.

The significance of elimination of noncardiomyocytes by apoptosis in MI has not been fully determined [28, 32]. Leukocytes and macrophages accumulate in the infarcted region to scavenge the necrotic tissue. Necrotic tissue is then replaced by granulation tissue. As repair proceeds, there is a decrease in cellularity, ending with the formation of a fibrotic scar. When the scavenging process is completed, inflammatory cells, which contain cytotoxic factors, must be eliminated promptly so that surviving tissue is not further damaged. The elimination of inflammatory cells by apoptosis appears reasonable, as toxic components are not released in the surrounding tissue [32], and has been confirmed in experimental models of acute inflammation [31]. Similarly, experimental studies have shown that the decrease in cellularity during the transformation of granulation tissue into a scar is also mediated by apoptosis [7, 27].

Much attention has been recently paid to caspase inhibition as a potential new treatment approach for ischemic cardiac disease [28, 34]. Experimental studies have shown that caspase inhibition reduces myocardial injury induced by ischemia and reperfusion [4, 16, 20–22, 34], but there is little information about the long-term effect of such treatment [15, 28]. To predict the long-term effect of treatment with caspase inhibitors, it is essential to understand the significance of activated caspase-3 in the evolution of MI. According to the results of our study, it may be expected that treatment with caspase inhibitors not only will affect myocyte loss but will also interfere with the clearance of neutrophils and other inflammatory cells and with the transformation of granulation tissue into a scar.

Acknowledgements This study was partially presented at the European Society of Cardiology Congress in Munich, Germany, August 28–September 1, 2004, and at the 25th International Congress of the International Academy of Pathology, Brisbane, Australia, October 10–15, 2004.

References

1. Abbate A, Biondi-Zoccai GGL, Baldi A (2002) Pathophysiologic role of myocardial apoptosis in post-infarction left ventricular remodeling. J Cell Physiol 193:145–153
2. Abbate A, Biondi-Zoccai GGL, Bussani R, Dobrina A, Camilot D, Feroce F, Rosiello R, Baldi F, Silvestri F, Biasucci LM, Baldi A (2003) Increased myocardial apoptosis in patients with unfavorable left ventricular remodeling and early symptomatic post-infarction heart failure. J Am Coll Cardiol 41:753–760
3. Anversa P (2000) Myocyte death in the pathological heart. Circulation 86:121–124
4. Chandrashekhar Y, Sen S, Anway R, Shuros A, Anand I (2004) Long-term caspase inhibition ameliorates apoptosis, reduces myocardial troponin-1 cleavage, protects left ventricular function, and attenuates remodeling in rats with myocardial infarction. J Am Coll Cardiol 43:295–301
5. Cowan MJ, Reichenbach D, Turner P, Thostenson C (1991) Cellular response of the evolving myocardial infarction after therapeutic coronary artery reperfusion. Human Pathol 22:154–163
6. De Boer RA, Van Veldhuisen DJ, Van Den Wijk J, Brouwer RM, de Jonge N, Cole GM, Suurmeijer AJ (2000) Additional use of immunostaining for active caspase 3 and cleaved actin and PARP fragments to detect apoptosis in patients with chronic heart failure. J Card Fail 6:330–337
7. Desmoulière A, Redard M, Darby I, Gabbiani G (1995) Apoptosis mediates the decrease in cellularity during the transition between granulation tissue and scar formation. Am J Pathol 146:56–66
8. Duan WR, Garner DS, Williams SD, Funckes-Shippy CL, Spath IS, Blomme EAG (2003) Comparison of immunohistochemistry for activated caspase-3 and cleaved cytokeratin 18 with the TUNEL method for quantification of apoptosis in histological sections of PC-3 subcutaneous xenografts. J Pathol 199:221–228
9. Eefting F, Rensing B, Wigman J, Pannekoek WJ, Liu WM, Cramer MJ, Lips DJ, Doevendans PA (2004) Role of apoptosis in reperfusion injury. Cardiovasc Res 61:414–426
10. Enari M, Sakahira H, Yokoyama H, Okawa K, Iwamatsu A, Nagata S (1998) A caspase-activated DNase that degrades DNA during apoptosis, and its inhibitor ICAD. Nature 1:43–50

11. Geske FJ, Gerschenson LE (2001) The biology of apoptosis. Human Pathol 32:1029–1038
12. Gottlieb RA, Burleson KO, Kloner RA, Babior BM, Engler RL (1994) Reperfusion injury induces apoptosis in rabbit cardiomyocytes. J Clin Invest 94:1621–1628
13. Gown AM, Willingham MC (2002) Improved detection of apoptotic cells in archival paraffin sections: immunohistochemistry using antibodies to cleaved caspase 3. J Histochem Cytochem 50:449–454
14. Green DR (2000) Apoptotic pathways: paper wraps stone blunts scissors. Cell 102:1–4
15. Hayakawa K, Takemura G, Kanoh M, Li YW, Koda M, Kawase Y, Maruyama R, Okada H, Minatoguchi S, Fujiwara T, Fujiwara H (2003) Inhibition of granulation tissue cell apoptosis during the subacute stage of myocardial infarction improves cardiac remodeling and dysfunction at the chronic stage. Circulation 108:104–109
16. Holly TA, Drincic A, Byun Y, Nakamura S, Harris K, Klocke FJ, Cryns VL (1999) Caspase inhibition reduces myocyte cell death induced by myocardial ischemia and reperfusion in vivo. J Mol Cell Cardiol 31:1709–1715
17. Itoh G, Tamura J, Suzuki M, Suzuki Y, Ikeda H, Koike M, Nomura M, Jie T, Ito K (1995) DNA fragmentation of human infarcted myocardial cells demonstrated by the nick end labeling method and DNA agarose gel electrophoresis. Am J Pathol 146:1325–1331
18. Jugdutt B, Idikio HA (2005) Apoptosis and oncosis in acute coronary syndromes: assessment and implications. Mol Cell Biochem 270:177–200
19. Krijnen PAJ, Nijmeijer R, Meijer CJLM, Visser CA, Hack CE, Niessen HWM (2002) Apoptosis in myocardial ischaemia and infarction. J Clin Pathol 55:801–811
20. Li HL, Karwatowska-Prokopczuk E, Mutomba M, Wu J, Karanewsky D, Valentino K, Engler RL, Gottlieb RA (2001) Pharmacology of caspase inhibitors in rabbit cardiomyocytes subjected to metabolic inhibition and recovery. Antioxid Redox Signal 3:113–123
21. McCully JD, Wakiyama H, Hsieh YJ, Jones M, Levitsky S (2004) Differential contribution of necrosis and apoptosis in myocardial ischemia–reperfusion injury. Am J Physiol Heart Circ Physiol 286:H1932–H1935
22. Mocanu MM, Baxter GF, Yellon DM (2000) Caspase inhibition and limitation of myocardial infarct size: protection against lethal reperfusion injury. Br J Pharmacol 130:197–200
23. Piro FR, di Gioia CRT, Gallo P, Giordano C, d'Amati G (2000) Is apoptosis a diagnostic marker of acute myocardial infarction? Arch Pathol Lab Med 124:827–831
24. Saraste A, Pulkki K, Kallajoki M, Henriksen K, Parvinen M, Voipio-Pulkki LM (1997) Apoptosis in human acute myocardial infarction. Circulation 95:320–323
25. Saraste A, Pulkki K (2000) Morphologic and biochemical hallmarks of apoptosis. Cardiovasc Res 45:528–537
26. Sharov VG, Sabbah HN, Shimoyama H, Goussev AV, Lesch M, Goldstein S (1996) Evidence of cardiocyte apoptosis in myocardium of dogs with chronic heart failure. Am J Pathol 148:141–149
27. Takemura G, Ohno M, Hayakawa Y, Misao J, Kanoh M, Ohno A, Uno Y, Minatoguchi S, Fujiwara T, Fujiwara H (1998) Role of apoptosis in the disappearance of infiltrated and proliferated interstitial cells after acute myocardial infarction. Circ Res 82:1130–1138
28. Takemura G, Fujiwara H (2004) Role of apoptosis in remodeling after myocardial infarction. Pharmacol Ther 104:1–16
29. Veinot JP, Gattinger DA, Fliss H (1997) Early apoptosis in human myocardial infarction. Human Pathol 28:485–492
30. Walker JA, Quirke P (2000) Viewing apoptosis through a "TUNEL". J Pathol 195:275–276
31. Webb PR, Wang KQ, Scheel-Toellner D, Pongracz J, Salmon M, Lord JM (2000) Regulation of neutrophil apoptosis: a role for protein kinase C and phosphatidylinositol-3-kinase. Apoptosis 5:451–458
32. Yaoita H, Ogawa K, Maehara K, Maruyama Y (2000) Apoptosis in relevant clinical situations: contribution of apoptosis in myocardial infarction. Cardiovasc Res 45:630–641
33. Zhao ZQ, Nakamura M, Wang NP, Wilcox JN, Shearer S, Ronson RS, Guyton RA, Vinten-Johansen J (2000) Reperfusion induces myocardial apoptotic cell death. Cardiovasc Res 45:651–660
34. Zhao ZQ (2004) Oxidative stress-elicited myocardial apoptosis during reperfusion. Curr Opin Pharmacol 4:159–165
35. Zidar N, Jeruc J, Balažic J, Štajer D (2005) Neutrophils in human myocardial infarction with rupture of the free wall. Cardiovasc Pathol 14:247–250

Virchows Arch (2006) 448: 80–84
DOI 10.1007/s00428-005-0068-2

ORIGINAL ARTICLE

Klaus Dirschmid · Claudia Platz-Baudin · Manfred Stolte

Why is the hyperplastic polyp a marker for the precancerous condition of the gastric mucosa?

Received: 28 February 2005 / Accepted: 16 August 2005 / Published online: 28 September 2005

Abstract It is well known from the older literature that gastric carcinomas are more likely to develop in a stomach containing hyperplastic polyps. The reason why such a stomach should represent a precancerous condition is, however, largely unexplained. The aim of this study was to determine the disorders of the gastric mucosa in which hyperplastic polyps occur. In 244 patients with hyperplastic polyp, in whom at least two additional biopsies each from the antrum and corpus were available, gastritis was classified on the basis of the updated Sydney System. In none of the 244 patients was the gastric mucosa found to be normal. The most common disorder, at 51.3%, was autoimmune gastritis of the corpus mucosa, while chronic active *Helicobacter pylori* (Hp) gastritis was seen in 37.3% of the patients. Of the patients with Hp gastritis, 56.1% had corpus-dominant Hp gastritis. Other forms were relatively rare: when A-gastritis, corpus-dominant Hp gastritis and any other form of Hp gastritis were lumped together as a precancerous condition, these changes were found in 88.6% of the patients with hyperplastic polyps of the stomach. In the presence of hyperplastic polyps of the gastric mucosa, additional biopsies obtained from the antrum and corpus should always be performed to obtain a basis for deciding whether to apply Hp eradication treatment as potential carcinoma prophylaxis.

Keywords Hyperplastic polyps · Gastritis · Precancerous condition

Introduction

Hyperplastic polyp of the gastric mucosa, the aetiopathogenesis of which still has not been clarified, is itself not considered to be a precancerous condition or lesion because carcinoma develops within it only in an average of 2.1% (range 0 to 8%) of the cases [4, 26]. From the earlier literature, however, it is known that the detection of such a polyp may be a marker for the risk of gastric carcinoma developing at some other site within the stomach [23]. For this reason, the presence of hyperplastic polyps of the stomach is considered to be a precancerous condition, and appropriate screening examinations are recommended. These older data suggest that the cause of the precancerous condition is to be sought in the status of the gastric mucosa in the antrum and corpus. However, few published reports are available of studies investigating the underlying disorder of the gastric mucosa in patients with hyperplastic polyp, and most of these studies stem from the period prior to the rediscovery of *Helicobacter pylori* (Hp) and before the introduction of the Sydney System of gastritis classification. Based on the results of these older studies, therefore, it can be concluded only indirectly that hyperplastic polyps very probably occur more frequently in atrophic autoimmune gastritis of the corpus mucosa and in Hp-induced gastritis [8, 12, 20].

Against this background, we investigated the antral and corpus mucosa at a distance from the polyps, with the aim of finding answers to the following open questions:

1. In what underlying diseases of the gastric mucosa do hyperplastic polyps develop?
2. Can these underlying diseases explain why hyperplastic polyps of the stomach is a precancerous condition?
3. Can any of these underlying disorders of the gastric mucosa be cured by treatment, with the potential for preventing the development of a gastric carcinoma?

Patients and methods

The status of the gastric mucosa of 244 patients with hyperplastic polyp, from whom at least two biopsies each were obtained concomitantly from the antrum and corpus for histological diagnosis, was retrospectively analysed. The diagnosis of hyperplastic polyp was established in the endoscopic polypectomy specimens of 25% of the patients and

K. Dirschmid (✉) · C. Platz-Baudin · M. Stolte
Institute of Pathology, Klinikum Bayreuth,
Preuschwitzer Str. 101,
95445 Bayreuth, Germany
e-mail: pathologie.klinikum-bayreuth@t-online.de
Tel.: +49-921-4005612
Fax: +49-921-4005609

Table 1 Age distribution of the patients

Age (years)	Number of patients	Percent
41–50	10	4.1
51–60	31	12.7
61–70	58	23.8
71–80	98	40.2
81–90	45	18.4
>90	2	0.8
Total	244	100.0

in the surgical polypectomy specimen in two patients. In all other patients, the hyperplastic polyps were diagnosed in forceps biopsies obtained from the polyps. Table 1 shows the age distribution of the patients, Table 2 the distribution of the location of the hyperplastic polyps within the stomach, and Table 3 the number of hyperplastic polyps per patient.

Histological methodology

The biopsy or polypectomy specimens were fixed in 10% formalin solution, dehydrated in the usual manner, and embedded in paraffin. After deparaffination, histological sections (4 μm thick, at least eight sections per tissue sample) were stained with haematoxylin and eosin and, if necessary, with the Warthin–Starry silver stain. The classification and grading of gastritis in the antrum and corpus were based on the updated Sydney System [6]. Corpus-dominant Hp gastritis was diagnosed whenever the grade and activity of the Hp gastritis in the corpus were at least medium grade and at least equally as pronounced as in the antrum. A not-yet atrophic autoimmune gastritis of the corpus mucosa was diagnosed on the basis of the criteria we previously published elsewhere and which have been confirmed by other authors [25, 28].

Results

In none of the patients with hyperplastic polyps was a normal gastric mucosa observed. Most commonly (51.3%), autoimmune gastritis of the corpus mucosa, mostly in the atrophic stage, was diagnosed (see Table 4).

In 37.3% of the patients, chronic active Hp gastritis was the most common underlying disease of the stomach in patients with hyperplastic polyps. More than half (56.1%) of these patients presented with corpus-dominant Hp gastritis.

Ex-Hp gastritis was diagnosed in 8.6%, lymphocytic gastritis in 0.8%, and Hp gastritis with additional lymphocytic gastritis in 0.8% of the patients. In 1.2% of the patients, it was not possible to classify the gastritis with certainty (see Table 4).

Analysis of the gastritis classification in relation to the location of the hyperplastic polyps in the antrum and corpus revealed no significant differences.

Table 2 Location of the hyperplastic gastric polyps

Location	Number of patients	Percent
Pylorus	5	2.1
Antrum	59	24.1
Intermediate zone	16	6.6
Corpus	125	51.2
Fundus	6	2.5
Cardia	6	2.5
Angulus	2	0.8
Multiple locations	13	5.3
Unknown	12	4.9
Total	244	100.0

Table 3 Number of hyperplastic polyps per patient

Number of polyps	Number of patients	Percent
1	198	81.1
2	21	8.6
3	9	3.7
4	6	2.5
5	1	0.4
>5	6	2.5
Unknown	3	1.2
Total	244	100.0

Discussion

On the basis of this retrospective analysis, the questions posed above can be answered as follows:

1. The most common underlying disease of the gastric mucosa in patients with hyperplastic polyp is autoimmune gastritis of the corpus mucosa and Hp gastritis, in particular gastritis of the corpus-dominant form.

Table 4 Classification of gastritis in the corpus in patients with hyperplastic polyp

	Number of patients	Percent
Chronic active Hp gastritis		
Antrum dominant (43.9%)	40	16.4
Corpus dominant (56.1%)	51	20.9
Ex-Hp gastritis	21	8.6
A-gastritis		
Pre-atrophic	2	0.8
Partially atrophic	48	19.7
Atrophic	75	30.8
Non-classifiable gastritis	3	1.2
Special forms		
Lymphocytic gastritis	2	0.8
Mixed lymphocytic and Hp gastritis	2	0.8
Total	244	100.0

2. This explains why the hyperplastic polyp of the gastric mucosa is a marker for a precancerous condition of the stomach.
3. The second most common underlying condition of the gastric mucosa in patients with hyperplastic polyp can be cured by Hp eradication therapy.

That atrophic autoimmune gastritis of the corpus mucosa is one of the possible underlying diseases in hyperplastic polyps can be deduced indirectly from the results of three older publications prior to the rediscovery of *H. pylori* and the introduction of the Sydney System classification of gastritis. As early as 1977, Elsborg et al. [8] described one or several "gastric mucosal polyps" in 25 of 68 patients with pernicious anaemia. In a comparison of 52 patients with hyperplastic polyp and patients with no such polyps, Laxen et al. [12] found atrophy of the corpus mucosa significantly more frequently in the former. Nakano et al. [20] reported corpus mucosal atrophy in 46 patients with hyperplastic polyps.

Our own observation that Hp gastritis is the second most common underlying disease in patients with hyperplastic polyps can be deduced from several studies with small numbers of patients.

In 35 patients with hyperplastic polyps and Hp gastritis, Ohkusa et al. [21] diagnosed chronic active and atrophic gastritis and observed regression of the polyps following Hp eradication in 12 of 17 patients. Ljubicic et al. [14] also reported regression of hyperplastic polyps following Hp eradication treatment in 16 of 21 patients with Hp gastritis. Following Hp eradication, regression of multiple polyps measuring up to 2.6 cm in diameter was noted in a case report [18].

A relevant comprehensive study has been published by Abraham et al. [1]. In 137 out of 160 patients with hyperplastic polyps, biopsies taken from gastric mucosa at some distance from the polyps in the antrum and corpus were examined.

This study is open to criticism on a number of points [27], for example, that the updated Sydney System was not taken into account and there was no subclassification of the Hp gastritis into corpus-dominant gastritis and A-gastritis (in the pre-atrophic stage). Gastritis was reported in 85% of these patients; however, with regard to the forms of gastritis that we consider of importance in hyperplastic polyps, the numbers cited differ considerably from our own. In the group described by Abraham et al. [1], Hp gastritis was found in 25% of the patients (in our case, 37.3%), and the percentage of autoimmune gastritis differed dramatically, with 12% of the patients in that study compared with 51.3% in our patient population. Furthermore, in our patients with hyperplastic polyps, no C-gastritis was found, in contrast to Abraham's study, in which it was observed in 20% of the patients. In our patients, hyperplastic polyps presented in the corpus/fundus part of the stomach in 53.5% and in the antrum in 24.1%, compared with 29% and 60%, respectively, in Abraham's study. Since just 50% of Abraham's patients had polyps measuring less than 5 mm in diameter, it is possible that they had foveolar hyperplasia. This possibility is supported by the frequent location of the polyps in the antrum and the high percentage of C-gastritis in that study. Furthermore, the age distribution of his patients showed a large range of 22–88 years, although hyperplastic polyps in patients younger than 50 years is very rare—in our own group of patients, only ten cases. All these discrepancies are difficult to explain, maybe, in part, due to genetic/environmental differences or rather because of different histological interpretation [27].

That hyperplastic polyps of the stomach is a precancerous condition was already known from earlier studies. In a follow-up study, Seifert et al. [23] detected gastric carcinoma in 8.5% of patients with hyperplastic polyps—not in the polyps themselves but in the gastric mucosa at some distance away. The development of a gastric carcinoma within a hyperplastic polyp is, in contrast, very rare [4, 22, 26, 31]. Dijkhuizen et al. [4] and Nakano et al. [20] demonstrate by molecular–pathological methods a certain risk for malignancy in hyperplastic polyps.

Our results show that the most common underlying disease in patients with hyperplastic polyps is autoimmune gastritis of the corpus mucosa. Autoimmune gastritis has long been considered to be a precancerous condition, admittedly with a highly variable incidence of gastric carcinoma development in follow-up investigations [30]. When hyperplastic polyps have been demonstrated, a diagnostic work-up of the matrix, with additional removal of two biopsies each from the antrum and corpus, should be carried out. If autoimmune gastritis is diagnosed in the non-atrophic stage [25], Hp eradication can result in a cure [19]. In the case of advanced autoimmune gastritis, there is a need for gastric biopsy screening examinations in addition to appropriate substitution therapy.

Even more important is the diagnosis of the matrix for the detection of the second most common underlying disease of the gastric mucosa, namely, Hp gastritis.

Although, on the basis of WHO criteria, Hp infection was already classified as definitely carcinogenic in humans in 1994 [10], the development of gastric carcinoma in underlying Hp infection is relatively rare, so that, initially, it is not easy to explain why gastric carcinomas develop more frequently in patients with hyperplastic polyps and Hp gastritis. This apparent contradiction can, however, be explained on the basis of our additional topographic grading of Hp gastritis in the antrum and corpus. While corpus-dominant Hp gastritis is relatively rare—accounting for 14–17% of all Hp infections [11, 13, 29]—in our study, it was seen in more than half of the patients with Hp gastritis. In several retrospective studies, we found this corpus-dominant Hp gastritis to be statistically significantly over-represented in patients with advanced gastric carcinoma [17] and early gastric carcinoma [15] and in first-degree relatives of patients with gastric carcinoma [16]. For this reason, this type of gastritis has been characterised as gastritis of the "gastric cancer phenotype" [24]. These retrospective studies were initially confirmed indirectly by the fact that, in comparison with controls with identical Hp prevalence, relatives of patients with gastric carcinoma significantly more frequently

have hypochlorhydria and atrophy of the gastric mucosa [7], both factors considered to represent an increased risk for the development of gastric carcinoma [9]. Furthermore, relatives of patients with gastric carcinoma are found to exhibit polymorphisms of the interleukin-1 gene family, which are responsible for marked production of acid, which can be seen as an explanation for the corpus-dominant Hp gastritis [5]. In their study of a family, Carneiro et al. [2] reported on hyperplastic polyposis and diffuse carcinoma of the stomach; they described the occurrence of hyperplastic changes/polyps in the non-neoplastic mucosa of E-cadherin mutation carriers [3].

The significance of corpus-dominant Hp gastritis for the development of a gastric carcinoma was confirmed by a large prospective Japanese study [29]. In that study, the relative risk of a gastric carcinoma developing in corpus-dominant gastritis was 34.5, while intestinal metaplasia (6.4) and atrophy (4.9) both represented for a much lower risk for gastric carcinoma.

In conclusion, our study shows that hyperplastic polyps of the stomach is a precancerous condition because of the most common underlying diseases in these patients, namely, atrophic autoimmune and Hp gastritis, in particular the corpus-dominant Hp gastritis. Future studies will have to show whether, in patients with hyperplastic polyp and Hp gastritis, gastric carcinoma prophylaxis is possible through Hp eradication.

References

1. Abraham SC, Singh VK, Yardley JH, Wu TT (2001) Hyperplastic polyps of the stomach. Associations with histologic patterns of gastritis and gastric atrophy. Am J Surg Pathol 25:500–507
2. Carneiro F, David L, Seruca R, Castedo S, Nesland JM, Sobrinho-Simoes M (1993) Hyperplastic polyposis and diffuse carcinoma of the stomach. A study of a family. Cancer 72:323–329
3. Carneiro F, Huntsman DG, Smyrk TC, Owen DA, Seruca R, Pharaoh P, Caldas C, Sorbrinho-Simoes M (2004) Model of the early development of diffuse gastric cancer in E-cadherin mutation carriers and its implications for patient screening. J Pathol 203:681–687
4. Daibo M, Itabashi M, Hirota T (1987) Malignant transformation of gastric hyperplastic polyps. Am J Gastroenterol 82:1016–1025
5. Dijkhuizen SMM, Entius MM, Clement MJ, Polak MM, van den Berg FM, Craanen ME, Slebos RJC, Offerhaus GJA (1997) Multiple hyperplastic polyps in the stomach: evidence for clonality and neoplastic potential. Gastroenterology 112:561–566
6. Dixon MF, Genta RM, Yardley JH, the Participants in the International Workshop on the Histopathology of Gastritis (1996) Classification and grading of gastritis: the updated Sydney system. Am J Surg Pathol 20:1161–1181
7. El-Omar EM, Carrington M, Chow WH, McColl KE, Bream SW, Young HA, Herrera S, Lissowska J, Yuan CC, Rothman N, Lanyon G, Martin M, Fraumeni JF, Rabkin CS (2000) Interleukin-1 polymorphisms associated with increased risk of gastric cancer. Nature 404:398–402
8. Elsborg L, Andersen D, Myrhe-Jensen O, Bastrup-Madsen P (1977) Gastric mucosal polyps in pernicious anaemia. Scand J Gastroenterol 12:49–52
9. Hansson LE, Nyren O, Hsing AW, Bergstrom R, Josefsson S, Chow WH, Fraumeni JF, Adami HO (1996) The risk of stomach cancer in patients with gastric or duodenal ulcer disease. N Engl J Med 335:242–249
10. International Agency for Research on Cancer (IARC) (1994) Schistosomes, liver flukes and *Helicobacter pylori*. Working group on the evaluation of carcinogenic risks to humans. IARC Monogr Eval Carcinog Risks Hum 61:177–241
11. Knight T, Wyatt JI, Wilson A, Greaves S, Newell D, Hengels K, Corlett M, Webb P, Forman D, Elder J (1996) *Helicobacter pylori* gastritis and serum pepsinogen levels in a healthy population: development of a biomarker strategy for gastric atrophy in high risk groups. Br J Cancer 73:819–824
12. Laxen F, Kekki M, Sipponen P, Siurala M (1983) The gastric mucosa in stomach with polyps: morphologic and dynamic evaluation. Scand J Gastroenterol 18:503–511
13. Leodolter A, Ebert M, Kahl S, Vieth M, Malfertheiner P (2003) Age-dependent prevalence of *H. pylori* associated gastritis phenotypes with increased risk for gastric cancer. Gastroenterology 124(Suppl):A648
14. Ljubicic N, Banic N, Kujundzic M, Antic Z, Vrkljan M, Kovacevic I, Hrabar D, Doko D, Doko M, Zowvak M, Mihatov S (1999) The effect of eradicating *Helicobacter pylori* infection on the course of adenomatous and hyperplastic gastric polyps. Eur J Gastroenterol Hepatol 11:722–730
15. Meining A, Bayerdörffer E, Müller P, Miehlke S, Lehn N, Hölzel D, Hatz R, Stolte M (1998) Gastric carcinoma risk index in patients infected with *Helicobacter pylori*. Virchows Arch 432:311–314
16. Meining A, Bayerdörffer E, Stolte M (1999) *Helicobacter pylori* gastritis of the gastric cancer phenotype in relatives of gastric carcinoma patients. Eur J Gastroenterol Hepatol 11:717–720
17. Miehlke S, Hackelsberger A, Meining A, Hatz, Lehn N, Malfertheiner P (1998) Severe expression of corpus gastritis is characteristic in gastric cancer patients infected with *Helicobacter pylori*. Br J Cancer 78:263–266
18. Mocek FW, Ward WW, Wolfson SE, Rumage WT, Wieman TJ (1994) Elimination of recurrent hyperplastic polyps by eradication of *Helicobacter pylori*. Ann Intern Med 120:1007–1008
19. Müller H, Rappel S, Wündisch T, Bayerdörffer E, Stolte M (2001) Healing of active, non-atrophic autoimmune gastritis by *H. pylori* eradication. Digestion 64:30–39
20. Nakano H, Persson B, Slezak P (1990) Study of the gastric mucosal background in patients with gastric polyps. Gastrointest Endosc 36:39–42
21. Ohkusa T, Takashimizu I, Fujiki K, Suzuki S, Shimoi K, Horiuchi T, Sakurazawa T, Ariake K, Ishiik, Kumagai J, Zanizawa T (1998) Disappearance of hyperplastic polyps in the stomach after eradication of *Helicobacter pylori*. Ann Intern Med 129:712–715
22. Orlowska J, Jarosz D, Pachlewski J, Butruk E (1995) Malignant transformation of benign epithelial gastric polyps. Am J Gastroenterol 90:2152–2159
23. Seifert E, Gail K, Weismüller J (1983) Gastric polypectomy—long term results (survey of 23 centers of Germany). Endoscopy 15:8–11
24. Sipponen P, Stolte M (1997) Clinical impact of routine biopsies of the gastric antrum and body. Endoscopy 29:671–678
25. Stolte M, Baumann H, Bethke B, Ritter M, Lauer E, Eidt H (1992) Active autoimmune gastritis without total atrophy of the glands. Z Gastroenterol 30:729–735
26. Stolte M, Sticht T, Eidt S, Ebert D, Finkenzeller G (1994) Frequency, location and age and sex distribution of various types of gastric polyps. Endoscopy 22:203–207
27. Stolte M (2001) Hyperplastic polyps of the stomach. Letter to the editor. Am J Surg Pathol 25:1342–1343
28. Torbenson M, Abraham SC, Boitnott J, Yardley JH, Wu TT (2002) Autoimmune gastritis: distinct histological and immunohistochemical findings before complete loss of oxyntic glands. Mod Pathol 15:102–109

29. Uemura M, Okamoto S, Yamamoto S, Matsumara N, Ymaguche I, Yamakido M, Taniyama K, Sasaki N, Schlemper RJ (2001) *Helicobacter pylori* infection and the development of gastric cancer. N Engl J Med 345:784–789
30. Ye W, Nyrén O (2003) Risk of cancers of the oesophagus and stomach by histology or subsite in patients hospitalised for pernicious anaemia. Gut 52:938–941
31. Zea-Iriarte WL, Sekine I, Istuno M, Makiyama K, Naito S, Nakayama T, Nishisawa-Takano JE, Hattori T (1996) Carcinoma in gastric hyperplastic polyps. A phenotypic study. Dig Dis Sci 41:377–386

Virchows Arch (2006) 448: 85–89
DOI 10.1007/s00428-005-0094-0

CASE REPORT

Florian Grabellus · Sien-Yi Sheu · Boris Schmidt · Cornelius Kuhnen · Michael Flasshove · Steffen Ruchholtz · Georg Taeger · Kurt Werner Schmid

Recurrent high-grade leiomyosarcoma with heterologous osteosarcomatous differentiation

Received: 19 July 2005 / Accepted: 9 September 2005 / Published online: 14 October 2005

Abstract Leiomyosarcomas (LM) of the soft tissue comprise approximately 5–10% of all soft tissue sarcomas. Besides the classic LM, several distinctly uncommon features of the cellular and growth patterns of LM have been described. The term "dedifferentiated LM" has rarely been used in the literature to describe soft tissue LM containing areas of undifferentiated, pleomorphic appearance or detectable heterologous differentiation. We report on a case of high-grade LM with almost entire transition to an osteosarcoma, which was classified as recurrent high-grade LM with heterologous osteosarcomatous differentiation. The identification of areas with osteosarcomatous dedifferentiation in soft tissue sarcomas can be of clinical importance because of a possible change in oncologic treatment strategies.

Keywords Sarcomas · Soft tissue

F. Grabellus (✉) · S.-Y. Sheu · K. W. Schmid
Institute of Pathology,
University Hospital of Essen,
University Duisburg-Essen,
Hufelandstrasse 55,
45122 Essen, Germany
e-mail: florian.grabellus@medizin.uni-essen.de
Tel.: +49-201-7233324
Fax: +49-201-7235926

B. Schmidt · S. Ruchholtz · G. Taeger
Department of Trauma Surgery,
University Hospital of Essen,
Essen, Germany

M. Flasshove
Department of Internal Medicine (Cancer Research),
University Hospital of Essen,
Essen, Germany

C. Kuhnen
Institute of Pathology,
University Hospital Bergmannsheil,
Bochum, Germany

Introduction

Leiomyosarcomas (LM) of the soft tissue are relatively infrequent malignant mesenchymal tumors in adults, which comprise approximately 5–10% of all soft tissue sarcomas. LM occur in the uterus, along the gastrointestinal tract and, to a lesser extent, in the soft tissues of the retroperitoneum, abdominal cavity, or the extremities. On histopathologic investigation, most LM consist of more or less uniform spindle cells that are arranged in bundles or fascicles, reminiscent of being of smooth muscle origin. Typical tumor cells have abundant eosinophilic cytoplasm and cigar-shaped nuclei. Besides this classic LM, several distinctly uncommon features of the cellular and growth patterns of LM have been described. These tumors may have schwannoma-like nuclear palisading, epitheloid changes, abundant pleomorphism, prominent inflammatory infiltrates, myxoid changes [19], or occasionally, the occurrence of CD68-positive osteoclastic giant cells [2, 11, 14].

Osteoclastic giant cells in soft tissue tumors are the hallmark of some benign and malignant so-called fibrohistiocytic tumors, like giant cell tumors of soft tissue (giant cell tumor with low malignant potential) or undifferentiated pleomorphic sarcomas with giant cells (giant cell malignant fibrous histiocytoma; [6]). These tumors occasionally exhibit metaplastic bone formation, which is uncommon for LM. Heterotopic bone formation can also be seen regularly in other entities of soft tissue sarcomas, like synovial sarcoma or malignant peripheral nerve sheath tumor, but the presence of malignant neoplastic osteoid or bone formation in soft tissue tumor should lead to the diagnosis of extraskeletal osteosarcoma [13].

LM as one part of tumors with dual lineage differentiation in combination with liposarcoma [20], rhabdomyosarcoma [18], and osteosarcoma [4] seem to be rare events and have only been reported sporadically.

We report on a case of LM of the soft tissue of the groin with transition to osteosarcoma within local recurrence.

Case report

A 35-year-old woman presented with a 10.8-cm maximum diameter lump of the right groin region. On histopathologic investigation of the specimen, an initial diagnosis of a high-grade LM was made (International Union Against Cancer (UICC), pT2b pNx pMx G3 R0; American Joint Committee on Cancer (AJCC), 4). An adjuvant local radiation treatment was temporarily stopped because of poor wound healing (19.8 Gy, single dose 1.8 Gy). Five and seven months later, the tumor showed local recurrences. After the first recurrence, a reconstruction of the soft tissue defect was achieved by the use of a rectus abdominis flap. Additionally, lung metastases were discovered 6 months after the first surgical intervention. Under chemotherapy with adriamycin and ifosfamide, a good response of the local tumor recurrence as well as of the pulmonary metastases could be seen. One year after the initial diagnosis of LM, the second local recurrence of the tumor was resected and investigated histopathologically.

Pathology

Gross pathology (second recurrence)

A soft tissue specimen measuring 20.8×18.2×10.0 cm, containing skin, subcutaneous tissue, and a musculocutaneous flap (M. rectus abdominis), was studied. Within the specimen, two 10.5- and 9.0-cm circumscribed tan-white tumors were detectable (Fig. 2a). Both tumors were cystic and contained a brown-red fluid.

Microscopic pathology

Primary tumor

Specimens of the primary tumor material could be classified as high-grade LM using light microscopy (Fig. 1a). This diagnosis was confirmed by positive immunohistochemical staining with α-smooth muscle actin (Dako, Glostrup, Denmark; dilution 1:1000, clone 1A4; Fig. 1b) and desmin antibodies (Dako; dilution 1:30, clone D33; Fig. 1c).

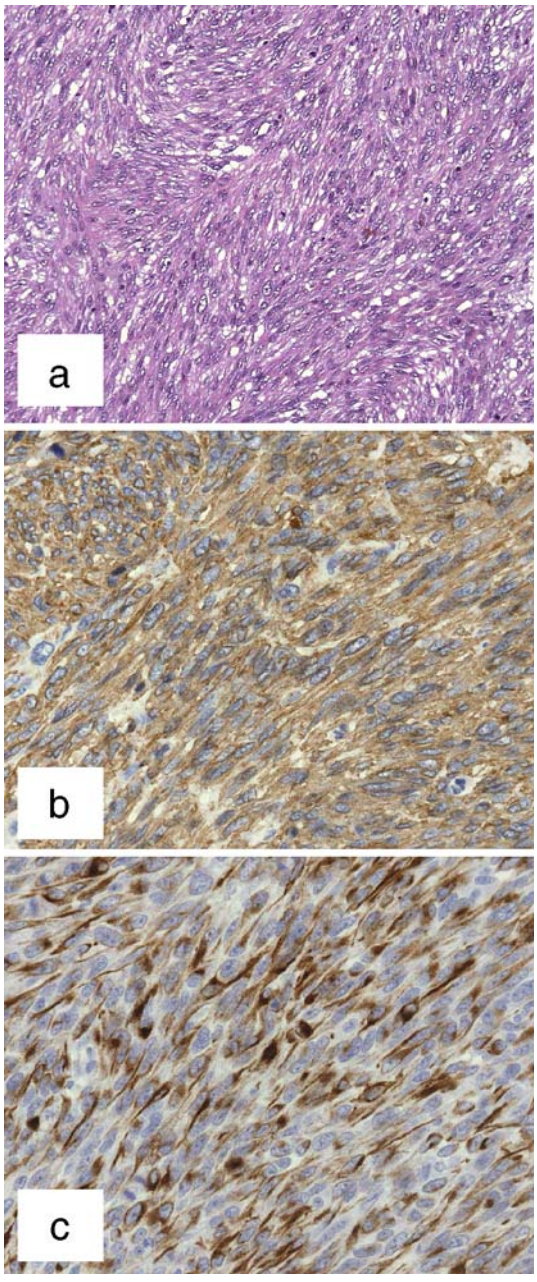

Fig. 1 **a** Light microscopic findings of the initially resected high-grade leiomyosarcoma (hematoxylin–eosin, H & E, ×200). **b** Immunohistochemical staining with smooth muscle actin antibody (×400). **c** Immunohistochemical staining with desmin antibody (×400)

Recurrent tumor

Microscopically, the recurrent tumor showed high cellularity and was composed of round irregular to pleomorphic cells with considerable mitotic activity and atypical mitotic figures. Neoplastic osteoid was deposited in a lacy, trabecular pattern and was focally mineralized (Fig. 2b). The tumor cells resembled malignant osteoblasts, and osteoclastic giant cells were frequently scattered throughout the tumor (Fig. 2c).

Only minor portions of the tumor exhibited a more fascicular arrangement of tumor cells, with spindle cells and elongated nuclei.

Immunohistochemically, the tumor cells of the osteosarcomatous part of the recurrent tumor stained negatively with antibodies against smooth muscle actin. Osteoclastic giant cells showed a positive reaction with a CD68 antibody (Dako; dilution 1:1200, clone PG-M1; Fig. 2d). More than 50% of the tumor cells of the spindled part of the tumor reacted positively with antibodies against smooth muscle actin.

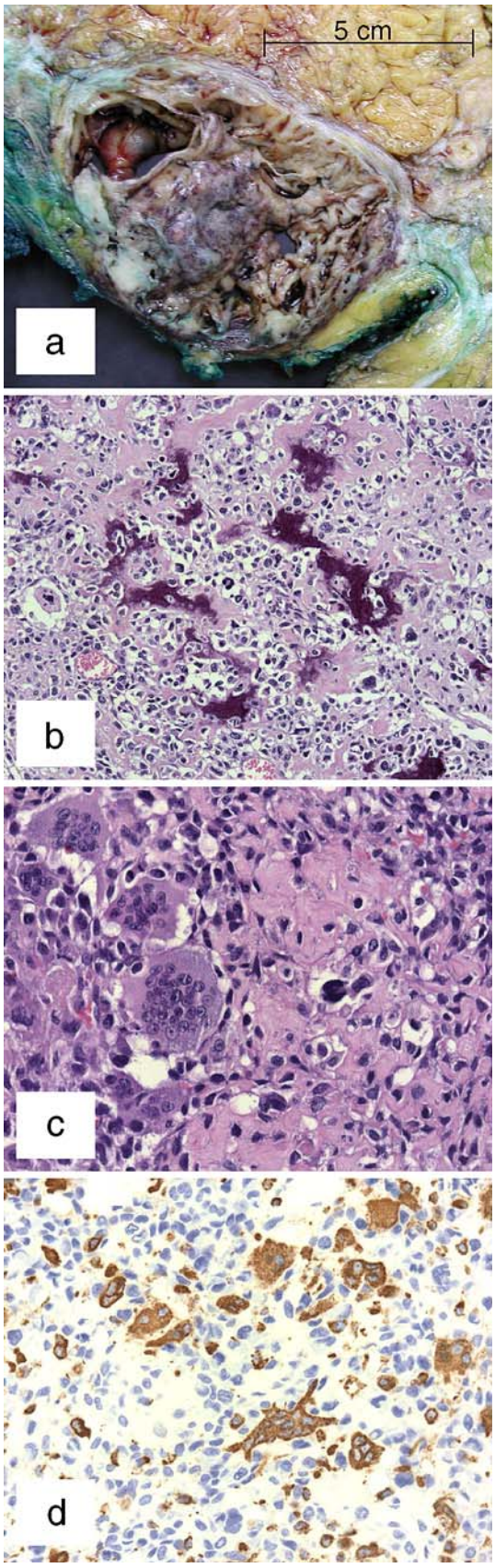

◀ **Fig. 2** **a** Macroscopy of recurrent tumor node. **b** Osteoid formation within the dedifferentiated area (H & E, ×200). **c** Osteoclastic giant cells (×400). **d** CD68 immunohistochemistry of osteoclastic giant cells (×400)

Discussion

Differentiation is the process whereby cells become specialized to execute specific functions and lose their ability to perform others, which means that these cells lose their so-called cell plasticity. Fully differentiated cells are generally mitotically inactive. In addition, the state of terminal differentiation was thought to be fixed, but it is now clear that differentiated cells may be capable of reentering the cell cycle on appropriate stimuli and that differentiation can be dynamically altered or even be reversed [9]. The cells with the most extensive potential of differentiation (plasticity) are stem cells, including mesenchymal stem cells. During dedifferentiation or retrodifferentiation, the expression of gene products associated with a differentiated phenotype and cell cycle regulation are reversed. The cells lose their special functions but regain cell plasticity. In cancer development, the expression of defects in the cellular control of the differentiation process and in the activation of pathways that initiate unregulated self-renewal is thought to be of etiological significance. In this context, it is noteworthy that stem cells and cancer cells have striking similarities, leading to the assumption that some cancers may arise from tissue stem cells [17], although dedifferentiation to more multipotent progenitor cells may

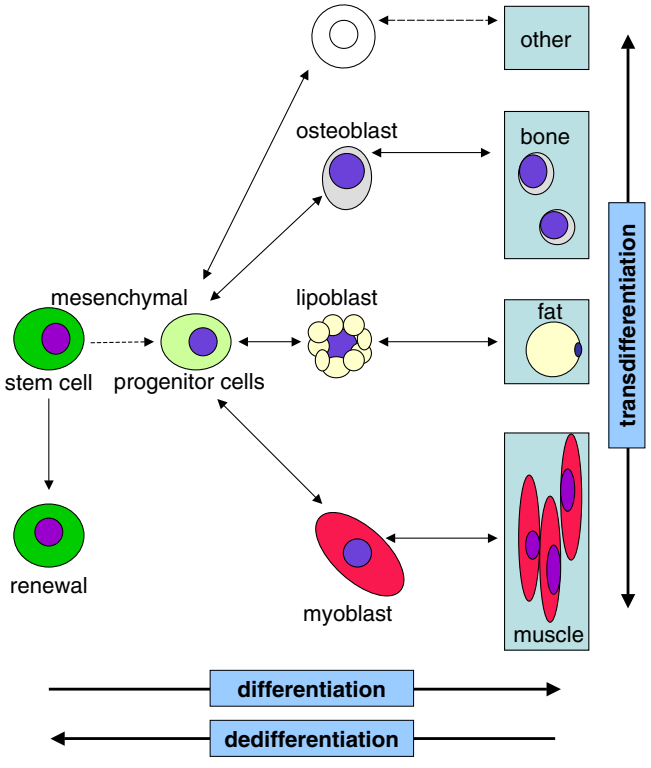

Fig. 3 Diagram of mesenchymal differentiation, dedifferentiation, and transdifferentiation

explain phenotypical change or transdifferentiation of tumor cells in dedifferentiated sarcomas (Fig. 3).

The concept of dedifferentiation in sarcomas has been best characterized for liposarcomas (and chondrosarcomas). In about 10% of cases, well-differentiated malignant adipocytic neoplasms undergo dedifferentiation. Dedifferentiation in liposarcomas classically means the transition of a well-differentiated liposarcoma to a nonlipogenic sarcoma with a higher grade of malignancy. This classical concept of dedifferentiation can be applied to the rare entity of dedifferentiated LM as well. The areas of dedifferentiation in these sarcomas are most frequently pleomorphic undifferentiated sarcomas (malignant fibrous histiocytomas, MFH) but can also exhibit a heterologous (*trans*-) differentiation [10, 22]. The concept of MFH as an entity on its own remains controversial since MFH lack the ability to express typical phenotypic markers. In recent years, it has been hypothesized that MFH originate from multipotent mesenchymal progenitor cells [7]. These findings may explain the high percentage of dedifferentiated liposarcomas with an MFH-like dedifferentiation as well as the phenomenon of divergent myosarcomateous or osteosarcomatous differentiation (transdifferentiation; [21]).

Tumors that contain two or more lineages of specialized differentiation have sometimes been described as "malignant mesenchymomas" in the past [3, 12, 15, 16]. Since the group of malignant mesenchymomas represents no homogeneous clinicopathological entity, and the majority of tumors considered to be mesenchymomas can be classified in other ways (especially dedifferentiated liposarcomas), this entity seems to be gradually disappearing. Nevertheless, malignant mesenchymoma as an entity on its own is still listed in the latest WHO (2002) classification of tumors of soft tissue and bone [6].

The use of the term "dedifferentiated LM" for soft tissue LM containing areas of nonspecific, poorly differentiated, pleomorphic appearance or detectable heterologous differentiation is uncommon, but according to the WHO classification, this diagnosis can be taken into consideration in those rare cases [6].

In the reported case, the transition from LM to osteosarcoma occurred in the second recurrence of a high-grade LM. This was proven by histopathological investigation of the primary tumor and both recurrent tumor manifestations. Minor portions of the second tumor recurrence still exhibited residual signs of leiomyogenic differentiation.

In our opinion, the diagnosis of a recurrent high-grade LM with heterologous osteosarcomatous differentiation is appropriate for this special case because the tumor gained the osteosarcomatous portion during progression and did not exhibit two lines of differentiation from the beginning, which might have suggested the diagnosis of malignant mesenchymoma. The term dedifferentiated LM may not be used for the reported tumor because this term is, strictly speaking, defined as a biphasic neoplasm composed of areas typical of a low-grade LM with a usually abrupt transition to high-grade sarcoma in which myogenic features are not obvious. This classical definition is mainly based on histomorphological and immunohistochemical criteria and cannot reflect the entire biological changes of a tumor. Therefore, the strict use of the definition seems to be problematic since heterologous differentiation in sarcomas may represent the consequence of a dedifferentiation process.

However, it is important to detail the different components of a tumor accurately when reporting about sarcomas with dual or multiple differentiations. For this reason, even recurrent soft tissue sarcomas should be extensively investigated in multiple tumor specimens from different tumor locations [5].

Because the described soft tissue tumor showed the morphology of an osteosarcoma in a high proportion (>95%), the case was reported to the clinicians as an extraskeletal osteosarcoma. A standardized therapeutic management of the extraosseous form of osteosarcoma does not exist to date and is discussed controversially in the literature. Ahmad et al. [1] reported on a cohort of 60 patients with extraskeletal osteosarcomas, concluding that extraskeletal osteosarcoma is "clinically and therapeutically distinct from osseous osteosarcoma," which should be treated similarly to high-risk soft tissue sarcomas. A recent publication showed a more favorable outcome obtained with a more aggressive multiagent chemotherapy like it is used for conventional skeletal osteosarcomas [8].

References

1. Ahmad SA, Patel SR, Ballo MT, Baker TP, Yasko AW, Wang X, Feig BW, Hunt KK, Lin PP, Weber KL, Chen LL, Zagars GK, Pollock RE, Benjamin RS, Pisters PW (2002) Extraosseous osteosarcoma: response to treatment and long-term outcome. J Clin Oncol 20:521–527
2. Aru A, Norup P, Bjerregaard B, Andreasson B, Horn T (2001) Osteoclast-like giant cells in leiomyomatous tumors of the uterus. A case report and review of the literature. Acta Obstet Gynecol Scand 80:371–374
3. Brady MS, Perino G, Tallini G, Russo P, Woodruff JM (1996) Malignant mesenchymoma. Cancer 77:467–473
4. Feeley C, Gallagher P, Lang D (2005) Osteosarcoma arising in a metastatic leiomyosarcoma. Histopathology 46:111–113
5. Fletcher CD (1994) The histological features of local recurrences of soft tissue sarcomas. Pathologe 15:196–200
6. Fletcher CDM, Unni KK, Mertens FE (eds) (2002) World Health Organization classification of tumours. Pathology and genetics of tumors of soft tissue and bone. IARC Press, Lyon
7. Gazziola C, Cordani N, Wasserman B, Carta S, Colombatti A, Perris R (2003) Malignant fibrous histiocytoma: a proposed cellular origin and identification of its characterizing gene transcripts. Int J Oncol 23:343–351
8. Goldstein-Jackson SY, Gosheger G, Delling G, Berdel WE, Exner GU, Jundt G, Machatschek JN, Zoubek A, Jurgens H, Bielack SS (2005) Extraskeletal osteosarcoma has a favourable prognosis when treated like conventional osteosarcoma. J Cancer Res Clin Oncol. DOI 10.1007/s00432-005-0687-7 (published online first: 26 May 2005)
9. Hass R (1994) Retrodifferentiation and cell death. Crit Rev Oncog 5:359–371
10. Henricks WH, Chu YC, Goldblum JR, Weiss SW (1997) Dedifferentiated liposarcoma: a clinicopathological analysis of 155 cases with a proposal for an expanded definition of dedifferentiation. Am J Surg Pathol 21:271–281
11. Insabato L, Di Vizio D, Ciancia G, Pettinato G, Tornillo L, Terracciano L (2004) Malignant gastrointestinal leiomyosarcoma and gastrointestinal stromal tumor with prominent osteoclast-like giant cells. Arch Pathol Lab Med 128:440–443

12. Kew CC, Putti TC, Razvi K (2004) Malignant mesenchymoma arising from a uterine leiomyoma in the menopause. Gynecol Oncol 95:712–715
13. Lidang JM, Schumacher B, Myhre JO, Steen NO, Keller J (1998) Extraskeletal osteosarcomas: a clinicopathologic study of 25 cases. Am J Surg Pathol 22:588–594
14. Mentzel T, Calonje E, Fletcher CD (1994) Leiomyosarcoma with prominent osteoclast-like giant cells. Analysis of eight cases closely mimicking the so-called giant cell variant of malignant fibrous histiocytoma. Am J Surg Pathol 18:258–265
15. Mentzel T, Fletcher CD (1994) Malignant mesenchymomas of soft tissue associated with numerous osteoclast-like giant cells mimicking the so-called giant cell variant of "malignant fibrous histiocytoma". Virchows Arch 424:539–545
16. Newman PL, Fletcher CD (1991) Malignant mesenchymoma. Clinicopathologic analysis of a series with evidence of low-grade behaviour. Am J Surg Pathol 15:607–614
17. Reya T, Morrison SJ, Clarke MF, Weissman IL (2001) Stem cells, cancer, and cancer stem cells. Nature 414:105–111
18. Roncaroli F, Eusebi V (1996) Rhabdomyoblastic differentiation in a leiomyosarcoma of the retroperitoneum. Hum Pathol 27: 310–313
19. Rubin BP, Fletcher CD (2000) Myxoid leiomyosarcoma of soft tissue, an underrecognized variant. Am J Surg Pathol 24:927–936
20. Suster S, Wong TY, Moran CA (1993) Sarcomas with combined features of liposarcoma and leiomyosarcoma. Study of two cases of an unusual soft-tissue tumor showing dual lineage differentiation. Am J Surg Pathol 17:905–911
21. Tosh D, Slack JM (2002) How cells change their phenotype. Nat Rev Mol Cell Biol 3:187–194
22. Weiss SW, Goldblum JR (eds) (2001) Enzinger and Weiss's soft tissue tumors, 4th edn. Mosby, St. Louis, MO

Virchows Arch (2006) 448: 90–94
DOI 10.1007/s00428-005-0093-1

CASE REPORT

Young-Hyeh Ko · Won-Seog Kim · Yoonjung Kim

Expression of CD56 antigen in Langerhans cell histiocytosis associated with T-lymphoblastic lymphoma in a same lymph node

Received: 22 December 2004 / Accepted: 6 February 2005 / Published online: 14 October 2005

Abstract Association of T-lymphoblastic lymphoma (LBL) and Langerhans cell histiocytosis (LCH) in the same lymph node is very rare. Herein, we report such two cases with expression of CD56 in Langerhans cells. Immunohistochemically, lymphoblasts were positive for anti-polyclonal CD3 antibody, CD34, CD7, CD99, and terminal deoxynucleotidyl transferase. LCH cells were positive for anti-S100 protein, CD1a, CD4, CD56, and CD68. Although those two populations were separated topographically, many histiocytes intermingled with lymphoblasts in the paracortex and a few lymphoblasts were scattered within the intrasinusoidal sheets of histiocytes. Neither admixed eosinophils nor multinucleated giant cells were observed. The pathogenetic mechanism of CD56 expression in LCH associated with LBL is discussed.

Keywords Langerhans cell histiocytosis · T-lymphoblastic lymphoma · CD56

Introduction

The CD56 antigen is a membrane glycoprotein encoded by a single gene located on 11q23-24 and is the most useful marker currently available for the identification of human natural killer (NK) cells [13]. CD56 also is expressed by a small subset of peripheral blood $CD3^+$ T cells and plasmacytoid dendritic cells (DCs) but not expressed on thymocytes, B cells, plasma cells, monocytes, Langerhans cell, or granulocytes. In the neoplasm of hematopoietic cells, CD56 is expressed in non-Hodgkin's lymphoma, of NK or T cell origin, and a subset of acute myelogenous leukemia [6]. Among DC neoplasm, except for recently described "agranular $CD4^+CD56^+$ hematodermic neoplasm" (blastic NK-cell lymphoma), expression of CD56 was not well investigated [1, 11].

Langerhans cell histiocytosis (LCH) may be associated with a wide range of neoplastic disorders, including malignant lymphoma, acute leukemia, melanoma, lung carcinoma, and other solid tumors, either at presentation or during the course of the diseases [3, 4]. The vast majority of malignant lymphoma showing such an association is a classical Hodgkin's lymphoma, and a minority corresponds to follicular lymphoma [3]. Association of T-lymphoblastic lymphoma (LBL) and LCH is rare, and only three such cases have been reported in the literature so far [8, 12].

We report herein two cases of $CD56^+$ LCH coexistent with T-LBL in the same lymph node.

Y.-H. Ko (✉)
Department of Pathology, Samsung Medical Center,
Sungkyunkwan University School of Medicine,
Kangnam-gu, Ilwon-dong 50,
135-710 Seoul, South Korea
e-mail: yhko@smc.samsung.co.kr
Tel.: +82-2-34102762
Fax: +82-2-34100025

W.-S. Kim
Department of Hematooncology, Samsung Medical Center,
Sungkyunkwan University School of Medicine,
Kangnam-gu, Ilwon-dong 50,
135-710 Seoul, South Korea

Y. Kim
Department of Pathology, Cheonan Hospital,
Soonchunyang University,
Ssangreong-dong,
366-1 Cheonan, South Korea

Clinical history

Case 1

A 59-year-old woman presented with epigastric pain and weight loss of 7 kg for 3 months. She was a housewife and had been healthy until she felt epigastric discomfort 3 months ago. On physical examination, no abnormal findings were noted except mild epigastric tenderness. There was neither organomegaly nor peripheral lymphadenopathy. Peripheral blood findings were the following: hemoglobin (Hb) 10.9 g/dl, hematocrit (Hct) 32.4%, platelets 567,000/μl, white blood cell (WBC) 8,300/μl with differentials of neutrophils 65.6%, lymphocytes 23.7%, eosinophils 0.9%, basophils 0.5%, and monocytes 9.3%. Blood chemistry revealed increased liver enzymes, including total bilirubin

1.6 mg/dl, aspartate transaminase 67 U/l, alanine transaminase 93 U/l, and alkaline phosphatase (ALP) 758 U/l.

On abdominal CT scan, an enlargement of multiple retroperitoneal lymph nodes below the renal vein was noted. The liver and spleen were unremarkable. An explolaparotomy was performed to obtain diagnostic tissue. On operation, enlarged lymph nodes were noted around the left renal vein, right iliac vessels, aorta, and hepatoduodenal ligament and measured up to 2×2×2.5 cm in dimensions. Biopsy was performed from lymph nodes in para-aortic, hepatoduodenal ligament, and left renal vein region and omentum. The aspiration smear of bone marrow revealed atypical terminal deoxynucleotidyl transferase (TdT)(+) blasts, which were counted up to 5% of all nucleated cells. Chemotherapy with cyclophosphamide, doxorubicin, vincristine, and prednisone regimen of four cycles was performed with complete remission. The disease relapsed and the patient died 2 years after the diagnosis.

Case 2

A 48-year-old man presented with intermittent fever, night sweat, and weight loss of 20 kg for 2 months. On physical examination, he had multiple enlarged lymph nodes, up to 2 cm in the neck, and splenomegaly. Peripheral blood showed anemia and pancytopenia. Hb was 9.0 g/dl, Hct was 26.4%, WBC was 1,400/μl with blast 14%, and platelets were 69,000/μl. Lactate dehydrogenase was 980 U/l, and ALP was 515 U/l. On CT scan, pulmonary, hilar, mediastinal, and mesenteric lymphadenopathy and splenomegaly were observed. Bone scan showed no significant abnormality. Biopsy from the neck lymph node was performed.

The patient received chemotherapy with methotrexate, dexamethasone, and vincristine, but his condition did not improve. The patient died of sepsis and *Pneumocystis carinii* pneumonia 1 month after diagnosis.

Materials and methods

The lymph node was fixed in 10% formalin and then embedded in paraffin. The 4-μm-thick sections were stained with hematoxylin and eosin. Paraffin sections were subjected to immunohistochemistry using an automated system (Techmate1000, Dakochemate). The antibody panel included CD2, CD3, CD4, CD5, CD7, CD8, CD1a, CD20, CD79a, CD10 (Novocastra), S100 protein, CD68, TdT, CD99, myeloperoxidase, CD34 (Dako), and CD56 (Monosan). All the immunohistochemical stains were performed after microwave antigen retrieval, for which the tissue sections were immersed in Coplin jars containing 0.01 M citrate buffer, pH 6.0, and subjected to heating for 20 min in a 625-W microwave.

For polymerase chain reaction (PCR) amplification of the T-cell antigen receptor–gamma (TCR-γ) locus in case 1, DNA was prepared by a standard proteinase K digestion and a phenol/chloroform extraction. A PCR analysis followed by single-strand conformational polymorphism was performed as previously described [15].

Results and discussion

Histological findings

Case 1 Normal architecture of the lymph node was destroyed by infiltration of two different populations (Fig. 1). One was medium to large histiocytes with eosinophilic cytoplasm and irregular nucleus showing nuclear folds. The cytoplasm of histiocytes was scanty to abundant in amount. The majority of histiocytes were aggregated in the marginal and cortical sinus. Neither admixed eosinophils nor multinucleated giant cells were observed. The other was small- to medium-sized lymphoblasts characterized by fine nuclear chromatin and high nuclear cytoplasmic ratio, which replaced paracortex and intimately abutted on the intrasinu-

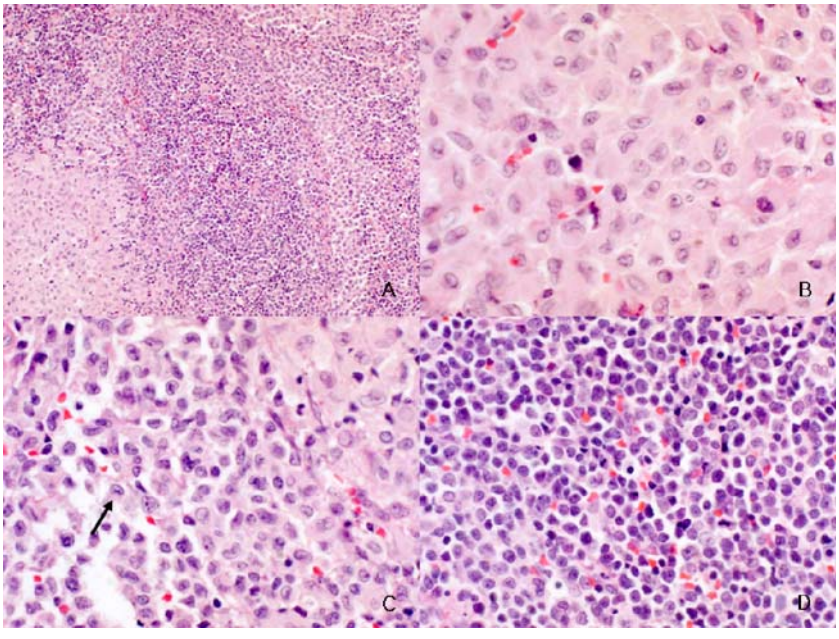

Fig. 1 Histological findings of case 1. **a** Pale sheets of Langerhans cells within sinuses alternating with dark zone of LBL in the paracortex. **b** Large Langerhans cells with abundant cytoplasm. **c** Medium-sized Langerhans cell (*arrow*) with nuclear folding. **d** LBL

soidal sheets of histiocytes. The nuclei were round or convoluted, and the cytoplasm was scanty. There was a few follicular remnants surrounded by lymphoblasts. Although those two populations were separated topographically, many histiocytes were scattered among lymphoblasts in the paracortex and a few lymphoblasts were observed within the intrasinusoidal sheets of histiocytes.

Case 2 Overall histological pattern of lymph node was similar to that described in case 1, with minor differences (Fig. 2). Infiltration of histiocytes was more extensive throughout the lymph node. The cells were aggregated in sinusoidal and perifollicular area and intermingled with lymphoblasts. The size of histiocytes was variable, most of them were large with abundant cytoplasm, but others were medium in size with scanty cytoplasm and had folded nuclei.

Immunohistochemical findings

In case 1, the histiocytes were positive for anti-CD4, anti-CD1a, anti-CD68, and anti-S100 protein antibody, and some of histiocytes were weakly positive for CD56. Majority of lymphoblasts were positive for TdT, CD99, and CD7. Several lymphoblasts expressed cytoplasmic CD3. CD34 was positive in many lymphoblasts. CD2, CD5, CD8, CD10, CD20, CD79a, myeloperoxidase, CD4, CD1a, CD68, and S100 protein were negative. CD56 was negative in majority of lymphoblasts but positive in a small number of lymphoblasts (Fig. 3).

In case 2, the immunoprofile of histiocytes was similar to that of case 1, with some differences. The histiocytes showed strong and uniform positive reaction for anti-S100 protein antibody, but expression of CD1a markedly decreased and was observed in a minority of histiocytes. CD56 staining was more intense and uniform, observed in a majority of intrasinusoidal and paracortical clusters of histiocytes as well as some lymphoblasts (Fig. 4).

To investigate the expression of CD56 in ordinary LCH, four cases of LCH without coexistent malignancy were stained with CD56 monoclonal antibody. All the cases showed no immunoreactivity on Langerhans cells.

T-cell receptor gene rearrangement

No monoclonality was identified for TCR-γ gene rearrangement.

Association of LCH and T-LBL has been firstly described by Quintanilla-Martinez et al. [12] in 1992. They reported three cases of prethymic adult LBL in the peripheral lymph nodes, two of them being coexistent with LCH. After that, the third case was reported in 2001, in which CD79a was aberrantly expressed in lymphoblastic component [8].

It is interesting that three tumors reported previously as well as two cases presented here belong to prethymic T-cell neoplasm according to the immunophenotype and gene rearrangement analysis. Two cases described by Quintanilla-Martinez et al. [12] showed an immunophenotype of TdT^+, human leukocyte antigen–DR $(HLA\text{-}DR)^+$, $CD34^+$, $CD71^+$, $CD38^+$, and $CD7^+$. TCR-β and TCR-γ gene rearrangement were germ line [12]. The patients had nodal disease but no peripheral blood involvement. The third case reported by Li et al. [8] also showed an immature T-cell phenotype (TdT^+, $cCD3^+$, $HLA\text{-}DR^+$, $CD34^+$, $CD38^+$, and $CD7^+$) with aberrant expression of CD79a. Other T- or B-cell markers were negative. T-cell receptor gene rearrangement was not examined. The patient presented with lymphadenopathy with B symptoms. Bone marrow was only partially involved. The phenotype of present cases were $CD7^+$, $CD34^+$, and TdT^+,

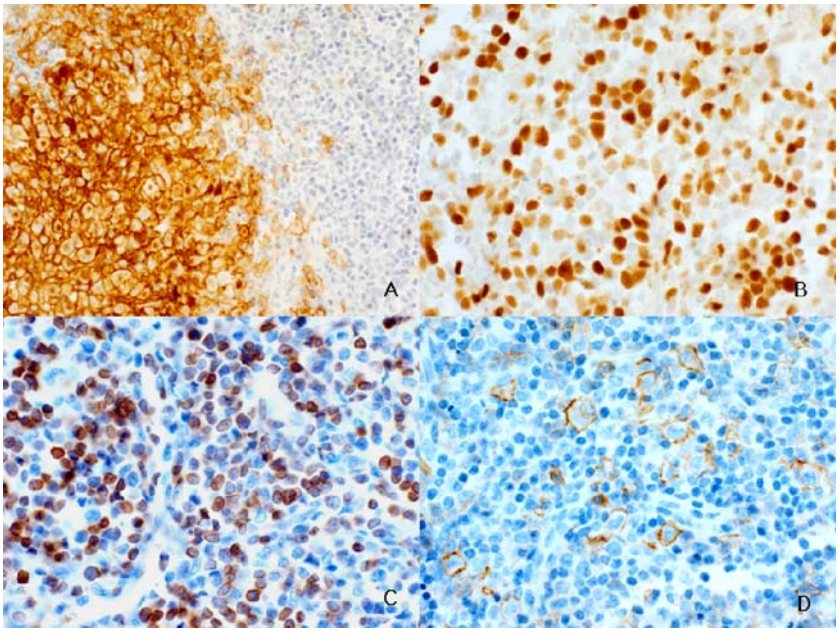

Fig. 2 Immunohistochemical findings of case 1. **a** CD1a. Strong expression in Langerhans cells and negative in LBL. **b** TdT. Positive in a majority of lymphoblasts. **c** CD3. Positive in a portion of lymphoblast. **d** CD56. Weak expression in scattered Langerhans cells

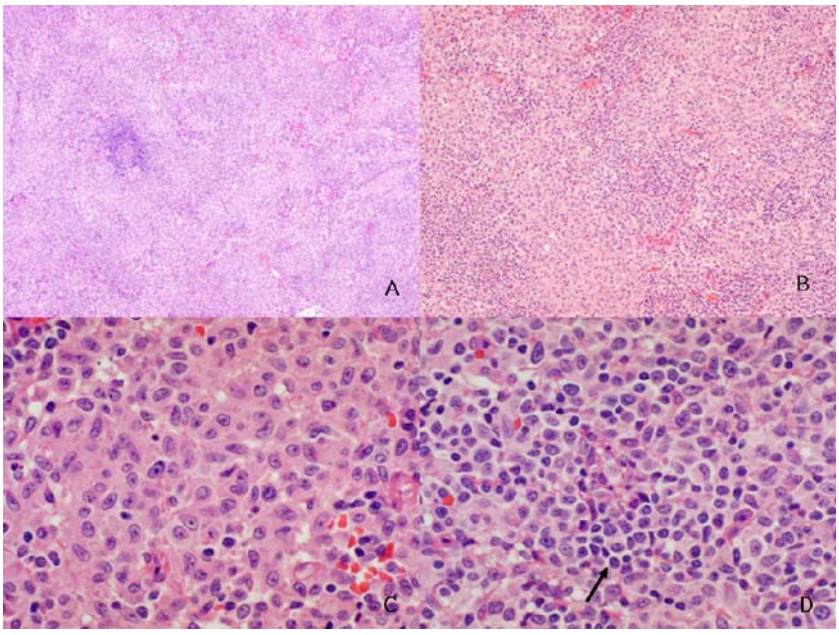

Fig. 3 Histological findings of case 2. **a** Vaguely nodular sheets of Langerhans cells throughout the lymph node. **b** Pale sheets of Langerhans cells alternating with dark zone of LBL **c** Langerhans cells with moderate cytoplasm. **d** LBL (*arrow*) intermingled with Langerhans cells

consistent with prothymocyte. Prothymocytes are the earliest identifiable T-cell precursors to appear in the bone marrow. In addition to TdT, HLA-DR, and CD34, prothymocytes express CD7, generally believed to be the first T-cell lineage-restricted antigen to appear during T-cell ontogeny [7]. In present cases, many lymphoblasts were positive for cCD3 but some lymphoblasts were negative for cCD3. The prothymocytes variably express cCD3. CD3 gene transcription begins during the prothymocyte stage, prior to entrance into the thymus, and cytoplasmic CD3 appears after CD7 but before CD2 [7]. Negative TCR-γ gene rearrangement further supports prethymic stage of differentiation. T-cell LBLs expressing the prothymocyte phenotype may not rearrange any TCR genes or may rearrange only the TCR-δ gene [7].

The reason why prethymic T-LBL is often associated with LCH is unknown.

Coexistence of LCH and malignant lymphoma with close topographic association suggests intimate pathogenetic relation. Magni et al. [9] showed an identical rearrangement of IgH gene in neoplastic Langerhans cell and B lymphocytes in the patient having concurrent nodal follicular lymphoma and cutaneous LCH and claimed that two lesions are derived from common progenitor cell. Because $CD34^{+}$ pleuripotent stem cells can develop into T cells, NK cells, and DCs in an appropriate cytokine environment in vitro [16], it is conceivable that T-LBL and LCH might share common progenitor. On the other hand, in cases reported previously, LCH was regressed when the primary malignancy was treated and had no influence on the treatment outcome of malignant lym-

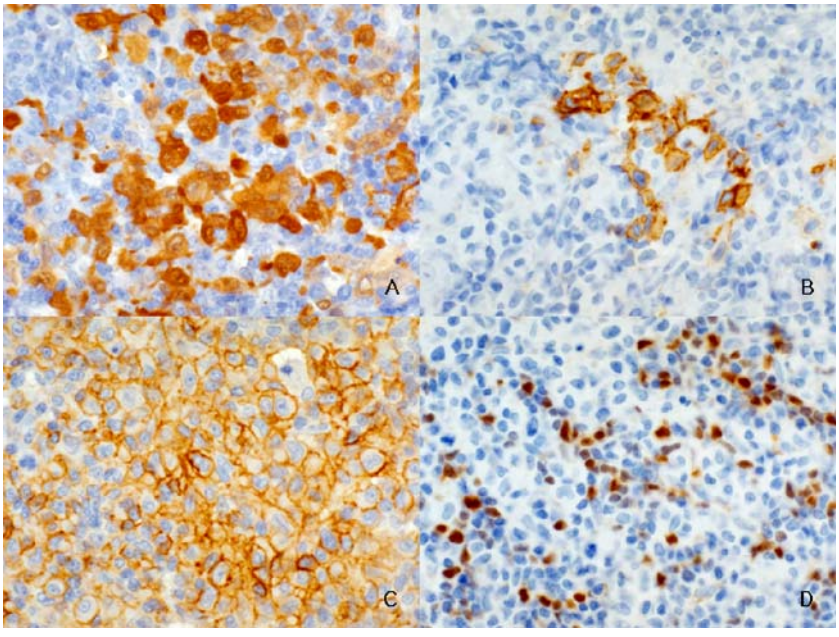

Fig. 4 Immunohistochemical findings of case 2. **a** S100 protein in the Langerhans cells. **b** CD1a. Weak and focal expression in Langerhans cells. **c** CD56. Langerhans cells showing strong positive immunoreaction. **d** TdT-positive lymphoblasts

phoma [3, 4, 8, 12]. LCH in this situation was thought to be passive accumulation of Langerhans cells by cytokine derived from lymphoma cells or Langerhans-cell-mediated immune response to the lymphoma cells.

Expression of CD56 in LCH is a unique finding that has not been described previously.

LCH is a clonal proliferative disorder of dendritic Langerhans cells, commonly involves the bone and skin, and less frequently other organs. Phenotypically, CD1a, S-100 protein, and peanut lectin agglutinin are the markers most consistently seen in paraffin section immunohistochemical studies, and in frozen section, CD2, cCD3, CD4, CD14, HLA-A, -B, -C, -DR are detected [6]. Expression of CD56 was not well studied in LCH as well as in LCH coexistent with other type of malignancies.

LCH cells share many features of early activated DCs that develop from immature DCs in contact with bacterial products [14]. Plasmacytoid DC, which is a normal counterpart of cutaneous $CD4^+CD56^+$ hematodermic neoplasm, seems to be the only subset expressing CD56 among DCs [1, 11]. It is conceivable that some Langerhans cells can be differentiated from plasmacytoid DCs in suitable cytokine environment. However, there is no direct evidence supporting that Langerhans cell is derived from $CD56^+$ plasmacytoid DC. Among DCs in human peripheral blood, Langerhans cell are derived from the $CD1a^+/CD11c^+$ DCs when cultured in the presence of granulocyte macrophage colony-stimulating factor $(GM\text{-}CSF)^+IL\text{-}4^+$ transforming growth factor beta 1 but not from the $CD1a^-CD11c^-$ DCs resembling plasmacytoid DCs [5].

It is worthy to note that the present two cases showed difference of CD1a and CD56 expression. CD56 expression was more extensive and stronger in case 2 than case 1, while the result of CD1a stain was reverse. Upon receipt of certain stimuli in vitro, LCs undergo a process of activation usually termed LC maturation. This process is characterized by downregulation of antigen uptake moieties, including CD1a and Birbeck granules, and massive upregulation of costimulatory molecules of T-cell activation such as CD40, CD54, CD80, and CD86 [10]. In this context, LCs showing weak CD1a/strong CD56 in case 2 seem to be more activated and mature cells than LCs showing strong CD1a/weak CD56 in case 1. Considering the CD56 negativity in ordinary CD1a/strong LCH as shown in our preliminary study and strong expression of CD56 in CD1a/weak case 2, CD56 in LCH associated with LBL might be upregulated by some cytokines or tumor antigens derived from lymphoma and the intensity depends on the degree of activation.

The clinical implication of CD56 expression in this situation is not known. Usually, CD56-expressing lymphoid malignancies pursue aggressive clinical course [2]. Although the patient in case 2 presented with more advanced disease and shorter survival compared to case 1, clinical observation of sufficient numbers of enrolled patients is required to reach any conclusion on prognostic significance of CD56 upregulation in LCH associated with LBL.

To summarize, we report the expression of CD56 antigen in LCH associated with T-LBL, which expands our understanding on the spectrum of CD56 expressing tumors.

References

1. Chaperot L, Bendriss N, Manches O, Gressin R, Maynadie M, Trimoreau F, Orfeuvre H, Corront B, Feuillard J, Sotto JJ, Bensa JC, Briere F, Plumas J, Jacob MC (2001) Identification of a leukemic counterpart of the plasmacytoid dendritic cells. Blood 97:3210–3217
2. Drenou B, Lamy T, Amiot L, Fardel O, Caulet-Maugendre S, Sasportes M, Diebold J, Le Prise PY, Fauchet R (1997) $CD3^-CD56^+$ non-Hodgkin's lymphomas with an aggressive behavior related to multidrug resistance. Blood 8:2966–2974
3. Egeler RM, Neglia JP, Puccetti DM, Brennan CA, Nesbit ME (1993) Association of Langerhans cell histiocytosis with malignant neoplasms. Cancer 71:865–873
4. Egeler RM, Neglia JP, Arico M, Favara BE, Heitger A, Nesbit ME, Nicholson HS (1998) The relation of Langerhans cell histiocytosis to acute leukemia, lymphomas, and other solid tumors. The LCH–Malignancy study group of the Histiocyte society. Hematol Oncol Clin North Am 12:369–378
5. Ito T, Inaba M, Inaba K, Toki J, Sogo S, Iguchi T, Adachi Y, Yamaguchi K, Amakawa R, Valladeau J, Saeland S, Fukuhara S, Ikehara S (1999) A $CD1a^+/CD11c^+$ subset of human blood dendritic cells is a direct precursor of Langerhans cells. J Immunol 163:1409–1419
6. Knowles DM (2001) Immunophenotypic markers useful in the diagnosis and classification of hematopoietic neoplasms. In: Knowles DM (ed) Neoplastic hematopathology, 2nd edn. Lippincott Williams and Wilkins, Philadelphia, pp 93–226
7. Knowles DM (2001) Lymphoblastic lymphoma. In: Knowles DM (ed) Neoplastic hematopathology, 2nd edn. Lippincott Williams and Wilkins, Philadelphia, pp 915–951
8. Li S, Borowitz MJ (2001) CD79a(+) T-cell lymphoblastic lymphoma with coexisting Langerhans cell histiocytosis. Arch Pathol Lab Med 125:958–960
9. Magni M, Di Nicola M, Carlo-Stella C, Matteucci P, Lavazza C, Grisanti S, Bifulco C, Pilotti S, Papini D, Rosai J, Gianni AM (2002) Identical rearrangement of immunoglobulin heavy chain gene in neoplastic Langerhans cells and B-lymphocytes: evidence for a common precursor. Leuk Res 26:1131–1133
10. Maurer D, Stingl G (2001) Langerhans cells. In: Lotze MT, Thomson AW (eds) Dendritic cells, Chapter 5. Academic, Somerset
11. Petrella T, Comeau MR, Maynadie M, Couillault G, De Muret A, Maliszewski CR, Dalac S, Durlach A, Galibert L (2002) 'Agranular $CD4^+CD56^+$ hematodermic neoplasm' (blastic NK-cell lymphoma) originates from a population of $CD56^+$ precursor cells related to plasmacytoid monocytes. Am J Surg Pathol 26:852–862
12. Quintanilla-Martinez L, Zukerberg LR, Harris NL (1992) Prethymic adult lymphoblastic lymphoma. A clinicopathologic and immunohistochemical analysis. Am J Surg Pathol 16: 1075–1084
13. Robertson MJ (1998) Natural killer cell clinical studies: surface antigens of human natural killer cells in health and disease. In: Kishimoto T, Kikutani H, von dem Borne AEGK et al (eds) Leukocyte typing VI: white cell differentiation antigens. Garland Publishing, New York, pp 327–329
14. Ricciardi-Castagnoli P, Granucci F (2002) Interpretation of complexity of innate immune responses by functional genomics. Nat Rev Immunol 2:881–888
15. Signoretti S, Murphy M, Cangi MG, Puddu P, Kadin ME, Loda M (1999) Detection of clonal T-cell receptor gamma gene rearrangements in paraffin-embedded tissue by polymerase chain reaction and nonradioactive single-strand conformational polymorphism analysis. Am J Pathol 154:67–75
16. Spits H, Blom B, Jaleco AC, Weijer K, Verschuren MC, van Dongen JJ, Heemskerk MH, Res PC (1998) Early stages in the development of human T, natural killer and thymic dendritic cells. Immunol Rev 165:75–86

Virchows Arch (2006) 448: 95–99
DOI 10.1007/s00428-005-0079-z

CASE REPORT

Juan Luis García · Cristina Robledo · E. Lumbreras · Teresa Flores · Luis Ramos · Jesús M. Hernández

Analysis of chromosomal imbalances in an elderly woman with a giant cell tumour

Received: 17 May 2005 / Accepted: 25 August 2005 / Published online: 12 October 2005

Abstract Giant cell tumour (GCT) remains one of the most obscure and intensely studied bone tumours. In an effort to resolve questions regarding the genesis and clinical outcome of GCT, advances have been made recently in the identification of chromosomal abnormalities implicated in the tumour. Fusion of telomeres is very frequent in GCT, and this process may be associated with chromosome instability and tumour development. However, little emphasis has been placed on chromosomal imbalances in the molecular characterization of this disease. Here, we report the case of an 83-year-old woman diagnosed with GCT where local recurrence was observed after 11 months of the resection. Cytogenetic studies of the GCT showed a modal number of 46 chromosomes with telomeric associations on 11p and dicentric chromosomes. Moreover, clonal abnormalities, such as del(17p) and losses of chromosomes 4, 13 and 18 and gains on chromosome 7, were also detected. Interestingly, comparative genomic hybridisation (CGH) analysis revealed chromosomal imbalances with gains on chromosomes 1p31-q44, 6q12-q23 and 12q15-q22. Thus, the use of CGH expanded the information obtained by conventional cytogenetics and demonstrated that chromosomal imbalances were associated with the recurrence of the GCT.

J. L. García (✉) · C. Robledo · E. Lumbreras · J. M. Hernández
Centro de Investigación del Cáncer (CIC),
Universidad de Salamanca–CSIC,
Salamanca, Spain
e-mail: jlgarcia@usal.es

T. Flores
Departamento de Anatomía Patológica, Hospital Universitario,
Salamanca, Spain

L. Ramos
Departamento de Traumatología, Hospital Universitario,
Salamanca, Spain

J. M. Hernández
Servicio de Hematología, Hospital Universitario,
Salamanca, Spain

Keywords Bone tumour · Giant cell tumour · Cytogenetics · CGH · Chromosomes

Introduction

Giant cell tumour (GCT) represents approximately 4% of all bone tumours and typically occurs in young women, although it has been observed in older subjects [17]. GCT preferentially involves the ends of the long bones and is characterized morphologically by three types of cells: (a) multinucleated giant cells–predominant type, (b) cells with a round morphology resembling monocytes and (c) spindle-shaped, fibroblast-like stromal cells. Recently, it has been suggested that the stromal cells may form a part of the neoplastic component, while the other cell types serve simply as the reactive component [11, 18]. Although 80% of GCTs is benign, local recurrences and metastases can occur, even in cases with a previous benign histology [9, 16]. For this reason, the WHO has classified GCT as an aggressive and potentially malignant lesion [3]. Clearly, histological features are not sufficient to predict the clinical outcome of this tumour, and other parameters are needed for an accurate prognosis.

The most recurrent karyotypic findings in GCT are telomeric associations (tas) that usually affect 11p, 15p, 19q and 21p[17], while numerical alterations are infrequently detected by conventional cytogenetic analysis [10]. This genetic profile differs from other bone tumours in which chromosomal imbalances (e.g. chondrosarcoma, osteosarcoma and chondroma) or recurrent structural rearrangements (e.g. Ewing sarcoma, aneurismal bone cysts and chondroma) are more frequent [10]. In the present study, we have analysed a recurrent GCT by comparative genomic hybridisation (CGH), which permitted us to detect extensive chromosomal imbalances. This novel observation suggests that chromosomal imbalances may predict recurrence of GCT, and thus, our study not only contributes to our basic understanding of this disease but it also reveals a potential new prognostic tool.

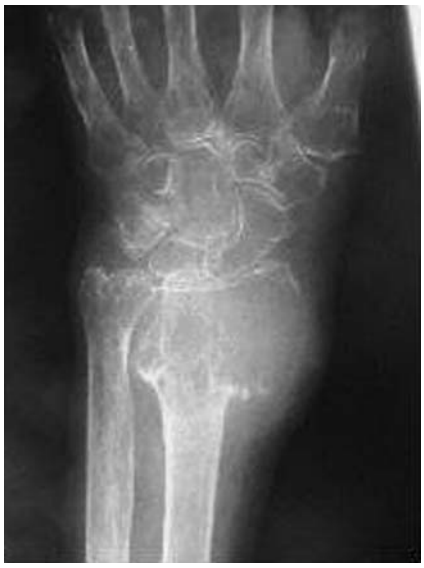

Fig. 1 X-ray film shows the stage 3 GCT of the distal radius

Clinical history

An 83-year-old female was evaluated for pain and immobility of her left wrist which developed over the course of 5 months and without previous trauma to the area. Radiographs revealed an osteolytic lesion in the distal epiphysis of the radius, with slightly precise edges and breakage of the cortex (Fig. 1). The local extension of the lesion was studied through computer tomography and magnetic resonance imaging. Marginal block resection was carried out at the distal end of the radius. Reconstruction was performed with wrist arthrodeses using an allograft of fibula and fixation with a plate. Histological examination of the biopsy specimens revealed GCT (Fig. 2). Eleven months following the resection, local recurrence in soft tissue was observed and a marginal resection was performed. Currently, the patient is free of symptoms with no evidence of tumour recurrence during a follow-up of 30 months.

Material and methods

A specimen of the biopsy was minced and disaggregated overnight in a solution of collagenase (400 UI/ml) and incubated in 3 ml DMEN/F12 (Gibco/BRL, UK) containing 10% fetal calf serum and 5% C02 atmosphere. The cytogenetic preparation and G-banding were performed according to routine cytogenetic procedures [12].

CGH analysis was performed as previously described [7]. Briefly, tumour DNA (test DNA) was labelled with biotin-16-deoxyuridine 5-triphosphate (dUTP) (Boehringer Mannheim, Mannheim, Germany), and the reference DNA was labelled with digoxigenin-11-dUTP (Boehringer Mannheim) by a standard nick-translation reaction. Equal amounts (21 μg) of labelled tumour and normal DNAs and 70 μg of unlabelled human Cot-1 DNA (Gibco/BRL, Gaithersburg, MD, USA) were co-hybridised to slides of human metaphase chromosome spread prepared from phytohaemagglutinin-stimulated lymphocytes from normal individuals. After hybridisation for 1 to 2 days in a moist chamber at 37°C, post-hybridisation washes were performed to a stringency of 0.1× saline sodium citrate at 42°C. Tumour and normal DNA were detected by avidin–fluorescein isothiocyanate and rhodamine-conjugated anti-digoxigenin, respectively. These slides were counterstained with 4,6-diamidino-2-phenylindole and mounted with an anti-fade solution. Image acquisition was performed with an epifluorescence microscope (Nikon MDR1000) equipped with a cooled charge-coupled device camera. The images were analysed with Quips CGH software (QUIPS, Vysis, Downers Grove, IL, USA).

The probes used for fluorescence in situ hybridisation (FISH) analyses were LSI p53 (17p13.1) Spectrum Orange and bacterial artificial chromosome (BAC) RP-11 611O2 which contains a DNA sequence specific for the MDM2 gene locus, mapping to 12q12 (RPCI-11 Human Male BAC Library). FISH studies were carried out following well-established methods [8].

Results

A benign tumour typically displays large numbers of evenly distributed multinucleated giant cells on a background of sheets of round to oval mononuclear cells lacking cytologic atypia and atypical mitotic figures (Fig. 2a,b). The neoplastic cells invade locally soft tissue (Fig. 2c).

Chromosomal analysis revealed that most cells were hypodiploidy, varying from 43 to 45 chromosomes, and the description of a representative karyotype was 41-

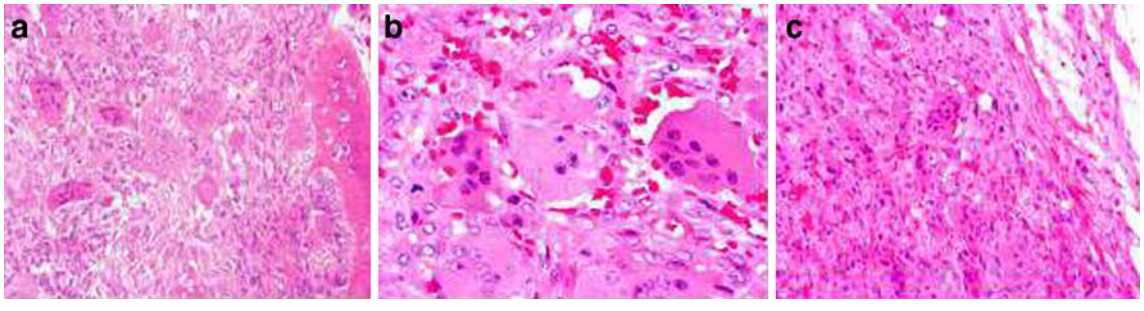

Fig. 2 Microscopic view a GCT from an 83-year-old woman. **a**, **b** Biopsy characterized by numerous multinucleated giant cells and oval mononuclear cells. **c** Peripheral areas showing the growth of the lesion with the permeation of the cortex and the extension to the soft tissue

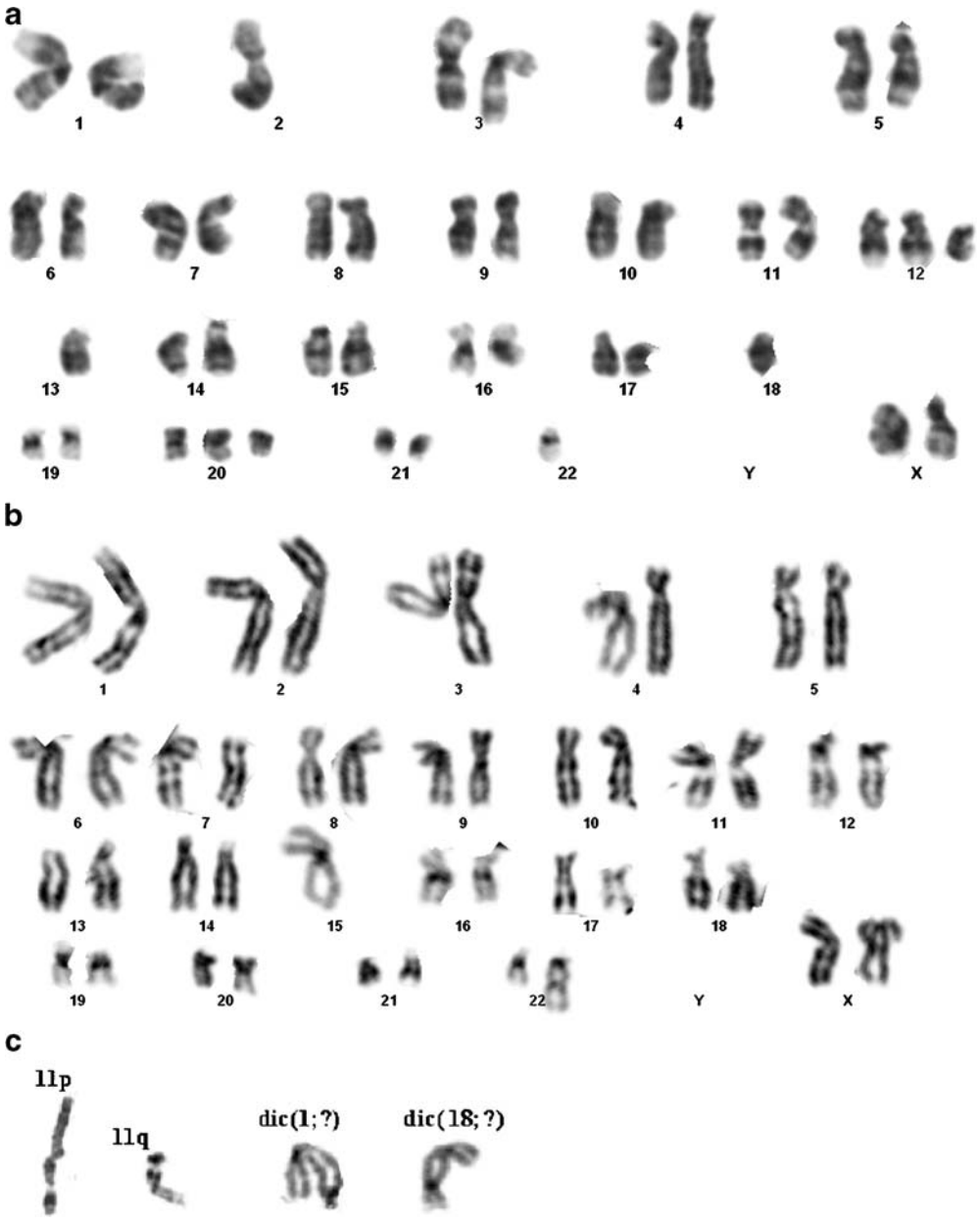

Fig. 3 **a** Representative karyotype showing 44,XX,−2,add(3)(q29),−13,del(17)(p13). **b** 46,XX,del(7)(q36),tas(15;15)(q11;q11),del(17)(p13),add(22)(13). **c** Partial karyotype of telomeric associations (tas) on 11p and 11q and dicentric chromosomes dic(1;?)(p;?) and dic(18;?)(p11;?)

46XX,−2[2],−4[3],+7[3],−13[3],del(17)(p12)[3],−18[4],−22[2] [cp10]/46XX [5]. In addition, no clonal dicentric chromosome (dic) or tas were observed on chromosomes 3p, 11p and 15q (Fig. 3).

Genomic DNA analysis of the tumour specimen by CGH revealed gains on 1p31-q44, 2q24-q34, 3q24-26, 4p15-q34, 5q14-q23, 6q12-q23, 7q31, 8q13-q21, 12q15-q22 and 13q14-q22. The losses were detected on 9q31-q34, 11q23-25, 12q23-q24, 14q31-32, 16, 17, 20q11-q13, 21 and 22 (Fig. 4).

Hybridisation with probe 17p showed that the 30% of cells displayed deletions of TP53 while 15% had three copies of 17p. Regarding the 12q region, all cells analysed contained two signals.

Discussion

Information about the genetic abnormalities underlying GCT has been limited to conventional cytogenetics which can identify tas and dic as the typical aberrations in this type of tumour [14]. These biomarkers, such as tas, have been implicated in chromosomal instability and tumorigenesis and could be responsible for the accumulation of other associated cytogenetic aberrations [1, 19]. However, the precise role of tas in the development of GCT and their molecular consequences are not fully understood. Along with tas, other karyotypic findings, such as clonal, structural and/or numerical changes, have been observed in GCT [3, 15]. Recently, a cytogenetic analysis of a CGT

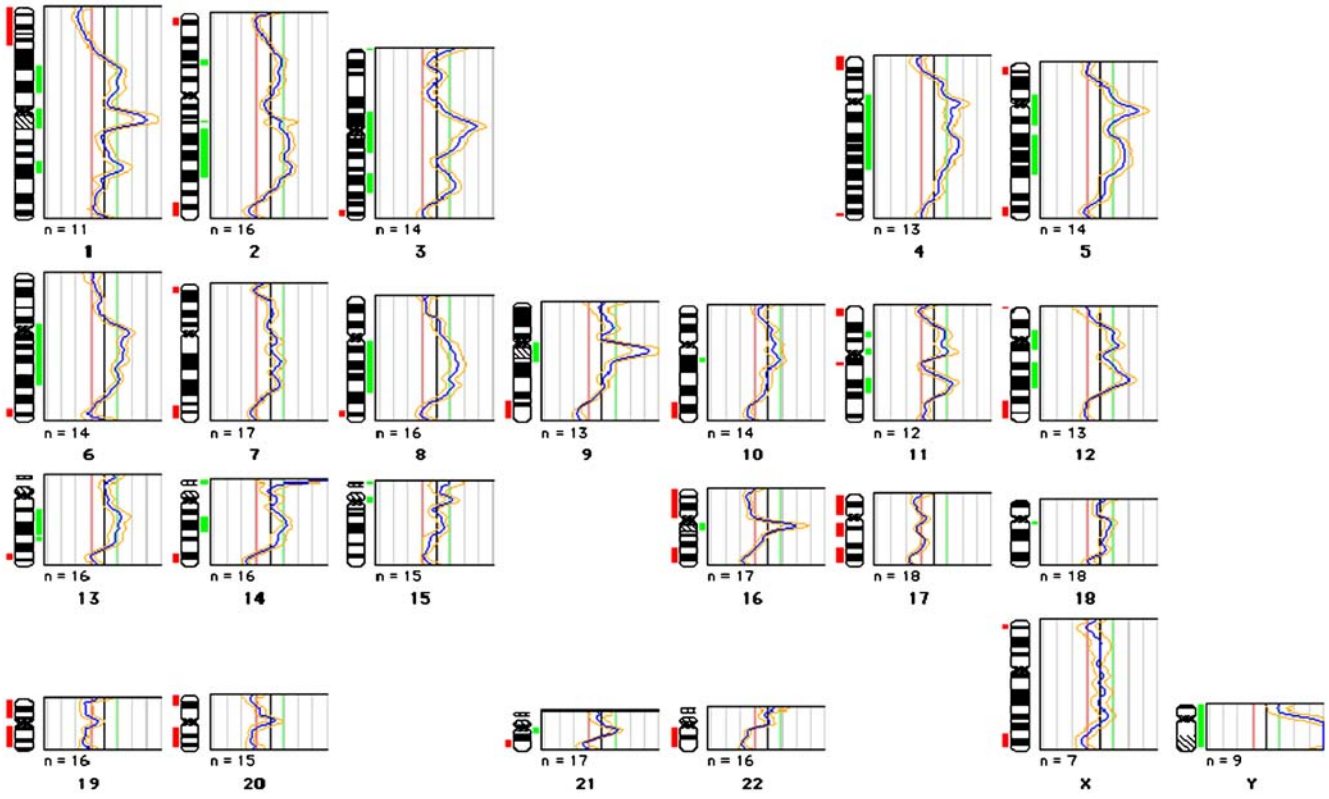

Fig. 4 Overview of chromosomal regions with gains or losses of genetic material in CGT tumours. CGH profile of case showing gains of 1p31-q44, 2q24-q34, 3q24-26, 4p15-q34, 5q14-q23, 6q12-q23, 7q31, 8q13-q21, 12q15-q22, 13q14-q22 and losses on 9q31-q34, 11q23-25, 12q23-q24, 14q31-32, 16, 17, 20q11-q13, 21 and 22. *Bars* to the left (*red*) and right (*green*) of each frame indicate losses and gains, respectively

reported a complex karyotype but without tas or dic aberration [11]. In the present study, we have used CGH to confirm and extend observations regarding the genetic changes associated with GCT. Clonal abnormalities were also detected in the current case and confirmed by FISH analysis. Furthermore, single or complex abnormalities could be observed. We noted changes on 17p that suggest the presence of a secondary aneurismal bone cyst component [15]; however, there was neither histological nor radiological evidence in this case of an aneurismal component.

We have found multiple genomic changes by CGH analysis, including gains on 1p32-q44, 6q12-q25 and 12q14-q22 and losses on 17p. Several reports concerning bone/cartilage-forming lesions or benign mesenchymal tumours have demonstrated associations with changes on 6q and 12q [1, 2]. In addition, gains on 1q, 6q and 12q have been associated with a subgroup of malignant bone fibrous histiocytoma of undifferentiated status, suggesting a possible role of these genomic alterations in GCT [4–6]. Recent molecular studies performed by loss of heterozygosity (LOH) revealed the accumulation of genetic abnormalities in primary and recurrent tumours, without any difference between the two groups [13]. LOH of 17p (close to p53 locus) was also observed in primary GCT and their lung metastases. Consistent with this, we have observed deletion on 17p by both CGH and FISH analysis, suggesting that this genetic abnormality may be associated with the recurrence of the tumour.

For predicting the clinical outcome of GCT, histological classification of the tumour has a limited prognostic value [16]. Recent data suggests that cytogenetic findings could be implicated in the course of the disease [3, 4]. Moreover, chromosomal loss is the most likely molecular event to occur in this disease and may represent a biomarker(s) of tumour progression [13]. Both types of abnormalities were observed in the patient of our study, and therefore, multiple chromosomal changes detected by cytogenetics and CGH could explain the local recurrence of GCT in the soft tissue, which occurred 11 months after removal of the original tumour.

In summary, through the use of the CGH technique, we have described for the first time the presence of chromosomal imbalances in a case of GCT. Further studies will be required to fully evaluate the clinical significance of our findings and to determine the specificity of this genetic profile.

Acknowledgements We would like to thank M. Angeles Hernández and M. Teresa Prieto for their excellent technical assistance and Deborah Burks for the English language.

This work was supported by Grants of Spanish FIS (01/3153).

References

1. Bale SJ, Chakravarti A, Greene MH (1986) Cutaneous malignant melanoma and familial dysplastic nevi: evidence for autosomal dominance and pleiotropy. Am J Hum Genet 38:188–196
2. Baruffi MR, Barbieri-Neto J, Pina-Nieto JM, Suerzut CE, Casartelli C (2002) Distinct norandom patterns of chromosomal deletions in giant-cell lesion of bone. Genet Mol Biol 25:265–270
3. Bridge JA, Mouron BJ, Neff JR, Bhatia PS (1991) Significance of chromosomal abnormalities in a malignant giant cell tumor of bone. Cancer Genet Cytogenet 57:87–92
4. Bridge JA, Neff JR, Bhatia PS, Sanger WG, Murphey MD (1990) Cytogenetic findings and biologic behavior of giant cell tumors of bone. Cancer 65:2697–2703
5. Buddingh EP, Naumann S, Nelson M, Neffa JR, Birch N, Bridge JA (2003) Cytogenetic findings in benign cartilaginous neoplasms. Cancer Genet Cytogenet 141:164–168
6. Chibon F, Mariani O, Derre J, Malinge S, Coindre JM, Guillou L, Lagace R, Aurias A (2002) A subgroup of malignant fibrous histiocytomas is associated with genetic changes similar to those of well-differentiated liposarcomas. Cancer Genet Cytogenet 139:24–29
7. Hernandez JM, Garcia JL, Gutierrez NC, Mollejo M, Martinez-Climent JA, Flores T, Gonzalez MB, Piris MA, San Miguel JF (2001) Novel genomic imbalances in B-cell splenic marginal zone lymphomas revealed by comparative genomic hybridization and cytogenetics. Am J Pathol 158:1843–1850
8. Hernandez JM, Schoenmakers EF, Dal Cin P, Michaux L, Van de Ven WJ, Van den Berghe H (1997) Molecular delineation of the commonly deleted segment in mature B-cell lymphoid neoplasias with deletion of 7q. Genes Chromosomes Cancer 18:147–150
9. Mirra JM (1989) Skelettsystem. In: Remmele W (ed) Pathologie band 5. Spinger, Berlin Heidelberg New York, pp 263–382
10. Mitelman F, Johansson B, Mertens F (2001) Mitelman database of chromosome aberrations in cancer. Internet Communication
11. Montero O, Salle MT, Guevara R, Olivera P, Maldonado V, Melendez-Zajgla J (2003) Cytogenetic analysis of the mononuclear cell component of giant cell tumors of bone. Cancer Genet Cytogenet 146:170–172
12. Qi H, Dal Cin P, Hernandez JM, Garcia JL, Sciot R, Fletcher C, Van Eyken P, De Wever I, Van den Berghe H (1996) Trisomies 8 and 20 in desmoid tumor. Cancer Genet Cytogenet 92:147–149
13. Rao UN, Goodman M, Chung WW, Swalski P, Pal R, Finkelstein S (2005) Molecular analysis of primary and recurrent giant cell tumors of bone. Cancer Genet Cytogenet 158:126–136
14. Schwartz HS, Jenkins RB, Dahl RJ, Dewald GW (1989) Cytogenetic analyses on giant-cell tumors of bone. Clin Ortop 250–260
15. Sciot R, Dorfman H, Brys P, Dal Cin P, De Wever I, Fletcher CD, Jonson K, Mandahl N, Mertens F, Mitelman F, Rosai J, Rydholm A, Samson I, Tallini G, Van den Berghe H, Vanni R, Willen H (2000) Cytogenetic–morphologic correlations in aneurysmal bone cyst, giant cell tumor of bone and combined lesions. A report from the CHAMP study group. Mod Path 13:1206–1210
16. Szendroi M (2004) Giant-cell tumour of bone. J Bone Joint Surg Br 86:5–12
17. Unni KK (1998) Dahlin's bone tumors: general aspect and data on 11087 cases, 5th edn. Lippincott-Raven, Philadelphia
18. Wulling M, Delling G, Kaiser E (2003) The origin of the neoplastic stromal cell in giant cell tumor of bone. Hum Pathol 34:983–993
19. Zheng MH, Siu P, Papadimitriou JM, Wood DJ, Murch AR (1999) Telomeric fusion is a major cytogenetic aberration of giant cell tumors of bone. Pathology 31:373–378

Virchows Arch (2006) 448: 100–104
DOI 10.1007/s00428-005-0072-6

CASE REPORT

Giulia Ottaviani · Anna Maria Lavezzi · Luigi Matturri

Sudden infant death syndrome (SIDS) shortly after hexavalent vaccination: another pathology in suspected SIDS?

Received: 10 May 2005 / Accepted: 23 August 2005 / Published online: 18 October 2005

Abstract Experts from panels of the European Agency for the Evaluation of Medical Products have investigated whether there might be a link between hexavalent vaccines and some cases of deaths that occurred. Participants included pathologists with experience in the field of vaccines and sudden infant death syndrome who conducted autopsies. However, to the best of our knowledge, little, if any, attention was paid to examination of the brainstem and the cardiac conduction systems on serial sections, nor was the possibility of a triggering role of the vaccine in these deaths considered. Herein we report the case of a 3-month-old female infant dying suddenly and unexpectedly shortly after being given a hexavalent vaccination. Examination of the brainstem on serial sections revealed bilateral hypoplasia of the arcuate nucleus. The cardiac conduction system presented persistent fetal dispersion and resorptive degeneration. This case offers a unique insight into the possible role of hexavalent vaccine in triggering a lethal outcome in a vulnerable baby. Any case of sudden unexpected death occurring perinatally and in infancy, especially soon after a vaccination, should always undergo a full necropsy study according to our guidelines.

Keywords Sudden infant death · SIDS · Hexavalent vaccine · Arcuate nucleus hypoplasia · Cardiac conduction system · Prolonged external cardiac massage

Prof. Luigi Matturri is a member of EMEA Pathologists Panel for evaluation of SUD (sudden unexpected death) cases reported for hexavalent vaccines.

G. Ottaviani · A. M. Lavezzi · L. Matturri (✉)
Institute of Pathology, University of Milan,
Via della Commenda 19,
Milan, 20122, Italy
e-mail: luigi.matturri@unimi.it
Tel.: +39-02-50320822
Fax: +39-02-50320823

Introduction

The European Agency for the Evaluation of Medical Products (EMEA) recently reviewed the safety of centrally authorized hexavalent vaccines. During the April 2003 meeting, it was concluded that there was no change in the benefit/risk profile of these products, and, therefore, no changes in the present conditions of use were recommended [4]. The Committee conducted a detailed review, in particular, of five reports of unexplained deaths in children occurring within 24 h of vaccination with a hexavalent vaccine. These reports were received as part of a routine post-marketing safety monitoring (pharmacovigilance) over a period of 2 1/2 years. During this time an estimated 8.7 million doses of vaccines corresponding to the vaccination of some three million children have been used worldwide [4]. Panels of experts investigated whether there might be a link between the vaccines and the deaths observed. Participants included pathologists with experience in the field of vaccines and sudden infant death syndrome (SIDS) who conducted autopsies. The EMEA's conclusions were that the causes of death remained unexplained. SIDS, viral infection, metabolic disorders, allergic reactions or airway obstruction were plausible but were not definitely proven to have been the cause of death [4]. However, to the best of our knowledge, during the mentioned post-mortem investigations, little, if any, attention was paid to examination of the brainstem and the cardiac conduction systems on serial sections, nor was the possibility of a triggering role of the vaccine in the lethal outcome considered.

Case report

A 3-month-old white female infant lost consciousness 1 h after being given a hexavalent vaccination. Emergency help was summoned and arrived quickly. Immediately, resuscitation efforts were attempted by external cardiac massage and assisted ventilation. One hour later the baby reached the hospital, where the resuscitation manoeuvres were

continued, followed by repeated administration of adrenaline and atropine. The baby remained unconscious, with persistent mydriasis, not reacting to light, and was pronounced dead 2 h after arrival at the hospital.

The baby was a firstborn child, born at term in the 42nd week of gestation by Caesarean section, with a birth weight of 3,300 g and an Apgar score of 9–10. The analysis of the placenta after birth was unremarkable. Her parents reported that shortly after birth, the baby had episodes of polypnoea, which was cured spontaneously, and the child continued in apparent good health until the day she received the hexavalent vaccine and then died suddenly. No previous ECG recordings were available. The 35-year-old mother had an unremarkable pregnancy, except for mild hypothyroidism, which required therapy. The baby was bottle-fed. There was no significant family history relevant to the case.

Post-mortem examination was requested with a clinical suspicion of SIDS. The case was analysed at the Institute of Pathology, University of Milan, where more in-depth examinations were performed, including a close study of the cardiac conduction system and the brainstem on serial sections [16, 19–21].

Methods

A complete autopsy was performed according to the autopsy protocol usually followed at our Institute of Pathology in case of sudden death, including careful examination of the cardiac conduction system and of the central and peripheral autonomic nervous structures involved in cardiorespiratory reflexogenesis [16, 19, 21].

The medulla oblongata was divided into three blocks. The first, cranial block, extended from the border between the medulla oblongata and pons up to the upper pole of the olivary nucleus. The second, intermediate block, corresponding to the submedian area of the inferior olivary nucleus, took the obex as the reference point and extended 2–3 mm above and below the obex itself. The third, caudal block, included the lower pole of the inferior olivary nucleus and the lower adjacent area of the medulla oblongata. The first and second blocks were sectioned in a cranial–caudal direction, and the third, in a caudal–cranial direction [13–16]. A fourth block was cut of the brainstem, including the ponto-mesencephalic portion, sectioned in a caudo–rostral direction [14, 16]. From each of these paraffin-embedded blocks, an average of 48 sections were obtained and were alternately stained using haematoxylin–eosin, Bielschowsky, and Klüver-Barrera stains [10, 13]. The pertinent nuclei were outlined, namely, the locus coeruleus, the parabrachial/Kölliker-Fuse complex in the pons; and the arcuate nucleus, the hypoglossus nucleus, the dorsal vagus motor nucleus, the tractus solitarii nucleus, the ambiguus nucleus, the trigeminal tractus and nucleus, and the ventrolateral reticular formation in the medulla oblongata [10, 13–16, 18].

After excluding the presence of gross cardiac malformations, the origin of the coronary arteries was carefully inspected. The heart chambers were regularly examined for pathologic changes in the atria, septa, ventricles, pericardium, endocardium and coronary arteries. Samples of the myocardium and the major coronary arteries were stained with haematoxylin–eosin and trichromic Heidenhain (Azan).

The cardiac conduction system was removed in two blocks: The first included the sino-atrial node and the crista terminalis, while the second contained the atrioventricular node, from the His bundle down to the bifurcation and bundle branches. These two blocks were serially cut at intervals of 40 μm (levels) and stained alternately with haematoxylin–eosin and Azan [14, 21].

Pathological findings

At autopsy, the baby was described as a well-developed, well-nourished white infant, with a body weight of 5,375 g and body length of 60 cm. Macroscopic examination did not reveal malformations, organ malposition or marks of violence. Results of the gross external and internal examinations were normal for the age and sex.

The study of the brainstem on serial sections revealed bilateral hypoplasia of the arcuate nucleus, as confirmed by two-dimensional morphometric reconstruction (Fig. 1). No abnormalities of the other cardiorespiratory medullary nuclei, namely, the dorsal vagus motor, the tractus solitarii, the ambiguus nucleus, the trigeminal nuclei, the ventrolateral reticular formation, locus coeruleus and the parabrachial/Kölliker-Fuse complex, were observed.

The heart weighed 28 g, and the cardiac diameters were the following: longitudinal 4 cm, transverse 4 cm, anteroposterior 3 cm. Gross cardiac examination revealed multiple dyschromic and brownish areas mainly located in the interventricular septum. Histologically, such areas presented wide myofibrillary injury, characterized by anisoinotrpism and contraction band necrosis typical of acute infarction. Myocardial haemorrhage was also detected. The coronaries were normally patent.

Histological examination of the cardiac conduction system showed islands of conduction tissue in the central

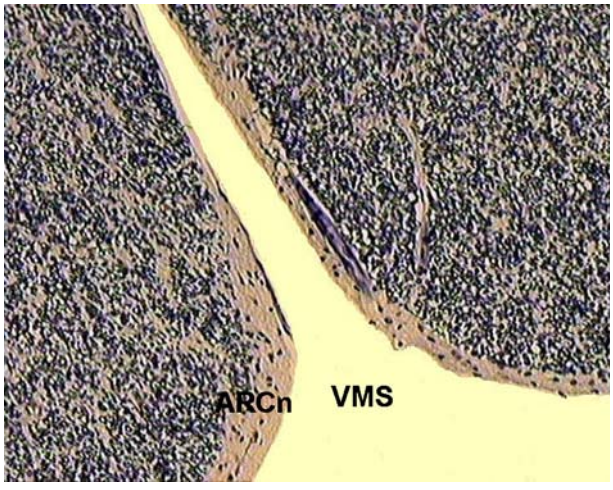

Fig. 1 Bilateral hypoplasia of the arcuate nucleus (ARCn). VMS Ventral medullary surface. Klüver-Barrera stain, ×25

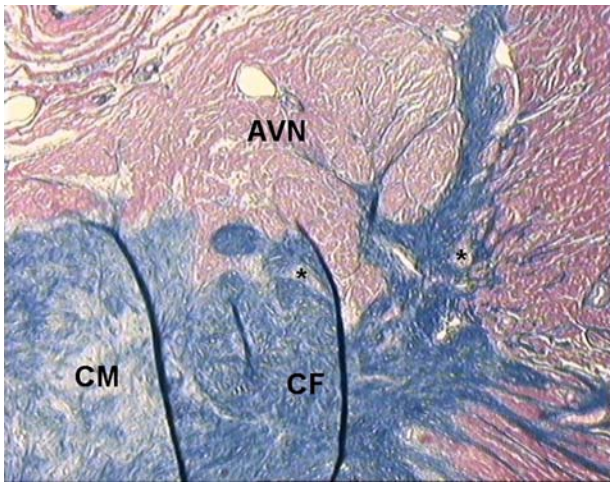

Fig. 2 The atrioventricular node (AVN) presents areas of fetal dispersion and resorptive degeneration. In the central fibrous body (CF), islets of junctional tissue (*) and initial cartilaginous metaplasia (CM) are detectable. Stain, ×25

fibrous body, known as persistent fetal dispersion and areas of resorptive degeneration [7, 21] in the atrioventricular node (Fig. 2).

No other significant pathologic changes were found. The post-mortem gross and microscopic examination corroborated the clinical diagnosis of SIDS.

Discussion

To reduce the number of injections needed to comply with paediatric vaccination requirements, a liquid hexavalent vaccine has been developed for primary booster vaccination of infants against diphtheria, tetanus, pertussis, poliomyelitis, *Haemophilus influenzae* type B and hepatitis B. Seroconversion or seroprotective titres of antibodies against multiple antigens have been achieved in a majority of infants following a primary series of three doses administered at 1- to 2-month intervals from 2 months of age, providing immunity against six important childhood diseases [11].

In the past there was concern that vaccinations might have a causal relationship with SIDS, particularly considering that the peak age for SIDS is 2–4 months, coincidental with the age for vaccinations. Many studies have shown that vaccines are not associated with an increased risk of SIDS [8, 24]. Some studies have even shown a reduced risk of SIDS associated with vaccinations [5]. Despite this, from time to time this controversy is reopened [3].

Recently, Brotherton et al. [2], considering that SIDS peaks at 2 months of age, when vaccination encounters are frequent, estimated the probability of vaccination within the last 24 h for a child who has died of SIDS as 1.3% and as 2.6% in the last 48 h. With the average number of SIDS deaths equal to 130 patients per year in Australia, they estimated that a case of SIDS will occur when vaccination was given in the last 24 h in 1.7 patients per year and within 48 h in 3.5 patients per year.

In 2003, the EMEA, through its scientific Committee for Proprietary Medicinal Products (CPMP), reviewed the safety of the centrally authorized hexavalent vaccines Hexavac and Infarix Hexa [4]. During the March and April 2003 meeting, the CPMP concluded the following:

1. Vaccination offers benefits to the individual child and to the general population.
2. The causes of death of the five children dead within 24 h of vaccination with a hexavalent vaccine remain unexplained, and it is not possible to establish a cause and effect association with hexavalent vaccines [4].

SIDS or crib death is defined as the sudden death of an infant under 1 year of age that remains unexplained after a thorough case investigation including performance of a complete autopsy, examination of the death scene, and a review of the clinical history [25].

The identification of a possible pathological basis of reflexogenic mechanisms in sudden, unexpected infant death necessarily requires examination of the brainstem nuclei and of the cardiac conduction system on serial sections according to the procedures described in the "Methods" section. The neuropathological and cardiovascular study necessary for the objective identification of the nature and location of each lesion, likely morphological substrata of death, requires examination of a large number of patients according to homogeneous and standardized criteria [15, 16]. It was proposed at the 7th International Conference on SIDS [12] that the current definition of SIDS as "the sudden death of an infant under one year of age which remains unexplained after a thorough case investigation, including the performance of a complete autopsy, examination of the death scene, and review of the clinical history" be modified to include the words "a complete autopsy with an in-depth histopathologic analysis of the cardiorespiratory innervation and specialized myocardium, performed only by an experienced, reliable pathologist".

More recently, Krous et al. [9] underlined that since the definition of SIDS originally appeared, an enormous amount of additional information has emerged, justifying the additional refinement of the definition of SIDS to incorporate epidemiologic features, risk factors, pathologic features, and ancillary test findings and that the definition of SIDS will be modified in the future to accommodate new understanding of sudden infant death.

Taken together, the abnormalities of the autonomous nervous and cardiac conduction systems described in the present case, as well as the review of the clinical history, represent a plausible basis for the diagnosis of SIDS [6, 13, 15].

Abnormalities in the morphological findings of the brainstem (Fig. 1) and cardiac conduction system (Fig. 2) similar to those detected in this case have already been proposed in infants dying suddenly and unexpectedly as possible morphological substrates for sudden reflexogenic infant death [6, 7, 13, 15, 16, 19, 21].

In this case, histological examination of the brainstem on serial sections revealed bilateral hypoplasia of the arcuate nucleus. In term fetuses, newborns and infants dying suddenly and unexpectedly, we have recently demonstrated a variety of structural defects of the arcuate nucleus, ranging from neuronal immaturity in a well-shaped structure to total agenesis [6, 13, 15, 16].

On one hand, the unexpected death of this vulnerable baby (infant with bilateral hypoplasia of the arcuate nucleus) could have been triggered by the hexavalent vaccination. This case is consistent with the triple-risk model of SIDS, a hypothesis comprising an underlying biological vulnerability to exogenous stressors and some triggering factors in a critical developmental period [6]. On the other hand, this case could be classified as a SIDS "gray zone" or borderline case, defined as a case in which it is difficult to establish whether the pathological findings are sufficiently severe to have caused the death. Recently, our examination of the brainstem of 103 patients of SIDS disclosed five SIDS gray zone cases in which only our further investigations on serial sections successfully identified anatomo-pathological findings likely representing the morphological substrates for a sudden reflexogenic death [20, 23].

Regarding the infarct-like myocardial lesions detected in this patient, two of the present authors have already pointed out, among the disadvantages of external cardiac massage, the not infrequent occurrence of damage to the myocardium and the cardiac conduction system [17, 22]. The compression of the heart between the spine and the sternum exerted by this maneuver causes a direct vertical pressure perpendicular to both the atrial and ventricular septa [17, 22]. In this case, the overinsistent external cardiac massage is responsible for the findings of the wide myofibrillary injury in the interventricular septum, as is typically seen in the contraction band degeneration of hyperacute infarction and as in many examples of myocardial biopsy [1].

In conclusion, the careful examination of the heart, cardiac conduction system and brainstem on serial sections was crucial to classify this case as SIDS and to identify the possible morphological substrates responsible for this lethal reflexogenic sudden death, that is, arcuate nucleus hypoplasia in the brainstem and persistent fetal dispersion and resorptive degeneration in the cardiac conduction system. All cases of sudden unexpected death occurring in infancy and perinatal age, especially soon after a vaccination, should always undergo an investigated necropsy study, according to our guidelines [14].

Acknowledgements The authors wish to express their gratitude to Mrs. Graziella Alfonsi for skillful technical cooperation.

This study was supported by the "Lino Rossi" Research Center for the study and prevention of unexpected perinatal death and sudden infant death syndrome (SIDS) funding (Rectorial Decree no. 225678 of 23/04/04) and by the Ministry of Foreign Affairs (joint project of particular relevance no. 269/P/0085087, "Anatomopathologic and genetic study of the unexplained perinatal death and SIDS"), Italy.

References

1. Atkinson JB, Virmani R (1991) The endomyocardial biopsy: techniques, indications and limitations. In: Virmani R, Atkinson JB, Fenoglio J (eds) Cardiovascular pathology. Saunders, Philadelphia, p 210
2. Brotherton JM, Hull BP, Hayen A, Gidding HF, Burgess MA (2005) Probability of coincident vaccination in the 24 or 48 hours preceding sudden infant death syndrome death in Australia. Pediatrics 15:e643–e646
3. National Health Federation (2001) Crib death (SIDS): are vaccinations the cause? National Health Federation, Monrovia, CA
4. EMEA (2003) EMEA reviews hexavalent vaccines: Hexavac and Infarnix Hexa. EMEA public statement, EMEA/8519/03, London, 28 April 2003. http://www.emea.eu.int
5. Essery SD, Raza MW, Zorgani A, MacKenzie DA, James VS, Weir DM et al (1999) The protective effect of immunization against diphtheria, pertussis and tetanus (DPT) in relation to sudden infant death syndrome. FEMS Immunol Med Microbiol 25:183–192
6. Filiano JJ, Kinney HC (1994) A perspective on neuropathologic findings in victims of sudden infant death syndrome: the triple risk model. Biol Neonate 65:194–197
7. James TN (1968) Sudden death in babies: new observations in the heart. Am J Cardiol 22:479–506
8. Jonville-Bera AP, Autret-Leca E, Barbeillon F, Paris-Liado J (2001) Sudden unexpected death in infants under 3 months of age and vaccination status—a case control study. J Clin Pharmacol 51:271–276
9. Krous HF, Beckwith JB, Byard RW, Rognum TO, Bajanowski T, Corey T, Cutz E, Hanzlick R, Keens TG, Mitchell EA (2004) Sudden infant death syndrome and unclassified sudden infant deaths: a definitional and diagnostic approach. Pediatrics 114: 234–238
10. Lavezzi AM, Ottaviani G, Rossi L, Matturri L (2004) Hypoplasia of the parabrachial/Kölliker-Fuse complex in perinatal death. Biol Neonate 86:92–97
11. Mallet E, Belohradsky BH, Lagos R, Gothefors L, Camier P, Carriere JP et al (2004) A liquid hexavalent combined vaccine against diphtheria, tetanus, pertussis, poliomyelitis, *Haemophilus influenzae* type B and hepatitis B: review of immunogenicity and safety. Vaccine 22:1343–1357
12. Matturri L, Lavezzi AM, Rossi L (2002) Proposal to modify the definition of SIDS, with regard to the post-mortem exam. In: Proceedings of the 7th International Conference on SIDS, Florence, 31 August 31–4 September 2002, p 103
13. Matturri L, Ottaviani G, Alfonsi G, Crippa M, Rossi L, Lavezzi AM (2004) Study of the brainstem, particularly the arcuate nucleus, in sudden infant death syndrome (SIDS) and sudden intrauterine unexplained death (SIUD). Am J Forensic Med Pathol 25:44–48
14. Matturri L, Ottaviani G, Alfonsi G, Rossi L, Lavezzi AM (2005) Guidelines in pathological and forensic-medical diagnostics of sudden unexpected infant (SIDS) and fetal death. Lombardy Region Project for Reduction of the Risk for SIDS and/or Sudden Fetal Death. http://users.unimi.it/~pathol/sids/linee_guida_e.html. Accessed 1 June 2005
15. Matturri L, Ottaviani G, Benedetti G, Agosta E, Lavezzi AM (2005) Unexpected perinatal death and sudden infant death syndrome (SIDS): anatomo-pathological and legal aspects. Am J Forensic Med Pathol 26:155–160
16. Matturri L, Ottaviani G, Lavezzi AM (2005) Techniques and criteria in pathologic and forensic-medical diagnostics of sudden unexpected infant and perinatal death. Am J Clin Pathol 124:259–268
17. Matturri L, Ottaviani G, Rossi L (2003) External cardiac massage in infants. Intensive Care Med 29:1199–1200
18. Olszewski J, Baxter D (1982) Cytoarchitecture of the human brain stem. Karger, Basel

19. Ottaviani G, Lavezzi AM, Rossi L, Matturri L (2004) Sudden unexpected death of a term fetus in an anticardiolipin positive mother. Am J Perinatol 21:79–83
20. Ottaviani G, Matturri L, Bruni B, Lavezzi AM (2005) Sudden infant death syndrome "gray zone" disclosed only by a study of the brain stem on serial sections. J Perinat Med 33:165–169
21. Ottaviani G, Matturri L, Rossi L, James TN (2003) Crib death: further support for the concept of fatal cardiac electrical instability as the final common pathway. Int J Cardiol 92:17–26
22. Ottaviani G, Rossi L, Matturri L (2005) Myocardial injury attributable to external cardiac massage in infants. Cardiology 1:25–29
23. Rossi L (1999) Bulbo-spinal pathology in neurocardiac sudden death of adults: a prognostic approach to a neglected problem. Int J Legal Med 112:83–90
24. Silvers LE, Ellenberg SS, Wise RP, Varricchio FE, Mootrey GT, Salive ME (2001) The epidemiology of fatalities reported to the vaccine adverse event reporting system 1990–1997. Pharmacoepidemiol Drug Saf 10:279–285
25. Willinger M, James LS, Catz C (1991) Defining the sudden infant death syndrome (SIDS): deliberations of an expert panel convened by the National Institute of Child Health Development. Pediatric Pathol 11:677–684

Virchows Arch (2006) 448: 105–106
DOI 10.1007/s00428-005-0088-y

LETTER TO THE EDITOR

Adjé Abbey-Toby · Marie-Pierre Vullierme · Alain Sauvanet · Philippe Ruszniewski · Pierre Bedossa · Anne Couvelard

A clear cell malignant gastrinoma of the pancreas with cytoplasmic accumulation of lipid droplets

Received: 1 July 2005 / Accepted: 31 August 2005 / Published online: 28 September 2005

Sir:
Well-differentiated endocrine tumours of the pancreas are usually diagnosed without difficulty by the presence of small eosinophilic cells with a characteristic disposition in cordons, solid nests, tubules and acini separated by a highly vascularised stroma. Clear cell endocrine tumours are rare in the pancreas in the absence of von Hippel–Lindau (VHL) disease, and changes resulting in clear cell appearance are poorly described. We report here the case of a sporadic, malignant clear cell gastrinoma of the pancreas with multiple hepatic metastasis and describe its specific imaging and histological appearances.

A 48-year-old woman with a Zollinger–Ellison syndrome, evidenced by epigastric pain, diarrhea, weight loss and presence of multiple gastroduodenal ulcers on endoscopy, was admitted to Beaujon Hospital. Laboratory tests revealed elevated levels of circulating chromogranin (5,933 ng/ml; N<100) and gastrin (319 pg/ml; N<80). The patient presented no personal or familial history of VHL disease or multiple endocrine neoplasia type 1 (MEN1). Ultrasound and computer tomography (CT) scan detected a 35-mm caudal mass of the pancreas associated with 18 liver metastases distributed in all lobes, measuring 3 to 25 mm. These lesions were hypoattenuated at CT scan, comprising enhanced CT (Fig. 1a,b). A left pancreatectomy associated with surgical ablation of the eight nodules of the left liver was initially performed, associated with a ligature of the right portal vein. Three months later, a right hepatic lobectomy, which took away ten other nodules, was done.

Grossly, the pancreatic tumour measured 35 mm, was multilobulated and firm. In the liver, the 18 nodules that measured 2 to 23 mm were well delimited. On cross-section, the nodules were yellow-tan. Microscopic examination revealed a lobular disposition of tumour cells presenting a large microvacuolated cytoplasm and well-defined cell borders. The finely vacuolated cytoplasms were not highlighted by Alcian blue and periodic acid Schiff (PAS) stains. The nuclei were round, with moderate atypia, and contained a small nucleoli (Fig. 1c). The stroma was often fibrotic. Mitoses were calculated as two per ten high-power fields; the index of proliferation ki67 (MIB-1 antibody, DAKO) was calculated at 3%. Necrosis and vascular invasion were absent. No lymph node metastasis was detected. Immunohistochemistry confirmed that most tumour cells expressed chromogranin (Fig. 1d), synaptophysin and gastrin (Fig. 1e). An examination of the oil-red-O staining showed that tumour cells contained numerous lipid droplets (Fig. 1f). Five years after the operation, there was no evidence of disease recurrence. The CT scan and levels of circulating chromogranin and gastrin were normal.

The morphological appearance of this endocrine tumour consisting in clear microvacuolated cells is highly distinctive. Endocrine tumour with clear cells has been rarely reported in the thyroid [1], in the adrenocortical gland, in the stomach, in the lung and in the gall bladder. In the pancreas, clear cell endocrine tumours are mostly described

A. Abbey-Toby
Department of Pathology, Bichat Hospital,
Paris, France

M.-P. Vullierme
Department of Radiology, Beaujon Hospital,
Clichy, France

A. Sauvanet
Department of Surgery, Beaujon Hospital,
Clichy, France

P. Ruszniewski
Department of Gastroenterology, Beaujon Hospital,
Clichy, France

P. Bedossa · A. Couvelard
Department of Pathology, Beaujon Hospital,
Clichy, France

A. Couvelard (✉)
Service d'Anatomie Pathologique, Hôpital Beaujon,
100 Boulevard du Général Leclerc,
92110 Clichy, France
e-mail: anne.couvelard@bjn.aphp.fr
Tel.: +33-1-40875462
Fax: +33-1-40870077

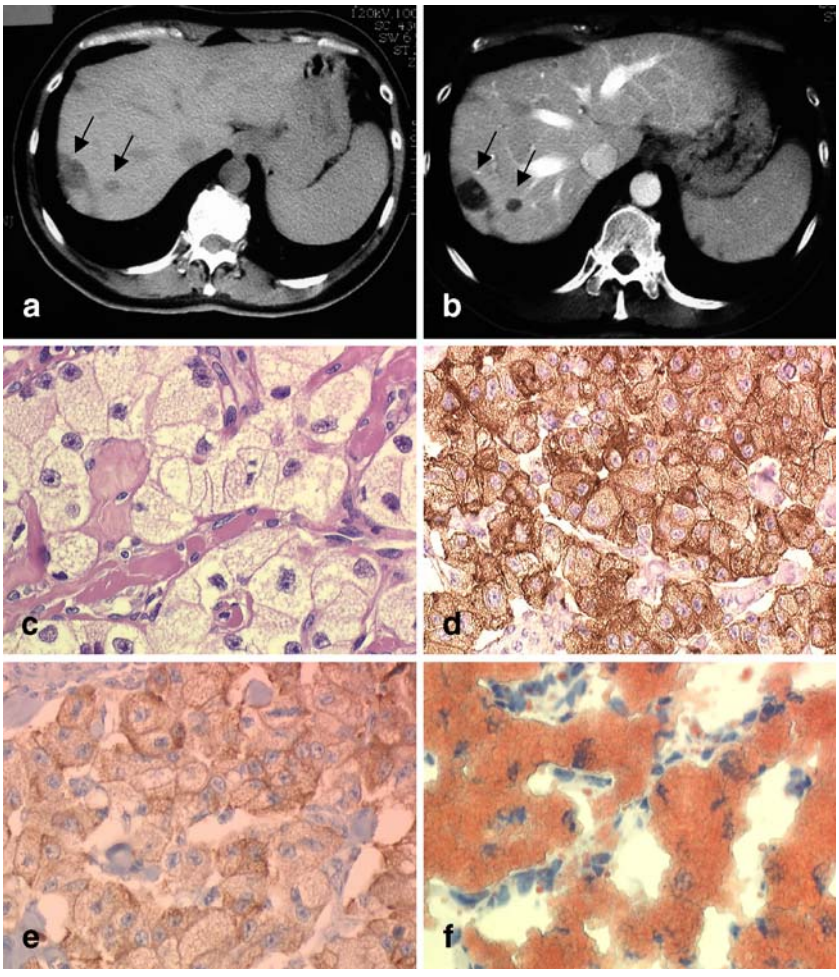

Fig. 1 **a** Unenhanced computer tomography (CT) scan of the liver: two strongly hypoattenuated lesions (*arrows*), the biggest suggesting steatosis component. **b** Enhanced CT scan of the liver at the same level of that in **a**. The two lesions are not enhanced. **c** High-power view of microvacuolated clear cells disposed in lobules. The vacuoles are not stained by periodic acid Schiff (original magnification ×400). **d** Tumour cells strongly express chromogranin (immunoperoxidase; original magnification ×200). **e** Most cells demonstrate reactivity for gastrin (immunoperoxidase; original magnification ×200). **f** The oil-red-O staining confirms the presence of numerous lipid droplets in the cytoplasm of most tumour cells (×300)

in VHL disease [6]. Only four cases of clear cell endocrine tumour have been described in pancreas without a VHL disease [2–5]. These four tumours were non-functional and were composed of cells containing lipid droplets associated with glycogen in one case [2]. One of these cases was described in a man with a history of MEN1 [5]. The present case is the first clear cell gastrinoma to be reported.

A clear cytoplasm can be the result of accumulation of glycogen, mucin or lipid. It can also be due to the swelling of mitochondria [1]. In our case, there was no evidence of accumulation of glycogen or mucin, as shown by the negativity of the PAS and Alcian blue colorations. However, tumour cells contained numerous lipid droplets highlighted by the oil-red-O staining. Interestingly, the hypoattenuated aspect at CT scan, which is unusual for endocrine tumours, was in accordance with the microscopic findings.

In conclusion, we report the first case of clear cell gastrinoma of the pancreas not associated with VHL disease, due to an accumulation of lipid droplets. Clear cell tumours are a diagnostic challenge for pathologists, and immunohistochemical detection of endocrine markers is essential to confirm the diagnosis. This tumour is important for the recognition and differentiation of mucinous carcinomas and metastases of renal carcinoma, especially in the liver. A clear cell "sugar" tumour, which can involve the pancreas, should also be eliminated.

References

1. Dickersin GR, Vickery AL Jr, Smith SB (1980) Papillary carcinoma of the thyroid, oxyphil cell type, "clear cell" variant: a light- and electron-microscopic study. Am J Surg Pathol 4 (5):501–509
2. Guarda LA, Silva EG, Ordonnez NG, Mackay B, Ibanez ML (1983) Clear cell islet cell tumor. Am J Clin Pathol 79:512–517
3. Namiq AL, Delcore R, Damjanov I (2003) Pathologic quiz case: clear cell tumor of the pancreas associated with hypercalcemia. Arch Pathol Lab Med 127(2):241–242
4. Nunobe S, Fukushima N, Yachida S, Shimada K, Kosuge T, Sakamoto M (2003) Clear cell endocrine tumor of the pancreas which is not associated with von Hippel–Lindau disease: report of a case. Surg Today 33(6):470–474
5. Ordonnez NG, Silva EG (1997) Islet cell tumor with vacuolated lipid-rich cytoplasm : a new histological variant of islet cell tumor. Histopathology 31:157–160
6. Terris B, Hammel P (2000) Pancreatic lesions in von Hippel–Lindau disease. Ann Pathol 20(2):124–129

Virchows Arch (2006) 448: 107–109
DOI 10.1007/s00428-005-0139-4

ACKNOWLEDGEMENT TO REFEREES

The Managing Editors are grateful to the following colleagues for generously giving their time in careful evaluation of the manuscript submitted to Virchows Archiv in 2005:

Adsay, N. Volkan, Detroit (USA)
Allory, Yves, Créteil (F)
Alves, Venancio, Sao Paulo (BR)
Amann, Kerstin, Erlangen (D)
Amann-Vesti, Beatrice, Zürich (CH)
Andea, Aleodor A., New York (USA)
Antonescu, Cristina, New York (USA)
Atkinson, Mike, München (D)

Bannasch, Peter, Heidelberg (D)
Barbareschi, Mattia, Trento (I)
Baretton, Gustavo, Dresden (D)
Barreto-Chaves, Maria Luiza, São Paulo (BR)
Baud, Laurent, Paris (F)
Becker, Karl-Friedrich, München (D)
Bertoni, Franco, Bologna (I)
Bevilacqua, Generoso, PISA (I)
Bohle, Rainer M., Gießen (D)
Bordi, Cesare, Parma (I)
Boss, Jochanan H., Haifa (IL)
Brabletz, Thomas, Erlangen (D)
Bralet, Marie-Pierre, Villejuif Cedex (F)
Brambilla, Elisabeth, Grenoble (F)
Bratthauer, Gary L., Washington DC (USA)
Brousset, Pierre, Toulouse (F)
Bruneval, Patrick, Paris. (F)
Bushara, Khalafalla O., Minneapolis (USA)
Büttner, Reinhard, Bonn (D)

Caduff, Rosmarie, Zurich (CH)
Capella, Carlo, Varese (I)
Carneiro, Maria Fatima, Porto (P)
Cassoni, Paola, Torino (I)
Cathomas, Gieri, Liestal (CH)
Cavazza, Alberto, Modena (I)
Cazals Hatem, Dominique, Clichy (F)
Chan, John K., Hong Kong (RC)
Chilosi, Marco, Verona (I)
Chu, Pao-Hsien, Taipei (D)
Clement, Sophie, Genf (CH)
Cleutjens, Jacques, Maastricht (NL)
Cohen, Arthur H., Los Angeles (USA)
Collan, Yrjö, Turku (FIN)
Collina, Guido, Bologna (I)
Couvelard, Anne, Clichy (F)
Cserni, Gábor, Kecskemét (H)
Cunha, Isabela Werneck, São Paulo (BR)
Cuvelier, Claude, Ghent (B)

Dahlstrom, Jane, Woden (AUS)
Dal Cin, Paola, Boston (USA)
Damiani, Stefania, Bologna (I)
Damjanov, Ivan, Kansas City (USA)
David, Leonor, Porto (P)
De Krijger, Ronald, Rotterdam (NL)
De Mascarel, Antoine, Pessac (F)
De Wolf-Peeters, Christiane, Leuven (B)
Deckert, Martina, Köln (D)
Dei Tos, Angelo P., Treviso (I)
DeLellis, Ronald A., Providence (USA)
Denk, Helmut, Graz (AUS)
Deshpande, Jaya, Mumbai (IND)
Desmouliere, Alexis, Bordeaux (F)
Diebold, Joachim, München (D)
Dienes, Hans Peter, Köln (D)
Dietmaier, Wolfgang, Regensburg (D)
Dizbay Sak, Serpil, Ankara (TR)
Doglioni, Claudio, Milano (I)
Drut, Ricardo, La Plata (RA)

Ebert, Andreas D., Berlin (D)
Eble, John N., Indianapolis (USA)
Ectors, Nadine, Leuven (B)
Eisenmenger, H., München (D)
Ensari, Arzu, Ankara (TR)

Facchetti, Fabio, Brescia (I)
Fadare, Oluwole, New Haven (USA)
Falconieri, Giovanni, Udine (I)
Fend, Falko, München (D)
Ferlicot, Sophie, Le Kremlin Bicètre (F)
Ferrero, Simone, Genoa (I)
Fisher, Cyril, London (GB)
Fléjou, Jean-Francois, Paris (F)
Fletcher, Christopher D.M., Boston (USA)
Folpe, A.L., Atlanta (USA)
Fornes, Paul, Paris (F)
Foschini, Maria Pia, Bologna (I)
Franchi, Alessandro, Firenze (I)
Fromenty, Brbard, Paris (F)

Gabbiani, Giulio, Genf (CH)
Galateau, Françoise, Caen (F)
Gale, Nina, Ljubljana (SLO)
Gaulard, Philippe, Creteil (F)
Genelhu, Marisa, Governador Valadares (BR)
Genta, Robert, Genf (CH)
Giordano, Giovanna, Parma (I)
Gobe, Glenda, Brisbane (A)
Godfraind, Catherine EE, Bruxelles (B)
Goto, Akiteru, Tokyo (J)
Gray, Françoise, Paris (F)
Greten, Tim, Hannover (D)
Grigioni, WF, Bologna (I)
Guski, Hans, Berlin (D)
Gütgemann, Ines, Bonn (D)

Hadchouel, Michelle, Kremlin-Bicêtre (F)
Harada, Oi, Matsumoto (J)
Hartmann, Arndt, Regensburg (D)
Hattori, Takenori, Shija (J)
Hattori, Hideo, Nagoya (J)
Hauptmann, Steffen, Halle a.d. Saale (D)
Hayes, Malcolm M., Vancouver (CDN)
Heinzmann, U., München (D)

Helpap, Burkhard, Singen (D)
Herbst, Hermann, Münster (D)
Hirose, Takanori, Moroyama (J)
Höfler, Gerald, Graz (A)
Hofman, Paul, Nice (F)
Hofstädter, Ferdinand, Regensburg (D)
Hogendoorn, P.C., Leiden (NL)
Horn, Lars-Christian, Leipzig (D)
Horny, Hans-Peter, Lübeck (D)
Hubscher, Stephan G., Birmingham (GB)
Hufnagl, Peter, Berlin (D)
Hung, Noelyn Anne, Dunedin (NZ)
Hytiroglou, Prodromos, Thessaloniki (GR)

Ichihara, Shu, Nagoya (J)

Jass, Jeremy, Montreal (CDN)
Jinno, Yoshio, Osaka (J)
Junker, Klaus, Bochum (D)

Kadar, Anna, Budapest (H)
Kalthoff, Holger, Kiel (D)
Kanitakis, Jean, Lyon (F)
Kankofer, Marta, Lublin (P)
Kasprzak, Aldina Anna, Poznan (P)
Kataoka, Horiaki, Kiyotake (J)
Keller, Gisela, München (D)
Kerjaschki, Dontscho, Wien (A)
Kern, Izidor, Golnik (SLO)
Kikuchi, Masahiro, Fukuoka (J)
Kim, Chong Jai, Seoul (ROK)
Kirchner, Thomas, Erlangen (D)
Klimstra, David, New York (USA)
Knisely, Alex, London (GB)
Knüchel-Clarke, Ruth, Aachen (D)
Knuuttila, Aija H., Helsinki (FIN)
Ko, Young H., Seoul (ROK)
Koelble, Konrad, Berlin (D)
Koerner, Frederick, Boston (USA)
Koike, Morio, Tokyo (J)
Kojiro, Masamichi, Kurume-shi (J)
Komminoth, Paul, Baden (CH)
Koop, Klaas, Leiden (NL)
Kreipe, Hans, Hannover (D)
Kremer, Markus, München (D)
Kristiansen, Glen, Berlin (D)
Kujawa, Marek, Warsaw (P)
Kuniyasu, Hiroki, Kashihara (J)
Kusafuka, Kimihide, Shizuoka (J)

La Rosa, Stefano, Varese (I)
Lacroix, Catherine, Le Kremlin Bicêtre (F)
Lakhani, Sunil R., Brisbane (AUS)
Lamovec, Janez, Ljubljana (SLO)
Langner, Cord, Graz (A)
Lax, Sigurd F., Graz (A)
Lazure, Thierry, Le Kremlin-Bicetre (F)
Lebail, Brigitte, Bordeaux (F)
Lebeau, Annette, München (D)
Lehr, Hans-Anton, Lausanne (CH)
Lehto, Veli-Pekka, Helsinki (FIN)
Leithner, Andreas, Graz (A)
Leoncini, Lorenzo, Siena (I)
Leong, Anthony S-Y, Newcastle (AUS)
Llombart-Bosch, Antonio, Valencia (E)
Löhr, J. - Matthias, Mannheim (D)
Longnecker, Daniel S., Lebanon (USA)
Löning, Thomas, Hamburg (D)
Looijenga, Leendert, Rotterdam (NL)
Lüttges, Jutta E., Saarbrücken (D)

Madigan, Michele, Sydney (AUS)
Magro, Gaetano, Catania (I)
Maheshwari, Amita, Mumbai (IND)
Maiorano, Eugenio, Bari (I)
Maode, Lai, Zhejiang (RC)
Martignoni, Guido, Verona (I)
Matias-Guiu, Xavier, Lleida (E)
Matturri, Luigi, Milano (I)
Meagher-Villemure, Kathleen, Lausanne (CH)
Menger, Michael D., Homburg/Saar (D)
Mentzel, Thomas, Friedrichshafen (D)
Merlio, Jean Philippe, Bordeaux (F)
Michal, Michal, Pilsen (CZ)
Miettinen, Markku, Washington (USA)
Mikuz, Gregor, Innsbruck (A)
Milde-Langosch, Karin, Hamburg (D)
Moch, Holger, Zürich (CH)
Molina, Thierry Jo, Paris (F)
Moll, Roland, Marburg (D)
Möller, Peter, Ulm (D)
Montironi, Rodolfo, Torrette di Ancona (I)
Moreau, Richard, Clichy (F)
Mortensen, Elin, Tromsø (N)
Mosquera, Jesus A., Maracaibo (YV)
Mukai, Kiyoshi, Tokyo (J)
Müller, Klaus-Michael, Bochum (D)
Müller-Hermelink, H.K., Würzburg (D)
Murer, Bruno, Mestre-Venezia (I)

Nabeshima, Kazuki, Fukuoka (J)
Nesi, Gabriella, Florence (I)
Niedobitek, Gerald, Erlangen (D)
Niesporek, Silvia, Berlin (D)
Nikkels, Peter G.J., Utrecht (NL)
Nishida, Naoki, Akita (J)
Nishioka, Hiroshi, Tokyo (J)
Noel, Laure-Helene, Paris (F)
Nogales, Francisco F., Granada (E)

Oberhuber, Georg, Überlingen (D)
Offerhaus, G.J.A., Amsterdam (NL)
Okabe, Hidetoshi, Otsu (J)
Oliveira, Maria José, Porto (P)
Ordonez, Nelson G., Houston (USA)
Ott, German, Würzburg (D)
Otterbach, Friedrich, Essen (D)
Oyama, Tetsunari, Gunma,
Ozturk, Evrim E.O., Ankara (TR)

Pakasa, Nestor, Le Puy en Velay (F)
Papotti, Mauro, Orbassano (Torino) (I)
Park, Young Nyun, Seoul (ROK)
Parwaresch, Reza, Kiel (D)
Paulus, Werner, Münster (D)
Peh, Suat-Cheng, Kuala Lumpur (MAL)
Pei, Hui, New Haven (USA)
Peres, Luiz Cesar, Ribeirao Preto (BR)
Perez-Ordonez, Bayardo, Toronto (CDN)
Perren, Aurel, Zürich (CH)
Petersen, Iver, Berlin (D)
Pfeifer, Lutz, Berlin (D)
Piaggesi, A, Pisa (I)
Piard, Françoise, Dijon (F)
Pileri, Stefano A., Bologna (I)
Pittenger, G, Norfolk (USA)
Popper, Helmut H., Graz (A)
Povysil, Ctibor, Prag (CZ)
Prat, Jaime, Barcelona (E)

Quaresma, Juarez AS, Belem (BR)
Quintanilla-Fend, Leticia, München (D)

Radford-Smith, Graham, Brisbane (AUS)
Ramos, Simone, Ribeirão Preto (BR)
Raphael, Martine, Paris (F)
Reifenberger, Guido, Düsseldorf (D)
Reis, Celso A., Porto (P)
Ribalta Farres, Teresa, Barcelona (E)
Ribeiro-Silva, Alfredo, Ribeirão Preto (BR)
Rindi, Guido, Parma (I)
Riva, Cristina, Varese (I)
Rodriguez-Justo, Manuel, London (GB)
Rosai, Juan, Milano (I)
Roskams, Tania, Leuven (B)

Rossi, Marcos A., Ribeirão Preto (BR)
Rudzki, Zbigniew, Krakow (PL)
Ruediger, Thomas, Würzburg (D)
Rüschoff, Josef, Kassel (D)
Rugge, Massimo, Padua (I)
Ruiter, Dirk J., Nijmegen (NL)

Sabah, Muna, Dublin (IRL)
Sabourin, Jean-Christophe Benoit, Villejuif (F)
Saeger, Wolfgang, Hamburg (D)
Sáez Artacho, Amparo, Sabadell (E)
Sandhyamani, Samavedam, Trivandrum (IND)
Santucci, Marco, Florenz (I)
Sapino, Anna, Torino (I)
Sarbia, Mario, München (D)
Sasaki, M., Kanazawa (J)
Scarpa, Aldo, Verona (I)
Schaff, Zsuzsa, Budapest (H)
Schlegel, Jürgen, München (D)
Schmid, Kurt, Essen (D)
Schmid, Roland M., München (D)
Schmitt-Gräff, Annette, Freiburg (D)
Schnalke, Thomas, Berlin (D)
Sciot, Raf, Leuven (B)
Scoazec, Jean-Yves, Lyon (F)
Seelentag, Walter, Lausanne (CH)
Sessa, Fausto, Varese (I)
Sesterhenn, Isabel, Wahington DC (USA)
Sheaff, Michael T., London (GB)
Shia, Jinru, New York (USA)
Sibony, Mathilde, Paris (F)
Sidoni, Angelo, Perugia (I)
Sivridis, Efthimios, Alexandroupolis (GR)
Skalova, Alena, Plzen (CZ)
Slootweg, P.J., Nijmegen (NL)
Soares, Paula, Porto (P)
Solcia, Enrico, Pavia (I)
Songqing, Fan, Changsha (RC)
Sotlar, Karl, Tübingen (D)
Spatz, Alain, Villejuif (F)
Stamenkovic, Ivan, Lausanne (CH)
Stanta, Giorgio, Trieste (I)
Stolte, Manfred, Bayreuth (D)
Suriano, Gianpaolo, Porto (P)
Susani, Martin, Wien (A)
Swerts, K, Ghent (B)
Szymas, Janusz, Poznan (PL)

Tagil, Magnus, Lund (S)
Tahara, Eiichi, Hiroshima (J)
Tallini, Giovanni, Bologna (I)
Tannapfel, Andrea, Leipzig (D)
Tavassoli, Fattaneh, New Haven (USA)
Terracciano, Luigi, Basel (CH)
Tham, E, Stockholm (S)
Thiene, Gaetano, Padua (I)
Timens, Wim, Groningen (NL)
Tot, Tibor, Falun (S)
Tran van Nhieu, Jeanne, Creteil (F)
Tsukamoto, Tetsuya, Nagoya (J)
Tyynella-Vesterinen, Jaana, Helsinki (FIN)

Uro-Coste, Emmanuelle, Toulouse (F)

Vainer, Ben, Copenhagen (DK)
Van den Oord, Joost J., Leuven (B)
Van der Waal, I., Amsterdam (NL)
Van Krieken, H.J.M., HB Nijmegen (NL)
Van Marck, Eric A.E., Antwerpen (Wilrijk) (B)
Viale, Giuseppe, Milan (I)
Vignaud, Jean-Michel, Nancy (F)
Villanacci, Vincenzo, Brescia (I)
Von Herbay, Axel, Harrow (GB)

Walch, Axel Karl, Neuherberg (D)
Wardelmann, Eva, Bonn (D)
Wassef, Michel, Paris (F)
Weichert, Wilko, Berlin (D)
Weinhäusel, Andreas, Seibersdorf (A)
Weirich, Gregor, München (D)
Wells, M., Sheffiled (GB)
Wendum, Dominique, Paris (F)
Werner, Martin, Freiburg (D)
Wick, Mark Robert, Charlottesville (USA)
Wittekind, Christian, Leipzig (D)
Woenckhaus, Christian, Ulm/Donau (D)
Wohlschlaeger, Jeremias, Essen (D)

Yagihashi, Soroku, Hirosaki (J)
Yan, Pu, Lausanne (CH)
Yasui, Wataru, Hiroshima (J)
Yu, DS, Taipei (RC)

Zaladek Gil, F, Sao Paulo (BR)
Zamboni, Giuseppe, Negrar-Verona (I)
Zareie, M, Amsterdam (NL)
Zatloukal, Kurt, Graz (A)
Ziol, Marianne, Bondy (F)
Zur Hausen, Axel, Freiburg (D)

Virchows Arch (2006) 448: 110
DOI 10.1007/s00428-006-0138-0

ANNOUNCEMENTS

6 May 2006
Problems in Breast Pathology
Malta College of Pathologists
Malta

Course Director
Professor J.G. Azzopardi

Scientific Secretariat
J. De Gaetano and V. Eusebi

9.00 Registration

Chair: J.G. Azzopardi (London/Malta) & Rosemary Millis (London)
9.30–10.00 Ian Ellis (Nottingham) : Prognostic factors: old versus new.
10.00–10.30 Gianni Bussolati (Torino) : The contribution of 3D models to the understanding of breast pathology.
10.30–11.00 Tibor Tot (Falun) : The theory of the sick lobe and the possible consequences.
11.00–11.30 Frederick Koerner (Boston) : The histogenesis of early breast carcinoma.
11.30–12.00 Tanya Tavassoli (New Haven) : To DIN or not to DIN, that is the question.
12.00–12.30 Discussion

Chair: J. Rosai (Milano) & G. Stamp (London)
14.30–15.00: James Connolly (Boston) : Present findings from the benign breast project of the nurses health study.
15.00–15.30: Stuart Schnitt (Boston) : Columnar cell lesions and flat epithelial atypia.
15.30–16.00 Hans Peterse (Amsterdam) : Ring carcinomas: the phenomenon of shift of cell polarization.
16.00–16.30: Thomas Krausz (Chicago) : Breast tumours. Race, loneliness and the pathologist.
16.30–17.00 : Werner Boecker (Muenster): The progenitor cell concept of breast epithelium and how it changes our understanding of proliferative breast disease.
17.00–17.30 : Sunil Lakhani (Brisbane): Myoepithelial cell and breast cancer.
17.30–18.00 : Vincenzo Eusebi (Bologna) : Salivary-like tumours of the breast.
18.00–18.30 : Juan Rosai (Milano) : The vascular lobule. A pitfall on the interpretation of vascular skin lesions following irradiation for breast carcinoma.

S.G. Silveberg (Baltimore) & Jane Dahlstrom
(Camberra) : Conclusive remarks

The congress fee is 30 ∈, that includes light lunch payable on the spot.

Scientific Organizer:
Dr. James De Gaetano
Pathology Department
St. Luke's Hospital
Gwardamangia
Malta
tel.n. xx356 25951117
e-mail james.degaetano@gov.mt

Venue and Hotel accomodation:
Hilton Hotel
Portomaso
St. Julians
Malta PTM01
Tel.n. XX 356 21383383
www.hilton.com.mt

15–16 June 2006
Thyroid Pathology for the Practicing Pathologist
15 rue de l'Ecole de Médecine, Paris,France

A 2-day course will take place in Paris again under the auspices of the French Division of the I.A.P.

This course will be given in English by Prof. M. Sobrinho-Simões (Porto) and Prof. R. Heimann (Brussels).

It will consist of lectures alternating with slide reviews and a slide seminar over a multihead microscope. The cases of this seminar will be sent (on CD) before the meeting.

The audience will be limited to 22 participants.
Course fees: 390 euros (320 euros for members of any I.A.P. division). The fees include registration, hand-out, CD of the slide seminar and coffee breaks.

For further information please contact
Mrs. M. Fontaniére
Administrative Secretary
French Division of the I.A.P.
32 Cours Albert Thomas
69008, Lyon, France
Fax: 33 4 78754311
e-mail: academie.pathologie@wanadoo.fr

Virchows Arch (2006) 448: 111–118
DOI 10.1007/s00428-005-0102-4

REVIEW ARTICLE

Antonio Lopez-Beltran · Gregor Mikuz · Rafael J. Luque · Roberta Mazzucchelli · Rodolfo Montironi

Current practice of Gleason grading of prostate carcinoma

Received: 5 October 2005 / Accepted: 17 October 2005 / Published online: 23 November 2005

Abstract The Gleason grading system remains one of the most powerful prognostic factors in prostate cancer and is the dominant method around the world in daily practice. It is based solely on the glandular architecture performed at low magnification. The Gleason grading system should be performed in needle core biopsies and radical prostatectomy specimens where it shows a reasonable degree of correlation between both specimens, and most importantly, it remains vital in the treatment decision-making process. This review summarizes the current status of Gleason grading in prostate cancer, incorporating recent proposals for the best contemporary practice of prostate cancer grading.

Keywords Prostate cancer · Gleason grade · Gleason score · Prostate biopsy · Radical prostatectomy

Introduction

The Gleason grading system for prostate cancer, named after Donald F. Gleason, is the predominant grading system around the world [21–23]. The Gleason grading system is based on glandular architecture which can be divided into five patterns of growth (also known as grades) with decreasing differentiation [10, 21–23]. The primary and secondary pattern or grade, i.e., the most prevalent and the second most prevalent pattern or grade is added to obtain a Gleason score or sum that is to be reported (see Appendix) [10, 21]. Nuclear atypia or cytoplasmic features are not evaluated. An important issue is that the initial grading of prostate carcinoma should be performed at low magnification using a 4× or 10× lens [16, 18]. Then one may proceed wit high-power objectives to look for rare fused glands or a few individual cells. Gleason grading of prostate cancer has changed over the years to adapt to needle biopsies and radical prostatectomy specimens that were unavailable at time when Gleason proposed his system [3, 4, 9, 14, 18, 19, 31, 32, 35, 36, 39, 48]. Issues on the application of the Gleason grading system in prostate cancer have been dealt with in recent consensus conferences organized under the auspices of the Uropathology Working Group (European Society of Pathology, ESP), the European Society of Uropathology (a full section office member of the European Association of Urology, EAU), and the Italian Society of Urology (SIU; Florence, Italy, June 2003; Palermo, Sicily, June 2005) [9, 39], World Health Organization (Lyon, France, December 2002; and Stockholm, Sweden, September 2004) [3, 14], and International Society of Urologic Pathology (San Antonio, TX, USA, March 2005) [18]. The authors of this review have been involved in the organization and participated in and contributed to these conferences. Important recommendations follow.

Gleason score as prognostic and predictive factor

Gleason grading remains as one of the most significant factors in the clinical decision-making activity both in needle biopsy specimens and after radical prostatectomy is performed; that is, it predicts pathological stage, margin status, biochemical failure, local recurrences, lymph node, disease progression, or distant metastasis after prostatec-

A. Lopez-Beltran (✉)
Department of Pathology, Faculty of Medicine,
Reina Sofia University Hospital
and Cordoba University Medical School,
Avda. Menendez Pidal s/n,
14004 Cordoba, Spain
e-mail: em1lobea@uco.es
Tel.: +34-957-218993
Fax: +34-957-218229

G. Mikuz
Department of Pathology,
University of Innsbruck School of Medicine,
Innsbruck, Austria

R. J. Luque
University Hospital of Jaen,
Jaén, Spain

R. Mazzucchelli · R. Montironi
Institute of Pathological Anatomy and Histopathology,
Polytechnic University of the Marche Region,
Ancona, Italy

tomy [3, 5–8, 11–13, 31, 32, 35]. Radiation therapy, radical prostatectomy, and other therapies are initially based on the Gleason score; in practice, Gleason scores of 7–10 are associated with worse prognosis, meanwhile Gleason scores of 5–6 are associated with lower progression rates after therapy [17, 19, 20]. In recent years, Gleason score has been included in clinical nomograms which are used with increasing frequency to predict disease progression [25–27, 30, 40, 44–48].

Reporting Gleason scores in prostate needle biopsies

Once carcinoma is detected in the needle biopsy, further descriptive information regarding the tumor type, Gleason score, and amount of cancer is necessary for management of the patient [35, 38]. As a recently indicated, the highest Gleason score was selected by most urologists to determine their treatment plan regardless of the overall involvement (Table 1) [35, 38, 45]. Some issues that need clarification follow.

Gleason scores 2–4

The diagnosis of Gleason scores 2–4 on needle biopsies should be made "rarely, if ever," and the reasons are compelling [18]: (1) Gleason scores 2–4 cancer is extraordinarily rare in needle biopsies as compared to transurethral resection (TURP) specimens, (2) poor reproducibility among experts [1, 2, 16], (3) the correlation with the prostatectomy score is poor, and (4) "low" Gleason scores of 2–4 may misguide clinicians into believing that there is an indolent tumor [20]. A recent consensus stated that a Gleason score of 1+1=2 is a grade that should not be diagnosed, regardless of the type of specimen with extremely rare exception, since most of these cases in the era of Gleason would today be referred to as adenosis (atypical adenomatous hyperplasia) because of improvement in recognizing basal cells [17, 18, 29]. Cribriform morphology is not allowed within Gleason pattern 2 [5].

Gleason pattern 3

Cribriform pattern 3 applies to round, well-circumscribed glands of the same size of normal glands, but only rare cribriform lesions satisfy these criteria. Therefore, the majority of cribriform patterns should be diagnosed as Gleason pattern 4. "Individual cells" would not be allowed within Gleason pattern 3 [5, 18, 19].

Gleason pattern 4 in Gleason score 7 tumors

The importance of the percentage of Gleason 4 pattern in Gleason score 7 tumors accumulates rapidly [18, 19, 34, 35, 40, 47, 49]. In recently generated nomograms, patients with Gleason score 4+3 vs 3+4 are stratified differently [30]. Whether or not the percentage of pattern 4 tumor should be included in the report remains optional at present time. Small, ill-defined glands with poorly formed glandular lumina also warrant the diagnosis of Gleason pattern 4 as stated by a recent consensus [18].

Gleason pattern 5

Comedonecrosis when seen in solid nests or cribriform masses should be regarded as Gleason pattern 5. However, the definition of comedonecrosis requires intraluminal necrotic cells and/or nuclear debris (karyorrhexis) [18].

Tertiary pattern

Another important change recently incorporated in current practice is the recognition and reporting of the tertiary pattern in needle biopsies [34, 43]. This includes tumors with patterns 3, 4, and 5 in various proportions on a biopsy. Tertiary patterns are uncommon, but when the worst Gleason grade is the tertiary pattern, it should influence the final Gleason score, and therefore, the primary pattern and

Table 1 Diagnostic reporting of Gleason score (see text)

General features
– Perform Gleason grading at low magnification using a 4× or 10× lens.
– Report primary pattern and secondary pattern and assign Gleason score.
– If only one pattern is present, double it to yield Gleason score. A Gleason score is usually assignable even if the cancer is extremely small.
– In a needle biopsy with more than 2 patterns (tertiary pattern), the worst pattern must be reflected in the Gleason score even if it is not the predominant or secondary pattern, use the rule "the most and the worst" (see text).
– In a radical prostatectomy with more than 2 patterns, the primary and secondary patterns must be reflected in the Gleason score. Add tertiary pattern as a note in the report.
– Provide Gleason score for each separately involved core when identified and give overall Gleason score when mixed in one container.
– In general, a diagnosis of Gleason scores 2–4 should not be made.
– Do not report Gleason score after hormonal or radiation therapy except if cancer shows no treatment effect.
Optional features
– Provide percent of tumor with Gleason pattern 4 in Gleason score 7.
– Provide percent of tumor with Gleason patterns 4 and 5 in tumors with Gleason scores 8–10.

the highest grade should be recorded following the rule of "the most and the worst" [18]. For example, a case with primary Gleason pattern 3, secondary pattern 4, and tertiary pattern 5 should be assigned a Gleason score of 8. These tumors should be classified overall as high grade (Gleason scores 8–10) [43, 46].

Needle biopsy with different cores showing different grades

This is related to a case when one or more of the cores shows pure high-grade cancer (i.e. Gleason score 4+4=8), and the other cores show pattern 3 (3+3, 3+4, or 4+3) cancer [18, 24, 27, 35]. If one reports the grades of each core separately, whereby the highest grade tumor (Gleason score 8) would typically be the one selected by the clinician as the grade of the entire case. Others give instead an overall score for the entire case. For example, in a case with Gleason score 4+4=8 on one core with pattern 3 (3+3=6, 3+4=7, 4+3=7), on other cores, the overall score for the entire case would be Gleason score 4+3=7 or 3+4=7, depending on whether pattern 4 or 3 predominated. Likewise, it was demonstrated that when one core is Gleason score 4+4=8 with other cores having pattern 3, the pathological stage at radical prostatectomy is comparable to cases with all needle cores having Gleason score 4+4=8 [3, 6–8, 18, 19]. The use of the highest core grade of the given case in cases where there are multiple cores of different grades advocated in current tables and nomograms gives additional support for giving cores a separate grade rather than an overall score for the entire case. This is the rationale of a recent survey in which 81% of urologists used the highest Gleason score on a positive biopsy, regardless of the overall percentage involvement, to determine treatment [45]. Consequently, it has been recommended to assign individual Gleason scores to separate cores as long as the cores were submitted in separate containers or the cores were in the same container yet specified by the urologist as to their location (i.e., by different color inks). In addition, one has the option to also give an overall score at the end of the case [33, 35].

In cases where a container contains multiple pieces of tissue and one cannot be sure if one is looking at an intact core, it is recommended that one should only give an overall score for that container [18].

Reporting Gleason scores in radical prostatectomies

In these specimens, one should assign the Gleason score based on the primary and secondary patterns with a comment if present on the tertiary pattern (Table 1) [3, 18, 19]. Specific issues follow.

Gleason scores 2–4

Gleason scores 2–4 are rarely seen as the grade of the main tumor in radical prostatectomies performed for stages T1c or T2 disease. These tumors are typically seen in multifocal incidental adenocarcinoma of the prostate found within the transition zone in TURP specimens [17–19]. The situation where Gleason scores 2–4 tumor represents the major tumor at radical prostatectomy performed for tumor incidentally found on TURP (stages T1a and T1b) is uncommon. In one study, Gleason scores 2–4 were the grade of the main tumor in 2% of the radical prostatectomy specimens; this represents a disproportionate number of T1a and T1b tumors, as compared to what would be currently seen in today's practice. All men with only Gleason scores 2–4 tumor at radical prostatectomy are cured [18, 19].

Gleason scores 5–6

It is important to recognize that the majority of tumors with Gleason scores 5–6 are cured after radical prostatectomy [18, 26].

Gleason score 7

Tumors with a Gleason score of 7 have a significantly worse prognosis than those with a Gleason score of 6. Given the adverse prognosis associated with Gleason pattern 4, one would expect that whether a tumor with Gleason score 3+4 vs 4+3 would influence prognosis [26]. There have been several studies addressing Gleason score 3+4 as compared to Gleason score 4+3 at radical prostatectomy, with somewhat conflicting results. In one study, they reported no significant survival advantage for Gleason pattern 3+4 over 4+3, but other study showed that Gleason score 3+4 vs 4+3 correlated with both stage and progression in men with serum PSA values less than 10 ng/ml and organ-confined disease [30, 47, 48]. Several other investigations have shown that Gleason score 4+3 has a worse prognosis. This is an issue in which much work needs to be done.

Gleason scores 8–10

Gleason scores 8–10 may account for only 7% of the grades seen at radical prostatectomy, but these patients have highly aggressive tumors with advanced stage such that they are not amenable to surgical therapy alone. Overall, patients with Gleason scores 8–10 at radical prostatectomy have a 15% chance of having no evidence of disease at 15 years following surgery [26, 33].

Percent Gleason pattern 4/5

The proportion of high-grade tumor as the preferred method for grading prostate cancer has been proposed, as it is predictive for progression at the extremes (greater than 70% or less than 20% of pattern 4/5) [12, 13]. It has been recently demonstrated that classifying tumors based on the combined percent of pattern 4/5 is more predictive than stratifying patients into Gleason score alone. Therefore, it has been recommended these data be included in the report [13].

Tertiary Gleason pattern

In radical prostatectomy, a higher proportion of cases are found to contain more than two grades, and over 50% of them contain at least three different grades [11, 18]. The progression rate of Gleason scores 5–6 tumor with a tertiary component of Gleason pattern 4 is almost the same as those of pure Gleason score 7 tumors. Gleason score 7 tumors with tertiary pattern 5 experience progression rates following radical prostatectomy approximating pure Gleason score 8 tumors [40, 43]. On the other hand, no such significance could be seen in cases of Gleason (4+4) score 8 with tertiary pattern 5; since Gleason score 8 tumors are already aggressive, the existence of pattern 5 elements adds no difference. These tumors should be graded routinely (primary and secondary patterns) with a comment in the report noting the presence of the tertiary element. In the setting of high-grade cancer (scores 8–10), one should ignore lower-grade patterns if they occupy less than 5% of the area of the tumor [35, 36, 38, 39].

Tumors with one predominant pattern and a small percentage of higher-grade tumor

Some controversy still exist on how to grade tumors, which are over 95% of one pattern, where there is only a very small percentage of higher-grade tumor. For example, a tumor composed of >95% Gleason pattern 3 and <5% pattern 4, some experts would assign a Gleason score 3+3=6, as it has been proposed that one needs over 5% of a pattern to be present for it to be incorporated within the Gleason score. Others might grade the tumor as Gleason score 3+4=7. It seems that the existence of a high-grade component, even if it constitutes less than 5% of the whole tumor, has a significant adverse influence [18, 20].

Radical prostatectomy specimens with separate tumor nodules

Radical prostatectomy specimens should be processed in an organized fashion where one can make some assessment as to whether one is dealing with a dominant nodule or separate tumor nodules and assign a separate grade to each dominant tumor nodule(s). Most often, the dominant nodule is the largest tumor, which is also the tumor associated with the highest stage and grade [35].

Grading variants and variations of adenocarcinoma of the prostate

A number of architectural or cytologic variations of carcinoma of the prostate have been described [15, 28, 35, 41, 42, 50]. These are descriptive terms used to assist pathologists avoid diagnostic pitfalls. Most of the times, one should grade the tumor solely based on the underlying architecture with some exceptions (Table 2). Variants of prostate cancer include ductal, mucinous (colloid), mucinous signet-ring cell, small cell carcinoma, sarcomatoid carcinoma, and some others (Table 2). The former three are diagnoses tenable only on examination of radical prostatectomy or TURP specimens. If seen in needle biopsy specimens, the diagnostic terminologies used are adenocarcinoma of prostate with ductal features, adenocarcinoma of prostate with signet-ring cell features, and adenocarcinoma of prostate with mucinous (colloid) differentiation. Small cell carcinoma and sarcomatoid carcinoma may be diagnosed on needle biopsies. Ductal adenocarcinoma should be graded as Gleason score 4+4=8 while retaining the diagnostic term of ductal adenocarcinoma to denote their unique clinical and pathological features. There is no

Table 2 Gleason grades in histological variants and variations of prostate cancer (see text)

Variants
– Ductal carcinoma [pattern 4]
– Small cell carcinoma [no grade applies]
– Mucinous (colloid) carcinoma [pattern 4 (some pattern 3) vs grade according to underlying pattern]
– Mucinous signet-ring cell carcinoma [no grade applies]
– Sarcomatoid carcinoma [no grade applies]
– Pleomorphic giant cell [pattern 5]
– Adenosquamous carcinoma [uncertain]
– Lymphoepithelioma-like [no grade applies]
– Basal cell/adenoid cystic carcinoma [no grade applies]
– Urothelial carcinoma (involving prostatic ducts and acini with or without stromal invasion) [no grade applies]
– Squamous cell carcinoma [no grade applies]
Variations
– Atrophic features [underlying glandular pattern]
– Pseudohyperplastic [pattern 3]
– Glomeruloid [pattern 3 or pattern 4]
– Collagenous micronodules (mucinous fibroplasia) [underlying glandular pattern (most pattern 3)]
– Focal acellular mucin extravasation [ignore mucin and use underlying glandular pattern]
– Foamy gland carcinoma [underlying glandular pattern (most pattern 3)]
– Non-mucinous signet-ring cell features (cytoplasmic vacuoles) [underlying glandular pattern (most pattern 4 or 5)]
– Hypernephroid [pattern 4]

consensus on how mucinous (colloid) carcinoma should be scored [18]. Some authors suggest that a Gleason score of 8 is to be assigned, while others recommend ignoring mucin and grading the tumor based on the underlying architectural pattern. Small cell, sarcomatoid, and mucinous signet-ring cell carcinomas should not be assigned a Gleason grade. It has been suggested that the rare pleomorphic giant cell carcinoma of the prostate should be assigned a pattern 5 (Table 2) [18, 28, 37].

Sources of discrepancies between needle biopsy and radical prostatectomy Gleason scores

Several studies have addressed the correlation between Gleason scores in needle biopsies and corresponding radical prostatectomy specimens [35]. In a recent meta-analysis from 18 studies, exact correlation of Gleason scores was found in 43% of cases and correlation plus or minus one Gleason score unit in 77% of cases. Undergrading of carcinoma in needle biopsy is the most common problem occurring in 42% of all reviewed cases, and overgrading is present in up to 15% of cases. In general, adverse findings on needle biopsy accurately predict adverse findings in the radical prostatectomy, whereas favorable findings on the needle biopsy do not necessarily predict favorable findings in the radical prostatectomy [35, 49].

Sampling error

This is related to the small sample of tissue inherent to needle biopsy [35]. The most common type of sampling error occurs when there is a higher-grade component present within the radical prostatectomy, which is not sampled on needle biopsy. This typically occurs when a needle biopsy tumor is graded as Gleason score 3+3=6, and in the prostatectomy exists a Gleason pattern 4 which was not sampled on the biopsy, thus resulting in a prostatectomy Gleason 3+4=7. In some instances, undergrading results from an attempt to grade very tiny areas of carcinoma, so-called minimal or limited adenocarcinoma. Overgrading can result from sampling error in cases where the high-grade pattern is present in needle biopsy, but it may only represent a very minor element in the radical prostatectomy specimen [35].

Borderline cases

There are some cases in the original description of the Gleason grading system that are right at the interface between two different patterns leading to interobserver and possibly intraobserver variability [21, 35].

Pathology error

A common pathology error is seen when pathologists assign a Gleason score of <4 on a needle biopsy which in fact was Gleason score 5–6 or higher. When there is a limited focus of small glands of cancer on needle biopsy, by definition, this is a Gleason pattern 3 or higher [35]. Gleason pattern 3 consists of small glands with an infiltrative pattern. Biopsying truly low-grade adenocarcinoma of the prostate could not result in just a few neoplastic glands but rather would be more extensive, as low-grade adenocarcinoma grows as nodules of closely packed rather than infiltrating glands. Undergrading may result from difficulty in recognizing an infiltrative growth pattern or failing to recognize the presence of small areas of gland fusion [35].

Pathologists' experience

With experience, pathologists recognize grading pitfalls; in particular, the fact that Gleason scores of 4 and lower are almost nonexistent in needle biopsy situation. Furthermore, small areas of fusion in the presence of a predominantly grade 3 background are recognized and will yield a Gleason score of 7 [35, 46].

Intraobserver and interobserver variability

Intraobserver variability of Gleason grade and exact agreement was reported in 43–78% of cases, and agreement within plus or minus one Gleason score unit was reported in 72–87% of cases. Gleason wrote that he duplicated exactly his previous histological scores approximately 50% times. Highly variable levels of interobserver agreement on Gleason scores have also been reported, with ranges of 36–81% for exact agreement and 69–86% within plus or minus one Gleason score unit [45–49].

Conclusions

The Gleason grading system is a powerful tool to predict response to therapy. The needle biopsy Gleason score correlates with virtually all other pathological and clinical parameters after radical prostatectomy. The Gleason score assigned to the tumor at radical prostatectomy is the most powerful predictor of progression and is very useful in stratifying patients for therapy. However, still significant deficiencies in the practice of this grading system exist. An important issue frequently missed by practicing pathologists is that the initial grading of prostate carcinoma should be performed at low magnification using a 4× or 10× lens. Keeping this in mind might help pathologists avoid

overgrade or undergrade prostate cancer in daily practice. Improvements in Gleason grading reproducibility can be achieved by recognizing problematic areas and educating physicians via meetings, courses, website tutorials, and publications.

Appendix

Gleason pattern 1 Nodule of separate, closely packed glands which do not infiltrate into adjacent benign prostatic tissue is very well circumscribed. The glands are of intermediate size and approximately equal in size and shape. The nucleus is typically small, and cytoplasm frequently is abundant and pale-staining. Nuclear and cytoplasm appearances are not taken into account in diagnosis. This pattern is exceedingly rare and usually seen in transition zone cancers (Fig. 1).

Gleason pattern 2 This pattern is characterized with round to oval glands with smooth ends. The glands are more loosely arranged and not quite as uniform in size and shape as those of Gleason pattern 1. There may be minimal invasion by neoplastic glands into the surrounding non-neoplastic prostatic tissue. The glands are of intermediate size and larger than those in Gleason pattern 1. The variation in glandular size and separation between glands is less than that seen in pattern 3. Although not evaluated in Gleason grading, the cytoplasm of Gleason pattern 2 cancers is abundant and pale-staining (Fig. 1). Gleason pattern 2 is usually seen in transition zone cancers but may occasionally be found in the peripheral zone.

Gleason pattern 3 This pattern is the most common pattern but is morphologically heterogeneous. The glands are infiltrative, and the distance between them is more variable than that in patterns 1 and 2. Malignant glands often infiltrate between adjacent non-neoplastic glands. The glands of pattern 3 vary in size and shape and are often angular (Fig. 1). Small glands are typical for pattern 3, but there may also be large and irregular glands. Each gland has an open lumen and is circumscribed by stroma. Cribriform pattern 3 is rare and difficult to distinguish morphologically from cribriform high-grade prostatic

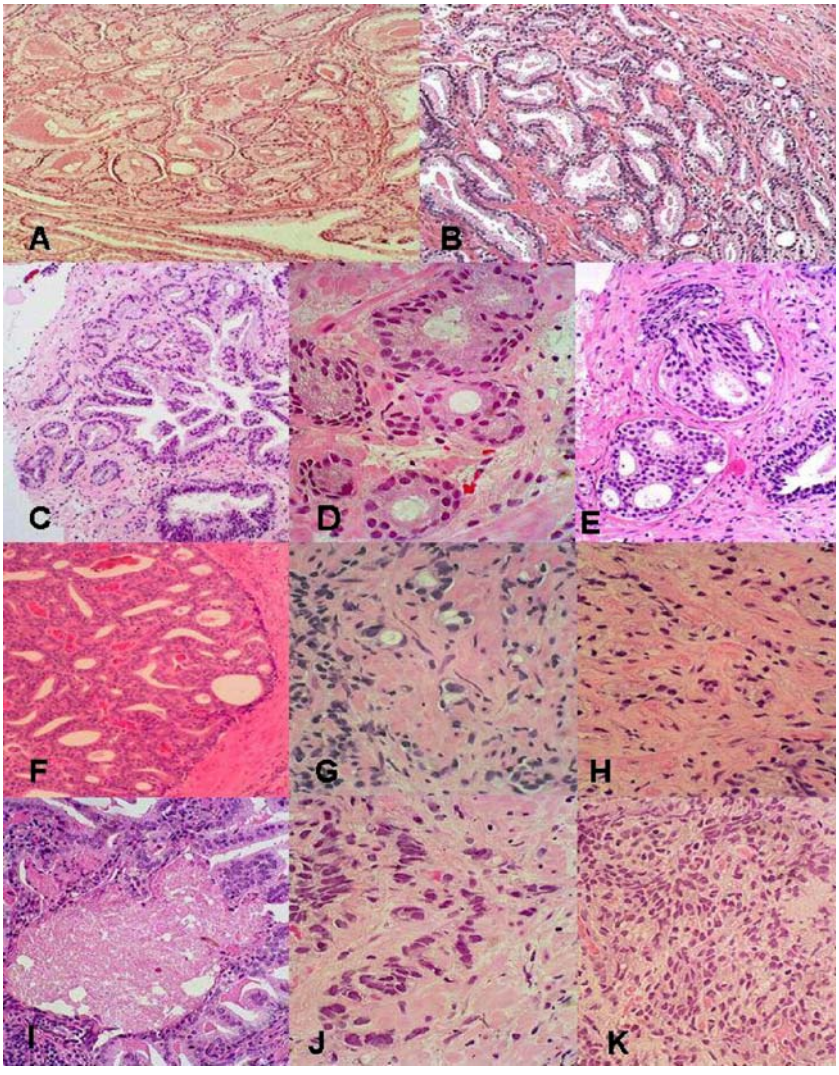

Fig. 1 Examples of Gleason patterns 1 (**a**) and 2 (**b**), Gleason pattern 3 (**c**–**e**), Gleason pattern 4 (**f**–**h**), and Gleason pattern 5 (**i**–**k**). **a**–**k** H & E staining

intraepithelial neoplasia (PIN). The latter shows the presence of basal cells. These are lacking in cribriform pattern 3 prostate cancer. This heterogeneous expression of Gleason grade 3 raised an initial subdivision in patterns A, B, and C, respectively.

Gleason pattern 4 Glands appear fused, cribriform, or they may be poorly defined and small. Fused glands are composed of a group of glands that are no longer completely separated by stroma (Fig. 1). The edge of a group of fused glands is scalloped, and there are occasional thin strands of connective tissue within this group. The hypernephroid pattern described by Gleason is a rare variant of fused glands with clear or very pale-staining cytoplasm. Cribriform pattern 4 glands are large or they may be irregular with jagged edges. As opposed to fused glands, there are no strands of stroma within a cribriform gland. Most cribriform invasive cancers should be assigned a pattern 4 rather than pattern 3. Poorly defined glands do not have a lumen that is completely encircled by epithelium.

Gleason pattern 5 This pattern is characterized with an almost complete loss of glandular lumina which are only occasionally present. The epithelium forms solid sheets, solid strands, or single cells invading the stroma; comedonecrosis may be present (Fig. 1). Care must be applied when assigning a Gleason pattern 4 or 5 to limited cancer on needle biopsy to exclude an artifact of tangential sectioning of lower-grade cancer.

Acknowledgement This work was supported by the Grant FIS 03/0952 (Madrid, Spain).

References

1. Allsbrook WC Jr, Mangold KA, Johnson MH, Lane RB, Lane CG, Amin MB, Bostwick DG, Humphrey PA, Jones EC, Reuter VE, Sakr W, Sesterhenn IA, Troncoso P, Wheeler TM, Epstein JI (2001) Interobserver reproducibility of Gleason grading of prostatic carcinoma: urologic pathologists. Hum Pathol 32: 74–80
2. Allsbrook WC Jr, Mangold KA, Johnson MH, Lane RB, Lane CG, Epstein JI (2001) Interobserver reproducibility of Gleason grading of prostatic carcinoma: general pathologist. Hum Pathol 32:81–88
3. Amin M, Boccon-Gibod L, Egevad L, Epstein JI, Humphrey PA, Mikuz G, Newling D, Nilsson S, Sakr W, Srigley JR, Wheeler TM, Montironi R (2005) Prognostic and predictive factors and reporting of prostate carcinoma in prostate needle biopsy specimens. Scand J Urol Nephrol Suppl 216:20–33
4. Amin MB, Grignon DJ, Humphrey PA, Srigley JR (2004) Gleason grading of prostate cancer: a contemporary approach. Lippincott Williams & Wilkins, Philadelphia, PA
5. Amin MB, Schultz DS, Zarbo RJ (1994) Analysis of cribriform morphology in prostatic neoplasia using antibody to high-molecular-weight cytokeratins. Arch Pathol Lab Med 118:260–264
6. Augustin H, Eggert T, Wenske S, Karakiewicz PI, Palisaar J, Daghofer F, Huland H, Graefen M (2004) Comparison of accuracy between the Partin tables of 1997 and 2001 to predict final pathological stage in clinically localized prostate cancer. J Urol 171:177–181
7. Babaian RJ, Troncoso P, Bhadkamkar VA, Johnston DA (2001) Analysis of clinicopathologic factors predicting outcome after radical prostatectomy. Cancer 91:1414–1422
8. Bailar JC 3rd, Mellinger GT, Gleason DF (1966) Survival rates of patients with prostatic cancer, tumor stage, and differentiation–preliminary report. Cancer Chemother Rep 50:129–136
9. Boccon-Gibod L, van der Kwast TH, Montironi R, Bono A (2004) Handling and pathology reporting of prostate biopsies. Eur Urol 46:177–181
10. Bostwick DG (1994) Gleason grading of prostatic needle biopsies. Correlation with grade in 316 matched prostatectomies. Am J Surg Pathol 18:796–803
11. Bostwick DG, Grignon DJ, Hammond ME, Amin MB, Cohen M, Crawford D, Gospadarowicz M, Kaplan RS, Miller DS, Montironi R, Pajak TF, Pollack A, Srigley JR, Yarbro JW (2000) Prognostic factors in prostate cancer. College of American Pathologists Consensus Statement 1999. Arch Pathol Lab Med 124:995–1000
12. Chan TY, Partin AW, Walsh PC, Epstein JI (2000) Prognostic significance of Gleason score 3+4 versus Gleason score 4+3 tumor at radical prostatectomy. Urology 56:823–827
13. Cheng L, Koch MO, Juliar BE, Daggy JK, Foster RS, Bihrle R, Gardner TA (2005) The combined percentage of Gleason patterns 4 and 5 is the best predictor of cancer progression after radical prostatectomy. J Clin Oncol 23:2911–2917
14. Eble JN, Sauter G, Epstein JI, Sesterhenn IA (2004) Pathology and genetics. Tumors of the urinary system and male genital organs. IARC, Lyon
15. Egan AJ, Lopez-Beltran A, Bostwick DG (1997) Prostatic adenocarcinoma with atrophic features: malignancy mimicking a benign process. Am J Surg Pathol 21:931–935
16. Egevad L, Allsbrook WC Jr., Epstein JI (2005) Current practice of Gleason grading among genitourinary pathologists. Hum Pathol 36:5–9
17. Epstein JI (2000) Gleason score 2–4 adenocarcinoma of the prostate on needle biopsy: a diagnosis that should not be made. Am J Surg Pathol 24:477–478
18. Epstein JI, Allsbrook WCJ, Amin MB, Egevad LL, and The ISUP Grading Committee (2005) The 2005 International Society of Urological Pathoogy (ISUP) consensus conference on Gleason grading of prostatic carcinoma. Am J Surg Pathol 29:1228–1242
19. Epstein JI, Amin M, Boccon-Gibod L, Egevad L, Humphrey PA, Mikuz G, Newling D, Nilsson S, Sakr W, Srigley JR, Wheeler TM, Montironi R (2005) Prognostic factors and reporting of prostate carcinoma in radical prostatectomy and pelvic lymphadenectomy specimens. Scand J Urol Nephrol Suppl:34–63
20. Epstein JI, Partin AW, Sauvageot J, Walsh PC (1996) Prediction of progression following radical prostatectomy. A multivariate analysis of 721 men with long-term follow-up. Am J Surg Pathol 20:286–292
21. Gleason DF (1966) Classification of prostatic carcinomas. Cancer Chemother Rep 50:125–128
22. Gleason DF (1977) Histologic grading and clinical staging of prostatic carcinoma. In: Tannenbaum M (eds) Urologic pathology: the prostate. Lea & Feibiger, Philadelphia, PA
23. Gleason DF, Mellinger GT (1974) Prediction of prognosis for prostatic adenocarcinoma by combined histological grading and clinical staging. J Urol 111:58–64
24. Grober ED, Tsihlias J, Jewett MA, Sweet JM, Evans AJ, Trachtenberg J, Robinette M, Nam RK (2004) Correlation of the primary Gleason pattern on prostate needle biopsy with clinico-pathological factors in Gleason 7 tumors. Can J Urol 11:2157–2162

25. Humphrey PA (2003) Prostate pathology. ASCP Press, Chicago, IL
26. Kattan MW, Eastham JA, Wheeler TM, Maru N, Scardino PT, Erbersdobler A, Graefen M, Huland H, Koh H, Shariat SF, Slawin KM, Ohori M (2003) Counseling men with prostate cancer: a nomogram for predicting the presence of small, moderately differentiated, confined tumors. J Urol 170:1792–1797
27. Kunz GM Jr, Epstein JI (2003) Should each core with prostate cancer be assigned a separate Gleason score? Hum Pathol 34:911–914
28. Lopez-Beltran A, Eble JN, Bostwick DG (2005) Pleomorphic giant cell carcinoma of the prostate. Arch Pathol Lab Med 129:683–685
29. Lopez-Beltran A, Qian J, Montironi R, Luque RJ, Bostwick DG (2005) Atypical adenomatous hyperplasia (adenosis) of the prostate: DNA ploidy analysis and immunophenotype. Int J Surg Pathol 13:167–173
30. Makarov DV, Sanderson H, Partin AW, Epstein JI (2002) Gleason score 7 prostate cancer on needle biopsy: is the prognostic difference in Gleason scores 4+3 and 3+4 independent of the number of involved cores? J Urol 167:2440–2442
31. Mazzucchelli R, Lopez-Beltran A, Scarpelli M, Montironi R (2002) Predictive factors in prostate needle biopsy. Pathologica 94:331–337
32. Mazzucchelli R, Santinelli A, Lopez-Beltran A, Scarpelli M, Montironi R (2002) Evaluation of prognostic factors in radical prostatectomy specimens with cancer. Urol Int 68:209–215
33. Mian BM, Troncoso P, Okihara K, Bhadkamkar V, Johnston D, Reyes AO, Babaian RJ (2002) Outcome of patients with Gleason score 8 or higher prostate cancer following radical prostatectomy alone. J Urol 167:1675–1680
34. Mills SE, Fowler JE Jr (1986) Gleason histologic grading of prostatic carcinoma. Correlations between biopsy and prostatectomy specimens. Cancer 57:346–349
35. Montironi R, Mazzuccheli R, Scarpelli M, Lopez-Beltran A, Fellegara G, Algaba F (2005) Gleason grading of prostate cancer in needle biopsies or radical prostatectomy specimens: contemporary approach, current clinical significance and sources of pathology discrepancies. BJU Int 95:1146–1152
36. Montironi R, Mazzucchelli R, Stramazzotti D, Scarpelli M, Lopez Beltran A, Bostwick DG (2005) Basal cell hyperplasia and basal cell carcinoma of the prostate: a comprehensive review and discussion of a case with c-erbB-2 expression. J Clin Pathol 58:290–296
37. Montironi R, Mazzucchelli R, van der Kwast T (2003) Morphological assessment of radical prostatectomy specimens. A protocol with clinical relevance. Virchows Arch 442:211–217
38. Montironi R, van der Kwast T, Boccon-Gibod L, Bono AV (2003) Handling and pathology reporting of radical prostatectomy specimens. Eur Urol 44:626–636
39. Montironi R, Scarpelli M, Lopez Beltran A (2004) Carcinoma of the prostate: inherited susceptibility, somatic gene defects and androgen receptors. Virchows Arch 444:503–508
40. Mosse CA, Magi-Galluzzi C, Tsuzuki T, Epstein JI (2004) The prognostic significance of tertiary Gleason pattern 5 in radical prostatectomy specimens. Am J Surg Pathol 28:394–398
41. Pacelli A, Lopez-Beltran A, Egan AJ, Bostwick DG (1998) Prostatic adenocarcinoma with glomeruloid features. Hum Pathol 29:543–546
42. Pan CC, Chiang H, Chang YH, Epstein JI (2000) Tubulocystic clear cell adenocarcinoma arising within the prostate. Am J Surg Pathol 24:1433–1436
43. Pan CC, Potter SR, Partin AW, Epstein JI (2000) The prognostic significance of tertiary Gleason patterns of higher grade in radical prostatectomy specimens: a proposal to modify the Gleason grading system. Am J Surg Pathol 24:563–569
44. Partin AW, Kattan MW, Subong EN, Walsh PC, Wojno KJ, Oesterling JE, Scardino PT, Pearson JD (1997) Combination of prostate-specific antigen, clinical stage, and Gleason score to predict pathological stage of localized prostate cancer. A multi-institutional update. JAMA 277:1445–1451
45. Rubin MA, Bismar TA, Curtis S, Montie JE (2004) Prostate needle biopsy reporting: how are the surgical members of the Society of Urologic Oncology using pathology reports to guide treatment of prostate cancer patients? Am J Surg Pathol 28: 946–952
46. Rubin MA, Dunn R, Kambham N, Misick CP, O'Toole KM (2000) Should a Gleason score be assigned to a minute focus of carcinoma on prostate biopsy? Am J Surg Pathol 24:1634–1640
47. Sakr WA, Tefilli MV, Grignon DJ, Banerjee M, Dey J, Gheiler EL, Tiguert R, Powell IJ, Wood DP (2000) Gleason score 7 prostate cancer: a heterogeneous entity? Correlation with pathologic parameters and disease-free survival. Urology 56: 730–734
48. Srigley JR, Amin M, Boccon-Gibod L, Egevad L, Epstein JI, Humphrey PA, Mikuz G, Newling D, Nilsson S, Sakr W, Wheeler TM, Montironi R (2005) Prognostic and predictive factors in prostate cancer: historical perspectives and recent international consensus initiatives. Scand J Urol Nephrol Suppl 216:8–19
49. Steinberg DM, Sauvageot J, Piantadosi S, Epstein JI (1997) Correlation of prostate needle biopsy and radical prostatectomy Gleason grade in academic and community settings. Am J Surg Pathol 21:566–576
50. Tran TT, Sengupta E, Yang XJ (2001) Prostatic foamy gland carcinoma with aggressive behavior: clinicopathologic, immunohistochemical, and ultrastructural analysis. Am J Surg Pathol 25:618–623

Virchows Arch (2006) 448: 119–126
DOI 10.1007/s00428-005-0058-4

ORIGINAL ARTICLE

Cinzia Azzoni · Lorena Bottarelli · Silvia Pizzi · Tiziana D'Adda · Guido Rindi · Cesare Bordi

Xq25 and Xq26 identify the common minimal deletion region in malignant gastroenteropancreatic endocrine carcinomas

Received: 29 June 2005 / Accepted: 3 August 2005 / Published online: 22 October 2005

Abstract Loss of heterozygosity (LOH) for markers on X chromosome are associated with malignancy in endocrine tumors of the stomach and pancreas. The aim of this work is to investigate low-grade, well-differentiated endocrine carcinomas (WDEC) vs high-grade, poorly differentiated endocrine carcinomas (PDEC) of the gastroenteropancreatic (GEP) tract for common deletion regions on X chromosome. We performed a comparative allelotyping analysis with 24 highly polymorphic markers for the X chromosome in 12 WDECs and 5 PDECs. Overall, the LOH frequency in all informative loci investigated was 59% in primary and 61% in metastasis, with a significantly higher rate in PDECs than in WDECs ($p<0.015$ for primary and $p<0.00005$ for metastasis). In both WDECs and PDECs, the small Xq25 region as defined by DXS8059, DXS8098, and DXS8009 markers showed higher LOH rate as compared to the rest of the chromosome markers ($p<0.04$). In addition, LOH was very frequently elevated also in DXS294 and in DXS102 loci mapping the chromosomal region Xq26. In no instances differences were found between primary tumors and metastases. Methylation analysis revealed that Xq25 loss preferentially occurred on the inactive X chromosome, a feature in agreement with findings from other human cancers suggesting escape of tumor suppressor genes to X chromosome inactivation at this region. Overall, our data indicate that the two chromosomal regions, Xq25 and Xq26, may participate to the malignant progression of GEP endocrine carcinomas.

Keywords X chromosome · Gastroenteropancreatic endocrine carcinomas · Loss of heterozygosity · Tumor suppressor genes

Introduction

Molecular and cytogenetic studies indicate that X chromosome is involved in the carcinogenesis and malignant progression of different types of human tumor. An increasing number of genes have been isolated as potentially responsible. Comparative genomic hybridization (CGH) analysis has demonstrated frequent gains on X chromosome that correlated with tumor progression in liver [38], stomach [33], and adrenal gland [32]. Conversely, X chromosome deletions have frequently been associated with the presence of metastases and/or worse prognosis in cancer of the breast [28], the uterine cervix [18], the ovary [6], and in papillary renal cell carcinoma [16]. These deletions are regarded as strong evidence for the occurrence of tumor suppressor genes (TSG) on this chromosome [6, 9, 16, 28, 29].

In our previous studies, allelic losses [loss of heterozygosity (LOH)] for just three microsatellite markers on X chromosome (DXS989 on p arm and DXS1003 and DXS1192 on q arm) were found to be restricted to foregut malignant endocrine tumors [9, 29]. These data were subsequently confirmed by Missiaglia et al. [25] who demonstrated a strong association between X chromosome markers LOH, aggressiveness, and shorter survival rates in 20 nonfunctioning pancreatic endocrine tumors (PETs). More recently, on this line, Chen et al. [4] found that X chromosome LOH frequently occurred in gastrinomas and was significantly associated with aggressive tumor growth and larger tumor size. On this basis, X chromosome LOH has been regarded as a potentially useful prognostic factor for aggressive growth in endocrine tumors of the upper

This study was supported by grants from the Italian Association for Cancer Research (AIRC), Milan; the Italian Ministry for University, Scientific and Technological Research (MURST grant number 2003063877-001); and the Italian Ministry of Health (grant number ICS060.2/RF00-57).

C. Azzoni · L. Bottarelli · S. Pizzi · T. D'Adda · G. Rindi · C. Bordi (✉)
Department of Pathology and Laboratory Medicine,
Section of Pathological Anatomy, University of Parma,
Via Gramsci 14,
43100 Parma, Italy
e-mail: cesare.bordi@unipr.it
Tel.: +39-0521-290386
Fax: +39-0521-292710

gastrointestinal tract and pancreas. Conversely, we and others demonstrated that poorly differentiated endocrine carcinomas (PDEC) of the stomach and the colon display similar genetic alterations indicating a site-independent genetic background for undifferentiated endocrine carcinomas at variance with well-differentiated endocrine carcinomas (WDECs) [12, 30].

In this work, we performed a high-resolution comparative allelotyping on X chromosome on WDECs vs PDECs of the gastroenteropancreatic (GEP) tract. Methylation analysis for CpG islands on Xq25 and immunohistochemistry for metalloproteinases 2 (MMP-2) and 9 (MMP-9) regulated by the myeloid elf-1 like factor gene (MEF) located at Xq26 were also performed. Our main aim was to identify minimal common deletion regions, ultimately indicating TSG possibly involved in the mechanism of malignancy in tumors of the GEP endocrine system.

Materials and methods

Patients and tissue specimens

Matched tumor and adjacent normal tissues were obtained from 17 female patients with malignant endocrine tumors of the pancreas and gastrointestinal tract collected in the files of the Department of Anatomic Pathology, University of Parma. According to the World Health Organization (WHO) criteria [36], in 12 patients, the tumors were WDECs (low grade malignant tumors, WHO class 2), and in five patients, the tumors were PDECs (high grade malignant tumors, WHO class 3). The age range of patients with WDEC was 43–73 years (mean 58.6), and with PDEC, 45–83 years (mean 70).

The main clinicopathological data of patients are summarized in Table 1. In eight cases, metastases were also analyzed (lymph node, cases #1, #2, #4, #6, #13, #14; liver, case #16, and both lymph node and liver, case #17). In two cases (#3 and #12), only liver metastases were available for the study. PDECs were either solitary (#13, #14, #15) or associated with adenocarcinoma (#16) or adenoma (#17). The primary tumor of patient #17 was not available for study, and DNA from liver and lymph node endocrine carcinoma metastases was used. In the two biphenotypic cases, the endocrine and nonendocrine tumor components occurred as separate masses with distinct morphology and were microdissected separately.

All tissue specimens were routinely formalin fixed and paraffin embedded. For 80% tumor cell enrichment, both normal and tumor tissues were microdissected from 5-μm sections stained with hematoxylin and DNA extracted using the QIAamp Tissue Kit (Qiagen GmbH, Hilden, Germany).

Polymerase chain reaction

DNA samples were microallelotyped for 24 polymorphic microsatellite markers covering the whole X chromosome (Table 2) selected from the Genome databases (http://www.gdb.org and http://www.geneatlas.org). Moreover, four microsatellite markers (D3S1621, D3S1100, D3S1478,

Table 1 Clinicopathological data of 17 female patients affected by malignant gastroenteropancreatic endocrine carcinomas

Type	Case	Age	Location	Metastases	Hormonal production	Syndrome
WDEC	1	47	Pancreas	N, L		NO
	2	63	Pancreas	N	Gastrin	NO
	3	51	Pancreas	L	PP	NO
	4	73	Pancreas	B, L	Somatostatin, glucagon	NO
	5	51	Pancreas	N, P	PP	NO
	6	43	Pancreas	N	Glucagon	NO
	7	75	Pancreas	P	PP	NO
	8	73	Pancreas	N		NO
	9	63	Pancreas	N		NO
	10	47	Stomach	N		NO
	11	70	Stomach	L	Serotonin	NO
	12	47	Duodenum	N, L	Gastrin	ZES/MEN-1
PDEC	13	83	Stomach	N		NO
	14	63	Colon	N		NO
	15	79	Colon	N, L		NO
	16[a]	80	Colon	N, L		NO
	17[b]	45	Colon	N, L		NO

WDEC Well-differentiated endocrine carcinoma, *PDEC* poorly-differentiated endocrine carcinoma, *N* lymph node, *L* liver, *P* peritoneum, *B* bone, *PP* pancreatic polypeptide, type of associated clinical syndrome: *ZES/MEN-1* Zollinger–Ellison syndrome/multiple endocrine neoplasia type 1, *NO* absence of associated syndrome (non functioning tumor)

[a]Associated with adenocarcinoma

[b]Associated with tubulo-villous adenoma

Table 2 Microsatellite marker set used for the allelotyping analysis on X chromosome and cytogenetic location

Microsatellite markers	Cytogenetic band	Geneatlas position[a] (bp)	UniSTS (NCBI)[a] position (bp)
DXS996	Xp22.3–p22.3	4.579.779	5.718.887
DXS207	Xp22.2–p22.2	14.112.607	15.188.763
DXS989	Xp22.13	21.564.927	22.944.099
DXS1237	Xp21.3–p21.2	30.390.426	31.745.042
MAOA.PCR1	Xp11.4–p11.3	41.474.541	43.359.613
DXS1003	Xp11.23	44.475.054	46.290.665
DXS1367	Xp11.3–p11.23	45.629.747	47.445.359
DXS1111	Xq12	61.995.658	67.811.398
DXS56	Xq13.2–q13.3	70.359.906	76.754.441
DXS738	Xq21.1–q21.1	–	–
DXS990	Xq21.33	86.401.205	89.918.106
DXS1153	Xq22.1–q22.3	–	98.452.635
DXS1220	Xq22.3–q23	107.802.910	114.431.063
DXS1001	Xq24	112.852.213	119.618.571
DXS8059	Xq24–q25	115.186.425	121.988.946
DXS8098	Xq24–q25	115.837.288	122.639.810
DXS8009	Xq25–q26	119.039.778	125.899.570
DXS1047	Xq25–q26	121.941.047	128.800.855
DXS692	Xq25–q26.2	124.850.440	131.710.249
DXS730	Xq26	130.696.964	137.556.978
DXS294	Xq26	–	–
DXS1192	Xq26	131.233.614	138.093.629
DXS102	Xq26	131.248.873	138.108.888
DXS731	Xq27–q28	139.986.141	146.878.018

[a]See "Materials and methods"

D3S1481) located on 3p chromosome were analyzed in the study. Forward primers were synthesized with a fluorescent tag (WellRed dyes from Research Genetics, Huntsville, AL, USA). DNA was amplified in a 25-μl reaction solution containing 2.5 μl of 10× buffer (Promega, Madison, WI, USA), 1 to 2 mM $MgCl_2$, 0.4 μmol/l primer pairs, 200 μM dNTPs, and 1.25 U Taq polymerase (Promega). Amplifications were performed using a 5-min initial denaturation at 95°C, followed by 35 cycles of 30″ at 94°C, 30″ at 53–64°C, and 1′ at 72°C; or by 40 cycles of 1′ at 94°C, 1′ at 55°C, and 2′ at 72°C (Table 2). The fluorescent-labeled polymerase chain reaction (PCR) products underwent electrophoresis on an automated DNA sequencer CEQ 2000XL (Beckman Coulter Inc., Fullerton, CA), and signals were analyzed using CEQ 2000XL analysis software (Beckman Coulter).

Definition of loss of heterozygosity

Allelic loss was defined as the ratio of relative allelic peak height in the tumor DNA to relative allelic peak height in the corresponding normal DNA. The formula employed for the calculation was (T2/T1)/(N2/N1), where T1 and N1 are the height values for the smaller allele, and T2 and N2 are the height values for the larger allele of the tumor (T) and normal (N) samples, respectively. For informative markers, LOH was scored when signal reduction for one allele was of 40% or more [2, 29].

Methylation-specific polymerase chain reaction

The methylation status of a CpG site located at position 225–226 of the DXS8059 microsatellite sequence was determined by methylation-specific PCR (MS-PCR) [28]. Genomic DNA (3 μg) was modified with sodium bisulfite as originally described by Herman et al. [14]. DNA modification was performed with the CpGenome DNA modification kit according to the manufacturer's instructions (Intergen Company, Oxford, UK). Primers for PCR amplification of the methylated (MA) allele were 59M2CF, 5′-TGTAGTTAGTTTGGTGTTTGTT-3′ and 8059MR, 5′-CAAACCAAAAATTCCCTCCG-3′, yielding a 97-bp fragment, whereas the primers for amplification of the unmethylated (UMA) allele were 59M2CF, 5′-TGTAGT TAGTTTGGTGTTTGTT-3′ and 8059N4R, 5′-AACCA CAAACCAAAAAATTCCCTCCA-3′, yielding a fragment of 102 bp. Genomic DNA positive controls were unmethylated DNA from normal lymphocytes for UMA allele and CpGenomeUniversal Methylated DNA for the MA allele (Intergen Company). Multiplexed PCR with all four primers was performed in a final volume of 25 μl in a mixture containing 125 μM each dNTP, 1.5 mM $MgCl_2$, 1 μM each of the primers, 0.05 U/μl of Thermo-Start DNA Polymerase (ABgene, Surrey, UK), and 50 ng of the bisulfite-modified DNA. MS-PCR cycling conditions were as follows: 15′ at 95°C, for DNA polymerase activation; 35 cycles each consisting of denaturation at 95°C for 30″, primer annealing at 54°C for 30″, and elongation at 72°C for

30″. MS-PCR products were analyzed by 3% metaphore gel electrophoresis. To determine whether the MA or UMA sequence of the DXS8059 marker was lost, normal ad tumoral tissues were compared for the intensity of MS-PCR bands corresponding to the methylated and unmethylated CpG sites using the Gel Doc software (Biorad). The following formula was employed: $(\text{alleleUMA/alleleMA})_{\text{NORM}}/(\text{alleleUMA/alleleMA})_{\text{TUM}}$. Values less than 1 were indicative of LOH on MA allele, and values greater than 1 were for LOH on UMA allele.

Immunohistochemistry

The following primary monoclonal antibodies were used: anti-metalloproteinase 2 (MMP-2, clone 1B4, Novocastra, Newcastle, UK; working dilution, 1/50); anti-metalloproteinase 9 (MMP-9, clone 2C3, Novocastra; working dilution, 1/50). Sections were treated with 10 mM citrate, pH 6.0, in a 750-W microwave oven for three 5′ cycles for antigen retrieval before immunostaining. Immunostaining was done with the streptavidin-biotin kit (LSAB2, Dakocytomation, Glostrup, Denmark) according to the manufacturer's specifications. Slides were counterstained with hematoxylin. Colon carcinomas served as positive control for MMP-2 and liver for MMP-9. Negative controls consisted of substituting normal mouse serum for the primary antibodies. The staining was scored as follows: no positive cells (−); <20% of the tumor cells staining positive (+); 20–50% of the tumor cells staining positive (++); >50% of the tumor cells staining positive (+++) [37].

Statistics

The data obtained in the primary tumors and metastases were evaluated separately and examined with χ^2 analysis and Fisher's exact test with the SPSS 11.5 statistical software package (SPSS, Inc., Chicago, IL). *P* values less than 0.05 were considered statistically significant, and two-sided *P* values were used.

Results

Microallelotyping analysis on X chromosome

The results of the LOH analysis are summarized in Table 3. In all 17 patients, LOH was detected for at least 1 of the 24 tested polymorphic markers mapping at the whole X chromosome. In one case (#13), LOH was identified with all microsatellites studied. Metastases showed the same

Table 3 Allelotyping results of 17 female patients with digestive malignant endocrine tumors (cases #1–12 WDEC, cases #13–17 PDEC)

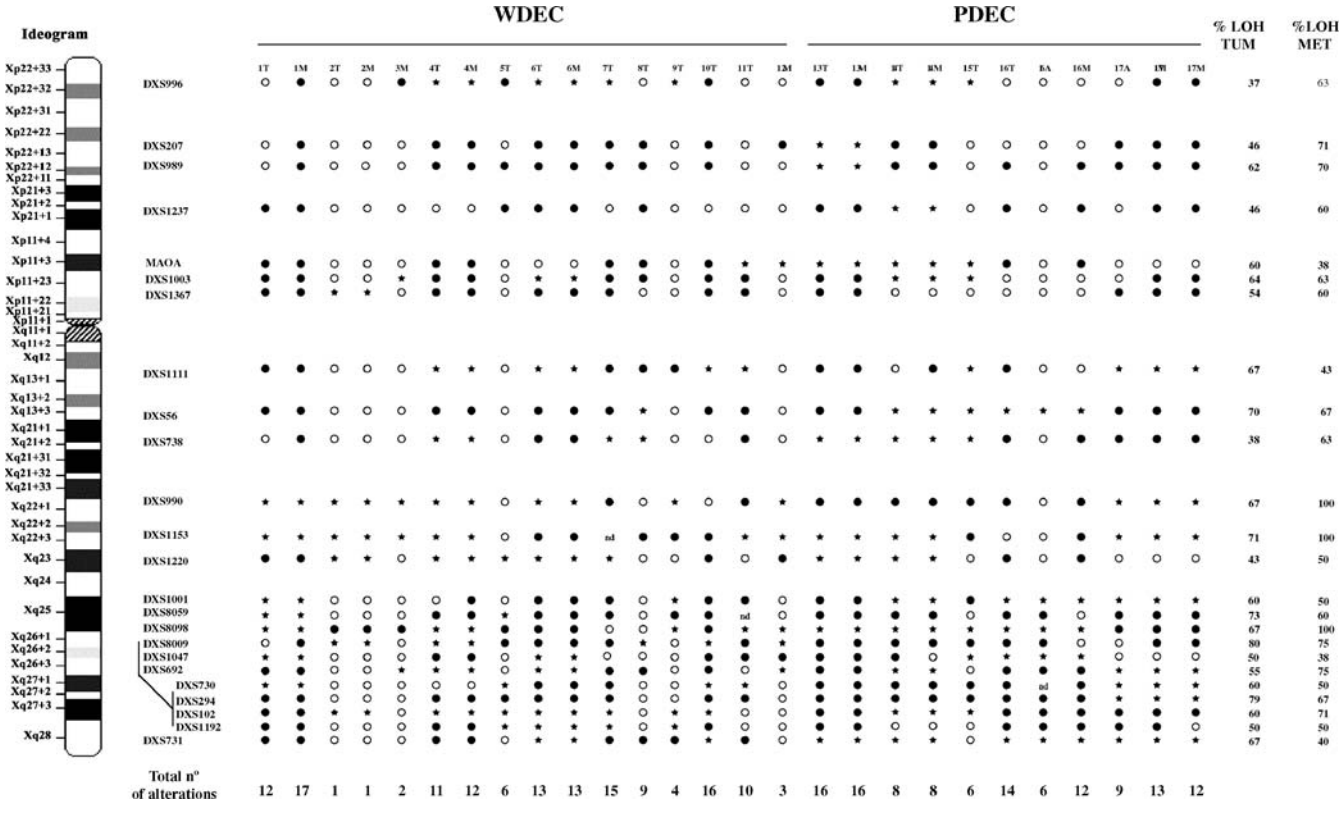

• LOH, ○ retention of heterozygosity, ★ noninformative, *nd* not determined, *T* primary tumor, *M* metastasis, *A* esocrine component

pattern of alterations as the primary tumors except in cases #1 and #4 in which allelic losses were found for additional loci (five in case #1; one in case #3). Overall, the LOH frequency for all informative loci investigated was 59% for primaries and 61% for metastases, with higher rates for PDECs as compared to WDECs primaries (72 vs. 55%, $p<0.015$) and metastases (81 vs. 48%, $p<0.00005$). The frequency of LOH at the individual 24 microsatellite loci varied from 39% in DXS996 locus to 82% in DXS8098 locus. The total degree of informativeness for the microsatellite markers used in the study was of 70% (38–93%), without any difference between WDEC (72%) and PDEC (66%).

Two common regions of deletion were identified on the long arm of X chromosome. Overall, the most frequent losses were observed at Xq25 region with a LOH frequency for DXS8059, DXS8098, and DXS8009 loci as high as 73, 67, and 80%, respectively, in primary tumors and 60, 100, and 75%, respectively, in metastases. No statistical significant difference was observed at any level between primary and metastatic tissues.

In particular, the LOH rate for primary carcinomas in the small region (of approximately 4.6 Mbp in length) defined by DXS8059 and DXS8009 was significantly higher than in the rest of the chromosome ($p<0.04$). No statistically significant differences were observed between WDECs and PDECs both in primary (68 vs. 87%, respectively) and metastatic tissues (64 vs. 83%, respectively). Moreover, DXS8098 was the only locus lost in WDEC case #2, whereas in case #3, its deletion was associated with a loss of only one of the other p-ter markers. Finally, all informative markers in this region were lost in nine cases (#1mt, #4, #5, #6, #10, #13, #14, #16, #17mt).

The overall frequency of LOH was elevated also for DXS294 (primary, 79% vs metastases, 67%) and DXS102 (primary, 60% vs metastases 71%) loci mapping the chromosomal region Xq26 (of approximately 1 Mbp in length). The rate of losses at these loci was significantly higher in PDEC (primary and metastasis 100%) than in WDEC (primary 62%, metastasis, 49%). For all cases investigated, the degree of markers' informativeness in the chromosomal regions at Xq25 and Xq26 was of 69 and 70% respectively, with no difference between WDECs and PDECs.

Other microsatellite markers with high LOH rate in WDECs and PDECs both in primary and metastatic tissues were DXS989 (62 and 70%), DXS56 (70 and 67%), DXS990 (67 and 100%), and DXS1153 (71 and 100%) located on Xp22.13, Xq13.2–13.3, Xq21.33, and Xq22.1–22.3 respectively. No statistically significant difference was observed in the LOH frequency of these microsatellite markers between WDECs and PDECs.

To evaluate the relation of allelic losses on X chromosome with those on 3p, reported by several studies [8, 15, 27, 31] to be associated with malignant progression, we have investigated four microsatellite markers of 3p (D3S1621, D3S1100, D3S1478, D3S1481). In our case, the overall 3p LOH rate was 48% in primary tumor and 37.5% in metastases with significant difference between primary PDECs (90%) and WDECs (19%) ($p<0.0003$). When the LOH rates at Xq25 and Xq26 were compared with those at 3p, an inverse correlation was found for WDECs (Xq25, $p<0.0007$; Xq26, $p<0.002$). Conversely, no differences were found for PDECs.

The nonendocrine component of the two biphenotypic tumors (#16, #17) consistently showed a lower number of LOH than its endocrine counterpart (Table 3).

Methylation analysis on X chromosome

Methylation analysis of CpG islands in microsatellite loci may provide information concerning chromosome inacti-

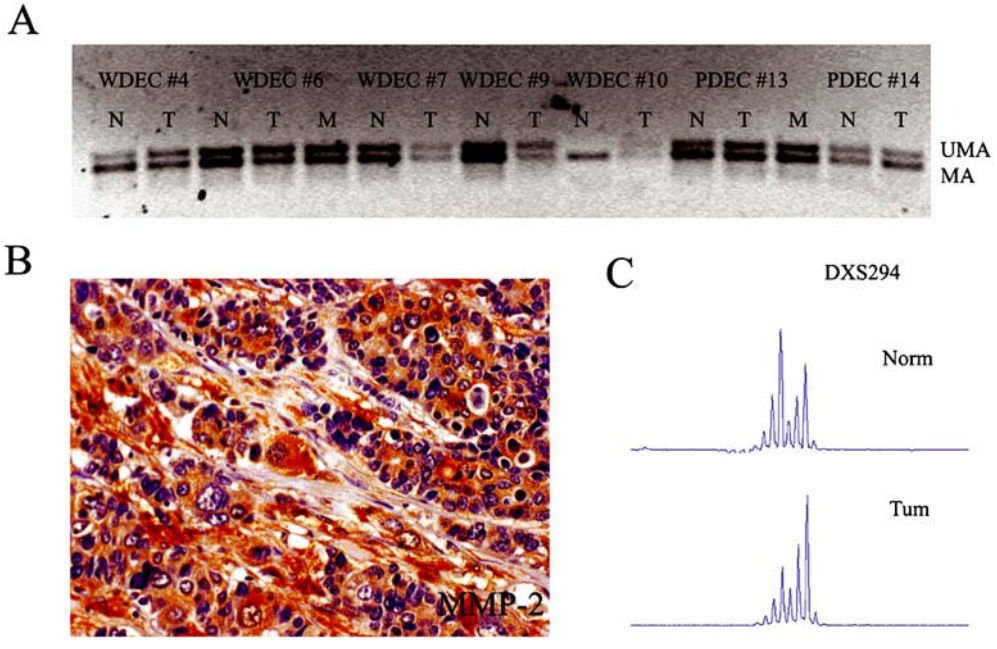

Fig. 1 **a** Results of methylation-specific PCR of a CpG site located at position 225–226 of the DXS8059 marker in malignant gastroenteropancreatic endocrine tumors. Analysis of the intensity of the bands using the Gel Doc software showed LOH of the methylated allele in all samples except the PDEC #14 (*N* normal, *T* tumor tissue, *M* metastatic tissue, *UMA* unmethylated allele, *MA* methylated allele). **b** Intense immunohistochemical expression of MMP-2 in a case of PDEC (#13). **c** Electropherograms of the same tumor showing LOH for DXS294 marker in tumoral tissue

Table 4 Immunohistochemical expression and LOH status in 10 female patients with gastroenteropancreatic endocrine carcinomas

Case #	Type	Xq25LOH	Methylation in Xq25	Xq26LOH	Immunohistochemical expression	
					MMP-2	MMP-9
2	Primary	Present	MA	Absent	+	−
3	Metastasis	Present	MA	Absent	−	−
6	Primary	Present	MA	Present	−	−
7	Primary	Present	MA	Present	+	−
9	Primary	Present	MA	Absent	+	−
11	Primary	Present	MA	Present	−	−
13	Primary	Present	MA	Present	+++	−
14	Primary	Present	UMA	Present	+	−
	Metastasis	Present	UMA	Present	−	−
15	Primary	Present	MA	Present	+++	+
16	Primary	Present	UMA	Present	−	+
	Metastasis	Present	UMA	Present	+	−

MA Methylated, *UMA* unmethylated

vation. To determine if the X copy undergoing LOH in our series of GEP carcinomas was active or inactive, we selected DXS8059 marker containing two CpG sites available for methylation analysis (Fig. 1) because the DXS8098 marker, which showed the highest rate of LOH in our series, does not contain any CpG site. The five WDECs (#4, #6, #7, #9, and #10) and the four PDECs (#13, #14, #16, and #17) which exhibited LOH at DXS8059 marker were analyzed (see Table 4). Our results showed that Xq25 LOH occurred in the active (unmethylated) allele of cases #14 and #16 and in the inactive allele of the remaining cases.

Immunohistochemistry

To determine the potential implication of myeloid elf-1 like factor (MEF), a putative tumor suppressor gene located on Xq26, tumor samples from 10 cases were investigated by immunohistochemistry for MMP-2 and MMP-9 that are negatively regulated by MEF. The immunohistochemical results are summarized in Table 4. The expression of MMP-2 was detected in 5/9 (56%) primary tumors, with strong positivity (+++) in two cases and weak and focal positivity (+) in three cases. The expression of MMP-9 was detected in 2/9 (22%) primary tumors, one of these showing moderate positivity (++), the other weak staining. No relation between MMP-2 or MMP-9 and Xq26 LOH was found (Table 4). It is worth noting, however, that the two cases with strong MMP-2 positivity showed Xq26 LOH (Fig. 1b).

Discussion

Different regions of X chromosome were shown to be deleted in malignant tumors of different organs including breast [28], uterine cervix [18], ovary [6], prostate [19], and kidney [16]. The present work shows high frequency of LOH on X chromosome in a series of malignant GEP endocrine primaries (59%) and metastases (61%), with a significantly higher LOH rate in PDEC (72% primaries and 81% metastases) than in WDEC (55% and 48%). This latter finding is in accordance with the results of a recent work by Furlan et al. [12] based on a microallelotyping analysis of chromosomes 1, 3, 5q, 6, 11, and 18, showing a significantly higher frequency of chromosomal derangements in PDECs than in WDECs of the GEP tract. Moreover, no recurrent allelic imbalance at specific chromosomal regions was detected in PDECs according to the primary anatomic site. Similar findings were also reported in a previous study from our laboratory [30]. The present results demonstrate that X chromosome is heavily involved in the chromosomal instability of PDECs.

Our study also aimed at assessing common deletion regions on X chromosome in an attempt to focus on potential TSGs implicated in endocrine tumor pathogenesis and malignancy. The existence of such genes is supported by the X chromosome involvement in the establishment of immortality and in the control of cell proliferation in vitro [21, 34].

Frequent X chromosome LOH has been detected in carcinomas of gallbladder [40], breast [28], ovary [6], and in renal oncocytomas [39]. In neuroendocrine tumors, X chromosome deletions have been reported in parathyroid [11], pancreatic, and gastric tumors [9, 25, 29]. Such losses were associated with malignancy in endocrine tumors of the stomach and pancreas, whereas they were virtually absent in benign neoplasms. However, the small number of markers tested in these studies did not allow to identify a common minimal chromosomal region of deletions [9, 29].

The present study of malignant GEP endocrine tumors relied on a panel of 24 polymorphic microsatellite markers on the whole X chromosome and demonstrated that the two chromosomal regions Xq25 and Xq26 were most frequently lost. The highest frequency of LOH (67% in primaries and 100% in metastases) was found for DXS8098 marker mapping on Xq25 between the two

other frequently deleted loci, DXS8059 and DXS8009 (73 and 80% in primaries and 60 and 75% in metastases, respectively). The same LOH pattern with the highest frequency of losses for DXS8098 and high LOH rates for DXS8009 and DXS8059 was reported in breast carcinomas and associated with larger tumor size, higher histological grade, and axillary lymph node metastasis [28].

For the development of neoplasia, complete inactivation of the tumor suppressor function is necessary in autosomal chromosomes requiring the inactivation of both alleles [22]. In the X chromosome, one of the two copies is almost entirely inactivated by DNA methylation during early development [28]. In the present study, we determined which copy, active or inactive, underwent loss of the Xq25 region. Our results showed that the loss occurs preferentially on the inactive X chromosome. Similar prevalence of Xq25 losses of the inactive Xq has been also reported in ovarian and breast carcinomas [5, 6, 28]. The most likely explanation for this phenomenon is that the putative tumor suppressor gene(s) in Xq25 escapes X inactivation and is expressed from both chromosomes or from the inactive X chromosome alone [28]. In addition, this hypothesis implies that if the putative TSG is expressed on the active X chromosome it may be inactivated by point mutations [28].

There are several putative tumor suppressor genes within the Xq25 chromosome region, here identified as frequently deleted. Among them, ODZ1 and SH2D1A appear as good candidates. ODZ1 encodes for Tenascin, an oligomeric glycoprotein of the extracellular matrix involved in morphogenetic movements, tissue patterning, repair, and tumor invasion [17, 24, 26]. SH2D1A was found mutated in the X-linked lymphoproliferative disease [23] and in associated non-Hodgkin lymphomas [3].

Additional X markers were also found frequently deleted in the present study, including DXS294 (79% in primaries and 67% in metastases) and DXS102 (60% in primaries and 71% in metastases), both mapping at Xq26. This chromosomal region appears to be involved in the development of different tumors including ovarian [6] and breast carcinomas [7] and endocrine tumors of the lung [10]. In ovarian carcinomas, Xq25–26.1 LOH has been associated with higher histological grade and advanced tumor stage [6].

Candidate tumor suppressor genes mapping at Xq26 are myeloid elf-1 like factor MEF and Glypican-3 (GPC-3). MEF (ELF4) is an ETS-transcription factor with tumor suppressive activity as demonstrated in cell lines of human nonsmall cell lung carcinoma [35]. MEF may have an important role in tumor differentiation and angiogenesis by suppressing the transcription and promoter activities of the genes encoding for the matrix metalloproteinases, MMP-2 and MMP-9, and interleukin-8 [13, 35]. In our study, the immunohistochemical expression of MMP-2 was intense in two PDECs only, both with Xq26 LOH, whereas MMP-9 was consistently negative with the exception of two cases showing weak positivity (Table 3). These results do not support the involvement of the tumor suppressor gene MEF in most GEP endocrine carcinomas. GPC-3 is a heparan sulfate proteoglycan linked to the cell membrane by a glycosyl–phosphatidylinositol anchor and is involved in the progression of several types of malignant tumors, including mesotheliomas, ovarian, and lung carcinomas [20].

Finally, several studies pointed out the significant association of 3p LOH with malignancy in GEP endocrine tumors [8, 15, 27, 31]. In the present study, 3p LOH rates were found inversely correlated with those at Xq25–26 in WDECs, indicating an independent involvement of the two chromosome regions in the pathogenesis of well-differentiated malignant endocrine neoplasms. On the contrary, no differences were found in PDECs in keeping with the high chromosomal instability of this type of tumors. In this study, 3p LOH rates in PDECs were higher than those found in previous investigations from our laboratory [30, 31]. The use of a larger number of 3p markers in the present study may justify such difference, indicating that PDECs have more extended allelic losses on 3p. As previously demonstrated, in fact, the extension of 3p LOH increases with tumor aggressiveness [1].

In conclusion, our data suggest that LOH on X chromosome is an important event in the carcinogenesis of GEP endocrine carcinomas and reveal the existence of two common chromosomal deletion regions, mapping at Xq25 and at Xq26 and harboring candidate tumor suppressor genes potentially involved in the progression and malignant behavior of these tumors.

Acknowledgements We wish to thank Mrs. Emilia Corradini for her histological assistance and Dott. Nicoletta Campanini for immunohistochemistry.

References

1. Barghorn A, Komminoth P, Bachmann D, Rutimann K, Saremaslani P, Muletta-Feurer S, Perren A, Roth J, Heitz PU, Speel EJ (2001) Deletion at 3p25.3–p23 is frequently encountered in endocrine pancreatic tumours and is associated with metastatic progression. J Pathol 194:451–458
2. Beckmann MW, Picard F, An HX, van Roeyen CR, Dominik SI, Mosny DS, Schnurch HG, Bender HG, Niederacher D (1996) Clinical impact of detection of loss of heterozygosity of BRCA1 and BRCA2 markers in sporadic breast cancer. Br J Cancer 73:1220–1226
3. Brandau O, Schuster V, Weiss M, Hellebrand H, Fink FM, Kreczy A, Friedrich W, Strahm B, Niemeyer C, Belohradsky BH, Meindl A (1999) Epstein–Barr virus-negative boys with non-Hodgkin lymphoma are mutated in the SH2D1A gene, as are patients with X-linked lymphoproliferative disease (XLP). Hum Mol Genet 8:2407–2413
4. Chen YJ, Vortmeyer A, Zhuang Z, Gibril F, Jensen RT (2004) X-chromosome loss of heterozygosity frequently occurs in gastrinomas and is correlated with aggressive tumor growth. Cancer 100:1379–1387
5. Cheng PC, Gosewehr JA, Kim TM, Velicescu M, Wan M, Zheng J, Felix JC, Cofer KF, Luo P, Biela BH, Godorov G, Dubeau L (1996) Potential role of the inactivated X chromosome in ovarian epithelial tumor development. J Natl Cancer Inst 88:510–518
6. Choi C, Cho S, Horikawa I, Berchuck A, Wang N, Cedrone E, Jhung SW, Lee JB, Kerr J, Chenevix-Trench G, Kim S, Barrett JC, Koi M (1997) Loss of heterozygosity at chromosome segment Xq25–26.1 in advanced human ovarian carcinomas. Genes Chromosomes Cancer 20:234–242

7. Choi C, Kim MH, Juhng SW (1998) Loss of heterozygosity on chromosome XP22.2–p22.13 and Xq26.1–q27.1 in human breast carcinomas. J Korean Med Sci 13:311–316
8. Chung DC, Smith AP, Louis DN, Graeme-Cook F, Warshaw AL, Arnold A (1997) A novel pancreatic endocrine tumor suppressor gene locus on chromosome 3p with clinical prognostic implications. J Clin Invest 100:404–410
9. D'Adda T, Candidus S, Denk H, Bordi C, Hofler H (1999) Gastric neuroendocrine neoplasms: tumour clonality and malignancy-associated large X-chromosomal deletions. J Pathol 189:394–401
10. D'Adda T, Bottarelli L, Azzoni C, Pizzi S, Bongiovanni M, Papotti M, Pelosi G, Maisonneuve P, Antonetti T, Rindi G, Bordi C (2005) Malignancy-associated X chromosome allelic losses in foregut endocrine neoplasms: further evidence from lung tumors. Mod Path 18:795–805
11. Farnebo F, Teh BT, Dotzenrath C, Wassif WS, Svensson A, White I, Betz R, Goretzki P, Sandelin K, Farnebo LO, Larsson C (1997) Differential loss of heterozygosity in familial, sporadic, and uremic hyperparathyroidism. Hum Genet 99:342–349
12. Furlan D, Cerutti R, Uccella S, La Rosa S, Rigoli E, Genasetti A, Capella C (2004) Different molecular profiles characterize well-differentiated endocrine tumors and poorly differentiated endocrine carcinomas of the gastroenteropancreatic tract. Clin Cancer Res 10:947–957
13. Hedvat CV, Yao J, Sokolic RA, Nimer SD (2004) MEF is a potent activator of interleukin-8 expression in hematopoietic cells. J Biol Chem 279:6395–6400
14. Herman JG, Graff JR, Myohanen S, Nelkin BD, Baylin SB (1996) Methylation-specific PCR: a novel PCR assay for methylation status of CpG islands. Proc Natl Acad Sci U S A 93:9821–9826
15. House MG, Herman JG, Guo MZ, Hooker CM, Schulick RD, Lillemoe KD, Cameron JL, Hruban RH, Maitra A, Yeo CJ (2003) Aberrant hypermethylation of tumor suppressor genes in pancreatic endocrine neoplasms. Ann Surg 238:423–431
16. Jiang F, Richter J, Schraml P, Bubendorf L, Gasser T, Sauter G, Mihatsch MJ, Moch H (1998) Chromosomal imbalances in papillary renal cell carcinoma: genetic differences between histological subtypes. Am J Pathol 153:1467–1473
17. Jones FS, Jones PL (2000) The tenascin family of ECM glycoproteins: structure, function, and regulation during embryonic development and tissue remodelling. Dev Dyn 218:235–259
18. Kersemaekers AM, van de Vijver MJ, Kenter GG, Fleuren GJ (1999) Genetic alterations during the progression of squamous cell carcinomas of the uterine cervix. Genes Chromosomes Cancer 26:346–354
19. Kibel AS, Faith DA, Bova GS, Isaacs WB (2003) Xq27–28 deletions in prostate carcinoma. Genes Chromosomes Cancer 37:381–388
20. Kim H, Xu GL, Borczuk AC, Busch S, Filmus J, Capurro M, Brody JS, Lange J, D'Armiento JM, Rothman PB, Powell CA (2003) The heparan sulfate proteoglycan GPC3 is a potential lung tumor suppressor. Am J Respir Cell Mol Biol 29:694–701
21. Klein CB, Conway K, Wang XW, Bhamra RK, Lin XH, Cohen MD, Annab L, Barrett JC, Costa M (1991) Senescence of nickel-transformed cells by an X chromosome: possible epigenetic control. Science 251:796–799
22. Knudson AGJ (1971) Mutation and cancer: statistical study of retinoblastoma. Proc Natl Acad Sci U S A 68:820–823
23. Latour S, Veillette A (2003) Molecular and immunological basis of X-linked lymphoproliferative disease. Immunol Rev 192:212–214
24. Minamitani T, Ariga H, Matsumoto K (2002) Adhesive defect in extracellular matrix tenascin-X-null fibroblasts: a possible mechanism of tumor invasion. Biol Pharm Bull 25:1472–1475
25. Missiaglia E, Moore PS, Williamson J, Lemoine NR, Falconi M, Zamboni G, Scarpa A (2002) Sex chromosome anomalies in pancreatic endocrine tumors. Int J Cancer 98:532–538
26. Murphy-Ullrich JE (2001) The de-adhesive activity of matricellular proteins: is intermediate cell adhesion an adaptive state? J Clin Invest 107:785–790
27. Nikiforova MN, Nikiforov YE, Biddinger P, Gnepp DR, Grosembacher LA, Wajchenberg BL, Fagin JA, Cohen RM (1999) Frequent loss of heterozygosity at chromosome 3p14.2–3p21 in human pancreatic islet cell tumours. Clin Endocrinol 51:27–33
28. Piao Z, Malkhosyan SR (2002) Frequent loss Xq25 on the inactive X chromosome in primary breast carcinomas is associated with tumor grade and axillary lymph node metastasis. Genes Chromosomes Cancer 33:262–269
29. Pizzi S, D'Adda T, Azzoni C, Rindi G, Grigolato P, Pasquali C, Corleto VD, Delle Fave G, Bordi C (2002) Malignancy-associated allelic losses on the X-chromosome in foregut but not in midgut endocrine tumours. J Pathol 196:401–407
30. Pizzi S, Azzoni C, Bassi D, Bottarelli L, Milione M, Bordi C (2003) Genetic alterations in poorly differentiated endocrine carcinomas of the gastrointestinal tract. Cancer 98:1273–1282
31. Pizzi S, Azzoni C, Bottarelli L, Campanini N, D'Adda T, Pasquali C, Rossi G, Rindi G, Bordi C (2005) RASSF1A promoter methylation and 3p21.3 loss of heterozygosity are features of foregut, but not midgut and hindgut, malignant endocrine tumours. J Pathol 206:409–416
32. Russell AJ, Sibbald J, Haak H, Keith WN, McNicol AM (1999) Increasing genome instability in adrenocortical carcinoma progression with involvement of chromosomes 3, 9 and X at the adenoma stage. Br J Cancer 81:684–689
33. Sakakura C, Mori T, Sakabe T, Ariyama Y, Shinomiya T, Date K, Hagiwara A, Yamaguchi T, Takahashi T, Nakamura Y, Abe T, Inazawa J (1999) Gains, losses, and amplifications of genomic materials in primary gastric cancers analyzed by comparative genomic hybridization. Genes Chromosomes Cancer 24:299–305
34. Sandberg AA (1983) The X chromosome in human neoplasia, including sex chromatin and congenital conditions with X-chromosome anomalies. In: Sandberg AA (ed) Cytogenetics of the mammalian X chromosome. Alan R. Liss, New York pp 459–498
35. Seki Y, Suico MA, Uto A, Hisatsune A, Shuto T, Isohama Y, Kai H (2002) The ETS transcription factor MEF is a candidate tumor suppressor gene on the X chromosome. Cancer Res 62:6579–6586
36. Solcia E, Capella C, Klöppel G, Heitz PU, Sobin LH, Rosai J (2000) Endocrine tumours of the gastrointestinal tract. In: Solcia E, Klöppel G, Sobin LH (eds) Histological typing of endocrine tumours. Springer, Berlin Heidelberg New York pp 61–68
37. Talvensaari-Mattila A, Paakko P, Hoyhtya M, Blanco-Sequeiros G, Turpeenniemi-Hujanen T (1998) Matrix metalloproteinase-2 immunoreactive protein: a marker of aggressiveness in breast carcinoma. Cancer 83:1153–1162
38. Terracciano LM, Bernasconi B, Ruck P, Stallmach T, Briner J, Sauter G, Moch H, Vecchione R, Pollice L, Pettinato G, Gurtl B, Ratschek M, De Krijger R, Tornillo L, Bruder E (2003) Comparative genomic hybridization analysis of hepatoblastoma reveals high frequency of X-chromosome gains and similarities between epithelial and stromal components. Human Pathol 34:864–871
39. Thrash-Bingham CA, Salazar H, Greenberg RE, Tartof KD (1996) Loss of heterozygosity studies indicate that chromosome arm 1p harbors a tumor suppressor gene for renal oncocytomas. Genes Chromosomes Cancer 16:64–67
40. Wistuba II, Tang M, Maitra A, Alvarez H, Troncoso P, Pimentel F, Gazdar AF (2001) Genome-wide allelotyping analysis reveals multiple sites of allelic loss in gallbladder carcinoma. Cancer Res 61:3795–3800

Virchows Arch (2006) 448: 127–134
DOI 10.1007/s00428-005-0062-8

ORIGINAL ARTICLE

Rahmawati Minhajat · Daisuke Mori · Fumio Yamasaki · Yasuo Sugita · Toshimi Satoh · Osamu Tokunaga

Endoglin (CD105) expression in angiogenesis of colon cancer: analysis using tissue microarrays and comparison with other endothelial markers

Received: 11 April 2005 / Accepted: 3 August 2005 / Published online: 22 September 2005

Abstract Some markers of angiogenic endothelial cells are emerging as targets of cancer therapy. The present study compares the expression of CD105 with that of other endothelial markers in all tissue layers during the development of colon cancer. We immunohistochemically analyzed the expression of the colon adenoma–carcinoma sequence by endothelial cells using a panel of eight endothelial markers. We examined sections from endoscopic mucosal resection and surgical resection of tubular adenoma (n=31), carcinoma in adenoma (n=11), and adenocarcinoma (n=34). Cylindrical cores were punched out from donor paraffin blocks of normal mucosa adjacent to tumors, from tumor lesions of mucosa, submucosa, muscularis propria, subserosa, and serosa, and from lymph node metastases. CD31 (PECAM-1) was universally expressed in the blood vessels of adenoma–carcinoma lesions as well as in normal mucosal vessels (80–95%), with no significant differences. In contrast, cancer-associated blood vessels (up to 80%) and cancer cells themselves expressed high levels of CD105. In normal mucosa, CD105 was weakly expressed in endothelial cells of capillaries (≦21%), and significant differences in its expression in endothelial cells between the normal mucosa and adenoma, carcinoma in adenoma, and adenocarcinoma were found. Flt-1, Flk-1, transforming growth factor-β1, transforming growth factor-β receptor II, and CD44 were strongly expressed in the cancer cells but were not expressed in the blood vessels. Vascular endothelial growth factor was expressed at <30% in the blood vessels of adenoma, carcinoma in adenoma, and carcinoma. Moreover, this study provided evidence that CD105 was expressed exclusively in endothelial blood vessels by double immunostaining of CD105 and D2-40. The present study shows that de novo blood vessels of colon cancer specifically express CD105. These findings provide the basis for novel antiangiogenic cancer therapies.

Keywords Colon tumor · CD105 · Tissue microarray · Angiogenesis · Endothelial markers

R. Minhajat · D. Mori · F. Yamasaki · Y. Sugita · T. Satoh · O. Tokunaga (✉)
Department of Pathology and Biodefense,
Faculty of Medicine, Saga University,
5-1-1 Nabeshima,
Saga, 849-8501, Japan
e-mail: tokunao@cc.saga-u.ac.jp
Tel.: +81-952-342230
Fax: +81-952-342055

Introduction

Colon cancer is a widespread human disease that is one of the major causes of morbidity and mortality worldwide [19]. Most colorectal carcinomas are considered to originate from precursor lesions (adenomas) [18]. Adenoma is thought to progress to carcinoma over many years because of multiple accumulated molecular alterations [25].

Angiogenesis is an important step in the process of cancer growth. It promotes metastatic spread by providing the means for cells to detach from the primary tumor and to travel in the bloodstream to distant metastatic sites. Moreover, the most important prognostic factor for colon cancer is the depth of cancer invasion. Cancer is always accompanied by angiogenesis as it grows and invades the surrounding tissues, and angiogenesis is a complex of endothelial cell growth and stem cell differentiation brought about by interactions of growth factors and their ligands.

Vascular endothelial growth factor (VEGF) is a potent mitogen and cytoprotective factor for vascular endothelial cells, and its receptors (VEGFR-1/Flt-1 and VEGFR-2/Flk-1), which are expressed exclusively by endothelial and neoplastic cells, have been documented [6, 11, 26].

CD105 is a receptor for transforming growth factor (TGF)-β1 and TGF-β3, and it modulates TGF-β signaling by interacting with TGF-β receptor I (TGF-βRI) and/or TGF-β receptor II (TGF-βRII) [22]. CD105 is predominantly expressed on cellular lineages within the vascular system and is overexpressed on proliferating endothelial cells. Several studies indicate that CD105 is involved in the development of blood vessels and that it represents a

powerful marker of neovascularization of various types of tumors, including colon cancer [1, 4, 8, 9, 17, 28]. CD105 is emerging as a prime vascular target of antiangiogenetic cancer therapy [10]. We reported that the predominantly CD105-positive microvessel count of polyploid-type early colon cancer is higher than that of nonpolyploid-type early cancer [20]. However, to our knowledge, the expression of CD105 in vessels of lesions invading all the various tissue layers during the colon adenoma–carcinoma sequence (adenoma, carcinoma in adenoma, and adenocarcinoma) has not been compared with that of other endothelial markers.

The use of tissue microarrays in colorectal carcinoma has been validated by analyzing the immunohistochemical expression of some markers [12]. We therefore compared the expression of CD105 in several hundred target spots with that of other endothelial markers in all tissue layers during the development of colon cancer using tissue microarrays and immunohistochemistry. To specifically differentiate the vascular expression of CD105 and CD31 as pan-endothelial markers, we compared them using double immunofluorescence. Additionally, to exclude the idea that the CD105-stained vessels represent lymphatic vessels, we performed a double immunohistochemistry of CD105 and D2-40, which has been reported as a new selective marker for lymphatic endothelial markers [13]. We also compared the vascular expression of the antibody between the normal mucosa adjacent to tumors and the neoplastic lesions.

Materials and methods

Tumor samples

Between 1998 and 2003, 36 consecutive resected colon samples and 40 endoscopic mucosal resection (EMR) samples from 76 patients (42 men, 34 women; age range 39–95 years) with colonic tumors were obtained from the files of the Department of Pathology, Faculty of Medicine, Saga University and its affiliated hospital. The specimens were formalin-fixed and paraffin-embedded, and the tumor was diagnosed from observations of sections stained with hematoxylin and eosin (H&E). Histological subtypes were classified according to the Japanese classification of colorectal carcinoma [29]: 31 tubular adenomas (10 mild, 10 moderate, and 11 severe atypias), 11 carcinomas in adenoma (focally expressed cancer cells in adenoma), and 34 adenocarcinomas (16 well, 16 moderate, and 2 poor differentiations). Table 1 shows the details of the patients and their diseases.

Tissue microarray

To identify the targets of core samples, we examined the microscopic features of each layer of invasion on slide sections and marked the locations to be punched out (Fig. 1).

Table 1 Clinicopathological data

Variable	Number
Number of patient	76
Age (years)	
Range (median)	39–95 (67)
Gender	
Male	42
Female	34
Histopathology	
Tubular adenoma	31
Mild atypia (low-grade dysplasia)	10
Moderate atypia	10
Severe atypia (high-grade dysplasia)	11
Carcinoma in adenoma	11
Adenocarcinoma	34
Well differentiated	16
Moderately differentiated	16
Poorly differentiated	2
Tissue cores	
Normal adjacent tumor	76
Depth of invasion	
Mucosa	76
Submucosa	33
Muscular propria	31
Subserosa	25
Serosa	6
Lymph nodes	11

Under a light microscope, we selected and marked areas of normal mucosa and representative tumor from each layer on H&E slides and corresponding paraffin blocks. The tissue microarrayer (Beecher Instruments, Sun Prairie, WI, USA) was used to prepare cylindrical cores of 1.5 mm in diameter. Cores were punched out from donor blocks and placed in recipient blocks.

Two array blocks of 258 cores were derived from the normal mucosa adjacent to tumors (n=76), from tumor lesions from mucosa (n=76), submucosa (n=33), muscular propria (n=31), subserosa (n=25), and serosa (n=6), and from lymph node metastases (n=11). The depth of each core depended on the extent of tumor cell invasion (Table 1). The array blocks were then incubated for 30 min at 37°C to improve adhesion between the cores and the paraffin of the recipient block.

Double immunostaining

For double immunofluorescence, the tissue array slides were deparaffinized and soaked in 0.01 M citrate buffer (pH 6.0) at 90°C for 40 min for antigen retrieval. The samples were treated with 10 mg/ml bovine serum albumin (BSA) to inhibit nonspecific antibody binding and then were incubated with the primary murine monoclonal antibody CD105 for 1 h at 37°C. After washing thrice

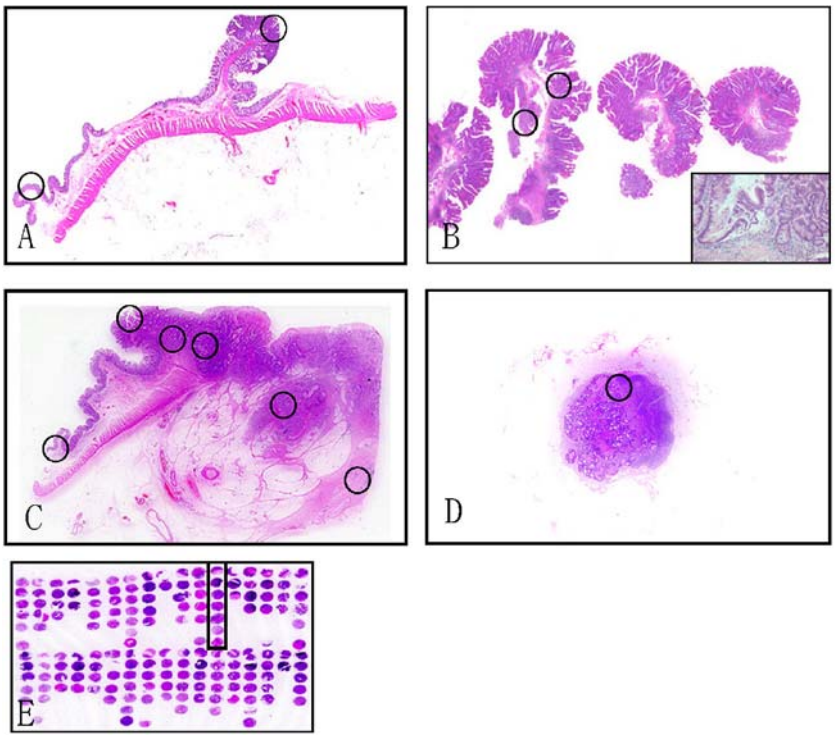

Fig. 1 Sources of punctured cores. Cores were punched out from the normal mucosa and neoplastic layer of adenoma at the mucosal level (**a** and **b**), carcinoma in adenoma (**b**), and normal mucosa, as well as in the mucosa, submucosa, muscular propria, subserosa, and serosa levels (**c**) of cancer tissues, and in lymph node metastasis (**d**). The box shows all layers from one advanced cancer in a representative tissue microarray (**e**). *Inset*: A transition area of adenoma (*left half*) and cancer (*right half*) in the right circle of **b**

with PBS (pH 7.2), the samples were incubated with fluorescein-isothiocyanate (FITC)-labeled secondary rabbit polyclonal antibody against murine immunoglobulin G (IgG) for 30 min at 37°C. To inactivate the primary and secondary antibodies, the samples were heated in the citrate buffer at 90°C for 15 min. This treatment made it possible to carry out the second immunoreaction with the monoclonal antibody. For the second immunoreaction, the same procedure was repeated; the samples were treated with 10 mg/ml BSA, incubated with another primary antibody CD31, and then incubated with rhodamine-labeled secondary antibody. After washing with PBS, FITC-labeled and rhodamine-labeled samples were examined using a fluorescence microscope (Olympus BX60, Tokyo, Japan). To detect nonspecific antibody binding, control sections were incubated with either normal murine or rabbit serum or PBS instead of primary antibody. No staining was observed in these control samples.

For double immunohistochemistry, after incubation with the first primary antibody CD105 and then washing with PBS, the alkaline-phosphatase-labeled secondary rabbit polyclonal antibody against murine IgG was reacted for 30 min at 37°C and visualized with the BCIP/NBT substrate system (Dako, USA), which produces a blue purple color. After microwave heating in ethylenediaminetetraacetic acid (EDTA; pH 8) for 5 min, the specimens were incubated with the second primary antibody (D2-40, mouse monoclonal antibody; Nichirei, Japan) for 3 h. The same procedure with the first step was repeated, and the expression of the second antibody was visualized with the New Fuchsin Substrate Kit (Nichirei), which produces a red color.

Immunohistochemistry

Sections from each array block were cut at a thickness of 4 μm. Briefly, the slides were placed at 60°C for 15 min, deparaffinized in xylene, and rehydrated in a series of graded alcohols. Thereafter, antigen retrieval was performed by microwave heating in EDTA (pH 8) for 6 min (for CD105, mouse monoclonal clone 4G11), then the slides were autoclaved (121°C) in EDTA (pH 8) for 5 min using the appropriate antibodies (for CD44, mouse monoclonal MH114; VEGF, mouse monoclonal clone C-1; Flt-1, rabbit polyclonal C-17; Flk-1, rabbit polyclonal N-931; TGF-β1, rabbit polyclonal V; and TGF-βRII, rabbit polyclonal L-21) and with proteinase K (Dako, Japan) for 10 min (for CD31, mouse monoclonal clone JC70A; Table 2). The sections were incubated with primary antibodies overnight at 4°C, washed, and incubated with goat antimouse or goat antirabbit Igs (EnVision Peroxidase; Dako) for 30 min at room temperature.

Histological assessment

Images of an immunostained section (×200) were captured on a computer (Windows XP, 7000 cl; Fujitsu) with a

Table 2 Used antibody

Antibody	Clone	Pretreatment	Dilution	Company
CD31	Mono	Proteinase K	×20	Dako
CD105	Mono	MW—EDTA	×50	Novocastra
CD44	Mono	AC—EDTA	×50	MBL
VEGF	Mono	AC—EDTA	×100	Santa Cruz
Flt-1	Poly	AC—EDTA	×200	Santa Cruz
Flk-1	Poly	AC—EDTA	×200	Santa Cruz
TGF-β1	Poly	AC—EDTA	×100	Santa Cruz
TGF-βRII	Poly	AC—EDTA	×200	Santa Cruz

Antigen retrieval method for immunohistochemistry
For double immunostaining, see "Materials and methods"
MW Microwave, *AC* citrate buffer

Nikon ACT-1 software by using a Nikon digital camera (DXm 1200) attached to an operator light microscope (Nikon Eclipse, E600). Assessment was performed on live images from each core. Endothelial staining of at least one blood vessel from each core was considered as a positive expression of the blood vessels. Staining of ≧10% of the neoplastic or normal epithelial cells was considered positive in neoplastic or normal epithelial cells. Positive immunoreactivity was graded as weak (+), moderate (++), and intense (+++).

Statistical analysis

Differences in the vascular endothelial expression of an antibody between a normal mucosa and neoplastic mucosal adenoma, carcinoma in adenoma, and adenocarcinoma from each layer were analyzed using the *t* test of independent samples. $P<0.05$ was considered significant.

Results

Double immunofluorescence staining revealed that CD31 (PECAM-1) was universally expressed in small blood vessels and capillaries. On the other hand, CD105 was rarely expressed in normal mucosal vessels; however, in the cancer tissue, CD105 was intensely expressed in newly formed numerous capillaries, which reflect angiogenesis (Fig. 2). After the demonstration that CD105 was specifically expressed in angiogenetic blood vessels, the detailed relationship between markers of blood vessels and tumor histology was assessed by immunohistochemistry.

CD31 was universally expressed in the blood vessels of all layers of adenoma, carcinoma in adenoma, and adenocarcinoma lesions (Fig. 3), as well as in those of normal mucosal blood vessels (80–95%) (Fig. 5). Vascular endothelial expression of CD31 in normal and neoplastic

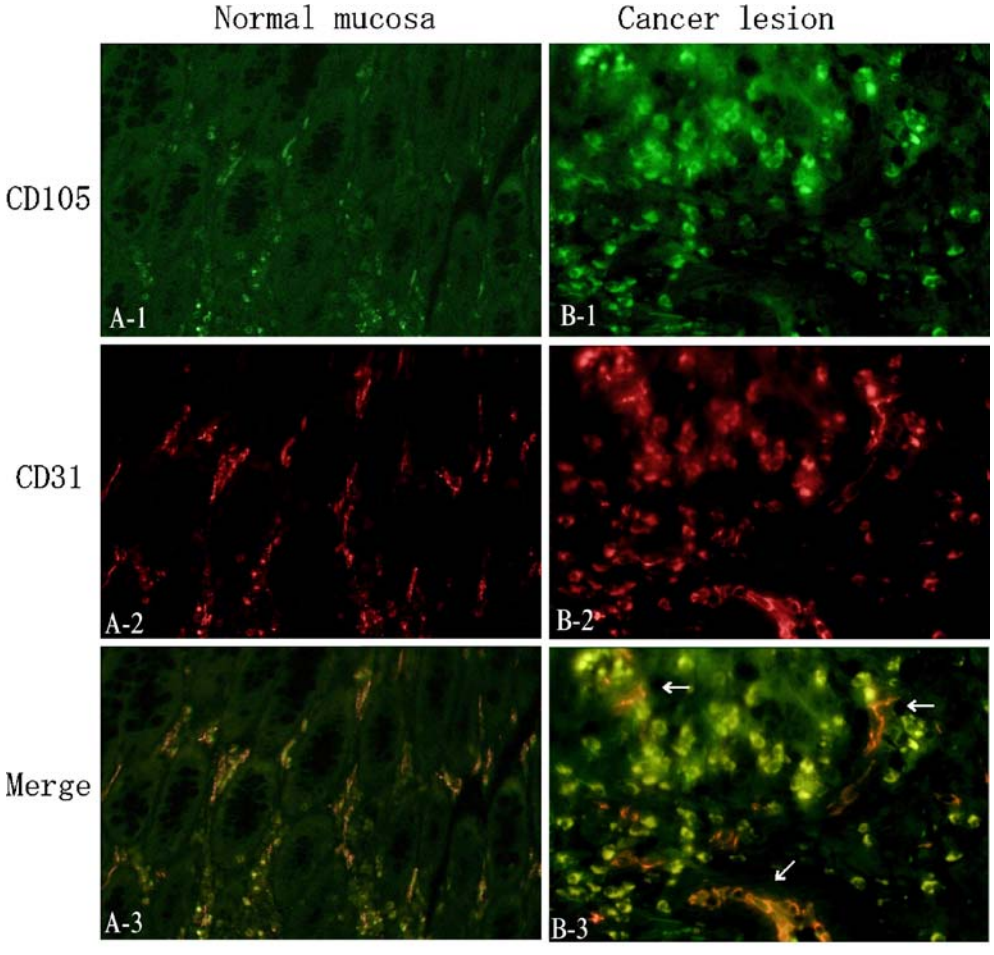

Fig. 2 Double immunofluorescence of CD105 and CD31. Normal mucosa (*upper layer*) and cancer lesion (*lower layer*). CD105 is rarely expressed in the normal mucosa (**a1**) and is intensely expressed in angiogenetic small blood vessels and capillaries (**b1**). An intense vascular expression of CD31 is universally noted in all large and small blood vessels and capillaries (**a2** and **b2**). Their characteristics are demonstrated in the merged images (**a3** and **b3**, *arrows*). Original magnification, ×200

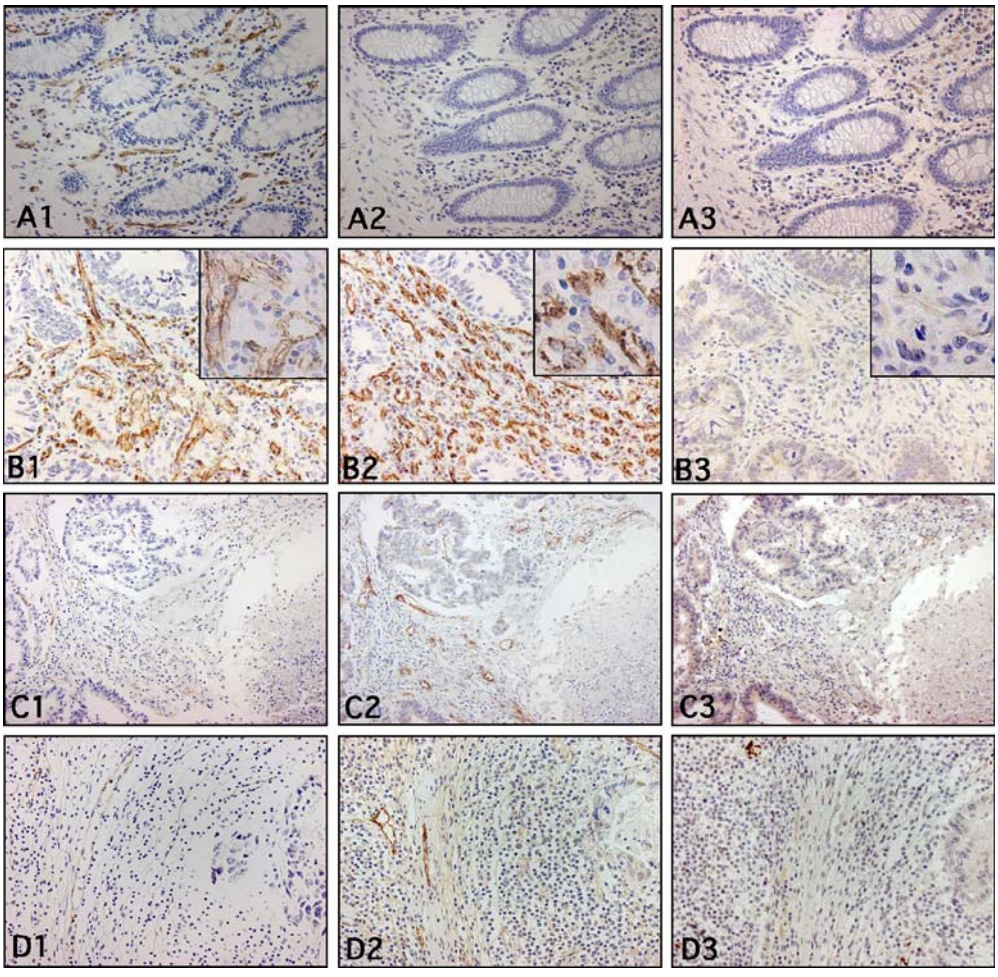

Fig. 3 Expression of CD31 (**a1**–**d1**), CD105 (**a2**–**d2**), and VEGF (**a3**–**d3**). Immunohistochemistry. Original magnification, ×200. Normal mucosa (**a1**–**a3**), neoplastic lesion at mucosal level (**b1**–**b3**), subserosal level (**c1**–**c3**), and lymph node metastasis (**d1**–**d3**) from 1.5-mm tissue cores of the same specimen. Intense vascular expression of CD31 (**a1**); absent expression of CD105 (**a2**) and VEGF (**a3**) in normal mucosa. Intense expression of CD31 (**b1**) in large blood vessels and CD105 (**b2**) in smaller blood vessels from serial sections. Cancer tissues expressed VEGF but not the blood vessels (**b3**). In subserosal layer and lymph node metastasis, only CD105 is expressed (**c2** and **d2**). *Inset*: Original magnification ×400

mucosal layers of adenoma, carcinoma in adenoma, and adenocarcinoma from all layers did not significantly differ (Fig. 5). CD105 was intensely expressed in vascular endothelial cells of neoplastic mucosal adenoma, carcinoma in adenoma, and various layers of adenocarcinoma at a level corresponding to the depth of cancer invasion. The CD105 expression was also seen in the cytoplasm of neoplastic epithelial cells (Fig. 3). CD105 was expressed by 30 and 54% of vascular endothelial cells in the neoplastic mucosa of adenoma and carcinoma in adenoma, respectively. Moreover, CD105 was also expressed in endothelial cells of blood vessels in neoplastic mucosa (65%), submucosa (72%), muscular propria (80%), subserosa (68%), serosa (50%) of adenocarcinoma, and lymph node metastasis (45%). In contrast, only 12, 18, and 21% of blood vessels in normal mucosal layers of adenoma, carcinoma in adenoma, and adenocarcinoma, respectively (Fig. 5), weakly expressed CD105, and its expression in normal epithelial cells was not found. Unlike CD31, vascular endothelial expression of CD105 significantly differed between the normal and neoplastic mucosal layers of adenoma, cancer in adenoma, adenocarcinoma lesions ($p<0.05$, $p<0.05$, and $p<0.0001$, respectively; Fig. 5). Additionally, by using a double immunostaining of CD105 and D2-40, our results demonstrated that CD105 was expressed exclusively in the endothelium of newly formed blood vessels within and around tumors from all layers, and no double-positive staining in the same vessels was found (Fig. 4).

VEGF was expressed on vascular endothelial cells (<30%) and in the cytoplasm of normal and neoplastic cells (<50%) throughout all layers of adenoma, cancer in adenoma, and adenocarcinoma. Vascular expression of VEGF

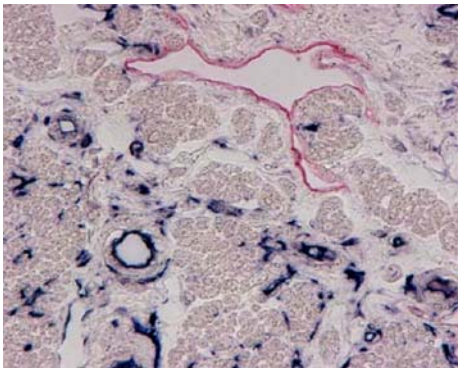

Fig. 4 Double immunostaining of CD105 (*blue purple*) and D2-40 (*red*). No apparent double labeling of CD105 and D2-40 in the vessels. Original magnification, ×200

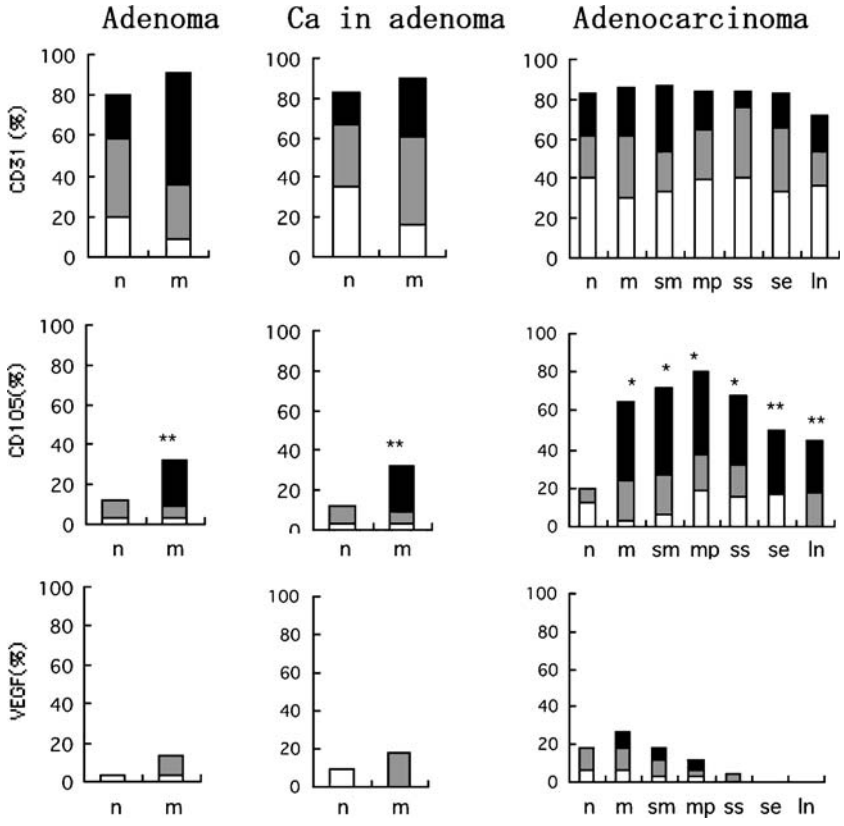

Fig. 5 Expression of CD31, CD105, and VEGF. Vascular endothelial cells express CD31, CD105, and VEGF throughout all tissue levels of colon adenoma, carcinoma in adenoma, and adenocarcinoma. Only CD105 significantly differs between the normal mucosa and adenoma or cancer (*middle three boxes*). CD31 (*upper boxes*) and VEGF (*lower boxes*) are not different between them. *n* Normal mucosa adjacent to the tumors at the level of tumor/cancer cells, *m* mucosal layers, *sm* submucosa, *mp* muscular propria, *ss* subserosa, *se* serosa. Significantly different: **p*<0.001 and ***p*<0.05. Grade of immunoreaction: (*rectangle*) weak, (*dotted rectangle*) moderate, and (*filled rectangle*) intense

was lost in the serosa of adenocarcinoma and lymph node metastasis. The expression of VEGF in the vascular endothelium did not significantly differ between normal and neoplastic mucosal layers of adenoma, cancer in adenoma, or adenocarcinoma (Fig. 5).

CD44 was not expressed in the vascular endothelium in normal tissues and in all layers of adenoma, carcinoma in adenoma, and adenocarcinoma, and was intensely expressed in the neoplastic cell membrane (Table 3). Flt-1 (cytoplasm and cell membrane), Flk-1 (cytoplasm and nuclei), TGF-β1 (cytoplasm), and TGF-βRII (cytoplasm and nuclei) were intensely expressed in neoplastic cells in all layers of adenoma, cancer in adenoma, and adenocarcinoma, but not in endothelial cells (Table 3).

Table 3 Immunohistochemical results

Markers	Vascular endothelial cells	Tumor cells
CD31	+[a]	−
CD105	+[a]	+ (cc)
CD44	−	+ (cm)
VEGF	+	+ (cc)
Flt-1	−	+ (cc, cm)
Flk-1	−	+ (cc, cn)
TGF-β1	−	+ (cc)
TGF-βRII	−	+ (cc, cn)

cc Cell cytoplasm, *cm* cell membrane, *cn* cell nucleus
[a]CD31 is mostly positive in preexisting larger blood vessels, whereas CD105 is positive in newly formed small blood vessels

Discussion

Endoglin (CD105), a cell membrane glycoprotein, was obviously upregulated in endothelial cells in de novo blood vessels of various tumors compared with those in normal tissues [3, 15, 16, 22, 27]. As far as we know, no study has compared the endothelial expression of CD105 with a lymphatic endothelium marker to exclude the idea that the CD105-stained vessels represent lymphatic vessels. The present study provides evidence that CD105 was expressed exclusively in the endothelium of newly formed blood vessels compared with D2-40, which was reported as a selective lymphatic endothelial marker [13]. Our results show no double-positive staining of CD105 and D2-40 in the same vessels (Fig. 4). CD105 is expressed in vascular endothelial cells of polypoid-type early colon cancer [20]. To our knowledge, the present study is the first to identify CD105 expression at levels corresponding to the depth of cancer invasion in the colon adenoma–carcinoma sequence (adenoma, carcinoma in adenoma, adenocarcinoma, and lymph node metastasis).

Angiogenesis always accompanies the development of cancer and metastasis, and the depth of tumor invasion of the colon wall determines the stage of cancer, which is a useful prognostic indicator and basis for the selection of appropriate therapy. We therefore considered that the expression of CD105 in each layer of the colon should be defined and compared with that of other angiogenetic markers. In this respect, we showed that CD105 was expressed at high levels in vascular endothelial cells in de novo blood vessels of the adenoma–carcinoma of the colon

and was weakly expressed (≦21%) in blood vessels of the normal mucosal layer. CD105 expression significantly differed between the normal mucosa and the corresponding layers of adenoma, carcinoma in adenoma, and adenocarcinoma ($p<0.05$, $p<0.05$, and $p<0.0001$, respectively), whereas CD31 and VEGF expression did not differ among them. This finding supports that of Akagi et al. [1], who showed that the expression of CD105 significantly differed from low-grade to high-grade adenoma and to carcinoma, whereas the MVD for a pan-endothelial marker (CD34) did not differ in the colorectal adenoma–carcinoma sequence. Moreover, when compared with CD31 and VEGF, CD105 was more intensely expressed in de novo microvessels (Fig. 3).

A higher expression of both VEGF and CD105 (MVD) correlates with a deeper invasion and lymph node metastasis in gastrointestinal cancer [30]. Our study also shows that CD105 expression is related to the depth of invasion, but not to VEGF expression (Fig. 3).

Flk-1 is expressed in the colon [24], lung [14], and prostate [2], and Flt-1 is expressed in pancreatic cancer [23, 26]. In contrast, we found that Flk-1 and Flt-1 were not expressed in vascular endothelial cells, whereas Flt-1 was intensely expressed in the cytoplasm and membrane of neoplastic cells and Flk-1 was found in the cytoplasm and nucleus of neoplastic cells.

Several studies have shown that CD31 is expressed in blood vessels in normal tissues, as well as in cancer tissues [1, 5, 7]. We found that 80–95% of the normal mucosa adjacent to the tumor and all layers in adenoma, carcinoma in adenoma, and adenocarcinoma expressed CD31.

One report describes that CD44 is expressed in the vascular endothelium [21]. However, we discovered a weak expression in lymphatic endothelial cells (data not shown) and an intense expression in normal and neoplastic cell membranes, but none in vascular endothelial cells.

The cytoplasm and nucleus of neoplastic cells expressed high levels of TGF-β1 and its receptor (TGF-βRII), whereas vascular endothelial cells expressed none.

These results confirm that CD105 was specifically expressed in de novo blood vessels of colon cancer.

References

1. Akagi K, Ikeda Y, Sumiyoshi Y, Kimura Y, Kinoshita J, Miyazaki M, Abe T (2002) Estimation of angiogenesis with anti-CD105 immunostaining in the process of colorectal cancer development. Surgery 131:S109–S113
2. Becker CM, Farnebo FA, Iordanescu I, Behonick DJ, Shih MC, Dunning P, Christofferson R, Mulligan RC, Taylor GA, Kuo CJ, Zetter BR (2002) Gene therapy of prostate cancer with the soluble vascular endothelial growth factor receptor Flk1. Cancer Biol Ther 1:548–553
3. Burrows FJ, Derbyshire EJ, Tazzari PL, Amlot P, Gazdar AF, King SW, Letarte M, Vitetta ES, Thorpe PE (1995) Up-regulation of endoglin on vascular endothelial cells in human solid tumors: implications for diagnosis and therapy. Clin Cancer Res 1:1623–1634
4. Cheryl AB, Jennifer JS, Miao J, Jill MJ, Jordan LM, Mary EM (2000) Endoglin expression as a measure of microvessel density in cervical cancer. Obstet Gynecol 96:224–228
5. Dales JP, Garcia S, Carpentier S, Andrac L, Ramuz O, Lavaut MN, Allasia C, Bonnier P, Charpin C (2004) Long-term prognostic significance of neoangiogenesis in breast carcinomas: comparison of Tie-2/Tek, CD105, and CD31 immunocytochemical expression. Hum Pathol 35:176–183
6. Faviana P, Boldrini L, Spisni R, Fontanini G et al (2002) Neoangiogenesis in colon cancer: correlation between vascular density, vascular endothelial growth factor (VEGF) and p53 protein expression. Oncol Rep 9:617–620
7. Feng D, Nagy JA, Pyne K, Dvorak HF, Dvorak AM (2004) Ultra-structural localization of platelet endothelial cell adhesion molecule (PECAM-1, CD31) in vascular endothelium. J Histochem Cytochem 52:87–101
8. Fonsatti E, Sigalotti L, Arslan P, Altomonte M, Maio M (2003) Emerging role of endoglin (CD105) as a marker of angiogenesis with clinical potential in human malignancies. Curr Cancer Drug Targets 3:427–432
9. Fonsatti E, Altomonte M, Arslan P, Maio M (2003) Endoglin (CD105): a target for anti-angiogenetic cancer therapy. Curr Drug Targets 4:291–296
10. Fonsatti E, Altomonte M, Nicotra MR, Natali PG, Maio M (2003) Endoglin (CD105): a powerful therapeutic target on tumor-associated angiogenetic blood vessels. Oncogene 22:6557–6563
11. Greenaway J, Connor K, Pederson HG, Coomber BL, LaMarre J, Petrik J (2004) VEGF and its receptor, Flk-1/KDR, are cytoprotective in the extravascular compartment of the ovarian follicle. Endocrinology 145:2896–2905
12. Jourdan F, Sebbagh N, Comperat E, Flejou JF (2003) Tissue microarray technology: validation in colorectal carcinoma and analysis of p53, hMLH1, and hMSH2 immunohistochemical expression. Virchows Arch 443:115–121
13. Kahn HJ, Marks A (2002) A new monoclonal antibody, D2-40, for detection of lymphatic invasion in primary tumors. Lab Invest 82:1255–1257
14. Kawaguchi T, Yamamoto S, Kudoh S, Goto K, Wakasa K, Sakurai M (1997) Tumor angiogenesis as a major prognostic factor in stage I lung adenocarcinoma. Anticancer Res 17:3743–3746
15. Kumar P, Wang JM, Bernabeu C (1996) CD105 and angiogenesis. J. Pathol 178:363–366
16. Li C, Gardy R, Seon BK, Duff SE, Abdalla S, Ranehan A, O'Dwyer ST, Haboubi N, Kumar S (2003) Both high intratumoral microvessel density determined using CD105 antibody and elevated plasma levels of CD105 in colorectal cancer patients correlate with poor prognosis. Br J Cancer 88:1424–1431
17. Li C, Guo B, Bernabeu C, Kumar C (2001) Angiogenesis in breast cancer: the role of transforming growth factor and CD105. Microsc Res Tech 4:437–449
18. Nasi A, Boulware D, Kaiser HE, Coppola D (2004) Flat and polyploid adenocarcinomas of the colorectum: a comparative histomorphologic analysis of 47 cases. Hum Pathol 35:604–611
19. Nicholl ID, Dunlop MG (1999) Molecular markers of prognosis in colorectal cancer. J Natl Cancer Inst 91:1267–1269
20. Okada K, Satoh T, Fujimoto K, Tokunaga O (2004) Interaction between morphology and angiogenesis in human early colorectal cancers. Pathol Int 54:490–497
21. Price EA, Coombe DR, Murray JC (1998) Endothelial CD44H mediates adhesion of a melanoma cell line to quiescent human endothelial cells in vitro. Int J Cancer 65:513–518
22. Duff SE, Li C, Garland JM, Kumar S (2003) CD105 is important for angiogenesis: evidence and potential applications. FASEB J 17:984–992
23. Siemann DW, Chaplin DJ, Horsman MR (2004) Vascular-targeting therapies for treatment of malignant disease. Cancer 100:2491–2499 [review]
24. Takahashi Y, Kitadai Y, Bucana CD, Cleary KR, Ellis LM (1995) Expression of vascular endothelial growth factor and its receptor, KDR, correlates with vascularity, metastasis, and proliferation of human colon cancer. Cancer Res 55:3964–3968

25. Volgestein B, Fearon ER, Hamilton SR (1988) Genetic alterations during colorectal-tumor development. N Engl J Med 319:525–532
26. Von Marschall Z, Cramer T, Hocker M, Burde R, Rosewicz S (2000) De novo expression of vascular endothelial growth factor in human pancreatic cancer: evidence for an autocrine mitogenic loop. Gastroenterology 119:1358–1372
27. Wang JM, Kumar S, Pye D, van Agthoven AJ, Krupinski J, Hunter RD (1993) A monoclonal antibody detects heterogeneity in vascular endothelium of tumours and normal tissues. Int J Cancer 54:363–370
28. Wilkstrom P, Lissbrant IF, Stattin P, Egevad L, Bergh A (2002) Endoglin (CD105) is expressed on immature blood vessels and is a marker for survival in prostate cancer. Prostate 51:268–275
29. Yasutomi M (ed) (1999) Japanese classification of colorectal carcinoma. Kanehara, Tokyo
30. Yu JX, Zhang XT, Liao YQ, Zhang QY, Chen H, Lin M, Kumar S (2003) Relationship between expression of CD105 and growth factors in malignant tumors of gastrointestinal tract and its significance. World J Gastroenterol 9:2866–2869

Virchows Arch (2006) 448: 135–141
DOI 10.1007/s00428-005-0059-3

ORIGINAL ARTICLE

Aija Knuuttila · Kowan J. Jee · Eero Taskinen · Henrik Wolff · Sakari Knuutila · Sisko Anttila

Spindle cell tumours of the pleura: a clinical, histological and comparative genomic hybridization analysis of 14 cases

Received: 3 June 2005 / Accepted: 3 August 2005 / Published online: 17 September 2005

Abstract We examined 14 spindle cell tumours of the pleura that were sent to a Mesothelioma Panel for re-evaluation after a primary suspicion of mesothelioma. The clinical, histological, immunohistochemical and CGH findings were investigated. Final diagnoses were eight sarcomatoid mesotheliomas (SM) and six non-mesotheliomas: two pulmonary sarcomatoid carcinomas, an epithelioid hemangioendothelioma, a malignant solitary fibrous tumour, a malignant pleural smooth muscle tumour and an extraskeletal osteosarcoma. Seven of the eight SM and two of the other six tumours presented with unilateral pleural effusion, dyspnoea, and chest pain, which are characteristic clinical findings in malignant mesothelioma. No single antibody used in the immunohistochemistry separated SM from other tumour types. The most frequently observed chromosomal losses in SM were 4q, 4p11-p13/p15, 6q and 13. Losses of 4p11-p13/p15 and 4q occurred in combination in four out of five SM with detectable chromosomal changes, but neither was found in any of the other tumours. Gain or high-level amplification of 5p was also common in SM. According to our results and literature, losses at 4p, 4q and 9p and gain at 5p are the chromosomal changes that best differentiate SM from pleural sarcomas and lung carcinomas. CGH analysis may help distinguish a cytokeratin-positive SM from a sarcomatoid carcinoma. Similarly, in the case of a cytokeratin-negative tumour, CGH analysis may disclose chromosomal changes characteristic of sarcomas or mesotheliomas.

Keywords Sarcomatoid mesothelioma · Spindle cell tumour of the pleura · CGH · Immunohistochemistry

A. Knuuttila
Department of Pulmonary Medicine,
Helsinki University Central Hospital,
Helsinki, Finland

K. J. Jee · E. Taskinen · H. Wolff · S. Knuutila · S. Anttila (✉)
Department of Pathology, HUSLAB and Haartman Institute,
University of Helsinki,
Helsinki, Finland
e-mail: sisko.anttila@ttl.fi
Tel.: +358-30-4742282
Fax: +358-30-4742021

H. Wolff · S. Anttila
Finnish Institute of Occupational Health,
Helsinki, Finland

Introduction

Differentiating sarcomatoid mesotheliomas (SM) from other spindle cell tumours of the pleura, e.g. pleural sarcomas and sarcomatoid carcinomas of the lung with invasion to the pleura, by morphological and immunohistochemical criteria is often difficult. The correct diagnosis also requires additional information from the clinical history, from imaging studies and from macroscopic surgical findings (e.g. diffuse vs localized pleural-based tumour mass).

The sarcomatoid differentiation is common in malignant mesotheliomas (MM) and occurs in pure form in SM as a component of biphasic mesothelioma or in association with a dense, collagen-rich, poorly cellular tumour tissue in desmoplastic MM. MM-associated immunohistochemical markers such as calretinin and cytokeratin 5/6 are useful in the differential diagnosis of epithelioid MM [6, 18]. However, neither calretinin nor cytokeratin 5/6 are uniformly sensitive markers for MM because they refer to the epithelioid component of the tumour and pure SM are often negative for both these antigens [1, 15]. The co-expression of cytokeratin and vimentin has been considered characteristic for all types of MM [4, 6]. However, pleomorphic and sarcomatoid carcinomas of the lung and other organs also express cytokeratin and vimentin. Furthermore, cytokeratin expression tends to decrease in poorly differentiated epithelial tumours, but some sarcomas may express cytokeratin.

Here we describe the clinical, histological, immunohistochemical and comparative genomic hybridization (CGH) findings of 14 primary spindle cell tumours of the pleura that have been sent for the evaluation of the Finnish Mesothelioma Panel. The aim of our study was to investigate

how these findings could be used in the differentiation between spindle cell tumours of the pleura, especially when diagnosing sarcomatoid type of MM.

Materials and methods

Tumour specimens

Fourteen spindle cell tumours of the pleura were drawn from the archives of the Finnish Mesothelioma Panel. They were sent for diagnostic re-evaluation because of a suspicion of pleural MM. The Finnish Mesothelioma Panel has four pathologist members, and it provides consultation services for problem cases but, as opposed to some other European Panels, does not collect all MM in its area. The Ethics Committee for Research in Occupational Health and Safety approved this study, and the National Authority for Medicolegal Affairs gave the permission to use the samples obtained for diagnostic purpose for research.

Immunohistochemistry

All 14 cases were immunostained with Techmate immunostainer for cytokeratin CAM5.2 (Becton Dickinson 349205, trypsin antigen retrieval; undiluted), vimentin (Dako, mouse anti-vimentin 7095; undiluted), calretinin (Zymed, rabbit anti-calretinin; 1:50 dilution, microwave antigen retrieval in citrate buffer, pH 6) and muscle actin (Dako, mouse anti-human muscle actin 7121; 1:10 dilution). In addition, six cases were stained for CD34 (Becton Dickinson 347660; 1:50 dilution, microwave antigen retrieval in citrate buffer, pH 6), S-100 (Dako, rabbit anti-S-100 H0066; undiluted) or cytokeratin 5/6 (Dako, mouse anti-cytokeratin 5/6 M7237; 1:50 dilution, microwave antigen retrieval in citrate buffer, pH 6); five cases for CEA (Dako, anti-human carcinoembryonic antigen H7096; undiluted, microwave antigen retrieval in citrate buffer, pH 6); four cases for CD15 (Becton Dickinson, mouse anti-human CD15 550382; 1:50 dilution, microwave antigen retrieval in citrate buffer, pH 6); three cases for Ber-EP4

Table 1 Clinical findings and asbestos exposure of the patients

Case number	Gender/ Age	Presenting symptoms	Survival	Occupation	Asbestos concentration[1]	Asbestos types
Non-mesothelioma spindle cell tumours						
Epithelioid hemangioendothelioma	F/72	Dyspnoea	9 years 5 months	Secretary	NA	
Spindle cell carcinoma	M/78	Arm pain, dyspnoea	3 months	Teacher	0.2[2]	Ant, amo/cro
Solitary fibrous tumour, malignant	M/54	Pleural effusion	17 months	Locksmith	0.1[2]	Ant
Pleomorphic carcinoma	M/73	Arm pain	6 months	Carpenter	16[3]	Cro, ant, amo
Malignant smooth muscle tumour	M/73	Chest pain, dyspnoea	3 months	Cement worker	1.1[3]	Ant, amo
Extraskeletal osteosarcoma	F/66	Pleural effusion	12 months	Sawmill worker	NA	
Sarcomatoid mesotheliomas						
SM1	M/58	Dyspnoea, CO_2 retention	2 months	Asbestos miner	NA	
SM2	M/67	Pleural effusion	10 months	General manager	NA	
SM3	M/88	Pleural effusion	6 months	Machine shop worker	9.1[3]	Cro, ant, amo, chr
SM4	M/74	Chest pain, pleural effusion	1 month	Maintenance man	0.3[2]	Ant, tre/act
SM5	M/83	Pleural effusion	6 months	Carpenter	3.1[2]	Ant, cro/amo
SM6	M/77	Pleural effusion	4 months	Mason	2.8[2]	Ant, amo/cro, tre
SM7	M/51	Chest pain, pleural effusion	12 months	Asbestos product worker	3.0[2]	Ant, amo/cro, chr
SM8	M/75	Chest pain, dyspnoea	8 months	Civil engineer	0.7[2]	Ant

Ant Anthophyllite, *cro* crocidolite, *amo* amosite, *chr* chrysotile, *tre* tremolite, *act* actinolite, *NA* not available
[1]Asbestos concentration: million fibres per gram dry tissue
[2]Method of asbestos analysis: scanning electron microscopy (SEM) with energy dispersive spectrometry (EDS)
[3]Method of asbestos analysis: scanning transmission electron microscopy (STEM) with energy dispersive spectrometry (EDS)

(Dako, mouse anti-human epithelial antigen M0804; 1:50 dilution, microwave antigen retrieval in citrate buffer, pH 6) and two cases for EMA (Dako, mouse anti-human epithelial membrane antigen M7097; undiluted), depending on the differential diagnosis.

Diagnoses

Three or four pathologists in the Panel made primary diagnoses in each of the 14 cases independently, and then all the cases were evaluated uniformly. Primarily, the independent diagnoses based on light microscopy and immunohistochemistry were certain or probable MM only in four cases, whereas in ten cases, the diagnoses varied from uncertain to opinions in favour of MM or other diagnoses. The clinical characteristics of the patients are given in Table 1. The symptoms mentioned are the main presenting symptoms at the time of diagnosis. The clinical and surgical/radiological/autopsy findings were classified either typical or unusual for MM (Table 2). The clinical findings were considered to be typical if the patient had the common clinical presentation of pleural MM including, e.g. unilateral pleural effusion with dyspnoea (known to be present in 80–90% of MM patients) and chest pain (present in 70% of MM patients), and the disease progressed typically for MM.Surgical and autopsy findings were considered typical when multiple pleural nodules or masses, more numerous on the parietal pleura but also involving the visceral pleura, or unilateral pleural effusion with pleural thickening was observed.

CGH analysis

CGH was performed as previously described by El-Rifai et al. [7]. Tumour DNA was labelled with FITC-dCTP and FITC-dUTP (DuPont, Boston, MA) and normal reference

Table 2 Summary of the clinical, histological and immunohistochemical findings

Histological diagnosis	Clinical features[1]	Surgical/radiological/ autopsy findings[2]	Histological pattern	Heterologous elements[3]	Cytokeratin- and vimentin-positive[4]	Calretinin-positive cells[5]
Non-mesothelioma spindle cell tumours						
Epithelioid hemangioendothelioma	Unusual: long survival	Unusual: large, cystic tumour, no effusion	Spindle cell	No	No	No
Spindle cell carcinoma	Unusual: arm pain	Unusual: pulmonary and renal metastases	Spindle cell–epithelial-like cell	No	No	No
Solitary fibrous tumour, malignant	Typical	Typical	Spindle cell	No	No	No
Pleomorphic carcinoma	Unusual: arm pain	Typical	Pleomorphic	No	No	No
Malignant smooth muscle tumour	Unusual: pain, no effusion	Unusual: contralateral pulmonary. metastases	Leiomyomatoid	Yes	No	No
Extraskeletal osteosarcoma	Typical	Typical	Pleomorphic	Yes	No	No
Sarcomatoid mesotheliomas						
SM1	Unusual: CO_2 retention	Unusual: liver metastases	Spindle cell	No	No	Yes
SM2	Typical	Typical	Spindle cell	No	No	No
SM3	Typical	Unusual: bilateral tumour, intestinal and renal metastases	Spindle cell	No	Yes	No
SM4	Typical	Typical	Angiosarcomatoid	No	No	Yes
SM5	Typical	Unusual: bilateral pleural thickening	Desmoplastic	No	Yes	No
SM6	Typical	Typical	Fibrosarcomatous	Yes	No	Yes
SM7	Typical	Typical	Spindle cell	No	Yes	No
SM8	Typical	Typical	Spindle cell–epithelial-like cell	No	Yes	Yes

[1]Symptoms, clinical findings and outcome: typical of mesothelioma; unusual in mesothelioma
[2]Surgical, radiological and/or autopsy findings: typical of mesothelioma; unusual in mesothelioma
[3]Osteoid and/or cartilaginous elements
[4]At least 50% of tumour cells positive for cytokeratin (CAM5.2) and vimentin
[5]Focal positive staining for calretinin in epithelial-like tumour cells

DNA with Texas-Red-dCTP and Texas-Red-dUTP (DuPont) in a standard nick-translation reaction. Hybridization mixture consisted of 1μg of labelled tumour DNA, 1μg of reference DNA and 20 μg unlabelled Cot-1 DNA, and hybridization was performed onto normal metaphase chromosomes in a moist chamber at 37°C for 48 h. After hybridization, the slides were washed and mounted with anti-fading medium containing a counterstain (Vector Laboratories, Burlingame, CA). CGH images were analysed using the ISIS digital image analysis system (MetaSystems, Altlussheim, Germany). Based on previous studies and control results, chromosomal regions were interpreted as over-represented (gained) when the red-to-green ratio exceeded 1.17 and under-represented (lost) when the ratio was less than 0.85. The region was considered as highly amplified when the ratio exceeded 1.5. Ninety-nine per cent confidence limits with 1% error probability were used to confirm the interpretation.

Results

Clinical findings

The main clinical features of the patients are given in Tables 1 and 2. Final diagnoses reached were eight SM and six non-MM, and they were confirmed by consensus after immunostaining of additional tissue blocks and taking clinical information into account. In this material, six out of 14 (44%) of the primarily proposed MM changed into other diagnoses after thorough diagnostic procedures and re-evaluation by the panel of pathologists. It was noticed that 4/6 non-MM presented with unusual clinical findings, such as absence of pleural effusion, and two had upper arm pain. Three of these six cases had radiological or surgical findings unusual for MM. Only one MM case had an unusual symptom presentation, having only dyspnoea and weakened general condition, whereas all others had either remarkable unilateral pleural effusion or chest pain or both. Among eight MM, three had autopsy findings unusual for MM, including two cases with widely spread metastases (liver, intestines and suprarenal) and one case with bilateral pleural tumour. These findings were not observed clinically during the patients' diagnostic work-ups. Two patients in the non-MM group and five in the MM group (62%) had a known work-related asbestos exposure (Table 1).

Immunohistochemistry

The results of immunohistochemical stainings are given in Tables 2 and 3. No single antibody used separated SM from other tumour types. The positive staining for calretinin in epithelioid-like tumour cells was seen in 4/8 SM (50%) but in none of the other tumours. Immunostaining for cytokeratin CAM5.2 occurred in 6/8 SM (75%) and in the two sarcomatoid carcinomas. All except one of the SM expressed muscle actin, but positive staining was also seen in the smooth muscle tumour and in one of the two sarcomatoid carcinomas. Co-expression of cytokeratin and vimentin was observed in 4/8 (50%) of the SM and in none of the other tumours (Table 2).

CGH results

DNA copy number changes were detected by conventional CGH in 11 of the 14 specimens as shown in Table 4. No changes were observed in two SM and in a malignant solitary fibrous tumour. There was no predominance of losses or gains in either SM or in the other spindle cell

Table 3 Immunohistochemical findings of the 14 tumours studied

Case number	CAM5.2	Vimentin	Calretinin	Muscle actin	CD34	S-100	CK5/6	EMA
Non-mesothelioma spindle cell tumours								
Epithelioid hemangioendothelioma	−	+	−	−	−	NA	NA	NA
Spindle cell carcinoma	+	(+)	−	(+)	NA	−	−	+
Solitary fibrous tumour, malignant	−	+	−	−	−	−	NA	NA
Pleomorphic carcinoma	(+)	+	−	−	−	−	−	NA
Malignant smooth muscle tumour	−	(+)	−	(+)	−	−	−	NA
Extraskeletal osteosarcoma	−	+	−	−	NA	(+)	NA	NA
Sarcomatoid mesotheliomas								
SM1	(+)	(+)	(+)	(+)	NA	−	NA	(+)
SM2	−	+	−	(+)	−	NA	NA	NA
SM3	+	+	−	−	NA	NA	−	NA
SM4	(+)	+	(+)	(+)	−	NA	−	NA
SM5	+	+	−	+	NA	NA	−	NA
SM6	−	+	(+)	+	−	NA	NA	NA
SM7	+	+	−	+	NA	NA	NA	NA
SM8	+	+	(+)	(+)	NA	NA	NA	NA

+, >50% of tumour cells positive; (+), <50% of tumour cells positive; −, 0–1% of tumour cells positive
NA not available

Table 4 CGH findings of the sarcomatoid mesotheliomas and non-mesothelioma spindle cell tumours of the pleura

Case number	Losses	Gains	High-level amplifications
Non-mesothelioma spindle cell tumours			
Epithelioid hemangioendothelioma	6q, 11p, 13, 20p, 22	None	7p11-pter, 7q11-34
Spindle-cell carcinoma	6q11-qter, 11, 13, 18, 20p, X11-pter	6p11-pter, 12q	1q, 9p11-p13, 9q11-qter, 12q22-qter
Solitary fibrous tumour, malignant	None	None	None
Pleomorphic carcinoma	6q, 9p12-pter	11q23-qter	3p13-pter, 4p, 20q
Smooth muscle tumour, malignant	10q, 13	19, 20	8q, 19q13.1-q13.3, 20q11-q13.1
Extraskeletal osteosarcoma	None	1q, 2, 7p15-pter, 20q	3p21-pter, 3q24-qter, 5p12-pter, 8q, 17q21-qter, 19, 20q11.2-qter
Sarcomatoid mesotheliomas			
SM1	6q, 9p21-pter, 11q14-qter, 13q13-31	1p31-pter, 1q11-qter, 7, 16, 18p, 20q	1p31.2-pter, 1q, 5p, 5q34-qter, 8, 16p, 18p11.22-pter, 19, 20q12-qter
SM2	4p11-p13, 4q, 6q, 9p, 13, 14	20q	5p12-pter, 20q13.1-qter
SM3	None	None	None
SM4	1p22-32, 4p11-15, 4q, 9p23-pter	1q21-qter, 8, 9q31-qter	None
SM5	None	5p	5p12-pter
SM6	None	None	None
SM7	4p11-p15, 4q, 6q11-q22, 13, Xp11-pter, Xq11-q22	1p32-p36, 5p, 7, 22	1q21-q24, 5p13-pter, 7p, 8q13-qter, 11, 12q22-qter, 17q22-qter, 22q
SM8	4p11-p15.2, 4q, 6q11-qter, 13, 18q	6p12-pter, 8, 12q24-qter, 17q21-qter	3p23-pter, 8q, 17q23-qter

tumours. In addition, high-level amplifications were observed in both groups.

In SM, losses of DNA sequences were observed in nine chromosomes. The chromosome arms most frequently lost were 4p11-13, 4p11-15, and 4q, which were observed in combination in 4/8 (50%) cases. The losses of 6q and chromosome 13 were also common in SM (4/8, 50%). In the other spindle cell tumours, losses of chromosome 4 were not observed, whereas losses of 6q and chromosome 13 were observed.

Table 5 Most common chromosomal changes in sarcomatoid mesotheliomas as compared to other relevant tumour types according to the literature

N/Tumour type	Reference	Losses at			Gain at
		4p (%)[1]	4q (%)[1]	9p (%)[1]	5p (%)[1]
All 41 sarcomatoid mesotheliomas		29	39	29	29
5/SM	[2]				
28/SM	[13]				
8/SM	Present study				
Sarcomas[2]					
51/Osteosarcoma	[3, 25]	0	8	10	10
37/Liposarcoma	[20, 23]	0	0	8	0
67/Synovial sarcoma	[24]	0	0	0	0
29/Leiomyosarcoma	[8]	0	10	16	7
Lung cancer[3]					
50/NSCLC	[21]	32	60	70	10

[1]Percentage of tumours with the chromosomal change
[2]Sarcomas most commonly detected in the pleural cavity or lung
[3]Non-small-cell carcinomas (NSCLC) were adenocarcinomas and squamous cell carcinomas of the lung; no CGH data available on pleomorphic carcinoma of the lung

Gain of DNA sequences was detected in 12 different chromosomes in SM and in 8 chromosomes in the other spindle cell tumours. High-level amplifications were common in SM as well as in the other spindle cell tumours. Most commonly, a high-level amplification was observed in 5p in SM (4/8, 50%), whereas, among other tumours, this high-level amplification was only seen in an extraskeletal osteosarcoma.

Discussion

We describe 14 cases of pleural spindle cell tumours, which were diagnostic challenges at the time of primary diagnosis. Clinical presentation of the disease together with the radiological and surgical findings seemed to be an important diagnostic clue. All except one SM presented with unilateral pleural effusion that required pleural drainage often repeatedly. SM patients also had dyspnoea and chest pain due to the tumour. The patients with other spindle cell tumours had more variable presenting symptoms, which included arm pain in two cases and chest pain and dyspnoea without pleural effusion in one case. Radiological and autopsy findings were also unusual for MM in three of the six non-MM spindle cell tumours: epithelioid hemangioendothelioma formed a large, cystic tumour and several smaller tumour nodules; spindle cell carcinoma had metastasized to the contralateral lung and kidney; and malignant smooth muscle tumour presented without pleural effusion. On the other hand, solitary fibrous tumour and extraskeletal osteosarcoma of the pleura had clinical and radiological findings similar to MM, whereas two of the SM had extrathoracic metastases in autopsy, and one of these patients had unusual CO_2 retention as a first disease symptom. The clinical symptom that separated the SM and non-MM group was arm pain that occurred in two patients with sarcomatoid carcinomas spread to the pleura.

The diagnosis of MM often relies on immunohistochemistry. As compared to the efficacy of immunohistochemical markers in confirming the diagnosis of epithelioid MM, their role in SM is not so clear. Calretinin and cytokeratin 5/6 are feasible immunohistochemical markers in discriminating between adenocarcinomas and epithelioid or biphasic MM, being positive in up to 100% of these type of MM and only focally positive in less than 10% of pulmonary adenocarcinomas [19]. In SM, calretinin expression has been demonstrated less often, the positive staining occurring in 20–70% of tumours [1, 11, 15], whereas cytokeratin 5/6 has not stained SM [15]. In the present study, half of the SM demonstrated focal positive staining for calretinin. We considered calretinin positive if the staining was seen in epithelioid-like cells and included both nuclear and cytoplasmic positivity. Lucas et al. [15] reported that calretinin staining reaction was less intense and more diffuse in SM than in the epithelioid MM, although 70% of the SM in their material were positive. We did not observe any calretinin positivity in the non-MM group, but Lucas et al. [15] reported 17% of sarcomas and 60% of sarcomatoid carcinomas to be calretinin-positive. Calretinin seems to be neither sensitive nor specific marker of SM.

Positive staining for cytokeratins has also been considered important in the diagnosis of MM. However, in two recent studies, the complete absence of cytokeratin staining in 15–23% of SM was reported [1, 15]. In our material, cytokeratin 8 (CAM5.2) stained 6/8 (75%) SM, but in two cases, less than half of the tumour cells were positive. In the non-MM group, spindle cell carcinoma was strongly cytokeratin-positive and pleomorphic carcinoma faintly positive. Altogether, other benign or malignant spindle cell tumours may also express cytokeratins [1, 5, 16], and they may be negative in SM.

Smooth muscle or myofibroblastic differentiation has been demonstrated in MM. Lucas et al. [15] reported that 60% of SM were smooth-muscle-actin-positive, but 58% of sarcomas and 10% of sarcomatoid carcinomas also stained positive in their material. In this study, all except one of the SM, a spindle cell carcinoma and a malignant smooth muscle tumour, were positive for smooth muscle actin. Thus, this further confirms that smooth muscle actin does not have much value in discriminating SM from other spindle cell tumours. In our case with extensive smooth muscle differentiation in a tumour encasing the lung, a diagnosis of malignant smooth muscle tumour of the pleura was made. Whether this type of tumour actually represents one type of SM is controversial [9, 17]. The presence of heterologous bone and cartilage in this tumour as well as asbestos exposure of the patient might favour the diagnosis of SM. However, the smooth muscle tumour of the pleura contained chromosomal losses at 10q and 13q, which are the most common losses described in soft tissue leiomyosarcomas [8], whereas loss at 10q is rare in SM [13].

The knowledge of chromosomal changes detectable by CGH in epithelioid and sarcomatoid MM is accumulating, although CGH so far has not been recommended as a diagnostic tool. In MM, on average, more losses and less gains and high-level amplifications have been reported in the literature as compared to carcinomas and sarcomas [2, 10, 22]. Furthermore, in a recent CGH study of 90 cases of MM, losses of chromosomal material were more common than gains, and SM were reported to have a fourfold higher number of amplifications than other MM subtypes [13]. In our study, gains were as frequent as losses both in the SM as well as in the other spindle cell tumours. High-level amplifications were also detected in both groups.

The most frequently observed losses in these eight SM were 4q, 4p11-p13/p15, 6q and 13, all these occurring in 50% of tumours. Losses of 4p11-p13/p15 and 4q occurred in combination in 4/5 SM with any detectable changes, but neither was found in any of the other tumours. In earlier cytogenetic analyses, losses at chromosomal regions 1p, 4q, 6q, 9p, 13q and 14q have been detected commonly in MM [10, 13, 14]. Among the non-MM spindle cell tumours, the loss of DNA was most often seen in 6q in the present study, but this finding was also common in SM. Losses on chromosome 6 and on 6q have also been reported in benign solitary fibrous tumours of the pleura and in mesodermomas (pleural MM with unusual meso-

dermal features), respectively [11, 12]. Gain or high-level amplification at 5p occurred in 4/6 SM, with detectable chromosomal gains in the present series. The chromosome arm 5p was also the most common site of gain or amplification in SM in the study of Krismann et al. [13]. This gain of chromosomal material has also been detected in about 10% of osteosarcomas and other soft tissue tumours (see references in Table 5), including our case of extraskeletal osteosarcoma of the pleura. Table 5 shows the most common chromosomal changes in SM as compared to other relevant tumour types according to the literature and our results. SM contain chromosomal aberrations characteristic of both epithelial tumours and sarcomas and thus differ from both groups.

In addition to morphological and immunohistochemical examinations, all clinical and radiological/surgical information as well as extensive tumour sampling, when possible, are necessary for the diagnosis of pleural spindle cell tumours. Immunostaining of several tumour blocks for cytokeratins and calretinin may be sufficient for the diagnosis of SM because it increases the likelihood of detecting small epithelioid, calretinin-positive areas, which confirm the diagnosis of MM. CGH analysis may help distinguish a cytokeratin-positive SM from a sarcomatoid carcinoma. Similarly, in the case of a cytokeratin-negative tumour, CGH analysis may disclose chromosomal changes characteristic of sarcomas or MM.

References

1. Attanoos RL, Dojcinov SD, Webb R, Gibbs AR (2000) Antimesothelial markers in sarcomatoid mesothelioma and other spindle cell neoplasms. Histopathology 37:224–231
2. Björkqvist A-M, Tammilehto L, Nordling S, Nurminen M, Anttila S, Mattson K, Knuutila S (1998) Comparison of DNA copy number changes in malignant mesothelioma, adenocarcinoma and large-cell anaplastic carcinoma of the lung. Br J Cancer 77:260–269
3. Brinkschmidt C, Blasius S, Bürger H, Simon R, Diallo R, Battmann A, Winkelmann W, Böcker W, Dockhorn-Dworniczak B (1998) Komparative genomische Hybridisierung (CGH) detektiert bisher nicht beschriebene amplifizierte chromosomale Abschnitte bei medullären high-grade Osteosarkomen. Verhandlungen der Deutschen Gesellschaft für Pathologie 82: 184–188
4. Carella R, DeLeonardi G, D'Errico A, Salerno A, Egater-Vigl E, Seebacher C, Donazzan G, Grigioni WF (2001) Immunohistochemical panels for differentiating epithelial malignant mesothelioma from lung adenocarcinoma: a study with logistic regression analysis. Am J Surg Pathol 25:43–50
5. Churg A, Colby TV, Cagle P, Corson J, Gibbs AR, Gilks B, Grimes M, Hammar S, Roggli V, Travis WD (2000) The separation of benign and malignant mesothelial proliferations. Am J Surg Pathol 24:1183–1200
6. Cury PM, Butcher DN, Fisher C, Corrin B, Nicholson AG (2000)Value of mesothelium-associated antibodies thrombomodulin, cytokeratin 5/6, calretinin and CD44H in distinguishing epithelioid pleural mesothelioma from adenocarcinoma metastatic to pleura. Mod Pathol 13:107–112
7. El-Rifai W, Larramendy ML, Björkqvist AM, Hemmer S, Knuutila S (1997) Optimization of comparative genomic hybridization using fluorochrome conjugated to dCTP and dUTP nucleotides. Lab Invest 77:699–700
8. El-Rifai W, Sarlomo-Rikala M, Knuutila S, Miettinen M (1998) DNA copy number changes in development and progression in leiomyosarcomas of soft tissues. Am J Pathol 153:985–990
9. Gibbs AR (1995) Smooth muscle tumours of the pleura. Histopathology 27:295–296
10. Knuutila S, Björkqvist AM, Autio K, Tarkkanen M, Wolf M, Monni O, Szymanska J, Larramendy ML, Tapper J, Pere H, El-Rifai W, Hemmer S, Wasenius WM, Vidgren V, Zhu Y (1998) DNA copy number amplifications in human neoplasms. Review of comparative genomic hybridization studies. Am J Pathol 152:1107–1123
11. Krismann M, Adams H, Jaworska M, Muller KM, Johnen G (2000) Patterns of chromosomal imbalances in benign solitary fibrous tumours of the pleura. Virchows Arch 437:248–255
12. Krismann M, Muller KM, Jaworska M, Johnen G (2000) Severe chromosomal aberrations in pleural mesotheliomas with unusual mesodermal features: CGH evidence for a mesothelioma subgroup. J Mol Diagn 2:209–216
13. Krismann M, Muller KM, Jaworska M, Johnen G (2002) Molecular cytogenetic differences between histological subtypes of malignant mesotheliomas: DNA cytometry and comparative genomic hybridization of 90 cases. J Pathol 197: 363–371
14. Lee WC, Testa JR (1999) Somatic genetic alterations in human malignant mesothelioma. Int J Oncol 14:181–188
15. Lucas DR, Pass HI, Madan SK, Adsay NV, Wali A, Tabaczka P, Lonardo F (2003) Sarcomatoid mesothelioma and its histological mimics: a comparative immunohistochemical study. Histopathology 42:270–279
16. Miettinen M, Limon J, Niezabitowski A, Lasota J (2001) Calretinin and other mesothelioma markers in synovial sarcoma: analysis of antigenic similarities and differences with malignant mesothelioma. Am J Surg Pathol 25:610–617
17. Moran CA, Suster S, Koss MN (1995) Smooth muscle tumours presenting as pleural neoplasms. Histopathology 27:227–234
18. Ordonez NG (1998) Value of calretinin immunostaining in differentiating epithelial mesothelioma from lung adenocarcinoma. Mod Pathol 11:929–933
19. Ordonez NG (2003) The immunohistochemical diagnosis of mesothelioma. A comparative study of epithelioid mesothelioma and lung adenocarcinoma. Am J Surg Pathol 27:1031–1051
20. Parente F, Grosgeorge J, Coindre J-M, Terrier P, Vilain O, Turc-Carel C (1999) Comparative genomic hybridization reveals novel chromosome deletions in 90 primary soft tissue tumors. Cancer Genet Cytogenet 115:89–95
21. Petersen I, Bujard M, Petersen S, Wolf G, Goeze A, Schwendel A, Langreck H, Gellert K, Reichel M, Just K, du Manoir S, Cremer T, Dietel M, Ried T (1997) Patterns of chromosomal imbalances in adenocarcinoma and squamous cell carcinoma of the lung. Cancer Res 57:2331–2335
22. Shivapurkar N, Virmani AK, Wistuba II, Milchgrub S, Mackay B, Minna JD, Gazdar AF (1999) Deletions of chromosome 4 at multiple sites are frequent in malignant mesothelioma and small-cell lung carcinoma. Clin Cancer Res 5:17–23
23. Szymanska J, Tarkkanen M, Wiklund T, Virolainen M, Blomqvist C, Asko-Seljavaara S, Tukiainen E, Elomaa I, Knuutila S (1996) Gains and losses of DNA sequences in liposarcomas evaluated by comparative genomic hybridization. Genes Chromosomes Cancer 15:89–94
24. Szymanska J, Serra M, Skytting B, Larsson O, Virolainen M, Åkerman M, Tarkkanen M, Huuhtanen R, Picci P, Bacchini P, Asko-Seljavaara S, Elomaa I, Knuutila S (1998) Genetic imbalances in 67 synovial sarcomas evaluated by comparative genomic hybridization. Genes Chromosomes Cancer 23:213–219
25. Tarkkanen M, Elomaa I, Blomqvist C, Kivioja AH, Kellokumpu-Lehtinen P, Böhling T, Valle J, Knuutila S (1999) DNA sequence copy number increase at 8q: a potential new prognostic marker in high-grade osteosarcoma. Int J Cancer 84:114–121

Virchows Arch (2006) 448: 142–150
DOI 10.1007/s00428-005-0063-7

ORIGINAL ARTICLE

Kuniaki Nakanishi · Hirotaka Matsuo · Yoshikatsu Kanai · Hitoshi Endou · Sadayuki Hiroi · Susumu Tominaga · Makio Mukai · Eiji Ikeda · Yuichi Ozeki · Shinsuke Aida · Toshiaki Kawai

LAT1 expression in normal lung and in atypical adenomatous hyperplasia and adenocarcinoma of the lung

Received: 27 April 2005 / Accepted: 15 August 2005 / Published online: 21 September 2005

Abstract No previous study has investigated neutral large amino acid transporter type 1 (LAT1) in normal lung cells, or in atypical adenomatous hyperplasia(s) (AAH) and nonmucinous bronchioloalveolar carcinoma(s) (NMBAC) of the lung. The authors examined: (1) the levels of *LAT1* mRNA/*glyceraldehyde-3-phosphate dehydrogenase* (*GAPDH*) mRNA in 41 normal lung tissues and 34 NMBAC using semiquantitative reverse transcription–polymerase chain reaction; (2) LAT1 mRNA and protein expressions in 35 normal lung tissues, 34 AAH (11 lesions were interpreted as low-grade AAH and 23 as high-grade AAH), and 43 NMBAC using in situ hybridization and immunohistochemistry; and (2) the association of the incidences of LAT1 mRNA and protein expressions with cell proliferation in these lesions. The level of *LAT1* mRNA/*GAPDH* mRNA (1) tended to be higher in NMBAC (12.0± 8.1) than in normal lung tissues (1.0±0.2), and (2) covered a much wider range (from 0 to 276) in NMBAC than in normal lung tissues (from 0 to 5.8), with six NMBAC having values higher than 7.0, while 5.8 was the highest value detected in normal lung tissues. In peripheral normal lung tissues, *LAT1* mRNA and protein were detected in bronchial surface epithelial cells and alveolar macrophages (but not in nonciliated bronchiolar epithelial cells, or in alveolar type I or type II cells). In bronchial surface epithelial cells, LAT1 protein appeared to be of a nodular type, which was considered to be a nonfunctional protein pattern. The incidences of positive expressions for *LAT1* mRNA and protein were 54.5 and 27.3% in low-grade AAH, 65.2 and 52.2% in high-grade AAH, and 65.1 and 79.1% in NM BAC, respectively. In the case of LAT1 protein expression, significant differences could be shown between total (low-grade plus high-grade) AAH and NMBAC, and between low-grade AAH and NMBAC. Thus, in terms of the incidence of LAT1 protein expression, high-grade AAH appeared intermediate between low-grade AAH and NMBAC. The Ki-67 labeling index (a cell proliferation score) was significantly higher in those AAH and NMBAC that were LTA1-protein-positive than in their LAT1-protein-negative counterparts. In conclusion, LAT1 expression may increase with the upregulation of metabolic activity and cell proliferation in high-grade AAH and NMBAC.

Keywords Atypical adenomatous hyperplasia · Pulmonary bronchioloalveolar carcinoma · Amino acid transporter · LAT1

K. Nakanishi (✉) · S. Hiroi · S. Tominaga · T. Kawai
Department of Pathology,
National Defense Medical College,
Tokorozawa, 359-8513, Japan
e-mail: nknsknak@ndmc.ac.jp
Tel.: +81-42-9951505
Fax: +81-42-9965192

H. Matsuo
Department of Physiology,
National Defense Medical College,
Tokorozawa, 359-8513, Japan

Y. Kanai · H. Endou
Department of Pharmacology and Toxicology,
School of Medicine, Kyorin University,
Tokyo, 181-8611, Japan

M. Mukai
Division of Diagnostic Pathology,
School of Medicine,
Keio University,
Tokyo, 160-8582, Japan

E. Ikeda
Department of Pathology,
School of Medicine,
Keio University,
Tokyo, 160-8582, Japan

Y. Ozeki
Department of Surgery,
National Defense Medical College,
Tokorozawa, 359-8513, Japan

S. Aida
Department of Laboratory Medicine,
National Defense Medical College,
Tokorozawa, 359-8513, Japan

Introduction

Nonmucinous bronchioloalveolar carcinoma(s) (NMBAC) of the lung is one of the major histological types of lung adenocarcinoma [24]. In the 1999 *World Health Organization international histologic classification of tumours* [25], it is defined as an adenocarcinoma with a pure bronchioloalveolar growth pattern and with no evidence of stromal, vascular, or pleural invasion. However, its histogenesis is not well-understood. Atypical adenomatous hyperplasia(s) (AAH) of the lung, which is classified among preinvasive lesions in the World Health Organization classification of lung and pleural tumours [25], is a proliferation of alveolar epithelial cells and is usually found incidentally in lungs surgically resected for lung cancer, predominantly in patients with adenocarcinoma.

Facilitated diffusion and active transport are responsible for the transport of substances such as glucose and amino acids. System L-amino acid transport mediates sodium-independent uptake of nonpolar branched-chain or aromatic neutral amino acids and is the major route by which mammalian cells take up nutritionally essential amino acids from extracellular fluids [2, 3, 5, 6]. Indeed, system L-amino acid transport plays a critical role in the absorption of amino acids by the intestine, kidney, and placenta. Recently, genes encoding proteins responsible for system L-amino acid transport have been cloned, and large amino acid transporter type 1 (LAT1) is the first member of the system L-amino acid transporter family to be identified [7, 10]. LAT1 requires covalent association with the heavy chain of 4F2 cell surface antigen (4F2hc) for its functional expression in plasma membrane [22]. Previous studies have shown LAT1 to be highly expressed in proliferating tissues, many tumor cell lines, and primary human tumors, but to be at barely detectable levels in adult tissues (except the brain, testis, and placenta), while 4F2hc is ubiquitous [2, 3, 5, 6, 8, 19–21, 23, 26]. Furthermore, overexpression of LAT1 in hepatocytes has been found to enhance their growth, leading Campbell and Thompson [1] to suggest that LAT1 may play an important role in cell growth. However, no study has yet investigated LAT1 expression in normal lung cells, or in AAH and NMBAC of the lung.

In this study, we took the opportunity to examine the expression of LAT1 mRNA and protein in normal lung cells, as well as in AAH and NMBAC. We investigated: (1) whether distributions of LAT1 mRNA and protein would be revealed in normal lung tissues; (2) whether LAT1 mRNA might be produced in normal lung tissues and NMBAC; (3) whether incidences of LAT1 mRNA and protein expressions might differ among normal lung tissues, precancerous lesions, and peripherally located adenocarcinomas; and (4) whether incidences of LAT1 mRNA and protein expressions would show associations with cell proliferation in these lesions. To those ends, we measured the levels of *LAT1* mRNA/*glyceraldehyde-3-phosphate dehydrogenase* (*GAPDH*) mRNA in 41 normal lung tissues and 34 NMBAC (measuring 30 mm or less in the greatest diameter) using a real-time reverse transcription–polymerase chain reaction (RT-PCR) approach. Furthermore, we examined the expressions of LAT1 mRNA and protein as well as cell proliferation index in 35 normal lung tissues, 34 AAH, and 43 bronchioloalveolar carcinomas (measuring 20 mm or less in the greatest diameter) using in situ hybridization and immunohistochemical approaches. Our goal was to obtain a better understanding of the relation of LAT1 expression to metabolic activity in normal lung cells, AAH, and NMBAC.

Materials and methods

From 1980 to 2002, the surgical pathology services of the National Defense Medical College Hospital (Tokorozawa, Japan) and the Keio University Hospital (Tokyo, Japan) received fresh frozen tissues of 41 normal lungs (resected from 41 patients with lung cancer) and 34 NMBAC of the lung (resected from 34 patients; measuring 30 mm or less in the greatest diameter), and also paraffin-embedded specimens of 34 AAH of the lung (resected from 19 patients) and 43 NMBAC of the lung (resected from 43 patients; measuring 20 mm or less in the greatest diameter). Of the 34 AAH lesions, 23 were interpreted as high-grade based on the findings of increased cellularity and cytological pleomorphism [14–17].

RT-PCR

Total mRNAs were obtained from the 41 normal lung tissues and 34 NMBAC (measuring 30 mm or less in the greatest diameter) that were available. Total RNA was isolated using acid guanidinium isothiocyanate–phenol–chloroform extraction and ethanol precipitation [4]. RT-PCR was performed using an amplification reagent kit (TaqMan EZRT-PCR kit; Applied Biosystems, Alameda, CA) with *LAT1* or *GAPDH* primers, as previously reported [18]. The *LAT1* and *GAPDH* primers were synthesized by an automated DNA synthesizer. The sense and antisense sequences of the *LAT1* primers were 5′-GTG ACG CTG GTG TAC GTG CT-3′ and 5′-GGG TGG ATC ATG GAG AGG AT-3′, respectively, while the sequence of the Taq Man probe was 5′-CTC CGT CAA TGG GTC CCT GTT CAC AT-3′. The cDNA amplification product was predicted to be a 251-bp fragment from positions 918 to 1,168 in the cDNA of *LAT1*. Primers were also synthesized to amplify the cDNA encoding *GAPDH*, a constitutively expressed gene, as a control. In the case of *GAPDH*, the sequences of the primers and TaqMan probe used were 5′-GAA GGT GAA GGT CGG AGT C-3′ (sense), 5′-GAA GAT GGT GAT GGG ATT TC-3′ (antisense), and 5′-CAA GCT TCC CGT TCT CAG CC-3′ (TaqMan probe). Both TaqMan probes were labeled at the 5′ end with the reporter dye molecule 6-carboxyfluorescein and at the 3′ end with the quencher dye 6-carboxytetramethylrhodamine. The re-

action master mix was prepared according to the manufacturer's protocol to give final concentrations of 1× reaction buffer, 300 μM 2′-deoxyadenosine 5′-triphosphate, 300 μM 2′-deoxycytidine 5′-triphosphate, 300 μM 2′-deoxyguanosine 5′-triphosphate, 600 μM 2′-deoxyuridine 5′-triphosphate, 3 mM $Mn(OAc)_2$, 0.1 U/μl *rTth* DNA polymerase, 0.01 U/μl AmpErase UNG, 200 nM AM primers, and 100 nM TaqMan probe. To perform PCR, the RT reaction was incubated at 60°C for 30 min, followed by incubation at 95°C for 5 min to deactivate AmpErase UNG. The present PCR employed was performed using 40 amplification cycles (using 1,000 ng of RNA for *LAT1* mRNA and 50 ng of RNA for *GAPDH* mRNA) at 95°C for 20 s and at 60°C for 1 min. For this, an ABI PRISM 7700 Sequence detector (Applied Biosystems) was used. Total RNA extracts from lung cancer were used as control templates (total RNA: 1,000, 200, 40, and 8 ng for *LAT1* mRNA; 200, 40, 8, and 1.6 ng for *GAPDH* mRNA). Increase in fluorescence was proportional to the concentration of the template in the present PCR (Fig. 2a). Threshold cycle was calculated by determining the point at which the fluorescence exceeded a threshold limit (ten times the standard deviation of the baseline). In other words, signals were regarded as positive if the fluorescence intensity exceeded ten times the standard deviation of the baseline fluorescence. A standard curve was obtained using the threshold cycles established separately for four wells for each applied RNA amount (Fig. 2b). PCR products were separated by electrophoresis in a 3% agarose gel then stained with ethidium bromide (Fig. 2c).

In situ hybridization

In situ hybridization was performed essentially as previously described [16]. Briefly, sections of 35 normal lung tissues, 34 AAH, and 43 NMBAC (measuring 20 mm or less in the greatest diameter) were treated with 0.2 N HCl for 20 min, incubated in 2× standard sodium citrate (SSC) for 10 min at 37°C, and incubated in 5 μg/ml proteinase K for 10 min at 37°C. Sections were subsequently post-fixed in 4% paraformaldehyde for 5 min, then incubated in 0.1 M triethanolamine buffer (pH 8.0) containing 0.25% (vol/vol) acetic anhydride for 10 min to prevent nonspecific binding due to oxidation of the tissue. Hybridization was carried out overnight at 42°C in 50% (vol/vol) deionized formamide, 5× Denhardt's solution, 5% (wt/vol) dextran sulfate, 2× SSC, 0.3 mg/ml salmon sperm DNA, 5 mM ethylenediaminetetraacetic acid, and 10 ng/ml biotin-labeled probes. After performing a final stringent wash at 37°C for 20 min, hybridization was detected immunologically. The *LAT1* cDNA probe used was a 251-bp fragment (obtained from positions 918 to 1,168 in the cDNA of *LAT1*) subcloned into the *Eco*RI site of a pGEM-T Easy Vector (Promega, Madison, WI). Antisense probes and corresponding sense probes were labeled with biotin using SP6 and T7 polymerases, respectively, by means of an RNA labeling kit (Roche Diagnostics, Mannheim, Germany).

Immunohistochemistry

We used polymer peroxidase method (EnVision+/HRP; Dako Cytomation, Denmark) on deparaffinized sections of

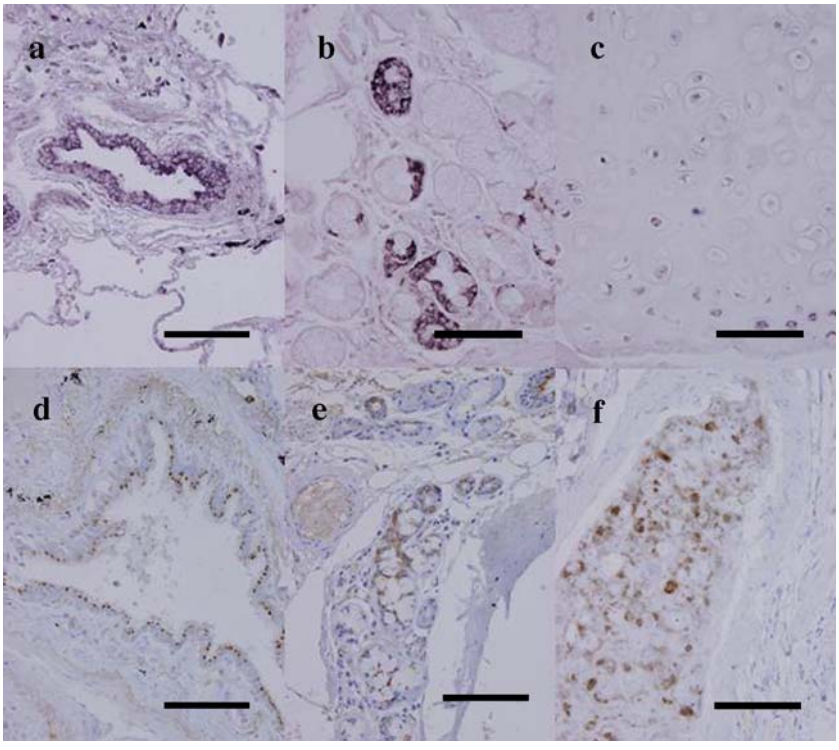

Fig. 1 LAT1 mRNA and protein expressions in normal lung tissues viz. bronchial surface epithelial cells in the bronchus (**a**, **d**), serous cells of the bronchial glands (**b**, **e**), and chondrocytes of the bronchial cartilage (**c**, **f**). *LAT1* mRNA appeared diffuse in the cytoplasm of positive cells within the normal lung. LAT1 protein was expressed as a single nodular spot in the cytoplasm of bronchial surface epithelial cells (**d**), while it was detected as a granular spreading pattern within the cytoplasm of lung components (**e**, **f**), except the bronchial surface epithelial cells. *Scale bar*, 100 μm

Table 1 Expressions of LAT1 mRNA and protein in normal lung

Anatomical site	Number of lesions	*LAT1* mRNA expression [*n* (%)]	LAT1 protein expression [*n* (%)]
Bronchus			
Surface epithelial cells	35	35 (100)	35 (100)
Nonciliated bronchiolar epithelial cells	35	0 (0)	0 (0)
Goblet cells	35	0 (0)	0 (0)
Chondrocytes of the bronchial cartilage	24	22 (91.7)	20 (83.3)
Bronchial glands			
Serous cells	23	15 (65.2)	17 (73.9)
Mucinous cells	23	0 (0)	0 (0)
Alveolar cells			
Type 1 cells	35	0 (0)	0 (0)
Type 2 cells	35	0 (0)	0 (0)
Alveolar macrophages	35	35 (100)	35 (100)

35 normal lung tissues, 34 AAH, and 43 NMBAC (measuring 20 mm or less in the greatest diameter), employing mouse monoclonal antibodies against LAT1 (1:20; clone no. 4D9; Transgenic, Kumamoto, Japan) and Ki-67 (1:20; clone no. Ki-55; Dako Cytomation, Tokyo, Japan). The sections received autoclave pretreatment of 0.05 M citrate buffer (pH 6.0) for 20 min before immunohistochemistry against both antibodies. For negative control, incubation step with the primary antibody was omitted. In absorption tests for LAT1, sections were treated with the primary antibody in the presence of LAT1 peptide.

Data analysis

For in situ hybridization and immunoreactivity analyses, staining was scored as: (−) negative reaction of tumor cells; (±) <10% of tumor area stained; (+) 11–25% stained; (2+) 26–50% stained; or (3+) ≥51% stained. The tumors in which stained tumor cells made up more than 25% of the

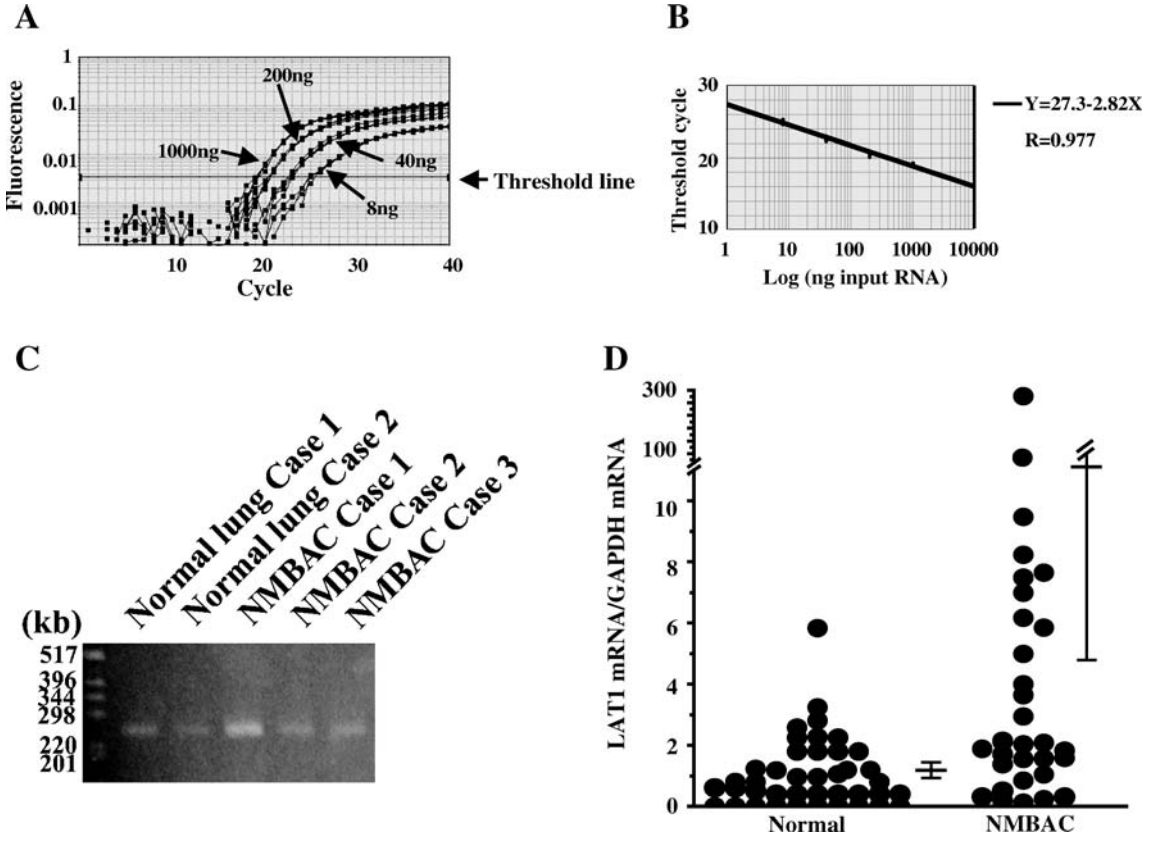

Fig. 2 Semiquantitative RT-PCR for *LAT1* mRNA. **a** Amplification plot obtained in real time using the semiquantitative RT-PCR method. Total RNA (1,000, 200, 40, and 8 ng) extracted from lung cancer was subjected to RT-PCR. **b** Standard curve for the threshold cycle of RT-PCR. The threshold cycle (obtained in quadruplicate) was plotted for each of the four RNA amounts applied. **c** Detection of PCR products. For instance, five PCR products (in two non-cancerous normal lung tissues and in tumors from three patients with peripherally located NMBAC) were detected at 251 bp. **d** Levels of *LAT1* mRNA/*GAPDH* mRNA in normal lung tissues (*n*=41) and NMBAC (*n*=34). When the actual "*LAT1* mRNA/*GAPDH* mRNA" value obtained for normal lung tissues in one individual patient was expressed as "1.0" and all other values were expressed in a relative manner, the mean ± SEM values obtained for the *LAT1* mRNA/*GAPDH* mRNA levels in 34 NMBAC and 41 normal lung tissues were 12.0±8.1 and 1.0±0.2, respectively. These levels tended to be higher for NMBAC than for normal lung tissues. Furthermore, 9 of 34 NMBAC (26.4%) had values higher than 5.8 (which was the highest value detected in the normal lung tissues)

tumor were graded as positive. For Ki-67 analysis, the percentage of nuclei exhibiting a positive immunoreaction (Ki-67 index) was determined based on immunoreactions in at least 1,000 cells.

Statistical analysis of differences in incidence between two groups was performed using chi-square analysis, while that of differences between two groups in levels of *LAT1* mRNA/*GAPDH* mRNA or the Ki-67 labeling index was performed using unpaired Student's *t* test. A value of $p<0.05$ was considered significant.

Results

Distributions of LAT1 mRNA and protein in normal lung

On in situ hybridization analysis, *LAT1* mRNA appeared diffuse in the cytoplasm of positive cells within the normal lung (Fig. 1). Detection of *LAT1* mRNA was as follows: 100% for bronchial surface epithelial cells (35 of 35 cases), 91.7% for chondrocytes of the bronchial cartilage (22 of 24 cases), 65.2% for serous cells of bronchial glands (15 of 23 cases), and 100% for alveolar macrophages (35 of 35 cases), but it was zero for nonciliated bronchiolar epithelial cells (Clara cells), goblet cells of the bronchus, mucinous cells of the bronchial glands, and alveolar type I or type II cells (Table 1, Fig. 1).

On immunohistochemistry analysis, LAT1 protein appeared granular in the cytoplasm of chondrocytes of the bronchial cartilage, serous cells of the bronchial glands, and alveolar macrophages within the normal lung (Fig. 1). In the cytoplasm of bronchial surface epithelial cells, however, the expression of LAT1 protein appeared as a single nodular spot, described as nodular-type staining, which was considered to represent an intracellularly localized nonfunctional protein. In the absorption test for LAT1 antibody, no LAT1 protein was detected using immunohistochemistry (data not shown). The following findings for LAT1 protein were similar to those described above for *LAT1* mRNA. LAT1 protein detection was as follows: 100% for bronchial surface epithelial cells (35 of 35 cases), 83.3% for chondrocytes of the bronchial cartilage (20 of 24 cases), 73.9% for serous cells of the bronchial glands (17 of 23 cases), and 100% for alveolar macrophages (35 of 35 cases), but it was zero for nonciliated bronchiolar epithelial cells (Clara cells), goblet cells of the bronchus, mucinous cells of the bronchial glands, and alveolar type I or type II cells (Table 1, Fig. 1).

Semiquantitative RT-PCR for *LAT1* mRNA in normal lung tissue and NMBAC

Polymerase chain reaction products were detected at 251 bp in noncancerous normal lung tissues and NMBAC (Fig. 2c). *GAPDH* mRNA levels (obtained using a total RNA of 50 ng for each sample) ranged from 0.72 to 18 ng (as control RNA levels). Therefore, semiquantitative RT-PCR for *LAT1* mRNA was performed using a total RNA of 1,000 ng for each sample. When the actual "*LAT1* mRNA/*GAPDH* mRNA" value obtained for normal lung tissues in one individual patient was expressed as "1.0" and all other values were expressed in a relative manner, the mean ±

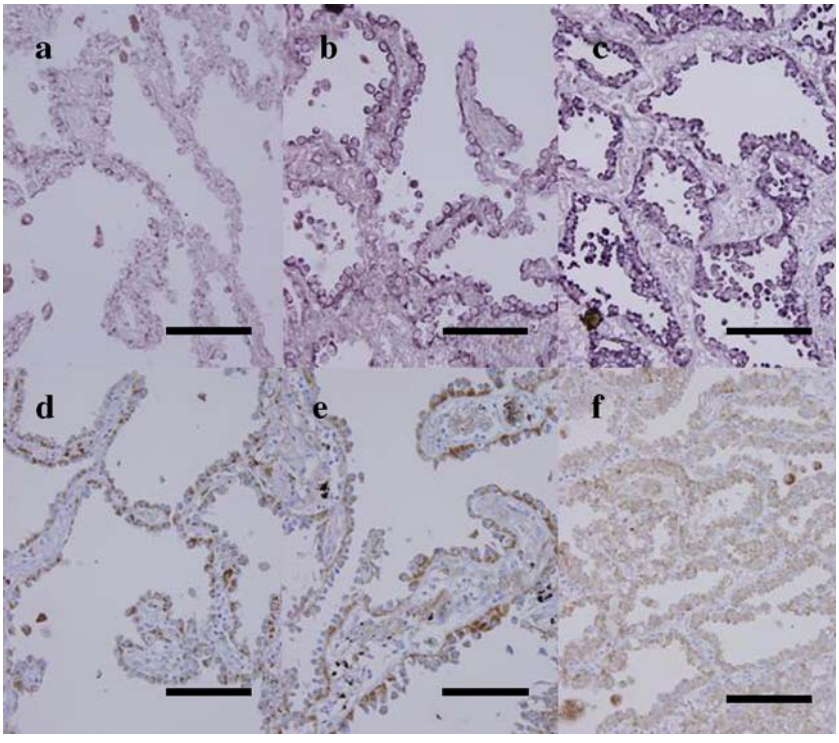

Fig. 3 LAT1 mRNA and protein expressions in low-grade AAH (*positive reaction*; **a**, **d**), high-grade AAH (*positive reaction*; **b**, **e**), and peripherally located NMBAC (*positive reaction*; **c**, **f**). *LAT1* mRNA was localized to within the cytoplasm of cells in AAH and NMBAC by in situ hybridization, whereas LAT1 protein was localized in the plasma membrane as well as the cytoplasm of cells in AAH and NMBAC by immunohistochemistry. *Scale bar*, 100 μm

Table 2 Expressions of LAT1 mRNA and protein in AAH and NMBAC of the lung

Lung condition	Number of lesions	*LAT1* mRNA expression [*n* (%)]	LAT1 protein expression [*n* (%)]
AAH			
Total	34	21 (61.8)	15 (44.1)*
Low grade	11	6 (54.5)	3 (27.3)**
High grade	23	15 (65.2)	12 (52.2)
NMBAC	43	28 (65.1)	34 (79.1)*,**

Statistical analysis was performed using chi-square analysis
*p=0.0015
**p=0.0010

standard error of the mean (SEM) values obtained for the *LAT1* mRNA/*GAPDH* mRNA levels in 34 NMBAC and 41 normal lung tissues were 12.0±8.1 and 1.0±0.2, respectively (Fig. 2d). These levels tended to be higher for NMBAC than for normal lung tissues, although a significant difference between normal lung tissues and NMBAC was not detected (p=0.13). The *LAT1* mRNA/*GAPDH* mRNA levels covered a much wider range (from 0 to 276) in NMBAC than in normal lung tissues (from 0 to 5.8). Moreover, six NMBAC had values higher than 7.0, whereas 5.8 was the highest value detected in the normal lung tissues.

Clinicopathological findings of AAH

There were 19 patients with a total of 34 AAH lesions. Nine of these 19 patients were male. Age at diagnosis was within the range 51–77 years, with a median age of 62 years. Among the 19 cases with 34 AAH lesions, 12 cases showed only one AAH lesion. Four of these 12 cases had only AAH lesions, without lung cancer. Among the 15 cases of lung cancer, there were 13 cases of adenocarcinoma, 1 case of squamous cell carcinoma, and 1 case of large cell carcinoma. Each AAH lesion in a patient with carcinoma was completely separated from the carcinoma by macroscopic examination, and in sections on a slide by microscopic examination. The diameter of the AAH lesions was within the range 1–20 mm, with a median diameter of 5 mm. In terms of diameter, there was no significant difference between low-grade AAH lesions (mean ± SD, 6.1±4.5 mm) and high-grade AAH lesions (mean ± SD, 6.1±3.9 mm). Of the 34 AAH lesions, 23 were interpreted as high-grade based on the findings of increased cellularity and cytological pleomorphism.

Expressions of LAT1 mRNA and protein in AAH and NMBAC

Expression of *LAT1* mRNA was confined to the cytoplasm of hyperplastic and neoplastic cells (Fig. 3). A positive *LAT1* mRNA expression was recognized in 61.8% of all AAH (21 of 34 lesions) [54.5% of low-grade AAH (6 of 11 lesions) and 65.2% of high-grade AAH (15 of 23 lesions)] and in 65.1% of NMBAC (28 of 43 lesions). LAT1 protein was detected in the cytoplasm and on the plasma membrane of hyperplastic and neoplastic cells (Fig. 3). The intensity of LAT1 protein staining sometimes varied within a given case. A positive LAT1 protein expression was recognized in 44.1% of all AAH (15 of 34 lesions) [27.3% of low-grade AAH (3 of 11 lesions) and 52.2% of high-grade AAH (12 of 23 lesions)] and in 79.1% of NMBAC (34 of 43 lesions). In the seven cases with multiple AAH (four cases with two AAH, two cases with four AAH, and one case with six AAH), the intensity and immunoreactive area varied among the multiple AAH in each case. The incidence of a positive expression for LAT1 protein was significantly different between total AAH and NMBAC, and between low-grade AAH and NMBAC (p=0.0015 and p=0.0010, respectively; Table 2).

Relationship between Ki-67 index and incidences of LAT1 mRNA and protein in AAH and NMBAC

The Ki-67 labeling index (taken as a cell proliferation score) increased from low-grade AAH (mean ± SEM, 1.6±0.3, ten lesions) to high-grade AAH (3.0±0.6, nine lesions) to NMBAC (7.4±0.7, 33 tumors). Significant differences were detected between total AAH and NMBAC, between low-grade AAH and NMBAC, and between high-grade AAH and NMBAC (p<0.0001, p<0.0001, and p=0.0062, respectively). The Ki-67 labeling index was significantly higher in those AAH and NMBAC that were positive for LAT1 protein than their LAT1-protein-negative counterparts (p=0.037 and p=0.034, respectively; Table 3).

Table 3 Ki-67 labeling index in AAH and NMBAC of the lung

Lung condition	Number of lesions	*LAT1* mRNA		LAT1 protein	
		Positive	Negative	Positive	Negative
AAH					
Total	19	2.7±0.4[a] (12)	1.5±0.4 (7)	3.2±0.6 (7)*	1.7±0.3 (12)*
Low grade	10	2.0±0.3 (6)	1.1±0.4 (4)	2.2±0.6 (3)	1.4±0.3 (7)
High grade	9	3.6±0.7 (6)	2.0±0.6 (3)	3.9±1.0 (4)	2.3±0.6 (5)
NMBAC	33	7.2±0.8 (22)	8.0±1.6 (11)	8.3±0.8 (25)**	4.7±0.9 (8)**

Statistical analysis was performed using an unpaired Student's t test
[a]Mean±SEM (number of cases)
*p=0.037
**p=0.034

Discussion

In the present study, we measured the levels of *LAT1* mRNA/*GAPDH* mRNA in normal lung tissues and NMBAC measuring 30 mm or less in the greatest diameter, and then applied in situ hybridization and immunohistochemistry to the normal lung, AAH, and NMBAC measuring less than 20 mm in diameter. Although the levels of *LAT1* mRNA/*GAPDH* mRNA failed to show a significant difference between normal lung tissues and NMBAC using semiquantitative RT-PCR, we observed that the incidence of a positive expression for LAT1 protein increased or tended to increase from low-grade AAH to high-grade AAH to NMBAC (with the incidence in high-grade AAH apparently being intermediate between those in low-grade AAH and NMBAC and tending to be closer to the latter than to the former). Furthermore, the Ki-67 labeling index (a cell proliferation score) was significantly higher in LTA1-protein-positive AAH and NMBAC than in their LAT1-protein-negative counterparts. Hence, our results are consistent with an upregulation of metabolic activity in both high-grade AAH and NMBAC alongside an upregulation of LAT1 protein.

It has previously been reported that LAT1 is expressed in some normal tissues, including the blood–brain barrier, activated lymphocytes, basal layer of the skin, proximal tubules of the kidney, placenta, and testis, and also in a variety of tumor cells such as glioma, breast cancer, bladder cancer, and colon cancer [8, 11, 19, 21, 23, 26]. To our knowledge, however, LAT1 expression has not previously been reported in the normal lung. We observed, using in situ hybridization and immunohistochemistry, that LAT1 mRNA and protein were expressed in a variety of lung components (including bronchial surface epithelial cells, serous cells of the bronchial glands, alveolar macrophages, and chondrocytes of the bronchial cartilage), although they were not detected in nonciliated bronchiolar epithelial cells (Clara cells), type I alveolar epithelial cells, type II alveolar epithelial cells, or mucinous cells of the bronchial glands. It should be noted that LAT1 protein in the bronchial surface epithelial cells was localized only to the cytoplasm, with a nodular pattern appearance that was considered to be nonfunctional (because it was not present on the plasma membrane). By semiquantitative RT-PCR, *LAT1* mRNA/*GAPDH* mRNA levels could be measured in 37 of 41 normal lung tissues, supporting the above results that were obtained using in situ hybridization and immunohistochemistry. Furthermore, the *LAT1* mRNA/*GAPDH* mRNA levels observed in normal lung tissues covered quite a wide range (from 0 to 5.8). This variety of levels may be due to heterogeneity or disproportionality among lung cell components.

In the present study, the *LAT1* mRNA/*GAPDH* mRNA values covered a much wider range (from 0 to 276) in NMBAC than in normal lung tissues (see above). In particular, six NMBAC (17.6%) had values higher than 7.0, and nine NMBAC (26.4%) had values higher than 5.8, which was the highest value obtained for the normal lung. Moreover, the mean NMBAC value tended to be higher than that obtained for normal lung tissues. Furthermore, *LAT1* mRNA was not detected in Clara cells or in type II alveolar epithelial cells in normal lung specimens using in situ hybridization. Based on these findings, the mean *LAT1* mRNA/*GAPDH* mRNA value may be lower in normal peripheral lung tissues (if we exclude cell components comprising central lung tissues, such as bronchial surface epithelial cells, serous cells of the bronchial glands, and chondrocytes of the bronchial cartilage) than in NMBAC. Furthermore, our immunohistochemical results indicate that bronchial surface epithelial cells in the central bronchi and peripheral bronchioles may produce a nonfunctional LAT1 protein (judging from the nodular-type cytoplasmic staining pattern), whereas the LAT1 protein is detected in the plasma membrane as well as in the cytoplasm in NMBAC. Thus, functional LAT1 protein may be produced at significantly higher levels in NMBAC than in normal lung tissues.

It is generally accepted that NMBAC was derived from nonbronchiolar epithelial cells (Clara cells) or type II alveolar epithelial cells, based on the phenotypic expression of neoplastic cells [9, 12]. In our in situ hybridization and immunohistochemical investigations, *LAT1* mRNA and protein were not detected in Clara cells or in type II alveolar epithelial cells in normal lung specimens. Campbell and Thompson [1], who transiently overexpressed LAT1 and 4F2hc (either alone or together) in nontransformed mouse hepatocytes, demonstrated that overexpression of LAT1 alone was sufficient to significantly increase system L transport activity in these hepatocytes, and that hepatic cells overexpressing LAT1 displayed a growth advantage relative to control cells under conditions involving limited arginine. Therefore, they suggested that LAT1 overexpression was an early event in hepatocarcinogenesis and that it provided neoplastic cells with selective growth or survival advantage, particularly under conditions of nutrient stress. Sang et al. [21] noted that TA1/E16, a partial sequence corresponding to LAT1, was expressed in rat-transformed cell lines and rat fetal liver, but not in adult liver. This led Campbell and Thompson [1] to propose that cells in which LAT1 was not normally expressed, such as hepatocytes, may acquire a growth advantage if LAT1 became constitutively expressed at some stage. This idea would support its involvement in the tumor growth of a lung adenocarcinoma if NMBAC acquired the ability to produce LAT1 during cancer development, although the induction of LAT1 expression may be an effect related to the upregulation of metabolic activity in AAH and NMBAC.

In the results obtained by in situ hybridization, the incidence of *LAT1* mRNA expression was relatively high (between 54.5 and 65.2%) in AAH and NMBAC, and no difference in the incidence of *LAT1* mRNA expression was detected between AAH and NMBAC. In contrast, the incidence of LAT1 protein expression increased or tended to increase from low-grade AAH to high-grade AAH to NMBAC, and a significant difference in its incidence was found between total AAH and NMBAC. The reason for this discrepancy between the incidence of *LAT1* mRNA (already high in low-grade AAH) and that of LAT1 protein

(progressive increase from low-grade AAH to high-grade AAH to NMBAC) is unclear. One possibility is that a rapid increase in *LAT1* mRNA may occur at the very early stage in the development of a lung carcinoma, with the subsequent synthesis of LAT1 protein occurring slowly throughout the development of this carcinoma. Another possibility is that, for reasons as yet unknown, LAT1 protein might be broken down more rapidly in the early stages of this development than in the later stages. Be that as it may, it would appear that *LAT1* mRNA expression may be a useful marker for evaluating early events in the pathogenesis of NMBAC. Furthermore, our results reveal a discrepancy between the incidence of *LAT1* mRNA (65.1%) and that of LAT1 protein (79.1%) in NMBAC. Although the reason for this discrepancy is as yet unclear, one possibility is that the probe used for in situ hybridization may be of lower sensitivity than the antibody used for immunohistochemistry. In addition, we reveal heterogeneities in expressions of LAT1 protein and mRNA among multiple AAH in individual cases, suggesting that AAH may be heterogeneous in terms of metabolic activity, cell growth, and the potential to progress to NMBAC. However, a limitation of this study was that we had only a small number (two cases) of NMBAC materials measuring 20 mm or less in the greatest diameter for RT-PCR, and no AAH. Moreover, the number of low-grade AAH lesions was lower than the number of high-grade AAH and NM BAC lesions. Confirmation of a role for LAT1 in AAH and NMBAC would need evidence from a large-scale study using molecular techniques.

In the present study, the Ki-67 labeling index increased from low-grade AAH to high-grade AAH to NMBAC, indicating a gain in proliferative activity from premalignant cells to malignant cells. These results are similar to findings described previously [9]. Furthermore, the Ki-67 labeling index was significantly higher in LTA1-protein-positive AAH and NMBAC than in their LAT1-protein-negative counterparts. These results suggest that the proliferating cells in AAH and NMBAC underwent an increase in their metabolism, with an associated upregulation of LAT1 protein.

In conclusion, the results of our study on LAT1 are consistent with high-grade AAH being a lesion closely associated with NMBAC of the lung. Furthermore, LAT1 protein overexpression in AAH and NMBAC shows a significant association with the Ki-67 labeling index, indicating an upregulation of metabolic activity. Finally, it is well-known that LAT1 requires 4F2hc for its functional expression. Furthermore, 4F2hc has been reported to induce cell proliferation and to be expressed in numerous tissues [20]. In the present study, we could not investigate the possible link between the functional role of 4F2hc and the overexpression of LAT1 (because a suitable 4F2hc antibody was not available to us). Therefore, further investigations of AAH, on a larger scale, will be necessary to establish whether 4F2hc expression at the plasma membrane correlates with metabolic activity and cell growth in AAH and NMBAC.

Acknowledgements We thank Dr. Robert Timms for correcting the English version of the manuscript. The anti-LAT1 antibody was supplied by Kumamoto Immunochemical Laboratory, Transgenic.

References

1. Campbell WA, Thompson NL (2001) Overexpression of LAT1/CD98 light chain is sufficient to increase system L-amino acid transport activity in mouse hepatocytes but not fibroblasts. J Biol Chem 276:16877–16884
2. Christensen HN (1990) Role of amino acid transport and countertransport in nutrition and metabolism. Physiol Rev 70:43–77
3. Chillaron J, Roca R, Valencia A, Zorzano A, Palacin M (2001) Heteromeric amino acid transporters: biochemistry, genetics, and physiology. Am J Physiol Renal Physiol 281:F995–F1018
4. Chomczyski P, Sacchi N (1987) Single-step method of RNA isolation by acid guanidium thiocyanate–phenol–chloroform extraction. Anal Biochem 162:156–159
5. Kanai Y, Endou H (2003) Functional properties of multispecific amino acid transporters and their implications to transporter-mediated toxicity. J Toxicol Sci 28:1–17
6. Kanai Y, Endou H (2001) Heterodimeric amino acid transporters: molecular biology and pathological and pharmacological relevance. Curr Drug Metab 2:339–354
7. Kanai Y, Segawa H, Miyamoto K, Uchino H, Takeda E, Endou H (1998) Expression cloning and characterization of a transporter for large neutral amino acids activated by the heavy chain of 4F2 antigen (CD98). J Biol Chem 273:23629–23632
8. Kim DK, Kanai Y, Choi HW, Tangtrongsup S, Chairoungdua A, Babu E, Tachampa K, Anzai N, Iribe Y, Endou H (2002) Characterization of the system L amino acid transporter in T24 human bladder carcinoma cells. Biochim Biophys Acta 1565: 112–121
9. Kitamura H, Kameda Y, Ito T, Hayashi H (1999) Atypical adenomatous hyperplasia of the lung. Am J Clin Pathol 111: 610–622
10. Mastroberardino L, Spindler B, Pfeiffer R, Skelly PJ, Loffing J, Shoemaker CB, Verrey F (1998) Amino-acid transport by heterodimers of 4F2hc/CD98 and members of a permease family. Nature 395:288–291
11. Matsuo H, Tsukada S, Nakata T, Chairoungdua A, Kim DK, Cha SH, Inatomi J, Yorifuji H, Fukuda J, Endou H, Kanai Y (2000) Expression of a system L neutral amino acid transporter at the blood–brain barrier. NeuroReport 11:3507–3511
12. Mori M, Rao SK, Popper HH, Cagle PT, Fraire AE (2001) Atypical adenomatous hyperplasia of the lung: a possible forerunner in the development of adenocarcinoma of the lung. Mod Pathol 14:72–84
13. Nakanishi K (1990) Alveolar epithelial hyperplasia and adenocarcinoma of the lung. Arch Pathol Lab Med 114:363–368
14. Nakanishi K, Kawai T, Kumaki F, Hiroi S, Mukai M, Ikeda E (2002) Expression of human telomerase RNA component (hTERC) and telomerase reverse transcriptase (hTERT) mRNA in atypical adenomatous hyperplasia of the lung. Hum Pathol 33:697–702
15. Nakanishi K, Kawai T, Kumaki F, Hiroi S, Mukai M, Ikeda E (2003) Survivin expression in atypical adenomatous hyperplasia of the lung. Am J Clin Pathol 120:712–719
16. Nakanishi K, Kawai T, Kumaki F, Hiroi S, Mukai M, Ikeda E, Koering CE, Gilson E (2003) Expression of mRNAs for telomeric repeat binding factor (TRF)-1 and TRF2 in atypical adenomatous hyperplasia and adenocarcinoma of the lung. Clin Cancer Res 9:1105–1111

17. Nakanishi K, Hiroi S, Kawai T, Suzuki M, Torikata C (1998) Argyrophilic nucleolar-organizer region counts and DNA status in bronchioloalveolar epithelial hyperplasia and adenocarcinoma of the lung. Hum Pathol 29:235–239
18. Nakanishi K, Uenoyama M, Tomita N, Morishita R, Kaneda Y, Ogihara T, Matsumoto K, Nakamura T, Maruta A, Matsuyama S, Kawai T, Aurues T, Hayashi T, Ikeda T (2002) Gene transfer of human hepatocyte growth factor into rat skin wounds mediated by liposomes coated with the sendai virus (hemagglutinating virus of Japan). Am J Pathol 161:1761–1772
19. Ohkame H, Masuda H, Ishii Y, Kanai Y (2001) Expression of L-type amino acid transporter 1 (LAT1) and 4F2 heavy chain (4F2hc) in liver tumor lesions of rat models. J Surg Oncol 78:265–271
20. Parmacek MS, Karpinski BA, Gottesdiener KM, Thompson CB, Leiden JM (1989) Structure, expression and regulation of the murine 4F2 heavy chain. Nucleic Acids Res 17:1915–1931
21. Sang J, Lim YP, Panzica M, Finch P, Thompson NL (1995) TA1, a highly conserved oncofetal complementary DNA from rat hepatoma, encodes an integral membrane protein associated with liver development, carcinogenesis, and cell activation. Cancer Res 55:1152–1159
22. Segawa H, Fukasawa Y, Miyamoto K, Takeda E, Endou H, Kanai Y (1999) Identification and functional characterization of a Na^+-independent neutral amino acid transporter with broad substrate selectivity. J Biol Chem 274:19745–19751
23. Shennan DB, Thomson J, Barber MC, Travers MT (2003) Functional and molecular characteristics of system L in human breast cancer cells. Biochim Biophys Acta 1611:81–90
24. Shimosato Y, Kodama T, Kameya T (1982) Morphogenesis of peripheral type adenocarcinoma of the lungs. In: Shimosato Y, Melamed MR, Nettesheim P (eds) Morphogenesis of lung cancer, vol 1. CRC Press, Boca Raton, FL, pp 65–89
25. Travis, WD, Colby TV, Corrin B, Shimosato T, Brambilla E (1999) World Health Organization international histologic classification of tumours. Histological typing of lung and pleural tumours, 3rd edn. Springer, Berlin Heidelberg New York, p 36
26. Wolf DA, Wang S, Panzica MA, Bassily NH, Thompson NL (1996) Expression of a highly conserved oncofetal gene, TA1/E16, in human colon carcinoma and other primary cancers: homology to *Schistosoma mansoni* amino acid permease and *Caenorhabditis elegans* gene products. Cancer Res 56:5012–5022

Virchows Arch (2006) 448: 151–159
DOI 10.1007/s00428-005-0049-5

ORIGINAL ARTICLE

Carsten Schrader · Peter Meusers · Günter Brittinger · Dirk Janssen · Afshin Teymoortash · Jens U. Siebmann · Reza Parwaresch · Markus Tiemann

Growth pattern and distribution of follicular dendritic cells in mantle cell lymphoma: a clinicopathological study of 96 patients

Received: 26 March 2005 / Accepted: 14 July 2005 / Published online: 17 August 2005

Abstract Mantle cell lymphoma (MCL) is an aggressive lymphoma with accepted risk factors such as proliferation markers. To date, the different follicular dendritic cell (FDC) patterns have never been analyzed in comparison with the overall survival time. Lymph node biopsy specimens from 96 patients were analyzed by conventional morphology and immunohistochemistry with antibodies against cluster differentiation (CD)20, CD5, CD23, cyclin D1, and FDC (Ki-M4P). Two groups can be distinguished with different FDC patterns: a nodular pattern in 79 cases and a diffuse pattern in 17 cases. A Kaplan–Meier analysis revealed significantly better survival for the nodular group (p=0.0312). This group was subdivided into a group with a nodular FDC pattern similar to the FDC distribution in primary follicles (PF-nodular in 72 cases) and one with a nodular FDC pattern resembling the colonization of germinal centers (GCs) by tumor cells (GC-nodular in seven cases). A Kaplan–Meier analysis showed that patients with MCL with a PF-nodular FDC pattern had a significantly better clinical outcome than patients with the other two patterns (p=0.0033). If only cases with classical cytology (n=79) were analyzed (blastoid types excluded), patients with a PF-nodular FDC pattern had a better clinical outcome (p=0.0008). The distribution of FDC in MCL is a diagnostic tool for identifying patients with a better clinical prognosis.

Keywords Mantle cell lymphoma (MCL) · Follicular dendritic cells (FDC) · Growth pattern

C. Schrader (✉)
II. Department of Internal Medicine and Hematology,
University Hospital of Schleswig-Holstein,
Kiel, Chemnitzstr. 33,
24116 Kiel, Germany
e-mail: c.schrader@med2.uni-kiel.de
Tel.: +49-431-16975220
Fax: +49-431-16971202

C. Schrader · D. Janssen · R. Parwaresch · M. Tiemann
Department of Hematopathology and Lymph Node Registry,
University Hospital of Schleswig-Holstein,
Kiel, Germany

P. Meusers · G. Brittinger
Division of Hematology, Department of Medicine,
University of Duisburg-Essen,
Duisburg-Essen, Germany

A. Teymoortash
Department of Otolaryngology, Head and Neck Surgery,
University of Marburg,
Marburg, Germany

J. U. Siebmann
Department of General Surgery,
University Hospital of Schleswig-Holstein,
Kiel, Germany

Introduction

Mantle cell lymphoma (MCL) has become a well-accepted entity since the diagnostic chromosomal translocation t(11;14) was first described [54]. This entity had been referred to as lymphocytic lymphoma of intermediate differentiation, intermediate lymphocytic lymphoma [52], or mantle-zone lymphoma [50] and was called centrocytic lymphoma in the Kiel classification [22]. The typical antigen constellation of centrocytes in this lymphoma includes the coexpression of cluster differentiation (CD)5 and CD20 and negativity for CD3, CD10, and CD23 [27, 38, 45, 47]. The term mantle cell lymphoma is based on the growth pattern in early stages of the disease. This is characterized by a nodular growth pattern of the lymphoma around residual reactive germinal centers (GCs), a so-called mantle-zone pattern [50]. Other patterns are nodular and diffuse [49, 55]. Corresponding to the growth pattern, dense networks of follicular dendritic cells (FDCs) have also been described in these lymphomas [3, 9, 55].

The function of these cells in the genesis and clinical course of MCL is not yet clear. To our knowledge, no study has been done on different FDC patterns and survival in patients with MCL. For this study, the paraffin-resistant monoclonal antibody Ki-M4P was used, which accurately detects FDC in lymph nodes [31].

We report on the growth pattern, and, for the first time, on the FDC pattern in MCLs in comparison with the clinical outcome of 96 patients enrolled in two multicenter prospective trials [4, 26].

Patients and methods

Patients

Lymph node biopsy specimens from 96 patients enrolled in two multicenter prospective trials (1975 and 1985) were included [4, 26]. The criterion for inclusion was a histopathological diagnosis of MCL verified by a reference pathologist of the European Mantle Cell Lymphoma Study Group (M.T. and R.P.). The diagnosis of MCL was made according to the morphological and immunological criteria specified by the European Lymphoma Task Force (ELTF) [55] and according to the criteria suggested by Banks et al. [3]. Table 1 shows the clinical characteristics of the patients.

Table 1 Clinical characteristics of 96 patients with MCL

Characteristics		*n*
Sex	male/female	74/22
Age	<60 years/>60 years	37/59
B symptoms	yes/no/NK	40/54/2
BM infiltration	yes/no/NK	61/34/1
Stage	1+2/3+4/NK	6/86/4
Status (WHO)	0–1/=2/NK	71/23/2
Extranodal	yes/no	84/12
LDH	normal/elevated/NK	73/14/9
IPI score	0–1/=2	21/75
Therapy	Ch+P/COP/CHOP/ Radiatio/no/NK	41/34/10/6/3/2
Cytology type	classical/blastoid	79/17

BM Bone marrow, *Stage* Ann Arbor stage, *Status* performance status, *Extranodal* extranodal involvement, *LDH* lactate dehydrogenase, *IPI* International Prognostic Index, *Ch* chlorambucil, *C* cyclophosphamide, *O* vincristine, *P* prednisone, *H* doxorubicin, *Radiatio* extended field irradiation alone, *NK* not known

Morphology

Histological sections from tissue biopsy specimens were stained with hematoxylin and eosin (H & E), Giemsa, and Gomori silver impregnation and reviewed.

Cytology

The cytology was classified into classical and blastoid subtypes [6, 49].

Growth pattern

The growth pattern of the tumor was divided into two different types (according to Weisenburger et al. [49] with modifications):

(1) nodular pattern (more than 50% nodular growth pattern) and
(2) diffuse pattern (more than 50% diffuse growth pattern).

Immunohistochemistry

Four-micrometer-thick sections were mounted on 3-aminopropoyltriethoxy-silane (APES)-coated slides and routinely processed. They were dewaxed in xylene and rehydrated in graded ethanol. The following antibodies were used for the immunohistochemical analysis: anti-CD3 (polyclonal rabbit antiserum, DAKO, Hamburg, Germany) [25], anti-CD5 (monoclonal, Novocastra, Newcastle, UK) [20], anti-CD20 (L26, monoclonal, DAKO) [24], anti-CD23 (monoclonal, Novocastra) [11], anticyclin D1 (monoclonal), anti-FDC (Ki-M4P, undiluted cell culture supernatant, Department of Hematopathology, University of Kiel, Germany) [30, 31], and Ki-67 (Ki-S5, undiluted cell culture supernatant, Department of Hema-

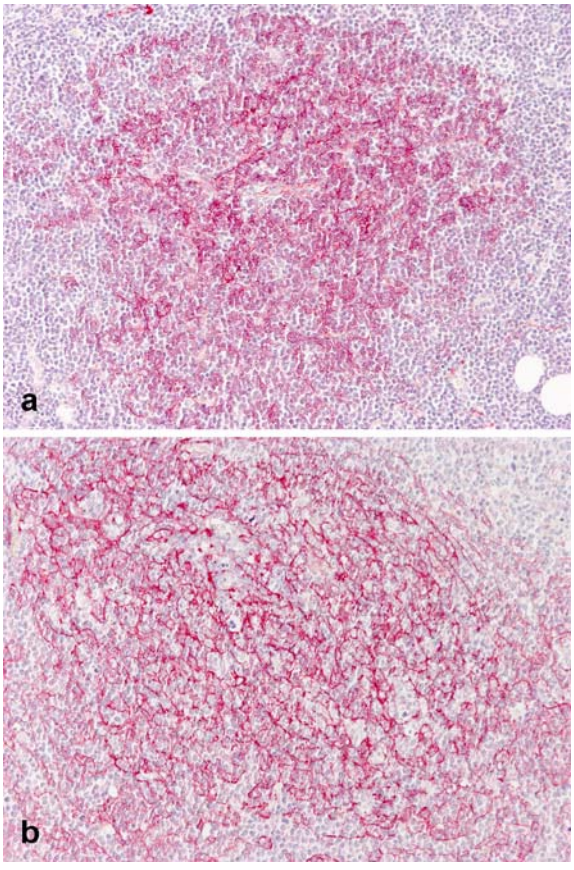

Fig. 1 Nodular FDC pattern in a lymph node infiltrated by MCL. **a** FDC pattern similar to primary follicles (PF-nodular) with weak Ki-M4P positivity, APAAP, ×200. **b** FDC pattern resembling colonized germinal centers (GC-nodular) with strong Ki-M4P positivity of preexisting FDC, APAAP, ×400

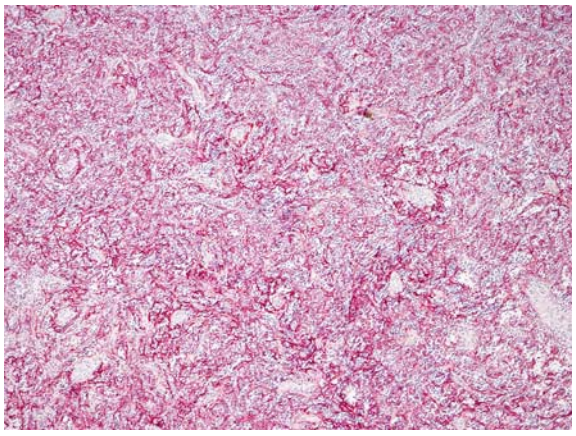

Fig. 2 Diffuse FDC pattern in a lymph node with MCL, Ki-M4P staining, APAAP, ×100

topathology, University of Kiel, Germany). Detection of the reactive epitopes in fixed material required previous antigen retrieval. For CD5, CD20, CD23, cyclin D1, and Ki-67, this was achieved by boiling the sections immersed in 0.01 M citric acid, pH 6.0, for 2 min and 30 s in a pressure cooker [2]. The CD3 epitope and the FDC were unmasked by digesting the sections with 0.02% protease XXIV (Sigma, Deisenhofen, Germany), pH 7.5, for 15 min at 37°C. Primary antibodies were then incubated on the sections for 60 min at room temperature. The immunoreactions were enhanced either by means of the avidin–biotin complex (ABC) technique [13] or the alkaline phosphatase antialkaline phosphatase (APAAP) method [8], followed by brief counterstaining with Mayer's hematoxylin. In the former case, endogenous peroxidase activity was previously blocked for 10 min in 30% hydrogen peroxide in methanol, biotinylated pig antirabbit immunoglobulin G (IgG) (E 353, DAKO) for the polyclonal anti-CD3 antibody, and the reaction was catalyzed by streptavidin-conjugated peroxidase using diaminobenzidine as a chromogen. For APAAP immunostaining, rabbit antimouse antiserum (Z 259, DAKO) was used as a secondary antibody, and naphthol-AS-biphosphate was used as a chromogen. Immunolabeling was evaluated by investigators blinded to the clinical information.

FDC distribution

Regarding the distribution of FDC, MCL was divided into two groups:

(1) nodular pattern (more than 50% nodular FDC pattern) (Fig. 1a and b) and
(2) diffuse pattern (more than 50% diffuse FDC pattern) (Fig. 2).

The nodular FDC pattern was subdivided into two different patterns according to the criteria of Annecy [55]:

(1) a nodular FDC pattern similar to the FDC distribution in primary follicles (PF-nodular, Fig. 1a) and
(2) a nodular FDC pattern resembling the colonization of GC by tumor cells (GC-nodular, Fig. 1b).

Controls

Tonsil samples from our routine files were used as positive controls.

Statistics

Statistical tests were computed using SPSS (version 10.0). Overall survival (OS) time was calculated from the date of diagnosis until death. Survival curves were estimated according to the Kaplan–Meier method and were compared by a log-rank test. p values of at most 0.05 were considered

Table 2 Results of the analysis of the growth pattern and the FDC pattern in 96 patients with MCL

Characteristics	Pattern	Number	Median (months)	3-year survival (%)	p value
Growth pattern (all cases)	Nodular	29	32.0	37.9	0.7468
	Diffuse	67	28.0	35.8	
Growth pattern (without blastoid type)	Nodular	29	32.0	37.9	0.4516
	Diffuse	50	28.8	34.0	
FDC pattern (all cases)	Nodular	79	32.0	42.9	0.0312
	Diffuse	17	21.2	29.4	
FDC pattern (without blastoid type)	Nodular	70	33.0	38.6	0.0021
	Diffuse	9	17.9	29.4	
FDC pattern (all cases)	PF-nodular	72	33.0	40.3	0.0033
	GC-nodular	7	14.4	28.6	
	Diffuse	17	21.2	29.4	
FDC pattern (without blastoid type)	PF-nodular	64	35.7	40.6	0.0008
	GC-nodular	6	19.9	33.3	
	Diffuse	9	17.9	22.2	

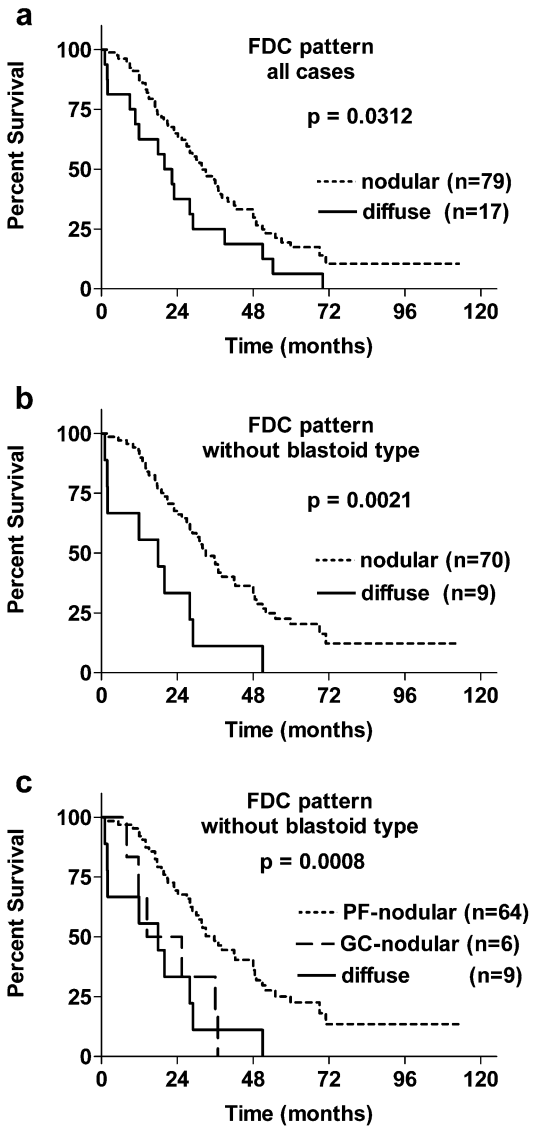

Fig. 3 Overall survival time of patients with MCL and different FDC patterns. **a** The analysis included all patients (*N*=96). The Kaplan–Meier analysis revealed a significant difference in the clinical outcome of patients with a nodular FDC pattern vs. diffuse pattern (p=0.0312). **b** Analysis of nodular and diffuse FDC pattern and exclusion of blastoid cytology types (n=79). The Kaplan–Meier analysis showed a significant difference for cases with a nodular FDC pattern (p=0.0021). **c** Analysis of two different nodular patterns and a diffuse FDC pattern without blastoid cytology types (n=79). The Kaplan–Meier analysis revealed a significant difference in the clinical outcome of patients with PF-nodular pattern and the other two (GC-nodular and GC-diffuse) patterns (p=0.0008)

to indicate statistical significance. The clinical parameters were compared by means of a multivariate Cox regression analysis using a stepwise conditional approach. Analysis of different prognostic parameters in comparison to the FDC distribution was done by likelihood quotient for all three FDC types and Fisher's Exact Test (two-tailed) for the two FDC types PF and GC.

Results

Clinical features

The clinical characteristics of the 96 patients are summarized in Table 1. The mean age at presentation was 63.4 years (range 41–86 years). The majority of patients were male, with a male to female ratio of 3.4:1 (74 males and 22 females). Most patients (89.5%) presented with advanced-stage disease (III or IV).

Histological findings

Cytology

The majority of cases (n=79, 82.3%) had a classical cytology with small- to medium-sized indented nuclei, moderately dispersed chromatin, and scanty pale cytoplasm [6, 22, 49]. In 17 cases (17.7%), a blastoid variant was observed [1, 6, 18, 37, 40, 49]. The median OS time of patients with classical MCL was 31.0 months compared to the blastoid group with 22.7 months (p=0.1226).

Growth pattern

The growth pattern was classified by conventional microscopy as nodular or diffuse. A nodular pattern was found in 29 patients (30.2%). In no case was the typical so-called mantle-zone pattern seen. A diffuse pattern was seen in 67 patients (69.8%). The Kaplan–Meier analysis did not show any significant differences between the growth pattern types (p=0.7468, Table 2). Excluding cases with blastoid cytology from the analysis of the growth pattern, as suggested by Fisher et al. [10], resulted in a smaller group of cases with a diffuse pattern (50 cases). Interestingly, all 17 cases with a blastoid cytology had a diffuse growth pattern. The relationship between OS time and the different patterns in this smaller group (nodular vs diffuse pattern without blastoid subtypes, Table 2, second group) was still not significant (p=0.4516).

Table 3 Results of the analysis of the growth pattern in relation to the FDC pattern in 96 patients with MCL

FDC pattern	Growth pattern	
	Nodular (n=29)	Diffuse (n=67)
PF-nodular (n=72)	25	47
GC-nodular (n=7)	2	5
Diffuse (n=17)	2	15

Immunohistochemistry

All cases fulfilled the immunophenotyping criteria for MCL, with coexpression of CD20 and CD5. Ninety cases (93.8%) were CD23-negative. In six cases (6.3%), the CD23 staining could not be analyzed. Ninety four cases (97.9%) stained positively for cyclin D1. In two cases (2.1%), the cyclin D1 staining could not be evaluated.

FDC distribution

The staining with the monoclonal antibody Ki-M4p clearly revealed the FDC pattern. The cases were first divided into a nodular (Fig. 1a and b) or diffuse (Fig. 2) FDC pattern according to the criteria of Annecy [55]. Patients with MCL and a nodular FDC pattern (n=79) had a significantly longer OS time (median 32.0 months, 3-year survival 41.4%) than patients with a diffuse FDC pattern (n=17, median 21.2 months, 3-year survival 29.4%, p=0.0312). In a second step, we analyzed the FDC pattern of the cases that did not have a blastoid cytology because this subtype normally has an aggressive clinical course. In this analysis, the nodular FDC pattern predicted a better clinical outcome than that of the diffuse group (Fig. 3b, median survival time 33 vs. 17.9 months, p=0.0021).

In the group with a nodular FDC pattern, two different types of FDC networks can be identified: (1) A nodular FDC pattern with an FDC distribution similar to PFs in lymphoid tissue (PF-nodular pattern, Fig. 1a). The staining showed faint Ki-M4p positivity with a mostly nodular network. This pattern was observed in 72 patients. (2) A nodular FDC pattern resembling the colonization of GCs by tumor cells, which was identified in seven patients. In these cases, strongly stained FDC, resembling preexisting GC-associated FDC networks, were seen (GC-nodular pattern, Fig. 1b). Patients with a GC-nodular pattern had a median OS time of only 14.4 months, in contrast to the PF-pattern group of 33.0 months. A significant difference in OS was seen between the PF-nodular and the other two patterns (GC-nodular and diffuse, p=0.0033). When blastoid subtypes were excluded, the differences became more evident (p=0.0008). Table 2 lists the results of the analysis of the growth and FDC patterns.

An analysis of the FDC distribution in relation to the growth pattern (Table 3) revealed a PF-FDC pattern in 25 of 29 cases (86%) with a nodular growth pattern. Forty seven of 72 cases (65%) with a PF-FDC pattern had a diffuse growth pattern, but the majority of cases with a diffuse FDC pattern (n=15) also had a diffuse growth pattern (88.2%, Table 3).

Due to the small number of GC-FDC pattern (n=6) and diffuse FDC pattern (n=9), the analysis of different prognostic factors in relation to the FDC distribution only has a limited statistical power, and the results had to be interpreted with caution. It revealed that only performance status and an International Prognostic Index (IPI) showed significant differences in each subgroup (Table 4). Interestingly, there was no difference in proliferation activity (Ki-67 index) in different FDC subtypes (p indicates not significant).

Complete clinical information of cases with classical cytology was available for multivariate analysis for only 62 out of 79 patients. A univariate analysis of this smaller group revealed that FDC distribution, Ki-67 index, IPI, age, and performance status [World Health Organization (WHO)] to be significant prognostic markers. In the multivariate Cox regression analysis, only FDC distribution (all three types and PF vs diffuse pattern), IPI, and the Ki-67 index were prognostic factors in our MCL patients (Table 5).

Table 4 Analysis of prognostic factors in relation to FDC distribution in 79 cases of MCL with classical cytology (without blastoid subtypes) out of 96 cases

	FDC distribution				
	PF-nodular	GC-nodular	Diffuse	p value (all FDC types)[a]	p value (PF+GC)[b]
Age					
<60	27	3	3	0.803	1.000
>60	37	3	6		
Sex					
Male	48	5	7	0.886	1.000
Female	16	1	2		
B symptoms					
Yes	23	4	4	0.363	0.206
No	39	2	5		
BM infiltration					
Yes	38	4	8	0.193	1.000
No	25	2	1		
Stage					
1+2	5	0	0	0.319	1.000
3+4	56	6	9		
Status (WHO)					
0–1	53	3	4	0.010	0.063
=2	9	3	5		
Extranodal					
Yes	55	6	8	0.416	1.000
No	9	0	1		
LDH					
<240	49	3	6	0.060	0.048
>240	7	3	3		
IPI					
0–1	20	0	0	0.007	0.173
=2	44	6	9		
Ki-67					
<10%	24	2	3	0.973	1.000
>10%	39	4	5		

BM Bone marrow, *Stage* Ann Arbor stage, *Status* performance status, *Extranodal* extranodal involvement, *LDH* lactate dehydrogenase, *IPI* International Prognostic Index

[a]Likelihood quotient

[b]Fisher's Exact Test (two-tailed)

Table 5 Uni- and multivariate Cox regression analysis of all prognostic factors with respect to overall survival in 62 MCL patients with complete available data out of 79 patients with classical MCL

Characteristics	Reference level	*p* value	
		Univariate	Multivariate
FDC distribution	PF-nodular vs. GC-nodular vs. diffuse	0.004	0.023
FDC distribution	PF vs. diffuse	0.009	0.010
FDC distribution	PF vs. GC	0.066	0.148
Growth pattern	Nodular vs. diffuse	0.567	0.188
International Prognostic Index	0–1 vs. =2	0.001	0.022
Ki-67 expression	0–10 vs. >10%	0.014	0.019
Age	<60 vs. >60	0.003	0.194
Bone marrow infiltration	Yes vs. no	0.096	0.751
Performance status (WHO)	0+1 vs. =2	0.041	0.793
LDH	Normal vs. elevated	0.136	0.309
Stage	1+2 vs. 3+4	0.270	0.601
B symptoms	Yes vs. no	0.653	0.653
Sex	Male vs. female	0.727	0.410
Extranodal involvement	Yes vs. no	0.227	0.890

Discussion

Mantle cell lymphoma was first described by Lennert, who called this lymphoma centrocytic lymphoma because of its morphology [21, 22]. Weisenburger identified this entity as an intermediate lymphocytic lymphoma [51, 53] and as mantle-zone lymphoma [48, 50]. Since the identification of the typical cytogenetic abnormality, the translocation t(11;14)(q13;32) [44, 46, 54], various cytological variants, e.g., blastoid types with an aggressive clinical course, have been described [6, 19, 29]. For this lymphoma, the typical growth pattern is a mantle-zone pattern, with tumor cells surrounding residual follicle centers. Additionally, a nodular and a diffuse growth pattern exist [6, 21, 52]. The clinical relevance of the different patterns is unclear. The mantle-zone pattern appears to have a significantly better prognosis [23]. Swerdlow et al. [39] described the pathological features in their study of 18 patients with MCL. They did not detect any differences between the different growth patterns that were of clinical relevance. Histologically, there seems to be a progression from a mantle-zone, to a nodular, and to a diffuse pattern [21, 23, 37]. In our study, 89.5% of the patients were in advanced stages (III and IV) of the disease, and the majority of cases (69.8%) had a diffuse growth pattern. Our results are in line with other studies revealing similar stages of the disease and growth patterns [9, 23, 37]. Lardelli et al. [18] investigated a group of 33 patients with MCL. The authors noticed a trend toward a prolonged median survival time for patients with MCL and mantle-zone pattern (77 months), but it did not reach statistical significance. A reason could be that the number of cases was too small.

In our study, we distinguished two types of growth pattern: a nodular and a diffuse pattern. The medium survival time in patients with a diffuse growth pattern was 28.0 months, in contrast to patients with a nodular architecture whose medium survival time was 32.0 months. Statistically, there was no significant difference in the OS time (p=0.7468). These results are comparable to the data of Argatoff et al. [1], who demonstrated in a large study of 80 patients a diffuse growth pattern in 78%, a nodular pattern in 16%, and a mantle-zone pattern in 6% of patients. There was no significant difference in the OS time between these three groups. In accordance with Fisher and coworkers [10], we also analyzed only the group with classical cytology without the clinically aggressive blastoid variants. Excluding these cases did not influence the statistical results. We conclude that the growth pattern of tumor cells in MCL is not a valid diagnostic tool for identifying patients with a poor prognosis.

In some studies on MCL, networks of FDC were mentioned [3, 9, 32, 37]. These FDC networks in MCL were well described by the ELTF [55]. They described the FDC network in combination with the growth pattern and mentioned, in addition to a nodular growth pattern without residual GCs and loosely structured FDC meshwork (PF pattern), cases with tight FDC clusters (GC pattern).

An FDC network is normally found in reactive lymph follicles [32]. The function of these FDCs in reactive lymph nodes is to present antigens to B cells [12, 15, 17, 42]. The FDC trap the antigen–antibody complexes and make immune-complex-coated bodies, the so-called iccosomes [5, 41]. The B cells endocytose these iccosomes, and the antigen is processed [43]. Networks of FDC have been observed not only in reactive lymphoid tissue but also in lymphoma [7, 28, 32, 35]. The interaction of FDC with normal B cells has been demonstrated in vitro [16, 36]. The interaction of FDC with lymphoma tumor cells has also been investigated [33, 34]. It was demonstrated that the FDC can influence the tumor cells in their environment through cytokines and prolong the entrance of these cells into apoptosis. The majority of proliferating lymphocytes was localized close to FDC. We analyzed the Ki-67 index in different FDC subtypes and could not observe significant proliferation differences, but due to the small number

of cases in the GC-FDC pattern and diffuse FDC groups, these results have only limited statistical power (Table 4).

To our knowledge, no study has investigated the FDC pattern in MCL in relation to the clinical outcome of patients. In our patients, we found both nodular and diffuse FDC patterns. Whereas the majority of cases have a diffuse pattern, the FDC pattern was mostly nodular (82.3%). The OS time was statistically longer (median 32.0 vs 21.1 months) than that for patients with MCL with a diffuse pattern (p=0.0312). If we exclude the blastoid variants from the analysis of the FDC pattern, the diffuse group only has a median OS time of 17.9 months, and the Kaplan–Meier analysis becomes more significant (p=0.0021). This effect is explained by the fact that the 17 cases with blastoid cytology had a longer median survival time of 22.7 months compared with the diffuse FDC group. Eight blastoid cases had a diffuse FDC network.

In the group with the nodular FDC pattern, we identified two different nodular patterns in accordance with the criteria of Annecy [55]. The first group showed a nodular FDC pattern, with an FDC distribution similar to a PF pattern in lymphoid tissue (Fig. 1a). This most frequent pattern was seen in 72 cases (75.0%). MCL patients with this PF-nodular pattern had a medium survival time of 33 months, in contrast to the second nodular FDC pattern, which resembles the colonization of GCs by tumor cells (GC-nodular). The GC-nodular pattern was only identified in seven cases. In these cases, strongly stained FDC resembling the FDC networks associated with preexisting GCs were seen (Fig. 1b). This pattern shows similarity to the follicular colonization first described in low-grade mucosa-associated lymphoid tissue (MALT) lymphomas by Isaacson and Wright [14]. The so-called FDC pattern of colonized GCs (GC-nodular) had the worst prognosis, with a medium survival time of 14.4 months. A significant difference in the OS of patients with MCL and different FDC networks was seen between the PF pattern and the other two (GC and diffuse) patterns in the analysis of all cases (p=0.0033, Table 2) and in that of cases without blastoid cytology (p=0.0008, Fig. 3c, Table 2). Multivariate analysis of the FDC distribution and other clinical parameters revealed that only FDC distribution, IPI, and the Ki-67 index are independent prognostic factors in our collective (Table 5).

The analysis of the relation between the FDC distribution and the growth pattern shows that the majority of cases (66.7%) with the PF-FDC pattern had a diffuse growth pattern (Table 3). Only 24 cases (33.3%) had a purely nodular architecture. Taking this into consideration, the analysis of the growth pattern has no predictive value about the FDC pattern. Only the immunohistochemical staining and the analysis of the FDC network distinguished between the FDC patterns.

From these results, we conclude that the interaction of FDC, or their distribution pattern, plays an important role in the clinical course of these malignant lymphomas. It is necessary to exclude aggressive cytological variants of MCL, like the blastoid subtype from the analysis of the FDC pattern, to better predict the clinical outcome of patients with MCL. The analysis of FDC distribution is a new independent prognostic marker in MCL.

Acknowledgements We would like to thank Mrs. K. Dege for language editing and T. Zwingers (Estimate GmbH, Augsburg) for assistance with the statistical calculations.

References

1. Argatoff LH, Connors JM, Klasa RJ, Horsman DE, Gascoyne RD (1997) Mantle cell lymphoma: a clinicopathologic study of 80 cases. Blood 89:2067–2078
2. Bankfalvi A, Riehemann K, Ofner D, Checci R, Morgan JM, Piffko J, Bocker W, Jasani B, Schmid KW (1994) Moist autoclaving. A simplified method for antigen unmasking. Pathologe 15:345–349
3. Banks PM, Chan J, Cleary ML, Delsol G, De Wolf-Peeters C, Gatter K, Grogan TM, Harris NL, Isaacson PG, Jaffe ES (1992) Mantle cell lymphoma. A proposal for unification of morphologic, immunologic, and molecular data. Am J Surg Pathol 16: 637–640
4. Brittinger G, Bartels H, Common H, Duhmke E, Fulle HH, Gunzer U, Gyenes T, Heinz R, Konig E, Meusers P (1984) Clinical and prognostic relevance of the Kiel classification of non-Hodgkin lymphomas results of a prospective multicenter study by the Kiel Lymphoma Study Group. Hematol Oncol 2:269–306
5. Burton GF, Kosco MH, Szakal AK, Tew JG (1991) Iccosomes and the secondary antibody response. Immunology 73:271–276
6. Campo E, Raffeld M, Jaffe ES (1999) Mantle-cell lymphoma. Semin Hematol 36:115–127
7. Carbone A, Poletti A, Manconi R, Gloghini A, Volpe R (1987) Heterogeneous in situ immunophenotyping of follicular dendritic reticulum cells in malignant lymphomas of B-cell origin. Cancer 60:2919–2926
8. Cordell JL, Falini B, Erber WN, Ghosh AK, Abdulaziz Z, MacDonald S, Pulford KA, Stein H, Mason DY (1984) Immunoenzymatic labeling of monoclonal antibodies using immune complexes of alkaline phosphatase and monoclonal anti-alkaline phosphatase (APAAP complexes). J Histochem Cytochem 32:219–229
9. Decaudin D, Bosq J, Munck JN, Bayle C, Koscielny S, Boudjemaa S, Bennaceur A, Venuat AM, Naccache P, Bendahmane B, Ribrag V, Carde P, Pico JL, Hayat M (1997) Mantle cell lymphomas: characteristics, natural history and prognostic factors of 45 cases. Leuk Lymphoma 26:539–550
10. Fisher RI, Dahlberg S, Nathwani BN, Banks PM, Miller TP, Grogan TM (1995) A clinical analysis of two indolent lymphoma entities: mantle cell lymphoma and marginal zone lymphoma (including the mucosa-associated lymphoid tissue and monocytoid B-cell subcategories): a Southwest Oncology Group study. Blood 85:1075–1082
11. Goff LK, Armitage RJ, Beverley PC (1988) Characterization of two CD23 monoclonal antibodies with reactivity distinct from other antibodies within this cluster of differentiation. Immunology 65:213–220
12. Hollmann C, Gerdes J (1999) Follicular dendritic cells and T cells: nurses and executioners in the germinal centre reaction. J Pathol 189:147–149
13. Hsu SM, Raine L, Fanger H (1981) Use of avidin–biotin–peroxidase complex (ABC) in immunoperoxidase techniques: a comparison between ABC and unlabeled antibody (PAP) procedures. J Histochem Cytochem 29:577–580

14. Isaacson P, Wright DH (1984) Extranodal malignant lymphoma arising from mucosa-associated lymphoid tissue. Cancer 53: 2515–2524
15. Kosco-Vilbois MH, Gray D, Scheidegger D, Julius M (1993) Follicular dendritic cells help resting B cells to become effective antigen-presenting cells: induction of B7/BB1 and upregulation of major histocompatibility complex class II molecules. J Exp Med 178:2055–2066
16. Kosco MH, Pflugfelder E, Gray D (1992) Follicular dendritic cell-dependent adhesion and proliferation of B cells in vitro. J Immunol 148:2331–2339
17. Lanzavecchia A (1985) Antigen-specific interaction between T and B cells. Nature 314:537–539
18. Lardelli P, Bookman MA, Sundeen J, Longo DL, Jaffe ES (1990) Lymphocytic lymphoma of intermediate differentiation. Morphologic and immunophenotypic spectrum and clinical correlations. Am J Surg Pathol 14:752–763
19. Laszlo T, Matolcsy A (1999) Blastic transformation of mantle cell lymphoma: genetic evidence for a clonal link between the two stages of the tumour. Histopathology 35:355–359
20. Ledbetter JA, Martin PJ, Spooner CE, Wofsy D, Tsu TT, Beatty PG, Gladstone P (1985) Antibodies to Tp67 and Tp44 augment and sustain proliferative responses of activated T cells. J Immunol 135:2331–2336
21. Lennert K, Mohri N, Stein H, Kaiserling E (1975) The histopathology of malignant lymphomata. Br J Haematol 31:193–203
22. Lennert K, Stein H, Kaiserling E (1975) Cytological and functional criteria for the classification of malignant lymphomata. Br J Cancer 31:29–43
23. Majlis A, Pugh WC, Rodriguez MA, Benedict WF, Cabanillas F (1997) Mantle cell lymphoma: correlation of clinical outcome and biologic features with three histologic variants. J Clin Oncol 15:1664–1671
24. Mason DY, Comans-Bitter WM, Cordell JL, Verhoeven MA, Van DJ (1990) Antibody L26 recognizes an intracellular epitope on the B-cell-associated CD20 antigen. Am J Pathol 136:1215–1222
25. Mason DY, Krissansen GW, Davey FR, Crumpton MJ, Gatter KC (1988) Antisera against epitopes resistant to denaturation on T3 (CD3) antigen can detect reactive and neoplastic T cells in paraffin embedded tissue biopsy specimens. J Clin Pathol 41:121–127
26. Meusers P, Engelhard M, Bartels H, Binder T, Fulle HH, Gorg K, Gunzer U, Havemann K, Kayser W, Konig E (1989) Multicentre randomized therapeutic trial for advanced centrocytic lymphoma: anthracycline does not improve the prognosis. Hematol Oncol 7:365–380
27. Molot RJ, Meeker TC, Wittwer CT, Perkins SL, Segal GH, Masih AS, Braylan RC, Kjeldsberg CR (1994) Antigen expression and polymerase chain reaction amplification of mantle cell lymphomas. Blood 83:1626–1631
28. Mori N, Oka K, Kojima M (1988) DRC antigen expression in B-cell lymphomas. Am J Clin Pathol 89:488–492
29. Ott G, Kalla J, Hanke A, Muller JG, Rosenwald A, Katzenberger T, Kretschmar R, Kreipe H, Muller-Hermelink HK (1998) The cytomorphological spectrum of mantle cell lymphoma is reflected by distinct biological features. Leuk Lymphoma 32:55–63
30. Parwaresch MR, Radzun HJ, Feller AC, Peters KP, Hansmann ML (1983) Peroxidase-positive mononuclear leukocytes as possible precursors of human dendritic reticulum cells. J Immunol 131:2719–2725
31. Parwaresch MR, Radzun HJ, Hansmann ML, Peters KP (1983) Monoclonal antibody Ki-M4 specifically recognizes human dendritic reticulum cells (follicular dendritic cells) and their possible precursor in blood. Blood 62:585–590
32. Petrasch S, Brittinger G, Wacker HH, Schmitz J, Kosco-Vilbois M (1994) Follicular dendritic cells in non-Hodgkin's lymphomas. Leuk Lymphoma 15:33–43
33. Petrasch S, Kosco M, Perez-Alvarez C, Schmitz J, Brittinger G (1992) Proliferation of non-Hodgkin-lymphoma lymphocytes in vitro is dependent upon follicular dendritic cell interactions. Br J Haematol 80:21–26
34. Petrasch S, Kosco M, Schmitz J, Wacker HH, Brittinger G (1992) Follicular dendritic cells in non-Hodgkin-lymphoma express adhesion molecules complementary to ligands on neoplastic B-cells. Br J Haematol 82:695–700
35. Petrasch S, Perez-Alvarez C, Schmitz J, Kosco M, Brittinger G (1990) Antigenic phenotyping of human follicular dendritic cells isolated from nonmalignant and malignant lymphatic tissue. Eur J Immunol 20:1013–1018
36. Petrasch SG, Kosco MH, Perez-Alvarez CJ, Schmitz J, Brittinger G (1991) Proliferation of germinal center B lymphocytes in vitro by direct membrane contact with follicular dendritic cells. Immunobiology 183:451–462
37. Pittaluga S, Wlodarska I, Stul MS, Thomas J, Verhoef G, Cassiman JJ, Van DB, De Wolf-Peeters C (1995) Mantle cell lymphoma: a clinicopathological study of 55 cases. Histopathology 26:17–24
38. Singh N, Wright DH (1997) The value of immunohistochemistry on paraffin wax embedded tissue sections in the differentiation of small lymphocytic and mantle cell lymphomas. J Clin Pathol 50:16–21
39. Swerdlow SH, Habeshaw JA, Murray LJ, Dhaliwal HS, Lister TA, Stansfeld AG (1983) Centrocytic lymphoma: a distinct clinicopathologic and immunologic entity. A multiparameter study of 18 cases at diagnosis and relapse. Am J Pathol 113: 181–197
40. Swerdlow SH, Zukerberg LR, Yang WI, Harris NL, Williams ME (1996) The morphologic spectrum of non-Hodgkin's lymphomas with BCL1/cyclin D1 gene rearrangements. Am J Surg Pathol 20:627–640
41. Szakal AK, Kosco MH, Tew JG (1988) A novel in vivo follicular dendritic cell-dependent iccosome-mediated mechanism for delivery of antigen to antigen-processing cells. J Immunol 140:341–353
42. Tew JG, Wu J, Fakher M, Szakal AK, Qin D (2001) Follicular dendritic cells: beyond the necessity of T-cell help. Trends Immunol 22:361–367
43. Tew JG, Wu J, Qin D, Helm S, Burton GF, Szakal AK (1997) Follicular dendritic cells and presentation of antigen and costimulatory signals to B cells. Immunol Rev 156:39–52
44. Tsujimoto Y, Yunis J, Onorato-Showe L, Erikson J, Nowell PC, Croce CM (1984) Molecular cloning of the chromosomal breakpoint of B-cell lymphomas and leukemias with the t(11;14) chromosome translocation. Science 224:1403–1406
45. Tworek JA, Singleton TP, Schnitzer B, Hsi ED, Ross CW (1998) Flow cytometric and immunohistochemical analysis of small lymphocytic lymphoma, mantle cell lymphoma, and plasmacytoid small lymphocytic lymphoma. Am J Clin Pathol 110:582–589
46. Van DB, Parloir C, David G, Michaux JL, Sokal G (1979) A new characteristic karyotypic anomaly in lymphoproliferative disorders. Cancer 44:188–195
47. Watson P, Wood KM, Lodge A, McIntosh GG, Milton I, Piggott NH, Proctor SJ, Taylor PR, Smith S, Jack F, Bell H, Steward M, Anderson JJ, Horne CH, Angus B (2000) Monoclonal antibodies recognizing CD5, CD10 and CD23 in formalin-fixed, paraffin-embedded tissue: production and assessment of their value in the diagnosis of small B-cell lymphoma. Histopathology 36:145–150
48. Weisenburger DD (1984) Mantle-zone lymphoma. An immunohistologic study. Cancer 53:1073–1080
49. Weisenburger DD, Armitage JO (1996) Mantle cell lymphoma —an entity comes of age. Blood 87:4483–4494
50. Weisenburger DD, Kim H, Rappaport H (1982) Mantle-zone lymphoma: a follicular variant of intermediate lymphocytic lymphoma. Cancer 49:1429–1438

51. Weisenburger DD, Linder J, Daley DT, Armitage JO (1987) Intermediate lymphocytic lymphoma: an immunohistologic study with comparison to other lymphocytic lymphomas. Human Pathol 18:781–790
52. Weisenburger DD, Nathwani BN, Diamond LW, Winberg CD, Rappaport H (1981) Malignant lymphoma, intermediate lymphocytic type: a clinicopathologic study of 42 cases. Cancer 48:1415–1425
53. Weisenburger DD, Sanger WG, Armitage JO, Purtilo DT (1987) Intermediate lymphocytic lymphoma: immunophenotypic and cytogenetic findings. Blood 69:1617–1621
54. Williams ME, Meeker TC, Swerdlow SH (1991) Rearrangement of the chromosome 11 bcl-1 locus in centrocytic lymphoma: analysis with multiple breakpoint probes. Blood 78: 493–498
55. Zucca E, Stein H, Coiffier B (1994) European Lymphoma Task Force (ELTF): report of the workshop on mantle cell lymphoma (MCL). Ann Oncol 5:507–511

Virchows Arch (2006) 448: 160–164
DOI 10.1007/s00428-005-0055-7

ORIGINAL ARTICLE

Joachim Arnemann · Omar Sultani · Dilek Hasgün · Wiltrud Coerdt

T-/H-cadherin (CDH13): a new marker for differentiating podocytes

Received: 31 January 2005 / Accepted: 27 July 2005 / Published online: 17 August 2005

Abstract Cadherin molecules are known to be involved in various biological processes other than cell adhesion such as morphogenesis, cell–cell communication, cell recognition or cell signalling. While the classical cadherin molecule is characterized by an extracellular moiety, a transmembrane region and a variable cytoplasmic domain, T-/H-cadherin differs from this pattern due to the absence of a transmembrane region and a cytoplasmic domain, respectively. Its extracellular moiety is bound to the apical cell membrane by a glycosyl–phosphatidyl–inositol anchor and localized to lipid raft domains. As its molecular function and expression pattern is still not fully understood, we used a newly generated anti-T-/H-cadherin antiserum to study immunohistochemically the expression of T-/H-cadherin during the differentiation of foetal human glomeruli. At the early capillary loop stage a strong apical signal comes up for visceral epithelial cells of Bowman's capsule, which begin to differentiate towards podocytes. At the advanced capillary loop stage, when podocytes have become part of the glomerular filtration barrier, the expression pattern, however, becomes more distinct and most likely restricted to the foot processes of the podocytes. We thus postulate a functional role of T-/H-cadherin for the differentiation of the podocytes and the formation of the glomerular capillary network.

J. Arnemann · W. Coerdt
Department of Paediatric Pathology,
Institute of Pathology, Johannes Gutenberg University Hospital,
Mainz, Germany

J. Arnemann · O. Sultani · D. Hasgün
Institute of Human Genetics,
Johann Wolfgang Goethe University Hospital,
Frankfurt, Germany

J. Arnemann (✉)
Institute of Pathology,
Johann Wolfgang Goethe University Hospital,
Theodor-Stern-Kai 7/Haus 6,
60590 Frankfurt, Germany
e-mail: Joachim_Arnemann@web.de
Tel.: +49-69-630183498
Fax: +49-69-63015241

Keywords T-/H-cadherin · GPI anchor · Human foetal kidney · Capillary loop stage · Podocytes

Introduction

Morphoregulatory processes, like embryonic development or differentiation of tissues and organs, as well as maintenance of tissue architecture, require, among others, cell–cell- or the cell–extracellular matrix interactions. In these, cell adhesion molecules or their macromolecular structures act as mediators, transforming their extracellular binding properties via an intracellular signal transduction pathway directly into a regulatory signal for the nucleus and its transcription machinery. Thus, adhesive processes influence the timing of cellular events, like differentiation, proliferation or cell migration.

Among the cell adhesion molecules, the still-growing family of cadherins is the most important [1]. Cadherins are Ca2+-dependant transmembrane-localized molecules. The so-called "classical," or type I, cadherin molecules, like E-cadherin, are characterized (a) by a well-defined extracellular region with a conserved HAV cell-adhesion recognition site (CAR) and extracellular Ca2+-binding cadherin domains, (b) by a transmembrane domain and (c) by an intracellular or cytoplasmic part, which links these molecules to the cytoskeleton and to various intracellular signalling pathways via binding, e.g. to catenin molecules.

An unusual member of the cadherin family is T-cadherin [6, 9], also known as H-cadherin [10] or CDH13, now referred to as T-/H-cadherin, which is characterized by the lack of several defined classical domains. Not only the transmembrane region and the cytoplasmatic tail are absent from the molecule but also the conserved CAR is missing. From these data, cellular properties have been noticed which differ from the classical cadherin molecules: First, T-/H-cadherin shows an apical instead of a baso-lateral localization. Second, the lack of a direct link to the cytoskeleton via catenin molecules excludes the β-catenin-directed signal transduction pathway from transcriptional regulation of T-/H-cadherin. Third, the absence of a func-

tional CAR and the lack of strong links to the cytoskeleton should exclude this molecule from homo- or heterophilic binding to other cadherin molecules in terms of cell–cell adhesion processes. Instead, the C-terminus of T-/H-cadherin is bound to a glycosyl–phosphatidyl–inositol (GPI) anchor [6] as part of a post-translational modification. Like other GPI-anchored molecules T-/H-cadherin thus localizes on defined domains of the plasma membrane, the so-called lipid rafts. Lipid rafts are of functional importance for the polarisation of epithelial cells, mainly by sorting out apical membrane proteins [8]. This process leads to a kind of compartmentation of the cell and, consequently, to the expression of defined signalling pathways. A specific form of lipid rafts are the caveolae, with their various caveoli proteins as main components. Furthermore, those caveolae, and T-/H-cadherin has been postulated to be a part of them, are regarded as organising centres for signal molecules [8]. A link to activation or inhibitory processes, e.g. of the Ras-/mitogen-activated protein kinase (Ras/MAPK) pathway, has been shown.

The function of T-/H-cadherin, however, is still controversially discussed, as it is supposed to be different in developmental stages, tissues and organs. While some authors [7] suggested a function for cell recognition, others [11] proposed a regulatory function in cellular signal transduction processes. Again, others demonstrated a negative regulation of cellular growth [9] or postulated a tumour suppressor function [10]. Recent data [12] even indicated towards a possible role in neo-vascularisation during tumour development, as T-/H-cadherin showed an overexpression in tumour-penetrating blood vessels.

As we are generally interested in the morphoregulatory function of the various members of the cadherin family, we produced an antiserum against a unique fragment from the N-terminal region to test T-/H-cadherin expression during foetal development of mice and humans.

Materials and methods

Expression of fusion protein and generation of antisera

A recombinant fragment of 56 amino acids (GSLQDIFK FARTSPVPRQKRSIVVSPILIPENQRQPFPRDVGKVV DSDRPEGSKFR), covering position 119 to 174 of the T-/H-protein, was cloned and expressed in the pATH3 expression system [5]. The fusion protein was purified by gel elution and submitted for the commercial immunisation of rabbits (SEQLAB, Göttingen, Germany).

Western blot analysis

For Western blot experiments proteins were extracted from cells, separated on 10% sodium dodecyl sulfate (SDS)–polyacrylamide gel electrophoresis (PAGE) gels and electroblotted onto nitrocellulose membrane (Hybond C; Amersham Pharmacia Biotech) according to standard protocols. The obtained blots were pre-incubated with non-fat milk (10% w/v) in Tris-buffer saline with Tween (TBST) (50 mM Tris–HCl, pH 7.4; 0.9% NaCl; and 0.05% Tween 20) and subsequently incubated for 1 h at room temperature (RT) with *anti-T-/H-cadherin* (*a-9002*) or *anti-caveolin-1* (Santa Cruz Biotechnology Inc.) antisera in TBST. After washing, membranes were incubated with an alkaline phosphate-labelled anti-rabbit immunoglobulin G (IgG) antibody for 1 h at RT. After washing in TBST signals were detected using the nitroblue tetrazolium (NBT)/5-bromo-4-chloro-3-indolyl phosphate (BCIP) system.

Immunohistochemistry

Briefly, paraffin sections of human foetal kidneys (weeks 20 and 21) were pretreated by the microwave method and subsequently incubated with *anti-T-/H-cadherin* (*a-9002*; 1:200) or *anti-caveolin-1* (Santa Cruz Biotechnology Inc.; 1:200), followed by incubation with a secondary biotynilated goat-anti-rabbit-antiserum (1:400; Sigma). The presence of bound antibodies was detected with the peroxidase-conjugated Avidin–Biotin Complex method (ABC Kit; Vector) using diaminobenzidine tetrahydrochloride (DAB) as a substrate according to standard protocols.

Results

The specificity of the obtained anti-T-/H-cadherin antiserum, *a-9002*, can be shown when immunoblots of fusion proteins and various protein extracts, e.g. from human kidney tissue and from the T-/H-cadherin expressing human embryonic kidney cell line *HEK 293*, were positively tested for a specific recognition pattern and a signal of predicted molecular weight (Fig. 1). The observed strong signals in human-kidney-derived protein lysates prompted us to analyse its cellular localization in more detail. We thus tested the expression pattern of T-/H-cadherin during human kidney development by means of immunohistochemistry.

The development and differentiation of the kidney is a complex process, which is characterized by a high level of gene activity, and thus, of increased regulatory pathways [3]. Different stages of kidney differentiation have been defined, like condensation stage, epithelial stage, tubulus

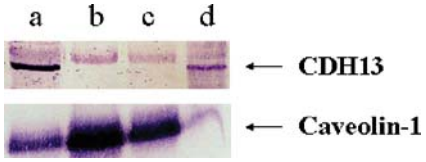

Fig. 1 **a** In immunoblot experiments the anti-T-/H-cadherin (CDH13) antiserum *a-9002* was positively tested in protein lysates of adult human kidney tissue (**a**) and of the human embryonic kidney cell line *HEK 293* (**d**), while samples of human adult lung (**b**) and testis tissue (**c**) were negative. **b** As a control for the specificity an antiserum against the broadly expressed caveolin-1 was run alongside it

differentiation stage or nephron differentiation stage. For our investigation foetal kidney specimens between the 20th and 22nd weeks of gestation, which were obtained for routine histopathological examinations, were selected, as at this stage, a cortex-to-medulla-orientated gradient from early to fully differentiated nephron stages can be found (Fig. 2a–c).

Immunohistochemical experiments showed distinct patterns of T-/H-cadherin expression. While there were no signals at all in the very early stages of nephron differentiation, namely, "comma-shape" and "S-shape" stages, a strong signal appears in the early phase of nephron differentiation, just before the glomerular capillary network differentiates, and extends to the final stage of glomerular capillary network differentiation. At the early stage the inner layer, or VEC, of Bowman's capsule shows a strong apical staining, with signals extending well into the lumina (Fig. 2d–f). These epithelial cells will differentiate into podocytes, which coat the glomerular capillary tuft.

With the ongoing differentiation of the glomerulus the continuous layer of VECs apparently disperses, and these cells, which begin to differentiate into podocytes with extended foot processes, move towards the endothelial cells of the invading capillaries. This can be shown by the punctate immunoreaction with the anti-T-/H-cadherin antiserum, where signals extend towards the capillaries (Fig. 2g–i). However, the overall impression is that the signal intensity should be slightly reduced. At this stage the podocytes have terminally differentiated and line the glomerular capillary network. These podocytes are part of the glomerular filtration barrier, which consists mainly of the capillary endothelial cells facing the circulating

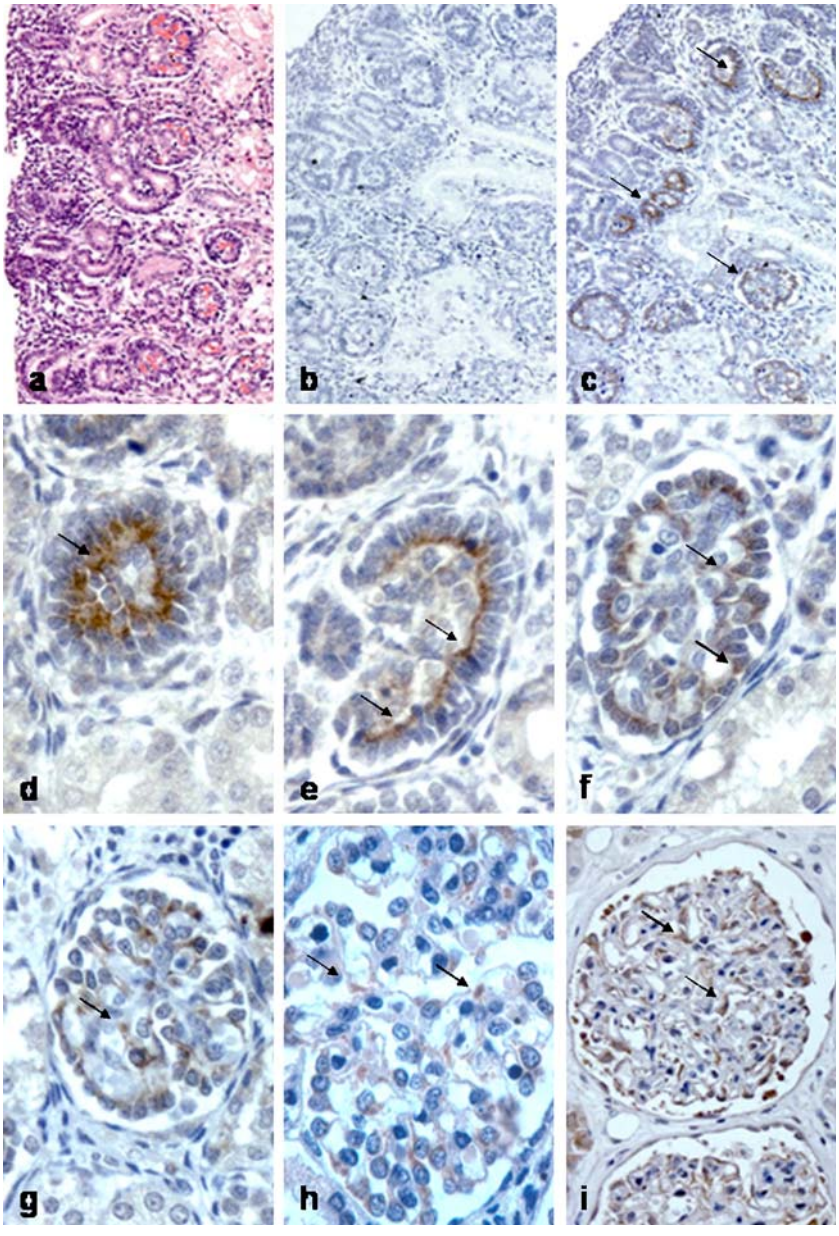

Fig. 2 Immunohistochemical localization (**b**–**i**) of T-/H-cadherin (CDH13) in various stages of human foetal kidney development using recombinant anti-T-/H-cadherin antiserum *a-9002*. **a** Hematoxylin and eosin (H & E) staining of the specimen; magnification ×200. **b** Negative control without any antiserum; magnification ×200. **c** Overview of the immunohistochemical staining pattern; note the various stages of differentiation oriented in cortex (*top*)–medulla (*bottom*) orientation; magnification ×200. **d**–**h** Sequential expression and localization of the T-/H-cadherin protein during early and advanced stages of glomerular capillary network differentiation; note the signal within the initially continuous, later dispersed, visceral layer of epithelial cells of Bowman's capsule, which differentiate into podocytes; magnification ×630. **i** Localization of the T-/H-cadherin protein in the terminally differentiated glomerulus of the adult kidney; note the dispersed and less dense signals within the glomerular capillary tuft; magnification ×400

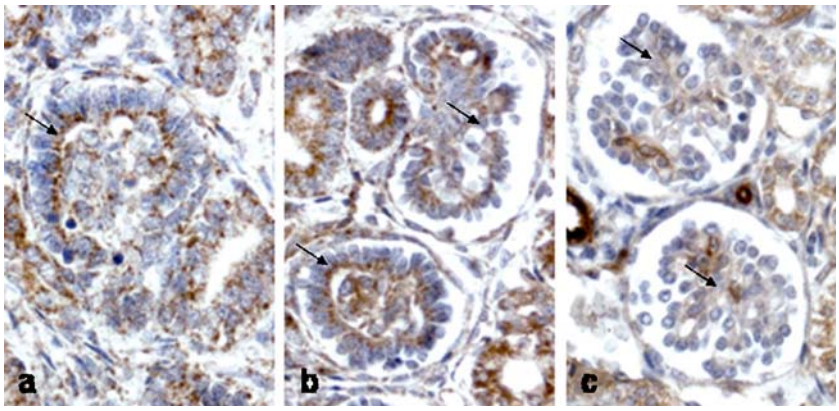

Fig. 3 Immunohistochemical localization of caveolin-1 in early and advanced stages (**a**–**c**) of human foetal kidney development using anti-caveolin-1 antiserum. Note as well the broader expression pattern of caveolin-1 as the almost identical pattern compared with anti-T/H-cadherin antiserum during glomerular capillary network differentiation. In early stages signals are present in the initially continuous, later dispersed, visceral layer of epithelial cells of Bowman's capsule; magnification ×630

blood, the glomerular basement membrane and the podocytes, facing the urinary space.

As the expression pattern obtained in this delicate stage of nephron differentiation is of particular interest for the pathologist working, e.g. on congenital nephrosis, we decided to run another well-defined marker, anti-caveolin-1, alongside it.

Caveolin proteins are the main components of caveolae, a specific organisation of lipid raft domains within the plasma membrane [8]. As the GPI-anchored T-/H-cadherin molecule localizes to lipid raft domains of the plasma membrane and potentially to caveolae, and as caveolin-1 has been shown to be expressed by podocytes and to be localized in the foot processes of the terminally differentiated podocytes, we chose the well-established marker caveolin-1 for comparison with the expression pattern of T-/H-cadherin.

Not only was the presence of caveolin-1 protein confirmed in immunoblot experiments with the abovementioned samples (Fig. 1) but also the obtained staining pattern of the podocytes were almost the same as for the anti T-/H-cadherin antiserum when tested on the same specimen by means of immunohistochemistry (Fig. 3a–c). This finding furthermore supports our observation that T-/H-cadherin protein should be localized to the foot processes of podocytes, leaving, however, the question of a possible function unsolved.

In all, we were able to demonstrate for the first time a distinct expression pattern of the T-/H-cadherin protein at defined stages of nephron differentiation.

Discussion

It should be noted that a signal for T-/H-cadherin protein first comes up in VEC at the early capillary loop stage, while previous stages are negative. The hereby observed high intensity, which is equivalent to a high amount of protein, indicates that it could well be linked to a defined differentiation step on the cellular level. We would like to speculate that its expression could well monitor the transition from VECs towards podocytes. The function of T-/H-cadherin is still unknown, but given that lipid rafts and their components are involved in the sorting of apical membrane proteins and compartmentation of the cell, T-/H-cadherin could well contribute to the differentiation of the foot processes, as the corresponding staining patterns of T-/H-cadherin and caveolin-1 suggest.

Papers published describe various members of the cadherin family as expressed in a hierarchical order during kidney development [4], similar to what has been previously described for the human epidermis [2]. Besides ubiquitously expressed classical cadherin molecules, like E-cadherin, certain cadherin molecules are expressed in narrow stage-specific limits.

Cadherin-11, for example, has a characteristic expression pattern in the early condensation stage of the kidney and is replaced by cadherin-4 (R-cadherin) and/or cadherin-6 (K-cadherin) during the epithelial stage, while during the tubulus stage, cadherin-16 [kidney-specific (KSP)-cadherin) is transcribed [4]. So far, T-/H-cadherin is the only published cadherin molecule with a specific expression pattern during the advanced nephron differentiation stage, and specifically in podocytes.

This is of special interest to the pathologist, as a disturbed differentiation can cause conditions like glomerulocystic kidney disease (OMIM #137920) or affect the volume of amniotic fluid by affecting the filtration rate. Oligo- or anhydramnion are conditions where malformations and malfunctions of the foetal kidney, besides maternal placenta insufficiency or early rupture of the foetal membrane, can cause the intra-uterine death of the foetus. Thus, one diagnostic criterion is the differentiation stage of the kidney, and particularly, of the nephrons. From this point of view the characterization and subsequent application of markers specific for this stage of differentiation should be of great help in histopathological evaluation.

In summary, the described pattern suggests that the epithelial podocytes are the expressing cell type during neph-

ron differentiation and that T-/H-cadherin should function as a kind of morphoregulatory molecule. We do not yet know what the specific function on the cellular level might be, but given that published data [12] suggest a possible role for T-/H-cadherin in the neo-vascularisation process during tumour growth, we would, like to speculate that it can have a similar role for the formation of the glomerular capillary network. However, this has to be proven experimentally in an animal model.

Acknowledgements We thank Jana Hoffmann for photographic work and Linda Tennant for critical reading of the manuscript. This work has been supported by a grant from the Riese-Stiftung to J.A.

The authors declare that the experiments comply with the current laws.

References

1. Angst BD, Marcozzi C, Magee AI (2001) The cadherin superfamily: diversity in form and function. J Cell Sci 114:629–641
2. Arnemann J, Sullivan KH, Magee AI, King IA, Buxton RS (1993) Stratification-related expression of isoforms of the desmosomal cadherins in human epidermis. J Cell Sci 104:741–750
3. Bard JBL (2002) Growth and death in the developing mammalian kidney: signals, receptors and conversations. BioEssays 24:72–82
4. Dahl U, Sjodin A, Larue L, Radice GL, Cajander S, Takeichi M, Kemler R, Semb H (2002) Genetic dissection of cadherin function during nephrogenesis. Mol Cell Biol 22:1474–1487
5. Dieckmann CL, Tzagoloff A (1985) Assembly of the mitochondrial membrane system. CBP6, a yeast nuclear gene necessary for synthesis of cytochrome b. J Biol Chem 260:1513–1520
6. Doyle DD, Goings GE, Upshaw-Earley J, Page E, Ranscht B, Palfrey HC (1998) T-cadherin is a major glycophosphoinositol-anchored protein associated with noncaveolar detergent-insoluble domains of the cardiac sarcolemma. J Biol Chem 273: 6937–6943
7. Koller E, Ranscht B (1996) Differential targeting of T- and N-cadherin in polarized epithelial cells. J Biol Chem 271:30061–30067
8. Kurzchalia TV, Parton RG (1999) Membrane microdomains and caveolae. Curr Opin Cell Biol 11:424–431
9. Kuzmenko YS, Kern F, Bochkov VN, Tkachuk VA, Resink TJ (1998) Density- and proliferation status-dependent expression of T-cadherin, a novel lipoprotein binding glycoprotein: a function in negative regulation of smooth muscle cell growth? FEBS Lett 434:183–187
10. Lee SW (1996) H-cadherin, a novel cadherin with growth inhibitory functions and diminished expression in human breast cancer. Nat Med 2:776–782
11. Philippova MP, Bochkov VN, Stambolsky DV, Tkachuk VA, Resink TJ (1998) T-cadherin and signal-transducing molecules co-localize in caveolin-rich membrane domains of vascular smooth muscle cells. FEBS Lett 429:207–210
12. Wyder L, Vitaliti A, Schneider H, Hebbard LW, Moritz DR, Wittmer M, Ajmo M, Klemenz R (2000) Increased expression of H/T-cadherin in tumor-penetrating blood vessels. Cancer Res 60:4682–4688

Virchows Arch (2006) 448: 165–171
DOI 10.1007/s00428-005-0056-6

ORIGINAL ARTICLE

Gary L. Bratthauer · Brian L. Strauss · Fattaneh A. Tavassoli

STAT 5a expression in various lesions of the breast

Received: 16 March 2005 / Accepted: 27 July 2005 / Published online: 19 August 2005

Abstract The seven signal transducer and activator of transcription (STAT) molecules are effectors of hormonal or cytokine stimulation through receptors. STAT 5a, isolated from prolactin-stimulated mammary cells, contributes to normal proliferation and is essential for mammary gland differentiation. Using a monoclonal antibody, we tested 100 formalin-fixed, paraffin-embedded breast tissues representing everything from simple hyperplasia to invasive carcinoma for the expression of STAT 5a in comparison to normal breast epithelial cells. Immunohistochemical analysis was performed following heat treatment in a pressure cooker. STAT 5a was found in endothelial cells, adipocytes, and leukocytes as well as in the cytoplasm and nucleus of normal epithelial cells, usual ductal hyperplasia, and benign lesions such as fibroadenoma. Myoepithelial cells and stromal fibroblasts failed to demonstrate any STAT 5a in addition to most atypical proliferations including in situ and invasive carcinomas. A few examples of lobular intraepithelial neoplasia and invasive carcinoma demonstrated some reactivity, albeit comparatively reduced. The absence of STAT 5a in the abnormal breast epithelial cells may indicate a defect contributory to the abnormal state.

Keywords Breast · Carcinoma · Immunohistochemistry · STAT 5a

The opinions or assertions contained herein are the private views of the authors and are not to be construed as official, or as reflecting the views of the Department of the Army, Department of the Air Force, or Department of Defense.

G. L. Bratthauer (✉) · B. L. Strauss · F. A. Tavassoli
Department of Gynecologic and Breast Pathology,
Armed Forces Institute of Pathology,
Washington, DC 20306-6000, USA
e-mail: bratthauer@afip.osd.mil
Tel.: +1-202-7821600
Fax: +1-202-7823939

Present address:
B. L. Strauss
Department of Pathology, Wilford Hall Medical Center,
Lackland Air Force Base,
San Antonio, TX 78236, USA

Present address:
F. A. Tavassoli
Department of Pathology, Yale University School of Medicine,
New Haven, CT 06520-8023, USA

Introduction

The seven signal transducer and activator of transcription (STAT) molecules are effectors of hormonal or cytokine stimulation through receptors. In unstimulated cells, STAT proteins exist largely in the cytoplasm as latent transcription factors. In response to exogenous factors, specific STATs undergo tyrosine phosphorylation, nuclear translocation, and DNA binding resulting in the transcriptional activation of distant target genes. There are many genes regulated by the STAT pathway that are required for cell growth, survival, differentiation, and motility [7].

STAT 5a, also called mammary growth factor, was isolated from prolactin-stimulated mammary cells, and is activated through the binding of prolactin to its receptor [17]. STAT 5a has been shown to be involved in integrin-mediated c-*fos* transcription and integrin-mediated adhesion affects control of cell cycle entry and inhibition of apoptosis [5]. In knockout mice that lack STAT 5a, the mammary gland does not develop properly [1, 14]. STAT 5a-deficient mice develop normally, but lobuloalveolar growth during pregnancy is aberrant [15].

It has been suggested that STAT 5a contributes to normal proliferation, and it has been shown that STAT 5a is essential for mammary gland differentiation in mice [15]. Furthermore, known defects in the Janus Kinase (JAK)/STAT pathway have led to the inhibition of growth restraint [19]. STAT 5a is also involved in adipocyte differentiation, its expression correlating with lipid accumulation, and it can be activated in the stroma by growth hormone and the epidermal growth factor [9, 24]. Recently, STAT 5a activation in breast cancer has been associated with a favorable prognosis [18].

Using a monoclonal antibody, we immunohistochemically tested different examples of breast disease for the expression of STAT 5a in comparison to normal breast ductal and lobular epithelial cells.

Materials and methods

For this study, 100 formalin-fixed, paraffin-embedded tissues representing various lesions of the breast were obtained from the files of the Armed Forces Institute of Pathology. The sections were reviewed for the presence of normal breast ductal and lobular epithelium, low-risk ductal intraepithelial neoplasia (DIN) (usual ductal hyperplasia), DIN 1 (atypical ductal hyperplasia), lobular intraepithelial neoplasia (LIN) (atypical lobular hyperplasia or lobular carcinoma in situ), DIN 1–3 (ductal carcinoma in situ), and invasive carcinoma [27]. Specimens were sectioned at 6 μm and then assayed with an antibody to STAT 5a (clone ST5a-2H2, Zymed Laboratories, South San Francisco, CA). Immunohistochemical analysis was performed as previously described [4]. Briefly, formalin-fixed, paraffin-embedded sections were heated at 70°C for 30 min and placed into a prewarmed pressure cooker in a solution of Reveal (Biocare Medical, Concord, CA) in which deparaffinization and antigen retrieval were performed simultaneously at 20 lb/in.^{2} for 3 min. Following depressurization, sections were placed into a prewarmed fresh solution of Reveal for 30 min before being rinsed in warm water. Endogenous peroxide and oxidative compounds were quenched by incubation in 5% H_2O_2 in methanol. Sections were rehydrated in Tris-buffered saline (TBS Plus, Biocare Medical) with 0.1% Tween 20 (DakoCytomation, Carpinteria, CA) added, prior to antibody application. Primary antibody incubations were performed for 60 min, with the ST5a-2H2 antibody diluted in TBS–Tween at 1:400. Detection reagents (ABC Universal Elite, Vector Laboratories Inc., Burlingame, CA) were applied for 45 min each, and all dilutions and intervening rinses were with TBS–Tween. Diaminobenzidine tetrahydrochloride (Sigma Chemical Co., St. Louis, MO) (0.08%) with 0.025% H_2O_2 added in a solution of TBS–Tween (DAB) served as the chromogenic substrate. Sections were allowed to develop in DAB for 12 min, counterstained with hematoxylin, dehydrated, and coverslipped with Permount (Fisher Chemical Co., Pittsburgh, PA) in xylene.

Assayed sections were examined for accurate interpretation of positive signal on a qualitative intensity scale. Tissues were regarded as positively expressing STAT 5a when qualitative intensity was at least 2 on a 4-point scale, and more than 20% of the cells were reactive. The cell type along with reaction product distribution was noted.

Results

The results are listed in Table 1. In normal mammary gland epithelium, STAT 5a was found to exist in the cytoplasm and the nucleus of about 80% of the luminal breast epithelial cells in the lobules and larger ducts (Fig. 1). Myoepithelial cells failed to demonstrate any STAT 5a, and stromal cell fibroblasts were also nonreactive. STAT 5a was, as expected, found in endothelial cells, adipocytes, and leukocytes [2, 12, 29].

Table 1 STAT 5a reactivity in various examples of breast epithelium

Histology	Total no. of cases	STAT 5a+no. of cases	%Positive
Normal/UDH	100	100[a]	100
Fibroadenoma	2	2	100
ADH (DIN 1)	14	0	0
LIN (ALH/LCIS)	25	8[b]	32
DCIS (DIN 1–3)	25	1[b]	4
Invasive Ca	30	5[c]	17

UDH Usual ductal hyperplasia, *ADH* Atypical ductal hyperplasia, *LIN* Lobular intraepithelial neoplasia, *ALH* Atypical lobular hyperplasia, *LCIS* Lobular carcinoma in situ, *DCIS* Ductal carcinoma in situ, *DIN* Ductal intraepithelial neoplasia

[a] Positive in 80% or more of cells

[b] Reactive but less so than surrounding normal cells

[c] Two tubular carcinomas and three invasive carcinomas with squamoid features and inflammation showed focally positive immunostaining

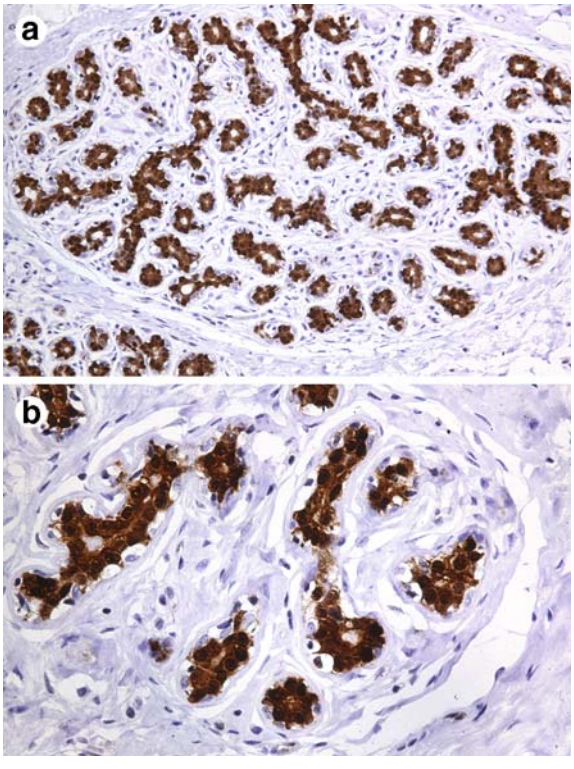

Fig. 1 **a** A normal breast lobule showing positive decoration for the presence of STAT 5a by immunohistochemistry (200×). **b** Normal breast lobule, immunohistochemical demonstration of STAT 5a in the cytoplasm and nucleus (400×)

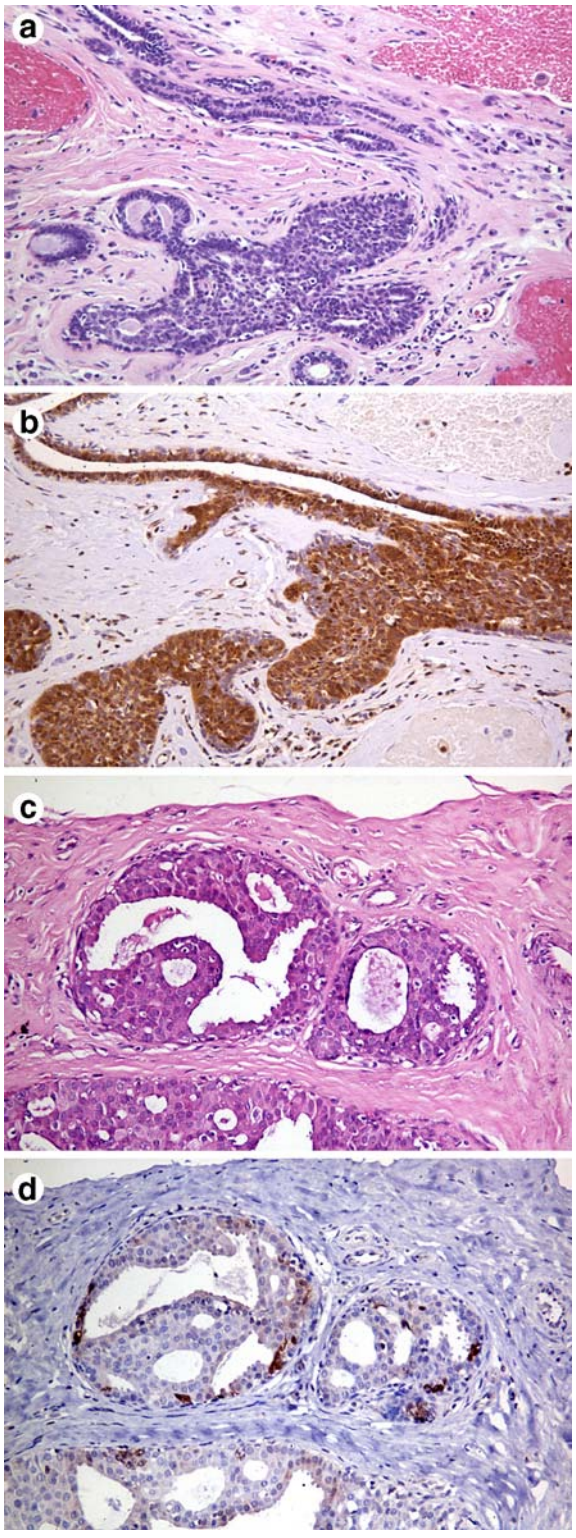

Fig. 2 **a** Hematoxylin and eosin (H&E) stain of a focus of low-risk DIN (usual ductal hyperplasia) (200×). **b** Immunohistochemical demonstration of STAT 5a in low-risk DIN (usual ductal hyperplasia) (200×). **c** H&E stain of a focus of DIN 1 (atypical ductal hyperplasia) (200×). **d** Immunohistochemical demonstration of the absence of STAT 5a in DIN 1 (atypical ductal hyperplasia) (200×). Note: scattered residual STAT 5a-positive normal epithelial cells

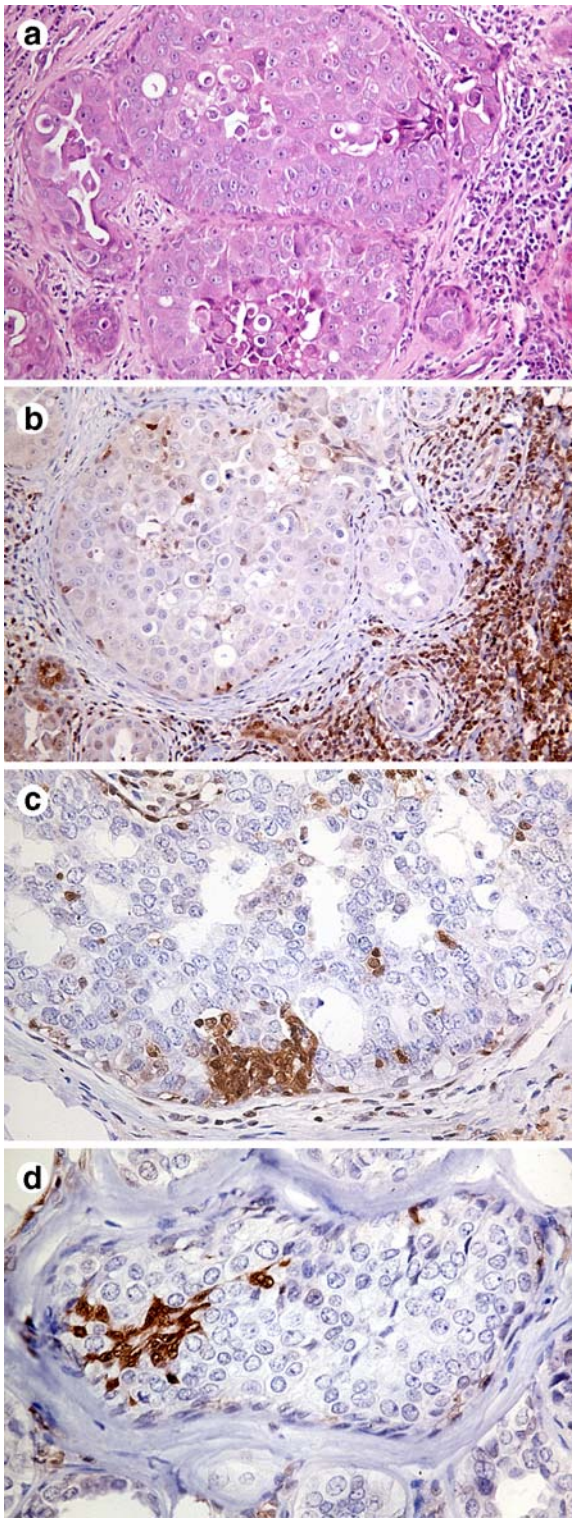

Fig. 3 **a** H&E stain of a focus of DIN 3 (ductal carcinoma in situ, grade 3) (200×). **b** Immunohistochemical demonstration of the absence of STAT 5a in the carcinoma (200×). Note: STAT 5a-positive inflammatory cells. **c**,**d** Immunohistochemical demonstration of the absence of STAT 5a in DIN 1 (ductal carcinoma in situ, grade 1) (400×). Note: residual STAT 5a-positive normal epithelial cells

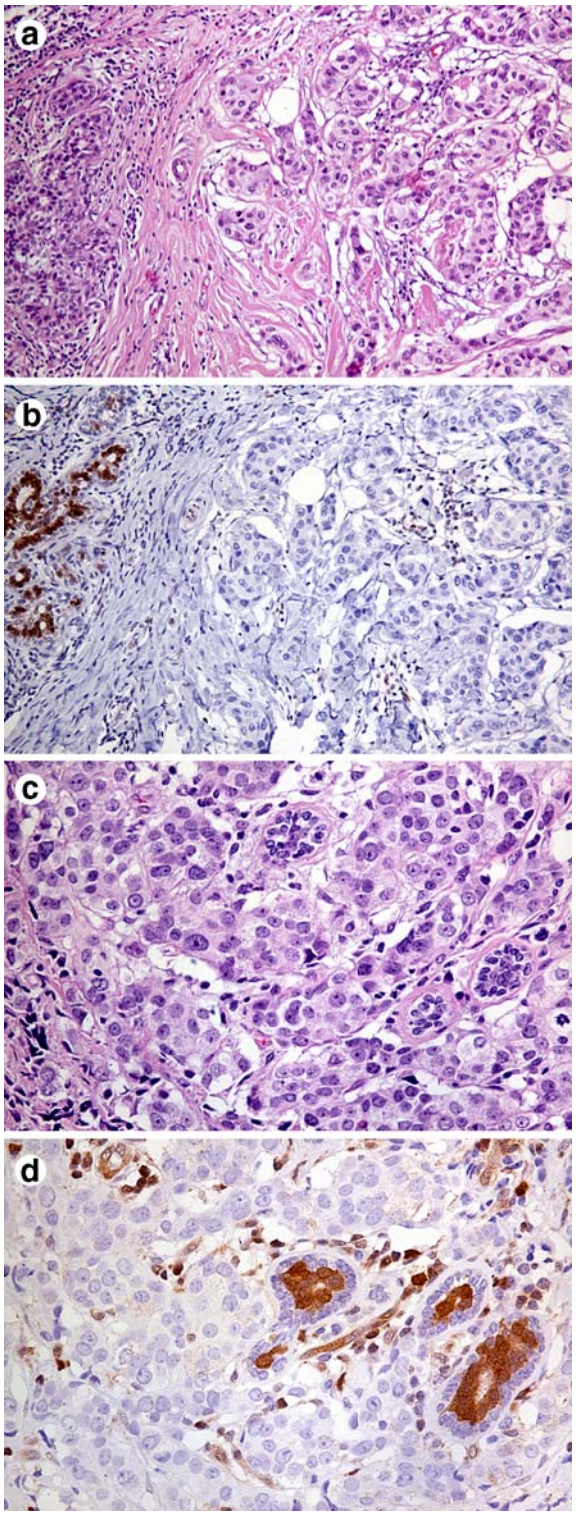

Fig. 4 **a** H&E stain of invasive ductal carcinoma (200×). **b** Immunohistochemical demonstration of the absence of STAT 5a in the carcinoma (200×). Note: adjacent normal STAT 5a-positive epithelial cells. **c** H&E stain of invasive ductal carcinoma (400×). **d** Immunohistochemical demonstration of the absence of STAT 5a in the carcinoma (400×). Note: entrapped normal STAT 5a-positive epithelial cells

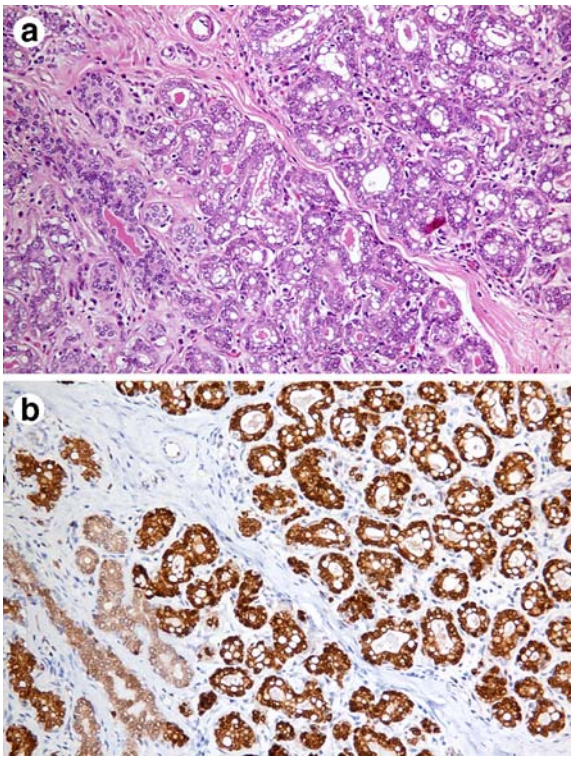

Fig. 5 **a** H&E stain of a focus of epithelial cell secretory change (200×). **b** Immunohistochemical demonstration of STAT 5a in the cells with secretory changes (200×). Note: intensity greater than that seen in neighboring epithelial cells

STAT 5a was detected in the cytoplasm and nucleus of epithelial cells in cases of usual ductal hyperplasia and in benign neoplasms such as fibroadenoma. However, in atypical proliferations, ductal carcinoma in situ (DIN 1–3) and in invasive carcinomas, the STAT 5a protein (with rare exceptions) was either not expressed or greatly reduced (Figs. 2, 3 and 4). It was absent in all cells with apocrine differentiation but was readily detected in cells undergoing secretory or lactational change. The reactivity in the secretory cells was often more intense than that seen in the surrounding normal cells, perhaps signaling a higher concentration of antigen in these cells (Fig. 5). Although most examples of LIN did not express STAT 5a, a few examples demonstrated some reduced reactivity. Also, two tubular carcinomas and three invasive carcinomas with squamoid features and inflammation exhibited focal reactivity (data not shown). This may be secondary to increased background STAT 5a in these cases, since it occurred only when the adjacent normal epithelial and inflammatory cells also showed increased STAT 5a expression as compared to STAT 5a-negative carcinomas. All control sections assayed with a normal mouse IgG in substitution for the STAT 5a antibody were nonreactive.

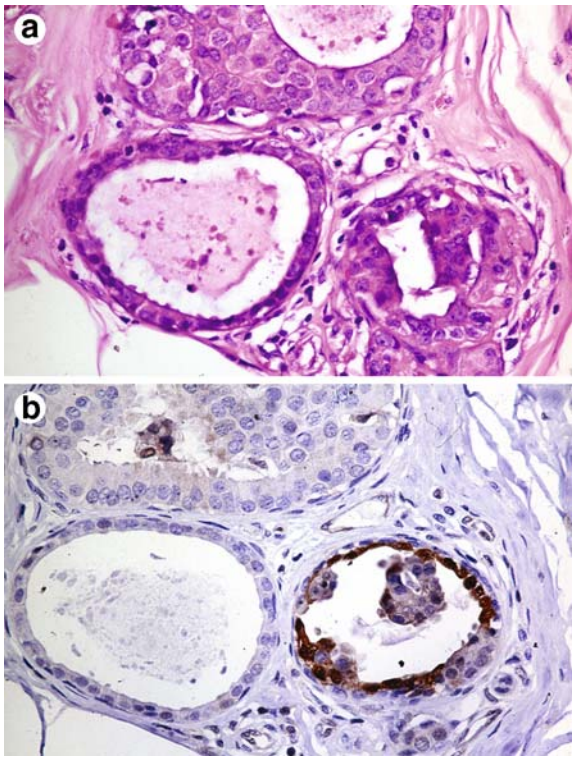

Fig. 6 **a** H&E stain showing small foci of DIN 1 Flat type (flat type epithelial atypia) and DIN 1 (atypical ductal hyperplasia) (400×). **b** Immunohistochemical detection of STAT 5a demonstrating its absence in these abnormal foci (400×)

Discussion

A reduction of STAT 5a was observed, associated with abnormal breast epithelial cells. The absence of STAT 5a in the abnormal breast epithelial cells may indicate a defect contributory to the abnormal state. Since STAT 5a is required for the development of breast lobules, repressors of its activation or inappropriate signaling through other mechanisms might alter the function and phenotype of these cells. Because the demonstrated expression was seen specifically in cells known from other studies to contain STAT 5a, it was reasoned that the reaction was specific for STAT 5a or a STAT 5a-like protein. In all of the sections, normal ductal and lobular epithelium reacted strongly in the cytoplasm and nucleus with the antibody to STAT 5a, serving as an internal control for cells with weak or absent staining.

STAT 5a expression may be affected by an abnormal genotype. Certain genomic deletions may affect the STAT 5a gene locus, found on chromosome 17q11, incidentally. However, it is also possible that any number of biochemical events involving STAT 5a may act to provide an atmosphere in which cellular transformation can occur. The absence of STAT 5a could result in aberrant signaling or suboptimal transcription of developmental, regulatory, or growth-restraining proteins contributing to altered (metaplastic or neoplastic) phenotypic differentiation.

Numerous reports implicate the suppression of STAT 5a in normal and disease processes [20, 22, 24]. Suppressors of cytokine signaling (SOCS) and protein inhibitors of activated STATs (PIAS) can suppress signal transduction by inhibiting the STAT pathway [10, 26, 28]. Activated SOCS can also stimulate cell proliferation and increase cell survival through the Ras signaling pathway [6]. Therefore, proliferation can occur through at least one mechanism that would inactivate STAT 5a in the process and, in fact, a recent study demonstrated increased SOCS gene expression in breast cancer [21].

The absence of STAT 5a in most abnormal breast epithelial cells including carcinomas is not something that has been widely noted, however. Because STAT 5a is a transcription factor, one might imagine that an over-expression or constitutive expression of STAT 5a would be seen in the uncontrolled growth of breast carcinomas like the reports of over-expression of STAT 3 in these tumors [3]. This has been reported in one study where 76% of the breast cancers examined showed phosphorylated STAT 5a to be present in the nucleus [8]. It has also been shown that in 65% of induced rat mammary gland tumors, STAT 5a was detected in the nucleus using phosphorylation-specific antibodies [23].

These data may seem, initially, to contradict the present findings. Antibody variability, however, can certainly make a difference in detection. Nevalainen et al. saw a decrease in activated STAT 5a in more aggressive breast cancers using a phosphor-specific antibody, while detection of the STAT 5a protein using another anti-STAT 5a was maintained [18]. In contrast, the report by Shan et al. [23] stated that high STAT 5a nuclear expression closely correlated with higher-grade carcinomas and identified a cytoplasmic location for STAT 5a in the normal rat mammary gland. Because the STAT 5a expression in this present study was seen in the nucleus, it was reasoned that at least some of the identified STAT 5a might be of an activated form. The ST5a-2H2 clone used for this study, while not described as an activation specific clone, demonstrated a lack of detection of STAT 5a in higher-grade lesions corroborating the results of Nevalainen et al. [18].

The ST5a-2H2 antibody is directed against the molecule's carboxy-terminus near where the active phosphorylation site is located. Some functional STAT 5a variants may exist that are not detectable with this antibody, and some naturally occurring splice site variants of STAT 5a have been shown to have the ability to suppress the transcriptional activity of the wild-type STAT 5a [30]. Also, a few early studies have pointed to distinct carboxy-terminal truncated forms of STAT 5a [13, 16]. If truncated forms were present in the tumor cells, they would not be visible with this antibody. Tantalizingly, a report examining the expression of various forms of STAT 5a in transgenic mice demonstrated that a carboxy-terminal truncated form of STAT 5a produced the most undifferentiated carcinomas in the mammary glands of these mice [11].

It was of interest to note that a relative over-expression of STAT 5a was observed in cells undergoing secretory change. This was considered unusual because cells under-

going apocrine differentiation (a secretory cell) were uniformly nonreactive. Perhaps the secretory nature of breast epithelium is dependent on viable STAT 5a, and the functional ability of the cell is lost when defects occur in this pathway leading to abnormal cell behavior. Also, the rare lesions showing some expression were either well-differentiated tubular carcinomas or tumors surrounded by a large amount of STAT 5a-positive inflammatory cells. Examples of LIN (merely an indicator of generalized risk) demonstrated the expression nearest to that of normal or hyperplastic samples, and in the study by Cotarla et al., the STAT 5a-positive tumors correlated with increased levels of differentiation [8]. This may indicate that STAT 5a function is maintained in lesions that are differentiated enough to allow normal processes to occur. These findings support STAT 5a as a marker of good prognosis, and the percentage of positive carcinomas reported by Nevalainen et al. is also similar to the number reported here [18]. In addition, a recent report described STAT 5a as a suppressor of invasion due to its loss associated with metastatic lesions and a relationship between STAT 5a and adhesion [25]. STAT 5a, then, has been alternately reported to be an active factor associated with breast carcinoma or acting almost like a tumor suppressor gene in the breast. The correlation of function and tumor grade with respect to STAT 5a expression as determined by the individual antibody employed will have to be investigated further.

Whether or not STAT 5a has an effect on the maintenance of the normal phenotype as it has an effect on the establishment of the normal phenotype is subject to conjecture. In most instances, abnormal cell growth can be identified by an absence of STAT 5a reactivity (Fig. 6). The St5a-2H2 antibody, therefore, might also have a possible clinical utility in distinguishing atypical ductal hyperplasia or grade one ductal carcinoma in situ (DIN 1) from usual ductal hyperplasia (low-risk DIN). Since STAT 5a is required for the normal development of breast lobules, repressors of its activation or inappropriate signaling through other mechanisms might alter the function and phenotype of breast epithelial cells.

Acknowledgements The authors gratefully acknowledge Mr. Doug Landry for the production of the figure files.

References

1. Akira S (1999) Functional roles of STAT family proteins: lessons from knockout mice. Stem Cells 17:138–146
2. Balhoff JP, Stephens JM (1998) Highly specific and quantitative activation of STATs in 3T3-L1 adipocytes. Biochem Biophys Res Commun 247(3):894–900
3. Berclaz G, Altermatt HJ, Rohrbach V, Siragusa A, Dreher E, Smith PD (2001) EGFR dependent expression of STAT 3 (but not STAT 1) in breast cancer. Int J Oncol 19(6):1155–1160
4. Bratthauer GL (1999) The avidin–biotin complex (ABC) method and other avidin–biotin binding methods. In: Javois LC (ed) Immunocytochemical methods and protocols, 2nd ed. Methods Mol Biol 115. Humana, Totowa, NJ, pp 203–214
5. Brizzi MF, Defillippi P, Rosso A, Venturino M, Garbarino G, Miyajima A, Silengo L, Tarone G, Pegoraro L (1999) Integrin-mediated adhesion of endothelial cells induces JAK2 and STAT 5a activation: role in the control of c-fos gene expression. Mol Biol Cell 10:3463–3471
6. Cacalano NA, Sanden D, Johnston JA (2001) Tyrosine-phosphorylated SOCS-3 inhibits STAT activation but binds to p120 RasGAP and activates Ras. Nat Cell Biol 3:460–465
7. Clevenger CV (2004) Roles and regulation of STAT family transcription factors in human breast cancer. Am J Pathol 165:1449–1460
8. Cotarla I, Ren S, Zhang Y, Gehan E, Singh B, Furth PA (2004) Stat5a is tyrosine phosphorylated and nuclear localized in a high proportion of human breast cancers. Int J Cancer 108 (5):665–671
9. Gallego MI, Binart N, Robinson GW, Okagaki R, Coschigano KT, Perry J, Kopchick JJ, Oka T, Kelly PA, Hennighausen L (2001) Prolactin, growth hormone, and epidermal growth factor activate STAT 5a in different compartments of mammary tissue and exert different and overlapping developmental effects. Dev Biol 229:163–175
10. Greenhalgh CJ, Hilton DJ (2001) Negative regulation of cytokine signaling. J Leukoc Biol 70:348–356
11. Iavnilovitch E, Cardiff RD, Groner B, Barash I (2004) Deregulation of Stat5 expression and activation causes mammary tumors in transgenic mice. Int J Cancer 112(4):607
12. Kagami S, Nakajima H, Suto A, Hirose K, Suzuki K, Morita S, Kato I, Sato Y, Kitamura T, Iwamoto I (2001) STAT 5a regulates T helper cell differentiation by several distinct mechanisms. Blood 97(8) 2358–2365
13. Kazansky AV, Raught B, Lindsey SM, Wang YF, Rosen JM (1995) Regulation of mammary gland factor/Stat5a during mammary gland development. Mol Endocrinol 9(11):1598–1609
14. Levy DE (1999) Physiological significance of STAT proteins: investigations through gene disruption in vivo. Cell Mol Life Sci 55:1559–1567
15. Miyoshi K, Shillingford JM, Smith GH, Grimm SL, Wagner KU, Oka T, Rosen JM, Robinson GW, Hennighausen L (2001) Signal transducer and activator of transcription (STAT) 5 controls the proliferation and differentiation of mammary alveolar epithelium. J Cell Biol 155:531–542
16. Mui AL, Wakao H, Harada N, O'Farrell AM, Miyajima A (1995) Interleukin-3, granulocyte-macrophage colony-stimulating factor, and interleukin-5 transduce signals through two forms of STAT5. J Leukoc Biol 57(5):799–803
17. Nevalainen MT, Xie J, Bubendorf L, Wagner KU, Rui H (2002) Basal activation of transcription factor signal transducer and activator of transcription (STAT 5) in nonpregnant mouse and human breast epithelium. Mol Endocrinol 16:1108–1124
18. Nevalainen MT, Xie J, Torhorst J, Bubendorf L, Haas P, Kononen J, Sauter G, Hallgeir R (2004) Signal transducer and activator of transcription-5 activation and breast cancer prognosis. J Clin Oncol 22(11):2053–2060
19. Pansky A, Hildebrand P, Fasler-Kan E, Baselgia L, Ketterer S, Beglinge C, Heim MH (2001) Defective Jak-STAT signal transduction pathway in melanoma cells resistant to growth inhibition by interferon alpha. Int J Cancer 85:720–725
20. Paukku K, Valgeirsdettir S, Saharinen P, Bergman M, Heldin CH, Silvennoinen O (2000) Platelet-derived growth factor (PDGF)-induced activation of signal transducer and activator of transcription (STAT) 5 is mediated by PDGF beta-receptor and is not dependent on c-Src, Fyn, Jak1 or Jak2. Biochem J 345:759–766
21. Raccurt M, Tam SP, Lau P, Mertani HC, Lambert A, Garcia-Caballero T, Li H, Brown RJ, McGuckin MA, Morel G, Waters MJ (2003) Suppressor of cytokine signalling gene expression is elevated in breast carcinoma. Br J Cancer 89(3):524–532
22. Schroeder MD, Rose-Hellekant TA, Sandgren EP, Schuler LA (2001) Dysregulation of mammary Stats 1, 3 and 5 and PRL receptors by overexpresssion of TGF-alpha. Mol Cell Endocrinol 175(1–2):173–183

23. Shan L, Yu M, Clark BD, Snyderwine EG (2004) Possible role of Stat5a in rat mammary gland carcinogenesis. Breast Cancer Res Treat 88(3):263–272
24. Stewart WC, Morrison RF, Young SL, Stephens JM (1999) Regulation of signal transducers and activators of transcription (STATs) by effectors of adipogenesis: coordinate regulation of STATs 1, 5a, and 5b with peroxisome proliferator-activated-receptor-gamma and C/AAAT enhancer binding protein-alpha. Biochim Biophys Acta 1452:188–196
25. Sultan AS, Xie J, LeBaron MJ, Ealley EL, Nevalainen MT, Rui H (2005) Stat5 promotes homotypic adhesion and inhibits invasive characteristics of human breast cancer cells. Oncogene 24:746–760
26. Tam SP, Lau P, Djiane J, Hilton DJ, Waters MJ (2001) Tissue-specific induction of SOCS gene expression by PRL. Endocrinology 142:5015–5026
27. Tavassoli FA (2005) Breast pathology: rationale for adopting the ductal intraepithelial neoplasia (DIN) classification. Nat Clin Pract Oncol 2:116–117
28. Tomic S, Chughtai N, Ali S (1999) SOCS-1, -2, -3: selective targets and functions downstream of the prolactin receptor. Mol Cell Endocrinol 158:45–54
29. Yahata Y, Shirakata Y, Tokumaru S, Yamasaki K, Sayama K, Hanakawa Y, Detmar M, Hashimoto K (2003) Nuclear translocation of phosphorylated STAT 3 is essential for vascular endothelial growth factor-induced human dermal microvascular endothelial cell migration and tube formation. J Biol Chem 278 (41):40026–40031
30. Yamashita H, Iwase H, Toyama T, Fujii Y (2003) Naturally occurring dominant-negative STAT 5 suppresses transcriptional activity of estrogen receptors and induces apoptosis in T47D breast cancer cells. Oncogene 22(11):1638–1652

Virchows Arch (2006) 448: 172–183
DOI 10.1007/s00428-005-0061-9

ORIGINAL ARTICLE

Ling Zheng · Raja Sinniah · Stephen I-Hong Hsu

In situ glomerular expression of activated NF-κB in human lupus nephritis and other non-proliferative proteinuric glomerulopathy

Received: 26 April 2005 / Accepted: 3 August 2005 / Published online: 5 October 2005

Abstract Nuclear Factor-κB (NF-κB) has been suggested to play a role in the cellular and molecular mechanisms underlying glomerular injury. We investigated the potential role of NF-κB activation in the pathogenesis of glomerular injury in 31 patients with class III–V lupus nephritis (LN), 14 patients with non-proliferative proteinuric glomerulopathy and six normal controls. The expression of NF-κB subunits p65 and p50, and the NF-κB regulated proinflammatory mediators tumor necrosis factor-α (TNF-α), interleukin-1β (IL-1β), interleukin-6 (IL-6) and intercellular adhesion molecule-1 (ICAM-1) as well as CD68 and synaptopodin was examined by Southwestern histochemistry (SWH) or immunohistochemistry. In contrast to non-proliferative glomerulopathy and normal controls, NF-κB activation (both p65 and p50) was enhanced in glomerular endothelial, mesangial cells or infiltrating cells in class IV LN, along with upregulation of TNF-α, IL-1β, IL-6 and ICAM-1 expression. Glomerular endothelial and mesangial activation of NF-κB and mesangial ICAM-1 expression correlated with disease activity and the level of glomerular macrophage infiltration. Podocyte NF-κB overactivation (predominantly p65) paralleled podocyte expression of TNF-α and IL-1β in patients with LN and non-proliferative glomerulopathy. Podocyte staining scores of NF-κB and p65 were positively correlated with the severity of proteinuria in LN and non-proliferative glomerulopathy. These results suggest a pathogenic role for NF-κB in glomerular injury by multiple mechanisms.

Keywords Glomerular disease · Nuclear factor-κB · Lupus nephritis · Proteinuria

Abbreviations IMN: idiopathic membranous nephropathy · ICAM-1: intercellular adhesion molecule-1 · IL-1β: interleukin-1β · IL-6: interleukin-6 · LN: lupus nephritis · MCD: minimal change disease · NF-κB: nuclear factor-kappaB · SWH: southwestern histochemistry · TNF-α: tumor necrosis factor-α

Introduction

In classic forms of immune-mediated glomerulonephritis such as lupus nephritis (LN), immune complex formation and deposition in the kidney result in intraglomerular inflammation with recruitment of leukocytes, and the activation and proliferation of resident renal cells [7]. Apart from macrophages, intrinsic glomerular cells have been demonstrated to be activated and to participate in the process of glomerular injury by the induction of in-

L. Zheng
Department of Pathology, National University of Singapore, Singapore, Singapore

Present address:
R. Sinniah
Department of Anatomical Pathology, Royal Perth Hospital, University of Western Australia,
Wellington Street Campus,
P.O. Box X22123 GPO Perth, 6847, Australia
Tel.: +61-08-9224-2244
Fax: +61-08-9224-2022

S. I-Hong Hsu
Department of Medicine, National University Hospital,
5 Lower Kent Ridge Road,
119074 Singapore, Singapore
e-mail: mdchsus@nus.edu.sg

S. I-Hong Hsu
Genome Institute of Singapore,
60 Biopolis St., Genome #02-014,
138672 Genome, Singapore

Present address:
S. I-Hong Hsu (✉)
Renal Division and Department of Medicine,
Brigham and Women's Hospital,
Harvard Institutes of Medicine,
Rm. 554, 77 Avenue Louis Pasteur
Boston, MA 02115, USA
e-mail: shsu@rics.bwh.harvard.edu
Tel.: +617-525-5878
Fax: +617-525-5965

flammatory mediators, including adhesion molecules and cytokines [6, 31, 33]. However, cellular and molecular mechanisms underlying glomerular cell activation have not been fully elucidated in human glomerulonephritis.

Transcription factor nuclear factor-κB (NF-κB) is a pleiotropic transcription factor regulating the gene expression of several adhesion molecules, cytokines and chemotatic proteins involved in inflammation, immune response and cell proliferation [4, 14, 24]. NF-κB belongs to the Rel family of five members: c-Rel, NF-κB1 (p50/p105), NF-κB2 (p52/p100), RelA (p65) and RelB. The DNA-binding nuclear form of NF-κB is a dimer, usually composed of p65 and p50 subunits. In resting cells, NF-κB exists in the cytoplasm, bound to its inhibitor IκB that functions to mask the nuclear localization sequence of NF-κB. In response to numerous stimuli, such as tumor necrosis factor (TNF-α) and interleukin-1β (IL-1β), phosphorylated IκB is disassociated from NF-κB and subsequently degraded by the proteasome pathway. Activated NF-κB, free from IκB, is then translocated from the cytosol into the nucleus, where it promotes the transcriptional activity of downstream target genes by binding to their promoters [11].

Recent studies suggest that NF-κB activation plays a pivotal role in the activation of mesangial cells and macrophages through the transcriptional induction of inflammatory mediators of glomerular inflammation and injury [20, 27]. NF-κB activation has been observed in several experimental and human glomerular diseases [2, 29, 38, 39]. Increased activation of NF-κB has been reported in rat glomeruli shortly after nephrotoxic serum administration, associated with the increased expression of NF-κB-regulated inflammatory mediator IL-1β, monocyte chemoattractant protein 1 and intracellular adhesion molecule-1 (ICAM-1), and the development of proteinuria [39]. In human IgA nephropathy and non-proliferative glomerulopathy such as minimal change disease (MCD) and idiopathic membranous nephropathy (IMN), NF-κB activation assessed by Southwestern histochemistry (SWH) has been observed in glomeruli, along with upregulated transcriptional activity of their downstream target genes [2, 28]. Although the presence of NF-κB activation in response to glomerular injury is indirectly mentioned in a study of a lupus-like mouse model [50], to our knowledge no report has documented the activation of NF-κB in the renal tissue of patients with LN.

Since in situ glomerular expression of NF-κB-responsive genes such as adhesion molecules and cytokines have been reported in experimental and human glomerulonephritis, including LN [5, 16, 23, 41, 49], we hypothesize that NF-κB activation may play a proinflammatory role in glomerular injury in LN. In this study, we examined the in situ expression of activated NF-κB, along with NF-κB-regulated proinflammatory mediators in the context of their potential role(s) in mediating glomerular injury, in human LN as well as non-proliferative proteinuric glomerulopathy.

Materials and methods

Patients

The Ethics Committee of the National University Hospital of Singapore (NUH) approved the use of human renal biopsy tissue for this study. Thirty-one patients who met the revised ACR criteria for SLE [42] and who had undergone diagnostic renal biopsy during the period from 1997 to 2000 participated in the study. Fourteen patients with non-proliferative proteinuric glomerulopathy (eight with IMN and six with MCD) and six samples of normal kidney tissue obtained from nephrectomies performed for treatment of renal cell carcinoma served as disease controls and normal controls, respectively. Tissue samples were obtained either by percutaneous renal biopsy at NUH, or through referral from local nephrologists to the NUH pathology department for definitive diagnosis. Data on proteinuria, serum creatinine and creatinine clearance at the time of biopsy were available for the majority of the patients. Clinical, demographic and histologic data are summarized in Table 1.

Biopsies containing less than five glomeruli were excluded from the present study. For light microscopy, the tissue samples were fixed in 4% paraformadehyde, embedded in paraffin, and 2-μm sections were cut and stained with hematoxylin and eosin, periodic acid-Schiff (PAS) reagent, Masson trichrome-silver impregnation (PAAG-MT). For direct immunofluorescence microscopy, a portion of the biopsy sample was snap-frozen, and 5-μm cryostat sections were cut and stained with fluorescein-isothiocyanated conjugated anti-IgG, IgA, IgM, C3, C1q and fibrinogen antibodies (Dako) in all cases.

Biopsies diagnosed as LN were classified according to the criteria defined by the International Society of Nephrology/Renal Pathology Society in 2003 [48]. The LN disease group consisted of two subjects with focal LN (class III), 23 with diffuse LN (class IV) and six with membranous LN (class V). The class IV group comprised two subjects with class IV-S (A) (diffuse segmental LN with active lesions), two with class IV-S (A/C) (diffuse segmental LN with active and chronic lesions), 15 with class IV-G (A) (diffuse global LN with active lesions) and four with class IV-G (A/C) (diffuse global LN with active and chronic lesions). The "activity index" and "chronicity index" were determined by the following histologic criteria proposed by Austin et al: mesangial cell proliferation, extracapillary lesions (cellular and fibrous crescents), leukocyte infiltration, karyorrhexis/fibrinous necrosis, hyaline deposits, glomerular sclerosis, interstitial inflammation and fibrosis and tubular atrophy [3]. Histologic classification of IMN was made according to the extent of glomerular membrane alterations revealed by silver staining or electron microscopy. The IMN disease group consisted of one subject with stage I, four subjects with stage I/II or II, and three subjects with stage III disease.

Table 1 Clinical, demographic and histopathologic features

Diagnosis and classification[a]	No. of patients (male: female)	Age (year)	Proteinuria (g/24 h)	Serum creatinine (mg/dl)	AI (score)	CI (score)	% Sclerosis	% Crescents	Glomerular CD68 (cells/GCS)
III	2 (1:1)	29±0	1.55±0.07	1.0	2.50±0.71	3.50±4.95	31.25±44.19	0±0	0.83±0.04
III (A)	1 (0:1)	29	1.5	1.0	2	0	0	0	0.857
III (C)	1 (0:1)	29	1.6	NA	3	7	61.25	0	0.8
IV	23 (2:21)	34.95±12.67	3.64±2.47	2.06±2.27	12.09±3.60	2.83±2.14	6.82±9.53	27.61±22.33	10.45±7.29*,**
IV-S (A)	2 (0:2)	36.5±16.26	1.5±0.54	0.68±0.02	6±0	1±1.41	0±0	0±0	2.95±2.89
IV-S (A/C)	2 (1:1)	28.5±9.19	2.67±0.47	0.70[b]	9±1.41	3±2.83	4.55±6.43	20.11±6.95	2.27[b]
IV-G (A)	15 (1:14)	35.33±14.27	4.09±2.66	1.76±1.19	13±2.95	2.13±1.25	6.49±9.23	26.26±20.92	13.80±6.82
IV-G (A/C)	4 (0:4)	36.33±6.11	3.52±2.66	4.45±4.51	13.25±4.11	5.75±2.63	12.54±13.22	49.89±19.03	5.38±2.30
V	6 (1:5)	28.5±10.13	3.78±3.58	0.97±0.35	3.67±1.51	3.67±3.08	9.46±13.37	0±0	2.57±1.50
Total LN	31 (4:27)	33.27±11.92	3.53±2.63	1.77±1.98	9.84±5.00	3.03±2.43	8.98±14.21	20.25±22.70	8.28±7.31
MCD	6 (5:1)	30.83±12.38	6.36±3.58	1.06±0.06	ND	ND	0±0	0±0	0.25±0.09
IMN	8 (5:3)	53.14±9.99	5.39±4.33	1.00±0.15	ND	ND	15.50±17.83	0.4±1.13	0.31±0.10

Data expressed as the mean±SD. To convert serum creatinine in mg/dl to μmol/l, multiply by 88.4
AI Activity index, *CI* chronicity index, *% Sclerosis* percentage of glomerular sclerosis, *% Crescents* percentage of glomerular crescents, *ND* not determined
*$P<0.05$ versus MCD and IMN; **$P<0.05$ versus class V LN
[a]ISN/RPS classification of lupus nephritis in 2003 [48]
[b]Data from one patient is unavailable

Immunohistochemistry

The mouse monoclonal antibody anti-human RelA/p65 (Chemicon International), which is directed against an epitope of p65 containing a nuclear localization signal, is specific for the detection of activated NF-κB [18, 28]. Polyclonal goat anti-human p50 (Santa Cruz Biotechnology, Santa Cruz, CA, USA) and monoclonal mouse anti-human synaptopodin (PP-44) (Progen, Heidelberg, Germany) were used in previous studies [28, 30]. Polyclonal rabbit anti-human TNF-α [35] and IL-1β were purchased from Rockland Immunochemicals (Gilbertsville, PA, USA), polyclonal rabbit anti-human IL-6 [26] was purchased from Endogen (Pierce Biotechnology, Rockford, IL, USA) and mouse anti-human ICAM-1 and CD68 were purchased from Santa Cruz Biotechnology (Santa Cruz, CA, USA) and Dako. The specificity of the antibodies was confirmed by their reactivity with specific human targets by immunoprecipitation and/or Western Blot analysis, as per manufacturer's description.

For the majority of primary antibodies, immunohistochemistry was conducted on paraformaldehyde-fixed paraffin sections with a two-step EnVision+ System peroxidase kit (Dako, Carpinteria, CA, USA) [37]. Except for CD68, slides were subjected to microwave antigen retrieval with wet heat at 98°C for 10 min under 150 W (Milestone Microwave System, Italy). We used 100 mmol/l pH 6.0 citrate buffer with anti-p65 and anti-p50; 10 mmol/l pH 6.0 citrate buffer was used with antibodies against TNF-α, IL-1β, IL-6, ICAM-1 and synaptopodin before peroxidase blocking. Slides were predigested with pronase for CD68 immunostaining. Endogenous peroxidase was blocked in 3% H_2O_2 for 30 min and sections were incubated with primary antibodies overnight at 4°C. After rinsing, horseradish peroxidase enzyme-labeled non-avidin–biotin polymer conjugated to goat anti-mouse or anti-rabbit was applied to the sections for detection of p65, TNF-α, IL-1β, IL-6, ICAM-1 and synaptopodin. Dako LSAB$^+$ Peroxidase Kit was employed to detect p50. Briefly, sections were incubated with 20% normal swine serum (Dako) for 30 min to block non-specific binding of proteins prior to incubation with primary antibodies. After rinsing, sections were incubated with biotinylated anti-goat immunoglobulin and horseradish peroxidase-conjugated streptavidin. 3,3′-Diaminobenzidine tetrahydrochloride (DAB) was used for colorimetric detection, followed by mild counterstaining with PAS reagents and Gill's haematoxylin. The specificity of primary antibodies or secondary antibodies was verified by the replacement of primary antibodies with equal concentrations of non-immune sera or by omitting primary antibodies. The positive control was tonsillitis tissue for detection of transcription factors and cytokines, and normal kidney tissue for detection of synaptopodin.

Southwestern histochemistry

SWH was performed as described previously [15, 28]. Complementary oligonucleotides containing consensus binding sequences for NF-κB were synthesized as follows: (sense) 5′-AGTTGAGGGGACTTTCCCAGGC-3′ and (anti-sense) 3′-TCAACTCCCCTGAAAGGGTCCG-5′ (Gibco-BRL, LifeTechnology, Gaithersburg, MD). After annealing (98°C for 10 min), the resulting double-stranded DNA probe was 3′-end labeled with digoxigenin (DIG oligonucleotide 3′-end labeling kit, Roche Dignostics).

Paraformaldehyde-fixed paraffin kidney sections (4 μm thick) were dewaxed and rehydrated. The preparations were incubated with levamisole (Sigma, St. Louis, MO, USA) to inhibit endogenous alkaline phosphatase activity and then fixed with 0.2% paraformaldehyde for 30 min at 28°C. Sections were subsequently digested with pepsin A (433 U/mg, Sigma) and washed twice in 4-(2-hydroxyethyl)-1-piperazineethanesulfonic acid (HEPES)–bovine serum albumin. The sections were incubated with 0.1 mg/ml DNase I in HEPES–bovine serum albumin for 30 min at 30°C. The labeled probes diluted to 100 pmol/l in HEPES–bovine serum albumin containing 0.5 μg/ml poly (dI-dC) (Roche Diagnostics) were applied to each slide overnight at 37°C. After incubation in blocking solution (0.01× SSC, 0.01% sodium dodecyl sulfate, 0.03% Tween 20, 0.1 mol/l maleic acid, 0.15 mol/l NaCl, pH 7.5), anti-digoxigenin antibody conjugated with alkaline phosphatase (1:250 in blocking solution, Roche) was added overnight at 4°C. The color reaction was developed using nitro blue tetrazolium (NBT/BCIP, Roche) according to the manufacturer's instructions. Slides were counterstained with mild PAS reagent minus haematoxylin. Double staining was performed to co-localize active NF-κB by SWH with immunostaining of TNF-α in selective cases. Sections were sequentially treated for SWH and IHC as described above.

The following conditions were carried out as negative controls: (1) absence of probe; (2) use of a mutant NF-κB probe (sense 5′- AGTTGAGGCTCCTTTCCCAGGC -3′; anti-sense 3′-GCAACTCCGAGGAAAGGGTCCG-5′); and (3) competition assays with a 200-fold excess of unlabeled NF-κB, followed by incubation with labeled probes.

Semi-quantitative histological analysis

Histological evaluation was performed under light microscopy by two independent pathologists (L.Z. and R.S.) who were left unaware of the clinical and demographic characteristics of the patients. The agreed-upon score was adopted for the final data set. In cases of disagreement in the scoring, the process was repeated and the final score was

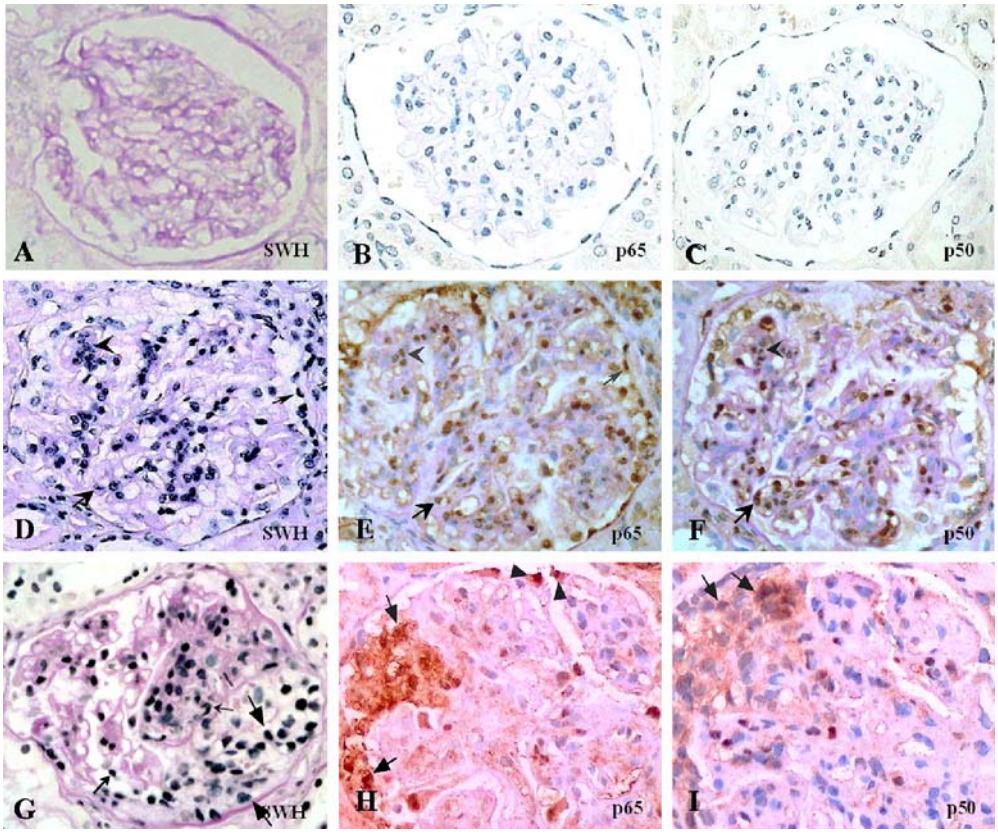

Fig. 1 Glomerular expression of activated NF-κB in normal controls and class IV LN. **A**–**C** Normal controls. NF-κB activation was barely detectable in normal glomeruli using Southwestern histochemistry (SWH) (**A**) and immunostaining of p65 (**B**) and p50 (**C**). SWH for NF-κB (**D**), p65 (**E**) and p50 (**F**) in a glomerulus from a patient with class IV-S (A/C) LN. Activated NF-κB is readily detected in glomerular endothelial cells (*open arrows*), mesangial cells (*open arrowheads*) and parietal epithelial cells (*small arrows*). **G** NF-κB activation in inflammatory infiltrates lying freely in capillary lumina or Bowman's space (*small arrows*), and cellular crescents (*large arrows*) in the SWH stained section from a patient with class IV-G (**A**) LN. Immunostaining of p65 (**H**) and p50 (**I**) in a glomerulus from a patient with class IV-G (A) LN. Podocytes displayed NF-κB activation predominantly in the form of p65 (**H**, *closed arrowheads*); cells in cellular crescents demonstrated immunoreactivity with both p65 and p50 (*arrows*). SWH with mild PAS counterstaining (NBT/BCIP; blue nuclei), p65 and p50 [DAB; brown nuclei; with haematoxylin plus mild periodic acid-Schiff (PAS) counterstaining]. Original magnification: ×400 (**H**, **I**); ×300 (**E**–**G**); ×200 (**A**–**D**)

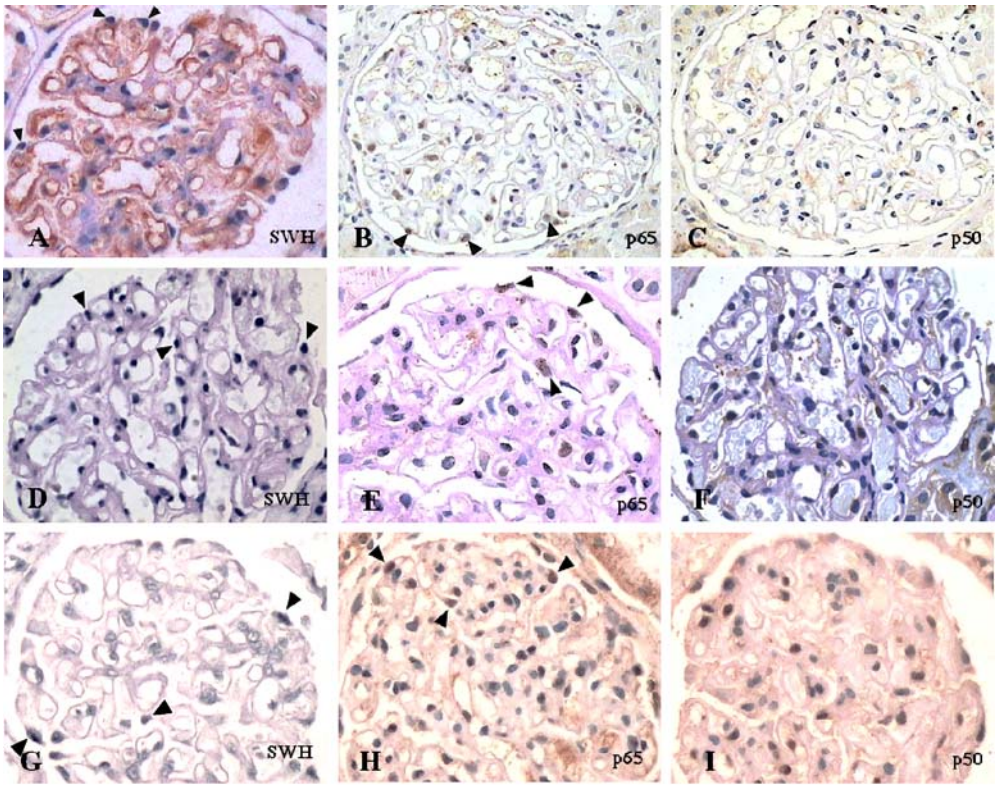

Fig. 2 Glomerular NF-κB activation in class V LN and non-proliferative glomerulopathy. (**A**–**C**) Glomeruli from a patient with class V LN. Double staining of NF-κB (SWH) and TNF-α (**A**) showed that podocyte NF-κB activation (*arrowheads*) co-localized with TNF-α immunostaining along glomerular capillary walls; a glomerulus from a patient with class V LN displayed predominant expression of p65 (**B**) in podocytes (*arrowheads*) in contrast to the lack of p50 (**C**) in podocytes. (**D**–**F**) Glomeruli from a patient with IMN. (**G**–**I**) Glomeruli from a patient with MCD. NF-κB activation was primarily observed in podocytes (*arrowheads*) in addition to endothelial cells in idiopathic membranous nephropathy (IMN) (**D**) and minimal change disease (MCD) (**G**). Podocytes demonstrated a predominant expression pattern of p65 (*arrowheads*), while both p65 and p50 were expressed in endothelial cells in IMN (p65, **E**; p50, **F**) and MCD (p65, **H**; p50, **I**). Original magnification: ×400 (**A**–**C**, **E**, **G**–**I**); ×300 (**D**, **F**)

Table 2 Semi-quantitative analysis of NF-κB activation in glomeruli

Diagnosis and classification[a]	Endo&MC (cells/GCS)			Podo (score)			PEC (cells/GCS)		
	NF-κB	p65	p50	NF-κB	p65	p50	NF-κB	p65	p50
III	24.83±9.43	7.37±6.78	10.33±5.28	3.5±0.71	4.5±0.71	0±0	8.12±1.59	0.92±1.29	0.55±0.64
IV	40.74±16.13***	11.01±10.86	20.25±15.09	3.81±1.21	3.73±1.45	0.14±0.64	7.31±5.14***	1.09±1.64	1.76±2.08
IV-S (A)	25.93±33.52	0±0	12.26±11.89	2.5±0.70	2.5±0.70	1.5±2.12	7.39±8.71	0±0	2.35±3.04
IV-S (A/C)	47.89±2.88	33.24[b]	29.83±7.30	3±0	3[b]	0±0	12.15±2.23	3.94[b]	10.57±12.15
IV-G (A)	42.88±13.84	12.24±10.12	22.88±16.75	4±1.04	4±1.14	0±0	6.37±4.39	1.32±1.74	2.03±2.30
IV-G (A/C)	36.51±20.27	6.33±8.08	9.61±2.81	4±1.83	3.5±2.64	0±0	8.37±7.42	0.15±0.24	0.75±1.31
V	22.83±9.14	12.36±11.85	6.81±6.08	3.8±1.79	3.4±1.95	0±0	4.40±0.66	0.37±0.38	0.17±0.21
Total LN	36.69±16.37*,**	11.04±10.61*,**	17.80±14.44*,**	3.79±1.26*	3.72±1.49*	0.10±0.56	6.88±4.64*,**	0.93±1.45	1.46±1.95
MCD	5.96±3.71*	3.65±4.91*	3.54±0.98	4±1.09*	3±0.63*	0±0	2.06±2.07*	1.28±0.99	1.11±0.57
IMN	5.75±4.41*	5.64±4.43*	6.58±4.13*	3.62±1.68*	3.4±1.41*	0±0	2.22±2.07*	0.88±0.71	1.03±0.71
NC	0±0	0±0	0±0	0.2±0.63	0±0	0±0	0±0	0±0	0±0

Data are expressed as mean±SD
Endo&MC Endothelial cell and mesangial cell, *Podo* podocyte, *PEC* parietal epithelial cell, *NC* normal controls
**P*<0.5 versus NC; ***P*<0.05 versus MCD and IMN; ****P*<0.05 versus class V LN
[a]ISN/RPS classification of LN in 2003 [48]
[b]Renal tissue from one patient was insufficient for staining

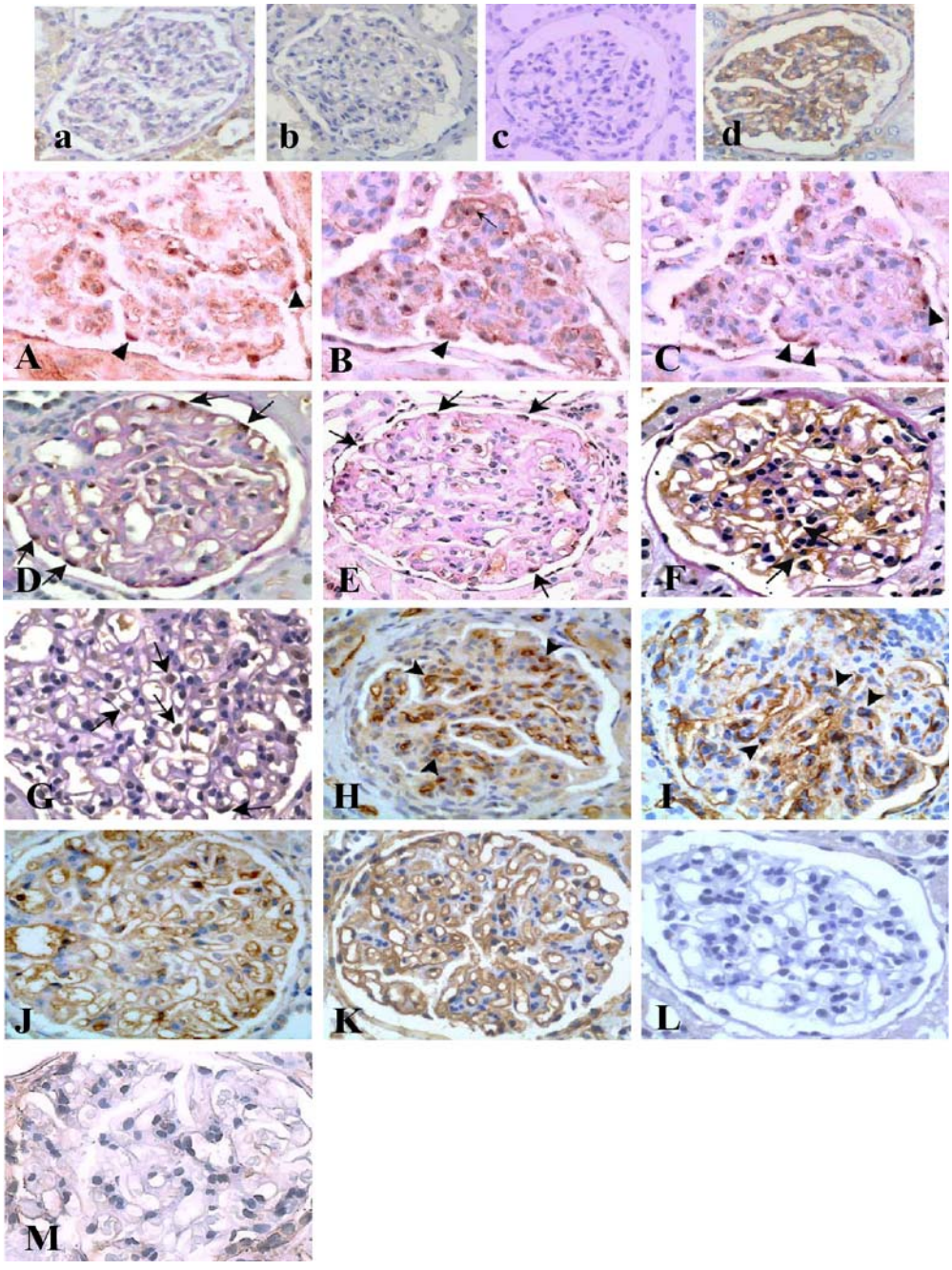

Fig. 3 Glomerular expression of TNF-α, IL-1β, IL-6 and ICAM-1 in normal and diseased human kidneys. Normal human kidney demonstrated sparse expression of TNF-α (**a**), IL-1β (**b**) and IL-6 (**c**), and constitutive expression of ICAM-1 along the inner wall of capillary loops (**d**). **A**–**C** Immunostaining of p65, TNF-α and IL-1β in a glomerulus from a patient with class IV-G (**A**). TNF-α (**B**) and IL-1β (**C**) were expressed in podocytes with activated p65 (**A**) (*arrowheads*); TNF-α expression was also observed in inflammatory leukocytes lying freely in capillary lumen (**B**, *long arrow*). **D**–**G** Expression of TNF-α and IL-1β was predominantly localized to podocytes on the outer aspect of glomerular capillaries (*arrows*) in class V LN (**D** for TNF-α, **E** for IL-1β) and MCD (**F** for TNF-α, **G** for IL-1β). **H**–**M** Abnormal expression of IL-6 (**H**) and ICAM-1 (**I**) was mainly located in mesangium from the patients with class IV-G (**A**) and class IV-G (**A**/**C**), respectively; no such abnormality was observed in class V LN (**J** for IL-6, **K** for ICAM-1) and MCD (**L** for IL-6, **M** for ICAM-1). Original magnification: ×400 (**A**–**C**, **L**, **M**); ×300 (**D**, **F**, **H**–**K**); ×200 (**E**); ×100 (**a**–**d**)

determined by consensus of both observers. Only glomeruli that were well preserved for conventional morphology were evaluated thoroughly. Extracapillary immunopositive cells, such as those found in fibrous crescents, or glomeruli with global sclerosis, were excluded from the count. The glomerular structures and cell components were identified morphologically by examination of consecutive sections with PAS and PAAG-MT. Additionally, most sections were mildly counterstained with PAS reagents after SWH or immunohistochemistry to allow for the identification of resident glomerular cell types by their anatomic features. Only cells lying within the mesangium, along the inner walls of glomerular capillaries and Bowman's capsule, were defined as mesangial, endothelial, and parietal epithelial cells (PEC), respectively. Cells along the outer aspect of glomerular capillary loops were defined as podocytes. Anatomically, cells lying freely either in capillary lumina or Bowman's space were considered as infiltrating leukocytes. The anatomic and morphologic features of inflammatory infiltrates were further confirmed by CD68 immunostaining of serial sections. For transcription factors, only cells stained with distinct blue nuclei (SWH) or brown nuclei (immunohistochemistry) stains were counted. Both the number of individual glomerular cells and the number of complete glomeruli were counted, respectively. The number of positively stained cells of each type was expressed as

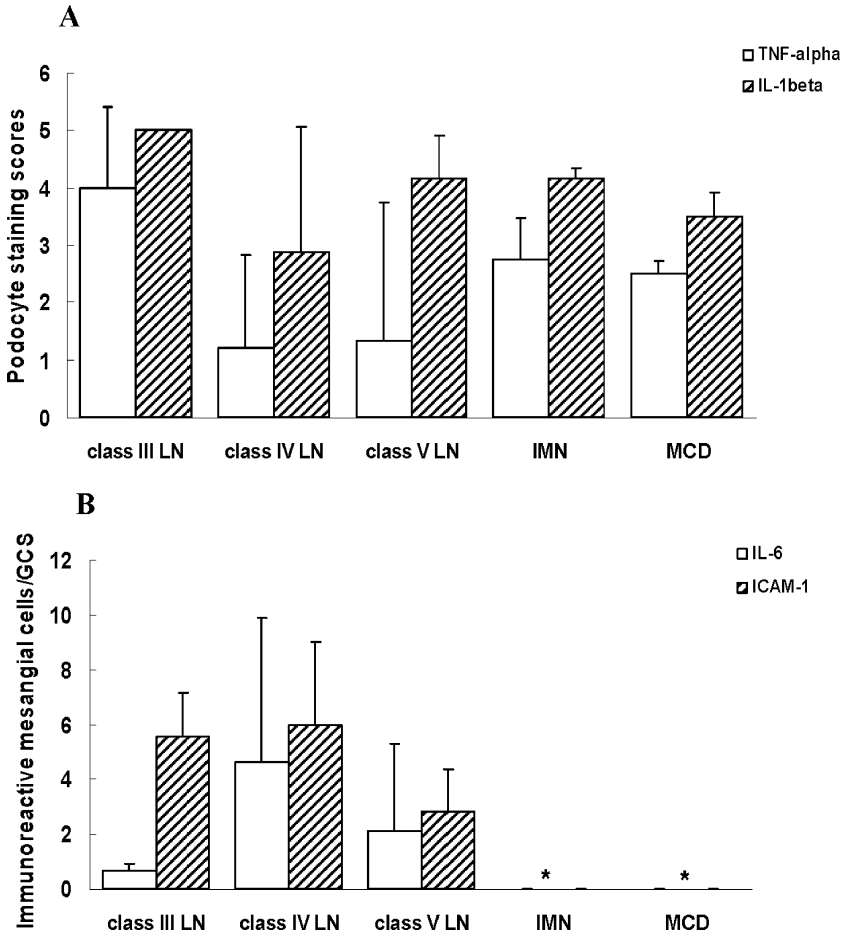

Fig. 4 Quantitative analysis of glomerular expression of TNF-α, IL-1β, IL-6 and ICAM-1 in diseased human kidneys. **A** Podocyte expression of TNF-α and IL-1β. No statistical difference in podocyte expression of TNF-α and IL-1β was observed between LN and non-proliferative glomerulopathy or between class IV and class V LN ($P>0.05$). **B** ICAM-1 expression in mesangium. Mesangial expression of IL-6 and ICAM-1 in LN was significantly higher than that in non-proliferative glomerulopathy ($P<0.05$); mesangial ICAM-1 expression in class IV LN significantly differed from that in class V LN ($P<0.05$). *No marker expression is detectable; the value of mesangial expression of ICAM-1 and IL-6 in normal control is zero and not shown in chart

the number of cells per glomerular cross-section (cells/GCS). For semi-quantitative analysis, glomerular endothelial and mesangial cells were counted together. In addition, a seven-point scoring system was employed for the evaluation of podocyte positive signals (NF-κB, p65, p50, TNF-α and IL-1β) in glomeruli that took both intensity and extent into account [34, 36]. Podocytes were primarily identified by architectural features revealed on light microscopy by mild PAS counterstaining. Synaptopodin staining of serial sections facilitated the evaluation of the extent of podocyte expression of various markers using SWH and immunohistochemistry. Briefly, the intensity was graded as 0 (no staining), 1+ (mild), 2+ (moderate), or 3+ (marked staining), while the extent of staining was graded as 1+ (1–25%), 2+ (26–50%), 3+ (51–75%), or 4+ (>75% of the glomerular tuft).

Statistical methods

Statistical analyses were performed using SigmaStat 3.1 programs (SPSS Inc.). The results were expressed as the mean±SD. Statistical significance was determined by one-way ANOVA, followed by Bonferroni's test for multiple comparisons among various groups. For non-parametric data, one-way ANOVA on ranks followed by Dunn's test was used for multiple comparisons test. Correlation was determined with Spearman's correlation coefficients. *P* values less than 0.05 were considered to be significant.

Results

Patients

Of the 31 LN subjects, 90.3% were female, and the average age was 33.1±12.1 years (range 15–59) at the time of LN diagnosis. The degree of proteinuria at the time of diagnostic renal biopsy, as determined by 24-h urine collection, was documented in 96.8% of LN patients, 100% of IMN patients and 83.3% of MCD patients. Clinical criteria for the diagnosis of nephrotic syndrome were met in 16 patients with LN (45.2%), five with IMN (62.5%) and five patients with MCD (83.3%). Serum creatinine was elevated in ten LN subjects (32.3%); all of the non-lupus glomerulopathy subjects had normal serum creatinine levels at the time of diagnostic renal biopsy.

In situ glomerular activation of NF-κB in normal and diseased kidneys

Activated NF-κB and its subunit p65/p50 were barely detectable by SWH in glomeruli of normal kidneys

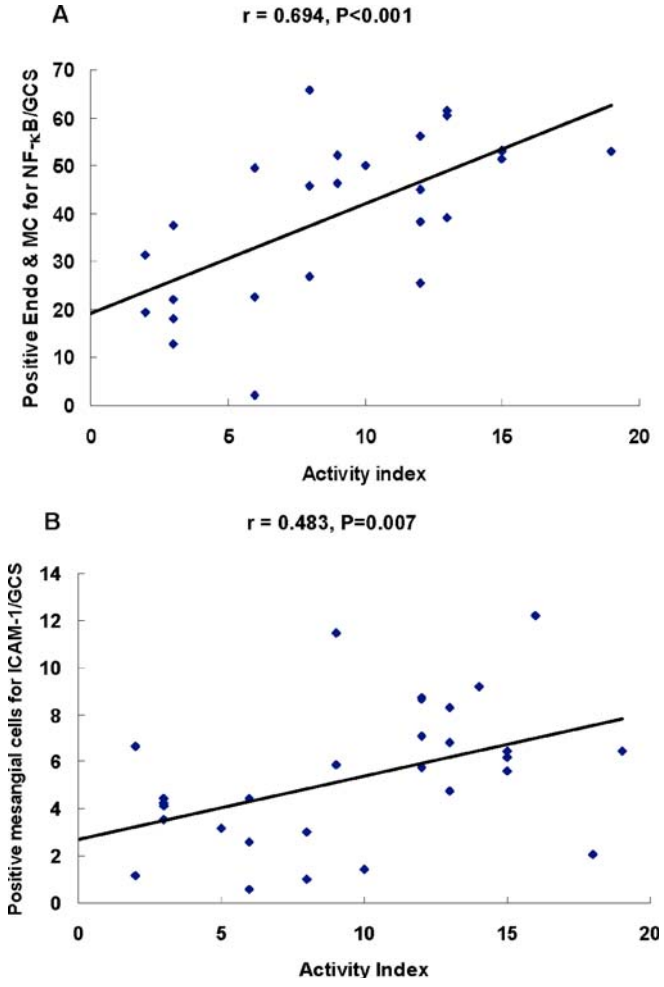

Fig. 5 Correlation analysis of the activity index with glomerular endothelial and mesangial NF-κB activation (**A**), as well as mesangial expression of ICAM-1 (**B**) in LN patients. *r*, Spearman's correlation coefficient

(Fig. 1A–C). In contrast, activated NF-κB was readily detected in all disease groups. Activated NF-κB was extensively expressed in resident glomerular cells (endothelia, mesangial cells, podocytes and PECs) as well as infiltrating macrophages in class IV LN (Fig. 1D–I). Simultaneous expression of p65 and p50 was readily observed in endothelial, mesangial cells and cellular crescents in a glomerulus from a patient with class IV LN (Fig. 1E,F,H,I), while p65 was the predominant form of NF-κB in podocytes in class IV LN (Fig. 1H,I). Inflammatory infiltrates lying freely in capillary lumina or Bowman's space were also observed in class IV LN (Fig. 1G). In class V LN and non-proliferative glomerulopathy, NF-κB activation was primarily noted in podocytes in addition to endothelial cells (Fig. 2A,D,G). In class V LN and non-proliferative glomerulopathy, podocyte NF-κB activation was predominantly in the form of p65 subunit (Fig. 2B,E,H), whereas p50 was mainly localized in endothelial cells if detectable (Fig. 2C,F,I). Semi-quantitative analysis showed that overwhelmingly high numbers of NF-κB-positive endothelial and mesangial cells and PECs were found in the class IV group; the number of these cells in LN group exceeded that in the non-proliferative glomerulopathy groups (Table 2). No statistically significant difference in the degree of podocyte NF-κB activation was detected between the LN and non-proliferative glomerulopathy comparison groups as a whole, nor between the IMN versus class V LN or class IV LN versus class V LN subgroups ($P>0.05$) (Table 2).

Glomerular expression of NF-κB-regulated pro-inflammatory mediators (TNF-α, IL-1β, IL-6 and ICAM-1)

An upregulation of TNF-α and IL-1β immunoreactivity was readily detected in glomeruli of inflammatory LN as compared to normal controls (Fig. 3a,b). Expression of TNF-α and IL-1β was detected in podocytes in a glo-

Table 3 Clinicopathologic correlation analysis of glomerular cell type-specific activation of NF-κB expression in LN patients

	Activity Index			Chronicity Index			Proteinuria		
	r	*P* Value	*N*	*r*	*P* value	*N*	*r*	*P* value	*N*
NF-κB Podo[a]	−0.095	0.616	30	0.095	0.616	30	0.749**	<0.001	28
p65 Podo[a]	0.002	0.992	29	0.253	0.185	30	0.663**	<0.001	29
p50 Podo[a]	0.161	0.441	25	−0.110	0.559	25	−0.183	0.381	25
NF-κB Endo&MC[b]	0.694**	<0.001	26	0.11	0.594	26	0.04	0.846	26
p65 Endo&MC[b]	0.142	0.481	27	0.324	0.099	27	−0.125	0.533	27
p50 End&MC[b]	0.355	0.082	25	−0.218	0.294	25	0.112	0.595	25
NF-κB PEC[b]	0.071	0.709	29	0.004	0.984	30	−0.201	0.287	30
p65 PEC[b]	0.260	0.173	29	0.083	0.668	29	−0.132	0.494	29
p50 PEC[b]	0.468*	0.01	29	−0.084	0.664	29	−0.179	0.353	29

Correlation was evaluated with Spearman's correlation coefficient
r Spearman's correlation coefficient, *Endo&MC* endothelial cell and mesangial cell, *Podo* podocyte, *PEC* parietal epithelial cell
*Correlation was significant at the 0.05 level (two-tailed)
**Correlation was significant at the 0.01 level (two-tailed)
[a]Score is described in Materials and methods
[b]Expressed as average number of immunoreactive cells per glomerular cross-section

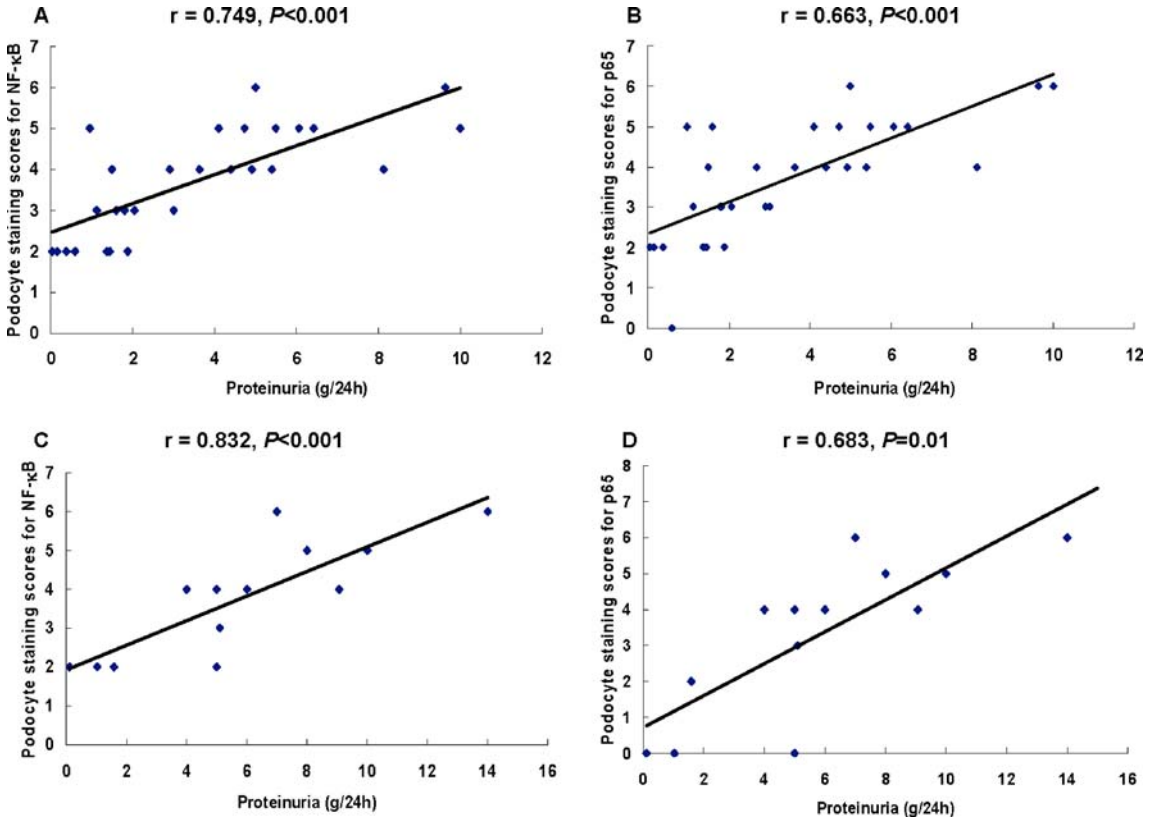

Fig. 6 Clinicopathologic correlation analysis of the magnitude of proteinuria with podocyte staining scores for NF-κB and p65 in both LN (**A**, **B**) and non-proliferative glomerulopathy (**C**, **D**). *r*, Spearman's correlation coefficient

merulus showing podocyte expression of p65, from a patient with class IV LN (Fig. 3A–C). Glomerular expression of TNF-α and IL-1β was also observed in infiltrating leukocytes, and, to a lesser extent, in other glomerular resident cells in class IV LN (Fig. 3B,C). In contrast to class IV LN, expression of both cytokines was primarily restricted to podocytes in class V LN (Fig. 3D,E) and non-proliferative glomerulopathy (Fig. 3F,G). Overall, no statistically significant difference in podocyte expression of TNF-α and IL-1β was found between LN and non-proliferative glomerulopathy (Fig. 4A).

Glomeruli of normal kidneys showed scant expression of IL-6 and constitutive ICAM-1 expression along the inner aspect of capillary loops (Fig. 3c,d). Expression of IL-6 and ICAM-1 in class V LN (Fig. 3J,K) and non-proliferative glomerulopathy (Fig. 3L,M) was indistinguishable from that observed in normal controls. Unlike TNF-α and IL-1β, enhanced expression ofICAM-1 and IL-6 was primarily localized in proliferative mesangial areas in the LN group, most evident in class IV LN (Figs. 3H,I and 4B).

Detection of the macrophage marker CD68 in glomeruli

CD68-positive cells, predominantly localized in capillary lumina and Bowman's space, were dramatically increased in number in glomeruli of class IV LN (Table 1), whereas fewer macrophages were detected in class V LN and macrophages were rarely seen in non-proliferative glomerulopathy (Table 1).

Clinicopathologic correlation analysis

In LN subjects, the number of endothelial and mesangial cells showing NF-κB activation by SWH was positively and strongly correlated with the activity index (Table 3 and Fig. 5A), whereas no correlation was found between the podocyte expression scores for NF-κB, p65 or p50 and the activity or chronicity indices (Table 3). The activity index was positively correlated with mesangial expression of ICAM-1 (Fig. 5B). In addition, the degree of glomerular macrophage infiltration was positively correlated with the number of endothelial and mesangial cells positive for NF-κB and p50, as well as with mesangial expression of ICAM-1 (Spearman's correlation coefficient r=0.49, P=0.02; r=0.50, P=0.02; r=0.53, P=0.03). Notably, podocyte NF-κB activation detected by SWH and podocyte p65 staining scores were positively correlated with the severity of proteinuria at the time of diagnostic renal biopsy in both the LN and non-proliferative disease groups (Table 3 and Fig. 6).

Discussion

NF-κB activation of glomerular cells has been investigated in experimental as well as human glomerulonephritis. Endothelial and mesangial activation of NF-κB has been previously reported in human IgA nephropathy with mesangial proliferation [2]. Numerous studies have shown that various experimental conditions modulating NF-κB activation result in a parallel modulation of proinflammatory molecule production in mesangial cells [27] and endothelial cells [8, 51]. Additionally, NF-κB activation has been reported in podocytes, parietal epithelial cells as well as crescents in experimental and human glomerulonephritis [2, 28, 29, 38]. NF-κB has also been implicated in the activation of macrophages in glomerulonephritis [31]. In the present study, we demonstrate for the first time that NF-κB is activated in glomerular resident cells and macrophages in human renal biopsies with LN.

In renal biopsies with LN (especially class IV LN), NF-κB activation in glomerular endothelial and mesangial cells was more remarkable than non-proliferative glomerulopathy (IMN and MCD), and was correlated with the activity index and the degree of glomerular macrophage infiltration. These observations suggest that NF-κB activation in multiple types of glomerular intrinsic cells may play a pathogenic role in glomerular inflammation and injury in LN. Furthermore, an upregulation of TNF-α and IL-1β was readily detected in inflammatory leukocytes and resident cells. IL-6 and ICAM-1 were mainly localized to the mesangium in parallel with NF-κB activation, in glomeruli of the class IV LN group. Our results are consistent with the findings of other groups [25, 41, 49].

The promoter regions of TNF-α, IL-1β, ICAM-1 and IL-6 contain at least one NF-κB consensus site that has been shown to be important for their transcription in monocytes and glomerular cells [6, 13, 43, 46]. Moreover, TNF-α itself can also stimulate NF-κB activation and subsequently induce downstream inflammatory mediators such as IL-1β, ICAM-1 and IL-6 in GN and rheumatoid arthritis [14, 43, 44]. Recent studies show that increased ICAM-1 expression by TNF-α activation of mesangial cells is one of the major pathways involved in monocyte adhesion to the mesangium [32], and that TNF-α, immunoglobulin aggregates and immune complex deposition increase NF-κB activation in mesangial cells [12, 40]. In the present study, we found a correlation between mesangial expression of ICAM-1 and both the activity index and the level of glomerular macrophage infiltration in class IV LN, in which mesangial immune complex deposits are frequently seen. This finding further supports the hypothesis that NF-κB activation of mesangial cells plays a proinflammatory role in glomerular injury by mediating their interactions with monocytes/macrophages through the induction of inflammatory mediators. Moreover, NF-κB activation and cytokine expression were observed in macrophages in class IV LN. The macrophage is believed to play an important role in amplifying inflammation through interactions with other renal cells in LN [9]. The results imply that NF-κB is a central regulator of a complex interaction network between glomerular resident cells and macrophages, mediated by inflammatory molecules in LN.

Another important finding in the present study is the detection of podocyte NF-κB overactivation, along with podocyte overexpression of the NF-κB-regulated proinflammatory cytokines TNF-α and IL-1β in subjects with LN. Notably, podocyte staining scores for NF-κB, as well as p65, the predominate subunit of NF-κB within podocytes, were positively correlated with the severity of proteinuria in LN. Similar findings were found in non-proliferative proteinuric glomerulopathy (IMN and MCD) that are characterized by podocyte injury. Our results suggest that NF-κB activation may be a generalized cellular response of the podocyte and associated with the development of proteinuria, an index of the severity of podocyte injury [45] in human glomerular diseases. However, evidence suggests that different immunopathogenic mechanisms underlie these associations in different disease groups as discussed below.

In immune-mediated class V LN or IMN, the deposits are located in the subepithelium, directly adjacent to the foot processes of podocytes. In the animal model of passive Heymann nephritis which closely resembles human membranous nephropathy, typical subepithelial immune deposits may trigger complement activation and stimulate adjacent podocytes to release inflammatory mediators associated with the subsequent development of proteinuria [19]. In passive Heymann nephritis, NF-κB activation and overexpression of downstream NF-κB-regulated genes is observed predominantly in podocytes at an early stage; inhibition of this pathway was shown to reduce proteinuria [29]. These studies support a contributory role for NF-κB activation as a downstream response to podocyte injury mediated by immune complex deposition in the pathogenesis of proteinuria as occurs in either idiopathic or secondary membranous nephropathy. By contrast, in class IV LN, immune deposits are largely located in the subendothelial or mesangial area, with little direct evidence that the podocyte is a primary target of the immune-mediated injury. Recent studies suggest that inflammatory cytokines such as TNF-α and/or IL-1β may induce the upregulation of nephrin expression and reorganization of the actin cytoskeleton, which is suggested to contribute to the development of proteinuria [17, 21, 22]. In this context, our observation of podocyte NF-κB activation likely results from glomerular inflammation in class IV LN. Additionally, podocyte NF-κB activation and overexpression of cytokines may be related to abnormally high levels of intraglomerular protein trafficking. Recent studies suggest a causal role of enhanced intraglomerular passage of proteins in the triggering of podocyte gene activation and podocyte architectural alterations [1]. MCD is a reversible condition not typically associated with visible evidence of glomerular inflammation or deposition of immunoglobulin or complement by light microscopy. It remains uncertain whether podocyte NF-κB activation is a causal mechanism of proteinuria in this disease. Putative circulating permeability factors may cause the loss of the glomerular permselectivity that leads to proteinuria in MCD [10]. Whether

podocyte NF-κB activation is involved in circulating permeability factors-induced proteinuria in MCD remains unproven.

Although the level of podocyte expression of the cytokines TNF-α and IL-1β in class IV LN did not differ from non-proliferative glomerulopathy, these cytokines produced by podocytes may play different roles under different disease conditions. In class IV LN, TNF-α and IL-1β produced by podocytes may have local proinflammatory effects on other glomerular resident cells as described above. Baseline levels of glomerular expression of ICAM-1 and IL-6 observed in MCD excludes the proinflammatory role of TNF-α and IL-1β by podocytes, although the latter may still play a non-inflammatory role in the pathogenesis of proteinuria, such as interruption of podocyte cell architecture (as suggested above) [17, 21, 22].

Recent studies suggest that different dimeric combinations formed by the NF-κB/Rel family of transcription factors offer the potential for fine-tuning of gene expression [47]. In the present study, p65 was observed to be the predominant NF-κB subunit in podocytes in all disease groups, while NF-κB subunit p65 and p50 were equally distributed in other types of glomerular cells in LN. The differential expression of inflammatory mediators such as ICAM-1 and IL-6 was also cell type-specific, exhibiting overexpression in endothelial or mesangial cells, but not in podocytes. The variable distribution of p65 and p50 subunits among different glomerular cell types suggests that NF-κB-responsive genes may be differentially regulated in a NF-κB subunit-specific manner in human glomerulonephritis.

In conclusion, our study illustrates the potential role of transcription factor NF-κB activation in glomerular injury in human LN and illustrates the possible role of molecular signaling in mediating glomerular injury in LN.

Acknowledgements We wish to acknowledge the support from National University of Singapore. This work was undertaken in the Special Histopathology laboratory in the Department of Pathology. We thank Dr. Koh Dow Rhoon for valuable advice and Dr. Thian Chai Lee (Johor Specialist Center, Malaysia) for his assistance in providing the clinical data on the biopsy cases included in the present study. This work was funded by Academic Research Fund Grant R-172-000-109-112 to R.S. and S.I.-H.H., and intramural funding from the Department of Medicine, National University of Singapore.

References

1. Abbate M, Zoja C, Morigi M, Rottoli D, Angioletti S, Tomasoni S, Zanchi C, Longaretti L, Donadelli R, Remuzzi G (2002) Transforming growth factor-beta1 is up-regulated by podocytes in response to excess intraglomerular passage of proteins: a central pathway in progressive glomerulosclerosis. Am J Pathol 161:2179–2193
2. Ashizawa M, Miyazaki M, Abe K, Furusu A, Isomoto H, Harada T, Ozono Y, Sakai H, Koji T, Kohno S (2003) Detection of nuclear factor-kappaB in IgA nephropathy using Southwestern histochemistry. Am J Kidney Dis 42:76–86
3. Austin HA, Muenz LR, Joyce KM, Antonovych TT, Balow JE (1984) Diffuse proliferative lupus nephritis: identification of specific pathologic features affecting renal outcome. Kidney Int 25:689–695
4. Baeuerle P (1998) Pro-inflammatory signaling: last pieces in NF-κB puzzle? Curr Biol 8:R19–R22
5. Boswell JM, Yui MA, Burt DW, Kelley VE (1988) Increased tumor necrosis factor and IL-1β gene expression in the kidneys of mice with lupus nephritis. J Immunol 141:3050–3054
6. Brennan DC, Jevnikar AM, Takei F, Reubin-Kelley VE (1990) Mesangial cell accessory functions: mediation by intercellular adhesion molecule-1. Kidney Int 38:1039–1046
7. Couser WG (1998) Pathogenesis of glomerular damage in glomerulonephritis. Nephrol Dial Transplant 13(Suppl 1):10–15
8. Eng E, Ballermann BJ (2003) Diminished NF-κB activation and PDGF-B expression in glomerular endothelial cells subjected to chronic shear stress. Microvasc Res 65:137–144
9. Foster MH, Kelley VR (1999) Lupus nephritis: update on pathogenesis and disease mechanisms. Semin Nephrol 19:173–181
10. Ghiggeri GM, Artero M, Carraro M, Perfumo F (2001) Permeability plasma factors in nephrotic syndrome: more than one factor, more than one inhibitor. Nephrol Dial Transplant 16:882–885
11. Ghosh S, May MJ, Kopp EB (1998) NF-κB and Rel proteins: evolutionarily conserved mediators of immune responses. Annu Rev Immunol 16:225–260
12. Gomez-Guerrero C, Lopez-Franco O, Suzuki Y, Sanjuan G, Hernandez-Vargas P, Blanco J, Egido J (2002) Nitric oxide production in renal cells by immune complexes: role of kinases and nuclear factor-kappaB. Kidney Int 62:2022–2034
13. Grassl C, Luckow B, Schlondorff D, Dendorfer U (1999) Transcriptional regulation of the interleukin-6 gene in mesangial cells. J Am Soc Nephrol 10:1466–1477
14. Guijarro C, Egido J (2001) Transcription factor-kappa B (NF-κB) and renal disease. Kidney Int 59:415–424
15. Hernandez-Presa MA, Gomez-Guerrero C, Egido J (1999) In situ non-radioactive detection of nuclear factors in paraffin sections by Southwestern histochemistry. Kidney Int 55:209–214
16. Herrera-Esparza R, Barbosa-Cisneros O, Villalobos-Hurtado R, Avalos-Diaz E (1998) Renal expression of IL-6 and TNF-α genes in lupus nephritis. Lupus 7:154–158
17. Huwiler A, Ren S, Holthofer H, Pavenstadt H, Pfeilschifter J (2003) Inflammatory cytokines upregulate nephrin expression in human embryonic kidney epithelial cells and podocytes. Biochem Biophys Res Commun 305:136–142
18. Kaltschmidt C, Kaltschmidt B, Henkel T, Stockinger H, Baeuerle PA (1995) Selective recognition of the activated form of transcription factor NF-kappa B by a monoclonal antibody. Biol Chem Hoppe-Seyler 376:9–16
19. Kerjaschki D, Neale TJ (1996) Molecular mechanisms of glomerular injury in rat experimental membranous nephropathy (Heymann nephritis). J Am Soc Nephrol 7:2518–2526
20. Kitamura M (2000) Adoptive transfer of nuclear factor-kappaB-inactive macrophages to the glomerulus. Kidney Int 57:709–716
21. Koop K, Eikmans M, Baelde HJ, Kawachi H, De Heer E, Paul LC, Bruijn JA (2003) Expression of podocyte-associated molecules in acquired human kidney diseases. J Am Soc Nephrol 14:2063–2071
22. Koukouritaki SB, Vardaki EA, Papakonstanti EA, Lianos E, Stournaras C, Emmanouel DS (1999) TNF-α induces actin cytoskeleton reorganization in glomerular epithelial cells involving tyrosine phosphorylation of paxillin and focal adhesion kinase. Mol Med 5:382–392
23. Lhotta K, Neumayer HP, Joannidis M, Geissler D, Konig P (1991) Renal expression of intercellular adhesion molecule-1 in different forms of glomerulonephritis. Clin Sci (Lond) 81:477–481
24. Li Q, Verma IM (2002) NF-κB regulation in the immune system. Nat Rev Immunol 2:725–734
25. Malide D, Russo P, Bendayan M (1995) Presence of tumor necrosis factor alpha and interleukin-6 in renal mesangial cells of lupus nephritis patients. Hum Pathol 26:558–564

26. Marenda SA, Aufdemorte TB (1995) Localization of cytokines in cholesteatoma tissue. Otolaryngol Head Neck Surg 112:359–368
27. Massy ZA, Guijarro C, O'Donnell MP, Kim Y, Kashtan CE, Egido J, Kasiske BL, Keane WF (1999) The central role of nuclear factor-kappa B in mesangial cell activation. Kidney Int Suppl 71:76–79
28. Mezzano SA, Barria M, Droguett MA, Burgos ME, Ardiles LG, Flores C, Egido J (2001) Tubular NF-κB and AP-1 activation in human proteinuric renal disease. Kidney Int 60:1366–1377
29. Mudge SJ, Paizis K, Auwardt RB, Thomas RJ, Power DA (2001) Activation of nuclear factor-kappa B by podocytes in the autologous phase of passive Heymann nephritis. Kidney Int 59:923–931
30. Niemir ZI, Stein H, Dworacki G, Mundel P, Koehl N, Koch B, Autschbach F, Andrassy K, Ritz E, Waldherr R, Otto HF (1997) Podocytes are the major source of IL-1 alpha and IL-1 beta in human glomerulonephritides. Kidney Int 52:393–403
31. Nikolic-Paterson DJ, Atkins RC (2001) The role of macrophages in glomerulonephritis. Nephrol Dial Transplant 16 (Suppl5):3–7
32. Pai R, Bassa B, Kirschenbaum MA, Kamanna VS (1996) TNF-alpha stimulates monocyte adhesion to glomerular mesangial cells. The role of intercellular adhesion molecule-1 gene expression and protein kinases. J Immunol 156:2571–2579
33. Pavenstadt H (2000) Roles of the podocyte in glomerular function. Am J Physiol Renal Physiol 278:173–179
34. Qiu LQ, Sinniah R, Hsu SI (2004) Role of differential and cell type-specific expression of cell cycle regulatory proteins in mediating progressive glomerular injury in human IgA nephropathy. Lab Invest 84:1112–1125
35. Qiu LQ, Sinniah R, Hsu SI (2004) Downregulation of Bcl-2 by podocytes is associated with progressive glomerular injury and clinical indices of poor renal prognosis in human IgA nephropathy. J Am Soc Nephrol 15:79–90
36. Rui-Mei L, Kara AU, Sinniah R (1998) In situ analysis of adhesion molecule expression in kidneys infected with murine malaria. J Pathol 185:219–222
37. Sabattini E, Bisgaard K, Ascani S, Poggi S, Piccioli M, Ceccarelli C, Pieri F, Fraternali-Orcioni G, Pileri SA (1998) The EnVision++ system: a new immunohistochemical method for diagnostics and research. Critical comparison with the APAAP, ChemMate, CSA, LABC, and SABC techniques. J Clin Pathol 51:506–511
38. Sakai N, Wada T, Furuichi K, Iwata Y, Yoshimoto K, Kitagawa K, Kokubo S, Kobayashi M, Takeda S, Kida H, Kobayashi K, Mukaida N, Matsushima K, Yokoyama H (2002) p38 MAPK phosphorylation and NF-κB activation in human crescentic glomerulonephritis. Nephrol Dial Transplant 17:998–1004
39. Sakurai H, Hisada Y, Ueno M, Sugiura M, Kawashima K, Sugita T (1996) Activation of transcription factor NF-κB in experimental glomerulonephritis in rats. Biochim Biophys Acta 1316:132–138
40. Satriano J, Schlondorff D (1994) Activation and attenuation of transcription factor NF-κB in mouse glomerular mesangial cells in response to tumor necrosis factor-alpha, immunoglobulin G, and adenosine 3′:5′-cyclic monophosphate. Evidence for involvement of reactive oxygen species. J Clin Invest 94:1629–1636
41. Takemura T, Yoshioka K, Murakami K, Akano N, Okada M, Aya N, Maki S (1994) Cellular localization of inflammatory cytokines in human glomerulonephritis. Virchows Arch 424: 459–464
42. Tan EM, Cohen AS, Fries JF, Masi AT, McShane DJ, Rothfield NF, Schaller JG, Talal N, Winchester RJ (1982) The 1982 revised criteria for the classification of systemic lupus erythematosus. Arthritis Rheum 25:1271–1277
43. Tomita N, Morishita R, Tomita S, Kaneda Y, Higaki J, Ogihara T, Horiuchi M (2001) Inhibition of TNF-α, induced cytokine and adhesion molecule. Expression in glomerular cells in vitro and in vivo by transcription factor decoy for NF-κB. Exp Nephrol 9:181–190
44. Tomita T, Takano H, Tomita N, Morishita R, Kaneko M, Shi K, Takahi K, Nakase T, Kaneda Y, Yoshikawa H, Ochi T (2000) Transcription factor decoy for NF-κB inhibits cytokine and adhesion molecule expressions in synovial cells derived from rheumatoid arthritis. Rheumatology (Oxford) 39:749–757
45. Tryggvason K, Wartiovaara J (2001) Molecular basis of glomerular permselectivity. Curr Opin Nephrol Hypertens 10:543–549
46. Udalova IA, Knight JC, Vidal V, Nedospasov SA, Kwiatkowski D (1998) Complex NF-κB interactions at the distal tumor necrosis factor promoter region in human monocytes. J Biol Chem 273:21178–21186
47. Udalova IA, Kwiatkowski D (2001) Interaction of AP-1 with a cluster of NF-κB binding elements in the human *TNF* promoter region. Biochem Biophys Res Commun 289:25–33
48. Weening JJ, D'Agati VD, Schwartz MM, Seshan SV, Alpers CE, Appel GB, Balow JE et al (2004) The classification of glomerulonephritis in systemic lupus erythematosus revisited. J Am Soc Nephrol 15:241–250
49. Wuthrich RP, Jevnikar AM, Takei F, Glimcher LH, Kelley VE (1990) Intercellular adhesion molecule-1 (ICAM-1) expression is upregulated in autoimmune murine lupus nephritis. Am J Pathol 136:441–450
50. Yu CC, Yang CW, Wu MS, Ko YC, Huang CT, Hong JJ, Huang CC (2001) Mycophenolate mofetil reduces renal cortical inducible nitric oxide synthase mRNA expression and diminishes glomerulosclerosis in MRL/lpr mice. J Lab Clin Med 138:69–77
51. Zoja C, Angioletti S, Donadelli R, Zanchi C, Tomasoni S, Binda E, Imberti B, te Loo M, Monnens L, Remuzzi G, Morigi M (2002) Shiga toxin-2 triggers endothelial leukocyte adhesion and transmigration via NF-κB dependent up-regulation of IL-8 and MCP-1. Kidney Int 62:846–856

Virchows Arch (2006) 448: 184–194
DOI 10.1007/s00428-005-0050-z

ORIGINAL ARTICLE

D. J. Schupp · B. P. Huck · J. Sykora · C. Flechtenmacher · M. Gorenflo · A. Koch · F.-U. Sack · M. Haass · H. A. Katus · H. E. Ulmer · S. Hagl · H. F. Otto · P. A. Schnabel

Right ventricular expression of extracellular matrix proteins, matrix-metalloproteinases, and their inhibitors over a period of 3 years after heart transplantation

Received: 6 April 2005 / Accepted: 15 July 2005 / Published online: 14 September 2005

Abstract Fibrillar collagens I and III, nonfibrillar collagen IV, and the glycoproteins fibronectin and laminin, are elements of the myocardial extracellular matrix (ECM). Alterations in the normal concentrations and ratios of these elements may reflect remodeling in response to physiologic stress. In the case of patients' post-heart transplantation (HTx), specific patterns of alteration may herald myocardial dysfunction. Right ventricular biopsies were taken from the same 28 HTx patients before implantation and 1 week, 2 weeks, and 1, 2, and 3 years after HTx. The above-noted five ECM proteins, six matrix metalloproteinases (MMPs) and two of their tissue inhibitors (TIMPs) were detected by immunohistochemistry and scored as cells per square millimeter or semiquantitatively. The total connective tissue fibers were detected by connective tissue stain and morphometry. Variations in these ECM components were followed in the same patient cohort over 3 years. In summary, during the first 2 weeks after HTx, a predominant increase in connective tissue occurred. Increases in MMP-8 and MMP-9 were found. By 3 years after transplantation, there was a decrease of connective tissue fibers and a significant reduction of all ECM components and an increase in MMPs and TIMPs. These findings may reflect a pattern of remodeling specific to the transplanted heart.

Keywords Extracellular matrix · Matrix metalloproteinases · Tissue inhibitors · Heart transplantation · Connective tissue fibers

D. J. Schupp · B. P. Huck · J. Sykora · C. Flechtenmacher · H. F. Otto · P. A. Schnabel (✉)
Department of Pathology,
University of Heidelberg,
INF 220/221,
69120 Heidelberg, Germany
e-mail: PhilippASchnabel@aol.com
Tel.: +49-6221-396496
Fax: +49-6221-565251

A. Koch · F.-U. Sack · S. Hagl
Department of Cardiac Surgery,
University of Heidelberg,
Heidelberg, Germany

M. Gorenflo · H. E. Ulmer
Department of Pediatric Cardiology,
University of Heidelberg,
Heidelberg, Germany

M. Haass · H. A. Katus
Department of Internal Medicine,
University of Heidelberg,
Heidelberg, Germany

Introduction

The myocardial extracellular matrix (ECM), which plays a significant role in maintaining the efficiency of cardiac function, contains numerous elements, including collagens I, III, and IV, and laminin and fibronectin. The ECM is not a static structure. It is a dynamic entity [4, 15, 34]. The myocardial fibrillar collagens such as Collagens I and III ensure structural integrity of the adjoining myocytes, provide the means by which myocyte shortening is translated into overall left ventricular pump function, and are essential for maintaining alignment of the myofibrils within the myocyte through a collagen–integrin–cytoskeletal myofibril relation [6, 17, 30, 34].

The ECM forms a continuum between different cell types within the myocardium and provides a structural supporting network to maintain myocardial geometry during the cardiac cycle [34]. Disruption or discontinuities within the fibrillar ECM network will result in a loss of normal structural support and continuity, resulting in myocyte fascicles being subjected to abnormal stress and strain patterns during the cardiac cycle, which, in turn, will result in changes in myocardial geometry and function. The identification and understanding of the enzyme systems responsible for ECM degradation within the myocardium have particular relevance in appreciating the process of rejection of transplanted hearts [7, 23, 28, 36].

The matrix metalloproteinases (MMPs) are a family of enzymes that degrade a wide variety of ECM components.

Different species of MMPs have been categorized on the basis of substrate specificity, and a body of evidence indicates that the MMPs play an important role in the tissue remodeling process [11, 46].

Interstitial collagenase, also known as MMP-1, degrades collagens I and III. Collagenase 3, which is also called MMP-13, also degrades collagens I and III. Gelatinase B, also known as MMP-9, degrades collagens I and IV. Stromelysin 1, also called MMP-3, degrades fibronectin, laminin, and collagens III and IV. It is also involved in MMP activation. The membrane-type-1-MMP (MT-MMP1), also known as MMP-14, degrades collagens I and III and fibronectin and laminin. It also activates pro-MMP-13. The extracellular activity of these enzymes is controlled at the level of gene expression, proenzyme activation, and interaction with specific tissue inhibitors of MPs (TIMP-1 and TIMP-2) [34]. MMP-8, which is also called neutrophil collagenase, or collagenase 2, degrades collagen I more than collagen III. It does not degrade collagen IV [25].

It has been demonstrated that TIMP-2 forms a complex with MT-MMPs, and that this complex enhances the activation of pro-MMP-2 [18]. It is assumed that the TIMPs bind directly to MMPs in a 1:1 fashion to inhibit them. It has been proposed that this ratio may change in hearts undergoing continued remodeling as a response to stress, suggesting a dysregulation of the normal compensatory remodeling response may lead to prolonged detrimental remodeling and subsequent myocardial dysfunction [20, 25, 34, 36]. For example, MMPs that are expressed at very low levels in normal myocardium such as MMP-13 and MT-MMP1 are substantially up-regulated in congestive heart failure [19]. Previous studies on hearts taken at the time of human heart transplantation (HTx) and at autopsy have provided evidence of collagenolytic activity in cardiac tissue that is consistent with MMP activity [14].

The purpose of the present study is to delineate the changes in the above-noted ECM protein components in the myocardium of transplanted hearts in a cohort of patients during the first 3 years following cardiac transplantation. For the purpose of helping to link the changes noted to the underlying physiologic process, we also performed an analysis of the changes in amounts of various cell types over this time by detecting and quantifying several cluster differentiation (CD) cell markers, namely, CDs 3, 4, 8, 15, 20, 57, 68, and 69.

Cluster differentiation 3 is a T cell marker which is important for early T cell differentiation. CD4 is a “T helper” cell marker. CD8 is a “killer T cell” marker. CD15 is present on myelomonocytes, monocytes, macrophages, and activated B and T cells. CD20 is present on B cells and is involved in their activation. CD57 is present on “natural killer” (NK) cells. CD68 is present on macrophages. CD69 is present on T cells, NK cells, monocytes, and platelets, and especially on activated T cells, B cells, and NK cells involved in inflammation.

Materials and methods

Patients

Right ventricular biopsies were taken from a group of 28 patients before implantation and 1 week, 2 weeks, 1, 2, and 3 years after HTx at the University of Heidelberg Medical Center (Departments of Cardiac Surgery, Internal Medicine, and Pediatric Cardiology), Heidelberg, Germany. They were embedded in Tissue Tek (Sakura, Netherlands, Batch #4583000) and stored at −72°C. Cryosections (4 μm) were cut at −20°C with Frigocut (Reichert-Jung Model 2700, Nussloch, Germany) and afterwards fixed in acetone.

The recipients’ mean age was 45.3 years, with a standard deviation (SD) of 16.9, ranging from 9 to 63 years; 26 were male, and 3 were female. Sixteen patients had suffered from dilated cardiomyopathy, ten from ischemic cardiomyopathy, one from transposition of the great vessels, one from tetralogy of Fallot, and one from double-outlet right ventricle. The donors’ mean age was 31.5 years, with an SD of 14.5, ranging from 10 to 55 years, with 20 being male and 9 being female; the cause of death was head trauma for 15, parenchymal intracranial bleeding for six, basilar arterial thrombosis for two, subarachnoid hemorrhage for one, ischemic stroke for one, gunshot wound to the head for one, status asthmaticus for one, thalamic tumor for one, and carbon monoxide poisoning for one. The intensive care of the donors averaged 3.5 days, with an SD of 3.5, ranging from 1 to 19 days.

All hearts were perfused with 2–4 l of histidine–tryptophan–ketoglutarate (HTK) solution (Custodiol, Dr. F. Koehler Chemie GmbH, Alsbach, Germany). The mean ischemic time period was 182 min, with an SD of 53.

Immunohistochemistry

The frozen sections were washed twice in phosphate-buffered saline (PBS) and then processed for 25 min with a mixture of CAS-Block, albumin, and γ-venin. The sections were then incubated for 1 h with a specific antibody. The following antibodies were used to show the ECM components, the MMPs, and their inhibitors:

MMP-1 (IHC) (Cat. # 551000, BD Biosciences BD PharMingen, San Diego, CA, USA), monoclonal mouse, 1:100;
MMP-8 (Ab-1) (Cat. # IM38L, Oncogene Research Products, Boston, MA, USA), monoclonal mouse, 1:20;
MMP-13 (Ab-5) (Cat. # IM79, Oncogene), monoclonal mouse, 1:20;
MMP-3 (Ab-5) (Cat. # RB-1589-PO, NeoMarker, Fremont, CA, USA), monoclonal mouse, 1:50;
MMP-9 (Ab-7) (Cat. # IM61, Oncogene), monoclonal mouse, 1:100;

MMP-14 (Ab-1) (Cat. # RB-1544-PO, NeoMarker), monoclonal mouse, 1:10;
TIMP- 1 (Ab-4) (Cat. # IM63 Oncogene), monoclonal mouse, 1:50;
TIMP-2 (Ab-4) (Cat. # IM82, Oncogene), monoclonal mouse, 1:100;
Collagen Type I (Cat. # 9 2150-0020, BioTrend, Köln, Germany), polyclonal rabbit, 1:100;
Collagen Type III (Ab 167M) (Cat. # MU 167-UC, BioGenex, San Ramon, CA, USA), monoclonal mouse, 1:400;
Collagen Type IV (Ab 379M) (Cat. # AM MU379-UC, BioGenex), monoclonal mouse, 1:100;
Fibronectin (AO 245) (Code # AO 245, DAKO, Denmark), polyclonal rabbit, 1:800;
Laminin (Cat. # PU078-UP, BioGenex), polyclonal rabbit, 1:50;
CD3 (Cat. # MCA1477, Serotec, Kidlington, England), monoclonal rat, 1:100;
CD4 (Cat. # M0716, DAKO), monoclonal mouse, 1:25;
CD8 (Cat. # M7103, DAKO), monoclonal mouse, 1:100;
CD15 (Cat. # M0733, DAKO), monoclonal mouse, 1:50;
CD20 (Cat. # M0755, DAKO), monoclonal mouse, 1:50;

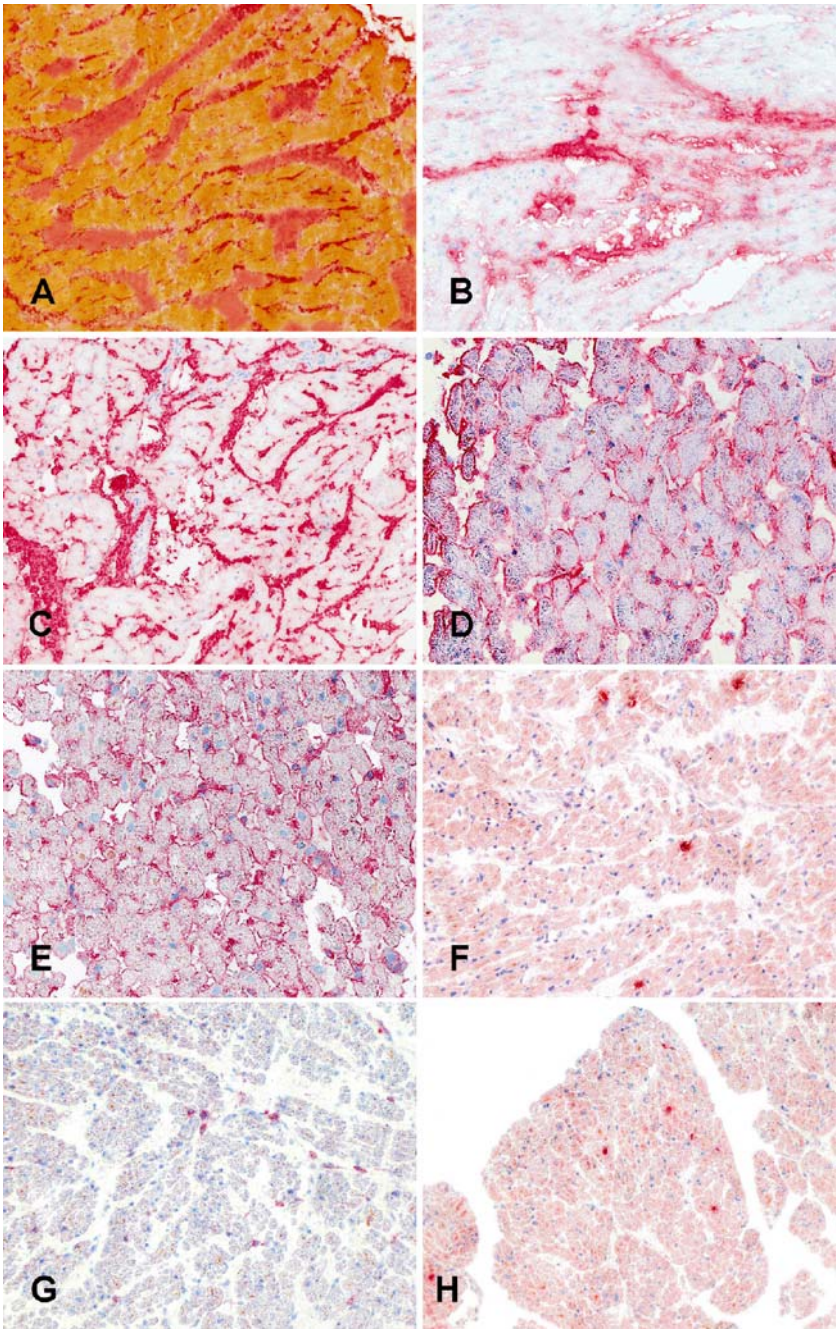

Fig. 1 **A** EvG staining showing the myocardium with cardiomyocytes (*yellow*/*amber*) and collagen fibers (*red*). Original magnification ×100. **B** Expression of collagen I, primarily perimysial. Stained with Fast Red and contrast staining with Hemalaun. Original magnification ×100. **C** Expression of collagen III, primarily perimysial and endomysial. Fast Red stain with Hemalaun was used for contrast staining. Original magnification ×100. **D** Expression of collagen IV framing the myocardial cells. Fast Red stain with Hemalaun was used for contrast staining. Original magnification ×200. **E** Expression of laminin, primarily endomysial. Fast Red with Hemalaun staining was used for contrast. Original magnification ×200. **F** Interstitial cells expressing MMP-1. Fast Red with Hemalaun staining was used for contrast. Original magnification ×100. **G** Interstitial cells expressing MMP-3. Fast Red with Hemalaun staining was used for contrast. Original magnification ×100. **H** Interstitial cells expressing MMP-8. Fast Red with Hemalaun staining was used for contrast. Original magnification ×100

CD57 (Cat. # 18-0167, Zymed Laboratories Inc, USA), monoclonal mouse, 1:100;
CD68 (Cat. # M0876, DAKO), monoclonal mouse, 1:100; and
CD69 (Cat. # sc-18880, Santa Cruz Biotechnology, USA), monoclonal mouse, 1:150.

All antibodies were diluted with common antibody diluent from BioGenex. For rabbit antibodies, as a negative control, rabbit immunoglobulin G (IgG) from DAKO (Code # X0936) was used. As a negative control for mouse, mouse Igs from DAKO (Code # Z0259) were used.

The sections were then washed twice in PBS. Afterwards, the second block (antibody diluent and goat serum) was applied and stayed on the sections for 20 min. The sections were incubated for 30 min with the second antibody. For rabbit antibodies, IgG biotin–antirabbit (Zymed, 1:400) was used. For mouse antibodies, a goat–antimouse supersensitive detection kit from BioGenex was used. Thereafter, they were washed twice again in PBS. Then, they were incubated with streptavidin–alkaline–phosphatase from the supersensitive detection kit (BioGenex). Again, they were washed twice in PBS, and then they were dyed with Fast Red, and the contrast staining was done by using Hemalaun. The connective tissue staining was done using Elastica van Gieson (EvG).

The tissue content of collagens I, III, and IV, laminin, and fibronectin were then semiquantitatively scored from 0 (without apparent staining) to 3 (demonstrating vigorous staining) [12]. This was performed by two independent investigators through 10, 20, and 40× objective lens on a

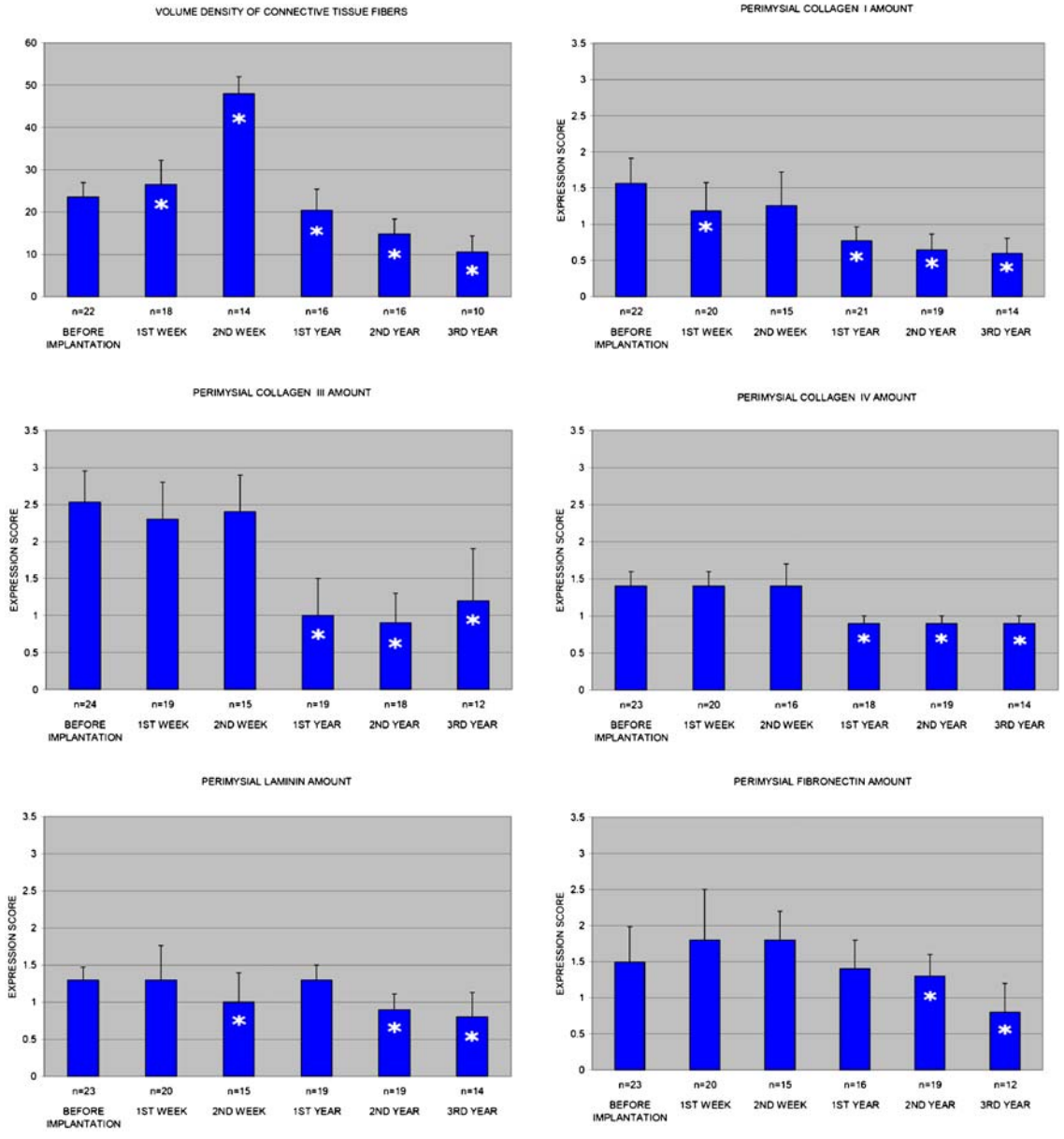

Fig. 2 Volume density of connective tissue fibers and the perimysial amount of collagen I, III, IV, laminin, and fibronectin. Mean±SD, * indicates $p<0.05$ (significant differences compared with values before implantation)

Zeiss Axioskope (Carl Zeiss AG, Jena, Germany) (Fig. 1). The investigators were blinded to patient identity and time of sample. Each slide was analyzed a total of three times, at least once by each investigator, and the results were averaged.

The cells with positive reaction (MMPs, TIMPs, and CD markers) were counted under the Zeiss microscope with 10× enlargement. The area of the sections, selected randomly and in an attempt to include reasonable myocardium and exclude artifact and large blood vessels, were measured with Optimas 5.2 (MediaCybernetics, Leiden, Netherlands), and the Hi Resolution CCD-IRIS camera (Sony, Tokyo, Japan) [15].

Morphometry

The morphometric analysis of EvG-stained sections was done with "random system sampling" on a grid through a light microscope using the point counting method [15, 43, 44]. This again involved random selection of microscopic fields which contain a high proportion of myocardium and no major vessels or color artifacts.

Statistics

The Wilcoxon signed rank test was applied for the MMPs, TIMPs, CDs, and volume density of connective tissue fibers. The sign test was used for collagen I, III, and IV, laminin, and fibronectin. p values of $p \leq 0.05$ were regarded as statistically significant.

Results

Connective tissue quality and morphometry

Collagen I is primarily expressed in the perimysium, as can be seen in Fig. 1B. Collagen III is expressed in the perimysium, and also, to some extent, the endomysium, as can be seen in Fig. 1C. The positively stained fibers in the perimysium and endomysium were counted. Collagen IV frames the myocytes, as can be seen in Fig. 1D.

The volume density of connective tissue fibers increased significantly from before implantation to the first and second week after transplantation. It decreased significantly from before implantation to 1, 2, and 3 years after transplantation (Fig. 2).

Matrix protein, MMP and TIMP, and CD immunohistochemistry

The results of the immunohistochemistry of the perimysial amounts of ECM components are indicated as scored data in Figs. 2 and 3, with the data on the CDs shown in Fig. 4.

The expression of collagen I decreased significantly in the first week after transplantation, as well as at 1, 2, and 3 years. The perimysial expression of Collagen III decreased significantly from before implantation at 1, 2, and 3 years.

The perimysial expression of Collagen IV decreased significantly from before implantation at 1, 2, and 3 years after HTx. The perimysial expression of laminin decreased significantly from before implantation at the second week, second year, and third year. The perimysial expression of fibronectin decreased significantly from before implantation at the second and third year after HTx.

The results of immunohistochemistry of the MMPs and TIMPs are shown in Fig. 3. The quantity of MMP-1-positive cells per square millimeter increased significantly from before implantation to the first, second, and third year after transplantation. MMP-8-positive cells increased significantly from before implantation to the first week, second week, and second year after transplantation. MMP-13-positive cells showed a significant decrease from before implantation to the second week, and then a significant increase to the first year, compared with preimplantation. The distribution of MMP-3 showed no significant changes from before implantation to the first 2 weeks or the first 3 years following transplantation. MMP-9 distribution increased significantly from before implantation to the first week, second week, and first year following HTx. MMP-14 (MT-MMP1) showed a significant increase in positive cells from before implantation to the third year.

The distribution of TIMP-1 showed a significant increase from before implantation to 2 and 3 years following HTx. TIMP-2 showed no significant changes from before implantation to the first 2 weeks or the first 3 years after transplantation.

Cluster differentiation 3+ cells, CD57+ cells, and CD69+ cells demonstrated no significant changes in number throughout the observation period. CD4+ cells registered a significant decrease in number from before implantation to the first week after transplantation. CD8+ cells decreased in number from before implantation to the second year following transplantation. CD15+ cells increased significantly in number at the first week, second week, and first year following transplantation when compared to preimplantation. CD20+ cells showed an increase in number at the second week following implantation. CD68+ cells showed significantly increased numbers at the first week, second week, and third year following implantation.

Rejection

Data on rejection were collected on all patients and graded according to the International Society for Heart and Lung Transplantation working formulation for HTx: grade 0, no rejection or equivocal rejection; grade 1, mild rejection; grade 2, focal moderate rejection; grade 3, multifocal or diffuse moderate rejection; and grade 4, severe rejection. In our patients, 196 (40.75%) achieved grade 0 rejection, 169 (35.14%) scored grade 1 rejection, 82 (17.04%) scored grade 2 rejection, 34 (7.07%) had grade 3 rejection, and 0 (0%) scored grade 4 rejection.

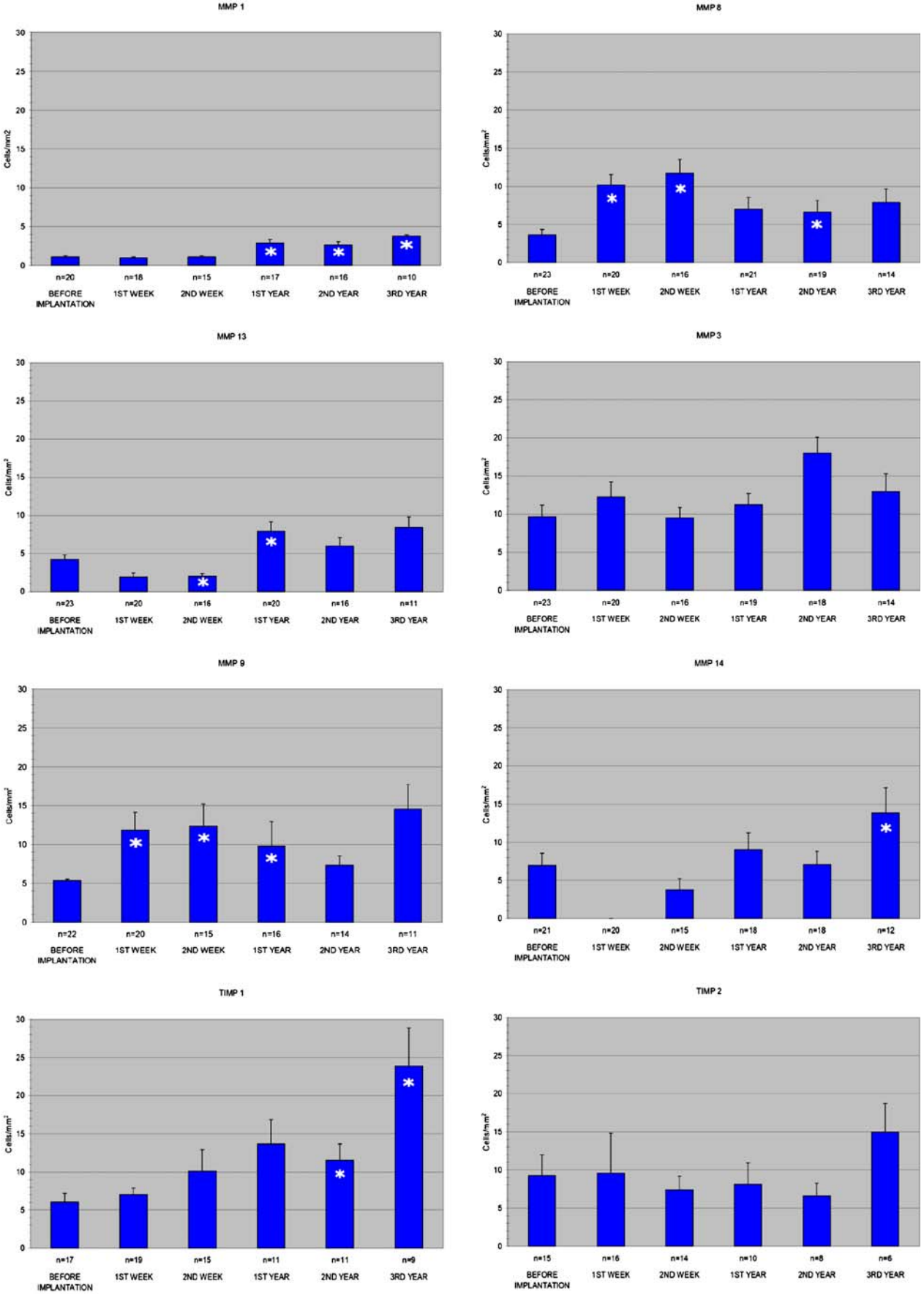

Fig. 3 Quantitative results: interstitial cells per area expressing MMP-1, MMP-8, MMP-13, MMP-3, MMP-9, MMP-14, and TIMP-1 and TIMP2. Mean±SEM, * indicates $p<0.05$ (significant differences compared with values before implantation)

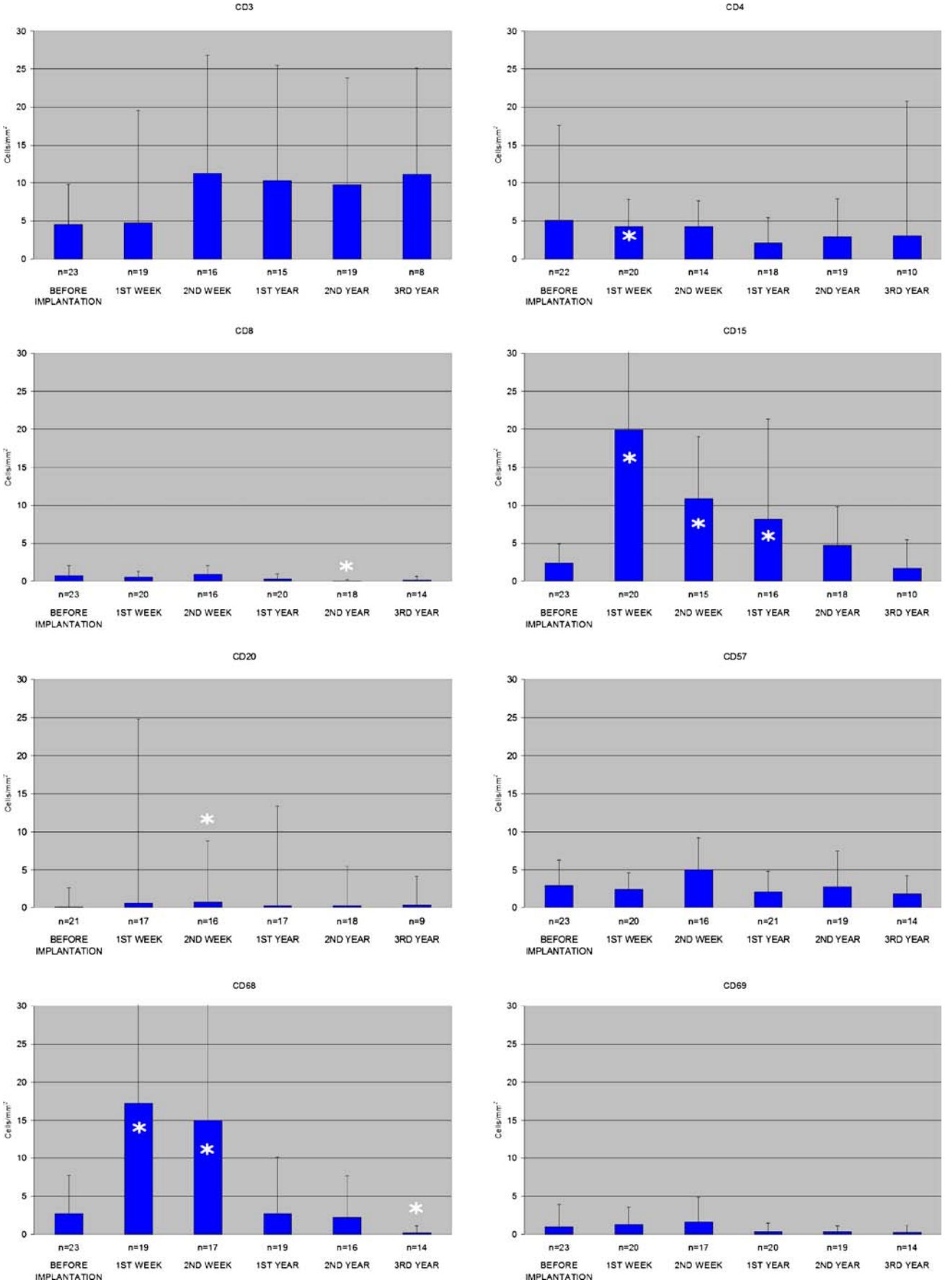

Fig. 4 Quantitative results: interstitial cells per area expressing CD3, CD4, CD8, CD15, CD20, CD57, CD68, and CD69. Mean±SEM, * indicates $p<0.05$ (significant differences compared with values before implantation)

Discussion

This study was designed to explore changes of the ECM components and the MMPs and TIMPs involved in the process of remodeling over a time period of 3 years following HTx, using the sequential biopsies of the same cohort of 28 patients over this time period. Only a few groups have looked at the ECM components and the enzymes involved in the structuring of the ECM after human HTx [7, 23]. To date, we are aware of no studies which have focused on a single cohort over such an extended time period.

The current study indicates increased expression in protein level of several MMPs, including MMP-1 and MMP-9, following HTx. Several studies have investigated changes at the level of ECM components, MMPs, and TIMPs occurring in dilated cardiomyopathy and congestive heart failure [10, 11, 20]. Differences in expression of these components are reported in different disease states [10, 11]. Increased MMP activity has been found within the left ventricle following the development of end-stage chronic heart failure [10, 11]. MMP-1 expression increased in ischemic and dilated cardiomyopathy but decreased in hypertrophic cardiomyopathy. MMP-9 expression increased in ischemic cardiomyopathy but decreased in dilated or hypertrophied cardiomyopathy [42].

We found a significant increase in MMP-13 from before implantation to 2 weeks and 1 year after human HTx. MMP-8 increased significantly in the first 2 weeks, whereas MT-MMP1 increased significantly from before implantation to 3 years after (Fig. 3). These findings are similar to those of a study looking at rodent hearts during induced ischemia, where an increase in MMP-13 predominated in the early postischemic period, while MMP-8 and MMP-14 (MT-MMP1) increased during late remodeling [27].

The observation that all MMP and TIMP species are not uniformly increased in patients with different forms of heart failure suggests that specific patterns of MMPs and TIMPs are expressed in the failing myocardium, depending on the type of stress undergone by the myocardium. The particular pattern observed in the current study may reflect the specific stresses which affect the transplanted heart and induce remodeling therein. We found increases in MMP-1, MMP-8, MMP-9, and MMP-13, a pattern similar to that seen previously specifically related to ischemia [27, 42].

Our study finds significant decreases in the perimysial amounts of laminin and fibronectin at 2 and 3 years posttransplantation [32]. Acute heart rejection has been associated with an early increase in the intermyocyte and endothelial deposition of laminin and fibronectin at the graft site, with their peak at 6 h after transplantation [7, 23].

Fibronectin has been thought of as a signal for graft-infiltrating cells and may play a key role in rejection [7, 23]. Macrophages have been found to likely be the primary source of fibronectin found in allograft rejection, although it has also been noted that a significant portion of fibronectin found in allografts comes from extravasation of plasma fibronectin [8, 9]. Of the cell markers we analyzed, it is known that CD68 and CD69, as well as CD4, are found on macrophages. We found a significant decrease in the number of CD68+ cells at 3 years posttransplantation and a significant decrease in fibronectin expression at 3 years, which may be related. While statistical significance was not reached, one can appreciate a trend toward similarity in the patterns seen on the respective charts (Figs. 3 and 4) of fibronectin, CD68, and CD69.

None of our patients experienced high-grade rejection. The expression of CD69 in peripheral blood lymphocytes has been directly correlated with the presence of rejection of HTx grafts [31]. In our study, CD69+ cell numbers did not change significantly throughout the study period.

At this point, it might also be helpful to briefly discuss the grade of rejection found on our patients and its relation to our data. Of all patient diagnostic samples, approximately 41% showed grade 0 rejection, 35% grade 1, 17% grade 2, 7% grade 3, and 0% grade 4 rejection. As a rejection grade of less than 3 does not normally prompt clinical intervention, our data are likely more representative of "healthier" postcardiac transplant patients.

Cluster differentiation 15+ cells showed significant increase in the first week following transplantation, subsequently decreasing in number to insignificance by the second year. There is little current literature regarding the role of CD15+ cells such as myelomonocytes in posttransplantation hearts. While none of our patients exhibited high-grade rejection, some did show evidence of lower-grade rejection, and the majority of these occurred within he first year. This might suggest a role of myelomonocytes in early low-grade rejection. Further investigation is warranted.

While significance was reached in decreases of numbers of CD4+ and CD8+ cells at 1 week and 2 years, respectively, their total numbers are low, and it is difficult to draw conclusions with respect to these changes.

These ECM components should be looked at as important and active participants in host immune responses leading to graft rejection. The majority of rejection episodes occur within the first 6 months after HTx [45]. Interstitial fibrosis has been found to rise within the first 2 months after heart transplant, with little additional change over the subsequent 5–6 years [2]. Our patients' follow-up over this time period of 3 years showed no severe complications, and this might be a good indicator for their favorable recovery.

All our patients have been transplanted very recently, and they all received angiotensin-converting enzyme (ACE) inhibitors, which may forestall remodeling and reduce fibrosis in the infarcted ventricle [22, 47]. This may have affected the patterns of ECM component expression found here, which may differ from the natural history of posttransplant myocardium.

Tissue inhibitors of MPs inhibit MMPs in a 1:1 stoichiometric manner [34], but this ratio has been found to be altered in situations of pathologic remodeling. We found that over the time period of 3 years following transplantation, the expression of the majority of MMPs and TIMP-1 increased, but the expression of TIMP-2 showed no significant changes. Other studies have discovered similar

trends in different pathological situations. Several studies found that MMP to TIMP ratios significantly increased in abdominal aortic aneurysms, Sjogren's syndrome, and chronic lung disease [3, 13, 37, 38]. One study found an up-regulation in MMP-9 and a down-regulation in TIMP-1 and TIMP-3, but no change in TIMP-2, in failing human hearts [20]. They noted that TIMP-1 responded to alterations in the ECM, whereas TIMP-2 provides a stable level of anti-MMP activity in tissue. Cardiac tissue of patients with ischemic cardiomyopathy similarly displayed no change in TIMP-2 [39, 40].

We found no significant change for TIMP-2, and only a significant increase from before implantation to 3 years for MMP-14 (Fig. 3). It is being said that TIMP-1 potentially inhibits the activity of most MMPs, with the exception of MMP-14 and MMP-2. TIMP-2 is thought to be a potential inhibitor of all MMPs except MMP-9 [34]. It has been discovered that pro-MMP-2 was gradually enhanced in mammalian fibrosarcoma cells by adding a small amount of exogenous TIMP-2 in a dose-dependent manner, but it was inhibited when an increased amount of TIMP-2 was added [25, 35]. MT-MMP has been shown to activate MMP-2/TIMP-2 complexes [35].

In our study, we found an increase in MMP-9 expression from before implantation to the first 2 weeks and the first year. Collagen IV decreased significantly in the first year (Fig. 2). Similarly, MMP-9, also called type-IV collagenase, showed a reverse correlation between its expression and the expression of type-IV collagen in gastric carcinomas [16]. There has been a reported robust increase in MMP zymographic activity in the failing human myocardium that was accompanied by a reduction in fibrillar collagen cross-link formation [14, 34]. Our study discovered similar trends, although immunohistochemistry was used rather than zymography. A similar increase in MMP has been found in early postinfarcted hearts, the early up-regulation of MMP activity after infarction thought to be strongly suggestive of involvement of MMPs in the repair process of the heart [34]. MMP-1, MMP-9, and to a lesser extent, MMP-3, may play an important role in the remodeling of the basement membrane and the ECM [34]. In nonhealing chronic and healing acute wound tissues, there have been reports of similar MMP-9 (gelatinase B) activity, contradicting former hypotheses that chronic ulcers are caused by excessive MMP-9 activity [24].

We found no significant change in the expression of MMP-3 over a 3-year time period (Fig. 3). MMP-3 has been found to be an activator of several precursors of MMPs such as pro-MMP-1, pro-MMP-3, and pro-MMP-9 [10, 26, 41]. MMPs are considered to be involved in the degradation of matrix components but also modulate collagen synthesis. This might be why some groups report an abundance in MMPs accompanied with increased fibrosis, such as those seen in failing hearts, and decreased MMP activity leading to reduced fibrosis [17, 21, 27]. Others have found that an increase in MMP activity and expression were concurrent with a reduction in total myocardial collagen content [14, 29, 33].

Finally, in our study, the volume density of connective tissue fibers increased over 2 weeks following transplantation and then decreased significantly at 1, 2, and 3 years after transplantation (Fig. 2). This initial increase has been marveled at before, as well as in other disease states such as renal failure and conduction system changes following HTx, and in the case of HTx, has been thought to be due to perioperative ischemia and reperfusion injury [1, 5, 19, 28]. Collagens I, III, and IV, and laminin and fibronectin, decreased significantly from before implantation to the second and third year (Fig. 2). MMP-1, MMP-8, MMP-13, MMP-9, MMP-14 (MT-MMP1), and TIMP-1 increased in the years following HTx, while MMP-3 and TIMP-2 showed no significant changes. Interestingly, in our data, while the total volume density of connective tissue fibers approximately doubles at 2 weeks when compared to preimplantation, the sum of the changes seen in individual components during this time period does not seem grossly proportional. This would suggest that other ECM components which we do not measure are contributing to the total connective tissue volume density increase. Further investigation with respect to the components involved during this time period may be warranted.

Our findings may reflect a pattern of remodeling similar to that observed in other scenarios after cardiac stress. It is thought that in the setting of congestive heart failure, initial remodeling following such stress probably represents a beneficial compensatory response, but that prolonged continued remodeling may be detrimental [7, 19, 22, 28, 34]. The decrease in structural ECM constituents observed here may reflect a decrease in the remodeling process over time, perhaps partly due to ACE inhibitor therapy. Further investigation into the factors contributing to this process of reverse remodeling may prove beneficial in increasing the survival of these posttransplant patients and in improving the outcome in patients with heart failure.

End note

Some limitations in this study should be recognized. Due to the large number of variables considered, the statistical power is decreased. This is, to our knowledge, the first study to follow a single cohort of posttransplantation patients for a long time period, and the goal of the study was to help delineate post-HTx ECM component changes over this time period. Further similar studies, perhaps utilizing zymography, mRNA quantification, etc., should be performed to help define more clearly the patterns of ECM component expression in such patients. Another limitation, difficult to eliminate in such studies, is the presence of medications such as ACE inhibitors, which are known to affect the remodeling process.

It should also be noted that the goal of this study was to provide general data regarding the changes in these ECM components over a long time period in postcardiac-transplantation patients and not necessarily to correlate these changes with the pathologic states (i.e., degree of rejection

or pretransplantation pathology) of the patients' hearts at the times of data collection. The comparisons provided in the Discussion with different disease states are meant as stimuli for further investigation rather than to suggest actual correlation with respect to our data.

Acknowledgements The authors thank Ms. G. Gorsberg for her excellent technical assistance, Ms. U. Horr for her help with the preparation of the photographs, and Dr. P.J. Dahlheimer for his assistance with computer issues. Funding: Forschungsfoerderungsprogramm der medizinischen fakultaet Heidelberg, projektnr. 150/2001

To the best of our knowledge, this study, at the time of its execution, was performed in compliance with the laws of Germany.

References

1. Amann K, Kronenberg G, Gehlen F, Wessels S, Orth S, Muenter K, Ehmke H, Mall G, Ritz E (1998) Cardiac remodelling in experimental renal failure—an immunohistochemical study. Nephrol Dial Transplant 13:1958–1966
2. Armstrong AT, Binkley PF, Baker PB, Myerowitz PD, Leier CV (1998) Quantitative investigation of cardiomyocyte hypertrophy and myocardial fibrosis over 6 years after cardiac transplantation. J Am Coll Cardiol 32:704–710
3. Asatsuma M, Ito S, Watanabe M, Takeishi H, Nomura S, Wada Y, Nakano M, Gejyo F, Igarashi A (2004) Increase in the ratio of matrix metalloproteinase-9 to tissue inhibitor of metalloproteinase-1 in saliva from patients with primary Sjogren's syndrome. Clin Chim Acta 345:99–104
4. Bosman FT, Stamenkovic I (2004) Functional structure and composition of the extracellular matrix. J Pathol 200:423–428
5. Calzolari V, Angelini A, Basso C, Livi U, Rossi L, Thiene G (1999) Histologic findings in the conduction system after cardiac transplantation and correlation with electrocardiographic findings. Am J Cardiol 84:756–759
6. Cleutjens JPM, Verluyten MJA, Smits JFM, Daemen MJAP (1995) Collagen remodeling after myocardial infarction in the rat heart. Am J Pathol 147:325–338
7. Coito AJ, Binder J, de Sousa M, Kupiec-Weglinski JW (1994) The expression of extracellular matrix proteins during accelerated rejection of cardiac allografts in sensitized rats. Transplantation 57:599–605
8. Coito AJ, Binder J, Brown LF, de Sousa M, Van de Water L, Kupiec-Weglinski JW (1995) Anti-TNF-alpha treatment downregulates the expression of fibronectin and decreases cellular infiltration of cardiac allografts in rats. J Immunol 154(6): 2949–2958
9. Coito AJ, Kupiec-Weglinski JW (2000) Extracellular matrix proteins in organ transplantation. Transplantation 69:2465–2473
10. Coker ML, Thomas CV, Clair MJ, Hendrick JW, Krombach RS, Galis ZS, Spinale FG (1998) Myocardial matrix metalloproteinase activity and abundance with congestive heart failure. Am J Physiol 274:H1516–H1523
11. Coker ML, Doscher MA, Thomas CV, Galis ZS, Spinale FG (1999) Matrix metalloproteinase synthesis and expression in isolated LV myocyte preparations. Am J Physiol 277:H777–H787
12. Edep ME, Shirani J, Wolf P, Brown DL (2000) Matrix metalloproteinase expression in nonrheumatic aortic stenosis. Cardiovasc Pathol 9:281–286
13. Ekekezie II, Thibeault DW, Simon SD, Norberg M, Merrill JD, Ballard RA, Ballard PL, Truog WE (2004) Low levels of tissue inhibitors of metalloproteinases with a high matrix metalloproteinase-9/tissue inhibitor of metalloproteinase 1 ratio are present in tracheal aspirate fluid of infants who develop chronic lung disease. Pediatrics 113(6):1709–1714
14. Gunja-Smith Z, Morales AR, Romanelli R, Woessner JF Jr (1996) Remodeling of human myocardial collagen in idiopathic dilated cardiomyopathy. Am J Pathol 148:1639–1648
15. Herpel E, Singer S, Flechtenmacher C, Pritsch M, Sack FU, Hagl S, Katus HA, Haass M, Otto HF, Schnabel PA (2005) Extracellular matrix proteins and matrix metalloproteinases differ between various right and left ventricular sites in end-stage cardiomyopathies. Virchows Arch 446:369–378
16. Kabashima A, Yao T, Sugimachi K, Tsuneyoshi M (2002) Relationship between biologic behavior and phenotypic expression in intramucosal gastric carcinomas. Human Pathol 33:80–86
17. Kim HE, Dalal SS, Young E, Legato MJ, Weisfeldt ML, D'Armiento J (2000) Disruption of the myocardial extracellular matrix leads to cardiac dysfunction. J Clin Invest 106:857–866
18. Kinoshita T, Sato H, Okada A, Ohuchi E, Imai K, Okada Y, Seiki M (1998) TIMP-2 promotes activation of progelatinase A by membrane-type 1 matrix metalloproteinase immobilized on agarose beads. J Biol Chem 273:16098–16103
19. Lee RT, Libby P (2000) Matrix metalloproteinases: not-so-innocent bystanders in heart failure. J Clin Invest Med 106: 827–828
20. Li YY, Feldman AM, Sun Y, McTiernan CF (1998) Differential expression of tissue inhibitors of metalloproteinases in the failing human heart. Circulation 98:1728–1734
21. Li YY, Feng YQ, Kadokami T, McTiernan CF, Draviam R, Watkins SC, Feldman AM (2000) Myocardial extracellular matrix remodeling in transgenic mice overexpressing tumor necrosis factor alpha can be modulated by anti-tumor necrosis factor alpha therapy. Proc Natl Acad Sci U S A 97:12746–12751
22. Libby P, Lee RT (2000) Matrix matters. Circulation 102:1874–1876
23. Maggard MA, Ke B, Wang T, Kaldas F, Seu P, Busuttil RW, Imagawa DK (1998) Effects of pravastatin on chronic rejection of rat cardiac allografts. Transplantation 65:149–155
24. Mirastschijski U, Impola U, Jahkola T, Karlsmark T, Agren MS, Saarialho-Kere U (2002) Ectopic localization of matrix metalloproteinase-9 in chronic cutaneous wounds. Human Pathol 33:355–364
25. Nagase H (1997) Activation mechanisms of matrix metalloproteinases. J Biol Chem 378:151–160
26. Ogata Y, Enghild JJ, Nagase H (1992) Matrix metalloproteinase 3 (stromelysin) activates the precursor for the human matrix metalloproteinase 9. J Biol Chem 267:3581–3584
27. Peterson JT, Li H, Dillon L, Bryant JW (2000) Evolution of matrix metalloprotease and tissue inhibitor expression during heart failure progression in the infarcted rat. Cardiovasc Res 46:307–315
28. Pickering JG, Boughner DR (1990) Fibrosis in the transplanted heart and its relation to donor ischemic time: assessment with polarized light microscopy and digital image analysis. Circulation 81:949–958
29. Rohde LE, Ducharme A, Arroyo LH, Aikawa M, Sukhova GH, Lopez-Anaya A, McClure KF, Mitchell PG, Libby P, Lee RT (1999) Matrix metalloproteinase inhibition attenuates early left ventricular enlargement after experimental myocardial infarction in mice. Circulation 99:3063–3070
30. Ross RS, Borg TK (2001) Integrins and the myocardium. Circ Res 88:1112–1119
31. Schowengerdt KO, Fricker FJ, Bahjat KS, Kuntz ST (2000) Increased expression of the lymphocyte early activation marker CD69 in peripheral blood correlates with histologic evidence of cardiac allograft rejection. Transplantation 69:2102–2107
32. Schupp DJ, Sykora J, Flechtenmacher CH, Huck BP, Koch A, Sack F-U, Haass M, Brockmeier K, Ulmer HE, Hagel S, Otto HF, Schnabel PA (2002) Right ventricular expression of laminin, fibronectin and collagens I, III, and IV over a period of 3 years after heart transplantation. Pathologica 94:71

33. Spinale FG, Coker ML, Thomas CV, Walker JD, Mukherjee R, Hebbar L (1998) Time-dependent changes in matrix metalloproteinase activity and expression during the progression of congestive heart failure: relation to ventricular and myocyte function. Circ Res 82:482–495
34. Spinale FG (2002) Matrix metalloproteinases-regulation and dysregulation in the failing heart. Circ Res 90:520–530
35. Strongin AY, Collier I, Bannikov G, Marmer BL, Grant GA, Goldberg GI (1995) Mechanism of cell surface activation of 72-kDa type IV collagenase. Isolation of the activated form of the membrane metalloprotease. Biol Chem 270:5331–5338
36. Suzuki J, Isobe M, Kawauchi M, Endoh M, Amano J, Takamoto S (2000) Altered expression of matrix metalloproteinases and tissue inhibitors of metalloproteinases in acutely rejected myocardium and coronary arteriosclerosis in cardiac allografts of nonhuman primates. Transpl Int 13:106–113
37. Sweet DG, Curley AE, Chesshyre E, Pizzotti J, Wilbourn MS, Halliday HL, Warner JA (2004) The role of matrix metalloproteinase -9 and -2 in development of neonatal chronic lung disease. Acta Paediatr 93:791–796
38. Tamarina NA, McMillan WD, Shively VP, Pearce WH (1997) Expression of matrix metalloproteinases and their inhibitors in aneurysms and normal aorta. Surgery 122:264–272
39. Thomas CV, Coker ML, Zellner JL, Handy JR, Crumbley AF, Spinale FG (1998) Increased matrix metalloproteinase activity and selective upregulation in LV myocardium from patients with end-stage dilated cardiomyopathy. Circulation 97:1708–1715
40. Tyagi SC, Campbell SE, Reddy HK, Tjahja E, Voelker DJ (1996) Matrix metalloproteinase activity expression in infarcted, noninfarcted and dilated cardiomyopathic human hearts. Mol Cell Biochem 155:13–21
41. Tyagi SC, Kumar SG, Haas SJ, Reddy HK, Voelker DJ, Hayden MR, Demmy TL, Schmaltz RA, Curtis JJ (1996) Post-transcriptional regulation of extracellular matrix metalloproteinases in human heart end-stage failure secondary to ischemic cardiomyopathy. J Mol Cell Cardiol 28:1415–1428
42. Tyagi SC (1998) Extracellular matrix dynamics in heart failure: a prospect for gene therapy. J Cell Biochem 68:403–410
43. Weibel ER (1979) Stereological methods, vol 1. Practical methods for biological morphometry. Academic, London
44. Weibel ER (1980) Stereological methods, vol 2. Theoretical foundations. Academic, London
45. Winters GL, Loh E, Schoen FJ (1995) Natural history of focal moderate cardiac allograft rejection. Circulation 91:1975–1980
46. Woessner JF (1991) Matrix metalloproteinases and their inhibitors in connective tissue remodeling. FASEB J 5:2145–2154
47. Yokoseki O, Yazuki Y, Suzuki J, Imamura H, Takenaka H, Isobe M (2000) Association of matrix metalloproteinase expression and left ventricular function in idiopathic dilated cardiomyopathy. Circ J 64:352–357

Virchows Arch (2006) 448: 195–199
DOI 10.1007/s00428-005-0053-9

ORIGINAL ARTICLE

Masanori Hisaoka · Hiroshi Hashimoto

Elastofibroma: clonal fibrous proliferation with predominant CD34-positive cells

Received: 20 June 2005 / Accepted: 22 July 2005 / Published online: 17 August 2005

Abstract Elastofibroma is a rare fibrous lesion that most commonly occurs in periscapular soft tissues and is characterized by accumulated abnormal elastic fibers. Although the lesion is generally regarded as a reactive process, an unusual fibroblastic pseudotumor, or as a fibroelastic tumor-like lesion, its etiology remains largely unknown. Recent cytogenetic demonstrations of chromosomal instability and some recurrent or clonal chromosomal changes have raised the possibility that the lesion represents a neoplastic process. We analyzed 14 cases of elastofibroma to further explore, morphologically and genetically, the characteristics of its cellular composition. The interspersed spindle or stellate cells showed a fibroblast-like appearance and were almost consistently positive for vimentin and frequently positive for CD34 and lysozyme immunohistochemically. No spindle cells of myofibroblastic phenotype were recognized. To assess the clonality of the lesions in female patients, the X-linked polymorphic human androgen receptor gene assay was performed using formalin-fixed, paraffin-embedded tissues. A nonrandom inactivation of the androgen receptor gene was detected in two informative cases. Thus, these findings suggest that CD34-positive mesenchymal cells are an integral component of elastofibroma, which represents a clonal fibrous proliferation.

Keywords Soft tissue · Immunohistochemistry · Electron microscopy · Molecular genetics

M. Hisaoka (✉) · H. Hashimoto
Department of Pathology and Oncology,
School of Medicine, University of Occupational
and Environmental Health,
1-1 Iseigaoka, Yahatanishi-ku,
Kitakyushu 807-8555, Japan
e-mail: hisaoka@med.uoeh-u.ac.jp
Tel.: +81-93-6917425
Fax: +81-93-6920189

Introduction

Elastofibroma is a benign fibrous proliferation that is characterized by its almost exclusive occurrence in the periscapular region of middle-aged or older individuals and, morphologically, by an admixture of excessive collagen and abnormal elastic fibers displaying a beaded or globular appearance. Although the lesion is generally assumed to be a fibrous pseudotumor or a reactive or degenerative process possibly due to repeated minor trauma or physical irritation [20], the true etiology or pathogenetic mechanism of elastofibroma still remains unknown. Interestingly, a genetic susceptibility to this lesion has been suggested by the facts that approximately one third of patients with the lesions in Okinawa had a family history of elastofibroma and that four members of a family had been recorded to have bilateral subscapular elastofibromas [10, 14].

Recently, Vanni et al. [19] reported the cytogenetic findings of three elastofibromas, in which they described chromosome instability as shown by various nonclonal structural changes frequently involving the short arm of chromosome 1. Subsequently, two other groups independently described clonal chromosomal aberrations, in addition to chromosome instability, and suggested a possible neoplastic origin for elastofibroma [2, 8]. In contrast to its peculiar extracellular matrix, the cellular composition of the lesion has, however, attracted little attention and has not been fully characterized. The interspersed spindle cells have been considered to be fibroblastic or myofibroblastic based largely on electron microscopic features [7, 13, 20].

To address these issues, we investigated the cellular composition of elastofibroma using a wide array of antibodies and assessed its clonality by analyzing X-chromosome inactivation as indicated by the methylation status of the X-chromosome-linked human androgen receptor gene.

Materials and methods

Fourteen cases of elastofibroma dorsi were selected from the files of the Department of Pathology and Oncology,

School of Medicine, University of Occupational and Environmental Health (Kitakyushu, Japan). The patients were seven women and seven men, with ages ranging from 45 to 79 years (mean 62.9 years). The lesions ranged in size from 3 to 11 cm (mean 6 cm). Periscapular soft tissues were obtained from four age-matched autopsy cases as controls.

Tissues were fixed in 10% formalin and embedded in paraffin. Deparaffinized 4-μm-thick sections of tissues were used for histological and immunohistochemical evaluations. In addition to hematoxylin–eosin and elastica van Gieson stains, immunohistochemical staining was performed using the following primary antibodies, with or without an appropriate antigen retrieval, and was accomplished with a labeled polymeric secondary antibody (the EnVision system; DAKO Cytomation, Kyoto, Japan), anti-vimentin (V9, 1:30; DAKO Cytomation), anti-CD34 (QBEnd-10, 1:100; Immunotech, Marseilles, France), anti-CD1a (O10, prediluted; Immunotech), anti-α-smooth muscle actin (1A4, 1:150; DAKO Cytomation), anti-muscle-specific actin (HHF35, 1:50; Enzo Diagnostics, New York, NY, USA), anti-desmin (D33, 1:100; DAKO Cytomation), anti-calponin (CALP, 1:50; DAKO Cytomation), anti-factor XIIIa (polyclonal, 1:500; Calbiochem, San Diego, CA, USA), anti-CD68 (KP-1, 1:100; DAKO Cytomation), anti-CD10 (56C6, 1:10; Novocastra, Newcastle upon Tyne, UK), anti-CD45RO (UCHL-1, 1:200; DAKO Cytomation), anti-S-100 protein (polyclonal, 1:500; DAKO Cytomation), anti-tropoelastin (polyclonal, 1:100; Elastin Product, Owensville, MO, USA), and anti-lysozyme (polyclonal, 1:500; DAKO Cytomation). In two cases, small pieces of the tissues were fixed in 4% formaldehyde and 1% glutaraldehyde, postfixed in 2% osmium tetroxide, and processed for transmission electron microscopy.

Genomic deoxyribonucleic acid (DNA) was extracted from the formalin-fixed, paraffin-embedded tissues of seven female patients and two female controls (one periscapular soft tissue and one myxoid liposarcoma) after overnight protein digestion by proteinase K (200 μg/ml) in a lysis buffer [20 mmol/l Tris–HCl, pH 8.0, 20 mmol/l ethylenediaminetetraacetic acid (EDTA), and 2% sodium dodecyl sulfate] at 55°C. The quality of the extracted DNA was assessed by polymerase chain reaction (PCR) using two sets of primers flanking 249- and 312-bp sequences of the β-*actin* gene. The primer sequences were as follows: forward (consensus) primer gtaaagcggccttggagtg and reverse primers ccagaggcgtacagggatag and ctcgtagatgggca cagtg. The cycling conditions were as follows: holding at 95°C for 9 min; 40 cycles of 95°C for 20 s, 57°C for 20 s, 72°C for 30 s; and holding at 72°C for 10 min. The crude DNA extract that was positive for β-*actin* gene in both PCRs was purified twice by extraction with phenol–chloroform–isoamyl alcohol (25:24:1, pH 6.7) and by eth-

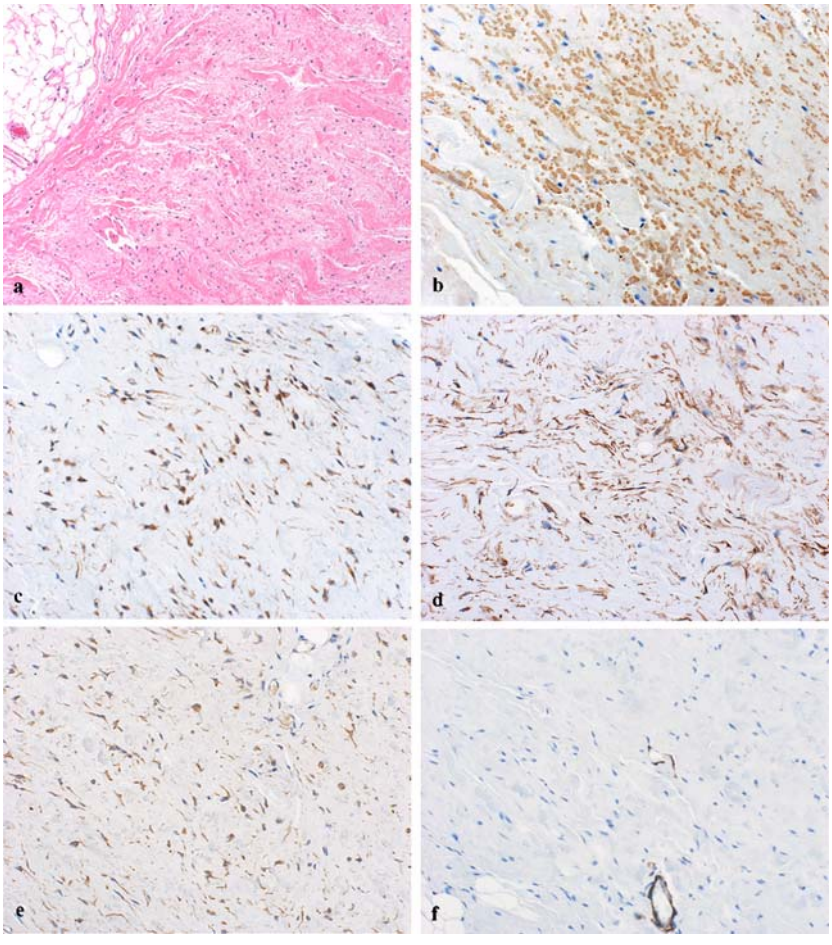

Fig. 1 Microscopic (**a**) and immunohistochemical (**b**–**f**) features of elastofibroma. Spindle or stellate cells are interspersed in an abundant fibrocollagenous stroma (**a**), in which numerous thick, globular, or beaded elastic fibers are present (tropoelastin) (**b**). Vimentin (**c**), CD34 (**d**), and lysozyme (**e**) are expressed in many spindle or stellate cells. They are negative for α-smooth muscle actin (**f**)

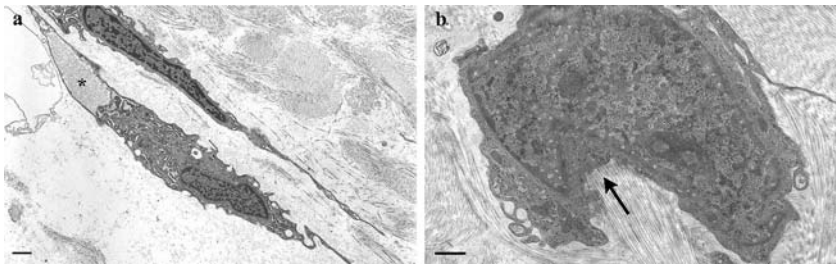

Fig. 2 Ultrastructural appearance of the spindle cells in elastofibroma. **a** The spindle cells have well-developed rough endoplasmic reticula and elongated cytoplasmic processes encircling the extracellular dense granular substance (*asterisk*; bar=1 μm). **b** The mesenchymal cells are often embedded in an abundant collagenous matrix. Collagen fibrils sometimes sprout from the cytoplasm (*arrow*; bar=1 μm)

anol precipitation. The precipitated DNA was recovered with TE buffer (10 mmol/l Tris–HCl and 1 mmol/l EDTA, pH 8.0) and further purified using a QIAquick spin column (Qiagen, Tokyo, Japan). Between 100 and 250 ng of DNA was incubated with 50 U of *Hha*I (Toyobo, Osaka, Japan), which cleaves the nonmethylated GCGC restriction site, overnight at 37°C. One microliter of DNA solution, with or without restriction enzyme digestion, was used as a template for PCR in the human androgen receptor gene assay (HUMARA). The primer sequences and cycling conditions of the PCR were described previously [3]. PCR products were size-fractionated by electrophoresis on polyacrylamide gels and visualized by silver staining. Images of the electrophoresis were scanned, and allele intensities were measured by densitometry.

Results

The lesions contained sparsely distributed spindle or stellate cells embedded in an abundant fibrocollagenous matrix with many thick, globular, or beaded elastic fibers, which were highlighted with elastica van Gieson staining and immunohistochemistry for tropoelastin (Fig. 1a,b). The abnormal elastic fibers were absent in periscapular soft tissues of controls. The spindle or stellate cells in elastofibroma were invariably positive for vimentin immunohistochemically (Fig. 1c). Besides, a large number (>50%) of them expressed CD34 in all the cases examined (Fig. 1d). The CD34-positive cells often had elongated or slender cytoplasms and were unevenly but randomly distributed throughout the lesion. Many lysozyme-positive spindle or stellate cells were also identified in all but two cases (Fig. 1e), in which the antigen was expressed in only less than 1% of the cells. A minor fraction (less than 5%) of the cells was positive for CD68 and/or factor XIIIa and showed relatively small, rounded, or stellate morphology, suggesting histiocytic cells. The other markers, including actin, calponin, and desmin, were consistently negative in elastofibroma cells (Fig. 1f). Vimentin- or CD34-positive spindle cells were also identified in periscapular fibroadipose tissues of controls, although most of them lacked the expression of lysozyme.

Ultrastructurally, the spindle or stellate cells scattered among the collagen bundles and large masses of dense granular or filamentous materials corresponding to abnormal elastic fibers often possessed irregularly indented nuclei, elongated cytoplasmic processes, well-developed or variably dilated rough endoplasmic reticula, rounded or fusiform mitochondria, and numerous intracytoplasmic filaments of the predominant intermediate type. The elongated cytoplasmic processes frequently encircled the extracellular granular material or were aligned parallel to the collagen bundles (Fig. 2a). Collagen fibrils occasionally sprouted from the cytoplasm or cell surfaces, reminiscent of collagen secretion (Fig. 2b). Many pinocytotic vesicles or lysosomes were seen in some of the spindle or stellate cells. Myofibroblastic cells with intracytoplasmic parallel filaments showing focal densities or subplasmalemmal attachment plaques or fibronexus were absent.

The extracted DNAs of four female patients were proven by PCR to be informative for β-*actin* gene and were subjected to HUMARA. In two cases with two distinct alleles loaded on the gel before *Hha*I digestion, the signal intensity of one allele was significantly reduced after enzymatic digestion (the ratios of peaks before and after *Hha*I digestion were 1.9 and 2.1, respectively), indicating the presence of a substantial population with a nonrandom inactivation of the gene (Fig. 3). The other two cases

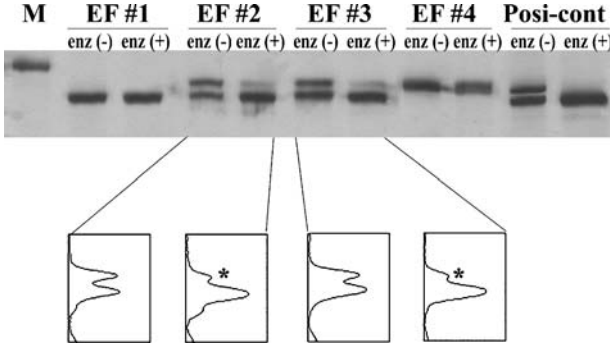

Fig. 3 HUMARA of elastofibromas (*EF1–4*) (posi-cont, myxoid liposarcoma). A significantly reduced intensity of one (*asterisk*) of the alleles after *Hha*I digestion is detectable in two elastofibromas (*EF2 and 3*)

showed a single allele before *Hha*I digestion and were considered uninformative.

Discussion

Despite the well-defined clinicopathological features, elastofibroma is an enigmatic entity of uncertain etiology. Its true nature and pathogenetic mechanism are still controversial. In contrast to the peculiar morphology of the abnormal elastic fibers, the interspersed spindle or stellate cells of the lesion have been poorly focused on probably because of their inconspicuous appearance.

Based primarily on ultrastructural features, the cells of elastofibroma are generally considered to be fibroblastic or myofibroblastic [7, 13, 20]. Abundant rough endoplasmic reticula, intracytoplasmic microfilaments, and pinocytotic vesicles have been described in elastofibroma cells, and such findings were also obtained from our electron microscopic observations. In addition to these features, Ramos et al. [13] reported a case of elastofibroma with cells attached ultrastructurally by a tight junction and suggested that it was a pseudotumor of myofibroblasts. However, essential morphological features of myofibroblasts, including bundles of microfilaments with focal densities (stress fibers) and cell-to-stroma attachment sites (fibronexus), have not been documented previously and were lacking in the two cases examined [15]. Moreover, consistently negative immunohistochemical reactivity to muscle actin, desmin, or calponin in our cases or those examined by Kayaselcuk et al. [6] could not support the view that elastofibroma is a myofibroblastic lesion.

It is noteworthy that the predominant cellular components of our elastofibromas are CD34-positive mesenchymal cells and that this finding has not been described previously in the English literature. CD34 is expressed in dendritic or fibroblast-like mesenchymal cells that almost ubiquitously distribute in the dermis and fibrocollagenous soft tissues, as well as in a wide variety of pathological conditions. Such CD34-positive mesenchymal cells are considered to act as potential "reserve" cells that are capable of endothelial, myoid, and adipocytic differentiation or myxoid or collagenous morphology [17]. Although biologic functions of CD34 expressed in the dendritic or fibroblast-like mesenchymal cells still remain unclear, CD34-mediated signal pathways or cell–matrix interactions may be involved in the pathogenesis of elastofibroma. Because of the lack of coexpression of CD1a, CD10, or CD45RO in the CD34-positive cells, it is difficult to further classify them into distinct subgroups of CD34-positive mesenchymal cells, such as peripheral blood fibrocytes and periadnexal fibroblasts (periglandular stromal cells) [1, 21].

Contrary to the observation by Kahn and Hanna [5], lysozymes—a group of 1,4-*N*-acetylmuramidases that break down bacterial proteoglycans by hydrolyzing cleavage—were frequently expressed in the spindle or stellate cells of the current elastofibromas. Although lysozymes are distributed in a wide variety of cells, including granulocytes, macrophages, and serous glands [12], fibroblastic or myofibroblastic mesenchymal cells usually lack their immunohistochemical expression, except for those isolated from human palatine tonsils [4]. Lysozymes have been detected in the abnormal elastic fibers of the skin associated with solar elastosis, aging, and pseudoxanthoma elasticum, as well as those in pulmonary emphysema, suggesting their pathogenetic role in degenerated or damaged elastic fibers [16, 18]. The aberrant expression of lysozymes in elastofibroma cells may be related to the production of abnormal or degenerated elastic fibers. Biologic properties of lysozymes expressed by elastofibroma cells should be further examined to address this point.

Another striking result of our study is that the nonrandom inactivation of X-linked androgen receptor gene was identified in two elastofibromas. This finding is in accordance with the clonal chromosomal aberrations in elastofibromas reported by Batstone et al. [2] and McComb et al. [8], who suggested that elastofibroma may represent a true neoplasm rather than a reactive process. Although the clonality of a given condition does not prove its neoplastic nature, this view may also be reinforced by repeated detection of chromosomal instability and by a gain of DNA copy number in a chromosomal region Xq in elastofibromas [2, 11, 19] because such chromosomal changes are commonly associated with various neoplastic processes. However, extreme lyonization or skewed random inactivation of the gene during embryogenesis may draw a false-positive result in HUMARA, although the phenomenon is rare and found only in a minority of healthy individuals [9]. Additional examples of elastofibroma should be examined to exclude this possibility.

In conclusion, our study demonstrates that vimentin/CD34-positive spindle or stellate mesenchymal cells are the major cellular components of elastofibromas and that myofibroblasts are not an integral component of the lesion. The nonrandom inactivation pattern of X-chromosome demonstrated by HUMARA provides further evidence that the lesion is a clonal or potentially neoplastic process.

Acknowledgements This work was partly supported by a grant provided by the Ichiro Kanehara Foundation.

References

1. Abe R, Donnelly SC, Peng T, Bucala R, Metz CN (2001) Peripheral blood fibrocytes: differentiation pathway and migration to wound sites. J Immunol 166:7556–7562
2. Batstone P, Forsyth L, Goodlad J (2001) Clonal chromosome aberrations secondary to chromosome instability in an elastofibroma. Cancer Genet Cytogenet 128:46–47
3. Javanovic L, Delahunt B, McIver B, Eberhardt HL, Grebe SKG (2003) Optimising restriction enzyme cleavage of DNA derived from archival histopathological samples: an improved HUMARA assay. Pathology 35:70–74
4. Honma M, Koizumi F, Wakaki K, Ochiai H (1995) Coexpression of fibroblastic, histiocytic and smooth muscle cell phenotypes on cultured adherent cells derived from human palatine tonsils: a morphological and immunocytochemical study. Pathol Int 45:903–913

5. Kahn HJ, Hanna WH (1995) “Aberrant elastic” in elastofibroma: an immunohistochemical and ultrastructural study. Ultrastruct Pathol 19:45–50
6. Kayaselcuk F, Demirhan B, Kayaselcuk U, Özedem ÖR, Tuncer I (2002) Vimentin, smooth muscle actin, desmin, S-100 protein, p53, and estrogen receptor expression in elastofibroma and nodular fasciitis. Ann Diagn Pathol 6:94–99
7. Kindblom L-G, Spicer SS (1982) Elastofibroma. A correlated light and electron microscopic study. Virchows Arch 396:127–140
8. McComb EN, Feely MG, Neff JR, Johansson SL, Nelson M, Bridge JA (2001) Cytogenetic instability, predominantly involving chromosome 1, is characteristic of elastofibroma. Cancer Genet Cytogenet 126:68–72
9. Mitterbauer G, Winkler K, Gisslinger H, Geissler K, Lechner K, Mannhalter C (1999) Clonality analysis using X-chromosome inactivation at the human androgen receptor gene (HUMARA). Evaluation of large cohorts of patients with chronic myeloproliferative diseases, secondary neutrophilia, and reactive thrombocytosis. Am J Clin Pathol 112:93–100
10. Nagamine N, Nohara Y, Ito E (1982) Elastofibroma in Okinawa: a clinicopathologic study of 170 cases. Cancer 50: 1794–1805
11. Nishio J, Iwasaki H, Ohjimi Y, Ishiguro M, Koga T, Isayama T, Naito M, Kikuchi M (2002) Gain of Xp detected by comparative genomic hybridization in elastofibroma. Int J Mol Med 10:277–280
12. Pinkus GS, Said JW (1977) Profile of intracytoplasmic lysozyme in normal tissues, myeloproliferative disorders, hairy cell leukemia, and other pathologic processes: an immunoperoxidase study of paraffin sections and smears. Am J Pathol 89: 351–366
13. Ramos CV, Gillespie W, Narconis RJ (1978) Elastofibroma. A pseudotumor of myofibroblasts. Arch Pathol Lab Med 102: 538–540
14. Schepel JAC, Wille J, Seldenrijk CA, van Ramshorst B (1998) Elastofibroma: a familial occurrence. Eur J Surg 164:557–558
15. Schürch W, Seemayer TA, Gabbiani G (1998) The myofibroblast. A quarter century after its discovery. Am J Surg Pathol 22:141–147
16. Shteyngart B, Chaiwiriyakul S, Wong J, Cantor JO (1998) Preferential binding of lysozyme to elastic fibers in pulmonary emphysema. Thorax 53:193–196
17. Silverman JS, Tamsen A (1998) Interactive CD34-positive fibroblasts and factor XIIIa-positive histiocytes in cutaneous mesenchymal tumors. Am J Dermatopathol 20:317–319
18. Suwabe H, Serizawa A, Kajiwara H, Ohkido M, Tsutsumi Y (1999) Degenerative processes of elastic fibers in sun-protected and sun-exposed skin: immunoelectron microscopic observation of elastin, fibrillin-1, amyloid P component, lysozyme and α1-antitrypsin. Pathol Int 49:391–402
19. Vanni R, Marras S, Faa G, Uccheddu A, Dal Cin P, Sciot R, Samson I, Van den Berghe H (1999) Chromosome instability in elastofibroma. Cancer Genet Cytogenet 111:182–183
20. Weiss SW, Goldblum JR (2001) Elastofibroma. In: Weiss SW, Goldblum JR (eds) Soft tissue tumors. Mosby, St. Louis, pp 286–289
21. Yamazaki K (2005) CD10- and CD34-positive periglandular stromal cells in pulmonary benign metastasizing leiomyoma with metaplastic adenomyomatous glands: an ultrastructural and immunohistochemical study. Virchows Arch 446:270–277

Virchows Arch (2006) 448: 200–203
DOI 10.1007/s00428-005-0051-y

CASE REPORT

Wenbin Huang · Xinhua Zhang · Dongjie Li · Jieyu Chen · Kui Meng · Yan Wang · Zengfeng Lu · Xiaojun Zhou

Osteoclast-rich tumor of the gastrointestinal tract with features resembling those of clear cell sarcoma of soft parts

Received: 24 May 2005 / Accepted: 22 July 2005 / Published online: 12 October 2005

Abstract Clear cell sarcoma is a high-grade sarcoma with morphological features resembling those of malignant melanoma. An osteoclast-rich tumor of the gastrointestinal tract with features resembling those of clear cell sarcomas of soft parts is very rare. Herein, we report an unusual stomach tumor with microscopic and immunohistochemical characteristics of an osteoclast-rich tumor of the gastrointestinal tract with features resembling those of clear cell sarcomas of soft parts. The tumor cells were predominantly oval, admixed with some round and spindle elements arranged in nests and fascicles, and admixed with scattered osteoclast-like multinucleated giant cells. Neoplastic cells were positive for S-100 protein, and osteoclast-like multinucleated giant cells were immunoreactive to CD68. The unusual morphology of the tumor caused significant diagnostic difficulties. The differential diagnosis included gastrointestinal stromal tumor, primary or metastatic melanoma, and epithelioid malignant peripheral nerve sheath tumor. To the best of our knowledge, this is possibly the second description of an osteoclast-rich tumor of the gastrointestinal tract with features resembling those of clear cell sarcomas of soft parts.

Keywords Stomach · Clear cell sarcoma · Melanoma · Osteoclast

W. Huang · X. Zhang · J. Chen · K. Meng · Y. Wang · Z. Lu · X. Zhou (✉)
Department of Pathology, Jinling Hospital,
Clinical School of Medical College,
Nanjing University,
305 Zhongshan East Road,
210002 Nanjing Jiangsu, PR China
e-mail: zhouxj@public1.ptt.js.cn
Tel.: +86-25-80860191
Fax: +86-25-80860191

D. Li
Department of Pathology,
Fuyang Maternity and Child Health Care Hospital,
236000 Fuyang Anhui, PR China

Introduction

Although gastrointestinal stromal tumors (GISTs) account for most mesenchymal tumors arising from within the gastrointestinal tract, clear cell sarcoma and primary or metastatic melanoma have been reported [1, 3, 5, 6, 8, 10, 13, 15–17]. This report describes a case of an osteoclast-rich tumor of the gastrointestinal tract with features resembling those of clear cell sarcomas of soft parts, with prominent clear cells and osteoclast-like multinucleated giant cells simulating clear cell sarcomas of soft parts. An osteoclast-rich tumor of the gastrointestinal tract with features resembling those of clear cell sarcomas of soft parts was reported originally as an entity by Zambrano et al. [20] in 2003. The tumor shows very similar microscopic features, which consist of nests of oval cells and osteoclast-like multinucleated giant cells. To the best of our knowledge, only one case of an osteoclast-rich tumor of the gastrointestinal tract with features resembling those of clear cell sarcomas of soft parts has been described to date. Our case is similar to that reported by Zambrano et al. In the English literature, this is only the second case to have arisen from the stomach.

Case report

A 40-year-old man presented with abdominal pain of 1 year duration. Radiographic and endoscopic studies revealed a large smooth submucosal mass at the transition of the body and the antrum of lesser curvature. On physical examination, no other lesions were detected, and no other black speck of melanoma was seen. A partial gastrectomy was performed. On laparotomy, a gastric tumor with multiple pathological lymph nodes was found.

Pathological findings

The specimen obtained through partial gastrectomy showed a tumor of size 30×30×20 mm, which extended

Table 1 Antibodies used

Antibody	Clone	Source	Dilution	Microwave pretreament
Vimentin	V9	Dako	Prediluted	−
S-100 protein	S1	Nova Castra	Prediluted	−
Melan-A	M2-7C10	Dako	1/100	+
HMB-45		Dako	1/150	+
CD34	QBEnd/10	Nova Castra	1/60	+
CD117	1DC3	SantaCruz	1/200	+
α-SMA	1A4	Dako	Prediluted	+
CK7	K72.2	Dako	1/100	+
CK5/6	D5/16B4	Dako	1/100	+
Synaptophysin	SVP38	Santa Cruz	Prediluted	−
CD1a	MTB1	Dako	1/50	+
CD68	KP1	Dako	1/50	+

transmurally and was adherent to surrounding tissues. The mucosa over the tumor was intact.

The specimen was fixed in a neutral buffered formalin and routinely processed, with tissue sections embedded in paraffin. The sections were cut into 4-μm-thick slices and stained with hematoxylin and eosin. Representative sections were also stained through the EnVision immunohistochemical technique. Immunohistochemical stains were performed with the antibodies listed in Table 1.

Microscopic examination showed a tumor on the muscularis propria and invading submucosa and serosa. The tumor cells were medium-sized, predominantly oval, and admixed with some round and spindle elements arranged in nests and fascicles (Fig. 1a). The cytoplasm was either clear or densely acidophilic (Fig. 1b). The nuclei were centrally located, of somewhat irregular contours, and either normochromatic or only slightly hyperchromatic. The mitotic index was 2.6/10 high power field (0.79 mm^{-2}). Cells with nuclear pseudoinclusions and small focal necrosis were observed. Melanin pigments were not seen. A striking feature in this case was the presence of scattered osteoclast-like multinucleated giant cells (Fig. 2a and b). The nuclei of these cells were bland and different from those of the tumor cells. The cytoplasm of some of these cells was focally foamy.

Immunohistochemistry with antibodies for vimentin, S-100 protein, Melan-A, HMB-45, CD34, CD117, α-SMA, CK7, CK5/6, Syn, CD1a, and CD68 was performed. A strong and diffuse reactivity of the neoplastic cells for vimentin and S-100 protein was observed (Fig. 3a); all other markers were negative. The osteoclast-like multinucleated giant cells were only positive for CD68 (Fig. 3b) but were negative for all other markers.

Discussion

An osteoclast-rich tumor of the gastrointestinal tract with features resembling those of clear cell sarcomas of soft parts was reported originally as an entity by Zambrano et al. [20] in 2003. These authors reported six cases of the lesions, with one case arising from the stomach and five cases arising from the duodenum and ileum. All the tumors showed very similar microscopic features consisting of nests of oval cells and osteoclast-like multinucleated giant cells. The neoplastic cells were positive for vimentin and showed reactivity for S-100 protein. Osteoclast-like multinucleated giant cells were positive for CD68 but negative for S-100 protein. Cytogenetic examination revealed a t(12;22)(q13;q12) chromosomal translocation. To the best of our knowledge, only one case of an osteoclast-rich tumor of the gastrointestinal tract with features resembling those of clear cell sarcomas of soft parts in the stomach has been described to date. Our case is similar to that reported by Zambrano et al. In the English literature, it is only the second case to have arisen from the stomach.

Based on morphology and particularly on immunohistochemical study, clear cell sarcoma is considered. Clear cell sarcoma presents as a slowly growing, quite often painful nodule in the distal extremities, especially the ankle

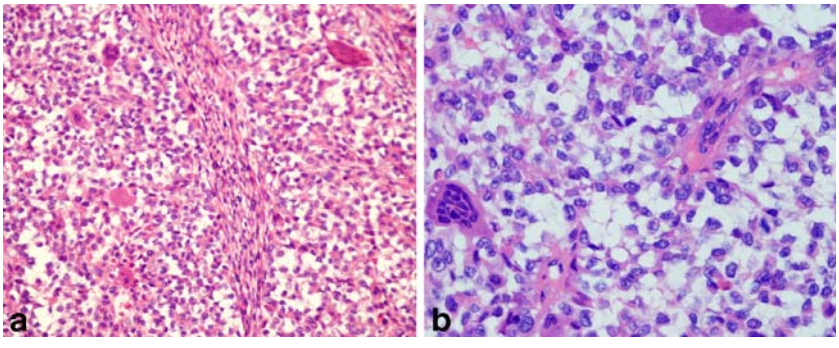

Fig. 1 Tumor cells arranged in nests (**a**). The cytoplasm is either clear or densely acidophilic (**b**)

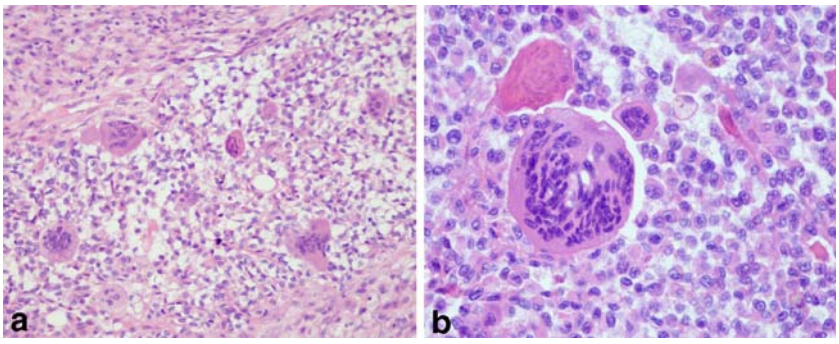

Fig. 2 Medium-sized tumor cells admixed with scattered osteoclast-like multinucleated giant cells (**a**). Higher-power view of osteoclast-like multinucleated giant cells within tumor cells (**b**)

and the foot, that is closely associated with fascial or tendoaponeurotic structures [4]. However, very rare examples at visceral locations have been described [5, 6, 13]. Microscopically, the distinguishing features of clear cell sarcoma are a clear cytoplasm, prominent nucleoli, the presence of multinucleated tumor giant cells rather than osteoclast-like multinucleated giant cells, a consistent immunoreactivity for S-100 protein, a common reactivity for HMB-45, and the presence of melanin and/or melanosomes in about half of the cases [20]. Some features of the osteoclast-rich tumor of the gastrointestinal tract resembling those of clear cell sarcomas of soft parts are similar to clear cell sarcoma but are negative for HMB-45 in immunohistochemistry, and no typical melanosomes can be found ultrastructurally. In addition, primary melanoma can arise from gastrointestinal mucosal sites, including the esophagus, anorectum, and small bowel [1, 3, 8, 16, 17]. Rarely, cases of primary melanoma of the stomach have been reported [10, 15]. Useful histological features used to recognize the melanocytic origin of the neoplasm are the presence of a correlation between the gastric mucosa and the tumor, cell pigmentation, and melanosomes found ultrastructurally.

In view of their location in the gastrointestinal tract and their mesenchymal appearance, an obvious consideration is that of GISTs and leiomyosarcomas. GISTs account for most mesenchymal tumors arising from within the gastrointestinal tract [2]. They arise most commonly within the walls of the stomach (65–70%) and the small intestines (30–45%) and are seen far less frequently in the esophagus, colon, and rectum, where myogenic tumors predominate [12]. They generally present in adults, with a peak incidence during the fifth and sixth decades, and are infrequent before the age of 40 years. Microscopically, there are two principal histological patterns: a spindle cell or epithelial character, or a combination of both in variable proportions. Immunohistochemically, GISTs may be positive for CD117, CD34, SMA, and S-100 protein. However, GISTs do not usually exhibit this high degree of S-100 protein immunoreactivity and are almost university positive for CD117 [19]. Recently, CD117-negative GISTs have been reported, but cytogenetic analysis shows the loss of chromosome 14 chromatid and 14q [11]. Furthermore, we are aware of only two cases of a CD117-positive GIST containing osteoclast-like multinucleated giant cells [7, 9]. In the English literature, only one case of epithelioid leiomyosarcoma with osteoclast-like multinucleated giant cells in the stomach has been reported [7, 18]. A diffuse strong staining for myogenic markers supports the diagnosis of leiomyosarcoma.

Extraskeletal neoplasms with osteoclast-like multinucleated giant cells are uncommon. They are most frequently reported in malignant epithelial tumors of the breasts and pancreas; quite rarely, they are reported in other sites, including soft tissue tumors. The significance of osteoclast-like multinucleated giant cells in tumors, as well as of their pathogenic mechanism of formation, remains obscure. Recent analyses of bone giant cell tumors reveal that neoplastic spindle cells may secrete a variety of cytokines and differentiation factors, including monocyte chemoattractant protein 1, osteoclast differentiation factor, and macrophage colony-stimulating factor. These molecules are monocyte chemoattractants and are essential for osteoclast differentiation, which suggests that the neoplastic spindle cells stimulate blood monocyte immigration into tumor tissues, enhancing their fusion into osteoclast-like multinucleated giant cells [14, 21].

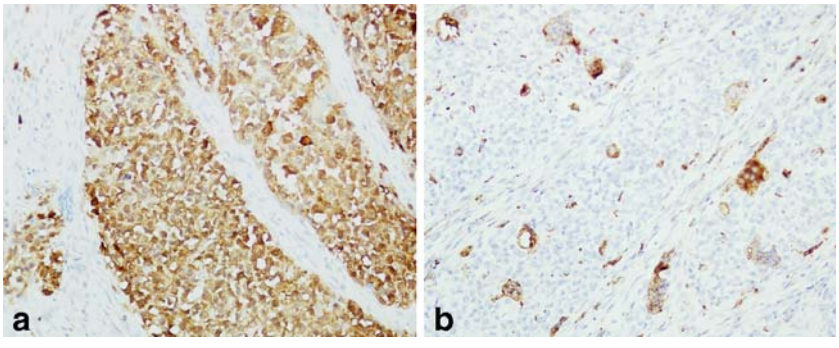

Fig. 3 The tumor cells are positive for S-100 protein (**a**). The osteoclast-like multinucleated giant cells within tumor cells are positive for CD68 (**b**)

Another differential diagnosis is epithelioid malignant peripheral nerve sheath tumor. Although the S-100 protein is usually positive in both, its distribution is diagnostically important: Whereas the osteoclast-rich tumor of the gastrointestinal tract with features resembling those of clear cell sarcomas of soft parts is diffusely and strongly positive for S-100 protein, the malignant peripheral nerve sheath tumor is only focally positive for this marker [13].

The histogenetic relationship between clear cell sarcoma and the osteoclast-rich tumor of the gastrointestinal tract with features resembling those of clear cell sarcomas of soft parts remains elusive. Morphological characters, an intense immunoreactivity for S-100 protein, and the cytogenetics of the two lesions share some similarities; however, our case and those of Zambrano et al. are both negative for HMB-45, and no typical melanosomes are clearly distinct ultrastructurally. This provides strong evidence that the osteoclast-rich tumor of the gastrointestinal tract with features resembling those of clear cell sarcomas of soft parts is indeed a separate and distinct entity that is somehow related to clear cell sarcomas of soft parts.

In conclusion, an osteoclast-rich tumor of the gastrointestinal tract with features resembling those of clear cell sarcomas of soft parts is a distinct type of gastrointestinal neoplasm. This neoplasm shares some features with clear cell sarcoma, but also has some important features that are different from the latter. The neoplasm is immunoreactive to the S-100 protein and is negative for CD117 and CD34, which have been segregated from GISTs.

References

1. Chalkiadakis G, Wihlm JM, Morand G, Weill-Bousson M, Witz JP (1985) Primary malignant melanoma of the esophagus. Ann Thorac Surg 39:473–475
2. Chan JKC (1999) Mesenchymal tumors of the gastrointestinal tract: a paradise for acronyms (STUMP, GIST, GANT, and now GIPACT). Implications of c-kit in genesis, and yet another of many emerging roles of the interstitial cell of Cajal in the pathogenesis of gastrointestinal disease. Adv Anat Pathol 6:19–40
3. Christova S, Meinhard K, Mihailov I, Alexiev B (1996) Three cases of primary malignant melanoma of the alimentary tact. Gen Diagn Pathol 142:63–67
4. Deenik W, Mooi WJ, Rutgers EJ, Peterse JL, Hart AA, Kroon BB (1999) Clear cell sarcoma of soft parts. A clinicopathological study of 30 cases. Cancer 86:969–975
5. Donner LR, Trompler RA, Dobin S (1998) Clear cell sarcoma of the ileum: the crucial role of cytogenetics for the diagnosis. Am J Surg Pathol 22:121–124
6. Ekfars TO, Kujari H, Isomäki M (1993) Clear cell sarcoma of tendons and aponeurosis in the duodenum: the first visceral case. Histopathology 22:255–259
7. Insabato L, Vizio DD, Ciancia G, Pettinato G, Tornillo L, Terracciano L (2004) Malignant gastrointestinal leiomyosarcoma and gastrointestinal stromal tumor with prominent osteoclast-like giant cells. Arch Pathol Lab Med 128:440–443
8. Kadivar TF, Vanek VW, Krishnan EU (1992) Primary malignant melanoma of the small bowel: a case study. Am Surg 58:418–421
9. Leung KM, Wong S, Chow TC, Lee KC (2002) A malignant gastrointestinal tumor with osteoclast-like giant cells. Arch Pathol Lab Med 126:972–974
10. Macak J (1998) Melanoma of the stomach: reality & fiction? Pathologica 90:388–390
11. Medeiros F, Corless CL, Duensing A, Hornick JL, Oliveira AM, Heinrich MC, Fletcher JA, Fletcher CD (2004) KIT-negative gastrointestinal stromal tumors: proof of concept and therapeutic implications. Am J Surg Pathol 28:889–894
12. Miettinen M, Sarlomo-Rikala M, Lasota J (1998) Gastrointestinal stromal tumours. Ann Chir Gynaecol 87:278–281
13. Pauwels P, Debiec-Rychter M, Sciot R, Vlasveld T, den Butter B, Hagemeijer A, Hogendoorn PC (2002) Clear cell sarcoma of the stomach. Histopathology 41:526–530
14. Quinn JM, Elliott J, Gillespie MT, Martin TJ (1998) A combination of osteoclast differentiation factor and macrophage-colony stimulating factor is sufficient for both human and mouse osteoclast formation in vitro. Endocrinology 139:4424–4427
15. Rao GM, Satyanarayana Y, Janaki M, Hayath MS (1999) Primary melanocarcinoma of stomach. Indian J Gastroenterol 18:176
16. Sachs DL, Lowe L, Chang AE, Carson E, Johnson TM (1999) Do primary small intestinal melanomas exist? Report of a case. J Am Acad Dermatol 41:1042–1044
17. Stranks G, Mathai J, Rowe-Jones D (1991) Primary malignant melanoma of the esophagus: case report and review of surgical pathology. Gut 32:828–829
18. Terada T, Endo K, Maeta H, Horie S, Ohta T (2000) Epithelioid leiomyosarcoma with osteoclast-like giant cells in the rectum. Arch Pathol Lab Med 124:438–440
19. van Roggen JFG, van Velthuysen MLF, Hogendoorn PCW (2001) The histopathological differential diagnosis of gastrointestinal stromal tumours. J Clin Pathol 54:96–103
20. Zambrano E, Reyes-Mugica M, Franchi A, Rosai J (2003) An osteoclast-rich tumor of gastrointestinal tract with features resembling clear cell sarcoma of soft parts: reports of 6 cases of a GIST simulator. Int J Surg Pathol 11:75–81
21. Zheng MH, Fan Y, Smith A, Wysocki S, Papadimitriou JM, Wood DJ (1998) Gene expression of monocyte chemoattractant protein-1 in giant cell tumors of bone osteoclastoma: possible involvement in $CD68^{+}$ macrophage-like cell migration. J Cell Biochem 70:121–129

Virchows Arch (2006) 448: 204–208
DOI 10.1007/s00428-005-0054-8

CASE REPORT

Katsuaki Sato · Yoshimichi Ueda · Aya Sakurai · Yoshimaro Ishikawa · Sachiko Kaji · Takayuki Nojima · Shogo Katsuda

Adenoid cystic carcinoma of the maxillary sinus with gradual histologic transformation to high-grade adenocarcinoma: a comparative report with dedifferentiated carcinoma

Received: 6 December 2004 / Accepted: 25 July 2005 / Published online: 17 August 2005

Abstract We report a unique case of adenoid cystic carcinoma (ACC) of the maxillary sinus, with gradual histologic transformation from lower-grade ACC (cribriform and tubular types) to high-grade adenocarcinoma (HGA) showing a sequential histologic spectrum via solid-type ACC. A 74-year-old man presented with swelling and mild pain of the right cheek. CT scan showed a mass measuring approximately 4 cm, with marked bone destruction in the right maxillary sinus. A surgically resected specimen revealed that the tumor was comprised of three different components: HGA and solid-type ACC in the central portion and lower-grade ACC in the periphery. The tumor was discriminated from a dedifferentiated carcinoma or hybrid tumor. Autopsy specimens also demonstrated both solid-type ACC and HGA components in the lung and spleen. Immunohistochemically, positive staining of p53 protein was detected on both solid-type ACC and HGA cells, but cyclin D1 and HER2/neu was only seen in HGA cells. Solid-type ACC cells were immunoreactive for CD117 (c-kit), but lower-grade ACC and HGA cells were negative. This case suggests that the overexpression of CD117, p53 protein, cyclin D1, and HER2/neu might be involved in the progression from lower-grade ACC to solid-type ACC and HGA.

Keywords Adenoid cystic carcinoma · Dedifferentiation · Hybrid tumors · Maxillary sinus · Transformation

K. Sato (✉) · Y. Ueda · A. Sakurai · Y. Ishikawa · S. Katsuda
Department of Pathophysiological and Experimental Pathology,
Kanazawa Medical University,
1-1 Daigaku, Uchinada, Kahoku-gun,
Ishikawa, 920-0293, Japan
e-mail: sato-k@kanazawa-med.ac.jp
Tel.: +81-76-2188119
Fax: +81-76-2862484

S. Kaji · T. Nojima
Department of Pathology and Laboratory Medicine,
Kanazawa Medical University,
Ishikawa, Japan

Introduction

Adenoid cystic carcinoma (ACC) is a specific type of adenocarcinoma, with a characteristic cribriform appearance that commonly occurs in the major and minor salivary glands. Patey and Thackray first reported that ACC with a solid growth pattern was associated with a worse prognosis than that of the cribriform type [12]. Perzin et al. described a more differentiated type of ACC, the tubular form, which is associated with a favorable prognosis [13]. Accordingly, ACCs are histologically classified into three subtypes: tubular, cribriform, and solid. The grading scheme that categorizes ACCs into three histologic grades is as follows: Grade 1—tubular and cribriform patterns without solid components, Grade 2—pure cribriform pattern or mixed with less than 30% of solid areas, and Grade 3—predominantly a solid pattern, and it is closely correlated with prognosis [15]. Therefore, the tubular- and cribriform-type ACCs are lower-grade, whereas solid-type ACC is higher grade.

Recently, cases have been reported of dedifferentiated ACC of the salivary gland and upper respiratory tract, which are rare variants of ACC [1, 2, 7, 9–11]. Dedifferentiation is defined as clonal evolution of a poorly differentiated or high-grade component arising within a low-grade carcinoma without histologic transition or spectrum from the original carcinoma [18], namely, as an abrupt transformation [11]. In all reported cases of dedifferentiated ACC, the low-grade component was tubular- or cribriform-type ACC, and high-grade areas demonstrated poorly differentiated adenocarcinoma or undifferentiated carcinoma. The two elements are clearly demarcated, although there is a transitional zone in some cases.

Although histologic progression from lower-grade ACC to solid-type ACC has previously been reported [16], there are no reports in the literature of transformation from solid-type ACC to high-grade adenocarcinoma (HGA) or undifferentiated carcinoma. The histologic appearance of solid-type ACC is variably sized solid islands of monomorphous tumor cells, which have small nuclei with fine chromatin and indistinct nucleoli, and scant cytoplasm

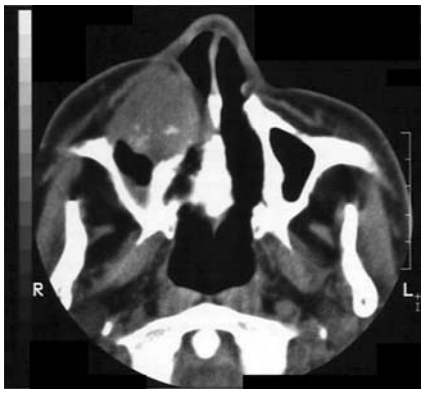

Fig. 1 CT scan shows a tumor with bone destruction in the right maxillary sinus

[3]. Immunohistochemical staining for cytokeratin of solid-type ACC demonstrated disproportionate ductal-cell proliferation. The HGA showed a more pleomorphic appearance, large nuclei, and infiltrative growth pattern. We present here a case of ACC with gradual transformation from lower-grade ACC to HGA with a continuous histologic spectrum via solid-type ACC. The immunohistochemical characteristics are also described and reviewed as compared with those of dedifferentiated ACC and hybrid carcinoma.

Clinical history

A 74-year-old man presented with swelling and mild pain of the right cheek, anosmia, and nasal bleeding for 6 months. CT scan demonstrated a mass approximately 4 cm in diameter, with marked bone destruction in the right maxillary sinus (Fig. 1). A needle biopsy specimen was diagnosed as poorly differentiated adenocarcinoma, and the mass was excised. Pulmonary and hepatic metastases were identified at follow-up 1 year later after the surgery. The patient died within 4 months following the development of metastases without any effect of chemotherapy. Autopsy was then performed.

Materials and methods

The whole surgically resected specimen was cut into 12 tissue blocks 5 mm thick for histologic and immunohistochemical examination. For light microscopic evaluation, all thin sections were stained with hematoxylin and eosin. Immunohistochemistry was performed on the deparaffinized tissue sections using the primary antibodies listed in Table 1 and the avidin-biotin-peroxidase complex method of Hsu and co-workers [6].

Results

The surgically resected specimen, measuring 7.5×5×3 cm, was comprised of the right maxillary tumor mass, the overlying skin, and the subcutaneous tissue. Grossly, the tumor was solid with a white or gray-tan appearance and was approximately 4 cm in diameter, with an indistinct margin and destruction of the maxillary bone wall.

Microscopically, the tumor was comprised of three distinct components. In the central portion of the tumor, HGA and solid-type ACC were the main components. HGA was comprised of highly malignant tumor cells with pleomorphic vesicular nuclei and relatively abundant amphophilic cytoplasm proliferating irregularly with loose solid nests (Fig. 2a) or infiltratively in a small tubular and cord-like pattern (Fig. 2b). Solid ACC was comprised of either solid nests of small duct-like structures with occasional comedo-like necrosis (Fig. 2c) or solid nests of larger tumor cells with vesicular nuclei with some ductular structures. There were transitional areas between HGA and solid-type ACC

Table 1 Immunohistochemical studies and findings

Antigens	Clone	Source	Dilution	Findings		
				Lower-grade ACC	Solid-type ACC	HGA
Cytokeratin	AE1/AE3	DakoCytomation (Glostrup, Denmark)	1:50	+	+	+
α-Smooth muscle actin	1A4	DakoCytomation	1:200	+	+	F+
S-100 protein	2A10	IBL (Takasaki, Japan)	1:50	+	+	+
P53 protein	Bp53-12	IBL	1:5,000	−	+	+
Cyclin D1	DSC-6	DakoCytomation	1:200	F+	F+	+
HER2/neu	CB11	Ventana (Tucson, AZ, USA)	Prediluted	−	−	+
CD117 (c-kit)	Polyclonal	DakoCytomation	1:80	−	+	−
Ki-67	MIB-1	DakoCytomation	1:50	5%	15%	30%
CEA	TF-3H8-1	Ventana	Prediluted	−	−	−
GCDFP-15	23A3	Novocastra (Newcastle upon Tyne, UK)	1:50	−	−	−
Androgen receptor	AR27	Novocastra	1:100	−	−	−
PSA	ER-PR8	DakoCytomation	1:20	−	−	−

ACC Adenoid cystic carcinoma, *HGA* high-grade adenocarcinoma, *F* focally

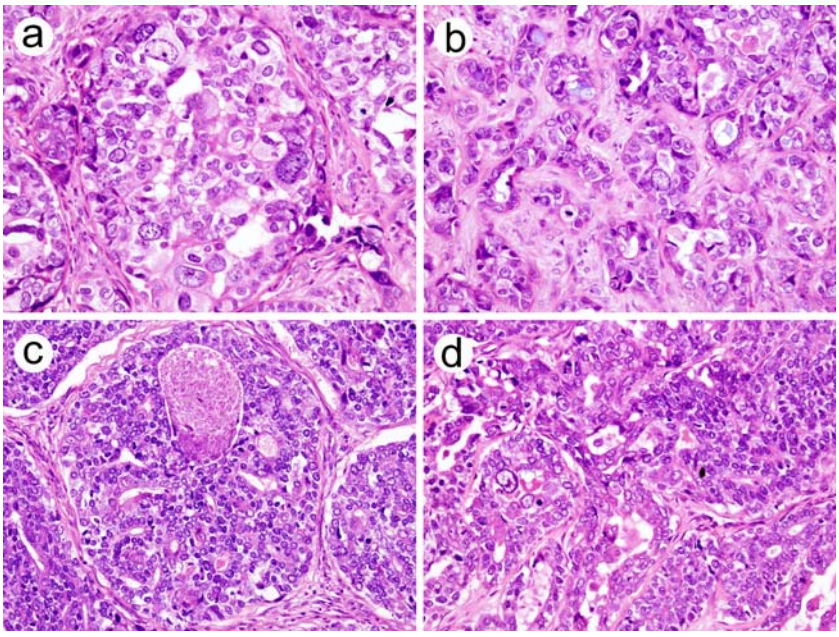

Fig. 2 Histopathological appearance of the tumor using hematoxylin and eosin stain. ×200. **a** and **b** High-grade adenocarcinoma. **c** Solid-type adenoid cystic carcinoma with comedo-like necrosis. **d** Transitional appearance from solid-type adenoid cystic carcinoma to high-grade adenocarcinoma

(Fig. 2d). In the periphery of the tumor, a lower-grade ACC component was identified. Small monomorphous cells were infiltratively proliferated with a cribriform or bicellular tubular pattern. Perineural invasion was frequently observed in the area.

The postmortem examination revealed metastases in the lungs, liver, spleen, bone marrow in the lumbar vertebrae, and right pulmonary hilar lymph nodes. Histopathological findings in the metastatic lesions of the lung and spleen were solid-type ACC and HGA, which were similar to those of the central parts of the primary maxillary lesion.

Table 1 summarizes the immunohistochemical findings of the present case. Immunohistochemically, ductal cells stained positively for cytokeratin (AE1/AE3) in all components. All components showed a positive reaction for α-smooth muscle actin, markers of myoepithelial cell differentiation, and S-100 protein. Ductal cells in HGA and solid-type ACC areas expressed positive immunoreactivity for S-100 protein. CD117 (c-kit) immunostaining showed a positive reaction only in solid-type ACC, with no positive staining in lower-grade ACC or HGA (Fig. 3a). The staining for p53 protein was positive in more than 50% of carcinoma cells both in the HGA and solid-type ACC areas, whereas it was negative in the lower-grade ACC portion (Fig. 3b). Cyclin D1 overexpression was demonstrated in approximately 30% of the tumor cells in the HGA component, but was only weakly and focally reactive in the ACC component (Fig. 3c). Membranous

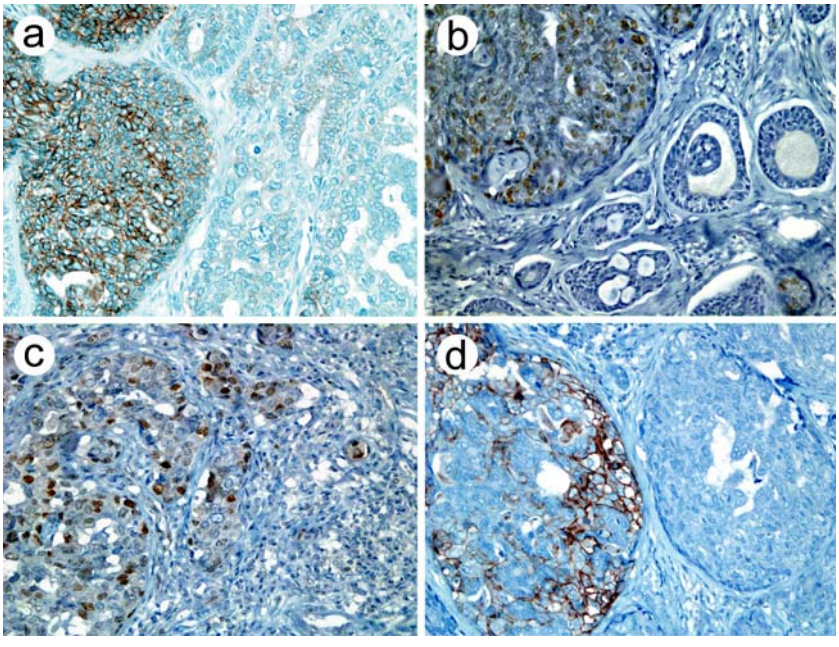

Fig. 3 Immunohistochemical findings of the tumor. ×200. **a** Solid-type adenoid cystic carcinoma cells with membranous expression for CD117 (*left*), which is negative in the high-grade adenocarcinoma cells (*right*). **b** Solid-type adenoid cystic carcinoma cells with nuclear expression for p53 protein (*left*), which is negative in the cribriform-type adenoid cystic carcinoma cells (*right*). **c** High-grade adenocarcinoma cells with nuclear expression for cyclin D1 (*left*), which is negative in the solid-type adenoid cystic carcinoma cells (*right*). **d** High-grade adenocarcinoma cells with membranous expression for HER2/neu (*left*), which is negative in the solid-type adenoid cystic carcinoma cells (*right*)

staining for HER2/neu was detected only in the HGA component (Fig. 3d). The Ki-67 (MIB-1) labeling index in lower-grade ACC, solid-type ACC, and HGA areas was approximately 5, 15, and 30%, respectively.

Discussion

The tumor in this case consisted of three different components: lower-grade (tubular and cribriform types) ACC, solid-type ACC, and HGA. We believe that gradual transformation from lower-grade ACC to HGA with a sequential histologic spectrum via solid-type ACC was involved in the tumor development. Discrimination from dedifferentiated carcinoma and hybrid carcinoma, which are organized with pleural carcinoma elements, is necessary in this unique case.

Dedifferentiation is recognized when a lower-grade malignant neoplasm abruptly transforms to a high-grade [11, 17], in which the high-grade component is juxtaposed to the original lesion or the original line of differentiation is lost [2]. This concept should be distinguished from malignancy arising from a benign tumor such as carcinoma ex pleomorphic adenoma, hybrid tumors, and transformation within a high-grade carcinoma to another high-grade pattern [18]. There are no previously reported cases of dedifferentiated ACC of the salivary glands and upper respiratory tract where a solid-type ACC area was mentioned [1, 2, 7, 9, 10], or accounted for only as a scant portion [11], which is consistent with the definition. The present case is unique in that the histologic features indicated a gradually successive transition from lower-grade to solid-type ACC and HGA. Histologic transformation from solid-type ACC to HGA corresponds to a transition from high-grade carcinoma to another high-grade carcinoma, which should discriminate from dedifferentiation.

Hybrid tumors are composed of two histologically distinct categories of tumor, each of which corresponds to an exactly defined tumor entity and an identical origin [14]. In the present case, the tumor components were lower-grade ACC, solid-type ACC, and HGA. Some of the tumor nests of the HGA component with comedo-like necrosis were superficially analogous to salivary duct carcinoma. However, dystrophic calcification, apocrine-like eosinophilic cytoplasm, coarse chromatin, and distinct single nucleolus, which are characteristic features of salivary duct carcinoma [18], were not observed. Immunoreactivity was not detected for CEA, GCDFP-15, androgen receptor, and prostate-specific antigen, which are frequently expressed in salivary duct carcinoma. Therefore, the HGA component was not assigned to a specific carcinoma entity and should be classified into adenocarcinoma NOS (not otherwise specified). The tumor in the present case could be differentiated from hybrid carcinoma.

Histologic transition from solid-type ACC to HGA is a characteristic finding in this case. Comedo-like necrosis and mitoses have appeared to a variable extent in solid-type ACC [3, 4] and were identified in the present case. In the HGA component, there were distinctive irregularly sized solid islands of highly pleomorphous tumor cells with vesicular large nuclei. There were transitional features between solid-type ACC and HGA. These morphological findings suggest that the increase in cellular atypism and pleomorphism in solid-type ACC might be involved in the initial stage of histologic transformation to HGA. In the autopsy specimens of the lung and spleen, histopathological findings of metastatic lesions showed the same pattern as the central portion of the surgical samples, i.e., combination of solid-type ACC and HGA, showing that solid-type ACC metastasized and then transformed to HGA. These findings also suggest a gradual successive transformation of tumor cells in this case.

Immunohistochemical studies and genetic analysis have been carried out for oncoprotein in dedifferentiated ACC and solid-type ACC. The Ki-67 labeling index was higher in dedifferentiated ACC than in that of lower-grade ACC [1, 2, 11]. The Ki-67 labeling index of solid-type ACC in the present case was between lower-grade ACC and HGA, demonstrating that proliferation activity increased in proportion to histologic progression from lower-grade ACC to solid-type ACC and HGA. CD117 (c-kit) expression was detected in ACC, which was intense in solid-type ACC [5]. Overexpression of p53 protein was detected by immunohistochemistry in six of nine cases (67%) [1, 2, 7, 9, 11], and that of cyclin D1 was detected in five of seven cases (71%) in previously reported dedifferentiated ACC cases [1, 2, 11]. Nagao et al. and Chau et al. reported dedifferentiated ACC cases with a p53 gene mutation [1, 11]. Immunohistochemical positive staining of HER2/neu has been demonstrated in three of five cases (60%) [1, 8, 10] of dedifferentiated ACC. Immunohistochemical expression of p53 protein [8] and p53 gene alterations [17] were markedly more frequent in solid-type ACC than lower-grade ACC. In our case, positivity for p53 protein was detected in both solid-type ACC and HGA cells, but immunoreactivity for cyclin D1 and HER2/neu were detected only in HGA cells. The molecular mechanisms of malignant transformation of ACC have not been clearly elucidated. Our case suggests that overexpression of CD117 (c-kit), p53 protein, cyclin D1, and HER2/neu are involved in the transformation from lower-grade ACC to solid-type ACC and HGA.

Acknowledgements We are grateful to Dr. Toshitaka Nagao, Department of Diagnostic Pathology, Tokyo Medical University, for providing useful comments.

References

1. Chau Y, Hongyo T, Aozasa K et al (2001) Dedifferentiation of adenoid cystic carcinoma: report of a case implicating p53 gene mutation. Human Pathol 32:1403–1407
2. Cheuk W, Chan JKC, Ngan RKC (1999) Dedifferentiation in adenoid cystic carcinoma of salivary gland: an uncommon complication associated with an accelerated clinical course. Am J Surg Pathol 23:465–472
3. Cleveland D, Abrams AM, Melrose RJ et al (1990) Solid adenoid cystic carcinoma of the maxilla. Oral Surg Oral Med Oral Pathol 69:470–478

4. Eby LS, Johnson DS, Baker HW (1972) Adenoid cystic carcinoma of the head and neck. Cancer 29:1160–1168
5. Holst VA, Marshall CE, Moskaluk CA, Frierson HF Jr (1999) KIT protein expression and analysis of c-kit gene mutation in adenoid cystic carcinoma. Mod Path 12:956–960
6. Hsu SM, Raine L, Fanger H (1981) Use of avidin-biotin-peroxidase complex (ABC) in immunoperoxidase techniques: a comparison between ABC and unlabeled antibody (PAP) procedures. J Histochem Cytochem 29:577–580
7. Ide F, Mishima K, Saito I (2003) Small foci of high-grade carcinoma cells in adenoid cystic carcinoma represent an incipient phase of dedifferentiation. Histopathology 43:604–606
8. Jia L, Esguerra RL, Tang X et al (2004) Prognostic value of apoptosis and apoptosis-associated proteins in salivary gland adenoid cystic carcinoma. Pathol Int 54:217–223
9. Kamio N, Tanaka Y, Mukai M et al (1997) A hybrid carcinoma: adenoid cystic carcinoma and salivary duct carcinoma of the salivary gland. An immunohistochemical study. Virchows Arch 430:495–500
10. Moles MA, Avila IR, Archilla AR (1999) Dedifferentiation occurring in adenoid cystic carcinoma of the tongue. Oral Surg Oral Med Oral Pathol Oral Radiol Endo 88:177–180
11. Nagao T, Gaffey TA, Serizawa H et al (2003) Dedifferentiated adenoid cystic carcinoma: a clinicopathologic study of 6 cases. Mod Path 16:1265–1272
12. Patey DH, Thackray AC (1958) The treatment of parotid tumors in the light of a pathological study of parotidectomy material. Br J Surg 45:477–487
13. Perzin KH, Gullane P, Clairmont AC (1978) Adenoid cystic carcinomas arising in salivary glands. A correlation of histologic features and clinical course. Cancer 42:265–282
14. Seifert G, Donath K (1996) Hybrid tumours of salivary glands. Definition and classification of five rare cases. Eur J Cancer B Oral Oncol 32:251–259
15. Szanto PA, Luna MA, Tortoledo ME et al (1984) Histologic grading of adenoid cystic carcinoma of the salivary glands. Cancer 54:1062–1069
16. Yamamoto Y, Saka T, Makimoto K et al (1992) Histological changes during progression of adenoid cystic carcinoma. J Laryngol Otol 106:1016–1020
17. Yamamoto Y, Virmani AK, Wistuba II et al (1996) Loss of heterozygosity and microsatellite alterations in p53 and RB genes in adenoid cystic carcinoma of the salivary gland. Human Pathol 27:1204–1210
18. Zarbo RJ (2002) Salivary gland neoplasia. A review for the practicing pathologist. Mod Path 15:298–323

Virchows Arch (2006) 448: 209–213
DOI 10.1007/s00428-005-0060-x

CASE REPORT

Christian E. Keller · Eugenia T. Gamboa · Arthur P. Hays · Jordan Karlitz · Gina Lowe · Peter H. R. Green · Govind Bhagat

Fatal CNS vasculopathy in a patient with refractory celiac disease and lymph node cavitation

Received: 31 May 2005 / Accepted: 3 August 2005 / Published online: 21 September 2005

Abstract Celiac disease is an enteropathy occurring in genetically predisposed individuals due to a dietary intolerance to gluten. Patients with celiac disease may develop a neurological disorder of unknown cause, although autoimmune mechanisms are suspected. We report on a 56-year-old man with celiac disease, who became refractory to a gluten-free diet and died of a rapidly progressive encephalopathy. Magnetic resonance imaging indicated focal lesions of the cerebellum and brainstem, and electrodiagnostic studies suggested an axonal neuropathy. Autopsy revealed a flattened small-bowel mucosa with intraepithelial lymphocytosis, a spectrum of degenerative changes of the intra-abdominal and mediastinal lymph nodes, including cavitary degeneration, and splenomegaly. Histologically, the lymph nodes showed pseudocyst formation and lymphocytic vasculitis with fibrinoid necrosis, and sections of the brain exhibited fibrinoid degeneration of small blood vessels, sparse perivascular lymphocytic infiltrates, and perivascular ischemic lesions. Identical T-cell clones were identified in the duodenum, stomach, lymph nodes, and spleen. This patient had an unusual neurological disorder related to a vasculopathy, probably mediated by a circulating neoplastic clone of activated T cells.

Keywords Celiac disease · Encephalopathy · Vasculopathy · Neuropathy

C. E. Keller · A. P. Hays · G. Bhagat
Department of Pathology, College of Physicians and Surgeons, Columbia University,
New York, NY, USA

E. T. Gamboa
Department of Neurology, College of Physicians and Surgeons, Columbia University,
630 West 168th Street,
New York, NY, USA

G. Lowe
Department of Radiology, College of Physicians and Surgeons, Columbia University,
New York, NY, USA

P. H. R. Green · J. Karlitz
Department of Medicine, College of Physicians and Surgeons, Columbia University,
New York, NY, USA

G. Bhagat (✉)
College of Physicians and Surgeons, Columbia University,
VC 14th, Room 236A 630 West 168th Street,
New York, NY 10032, USA
e-mail: gb96@columbia.edu
Tel.: +1-212-3421323
Fax: +1-212-3052301

Introduction

Celiac disease is an immune-mediated, small intestinal enteropathy triggered by ingestion of gluten, the storage protein of wheat and related grains [30]. The disease is occasionally associated with disorders of the nervous system, including cerebellar ataxia, seizures, migraine headaches, and peripheral neuropathy [5, 27]. Little is known about the pathogenesis of these neurological disorders as autopsies are rarely performed in such individuals [4, 11, 13, 17, 22, 26, 28]. We describe an unusual case of fatal subacute encephalopathy due to a small vessel angiopathy in a patient with refractory celiac disease complicated by mediastinal and mesenteric lymph node cavitation (MLNC).

Clinical history

A 56-year-old man presented with a history of diminished appetite, diarrhea, and profound weight loss (70 lbs). He had been diagnosed with celiac disease 2.5 years earlier based on positive endomysial antibodies, a duodenal biopsy that revealed total villous atrophy with intraepithelial lymphocytosis, and response to a gluten-free diet. A strict gluten-free diet led to a diminution of symptoms and weight gain (58 lbs), and he returned to his usual state of health. He did well for more than a year, but became symptomatic again despite strict adherence to a gluten-free diet. On admission to the hospital, he complained of decreased appetite, nausea, diarrhea, weight loss, and mental

confusion. Examination revealed a cachectic man with bitemporal wasting, hypotension, tachycardia, and a fever of 101.9°F (38.8°C). Routine blood tests, including serum iron, folate, vitamin B12, and vitamin E levels, were normal. He had a low serum sodium level (128 mM/l) and elevations of total bilirubin (3.1 mg/dl), alkaline phosphatase (550 U/l), and serum ferritin (854 ng/ml). Antigliadin, anti-endomysial, and antinuclear antibodies were negative as was a serologic test for HIV. Urine, blood, and stool cultures were negative. An upper gastrointestinal series revealed dilatation of the small intestine, while an abdominal ultrasound and computerized tomography (CT) scan were normal. A repeat duodenal biopsy exhibited total villous atrophy and persistent intraepithelial lymphocytosis without morphologic evidence of collagenous sprue, lymphoma, or infection; gastric biopsies demonstrated lymphocytic gastritis. The patient received total parenteral nutrition, intravenous steroids, and azathioprine. Neurological examination showed diffuse muscle wasting and weakness (3/5 in the legs and 4/5 in the arms). He had diminished pain sensation in a glove–stocking distribution and areflexia with evidence of an axonal neuropathy on electrodiagnostic studies. Dysmetria and ataxia were detected. A CT scan of the brain was normal except for an ill-defined lucency in the left medial occipital lobe, attributed to focal atrophy. Lumbar cerebrospinal fluid (CSF) had a glucose level of 59 mg/dl, protein 244 mg/dl and one white blood cell. A venereal disease research laboratory test was nonreactive, and cultures for viruses, fungi, and bacteria were negative as were the results of polymerase chain reaction (PCR) for mycobacteria and herpes simplex virus.

The patient deteriorated neurologically with onset of brainstem dysfunction, progression of the peripheral neuropathy, and seizures. He received intravenous immunoglobulin (30 g daily for 3 days) with minimal improvement. On the 14th hospital day, magnetic resonance (MR) imaging demonstrated an area of T2 hyperintensity involving the right cerebellar hemisphere, pons, midbrain, and thalamus (Fig. 1a). Contrast enhancement was observed along the periphery of the lesions (Fig. 1b). Repeat CSF examination showed 15 cells (lymphocytes and monocytes). Despite aggressive treatment, including intravenous antibiotics, intravenous steroids, and infusions of gamma globulin, the disorder progressed, and the patient died 6 weeks after the onset of his neurological disorder.

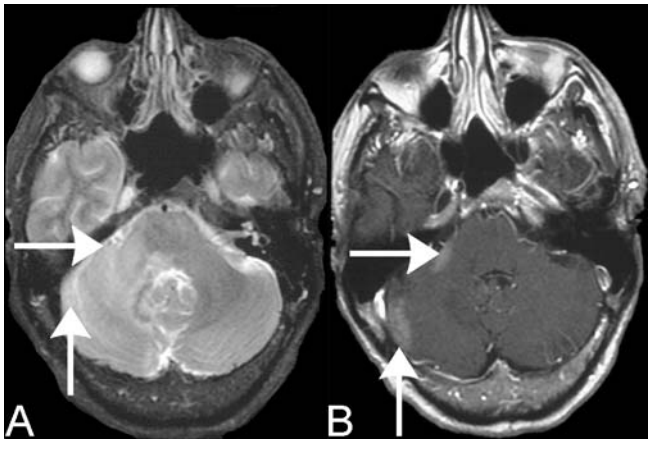

Fig. 1 Axial brain MR images. **a** T2-weighted image shows increased signal in the right pons, brachium pontis, and cerebellum (*arrows*). **b** Postcontrast T1-weighted image demonstrates enhancement along the lateral aspect of the signal abnormality (*arrows*)

Materials and methods

Morphologic assessment was performed using hematoxylin and eosin stained, formalin-fixed, paraffin-embedded tissue sections (3 μ). Sections of the brain were also stained with Bielschowsky, Gomori methenamine silver, periodic acid Schiff with and without diastase digestion, Ziehl–Neelsen (acid fast bacteria), Gram, Giemsa, and Warthin–Starry stains. The following primary antibodies were used for immunohistochemical staining: CD2 (dilution 1:100; Novocastra, Burlingame, CA, USA), CD3 (dilution 1:800; Dako, Carpinteria, CA, USA), CD4 (dilution 1:50; Novocastra), CD5 (dilution 1:50; Novocastra), CD7 (dilution 1:200; Novocastra), CD8 (dilution 1:40; Dako), TIA-1 (dilution 1:1000; Dako), granzyme B (dilution 1:20; Chemicon, Temecula, CA, USA), perforin (dilution 1:50; Novocastra), CD30 (dilution 1:50; Dako), and C4d (dilution 1:100; ALPCO, Windham, NH, USA). The Envision plus system (Dako) was used for detection. Immunofluorescent (IF) staining was performed after pronase (*Streptomyces griseus*, 50,000 units; Calbiochem, La Jolla, CA, USA) pretreatment (0.03 g/ml for 10 min in TRIS buffer at 37°C) of paraffin-embedded tissue sections using the following fluorescein isothiocyanate–labeled antibodies: IgM, IgG, IgA, C3, C1q, fibrinogen, and albumin (Dako). PCR for T-cell receptor-γ (TCR-γ) gene rearrangement followed by polyacrylamide gel electrophoresis and heteroduplex analysis was performed according to the method of Bottaro et al. [3].

Results

A premortem right cerebellar hemisphere biopsy (performed on hospital day 15) demonstrated small vessel angiopathy, rare occlusive fibrin thrombi, and confluent areas of perivascular ischemic injury. Fibrinoid material was present in the vessel walls and perivascular areas accompanied by edema and an infiltrate of macrophages. Only sparse perivascular lymphocytes were noted in the neural tissue and leptomeninges. Histochemical stains and electron microscopy did not reveal any microorganisms.

Postmortem examination was significant for cachexia, hepatomegaly (2,750 g), and mild splenomegaly (210 g); no distinct mass lesions were identified in any organ. Sections of the duodenum and jejunum showed total villous atrophy (Fig. 2a) and a moderate intraepithelial lymphocytosis (Fig. 2a, insert). Although the intraepithelial lymphocytes lacked morphological atypia, they had an abnormal phenotype: CD2+, CD3+, CD5−, CD7+, CD4−, CD8−, CD30−, TIA-1+, granzyme B+, and perforin+.

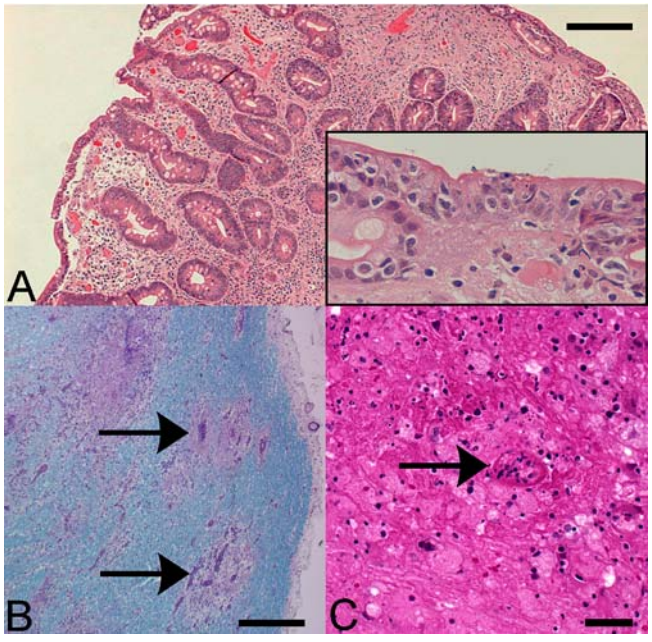

Fig. 2 Duodenum (**a**) and transverse sections of the pons (**b** and **c**). **a** Total villous atrophy and crypt hyperplasia. Hematoxylin & eosin, *bar*=500 μm. *Inset*: intraepithelial lymphocytosis. Hematoxylin & eosin. **b** The basis pontis exhibits small perivascular areas of ischemic injury (*arrows*) as reflected by loss of myelin. Luxol fast blue–periodic acid Schiff, *bar*=500 μm. **c** Fibrinoid material is present in the vessel wall (*arrow*) and the surrounding neural tissue accompanied by macrophages. Hematoxylin & eosin, *bar*=50 μm

Mesenteric, para-aortic, and hilar lymph nodes showed a spectrum of histologic alterations from multifocal paracortical histiocytic aggregates to lymphocyte depletion and chylous pseudocyst formation to fibrosis and atrophy. In addition, numerous lymph nodes showed lymphocytic vasculitis of small-sized vessels with fibrinoid necrosis (Fig. 3a). The lymphocytes surrounding and infiltrating the vessel walls had the same immunophenotype as the intraepithelial lymphocytes, and there was no evidence of immune-complex deposition on staining for the different immunoglobulin heavy chains and complement components C1q, C3, and C4d. The amorphous fluid in the cavitary lymph nodes showed scattered clumps of fibrinogen by IF staining (Fig. 3c) that stained bright red with a trichrome stain (Fig. 3b). Apoptotic paracortical lymphocytes were also seen in the areas infiltrated by the atypical lymphocytes. Sections of the spleen showed marked white pulp depletion and a sparse red pulp infiltrate of small lymphocytes. PCR analysis for TCR-γ gene rearrangement demonstrated clonal T-cell products of similar molecular weight with the V10/11 family primers in the small intestine, stomach, lymph nodes, and spleen (Fig. 4).

Sections of the cerebellum revealed widespread loss of Purkinje cells and neurons of the dentate nucleus and astrocytosis, in addition to the histologic changes observed in the premortem biopsy. Microscopic lesions similar to the premortem cerebellar biopsy were also detected in the right pons (Fig. 2b,c), midbrain, thalamus, and basal ganglia. The spinal cord exhibited mild degeneration of the pyramidal tracts and the posterior columns with loss of myelinated nerve fibers in the nerve roots. No peripheral nerves were examined. Nearly all the perivascular lymphocytes were T cells, but no inflammatory cell infiltrates were noted within the blood vessel walls. Due to the paucity of the lymphocytic infiltrate, the immunophenotype of these cells

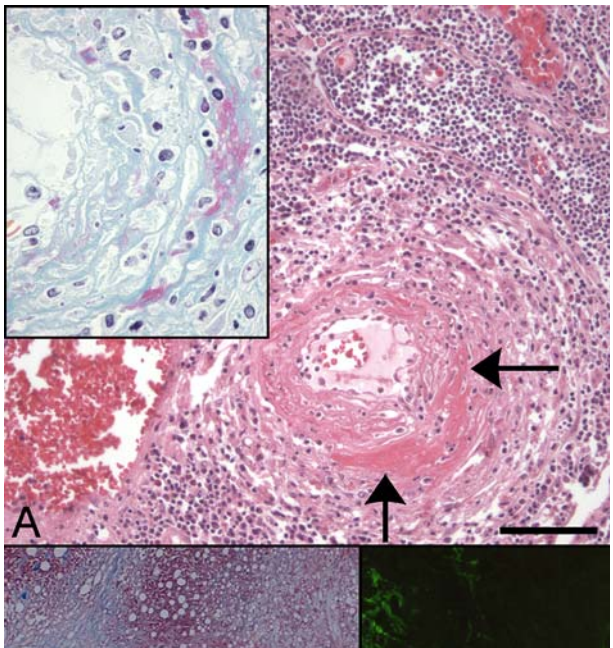

Fig. 3 Lymph node paracortex (**a**) and lymph node pseudocyst (**a** and **b**). **a** Small caliber blood vessel with an "onion-skin" appearance, infiltrating lymphocytes, and fibrin extravasate in the vessel wall (*arrows*). Hematoxylin & eosin, *bar*=100 μm. *Inset*: Lendrum stain highlights fibrin deposits. **b** Lymph node pseudocyst containing amorphous, granular, and flocculent material (chyle). Trichrome stain, *bar*=100 μm. **c** IF stain for fibrinogen

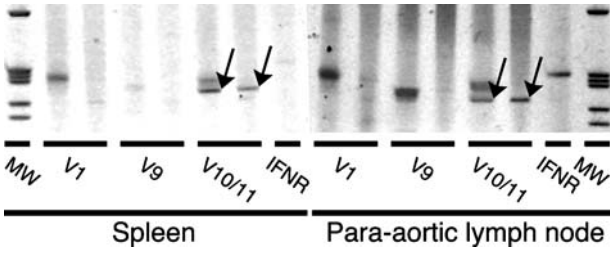

Fig. 4 Results of PCR heteroduplex analysis for TCR-γ gene rearrangement from patient's spleen and para-aortic lymph node (*arrows* indicate monoclonal products of similar molecular weight with the V10/11 primers). The first lane of every primer type was loaded with half of the PCR product run directly and the second lane with the remaining PCR product after heat denaturation and reannealing (heteroduplex analysis). *MW* Molecular weight, *IFNR* interferon receptor (control for DNA quality)

could not be determined reliably, and PCR for TCR-γ gene rearrangement of the brain tissue yielded unamplifiable DNA, possibly due to prolonged formalin fixation (1 week).

Discussion

Our patient had refractory celiac disease, based on an initial response to gluten-free diet with subsequent loss of responsiveness to the diet [29]. He subsequently developed a rapidly evolving fatal encephalopathy caused by an acute small-vessel angiopathy, superimposed on a subacute degeneration of the cerebellum and a peripheral neuropathy. The patient was receiving corticosteroids and antimicrobial treatment when he developed neurological symptoms, but cultures, PCR analysis, histologic exam, and electron microscopy ruled out an opportunistic infection. Autopsy revealed mild splenomegaly and a spectrum of destructive changes of the intra-abdominal and mediastinal lymph nodes, including chylous pseudocyst formation in numerous mesenteric lymph nodes, the latter consistent with MLNC [20, 25]. The small-bowel mucosa was flattened, and a clonal expansion of intraepithelial lymphocytes was observed. These lymphocytes lacked morphologic atypia but had an aberrant phenotype (CD4-CD8-). Generalized gastrointestinal mucosal and extraintestinal spread of clonal T cells to the blood and other organs, in the absence of a morphologically overt lymphoma, has been described in patients with refractory celiac disease [9, 10, 31], and many of these patients are believed to have a cryptic enteropathy-associated T-cell lymphoma (EATL) [8, 9].

The pathogenesis of MLNC is unclear; the two extant theories have proposed lymph node damage either due to chronic immune stimulation [18] or the consequence of complement-mediated endothelial damage due to vascular immune complex deposition [23]. Moreover, none of the reported cases of MLNC have documented extra-abdominal lymph node involvement or the presence of a clonal T-cell population within the lymph nodes. Our findings suggest that vascular damage and lymphocyte depletion of secondary lymphoid organs in our case could have been mediated by circulating activated T cells that originated from the small-bowel epithelial compartment. It remains unclear, however, whether cytokines or a contact-mediated mechanism (or both) were responsible for endothelial damage and bystander killing of lymphocytes.

Numerous neurological disorders have been associated with celiac disease [6, 11, 16], and patients with refractory sprue are at the greatest risk for developing these complications [26]. However, the prevalence of these disorders is not known, and an etiologic link with celiac disease remains controversial. Holmes [19] estimated that 6% of patients with celiac disease have neurological disorders. The most common neurological syndromes include cerebellar ataxia and peripheral neuropathy [17, 27]. Of all patients with ataxia, 50% or more have a coexisting neuropathy, usually caused by axonal degeneration [5, 17]. Both disorders often progress slowly [5, 7, 17], although, occasionally, the encephalopathy is rapid and fatal within a few weeks of onset as in our patient [24]. The cause of neurologic dysfunction remains unknown, but a link with HLA-DQ2 in a large percent of patients with gluten sensitivity and cerebellar ataxia suggests an underlying genetic predisposition [5, 7]. The presence of anti-ganglioside antibodies in a high proportion of patients who have peripheral neuropathies is also supportive of an autoimmune etiology [1].

A wide spectrum of histologic changes of the central nervous system (CNS) have been reported in patients with celiac-disease-associated neurological disorders [4, 11, 13, 17, 22, 26], but Purkinje cell loss and astrocytosis with or without a coexistent neuropathy are the most common finding. Less frequent pathologic features include perivascular lymphocytic infiltrates and reactive changes in endothelial cells of small vessels. Isolated CNS vasculitis has only been reported in one instance [28]. Our patient showed histologic signs of small blood vessel injury of the brain with marked perivascular edema, exudation of fibrin, and ischemic injury of the neural tissue. These findings are similar to those reported in a minority of patients who die due to a cerebral disorder associated with systemic lupus erythematosus [12, 21]. CNS vasculopathy mediated by a clonal circulating T-cell population has not been reported in any of the 21 published studies of celiac disease, where autopsy data was provided.

There are no standardized treatment regimens for celiac-disease-associated CNS complications or neuropathies, and gluten-free diet, the mainstay therapy, often fails to prevent or ameliorate neurological complications [26, 27]. A beneficial response to early dietary intervention, after the onset of neurological complications, has been reported in some patients with neuropathies [15]. Since the vast majority of patients with neurological symptoms do not have a detectable hypovitaminosis, treatment with vitamins (i.e. vitamin B12, folic acid, or vitamin D) is deemed to be of little value [26, 27]. An improvement in symptoms was reported for a patient with cerebral vasculitis, treated with prednisone and cyclophosphamide [28], and for a patient with a brainstem–cerebellar syndrome, who was treated with prednisone alone [14]. Similar immunosuppressive regimens, however, have failed to halt or revert the neurological manifestations of other patients [2, 24, 26].

In summary, we describe a patient with refractory celiac disease who had a CNS disorder due to a small vessel vasculitis in association with MLNC, both possibly linked to the presence of a circulating clone of activated T cells, conceivably representing a cryptic EATL.

References

1. Alaedini A, Green PH, Sander HW, Hays AP, Gamboa ET, Fasano A, Sonnenberg M, Lewis LD, Latov N (2002) Ganglioside reactive antibodies in the neuropathy associated with celiac disease. J Neuroimmunol 127:145–148
2. Beyenburg S, Scheid B, Deckert-Schluter M, Lagreze HL (1998) Chronic progressive leukoencephalopathy in adult celiac disease. Neurology 50:820–822

3. Bottaro M, Berti E, Biondi A, Migone N, Crosti L (1994) Heteroduplex analysis of T-cell receptor gamma gene rearrangements for diagnosis and monitoring of cutaneous T-cell lymphomas. Blood 83:3271–3278
4. Brucke T, Kollegger H, Schmidbauer M, Muller C, Podreka I, Deecke L (1988) Adult coeliac disease and brainstem encephalitis. J Neurol Neurosurg Psychiatry 51:456–457
5. Burk K, Bosch S, Muller CA, Melms A, Zuhlke C, Stern M, Besenthal I, Skalej M, Ruck P, Ferber S, Klockgether T, Dichgans J (2001) Sporadic cerebellar ataxia associated with gluten sensitivity. Brain 124:1013–1019
6. Bushara KO (2005) Neurologic presentation of celiac disease. Gastroenterology 128:S92–S97
7. Bushara KO, Goebel SU, Shill H, Goldfarb LG, Hallett M (2001) Gluten sensitivity in sporadic and hereditary cerebellar ataxia. Ann Neurol 49:540–543
8. Carbonnel F, Grollet-Bioul L, Brouet JC, Teilhac MF, Cosnes J, Angonin R, Deschaseaux M, Chatelet FP, Gendre JP, Sigaux F (1998) Are complicated forms of celiac disease cryptic T-cell lymphomas? Blood 92:3879–3886
9. Cellier C, Delabesse E, Helmer C, Patey N, Matuchansky C, Jabri B, Macintyre E, Cerf-Bensussan N, Brousse N (2000) Refractory sprue, coeliac disease, and enteropathy-associated T-cell lymphoma. French Coeliac Disease Study Group. Lancet 356:203–208
10. Cellier C, Patey N, Mauvieux L, Jabri B, Delabesse E, Cervoni JP, Burtin ML, Guy-Grand D, Bouhnik Y, Modigliani R, Barbier JP, Macintyre E, Brousse N, Cerf-Bensussan N (1998) Abnormal intestinal intraepithelial lymphocytes in refractory sprue. Gastroenterology 114:471–481
11. Cooke WT, Smith WT (1966) Neurological disorders associated with adult coeliac disease. Brain 89:683–722
12. Ellis SG, Verity MA (1979) Central nervous system involvement in systemic lupus erythematosus: a review of neuropathologic findings in 57 cases, 1955–1977. Semin Arthritis Rheum 8:212–221
13. Finelli PF, McEntee WJ, Ambler M, Kestenbaum D (1980) Adult celiac disease presenting as cerebellar syndrome. Neurology 30:245–249
14. Ghezzi A, Filippi M, Falini A, Zaffaroni M (1997) Cerebral involvement in celiac disease: a serial MRI study in a patient with brainstem and cerebellar symptoms. Neurology 49:1447–1450
15. Gobbi G, Bouquet F, Greco L, Lambertini A, Tassinari CA, Ventura A, Zaniboni MG (1992) Coeliac disease, epilepsy, and cerebral calcifications. The Italian Working Group on Coeliac Disease and Epilepsy. Lancet 340:439–443
16. Green PH, Alaedini A, Sander HW, Brannagan TH III, Latov N, Chin RL (2005) Mechanisms underlying celiac disease and its neurologic manifestations. Cell Mol Life Sci 62:791–799
17. Hadjivassiliou M, Grunewald RA, Chattopadhyay AK, Davies-Jones GA, Gibson A, Jarratt JA, Kandler RH, Lobo A, Powell T, Smith CM (1998) Clinical, radiological, neurophysiological, and neuropathological characteristics of gluten ataxia. Lancet 352:1582–1585
18. Holmes GK (1986) Mesenteric lymph node cavitation in coeliac disease. Gut 27:728–733
19. Holmes GK (1997) Neurological and psychiatric complications of coeliac disease. In: Gobbi G, Andermann F, Naccarato S, Banchini G (eds) Epilepsy and other neurological disorders in coeliac disease. John Libbey, London, pp 251–264
20. Howat AJ, McPhie JL, Smith DA, Aqel NM, Taylor AK, Cairns SA, Thomas WE, Underwood JC (1995) Cavitation of mesenteric lymph nodes: a rare complication of coeliac disease, associated with a poor outcome. Histopathology 27:349–354
21. Johnson RT, Richardson EP (1968) The neurological manifestations of systemic lupus erythematosus. Medicine (Baltimore) 47:337–369
22. Kinney HC, Burger PC, Hurwitz BJ, Hijmans JC, Grant JP (1982) Degeneration of the central nervous system associated with celiac disease. J Neurol Sci 53:9–22
23. Le Quellec A, Ciurana AJ, Greth I, Eliaou JF, Pages A (1990) Hemorrhagic necrosis of the mesenteric lymph nodes in adult celiac disease. Physiopathologic interpretation of 1 case. Ann Pathol 10:194–197
24. Luostarinen L, Pirttila T, Collin P (1999) Coeliac disease presenting with neurological disorders. Eur Neurol 42:132–135
25. Matuchansky C, Colin R, Hemet J, Touchard G, Babin P, Eugene C, Bergue A, Zeitoun P, Barboteau MA (1984) Cavitation of mesenteric lymph nodes, splenic atrophy, and a flat small intestinal mucosa. Report of six cases. Gastroenterology 87:606–614
26. Muller AF, Donnelly MT, Smith CM, Grundman MJ, Holmes GK, Toghill PJ (1996) Neurological complications of celiac disease: a rare but continuing problem. Am J Gastroenterol 91:1430–1435
27. Pengiran Tengah DS, Wills AJ, Holmes GK (2002) Neurological complications of coeliac disease. Postgrad Med J 78:393–398
28. Rush PJ, Inman R, Bernstein M, Carlen P, Resch L (1986) Isolated vasculitis of the central nervous system in a patient with celiac disease. Am J Med 81:1092–1094
29. Ryan BM, Kelleher D (2000) Refractory celiac disease. Gastroenterology 119:243–251
30. Sollid LM (2002) Coeliac disease: dissecting a complex inflammatory disorder. Nat Rev Immunol 2:647–655
31. Verkarre V, Asnafi V, Lecomte T, Patey Mariaud-de Serre N, Leborgne M, Grosdidier E, Le Bihan C, Macintyre E, Cellier C, Cerf-Bensussan N, Brousse N (2003) Refractory coeliac sprue is a diffuse gastrointestinal disease. Gut 52:205–211

Virchows Arch (2006) 448: 214–217
DOI 10.1007/s00428-005-0067-3

CASE REPORT

Frank Traub · Karin Sickmann · Mathewos Tessema · Ludwig Wilkens · Hans H. Kreipe · Kenji Kamino

Nephroblastomatosis and loss of *WT1* expression associated with trisomy 13

Received: 1 June 2005 / Accepted: 16 August 2005 / Published online: 22 September 2005

Abstract Trisomy 13 (Pätau's syndrome) is a rare finding in newborns. The life span of babies affected by this chromosome abnormality is severely shortened, and multiple, partly severe malformations occur. In this study, we report on an unborn with trisomy 13 (artificially aborted on the 24th week) which showed, among other typical deformities, bilateral nephrogenic rests (nephroblastomatosis). Using molecular analysis, a loss of Wilms' tumor gene 1 (*WT1*) transcript and a biallelic expression of insulin growth factor 2 (*IGF2*) could be revealed. To our knowledge, this is the first reported case of trisomy 13 which showed this type of anomaly and gene expression findings.

Keywords Trisomy 13 · Nephroblastomatosis · Wilms' tumor · Gene expression

Introduction

Trisomy 13 (Pätau's syndrome) was first described by Pätau in 1960 as a chromosome abnormality due to an extra copy of the 13th chromosome [9]. It occurs in approximately 1/5,000 to 1/15,000 live births. Infants affected with trisomy 13 tend to be small at birth and have a microcephaly with sloping forehead. A holoprosencephaly is common and a myelo-meningocele is found in almost 50% of cases. Usually the child suffers from severe mental retardation, and seizures are common. Deformities of the eye, including microphthalmia, coloboma, and retinal dysplasia, frequently occur. Cleft lip, cleft palate, or both are present in most cases. Defects of the heart, like ventricular–septal defect, atrial–septal defect, patent ductus arteriosus, and dextrocardia, are frequently observed. Capillary hemangiomas, especially on the forehead in the midline, may also be present. The genitalia are frequently abnormal in both sexes. A single transverse crease on the palm, polydactyl, and hyperconvex, narrow fingernails are common. Hematologically, there is an increased frequency of nuclear projection in polymorph nuclear leukocytes and a persistence of fetal hemoglobin [5].

Nephrogenic rests are the consequence of residual metanephric tissue in a fully developed kidney. They usually occur along the perimeter of a mature renal lobe (perilobar), within the lobe itself (intralobar), or both (combined). Nephrogenic rests can be grossly obvious or microscopically discrete. Nephroblastomatosis designates nephrogenic rests that are multifocal or diffuse and implies more extensive disease. Universal (panlobar) nephroblastomatosis denotes complete replacement of the renal lobe by nephrogenic tissue. The fate of nephrogenic rests and nephroblastomatosis varies and includes hyperplasia, sclerosis, dormancy, obsolescence, or neoplasia [3]. Evidence strongly suggests that neoplastic transformation of nephrogenic rests results in Wilms' tumor (nephroblastoma). Nephrogenic rests frequently occur in the setting of Wilms' tumor; perilobar rests show a strong association with synchronous bilateral Wilms' tumors, whereas intralobar rests are more strongly associated with metachronous tumors [3]. Genetic studies have shown that nephrogenic rests often share many of the same chromosomal defects as Wilms' tumor, which provides further evidence that they are precursor lesions [1].

Case report

The pregnancy of a 31-year-old white woman (2 G/0 P) had been uneventful. Routine ultrasound scan in the 20th week of pregnancy revealed multiple malformations of the fetus.

F. Traub · K. Sickmann · M. Tessema · L. Wilkens · H. H. Kreipe · K. Kamino
Institute of Pathology, Medizinische Hochschule Hannover,
Carl-Neuberg-Str. 1,
D-30625 Hanover, Germany

L. Wilkens · K. Kamino (✉)
Institute of Cell and Molecular Pathology,
Medizinische Hochschule Hannover,
Carl-Neuberg-Str. 1,
D-30625 Hanover, Germany
e-mail: Kamino.Kenji@MH-Hannover.de
Tel.: +49-511-5324524
Fax: +49-511-5325721

An amniocentesis was performed and showed trisomy 13. After a lengthy discussion, the mother decided on an induced abortion on the 24th week of gestation. The family history was free of any noteworthy findings.

Pathologic findings

The male fetus measured 30.3 cm in crown–heel length and 3.8 cm in foot length and weighed 520 g. The head was reduced in size, with a circumference of 18.1 cm. As external anomalies, a unilateral cleft lip and palate as well as a significant hypertelorism and dysplasia of the ears were present. The external genitals were hypoplastic. The brain was very fragile, weighed approximately 70 g, and showed some unspecific dysplasia of the cerebellum and an aberration of the brain stem. The kidneys were enlarged (right 10 g, left 4 g, normal 3.5±0.7 g) and revealed hydronephrosis with hydroureter and showed polycystic dysplasia (Potter IIa). The cutting surface displayed bilateral diffuse peri- and intralobar nephroblastomatosis (histological image, Fig. 2). Further findings were hypoplastic lungs and a Meckel's diverticulum.

A fluorescence in situ hybridization (FISH) analysis of the lung tissue for chromosome 13 was performed to confirm the amniocentesis finding (Fig. 1).

Materials and methods

For histological analysis, 3-μm paraffin sections of all organs were stained routinely with hematoxylin and eosin. The histological evaluation was carried out using a light microscope (Fig. 2).

FISH was performed as described in detail earlier [16]. In brief, a 5-μm histological section was deparaffinized and pretreated, and hybridization was carried out with 13q14 (RB1, Abbott, Wiesbaden, Germany). Counterstaining was performed with 5 μl DAPI (Qbiogene, Heidelberg, Germany) and Vectashield antifade (Vector Laboratories, Burlington, USA). Evaluation of signals was carried out with an epifluorescence microscope (Axioskop 2, Zeiss, Oberkochen, Germany).

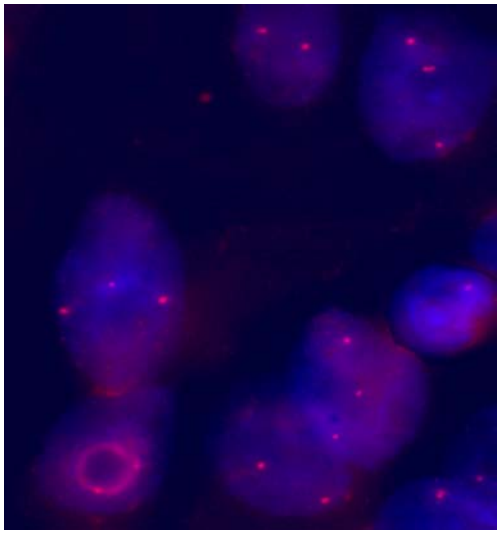

Fig. 1 To confirm the diagnosis of trisomy 13, FISH for chromosome 13 in lung tissue was performed. Three signals are clearly visible per cell

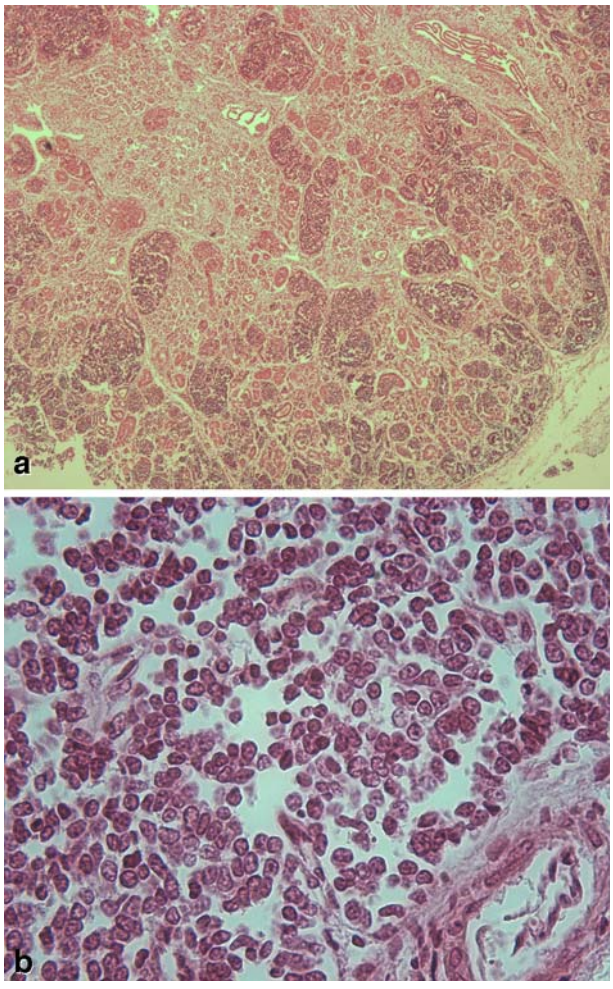

Fig. 2 **a** Multiple peri- and intralobar nephrogenic rests which are partly well and partly poorly circumscribed. Hematoxylin and eosin, original magnification 45×. **b** High-power magnification of an intralobular nephrogenic rest, consisting of round to oval, slightly pleomorphic cells with scanty cytoplasm. Hematoxylin and eosin, original magnification 400×

To assess basic genetic changes in nephrogenic rests, the mRNA expression of the tumors and the surrounding healthy tissue was investigated using the PALM Laser-MicroBeam System (P.A.L.M., Germany), which enables contact-free isolation of defined cell populations. A total of 35 histologically mature respectively forming glomeruli and adjacent tubuli as well as an equal area of nephrogenic rests were microdissected. Total RNA was extracted using phenol–chloroform precipitation and transcribed into complementary DNA. All techniques have been described previously by Lehmann et al. [7] and are well established in our laboratory.

PCR primers for expression of Wilms' tumor gene 1 (*WT1*), adult skeletal muscle gene (*H19*), insulin growth factor 2 (*IGF2*), and *β-Gus* were used (Table 1). The target

Table 1 Primer sequences used in this study

Gene	Sequence (5′ to 3′)
H19	CAACCACTGCACTACCTGACTCAG
	GTCTTTGATGTTGGGCTGATGAG
IGF2	GAGTCCCTGAACCAGCAAAGAG
	CCGTGAGAAGGGAGATGGC
WT1	CAGGCAGCACAGTGTGTGAAC
	TCCAGGCACACCTGGTAGT
β-Gus	CTCATTTGGAATTTTGCCGATT
	CCGGAGTGAAGATCCCCTTTTTA

genes for molecular investigation were chosen because of their supposed roles in Wilms' tumor development: *β-Gus* was used as positive DNA input control.

To screen for known polymorphism in *H19* and *IGF2*, genomic DNA was extracted from lung and normal kidney tissue and analyzed using restriction enzyme digestion described in detail by Tessema et al. [14]. For the imprinting analysis, restriction enzymes *Apa*I (*IGF2*) and *Alu*I (*H19*) were used according to the manufacturer's instructions (Fermentas GmbH, Germany).

Results

For *WT1*, an expression was detected in forming glomeruli and mature ones as well as in surrounding tubuli, but in the nephrogenic rests, no expression was detectable (Fig. 3). Concerning *IGF2* and *H19*, RNA expression was found in all examined tissues. Because it is known that *H19* and *IGF2* are imprinted genes and, thus, normally only one allele is expressed (*IGF2* paternal, *H19* maternal), restriction enzyme digestion was used to screen for polymorphisms. Heterozygosity for *IGF2* and homozygosity for *H19* were observed in lung and normal kidney tissues. Concerning *IGF2*, monoallelic expression (imprinting) was found in the normal tissue, whereas a biallelic expression was observed in the nephrogenic rests (Fig. 3b).

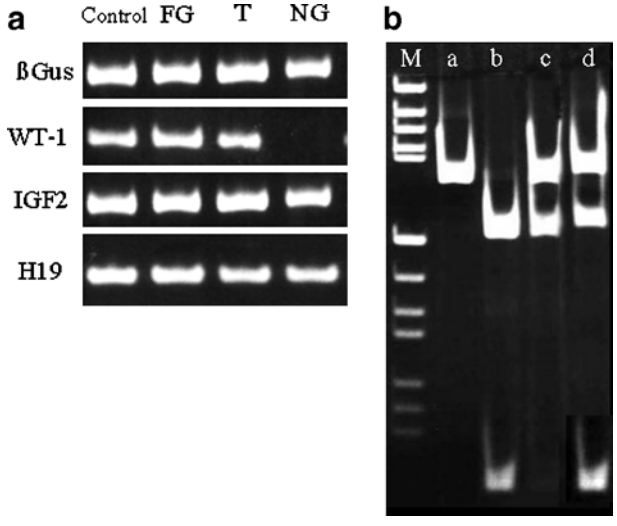

Fig. 3 **a** Expression of *WT1*, *IGF2*, *H19*, and *β-Gus* in different compartments. *FG* Forming glomeruli, *T* tubuli, *NG* nephrogenic rests. The loss of *WT1* expression in NG is obvious. **b** Imprinting analysis of *IGF2*. *Lanes a* and *b* show different polymorphism restriction products (control). *Lane c* shows that the two different alleles are present on DNA level (heterozygosity). In *lane d*, expression of *IGF2* mRNA is shown (NG tissue). Because two bands are visible, *IGF2* must be biallelically expressed. Controls of normal tissue show only one band (data not shown)

Discussion

An interesting aspect of the pathogenesis of nephroblastoma is the presence of immature embryonic nephrogenic rests and the genetic relationship between these entities. Nephroblastomas are assumed to develop from nephrogenic rests by accumulating genetic alterations and are considered as subclones of nephrogenic rests. The heterogenous genetic pathogenesis of Wilms' tumors has already been the focus of extensive research [12]. So far, a lower level of *WT1* gene transcripts in tumors has been revealed and a correlation of *WT1* mutations with stromal-predominant histology of nephroblastomas could be demonstrated [1]. The role of *WT1* in renal development and maturation of blastema cells suggests that abnormalities of this gene may be involved in the persistence of blastema and hence have a role in the early pathogenesis of Wilms' tumors [11]. Consistent with such pervious results, in the unborn fetus presented in this article, transcripts of *WT1* were not detected in the nephrogenic rests but expression was found in the adjacent tissue.

Other genes, including *H19* and *IGF2* (located at 11p15 downstream of *WT1*) and a putative *WT2* at the same location, are likely to be involved in the pathogenesis of Wilms' tumors. *H19* is a developmentally regulated gene with putative tumor suppressor activity, and loss of *H19* expression may be involved in Wilms' tumorigenesis [4]. Drummond et al. (1992) could demonstrate that the *WT1* gene product binds to multiple sites in the promoter region of *IGF2* and acts as a potent transcription repressor in vivo [2]. In a report from Reeve et al., it is stated that in Wilms' tumors, an overexpression of the *IGF2* protein is found [10]. Others reported a loss of imprinting of *IGF2* in sporadic Wilms' tumors and in a group of patients with Beckwith–Wiedemann syndrome [15]. In the present unborn, we were able to detect biallelic expression of *IGF2*, and *WT1* RNA expression was not measurable with the chosen setup in the nephrogenic rests. These findings support the assumption that a loss of *WT1* causes an *IGF2* overexpression and acts as a repressor for *IGF2* transcription. The data from the literature and our results suggest that the loss of *WT1* and the overexpression of *IGF2* possibly support the development of nephrogenic rest to a nephroblastoma.

Concerning the combination of Wilms' tumor and chromosomal aberration, there is the WAGR syndrome showing aniridia, hemihypertrophy, genitourinary dysplasia, mental retardation and other congenital anomalies, and Wilms' tumor [8]. It is well known that this syndrome is associated

with a deletion of chromosomal segment 11p13 on which also the *WT1* gene is located.

Up to now, only two reports of trisomy 13 and nephroblastomatosis, with respect to Wilms' tumor, are to be found in the literature, but no molecular findings are reported [6, 13]. Thus, the question whether the parallel occurrence of trisomy 13 and nephroblastomatosis is a coincidence or whether there is a link between both abnormalities has to be resolved by further investigations.

References

1. Charles AK, Brown KW, Berry PJ (1998) Microdissecting the genetic events in nephrogenic rests and Wilms' tumor development. Am J Pathol 153(3):991–1000
2. Drummond IA, Madden SL, Rohwer-Nutter P, Bell GI, Sukhatme VP, Rauscher FJ III (1992) Repression of the insulin-like growth factor II gene by the Wilms tumor suppressor WT1. Science 257(5070):674–678
3. Hennigar RA, O'Shea PA, Grattan-Smith JD (2001) Clinicopathologic features of nephrogenic rests and nephroblastomatosis. Adv Anat Pathol 8(5):276–289
4. Hu JF, Vu TH, Hoffman AR (1997) Genomic deletion of an imprint maintenance element abolishes imprinting of both insulin-like growth factor II and H19. J Biol Chem 272(33): 20715–20720
5. Jones KL (1997) Trisomy 13 syndrome. In: Jones KJ (ed) Smith's recognizable patterns of human malformation, 5th edn. Saunders, Philadelphia, pp 18–19
6. Keshgegian AA, Chatten J (1979) Nodular renal blastema in trisomy 13. Arch Pathol Lab Med 103:73–75
7. Lehmann U, Glockner S, Kleeberger W, von Wasielewski HF, Kreipe H (2000) Detection of gene amplification in archival breast cancer specimens by laser-assisted microdissection and quantitative real-time polymerase chain reaction. Am J Pathol 156(6):1855–1864
8. Miller RW, Fraument JF Jr, Manning MD (1964) Association of Wilms's tumor with aniridia, hemihypertrophy and other congenital malformations. N Engl J Med 270:922–927
9. Patau K, Smith DW, Therman E, Inhorn SL, Wagner HP (1960) Multiple congenital anomaly caused by an extra autosome. Lancet 9:790–793
10. Reeve AE, Eccles MR, Wilkins RJ, Bell GI, Millow LJ (1985) Expression of insulin-like growth factor-II transcripts in Wilms' tumour. Nature 317(6034):258–260
11. Schumacher V, Schuhen S, Sonner S, Weirich A, Leuschner I, Harms D, Licht J, Roberts S, Royer-Pokora B (2003) Two molecular subgroups of Wilms' tumors with or without WT1 mutations. Clin Cancer Res 9(6):2005–2014
12. Strong LC (2003) The two-hit model for Wilms' tumor: where are we 30 years later? Genes Chromosomes Cancer 38(4):294–299
13. Sweeney H, Pelegano J (2000) Wilms tumor in a child with trisomy 13. J Pediatr Hematol Oncol 22(2):171–172
14. Tessema M, Langer F, Bock O, Seltsam A, Hasemeier B, Kreipe H, Lehmann U (2005) Down-regulation of the IGF-2/H19 locus during normal and malignant hematopoiesis is independent of the imprinting pattern. Int J Oncol 26(2):499–507
15. Weksberg R, Shen DR, Fei YL, Song QL, Squire J (1993) Disruption of insulin-like growth factor 2 imprinting in Beckwith–Wiedemann syndrome. Nat Genet 5(2):143–150
16. Wilkens L, Gerr H, Gadzicki D, Kreipe H, Schlegelberger B (2005) Standardized fluorescence in situ hybridisation in cytological and histological specimens. Virchows Archiv (in press)

Virchows Arch (2006) 448: 218–222
DOI 10.1007/s00428-005-0143-8

CASE REPORT

Catherine Guettier · Pierre Validire · Dominique Emilie · Viviane Tricottet · Mylène Sebagh · Aurora Anjo · Jean-Louis Misset · Michel Reynes

Follicular dendritic cell tumor of the mediastinum: expression of fractalkine and SDF-1α as mast cell chemoattractants

Received: 27 November 2005 / Accepted: 5 December 2005 / Published online: 12 January 2006

Abstract Follicular dendritic cell tumor (FDCT) is a rare tumor mainly located in laterocervical lymph nodes. We report one case of mediastinal FDCT associated with a history of bullous skin disease and clinically obvious immunosuppression. This tumor was characterized by heavy mast cell infiltration. Mast cells were in close relationship with tumor cells as demonstrated by ultrastructural examination and their presence are probably related with the strong expression of mast cell chemoattractants as fraktalkine and stromal cell-derived factor-1α by tumor cells. The long follow-up period of more than 17 years allowed to us assess the relatively indolent evolution of this tumor characterized by three slowly growing local recurrences without metastasis.

Keywords Follicular dendritic cell tumor · Mediastinum · Mast cells · Fractalkine · SDF-1α

C. Guettier (✉) · V. Tricottet · M. Sebagh · M. Reynes
Department of Pathology,
Assistance Publique des Hôpitaux de Paris (AP–HP),
Hôpital Paul Brousse,
12 avenue Paul Vaillant-Couturier,
UPRES 3541 Université PARIS XI,
Villejuif cedex 94804, France
e-mail: catherine.guettier@pbr.ap-hop-paris.fr
Tel.: +33-1-45593018

P. Validire
Department of Pathology Institut Mutualiste Montsouris
42 boulevard Jourdan,
Paris cedex, 75674, France

D. Emilie
Institut Paris–Sud sur les Cytokines Hôpital Antoine Béclère
157 rue de la Porte de Trivaux,
Clamart 92141, France

A. Anjo
ICIG Hôpital Paul Brousse,
Villejuif, France

J.-L. Misset
FMSIT, Assistance Publique des Hôpitaux de Paris,
Hôpital Paul Brousse,
Villejuif, France

Introduction

Follicular dendritic cell tumor (FDCT) is an uncommon tumor, usually affecting laterocervical lymph nodes. Among the nearly 70 cases reported hitherto in the literature, 11 cases are of mediastinal localization [1, 3, 4, 6, 9, 10, 14].

We report one additional case of mediastinal FDCT occurring in a patient with a long-lasting history of bullous skin disease diagnosed as pemphigus vulgaris and clinically obvious immunosuppression. This case is characterized by the unusual presence of numerous mast cells in close relationship with tumor cells as demonstrated by ultrastructural examination. The tumor had a relatively indolent behavior because the patient is still alive after a 17-year follow-up despite three local recurrences after several years of latency.

Clinical history

The patient, a 45-year-old male Italian was referred to our institution for recurrence of a mediastinal mass. He had a long history of pemphigus vulgaris treated with corticoids since 1985. Complete surgical excision of a mediastinal mass of 10 cm in size from anterior and median mediastinum was performed in Italy in March 1987; the histological diagnosis was diffuse mixed B cell lymphoma. At this time, there was neither abdominal nor peripheral lymphadenopathy and bone marrow biopsy was negative. Chemotherapy was delayed for 4 months because of the occurrence of visceral leishmaniosis. The patient finally received six cures of Cytoxan, hydroxydaunomycin (Adriamycin), vincristine (Oncovin), and prednisone from July 1987 to February 1988. In May 1988, a chest CT scan on follow-up disclosed a residual mediastinal mass of 2 cm large associated with a parenchymal nodule in Nelson's lobe. Both lesions were surgically removed; the histological diagnosis of tuberculosis was confirmed by bacteriological results identifying *Mycobacterium Tuberculosis* from culture. In April 1989, a new chest CT scan showed again a 2.5-cm large mass located in the anterior medias-

tinum. This lesion remained stable at least until 1992. At this time, chronic hepatitis C was diagnosed. Then the patient was followed up for 8 years by chest X-ray.

A chest CT scan performed in November 2000 showed a large polylobated mediastinal tumor of 15 cm rising to the left subclavicular area. Clinical examination was otherwise normal without any sign of compression. There was no cutaneous or mucosal blistering lesion. A surgical biopsy of the subclavicular tumor extension was rapidly performed and the histological diagnosis of FDCT led to the decision to undergo surgical resection, which was performed in January 2001. The tumor was encapsulated and could be totally excised in two parts. The patient recovered uneventfully after the operation.

He came back 2 years later in March 2003 for a left cervical mass of 7 cm in size close to the thyroid. This new lesion was considered to have developed from seeding on the biopsy tract and was surgically removed. A new small and asymptomatic paraesophageal tumor was disclosed on CT scan in December 2003. The patient was followed up for one additional year until the onset of compression symptoms led to a new surgical thoracic procedure successfully performed in December 2004.

Material and methods

All techniques were performed on samples from the mediastinal tumor removed in 2001.

Immunohistochemistry

Immunohistochemical studies were performed on paraffin and frozen sections using a labeled streptavidin biotin technique with the following antibodies (1) on paraffin sections: KL1 (Immunotech), anti-epithelial membrane antigen (EMA), anti-vimentin, anti-smooth-muscle actin, antidesmine, CD20, CD3, CD 68, anti-human leukocyte antigen anti-(HLA)-DR, anti-PS100, anti-neuron-specific enolase (NSE), CD31, CD34, c-kit (CD117), CD1a, anti-lysozyme, anti-latent membrane protein (LMP)1, CD35, CNA42, CD21 (Dakopatts), and antiepidermal growth factor receptor (EGFr) (31G7—Zymed) and (2) on frozen sections: CD35, anti-HLA-DR, CD23 (Dakopatts), anti-stromal cell-derived factor-1α (SDF-1α) [2], and anti-fractalkine (CX3C) (Chemocentrix). Antifractalkine and anti-SDF1 immunostaining was performed on control tissues, i.e., normal lymph node and fetal liver. Antigen retrieval was achieved on paraffin sections by steaming in citrate buffer pH 6.1 prior to incubation with all antibodies except anti-actin, anti-LMP1, anti-PS100, and anti-lysozyme, and by protease digestion for anti-LMP1.

In situ hybridization

Non-isotopic in situ hybridization for Epstein–Barr virus-encoded RNA (EBER) was performed on paraffin sections using fluorescein isothiocyanate-conjugated PNA probe for EBER and detection kit from Dakopatts.

Electron microscopy

Tissue samples fixed in a 2.5% glutaraldehyde solution were postfixed in osmium tetroxide and embedded in epoxy resin. Ultrathin sections were cut and contrasted with uranyl acetate and lead citrate after the selection of appropriate blocks on semithin sections examination. The ultrathin sections were examined using a JEOL transmission electron microscope JEM 100C.

Results

Gross findings

The resection specimen of the mediastinal mass was composed of two parts weighting 410 and 130 g and measuring 12×9×8 and 9×6×5 cm, respectively. The tumor was well limited by a thin capsule. On the cut section, it was homogeneously whitish and firm without any necrotic or hemorrhagic area. A normal residual thymus of 9 cm in its highest dimension was identified at the right edge of the mass. The recurrent cervical lesion removed in March 2003 was a well-limited mass of 6 cm in size with the same gross aspect. In December 2004, the surgical specimens consisted of a paraesophageal and a cervical tumor measuring 6×5×4.5 and 4×2.5×2.5 cm.

Histological findings

The mediastinal mass and the recurrent lesions showed the same histological pattern. The tumor cells were spindle or ovoid with a moderate amount of lightly eosinophilic cy-

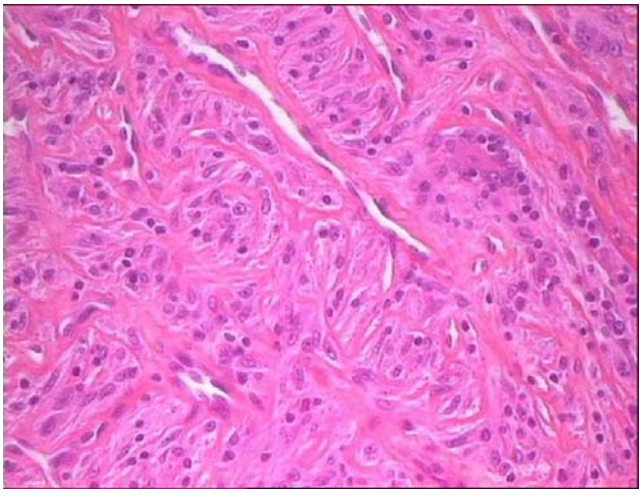

Fig. 1 Spindle cells organized in short fascicles intermingled with thin collagen bundles (HE: original magnification ×400)

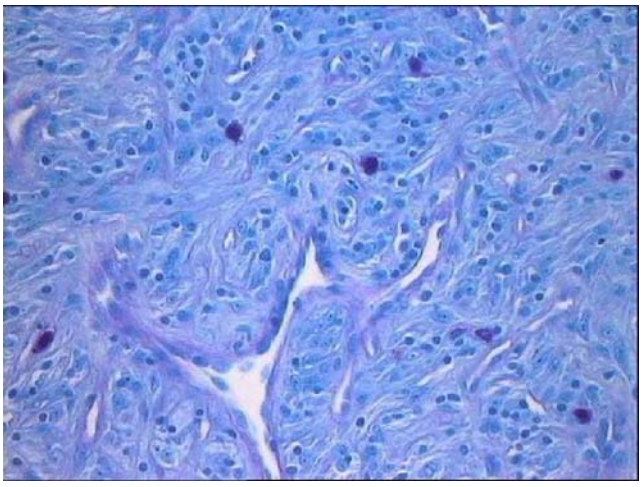

Fig. 2 Giemsa staining highlighting the presence of numerous mast cells in addition to small lymphocytes and plasma cells (Giemsa: original magnification ×400)

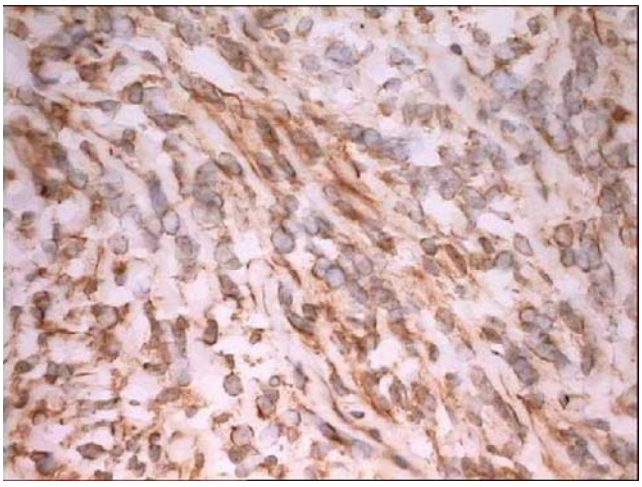

Fig. 4 Strong cytoplasmic and membranous staining of tumor cells with antifractalkine antibody (Immunoperoxidase: original magnification ×400)

toplasm; they were arranged in short fascicles intermingled with numerous bundles of hyaline collagen (Fig. 1). Their nuclei were often irregularly folded with clear nucleoplasm and one or two nucleoli that are small to medium in size. Nuclear atypia were mild. Mitotic count was low, less than 1 mitosis per 10 high-power fields. Frequent binucleated cells and occasional symplasmic elements with abundant eosinophilic cytoplasm were seen. There was no necrotic change.

The entire tumor was sprinkled with a heavy population of small lymphocytes, often cuffing around blood vessels. In addition, numerous mast cells highlighted on Giemsa staining were present (Fig. 2). Plasma cells were rare.

The vasculature was represented by a rich network of small blood vessels, some of them with hyalinized wall. There was no residual lymphoid tissue within the mass. The adjacent thymus was histologically normal.

On review, the histological pattern of the first mediastinal tumor removed in 1987 was exactly similar and the revised diagnosis for this tumor was FDCT.

Immunohistochemistry and in situ hybridization

Tumor spindle cells were strongly positive for vimentin and CD68 and negative for cytokeratin, EMA, alpha-actin, desmin, NSE, PS100, CD31, CD34, c-kit, CD1a, and lysozyme. They expressed all known markers of follicular dendritic cells: HLA-DR, CNA42, CD35, CD21 (Fig. 3), and CD23. Anti-EGFr staining was strongly positive on most tumor cells with a membrane pattern. The small lymphocytes were a mixture of CD20-positive B cells and CD3-positive T cells. The background cells also included numerous c-kit positive mast cells. LMP1 immunostaining was negative.

Antifractalkine antibody demonstrated a strong cytoplasmic and membranous positivity of tumor cells (Fig. 4) and of endothelial cells. On lymph node control sections, endothelial cells, interdigitating dendritic cells, and follicular dendritic cells were positive for fractalkine.

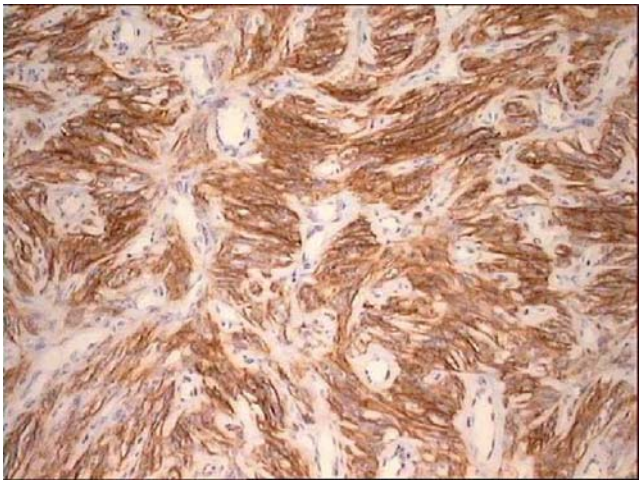

Fig. 3 Tumor cells showing strong immunoreactivity for CD21 (Immunoperoxidase: original magnification ×200)

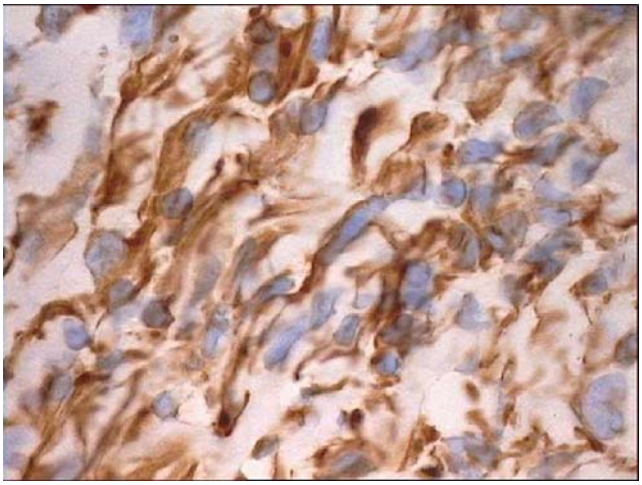

Fig. 5 Strong cytoplasmic and membranous staining of tumor cells with anti-SDF-1α antibody (Immunoperoxidase: original magnification ×1,000)

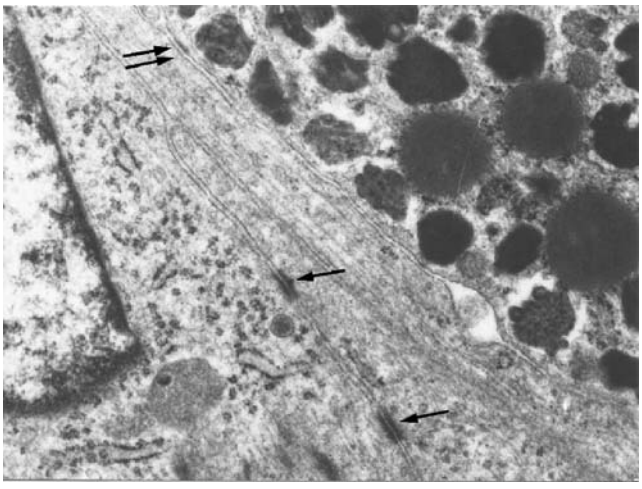

Fig. 6 Electron microscopy showing tumor cells with long and complex interdigitating processes with some desmosome-like junctions (*arrow*). Mast cell at the top containing granules at different stages of maturation and connected to a tumor cell process by a semijunction (*double arrow*) 1 cm=0.5μ

Anti-SDF1 antibody disclosed a membranous and cytoplasmic staining of tumor cells and endothelial cells (Fig. 5). On the fetal liver section, SDF1 was strongly expressed on epithelial ductal cells. Tumor cells were negative for EBER probe.

Ultrastructural findings

The tumor cells had numerous interwoven long villous processes, which were sometimes connected by desmosome-like junctions. The cytoplasm did not contain myofilaments.

The numerous mast cells had granules at different stages of maturation. Some mature granules were close to the cytoplasmic cell membrane. Mast cells were close to the tumor cells and frequently their villous processes were intermingled with those of tumor cells. Few semijunctions of the mast cell membrane were present at the contact with the tumor cells (Fig. 6).

Discussion

FDCT are rare tumors, the majority occurring in latero-cervical lymph nodes. Around 15% of all published cases arose or involved the mediastinum [1, 3, 4, 6, 9, 10, 13]. Four among these cases complicated a Castleman's disease [3, 10]. A special form of pemphigus called paraneoplastic pemphigus was described in association with FDCT arising or not from Castleman's disease [16]. In 1985, at the time when the diagnosis of pemphigus vulgaris was made in our patient, the paraneoplastic pemphigus was not yet described and the autoantibodies specific for this disease were not characterized. No serum contemporary with the skin disease was available for our patient to test retrospectively these autoantibodies. Nevertheless, the lack of parallelism between the evolution of the skin bullous disease and the mediastinal tumor is not in favor of a paraneoplastic process.

The expression of EGFr by tumor cells is in agreement with recently published data, which showed that nearly 90% of FDCT expressed EGFr and could be useful for therapeutic approach [17].

Reactive inflammatory cells in FDCT usually consist of small lymphocytes of T cell phenotype and plasma cells. The presence of numerous mast cells scattered all over the tumor is a previously unreported morphological feature in FDCT. At the ultrastructural level, the mast cells were in very close relationship with tumor cells and appeared in a state of active secretion This feature prompted us to look for the expression of chemokines acting as mast cell chemoattractants such as fractalkine and SDF-1α. Fractalkine is a CX3C chemokine constitutively expressed in diverse cell types including follicular dendritic cells within hyperplastic lymph nodes [5]. SDF-1α mRNA and protein are expressed by FDC-like cells in culture [7]. Both chemokines were strongly and diffusely expressed on tumor cells. Because mast cells express both CX3CR1 receptor for fractalkine and CXCR4 receptor for SDF-1α [8, 12] and fractalkine was shown to have in vitro chemotactic activity toward mast cells [11], the expression of fractalkine and SDF-1α is likely to be responsible for the presence of mast cells in close relationship with the tumor cells. Ultrastructural features in our case suggest that mast cells are in a state of active secretion. Mast cell infiltrations of various degrees were described in other types of nonepithelial tumors such as leiomyomas and leiomyosarcomas in the uterus [19], soft-tissue sarcomas [18], and more recently in the myxoid epithelioid variant of gastrointestinal tumor [15]. The presence of mast cells would be associated with better prognosis in some of these tumors [18, 19] and could also be a marker for a more indolent course of FDCT. FDCTs are considered as an intermediate-grade sarcoma associated with recurrence, metastatic, and mortality rates of 43, 24, and 17%, respectively [1]. We have followed up on our patient for an exceptionally long period of 17 years while most reported cases have follow-up data with a time interval inferior to 5 years. After an initial treatment consisting of surgical complete excision and adjuvant chemotherapy that is active against lymphoma, he experienced three slowly growing local recurrences at 13, 16 and 17 years without evidence of metastasis despite the large tumor size at the first recurrence. In the largest retrospective study of FDCT [1], only intraabdominal location and nuclear pleomorphism are significantly associated with a higher rate of recurrence, metastasis, or death. In addition, large sized tumors (>6 cm), the presence of coagulative necrosis, abnormal mitoses, high mitotic activity, and lack of adjuvant therapy are likely to be morphologic predictors of unfavorable events [1, 13]; our patient met only the first of these criteria. Very few data are available concerning specifically the course of mediastinal FDCT but in most reported cases, tumors exhibit histological signs of aggressive growth [6], which is not the case for our patient.

To the best of our knowledge this is the first demonstration of the expression of fractalkine and SDF-1α on the tumoral counterpart of follicular dendritic cells. Other FDCT have to be tested to determine the accuracy of fractalkine and SDF-1α as diagnosis markers for this type of tumor, which is often a difficult diagnostic challenge.

Acknowledgements The authors thank Prof. Thierry Molina from the Department of Pathology Hôtel-Dieu AP-HP Paris and Dr Agnès Carlotti from the Department of Pathology Paul Brousse Hospital AP-HP for helpful diagnostic discussions, and Ingrid Durand-Gasselin from Institut Paris-Sud sur les Cytokines Hôpital Antoine Béclère - Clamart for technical assistance.

References

1. Chan JK, Fletcher CD, Nayler SJ, Cooper K (1997) Follicular dendritic cell sarcoma. Clinicopathologic analysis of 17 cases suggesting a malignant potential higher than currently recognized. Cancer 79:294–313
2. Coulomb-L'Herminé A, Amara A, Schiff C, Durand-Gasselin I, Foussat A, Delaunay T, Chaouat G, Capron F, Ledee N, Galanaud P, Arenzana-Seisdedos F, Emilie D (1999) Stromal cell-derived factor 1 (SDF-1) and antenatal human B cell lymphopoiesis: expression of SDF-1 by mesothelial cells and biliary ductal plate epithelial cells. Proc Natl Acad Sci U S A 96:8585–8590
3. Desai SB, Pradhan SA, Chinoy RF (2000) Mediastinal Castleman's disease complicated by follicular dendritic cell tumour. Indian J Cancer 37:129–132
4. Fassina A, Marino F, Poletti A, Rea F, Pennelli N, Ninfo V (2001) Follicular dendritic cell tumor of the mediastinum. Ann Diagn Pathol 5:361–367
5. Foussat A, Coulomb-L'Hermine A, Gosling J, Krzysiek R, Durand-Gasselin I, Schall T, Balian A, Richard Y, Galanaud P, Emilie D (2000) Fractalkine receptor expression by T lymphocyte subpopulations and in vivo production of fractalkine in human. Eur J Immunol 30:87–97
6. Grogg KL, Lae ME, Kurtin PJ, Macon WR (2004) Clusterin expression distinguishes follicular dendritic cell tumors from other dendritic cell neoplasms: report of a novel follicular dendritic cell marker and clinicopathologic data on 12 additional follicular dendritic cell tumors and 6 additional interdigitating dendritic cell tumors. Am J Surg Pathol 28:988–998
7. Husson H, Carideo EG, Cardoso AA, Lugli SM, Neuberg D, Munoz O, de Leval L, Schultze J, Freedman AS (2001) MCP-1 modulates chemotaxis by follicular lymphoma cells. Br J Haematol 115:554–562
8. Juremalm M, Hjertson M, Olsson N, Harvima I, Nilsson K, Nilsson G (2000) The chemokine receptor CXCR4 is expressed within the mast cell lineage and its ligand stromal cell-derived factor-1alpha acts as a mast cell chemotaxin. Eur J Immunol 30:3614–3622
9. Krober SM, Marx A, Aebert H, Dohmen BM, Kaiserling E (2004) Sarcoma of follicular dendritic cells in the dorsal mediastinum. Hum Pathol 35:259–263
10. Lin O, Frizzera G (1997) Angiomyoid and follicular dendritic cell proliferative lesions in Castleman's disease of hyaline-vascular type: a study of 10 cases. Am J Surg Pathol 21:1295–1306
11. Papadopoulos EJ, Fitzhugh DJ, Tkaczyk C, Gilfillan AM, Sassetti C, Metcalfe DD, Hwang ST (2000) Mast cells migrate, but do not degranulate, in response to fractalkine, a membrane-bound chemokine expressed constitutively in diverse cells of the skin. Eur J Immunol 30:2355–2361
12. Papadopoulos EJ, Sassetti C, Saeki H, Yamada N, Kawamura T, Fitzhugh DJ, Saraf MA, Schall T, Blauvelt A, Rosen SD, Hwang ST (1999) Fractalkine, a CX3C chemokine, is expressed by dendritic cells and is up-regulated upon dendritic cell maturation. Eur J Immunol 29:2551–2559
13. Perez-Ordonez B, Erlandson RA, Rosai J (1996) Follicular dendritic cell tumor: report of 13 additional cases of a distinctive entity. Am J Surg Pathol 20:944–955
14. Perez-Ordonez B, Rosai J (1998) Follicular dendritic cell tumor: review of the entity. Semin Diagn Pathol 15:144–154
15. Sakurai S, Hasegawa T, Sakuma Y, Takazawa Y, Motegi A, Nakajima T, Saito K, Fukayama M, Shimoda T (2004) Myxoid epithelioid gastrointestinal stromal tumor (GIST) with mast cell infiltrations: a subtype of GIST with mutations of platelet-derived growth factor receptor alpha gene. Hum Pathol 35:1223–1230
16. Seishima M, Oda M, Oyama Z, Yoshimura T, Yamazaki F, Aoki T, Nei M, Hashimoto T (2004) Antibody titers to desmogleins 1 and 3 in a patient with paraneoplastic pemphigus associated with follicular dendritic cell sarcoma. Arch Dermatol 140:1500–1503
17. Sun X, Chang K-C, Abruzzo LV, Lai R, Younes A, Jones D (2003) Epidermal growth factor receptor expression in follicular dendritic cells: a shared feature of follicular dendritic cell sarcoma and Castleman's disease. Hum Pathol 34:835–840
18. Tomita Y, Aozasa K, Myoui A, Kuratsu S, Uchida A, Ono K, Matsumoto K (1993) Histologic grading in soft-tissue sarcomas. An analysis of 194 cases including AgNOR count and mast-cell count. Int J Cancer 54:194–199
19. Yavuz E, Gulluoglu MG, Akbas N, Tuzlali S, Ilhan R, Iplikci A, Akhan SE (2001) The values of intratumoral mast cell count and Ki-67 immunoreactivity index in differential diagnosis of uterine smooth muscle neoplasms. Pathol Int 51:938–941

Virchows Arch (2006) 448: 223–227
DOI 10.1007/s00428-005-0126-9

CASE REPORT

Klaus Willenbrock · Susanne Kriener · Sabine Oeschger · Martin-Leo Hansmann

Nodular lymphoid lesion of the liver with simultaneous focal nodular hyperplasia and hemangioma: discrimination from primary hepatic MALT-type non-Hodgkin's lymphoma

Received: 28 July 2005 / Revised: 15 September 2005 / Accepted: 21 September 2005 / Published online: 6 December 2005

Abstract Nodular lymphoid lesion (NLL) of the liver is a rare but unique entity and has also been termed reactive lymphoid hyperplasia of the liver. We describe the histological, immunohistochemical and molecular biologic findings of a case with NLL and two other tumors of the liver. The nodular lymphoid mass found in the liver was composed of heterogeneous small lymphocytes forming reactive follicles. Plasma cells, few immunoblasts, centroblasts, few macrophages, epithelioid cells, and giant cells were seen. The lymphoid infiltrate displaced the adjacent hepatic parenchyma. By immunohistochemistry and molecular studies, the lymphocytes were found to be polyclonal. The diagnosis of NLL was made. In addition to NLL, focal nodular hyperplasia and hemangioma were detected. The discrimination of NLL from primary hepatic malignant non-Hodgkin's lymphoma of mucosa- associated lymphoid tissue-type may pose diagnostic difficulties and may require the use of immunohistochemical and molecular techniques. The simultaneous occurrence of NLL with focal nodular hyperplasia and hemangioma in the liver has not been described before.

Keywords Liver neoplasms · Non-Hodgkin's lymphoma · Pseudolymphoma

Introduction

Nodular lymphoid lesion (NLL) is a rare condition observed in the liver. It is characterized by a nodular mass that displaces the normal parenchyma of the liver and is composed of lymphoid tissue with reactive follicles. NLL is a benign lesion, which has to be distinguished from malignant non-Hodgkin's lymphoma (NHL). The discrimination from primary hepatic lymphoma of the mucosa-associated lymphoid tissue (MALT) type, as introduced by Isaacson et al. in 1995 [4], is especially crucial and may pose considerable problems relying on conventional histological examination alone.

The case presented here displays three different benign liver tumors. In addition to NLL, focal nodular hyperplasia and hemangioma were detected. To the best of our knowledge, this is the first report of a simultaneous occurrence of these tumors in the liver.

K. Willenbrock (✉) · S. Kriener · S. Oeschger · M.-L. Hansmann
Senckenbergisches Institut für Pathologie,
Klinikum der Johann Wolfgang Goethe-Universität,
Theodor-Stern-Kai 7,
60590 Frankfurt am Main, Germany
e-mail: Willenbrock@em.uni-frankfurt.de
Tel.: +49-69-63015761
Fax: +49-69-63015241

Clinical history

A 36-year-old female patient was referred to the department of surgery with two tumors of the liver involving segments VII and VIII. The liver lesions had been detected by computed tomography, which had been performed as screening because of an ovarian cyst. The abdomen was soft on palpation with no pain on pressure and no palpable tumor. An open excisional biopsy of the two tumors was performed to rule out malignancy and establish a definite diagnosis. NHL could not be definitively ruled out in intraoperative frozen section histology. Therefore, a staging procedure was performed with the excision of representative lymph nodes from the pancreas, hepatoduodenal ligament, and mesentery of the small bowel. The postoperative course was uneventful.

Material and methods

Tissue was fixed in 4% buffered formalin, processed and embedded in paraffin. Five-micron sections were stained with hematoxylin and eosin. In addition, Giemsa and Ziehl–Neelsen staining were performed.

Immunohistochemical staining was performed on an automatic immunostainer (Autostainer 720, LabVision, Fremont, CA) by a labeled streptavidin biotin method

using alkaline phosphatase with fast red as chromogen. The following antibodies were applied: CD3 (PS1, Novocastra, Newcastle upon Tyne, UK), CD20 (L26, DakoCytomation, Glostrup, Denmark), immunoglobulin (Ig) κ and λ light chains (rabbit antihuman, Dako), and pan-cytokeratin (MNF116, Dako). Slides were pretreated by pressure cooking in 1 mM EDTA pH 8.0 for 45 sec for cytokeratin-, CD3-, and CD20-staining and by enzymatic digest with protease for 13 min (Protease XI, concentration 0,125%, Sigma-Aldrich, Munich, Germany) for staining of Ig light chains.

For polymerase chain reaction (PCR)-amplification of Ig-heavy chain (IgH) and T cell receptor γ (TCR-γ) chain gene rearrangements, the BIOMED-2 primer sets were used as recommended [17]. The length distribution of PCR fragments amplified was analyzed on an automated sequencer using the GeneScan software (ABI-prism 3100, Applied Biosystems, Darmstadt, Germany).

Results

A subcapsular specimen of 3.5×2.5×2-cm size was obtained from liver segment VIII. The cut surface displayed a brownish tumor of 1.8-cm diameter beneath the capsule. Upon macroscopic examination, the lesion seemed well-circumscribed, without a capsule or pseudocapsule. Histologically, the entire tumor consisted predominantly of mononuclear cells with formation of some lymph follicles (Fig. 1a,b). Between the follicles were small lymphocytes and plasma cells, few immunoblasts, some epithelioid cells, and giant cells (Fig. 1f). The lymphoid infiltrate displaced the hepatic parenchyma in a serpiginous fashion.

In the immunohistochemical investigation, the follicles contained $CD20^+$ centrocytic and some centroblastic B lymphocytes (Fig. 1c). B cells and plasma cells were polyclonal in κ and λ light chain stainings. The interfollicular area showed a mixed population of $CD3^+$ T cells (Fig. 1c,d) and

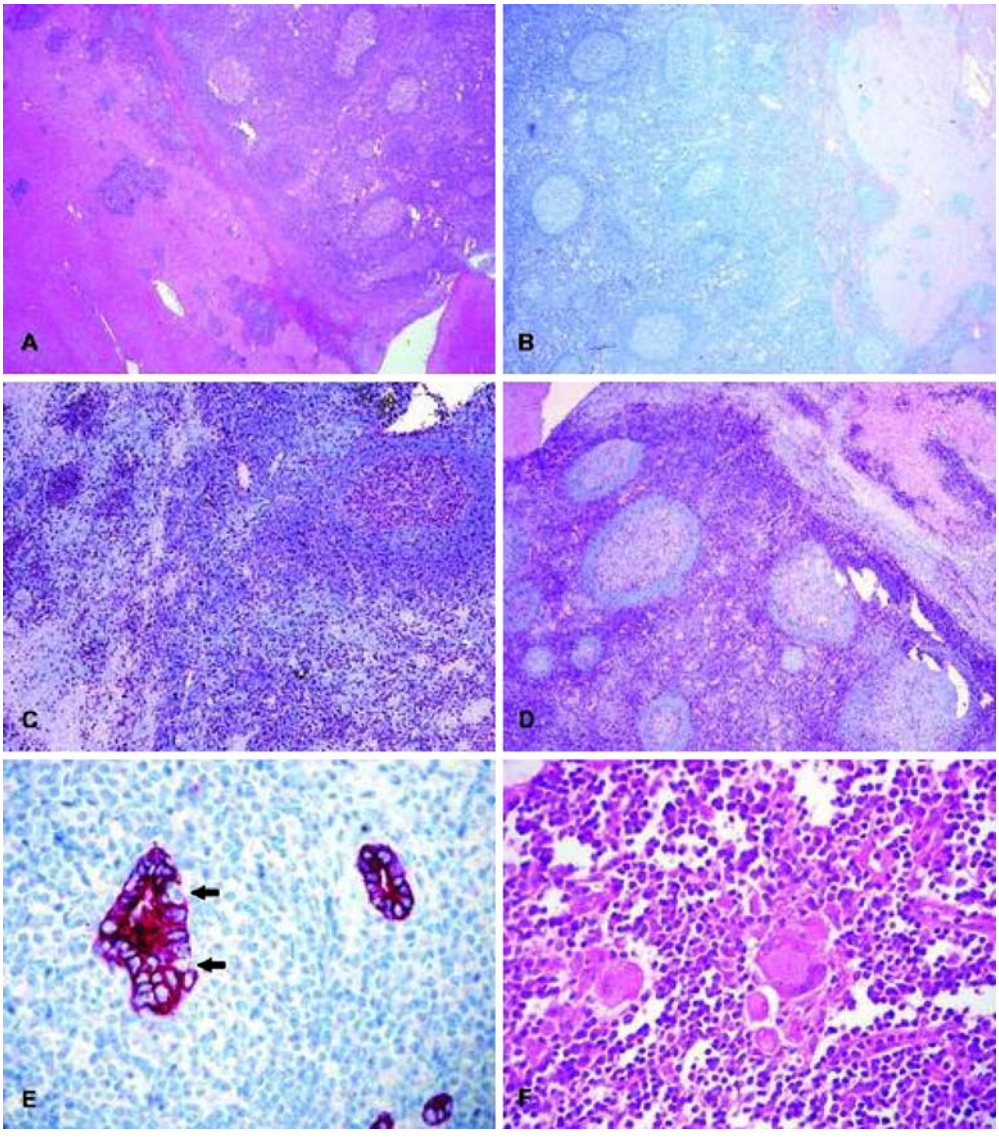

Fig. 1 Specimen from liver segment VIII. **a**, **b** A lymphoid mass is displacing and infiltrating the liver (HE/Giemsa, ×20). Reactive follicles are present. **c** Mixed infiltrate of $CD20^+$ B cells (**c**, CD20, ×40) and **d** $CD3^+$ T cells (**d**, CD3, ×40) in between the follicles. **e** Bile ductules are strongly stained by pan-cytokeratin antibodies (×400). Lymphoepithelial lesions are indicated by *arrows*. **f** Epithelioid cells and giant cells in the interfollicular area (HE, ×200)

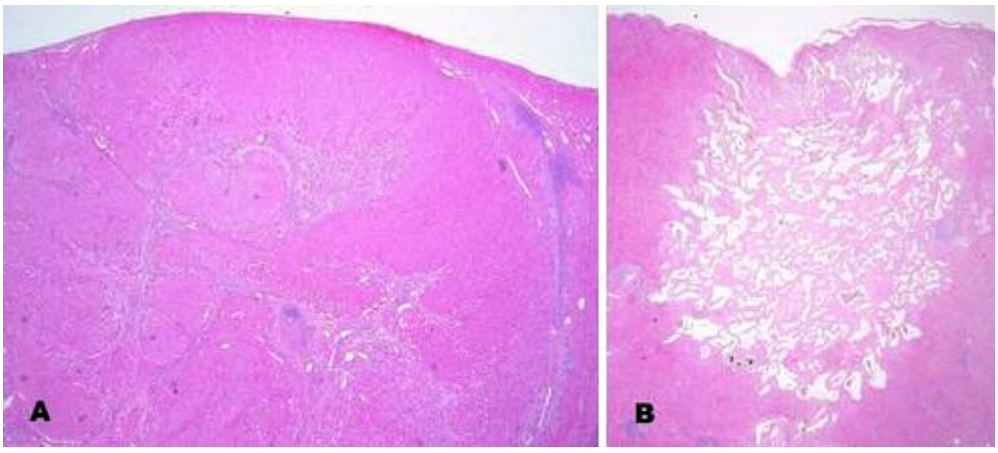

Fig. 2 **a** Focal nodular hyperplasia in liver segment VII (HE, ×20). **b** Cavernous hemangioma in liver segment VIII (HE, ×20)

$CD20^+$ B lymphocytes. Remnants of lymphoid sinus structures were not apparent. Bile ductules were found near the margin of the lesion within the lymphoid infiltrate, showing focal epithelial cell injury in cytokeratin staining (Fig. 1e). Ziehl-Neelsen staining was negative for mycobacteria.

A second tumor of 0.3-cm diameter was found subcapsular in the adjacent tissue of this specimen. Histologically, it consisted of irregular blood vessels with inconspicuous endothelial cells (Fig. 2b). The diagnosis of hemangioma was made.

The specimen from liver segment VII measured 4 × 3.5 × 1.5 cm and contained a tumor of 1.5-cm diameter. The tumor was brownish and had a central scar. Microscopically, it displayed nodular hyperplastic hepatic parenchyma. The nodules were separated by fibrous septa that formed a central scar. Numerous bile ductules were present in the connective tissue. At the tumor margins and in the stroma, aggregates of lymphocytes and plasma cells were observed (Fig. 2a). Taken together, the tumor showed the typical morphology of focal nodular hyperplasia (FNH).

In the liver parenchyma surrounding the tumors, the portal fields were infiltrated by few lymphocytes and plasma cells. A punch biopsy obtained from the left lobe of the liver showed normal liver tissue without an increased number of inflammatory cells. Granulomas were absent.

Lymph nodes excised from three different locations in the abdomen (peripancreatic, hepatoduodenal ligament, and

Table 1 Reports of nodular lymphoid lesions of the liver in the literature

Reference	Age	Sex	Size mm	Special histological features	Accompanying disease
Isobe et al. [5]	59	f	ns		Diabetes mellitus
Ohtsu et al. [11]	42	f	15		Chronic hepatitis B, interferon-alpha therapy
Katayanagi et al. [6]	66	f	15		Diabetes mellitus
Tanizawa et al. [16]	67	f	20	Hyalinized interfollicular spaces, hyalinized vessels, angiofollicular structures	'Abnormal liver function'
Kim et al. [7]	72	m	17		Chronic hepatitis C
Sharifi et al. [15]	52	f	4	Lymphoepithelial lesions, hyalinized material, thick walled arterioles	Primary biliary cirrhosis
	56	f	15	Epithelioid cells, rare lymphoid follicles	CREST syndrome
	56	m	7	Lymphoepithelial lesions, giant cells, hyalinized material	Allergic drug-induced hepatitis
Nagano et al. [10]	47	f	10		Hashimoto thyroiditis, hemangioma of the liver
Okubo et al. [12]	49	f	20		Sjögren's syndrome
Present case	36	f	18	Lymphoepithelial lesions, giant cells, epithelioid cells	FNH, hemangioma of the liver

f Female; *m* male; *CREST* Calcinosis cutis, Raynaud's syndrome, esophageal dysmotility, sclerodactyly, teleangiectasia; *FNH* focal nodular hyperplasia; *ns* not specified

mesentery of the small bowel) displayed a normal lymph node architecture. Sinuses were dilated with features of vascular sinus transformation. Interfollicular zones were prominent. No atypical infiltrate or granuloma was observed.

Fragment length analysis of amplified IgH and TCR-γ fragments was performed to assess clonality of B and T lymphocytes in the liver lesion from segment VIII. A polyclonal pattern of IgH and TCR-γ gene rearrangements was observed (not shown).

Discussion

Many lymphoid tumors formerly called pseudolymphoma have been attributed to NHL of MALT-type in recent years. However, some truly reactive nonneoplastic lesions remain, for which the term NLL seems appropriate. Reports in the literature about such lesions in the liver are rare (Table 1). Sharifi et al. [15] published three cases of NLL in 1999, describing similar features as found in the case presented here. Reactive lymphoid follicles were surrounded by a heterogeneous cellular infiltrate, displacing and invading surrounding hepatic tissue. Few lymphoepithelial lesions were present and in one case Ig-light chain restriction was observed by immunohistochemistry. However, there was no evidence of a monoclonal B cell population by molecular genetic analysis. One case in that series contained some scattered epithelioid cells and giant cells, as did the case presented here. An underlying chronic inflammatory process as a probable cause of the disease, as reported by Sharifi et al. [15], was not apparent in the case presented here (Table 1).

NLL has to be distinguished from B cell NHL of MALT-type. First described in 1983 by Isaacson and Wright [3] in the stomach, lung, thyroid, and salivary gland, MALT-type lymphomas have also been reported in numerous other body sites [19]. They recapitulate the features of the mucosa-associated lymphoid tissue and often occur at sites otherwise devoid of such [2]. In 1995, Isaacson et al. [4] published a series of four low-grade NHL of MALT-type of the liver. Since then, a number of small series and sporadic cases of primary hepatic MALT-type lymphoma have been reported [1, 8, 9, 13, 18, 19]. All of these cases displayed a nodular mass of lymphoid tissue with lymphoid follicles and a proliferation of heterogeneous small B cells. Lymphoepithelial lesions were usually present. Primary biliary cirrhosis or chronic hepatitis preceding and accompanying the lymphoma was reported in a few cases [4, 9, 13, 18]. In most cases of primary hepatic MALT-type lymphoma, evidence of B cell clonality was based on Ig-light chain restriction detected by immunohistochemistry. Only in single cases, clonality of lymphocytes was assessed by a molecular gene rearrangement study [8].

At first glance, the case presented here seems to resemble NHL of MALT-type. However, a mixed infiltrate of B and T cells and no restriction of Ig-light chains was seen by immunohistochemistry. A polyclonal B cell pattern was observed by molecular fragment length analysis of rearranged IgH genes. In a needle biopsy of the liver no underlying inflammatory process was apparent. Normal histology of abdominal lymph nodes from various sites ruled out systemic disease. Therefore, the diagnosis of NLL of the liver seems justified in this case.

In the case presented here, NLL occurred simultaneously with FNH and hemangioma. FNH with a lymphoma-like presentation has been reported before. Schmitz et al. [14] described a case with a single lesion of the liver displaying typical FNH-like features with a central scar by radiological examination. Histologically, a lymphoma-like infiltrate was found in a biopsy of that tumor. Here, FNH and the lymphoid lesion were found separate from each other and the latter did not display a central scar or other histological features of FNH. Thus, it is unlikely that the lymphoid tumor represents an unusual appearance of FNH. Because FNH and hemangioma are both lesions frequently found in the liver, their simultaneous appearance with NLL is most likely coincidental.

The rareness of both NLL and MALT-type non-Hodgkin's lymphoma of the liver and their similarity in many histological features may pose considerable problems in their distinction. The growth of prominent centrocyte-like B cells in a marginal zone pattern and assessment of clonality by immunohistochemical and molecular genetic investigations may be the best discriminating findings. NLL of the liver is a benign process that is adequately treated by local excision. In cases like this, the erroneous diagnosis of low-grade NHL may only be avoided by a thorough histological examination and the use of immunohistochemical and molecular genetic techniques.

References

1. Bronowicki JP, Bineau C, Feugier P, Hermine O, Brousse N, Oberti F, Rousselet MC, Dharancy S, Gaulard P, Flejou JF, Cazals-Hatem D, Labouyrie E (2003) Primary lymphoma of the liver: clinical-pathological features and relationship with HCV infection in French patients. Hepatology 37:781–787
2. Isaacson P, Müller-Hermelink HK, Piris MA, Berger F, Nathwani BN, Swerdlow SH, Harris NL (2001) Extranodal marginal zone B cell lymphoma of mucosa-associated lymphoid tissue (MALT lymphoma). In: Jaffe ES, Harris NL, Stein H, Vardiman JW (eds) World Health Organization Classification of tumours. Pathology and genetics of tumours of haematopoietic and lymphoid tissue. IARC, Lyon, pp 157–160
3. Isaacson P, Wright DH (1984) Extranodal malignant lymphoma arising from mucosa-associated lymphoid tissue. Cancer 53:2515–2524
4. Isaacson PG, Banks PM, Best PV, McLure SP, Müller-Hermelink HK, Wyatt JI (1995) Primary low-grade hepatic B cell lymphoma of mucosa-associated lymphoid tissue (MALT)-type. Am J Surg Pathol 19:571–575
5. Isobe H, Sakamoto S, Sakai H, Masumoto A, Sonoda T, Adachi E, Nawata H (1993) Reactive lymphoid hyperplasia of the liver. J Clin Gastroenterol 16:240–244
6. Katayanagi K, Terada T, Nakanuma Y, Ueno T (1994) A case of pseudolymphoma of the liver. Pathol Int 44:704–711
7. Kim SR, Hayashi Y, Kang KB, Soe CG, Kim JH, Yang MK, Itoh H (1997) A case of pseudolymphoma of the liver with chronic hepatitis C. J Hepatol 26:209–214
8. Kirk CM, Lewin D, Lazarchick J (1999) Primary hepatic B cell lymphoma of mucosa-associated lymphoid tissue. Arch Pathol Lab Med 123:716–719

9. Maes M, Depardieu C, Dargent JL, Hermans M, Verhaeghe JL, Delabie J, Pittaluga S, Troufleau P, Verhest A, De Wolf-Peeters C (1997) Primary low-grade B cell lymphoma of MALT-type occurring in the liver: a study of two cases. J Hepatol 27:922–927
10. Nagano K, Fukuda Y, Nakano I, Katano Y, Toyoda H, Nonami T, Nagasaka T, Hayakawa T (1999) Reactive lymphoid hyperplasia of liver coexisting with chronic thyroiditis: radiographical characteristics of the disorder. J Gastroenterol Hepatol 14:163–167
11. Ohtsu T, Sasaki Y, Tanizaki H, Kawano N, Ryu M, Satake M, Hasebe T, Mukai K, Fujikura M, Tamai M, et al (1994) Development of pseudolymphoma of liver following interferon-alpha therapy for chronic hepatitis B. Intern Med 33:18–22
12. Okubo H, Maekawa H, Ogawa K, Wada R, Sekigawa I, Iida N, Maekawa T, Hashimoto H, Sato N (2001) Pseudolymphoma of the liver associated with Sjogren's syndrome. Scand J Rheumatol 30:117–119
13. Prabhu RM, Medeiros LJ, Kumar D, Drachenberg CI, Papadimitriou JC, Appelman HD, Johnson LB, Laurin J, Heyman M, Abruzzo LV (1998) Primary hepatic low-grade B cell lymphoma of mucosa-associated lymphoid tissue (MALT) associated with primary biliary cirrhosis. Mod Pathol 11:404–410
14. Schmitz D, Köhler HH, Heussel CP, Löhr HF, Galle PR (2001) Lymphoma-simulating presentation of focal nodular hyperplasia (FNH) of the liver. Z Gastroenterol 39:219–224
15. Sharifi S, Murphy M, Loda M, Pinkus GS, Khettry U (1999) Nodular lymphoid lesion of the liver: an immune-mediated disorder mimicking low-grade malignant lymphoma. Am J Surg Pathol 23:302–308
16. Tanizawa T, Eishi Y, Kamiyama R, Nakahara M, Abo Y, Sumita T, Kawano N (1996) Reactive lymphoid hyperplasia of the liver characterized by an angiofollicular pattern mimicking Castleman's disease. Pathol Int 46:782–786
17. van Dongen JJ, Langerak AW, Brüggemann M, Evans PA, Hummel M, Lavender FL, Delabesse E, Davi F, Schuuring E, Garcia-Sanz R, van Krieken JH, Droese J, Gonzalez D, Bastard C, White HE, Spaargaren M, Gonzalez M, Parreira A, Smith JL, Morgan GJ, Kneba M, Macintyre EA (2003) Design and standardization of PCR primers and protocols for detection of clonal immunoglobulin and T cell receptor gene recombinations in suspect lymphoproliferations: report of the BIOMED-2 Concerted Action BMH4-CT98-3936. Leukemia 17:2257–2317
18. Ye MQ, Suriawinata A, Black C, Min AD, Strauchen J, Thung SN (2000) Primary hepatic marginal zone B cell lymphoma of mucosa-associated lymphoid tissue type in a patient with primary biliary cirrhosis. Arch Pathol Lab Med 124:604–608
19. Zucca E, Conconi A, Pedrinis E, Cortelazzo S, Motta T, Gospodarowicz MK, Patterson BJ, Ferreri AJM, Ponzoni M, Devizzi L, Giardini R, Pinotti G, Capella C, Zinzani PL, Pileri S, Lopez-Guillermo A, Campo E, Ambrosetti A, Baldini L, Cavalli F (2003) Nongastric marginal zone B cell lymphoma of mucosa-associated lymphoid tissue. Blood 101:2489–2495

Virchows Arch (2006) 448: 228–231
DOI 10.1007/s00428-005-0148-3

CASE REPORT

Simonetta Piana · Silvia Asioli · Moira Foroni

Oncocytic adenocarcinoma of the rectum arising on a villous adenoma with oncocytic features

Received: 6 October 2005 / Accepted: 15 December 2005 / Published online: 1 February 2006

Abstract Rectal adenocarcinoma with diffuse oncocytic features is a very rare lesion, having been reported only once in the English literature. We describe a case of oncocytic adenocarcinoma of the rectum, associated with a villous adenoma, arising on a 66-year-old man. On histological examination, the adenocarcinoma was composed of neoplastic glands lined by a strongly eosinophilic, granular epithelium that deeply infiltrated the rectal wall. Some basophilic calcifications were present in the gland lumina. Superficially, a villous adenoma with high-grade dysplasia was evident; adenomatous cells showed focal eosinophilic changes, consisting of a large granular cytoplasm, an oval atypical nucleus, and a prominent nucleolus. Immunohistochemically, neoplastic glands reacted strongly with antimitochondria antibody, carcinoembryonic antigen, cytokeratin 20, p53, and CDX2. Molecular alterations observed in oncocytic changes and their significance with regards to neoplastic transformation are briefly discussed.

Keywords Adenocarcinoma · Rectum · Oncocytic tumor · Mitochondria · Immunohistochemistry

Introduction

Adenocarcinomas of the large bowel are very common malignant neoplasias. Many histological subtypes have been described (mucinous, signet-ring cell, small cell, squamous cell, adenosquamous, medullary, and undifferentiated) [21] and have been included in the World Health Organization histological classification of tumors of the colon and rectum [5]. Nevertheless, an oncocytic variant of colorectal adenocarcinoma has been reported only once [20], and very few cases of oncocytic adenocarcinoma of the stomach have been collected recently [25]. Although oncocytic changes can be present in many gastrointestinal neoplasias [16], from an analysis of pertinent literature, it is clear that pure oncocytic neoplasias are far rarer in the gastrointestinal tract than in other sites.

In the present case, an oncocytic adenocarcinoma arising on a precursor lesion (a villous adenoma) with oncocytic changes is described. Extension of oncocytic modifications may allow to define a new histological subtype among colorectal adenocarcinomas.

Clinical history

A 66-year-old man presented for spontaneous rectal bleeding. He had no previous history of inflammatory bowel disease. During echoendoscopy, a large vegetating neoplasia was found in the rectum, extending from 5 to 13 cm above the pectinate line. On ultrasound examination, it apparently infiltrated the submucosa, with no extension into the tunica muscularis; no regional enlarged lymph nodes were found. Multiple biopsies were taken with superficial sampling. On histological examination, the lesion resulted in a villous adenoma with high-grade dysplasia. The patient underwent an endoscopic resection of the rectum and of regional lymph nodes, with subsequent sigmoidostomy. The patient was disease-free after 3 months.

Materials and methods

The specimens were routinely formalin-fixed, paraffin-embedded, and cut overnight. Microscopic slides were stained with hematoxylin-eosin and periodic acid-Schiff. Immunohistochemical stainings were performed using the labeled streptavidin-biotin method in a Lab Vision auto-

S. Piana · S. Asioli · M. Foroni
Department of Pathology, Arcispedale Santa Maria Nuova,
Viale Risorgimento 80,
42100 Reggio Emilia, Italy

S. Piana (✉)
Department of Pathology, Arcispedale Santa Maria Nuova,
Room 1.030, Viale Risorgimento 80,
42100 Reggio Emilia, Italy
e-mail: SIMONETTA.PIANA@ASMN.RE.IT
Tel.: +39-522-295919
Fax: +39-522-296945

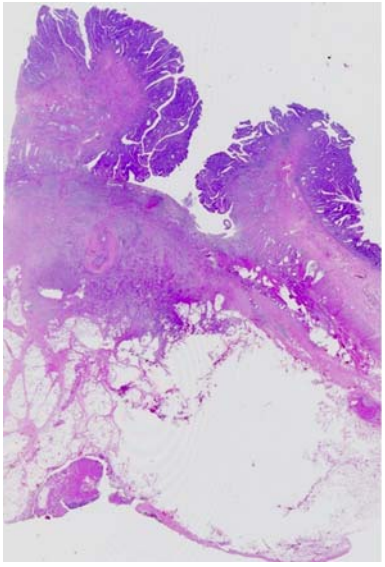

Fig.1 Low-power view of the neoplasia, with a central ulcerated area rimmed by vegetating tissue

stainer (Fremont, CA, USA), with the following antibodies: CDX2 (BioGenex, California, USA), carcinoembryonic antigen (CEA; DakoCytomation, Glostrup, Denmark), chromogranin A (DakoCytomation), cytokeratin 7 (NeoMarkers, California, USA), cytokeratin 20 (NeoMarkers), Ki-67 (DakoCytomation), antimitochondria antibody (BioGenex), p53 (DakoCytomation), and bcl-2 (NeoMarkers). An appropriate positive control was used.

Results

Macroscopically, a centrally ulcerated tumor (8 cm in the greatest axis) was present (Fig. 1), replacing the whole rectal circumference. On histological examination, the lesion was a moderately differentiated adenocarcinoma, consisting of irregular, branching glands lined by cells

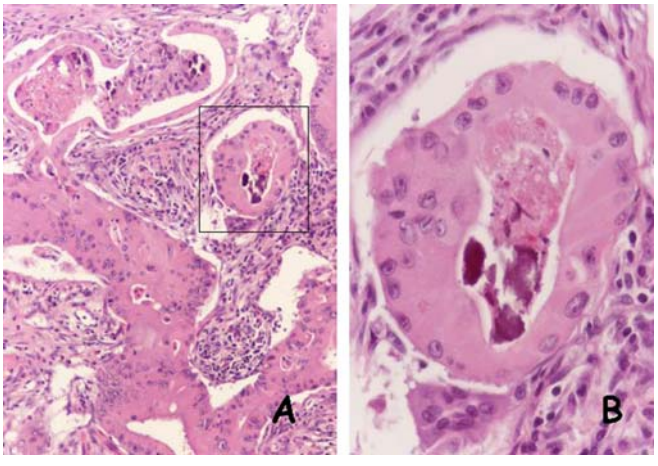

Fig.2 **a** Infiltrating glands lined by oncocytic cells and containing some calcifications. **b** High-power view of a neoplastic gland with intraluminal calcifications

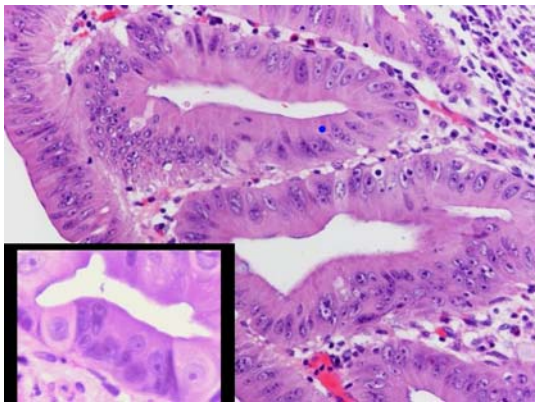

Fig.3 Adenomatous glands lined by columnar cells with a finely granular, eosinophilic cytoplasm and with an oval-to-round nucleus (*inset*)

with a finely granular, eosinophilic cytoplasm, a round nucleus, and a prominent nucleolus (Fig. 2a). Many glands contained nuclear debris and microcalcifications (Fig. 2b). The adenocarcinoma invaded through the muscularis propria into nonperitonealized perirectal tissues and reached the radial margins; distal surgical margins were tumor-free. Neither mitoses, nor vascular invasion, nor foci of usual colorectal adenocarcinoma were noted. Around the infiltrating carcinoma, a villous adenoma was found with high-grade dysplasia (Fig. 3); the glands were lined by cells with a large, granular, eosinophilic cytoplasm and an oval-to-round nucleus (Fig. 3). A transition between a classical adenomatous epithelium and these unusual eosinophilic cells was evident. Residual mucosa was unremarkable. Seventeen regional lymph nodes were found, with no evidence of metastasis. According to the American Joint Committee on Cancer, the pathologic tumor stage was pT3N0-R1.

On immunohistochemistry, the adenocarcinomatous component reacted strongly with antimitochondria antibody (Fig. 4a), cytokeratin 20, and CEA. The adenomatous component was diffusely positive with cytokeratin 20 and CEA, whereas the antimitochondria antibody reacted focally (Fig. 4b). Ki-67 was positive in 3 and 30% of neoplastic cells in the adenocarcinoma (Fig. 5a) and adenoma, respectively.

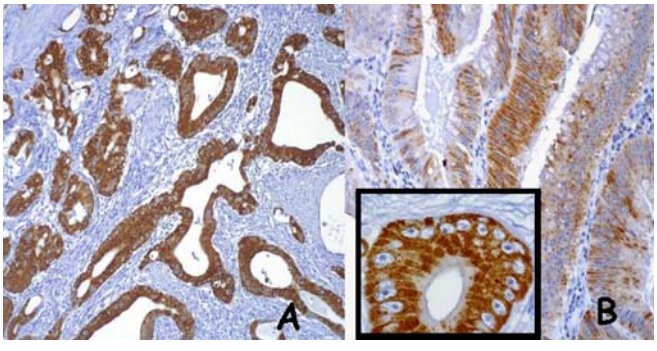

Fig.4 The antimitochondria antibody is diffusely positive either in the adenocarcinoma (**a**) or in the villous adenoma (**b**), with a granular cytoplasmic pattern (*inset*)

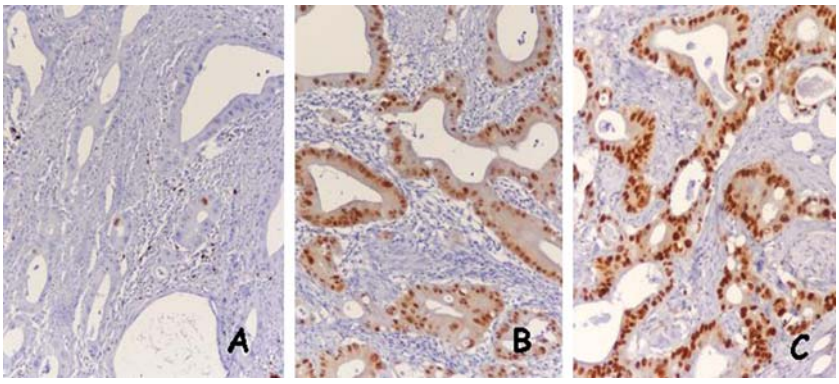

Fig.5 The Ki-67 rate is very low in infiltrating adenocarcinoma (**a**). All neoplastic cells display strong immunoreactivity with CDX2 (**b**) and p53 (**c**)

Intranuclear immunoreactivity for CDX2 (Fig. 5b) and p53 (Fig. 5c) was noted either in the adenocarcinoma and in the adenoma; in the former, p53 was much stronger than in the latter. Cytokeratin 7 and bcl-2 were unexpressed either in the adenocarcinoma or in the villous adenoma.

Discussion

Oncocytic cellular changes, by definition [6], are morphologically characterized by a finely granular, wide, and eosinophilic cytoplasm and a round nucleus with an evident nucleolus. The "swollen" appearance of oncocytes and their granularity in histological sections are due to the accumulation of mitochondria. Although oncocytic metaplasia is quite common in some epithelia (i.e., intercalated ducts of the salivary glands, or the follicular thyroid epithelium in Hashimoto's thyroiditis), the terms *oncocytoma* and *oncocytic carcinoma* usually designate tumors that mostly consist of oncocytic cells. How accumulation of mitochondria leads to neoplasia is still an object of debate, but many advances have been achieved in the comprehension of oncocytic tumors in recent years. Most recent review articles on oncocytic neoplasias-some of which offer an exhaustive explanation of biochemical mechanisms underlying mitochondrial accumulation [26]-deal with oncocytic (Hürthle cell) tumors of the thyroid gland [12, 24]. In an oversimplified way, oncocytic transformation is due to an alteration of mitochondrial DNA, probably following oxidative stress, which causes a defective function of organelles and leads to a compensatory increase in cellular mitochondrial content. This degenerative aging process is likely to be the same in all tissues undergoing oncocytic transformation; in fact, it is not possible to morphologically distinguish thyroid oncocytic cells from, for example, renal oncocytic cells. The first case of oncocytic adenocarcinoma of the rectum has been described by Piscitelli et al. [20]. Since then, no other similar cases have been reported in the large bowel, even though oncocytic neoplasias are frequently observed in many sites [3, 15, 17, 22, 28]. Only focal oncocytic changes have been observed in ordinary carcinomas of the gastrointestinal tract [16], and ten cases of gastric oncocytic adenocarcinoma have been extensively discussed recently [25]. Máximo and Sobrinho-Simões [12] suggest that, in the digestive and respiratory tracts, cellular turnover is too high to allow the accumulation of abnormal mitochondria; this would explain the exceptional occurrence of oncocytic tumors in these areas.

The present case is almost completely superimposable on the first described, as it is an oncocytic, infiltrating adenocarcinoma of the rectum, focally containing small basophilic microcalcifications. Some points of distinction are (1) the complete absence of areas of conventional colorectal adenocarcinoma and (2) the presence of a villous adenoma, which exhibits focal oncocytic changes as well. On immunohistochemistry, neoplastic cells are positive for antimitochondria antibody, diffusely in infiltrative glands and focally in the adenoma. They also have a typical colonic phenotype, with immunoreactivity to CDX2, CEA, and cytokeratin 20. Immunohistochemical evaluation of proliferative activity by Ki-67 antibody shows a very low rate in the adenocarcinomatous component, in comparison with that in the villous adenoma. This is not in keeping with the data reported by many papers [2, 7, 8, 23, 27], where the Ki-67 index is higher in carcinomas than in adenomas; it also contrasts with the deep penetration of proliferating cells through the rectal wall.

An alternative explanation for tumor growth (and the high stage of the neoplasia) is blockage of apoptotic cell death. Bcl-2 belongs to a family of genes that regulates cell death [1]; it is expressed in several normal and neoplastic tissues, mostly in developing epithelia [9, 10]. Interestingly, in thyroid carcinomas, bcl-2 expression varies according to the degree of differentiation and results in the absence of anaplastic carcinomas [11, 18, 19] and oncocytic tumors [13, 14]. Since bcl-2 is localized in the outer mitochondrial membrane, it is likely that mitochondrial anomalies cause reduced bcl-2 expression [12]. As mitochondria are also involved in the initiation of apoptosis [4] by a complex biochemical switch, it has been suggested that abnormal mitochondria are unable to start apoptosis itself [12].

In oncocytic thyroid tumors, p53 expression is evident in a high proportion of cases, either adenomas and carcinomas, but its biological significance is still unclear [13]. In the present case, p53 was strongly expressed, but its correlation with oncocytic transformation and low proliferative rate is unknown.

In conclusion, the pathogenesis of oncocytic transformation is still unresolved either in the thyroid gland, where it is

very common, or in the present case. So far, it is not possible to say whether oncocytic changes or intraluminal calcifications have functional implications in colorectal adenocarcinoma. Indeed, even though no prognostic considerations can be performed, oncocytic colorectal adenocarcinoma may constitute more than a morphological curiosity.

References

1. Boise LH, Gonzales-Garcia M, Postema CE et al (1993) Bcl-x, a bcl-2 related gene that functions as a dominant regulator of apoptotic cell death. Cell 74:597-607
2. Carr NJ, Monihan MJ, Nzeako UC, Murakata LA, Sobin LH (1995) Expression of proliferative cell nuclear antigen in hyperplastic polyps, adenomas and inflammatory cloacogenic polyps of the large intestine. J Clin Pathol 48:46-52
3. Damiani S, Dina R, Eusebi V (1999) Eosinophilic and granular cell tumors of the breast. Semin Diagn Pathol 16:117-125
4. Green Dr, Reed JC (1998) Mitochondria and apoptosis. Science 281:1309-1312
5. Hamilton SR, Aaltonen LA (eds) (2000) World Health Organization classification of tumours. Pathology and genetics of tumours of the digestive system. IARC Press, Lyon
6. Hamperl H (1962) Onkocyten und onkocytome. Virchows Arch Pathol Anat 335:452-483
7. Johnston PG, O'Brien MJ, Dervan P, Carney DN (1989) Immunohistochemical analysis of cell kinetic parameters in colonic adenocarcinomas, adenomas, and normal mucosa. Hum Pathol 20:696-700
8. Kikuchi Y, Dinjens WNM, Bosman FT (1997) Proliferation and apoptosis in proliferative lesions of the colon and rectum. Virchows Arch 431:111-117
9. Lu QL, Poulson R, Wong L et al (1993) Bcl-2 expression in adult and embryonic non-haematopoietic tissues. J Pathol 169:431-437
10. Lu QL, Abel P, Foster CS et al (1996) Bcl-2 role in epithelial differentiation and oncogenesis. Hum Pathol 27:102-110
11. Manetto V, Lorenzini R, Cordon-Carlo C et al (1997) Bcl-2 and bax expression in thyroid tumours. Virchows Arch 430:125-139
12. Máximo V, Sobrinho-Simões M (2000) Hürthle cell tumours of the thyroid. A review with emphasis on mitochondrial abnormalities with clinical relevance. Virchows Arch 437:107-115
13. Müller-Hocker J (1999) Immunoreactivity of p53, Ki-67 and bcl-2 in oncocytic adenomas and carcinomas of the thyroid gland. Hum Pathol 30:926-933
14. Müller-Hocker J (2000) Expression of BCL-2, Bas and Fax in oxyphilic (Askanazy) cells of Hashimoto thyroiditis. Virchows Arch 436:602-607
15. Nappi O, Ferrara G, Wick MR (1999) Neoplasms composed of eosinophilic polygonal cells: an overview with consideration of different cytomorphologic patterns. Semin Diagn Pathol 16:82-90
16. Papotti M, Cassoni P, Taraglio S, Bussolati G (1999) Oncocytic and oncocytoid tumors of the exocrine pancreas, liver, and gastrointestinal tract. Semin Diagn Pathol 16:126-134
17. Paulino AFG, Huvos AG (1999) Oncocytic and oncocytoid tumors of the salivary glands. Semin Diagn Pathol 16:98-104
18. Pilotti S, Collini P, del Bo R et al (1994) A novel panel of antibodies that segregates immunocytochemically poorly differentiated carcinoma from undifferentiated carcinoma of the thyroid gland. Am J Surg Pathol 18:1054-1064
19. Pilotti S, Collini, Rilke F et al (1994) Bcl-2 protein expression in carcinomas originating from the follicular epithelium of the thyroid gland. J Pathol 172:337-342
20. Piscitelli D, Ingravallo G, Resta L, Fiore MG, Maiorano E (2003) Oncocytic adenocarcinoma of the rectum with diffuse intraluminal microcalcifications: the first reported case. Virchows Arch 443:579-582
21. Riddell RH, Petras RE, Williams GT, Sobin LH (2002) Tumors of the intestines. In: Atlas of tumor pathology, third series, fascicle 32. Armed Forces Institute of Pathology, Washington
22. Reuter VE (1999) Renal tumors exhibiting granular cytoplasm. Semin Diagn Pathol 16:135-145
23. Saleh HA, Jackson H, Khatib G, Banerjee M (1999) Correlation of bcl-2 oncoprotein immunohistochemical expression with proliferation index and histopathologic parameters in colorectal neoplasia. Pathol Oncol Res 5:273-279
24. Sobrinho-Simões M, Máximo V, Vieira de Castro I, Fonseca E, Soares P, Garcia-Rostan G et al (2005) Hürthle (oncocytic) cell tumors of thyroid: etiopathogenesis, diagnosis and clinical significance. Int J Surg Pathol 13:29-35
25. Takubo K, Honma N, Sawabe M, Arai T, Izumiyama-Shimomura N, Kammori M, Sasajima K, Esaki Y (2002) Oncocytic adenocarcinoma of the stomach. Parietal cell carcinoma. Am J Surg Pathol 26:458-465
26. Tallini G (1998) Oncocytic tumours. Virchows Arch 433:5-12
27. Yang H, Hsu P, Chan S, Lee JC, Shin JS, Chow NH (1996) Growth kinetics of colorectal adenoma-carcinoma sequence: an immunohistochemical study of proliferating cell nuclear antigen expression. Hum Pathol 27:1071-1076
28. Young RH, Scully RE (1999) Oxyphilic tumors of the female and male genital tracts. Semin Diagn Pathol 16:146-161

Virchows Arch (2006) 448: 232–235
DOI 10.1007/s00428-005-0149-2

CASE REPORT

Ksenya V. Shelekhova · Dmitry V. Kazakov · Ondrej Hes · Vladislav Treska · Michal Michal

Phosphaturic mesenchymal tumor (mixed connective tissue variant): a case report with spectral analysis

Received: 8 December 2005 / Accepted: 19 December 2005 / Published online: 31 January 2006

Abstract We present a further case of a rare mesenchymal neoplasm termed phosphaturic mesenchymal tumor (mixed connective tissue variant). The patient was a 42-year-old man with a long history of osteomalacia of unknown etiology with pathological bone fracture, abnormality of parathyroid glands, kyphosis, scoliosis, and spondylosis. Laboratory investigation disclosed hypophosphatemia, elevated serum alkaline phosphatase activity, and normal serum calcium level. The patient had a soft tissue mass in the right inguinal area, measuring 11×6×5 cm, which was previously interpreted as a calcified hematoma on sonography. The tumor was surgically removed. Grossly, the tumor was well circumscribed, unencapsulated, and had soft to dense consistency. The cut surface had a variegated appearance due to the presence of large hemorrhagic areas admixed with foci of grey-yellow tissue. Histologically, the tumor was composed of primitive mesenchymal cells, osteoclast-like cells, and cells showing myofibroblastic features without cytologic atypia. There were a well developed vascular network, microcystic areas, and poorly formed cartilaginous foci. Unusual and hitherto unpublished prominent features were flower-like, slate-gray crystals, widespread hemosiderin deposits and large areas of hemorrhages, with the latter comprising approximately 60% of the tumor. A spectral analysis indicated that chemically, the crystals mainly consisted of calcium phosphate and sodium nitrate.

K. V. Shelekhova
Department of Pathology, Petrov's Institute of Oncology,
Saint-Peterburg, Russia

D. V. Kazakov · O. Hes · M. Michal (✉)
Sikl's Department of Pathology, Charles University,
Medical Faculty Hospital,
Alej Svobody 80,
304-60 Pilsen, Czech Republic
e-mail: michal@medima.cz
Tel.: +420-603-886633
Fax: +420-377-104650

V. Treska
Department of Surgery, Charles University,
Medical Faculty Hospital,
Pilsen, Czech Republic

Keywords Phosphaturic mesenchymal tumor · Ultrastructural findings · Spectral analysis · Hemorrhages · Crystal · Osteomalacia · Rickets

Introduction

Phosphaturic mesenchymal tumor (mixed connective tissue variant) (PMTMCT) is the most frequent variant of a "heterogeneous" group of rare mesenchymal tumors, which often cause osteomalacia or rickets and are accompanied by specific biochemical abnormalities such as hypophosphatemia, hyperphosphaturia, elevated alkaline phosphatase activity, and low or inappropriately normal circulating 1.25 $(OH)_2D$ levels. Classic PMTMCT has unique morphologic features. The tumors are mainly composed of small, bland, spindled cells embedded in a distinctively "grungy", calcified, myxoid matrix, also often containing fat, microcysts, areas of hemorrhage, osteoclasts, foci of poorly developed cartilage, osteoid, or bone. The vascularity is often prominent, and focally it resembles that seen in hemangiopericytoma. The tumors typically follow a benign clinical course. After neoplasm resection, the serum phosphate concentration usually returns to normal values [1, 3–5, 7–9].

We describe a case of PMTMCT, including the clinicopathologic features, ultrastructural findings, and results of spectral analysis of the lesional tissue.

Case report

A 42-year-old man presented in 2004 with a soft tissue mass in the right inguinal area that had been detected by somatostatin receptor scintigraphy during a recent hospitalization. His medical history was significant for a pathological fracture of the ulnar bone in 1995, with a protracted unsuccessful healing, requiring an operation in 1997. He was also followed up and treated for hypophosphatemia and osteomalacia of unknown etiology. No abnormality of parathyroid glands was previously found.

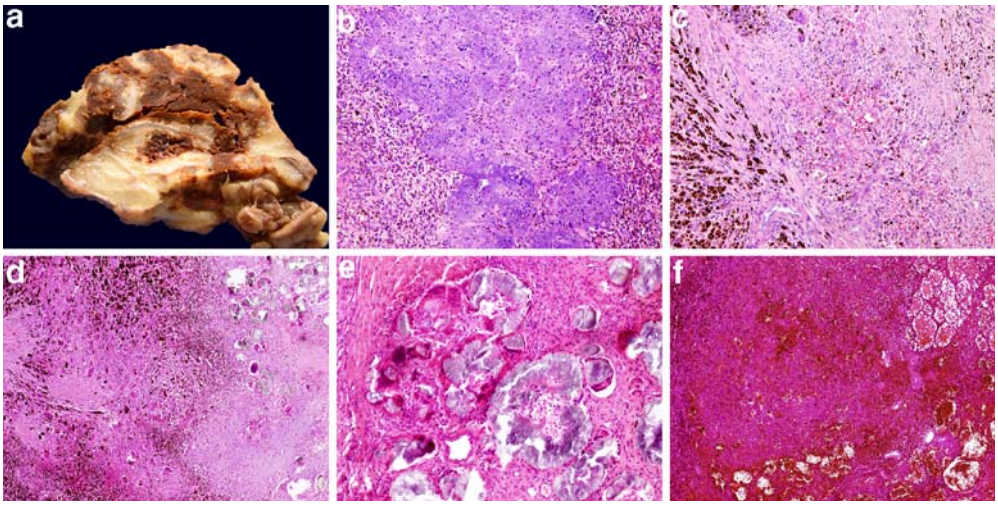

Fig. 1 **a** The cut surface of the tumor with extensive areas of hemorrhage. **b** Typical cells of phosphaturic mesenchymal tumor (mixed connective tissue variant). **c** Spindle-cell proliferation, hemosiderin deposits and osteoclast-like giant cells. **d** Numerous crystals and plentiful hemosiderin deposits. **e** Flower-like, slate-gray appearance of the crystals. **f** Prominent hemorrhage and vascular structures

Previous radiological investigations detected various skeletal abnormalities. Radiographic images consistent with osteomalacia were pseudofractures (Looser zone) in the distal diaphysis of the ulnar bone, ventral surface of S1, 12th rib, proximal metaphysis of both femurs, and superior pubic ramus. He had also kyphosis, scoliosis, and spondylosis L5. It is interesting to note that the sonographic investigation performed 6 months before the presentation disclosed a 4×7.8 cm mass in the right inguinal area, which was interpreted as a calcified hematoma.

Laboratory tests revealed a serum phosphate level of 0.55 mmol/l (normal range, 0.7–1.6l). Serum alkaline phosphatase was moderately elevated. Serum calcium was normal.

The patient was administered a long-term phosphate therapy and vitamin D. The soft tissue mass was surgically removed. After the operation, technetium-99 m 2-methoxyisobutyl isonitrile scintigraphy of parathyroid glands revealed a lesion, measuring 1.8×1.0×1.6 cm. Histologically, the parathyroid lesion proved to be an adenoma.

The patient is alive without signs of recurrence of the soft tissue tumor and the parathyroid gland adenoma 15 months after the surgery.

Materials and methods

Tissues were fixed in glutaraldehyde, then in osmium tetroxide and embedded into the Spurr's resin for ultrastructural study. Specimens were examined with a Philips (Eindhoven, The Netherlands) EM 208S electron microscope. X-ray fluorescence spectrometry was performed at the Institute of Geochemistry, Mineralogy and Mineral Resources, Faculty of Science, Charles University, Prague,

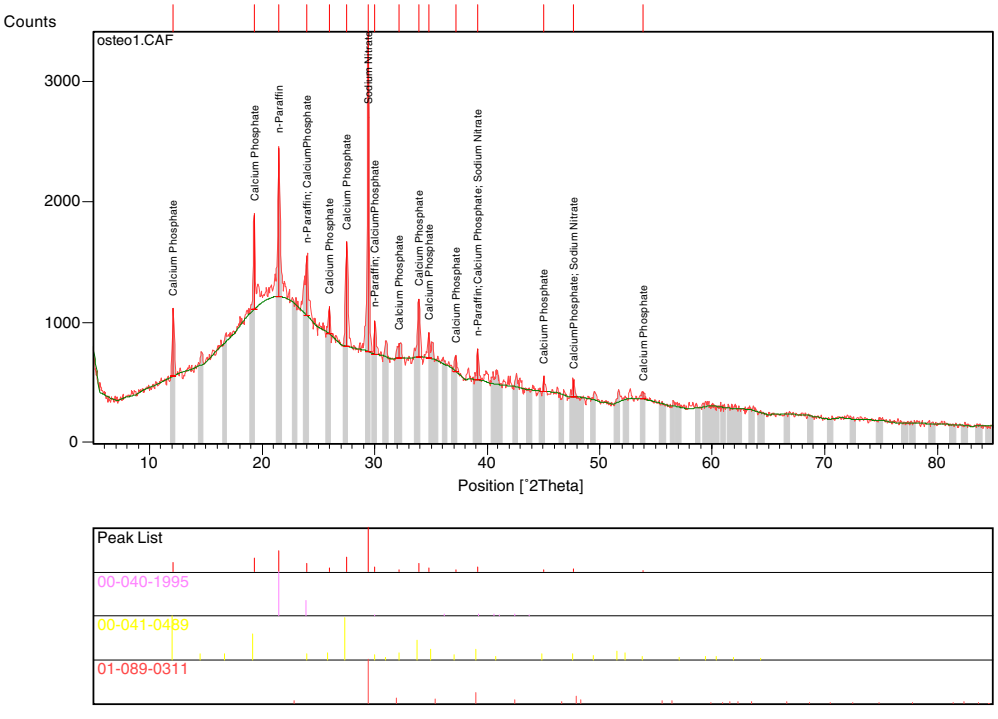

Fig. 2 The results of spectral analysis of the lesional tissue. Calcium phosphate and sodium nitrate predominate (see also Table 1)

Czech Republic using the standard hardware (X'Pert Pro) and software (X'Pert HighScore 1.0d) supplied by PANalytical B.V., Almelo, The Netherlands.

Pathological findings

As can be seen, the tumor was a well circumscribed, unencapsulated mass that measured 11×6×5 cm. It had a soft to dense consistency. The cut surface had a variegated appearance due to the presence of large hemorrhagic areas admixed with foci of grey-yellow tissue (Fig. 1a). There was no necrosis.

Histopathologically, the tumor was separated into nodules by septa. The margins of the tumor appeared well delimited from the surrounding muscle, fat, and fibrous tissues. The neoplasm had an appearance of a typical PMTMCT (Fig. 1b). The tumor was composed of small, spindle to oval cells that grew in sheets. There were also clusters of osteoclast-like giant cells, microcystic areas, and poorly formed cartilaginous foci (Fig. 1c). Neither cellular or nuclear pleomorphism nor atypical mitotic figures were found. There were many crystals within the tumorous mass (Fig. 1d). They had a flower-like, slate-gray appearance (Fig. 1e). The vascular network was prominent and consisted of thin-walled capillaries, sinusoids, and lacunae (Fig. 1f). There were also areas of wide-open vascular lumens with a regular endothelial lining stuffed with erythrocytes (Fig. 1f). There were also extensive areas of hemorrhage and hemosiderosis, and these comprised at least 60% of the tumor (Fig. 1c,d,f).

Ultrastructural findings

Electron microscopy had shown osteoclast-like cells, and irregular, primitive-appearing stromal cells with markedly convoluted nuclei, organelle-poor cytoplasm, and occasional stretches of basal lamina. The third type of cells showed myofibroblastic features. These cells disclosed irregular, stellate cellular outlines, partly enveloped by a basal lamina and pinocytotic vesicles. Their cytoplasm contained abundant cisterns of rough endoplasmic reticulum, variable numbers of mitochondria, microfilaments, and dense bodies. The myxoid intercellular matrix was composed of collagen fibers and granules that sometimes formed globular aggregates. There were numerous granules of hemosiderin within the matrix. The blood vessels appear to represent normal capillaries and venules with myxoid walls.

Spectral analysis

Calcium phosphate and sodium nitrate were the dominant substances in the lesional tissue (Fig. 2, Table 1).

Table 1 The results of spectral analysis of the lesional tissue. Calcium phosphate and sodium nitrate were found to be the predominant substances (see also Fig. 2)

Reference Code	Score	RIR	Compound name	Chemical formula	SemiQuant (%)
00-040-1995	52	0.000	*n*-Paraffin	$(CH_2)_x$	–
00-041-0489	36	0.000	Calcium phosphate	$Ca_2P_2O_7$	–
01-089-0311	27	2.290	Sodium nitrate	$Na(NO_3)$	–

Discussions

Our case is unusual in that the tumor exhibited large areas of hemorrhage, prominent hemosiderosis, and widespread crystals, which altogether often masked the tumor itself. Although prominent vascularity and focal hemorrhages are said to be typical histologic features of PMTMCT, such massive hemorrhages were not found in the English language literature. Coupled with the crystal deposits, which is another hitherto unpublished occurrence, this feature probably explains the diagnostic error of the sonographic examination (misinterpreted as calcified hematoma) in our case, and may also be a potential diagnostic pitfall histologically. Otherwise, the lesion in our patient manifested typical histologic and ultrastructural features.

The coexistence of parathyroid hyperfunction and oncogenic osteomalacia, including osteomalacia caused by PMTMCT, is rare. It has been found in approximately 10% of cases of osteomalacia [6]. All those patients with impaired parathyroid function received anorganic phosphate supplements, which may have stimulated parathyroid hormone secretion and ultimately led to parathyroid autonomy [2, 6]. Microscopic examination showed hyperplasia/adenoma of parathyroid glands [2, 6]. The data from our case are consistent with this hypothesis.

To our knowledge, this is the first report in which a spectral analysis of matrix dystrophic calcification was performed. It demonstrated that the crystals within the tumorous mass were made up of calcium phosphate and sodium nitrate mainly.

In summary, we have described a case of PMTMCT with unusual secondary changes of the lesional tissue such as prominent hemorrhage, hemosiderosis, and formation of crystals. Clinicians and pathologists should be aware of these features because it may prevent a diagnostic pitfall.

Acknowledgement The authors wish to thank Dr. Marek Chvátal from the Institute of Geochemistry, Mineralogy and Mineral Resources, Faculty of Science, Charles University, Prague, Czech Republic, who performed the spectral analysis.

References

1. Cehreli CA, Alakavuklar MN, Cavdar C (1994) Oncogenous osteomalacia: report of a case. Acta Oncol 33:975–976
2. Firth RG, Grant CS, Riggs BL (1985) Development of hypercalcemic hyperparathyroidism after long-term phosphate supplementation in hypophosphatemic osteomalacia: report of two cases. Am J Med 78:669–673
3. Folpe AL, Fanburg-Smith JC, Billings SD, Bisceglia M, Bertoni F, Cho JY, Econs MJ, Inwards CY, Jan de Beur SM, Mentzel T, Montgomery E, Michal M, Miettinen M, Mills SE, Reith JD, O'Connell JX, Rosenberg AE, Rubin BP, Sweet DE, Vinh TN, Wold LE, Wehrli BM, White KE, Zaino RJ, Weiss SW (2004) Most osteomalacia-associated mesenchymal tumors are a single histopathologic entity: an analysis of 32 cases and a comprehensive review of the literature. Am J Surg Pathol 28:1–30
4. McClure J, Smith PS (1987) Oncogenic osteomalacia. J Clin Pathol 40:446–453
5. Papotti M, Foschini MP, Isaia G, Rizzi G, Betts CM, Eusebi V (1988) Hypophosphatemic oncogenic osteomalacia: report of three new cases. Tumori 74:599–607
6. Reid IR, Teitelbaum SL, Dusso A, Whyte MP (1987) Hypercalcemic hyperparathyroidism complicating oncogenic osteomalacia: effect of successful tumor resection on mineral homeostasis. Am J Med 83:350–354
7. Weidner N, Santa Cruz D (1987) Phosphaturic mesenchymal tumors: a polymorphous group causing osteomalacia or rickets. Cancer 59:1442–1454
8. Weidner N (1991) Review and update: oncogenic osteomalacia-rickets. Ultrastruct Pathol 15:317–333
9. Yang IM, Park YK, Hyun YJ (1997) Oncogenic osteomalacia caused by a phosphaturic mesenchymal tumor of the oral cavity: a case report. Korean J Intern Med 12:89–95

Virchows Arch (2006) 448: 236–238
DOI 10.1007/s00428-005-0135-8

LETTER TO THE EDITOR

J. G. P. Murphy · R. Lonsdale · D. Premachandra · H. B. Hellquist

Salivary hybrid tumour: adenoid cystic carcinoma and basal cell adenocarcinoma

Received: 3 November 2005 / Accepted: 17 November 2005 / Published online: 13 January 2006

Dear Editor,

Hybrid tumours of the salivary glands are very rare and since their description and definition by Seifert and Donath in 1996 [7], only some 25 cases have been reported [1–10]. A salivary hybrid tumour comprises two different tumour entities, each of which conforms to an exactly defined tumour category, arising within the same topographical area [7]. Most reported cases are carcinomas, either with one or both components being malignant. Benign variants are also described, e.g. combination of basal cell adenoma and canalicular adenoma [7].

We present the fine needle aspirate and histological features of a hybrid tumour arising in the parotid gland of a 68-year-old woman. The tumour is, to the best of our knowledge, a hitherto undescribed variant of salivary hybrid tumour, showing features of both adenoid cystic carcinoma and basal cell adenocarcinoma. The patient presented with a rapidly growing mass in the right parotid gland, and 4 weeks prior to seeking medical advice the mass had become tender and erythematous. When seen in the clinic the mass measured 4×4×3 cm and was located in the body of the parotid anterior to the tragus. The fine needle aspirate was highly cellular with large, branching, basaloid cell clusters and a dispersed population of oval bare nuclei and intact cells with scant cytoplasm (Fig. 1). Most of the cells had small prominent nucleoli. There were eosinophilic hyaline globules and finger-like structures of basement-membrane-like material associated with some epithelial clusters. The fine-needle aspirate suggested a basaloid neoplasm. There were some features of adenoid cystic carcinoma (spherical globules of basement membrane material surrounded by tumour cells), while other features (cohesive basaloid cells associated with hyaline stromal material and frequent bare nuclei) suggested a basal cell neoplasm (basal cell adenoma/basal cell adenocarcinoma). The patient subsequently underwent total parotidectomy with preservation of the facial nerve and had an uneventful postoperative recovery. Follow-up 3 months later showed no residual disease and she died 5 months later of unrelated causes.

The excised parotid gland contained a whitish, somewhat fleshy tumour measuring 22 mm that microscopically showed two distinct histological components (Fig. 2). The larger part of the tumour, approximately 75%, consisted of an adenoid cystic carcinoma with a mixture of cribriform and tubular growth patterns, with both "punched-out" pseudocysts and some true cysts. However, a solid growth pattern predominated. Here, the flat and spindle-shaped myoepithelial cells with scanty cytoplasm grew in nests and strands with interspersed ductal formations, and the tumour sheets were situated in rather sparse strands of stroma. Mitotic figures were rare (Fig. 3). The other smaller part of the tumour showed features of basal cell adenocarcinoma with invasive lobules composed of basaloid cells with a palisading outer layer. The majority of these cells had basophilic vesicular nuclei and scant cytoplasm. There were also larger cells with paler nuclei towards the centre of the tumour nests. Many of the tumour lobules were surrounded by a thick hyaline membrane with features of the membranous type of basal cell adenocarcinoma (Fig. 4). In yet other areas the trabecular type of basal cell adenocarcinoma was present where basaloid cells formed thin anastomosing cords (two or three cell layers only). There were also more solid areas with virtually no ductal structures. The two tumours shared a similar myoepithelial immunophenotype with variable immunopositivity for S-100, smooth muscle actin, keratins

J. G. P. Murphy · R. Lonsdale · H. B. Hellquist (✉)
The Cotman Centre,
Department of Cellular Pathology,
Norfolk and Norwich University Hospital,
Colney Lane,
Norwich, NR4 7UB, UK
e-mail: henrik.hellquist@nnuh.nhs.uk
Tel.: +44-1603-286942
Fax: +44-1603-286017

D. Premachandra
Department of Surgery,
James Paget NHS Healthcare Trust,
Gorleston,
Great Yarmouth, NR31 6LA, UK

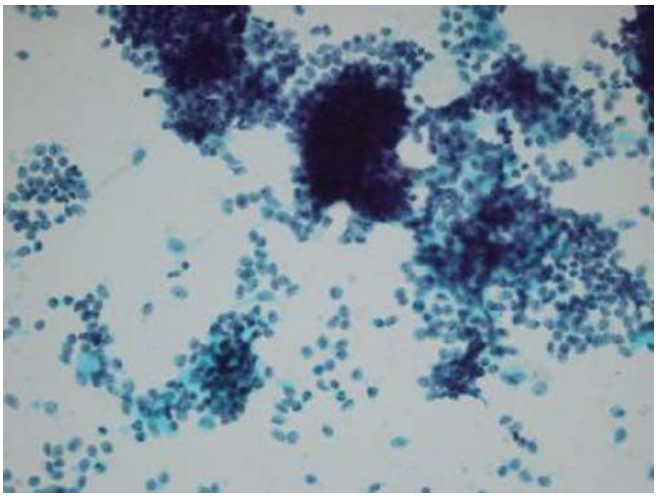

Fig. 1 Basaloid cell groups with a cribriform architecture associated with a dispersed population of oval bare nuclei and intact cells with scant cytoplasm. Spherical hyaline globules are also present

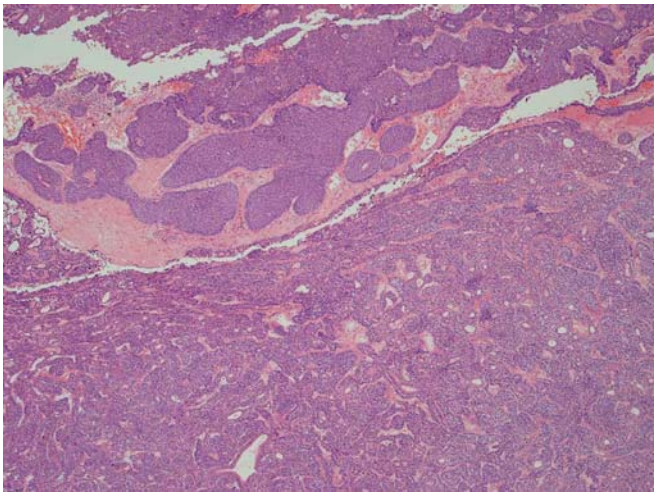

Fig. 2 Salivary hybrid tumour. Basal cell adenocarcinoma (*top*) bordering adenoid cystic carcinoma (*bottom*)

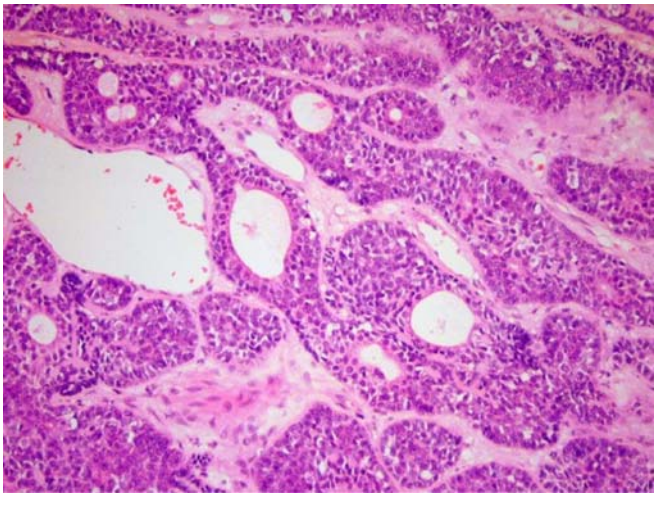

Fig. 3 Adenoid cystic carcinoma. Cribriform growth pattern with pseudocysts and some true cysts

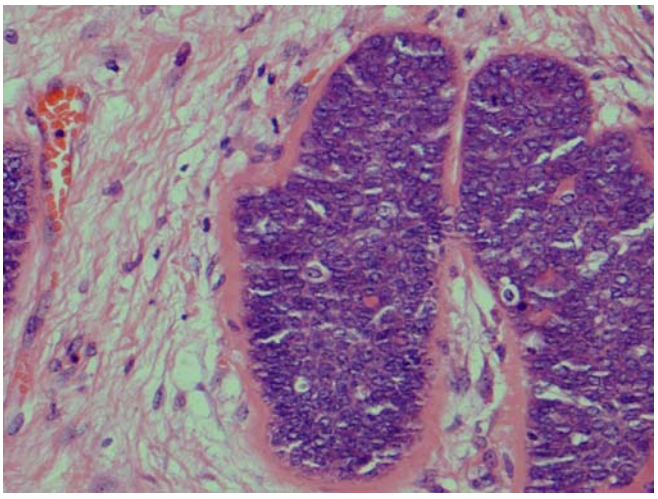

Fig. 4 Basal cell adenocarcinoma. Invasive lobules of basaloid cells with a palisaded outer layer, surrounded by a thick basement membrane

(pankeratin MNF 116, CK7, CK5D3 and EMA) and myosin heavy chain. The ductal cells of the adenoid cystic carcinoma were strongly positive for MNF 116, CK5D3 and CK7, and positive for EMA. The basal cell adenocarcinoma was EMA negative but showed a more intense MNF 116 expression than did the non-ductal parts of the adenoid cystic carcinoma. The Ki-67 labelling index varied in different areas from 8 to 14% in the adenoid cystic component, whilst being between 4 and 7% in the basal cell adenocarcinoma.

Hybrid salivary gland tumours are rare, accounting for less than 0.1% of all salivary gland tumours [7]. The small number of reported cases makes prognostic assessment and clinical management of these tumours difficult, but management is guided by the most aggressive component. The fine-needle aspirate showed both features of basaloid neoplasm and adenoid cystic carcinoma, underlining its value in the clinical management of salivary gland tumours. The malignant tumour types most frequently found as components of hybrid salivary tumours are adenoid cystic carcinoma, epithelial–myoepithelial carcinoma and salivary duct carcinoma. The most commonly described hybrid is adenoid cystic carcinoma and epithelial–myoepithelial carcinoma [1–10]. As it is not unusual to see varying architectural patterns within individual salivary gland tumours, e.g. cribriform, tubular and solid patterns with adenoid cystic carcinoma, it is important to distinguish this common variation from a true hybrid salivary gland tumour, showing diagnostic criteria for two or more salivary neoplasms.

References

1. Chetty R, Medley P, Essa A (2000) Hybrid carcinomas of salivary glands. Arch Pathol Lab Med 124:494–496

2. Croitoru CM, Suarez PA, Luna MA (1999) Hybrid carcinomas of salivary glands. Report of 4 cases and review of the literature. Arch Pathol Lab Med 123:698–702
3. Kamio N, Tanaka Y, Mukai M, Ikeda E, Kuramochi S, Fujii M, Hosoda Y (1997) A hybrid carcinoma: adenoid cystic carcinoma and salivary duct carcinoma of the salivary gland. An immunohistochemical study. Virchows Arch 430:495–500
4. Nagao T, Sugano I, Ishida Y, Asoh A, Munakata S, Yamazaki K, Konno A, Iwaya K, Shimizu T, Serizawa H, Ebihara Y (2002) Hybrid carcinomas of the salivary glands: report of nine cases with clinicopathologic, immunohistochemical, and p53 gene alteration analysis. Mod Pathol 15:724–733
5. Piana S, Damiani S, Asioli S, Magrini E, Barberi W, Cavazza A (2004) Epstein–Barr positive lymphoepithelial carcinoma and epi-myopepithelial cell carcinoma of the parotid gland: a hitherto unreported example of hybrid tumour. Virchows Arch 445:425–428
6. Ruiz-Godoy LM, Mosqueda-Taylor A, Suarez-Roa L, Poitevin A, Bandala-Sanchez E, Meneses-Garcia A (2003) Hybrid tumours of the salivary glands. A report of two cases involving the palate and a review of the literature. Eur Arch Otorhinolaryngol 260:312–315
7. Seifert G, Donath K (1996) Hybrid tumours of salivary glands. Definition and classification of five rare cases. Eur J Cancer Oral Oncol 32:159–251
8. Snyder ML, Paulino AF (1999) Hybrid carcinoma of the salivary gland: salivary duct adenocarcinoma and adenoid cystic carcinoma. Histopathology 35:380–383
9. Woo JS, Kwon SY, Jung KY, Kim I (2004) A hybrid carcinoma of epithelial–myoepithelial carcinoma and adenoid cystic carcinoma in maxillary sinus. J Korean Med Sci 19:462–465
10. Zardawi IM (2000) Hybrid carcinoma of the salivary gland. Histopathology 37:283–284

Virchows Arch (2006) 448: 239
DOI 10.1007/s00428-005-0128-7

LETTER TO THE EDITOR

David B. Weinreb

Re: Detection of JC virus sequences in colorectal cancers in Japan

Received: 18 October 2005 / Accepted: 26 October 2005 / Published online: 20 December 2005

To the Editors:

We read "Detection of JC virus DNA sequences in colorectal cancers in Japan" by Hori et al. with great excitement. These authors offer convincing evidence that polyoma T antigen may be integrated into the cellular genome of colon carcinoma tissues, although the T-antigen protein is not expressed [4]. We enthusiastically agree with their conclusions and would like to offer additional data to advance this discussion.

First, we have investigated the presence of polyomavirus (PV) T antigen in tumors by immunohistochemistry (IHC), using a primary antibody that reacts with the large T antigen of both the JC and BK viruses [1, 5]. T antigen was not detected in any of 50 cases of colon carcinoma, 18 cases of gastric cancer, or 15 cases of bladder carcinoma.

In addition, we examined by IHC the presence of T antigen in six cases of polyoma virus nephropathy (PVN) in renal transplant patients. In all of these six patients, robust nuclear staining specific for T antigen was observed in scattered tubular cells. The infected tubular cells were characterized by distinct cytopathological features, including anisonucleosis, hyperchromasia with clumped chromatin, and intranuclear inclusions. Such cellular changes represent a "permissive" infection, i.e., a state of viral replication. These histopathological features are absent in our 83 cases of carcinoma.

We agree with these authors that if PV is present in tumors, it is likely to be integrated into the cellular genome, representing a "nonpermissive" infection in which viral replication does not occur.

We conclude that future IHC studies of tumors are likely to be uninformative because we fail to detect viral antigens in nonpermissive infections, which are precisely the category of infections hypothesized to drive oncogenesis. Although recent studies have detected T antigen by IHC in esophageal [2] and colon [3] carcinoma, it remains to be seen whether these data truly represent evidence for a viral etiology in these tumors, or, alternatively, a sequelae of the patient's immunocompromised state.

We look forward to hearing the results of future studies from Dr. Hori's team.

References

1. Del Valle L, Gordon J, Assimakopoulou M, Enam S, Geddes JF, Varakis JN, Katsetos CD, Croul S, Khalili K (2001) Detection of JC virus DNA sequences and expression of the viral regulatory protein T-antigen in tumors of the central nervous system. Cancer Res 61:4287–4293
2. Del Valle L, White MK, Enam S, Oviedo SP, Bromer MQ, Thomas RM, Parkman HP, Khalili K (2005) Detection of JC virus DNA sequences and expression of viral T antigen and agnoprotein in esophageal carcinoma. Cancer 103(3):516–527
3. Enam S, Del Valle L, Lara C, Gan DD, Ortiz-Hidalgo C, Palazzo JP, Khalili K (2002) Association of human polyomavirus JCV with colon cancer: evidence for interaction of viral T-antigen and beta-catenin. Cancer Res 62(23):7093–7101
4. Hori R, Murai Y, Tsuneyama K, Abdel-Aziz HO, Nomoto K, Takahashi H, Cheng CM, Kuchina T, Harman BV, Takano Y (2005) Detection of JC virus DNA sequences in colorectal cancers in Japan. Virchows Arch 14:1–8
5. Mann RS, Carroll RB (1984) Cross-reaction of BK virus large T antigen with monoclonal antibodies directed against SV40 large T antigen. Virology 138:379

D. B. Weinreb (✉)
School of Medicine,
Mount Sinai Hospital,
Room 11C1, 50 East 98th Street,
New York, NY 10029, USA
e-mail: David.weinreb@mssm.edu
Tel.: +1-917-8339472

Virchows Arch (2006) 448: 240
DOI 10.1007/s00428-006-0156-y

ANNOUNCEMENTS

6 May 2006
Problems in Breast Pathology
Malta College of Pathologists
Malta

Course Director
Professor J.G. Azzopardi

Scientific Secretariat
J. De Gaetano and V. Eusebi

9.00 Registration

Chair: J.G. Azzopardi (London/Malta) & Rosemary Millis (London)
9.30–10.00 Ian Ellis (Nottingham) : Prognostic factors: old versus new.
10.00–10.30 Gianni Bussolati (Torino) : The contribution of 3D models to the understanding of breast pathology.
10.30–11.00 Tibor Tot (Falun) : The theory of the sick lobe and the possible consequences.
11.00–11.30 Frederick Koerner (Boston) : The histogenesis of early breast carcinoma.
11.30–12.00 Tanya Tavassoli (New Haven) : To DIN or not to DIN, that is the question.
12.00–12.30 Discussion

Chair: J. Rosai (Milano) & G. Stamp (London)
14.30–15.00: James Connolly (Boston) : Present findings from the benign breast project of the nurses health study.
15.00–15.30: Stuart Schnitt (Boston) : Columnar cell lesions and flat epithelial atypia.
15.30–16.00 Hans Peterse (Amsterdam) : Ring carcinomas: the phenomenon of shift of cell polarization.
16.00–16.30: Thomas Krausz (Chicago) : Breast tumours. Race, loneliness and the pathologist.
16.30–17.00 : Werner Boecker (Muenster): The progenitor cell concept of breast epithelium and how it changes our understanding of proliferative breast disease.
17.00–17.30 : Sunil Lakhani (Brisbane): Myoepithelial cell and breast cancer.
17.30–18.00 : Vincenzo Eusebi (Bologna) : Salivary-like tumours of the breast.
18.00–18.30 : Juan Rosai (Milano) : The vascular lobule. A pitfall on the interpretation of vascular skin lesions following irradiation for breast carcinoma.

S.G. Silveberg (Baltimore) & Jane Dahlstrom
(Camberra) : Conclusive remarks
The congress fee is 30 ∈, that includes light lunch payable on the spot.

Scientific Organizer:
Dr. James De Gaetano
Pathology Department
St. Luke's Hospital
Gwardamangia
Malta
tel.n. xx356 25951117
e-mail james.degaetano@gov.mt

Venue and Hotel accomodation:
Hilton Hotel
Portomaso
St. Julians
Malta PTM01
Tel.n. XX 356 21383383
www.hilton.com.mt

Diagnostic histopathology of breast disease
at Hammersmith Hospital (Imperial College),
London, UK

A week–long course designed for pathologists at Consultant and Senior Trainee level. The course provides a comprehensive coverage of the Histopathology of Breast Disease, with special emphasis on areas that pose diagnostic difficulties. The participants will be given ample time to study histological preparations, followed by illustrated discussion of the cases. There will also be several daily talks dealing with specific topics, given by eminent breast pathologists and followed by discussions. The topics will include update on reporting breast biopsies, immunohistochemistry, hormone receptors and HER2 assessment, Sentinel lymph node biopsy, dealing with the gross specimen, prognostic factors, proliferative lesions/ carcinoma in situ, problems in breast pathology and interpretation of breast core biopsies. The faculty will include Ian Ellis, Christopher Elston, Andrew Hanby, Andrew Lee, Sarah Pinder and Sami Shousha.

Further further information please contact
Wolfson Conference Centre
Hammersmith Hospital
Du Cane Road
London W12 ONN, UK
Tel: +44-20-83833117/3227/3245;
Fax: +44-20-83832428;
e-mail: wcc@imperial.ac.uk

15–16 June 2006
Thyroid Pathology for the Practicing Pathologist
15 rue de l'Ecole de Médecine, Paris,France

A 2-day course will take place in Paris again under the auspices of the French Division of the I.A.P.

This course will be given in English by Prof. M. Sobrinho-Simões (Porto) and Prof. R. Heimann (Brussels).

It will consist of lectures alternating with slide reviews and a slide seminar over a multihead microscope. The cases of this seminar will be sent (on CD) before the meeting.

The audience will be limited to 22 participants.
Course fees: 390 euros (320 euros for members of any I.A.P. division). The fees include registration, hand-out, CD of the slide seminar and coffee breaks.

For further information please contact
Mrs. M. Fontaniére
Administrative Secretary
French Division of the I.A.P.
32 Cours Albert Thomas
69008, Lyon, France
Fax: 33 4 78754311
e-mail: academie.pathologie@wanadoo.fr

Virchows Arch (2006) 448: 241–247
DOI 10.1007/s00428-005-0103-3

REVIEW ARTICLE

Giuseppe Viale · Mauro G. Mastropasqua · Eugenio Maiorano · Giovanni Mazzarol

Pathologic examination of the axillary sentinel lymph nodes in patients with early-stage breast carcinoma: current and resolving controversies on the basis of the European Institute of Oncology experience

Received: 17 October 2005 / Accepted: 17 October 2005 / Published online: 24 November 2005

Abstract Several controversial aspects of sentinel lymph node biopsy (SLNB) for patients with early-stage, node-negative breast carcinoma have been dealt with and resolved in the past decade since its introduction. Unfortunately, however, there is still no consensus on how best to examine sentinel lymph nodes (SLN) histologically. As a consequence, the protocols for SLN examination are remarkably variable in different institutions, leading to a very poor reproducibility of the data stemming from investigations on series of patients whose SLNs have been evaluated according to diverse protocols. Patient outcomes, however, can be optimised only by standardization of the whole procedure of SLNB, with particular reference to the histopathologic scrutiny. Lack of a standardized histopathologic protocol likely derives also from the uncertainties about the clinical implications of minimal lymph node involvement (isolated tumour cells and micrometastases) with regard both to the risk of additional metastases to non-sentinel lymph nodes of the same basin and to the prognostic value for patients' survival. This review aims at highlighting some of the controversial issues of the histopathologic examination of the SLNs, including the number of sections and cutting intervals, the use of immunohistochemistry and the role of molecular biology assays.

G. Viale (✉) · M. G. Mastropasqua · G. Mazzarol
Department of Pathology and Laboratory Medicine,
European Institute of Oncology,
Via Ripamonti, 435,
20141 Milan, Italy
e-mail: giuseppe.viale@ieo.it
Tel.: +39-02-57489419
Fax: +39-02-57489417

G. Viale
School of Medicine, University of Milan,
Milan, Italy

E. Maiorano
Department of Pathological Anatomy, University of Bari,
Bari, Italy

Keywords Breast carcinoma · Sentinel node biopsy · Micrometastasis

Introduction

Over the past decade, lymphatic mapping and axillary sentinel lymph node biopsy (SLNB) have been increasingly adopted for staging with minimal morbidity patients with node-negative, early-stage breast carcinoma. Since the procedure was introduced, several problem aspects and controversial issues have been dealt with and resolved, while others still remain open. The studies reported thus far support the validity and safety of SLNB in different clinical scenarios where they were formerly questioned, as for patients with previous surgical biopsy/lumpectomy or with multicentric breast carcinomas [39] and for patients treated with neoadjuvant chemotherapy [27]. The safety of the procedure in pregnant women and the accuracy of a second SLNB for relapsing tumours following conservative surgical treatment inclusive of SLNB remain to be assessed.

Several methodological issues regarding the site of tracer injection, the type of tracer, and the surgical identification and removal of the sentinel lymph node (SLN) have also been clarified, and guidelines or procedures for lymphatic mapping and SLN removal have been agreed upon. It is surprising that, despite its pivotal role in determining the accuracy and hence the clinical utility of SLNB, the histopathologic examination of SLN largely remains an unresolved issue.

To be effective in properly staging with minimal morbidity patients with clinically node-negative breast malignancies, the SLNB must rely upon a very accurate histopathologic examination of the SLNs [7, 42, 45]. It is indeed intuitive that the detection rate of metastatic tumour depends on the accuracy and extent of the histopathologic evaluation, i.e. the number of sections scrutinized. The lack of universally adopted protocols for the examination of SLNs resulted in a wide heterogeneity of the procedures currently used in different institutions, and in several guide-

lines or recommendations issued by scientific organizations at the local or international level. Unfortunately, this led to a very poor reproducibility of the data stemming from investigations on different series of patients whose SLNs have been evaluated according to different protocols. As a result, despite almost a decade of investigations on SLNB and several thousand patients enrolled in clinical studies, a number of questions still remain unanswered. Among these, the most important is whether or not the histopathologic examination of SLNs should aim at detecting even minimal lymph node involvement (isolated tumour cells and micrometastases) using all the available technological resources, from the traditional step sectioning with or without immunohistochemical detection of specific tumour cell markers to more sophisticated assays [e.g. reverse-transcription polymerase chain reactions (RT-PCR)]. This question, however, may only be addressed properly after the clinical implications of minimal lymph node involvement are definitively assessed, with regard both to the risk of additional metastases to non-sentinel lymph nodes of the same basin and to the prognostic value of isolated tumour cells (ITC) and micrometastases for patients' survival [18, 38]. Indeed, due to the lack of a standardized histopathologic examination, the clinical implications of minimal SLN involvement are still debated, with some studies documenting an important risk of additional involvement of higher-echelon lymph nodes and of unfavourable clinical outcome, at variance with the results of other investigations [9, 10, 17, 23–25, 30, 32, 33, 35].

Due to the uncertainty on the clinical implications of minimal SLN involvement, individual institutions have reserved the right to devise their own protocol for SLN examination according to the available resources and the cost/benefit analysis. A recent survey of the protocols used in Europe for the histopathologic examination of axillary SLNs of breast carcinoma patients has unveiled remarkable differences among the 240 laboratories that responded to the questionnaire, with the reporting of 123 somewhat different histological protocols. Almost 12% of the responding laboratories examined only one level per SLN, whereas all the other laboratories performed a multilevel assessment, ranging from the evaluation of 2–5 levels to more than 100 levels separated by 40-μm cutting intervals. Patient outcomes, however, can be optimised only by standardization of the whole procedure of SLNB, with particular reference to the histopathologic scrutiny [8, 22].

The histopathologic examination of SLN

The very first histopathologic approaches to SLN examination did not differ from the routine assessment of the regional lymph node status, based on the evaluation of a single or very few sections cut from frozen (in case of intraoperative diagnosis) or paraffin-embedded lymph nodes. As expected, however, the high false-negative rate of this traditional approach was soon highlighted by the first reports on the higher accuracy of a more extensive histopathologic examination of SLNs.

Subsequently, a large series of studies aimed at assessing the benefit of a more extensive histopathologic examination of SLNs. Endpoint of the studies was to increase the positive and negative predictive value of the SLNB by using more demanding histopathologic protocols based on sub-serial sectioning of the entire SLNs and the use of ancillary immunohistochemical staining techniques [21] that however had to be cost-effective and not exceeding the workload capacity of the laboratory. It is self-evident that the cost/benefit analyses of an extensive examination of SLNs vary according to several parameters, including the number of patients evaluated, the amount of the reimbursement and the availability of dedicated personnel and instrumentation. As a rule, the detection rate of metastases depends on the number of sections examined from the entire lymph node, so that the prevalence of SLN involvement in a given series of patients depends on the adopted histopathologic protocol. To ensure optimisation of patients' management in different institutions, however, a standardized protocol should be agreed upon [46, 49].

We have devised one of the most demanding protocols for SLN examination of breast carcinoma patients, which requires the histopathologic scrutiny of the entire SLN by step sectioning at very thin cutting intervals. According to this protocol, which is suitable for both frozen and paraffin-embedded lymph nodes, the SLN is bisected along the longest axis or cut into 2- to 3-mm slices if thicker than 5 mm (thinner lymph nodes are processed uncut). In handling the lymph node, special attention should be paid to preserve intact the nodal capsule and the peripheral sinuses, where many metastatic foci may be first seen. Sections are then cut at 50- to 100-μm intervals until the complete examination of the lymph node by scanning individual sections at 100× magnification. Spare sections for immunohistochemistry were formerly cut at each level, but now we perform immunohistochemical reactions on destained sections whenever deemed necessary to confirm the metastatic nature of morphologically atypical cells (approximately 5% of the cases).

The need for a complete examination of the SLN derives from the observation that while larger (macro-)metastases, measuring 2 mm or more, are detected in the vast majority of the cases in the very first sections cut from the middle areas of the nodes, smaller (micro-)metastasis, measuring less than 2 mm, are more randomly distributed throughout the SLN and cannot be reliably detected by the examination of the sections from the central portions of the node. The choice of cutting step sections at 50- to 100-μm intervals is dictated by the aim of identifying even a minimal lymph node involvement (ITC and micrometastases), which could escape detection by sectioning the node at wider cutting intervals [45, 46].

That such a labour-intensive protocol could not be followed by many other institutions is intuitive, especially when considering that the clinical implications of minimal SLN involvement are still controversial. Thus it is not surprising that recommendations for SLN examination issued by nationwide or international organizations suggest more affordable protocols [8, 22], which re-emphasize the

need for a complete examination of the node, but allow cutting intervals ranging from 0.5 [22] to 1 mm [8]. The rationale for defining these minimal requirements is only to assure the detection of macrometastases and not to search for minimal lymph node involvement by ITC or micrometastases. Accordingly, use of ancillary diagnostic techniques, such as immunohistochemistry or molecular biology assays, is not recommended. Similar conclusions were reached by the panelists of the Consensus Conference held in Philadelphia in 2001 [37]. Whether these recommendations will be maintained or changed depends mainly on the future progresses in unveiling the clinical implications of minimal lymph node involvement.

Workload for the department of pathology

At first glance, any protocol for a more or less extensive examination of SLNs looks very worrisome for the increased workload for both the histo-technicians and the pathologists. In several institutions, the pathologists' reaction to the implementation of the SLNB for breast carcinoma patients is to declare the unavailability of sufficient human and/or instrumental resources for an extensive examination of the SLNs. This might well be true in rare instances, but in the majority of the cases, the SLN workload should be affordable.

The above-described protocol for SLN examination implemented at the European Institute of Oncology requires that approximately 60 sections are cut from each individual 0.5-cm-thick SLN and examined histologically. This might well seem a painstaking procedure, not affordable in many other centres. The first reaction, however, could be mitigated by considering that in about 70% of the cases, the SLN will be free of metastases, thus preventing any further axillary treatment. In these circumstances, the workload for SLN examination will be counterbalanced by the avoidance of embedding, trimming, cutting and examining sections from each of the 20–30 lymph nodes retrieved by complete axillary clearing.

In approximately 60% of the positive SLNB, the size (>2 mm) of the metastases will allow their detection in the very first sections of the SLN (obtained from the central portion of the nodes, after bisection) or even by touch cytology, and the examination of further sections will be spared. Although these patients will undergo completion axillary dissection, the additional workload for SLN examination may indeed be very limited. In the remaining 40% of the cases, the SLN will be minimally involved by micrometastases or isolated tumour cells whose detection requires a complete examination of the SLN by step sectioning. The diagnosis of minimal SLN involvement will be followed—at least in some institutions—by completion axillary dissection, resulting in a net increase in the workload for the laboratory. It should be noted, however, that this applies to only about 12% of the patients with early-stage breast carcinoma.

From our experience with more than 8,000 SLNB examined in the last 9 years, we have calculated that our procedure implies an overall additional workload for the laboratory of approximately ten sections per treated patient (considering that almost 75% of the patients undergo SLNB). A slight modification of the protocol (i.e. cutting step sections of the whole SLN at 100-μm intervals) would be enough to eliminate the need for any additional section. These figures depend on the fact that we routinely scrutinize non-sentinel axillary lymph nodes by examining three to six sections per node. The mean number of SLN per patient is 1.5 (median 1 SLN/patient), the mean number of lymph nodes retrieved by axillary dissection is 27, and the patients with minimal SLN involvement are offered randomisation in a clinical trial comparing axillary dissection with no further treatment. Needless to say, the above conditions vary in different institutions because the mean yield of a completion axillary dissection, the number of sections examined from non-sentinel axillary lymph nodes, the mean number of SLN removed per patients and the mean thickness of the SLNs are highly variable and prevent any general statement to be made. The take-home message, however, is that a truly extensive histopathologic examination of SLNs may well have a lower impact on the global workload of pathology departments than figured and feared at first glance.

False-negative and false-positive SLNB

The assessment of SLN status may be affected by both false-negative and false-positive histopathologic results.

A false-negative SLNB is almost invariably due to a less-than-optimal scrutiny of the SLN, either because of the number of evaluated sections is not high enough to be truly representative of the node status or because metastases escape recognition by the pathologist. The issue of a variable detection rate of metastases according to the more or less extensive examination of the SLNs has been dealt with in the preceding paragraphs. It is quite uncommon for an experienced pathologist to overlook lymph node metastases. There are instances, however, where small and/or morphologically unusual metastases from breast carcinoma may be misinterpreted as non-neoplastic resident cells, most likely nevus cells [34], epithelioid histiocytes of granulomatous lymphadenitis or vessels with high endothelial lining, especially when examining frozen tissue sections. To avoid misdiagnoses, use of ancillary immunohistochemical techniques for specific markers of the epithelial lineage (i.e. cytokeratins) may be extremely useful. These techniques may also be applied to intraoperative frozen section diagnosis, taking advantage of commercially available reagents that allow the reaction to be completed in less than 20 min [5, 41].

Less attention has been paid to the risk of false-positive identification of SLN metastases, although this would imply unwarranted lymph node dissection and improper adjuvant treatments.

Carter et al. [4] first warned of the possible occurrence of passive transport to the axillary lymph node of normal (and neoplastic) breast tissue following diagnostic needle

procedures on the breast. Chiu et al. [6] emphasized inaccurate immunohistochemical procedures as a potential source of false-positive SLNB. Furthermore, the immunoreactivity for low-molecular-weight cytokeratins of fibroblastic reticulum cells invariably present in normal lymph nodes [11, 14] may be responsible for a false identification of metastatic cells. A more subtle cause of false-positive identification of breast metastases is the possible occurrence of benign-appearing breast tissue in the lymph node capsule and/or parenchyma.

The occurrence of ectopic non-neoplastic tissue within lymph nodes is a well-recognized phenomenon, especially for thyroid or salivary structures within latero-cervical lymph nodes or nevus cells in lymph nodes from different basins [13]. Mammary glands are the ectopic epithelial structures most frequently detected within axillary lymph nodes [19], and at variance with most of the aforementioned examples that occur intra-parenchimally, these are commonly seen in capsular or sub-capsular locations or in the peri-nodal fat tissue. Occasionally, the ectopic tissue has been interpreted as metastatic, thus leading to over-staging and, eventually, over-treatment of the patients [13, 19].

We [26] first reported on the occurrence of benign epithelial inclusions of ectopic breast tissue in axillary SLNs of seven breast carcinoma patients, with remarkably different morphological features. Indeed, these benign epithelial inclusions may undergo proliferative changes similar to those encountered in fibrocystic disease (florid duct hyperplasia and sclerosing adenosis), making the differential diagnosis with true metastases very difficult. Again, use of appropriate immunohistochemical reactions for specific markers (e.g. p63, smooth-muscle myosin, calponin) of the myoepithelial cell component, invariably present in benign inclusions and absent in metastatic breast carcinoma, is instrumental in reaching the correct diagnosis, but the examining pathologist should be fully aware of the possible occurrence of such benign inclusions.

Predicting the status of non-sentinel lymph nodes

The extensive examination of SLNs has significantly increased the detection rate of minimal lymph node involvement, and the question has now arisen whether or not micrometastases or ITC only in the SLN predict a risk for additional non-sentinel node metastases high enough to justify completion axillary dissection for these patients. Previous studies had suggested that breast carcinoma patients with minimal SLN involvement could indeed be spared axillary surgery because of an alleged negligible risk of additional metastases, but we and other authors documented a 20–24% risk of involvement of further-echelon lymph nodes in patients with micrometastatic SLNs [40, 49].

More recently, we evaluated a large series of patients with positive SLN biopsy followed by completion axillary dissection, showing that of the 116 patients with ITC only in the SLN, 17 (14.7%) had further axillary involvement, as did 68 (21.4%) of the 318 patients with SLN micrometastases (0.2–2 mm in size) [47]. The prevalence of additional metastases was not significantly different between these two groups of patients (P=0.15), whereas patients with macrometastatic disease in the SLNs showed a significantly higher proportion of non-sentinel lymph node metastases, which were detected in 50.3% (399/794) of the cases (P<0.0001). However, when the patients with SLN micrometastases were further stratified according to the size of the micrometastases (up to 1 vs 1–2 mm), those with larger micrometastases showed a significantly higher prevalence of additional metastases (30.2 vs 17.0; P=0.01), thus confirming previous data [17, 47]. To summarize, patients with a positive SLN biopsy can be stratified in three groups at significantly different risk for involvement of non-sentinel lymph nodes. Patients with ITC or small (up to 1 mm) micrometastases in the SLN have the lowest risk of additional metastases (16.2%), which increases to 30.2 and 50.3% for patients with 1–2 mm micrometastases or larger metastases, respectively.

In each subgroup of patients with SLN metastases, the identified additional metastases to non-sentinel lymph nodes were mostly of the macrometastatic type, i.e. larger than 2 mm [47], most likely because the non-sentinel nodes were scrutinized with a limited number of sections (3–6) and at least some micrometastases or ITCs were likely missed. Therefore, completion axillary dissection in all the patients with positive axillary SLN biopsy may add clinically meaningful information because in the vast majority of the cases, including those with ITC only or micrometastases in the SLNs, non-sentinel nodes will be shown to harbour metastases larger than 2 mm.

To ascertain whether the identification of minimal SLN involvement (with the associated risk of additional non-sentinel lymph node metastases) is per se informative enough to plan an effective adjuvant treatment without the need for further axillary surgery, the International Breast Cancer Study Group has launched a randomised clinical trial (IBCSG trial 23-01), whereby patients with micrometastatic disease or ITC only in the SLN are randomised to further axillary surgery or follow-up. Primary endpoint of the trial is disease-free survival; secondary endpoints are overall survival and quality of life.

Tumour mRNA markers

The ever-increasing adoption of SLNB for staging patients with minimal morbidity has raised the question of how best to evaluate the SLN to minimize the risk of false-negative results. Owing also to the lack of standardized and widely accepted protocols for a truly extensive histopathological examination of SLN, the relative merits of alternative assays based on the identification of tumour-specific mRNA markers over traditional histological or immunohistochemical methods have been extensively exploited. Initially, qualitative RT-PCR experiments documented that several mRNA markers, either alone or in multimarker assays,

were indeed suitable for a high-sensitivity detection of metastatic breast cancer or melanoma in sentinel or non-sentinel lymph nodes [2, 3, 28, 31].

The specificity of the assays, however, was less satisfactory, with a high prevalence of positive assays in histologically unaffected lymph nodes and also in lymph nodes obtained from patients without malignancies [2]. Because a possible cause of false-positive identification of lymph node metastases by RT-PCR assays might be the illegitimate expression of low levels of target mRNAs by non-neoplastic cells, real-time quantitative RT-PCR (qRT-PCR) assays have been developed to correctly identify lymph node metastases according to a threshold level of mRNA expression [15, 20, 29, 36, 48]. Very recently, dedicated kits and instruments for "rapid" quantitative RT-PCR assays have also become commercially available for the intraoperative detection of SLN metastases from breast carcinoma.

A critical reappraisal of the investigations dealing with the identification of breast carcinoma mRNA markers in axillary sentinel and non-sentinel nodes, however, still challenges the possible application of qRT-PCR assays in the clinical practice. Indeed, in the studies with the largest series of patients evaluated, the overall concordance between qRT-PCR assays for individual or multiple mRNA markers and morphological or immunohistochemical findings ranges from 73.2 [15] to 95.7% [48]. Discrepancies include both false-negative qRT-PCR results, with histologically detected metastases escaping identification by the assays and still positive assays in lymph nodes not harbouring any morphologically identifiable metastasis.

Besides the choice of the molecular assay (qualitative vs quantitative RT-PCR), a most likely cause for the discrepancies between morphological and molecular findings is the sampling procedure, with part (or half) of the lymph node being subjected to molecular biology assays and another part to morphological and immunohistochemical examination. As a consequence, the smallest tumour deposits (micrometastases and ITC) may remain confined exclusively to the sample undergoing one assay, escaping detection by the other.

To minimize the effects of sampling on the final results, we have combined RT-PCR assays with our procedure whereby axillary SLNs of patients with breast carcinoma are snap frozen and examined completely by step sectioning at 50-μm intervals. While the frozen sections are examined histologically (including immunohistochemical testing), the interval tissue is subjected to RT-PCR assays. Applying this procedure, we have previously examined 146 axillary SLNs from 123 patients for the detection of five different mRNA tumour markers (cytokeratin 19, CEA, mammaglobin 1, MUC-1 and maspin) by qualitative RT-PCR assays [28]. When analysed individually, the general concordance with the histopathologic findings ranged from 78.8 to 83.6%, with none of the different markers attaining a sensitivity higher than 77.8%. Mammaglobin (MGB1) was the mRNA marker most closely correlated with the histopathologic findings, with a sensitivity of 77.8% and a specificity of 86.1%. We have more recently evaluated the effectiveness of a real-time qRT-PCR assay for MGB1 mRNA in the detection of lymph node metastases in a retrospective series of 81 axillary SLNs from 72 patients, for which the results of the previous qualitative assays were known, and validated the results in a prospective series of 61 SLNs from 61 newly diagnosed breast carcinoma patients.

In our experimental conditions, qRT-PCR assays were indeed more accurate than conventional RT-PCR in assessing the status of axillary SLNs: four of the six false-negative cases in conventional RT-PCR assays turned positive in qRT-PCR experiments, whereas two of the five false-positive cases in conventional RT-PCR assays turned negative in qRT-PCR experiments. Accordingly, qRT-PCR assays were superior to qualitative RT-PCR in terms both of specificity and of sensitivity.

The results were compared with the histopathological findings obtained by a very extensive examination of the same lymph nodes, specifically designed to minimize the possible effects of the sampling procedures on the correlation between morphological and molecular data. The overall concordance with histopathological findings was 93.8 and 93.4% in the retrospective and validation series, respectively, well in line with previous findings from qRT-PCR assays of individual or multiple tumour markers, indicating a concordance ranging from 73.2 [15] to 95.7% [48]. The overall sensitivity of the assay in the two combined series was 88.5% and the specificity 94.8%, with a PPV of 79.3% and an NPV of 97.3%. The false-negative rate of the assay (11.6% or 3/26 histologically positive SLN), and the rate of positive detection of MGB1 mRNA (5.2% or 6/116) in lymph nodes not harbouring any histologically identifiable metastasis, however, question its use in the clinical practice as an alternative to the histopathological examination of the SLN. In the above study, we compared the qRT-PCR findings with a very extensive histopathological evaluation of the SLN, which makes it unlikely that the molecular assay actually identifies true metastases missed at the morphological scrutiny. Whether the molecular assay may be a valuable and cost-effective tool for the identification of breast cancer metastases in axillary SLN that are not subjected to a very extensive histopathologic examination remains to be evaluated.

Epilogue

This review focused on some controversial issues of the histopathologic assessment of SLN status, with special reference to the assumption that the detection of even minimal lymph node involvement may be clinically relevant, both for immediate surgical intervention on further-echelon lymph nodes and for prognostic/predictive evaluations.

The mere occurrence of tumour cells in the regional lymph nodes, however, may not be an invariable predictor of clinical progression of the disease. The results of randomised trials [43, 44, 50] have shown that the observed number of breast carcinoma patients with clinically overt axillary

progression of the disease is much lower than expected based on either the false-negative rate of the sentinel lymph node biopsy or the known prevalence of metastasis to axillary lymph nodes. This suggests that metastatic cells may not progress to clinical disease in all patients and that only some of them have the capability of sustaining tumour progression, consistent with the hypothesis that cancer growth and progression, and hence the clinical outcome of the disease, are dependent on the activation of tumorigenic stem/progenitor breast cancer cells [1, 12].

The stem/progenitor cell theory of carcinogenesis and tumour progression conflicts with the traditional stochastic approach, by which all tumour cells in a given patient share the same potential for progression. According to the stochastic approach, prognosis is dictated by the actual amount of invasive or metastatic tumour cells, and the therapeutic interventions are intended to minimize their number. This leads pathologists to evaluate painstakingly tumour burden and count tumour cells, using all the possible ancillary techniques to identify even individual tumour cells. This attitude may not be truly rewarding. Indeed, the progenitor/stem cell theory predicts that only some (and possibly a minor percentage of) tumour cells are actually responsible for tumour progression and clinical outcome, and that all efforts should be made to target these cells with specific interventions [16]. Thus, what is now needed is to unveil specific markers of the tumorigenic cells that would allow their identification and quantitation in clinical specimens and to re-evaluate the prognosis by alternative means.

References

1. Al-Hajj M, Wicha MS, Benito-Hernandez A, Morrison SJ, Clarke MF (2003) Prospective identification of tumorigenic breast cancer cells. Proc Natl Acad Sci U S A 100:3983–3988
2. Bostick PJ, Chatterjee S, Chi DD, Huynh KT, Giuliano AE, Cote R, Hoon DS (1998) Limitations of specific reverse-transcriptase polymerase chain reaction markers in the detection of metastases in the lymph nodes and blood of breast cancer patients. J Clin Oncol 16:2632–2640
3. Branagan G, Hughes D, Jeffrey M, Crane-Robinson C, Perry PM (2002) Detection of micrometastases in lymph nodes from patients with breast cancer. Br J Surg 89:86–89
4. Carter BA, Jensen RA, Simpson JF, Page DL (2000) Benign transport of breast epithelium into axillary lymph nodes after biopsy. Am J Clin Pathol 113:259–265
5. Chilosi M, Lestani M, Pedron S, Montagna L, Benedetti A, Pizzolo G, Menestrina F (1994) A rapid immunostaining method for frozen sections. Biotech Histochem 69:235–239
6. Chiu A, Hoda SA, Yao DX, Rosen PP (2001) A potential source of false-positive sentinel nodes: immunostain misadventure. Arch Pathol Lab Med 125:1497–1499
7. Cote RJ, Peterson HF, Chaiwun B, Gelber RD, Goldhirsch A, Castiglione-Gertsch M, Gusterson B, Neville AM (1999) Role of immunohistochemical detection of lymph-node metastases in management of breast cancer. International Breast Cancer Study Group. Lancet 354:896–900
8. Cserni G, Amendoeira I, Apostolikas N, Bellocq JP, Bianchi S, Boecker W, Borisch B, Connolly CE, Decker T, Dervan P, Drijkoningen M, Ellis IO, Elston CW, Eusebi V, Faverly D, Heikkila P, Holland R, Kerner H, Kulka J, Jacquemier J, Lacerda M, Martinez-Penuela J, De Miguel C, Peterse JL, Rank F, Regitnig P, Reiner A, Sapino A, Sigal-Zafrani B, Tanous AM, Thorstenson S, Zozaya E, Fejes G, Wells CA (2004) Discrepancies in current practice of pathological evaluation of sentinel lymph nodes in breast cancer. Results of a questionnaire based survey by the European Working Group for Breast Screening Pathology. J Clin Pathol 57:695–701
9. de Widt-Levert L, Tjan-Heijnen V, Bult P, Ruers T, Wobbes T (2003) Stage migration in breast cancer: surgical decisions concerning isolated tumour cells and micro-metastases in the sentinel lymph node. Eur J Surg Oncol 29:216–220
10. den Bakker MA, van Weeszenberg A, de Kanter AY, Beverdam FH, Pritchard C, van der Kwast TH, Menke-Pluymers M (2002) Non-sentinel lymph node involvement in patients with breast cancer and sentinel node micrometastasis; too early to abandon axillary clearance. J Clin Pathol 55:932–935
11. Doglioni C, Dell'Orto P, Zanetti G, Iuzzolino P, Coggi G, Viale G (1990) Cytokeratin-immunoreactive cells of human lymph nodes and spleen in normal and pathological conditions. An immunocytochemical study. Virchows Arch A Pathol Anat Histopathol 416:479–490
12. Dontu G, Abdallah WM, Foley JM, Jackson KW, Clarke MF, Kawamura MJ, Wicha MS (2003) In vitro propagation and transcriptional profiling of human mammary stem/progenitor cells. Genes Dev 17:1253–1270
13. Fisher CJ, Hill S, Millis RR (1994) Benign lymph node inclusions mimicking metastatic carcinoma. J Clin Pathol 47:245–247
14. Franke WW, Moll R (1987) Cytoskeletal components of lymphoid organs. I. Synthesis of cytokeratins 8 and 18 and desmin in subpopulations of extrafollicular reticulum cells of human lymph nodes, tonsils, and spleen. Differentiation 36:145–163
15. Gillanders WE, Mikhitarian K, Hebert R, Mauldin PD, Palesch Y, Walters C, Urist MM, Mann GB, Doherty G, Herrmann VM, Hill AD, Eremin O, El-Sheemy M, Orr RK, Valle AA, Henderson MA, Dewitty RL, Sugg SL, Frykberg E, Yeh K, Bell RM, Metcalf JS, Elliott BM, Brothers T, Robison J, Mitas M, Cole DJ (2004) Molecular detection of micrometastatic breast cancer in histopathology-negative axillary lymph nodes correlates with traditional predictors of prognosis: an interim analysis of a prospective multi-institutional cohort study. Ann Surg 239:828–840
16. Glinsky GV, Berezovska O, Glinskii AB (2005) Microarray analysis identifies a death-from-cancer signature predicting therapy failure in patients with multiple types of cancer. J Clin Invest 115:1503–1521
17. Guenther JM, Hansen NM, DiFronzo LA, Giuliano AE, Collins JC, Grube BL, O'Connell TX (2003) Axillary dissection is not required for all patients with breast cancer and positive sentinel nodes. Arch Surg 138:52–56
18. Hermanek P, Hutter RV, Sobin LH, Wittekind C (1999) International Union Against Cancer. Classification of isolated tumor cells and micrometastasis. Cancer 86:2668–2673
19. Holdsworth PJ, Hopkinson JM, Leveson SH (1988) Benign axillary epithelial lymph node inclusions—a histological pitfall. Histopathology 13:226–228
20. Inokuchi M, Ninomiya I, Tsugawa K, Terada I, Miwa K (2003) Quantitative evaluation of metastases in axillary lymph nodes of breast cancer. Br J Cancer 89:1750–1756
21. Karsten U, Stosiek P (2002) Fast and sensitive immunodetection of carcinoma cells in sentinel nodes. Virchows Arch 440:325–329

22. Kuehn T, Bembenek A, Decker T, Munz DL, Sautter-Bihl ML, Untch M, Wallwiener D, Consensus Committee of the German Society of Senology (2005) A concept for the clinical implementation of sentinel lymph node biopsy in patients with breast carcinoma with special regard to quality assurance. Cancer 103:451–461
23. Lawrence WD, Association of Directors of Anatomic and Surgical Pathology (2001) ADASP recommendations for processing and reporting of lymph node specimens submitted for evaluation of metastatic disease. Virchows Arch 439:601–603
24. Lee AH, Ellis IO, Pinder SE, Elston CW (2000) Pathological assessment of sentinel lymph-node biopsies in patients with breast cancer. Virchows Arch 436:97–101
25. Liang WC, Sickle-Santanello BJ, Nims TA (2001) Is a completion axillary dissection indicated for micrometastases in the sentinel lymph node? Am J Surg 182:365–368
26. Maiorano E, Mazzarol GM, Pruneri G, Mastropasqua MG, Zurrida S, Orvieto E, Viale G (2003) Ectopic breast tissue as a possible cause of false-positive axillary sentinel lymph node biopsies. Am J Surg Pathol 27:513–518
27. Mamounas EP, Brown A, Anderson S, Smith R, Julian T, Miller B, Bear HD, Caldwell CB, Walker AP, Mikkelson WM, Stauffer JS, Robidoux A, Theoret H, Soran A, Fisher B, Wickerham DL, Wolmark N (2005) Sentinel node biopsy after neoadjuvant chemotherapy in breast cancer: results from National Surgical Adjuvant Breast and Bowel Project Protocol B-27. J Clin Oncol 23:2694–2702
28. Manzotti M, Dell'Orto P, Maisonneuve P, Zurrida S, Mazzarol G, Viale G (2001) Reverse transcription-polymerase chain reaction assay for multiple mRNA markers in the detection of breast cancer metastases in sentinel lymph nodes. Int J Cancer 95:307–312
29. Mitas M, Mikhitarian K, Walters C, Baron PL, Elliott BM, Brothers TE, Robison JG, Metcalf JS, Palesch YY, Zhang Z, Gillanders WE, Cole DJ (2001) Quantitative real-time RT-PCR detection of breast cancer micrometastasis using a multigene marker panel. Int J Cancer 93:162–171
30. Nos C, Harding-MacKean C, Freneaux P, Trie A, Falcou MC, Sastre-Garau X, Clough KB (2003) Prediction of tumour involvement in remaining axillary lymph nodes when the sentinel node in a woman with breast cancer contains metastases. Br J Surg 90:1354–1360
31. Ouellette RJ, Richard D, Maicas E (2004) RT-PCR for mammaglobin genes, MGB1 and MGB2, identifies breast cancer micrometastases in sentinel lymph nodes. Am J Clin Pathol 121:637–643
32. Rahusen FD, Torrenga H, van Diest PJ, Pijpers R, van der Wall E, Licht J, Meijer S (2001) Predictive factors for metastatic involvement of nonsentinel nodes in patients with breast cancer. Arch Surg 136:1059–1063
33. Reynolds C, Mick R, Donohue JH, Grant CS, Farley DR, Callans LS, Orel SG, Keeney GL, Lawton TJ, Czerniecki BJ (1999) Sentinel lymph node biopsy with metastasis: can axillary dissection be avoided in some patients with breast cancer? J Clin Oncol 17:1720–1726
34. Ridolfi RL, Rosen PP, Thaler H (1977) Nevus cell aggregates associated with lymph nodes: estimated frequency and clinical significance. Cancer 39:164–171
35. Sachdev U, Murphy K, Derzie A, Jaffer S, Bleiweiss IJ, Brower S (2002) Predictors of nonsentinel lymph node metastasis in breast cancer patients. Am J Surg 183:213–217
36. Schroder CP, Ruiters MH, de Jong S, Tiebosch AT, Wesseling J, Veenstra R, de Vries J, Hoekstra HJ, de Leij LF, de Vries EG (2003) Detection of micrometastatic breast cancer by means of real time quantitative RT-PCR and immunostaining in perioperative blood samples and sentinel nodes. Int J Cancer 106: 611–618
37. Schwartz GF, Giuliano AE, Veronesi U, Consensus Conference Committee (2002) Proceedings of the consensus conference on the role of sentinel lymph node biopsy in carcinoma of the breast, April 19–22, 2001, Philadelphia, Pennsylvania. Cancer 94:2542–2551
38. Singletary SE, Greene FL, Sobin LH (2003) Classification of isolated tumour cells: clarification of the 6th edn of the American Joint Committee on Cancer Staging Manual. Cancer 98:2740–2741
39. Tousimis E, Van Zee KJ, Fey JV, Hoque LW, Tan LK, Cody HS 3rd, Borgen PI, Montgomery LL (2003) The accuracy of sentinel lymph node biopsy in multicentric and multifocal invasive breast cancers. J Am Coll Surg 197:529–535
40. Turner RR, Chu KU, Qi K, Botnick LE, Hansen NM, Glass EC, Giuliano AE (2000) Pathologic features associated with non-sentinel lymph node metastases in patients with metastatic breast carcinoma in a sentinel lymph node. Cancer 89:574–581
41. Veronesi U, Paganelli G, Galimberti V, Viale G, Zurrida S, Bedoni M, Costa A, de Cicco C, Geraghty JG, Luini A, Sacchini V, Veronesi P (1997) Sentinel-node biopsy to avoid axillary dissection in breast cancer with clinically negative lymph-nodes. Lancet 349:1864–1867
42. Veronesi U, Paganelli G, Viale G, Galimberti V, Luini A, Zurrida S, Robertson C, Sacchini V, Veronesi P, Orvieto E, De Cicco C, Intra M, Tosi G, Scarpa D (1999) Sentinel lymph node biopsy and axillary dissection in breast cancer: results in a large series. J Natl Cancer Inst 91:368–373
43. Veronesi U, Paganelli G, Viale G, Luini A, Zurrida S, Galimberti V, Intra M, Veronesi P, Robertson C, Maisonneuve P, Renne G, De Cicco C, De Lucia F, Gennari R (2003) A randomized comparison of sentinel-node biopsy with routine axillary dissection in breast cancer. N Engl J Med 349:546–553
44. Veronesi U, Galimberti V, Mariani L, Gatti G, Paganelli G, Viale G, Zurrida S, Veronesi P, Intra M, Gennari R, Rita Vento A, Luini A, Tullii M, Bassani G, Rotmensz N (2005) Sentinel node biopsy in breast cancer: early results in 953 patients with negative sentinel node biopsy and no axillary dissection. Eur J Cancer 41:231–237
45. Viale G, Bosari S, Mazzarol G, Galimberti V, Luini A, Veronesi P, Paganelli G, Bedoni M, Orvieto E (1999) Intraoperative examination of axillary sentinel lymph nodes in breast carcinoma patients. Cancer 85:2433–2438
46. Viale G, Maiorano E, Mazzarol G, Zurrida S, Galimberti V, Luini A, Renne G, Pruneri G, Maisonneuve P, Veronesi U (2001) Histologic detection and clinical implications of micrometastases in axillary sentinel lymph nodes for patients with breast carcinoma. Cancer 92:1378–1384
47. Viale G, Maiorano E, Pruneri G, Mastropasqua MG, Valentini S, Galimberti V, Zurrida S, Maisonneuve P, Paganelli G, Mazzarol G (2005) Predicting the risk for additional axillary metastases in patients with breast carcinoma and positive sentinel lymph node biopsy. Ann Surg 241:319–325
48. Weigelt B, Verduijn P, Bosma AJ, Rutgers EJ, Peterse HL, van't Veer LJ (2004) Detection of metastases in sentinel lymph nodes of breast cancer patients by multiple mRNA markers. Br J Cancer 90:1531–1537
49. Wong SL, Edwards MJ, Chao C, Tuttle TM, Noyes RD, Woo C, Cerrito PB, McMasters KM, University of Louisville Breast Cancer Sentinel Lymph Node Study Group (2001) Predicting the status of the nonsentinel axillary nodes: a multicenter study. Arch Surg 136:563–568
50. Zurrida S, Orecchia R, Galimberti V, Luini A, Giannetti I, Ballardini B, Amadori A, Veronesi G, Veronesi U (2002) Axillary radiotherapy instead of axillary dissection: a randomized trial. Italian Oncological Senology Group. Ann Surg Oncol 9:156–160

Virchows Arch (2006) 448: 248–255
DOI 10.1007/s00428-005-0112-2

ORIGINAL ARTICLE

Katharina Glatz-Krieger · Udo Spornitz · Alain Spatz · Michael J. Mihatsch · Dieter Glatz

Factors to keep in mind when introducing virtual microscopy

Received: 17 June 2005 / Accepted: 4 October 2005 / Published online: 22 November 2005

Abstract Digitization of glass slides and delivery of so-called virtual slides (VS) emulating a real microscope over the Internet have become reality due to recent improvements in technology. We have implemented a virtual microscope for instruction of medical students and for continuing medical education. Up to 30,000 images per slide are captured using a microscope with an automated stage. The images are post-processed and then served by a plain hypertext transfer protocol (http)-server. A virtual slide client (vMic) based on Macromedia's Flash MX, a highly accepted technology available on every modern Web browser, has been developed. All necessary virtual slide parameters are stored in an XML file together with the image. Evaluation of the courses by questionnaire indicated that most students and many but not all pathologists regard virtual slides as an adequate replacement for traditional slides. All our virtual slides are publicly accessible over the World Wide Web (WWW) at http://vmic.unibas.ch. Recently, several commercially available virtual slide acquisition systems (VSAS) have been developed that use various technologies to acquire and distribute virtual slides. These systems differ in speed, image quality, compatibility, viewer functionalities and price. This paper gives an overview of the factors to keep in mind when introducing virtual microscopy.

Keywords Telepathology · Virtual slides · Virtual microscopy · Continuing medical education

Abbreviations NA: Numerical aperture · VM: Virtual microscope · VS: Virtual slide · VSAS: Virtual slide acquisition system · VSS: Virtual slide system · WWW: World Wide Web

Universal resource locators (URLs) visited at the time of writing (June 2005) may change or vanish with lapse of time. Therefore and because of usability, we have created a web page with all URLs that will be updated on a regular basis: http://kathrin.unibas.ch/pub/2005–06.

K. Glatz-Krieger · M. J. Mihatsch
Institute for Pathology,
University Hospital of Basel,
Basel, Switzerland

U. Spornitz
Anatomical Institute,
University of Basel,
Basel, Switzerland

A. Spatz
Institute Gustave Roussy,
Villejuif, France

D. Glatz
IT Department,
University of Basel,
Basel, Switzerland

K. Glatz-Krieger (✉)
Institut für Pathologie,
Schönbeinstrasse 40,
CH-4031 Basel, Switzerland
e-mail: Katharina.Glatz@unibas.ch
Tel.: +41-61-2652880

Introduction

Only recently, advances in computer technology have been made that allow to digitize a complete glass slide. Such virtual slides (VS) can be accessed over the World Wide Web (WWW), making them available to a large audience. Since 1998, several virtual slide systems (VSS) have been developed by different commercial and academic bodies (http://www.pathmax.com/apiii/exp.html, http://141.214.6.12/cyberscope631) [1–4, 6, 10, 15, 18, 20, 21, 23, 24, 26]. The value of these virtual microscopes varies considerably depending on the technology used for image acquisition, processing, delivery and viewer functionality. Only few sites are publicly available over the Internet (http://interpath1.uio.no/telemedisin/WebInterPath/interpathindex.htm, http://www.bacuslabs.com, http://virtualmicroscope.osu.edu/virtual.htm, http://neuroinformatica.com, http://images.scanscope.com, http://www.telepathology.dcu.ie/vps02.php3?hits=, http://www2.primed.helsinki.fi/webmicroscope/atlases/breast/brcatlas_start.asp). An outstanding collection of

more than 900 VS is accessible for public use and education from the University of Iowa (http://www.path.uiowa.edu/virtualslidebox).

There is no generally accepted definition of the term "virtual microscopy". In the past, this term has variably been used for sending single images to a colleague by e-mail, for online atlases containing large single images or for image collections showing various sectors of a slide at different magnifications. Only recently, it became possible to digitize entire slides at high magnification, allowing exploration of the tissue on a computer screen in a manner analogous to a real microscope, thus justifying the designation "virtual microscope". We advocate the restricted use of the term "virtual slide" for completely digitized slides at full resolution (scanned at 20× or higher), allowing the pathologist to make a clear-cut diagnosis. Similarly, a virtual microscope should provide at least the functionality of a real microscope (scrolling and zooming of the VS) and may offer additional functionalities like Web accessibility, annotations or automated image analysis.

We have developed a VSS called vMic for public WWW access (http://vmic.unibas.ch). Emphasis was laid on open standards and maximal image quality still allowing for reasonable download times. In an earlier paper, we discussed the theoretical aspects of virtual microscopy [9]. We now report on the first successful applications of vMic in teaching. The parameters to be considered when planning the implementation/acquisition of a VSS are discussed extensively.

Construction of the virtual slide system

We have built a high-quality/low-cost VSS based on the theoretical requirements described in detail earlier [9]. In short, a typical setup for a VSS consists of a virtual slide acquisition system (VSAS), a server that delivers the VS via Internet/WWW to the user and a viewer—preferably a Web-based version.

The demands for our VSAS were:

- Highest possible image quality
- Use of standard components available on the market
- Least possible effort for custom developments (software)
- Highest possible reusability of the investment

Our VSAS consists of commercially available components (Table 1) and includes: a microscope with a robotic stage, high-quality objectives, and a camera for slide acquisition. An acquisition software moves the stage and acquires the images. Due to limitations of the mechanical precision of components (motorized stage, camera mounting, reproducibilitiy, hysteresis, thermal drift, different *z*-positions due to autofocus), the creation of a nearly seamless VS is very tedious when using a standard robotic microscope [23]. In order to circumvent time-consuming calibrations, overlaps of about 3–5 μm at 40× magnification at the intersection of two individual images were deliberately chosen for our VSAS. For viewing the digitized slides in a Web browser, a Flash application was developed that allows the examination of the slides at different magnifications and to move continuously within a slide, closely emulating the functionality of a real microscope. In addition, the user may directly jump to regions of interest guided by an overview image with a cross and a rectangle indicating the current viewing position (Fig. 1). Annotations describe regions of interest and link to extra information on the Web.

Table 1 Components of the vMic slide acquisition system

Microscope	Zeiss Axioskop 2 mot plus
Objectives	Zeiss Plan Apochromat 40×/0.95 for scanning the slides, Zeiss Neofluar 2.5 for overviews
Motorized stage	Maerzhaeuser stage SCAN 75*50
Stage controller	Ludl Controller MAC5000
Camera	Zeiss AxioCam HRc
Software	Zeiss KS400 (includes a macro language enabling to programme a VSAS)
Computers	2 computers with P4/2.4 GHz; one as the capturing system, the second for post-processing

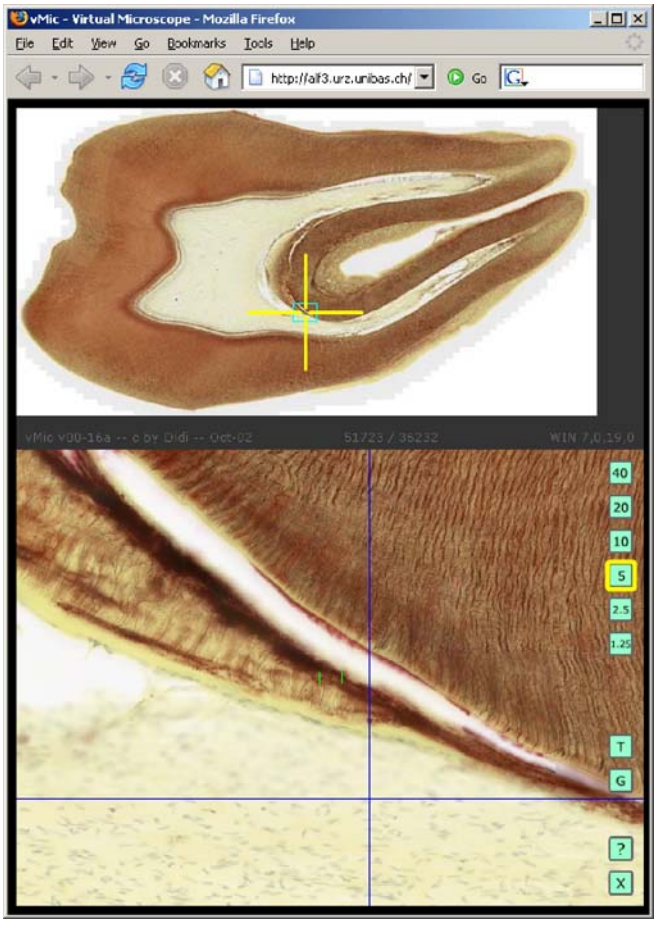

Fig. 1 Virtual slide of the Oral Histology course: The *upper part* of the vMic viewer shows an overview of a molar tooth. A *blue frame* plus *yellow crosshairs* indicate the field of view that is shown at 5× magnification in the lower part

The optical parameters of the VSAS have been chosen to match the limitation of the optical resolution [9]. Maximal image quality was achieved at the cost of low acquisition speed. Each single image was autofocussed, and the AxioCam was set to scan mode at 1,300*1,030 pixel, providing full colour information for each pixel.

To reduce capturing time, a mask representing the region of interest was predefined to guide the roboter.

The captured images were post-processed with Java-scripted Adobe Photoshop. This step included correction of colour and gradation as well as applying an unsharp mask. The latter was only applied to the lightness channel in Lab space, generating crisper images without introducing unwanted colour artefacts. Details of post-processing are illustrated at http://kathrin.unibas.ch/pub/2005–06. Finally, a multi-resolution stack was produced and transferred to the Web server. The viewer (vMic, http://vmic.unibas.ch) and the server have been described in detail previously [9]. Capturing as well as post-processing may last for several hours depending on the slide size and the number of images taken. The components of the described system adhere to open standards and are interchangeable with further developments in the field.

vMIC applications in teaching

After its introduction, vMic (http://vmic.unibas.ch) has primarily been used for teaching purposes: as a component of an online histopathology course for medical students (http://alf3.urz.unibas.ch/hipaku), in a "virtual histology" laboratory for students in dentistry (http://oralhisto.unibas.ch) and in three slide seminars for surgical pathologists (http://vmic.unibas.ch/patho/seminar). The slide seminars had all been organized by sections of the International Academy of Pathology.

Histology course for students in dentistry

Students in dentistry have traditionally been taught dental histology by means of introductory lectures and practical hands-on microscopy courses. A professor of anatomy taught histology showing microscopic slides on a microscope projected with a video projector. Every student needed a microscope and a set of glass slides for the laboratory sessions. Many of these valuable glass slides had already been lost, broken, or faded because of prolonged storage and recurrent intensive exposure to the microscopic illumination. Some of the slides used in this course were very old and could not be replaced due to lack of technicians trained in the various technologies required for the preparation of dental tissues. Furthermore, the procedures applied in the production of some of the slides, e.g. grinding of enamel, is very time consuming, and human resources are scarce. In order to avoid further loss of valuable material, a selection of the best slides used during the course was digitized and the course was moved from the microscopy lab to a computer room. Every student now has identical material of optimal quality to study on a monitor, and the instructor can indicate the coordinates of the area under discussion. Prior to examinations, students may review the slides at home or at one of the numerous public computer workstations offered by the university. Individual use of the course is alleviated by an information sheet provided as a "PDF" file that can be downloaded. The new course (http://oralhisto.unibas.ch) was held for the first time during the winter semester 2003/2004. On average, 85% (29/34) of the students in dentistry participated in each virtual microscopy session. Overall, the students were highly satisfied with the new teaching method. The course had been evaluated with an online questionnaire after the last virtual microscope session (Table 2). Remarkably, the students rated image quality of vMic equal (6×) or even superior (7×) to the image quality of their traditional microscopes, whereas no student indicated the reverse. Last but not least, the grades for the histology exams went up from an average of 5.1 to 5.3 (6 being the highest grade). This, however, might be due to various not course-related factors and certainly needs further evaluation.

Histology course for medical students

We have included some of the more than 900 VS of the virtual slidebox of histopathology (http://www.path.uiowa.edu/virtualslidebox) and few vMic slides in our Web-based histopathology course for medical students (http://alf3.urz.unibas.ch/hipaku).

Traditional slide seminar with additional virtual slides

For the course "Diagnosis of Melanocytic Lesions: Common Problems for the Practicing Pathologist" of the French section of the International Academy of Pathology, VS had been produced in addition to traditional slides. The two courses held in Paris in December 2003 and in November 2004 had been organized by R.L. Barnhill, M.G. Cook, D. J. Ruiter and A. Spatz. The main topic of this annual course is melanocytic lesions that are known for their highly variable appearance in different step sections. Therefore, it was in many cases impossible to provide a set of glass slides for each of the around 80 to 100 participants showing all the diagnostic details of the 12 cases discussed during the 1-day course meeting. In order to circumvent this problem, a representative step section of each course slide was digitized and made available for viewing via the Internet of all the participants prior to the course meeting (http://vmic.unibas.ch/patho/seminar).

Traditional slide seminar with virtual slides (without glass slides)

Transplant pathology was the main topic of the 88th annual meeting of the German Society of Pathology in Rostock in June 2004. On this occasion, the German section of the

Table 2 Evaluation of oral histology course and slide seminars (Paris 2003/04 and Rostock 2004) by participants

	Oral Histology students	Paris Dermatopathology	Rostock Renal Pathology
The download time for the individual image segments is… (The type of internet connection used by the respondents is indicated in brackets. All students had a LAN connection.)			
Fast	3	2 (2 T1)	2 (2 ?)
OK	9	9 (2 ISDN, 5 ADSL, 2 ?)	7 (4 T1, 2 ?, 1 ISDN)
Slow	1	13 (4 ISDN, 3 ADSL, 6 ?)	2 (1 ISDN, 1 Modem)
Inacceptably slow	0	3 (1 modem, 1 ADSL, 1 ISDN)	0
Making a diagnosis on a VS compared to a traditional slide is…			
Easier	3	0	0
Comparable	9	6	4
More difficult	1	17	7
Impossible	0	2	0
Would you like VS seminars in addition to the conventional seminars?			
Yes	–	20	8
No	–	6	3
For future conventional slide seminars, I would prefer…			
VS as a supplement	–	18	7
VS only	–	4	4
Traditional slides only	–	2	0
For what purposes would you like to use a virtual microscope? (all that apply)			
Slide seminars	–	26	8
Other kinds of online education	–	25	9
Online consultation (second opinion) as consulter	–	12	7
Online consultation (second opinion) as expert	–	3	5
I will not use virtual microscopy	–	4	0

Some participants of slide seminars did not answer all of the questions. Therefore, the number of respondents for each question varies

International Academy of Pathology organized a slide seminar exclusively with VS. As needle biopsies of the kidney are very small, slide seminars with many participants on this topic were not feasible to date owing to lack of sufficient tissue. The six seminar cases represented various conditions of kidney transplant pathology. The slides were contributed by three specialists in the field—M.J. Mihatsch, H. Regele, and H.-J. Gröne—who discussed their cases on the occasion of the course meeting in Rostock. The slides were published online 1 month prior to the course meeting. The participants could either view the cases at home or at a computer station in Rostock.

The participants of the slide seminars were asked to answer a questionnaire about vMic (Table 2). While most respondents expressed positive opinions about the virtual microscope ("it is the future"), others were more sceptic ("probably useful for slide seminars but not yet good enough for consultation"). The image quality of the VS was rated as either excellent (62%) or good (38%). Nobody had voted for moderate or poor.

All slide seminars are publicly accessible (http://vmic.unibas.ch/patho/seminar).

Added value of virtual slides

VS should not simply be regarded as a mere replacement of traditional glass slides. This new technology offers several advantages and applications to pathology that could not be provided before [3–5, 7, 8, 10, 12, 15, 16, 18–22, 24, 26]. The overview image facilitates orientation within a given section (Fig. 1). Annotations that lead the user to a specific location within the slide are a valuable tool not only in the teaching setting but also for consultations. The one-time digitization of the histological glass slides for teaching purposes is much less time consuming and expensive than the production of a traditional slide set that additionally comprises the replacement of lost, broken or faded sections and delivery. The decision about which cases are to be presented in a course no longer depends on the availability of a large amount of representative tissue but exclusively on didactics. Cytopathology courses [7, 19, 27] or slide seminars in subspecialties traditionally relying on small biopsy samples or needle biopsies such as haematopathology, dermatopathology (http://vmic.unibas.ch/patho/seminar, http://www.pathmax.com/apiii/exp.html), hepatopathology or nephropathology (http://vmic.unibas.ch/patho/seminar) can now be offered to a large audience. For digitization, a step section representative of the lesion and of best quality is chosen. The fact that the best possible identical step section of a given lesion is allocated to all users is not only desirable for teaching purposes but represents an optimal condition for consensus conferences in research settings [26] or measures of quality control [7, 17]. A group of experts from any part of the world can use the "virtual multi-header microscope" to examine a slide together via the WWW.

Consumer needs

If virtual microscopy is to be widely accepted by pathologists for diagnostic purposes, image quality and functionality should be comparable to that of a traditional microscope. The acceptance of Web-based technology is generally very high in the student population. The improvement of technology should be paralleled by increasing computer competency of the upcoming generation of pathologists [11, 14]. Students have already been shown to rate the quality of images and navigation of a virtual microscope equal to or even better than a real microscope [2, 10, 18]. While real slides need adjustments of focus, lighting and condensor, VS are always ready to use. In contrast, most pathologists found it more difficult to make a diagnosis on vMic slides than with traditional slides. This is probably due in part to unfamiliarity with this new technology and in part to a rather small display and delayed response time when using slow Internet connections.

When we developed vMic, we decided to obtain the highest possible image quality accepting increased time requirements for image acquisition and download. It has to be taken into account that rating of image quality not only depends on the virtual microscope but also on the quality of the computer screen of the user and the quality of the physical microscope vMic is compared to. Due to limited budgets for medical education, microscopes in student labs normally do not feature best-of-breed optics to minimize costs, while VS can be maximized for quality. The latter probably explains why more than half of students in dentistry rated vMic images as superior to a real microscope image.

The overall quality of a VSS will not only be measured by its visual quality and its ability to perfectly emulate a traditional microscope but will also depend on additional functionalities like annotations, automatized slide analysis or discussion tools.

Considerations for acquisition/implementation of a virtual slide system

Nowadays, many companies offer VSAS or even complete VSS (http://www.soft-imaging.de/rd/english/3412.htm, http://www.telepathologycity.com/systems.htm). They foster different technological approaches, and the price tag varies by a factor of 6 and more. The following discussion of the most relevant parameters in virtual microscopy is intended to help institutions that plan to establish their own VSS.

Acquisition speed

One obvious and central weakness of most existing VSAS is acquisition speed. As long as the system is only planned to serve educational purposes (e.g. vMic, http://vmic.unibas.ch), this shortcoming may be acceptable. A single scan may last for hours. However, if VS are to be introduced in routine diagnostics, a very fast and automated system—mostly at a higher price—is mandatory.

Four systems that meet the latter conditions are (incomplete list of available products):

- DMetrix DX-40 scanner (first systems delivered in 2004; http://www.dmetrix.net)
- Olympus .Slide (pronounced dot-slide; available since beginning of 2005; http://www.soft-imaging.de/rd/english/3412.htm)
- Aperio ScanScope (available since more than 1 year ago; http://images.scanscope.com)
- InterScope Xcellerator (http://www.interscopetech.com)

The most promising technology is the one used in the DX-40 scanner from DMetrix. This VSAS consists of an array of multiple miniaturized microscopes allowing for ultra-rapid digitization of a whole slide in less than a minute [26].

20× vs 40× objective

In traditional settings, 40× objectives with a numerical aperture (NA) of 0.75 are used for diagnostic purposes. A 40× Plan Apochromat objective (normally used to take images) has up to NA=0.95, providing higher lateral resolution, while depth of sharpness is reduced. A 20× Plan Apochromat objective with NA=0.75 results in the same lateral resolution as a standard 40× objective used for diagnostics.

Some suppliers therefore argue that by using a 20× Plan Apochromat instead of a 40× objective, the scanning time would be reduced by a factor of 4 without cutting on image quality and resolution of the resulting VS. Yet, that claim is only true when comparing two objectives with the same NA. A 40×/NA=0.95 clearly provides higher lateral resolution. Furthermore, the resolution of the camera must be considered as commented on in the next section.

Video camera vs still camera and camera resolution

Video cameras are in general faster than still cameras. They can grab up to 30 images per second, whereas still cameras take up to 1 sec per image. On the other hand, still cameras deliver up to 12 to 20 megapixels per image, whereas video cameras are limited to about 0.3 to 1.3 megapixels per image (640*480 to 1,300*1,030).

Dedicated VS scanners may also use specialized sensors (Aperio, http://images.scanscope.com; DMetrix, http://www.dmetrix.net).

For optimal colour information, the red, green and blue (RGB) component of light should be collected at each pixel. Many charge coupled device (CCD)-chips use a so-called Bayer mask instead (Fig. 2), which reduces colour information significantly.

Three types of technology are available to gather colour information for every single pixel: (a) three-chip cameras—

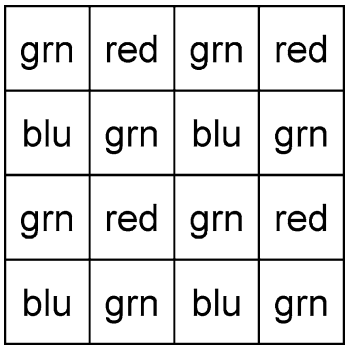

Fig. 2 Bayer mask. Chequer-board-like filter for RGB (red, green, blue). The intensity of each pixel of the sample is measured at one wavelength (colour) only. Full colour information will then be interpolated, not really measured

the light path is split and RGB components are captured each on a separate chip, (b) scan mode—a sensor is equipped with a Bayer mask and the whole chip is piezoelectrically repositioned four times per image to measure each component separately (e.g. AxioCam HR; image comparison, (http://alf3.urz.unibas.ch/patho/pub/axiocam.pdf), (c) three-pass mode—the sensor scans the sample in three successive scans each time using a different illumination for red, green and blue (e.g. DX-40, (http://www.dmetrix.net).

As a rule of thumb, approximately 1 to 1.5 megapixels are needed when taking pictures with a 40× objective and a standard camera to match the optophysical resolution of a standard microscope [9]. Increasing the resolution of the camera above this value increases image size without yielding more information and should therefore be avoided. When using a 20× Plan Apochromat objective for slide scanning, the camera resolution should be four times higher because the field of view is four times larger than with a 40× objective. Otherwise, image information is lost.

Single/multiple focus planes and *z*-sharpening

A major drawback of most VS is the lack of multiple focus planes that allow the pathologist and even more so the cytologist to slightly change focus from the main focus plain within the *z*-axis. Therefore, information contained within a real slide is lost in the VS due to a reduced depth of sharpness. To avoid this drawback, two different approaches have been realized, both scanning the slide at multiple focus planes, but:

(a) Delivers the additional planes on request to the browser (e.g. Bacus Laboratories WebSlide, (http://www.bacuslabs.com).
(b) *z*-sharpening: a software algorithm extracts the sharpest areas from the different focal planes and combines them to a synthesised image with a high depth of sharpness (e.g. Olympus. Slide, http://www.soft-imaging.de/rd/english/3412.htm; DMetrix, http://www.dmetrix.net—announced as a future feature).

Both approaches significantly increase total scanning time. Bacus' WebSlide more closely simulates a real microscope—at the cost of increased download time and a magnitude of storage.

It remains to be evaluated which of the two approaches will lead to more accurate diagnoses with comparative studies of the two methods.

Single large image file vs matrix with thousands of images

Scanning large samples results in dozens of gigabytes of raw data. Advances in computer technology are by and by overcoming the problems arising from handling single large image files. However, only few software tools are able to handle (analysis, post-processing) such huge image files yet. For Web delivery, special server processes are needed for single-file VS, whereas matrices of small files can be served using a standard http demon.

Dynamic downsizing vs pyramidal multi-resolution stack

Two different approaches are used to view VS at different magnifications. Some systems only store the highest resolution on disk. For viewing VS at smaller magnifications, the image is dynamically downsized. This might be appropriate for a single-user system. However, in a multi-user and multi-access system, which is true for most Web applications, dynamical downsizing raises unnecessary high demands to the server [3]. A pyramidal stack stores images at different resolutions [9]. Most VSS use a pyramidal approach. In the case of vMic, this requires less than 12% additional storage space.

Proprietary systems vs open standards

Unfortunately, many suppliers offer VSS that use proprietary image file formats and viewers. Some have adopted Zoomify's technology (http://www.zoomify.com/customers). Although this is also a proprietary image file format, a low-cost developer kit enables the development of own viewers optimized for teaching, research or diagnostics. For maximal compatibility, VSAS should be able to export VS as a matrix of single-image files in a standard format.

It would be advantageous if image acquisition was decoupled from image delivery. This would not only foster interchange of VS but also the independent development of value-adding viewer applications for education, research and diagnostics. Open standards in the delivery of VS are the precondition for the construction of a semantic web of pathology (http://www.w3.org/2001/sw, http://www.inf.fu-berlin.de/inst/ag-nbi/research/swpatho/icwe04.pdf).

Sufficient image quality vs best possible quality

Most VSAS are designed to reach reasonable diagnostic quality allowing the pathologist to make a reliable diagnosis [4, 16, 20, 26]. Depending on the application, this approach is absolutely adequate since it minimizes storage space, scanning time and expenditures for optics. vMic on the other hand aims at maximal quality that is reached when equalling the optophysical limitations of the microscope (40×, NA=0.95). With the advent of improved technologies, maximal quality will sooner or later be standard, although minimal diagnostic quality will still be good enough in the future.

Overlapping images vs seamless images

Producing seamless VS using standard microscope technologies demands tedious alignment procedures [23] or time-consuming software stitching.

Dedicated VSAS (DMetrix, http://www.dmetrix.net; Olympus, (http://www.soft-imaging.de/rd/english/3412.htm; Aperio, http://images.scanscope.com) produce seamless VS. Our user surveys have shown that overlaps are accepted by students and pathologists and are not regarded as a drawback in the use of VS.

Purpose of application

If VS are to be used for educational purposes, a low-cost solution may do since scanning time is not critical and overlaps are accepted by the users. VS in daily diagnostics as introduced at the University of Arizona [26] require a high throughput instrument including many terabyte of disk space.

First test, then buy

Some suppliers do not like customers to test their systems before purchase. Some of the systems we have evaluated would never have been able to deliver a VS. Most of the times, additional implementing work is needed depending on the user preferences. Before investing in an expensive VS equipment, the intended uses should be worked out and the possibility to test the system should be demanded from the supplier.

Outlook

Due to additional functionalities that a physical microscope cannot provide, virtual microscopy is a promising new tool, offering a wide range of new applications in the fields of education, research, diagnosis and quality control (http://www.bacuslabs.com, http://virtualmicroscope.osu.edu) [2, 4, 7, 10, 13, 15, 18, 20, 24, 26, 27].

High-speed broadband Internet connections are expected to be available in most laboratories soon, allowing most pathologists and students to profit from publicly accessible sites.

Storing information contained in a single VS (one focal plane only) takes up to ten CD-ROMs or one DVD. Replacing physical slide archives by digital archives is therefore not reasonable at present but will probably be possible within the next decades.

Fast slide-processing time is essential if VS are to be widely used for routine diagnostic pathology including intra-operative frozen sections and second-opinion consultations. The advent of easy-to-handle ultra-rapid slide scanners [25] will ensure a fast propagation of this most recent application in telepathology.

By participating in VS seminars, every pathologist can make a first step towards mastery of this trend-setting technique. The use of vMic (http://vmic.unibas.ch) slides is free of charge and does not require registration, allowing everyone to gain first experiences with a new way of looking at histology slides.

Acknowledgements The authors thank Drs. Ray Barnhill, Martin Cook, Dirk Ruiter, Heinz Regele and Hermann-Josef Gröne for the contribution of cases for the VS seminars. This work has been supported by a grant of the University of Basel.

References

1. Afework A, Beynon MD, Bustamante F, Cho S, Demarzo A, Ferreira R, Miller R, Silberman M, Saltz J, Sussman A, Tsang H (1998) Digital dynamic telepathology—the virtual microscope. Proc AMIA Symp: 912–916
2. Blake CA, Lavoie HA, Millette CF (2003) Teaching medical histology at the University of South Carolina School of Medicine: transition to virtual slides and virtual microscopes. Anat Rec B New Anat 275:196–206
3. Catalyurek U, Beynon MD, Chang C, Kurc T, Sussman A, Saltz J (2003) The virtual microscope. IEEE Trans Inf Technol Biomed 7:230–248
4. Costello SS, Johnston DJ, Dervan PA, O'Shea DG (2003) Development and evaluation of the virtual pathology slide: a new tool in telepathology. J Med Internet Res 5:e11
5. Dee FR, Lehman JM, Consoer D, Leaven T, Cohen MB (2003) Implementation of virtual microscope slides in the annual pathobiology of cancer workshop laboratory. Hum Pathol 34:430–436
6. Demichelis F, Barbareschi M, Dalla Palma P, Forti S (2002) The virtual case: a new method to completely digitize cytological and histological slides. Virchows Arch 441:159–164
7. Demichelis F, Della Mea V, Forti S, Dalla Palma P, Beltrami CA (2002) Digital storage of glass slides for quality assurance in histopathology and cytopathology. J Telemed Telecare 8:138–142
8. Giltnane JM, Rimm DL (2004) Technology Insight: identification of biomarkers with tissue microarray technology. Nature Clinical Practice Oncology 1:104–111
9. Glatz-Krieger K, Glatz D, Mihatsch MJ (2003) Virtual slides: high-quality demand, physical limitations, and affordability. Hum Pathol 34:968–974
10. Harris T, Leaven T, Heidger P, Kreiter C, Duncan J, Dick F (2001) Comparison of a virtual microscope laboratory to a regular microscope laboratory for teaching histology. Anat Rec 265:10–14
11. Harrison JH Jr, Stewart J 3rd (2003) Training in pathology informatics: implementation at the University of Pittsburgh. Arch Pathol Lab Med 127:1019–1025

12. Heidger PM Jr, Dee F, Consoer D, Leaven T, Duncan J, Kreiter C (2002) Integrated approach to teaching and testing in histology with real and virtual imaging. Anat Rec 269:107–112
13. Helin H, Lundin M, Lundin J, Martikainen P, Tammela T, van der Kwast T, Isola J (2005) Web-based virtual microscopy in teaching and standardizing Gleason grading. Hum Pathol 36:381–386
14. Henricks WH, Boyer PJ, Harrison JH, Tuthill JM, Healy JC (2003) Informatics training in pathology residency programs: proposed learning objectives and skill sets for the new millennium. Arch Pathol Lab Med 127:1009–1018
15. Kumar RK, Velan GM, Korell SO, Kandara M, Dee FR, Wakefield D (2004) Virtual microscopy for learning and assessment in pathology. J Pathol 204:613–618
16. Leong FJ, McGee JO (2001) Automated complete slide digitization: a medium for simultaneous viewing by multiple pathologists. J Pathol 195:508–514
17. Leong FJ, Graham AK, Schwarzmann P, McGee JO (2000) Clinical trial of telepathology as an alternative modality in breast histopathology quality assurance. Telemed J E Health 6:373–377
18. Marchevsky AM, Relan A, Baillie S (2003) Self-instructional "virtual pathology" laboratories using web-based technology enhance medical school teaching of pathology. Hum Pathol 34:423–429
19. Marchevsky AM, Wan Y, Thomas P, Krishnan L, Evans-Simon H, Haber H (2003) Virtual microscopy as a tool for proficiency testing in cytopathology: a model using multiple digital images of Papanicolaou tests. Arch Pathol Lab Med 127:1320–1324
20. Molnar B, Berczi L, Diczhazy C, Tagscherer A, Varga SV, Szende B, Tulassay Z (2003) Digital slide and virtual microscopy based routine and telepathology evaluation of routine gastrointestinal biopsy specimens. J Clin Pathol 56:433–438
21. Okada DH, Binder SW, Felten CL, Strauss JS, Marchevsky AM (1999) "Virtual microscopy" and the internet as telepathology consultation tools: diagnostic accuracy in evaluating melanocytic skin lesions. Am J Dermatopathol 21:525–531
22. Romer DJ, Suster S (2003) Use of virtual microscopy for didactic live-audience presentation in anatomic pathology. Ann Diagn Pathol 7:67–72
23. Romer DJ, Yearsley KH, Ayers LW (2003) Using a modified standard microscope to generate virtual slides. Anat Rec 272B:91–97
24. Steinberg DM, Ali SZ (2001) Application of virtual microscopy in clinical cytopathology. Diagn Cytopathol 25:389–396
25. Weinstein RS, Descour MR, Liang C, Bhattacharyya AK, Graham AR, Davis JR, Scott KM, Richter L, Krupinski EA, Szymus J, Kayser K, Dunn BE (2001) Telepathology overview: from concept to implementation. Hum Pathol 32:1283–1299
26. Weinstein RS, Descour MR, Liang C, Barker G, Scott KM, Richter L, A. KE, Bhattacharyya AK, Davis JR, Graham AR, Rennels M, Russum WC, Goodall JF, Zhou P, Olszak AG, Williams BH, Wyant JC, Bartels PH (2004) An array microscope for ultrarapid virtual slide processing and telepathology. Design, fabrication, and validation Study. Hum Pathol 35:1303–1314
27. Zito FA, Marzullo F, D'Errico D, Salvatore C, Digirolamo R, Labriola A, Pellecchia A (2004) Quicktime virtual reality technology in light microscopy to support medical education in pathology. Mod Pathol 17:728–731

Virchows Arch (2006) 448: 256–261
DOI 10.1007/s00428-005-0116-y

ORIGINAL ARTICLE

Maria P. Foschini · Alberto Righi · Maria C. Cucchi · Teresa Ragazzini · Stefano Merelli · Bruna Santeramo · Vincenzo Eusebi

The impact of large sections and 3D technique on the study of lobular in situ and invasive carcinoma of the breast

Received: 5 October 2005 / Accepted: 10 October 2005 / Published online: 3 December 2005

Abstract The aim of the present study was to investigate the type of intraglandular spread of lobular neoplasia (LN) and its relationship with invasive lobular carcinoma (ILC) through three-dimensional (3D) stereomicroscopy and analyses of large histological sections (histological macrosections, HM). Fifteen cases showing multiple foci of in situ LN and/or ILC (1 pure LN, 12 LN+ILC, and 2 pure ILC) constituted the basis of the present study. Thirteen cases were treated with mastectomy (including the case of pure LN), and two cases were treated with quadrantectomy. In all cases, large parallel 5-mm-thick sections were embedded in paraffin and stained with hematoxylin and eosin (H&E). Selected large paraffin blocks were investigated with stereomicroscopy. The H&E-stained HM were then compared with the corresponding tissues examined using stereomicroscopy. (1) LN was multicentric in nine cases. (2) The average maximum distance among LN foci was 37.9 mm, while the average maximum distance among ILC areas was 58.2 mm. (3) On 3D examination, LN-filled acini and ducts appeared dilated. When "Pagetoid spread" was present, the ducts were lined by a continuous layer of neoplastic epithelium. (4) No anastomoses between lobes were observed in the two cases where glandular trees were visualized. (5) In 12 cases, ILC areas enveloped ducts and acini affected by LN—an association that was more than coincidental. (6) Multicentric ILC areas not associated with LN indicated vascular spread. It is concluded that the information given in LN and ILC, obtained by analyses of large histological sections, is far superior than that obtained by analyses of conventional histological sections, which underestimate multiple distant small foci of invasion. 3D sections are useful in understanding the architecture of specific lesions.

Keywords Invasive lobular carcinoma · Lobular neoplasia · Large sections · Macrosections

This work was financed by grants from the Universisty of Bologna (ex 60%; M.P. Foschini and V. Eusebi) and by grant 2002064975 (Cofin 2002) from the Ministry of University and Research, Rome.

M. P. Foschini · A. Righi · T. Ragazzini · V. Eusebi
Section of Anatomic Pathology,
Department of Oncological Sciences,
University of Bologna, Bellaria Hospital,
Bologna, Italy

M. C. Cucchi
Section of Oncologic Surgery,
Department of Oncological Sciences,
University of Bologna, Bellaria Hospital,
Bologna, Italy

S. Merelli
Section of Plastic Surgery,
Department of Oncological Sciences,
University of Bologna, Bellaria Hospital,
Bologna, Italy

B. Santeramo
Department of Surgery,
Clinica Villa Laura,
Bologna, Italy

V. Eusebi (✉)
Anatomia Patologica,
Ospedale Bellaria,
Via Altura, 3,
40139 Bologna, Italy
e-mail: Vincenzo.Eusebi@ausl.bologna.it
Tel.: +39-51-6225523
Fax: +39-51-6225759

Introduction

Large histological sections (histological macrosections, HM) and three-dimensional (3D) stereomicroscopy allow the visualization of the entire mammary glandular tree. 3D studies were originally applied to mouse breast tissues and gave relevant insights into the development of normal breasts [1, 9].

The site of origin of ductal carcinoma in situ (DCIS)/ductal intraepithelial neoplasia (DIN) is believed to be the terminal ductal lobular unit (TDLU) [21], and the type of intraglandular spread of DCIS/DIN in terms of unifocality or multifocality has been repeatedly shown [7, 11]. Accordingly, well-differentiated DCIS recognizes a multifocal

discontinuous type of growth, with gaps of noninvolved ductal walls located between two neoplastic foci. On the contrary, poorly differentiated DCIS spreads along the ducts in a continuous unifocal fashion without visible gaps [7, 11]. The correlation between mammography and pathology is also enhanced by HM and 3D studies [19]. 3D reconstruction of the breast glandular tree, recently aided by computers, has allowed a better understanding of the normal glandular structure of the breast, which is subdivided into lobes (anatomical structures that are independent of one another) [10, 13]. Lobes vary from 11 to 48 (median, 27) [10] and do not have apparent anastomoses among themselves.

To date, lobular carcinoma, either in situ (lobular neoplasia, LN) or invasive (invasive lobular carcinoma, ILC) [22], has never been studied at the 3D level and, to our surprise, there has only been one study that used HM on ILC, but it did not mention LN [17].

During routine practice, it is common to observe cases containing multiple foci of LN or ILC located far away from one another, but the multifocality (here defined according to Tot [17] as multiple foci in the same lobe) or multicentricity (here defined according to Tot [17] as multiple foci present in different lobes) of LN is a highly controversial issue in the literature. Foote and Stewart [8] stated that LN is always a disease of multiple foci. Subsequent reports have confirmed that multicentric LN is identified in 60–80% of mastectomy specimens [16]. These conflicting results probably are consequent to the fact that, in routine practice, biopsy provides only a limited tissue sample and, thus, the process cannot be visualized in its entire extension.

The purpose of the present study is to investigate the intraglandular spread, size, and multifocality and/or multicentricity of LN and ILC, using HM and 3D stereomicroscopy.

Materials and methods

Fourteen cases that have undergone preoperative diagnostic procedures [either fine needle aspiration cytology or core biopsy (CB)] for palpable nodules, which in turn have led to diagnostic categories of positive (13 cases) or suspicious for malignancy (1 case) [3], were randomly selected for this study from the files of the Section of Anatomic Pathology of the University of Bologna at Bellaria Hospital. Two cases were pure ILC and 12 cases showed LN and ILC simultaneously.

An additional case of pure LN diagnosed by histology of tissues excised for reduction mastoplasty was also included in the study.

On mammography, no calcifications were visible in all cases. The only criterion of selection was the processing of cases using the procedure for macrosections (see below).

The diagnostic criteria of LN (also called lobular in situ neoplasia, LIN) and ILC were in consonance with current histological criteria [22]. Accordingly, E-cadherin immunostaining (monoclonal, clone HECD-1, dilution 1:1,000; Zymed) yielded negative results in all cases. Twelve cases underwent mastectomy, the case of pure LN was treated with bilateral subcutaneous mastectomy, and two cases were treated with quadrantectomy. Axillary dissection was performed in 11 cases.

Specimens were received fresh. In all cases, large parallel 5-mm-thick slices (also called macrosections) were obtained. Care had been taken to slice each section, which included the nipple, perpendicularly to the skin during mastectomy. Slices were then formalin-fixed and paraffin-embedded. From each large block, hematoxylin and eosin (H&E)-stained HM were obtained [9] and used for routine histology.

For 3D stereomicroscopy study, large paraffin blocks were selected with the guidance of a related large H&E

Table 1 Clinical data

Case	Age (years)	Surgical procedure	Laterality	Histological ILC subtype	Mets
1	56	Mastectomy	U R	Pleomorphic	Axly +
2	44	Mastectomy	U L	Pleomorphic	Axly + Men
3	41	SC mastectomy	B		ND
4	61	Mastectomy	U L	Classic	Axly
5	53	Quadrantectomy	U L	Classic	No Axly mets
6	63	Mastectomy	U L	Pleomorphic	Axly +
7	72	Mastectomy	U L	Pleomorphic	ND
8	69	Mastectomy	U R	Pleomorphic	Axly +
9	56	Mastectomy	U L	Pleomorphic	Axly +
10	74	Mastectomy	U R	Classic	Axly +
11	46	Mastectomy	U R	Classic	Axly +
12	85	Quadrantectomy	U	Classic	ND
13	77	Mastectomy	U L	Pleomorphic	No Axly mets
14	87	Mastectomy	U L	Classic	ND
15	50	Mastectomy	U L	Pleomorphic	Axly +

SC Subcutaneous, *U* unilateral, *B* bilateral, *R* right breast, *L* left breast, *Mets* metastases at presentation, *Axly* axillary lymph nodes, *Men* meningeal metastases, *ND* axillary dissection not performed

Table 2 Summary of pathological data

Case	LN foci (*n*)	LN *D* (mm)	ILC foci (*n*)	ILC *D* (mm)	ILC (mm)[a]	LN in ILC
1	49	60	4	15	47	39
2	9	32	19	67	20	4
3 R	77	112	–	–		
3 L	1		–	–		
4	21	44	2	10	38	10
5	27	32	1	0	10	15
6	5	22	>100	50		5
7	3	24	1	0	30	3
8	2	5	>100	130	70	2
9	3	12	9	85	68	3
10	49	44	2	13	40	49
11	2	17	21	55	30	2
12	50	36	4	70	40	38
13	–	–	19	64	16	0
14	14	15	1	0	45	14
15	–	–	8	82	21	–

R Right breast, *L* left breast, *n* number, *LN D* maximum distance between LN foci, *ILC D* maximum distance between ILC areas, *LN* lobular neoplasia, *ILC* invasive lobular carcinoma
[a]The size of the greatest area is reported

section. Selected blocks were then deparaffinized. Paraffin was melted in a hot bath at 60°C (3–4 h) and subsequently immersed in xylene (four times) for at least 24 h to remove residual paraffin [6]. Tissues were then rehydrated as follows: 50% absolute alcohol and 50% xylene (1 h), absolute alcohol (2 h), and 70% alcohol (2 h). Finally, blocks were washed overnight in distilled water, stained in Harris' hematoxylin for 4–5 min, rinsed in tape water for 10 min, and immersed in four baths of acid alcohol for 8 min each. Then tissues were dehydrated, through a graded series of alcohol to xylene, and finally immersed in methyl salicylate for one night.

3D examination was performed using a stereomicroscope (Nikon, Tokyo, Japan). The H&E-stained large histological slide was used to retrace the lesions to examine corresponding cleared tissues.

In all cases, the number of LN foci (focus is defined here as neoplastic cells located within, at least, a space of one another) and the number of ILC areas (area is defined here as a clump, sheet, or nest of ILC cells), independently of their size, were counted. The distance between foci and areas was assessed microscopically using calibrated lenses on large histological slides.

Results

Clinical data are summarized in Table 1. All patients were female, with age ranging from 41 to 87 years (mean, 62 years). Twelve cases showed LN and ILC at the same time, while one case (case 3) showed only bilateral LN. Pure ILC was present in two cases.

All LN foci showed features of LIN 2, as recently subtyped [22]. ILC was of the classic type in six cases and was of the pleomorphic type [5] in eight cases.

Number of LN foci With the exception of the two ILC cases that did not contain LN foci, all the other cases, as seen in HM, ranged from a maximum of 77 LN foci randomly distributed throughout the whole section of the right breast in case 3 to a minimum of 2 foci in cases 8 and 11 (mean, 23.9 foci) (Table 2 and Fig. 1). Case 3, the only one that had undergone bilateral mastectomy, had only one focus of LN in the contralateral breast. In no fewer than seven cases was the number of LN foci higher than ten (53.8%).

Distance between LN foci as measured on HM The maximum space between the most distant LN foci ranged from 112 mm in the right breast of case 3 (Fig. 1) to 5 mm in the breast of case 8 (mean, 37.9 mm). The maximum space was greater than 20 mm in not less than nine cases (69%).

Number of ILC areas The number of ILC areas in the 14 cases ranged from 1 (in three cases, 21.4%) to more than 100 (in two cases, 20.7%). The areas were diffusely spread throughout the breast tissues of the various cases and, as general rule, there was a dominant larger-sized area in each case (see Table 2 and Fig. 2a). When multiple ILC areas were present in the same cases, diffuse vascular in-

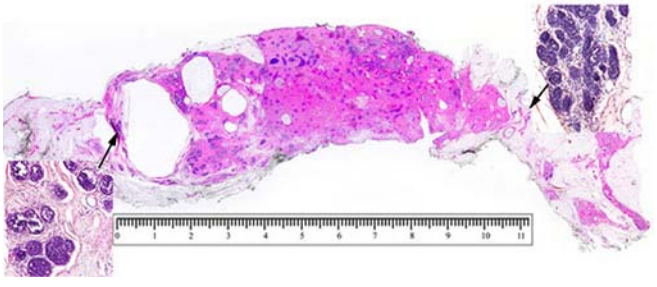

Fig. 1 Case 3: subcutaneous mastectomy. In this case, 77 foci of LN were observed. The maximum distance between LN foci was 112 mm. In both *insets*, LN involvement of acini is evident

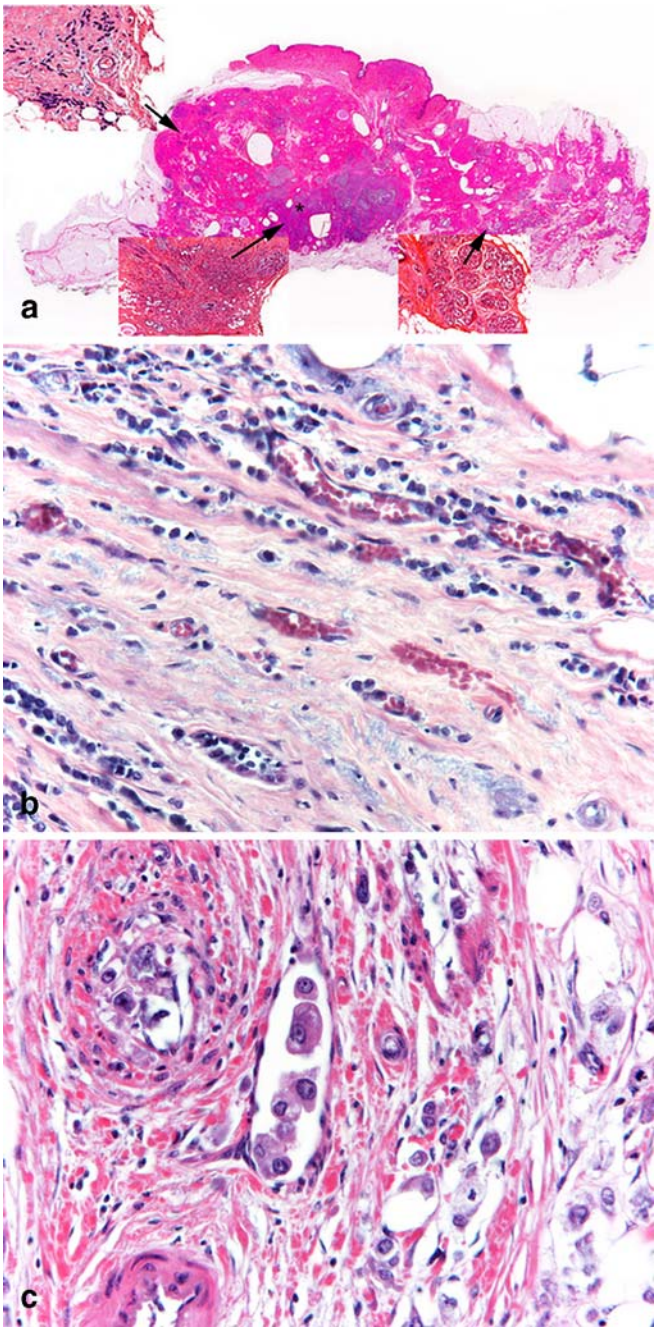

Fig. 2 Case 2. **a** In this case, LN foci (*lower right inset*), multiple ILC areas (*upper inset*), and ILC intermingled with LN (*lower left inset*) are present. (*) A dominant large area is evident. **b** Neoplastic invasive cells are located in perivascular spaces reminiscent of Hartveit's prelymphatic labyrinth. **c** In the center, neoplastic cells are clearly evident in a small vessel. *Right*: there are cells located in spaces suggestive of Hartveit's channels

vasion or invasion of Hartveit's pseudovascular channels [2] was observed (cases 2, 6, 8, 9, 11, 13, and 15) (Fig. 2b,c).

Distance between ILC areas as measured on HM The maximum distance of uninvolved tissue between the most distant ILC areas ranged from 10 to 130 mm (mean, 58.2 mm). The size of the largest ILC areas in each case ranged from 10 to 70 mm (mean, 36.7 mm).

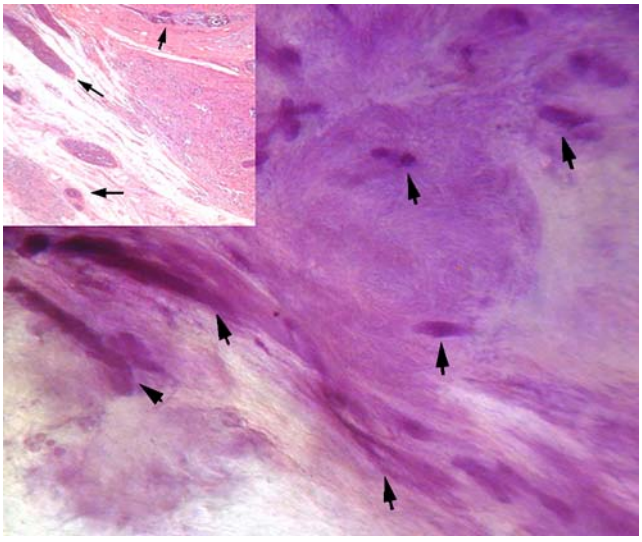

Fig. 3 Case 4: LN foci (*arrows*) immersed in ILC cells. On 3D stereomicroscopy, the invasive area shows a "cloudy" appearance with evanescent margins. *Inset*: the corresponding area at HM shows LN (*arrows*) intermingled with ILC

Relationship between LN foci and ILC areas In no fewer than ten cases most of the LN foci were located within the largest sized area of ILC, enveloped by and immersed in invasive neoplastic cells (Fig. 3). Nevertheless, in five of such cases (cases 1, 2, 4, 5, and 12), some foci (5–12 foci) of LN were independent of ILC areas. On the contrary, in nine cases, several ILC areas located far from the largest area of ILC did not contain LN foci.

A total of 234 foci of LN were observed in the 12 cases where LN and ILC were present at the same time, and it appeared that 184 LN (78.6%) were located inside ILC areas.

Three-dimensional study On 3D examination, lobular acini of LN were enlarged and globoid, and the related TDLU

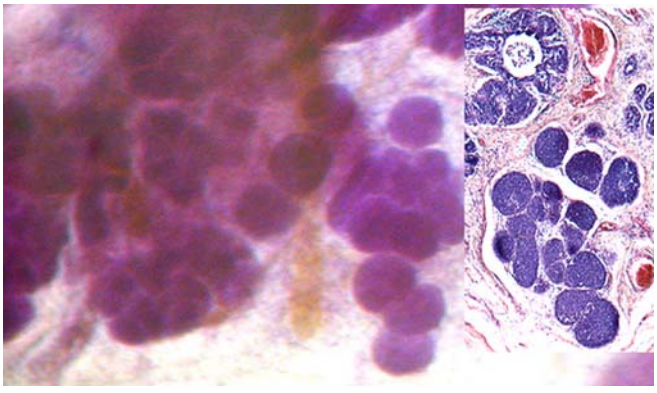

Fig. 4 Case 3: the 3D appearance of LN shows the uniform growth of neoplastic cells in acini (as also shown in the *inset* from the same area) as seen with HM

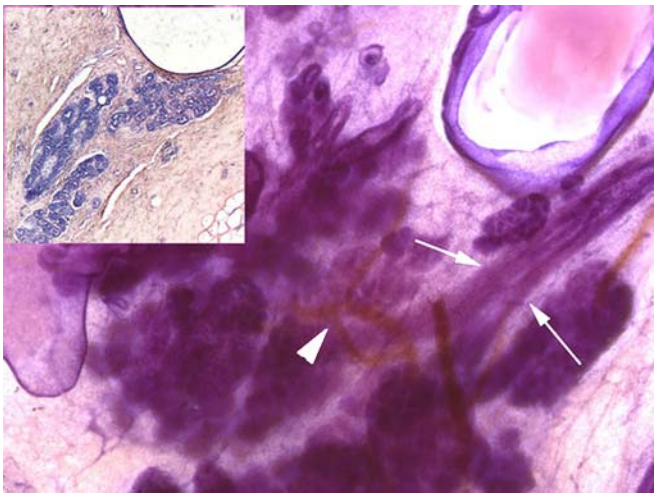

Fig. 5 Case 5: at 3D level, Pagetoid spread manifests as a continuous intramural growth along the duct (*arrows*). The *arrowhead* shows serpiginous vessels. *Inset*: the corresponding histological section as seen with HM

appeared completely filled by neoplastic cells (Fig. 4). No anastomoses between different subsegmental ducts were observed.

LN spread intramurally along larger ducts from acini, presenting the features of "Pagetoid spread" in two cases (cases 3 and 5) (Fig. 5). The spread showed a continuous pattern of growth, and no gaps of noninvolved glandular walls were visible. Duct walls appeared as thickened, bluish structures (Fig. 5). ILC appeared as finely granular, bluish areas that resembled clouds with fading margins. ILC "clouds" (Fig. 6) enveloped ducts and lobules affected by LN (Fig. 3) and also contained numerous vessels.

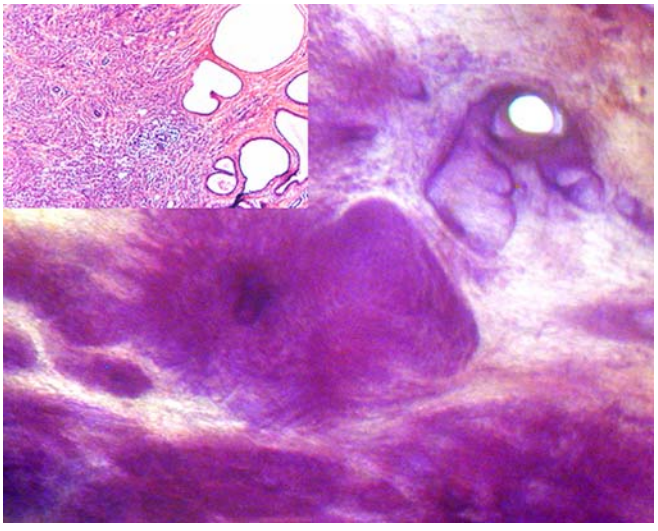

Fig. 6 Case 10: invasive carcinoma appears on 3D stereomicroscopy as bluish, irregular "clouds." *Inset*: the same area as seen in "conventional" histology

Discussion

Since the seminal paper of Foote and Stewart [8] in which it was stated that all LN recognize multiple foci of growth, multicentricity in LN has been shown in as many as 85% of patients [15]. This is in keeping with the present data in which the 13 cases containing LN showed a wide range of multiple foci varying from 2 to 77 (mean, 23.9) in various cases, with no fewer that seven cases (53.8%) having ten or more foci.

Tot [18] has suggested that DCIS usually arises in one "sick" lobe only. This in view of the fact that the maximum distance between different foci of DCIS does not exceed 10 mm in most of the cases [7]—a measurement that probably corresponds to the width of most lobes, although it has been suggested that lobes are of different sizes and can extend from 2 to 23% of the breast volume [10].

The maximum distance between LN foci in the present cases varied from 5 to 112 mm (mean, 37 mm); in addition, in nine cases (69%), the maximum distance was no less than 20 mm. This probably indicates that, in most LN, more that one lobe is affected by the tumor (not to mention case 3 in which virtually all lobes from the same breast were involved).

No anastomoses between lobes were found in the 3D study of the cases in which entire lobes could be visualized—a finding also corroborated by previous works [10]. A continuous type of spread along the breast glandular tree, similar to that observed in poorly differentiated DCIS [7, 11], was seen in the two cases in which Pagetoid spread was found.

Invasive areas, with the exception of three cases that were unifocal (21.4%), were multiple in the same breast. There were as many as more than 100 areas in one case, and these averaged 20.7 in different patients. In cases with multiple involvement, the distance between the farthest-apart areas ranged from 10 to 130 mm. These data are in keeping with the only available study on macrosections of 130 cases of ILC, in which it was found that 39% of cases were unifocal, while the remaining cases were widespread lesions [17].

In the ILC areas of the present cases, the most frequent feature was that of LN immersed in and surrounded by ILC cells in 78.6% of the instances—an association so relevant that it cannot indicate a fortuitous phenomenon [14].

Furthermore, it has been shown in a literature review of 493 cases of pure LN diagnosed with CB that the presence of invasive breast cancer was underestimated in 18% of patients [4]. This further indicates, as shown in the present cases, that LN and LCI are widespread lesions that cannot all be represented in the limited materials obtained by CB. To adequately map a quadrant or a whole breast, numerous conventional histological blocks are required, making routine examination an expensive and time-consuming procedure [9]. Jackson et al. [12] compared two series: one studied with conventional histology and the other studied with HM. With the latter, the size of the invasive carcinoma could be determined for all cases. In contrast, size could be measured for only 63% of the 99 cases studied with

conventional small blocks. The size measured with HM was larger than that measured with conventional blocks; DCIS was also found more frequently, in association with invasive carcinomas, in specimens assessed by HM (80%) than in cases processed using small blocks (63%).

In nine cases in which ILC areas were devoid of LN, neoplastic cells were frequently seen in vessels or in spaces of Hartveit's prelymphatic labyrinth [2], suggesting that multicentric invasive carcinoma without LN is more probably an expression of intramammary metastases.

Admittedly, the number of cases studied here is small, and a selection bias of some sort is present, reflecting the high incidence of pleomorphic ILC observed in eight cases. Six cases were classic ILC, with an average of five ILC areas per case, while the eight pleomorphic cases showed, on average, 32 areas per case. Therefore, it appears that pleomorphic lobular carcinomas are neoplasms different from classic ILC, as shown by the fact they are aggressive tumors, as previously suggested [5, 20] and recently demonstrated by Tot [17].

Nevertheless, in spite of the limited number of cases, the data obtained in the present cases indicate the following:

1. LN equally involves ducts and acini, and Pagetoid spread appears as a thickening of the ductal walls in which the cells spread in a continuous fashion, as shown in 3D stereomicroscopy. No anastomoses between lobes were observed in the two cases in which the glandular trees were visualized.
2. LN observed in the present cases often appeared as a true multicentric lesion, affecting different breast lobes. This finding would probably indicate that there is a near-germline commitment of the breast epithelium to neoplastic transformation [18], although this view has to be further proven.
3. Conventional histological slides clearly would have underestimated ILC areas, as the mean distance between ILC areas was 5.8 cm.
4. ILC contained numerous LN foci (78.6% of LN), suggesting the existence of a direct relation between the two lesions in which LN might be the precursor of ILC.
5. In addition, the presence of multiple areas of pure ILC is probably the result of intramammary metastases in transit, as numerous cells are observed in vessels or Hartveit's spaces.

In conclusion, larger series of LN and ILC, which appear to be more and more necessary to better understand the extent of breast tumors, have to be studied using HM.

Acknowledgement The experiments complied with the laws of the state (Italy) in which they were performed.

References

1. Dalton AJ (1949) Histogenesis of the mammary gland of the mouse. In: Moulton FR (ed) A symposium on mammary tumors in mice. American Association for the Advancement of Science, Washington, pp 39–46
2. Damiani S, Peterse JL, Eusebi V (2002) Malignant neoplasms infiltrating "pseudoangiomatous" stromal hyperplasia of the breast: an unrecognized pathway of tumor spread. Histopathology 41:208–215
3. Ellis IO, Humphreys S, Michell M, Pinder SE, Wells CA, Zakhour HD (2004) Guidelines for breast needle core biopsy handling and reporting in breast screening assessment. J Clin Pathol 57:897–902
4. Elsheikh TM, Silverman JF (2005) Follow-up surgical excision is indicated when breast core needle biopsies show atypical lobular hyperplasia or lobular carcinoma in situ. A correlative study of 33 patients with review of the literature. Am J Surg Pathol 29:534–543
5. Eusebi V, Magalhaes F, Azzopardi JG (1992) Pleomorphic lobular carcinoma of the breast: an aggressive tumor showing apocrine differentiation. Hum Pathol 23:655–662
6. Faverly DRG, Holland R, Burgers L (1992) An original stereomicroscopic analysis of the mammary glandular tree. Virchows Arch 421:115–119
7. Faverly DRG, Burgers L, Bult P, Holland R (1994) Three dimensional imaging of mammary ductal carcinoma in situ: clinical implications. Semin Diagn Pathol 11(3):193–198
8. Foote FW, Stewart FW (1941) Lobular carcinoma in situ. Am J Pathol 17:491–500
9. Foschini MP, Tot T, Eusebi V (2002) Large-section (macrosection) histologic slides. In: Silverstein MJ (ed) Ductal carcinoma in situ of the breast. Lippincott, Philadelphia, pp 249–524
10. Going JJ, Moffat DF (2004) Escaping from flatland: clinical and biological aspects of human mammary duct anatomy in three dimensions. J Pathol 203:538–544
11. Holland R, Faverly DRG (2002) The local distribution of ductal carcinoma in situ of the breast: whole-organ studies. In: Silverstein MJ (ed) Ductal carcinoma in situ of the breast, chap 19. Lippincott, Philadelphia, pp 240–248
12. Jackson PA, Merchant W, McCormick CJ, Cook MG (1994) A comparison of large block macrosectioning and conventional techniques in breast pathology. Virchows Arch 425:243–248
13. Ohtake T, Kimijima I, Fukushima T et al (2001) Computer-assisted complete three-dimensional reconstruction of the mammary ductal/lobular systems. Cancer 91:2263–2272
14. Page DL, Schuyler PA, Dupont WD, Jensen RA, Plummer WD Jr, Simpson JF (2003) Atypical lobular hyperplasia as a unilateral predictor of breast cancer risk: a retrospective cohort study. Lancet 361:125–129
15. Rosen PP, Kosloff C, Lieberman PH, Adair F, Braun DW (1978) Lobular carcinoma in situ of the breast. Am J Surg Pathol 2:225–252
16. Schnitt SJ, Morrow M (1999) Lobular carcinoma in situ: current concepts and controversies. Semin Diagn Pathol 16(3): 209–223
17. Tot T (2003) The diffuse type of invasive lobular carcinoma of the breast: morphology and prognosis. Virchows Arch 443: 718–724
18. Tot T (2005) DCIS, cytokeratins, and the theory of the sick lobe. Virchows Arch 447:1–8
19. Tot T, Tabar L, Dean PB (2000) The pressing need for better histologic–mammographic correlation of the many variations in normal breast anatomy. Virchows Arch 437:338–344
20. Weidner N, Semple JP (1992) Pleomorphic variant of invasive lobular carcinoma of the breast. Hum Pathol 23:1167–1171
21. Wellings SR, Jensen HM (1973) On the origin and progression of ductal carcinoma in the human breast. J Natl Cancer Inst 50: 1111–1118
22. WHO (2203). Tumours of the breast and female genital organs. In: Tavassoli FA, Devilee P (Kleihues P, Sobin L) (eds). WHO classification of tumours, 3rd (5th) edn. IARC Press, Lyon

Virchows Arch (2006) 448: 262–268
DOI 10.1007/s00428-005-0111-3

ORIGINAL ARTICLE

Francesca Minnei · Charlotte Wetzels · Gert De Hertogh · Peter Van Eyken · Nadine Ectors · Rossano Ambu · Gavino Faa · Anne Marie Kochuyt · Karel Geboes

Chronic urticaria is associated with mast cell infiltration in the gastroduodenal mucosa

Received: 26 September 2005 / Accepted: 28 September 2005 / Published online: 3 December 2005

Abstract Chronic urticaria (CU) is characterized by recurrent itching skin eruptions caused by mast cell degranulation. Relapses can be provoked by food intake. The aim of this study was to investigate if the mast cell number in the gastroduodenal mucosa is increased in CU patients, and whether mast cell counting by pathologists is clinically useful. We defined two study groups: 50 disease controls (16 Belgians and 34 Italians) and 43 Belgian CU patients. Mast cells were detected using immunohistochemistry for tryptase and CD117. The mast cell number in the disease controls was 20.2/high-power filed (HPF; 133.3/mm^2) in the stomach and 32.5/HPF (209.2/mm^2) in the duodenum. There was no difference between Belgian and Italian controls, indicating that dietary habits have no influence on the normal gastroduodenal mast cell number. In CU patients, mast cell numbers were significantly higher: 32.4/HPF (186.0/mm^2) in the stomach (P<0.0001) and 44.8/HPF (246.0/mm^2) in the duodenum (P=0.0002). CU is thus associated with mast cell infiltration in the gastroduodenal mucosa, even if patients do not have gastrointestinal symptoms. Mast cell counting in gastroduodenal biopsies of CU patients can be useful in selecting patients who may respond to a therapy with intestinal mast-cell-stabilizing agents.

Keywords Mast cell · Chronic urticaria · Stomach · Duodenum · Nutrition

F. Minnei · R. Ambu · G. Faa
Dipartimento di Citomorfologia,
Divisione di Anatomia Patologica,
Università degli Studi di Cagliari,
Via Ospedale 46,
09100 Cagliari, Italy

C. Wetzels · G. De Hertogh · P. Van Eyken · N. Ectors · K. Geboes (✉)
Department of Morphology and Molecular Pathology,
University Hospitals, K.U. Leuven,
Minderbroedersstraat 12,
3000 Louvain, Belgium
e-mail: karel.geboes@uz.kuleuven.ac.be
Tel.: +32-16-336584
Fax: +32-16-336548

A. M. Kochuyt
Department of Allergy and Clinical Immunology,
University Hospitals,
K.U. Leuven, Herestraat 49,
3000 Louvain, Belgium

Introduction

Urticaria is a very common skin disease characterized by the sudden appearance of smooth, raised, red, pink or white bumps and wheals of varying sizes almost anywhere on the skin (Fig. 1). The lesions usually last for several hours and then disappear without therapy [22]. About 20% of the general population has at least one episode of urticaria during their lifetime. When the disease lasts for more than 6 weeks and the skin eruptions occur at least twice a week, the condition is called chronic urticaria (CU) [15]. The aetiology of CU is unclear in most cases. Epidemiological studies show that it occurs most often in middle-aged women, but it can affect all ages, genders and races. Hidden or overt infections, abdominal disorders, and in some cases, mental strain have been associated with the disease. The skin lesions of CU are caused by vasoactive mediators released through specific or non-specific mast cell degranulation in the skin or elsewhere. CU patients are particularly susceptible to the non-specific histamine-releasing effect of pseudoallergenic substances in various foods and drugs, and the success rate of pseudoallergen-free diets varies between 30 and 50% [5, 27]. It is conceivable that food pseudoallergens induce non-specific mast cell degranulation, rather in the gastrointestinal tract than elsewhere. Activation of many intestinal mast cells may then result in enough histamine release to cause urticaria either directly or indirectly.

Mast cells are involved in numerous inflammatory and immunologic processes. They are part of our innate defence against bacterial and parasitic infections, and they play a role in the induction of the acquired immune response [12]. They store and release various mediators

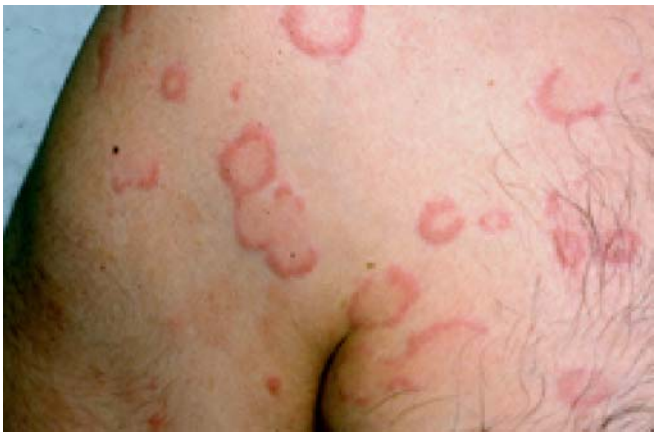

Fig. 1 Bumps and wheals of varying sizes in a patient with chronic urticaria

including histamine, tryptase, fibroblast growth factor-2, vascular endothelial growth factor and nerve growth factor. Histamine causes blood vessels to widen and leak fluid into the surrounding tissue, thereby producing swelling. Histamine also binds on the H1 receptors of neurons, which results in an itching sensation.

Another substance released upon mast cell degranulation is β-tryptase, which is a mast-cell-specific product. In humans, there is a constitutive low-grade release of α-tryptase from mast cells. Therefore, the determination of baseline serum tryptase, which measures both α- and β-tryptase, may be used to estimate the mast cell load. In CU patients, baseline levels of histamine and tryptase are higher than in normals [4, 14]. This may result either from mast cell activation or from a higher number of mast cells in the skin or elsewhere. Haas et al. [13] report an increase in mast cells in lesional and non-lesional skin of CU patients with classical histochemical staining methods. However, recent studies that have used immunohistochemical techniques with specific monoclonal antibodies to mast cell tryptase have not confirmed these findings [6, 21].

In the normal human gastrointestinal tract, mast cells are mainly located in the mucosal lamina propria. In the submucosa, mast cell density is lower, while the muscularis propria and serosa contain only negligible quantities of mast cells. Immunohistochemical data on gastroduodenal mast cell numbers in healthy subjects are however very scarce. The mast cell number in the digestive tract has been studied in mast-cell-related diseases such as systemic mastocytosis, and in other conditions like coeliac disease. Results are contradictory with either the reported increase or decrease [1, 7, 8, 10, 20, 24]. At this moment, little is known about mast cell numbers in the gastroduodenal mucosa in CU. The aim of this study is threefold: (1) to determine by immunohistochemical techniques the mast cell number in the normal gastroduodenal mucosa, (2) to investigate whether different dietary habits influence the mast cell number in normal subjects and (3) to determine whether the number of mast cells is increased in the gastroduodenal mucosa of CU patients because this could be of importance for the therapy for CU.

Materials and methods

Patients

The patient group consisted of 43 Belgian subjects (M/F ratio 15:28, age range 16–77 years, median age 45 years) with CU referred to the Department of Allergy and Clinical Immunology in our hospital. CU was defined as urticarial lesions appearing at least twice a week for more than 6 weeks. In 42 out of 43 patients, the baseline serum tryptase level was determined with the UniCAP-Tryptase fluoro-immunoassay (Pharmacia-Upjohn, Sweden). In 1 patient, tryptase was not measured because of an administrative error. A gastroduodenoscopy was performed prospectively as part of the investigative procedure in all patients, whether gastrointestinal symptoms were present (n=30) or not (n=13). One patient had been treated for *Helicobacter pylori* (Hp) infection in the months preceding the endoscopy. Biopsies were taken from the gastric corpus, the antrum and/or the duodenum. A urea breath test was included in the diagnostic work up after the start of the study and was performed in 25 out of 43 patients. All patients were questioned for the presence of rhinitis, asthma and food allergic or pseudoallergic symptoms. They were also asked to report on intolerance reactions to food pseudoallergens such as additives, histamine-releasing agents and alcoholic drinks. They were prospectively investigated by skin prick tests (SPT) with a screening panel including pollen of grasses, trees and weeds, with house dust mite, moulds, cat, dog and with food allergens in patients with a positive history. Specific IgE determinations (CAP system, Pharmacia-Upjohn) for respiratory and/or food allergens were performed in patients with a negative SPT. Patients with a positive history and at least one positive SPT or CAP-test were considered as “atopic”, whereas the other patients were designated as “non-atopic”.

Disease controls

A control group of 16 Belgian and 34 Italian (Sardinian) subjects (M/F 17:33, age range 6–72 years, median age 45 years) without urticaria underwent upper endoscopy for abdominal pain, pyrosis, weight loss or anaemia. Biopsies were taken from the gastric corpus, the antrum and/or the duodenum where appropriate. All disease controls were tested for coeliac disease: serology was negative in all cases except for 1 Italian subject having a positive anti-gliadin but negative anti-endomysium Ab test.

Biopsy evaluation

All biopsy specimens were fixed in 10% buffered formalin, routinely processed and embedded in paraffin. Haematoxylin–eosin (HE) stained sections were examined for routine diagnosis using the Sydney system for gastric biopsies [9].

Immunohistochemical detection of tryptase and CD117 (c-kit) was chosen as the preferred method for identification of mast cells. For tryptase detection, a 1:100 diluted monoclonal mouse–antihuman mast cell tryptase antibody solution (DakoCytomation, clone AA1) was applied for 30 min at room temperature after proteolytic enzyme digestion with trypsin. The reaction was completed by adding avidin–biotin–peroxidase complex and 3,3′diaminobenzidine (DAB) chromogen. CD117 was detected with a 1:250 diluted polyclonal rabbit–antihuman antibody solution (DakoCytomation, code no. A4502). Antigen retrieval was by boiling the dewaxed paraffin sections in 0.01 M Tris–EDTA solution (pH 9) for 30 min. The reaction was completed by addition of peroxidase-labelled anti-rabbit EnVision + Reagent (DakoCytomation) and DAB chromogen. Sections were faintly counterstained with Harris haematoxylin. Mast cells were counted by two pathologists (F.M. and C.W.) on a Zeiss light microscope. Only cells with a visible nucleus and unequivocal cytoplasmic or membranous staining were considered as mast cells. Differential diagnosis with Cajal cells was by cell shape (rounded instead of elongated) and by location. Counting was done only in vertically oriented tissue pieces. Mast cells were counted in five high-power fields (HPF; surface area of 1 HPF at magnification ×400 = 0.229 mm^2) and also in 5-μm grids composed of 100 small squares (surface area of 1-μm grid at magnification ×400 = 0.090 mm^2), enabling us to express the results as mean mast cell number per millimeter squared. The optical field of the microscope was positioned at the superficial part of the mucosa, so that as much lamina propria as possible was included.

Biopsies were also stained immunohistochemically for Hp in all CU patients and in the disease controls when appropriate. Hp staining was done using a 1:40 diluted polyclonal rabbit–anti-Hp antibody solution (DakoCytomation, code no. B0471) applied for 30 min at room temperature after heat-induced epitope retrieval by boiling the dewaxed paraffin sections in 0.01 M citrate solution (pH 6) for 30 min. The reaction was completed by addition of peroxidase-labelled anti-rabbit EnVision + Reagent (DakoCytomation) and DAB chromogen.

Statistical methods

All statistical analyses were performed using non-parametric tests (Mann–Whitney test and Spearman's rank correlation). *P* values less than 0.05 were considered statistically significant.

Results

Endoscopic findings

Upper endoscopy was normal in all disease controls. In the CU patients, there were no endoscopic abnormalities in 28/43 subjects. Twelve CU patients had signs of reflux oesophagitis, 1 showed gastric mucosal hyperaemia, 1 had a gastric ulcer suspicious for malignancy and 1 had a duodenal ulcer.

Pathological findings

Examination of the HE-stained sections showed normal gastric and duodenal biopsies in all disease controls. Twenty-seven CU patients had stomach and/or duodenal biopsies within normal limits. Otherwise, there were 4 cases of inactive chronic gastritis, 4 cases of active chronic gastritis, 4 cases of reactive gastropathy, 1 with fundic gland polyps, 1 with gastric adenocarcinoma and 2 with benign duodenal ulcers.

Immunohistochemistry for Hp was positive in 3 CU patients, 2 of whom had a positive breath test (no breath test was performed in the third). On the other hand, there were 2 CU patients with a positive breath test but with a negative Hp stain. Thus, there were 5 CU patients with Hp infection (4 of them had active chronic gastritis).

Immunohistochemistry allowed unequivocal identification and counting of mast cells in well-oriented biopsies. The tryptase stain showed granular positivity in the cytoplasm (Fig. 2), while CD117 was present in the cell membrane. Since mast cell numbers obtained by CD117

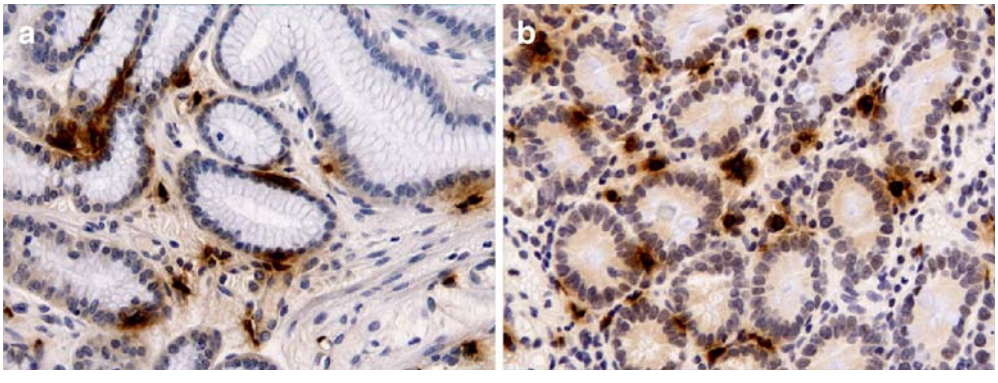

Fig. 2 **a** Cytoplasmic staining of mast cells in the stomach [immunohistochemistry (IHC) for tryptase, original magnification ×400]. **b** Cytoplasmic staining of mast cells in the duodenum (IHC for tryptase, original magnification ×400)

Table 1 Mean mast cell numbers per HPF and per mm^2 in disease controls and CU patients[a]

Disease controls			CU patients		
	per HPF	per mm^2		per HPF	per mm^2
Stomach			Stomach		
All (*n*=20)	20.2±6.2 [17.4–22.9]	133.3±36.6 [117.3–149.4]	All (*n*=38)	32.4±9.4 [29.5–35.4]	186.0±46.9 [171.1–200.9]
Belgian (*n*=15)	20.7±6.5		All, normal[b] (*n*=20)	30.4±9.6 [26.2–34.6]	173.9±41.0 [155.9–191.9]
Italian (*n*=5)	18.4±5.3				
Duodenum			Duodenum		
All (*n*=35)	32.5±9.2 [29.4–35.6]	209.2±61.6 [188.8–229.6]	All (*n*=36)	44.8±16.9 [39.2–50.3]	246.0±89.2 [216.8–275.1]
Belgian (*n*=6)	32.0±10.2		All, normal[b] (*n*=27)	45.2±18.2 [38.4–52.1]	248.6±95.1 [212.7–284.4]
Italian (*n*=29)	32.6±9.2				

[a]Mean±standard deviation (95% confidence interval)
[b]Normal = biopsies histologically normal

stain were comparable to those obtained by tryptase stain (data not shown), all counts were performed on the tryptase stainings. The mean mast cell number for all disease controls together was 20.2/HPF (133.3/mm^2) in the stomach and 32.5/HPF (209.2/mm^2) in the duodenum (95% confidence intervals for mean mast cell numbers; see Table 1). There was no significant difference between Belgian and Italian controls either in the stomach (Mann–Whitney test, P=0.49) or in the duodenum (P=0.76).

The mean mast cell number for all CU patients was 32.4/HPF (186.0/mm^2) in the stomach and 44.8/HPF (246.0/mm^2) in the duodenum. Both in the stomach and in the duodenum, the mean mast cell number was significantly higher in the CU patients than that in the disease controls (Mann–Whitney test, P<0.0001 and P=0.0002, respectively; Figs. 3 and 4). The difference between CU patients and disease controls was more pronounced in the stomach than in the duodenum (a 61.0% increase in mast cell number in CU patients vs disease controls in the stomach vs a 37.8% increase in the duodenum). The mast cell number in the stomach was not significantly different between CU patients with (29.4/HPF) and without (32.9/HPF) Hp infection (Mann–Whitney test, P=0.3574). When all 20 histologically normal stomach biopsies from CU patients were compared with the control biopsies, the mean mast cell number was still significantly higher in the CU patients (Mann–Whitney test, P=0.0006). The same was found when 27 histologically normal duodenum biopsies from CU patients were compared with their corresponding control biopsies (P=0.0007).

Relation of mast cell number to atopy, food allergy or pseudoallergy in CU patients

An atopic constitution was demonstrated in 11/43 CU patients. Atopic patients did not differ from non-atopic patients with regard to the gastric or duodenal mast cell numbers (P=0.8553 and 0.4126, respectively).

In 4 of the 11 atopic patients, an IgE-mediated food allergy was detected. In these 4 patients, there was a trend towards higher mast cell numbers in stomach (P=0.0750)

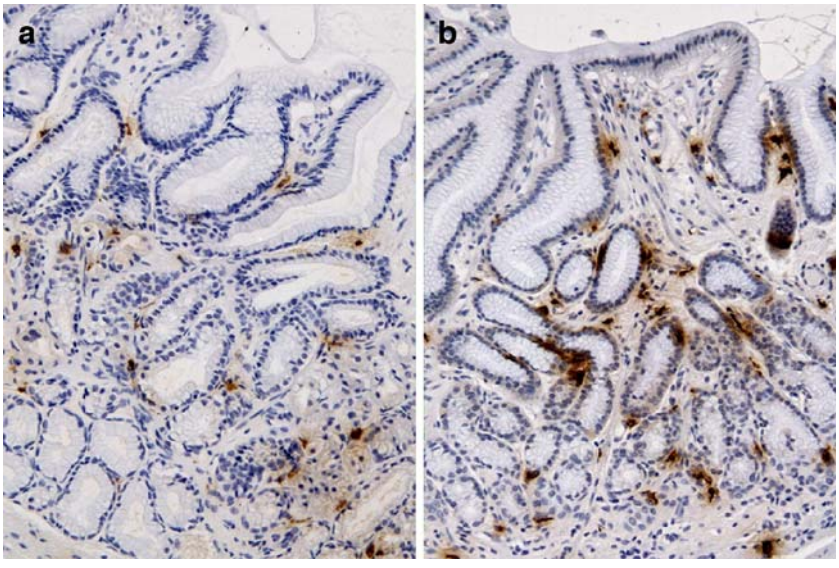

Fig. 3 **a** Stomach from control subject (tryptase, original magnification ×200). **b** Stomach from CU patient (tryptase, original magnification ×200)

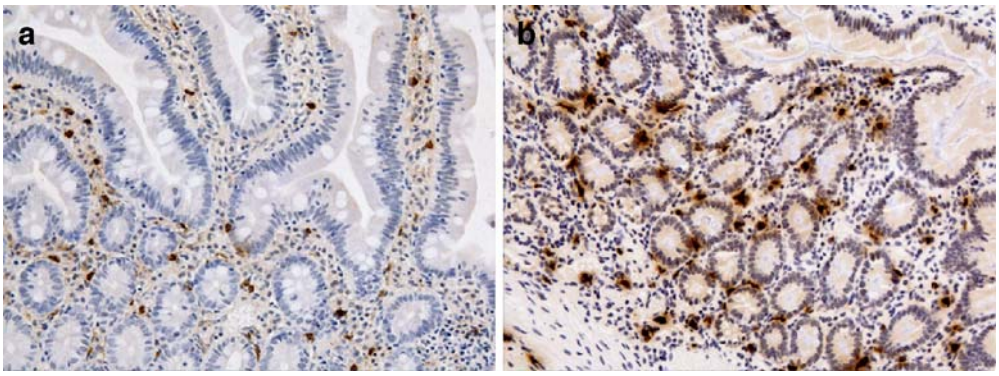

Fig. 4 **a** Duodenum from control subject (tryptase, original magnification ×200). **b** Duodenum from CU patient (tryptase, original magnification ×200)

than in the non-food allergic patients, but statistical significance was not reached probably because of the low number of food allergic patients.

Fourteen CU patients had a history of food pseudoallergen-induced aggravation of their disease. In these 14 patients, we surprisingly found a lower stomach mast cell number than in those without food pseudoallergy (P=0.0252).

Correlation of mast cell number with baseline tryptase levels in CU patients

Baseline tryptase levels were normal (≤11.5 μg/l) in 38 out of 42 CU patients. The mean value for all patients was 7.2 μg/l (range 2.3–21.9 μg/l). There was no correlation between the gastric or duodenal mast cell number and the baseline tryptase levels (P values for the Spearman's rank correlation were 0.8998 in the stomach and 0.3982 in the duodenum).

Discussion

In this study, we investigated whether CU, a mast-cell-related disorder which is often aggravated by the intake of pseudoallergen-containing foods, might be associated with mast cell infiltration in the gastrointestinal mucosa. Classically, mast cells have been identified by metachromatic stains such as Giemsa or toluidine blue. We chose to detect them by immunohistochemistry for tryptase and CD117, as these methods are more sensitive and specific [16]. Tryptase is present in the cytoplasmatic granules of the mast cells, and CD117 is located in the cell membrane. Positive staining results for tryptase may be more specific for mast cells [25]. Moreover, other authors have found that the results of tryptase and CD117 stains (with antigen retrieval) show a highly significant correlation, so that staining for mast cell tryptase alone apparently is sufficient [20]. Thus, we eventually chose to count mast cells in the tryptase stains. Unfortunately, there are only few authors mentioning normal values obtained by immunohistochemical methods, and their results are variable [7, 20]. We were therefore compelled to determine first the normal values in a disease control group. As there are no data available on the potential effect of different dietary habits on gastrointestinal mast cell number, we have included in the disease control group both Belgian and Italian (Sardinian) subjects. Italian dietary habits differ from the Belgian by the use of olive oil "extra vergine", more seafood, more fresh vegetables, more wine, less beer and less food additives.

In the disease control group, we found a mean mast cell number of 20.2/HPF (133.3/mm^2) for the stomach and 32.5/HPF (209.2/mm^2) for the duodenum. Variability was somewhat larger in the duodenal mucosa; 95% confidence intervals were non-overlapping, however. The larger number in the duodenum may have been caused by selection bias: control subjects often had duodenal biopsies taken to rule out coeliac disease, a condition in which mast cell numbers may be increased [23, 26]. However, this cause is not plausible since all controls had normal duodenal histology, and all but one had normal antigliadin and anti-endomysium Ab tests. Our normal value for the duodenum is comparable to the 204.2/mm^2 found by Crivellato et al. [7]. In contrast, Siegert et al. [20] found a higher mast cell number in the normal stomach than we did (331.9/mm^2 in the corpus and 251.9/mm^2 in the antrum). This may be due to a different positioning of the optical field of the microscope: we chose to count mast cells predominantly in the superficial part of the mucosa, with the aim of including as much lamina propria as possible. Our way of positioning also tends to minimize possible differences between corpus and antrum biopsies.

We found that there was no significant difference between Belgian and Italian controls for mean mast cell numbers either in the stomach or the duodenum. Different dietary habits therefore seem to have no influence on the mast cell number in the gastroduodenal mucosa. This result also allowed us to compare the CU patient group (which is exclusively Belgian) with all disease controls (Italian as well as Belgian).

When compared to the disease control group, our CU patients demonstrated a significantly increased mast cell number in the stomach and the duodenum. Liutu et al. [17] found no significant differences in gastric mucosal mast cell numbers between patients with and without CU. However, they only used the less sensitive toluidine blue staining method. Mast cell numbers in the gastroduodenal mucosa have also been determined in mast-cell-related diseases like systemic mastocytosis and urticaria pigmentosa, again with varying results [8, 10, 20].

Gastrointestinal mast cell infiltration in CU may be primary or secondary to concomitant disorders. An increased number of gastrointestinal mast cells has indeed been described in several infectious or non-infectious types of gastritis, with a correlation between the mast cell number and the density of the polynuclear and mononuclear cell infiltrates [3]. In our study, however, there was no relation between the occurrence of a histological abnormality and mast cell counts. Indeed, even CU patients with histologically normal biopsies showed a significantly higher mast cell number in the stomach and the duodenum than disease controls. Hp infection, which is associated with reactive mucosal mast cell infiltration in the stomach [11, 18], is often reported as a possible cause of CU. In our CU patient group, the prevalence of Hp infection was 8% (3/38) with immunostaining and 24% (6/25) with the urea breath test. CU patients with and without Hp infection did not differ in the degree of mast cell infiltration in the stomach.

An increase in the number of intestinal mast cells has also been described in patients with food allergy by some authors [19] but was not confirmed by others [1]. Some reports even mention an increase in intestinal mast cells in atopic subjects with only inhalant allergy [2]. We were able to exclude that atopy and food allergy were the factors that determined intestinal mast cell infiltration in our CU patients. We may conclude that the observed increase in intestinal mast cell numbers in CU patients is directly connected with the disorder itself rather than being part of an inflammatory cell response.

That food allergens are able to cause local degranulation of mast cells has been proven during segmental mucosal challenges [19]. Likewise, one might expect food pseudoallergens to have a similar local effect on mast cells and to cause urticaria by intestinal mast cell degranulation. We therefore expected a higher mast cell number in CU patients with a history of food pseudoallergy than in those without, but we surprisingly found the opposite. This can be explained in different ways. First, the diagnosis of food pseudoallergy is very difficult and the sensitivity of history-taking is low. Ideally, the results of elimination diets should have been taken into account. Second, it could be that there is indeed no relation between mast cell infiltration and food-induced aggravation of CU. Further studies are needed to clarify this.

Determination of baseline tryptase is currently used to estimate the mast cell load. Clearly, elevated levels were found in only 4 out of 42 (10%) of our CU patients. The mean level of 7.2 μg/l in our study is comparable with the level in Hidvegi et al.'s [14] patients and is significantly higher than that in their control group. We did not find a correlation between baseline tryptase levels and intestinal mast cell numbers, which means that peripheral tryptase levels are probably not affected by local mast cell infiltration but predominantly reflect the total body mast cell load.

In conclusion, we showed that CU is associated with gastroduodenal mast cell infiltration. We strongly suppose that there is a causal relation between both phenomena, but at this stage, it is impossible to establish the exact relationship. CU could indeed be the consequence as well as the cause of the reactive mast cell infiltration. This has still to be investigated. Further studies are also needed to establish whether it is justified to take endoscopic biopsies for tryptase and CD117 stainings in the absence of clear endoscopic lesions in CU patients without gastrointestinal symptoms. The finding of increased mast cell numbers might on the other hand be helpful in directing therapy towards strategies that could prevent intestinal mast cell degranulation. These patients might, for example, benefit more from pseudoallergen-free elimination diets, from H_2-antihistamines or from mast cell stabilizers as disodium-chromoglycate than CU patients with normal mast cell numbers.

References

1. Augustin M, Karttunen TJ, Kokkonen J (2001) TIA1 and mast cell tryptase in food allergy of children: increase of intraepithelial lymphocytes expressing TIA1 associates with allergy. J Pediatr Gastroenterol Nutr 32:11–18
2. Bagnato GF, Di Cesare E, Caruso RA, Gulli S, Cugliari A, Morabito Lo Prete A, Previti M, Muscara M, Bottari M (1995) Gastric mucosal mast cells in atopic subjects. Allergy 50:322–327
3. Beil WJ, Schulz M, McEuen AR, Buckley MG, Walls AF (1997) Number, fixation properties, dye-binding and protease expression of duodenal mast cells: comparisons between healthy subjects and patients with gastritis or Crohn's disease. Histochem J 29:759–773
4. Bruno G, Andreozzi P, Magrini L, Graf U, Santangelo G, Zaino S (2001) Mast cell activation in acquired chronic urticaria–angioedema. Sci Total Environ 270:77–81
5. Buhner S, Reese I, Kuehl F, Lochs H, Zuberbier T (2004) Pseudoallergic reactions in chronic urticaria are associated with altered gastroduodenal permeability. Allergy 59:1118–1123
6. Caproni M, Volpi W, Macchia D, Giomi B, Manfredi M, Campi P, Cardinali C, D'Agata A, Fabbri P (2003) Infiltrating cells and related cytokines in lesional skin of patients with chronic urticaria and positive autologus serum skin test. Exp Dermatol 12:621–628
7. Crivellato E, Finato N, Isola M, Ribatti D, Beltrami CA (2003) Low mast cell density in the human duodenal mucosa from chronic inflammatory duodenal bowel disorders is associated with defective villous architecture. Eur J Clin Invest 33:601–610
8. Debeuckelaere S, Schoors DF, Devis G (1991) Systemic mast cell disease: a review of the literature with special focus on the gastrointestinal manifestations. Acta Clin Belg 46:226–232
9. Dixon MF, Genta RM, Yardley JH, Correa P (1996) Classification and grading of gastritis. The updated Sydney System. International workshop on the histopathology of gastritis, Houston 1994. Am J Surg Pathol 20:1161–1181
10. Ferguson J, Thompson RP, Greaves MW (1988) Intestinal mucosal mast cells: enumeration in urticaria pigmentosa and systemic mastocytosis. Br J Dermatol 119:573–578
11. Furusu H, Murase K, Nishida Y, Isomoto H, Takeshima F, Mizuta Y, Hewlett BR, Riddel RH, Kohno S (2002) Accumulation of mast cell and macrophages in focal active gastritis of patients with Crohn's disease. Hepatogastroenterology 49:639–643
12. Gemmel E, Carter CL, Seymour GJ (2004) Mast cell in human peridontal disease. J Dent Res 83:384–387
13. Haas N, Toppe E, Henz BM (1998) Microscopic morphology of different types of urticaria. Arch Dermatol 134:41–46

14. Hidvegi B, Nagy E, Szabo T, Temesvari E, Marschalko M, Karpati S, Horvath A, Gergely P (2003) Correlation between T-cell and mast cell activity in patients with chronic urticaria. Int Arch Allergy Immunol 132:177–182
15. Kozel MM, Sabroe RA (2004) Chronic urticaria: aetiology, management and current and future treatment options. Drugs 64:2515–2536
16. Li CY, Dry SM (2004) Are c-kit and mast cell tryptase more effective at identifying mucosal mast cell in GI biopsies? Mod Pathol 17(Suppl 1):121A
17. Liutu M, Kalimo K, Kalimo H, Uksila J, Leino R (2004) Mast cells and IgE-containing cells in gastric mucosa of *Helicobacter pylori* infected and non-infected patients with chronic urticaria. J Eur Acad Dermatol Venereol 18:69–72
18. Nakajima S, Krishnan B, Ota H, Segura AM, Hattori T, Graham DY, Genta RM (1997) Mast cell involvement in gastritis with or without *Helicobacter pylori* infection. Gastroenterology 113: 746–754
19. Reimann HJ, Ring J, Ultsch B, Wendt P (1985) Intragastral provocation under endoscopic control (IPEC) in food allergy: mast cell and histamine changes in gastric mucosa. Clin Allergy 15:195–202
20. Siegert SI, Diebold J, Ludolph-Hauser D, Lohrs U (2004) Are gastrointestinal mucosal mast cells increased in patients with systemic mastocytosis? Am J Clin Pathol 122:560–565
21. Smith CH, Kepley C, Schwartz LB, Lee TH (1995) Mast cell number and phenotype in chronic idiopathic urticaria. J Allergy Clin Immunol 96:360–364
22. Staumont-Salle D, Piette F, Delaporte E (2003) Etiological diagnosis and treatment of chronic urticaria. Rev Med Interne 24:34–44
23. Strobel S, Busuttil A, Ferguson A (1983) Human intestinal mucosal mast cells: expanded population in untreated coeliac disease. Gut 24:222–227
24. Suranyi Y, Freier S, Faber J, Dollberg L (1986) Intestinal mast cells in different stages of celiac disease. Isr J Med 22:370–375
25. Walls AF, Jones DB, Williams JH, Church MK, Holgate ST (1990) Immunohistochemical identification of mast cells in formaldehyde-fixed tissue using monoclonal antibodies specific for tryptase. J Pathol 162:119–126
26. Wingren U, Hallert C, Norrby K, Enerback L (1986) Histamine and mucosal mast cells in gluten enteropathy. Agents Actions 18:266–268
27. Zuberbier T (2001) The role of allergens and pseudoallergens in urticaria. J Investig Dermatol Symp Proc 6(2):132–134

Virchows Arch (2006) 448: 269–276
DOI 10.1007/s00428-005-0107-z

ORIGINAL ARTICLE

Irina P. Eide · Toril Rolfseng · Christina V. Isaksen · Reidun Mecsei · Borghild Roald · Stian Lydersen · Kjell Å. Salvesen · Nina K. Harsem · Rigmor Austgulen

Serious foetal growth restriction is associated with reduced proportions of natural killer cells in decidua basalis

Received: 21 September 2005 / Accepted: 26 October 2005 / Published online: 19 November 2005

Abstract Extravillous trophoblasts are major participants in placental development and remodelling of spiral arteries. Trophoblast invasion is regulated by maternal immune cells, and abnormal leucocyte subpopulation composition has been reported in implantation failure. In pre-eclampsia (PE), with or without foetal growth restriction (FGR), superficial trophoblast invasion and insufficient remodelling of spiral arteries are common findings. In the present study, we have compared spiral artery remodelling and leucocyte composition in decidual tissue from 30 cases (PE=8, FGR=5, PE + FGR=17) and 31 controls. Six histological remodelling criteria were established, and each pregnancy obtained a remodelling score. Numbers of natural killer (NK) cells ($CD56^+$), T cells ($CD3^+$) and activated ($CD25^+$ or $CD69^+$) leucocytes were determined and related to total leucocyte ($CD45^+$) numbers in serial sections. Cases demonstrated significantly impaired spiral artery remodelling, inappropriate placental growth and reduced NK cell proportions, as compared to controls (P=0.02, P<0.001 and P=0.01, respectively). Reduced NK cell proportion was primarily found in pregnancies complicated by FGR, with or without PE, and a significant positive correlation was observed between NK cell proportion, trophoblast infiltration and placental growth. Our in vivo observations support the hypothesized association between NK cells, impaired placental development and pathogenesis of PE/FGR.

Keywords Pregnancy · Foetal growth restriction · Pre-eclampsia · Spiral artery · Activation markers

I. P. Eide (✉) · T. Rolfseng · R. Austgulen
Department of Cancer Research and Molecular Medicine,
Norwegian University of Science and Technology,
Medisinsk Teknisk Forskningssenter,
Olav Kyrres gt. 3,
7489 Trondheim, Norway
e-mail: irina.p.eide@ntnu.no
Tel.: +47-73-550290
Fax: +47-73-598801

C. V. Isaksen · K. Å. Salvesen
Department of Laboratory Medicine,
Children's and Women's Health,
Norwegian University of Science and Technology,
Trondheim, Norway

R. Mecsei
Department of Medical Laboratory Technology,
Sør-Trøndelag University College,
Trondheim, Norway

B. Roald
Department of Pathology, Ullevål University Hospital,
Oslo, Norway

S. Lydersen
Unit of Applied Clinical Research,
Department of Cancer Research and Molecular Medicine,
Norwegian University of Science and Technology,
Trondheim, Norway

N. K. Harsem
Department of Obstetrics and Gynecology,
Ullevål University Hospital,
Oslo, Norway

Introduction

A complicated and gestation-related interaction between cells of foetal and maternal origin, hormones, growth factors and matrix components is a prerequisite for successful implantation and subsequent placental development [3, 12, 30]. Effector cells and molecules of the maternal immune system are key participants, and decidual leucocytes may both promote and limit placental development through influencing trophoblast survival, invasion, proliferation and differentiation. Endometrial arteries undergo structural alterations to increase blood flow to the intervillous space [11, 28]. The cellular mechanisms of spiral artery remodelling are unknown, but the role of extravillous trophoblast (EVT) in this process is well recognized [19, 28].

Dramatic changes take place in the composition of uterine leucocyte subpopulations following implantation; natural killer (NK) cells emerge as the most prominent subpopulation [18, 26], constituting 50–70% of total leu-

cocyte numbers in the beginning of pregnancy, with decreasing numbers towards term [18, 26]. The uterine (u)NK cells are highly specialized and regulate trophoblast invasion and spiral artery remodelling by NK receptor recognition of trophoblast-expressed proteins with subsequent cytokine production [12, 18, 26]. Macrophages, T and B cells constitute approximately 15, 10 and 2%, respectively, of uterine leucocyte population, and their proportions remain fairly stable throughout pregnancy [2, 18]. The pregnancy-associated intrauterine immune response also implies reduced leucocyte activation, as assessed by down-regulated expression of the T-cell receptors and activation markers CD69, human leucocyte antigen–DR, CD45DR and CD25 (interleukin-2 receptor α) [10, 27].

Implantation failure and incomplete remodelling of spiral arteries may result in placental hypoperfusion, causing pre-eclampsia (PE) and/or foetal growth restriction (FGR) [8, 28]. Several studies suggest that implantation failure may be ascribed to altered composition and/or function of decidual leucocytes [21, 22, 29, 32], but only two studies have focused on changes associated with PE and/or FGR. One study reported increased NK cell and cytotoxic T-cell numbers among cases [36], whereas the other has found altered uNK phenotype and cytokine profile in the disease group [39].

Decidual leucocytes, and especially NK cells, seem to play an important role in placental development and remodelling of spiral arteries. The aim of the present investigation was to study leucocyte composition in decidual tissues and relate findings to remodelling assessment. Tissues from cases with assumed reduced remodelling of spiral arteries (PE and/or FGR) were compared to normal controls, using immunohistochemical techniques.

Materials and methods

Study groups

Suspected placental disease due to insufficient implantation and remodelling of spiral arteries was the major criterion for inclusion of women into the case group of the study. Thus, women with pregnancies complicated by PE and FGR, alone or in combination, were included. Decidual tissue was collected at delivery by vacuum aspiration of the placental bed, and, for technical reasons, collection of material had to be done during caesarean section (CS) [16, 34]. Thus, only women who delivered by CS were included. In the case group, CS was done on clinical indications, whereas the controls were undergoing CS for various reasons considered irrelevant to the aim of this study. FGR was identified as FGR assessed by prenatal ultrasound measures and birth weight confirmation [24]. A birth weight ≤2 standard deviation (SD), corresponding to the 2.5 centile for gestational age, was used as FGR criterion. PE was defined as persistent hypertension (blood pressure of ≥140// 90 mmHg) plus proteinuria (≥0.3 g/d or ≥2+ according to a dipstick test), developing after 20 weeks of pregnancy [1]. The study was approved by the Regional Committee for Medical Research Ethics. Specimens were collected at St. Olavs Hospital, the University Hospital of Trondheim from 2002 to 2004. Informed consent was obtained from all participants. Pregnancies with chromosomal aberrations, foetal and placental structural abnormalities or suspected perinatal infections were not included.

Sixty-one women were included in the study (30 cases, 31 controls). Five cases suffered from FGR alone, 17 had PE and FGR in combination and 8 women received the diagnosis PE without FGR (Table 1). Cases and controls differed significantly with respect to several clinical manifestations, among those gestational age at delivery, birth weight and placental weight (Table 1).

Tissue collection and preparation

Decidual tissue was obtained by vacuum suction of the placental bed after the placenta was delivered [16, 34]. The collected tissue was fixed in 10% neutral-buffered formalin, paraffin embedded and cut in sections at 4 μm on a motorised rotation microtome. One section, stained with haematoxylin, erythrosine and saffron (HES), was used for quality control of the tissue collected. Only specimens containing EVT (decidua basalis) were included for further studies. Three (4.6%) of the 65 collected samples consisted mostly of blood or placental tissue and were rejected at this stage. Placental weight was registered, and the placental weight ratio (PWR; observed placental weight/expected placental weight) was calculated. The expected placental weight was obtained from the placental weight standards given by Benirschke and Kaufmann [4]. All placentas enrolled were examined by a pathologist, in accordance with established routines.

Spiral artery remodelling, visualization and assessment

Remodelling of spiral arteries was examined in two sections from each individual; one HES-stained and a second stained with monoclonal antibodies (mAbs) against trophoblasts [anti-cytokeratin 7 (anti-CK7), clone OV-TL 12/30, diluted 1:300; DakoCytomation, Glostrup, Denmark] and against smooth muscle cells (anti-actin, clone HHF35; Ventana Medical Systems Inc., Tucson, AZ, USA). Double immunostaining was performed in an automated slide stainer (Ventana ES, Ventana Medical Systems Inc.) after deparaffination, rehydration and heat-induced antigen retrieval. The staining procedure was divided in two: anti-CK7 was added in the first step, whereas the second step was initiated with anti-actin. The secondary antibodies in both steps were biotinylated (with a streptavidin–biotin complex), and the binding sites were visualized by a 3c3-diaminobenzidine HCl (DAB) chromogen in the first step (iVIEW DAB Detection Kit, Ventana Medical Systems Inc.) and alkaline phosphatase in the second step (Ventana Enhanced Alkaline Phosphatase RED Detection Kit, Ventana Medical Systems Inc.). All sections were counterstained in haematoxylin.

Table 1 Clinical information

	FGR (*n*=5)	FGR + PE (*n*=17)	PE (*n*=8)	Controls (*n*=31)
Maternal age (years)	34±6	29±5	29±5	31±5
Gestational age (weeks)	33±6*	31±3**	35±2**	39±1
Systolic blood pressure (mmHg)	139±9*	171±9**	169±17**	121±12
Diastolic blood pressure (mmHg)	82±14*	100±6**	98±12**	71±14
Birth weight (g)	1327±846**	1223±363**	2318±378**	3673±512
Placental weight (g)	290±132**	263±51**	476±62**	645±143
PWR	0.83±0.23**	0.87±0.15**	1.28±0.13	1.45±0.33

Values are expressed as means±SDs, unless stated otherwise. All case groups were compared to controls
FGR Foetal growth restriction, *PE* pre-eclampsia, *PWR* placental weight ratio (observed placental weight/expected placental weight)
*P<0.05; **P<0.001

For arteries to be included for assessment, the presence of a defined lumen and a visible vessel wall was required. The remodelling process of each artery was scored, according to eight criteria (Table 2). Six of the criteria were used primarily to grade the remodelling process [i.e., trophoblast infiltration (Fig. 1a,e), trophoblast replacement of the endothelial layer (Fig. 1c), lumen diameter (defined as the most-narrow-measured lumen in a vessel; Fig. 1b), presence and characteristics of smooth muscle cells in the vessel wall (Fig. 1c)]. The remaining two were included to cover pathological vessel alterations [acute atherosis (Fig. 1f) and endothelial activation/thrombosis (not shown)]. The HES-stained section was used for evaluation of the vessel diameter, amount of fibrinoid in the vessel wall, acute atherosis and endothelial activation/thrombosis (Fig. 1b,d,f), whereas all other criteria were assessed in the CK7/actin-immunostained sections (Fig. 1a,c,e).

The remodelling scores obtained by each artery were added up to a sum-remodelling index for each artery. When arterial cross sections were closely located and considered loops of the same tortuous vessel, the sum-remodelling index of the artery was calculated as the mean of all scores given to its loops. Finally, the mean score for each criterion in each pregnancy was calculated (by including assessment scores from all arteries found in that decidual section), and these scores were used for comparison between cases and controls.

Leucocyte population

Six serial sections were used for immunostaining with mAbs towards leucocyte markers. Sections were cut at 4 μm; that is, the first and the last sections were approximately 20 μm apart. This implies that the lymphocytes (7–15 μm in size)

Table 2 Criteria for assessment of spiral arteries

Criteria	Grade				
	0	1	2	3	4
Remodelling criteria					
Trophoblast infiltration		In decidua, but not adjacent to arteries	Adjacent to vessel wall	In arterial wall	Endothelial cells replaced
Trophoblast replacement[a]	None	<25	25–50	50–75	>75
Lumen diameter (μm)	<25	25–50	50–100	100–200	>200
Fibrinoid in vessel wall[b]	Not present	<25	25–50	50–75	>75
Smooth muscle cells in vessel wall[c]	++++	+++	++	+	Not present
Bundles[d] of muscle cells	Present	Not present			
Pathological alterations					
Acute atherosis[e]	No	<25	25–50	50–75	>75
Endothelial activation/thrombosis[f]	Flat endothelium	Endothelial activation	Signs of thrombosis	Partial thrombosis	Occluding thrombosis

Every cross section was evaluated according to the eight criteria given in Table 1
[a]Trophoblast replacement is given as a visually estimated percentage of the endothelial layer of the inner vessel wall
[b]Fibrinoid replacement is given as a visually estimated percentage of vessel wall area replaced by fibrinoid
[c]The occurrence of smooth muscle cells in vessel wall was quantified; +,++,+++ and ++++ indicate the spread of muscle cells in vessel wall quadrants
[d]A muscle bundle consists of several (>5) smooth muscle cells, closely attached together. The parameter was categorized as present/not present for each vessel
[e]Acute atherosis is defined by the presence of lipid-laden cells in the intima layer of the vessel wall, given as a percentage of the lumen circumference
[f]Endothelial activation is defined by the presence of prominence, basophilia and vacuolization of endothelial cells of the inner vessel wall

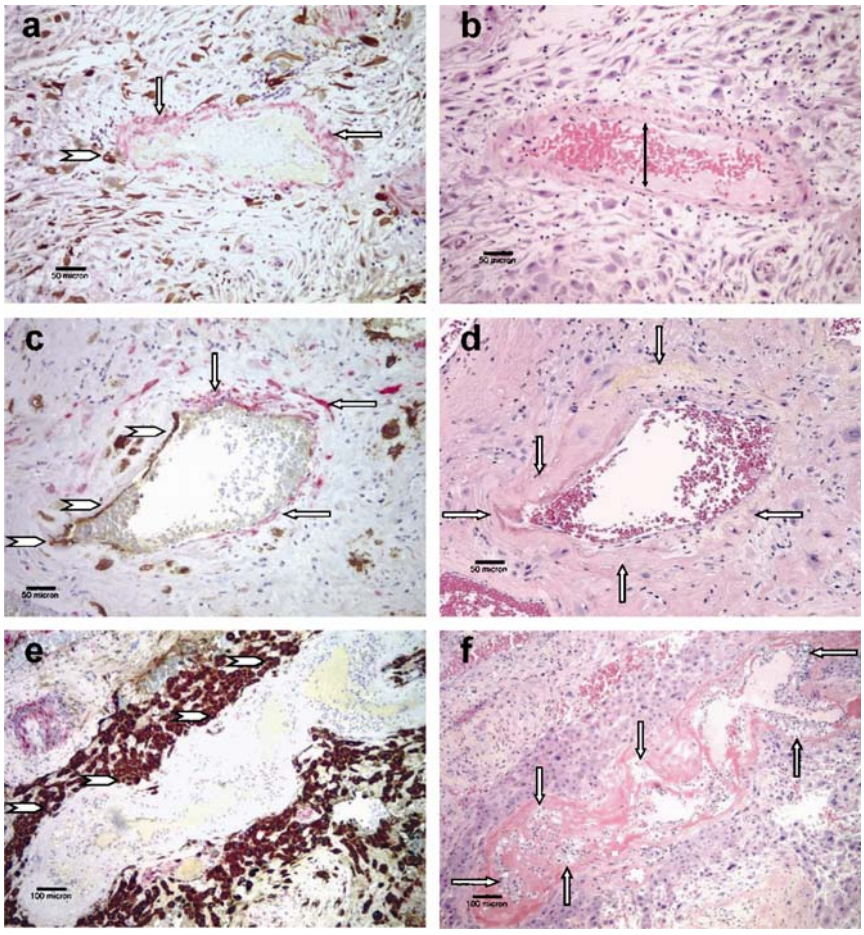

Fig. 1 **a**–**f** Remodelling of spiral arteries was assessed in sections double-stained with mAbs against trophoblasts (anti-CK7, *brown colour*) and against smooth muscle cells (anti-actin, *red colour*) (**a**, **c**, **e**) and in HES-stained sections (**b**, **d**, **f**). The decidual tissue photographed was collected from two women with PE + FGR (**a**–**b** and **e**–**f**) and from one control (**c**–**d**). Remodelling parameters were given the following scores: trophoblast infiltration—score 2, adjacent to vessel wall ("fx1") (**a**, **e**); trophoblast replacement—score 2, 25–50% of the endothelial layer is replaced by trophoblasts ("fx1") (**c**); lumen diameter 100 μm—score 3 (**b**); fibrinoid in vessel wall—score 4, more than 75% of vessel wall area is replaced by fibrinoid ("fx2") (**d**); smooth muscle cells in vessel wall—score 2, present in two quadrants ("fx2") (**c**); bundles of muscle cells—score 0, more than five smooth muscle cells closely attached together ("fx2") (**a**). In addition, acute atherosis was scored 4, lipid-laden cells in more than 75% of the intima layer of vessel circumference ("fx2") (**f**). **a**–**d**, ×200; **e**–**f**, ×100

found on section no. 1 would not be the same as those observed on section no. 6. The mAb against CD45 (clone F7.2.38, diluted 1:400; DakoCytomation) was used as a common leucocyte marker, and the number of CD45 positive ($CD45^+$) cells was used as the denominator to calculate the proportion of other markers. Due to this and the distance between section no. 1 and no. 6, mAb against CD45 was added to section no. 3. mAb against CD3, T-cell marker (clone F7.2.38, diluted 1:50; DakoCytomation), was added to section no. 1. NK cells were detected by mAb against CD56 (clone 123C3, diluted 1:20; Monosan, Uden, the Netherlands), and the antibody was added to section no. 2, whereas mAb against CD16 [clone 16CO2(2H7), diluted 1:75; Neo Markers, Fremont, CA, USA] (detects NK cells, macrophages, granulocytes) was used for staining of section no. 4. MAbs against the cell activation markers CD25 (clone 4C9, diluted 1:150, Novocastra, Newcastle, UK) (T and B cells) and CD69 (clone CH11, diluted 1:25; Novocastra) (T and B cells, NK cells, granulocytes) were added to section no. 5 and no. 6, respectively.

The leucocyte marker staining was performed in an automated slide stainer (DakoCytomation) after deparaffination, rehydration and heat-induced antigen retrieval. Endogenous peroxidase activity was blocked, and primary antibodies were added. Incubation time for all mAbs was 30 min, with the exception of mAb against CD69 (60-min incubation). Secondly, a peroxidase-conjugated polymer with antibodies against rabbit/mouse (ChemMate Dako Envision Detection Kit Peroxidase/DAB, DakoCytomation) was used, according to manufacturer's standard procedure. Antibody diluent without antibody was used as a control for non-specific staining. Paraffin-embedded sections of tonsil tissue were used as positive controls for all antibodies. The sections were counterstained in haematoxylin.

Cells stained positively with the different leucocyte markers were counted in identical areas of all serial sections. The area selected was determined on the basis of the following criteria: the area should contain at least 250 $CD45^+$ cells (to provide cell numbers that were statistically sufficient for comparisons between groups), only small amounts of maternal blood should be present, and the defined area should easily be reproduced from section to section. Areas fulfilling these criteria were demarcated with Indian ink in all sections of each series. Two observers counted positive cells simultaneously, independently and blindly for case/control status, after consensus on inclusion criteria for the different leucocyte populations was reached (Fig. 2). Counting was performed at 400× magnification, using a 13×13-mm reticule.

The total cell number used for calculation of the leucocyte subpopulation proportion was obtained by two different approaches: in the first alternative, all $CD45^+$ cells were counted (n=$CD45^+$ leucocytes), whereas in the second, only $CD45^+$ cells with lymphocyte appearance

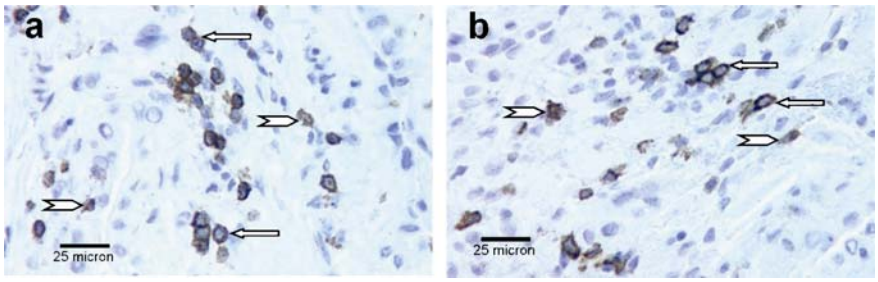

Fig. 2 **a**–**b** Immunostaining with mAbs against CD45 (common leucocyte marker) (**a**) and against CD56 (NK marker) (**b**) was performed on formalin-fixed, paraffin-embedded serial sections. Tissue fields containing at least 250 $CD45^+$ cells were included in assessment, and cell proportions were calculated, with the $CD45^+$ counts as the denominator. Only positive cells with distinguishable nuclei were counted. The photos demonstrate cells included in ("fx2") and excluded from ("fx1") counting. **a**–**b**, ×400

were included (n=$CD45^+$ lymphocytes). Ratios between $CD3^+$, $CD56^+$, $CD16^+$, $CD25^+$ and $CD69^+$ cells and both leucocyte numbers ($CD45^+$ leucocytes and $CD45^+$ lymphocytes) were calculated for each individual. In addition, the ratios between $CD16^+$ and $CD56^+$ cells were calculated. The results are given as means±SDs.

Statistical analysis

Results are expressed as the mean of groups±the corresponding SD. The Mann–Whitney test was used for comparison between groups, and Spearman's ranked correlation test was used to examine correlation between spiral artery remodelling and leucocyte subpopulation composition. P<0.05 was considered to be significant. SPSS version 12 was used for all statistical analyses.

Results

Spiral artery remodelling

Most sections (89%) contained one or more loops of uteroplacental arteries (remodelled spiral arteries) in decidua basalis. The number of arteries on each section varied from 1 to 15 (4±3), and the number of loops belonging to one spiral artery varied from 1 to 17 (4±3). The number of spiral arteries found in sections did not differ between the case and control groups. In seven sections (PE, 2; FGR + PE, 1; controls, 4), no arteries were found, and accordingly, these pregnancies were excluded from the spiral artery remodelling classification.

The overall case group demonstrated insufficient remodelling of uteroplacental arteries, as expressed by comparison of sum-remodelling indexes of cases (8.8±3.3) and controls (11.1±3.3, P=0.02). When the separate remodelling criteria were considered, vessel lumen, trophoblast invasion and endothelial replacement seemed, in order of appearance, to give the best discrimination between cases (2.5±0.5, 1.9±0.6, 0.1±0.2) and controls (2.9±0.4, 2.8±0.7, 0.5±0.5; all Ps<0.01). In contrast, fibrinoid replacement and muscle cells (either separate or in bundles) did not differ between study groups (data not shown).

Acute atherosis was observed more frequently among cases (1.0±1.0) compared with controls (0.3±0.5, P<0.01), whereas endothelial activation/thrombosis did not differ significantly between the overall case group and controls (data not shown).

Placental weight and placental histology

The ratio between observed and expected placental weight (PWR) reflects placental growth conditions. The PWR among controls (1.5±0.3) was significantly higher than that found in cases (1.0±0.3, P<0.001). Pregnancies with FGR alone and in combination with PE were associated with significantly reduced placental growth as compared to normal pregnancies (both Ps<0.001), while in pregnancies with isolated PE, PWR did not differ significantly from controls. Furthermore, a positive association was found between PWR and trophoblast invasion (P=0.02) and trophoblast replacement (P=0.03).

Morphological alterations in the placenta were more frequent among cases than controls; 13 (43%) cases demonstrated advanced villous maturation, as compared to three (10%) controls. Multiple infarcts (involving more than 15% of the placental volume) were found in four (13%) cases (all of them from the FGR ± PE subgroup) and none in controls. Placental histology was described as normal in five (16%) cases and 17 (55%) controls.

Leucocyte subpopulations and cell activation

The proportion of NK cells (with the $CD45^+$ leucocyte numbers as the denominator) was significantly lower in the overall case group (18.5±10.4%), as compared with controls (26.8±13.7%, P=0.01; Fig. 3). Pregnancies complicated with FGR had the lowest NK cell ratio as compared with controls (P=0.01; Fig. 3). The reduction was less pronounced in pregnancies complicated with PE, and the proportion of NK cells in this group did not differ significantly from controls (Fig. 3). The proportions of CD3 and CD16 positive cells did not differ between cases and controls, neither overall nor in subgroups (Fig. 3). The CD16/CD56 ratios were increased in cases (all cases 0.13±0.10, PE 0.10±0.09, FGR 0.16±0.13, PE + FGR 0.14±0.10) but did not differ significantly from that found in controls (0.11±0.11).

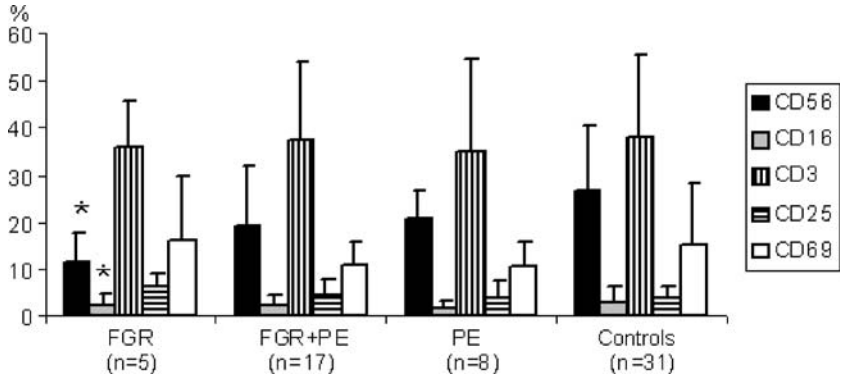

Fig. 3 Proportions (%) of $CD56^+$ (NK cells), $CD3^+$ (T cells), $CD16^+$(NK cells, macrophages, granulocytes), $CD25^+$ and $CD69^+$ (leucocyte activation markers) leucocytes, as related to the total number of $CD45^+$ (common leucocyte marker) cells, in formalin-fixed, paraffin-embedded serial sections of decidual tissue obtained from women at delivery. One case group suffered from foetal growth restriction (*FGR*), a second had FGR and pre-eclampsia (*PE*) and in the third, PE was the only diagnosis. All case groups were compared to controls. Results are displayed as mean values, with the corresponding SD. *$P<0.05$

When leucocyte proportions were calculated as proportions of $CD45^+$ lymphocyte numbers, similar results were obtained. For NK cells, the proportions were 28.0±15.3% among cases and 40.9±18.6% among controls ($P<0.01$). Both the case group with isolated FGR and the FGR + PE group demonstrated significantly reduced NK cell proportions when NK cell counts were related to $CD45^+$ lymphocyte numbers ($P=0.02$ and 0.03, respectively), whereas in the isolated PE group, the reduction was not significant.

Cell activation, as assessed by expression of CD25 and/or CD69, was neither increased in association with FGR nor with PE. A higher expression of CD25 was found in the group with isolated FGR ($P=0.04$), whereas all other comparisons between study groups and controls demonstrated no significant differences in CD25 and/or CD69 expression (Fig. 3).

NK cell proportion, spiral artery remodelling and placental growth

A positive correlation was observed between NK cell proportion and trophoblast infiltration in pregnancies complicated with FGR, i.e., FGR ± PE ($P=0.03$). With reference to study groups, this correlation was statistically confirmed by the FGR + PE group ($P=0.04$) but not by the group with isolated FGR ($P=1.0$). Furthermore, a positive association was observed between NK cell proportion and PWR in both cases and controls ($P=0.01$).

Discussion

In this study, we have investigated the leucocyte subpopulation composition in the decidual tissue collected from women at delivery with pregnancies complicated with PE and FGR, alone or in combination. Tissue was obtained by vacuum suction of the placental bed during CS, a procedure which provides representative material for studies of feto-maternal interactions in the decidua basalis [16, 34]. Cases demonstrated a reduced proportion of NK cells, as compared to controls. The reduction was primarily found in pregnancies complicated with FGR, whereas the association between NK cell proportion and PE was less pronounced.

uNK cell numbers decrease from mid-gestation towards term [26]. It is a general problem in research on human reproduction that it is impossible to obtain normal, age-matched controls. As a rule, non-PE/FGR pregnancies with preterm deliveries are complicated by other pathological conditions that may put influence upon observations. In our study, we found a reduced NK cell proportion in the case group, although their mean gestational age was 6 weeks lower than that of controls, suggesting that differences would have been even more pronounced if comparisons could have been done between gestational age-matched cases and controls.

Several lines of evidence suggest that uNK cells have major roles in implantation and placental development [21, 26]. It is a general assumption that these cells are recruited to decidua from peripheral blood by homing mechanisms [9]. Various signals from decidua (cytokines, chemotactic signals, protease inhibitors) probably coordinate this process [37] and influence the composition of decidual leucocytes which differ significantly from both that in peripheral blood and other tissues [25]. Decidual leucocytes play major roles in implantation and trophoblast invasion [12]. Reduced NK cell numbers have been reported in spontaneous abortion [13, 17, 22, 29, 32, 40], but we know little about the role of NK cells in the implantation failure associated with PE and/or FGR [36, 39]. Stallmach et al. [36] have studied leucocyte composition in decidual tissue from PE and/or FGR pregnancies and conclude that NK cell numbers are increased. This contradicts our results, but a comparison between leucocyte subpopulation proportions calculated in the two studies may be difficult; Stallmach et al. [36] used lymphocyte (i.e., $CD56^+$ and $CD3^+$ cells) numbers as denominator, whereas our results were based on leucocyte ($CD45^+$) counts. However, since cases in the present study demonstrated a reduced NK cell proportion, even when we used lymphocyte numbers as denominator, we anticipate that the results in fact are diverging. The size of the areas used for counting of leucocytes in our study was defined by $CD45^+$

cell numbers; at least 250 $CD45^+$ cells should be present. Both size of areas (7.0±4.0 mm^2) and leucocyte densities (120±58/mm^2) varied from case to case. Thus, cell proportions seem the most adequate measure for comparisons between groups. However, cases also demonstrated a reduced number of NK cells when absolute numbers were assessed ($CD56^+$ cells/mm^2, 19±12), as compared to that found in controls (30±15, P=0.002). These observations differ from the results obtained of Stallmach et al. [36], but comparisons should be done with caution, since both size and localization of selected areas in the two studies differ. A couple of discrepancies between the two studies should be taken into consideration. The study of Stallmach et al. [36] differed from ours with regard to gestational age (cases 33 vs 32 weeks, controls 36 vs 39 weeks), and they used less severe criteria for defining FGR. Since decidual leucocyte composition may vary both by gestational age and with FGR [26], comparisons should be done with caution. Others have reported changes in leucocyte phenotype, cytotoxicity and cytokine production in women with PE ± FGR, both in peripheral blood [14, 15, 23, 31] and decidual tissue [36, 39]. A shift from the $CD56^+CD16^-$ towards the more cytotoxic $CD56^+CD16^+$ NK cell phenotype and increased cytokine production have been reported in decidual lymphocytes in PE [39]. Results were obtained by flow cytometric analysis of lymphocytes isolated from decidual tissue at delivery [39]. Our results may suggest similar changes, but $CD16^+$/$CD56^+$ proportions were not significantly increased among cases. The increased cytotoxicity and cytokine production previously reported may indicate cell activation in PE [39]. However, we found no convincing cell activation in cases, as assessed by CD25 and CD69 expression. A significant increase in CD25 expression was observed when the group of isolated FGR cases was compared to controls (P=0.04), but one should take the small number of cases (n=5) in this group into account. In accordance with this, the positive association between increased CD25 expression and FGR was not maintained when all pregnancies complicated by FGR (n=23) were included in analysis. Increased numbers of $CD25^+$ decidual leucocytes have been reported in women with recurrent abortions [29], but as far as we know, this is the first study to assess CD25 expression in decidual tissues in PE ± FGR. CD69 expression did not differ between cases and controls, in accordance with previous reports [39].

Implantation failure and placental disease may underlie both PE and FGR, and several studies have demonstrated insufficient remodelling [6–8, 20, 28] and reduced placental weight [35] in PE/FGR. Our data support previously published observations; the remodelling scores and PWRs among cases were reduced. The PWR in the control group was higher than expected (1.5). This may be due to the high proportion of large babies in the control group (3673±512), and that large babies have large placentas [5]. In addition, our preparation of placentas before weighing differed from that used to establish expected weight standards [4]; our placentas were weighed together with the umbilical cord and membranes after early umbilical cord clamping, whereas standard placental weight was achieved after trimming off the chorion leave and cutting the cord near the chorionic plate. The different procedures may explain the elevated PWR in our study but do not influence comparison between cases and controls.

Furthermore, correlation analysis of leucocyte counts, remodelling criteria and clinical data of both cases and controls revealed interesting, and hypothesis-generating, associations; both NK cell proportions and trophoblast invasion were positively linked to placental growth. In pregnancies with FGR, with or without PE, we also detected a significant correlation between NK cell proportion and trophoblast infiltration. Our in vivo data support the hypothesized central role of NK cells in regulating trophoblast invasion [33, 36, 38], and the reduced NK cell proportions found among cases, especially in FGR pregnancies, suggest that reduced proportions of NK cells may be part of the impaired placental development and pathogenesis of the disease.

The insufficient implantation underlying PE takes place in the beginning of pregnancy, while the clinical manifestations of the disease appear at mid-gestation or towards term. First trimester decidual leucocyte populations may be examined in specimens collected from abortions, but such material cannot be applied for PE/FGR investigation, since we have no information about possible future development of PE/FGR in the terminated pregnancy. Due to the lack of availability of PE/FGR tissue from early pregnancy, tissue samples collected at birth are probably the best in vivo material there is. Since we observed a positive association between impaired spiral artery remodelling and reduced NK cell numbers, it is tempting to suggest that recruitment and composition of decidual leucocytes may have been altered at the early stages of pregnancy. However, due to the time passed between implantation and tissue collection, it is a matter of speculation whether the changes found reflect mechanisms involved in pathogenesis of the disease studied or represent abnormalities occurring as a consequence of the disease. Both possibilities are left open. In future investigations, we plan to transfer the present in vivo observations to appropriate in vitro settings, examining phenotype and function of decidual leucocytes isolated from normal and PE/FGR pregnancies.

Acknowledgements Tove Noren (Department of Pathology, Ullevål University Hospital, Oslo, Norway) performed the double staining with mAb CK7 and mAb actin. The study was supported by the Norwegian University of Science and Technology and St. Olavs Hospital HF.

References

1. 2000 Report of the National High Blood Pressure Education Program Working Group on High Blood Pressure in Pregnancy. Am J Obstet Gynecol 183:S1–S22
2. Abadia-Molina AC, Ruiz C, Montes MJ, King A, Loke YW, Olivares EG (1996) Immune phenotype and cytotoxic activity of lymphocytes from human term decidua against trophoblast. J Reprod Immunol 31:109–123
3. Aplin JD, Kimber SJ (2004) Trophoblast-uterine interactions at implantation. Reprod Biol Endocrinol 2:48

4. Benirschke K, Kaufmann P (2000) Pathology of the human placenta. Springer, Berlin, Heidelberg, New York
5. Bouw GM, Stolte LA, Baak JP (1976) Quantitative morphology of the placenta. I. Standardization of sampling. Eur J Obstet Gynecol Reprod Biol 6:325–331
6. Brosens I (1988) The utero-placental vessels at term—the distribution and extent of physiological changes. Trophobl Res 3:61–67
7. Brosens I, Dixon HG, Robertson WB (1977) Fetal growth retardation and the arteries of the placental bed. Br J Obstet Gynaecol 84:656–663
8. Brosens JJ, Pijnenborg R, Brosens IA (2002) The myometrial junctional zone spiral arteries in normal and abnormal pregnancies: a review of the literature. Am J Obstet Gynecol 187:1416–1423
9. Bulmer JN, Lash GE (2005) Human uterine natural killer cells: a reappraisal. Mol Immunol 42:511–521
10. Chao KH, Wu MY, Yang JH, Chen SU, Yang YS, Ho HN (2002) Expression of the interleukin-2 receptor alpha (CD25) is selectively decreased on decidual CD4+ and CD8+ T lymphocytes in normal pregnancies. Mol Hum Reprod 8:667–673
11. Craven CM, Morgan T, Ward K (1998) Decidual spiral artery remodelling begins before cellular interaction with cytotrophoblasts. Placenta 19:241–252
12. Croy BA, Chantakru S, Esadeg S, Ashkar AA, Wei Q (2002) Decidual natural killer cells: key regulators of placental development (a review). J Reprod Immunol 57:151–168
13. Dosiou C, Giudice LC (2005) Natural killer cells in pregnancy and recurrent pregnancy loss: endocrine and immunologic perspectives. Endocr Rev 26:44–62
14. Gervasi MT, Chaiworapongsa T, Pacora P, Naccasha N, Yoon BH, Maymon E, Romero R (2001) Phenotypic and metabolic characteristics of monocytes and granulocytes in preeclampsia. Am J Obstet Gynecol 185:792–797
15. Halim A, Kanayama N, El Maradny E, Maehara K, Bhuiyan AB, Terao T (1996) Correlated plasma elastase and sera cytotoxicity in eclampsia. A possible role of endothelin-1 induced neutrophil activation in preeclampsia–eclampsia. Am J Hypertens 9:33–38
16. Harsem NK, Staff AC, He L, Roald B (2004) The decidual suction method: a new way of collecting decidual tissue for functional and morphological studies. Acta Obstet Gynecol Scand 83:724–730
17. Hill JA, Melling GC, Johnson PM (1995) Immunohistochemical studies of human uteroplacental tissues from first-trimester spontaneous abortion. Am J Obstet Gynecol 173:90–96
18. Hunt JS, Petroff MG, Burnett TG (2000) Uterine leukocytes: key players in pregnancy. Semin Cell Dev Biol 11:127–137
19. Kam EP, Gardner L, Loke YW, King A (1999) The role of trophoblast in the physiological change in decidual spiral arteries. Hum Reprod 14:2131–2138
20. Kaufmann P, Black S, Huppertz B (2003) Endovascular trophoblast invasion: implications for the pathogenesis of intrauterine growth retardation and preeclampsia. Biol Reprod 69:1–7
21. King A, Burrows T, Verma S, Hiby S, Loke YW (1998) Human uterine lymphocytes. Hum Reprod Update 4:480–485
22. Lachapelle MH, Miron P, Hemmings R, Roy DC (1996) Endometrial T, B, and NK cells in patients with recurrent spontaneous abortion. Altered profile and pregnancy outcome. J Immunol 156:4027–4034
23. Mahmoud F, Omu A, Abul H, El-Rayes S, Haines D (2003) Lymphocyte subpopulations in pregnancy complicated by hypertension. J Obstet Gynaecol 23:20–26
24. Marsal K, Persson PH, Larsen T, Lilja H, Selbing A, Sultan B (1996) Intrauterine growth curves based on ultrasonically estimated foetal weights. Acta Paediatr 85:843–848
25. Moffett A, Regan L, Braude P (2004) Natural killer cells, miscarriage, and infertility. BMJ 329:1283–1285
26. Moffett-King A (2002) Natural killer cells and pregnancy. Nat Rev Immunol 2:656–663
27. Morii T, Nishikawa K, Saito S, Enomoto M, Ito A, Kurai N, Shimoyama T, Ichijo M, Narita N (1993) T-cell receptors are expressed but down-regulated on intradecidual T lymphocytes. Am J Reprod Immunol 29:1–4
28. Pijnenborg R (1998) The origin and future of placental bed research. Eur J Obstet Gynecol Reprod Biol 81:185–190
29. Quack KC, Vassiliadou N, Pudney J, Anderson DJ, Hill JA (2001) Leukocyte activation in the decidua of chromosomally normal and abnormal fetuses from women with recurrent abortion. Hum Reprod 16:949–955
30. Robertson SA, Redman CW, McCracken SA, Hunt JS, Dimitriadis E, Moffett-King A, Chamley L (2003) Immune modulators of implantation and placental development—a workshop report. Placenta 24(Suppl A):S16–S20
31. Sakai M, Shiozaki A, Sasaki Y, Yoneda S, Saito S (2004) The ratio of interleukin (IL)-18 to IL-12 secreted by peripheral blood mononuclear cells is increased in normal pregnant subjects and decreased in pre-eclamptic patients. J Reprod Immunol 61:133–143
32. Sehmsdorf US, Zenclussen AC, Arck P, Hertwig K, Joachim RA, Klapp B, Hildebrandt MO (2004) Human miscarriage is associated with increased number of CD26 decidual lymphocytes. Scand J Immunol 59:400–407
33. Sindram-Trujillo AP, Scherjon SA, van Hulst-van Miert PP, van Schip JJ, Kanhai HH, Roelen DL, Claas FH (2003) Differential distribution of NK cells in decidua basalis compared with decidua parietalis after uncomplicated human term pregnancy. Hum Immunol 64:921–929
34. Staff AC, Ranheim T, Khoury J, Henriksen T (1999) Increased contents of phospholipids, cholesterol, and lipid peroxides in decidua basalis in women with preeclampsia. Am J Obstet Gynecol 180:587–592
35. Stallmach T, Hebisch G (2004) Placental pathology: its impact on explaining prenatal and perinatal death. Virchows Arch 445: 9–16
36. Stallmach T, Hebisch G, Orban P, Lu X (1999) Aberrant positioning of trophoblast and lymphocytes in the feto-maternal interface with pre-eclampsia. Virchows Arch 434:207–211
37. Trundley A, Moffett A (2004) Human uterine leukocytes and pregnancy. Tissue Antigens 63:1–12
38. von Rango U, Classen-Linke I, Kertschanska S, Kemp B, Beier HM (2001) Effects of trophoblast invasion on the distribution of leukocytes in uterine and tubal implantation sites. Fertil Steril 76:116–124
39. Wilczynski JR, Tchorzewski H, Banasik M, Glowacka E, Wieczorek A, Lewkowicz P, Malinowski A, Szpakowski M, Wilczynski J (2003) Lymphocyte subset distribution and cytokine secretion in third trimester decidua in normal pregnancy and preeclampsia. Eur J Obstet Gynecol Reprod Biol 109:8–15
40. Yamamoto T, Takahashi Y, Kase N, Mori H (1999) Role of decidual natural killer (NK) cells in patients with missed abortion: differences between cases with normal and abnormal chromosome. Clin Exp Immunol 116:449–452

Virchows Arch (2006) 448: 277–287
DOI 10.1007/s00428-005-0118-9

ORIGINAL ARTICLE

Erika Rosivatz · Karl-Friedrich Becker · Elisabeth Kremmer · Christina Schott · Kareen Blechschmidt · Heinz Höfler · Mario Sarbia

Expression and nuclear localization of Snail, an E-cadherin repressor, in adenocarcinomas of the upper gastrointestinal tract

Received: 18 October 2005 / Accepted: 18 October 2005 / Published online: 17 November 2005

Abstract Transcriptional E-cadherin down-regulation can be mediated by Snail, a zinc finger transcription factor. To be able to examine nuclear Snail immunoreactivity in archival human cancers, we established a monoclonal antibody against the purified human Snail protein. The specificity of the selected rat antibody Sn9H2 was demonstrated by Western blot analysis using extracts from different cell lines and by immunofluorescence and immunohistochemistry of primary tissues. Subsequently, a series of 340 adenocarcinomas of the upper gastrointestinal tract, including tumours from the oesophagus (n=154), cardia (n=102) and stomach (n=84), arranged in tissue microarrays, were examined for Snail expression and were correlated to E-cadherin expression and clinico-pathological parameters. Nuclear Snail immunoreactivity was seen in 27 tumours (7.9%) and tended to be more frequent in oesophageal adenocarcinomas (11.1%) than in cardiac (6.9%) or gastric (3.6%) carcinomas (p=0.0428). In 35% of the Snail-positive cases, E-cadherin immunoreactivity was lost. No correlation was found for nuclear Snail expression and tumour grade, Lauren's classification, WHO classification, tumour stage and tumour size. The pattern of Snail expression observed with our new hybridoma, Sn9H2, which is currently the only antibody that reacts with endogenous nuclear (active) Snail, suggests only a minor role of Snail in tumours of the upper gastrointestinal tract.

Keywords Cell adhesion · Gastric cancer · Oesophagus cancer · Differentiation

E. Rosivatz · K.-F. Becker (✉) · C. Schott · K. Blechschmidt · H. Höfler · M. Sarbia
Institut für Pathologie, Technische Universität München, Trogerstrasse 18, 81675 München, Germany
e-mail: kf.becker@lrz.tum.de
Tel.: +49-89-41404591
Fax: +49-89-41404915

E. Kremmer
Institute of Molecular Immunology, GSF-National Research Centre for Environment and Health, Marchioninistrasse 25, 81377 München, Germany

H. Höfler
Institute of Pathology, GSF-National Research Centre for Environment and Health, 85764 Neuherberg, Germany

Present address:
E. Rosivatz
Department of Biological Sciences, Imperial College London, London SW7 2AY, UK

Introduction

The cell adhesion molecule and tumour suppressor gene E-cadherin [online Mendelian Inheritance in Man (OMIM) 192090] is well known to play a crucial role during the progression of human cancer [24]. E-cadherin function is required for the maintenance of normal epithelial tissue architecture and the stabilization of adherens junctions [36]. Its inactivation in carcinomas can disrupt these junctional complexes, resulting in marked phenotypic changes and the acquisition of invasive growth [15, 49]. Immunohistochemical studies have demonstrated that reduced or absent E-cadherin immunoreactivity is common in most cancers, including carcinomas of the oesophagus and stomach [8, 24, 42]. Direct transcriptional repression by zinc finger transcription factors such as Snail [3, 12], Slug [10, 21], Zeb1 (deltaEF1; [20]), Zeb2 (Sip1; [13]) or the basic helix–loop–helix transcription factor E12/E47 [35] is one of the mechanisms that may be responsible for reduced E-cadherin immunoreactivity.

Here, we focus our analysis on the transcription factor Snail, which was first described in *Drosophila* in 1984 [19]. Snail homologues were subsequently found in other species as well, including mouse and human. Snail triggers epithelial–mesenchymal transition (EMT) during embryonic development. Its role during gastrulation and in the delamination of the neural crest from the neural tube has been well established in the mouse (reviewed in [32]).

Since EMT is frequently observed in human tumours [23, 46], Snail has been analysed in carcinoma cells in culture if there is evidence of a functional role during tumour invasion and metastasis. Indeed, it has been shown that Snail directly binds to the E-boxes present in the E-cadherin promoter, resulting in the down-regulation of promoter activity in vitro. Moreover, the transfection of Snail in E-cadherin-positive carcinoma cells induced a full EMT with the down-regulation of E-cadherin and other epithelial marker genes, such as occludin [25], and the up-regulation of mesenchymal markers, including vimentin and fibronectin [3, 12]. Importantly, Snail-expressing cells became invasive after transfection, supporting its role in tumour progression. Snail not only induces invasion but also blocks the cell cycle and confers resistance to cell death [48].

On the mRNA level, Snail is expressed in invasive cells of tumours induced in the mouse skin [12]. In humans, Snail mRNA expression has been detected in biopsies or resected tissue samples from patients with breast cancer [9, 17], gastric cancer [39] and hepatocellular carcinomas [27, 45] and in melanoma cell lines [37]. In colon cancer, Snail mRNA was either found to be expressed [33] or to be absent [40]. Because no Snail-specific antibodies suitable for immunohistochemical analysis of the active, i.e. nuclear localized, molecule have been available so far, evidence for functional Snail protein expression in primary human tumours and tissues is missing. Until now, a direct cellular comparison between E-cadherin down-regulation and endogenous nuclear Snail expression at the protein level in cancer tissues has not been possible.

To analyse nuclear Snail immunoreactivity in human cancers, we established a monoclonal antibody (mAb) in rats against purified human Snail protein. The specificity of the antibody was demonstrated by Western blot, immunofluorescence and immunohistochemistry of cells and primary human tissues. Subsequently, we analysed a series of 340 adenocarcinomas from the upper gastrointestinal tract, i.e. primary carcinomas of the oesophagus, the gastric cardia and the stomach, arranged in tissue microarrays (TMA), for nuclear Snail expression. We compared Snail and a variety of histopathological and clinical parameters and found that Snail expression is significantly more frequent in oesophageal than in cardiac or gastric adenocarcinomas. In 7 out of 20 Snail-positive cases, the expression of Snail in tumour cells was associated with a concomitant loss of E-cadherin expression. No correlation was found between the expression of Snail and tumour grade, tumour stage and histological tumour type according to Lauren's and WHO classification.

Materials and methods

Cell lines

The following cell lines were used: MCF7 (mammary gland, breast epithelium), HTB-135 (stomach carcinoma) and GC2957 (stomach carcinoma). MCF7 and HTB-135 cells were cultured in Dulbecco's Modified Eagle's Medium (DMEM), 10% foetal calf serum (FCS) and 2.5 ml penicillin/streptomycin (#15140-122, Gibco; 10,000 units/ml penicillin G sodium/10,000 μg/ml streptomycin sulphate). The E-cadherin-positive cell line GC2957 was cultured in RPMI 1640 (#31870-025, Gibco), 20% FCS, 25 mM 4-(2-hydroxyethyl)-1-piperazineethanesulfonic acid (HEP ES) and 2.5 ml penicillin/streptomycin. MCF7 cells have been reported to express both E-cadherin and Snail [14]. HTB-135 cells are E-cadherin negative and Snail positive (E. Rosivatz, unpublished observation).

Cloning of human Snail cDNA

The cDNA coding for human Snail (SNAI1, OMIM 604238, RefSeq 005985) was amplified by reverse transcription-polymerase chain reaction (RT-PCR) from MDA-MB-435S human mammary carcinoma cells known to express Snail mRNA [3, 12]. Recently, evidence was provided that this cell line is of melanocytic origin [38]. The upstream (5′-CAT ATG CCG CGC TTT CCT CGT CAG G-3′) and downstream (5′-AAG CTT TGC GGG GAC ATC CTG AGC AG-3′) primers used for the amplification of a 802-bp sequence were designed to contain an *Nde*I site and a *Hin*dIII site, respectively. After gel purification of the amplification product, the Snail sequence was cloned using the *Nde*I and *Hin*dIII sites and standard methods into a modified expression vector, pHAT, in-frame with the so-called histidine affinity tag (HAT) sequence (BD Biosciences Clontech, Palo Alto, USA). The original pHAT vector was modified (Jörg Mages, Technical University Munich, Germany, unpublished data) to contain the His tag at the C terminus, instead of the N terminus, of the recombinant protein. The construct was sequenced to exclude sequence alterations that may have occurred during amplification. The recombinant vector, now termed pSnail1HAT, was expressed in bacteria, and the resultant His-tagged protein was purified from inclusion bodies using a talon metal resin (BD Biosciences Clontech) under denaturing conditions using 8 M urea. For the expression of recombinant His-tagged Snail in human tumour cell lines, full-length 6× His-tagged Snail from pSnail1HAT flanked by the *Xba*I/*Kpn*I restriction sites were ligated into the pBK-CMV vector (#212209, Stratagene; GenBank accession no. U37573).

Cell transfection

The day before transfection, 1×10^5 cells per well of a six-well plate were seeded in 2 ml of appropriate growth medium. Cells were grown to 70% confluency for approximately 24 h. For the preparation of solution A, 1 μg plasmid DNA was diluted in 100 μl Optimem (#31985, Invitrogen) for each transfection and mixed gently. For the preparation of solution B, 15 μl Lipofectamine (#18324-012, Invitrogen) reagent was diluted in 100 μl Optimem for each transfection and mixed. Solutions A and B were

combined, mixed gently and incubated at room temperature for 45 min to allow the formation of DNA–liposome complexes. For each transfection, 800 μl Optimem was added to the DNA–liposome complexes and gently mixed. Growth medium was aspirated from the cells, and the diluted transformation mix was added drop by drop. The cells were incubated with the complexes for 6 h at 37°C in a CO_2 incubator. Following incubation, 1 ml of growth medium (containing twice the normal concentration of serum) was added without removing the transfection mixture.

Twenty-four hours following the start of transfection, the medium was replaced with normal growth medium. An assay for transient gene expression was carried out 48 h after the start of transfection. Alternatively, 72 h after the start of transfection, cells were passaged 1:10 into a selective medium to achieve stable clones.

Quantitative real-time RT-PCR

RNA extraction from the cell lines, RT, quantitative real-time PCR and quantitation of Snail and E-cadherin mRNA expression were done as previously described [39] and were used here without modification. The primers and probes were designed to span an intron to exclude annealing to genomic DNA. Amplicon size was kept below 100 bp. Glyceraldehyde 3-phosphate dehydrogenase (GAPDH) was included as a housekeeping gene control to correct for equal RNA amounts. We then calculated relative amounts of mRNA by the standard curve method in relation to GAPDH levels. The TaqMan runs were done in triplicate and repeated in an independent experiment.

Western blot

For Western blot analysis using hybridoma supernatant Sn9H2 to detect Snail protein, extracts from the MCF7 and GC2957 cells, as well as extracts from fresh, frozen human placenta, were prepared using a 1:1 mixture of 2× sodium dodecyl sulfate (SDS) electrophoresis buffer (120 mM Tris pH 6.8, 4% SDS, 16% glycerol, 2% beta-mercaptoethanol) and tissue protein extraction reagent (T-PER, Pierce, Rockford, IL, USA). Twenty micrograms of total protein was used for SDS-polyacrylamide gel electrophoresis (PAGE). Protein detection was performed using a peroxidase-coupled secondary antibody (ECL-Western, Amersham, Germany).

Immunofluorescence analysis of HTB-135 gastric cancer cells

Cells were grown on glass cover slips for 24 h and subsequently rinsed briefly in phosphate-buffered saline (PBS). For cell fixation, cover slips were immersed in freshly prepared 3.7% para-formaldehyde for 30 min, followed by 3× washes in PBS. The cover slips were incubated in 0.25% Triton X-100/PBS for 5 min at room temperature for cell permeabilization and then placed cell-side up in a petri dish and covered with blocking buffer [1% bovine serum albumin (BSA) in PBS] for 30 min. After removing the blocking buffer, primary antibodies [Sn9H2, 1:10 in blocking buffer; anti-His-tag (#70796-3, Novagen), 1:500 in blocking buffer] were distributed on the cover slip and incubated at 4°C for 16 h (Sn9H2) or at room temperature for 2 h (anti-His-tag), followed by 3× washes with PBS. Secondary antibodies conjugated to a fluorochrome [anti-rat fluorescein isothiocyanate (FITC), #112-069-044, Jackson laboratories; anti-mouse tetramethyl rhodamine isothiocyanate (TRITC), #115-026-044, Jackson Laboratories] were distributed on the cover slips and incubated for 1 h at room temperature. Cover slips were washed 3× with PBS and inverted onto slides containing 10 μl of mounting medium from Antifade kit (#S-2828, MoBiTec GmbH, Germany). Excess mounting medium was removed, and the edges were sealed and dried before the analysis of immunofluorescence using a Zeiss Axiovert microscope.

Generation of a rat mAb, Sn9H2, against human Snail

Purified His-tagged human Snail protein (50 μg) was injected both intraperitoneally and subcutaneously into Lou/C rats using CPG2006 (TIB MOLBIOL, Berlin, Germany) as adjuvant. After an 8-week interval, a final boost was given intraperitoneally and subcutaneously 3 days before fusion. The fusion of the myeloma cell line P3X63–Ag8.653 with the rat immune spleen cells was performed essentially as described [28]. Hybridoma supernatants were tested in a solid-phase immunoassay using the His-tagged protein that was used for immunization (10 μg/ml) adsorbed to polystyrene microtiter plates. An irrelevant His-tagged protein served as a negative control. Bound rat mAbs were detected with a cocktail of biotinylated mouse mAbs against the rat immunoglobulin G (IgG) heavy chains [α-IgG1, α-IgG2a and α-IgG2b (ATCC, Manassas, VA, USA) and α-IgG2c (Ascenion, Munich, Germany)]. The biotinylated mAbs were visualized with peroxidase-labelled Avidin (Alexis, Grünberg, Germany) and *o*-phenylenediamine as chromogen in the peroxidase reaction. The clone designated Sn9H2 (rat IgG2) was stably subcloned and used for further analysis.

Immunohistochemical analysis

After standard pressure-cooker-based antigen retrieval with citric acid pretreatment, 2-μm sections were incubated in goat serum to block nonspecific reactivity. For the detection of Snail-specific immunoreactivity, the specimens were incubated with diluted Sn9H2 hybridoma supernatant (1:20 in 1% BSA in PBS) for 2 h at room temperature. Bound antibodies were detected using the avidin–biotin complex (ABC) peroxidase method (ABC Elite Kit, Vector, Burlingame, CA, USA). Final staining was developed with the Sigma FAST DAB peroxidase substrate kit (Sigma, Deisenhofen, Germany). Haemalaun was used for counterstaining. In addition, E-cadherin immunoreactivity was

detected using the mAbs HECD-1 (Alexis) or clone 34 (#C37020, Transduction Laboratories, Lexington, KT, USA), both of which are known to react with human E-cadherin and to work on archival material. Subsequently, adenocarcinomas from the upper gastrointestinal tract arranged in TMA (see below) were analysed in exactly the same way. For the analysis of cancer samples, non-tumourous epithelium was used as positive control for E-cadherin immunoreactivity. Sections of placenta tissue were used as positive control for Sn9H2.

Immunohistochemical analysis of upper gastrointestinal adenocarcinomas

The analysis was based on 266 patients with adenocarcinomas of the upper gastrointestinal tract who underwent surgical resection without prior radio- and/or chemotherapy between January 1983 and January 2003 at the University of Düsseldorf, Germany. Additionally, 101 patients with oesophageal adenocarcinomas who underwent resection without prior radio- and/or chemotherapy between January 1991 and January 2004 at the Technical University of Munich, Germany, were included. Of the patients, 292 (79.6%) were men. The age of the patients ranged between 29 and 90 years (median 63 years). Together, the series consisted of 158 oesophageal, 108 cardiac and 101 gastric adenocarcinomas. Differentiation between oesophageal and cardiac adenocarcinomas done by a senior pathologist (MS) based on a review of the original macroscopic pathologic descriptions of the operation specimens according to standard criteria [43]. Tumours that had their epicenters in the oesophagus were regarded as oesophageal in origin, and tumours that had their epicenters in the cardia were regarded as cardiac in origin. Staging was performed according to the current tumor, node and metastasis (TNM) classification [44]. Histological typing included Lauren's classification [29] and the current WHO classification for gastric carcinomas [22]. Grading was performed according to the current WHO classification. Signet-ring cell carcinomas and mucinous carcinomas were categorized as G3.

Accordingly, 116 tumours (31.6%) were in stage I, 105 in stage II (28.6%), 110 in stage III (30.0%) and 36 in stage IV (9.8%). According to Lauren's classification, 26 tumours (7.1%) belonged to the diffuse type, 274 (74.7%) to the intestinal type and 67 (18.3%) to the mixed type. According to the WHO classification, this series included 56 signet-ring cell carcinomas (15.3%), 4 papillary adenocarcinomas (1.1%), 7 mucinous adenocarcinomas (1.9%) and 300 tubular adenocarcinomas (81.7%). Twelve tumours were graded as G1 (3.3%), 131 as G2 (35.7%) and 224 as G3 (61.0%). Tumour size (largest diameter) ranged between 5 and 185 mm (median 50).

Construction of TMA

For each of the 367 adenocarcinomas, one paraffin block was selected, and representative, non-necrotic tumour areas were marked on Haemalaun–Eosin-stained slides from these blocks. Three tissue cylinders with a diameter of 0.6 mm per tumour were punched from these areas and brought into a recipient paraffin block using a tissue arraying instrument (Beecher Instruments, Silver Spring, MD). In the case of signet-ring cell carcinomas, six, instead of three, biopsies were sampled. A sample template designating the sample location by case number was created. Four-micrometer sections from the TMA were used for the subsequent immunohistochemical investigations.

The immunohistological evaluation of Snail expression in TMAs was performed by a senior pathologist (MS). A tumour was considered positive for Snail expression if, in at least one tumour, a sample nuclear expression of Snail was detectable. A positive immunoreactivity was confirmed using whole-tissue sections from the corresponding donor block.

Statistical analysis

The analysis of the expression of Snail and a variety of clinico-pathological parameters, such as tumour stage, nodal status, tumour grade, tumour size, tumour type (according to Lauren and WHO) and location of the primary tumour, was performed according to the chi-square exact test.

Results

To analyse Snail protein expression in human cell lines and tissues, and for the determination of intracellular localization, mAbs were produced in rats against a purified His-tagged human Snail protein. Hybridoma supernatants were tested in a solid-phase immunoassay against the specific protein. Hybridoma Sn9H2 of rat IgG2a subclass was selected for further analysis.

Antibody specificity

Hybridoma supernatant Sn9H2 detected a single protein band at approximately 32 kDa in the *Escherichia coli* inclusion body preparation that was used for protein purification and in the E-cadherin-negative gastric cancer cell line HTB-135 (Fig. 1a). A protein band of very similar molecular weight was seen using a mAb against the tag (anti-His) in the inclusion body preparation that is absent in the HTB-135 cell extract. After the transient transfection of human Snail cDNA fused to the histidine affinity tag sequence in HTB-135 gastric cancer cells, hybridoma supernatant Sn9H2, indirectly detected by an FITC-labelled secondary anti-rat antibody, reacted with a protein that is located in the cytoplasm and strongly in the nucleus (Fig. 1b). Using the anti-His antibody and a rhodamine-labelled secondary antibody, immunofluorescence was exclusively seen in the nucleus, suggesting that exogenously expressed His-tagged Snail is retained within the nucleus while endogenously expressed Snail is localized also in the cytoplasm.

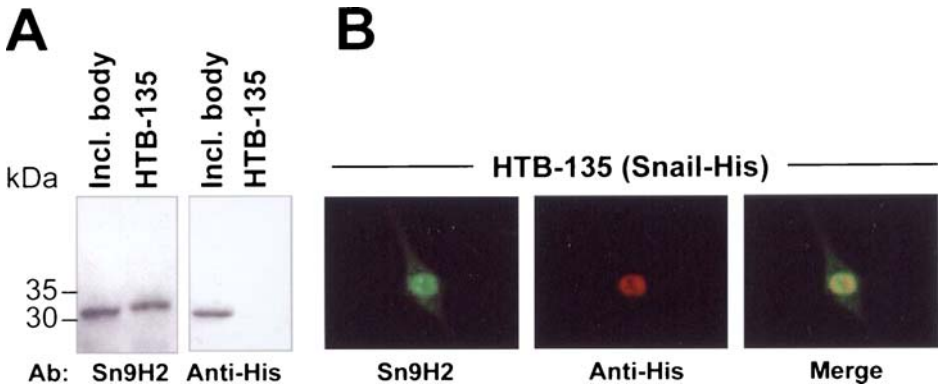

Fig. 1 Analysis of hybridoma supernatant Sn9H2. **a** Western blot. Inclusion body preparation from the transfected *E. coli* strain used to purify Snail protein and a lysate from an E-cadherin-negative gastric cancer cell line, HTB-135, were examined for Snail expression. Protein bands at approximately 32 kDa were observed in both lysates using hybridoma supernatant Sn9H2. An antibody against the His tag, anti-His, detected only a protein band in the *E. coli* lysate. **b** Intracellular localization of endogenously and exogenously expressed Snail. The distribution of Snail in Snail-His-transfected HTB-135 cells was observed by immunocytochemical staining with hybridoma supernatant Sn9H2 or anti-His antibody, followed by fluorescein isothiocyanate (FITC)-labelled or tetramethyl rhodamine isothiocyanate (TRITC)-labelled secondary antibodies, respectively. Immunofluorescence was visualized and captured with fluorescence microscopy. Endogenously expressed Snail was detected within the nucleus and the cytoplasm; exogenously expressed Snail was seen only in the nucleus

To prove a functional effect of Snail in E-cadherin-positive gastric cancer cells and to provide additional evidence for the specificity of the novel hybridoma supernatant Sn9H2, we analysed GC2957 gastric cancer cells. Using anti-Snail antibody Sn9H2, we were able to detect a band of about 32 kDa in GC2957 cells, suggesting the expression of low levels of endogenous Snail (Fig. 2a). Using real-time quantitative RT-PCR, we were able to detect only traces of Snail mRNA in GC2957 cells, whereas high levels of Snail mRNA were found in HTB-135

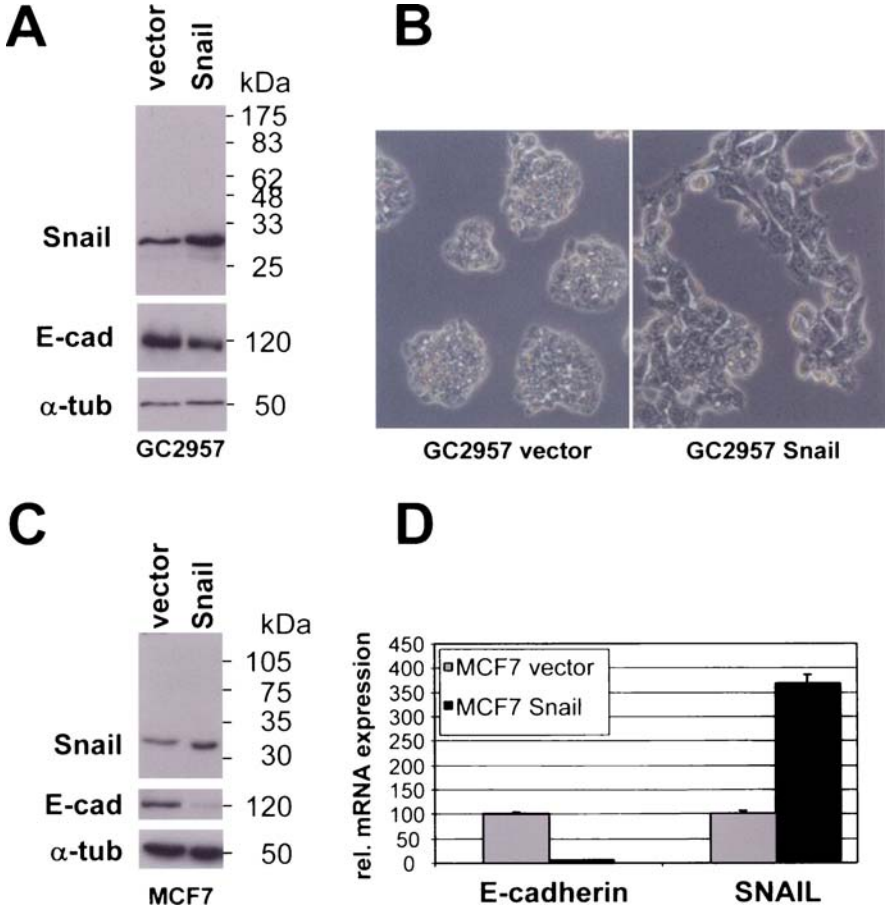

Fig. 2 Hybridoma supernatant Sn9H2 detects a functional Snail protein. E-cadherin-positive gastric cancer cells GC2957 (**a**, **b**) and MCF7 mammary cells (**c**, **d**) were transfected with vector as control or with Snail-His. **a** Western blot demonstrating the overexpression of Snail and the reduction of E-cadherin in the Snail-transfected cells. Alpha-tubulin was used as protein loading control. **b** Snail overexpression resulted in cell scattering. **c** Western blot showing the reduction of E-cadherin after Snail overexpression. No change is seen for alpha-tubulin. **d** Quantitative real-time RT-PCR demonstrates the reduction of E-cadherin expression by 95% after 3.7-fold Snail overexpression at the mRNA level. Results are representative of two independent transfection experiments done in triplicates and measured 48 h after transfection. The mRNA levels of vector-transfected cells are set to 100%; the mean ± standard deviation is shown

gastric cancer cells (data not shown). After the overexpression of Snail in GC2957 cells, the 32-kDa band increased in intensity, and E-cadherin levels were reduced. Alpha-tubulin expression was used to show equal protein loading. Despite low but detectable levels of Snail mRNA and protein, GC2957 cells formed cellular contacts and grew in epithelial-like structures. The overexpression of Snail, however, resulted in cell scattering (Fig. 2b).

After the transfection of another E-cadherin-positive cell line, MCF7 mammary cells, the 32-kDa band detected by hybridoma supernatant Sn9H2 became stronger, less E-cadherin protein was present, and levels for alpha-tubulin did not change significantly (Fig. 2c). Quantitative real-time RT-PCR demonstrated 95% reduced E-cadherin and 3.7-fold increased Snail mRNA levels upon transfection with the Snail cDNA (Fig. 2d).

These results indicate that the overexpression of a functional Snail protein resulting in E-cadherin down-regulation and cell scattering can be visualized using hybridoma supernatant Sn9H2.

Immunohistochemistry using human placenta as test system

After having rigorously demonstrated antibody specificity by Western blot and immunofluorescence, we tested if hybridoma supernatant Sn9H2 may react with formalin-fixed and paraffin-embedded tissues. As a test system, we used human placenta, as this tissue was reported to be Snail-mRNA-positive using Northern blot analysis [34]. Using Western blot analysis, we detected a protein band at about 32 kDa in extracts of human placenta, confirming Snail expression in this tissue on the protein level but without providing information about which cell types are Snail positive (Fig. 3a). In human placenta, two morphologically

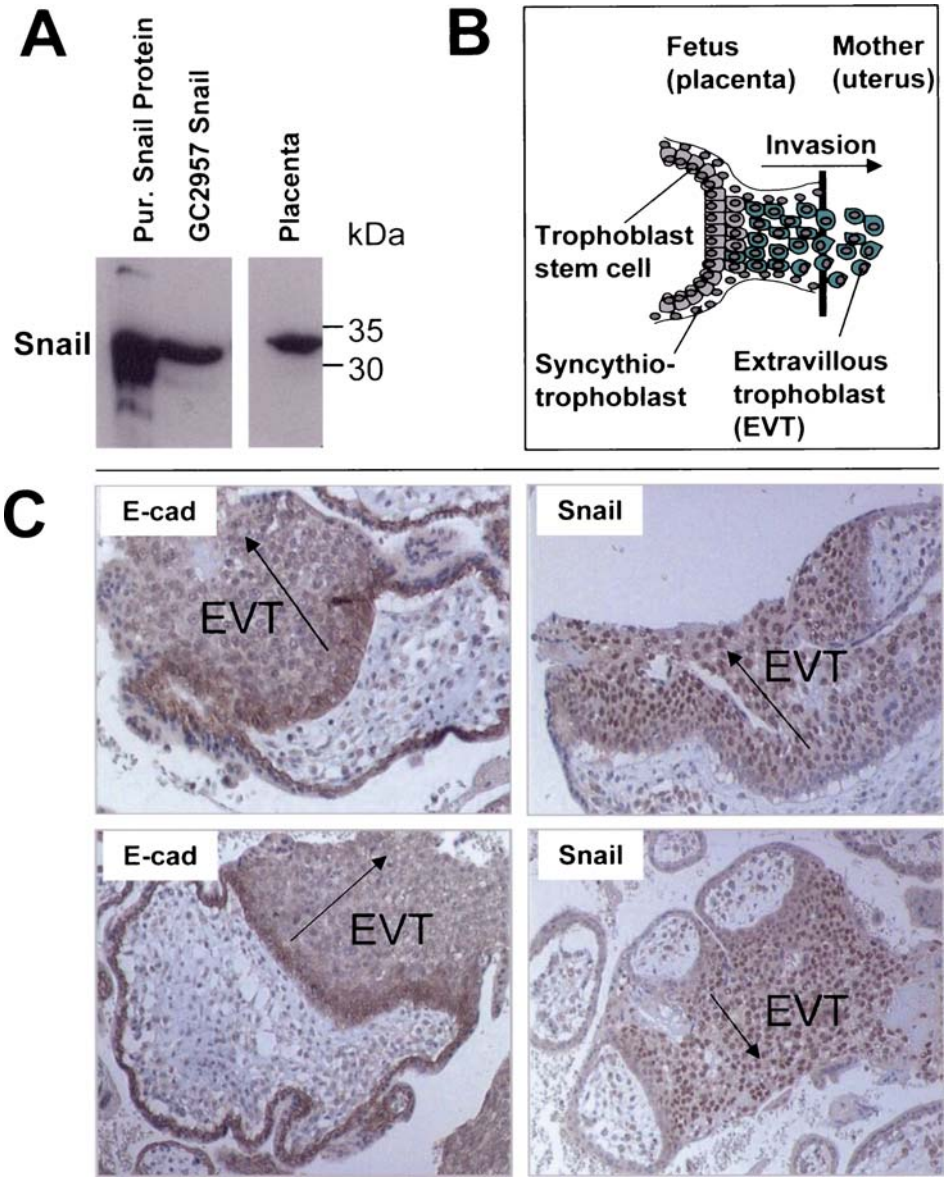

Fig. 3 Hybridoma supernatant Sn9H2 detects a nuclear protein in invasive trophoblasts in placenta. **a** Western blot showing Snail expression in placenta; the molecular weight is compared with the purified protein and Snail-transfected GC2957 gastric cancer cells. **b** Diagram of human placenta demonstrating the different cell types, e.g. non-invasive trophoblast stem cells and invasive EVT. **c** Immunoreactivity of Snail and E-cadherin in formalin-fixed and paraffin-embedded placenta. Nuclear Snail immunoreactivity is seen in invasive EVT; E-cadherin is localized at the cell membrane of trophoblast stem cells and reduced or absent in invasive EVT. (The *arrow* indicates the direction of invasion.)

distinct cell populations that differentiate from cytotrophoblast stem cells can be identified: (a) villous cytotrophoblasts are immotile cells that fuse to form a syncytium overlying the cytotrophoblast stem cells, and (b) extravillous cytotrophoblasts become invasive and invade the endometrium and, eventually, its arterial system. Thus, in placenta, both invasive (extravillous cytotrophoblasts) and non-invasive (cytotrophoblast stem cells) cells are present (Fig. 3b). These different cell types may be optimally suited for the determination of Snail immunoreactivity using formalin-fixed and paraffin-embedded archival material and, consequently, for the demonstration of the usefulness of hybridoma supernatant Sn9H2 for immunohistochemical analysis. As can be seen in Fig. 3c, hybridoma supernatant Sn9H2 exclusively reacts with invasive extravillous trophoblasts (EVT), while trophoblast stem cells are not stained. The immunoreactivity is clearly nuclear, a finding that is in line with Snail's function as a transcriptional repressor. In contrast, membranous E-cadherin immunoreactivity is seen preferentially in trophoblast stem cells; invasive trophoblasts only show a very faint reaction or they are E-cadherin negative. These very encouraging results enabled us to perform the first analysis for nuclear Snail immunoreactivity of a larger series of primary human carcinomas.

Analysis of nuclear Snail immunoreactivity in primary adenocarcinomas of the upper gastrointestinal tract

According to the immunohistochemical analyses based on TMAs, 27 tumours were considered positive for Snail expression while 313 were considered negative. Immunoreactivity for Snail in the tumour cells was found exclusively

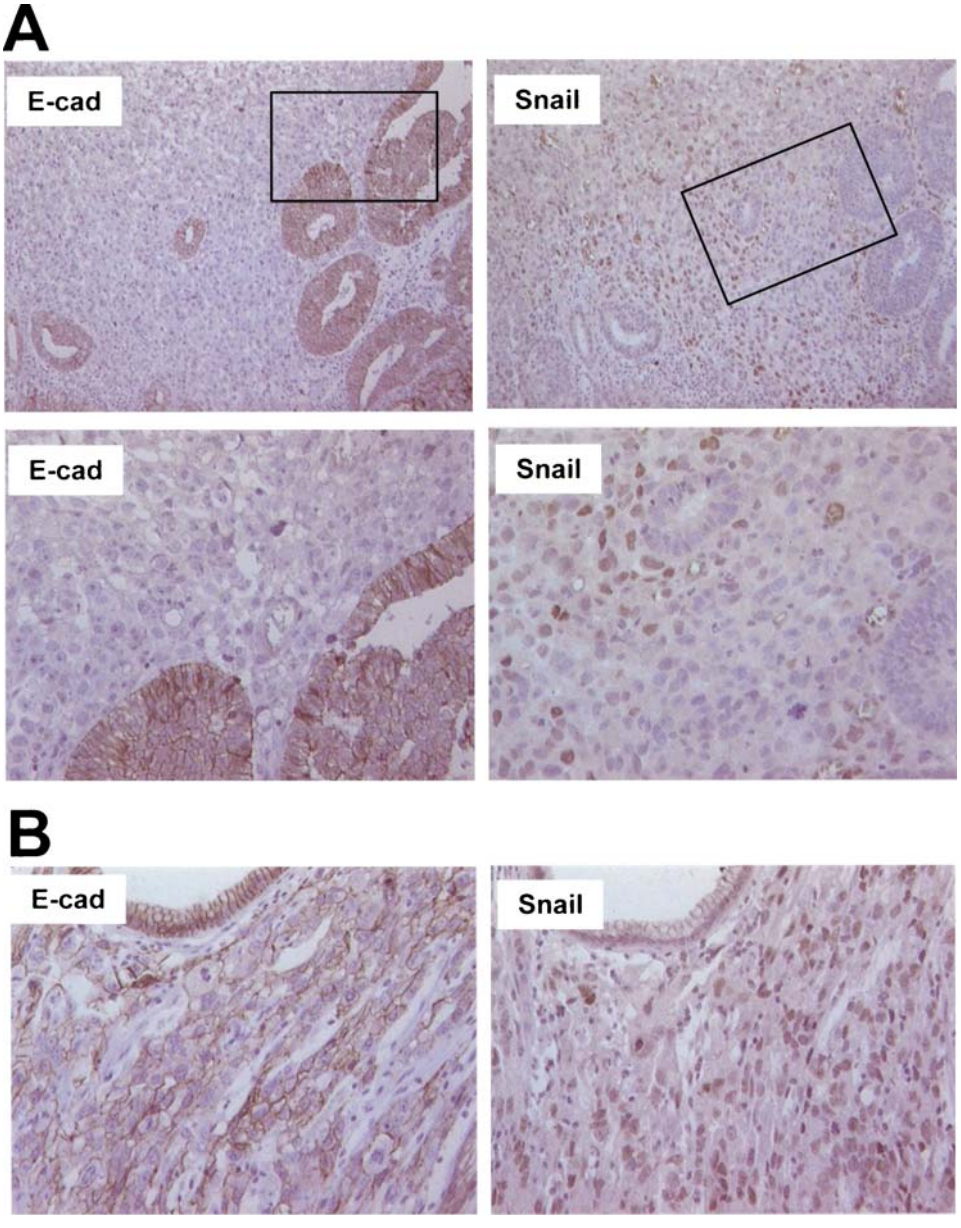

Fig. 4 Snail and E-cadherin immunoreactivity in cancers of the upper gastrointestinal tract. **a** This undifferentiated tumour shows an inverse correlation of Snail and E-cadherin expression. The *rectangles* indicate areas that are shown at higher magnification below the *upper panel*. *Upper panel*, ×100; *lower panel*, ×200. **b** Tumour cells in this tumour show coexpression of Snail and E-cadherin

Table 1 Correlation between the expression of snail in 340 adenocarcinomas of the upper gastrointestinal tract and various clinico-pathologic parameters

	Snail expression		*p* Value
	Negative (%)	Positive (%)	
Tumour differentiation			NS
G1/G2	123 (91.1)	12 (8.9)	
G3	190 (92.7)	15 (7.3)	
Lauren's classification			NS
Intestinal	240 (91.3)	23 (8.7)	
Diffuse	20 (90.9)	2 (9.1)	
Mixed	53 (96.4)	2 (3.6)	
WHO classification			NS
Adenocarcinoma (tubular, papillary, mucinous)	271 (91.6)	25 (8.4)	
Signet-ring cell carcinoma	42 (95.5)	2 (4.5)	
Tumour location			p=0.0428[a]
Oesophagus	137 (88.9)	17 (11.1)	
Cardia	95 (93.1)	7 (6.9)	
Stomach	81 (96.4)	3 (3.6)	
Stage			NS
I/II	182 (91.0)	18 (9.0)	
III/IV	131 (93.6)	9 (6.4)	
Tumour size			NS
≤5 cm	160 (93.0)	12 (7)	
>5 cm	151 (89.9)	17 (10.1)	

NS Not significant
[a]Chi square test. Oesophageal carcinomas vs cardiac and gastric carcinomas

nuclear. Twenty-seven cases had to be excluded from further analysis because either only non-cancerous tissue was present in all three punches or all tissue samples had been lost during immunohistochemical staining. Besides cancer cells, immunoreactivity for Snail was found consistently in a small subset of stromal cells (inside and outside of the tumours), i.e. fibroblasts and endothelial cells. This expression tended to be accentuated in areas of mucosal erosion or ulceration.

To validate immunohistochemical analyses based on TMAs, whole-tissue sections from the donor blocks of the 27 Snail-positive carcinomas were immunohistochemically stained for Snail. Analysis of whole-tissue sections confirmed Snail expression in all cases considered to be positive based on TMA analysis. Figure 4 shows examples of some of these cases. Immunohistochemical analysis of whole-tissue sections allowed the semiquantitative assessment of Snail expression. In 14 tumours, 5–25% of the tumour cells were Snail positive; in 4 tumours, 26–50% of the tumour cells were Snail positive; in 1 tumour, the percentage of Snail-positive tumour cells was 51–75%, and in 1 tumour, the percentage was 76–100%.

To analyse the correlation between the expression of Snail and E-cadherin, serial whole-tissue sections of only 20 Snail-positive carcinomas were also immunohistochemically stained for E-cadherin. Of these 20 Snail-positive carcinomas, only 7 showed a loss of E-cadherin expression in the tumour area where Snail expression was detectable (Fig. 4), indicating no clear correlation between Snail up-regulation and E-cadherin down-regulation.

Correlation of Snail expression and clinico-pathological parameters

The expression of Snail in adenocarcinomas from the upper gastrointestinal tract was not correlated with a variety of clinico-pathological parameters, such as tumour grade, Lauren's classification, WHO classification, tumour stage and tumour size (Table 1). However, the expression of Snail was significantly more frequent in oesophageal adenocarcinomas (11.1%) than in cardiac (6.9%) or in gastric (3.6%) carcinomas (p=0.0428).

Discussion

A hallmark in disease progression of epithelial cancers is the functional loss of the homophilic cell adhesion molecule E-cadherin, altering both the physical attachment of cells and the regulatory signals transmitted through cytoplasmic adapter molecules. Reduced or lack of E-cadherin immunoreactivity has been observed in many types of cancers and correlated with histopathological and clinical features, such as tumour dedifferentiation, invasive growth, lymph node metastasis and a worse patient prognosis [24]. The main mechanisms resulting in a loss of E-cadherin function include loss of heterozygosity (LOH) in combination with gene mutations [50], promoter hypermethylation [18, 31], enhanced degradation due to HAKAI, a c-Cbl-like protein [16], down-regulation by the RON tyrosine kinase [2], down-regulation by the transmembrane molecule dysadherin [26] and proteolytic degradation by matrix metalloproteases [30]. While E-cadherin gene mutations are found in diffuse-type gastric cancer [4, 5] and in invasive lobular breast cancer [6], they are rare in other cancers [7] and may not account for the majority of E-cadherin inactivations seen in human cancer tissues.

Recent reports highlighted the significance of EMT regulators that directly repress E-cadherin transcription. Several transcription factors, including the zinc finger transcription factor Snail [3, 12], the Snail-related molecule Slug [10, 21], Zeb2 (Sip1; [13]), Zeb1 [20] and E12/47 [35], may bind to E-box elements present in E-cadherin's promoter, resulting in transcriptional down-regulation. In various types of cancers and cell lines, the increased expression of Snail mRNA has been correlated with the loss of or reduced E-cadherin expression, although in several systems, a coexpression of Snail and E-cadherin was observed [14]. In the current study, we transfected two different cell lines with human Snail and found a concomitant reduction in E-cadherin levels, indicating the expression of a functional Snail molecule.

Most studies analysing Snail expression have been performed at the mRNA level, possibly because only a few commercial antibodies that react with human Snail protein

are available. Using an in-house-made polyclonal antibody against mouse Snail, Dominguez et al. [14] detected a doublet band in Western blot analysis (15% gel) at about 32 kDa in extracts from Snail-transfected HTB-29 and Madin-Darby canine kidney (MDCK) cells (80 μg of a cell extract per lane was used). They postulated a modification of the snail protein (phosphorylation) that may be responsible for the upper band seen in the blot and may regulate nuclear localization. We showed here that in E-cadherin-negative HTB-135 gastric cancer cells, endogenously expressed Snail seems to be localized in the nucleus and in the cytoplasm, whereas exogenously expressed Snail is seen exclusively in the nucleus. When we double our cell lysates from HTB-135 cells (40 μg total protein instead of 20 μg) and extend film exposure time (10 s instead of 5 s), a second smaller band is visible in Western blots (not shown). In extracts from human placenta, however, only one band is seen, migrating at the same position as the purified human protein and most likely corresponding to the "upper" band. In this tissue, Snail immunoreactivity appeared exclusively nuclear (Fig. 3).

When we used commercial anti-Snail antibodies used by others (e.g. [47, 48]), they did not work (data not shown). In addition, none of those could be applied for analysis of Snail nuclear immunoreactivity in archival human tissues so far. Therefore, we generated a rat mAb, termed Sn9H2, against human Snail that works excellently in Western blotting and can be used for immunohistochemical analysis of human tissue samples and, although not yet tested, possibly for immunoprecipitation and chromatin immunoprecipitation studies. The specificity of the antibody was demonstrated by Western blot analysis, immunofluorescence and immunohistochemical analysis of appropriate test systems, such as transfected cells in a culture expressing functional Snail and invasive trophoblasts from human placenta. With our new antibody, a direct correlation between E-cadherin repression and Snail neoexpression can now be analysed in cell lines and tissues, even after formalin fixation. In some cell lines, there is a coexpression of E-cadherin and Snail. A forced overexpression of Snail, however, resulted in the reduction of E-cadherin, suggesting some dosage effect. This may explain the failure to find a concomitant reduction of E-cadherin in every Snail-positive case (see "Results").

To start with an evaluation of Snail immunoreactivity in human cancers, we chose adenocarcinomas of the upper gastrointestinal tract, i.e. tumours that arise in the oesophagus, in the cardia or in the stomach. Today, it is generally accepted that the majority of carcinomas of the upper gastrointestinal tract develop through an accumulation of somatic genetic and epigenetic changes, such as point mutations and/or LOH in the *p53* gene, promoter methylation of $p16^{ink4A}$ and amplification and overexpression of cyclin D1, epidermal growth factor receptor (EGFR) and c-erbB-2. In addition, the expressions of E-cadherin and adenomatous polyposis coli (APC) were frequently found to be altered (for review, see [41]). We found Snail immunoreactivity in about 8% of the 340 cases analysed. No statistically significant correlation to the pathological and clinical data evaluated was seen. However, Snail immunoreactivity was more frequently detected in oesophageal cancers compared with cardia or gastric cancers, although only with marginal statistical significance. From the 154 analysed cases with oesophageal cancers, 17 (11%) were found to express Snail. In the gastric cancers analysed, only 4% Snail-positive tumours were detected. In a previous study, using quantitative real-time RT-PCR, we found Snail mRNA overexpression preferentially in diffuse-type gastric cancers [39]. However, analysing a much larger series of tumours, as was done in the current study, we did not find a statistical correlation between Snail immunoreactivity and Lauren's classification (diffuse vs intestinal).

Epithelial–mesenchymal transition mediated by Snail is considered to be a local event occurring at certain sites within an invasive tumour; EMT is typically seen at the invasion front [11]. Interestingly, Snail mRNA was not detected in a series of microdissected colon cancers in one study [40] but was reported to be overexpressed in another [33]. As mentioned in the "Results" section, some fibroblasts and endothelial cells showed Snail immunoreactivity. Even after careful tissue microdissection, it cannot be excluded that non-tumourous cells, such as fibroblasts or endothelial cells, are present in the tissue samples and may have contributed to the results of mRNA studies. Hybridoma Sn9H2 can now aid to solve some discrepancies that may have arisen in quantitative real-time RT-PCR analysis of primary tumours.

Using in situ hybridisation, Blanco et al. [9] found Snail mRNA expression in scarce fibroblastic cells present in stromal regions of breast cancers. In the same study, 9 out of 21 breast cancers expressed Snail mRNA, inversely correlating with the grade of differentiation of the tumours [9]. The authors concluded that Snail may be a marker of metastatic potential. While estrogen receptor signalling via metastasis associated gene 3 (MTA3) up-regulation was demonstrated to play a role in Snail inhibition in breast cancer [17], the mechanisms for Snail regulation in cancers of the upper gastrointestinal tract are currently unknown. Recently, the human Snail promoter was characterized, demonstrating an induction of Snail transcription by integrin linked kinase (ILK) and the oncogenes Ha-ras and v-Akt [1]. In addition, extracellular signal-regulated kinase (ERK) and NFkappaB/p65 also stimulated Snail transcription [1]. In an elegant paper, Zhou et al. [51] demonstrated a role for glycogen synthase kinase-3beta (GSK-3beta) in the regulation of Snail function. The authors found that GSK-3beta binds to and phosphorylates Snail at two consensus motifs to regulate both ubiquitination and subcellular localization. Nuclear immunoreactivity, however, indicative of active Snail was apparently not seen in 134 breast cancer samples analysed. Thus, our hybridoma Sn9H2, which, to our knowledge, is currently the only antibody that reacts with endogenous nuclear Snail, may be a valuable tool in determining the percentage of active Snail in archival human cancers. As soon as antibodies for other active E-cadherin repressors suitable for immunohistochemistry of archival human tissues are available, the relative contribution of each of these repressor molecules in

E-cadherin silencing can be analysed in defined sets of human tumours.

In conclusion, we generated a mAb against human Snail and showed nuclear expression in a subset of adenocarcinomas of the upper gastrointestinal tract. Snail's role in these tumours and mechanisms of its regulation, e.g. signalling pathways known to induce EMT, however, have to be established.

Acknowledgements We thank M. Blöchinger and M. Bekesch for excellent technical assistance, J. Mages for providing the modified pHAT vector, and R. Langer for help with some tissues. The E-cadherin-positive gastric cancer cell line GC2957 was kindly provided by R. Seruca, IPATIMUP-Porto. This work is supported by a grant from the Deutsche Krebshilfe (grant no. 10-2012-Be3) to KFB and HH.

References

1. Barbera MJ, Puig I, Dominguez D, Julien-Grille S, Guaita-Esteruelas S, Peiro S, Baulida J, Franci C, Dedhar S, Larue L, Garcia De Herreros A (2004) Regulation of Snail transcription during epithelial to mesenchymal transition of tumour cells. Oncogene 23:7345–7354
2. Bardella C, Costa B, Maggiora P, Patane' S, Olivero M, Ranzani GN, De Bortoli M, Comoglio PM, Di Renzo MF (2004) Truncated RON tyrosine kinase drives tumour cell progression and abrogates cell–cell adhesion through E-cadherin transcriptional repression. Cancer Res 64:5154–5161
3. Batlle E, Sancho E, Franci C, Dominguez D, Monfar M, Baulida J, Garcia De Herreros A (2000) The transcription factor Snail is a repressor of E-cadherin gene expression in epithelial tumour cells. Nat Cell Biol 2:84–89
4. Becker KF, Atkinson MJ, Reich U, Becker I, Nekarda H, Siewert JR, Hofler H (1994) E-cadherin gene mutations provide clues to diffuse type gastric carcinomas. Cancer Res 54:3845–3852
5. Becker KF, Kremmer E, Eulitz M, Becker I, Handschuh G, Schuhmacher C, Muller W, Gabbert HE, Ochiai A, Hirohashi S, Hofler H (1999) Analysis of E-cadherin in diffuse-type gastric cancer using a mutation-specific monoclonal antibody. Am J Pathol 155:1803–1809
6. Berx G, Cleton-Jansen AM, Strumane K, de Leeuw WJ, Nollet F, van Roy F, Cornelisse C (1996) E-cadherin is inactivated in a majority of invasive human lobular breast cancers by truncation mutations throughout its extracellular domain. Oncogene 13:1919–1925
7. Berx G, Becker KF, Hofler H, van Roy F (1998) Mutations of the human E-cadherin (CDH1) gene. Hum Mutat 12:226–237
8. Birchmeier W, Behrens J (1994) Cadherin expression in carcinomas: role in the formation of cell junctions and the prevention of invasiveness. Biochim Biophys Acta 1198:11–26
9. Blanco MJ, Moreno-Bueno G, Sarrio D, Locascio A, Cano A, Palacios J, Nieto MA (2002) Correlation of Snail expression with histological grade and lymph node status in breast carcinomas. Oncogene 21:3241–3246
10. Bolos V, Peinado H, Perez-Moreno MA, Fraga MF, Esteller M, Cano A (2003) The transcription factor slug represses E-cadherin expression and induces epithelial to mesenchymal transitions: a comparison with Snail and E47 repressors. J Cell Sci 116:499–511
11. Brabletz T, Jung A, Reu S, Porzner M, Hlubek F, Kunz-Schughart LA, Knuechel R, Kirchner T (2001) Variable beta-catenin expression in colorectal cancers indicates tumour progression driven by the tumour environment. Proc Natl Acad Sci U S A 98:10356–10361
12. Cano A, Perez-Moreno MA, Rodrigo I, Locascio A, Blanco MJ, del Barrio MG, Portillo F, Nieto MA (2000) The transcription factor Snail controls epithelial–mesenchymal transitions by repressing E-cadherin expression. Nat Cell Biol 2:76–83
13. Comijn J, Berx G, Vermassen P, Verschueren K, van Grunsven L, Bruyneel E, Mareel M, Huylebroeck D, van Roy F (2001) The two-handed E box binding zinc finger protein SIP1 downregulates E-cadherin and induces invasion. Mol Cell 7:1267–1278
14. Dominguez D, Montserrat-Sentis B, Virgos-Soler A, Guaita S, Grueso J, Porta M, Puig I, Baulida J, Franci C, Garcia de Herreros A (2003) Phosphorylation regulates the subcellular location and activity of the Snail transcriptional repressor. Mol Cell Biol 23:5078–5089
15. Frixen UH, Behrens J, Sachs M, Eberle G, Voss B, Warda A, Lochner D, Birchmeier W (1991) E-cadherin mediated cell–cell adhesion prevents invasiveness of human carcinoma cells. J Cell Biol 113:173–185
16. Fujita Y, Krause G, Scheffner M, Zechner D, Leddy HE, Behrens J, Sommer T, Birchmeier W (2002) Hakai, a c-Cbl-like protein, ubiquitinates and induces endocytosis of the E-cadherin complex. Nat Cell Biol 4:222–231
17. Fujita N, Jaye DL, Kajita M, Geigerman C, Moreno CS, Wade PA (2003) MTA3, a Mi-2/NuRD complex subunit, regulates an invasive growth pathway in breast cancer. Cell 113:207–219
18. Graff JR, Herman JG, Lapidus RG, Chopra H, Xu R, Jarrard DF, Isaacs WB, Pitha PM, Davidson NE, Baylin SB (1995) E-cadherin expression is silenced by DNA hypermethylation in human breast and prostate carcinomas. Cancer Res 55:5195–5199
19. Grau Y, Carteret C, Simpson P (1984) Mutations and chromosomal rearrangements affecting the expression of Snail, a gene involved in embryonic patterning in Drosophila melanogaster. Genetics 108:347–360
20. Guaita S, Puig I, Franci C, Garrido M, Dominguez D, Batlle E, Sancho E, Dedhar S, De Herreros AG, Baulida J (2002) Snail induction of epithelial to mesenchymal transition in tumour cells is accompanied by MUC1 repression and ZEB1 expression. J Biol Chem 277:39209–39216
21. Hajra KM, Chen DY, Fearon ER (2002) The SLUG zinc-finger protein represses E-cadherin in breast cancer. Cancer Res 62:1613–1618
22. Hamilton SR, Aaltonen LA (eds) (2000) World Health Organisation. Classification of tumours. Pathology and genetics of tumours of the digestive system. Lyon: IARC Press
23. Hay ED (1995) An overview of epithelio-mesenchymal transformation. Acta Anat (Basel) 154:8–20
24. Hirohashi S (1998) Inactivation of the E-cadherin-mediated cell adhesion system in human cancers. Am J Pathol 153:333–339
25. Ikenouchi J, Matsuda M, Furuse M, Tsukita S (2003) Regulation of tight junctions during the epithelium–mesenchyme transition: direct repression of the gene expression of claudins/occludin by Snail. J Cell Sci 116:1959–1967
26. Ino Y, Gotoh M, Sakamoto M, Tsukagoshi K, Hirohashi S (2002) Dysadherin, a cancer-associated cell membrane glycoprotein, down-regulates E-cadherin and promotes metastasis. Proc Natl Acad Sci U S A 99:365–370
27. Jiao W, Miyazaki K, Kitajima Y (2002) Inverse correlation between E-cadherin and Snail expression in hepatocellular carcinoma cell lines in vitro and in vivo. Br J Cancer 86:98–101
28. Kremmer E, Kranz BR, Hille A, Klein K, Eulitz M, Hoffmann-Fezer G, Feiden W, Herrmann K, Delecluse HJ, Delsol G, Bornkamm GW, Mueller-Lantzsch N, Grassert FA (1995) Rat monoclonal antibodies differentiating between the Epstein-Barr virus nuclear antigens 2A (EBNA2A) and 2B (EBNA2B). Virology 208:336–342
29. Lauren P (1965) The two histological main types of gastric carcinoma: diffuse and so-called intestinal-type carcinoma. Acta Pathol Microbiol Scand 64:31–49

30. Lochter A, Galosy S, Muschler J, Freedman N, Werb Z, Bissell MJ (1997) Matrix metalloproteinase stromelysin-1 triggers a cascade of molecular alterations that leads to stable epithelial-to-mesenchymal conversion and a premalignant phenotype in mammary epithelial cells. J Cell Biol 139:1861–1872
31. Machado JC, Oliveira C, Carvalho R, Soares P, Berx G, Caldas C, Seruca R, Carneiro F, Sobrinho Simoes M (2001) E-cadherin gene (CDH1) promoter methylation as the second hit in sporadic diffuse gastric carcinoma. Oncogene 20:1525–1528
32. Nieto MA (2002) The Snail superfamily of zinc-finger transcription factors. Nat Rev Mol Cell Biol 3:155–166
33. Palmer HG, Larriba MJ, Garcia JM, Ordonez-Moran P, Pena C, Peiro S, Puig I, Rodriguez R, De La Fuente R, Bernad A, Pollan M, Bonilla F, Gamallo C, De Herreros AG, Munoz A (2004) The transcription factor SNAIL represses vitamin D receptor expression and responsiveness in human colon cancer. Nat Med 10:917–919
34. Paznekas WA, Okajima K, Schertzer M, Wood S, Jabs EW (1999) Genomic organization, expression, and chromosome location of the human Snail gene (SNAI1) and a related processed pseudogene (SNAI1P). Genomics 62:42–49
35. Perez-Moreno MA, Locascio A, Rodrigo I, Dhondt G, Portillo F, Nieto MA, Cano A (2001) A new role for E12/E47 in the repression of E-cadherin expression and epithelial–mesenchymal transitions. J Biol Chem 276:27424–27431
36. Perez-Moreno M, Jamora C, Fuchs E (2003) Sticky business: orchestrating cellular signals at adherens junctions. Cell 112: 535–548
37. Poser I, Dominguez D, de Herreros AG, Varnai A, Buettner R, Bosserhoff AK (2001) Loss of E-cadherin expression in melanoma cells involves up-regulation of the transcriptional repressor Snail. J Biol Chem 276:24661–24666
38. Rae JM, Ramus SJ, Waltham M, Armes JE, Campbell IG, Clarke R, Barndt RJ, Johnson MD, Thompson EW (2004) Common origins of MDA-MB-435 cells from various sources with those shown to have melanoma properties. Clin Exp Metastasis 21:543–552
39. Rosivatz E, Becker I, Specht K, Fricke E, Luber B, Busch R, Hofler H, Becker KF (2002) Differential expression of the epithelial–mesenchymal transition regulators Snail, SIP1, and twist in gastric cancer. Am J Pathol 161:1881–1891
40. Rosivatz E, Becker I, Bamba M, Schott C, Diebold J, Mayr D, Hofler H, Becker KF (2004) Neoexpression of N-cadherin in E-cadherin positive colon cancers. Int J Cancer 111:711–719
41. Sarbia M, Becker KF, Hofler H (2004) Pathology of upper gastrointestinal malignancies. Semin Oncol 31:465–475
42. Shiozaki H, Tahara H, Oka H, Miyata M, Kobayashi K, Tamura S, Iihara K, Doki Y, Hirano S, Takeichi M (1991) Expression of immunoreactive E-cadherin adhesion molecules in human cancers. Am J Pathol 139:17–23
43. Siewert JR, Stein H (1998) Classification of adenocarcinoma of the esophago–gastric junction. Br J Cancer 85:1457–1459
44. Sobin LH, Wittekind Ch (eds) (2002) TNM classification of malignant tumours, 6th edn. Wiley, New York
45. Sugimachi K, Tanaka S, Kameyama T, Taguchi K, Aishima S, Shimada M, Sugimachi K, Tsuneyoshi M (2003) Transcriptional repressor Snail and progression of human hepatocellular carcinoma. Clin Cancer Res 9:2657–2664
46. Thiery JP (2002) Epithelial–mesenchymal transitions in tumour progression. Nat Rev Cancer 2:442–454
47. Timmerman LA, Grego-Bessa J, Raya A, Bertran E, Perez-Pomares JM, Diez J, Aranda S, Palomo S, McCormick F, Izpisua-Belmonte JC, de la Pompa JL (2004) Notch promotes epithelial–mesenchymal transition during cardiac development and oncogenic transformation. Genes Dev 18:99–115
48. Vega S, Morales AV, Ocana OH, Valdes F, Fabregat I, Nieto MA (2004) Snail blocks the cell cycle and confers resistance to cell death. Genes Dev 18:1131–1143
49. Vleminckx K, Vakaet L Jr, Mareel M, Fiers W, van Roy F (1991) Genetic manipulation of E-cadherin expression by epithelial tumour cells reveals an invasion suppressor role. Cell 66:107–119
50. Vos CB, Cleton-Jansen AM, Berx G, de Leeuw WJ, ter Haar NT, van Roy F, Cornelisse CJ, Peterse JL, van de Vijver MJ (1997) E-cadherin inactivation in lobular carcinoma in situ of the breast: an early event in tumourigenesis. Br J Cancer 76:1131–1133
51. Zhou BP, Deng J, Xia W, Xu J, Li YM, Gunduz M, Hung MC (2004) Dual regulation of Snail by GSK-3beta mediated phosphorylation in control of epithelial–mesenchymal transition. Nat Cell Biol 6:931–940

Virchows Arch (2006) 448: 288–294
DOI 10.1007/s00428-005-0117-x

ORIGINAL ARTICLE

Abbas Agaimy · Peter H. Wünsch

Sporadic Cajal cell hyperplasia is common in resection specimens for distal oesophageal carcinoma

A retrospective review of 77 consecutive surgical resection specimens

Received: 11 October 2005 / Accepted: 20 October 2005 / Published online: 25 November 2005

Abstract Interstitial cell of Cajal (ICC) hyperplasia has been documented in conditions associated with multiple gastrointestinal stromal tumours (GISTs) (familial GIST syndromes, Carney's triad and von Recklinghausen's disease) and rarely in the vicinity of sporadic GISTs. The incidence of sporadic ICC hyperplasia and the so-called seedling leiomyoma (SLM) of the lower oesophagus has not been studied in the KIT era. In a retrospective review of 77 consecutive, routinely processed oesophagogastric resection specimens for distal oesophageal carcinoma, we found foci of ICC hyperplasia in 7 of 77 (9.1%) cases and foci of SLM in 17 of 77 (22%) cases. Two types of ICC hyperplasia were recognized: a non-circumscribed type and a nodular expansile type with peripherally compressed myenteric neural tissues. All cases of ICC hyperplasia were vimentin^{+}/CD34^{+}/CD117^{+}. SLMs were desmin^{+}/vimentin^{-}/CD34^{-}/CD117^{-}, similar to smooth muscles of the gut wall. In a prospective study of 32 non-carcinomatous specimens from age-matched patients (mostly autopsy cases), we found SLMs in only one case, but we were unable to detect ICC hyperplasia in any of the cases. We concluded that sporadic KIT-positive spindle-cell hyperplasia and SLMs were unexpectedly common in distal oesophageal specimens harbouring carcinomas. The possible mechanisms leading to the development of these putative precursor lesions will be discussed.

Keywords ICC hyperplasia · GIST precursor · Seedling leiomyoma

A. Agaimy (✉) · P. H. Wünsch
Institute of Pathology, Klinikum Nürnberg,
Prof.-Ernst-Nathan-Strasse 1,
90419 Nürnberg, Germany
e-mail: abbas.agaimy@klinikum-nuernberg.de
Tel.: +49-911-3982533
Fax: +49-911-3982121
e-mail: wuensch@klinikum-nuernberg.de

Introduction

Gastrointestinal stromal tumours (GISTs) are the most common primary mesenchymal neoplasms of the tubular gastrointestinal (GI) tract [6, 21, 31]. GISTs arise predominantly in the stomach (60–70%), followed by the small intestine (20–25%), the colorectum (10%) [19, 21, 31] and the oesophagus (1–3%) [7, 18, 31]. Extragastrointestinal GISTs are vanishingly rare [26]. At our department, no case of primary oesophageal GIST was found among more than 200 GISTs (unpublished data). GISTs are KIT-signaling-driven neoplasms caused by gain-of-function mutations of *c-kit* or platelet-derived growth factor receptor alpha (*PDGFRA*) oncogenes leading to tumorigenesis through a ligand-independent activation of type III receptor tyrosine kinases [11–14, 17, 33]. Small (measuring less than 1 cm) incidental GISTs were found to harbour *c-kit* mutations [5]. Bland spindle-cell proliferations forming a diffuse band or minute nodules in the region of the myenteric plexus of Auerbach [also called interstitial cell of Cajal (ICC) hyperplasia] have been documented in rare cases of multiple familial GISTs caused by germline mutations of *c-kit* or *PDGFRA* genes [3, 8, 12], in a case of Carney's triad [25], in a case of congenital intestinal neuronal dysplasia [10], in von Recklinghausen's disease [2, 30, 32] and (extremely rare) in the vicinity of sporadic GISTs [15]. Diffuse ICC hyperplasia was found to be polyclonal in nature in one reported case [3]. Precursor lesions for sporadic GISTs have not been well characterized. We recently observed microscopic KIT-positive stromal nodules (ICC hyperplasia) in the vicinity of adenocarcinomas involving the lower oesophagus and the sigmoid colon (one case each) as collision tumours (unpublished data). To our knowledge, the incidence and clinicopathological features of ICC hyperplasia as putative precursor lesions for sporadic GISTs have not been studied in detail before. Seedling leiomyomas (SLMs) are minute (microscopic) lesions of smooth muscle tissues found incidentally in the muscularis propria of the lower oesophagus.

Table 1 Clinicopathological features of cases with ICC hyperplasia

Case number	Age and gender	Cancer type	Number	Size (mm)	Immunoprofile
1	66 ♀	SCC	1	0.4	Vimentin$^+$/CD117$^+$/CD34$^+$
2	69 ♂	BACA	1	0.4	Vimentin$^+$/CD117$^+$/CD34$^+$
3	60 ♂	SCC	1	0.6	Vimentin$^+$/CD117$^+$/CD34$^+$
4	73 ♂	SCC	1	1.0	Vimentin$^+$/CD117$^+$/CD34$^+$
5	75 ♀	SCC	1	1.0	Vimentin$^+$/CD117$^+$/CD34$^+$
6	61 ♂	BACA	1	1.0	Vimentin$^+$/CD117$^+$/CD34$^+$
7	61 ♂	BACA	1	1.0	Vimentin$^+$/CD117$^+$/CD34$^+$

SCC Squamous cell carcinoma, *BACA* Barrett's adenocarcinoma

Materials and methods

Seventy-seven non-selected oesophageal/oesophagogastric surgical resection specimens for carcinoma of the distal oesophagus or the oesophagogastric junction were retrieved retrospectively from surgical pathology files at the Institute of Pathology of Nuremberg's Clinic Centre. All hematoxylin and eosin (H&E)-stained slides were systematically reviewed by the first author, looking for the presence of minute spindle-cell lesions in the muscle coat on the oesophageal side of the specimen. At the same time, the presence of minute leiomyomatous nodules in the muscularis propria corresponding to so-called SLMs was recorded. If present, the number, size, location in the outer or inner muscle coat, shape, circumscription, cell type and relationship of the lesion to the myenteric plexus were recorded. Case selection was based on H&E-stained sections only. No serial sectioning or blind immunostaining for enhanced detection was performed. Immunohistochemistry was then performed on fresh-cut sections using the ABC-DAB method and the following primary antibodies: vimentin (1:50; Linaris), smooth muscle actin (1:200; Dako), desmin (1:250; Dako), h-caldesmon (1:125; Dako), CD117 (1:50; Dako), CD34 (1:200; Zytomed), S-100 (1:2,500; Dako), neurofilament (1:500; Dako), synaptophysin (1:500; Biogenics), bcl-2 (1:200; Dako) and Ki67 (MiB-1) (1:150; Dako). For validation of results, 32 additional specimens from age-matched patients without oesophageal or gastric cancer were collected (autopsy cases) and studied in a manner similar to that performed with six to eight tissue sections taken from the entire oesophagogastric junction.

Results

Four to 19 (mean, 8) H&E-stained sections were available in all cases. The study group included 63 men and 14 women (M:F, 4.5:1) aged 39–81 years (mean age, 62 years). Forty patients (52%) had squamous carcinoma, 35 (45%) had Barrett's carcinoma and 2 (1.3%) had neuroendocrine carcinoma and adenosquamous carcinoma (one each).

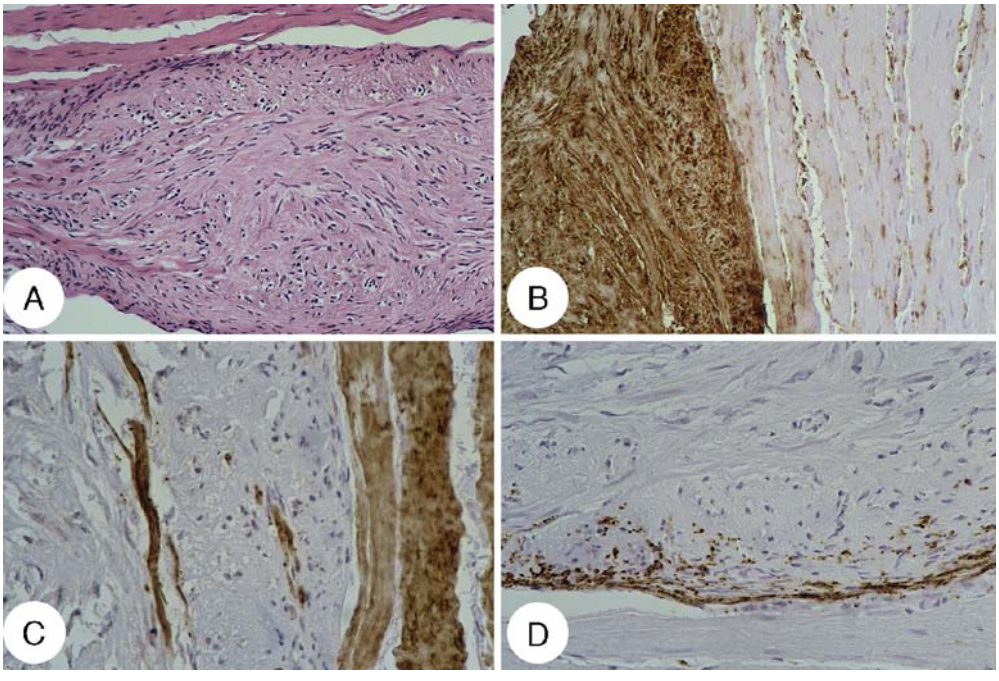

Fig. 1 Nodular-type ICC hyperplasia with typical cytomorphological features of spindle-type GIST (**a**); strong reactivity for CD34 in the same lesion (**b**); lack of reactivity for desmin (note strongly staining muscle fibres) (**c**); synaptophysin-reactive compressed neural cells at the periphery of the lesion (**d**)

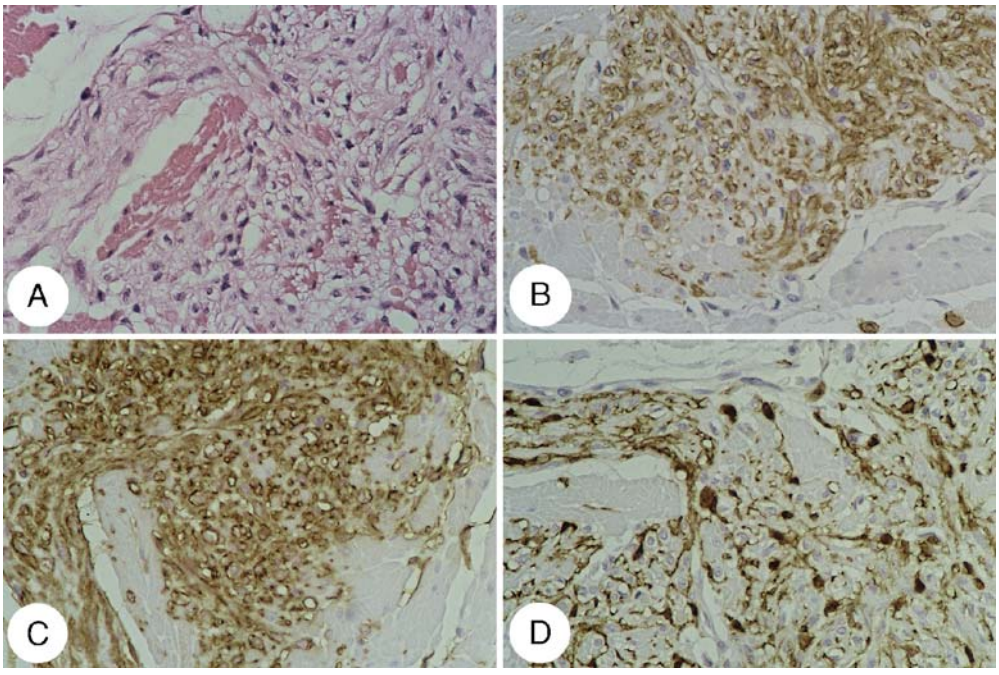

Fig. 2 Non-circumscribed ICC hyperplasia with short spindle cells infiltrating between smooth muscle fibres and along a small autonomic nerve at the left border of the field (**a**); strong reactivity for CD117 (**b**) and CD34 (**c**); coexpression of S-100 protein (**d**)

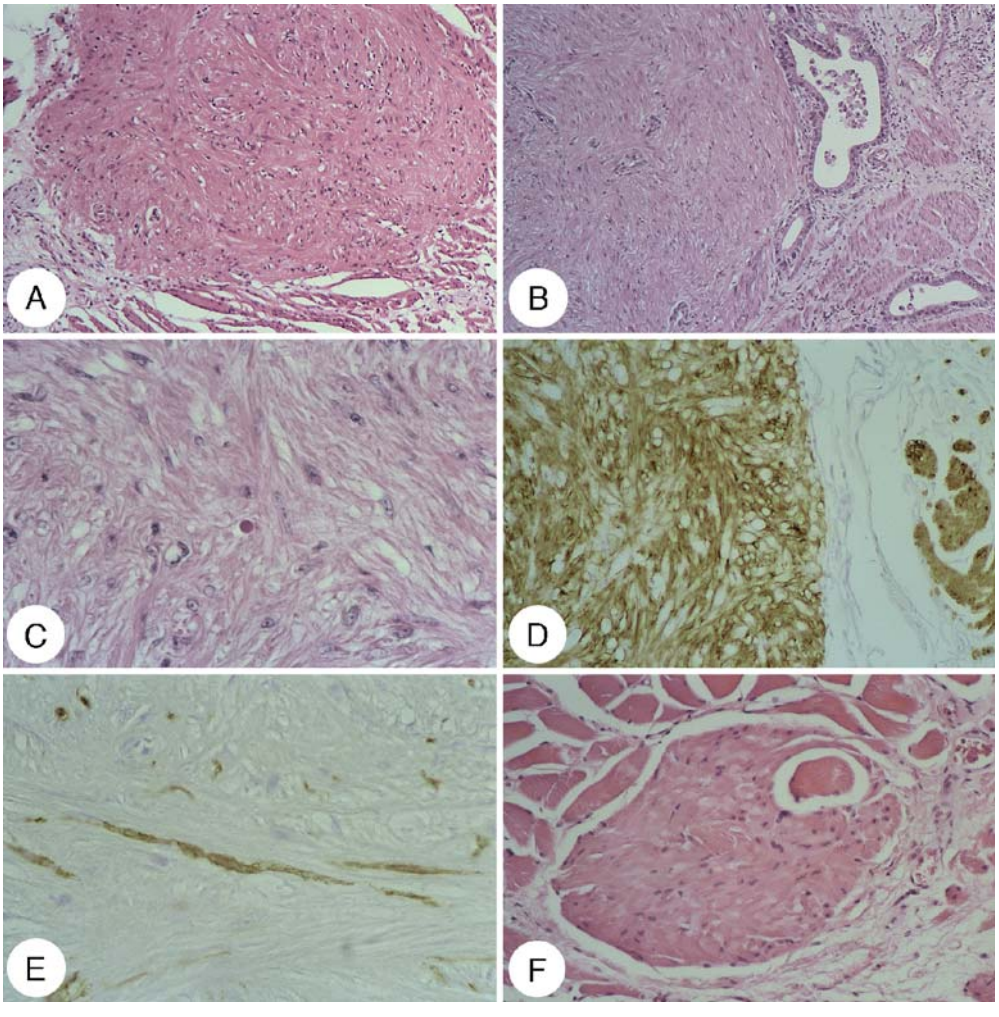

Fig. 3 SLM of the oesophagus showing nodular circumscription and striking similarity to surrounding original muscle tissues (**a**); perifocal adenocarcinomatous glands sparing the leiomyomatous nodule (**b**); brightly eosinophilic cytoplasm with characteristic hyaline globule (in the centre of the field) (**c**); strong desmin expression (*left*) similar to normal muscle tissue (*right*) (**d**); isolated CD117-reactive spindle cells, probably ICCs (**e**); nodular transformation of normal smooth muscle in the external coat of the middle and proximal oesophagus, mimicking SLM (**f**)

Table 2 Clinicopathological features of oesophageal SLMs

Case number	Age and gender	Cancer type	Number	Size (mm)	Location
1	75 ♂	SCC	1	0.4	INT
2	68 ♀	SCC	3	0.1–2	INT
3	61 ♂	SCC	2	0.5–12	INT
4	64 ♂	SCC	1	1	INT
5	50 ♂	SCC	2	2	INT
6	64 ♂	BACA	1	5	INT
7	66 ♀	SCC	1	0.5	IM
8	74 ♂	BACA	3	0.2	INT
9	66 ♂	SCC	1	1	INT
10	65 ♂	BACA	1	1	INT
11	62 ♂	BACA	7	0.1–5	IM
12	75 ♂	BACA	1	0.5	INT
13	39 ♂	BACA	1	1	INT
14	75 ♀	SCC	1	1	INT
15	67 ♂	BACA	1	1	INT
16	71 ♂	BACA	3	1	INT
17	61 ♂	BACA	6	1	INT

SCC Squamous cell carcinoma, *BACA* Barrett's adenocarcinoma, *INT* internal muscle layer, *IM* intermuscular region (plane of the plexus of Auerbach), ♂ male, ♀ female

ICC hyperplasia

Minute spindle-cell lesions with features of ICC hyperplasia at the H&E level were found in seven cases (9.1%). Clinicopathological and immunohistochemical features of the seven cases were summarized in Table 1. There were five men and two women (M:F, 2.5:1) aged 60–75 years (mean, 67 years). Associated cancers were squamous carcinoma in four cases and Barrett's carcinoma in three cases. The size of the lesion varied from 0.4 to 1.0 mm (mean size, 0.7 mm). All lesions were of the spindle-cell type and were located either in the external muscle coat (two cases), the internal layer (two cases) or in the intermuscular region abutting the myenteric plexus (three cases). Two of the lesions showed an expansile (nodular, circumscribed) pattern of growth—with cytomorphology similar to that of usual GISTs (Fig. 1a); with strong reactivity for vimentin, CD117 (not shown) and CD34 (Fig. 1b); but without expression of myogenic (Fig. 1c) or neurogenic markers (Fig. 1d). The remaining five lesions had irregular borders with enclosed muscle fibres between lesional cells (Fig. 2a) and had strong immunoreactivity for CD117 (Fig. 2b), CD34 (Fig. 2c) and S-100 (Fig. 2d). They were negative for synaptophysin, neurofilament, bcl-2, SMA, desmin and h-caldesmon (not shown). No mitoses or cellular atypia were seen in any of the lesions. Ki67 (MiB-1) decorated isolated lesional cells (not shown). Two non-circumscribed lesions with prominent S-100 reactivity were negative for neurofilament and synaptophysin, indicating true S-100 expression in lesional cells. Expansile lesions revealed compressed neural tissues at the periphery of the lesion that were reactive for S-100 (not shown) and synaptophysin (Fig. 1d).

Seedling leiomyomas

Seventeen cases (22%) harboured one or more well-differentiated smooth muscle micronodules with a bright eosinophilic fibrillary cytoplasm typical of smooth muscle cells (Fig. 3a–c). Patients included 14 men and 3 women (M:F, 4.7: 1) aged 39–75 years (mean age, 65 years). Associated cancers were eight cases of squamous carcinoma and nine cases of Barrett's carcinoma. All lesions (except two in the intermuscular region) were located in the inner (circular) muscle layer. In one case, a gastric-side SLM was found (in another case, a submucosal lipoma of the cardia was also found). In three cases, an initial gastric fundic GIST (ICC hyperplasia) was also seen (not shown). More than one SLM (two to six lesions) were found in seven cases (41%). The size of the lesions ranged from 0.1 to 5.0 mm, with one case having, in addition, a 12-mm-large intramural oesophageal leiomyoma that was submitted for frozen section. Immunohistochemically, all SLMs were identical to the gut wall musculature (muscularis mucosae and propria), which was strongly positive for smooth muscle actin, h-caldesmon and desmin (Fig. 3d), but was negative for vimentin, CD117, CD34 and S-100 protein. However, scattered CD117-immunoreactive spindle cells probably representing overrun ICCs were seen in most SLMs and were occasionally prominent (Fig. 3e). In the upper and middle oesophagus, where smooth and striated muscle fibres in the external layer were in close contact, smooth muscle fibres commonly showed a nodular configuration, thus simulating SLM (Fig. 3f).

Control cases

Specimens from 32 patients aged 49–86 years (mean age, 69 years) were extensively examined. All cases were negative for ICC hyperplasia. Only one case revealed five SLMs (<1 mm) in the internal muscle coat. Another case contained a 2-mm sclerosing minute spindle-cell GIST (ICC hyperplasia) on the gastric side of the specimen (fundus), and a third one (HIV-positive) had multiple extramural leiomyomas of the distal oesophagus measuring up to 3.0 cm.

Discussion

The most common primary mesenchymal neoplasms of the tubular GI tract [6, 19, 21, 31] are GISTs, followed by benign polypoid leiomyomas of the muscularis mucosae of the colon and rectum [20]. The vast majority of GISTs occur in the stomach and small intestine [19, 21, 31]. Colorectal GISTs are rare, comprising less than 10% [19, 21, 31]. GISTs primary in the oesophagus are exceptionally rare and are considered to represent less than 1–3% of GISTs [7, 18, 19, 31]. The reason for this striking variability in the incidence of GISTs among the different parts of the GI tract is unknown. Very rare cases of oesophageal GISTs have been reported to occur following irradiation

[23], or in association with HIV infection [24]. GISTs are thought to arise from, or differentiate along, ICCs [9, 15, 27, 29]. ICCs form a network around the myenteric plexus of Auerbach and between muscle fibres of the muscularis propria [28]. Most GISTs show an immunoprofile similar to that of ICCs (vimentin$^+$, CD117$^+$ and CD34$^+$). Abnormalities of the myenteric plexus with focal or diffuse proliferation of KIT-positive spindle cells (ICC hyperplasia) have been demonstrated in conditions known to predispose to multiple GISTs, as in cases of germline mutations of *c-kit* or *PDGFRA* [3, 8, 12], von Recklinghausen's disease [2, 30, 32] and Carney's triad [25]. The finding of ICC hyperplasia explains the development of multiple GISTs in such conditions, possibly because ICC hyperplasia represents a preneoplastic lesion. Diffuse ICC hyperplasia was found to be polyclonal in nature [3]. Precursor lesions for sporadic GISTs have not been well defined. The only two available studies dealing with putative mesenchymal precursor lesions in the stomach (so-called gastric microleiomyoma) have preceded the KIT era and therefore contained a mixture of both small GISTs and true microleiomyomas [22, 34]. Grossly recognizable, incidentally found GISTs measuring less than 1 cm were found to harbour *c-kit*-activating mutations and were considered to represent early GISTs [5]. Although diminutive lesions consisting of KIT-positive spindle cells have been rarely recognized in the vicinity of sporadic GISTs [15], there was no report describing in detail the clinicopathological features and the incidence of microscopic sporadic ICC hyperplasia. In the current study, we found ICC hyperplasia in 9.1% of routinely processed oesophageal resection specimens for carcinomas involving the lower third of the oesophagus, which is an unexpectedly high incidence, given that all cases have been routinely processed without extensive or systematic sectioning to enhance detection. No significant association with a specific cancer type (squamous carcinoma vs Barrett's carcinoma) or a previous irradiation was found. Similarly, we found a high incidence (22%) of minute leiomyomatous microlesions, the so-called SLMs, involving the internal muscularis propria of the lower oesophagus. It is well known that the incidence of microleiomyoma varies greatly, depending on the methodology used in a given study [34]. No case of SLM involving the outer muscle coat could be found. With the exception of a few cases of SLMs and two cases of ICC hyperplasia (featuring collision with the associated cancer), ICC hyperplasia and SLMs in this study involved tumour-free lamina muscularis propria surrounding carcinomatous tissues proximally or distally (mostly in sections submitted from the tumour). Given the relatively high incidence of these GIST tumourlets, in contrast to vanishingly rare clinical oesophageal GISTs, it seems very likely that these microscopic lesions mostly represent reactive, self-limiting lesions that probably do not harbour determinant genetic alterations to evolve into true neoplasms. The mechanisms and aetiopathogenetic factors behind the development of these unusual lesions in this peculiar microanatomical region of the GI tract and their association with carcinomas remain unknown. A synchronous occurrence of GISTs and other types of cancer in the GI tract, either at the same site or involving different parts, is well documented in the literature [1, 16]. Possible explanations for the association of ICC hyperplasia with cancer could be that either: (1) a field effect by a specific carcinogen acts on two different tissue types, initiating histogenetically different neoplasms/lesions (ICC hyperplasia and carcinoma); or (2) the second lesion (ICC hyperplasia) could be induced by growth factors or specific mitogens produced by neighbouring carcinoma and released in the surrounding interstitial microenvironment; and/or (3) a yet unidentified motility-related mechanism caused by the coexisting cancer or its initiating factors may act on and stimulate the proliferative dynamic of ICCs to initiate such reactive (hyperplastic) lesions. The fourth possibility—that ICC hyperplasia represents a mere incidental finding—is disputed by the relatively high incidence in carcinoma specimens and its rarity or virtual absence in our autopsy series, but this must be confirmed in further studies investigating a large number of cases. The significant temporal difference between the two lesions (well-developed carcinoma vs initial mesenchymal proliferation) argues against the first hypothesis (cogenesis), as it is expected that both lesions would be at comparable clinical stages if they had been initiated by the same causal agent or cofactor. If ICC hyperplasia could be induced by locally acting growth factors or mitogens produced by the associated cancer, it is convenient to expect similar lesions in the vicinity of carcinomas in the remainder of the GI tract, especially in the large intestine where carcinomas are more common, but ICC hyperplasia in the large bowel is exceedingly rare (unpublished data). Among hundreds of colonic resection specimens, most of them containing carcinomas, we observed minute GISTs (ICC hyperplasia) in only three cases—all of them in the sigmoid colon and with only one lesion associated with carcinoma (unpublished data). Accordingly, it is likely that ICC hyperplasia is initiated by more than one causal factor; some of them may be site-dependent. Experimental studies have demonstrated that certain carcinogens used to induce gastric carcinoma in rats have also induced gastric leiomyosarcoma, but only after the addition of other specific cofactors such as aspirin and stress [4]. Furthermore, microanatomical peculiarities of the oesophagogastric junction and its involvement in a specialized motoric function due to the presence of sphincteric structures and the unique presence of the oblique muscle layer in the post-sphincteric region of the gastric fundus may be involved in some way in the very early initiation or promotion of these probably reactive mesenchymal proliferations. Actually, the presence of the oblique muscle layer in the stomach has been suggested as a possible cofactor in the pathogenesis of the so-called microleiomyoma [22, 34].

The relatively high incidence of ICC hyperplasia in the distal oesophagus correlates with an even higher one for gastric fundic ICC hyperplasia (unpublished data). However, in contrast to a high incidence of sporadic gastric ICC hyperplasia that parallels the high incidence of GISTs in the stomach, oesophageal ICC hyperplasia is probably only rarely preneoplastic, given the very rare occurrence of oesophageal GISTs. The striking variance in the incidence of both clinical GISTs and their presumable precursor

lesions (ICC hyperplasia) in different parts of the GI tract may indicate great heterogeneity in the commitment of ICCs and the presence of diverse subpopulations of ICCs possessing greatly varying proliferative and neoplastic potentials. Future studies may contribute to our understanding of the pathogenetic mechanisms involved in the initiation and development of sporadic ICC hyperplasia in this part of the GI tract and their relationship to clinical GISTs.

In our study, considering the mean age of 35 years for patients with clinical oesophageal leiomyomas [18] compared to the mean age of 65 years for those with SLMs, it seems unlikely that SLMs are regular precursor lesions for clinical leiomyomas. In this study, we found only one case with both SLM and clinical leiomyoma at the same site. The exclusive occurrence of SLMs in the internal muscle coat is in accordance with a reactive process that is possibly related to disturbed motility functions and other cofactors. The fate of oesophageal ICC hyperplastic lesions and SLMs is unknown. Rare lesions (ICC hyperplasia) may evolve into true neoplasms through acquisition of additional genetic alterations. Gastric ICC hyperplasia evolves mostly through a course of extensive hyalinization with dystrophic calcification, and only a minority of them may transform into true GISTs, either of the spindle-cell type or the epithelioid-cell type (unpublished data).

The histopathological differential diagnosis of ICC hyperplasia in our study included neuroma-like neural hyperplasia and hypertrophic nerve fibres related to neoadjuvant radiotherapy, focally cellular stromal desmoplasia with prominent myofibroblasts and focal spindling of squamous carcinoma. SLMs are readily recognizable, as they show features of well-differentiated smooth muscle cells similar to normal muscle tissues of the gut wall and they will not be mistaken for ICC hyperplasia if one is familiar with them. However, in the middle and upper oesophagus, where both smooth muscle and striated muscle cells are intimately associated in the outer muscle coat, the smooth muscle component usually takes a somewhat nodular configuration and should be distinguished from SLMs. Furthermore, SLMs are almost exclusive to the internal muscle coat, and their occurrence in the outer layer should be questioned.

In summary, we reported the occurrence of sporadic ICC hyperplasia in 9.1%—and SLMs in 22%—of routinely processed distal oesophageal resection specimens harbouring carcinomas. This high incidence is in favour of a reactive self-limiting process. SLMs are probably unrelated to most clinical leiomyomas of the oesophagus. However, a subset of ICC hyperplasias may represent facultative precursor lesions for sporadic GISTs in a hyperplasia–neoplasia sequence. Further studies are needed to elucidate the molecular–genetic profile (and hence the biological significance) of these microlesions, their initiating mechanisms and their possible role in very early events in tumourigenesis of sporadic GISTs and leiomyomas.

References

1. Agaimy A, Wuensch PH (2005) Gastrointestinal stromal tumours in patients with other-type cancer: a mere co-incidence or an etiological association? A study of 97 GIST cases. Z Gastroenterol 43:1025–1030
2. Andersson J, Sihto H, Meis-Kindblom JM, Joensuu H, Nupponen N, Kindblom L-G (2005) NF1-associated gastrointestinal stromal tumors have unique clinical, phenotypic, and genotypic characteristics. Am J Surg Pathol 29:1170–1176
3. Chen H, Hirota S, Isozaki K, Sun H, Ohashi A, Kinoshita K, O'Brien P, Kapusta L, Dardick I, Obayashi T, Okasaki T, Shinomura Y, Matsuzawa Y, Kitamura Y (2002) Polyclonal nature of diffuse proliferation of interstitial cells of Cajal in patients with familial and multiple gastrointestinal stromal tumours. Gut 51:793–796
4. Cohen A, Geller SA, Horowitz I, Toth LS, Werther JL (1984) Experimental models for gastric leiomyosarcoma. The effects of *N*-methyl-*N*′-nitro-*N*-nitrosoguanidine in combination with stress, aspirin, or sodium taurocholate. Cancer 53:1088–1092
5. Corless CL, McGreevey L, Haley A, Town A, Heinrich MC (2002) KIT mutations are common in incidental gastrointestinal stromal tumors one centimeter or less in size. Am J Pathol 160:1567–1572
6. Fletcher CDM, Berman JJ, Corless C, Gorstein F, Lasota J, Longley B, Miettinen M, Oleary T, Remotti H, Rubin BP, Shmookler B, Sobin LH, Weiss SW (2002) Diagnosis of gastrointestinal stromal tumors: a consensus approach. Hum Pathol 33:459–465
7. Gouveia AM, Pimenta AP, Lopes JM, Copelinha AF, Ferreira SS, Valbuena C, Oliveira MC (2005) Esophageal GIST: therapeutic implications of an uncommon presentation of a rare tumor. Dis Esophagus 18:70–73
8. Handra-Luca A, Flejou J-F, Molas G, Sauvanet A, Belghiti J, Degott C, Terris B (2001) Familial multiple gastrointestinal stromal tumours with associated abnormalities of the myenteric plexus layer and skeinoid fibres. Histopathology 39:359–363
9. Herrera GA, Pinto de Moraes H, Grizzle WE (1984) Malignant small bowel neoplasm of enteric plexus derivation (plexosarcoma). Dig Dis Sci 29:275–284
10. Jeng Y-M, Mao T-L, Hsu W-M, Huang S-F, Hsu HC (2000) Congenital interstitial cell of Cajal hyperplasia with neuronal intestinal dysplasia. Am J Surg Pathol 24:1568–1572
11. Hirota S, Isozaki K, Moriyama Y et al (1998) Gain-of-function mutations of *c-kit* in human gastrointestinal stromal tumors. Science 279:577–580
12. Hirota S, Okazaki T, Kitamura Y et al (2000) Cause of familial and multiple gastrointestinal autonomic tumor with hyperplasia of interstitial cells of Cajal is germline mutation of the *c-kit* gene. Am J Surg Pathol 24:326–327
13. Hirota S (2001) Gastrointestinal stromal tumors: their origin and cause. Int J Clin Oncol 6:1–5
14. Hirota S, Ohashi A, Nishida T, Isozaki K, Kinoshita K, Shinomura Y, Kitamura Y (2003) Gain-of-function mutations of platelet-derived growth factor receptor α gene in gastrointestinal stromal tumors. Gastroenterology 125:660–667
15. Kindblom L-G, Remotti HE, Aldenborg F et al (1998) Gastrointestinal pacemaker cell tumor (GIPACT): gastrointestinal stromal tumors show phenotypic characteristics of the interstitial cells of Cajal. Am J Pathol 152:1259–1269
16. Maioranna A, Fante R, Maria Cesinaro A, Adriana Fano R (2000) Synchronous occurrence of epithelial and stromal tumors in the stomach: a report of 6 cases. Arch Pathol Lab Med 124:682–686
17. Medeiros F, Corless CL, Duensing A, Hornick JL, Oliveira AM, Heinrich MC, Fletcher JA, Fletcher CDM (2004) KIT-negative gastrointestinal stromal tumors. Proof of concept and therapeutic implications. Am J Surg Pathol 28:889–894

18. Miettinen M, Sarlomo-Rikala M, Sobin LH, Lasota J (2000) Esophageal stromal tumors. A clinicopathologic, immunohistochemical and molecular genetic study of 17 cases and comparison with esophageal leiomyomas and leiomyosarcomas. Am J Surg Pathol 24:211–222
19. Miettinen M, Lasota J (2001) Gastrointestinal stromal tumors—definition, clinical, histological, immunohistochemical and molecular genetic features and differential diagnosis. Virchows Arch 438:1–12
20. Miettinen M, Sarlomo-Rikala M, Sobin LH (2001) Mesenchymal tumors of the muscularis mucosae of the colon and rectum are benign leiomyomas that should be separated from gastrointestinal stromal tumors—a clinicopathologic and immunohistochemical study of eighty eight cases. Mod Pathol 14:950–956
21. Miettinen M, Lasota J (2003) Gastrointestinal stromal tumors (GISTs): definition, occurrence, pathology, differential diagnosis and molecular genetics. Pol J Pathol 54:3–24
22. Mikami T, Terada T, Nakamura K, Okayasu I (1997) The gastric hypercellular microleiomyoma as a precursor lesion for clinical gastrointestinal stromal tumors. Hum Pathol 28:1355–1360
23. Miller PR, Jackson SL, Pineau BC, Levine EA (2000) Radiation-induced gastrointestinal stromal sarcoma of the esophagus. Ann Thorac Surg 70:660–662
24. Padula A, Chin NW, Azeez S, Resetkova E, Andriko JA, Miettinen M (2005) Primary gastrointestinal stromal tumor of the esophagus in an HIV-positive patient. Ann Diagn Pathol 9:49–53
25. Perez-Atayde AR, Shamberger RC, Kozakewich HW (1993) Neuroectodermal differentiation of the gastrointestinal tumors in the Carney triad. Am J Surg Pathol 17:706–714
26. Reith JD, Goldblum JR, Lyles RH, Weiss SW (2000) Extragastrointestinal (soft tissue) stromal tumors: an analysis of 48 cases with emphasis on histologic predictors of outcome. Mod Pathol 13:577–585
27. Robinson TL, Sircar K, Hewlett BR, Chorneyko K, Riddell RH, Huizinga JD (2000) Gastrointestinal stromal tumors may originate from a subset of CD34-positive interstitial cells of Cajal. Am J Pathol 156:1157–1163
28. Rumessen JJ, Thuneberg L (1991) Interstitial cells of Cajal in human small intestine. Ultrastructural identification and organisation between the main smooth muscle layers. Gastroenterology 100:1417–1431
29. Sircar K, Hewlett BR, Huizinga JD, Chorneyko K, Berezin I, Riddell RH (1999) Interstitial cells of Cajal as precursors of gastrointestinal stromal tumors. Am J Surg Pathol 23:377–389
30. Takazawa Y, Sakurai S, Sakuma Y et al (2005) Gastrointestinal stromal tumors in neurofibromatosis type I (von Recklinghausen's disease). Am J Surg Pathol 29:755–763
31. Tran T, Davila JA, El-Serag HB (2005) The epidemiology of malignant gastrointestinal stromal tumors: an analysis of 1,458 cases from 1992 to 2000. Am J Gastroenterol 100:162–168
32. Walsh NM, Bodurtha A (1990) Auerbach's myenteric plexus. A possible site of origin for gastrointestinal stromal tumors in von Recklinghausen's neurofibromatosis. Arch Pathol Lab Med 114:522–525
33. Wardelmann E, Hrychyk A, Merkelbach-Bruse S, Pauls K, Goldstein J, Hohenberger P, Losen I, Manegold C, Buttner R, Pietsch T (2004) Association of platelet-derived growth factor receptor alpha mutations with gastric primary site and epithelioid or mixed cell morphology in gastrointestinal stromal tumors. J Mol Diagn 6:197–204
34. Yamada Y, Kato Y, Yanagisawa A, Sugano H (1988) Microleiomyoma of human stomach. Hum Pathol 19:569–572

Virchows Arch (2006) 448: 295–300
DOI 10.1007/s00428-005-0105-1

ORIGINAL ARTICLE

Kukka Heiskala · Jill Giles-Komar · Marja Heiskala · Leif C. Andersson

High expression of RELP (Reg IV) in neoplastic goblet cells of appendiceal mucinous cystadenoma and pseudomyxoma peritonei

Received: 9 August 2005 / Accepted: 26 September 2005 / Published online: 2 December 2005

Abstract The regenerating protein (Reg)-like protein (RELP, also known as Reg IV) is a recently characterized fourth member of the human Reg protein family. The Reg proteins are small, about 20-kD-sized, secretory proteins of C-lectin type. The previously known Reg proteins have been functionally implicated in regeneration, proliferation, and differentiation of the pancreas, liver, and gastrointestinal mucosa. To study the tissue expression of RELP, we raised a monoclonal antibody to RELP. By immunohistochemistry and in situ hybridization, we found a robust de novo expression of RELP in the neoplastic goblet cells of appendiceal mucinous cystadenomas and in the epithelial implants of pseudomyxoma peritonei (PMP). Our findings indicate that RELP serves as a marker for appendiceal mucinous cystadenomas and PMP, and that RELP may contribute to the pathogenesis of these disorders.

Keywords Pseudomyxoma peritonei · RELP (Reg IV) · Reg proteins · CDX2 · Intestinal mucin

K. Heiskala · L. C. Andersson (✉)
Department of Pathology,
Haartman Institute University of Helsinki
P.O. Box 21 (Haartmaninkatu 3),
FIN-00014 Helsinki, Finland
e-mail: Leif.Andersson@helsinki.fi
Tel.: +358-9-19126510
Fax: +358-9-19126675

K. Heiskala · L. C. Andersson
HUSLAB, Division of Pathology,
Helsinki, Finland

J. Giles-Komar
Centocor, Inc.,
Malvern, PA, USA

M. Heiskala
Cell Therapeutics, Inc.
Seattle, WA, USA

Abbreviations RELP: Reg-like protein · Reg: regenerating · PMP: pseudomyxoma peritonei · EIA: enzyme immunoassay

Introduction

Pseudomyxoma peritonei (PMP) is a rare disorder characterized by progressive accumulation of viscous, mucinous ascites in the peritoneal cavity. The gelatinous ascites is produced by disseminated implants of mucinous epithelium on the peritoneal surfaces and omentum. The incidence of PMP is two times as high in women as in men. Therefore, there has been some controversy about the role of ovarian mucinous neoplasms as a potential origin of PMP. Recent immunohistochemical and molecular genetic studies indicate, however, that a dissemination of epithelium from mucinous cystadenomas of the appendix is a common cause of PMP in women. The occurrence of synchronous ovarian mucinous tumors in PMP can, in most instances, be regarded as implants of mucinous epithelium of appendiceal derivation (for review, see: [3, 7]). In rare cases, as recently described by Ronnett and Seidman [13], ovarian teratomas containing elements of mucinous appendiceal epithelium may give rise to PMP. The appendiceal origin is further supported by the high expression of the intestinal mucin MUC2 and the intestinal-specific homeobox gene CDX2 in PMP [10, 16].

The mucinous change in appendix or mucinous cystadenoma, previously called mucocele, is histologically characterized by extensive mucosal replacement of abundant mucin-producing goblet cells. Despite a usually well-differentiated morphology, cytogenetic studies have revealed monoclonal loss of heterozygoity, indicating the true neoplastic nature of appediceal mucinous cystadenomas [3, 7].

The regenerating (Reg) proteins belong to a group of calcium-dependent, c-type lectins. The 17 Reg proteins of various mammalian species recognized so far are small (about 20 kD) secreted proteins of four superfamilies, now called Regs I–IV. The Reg proteins have been functionally implicated as growth factors and antiapoptotic “survival

factors" for pancreatic islets and neural cells, as acute phase reactants modifying inflammation, and as regeneration factors stimulating mucosal repair of the gastrointestinal tract.

The genes for the three previously known human Reg proteins (Reg I–III, also called Reg1a or Lithostatin A, Lithostatin B, and pancreatitis-associated protein) are clustered in tandem on chromosome 2p12 (reviewed in [18]). Hartupee et al. [2] and Kämäräinen et al. [4] independently identified, cloned, and characterized a fourth member of the human Reg family called Reg IV or Reg-like protein (RELP). The gene for RELP has a different chromosomal location on p12–13, and encodes a secreted protein of 158 amino acids that shows about 45% similarity with the Reg I–III proteins [4].

In situ hybridization revealed a restricted expression of RELP in the neuro-endocrine cells of normal intestinal epithelium. By immunohistochemical staining of RELP with rabbit antibodies, we demonstrated a coexpression of RELP and chromogranin A in selected cells in the crypt epithelium of small intestinal mucosa [4]. A strongly up-regulated expression of RELP was found in the goblet cells in areas of intestinal metaplasia in the gastric mucosa and in Barrett's esophagus [4]. Hartupee et al. [2] reported an accumulation of Reg IV message in colon mucosa from patients with inflammatory bowel diseases. We used immunohistochemistry and found a strong expression of RELP protein in the goblet cells of inflamed intestinal mucosa in Crohn's disease and in ulcerative colitis [4].

In situ hybridization has revealed up-regulated expressions of RELP message in colorectal adenomas and colorectal cancer [15, 19]. Oue et al. [11] recently performed a serial analysis of gene expression on samples from primary gastric cancers and found that RELP was one of the most prominently up-regulated genes in the schirrous type of gastric cancer [11].

Taken together, previous findings indicate that the up-regulated expression of RELP associates with preneoplastic and neoplastic changes in the gastrointestinal mucosa. Given our previous observations on the accumulation of RELP in metaplastic goblet cells in the gastric mucosa, we asked whether RELP is also expressed in the neoplastic goblet cells of appendiceal mucinous cystadenomas and PMP. Here we report the expression of RELP in appendiceal mucinous cystadenomas and in PMP in relation to other intestinal marker proteins.

Materials and methods

Formalin fixed and paraffin-embedded specimens were collected from the archives of the Department of Pathology, Haartman Institute, University of Helsinki. All patients were of Finnish, Caucasian origin. The PMP samples conformed to the classification of Ronnett et al. [12] of disseminated peritoneal adenomucinosis type. Cases representing peritoneal mucinous carcinosis with or without intermediate/discordant features were not included. The data are summarized in Table 1.

Monoclonal antibodies to RELP

Monoclonal antibodies to RELP have not been reported previously. The RELP coding complementary DNA (cDNA) sequence was amplified by polymerase chain reaction (PCR) and cloned into an expression vector by replacing human immunoglobulin G1 (IgG1) variable region sequence with RELP coding sequence. The human IgG1 heavy chain secretion signal and the N-terminal amino acids of the variable region, glutamine (Gln)-isoleucine (Ile)-glutamine (Gln), are retained on the recombinant protein. Human IgG1 hinge, calponin homology 2 (CH2), and CH3 domains are C-terminal to the RELP coding sequence. SP2/0 myeloma cells were transfected by electroporation with the RELP plasmid, and clonal cell lines that stably secrete the protein were isolated. The recombinant RELP protein was purified by protein A column chromatography.

Mice were immunized with 50 μg of RELP/Fc protein mixed with adjuvant until IgG titers of 1:50,000 were achieved. Three days prior to fusion the mice were injected with 10 mg of RELP in phosphate buffered saline (PBS), administered intravenously. The splenocytes were harvested and fused at a 1:1 ratio with FO murine myeloma cells with a polyethylene glycol 3,000 solution. To assess hybridoma supernatant activity, solid phase enzyme immunoassays (EIA) were performed. RELP/Fc protein or a control Fc construct were coated overnight on to 96-well EIA plates. After washing, the wells were then blocked with 1% bovine serum albumin in PBS. Undiluted supernatants from the growth-positive hybridomas were incubated on both Fc protein coated plates and then probed with horseradish peroxidase (HRP)-labeled goat antimouse IgG Fc-specific antibody. HRP substrate solution was added, and the absorbance was measured at 490 nm by an automated plate spectrophotometer. Only clones specifically reactive to RELP/Fc and not to the negative-control Fc protein were expanded in tissue culture and subcloned. Monoclonal supernatants were purified using protein A.

Mouse monoclonal antibodies to the human mucins-MUC2, mucin 5 subtypes A and C (MUC5AC), and MUC6 were obtained from Novocastra Laboratories Ltd (Newcastle upon Tyne, UK). Monoclonal anti-CDX2 antibody was obtained from BioGenex (San Ramon, CA). Secondary antibody, HRP-conjucated Rabbit antimouse immunoglobulin (IgG), was obtained from Dako (Glostrup, Denmark).

Immunohistochemistry

Four-μm sections from formalin-fixed, paraffin-embedded tissues were mounted on 3-aminopropyl-triethoxysilane-coated slides (Sigma), deparaffinized, and heated twice for 5 min in a microwave oven (650 W) before exposure to the

Table 1 Patient data and summary of the staining results

Appendix						
Patient number	Sex/age	RELP	CDX2	MUC2	MUC5	MUC6
Normal						
1	F20	+	2+	+	−	−
2	M28	+	3+	+	−	−
Normal/adenoma						
3	F58	+/3+	3+/2+	+/2+	−/2+	−/+
4	F61	+/3+	2+/2+	+/2+	−/2+	−/+
5	F68	+/3+	3+/2+	+/2+	+/2+	−/+
6	M59	+/3+	2+/2+	+/2+	−/2+	−/−
Adenoma						
7	F49	2+	2+	3+	2+	+
8	F50	3+	3+	3+	3+	−
9	F55	3+	2+	3+	2+	+
10	M49	3+	2+	2+	+	−
11	M53	2+	2+	2+	+	−
12	M91	3+	+	3+	3+	−
Pseudomyxoma peritonei						
13	F50	2+	2+	2+	3+	−
14	F52	3+	2+	3+	3+	−
15	F55	2+	2+	3+	2+	−
16	F72	+	2+	2+	2+	−
17	F77	2+	2+	3+	2+	−
18	F78	2+	2+	2+	2+	−
19	M39	2+	2+	3+	2+	−
20	M38	+	2+	3+	3+	−
21	M69	+	2+	3+	2+	−

Appendixes of patient numbers 1 and 2 are normal appendixes. Normal/adenoma (numbers 3–6) are cases where the proximal part of appendix was morphologically normal while the distal portion contained mucinous adenoma. Sections from both parts were mounted and stained on the same slide. Adenoma (numbers 7–12) are appendixes with only mucinous adenoma. PMP (numbers 13–21) are sections of epithelial implants from pseudomyxoma peritonei. Number 14 represents implants from number 8, and number 15 represents implants from number 7
MUC5 MUC5AC

first antibody (monoclonal mouse anti-RELP antibody, dilution 1:500). EliteKit (Vectastain, Vector Laboratories, Burlingame, CA) was used for immunoperoxidase staining, visualized with 3-amino-9-ethylcarbazole (Sigma).

In situ hybridization

We prepared probes by using the TA cloning kit (Invitrogen, San Diego, CA) ligating a polymerase chain reaction-amplified 0.4-kilobase RELP cDNA insert into the pCR-II vector (Invitrogen). The templates for RELP antisense or sense RNA probes were generated by linearizing the appropriate vector construct (3′ to 5′, or 5′ to 3′, respectively). The RNA Labeling Kit of Boehringer–Mannheim (Mannheim, Germany) was used according to the manufacturer's instructions to generate digoxigenin-labeled RNA probes by in vitro transcription.

Treatment of sections for in situ hybridization

Tissue sections were deparaffinized as before and specially prepared for in situ hybridization. Prior to hybridization, the sections were treated with 0.3% triton X-100 and then with 10 mg/ml proteinase K for 15 min at 37°C. The sections were then postfixed with 4% paraformaldehyde for 5 min. After acetylation of the section [2×5 min with triethylamine buffer containing 0.25% acetic anhydride (v/v)], they were incubated with a prehybridization buffer [4× sodium chloride–sodium citrate (SSC) containing 50% deionized formamide] for 15 min at 37°C.

The prehybridization buffer was drained and sections were overlaid with hybridization buffer (Sigma, St. Louis, MI) containing 10 ng of digoxigenin-labeled RNA probe. Sections were covered with plastic coverslips and incubated in a humid chamber at 42°C overnight.

After hybridization, the coverslips were removed and the sections were washed at 37°C twice in 2× SSC for 15 min each then twice with 1× SSC for another 15 min each. Unbound RNA probe was digested with a NaCl–Tris HCl–ethylenediaminetetraacetic acid buffer containing 20 μg/ml of ribonuclease A at 37°C; the sections were washed twice with 0.1× SSC for 30 min each. The labeled probe was detected using the digoxigenin nucleic acid detection kit (Roche, Germany) according to the manufacturer's instructions.

Results

Staining of sections from normal appendix with monoclonal antibody to RELP revealed exclusive expression in scattered cells in the crypt epithelium (Fig. 1b). We have earlier shown that the cells strongly expressing RELP in normal intestinal mucosa codistribute with cells expressing chromogranin A as a marker of neuro-endocrine differen-

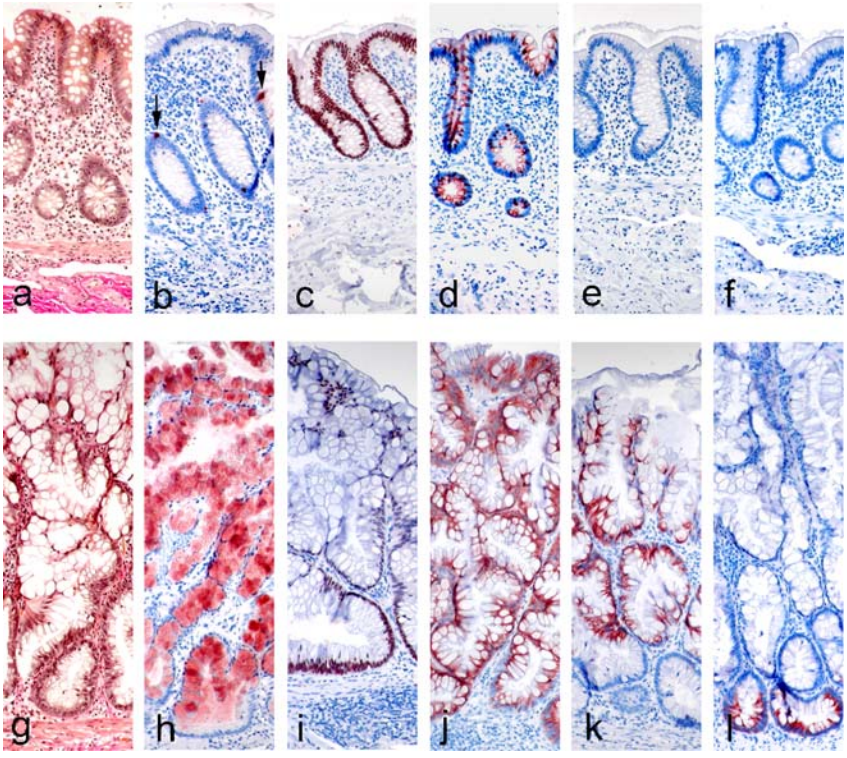

Fig. 1 Sections from proximal appendix with normal mucosa (case number 5 in Table 1) (**a**–**f**), and from mucinous cystadenoma in the distal end of the same appendix (**g**–**l**), stained with van Gieson trichrome stain (**a** and **g**) and immunohistochemically with antibodies to RELP (**b**, *arrow heads*, and **h**), CDX2 (**c** and **i**), MUC2 (**d** and **j**), MUC5AC (**e** and **k**), and MUC6 (**f** and **l**). Original magnification ×100

tiation [4]. The nuclei of the normal appendiceal epithelium stained strongly for CDX2. Normal goblet cells stained for MUC2 but not for RELP. The MUC2 staining was confined to the perinuclear region and along the cellular membrane (Fig. 1d). A weak staining for MUC5AC was seen locally in a morphologically normal mucosa in one case, while expression of MUC6 was not evident in the sections from normal appendix (Fig. 1e,f).

A strong expression of RELP was seen throughout in the mucin-containing goblet cells of appendiceal mucinous cystadenomas (Fig. 1h). Higher magnifications revealed a slightly granular staining of the goblet content for RELP. The nuclei of the adenomatous mucosa stained for CDX2. MUC2 was also strongly expressed in all cells of the adenomatous epithelium (Fig. 1j). The intracellular staining for MUC2 was mainly seen in the perinuclear, basal, and lateral portions of the goblet cells, and hence, did not fully co-distribute with the staining for RELP.

In contrast to the normal appendiceal mucosa, the adenomatous epithelium stained strongly for MUC5AC. The antibodies to MUC5AC decorated the goblet cells of the upper, luminal portion of the adenomatous mucosa, while the deepest glands did not contain the antibodies to MUC5AC (Fig. 1k). Staining for MUC6 was restricted to the basal, MUC5AC-negative glands in five out of six adenomas that came from women. The epithelium of the basal glands in three appendiceal cystadenomas from male patients did not stain for MUC6 (Fig. 1, Table 1). Immunohistochemical staining of epithelial implants from PMP also revealed a strong expression of RELP in the mucin-producing cells (Fig. 2b). The staining pattern was virtually identical to that seen in the epithelium of appendiceal mucinous cystadenoma. As reported earlier by O'Connell et al. [10], the epithelial cells of PMP stained throughout for MUC2. As in appendiceal mucinous cystadenomas, the intracellular distribution of MUC2 appeared mainly at the

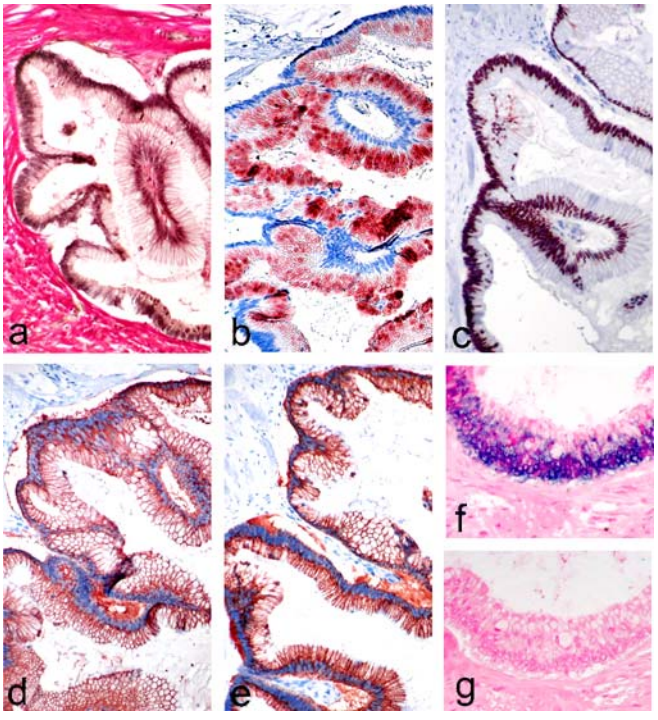

Fig. 2 Sections of epithelial implants of PMP stained with van Gieson's trichrome stain (**a**) and immunohistochemically with antibodies to RELP (**b**), CDX2 (**c**), MUC2 (**d**), and MUC5AC (**e**). Original magnification ×100. In situ hybridization of PMP epithelium with antisense RELP probe (**f**) and with control, sense probe (**g**). Original magnification ×200

perinuclear and baso-lateral areas of the goblet cells (Fig. 2c,d). The PMP epithelium also stained for MUC5AC (Fig. 2e), while no staining was seen for MUC6 in the nine cases of PMP investigated in this study (Table 1).

To confirm the local production of RELP in the PMP epithelium, in situ hybridization was carried out with antisense and sense RNA probes to RELP. As shown in Fig. 2f, a strong signal indicating accumulation of RELP messenger RNA was seen in PMP epithelium, while no signal was obtained from consecutive sections using the sense (control) probe.

Discussion

We have employed a novel monoclonal antibody and in situ hybridization to demonstrate a strong expression of RELP in the neoplastic goblet cells of appendiceal cystadenoma and epithelial implants of PMP. However, it appears unlikely that the robust expression of RELP is a consequence of neoplastic transformation because we have previously reported a strong staining for RELP in non-neoplastic, reactive mucosal goblet cells in inflammatory bowel diseases and in metaplastic goblet cells. Goblet cells of normal intact intestinal mucosa did not express RELP at levels discernible by immunohistochemistry or by in situ hybridization [4]. RELP and MUC5AC displayed a similar expression profile, albeit with a different intracellular distribution. Therefore, convergent mechanisms appear to regulate the de novo acquisition of goblet cell phenotype and activation of expression of the RELP and MUC5AC genes. The molecular details of these events, however, are still poorly understood.

Yamamoto et al. [16] recently provided experimental data to show that the homeodomain protein CDX2 acts as a transcriptional activator to regulate the expression of MUC2 in transfected COS-7 cells. Moreover, Mutoh et al. [8] generated transgenic (TG) mice in which ectopic expression of CDX2 was targeted to the gastric mucosa under the promoter of the noncatalytic subunit of the rat H+/K+-adenosine triphosphatase gene. They found that the TG mice developed a progressive loss of parietal cells and eventually showed intestinal metaplasia of the entire gastric mucosa. The same authors recently reported a progress from intestinal metaplasia to adenomatous polyps and to invasive gastric cancer in the same TG mice with targeted gastric overexpression of CDX2 [9]. However, it seems unlikely that CDX2 alone regulates the transcription of the RELP gene in appendiceal mucinous adenomas and PMP, because a strong nuclear staining for CDX2 is seen in normal intestinal epithelium, including normal goblet cells, which lack RELP expression.

RELP is abundantly present in normal intestinal neuroendocrine cells. Therefore, we performed immunohistochemistry of appendiceal carcinoid tumors and found expression of RELP in solid and, in particular, in goblet cell variants of the tumor (manuscript in preparation). Interestingly, appendiceal carcinoid tumors show a similar female preponderance as mucinous adenomas and PMP do [13]. Given the expression of RELP in both tumors, it is tempting to speculate about a common cellular origin of these neoplasms.

Coexpression of MUC5AC and RELP was seen in the goblet cells of PMP. In the appendiceal mucinous cystadenomas, however, RELP homogeneously stained the entire transformed mucosa, while positivity for MUC5AC was seen in its upper, luminal portion, leaving the deepest glands unstained. Adenomatous epithelium in the basal glands stained for MUC6 in five out of six appendiceal mucinouos cystadenomas from women, while no reactivity for MUC6 was seen in the adenomas from men. Although the material is too limited to allow any firm conclusions, it is interesting to notice that steroid hormones influence the expression of MUC6 in breast cancer cells [1]. This might have some bearing on the higher female incidence of appendiceal mucinous cystadenomas and PMP.

MUC6 was absent in all ten cases of PMP, while a strong expression of MUC5AC was detected. This might indicate that subclones expressing MUC5AC have a higher propensity for intraperitoneal implantation. The MUC5AC-positive subclones may also be better adjusted for growth and/or survival under poorly oxygenated conditions, like inside the mucous masses of PMP. The MUC5AC-containing goblet cells are also located in the upper portion of the appendiceal adenomatous mucosa, furthest away from the circulation.

The functional significance of the strongly up-regulated expression of RELP in inflammatory, metaplastic, and neoplastic goblet cells remains to be clarified. Because RELP, like other known members of the Reg protein family, is a secreted protein, it may be a ligand for a still unidentified receptor mediating signals in a paracrine or autocrine fashion. A receptor for the homologous Reg I, RegR was cloned by Kobayashi et al. [6]. Reg IR is a 919 amino acid transmembrane protein, which shows homology to the human multiple exostoses-like gene. RegR has been found on beta cells of pancreatic islets and in rat gastric mucosa where it mediates proliferative signals [5]. A corresponding receptor for RELP remains to be identified.

Taken together, we show here a strong de novo expression of RELP in the neoplastic goblet cells of appendiceal mucinous cystadenomas and PMP. RELP may serve as a clinical and immunohistochemical marker for these disorders. Our recent observations indicate that RELP displays relative specificity for neoplastic goblet cells of intestinal derivation. Immunohistochemical staining of 73 ovarian tumors with mucinous differentiation revealed some degree of positivity in 15 cases (20%) (unpublished observations). Further studies are in progress to elucidate the pathogenetic role of RELP expression in neoplastic and metaplastic goblet cells in the gastrointestinal tract.

Acknowledgements We thank Jill Carton, Centocor, Inc for preparing the immunogen for mab generation and Anu Harju for technical assistance. This work was supported by The Finnish Academy of Sciences, The Finnish Cancer Foundation, Biocentrum Helsinki, and Finska Läkaresällskapet.

The experiments reported in this manuscript comply with the current laws of Finland.

References

1. de Bolòs C, Gumà M, Barranco C, Garrido M, Kim YS, Real FX (1998) MUC6 expression in breast tissues and cultured cells: abnormal expression in tumors and regulation by steroid hormones. Int J Cancer 77:193–199
2. Hartupee JC, Zhang H, Bonaldo MF, Soares MB, Dieckgraefe BK (2001) Isolation and characterization of a cDNA encoding a novel member of the human regenerating protein family: Reg IV. Biochim Biophys Acta 1518:287–293
3. Hinson FL, Ambrose NS (1998) Pseudomyxoma peritonei. Br J Surg 85:1332–1339
4. Kämäräinen M, Heiskala K, Knuutila S, Heiskala M, Winqvist O, Andersson LC (2003) RELP, a novel human reg-like protein with up-regulated expression in inflammatory and metaplastic gastrointestinal mucosa. Am J Pathol 163:11–20
5. Kazumori H, Ishinara S, Fukuda R, Kinoshita Y (2002) Localization of reg receptor in rat fundic mucosa. J Lab Clin Med 139:101–108
6. Kobayashi S, Akiyama T, Nata K, Abe M, Tajima M, Shervani NJ, Unno M, Matsuno S, Sasaki H, Takasawa S, Okamoto H (2000) Identification of a receptor for reg (regenerating gene) protein, a pancreatic B-cell regeneration factor. J Biol Chem 275:10723–10726
7. Moran BJ, Cecil TD (2003) The etiology, clinical presentation and management of pseudomyxoma peritonei. Surg Oncol Clin N Am 12:585–603
8. Mutoh H, Hakamata Y, Sato K, Eda A, Yanaka I, Honda S, Osawa H, Kaneko Y, Sugano K (2002) Conversion of gastric mucosa to intestinal metaplasia in Cdx2-expressing transgenic mice. Biochem Biophys Res Commun 294:470–479
9. Mutoh H, Sakurai S, Satoh K, Tamada K, Kita H, Osawa H, Tomiyama T, Sato Y, Yamamoto H, Isoda N, Yoshida T, Ido K, Sugano K (2004) Development of gastric carcinoma from intestinal metaplasia in Cdx2-transgenic mice. Cancer Res 64:7740–7747
10. O'Connell JT, Tomlinson JS, Roberts AA, McGonigle KF, Barsky SH (2002) Pseudomyxoma peritonei is a disease of MUC2-expressing goblet cells. Am J Pathol 161:551–564
11. Oue N, Hamai Y, Mitani Y, Matsumura S, Oshimo Y, Aung PP, Kuraoka K, Nakayama H, Yasui W (2004) Gene expression profile of gastric carcinoma: identification of genes and tags potentially involved in invasion, metastasis, and carcinogenesis by serial analysis of gene expression. Cancer Res 64:2397–2405
12. Ronnett BM, Yan H, Kurman RJ, Shmookler BM, Wu L, Sugarbaker PH (2001) Patients with pseudomyxoma peritonei associated with disseminated peritoneal adenomucinosis have a significantly more favourable prognosis than patients with peritoneal mucinous carcinomatosis. Cancer 92:85–91
13. Ronnet BM, Seidman JD (2003) Mucinous tumors arising in ovarian mature cystic teratomas. Am J Surg Pathol 27:650–657
14. Sandor A, Mordlin IM (1998) A retrospective analysis of 1,570 appendiceal carcinoids. Am J Gastroenterol 93:422–428
15. Violette S, Festor E, Pandrea-Vasile I, Mitchell V, Adida C, Dussaulx E, Lacorte JM, Chambaz J, Lacasa M, Lesuffleur T (2003) Reg IV, a new member of the regenerating gene family, is overexpressed in colorectal carcinomas. Int J Cancer 103:185–193
16. Werling RW, Yaziji H, Bacchi CE, Gown AM (2003) CDX2, a highly sensitive and specific marker of adenocarcinomas of intestinal origin. Am J Surg Pathol 27:303–310
17. Yamamoto H, Bai QB, Yuasa Y (2003) Homeodomain protein CDX2 regulates goblet-specific *MUC2* gene expression. Biochem Biophys Res Commun 300:813–818
18. Zhang Y, Ding L, Lai M (2003) Reg gene family and human diseases. World J Gastroenterol 9:2635–2641
19. Zhang Y, Lai M, Lv B, Gu X, Wang H, Zhu Y, Zhu Y, Shao L, Wang G (2003) Overexpression of Reg IV in colorectal adenoma. Cancer Lett 200:69–76

Virchows Arch (2006) 448: 301–305
DOI 10.1007/s00428-005-0104-2

ORIGINAL ARTICLE

Shih-Ming Jung · Hsin-Chiung Lin · Pao-Hsien Chu · Hsien-Hwa Wu · Tzu-Fang Shiu · Shang Lang Huang · Chyong-Huey Lai

Expression of cell cycle-regulatory proteins, MIB-1, p16, p53, and p63, in squamous cell carcinoma of conjunctiva: not associated with human papillomavirus infection

Received: 26 July 2005 / Accepted: 26 October 2005 / Published online: 3 December 2005

Abstract Squamous cell carcinoma (SCC), the most common primary malignant tumor of the conjunctiva, has a variable clinical presentation and immunohistochemical profile. Abundant cell cycles exist, including MIB-1 (Ki67 antigen), p16, p53, and p63, within the conjunctiva SCC. This investigation first reports the expressions of cell cycle markers in SCC. A retrospective study was conducted between December 1976 and June 2004, comprising 13 consecutive patients with conjunctiva SCC who were treated with surgical excision. Detailed clinical parameters were also reviewed. Overexpression of MIB-1, p16, p53, and p63 genes were studied by immunohistochemistry. Genechip containing 39 subtypes was used to elucidate human papillomavirus (HPV). The study group contained 13 (100%) men, with a mean age of 68±18 years and follow-up period of 20±17 months. The sample included four (33%) SCC located in the left eye and two (17%) recurrent SCC. Overexpression of the p53 and p63 was considerably higher than that of the p16 (P<0.01). HPV DNA was not detected in any of the 13 cases. This work first examined the immunohistochemical overexpression of cell cycle (MIB-1, p16, p53, and p63) in SCC. This investigation then showed that the expression of cell cycles in SCC was associated with key tumor clinicopathological features. This approach can help distinguish the potential roles of cell cycle in the development of SCC.

Keywords Cell cycle · Conjunctiva · Human papillomavirus · MIB-1 · p16 · p53 · p63 · Squamous cell carcinoma

S.-M. Jung
Department of Pathology,
Chang Gung University,
Taipei, Taiwan

H.-C. Lin
Department of Ophthalmology,
Chang Gung Memorial Hospital,
Chang Gung University,
Taipei, Taiwan

P.-H. Chu (✉) · H.-H. Wu · T.-F. Shiu
The First Cardiovascular Division,
Department of Internal Medicine,
Chang Gung Memorial Hospital,
School of Medicine, Chang Gung University,
199 Tun-Hwa North Road,
Taipei 105, Taiwan
e-mail: pchu@adm.cgmh.org.tw
Tel.: +886-3-3281200
Fax: +886-3-3271192

Introduction

Squamous cell carcinoma (SCC) is the most common neoplasm of the conjunctiva. SCC also is associated with numerous cell cycle genes [1, 16, 22]. Cell cycle genes vary during cell proliferation and apoptosis [8, 9, 19, 20, 24–26]. The expression of cell cycle genes in SCC previously has never been clarified. To our knowledge, detailed immunohistochemical analysis of the cell cycle genes, the proliferating MIB-1 (Ki67 antigen), and apoptotic p16, p53, and p63 activities of conjunctiva SCC have not been performed.

At least 90% of the basal cells in limbal and peripheral corneal epithelia synchronously progress through the cell cycle. MIB-1 is a marker of actively cycling cells. Actively proliferating cells were identified with anti-Ki67, a marker of the late G1-M phase of the cell cycle [15]. There are two families of cyclin-dependent kinase inhibitors identified. The CIP/KIP family includes p21, p27, and p57, while the INK4 family consists of p16, p15, p18, and p19 [24, 26]. The expression of p16, p53, and p63 are dramatically altered during wound endothelium, suggesting that they may be involved in the changes in cell proliferation observed during carcinogenesis [6]. Moreover, the central role of human papillomavirus (HPV)-16 and HPV-18 in the oncogenesis of conjunctival cancers has been debated for a decade [6, 11–13, 17, 18, 21].

The purpose of the current study was to identify differences in cell cycle protein, MIB-1, p16, p53, and p63 expression in conjunctiva SCC that would express the proliferative and apoptotic capacities. This investigation

then attempted to determine whether the expression of cell cycle in SCC was associated with main clinicopathological features and HPV infection.

Materials and methods

This retrospective study conducted between December 1976 and June 2004 included 13 consecutive patients with SCC who were treated by surgical excision. Detailed clinical parameters were also reviewed [2–4]. The clinical charts displayed data on age, sex, presenting symptoms, and surgical procedures. Follow-up data were gathered from clinical records and standardized telephone interviews. In addition, tumor size and morphologic features were retrieved from the surgical pathology reports. All sections were stained with hematoxylin–eosin and examined for the presence of vascular proliferation, inflammation, cellularity, and fibrosis. The clinical and pathologic features of the SCC were analyzed statistically to identify morphological features related to recurrence and patient age on diagnosis.

Immunohistochemical staining for cell cycle: MIB-1, p16, p53, and p63

Cell cycle markers, including MIB-1, p16, p53, and p63, were studied immunohistochemically in 12 patients of conjunctiva SCC. Formalin-fixed, paraffin-embedded tissues were cut into 4-μm sections and mounted on glue-coated slides. Slides were deparaffinized in xylene, rehydrated in graded alcohols, and prepared by pressure cooker for 3 min. All slides were treated by tris–EDTA 1 nM pH 9.0 for MIB-1, 1 nM pH 8.0 for p16, 10 nM pH 6.0 for p53, and 1 nM pH 8.0 for p63. The various primary antibodies (MIB-1, 1:100, monoclonal, DakoCytomation; p16, 1:50, monoclonal, Santa Cruz; p53 1:50, DakoCytomation; p63 1:25, DakoCytomation) were applied for immunochemical stains according to the instruction of the manufacturer.

MIB-1 labeling index (%) was determined by counting positive cells per 100 squamous cells. The immunoreactivity was scored semiquantitatively as follows: weak or 0 (<10%) or 1+ (1–20%); moderate or 2+ (21–40%); and strong or 3+ (41–100%) nuclei per 100 nuclei. Stained cells with scale 0 or 1+ were classified as immunonegative, while those with scale 2+ or 3+ were considered immunopositive [16, 19, 22].

Genomic DNA extraction and electrophoresis

Genomic DNA was extracted using proteinase K and the phenol chloroform extraction method [7]. Samples were further purified through the use of a DNAeasy kit (Qiangen Inc., Venlo, The Netherlands). Finally, 1 μg of DNA solution was eluted, and 1 μg of the aliquot was used for polymerase chain reaction (PCR) amplification.

HPV genotyping by genechip

The SPF1/GP6+ consensus primers were used to amplify a fragment of approximately 184 bp in L1 open-reading frame first. Next, each PCR experiment was performed with several positive and negative controls [7]. The quality of isolated DNA was checked with glyceraldehyde-3-phosphate dehydrogenase (GAPDH) PCR. The resulting amplimers of 15 μg were then hybridized with an HPV genechip (Easychip HPV Genotyping Array, King Car Taiwan). Thirty-nine types of HPV ligonucleotide probes of 20- and 30-mer, with an approximately 100–200 poly-T tail, were immobilized on a nylon membrane [7].

Table 1 The basic clinical parameters of the squamous cell carcinoma in conjunctiva

Patient	Age/sex/eye	Main symptoms	Location	Treatment	Outcome
1	20/M/L	Recurrent red eye for 4 years	Limbus	Excision + keratectomy	No recurrence in 24 months
2	76/M/R	Decreased VA	Limbus	Excision + AMT + MMC	No recurrence in 9 months
3	77/M/R	Mass	Limbus	Excision + MMC	No recurrence in 6 months
4	73/M/R	Red eye, blurry	Limbus	Excision + MMC	No recurrence in 26 months
5	60/M/R	Red eye	Bulbar conjunctiva	RT	Persistent of tumor in 12 months, no systemic metastases
6	59/M/R	Recurrent tumor 9 years earlier	Limbus	RT	Persistence of tumor mass 20 months, no systemic metastases
7	70/M/R	Foreign body sensation	Limbus	Excision + cryo	No recurrence in 5 months
8	63/M/R	Red eye	Limbus	Excision + cryo + AMT	No recurrence
9	89/M/R	Mass	Limbus	Excision + cryo exenteration + RT	Recurrence in 1 months, no recurrence after exenteration in 24 months
10	81/M/R	Mass	Limbus	Excision + AMT	No recurrence in 58 months
11	62/M/R	Red eye	Limbus	Excision + AMT	No recurrence 36 months
12	83/M/R	Red eye	Limbus	Excision + AMT + MMC	No recurrence in 24 months
13	62/M/R	Red eye	Limbus	Excision + AMT	No recurrence 36 months

AMT amniotic membrane transplantation, *Cryo* cyosection, *MMC* mitomycin C, *RT* radiotherapy, *VA* visual acuity

Statistical comparisons were conducted using the Fisher exact test, Student *t* test for unpaired data, and Pearson correlation.

Results

Clinical findings

The patients comprised 13 (100%) men with a mean age of 20.3±16.5 years Table 1. The presentations included seven red eyes (58%), one decreased visual ability (8%), and three orbital masses (25%). Notably, the sample included four SCC (33%) located in the left eye and two (17%) recurrence. Eight patients were diagnosed first during operative biopsy, and two were current SCC patients. These patients were followed-up for an average of 20.3± 16.5 months (median, 32 months).

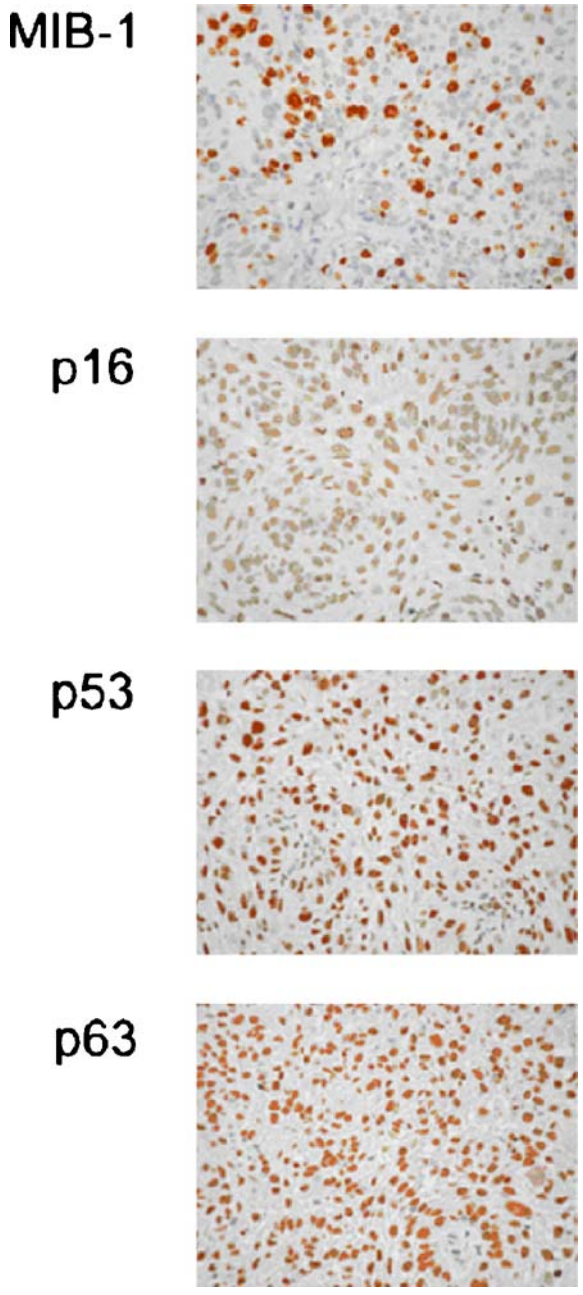

Fig. 1 The representative positive staining of MIB-1, p16, p53, and p63 to show the location and staining percentage in conjunctiva SSC (×400)

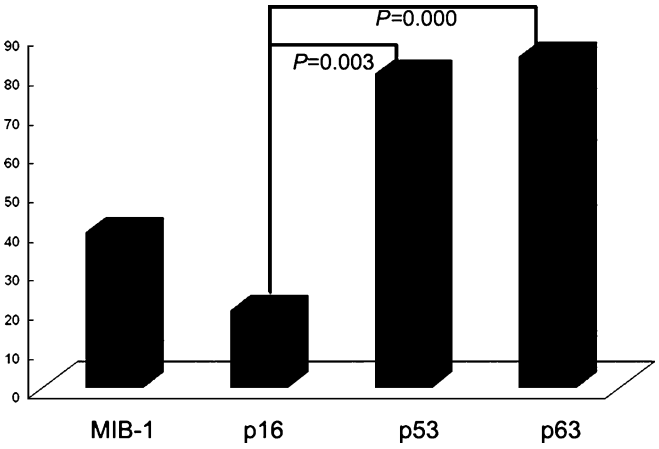

Fig. 2 Cell percentage of the various cell cycles staining in conjunctiva SSC

Expression of MIB-1, p16, p53, and p63 in squamous cell carcinoma

All SCC express immunopositive cell cycle genes, including all MIB-1, p16, p53, and p63 in 13 patients. Most positive MIB-1 staining was limited in the basal layer, but the p16/53/63 showed infiltration in the subepithelial cells (Fig. 1). Stained cell percentage is MIB-1 (41.0+ 18.6%), p16 (19.1+24.7%), p53 (83+8.1%), and p63 (86.7+ 8.6%), respectively (Fig. 2).

The percentage of expression of the p53 (80.0%) and p63 (84.6%) had higher expression than p16 (19.8%) (P=0.003 and P=0.000, respectively). However, p53 and p63 do not differ significantly (P=0.339).

Negative detection of HPV in SCC

Detection limit of this assay was determined by serial dilution of plasmid DNA containing the specific segment of L1 open-reading frame, using 39 HPV types and cell lines containing known HPV genotype, such as HeLa and CaSki cells, including between 10 and 100 copies per sample. None of the sample (0%) HPV-type DNA sequences were detected on the genechip.

Discussion

During corneal epithelial wound repair, cells migrating to cover the wound area exhibit a drastic reduction in proliferative activity [25]. In contrast, cells distal to the original wound exhibit a greatly enhanced level of pro-

liferative activity. At least 90% of the basal cells in limbal and peripheral corneal epithelia synchronously progress through the cell cycle. These inhibitors specifically block cells in the G1 phase of the cell cycle [1, 16, 19]. This study aimed to investigate the correlation between MIB-1, cell proliferative activity, and p16, p53, and p63 overexpression in conjunctiva SCC.

Positive staining of MIB-1, indicating cycling cells, was about 41% conjunctiva SCC in our study. Actively proliferating cells were identified with anti-MIB-1, a marker of the late G1-M phase of the cell cycle. It implies that the SCC maintains ability of proliferation well.

The expression of p16-form INK4 family is dramatically altered during wound SCC, suggesting that they may be involved in the changes in cell proliferation observed during carcinogenesis [8, 26]. The staining of p16 was the lowest among apoptotic markers, p16, p53, and p63 in conjunctiva SCC.

The p53 family—p53, p63, and p73—functions as transcription factors that play a major role in regulating the response of mammalian cells to stressors and damage, in part through the transcriptional activation of genes involved in cell cycle control, DNA repair, senescence, angiogenesis, and apoptosis. The strong positive p53 and p63 in this study indicate the malignancy of SCC.

The p53 protein is essential for the regulation of cell proliferation, and its aberrant accumulation is usually seen in malignant tumors [5]. The overexpression of p53 protein is an early event in head and neck carcinogenesis and may represent a biomarker for patients with preinvasive lesions. Mutation of the p53 tumor suppressor gene, often accompanied by overexpression of mutant p53 protein, is the most frequent molecular genetic event described thus far in human cancers. Overexpression of p53 protein (which is either wild type in sequence or mutant) is abnormal.

The p63 transcription factor, a p53 homolog, is essential for regenerative proliferation in epithelial development. Overrepresentation of p63 locus at chromosomal 3q27–29 was a typical finding in SCC. Within the cornea, nuclear p63 is expressed by the basal cells of the limbal epithelium. The identification of p63 as a keratinocyte stem cell marker will be of practical importance for the clinical application of epithelial cultures in cell therapy as well as for studies on epithelial tumorigenesis [23]. In contrast to the tumor suppressive function of p53, overexpression of select p63 splice variants is observed in many squamous carcinomas, suggesting that p63 may act as an oncogene [14, 23].

The results indicate that defects in the p16, p53, and p63 pathways are essential for the malignant transformation of conjunctiva epithelial cells. Molecular footprints at the sites of p53/63 mutations and p16 deletions further indicate that DNA repair activities for G/C to T/A. Transversion and nonhomologous end-joining of double-stranded DNA breaks play important roles in the accumulation of genetic alterations in lung cancer cells [10].

It is well known that HPV, which inactivates p53, is involved in the development of cervical squamous carcinoma, and the Rb inactivation probably contributes to the high $p16^{INK4a}$ expression in cervical cancer [8, 24]. Although infection of conjunctival epithelium with HPV is thought to be one of the important factors in the development of SCC [11–13, 17, 18], HPV DNA was not detected in any of these 13 cases as compared to some previous studies [17, 18]. Furthermore, HPV subtyping analysis showed that high risk HPV DNA was not present in any of these patients. It is probably associated with geographic regions, lifestyle, or HPV detection multiply methods [11–18]. The above findings strongly support that the SCC of conjunctiva is not associated with HPV infection.

Limitation

We acknowledge two limitations of our study. One is that the number of patients was small, and the other was that the follow-up period was relatively short. We conduct a prospective work to determine the role of cell cycle proteins in conjunctiva SCC.

Conclusion

MIB-1, p16, p53, and p63 may be useful markers of conjunctiva SCC and should be considered in the following up of conjunctiva SCC patients. The expressions of these cell cycles are not related to HPV infection.

Acknowledgements Dr. Chu is supported by NHRI, Taiwan (NHRI-EX91-9108SC, NHRI-EX92-9108SC, NHRI-EX-93-9108SC, and NHRI-EX94-9108SC), the National Sciences Council, Taiwan (NSC 94-2222-B-182-036), and CMRPG32057 from Chang Gung Memorial Hospital, Taiwan. Dr. Jung is supported by CMRPG33044 from Chang Gung Memorial Hospital, Taiwan. Dr. Lai is supported by research grants NSC 93-2314-B-182-036 from the National Sciences Council, Taiwan.

References

1. Aoki S, Kubo E, Nakamura S, Tsuzuki A, Tsuzuki S, Takahashi Y, Akagi Y (1998) Possible prognostic markers in conjunctival dysplasia and squamous cell carcinoma. Jpn J Ophthalmol 42: 256–261
2. Chu PH, Jung SM, Yeh TS, Yeh CH, Wang CL (2004a) Mucin genes expression in cardiac myxoma. Int J Clin Pract 58:306–309
3. Chu PH, Jung SM, Wu HH, Wu S, Chien LY, Hsueh C, Chu JJ, Lee YS (2004b) Apoptosis in primary cardiac tumor. Int J Clin Pract 58:564–567
4. Chu PH, Jung SM, Yeh TS, HC Lin, Chu JJ (2005) MUC1, MUC2 and MUC5AC expressions in cardiac myxoma. Virchows Arch 446:52–56
5. Dushku N, Hatcher SL, Albert DM, Reid TW (1999) p53 expression and relation to human papillomavirus infection in pingueculae, pterygia, and limbal tumors. Arch Ophthalmol 117:1593–1599
6. Eng HL, Lin TM, Chen SY, Wu SM, Chen WJ (2002) Failure to detect human papillomavirus DNA in malignant epithelial neoplasms of conjunctiva by polymerase chain reaction. Am J Clin Pathol 117:429–436

7. Huang HJ, Huang SL, Lin CY, Lin RW, Chao FY, Chen MY et al (2004) Human papillomavirus genotyping by a polymerase chain reaction-based genechip method in cervical carcinoma treated with neoadjuvant chemotherapy plus radical surgery. Int J Gynecol Cancer 14:639–649
8. Joseph A, Powell-Richards AO, Shanmuganathan VA, Dua HS (2004) Epithelial cell characteristics of cultured human limbal explants. Br J Ophthalmol 88:393–398
9. Joyce NC, Harris DL, Mello DM (2002) Mechanisms of mitotic inhibition in corneal endothelium: contact inhibition and TGF-beta2. Invest Ophthalmol Vis Sci 43:2152–2159
10. Massion PP, Taflan PM, Jamshedur Rahman SM, Yildiz P, Shyr Y, Edgerton ME, Westfall MD, Roberts JR, Pietenpol JA, Carbone DP, Gonzalez AL (2003) Significance of p63 amplification and overexpression in lung cancer development and prognosis. Cancer Res 63:7113–7121
11. Moubayed P, Mwakyoma H, Schneider DT (2004) High frequency of human papillomavirus 6/11, 16, and 18 infections in precancerous lesions and squamous cell carcinoma of the conjunctiva in subtropical Tanzania. Am J Clin Pathol 122:938–943
12. Nakamura Y, Mashima Y, Kameyama K, Mukai M, Oguchi Y (1997) Detection of human papillomavirus infection in squamous tumours of the conjunctiva and lacrimal sac by immunohistochemistry, in situ hybridisation, and polymerase chain reaction. Br J Ophthalmol 81:308–313
13. Odrich MG, Jakobiec FA, Lancaster WD, Kenyon KR, Kelly LD, Kornmehl EW, Steinert RF, Grove AS Jr, Shore JW, Gregoire L et al (1991) A spectrum of bilateral squamous conjunctival tumors associated with human papillomavirus type 16. Ophthalmology 98:628–635
14. Pellegrini G, Dellambra E, Golisano O, Martinelli E, Fantozzi I, Bondanza S, Ponzin D, McKeon F, De Luca M (2001) p63 identifies keratinocyte stem cells. Proc Natl Acad Sci U S A 98:3156–3161
15. Petroll WM, Jester JV, Bean J, Cavanagh HD (1998) Labeling of cycling corneal endothelial cells during healing with a monoclonal antibody to the Ki67 antigen (MIB-1). Cornea 18:98–108
16. Reszec J, Kanczuga-Koda L, Sulkowska M, Koda M, Cylwik J, Barwijuk-Machala M, Sulkowski S (2004) An evaluation of Ki-67 and PCNA expression in conjunctival and eyelid tumours. Folia Morphol (Warsz) 63:95–98
17. Saegusa M, Takano Y, Hashimura M, Okayasu I, Shiga J (1995) HPV type 16 in conjunctival and junctional papilloma, dysplasia, and squamous cell carcinoma. J Clin Pathol 48:1106–1110
18. Scott IU, Karp CL, Nuovo GJ (2002) Human papillomavirus 16 and 18 expression in conjunctival intraepithelial neoplasia. Ophthalmology 109:542–547
19. Senoo T, Joyce NC (2000) Cell cycle kinetics in corneal endothelium from old and young donors. Invest Ophthalmol Vis Sci 41:660–667
20. Staunton MJ, Gaffney EF (1995) Tumor type is a determinant of susceptibility to apoptosis. Am J Clin Pathol 103:300–307
21. Tulvatana W, Bhattarakosol P, Sansopha L, Sipiyarak W, Kowitdamrong E, Paisuntornsug T, Karnsawai S (2003) Risk factors for conjunctival squamous cell neoplasia: a matched case-control study. Br J Ophthalmol 87:396–398
22. Weissman SS, Char DH, Herbort CP, Ostler HB, Kaleta-Michaels S (1992) Alteration of human conjunctival epithelial proliferation. Arch Ophthalmol 110:357–359
23. Westfall MD, Pietenpol JA (2004) p63: molecular complexity in development and cancer. Carcinogenesis 25:857–864
24. Zieske JD (2002) Expression of cyclin-dependent kinase inhibitors during corneal wound repair. Prog Retin Eye Res 19:257–270
25. Zieske JD, Guimaraes SR, Hutcheon AE (2001) Kinetics of keratocyte proliferation in response to epithelial debridement. Exp Eye Res 72:33–39
26. Zieske JD, Francesconi CM, Guo X (2004) Cell cycle regulators at the ocular surface. Exp Eye Res 78:447–456

Virchows Arch (2006) 448: 306–310
DOI 10.1007/s00428-005-0099-8

ORIGINAL ARTICLE

R. Awasthi · J. K. O'Neill · C. E. Keen · P. T. L. Sarsfield · V. S. Devaraj · C. A. Stone · M. E. F. Smith

Biphasic solitary fibrous tumour: a report of two cases with epithelioid features

Received: 6 May 2005 / Accepted: 19 September 2005 / Published online: 22 October 2005

Abstract We present two cases of solitary fibrous tumour (SFT) showing biphasic morphology with a spectrum of malignant epithelioid components. Slides prepared from formalin-fixed and paraffin-embedded tissue from both cases were stained with haematoxylin and eosin and by immunohistochemistry. Interphase fluorescent in situ hybridisation studies were performed in both cases using paraffin-embedded tissue to look for the t(X;18) translocation, thereby to exclude synovial sarcoma. Both cases showed biphasic morphology with some areas having typical benign spindled SFT morphology (including CD34 expression) and other areas having a malignant epithelioid appearance. In one of the cases, the epithelioid area, which was well circumscribed and showed packeting of cell groups, demonstrated expression of cytokeratin and epithelial cadherin but not of CD34. In the second case, the immunophenotype of the epithelioid component was similar to that of the benign SFT component. These findings suggest that epithelioid change in SFT shows a range of differentiation at one end, similar to that of a standard SFT, and at the other end, possibly acquiring epithelial characteristics.

R. Awasthi · C. E. Keen · P. T. L. Sarsfield
Department of Histopathology,
Royal Devon and Exeter Hospital,
Barrack Road,
EX2 5DW Exeter, UK

J. K. O'Neill · V. S. Devaraj · C. A. Stone
Department of Plastic Surgery,
Royal Devon and Exeter Hospital,
Barrack Road,
EX2 5DW Exeter, UK

M. E. F. Smith (✉)
Department of Histopathology,
Derriford Hospital,
Derriford Road,
PL6 8DH Plymouth, UK
e-mail: mark.smith@phnt.swest.nhs.uk
Tel.: +44-1752-792361
Fax: +44-1752-763590

Keywords Solitary fibrous tumour · Biphasic · Epithelioid · Epithelial differentiation · Cytokeratin

Introduction

Solitary fibrous tumour (SFT) is an uncommon mesenchymal tumour usually arising from the visceral pleura but also at various extrapleural sites such as the peritoneum, retroperitoneum, mediastinum and orbit. Benign tumours significantly outnumber malignant ones. Epithelioid morphology in SFT has only very occasionally been described [3, 5, 6]. We present two cases of SFT showing distinct biphasic morphology and demonstrating a range of epithelioid differentiation.

Materials and methods

The slides of formalin-fixed and paraffin-embedded tissue were stained with haematoxylin and eosin. The immunohistochemical staining (primary antibodies listed in Table 1) was performed using a Vector Elite avidin–biotin complex method. Fluorescent in situ hybridisation (FISH) studies investigating the presence of a t(X;18) translocation in the tumours were purchased from the Institute of Human Genetics, Newcastle-upon-Tyne Hospitals, UK. The interphase FISH study was carried out by the Institute on 100 nuclei from disaggregated paraffin-embedded tissue using the Vysis SYT probe to investigate the translocation.

Clinical history

Case 1

A 63-year-old woman presented with a non-tender swelling in the posterior part of the right side of her neck. She was otherwise well with no significant past medical history. There was no limitation of cervical spine movement, and she had no neurological deficit in the upper or lower limbs.

Table 1 Antibodies used in the study

Specificity	Antibody	Pretreatment	Dilution	Incubation time (min)	Source/reference
AUA-1	AUA-1	T	1:100	30	Skybio[a]
Ber-EP4	Ber-EP4	T	1:40	30	Dako[b]
Bcl-2	124	MW	1:600	30	Dako
Calretinin	5A5	PC	1:300	45	Novocastra[c]
Collagen type IV	CIV 22.1(1).	MW	1:200	30	Dako
Cytokeratin	MNF116	T	1:100	60	Dako
Cytokeratin 5/6	D5/16 B4	MW	1:1000	30	Dako
Cytokeratin	AE1/AE 3	PC	1:40	60	Novocastra
CD34	Q Bend 10	MW	1:400	30	Skybio
CD99	HO36-1.1	PC	1:200	60	Novocastra
Desmin	DE-R-11	MW	1:1200	30	Dako
E-cadherin	HECD-1	PC	1:200	60	British Biotech[d]
EMA	E 29	T	1:800	45	Dako
Laminin	Polyclonal	T	1:100	30	SIGMA[e]
SMA	IA-4	MW	1:500	30	Dako
S-100	Polyclonal	T	1:6000	30	Dako
Vimentin	Monoclonal	MW	1:4000	30	Dako

MW Microwave, *PC* pressure cooker, *T* trypsin treatment
[a]Skybio, Bedfordshire, UK
[b]Dakocytomation, Cambridgeshire, UK
[c]Novocastra, Newcastle-upon-Tyne, UK
[d]British Technology, Oxford, UK
[e]SIGMA, Dorset, UK

An ultrasound scan was performed which confirmed a 40×20-mm mass. A magnetic resonance imaging (MRI) scan showed the presence of a well-defined, multilobulated mass within the substance of the deep transverse spinal muscle, lying deep to splenius capitis and scalene muscles and abutting the vertebral laminae of C3 to C5. No extension into the neural canal was identified. A needle core biopsy from the mass was considered to be suggestive of synovial sarcoma. Tumour excision necessitated peeling the tumour off the laminae of C3 to C5 in a subperiosteal plane. The patient was referred for radiotherapy.

Case 2

A 57-year-old man presented with an approximately 100-mm mass in the left ischiorectal fossa, which, although present for the last 15 years, had started growing over the previous 6 months. An MRI scan demonstrated a 100×80×60-mm lobulated mass located within the fat of the left ischiorectal fossa, displacing the rectum to the right and the levator muscles superiorly. These findings suggested a soft tissue sarcoma. No evidence of metastatic malignancy was seen on staging CT scan. An ultrasound-guided core biopsy was performed, which showed a biphasic tumour with spindled and epithelioid elements suggestive of an SFT. The tumour was excised. At operation, the tumour was located in a separate plane from rectum, bladder and prostate and was removed without disturbance of these structures.

Results

Case 1

The resected tumour was ovoid and lobulated, measuring 40×35×20 mm (Fig. 1a). Histologically, a biphasic pattern, with spindled and epithelioid components, was confirmed (Fig. 1b–d). The morphology of the spindle cell component was typical of SFT having variable sclerosis and variable cellularity and showing a haemangiopericytomatous vasculature (Fig. 1b,c). Focal stromal myxoid change was present. There was generally a low mitotic count [2/10 high-power field (HPF)], but in more cellular, non-epithelioid areas, the mitoses rose to 4/10 HPF. Focal microcalcification was also noted within the benign SFT area. The histological appearance of SFT was confirmed by immunohistochemistry, which in spindled areas showed strong and diffuse CD34 expression (Fig. 2a). The spindled tumour cells expressed Bcl-2 and vimentin but not cytokeratin (MNF116 and AE1/AE3) (Fig. 2b), CD99 or epithelial cadherin (E-cadherin). Type IV collagen and laminin were seen, mainly associated with the blood vessels in the spindled area with minor extension of fibres around the tumour cells.

The epithelioid tumour component arose within a distinct, pale yellow nodule approximately 20×15×10 mm in diameter (Fig. 1a). Its large cells had abundant eosinophilic or clear cytoplasm and vesicular pleomorphic nuclei with prominent nucleoli. They were packeted and arranged in sheets (Fig. 1d). Some multinucleate, osteoclast-like giant

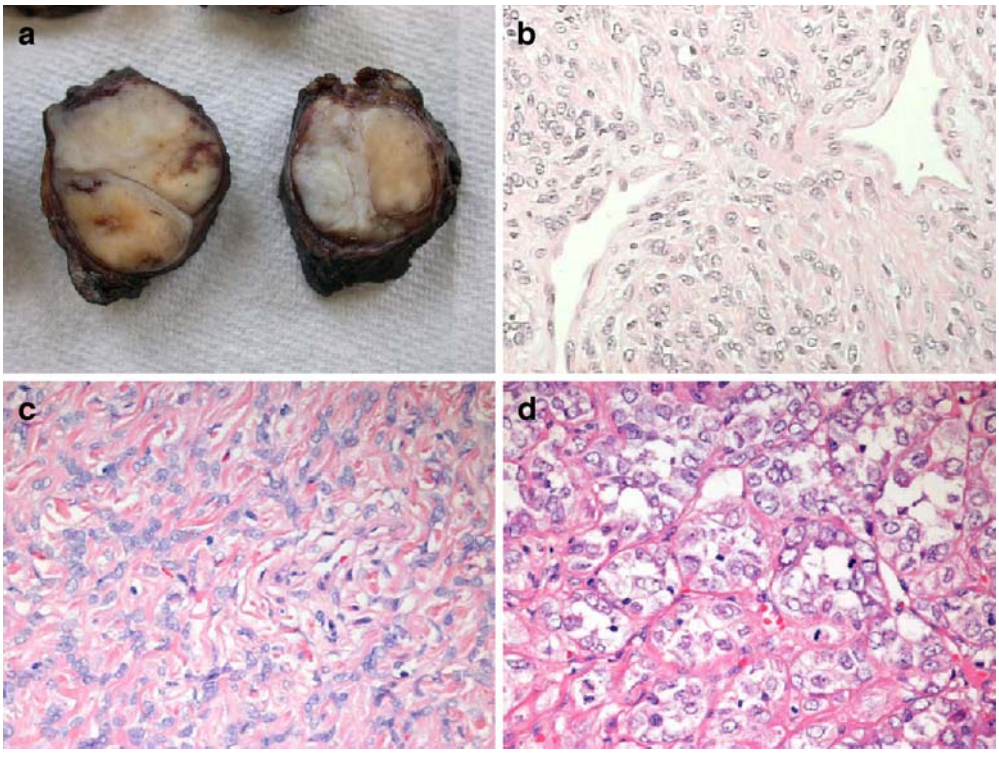

Fig. 1 Case 1. Tumour showing a pale yellow nodule (microscopically corresponding to malignant epithelioid component) within firm, pale tissue (**a**). The spindle cell tumour component shows typical benign SFT with intervening collagen and a haemangiopericytic vasculature (**b**, **c**). The malignant epithelioid component shows large cells with clear cytoplasm and a packeted arrangement (**d**)

cells were present within the nodule. Mitoses were frequent in the epithelioid area (up to 11 mitoses/10 HPF) and were occasionally abnormal. No necrosis was present. Both spindled and malignant epithelioid areas were generally distinct (Fig. 2a,b), but focally, the two tumour patterns merged with an indistinct transition.

The malignant epithelioid cells showed diffuse cytokeratin expression with strong intensity using MNF116 (Fig. 2b) and moderate to strong intensity using AE1/AE3. They showed diffuse E-cadherin (Fig. 2c) and focal CD99; CD34 (Fig. 2a), Bcl-2 and vimentin were negative. The packeted appearance of the epithelioid tumour was accentuated by collagen type IV and laminin expression around the periphery of epithelioid cell groups. Other immunohistochemical stains performed that were negative in both epithelioid and spindle areas were epithelial membrane antigen (EMA), S-100, desmin, smooth muscle actin (SMA), BerEP-4, calretinin, AUA-1 and CK5/6. In the FISH analysis, there was no evidence of a split signal, a finding consistent with the absence of a t(X;18) translocation.

Case 2

Macroscopically, the excised tumour had well-circumscribed margins and was multilobulated and very vascular. It measured 120×70×65 mm. Microscopically, it showed a biphasic pattern. One component, comprising approximately 50% of total tumour bulk, showed classical benign SFT (Fig. 3a, b) with a haemangiopericytomatous vasculature and hardly any mitoses (0/10 HPF). The other component was very variable, comprising areas with round cell and epithelioid cell morphology. Focally, these comprised

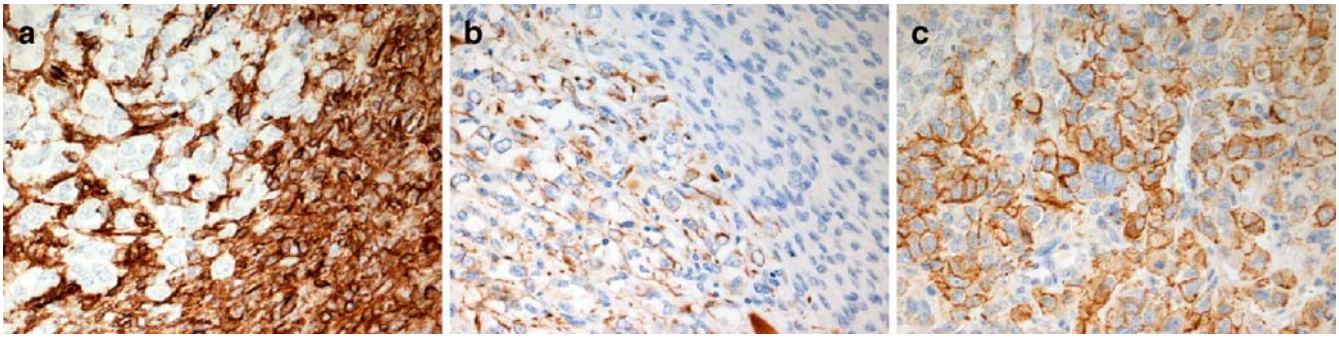

Fig. 2 Case 1. Closely apposed spindled and epithelioid cells are seen, showing strong and diffuse CD34 positivity in the former and none in the latter (**a**). The epithelioid tumour shows strong cytokeratin expression (MNF116), whereas the spindled tumour is negative (**b**). The epithelioid area shows variable E-cadherin positivity (**c**)

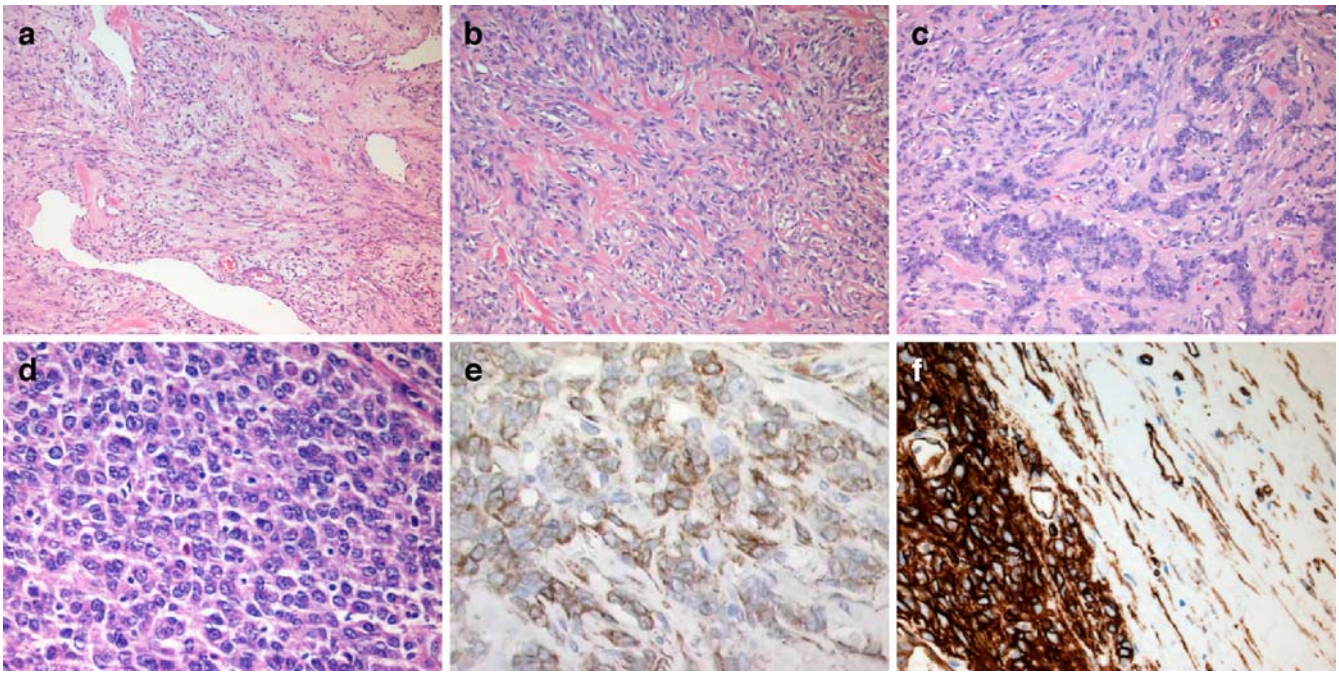

Fig. 3 Case 2. Typical benign SFT areas (**a**, **b**). A biphasic area (**c**) with strands of epithelioid cells intermixed with spindled cells. Sheets of round/epithelioid cells (**d**). Cytokeratin positivity (AE1/AE3) is present in epithelioid cells (**e**). CD34 positivity is present in both epithelioid and spindle cell components (**f**)

strands of cohesive cells intermixed with the spindle cell components (Fig. 3c). Elsewhere, there were sheets of round/epithelioid cells (Fig. 3d). Given the raised mitotic count (up to 5/10 HPF), extensive infiltration of peripheral fat and the presence of focal moderate nuclear pleomorphism in this component, the tumour was regarded as malignant. No well-marked packeting was identified, and the epithelioid appearance of the sheets of cells was less marked than was seen in case 1. Focal necrosis was identified. Immunohistochemical staining revealed that a proportion of tumour cells in both the epithelioid and spindled areas stained positively with cytokeratin antibodies (AE1/AE3) (Fig. 3e), though cytokeratin detected by MNF116 was restricted to the spindled area. The entire umour stained strongly with CD34 (Fig. 3f), Bcl-2 and vimentin but was negative for E-Cadherin, S-100 and desmin. EMA was focally positive in benign spindled cells but was negative in epithelioid cells. Focal, weak positivity for CD99 was seen in both components. Laminin and collagen type IV showed vascular staining in both components with extension of fibres around spindle cells, but epithelioid cells were completely negative. The FISH analysis showed no evidence of a split signal, a finding consistent with the absence of the t (X;18) translocation.

Discussion

Two biphasic SFTs with focal epithelioid appearance are described. Epithelioid change in SFT has only very rarely been reported. A cytokeratin-expressing mediastinal tumour arising in a 74-year-old man and an ischioanal fossa lesion arising in a 67-year-old man have been advanced as examples [5, 6]. In addition, a malignant SFT that did not express cytokeratin has been briefly described as showing ‘solid sheets of epithelioid-like cell clusters’ [3].

The histological distinction of epithelioid SFT from other epithelioid tumours, such as carcinosarcoma, malignant mesothelioma, synovial sarcoma and thymoma, may be very difficult, the more so if the SFT expresses cytokeratin [2]. Careful histological assessment of epithelioid SFT is required to identify any accompanying typical spindled SFT component, a feature we presently regard as being important in establishing a diagnosis. We note, however, that a spindled SFT area was either absent [6] or was, at most, exceedingly minor [5] in some previous reports of epithelioid SFT. A panel of immunostains appropriate for the differential diagnosis noted above is of use in identifying tumours of non-SFT type or in confirming an SFT-compatible phenotype (CD34-, Bcl-2- and CD99-positive). Occasionally, molecular biologic techniques may be of use as in the demonstration that all eight tumours lacked the t (X;18) translocation, a finding that further helped exclude a diagnosis of synovial sarcoma.

In case 1, there was well-demarcated, focal but extensive epithelioid change associated with malignant transformation, arising in an otherwise histologically typical benign SFT. The epithelioid component was characterised by a modulation of antigen expression with the loss of CD34 and vimentin and acquisition of cytokeratin and E-cadherin. This profound antigen modulation suggests a shift of differentiation pattern. It should be noted that E-cadherin is commonly expressed in soft tissue tumours in two contexts, as true epithelial differentiation such as is seen in synovial sarcoma, epithelioid sarcoma and glandular malignant peripheral nerve sheath tumours (PNSTs) and as a marker

of Schwannian/melanocytic differentiation as is seen, for example, in epithelioid malignant PNST or clear cell sarcoma [4, 7, 8]. SFTs are not of Schwannian/melanocytic derivation and, in keeping with this, are S-100-negative. The expression of E-cadherin in the epithelioid SFT (case 1) described herein therefore supports the presence of epithelial differentiation. Indeed, the epithelioid phenotype, cytokeratin and E-cadherin expression and loss of CD34 and vimentin are all features consistent with epithelial differentiation, though it is recognised that ultrastructural analysis would be required for unequivocal demonstration of epithelial features. In this context, the ultrastructural demonstration of 'primitive desmosomes' in SFTs suggests a restricted degree of epithelial differentiation even in standard SFTs [1]. We suggest that a greater degree of epithelial differentiation may have been present in case 1 of this report. In contrast, in case 2, the lack of E-cadherin and the retention of CD34 suggest that overt epithelial differentiation was not present.

Though the genetic and epigenetic abnormalities underlying epithelioid change in SFT are not known, the expression of E-cadherin in case 1 may have contributed to directing an epithelioid pattern rather than merely reflecting it, the expression of E-cadherin having a recognised role in conferring an epithelioid appearance to tumour cells [7, 9].

In conclusion, we present two cases of epithelioid SFT. Our studies suggest that a variable degree of epithelial differentiation may be present in these tumours.

References

1. Amo-Takyi BK, Gunther K, Peters I, Mittermayer C, Eblenkamp M, Tietze L (2001) Benign solitary fibrous pleural tumour. Evidence of primitive features and complex genomic imbalances, including loss of 20q. APMIS 109:601–606
2. Cavazza A, Rossi G, Agostini L, Roncella S, Ferro P, Fedeli F (2003) Cytokeratin-positive malignant solitary fibrous tumour of the pleura: an unusual pitfall in the diagnosis of pleural spindle cell neoplasms. Histopathology 43:606–608
3. Hanau CA, Miettinen M (1995) Solitary fibrous tumour: histological and immunohistochemical spectrum of benign and malignant variants presenting at different sites. Hum Pathol 26:440–449
4. Laskin WB, Miettinen M (2002) Epithelial-type and neural-type cadherin expression in malignant noncarcinomatous neoplasms with epithelioid features that involve the soft tissues. Arch Pathol Lab Med 126:425–431
5. Marchevsky AM, Varshney D, Fuller C (2003) Mediastinal epithelioid solitary fibrous tumour. Arch Pathol Lab Med 127: e212–e215
6. Mourra N, Lewin M, Sautet A, Parc R, Flejou JF (2005) Epithelioid solitary fibrous tumour in the ischioanal fossa. Virchows Arch 446:674–676
7. Sato H, Hasegawa T, Abe Y, Sakai H, Hirohashi S (1999) Expression of E-cadherin in bone and soft tissue sarcomas: a possible role in epithelial differentiation. Hum Pathol 30:1344–1349
8. Smith MEF, Cowley GP, Dogan A, Weiss SW, Fisher C (1994) E-cadherin is a differentiation antigen of normal Schwann cells and is expressed in epithelioid Schwann cell tumours. J Pathol 173:181A
9. Smith MEF, Pignatelli M (1997) The molecular histology of neoplasia: the role of the cadherin/catenin complex. Histopathology 31:107–111

Virchows Arch (2006) 448: 311–318
DOI 10.1007/s00428-005-0098-9

ORIGINAL ARTICLE

Yoshihiro Adachi · Tamotsu Takeuchi · Hiroshi Sonobe · Yuji Ohtsuki

An adiponectin receptor, T-cadherin, was selectively expressed in intratumoral capillary endothelial cells in hepatocellular carcinoma: possible cross talk between T-cadherin and FGF-2 pathways

Received: 27 May 2005 / Accepted: 14 September 2005 / Published online: 5 November 2005

Abstract T-cadherin is a unique receptor of adiponectin, which plays a critical role in various angiogenesis. In the present study, T-cadherin expression in tumor vessels of hepatocellular carcinoma (HCC) and, subsequently, the molecular mechanism, which induced T-cadherin expression in sinusoidal endothelial cells were investigated. Sinusoidal endothelium in nontumorous liver, chronic hepatitis, or liver cirrhosis expressed little or no T-cadherin. By contrast, T-cadherin was found in intratumoral capillary endothelial cells of 34 out of 63 HCC specimens. In positive cases, focal T-cadherin expression was found in well-differentiated HCC, whereas diffuse and intense T-cadherin expression was observed in poorly differentiated HCC specimens. T-cadherin was much expressed in intratumoral capillary endothelial cells in a less differentiated HCC region than that in a well-differentiated region in five specimens, in which various differentiated HCC components were coexistent. In a double-cell chamber assay, fibroblast growth factor-2 appeared to have a critical role to induce T-cadherin in cultured liver sinusoidal endothelial cells. The present finding indicated that T-cadherin was selectively expressed in intratumoral capillary endothelial cells of many HCCs, increasingly expressed as tumor progression, and T-cadherin may have a positive role in angiogenesis of HCC. In addition, cross talk between the signal pathways mediated by fibroblast growth factor-2 and adiponectin was suggested.

Y. Adachi · T. Takeuchi (✉) · Y. Ohtsuki
Department of Pathology, Kochi Medical School,
Nankoku, Kochi 783-8505, Japan
e-mail: takeutit@med.kochi-ms.ac.jp
Tel.: +81-88-8802335
Fax: +81-88-8802336

H. Sonobe
Department of Laboratory Medicine and Pathology,
National Hospital Organization, Fukuyama Medical Center,
Okinogami 4-14-17, Fukuyama,
Hiroshima 720-8520, Japan

Keywords T-cadherin · Adiponectin · Hepatocellular carcinoma · Neovascularization

Introduction

Tumor neovascularization is a critical event in various types of malignant tumor growth [3]. Hepatocellular carcinoma (HCC), in particular, is a hypervascular neoplasm, and many approaches that involve the interruption of blood supply have been used for patients with HCC. The intratumoral endothelial cells in HCC have morphological characteristics intermediate between those of ordinary capillary endothelium and the sinusoidal endothelium in normal liver [30]. Sinusoidal endothelium in HCC lost the phenotypes peculiar to liver and acquired the characteristics of capillary endothelial cells with progression of tumor dedifferentiation [22]. A cross talk between hepatic sinusoidal endothelial cells and juxtaposed hepatocytes play a role for the phenotype change and maintenance of sinusoidal endothelial growth and differentiation [6]. Especially, endothelial-cell growth factors, including vascular endothelial growth factor (VEGF) and fibroblast growth factor-2 (FGF-2), which is secreted from normal or neoplastic hepatocytes, is believed to regulate the endothelial cell growth by a paracrine manner. Therefore, it is important to unravel the molecules, which are involved in a cross talk between HCC cells and intratumoral capillary endothelial cells, to regulate the tumor neovascularization in HCC.

T-cadherin (also referred to as CDH13 or H-cadherin) is a unique cadherin cell adhesion molecule that is anchored to the cell-surface membrane through a glycosyl phosphatidylinositol (GPI) moiety [26]. The T-cadherin amino acid motif has been well conserved through evolution in vertebrates relative to other classical cadherins [35]. However, T-cadherin lacks the cytoplasmic domain, which is critical for homophilic binding through interaction with submembrane cytoskeletal proteins in classical cadherin molecules [21]. There are also several reports which sug-

gest that T-cadherin plays an important role in signal transduction apart from cell–cell adhesion [9, 15, 34, 43]. In line with this speculation, recently, T-cadherin was identified as a novel receptor for hexametric and high-molecular-weight (HMW) isoforms of adiponectin, which has significant effects on angiogenesis [10]. Interestingly, murine T-cadherin was selectively expressed in transplanted tumor vessels in mice, and murine T-cadherin was believed to be a pivotal molecule for tumor neovascularization [24, 42]. However, there are still few reports that describe T-cadherin expression in intratumoral capillary endothelial cells in human tumors.

We have examined T-cadherin expression in various human malignant tumors, and here, we report that T-cadherin was selectively expressed in intratumoral capillary endothelial cells of HCC but not in sinusoidal endothelial cells in noncancerous liver. We also describe the relationship of T-cadherin expression with FGF-2.

Materials and methods

Antibodies, tissue samples, and immunohistochemical staining

Details of the procedures used to prepare rabbit-specific antibody to human T-cadherin and immunohistochemical staining were described previously [33]. Briefly, rabbits were immunized with human T-cadherin peptide QRQPF PRDVGKVVDSDRPERSKFRLTGKGVD. Antibody was purified by affinity chromatography using the same peptide. We verified the specificity of the antibody through Western immunoblotting by using various human tissue extracts. Control normal rabbit immunoglobulin (Ig)G was also prepared in our laboratory. Specific antibody to human LYVE-1 and CD34 were purchased from RELIA*Tech* GmbH (Braunschweig, Germany) and Becton Dickinson Immunocytometry Systems (San Jose, CA), respectively.

We examined archival liver tissue specimens that comprised a spectrum of noncancerous liver, liver cirrhosis, and HCC. We examined 63 HCC specimens, which contain a uniform differentiation type. The pathological features of the specimens are summarized in Table 1. All tissue specimens were untreated prior to resection, obtained from pathology files, and classified according to the World Health Organization classification [7]. In the present study, we focused on T-cadherin expression in liver tissues affected with viral infection when we examined HCC specimens. The differentiation in HCC was assessed based on the examination of hematoxylin–eosin (H & E)-stained sections according to Edmonson's grading [5]. Briefly, well-differentiated HCC was composed of tumor cells with minimal atypia and an increased nuclear/cytoplasmic ratio. Tumor cells were arranged in uniformly thin trabeculae. By contrast, in moderately differentiated HCC, tumor cells harboring the abundant eosinophilic cytoplasm and round nuclei were arranged in trabeculae of three or more cells in thickness. Giant tumor cells are more numerous in moderately differentiated HCC. In poorly differentiated HCC, tumor cells have intense hyperchromatic nuclei and little cytoplasm without demonstrating a trabecular pattern. Pleomorphism and bizarre giant cells were frequently found in poorly differentiated HCC. We also examined five HCC specimens, which composed variously differentiated HCC regions in individual tissue slides. After antigen retrieval by autoclaving with citrate buffer (pH 6.0), the tissues were immunostained with affinity-purified antihuman T-cadherin peptide or control antibody using a streptavidin biotin complex peroxidase kit (DAKO LABS Kit; Dakopatts, Kyoto, Japan). In several experiments, anti-T-cadherin antibody was preadsorbed with human T-cadherin peptide, which was used for immunization.

To evaluate the immunostained specimens, the entire tumor section was scanned at low magnification (×40) to find the areas in which the tumor necrosis is absent. Next, we counted the percentage of endothelial cells positive in ten high-powered fields (HPFs) (×200). In preliminary experiments, reproducibility was poor in the specimens when less than 10% of the cells were stained in a section. In these cases, intratumoral capillary endothelial cells in other HCC areas sometimes did not exhibit staining with anti-T-

Table 1 Relationship between expression of T-cadherin in intratumoral capillary endothelium of HCC and various histopathological features

Variant	T-cadherin expression		
	Positive	Negative	Significance
Differentiation			
Poor	16	6	Present[a]
Moderate	15	14	
Well	3	9	
Adjacent tissues to HCC			
Cirrhosis	23	20	NS
Hepatitis	11	9	
Tumor size			
>5 cm	8	6	NS
>3 cm, <5 cm	19	16	
<3 cm	7	7	
Capsule			
Present	24	21	NS
Absent	10	8	
Portal invasion			
Present	8	11	NS
Absent	26	18	
Intrahepatic metastasis			
Present	12	8	NS
Absent	22	21	
Etiology			
HBV	16	15	NS
HCV	18	14	

NS Not significant, *HCC* hepatocellular carcinoma, *HBV* hepatitis B virus, *HCV* hepatitis C virus

[a]Significant differences, p=0.027, were observed between poorly, moderately, and well-differentiated HCC, whereas p=0.007 between well- and poorly differentiated HCC

cadherin antibody. Therefore, we considered a specimen to be positive when we observed T-cadherin staining in more than 10% of intratumoral capillary endothelial cells. Finally, two authors reviewed the immunostains independently and drew concordant interpretations.

Assessment of microvessel density

Sections were immunohistochemically stained with antihuman CD34 antibody and examined at low-power magnification (×100) to identify the areas with the highest density of CD34-positive vessels. In each case, the most vascularized area was selected, and microvessels in five HPFs (×200) were counted. Finally, the mean microvessel count of the five most vascular areas was taken as the microvessel density, which was expressed as the absolute number of microvessels/HPF.

In situ hybridization

Details of the in situ hybridization procedures were described previously [34]. Antisense digoxigenin-labeled RNA probes to human T-cadherin were generated by promoter-mediated in vitro transcription using a digoxigenin RNA labeling kit (Boehringer Mannheim GmbH, Germany). Two hundred thirty base pairs of human T-cadherin cDNA were amplified by polymerase chain reaction (PCR) and subcloned into a pGEM-T easy vector (Promega, Madison, WI). We also used sense digoxigenin-labeled RNA probes as a negative control. Digoxigenin-labeled probes were finally visualized using a digoxigenin DNA detection kit (Boehringer). The experimental condition was assessed by using human brain tissues in which T-cadherin mRNA is abundantly expressed.

Double-chamber cell cultures

Human cultured Hep G2 cells were maintained in our laboratory in Dulbecco's medium (Life Technologies, Grand Island, NY) containing 10% heat-inactivated fetal bovine serum (FBS) and 50 μg/ml gentamycin (Life Technologies). Normal human liver sinusoidal microvascular endothelial cells were purchased from the Applied Cell Biology Research Institute (Kirkland, WA) and cultured with cell systems complete (CS-C) medium (Cell Systems, Kirkland, WA). In double-chamber cell cultures using Transwell polycarbonate membrane (Corning Costar Co. Ltd., Cambridge, MA), 1×10^3 Hep G2 and 1×10^4 normal liver sinusoidal endothelial cells were cultured with CS-C medium in upper and lower dishes, respectively, as shown in Fig. 5. Neutralizing goat anti-FGF-1 and goat antihuman VEGF-165 and VEGF-121 antibodies were purchased from Genzyme/Techne (MPLS, Minneapolis, MN). Neutralizing murine monoclonal anti-FGF-2 was purchased from Wako Pure Chemical Industries, Ltd. (Osaka, Japan). Normal goat IgG and murine monoclonal antibody directed against *Trichosporon beigelii*, which were prepared in our labora-

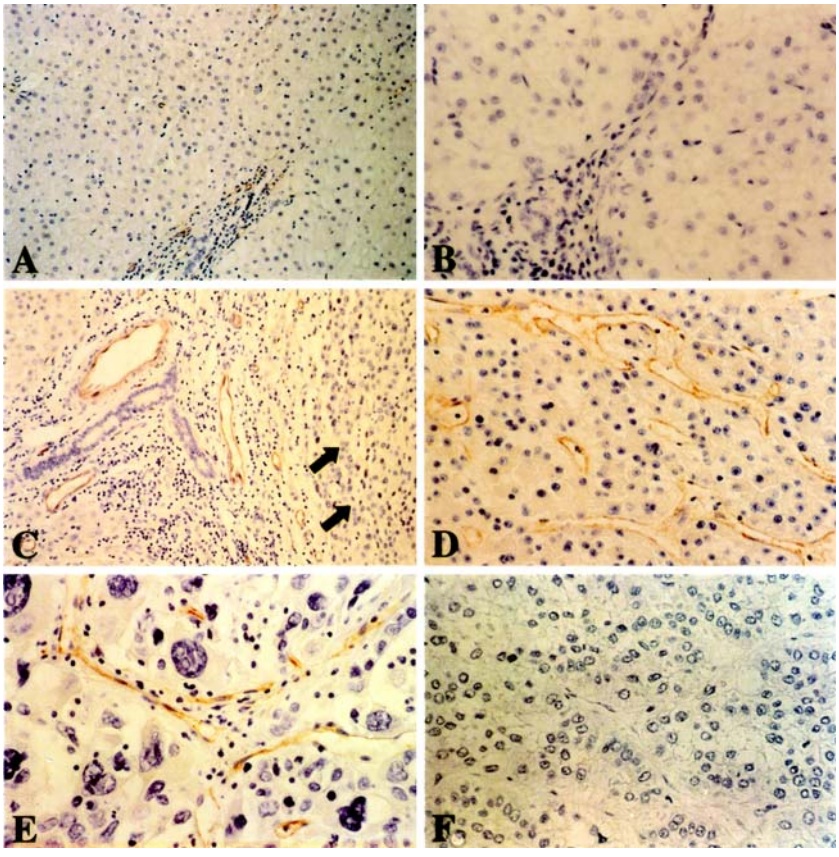

Fig. 1 Representative immunohistochemical staining of noncancerous liver and HCC tissues with anti-T-cadherin antibody. Hepatocytes and sinusoidal endothelial cells in noncancerous liver were not stained with anti-T-cadherin antibody (**a**). T-cadherin expression was not observed in sinusoidal endothelial cells in liver cirrhosis (**b**). Intratumoral capillary endothelial cells of 9 of 12 well-differentiated HCC specimens did not express a detectable level of T-cadherin (**c**; *arrow* indicates well-differentiated HCC region in liver cirrhosis specimen). T-cadherin expression was restricted in the artery or large vessels in Glisson's sheath. T-cadherin expression was observed in intratumoral capillary endothelial cells in moderately to poorly differentiated HCC (**d** and **e**). Preadsorption with T-cadherin peptide eliminated staining of endothelium (**f**). Note that HCC cells were not stained with anti-T-cadherin antibody (**c**–**e**). Original magnifications were ×100 (**a** and **c**), ×200 (**b**, **d**, and **f**), and ×640 (**e**)

tories, were also used as control antibodies. Notably, a previous study demonstrated that this murine monoclonal antibody does not react with human tissues, including liver tissues [32]. Antibodies were added to the lower dishes at a final concentration of 10 μg/ml. After culturing for 2 days, liver sinusoidal endothelial cells were harvested. T-cadherin expression was examined by Western immunoblotting as previously described [27]. To exclude the effect of additive in the CS-C medium, the cells were also cultured with Dulbecco's modified Eagle's media (DMEM) and 10% FBS in several experiments.

Several previous studies demonstrated that cultured HCC cells, including Hep-G2-cell-expressed FGF-2 [1]. We also confirmed that cultured Hep G2 cells in our laboratory also secreted FGF-2 by using enzyme-linked immunosorbent assay (ELISA). Briefly, Hep G2 cells were plated in 96-well culture dish plates and allowed to grow at full sheet in DMEM and 10% FBS. After 24 h, the culture medium was changed to DMEM without FBS and further incubated for 2 days. Finally, FGF-2 in culture supernatants were quantified using a standard sandwich ELISA kit (Quantikine FGF basic, R&D Systems Inc, Minneapolis, MN) following the manufacturer's instructions.

Results

T-cadherin was expressed in tumor endothelial cells of HCC

The results of immunohistochemical staining of human HCC are summarized in Table 1, and representative cases are demonstrated in Fig. 1. T-cadherin expression was restricted in the arterial endothelium and not observed in hepatocytes or in the sinusoidal endothelium of nontumorous liver tissues (Fig. 1a). Neither hepatocytes nor sinusoidal endothelial cells of liver cirrhosis were stained with anti-T-cadherin antibody (Fig. 1b). In contrast, staining with anti-T-cadherin antibody was observed in tumor sinusoidal endothelium of 34 out of 63 specimens, where a specimen is considered T-cadherin-positive when more than 10% of tumor vessels are stained. Notably, T-cadherin expression was not uniform but instead was observed focally (less than 30%) in three positive well-differentiated HCC cases. By contrast, T-cadherin was diffusely (more than 80%) expressed in most moderately positive to poorly differentiated HCC specimens. Preadsorption of antibody with T-cadherin peptide eliminated all staining (Fig. 1f) and verified the specificity of the antibody used in the present study.

Next, we asked whether T-cadherin expression was related to pathological factors of HCC. T-cadherin staining was related to differentiation of HCC. Three of 12 (25%), 15 of 29 (52%), and 16 of 22 (73%) HCC specimens diagnosed as well, moderately, and poorly differentiated types, respectively, were positive for T-cadherin staining (Fig. 1c–e). Significant differences were observed between well- and poorly differentiated HCC (p=0.007). However, all other pathological parameters, including the status of nonneoplastic liver tissues adjacent to HCC (cirrhosis or hepatitis) examined, were not significantly related to T-cadherin expression (Table 1).

We further examined five tissue specimens, which contained variously differentiated HCC components. Interestingly, T-cadherin expression was again much found in a less-differentiated region in individual specimens (Fig. 2).

A previous study clearly demonstrated that liver sinusoidal endothelial cells also expressed LYVE-1, whereas

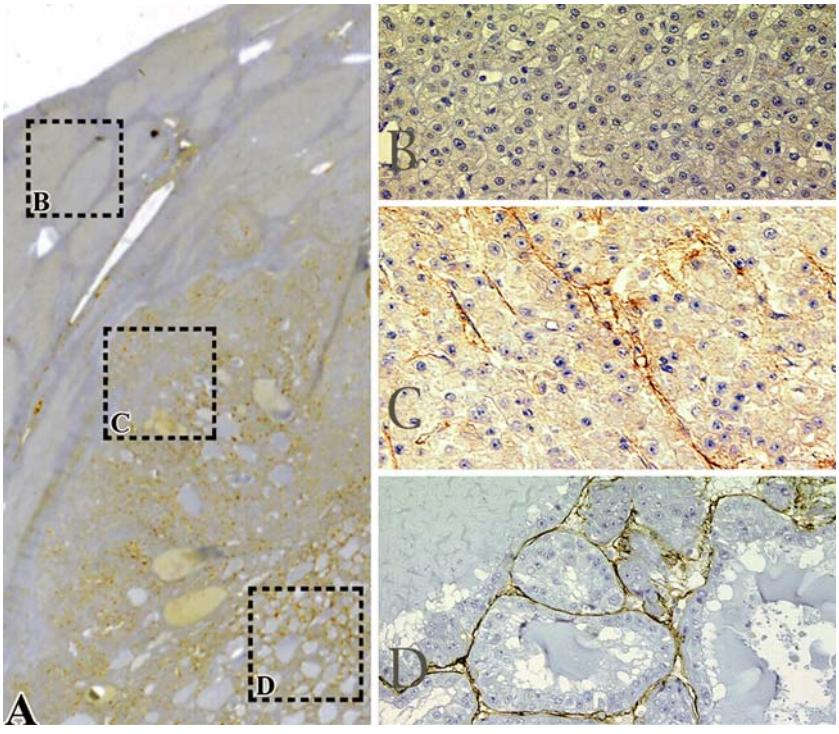

Fig. 2 Representative immunohistochemical staining of HCC tissues, which contained various differentiated cancer foci, with anti-T-cadherin antibody. In this tissue specimen, moderately differentiated HCC, in which pseudoglandular proliferation was observed, was found in the center of a well-differentiated HCC region (**a**). Note that sinusoidal endothelial cells in noncancerous liver cirrhosis were not stained with anti-T-cadherin antibody (**b**). In contrast, immunoreactivity was focally found in well-differentiated HCC (**c**), whereas almost all intratumoral capillary endothelial cells were strongly stained in a moderately differentiated region (**d**). Original magnifications were ×4 (**a**), ×100 (**d**), ×200 (**b**), and ×400 (**c**)

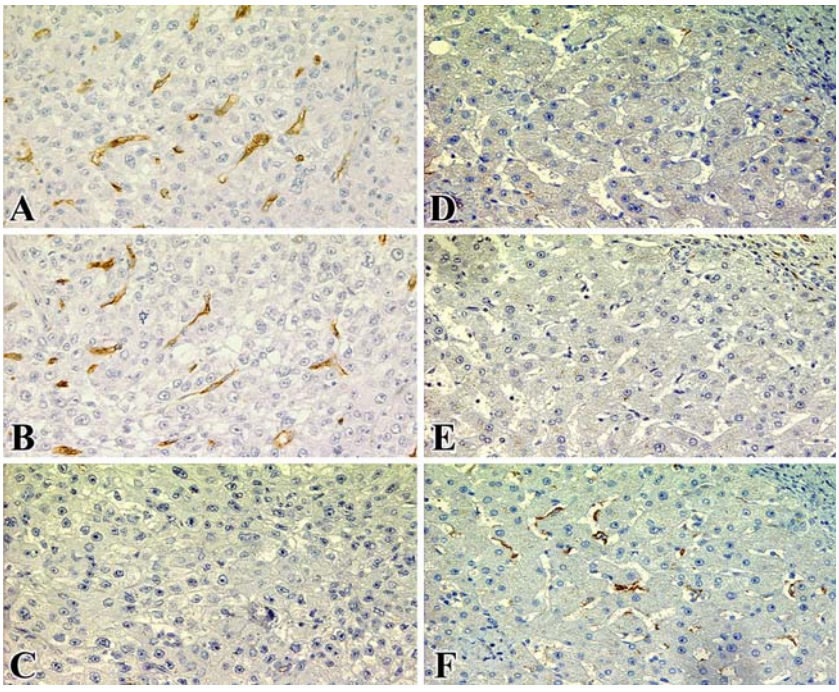

Fig. 3 T-cadherin, CD34, and LYVE-1 expression in HCC (**a**–**c**) and chronic hepatitis (**d**–**e**). In this HCC tissue specimen, both T-cadherin (**a**) and CD34 (**b**) immunoreactivity was observed in intratumoral capillary endothelial cells. By contrast, any significant LYVE-1 immunoreactivity was not found in HCC specimen (**c**). Neither T-cadherin (**d**) nor CD34 expression was found in chronic hepatitis specimens, whereas LYVE-1 was barely expressed in sinusoidal endothelial cells in chronic hepatitis (**f**). Original magnifications were ×200

intratumoral capillary endothelial cells expressed little LYVE-1 [20]. In the present study, we examined the correlation of LYVE-1 and T-cadherin expression. As previously reported by Mouta Carreira et al. [20], LYVE-1 was barely expressed in intratumoral endothelial cells in HCC. Any significant overlap expression of T-cadherin and LYVE-1 was not observed in intratumoral capillary endothelial cells in HCC specimens. The median tumor microvascular density of T-cadherin-positive HCC was 56.6, whereas the median tumor microvascular density of T-cadherin-negative HCC was 59.4. Thus, any significant correlation between T-cadherin expression and the microvascular density was observed in the present study. Representative results were demonstrated in Fig. 3.

These findings indicate that T-cadherin molecules were selectively expressed in a tumor surrounding sinusoidal endothelial cells of HCC, especially in poorly differentiated HCC. Since less differentiated HCC may be developed from a well-differentiated HCC region in an individual patient, T-cadherin expression may be increasingly induced in sinusoidal endothelial cells as the tumor progressed.

mRNA expression in tumor endothelial cells

Our ongoing experiments demonstrated that soluble T-cadherin molecules were present in serum using the sensitive sandwich ELISA assay (unpublished data). Consequently, we examined the possibility that soluble T-cadherin molecules adhered to tumor endothelium using in situ hybridization. Positive signals were observed in tumor sinusoidal

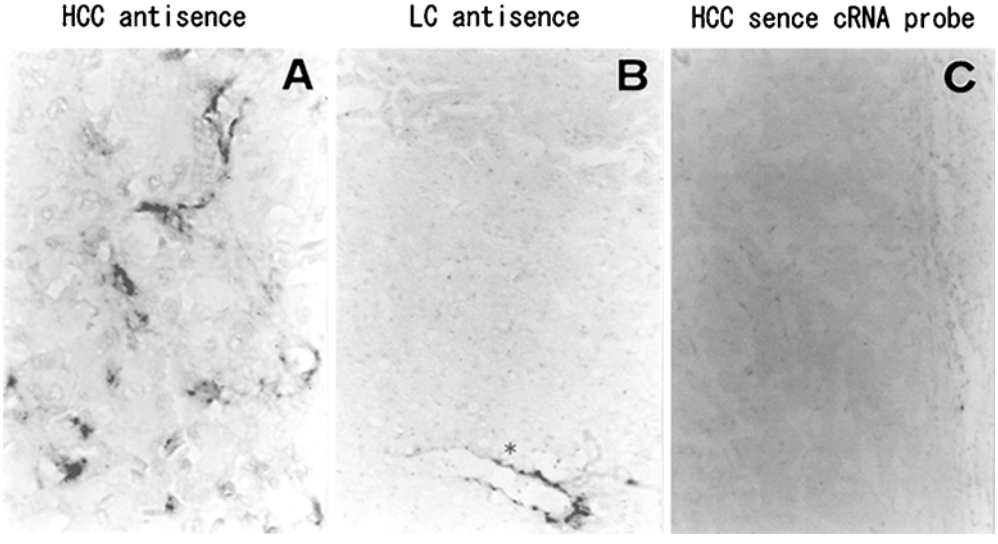

Fig. 4 In situ hybridization of human HCC (**a** and **c**) and liver cirrhosis specimens from the same patient (**b**). Tumor sinusoid endothelium demonstrated positive signals with the antisense T-cadherin probe (**a**). However, positive signals were not observed in liver cirrhosis specimens except in arterial endothelium (indicated by *) in Glisson's sheath (**b**). No significant signals were detected with sense probe in HCC specimens (**c**). Original magnification was ×400 (**a**–**c**)

endothelium of HCC specimens with the antisense cRNA probe of T-cadherin (Fig. 4a). Artery endothelial cells, but not sinusoidal endothelium from liver cirrhosis, were stained with the antisense probe (Fig. 4b). No significant reactivity was observed with the control sense cRNA probe (Fig. 4c). These results indicate that tumor endothelial cells express T-cadherin mRNA, and consequently, we excluded the possibility that partially degraded or soluble T-cadherin were adsorbed at the cell surface of tumor endothelial cells. Notably, we did not detect T-cadherin mRNA in nonneoplasmic hepatocytes or HCC cells.

Double-chamber cell culture

As described in the "Introduction," VEGF and FGF-2 regulate the endothelial cell growth in HCC by a paracrine manner. We speculated that T-cadherin was also an important molecule, which played a role in the VEGF- or FGF-2-mediated cross talk between neoplastic hepatocytes and sinusoidal endothelial cells. Therefore, we decided to investigate the induction of T-cadherin on sinusoidal endothelial cells by using a double-chamber cell culture.

Cultured nontumorous liver sinusoidal endothelial cells did not express T-cadherin (Fig. 5a). In contrast, sinusoidal endothelial cells in lower compartments of the double-chamber cell culture, in which the upper chamber contained Hep G2 HCC cells, expressed T-cadherin, as shown in Fig. 5b. Therefore, we conclude that humoral factors secreted from Hep G2 HCC cells induced expression of T-cadherin molecules in liver sinusoidal endothelial cells.

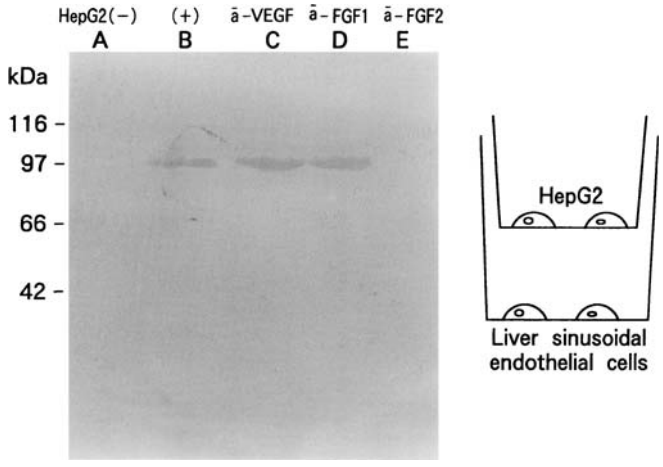

Fig. 5 Western immunoblotting of cultured liver sinusoidal endothelial cells. Double-chamber culture was performed as illustrated in the *right column* with or without Hep G2 cells. No significant band was detected in cultured human liver sinusoidal cells alone by Western immunoblotting by using anti-T-cadherin antibody (**a**). In contrast, an approximately 100-kDa band was observed in liver sinusoidal cells when they were double-chamber-cultured with Hep G2 human HCC cells (**b**). An identical 100-kDa band was also observed in sinusoidal endothelial cells in double-chamber culture with neutralizing antibody to VEGF and FGF-1 (**c** and **d**, respectively). However, neutralizing antibody to FGF-2 markedly reduced T-cadherin expression in sinusoidal endothelial cells in double-chamber culture (**e**) even in the presence of Hep G2 in the upper chamber

Neither neutralizing anti-FGF-1 nor VEGF were able to inhibit induction of T-cadherin in sinusoidal endothelial cells (Fig. 5c and d, respectively). In contrast, neutralizing anti-FGF-2 inhibited T-cadherin expression in double-chamber cell cultures, as shown in Fig. 5e. ELISA assay clearly demonstrated that cultured Hep G2 secreted FGF-2. Neither control goat IgG nor murine monoclonal antibody inhibited T-cadherin expression in double-chamber cell cultures. Although we could not exclude the possibility that other humoral factors were also involved in T-cadherin expression, it is likely that FGF-2 plays a critical role in the induction of T-cadherin molecules in sinusoidal endothelial cells.

In addition, there are two major forms of T-cadherin, a mature 100-kDa molecule and a premature partially processed 130-kDa molecule. The present data indicate that mature T-cadherin molecules were induced in cultured sinusoidal endothelial cells in the double-chamber assay and validated again the specificity of the antibody used in this study.

The consistent result was obtained by using DMEM supplemented with 10% FBS instead of CS-C medium.

Discussion

T-cadherin is believed to be a tumor suppressor gene, the promoter region of which is often hypermethylated in a wide variety of malignant tumors (see 35 for a review). T-cadherin is silenced in the tumor cells of the breast, lung, urinary bladder, colon, skin, chronic myeloid leukemia, and pancreas [14, 17, 28, 29, 31, 36, 37, 40, 41]. In contrast, Riou et al. [27] demonstrated that the mRNA expression of the CDH13 gene is higher in HCC than in normal or nontumorous liver tissues using real-time quantitative PCR. Is T-cadherin overexpressed in HCC cells? The answer to this question is currently unknown since, to our knowledge, there is no research available that demonstrates the precise T-cadherin distribution in noncancerous liver and HCC tissues.

The immunohistochemical staining presented here demonstrates that T-cadherin was not expressed in nonneoplasmic hepatocytes or HCC cells but selectively expressed in intratumoral capillary endothelial cells. It is likely that highly sensitive PCR can detect T-cadherin mRNA expression in the tumor endothelium of HCC tissues. However, this would not mean that T-cadherin is overexpressed in HCC cells. We suggest that T-cadherin overexpression in tumor endothelium should be considered when examining whether T-cadherin was silenced in malignant tumors. Silencing of T-cadherin expression may be overwhelmed in the presence of T-cadherin expressed in the tumor endothelium. To elucidate these problems, immunohistochemical or in situ hybridization should be performed in parallel.

The present findings indicated that T-cadherin might be increasingly expressed in tumor surrounding sinusoidal endothelial cells as HCC progressed. Therefore, it is likely that T-cadherin may positively mediate tumor angiogenesis in HCC. Recently, T-cadherin appeared to be a receptor for

hexametric and HMW forms of adiponectin [10]. Adiponectin is a kind of adipocytokine, and it is found in the serum in trimer, hexamer, and HMW forms. Regarding the effect of adiponectin on neovascularization, several discordant results have been reported (see 8 for a review). Hexametric and HMW forms of adiponectin activate NF-κB activity [39] and inhibit apoptosis of endothelial cells [13]. Full-length adiponectin stimulates the differentiation of human-umbilical-vein endothelial cells into a capillary-like structure [25]. Adiponectin can also stimulate new blood vessel growth by promoting cross talk between adenosine monophosphate (AMP)-activated protein kinase and Akt signaling [25]. In contrast, recombinant adiponectin induces apoptosis in endothelial cells and inhibits tumor neovascularization [2]. T-cadherin bound hexametric and HMW adiponectin, but it did not bind to trimetric or bacterial-recombinant adiponectin [10]. Combined together, we speculate that T-cadherin molecules on tumor endothelial cells may bind hexamer and/or HMW adiponectin, activate NF-κB, and prevent apoptosis of tumor endothelial cells during reorganization and angiogenesis of tumor vessels. However, we cannot discriminate the possibility that T-cadherin in intratumoral capillary endothelial cells play a role in tumor angiogenesis by an unknown mechanism, which is apart from the role of an adiponectin receptor. However, it may be unlikely that T-cadherin in intratumoral endothelial cells directly interacted with other cadherin molecules since each cadherin molecule has a homophilic binding activity. In fact, a previous study demonstrated that no systematic difference in VE-cadherin, another endothelial cell cadherin molecule [38], was found between HCC and nontumorous liver tissues [4].

The present study indicated that FGF-2 might play an important role in the induction of T-cadherin in liver sinusoidal endothelial cells. Several studies have reported that FGF-2 secreted from HCC cells plays an important role in angiogenesis of HCC [16, 18, 23]. Motoo et al. immunohistochemically examined HCC and found that capillarized sinusoids were significantly more numerous in FGF-positive cases than in FGF-negative cases [19]. Notably, plasma levels of FGF-2 were elevated to a greater extent in HCC patients compared to patients with chronic hepatitis and liver cirrhosis [12]. Combined with these previous studies, we suggest that FGF-2 secreted from HCC cells may facilitate T-cadherin (a unique adiponectin receptor) expression in the tumor endothelium by a paracrine manner and attribute the tumor neovascularization to activate the adiponectin-dependent pathway. Notably, Ivanov et al. recently reported that exogenously overexpressed T-cadherin stimulated the proliferation of human umbilical endothelial cells [11].

In conclusion, the current study presents three key results. First, T-cadherin expression was restricted to the arterial endothelium in noncancerous liver tissues and was not expressed in hepatocytes or HCC cells. Second, T-cadherin was selectively expressed in intratumoral capillary endothelial cells in many HCC specimens and may be increasingly expressed as the tumor progressed. Last, FGF-2 appeared to play a critical role to induce T-cadherin on sinusoidal endothelial cells; thus, a cross talk between adiponectin-T-cadherin and FGF-2 pathways is suggested.

Acknowledgements We thank Mr. Yamaguchi, Takuya, Ms. Nakamura, Naoyo (Department of Pathology, Kochi Medical School), and Ms. Matumura, Rumi (Division of Molecular Biology, Kochi Medical School) for skillful technique. This study was supported by grants from the Ministry of Education of Japan (KAKEN 12670165, 13670177, and 17590270) and the Medical Research Fund of Kochi Medical School.

References

1. Asada N, Tanaka Y, Hayashido Y, Toratani S, Kan M, Kitamoto M, Nakanishi T, Kajiyama G, Chayama K, Okamoto T (2003) Expression of fibroblast growth factor receptor genes in human hepatoma-derived cell lines. In Vitro Cell Dev Biol Anim 39:321–328
2. Bråkenhielm B, Veitonmäki N, Cao R, Kihara S, Matsuzawa Y, Zhivotovsky B, Fukuhashi T, Cao Y (2004) Adiponectin-induced antiangiogenesis and antitumor activity involve caspase-mediated endothelial cell apoptosis. Proc Natl Acad Sci U S A 101:2476–2481
3. Carmeliet P, Jain RK (2000) Angiogenesis in cancer and other diseases. Nature 407:249–257
4. Chen X, Cheung ST, So S, Fan ST, Barry C, Higgins J, Lai KM, Ji J, Dudoit S, Ng IO, Van De Rijn M, Botstein D, Brown PO (2002) Gene expression patterns in human liver cancers. Mol Biol Cell 13:1929–1939
5. Edmonson HA, Steiner PE (1954) Primary carcinoma of the liver: a study of 100 among 489,000 necropsies. Cancer (Phila), 7:462–503
6. Edwards S, Lalor PF, Nash GB, Rainger GE, Adams DH (2005) Lymphocyte traffic through sinusoidal endothelial cells is regulated by hepatocytes. Hepatology 41:451–459
7. Gibson JB, Sobin LH (1978) Histological typing of tumors of the liver, biliary tract and pancreas. In: International Histological Classification of Tumors. World Health Organization, Geneva 19–25
8. Goldstein BJ, Scalia R (2004) Adiponectin: a novel adipokine linking adipocytes and vascular function. J Clin Endocrinol Metab 89:2563–2568
9. Huang ZY, Wu Y, Hedrick N, Gutmann DH (2003) T-cadherin-mediated cell growth regulation involves G2 phase arrest and requires p21(CIP1/WAF1) expression. Mol Cell Biol 23:566–578
10. Hug C, Wang J, Ahmad NS, Bogan JS, Tsao TS, Lodish HF (2004) T-cadherin is a receptor for hexameric and high-molecular-weight forms of Acrp30/adiponectin. Proc Natl Acad Sci U S A 101:10308–10313
11. Ivanov D, Philippova M, Allenspach R, Erne P, Resink T (2004) T-cadherin upregulation correlates with cell-cycle progression and promotes proliferation of vascular cells. Cardiovasc Res 64:132–143
12. Jin-no K, Tanimizu M, Hyodo I, Kurimoto F, Yamashita T (1997) Plasma level of basic fibroblast growth factor increases with progression of chronic liver disease. J Gastroenterol 32:119–121
13. Kobayashi H, Ouchi N, Kihara S, Walsh K, Kumada M, Abe Y, Funahashi T, Matsuzawa Y (2004) Selective suppression of endothelial cell apoptosis by the high molecular weight form of adiponectin. Circ Res 94:27–31
14. Lee SW (1996) H-cadherin, a novel cadherin with growth inhibitory functions and diminished expression in human breast cancer. Nat Med 2:776–782

15. Li X, Massa PE, Hanidu A, Peet GW, Aro P, Savitt A, Mische S, Li J, Marcu KB (2002) IKKalpha, IKKbeta, and NEMO/IKKgamma are each required for the NF-kappa B-mediated inflammatory response program. J Biol Chem 277:45129–45140
16. Maret A, Galy B, Arnaud E, Bayard F, Prats H (1995) Inhibition of fibroblast growth factor 2 expression by antisense RNA induced a loss of the transformed phenotype in a human hepatoma cell line. Cancer Res 55:5075–5079
17. Maruyama R, Toyooka S, Toyooka KO, Harada K, Virmani AK, Zochbauer-Muller S, Farinas AJ, Vakar-Lopez F, Minna JD, Sagalowsky A, Czerniak B, Gazdar AF (2001) Aberrant promoter methylation profile of bladder cancer and its relationship to clinicopathological features. Cancer Res 61: 8659–8663
18. Mise M, Arii S, Higashituji H, Furutani M, Niwano M, Harada T, Ishigami S, Toda Y, Nakayama H, Fukumoto M, Fujita J, Imamura M (1996) Clinical significance of vascular endothelial growth factor and basic fibroblast growth factor gene expression in liver tumor. Hepatology 23:455–464
19. Motoo Y, Sawabu N, Yamaguchi Y, Terada T, Nakanuma Y (1993) Sinusoidal capillarization of human HCC: possible promotion by fibroblast growth factor. Oncology 50:270–274
20. Mouta Carreira C, Nasser SM, di Tomaso E, Padera TP, Boucher Y, Tomarev SI, Jain RK (2001) LYVE-1 is not restricted to the lymph vessels: expression in normal liver blood sinusoids and down-regulation in human liver cancer and cirrhosis. Cancer Res 61:8079–8084
21. Nagafuchi A, Takeichi M (1988) Cell binding function of E-cadherin is regulated by the cytoplasmic domain. EMBO J 7:3679–3684
22. Nakamura S, Muro H, Suzuki S, Sakaguchi T, Konno H, Baba S, Syed AS (1997) Immunohistochemical studies on endothelial cell phenotype in hepatocellular carcinoma. Hepatology 26:407–415
23. El-Assal ON, Yamanoi A, Ono T, Kohno H, Nagasue N (2001) The clinicopathological significance of heparanase and basic fibroblast growth factor expressions in HCC. Clin Cancer Res 7:1299–1305
24. Oshima RG, Lesperance J, Munoz V, Hebbard L, Ranscht B, Sharan N, Muller WJ, Hauser CA, Cardiff RD (2004) Angiogenic acceleration of Neu induced mammary tumor progression and metastasis. Cancer Res 64:169–179
25. Ouchi N, Kobayashi H, Kihara S, Kumada M, Sato K, Inoue T, Funahashi T, Walsh K (2004) Adiponectin stimulates angiogenesis by promoting cross-talk between AMP-activated protein kinase and Akt signaling in endothelial cells. J Biol Chem 279:1304–1309
26. Ranscht B, Dours-Zimmermann MT (1991) T-cadherin, a novel cadherin cell adhesion molecule in the nervous system, lacks the conserved cytoplasmic region. Neuron 7:391–402
27. Riou P, Saffroy R, Comoy J, Gross-Goupil M, Thiery JP, Emile JF, Azoulay D, Piatier-Tonneau D, Lemoine A, Debuire B (2002) Investigation in liver tissues and cell lines of the transcription of 13 genes mapping to the 16q24 region that are frequently deleted in hepatocellular carcinoma. Clin Cancer Res 8:3178–3186
28. Roman-Gomez J, Castillejo JA, Jimenez A, Cervantes F, Boque C, Hermosin L, Leon A, Granena A, Colomer D, Heiniger A, Torres A (2003) Cadherin-13, a mediator of calcium-dependent cell–cell adhesion, is silenced by methylation in chronic myeloid leukemia and correlates with pretreatment risk profile and cytogenetic response to interferon alfa. J Clin Oncol 21:1429–1472
29. Sakai M, Hibi K, Koshikawa K, Inoue S, Takeda S, Kaneko T, Nakao A (2004) Frequent promoter methylation and gene silencing of CDH13 in pancreatic cancer. Cancer Sci 95:588–591
30. Sakamoto M, Ino Y, Fujii T, Hirohashi S (1993) Phenotype changes in tumor vessels associated with the progression of hepatocellular carcinoma. Jpn J Clin Oncol 23:98–104
31. Sato M, Mori Y, Sakurada A, Fujimura S, Horii A (1998) The H-cadherin (CDH13) gene is inactivated in human lung cancer. Hum Genet 103:96–101. Erratum in: Hum Genet (1998) 103:532
32. Takeuchi T, Kobayashi M, Moriki T, Miyoshi I (1988) Application of a monoclonal antibody for the detection of *Trichosporon beigelii* in paraffin-embedded tissue sections. J Pathol 15: 23–27
33. Takeuchi T, Misaki A, Chen BK, Ohtsuki Y (1999) H-cadherin expression in breast cancer. Histopathology 35:87–88
34. Takeuchi T, Misaki A, Liang S-B, Tachibana A, Hayashi N, Sonobe H, Ohtsuki Y (2000) Expression of T-cadherin (CDH13, H-cadherin) in human brain and its characteristics as a negative growth regulator of EGF in neuroblastoma cells. J Neurochem 74:1489–1497
35. Takeuchi T, Ohtsuki Y (2001) Recent progress of T-cadherin (CDH13, H-cadherin) research. Histol Histopathol 16:1287–1293
36. Takeuchi T, Liang SB, Matsuyoshi N, Zhou S, Miyachi Y, Sonobe H, Ohtsuki Y (2002a) Loss of T-cadherin (CDH13, H-cadherin) expression in cutaneous squamous cell carcinoma. Lab Invest 82:1023–1029
37. Takeuchi T, Liang SB, Ohtsuki Y (2002b) Downregulation of expression of a novel cadherin molecule, T-cadherin, in basal cell carcinoma of the skin. Mol Carcinog 35:173–179
38. Salomon D, Ayalon O, Patel-King R, Hynes RO, Geiger B (1992) Extrajunctional distribution of N-cadherin in cultured human endothelial cells. J Cell Sci 102:7–17
39. Tsao TS, Murrey HE, Hug C, Lee DH, Lodish HF (2002) Oligomerization state-dependent activation of NF-kappa B signaling pathway by adipocyte complement-related protein of 30 kDa (Acrp30). J Biol Chem 277:29359–29362
40. Toyooka KO, Toyooka S, Virmani AK, Sathyanarayana UG, Euhus DM, Gilcrease M, Minna JD, Gazdar AF (2001) Loss of expression and aberrant methylation of the CDH13 (H-cadherin) gene in breast and lung carcinomas. Cancer Res 61:4556–4560
41. Toyooka S, Toyooka KO, Harada K, Miyajima K, Makarla P, Sathyanarayana UG, Yin J, Sato F, Shivapurkar N, Meltzer SJ, Gazdar AF (2002) Aberrant methylation of the CDH13 (H-cadherin) promoter region in colorectal cancers and adenomas. Cancer Res 62:3382–3386
42. Wyder L, Vitaliti A, Schneider H, Hebbard LW, Moritz DR, Wittmer M, Ajimo M, Klemenz R (2000) Increased expression of H/T-cadherin in tumor penetrating blood vessels. Cancer Res 60:4682–4688
43. Zhou S, Matsuyoshi N, Liang SB, Takeuchi T, Ohtsuki Y, Miyachi Y (2002) Expression of T-cadherin in basal keratinocytes of skin. J Invest Dermatol 118:1080–1084

Virchows Arch (2006) 448: 319–324
DOI 10.1007/s00428-005-0092-2

ORIGINAL ARTICLE

Eva Compérat · Philippe Camparo · Rachel Haus · Emmanuel Chartier-Kastler · Stephane Bart · Annick Delcourt · Alain Houlgatte · Richard François · Fréderique Capron · Annick Vieillefond

Immunohistochemical expression of p63, p53 and MIB-1 in urinary bladder carcinoma. A tissue microarray study of 158 cases

Received: 9 December 2004 / Accepted: 6 February 2005 / Published online: 8 November 2005

Abstract P63 is a member of the p53 family, which plays a role in the differentiation of urothelium and is supposed to play a role in urothelial carcinogenesis. P53 and MIB-1 are recognised in many studies as predictive markers of progression, but few studies in the literature have examined p63. The aims of our study were to explore the expression of p63 in bladder carcinomas and to compare this expression to p53 and MIB-1, as well as to stage and grade. Tissue microarrays were performed on 158 urothelial carcinomas (56 pTa, 45 pT1 and 57≥pT2). Immunohistochemical studies were performed with p63, p53 and MIB-1 antibodies. In our study we observed that p63 immunostaining is present in all cell layers in papillary urothelial neoplasm of low malignant potential (PUNLMP), but partially lost in non-invasive papillary urothelial carcinoma low grade (NILGC) and in pT1/≥pT2 bladder cancers. P53 and MIB-1 displayed lower expression in PUNLMP/NILGC vs non-invasive papillary urothelial carcinoma high grade (NIHGC)/pT1, but there was no correlation between the expression of p63, p53 and MIB-1. Our study demonstrates that p63 expression distinguishes between PUNLMP/NILGC and NIHGC/pT1 (p=4.10^5). A statistical difference disserving pTa and pT1/≥pT2 with a statistical significance (p<10^{-6}) could also be observed. P63 should be considered as an additional biomarker that might help pathologists to classify their patients.

Keywords Bladder cancer · Immunohistochemistry · MiB-1 · p53 · p63

E. Compérat (✉) · E. Chartier-Kastler · S. Bart · A. Delcourt · R. François · F. Capron
Service Central d'Anatomie et Cytologie Pathologiques et d'Urologie Hôpital La Pitié-Salpêtrière 83, Bd de l'Hôpital,
75013 Paris, France
e-mail: evacomperat@yahoo.fr
Tel.: +33-1-58411465

P. Camparo · R. Haus · A. Houlgatte
Service Central d'Anatomie et Cytologie Pathologiques et d'Urologie,
Departement d'Epidemiologie et de Santé Publique Nord,
Hôpital d'Instructions des Armée Val-de Grace,
74 boulevard Port Royal,
75230 Paris, France

A. Vieillefond
Service Central d'Anatomie et Cytologie Pathologiques
Groupe hospitalier Cochin,
Saint Vincent de Paul 27,
rue du Faubourg Saint Jaques,
75679 Paris, Cedex 14, France

Introduction

Urothelial carcinomas (UC) are divided into three groups: pTa, pT1 and ≥pT2 disease, regarding the local extension. PTa bladder cancers have a variable recurrence rate and progression [13, 16, 20, 40]. In papillary urothelial neoplasm of low malignant potential (PUNLMP) or non-invasive papillary urothelial carcinoma low grade (NILGC), recurrence varies from 25 to 70%, and few progress towards higher grade or invasive tumors. On the other hand, 15 to 20% of pTa non-invasive papillary urothelial carcinoma high grade (NIHGC) and up to 30% of pT1 tumors develop towards pT2, with muscular invasion and poor clinical outcome [16, 33]. To date, although many investigations have been made, no immunohistochemical marker has proved to be specific to predict clinical outcome in patients with NIHGC or pT1 urothelial carcinomas [32].

p63 is a member of the p53 family located on chromosome 3q27–28. Several studies have shown that p63 seems to play a key role in differentiation of transitional epithelium [44, 48]. Two main isoforms (TAp63 and ΔNp63) with different functions are known. It seems that TAp63 isoform is required for initiation of epithelial stratification and maintains a proliferative potential of basal cell, while ΔNp63 allows cells to respond to signals required for maturation.

In normal bladder, TAp63 has been shown to be expressed in basal cells, whereas ΔNp63 is absent or weakly expressed in these cells [3, 28]. In bladder carcinomas, elevated expression of ΔNp63 and decreased expression of

TAp63 has been observed [28]. These results suggest that ΔNp63 might contribute to progression of bladder carcinomas. Some authors have proposed that p63 could therefore be a prognostic marker. But results of variation in p63 expression and its role in bladder cancer development still remains controversial [17, 19, 28, 44].

As a member of the p53 family, p63 shows strong structural similarities with p53 [8], and biochemical interactions of these two proteins exist [21, 24]. *p53* gene is a well-known tumor suppressor gene that play a key role in cellular damage response and cell-cycle arrest [22]. Loss of p53 function is a frequent finding in all kind of cancers where mutant inactive forms may easily be detectable.

Proliferation index Ki-67 (MIB-1), a marker for cellular proliferation, is a nuclear protein complex expressed in the G1, S, G2 and M phases of the cell cycle of proliferating cells.

Immunohistochemical investigations with p53 and MIB-1 have shown to be predictive markers in the progression of bladder cancer [34, 37, 47]. p53 over-expression has shown to be associated with grade and stage [12, 39] and correlated with recurrence in pTa and T1 cancers as well as tumor progression [12, 22, 37], but its association with overall survival and clinical outcome is still controversial [12, 22]. Studies concerning MIB-1 have underlined the predicting potential of MIB-1 concerning recurrence rates especially in PUNLMP [35, 44]. Increased and diffuse-labelling index of MIB-1 is observed in non-invasive high-grade and invasive high-grade carcinomas [10, 11]. Taken together, p53 and MIB-1 seem to be powerful predictors of tumor recurrence for patients especially with non-muscle invasive transitional cell carcinoma [34].

Using tissue micro arrays (TMA) for immunohistochemical studies has been proven to be a very useful tool in exploration of large series of different tumors of tissues [14, 27, 30].

The aim of our study was to see whether (1) p63 expression varied according to grade and stage of bladder cancer, (2) there was a correlation between p63, p53 and MIB-1 expressions and (3) at least whether there existed a difference in the expression of p63 between the groups PUNLMP/NILGC vs NIHGC/pT1 and ≥pT2.

Materials and methods

This retrospective study concerned 158 patients who underwent either transurethral resection of non-invasive bladder tumors by transurethral resection or cystectomy for invasive bladder cancer between 2001 and 2004 in our establishments. We excluded from our study papillomas and carcinoma in situ as well as reactive atypia and dysplasia, because it is difficult to interpret these lesions with the TMA technique.

All tumor specimen and TMAs with immunohistochemical staining were evaluated by two experimental independent pathologists (E.C. and P.C.). The nuclear grading and the pT stage were adjusted according to the World Health Organization guidelines 2004 [45] into the following groups: pTa, (distinguishing PUNLMP, NILGC, NIHGC), pT1 and ≥pT2. The group ≥pT2 concerned pT2 to pT4 bladder cancers. Metastatic progression was not distinguished. The control group composed of 12 cases of non-tumoral bladder specimen from spinal cord-injuries patients were explored.

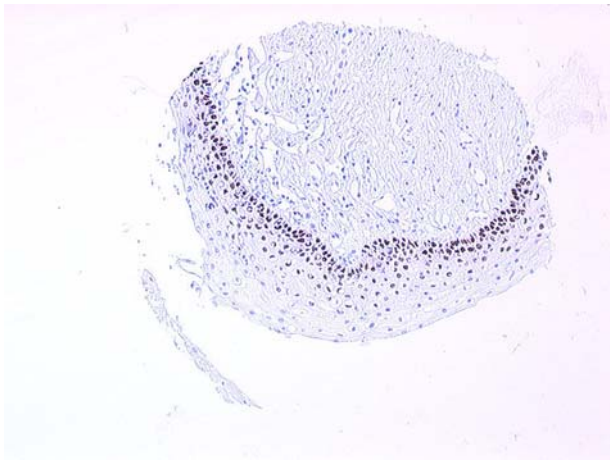

Fig. 1 Nuclear staining of p63 basal cell layers

Different TMAs have been confected for each pTa, pT1 and ≥pT2. At least three cylindrical score biopsies of 0.6 cm in diameter have been taken from each tumor. Different sites of each tumor were chosen and arrayed in a paraffin tissue bloc. Only scores with at least 200 malignant cells were scored. TMA sections (4 μm) were de-paraffinized and rehydrated, and immunohistochemistry was performed using the modified streptavidin–biotin–peroxidase method and diaminobenzidine as chromogen; an antigenic retrieval was used if necessary. The panel of antibodies included p63 (monoclonal, clone 4A4; Dako, 1/100), p53 (monoclonal, clone DO-7; Dako, ready to use) and MIB-1 (monoclonal; Dako, 1/50). Positive and negative controls were performed for each antibody. The evaluation of immunoreactivity was procured as follows: 200 cells were counted for each cylindrical score. p63 staining was considered positive if nuclear percentage

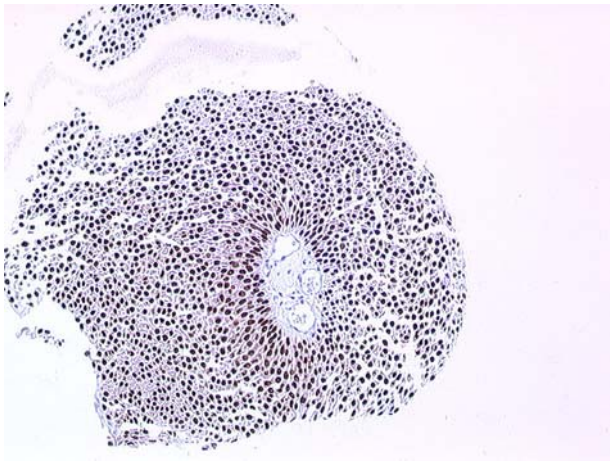

Fig. 2 Strong staining of all cell layers in pTa tumor (×100)

Table 1 Percentage of p63 in different stages

p63 (%)	pTa, *n*=56 (%)	pT1, *n*=45 (%)	pT2, *n*=57 (%)
0 (<10)	0/56 (0)	6/45 (13)	13/57 (23)
1 (10–80)	4/56 (7)	15/45 (34)	26/57 (46)
2 (>80)	52/56 (93)	24/45 (53)	18/57 (31)
Total	56 (100.0)	45 (100.0)	57 (100.0)

Table 2 Percentage of p63 in different grades

p63 (%)	PUNLMP, *n*=22 (%)	NILGC, *n*=26 (%)	NIHGC, *n*=8 (%)
<10	0 (0)	0 (0)	0 (0)
10–80	0 (0)	3 (12)	1 (12)
>80	22 (100)	23 (88)	7 (88)
Total	22 (100)	26 (100)	8 (100)

between 0 (stained cells <10%), 1 (>10% stained cells <80%) and 2 (stained cells >80–100%) was assessed. Regarding p53, tumors with nuclear immunoreactivity of more than 10% were considered positive according to other pervious studies [26, 27, 47].

For MIB-1, we evaluated the percentage of nuclear staining. MIB-1 staining of more than 10% was considered as positive.

Chi-square test was performed to compare categorical variables with the status of p63, p53 and MIB-1 expression.

Results

The population concerned 41 females and 117 males, mean age 68.5 years (extremes 38–94).

Stage pTa was present in 56 cases (36%) with 22/56 (39%) PUNLMP, 26/56 (47%) NILGC and 8/56 (14%) NIHGC. Forty-five cases (28%) were pT1, and 57 (36%) cases were ≥pT2.

p63

p63 expression in control bladder specimen displayed staining only on the basal layer; staining was always nuclear (Fig. 1). No staining was seen on smooth muscle cells, adipocytes or neural cells. Nuclear staining of lymphoid cells was rarely observed. The superficial layer constituted of umbrella cells never showed any immunoexpression.

In the pTa group, expression of p63 was always nuclear; cytoplasmic staining was rare and not considered. In 52/56 (93%) pTa cases, expression of p63 was homogenous, and intensity was considered as 2. Three NILGC and one NIHGC displayed a weaker heterogeneous expression; the percentage of stained cells in these cases was between 10 and 70% (score 1) (Fig. 2). In pT1 urinary bladder cancers, p63 staining was more heterogeneous. Six/forty-five cases (13%) lost p63 expression, 15/45 (34%) displayed weak staining (score 1) and 24/45 (53%) showed strong homogenous staining (score 2). These results are summarized in Table 1. Usually, loss of expression could be observed predominantly in the upper layers of transitional epithelium and could concern up to six layers, although punctual expression of p63 could be seen. In ≥pT2 cases, no immunostaining was observed in 13/57 (23%) cases, weak staining was seen in 26/57 (46%), and strong staining could be observed in 18/57 (31%) (Fig. 3).

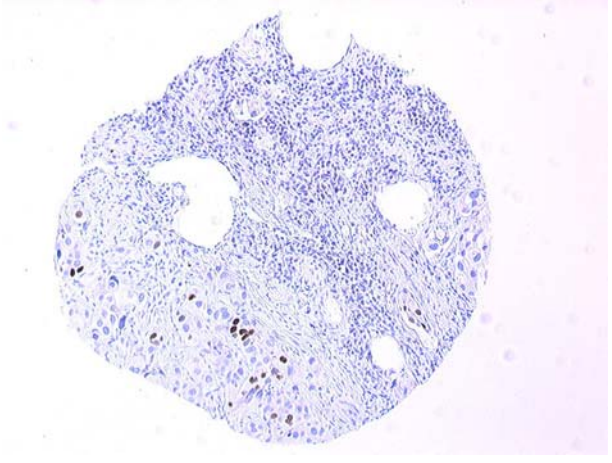

Fig. 3 Loss of p63 expression in ≥pT2 tumor (×100)

Statistical significant difference was found between PUNLMP/NILGC and NIHGC/pT1 groups (p=4.10^{-5}). Between pTa, pT1 and >pT2, statistical significant difference was also observed. p63 expression in pTa showed more often score 2 than pT1 and pT2 cases together (p<10−6), while p63 expression was more often score 1 in pT2 group vs pTa and pT1 (p=2.10^{-5}). According to the grade, no significant difference could be observed (p=1). Table 2 summarizes p63 expression in different grades of pTa.

p53

No p53 immunoreactivity was found in normal samples. Concerning the pTa group, p53 displayed nuclear expression in 7/22 PUNLMP (32%), in 10/26 NILGC (38%) and in 6/8 NIHGC (75%); expression was observed in 20–80% tumor cells. pT1 specimen showed expression in 37/45 (84%) cases and ≥pT2 specimen in 41/57 cases (72%).

Statistical significant difference was seen between pTa, pT1 and =pT2 (p=2.10^{-5}), with a stronger expression in the pT1 and pT2 groups.

Table 3 p53 and MIB-1 immunostaining

Positive antibody expression, (+/n)	PUNLMP/ NILGC, *n*=48 (%)	NIHGC, *n*=8 (%)	pT1, *n*=45 (%)	≥pT2, *n*=57 (%)
P53	17/48 (35)	6/8 (75)	37/45 (84)	41/57 (72)
MIB-1	2/48 (4)	2/8 (25)	32/45 (71)	45/57 (79)

Table 4 Comparison between p63 and p53 in global population

	p63<80%	p63>80%	Total (%)
p53<10%	16	40	56 (35)
P53>10%	48	54	102 (65)
Total (%)	64 (40)	94 (60)	158 (100)

No statistical significant difference could be observed between PUNLMP to NILGC/NIHGC (p=0, 25). Comparison between PUNLMP/NILGC vs NIHGC/pT1 showed statistical significant difference with 17/48 (35%) cases positive in the first group and 43/53 (83%) cases positive in the second group (p=10^{-6}).

MIB-1

No immunoreactivity was found in normal samples for MIB-1.

In bladder tumors, 75/157 (47%) displayed MIB-1 immunoreactivity. In the pTa group, 1/22 (2%) PUNLMP, 1/26 (3%) NILGC and 2/8 NIHGC (25%) displayed increased immunoreactivity with nuclear staining between 10 and 20%. In the pT1 group, two cases (3%) could not be evaluated, because of loss of transitional epithelium in TMA. Eleven/forty-five cases (24%) did not show any MIB-1 expression, and 32/45 (71%) displayed expression in more than 10% of tumor cells. In the ≥pT2 group of bladder cancers, MIB-1 was not expressed in 12/57 (21%) of the cases. Forty-five/fifty-seven (79%) cases showed staining between 10 and 100%.

By comparing pTa, pT1 and ≥pT2, statistical significance could be observed (p<10^{-4}) with a stronger expression in pT1 and ≤pT2 groups.

No statistical significant difference could be observed between PUNLMP to NILGC/NIHGC (p=0, 44). A statistical significant difference could be observed between PUNLMP/NILGC vs NIHGC/pT1, with a stronger expression in the second group (p=10^{-8}).

Table 3 summarizes the distribution of p53/MIB-1 immunostaining in pTa, pT1 and ≥pT2 bladder tumors.

By comparing in pTa, pT1 and ≥pT2 groups, no relation between p63, p53 and Mib-1 expressions could be found (Table 4).

Discussion

At presentation, 70–80% of bladder tumors are non-muscle invasive papillary tumors pTa or pT1. Recurrences are frequent, often during many years. Progression to muscle invasion occurs in about 15–20% of cases [12], taken all different groups of pTa (PUNLMP, NILGC, NIHGC). Especially, NIHGC has a high rate of progression that varies between 23 and 65% in different studies [20, 40]. pT1 tumors progress in up to 30% of cases [16]. Papillary non-invasive and invasive bladder tumors are believed to have different natural histories, and the proposed pathways concerning papillary tumors is hyperplasia, which develops to urothelial atypia and at least to papillary tumors [16, 33]. The pathway for muscle invasive tumors is proposed as follows by atypia, dysplasia, carcinoma in situ and invasive disease [33]. The debate about choice of treatment, especially for pT1 tumors, is very difficult, as it is not completely clear whether all these tumors display a real aggressive behaviour. It would be important to find reliable markers to predict clinical outcome of urothelial tumors especially in pTa and pT1 groups [16].

p63 is a member of the p53 family, which seems to react by a pathway distinct from p53 [25, 28]. p63 is a protein that is expressed by epithelial cells of stratified epithelia, such as skin oesophagus and exocervix as well as in basal cell layers of different tissues such as breast, prostate and lung [3, 38, 48]. Over-expression of p63 has been observed in squamous cell carcinomas [4, 6, 23]. Recently, Wu et al. [46] reported that p63 can regulate a wide range of downstream gene targets with various cellular functions, including cell cycle control, stress and signal transduction. Some authors reported the potential role on phosphoinositidine-3-kinase (PI3K) pathway under the control of epithelial growth factor receptor (EGFR) [1, 2], beta-catenin, uroplakin III [17, 18] and vascular endothelial growth factor (VEGF) [36].

It has been shown that p63 plays a role in urothelial differentiation [44], but seems also to play a role in bladder carcinogenesis. Park et al. [28] have shown an under-expression of one of the major isotypes TAp63, which contains a transactivation domain, while ΔNp63, which lacks the transactivation domain, seems to be over-expressed.

In this study, we have shown that a majority of transitional cell carcinoma [139/158 (88%)] cases express p63 in all cell layers. These results [15, 19, 28, 44, 49] are corresponding to those observed in squamous cell carcinomas of the oesophagus [4, 7] and lung [23].

Moreover, our study confirms a decrease in p63 expression during bladder cancer development from pTa, especially from low-grade to high-grade neoplasms, via pT1 to ≥pT2 (p=2.10^{-5}). These results confirm previous observations made in oesophageal squamous cell carcinomas [4] and transitional cell carcinomas [44, 49], but differ from those of Park et al. [28] who failed to determine statistical difference in ΔNp63 expression between pTa, pT1 or ≥pT2.

Our study demonstrates clearly for the first time that p63 expression distinguishes between PUNLMP/NILGC and NIHGC/pT1 (p=4.10^{-5}). The loss of p63 expression in NIHGC might be useful to help to differentiate them from NILGC as an additional factor, if morphological criterions are not sufficient. We also observed a statistical difference between pTa and pT1/≥pT2 with a statistical significance (p<10^{-6}). However, the NIHCG group did not include enough cases to conclude.

Meanwhile, we failed to determine any statistical correlation between survival and p63 expression. Longer follow up may be necessary to assess these results.

On the other hand, we explored the p53 activity in our different samples. As p53 seems to regulate ΔNp63 promoter activity [8, 41] and inversely ΔNp63 inhibits p53 transcription activation [4, 8, 21, 24], we studied the relationship between p53 and p63 expression in bladder cancer.

p53 is over-expressed in numerous malignancies. In transitional carcinomas, p53 expression seems to be able to identify patients with high risk for recurrence in pTa or pT1 tumors [37, 45]. Several studies have documented a sensitive reduction of progression-free interval for p53-positive tumors, with a significant relation of tumor progression [5, 35, 43]. Recent studies concerning tumors of the upper urinary tract [49] and bladder [22, 34] showed that increased p53 expression is significantly associated with advanced tumor stages and poor prognosis. Our results confirm these findings. We have shown p53 expression in PUNLMP and NILGC in 31 and 38%, respectively. In the opposite, NIHGC and pT1 display p53 expression in already 75 and 84% of cases, respectively ($p=10^{-6}$).

Meanwhile, no correlation could be found between p63 and p53 expression in bladder cancer (Table 4), suggesting that p63 and p53 play a role in carcinogenesis by different pathways. These results confirm previous studies concerning bladder carcinoma [44], oesophagus carcinomas [7, 42], lung carcinomas [29], while controversial in breast carcinomas [8, 33].

Proliferation marker MIB-1 has been studied by several trials. Santos et al. [35] have shown that MIB-1-positive tumors have a worse course of disease. Yan et al. [47] observed that MIB-1 could be used to identify patients with high risk for recurrence. Helpap and Köllermann [10] have shown that pattern and intensity of staining for MIB-1 and 34βE12 might help to distinguish grades. Disturbance of urothelium's stratification and diffuse-labelling pattern by CK34βE14 and MIB-1 seem to predict higher recurrence rates [11].

The loss of p63 expression in NIHGC might be used to help to differentiate them from NILGC. Our study shows that there exists a relationship between MIB-1 expression and stage. The expression of MIB-1 between the different stages pTa, pT1 and ≥pT2 showed significant differences. pT1 disease displayed MIB-1 expression in 71% of cases and in 79% of ≥pT2 patients, while only 8% of pTa showed increased MIB-1 expression ($p<0{,}0001$). No correlation could be observed between p63, p53 and MIB-1 staining.

Conclusion

Our study compares p63 expression in pTa (PUNLMP, NILGC, NIHGC), pT1 and ≥pT2. We clearly show for the first time that p63 immunostaining is present in all cell layers in PUNLMP and NILGC, but already partially lost in NIHGC and pT1 bladder cancers. Further studies have to investigate the role of p63 in bladder carcinogenesis and its prognostic value especially by focussing on NIHGC.

Acknowledgement Brigitte Radenen is acknowledged for excellent technical assistance.

References

1. Barbieri CE, Barton CE, Pietenpol JA (2003) Delta Np63 alpha expression is regulated by the phosphoinositide 3-kinase pathway. J Biol Chem 278:51408–51414
2. Cho NH, Kim YB, Park TK, Kim GE, Park K, Song KJ (2003) P63 and EGFR as prognostic predictors in stage IIB radiation-treated cervical squamous cell carcinoma. Gynecol Oncol 91: 346–353
3. DiComo CJ, Urist MJ, Babayan I, Drobnjak M, Hedvat CV, Teruya-Feldstein J, Pohar K, Hoos A, Cordon-Cardo C (2002) p63 expression profiles in human normal and tumor tissue. Clin Cancer Res 8:494–501
4. Geddert H, Kiel S, Heep HJ, Gabbert HE, Sarbia M (2003) The role of p63 and deltaNp63 (p40) protein expression and gene amplification in esophageal carcinogenesis. Hum Pathol 34: 850–856
5. Habuchi T, Kinoshita H, Yamada H, Knowles M (1995) Oncogene amplification in urothéliale cancers with p53 gene mutation or MDM2 amplification. J Natl Cancer Inst 86:1331–1335
6. Hagiwara K, McMenamin MG, Miura K, Harris CC (1999) Mutational analysis of the p63/p73L/p51/p40/CUSP/KET gene in human cancer cell lines using intronic primer. Cancer Res 59: 14165–14169
7. Hara T, Kijima H, Yamamoto S, Kenmochi T, Kise Y, Tanaka H, Chino O, Shimada H, Takazawa K, Tanaka M, Inokuchi S, Makuuchi H (2004) Ubiquitous p63 expression in human esophageal squamous cell carcinoma. Int J Mol Med 14:169–173
8. Harmes DC, Bresnick E, Lubin EA, Watson JK, Heim KE, Curtin JC, Suskind AM, Lamb J, DiRenzo J (2003) Positive and negative regulation of deltaN-p63 promoter activity by p53 and deltaN-p63-alpha contributes to differential regulation of p53 target genes. Oncogene 22:7607–7616
9. Harms K, Nozell S, Chen X (2004) The common and distinct target genes of the p53 family transcription factors. Cell Mol Life Sci 61:822–842
10. Helpap B, Köllermann J (1999) Proliferative pattern of exophytic and superficially invasive and non-invasive low grade urothelial carcinomas. Hum Pathol 30:145–150
11. Helpap B, Köllermann J (2000) Assessment of basal cell status and proliferative patterns in flat and papillary urothelial lesions: a contribution to the new WHO classification of urothelial tumors of the urinary bladder. Hum Pathol 31:745–750
12. Helpap B, Schmitz-Dräger B, Hamilton PW, Muzzonigro G, Galosi AB, Kurth KH, Lubaroff D, Waters D, Droller MJ (2003) Molecular pathology of non-invasive urothéliale carcinomas (part I). Virchows Arch 442:309–316
13. Holmang S, Johansson SL (2002) Stage Ta-T1 bladder cancer: the relationship between findings at first follow-up cystoscopy and subsequent recurrence and progression. J Urol 167:1634–1637
14. Jourdan F, Sebbagh N, Compérat E, Mourra N, Flahault A, Olschwang S, Hamelin R, Fléjou JF (2003) Tissue microarray technology: validation in colorectal carcinoma and analysis of p53, hMLH1 and hMSH2 immunohistochemical expression. Virchows Arch 443:115–121
15. Kaufmann O, Fietze E, Mengs J, Dietel M (2001) Value of p63 and cytokeratin 5/6 as immunohistochemical markers for the differential diagnosis of poorly differentiated and undifferentiated carcinomas. Am J Clin Pathol 116:823–830
16. Knowles M (2001) What we could do now: molecular pathology of bladder cancer. J Clin Pathol 54:215–221

17. Koga F, Kawakami S, Fujii Y, Saito K, Ohtsuka Y, Iwai et al (2003) Impaired p63 expression associates with poor prognosis and uroplakin III expression in invasive urothéliale carcinoma of the bladder. Clin Cancer Res 9:5501–5507
18. Koga F, Kawakami S, Kumagai J, Takizawa T, Ando N, Arai G, Kageyama Y, Kihara K (2003) Impaired Delta Np63 expression associates with reduced beta-catenin and aggressive phenotypes of urothelial neoplasms. Br J Cancer 88:740–747
19. Langner C, Ratschek M, Tsybrovskyy O, Schips L, Zigeuner R (2003) P63 immunoreactivity distinguishes upper urinary tract transitional-cell carcinoma and renal-cell carcinoma even in poorly differentiated tumors. J Histochem Cytochem 51:1097–1099
20. Lebret T, Bohin D, Kassardjan Z, Herve JM, Molinie V, Barre P, Lugagne PM, Botto H (2000) Recurrence, progression and success in stage Ta grade 3 bladder tumors treated with low dose bacillus Calmette–Guerin instillations. J Urol 163:63–67
21. Little NA, Jochemsen AG (2002) p63. Int J Biochem Cell Biol 34:6–9
22. Lu ML, Wikman F, Orntoft T, Charytonowicz E, Rabbani F, Zhang Z, Dalbagni G, Pohar KS, Yu G, Cordon-Cardo C (2002) Impact of alterations affecting the p53 pathway in bladder cancer on clinical outcome assessed by conventional and array-based methods. Clin Cancer Res 8:171–179
23. Massion PP, Taflan PM, Jamshedur Rahman SM, Yildiz P, Shyr Y, Edgerton ME, Westfall MD, Roberts JR, Pietenpol JA, Carbone DP, Gonzalez AL (2003) Significance of p63 amplification and overexpression in lung cancer development and prognosis. Cancer Res 63(21):7113–7121
24. Melino G, Lu X, Gasco M, Crook T, Knight RA (2003) Functional regulation of p73 and p63: development and cancer. Trends Biochem Sci 28:663–670
25. Moll U (2003) The role of p63 and p73 in tumor formation and progression: coming of age towards clinical usefulness. Clin Cancer Res 9:5437–5441
26. Nakanishi K, Kawai T, Torikata C (1996) Immunohistochemical evaluation of p53 oncoprotein in transitional cell carcinoma of the upper urinary tract. Hum Pathol 27:1336–1340
27. Nocito A, Bubendorf L, Tinner EM, Süss K, Wagner U, Forster T, et al (2001) Microarrays of bladder cancer tissue are highly representative of proliferation index and histological grade. J Pathol 194:349–357
28. Park BJ, Lee SJ, Lee KSJ, Lee CH, Chang SG, Park JH et al (2000) Frequent alteration of p63 expression in human primary bladder carcinomas. Cancer Res 60:3370–3374
29. Pelosi G, Pasini F, Olsen Stenholm C, Pastorino U, Maisonneuve P, Sonzogni A, Maffini F, Pruneri G, Fraggetta F, Cavallon A, Roz E, Iannucci A, Bresaola E, Viale G (2002) p63 immunoreactivity in lung cancer: yet another player in the development of squamous cell carcinomas? J Pathol 198:100–109
30. Reis-Filho JS, Simpson PT, Martins A, Preto A, Gärtner F, Schmitt FC (2003) Distribution of p63, cytokeratins 5/6 and cytokeratin 14 in 51 normal and 400 neoplastic human tissue samples using TARP-4 multi-tumor tissue microarray. Virchows arch 443:122–132
31. Ribeiro-Silva A, Zambelli Ramalho LN, Britto Garcia S, Zucoloto S (2003) The relationship between p63 and p53 expression in normal and neoplastic breast tissue. Arch Pathol Lab Med 127:336–340
32. Richter J, Jiang F, Gorog JP (1997) Marked genetic differences between stage pTa and stage pT1 papillary bladder cancer detected by comparative genomic hybridization. Cancer Res 57:2860–2864
33. Sandberg AA (2002) Cytogenetics and molecular genetics of bladder cancer: a personal view. Am Med Genet 115:173–182
34. San Miguel Fraile P, Anton Badiola I, Ortiz Rey JA, Alvarez Alvarez C, Fernandez Costas A, Lago Fernandez M, Pelaez Boismorand E, Zungri Telo E, De La Fuente Buceta A (2003) Comparative study of the expression of p53, Ki-67, bcl-2 and CK20 in superficial transitional carcinoma of the bladder: correlation with recurrence, histological grade, and clinical stage. Actas Urol Esp 27:587–593
35. Santos L, Amaro T, Costa C, Pereira S, Bento MJ, Lopes P et al (2003) Ki-67 index enhances the prognostic accuracy of the urothéliale superficial bladder carcinoma risk group classification. Int J Cancer 105:267–272
36. Senoo M, Matsumura Y, Habu S (2002) TAp63gamma (p51A) and dNp63alpha (p73L), two major isoforms of the p63 gene, exert opposite effects on the vascular endothelial growth factor (VEGF) gene expression. Oncogene 21:2455–2465
37. Shariat SF, Kim J, Raptidis G, Ayala G, Lerner S (2003) Association of p53 and p21 expression with clinical outcome in patients with carcinoma in situ of the urinary bladder. Urology 61:1140–1145
38. Signoretti S, Waltregny D, Dilks J, Isaac B, Lin D, Garraway L, Yang A Montironi R, McKeon F, Loda M (2000) p63 is a prostate basal cell marker and is required for prostate development. Am J Pathol 157:1769–1775
39. Smith ND, Rubenstein JN, Eggener SE, Kozlowski JM (2003) The p53 tumor suppressor gene and nuclear protein: basic science review and relevance in the management of bladder cancer. J Urol 169:1219–1228
40. Soloway MS, Sofer M, Vaidya A (2002) Contemporary management of stage T1 transitional cell carcinoma of the bladder. J Urol 167:1573–1583
41. Strano S, Fontemaggi G, Costanzo A, Rizzo MG, Monti O, Baccarini A, Del Sal G, Levrero M, Sacchi A, Oren M, Blandino G (2002) Physical interaction with human tumor-derived p53 mutants inhibits p63 activities. J Biol Chem 277:18817–18826
42. Thurfjell N, Coates PJ, Uusitalo T, Mahani D, Dabelsteen E, Dahlqvist A, Sjostrom B, Roos G, Nylander K (2004) Complex p63 mRNA isoform expression patterns in squamous cell carcinoma of the head and neck. Int J Oncol 25(1):27–35
43. Tiguert R, Lessard A, So A, Fradet Y (2002) Prognostic markers in muscle invasive bladder cancer. World J Urol 20:190–195
44. Urist M J, Di Como CJ, Lu ML, Charytonowicz E, Verbel D, Crum CP et al (2002) Loss of p63 expression is associated with tumor progression in bladder cancer. Am J Pathol 161:1199–1206
45. World Health Organization Classification of Tumors (2004) Tumors of the urinary system and male genital organs. In: Eble J et al (eds) IARC, Lyon
46. Wu G, Nomoto S, Hoque MO, Dracheva T, Osada M, Lee CC, Dong SM, Guo Z, Benoit N, Cohen Y, Rechthand P, Califano J, Moon CS, Ratovitski E, Jen J, Sidransky D, Trink B (2003) DeltaNp63alpha and TAp63alpha regulate transcription of genes with distinct biological functions in cancer and development. Cancer Res 63:2351–2357
47. Yan Y, Andriole GL, Humphrey PA, Kibel AS (2002) Patterns of multiple recurrences of superficial (Ta/T1) transitional cell carcinomas of bladder and effects of clinicopathologic and biochemical factors. Cancer 95:1239–1246
48. Yang A, Schweitzer R, Sun D, Kaghad M, Walker N, Bronson RT, Tabin C, Sharpe A, Caput D, Crum C, McKeon F (1999) p63 is essential for regenerative proliferation in limb, craniofacial, and in epithelial development. Nature 398:714–718
49. Zigeuner R, Tsybrovskyy O, Ratschek M, Rehak P, Lipsky K, Langner C (2004) Prognostic impact of p63 and p53 expression in upper urinary tract transitional cell carcinomas. Urology 63:1079–1083

Virchows Arch (2006) 448: 325–330
DOI 10.1007/s00428-005-0129-6

ORIGINAL ARTICLE

Cord Langner · Gerhild Rupar · Sebastian Leibl · Georg Hutterer · Thomas Chromecki · Gerald Hoefler · Peter Rehak · Richard Zigeuner

Alpha-methylacyl-CoA racemase (AMACR/P504S) protein expression in urothelial carcinoma of the upper urinary tract correlates with tumour progression

Received: 19 September 2005 / Accepted: 27 October 2005 / Published online: 29 November 2005

Abstract Alpha-methylacyl-CoA racemase (AMACR/P504S) is a useful biomarker of prostate cancer. We evaluated the expression of AMACR in upper urinary tract urothelial carcinomas with respect to associations with tumour stage, grade and metastasis-free survival. A total of 268 tumours were investigated immunohistochemically using a tissue microarray technique. AMACR expression was noted in 127 of 261 (48.7%) evaluated tumours and was associated with high tumour stage [58 of 139 (41.7%) pTa/pT1 vs. 69 of 122 (56.6%) pT2–pT4, P=0.019] and high tumour grade [44 of 137 (32.1%) low vs. 83 of 124 (66.9%) high grade, P<0.001]. In addition, AMACR expression was associated with the presence of tumour necrosis (P<0.001) and marked stromal desmoplasia (P=0.0026). This correlation indicates that increased AMACR expression might be related to hypoxia-induced changes in cancer cell metabolism, such as increased dependence on fatty acid oxidation for energy generation. Progressive disease was observed in 73 of 183 (39.9%) patients with solitary invasive carcinomas and was associated with AMACR expression (P=0.017). Multivariate analysis, however, proved only pT-stage >1 (P<0.001) and high tumour grade (P<0.001) to be independent predictors of patient outcome. In conclusion, AMACR expression correlated with advanced tumour stage and grade and may serve as an additional prognostic indicator in upper urinary tract urothelial cancer.

Keywords Urothelial carcinoma · Transitional cell carcinoma · Upper urinary tract · Alpha-methylacyl-CoA racemase (AMACR) · Prognosis

C. Langner (✉) · G. Rupar · S. Leibl · G. Hoefler
Institute of Pathology, Medical University Graz,
Auenbruggerplatz 25,
A-8036 Graz, Austria
e-mail: cord.langner@meduni-graz.at
Tel.: +43-316-38583665
Fax: +43-316-384329

G. Hutterer · T. Chromecki · R. Zigeuner
Department of Urology, Medical University Graz,
Auenbruggerplatz 7,
A-8036 Graz, Austria

P. Rehak
Department of Surgery,
Division of Biomedical
Engineering & Computing,
Medical University Graz,
Auenbruggerplatz 29,
A-8036 Graz, Austria

Introduction

Upper urinary tract urothelial carcinoma (UC) accounts for approximately 5% of all urothelial and for 10% of all renal cancers [1]. TNM-stage and tumour grade are well-known prognostic factors [2]. Assessment of tumour grade, however, may show considerable variation due to inter-observer variability [3, 4]. Therefore, the discovery of new prognostic markers represents an important step for the evaluation of affected patients, not only to predict disease evolution and thus aiding surveillance strategies, but also to identify subgroups that might benefit from adjuvant cancer therapy.

Alpha-methylacyl-CoA racemase (AMACR), formerly known as P504S, is a mitochondrial and peroxisomal enzyme involved in the beta-oxidation of branched fatty acids and bile acid intermediates [5]. Specifically, AMACR catalyses the conversion of (2R) alpha-methyl branched chain fatty acyl-CoAs to their (S) stereoisomers. Only stereoisomers with the 2-methyl group in the (S) position can be metabolised by peroxisomal oxidases, the first enzymes in the beta-oxidation pathway [6, 7]. Immunohistochemically, moderate to strongly positive staining with AMACR has been demonstrated in a wide variety of normal human tissues, including hepatocytes, the epithelium of proximal renal tubules and glomeruli, as well as acinar and ductal cells of major salivary glands. Moreover, strong immmunohistochemical staining for AMACR has been demonstrated in most carcinomas arising from these organs [8] and, additionally, in some neoplasms originating from tissue normally lacking AMACR expression, such as prostate [9] and colorectal cancer [10, 11].

With respect to prostate cancer, several groups have shown that AMACR represents a new important biomarker, as it is upregulated in the vast majority of cancer and prostatic intraepithelial neoplasia lesions, which is in sharp contrast to the near-complete lack of expression in both normal and hyperplastic prostate glands [9, 12–15]. Thus, immunohistochemical AMACR staining, alone or in combination with negative staining for a basal cell marker, such as 34betaE12 or p63, has recently been proven useful in the assessment of difficult prostate needle biopsies [16–18].

Recently, AMACR expression has been detected in a subset of UCs [8, 19–21]. However, data systematically correlating AMACR expression with tumour stage and grade as well as patient outcome are currently lacking. Therefore, we evaluated the expression of AMACR in upper urinary tract UCs with special emphasis on associations with tumour stage and grade as well as prognostic significance.

Materials and methods

Case selection

A total of 268 consecutive upper urinary tract UCs (169 pelvic and 99 ureteral tumours) from 239 consecutive patients (108 females, 131 males; ratio 1:1.2) operated between 01/1984 and 12/2004 were retrieved from the archives of our institute. Mean and median age of patients was 69.8 and 70.8 (range 39–89) years, respectively. pT-stages were adjusted according to the UICC 2002 issue of the TNM-system [22]. Grading was performed according to the recently published two-tiered WHO grading system, corresponding to the WHO/ISUP consensus classification [23]. For the correlation of pathological findings with metastasis-free survival, all non-invasive cancers (41 tumours) and all tumours from patients with multiple invasive cancers (37 tumours) were excluded resulting in a group of 190 UCs (134 pelvic and 56 ureteral tumours) from 190 patients (77 females, 113 males; ratio 1:1.5). The patients either underwent nephroureterectomy with bladder-cuff resection (n=130), nephrectomy alone (n=40), or distal ureteral resection with reimplant (n=20) and did not receive adjuvant therapy. Follow-up regimen included abdominal ultrasound and cystoscopy at 3-month intervals for the first 3 years, at 6-month intervals for the subsequent two years and yearly thereafter as well as chest X-ray and computerised tomography at 6-month intervals for the first 3 years and yearly thereafter. Two cases of non-neoplastic pelvic urothelium, two cases of urothelial dysplasia (intraurothelial neoplasia) and two cases of urothelial carcinoma in situ were investigated for comparison. All procedures were in accordance with the ethical standards established by our institution. Informed consent is not required for retrospective analyses dealing with archive material obtained during routine medical treatment.

Immunohistochemistry

For immunohistochemical evaluation, a tissue microarray technique was used. The details of this technique have been described previously [24]. Briefly, tissue microarrays (TMAs) were constructed using a manual tissue arraying instrument (Beecher, Silver Spring, MD). At least three cylindrical core biopsies, 0.6 mm in diameter, were taken from different sites of each tumour and arrayed in a recipient paraffin TMA block. Four micrometer TMA sections were deparaffinised by xylene, rehydrated in graded alcohols, treated for 5 min with 1% H_2O_2, and submitted to microwave epitope retrieval (30 min, 160 W in 0.1 M TRIS–HCl buffer, pH 9.5, containing 5% urea). For the detection of AMACR, sections were incubated for 30 min with the rabbit polyclonal antibody P504S (1:100; Biocare Medical LLC, Walnut Creek, CA, USA) using an automated immunostainer (DAKO-Autostainer, Universal Staining System, DAKO, Glostrup, Denmark). Binding of the primary antibodies was assessed by the DAKO ChemMate detection kit.

Immunohistochemical evaluation and controls

Immunoreactivity was assessed by two investigators (G.R. and C.L.) who were blinded to clinicopathologic data using a semiquantitative scoring system. Discrepancies were resolved by simultaneous reexamination of the slides by both investigators using a double-headed microscope. A distinct granular cytoplasmic staining was considered positive, and immunoreactivity was categorised as "focal" (<10% of tumour cells positive), "moderate" (10–50%), or "extensive" (>50%). Slides of prostate adenocarcinoma known to express AMACR served as positive control. Negative controls included omission of the primary antibody and incubation with DAKO ChemMate Antibody Diluent (Code No. S 2022).

Statistical analysis

Subgroups according to pT-stage and tumour grade were compared with respect to possible differences in immunoreactivity using the Fisher's exact test. Disease-free survival was assessed using the Kaplan–Meier method and compared by the log-rank test. For multivariate testing, a Cox's proportional hazards regression model was performed. All reported P values were two-sided with significance at P<0.05.

Results

Histopathology

Stage pTa was present in 41 (15.3%), pT1 in 102 (38.1%), pT2 in 37 (13.8%), pT3 in 80 (29.9%), and pT4 in eight

Table 1 Upper urinary tract urothelial carcinomas related to tumour stage (pTa–pT4) and tumour grade [low grade (LG) and high grade (HG)]

	All tumours		Pelvic tumours		Ureteral tumours	
	n	%	*n*	%	*n*	%
pTa	41	15.3	19	11.2	22	22.2
pT1	102	38.1	60	35.5	42	42.4
pT2	37	13.8	20	11.8	17	17.2
pT3	80	29.9	62	36.7	18	18.2
pT4	8	3.0	8	4.7	–	–
LG	141	52.6	84	49.7	57	57.6
HG	127	47.4	85	50.3	42	42.4
Total	268	100	169	100	99	100

(3.0%) cases, respectively. There were 141 (52.6%) low- and 127 (47.4%) high-grade cases. Pelvic and ureteral UCs showed a comparable distribution regarding the different categories (Table 1). High tumour grade was associated with high tumour stage [53 of 139 (38.1%) pT1/pT2 vs. 74 of 88 (84.1%) pT3/pT4, $P<0.001$]; no high-grade tumours were detected among non-invasive cancers. Tumour necrosis was noted in 113 (42.2%), a marked desmoplastic stromal response in 71 (26.5%) and focal squamous differentiation in 47 of 261 (17.5%) tumours, respectively.

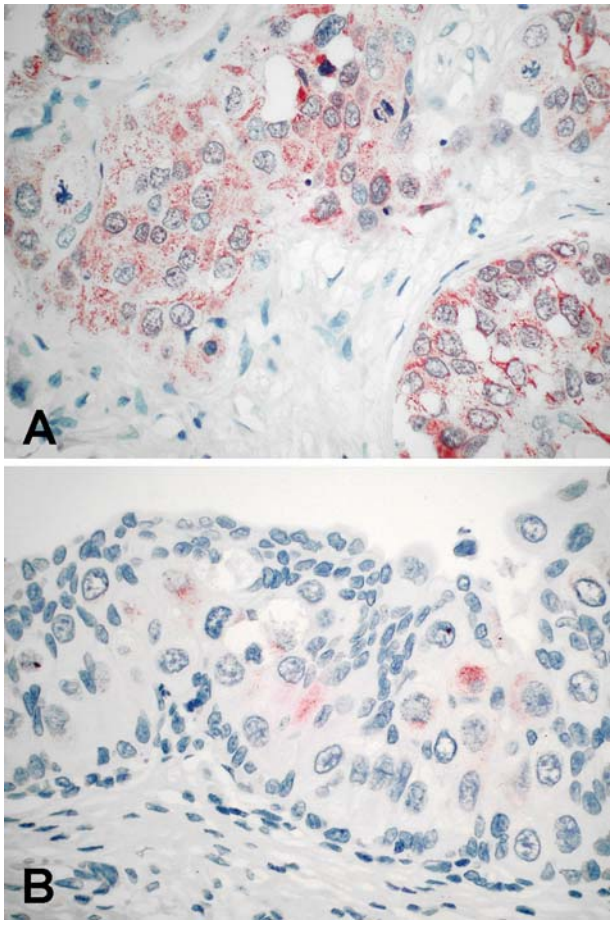

Fig. 1 Distinct finely granular cytoplasmic AMACR immunostaining in a high-grade urothelial carcinoma of the upper urinary tract ((**a**), original ×100). Note focal, though specific, labelling in urothelial carcinoma in situ ((**b**), original ×200)

Immunohistochemistry

Cancer tissue allowing a reliable evaluation of AMACR immunoreactivity was present in 261 of 268 (97.4%) cases. Overall, distinct finely granular cytoplasmic AMACR immunoreactivity was noted in 127 of 261 (48.7%) tumours, with 32 (12.3%) cases showing only focal staining, whereas 53 (20.3%) cases showed extensive staining (Fig. 1a). Urothelial carcinoma in situ revealed distinct AMACR positivity of single cancer cells (Fig. 1b), whereas non-neoplastic urothelium and urothelial dysplasia lacked specific labelling.

AMACR expression was associated with high tumour stage [58 of 139 (41.7%) pTa/pT1 vs. 69 of 122 (56.6%) pT2–pT4, $P=0.019$] and high tumour grade [44 of 137 (32.1%) low grade vs. 83 of 124 (66.9%) high grade, $P<0.001$). Pelvic and ureteral UCs showed comparable staining results regarding the different tumour categories (Table 2).

AMACR expression was associated with the presence of tumour necrosis. Thus, 69 of 111 (62.2%) UCs with necrosis showed AMACR immunoreactivity, compared with 58 of 150 (38.7%) UCs without necrosis ($P<0.001$). In addition, AMACR immunoreactivity was associated with the amount of intratumoural stromal response, as 44 of 69 (63.8%) UCs with marked desmoplastic stromal response showed specific labelling, compared with 83 of 192 (43.2%) UCs lacking marked desmoplasia ($P=0.0026$). Finally, AMACR immunoreactivity was also associated with squamous morphology. Thus, 29 of 46 (63%) UCs with focal squamous differentiation were immunostained, compared with 98 of 215 (45.6%) pure urothelial cancers ($P=0.035$).

Table 2 AMACR expression in upper urinary tract urothelial carcinomas related to tumour stages (pTa–pT4) and tumour grades [low grade (LG) and high grade (HG)]

	All tumors		Pelvic tumors		Ureteral tumors	
	n	%	*n*	%	*n*	%
pTa	11/39	28.2	6/18	33.3	5/21	23.8
pT1	47/100	47	27/58	46.6	20/42	47.6
pT2	18/37	48.6	7/20	35	11/17	64.7
pT3	45/77	58.4	34/61	55.7	11/16	68.8
pT4	6/8	75	6/8	75	–	–
LG	44/137	32.1	29/82	35.4	15/55	27.3
HG	83/124	66.9	51/83	61.4	32/41	78
Total	127/261	48.7	80/165	48.5	47/96	49

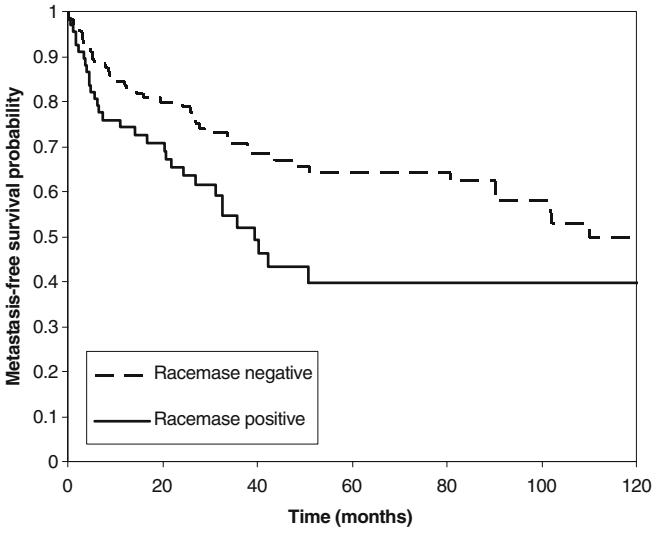

Fig. 2 Metastasis-free survival (months) in patients with upper urinary tract urothelial carcinomas related to the presence of AMACR immunoreactivity (P=0.017, log-rank test)

Survival analysis

Follow-up data were available for 183 of 190 (96.3%) patients with solitary invasive UCs. After a mean and median follow-up of 47 and 30 months, respectively, progressive disease was observed in 73 of 183 (39.9%) patients including 57 patients who died from cancer and 16 patients who currently are alive with metastatic disease. The lung was the most common site of metastasis. Mean time to progression was 23 months (median 14, range 0–110). A total of 26 patients died from causes not related to upper urinary tract cancer.

The development of distant metastases was associated with the presence of AMACR immunoreactivity. Thus, 32 of 69 (46.4%) patients with UCs with AMACR expression developed disease progression, compared with 41 of 114 (36%) patients with UCs without AMACR expression (P=0.017, log-rank test; Fig. 2).

In a Cox's proportional hazards regression model including patient age, gender, tumour stage, tumour grade and AMACR expression, however, only pT-stage >1 (P<0.001, risk ratio [RR]=7.32, 95% confidence interval [CI]=3.32–16.13) and high tumour grade (P<0.001, RR=3.64, 95% CI 1.82–7.28) proved to be independent predictors of metastatic disease, whereas AMACR immunoreactivity lacked independent influence on patient outcome.

Discussion

To the best of our knowledge, this is the first study which correlates the expression of AMACR in urothelial cancer with tumour stage, tumour grade and patient outcome. In our series, AMACR is expressed in about 50% of upper urinary tract tumours, with 20% of cases showing extensive immunostaining. The number of positive cells is higher compared to bladder cancers showing staining in 12–31% [8, 19] and as reported in a single former study regarding pelvic UCs with 12% positivity [20]. These studies, however, only included small numbers of patients and detailed information regarding tumour stage and grade was not given.

In our samples, extensive AMACR expression was detected predominantly in high-stage and high-grade tumours. This is an important finding with respect to differential diagnosis, and pathologists should be aware of AMACR immunoreactivity in poorly differentiated UCs in situations requiring the differentiation from poorly differentiated prostate cancer. In select cases, p63 may serve as an additional biomarker, as it is nearly always expressed in urothelial tumours [25], but constantly absent in prostate cancers.

Comparable results to ours have only been very recently reported for breast cancer. Witkiewicz et al. [26] showed AMACR overexpression in 42 of 160 (26%) invasive breast carcinomas and observed stronger AMACR expression in high-grade compared with low-grade tumours. However, AMACR expression in 25–69% of clear cell and in 100% of papillary renal cell cancers was independent of tumour stage and Fuhrman nuclear grade [20, 27]. Comparable data have been obtained from prostate cancer. Most authors agree that there is no association between AMACR immunoreactivity and established histoprognostic factors, such as Gleason score, pathological stage, or the Ki67 labelling index as a marker of tumour cell proliferation [28]. In contrast, in colorectal cancer, two investigations showed a weaker AMACR expression in high-grade compared with low-grade tumours [21, 29].

The reason why AMACR is predominantly expressed in high-grade UCs as well as high-grade breast cancers is not clear. As AMACR is involved in the beta-oxidation of branched-chain fatty acids, it may be speculated that increased expression might lead to the generation of radical species causing genetic instability and damage of cellular membranes. However, it is not clear whether AMACR is directly involved in cancer initiation and/or progression or if it rather represents an epiphenomenon indicating the use of an alternative pathway for providing energy in neoplastic cells. The latter interpretation may be supported by our finding that tumours showing foci of necrosis and/or marked desmoplastic stromal response revealed strong AMACR immunostaining. Desmoplasia has been shown to correlate with hypoxia of tumour cells in breast cancer [30] and may thus lead to changes in tumour cell metabolism, such as increased dependence on fatty acid oxidation for energy generation.

A systematic review of the literature shows that AMACR expression has so far only been systematically correlated with patient outcome in prostate cancer. Data, however, are contradictory. While Rhodes et al. [31] did not find an association between AMACR expression and recurrence-free survival, Rubin et al. [32] recently observed an association between decreased AMACR ex-

pression and increased rate of biochemical recurrence and cancer-related death. TNM-stage and tumour grade are well-established prognostic indicators of upper urinary tract UCs. According to our study, AMACR may be used as an additional indicator of unfavourable prognosis that, however, lacked independent influence on patient outcome.

Acknowledgements The authors are grateful to Mrs. M. Gogg-Kamerer, Mrs. M. Lindbauer, Mr. M. Al-Effah, and Mr. R. Christof for excellent technical assistance. Part of this work was supported by the FP6 European Union Project "Peroxisomes" (LSHG-CT-2004-512018, G.H.).

References

1. Genega EM, Porter CR (2002) Urothelial neoplasms of the kidney and ureter. An epidemiologic, pathologic, and clinical review. Am J Clin Pathol 117(Suppl):S36–S48
2. Hall MC, Womack S, Sagalowsky AI, Carmody T, Erickstad MD, Roehrborn CG (1998) Prognostic factors, recurrence, and survival in transitional cell carcinoma of the upper urinary tract: a 30-year experience in 252 patients. Urology 52:594–601
3. Bol MG, Baak JP, Buhr-Wildhagen S, Kruse AJ, Kjellevold KH, Janssen EA, Mestad O, Ogreid P (2003) Reproducibility and prognostic variability of grade and lamina propria invasion in stages Ta, T1 urothelial carcinoma of the bladder. J Urol 169: 1291–1294
4. Tosoni I, Wagner U, Sauter G, Egloff M, Knonagel H, Alund G, Bannwart F, Mihatsch MJ, Gasser TC, Maurer R (2000) Clinical significance of interobserver differences in the staging and grading of superficial bladder cancer. BJU Int 85:48–53
5. Ferdinandusse S, Denis S, IJlst L, Dacremont G, Waterham HR, Wanders RJ (2000) Subcellular localization and physiological role of alpha-methylacyl-CoA racemase in humans. J Lipid Res 41:1890–1896
6. Cuebas DA, Phillips C, Schmitz W, Conzelmann E, Novikov DK (2002) The role of alpha-methylacyl-CoA racemase in bile acid synthesis. Biochem J 363:801–807
7. Wanders RJ, Vreken P, Ferdinandusse S, Jansen GA, Waterham HR, van Roermund CW, van Grunsven EG (2001) Peroxisomal fatty acid alpha- and beta-oxidation in humans: enzymology, peroxisomal metabolite transporters and peroxisomal diseases. Biochem Soc Trans 29:250–267
8. Jiang Z, Fanger GR, Woda BA, Banner BF, Algate P, Dresser K, Xu J, Chu PG (2003) Expression of alpha-methylacyl-CoA racemase (P504S) in various malignant neoplasms and normal tissues: a study of 761 cases. Hum Pathol 34:792–796
9. Jiang Z, Woda BA, Wu CL, Yang XJ (2004) Discovery and clinical application of a novel prostate cancer marker: alpha-methylacyl-CoA racemase (P504S). Am J Clin Pathol 122:275–289
10. Chen ZM, Ritter JH, Wang HL (2005) Differential expression of alpha-methylacyl coenzyme A racemase in adenocarcinomas of the small and large intestines. Am J Surg Pathol 29:890–896
11. Jiang Z, Fanger GR, Banner BF, Woda BA, Algate P, Dresser K, Xu J, Reed SG, Rock KL, Chu PG (2003) A dietary enzyme: alpha-methylacyl-CoA racemase/P504S is overexpressed in colon carcinoma. Cancer Detect Prev 26:422–426
12. Gelmann EP, Semmes OJ (2004) Expression of genes and proteins specific for prostate cancer. J Urol 172:23–26
13. Halvorsen OJ, Oyan AM, Bo TH, Olsen S, Rostad K, Haukaas SA, Bakke AM, Marzolf B, Dimitrov K, Stordrange L, Lin B, Jonassen I, Hood L, Akslen LA, Kalland KH (2005) Gene expression profiles in prostate cancer: association with patient subgroups and tumour differentiation. Int J Oncol 26:329–336
14. Varma M, Jasani B (2005) Diagnostic utility of immunohistochemistry in morphologically difficult prostate cancer: review of current literature. Histopathology 47:1–16
15. Zha S, Ferdinandusse S, Denis S, Wanders RJ, Ewing CM, Luo J, De Marzo AM, Isaacs WB (2003) Alpha-methylacyl-CoA racemase as an androgen-independent growth modifier in prostate cancer. Cancer Res 63:7365–7376
16. Browne TJ, Hirsch MS, Brodsky G, Welch WR, Loda MF, Rubin MA (2004) Prospective evaluation of AMACR (P504S) and basal cell markers in the assessment of routine prostate needle biopsy specimens. Hum Pathol 35:1462–1468
17. Hameed O, Sublett J, Humphrey PA (2005) Immunohistochemical stains for p63 and alpha-methylacyl-CoA racemase, versus a cocktail comprising both, in the diagnosis of prostatic carcinoma: a comparison of the immunohistochemical staining of 430 foci in radical prostatectomy and needle biopsy tissues. Am J Surg Pathol 29:579–587
18. Jiang Z, Li C, Fischer A, Dresser K, Woda BA (2005) Using an AMACR (P504S)/34betaE12/p63 cocktail for the detection of small focal prostate carcinoma in needle biopsy specimens. Am J Clin Pathol 123:231–236
19. Suh N, Yang XJ, Tretiakova MS, Humphrey PA, Wang HL (2005) Value of CDX2, villin, and alpha-methylacyl-CoA racemase immunostains in the distinction between primary adenocarcinoma of the bladder and secondary colorectal adenocarcinoma. Mod Pathol 18:1217–1222
20. Tretiakova MS, Sahoo S, Takahashi M, Turkyilmaz M, Vogelzang NJ, Lin F, Krausz T, Teh BT, Yang XJ (2004) Expression of alpha-methylacyl-CoA racemase in papillary renal cell carcinoma. Am J Surg Pathol 28:69–76
21. Zhou M, Chinnaiyan AM, Kleer CG, Lucas PC, Rubin MA (2002) Alpha-methylacyl-CoA racemase: a novel tumor marker over-expressed in several human cancers and their precursor lesions. Am J Surg Pathol 26:926–931
22. Sobin LH, Wittekind C (eds) (2002) TNM classification of malignant tumors, 6th edn. Wiley-Liss, New York
23. Lopez-Beltran A, Sauter G, Gasser T, Hartmann A, Schmitz-Dräger BJ, Helpap B, Ayala AG, Tamboli P, Knwles MA, Sidransky D, Cordon-Cardo C, Jones PA, Cairns P, Simon R, Amin MB, Tyczynski JE (2004) Tumours of the urinary system. Infiltrating urothelial carcinoma. In: Eble JN, Sauter G, Epstein JI, Sesterhenn IA (eds) World Health Organization classification of tumours. Pathology and genetics. Tumours of the urinary system and male genital organs. IARC, Lyon, pp 93–109
24. Kononen J, Bubendorf L, Kallioniemi A, Barlund M, Schraml P, Leighton S, Torhorst J, Mihatsch MJ, Sauter G, Kallioniemi OP (1998) Tissue microarrays for high-throughput molecular profiling of tumor specimens. Nat Med 4:844–847
25. Langner C, Ratschek M, Tsybrovskyy O, Schips L, Zigeuner R (2003) P63 immunoreactivity distinguishes upper urinary tract transitional-cell carcinoma and renal-cell carcinoma even in poorly differentiated tumors. J Histochem Cytochem 51:1097–1099
26. Witkiewicz AK, Varambally S, Shen R, Mehra R, Sabel MS, Ghosh D, Chinnaiyan AM, Rubin MA, Kleer CG (2005) Alpha-methylacyl-CoA racemase protein expression is associated with the degree of differentiation in breast cancer using quantitative image analysis. Cancer Epidemiol Biomarkers Prev 14:1418–1423
27. Lin F, Brown RE, Shen T, Yang XJ, Schuerch C (2004) Immunohistochemical detection of P504S in primary and metastatic renal cell carcinomas. Appl Immunohistochem Mol Morphol 12:153–159
28. Evans AJ (2003) Alpha-methylacyl-CoA racemase (P504S): overview and potential uses in diagnostic pathology as applied to prostate needle biopsies. J Clin Pathol 56:892–897

29. Kuefer R, Varambally S, Zhou M, Lucas PC, Loeffler M, Wolter H, Mattfeldt T, Hautmann RE, Gschwend JE, Barrette TR, Dunn RL, Chinnaiyan AM, Rubin MA (2002) Alpha-methylacyl-CoA racemase: expression levels of this novel cancer biomarker depend on tumor differentiation. Am J Pathol 161:841–848
30. Colpaert CG, Vermeulen PB, Fox SB, Harris AL, Dirix LY, Van Marck EA (2003) The presence of a fibrotic focus in invasive breast carcinoma correlates with the expression of carbonic anhydrase IX and is a marker of hypoxia and poor prognosis. Breast Cancer Res Treat 81:137–147
31. Rhodes DR, Sanda MG, Otte AP, Chinnaiyan AM, Rubin MA (2003) Multiplex biomarker approach for determining risk of prostate-specific antigen-defined recurrence of prostate cancer. J Natl Cancer Inst 95:661–668
32. Rubin MA, Bismar TA, Andren O, Mucci L, Kim R, Shen R, Ghosh D, Wei JT, Chinnaiyan AM, Adami HO, Kantoff PW, Johansson JE (2005) Decreased alpha-methylacyl-CoA racemase expression in localized prostate cancer is associated with an increased rate of biochemical recurrence and cancer-specific death. Cancer Epidemiol Biomarkers Prev 14:1424–1432

Virchows Arch (2006) 448: 331–336
DOI 10.1007/s00428-005-0091-3

ORIGINAL ARTICLE

Yoon-La Choi · So Young Kang · Young Kee Shin · Jong Sun Choi · Seok Hyung Kim · Sun-Joo Lee · Duk-Soo Bae · Geunghwan Ahn

Aberrant hypermethylation of *RASSF1A* promoter in ovarian borderline tumors and carcinomas

Received: 19 November 2004 / Accepted: 5 February 2005 / Published online: 29 November 2005

Abstract The newly identified 3p21.3 tumor suppressor gene *RASSF1A* is inactivated by hypermethylation in variable solid tumors, including those of the lung, breast, prostate, kidney, and ovary. The purpose of this study was to evaluate the methylation status of *RASSF1A* in various types and stages of ovarian epithelial tumors. We analyzed the DNA methylation status of ovarian tumors using methylation-specific polymerase chain reaction in 54 frozen ovarian tumor tissues and in 97 cases of archival ovarian serous epithelial tumors using a microdissection procedure. Hypermethylation statuses were examined vs clinicopathologic findings. *RASSF1A* promoter methylation rates in the various types of fresh ovarian tissues were as follows: serous cystadenoma (1/5), serous tumor of borderline malignancy (2/7), serous adenocarcinoma (4/10), mucinous cystadenoma (0/5), mucinous tumor of borderline malignancy (2/7), mucinous adenocarcinoma (3/6), transitional-cell carcinoma (1/3), clear-cell carcinoma (3/3), and malignant müllerian mixed tumor (3/3). In archived serous tumor tissues, *RASSF1A* promoter hypermethylation was detected in serous cystadenoma (1/6, 16.6%), serous tumor of borderline malignancy (20/41, 48.8%), and in serous adenocarcinoma (25/50, 50%). The status of *RASSF1A* hypermethylation in borderline tumors was found to correlate statistically with the presence of microinvasion (p=0.002), peritoneal implant (p<0.001), and bilaterality (p=0.019). The *RASSF1A* promoter hypermethylation was frequently found in borderline tumors and carcinomas, suggesting that *RASSF1A* promoter hypermethylation may be a useful molecular marker for the early detection of ovarian tumors.

Keywords *RASSF1* · Ovarian tumor · Borderline · Tumor suppressor gene · Methylation

Y.-L. Choi · S. Y. Kang · J. S. Choi · G. Ahn (✉)
Department of Pathology, Samsung Medical Center,
Sungkyunkwan University School of Medicine,
Seoul, South Korea
e-mail: g.ahn@samsung.com
Tel.: +82-2-34102809
Fax: +82-2-34100025

Y. K. Shin
Department of Pharmacy, Research Institute of Pharmaceutical Science, College of Pharmacy, Seoul National University,
Seoul, South Korea

S. H. Kim
Department of Pathology, College of Medicine,
Chungbuk National University,
Chungbuk, South Korea

S.-J. Lee · D.-S. Bae
Department of Obstetrics and Gynecology,
Samsung Medical Center,
Sungkyunkwan University School of Medicine,
Seoul, South Korea

Introduction

Ovarian carcinoma is the leading cause of death due to female genital malignancy, and more than half of ovarian carcinoma patients are diagnosed with advanced-stage disease [13]. A family history of breast and/or ovarian cancer increases the lifetime risk by 40%, and mutations in the *BRCA1* gene increase the risk by 63% in hereditary forms of the disease [6, 12]. However, most cases of ovarian carcinoma are sporadic. A poor understanding of the biology of sporadic forms of the disease, imperfect screening markers, and few symptoms or warning signs of early-stage disease contribute to early-detection failure.

The debate about the diagnostic features, terminology, and treatment of ovarian borderline tumors continue [16]. Ovarian borderline tumors are subtypes of ovarian-surface epithelial stromal tumors, which are noninvasive and are associated with a much better prognosis than ovarian carcinoma. Microinvasion or invasive implants have been shown to be significant in the mortality of borderline ovarian tumors [2, 3, 5, 17], which are best, although not always effectively, treated by chemotherapy. The sequential progression of serous tumors from serous adenomas through borderline tumor to adenocarcinoma has not been well established, and many investigators are pursuing ac-

tivities to detect and explain these carcinomatous changes. Until now, no well-recognized early molecular events have been reported in borderline tumors.

Epigenetic gene alterations such as aberrant promoter methylation are common and important mechanisms of tumorigenesis and may be mechanistic alternatives to gene mutations for the formation of ovarian tumors. An example is provided by the tumor suppressor gene *RASSF1A* (Ras association domain family 1A gene) and its common homozygous deletion at 3p21.3, which is frequently inactivated in a variety of primary human cancers, including lung cancer (30–80%), breast cancer (49–62%), and renal-cell cancer (23–91%). Among female genital-tract tumors, a high frequency of loss of heterozygosity (LOH) for 3p is found in cervical and ovarian carcinoma [15], and in ovarian tumors, the deletion of the short arm of chromosome 3 is a frequent genetic alteration [7]. Until now, only three reports on the hypermethylation rate of *RASSF1A* have been published in ovarian tumors (Table 1). Yoon et al. analyzed 20 ovarian tumors for *RASF1A* methylation, and 8 of 20 tumors (40%) were found methylated [21]; similarly, Rathi et al. [14] reported a rate of 41%. In contrast to this, Agathanggelou et al. found a methylation rate of only 10% in ovarian cancer [1]. However, in these studies, *RASSF1A* methylation was not examined in benign and borderline tumors and was not compared with clinicopathologic parameters. Consequently, we investigated the methylation status of *RASSF1A* in ovarian tumors at various stages.

Table 1 Methylation of the *RASSF1A* gene in ovarian tumors

Histologic type	Methylation	Reference
Ovarian tumor	8/20 (40%)	Yoon et al. [21]
Ovarian carcinoma	8/16 (50%)	
Poorly differentiated	4/7 (57%)	
Moderately differentiated	1/3 (33%)	
Well differentiated	3/3 (100%)	
Unknown	0/3 (0%)	
Ovarian fibroma	0/1 (0%)	
Lipoma	0/1 (0%)	
Unclassified	0/2 (0%)	
Normal tissue	0/10 (0%)	
Ovarian epithelial tumor	2/21 (10%)	Agathanggelou et al. [1]
Ovarian carcinoma	20/49 (41%)	Rathi et al. [14]
Papillary serous	17/32 (53%)	
Endometrioid	3/7 (43%)	
Mucinous	0/2 (0%)	
Clear cell	0/2 (0%)	
Other adenocarcinoma	0/6 (0%)	
Nonmalignant ovarian tissue	5/39 (15%)	

Materials and methods

Tissue samples

Fifty-four nonmicrodissected frozen ovarian tumors were collected from patients at the Samsung Medical Center. All samples were stored at −70°C, and formalin-fixed and paraffin-embedded tissue blocks representative of serous carcinoma, borderline tumors, and serous adenoma in 97 cases were obtained from the Department of Pathology. Detailed patient demographic and clinical information was obtained by reviewing medical records. Histologic classifications were established according to the World Health Organization (WHO) criteria, and tumor stage was established according to the Federation of International Gynecological Oncologists of classification. Two cases of normal ovarian tissue were collected from patients without cancer undergoing bilateral salpingo-oophorectomy at the time of surgery for benign gynecological disease. All samples were collected after obtaining appropriate institutional Review Board consent.

Microdissection and DNA extraction

Surgically resected fresh tumor tissues were macroscopically dissected to separate tumorous and nontumorous tissues. DNA from 100 mg (or more) frozen tissue specimens were obtained by overnight digestion with 200 μg/ml proteinase K at 50°C by following the manufacture's instructions (Qiagen). Each paraffin-embedded ovarian tissue block was used to prepare a 10-μ tissue section. Sections were stained with hematoxylin to confirm the histological presence of tumor. Tumor areas were carefully microdissected from normal surrounding stromal tissues, placed in an Eppendorf tube, deparaffinized overnight at 63°C in xylene, and then vortexed vigorously. After centrifuging at full speed for 5 min, the supernatant was removed, and ethanol was added to remove residual xylene, and then ethanol was removed by centrifugation. After ethanol evaporation, the obtained tissue pellets were resuspended in lysis buffer (Qiagen), and DNA was isolated according to the manufacturer's instructions (Qiagen).

Methylation analysis

The methylation status of the promoter region was determined by methylation-specific polymerase chain reaction (PCR) (MSP), which distinguishes unmethylated alleles from methylated alleles. Genomic DNA (2 μg) was denatured in NaOH (0.3 M) for 15 min at 37°C. Cytosines were sulfonated in sodium bisulfite (3.12 M; Sigma) and hydroquinone (5 mM; Sigma) in a thermocycler for 30 s at 99°C and for 15 min at 50°C for 20 cycles. The DNA samples were then desalted through a column (Wizard DNA Clean-Up System, Promega), desulfonated in NaOH (0.3 M) and precipitated. We amplified DNA sequences by mixing bisulfite-treated DNA (100 ng) with 50 pmol of primer MU379 (5′-GTTTTGGTAGTTTAATGAGTTTAG GTTTTTT-3′) and 50 pmol primer of ML730 (5′-AC CCTCTTCCTCTAACACAATAAAACTAACC-3′) in a re-

Table 2 Summary of the methylation status of *RASSF1A* in ovarian tissues

Tissue	Diagnosis	Methylation of *RASSF1A*
Frozen	Normal	0/5 (0%)
	Serous	
	Adenoma	1/5 (20.0%)
	Borderline	2/7 (28.6%)
	Carcinoma	4/10 (25.0%)
	Mucinous	
	Adenoma	0/5 (0%)
	Borderline	2/7 (28.6%)
	Carcinoma	3/6 (50.0%)
	Transitional-cell carcinoma	1/3 (33.3%)
	Clear-cell carcinoma	3/3 (100%)
	Malignant müllerian mixed tumor	3/3 (100%)
Archival	Serous	
	Adenoma	1/6 (16.6%)
	Borderline	20/41 (48.8%)
	Carcinoma	25/50 (50.0%)

action buffer (100 μl) containing deoxynucleoside 5c-triphosphates (dNTPs) (200 μM each) and *Taq* polymerase (Boehringer) at 95°C for 1 min, 55°C for 1 min, and at 74°C for 2 min for 30 cycles. Seminested PCR was performed using DNA (100 ng) of the amplified products and the internal primer ML561 (5′-CCCCACAATCCCTACACC-CAAAT-3′) and primer MU379 using the PCR conditions described above. Placental-tissue DNA treated in vitro with *Sss*I methyltransferase was used as a positive control for amplification of methylated alleles. Water blanks without added DNA were included as negative PCR controls in each assay. PCR products were loaded directly onto 2% agarose gels, stained with ethidium bromide, and visualized under ultraviolet illumination. A portion of the PCR products were purified using a QIAquick PCR purification kit (Qiagen) and directly sequenced to confirm methylation.

Statistical analysis

Associations between *RASSF1A* methylation and clinicopathologic parameters were analyzed using the Student's *t* test for continuous variables or Fisher's exact test (or the Pearson chi test) for categorical variables. The effects of *RASSF1A* methylation on patient survival were estimated using the Kaplan–Meier method, and differences between the survival curves of the two groups were analyzed using the log-rank test. Quoted *p* values were based on two-sided statistical analysis.

Results

To elucidate the status of *RASSF1A* during ovarian cancer pathogenesis, we analyzed the methylation status of *RASSF1A* promoter in various ovarian tissues. All of the tumors analyzed were of epithelial origin and were classified based on histologic subtype, as shown in Table 2. Initially, the analysis was performed using frozen tissues, and a high frequency (24–100%) of *RASSF1A* promoter hypermethylation was detected. The *RASSF1A* methylation rates in various types of fresh ovarian tissue were serous cystadenoma (1/5), serous tumor of borderline malignancy (2/7), serous adenocarcinoma (4/10), mucinous cystadenoma (0/5), mucinous tumor of borderline malignancy (2/7), mucinous adenocarcinoma (3/6), transitional-cell carcinoma (1/3), clear-cell carcinoma (3/3), and malignant mixed müllerian tumor (3/3) (Table 2). Agarose gel electrophoresis of representative MSP products is shown in Fig. 1. *RASSF1A* methylation was confirmed by direct sequencing of the *RASSF1A* MSP product in seven samples. All samples were methylated at the 12 cytosine–

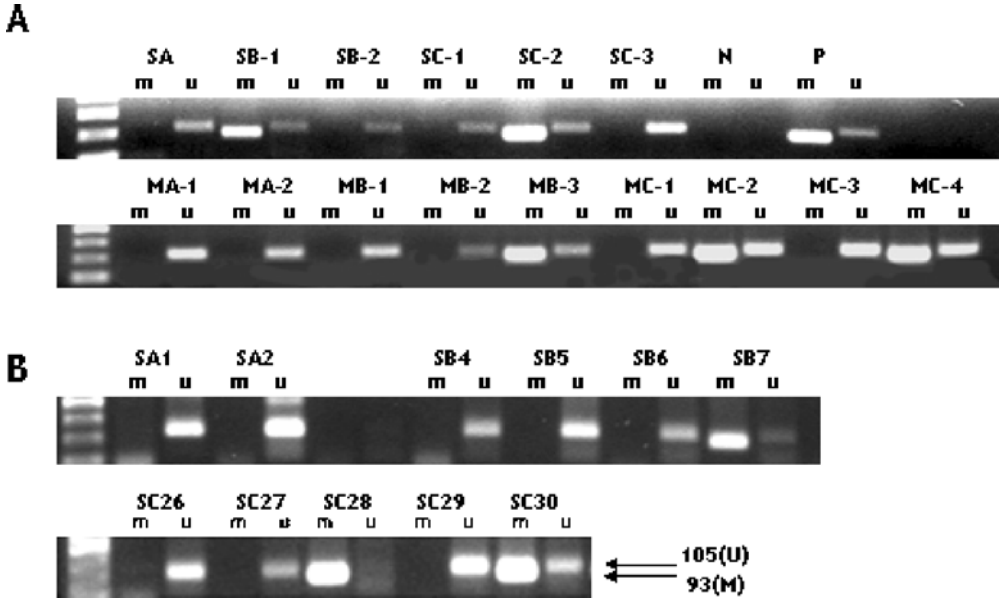

Fig. 1 Agarose gels showing representative products of MS-PCR analysis in ovarian tumors. *P* is positive control, i.e., artificially methylated DNA, and *N* (water blank) is negative PCR control. The methylated status of the *RASSF1A* CpG island is indicated as methylated (*m*) and unmethylated (*u*). The sizes of the methylation- and unmethylation-specific products were 93 and 105 bp, respectively. *SA*, serous adenoma; *SB*, serous borderline tumor; *SC*, serous carcinoma; *MA*, mucinous adenoma; *MB*, mucinous borderline tumor; and *MC*, mucinous carcinoma. **a** Frozen tissue. **b** Archival tissue

phosphate–guanine (CpG) sites contained in the amplicon (data not shown). The methylated form was composed of 96 base pairs, and the unmethylated form was composed of 106 base pairs; in normal ovarian tissues, hypermethylation was not detected (0/5). We found that one case of serous adenoma and some portions of borderline tumors had an aberrant *RASSF1A* methylation. We than extended the study to include archival tissue. All 97 archived paraffin tissues were evaluated, and *RASSF1A* methylation was detected in serous cystadenoma (1/6, 16.6%), serous tumor of borderline malignancy (20/41, 48.8%), and in serous adenocarcinoma (25/50, 50.0%) (Table 2). The most interesting finding was that borderline tumors and carcinomas have similar methylation rates. Moreover, methylation status was statistically correlated with several clinicopathologic parameters in borderline tumors: ascites at diagnosis (p=0.027), surface involvement (p<0.001), bilaterality (p=0.019), microinvasion (p=0.027), and implant (p=0.001) (Table 3). When implant cases were divided into two groups of noninvasive and invasive implants, methylation status was significant in only noninvasive implant cases (p=0.001). Because the number of cases with invasive implant was so small (n=4), the methylation status was inconclusive.

In carcinomas, *RASSF1A* promoter methylation was more frequent in advanced-stage cases, but this was not significant because of the limited number of cases in stages I–II (Table 4). Also, we examined the correlation between patient survival and *RASSF1A* methylation status, but we found no significant relation.

Table 3 Association of methylation status of *RASSF1A* promoter with clinicopathologic features in serous ovarian borderline tumors

Variables	*RASSF1A*		
	Methylated (%)	Unmethylated (%)	p
Mean age (years)	50.0±14.7	45.3±13.8	0.297[a]
Tumor size (cm)	11.1±6.5	8.7±3.5	0.114[a]
Stage			
I (31/41)	13/31 (41.9)	18/31 (58.1)	
II (4/41)	2/4 (50.0)	2/4 (50.0)	
III (6/41)	5/6 (83.3)	1/6 (16.7)	0.076[b]
Ascites			
Present (10/41)	8 (80.0)	2 (20.0)	
Absent (31/41)	12 (38.7)	19 (61.3)	0.027[b]
Surface involvement			
Present (17/41)	14 (82.4)	3 (17.6)	
Absent (24/41)	6 (25.0)	18 (75.0)	0.000[b]
Bilaterality			
Bilateral (15/41)	11 (73.3)	4 (26.7)	
Unilateral (26/41)	9 (34.62)	17 (65.3)	0.019[b]
Microinvasion			
Present (10/41)	8 (80.0)	2 (20.0)	
Absent (31/41)	12 (38.7)	19 (61.3)	0.027[b]
Implant			
Present (16/41)	13 (81.3)	3 (18.8)	
Absent (25/41)	7 (28.0)	18 (72.0)	0.001[b]

[a]Student's t test
[b]Fisher's exact test

Table 4 Association of methylation status of *RASSF1A* promoter with clinicopathologic features in serous ovarian carcinomas

Variables	*RASSF1A*		
	Methylated (%)	Unmethylated (%)	p
Mean age (years)	55.9±10.1	52.3±11.9	0.253[a]
Age (years)			
0–49 (16/50)	7/16 (43.8)	9/16 (56.3)	
50+ (34/50)	18/34 (52.9)	16/34 (37.2)	0.381[b]
Stage			
I–II (3/50)	1/3 (33.3)	2/3 (66.7)	
III–IV (47/50)	24/47 (51.1)	23/47 (48.9)	0.500[c]
Ascites			
Absent (9/50)	5/9 (55.6)	4/9 (44.4)	
Present (41/50)	20/41 (48.8)	21/41 (51.2)	0.500[c]
Outcome of primary surgery			
<2 cm (20/50)	10/20 (50.0)	10/20 (50.0)	
≥2 cm (30/50)	15/30 (50.0)	15/30 (50.0)	

[a]Student's t test
[b]χ^2 test (asymptotic significance, two-sided)
[c]Fisher's exact test

Discussion

The hypermethylation rate of *RASSF1A* has been extensively studied in variable solid tumors. Whereas we did not study *RASSF1A* gene expression, previous studies have demonstrated that the inactivation of the expression of *RASSF1A* is highly correlated with the methylation of its promoter. Thus, the frequent methylation of the *RASSF1A* gene suggests that it plays a role in ovarian tumorigenesis, especially in the development of epithelial proliferation to form a borderline tumor. Although one [1] report of *RASSF1A* gene in ovarian tumor produced conflicting results, our results are in agreement with the 40 and 41% incidences of hypermethylation in ovarian tumors observed by Yoon et al. [21] and Rathi et al. [14], respectively.

Our findings on *RASSF1A* hypermethylation in ovarian tumors are interesting for several reasons. First, this hypermethylation occurs at an early stage of ovarian tumorigenesis (i.e., in borderline tumors), and this represents the first example of epigenetic inactivation of this tumor suppressor gene at a high prevalence in an early lesion. This contrasts with the genetic inactivation of the major tumor suppressor gene, p53, which generally occurs in late-stage advanced carcinomas. Recently, several reports have demonstrated an early role for *RASSF1A* methylation in the tumorigenesis of thyroid, lung, and breast cancer and suggested its use as a molecular marker of early detection [8, 19, 20]. Ibanez de Caceres et al. [9] also reported the results of *RASSF1A* hypermethylation in serum, plasma, and peritoneal fluid from ovarian cancer patients. They concluded that promoter hypermethylation

was a common and relatively early event in ovarian tumorigenesis that could be detected in the serum DNA from patients with ovary-confined (stage IA or B) tumors in a cytologically negative peritoneal fluid. Results of the present study correspond with the results of earlier studies. Second, the prevalence of *RASSF1A* promoter methylation is similar in borderline tumors and in serous carcinomas. The tumor suppressor role of the *RASSF1A* gene may be involved during the stage of epithelial proliferation rather than during the invasion or metastasis of advanced carcinomas. The progression from a serous borderline tumor to adenocarcinoma remains controversial [16]. However, this *RASSF1A* methylation pattern supports the hypothesis that some proportion of serous carcinomas originate from serous borderline tumors. Third, we observed for the first time that *RASSF1A* methylation occurs more frequently in advanced borderline tumors, i.e., in cases with ascites at diagnosis, surface involvement, bilaterality, microinvasion, and peritoneal implants. There was no significant correlation between *RASSF1A* methylation status and invasive implant, which is a prognostic factor of borderline tumors.

Clinically, it is still controversial whether aberrant *RASSF1A* methylation in human cancer is associated with clinicopathologic features. During breast cancer progression, *RASSF1A* inactivation is common in grade I tumors; *RASSF1A* methylation may thus be an early event [4]. No statistically significant association has been found between *RASSF1A* methylation and age, stage, tumor histology, recurrence/metastasis, or overall survival in patients with bladder cancer or childhood neoplasia [11, 19]. In our study, there was no relationship between *RASSF1A* promoter methylation and stage or survival in carcinomas. It appears that this frequent and ubiquitous epigenetic alteration may potentially be a very early and critical event deregulating apoptosis and cell cycle progression in ovarian epithelial tumors rather than invasiveness or metastasis.

Based on the above, we propose that the epigenetic inactivation of the tumor suppressor gene *RASSF1A*, through aberrant promoter methylation, may play an important role in the formation of borderline tumors and in their progression to adenocarcinoma. Aberrant *RASSF1A* methylation may lead to progressive clonal expansion in borderline tumors, and when the accumulation of such methylation reaches a critical level, or perhaps when an additional genetic/epigenetic alteration occurs, this may subsequently lead to malignant transformation to adenocarcinoma. Although many details of how *RASSF1A* inactivation by hypermethylation contributes to ovarian tumorigenesis remain unknown, its hypermethylation in a subgroup of serous adenocarcinoma suggests that the role of *RASSF1A* methylation may be both critical and indispensable for the formation or progression of this subgroup of ovarian cancers.

Recently, Song et al. [18] found evidence of the tumor suppressor function of *RASSF1A*. He found that *RASSF1A* regulates mitosis by inhibiting the mitogenic APC-Cdc20 complex. *RASSF1A* localized to microtubules during the interphase and to centrosomes and the spindle during mitosis. Cells without *RASSF1A* divided faster than normal controls, and *RASSF1A* knock-down cells using siRNA showed more abnormal mitotic figures. An in vivo study also revealed larger tumor sizes in *RASSF1A*-negative mice. Thus, we suggest that the loss of *RASSF1A* protein function by hypermethylation increases the speed of the cell cycle, which increases the likelihood of genetic mutation. The most characteristic feature of borderline tumors is the proliferation of epithelium. Therefore, the frequent loss of *RASSF1A* protein in borderline tumors may be self-explanatory. Progression to malignancy results from accumulated damage to both oncogenes and tumor suppressor genes. It would appear that such silencing of a normal tumor suppressor gene is responsible for the proliferation of ovarian epithelial cells.

Initially, we worked with frozen tissues; however, cellular heterogeneity was a common problem that precludes accurate DNA analysis in human tissue samples, i.e., a mixture of neoplastic and nonneoplastic cells such as supporting stromal cells, inflammatory cells, and preexisting original tissue [10]. Moreover, the natures of heterogeneous cells may obscure the results of molecular assays, depending on the ratio of neoplastic to nonneoplastic genomic DNA and the sensitivity of the tests. Although MSP is a highly sensitive technique for the detection of targeted DNA, the relative amounts of competing DNAs present is an important factor. Nonmicrodissected tissue did not represent the homogenous ovarian epithelium or adenoma component even in carcinoma, and thus, results can be distorted by the relatively predominant stromal component. Previous studies have also used nonmicrodissected frozen tissues. Thus, we collected tumor DNA by microdissecting archival tissues and minimized stromal tissue contamination. The rate of methylation in archival tissue was higher than in frozen tissue, which stresses the importance of microdissection when an analysis is peformed using PCR, since surrounding stromal tissue may mask tumor-specific changes, especially in borderline cases.

Several conclusions may be drawn from this study. First, the *RASSF1A* hypermethylation rate is infrequent in normal and benign tumors. Moreover, the different hypermethylation frequencies in benign and malignant tumors suggest that in ovarian tumors *RASSF1A* silencing is an epigenetic alteration related to tumor progression. Finally, the frequent hypermethylation rate observed in borderline tumors suggests the possibility that the inactivation of *RASSF1A* may be a relatively early event in ovarian tumorigenesis.

Acknowledgements This work was supported in part by Samsung Biomedical Research Institute grant no. SBRI CA32161.

References

1. Agathanggelou A, Honorio S, Macartney DP, Martinez A, Dallol A, Rader J, Fullwood P, Chauhan A, Walker R, Shaw JA, Hosoe S, Lerman MI, Minna JD, Maher ER, Latif F (2001) Methylation associated inactivation of RASSF1A from region 3p21.3 in lung, breast and ovarian tumours. Oncogene 20: 1509–1518

2. Bell DA, Weinstock MA, Scully RE (1988) Peritoneal implants of ovarian serous borderline tumors. Histologic features and prognosis. Cancer 62:2212–2222
3. Bell KA, Smith Sehdev AE, Kurman RJ (2001) Refined diagnostic criteria for implants associated with ovarian atypical proliferative serous tumors (borderline) and micropapillary serous carcinomas. Am J Surg Pathol 25:419–432
4. Dammann R, Yang G, Pfeifer PF (2001) Hypermethylation of the CpG island of Ras association domain family 1A (RASSF1A), a putative tumor suppressor gene from the 3p21.3 locus, occurs in a large percentage of human breast cancers. Cancer Res 61:3105–3109
5. de Nictolis M, Montironi R, Tommasoni S, Carinelli S, Ojeda B, Matias-Guiu X, Prat J (1992) Serous borderline tumors of the ovary. A clinicopathologic, immunohistochemical, and quantitative study of 44 cases. Cancer 70:152–160
6. Ford D, Easton D (1995) The genetics of breast and ovarian cancer. Br J Cancer 72:805–812
7. Fullwood P, Marchini S, Rader JS, Martinez A, Macartney D, Broggini M, Morelli C, Barbanti-Brodano G, Maher ER, Latif F (1999) Detailed genetic and physical mapping of tumor suppressor loci on chromosome 3p in ovarian cancer. Cancer Res 59:4662–4667
8. Honorio S, Agathanggelou A, Schuermann M, Pankow W, Viacava P, Maher ER, Latif F (2003) Detection of RASSF1A aberrant promoter hypermethylation in sputum from chronic smokers and ductal carcinoma in situ from breast cancer patients. Oncogene 22:147–150
9. Ibanez de Caceres I, Battagli C, Esteller M, Herman JG, Dulaimi E, Edelson MI, Bergman C, Ehya H, Eisenberg BL, Cairns P (2004) Tumor cell-specific BRCA1 and RASSF1A hypermethylation in serum, plasma, and peritoneal fluid from ovarian cancer patients. Cancer Res 64:6476–6481
10. Lee JY, Dong SM, Kim SY, Yoo NJ, Lee SH, Park WS (1998) A simple, precise and economical microdissection technique for analysis of genomic DNA from archival tissue sections. Virchows Arch 433:305–309
11. Lee MG, Kim HY, Byun DS, Lee SJ, Lee CH, Kim JI, Chang SG, Chi SG (2001) Frequent epigenetic inactivation of RASSF1A in human bladder carcinoma. Cancer Res 61: 6688–6692
12. Murdoch WJ (1996) Ovarian surface epithelium, ovulation and carcinogenesis. Biol Rev Camb Philos Soc 71:529–543
13. NIH consensus conference (1995) Ovarian cancer. Screening, treatment and follow-up. NIH Consensus Development Panel on Ovarian Cancer. JAMA 273:491–497
14. Rathi A, Virmani AK, Schorge JO, Elias KJ, Maruyama R, Minna JD, Mok SC, Girard L, Fishman DA, Gazdar AF (2002) Methylation profiles of sporadic ovarian tumors and nonmalignant ovaries from high-risk women. Clin Cancer Res 8:3324–3331
15. Rimessi P, Gualandi F, Morelli C, Trabanell C, Wu Q, Possati L, Montesi M, Barrett JC, Barbanti-Brodano G (1994) Transfer of human chromosome 3 to an ovarian carcinoma cell line identifies three regions on 3p involved in ovarian cancer. Oncogene 9:3467–3474
16. Russell SE, McCluggage WG (2004) A multistep model for ovarian tumorigenesis: the value of mutation analysis in the KRAS and BRAF genes. J Pathol 203:617–619
17. Silva EG, Kurman RJ, Russell P, Scully RE (1996) Symposium: ovarian tumors of borderline malignancy. Int J Gynecol Pathol 15:281–302
18. Song MS, Song SJ, Ayad NG, Chang JS, Lee JH, Hong HK, Lee H, Choi N, Kim J, Kim H, Kim JW, Choi EJ, Kirschner MW, Lim DS (2004) The tumour suppressor RASSF1A regulates mitosis by inhibiting the APC-Cdc20 complex. Nat Cell Biol 6:129–137
19. Wong IH, Chan J, Wong J, Tam PK (2004) Ubiquitous aberrant RASSF1A promoter methylation in childhood neoplasia. Clin Cancer Res 10:994–1002
20. Xing M Cohen Y, Mambo E, Tallini G, Udelsman R, Ladenson PW, Sidransky D (2004) Early occurrence of RASSF1A hypermethylation and its mutual exclusion with BRAF mutation in thyroid tumorigenesis. Cancer Res 64:1664–1668
21. Yoon JH, Dammann R, Pfeifer GP (2001) Hypermethylation of the CpG island of the RASSF1A gene in ovarian and renal cell carcinomas. Int J Cancer 94:212–217

Virchows Arch (2006) 448: 337–343
DOI 10.1007/s00428-005-0089-x

ORIGINAL ARTICLE

Raphael Schiffmann · Amy Rapkiewicz · Mones Abu-Asab · Markus Ries · Hasan Askari · Maria Tsokos · Martha Quezado

Pathological findings in a patient with Fabry disease who died after 2.5 years of enzyme replacement

Received: 22 June 2005 / Accepted: 31 August 2005 / Published online: 29 November 2005

Abstract We describe the postmortem findings of a 47-year-old man with Fabry disease, an X-linked glycolipid storage disorder, who was on enzyme replacement therapy with recombinant α-galactosidase A for more than 2 years. The patient had widespread atherosclerotic coronary artery disease that culminated in a massive acute myocardial infarction. Atherosclerotic lesions were seen in the right and left coronary systems, aorta, and the basilar artery. Typical Fabry cardiomyopathy and glomerular nephropathy were found. With the exception of vascular endothelial cells, extensive glycolipid storage deposits were seen in all vascular and nonvascular cells and organ systems. We conclude that, at least in this patient, repeated infusions with α-galactosidase A over a prolonged period did not appreciably clear storage material in cells other than vascular endothelial cells. These findings also illustrate accelerated atherosclerosis in susceptible patients with Fabry disease.

Keywords Fabry disease · Lysosomes · Atherosclerosis · Myocardial infarction · Enzyme replacement therapy · Glycolipids

R. Schiffmann · M. Ries · H. Askari
Developmental and Metabolic Neurology Branch,
National Institute of Neurological Disorders and Stroke,
National Institutes of Health,
Bethesda, MD, USA

R. Schiffmann (✉)
National Institutes of Health,
Room 3D03, Building 10, 9000 Rockville Pike,
Bethesda, MD 20892-1260, USA
e-mail: RS4e@nih.gov
Tel.: +1-301-4961465
Fax: +1-301-4808354

A. Rapkiewicz · M. Abu-Asab · M. Tsokos · M. Quezado
Laboratory of Pathology, National Cancer Institute,
National Institutes of Health,
Bethesda, MD, USA

Introduction

Fabry disease, an X-linked systemic disorder caused by a deficiency of the lysosomal enzyme α-galactosidase A, results in a failure to metabolize α-D-galactosyl moieties [4]. This abnormality leads to the systemic deposition of glycosphingolipids, particularly globotriaosylceramide (Gb_3) [5]. In adulthood, progressive renal failure, strokes, and heart disease develop, leading to death at a median age of 50–55 years. In the past 5 years, enzyme replacement therapy (ERT) with recombinant α-galactosidase A has been added to the standard therapeutic regimen [8, 17, 18, 22]. Targeted primarily to reverse vasculopathy of Fabry disease, ERT has been shown to markedly reduce the cellular storage deposition in vascular endothelial cells [22]. Its long-term clinical effects, however, remain to be fully assessed. No extensive pathological analysis in patients on long-term ERT has been reported thus far. We present in this report the autopsy results of a 47-year-old man who was on ERT for more than 2 years and died suddenly.

Case report

The patient was a 47-year-old man who was diagnosed with Fabry disease at age 19 with α-galactosidase A activity of 1.3% of normal controls. Since 5 years of age, he suffered from episodes of fever and acroparesthesia, hypohidrosis, poor heat and exercise tolerance, diarrhea with abdominal cramps, and bouts of depression. At 35, he developed an acute onset of right-sided weakness and difficulty with word finding. A CT scan revealed a large anterior parietal infarct, and a left carotid angiogram showed marked narrowing of mid-sylvian branches of the left middle cerebral artery (MCA) with an area of avascularity in the left anterior parietal lobe. He was put on oral warfarin therapy with no apparent stroke recurrence. His most recent head MRI scan showed old left encephalomalacia in the left frontal lobe along with white matter

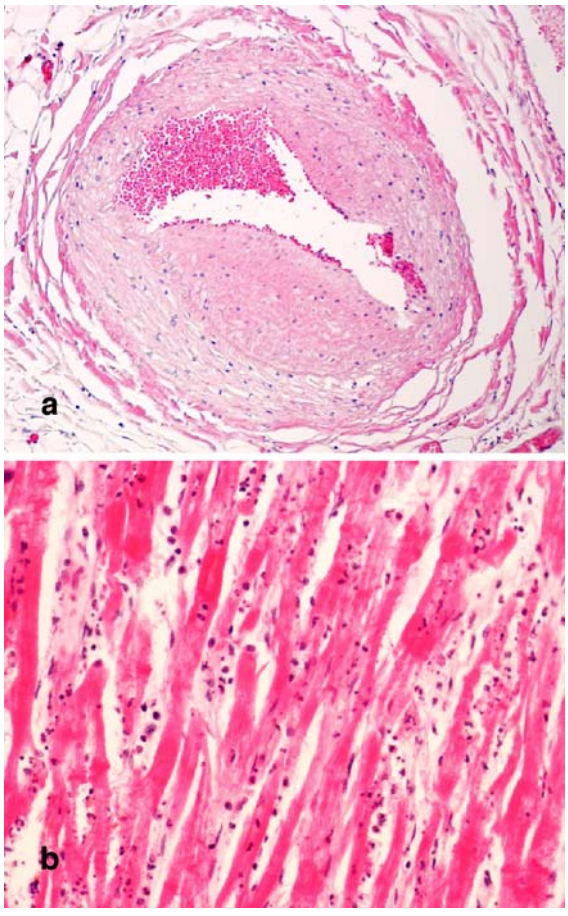

Fig. 1 Cardiovascular findings. **a** Section of the left coronary artery showing a marked intimal proliferation and stenosis of the lumen. Hematoxylin and eosin (H & E), ×20. **b** Representative section of the anterior portion of the left ventricle showing coagulative necrosis of the muscle with wavy fibers and a dense polymorphonuclear leukocytic infiltrate. H & E, ×20

hyperintense lesions on T2 and fluid-attenuated inverse recovery (FLAIR) images on the left.

He had no hypertension. His renal function was normal until age 37 when his serum creatinine was found to be 1.4 mg/dL (normal 0.9–1.4) with a creatinine clearance of 78 mL/min. He had mild-to-moderate proteinuria with variable 24-h protein excretion of up to 1.2 g/24 h. At age 43, his serum creatinine level was 1.5 mg%. His total blood cholesterol at age 20 was 189 mg/dL. At age 36, it was 201 mg/dL, and his HDL and triglyceride levels were 87 mg/dL and 92 mg/dL, respectively. At age 43, total cholesterol was 241 mg/dL, LDL level was 161 mg/dL, and HDL level was 24 mg/dL.

Other abnormalities noted were bilateral pedal edema, mild-to-moderate bilateral high-frequency hearing loss, sinus bradycardia and left ventricular hypertrophy in the electrocardiogram, and mild mitral and tricuspid valve regurgitation.

His therapy included Coumadin and carbamazepine. In addition, he received intravenous α-galactosidase A infusions (agalsidase beta; Genzyme Corporation, Cambridge, MA) at a dosage of 1 mg/kg every 2 weeks for the last 2.5 years of his life.

He first complained of sharp chest pain at age 40, lasting about 30 s (not precipitated by exertion). He complained mostly of burning chest pain on and off in the years prior to his death. One week prior to his death, he again reported a burning discomfort on his chest, which increased with physical activity. He refused to seek medical attention and shortly thereafter was found dead.

Regarding his family history, his mother, two sisters, and a brother were affected by Fabry disease. Two of his maternal uncles died of the same disease. One died of a cardiac cause at age 39 and another maternal uncle died of stroke at age 47. Another cousin with Fabry disease died of myocardial infarction at age 53.

Pathological findings

The postmortem interval was approximately 32 h before an unrestricted autopsy was performed. Only the pertinent findings will be described.

The heart weighed 520 g with approximately 30–50 mL of pericardial fluid. The right dominant coronary arterial systems showed marked atheromas with calcifications. The left ventricular wall thickness was 1.7 cm (normal 1.0–1.5 cm). Sections of the left coronary arterial system showed significant intimal atheromas with intimal proliferation and calcifications with reduction of the luminal diameter of up to 95% in some regions (Fig. 1a). The right coronary artery also showed significant intimal atheromas and calcification with reduction of the interior diameter of up to 50%. Microscopically, portions of the anterior free wall of the left ventricle showed an inflammatory infiltrate consisting predominately of neutrophils with necrosis of the myocardium (Fig. 1b). Additional sections of the anterior wall distant from the inflammatory infiltrate showed a significant patchy, fibrous scarring of the myocardium. Ultrastructural analysis showed the heart muscle separated by thin strands of fibrosis (Fig. 2). The myocytes showed focal loss of filaments and increased number of mitochondria containing tubulovesicular cristae and dense aggregates. Numerous lamellar inclusions were found in myocytes and fibroblasts. Inclusions were only rarely seen in endothelial cells (Fig. 2d).

The intimal surface of the aorta showed marked atherosclerotic ulcerative plaques. The orifices of major arteries were widely patent.

The lungs were heavy and consolidated with blood-tinged pulmonary edema. Pulmonary hemorrhage was identified in the peripheral hilar region of the right and left lung. Microscopic examination showed significant congestion, with hemorrhage into the bronchioles and spilling into the alveolar spaces with distal necrosis/infarction of the parenchyma. Other sections from the consolidated lung showed areas of frothy, eosinophilic cell-free fluid filling the alveolar spaces and scattered, admixed hemosiderin-laden macrophages.

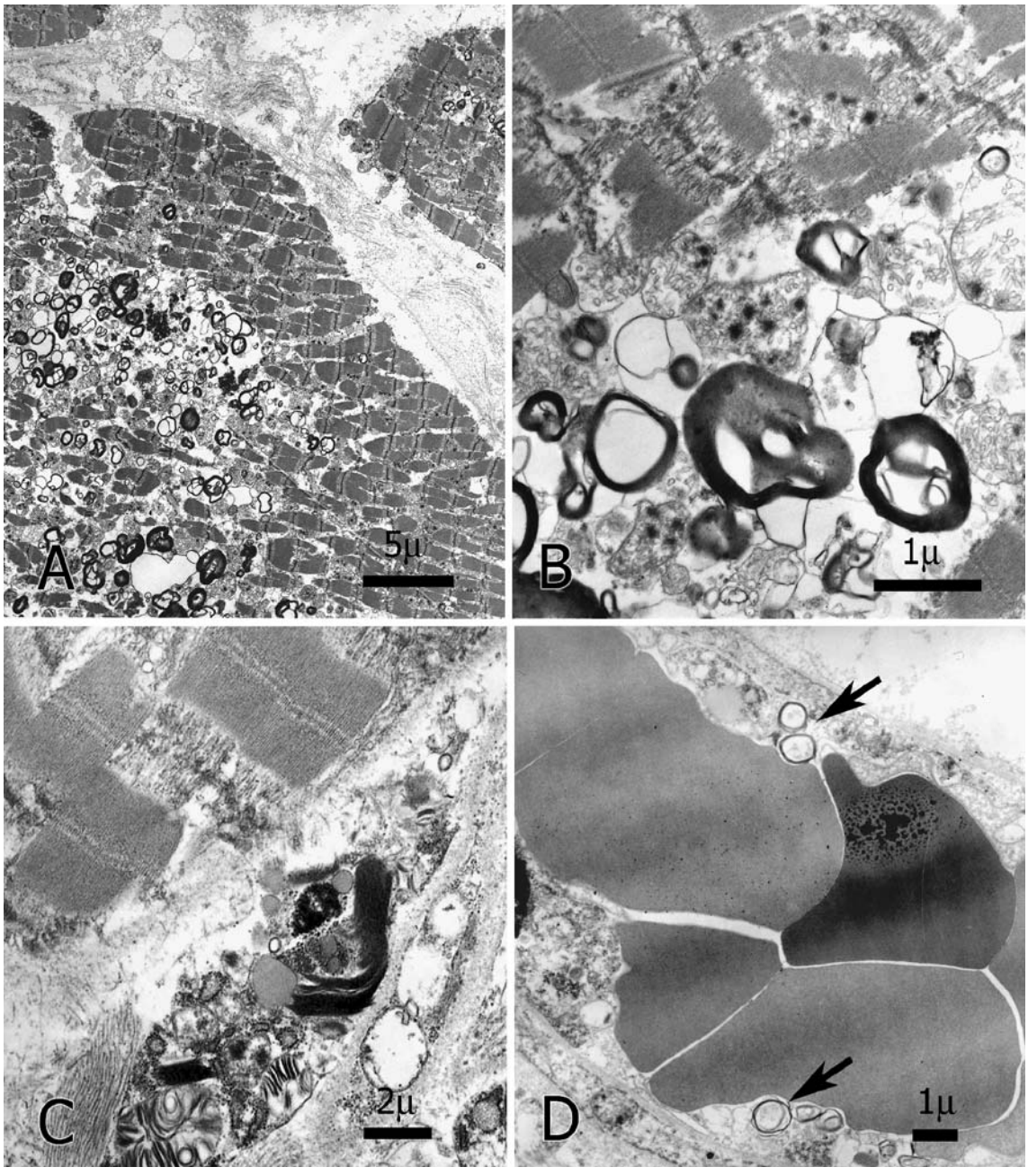

Fig. 2 Ultrastructure of the heart. **a** Large aggregates of concentric lamellated cytoplasmic inclusions displace cardiac myofibrils to the periphery of the cell. Interstitial fibrosis and increased numbers of mitochondria are secondary features of the cardiomyopathy. **b** Higher magnification of the lamellar inclusions and the accumulated mitochondria. The latter exhibit tubulovesicular cristae and cell size variation. **c** The myelinoid inclusions sometimes consisted of parallel-stacked lamellae with a zebra-like pattern. **d** Inclusions were only rarely present in endothelial cells of adjacent interstitial capillaries (*arrows*)

The right kidney weighed 140 g and the left one weighed 184 g. The pelvis and calices of both kidneys were markedly dilated with thinning of the renal cortical parenchyma. Microscopically, glomeruli were either normal with occasional mesangial widening or sclerosis (Fig. 3). At the ultrastructural level, numerous lamellar inclusions were present in the glomerular epithelium and tubular epithelial cells. Only an occasional inclusion was seen in endothelial cells of glomerular capillaries (Fig. 4). Glycolipid deposits were not seen in peritubular capillary endothelial cells and only rarely seen in mesangial cells (not shown).

The fixed brain weighed 1,520 g. The left cerebral hemisphere showed a cystic cavity area in the frontoparietal lobes corresponding to an old infarct in the left MCA territory. Microscopically, this area was characterized by abnormal brain parenchyma with abundant reactive astrocytes, few foamy macrophages containing hemosiderin,

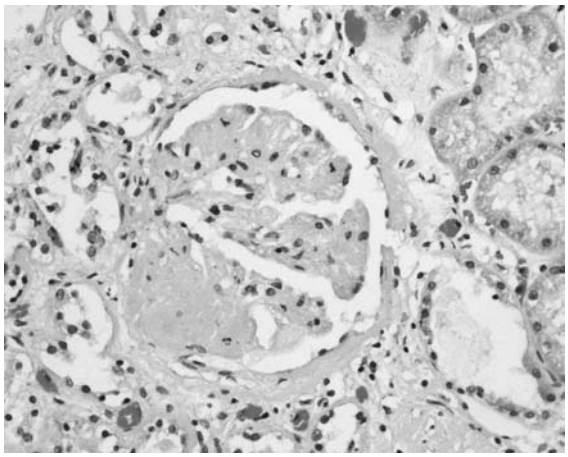

Fig. 3 Representative section of the renal cortex showing a glomerulus with focal mesangial sclerosis. H & E, ×40

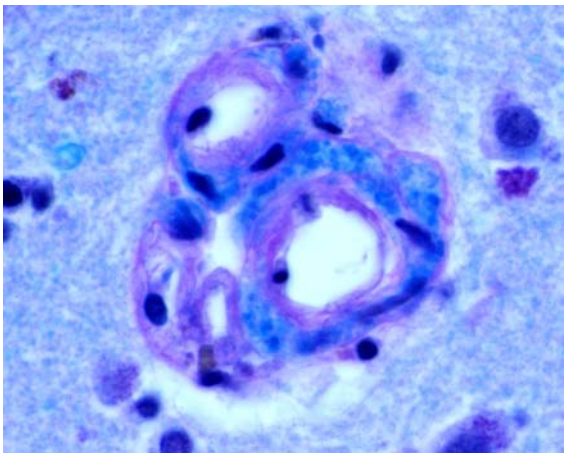

Fig. 5 Intracerebral blood vessels with Luxol fast blue (LFB)-stained deposits within vacuolated smooth muscle/adventitial cells. LFB–period acid Schiff (PAS), ×100 oil

and calcification. The basilar artery was atherosclerotic. Luxol fast blue (LFB)-stained deposits were found in blood vessels, mostly in the smooth muscle cells of the media and adventitia and little or none in endothelial cells (Fig. 5). Similar results were obtained by electron microscopy (Fig. 6). Neuronal storage was also observed in various areas including the hypothalamus (Fig. 7a), brainstem, and spinal cord. Sections of the paraspinal ganglia showed prominent neuronal distention with accumulating storage deposits (Fig. 7b).

Discussion

We describe herein the pathological abnormalities of a 47-year-old man with Fabry disease who died of acute myocardial infarction associated with nonhypertensive atherosclerotic coronary artery disease. Other significant findings at autopsy were the characteristic Fabry cardiomyopathy with increased cardiac mass by both weight and arterial wall thickness, as well as microscopic fibrosis and marked cellular storage. Typical primary and secondary findings of Fabry disease were also found in the kidney, the brain, and the paraspinal sensory ganglia.

A number of autopsy and pathological reports of patients with Fabry disease have been published [6, 7, 10, 20, 21]. The pathological findings in this patient showed an almost complete absence of glycolipid deposits in vascular endothelial cells attributable to the agalsidase beta infusions. Similar findings of predominant clearing of capillary endothelial cells were described in kidney biopsy material in the pivotal trial of agalsidase beta [21]. The presence of marked storage in other cells, including smooth muscle cells and pericytes of the vascular system, as well as in

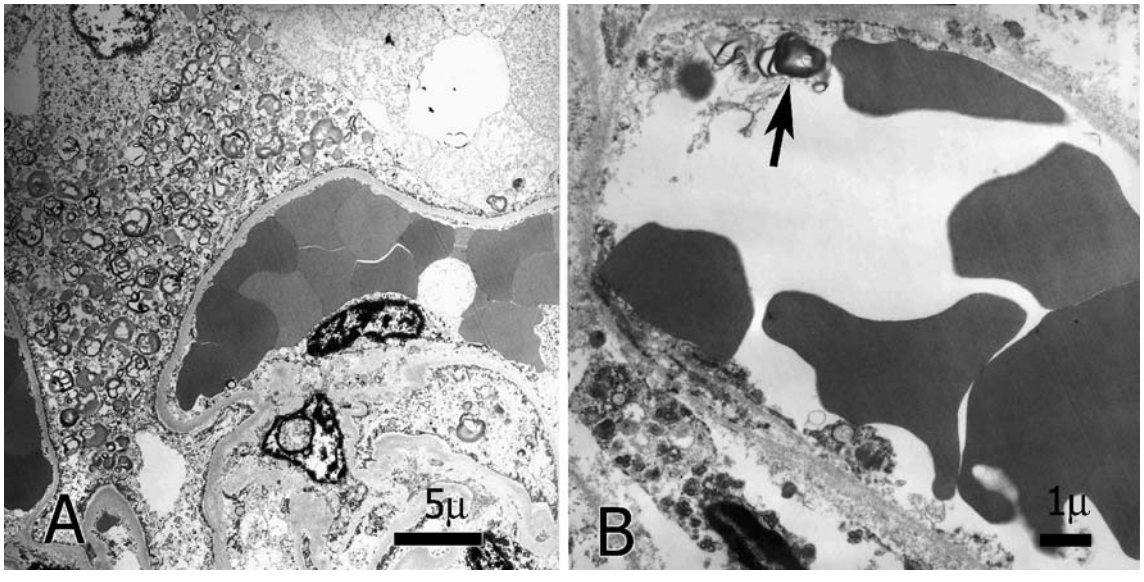

Fig. 4 Ultrastructure of the kidney. **a** Abundant lamellar inclusions in the glomerular epithelial cells (podocytes) and tubular epithelial cells (not shown). **b** On the other hand, only an occasional inclusion was identified in the glomerular capillary endothelial cells (*arrow*)

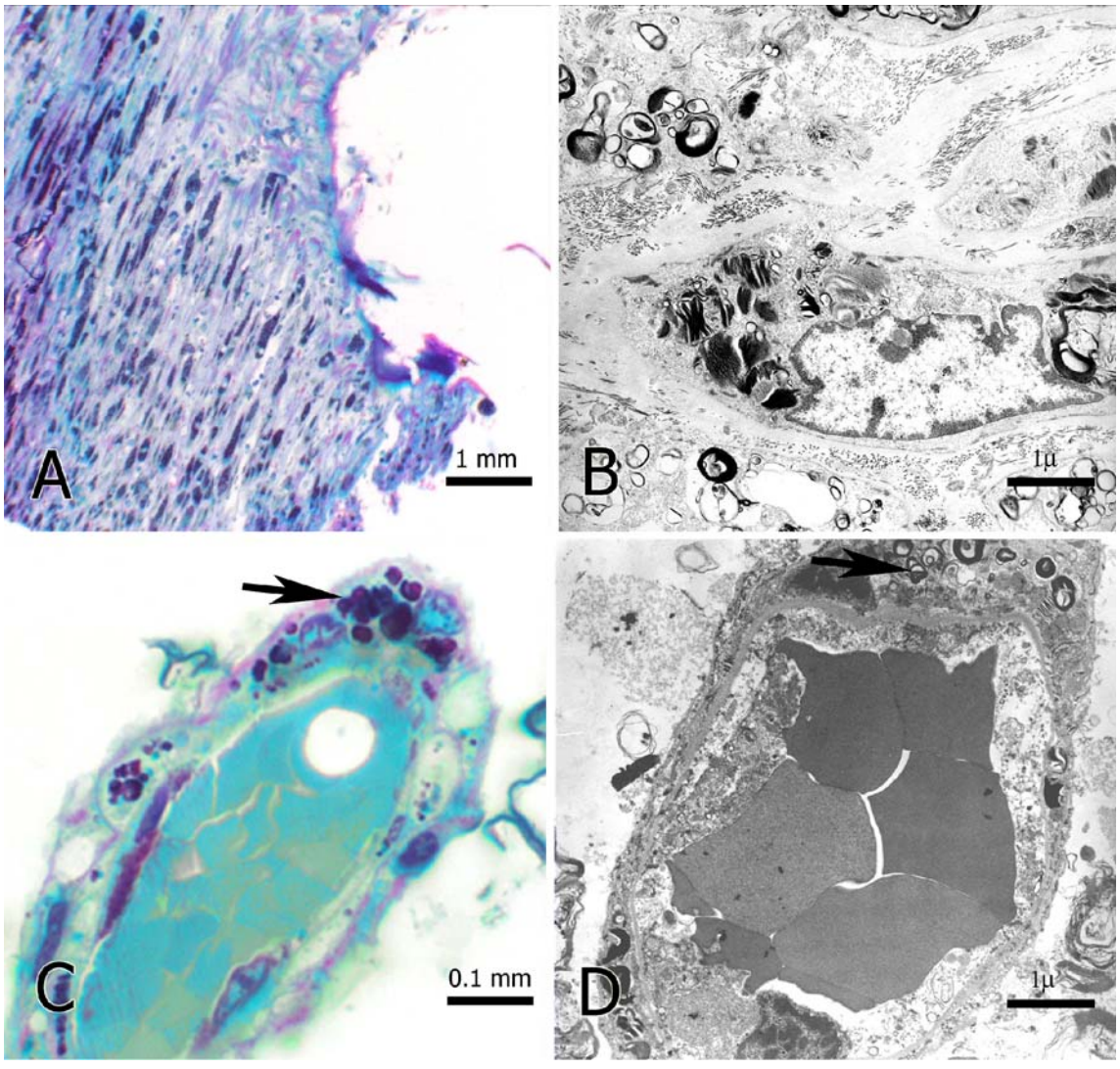

Fig. 6 Ultrastructure of the brain. The smooth muscle cells in the wall of a cerebral vessel shown in a semithin section in **a** (toluidine blue/fuchsin stain) are loaded with lamellar inclusions exhibiting concentric and zebra-like patterns at the ultrastructural level (**b**). Another semithin section (**c**) shows a capillary identified within the cerebral tissue, which exhibits many Fabry-type inclusions in pericytes (*arrows*) but lacks endothelial cell inclusions (**d**)

nonvascular cells, after more than 2 years of enzyme infusions suggests that the infused enzyme has limited access to nonvascular endothelial cells. If so, this may constitute a significant limitation of this therapeutic approach. We cannot however exclude the fact that greater storage clearance is achieved in other patients. Efforts to modify recombinant α-galactosidase A or the development of other therapeutic strategies may achieve more complete clearing of storage material. The partial clearance of glycolipid deposits from the vascular tree may explain in part the clinical impression that the incidence of strokes is not reduced in the first few years after α-galactosidase A infusions.

The involvement of the coronary arteries in Fabry disease has been previously recognized [1, 7, 9, 12], although minimized by others [19]. In addition, the possibility of accelerated atherosclerosis in Fabry disease has been previously mentioned [11, 13, 15]. Reported autopsies have shown that these coronary lesions are similar to typical atherosclerosis except that they are concentric with a white discoloration rather than the eccentric yellowish characteristics of atherosclerotic plaques [1].

The severe atherosclerotic disease seen in this patient that culminated in a fatal coronary event could be coincidental to the Fabry disease process. Nevertheless, we increasingly recognize fixed coronary artery disease among our Fabry disease patient population. For example, five men with Fabry disease from a group of 38 patients who participated in enzyme replacement trials (age range 19–49, not including this patient) were found to have symptomatic fixed coronary artery disease requiring coronary bypass or angioplasty (three patients). In addition, we found that random (not during acute events) blood levels of myeloperoxidase (MPO) in patients with Fabry disease are significantly higher than controls [15]. MPO has been associated with the atherosclerosis process, endothelial dysfunction, and acute coronary events, and it

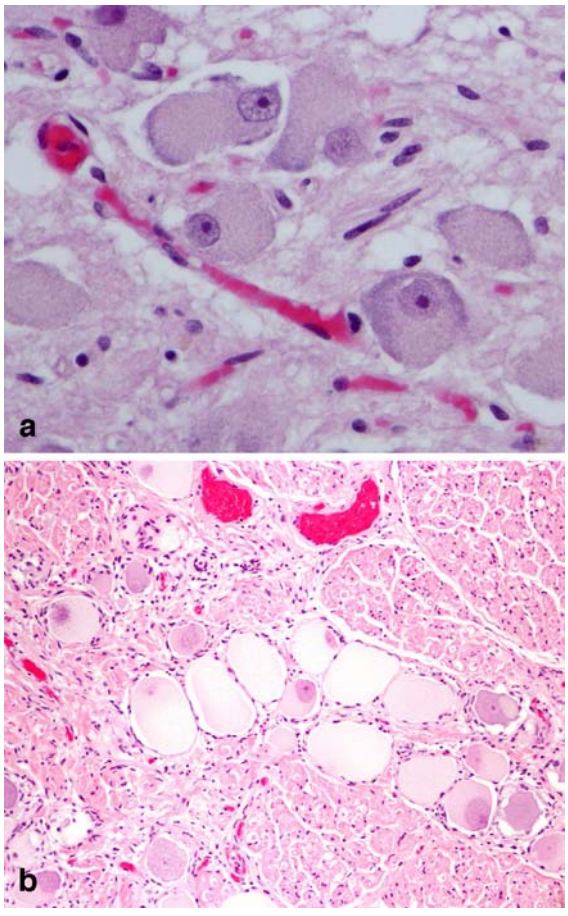

Fig. 7 **a** Storage in neurons. Hypothalamic nuclei showing neuronal storage. H & E, ×40. **b** Dorsal root ganglia showing swollen storage neurons. H & E, ×20

was recently shown to modify apo A-1 HDL cholesterol to make it more likely to accumulate in macrophages [16]. Evidence for excess production of reactive oxygen species, such as superoxide in Fabry disease, has also accumulated [14, 15]. Recently, another group has shown that aortic atherosclerosis in mice deficient in both apo E and α-galactosidase A is markedly accelerated compared with either of those mouse models alone [3]. Together, this clinical and experimental evidence suggests that the process of atherosclerosis may be accelerated in Fabry disease. It is likely therefore that other factors in combination with α-galactosidase A deficiency render certain patients with Fabry disease susceptible to atherosclerosis. Indeed, we have recently shown that polymorphisms of genes known to be risk factors for stroke modify the likelihood of developing cerebral ischemic lesions in Fabry disease [2]. Therefore, a number of genetic factors may modulate the interaction between the α-D-galactosyl glycolipid accumulation and vascular plaque formation. Additional investigation is necessary to confirm and further characterize this process.

Acknowledgements We thank Dr. Kristen Carr for her participation in the autopsy of this patient. This work was supported by the Intramural program of National Institute of Neurological Disorders and Stroke, NIH.

References

1. (1984) Case 2-1984: Fabry's disease. N Engl J Med 310:1607
2. Altarescu G, Moore DF, Schiffmann R (2005) Effect of genetic modifiers on cerebral lesions in Fabry disease. Neurology 64:2148–2150
3. Bodary PF, Shen Y, Vargas FB, Bi X, Ostenso KA, Gu S, Shayman JA, Eitzman DT (2005) Alpha-galactosidase A deficiency accelerates atherosclerosis in mice with apolipoprotein E deficiency. Circulation 111:629–632
4. Brady RO, Gal AE, Bradley RM, Martensson E, Warshaw AL, Laster L (1967) Enzymatic defect in Fabry's disease. Ceramidetrihexosidase deficiency. N Engl J Med 276:1163–1167
5. Desnick RJ, Ioannou YA, Eng CM (2001) a-Galactosidase A deficiency: Fabry disease. In: Scriver CR, Beaudet AL, Sly WS, Valle D (eds) The metabolic and molecular bases of inherited disease, 8th edn. McGraw-Hill, New York, pp 3733–3774
6. Duncan C, McLeod GM (1970) Angiokeratoma corporis diffusum universale (Fabry's disease): a case with gross myocardial involvement. Australas Ann Med 19:58–61
7. Elleder M (2003) Sequelae of storage in Fabry disease—pathology and comparison with other lysosomal storage diseases. Acta Paediatr Suppl 92:46–53; discussion 45
8. Eng CM, Guffon N, Wilcox WR, Germain DP, Lee P, Waldek S, Caplan L, Linthorst GE, Desnick RJ (2001) Safety and efficacy of recombinant human alpha-galactosidase A—replacement therapy in Fabry's disease. N Engl J Med 345:9–16
9. Fisher EA, Desnick RJ, Gordon RE, Eng CM, Griepp R, Goldman ME (1992) Fabry disease: an unusual cause of severe coronary disease in a young man. Ann Intern Med 117:221–223
10. Gadoth N, Sandbank U (1983) Involvement of dorsal root ganglia in Fabry's disease. J Med Genet 20:309–312
11. Kampmann C, Wiethoff CM, Martin C, Wenzel A, Kampmann R, Whybra C, Miebach E, Beck M (2002) Electrocardiographic signs of hypertrophy in fabry disease-associated hypertrophic cardiomyopathy. Acta Paediatr Suppl 91:21–27
12. Kotnik J, Kotnik F, Desnick RJ (2005) Fabry disease. A case report. Acta Dermatovenerolog Alp Panon Adriat 14:15–19
13. Linhart A, Lubanda JC, Palecek T, Bultas J, Karetova D, Ledvinova J, Elleder M, Aschermann M (2001) Cardiac manifestations in Fabry disease. J Inherit Metab Dis 24:75–83; discussion 65
14. Moore DF, Scott LT, Gladwin MT, Altarescu G, Kaneski C, Suzuki K, Pease-Fye M, Ferri R, Brady RO, Herscovitch P et al (2001) Regional cerebral hyperperfusion and nitric oxide pathway dysregulation in Fabry disease: reversal by enzyme replacement therapy. Circulation 104:1506–1512
15. Moore DF, Ye F, Brennan ML, Gupta S, Barshop BA, Steiner RD, Rhead WJ, Brady RO, Hazen SL, Schiffmann R (2004) Ascorbate decreases Fabry cerebral hyperperfusion suggesting a reactive oxygen species abnormality—an arterial spin tagging study. J Magn Reson Imaging 20:674–683
16. Nguyen TT, Gin T, Nicholls K, Low M, Galanos J, Crawford A (2005) Ophthalmological manifestations of Fabry disease: a survey of patients at the Royal Melbourne Fabry Disease Treatment Centre. Clin Experiment Ophthalmol 33:164–168
17. Schiffmann R, Floeter MK, Dambrosia JM, Gupta S, Moore DF, Sharabi Y, Khurana RK, Brady RO (2003) Enzyme replacement therapy improves peripheral nerve and sweat function in Fabry disease. Muscle Nerve 28:703–710

18. Schiffmann R, Kopp JB, Austin HA III, Sabnis S, Moore DF, Weibel T, Balow JE, Brady RO (2001) Enzyme replacement therapy in fabry disease: a randomized controlled trial. JAMA 285:2743–2749
19. Senechal M, Germain DP (2003) Fabry disease: a functional and anatomical study of cardiac manifestations in 20 hemizygous male patients. Clin Genet 63:46–52
20. Tabira T, Goto I, Kuroiwa Y, Kikuchi M (1974) Neuropathological and biochemical studies in Fabry's disease. Acta Neuropathol 30:345–354
21. Thurberg BL, Rennke H, Colvin RB, Dikman S, Gordon RE, Collins AB, Desnick RJ, O'Callaghan M (2002) Globotriaosylceramide accumulation in the Fabry kidney is cleared from multiple cell types after enzyme replacement therapy. Kidney Int 62:1933–1946
22. Wilcox WR, Banikazemi M, Guffon N, Waldek S, Lee P, Linthorst GE, Desnick RJ, Germain DP (2004) Long-term safety and efficacy of enzyme replacement therapy for Fabry disease. Am J Hum Genet 75:65–74

Virchows Arch (2006) 448: 344–353
DOI 10.1007/s00428-005-0066-4

ORIGINAL ARTICLE

Anna Maria Chiaravalli · Maddalena Feltri · Valentina Bertolini · Elena Bagnoli · Daniela Furlan · Roberta Cerutti · Raffaele Novario · Carlo Capella

Intratumour T cells, their activation status and survival in gastric carcinomas characterised for microsatellite instability and Epstein–Barr virus infection

Received: 15 June 2005 / Accepted: 16 August 2005 / Published online: 27 October 2005

Abstract Gastric carcinomas (GCs) with high microsatellite instability (MSI) or an Epstein–Barr virus (EBV) infection are prevalently poorly differentiated adenocarcinomas with abundant lymphoid infiltration. The aims of the study were to clarify (1) if tumour-infiltrating lymphocytes (TILs) and cytotoxic-activated TILs are associated with a better clinical outcome in patients with GCs characterised for the presence of MSI and EBV; (2) if the nature and the activation status of TILs are involved in tumour cell apoptosis, evaluated using the M30 antibody, directed against a fragment of cytokeratin-18 caspase-cleaved during early steps of epithelial cell apoptosis. The immunophenotype of TILs and the tumour cell apoptosis were analysed with immunohistochemistry in 96 GCs, including 35 MSI GCs, and 61 GCs without MSI [microsatellite stable (MSS)], 17 of which were EBV+. MSI and MSS/EBV+ GCs displayed a significantly higher mean number of cytotoxic-activated TILs and apoptotic tumour cells than MSS/EBV− GCs (CD8+ TILs/HPF, 21.7 and 69.6 vs 6.4; T-cell intracellular antigen (TIA)-1+ TILs/HPF, 16.7 and 32.05 vs 5.2; granzyme B+ TILs/HPF, 7.5 and 8.6 vs 0.8; perforin+ TILs/HPF, 5.9 and 9.2 vs 0.9; and M30 IR tumour cells, 5.9 and 2.9 vs 2.3%). In addition to the most reliable clinico-pathological parameters (lymph node status, depth of tumour invasion and tumour stage), a univariate analysis showed that the presence of CD3+ TILs higher than 14.9 (p=0.01), CD8+ TILs higher than 9.5 (p<0.05) and MSI (p=0.02) were associated with better overall patient survival. Using a Cox regression model, only a high number of CD3+ TILs (p=0.02) and a low tumour stage (p=0.00001) were identified as independent prognostic factors. In conclusion, our study demonstrates that a high number of CD3+ and CD8+ TILs is a characteristic of MSI- and EBV-associated GCs and represents a favourable prognostic factor, independently of the pathogenesis of GCs.

Keywords Gastric carcinoma · Microsatellite instability · Epstein–Barr virus · Tumour-infiltrating lymphocytes · Activated cytotoxic T cells · Survival

A. M. Chiaravalli · M. Feltri · V. Bertolini · E. Bagnoli · D. Furlan · R. Cerutti · C. Capella
Department of Human Morphology,
Section of Anatomic Pathology,
University of Insubria and Ospedale di Circolo,
Varese, Italy

A. M. Chiaravalli (✉)
Department of Pathology, Ospedale di Circolo,
viale Borri 57,
21100 Varese, Italy
e-mail: annamaria.chiaravalli@tin.it
Tel.: +39-332-264557
Fax: +39-332-262313

R. Novario
Department of Clinical and Biological Science,
University of Insubria,
Varese, Italy

Introduction

Over the past 10 years, accumulating evidence has indicated that a pronounced intratumour inflammatory reaction plays a crucial role in host response to cancer. Various inflammatory elements (dendritic cells, macrophages, granulocytes and lymphocytes) have been found in the tumour micro-environment, both in supporting stroma and among epithelial cells in tumour nests.

The presence of tumour-infiltrating lymphocytes (TILs) has been shown to correlate with a favourable prognosis in several human malignancies such as melanoma and ovarian, prostatic, renal-cell, breast and colorectal carcinomas [12, 25, 27, 38, 42]. The presence of abundant lymphocytic tumour infiltration is a peculiar histological feature common to gastric carcinomas (GCs), both with Epstein–Barr virus (EBV) infection [4, 28, 37] and with a high level of microsatellite instability (MSI) [4, 34].

The immune response to cancer cells may be mediated by non-specific natural killer (NK) cells [30] or by cancer-specific lymphocytes, which are usually CD8-positive [2, 31].

In GCs, a high level of NK infiltration was significantly associated with a better prognosis of disease [14].

In MSI colorectal carcinomas, the intratumour lymphocytes have been demonstrated to be prevalently cytotoxic-activated T cells [7]. Their presence could be responsible for the increased apoptosis of tumour cells observed in these tumours, although Michael-Robinson et al. [23] demonstrated that TILs and apoptosis are independent characteristics of MSI tumours.

In the present investigation, we studied a series of GCs characterised for MSI status and EBV infection with the aims of clarifying whether TILs are associated with a better clinical outcome in GC patients and of defining the nature and the activation status of TILs in the different subtypes of GCs.

Materials and methods

Case selection The study included 96 cases of sporadic advanced GCs (Table 1) operated on at the University Hospital of Varese between January 1980 and June 1999.

Table 1 Clinico-pathological data of 96 gastric carcinomas

Feature	MSI [number of cases (%)]	MSS/EBV− [number of cases (%)]	MSS/EBV+ [number of cases (%)]	Total [number of cases (%)]
Number of cases	35 (36)	44 (46)	17 (18)	96
Male/female	21/14 (1.5)	24/20 (1.2)	12/5 (2.4)	57/39 (1.5)
Mean age (range), years	68.5 (49–82)	64.4 (43–84)	64.7 (42–86)	66.4 (42–86)
Tumour location				
Cardias	2 (6)	2 (4.5)	3 (18)	7 (7.5)
Body/fundus	6 (17)	9 (20)	8 (47)	23 (24)
Antrum/body antrum	27 (77)	30 (68)	1 (6)	58 (60.5)
Stump	0	1 (2)	5 (29)	6 (6)
Unknown		2 (4.5)		2 (2)
Diameter (range), mm	58.6 (30–100)	39.7 (20–70)	60.3 (40–90)	50 (20–100)
Histology				
Carneiro classification				
Glandular	23 (66)	31 (70)	7 (41)	61 (64)
Solid	5 (14)	2 (5)	5 (29.5)	12 (12)
Mixed	7 (20)	11 (25)	5 (29.5)	23 (24)
Lauren classification				
Intestinal	28 (80)	37 (84)	11 (65)	76 (80)
Diffuse	2 (6)	1 (2)	1 (6)	4 (4)
Unclassified	5 (14)	6 (14)	5 (29)	16 (16)
Grading				
G1	1 (3)	3 (7)	0	4 (4.2)
G2	8 (23)	27 (61)	0	35 (36.5)
G3	26 (74)	14 (32)	17 (100)	57 (59.3)
Node metastases				
Yes	18 (51)	31/43 (72)	14 (82)	63/95 (66)
No	17 (49)	12/43 (28)	3 (18)	32/95 (34)
Stage				
I	15	9	3	27
II	10	13	8	31
III	9	18	3	30
IV	1	4	3	8
Follow-up				
Alive	7 (20)	4 (9)	5 (29)	16 (17)
Alive (60 months)	21 (59)	8 (46)	14 (32)	43 (45)
Dead because of disease	14 (40)	27 (62)	9 (53)	50 (52)
Dead because of other causes	14 (40)	13 (29)	3 (18)	30 (31)
CD3+ TILs				
Mean value	30.7	6.58	100.04	31.6
Median value	27.7	2.5	85.7	14.9
Range	(1.6–77)	(0–30.4)	(43.3–254)	(0–254)

The majority of the tumours were from a series of 185 cases which had previously been examined for the presence of high MSI, expression of hMSH2 and hMLH1 proteins and EBV infection with in situ hybridisation for EBER-1 [4]. In particular, 35 MSI and 31 microsatellite stable (MSS) GCs were selected for the presence of abundant lymphoid infiltration, while 20 cases, showing a less abundant lymphoid infiltrate, were selected from the remaining consecutive MSS glandular carcinomas. Ten other cases were added to the series because they were known to be EBV-positive. Altogether, 35 cases were MSI, and 61 were MSS carcinomas, 17 of which were positive for EBV.

The tumours were classified, according to the criteria outlined by Carneiro et al. [3], as glandular, solid or mixed types and according to the Lauren criteria [19]. The tumour stage was assessed using the tumour node metastases (TNM) system defined by the International Union Against Cancer [35]. The clinico-pathological data of the GCs, characterised for MSI status and EBV infection, are summarised in Table 1.

All patients were followed-up either until death or for a median period of 150 months (range 42–238 months); information was obtained from the Lombardy Tumour Register and from the record offices of local authorities. The mean overall follow-up was 64.3 months (range 0–238).

Immunohistochemical study The characterisation of TILs was performed on formalin-fixed, paraffin-embedded materials using the avidin–biotin–peroxidase complex (ABC) methods. Briefly, sections were deparaffinised, rehydrated and, for selected antigens, pre-treated with different antigen-retrieval solutions in a domestic 750-kW microwave oven (see Table 2). Endogenous peroxidase activity was quenched in 3% H_2O_2 in water for 10 min. Primary antibodies (listed in Table 2) were applied overnight at 4°C. Sections were then incubated with biotinylated anti-mouse immunoglobulins and with ABC peroxidase complex, each for 1 h at room temperature.

Immunoreactive intraepithelial lymphocytes were counted at 400× (Leitz, Laborlux K; field area 0.173 mm^2) in ten consecutive fields, selecting areas containing the maximal number of neoplastic cells with minimal reactive stroma and necrosis. The mean value of immunoreactive TILs per high-power field was reported. Only the immunoreactive lymphocytes in direct contact with tumour cells were included in the count.

The apoptotic index was expressed as the percentage of M30 immunoreactive cells per 2,000 tumour cells counted in the ten most positive fields at 200×. Areas of intraglandular or superficial necrosis were not considered for the evaluation of the apoptotic index.

Statistical analysis The statistical significance of the results was evaluated using the Wilcoxon rank-sum test for unpaired data, chi-square test and Fisher's Exact Test. The correlation of patient survival with the immunohistochemical and clinico-pathological data was estimated using the Kaplan–Meier product limit method, and statistical differences were tested using the log-rank test. A multivariate analysis was performed with the Cox proportional-hazard regression model.

Results

Clinical and pathological features

The clinico-pathological data of the GCs are summarised in Table 1. There were slightly more males (male to female

Table 2 List of primary antibodies used

Mouse monoclonal antibody	Clone	Specificity	Working dilution	Treatment	Manufacturer
CD3	PS1	ε chain of T-cell receptor	1/100	MW 5 min ×2 EDTA, pH 10	Biogenex (San Ramon, CA, USA)
CD8	4B11	Membrane glycoprotein of CTLs	1/20	MW 5 min ×4 EDTA, pH 8	Novocastra (Newcastle, UK)
Granzyme B	GrB-7	Serine protease of NK cells and CTLs	1/20	MW 5 min ×2 CB, pH 6	Monosan (Uden, Netherlands)
CD57	HNK-1	Membrane glycoprotein of NK cells and T-cell subset	1/20		Becton-Dickinson (San Jose, CA, USA)
Perforin	KM585 (P1-8)	Pore-forming protein of NK cells and CTLs	1/1,000	MW 5 min ×4 EDTA, pH 8	Kamiya (Seattle, WA, USA)
TIA-1	26gA10F5 (TIA-1)	T-cell intracellular antigen also present in NK cells	1/1,000	MW 5 min ×2 EDTA, pH 8	Immunotech (Marseilles, France)
M30 CytoDEATH	M30	Caspase-derived CK18 fragment	1/100	MW 5 min ×2 CB, pH 6	Roche (Mannheim, Germany)

MW Microwave, *CB* citrate buffer, *CTLs* cytotoxic T-lymphocytes

ratio 2.4:1) with MSS/EBV+ cancers compared to MSI and MSS/EBV− cancers (male to female ratios 1.5:1 and 1.2:1, respectively).

Both MSI and MSS/EBV− carcinomas were more frequent in the antrum (77 and 68%, respectively), whereas MSS/EBV+ carcinomas were prevalently located in the gastric fundus (47%) and in the gastric stump (29%) ($p<0.001$).

Tumour size varied in diameter from 20 to 100 mm. The mean diameters were 58.6, 60.3 and 39.7 mm for MSI, MSS/EBV+ and MSS/EBV− carcinomas, respectively.

Histologically, 64% of all tumours were glandular carcinomas. In particular, 74% of MSI and all the MSS/EBV+ cases were poorly differentiated, whereas 61% of MSS/EBV− were moderately differentiated carcinomas (Fig. 1). According to Lauren's criteria [19], 80% of tumours were intestinal, and only 4% were diffuse GCs; 16% of cases were unclassified.

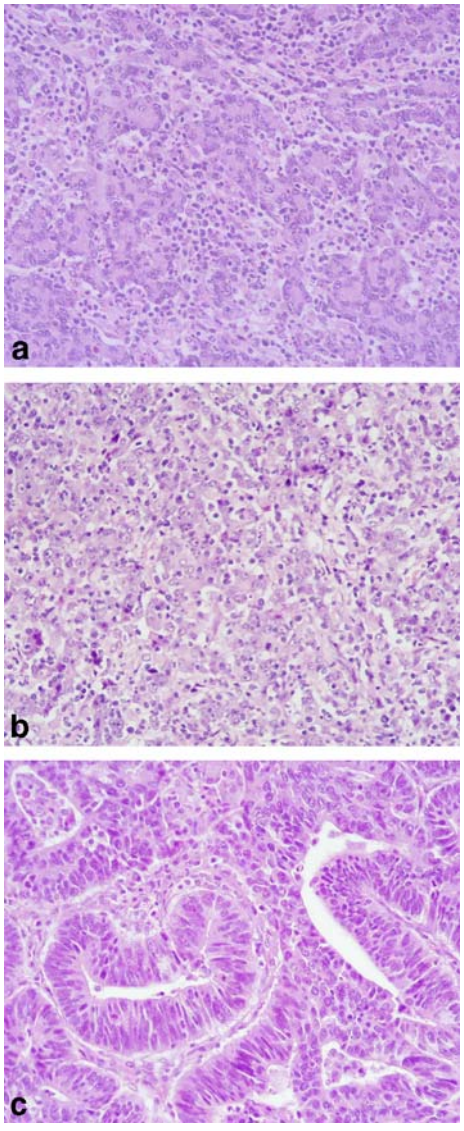

Fig. 1 Gastric carcinoma with microsatellite instability (**a**), EBV infection (**b**) and without microsatellite instability and EBV infection (**c**) (haematoxylin and eosin stain, original magnification ×200)

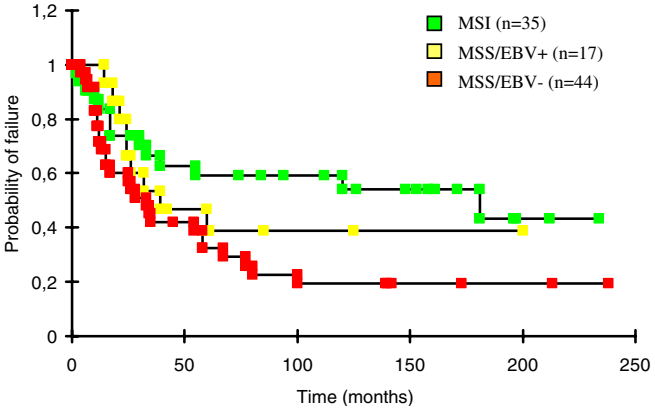

Fig. 2 Failure time according to MSI and EBV status [log-rank chi-square 6.35 ($p=0.0417$)]

At diagnosis, MSS/EBV− and MSS/EBV+ carcinomas showed lymph node metastases in 31 of 43 (72%) and 14 of 17 (82%) cases, whereas they were present in only 18 of 35 (51%) MSI carcinomas ($p<0.05$).

Fifty (52%) patients died of disease after an average time of 32.5 months (range 2–181), including 14 (40%) patients with MSI, 27 (62%) with MSS/EBV− and 9 (53%) with MSS/EBV+ carcinomas.

Thirty (31%) patients died of other causes (mean follow up 46.5 months, range 0–212), and only 16 patients (17%) were still alive at the last follow-up after a mean time of 150 months (range 42–238).

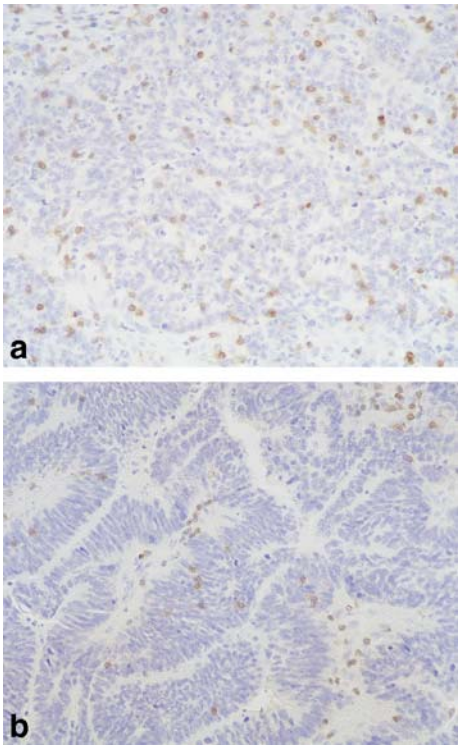

Fig. 3 CD3 immunoreactive tumour-infiltrating lymphocytes in MSI (**a**) and MSS/EBV− (**b**) gastric carcinomas (immunoperoxidase; original magnification ×200)

Table 3 Immunophenotype of TILs and apoptosis of tumour cells in 72 gastric carcinomas

	MSI	MSS/EBV−	MSS/EBV+	*p* value
Number of cases	35	24	13	
CD3[a,b]	30.7[$#] (1.6–77)	6.6[$°] (0–30.4)	100[°#] (43.3–254)	$p<0.001^{\$°\#}$
CD8[a]	21.7[$#] (2.1–56)	6.4[$°] (0.3–23.7)	69.6[°#] (26–118.7)	$p<0.001^{\$°\#}$
TIA-1[a]	16.7[$#] (0.4–59.5)	5.2[$°] (0–29.1)	32.05[°#] (3–84.6)	$p<0.001^{\$°}$ $p<0.05^{\#}$
Granzyme B[a]	7.5[$] (0–27.3)	0.8[$°] (0–5.1)	8.6° (0.3–27.5)	$p<0.001^{\$°}$
Perforin[a]	5.9[$] (0–25.1)	0.9[$°] (0–5.4)	9.2° (0–18.7)	$p<0.05^{°}$ $p<0.001^{\$}$
CD57[a]	3.1[$#] (0–31.4)	0.8[$°] (0.1–22.2)	4.20[°#] (1–13.9)	$p<0.01^{\$°\#}$
M30[c]	5.9[$] (0.05–19.5)%	2.3[$°] (0.05–29.2)%	2.9° (0.05–17.95)%	$p<0.01^{\$°}$

[a]Mean value and range of immunoreactive TILs
[b]CD3 was counted on 96 gastric carcinomas
[c]Mean percentage and range of tumour immunoreactive cells
[$,#,°]Indicators for statistical evaluation

The survival curves (Fig. 2) showed a significantly different prognosis in the three groups ($p<0.05$). In particular, the overall survival was significantly higher for patients with MSI than with MSS/EBV− GCs ($p=0.01$). The mean 5-year survival was 59, 46 and 32% for MSI, MSS/EBV+ and MSS EBV− GCs, respectively.

Characterisation of lymphoid infiltration

Lymphocytes were present both within tumour-cell nests and in peritumoural stroma. CD3+ intraepithelial TILs varied in number from 0 to 254 in a high-power microscopic field (mean value 31.6, median value 14.9).

The mean number of CD3+ TILs was 30.7 (range 1.6–77), 6.6 (range 0–30.4) and 100 (range 43.3–254) in MSI, MSS/EBV− and MSS/EBV+, respectively, and the differences were statistically significant ($p<0.001$; Fig. 3).

The nature and the activation status of TILs were analysed in a subset of GCs, selected because sufficient material was available for study, and the immunohistochemical results are summarised in Table 3. The majority of TILs showed an intense CD8 immunoreactivity. CD8+ TILs varied from 0.3 to 118.7 cells per field, the mean value being 25.5 and the median value being 14.6. The mean numbers of CD8+ TILs in MSI (21.7; range 2.1–56) and in MSS/EBV+ (69.6; range 26–118.7) GCs were significantly higher ($p<0.001$) than those found in MSS/EBV− cases (6.4; range 0.3–23.7).

A minimal number of TILs was composed of NK cells. The number of CD57+ TILs was significantly higher ($p<0.01$) in MSS/EBV+ (mean value 4.2) than in MSS/EBV− (mean value 0.8) or in MSI (mean value 3.1) GCs.

The presence of cytotoxic cells was confirmed by the expression of T-cell intracellular antigen (TIA-1) in the cytoplasmic granules in a considerable proportion of TILs. The mean number of TIA-1+ TILs was significantly higher in MSS/EBV+ (32.05; range 3–84.6) than that observed in MSS/EBV− (5.2; range 0–29.1; $p<0.001$) and MSI (16.7; range 0.4–59.5; $p<0.05$) GCs.

The activation status of TILs was assessed on the basis of immunoreactivity for granzyme B and perforin. The number of granzyme B+ TILs (Fig. 4) was significantly higher ($p<0.001$) in MSI and in MSS/EBV+ than in MSS/EBV− GCs (mean values 7.5 and 8.6, respectively, vs 0.8). Perforin+ TILs were also significantly more numerous in MSI GCs and in MSS/EBV+ than in MSS/EBV− tumours (mean values 5.9 and 9.2, respectively, vs 0.9; $p<0.001$ and $p<0.05$).

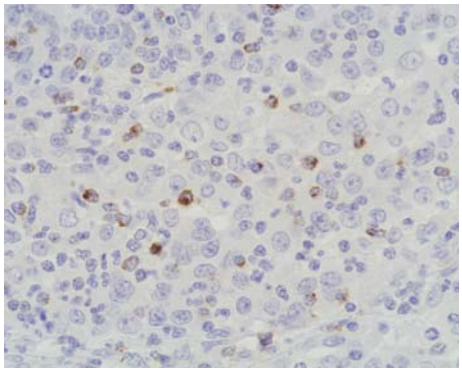

Fig. 4 Granzyme B immunoreactive tumour-infiltrating lymphocytes in EBV+ gastric carcinoma (immunoperoxidase, original magnification ×400)

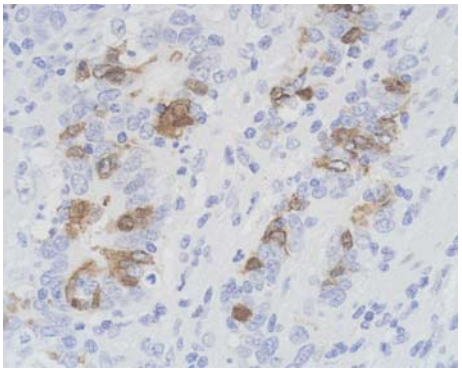

Fig. 5 Apoptotic cells immunoreactive for M30 CytoDEATH antibody in a microsatellite-instable gastric carcinoma (immunoperoxidase, original magnification ×400)

Table 4 Relationships of age, sex, Carneiro and Lauren classification, tumour site, pT, pN, stage, EBV status, MSI status, diameter, CD3+ TILs and CD8+ TILs with survival

Feature	Number of cases (%)	Relative risk (95% CI)	*p* value
Age (years)			
≤66	44 (46)	1.06	0.8356
>66	52 (54)		
Sex			
Male	57 (59)	1.14	0.6510
Female	39 (41)		
Histology			
Carneiro classification			
Glandular/solid	73 (76)	1.73	0.0689
Mixed	23 (24)		
Lauren classification			
Intestinal	76 (80)	1.05	0.04
Diffuse	4 (4)		
Unclassified	16 (16)		
Tumour site			
Cardias	7 (8)	1.07	0.0859
Corpus/fundus	23 (24)		
Antrum/corpus antrum	58 (60)		
Stump	6 (6)		
Unknown	2 (2)		
pT			
pT2	69 (72)	2.70	0.0003
pT3/pT4	27 (28)		
pN			
pN0	32/95 (34)	4.21	<0.0001
pN1/pN2	63/95 (66)		
Stage			
I	27 (28)	2.43	<0.0001
II	31 (33)		
III	30 (31)		
IV	8 (8)		
EBV status			
Negative	78 (81)	1.25	0.5379
Positive	18 (19)		
MSI status			
Negative	61 (64)	1.94	0.0290
Positive	35 (36)		
Diameter, mm			
≤50	58 (66)	1.54	0.1381
>50	29 (34)		
CD3+ TILs			
≤14.9	48 (50)	2.03	0.0115
>14.9	48 (50)		
CD8+ TILs			
≤9.5	31 (44)	2.09	0.0265
>9.5	40 (56)		

Apoptosis of tumour cells

To assess the apoptotic index of tumour cells, GCs were immunostained with the M30 CytoDEATH antibody that recognises a fragment of cytokeratin-18 cleaved by a caspase at the beginning of the apoptotic process. Tumour cells showed an intense and variable cytoplasmic M30 immunoreactivity in relation to the apoptotic stage of the cell (Fig. 5). At the beginning of the apoptotic process, in cells which were still histologically normal, the immunoreactivity was distributed throughout the cytoplasm, whereas in damaged cells, the immunoreactivity was localised in granules, which varied in size and number, within the cytoplasm.

The distribution of M30 immunoreactive tumour cells differed among the various tumours; in some cases, M30+

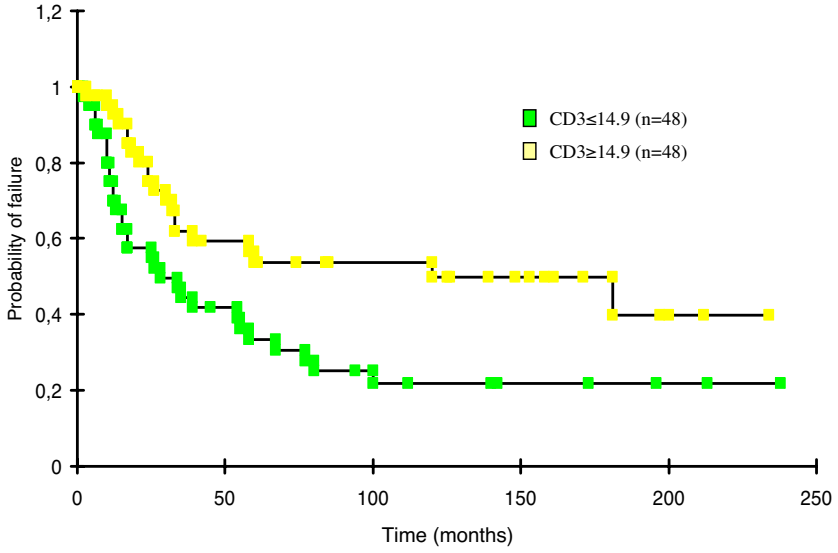

Fig. 6 Failure time according to CD3+ TILs [relative risk 2.03; log-rank chi-square 6.38 (p=0.0115)]

cells were dispersed throughout the tumour, while in other cases, they were localised near necrotic areas or within the glandular lumens. The mean percentage of M30+ cells varied from 0.05 to 29.2% (Table 3). M30+ cells were more frequent in MSI and in MSS/EBV+ than in MSS/EBV− GCs (mean percentages 5.9 and 2.9, respectively, vs 2.3; p<0.01).

Necrotic areas and intraglandular abscesses, frequently observed in MSS/EBV+ GCs, were always M30-negative.

Correlation with survival

A univariate analysis (Table 4) revealed that the low-tumour stage (p<0.0001), the absence of node metastases (pN, p<0.0001), the low depth of tumour invasion (pT, p<0.0003), the intestinal type (p=0.04), the presence of MSI (p=0.02) and high numbers of CD3+ TILs and CD8+ TILs correlated with survival. In particular, carcinomas with CD3+ TILs higher than 14.9 (Fig. 6) and CD8+ TILs higher than 9.5 (Fig. 7) were associated with a significantly improved survival (p=0.01 and p<0.05, respectively).

The presence of intratumoural CD8+-activated lymphocytes (perforin >1.5 and granzyme B >1.75) was also statistically significant (p<0.01).

On the basis of a Cox regression analysis, only a low tumour stage (p<0.00001) and a high number of CD3+ TILs (p=0.02) were identified as independent prognostic factors (Table 5).

Discussion

Abundant TILs seem to be associated with a more favourable prognosis in various malignancies, including melanomas and breast, renal, colorectal and GCs [12, 25, 27, 38, 42]. Tumour-associated lymphocytes show oligoclonal expansion [13], exhibit tumour-specific cytotoxic activity in vitro [32] and recognise tumour-specific antigens [17, 29, 33].

The prognostic significance of lymphocytic infiltration in gastric cancer was first emphasised by MacCarty and Mahle [21]. In 1976 Watanabe and colleagues [39] ob-

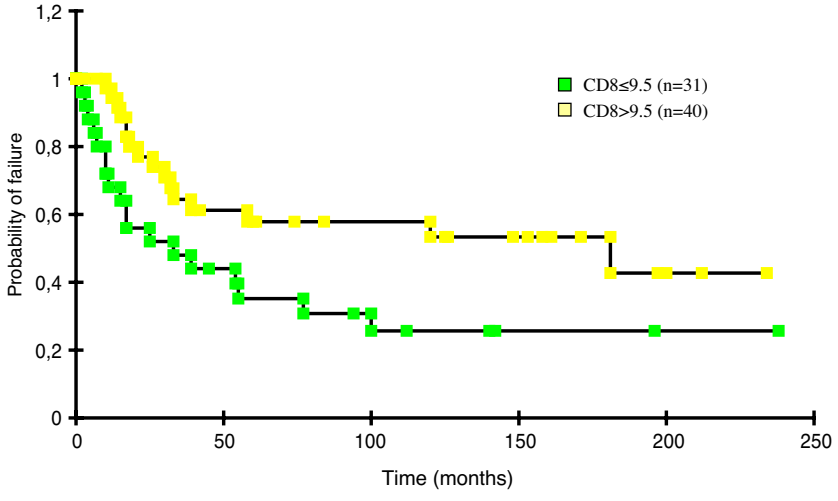

Fig. 7 Failure time according to CD8+ TILs (relative risk 2.09, log-rank chi-square 4.92 (p=0.0265)]

Table 5 Multivariate Cox proportional-hazard analysis of overall survival

Feature	Beta	Standard error	*Z* value	*p* value	EXP (beta)	Partial first derivate
Stage	0.7538	0.1544	4.881	0.00001	2.1251	1.53E-05
MSI status	0.2789	0.3454	0.8077	0.2096	1.321	4.77E-06
CD3+ TILs	0.805	0.4245	1.8936	0.029	2.2367	5.72E-06
CD8+ TILs	0.1326	0.4538	0.2923	0.385	1.1418	6.68E-06

served a high survival rate among patients with GCs with lymphoid stroma. With the aim of evaluating the prognostic significance of TILs, we selected, from a series of consecutive GCs, those showing abundant lymphoid infiltration. The MSS/EBV− and MSS/EBV+ groups were enriched in number to be better comparable. Our study, with the limit that our cases were partly selected, seems to indicate that the presence of intratumoural T cells correlates with the clinical outcome of advanced gastric cancer after apparently radical surgery. In a series of 96 patients with advanced GCs, cancer-specific survival of patients appeared to be increased by a factor of approximately 2 if more than 14.9 CD3+ TILs or more than 9.5 CD8+ TILs were present per high-power microscopic field. A univariate analysis showed that, in addition to clinico-pathological parameters including stage, lymph node status, depth of tumour invasion, histological type and MSI status, TIL count was significantly correlated with patient survival. A Cox regression analysis confirmed TILs as an independent prognostic factor together with stage.

Two types of GCs are characterised by a large number of TILs: the MSI- and the EBV-associated GCs [16, 28, 34, 37].

Like patients with sporadic MSI colorectal cancers [8, 11, 40], patients with sporadic MSI GCs apparently have a better survival rate than patients with MSS tumours [34, 41]. EBV-positive GCs have sometimes been associated with a survival advantage [5, 16, 36]. However, in 1994, Nakamura et al. [26] observed that, among GCs with lymphoid stroma, there was no significant difference in the 5-year survival rate between cases with EBV-positive and EBV-negative GCs.

The molecular characteristics of tumours that elicit an enhanced immune response are unclear, but the increased production of abnormal peptides seems to be the more probable hypothesis to explain this phenomenon. In patients with MSI colorectal carcinomas with abundant T-cell infiltration, Ishikawa et al. [15] demonstrated the production of specific antibodies against an abnormal fragment of CDX2 protein found in tumour tissue. The aberrant protein is produced by a frameshift mutation in the microsatellite sequence of the CDX2 coding region. This study seems to support the hypothesis that, in MSI tumours, the alteration of the mismatch repair system is responsible for the production, by tumour cells, of abnormal tumour-specific peptides which recruit lymphocytes in the tumour and induce an immune response.

A similar mechanism can operate in EBV-positive tumours, where the recruitment of TILs could be the consequence of the production by a virus, via tumour cells, of abnormal peptides, although this hypothesis has not been demonstrated yet. As a matter of fact, in their paper, Kuzushima and colleagues [18] observed that CD8-infiltrating lymphocytes did not recognise EBNA−1 and BRAF antigens produced by tumour cells.

The nature and the activation status of TILs in our cases of GCs seem to be similar to that observed by Dolcetti et al. [7] in MSI colorectal carcinomas. In both MSS/EBV+ and MSI GCs, the majority of TILs was represented by cytotoxic CD8+ cells. A minor component of TILs was represented by NK CD57+ cells. Cytotoxic effector CD8+ and NK cells are characterised by the presence of TIA-1 immunoreactive granules in their cytoplasms, independently of their activation status. TIA-1 protein is crucial for DNA fragmentation and the apoptotic process [1]. In our study, the mean value was significantly higher in MSS/EBV+ and MSI than in MSS/EBV− GCs.

The production and secretion of granzyme B and perforin are indispensable for the activation of cytotoxic and NK lymphocytes. In the presence of Ca^{++}, the monomers of perforin are released by the killer lymphocytes and inserted into the membrane of target cells, where they form membrane pores which promote the entry of cytolytic enzymes, in particular, TIA-1 and granzyme B [20].Granzyme B is a granule-associated serine protease that triggers the apoptotic cascade, probably by activating caspases 10, 3 and 7 [9].

Both perforin+ and granzyme B+ TILs were significantly more numerous in MSS/EBV+ and MSI than in MSS/EBV− GCs, suggesting that the activation of cytotoxic cells is a specific event priming the apoptotic process in MSS/EBV+ and MSI GCs.

The M30 monoclonal antibody identifies epithelial apoptotic cells and has been previously used by Michael-Robinson et al. [24] to evaluate the apoptotic index in MSI colorectal carcinomas. This antibody binds to the caspase-cleaved fragment of cytokeratin-18 during the early steps of epithelial cell apoptosis. The demonstration that apoptosis of neoplastic cells was significantly more frequent in MSI (5.87%) and in MSS/EBV+ (2.95%) than in MSS/EBV− (2.26%) GCs supports the hypothesis that, in these tumours, TILs play a crucial role in the increased apoptotic cell death of neoplastic cells.

As for the difference between MSI and MSS/EBV+ GCs, it is worth noting that, although CD3+, CD8+ and TIA-1+ TILs were significantly higher in MSS/EBV+ than in MSI GCs, the percentage of activated TILs, as well as the apoptotic index of tumour cells, were not significantly different between the two subsets of GCs. These data might explain the absence of a significant difference in prognosis between patients with MSS/EBV+ and MSI GCs.

In our study, the prognosis of MSS/EBV+ cases appears to be better than that of MSS/EBV− cases, although the difference is not statistically significant. In addition, the prognosis of patients with MSI+ GCs appears to be better than that of patients with MSS/EBV+ GCs. Previous studies examining the correlation between survival and EBV infection in GCs did not consider the MSI status [5, 16, 22] with the exception of that of Grogg et al. [10]. In this context, it is important to underline that in our study, all the MSI GCs are EBV-negative, in agreement with the findings of previous investigations [6, 10]. In addition, our results confirm that MSI GCs are associated with a significantly better prognosis than that of the MSS GCs, and particularly, of MSS/EBV− GCs.

In conclusion, our study demonstrates that the presence of a high number of CD3+ TILs is a favourable prognostic factor, independently of the pathogenesis of GCs. EBV-positive and MSI GCs are two subsets of tumours characterised by a similar intratumour lymphocytic infiltration prevalently composed of activated cytotoxic CD8+ cells. The relatively better prognosis of these subsets of GCs seems to be related to the increased host immune response against abnormal peptides, probably produced by the virus infection or by the presence of an altered mismatch repair system.

Acknowledgements The authors thank Prof. E. Solcia for his helpful suggestions.

References

1. Anderson P, Nagler-Anderson C, O'Brein C, Levine H, Watkins S, Slayter HS, Blue ML, Schlossman SF (1990) A monoclonal antibody reactive with a 15-kDa cytoplasmic granule-associated protein defines a subpopulation of Cd8+ T lymphocytes. J Immunol 144:574–582
2. Boon T, Cerottini JC, Van den Eynde B, van der Bruggen P, Van Pel A (1994) Tumor antigens recognized by T lymphocytes. Annu Rev Immunol 12:337–365
3. Carneiro F, Seixas M, Sobrinho-Simoes M (1995) New elements for an updated classification of carcinomas of the stomach. Pathol Res Pract 191:571–584
4. Chiaravalli AM, Cornaggia M, Furlan D, Capella C, Fiocca R, Tagliabue G, Klersy C, Solcia E (2001) The role of histological investigation in prognostic evaluation of advanced gastric cancer. Analysis of histological structure and molecular changes compared with invasive pattern and stage. Virchows Arch 439:158–169
5. Cho MY, Kim TH, Yi SY, Jung WH, Park KH (2004) Relationship between Epstein–Barr virus encoded RNA expression, apoptosis and lymphocytic infiltration in gastric carcinoma with lymphoid-rich stroma. Med Princ Pract 13:353–360
6. Chong JM, Fukayama M, Hayashi Y, Takizawa T, Koike M, Konishi M, Kikuchi-Yanoshita R, Miyaki M (1994) Microsatellite instability in the progression of gastric carcinoma. Cancer Res 54:4595–4597
7. Dolcetti R, Viel A, Doglioni C, Russo A, Guidoboni M, Capozzi E, Vecchiato N, Macrì E, Fornasarig M, Boiocchi M (1999) High prevalence of activated intraepithelial cytotoxic T lymphocytes and increased neoplastic cell apoptosis in colorectal carcinomas with microsatellite instability. Am J Pathol 154(6):1805–1813
8. Elsaleh H, Powell B, Soontrapornchai P, Joseph D, Goria F, Spry N, Iacopetta B (2000) p53 gene mutation, microsatellite instability and adjuvant chemotherapy: impact on survival of 388 patients with Duke's C colon carcinoma. Oncology 58:52–59
9. Froelich CJ, Dixit VM, Yang X (1998) Lymphocyte granule-mediated apoptosis: matter of viral mimicry and deadly proteases. Immunol Today 19:30–36
10. Grogg KL, Lohse CM, Shane Pankratz V, Halling KC, Smyrk TC (2003) Lymphocyte-rich gastric cancer: association with Epstein–Barr virus, microsatellite instability, histology, and survival. Mod Pathol 16 (7):641–651
11. Gryfe R, Kim H, Hsieh ETK, Aronson MD, Holowaty EJ, Bull SB, Redston M, Gallinger S (2000) Tumor microsatellite instability and clinical outcome in young patients with colorectal cancer. N Engl J Med 342:69–77
12. Halpern AC, Schuchter LM (1997) Prognostic models in melanoma. Semin Oncol 24(Suppl 4):S2–S7
13. Hayashi K, Yonamine K, Masuko-Hongo K, Iida T, Yamamoto K, Nishioka K, Kato T (1999) Clonal expansion of T cells that are specific for autologous ovarian tumor among tumor-infiltrating T cells in humans. Gynecol Oncol 74:86–92
14. Ishigami S, Natsugoe S, Tokuda K, Nakajo A, Che X, Iwashige H, Aridome K, Hokita S, Aikou T (2000) Prognostic value of intratumoral natural killer cells in gastric carcinoma. Cancer 88:577–583
15. Ishikawa T, Fujita T, Suzuki Y, Okabe S, Yuasa Y, Iwai T, Kawakami Y (2003) Tumor-specific immunological recognition of frameshift mutated peptides in colon cancer with microsatellite instability. Cancer Res 63:5564–5572
16. Kijima Y, Ishigami S, Hokita S, Koriyama C, Akiba S, Eizuru Y, Aikou T (2003) The comparison of the prognosis between Epstein–Barr virus (EBV)-positive gastric carcinomas and EBV-negative ones. Cancer Lett 200:33–40
17. Kooi S, Freedman RS, Rodriguez-Villanueva J, Platsoucas CD (1993) Cytokine production by T-cell lines derived from tumor-infiltrating lymphocytes from patients with ovarian carcinoma: tumor-specific immune responses and inhibition of antigen-independent cytokine production by ovarian tumor cells. Lymphokine Cytokine Res 12:429–437
18. Kuzushima K, Nakamura S, Nakamura T, Yamamura N, Yokoyama N, Fujita M, Kiyono T, Tsurumi T (1999) Increased frequency of antigen-specific CD8+ cytotoxic lymphocytes infiltrating an Epstein–Barr virus associated gastric carcinoma. J Clin Invest 140:163–171
19. Lauren P (1965) The two histological main type of gastric carcinoma: diffuse and so-called intestinal-type carcinoma. Acta Pathol Microbiol Scand 64:31–49
20. Liu B, Nicolaides NC, Markowitz S, Willson JK, Parsons RE, Jen J, Papadopulos N, Peltomaki P, de la Chapelle A, Hamilton SR, Kinzler KW, Vogelstein B (1995) Mismatch repair gene defects in sporadic colorectal cancers with microsatellite instability. Nat Genet 9:48–55
21. MacCarty WC, Mahle AE (1921) Relation of differentiation and lymphocytic infiltration to postoperative longevity in gastric carcinoma. J Lab Clin Med 6:473–480
22. Matsunou H, Konishi F, Hori H, Ikeda T, Sasaki K, Hirose Y, Yamamichi N (1996) Characteristics of Epstein–Barr virus-associated gastric carcinoma with lymphoid stroma in Japan. Cancer 77:1998–2004
23. Michael-Robinson JM, Biemer-Huttmann A-E, Purdie DM, Walsh M, Simms LA, Biden KG, Young JP, Leggett BA, Jass JR, Radford-Smith GL (2001) Tumor infiltrating lymphocytes and apoptosis are independent features in colorectal cancer stratified according to microsatellite instability status. Gut 48:360–366
24. Michael-Robinson JM, Reid LE, Purdie DM, Biemer-Huttmann A-E, Walsh MD, Pandeya N, Simms LA, Young JP, Leggett BA, Jass JR, Radford-Smith GL (2001) Proliferation, apoptosis and survival in high-level microsatellite instability sporadic colorectal cancer. Clin Cancer Res 7:2347–2356

25. Naito Y, Saito K, Shiiba K, Ohuci A, Saigenji K, Nagura H, Ohtani H (1998) CD8+ T cells infiltrated within cancer cell nests as prognostic factor in human colorectal cancer. Cancer Res 58:3491–3494
26. Nakamura S, Ueki T, Yao T, Ueyama T, Tsuneyoshi M (1994) Epstein–Barr virus in gastric carcinoma with lymphoid stroma. Cancer 73:2239–2249
27. Nakano O, Sato M, Naito Y, Suzuki K, Orikasa S, Aizawa M, Suzuki Y, Shintaku I, Nagura H, Ohtani H (2001) Proliferative activity of intratumoral CD8(+) T-lymphocytes as prognostic factor in human renal cell carcinoma: clinicopathologic demonstration of antitumor immunity. Cancer Res 61:5132–5136
28. Oda K, Tamaru J, Takenouchi T, Mikata A, Nunomura M, Saitoh N, Sarashina H, Nakajima N (1993) Association of Epstein–Barr virus with gastric carcinoma with lymphoid stroma. Am J Pathol 143:1063–1071
29. Peoples GE, Goedegebuure PS, Smith R, Linehan DC, Yoshino I, Eberlein TJ (1995) Breast and ovarian cancer-specific cytotoxic T lymphocytes recognize the same HER2/neu-derived peptide. Proc Natl Acad Sci U S A 17:432–436
30. Pross HF, Lotzova E (1993) Role of natural killer cells in cancer. Nat Immunol 12:279–292
31. Saeterdal I, Gjertsen MK, Straten P, Eriksen JA, Gaudernack G (2001) A TGRFβRII frameshift-mutation-derived CTL epitope recognised by HLA-A2-restricted $CD8^+$ T cells. Cancer Immunol Immunother 50:469–476
32. Santin AD, Bellone S, Ravaggi A, Pecorelli S, Cannon MJ, Parham GP (2000) Induction of ovarian tumor-specific CD8+ cytotoxic T lymphocytes by acid-eluted peptide-pulsed autologous dendritic cells. Obstet Gynecol 96:422–30
33. Santin AD, Hermonat PL, Ravaggi A, Bellone S, Roman JJ, Smith CV, Pecorelli S, Radominska-Pandya A, Cannon MJ, Parham GP (2001) Phenotypic and functional analysis of tumor-infiltrating lymphocytes compared with tumor-associated lymphocytes from ascitic fluid and peripheral blood lymphocytes in patients with advanced ovarian cancer. Gynecol Obstet Invest 51:254–261
34. Seruca R, Santos NR, David L, Constancia M, Barroca H, Carneiro F, Seixas M, Peltomaki P, Lothe R, Sobrinho-Simoes M (1995) Sporadic gastric carcinomas with microsatellite instability display a particular clinicopathologic profile. Int J Cancer 64:32–36
35. Sobin LH, Wittekind C (eds) (2002) TNM classification of malignant tumors, 6th edn. Wiley-Liss, New York
36. Stracca-Pansa V, Menegon A, Donisi PM, Bozzola L, Fedeli F, Quarto F, Nappi O, Pettinato G (1995) Gastric carcinoma with osteoclast-like giant cells. Report of four cases. Am J Clin Pathol 103:453–459
37. Tokunaga M, Land CE, Uemura Y, Tokudome T, Tanaka S, Sato E (1993) Epstein–Barr virus in gastric carcinoma. Am J Pathol 143:1250–1254
38. Vesalainen S, Lipponen P, Talia M, Syrjanen K (1994) Histological grade, perineural infiltration, tumor-infiltrating lymphocytes and apoptosis as determinants of long-term prognosis in prostatic adenocarcinoma. Eur J Cancer 30A:1797–1803
39. Watanabe H, Enjoji M, Imai T (1976) Gastric carcinoma with lymphoid stroma. Cancer 38:232–243
40. Wright CM, Dent OF, Barker M, Newland RC, Chapuis PH, Bokey EL, Young JP, Leggett BA, Jass JR, Macdonald GA (2000) Prognostic significance of extensive microsatellite instability in sporadic clinicopathological stage C colorectal cancer. Br J Surg 87:1197–1202
41. Yamamoto H, Perez-Piteira J, Yoshida T, Terada M, Itoh F, Imai K, Perucho M (1999) Gastric cancers of the microsatellite mutator phenotype display characteristic genetic and clinical features. Gastroenterology 116:1348–1357
42. Zhang L, Conejo-Garcia JR, Katsaros D, Gimotty PA, Massobrio M, Regnani G, Makrigiannakis A, Gray H, Schlienger K, Liebman MN, Rubin SC, Coukos G (2003) Intratumoral T cells, recurrence, and survival in epithelial ovarian cancer. N Engl J Med 348:203–213

Virchows Arch (2006) 448: 354–360
DOI 10.1007/s00428-005-0064-6

ORIGINAL ARTICLE

Seiji Naganuma · Hiroshi Itoh · Shuichiro Uchiyama · Koki Nagaike · Hiroyuki Tanaka · Yutaka Akiyama · Kazuo Chijiiwa · Hiroaki Kataoka

Nuclear translocation of H2RSP is impaired in regenerating intestinal epithelial cells of murine colitis model

Received: 25 May 2005 / Accepted: 15 August 2005 / Published online: 28 September 2005

Abstract Hepatocyte growth factor activator inhibitor type 2-related small peptide (H2RSP) is a recently identified nuclear peptide that is abundantly expressed in the gastrointestinal tract. In this study, we analyzed the expression of H2RSP in normal and injured intestinal mucosa in a murine experimental colitis induced by oral administration of 2.5% dextran sodium sulfate. Results of immunohistochemistry and in situ hybridization showed that H2RSP was expressed predominantly in the epithelium of normal intestine. Whereas H2RSP was localized in the cytoplasm of cells in the crypt, it was translocated into the nuclei of the surface epithelial cells. In injured intestine, H2RSP was detected in the cytoplasm of regenerating epithelial cells, and the nuclear translocation was impaired even in the surface epithelium. However, the mRNA level was not significantly altered in these cells by real-time reverse transcription–polymerase chain reaction using total RNAs obtained from the fractionated mucosal tissue samples prepared by laser-captured microdissection technique. On the other hand, H2RSP mRNA was significantly upregulated in the stromal cells of injured intestinal mucosa compared with those in normal mucosa, which shows cytoplasmic localization of H2RSP. These circumstantial evidences suggest that the nuclear translocation of H2RSP may be related to a signaling involved in the transition from cellular proliferation to differentiation.

S. Naganuma · H. Itoh · S. Uchiyama · K. Nagaike · H. Tanaka · Y. Akiyama · H. Kataoka (✉)
Section of Oncopathology and Regenerative Biology, Department of Pathology, Faculty of Medicine, University of Miyazaki, 5200 Kihara, Kiyotake, Miyazaki, 889-1692, Japan
e-mail: mejina@fc.miyazaki-u.ac.jp
Tel.: +81-985-852809
Fax: +81-985-856003

S. Naganuma · S. Uchiyama · K. Nagaike · K. Chijiiwa
First Department of Surgery, Faculty of Medicine, University of Miyazaki, 5200 Kihara, Kiyotake, Miyazaki, 889-1692, Japan

Keywords H2RSP · Nuclear translocation · Experimental colitis · Cellular differentiation · Mouse

Introduction

Hepatocyte growth factor (HGF) activator inhibitor type 2 (HAI-2)-related small peptide (H2RSP) is a small nuclear peptide recently identified during the search for splicing variant forms of human HAI-2 [3]. HAI-2 is a Kunitz-type serine proteinase inhibitor that regulates the activity of HGF activator (HGFA), a serine proteinase responsible for proteolytic processing of immature single-chain HGF into mature two-chain HGF [2, 5, 6]. Chimeric mRNA was transcribed from *HAI-2* and *H2RSP* genes in some human tissues [3], but it was not detected in any mouse tissues even by a sensitive reverse transcription–polymerase chain reaction (RT-PCR) analysis [10]. Thus, it is unlikely that H2RSP is directly involved in the regulation of HGF activation, at least in mice, and so far, biological roles of H2RSP have been poorly understood. H2RSP is identical to immortalization-upregulated protein-1 (IMUP-1), which was identified as one of the mRNAs upregulated in SV40-immortalized fibroblasts compared with senescent fibroblasts [8]. Thus, H2RSP/IMUP-1 may have a role in cellular proliferation.

H2RSP mRNA was detected abundantly in various tissues including the gastrointestinal tissues, and the predicted amino acid sequence contained a potential nuclear localization signal (NLS) in the lysine-rich region of exon 4 [3, 10]. Transfection study and preliminary immunohistochemical analysis revealed that H2RSP was actually translocated into the nucleus in vitro and was detected in the nuclei of the differentiated surface epithelial cells of normal gastrointestinal mucosa [3, 10]. However, little is known regarding the function of H2RSP in the gastrointestinal epithelium. In this study, to obtain a better understanding of the role of H2RSP in the gastrointestinal epithelial cells, we investigated the expression and localization of H2RSP along with mucosal injury and subsequent regeneration phase by using a mouse model of experimental colitis.

Materials and methods

Induction of experimental colitis in mice

C57BL/6 mice were purchased from Charles River Japan (Atsugi, Japan) and kept on standard chow diet ad libitum in a specific pathogen-free condition. Mice matched for age (8–10 weeks), sex, and body weight (20–25 g) were used for all experiments, which were approved by the Animal Care Committee of University of Miyazaki. Experimental colitis was induced by oral administration of 2.5% (w/v) dextran sodium sulfate (DSS; mol. wt.=40 kDa; ICN Biomedicals, Aurora, OH) in drinking water as described previously [1, 4]. To assess the recovery after DSS-induced colitis, mice were treated with 2.5% DSS in drinking water for 7 days, and then drinking water was changed to distilled water without DSS for the following days. Mice were sacrificed by cervical dislocation under ether anesthesia 7, 10, 14, and 21 days after DSS administration.

Preparation of tissue samples

Mouse colorectal tissue was immediately removed after death and divided into two pieces. One piece was fixed in freshly prepared 4% paraformaldehyde in phosphate-buffered saline (PBS) for 16 h and then soaked in 10% sucrose in PBS for 1 h, 15% for 1 h, and 20% for 2 h. Frozen and paraffin sections 3 μm thick were prepared for in situ hybridization (ISH) and immunohistochemistry, respectively. Another piece was immediately embedded in OCT compound (Sakura Fintek, Inc., Torrance, CA) and snap-frozen with liquid nitrogen. Frozen sections 5 μm thick were prepared with a clean blade and mounted on glass slides coated with a thermoplastic membrane (Matsumani Glass Ind., Ltd., Osaka, Japan). They were fixed in 70% alcohol, stained briefly with Truidin blue, and processed for the laser-captured microdissection (LCM) of desired tissue elements as described below.

Preparation of anti-H2RSP antibody and immunoblot analysis

Glutathione *S*-transferase (GST)–human H2RSP (hH2RSP) fusion protein was produced using the pGEX expression vector (Amersham Pharmacia Biotech, Buckinghamshire, UK) and full-length hH2RSP cDNA and purified using glutathione Sepharose 4B according to the manufacturer's instructions. The recombinant hH2RSP was generated from GST–hH2RSP by digestion with PreScission protease (Amersham) and purified by the batch method using glutathione Sepharose 4B again. To evaluate the purity of recombinant hH2RSP, the sample obtained in each purification step was subjected to sodium dodecyl sulfate–polyacrylamide gel electrophoresis (SDS-PAGE) using a 4–12% gradient gel under reducing condition. Anti-hH2RSP rabbit antiserum was raised against the finally purified recombinant hH2RSP, and then its IgG fraction [polyclonal antibody (pAb)] was affinity purified. To confirm whether anti-hH2RSP also recognized mouse H2RSP (mH2RSP), immunoblot analysis was performed using GST–hH2RSP and GST–mH2RSP fusion proteins, which were prepared as described above. SDS-PAGE was performed under a reducing condition using 4–12% gradient gel. After electrophoresis, the proteins were transferred electrophoretically onto an Immobilon membrane (Millipore, Bedford, MA). After blocking the nonspecific binding sites with 5% nonfat dry milk in 50 mM Tris–HCl (pH 7.5), 150 mM NaCl, and 0.05% Tween 20, the membrane was incubated with anti-hH2RSP pAb diluted in buffer containing 1% bovine serum albumin (BSA) at 4°C overnight, followed by washing in the buffer three times and incubation with peroxidase-conjugated secondary antibody diluted in buffer with 1% BSA for 30 min at room temperature. The labeled proteins were visualized with a chemiluminescence reagent (PerkinElmer Life Sciences).

Immunohistochemical study

In addition to anti-hH2RSP pAb generated in this study, anti-human Ki-67 monoclonal antibody (mAb), namely, MIB-1, which cross-reacts with mouse Ki-67, was purchased from Immunotech Inc. (Westbrook, ME) to detect the proliferating epithelial cells. Deparaffinized and rehydrated serial sections were subjected to antigen retrieval by autoclaving for 5 min in 10 mM citrate buffer (pH 6.0). After treatment with 3% H_2O_2 in PBS for 10 min followed by washing in PBS twice, the sections were incubated with 3% BSA and 10% goat serum (DAKO, Carpinteria, CA) in PBS for 1 h at room temperature to block the nonspecific binding. Subsequently, the sections were incubated with anti-hH2RSP pAb (5 μg/ml) or anti-Ki-67 monoclonal antibody (×50 dilution) in PBS/1% BSA at 4°C overnight. After washing in PBS three times, the sections were incubated with Envision-labeled polymer reagents (DAKO) for 15 min at room temperature. After washing in PBS three times, the sections were visualized with nickel/cobalt-3,3′-diaminobenzidine (ImmunoPure Metal-Enhanced DAB Substrate Kit; Pierce, Rockford, IL) and counterstained with Mayer's hematoxylin.

In situ hybridization

A 525-bp cDNA fragment corresponding to bases 9–533 of mH2RSP cDNA sequence was generated by a polymerase chain reaction (PCR) [10]. The PCR product was subcloned into pBluescript II SK(+) (Stratagene, La Jolla, CA). In vitro transcription was carried out to produce digoxigenin (DIG)-labeled riboprobes, according to the manufacturer's protocols (Roche Diagnostics GmbH, Penzberg, Germany). The sense-strand probe was used as a negative control. In situ hybridization was performed using a fully automated ISH system, Ventana's HX System Discovery, and RiboMap System (Ventana, Yokohama, Japan) according to the manufacturer's instructions. Briefly, after the pretreatment step

(fixation, acid treatment, and conditioning without protease treatment), the sections were applied for hybridization using 1 ng per slide of DIG-labeled probe at 65°C for 6 h. After the hybridization, signals were detected by biotin-labeled anti-DIG antibody. The reaction was detected with BlueMap Kit and counterstained with nuclear fast red.

LCM and following real-time RT-PCR analysis

Sections prepared as above were subjected to LCM using a Leica SVS LMD System (Leica Microsystems, Wetzlar, Germany). Under microscopic guidance, epithelial cells on the mucosal surface, epithelial cells at the crypt base, epithelial cells showing restitution, and interstitial cells were selectively dissected in normal, injured, and regenerating colorectal tissues by focal melting of the membrane through laser activation. Total RNAs were extracted from thickly sliced nonfixed frozen sections (10 μm×5 slices per tissue sample) by Trizol reagent (Life Technologies Inc., Gaithersburg, MD) according to the manufacturer's instructions. Alternatively, tissue fragments obtained by LCM were dropped by gravity into cap tubes filled with lysis solution of RNAqueous-Micro kit (Ambion Inc., Austin, TX) under microscopic inspection. For RT-PCR, 1 μg each of total RNA was reverse-transcribed by $pd(N)_6$ and pdT_{12} mixed primers and SuperScript II reverse transcriptase (Life Technologies Inc.). The resulting cDNA was subjected to real-time PCR on a LightCycler with a master mix of LightCycler DNA master SyberGreen I (Roche Diagnostics, Mannheim, Germany) according to the manufacturer's instructions. The thermal cycle profile was 10 s at 95°C, 15 s at 65°C, and 12 s at 72°C for 40 cycles. Product amplification specificity was determined by melting curve analysis and agarose gel electrophoresis. The amount of mRNA per sample was expressed as percentage of control β-actin mRNA. Primer sequences of mH2RSP and mouse β-actin were as follows: mH2RSP forward primer, 5′-GTCTCTGGCAGCTCCTCCGA-3′; mH2RSP reverse primer, 5′-GGTTTCTTGGCCTTGTCTGA-3′; β-actin forward primer, 5′-AGAGGGAAATCGTGCGTGAC-3′; β-actin reverse primer, 5′-CAATAGTGATGACCTGGCCGT-3′.

Statistical analysis

Data were presented as mean±SEM. Parametric data were analyzed using Student's *t* test. An associated probability (*p* value) of less than 0.05 was considered significant. All statistical analysis was performed with Statview 5.0 program (Brainpower Inc., Calabasas, CA).

Results

Expression of H2RSP in normal mouse intestine

We first confirmed that anti-hH2RSP pAb generated in this study also recognized mH2RSP by immunoblot analysis (Fig. 1a). Immunoreacted bands were found in the lanes loading GST–hH2RSP (0.05 μg/lane) and GST–mH2RSP (0.1 μg/lane), whereas no positive band was found in the lane loading 5 μg of GST. Subsequently, immunohistochemical staining using this antibody was performed for mouse intestinal tissues. In normal murine small intestine (Fig. 1b) and colon tissues (Fig. 1c), H2RSP was localized mainly in the cytoplasm of the epithelial cells at the crypt base. These cells were also positive for MIB-1, suggesting proliferating epithelial cells (Fig. 1c, right). On the other hand, in the surface epithelial cells, which were considered as differentiated cells, H2RSP was mainly localized in the

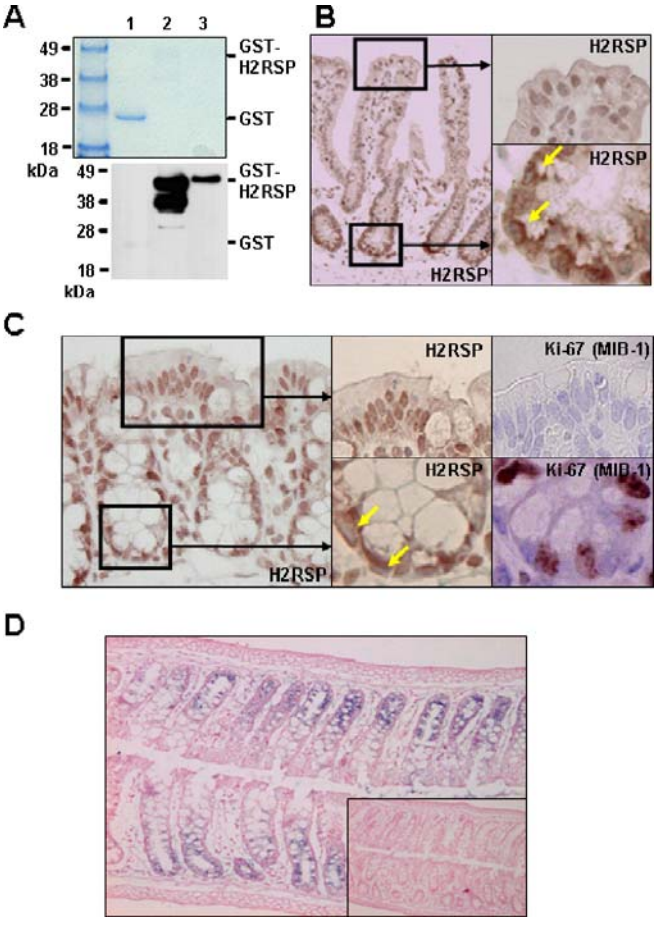

Fig. 1 **a** Immunoblot analysis for confirmation of anti-hH2RSP pAb cross-reactivity to mH2RSP. Immunoreacted bands were found in the lanes loading GST–hH2RSP (*lane 2*; 0.05 μg/lane) and GST–mH2RSP (*lane 3*; 0.1 μg/lane), whereas no positive band was found in the lane loading 5 μg of GST (*lane 1*). SDS-PAGE stained by Coomassie brilliant blue (*upper panel*) followed by Western blot analysis (*lower panel*). **b** Immunohistochemical staining of H2RSP for normal mouse small intestine. H2RSP was localized mainly in the cytoplasm of the epithelial cells in the crypt base (*arrows*) and in the nuclei of the surface epithelium. **c** Immunohistochemistry for normal colon. Similar to small intestine, H2RSP was localized in the cytoplasm of the epithelial cells in the crypt (*arrows*), which were positive for MIB-1 representing proliferating cells, and in the nucleus of the surface epithelial cells, which were negative for MIB-1 representing mature differentiated cells. **d** In situ hybridization of normal colon. H2RSP mRNA was detected in the epithelial cells of the lower part of the crypt by ISH. Negative control (sense-strand probe) is also shown in the *inset*

nuclei (Fig. 1b,c). These immunostaining patterns were essentially similar to those observed in human tissues (Uchiyama et al., manuscript in preparation), indicating the cross-reactivity and specificity of the antibody used in this study. In situ hybridization analysis also confirmed the existence of H2RSP mRNA in the epithelial cells, and the signal appeared to be stronger in the cells in the lower part of the crypt (Fig. 1d). These results indicated that H2RSP was expressed by the intestinal epithelial cells, localized in the cytoplasm of the cells in the crypt, and translocated gradually into the nuclei of surface epithelial cells possibly along with the cellular differentiation.

Expression of H2RSP in injured and regenerating intestinal mucosa

To assess the in vivo role of H2RSP in the intestinal mucosa, we used a murine experimental model of colitis induced by oral administration of 2.5% DSS for 7 days and examined the patterns of H2RSP expression during the course of the colitis from acute ulcerating phase to regenerating phase. Figure 2 showed representative histological findings of the colonic mucosa 7, 10, 14, and 21 days after the start of oral DSS administration. On day 7 (termination of DSS administration; Fig. 2a), mucosal ulceration and infiltration of various inflammatory cells were seen throughout the colon, although focal epithelial restitution was also noted. Then, the repair of ulcerated mucosa was gradually observed on days 10 and 14 (3 and 7 days after the termination of DSS treatment, respectively). On day 10 (Fig. 2b), epithelial restitution was almost completed, and the mucosal structure was partly repaired. Proliferation of fibroblastic cells and infiltration of inflammatory cells were also seen. On day 14 (Fig. 2c), the mucosa was almost regenerated, although depletion of goblet cells and infiltration of chronic inflammatory cells were still observed in the mucosa. On day 21 (14 days after the termination of DSS treatment; Fig. 2d), the mucosa was completely regenerated, and the histological feature was not distinguishable from those of normal colonic mucosa, except for mild destruction of the crypts.

Immunohistochemically, accumulation of H2RSP was observed in the cytoplasm (but not in the nucleus) of the regenerating epithelial cells showing restitution on day 10 (Fig. 3a). On day 14, in the late phase of regeneration, the nuclear localization of H2RSP became evident, showing nuclear H2RSP immunoreactivity in two thirds to three fourths of the surface epithelial cells. Some goblet cells were observed, which also showed nuclear localization of H2RSP (Fig. 3b). On day 21, most surface epithelial cells showed nuclear localization of H2RSP (Fig. 3b). Interestingly, interstitial cells of the injured mucosa, which were mainly infiltrating inflammatory cells and proliferated myofibroblastic cells, also showed positive immunoreactivity of H2RSP (Fig. 3a). In these interstitial cells of injured mucosa, H2RSP was localized predominantly in the cytoplasm, whereas only weak nuclear staining was observed in the mononuclear cells in normal mucosa (Fig. 3c). In situ hybridization revealed strong expression of H2RSP mRNA in regenerative epithelial cells on day 10, even on the mucosal surface, as well as in the stromal cells on day 7 (Fig. 3d). These results indicated that H2RSP was upregulated in injured and regenerating mucosa and that the nuclear translocation of H2RSP was impaired in the regenerative epithelial cells and in the proliferating and/or infiltrating stromal cells.

Real-time RT-PCR analysis for H2RSP mRNA expression during DSS-induced mouse colitis

We then performed a quantification analysis of H2RSP mRNA on each designated day along with the course of DSS-induced colitis by real-time RT-PCR (Fig. 4a). Total expression level of H2RSP mRNA was significantly increased on days 7 and 10 ($p<0.005$, compared with control) when the inflammatory reactions were obvious and subsequent regenerative processes were gradually undergoing in the mucosa. This upregulation of H2RSP was not ob-

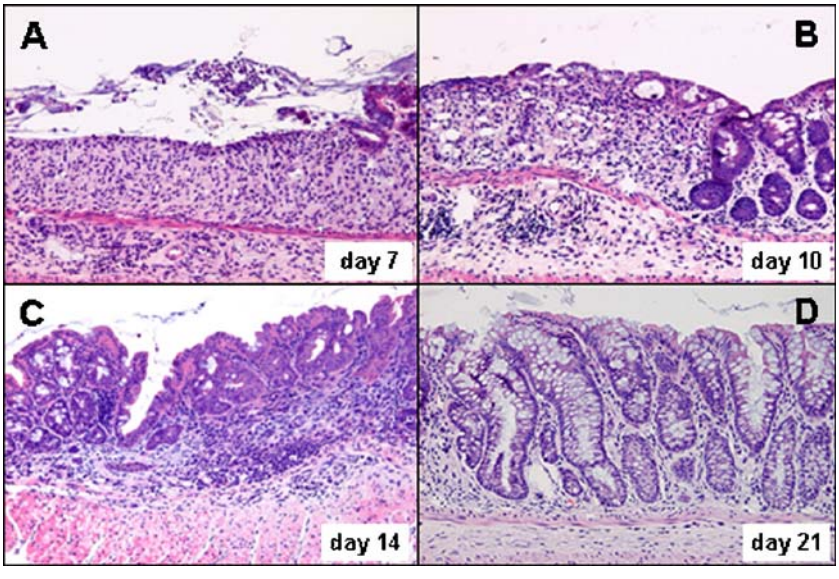

Fig. 2 Histology of colonic mucosa 7 (**a**), 10 (**b**), 14 (**c**), and 21 (**d**) days after the start of oral DSS administration. On day 7 (termination of DSS administration), mucosal ulceration with infiltration of various inflammatory cells was seen throughout the colon, although focal epithelial restitution was also noted. Mucosal ulceration was gradually recovered on days 10 and 14 (3 and 7 days after the termination of DSS treatment, respectively). On day 21 (14 days after the termination of DSS treatment), the mucosa was completely regenerated, and the histological feature was not distinguishable from those of normal colonic mucosa

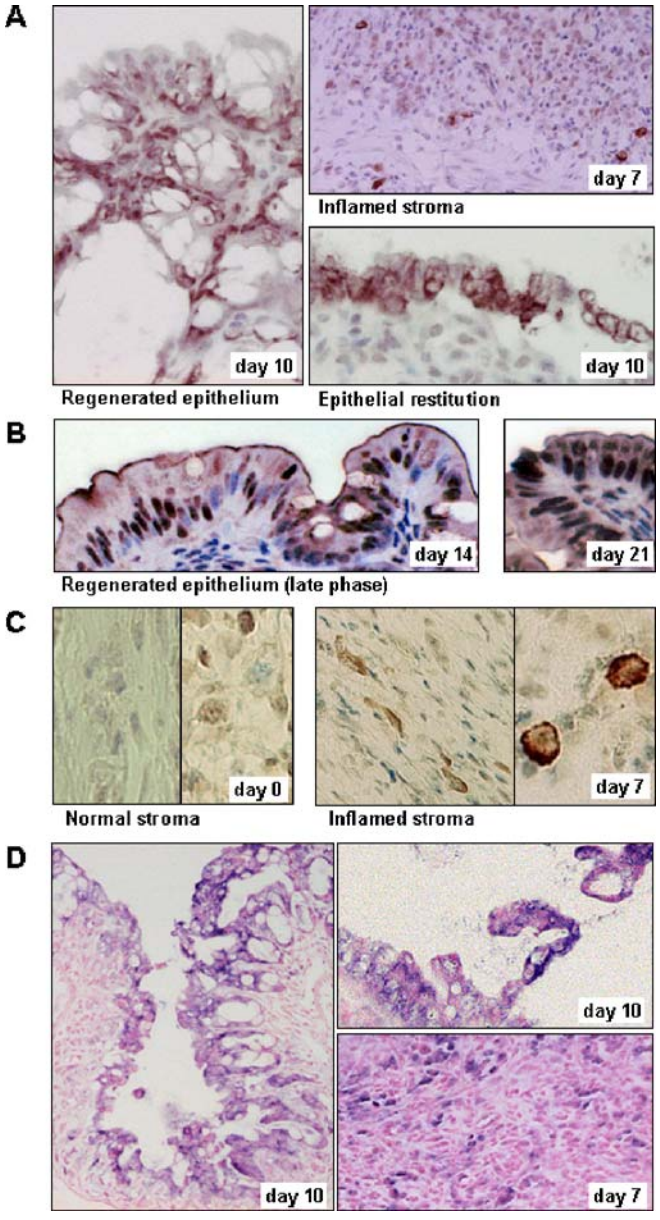

Fig. 3 Immunohistochemistry (**a**–**c**) and ISH (**d**) of H2RSP in injured and regenerating mucosal tissue after DSS administration. Upregulation and accumulation of H2RSP were observed in the cytoplasm (but not in the nucleus) of the epithelial cells showing restitution and regeneration 3 days after the termination of DSS administration (day 10; **a**). On day 14 (7 days after the termination of DSS administration), considerable regeneration had occurred, and the nuclear localization of H2RSP became evident. Some goblet cells were observed showing nuclear localization of H2RSP. However, part of the surface epithelial cells still showed the cytoplasmic localization (**b**). On day 21, most surface epithelial cells showed nuclear localization of H2RSP (**b**). On day 7 (termination of DSS administration), interstitial cells, mainly infiltrating inflammatory cells and myofibroblastic cells in the injured mucosa, were also positively stained with H2RSP (**a**). These stromal cells showed cytoplasmic H2RSP localization (**c**). In situ hybridization revealed strong expression of H2RSP mRNA in regenerative epithelial cells even on the surface and in the stromal cells in injured mucosa (**d**)

served on day 14, when mucosal regeneration had been almost completed, and the mRNA level of H2RSP was comparable with that of normal control. We next examined the mRNA levels of H2RSP in fractionated samples of mice with (day 10) and without (control) DSS treatment. By using LCM, epithelial cells on the surface of mucosa, those in the crypt, those showing restitution, and mucosal stromal cells were obtained separately, and total RNA was prepared

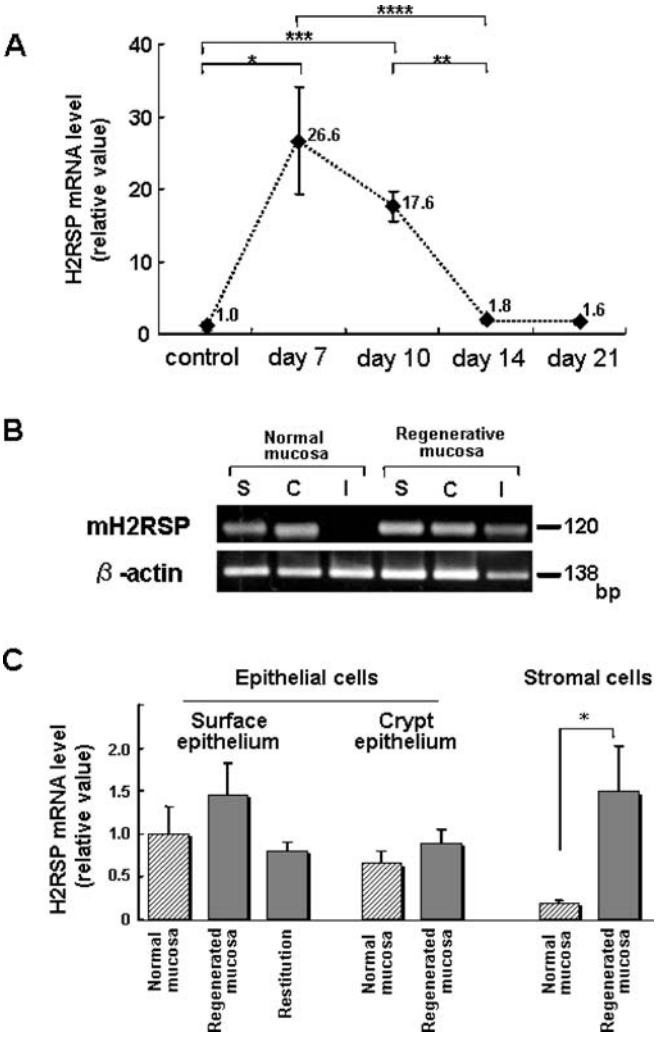

Fig. 4 **a** Real-time RT-PCR analysis of H2RSP mRNA expression during the course of DSS-induced colitis. Total expression level of H2RSP mRNA was significantly increased on days 7 and 10, when the regenerative processes were undergoing and inflammatory reaction was seen in the mucosa. This upregulation of H2RSP disappeared on day 14, when mucosal regeneration was almost complete, and the mRNA level of H2RSP was comparable with that of normal control. *p=0.004, **p=0.002, ***p=0.003, ****p=0.003. **b** Agarose gel electrophoresis of RT-PCR for H2RSP mRNA expression in fractionated samples obtained by LCM. Note that the band representing mRNAs of the interstitial cells was detectable in the regenerative but not in normal mucosa. *S* Epithelial cells on the mucosal surface, *C* epithelial cells in the crypt, *I* interstitial cells. **c** Real-time RT-PCR analysis of H2RSP mRNA expression in fractionated samples obtained by LCM. The expression level of mH2RSP mRNA was modestly increased in regenerating epithelial cells, both on the surface and in the crypt, but the differences were not statistically significant. The epithelial cells showing restitution do not show enhanced H2RSP mRNA expression. On the other hand, the H2RSP mRNA level of stromal cells was significantly upregulated in regenerative and inflamed mucosa compared with normal control mucosa. *p=0.004

from each fraction. Then the expression level of H2RSP mRNA was analyzed in each sample (Fig. 4b,c). The mRNA levels of H2RSP were modestly increased in regenerated epithelial cells compared with corresponding epithelial cells of normal mucosa; however, the differences were not statistically significant. The epithelial cells showing restitution did not show altered level of H2RSP mRNA compared with the normal surface epithelium. However, the mRNA level in the mucosal stromal cells was significantly upregulated in the regenerating mucosal tissue compared with normal control mucosa ($p<0.005$). Therefore, a large proportion of increased H2RSP mRNA in the regenerating and inflamed mucosa was derived from the reactive stromal cells.

Discussion

In this study, we analyzed the subcellular localization of H2RSP in normal, injured, and regenerating intestinal tissues using a murine experimental colitis model. Immunohistochemically, H2RSP was localized in the cytoplasm of the proliferating epithelial cells at the crypt base and then translocated into the nuclei of the mature and differentiated epithelial cells at the surface. Of particular interest was the observation that this nuclear translocation was significantly impaired in the regenerating epithelium, showing epithelial restitution as well as cellular proliferation. Therefore, it is intriguing to speculate that the nuclear translocation of H2RSP in the intestinal epithelial cells serves as a signal for the transition from proliferating phase to growth arrest followed by terminal differentiation. In situ hybridization study showed that H2RSP mRNA was strongly detectable in the MIB-1-positive proliferating epithelial cells in the crypt in normal intestine, and the surface-differentiated epithelial cells showed less amounts of H2RSP mRNA. However, real-time RT-PCR analysis revealed that comparable amounts of H2RSP mRNA were also present in the surface-differentiated epithelial cells. We assumed that hybridization of riboprobe to the cellular mRNA may be interfered with in some fashion by mucin produced by the goblet cells of the mucosal surface. Indeed, strong ISH signal was observed in the surface epithelial cells of the regenerating mucosa, in which goblet cells were severely depleted.

In addition to the epithelial cells, the stromal cells of injured mucosa, but not of normal mucosa, also expressed H2RSP abundantly. In DSS-induced colitis, the levels of H2RSP mRNA were significantly increased on days 7 and 10, and most of the increased mRNA in these mucosal tissues appeared to be derived from the stromal cells. Morphologically, these H2RSP-expressing stromal cells were infiltrated inflammatory cells and proliferating fibroblastic (myofibroblastic) cells. In this regard, IMUP-1, an identical peptide with H2RSP, has been identified as one of the mRNAs upregulated in SV40-immortalized fibroblasts compared to senescent WI-38 fibroblasts [8]. This characteristic of IMUP-1 may be consistent with our present observation that H2RSP was upregulated in proliferating fibroblastic cells in response to tissue injury. Notably, H2RSP was localized in the cytoplasm of these interstitial cells, but not in the nuclei. Therefore, H2RSP might be upregulated in various types of cells showing proliferation and/or active migration accompanying its confined localization in the cytoplasm.

H2RSP is a small peptide containing the effective bipartite basic type NLS in the lysine-rich region of exon 4 [3, 10]. However, no apparent motif of known nuclear proteins interacting with DNA homologous to the predicted amino acid sequence of H2RSP was found in the NCBI database. Thus, it is unlikely that H2RSP directly interacts with nuclear DNA, and the precise function of H2RSP in the nucleus remains unclear at present. H2RSP may interact with ribosomal RNA because H2RSP was especially located in the nucleolus [3, 10], and IMUP-1, a peptide homologous to H2RSP, indeed bound to poly r(G) in vitro [8]. Recently, it has been shown that most of the genes involved in cellular proliferation, RNA splicing and transport, and protein translation are downregulated along with the maturation of colonic epithelial cells by gene expression profiling [9]. H2RSP may be a promising additional candidate for the signaling molecule involved in the transition from proliferation to terminal differentiation and growth arrest in gastrointestinal epithelial cells, acting in the nucleus, having a reciprocal function to the proliferation-initiating molecule such as musashi-1, an RNA-binding protein expressed in stem and early-lineage progenitor cells in mouse intestinal epithelial cells [7, 11, 12].

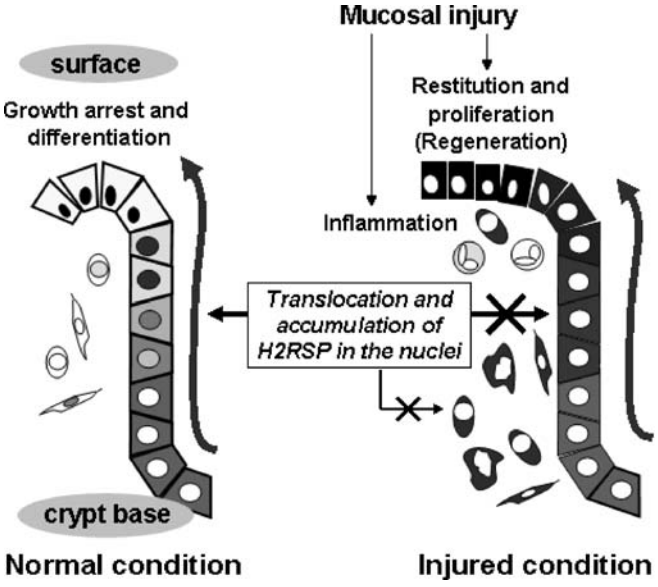

Fig. 5 Schematic of H2RSP immunolocalization and immunoreactivity in normal and injured mucosal tissues of murine intestine. Localization and intensity of H2RSP immunoreactivity are indicated as a gradation of gray to black shading. In normal intestinal epithelium, H2RSP is translocated into the nucleus along with the differentiation of epithelial cells (*left*). This nuclear translocation is impaired in regenerating epithelial cells showing restitution and proliferation, and the regenerated epithelial cells show increased intensity of H2RSP immunoreactivity (*right*). H2RSP is also upregulated in reactive stromal cells of injured mucosa, which also shows confined cytoplasmic localization in these cells

The summary of H2RSP immunolocalization in normal and injured intestinal mucosa is shown in Fig. 5. In normal intestinal epithelium, H2RSP is present in the nuclei of differentiated surface epithelial cells, whereas its subcellular localization is confined in the cytoplasm in the crypt base. Therefore, H2RSP may be translocated into the nucleus along with the differentiation of epithelial cells. In injured mucosa, the nuclear translocation of H2RSP is impaired in epithelial cells, and these cells undertake subsequent restitution and regeneration. These circumstantial evidences suggest a possible role of nuclear translocation of H2RSP in a signal related to the transition from proliferation to differentiation of intestinal epithelial cells. H2RSP is also upregulated in interstitial cells, such as proliferating fibroblastic cells and infiltrating inflammatory cells, in response to mucosal injury, and H2RSP shows preferred cytoplasmic localization in these reactive stromal cells as observed in the regenerating epithelial cells. To clarify the mechanism underlying the nuclear translocation of H2RSP and its precise function in the nucleus, further detailed experiments are underway in our laboratory.

Acknowledgements The authors thank Mr. T. Miyamoto and Mrs. Y. Nomura for their skillful technical assistance.

This study is supported in part by Grant-in-Aid for Scientific Research (B) 17390116 and (C) 17590354 and the 21st Century COE program (Life Science) from the Ministry of Education, Science, Sports and Culture, Japan, and grants from the Novartis Foundation (Japan) for the promotion of science and the Naito Foundation.

References

1. Itoh H, Beck PL, Inoue N, Xavier R, Podolsky DK (1999) A paradoxical reduction in susceptibility to colonic injury upon targeted transgenic ablation of goblet cells. J Clin Invest 104:1539–1547
2. Itoh H, Yamauchi M, Kataoka H, Hamasuna R, Kitamura N, Koono M (2000) Genomic structure and chromosomal localization of the human hepatocyte growth factor activator inhibitor type 1 and 2 genes. Eur J Biochem 267:3351–3359
3. Itoh H, Kataoka H, Yamauchi M, Naganuma S, Akiyama Y, Nuki Y, Shimomura T, Miyazawa M, Kitamura N, Koono M (2001) Identification of hepatocyte growth factor activator inhibitor type 2 (HAI-2)-related small peptide (H2RSP): its nuclear localization and generation of chimeric mRNA transcribed from both HAI-2 and H2RSP genes. Biochem Biophys Res Commun 288:390–399
4. Itoh H, Naganuma S, Takeda N, Miyata S, Uchinokura S, Fukushima T, Uchiyama S, Tanaka H, Nagaike K, Shimomura T, Miyazawa K, Yamada G, Kitamura N, Koono M, Kataoka H (2004) Regeneration of injured intestinal mucosa is impaired in hepatocyte growth factor activator-deficient mice. Gastroenterology 127:1423–1435
5. Kataoka H, Itoh H, Nuki Y, Hamasuna R, Naganuma S, Kitamura N, Shimomura T (2002) Mouse hepatocyte growth factor (HGF) activator inhibitor type 2 lacking the first Kunitz domain potently inhibits the HGF activator. Biochem Biophys Res Commun 290:1096–1100
6. Kawaguchi T, Qin L, Shimomura T, Kondo J, Matsumoto K, Denda K, Kitamura N (1997) Purification and cloning of hepatocyte growth factor activator inhibitor type 2, a Kunitz-type serine protease inhibitor. J Biol Chem 272:27558–27564
7. Kayahara T, Sawada M, Takaishi S, Fukui H, Seno H, Fukuzawa H, Suzuki K, Hiai H, Kageyama R, Okano H, Chiba T (2003) Candidate markers for stem and early progenitor cells, Musashi-1 and Hes1, are expressed in crypt base columnar cells of mouse small intestine. FEBS Lett 535:131–135
8. Kim JK, Ryll R, Ishizuka Y, Kato S (2000) Identification of cDNAs encoding two novel nuclear proteins, IMUP-1 and IMUP-2, upregulated in SV40-immortalized human fibroblasts. Gene 257:327–334
9. Mariadason JM, Arango D, Corner GA, Arañes MJ, Hotchkiss KA, Yang W, Augenlicht LH (2002) A gene expression profile that defines colon cell maturation in vitro. Cancer Res 62:4791–4804
10. Naganuma S, Itoh H, Uchiyama S, Tanaka H, Nagaike K, Miyata S, Uchinokura S, Nuki Y, Akiyama Y, Chijiiwa K, Kataoka H (2003) Characterization of transcripts generated from mouse hepatocyte growth factor activator inhibitor type 2 (HAI-2) and HAI-2-related small peptide (H2RSP) genes: chimeric mRNA transcribed from both HAI-2 and H2RSP genes is detected in human but not in mouse. Biochem Biophys Res Commun 302:345–353
11. Okano H, Imai T, Okabe M (2002) Musashi: a translational regulator of cell fate. J Cell Sci 115:1355–1359
12. Potten CS, Booth C, Tudor GL, Booth D, Brady G, Hurley P, Ashton G, Clarke R, Sakakibara S, Okano H (2003) Identification of a putative intestinal stem cell and early lineage marker; musashi-1. Differentiation 71:28–41

Virchows Arch (2006) 448: 361–365
DOI 10.1007/s00428-005-0108-y

CASE REPORT

Annette Zimpfer · Martin C. Freund · Stephan Dirnhofer · Eberhard Gunsilius · Berthold Streubel · Andreas Chott · Alexandar Tzankov

Marginal zone lymphoma of the lacrimal gland spreading to the lung and the bone marrow 11 years after first symptoms

Received: 5 August 2005 / Accepted: 23 September 2005 / Published online: 17 November 2005

Abstract We report on the case of a 52-year-old male presenting with an extranodal marginal zone lymphoma of the mucosa-associated tissue (MALT lymphoma) in the lung 11 years after radiotherapy for a MALT lymphoma of the lacrimal gland, which was primarily diagnosed as dacryoadenitis. Both tumors were investigated by immunohistochemistry and molecular techniques demonstrating their clonal genetic relationship. Both harbored the t(14;18)(q32;q21) and a trisomy 3 and showed identical immunoglobulin heavy-chain gene rearrangements. At the time of pulmonary relapse, clonal CD20- and CD43-positive bone marrow B lymphocytes were detected as well. The elaboration of this case emphasizes the importance of the combined use of modern diagnostic methods for establishment of correct diagnosis of MALT lymphomas at late relapses, which is essential for proper patient management.

A. Zimpfer · S. Dirnhofer
Institute of Pathology, University of Basel,
Basel, Switzerland

M. C. Freund
Department of Radiology,
Medical University of Innsbruck,
Innsbruck, Austria

E. Gunsilius
Department of Hematology and Oncology,
Medical University of Innsbruck,
Innsbruck, Austria

B. Streubel · A. Chott
Institute of Pathology, Medical University of Vienna,
Vienna, Austria

A. Tzankov (✉)
Institute of Pathology,
Medical University of Innsbruck,
Muellerstr. 44,
4020 Innsbruck, Austria
e-mail: Alexandar.Tzankov@uibk.ac.at
Tel.: +43-512-5073692
Fax: +43-512-582088

Keywords MALT lymphoma · Tear gland · Lung · Late relapse · t(14;18)(q32;q21) · Trisomy 3

Introduction

Lymphomas arising in the ocular adnexa, including the conjunctiva, eyelid, lacrimal gland, and orbit, are infrequent and account for approximately 8–12% of all ocular adnexal tumors [3, 7, 8, 10, 18]. They represent the malignant counterpart of a spectrum of ocular adnexal lymphoproliferative lesions [3, 9, 10]. The extranodal marginal zone B-cell lymphoma of mucosa-associated tissue (MALT lymphoma) represents the most common lymphoma subtype at this site and shows a rising incidence in the last decade [1, 3, 13]. Usually, MALT lymphomas have an indolent clinical course but, especially nongastric ones, frequently recur and, occasionally, transform into an aggressive disease [7, 8, 10, 15, 18, 19]. Thus, a closed lifelong follow-up with half-yearly examinations is currently recommended [15]. Late recurrences of MALT lymphoma are mainly documented on a single-case basis, with cases insufficiently studied at the molecular level [2, 4, 12, 19]. Recently, the thus far best-proved follow-up cohort of 86 MALT patients with 37% relapses observed within a median observation period of 47 months was published [15]. Interestingly, these patients did not show evidence for a cytogenetic progression in the recurrent lesions [15].

Here, we report an additional molecularly documented case of MALT lymphoma of the lacrimal gland that recurred after more than 130 months. Recurrence of MALT lymphoma of the lacrimal gland after such a long interval has never been reported before.

Clinical history

In 1994, a 41-year-old male patient was admitted to the ENT unit of our hospital for swelling of the upper eyelid and exophthalmia on the left side. The biopsy performed at

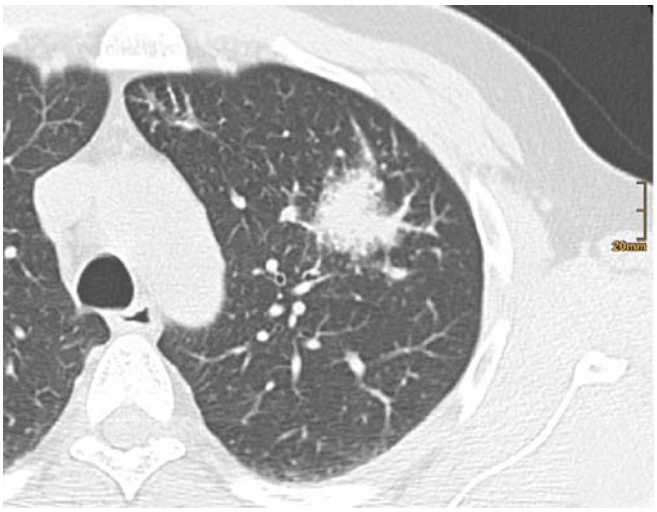

Fig. 1 Computerized imaging of the thorax showing large opacity in the upper left lung lobe and additional smaller lesions in both lungs

that time showed a "lymphoepithelial dacryoadenitis." An underlying MALT lymphoma was also discussed, but the lymphoid cells did not immunohistochemically show a clear-cut clonal light-chain restriction, so that a reactive process was favored. The patient was successfully treated with steroids, but the symptoms recurred after taking off the treatment. Then, radiotherapy was performed (cumulative dose 20 Gy) leading to complete remission. In 2004, the patient was planned to undergo reconstructive vascular surgery due to peripheral arterial occlusive disease grade II. The patient reported nicotine abuse of 60 pack years and complained about a productive cough for 1 month. A 3×5-cm large opacity in the upper left lung lobe was discovered on a routine chest x-ray. Further evaluation by CT showed additional smaller lesions in both lungs (Fig. 1). Nodal status, laboratory findings, and ^{18}F-fluorodeoxyglucose positron emission tomography (PET) were inconspicuous. Multiple CT-guided percutaneous large-core biopsies of the pulmonary nodule were performed with a 16-gauge cutting needle with 2.2-cm cutting length inserted into a 15-gauge coaxial needle as described [11]. Pulmonary recurrence of a MALT lymphoma of the lacrimal gland was diagnosed (see "Results"). The patient was given a combined radiochemotherapy with fludarabine and involved-field irradiation. At the time of last control (June 2005), he was in complete remission.

Methods

Immunohistochemistry

Four-meter-thick sections from the formalin-fixed paraffin-embedded tissue samples were immunohistochemically analyzed using an automated immunostainer (Nexes, Ventana, Tucson, AZ, USA). The streptavidin–biotin–peroxidase technique with diaminobenzidine as chromogen was applied. The primary antibodies were diluted in 1% solution of bovine serum albumin in phosphate-buffered saline (pH 7.4) and incubated for 30 min at room temperature. The primary antibodies, their dilutions, and pretreatment conditions are listed in Table 1.

Fluorescent in situ hybridization analysis

Formalin-fixed paraffin-embedded tissue was used for fluorescent in situ hybridization (FISH). For a reliable interpretation of the hybridization signals, we preferred analysis of single-cell suspensions to thin sections [16]. FISH was performed on interphases with the following probe sets: for rearrangements of *BCL10*, BACs RP11-1077C10 and RP11-36L4 (SpectrumGreen) centromeric to *BCL10* and RP11-1080I1 and RP11-40K4 (SpectrumOrange) telomeric to *BCL10*; and for the detection of translocations of *MALT1*, dual-color break-apart rearrangement probes (Vysis, Downer's Grove, IL, USA). As a result of this probe design, any translocation of *MALT1* should produce separate orange and green signals. For the iden-

Table 1 Primary antibodies, dilutions, and pretreatment conditions

Antibody	Source	Dilution	Retrieval
CD5	Novocastra	1:150	Citrate buffer, pH 6, wet autoclave, 121°C, 5 min
CD10	Novocastra	1:50	Citrate buffer, pH 6, wet autoclave, 121°C, 5 min
CD20	DAKO	1:700	Citrate buffer, pH 6, microwave oven, 800 W, 10 min
CD43	PharMingen	1:200	0.1% pronase, 4 min
CD138	DAKO	1:200	Citrate buffer, pH 6, microwave oven, 800 W, 10 min
IgM	DAKO	1:20,000	0.1% pronase, 8 min
IgG	DAKO	1:20,000	0.1% pronase, 4 min
κ	DAKO	1:16,000	0.1% pronase, 4 min
λ	DAKO	1:40,000	0.1% pronase, 4 min
Bcl-2	DAKO	1:50	Citrate buffer, pH 6, wet autoclave, 121°C, 5 min
Bcl-6	DAKO	1:40	Citrate buffer, pH 6, wet autoclave, 121°C, 5 min
Ki-67	DAKO	1:100	Citrate buffer, pH 6, wet autoclave, 121°C, 5 min
Cyclin D1	Novocastra	1:20	Citrate buffer, pH 6, wet autoclave, 121°C, 5 min

tification of the t(14;18)(q32;q21) involving the immunoglobulin heavy-chain *IGH* and *MALT1* genes, P1 artificial chromosome (PAC) 152M5 (SpectrumOrange-labeled) spanning the *MALT1* gene and flanking regions and bacterial artificial chromosome (BAC) 158A2 were used [16]. For the detection of trisomies 3 and 18, we applied centromere-specific probes for the chromosomes 3 (SpectrumOrange) and 18 (SpectrumGreen) (Vysis).

Detection of t(11;18) by reverse transcription-polymerase chain reaction

RNA was isolated from archival formalin-fixed paraffin-embedded lymphoma tissues. Total RNA was extracted from 10-μm sections. First-strand cDNA synthesis and reverse transcription-polymerase chain reaction (RT-PCR) for the detection of the *API2–MALT1* fusion transcript were performed as described elsewhere [17].

Clonality analysis

DNA extraction from the formalin-fixed paraffin-embedded tissue samples from the lung, bone marrow, and lacrimal gland as well as analysis of *IGH* gene rearrangements was performed as described elsewhere [5].

Results

The core biopsies from the lung lesion showed a diffuse interstitial small lymphocytic infiltrate composed of centrocytoid, centroblastoid, and plasmacytoid cells surrounding the bronchioles and the vessels (Fig. 2). Partial destruction of the alveolar lung parenchyma and accumulation of foamy macrophages were present as well. Immunohistochemically, the cells stained positively for CD20 (Fig. 3), CD43, IgM, and bcl-2 and remained negative for CD5, CD10, CD23, IgG, bcl-6, and cyclin D1. The plasmacytoid component was CD138 positive and κ-light-chain-restricted. The proliferation fraction (Ki-67) was 5%. The work-up of the primary tumor of the lacrimal gland revealed identical immunohistochemical results.

The biopsy specimens from the lacrimal gland and from the lung were analyzed by FISH for the presence of *MALT1* and *BCL10* rearrangements as well as for trisomies 3 and 18. Three hundred cells per biopsy (lung and ocular adnexa) were investigated. Signals for *BCL10* and centro-

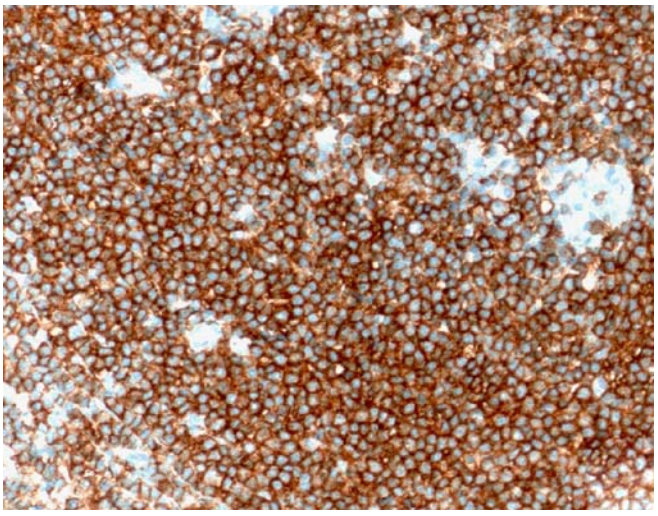

Fig. 3 Immunohistochemical staining for CD20 displaying strong membranous positivity of the lymphoid infiltrate (streptavidin–biotin–peroxidase technique with diaminobenzidine as chromogene, ×200)

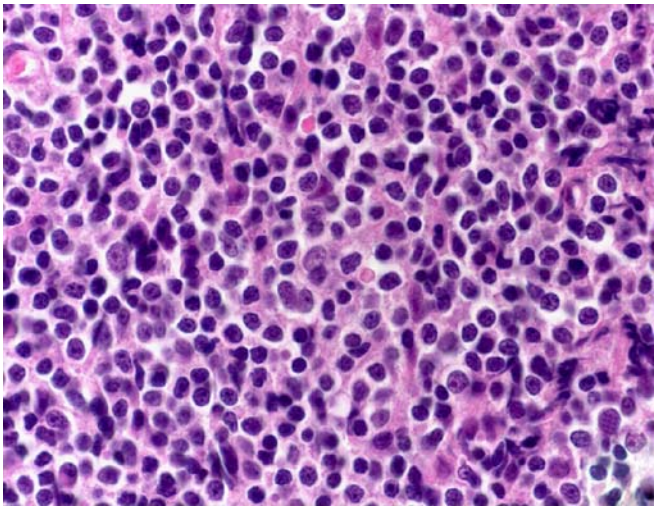

Fig. 2 Detailed morphological view of the lung biopsy showing a diffuse, predominantly small lymphocytic infiltrate with occasional plasma cells and isolated blasts (e.g., lower left corner) with destruction of the preexisting parenchyma (H & E stain, ×400)

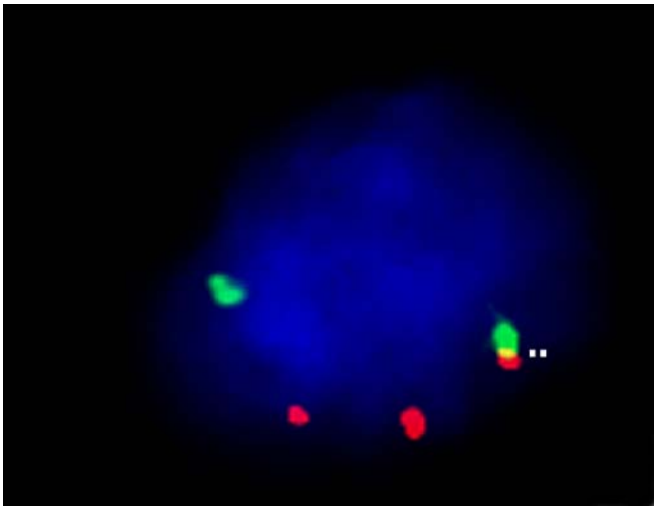

Fig. 4 Fluorescent in situ hybridization with probes for *IGH* (*green signals*) and *MALT1* (*red signals*) demonstrating *IGH*/*MALT1* fusion (⋯) corresponding to t(14;18) involving *IGH* and *MALT1*. The t(14;18) was detected in the biopsies from the lung (2004) and the ocular adnexa (1994), ×1000

mere 18 were inconspicuous. Centromere 3 probes revealed three signals in 166 out of 300 cells in the lung and 132 out of 300 cells in the ocular adnexa. In the FISH with probes flanking *MALT1*, a split signal indicating a rearrangement of *MALT1* was seen in both biopsies. RT-PCR was negative for the t(11;18) involving *API2* and *MALT1*. In contrast, FISH with probes for *IGH* and *MALT1* demonstrated *IGH*/*MALT1* fusion signals proving a t(14;18) in each lung (174/300 cells) and ocular adnexal (121/300 cells) biopsies. In conclusion, a t(14;18)(q32;q21) involving *IGH* and *MALT1* (Fig. 4) together with a trisomy 3 was detected in both biopsies of the patient. This constellation pointed to the presence of the same clone (see also next paragraph) in both the primary MALT lymphoma of the lacrimal gland and the lung lesion 11 years after the initial diagnosis.

Interstitial small CD20- and CD43-positive B-cell lymphocytosis in the bone marrow harboring the same *IGH* gene rearrangement as suggested by the identical pattern of PCR products migration in the polynat gel as the pulmonary lesion and the lacrimal gland was detected in the staging trephine biopsy from 2004. The gastric and colic biopsies were inconspicuous.

Discussion

Lymphoid proliferations of the ocular adnexa are categorized in reactive lesions such as reactive lymphoid hyperplasia and atypical lymphoid hyperplasia as well as lymphomas such as MALT lymphoma. They cannot be diagnosed accurately based solely on clinical and imaging criteria [1, 3, 7]. In the past, many of these lesions were considered benign based on their low-grade histological features. However, by the recognition of MALT lymphoma [7] and applying modern molecular techniques, many lymphocytic proliferations formerly classified as benign or atypical lymphoid hyperplasia would now be diagnosed as MALT lymphoma [1]. Immunohistochemistry, flow cytometry, and in situ hybridization for light-chain restriction and PCR analysis of *IGH* rearrangements, as in the present case, proved to be very helpful in achieving a more accurate diagnosis. Meanwhile, distinct recurrent chromosomal aberrations in MALT lymphomas are recognized such as, e.g., t(11;18)(q21;q21) in gastric marginal zone lymphomas [16]. There is a correlation between the presence of a specific translocation and anatomical site of the MALT lymphoma [17]. In gastric and pulmonary lymphomas, t(11;18)(q21;q21) can be predominantly identified, whereas t(14;18)(q32;q21) is most commonly found in lesions of the ocular adnexa, salivary glands, and skin [17]. Concomitantly, t(11;18)(q21;q21) in MALT lymphomas of the ocular adnexa seem to be rare [17]. Numerical aberrations such as trisomies 3 or 18 occur most frequently in MALT lymphomas of the intestine and salivary glands [17] but can be found beside t(14;18)(q32;q21) in ocular MALT lymphomas as well [16]. This distribution of distinct translocations at different anatomical sites is supported by the findings in our patient. In 2004, he suffered from a MALT lymphoma in/of the lung carrying a t(14;18)(q32;q21) and a trisomy 3, a constellation rather not typical for a primary pulmonary MALT lymphoma. Indeed, 11 years before, he was diagnosed to suffer from steroid-treatment-resistant lymphoepithelial dacryoadenitis, showing on reevaluation the same chromosomal aberrations as the pulmonary lymphoma. Nevertheless, the initial misinterpretation did not prevent a correct clinical management. Since the lacrimal gland lesion recurred after withdrawal of steroids, the patient was given radiotherapy leading to complete remission. Interestingly, at the time of recurrence, a PET was performed but the pulmonary lesions remained silent, a constellation rather typical for marginal zone lymphomas [6], so that the correct diagnosis was established by means of morphological analysis supported by modern molecular techniques. Even more, we identified virtually identical clonal *IGH* rearrangements in the pulmonary and lacrimal lesions and a suspicious interstitial CD20- and CD43-positive small bone marrow lymphocyte population at the time of recurrence. Importantly, this finding was critically considered by the treating physicians when choosing a multimodal systemic (chemotherapy) and local (involved-field irradiation) therapy regimen.

Late recurrences in MALT lymphomas were till recently [15] poorly documented particularly at the molecular level being mainly single-case reports [2, 4, 12, 19]. The median period between first diagnosis and relapse reportedly varies between several months and decades [2, 4, 12, 15, 19]. In the present case, the late pulmonary recurrence of a primary MALT lymphoma of the lacrimal gland was diagnosed after 11 years, with both tumors harboring identical genetic aberrations. Similarly, late recurrences after more than 10 years have been accurately documented in only four cases of MALT lymphomas of the parotid gland as well of the stomach and lung [4, 15]. The reason for this behavior of MALT lymphomas is unclear but underlines their unpredictable course, probably due to higher rates of silent initial multiorgan spread [14]. Though mostly diagnosed at stage IE and often responding to unimodal therapy [12], ocular MALT lymphomas are malignant tumors that can recur even more than a decade after initial diagnosis and/or spread to other MALT organs and to the bone marrow. Our case study emphasizes the feasibility of modern histopathological diagnostic tools for proper diagnosis of MALT lymphomas at late relapses and underscores the importance of extensive staging, paying particular attention to other organs with MALT and bone marrow as well as lifelong follow-up in such patients, which is essential for their appropriate management.

References

1. Auw-Haedrich C, Coupland SE, Kapp A, Schmitt-Graff A, Buchen R, Witschel H (2001) Long term outcome of ocular adnexal lymphoma subtyped according to the REAL classification. Revised European and American Lymphoma. Br J Ophthalmol 85:63–69

2. Cho EY, Han JJ, Ree HJ, Ko YH, Kang YK, Ahn HS, Ahn SD, Park CJ, Huh J (2003) Clinicopathologic analysis of ocular adnexal lymphomas: extranodal marginal zone B-cell lymphoma constitutes the vast majority of ocular lymphomas among Koreans and affects younger patients. Am J Hematol 73:87–96
3. Coupland SE, Krause L, Delecluse HJ, Anagnostopoulos I, Foss HD, Hummel M, Bornfeld N, Lee WR, Stein H (1998) Lymphoproliferative lesions of the ocular adnexa. Analysis of 112 cases. Ophthalmology 105:1430–1441
4. Dunphy CH, Grosso LE, Rodriquez JJ, Dunphy FR (1996) Bilateral mucosa-associated lymphoid tissue lymphomas of parotid glands: a 13-year interval. Mod Pathol 9:560–565
5. Fong D, Kaiser A, Spizzo G, Gastl G, Tzankov A (2005) Hodgkin's disease variant of Richter's syndrome in chronic lymphocytic leukaemia patients previously treated with fludarabine. Br J Haematol 129:199–205
6. Hoffmann M, Kletter K, Becherer A, Jager U, Chott A, Raderer M (2003) 18F-fluorodeoxyglucose positron emission tomography (18F-FDG-PET) for staging and follow-up of marginal zone B-cell lymphoma. Oncology 64:336–340
7. Isaacson P, Wright DH (1984) Extranodal malignant lymphoma arising from mucosa-associated lymphoid tissue. Cancer 53:2515–2524
8. Isaacson P, Norton A (1994) Extranodal lymphomas. Churchill Livingstone, Edinburgh
9. Jenkins C, Rose GE, Bunce C, Wright JE, Cree IA, Plowman N, Lightman S, Moseley I, Norton A (2000) Histological features of ocular adnexal lymphoma (REAL classification) and their association with patient morbidity and survival. Br J Ophthalmol 84:907–913
10. Knowles DM, Jakobiec FA, McNally L, Burke JS (1990) Lymphoid hyperplasia and malignant lymphoma occurring in the ocular adnexa (orbit, conjunctiva, and eyelids): a prospective multiparametric analysis of 108 cases during 1977 to 1987. Human Pathol 21:959–973
11. Lucidarme O, Howarth N, Finet JF, Grenier PA (1998) Intrapulmonary lesions: percutaneous automated biopsy with a detachable, 18-gauge, coaxial cutting needle. Radiology 207: 759–765
12. Matsuo T, Yoshino T (2004) Long-term follow-up results of observation or radiation for conjunctival malignant lymphoma. Ophthalmology 111:1233–1237
13. Mitterlechner T, Fiegl M, Mühlböck H, Oberaigner W, Dirnhofer S, Tzankov A (2005) Epidemiology of non-Hodgkin-lymphomas in Tyrol/Austria from 1991 through 2000. J Clin Pathol (in press) DOI: 10.1136/Jcp.2005.026815
14. Raderer M, Vorbeck F, Formanek M, Osterreicher C, Valencak J, Penz M, Kornek G, Hamilton G, Dragosics B, Chott A (2000) Importance of extensive staging in patients with mucosa-associated lymphoid tissue (MALT)-type lymphoma. Br J Cancer 83:454–457
15. Raderer M, Streubel B, Woehrer S, Puespoek A, Jaeger U, Formanek M, Chott A (2005) High relapse rate in patients with MALT lymphoma warrants lifelong follow-up. Clin Cancer Res 11:3349–3352
16. Streubel B, Lamprecht A, Dierlamm J, Cerroni L, Stolte M, Ott G, Raderer M, Chott A (2003) T(14;18)(q32;q21) involving IGH and MALT1 is a frequent chromosomal aberration in MALT lymphoma. Blood 101:2335–2339
17. Streubel B, Simonitsch-Klupp I, Mullauer L, Lamprecht A, Huber D, Siebert R, Stolte M, Trautinger F, Lukas J, Puspok A, Formanek M, Assanasen T, Muller-Hermelink HK, Cerroni L, Raderer M, Chott A (2004) Variable frequencies of MALT lymphoma-associated genetic aberrations in MALT lymphomas of different sites. Leukemia 18:1722–1726
18. Thieblemont C, Bastion Y, Berger F, Rieux C, Salles G, Dumontet C, Felman P, Coiffier B (1997) Mucosa-associated lymphoid tissue gastrointestinal and nongastrointestinal lymphoma behavior: analysis of 108 patients. J Clin Oncol 15: 1624–1630
19. Uno T, Isobe K, Shikama N, Nishikawa A, Oguchi M, Ueno N, Itami J, Ohnishi H, Mikata A, Ito H (2003) Radiotherapy for extranodal, marginal zone, B-cell lymphoma of mucosa-associated lymphoid tissue originating in the ocular adnexa: a multiinstitutional, retrospective review of 50 patients. Cancer 98:865–871

Virchows Arch (2006) 448: 366–368
DOI 10.1007/s00428-005-0119-8

CASE REPORT

R. K. Hejmadi · D. Gey van Pittius · M. Stephens · R. Chasty · M. Braithwaite

Angiolymphoid hyperplasia with eosinophilia (epithelioid haemangioma) occurring within multiple deep lymph nodes and presenting with weight loss and raised CA-125 levels

Received: 9 October 2005 / Accepted: 11 October 2005 / Published online: 29 November 2005

Abstract We report a case of angiolymphoid hyperplasia with eosinophilia (epithelioid haemangioma) involving multiple deep mediastinal, abdominal and intramammary lymph nodes in a 52-year-old woman with weight loss and raised CA-125 levels. The unusual clinical presentation with raised CA-125 levels and its occurrence within multiple deep visceral lymph nodes has never been reported in literature.

Keywords Epithelioid haemangioma · Raised CA-125 · Vascular lesion

Introduction

Epithelioid haemangiomas are circumscribed, superficial vascular lesions occurring in the dermis and subcutaneous tissue and clinically presenting as small red pruritic plaques [5]. Occasionally, they are reported in soft tissue, bone and vessels [3]. These lesions show specific histological features and carry a benign clinical behaviour [5].

Clinical history, material and methods and results

A 52-year-old woman presented with weight loss of approximately 6 kg over a period of 3 months. Clinical examination showed no significant findings, in particular, she was apyrexic and had no enlarged peripheral lymph nodes or hepatosplenomegaly. A detailed gynaecological examination showed no abnormality. She was a smoker and smoked ten cigarettes a day. Biochemical investigations showed a raised erythrocyte sedimentation rate of 80 and raised CA-125 levels, which initially measured 158 U/ml and later 190 U/ml (normal less than 35 U/ml). Haematological investigations showed a raised absolute eosinophil count of 4.26×10^9/l (normal 0.65×10^9/l). Chest x-ray showed mediastinal widening. Computerised tomography (CT) scans showed numerous enlarged lymph nodes in the upper central mediastinum, paratracheal, subcarinal and right paracardiac regions (Fig. 1). The largest node measured up to 2.2×1.8 cm. A few smaller abdominal nodes were seen in the coeliac, peripancreatic and para-aortic areas, the largest node measured 1×1.8 cm. No pelvic abnormality was identified. The overall imaging findings suggested a lymphoma. Biopsies from the mediastinal and paratracheal lymph nodes were performed. Multiple tissue pieces measuring 13 and 15 mm in aggregate were received. Both biopsies comprised abundant varying sized proliferating vessels arranged in a fibrotic stroma with numerous incorporated eosinophils and few haemosiderin-containing histiocytes. The endothelial cells lining the vessels showed a striking epithelioid/histiocytoid morphology with large ovoid nuclei, small nucleoli and abundant eosinophilic cytoplasm (Figs. 2 and 3). No Reed–Sternberg cells were seen, and no parasites were identified. One of the biopsies included lymphoid tissue with follicular hyperplasia. On immunohistochemical staining, the epithelioid cells were positive for CD31 (1:20, clone JC70A, Dako, England) (Fig. 4) and CD34 (1:25, QBend10, Novocastra, England) and were negative for Cam 5.2 (1:5, Becton and Dickinson, England). The differential diagnosis was between epithelioid haemangioma (angiolymphoid hyperplasia with eosinophilia) and Kimura's disease. The microscopic features of prominent epithelioid cells lining small blood vessels accompanied by a heavy infiltrate of eosinophils favoured a diagnosis of epithelioid haemangioma; however, the presence of blood eosinophilia was described more commonly in Kimura's disease. Following

R. K. Hejmadi (✉)
Department of Histopathology, Central Pathology Laboratory,
University Hospital of North Staffordshire,
Hartshill Road, Hartshill,
Stoke-on-Trent, Staffordshire, ST4 7PA, UK
e-mail: rhej10@hotmail.com
Tel.: +44-1782-554662
Fax: +44-1782-554664

D. G. van Pittius · M. Stephens · R. Chasty · M. Braithwaite
University Hospital of North Staffordshire,
Stoke-on-Trent, Staffordshire, UK

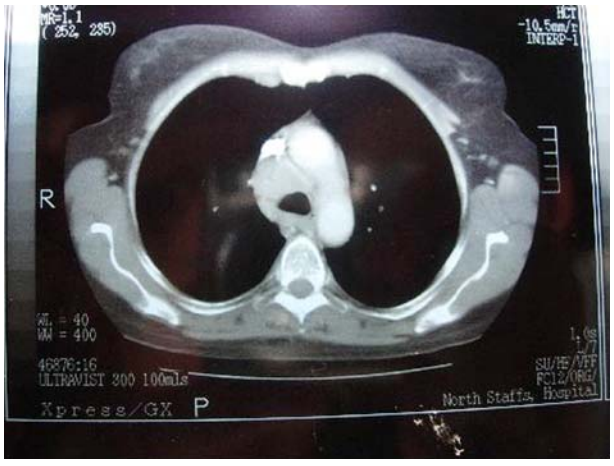

Fig. 1 CT scan of mediastinum showing enlarged nodular mass between the superior vena cava and trachea

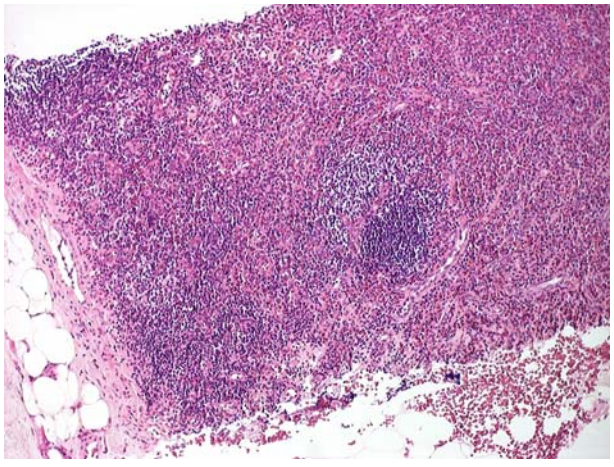

Fig. 2 Histology showing lymph node with capsule and lymphoid cells on the left and epithelioid haemangioma on the right (H & E, ×10)

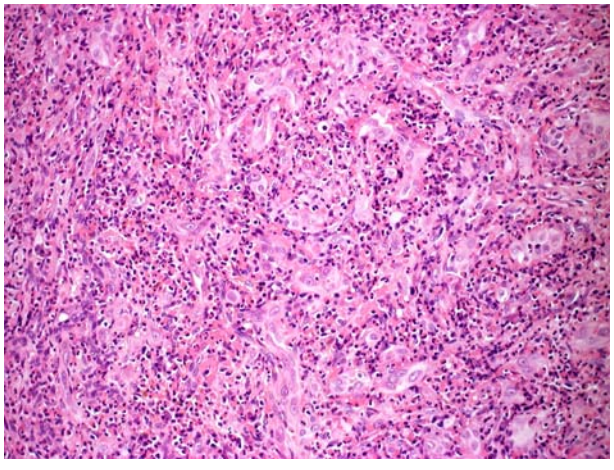

Fig. 3 Histology showing varying sized blood vessels lined by epithelioid cells. Numerous eosinophils are present in the background stroma. H & E, ×20

an expert referral, the case was diagnosed as an epithelioid haemangioma. Eleven months later, routine mammographic examination showed a shadow in the upper outer quadrant of her left breast. Ultrasound needle core biopsy which was subsequently performed showed partly effaced lymph node tissue with histological features of an epithelioid haemangioma as described earlier.

A year later, on follow-up, she was clinically stable and asymptomatic. On the CT scan, the nodes appeared stable without any increase in size.

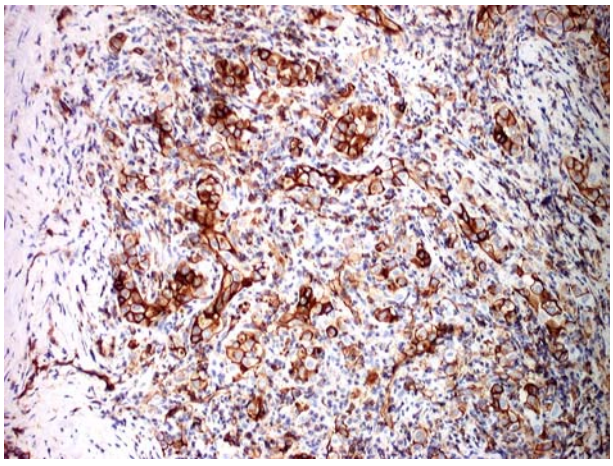

Fig. 4 Immunohistochemistry showing positive CD31 staining for epithelioid endothelial cells (×20)

Discussion

Epithelioid haemangioma is a distinct vascular lesion described initially by Wells and Whimster [6] in 1969 as subcutaneous angiolymphoid hyperplasia with eosinophilia. Contrary to our case, these lesions most commonly occur as solitary lesions in the dermal and subcutaneous regions over the head and neck [5]. Less commonly, they are known to occur at multiple superficial sites [2] and occasionally have also been reported in soft tissues, bone and vessels [3]. To the best of our knowledge, epithelioid haemangiomas have not been described in multiple deep mediastinal, abdominal and intramammary locations.

Our case presented with weight loss and, following a detailed investigation, also showed raised CA-125 levels. CA-125 levels are commonly raised in gynaecological malignancies; nevertheless, they can be raised in a few non-gynaecological benign conditions [1]. In our case, there was no evidence of gynaecological disease. Raised CA-125 levels and weight loss have not been described in epithelioid haemangiomas [1]. In this case, the weight loss and the rise in CA-125 levels are unexplained. On the CT scan, the multiple enlarged mediastinal and abdominal nodes, in addition to weight loss and raised CA-125 levels, are features clinically suggestive of a lymphoma or metastatic malignancy. The role of biopsy was crucial since the histological features were diagnostic of epithelioid haemangioma. The unusual site and the distribution of disease combined with the histological features also raised the differential diagnosis of Kimura's disease, Hodgkin lymphoma and parasitic infections. The morphological and

immunohistochemical features excluded Hodgkin lymphoma, and no parasites were identified. Kimura's disease is endemic in the Asian population and is often present in Oriental males as nodules not confined to the head and neck with high incidence of contiguous lymphadenopathy [5]. Presence of blood eosinophilia, although known to occur in both conditions, has been described more commonly in Kimura's disease [5]. Kimura's disease and epithelioid haemangioma both have an eosinophil-rich lymphoid infiltrate [5]. However, a prominent vascular component lined by plump epithelioid endothelial cells is characteristic of epithelioid haemangioma [5]. This feature is classically absent in Kimura's disease, in which the inflammatory infiltrate typically overshadows vessels lined by more attenuated endothelial cells [5]. Kimura's disease and epithelioid haemangiomas were formerly thought to be identical but are now regarded as two entirely unrelated lesions [4, 5]. Our case further blurs the division of these entities with an unusual presentation of epithelioid haemangioma. Another entity that should be excluded on morphological grounds is epithelioid haemangioendothelioma [2]. In our case, the absence of pleomorphism in the endothelial cells excludes the possibility of a haemangioendothelioma.

Our main aim is to report a unique case of angiolymphoid hyperplasia with eosinophilia (epithelioid haemangioma) occurring in multiple deep lymph nodes within the mediastinum, abdomen and intramammary locations with an unusual clinical presentation of weight loss and raised CA-125 levels. Both these aspects were never described previously.

Acknowledgement We thank Professor CDM Fletcher (Brigham and Women's Hospital, USA) for his expert histological opinion in this case.

References

1. Buamah P (2000) Benign conditions associated with raised CA-125 concentration. J Surg Oncol 75:264–265
2. Olsen TG, Helwig EB (1985) Angiolymphoid hyperplasia with eosinophilia. A clinicopathologic study of 116 cases. J Am Acad Dermatol 12:781–796
3. Rosai J, Gold J, Landry R (1979) The histiocytoid haemangiomas. A unifying concept embracing several previously described entities of skin, soft tissue, large vessels, bone and heart. Hum Pathol 10:707–730
4. Urabe A, Tsuneyoshi M, Enjoji M (1987) Epithelioid haemangioma versus Kimura's disease. A comparative clinicopathologic study. Am J Surg Pathol 11:758–766
5. Weiss SA, Goldblum JR (2001) Benign tumors and tumor-like conditions of blood vessels. In: Enzinger FM, Weiss SW (eds) Soft tissue tumours, 4th edn. Mosby, St. Louis, pp 837–889
6. Wells GC, Whimster IW (1969) Subcutaneous angiolymphoid hyperplasia with eosinophilia. Br J Dermatol 81:1–15

Virchows Arch (2006) 448: 369–374
DOI 10.1007/s00428-005-0115-z

CASE REPORT

Boris Dominik Jülg · Sven Weidner · Doris Mayr

Pulmonary manifestation of a Langerhans cell sarcoma: case report and review of the literature

Received: 4 October 2005 / Accepted: 10 October 2005 / Published online: 22 November 2005

Abstract In the following, we describe the very rare case of Langerhans cell sarcoma (LCS) in the lung. Throughout the medical literature, only a few cases have been published, and, to the best of our knowledge, this is the first case to be reported in Germany. The patient was an 81-year-old man who showed symptoms such as chronic cough and weight loss. Clinical examination including needle biopsy indicated a high possibility of carcinoma in the right lung and in the mediastinum; however, the final histopathological diagnosis after immunohistochemistry gave evidence of LCS. LCS is a neoplastic proliferation of Langerhans cells with malignant cytological features exhibiting a very aggressive behaviour. LCS can be distinguished from other carcinomas, lymphomas and sarcomas by the typical morphological features of Langerhans cells and the immunophenotype with a consistent expression of S-100 protein and CD1a. In contrast to Langerhans cell histiocytosis, the LCS consists of Langerhans cells with high atypia and a very high mitotic rate.

Keywords Langerhans cell sarcoma · Histiocytosis · S-100 protein · CD1a

Introduction

Neoplasms deriving from dendritic or histiocytic cells occur rarely. These cells are members of the family of immune accessory cells whose primary role is to present antigen to lymphocytes. Although they share a common CD34+ stem cell with macrophages, the lineage is separate. Parts of the family are Langerhans cells of the skin, interdigitating cells and veiled cells, which are regarded as different stages of evolution of the same cell type [10]. Others are the follicular dendritic cells, which are presumably derived from lymph node stromal cells rather than from a haematopoetic precursor cell, although this is still under discussion. In addition, interstitial dendritic cells can be distinguished, which represent the counterpart of Langerhans cells in parenchymal organs [9]. The World Health Organization (WHO) classification of histiocytic and dendritic cell neoplasms differentiates between histiocytic sarcoma, Langerhans cell histiocytosis, Langerhans cell sarcoma, interdigitating dendritic cell sarcoma/tumour, follicular dendritic cell sarcoma (FDCS)/tumour and dendritic cell sarcoma, not otherwise specified [12]. To distinguish the different types, a combination of morphologic and immunophenotypic characterization is necessary. Langerhans cells are positive for CD1a and S-100 protein, negative for CD21, CD35 and CD68, and show Birbeck granules (subdomains of the endosomal-recycling compartment) ultrastructurally. Veiled cells show the same phenotype as Langerhans cells, but have neither Birbeck granules nor complex interdigitating cellular junctions. Interdigitating dendritic cells are positive for S-100 protein and CD68 and negative for CD1a, CD21 and CD35, thus revealing complex interdigitating cellular junctions. The follicular dendritic cells are CD21+, CD35+, CD1a− and S-100 protein+ or −, and they show desmosomes ultrastructurally [12].

Especially neoplasms of the Langerhans cell phenotype occur rarely; hence, only 14 cases of Langerhans cell sarcoma (LCS) have been reported in previous research (see Table 1). Usually LCSs show a multi-organ involvement, including lymph nodes, liver, spleen, lung and bone. This paper reports a case of an LCS arising in the lung of an 81-year-old man and reviews the existing literature concerning these neoplasms.

Case report

An 81-year-old white man was seen at the Medizinische Poliklinik, Ludwig-Maximilian-University, Munich, reporting a chronic cough which he had first noticed 3 months before and a weight loss of 10 kg over the last

B. D. Jülg (✉) · S. Weidner
Medizinische Poliklinik, Ludwig Maximilian University,
80336 Munich, Germany
e-mail: boris.juelg@med.uni-muenchen.de
Tel.: +49-89-51603556
Fax: +49-89-51603379

D. Mayr
Institute of Pathology, Ludwig Maximilian University,
Munich, Germany

Table 1 Summary of reported cases of Langerhans cell sarcoma

Authors	Gender/age (year)	Site/symptoms	Therapy	Outcome
Wood et al. [13]	M/71	Cutaneous, lung	Chemotherapy	Died of disease at 2 months
Elleder et al. [3]	F/NA	Cutaneous and mucosal tumors	NA	NA
Delabie et al. [2]	F/23	Inguinal, iliac and retroperitoneal adenopathies + skin lesions + interstitial lung involvement	Chemotherapy	Died of disease
Tani et al. [11]	F/49	Skin, inguinal adenopathy	Chemotherapy	Died of disease
Lauritzen et al. [8]	M/38	Skin, lymph nodes, lung	Chemotherapy	Partial remission after 12 months
Itoh et al. [6]	F/74	Skin (erythematous plaque), axillary adenopathy	Surgery + radiotherapy + Chemotherapy	Died at 14 months
Pileri et al. [9]	F/17	Cervical, groin, iliac and retroperitoneal adenopathies + systemic symptoms	Chemotherapy + radiotherapy on the abdomen	Alive in complete remission
	M/46	Submandibular and left cervical adenopathies	Chemotherapy	Alive with disease
	M/28	Fever + cytopenia + anterior mediastinal mass + hepatosplenomegaly	None	Died at 3 weeks
	F/50	Skin (multiples nodules)	NA	NA
	F/10	Skin (single nodule)	Surgery + radiotherapy	Alive in complete remission
	F/65	Generalized adenopathies + hepatosplenomegaly + lung lesions	Chemotherapy	Died of disease
	M/72	Fever, mediastinal and axillary adenopathies + lung nodules + rib fractures + CNS lesions	Chemotherapy	Died of disease
	F/50	Polyostotic bone lesions (skull and right occipital region)	Surgery	Alive in complete remission
Present case	M/81	Mediastinal mass + interstitial lung involvement	Chemotherapy	Died at 4 weeks

F Female, *M* male, *NA*, not available, *CNS* central nervous system

4 months. Physical examination revealed a pulmonary infiltration, which, on computed tomography (CT) scan (Fig. 1) was identified as a mass lesion occupying the lower lobe of the right lung and mediastinum with radiologic signs of a generalized lymphangitic spread (Fig. 2). Laboratory data on admission were within normal limits except for a leukocytosis with 24 G/l (4-11G/l), an elevated C-reactive protein with 11.4 mg/dl (<0.50 mg/dl) and a hyponatremia of 125 mmol/l (135–145 mmol/l). The patient's lingering smoking habit and the clinical results raised the suspicion of a bronchogenic carcinoma causing a paraneoplastic syndrome of inappropriate anti-diuretic hormone (SIADH) secretion. A bronchoscopy was performed, revealing a tumoural lesion located in the right main bronchus. A biopsy was performed, and the specimen was sent to the Institute of Pathology, University of Munich, for histological examination.

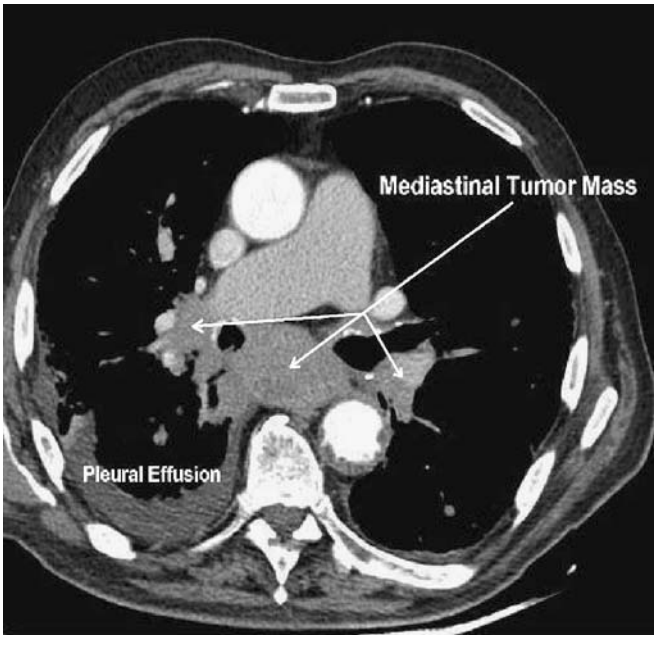

Fig. 1 CT scan of the chest showing a mass in the mediastinum and a small pleura effusion of the right lung

Materials and methods

The paraffin-embedded 13 specimens (diameter together 1 cm) were cut at 2–3 μm and mounted on SuperFrost/Plus microscopic slides (Menzel, Germany). After deparaffiniza-

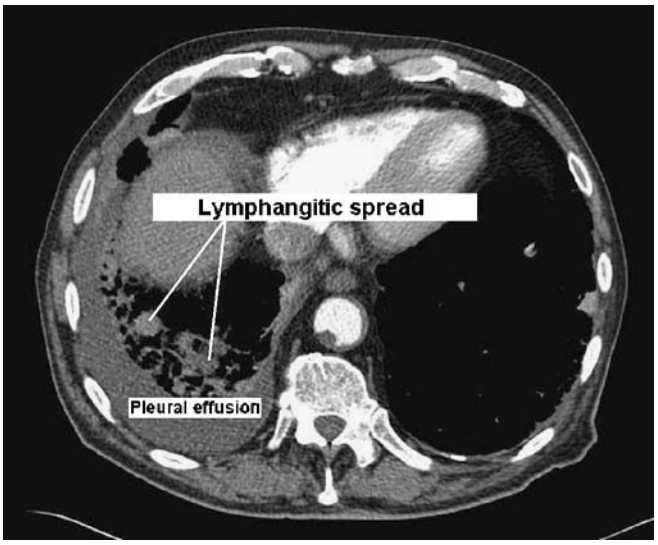

Fig. 2 Lymphangitic spread

tion and rehydration, staining for haematoxylin–eosin, giemsa, iron, silver and elastic van Gieson (EVG) as well as immunohistochemical assays for a wide panel of antibodies were performed by standard methods (see Table 2).

For electron microscopy, following deparaffinization, the tissue was buffered in osmium tetroxide, dehydrated in ethanol and embedded in EPON 812 (SERVA Electrophoresis GmbH, Heidelberg, Germany). To gain a first overall impression, methylene/azur staining of tissue sections with 0.5 μm were performed, then ultrathin sections with 80–100 nm were prepared, stained with uranyl acetate–lead citrate and examined using a transmission electron microscope (EM420; Philips, Eindhoven, the Netherlands).

Pathological findings

Microscopy

The specimens consisted of multiple parts of a highly cellular tumour, which was composed of enlarged round cells arranged primarily in compact, cohesive pattern. The neoplastic cells had lightly eosinophilic and partly vacuolized cytoplasm with ill-defined cell borders. The tumour cell nuclei were large and very variable in size. They ranged between round and oval, grooved and lobulated with delicate membranes, showing chromatin abnormalities and prominent nucleoli (see Fig. 3). The mitotic rate was very high. Partial necrosis surrounded by a granulocytic infiltration was identified. The neoplasm was not encapsulated and extended up to the epithelium. A characteristic feature of the tumour was the presence of small mature lymphocytes, a few plasma cells and very few eosinophils dispersed throughout the process. The remaining lung and the bronchial mucosa were unremarkable.

Table 2 Primary antibodies used with their marked cells, dilution, source, system and results in tumor cells

Antibody	Marker	Dilution	Source	System	Clone	Results
CD1a	Langerhans	Cells 1:20	Novocastra	LSAB	MTB1	+++
CD3	Lymphocytes (T type)	1:300	DakoCytomation	LSAB	F7.2.38	−
CD4	Lymphocytes (T type)	1:40	Biozol	LSAB	4B12	+
CD8	Lymphocytes (T type)	1:100	DakoCytomation	LSAB	C8/144 B	−
CD20	Lymphocytes (B type)	1:60	Immunotech	APAAP	L26	−
CD25	Activated lymphocytes	1:250	Quartett	LSAB	IL2R	−
CD30	Activated lymphocytes	1:150	Novocastra	LSAB	1G12	−
CD34	Haematopoetic progenitor cells	1:60	Serotec	APAAP	QBEND 10	−
CD45	Leukocyte common antigen	1:150	DakoCytomation	APAAP	2B11 + PD7/26 +	+
CD56	Natural killer cells	1:50	Novocastra	LSAB	1B6	−
CD68	Pan-macrophage	1:100	DakoCytomation	APAAP	KP1	+
CD79a	Lymphocytes (B type)	1:30s	Eurodiagnostics	APAAP	MB1	−
MPO	Myeloperoxidase	1:1500	DakoCytomation	LSAB	Polyclonal	−
S100	Dendritic cell	1:400	DakoCytomation	LSAB	Polyclonal	+++
Ki-67	Antigen proliferation marker	1:50	DakoCytomation	APAAP	MIB-1	70%
Aktin	α-Smooth muscle actin	1:500	Cymbus	LSAB	ASM-1	−
Pancytokeratin	Epithelial cells	1:1200	BMA-Dianova	APAAP	Lu-5	−
Vimentin	Stroma cells	1:100	DakoCytomation	APAAP	V9	+
HMB45	Melanoma	1:100	ENZO	LSAB	HMB45	−
Melan A	Melanoma	1:1500	Biogenex	LSAB	A103	−
TTF1	Thyroid transcription factor	1:100	DakoCytomation	APAAP	8G7G3/1	−
Chromogranin	Neuroendocrine cells	1:100	Novocastra	LSAB	DAK-A3	−

LSAB Avidin–biotin complex (Dako), *APAAP* alkaline phosphatase–anti-alkaline phosphatase (Dako), + weak reactivity, ++ moderate reactivity, +++ strong reactivity, − negative reactivity

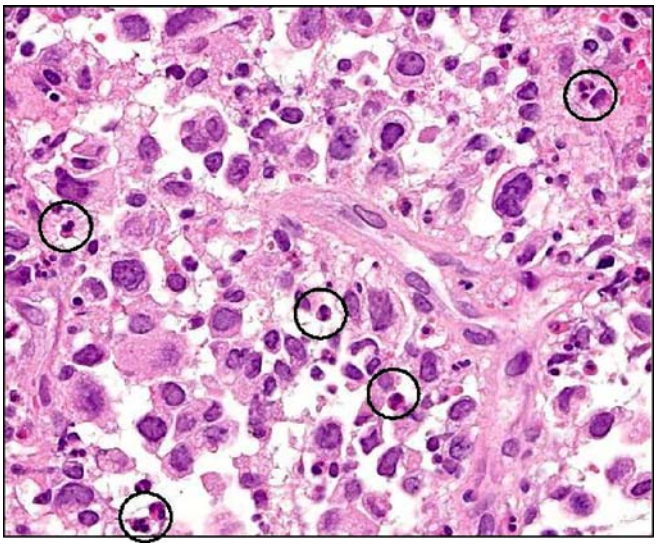

Fig. 3 Haematoxylin–eosin staining, magnification 40× objective, *black circles* mark eosinophiles

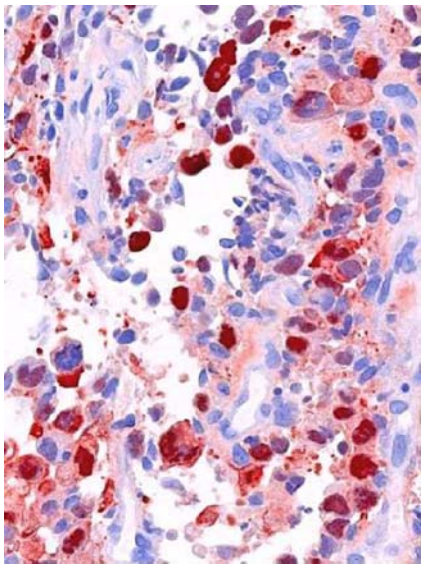

Fig. 5 S-100 protein staining, magnification 40× objective

Immunohistochemistry

The immunohistochemical results are summarized in Table 2. Tumour cells were strongly positive for CD1a and S-100 protein (see Figs. 4 and 5), as well as slightly positive for Vimentin. Focally, there was a very weak expression of CD45, CD68 and CD4. The proliferation marker Ki67 reached 70% (Fig. 6). The tumour cells failed to express Pancytokeratin, thyroid transcription factor (TTF1), HMB-45, Melan A, Aktin, CD3, CD25, CD 30, CD 34 and Chromogranin.

Electron microscopy

Ultrastructural examination showed round tumour cells with regular substructures suitable to Langerhans cells morphology. The cytoplasm of the cells contained non-branching, rough endoplasmic reticulum and small mitochondria.

Birbeck granules could not be identified, possibly due to the fact that the biopsy was previously paraffin embedded and damaged during the fixation process.

Diagnosis

In consideration of histomorphological findings and immunohistochemical staining, a tumour of Langerhans cell origin was diagnosed 1 week after admission to the hospital. The malignant cytologic features and the very high proliferation rate suggested a Langerhans cell sarcoma. The absence of Birbeck granules was explained by the unavailable examination of fresh tissue and the reduced quality of the biopsy.

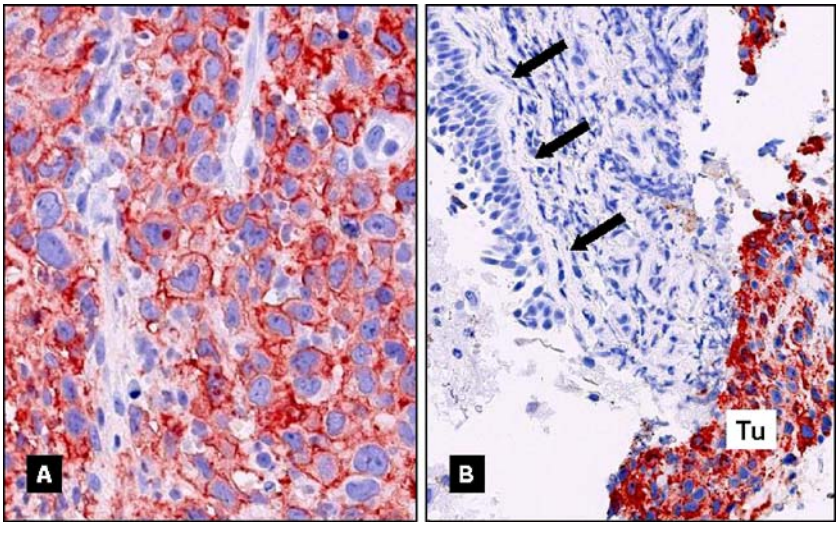

Fig. 4 Immunohistrochemistry for CD1a, magnification **a** 100× objective, **b** 40× objective; *black arrows* mark CD1a-negative bronchial epithelium; *Tu*, tumor

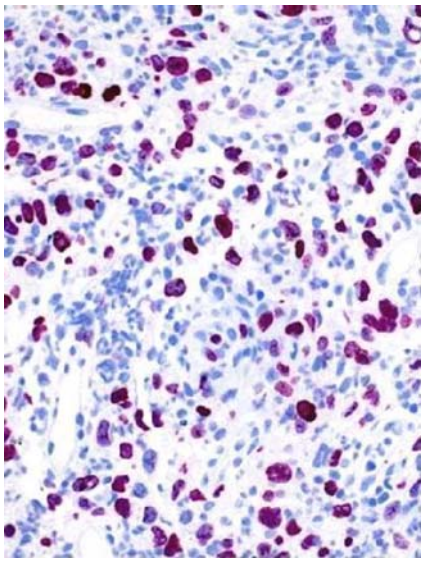

Fig. 6 Ki-67 antigen staining, magnification 40×

Treatment

After diagnosis of a Langerhans cell sarcoma (LCS), the existence of other manifestation sites of the LCS besides suspicious lymph nodes para-aortal and cervical (up to 2 cm) was excluded by brain and abdominal CT scans as well as by skeletal szintigraphy. Particularly the skin was normal. Chemotherapy was started using cyclophosphamide, prednisolone, adriamycin and vincristin (CHOP) in a standard dose adapted to the common lymphoma treatment protocols. Due to the tumoural growth, a stenosis of the right middle lobe bronchus had caused a retention pneumonia. Therefore, a second bronchoscopy was performed to accomplish a laser photocoagulation combined with an endotracheal after loading therapy. Following initial recovery, 10 days after the first cycle of CHOP, the patient developed a severe neutropenia with multiple infectious complications, in particular, a fungal infection of the lung. Despite extensive anti-microbial and anti-fungal therapy, the patient's general condition worsened, and he died of severe infectious complications 1 week later. An autopsy was not permitted by his family.

Discussion

Neoplasms of dendritic or histiocytic cells are extremely rare [4]. To the best of our knowledge, Wood et al. [13] published the first case report of a LCS in 1984. His 71-year-old patient showed a diffuse pulmonary infiltration alongside multiple nodules of the skin, each with an infiltration by Langerhans cells in histological specimens [13].

In 1991 Ben-Ezra et al. [1] reported the results of a study of 31 patients with a neoplasm of Langerhans cells. Taking into account characterized morphology and clinical course, they divided the patients into four groups. In this case, immunohistochemical staining for CD1a on paraffin-embedded material was not possible. Hence, the Langerhans cells had to be identified by finding Birbeck granules. Subsequently, they came to the conclusion that some of the patients suffered under a malignant Histiocytosis X, indicated by highly atypical cytological features and a very aggressive course [1].

Nowadays, antibodies suitable for tissue immunohistochemistry and molecular genetic methods permit the identification of the cell of origin of the different types of histiocytic or dendritic neoplasms.

Malignant disorders of these cell lines derive from immune accessory cells of the peripheral lymphoid tissue. The majority of them involve lymph nodes, with a few cases reported in extranodal sites, like the lung or the skin [9]. The aforementioned neoplasms, in particular histiocytic or Langerhans cell sarcomas, behave in the typical biological way of malignant tumours, i.e. a locally aggressive solitary mass with the ability to recur and metastasize. Among dendritic-cell sarcomas, several subtypes are distinguished: sarcomas deriving from interdigitating reticulum cells and follicular dendritic cells described in several locations, such as lymph nodes, liver, skin and the bowel. Seventy-two cases of FDCS and interdigitating reticulum cell sarcoma (IDDCS) have been well documented [5]. Sarcomas of histiocytes, as well as sarcomas with Langerhans cell-like differentiation, have been described as bonafide neoplasms with aggressive features and poor response to therapy, occurring in a wide age range, including infants, children and adults. Nevertheless, differentiation between both cell types is possible by morphological, immunohistochemical and ultrastructural methods. Some researchers assume that the distinction is of no great significance, because the clinical behaviour of histiocytic sarcomas and Langerhans cell sarcomas appears similar [7].

In this case report, we are presenting a patient with a pulmonary tumour showing the immunohistochemical features (CD1a+, S-100 protein+ and only very weak CD68+) of a neoplastic proliferation of Langerhans cells. Due to technical reasons, no Birbeck granules could be identified, and, according to the WHO classification of histiocytic and dendritic cell neoplasms, Birbeck granules should theoretically be present in all cases of LCS in which "adequate examination can be carried out" [12], meaning that tumours with the abovementioned features and with no evidence of Birbeck granules should be classified as "dendritic cell sarcoma, not otherwise specified". Although this is probably a non-existent entity if cases are well studied. In our case, the tumour showed overtly malignant cytological features of Langerhans cells and a very high proliferation rate and was therefore classified as a Langerhans cell sarcoma. The absence of Birbeck granules was explained by the unavailable examination of fresh tissue and the reduced quality of the biopsy. The occurrence of Langerhans cells in the setting of other malignancies, as it has been described for cancer of the larynx [14], could be excluded due to the malignant phenotype of the Langerhans cells in this case.

Until the current day, a total of 15 cases considered as LCS, including the present case, have been reported and reviewed in medical literature [2, 3, 6, 8, 9, 11, 13]. In these

few cases, a wide diversity concerning age, site of occurrence, progression and applied treatments has been observed. The age ranges from 10 to 81 years, with a median age of 48 years and a female predominance (1:1.5). In nearly every case, lymph nodes were involved, although cases with extranodular sites were also published [9]. In most cases, chemotherapy was an essential part of the treatment, in particular, the use of drug combinations known for their efficiency in the treatment of lymphatic neoplasms are described. Overall, LCSs impress with their poor outcome. From 13 patients on whom follow-up data were available, eight (61.5%) died of their disease, only three (23%) patients survived in complete remission, one (7.7%) patient reached a partial remission and one (7.7%) patient lived with the disease.

Due to the small number of cases, no organized series of treatments for adults have been published. The diversity of applied treatments reported in medical literature makes it almost impossible to define an optimal strategy. Nevertheless, successful treatment is feasible with a variety of chemotherapy regimens. It is claimed that chemotherapy including steroids may help slow or even stop the progression of LCS.

To the best of our knowledge, only few cases of LCS have been documented in the English literature; however, we were unable to find any comparable case report in Germany. Our patient was an elderly man with an unusual case of LCS initially localized in the lung and mediastinum. Due to the advanced stage of the disease, an intensive therapy with chemotherapeutics and bronchoscopic interventions could not stop the progression of the tumour, and the patient died of respiratory insufficiency and severe infectious complications. Unfortunately the patient's family did not agree to an autopsy. Subsequently, the supposed extension of disease could not be examined.

Acknowledgement Prof. Müller-Höcker, Institute of Pathology, University of Munich, is acknowledged.

References

1. Ben-Ezra J, Bailey A, Azumi N et al (1991) Malignant histiocytosis X. A distinct clinicopathological entity. Cancer 68 (5):1050–1060
2. Delabie J, De Wolf-Peeters C, De Vos R et al (1991) True histiocytic neoplasm of Langerhans' cell type. J Pathol 163 (3):217–223
3. Elleder M, Fakan F, Hula M (1986) Pleiomorphous histiocytic sarcoma arising in a patient with histiocytosis X. Neoplasma 33 (1):117–128
4. Favara BE, Feller AC (1997) Contemporary classification of histiocytic disorders. Medical and pediatric. Oncology 29:157–166
5. Fonseca R, Yamakawa M, Nakamura S et al (1998) Follicular dendritic cell sarcoma and interdigitating reticulum cell sarcoma: a review. Am J Hematol 59(2):161–167
6. Itoh H, Miyaguni H, Kataoka H et al (2001) Primary cutaneous Langerhans cell histiocytosis showing malignant phenotype in an elderly woman: report of a fatal case. J Cutan Pathol 28 (7):371–378
7. Jason L, Hornick ES, Jaffe CD et al (2004) Extranodal histiocytic sarcoma: clinicopathologic analysis of 14 cases of a rare epithelioid malignancy. Am J Surg Pathol 28:1133–1144
8. Lauritzen AF, Delsol G, Hansen NE et al (1994) Histiocytic sarcomas and monoblastic leukemias. A clinical, histologic, and immunophenotypical study. Am J Clin Pathol 102(1):45–54
9. Pileri SA, Grogan TM, Harris NL et al (2002) Tumours of histiocytes and accessory dendritic cells: an immunohistochemical approach to classification from the International Lymphoma Study Group based on 61 cases. Histopathology 41:1–29
10. Pillay K, Solomon R, Daubenton JD, Sinclair-Smith CC (2004) Interdigitating dendritic cell sarcoma: a report of four paediatric cases and review of the literature. Histopathology 44(3):283–291
11. Tani M, Ishii N, Kumagai M et al (1992) Malignant Langerhans cell tumour. Br J Dermatol 126(4):398–403
12. Travis WD, Brambilla E, Müller-Hermelink HK, Harris CC (2004) WHO, pathology & genetics. Tumours of the lung, pleura, thymus and heart. IARC Press, Lyon
13. Wood C, Wood GS, Deneau DG et al (1984) Malignant histiocytosis X. Report of a rapidly fatal case in an elderly man. Cancer 54(2):347–352
14. Yilmaz T, Gedikoglu G, Celik A et al (2005) Prognostic significance of Langerhans cell infiltration in cancer of the larynx. Otolaryngol Head Neck Surg 132(2):309–316

Virchows Arch (2006) 448: 375–378
DOI 10.1007/s00428-005-0127-8

CASE REPORT

Wilfried Roth · Dietrich Bucsenez · Hendrik Bläker · Irina Berger · Philipp A. Schnabel

Misalignment of pulmonary vessels with alveolar capillary dysplasia: association with atrioventricular septal defect and quadricuspid pulmonary valve

Received: 12 October 2005 / Accepted: 25 October 2005 / Published online: 6 December 2005

Abstract Misalignment of pulmonary vessels (MPV) with alveolar capillary dysplasia (ACD) is a complex congenital vascular abnormality in newborn infants. This condition is often associated with persistent pulmonary hypertension, which leads to severe respiratory distress and finally to the death of the newborn. Here, two cases of MPV with ACD are reported that were associated with atrioventricular septal defects. Both cases showed a combination of a large atrial septal defect and a smaller subvalvular ventricular septal defect. In one newborn, the cardiac malformation was accompanied by a quadricuspid pulmonary valve. These cases emphasize the importance of considering MPV with ACD a possible cause for pulmonary hypertension in the newborn, especially when a concomitant atrioventricular septal defect could represent an alternative explanation for the pulmonary hypertension.

Keywords Alveolar capillary dysplasia · Misalignment of lung vessels · Persistent pulmonary hypertension of the neonate · Atrioventricular septal defects · Quadricuspid pulmonary valve

W. Roth · H. Bläker · I. Berger · P. A. Schnabel
Institute of Pathology, University Hospital,
Im Neuenheimer Feld 220/221,
69120 Heidelberg, Germany

W. Roth (✉)
German Cancer Research Center (DKFZ),
Im Neuenheimer Feld 280,
69120 Heidelberg, Germany
e-mail: Wilfried.Roth@med.uni-heidelberg.de
Tel.: +49-6221-562647
Fax: +49-6221-423630

D. Bucsenez
University Children's Hospital,
Im Neuenheimer Feld 153,
69120 Heidelberg, Germany

Introduction

Persistent pulmonary hypertension of the newborn (PPHN) is caused by a variety of diseases including pneumonia, hyaline membrane disease, meconium aspiration, fetal hypoxia or surfactant deficiency. Similarly, congenital heart diseases such as ventricular septal defects, patent ductus arteriosus Botalli or the transposition of great arteries result in high pressure and increased flow in the pulmonary circulation. In rare cases, PPHN is the consequence of a misalignment of pulmonary vessels (MPV) with or without alveolar capillary dysplasia (ACD) [10]. Morphologically, MPV is characterized by pulmonary veins being closely associated with pulmonary arteries and bronchi (for review, see [8]). In contrast, ACD is caused by a loss of alveolar capillaries and dysplasia of alveolar walls leading to a severe impairment of the normal air–blood barrier. In most cases, ACD is associated with MPV [11], but there have also been reports of ACD without MPV [4]. To date, 73 cases of MPV/ACD are reported in the English literature. This congenital disease presents clinically as pulmonary hypertension of the newborn infants, with the cardinal symptom being respiratory failure [7]. Moreover, MPV with ACD is often accompanied by other congenital abnormalities, e.g. of the cardiovascular system or gastrointestinal tract. The present report describes two newborn infants presenting with PPHN caused by MPV with ACD. Both had a concomitant atrioventricular septal defect (AVSD); in one case it was associated with a quadricuspid pulmonary valve.

Clinical history

Case 1 A full-term, 3,130-g baby girl was delivered after a normal pregnancy. One day after delivery, she developed increasing respiratory distress and cyanosis. Echocardiography showed an atrioventricular septal defect with a large atrial and a small ventricular (approximately 3 mm) component. Cardiac catheterization confirmed the diagnosis of atrioventricular septal defect and pulmonary hypertension (pulmonary wedge pressure of 8 mmHg). The respiratory

distress deteriorated, and, because of suspected neonatal sepsis, antibiotic treatment was started. Despite aggressive management of pulmonary hypertension with sedation, analgesia, 100% oxygen, relaxation, hyperventilation, NO inhalation, intravenous prostacyclin and catecholamines, the cardiopulmonary status progressively deteriorated, and the infant expired on the 30th day.

Case 2 A dystrophic newborn girl was delivered in week 38 of the pregnancy. Echocardiography showed an atrioventricular septal defect with a large atrial and a medium-sized ventricular (approximately 5 mm) component and a severe right-to-left shunt. Seven hours after delivery, the newborn showed rapid ventilatory deterioration and a progressive, severe cyanosis. After pulmonary hypertension was diagnosed, 100% oxygen, relaxation, analgesia, sedation, hyperventilation, NO inhalation, intravenous prostacyclin and catecholamines were administered. Genetic testing resulted in the diagnosis of a triple X mosaic constellation (47,XXX). The subsequent course was complicated by oliguria and a capillary leak syndrome, renal vein thrombosis and septicaemia. The newborn died in protracted cardiac failure and due to the capillary leak syndrome on day 23.

Materials and methods

After the autopsy of the newborn infants, several tissue samples from the lungs and other organs were fixed in formalin and embedded in paraffin: case 1 (autopsy limited to thoracic organs): heart, three samples; lungs, eight samples; thymus, one sample; case 2: heart, three samples; lungs, five samples; liver, one sample; spleen, one sample; kidneys, two samples; bone tissue, one sample. Microscopic examination of paraffin-embedded sections (2–3 μm) was performed following standard staining procedures with hematoxylin and eosin, Elastica van Gieson or Masson's trichrome. Immunohistochemical staining was performed using a Techmate 500+ automated immunostainer (Dako-Cytomation, Hamburg, Germany) with an avidin–biotin complex peroxidase-detection system. The antibody specific for human muscle actin (HHF35, dilution 1:2) was obtained from Loxo (Dossenheim, Germany). Negative controls included sections in which the primary antibody was omitted.

Results

In the autopsy, case 1 presented with an atrioventricular septal defect, which was approximately 9 mm in diameter (Fig. 1a). The major defect was found in the atrial septum, whereas a minor cleft-like lesion (approximately 4 mm in diameter) extended to the ventricular septum and disrupted the common atrioventricular valve (arrow). The right atrium and ventricle were dilated, and the right ventricle wall showed a substantial hypertrophy (0.6 cm, right ventricle; 0.4 cm, left ventricle). The weight of the heart was slightly increased (25 g). The pulmonary valve was quadricuspid without signs of pulmonary stenosis (Fig. 1b). The aortic valve did not show any abnormalities. The lungs showed a marked increase of consistency and weighed 40 g (right) and 50 g (left). The other organs did not exhibit any abnormal findings in the macroscopic examination. Case 2 showed an atrioventricular septal defect very similar to the one described for case 1 except for the slightly bigger size of the ventricular component (diameter, 6 mm). The pulmonary valve was normally tricuspid. However, the intestinal tract exhibited the characteristics of a malrotation type I, with the caecum located in the right upper abdomen.

On histological examination, the lungs of both cases showed very similar morphological alterations. The small pulmonary veins were closely accompanied by muscular arteries and bronchi, partly sharing a common adventitial envelope (Fig. 2a). Even very peripheral pulmonary arterioles showed strong muscularization as demonstrated by immunohistochemical detection of smooth muscle actin (Fig. 2b). The diameter of arteries and arterioles at the level of the terminal and respiratory bronchioli ranged between 100 and 150 and 30 and 60 μm, respectively. There was no evidence of intimal hyperplasia, advanced stages of plexogenic arteriopathy or AV fistula. In contrast, pulmonary venules tended to be wide and thin-walled. The number of

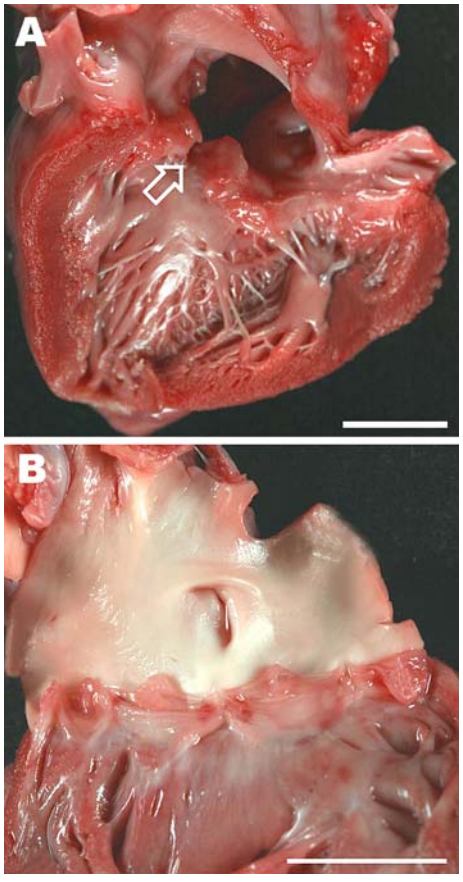

Fig. 1 **a** Atrioventricular septal defect with a large defect of the atrial septum and a smaller, cleft-like defect in the upper ventricular septum (*arrow*). **b** Quadricuspid pulmonary valve. Scale bar=1 cm

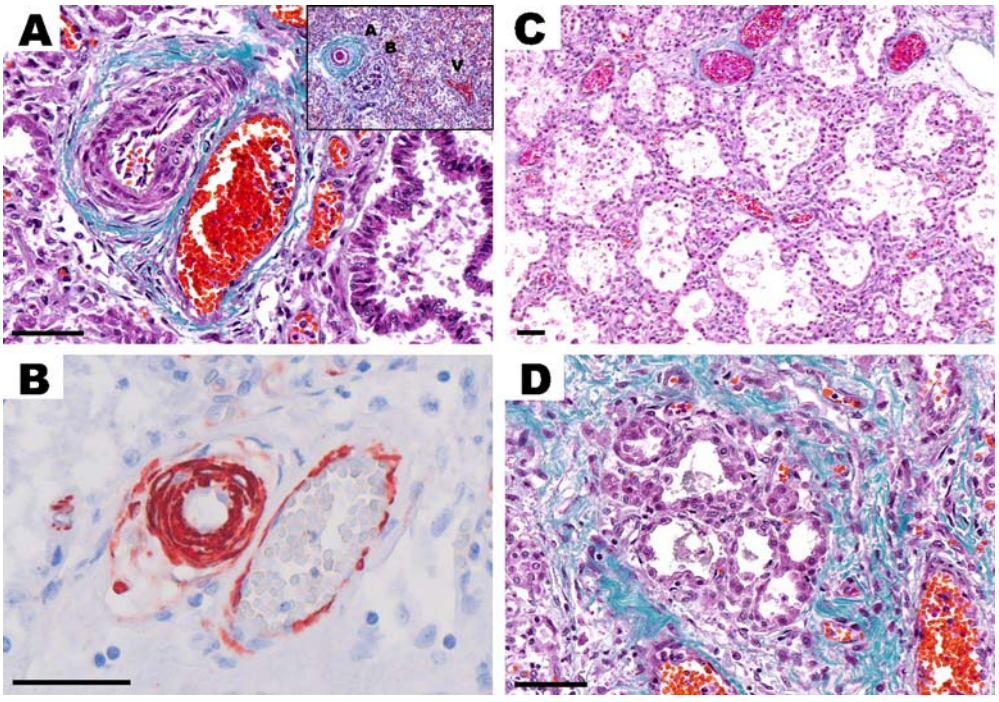

Fig. 2 **a** Lung tissue from the upper right lobe showing misalignment of pulmonary vessels: close apposition of a pulmonary artery and a pulmonary vein with partly common adventitia. The pulmonary vein, normally located within the lung septa, lies between the artery (*left*) and a bronchus (*right*) (Masson's trichrome, ×200). *Inset*: In contrast, lung tissue of a newborn without pulmonary disease demonstrates the normal lung architecture: arteries (**a**) are accompanied by bronchi (**b**), whereas veins run separately. **b** Immunohistochemical detection of smooth muscle actin demonstrates the anomalous placement of a thin-walled venule lying directly adjacent to an arteriole showing muscularization and medial hypertrophy (×350). **c**, **d** Lung tissue exhibiting alveolar capillary dysplasia: thickened alveolar septa with interstitial fibrosis and a reduction of alveolar capillaries. Normal alveoli are replaced by irregular air spaces which are lined by a cuboidal epithelium (**c** H&E, ×60; **d** Masson's trichrome, ×200). Scale bar=100 μm

alveolar capillaries was reduced, and the alveolar septa showed marked thickening, producing irregularly formed air spaces (Fig. 2c). These spaces were lined by a cuboidal epithelium (Fig. 2d). In general, there was diffuse prominent interstitial and periadventitial lung fibrosis. The histological examination of the heart (case 1) showed marked myocyte hypertrophy in the right ventricle wall, partly accompanied by bizarre nuclei of myocytes.

Discussion

ACD and MPV were first described by Janney et al. [7] and Wagenvoort [11], respectively. Both conditions mostly occur together and might represent two different manifestations of the same developmental disease. The precise aetiology of this disease is not known, but alveolar proteinosis due to a mutation in the surfactant protein B gene has been suggested to play an important role [12]. Although most cases of MPV with ACD are sporadic, there are also reports of familial cases that point to the relevance of genetic mutations [1, 3, 6]. The present report describes two newborn infants who clinically presented with PPHN and died of respiratory decompensation shortly after delivery. Both patients had the typical microscopic features of MPV and ACD. Both cases reported here showed very similar atrioventricular septal defects, and in one case, this defect was accompanied by a quadricuspid pulmonary valve. Many of the reported MPV/ACD cases are associated with other anomalies (for review, see [2]). The cardiac abnormalities in newborns with MPV with ACD include hypoplastic left heart syndrome, bicuspid aortic valve and coarctation of the aorta [4, 9]. To our knowledge, the association of MPV/ACD, AVSD and quadricuspid pulmonary valve has not been reported before. Moreover, the cases described in the present report are of particular clinical interest, since both MPV/ACD and ventricular septal defects are accompanied by pulmonary hypertension. In the case of pulmonary hypertension due to a ventricular septal defect, histological examination shows media hypertrophy of muscular arteries, muscularization of arterioles, and plexiform lesions, but not misalignment of lung vessels or alveolar dysplasia [5]. Moreover, although morphological changes in bronchopulmonary dysplasia in the infant respiratory distress syndrome (IRDS) can resemble those in ACD, the reduction (or even loss) of capillaries is much more prominent in ACD. In cases with pulmonary hypertension and known ventricular septal defects, MPV with ACD has to be considered as an infrequent, but yet important differential diagnosis. A lung biopsy should be performed to histologically confirm MPV with ACD.

References

1. Abdallah HI, Karmazin N, Marks LA (1993) Late presentation of misalignment of lung vessels with alveolar capillary dysplasia. Crit Care Med 21:628–630
2. Alameh J, Bachiri A, Devisme L, Truffert P, Rakza T, Riou Y, Manouvrier S, Lequien P, Storme L (2002) Alveolar capillary dysplasia: a cause of persistent pulmonary hypertension of the newborn. Eur J Pediatr 161:262–266
3. Boggs S, Harris MC, Hoffman DJ, Goel R, McDonald-McGinn D, Langston C, Zackai E, Ruchelli E (1994) Misalignment of pulmonary veins with alveolar capillary dysplasia: affected siblings and variable phenotypic expression. J Pediatr 124:125–128
4. Garola RE, Thibeault DW (1998) Alveolar capillary dysplasia, with and without misalignment of pulmonary veins: an association of congenital anomalies. Am J Perinatol 15:103–107
5. Gorenflo M, Ullmann M, Sebening C, Brockmeier K, Hagl S, Ulmer HE, Otto HF, Schnabel PA (2002) The index of pulmonary vascular disease in children with congenital heart disease: relationship to clinical and haemodynamic findings. Virchows Arch 441:264–270
6. Gutierrez C, Rodriguez A, Palenzuela S, Forteza C, Rossello JL (2000) Congenital misalignment of pulmonary veins with alveolar capillary dysplasia causing persistent neonatal pulmonary hypertension: report of two affected siblings. Pediatr Dev Pathol 3:271–276
7. Janney CG, Askin FB, Kuhn C 3rd (1981) Congenital alveolar capillary dysplasia—an unusual cause of respiratory distress in the newborn. Am J Clin Pathol 76:722–727
8. Pucci A, Zanini C, Ferrero F, Arisio R, Valori A, Abbruzzese P, Forni M (2003) Misalignment of lung vessels: diagnostic role of conventional histology and immunohistochemistry. Virchows Arch 442:597–600
9. Rabah R, Poulik JM (2001) Congenital alveolar capillary dysplasia with misalignment of pulmonary veins associated with hypoplastic left heart syndrome. Pediatr Dev Pathol 4:167–174
10. Tibballs J, Chow CW (2002) Incidence of alveolar capillary dysplasia in severe idiopathic persistent pulmonary hypertension of the newborn. J Paediatr Child Health 38:397–400
11. Wagenvoort CA (1986) Misalignment of lung vessels: a syndrome causing persistent neonatal pulmonary hypertension. Hum Pathol 17:727–730
12. Wallot M, Wagenvoort C, deMello D, Muller KM, Floros J, Roll C (1999) Congenital alveolar proteinosis caused by a novel mutation of the surfactant protein B gene and misalignment of lung vessels in consanguineous kindred infants. Eur J Pediatr 158:513–518

Virchows Arch (2006) 448: 379–380
DOI 10.1007/s00428-005-0114-0

LETTER TO THE EDITOR

Gaetano Magro · Marina Paola Gardiman · Maria Rosa Lopes · Michal Michal

Small-cell variant of renal oncocytoma with dominating solid growth pattern: a potential diagnostic pitfall

Received: 22 September 2005 / Accepted: 5 October 2005 / Published online: 16 November 2005

Keywords Oncocytoma · Small cell variant · Kidney

Dear Editor,

Renal oncocytoma is a distinct benign renal tumour accounting approximately for 4% of all renal tumours. This neoplasm is easily recognizable in its classic form—polygonal cells with abundant granular eosinophilic cytoplasm, arranged in tubuloalveolar cystic pattern—whereas diagnostic difficulties may arise when it exhibits small cells with scant cytoplasm and hyperchromatic nuclei (so-called "oncoblasts") [2]. Although these small cells are rarely detectable in an otherwise classic renal oncocytoma [1, 3], there is the possibility that they may represent the dominating cell component [2]. One of us (MM), by reviewing a large series of renal oncocytomas, found only 3 out of 134 tumours with a prominent (80% of the entire tumours in two cases and 50% in the other case) small-cell component, and the term "small-cell variant of renal oncocytoma" was proposed for these cases [2]. We report a rare case of renal oncocytoma with a predominant small-cell component, accounting for about 80% of the entire tumour. The unusual extensive solid growth pattern of the tumour may represent a potential diagnostic pitfall with primary or metastatic malignant small cell tumours.

A 58-year-old woman presented with a vague right-flank pain. Ultrasonography and computerized tomography examination revealed a renal mass, measuring 3.5 cm in greatest dimension and located in the upper pole. A radical nephrectomy with abdominal lymph node dissection was performed. Grossly, a well-circumscribed, nonencapsulated tumour mass, tan in colour, was observed. No central scar or haemorraghic or necrotic areas were seen. Histologically, the tumour was mainly (about 80% of the entire tumour) composed of small cells with scant pale to slightly eosinophilic cytoplasm and small hyperchromatic round-shaped nuclei, arranged in a solid growth pattern (Fig. 1a,b). Only focally, the tumour cells exhibited a tubular and alveolar growth pattern. After an extensive search, in some tumour areas, we observed that neoplastic small cells gradually merged with larger cells with abundant granular eosinophilic cytoplasm similar to oncocytes as seen in classic oncocytoma (Fig. 1c). In other areas, the transition between the small cells and the classic oncocytes was abrupt (Fig. 1d). Only the small foci of tumour were composed exclusively of typical oncocytes (Fig. 1e). Nuclear pleomorphism was focally observed in classical oncocytes, as well as binucleation. Mitoses, necrosis, and nuclear pleomorphism were absent. Perirenal adipose tissue invasion and lymph node metastasis were not seen. The patient is well, without evidence of tumour after a 2-year follow-up. Immunohistochemical analyses revealed a faint immunoreactivity to antimitochondrial antibody MITO-113 (Biogenex) in the small-cell component (Fig. 1f), whereas a stronger staining was observed in typical oncocytes. All neoplastic cells were positive to epithelial membrane antigen and pancytokeratins. No reactivity was obtained with chromogranin A, synaptophysin, CD56, neuron-specific enolase, leucocyte common antigen, CD34 and CD99. Differential diagnosis mainly revolved around malignant small-cell tumours. Among these, metastatic or primary neuroendocrine carcinomas (small cell

G. Magro (✉)
Dipartimento G.F. Ingrassia, Anatomia Patologica,
Università di Catania,
Via S. Sofia 87,
95123 Catania, Italy
e-mail: g.magro@unict.it
Tel.: +39-95-3782024
Fax: +39-95-3782023

M. P. Gardiman
Dipartimento Scienze Oncologiche,
Anatomia Patologica, Università di Padova,
Padua, Italy

M. R. Lopes
Unità Operativa di Urologia,
Ospedale Vittorio Emanuele di Gela,
Caltanissetta, Italy

M. Michal
Sikl's Department of Pathology,
Charles University Hospital,
Pilsen, Czech Republic

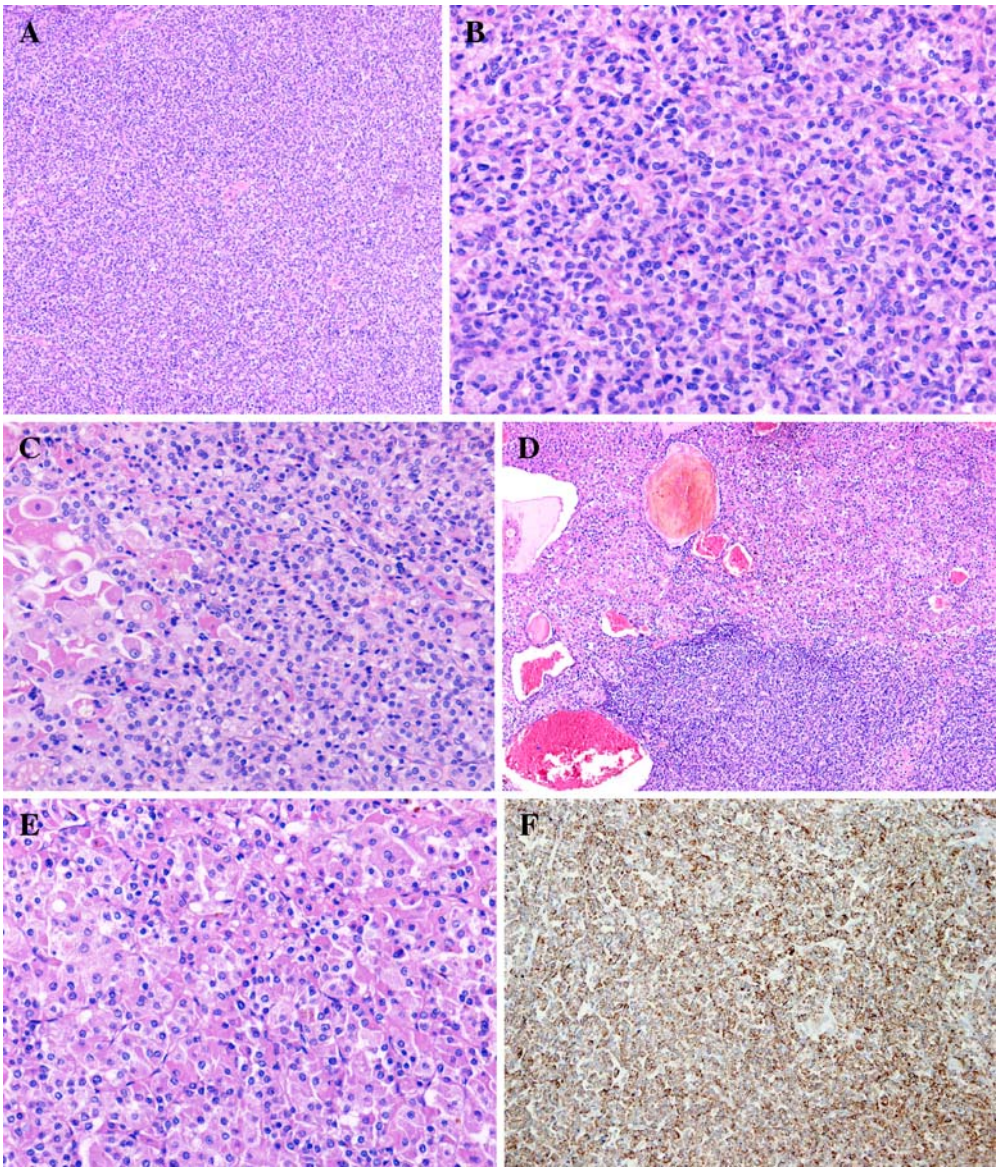

Fig. 1 **a** Low-power magnification showing a small-cell tumour with solid growth pattern. **b** At higher magnification, cells with scant pale to slightly eosinophilic cytoplasm and hyperchromatic nuclei are seen. **c** Tumour area showing small cells intermingling with typical oncocytes as seen in renal oncocytoma. **d** Abrupt transition between small-cell component and typical area of oncocytoma. **e** High magnification of oncocytic tumour component identical to the classic renal oncocytoma. **f** Cytoplasmic immunostaining with the antimitochondrial antibody MITO-113 is less strong in the small cells than in the larger ones (typical oncocytes)

carcinoma of renal parenchyma; pelvis urothelial carcinoma with small-cell or neuroendocrine features) and primitive or metastatic neuroectodermal tumour (Ewing's sarcoma) need to be excluded. Unlike these malignant tumours, our case failed to have high mitotic activity, necrosis and immunostaining for neuroendocrine markers and CD99, respectively.

Although the possibility that a renal oncocytoma is composed exclusively of small cells does exist, the present case, along with the three previously reported in the literature [2], suggests that a thorough tissue sampling and careful identification of typical oncocytes, even if as a minor cellular population of the tumour, is the diagnostic key of the small-cell variant of oncocytoma. In addition, the present case, providing evidence that such a rare variant may have a dominating solid growth pattern, widens the morphological spectrum of renal oncocytoma, preventing a potential misdiagnosis of malignancy.

References

1. Amin MB, Crotty TB, Tickoo SK, Farrow G (1997) Renal oncocytoma. A reappraisal of morphologic features with clinicopathologic findings in 80 cases. Am J Surg Pathol 21:1–12
2. Hes O, Michal M, Boudova L, Mukensnabl, Kinkor Z, Miculka P (2001) Smal cell variant of renal oncocytoma—a rare and misleading type of benign renal tumour. Int J Surg Pathol 9:215–222
3. Perez-Ordonez B, Hamed G, Campbell S, Erlandson RA, Russo P, Gaudin PB, Reuter VE (1997) Renal oncocytoma: a clinicopathologic study of 70 cases. Am J Surg Pathol 21:871–883

Virchows Arch (2006) 448: 381–383
DOI 10.1007/s00428-005-0106-0

LETTER TO THE EDITOR

Gabriella Kiss · Judit Kelemen · Miklós Bély · Péter Vértes

Clinically diagnosed fatal cerebral vasculitis in long-standing juvenile rheumatoid arthritis

Received: 6 September 2005 / Accepted: 26 September 2005 / Published online: 22 November 2005

Keywords Juvenile rheumatoid arthritis · Cerebral vasculitis · Immunoglobulin therapy

Dear Editor,

Systemic vasculitis is one of the most common extra-articular manifestations of rheumatoid arthritis (RA) [1], although it is less frequent in juvenile RA (JRA).

We report a case of JRA with systemic vasculitis. The patient spent a total of 2 years and 8 months in hospitals over the 39-year course of her disease until she finally died of autoimmune cerebral vasculitis.

The female patient's (born in 1942) polyarthritis and carditis started in 1954 and required several hospitalizations. In 1991, chronic vasculitis was suspected because of cutaneous lesions. In September 1992, she was hospitalized with left side hemiparesis attributed to cerebral arterial thrombosis. In July 1993, she was admitted as an emergency case for partly encrusted pustules of the gluteal region, the posterior thighs and lower arms.

G. Kiss (✉)
Intensive Care Unit,
National Institute of Rheumatology and Physiotherapy,
Frankel Leo u. 17-19,
1023 Budapest, Hungary
e-mail: bszende@korb1.sote.hu
Tel.: +36-1-260451

G. Kiss
Üllői u. 55,
1091 Budapest, Hungary

J. Kelemen · P. Vértes
Department of Rheumatology A,
National Institute of Rheumatology and Physiotherapy,
Frankel Leo u. 17-19,
1023 Budapest, Hungary

M. Bély
Department of Pathology,
National Institute of Rheumatology and Physiotherapy,
Frankel Leo u. 17-19,
1023 Budapest, Hungary

She became withdrawn, lost sphincter control, without localizing neurological signs and symptoms. She was transferred to our Medical Intensive Care Unit (MICU) with the suspected diagnosis of cerebral oedema. Bacteriologic examination of the pharynx revealed *Staphylococcus aureus*. The CT scan showed small multiple foci of decreased density in the cerebral white matter (Fig. 1; Dr. K. Urbanek, Central Institute of Radiology, Budapest). Cerebral vasculitis was diagnosed as part of the basic immunologic disorder. Considering the pustulous skin process and the presence of staphylococcus in the pharynx, we decided against combined immunosuppressive therapy.

In the third week of hospitalization, she gradually became comatose. She was given continuous antibiotic treatment (125 mg Solu-Medrol) combined with intravenous administration of immunoglobulin (6 U Sandoglobulin). The patient became comatose and died. The main clinical and laboratory data of the 39-year case history are summarized in Table 1.

At autopsy, non-specific chronic synovitis was found in small articular deformities and in the synovial membranes of the knees and elbows. These and the fibrous pleural and pericardial adhesions, signs of polyserositis, support the diagnosis of JRA. Histologically, vasculitis was found in the areas of the scattered subcutaneous haemorrhages. Vasculitis was detected in the striated muscles, the ovaries, the periadrenal adipose tissue and the brain (Fig. 2). The vasculitis was mainly non-specific, showing acute and also chronic signs of inflammation such as fibrionoid necrosis, perivascular fibrosis and lymphocytic infiltration, and was focally accompanied by thrombosis and haemorrhage. The vasculitis was mainly localized to the arterioles and small arteries of the white matter of all lobes. Corresponding to the vascular lesions, multiple microscopic foci of liquefaction necrosis of various pathological stages corresponded to the hypodense, patchy alterations shown by the CT scan. Further major autopsy findings included mild secondary amyloidosis, above all, in the heart. No gross or microscopic evidence of sepsis was found.

Autopsy confirmed the clinical diagnosis of immune vasculitis in the JRA patient. Cerebral manifestation of immune vasculitis is relatively uncommon in RA. In our case, the

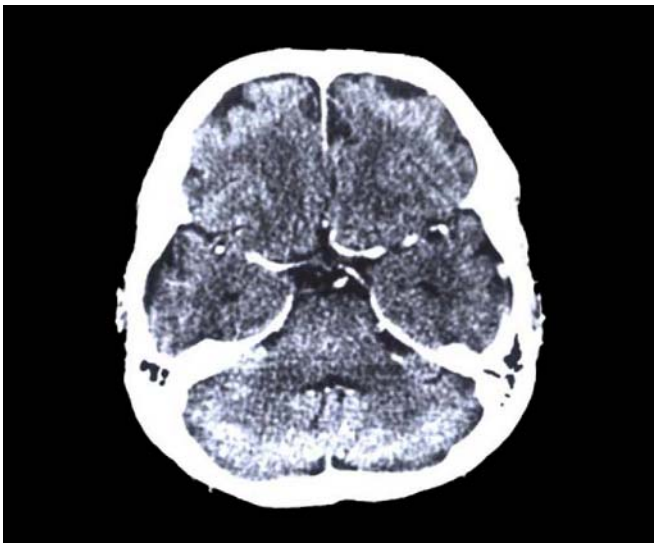

Fig. 1 Multiple foci of decreased density on CT scan in the white matter

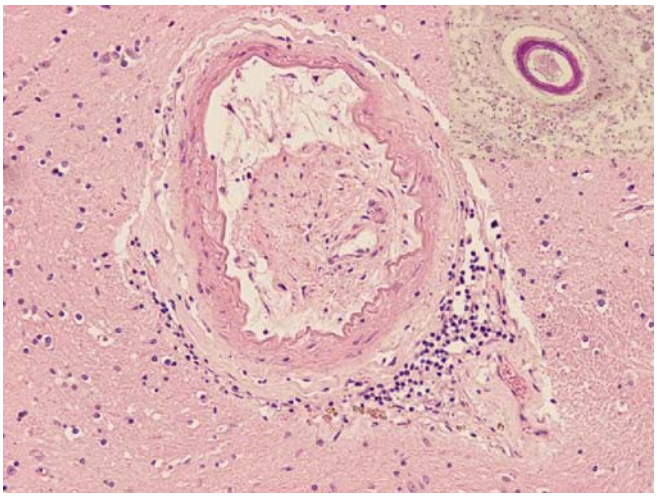

Fig. 2 Small intracerebral artery. Note the re-canalized thrombus, perivascular fibrosis and perivascular lymphocytic infiltration [haematoxylin–eosin (H & E), ×150]. *Inset*: necrotizing arteritis of a small intracerebral artery. See also liquefaction necrosis around the vessel [periodic acid–Schiff (PAS), ×300]

diagnosis of cerebral vasculitis was established on the basis of clinical data and CT findings. The differential diagnosis of infection or septic complication is always a challenge in immunopathologic diseases. In our case, the pyoderma, positive pharyngeal bacteriology and later pseudomonas positivity represented this diagnostic problem.

Table 1 Clinical course

	Year								
	1954/1956	1957	1972	1979/1982	1983	1987/1991	1992	April 1993	August 1993–September 1993
Diagnosis/clinical symptoms	Swelling of both ankles, MCPJs, PIPJs	Carditis, JIA: knees, shoulder, temporomandibular joints	JIA, iatrogenic Cushing's syndrome	JIA: hip, wrist, elbow, hypacidic gastritis	JIA, overlap SLE, muscle pain, hair loss	JIA, keratoconjunctivitis sicca, corneal ulcer, osteoporosis, nephrolithiais	JIA, cerebral thrombosis, hemiparesis (left side), spondylosis, keratoconjunctivitis	JIA, keratoconjunctivitis sicca, uterus myoma, cholelithiasis	JIA, cerebral oedema, pyoderma
Laboratory findings									
ESR (mm/h)		28–102	28	20–100	48	45–115	66	40	61–70
WBC (G/l)		10.8	6.6	3.0–8.0	3.8	4.1–7.9	4.9	4.6	4.6–20.6
Platelet					280	300		376	470–711
Latex fixation			++	Negative	+++	+/+++		+++	+++
CRP		128–296			256	32–80		27	56
Waaler–Rose		32–64		8	256	512		16	32
ANF				l:10++	l:10++	l:10++		Negative	
LE cell				Negative	+++				
IC					234				

JIA juvenile idiopathic arthritis, *MCPJs* metacarpophalangeal joints, *PIPJs* proximal interphalangeal joints, *SLE* systemic lupus erythematosus, *ESR* erythrocyte sedimentation rate, *WBC* white blood cell, *CRP* C-reactive protein, *ANF* antinuclear factor, *LE* lupus erythematosus, *IC* immune complex
+, ++, +++ intensity of the reaction

In 1990, Schuschke et al. [2] published a case of JRA with fatal cerebral vasculitis, directing our attention to the possibility of such an alteration in JRA. Though in his case all modern imaging techniques were used, the diagnosis was made only at autopsy. In 1989, Moore [3] reported five cases of cerebral immune vasculitis treated successfully with high doses of corticosteroid and cyclophosphamide.

In an autopsy series of 161 RA cases, Bély and Apáthy [4] found 36 cases (22.4%) of systemic vasculitis, 3 of them with cerebral manifestations (8.6 relative percentage).

Referring to the work of Moore [3], in the presence of vasculitis in RA (JRA), higher doses of steroid in combination with immunosuppressive therapy are mandatory. If this treatment is prevented by multifocal bacterial infection, the intravenous administration of highly purified gamma-globulin has to be considered [5].

Our clinical and pathological findings point to the possibility of a rare manifestation of autoimmune cerebral vasculitis related to JRA. The diagnosis may be established in vivo and has a major impact on therapy.

References

1. Bély M, Apáthy Á (1993) Krankheitsmodifizierende Faktoren bei chronischer Polyarthritis: Über Zusammenhänge zwischen generalisierter Vaskulitis, sekundärer Amyloidose, septischen Infektionenen und Auftreten von miliaren epitheloidzelligen Granulomen. Eine Untersuchung am Autopsiegut. Zentralbl Pathol 139:51–60
2. Schuschke HJ, Meister P, Pitzl H (1990) Fataler Verlauf einer juvenilen chronischen Arthritis. Klin Pediatr 202:365–367
3. Moore PM (1989) Diagnosis and management of isolated angiitis of the central nervous system. Neurology 39:167–173
4. Bély M, Apáthy A (1994) Systemic vasculitis in rheumatoid arthritis. Rheumatology 8:221–240
5. Smith RW, Ellison DW, Jenkins EA, Gallagher PJ, Cawley MID (1994) Cerebellum and brainstem vasculopathy in systemic lupus erythematosus: two clinico-pathological cases. Ann Rheum Dis 53:327–330

Virchows Arch (2006) 448: 384
DOI 10.1007/s00428-006-0172-y

ANNOUNCEMENTS

6 May 2006
Problems in Breast Pathology
Malta College of Pathologists
Malta

Course Director
Professor J.G. Azzopardi

Scientific Secretariat
J. De Gactano and V. Euscbi

9.00 Registration

Chair: J.G. Azzopardi (London/Malta) & Rosemary Millis (London)
9.30–10.00 Ian Ellis (Nottingham) : Prognostic factors: old versus new.
10.00–10.30 Gianni Bussolati (Torino) : The contribution of 3D models to the understanding of breast pathology,
10.30–11.00 Tibor (Tot) (Falun) : The theory of the sick lobe and the possible consequences.
11.00–11.30 Frederick Koerner (Boston) : The histogenesis of early breast carcinoma,
11.30–12.00 Tanya Tavassoli (New Haven) : To DIN or not to DIN, that is the question.
12.00–12.30 Discussion

Chair: J Rosai (Milano) & G. Stamp (London)
14.30–15.00: James Connoly (Boston): Present findings from the benign breast project of the nurses health study.
15.00–15.30 Stuart Schnitt (Boston) : Columnar cell lesions and flat epithelial atypia.
15.30–16.00 Hans Peterse (Amsterdam): Ring carcinomas: the phenomenon of shift of cell polarization.
16.00–16.30: Thomas Krausz (Chicago) : Breast tumours, Race, loneliness and the pathologist.
16.30–17.00 : Werner Boecker (Muenster): The progenitor cell concept of breast epithelium and how it changes our understanding of profilerative breast disease.
17.00–17.30 : Sunil Lakhani (Brisbane): Myoepithelial cell and breast cancer.
17.30–18.00 : Vincenzo Euscbi (Bologna) : Salivary-like tumours of the breast.
18.00–18.30 : Juan Rosai (Milano) : The vascular lobule. A pitfall on the interpretation of vascular skin lesions following irradiation for breast carcinoma.

S.G. Silveberg (Baltimor) & Jane Dahlstrom
(Camberra) : Conclusive remarks

The congress fee is 30 ∈, that includes light lunch payable on the spot.

Scientific Organizer:
Dr. James De Gaetano
Pathology Department
St. Luke's Hospital
Gwardamangia
Malta
tel.n. xx356 Z5951117
e-mail james.degaetano@gov.mt

Venue and Hotel accomodation:
Hilto Hotel
Portomaso
St. Julians
Malta PTM01
Tel.n. XX 356 21383383
www.hilton.com.mt

8–12 May 2006
Diagnostic histopathology of breast disease at Hammersmith Hospital (Imperial College), London, UK

A week-long course designed for pathologists at Consultant and Senior Trainee level. The course provides a comprehensive coverage of the Histopathology of Breast Disease, with special emphasis on areas that pose diagnostic difficulties. The participants will be given ample time to study histological preparations, followed by illustrated discussion of the cases. There will also be several daily talks dealing with specific topics, given by eminent breast pathologists and followed by discussions. The topics will include update on reporting breast biopsies, immunohistochemistry, hormone receptors and HER2 assessment, Sentinel lymph node biopsy, dealing with the gross specimen, prognostic factors, proliferative lesions/carcinoma in situ, problems in breast pathology and interpretation of breast core biopsies. The faculty will include Ian Ellis, Christopher Elston, Andrew Hanby, Andrew Lee, Sarah Pinder and Sami Shousha.

For further information please contact
Wolfson Conference Centre
Hammersmith Hospital
Du Cane Road
London W12 ONN, UK
Tel: +44-20-83833117/3227/3245;
Fax: +44-20-83832428;
e-mail: wcc@imperial.ac.uk

15–16 June 2006
Thyroid Pathology for the Practicing Pathologist
15 rue de l'Ecole de Médecine, Paris, France

A 2-day course will take place in Paris again under the auspices of the French Division of the L.A.P.

This course will be given in English by Prof. M. Sobrinho-Simōcs (Porto) and Prof. R. Heimann (Brussels).

It will consist of lectures alternating with slide reviews and a slide seminar over a multihead microscope. The cases of this seminar will be sent (on CD) befor the meeting.

The audience will be limited to 22 partcicpants.
Course fees: 390 euros (320 euros for members of any I.A.P. division).
The fees include registration, hand-out, CD of the slide seminar and coffee breaks.

For further information please contact
Mrs. M. Fontaniére
Administrative Secretary
French Division of the I.A.P.
32 Cours Albert Thomas
69008, Lyon, France
Fax: 33 4 78754311
e-mail: academic.pathologie@wanadoo.fr

Virchows Arch (2006) 448: 385–393
DOI 10.1007/s00428-006-0162-0

REVIEW ARTICLE

Kurt Werner Schmid · Nadir Rashad Farid

How to define follicular thyroid carcinoma?

Received: 23 September 2005 / Accepted: 20 December 2005 / Published online: 28 February 2006

Abstract The appropriate diagnosis of follicular thyroid carcinoma (FTC) still depends on its histological discrimination from follicular adenoma (including the distinction of benign from malignant oncocytic variants), papillary thyroid carcinoma (particularly from the follicular variants) and poorly differentiated thyroid carcinoma. The use of immunohistochemical markers contributed only marginally to better defining FTC. The introduction of the micro array technique, however, may offer the possibility of getting a better insight into the natural history, as well as predicting the clinical course, of a given thyroid nodule. This review attempts to recapitulate common standards in the diagnosis of FTC, to summarise current molecular data available to distinguish FTC from other benign and malignant tumours and, finally, to outline future perspectives to define FTC on its specific genetic features.

Keywords Follicular thyroid carcinoma · Follicular adenoma · Papillary thyroid carcinoma · Poorly differentiated thyroid carcinoma · Microarray

Introduction

According to the recently published WHO classification of thyroid tumours [89], follicular thyroid carcinoma (FTC) is defined as a "malignant epithelial tumour showing evidence of follicular cell differentiation but lacking the diagnostic features of thyroid papillary carcinoma". The follicular cell differentiation of FTC can be easily confirmed by thyroglobulin immunohistochemistry; the assessment of the two remaining criteria [proof of malignancy and exclusion of a papillary thyroid carcinoma (PTC)], however, is based on histological features, which still represent the gold standard for the recognition of FTC. Thus, FTC would have to be distinguished both from follicular adenoma (FA) and PTC with a predominantly follicular architecture. Both differential diagnoses may cause severe problems for the surgical pathologist.

To distinguish FA from encapsulated FTC, numerous tissue blocks have to be prepared in a standardised manner [61, 67, 72] and investigated to demonstrate or exclude vascular invasion and/or a capsular breakthrough as the decisive hallmarks of malignancy [20, 34, 65]. FTC with unusual growth patterns may resemble medullary thyroid carcinoma or metastasis to the thyroid, and thus require immunohistochemical stains for the demonstration of its follicular cell differentiation. The lack of appreciation of the diagnostic nuclear features of PTC, particularly in encapsulated tumours, may either lead to the misdiagnosis of an FTC or that of a benign FA. Occasionally, follicular tumours with definite vascular and/or capsular invasion may show nuclear features suggestive of a PTC; for those cases, Williams [91] suggested the term "well differentiated carcinoma not otherwise specified (NOS)". In contrast to PTC, FTC almost exclusively spreads via the blood stream; due to its usually slow growing rate within the thyroid, the presence of lung or bone metastases may be the first clinical manifestation of FTC.

FTC is traditionally subdivided into two categories with distinctly different biological behaviour [27, 89]. The first type comprises completely encapsulated tumours, grossly resembling thyroid FA, which can only be identified by careful histological examination (*minimally invasive FTC*). The second type comprises diffusely infiltrating non-encapsulated carcinomas or (partly) encapsulated tumours with marked tissue or vascular invasion (*widely invasive FTC*). The differential diagnosis between widely and minimally

K. W. Schmid (✉)
Institute of Pathology, University of Essen Medical School,
Member of the West German Cancer Center Essen (WTZE),
Hufelandstraβe 55,
D-45122 Essen, Germany
e-mail: kw.schmid.pathologie@uni-essen.de
Tel.: +49-201-7232890
Fax: +49-201-7235926

N. R. Farid
Osancor Biotech Inc,
Watford, Herts WD17 3BY, UK

invasive FTC is usually straightforward because there is only minimal histological overlap between these two types of FTC. Minimally invasive FTC, however, has to be distinguished from FA by demonstrating vascular and/or capsular invasion (for the details of the histological criteria, see below). It has to be emphasised that both types of FTC are well differentiated thyroid carcinomas; particularly, widely invasive FTC has to be distinguished from poorly differentiated thyroid carcinoma (PDTC [14, 63, 85]), which is nowadays commonly accepted as an independent thyroid cancer entity [89], both clinically and morphologically different from differentiated FTC and PTC.

It still remains unclear whether FTC arises from pre-existing FA or not. Epidemiological and demographic data, showing that the incidence of FTC parallels that of FA in relationship to known environmental factors (particularly the dietary iodine intake) and the fact that FTC occurs in a later age group than FA, suggest that FTC may develop from FA in a sequential progressive manner ("linear tumour progression model"). This concept is also supported by the exceptionally rare occurrence of follicular "microcarcinoma" and the obvious identical cytological appearance of FA and (minimally invasive) FTC. Additionally, as pointed out by Wynford-Thomas [92], there is no supportive evidence for an alternative pathway, i.e., that FTC and FA arise independently from normal thyroid follicular cells. A third model assumes that progression from FA to FTC is only possible within a critical time window, during which an early adenoma may be irreversibly transformed to ultimately become FTC, or after which it is refractory and becomes an end-stage lesion presenting clinically as an adenoma ("time-restricted model" [92]).

Specific markers for the diagnosis of FTC would be most desirable; in the past, a variety of histochemical, immunohistochemical and molecular markers have been proposed to support the diagnosis of FTC. However, the assessment of the specificity of a given marker is hampered by the fact that each marker candidate has to be related to its presence or absence in the respective "nodule", the diagnosis of which was originally based on the above-outlined *histological* criteria.

The "tumour stages" (i.e., FA or FTC) of the linear tumour progression model (and the time-restricted model) are due to the accumulation of genetic alterations. However, the genetic defect ultimately leading to malignancy has to occur in a certain time period (months? years?) before vascular and/or capsular invasion, as the histological hallmarks for the diagnosis of FTC, are fully developed. Thus, a follicular neoplasm, which, due to its lack of vascular and/or capsular invasion, has to be histologically classified as FA may already exhibit one or several molecular alteration(s) associated with FTC. On the other hand, it cannot be excluded that some follicular neoplasms, despite showing vascular and/or capsular invasion and thus histologically classified as FTC, may represent a subtype of FA never able to metastasise. The exceptionally favourable prognosis, particularly of minimally invasive FTC [63, 68], is highly suggestive that a (substantial) proportion of patients with histologically proven (minimally invasive) FTC may be unnecessarily treated by thyroidectomy, lymphadenectomy and subsequent radioiodine administration.

The aim of this review is to summarise the histological criteria as the present gold standard in defining FTC and to critically comment on various parameters proposed to distinguish FTC from FA (including the distinction of benign from malignant oncocytic variants), PTC and PDTC.

Differentiating FTC from FA

Due to the favourable prognosis of thyroid cancer, data on its epidemiology depend to a high degree both on clinical screening efforts and the accuracy of the diagnostic methods applied; this is reflected by the broad range of incidence and survival data available from various national thyroid cancer registries. In general, thyroid cancer is rather uncommon, making up only approximately 1% of all human malignancies [76]. Nevertheless, it is the most common endocrine malignancy and its rate of increase is the fastest of all malignancies in women. However, because thyroid nodules are frequently found (up to 50% of the population in areas with iodine deficiency [89]), the assessment of a possible malignant nature of a thyroid nodule represents not only a medical but also an economical problem. In some iodine-deficient endemic goitre areas, FTC constitutes up to 40% of thyroid cancers [28, 32, 64, 90], whereas it occurs distinctly less frequently (5–25%) in non-endemic areas [46]. FTC occurs in an older age group than PTC, with the peak incidence in 60–70-year-old individuals. Just as with PTC, FTC is 2–4 times more frequently found in women than men. FTC seems to be rare in children and young adults. FTC may be exceptionally rarely associated with familial syndromes, these include Cowden's disease (inherited mutations of the PTEN tumour suppressor gene) and the Carney complex.

At least 50% of FTCs are classified as minimally invasive. This figure represents a shift towards a higher proportion of minimally invasive FTCs amongst all FTCs, most likely reflecting the acceptance of PDTC as an independent clinico-pathological entity leading to a decrease of widely invasive FTC. Two decades ago, minimally invasive FTCs accounted for approximately 40% or less amongst all FTCs [28, 68].

The true incidence of FA is difficult to assess because there are no easily reproducible criteria to distinguish FA from hyperplastic nodules. However, clonality studies [6, 19, 26, 33, 81] have revealed that as many as 60% of thyroid nodules are monoclonal, and thus represent FA. The major task for the surgical pathologist is to meticulously exclude malignancy in each nodule even in multi-nodular goitre.

Grossly FTCs may form a mass ranging from a sharply demarcated nodule of usually more than 1 cm and up to several centimetres in diameter to a diffusely infiltrating tumour replacing a whole thyroid lobe. The latter tumours may macroscopically show extension beyond the thyroid capsule. These two growth patterns usually correspond to the encapsulated and widely invasive types of FTC, respectively.

Microscopically FTCs are composed of follicular, and rarely trabecular, and/or solid growth patterns which cannot be distinguished from the growth patterns seen in FA. The diagnosis of minimally invasive FTC entirely depends on the demonstration of limited vascular invasion and/or localised tumour invasion through its capsule. Widely invasive FTC shows extensive infiltration of the surrounding non-neoplastic tissue(s). Some of the latter may contain remnants of a tumour capsule strongly suggestive that widely invasive FTC most likely develops from encapsulated tumours. When follicular differentiation is poorly developed or even absent, the carcinoma should be preferentially diagnosed as a PDTC [89].

The histological criteria for the diagnosis of minimally invasive FTCs are summarised in Table 1. The controversy of whether capsular breakthrough and vascular invasion are equally associated with metastatic spread is reflected by the fact that some authors apply the term "minimally invasive FTC" only for tumours with capsular invasion, whereas tumours with vascular invasion have been called "encapsulated angioinvasive FTC" [31, 36]. Other features suggesting malignancy, such as high cellularity, an increased mitotic rate, architectural and cellular atypia, foci of necrosis, etc., may be present and should undergo prompt, careful, histological examination; none of these features, however, are sufficient by themselves for the diagnosis of malignancy. In some cases, it may be impossible to ultimately decide whether an encapsulated follicular tumour shows vascular and/or capsular invasion or not; for those cases, Williams suggested the term "follicular tumours of uncertain malignant potential" [91].

Occasionally, FAs without vascular and/or capsular invasion show a pronounced cellular proliferation, less regular cytology, or unusual histologic patterns; these tumours have been referred to as "atypical adenomas" [27]. Several studies have provided unequivocal evidence that atypical adenomas pursue a biologically benign course and do not metastasise or recur [28, 34]. Rosai and co-workers quite correctly stated that the diagnosis of an "atypical adenoma" has become a "wastebasket term for too many pathologists"; they suggested designating these lesions as "hypercellular adenomas" [61]. According to the WHO classification [89], the "use of the term atypical adenoma is discouraged". We suggest avoiding the term "atypical adenoma" because it does not indicate a lesion that (even occasionally) behaves biologically "atypically".

In contrast to the minimally invasive type, widely invasive FTC is easy to distinguish from benign lesions. Widely invasive FTC shows a variable range of solid and trabecular areas intermingled with areas showing a follicular pattern. The tumour may consist of several or multiple nodules of variable size. Between the nodules, broad bands of fibrous tissue may sometimes be present; vascular invasion is usually easy detectable within these bands. Tumour infiltration beyond the thyroid capsule is a regular finding in widely invasive FTC. As noted before, widely invasive FTC, in particular, needs to be distinguished from PDTC [89], although the respective criteria are still far from established (for detailed discussion, see below).

The distinction of FA from FTC may cause considerable histologic problems and cannot be made reliably on cytological specimens [89]. Thus, the identification of genes whose products can be held up as a molecular signature would be a most welcome addition to the diagnostic armamentarium available.

FTCs harbour a number of chromosomal abnormalities and chromosomal imbalances (for an overview, see [89]) which can be detected by comparative genomic hybridisation (CGH). However, CGH is not a practical technique to be performed on large numbers of specimens. Some authors have, however, focussed their efforts on gene mapping in areas of loss of heterozygozity (LOH), for further studies in FTC. Aldred et al. [4] selected genes from chromosomal regions reported to exhibit LOH in FTC. Because of the nature of the question asked, the authors concentrated on down-regulated genes, detecting three genes (caveolin-1, caveolin-2 and GDF10/BMP3b) localised to two chromosomal regions (7q31.1 and 10q11.1), which were found to be coordinately down-regulated. Following the theme of bone morphogenesis signalling and possible interaction with GDF10/BMP3b, they further selected glycipan-3 (Xq26.1) and chordin-like (Xq22) for analysis. The expression of each

Table 1 Histological criteria for the diagnosis of minimally invasive FTC

Vascular invasion
Tumour plug or polyp in a sub-endothelial location within a vein (not a capillary; thus, the immunohistochemical demonstration of endothelial cells is not necessary) in or immediately beyond the tumour capsule; vascular invasion within the tumour has no diagnostic or prognostic implication
The tumour cell cluster protruding into is usually, but not necessarily, covered by endothelium
The tumour thrombus does not necessarily have to be attached to the vessel wall; tumour cell clusters without endothelial covering and freely situated in the vessel lumen, however, most likely represent artefacts
Capsular breakthrough
Penetration of the tumour through the whole capsule, deflecting the collagen fibres of the capsule
Contact of the tumour with the surrounding non-neoplastic thyroid tissue
A concomitant vascular invasion is not required even if metastases are already present at the time of diagnosis
Tumour foci within the capsule are not sufficient for the diagnosis of minimally invasive FTC. They represent, most likely, tumour trapping and distortion by fibrosis

Vascular invasion and capsular breakthrough may occasionally occur simultaneously

of these genes was reduced in at least 79% of FTC samples. The fact that a reduced expression of three genes involved in bone morphogenesis signalling was also found in FA and multi-nodular goitre (as well as glycipan 3 in PTC) substantially limits the utility of these genes in differentiating FA from FTC. Nevertheless, gene expression analysis of these three genes may be helpful as part of a diagnostic panel to differentiate FA from FTC. Another bone morphogenic factor, BMP7, which is part of the tumour necrosis factor signalling pathway, is decreased in FTC, whereas a negative regulator of that signalling pathway, the BMP and activin membrane-bound inhibitor, was found to be up-regulated in FTC [57, 58]. Rearrangements of the peroxisome proliferator-activated receptor gamma (PPARγ) are a regular feature of thyroid follicular tumours with a pronounced preponderance for FTC; because these rearrangements may also occur with a lower frequency in FA, they are not specific for FTC [53]. Aldred et al. [3] showed that PPARγ gene expression was reduced in FTC even in those samples not showing PPARγ/PAX8 rearrangement; they attributed the reduction in the expression of this gene to changes in one or more regulatory proteins acting upstream from PPARγ, and which they had not identified. The reduction in expression of PPARγ was, however, also found to extend to PTC and oncocytic thyroid neoplasms. Marques et al. [39] have recently reported that PPARγ-negative FTC presented a more aggressive course, and that the follicular variants of PTC (FVPTC) are more likely than classic PTC to be PPARγ-negative.

Cerutti et al. [16] used serial analysis of gene expression to focus on four genes that correctly categorised benign as opposed to malignant follicular thyroid lesions. Two of these genes have been previously described by Barden et al. [7] to be up-regulated in FTC (DDTI3) and FA (putative *Emu*1), although only the former was found to discriminate between FTC and FA. ARG2, whose expression was reported to be increased in FTC [16], but not in FA, was found to be up-regulated in PTC, too [58, 59]. Whilst AGR2 thus seems to lack specificity to distinguish FTC from PTC, it may be helpful in the context of follicular tumours. Additionally, a specific increase in the expression of aconitase 1 (ACOI) and PCSK2 in FTC was noted; although only the latter has been so far pursued with confirmatory real-time PCR. Takano and co-workers demonstrated that the *decrease* in TFF3 transcript abundance was significantly reduced in FTC, particularly when expressed as a ratio of galectin-3 in the same sample [77, 78].

One of the authors [57] has demonstrated the over-expression of TRIB1, PCSK2, MET, RAP1 GA1, LGALS3 and ACO1 in FTC compared to that in FA. The importance of PCSK2 and ACO1 in differentiating between these two lesions was also recognised in the study by Cerutti et al. [16].

In an exemplary study, Weber et al. [88] honed in on three genes, CyclinD2, PCSK2 and PLAB, that they found to differentiate FTC from FA with 100% sensitivity, 94.7% specificity and 96.7% accuracy. The combination of three genes was less efficient in the identification of FVPTC, and the authors had to include genes specific for PTC to make the distinction. While this study included many samples and submitted the results to careful unbiased analysis, it does not exclude that some of the other genes identified that were used in combinations cannot be used as diagnostics of FTC.

Differentiating FTC from PTC

PTC is defined as a malignant tumour showing evidence of follicular differentiation and characterised by distinctive nuclear features [89]. PTC regularly shows a broad spectrum of special features concerning its growth patterns, cell types, and stromal reactions. Because papillary structures may be found occasionally in nodular goitres, FA and FTC, the diagnosis of PTC ultimately entirely depends on its nuclear features (ground-glass appearance, irregularity of nuclear contours, grooves, pseudo-inclusions). The appreciation of the nuclear features of PTC is crucially dependent on tissue processing (fixative, duration of fixation, thickness of sections). Finally, the diagnosis of PTC relies on the extent of the nuclear features which should be present in "a significant proportion of the neoplasm" [84, 89]; it must be clearly stated that particularly the diagnosis of encapsulated PTC regularly depends on a considerable subjective judgement.

The majority of tumours representing FVPTC are encapsulated, composed of small- to medium-sized follicles and completely lack papillary structures. FVPTC may be occasionally found with a diffuse or multi-nodular growth pattern. Rarely, FVPTC can be composed predominantly or exclusively of macro-follicles [1]. FVPTC and its variants may cause, if the nuclear features of PTC are insufficiently appreciated, severe problems in the differentiation from FTC, FA or even multi-nodular goitre.

A number of immunohistochemical markers have been proposed to confirm the diagnosis of PTC; these include, amongst others, cytokeratin 19, HBME-1 and galectin-3 [10, 17]. However, neither of these "markers" reliably distinguishes PTC from FTC.

Finley et al. [22] extended their previous experience (compare to Barden et al. [7]) to array RNA from a set of tumours including PTC, FVPTC, FA and hyperplastic nodules. They selected five genes: AM, MET, TROP-2, NRP2 and TFF3. Although they have suggested a high degree of specificity and sensitivity, in both studies, FVPTC frequently clustered with benign adenomas. Among the genes that were found up-regulated in carcinoma but were not further pursued are HVH3, TIMP, HGFR, CPP1, AHR and HLA-DQB, and those in adenomas are CRABP1, THBS4, DPPX, MT1, PDDR, MT2-MMP and RNS1; these genes may be further candidates to select PTC from follicular tumours. Chevillard et al. [18] identified 155 genes that were differentially expressed between normal thyroid and both benign and malignant tumours; 75 genes separated follicular lesions from FVPTC and 43 genes separated FTC from FA. Hierarchical clustering was able to further separate between FVPTC and classic PTC. Platelet-derived growth

factor gene profiling was found to be useful for the identification of PTC [93], which may also be helpful for differentiating FTC from PTC.

The Columbus (Ohio) group [3, 4] has recently put to the test the notion that five genes might distinguish between FTC and PTC: PTC showed increased expression of CITED1, CLDN10 and IGFBP6, but no change in CAV1 or CAV2, whereas FTC showed decreased expression of IGFBP6 and CAV1and/or CAV2, but no change in CLDN10. These promising results, however, need to be verified in larger samples in a prospective series. As already discussed above, Weber et al. [88] from the same group has extended the notion of selecting a few important genes to separate FTC from FA.

Differentiating the oncocytic variants of FA and FTC from non-oncocytic FTC

Histologically oncocytic or Hürthle cell tumours of the thyroid are predominantly (at least 75%) composed of oncocytic cells (WHO). As recently pointed out by Sobrinho-Simoes et al. [75], there is sufficient clinico-pathological evidence to support the concept that every type of thyroid neoplasm (FA, FTC, PTC and poorly differentiated carcinoma) has its oncocytic counterpart; thus, the presence of oncocytic cells should not interfere with the diagnostic criteria of PTC (nuclear characteristics), FA and FTC (vascular and/or capsular invasion).

Macroscopically oncocytic tumours show a distinct mahagony brown appearance; microscopically oncocytic cells are characterised by a hyper-chromatic and pleomorphic nucleus with a generally prominent nucleolus, as well as a granular, brightly eosinophilic cytoplasm containing up to 5,000 mitochondria [41, 50, 74]. The majority of these tumours show a follicular, trabecular and/or solid architecture [35, 61], exhibit a rather uniform oxyphilia throughout the tumour [30] and produce thyroglobulin [29]; they are thus considered to belong to the "follicular family" (FA and FTC) of thyroid tumours [89]. In oncocytic tumours with a predominantly papillary pattern, the diagnosis of an oncocytic papillary carcinoma should only be made if the nuclear features of conventional papillary carcinoma are present [27, 41, 89]; the oncocytic variant of PTC is regarded as a rather uncommon thyroid malignancy [11, 38, 61, 66, 89].

In the 1950s, the American Cancer Society recommended that all oncocytic thyroid tumours should be regarded as malignant; subsequently, it was unequivocally proven that encapsulated oncocytic tumours, as other encapsulated follicular neoplasms, only behave clinically malignant if vascular and/or capsular invasion can be histologically demonstrated [15, 79]. Amongst encapsulated oncocytic tumours, the percentage of tumours showing vascular and/or capsular invasion (thus representing the oncocytic variant of FTC) is considerably higher than the percentage of non-oncocytic FTCs amongst encapsulated non-oncocytic tumours [12, 15, 21, 45, 55, 87]. The rate of metastasis [89], as well as the overall mortality [15], of patients with oncocytic carcinomas was reported to be higher when compared to conventional FTC [34]; other studies failed to demonstrate a higher malignant potential of oncocytic carcinomas [21, 75, 85]. A less favourable outcome of patients suffering from oncocytic carcinoma is most likely related to a decreased responsiveness of oncocytic carcinomas to radioiodine treatment as a consequence of the decreased iodine uptake and hormone synthesis of oncocytic cells [41, 83].

The knowledge about the mechanism(s) leading to oncocytic thyroid tumours has substantially improved over the past few years (reviewed by Sobrinho-Simoes et al. [75]). The accumulation of mitochondria in oncocytic cells may be due to (1) a primary alteration of the mitochondrial DNA that encodes mitochondrial enzymes [40–42, 48, 79] or (2) somatic or point mutations of nuclear genes encoding for enzymes of the mitochondrial respiratory chain or the Krebs cycle [41]. It has been proposed that if the genetic alterations responsible for the accumulation of abnormal mitochondria occur in already transformed neoplastic cells, the resulting tumour will morphologically, biochemically and clinically correspond to an FTC or PTC; if the mitochondrial alterations occur in a yet non-transformed cell, subsequent further mutations will lead to a "primary" oncocytic neoplasm (showing exclusively Hürthle cell features) [30, 75].

Multiple tumours are found in approximately 20% of patients with oncocytic thyroid neoplasms [30]; those tumours are less frequently malignant than solitary oncocytic tumours. The occurrence of multiple oncocytic thyroid tumours with the same phenotype is strongly suggestive of a germ line alteration [30]. Familial clustering of oncocytic tumours has been reported [55, 69], and consistent cytogenetic alterations have been mapped to chromosome 19p13.2 [13, 25]; however, the exact gene(s) responsible has yet to be identified [43]. The BRAF V600E mutation has been demonstrated in approximately 50% of both conventional PTC and the oncocytic variant of PTC [73, 82]. PTC-specific RET rearrangements have been demonstrated in 4 out of 5 oncocytic PTCs and 7 out of 27 oncocytic carcinomas with a solid/trabecular growth pattern, but not in oncocytic carcinomas exhibiting a follicular architecture [49].

Concerning gene profiling, Baris et al. [8, 9], studying a large number of oncocytic thyroid tumours, were able to identify gene clusters involved in mitochondrial biogenesis and oxidative metabolism, in common with oncocytic tumours of other organs. Genes down-regulated but not further studied include IFIM1, DUP1, TNFSF1, CAV1 and GJA1, which appear to be differentially regulated in FTC. Genes noted to be over-expressed include DDIT3 (see above), CCNG2, BDNF, THBS3, LMO2, DDX24 and CRABP1, which were found to feature in thyroid carcinogenesis. Thomas et al. [80] recently showed that ACO1, PCTAIRE protein kinase and ced homolog reliably distinguish oncoctyic tumours from non-oncocytic thyroid tumours. In contrast to the high frequency of retinoblastoma (Rb) protein loss in other malignant thyroid tumours, this crucial regulator of the cell cycle and cell fate is apparently

unaltered in oncocytic tumours [5]. The persistence of wild-type Rb may be essential to the metabolic and proliferative characteristics of oncocytic tumours and may be reminiscent of the mandatory role of wild-type Rb in thyroid cancer with up-regulated CyclinD1 [71].

Differentiating FTC from PDTC

PDTC is defined as a "follicular cell neoplasm that show limited evidence of structural follicular cell differentiation and occupy both morphologically and behaviourally an intermediate position between differentiated (FTC and PTC) and undifferentiated (anaplastic) carcinomas" [62, 89]. Although recognised for more than 20 years as an aggressive type of thyroid carcinoma [14, 63], the diagnosis of PDTC is still not familiar to many surgical pathologists. This may be the most important reason for the observed considerable variations in its different prevalence rates among different geographic regions. The aetiology of PDTC is obscure; pre-existing differentiated tumour areas suggest that some PDTCs have developed from differentiated carcinomas of follicular cell origin (FTC or PTC). Others most likely arise de novo [56]. According to the literature, the morphological appearance of PDTC is highly variable [14, 37, 54, 63, 84, 89].

The major problem in distinguishing FTC from PDTC is caused by rather poorly defined criteria to set the threshold between differentiated carcinoma (both FTC and PTC) and PDTC. The diagnosis of PDTC was based by some authors on growth patterns, whilst others used histologic patterns and/or cytologic features. A variety of immunohistochemical markers, including thyroglobulin, TTF-1, high-molecular-weight cytokeratins, HBME-1 and galectin-3, do not reliably distinguish PDTC from differentiated thyroid carcinoma [60]. As recently reviewed by Albores-Saavedra and Carrick [2], the various growth patterns (insular, trabecular and/or solid) suggested for the diagnosis of PDTC, may also be present in hyperplastic nodules, FA and FTC. The cytologic features of PDTC are regularly found to be similar to or overlapping with those of FTC and PTC; moreover cytologic atypia, mitotic rate and necrosis do not necessarily reflect cell differentiation, particularly in endocrine organs. Thus, Albores-Saavedra and Carrick [2] concluded that the majority of PDTCs represent examples of FTC or PTC with unusual growth patterns; they strongly emphasised that an aggressive clinical course of a given thyroid carcinoma does not justify its inclusion in the category of PDTC.

However, according to the WHO classification [89], PDTC should be treated as a separate entity because of its clinical significance. Volante and co-workers [85] proposed insular characteristics, trabecular and/or solid growth patterns, association with vascular invasion, necrotic areas and/or infiltration of adjacent non-neoplastic tissues, as the main diagnostic features of PDTC. The same group [86] recently showed that patients of ages >45 years, with the presence of necrosis (either focal or extensive) and with mitotic counts >3 per 10 HPF are associated with a more aggressive clinical behaviour of PDTC.

In accordance with others [2], we believe that the morphological diagnosis of PDTC should be based on the above-outlined growth patterns, easily recognisable mitoses and a characteristically focal thyroglobulin immunoreactivity in less than 20% of tumour cells. The occurrence of small foci of PDTC within an otherwise well-differentiated FTC should be reported; it remains to be elucidated whether this finding is associated with a clinical significance.

Because the diagnostic criteria of PDTC are far from being well established, molecular and/or genetic markers would be most welcome [52]. At least 30% of PDTCs show mutations of TP53 [70], approximately 50% show H-, K- or N-RAS mutations. The latter mutations are regularly found in PDTC as multiple activation mutations that are virtually never seen in differentiated thyroid carcinomas [24]. Very rarely, PDTCs express rearranged tyrosine kinase genes such as RET/PTC or NRTK1 [51]. An interesting candidate for a genetic trigger of thyroid tumour dedifferentiation is β-catenin; β-catenin point mutations (in exon 3 of the CTNNB1 gene) block β-catenin's degradation, resulting in a β-catenin accumulation in the nucleus and constitutive activation of target gene expression. CTNNB1 point mutations have so far only been reported in PDTC and anaplastic thyroid carcinomas, but not in FTC and PTC [23, 47]. As the questions of disease stage or disease progression have not been posed in the studies done to date, it is difficult to assign a role to oncogenes or tumour suppressor genes that show gene expression, except that these genes are related to malignant thyroid subtypes. The lack of uniform histologic criteria for PDTC is, of course, limiting the search for genetic mutations, chromosomal abnormalities and gene expression profiling.

Future perspectives for the definition of FTC

The questions asked in gene expression studies done to date were: (1) can gene expression profiling distinguish between benign and malignant thyroid nodules, (2) does this approach ultimately allow distinguishing between FA and FTC and (3) does PTC have a gene expression profile distinct from normal thyroid? The majority of gene expression studies cited in this overview were exploratory

Table 2 Genes whose expressions are useful in the diagnosis of FTC

Up-regulated in FTC	Down-regulated in FTC
PCSK2[a]	*TFF3*
TRIB1[a]	*BMP7*
Cyclin D2	*CAV1*
ACO1	*CAV2*
ARG2	*IGFBP6*
PLAB	
LGAL3	
DDIT3	
MET1	

[a]First identified by one of the authors (N.R. Farid)

or "scouting" inquiries. The performance of derivative studies with proper definitions of variables, sufficient numbers of cases included and uniformity of techniques, data acquisition and analysis are largely awaited. To date, the approach of Weber and co-workers [87], as applied to follicular tumours, satisfies most of these criteria.

We feel the time is now ripe to mount concerted collaborative efforts to concentrate on gene products that particularly differentiate between FA and FTC (Table 2). The variation in the expressions of these genes should show a high prevalence in one lesion or the other, and thus offer a high degree of specificity. From a pragmatic viewpoint, it does not matter whether the variation in the expression of these genes spills over to multi-nodular goitre or PTC. The designated genes should be tested either prospectively in a large number of samples from different centres using cDNA array (prepared in one source and distributed to participating laboratories) or with real-time PCR using standardised protocols. Sample preparation, assessment of histological criteria and data capture should follow protocols generally agreed upon, with the raw data being sent to a central coordinating centre. Once a minimum of 5–10 genes have been identified as diagnostics, a prospective study on fine-needle aspiration biopsies of the thyroid should be performed: needle washings would be delivered to an RNA extraction solution and be further processed if the cytology does not show evidence of PTC. Recent progress in real-time PCR technology allows for an economic examination of a large number of genes [44]. One can thus take advantage of the diagnostic concurrence of a larger number of samples.

References

1. Albores-Saavedra J, Gould E, Vardaman C, Vuitch F (1991) The macrofollicular variant of papillary thyroid carcinoma: a study of 17 cases. Hum Pathol 22:1195–1205
2. Albores-Saavedra J, Carrick K (2004) Where to set the threshold between well differentiated and poorly differentiated follicular carcinomas of the thyroid. Endocr Pathol 15:297–305
3. Aldred MA, Ginn-Pease ME, Morrison CD, Popkie AP, Gimm O, Hoang-Vu C, Krause U, Dralle H, Jhiang SM, Plass C, Eng C (2003) Caveolin-1 and caveolin-2, together with three bone morphogenetic protein-related genes, may encode novel tumor suppressors down-regulated in sporadic follicular thyroid carcinogenesis. Cancer Res 63:2864–2871
4. Aldred MA, Huang Y, Liyanarachchi S, Pellegata NS, Gimm O, Jhiang S, Davuluri RV, de la Chapelle A, Eng C (2004) Papillary and follicular thyroid carcinomas show distinctly different microarray expression profiles and can be distinguished by a minimum of five genes. J Clin Oncol 22:3531–3539
5. Anwar F, Emond MJ, Schmidt RA, Hwang HC, Bronner MP (2000) Retinoblastoma expression in thyroid neoplasms. Mod Pathol 13:562–569
6. Apel RL, Ezzat S, Bapat BV, Pan N, LiVolsi VA, Asa SL (1995) Clonality of thyroid nodules in sporadic goiter. Diagn Mol Pathol 4:113–121
7. Barden CB, Shister KW, Zhu B, Guiter G, Greenblatt DY, Zeiger MA, Fahey TJ 3rd (2003) Classification of follicular thyroid tumors by molecular signature: results of gene profiling. Clin Cancer Res 9:1792–1800
8. Baris O, Savagner F, Nasser V, Loriod B, Granjeaud S, Guyetant S, Franc B, Rodien P, Rohmer V, Bertucci F, Birnbaum D, Malthiery Y, Reynier P, Houlgatte R (2004) Transcriptional profiling reveals coordinated up-regulation of oxidative metabolism genes in thyroid oncocytic tumors. J Clin Endocrinol Metab 89:994–1005
9. Baris O, Mirebeau-Prunier D, Savagner F, Rodien P, Ballester B, Loriod B, Granjeaud S, Guyetant S, Franc B, Houlgatte R, Reynier P, Malthiery Y (2005) Gene profiling reveals specific oncogenic mechanisms and signaling pathways in oncocytic and papillary thyroid carcinoma. Oncogene 24:4155–4461
10. Bartolazzi A, Gasbarri A, Papotti M, Bussolati G, Lucante T, Khan A, Inohara H, Marandino F, Orlandi F, Nardi F, Vecchione A, Tecce R, Larsson O (2001) Application of an immunodiagnostic method for improving preoperative diagnosis of nodular thyroid lesions. Lancet 357:1644–1650
11. Berho M, Suster S (1997) The oncocytic variant of papillary carcinoma of the thyroid: a clinicopathologic study of 15 cases. Hum Pathol 28:47–53
12. Bronner MP, LiVolsi VA (1988) Oxyphilic (Askanazy/Hürthle cell) tumors of the thyroid: microscopic features predict biological behaviour. Surg Pathol 1:137–150
13. Canzian F, Amati P, Harach HR, Kraimps JL, Lesueur F, Barbier J, Levillain P, Romeo G, Bonneau D (1998) A gene predisposing to familial thyroid tumors with cell oxyphilia maps to chromosome 19p13.2. Am J Hum Genet 63:1743–1748
14. Carcangiu ML, Zampi G, Rosai J (1984) Poorly differentiated ("insular") thyroid carcinoma. A reinterpretation of Langhans' "wuchernde Struma". Am J Surg Pathol 8:655–668
15. Carcangiu ML, Bianchi S, Savino D, Voynick IM, Rosai J (1991) Follicular Hurthle cell tumors of the thyroid gland. Cancer 68:1944–1953
16. Cerutti JM, Delcelo R, Amadei MJ, Nakabashi C, Maciel RM, Peterson B, Shoemaker J, Riggins GJ (2004) A preoperative diagnostic test that distinguishes benign from malignant thyroid carcinoma based on gene expression. J Clin Invest 113:1234–1242
17. Cheung CC, Ezzat S, Freeman JL, Rosen IB, Asa SL (2001) Immunohistochemical diagnosis of papillary thyroid carcinoma. Mod Pathol 14:338–342
18. Chevillard S, Ugolin N, Vielh P, Ory K, Levalois C, Elliott D, Clayman GL, El-Naggar AK (2004) Gene expression profiling of differentiated thyroid neoplasms: diagnostic and clinical implications. Clin Cancer Res 10:6586–6597
19. Chung DH, Kang GH, Kim WH, Ro JY (1999) Clonal analysis of a solitary follicular nodule of the thyroid with the polymerase chain reaction method. Mod Pathol 12:265–271
20. D'Avanzo A, Treseler P, Ituarte PH, Wong M, Streja L, Greenspan FS, Siperstein AE, Duh QY, Clark OH (2004) Follicular thyroid carcinoma: histology and prognosis. Cancer 100:1123–1129
21. Evans HL, Vassilopoulou-Sellin R (1998) Follicular and Hurthle cell carcinomas of the thyroid: a comparative study. Am J Surg Pathol 22:1512–1520
22. Finley DJ, Zhu B, Barden CB, Fahey TJ III (2004) Discrimination of benign and malignant thyroid nodules by molecular profiling. Ann Surg 240:425–437
23. Garcia-Rostan G, Camp RL, Herrero A, Carcangiu ML, Rimm DL, Tallini G (2001) Beta-catenin dysregulation in thyroid neoplasms: down-regulation, aberrant nuclear expression, and CTNNB1 exon 3 mutations are markers for aggressive tumor phenotypes and poor prognosis. Am J Pathol 158:987–996
24. Garcia-Rostan G, Zhao H, Camp RL, Pollan M, Herrero A, Pardo J, Wu R, Carcangiu ML, Costa J, Tallini G (2003) ras mutations are associated with aggressive tumor phenotypes and poor prognosis in thyroid cancer. J Clin Oncol 21:3226–3235
25. Harach HR, Lesueur F, Amati P, Brown A, Canzian F, Kraimps JL, Levillain P, Menet E, Romeo G, Bonneau D (1999) Histology of familial thyroid tumours linked to a gene mapping to chromosome 19p13.2. J Pathol 189:387–393

26. Harrer P, Broecker M, Zint A, Schatz H, Zumtobel V, Derwahl M (1998) Thyroid nodules in recurrent multinodular goiters are predominantly polyclonal. J Endocrinol Invest 21:380–385
27. Hedinger C, Williams ED, Sobin LH (1988) Histological typing of thyroid tumours. International histological classification of tumours. Springer, Berlin Heidelberg New York
28. Hofstädter F (1980) Frequency and morphology of malignant tumours of the thyroid before and after the introduction of iodine-prophylaxis. Virchows Arch A Pathol Anat Histol 385:263–270
29. Johnson TL, Lloyd RV, Burney RE, Thompson NW (1987) Hurthle cell thyroid tumors. An immunohistochemical study. Cancer 59:107–112
30. Katoh R, Harach HR, Williams ED (1998) Solitary, multiple, and familial oxyphil tumours of the thyroid gland. J Pathol 186:292–299
31. Kesmodel SB, Terhune KP, Canter RJ, Mandel SJ, LiVolsi VA, Baloch ZW, Fraker DL (2003) The diagnostic dilemma of follicular variant of papillary thyroid carcinoma. Surgery 134:1005–1012
32. Kober F, Wolf G, Depisch D, Galvan G, Keminger K, Ladurner D, Langsteger W, Ogris E, Pimpl W, Roka R, Schmalzer E, Schmid KW, Tuchmann A (1990) Schilddrüsenkarzinom. In: Steindorfer P (ed) Manual der chirurgischen Krebstherapie. Springer, Berlin Heidelberg New York, pp 35–48
33. Krohn K, Paschke R (2002) Somatic mutations in thyroid nodular disease. Mol Genet Metab 75:202–208
34. Lang W, Choritz H, Hundeshagen H (1986) Risk factors in follicular thyroid carcinomas. A retrospective follow-up study covering a 14-year period with emphasis on morphological findings. Am J Surg Pathol 10:246–255
35. LiVolsi VA (1990) Surgical pathology of the thyroid. Major problems in pathology, vol 22. Saunders, Philadelphia
36. LiVolsi VA (2003) Pure versus follicular variant of papillary thyroid carcinoma: clinical features, prognostic factors, treatment, and survival. Cancer 98:1997–1998
37. Ljungberg O, Bondeson L, Bondeson AG (1984) Differentiated thyroid carcinoma, intermediate type: a new tumor entity with features of follicular and parafollicular cell carcinoma. Hum Pathol 15:218–228
38. Mai KT, Elmontaser G, Perkin DG, Thomas J, Stinson WA (2005) Benign Hürthle cell adenoma with papillary architecture: a benign lesion mimicking oncocytic papillary carcinoma. Int J Surg Pathol 13:37–41
39. Marques AR, Espadinha C, Frias MJ, Roque L, Catarino AL, Sobrinho LG, Leite V (2004) Underexpression of peroxisome proliferator-activated receptor (PPAR)gamma in PAX8/PPAR gamma-negative thyroid tumours. Br J Cancer 91:732–738
40. Maximo V, Sores P, Rocha AS, Sobrinho-Simoes M (1998) The common deletion of mitochondrial DNA is found in goiters and thyroid tumors with and without oxyphil cell change. Ultrastruc Pathol 22:271–273
41. Maximo V, Sobrinho-Simoes M (2000) Hurthle cell tumours of the thyroid. A review with emphasis on mitochondrial abnormalities with clinical relevance. Virchows Arch 437:107–115
42. Maximo V, Soares P, Lima J, Cameselle-Teijeiro J, Sobrinho-Simoes M (2002) Mitochondrial DNA somatic mutations (point mutations and large deletions) and mitochondrial DNA variants in human thyroid pathology: a study with emphasis on Hurthle cell tumors. Am J Pathol 160:1857–1865
43. Maximo V, Botelho T, Capela J, Soares P, Lima J, Taveira A, Amaro T, Barbosa AP, Preto A, Harach HR, Williams D, Sobrinho-Simoes M (2005) Somatic and germline mutation in GRIM-19, a dual function gene involved in mitochondrial metabolism and cell death, is linked to mitochondrion-rich (Hurthle cell) tumours of the thyroid. Br J Cancer 92:1892–1898
44. Mazzanti C, Zeiger MA, Costouros NG, Umbricht C, Westra WH, Smith D, Somervell H, Bevilacqua G, Alexander HR, Libutti SK (2004) Using gene expression profiling to differentiate benign versus malignant thyroid tumors. Cancer Res 64:2898–2903
45. McDonald MP, Sanders LE, Silverman ML, Chan HS, Buyske J (1996) Hurthle cell carcinoma of the thyroid gland: prognostic factors and results of surgical treatment. Surgery 120:1000–1004
46. Mendelsohn G (1988) Pathology of thyroid disease. In: Mendelsohn G (ed) Diagnosis and pathology of endocrine disease. J.B. Lippincott, Philadelphia, pp 37–117
47. Miyake N, Maeta H, Horie S, Kitamura Y, Nanba E, Kobayashi K, Terada T (2001) Absence of mutations in the beta-catenin and adenomatous polyposis coli genes in papillary and follicular thyroid carcinomas. Pathol Int 51:680–685
48. Müller-Hocker J, Jacob U, Seibel P (1998) Hashimoto thyroiditis is associated with defects of cytochrome-c oxidase in oxyphil Askanazy cells and with the common deletion (4,977) of mitochondrial DNA. Ultrastruct Pathol 22:91–100
49. Musholt PB, Imkamp F, von Wasielewski R, Schmid KW, Musholt TJ (2003) RET rearrangements in archival oxyphilic thyroid tumors: new insights in tumorigenesis and classification of Hurthle cell carcinomas? Surgery 134:881–889
50. Nesland JM, Sobrinho-Simoes MA, Holm R, Sambade MC, Johannessen JV (1985) Hurthle-cell lesions of the thyroid: a combined study using transmission electron microscopy, scanning electron microscopy, and immunocytochemistry. Ultrastruct Pathol 8:269–290
51. Nibu K-I, Otsuko N, Nakao K, Sugasawa M, Rothstein JL (2005) RET/PTC fusion gene rearrangements in Japanese thyroid carcinomas. Eur Arch Otorhinolaryngol 262:368–373
52. Nikiforov YE (2004) Genetic alterations involved in the transition from well-differentiated to poorly differentiated and anaplastic thyroid carcinoma. Endocr Pathol 15:319–327
53. Nikiforova MN, Lynch RA, Biddinger PW, Alexander EK, Dorn GW, Tallini G, Kroll TG, Nikiforov YE (2003) Ras point mutations and PAX8-PPAR gamma rearrangements in thyroid tumours: evidence for distinct molecular pathways in thyroid follicular carcinoma. J Clin Endocrinol Metab 88:2318–2326
54. Papotti M, Botto Micca F, Favero A, Palestini N, Bussolati G (1993) Poorly differentiated thyroid carcinomas with primordial cell component. A group of aggressive lesions sharing insular, trabecular, and solid patterns. Am J Surg Pathol 17:291–301
55. Papotti M, Torchio B, Grassi L, Favero A, Bussolati G (1996) Poorly differentiated oxyphilic (Hurthle cell) carcinomas of the thyroid. Am J Surg Pathol 20:686–694
56. Pilotti S, Collini P, Mariani L, Placucci M, Bongarzone I, Vigneri P, Cipriani S, Falcetta F, Miceli R, Pierotti MA, Rilke F (1997) Insular carcinoma: a distinct de novo entity among follicular carcinomas of the thyroid gland. Am J Surg Pathol 21:1466–1473
57. Puskas LG, Farid NR (2004) Gene expression in thyroid tumors. In: Farid NR (ed) The molecular basis of thyroid cancer. Kluwer, Boston, pp 265–271
58. Puskas LG, Juhasz F, Farid NR (2004) Microarray study of malignant and benign nodular thyroid tissue. In: 86th annual meeting of the Endocrine Society, Abstract P2, New Orleans, p 183
59. Puskas LG, Juhasz F, Zarva A, Hackler L Jr, Farid NR (2005) Gene profiling identifies genes specific for well-differentiated epithelial thyroid tumors. Mol Cell Biol 51:177–186
60. Raphael SJ (2002) The meanings of markers: ancillary techniques in diagnosis of thyroid neoplasia. Endocr Pathol 13:301–311
61. Rosai J, Carcangiu ML, DeLellis RA (1992) Tumors of the thyroid gland. Atlas of tumor pathology, 3rd series, vol 5. AFIP, Washington, DC
62. Rosai J (2004) Poorly differentiated thyroid carcinoma: introduction to the issue, its landmarks, and clinical impact. Endocr Pathol 15:293–296
63. Sakamoto A, Kasai N, Sugano H (1983) Poorly differentiated carcinoma of the thyroid. A clinicopathologic entity for a high-risk group of papillary and follicular carcinomas. Cancer 52:1849–1855
64. Schmid KW, Tötsch M, Hittmair A, Feichtinger H, Ladurner D, Hofstädter F (1989) Frequency of medullary thyroid carcinoma in an endemic area. Mod Pathol 2:90–93

65. Schmid KW, Tötsch M, Öfner D, Böcker W, Ladurner D (1997) Minimally invasive follicular thyroid carcinoma. A clinicopathological study. In: Schmid KW, Böcker W (eds) Thyroid pathology. Current topics in pathology. Springer, Berlin Heidelberg New York, pp 37–44
66. Schmid KW (1998) Does the encapsulated oxyphilic variant of papillary thyroid carcinoma really exist? J Pathol 184:31A
67. Schmid KW, Sheu S-Y, Görges R, Ensinger C, Tötsch M (2003) Tumoren der Schilddrüse. Pathologe 24:357–372
68. Schröder S (1988) Pathologie und Klinik maligner Schilddrüsentumoren. Gustav Fischer Verlag, Stuttgart
69. Shaha AR, Loree TR, Shah JP (1995) Prognostic factors and risk group analysis in follicular carcinoma of the thyroid. Surgery 118:1131–1136
70. Shahedian B, Shi Y, Zou M, Farid NR (2001) Thyroid carcinoma is characterized by genomic instability: evidence from p53 mutations. Mol Genet Metab 72:155–163
71. Shi Y, Zou M, Varkondi E, Nagy A, Kozma L, Farid NR (2001) Cyclin D1 in thyroid carcinomas. Thyroid 10:741–746
72. Sneed DC (1999) Protocol for the examination of specimens from patients with malignant tumors of the thyroid gland, exclusive of lymphomas. Arch Pathol Lab Med 123:45–49
73. Soares P, Trovisco V, Rocha AS, Lima J, Castro P, Preto A, Maximo V, Botelho T, Seruca R, Sobrinho-Simoes M (2003) BRAF mutations and RET/PTC rearrangements are alternative events in the etiopathogenesis of PTC. Oncogene 22:4578–4580
74. Sobrinho-Simoes MA, Nesland JM, Holm R, Sambade MC, Johannessen JV (1985) Hurthle cell and mitochondrion-rich papillary carcinomas of the thyroid gland: an ultrastructural and immunocytochemical study. Ultrastruct Pathol 8:131–142
75. Sobrinho-Simoes M, Maximo V, Castro IV, Fonseca E, Soares P, Garcia-Rostan G, Oliveira MC (2005) Hurthle (oncocytic) cell tumors of thyroid: etiopathogenesis, diagnosis and clinical significance. Int J Surg Pathol 13:29–35
76. Stewart BW, Kleihues P (2003) World cancer report. IARC Press, Lyon, pp 257–260
77. Takano T, Miyauchi A, Yoshida H, Kuma K, Amino N (2004) High-throughput differential screening of mRNAs by serial analysis of gene expression: decreased expression of trefoil factor 3 mRNA in thyroid follicular carcinomas. Br J Cancer 90:1600–1605
78. Takano T, Miyauchi A, Yoshida H, Kuma K, Amino N (2005) Decreased relative expression level of trefoil factor 3 mRNA to galectin-3 mRNA distinguishes thyroid follicular carcinoma from adenoma. Cancer Lett 219:91–96
79. Tallini G (1998) Oncocytic tumours. Virchows Arch 433:5–12
80. Thomas D, Lizyness M, Kuick R, Sanders D, Misek D, Hanash S, Nikiforov Y, Koenig R, Giorando TJ (2004) Gene expression signature of oncocytic (Hurthle cell) thyroid carcinoma. Thyroid 14:713
81. Thomas GA, Williams D, Williams ED (1989) The clonal origin of thyroid nodules and adenomas. Am J Pathol 134:141–147
82. Trovisco V, Soares P, Preto A, de Castro IV, Lima J, Castro P, Maximo V, Botelho T, Moreira S, Meireles AM, Magalhaes J, Abrosimov A, Cameselle-Teijeiro J, Sobrinho-Simoes M (2005) Type and prevalence of BRAF mutations are closely associated with papillary thyroid carcinoma histotype and patients' age but not with tumour aggressiveness. Virchows Arch 446:589–595
83. Valenta LJ, Michel-Bechet M, Warshaw JB, Maloof F (1974) Human thyroid tumors composed of mitochondrion-rich cells: electron microscopic and biochemical findings. J Clin Endocrinol Metab 39:719–733
84. Vickery AL Jr, Carcangiu ML, Johannessen JV, Sobrinho-Simoes M (1985) Papillary carcinoma. Semin Diagn Pathol 2:90–100
85. Volante M, Landolfi S, Chiusa L, Palestini N, Motta M, Codegone A, Torchio B, Papotti MG (2004) Poorly differentiated carcinomas of the thyroid with trabecular, insular, and solid patterns: a clinicopathologic study of 183 patients. Cancer 100:950–957
86. Volante M, Cavallo GP, Papotti M (2004) Prognostic factors of clinical interest in poorly differentiated carcinomas of the thyroid. Endocr Pathol 15:313–317
87. Watson RG, Brennan MD, Goellner JR, van Heerden JA, McConahey WM, Taylor WF (1984) Invasive Hurthle cell carcinoma of the thyroid: natural history and management. Mayo Clin Proc 59:851–855
88. Weber F, Shen L, Aldred MA, Morrison CD, Frilling A, Saji M, Schuppert F, Broelsch CE, Ringel MD, Eng C (2005) Genetic classification of benign and malignant follicular neoplasm based on a 3-gene combination. J Clin Endocrinol Metab 90:2512–2521
89. DeLellis RA, Lloyd RV, Heitz PU, Eng C (eds) (2004) WHO histological classification of thyroid and parathyroid tumours. World Health Organization classification of tumours. Pathology & genetics. Tumours of endocrine organs. IARC Press, Lyon, pp 49–123
90. Williams ED, Doniach I, Bjarnson O, Michie W (1977) Thyroid cancer in an iodine rich area. Cancer 39:215–222
91. Williams ED (2000) Guest editorial: two proposals regarding the terminology of thyroid tumors. Int J Surg Pathol 8:181–183
92. Wynford-Thomas D (1994) Thyroid cancer. In: Lemoine N, Neoptolemos J, Cooke T (eds) Cancer. A molecular approach. Blackwell Scientific Publications, Oxford, pp 192–222
93. Yano Y, Uematsu N, Yashiro T, Hara H, Ueno E, Miwa M, Tsujimoto G, Aiyoshi Y, Uchida K (2004) Gene expression profiling identifies platelet-derived growth factor as a diagnostic molecular marker for papillary thyroid carcinoma. Clin Cancer Res 10:2035–2043

Virchows Arch (2006) 448: 394–398
DOI 10.1007/s00428-005-0147-4

ORIGINAL ARTICLE

Y. Kapran · J. Bauersfeld · M. Anlauf ·
B. Sipos · G. Klöppel

Multihormonality and entrapment of islets in pancreatic endocrine tumors

Received: 7 December 2005 / Accepted: 8 December 2005 / Published online: 18 January 2006

Abstract We analyzed pancreatic endocrine tumors (PETs) from 200 patients for the incidence of multihormonality and entrapped islets and correlated the results with clinicopathological features. Our series included 86 cases (43%) of functioning PET and 114 cases (57%) of nonfunctioning PET. Classified according to the WHO classification, there were 32 well-differentiated benign PETs, 85 well-differentiated PETs with uncertain behavior, and 83 well-differentiated malignant PETs. All tumors were immunostained for pancreatic hormones (insulin, glucagon, somatostatin, and pancreatic polypeptide) and for additional hormones such as gastrin, vasoactive intestinal polypeptide, calcitonin, seratonin, and adrenocorticotropic hormone. Multihormonality was found in 34% of all PETs and it was a frequent finding in the tumors of the uncertain behavior (38.8%) group. Islet entrapment was found in 57 tumors (28.5%) and was significantly more frequent in PETs with uncertain and malignant behavior than benign ones (p=0.01). In 57 cases, we also investigated whether ductule entrapment accompanied islet entrapment. Of these 57 tumors, 45 (79%) tumors had accompanying ductule entrapment. Ductule entrapment did not show significant correlation with malignancy and was a more frequent finding in nonfunctioning tumors. We conclude that the incidence of multihormonality in PETs is not as high as suggested previously and islet entrapping may reflect aggressive tumor growth and may be a complementary criterion for predicting the biological behavior of PETs.

Keywords Pancreas · Endocrine tumor · Multihormonality · Islet entrapment · Malignancy

Y. Kapran (✉)
Department of Pathology, Istanbul Medical Faculty,
Istanbul University,
34390 Capa, Istanbul, Turkey
e-mail: ykapran@hotmail.com
Tel.: +90-212-4142398

J. Bauersfeld · M. Anlauf · B. Sipos · G. Klöppel
Department of Pathology, University of Kiel,
Kiel, Germany

Introduction

Pancreatic endocrine tumors (PETs) often show a heterogeneous composition. First, they may not only be composed of one cell type producing one hormone but may be multihormonal, i.e., displaying various cell types expressing different hormones [3, 6, 8–12, 18, 21]. Second, they may show ductules, either as a true neoplastic component (mixed ductal–endocrine carcinoma) or as a non-neoplastic component (PETs with entrapped ductules) [1, 4, 13, 16, 20]. Third, they may contain islets, which are thought to be entrapped by the growing tumor [20].

In this paper, we studied the incidence of multihormonality and entrapped islets and ductules in a large series of PETs of differing biology. The results were then correlated with malignancy, as defined by the WHO criteria, and functional properties such as the presence of a hormonal syndrome. This study should enable us to find an answer to the following questions: (1) Can the relatively high figures on multihormonality reported in the literature [3, 11] be confirmed and, if not, could the presence of these entrapped islets have caused the immunohistochemical findings to be misinterpreted with regard to the hormonal/multihormonal profile in PETs? (2) Can the occurrence of multihormonality and/or entrapped islets serve as an additional criterion in the identification of malignant PETs?

Materials and methods

Patients and tissues

We analyzed 200 PETs retrieved from the surgical pathology files and consultation files of the Department of Pathology of the University of Kiel. The tumor material was collected between the years 1972 and 2000. The PETs had been surgically removed from 200 patients. Clinical data (age, sex, and hormonal syndrome) and data on tumor size, metastasis, and gross local invasion at the time of diagnosis were obtained from the patients' records. Detailed pathologic data, including angioinvasion, perineural

invasion, and mitotic index, were obtained by reviewing the slides from the available blocks (mean number 1.5, range 1–5). The tumors were classified according to the WHO classification of tumors of the endocrine pancreas [19]. Tumors confined to the pancreas, smaller than 2 cm in diameter without perineural and angioinvasion, less than two mitosis per ten high power fields (HPF) and <2% Ki-67 were classified as well-differentiated endocrine tumors showing benign behavior. Tumors fulfilling one of the criteria, tumor size ≥2 cm diameter, two to ten mitosis per ten HPF, angioinvasion, perineural invasion, and >2% Ki-67, were classified as well-differentiated endocrine tumors with uncertain behavior. A diagnosis of malignancy was based on gross local invasion and/or metastasis.

The tumor tissue had been fixed in either 10% formaldehyde or Bouin's solution and embedded in paraffin. Deparaffinized sections from all available tissue blocks were cut and stained with hematoxylin and eosin and periodic acid–Schiff.

Immunohistochemistry

Three-micrometer sections were cut from one representative block per case for immunostaining for chromogranin A (CGA, monoclonal antibody, Ventana Medical systems, Tucson, AZ, USA, 1:2), synaptophysin (polyclonal antibody, DakoCytomation, Glostrup, Denmark, 1:50), Ki-67 (monoclonal antibody, DakoCytomation, 1:100), insulin (monoclonal antibody, Biogenex, San Ramon, CA, USA, 1:40), glucagon (polyclonal antibody, Biogenex, 1:60), somatostatin (polyclonal antibody, DakoCytomation, 1:200), pancreatic polypeptide (PP, polyclonal antibody, DakoCytomation, 1:5000), proinsulin (monoclonal, Hy-Test, Turku, Finland, 1:1000). gastrin (polyclonal, Paesel, Frankfurt, Germany, 1:3000), vasoactive intestinal polypeptide (VIP, polyclonal, Zymed, San Francisco, CA, USA, 1:10), serotonin (monoclonal antibody, DakoCytomation, 1:20), calcitonin (polyclonal antibody, DakoCytomation, 1:500), and adrenocorticotropic hormone (ACTH, monoclonal, DakoCytomation, 1:500). Staining for growth hormone releasing hormone (GRH, polyclonal, Biotrend, Cologne, Germany, 1:100) was performed on only one tumor that was associated with acromegaly. Immunostaining was carried out using the avidin–biotin peroxidase

Table 1 Multihormonality in pancreatic endocrine tumors

Tumor type	Number of patients (*n*)	Multihormonality (%)
Functioning		
Insulinoma	62	
Benign behavior	30	8 (26.6)
Uncertain behavior	20	9 (45)
Malignant	12	6 (50)
Gastrinoma	10	
Benign behavior	1	1 (100)
Uncertain behavior	2	1 (50)
Malignant	7	4 (57)
Glucagonoma	5	
Uncertain behavior	1	1 (100)
Malignant	4	2 (50)
Vipoma	5	
Malignant	5	1 (20)
ACTHoma	3	
Malignant	3	1 (33.3)
GRHoma	1	
Uncertain behavior	1	–
Total	86	34 (37.2)
Nonfunctioning		
Benign behavior	1	–
Uncertain behavior	61	22 (36)
Malignant	52	12 (23)
Total	114	34 (22.8)
Total	200	68 (34)

Table 2 Clinicopathologic data on 200 pancreatic endocrine tumors and frequency of islet entrapment

Tumor type	Number of patients	Mean age (years)	Sex (M:F)	Mean tumor size (cm)	No. of tumors showing islet entrapment (%)
Functioning					
Insulinoma	62				
Benign behavior	30	50.7	10:20	1.3	2 (6.7)
Uncertain behavior	20	48.5	13:7	2.1	4 (20)
Malignant	12	53.7	6:6	4	7 (58)
Gastrinoma	10				
Benign behavior	1	32	0:1	1.5	
Uncertain behavior	2	54	1:1	3.5	
Malignant	7	45.2	3:4	4.4	2 (29)
Glucagonoma	5				
Uncertain behavior	1	58	0:1	4	
Malignant	4	47.7	1:3	5.7	
Vipoma	5				
Malignant	5	59	3:2	5.9	
ACTHoma	3				
Malignant	3	46	1:2	2.7	2 (67)
GRHoma	1				
Uncertain behavior	1	65	0:1	2.2	
Total	86	50.4	38:48	2.7	17 (20)
Nonfunctioning					
Benign behavior	1	50	0:1	1.5	
Uncertain behavior	61	56	25:36	5.5	17 (27.8)
Malignant	52	52.7	26:26	5.6	23 (44.2)
Total	114	52.7	51:63	3.4	40
Total	200				57 (28.5)

complex method, as described previously [17]. The slides were subjected to pressure cooker treatment for 3.5 min prior to synaptophysin, VIP, and Ki-67 immunostaining.

Assessment of multihormonality and entrapment of islets and ductules

The percentage of tumor cells positive for each hormone was ascertained by monitoring the tumor tissue and was scored semiquantitatively. Positive immunostaining was recorded if more than 1% of the tumor cells (i.e., more than three to five cells) reacted with one of the hormonal peptide antibodies. Islets entrapped in the tumor were identified by their histopathological features and/or the spatial distribution of immunohistochemically identified islet cell types compatible with the cell composition of a normal islet. Ductule entrapment was defined as the presence of ductular components within the tumor.

Statistical analysis

Statistical analysis was performed using SPSS 11.0 for Windows. Chi square, Fischer's exact test and Student's *T* test and multivariate analysis were used to compare variables where appropriate. Differences with *p* values of less than 0.05 were regarded as significant.

Results

Of the 200 PETs in our series, 32 were well-differentiated PETs with benign behavior, 85 were well-differentiated PETs with uncertain behavior, and 83 were well-differentiated endocrine carcinomas. There were 111 female (55.5%) and 89 male (44.5%) patients with ages ranging from 3 to 88 years (mean 52.7 years). In 86 cases (43%), the tumors were functioning (i.e., associated with a hormonal syndrome), and in 114 cases (57%), they were nonfunctioning. Among the functioning group, 62 cases were classified as insulinoma (72%), ten cases as gastrinoma (5.8%), five cases as VIPoma (5.8%), five cases as glucagonoma (5.8%), three cases as ACTHoma (3.5%), and one case as GRHoma (1.2%).

Table 1 summarizes the data on multihormonality in PETs. The incidence of multihormonality was 34% for all PETs. In the functioning group, 39.5% of the tumors were multihormonal. In the non-functioning group, the incidence of multihormonality and monohormonal expression was 29.8 and 37.7%, respectively. In the nonfunctioning multihormonal tumors, 19.3% of them expressed two and 9.6% of them expressed three hormone peptides. Among the functioning group, malignant gastrinomas, malignant glucagonomas, and malignant insulinomas had the highest incidence of multihormonality (57, 50 and 50%, respectively). Except for one VIPoma, the hormone causing the syndrome could be localized in all functioning tumors. Somatostatin was the most frequently expressed hormone among the multihormonal tumors, followed by PP and glucagon. Multihormonal expression was observed in 9 of 32 (28%) benign tumors, 33 of 85 (38.8%) tumors of uncertain behavior, and 26 of 83 (31.3%) malignant tumors. There was a random distribution of the various hormone-positive cells in the multihormonal tumors.

Table 2 shows the clinicopathologic features of PETs and the distribution of the tumors with entrapped islets. Fifty-seven tumors (28.5%) had entrapped islets. They

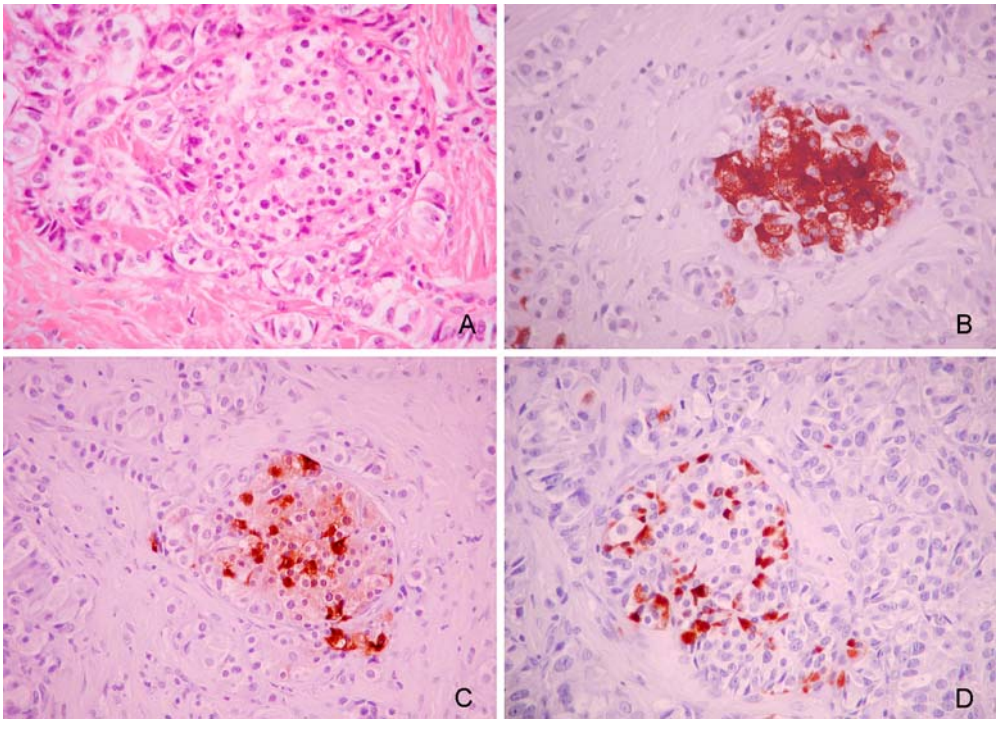

Fig. 1 **a** Malignant PET with an entrapped islet (H.E.). **b–d** Normal distribution of islet cell type hormone antibodies highlight the islet entrapped by neoplastic cells negative for the antibodies (insulin, glucagon, and pancreatic polypeptide, respectively)

were generally found at the tumor periphery and only rarely in the more central portion of the tumors (Fig. 1a). Islet entrapment was a more frequent finding in tumors with uncertain behavior (21 of 85) and malignant tumors (34 of 83) than in benign tumors (2 of 32) (p=0.01). The mean size of the tumors with islet entrapment was 3.98±2.86 cm (range 1–15 cm) and that of tumors without islet entrapment was 4.55±3.59 cm (range 0.8–15 cm), which was not statistically significant. On multivariate analysis, islet entrapment was not significant when compared to other parameters such as angioinvasion, perineural invasion, mitotic index, and Ki-67 index.

Multihormonality was detected in 35% of the tumors that had entrapped islets, but there was no association between multihormonality and islet entrapment. Of the tumors with islet entrapment, 70% belonged to the nonfunctioning group, and this was statistically significant (p=0.017). In the functioning tumors, islet entrapment was most frequent in ACTHoma, followed by malignant insulinomas. In 57 cases showing entrapped islets, we also investigated the entrapment of ductules. It was found that 45 tumors had both islet and ductule entrapment (79%), demonstrating a close association between entrapped ductules and islets. Entrapped ductules were observed in 14 of 17 (82.4%) functioning and 31 of 40 (77.5%) nonfunctioning tumors. There was no association between ductule entrapment and malignancy.

Discussion

It is well established that PETs can produce more than one immunohistochemically detectable peptide hormone. The incidence rates reported in the literature range from 33 to 69% [3, 9, 10, 12], with a mean value above 50%. In our series, the incidence of multihormonality was 34% for all tumors, both the functioning and nonfunctioning ones. Mukai et al. [12] observed a similar incidence of multihormonality (33%) to that in our study and underlined the importance of islet entrapment in the evaluation of multihormonality. We therefore investigated the incidence of entrapped islets in PETs and found islet entrapment in 28.5% of the cases in our series. As the incidence rate of 34% for multihormonality and of 28.5% for islet entrapment add up to 62.5%, which compares well with the mean incidence rate of 54% that can be extracted from the literature, it is conceivable that entrapped islets with their various cell types may have falsely been considered to be multihormonal tumor cells in some of the early studies. Multihormonality in PETs therefore seems to be somewhat rarer than has previously been thought.

Entrapped islets were most often found at the periphery of the PETs. In some PETs, we recognized entrapped islets already in the hematoxylin- and eosin-stained sections because the islet cells were smaller and more regular in size and shape than the surrounding tumor cells. In most PETs, however, the entrapped islets were only detected in the immunostainings for the four pancreatic hormones, which clearly revealed the typical cellular composition of islets, depending on the location of the tumor in the pancreas [5]. Difficulties only arose in those tumors in which the outline of an entrapped islet was blurred and indistinct, suggesting the existence of multihormonal tumor cells in its immediate vicinity. We identified such cases as entrapped islets if the adjacent immunostainings revealed that the cells that seemed to have left the islets remained in direct contact with the otherwise typically composed islet core.

Apart from the entrapment of islets, PETs may also entrap ductules. It has always been the question whether these ductules are a neoplastic or nonneoplastic component of the PETs. There is indeed an infrequently encountered group of tumors clearly consisting of both neoplastic ducts and endocrine cells, i.e., mixed exocrine–endocrine carcinomas [14]. In the remaining cases, however, it was often difficult to identify the entrapped ductules as either neoplastic or nonneoplastic. Reid et al. [16] suggested that these ductules should be considered entrapped ducts showing some degree of proliferation, while Deshpande et al. [2] suggested that they should be considered to be neoplastic resulting from transdifferentiation of the endocrine cells. In a recent study, it was confirmed on the basis of clonality and immunohistochemistry that the ductular component is entrapped rather than a neoplastic phenomenon [20]. We think that the significant correlation between islet and ductule entrapment encountered in our series also supports the latter concept. Additionally, in their study, Deshpande et al. [2] reported that ductules were more frequently observed in insulinomas. In our large series of PETs, we found a similar incidence of ductules in both insulinomas and nonfunctioning tumors. Hence, our study did not confirm the association between ductules and insulinomas. It is probably related to the relative frequency of insulinomas in the study in question.

In the WHO classification of well-differentiated PETs, metastasis and gross local invasion were accepted as the definite criteria of malignancy [19]. Angioinvasion, perineural invasion, tumor size, proliferative activity, and mitotic index have also been reported to be associated with aggressive tumor growth [7, 15]. In this paper, we can add islet entrapment as a further criterion suggesting malignancy, as our study showed that islet entrapment was significantly more common in malignant PETs than in their benign counterparts. It may be argued that islet entrapment is correlated with tumor size, as the chance that islets will be entrapped may increase as the tumor grows. However, a comparison of the size of tumors that contained islets with that of tumors that did not failed to reveal any significant correlation. Although islet entrapment is not an independent indicator of malignancy when compared with other parameters such as angioinvasion and perineural invasion, it should alert the observer to the possibility that the tumor may behave aggressively.

In summary, we found a lower incidence of multihormonality in PETs than in earlier studies and conclude that the presence of entrapped islets may have caused the immunohistochemical findings to be misinterpreted with

regard to the hormonal and multihormonal profile of these tumors. Moreover, islet entrapment may be suggestive of malignancy in PETs.

Acknowledgements We would like to thank Maike Pacena and Anja Bredtmann for their excellent technical assistance, Dr. Nadir Arican for help with the statistics, and Kay Dege for editing the manuscript.

References

1. Chatelain D, Parc Y, Christin-Maitre S, Parc R, Flejou JF (2002) Mixed ductal–pancreatic polypeptide-cell carcinoma of the pancreas. Histopathology 41:122–126
2. Deshpande V, Selig MK, Nielsen GP, Fernandez-del Castillo C, Lauwers GY (2003) Ductulo-insular pancreatic endocrine neoplasms. Clinicopathologic analysis of a unique subtype of pancreatic endocrine neoplasms. Am J Surg Pathol 27:461–468
3. Heitz PU, Kasper M, Polak JM, Klöppel G (1982) Pancreatic endocrine tumours. Immunohistochemical analysis of 125 tumours. Hum Pathol 13:263–271
4. Klöppel G (2000) Mixed exocrine–endocrine tumors of the pancreas. Semin Diagn Pathol 17:104–108
5. Klöppel G, In't Veld PA, Komminoth P, Heitz PU (1998) The endocrine pancreas. In: Kovacs K, Asa SL (eds) Functional endocrine pathology, 2nd edn. Blackwell, Boston, pp 415–487
6. Kruseman AC, Knijnenburg G, de la Riviere GB, Bosman FT (1978) Morphology and immunohistochemically-defined endocrine function of pancreatic islet cell tumours. Histopathology 2:389–399
7. La Rosa S, Sessa F, Capella C, Riva C, Leone BE, Klersy C, Rindi G, Solcia E (1996) Prognostic criteria in nonfunctioning pancreatic endocrine tumours. Virchows Arch 429:323–333
8. Larsson LI, Grimelius L, Håkanson R, Rehfeld JF, Stadil F, Holst J, Angervall L, Sundler F (1975) Mixed endocrine pancreatic tumors producing several peptide hormones. Am J Pathol 79:271–284
9. Le Bodic MF, Heymann MF, Lecomte M, Berger N, Berger F, Louvel A, De Micco C, Patey M, De Mascarel A, Burtin F, Saint-Andre JP (1996) Immunohistochemical study of 100 pancreatic tumors in 28 patients with multiple endocrine neoplasia, type I. Am J Surg Pathol 20:1378–1384
10. Liu TH, Tseng HC, Zhu Y, Zhong SX, Chen J, Cui QC (1985) Insulinoma: an immunohistochemical and morphologic analysis of 95 cases. Cancer 56:1420–1429
11. Liu TH, Zhu Y, Cui QC, Cai LX, Ye SF, Zhong SX, Jia HP (1992) Nonfunctioning pancreatic endocrine tumors. An immunohistochemical and electron microscopic analysis of 26 cases. Pathol Res Pract 188:191–198
12. Mukai K, Greider MH, Grotting JC, Rosai J (1982) Retrospective study of 77 pancreatic endocrine tumors using the immunoperoxidase method. Am J Surg Pathol 6:387–399
13. Ohike N, Jürgensen A, Pipeleers-Marichal M, Klöppel G (2003) Mixed ductal–endocrine carcinomas of the pancreas and ductal adenocarcinomas with scattered endocrine cells: characterization of the endocrine cells. Virchows Arch 442:258–265
14. Ohike N, Kosmahl M, Klöppel G (2004) Mixed acinar–endocrine carcinoma of the pancreas: a clinicopathological study and comparison with acinar-cell carcinoma. Virchows Arch 445:231–235
15. Pelosi G, Bresaola E, Bogina G, Pasini F, Rodella S, Castelli P, Iacono C, Serio G, Zamboni G (1996) Endocrine tumors of the pancreas: Ki-67 immunoreactivity on paraffin sections is an independent predictor for malignancy: a comparative study with proliferating-cell nuclear antigen and progesterone receptor protein immunostaining, mitotic index, and other clinicopathologic variables. Hum Pathol 27:1124–1134
16. Reid JD, Yuh SL, Petrelli M, Jaffe R (1982) Ductuloinsular tumors of the pancreas: a light, electron microscopic and immunohistochemical study. Cancer 49:908–915
17. Sipos B, Möser S, Kalthoff H, Török V, Löhr M, Klöppel G (2003) A comprehensive characterization of pancreatic ductal carcinoma cell lines: towards the establishment of an in vitro research platform. Virchows Arch 442:444–452
18. Solcia E, Capella C, Buffa R, Usellini L, Fiocca R, Sessa F, Tortora O (1984) The contribution of immunohistochemistry to the diagnosis of neuroendocrine tumors. Semin Diagn Pathol 1:285–296
19. DeLellis RA, Lloyd RV, Heitz PU, Eng C (2004) Pathology and genetics of tumours of endocrine organs. WHO classification of tumours, 1st edn. IARC Press, Lyon
20. van Eeden S, de Leng WWJ, Offerhaus GJA, Morsink FH, Weterman MAJ, De Krijger RR, Klöppel G, Klimstra DS (2004) Ductuloinsular tumors of the pancreas. Endocrine tumors with entrapped nonneoplastic ductules. Am J Surg Pathol 28:813–820
21. Yamaguchi K, Enjoji M (1992) Endocrine neoplasms of the pancreas: a clinicopathologic study of 24 cases and immunohistochemical remarks. Jpn J Surg 22:305–312

Virchows Arch (2006) 448: 399–406
DOI 10.1007/s00428-005-0113-1

ORIGINAL ARTICLE

Andreas Tartaglia · Guida M. Portela-Gomes · Kjell Öberg · Paolo Vezzadini · Maria P. Foschini · Mats Stridsberg

Chromogranin A in gastric neuroendocrine tumours: an immunohistochemical and biochemical study with region-specific antibodies

Received: 27 July 2005 / Accepted: 4 October 2005 / Published online: 12 January 2006

Abstract The aim of the present study was to investigate ECLomas and enterochromaffin-like (ECL) cell hyperplasia in gastric human mucosa regarding the immunohistochemical expression of chromogranin A (CgA) epitopes and to measure the same CgA epitopes in plasma samples. Eight gastric biopsies from ECLomas, seven of type I and one of type III, and biopsies from one patient showing only ECL cell hyperplasia were included in the study. Our results revealed a varying expression of region-specific CgA epitopes in the ECLomas regarding both the frequency of immunoreactive cells and intensity of immunoreactivity. CgA284–301 (pancreastatin) was not revealed in any neoplasm, whereas CgA361–372 (catestatin) was expressed in all ECLomas. However, the number of immunoreactive cells to vesicular monoamino transporter 2 (VMAT 2) or the commercial monoclonal CgA (CgA250–284) antibodies were generally higher. The plasma concentrations of the region-specific CgA radioimmunoassays differed considerably, with highest concentrations of CgA1–17 and CgA116–130 epitopes and the lowest with the CgA17–37, CgA63–76, CgA238–247 and CgA441–424 epitopes. No relationship was found between tissue expression and plasma concentration of CgA epitopes. In conclusion, this study shows that VMAT 2 and the commercial CgA antibodies seem more useful for histopathological diagnosis of ECLomas than the antibodies to the other CgA regions.

Keywords Chromogranin A · ECLomas · Enterochromaffin-like cells

A. Tartaglia (✉) · P. Vezzadini
Department of Medicine and Gastroenterology,
Bellaria Hospital, University of Bologna,
Via Altura 3,
40139 Bologna, Italy
e-mail: andreastartaglia@hotmail.com
Tel.: +39-051-6225356
Fax: +39-051-6225083

G. M. Portela-Gomes
Centre of Nutrition, University of Lisbon,
Lisbon, Portugal

G. M. Portela-Gomes
Department of Genetics and Pathology,
University of Uppsala,
Uppsala, Sweden

K. Öberg · M. Stridsberg
Department of Medical Sciences, Clinical Chemistry,
University Hospital,
Uppsala, Sweden

M. P. Foschini
Section of Anatomic Pathology at Bellaria Hospital,
University of Bologna,
Bologna, Italy

Introduction

Chromogranin A (CgA) is a glycoprotein consisting of 439 amino acids, which is located in the secretory granules of neuroendocrine (NE) cells and has been widely used as a general NE cell marker in histopathological diagnosis [18]. CgA is released together with hormones and has therefore also been used as a circulating marker for the clinical diagnosis of NE tumours and to evaluate the response to medical treatment in the follow-up of the patients [21].

The primary amino acid sequence of human CgA contains ten potential cleavage sites for specific endogenous proteases [2, 8]. Various CgA-related peptides have been identified biochemically and they are, from the N-terminal to the C-terminal region of the molecule, vasostatins (amino acid sequences 1–17/113) [6, 13], chromostatin (124–143) [10], chromacin (173–194) [35], pancreastatin (250–301) [36], WE-14 (316–329) [5], catestatin (361–372) [19], parastatin (347–419) [9] and GE-25 (367–391) [15]. The immunohistochemical expression of various CgA epitopes has been shown to vary in different human NE cells and tumours and may be of help in the characterization of some neuroendocrine tumours [22–25]. The occurrence of CgA-related peptides in human plasma has also been reported in patients with NE tumours [34].

The enterochromaffin-like (ECL) cells are the predominant NE cell type in the gastric corpus mucosa. This cell

type synthetises histamine, which is localised in the secretory granules together with various proteins, among other CgA. This cell type may give rise to neoplastic lesions ("ECLomas"), which have been divided into three subgroups: types I, II and III [27, 28, 31, 33]. Type I is a mostly benign NE tumour, usually multiple and associated with ECL cell hyperplasia due to hypergastrinaemic chronic atrophic gastritis, with or without pernicious anaemia. Type II shows the same neoplastic–hyperplastic pattern in corpus mucosa as type I and is due to hypergastrinaemia caused by gastrinoma (Zollinger–Ellison syndrome, MEN I syndrome). Evidence has been provided that ECLomas type I and II can develop through a sequence of ECL cell hyperplasia, followed by dysplasia and neoplasia [4, 38,]. Type III is a solitary neoplasm, often large and mostly with a malignant behaviour. This tumour is not associated with hypergastrinaemia or any specific gastric pathology, as described for the two other tumour types. Rarely, ECLomas type III induce an atypical carcinoid syndrome, which has been linked to histamine production [29].

The aim of the present investigation was to study the immunohistochemical expression of various CgA epitopes in ECLomas and ECL cell hyperplasia and to measure the same CgA epitopes in plasma samples from the patients included in the study.

Materials and methods

Patients

This study includes gastric biopsies from the oxyntic mucosa of the eight patients with ECLoma and the patient with only ECL cell hyperplasia subsequently observed at the Section of Anatomic Pathology at Bellaria Hospital during a 7-year period, from 1994 to 2001. At the initial gastroscopy with gastric biopsies, atrophic gastritis was observed in eight of the nine patients, and in seven of these, solitary or multiple polypoid lesions were seen. In one patient (no. 8), a solitary tumour was found without signs of atrophic gastritis. In another patient (no. 3), two polyps were removed initially. Table 1 summarises some features of the tumours in the individual patients, including the presence of ECL cell hyperplasia, pernicious anaemia and other endocrine diseases. None of the patients had signs of atypical carcinoid syndrome. Before gastroscopy, no patients had been receiving medication to decrease or inhibit gastric acid secretion.

Follow-up

A follow-up gastroscopy was performed annually in all the patients except nos. 5 and 6. Patient no. 1 underwent total gastrectomy some months after polypectomy for recurrence of numerous mucosal polyps, ranging from 3 to 8 mm in diameter. The surgical treatment was decided and performed in another hospital. In patient no. 2, the initial gastroscopy was performed in 1997, revealing multiple polyps (diameter ranging from 3 to 10 mm). Endoscopic resection of polyps was performed at yearly intervals during the initial 5 years of follow-up, with the histological diagnosis of carcinoid tumours and ECL cell hyperplasia in the surrounding mucosa. This patient had high concentrations of serum gastrin (maximum 744 pmol/l) during the initial 5 years of follow-up. Somatostatin analogue (lanreotide, 60 mg monthly) was administered from February 2002 up to now due to the

Table 1 Initial tumour features, histopathological conditions and serum gastrin levels in patients with ECLomas type I and III

Case number	1 F age 69	2 F age 56	3 M age 61	4 M age 72	5 F age 88	6 M age 93	7 F age 56	8 F age 52	9 M age 70
Tumour(s) identified at the initial gastroscopy	Multiple	Multiple	Multiple	Multiple	Multiple	Solitary	Multiple	Solitary	–
Location of tumour(s)	Fundus-corpus	Fundus-corpus	Corpus	Corpus	Corpus	Corpus	Corpus	Corpus	–
ECL cell hyperplasia	Yes	Yes	Yes	Yes	Yes	Yes	Yes	No	Yes
Chronic atrophic gastritis	Yes	Yes	Yes	Yes	Yes	Yes	Yes	No	Yes
Pernicious anaemia	Yes	Yes	Yes	Yes	Yes	No	Yes	No	No
Serum gastrin levels (pmol/l)	425.6	743.5	806.5	521	1,406	271.7	1,385.6	13	343.2
Other endocrine diseases	No	Chronic thyroiditis, hyperparathyroidism	No	No	No	No	Chronic thyroiditis, hyperparathyroidism	No	No
Follow-up time (years)	3	7	4	9	–	0.7	5	9	5

F Female, *M* male, *ECL* enterochromaffin-like

recurrence of carcinoids. Shortly after the treatment was initiated, a marked and persistent decrease in serum gastrin (<100 pmol/l) was observed. The tumour polyps regressed and have not recurred till now. Histologic examination of random biopsy specimens of corpus-fundus mucosa showed ECL cell hyperplasia, but no dysplasia. Patients no. 3 and no. 4 showed persistent ECL cell hyperplasia with dysplasia, but no further tumour polyps have been verified by examination at the subsequent yearly gastroscopies until 2004. Patient no. 5 displayed multiple microcarcinoids of about 0.5 mm in size and ECL cell hyperplasia at the initial gastroscopy in 1996, but this patient refused follow-up and medical treatment. Patient no. 6, an old man, showed at gastroscopy a single gastric polyp with chronic atrophic gastritis, associated with hypergastrinaemia. This patient died in 2003 due to heart failure; therefore, plasma CgA epitopes were not analysed. Patient no. 7 had multiple gastric carcinoids (diameter ranging from 0.6 to 10 mm) and ECL cell hyperplasia in 1997. The polyps were extirpated but recurred in the following year. At follow-up, recurrent microcarcinoids were found at each control and serum gastrin concentrations were elevated; no medical treatment has been given. Patient no. 8 had a large (1.5 cm in diameter) solitary ECLoma of type III according to Solcia classification [33] and normal gastrin plasma concentrations. No signs of recurrences were found in a 9-year follow-up after perendoscopic polypectomy. Patient no. 9 displayed linear and nodular ECL cell hyperplasia and hypergastrinaemia in 1999, but did not develop any visible gastric tumours during a 5-year follow-up. None of the patients alive has revealed signs of lymph node or distant metastasis.

Tissue specimens

The tumour specimens were routinely fixed in 10% buffered formalin for 18–20 h at room temperature and processed to paraffin. Sections (5 μm thick) were cut and attached to poly-L-lysine-coated glass slides. Haematoxylin–eosin was used as a routine staining. Corpus mucosa from surgical specimens of two patients operated for adenocarcinoma were included as non-neoplastic controls. The specimens were taken from macroscopically normal tissue at least 2 to 5 cm from the neoplasm.

Immunohistochemistry

Sections from the tumours were characterised by a monoclonal CgA antibody (LK2H10, Biogenex Laboratories, San Ramon, CA) and a rabbit polyclonal antibody against vesicular monoamino transporter 2 (VMAT 2) (AB1767, Chemicon International, Temecula, CA). All tissue sections were immunostained with the various CgA region-specific antibodies. The production of CgA region-specific antibodies and their dilutions for immunohistochemistry have been described earlier [24]. The streptavidin–biotin complex (Vectastatin Elite Kit, Vector Laboratories, Burlingame, CA) technique [14] was applied as a single immunostain, with 3-amino-9-ethylcarbazole (Sigma Chemical Co., St. Louis, MO) as chromogen. All the sections were pretreated in a microwave oven three times for 5 min at 750 W, using a citrate buffer (pH 6.0) as a retrieval solution.

Before applying the respective primary antibodies, all the sections were incubated with normal goat serum for 30 min at room temperature, at a dilution of 1:5. Then the sections were incubated with the primary antibodies overnight at 4°C. The region-specific antibodies used have been previously characterized [24].

The sections were incubated with biotinylated anti-rabbit IgG as secondary antibodies (Vector Laboratories) diluted 1:200 for 45 min at room temperature followed by the streptavidin–biotin complex (ABC) for 45 min. Subsequently, the sections were transferred to a solution containing 6 ml of 3-amino-9-ethylcarbazole, 44 ml of acetate buffer and 10 μl of H_2O_2 for about 5 min. After washing with tap water, the sections were counterstained with Mayer's haematoxylin–eosin and mounted with glycerine jelly. Between each staining step, the sections were carefully washed with PBS. The control staining entailed replacement of the first layer of antibodies by pre-immune anti-rabbit antibodies, at a dilution of 1:800.

Plasma samples

About 2–3 weeks before the initial gastroscopy, blood samples were collected from all patients, after overnight fasting, for measurements of gastrin in plasma, performed by a radioimmunoassay as previously described [16].

After an overnight fast, blood for measurements of CgA region-specific epitopes was also collected from seven of the patients. This collection was performed in 2002, i.e. at a varying time after the initial gastroscopy and removal of the tumours. Blood samples were collected in heparin-containing tubes, and plasma samples were divided into aliquots and stored at −20°C until performing the radioimmunoassay. Concentrations of the region-specific CgA epitopes were measured by specific assays as previously described [34].

Ethics

Informed consent to the examinations was obtained from each of the nine patients included in this study after full explanation of the purpose and the nature of all procedures. The study was approved by the local ethical committee.

Results

The examined biopsy sections from eight of the nine patients showed tumours expressing CgA and VMAT 2 immunoreactivity (Fig. 1a,f), i.e. the tumours represented ECLomas.

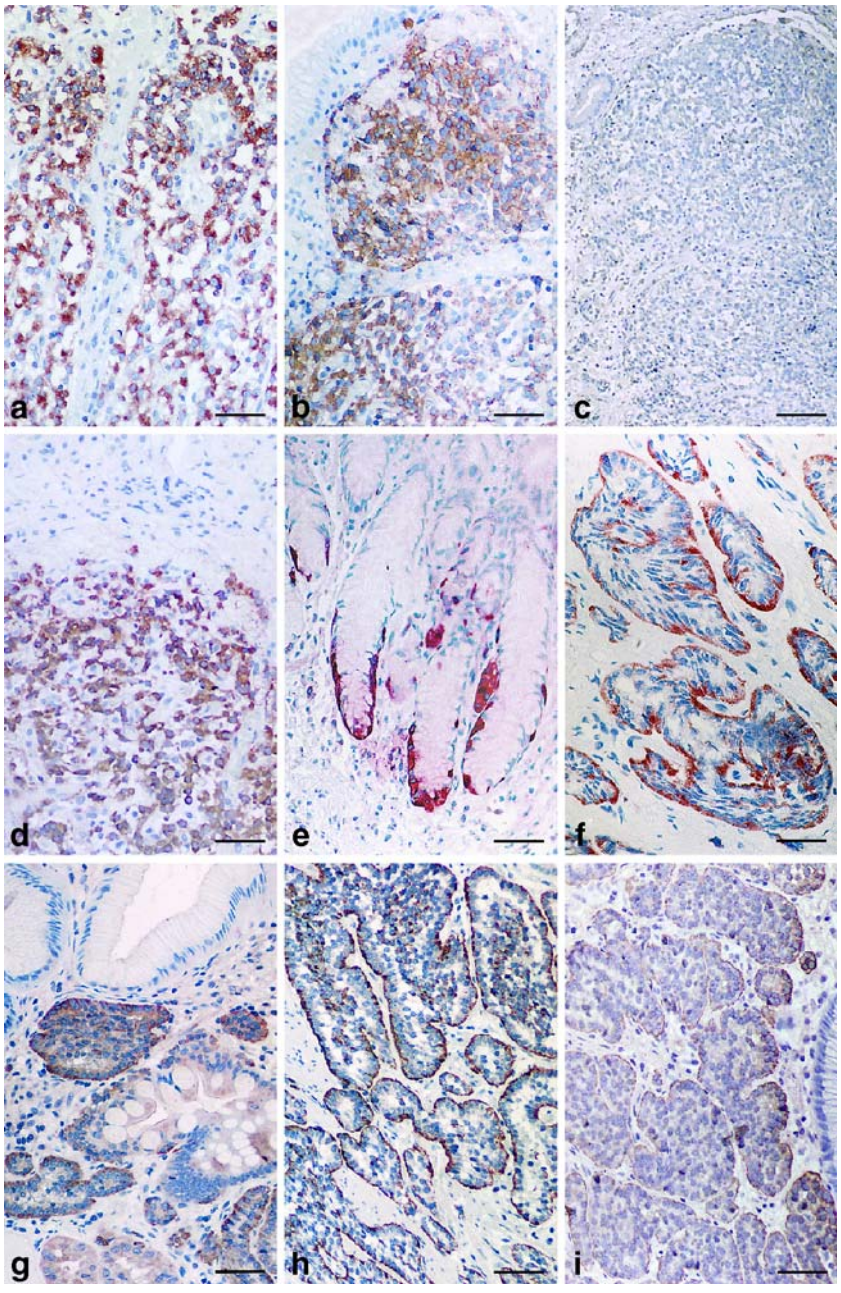

Fig. 1 **a** Type I ECLoma immunostained with antibodies to VMAT 2, showing a strong immunoreactivity in all ECL cells. Bar=30 μm **b** The same type I ECLoma as in (**a**), displaying mainly strong immunoreactivity to fragment CgA100–113. *Top left*: epithelium from normal oxyntic mucosa is seen. Bar=30 μm **c** The same type I ECLoma as in (**a**) immunostained with antibodies against fragment CgA284–301 (pancreastatin). No immunoreactive cells are visible. *Top left*: a remnant of normal glandular structures. Bar=60 μm **d** The same type I ECLoma as in (**a**) immunostained with antibodies raised against fragment CgA176–195 (chromacin). More than half of the ECL cells displayed immunoreactivity. Bar=30 μm **e** Human oxyntic mucosa exhibiting ECL cell linear hyperplasia with antibodies raised against fragment CgA176–195 (chromacin). Bar=50 μm **f** Type III ECLoma demonstrating immunoreactivity to VMAT 2, mainly in the periphery of the neoplastic nests. Bar=30 μm **g** ECLoma type I displaying moderate immunoreactivity to fragment CgA116–130 (chromostatin), mainly in the periphery of the tumour nests. At the top, normal epithelium is seen, and centrally there are two metaplastic intestinal glands containing numerous goblet cells. Bar=30 μm **h** The same type III ECLoma as in (**f**) showing strong immunoreactivity to fragment CgA361–372 (catestatin), mainly in the periphery of the neoplastic nests. Bar=30 μm **i** The same type III ECLoma as in (**f**) demonstrating weak immunoreactivity to fragment CgA63–76 (vasostatin). Bar=30 μm

Seven of these were associated with focal hyperplasia of cells expressing these two proteins; the tumours in these cases represented ECLomas of type I. The ECLomas type I varied in size between 1 and 4 mm and were located in the mucosa. The biopsies did not permit estimation of the depth of the tumour growth. The pattern varied between solid, trabecular and cell nests; sometimes the tumour revealed more than one growth pattern. The biopsies from the large

solitary tumour (no. 8) did not display ECL cell hyperplasia in the surrounding mucosa, i.e. this tumour represented an ECLoma type III. This ECLoma type III showed a trabecular and solid arrangement and did not invade the submucosa nor the muscolaris propria. The biopsies from one patient (no.9) contained only linear and nodular ECL cell hyperplasia without tumour.

The immunoreactivity to the commercial monoclonal CgA and VMAT 2 antibodies in the ECLomas and ECL cell hyperplasia (see Tables 2 and 3) was present in varying frequency, ranging from a moderate number of the cell population to the majority; the intensity of the immunostaining also varied, from weak to strong. The number of immunoreactive cells to these two antibodies was generally higher than that to the region-specific CgA epitopes.

Region-specific CgA epitopes

ECLomas type I The ECLomas expressed between two and nine CgA epitopes. CgA361–372 (Fig. 1h) was expressed in all ECLomas, CgA63–76 (Fig. 1i) in all but one tumour, while CgA284–301 antibody (pancreastatin) (Fig. 1c) was lacking in all cases. The expression of the other epitopes varied. The intensity of the immunostaining reaction with the respective antibody varied remarkably, both between the tumours and within the same tumour (Fig. 1b,d,g) (see Table 2).

ECL cell hyperplasia The expression of CgA epitopes varied in the hyperplastic ECL cells. CgA176–195 (Fig. 1e), 238–247 and 441–424 were expressed in almost all cases, whereas CgA17–38 was not expressed in any case. In general, the immunoreactivity of region-specific CgA antibodies in the hyperplastic ECL cells agreed only partly with that displayed by the ECLomas. Some CgA epitopes were expressed in the tumours but not in the hyperplastic areas (e.g. CgA17–38) and vice-versa (see Table 3).

ECLoma type III Four of the CgA sequences were demonstrated in the ECLoma type III. The frequency of immunoreactive cells varied as well as the staining intensity in different regions of the tumours.

Normal mucosa In the two cases of normal oxyntic mucosa, only four CgA epitopes were expressed (CgA100–113, CgA176–195, CgA324–337 and CgA250–284), mainly with moderate staining intensity. With the other region-specific antibodies, virtually no immunoreactive cells were demonstrated.

Table 2 Co-localization of chromogranin-A-related peptides and VMAT 2 in ECLomas using region-specific antibodies

Case number	1	2a[a]	2b[a]	3a[b]	3b[b]	4	5	6	7	8
ECLomas	Type I	Type I	Type I	Type I	Type I	Type I	Type I	Type I	Type I	Type III
CgA1–17 N-terminal vasostatin	++/*	–	+/*	–	–	++/**	+(+)/**	+/*	–	–
CgA17–38 mid-vasostatin	++/*	++/*	+/*	++/*	–	–	–	–	–	–
CgA63–76 mid-vasostatin	+++/**	++/**	++/*(*)	+++/** (*)	–	+++/***	+(+)/**	+/**	+/**	+/**
CgA100–113 C-terminal vasostatin	–	–	–	++/***	–	+++/***	+/*	–	–	–
CgA116–130 chromostatin	++/*	–	–	+++/***	–	++/*	+(+)/*	–	+(+)/*(*)	++/**
CgA176–195 chromacin	–	–	+++/***	–	–	++/**	–	–	+/**	–
CgA238–247	+++/***	–	++/**	++/*	–	+++/***	+(+)/**	++/**	++/**	+/*
CgA284–301 C-terminal pancreastatin	–	–	–	–	–	–	–	–	–	–
CgA324–337	–	++/**	–	+++/*	+++/** (*)	+/**	–	–	–	–
CgA361–372 catestatin (N-terminal parastatin)	++/**	++/**	++/*	++/*	++/**(*)	++/***	+(+)/**	+(+)/**	+(+)/***	+++/***
CgA375–384 mid-parastatin	–	++/**	–	++/**(*)	–	–	++/**	–	+/*	–
CgA441–424 C-terminal parastatin	–	+++/*	++/*	+++/**	–	–	+++/**	++/**	+/**	–
MabCgA CgA250–284 N-terminal pancreastatin	++	+	–	+++/***	+++/***	++(+)/***	+++/* (*)	+++/**	+++/*(*)	+++/* (*)
VMAT 2	++/**	++/**	–	+++/*(*)	+++/** (*)	+++/***	+++/***	+++/** (*)	+++/** (*)	+++/***

–, no immunoreactive cells; +, <10% positive cells; ++, 10–50% positive cells; +++, >50% positive cells; *, weak intensity; **, moderate intensity; ***, strong intensity

[a]Two bioptical specimens removed in two different occasions from the same patient

[b]Two bioptical specimens obtained from the same patient at the same time

Table 3 Co-localization of chromogranin-A-related peptides and VMAT 2 in ECL cell hyperplasia using region-specific antibodies

Case number	1	2a[a]	2b[a]	3b[b]	4	5	7	9
ECL cell hyperplasia	Type I	Type I	Type I	Type I	Type I	Type I	Type I	ECL hyperplasia
CgA1–17 N-terminal vasostatin	–	–	–	–	***	–	–	–
CgA17–38 mid-vasostatin	–	–	–	–	–	–	–	–
CgA63–76 mid-vasostatin	–	–	**	***	***	***	–	***
CgA100–113 C-terminal vasostatin	–	–	–	***	***	–	–	–
CgA116–130 chromostatin	–	–	–	–	**	***	**	**
CgA176–195 chromacin	***	–	**	**	***	**	***	***
CgA238–247	***	*	**	**	***	**	–	**
CgA284–301 C-terminal pancreastatin	*	–	–	–	–	–	–	–
CgA324–337	**	–	–	*	**	–	–	–
CgA361–372 catestatin (N-terminal parastatin)	–	***	–	**	–	–	***	***
CgA375–384 mid-parastatin	–	–	–	*	**	–	–	**
CgA441–424 C-terminal parastatin	**	*	*	**	*	***	–	**
MabCgA CgA250–284 N-terminal pancreastatin	**	–	**	***	***	***	***	***
VMAT 2	–	–	–	**	–	***	***	***

–, no immunoreactive cells; +, <10% positive cells; ++, 10–50% positive cells; +++, >50% positive cells; *, weak intensity; **, moderate intensity; ***, strong intensity

[a]Two bioptical specimens removed in two different occasions from the same patient

[b]Two bioptical specimens obtained from the same patient at the same time

Circulating concentrations of gastrin and chromogranin A epitopes

Serum gastrin values were raised in all patients with the exception of the type III ECLoma patient (no. 8) (reference range 11–55 pmol/l). The plasma concentrations of the region-specific CgA radioimmunoassays differed considerably between the 11 different assays. In general, the CgA1–17 and CgA116–130 assays displayed the highest levels. The plasma concentrations of CgA17–37, CgA63–76, CgA238–247 and CgA441–424 were very low compared with the other assays, while the other epitopes were measured in intermediate concentrations (Fig. 2).

Discussion

The present study is the first investigation of ECLomas regarding the immunohistochemical expression of various region-specific epitopes of the CgA molecule. The study was performed on biopsies removed at the initial gastroscopy. Plasma concentration of these CgA epitopes were performed in samples collected after removal of the tumours.

ECL cells are the main endocrine cell type in the corpus mucosa and display CgA immunoreactivity [32, 37]. However, this immunostain also visualizes other NE cells such as the enterochromaffin (serotonin-containing)

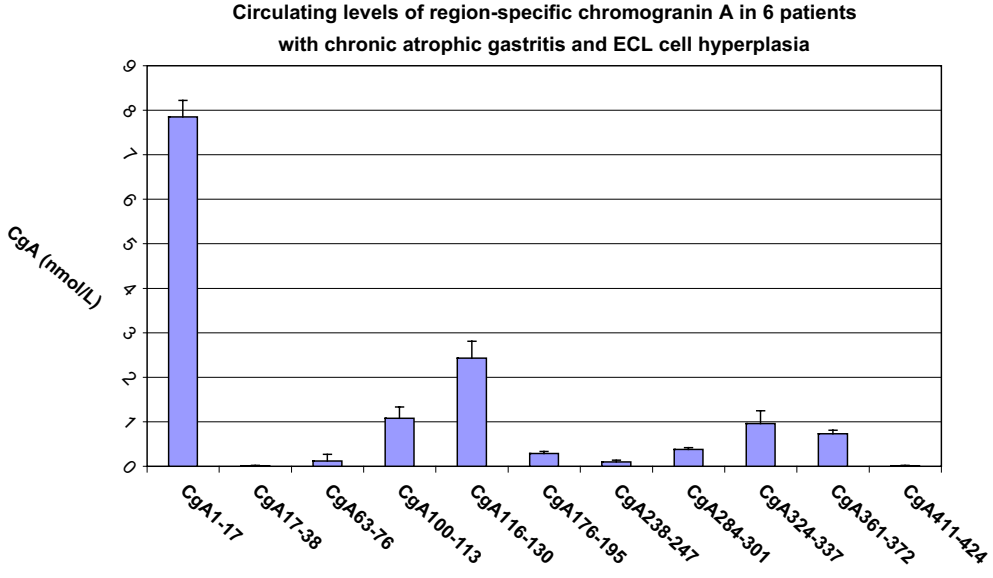

Fig. 2 Plasma concentrations of 11 region-specific CgA epitopes in six patients with chronic atrophic gastritis and ECL cell hyperplasia. Values are expressed as mean±SEM

cells. With the introduction of VMAT 2, a more specific characterization of ECL cells can be obtained [7]. The ECLomas type I and type II arise in a hypergastrinaemic condition in a stepwise evolution of hyperplasia (diffuse, linear, nodular) through dysplasia to intramucosal ECLomas, which, later on, may acquire full invasive properties [20, 39]. In type I ECLomas, the absence or marked decrease in gastric acid secretion, caused by chronic atrophic gastritis with or without pernicious anaemia [3, 40], leads to G cell hyperplasia and hypergastrinaemia. In type II ECLomas, the hypergastrinaemia is caused by a gastrinoma (Zollinger–Ellison syndrome, MEN 1 syndrome) [1, 30].

None of our patients with type I ECLoma developed metastasis. One explanation may be that most of them are small and located in the mucosa and submucosa. Type III ECLoma is not related to hypergastrinaemia and has a more malignant behaviour than the other two types [11, 26]. However, our patient with type III ECLoma had no sign of recurrent disease or metastasis during the 9-year follow-up.

In the present investigation, plasma concentration of gastrin and 11 CgA region-specific epitopes were measured in six of the patients. Gastrin concentrations reflect the initial condition and show increased values, which are in line with the patients' condition of chronic atrophic gastritis. The concentration of region-specific epitopes reflects a later stadium of the patients' gastric disease, with various degrees of ECL cell hyperplasia.

All CgA regions except one (CgA284–301; pancreastatin) were identified in one or more tumours, but the frequency and staining intensity varied within, as well as between, the tumours. The antibodies raised against the sequences CgA63–76 (vasostatin) and especially CgA361–372 (catestatin) visualized more neoplastic cells than did the other region-specific antibodies. However, the number of cells expressing either VMAT 2 or the commercial monoclonal CgA (CgA250–284) antibodies were generally higher than when the antibodies to other CgA regions were used. The staining pattern of the hyperplastic ECL cells agreed only partly with that of the ECLomas; some CgA epitopes were expressed in the tumours but not in the hyperplastic areas and vice-versa.

The variation in CgA region-specific expression patterns reflects the available epitopes. The weak or negative immunoreaction with some of the antibodies may indicate that the epitopes in question are masked by other granule-related proteins or that the 3-D molecule structure has hidden some epitopes. Other causes for the various expression of epitopes may be the lack of transcription of some molecule regions or abnormal splicing of the CgA mRNA. Another explanation may be that the pattern is related to specific post-translational processing.

ECL cell function is poorly documented clinically by combined immunohistochemical and RIA studies. Although in our study we were unable to obtain tissue and blood samples at the same period of time, it is of interest to note that molecule regions weakly expressed immunohistochemically were found in higher concentration in the plasma. On the other hand, CgA epitopes causing intense immunostaining in tissue sections (i.e. CgA63–76, 238–47, 441–424) were detected in low concentration in plasma. It appears likely that these findings may indicate different cleavage sites of the CgA molecule or may reflect, respectively, either a rapid peptide synthesis and release with a too low concentration in the ECL cells or a low release of the molecule fragments with a high concentration in the ECL cells.

In our study, the CgA284–301 sequence, pancreastatin, was the only examined sequence which could not be demonstrated immunohistochemically in either ECL neoplastic or hyperplastic cells. Furthermore, plasma concentrations of CgA284–301 were rather low, which indicate that this part of the molecule is not important in hyperplastic gastric conditions. In rat stomach, however, ECL cells have been shown to be an important source of circulating pancreastatin [12]. This difference can be either a true species difference, with different processing of the CgA molecule, or the effect of antibody specificity.

Of particular interest was that our CgA361–372 (catestatin) antibody was expressed in all ECLomas. Different biological activity has been attributed to catestatin. In addition to inhibiting catecholamine release [19], catestatin has more recently been reported to have a concentration-dependent effect on histamine release [17]. This finding in the present study may be related to the stimulatory role of catestatin on histamine release from the histamine-producing ECL neoplastic cells.

In conclusion, this study shows a variation of the tissue expression and plasma concentrations of different CgA epitopes in ECLomas type I and ECL cell hyperplasia. VMAT 2 and the commercial CgA antibodies stain more tumour cells than the antibodies to the other CgA regions and therefore seem more appropriate for the histopathological diagnosis of ECLomas, especially VMAT 2, which is more specific compared to CgA. Our investigation shows that CgA361–372 (catestatin) is the only CgA region expressed in all ECLomas, but further studies are necessary to clarify if the expression of catestatin may be a helpful complement in the characterization of ECLomas, as our study suggests.

References

1. Cadiot G, Lehy T, Mignon M (1993) Gastric endocrine cell proliferation and fundic argyrophil carcinoid tumors in patients with the Zollinger–Ellison syndrome. Acta Oncol 32:135–140
2. Conlon JM, Hamberger B, Grimelius L (1992) Isolations of peptides arising from the specific post-translational processing of chromogranin A and chromogranin B from human pheochomocytoma tissue. Peptides 13:639–644
3. Creutzfeldt W (1988) The achlorydria-carcinoid sequence: role of gastrin. Digestion 39:61–79
4. Cui G, Qvigstad G, Falkmer S, Sandvik AK, Kawase S, Waldum HL (2000) Spontaneous ECLomas in cotton rats (*Sigmodon hispidus*): tumors occurring in hypoacidic/hypergastrinaemic animals with normal parietal cells. Carcinogenesis 21:23–27

5. Curry WJ, Shaw C, Johnston CF, Thim L, Buchanan KD (1992) Isolation and primary structure of a novel chromogranin A-derived peptide, WE-14, from a human midgut carcinoid tumour. FEBS Lett 301:319–321
6. Drees BM, Rouse J, Johnson J, Hamilton JW (1991) Bovine parathyoid glands secrete a 26-kDa N-terminal fragment of chromogranin-A which inhibits parathyroid cell secretion. Endocrinology 129:3381–3387
7. Eissele R, Anlauf M, Schafer MK, Eiden LE, Arnold R, Weihe E (1999) Expression of vesicular monoamine transporters in endocrine hyperplasia and endocrine tumors of the oxyntic stomach. Digestion 60:428–439
8. Eskeland NL, Zhou A, Dinh TQ, Wu H, Parmer RJ, Mains RE, O'Connor DT (1996) Chromogranin A processing and secretion: specific role of endogenous and exogenous prohormone convertases in the regulated secretory pathway. J Clin Invest 98:148–156
9. Fasciotto BH, Trauss CA, Greely GH, Cohn DV (1993) Parastatin (porcine chromogranin A 347–419), a novel chromogranin A-derived peptide, inhibits parathyroid cell secretion. Endocrinology 133:461–466
10. Galindo E, Rill A, Bader MF, Aunis D (1991) Chromostatin, a 20-amino acid peptide derived from chromogranin A, inhibits chromaffin secretion. Proc Natl Acad Sci U S A 88:1426–1430
11. Granberg D, Wilander E, Stridsberg M, Granerus G, Skogseid B, Öberg K (1998) Clinical symptoms, hormone profiles, treatment, and prognosis in patients with gastric carcinoids. Gut 43:223–228
12. Hakanson R, Ding KQ, Norlen P, Chen D (1995) Circulating pancreastatin is a marker for the enterochromaffin-like cells of the rat stomach. Gastroenterology 108:1445–1452
13. Helle KB, Aardal S, Reed RK, Elsayed S (1990) N-terminal fragment of bovine chromogranin A inhibits the contractile response to endothelin-1 in human venous and arterial isolated fragments. J Physiol (London) 430:40P
14. Hsu SM, Raine T, Fanger H (1981) Use of avidin–biotin–peroxidase complex (ABC) in immunoperoxidase techniques: a comparison between ABC and unlabeled antibody (PAP) procedures. J Histochem Cytochem 29:577–580
15. Kirchmair R, Leitner B, Fischer-Colbrie R, Marksteiner J, Hogue-Angeletti R, Winkler H (1995) Large variations in the proteolytic formation of a chromogranin A-derived peptide (GE-25) in neuroendocrine tissues. Biochem J 310:331–336
16. Kleveland PM, Haugen SE, Waldum HL (1985) The preparation of bioactive 125I-gastrin, using Iodo-gen as oxidizing agent, and the use of this tracer in receptor studies. Scand J Gastroenterol 20:569–576
17. Krüger PG, Mahata SK, Helle KB (2003) Catestatin (CgA344–364) stimulates rat mast cell release of histamine in a manner comparable to mastoparan and other cationic charged neuropeptides. Regul Pept 114:29–35
18. Lloyd RV, Wilson BS (1983) Specific endocrine tissue marker defined by a monoclonal antibody. Science 222:628–630
19. Mahata SK, O'Connor DT, Mahata M, Yoo SH, Taupenot L, Wu H, Gill BM, Parmer RJ (1997) Novel autocrine feedback control of catecholamine release. A discrete chromogranin A fragment is a noncompetitive nicotinic cholinergic antagonist. J Clin Invest 100:1623–1633
20. Muller J, Kirchner T, Muller-Hermelink HK (1987) Gastric endocrine cell hyperplasia and carcinoid tumors in atrophic gastritis type A. Am J Surg Pathol 11:909–917
21. O'Connor DT, Takiyyuddin MA, Cervenka JH, Parmer RJ, Barbosa JA, Chang YM, Hsiao RJ (1990) Circulating chromogranin A as a diagnostic tool in clinical chemistry. Acta Histochem Suppl 38:27–33
22. Portela-Gomes GM, Stridsberg M (2001) Selective processing of chromogranin A in the different islet cells in human pancreas. J Histochem Cytochem 49:483–490
23. Portela-Gomes GM, Stridsberg M (2002) Chromogranin A in the human gastrointestinal tract: an immunocytochemical study with region specific antibodies. J Histochem Cytochem 50:1487–1492
24. Portela-Gomes GM, Grimelius L, Johansson H, Wilander E, Stridsberg M (2001) Chromogranin A in human neuroendocrine tumors—an immunohistochemical study with region-specific antibodies. Am J Surg Pathol 25:1261–1267
25. Portela-Gomes GM, Grimelius L, Stridsberg M, Puppa G, Bresaola E, Viale G, Pelosi G (2005) Expression of amino acid sequences of the chromogranin A molecule and synaptic vesicle protein 2 in neuroendocrine tumors of the lung. Virchows Arch 446:604–612
26. Qvigstad G, Falkmer S, Westre B, Waldum HL (1999) Clinical and histopathological tumour progression in ECL cell carcinoids ("ECLomas"). APMIS 107:1085–1092
27. Rappel S, Altendorf-Hofmann A, Stolte M (1995) Prognosis of gastric carcinoid tumours. Digestion 56:455–462
28. Rindi G, Bordi C, Rappel S, La Rosa S, Stolte M, Solcia E (1996) Gastric carcinoids and neuroendocrine carcinomas: pathogenesis, pathology, and behavior. World J Surg 20:168–171
29. Roberts LJ 2nd, Bloomgarden ZT, Marney SR Jr, Rabin D, Oates JA (1983) Histamine release from a gastric carcinoid: provocation by pentagastrin and inhibition by somatostatin. Gastroenterology 84:272–275
30. Robinson M (1999) Review article: current perspectives on hypergastrinaemia and enterochromaffin-like-cell hyperplasia. Aliment Pharmacol Ther13:5–10
31. Simonsson M, Eriksson S, Hakanson R, Lind T, Lonroth H, Lundell L, O'Connor DT, Sundler F (1988) Endocrine cells in the human oxyntic mucosa—a histochemical study. Scand J Gastroenterol 23:1089–1099
32. Solcia E, Capella C, Sessa F, Rindi G, Cornaggia M, Riva C, Villani L (1986) Gastric carcinoids and related endocrine growths. Digestion 35:3–22
33. Solcia E, Bordi C, Creutzfeldt W, Dayal Y, Dayan AD, Falkmer S, Grimelius L, Havu N (1988) Histopathological classification of nonantral gastric endocrine growths in man. Digestion 41:185–200
34. Stridsberg M, Eriksson B, Öberg K, Janson ET (2004) A panel of 11 region-specific radioimmunoassays for measurement of human chromogranin A. Regul Pept 117:219–227
35. Strub JM, Sorokine O, Van Dorsselaer A, Aunis D, Metz-Boutigue MH (1997) Phosphorylation and O-glycosylation sites of bovine chromogranin A from adrenal medullary chromaffin granules and their relationship with biological activities. J Biol Chem 272:11928–11936
36. Tatemoto K, Efendic S, Mutt V, Makk G, Feistner GJ, Barchas JD (1986) Pancreastatin, a novel pancreatic peptide that inhibits insulin secretion. Nature (London) 324:476–478
37. Thomas RM, Baybick JH, Elsayed AM, Sobin LH (1994) Gastric carcinoids—an immunohistochemical and clinicopathologic study of 104 patients. Cancer 73:2053–2058
38. Waldum HL, Brenna E, Sandvik AK (1998) Relationship of ECL cells and gastric neoplasia. Yale J Biol Med 71:325–335
39. Waldum HL, Sandvik AK, Idle JR (1998) Gastrin is the most important factor in ECL tumorigenesis. Gastroenterology 114: 1113–1115
40. Wilander E, Nordgren H, Öberg K (1986) Nonantral gastric carcinoid tumours associated to hypergastrinaemia. Acta Med Scand 219:393–397

Virchows Arch (2006) 448: 407–411
DOI 10.1007/s00428-005-0145-6

ORIGINAL ARTICLE

I. Gütgemann · S. Haas · J. P. Berg · H. Zhou
R. Büttner · H.-P. Fischer

CD56 expression aids in the differential diagnosis of cholangiocarcinomas and benign cholangiocellular lesions

Received: 22 September 2005 / Accepted: 7 December 2005 / Published online: 13 January 2006

Abstract CD56 (neuronal cell adhesion molecule, N-CAM) has been reported in neuroendocrine tumours and as a marker of reactive biliary epithelial cells. However, up to date, it is not used to distinguish malignant from non-malignant biliary lesions. In this study, we systematically examined CD56 expression on 98 tumours arising from the biliary tree as well as intrahepatic conditions with reactive neoductules. When neuroendocrine carcinomas are excluded, only 4 of 32 (12.5%) cholangiocarcinomas expressed CD56, 2 of which showed clear cell morphology. Reactive bile ductules adjacent to cirrhotic nodules as well as in focal nodular hyperplasia were CD56 positive. Twelve of 17 (70.5%) bile duct adenomas were CD56 positive, whereas von Meyenburg complexes expressed CD56 only very focally in less than 5% of lesional cells. Bile duct cysts were negative for CD56 with the exception of focally interspersed neuroendocrine cells, similar to that seen in segmental bile ducts. Thus, if van Meyenburg complexes are excluded, CD56 can be used to differentiate intrahepatic non-neoplastic from neoplastic proliferations, which is a helpful diagnostic tool in small liver biopsies.

Keywords CD56 · N-CAM · Cholangiocarcinoma · Bile ductules

Introduction

The distinction of cholangiocarcinoma from reactive bile ductules can be a challenge if performed on morphological grounds only. Most often, the clinical picture and macroscopic evaluation of the specimen are helpful, as cholangiocarcinomas present late and as intra- or extrahepatic mass forming lesions. However, diagnostic challenges exist, such as with periductal infiltrating types [13] or well-differentiated carcinomas in small liver biopsies. In contrast to cholangiocarcinomas, reactive bile ductules are most often found in liver biopsies showing chronic hepatitis or adjacent to cirrhotic nodules. Sometimes, bile ductules are found adjacent to a malignant tumour or in liver biopsies that are non-representative of the tumour to be sampled.

Histologically, invasive growth pattern and cytology of bile duct cells with high nuclear-cytoplasmatic ratio, pleomorphic, irregular and hyperchromatic nuclei, prominent nucleoli or brisk mitotic activity, help to distinguish neoplastic from reactive lesions. However, in some cases, this distinction becomes difficult, especially when small liver biopsies are reviewed or when cytological atypia is minimal. In such cases, the diagnosis perhaps "cannot exclude malignancy". Thus, to separate benign from malignant biliary epithelium, novel markers are needed. In this study, we describe CD56, previously designated as neuronal cell adhesion molecule (N-CAM), as one such marker. CD56 has also been demonstrated to be expressed on regenerating bile duct epithelium [16], in the setting of alcoholic liver disease [3], congenital and acquired liver disease [9], primary sclerosing cholangititis [16], extrahepatic biliary atresia [15], cholestatic liver disease [12], and during early developmental stages of the ductal plate in fetal livers [5]. However, what has been lacking is a systematic comparison of CD56 on tumours and tumour-like lesions of the cells of the biliary tract and its evaluation as a diagnostic marker.

Methods

Surgical specimens

The study material comprised 98 cases, including 23 intrahepatic cholangiocarcinomas, 9 adenocarcinomas of the extrahepatic bile ducts, 17 bile duct adenomas, 16 von Meyenburg complexes, 8 bile duct cysts and 2 mucinous

I. Gütgemann (✉) · S. Haas · J. P. Berg · H. Zhou ·
R. Büttner · H.-P. Fischer
Institute of Pathology, University of Bonn (UKB),
Sigmund-Freud-Str. 25,
53105 Bonn, Germany
e-mail: ines.guetgemann@ukb.uni-bonn.de
Tel.: +49-228-2876968
Fax: +49-228-2875030

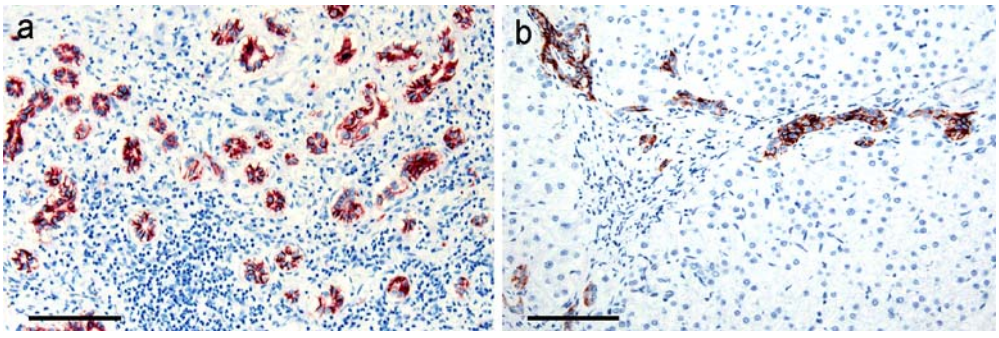

Fig. 1 CD56 is strongly and diffusely expressed in reactive neoductules adjacent to a cirrhotic nodule (**a**) and within neoductules in focal nodular hyperplasia (**b**) (DAB, ×200, *scale bar* = 100 μm)

cystadenomas. Furthermore, 10 cases of end-stage cirrhosis, 10 cases of focal nodular hyperplasia (FNH) and 11 cases of intrahepatic metastases of colorectal adenocarcinomas were included. Paraffin-embedded tissue that was collected during the period of 1991–2005 was retrieved from the files of the Department of Pathology, University of Bonn. Histologic grade of intrahepatic cholangiocarcinomas and adenocarcinomas of the extrahepatic bile ducts ranged from well (8), over moderately (14) to poorly differentiated (6).

Immunohistochemistry

Tissues were fixed in neutral buffered formalin and embedded in paraffin for histologic processing. Tissue sections were stained with haematoxylin and eosin for conventional histology. Representative paraffin-fixed tissue blocks were cut and processed for immunohistochemical studies using an immunostainer (Techmate 500; DAKO). Sections were stained using anti-CD56/NCAM (1:50 dilution, DAKO), anti-CK7 (1:500, DAKO), anti-HepPar 1 (1:250, DAKO), anti-chromogranin (1:500, DAKO) and anti-synaptophysin (1:10, DAKO). The antigen–antibody binding was visualized by means of the avidin–binding complex (ABC method), using 3-amino-9-ethylcarbazol (AEC) as a chromogen. Appropriate positive and negative controls were run concurrently. Diagnosis and interpretation of immunohistochemical stains were confirmed by two independent pathologists.

Results

Normal segmental bile ducts express very little CD56. In contrast, reactive neoductules are positive for CD56, as seen in fibrous bands in cirrhosis (Fig. 1a) and in FNH (Fig. 1b).

Most cholangiocarcinomas were CD56 negative (Fig. 2a,b). Only 4 of 32 cases (12.5%) of cholangiocarcinomas were CD56 positive, all of which were negative for the neuroendocrine markers chromogranin and synaptophysin. Of these four CD56-positive tumours, two showed clear cell morphology and immunohistochemical markers consistent with cholangiocellular origin. The remaining two CD56-positive cholangiocarcinomas were both intra-

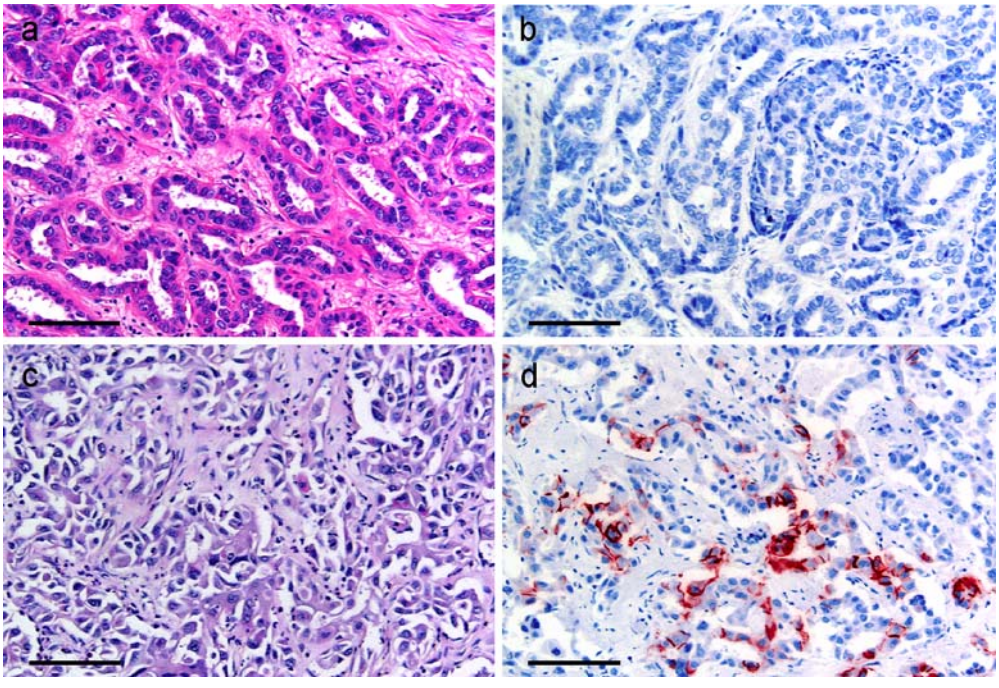

Fig. 2 CD56 expression in intrahepatic cholangiocarcinoma: These carcinomas are mostly negative for CD56 (**a**, **b**) and rarely focally positive for CD56 (**c**, **d**) (*left*: H & E, *right*: DAB, ×200, *scale bar* = 100 μm)

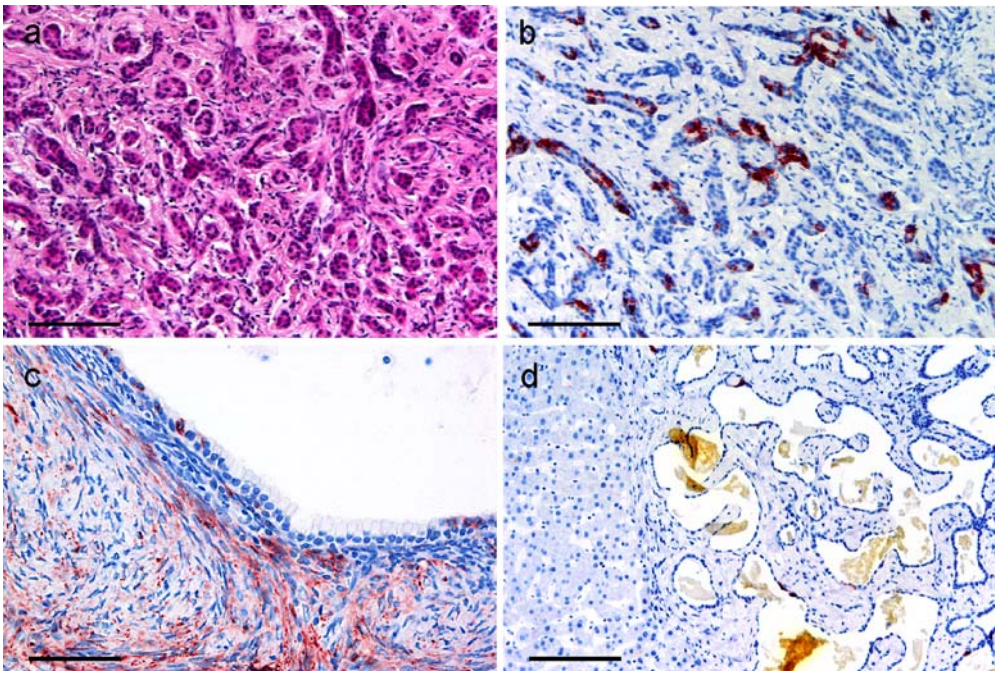

Fig. 3 CD56 expression in benign tumours and tumour-like lesions: In bile duct adenoma (**a**, **b**), focal expression is also seen in flattened epithelium of mucinous cystadenoma and in ovarian type stroma (**c**) and in von Meyenburg complexes (**d**) (*left*: H & E, *right*: DAB, ×200, *scale bar* = 100 μm)

hepatic, moderately differentiated and showed very focal CD56 expression. The first case had tubular and solid architecture (Fig. 2c,d), and the second case had a trabecular growth pattern with intensive desmoplastic stroma.

Eleven intrahepatic metastases of colorectal adenocarcinomas were negative for CD56. Benign tumours and tumour-like lesions showed a somewhat diverse staining pattern with anti-CD56.

In bile duct adenomas, 12 of 17 lesions showed at least partial expression of CD56 (Fig. 3a,b). All eight bile duct cysts examined were either negative or showed very focal staining. Mucinous cystadenomas were negative on most of the epithelium; however, especially in flattened epithelium, CD56 was expressed focally as well as in ovarian type stroma cells (Fig. 3c). The majority of von Meyenburg complexes showed very focal CD56 expression in cells lying in between biliary cells (Fig. 3d), similar as the staining pattern observed in segmental bile ducts. The summary of the results in Table 1 highlights the observation that CD56 expression is mostly seen in benign cholangiocellular lesions.

Table 1 CD56 expression in malignant and benign cholangiocellular lesions

	Positive	Negative
Cholangiocarcinoma, intrahepatic	4[a]	28
Adenocarcinoma of the extrahepatic bile ducts	0	9
Bile duct adenoma	12	5
Bile duct cyst	0	8
Mucinous cystadenoma	0	2
von Meyenburg complex	0	16[b]
Focal nodular hyperplasia (neoductules)	10	0
Cirrhosis (neoductules)	10	0

Negative: CD56 staining in less than 5% of lesional cells. Positive: CD56 staining in more than 5% of lesional cells

[a]Two of these carcinomas were clear cell cholangiocarcinomas

[b]Twelve of 16 cases showed focal CD56 expression in less than 5% of lesional cells

Discussion

The distinction of malignant vs benign cholangiocellular proliferations in the liver is of utmost importance since cholangiocarcinomas carry a poor prognosis and high mortality. Lesions that can be mistaken for a cholangiocelullar carcinoma are reactive neoductules and bile duct adenomas, also designated as peribiliary gland hamartomas [2, 8]. The pattern of growth does not always distinguish malignant from benign ductular epithelium, as cholangiocarcinoma can be found immediately adjacent to and confluent with adjacent hepatic parenchyma. Also, reactive neoductules occur in direct contact with hepatocytes as seen in cirrhosis (Fig. 1a) and FNH (Fig. 1b), a benign hepatic lesion thought to occur due to aberrant vascular supply. Furthermore, neoductules may show cytological atypia, making the distinction from a malignant glandular proliferation difficult. Especially in small liver biopsies, the architecture may not be of aid in recognizing reactive neoductules.

Cholangiocarcinomas arise from the biliary epithelium anywhere along the biliary ductal system. In this study, we show that reactive neoductules in the liver are CD56 positive, whereas most malignant tumours arising from bile duct epithelium are CD56 negative. Exceptions do exist, however, including cholangiocarcinomas with clear cell differentiation, that are CD56 positive.

Reactive bile ductules can both represent a metaplastic change of hepatocytes and reflect a proliferation of resident bile duct cells or precursor cells thereof. In FNH, evidence

exists for a metaplastic change of resident hepatocytes [6, 7]. We could show in this study that both metaplastic neoductules in FNH, as well as reactive bile duct proliferations, are characterized by expression of CD56. Interestingly, in vitro, mature hepatocytes are able to transdifferentiate into bile duct cells [11]. In cholestatic liver disease, CD56 expression in reactive bile ductules has been correlated with neuroendocrine differentiation of such cells [12].

Bile duct cysts are negative or focally positive for CD56, similar to normal bile ducts. Fortunately, bile duct cysts are easily distinguished from malignant tumours by macroscopic and microscopic findings alone.

In our study, CD56 is partially positive in a substantial number of bile duct adenomas, thus enabling a distinction from malignant counterparts. Bile duct adenomas have also been designated peribiliary gland hamartoma due to the observation that they resemble peribiliary glands rather than bile ducts [2]. Typically, in older lesions, hyalinized stroma develops to compress glands, a feature that must not be mistaken for desmoplastic stroma. Also helpful are the presence of pre-existing portal areas and the absence of cytologic features of malignancy and lymphatic or vascular invasion. In difficult cases, however, CD56 can confirm the diagnosis of a benign lesion.

In contrast to bile duct adenomas, von Meyenburg complexes show mostly negativity for CD56, with the exception of less than 5% cells that are located in between biliary epithelial cells. von Meyenburg complexes are thought to represent developmental anomalies. Helpful are location and multifocality as well as their size of less than 5 mm. von Meyenburg complexes can be easily distinguished from cholangiocarcinomas, as they frequently lie underneath or in close proximity to the liver capsule. Histologically, they are found paraportal and sometimes contain bile, thus distinguishing them from bile duct adenoma. Most often, diagnosis is straightforward on morphologic grounds. However, one needs to take into account negative or only focal expression of CD56 in von Meyenburg complexes when using CD56 as a diagnostic tool.

In contrast to the benign lesions mentioned above, the great majority of cholangiocarcinomas are CD56 negative. Exceptions in this study include the two carcinomas with clear cell differentiation. Clear cell cholangiocarcinomas represent a rare variant that is recognized on morphologic and immunohistochemical grounds [10, 14]. Second, metastases of neuroendocrine carcinomas need to be excluded prior to interpretation of CD56 staining in the evaluation of benign and malignant intrahepatic lesions [4]. Neuroendocrine differentiation can be excluded best by performing a chromogranin or synaptophysin stain. Third, CD56 expression has been observed on cholangiocarcinomas that arise in a background of hepatitis B and C infection [1]. The authors describe that these CD56-positive variants are unlikely to metastasize and more frequently show venous invasion, perineural invasion and intrahepatic metastases. Most of these carcinomas were undifferentiated, thus not posing a problem in misdiagnosis of a benign lesion. In this study, all cholangiocarcinomas examined arose in non-cirrhotic liver tissue and without clinical evidence of hepatitis B or C infection.

In conclusion, CD56 expression, when observed in biliary epithelial cells, is likely reflecting the benign nature of the lesion examined. Clear cell cholangiocellular and neuroendocrine carcinomas should be excluded on morphologic and immunohistochemical grounds. CD56 represents an important diagnostic tool helpful in distinguishing malignant and benign tumours arising from the biliary tree.

References

1. Asayama Y, Aishima S, Taguchi K, Sugimachi K, Matsuura S, Masuda K, Tsuneyoshi M (2002) Coexpression of neural cell adhesion molecules and bcl-2 in intrahepatic cholangiocarcinoma originated from viral hepatitis: relationship to atypical reactive bile ductule. Pathol Int 52:300–306
2. Bhathal PS, Hughes NR, Goodman ZD (1996) The so-called bile duct adenoma is a peribiliary gland hamartoma. Am J Surg Pathol 20:858–864
3. Chedid A, Mendenhall CL, Moritz TE (1999) The antigenic heterogeneity of the bile duct epithelium in alcoholic liver disease. VA Cooperative Study Group 275. Arch Pathol Lab Med 123:411–414
4. Chu PG, Arber DA, Weiss LM (2003) Expression of T/NK-cell and plasma cell antigens in nonhematopoietic epithelioid neoplasms. An immunohistochemical study of 447 cases. Am J Clin Pathol 120:64–70
5. Fabris L, Strazzabosco M, Crosby HA, Ballardini G, Hubscher SG, Kelly DA, Neuberger JM, Strain AJ, Joplin R (2000) Characterization and isolation of ductular cells coexpressing neural cell adhesion molecule and Bcl-2 from primary cholangiopathies and ductal plate malformations. Am J Pathol 156:1599–1612
6. Fischer HP, Lankes G (1991) Morphologic correlation between liver epithelium and mesenchyme allows insight into histogenesis of focal nodular hyperplasia (FNH) of the liver. Virchows Arch B Cell Pathol Incl Mol Pathol 60:373–380
7. Fischer HP, Meybehm M, Zhou H, Schoch J (1995) Hepatic neoductules. Verh Dtsch Ges Pathol 79:36–46
8. Ishak KG, Goodman ZD, Stocker JT (1999) Tumors of the liver and intrahepatic bile ducts. Armed Forces Institute of Pathology, Washington, DC, pp 1–356
9. Libbrecht L, Cassiman D, Desmet V, Roskams T (2001) Expression of neural cell adhesion molecule in human liver development and in congenital and acquired liver diseases. Histochem Cell Biol 116:233–239
10. Logani S, Adsay V (1998) Clear cell cholangiocarcinoma of the liver is a morphologically distinctive entity. Human Pathol 29:1548–1549
11. Nishikawa Y, Doi Y, Watanabe H, Tokairin T, Omori Y, Su M, Yoshioka T, Enomoto K (2005) Transdifferentiation of mature rat hepatocytes into bile duct-like cells in vitro. Am J Pathol 166:1077–1088

12. Roskams T, van den Oord JJ, De Vos R, Desmet VJ (1990) Neuroendocrine features of reactive bile ductules in cholestatic liver disease. Am J Pathol 137:1019–1025
13. Sasaki A, Aramaki M, Kawano K, Morii Y, Nakashima K, Yoshida T, Kitano S (1998) Intrahepatic peripheral cholangiocarcinoma: mode of spread and choice of surgical treatment. Br J Surg 85:1206–1209
14. Tihan T, Blumgart L, Klimstra DS (1998) Clear cell papillary carcinoma of the liver: an unusual variant of peripheral cholangiocarcinoma. Human Pathol 29:196–200
15. Torbenson M, Wang J, Abraham S, Maitra A, Boitnott J (2003) Bile ducts and ductules are positive for CD56 (N-CAM) in most cases of extrahepatic biliary atresia. Am J Surg Pathol 27:1454–1457
16. Van Den Heuvel MC, Slooff MJ, Visser L, Muller M, De Jong KP, Poppema S, Gouw AS (2001) Expression of anti-OV6 antibody and anti-N-CAM antibody along the biliary line of normal and diseased human livers. Hepatology 33:1387–1393

Virchows Arch (2006) 448: 412–421
DOI 10.1007/s00428-005-0136-7

ORIGINAL ARTICLE

Yoshio Jinno · Haruo Ohtani · Shiro Nakamura · Motoji Oki · Kiyoshi Maeda · Kohei Fukushima · Hiroshi Nagura · Nobuhide Oshitani · Takayuki Matsumoto · Tetsuo Arakawa

Infiltration of CD19$^+$ plasma cells with frequent labeling of Ki-67 in corticosteroid-resistant active ulcerative colitis

Received: 3 August 2005 / Accepted: 17 November 2005 / Published online: 25 January 2006

Abstract Abnormalities in humoral immunity are implicated in the pathogenesis of ulcerative colitis. However, the detailed mechanisms of B-cell activation in the locale remain unaccounted for. We analyzed ulcerative colitis from the standpoint of lymphocytic expansion in the loco. Intestinal specimens obtained at surgery from 30 patients with ulcerative colitis treated with corticosteroids and 15 with Crohn's disease were analyzed by immunohistochemistry and flow cytometry. Ulcerative colitis was characterized by a diffuse distribution of Ki-67$^+$ small round cells particularly in the ulcer base (that were CD19$^+$ and CD20$^-$), with a significant number of them also CD138$^+$. Immunoelectron microscopy for CD19 revealed an abundance of rough endoplasmic reticulum in the cytoplasm. These indicated that they are of immature plasma lineage cells. By contrast, plasma cells in Crohn's disease were negative for CD19, and the labeling for Ki-67 was infrequent, showing mature phenotype. Flow cytometry revealed an occurrence of CD19$^+$ and CD20$^-$ cells in ulcerative colitis but not in Crohn's disease. The labeling index of Ki-67 among CD19$^+$ plasma cells was positively correlated with the clinical activity of ulcerative colitis. High labeling of Ki-67 in CD19$^+$ plasma cells is specific for active ulcerative colitis that was resistant to medical treatment by corticosteroids.

Keywords Ulcerative colitis · Ki-67 · B-lineage cells · Plasma cells

Y. Jinno · S. Nakamura · N. Oshitani · T. Matsumoto · T. Arakawa
Department of Gastroenterology,
Osaka City University Graduate School of Medicine,
Osaka, Japan

H. Ohtani (✉)
Department of Pathology,
National Hospital Organization Mito Medical Center,
Ibaraki, Japan
e-mail: hohtani@mito.hosp.go.jp

M. Oki
Department of Gastroenterology,
Tohoku University Graduate School of Medicine,
Sendai, Japan

K. Maeda
Surgical Oncology,
Osaka City University Graduate School of Medicine,
Osaka, Japan

K. Fukushima
Department of Surgery,
Tohoku University Graduate School of Medicine,
Sendai, Japan

H. Ohtani · H. Nagura
Department of Pathology,
Tohoku University Graduate School of Medicine,
Sendai, Japan

Y. Jinno (✉) · T. Matsumoto
Department of Internal Medicine, Division of Gastroenterology,
Hyogo College of Medicine,
Nishinomiya, Japan
e-mail: jinno@hyo-med.ac.jp

Introduction

Ulcerative colitis and Crohn's disease comprise idiopathic inflammatory bowel disease (IBD). Immunologic abnormalities have been implicated in the pathogenesis of IBD, and immunosuppressive therapies are, at least in part, effective for the treatment of IBD. In Crohn's disease, T-helper type 1 (Th1)-shifted overactivation of cellular immunity is closely involved in its pathogenesis together with the abnormality of macrophages [1, 16]. Recent reports indicated that mutation of nucleotide-binding oligomerization domain 2 (NOD2), a key mediator of innate host defense in the intestinal mucosa, is involved in the pathogenesis of Crohn's disease [4, 15]. As for ulcerative colitis, in turn, overactivation of humoral immunity is implicated in its pathogenesis. Halstensen et al. [9] reported accumulation of immunoglobulin G (IgG) and activated complement complex on colonic epithelial cells in ulcerative colitis. Lamina propria lymphocytes contain activated B-cell subsets [24], which are considered to be important sources of increased immunoglobulins, including autoantibodies in ulcerative colitis [5]. Therefore, acute exac-

erbation of ulcerative colitis is thought to be accompanied by massive, local activation of humoral immune responses. However, little is known about the mechanisms and processes of B-lineage cell activation in the affected intestinal mucosa in ulcerative colitis.

One of the clues to assess the dynamics of lymphocytes in the locale, particularly clonal expansion after possible antigenic stimuli, is to analyze the proliferative activity of lymphocytes by double staining of a lymphoid cell marker and Ki-67, one of the representative cell-proliferation-associated nuclear antigens [8]. This histochemical method was introduced by Saiki et al. in a study on immune responses in Epstein–Barr-virus-associated gastric cancer [18]. In IBD, Ki-67 has been used to assess the proliferative activity of epithelial cells in dysplasia [10, 12]. Fell et al. applied double staining of Ki-67 and lymphoid cell marker to the analysis of lamina propria lymphocytes (LPLs) in IBD without referring to B cells [6].

We already reported the presence of a high labeling index of Ki-67 in $CD19^{+}$ and $CD138^{+}$ cells in inflamed vermiform appendix in patients with ulcerative colitis [11]. However, analyses in the colon were not performed. The present paper performed detailed morphological analyses to report that Ki-67 labeling in lymphoid cells is one of the predominant features of ulcerative colitis, particularly in the ulcer base, and that these proliferating cells were identified as plasma cells. We discuss the possible significance of these novel findings in the pathogenesis of ulcerative colitis.

Materials and methods

Tissue

Tissue specimens were obtained during surgical operations performed on 30 patients with ulcerative colitis and 15 patients with Crohn's disease at Osaka City University Hospital and Tohoku University Hospital. All patients were Japanese. All ulcerative colitis patients had total colitis, which was treated with corticosteroids. The average of total prednisolone dose at the time of operation was 16,731 mg

Table 1 The list of all patients with ulcerative colitis and steroid doses

Dose of steroids before operation					
No.	Age (years)	Gender (M/F)	Type	Daily dose (mg/day)	Total dose (mg)
1	27	F	Total colitis	60	6,000
2	35	F	Total colitis	10	28000
3	32	M	Total colitis	20	24,000
4	21	M	Total colitis	10	22000
5	32	M	Total colitis	60	15,000
6	22	M	Total colitis	30	27000
7	21	F	Total colitis	60	15,000
8	16	F	Total colitis	60	22000
9	21	F	Total colitis	40	15,000
10	28	F	Total colitis	60	10000
11	53	F	Total colitis	50	12,000
12	33	F	Total colitis	30	12000
13	29	M	Total colitis	5	30,000
14	32	M	Total colitis	20	23,000
15	22	F	Total colitis	20	25,000
16	23	M	total colitis	60	18,000
17	21	M	total colitis	50	18,000
18	43	F	total colitis	60	11,000
19	23	M	total colitis	20	20,000
20	74	M	total colitis	60	500
21	28	F	total colitis	60	6,000
22	37	F	total colitis	40	21,000
23	48	F	total colitis	60	7,000
24	11	M	total colitis	60	420
25	17	F	total colitis	40	12,000
26	51	F	total colitis	15	23,000
27	25	F	total colitis	20	18,000
28	49	M	total colitis	35	23,000
29	64	F	total colitis	60	18,000
30	46	F	total colitis	60	20,000

F Female, *M* male

Table 2 The method to calculate the clinical activity index of ulcerative colitis

Variable	Right at your correlation	Weight
X_1 (bloody stool)		$\times 60 = Y_1$
Little or none	0	
Present	1	
X_2 (bowel movements/day)		$\times 13 = Y_2$
≤4	1	
5–7	2	
≥8	3	
X_3 (ESR mm/h)		$\times 0.5 = Y_3$
X_4 (Hb g/dl)		$\times -4 = Y_4$
X_5 (albumin g/dl)		$\times -15 = Y_5$
Constant		200

$$\mathrm{AI} = \sum_{i-1}^{5} Yi + 200$$

Adopted from Seo et al. [19]
ESR Erythrocyte sedimentation rate, *Hb* blood hemoglobin

(420–30,000 mg), and the average dose of recent prednisolone was 41 mg/day (5–60) (Table 1). Patients with Crohn's disease included ten cases with ileocolitis, two with ileitis, and three with colitis. For preoperative treatments, all patients with Crohn's disease were treated with total parenteral nutrition [22], with only one patient receiving corticosteroid therapy. Nonneoplastic, large, and small intestinal tissues were taken from five patients with colon cancer. Tissue samples of ischemic colitis were obtained from three patients during surgical operations.

Fixation

Immediately after surgical resection, fresh tissue samples, 5×5×2 mm in size, were fixed in periodate-lysine-2% paraformaldehyde (PLP) at 4°C for 6 h followed by sequential washing in phosphate-buffered saline (PBS) containing 10, 15, and 20% sucrose for 4 h in each step. The specimens were embedded in an OCT compound (Miles, Elkhart, IN), rapidly frozen in dry ice–acetone, and stored at −80°C until use.

Immunohistochemistry

PLP-prefixed frozen sections were used with the peroxidase-labeled dextran polymer method (Envision staining kit; DAKO, Kyoto, Japan). The chromogen was 3′, 3-diaminobenzidine tetrahydrochloride (DAB) (Dojin, Kumamoto, Japan). Primary antibodies used were mouse monoclonal antibody against CD3 (clone UCTH1, applied at 1:200; Immunotech, Marseille, France), CD19 (clone HD37, 1:200; DakoCytomation, Glostrup, Denmark), CD20 (L26, 1:200; DAKO, California, USA), CD138 (clone MI15, 1:200; DAKO), Ki-67 (clone MIB1, 1:100; DAKO), follicular dendritic cell (FDC, clone CAN.42, 1:500; DAKO) and polyclonal antibodies against IgA (1:2,000; DAKO), IgG (1:2,000; DAKO), and IgM (1:200; DAKO). For Ki-67 staining, the sections were heat-treated in 0.1 M citrate buffer (pH 6.0) at 97°C for 15 min for antigen retrieval. The specificity of immunoreactivity was confirmed by replacing the primary antibodies with isotype-matched control antibodies at the

Table 3 List of each parameter of the clinical activity of 19 cases of ulcerative colitis

Age (years)	Gender (M/F)	Bloody stool	Bowel movements (per day)	ESR (mm/h)	Hb (g/dl)	Albumin (g/dl)	Activity index	Ki-67 labeling index in $CD19^+$ cells
43	F	+	>10	56	12.3	2.7	237.3	55
23	M	−	3	24	9.6	3.2	138.6	17.7
74	M	+	>10	74	11.2	2.3	256.7	63.3
28	F	+	>10	62	9.3	2.7	252.3	55.8
37	F	−	3	23	13.8	3.9	107.8	31.7
48	F	+	>10	61	8.8	2.7	253.8	55.8
11	M	+	7	78	8.7	2.3	255.7	75.8
17	F	+	>10	34	10.1	2.8	233.6	75.8
51	F	+	6	24	9.7	2.2	224.2	29.9
25	F	+	>10	49	15.4	2.3	227.4	41.1
49	M	+	>10	38	11.9	2.4	234.4	43.2
64	F	+	7	48	10.1	2.8	227.6	37.1
46	F	+	10	28	7.8	2.4	245.8	56.9
32	M	+	3	8	17.2	4.2	146.8	16.7
21	M	−	3	13	9.5	3.2	133.5	20
21	F	+	10	52	8.7	3.1	243.7	35.3
16	F	+	10	17	10.5	2.7	225	45.5
21	F	+	10	81	8.8	2.7	263.8	51.7
53	F	+	6	75	12.7	2.2	252.7	64.1

ESR Erythrocyte sedimentation rate, *Hb* blood hemoglobin, *F* female, *M* male

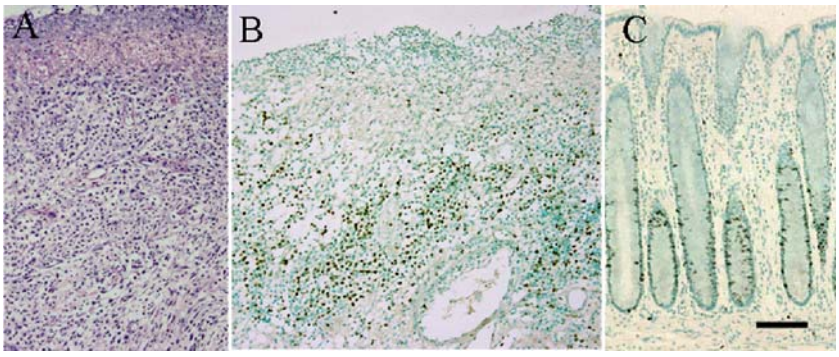

Fig. 1 Immunostaining of Ki-67. **a** Hematoxylin and eosin stain of ulcer base. Scale bar, 100 μm. **b** Ulcer base of ulcerative colitis. **c** Normal colonic mucosa. Note the diffuse occurrence of Ki-67$^+$ small round cells in ulcer base of ulcerative colitis contrasted by nearly no expression of Ki-67 in inflammatory infiltrate in normal colonic mucosa

same concentration (DAKO), and sections were counterstained with methyl green.

Morphometric analyses of Ki-67$^+$ cells

We counted the number of Ki-67$^+$ mononuclear cells in a unit area of 0.0625 mm^2 that corresponded to one microscopic grid area in a ×400 field. Three representative grids were observed in each patient, and the average count was calculated. The labeling of Ki-67 in the epithelial cells was carefully excluded. The counting was done by two independent observers, and the correlation coefficient between the results of both observers was 0.79. The areas we measured were the inflamed mucosa without erosions of ulcerative colitis (n=25) and Crohn's disease (n=15), the ulcer base (granulation tissue in the bottom area of the open ulcer) of ulcerative colitis (n=30), Crohn's disease (n=15), ischemic colitis (n=3), and the mucosa of normal colon (n=5). The differences among these groups were tested by the Kruskal–Wallis test and multiple comparison (SPSS version 11.0, SPSS, Tokyo, Japan).

Counting of the germinal centers

The number of germinal centers was counted by microscopic field (×40) of H & E-stained inflamed ulcerative colitis and Crohn's disease and non-IBD tissues. The whole length of tissue was searched for the germinal center, calculating the number per unit length (1 mm).

Double staining of Ki-67 and lymphocyte marker (enzyme-linked method)

We performed double immunohistochemistry for CD3, 19, or 20, and Ki-67 with minor modifications from Saiki et al. [18]. First, sections were processed for CD3, 19, or 20 with DAB as a chromogen using an EnVision kit (DAKO). After heat-antigen retrieval of Ki-67 antigen, sections were stained with anti-Ki-67 with True Blue (Kirkegard & Perry Laboratories, Gaithersburg, MD, USA) as a chromogen. The labeling index was defined as the percentage of double-positive cells for Ki67$^+$ and each lymphocyte marker among the total numbers of corresponding lymphocytes in a unit area. The method of counting was the same as that of Ki67-positive mononuclear cells.

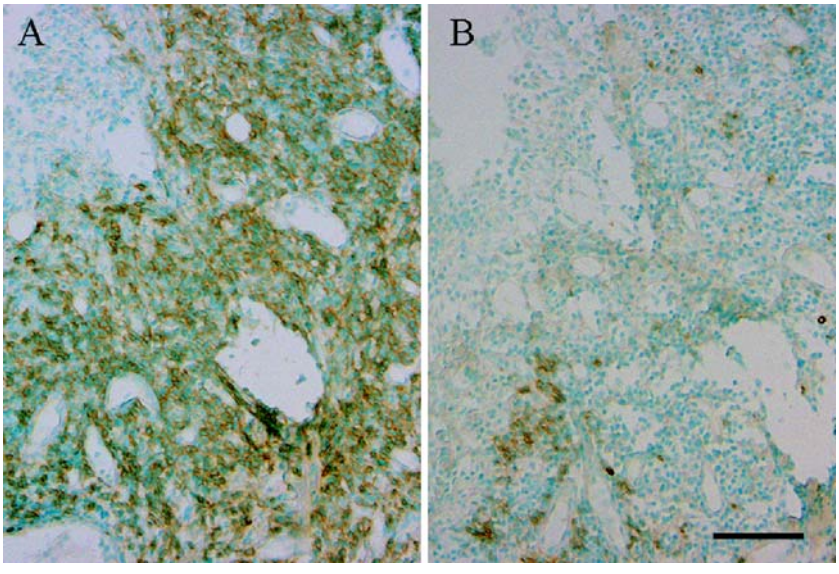

Fig. 2 Immunostaining of CD19 (**a**) and CD20 (**b**) in ulcer base of ulcerative colitis. Note abundance of CD19$^+$ cells contrasted by scantiness of CD20$^+$ cells. Counterstained with methyl green. Scale bar, 100 μm

Double staining of CD19 and CD138

We performed double staining for CD19 and CD138 (plasma cell marker) [23] by both enzyme-linked and immunofluorescent immunohistochemistry. The details of the enzyme-linked method have been described above. For double-labeling immunofluorescent microscopy (performed in four representative cases), fresh frozen sections were fixed in cold acetone for 10 min at 4°C. The sections were sequentially incubated with 10% normal goat serum, mouse monoclonal anti-CD138 antibody (1:8, 11 μg/ml; DAKO), biotinylated goat antimouse immunoglobulin antibody (1:200, 5 μg/ml; Jackson ImmunoResearch, West Grove, PA, USA), and Alexa Fluor 594-conjugated streptavidin (1:100, 10 μg/ml; Molecular Probes Europe, Leiden, the Netherlands) for 15, 30, 20, and 15 min, respectively. After incubation with 10% normal mouse serum, the sections were incubated with fluorescein isothiocyanate (FITC)-conjugated anti-CD19 antibody (1:1; Pharmingen), rabbit anti-FITC antibody (1:40, 10 μg/ml; Molecular Probe), and Alexa Fluor 488-conjugated goat antirabbit immunoglobulin (1:100, 20 μg/ml; Molecular Probe) for 30, 20, and 20 min, respectively. The negative control included replacement of the first- and second-step primary antibodies with isotype-matched control antibodies (IgG1) (DAKO). The specimens were observed with a Nikon Eclipse E800 microscope equipped with band-pass filters for double immunofluorescent microscopy. The fluorescent images were captured with a cooled charge-coupled device (CCD) camera and processed on a personal computer.

Flow cytometry

The procedures for purification of lamina propria mononuclear cells (LPMCs) have been described elsewhere [3, 7, 25]. In brief, mucosal strips were denuded of epithelial cells by ethylenediamine tetraacetate (EDTA) treatment, cut into 5-mm-thick pieces, and digested by collagenase (0.1 mg/ml) (Wako Co. Ltd., Osaka, Japan), for 8 h at 37°C. LPMCs were isolated by means of a Lymphoprep (Nycomed, Oslo, Norway) gradient. The purity (ratio of LPMCs) and viability (ratio of trypan-blue-negative, nonprickled cells) were microscopically evaluated, which were consistently greater than 90%. Cell surfaces were stained with FITC- or PE-labeled anti-CD19 and CD20 (Beckton Dickinson). After staining, flow cytometric analysis was carried out on a FACScalibur (Beckton Dickinson).

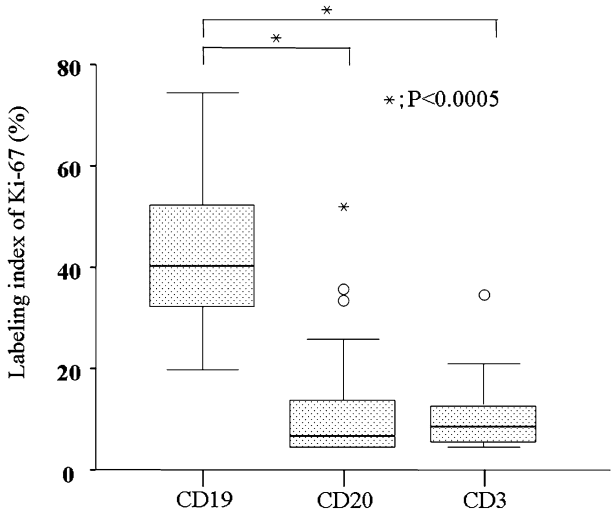

Fig. 4 Comparison of labeling index of Ki-67 among $CD19^+$, $CD20^+$, and $CD3^+$ cells in ulcer base of ulcerative colitis analyzed by double-labeling immunohistochemistry

Immunoelectron microscopy

The preembedding, immunoperoxidase method was applied to PLP-fixed, frozen sections as described previously [18].

Clinical activity of ulcerative colitis

We adopted the activity index of Seo et al., an improved version of the clinical activity of Truelove and Witts, because it is clearly quantitative [19, 21]. The activity index was calculated in 19 cases from which sufficient

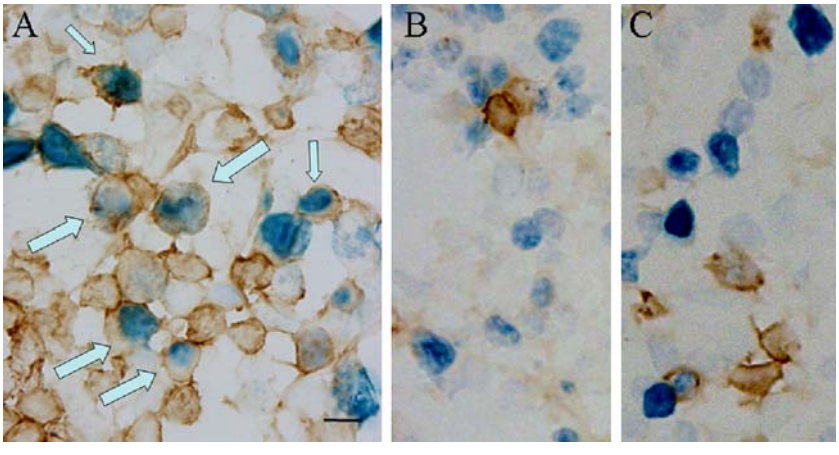

Fig. 3 Double staining of lymphocyte marker and Ki-67. **a** CD19 (*brown*) and Ki-67 (*blue*) in ulcer base of ulcerative colitis. Scale bar, 10 μm. Note most Ki-67 reactivity in the nucleus is expressed in cells immunoreactive for CD19 on the cell surface (*arrows*). **b** CD3 (*brown*) and Ki-67 (*blue*) in ulcer base of ulcerative colitis. **c** CD20 (*brown*) and Ki-67 (*blue*) in ulcer base of ulcerative colitis. Note that Ki-67 reactivity is not colocalized with CD3 or CD20

clinical data were obtained (Table 2). The parameters included bloody stool, erythrocyte sedimentation rate, blood hemoglobin, and serum albumin (Table 3). The correlation between this index and the proliferative activity of lymphocytes was tested by the Spearman's test (SPSS).

Results

Distribution of Ki-67$^+$ lymphoid cells

The occurrence of Ki-67$^+$ small round cells was frequently observed, particularly in granulation tissue in the ulcer base, as a diffuse pattern (Fig. 1a,b). It was notable that this labeling for Ki-67 was not usually associated with a follicular pattern. By contrast, the labeling of Ki-67$^+$ in small round cells in Crohn's disease showed mainly a follicular pattern with a sporadic positivity in small round cells in ulcer bases. This clearly indicated that the labeling in Crohn's disease was mostly confined to germinal centers, typical areas of B-cell proliferation. In ischemic colitis, Ki67$^+$ small round cells were only sporadically observed. In the normal colonic mucosa, Ki67$^+$ small round cells were quite infrequent in the lamina propria except in the areas of lymphoid follicles (Fig. 1c).

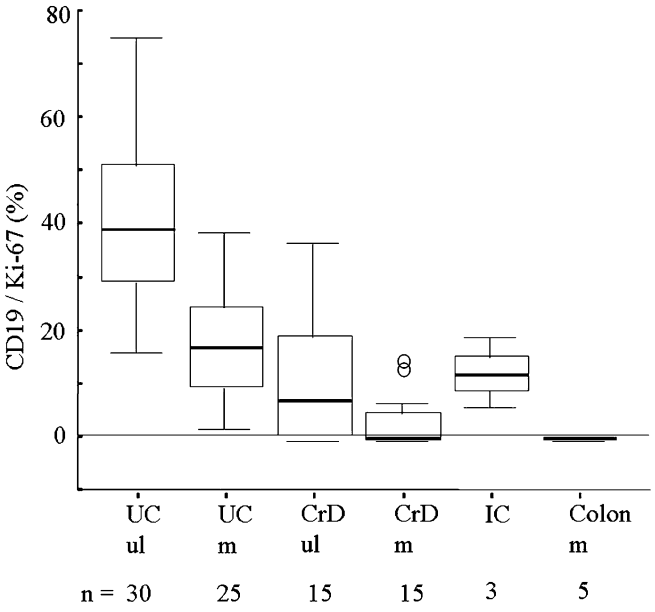

Fig. 6 Comparison of the labeling index of Ki-67 among CD19$^+$ cells analyzed by double-labeling immunohistochemistry. The percentage of CD19$^+$ and Ki-67$^+$ cells among total CD19$^+$ cells was significantly higher in ulcer base of ulcerative colitis than any other groups by multiple comparison (P<0.001 in all). *ul*, ulcer; *m*, mucosa; *IC*, ulcer base of ishemic colitis; *UC*, ulcerative colitis; *CrD*, Crohn's disease

Ki-67$^+$ round cells were identified as CD19$^+$ and CD20$^-$ B-lineage cells

To identify the cell types, we first performed immunohistochemistry. The ulcer base of ulcerative colitis abounded of CD19$^+$ cells, contrasted by the scarcity of CD20$^+$ cells or CD3$^+$ cells (Fig. 2). Next, double staining clearly revealed that it was CD19$^+$ cells that showed a higher frequency of Ki-67 positivity in the ulcer base of ulcerative colitis as compared with CD3$^+$ and CD20$^+$ cells (Figs. 3 and 4). This suggests an active proliferation of B-lineage cells that showed an unusual phenotype of CD19$^+$ and CD20$^-$ in the ulcer base of ulcerative colitis. This unusual immunophenotype was contrasted by that of B cells in germinal cen-

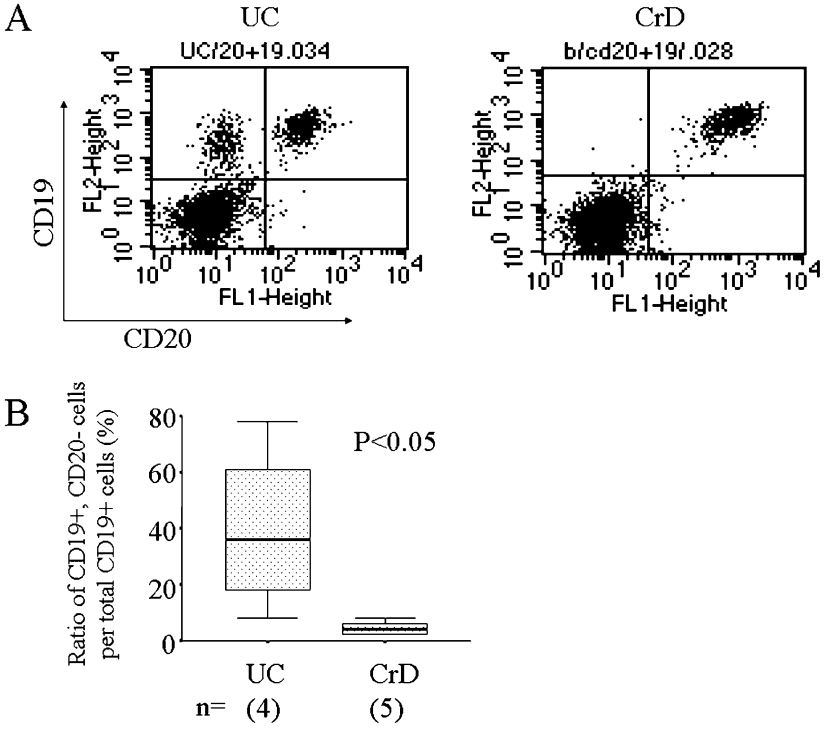

Fig. 5 **a** Example of flow cytometry using freshly prepared lamina propria lymphocytes. CD19$^+$ and CD20$^-$ cells were detected in ulcerative colitis, not in Crohn's disease. **b** Comparison of the ratio of CD19$^+$ and CD20$^-$ cells among total CD19$^+$ cells between ulcerative colitis and Crohn's disease. *UC*, ulcerative colitis; *CrD*, Crohn's disease

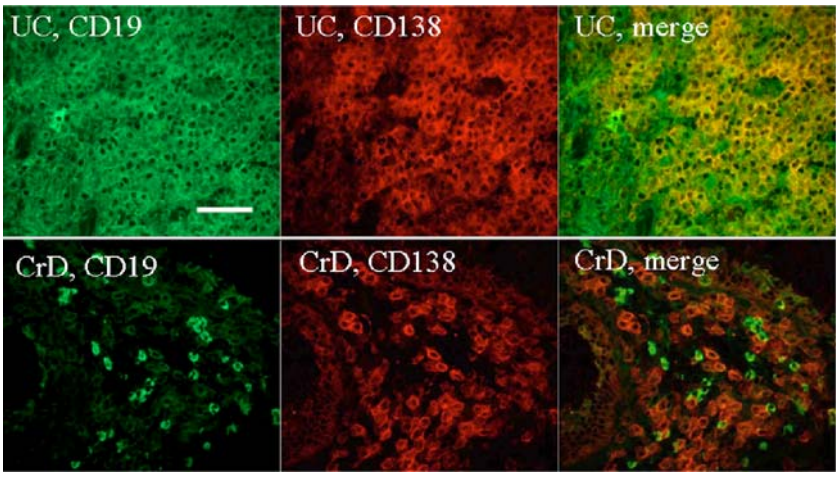

Fig. 7 Double labeling immunofluorescent microscopy for CD19 (*green*) and CD138 (*red*) in ulcer bases of ulcerative colitis and Crohn's disease. Note that most $CD138^+$ cells are double-positive for CD19 (*orange*) in ulcerative colitis (*upper panel*) but not in Crohn's disease (*lower panel*). Scale bar, 50 μm

ters, where $CD19^+$ and $CD20^+$ B cells of usual phenotype frequently express Ki-67 positivity. Labeling of Ki-67 in $CD19^+$ and $CD20^-$ B cells was also observed in the inflamed mucosa of ulcerative colitis at a lower rate (vide infra for details).

Flow cytometry was performed to check the occurrence of such $CD19^+$ and $CD20^-$ cells. Approximately 20% of $CD19^+$ cells showed the phenotype of $CD19^+$ and $CD20^-$ in ulcerative colitis mucosa, contrasted by a predominance of $CD19^+$ and $CD20^+$ phenotype in Crohn's disease mucosa (Fig. 5a,b). Due to technical difficulty, areas of the ulcer base were not analyzed.

High labeling index of Ki-67 among $CD19^+$ cells was specific for ulcerative colitis, particularly the ulcer base

To check the specificity of our findings, we compared the labeling index of Ki-67 in diffusely distributed $CD19^+$ cells among different diseases. As shown in Fig. 6, this labeling index was significantly higher in the ulcer base of ulcerative colitis (approximately 40% on average) than in the inflamed mucosa of ulcerative colitis, the ulcer base of Crohn's disease, the ulcer base of ischemic colitis, and the inflamed mucosa of Crohn's disease (Fig. 6). In Crohn's disease, no significant difference was noted between the labeling index of Ki-67 in $CD19^+$ cells between the small and large intestines. This analysis clearly indicated the specific occurrence of $Ki67^+$ and $CD19^+$ cells in the ulcer base of ulcerative colitis.

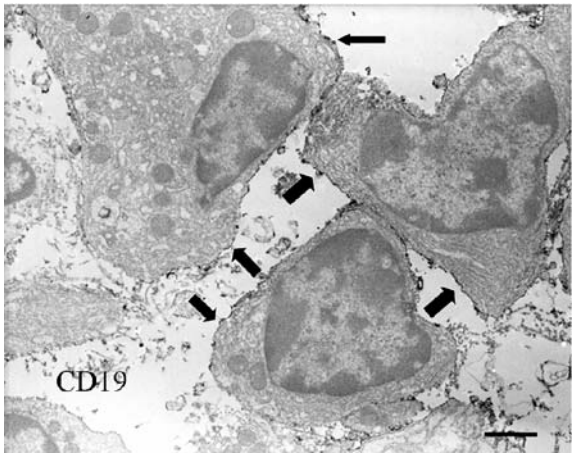

Fig. 8 Immunoelectron microscopy for CD19 in ulcer base of ulcerative colitis. Immunoreactivity along the plasma membrane is expressed by *black arrows*. $CD19^+$ cells had eccentrically located nuclei and abundant rough endoplasmic reticula, a feature of plasma cells. Scale bar, 1μm

Identification of $CD19^+$ and $CD20^-$ B-lineage cells as plasma cells

Basal plasmacytosis is one of the most important features of ulcerative colitis [20]. To search for the relationship to plasma cells, we performed double-labeling immunofluorescent microscopy for CD19/CD138 in two representative cases of ulcerative colitis and two cases of Crohn's disease. In the ulcer base of ulcerative colitis, approximately 60% of $CD19^+$ cells were double-positive for CD138, a marker of plasma cells (Fig. 7a–c). Nearly identical results were

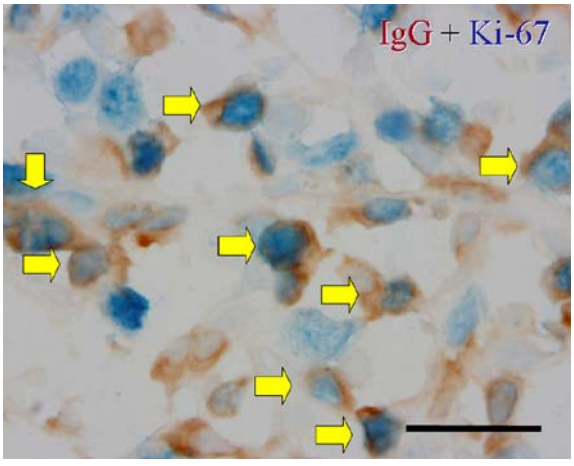

Fig. 9 Double-labeling enzyme-linked immunohistochemistry for IgG (*brown*) and Ki-67 (*blue*) in ulcer base of ulcerative colitis. *Arrows*, double-positive cells

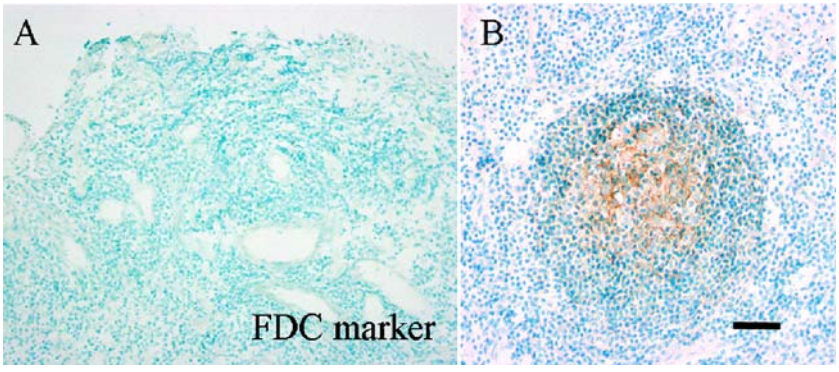

Fig. 10 Immunostaining of follicular dendritic cell (*FDC*) marker (clone CAN.42). **a** Ulcer base of UC lacks FDC. **b** Positive control of FDC staining in a germinal center in lymphoid tissue in Crohn's disease. Scale bar, 50 μm (×200)

obtained in the inflamed mucosa of ulcerative colitis. By contrast, $CD138^+$ plasma cells in Crohn's disease lacked the reactivity for CD19 (Fig. 7d–f). The same results were obtained by double-labeling enzyme-linked immunohistochemistry for CD19 and CD138 in ten cases of ulcerative colitis and five cases of Crohn's disease (data not shown). Immunoelectron microscopy confirmed that most of the $CD19^+$ cells in the ulcer base and inflamed mucosa of ulcerative colitis showed a differentiation toward plasma cells because they had eccentrically located nuclei and abundant rough endoplasmic reticula (Fig. 8). There were a few $CD19^+$ cells with typical lymphocytic features. These two observations suggested that $CD19^+$ and $CD20^-$ B-lineage cells in ulcerative colitis belong to plasma cells. The labeling index of Ki-67 of $CD138^+$ cells was lower (30% on average) than that of $CD19^+$ cells (45% on average) ($P<0.01$) in the ulcer base of ulcerative colitis. This suggested that $CD138^+$ cells belong to more mature plasma cells than the total $CD19^+$ cells do. Collectively, our data clearly showed that one of the most pathognomonic changes for ulcerative colitis is observed in its ulcer base rather than in the inflamed mucosa, where proliferating $CD19^+$ plasma cells were abundant.

Immunoglobulin type

With plasma cell features revealed, we next analyzed the immunoglobulin type. Double staining of immunoglobulins and Ki-67 in six representative cases revealed that Ki-67 positivity appeared in IgG^+ or IgA^+ cells but not in IgM^+ cells in the ulcer base of UC (Fig. 9).

Ulcer base lacks FDCs and germinal centers

To check the microenvironments in the ulcer base in ulcerative colitis, we searched for FDCs that characterize germinal centers. Despite the abundance of plasma cells, the ulcer base of ulcerative colitis lacked FDCs, except sparsely distributed germinal centers (Fig. 10a,b), and

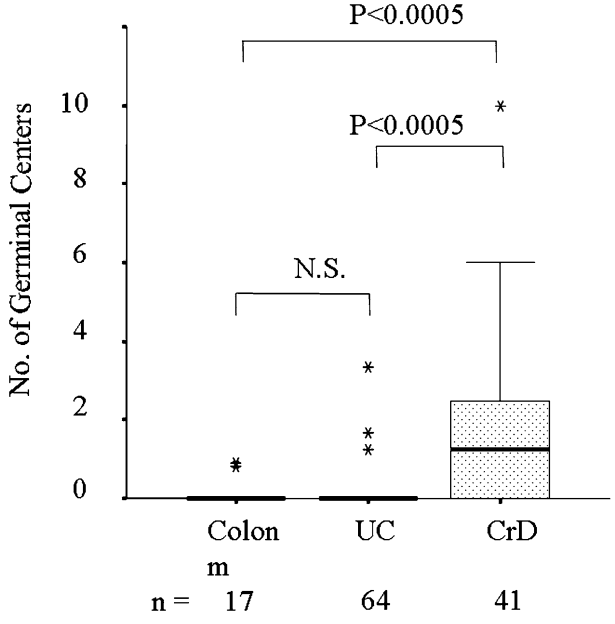

Fig. 11 Results of quantification of germinal centers. *m*, mucosa; *UC*, ulcerative colitis; *CrD*, Crohn's disease. Note that there was no increase in germinal centers in ulcerative colitis

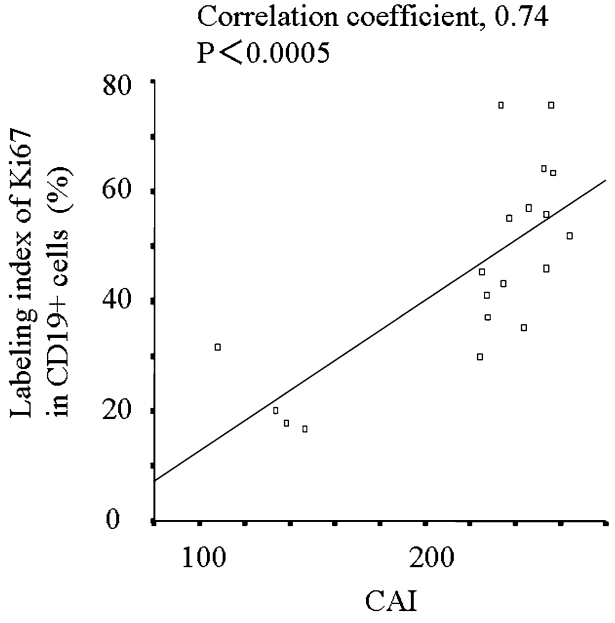

Fig. 12 Positive correlation between the labeling index of Ki-67 among $CD19^+$ cells in the ulcer base of ulcerative colitis and the clinical activity of ulcerative colitis

ulcerative colitis tissues showed no increase in germinal centers as compared with normal colonic tissue (Fig. 11).

The labeling index of Ki-67 in $CD19^+$ cells is correlated with the clinical activity of ulcerative colitis

We next searched for a possible clinical implication of our findings. There was a significant positive correlation between the labeling index of Ki-67 among $CD19^+$ cells in the ulcer base of ulcerative colitis and the clinical activity of ulcerative colitis at the time of operation (Fig. 12). This suggested that active proliferation of $CD19^+$ plasma cells that were resistant to medical treatment with corticosteroids takes place in the ulcer base of active ulcerative colitis. In contrast to this, there was no such significant correlation observed as far as plasma cells in the inflamed mucosa were concerned (data not shown), underscoring the importance of these changes in the ulcer base of ulcerative colitis.

Discussion

To the best of our knowledge, the present study documented for the first time the specific occurrence of $CD19^+$ plasma cells that showed higher labeling of Ki-67 in the ulcer base of ulcerative colitis. Previous studies on the subsets of lymphocytes in ulcerative colitis dealt with either CD19 or CD20, and no reports compared the distribution changes of the two markers. We compared the two markers to detect the widely spread distribution of $CD19^+$ and $CD20^-$ cells in ulcerative colitis. A considerable number of them were further positive for CD138. Together with immunoelectron microscopic features, we judged that they belong to plasma cells. Since CD19 is positive in early (or immature) plasma cells [13], $CD19^+$ plasma cells in ulcerative colitis included a considerable number of immature plasma cells. The higher labeling of Ki-67 that suggests the proliferative activity in these cells was consistent with this immaturity. These changes were specific for ulcerative colitis because most $CD138^+$ plasma cells in Crohn's disease belonged to $CD19^-$ and $CD138^+$ mature plasma cells that lacked proliferative activity.

The most prominent changes we observed took place in the ulcer base of ulcerative colitis. Caution must be exercised in this explanation because inflammatory reactions occurring in the ulcer base have been generally regarded as secondary changes after the breakdown of the mucosal barrier in ulcerative colitis. Our data here, however, suggest that higher occurrence of Ki-67 in $CD19^+$ plasma cells in the ulcer base of ulcerative colitis is not secondary, but at least in part, ulcerative-colitis-specific, since similar findings were not detected in Crohn's disease or ischemic colitis even in the areas of ulceration or actively inflamed mucosa. The positive correlation between the labeling index of Ki-67 of $CD19^+$ plasma cells in the ulcer base and the clinical severity of ulcerative colitis further underscores this notion. Collectively, our findings here indicated the importance of abnormalities in the humoral immunity in ulcerative colitis that takes place mainly in the ulcer base and partly in the inflamed mucosa. These reactions by plasma cells would possibly induce an overactivation of humoral immune responses, including autoantibody production.

Next, we considered possible differentiation pathways of plasma cells we observed. To date, three pathways have been proposed for the differentiation of B cells: (a) the pathway via follicles in lymph nodes or gut-associated lymphoid tissue (GALT) (the main pathway) [17], (b) the extrafollicular pathway via splenic marginal zone B-cells–plasmablasts, which shows a high proliferative activity [14], and (c) the B-1 cell pathway that is independent of T cells, which is observed in the peritoneal and pleural cavities [2]. As shown in the results, the proliferation of plasma cells in the present study took place without new formation of the germinal centers. This indicated that these plasma cells are in a distinct maturational pathway from the ordinary one in GALT [17]. The origin of these plasma cells remains to be clarified in future studies.

In conclusion, our study revealed frequent labeling for Ki-67 in $CD19^+$ plasma cells (immature plasma cells), which is specific for ulcerative colitis, particularly in the ulcer base. We need further analysis to clarify the mechanisms of plasma-cell responses in ulcerative colitis at various stages with or without medical treatments, which will surely contribute to a better understanding of the pathogenesis of ulcerative colitis.

Acknowledgements The authors wish to thank Dr. Atsuo Kitano, Dr. Yukio Nishiguchi, Yoshitaka Kinouchi, and Iwao Sasaki for helpful discussions. This work was supported in part by grants-in-aid for cancer research and a grant for intractable inflammatory bowel disease from the Ministry of Health, Labor, and Welfare, Japan.

References

1. Baldassano RN, Schreiber S, Johnston RB Jr, Fu RD, Muraki T, MacDermott RP (1993) Crohn's disease monocytes are primed for accentuated release of toxic oxygen metabolites. Gastroenterology 105:60–66
2. Berland R, Wortis HH (2002) Origins and functions of B-1 cells with notes on the role of CD5. Annu Rev Immunol 20:253–300
3. Bull DM, Bookman MA (1977) Isolation and functional characterization of human intestinal mucosal lymphoid cells. J Clin Invest 59: 966–974
4. Cario E (2005) Bacterial interactions with cells of the intestinal mucosa: toll-like receptors and NOD2. Gut 54:1182–1193
5. Das KM, Dubin R, Nagai T (1978) Isolation and characterization of colonic tissue-bound antibodies from patients with idiopathic ulcerative colitis. Proc Natl Acad Sci U S A 74:4523–4532
6. Fell JME, Walker-Smith JA, Spencer J, Macdonald TT (1996) The distribution of dividing T cells throughout the intestinal wall in inflammatory bowel disease. Clin Exp Immunol 104:280–285
7. Fiocchi C (1985) Lymphoid cells of the gastrointestinal tract. Isolation procedures. Acta Chir Scand Suppl 525: 11–23

8. Gerdes J, Li L, Schlueter C, Duchrow M, Wohlenberg C, Gerlach C, Stahmer I, Kloth S, Brandt E, Flad HD (1991) Immunobiochemical and molecular biologic characterization of the cell proliferation-associated nuclear antigen that is defined by monoclonal antibody Ki-67. Am J Pathol 138:867–873
9. Halstensen TS, Das KM, Brandtzaeg P (1993) Epithelial deposits of immunoglobulin G1 and activated complement colocalise with 40kD putative autoantigen in ulcerative colitis. Gut 34:650–657
10. Iatropoulos MJ, Williams GM (1996) Proliferation markers. Exp Toxicol Pathol 48:175–181
11. Kawachiya T, Oshitani N, Jinno Y, Watanabe K, Nakamura S, Fujiwara Y, Higuchi K, Maeda K, Nishiguchi Y, Hirakawa K, Matsumoto T, Arakawa T (2005) Significance of increased proliferation of immature plasma cells in the appendix of patients with ulcerative colitis. Int J Mol Med 15:417–423
12. Kullmann F, Fadale M, Gross V, Knuchel R, Bocker T, Steinbach P, Scholmerich J, Ruschoff J (1996) Expression of proliferating cell nuclear antigen (PCNA) and Ki-67 in dysplasia in inflammatory bowel disease. Eur J Gastroenterol Hepatol 8:371–379
13. Leonard JP, Schattner EJ, Coleman M (2001) Biology and management of mantle cell lymphoma. Curr Opin Oncol 13: 342–347
14. MacLennan I, Vinuesa C (2002) Dendritic cells, BAFF, and APRIL: innate players in adaptive antibody responses. Immunity 17:235–238
15. Meinzer U, Hugot JP (2005) NOD2 and Crohn's disease: many connected highways. Lancet 365:1752–1754
16. Monteleone I, Vavassori P, Biancone L, Monteleone G, Pallone F (2002) Immunoregulation in the gut: success and failures in human disease. Gut 50(Suppl 3):III60–64
17. Nagler-Anderson C (2001) Man the barrier! Strategic defenses in the intestinal mucosa. Nat Rev Immunol 1:59–67
18. Saiki Y, Ohtani H, Naito Y, Miyazawa M, Nagura H (1996) Immunophenotypic characterization of Epstein–Barr virus-associated gastric carcinoma: massive infiltration by proliferating CD8+ T-lymphocytes. Lab Invest 75:67–76
19. Seo M, Okada M, Yao T, Ueki M, Arima S, Okumura M (1992) An index of disease activity in patients with ulcerative colitis. Am J Gastroenterol 87:971–976
20. Tibble JA, Sigthorsson G, Foster R, Forgacs I, Bjarnason I (2002) Use of surrogate markers of inflammation and Rome criteria to distinguish organic from nonorganic intestinal disease. Gastroenterology 123:450–460
21. Truelove SC, Witts LJ (1959) Cortisone and corticotrophin in ulcerative colitis. Br Med J 14:387–394
22. Tsujikawa T, Satoh J, Uda K, Ihara T, Okamoto T, Araki Y, Sasaki M, Fujiyama Y, Bamba T (2000) Clinical importance of n-3 fatty acid-rich diet and nutritional education for the maintenance of remission in Crohn's disease. J Gastroenterol 35:99–104
23. Wijdenes J, Dore JM, Clement C, Vermot-Desroches C (2002) CD138. J Biol Regul Homeost Agents 16:152–155
24. Yacyshyn BR (1993) Activated CD19+ B cell lamina propria lymphocytes in ulcerative colitis. Immunol Cell Biol 71:265–274
25. Youngman KR, Simon PL, West GA, Cominelli F, Rachmilewitz D, Klein JS, Fiocchi C (1993) Localization of intestinal interleukin 1 activity and gene expression to lamina propria cells. Gastroenterology 104:749–758

Virchows Arch (2006) 448: 422–427
DOI 10.1007/s00428-005-0110-4

ORIGINAL ARTICLE

Takamitsu Sasaki · Kiyomu Fujii · Kazuhiro Yoshida · Hideo Shimura · Tomonori Sasahira · Hitoshi Ohmori · Hiroki Kuniyasu

Peritoneal metastasis inhibition by linoleic acid with activation of PPARγ in human gastrointestinal cancer cells

Received: 28 September 2005 / Accepted: 29 September 2005 / Published online: 16 December 2005

Abstract The effect on peritoneal metastasis of linoleic acid (LA) was examined using in vitro treatment of cancer cells and mouse peritoneal metastasis models. Firstly, cell growth of MKN28 human gastric cancer cells and Colo320 human colon cancer cells was suppressed by LA in a dose-dependent manner with increment of apoptosis. LA-induced growth inhibition was recovered by the exposure to antisense *S*-oligodeoxynucleotide for peroxisome proliferator-activated receptor gamma (PPARγ) or 15-lipoxygenase-1, which converts LA to PPARγ ligands. LA significantly inhibited invasion into type-IV collagen-coated membrane of MKN28 and Colo320 cells ($p<0.05$). BALB/c *nu/nu* mice inoculated with MKN28 and Colo320 cells into their peritoneal cavities were administrated with LA intraperitoneally (weekly, four times). The LA treatment significantly diminished the number of metastatic foci of both cells in the peritoneal cavity ($p<0.05$). Protein production in MKN28 and Colo320 cells treated with LA showed a decrease of epidermal growth factor receptor and an increase of Bax. These findings suggest that LA inhibits invasion and metastasis of human gastric and colon cancer cells by nondietary administration.

T. Sasaki · K. Fujii · T. Sasahira · H. Ohmori · H. Kuniyasu (✉)
Department of Molecular Pathology,
Nara Medical University,
Kashihara, Japan
e-mail: cooninh@zb4.so-net.ne.jp
Tel.: +81-744-223051
Fax: +81-744-257308

K. Yoshida
Department of Surgical Oncology,
Research Institute for Radiation Biology and Medicine,
Hiroshima University,
Hiroshima, Japan

H. Shimura
First Department of Surgery,
Fukuoka University School of Medicine,
Fukuoka, Japan

Keywords Peritoneal metastasis · Linoleic acid · Peroxisome proliferator-activated receptor gamma · 15-Lipoxygenase-1 · Gastrointestinal cancer

Abbreviations LA: Linoleic acid · ODN: Oligodeoxynucleotide · PPAR: Peroxisome proliferator-activated receptor · LOX: Lipoxygenase · EGFR: Epidermal growth factor receptor · PG: Prostaglandin · HODE: Hydroxyoctadecadienoic acid · OXO: Oxooctadecadienoic acid · CLA: Conjugated linoleic acid · PBS: Phosphate-buffered saline

Introduction

Linoleic acid (LA) is an ω-6 polyunsaturated fatty acid, which is a precursor of prostaglandin (PG) yielding PGE2 by enzymatic process with cyclooxygenase-2. PGE2 plays a pivotal role in carcinogenesis due to its properties of pro-inflammation, proproliferation, and immunosuppression [5, 14]. The carcinogenic effect of dietary LA is already evident in rodent colon carcinogenesis models [3, 12, 13, 20]. However, molecular biological direct effects of LA are poorly understood.

Oxidative metabolites of LA by 15-lipoxygenase-1 (LOX 15), in particular 9-hydroxyoctadecadienoic acid (9-HODE), 13-hydroxyoctadecadienoic acid (13-HODE), and 13-oxooctadecadienoic acid (13-OXO), have biological effects as a peroxisome proliferator-activated receptor gamma (PPARγ) ligand [10]. PPARγ possesses an anticarcinogenic effect in colon cancer. Synthesized PPARγ ligands including troglitazon are shown to be effective chemopreventive agents in a rat model of carcinogenesis and in azoxymethane (AOM)-induced colon cancer in mice [11]. Conjugated LA (CLA) is composed of positional tereoisomers of octadecadienoate (18:2), whose chemoprotective properties are studied in experimental cancer models and in vitro examinations [2, 9]. CLA induces apoptosis in cancer cells by activation of PPARγ as a ligand. A decrease of PPARγ is associated with metastasis [1, 17]. If LA provides PPARγ ligands, LA might act as an anticarcinogenic and antimetastatic agent.

Peritoneal metastasis of cancer is a terminal condition of human gastrointestinal cancer, difficult to be treated, and worsens quality of patients' life [15, 16, 18]. Differently from metastasis to solid organs, cancer cells in peritoneal metastasis can be treated with anticancer agents directly delivered by intraperitoneal administration. To elucidate direct effects of LA in cancer cells, we used the peritoneal metastasis models in this study.

Materials and Methods

Cell culture

A human gastric cancer cell line, MKN28, was kindly provided by Dr. W. Yasui (Hiroshima University Graduate School, Hiroshima, Japan). A human colon cancer cell line, Colo320, was provided by American Tissue and Cell Culture. The cells were routinely maintained in RPMI-1640 (Sigma Chemical Co., St. Louis, MO, USA) containing 10% fetal bovine serum (FBS, Sigma Chemical Co.) under the condition of 5% CO_2 in air at 37°C. LA (Calbiochem, Darmstadt, Germany) was dissolved with 70% ethanol (50 μg/μl). For negative control, same amount of 70% ethanol was used.

Cell growth

Cells were harvested from 80% confluent monolayer cultures by a brief trypsinization with 0.1% trypsin and 0.1% EDTA (Sigma Chemical Co.). The cells were seeded at density of 10,000 cells/well of 24-well tissue culture plates and treated under the conditions mentioned in "Results." The cell number was counted by an autocytometer (Sysmecs, Kobe, Japan) at 24, 48, and 72 h after the treatment. Apoptotic cells were confirmed by the Giemsa staining. One thousand cells were observed to measure apoptotic cell percentage. Each experiment was repeated three times.

Antisense phosphorothioate (*S*)-oligodeoxynucleotide assay

The 18-mer *S*-oligodeoxynucleotide (*S*-ODN) for the antisense sequence from the 1st to the 18th nucleotide of LOX15 and PPARγ cDNA coding region were synthesized and purified by reverse-phase high-performance liquid chromatography (Sigma Genosys, Ishikari, Japan). The sequence of LOX15 was 5′-CCA TAT AGA TCT GAA T-3′ and that of PPARγ was 5′-CCT GGG GTA AGG TCG G-3′. Each sense sequence 18-mer was for negative control. The cells were pretreated with 3 μM antisense or sense *S*-ODN for 6 days, with medium exchanges and additions of antisense or sense *S*-ODN every 2 days. After that, the cells were used for further experiments.

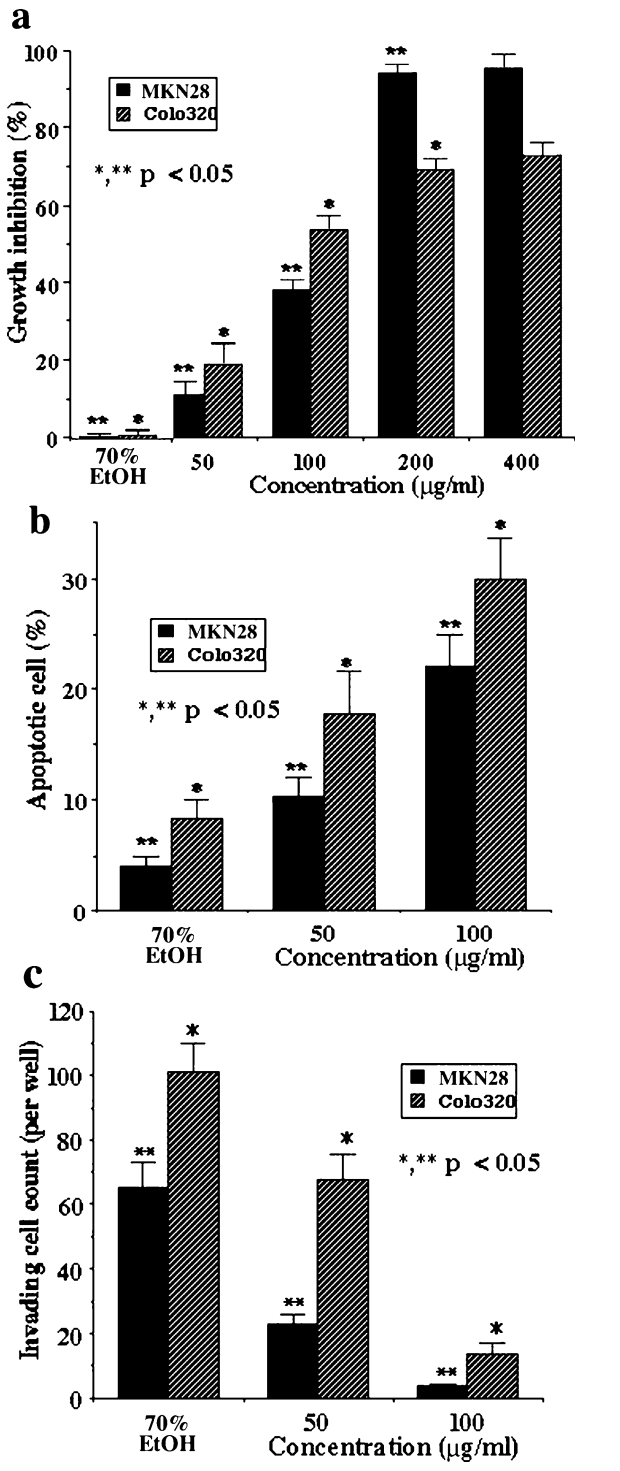

Fig. 1 Effects of linoleic acid (LA) on growth, apoptosis, and invasion in MKN28 and Colo320 cells. **a** Cell growth inhibition by LA. Cell growth inhibition by 200 and 400 μg/ml LA is significantly higher than that by 50 or 100 μg/ml LA in both cell lines (*·**$p<0.05$). **b** Percentage of apoptotic cells induced by LA. Apoptotic cells were counted from 1000 cells examined by the Giemsa staining. The apoptotic cells were significantly increased compared with nontreated cells (*·**$p<0.05$). **c** In vitro invasion assay of LA-treated cells. Invading cells were significantly decreased compared with nontreated cells (*·**$p<0.05$). **a**–**c** Seventy percent ethanol, 70% EtOH, a solvent for LA, was used as a negative control. *Bar*, mean of three independent experiment. *Error bar*, standard deviation

Reverse transcriptase-polymerase chain reaction

PPARγ and LOX5 mRNA expression was assessed with reverse transcriptase-polymerase chain reaction (RT-PCR) using 0.5 μg of total RNA extracted by an RNeasy kit (Qiagen, Hilden, Germany). Primer sets for LOX15 were as follows: upper, 5′-CGC ACG GGG CAA GGA GAC-3′; lower, 5′-TGA CCA CAC CAG AAA ATC-3′. Primer sets for PPARγ were as follows: upper, 5′-GCC ATC CGC ATC TTT CAG-3′; lower, 5′-CCC CAT CTT TAT TCA TCA-3′. PCR products were electrophoresed in a 2% agarose gel and stained with ethidium bromide. β-Actin mRNA was also amplified for internal control. The experiment was repeated twice.

Animal model

BALB/c *nu/nu* athymic mice were purchased from Japan SLC Inc. (Shizuoka, Japan). The mice were maintained according to institutional guidelines approved by the Committee for Animal Experimentation of Nara Medical University, in accordance with the current regulations and standards of the Ministry of Health, Labour, and Welfare. The mice were used according to the institutional guidelines when they were 5 weeks old. Cells were briefly trypsinized and washed with PBS, three times. Cells suspended with PBS were injected into the peritoneal cavity by 1×10^7 in each mouse. Ten mice were injected for each group. After the inoculation, LA (100 μg in 1 ml PBS)

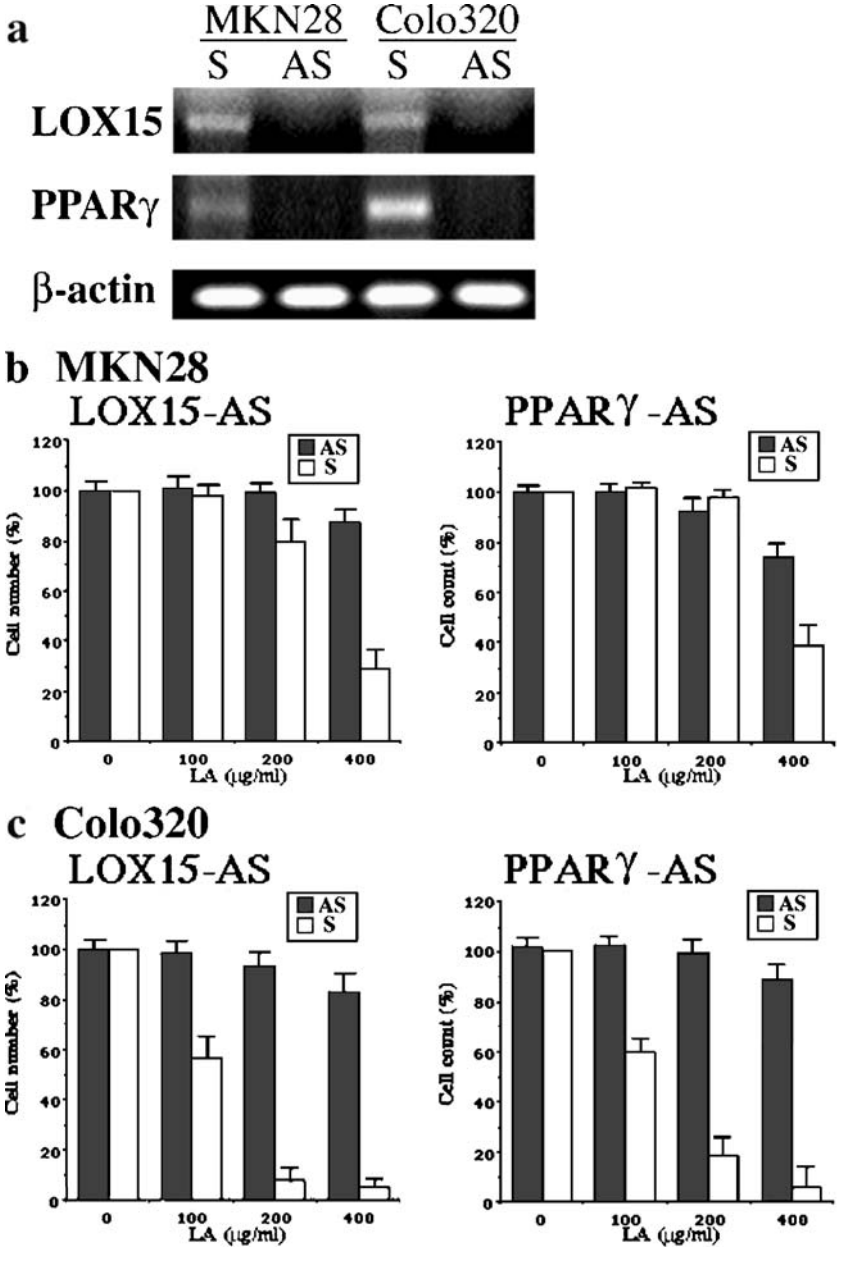

Fig. 2 Effect of antisense *S*-oligodeoxynucleotide (*S*-ODN) for LOX15 or peroxisome proliferator-activated receptor gamma (PPARγ) growth in MKN28 and Colo320 cells. (**a**) mRNA expression of LOX15 and PPARγ in MKN28 and Colo320 cells exposed to sense and antisense *S*-ODNs. β-Actin was detected for internal control. Cell growth inhibition by LA in MKN28 (**b**) and Colo320 (**c**) cells exposed to antisense (*AS*) or sense (*S*) *S*-ODN. Growth inhibition by LA was significantly reduced by antisense treatment (*$p<0.01$, **$p<0.05$). *Bar*, mean of three independent experiment. *Error bar*, standard deviation

was weekly injected into the peritoneal cavity four times. Then, those mice were killed to count the number of metastatic foci in the peritoneal cavity.

Immunoblot analysis

Whole-cell lysates were prepared as described previously [6]. Fifty-microgram lysates were subjected to the immunoblot analysis in 12.5% sodium dodecyl sulfate-polyacrylamide gels followed by electrotransfer onto nitrocellulose filters. The filters were incubated with primary antibodies and then with peroxidase-conjugated IgG antibodies (Medical and Biological Laboratories, Nagoya, Japan). An α-tubulin antibody was used to assess the levels of protein loaded per lane (Oncogene Research Products, Cambridge, MA, USA). The immune complex was visualized by the ECL Western blot detection system (Amersham, Aylesbury, UK). Anti-epidermal growth factor receptor (anti-EGFR) and anti-Bax (Santa Cruz Biotechnology, Santa Cruz, CA, USA) were used as the primary antibodies.

Statistical analysis

Statistical significance was examined by the two-tailed Fisher's exact test, the two-tailed chi-square test, and the two-tailed, unpaired Mann–Whitney test using the InStat Software (GraphPad Software, Los Angels, CA, USA). The statistical significance was defined as a two-sided p value of less than 0.05.

Results

Effect of LA on growth, apoptosis, and invasion in MKN28 and Colo320 cells

We firstly examined the growth inhibitory effect on cancer cells by LA in vitro (Fig. 1a). LA treatment showed growth inhibition in MKN28 and Colo320 cells in a dose-dependent manner. MKN28 cells respectively showed 97 and 98% growth inhibition by treatments with concentrations of 200 and 400 μg/ml. Colo320 cells showed 73% inhibition by 400 μg/ml LA. LA induces apoptosis on MKN28 and Colo 320 cells (Fig. 1b). Treatment with 100 μg/ml of LA induced apoptosis in MKN28 and Colo320 cells to 22 and 28%, respectively. The induction of apoptosis by LA showed a dose-dependent manner. MKN28 and Colo320 cells were examined invasive for capacity by in vitro invasion assay using culture inserts with type-IV collagen-coated membrane (Fig. 1c). The treatment with 100 μg/ml of LA decreases invading cell number in MKN28 and Colo320 cells to 5 and 17%, respectively, compared with those in nontreated cells. The LA-induced inhibition of invasion showed a dose-dependent manner.

Effect of antisense *S*-ODN for LOX15 or PPARγ growth inhibition of LA

To test the hypothesis that LA is metabolized by LOX15 to PPARγ ligands to cause growth inhibitory effect, MKN28 and Colo320 cells were treated with LA under an exposure to sense or antisense *S*-ODNs for LOX15 or PPARγ (Fig. 2). Constitutive expression of LOX15 and PPARγ was suppressed by exposure to each specific antisense *S*-ODN (Fig. 2a). The exposure to antisense *S*-ODNs for LOX15 significantly reduced the growth inhibition by LA in MKN28 and Colo320 cells (Fig. 2b). The exposure to antisense *S*-ODNs for PPARγ also significantly reduced the growth inhibition by LA in MKN28 and Colo320 cells (Fig. 2c).

Effect of LA on peritoneal colonization of MKN28 and Colo320 cells

We next examined the effect of LA on metastasis of MKN28 and Colo320 cells using nude mice models (Fig. 3a). MKN-28 and Colo320 cells were inoculated by 1×10^7 in the peritoneal cavity of BALB/c nude mice. After the inoculation, the mice were intraperitoneally administrated with LA (100 μg in 1 ml PBS), weekly, four times. The treatment with

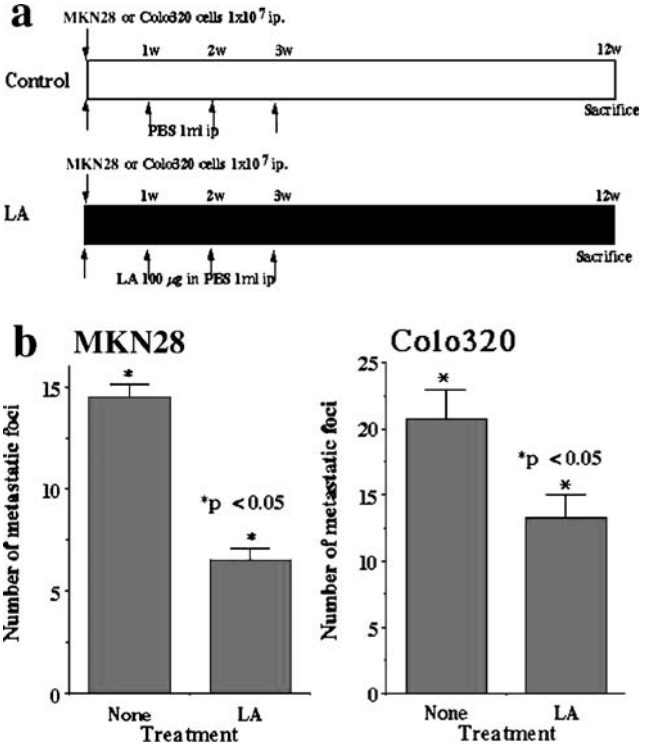

Fig. 3 Effect of LA on peritoneal colonization of MKN28 and Colo320 cells. **a** Experimental design of peritoneal metastasis. Cells (1×10^7) were inoculated into the peritoneal cavity. **b** Number of metastatic foci in the peritoneum. Number of metastatic foci was significantly reduced by LA treatment (*p<0.05). *Bar*, mean of ten mice. *Error bar*, standard deviation

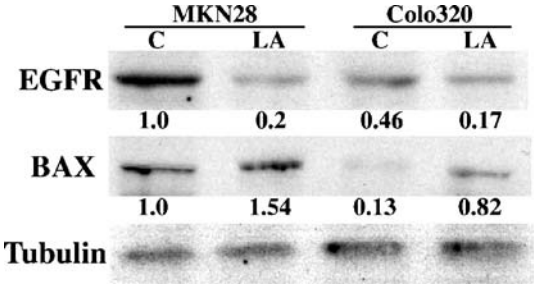

Fig. 4 Effect of LA on production of epidermal growth factor receptor (EGFR) and Bax in MKN28 and Colo320 cells. Protein production of EGFR and Bax was examined by the immunoblotting. Tubulin was detected for internal control. Protein levels are compensated by internal control and standardized by the level in nontreated MKN28 cells, which is set to 1.0. The experiment was repeated twice

LA did not affect body weight of these mice. In 12 weeks after the inoculation, the number of the colonized foci of cancer cells was counted (Fig. 3b). In MKN28 cells, 14±1 per rat of colonized foci were observed in untreated mice, whereas colonizations were decreased to 7±1 foci per rat by the treatment with LA. In Colo320 cells, 21±3 per rat of colonized foci were observed in untreated mice, whereas colonizations were reduced to 13±2 foci per rat by the treatment with LA.

Effect of LA on production of metastasis-related proteins in MKN28 and Colo320 cells

Finally, we examined protein levels in LA-treated MKN28 and Colo320 cells (Fig. 4). In LA-treated MKN28 and Colo320 cells, a decrease of EGFR protein and an increase of Bax were detected. EGFR protein levels in LA-treated MKN28 and Colo320 cells were decreased to 20 and 37%, respectively, compared with those of nontreated cells. In contrast, Bax protein levels in LA-treated MKN28 and Colo320 cells were increased to 154 and 631%, respectively, compared with those of nontreated cells.

Discussion

In the present study, we examined the direct effects of LA on growth, invasion, apoptosis, and metastasis of cancer cells in vitro and in vivo. Our results showed that LA inhibits cell growth and invasion and induces apoptosis with direct exposure to cancer cells. Moreover, LA inhibited cancer cell colonization in the peritoneal cavity. In addition, LA treatment provided the alteration of protein levels of metastasis-related genes. Thus, we can conclude from the data that LA has antimetastatic effect.

We hypothesized that LA is a PPARγ ligand precursor and that LA metabolites by LOX15, 13-HODE, and 13-OXO have ligand activity for PPARγ [10]. To confirm this hypothesis, we inactivated PPARγ by specific antisense *S*-ODN. The result showed that the inhibition of growth and invasion and the induction of apoptosis by LA were abogated by exposure to antisense *S*-ODN for PPARγ. Moreover, the decrease of LOX15 expression by exposure to antisense *S*-ODN for LOX15 suppressed the inhibition of growth and invasion and the induction of apoptosis by LA. These findings support our hypothesis that LA acts as a PPARγ ligand precursor. We also examined a PPARγ ligand, CLA, for suppression of peritoneal metastasis of MKN28 and CoLo320 cells, which showed same inhibitory effect to LA. However, its efficacy was 10^3 times stronger than LA (data not shown). It suggests that LA metabolites might be weaker agonists of PPARγ.

PPARγ is a multifunctional nuclear receptor. Activation of PPARγ by synthesized PPARγ ligands provided growth inhibition and apoptosis in cancer cells. Some reports show that down-regulation of EGFR and up-regulation of Bax are associated with antiproliferative and proapoptotic effects [4, 7, 8]. In the present study, we confirmed that LA decreased EGFR expression and increased Bax expression in both MKN28 and CoLo320 cells. A recent report shows that PPARγ is also associated with inhibition of colon cancer metastasis [19]. Metastasis of HT-29 human colon cancer cells is inhibited by thiazolidinedione through induction of terminal differentiation. We examined the alteration of differentiation status of MKN28 and Colo320 cells by LA, testing protein levels of p21waf1; however, no remarkable change was detected (data not shown).

In the present study, we showed the inhibitory effect of PPARγ on peritoneal metastasis and the activation of PPARγ by LA. The results suggest that PPARγ is a key target of metastasis therapeutics. It is necessary to test the suppression of metastasis by dietary LA on animal models.

Acknowledgements The authors thank Kaori Isobe for expert assistance with the preparation of this manuscript. This research was supported by Grant-in-Aid for Scientific Research from Japan Society for the Promotion of Science and Grant-in-Aid for Scientific Research from Mitsui Memorial Fund.

References

1. Badawi AF, Eldeen MB, Liu Y, Ross EA, Badr MZ (2004) Inhibition of rat mammary gland carcinogenesis by simultaneous targeting of cyclooxygenase-2 and peroxisome proliferator-activated receptor γ. Cancer Res 64:1181–1189
2. Belury MA (2002) Inhibition of carcinogenesis by conjugated linoleic acid: potential mechanisms of action. J Nutr 132:2995–2998
3. Chang WC, Chapkin RS, Lupton JR (1997) Predictive value of proliferation, differentiation and apoptosis as intermediate markers for colon tumorigenesis. Carcinogenesis 18:721–730
4. Chen A, Xu J (2004) Activation of PPARγ by curcumin inhibits Moser cell growth and mediates the suppression of the gene expression of cyclinD1 and EGFR. Am J Physiol Gastrointest Liver Physiol 14:14
5. Gupta RA, Dubois RN (2001) Colorectal cancer prevention and treatment by inhibition of cyclooxygenase-2. Nat Rev Cancer 1:11–21

6. Kuniyasu H, Yasui W, Kitahara K, Naka K, Yokozaki H, Akama Y, Hamamoto T, Tahara H, Tahara E (1997) Growth inhibitory effect of interferon-beta is associated with the induction of cyclin-dependent kinase inhibitor p27Kip1 in a human gastric carcinoma cell line. Cell Growth Differ 8:47–52
7. Liu JJ, Huang RW, Lin DJ, Peng J, Wu XY, Lin Q, Pan XL, Song YQ, Zhang MH, Hou M, Chen F (2005) Expression of survivin and bax/bcl-2 in peroxisome proliferator activated receptor-γ ligands induces apoptosis on human myeloid leukemia cells in vitro. Ann Oncol 10:10
8. Majumder B, Wahle KW, Moir S, Schofield A, Choe SN, Farquharson A, Grant I, Heys SD (2002) Conjugated linoleic acids (CLAs) regulate the expression of key apoptotic genes in human breast cancer cells. FASEB J 16:1447–1449
9. Miller A, Stanton C, Devery R (2002) *Cis* 9, *trans* 11- and *trans* 10, *cis* 12-conjugated linoleic acid isomers induce apoptosis in cultured SW480 cells. Anticancer Res 22:3879–3887
10. Nagy L, Tontonoz P, Alvarez JG, Chen H, Evans RM (1998) Oxidized LDL regulates macrophage gene expression through ligand activation of PPARγ. Cell 93:229–240
11. Osawa E, Nakajima A, Wada K, Ishimine S, Fujisawa N, Kawamori T, Matsuhashi N, Kadowaki T, Ochiai M, Sekihara H, Nakagama H (2003) Peroxisome proliferator-activated receptor γ ligands suppress colon carcinogenesis induced by azoxymethane in mice. Gastroenterology 124:361–367
12. Rao CV, Hirose Y, Indranie C, Reddy BS (2001) Modulation of experimental colon tumorigenesis by types and amounts of dietary fatty acids. Cancer Res 61:1927–1933
13. Reddy BS, Burill C, Rigotty J (1991) Effect of diets high in ω-3 and ω-6 fatty acids on initiation and postinitiation stages of colon carcinogenesis. Cancer Res 51:487–491
14. Singh J, Hamid R, Reddy BS (1997) Dietary fat and colon cancer: modulation of cyclooxygenase-2 by types and amount of dietary fat during the postinitiation stage of colon carcinogenesis. Cancer Res 57:3465–3470
15. Sugarbaker PH (2002) New responsibilities in the management of colorectal cancer with peritoneal seeding. Cancer Invest 20:1118–1122
16. Sugarbaker PH, Yu W, Yonemura Y (2003) Gastrectomy, peritonectomy, and perioperative intraperitoneal chemotherapy: the evolution of treatment strategies for advanced gastric cancer. Semin Surg Oncol 21:233–248
17. Terashita Y, Sasaki H, Haruki N, Nishiwaki T, Ishiguro H, Shibata Y, Kudo J, Konishi S, Kato J, Koyama H, Kimura M, Sato A, Shinoda N, Kuwabara Y, Fujii Y (2002) Decreased peroxisome proliferator-activated receptor γ gene expression is correlated with poor prognosis in patients with esophageal cancer. Jpn J Clin Oncol 32:238–243
18. Vogel I, Kalthoff H (2001) Disseminated tumour cells. Their detection and significance for prognosis of gastrointestinal and pancreatic carcinomas. Virchows Arch 439:109–117
19. Yoshizumi T, Ohta T, Ninomiya I, Terada I, Fushida S, Fujimura T, Nishimura G, Shimizu K, Yi S, Miwa K (2004) Thiazolidinedione, a peroxisome proliferator-activated receptor-γ ligand, inhibits growth and metastasis of HT-29 human colon cancer cells through differentiation-promoting effects. Int J Oncol 25:631–639
20. Zhou S, Wang G, Chen B, Wang P (2000) Effect of dietary fatty acids on tumorigenesis of colon cancer induced by methyl nitrosourea in rats. J Environ Pathol Toxicol Oncol 19:81–86

Virchows Arch (2006) 448: 428–434
DOI 10.1007/s00428-005-0120-2

ORIGINAL ARTICLE

Phyu Phyu Aung · Yoshitsugu Mitani · Yuichi Sanada · Hirofumi Nakayama · Keisuke Matsusaki · Wataru Yasui

Differential expression of claudin-2 in normal human tissues and gastrointestinal carcinomas

Received: 3 October 2005 / Accepted: 10 October 2005 / Published online: 17 November 2005

Abstract Claudins are involved in the formation of tight junctions in epithelial and endothelial cells. Claudins form a family of 24 members displaying organ- and tissue-specific patterns of expression. In the present study, we evaluated the specificity of the claudin-2 expression in various normal human tissues and gastrointestinal cancers by quantitative reverse transcriptase–polymerase chain reaction and immunohistochemistry. In 14 various normal tissues, *claudin-2* mRNA was expressed in the kidney, liver, pancreas, stomach, and small intestine; the highest level of which was detected in the kidney. Colorectal cancers (CRCs) expressed *claudin-2* mRNA at high levels. Immunohistochemical analysis of claudin-2 in 146 gastric cancers (GCs) and 99 CRCs demonstrated claudin-2 expression in 2.1% of GCs and 25.3% of CRCs, respectively. There was no obvious correlation between claudin-2 expression and clinicopathological parameters of CRCs. These results suggest that the expression of claudin-2 may involve organ specificity, and increased expression of claudin-2 may participate in colorectal carcinogenesis.

Keywords Claudin-2 · Gastric · Colorectal cancers

P. P. Aung · Y. Mitani ·
Y. Sanada · H. Nakayama · W. Yasui (✉)
Department of Molecular Pathology,
Graduate School of Biomedical Sciences,
Hiroshima University,
1-2-3 Kasumi, Minami-ku,
Hiroshima 734-8551, Japan
e-mail: wyasui@hiroshima-u.ac.jp
Tel.: +81-82-2575145
Fax: +81-82-2575149

K. Matsusaki
Department of Surgery,
Hofu Institute of Gastroenterology,
14-33 Ekiminami, Hofu,
Yamaguchi 747-0801, Japan

Introduction

Claudin-1 and claudin-2 were the first members of the transmembrane tetraspan family of proteins identified as being involved in tight junction formation with the reruitment of occludin [4] and binding to other tight junction constituents [8]. Claudins form a family of at least 24 members displaying organ- and tissue-specific patterns of expression [9, 17]. Among the claudin family members, expression of claudin-2 is found in the liver, pancreas, and gut in normal rat tissues [17]. Claudin-2 expression is ubiquitous in the epithelial cells at the crypts of the small intestine but restricted to the undifferentiated cell compartment of the colon in rats [17]. Claudin-2 is also known to be expressed in mouse nephron [3, 9]. However, the expression pattern of claudin-2 remains to be elucidated in normal human tissues.

Gastrointestinal cancers including gastric cancer (GC) and colorectal cancer (CRC) are the most common malignancies worldwide. A better knowledge of changes in gene expression during gastrointestinal carcinogenesis may lead to new paradigms and possible improvements in diagnosis, treatment, and prevention. On the other hand, relatively little is known about the expression of claudins in human tumors, and only little information is available on the influence of claudin expression on tumor behavior. It was reported that the expression of claudin-7 was decreased in high-grade breast cancer [10]. Overexpression of claudin-4 has been found in pancreatic adenocarcinoma and its precursor lesions [15, 22], while overexpression of claudin-3 and claudin-4 has been found in prostate and ovarian carcinomas [7, 13]. Concerning the expression of claudin-2 in tumor tissue, it has been reported that claudin-2 expression was detected in 98 (52%) of 188 breast carcinomas [20]. There is one report showing claudin-2 expression in gastrointestinal tumors, but the sample number was small [21].

In the present study, the expression of claudin-2 was investigated in various normal tissues, GCs, and CRCs by

quantitative reverse transcriptase–polymerase chain reaction (RT-PCR) and immunohistochemistry. The aim of this study is to clarify whether claudin-2 expression is specific for cancer by comparing the expression level of claudin-2 in various normal tissues with that in cancer tissues.

Materials and methods

Tissue samples

For quantitative RT-PCR, five GCs and nine CRCs were used. The samples were obtained at the time of surgery at the Hiroshima University Hospital and affiliated hospitals. We confirmed microscopically that the tumor specimens consisted mainly (>50%) of carcinoma tissue. Samples were frozen immediately in liquid nitrogen and stored at −80°C until use. Noncancerous samples of the heart, lung, stomach, small intestine, colon, liver, pancreas, kidney, bone marrow, peripheral leukocytes, spleen, skeletal muscle, brain, and spinal cord were purchased directly from Clontech (Palo Alto, CA, USA).

For immunohistochemical analysis, we used archival formalin-fixed, paraffin-embedded tissues from 245 patients who had undergone surgical excision or removal of the tumor by polypectomy for GC (n=146) and CRC (n=99). The 146 GCs were either histologically classified (n=85) or poorly (n=61) differentiated. Ninety-nine CRCs were either histologically classified (n=47) or moderately (n=45) or poorly (n=7) differentiated. Tumor staging was carried out according to the tumor–node–metastasis (TNM) staging system [12]. Because written informed consent was not obtained, for strict privacy protection, identifying information for all samples was removed before analysis; the procedure was in accordance with the Ethical Guidelines for Human Genome/Gene Research enacted by the Japanese Government.

Cell lines

Eight cell lines derived from human GC were used. The TMK-1 cell line was established in our laboratory [16]. Five GC cell lines of the MKN series were kindly provided by Dr. T. Suzuki. KATO-III and HSC-39 cell lines were kindly provided by Dr. M. Sekiguchi and Dr. K. Yanagihara [25], respectively. All cell lines were maintained in RPMI 1640 (Nissui Pharmaceutical Co., Ltd., Tokyo, Japan) containing 10% fetal bovine serum (Whittaker, Walkersville, MA, USA) in a humidified atmosphere of 5% CO_2 and 95% air at 37°C.

Quantitative RT-PCR analysis

Total RNA was extracted with an RNeasy Mini kit (Qiagen, Valencia, CA, USA), and 1 μg of total RNA was converted to cDNA with a First-Strand cDNA Synthesis kit (Amersham Pharmacia, Little Chalfont, UK). PCR was performed with an SYBR Green PCR Core Reagents kit (Applied Biosystems, Foster City, CA, USA). Real-time detection of the emission intensity of SYBR green bound to double-stranded DNA was performed with an ABI PRISM 7700 Sequence Detection System (Applied Biosystems) as described previously [11]. *Claudin-2* cDNA and internal control cDNAs [β-actin gene (*ACTB*) and glyceraldehyde-3-phosphate dehydrogenase (*GAPDH*)] were PCR-amplified separately. Relative gene expression was determined by the threshold cycles for the *claudin-2* and *ACTB* or *GAPDH* genes. Reference samples (GC cell line, KATO-III) were included on each assay plate to verify plate-to-plate consistency. Plates were normalized to each other by these reference samples. PCR amplification was performed according to the manufacturer's instructions in 96-well optical trays with caps with a 25-μl final reaction mixture. Quantitative RT-PCRs were performed in triplicate for each sample primer set, and the mean of the three experiments was used as the relative quantification value. *Claudin-2* primer sequences are forward primer 5′-TCCCCAAACCC ACTAATCACA-3′ and reverse primer 5′-CCAACCTCAG CCAGAGAGAGG-3′. *ACTB* primer sequences were 5′-T CACCGAGCGCGGCT-3′ and 5′-TAATGTCACGCAC GATTTCCC-3′ [11]. *GAPDH* primer sequences were 5′-GGTGAAGGTCGGAGTCAACG-3′ and 5′-AGAGTTAA AAGCAGCCCTGGTG-3′. The units are arbitrary, and we calculated *claudin-2* mRNA expression by standardization to 1.0 μg total RNA from KATO-III as 1.0. We found a similar result in both quantitative RT-PCR analyses of *claudin-2* and *ACTB* or *GAPDH* of 8 GC cell lines, 14 various normal tissues, 5 GC tissues, and 9 CRC tissues. Therefore, throughout this article, we will describe and discuss the results obtained using *ACTB* as an internal control in quantitative RT-PCR analysis.

Western blot analysis

Preparation of whole cell lysates from GC cell lines was made and Western blotting was performed as described previously [26]. Protein concentrations were determined by Bradford protein assay (Bio-Rad, Hercules, CA, USA) with bovine serum albumin used as the standard. Lysates (20 μg) were solubilized in Laemmli's sample buffer by boiling and then subjected to 12% sodium dodecyl sulfate–polyacrylamide gel electrophoresis (SDS-PAGE) followed by electrotransfer onto a nitrocellulose filter. Anti-claudin-2 polyclonal antibody was purchased from Zymed (South San Francisco, CA, USA), and anti-β-actin mouse monoclonal antibody was purchased from Sigma (USA). Peroxidase-conjugated anti-rabbit IgG and anti-mouse IgG was used in the secondary reaction, respectively. The immunocomplex was visualized with an ECL Western Blot Detection System (Amersham Pharmacia Biotech).

Immunohistochemistry

A Dako LSAB kit (Dako, Carpinteria, CA, USA), which is based on the LSAB method, was used for the immunohistochemical analysis. In brief, microwave pretreatment in citrate buffer was performed for 15 min to retrieve antigenicity. After blocking the peroxidase with 3% H_2O_2–methanol for 10 min, sections were incubated with antibody/rabbit polyclonal anti-claudin-2, 1:100 (Zymed).

Sections were treated consecutively at room temperature with primary antibody for 2 h, followed by sequential 10 min incubation with biotinylated anti-rabbit IgG and peroxidase-labeled streptavidin. Staining was completed after 10 min incubation with the substrate–chromogen solution. The sections were counterstained with 0.1% hematoxylin. The results of staining with each antibody were evaluated with reference to the percentage of stained cancer cells. The results of immunohistochemistry were graded as follows: "−," 0% to 25% of tumor cells showed immunoreactivity; "+," 25–50% of tumor cells showed immunoreactivity; "++," more than 50% of tumor cells showed immunoreactivity. We regarded "++" as positive throughout this report.

Statistical methods

Associations between clinicopathologic parameters and claudin-2 expression were analyzed by Fisher's exact test. *P* values less than 0.05 were considered statistically significant.

Results

Measurement of mRNA expression of *claudin-2* in various normal tissues, GCs, and CRCs by quantitative RT-PCR

To measure the expression levels of *claudin-2* mRNA, we performed quantitative RT-PCR on 5 GCs, 5 CRCs, and 14 normal tissue samples (heart, lung, stomach, small intestine, colon, liver, pancreas, kidney, bone marrow, peripheral leukocytes, spleen, skeletal muscle, brain, and spinal cord). The results are shown in Fig. 1. In general, the expression levels in CRCs were higher than those in GCs and normal tissues. Among the 14 normal tissues mentioned, the highest level of expression was detected in the kidney. Although obvious expression of *claudin-2* was also detected in the liver, pancreas, stomach, and small intestine, it was not as high as compared with the kidney. In the lung and skeletal muscle, a faint expression of *claudin-2* was found. There was no expression in the remaining normal tissues. Expression levels of *claudin-2* were not so different between normal stomach and GCs. While no expression of *claudin-2* was found in normal colon, two of five CRCs expressed *claudin-2* at significantly higher levels (more than 5 arbitrary units).

Expression and localization of claudin-2 in cancer cell lines

To confirm the mRNA expression of *claudin-2* in cancer cells, we performed quantitative RT-PCR in eight GC cell

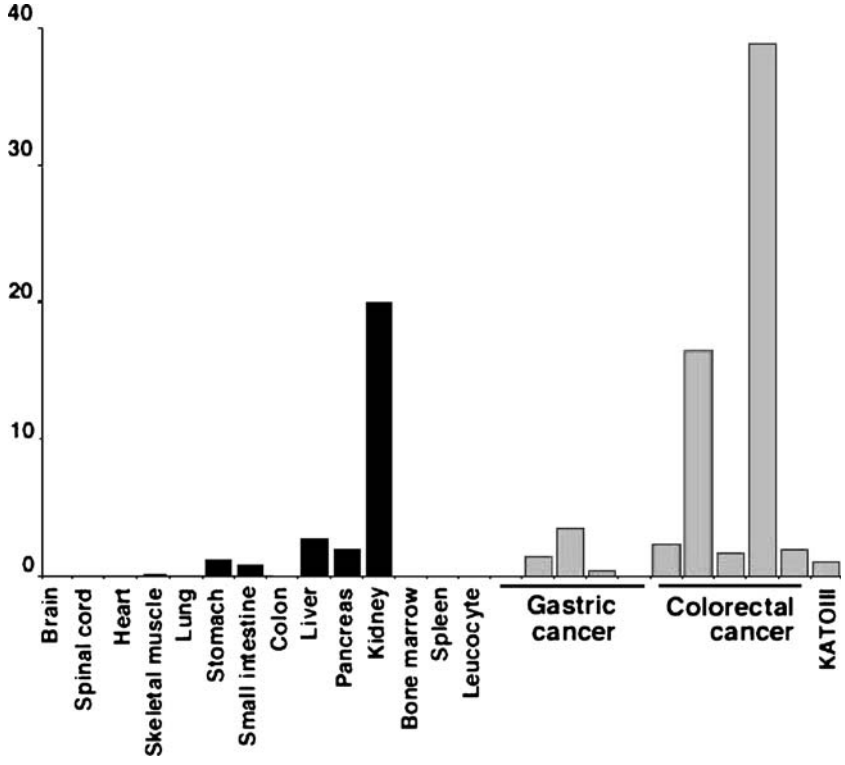

Fig. 1 Quantitative RT-PCR analysis of *claudin-2* in 14 various normal tissues as well as in 5 GC and 5 CRC samples. Among the various normal tissues, the highest level of *claudin-2* expression was found in the kidney; low expression was detected in the stomach, small intestine, liver, and pancreas; and faint expression was seen in the lung and skeletal muscle. In GCs, the expression levels were not so different from that in normal stomach. In CRCs, the expression levels were higher than those in normal colon

lines. As shown in Fig. 2a, an obvious expression of *claudin-2* was detected in MKN-45, MKN-74, and KATO-III, whereas only a low level of expression was seen in HSC-39; there was no expression detected in the remaining four GC cell lines. The anti-claudin-2 antibody detected an approximately 22-kDa band on Western blot of cell extracts from MKN-45, MKN-74, and KATO-III (Fig. 2b). We also confirmed these results by immunohistochemical staining in MKN-28 and MKN-45 cell lines. Claudin-2 staining was detected in cell membranes in MKN-45 cells but not in MKN-28 cells (Fig. 2c). Thus, this antibody was considered to be useful in the detection of claudin-2 protein in situ.

Expression and localization of claudin-2 in CRC tissues

To predict the sensitivity of anti-claudin-2 rabbit polyclonal antibody in immunohistochemistry, we examined the mRNA expression and protein expression of claudin-2 in an additional four CRC tissues. Firstly, we performed quantitative RT-PCR to detect *claudin-2* mRNA expression level and found an obvious expression of *claudin-2* (more than 5 arbitrary units) in three of four examined CRC tissue samples (Fig. 3a). The anti-claudin-2 antibody detected an approximately 22-kDa band on Western blot of protein extracts from the three CRC tissues, which showed obvious high expression in quantitative RT-PCR analysis (Fig. 3b). We also confirmed these results by immunohistochemical staining. Claudin-2 staining was detected in cell membranes of the same three CRC tissue samples, which expressed claudin-2 at a significantly higher level in both quantitative RT-PCR and Western blotting analyses (Fig. 4c). Therefore, in these CRC tissue samples, we found a good correlation between mRNA and protein levels. This result also suggests that in immunohistochemical analysis, our antibody may detect claudin-2 protein expression at levels higher than 5 arbitrary units measured by quantitative RT-PCR analysis.

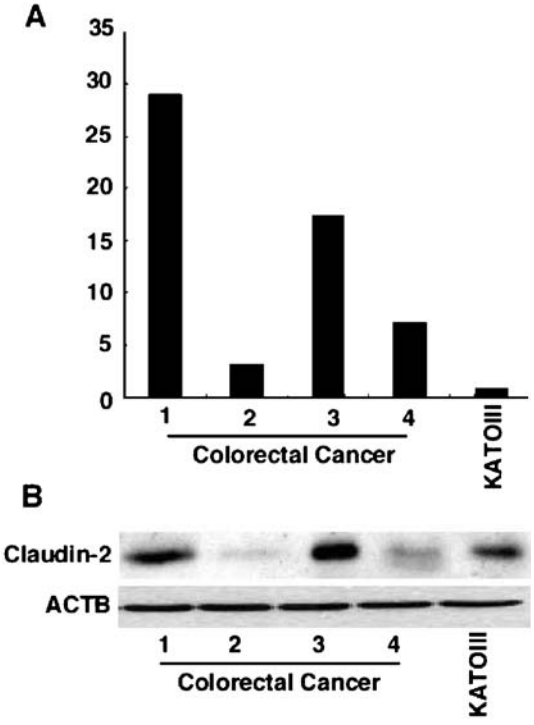

Fig. 3 Expression of claudin-2 in CRC tissue samples. Claudin-2 expression was analyzed at the mRNA level by quantitative RT-PCR (**a**) and at the protein level by Western analysis (**b**)

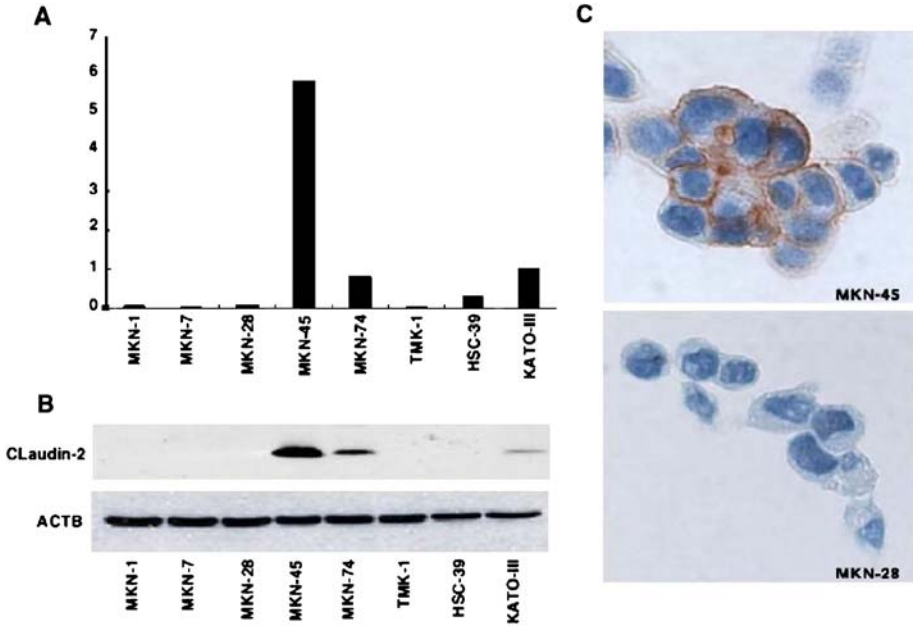

Fig. 2 Expression and localization of claudin-2 in GC cell lines. Claudin-2 expression was analyzed at the mRNA level by quantitative RT-PCR (**a**) and at the protein level by Western analysis (**b**) and immunohistochemistry (**c**); claudin-2 immunoreactivity was evident in the cell membranes of MKN-45 cells but not MKN-28 cells

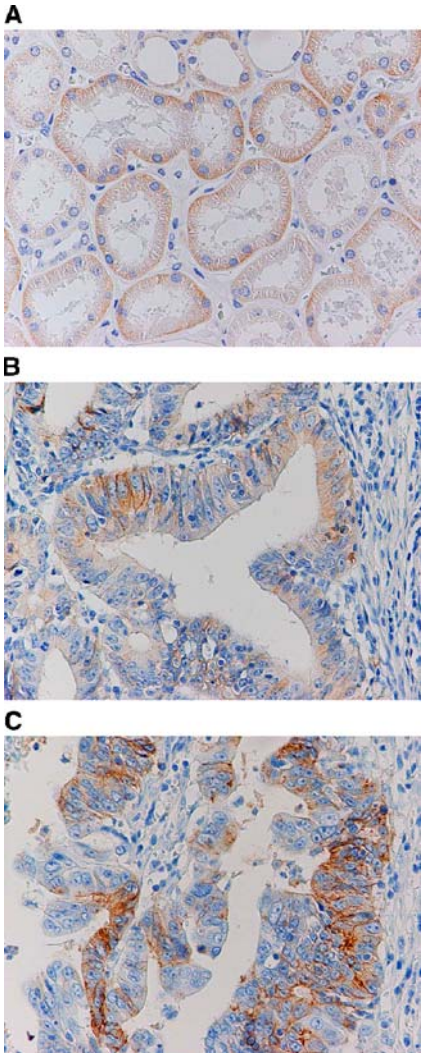

Fig. 4 Immunohistochemical analysis of claudin-2 in normal kidney (as a control) as well as in GC and CRC tissues. Staining for claudin-2 was observed in the basal membranes of the proximal tubule of the kidney (**a**), the cellular membrane of GC cells forming a tubular structure (**b**), and the cellular membrane of CRC cells forming a papillotubular structure (**c**). **c** is case number 1, which expressed *claudin-2* at a high level (more than 5 arbitrary units measured by quantitative RT-PCR), as shown in Fig. 3a,b. Original magnification was ×400

Expression of claudin-2 protein in GCs and CRCs by immunohistochemistry

We then examined the expression of claudin-2 protein in 146 GC and 99 CRC samples by immunohistochemistry. Immunostaining was also performed in normal kidney to serve as a positive control because our real-time RT-PCR revealed a high expression level and a previous report showed claudin-2 expression in mouse nephron. In the kidney, claudin-2 positivity was found strongest in the basal membranes of the proximal tubule, which is consistent with the result of previous reports [3, 9] (Fig. 3a). No obvious staining of claudin-2 was found in normal liver, stomach, and small and large intestines (data not shown). Of the 146 cases of GC, only 3 (2.1%) were positive for claudin-2. Immunoreactivity of claudin-2 was mainly observed in the cell membranes of GC cells forming a tubular structure (Fig. 3b). In CRCs, 25 (25.3%) of 99 cases were positive for claudin-2. Claudin-2 was mainly localized in the cell membranes of tumor cells forming a papillotubular structure (Fig. 3c).

We analyzed the relation between the expression of claudin-2 and clinicopathologic characteristics of CRC. There was no clear correlation between claudin-2 staining and clinicopathological parameters such as location, T grade, N grade, M grade, stage, and histologic differentiation (Table 1).

Table 1 Relation between claudin-2 protein expression and clinicopathologic characteristics in CRCs

	Claudin-2 expression	*P* value[a]
Location		
Right	8/32 (25.0%)	1.0000
Left	17/67 (25.4%)	
T grade		
T1/2	7/29 (24.1%)	1.0000
T3/4	18/70 (25.7%)	
N grade		
N0	17/58 (29.3%)	0.3494
N1/2	8/41 (19.5%)	
M grade		
M0	25/95 (26.3%)	0.5695
M1	0/4 (0.0%)	
Stage		
I	6/25 (24.0%)	0.1453
II	11/33 (33.3%)	
III	8/37 (21.6%)	
IV	0/4 (0.0%)	
Histology		
Well	14/47 (29.8%)	0.4774
Moderate	9/45 (20.0%)	
Poor	2/7 (28.6%)	

[a]Fisher's exact test

Discussion

Cellular tight junctions are structures that help preserve the integrity of cellular layers and regulate their permeability [23, 24]. It may be hypothesized that changes in expression of tight junctional proteins can lead to cellular disorientation and detachment, which are commonly seen in neoplasia. In this study, we demonstrated for the first time the expression of *claudin-2* mRNA in normal human kidney, liver, pancreas, and so on. Among these, the highest level of expression was detected in the kidney. In addition, an obvious expression of *claudin-2* was also detected in the stomach and small intestine. These results are consistent with a previous report in rat and mice; *claudin-2* is expressed in nephron, liver, pancreas, and gut

[3, 17]. We found a basal expression of claudin-2 in kidney tubules, although claudin-2 is not a known basal membrane protein and tight junctions are not known to be in the region of basal membrane. We could not explain well this unusual expression. However, it has been already published by Kiuchi-Saishin et al. [9] that claudin-2, claudin-10, and claudin-11 were clearly concentrated at the tight junction of epithelial cells of the proximal tubules. Among these, only claudin-2 seemed to be distributed along basal plasma membranes in addition to tight junction. This staining is specific for claudin-2 because the kidneys of claudin-2-deficient mice demonstrated no such staining (Furuse et al., unpublished data) [9].

We also investigated claudin-2 expression in 146 GC and 99 CRC cases to evaluate their differential expression of claudin-2 in gastrointestinal cancers. In previous studies, type-specific expression of claudin-1, claudin-2, claudin-3, claudin-4, claudin-5, and claudin-7 has been detected in various types of cancers including carcinomas of breast, pancreas, liver, esophagus, etc. [20, 21]. Soini [21] also analyzed claudin-2 expression in a small number of GCs and CRCs by using the monoclonal anticlaudin-2 antibody and reported that 12 of 13 GCs (92%) and 9 of 11 CRCs (82%) were positive for claudin-2. No method other than immunohistochemistry was utilized. In our study, the frequency of claudin-2 expression in GC and CRC was much lower as compared to the above studies, partly due to the different antibody used. However, our immunohistochemistry must be precise even if it was not so sensitive because we have found a good correlation between levels of *claudin-2* mRNA expression and protein expression by immunostaining and Western analysis of not only GC cell lines but also CRC tissues, as shown in Figs. 2, 3, and 4c. Our antibody may detect claudin-2 expression at levels higher than 5 arbitrary units, as measured by quantitative RT-PCR. In situ hybridization experiments may help detect the expression of claudin-2 with high sensitivity. We will perform it in a future study of claudin-2.

The results of the present study demonstrated that expression of claudin-2 was detected in CRCs, whereas no expression of claudin-2 was detected in normal colon. We did not find any significantly different expression between GC and normal stomach. Therefore, the participation of claudin-2 in tumorigenesis may involve organ specificity. Claudin species have been found to be the major constituents of tight junction strands [2, 5, 9, 19]. The presence of junctional claudin-2 causes the formation of cation-selective channels sufficient to transform a "tight" junction into a "leaky" one [1]. In carcinogenesis of CRC, claudin-2 may contribute to an easier leak of tight junctions in between neoplastic cells. Although we observed claudin-2 staining mainly in the neoplastic cells forming a tubular or papillary structure in both GCs and CRCs, we did not find any significant correlation between claudin-2 protein expression and histological differentiation. Moreover, we could not find any correlation with tumor advancement. Therefore, increased expression of claudin-2 may participate in the development but not in the progression of CRCs, although the exact mechanism is unknown. It has been shown that human claudin-2 promoter activity is positively regulated by the caudal-related homeobox gene (*CDX2*), as well as by the hepatocyte nuclear factor-1 alpha isoform (HNF-1α) [18]. A published study has shown the presence of functional cross talk between *CDX2* and the Wnt pathway in the positive regulation of claudin-2 expression [14]. These regulations may be the cause of the involvement of claudin-2 in colorectal carcinogenesis. In fact, abnormalities in Wnt signaling, including β-catenin/TCF, have been shown to participate in the pathogenesis of CRC [6]. Further studies are needed to explore the exact mechanism of claudin-2 involvement in gastrointestinal tumor pathology.

Acknowledgements This work was supported, in part, by Grants-in-Aid for Cancer Research from the Ministry of Education, Culture, Science, Sports, and Technology of Japan and from the Ministry of Health, Labor, and Welfare of Japan. We thank Mr. Masayoshi Takatani and Ms. Mutsumi Ueda for excellent technical assistance and advice. We thank the Analysis Center of Life Science, Hiroshima University, for the use of their facilities. The experiments in this study were in accordance with the Ethical Guidelines for Human Genome/Gene Research enacted by the Japanese government.

References

1. Amasheh S, Meiri N, Gitter AH, Schoneberg T, Mankertz J, Schulzke JD, Fromm M (2002) Claudin-2 expression induces cation-selective channels in tight junctions of epithelial cells. J Cell Sci 115:4969–4976
2. Colegio OR, Van Itallie C, Rahner C, Anderson JM (2003) Claudin extracellular domains determine paracellular charge selectivity and resistance but not tight junction fibril architecture. Am J Physiol Cell Physiol 284:C1346–C1354
3. Enck AH, Berger UV, Yu AS (2001) Claudin-2 is selectively expressed in proximal nephron in mouse kidney. Am J Physiol Renal Physiol 281:F966–F974
4. Furuse M, Sasaki H, Fujimoto K, Tsukita S (1998) A single gene product, claudin-1 or -2, reconstitutes tight junction strands and recruits occludin in fibroblasts. J Cell Biol 143:391–401
5. Furuse M, Sasaki H, Tsukita S (1999) Manner of interaction of heterogeneous claudin species within and between tight junction strands. J Cell Biol 147:891–903
6. Gaspar C, Fodde R (2004) APC dosage effects in tumorigenesis and stem cell differentiation. Int J Dev Biol 48(5–6):377–386
7. Hough CD, Sherman-Baust CA, Pizer ES, Montz FJ, Im DD, Rosenshein NB, Cho KR, Riggins GJ, Morin PJ (2000) Large-scale serial analysis of gene expression reveals genes differentially expressed in ovarian cancer. Cancer Res 60(22):6281–6287
8. Itoh M, Furuse M, Morita K, Kubota K, Saitou M, Tsukita S (1999) Direct binding of three tight junction-associated MAGUKs, ZO-1, ZO-2, and ZO-3, with the COOH termini of claudins. J Cell Biol 147:1351–1363
9. Kiuchi-Saishin Y, Gotoh S, Furuse M, Takasuga A, Tano Y, Tsukita S (2002) Differential expression patterns of claudins, tight junction membrane proteins, in mouse nephron segments. J Am Soc Nephrol 13:875–886
10. Kominsky SL, Argani P, Korz D, Evron E, Raman V, Garrett E, Rein A, Sauter G, Kallioniemi OP, Sukumar S (2003) Loss of the tight junction protein claudin-7 correlates with histological grade in both ductal carcinoma in situ and invasive ductal carcinoma of the breast. Oncogene 22(13):2021–2033

11. Kondo T, Oue N, Yoshida K, Mitani Y, Naka K, Nakayama H, Yasui W (2004) Expression of POT1 is associated with tumor stage and telomere length in gastric carcinoma. Cancer Res 64:523–529
12. Lauren P (1965) The two histological main types of gastric carcinoma: diffuse and so-called intestinal-type carcinoma an attempt at a histo-clinical classification. Acta Pathol Microbiol Scand 64:31–49
13. Long H, Crean CD, Lee WH, Cummings OW, Gabig TG (2001) Expression of Clostridium perfringens enterotoxin receptors claudin-3 and claudin-4 in prostate cancer epithelium. Cancer Res 61(21):7878–7881
14. Mankertz J, Hillenbrand B, Tavalali S, Huber O, Fromm M, Schulzke JD (2004) Functional crosstalk between Wnt signaling and Cdx-related transcriptional activation in the regulation of the claudin-2 promoter activity. Biochem Biophys Res Commun 314:1001–1007
15. Michl P, Barth C, Buchholz M, Lerch MM, Rolke M, Holzmann KH, Menke A, Fensterer H, Giehl K, Lohr M, Leder G, Iwamura T, Adler G, Gress TM (2003) Claudin-4 expression decreases invasiveness and metastatic potential of pancreatic cancer. Cancer Res 63(19):6265–6271
16. Ochiai A, Yasui W, Tahara E (1985) Growth-promoting effect of gastrin on human gastric carcinoma cell line TMK-1. Jpn J Cancer Res 76:1064–1071
17. Rahner C, Mitic LL, Anderson JM (2001) Heterogeneity in expression and subcellular localization of claudins 2, 3, 4, and 5 in the rat liver, pancreas, and gut. Gastroenterology 120:411–422
18. Sakaguchi T, Gu X, Golden HM, Suh E, Rhoads DB, Reinecker HC (2002) Cloning of the human claudin-2 5′-flanking region revealed a TATA-less promoter with conserved binding sites in mouse and human for caudal-related homeodomain proteins and hepatocyte nuclear factor-1alpha. J Biol Chem 277:21361–21370
19. Sasaki H, Matsui C, Furuse K, Mimori-Kiyosue Y, Furuse M, Tsukita S (2003) Dynamic behavior of paired claudin strands within apposing plasma membranes. Proc Natl Acad Sci U S A 100:3971–3976
20. Soini Y (2004) Claudins 2, 3, 4, and 5 in Paget's disease and breast carcinoma. Hum Pathol 35:1531–1536
21. Soini Y (2005) Expression of claudins 1, 2, 3, 4, 5 and 7 in various types of tumors. Histopathology 46:551–560
22. Terris B, Blaveri E, Crnogorac-Jurcevic T, Jones M, Missiaglia E, Ruszniewski P, Sauvanet A, Lemoine NR (2002) Characterization of gene expression profiles in intraductal papillary-mucinous tumors of the pancreas. Am J Pathol 160(5):1745–1754
23. Tsukita S, Furuse M (2000) Pores in the wall: claudins constitute tight junction strands containing aqueous pores. J Cell Biol 149:13–16
24. Tsukita S, Furuse M (2002) Claudin-based barrier in simple and stratified cellular sheets Curr Opin Cell Biol 14(5):531–536
25. Yanagihara K, Seyama T, Tsumuraya M, Kamada N, Yokoro K (1991) Establishment and characterization of human signet ring cell gastric carcinoma cell lines with amplification of the c-myc oncogene. Cancer Res 51:381–386
26. Yasui W, Ayhan A, Kitadai Y, Nishimura K, Yokozaki H, Ito H, Tahara E (1993) Increased expression of p34cdc2 and its kinase activity in human gastric and colonic carcinomas. Int J Cancer 53:36–41

Virchows Arch (2006) 448: 435–441
DOI 10.1007/s00428-005-0132-y

ORIGINAL ARTICLE

Gou Yamamoto · Tarou Irie · Tadateru Aida · Yuuki Nagoshi · Reiko Tsuchiya · Tetsuhiko Tachikawa

Correlation of invasion and metastasis of cancer cells, and expression of the RAD21 gene in oral squamous cell carcinoma

Received: 31 July 2005 / Accepted: 28 October 2005 / Published online: 14 January 2006

Abstract Although RAD21 is involved in the repair of double-strand breaks in DNA and is essential for mitotic growth, its role in cancer has been unclear. In this study, the relevance of RAD21 gene expression to the invasion and metastasis of oral squamous cell carcinoma was clarified using laser microdissection and real-time polymerase chain reaction (PCR). Using two different metastatic potential oral squamous cells [high-metastatic-potential squamous cell carcinoma cells (SAS-Ly) and low-metastatic-potential squamous cell carcinoma cells (SAS)], the relation of RAD21 gene expression to apoptosis, invasion, and metastasis was examined. The results showed that RAD21 gene expression was significantly decreased in oral squamous cell carcinoma when it expressed the INFβ and INFγ invasion patterns in comparison with the INFα invasion pattern ($p<0.01$). In addition, in comparison with SAS cells, SAS-Ly cells indicated tolerance to cell death induced by an apoptosis induction reagent, while the expression level of the RAD21 gene in SAS cells was increased by the apoptosis induction reagent. However, in SAS-Ly cells, the reagent induced no significant difference. Our findings indicate that the RAD21 gene was closely related to the invasion and metastasis of cancer cells.

Keywords Invasion · Lymph node metastasis · Oral cancer · Apoptosis · RAD21

Abbreviation DEPC: Dietyl pyrocarbonate

G. Yamamoto (✉) · T. Irie · T. Aida · Y. Nagoshi · R. Tsuchiya · T. Tachikawa
Department of Oral Pathology and Diagnosis,
School of Dentistry, Showa University,
Hatanodai 1-5-8, Shinagawaku,
Tokyo 142-8555, Japan
e-mail: gd0021@dent.showa-u.ac.jp
Tel.: +81-3-37848169
Fax: +81-3-37842870

Introduction

RAD21 is one of the four subunits of cohesin, the latter of which holds sister chromatids together until anaphase [8, 23]. Cohesin is combined with the chromosome in the G1 phase and holds the sister chromatids until RAD21 is cleaved by separase during the onset of anaphase, with these cleavages allowing chromosomal separation [9, 17, 18, 24, 33]. When RAD21 was knocked out of chicken DT40 cells, it caused premature sister chromatid separation [30]. When RAD21 is mutated at the cleavage site by separase, not only chromosome segregation but also cell division is inhibited [16]. In light of the above fact, RAD21 may play an important role in faithful and stabilized chromosomal separation. Recently, it has been shown that the degradation product formed by the C-terminal cleavage of RAD21 by caspases 3 and 7 becomes a factor which induces apoptosis [13, 26]. In addition, in regard to the association of tumor formation and RAD21, the expression level of the RAD21 gene is suppressed by hypoxia in liver cancer and mammary cancer cells [31], the RAD21 gene is over-expressed in prostate cancer cells [27], and it has been reported that RAD21 gene expression is induced by the BRCA1 gene which is a tumor suppressor gene in breast cancer cells [3]. However, the relation between the RAD21 gene and cancer remains unclear. In the present study, the relevance of the RAD21 gene to the invasion and metastasis of squamous cell carcinoma was investigated in carcinoma tissue samples using laser microdissection and real-time polymerase chain reaction (PCR). RAD21's relevance to cancer cell invasion was investigated using the high (SAS-Ly) and low (SAS) metastatic potentials of the squamous cell carcinoma cell line.

Materials and methods

Cell culture

The SAS cell, a poorly differentiated squamous cell carcinoma cell line, was derived from human tongue primary

lesion [32]. The SAS-Ly cell with high lymph node metastatic potential was established in our department from SAS by repetition of orthotopic implantation to the tongue of the nude mouse [2]. Cells were cultured in Dulbecco's Modified Eagle medium nutrient mixture F-12 ham (SIGMA) supplemented with 10% fetal bovine serum, 50 units/ml penicillin, and 50 μg/ml streptomycin, in a humidified atmosphere, 5% CO_2, at 37°C.

Drug treatment

Actinomycin D and trichostatin A were purchased from Sigma. Actinomycin D was kept as a 1.25-mg/ml solution in ethanol at 4°C, and trichostatin A was an 8.3-mM solution in ethanol at −20°C. SAS and SAS-Ly cells at subconfluent states were treated with these drugs at the desired final concentration and duration. Control cells were treated with the vehicle (ethanol) used to dilute actinomycin D and trichostatin A.

Frozen sample preparation for laser microdissection

Tumor specimens were obtained at surgery from 28 patients with oral squamous cell carcinoma (Table 1). The extracted tissues were embedded in OCT compound and frozen in isopentane cooled in liquid nitrogen. The specimens were then made into frozen blocks, which were sliced using a cryomicrotome (MICROM) at 7-μm thickness for microdissection.

RNA isolation

Total RNA was extracted from the cultured cells by TRIzol reagent (Invitrogen). After phenol/chloroform extraction and ethanol precipitation, RNA was resuspended in dietyl pyrocarbonate (DEPC)-treated water. For total RNA extraction using laser microdissection, the frozen sections were placed at room temperature for 5 min and fixed in 100% methanol for 3 min. After washing with RNase-free water, the sections were stained with 1% toluidine blue. After they were air-dried, the sections were microdissected by means of a PALM Micro Beam (P.A.L.M. Microlaser Technologies). The target areas were the invasive areas in primary lesion and regional lymph node metastasis of squamous cell carcinoma. The invasion pattern of each case was determined in terms of the classification (pattern of infiltration, INF) of the cancer handling convention of Japan [20, 21]. The patterns are regarded as INFα if the cancer nest grows expansively and a clear circumference boundary can be seen between the cancer and the surrounding tissue. INFβ is intermediate between INF-alpha and INFγ. INFγ shows an infiltrative growth pattern and the boundary with the circumference tissue is indistinct. From the type of well-differentiated regions that form a cancer pearl, we removed the keratinized area in advance. The number of microdissected cells was estimated to be about 700–2,500 cells for each sample. The total RNA that had been extracted from each population of laser-microdissected cells was independently extracted by means of our previously described method [19]. Extracted total RNA was resuspended in DEPC-treated water.

Table 1 Summary of clinicopathological findings

Case	Age	Sex	Site	INF	Metastasis
1	76	M	T		
2	71	M	T		
3	67	M	T		
4	44	M	T		
5	71	F	G		
6	61	F	G		
7	71	M	T		
8	69	M	T		
9	53	F	FM		
10	64	M	T		
11	41	F	T		
12	73	F	BM		
13	64	M	T		
14	75	M	T		
15	54	M	G		
16	72	M	G		
17	52	M	G		
18	72	F	BM		
19	82	F	BM		
20	59	M	T		
21	59	F	G		
22	61	M	T		
23	34	M	T		
24	56	M	FM		
25	70	M	T		
26	76	M	L		Lymph node of case No. 1
27	72	F	L		Lymph node of case No. 18
28	71	F	L		
29	56	M	L		
30	77	M	L		

T Tongue, *BM* buccal mucosa, *G* gingiva, *FM* floor of mouth, *L* lymph node metastasis, *INF* pattern of infiltration

Real-time quantitative PCR

Using 40–50 ng total RNA of the cells and all RNA extracted from the frozen sections, cDNA was made by reverse transcription with Sensiscript RT (QUIAGEN) and oligo d $(T)_{16}$ primer (QUIAGEN). The PCR reactions were performed using an ABI PRISM 7000 Sequence Detection System (Applied Biosystems Japan) apparatus employing QuantiTect SYBR Green PCR (QIAGEN). Each 30-μl reaction mixture contained 15 μl of 2× QuantiTect SYBR Green PCR Master Mix, sense primer (1 μM), antisense primer (1 μl), 2 μl of template cDNA, and RNase-free water. The PCR conditions were as follows: initial denaturation at 95°C for 15 min, 50 cycles at 94°C for

15 s, 57°C for 30 s, and 72°C for 30 s. The primers are described below:RAD21 (GenBank accession no. NM_006265)(5′-TGGGTTGTGTTTGTGTTCTG-3′, 5′-TCAAGAGGGTGACCATTGTT-3′ and GAPDH (5′-CGACCACTTTGTCAAGCTCA-3′, 5′-CAGTTGCCATG TAGACCCCT-3′). Standard curves were generated using serial dilutions (1–0.0001) of known quantities of tumor cells cDNA. In addition, melting curve analysis was used to ensure the purity of the amplified PCR product. The relative expression of RAD21 was calculated by dividing the value by the GAPDH value of each sample.

Fluorogenic cell viability assay

Cell viability was assessed using a FluoDia T70 OTSTKA ELECTRONICS apparatus employing CellTiter-Blue Cell Viability Assay, Promega according to the manufacturer's directions. The 5×10^4 cells were seeded into each well of a 96-well microtiter plate. After culturing overnight, various concentrations of drugs, as indicated in the figure, were added to the wells and incubated for 24 h in a humidified atmosphere, 5% CO_2, at 37°C. A blank control, consisting of CellTiter-Blue Reagent and cell culture medium without cells, was used as a measure of background fluorescence associated with the culture system. The control used vehicle-treated cells with CellTiter-Blue Reagent. After incubation, fluorescence was measured and cell viability as a percentage of untreated cells was calculated.

Results

The expression of RAD21 gene in oral squamous cell carcinoma of various invasion patterns and regional lymph node metastasis in vivo

Using the laser microdissection method, the cancer cell that corresponds to each invasion pattern is procured from the invasion front in the primary lesion (Fig. 1). The expression

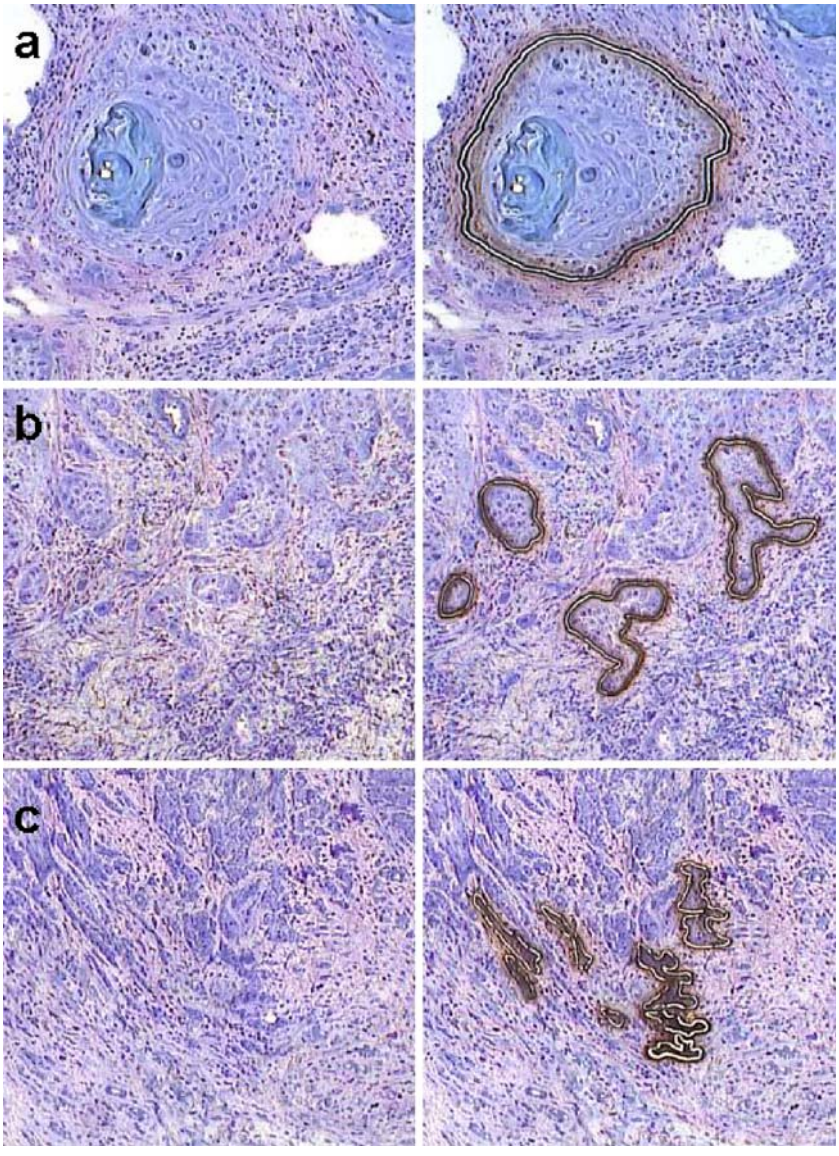

Fig. 1 Procurement of the target tissue from the frozen section by the laser microdissection method. **a** INFα, **b** INFβ, and **c** INFγ. Laser microdissection was performed by PALM Micro Beam (P.A.L.M. Microlaser Technologies) after staining in 1% toluidine blue. For the left-hand side, before the cut by laser and for the right-hand ride are after a cut

level of the RAD21 gene was examined by means of real-time PCR. As a result, the expression level of the RAD21 gene decreased significantly ($p<0.01$) in the areas that showed the invasion patterns of INFβ and INFγ in comparison with the areas that showed the INFα invasion pattern (Fig. 2, Table 2).

In regional lymph node metastasis, the expression level of the RAD21 gene also decreased similar to the INFγ invasion pattern (Fig. 2, Table 2).

Table 2 Relation of RAD21 gene expression in various invasion pattern and lymph node metastasis

	p value
INFα vs INFβ	<0.01
INFα vs INFγ	<0.01
INFα vs LN	<0.01
INFβ vs INFγ	NS
INFβ vs LN	<0.05
INFγ vs LN	NS

LN Regional lymph node metastasis, *NS* not significant

Invasion pattern of culture cells transplanted in a nude-mouse tongue

It was shown in our previous report that the invasion potential of SAS-Ly cells is higher than that of SAS cells [2]. When both types of cell were transplanted to the lingua1 edge region of nude mice (BALB/C-nu/nu), the SAS-Ly cell showed an invasive growth pattern to the circumference tissue, and the invasion pattern corresponded to INFγ. Meanwhile, the SAS cells showed an expansive growth pattern to the circumference tissue, with the invasion pattern corresponding to INFα (Fig. 3).

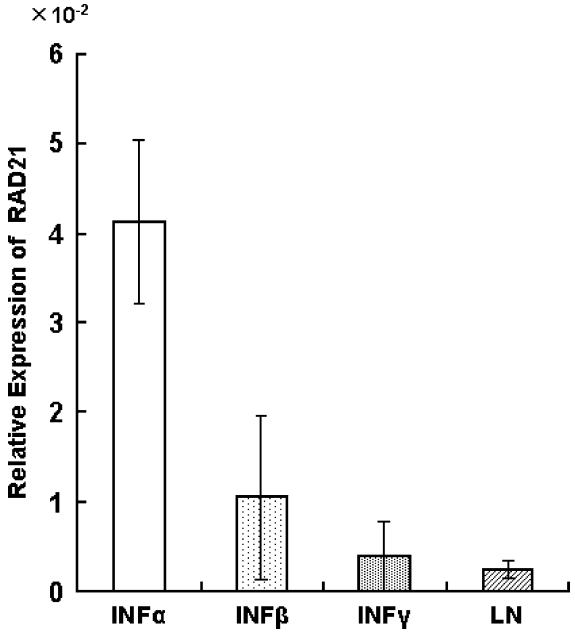

Fig. 2 The expression level of the RAD21 gene by laser microdissection and real-time quantitative PCR. The relative expression of RAD21 gene was calculated by dividing the value by the GAPDH value of each sample. At the infiltrating edge of the oral squamous cell carcinoma, the RAD21 gene expression was decreased in the area that showed the invasion patterns of INFβ (n=8) and INFγ (n=10) in comparison with the area of INFα (n=7). In regional lymph node metastasis (LN, n=5), the RAD21 gene expression was also decreased similar to the INFγ invasion pattern. *Bars* ±SD

The expression level of the RAD21 gene of high-metastatic-potential squamous cell carcinoma cells (SAS-Ly) and low-metastatic-potential squamous cell carcinoma cells (SAS)

The expression level of RAD21 gene in SAS cells and SAS-Ly cells with the different invasion patterns was analyzed. The RAD21 gene of the SAS-Ly cell significantly decreased in comparison with the SAS cell ($p<0.05$) (Fig. 4). It was confirmed that the expression levels of the

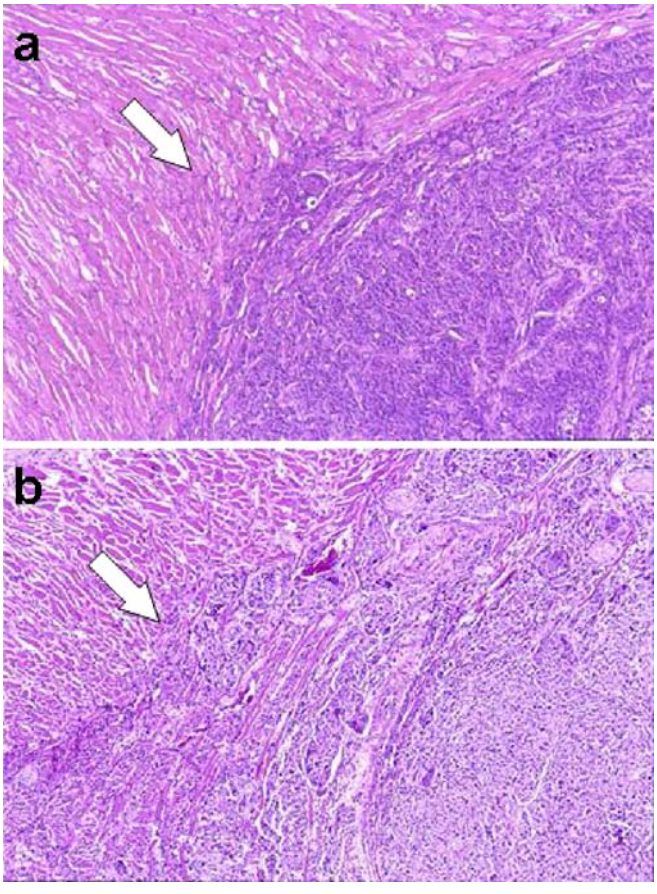

Fig. 3 The histological pattern of infiltration in a nude-mouse tongue, transplanted SAS and SAS-Ly. **a** SAS and **b** SAS-Ly. Transplanted to the nude mouse, as compared with the SAS cells, showing the invasion pattern of INFα with a comparatively clear boundary with a circumference. The SAS-Ly cells showed the invasion pattern of INFγ (indicated by a *white arrow*)

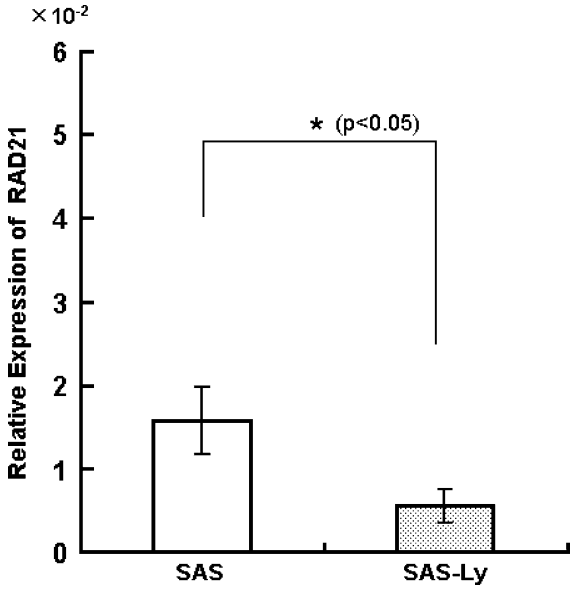

Fig. 4 The expression level of the RAD21 gene in SAS and SAS-Ly. The SAS cells and the SAS-Ly cells were used. The relative expression of the RAD21 gene was calculated by dividing the value by the GAPDH value of each sample. As compared with the SAS cells, the expression level of the RAD21 gene decreased significantly ($p<0.05$) by the SAS-Ly cells of higher invasion potential. Each point represents a mean of triplicates. *Bars* ±SD (*$p<0.05$)

RAD21 gene in invasion and metastasis in vitro correlated with those in vivo.

Resistance to cell death induced by apoptosis induction reagents in SAS and SAS-Ly

The results of a cell survival test showed that the population of SAS cells decreased to a greater degree than that of SAS-Ly cells by treatments with actinomycin D and trichostatin A. SAS-Ly cells with high metastatic potential showed resistance to apoptosis (Fig. 5).

Effect of apoptosis induction reagents on the expression level of the RAD21 gene in SAS and SAS-Ly

The optimum concentration and time was determined using the SAS cells. After the SAS cells and SAS-Ly cells were treated with 0.5 ug/ml actinomycin D and 1,000 nM trichostatin A for 24 h, RAD21 gene expression quantity was measured. As a result, though RAD21 gene expression was significantly increased in the SAS cells treated with the apoptosis induction reagent, a change in the expression of the gene was not recognized in the SAS-Ly cells (Fig. 6).

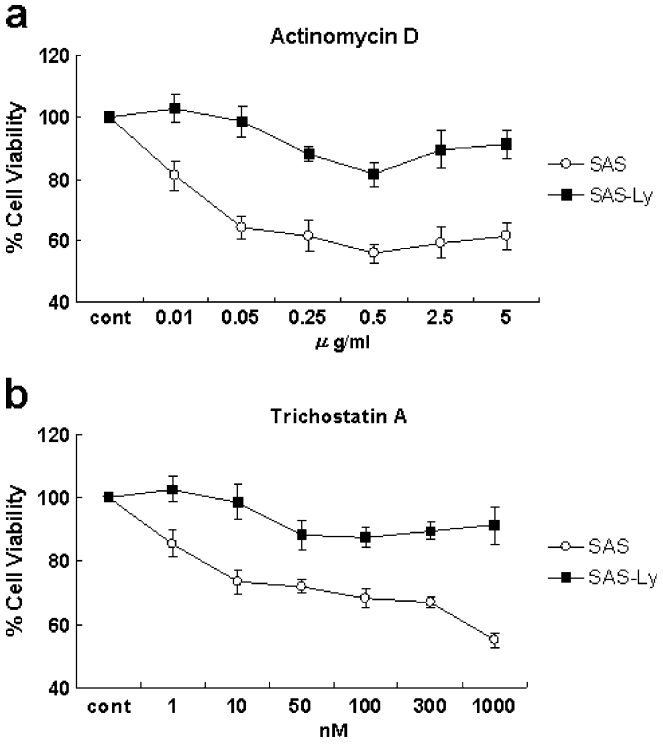

Fig. 5 The cell survivability with the apoptosis induction reagents in SAS and SAS-Ly. SAS and SAS-Ly were used. **a** Dose-related apoptosis in SAS and SAS-Ly treated with increasing concentration of actinomycin D (0.01 to 5 μg/ml) for 24 h. **b** Treated with trichostatin A (1 to 1,000 nM) for 24 h. The *X*-axis expresses the concentration of a reagent and the *Y*-axis expresses the rate of a survival cell to control. The concentration to which resistance to apoptosis induction reagents was shown in SAS-Ly was compared with SAS. Each point represents a mean of triplicates. *Bars* ±SD

Discussion

We studied the relation between the invasion pattern of squamous cell carcinoma and the expression level of the RAD21 gene using the laser microdissection method and real-time PCR in surgical material. It became clear that the expression level of the RAD21 gene decreased as the invasion pattern of squamous cell carcinoma changed to INFγ from INFα. It is known that the expression level of the RAD21 gene is down-regulated under hypoxia in many human tumor cells [31]. As well, hypoxia in malignant tumor tissue is more concerned in development of the aggressive character and metastasis of malignant tumor cells [1, 6, 7, 10, 12, 29]. It has been shown that the lowering of oxygen partial pressure in the tumor correlates with prognosis in squamous cell carcinoma of the head and neck [11]. In regard to the biological significance of the invasion pattern, it is known that in oral squamous cell carcinoma, similar to cancer in other organs, an invasive growth pattern such as INFγ indicates high lymph node metastasis frequency and poor prognosis, as compared with

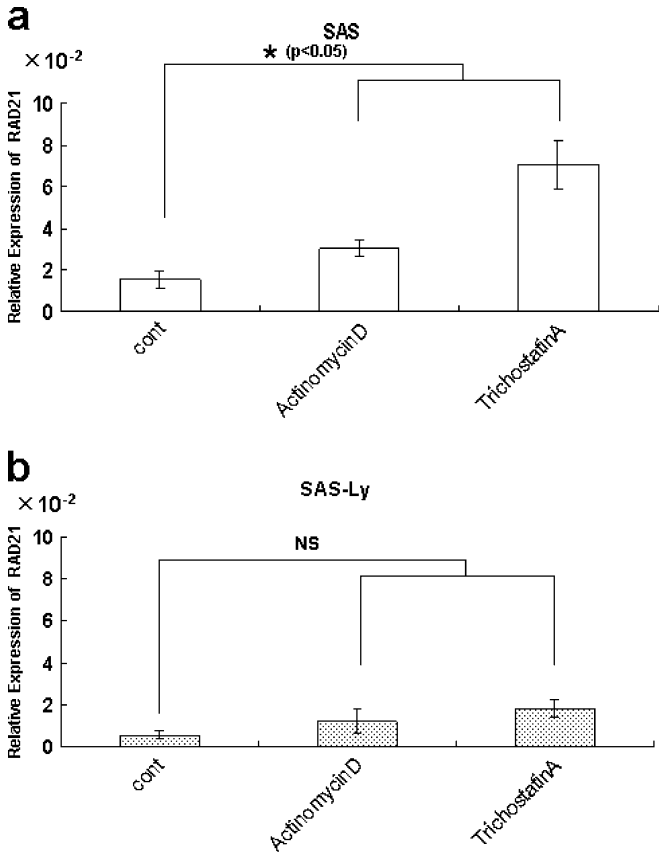

Fig. 6 The expression level of the RAD21 gene in SAS and SAS-Ly treated with apoptosis induction reagents. **a** SAS and **b** SAS-Ly. The SAS cells and the SAS-Ly cells were treated with actinomycin D (0.5 μg/ml) and trichostatin A (1,000 nM) for 24 h. The relative expression of the RAD21 gene was calculated by dividing the value by the GAPDH value of each sample. The expression level of the RAD21 gene increased significantly ($p<0.05$) in the SAS cells with apoptosis induction reagents. In SAS-Ly, although the increase was shown, there was no significant difference. Each point represents a mean of triplicates. *Bars* ±SD, *NS* not significant (*$p<0.05$)

the cancer which shows an expansive growth pattern such as INFα [4, 22, 25]. Actually, the case of INFγ showed a lot of metastasis in the case we had used (Table 1). Based on the above reports and the results of our study, the RAD21 gene might be related to the development of an invasive pattern. Simultaneously, these results suggest the possibility that the invasion pattern of squamous cell carcinoma reflects the hypoxia in the tumor tissue.

In regional lymph node metastasis, the expression level of the RAD21 gene decreased similarly to the INFγ invasion pattern. This result supports the possibility that cancer cells with high invasion potential cause lymph node metastasis in relation to hypoxic condition.

Further, we analyzed the relation of RAD21 gene expression to invasion and metastasis potential using high (SAS-Ly) and low (SAS) metastatic squamous cell carcinoma cell lines. It became clear that SAS-Ly cells showed an invasive growth pattern similar to INFγ in grafts to the nude mouse, and that SAS cells showed an expansive growth pattern similar to INFα. This result shows that these cell lines have the phenotype reflecting the invasion pattern in vivo, and that the invasion pattern and metastasis are closely related in the cultured cells. In addition, the lower RAD21 gene expression level in SAS-Ly cells than in SAS cells supports the analytical result regarding the quantity of RAD21 gene expression in cancer cells of each invasion pattern of the squamous cell carcinoma tissue. This seems to suggest more firmly that RAD21 is closely related to the potential for invasion and metastasis in oral squamous cell carcinoma.

The RAD21 gene has been identified, by means of the differential display method, as the gene which is down-regulated in the hypoxia [31]. This suggests the possibility that the decrease of the expression level of the RAD21 gene affects various intracellular changes in the hypoxia. In solid tumors, hypoxic condition concerns a selection of the apoptosis-resistant cells, and it has been indicated to be important for progression of tumor cells [15]. As well, hypoxia directly induces the cell's apoptotic resistance [5, 14, 34]. In addition, it has been shown that the angiogenesis of cancer and the apoptosis of cancer cells correlate inversely in squamous cell carcinoma of the head and neck. These are considered to be the results of apoptotic resistance induced by hypoxia in cancer cells [28].

RAD21 is cleaved by caspase 3, and it has become clear that the degradation product in the C-terminal site induces apoptosis, so the RAD21 gene plays an important role in apoptosis [13, 26]. These reports suggest that the apoptotic resistance of the tumor cell and the down-regulation of the RAD21 gene are closely related. Our results supports this: the proportion of cell death due to the apoptosis induction reagent in high-metastatic-potential squamous cell carcinoma cells is lower than in low-metastatic-potential squamous cell carcinoma cells. As well, in SAS cells, the expression level of the RAD21 gene was increased by apoptosis induction, but it lead to no significant change in SAS-Ly cells at the gene expression level. These results indicate the possibility that the decrease of the RAD21 expression level in SAS-Ly cells is a direct cause of apoptotic resistance. Finally, our findings suggest that the RAD21 gene plays an important role in the invasion and metastasis of cancer cells.

Acknowledgements This work was supported in part by the Showa University Grant-in-Aid for Innovative Collaborative Research Projects, the High-Technology Research Center Project and Characteristic Education from the Ministry of Education, Culture, Sports, Science and Technology of Japan.

References

1. Acs G, Zhang PJ, Rebbeck TR, Acs P, Verma A (2002) Immunohistochemical expression of erythropoietin and erythropoietin receptor in breast carcinoma. Cancer 95:969–981
2. Aida T, Irie T, Tachikawa T (2001) Establishment and characterization of human oral squamous cell carcinoma cell line with highly lymph node metastatic potential. J Jpn Soc Oral Tumor 13:301–306

3. Atalay A, Crook T, Ozturk M, Yulug IG (2002) Identification of genes induced by BRCA1 in breast cancer cells. Biochem Biophys Res Commun 299:839–846
4. Baba H, Ohshiro T, Yamamoto M, Endo K, Adachi E, Kakeji Y, Kohnoe S, Maehara Y, Sugimachi K (1997) Clinicopathological characteristics of stage 1 gastric cancer: comparison of macroscopic and microscopic findings. Hepatogastroenterology 44:554–558
5. Baek JH, Jang JE, Kang CM, Chung HY, Kim ND, Kim KW (2000) Hypoxia-induced VEGF enhances tumor survivability via suppression of serum deprivation-induced apoptosis. Oncogene 19:4621–4631
6. Beavon IR (1999) Regulation of E-cadherin: does hypoxia initiate the metastatic cascade? Mol Pathol 52:179–188
7. Beavon IR (2000) The E-cadherin–catenin complex in tumour metastasis: structure, function and regulation. Eur J Cancer 36:1607–1620
8. Birkenbihl RP, Subramani S (1992) Cloning and characterization of rad21, an essential gene of *Schizosaccharomyces pombe* involved in DNA double-strand-break repair. Nucleic Acids Res 20:6605–6611
9. Birkenbihl RP, Subramani S (1995) The rad21 gene product of *Schizosaccharomyces pombe* is a nuclear, cell cycle-regulated phosphoprotein. J Biol Chem 270:7703–7711
10. Brizel DM, Scully SP, Harrelson JM, Layfield LJ, Bean JM, Prosnitz LR, Dewhirst MW (1996) Tumor oxygenation predicts for the likelihood of distant metastases in human soft tissue sarcoma. Cancer Res 56:941–943
11. Brizel DM, Sibley GS, Prosnitz LR, Scher RL, Dewhirst MW (1997) Tumor hypoxia adversely affects the prognosis of carcinoma of the head and neck. Int J Radiat Oncol Biol Phys 38:285–289
12. Cairns RA, Kalliomaki T, Hill RP (2001) Acute (cyclic) hypoxia enhances spontaneous metastasis of KHT murine tumors. Cancer Res 61:8903–8908
13. Chen F, Kamradt M, Mulcahy M, Byun Y, Xu H, McKay MJ, Cryns VL (2002) Caspase proteolysis of the cohesin component RAD21 promotes apoptosis. J Biol Chem 277:16775–16781
14. Dong Z, Wang JZ, Yu F, Venkatachalam MA (2003) Apoptosis-resistance of hypoxic cells: multiple factors involved and a role for IAP-2. Am J Pathol 163:663–671
15. Graeber TG, Osmanian C, Jacks T, Housman DE, Koch CJ, Lowe SW, Giaccia AJ (1996) Hypoxia-mediated selection of cells with diminished apoptotic potential in solid tumours. Nature 379:88–91
16. Hauf S, Waizenegger IC, Peters JM (2001) Cohesin cleavage by separase required for anaphase and cytokinesis in human cells. Science 293:1320–1323
17. Hirano T (2000) Chromosome cohesion, condensation, and separation. Annu Rev Biochem 69:115–144
18. Hoque MT, Ishikawa F (2001) Human chromatid cohesin component hRad21 is phosphorylated in M phase and associated with metaphase centromeres. J Biol Chem 276:5059–5067
19. Irie T, Tsutiya R, Yamamoto G, Maeda Y, Tachikawa T (2000) Expression analysis of mRNAs in oral squamous cell carcinoma using laser microdissection (laser pressure cell transfer type) and semiquantitative RT-PCR. J Showa Univ Dent Soc 21:75–81
20. Japanese Research Society for Gastric Cancer (1995) Japanese classification of gastric carcinoma, first English edition. Kanehara, Tokyo
21. Japanese Research Society for Corolectal Cancer (1995) Japanese classification of colorectal carcinoma, first English edition. Kanehara, Tokyo
22. Kumagai S, Kojima S, Imai K, Nakagawa K, Yamamoto E, Kawahara E, Nakanishi I (1994) Immunohistologic distribution of basement membrane in oral squamous cell carcinoma. Head Neck 16:51–57
23. Michaelis C, Ciosk R, Nasmyth, K (1997) Cohesins: chromosomal proteins that prevent premature separation of sister chromatids. Cell 91:35–45
24. Nasmyth K, Peters JM, Uhlmann F (2000) Splitting the chromosome: cutting the ties that bind sister chromatids. Science 288:1379–1385
25. Nishida T, Tanaka S, Haruma K, Yoshihara M, Sumii K, Kajiyama G (1995) Histologic grade and cellular proliferation at the deepest invasive portion correlate with the high malignancy of submucosal invasive gastric carcinoma. Oncology 52:340–346
26. Pati D, Zhang N, Plon SE (2002) Linking sister chromatid cohesion and apoptosis: role of Rad21. Mol Cell Biol 22:8267–8277
27. Porkka KP, Tammela TL, Vessella RL, Visakorpi T (2004) RAD21 and KIAA0196 at 8q24 are amplified and overexpressed in prostate cancer. Genes Chromosomes Cancer 39:1–10
28. Riedel F, Gotte K, Bergler W, Hormann K (2001) Inverse correlation of apoptotic and angiogenic markers in squamous cell carcinoma of the head and neck. Oncol Rep 8:471–476
29. Schwickert G, Walenta S, Sundfor K, Rofstad EK, Mueller-Klieser W (1995) Correlation of high lactate levels in human cervical cancer with incidence of metastasis. Cancer Res 55:4757–4759
30. Sonoda E, Matsusaka T, Morrison C, Vagnarelli P, Hoshi O, Ushiki, T, Nojima K, Fukagawa T, Waizenegger IC, Peters JM, Earnshaw WC, Takeda S (2001) Scc1/Rad21/Mcd1 is required for sister chromatid cohesion and kinetochore function in vertebrate cells. Dev Cell 1:759–770
31. Sook Kim M, Hyen Baek J, Bae MK, Kim KW (2001) Human rad21 gene, *hHR21*(SP), is downregulated by hypoxia in human tumor cells. Biochem Biophys Res Commun 281:1106–1112
32. Takahashi K, Kanazawa H, Akiyama Y, Tazaki S, Takahara M, Muto T, Tanzawa H, Sato K (1989) Establishment and characterization of a cell line (SAS) from poorly differentiated human squamous cell carcinoma of the tongue. J Jpn Stomatol Soc 38:20–28
33. Uhlmann F, Lottspeich F, Nasmyth K (1999) Sister-chromatid separation at anaphase onset is promoted by cleavage of the cohesin subunit Scc1. Nature 400:37–42
34. Volm M, Koomagi R (2000) Hypoxia-inducible factor (HIF-1) and its relationship to apoptosis and proliferation in lung cancer. Anticancer Res 20:1527–1533

Virchows Arch (2006) 448: 442–448
DOI 10.1007/s00428-005-0137-6

ORIGINAL ARTICLE

Andrea Ambrosini-Spaltro · Fabrizio Salvi · Christine M. Betts · Giovanni P. Frezza · Antonio Piemontese · Pietro Del Prete · Cristina Baldoni · Maria P. Foschini · Giuseppe Viale

Oncocytic modifications in rectal adenocarcinomas after radio and chemotherapy

Received: 17 November 2005 / Revised: 17 November 2005 / Accepted: 18 November 2005 / Published online: 20 December 2005

Abstract The purpose of the study is to highlight oncocytic modifications in rectal adenocarcinomas and evaluate a possible correlation with preoperative radiochemotherapy (RCT). Twenty-eight cases of advanced rectal carcinoma, treated preoperatively by 5-fluorouracil (200–225 mg/m^2) and 44–46 Gy in 22–23 fractions, were studied. All patients underwent biopsy before RCT. Surgery was performed within 6 weeks after RCT. In all cases oncocytic modifications were searched for on hematoxylin and eosin (H&E) and at immunohistochemistry using an antimitochondrial antibody. In addition, in two cases, both pre- and post-RCT tissues were examined at electron microscopy. All tumors were adenocarcinomas. In pre-RCT biopsies, oncocytic changes were difficult to find on H&E, while the antimitochondrial antibody strongly stained numerous neoplastic cells (mean 48.4%). In post-RCT surgical specimens, oncocytic changes were detected in 24 out of 28 cases on H&E and the antimitochondrial antibody stained most of the residual neoplastic cells (mean 76.7%). Ultrastructural examination revealed large and bizarre mitochondria inside tumor cells both in pre- and post-RCT tissues. In conclusion, the present data suggest that rectal adenocarcinomas are "mitochondrion-rich" tumors. After preoperative RCT, residual neoplastic cells acquire a definite oncocytic phenotype.

Keywords Mitochondria · Oncocyte · Rectum · Adenocarcinoma · Drug-resistance

A. Ambrosini-Spaltro · M. P. Foschini (✉)
Section of Anatomic Pathology "M. Malpighi",
University of Bologna, Bellaria Hospital,
Via Altura 3,
40139 Bologna, Italy
e-mail: Mariapia.foschini@ausl.bologna.it
Tel.: +39-051-6225523
Fax: +39-051-6225759

F. Salvi · G. P. Frezza
Unit of Radiotherapy, Bellaria Hospital,
Bologna, Italy

C. M. Betts
Department of Experimental Pathology,
University of Bologna,
Bologna, Italy

A. Piemontese
Department of Gastroenterology, Bellaria Hospital,
Bologna, Italy

P. Del Prete
Department of General Surgery, General Hospital, Budrio,
Bologna, Italy

C. Baldoni
Unit of Anatomic Pathology, Maggiore Hospital,
Bologna, Italy

G. Viale
Post-graduate Medical School in Anatomic Pathology,
University of Milan,
Milan, Italy

Introduction

Since the first definition given by Hamperl in 1894 [12], oncocytes are traditionally described as cells with abundant, granular, and eosinophilic cytoplasm on the basis of optical microscopic appearance at hematoxylin and eosin (H&E). Immunohistochemical and ultrastructural studies revealed that the cytoplasm of these cells is mainly composed of mitochondria [3, 7, 31]. Furthermore, many tumors present focal oncocytic differentiation, however, in oncocytomas or oncocytic tumors (both benign and malignant lesions), at least 75% of the constituent neoplastic cells are oncocytes [40]. Immunohistochemical examination with antimitochondrial monoclonal antibody provides helpful evaluation for diagnosis [26, 41]. Oncocytomas are diffusely distributed in various organs, although the most frequent sites of origin are thyroid, salivary glands, and kidney [39]. To the best of our knowledge, rare carcinomas with oncocytic changes were described in the gastrointestinal tract [25], although only one oncocytoma arising in the rectum was reported [27].

During histological evaluation of tumors from patients treated with preoperative radiochemotherapy (RCT) for

locally advanced rectal carcinoma, we noted a peculiar differentiation toward an oncocytic phenotype. Thus, the aim of the present study is to consider oncocytic differentiation in colorectal adenocarcinoma and to evaluate the possible correlation between oncocytic differentiation and response to preoperative RCT.

Materials and methods

Patients

From January 2000 to February 2005, a total of 28 cases of rectal carcinoma (20 men, eight women) were preoperatively treated with concomitant radiotherapy and chemotherapy at the Department of Oncological Sciences, Bellaria Hospital, University of Bologna (Italy). The clinical assessment and the tumor stage prior to RCT were estimated by physical examination, colonoscopy with rectal biopsy, endorectal ultrasound, abdominopelvic computed tomography (CT) scan, and chest X-ray. Radiotherapy consisted of an external beam irradiation given by means of three orthogonal fields (posterior–anterior, left lateral, right lateral) with a total dose of 44–46 Gy, subdivided in 22–23 fractions, and distributed in the course of about 1 month. Simultaneously (for approximately 32–33 days), patients were treated with 5-fluorouracil (5FU) (200–225 mg/m^2) by continuous intravenous infusion. Four to 6 weeks after completion of RCT, patients underwent either an anterior resection (20 patients), or abdominoperineal resection (six patients); an anterior resection with left hemicolectomy and an abdominoperineal resection with radical cystectomy were also performed (one patient each). Surgical specimens were evaluated for residual disease, depth of tumor penetration, and lymph node metastasis according to the tumor-node-metastasis staging [35]. Pathological stage after RCT (tumor classification after neoadjuvant therapy) was then compared with the clinical stage as previously assessed.

Control cases

As controls, 14 surgical specimens of colon adenocarcinoma (four ascending colon, five transverse colon, five sigmoid colon) not treated with preoperative RCT were retrieved from the Anatomic Pathology files of University of Bologna, at Bellaria Hospital, for study and search for oncocytic differentiation.

Histology and immunohistochemistry

All tissues were fixed in 4% buffered formalin and paraffin embedded according to a routine procedure. From each block, sections were stained with H&E and with antimitochondrial antibody (BioGenex, clone 113-1, dilution 1:500). The processing was carried out using the Ventana BenchMark automated stainer.

On H&E, oncocytic differentiation was diagnosed when cells had intense and granular cytoplasmic eosinophilia and nuclei showed granular chromatin and prominent nucleoli.

Finely granular cytoplasmic immunostaining observed in stromal fibroblasts and in nonneoplastic epithelial cells was considered as internal control. Positive oncocytic counting was performed both on the preoperative small biopsies and in the surgical specimens containing residual cells within fibrous tissues. We decided to count 200 consecutive cells to obtain a quantitative evaluation of the immunohistochemical results.

Ultrastructure

In two cases, ultrastructural investigation was performed, both pretreatment biopsy and posttreatment surgical specimen. Tissues were retrieved from paraffin blocks. Samples were deparaffined; rehydrated; fixed in phosphate-buffered 2.5% glutaraldehyde and 1% osmium tetroxide; dehydrated in alcohol and propylene oxide; and embedded in Epon 812. Thin sections were stained with uranyl acetate and Reynolds' lead citrate and observed in a Phillips CM 10 TEM.

Results

Tumor stage and pathologic response

The total of 28 patients was composed of 20 males and eight females, with a median age at surgery of 66 years.

The pretreatment clinical stage, evaluated by endorectal ultrasound and abdominopelvic CT scan revealed: (1) five stage T2 tumors, 17.9%; (2) 21 stage T3 tumors, 75%; and (3) two stage T4 tumors, 7%. Possible lymph node metastasis was found in 15 (53.6%) cases. All T2 tumors were located very close to the anorectal junction, and preoperative RCT was performed in the attempt to reduce the size, avoiding abdominoperineal resection.

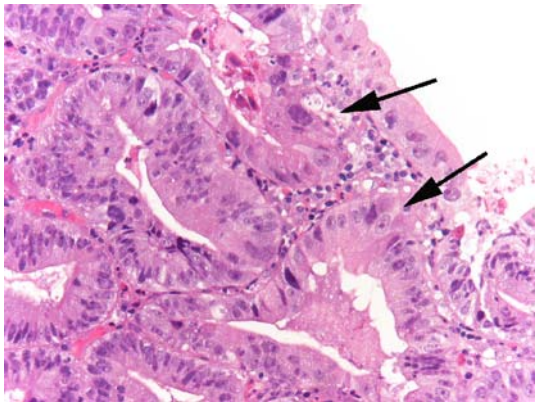

Fig. 1 Case No. 4, pretreatment biopsy, H&E. The lesion is composed of adenocarcinoma; rare cells with modifications reminiscent of oncocytic features are visible (*arrows*)

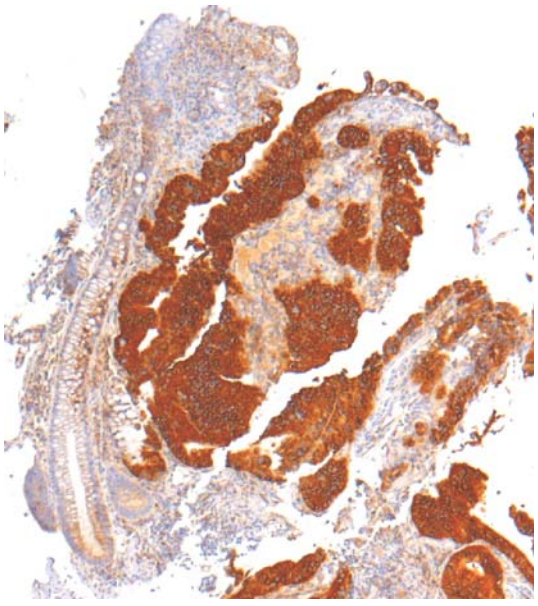

Fig. 2 Case No. 4, pretreatment biopsy. Immunohistochemistry with antimitochondrial antibody shows that most of the neoplastic cells are rich in mitochondria. Adjacent normal mucosa, present in the *left corner*, shows a definitely weaker staining

After RCT, pathological examination of surgical specimens detected: (1) one stage T0 tumor, 3.6%; (2) three stage T1 tumors, 10.7%; (3) ten stage T2 tumors, 35.7%; (4) 13 stage T3 tumors, 46.4%; and (5) one stage T4 tumor, 3.6%. Histological staging performed on the surgically resected specimen showed complete regression in one (3.6%) patient and down-staging in 13 (46.4%) patients.

Morphologic analysis before and after treatment

Pretreatment biopsies Twenty-seven patients were diagnosed with invasive, conventional type, adenocarcinoma

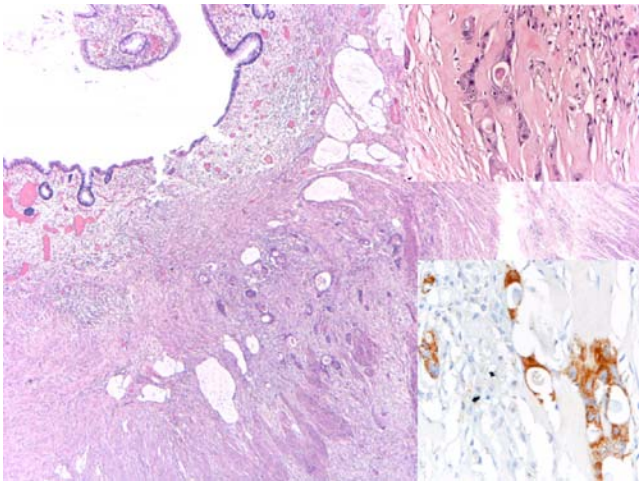

Fig. 3 Case No. 21, posttreatment surgical specimen, H&E. Rare neoplastic cells remain among fibrous tissue. Residual cells show clear oncocytic modifications (*upper right inset*), as revealed by antimitochondrial antibody (*lower right inset*)

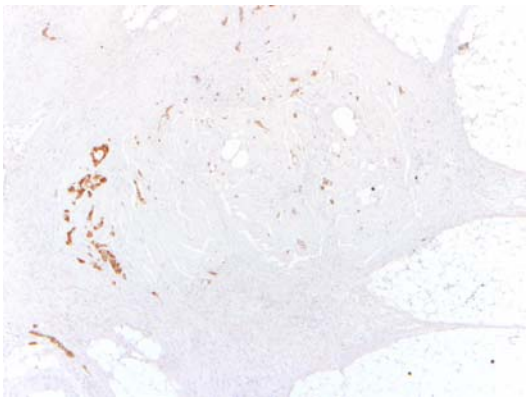

Fig. 4 Case No. 21, posttreatment surgical specimen. At low power view, antimitochondrial antibody stains residual neoplastic cells

(nine well-differentiated, 15 moderately differentiated, and three poorly differentiated) and one was diagnosed with mucinous adenocarcinoma. On H&E, neoplastic cells with oncocytic differentiation were detectable in 16 cases where they composed 3 to 20% (mean, 5.3%) of the neoplastic population (Fig. 1). Antimitochondrial antiserum strongly stained 5 to 100% (mean, 48.4%) of the neoplastic cells (Fig. 2).

Posttreatment surgical specimens Twenty-four patients were diagnosed with invasive, conventional type adenocarcinoma (15 moderately differentiated, two well-differentiated, five poorly differentiated, and two with scattered

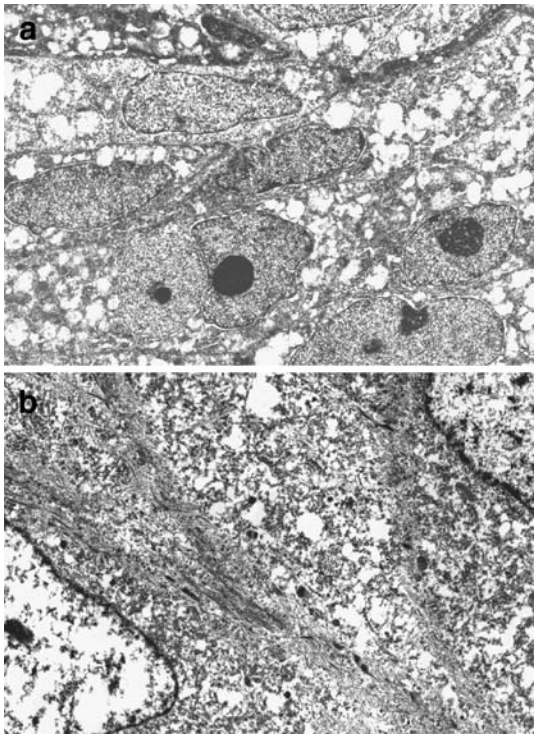

Fig. 5 On ultrastructure, numerous mitochondria are visible in the cytoplasm of the neoplastic cells both in pretreatment (**a**) and in posttreatment (**b**) tissues

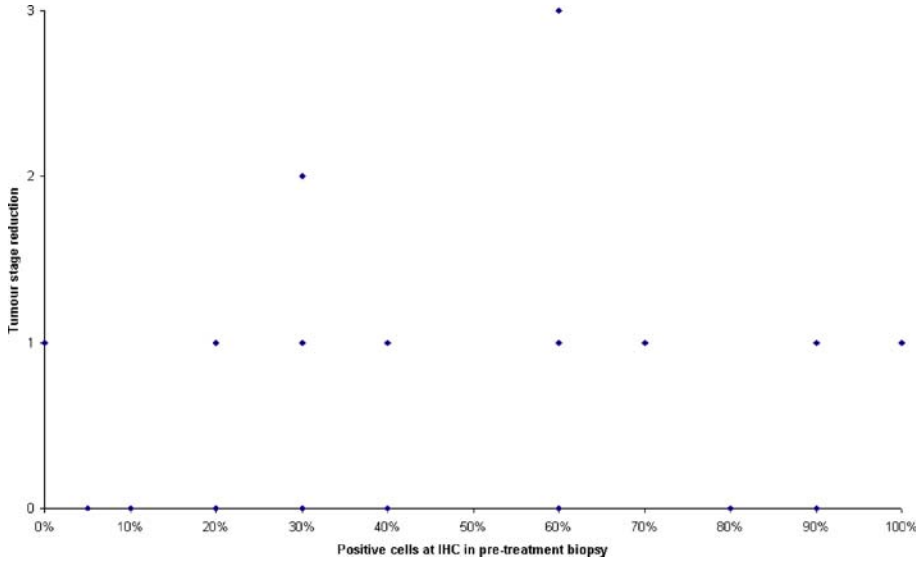

Fig. 6 Cells positive for antimitochondrial antibody at immunohistochemistry (IHC) in pretreatment biopsy and tumor stage reduction (see text)

neoplastic cells only) and three were diagnosed with mucinous adenocarcinoma. In one case, a complete pathologic response was documented. Neoplastic cells with oncocytic differentiation were detectable on H&E in 24 cases where they constituted 10 to 100% (mean, 54.4%) of the residual neoplastic population. Antimitochondrial-positive neoplastic cells varied from 5 to 100% (mean, 76.7%). The two cases with scattered residual neoplastic cells exhibited a definite oncocytic differentiation on H&E and a strong immunoreactivity to antimitochondrial antiserum (Figs. 3 and 4).

Ultrastructure

Ultrastructural examination revealed similar alterations in mitochondrial morphology, both in pretreatment biopsies and in posttreatment surgical specimens. Mitochondria were numerous, closely packed, large, swollen, and bizarre in shape; nucleoli were prominent. The same alterations were more pronounced and appeared more evident in surgical specimens after RCT (Fig. 5).

Control cases

Oncocytic modifications were identifiable on H&E in 14 cases. Oncocytic cells composed 5 to 30% of neoplastic cells (mean 10.7%). Immunoreactivity for antimitochondrial antiserum was present in all cases with the percentage of positive cells varying from 20 to 80% (mean 64.3%).

Additional modifications observed in posttreatment surgical specimens

In surgical specimens of post-RCT rectal carcinomas, eight cases (28.6%) showed mucinous modifications and two cases acquired a definite mucinous phenotype. The case diagnosed as mucinous adenocarcinoma in pretreatment biopsy did not show features of regression or modifications of histotype after RCT.

Clinical correlations

The percentage of mitochondrial antigen positive neoplastic cells detected in pretreatment biopsies was correlated to the tumor stage reduction induced by RCT. Tumor stage reduction was evaluated by the comparison between pretreatment clinical staging and posttreatment pathological staging. Data collected are illustrated in Fig. 6. Correlation index calculated for the two variable groups was 0.03896. Statistical analysis did not show any statistically significant correlation.

Discussion

In the present study, a series of preoperative RCT led to a stage reduction of the tumor in 13 (46.4%) out of 28 patients. Complete regression was achieved in only one case (3.6%) while 14 (50%) out of 28 patients with rectal adenocarcinoma were not affected by preoperative treatment. These data are consistent with previously published series where a complete response after RCT was observed in only 5 to 10% of the cases [11, 29, 42, 43]. Preoperative RCT can reduce tumor mass in rectal carcinomas and improve surgery efficacy, although the magnitude of this benefit is relatively small. Understanding the reasons for partial response to preoperative RCT is of utmost importance and numerous studies have already addressed this issue [2, 8, 9, 14, 19, 20, 23, 30, 44]. It was shown that radiotherapy may induce changes at the genetic level [21, 22], particularly in those genes regulating proliferation, apoptosis, and tissue repair. This might explain the morphological modifications observed in tissues after RCT.

Regarding the colorectal site, many authors have analyzed morphological features following RCT or radiotherapy alone. Extensive fibrosis, mucous lakes, thickening of the intima, and media layers of blood vessels are well-documented features [4, 45]. Nagtegaal et al. [22] documented mucinous changes in irradiated rectal carcinomas. Increased number of endocrine cells following RCT in rectal cancer were also reported [33, 32]. Similar aspects were also observed in our cases.

To the best of our knowledge, oncocytic modifications after RCT in colorectal adenocarcinomas were never extensively investigated, although tumor epithelial cells with marked eosinophilic cytoplasm were described [17, 32]. Even after short-term preoperative radiotherapy (25 Gy in 5–7 days), epithelial cells in the crypts displayed an intensive eosinophilic cytoplasm [15]. It is possible to hypothesize that the intense cytoplasmic eosinophilia previously identified is comparable to the oncocytic modifications observed here.

The present cases show that colorectal adenocarcinomas are characterized by numerous mitochondrion-rich neoplastic cells. These cells, even if not clearly recognizable on H&E, became more evident after immunostaining with antimitochondrial antiserum. In the pretreatment biopsies, a mean of 48.4% of antimitochondrial antibody positive cells was observed. This finding was confirmed in surgical specimens of the 14 untreated colon adenocarcinomas ("control cases") where a mean of 64.3% cells positive to antimitochondrial antiserum was detected. Thus, colorectal adenocarcinomas may be considered "mitochondrion-rich" tumors [3, 5].

True oncocytic modifications became evident in surgical specimens of rectal adenocarcinomas after RCT where a mean of 54.4% of neoplastic cells showed the typical features of oncocytes on H&E and a mean of 76.7% of neoplastic cells was strongly positive to antimitochondrial immunostaining. In surgical specimens from two cases that underwent a marked reduction of neoplastic population, the residual neoplastic cells were oncocytic.

Oncocytic modifications due to radiotherapy were described in the literature in various organs. Busuttil [1] described similar alterations in 48 specimens of salivary glands after irradiation. In seven irradiated adenomas of a pituitary gland, diffuse fibrosis was found and some irradiated pituitary cells showed cytoplasmic immunoreactivity for mitochondrial protein, mimicking oncocytes [24]. Oncocyte differentiation was also observed after metyrapone therapy in adrenal cortex [38]. Oncocytic modifications observed and related abundance in mitochondria may represent one of the factors responsible for resistance to RCT.

The mechanism of mitochondriogenesis is a complex phenomenon resulting in the synthesis of membrane phospholipids, DNA replication and expression of the mitochondrial genome and of genes encoding for mitochondrial proteins [46].

Possible mechanisms for oncocytic cell increase might be: (1) differentiation of epithelial neoplastic cells toward an "oncocyte-appearance" phenotype and (2) selective proliferation of oncocytes within tumor cells due to their resistance to RCT.

Neoplastic cells may acquire an oncocytic phenotype after radiation therapy as a response to injury (so-called "secondary oxyphilia") [36]. It was observed that ionizing radiation and other oxidants increase mitochondrial gene expression and its activity. After irradiation, expression of mitochondrially encoded genes, mitochondrial membrane potential, and ATP production were enhanced in a cell line derived from glioblastoma [10]. Furthermore, the viability of this cell line after exposure to irradiation was high, suggesting a possible protective role against additional oxidative damage. Studies conducted with cationic hexakis (2-methoxyisobutylisonitrile)-technetium-99 m (^{99m}Tc-MIBI), an agent that accumulates in mitochondria of various cells and tissues of high mitochondrial metabolic activity, have shown an increase of mitochondrial membrane potentials and mitochondrial metabolic activity in cancer cell lines after irradiation [6]. Mitochondria may be metabolically activated after RCT and become larger and swollen, determining an oncocytic appearance on H&E.

On the other hand, oncocytic differentiation detected in pretreatment biopsies may be responsible for resistance to RCT itself. This was observed in carcinomas of the thyroid exhibiting oncocytic appearance that are less responsive to radioactive iodine [18]. Homoplasmic mitochondrial DNA (mtDNA) somatic mutations were detected in colorectal cancer [28]. Experimental studies have shown that damage to mtDNA and to the mitochondrial respiratory chain may change the response of tumor cells to anticancer drugs [3, 47]. The antioxidant enzyme manganese superoxide dismutase (MnSOD), located in mitochondria, seemed to be one of the most effective enzymes in protecting cells against ionizing radiation damage [37]. Overexpression of MnSOD improves the survival of cells exposed to gamma radiation [13]. Mitochondrial somatic mutations in the D-loop region—a noncoding sequence of the mitochondrial genome—was described in colorectal cancer not only as potential tumor marker and an independent prognostic factor, but as a factor of resistance to adjuvant chemotherapy with 5FU, suggesting a central role of the mitochondria in drug resistance [16].

In conclusion, we demonstrated that colorectal adenocarcinomas are mitochondrion-rich tumors. Although oncocytic features were difficult to identify on H&E, immunohistochemical and ultrastructural studies revealed their abundance of mitochondria. After preoperative RCT, residual neoplastic cells of rectal adenocarcinomas exhibited a definite oncocytic phenotype, as evaluated by both H&E and immunohistochemistry along with ultrastructure. The oncocytic component and mitochondria enrichment may be considered to be among the factors responsible for the resistance to preoperative RCT.

References

1. Busuttil A (1977) Irradiation-induced changes in human salivary glands. Clin Otolaryngol Allied Sci 2:199–206

2. Chapet O, Romestaing P, Mornex F, Souquet JC, Favrel V, Ardiet JM, D'Hombres A, Gerard JP (2005) Preoperative radiotherapy for rectal adenocarcinoma: which are strong prognostic factors? Int J Radiat Oncol Biol Phys 61:1371–1377
3. Damiani S, Eusebi V, Losi L, D'Adda T, Rosai J (1998) Oncocytic carcinoma (malignant carcinoma) of the breast. Am J Surg Pathol 22:221–230
4. Dworak O, Keilholz L, Hoffmann A (1997) Pathological features of rectal cancer after preoperative radiochemotherapy. Int J Colorectal Dis 12:19–23
5. Foschini MP, Macchia S, Losi L, Dei Tos AP, Pasquinelli G, Di Tommaso L, Del Duca S, Roncaroli F, Dal Monte PR (1998) Identification of mitochondria in liver biopsies. A study by immunohistochemistry, immunogold and Western blot analysis. Virchows Arch 433:267–273
6. Furuta M, Nozaki M, Kawashima M, Iimuro M, Okayama A, Fukushima M, Natsui S, Souma R, Jinnai M (2004) Monitoring mitochondrial metabolism in irradiated human cancer cells with ^{99m}Tc-MIBI. Cancer Lett 212:105–111
7. Ghadially FN (1988) Ultrastructural pathology of the cell and matrix, 3rd edn, vol 1. Butterworth, London, UK, pp 260–265 (Chapter 3)
8. Ghadimi BM, Grade M, Difilippantonio MJ, Varma S, Simon R, Montagna C, Füzesi L, Langer C, Becker H, Liersch T, Ried T (2005) Effectiveness of gene expression profiling for response prediction of rectal adenocarcinomas to preoperative chemoradiotherapy. J Clin Oncol 23:1826–1838
9. Giralt J, Eraso A, Armengol M, Rosselló J, Majó J, Ares C, Espin E, Benavente S, de Torres I (2002) Epidermal growth factor receptor is a predictor of tumor response in locally advanced rectal cancer patients treated with preoperative chemotherapy. Int J Radiat Oncol Biol Phys 54:1460–1465
10. Gong B, Chen Q, Almasan A (1998) Ionizing radiation stimulates mitochondrial gene expression and activity. Radiat Res 150:505–512
11. Hahnloser D, Nelson H, Gunderson LL, Hassan I, Haddock MG, O'Connell MJ, Cha S, Sargent DJ, Horgan A (2003) Curative potential of multimodality therapy for locally recurrent rectal cancer. Ann Surg 237:502–508
12. Hamperl H (1931) Beiträge zur normalen und pathologischen Histologie menschlicher Speicheldrüsen. Z Mikrosk Anat Forsch 27:1–55
13. Hirose K, Longo DL, Oppenheim JJ, Matsushima K (1993) Overexpression of manganese superoxide dismutase promotes the survival of tumor cells exposed to interleukin-1, tumor necrosis factor, selected anticancer drugs, and ionizing radiation. FASEB J 7:361–368
14. Komuro Y, Watanabe T, Tsurita G, Muto T, Nagawa H (2005) Evaluating the combination of molecular prognostic factors in tumor radiosensitivity in rectal cancer. Hepatogastroenterology 52:666–671
15. Leupin N, Curschmann J, Kranzbuhler H, Maurer C, Laissue J, Mazzucchelli L (2002) Acute radiation colitis in patients treated with short-term preoperative radiotherapy for rectal cancer. Am J Surg Pathol 26:498–504
16. Lièvre A, Chapusot C, Bouvier AM, Zinzindohoué F, Piard F, Roignot P, Arnould L, Beaune P, Faivre J, Laurent-Puig P (2005) Clinical value of mitochondrial mutations in colorectal cancer. J Clin Oncol 23:3517–3525
17. Mai KT, Carnat T (2004) Mucinous and immunohistochemical changes of colonic adenocarcinoma secondary to chemoradiotherapy. Histopathology 45:91–93
18. Máximo V, Sobrinho-Simões M (2000) Hurtle cell tumours of the thyroid. A review with emphasis on mitochondrial abnormalities with clinical relevance. Virchows Arch 437:107–115
19. McLeod HL, Murray GI (1999) Tumour markers of prognosis in colorectal cancer. Br J Cancer 79:191–203
20. Myerson RJ, Singh A, Birnbaum EH, Fry RD, Fleshman JW, Kodner IJ, Lockett MA, Picus J, Walz BJ, Read TE (2001) Pretreatment clinical findings predict outcome for patients receiving preoperative radiation for rectal cancer. Int J Radiat Oncol Biol Phys 50:665–674
21. Nagtegaal ID, Gaspar CGS, Peltenburg LTC, Marijen CAM, Kepiteijn E, van de Velde CJH, Fodde R, van Krieken JHJM (2005) Radiation induces different changes in expression profiles of normal rectal tissue compared with rectal carcinoma. Virchows Arch 446:127–135
22. Nagtegaal ID, Gaspar CGS, Marijen CAM, van de Velde CJH, Fodde R, van Krieken JHJM (2004) Morphological changes in tumour type after radiotherapy are accompanied by changes in gene expression profile but not in clinical behaviour. J Pathol 204:183–192
23. Nehls O, Klump B, Holzmann K, Lammering G, Borchard F, Gruenagel HH, Gaco V, Gregor M, Porschen R (1999) Influence of p53 status on prognosis in preoperatively irradiated rectal carcinoma. Cancer 85:2541–2548
24. Nishioka H, Hirano A, Haraoka J, Nakajima N (2002) Histological changes in the pituitary gland and adenomas following radiotherapy. Neuropathology 22:19–25
25. Papotti M, Cassoni P, Taraglio S, Bussolati G (1999) Oncocytic and oncocytoid tumors of the exocrine pancreas, liver, and gastrointestinal tract. Semin Diagn Pathol 16:126–134
26. Papotti M, Gugliotta P, Forte G, Bussolati G (1994) Immunocytochemical identification of oxyphilic mitochondrion-rich cells. Appl Immunohistochem 2:261–267
27. Piscitelli D, Ingravallo G, Resta L, Fiore MG, Maiorano E (2003) Oncocytic adenocarcinoma of the rectum with diffuse intra-luminal microcalcification: the first reported case. Virchows Arch 443:579–582
28. Polyak K, Li Y, Zhu H, Lengauer C, Willson JK, Markowitz SD, Trush MA, Kinzler KW, Vogelstein B (1998) Somatic mutations of the mitochondrial genome in human colorectal tumours. Nat Genet 20:291–293
29. Rödel C, Grabenbauer GG, Matzel KE, Schick C, Fietkau R, Papadopoulos T, Martus P, Hohenberger W, Sauer R (2000) Extensive surgery after high-dose preoperative chemoradiotherapy for locally advanced recurrent rectal cancer. Dis Colon Rectum 43:312–319
30. Rödel C, Grabenbauer GG, Papadopoulos T, Bigalke M, Günther K, Schick C, Peters A, Sauer R, Rödel F (2002) Apoptosis as a cellular predictor for histopathologic response to neoadjuvant radiochemotherapy in patients with rectal cancer. Int J Radiat Oncol Biol Phys 52:294–303
31. Roth SI, Olen E, Hansen LS (1962) The eosinophilic cells of the parathyroid (oxyphilic cells), salivary (oncocytes), and thyroid (Hürtle cells) glands. Light and electron microscopic observations. Lab Invest 11:933–941
32. Shia J, Guillem JG, Moore HG, Tickoo SK, Qin J, Ruo L, Suriawinata A, Paty PB, Minsky BD, Weiser MR, Temple LK, Wong WD, Klimstra DS (2004) Patterns of morphologic alterations in residual rectal carcinoma following preoperative chemoradiation and their association with long-term outcome. Am J Surg Pathol 28:215–223
33. Shia J, Tickoo SK, Guillem JG, Qin J, Nissan A, Hoos A, Stojadinovic A, Ruo L, Wong WD, Paty PB, Weiser MR, Minsky BD, Klimstra DS (2002) Increased endocrine cells in treated rectal adenocarcinomas. A possible reflection of endocrine differentiation in tumor cells induced by chemotherapy and radiotherapy. Am J Surg Pathol 26:863–872
34. Singh KK, Russel J, Sigala B, Zhang Y, Williams J, Keshav KF (1999) Mitochondrial DNA determines the cellular response to cancer therapeutic agents. Oncogene 18:6641–6646
35. Sobin LH, Wittekind Ch (eds) (2002) TNM classification of malignant tumours. Wiley, New York
36. Sobrinho-Simões M, Máximo V, Vieira de Castro I, Fonseca E, Soares P, Garcia-Rostan G, Cardoso de Oliveira M (2005) Hürtle (oncocytic) cell tumors of thyroid: etiopathogenesis, diagnosis and clinical significance. Int J Surg Pathol 13:29–35
37. Sun J, Chen Y, Li M, Ge Z (1998) Role of antioxidants enzymes in ionizing radiation resistance. Free Radic Biol Med 24:586–593
38. Suvarna SK, Stephenson TJ (2001) Oxyphilic metaplasia of adrenal cortex secondary to metyrapone therapy. Histopathology 39:546–547

39. Tallini G (1998) Oncocytic tumours. Virchows Arch 433:5–12
40. Tallini G, Carcangiu ML, Rosai J (1992) Oncocytic neoplasm of the thyroid gland. Acta Pathol Jpn 42:305–315
41. Tickoo SK, Amin MB, Linden MD, Lee MW, Zarbo RJ (1997) Antimitochondrial antibody (113-1) in the differential diagnosis of granular cells tumors. Am J Surg Pathol 21:922–930
42. Valentini V, Morganti AG, De Franco A, Coco C, Ratto C, Battista Doglietto G, Trodella L, Ziccarelli L, Picciocchi A, Cellini N (1999) Chemoradiation with or without intraoperative radiation therapy in patients with locally recurrent rectal carcinoma: prognostic factors and long term outcome. Cancer 86:2612–2624
43. Vermaas M, Ferenschild FT, Nuyttens JJ, Marinelli AW, Wiggers T, van der Sijp JR, Verhoef C, Graveland WJ, Eggermont AM, de Wilt JH (2005) Preoperative radiotherapy improves outcome in recurrent rectal cancer. Dis Colon Rectum 48:918–928
44. Willett CG, Warland G, Coen J, Shellito PC, Compton CC (1995) Rectal cancer: the influence of tumor proliferation on response to preoperative irradiation. Int J Radiat Oncol Biol Phys 32:57–61
45. Wittekind C, Tannapfel A (2003) Regressionsgrading des präoperativ-radiochemotherapierten Rektumkarzinoms. Eine Bestandsaufnahme. Pathologe 24:61–65
46. Wrutniak-Cabello C, Casas F, Cabello G (2001) Thyroid hormone action in mitochondria. J Mol Endocrinol 26:67–77
47. Xu R, Pelicano H, Zhou Y, Carew JS, Feng L, Bhalla KN, Keating MJ, Huang P (2005) Inhibition of glycolysis in cancer cells: a novel strategy to overcome drug resistance associated with mitochondrial respiratory defect and hypoxia. Cancer Res 65:613–621

Virchows Arch (2006) 448: 449–458
DOI 10.1007/s00428-005-0124-y

ORIGINAL ARTICLE

L. Krsková · M. Mrhalová · D. Sumerauer · R. Kodet

Rhabdomyosarcoma: molecular diagnostics of patients classified by morphology and immunohistochemistry with emphasis on bone marrow and purged peripheral blood progenitor cells involvement

Received: 8 September 2005 / Accepted: 21 September 2005 / Published online: 20 December 2005

Abstract Two histologically distinct subtypes of rhabdomyosarcomas (RMS), embryonal and alveolar, are different in many aspects, such as age distribution, primary site, and clinical outcome. We analyzed a group of 30 patients with RMS. The aim was to broaden the spectrum of diagnostic tools in evaluating the primary tumors, their recurrences and/or metastases, and to extend the diagnostic boundary to bone marrow and purged peripheral progenitor blood cell samples. We have performed the RT-PCR assay to analyze RMS for the presence of expression of *MyoD1* gene and for the presence of chimeric transcripts PAX3/FKHR or PAX7/FKHR. *MyoD1* gene expression was found in all 30 patients in samples from primary tumors. The chimeric transcripts PAX/FKHR were identified in 13 of 15 patients with alveolar RMS. Furthermore, the fusion transcript PAX7/FKHR was identified in 2 of 15 patients with RMS classified as embryonal by histology. Bone marrow samples (12) and peripheral blood progenitor cell specimens (13) in ten patients were examined by RT-PCR. We were able to identify 7 patients with bone marrow involvement and/or with contamination of peripheral blood progenitor cells by the tumor cells. We demonstrate that employing molecular diagnostics has an impact on staging, therapy monitoring and recognition of malignant cells at the tumor resection margins.

L. Krsková (✉) · M. Mrhalová · R. Kodet
Department of Pathology and Molecular Medicine,
2nd Medical School,
Charles University and Faculty Hospital in Motol,
Prague, Czech Republic
e-mail: lenka.krskova@lfmotol.cuni.cz
Tel.: +420-2-24435650
Fax: +420-2-24435620

D. Sumerauer
Department of Pediatric Hematology and Oncology,
2nd Medical School,
Charles University and Faculty Hospital in Motol,
Prague, Czech Republic

Keywords Rhabdomyosarcoma · Immunohistochemistry · Molecular diagnosis · RT-PCR · Bone marrow · Peripheral blood progenitor cells

Introduction

Rhabdomyosarcomas (RMS) constitute a heterogeneous spectrum of tumors with respect to clinical behavior and also with respect to tumor morphology [36]. They are frequently composed of primitive cells, which show only a subtle evidence of a lineage-specific differentiation, but they may mature and in some cases may reach a stage close to terminal differentiation resembling myotubes of a developing skeletal muscle. Most RMS in childhood are of two histological subtypes—embryonal (80%) and alveolar (20%), which have distinct clinicopathological features [33]. Alveolar and undifferentiated variants portend an unfavorable prognosis [33, 42]. Because of a broad spectrum of tumor morphology and some overlapping features between the alveolar/undifferentiated and embryonal forms, it may be difficult to classify some of these tumors into an individual category. A standard approach to the diagnosis requires utilization of histology and immunohistochemistry [25, 30, 35], cytogenetical analysis, and molecular techniques [1, 2, 14, 16, 26, 28, 37, 45]. The immunohistochemical profile of RMS is well characterized. The embryonal and alveolar RMS share a similar spectrum of protein expression such as cytoskeletal filaments (vimentin, desmin), muscle-specific cytoplasmic proteins such as myoglobin, contractile filaments (actin, myosin), and regulatory proteins of muscle-specific differentiation (myoD1, myogenin).

The discovery of myogenic determination (*MyoD*) gene family has provided an insight in the regulation of myogenesis and has prompted a search for applicable markers that may assist in the diagnosis of RMS [7, 39]. The *MyoD* gene was first identified by virtue of its ability to convert nonmuscle cells into muscle cells [12]. The genes of the MyoD family represent a nodal point of early myogenesis by up-regulating the expression of other myogenic genes,

such as those coding for desmin, creatine kinase, and myosin [48]. Among the MyoD family genes, the expression of MyoD1 has been found to be the most consistent molecular feature of RMS. MyoD1 protein is a member of a basic helix-loop-helix protein family with nuclear localization and maps on chromosome 11p15. It is a DNA-binding nuclear protein that initiates muscle differentiation in mesenchymal stem cells at the earliest stage of their commitment to the striated muscle phenotype [31]. Although MyoD1 is an excellent molecular marker, there are problems with its immunohistochemical detection in histopathology; another member of myogenic transcriptional regulators, myogenin, is on the protein level consistently detectable in RMS [13].

Most cases of alveolar RMS are characterized by a chromosomal translocation t(2;13)(q35;q14) involving the *PAX3* gene at 2q and the *FKHR* gene at 13q. The *FKHR* gene is coding for a protein of the forkhead family of transcription factors. The FKHR protein contains a central forkhead DNA-binding domain, which is found in a number of different transcription factors including hepatic nuclear factor 3 and interleukin binding factor [17]. The *PAX3* gene is a member of a family of evolutionarily conserved and developmentally regulated genes coding for transcription factors [40]. PAX3 protein contains two discrete DNA-binding domains, a paired box and a paired-type homeodomain, and displays a unique coordinate DNA-binding specificity. This protein is expressed exclusively during embryogenesis, and it is thought to be important in the development of mesenchymal precursors destined to become myoblasts. In muscle progenitor cells, PAX3 is expressed even earlier than myogenic transcription factors, such as MyoD1 and Myf5, and gradually declines during muscle differentiation [5]. The fusion protein PAX3/FKHR exhibits an increased transcriptional potency relative to PAX3 due to swapping of PAX3 and FKHR C-terminal transactivation domains. Cell culture experiments demonstrated that the PAX3/FKHR protein has the capacity to induce phenotypic changes, including cellular transformation and inhibition of myogenic differentiation [10]. Some cases of alveolar RMS have been characterized by a variant translocation t(1;13)(q36;p14), which fuses the *PAX7* gene with FKHR [11, 15, 42]. This chimeric gene transcript is similar in structure and function to that of the PAX3/FKHR. The tumors with the PAX7/FKHR fusion transcript show a predilection for younger patients and appear to have a more favorable prognosis [3, 4].

In this study, we present data on 30 patients with RMS characterized by morphology and by immunohistochemistry. We bring some insights on the specificity of the reverse transcriptase polymerase chain reaction (RT-PCR) assay for the detection of the *MyoD1* gene expression and on the practical diagnostic utilization of molecular events such as the demonstration of the t(2;13)-encoded PAX3/FKHR chimeric transcript and t(1;13)-encoded PAX7/FKHR fusion transcript in primary tumors, bone marrow specimens, and in purged peripheral blood stem cells intended for autologous transplantation.

Material and methods

Seventy-two samples from 30 patients with histological diagnosis of RMS were analyzed (Table 1). All samples from the primary tumors and their recurrences were obtained from fresh tissue, snap frozen and stored at −80°C. All specimens were from the Pediatric Tumor Registry in the Department of Pathology and Molecular Medicine in Prague. Samples of bone marrow or peripheral blood progenitor cells (PBPCs) were collected in ethylenediaminetetraacetate (EDTA) at the time of tumor diagnosis and, in some cases, during chemotherapy. The tumors were diagnosed by light microscopy using hematoxylin and eosin staining complemented by immunohistochemistry. A panel of primary antibodies included vimentin, desmin, sarcomeric actin, MyoD1 protein, myogenin, and anti-CD99 (all obtained from DakoCytomation, Glostrup, Denmark). Super sensitive kit using alkaline phosphatase–antialkaline phosphatase and fast red (BioGenex, San Ramon, CA, USA) was utilized to visualize the results.

RNA extraction

RNA was extracted from 10×5 μm thick sections of the frozen tumor tissue or from bone marrow samples using Tri-Reagent (Invitrogen Corporation, Carlsbad, CA) according to the manufacturer's instructions.

Polymerase chain reaction analysis

A total of 1 μg of RNA was reverse-transcribed in a 20 μl reaction volume using 10 pmol of random hexamers as primers and 1 μl of Moloney murine leukemia virus (MMLV) Reverse Transcriptase (Life Technologies, Inc., Gaithersburg, USA) according to the manufacturer's instructions. Reverse transcription included an incubation period of 60 min at 42°C.

Two microliters of cDNA products was then tested for the expression of the regulation gene *MyoD1* (F-MyoD1: 5'AGC ACT ACA GCG GCG ACT, R-MyoD1: 5'GCG ACT CAG AAG GCA CGT C, MyoD1 cDNA probe: 5' GCT ACG AAG GCG CCT ACT ACA ACG AGG CGC) and for the presence of the t(2;13) and t(1;13) translocations using seminested PCR with primers PAX3, PAX7, FKHR-A, and FKHR-B (PAX3: 5' AGC TAT ACA GAC AGC TTT GT, PAX7: 5' GCT TCT CCA GCT ACT CTG AC, FKHR-A: 5' CTC TGG ATT GAG CAT CCA CC, FKHR-B: 5' TCC AGT TCC TTC ATT CTG CA).

Each PCR reaction was carried out with an initial denaturation step at 95°C for 5 min, annealing for 30 s, and extension at 72°C for 30 s, followed by 30 cycles of denaturation at 95°C for 15 s, annealing for 5 s, and extension at 72°C for 5 s. Undiluted PCR product (1 μl) was added to the seminested reaction mix for the second round of 30 cycles. The quality of the isolated RNA was assayed with the A2 and A3 oligonucleotide primers to detect the

Table 1 Characteristics of the patients

Patient number	Age (years)	Sex	Histology	Translocation	Fusion type	MyoD1	Follow-up (years)	Outcome
1	7	F	A-RMS	t(2;13)	PAX3	+	5.5	AW
2	6.5	M	A-RMS	t(2;13)	PAX3	+	5.5	DD
3	14	F	A-RMS	t(2;13)	PAX3	+	4	AW
4	9	F	A-RMS	t(2;13)	PAX3	+	4	AD
5	10	F	A-RMS	t(2;13)	PAX3	+	2.5	AW
6	2.5	F	A-RMS	–	–	+	7.5	DD
7	7	F	A-RMS	t(2;13)	PAX3	+	1	DD
8	10.5	M	A-RMS	t(1;13)	PAX7	−	2	DD
9	18	F	A-RMS	t(2;13)	PAX3	+	8.5	AW
10	13	M	A-RMS	t(2;13)	PAX3	+	5 months	DD
11	3.5	F	A-RMS	t(2;13)	PAX3	+	8	AW
12	1 month	M	A-RMS	–	–	+	1 month	DD
13	13.5	F	A-RMS	t(2;13)	PAX3	+	4	DD
14	6.5	M	A-RMS	t(1;13)	PAX7	+	4	DD
15	2.5	F	A-RMS	t(1;13)	PAX7	+	3	DD
16	10	M	E-RMS	–	–	+	1.5	DD
17	2	M	E-RMS	–	–	+	4.5	AW
18	10.5	M	E-RMS	–	–	+	4	DD
19	0.5	F	E-RMS	–	–	+	3.5	AW
20	17.5	M	E-RMS	–	–	+	2	DD
21	1	F	E-RMS	–	–	+	3.5	AW
22	14.5	F	E-RMS	–	–	+	2	DD
23	1	M	E-RMS	t(1;13)	PAX7	+	6.5	AW
24	6	F	E-RMS	–	–	+	5.5	AW
25	5	M	E-RMS	–	–	+	18	DOC
26	4	F	E-RMS	–	–	+	2	DD
27	7.5	M	E-RMS	–	–	+	6.5	AD
28	10	F	E-RMS/A-RMS	t(1;13)	PAX7	+	1.5	DD
29	8.5	F	E-RMS	–	–	+	Lost	Lost
30	4	F	E-RMS	–	–	+	1	DD

A-RMS alveolar histology, *AD* alive with disease, *AW* alive and well, *DD* died of tumor progression, *E-RMS* embryonal histology, *E-RMS/A-RMS* residual tumor with alveolar histology after chemotherapy, *F* female, *M* male

ubiquitously expressed cABL kinase (primers A2: 5' TTC AGC GGC CAG TAG CAT CTG ACT T and A3: 5' TGT GAT TAT AGC CTA AGA CCC GGA GCT TTT). Negative controls lacking either RNA or RT were routinely included. Products were identified using 1.5% agarose gel electrophoresis and ethidium bromide staining.

The specificity of the PCR products was confirmed by Southern blot hybridization using AlkPhos Direct Kit (Amersham Biosciences Trading GmbH, Austria) according to the manufacturer's instructions.

Results

Morphology

The embryonal RMS were characterized by a variable cellularity and haphazard cell orientation. Rhabdomyoblastic differentiation was discernible in 12 cases (Fig. 1a). Three cases were characterized as a botryoid subtype. None of the cases had features of the spindle cell variant [29]. Alveolar RMS had a typical appearance of predominantly round-celled tumors with a characteristic pattern of tumor cell adhesion to the fibrovascular stroma. Two cases had an almost entirely solid morphology, but the alveolar pattern was still focally discernible (Fig 1b). On the basis of the morphological examination of the primary tumors, the original classification was that of embryonal RMS in 15 patients and alveolar RMS also in 15 patients. The distribution of cases with embryonal and alveolar RMS differs from that known from a large series of cases [33] and may be caused, at least partially, by patient distribution in health service referral centers.

Immunohistochemical findings

The results of immunohistochemical staining are summarized in Table 2. Tumor cells stained positively for vimentin and desmin in the majority of cases tested and

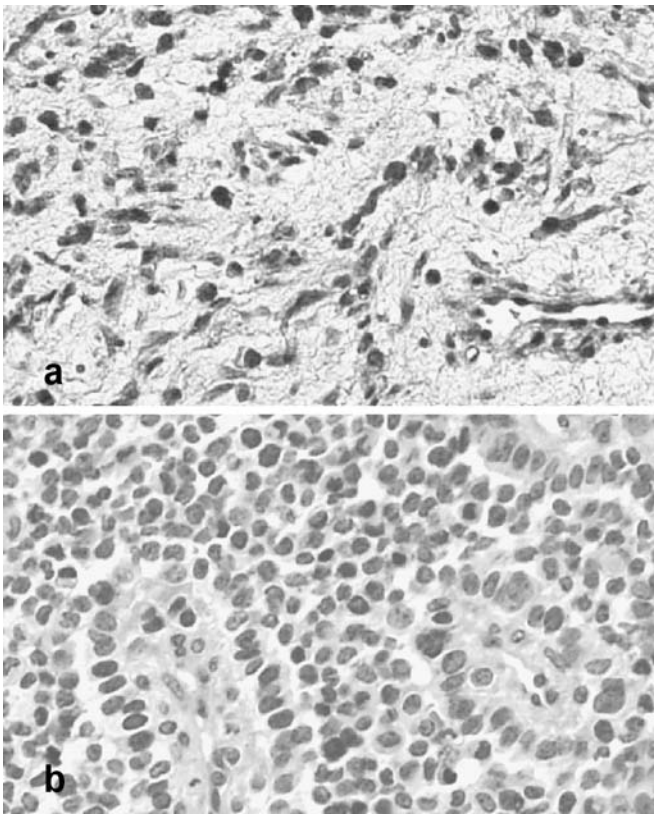

Fig. 1 **a** Embryonal RMS showing haphazardly oriented primitive and maturating tumor cells in a loose stroma, original magnification ×100. **b** Alveolar RMS with perivascular palisading of the tumor cells and solid arrangement of the remaining sheets of undifferentiated tumor cells, original magnification ×200

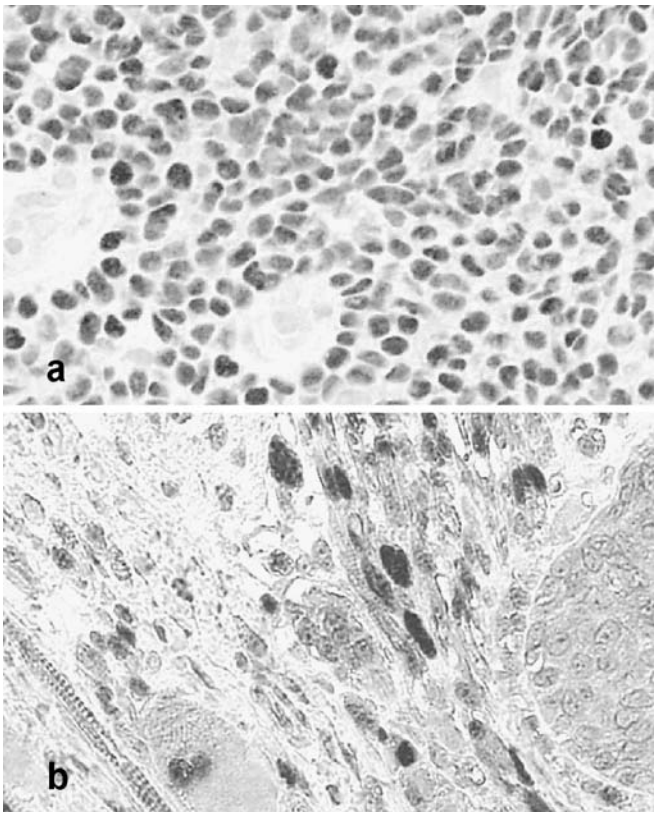

Fig. 2 Immunohistochemical staining demonstrating myogenin. **a** Alveolar RMS is uniformly positive in the tumor cell nuclei, original magnification ×200. Alkaline phosphatase–antialkaline phosphatase, fast red. **b** Undifferentiated tumor cells of embryonal RMS of the urinary bladder show occasional nuclear positivity. The more differentiated tumor cells with abundant cytoplasm are weakly stained or negative, original magnification ×200

less frequently for sarcomeric actin. In addition, rhabdomyoblasts were positive for myogenin in 90% of cases (27/30) and MyoD1 in 60% (18/30). The intensity of myogenin positivity was uniform and strong in alveolar RMS regardless of the degree of differentiation, and even cases with no myoblastic maturation at the hematoxylin–eosin staining level were positive (Fig. 2a). In embryonal RMS, the staining for myogenin varied in individual tumor cells, and they were generally less positive than in the alveolar RMS (Fig. 2b). MyoD1 was positive in a smaller percentage of cases, the pattern of staining was not distinctive when embryonal and alveolar RMS were compared. Moreover, in some cases, the expression of MyoD1 was weak, most likely due to inadequate formalin fixation or other technical problems prior to the immunohistochemical procedure. All tumors were negative for CD99.

Molecular findings

All 30 RMS samples from primary tumors expressed the MyoD1 transcript, which hybridized to the 3' end of the MyoD1 cDNA probe. The absence of MyoD1 expression confirmed by negative RT-PCR and Southern Blot hybridization with non-radioactive-labeled cDNA probe was detected in one patient (case 20) with embryonal RMS after chemotherapy (Fig. 3). This tumor also failed to manifest nuclear immunoreactivity for MyoD1 and myogenin.

The t(2;13) and t(1;13) translocations were identified in cases of RMS having alveolar histology. The fusion transcript PAX3/FKHR indicating the translocation t(2;13) was found in ten patients with the diagnosis of alveolar RMS (Fig. 4), and the fusion transcript PAX7/FKHR indicating the t(1;13) was detected in three histologically diagnosed

Table 2 Results of immunohistochemistry (RMS diagnosed by morphology prior to reclassification of two cases of embryonal RMS into alveolar RMS)

Tumor type	Vimentin	Desmin	SA	Myogenin	MyoD1	CD99
RMS-A	14/15	14/15	9/15	14/15	11/15	0/15
%	93.3	93.3	60	93.3	73.3	0
RMS-E	15/15	13/15	11/15	13/15	7/15	0/15
%	100	86.7	73.3	86.7	46.7	0

SA sarcomeric actin

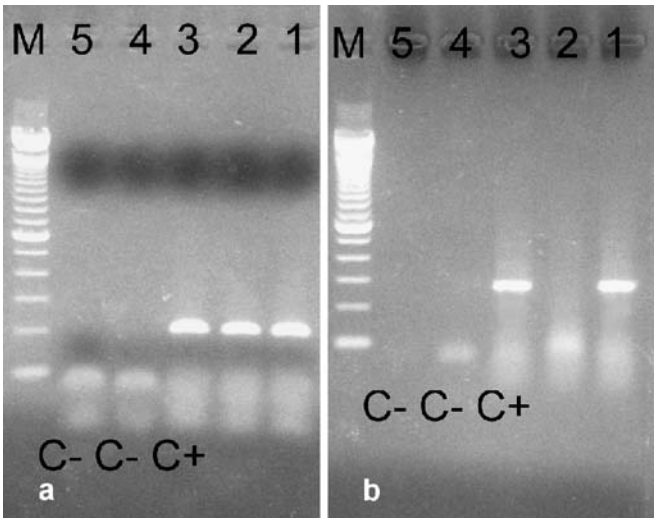

Fig. 3 RT-PCR analysis of RMS (case 20) for the transcription of MyoD1. **a** c-ABL RNA was amplified as a control for amplifiable RNA (209 bp). Lines: *1* expression c-ABL in the primary tumor, *2* expression c-ABL in the residual tumor after chemotherapy, *3* positive control for c-ABL transcript, *4* negative control for reverse transcription, *5* negative control for PCR. **b** Lines: *1* expression of MyoD1 in the primary tumor (264 bp), *2* absence of MyoD1 transcript in the residual tumor after chemotherapy, *3* positive control for MyoD1 transcript, *4* negative control for reverse transcription, *5* negative control for PCR

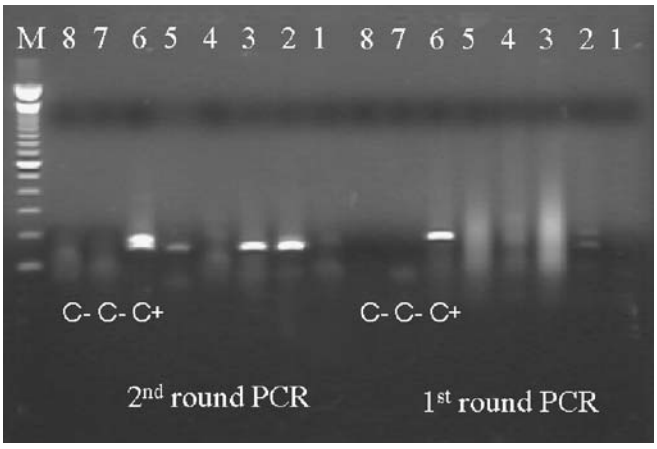

Fig. 4 Detection of the PAX3/FKHR transcript in bone marrow samples and PBPC (case 4, patient with alveolar RMS) using nested RT-PCR (188 bp first round RT-PCR and 158 bp second round RT-PCR). Lines: *1* negative sample of bone marrow after chemotherapy, *2* PAX3/FKHR transcript in the bone marrow sample at the time of the tumor recurrence, *3* PAX3/FKHR transcript in PBPC sample, *4* negative sample of the peripheral blood, *5* PAX3/FKHR transcript in PBPC sample after purging, *6* positive control for the PAX3/FKHR transcript, *7* negative control for reverse transcription, *8* negative control for PCR

alveolar RMS. Furthermore, the fusion transcript PAX7/FKHR, suggesting the diagnosis of alveolar RMS, was found in 2 of 15 patients with RMS classified as embryonal by histology.

One of the latter patients (case 28) had no evidence of alveolar differentiation in the first biopsy, but the morphological features of alveolar RMS were revealed in the second biopsy taken from a residual tumor after chemotherapy (Fig. 5). This tumor was reclassified as mixed RMS; the alveolar component was most probably disclosed by a more extensive tissue sampling, although the possibility that the treatment induced changes in the tumor may have played a role. The other patient (case 23) had the tumor composed of a relatively uniform mixture of undifferentiated short spindle cells and round cells organized in diffuse sheets (Fig. 6). The vasculature and the stroma were inconspicuous. There was a tissue edema diminishing the tumor cell density. The myoblastic differentiation was apparent only at a level detected by immunohistochemistry (variably positive desmin and myogenin). The case was considered to fit the diagnosis of embryonal RMS at the time of diagnosis. After establishing the PAX7/FKHR fusion transcript, we reevaluated the findings, and, admittedly, some features of the tumor may fulfill the criteria of the so-called solid alveolar category [44]. The presence of spindle cells was, however, unusual.

Two cases had alveolar morphology, but there was no evidence of either t(2;13) or t(1;13) fusion transcripts. The first fusion-negative case was a patient with a congenital manifestation of alveolar RMS (case 12). The second was a 2-year-old girl (case 6) with botryoid RMS in the vagina. This patient had no evidence of alveolar differentiation in the first biopsy (from the vagina), but the morphological features of alveolar RMS were revealed in the biopsy taken from a metastastatic disease in the inguinal lymph node 14 months after diagnosis and from lung metastasis 5 years later.

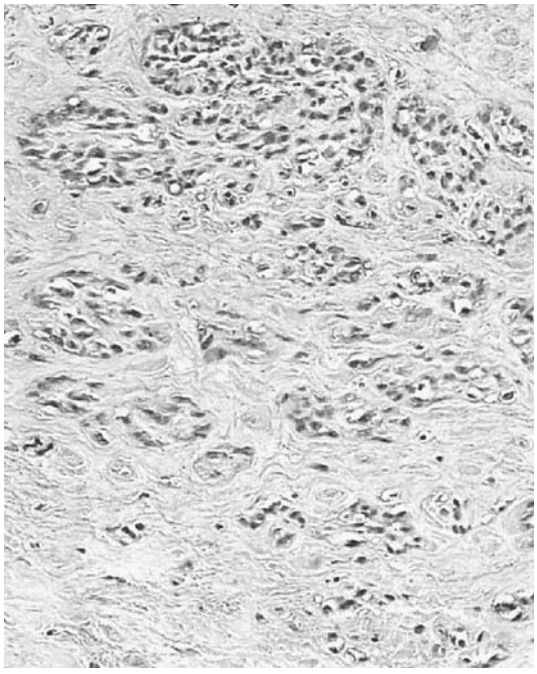

Fig. 5 Case 28. The original diagnosis was that of embryonal RMS. The post-therapy excision of the residual tumor showed a hyaline stroma with foci of the tumor having solid alveolar appearance, original magnification ×50. RT-PCR revealed PAXPAH7/FKHR fusion transcript in this patient, confirming the diagnosis of alveolar RMS

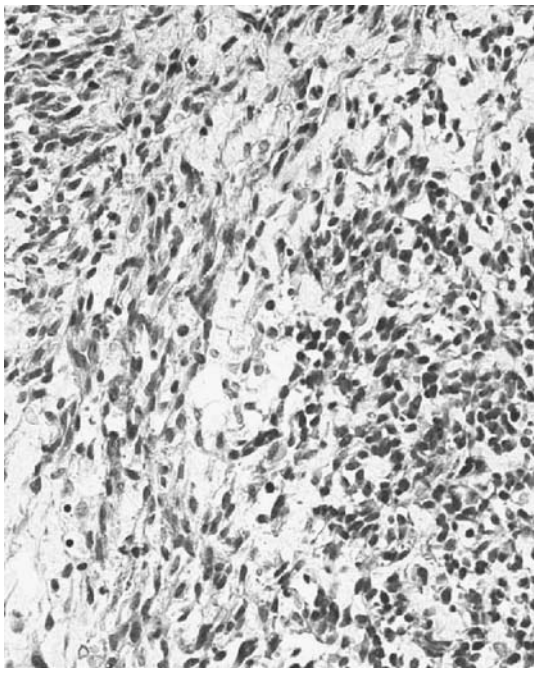

Fig. 6 Case 23. The tumor was composed of a mixture of round and spindle cells with a haphazard orientation. The tissue edema present in the tumor separated the cells in a similar fashion as seen in some embryonal RMS. The fibrovascular stroma was inconspicuous, and no features of alveolar morphology were revealed after sampling the entire tumor mass, original magnification ×100. The original morphological interpretation was that of embryonal RMS. RT-PCR revealed PAX/FKHR fusion transcript. The diagnosis was then reevaluated, and the tumor was reclassified as "solid alveolar RMS" with awareness that such tumors may need further analysis in future

In one patient with alveolar RMS (case 13), the presence of the PAX3/FKHR fused gene was detected in the primary tumor and in two subsequent recurrences. We used RT-PCR to identify malignant cells in the resection margin of the tumor at the time of the second recurrence. Two of nine samples taken from the tumor margin, which were shown to be microscopically free of tumor or uncertain whether they contain tumor cells or not on frozen section histology, revealed the fusion transcript PAX3/FKHR of the same size as detected in the primary tumor. In this patient, bone marrow aspirates were also positive for the fusion transcript in the nested RT-PCR.

Although the number of patients with alveolar RMS was small to analyze clinical data such as the differences of the primary tumor sites and the outcome of the patients, we noticed that the age of patients with the PAX7/FKHR fusion was lower than the age of patients with PAX3/FKHR rearrangement. For the former group, it ranged from 1 to 10.5 years (median 6.5 years), while the latter group had the age range from 3.5 to 18 years (median 9.5 years).

Bone marrow samples

Bone marrow samples (12) and PBPC samples (13) in ten patients with alveolar RMS were examined by the RT-PCR technique using the specific primers.

Six of 12 bone marrow samples (from four patients) and 7 of 13 PBPC samples (from five patients) were shown to be positive for the fusion transcript. Four patients had the PAX3/FKHR and two had the PAX7/FKHR fusion product of the same size as detected previously in the primary tumors. One patient with the PAX3/FKHR fusion transcript (case 3) had no detectable fusion transcript in bone marrow samples at the time of diagnosis, but we found the MyoD1 transcript. A relatively weak transcript PAX3/FKHR was repeatedly detected in the primary tumor. Cytogenetic analysis performed in this patient failed to demonstrate t(2;13), probably because der(2) was lost and the small der(13) could not be identified. The cytogenetic analysis of the bone marrow samples showed tetra- and octaploidy. The discrepant findings may be explained by an existence of one clone carrying t(2;13) and by an appearance of secondary clones with different ploidy status and secondary chromosomal changes.

Follow up of patients with bone marrow and PBPC samples tested by RT-PCR is summarized in Table 3. Of the seven patients in whom we were able to identify bone marrow involvement or contamination of PBPCs by the tumor cells, six died of progressive disease, and one lives with a complete remission 3 years after the treatment start. Three patients had no detectable tumor by RT-PCR technique in the bone marrow. Two patients are alive without evidence of the disease. One patient, a boy aged 6 years, had a primary tumor of the paranasal sinuses. His recurrent tumor infiltrated the orbit. The therapy at the time of the tumor recurrence included surgical excision, chemothera-

Table 3 Follow-up of patients with bone marrow and PBPC samples tested by RT-PCR

Case	Fusion product in primary tumor	Bone marrow	PBPC	Follow-up
1	PAX3/FKHR+	−	ND	AW
2	PAX3/FKHR+	+	–	DD
			–	
			–	
			+	
3	PAX3/FKHR+	+−	ND	AW
4	PAX3/FKHR+	−	+	DD
		+	+	
		–		
		+		
5	PAX3/FKHR+	−	ND	DD
8	PAX7/FKHR+	+	+	DD
10	PAX3/FKHR+	ND	+	DD
			–	
13	PAX3/FKHR+	+	−	DD
		+	+	
14	PAX7/FKHR+	−	−	DD
15	PAX7/FKHR+	ND	+	DD

+− PAX3/FKHR negative but MyoD1 positive in a bone marrow sample, *AW* alive and well, *DD* died of tumor progression, *ND* not done, *PBPC* peripheral blood progenitor cells

py, and autologous stem cell transplantation. His bone marrow and peripheral progenitor cells at the time of the recurrent disease showed no evidence of the fusion product PAX7/FKHR. The patient died of a local progression of the tumor 7 months after autologous stem cell transplantation.

Discussion

RMS represent a group of sarcomas challenging investigators for decades to improve their diagnostic approach. Histological classification is well established [33, 34], but in practical diagnostics, there are many causes why the diagnosis is not always straightforward. One of diagnostic caveats in RMS rests in overlapping features between the subsets of RMS, and an incorrect interpretation of histological findings may lead to a choice of inadequate treatment intensity. Current treatment of patients with RMS is based on histopathology subtype, staging, size, and patient's age, those with advanced disease and unfavorable histology (alveolar RMS) require a more aggressive approach.

The immunohistochemical investigations are helpful and are performed routinely virtually in all cases of RMS and related neoplasms. In this study, we may confirm observations showing that there are differences between a strong and uniform pattern of myogenin positivity in alveolar RMS, whereas the pattern in embryonal RMS is more heterogeneous [6, 13, 27]. As has been pointed out, the difference in the intensity of staining cannot be used as a sole criterion discriminating the alveolar from embryonal RMS [6]. The problem with interpreting immunohistochemistry for myogenin, and for MyoD1, also arises in samples showing post-therapy changes. It has been demonstrated that skeletal muscle, especially regenerating or atrophic muscle fibers, may display myogenin positivity [6]. Such a phenomenon may be misleading in the interpretation of the local residual disease when investigated by morphology alone. The most frequent subtypes in children, alveolar and embryonal RMS, are entities associated with different genomic changes. Therefore, molecular analysis helps to define the nature of these tumors more precisely.

All 30 patients with RMS analyzed in this study expressed the MyoD1 transcript in their primary tumors. The absence of MyoD1 expression using RT-PCR and Southern Blot hybridization with a non-radioactive-labeled cDNA probe was detected only in one patient with embryonal RMS after treatment. This residuum of the tumor failed to manifest nuclear immunoreactivity for MyoD1 and myogenin in spite of the presence of well-defined myoblasts in the tissue. The tumor cell differentiation was particularly pronounced in tissues obtained from postchemotherapy patients, and their tumors were often composed of differentiated rhabdomyoblast, a phenomenon recognized by other authors [8, 9]. Downregulation of nuclear regulatory proteins myogenin and MyoD1 in therapy-induced differentiation of rhabdomyoblasts has been noticed by Wang et al. [47].

Data on specificity of MyoD1 expression are contradictory. Frascella et al. [19] considered MyoD1 a sensitive and specific marker for the molecular diagnosis of RMS. In our study, in accordance with observations published by Gattenloehner et al. [21], we found that the MyoD1 transcript is not entirely specific for RMS. We found weak expression of MyoD1 in normal skeletal muscles. Furthermore, other neoplasms used as a control tissue (teratomas, synovial sarcoma, Ewing tumor/primitive neuroectodermal tumor (PNET), some non-Hodgkin's B cell lymphomas) revealed MyoD1 expression (data not shown). To test the specificity and to minimize the possibility of PCR contamination, we analyzed peripheral bloods and bone marrow aspirates without tumor cell contamination, all of them with negative results of MyoD1 expression. We also analyzed, simultaneously with samples of RMS, other neoplasms (epiteloid sarcoma, aggressive fibromatosis, non-Hodgkin's T cell lymphomas, and carcinomas) which were negative for all tested molecules by RT-PCR. This diminishes the usefulness of MyoD1 investigation in the diagnosis of RMS. Further studies are necessary to address this issue.

Chimeric transcripts and gene fusions can be detected in samples by RT-PCR and are of a great diagnostic significance in RMS. The molecular analysis appears superior to classical cytogenetics, because conventional karyotyping of these tumors is often unyielding [18].

Using RT-PCR, we disclosed PAX/FKHR transcripts in primary RMS in 13 of 15 patients diagnosed as alveolar RMS by histology, which underscores a good correlation between morphological and molecular diagnostics. Two patients with alveolar histology were, however, negative for PAX3/FKHR and PAX7/FKHR transcripts. It is possible that these cases harbored an uncommon variant translocation associated with alveolar RMS such as t(2;11)(q37;q13) [31], t(8;13)(p21;q14) [15], t(2;2)(q35;p23) [46], or had other types of genetic abnormalities that led to the activation of oncogenic pathways as do PAX-FKHR oncoproteins. Two tumors with t(1;13) were diagnosed originally as embryonal RMS by histology. Reexamination of the original material in one patient revealed embryonal type of RMS at presentation with no alveolar features, although multiple samples were taken. After chemotherapy, the residual tumor showed a hyalinized tumor with a focus of a well-defined alveolar RMS, which was underestimated at the time of the residual tumor description. Following the molecular analysis revealing the PAX7/FKHR fusion transcript, the tumor was reclassified as mixed embryonal/alveolar RMS. The second case diagnosed as embryonal RMS retained its morphology as observed in the biopsy of the recurrent tumor, and we were unable to redefine this tumor as a classical alveolar type. The tumor best fitted the category described by Tsokos [44] as a solid alveolar form, although the mixture of undifferentiated round and spindle cells would be rather uncommon for this subtype. Such cases should be possibly classified separately until more detailed data on their molecular profile are gathered.

The potential clinical value of determining minimal (submicroscopical) residual disease in situ by detection of fusion transcripts PAX3/FKHR and PAX7/FKHR by nested RT-PCR was confirmed by our findings, showing

fusion transcripts in microscopically tumor-free resection borders. The tendency to recur locally often observed in RMS may well find its explanation in tumor cells located distant from the main tumor mass and obscured from microscopical identification. This approach also helps to distinguish residual tumor cells with advanced differentiation (post-therapy changes) from atrophic and regenerating muscle cells at the site of the tumor removal.

Fusion transcripts generated through chromosomal translocations have been demonstrated to represent excellent targets for monitoring minimal residual disease in hematological malignancies [20, 32, 43]. Many studies suggest a direct correlation between the numbers of residual tumor cells and the prognosis of the patients. Dissemination of tumor cells in the bone marrow and peripheral blood has been observed also in patients with solid malignancies [22, 49]. The presence of metastases is the most adverse prognostic factor in RMS [38], and the bone marrow is a frequent site of tumor dissemination, particularly in the alveolar subtype [23, 41]. Assessment of bone marrow dissemination by light microscopy has a limited sensitivity. Using the RT-PCR technique, we were able to identify bone marrow involvement in 7 of 12 bone marrow samples and in 7 of 13 PBPC samples. Assessment of a potential tumor cell infiltration of bone marrow grafts or PBPCs destined for stem cell transplantation after myeloablative regimen is important for a selection of tumor cell-free grafts.

The prognostic value of the identification of fusion transcripts in bone marrow aspirates or in PBPC samples has to be proven in further prospective studies. Our results detecting the fusion transcripts typical of alveolar RMS in the bone marrow and PBPC suggest that patients with positive findings are at a high risk of the tumor progression. Similarly, results described by Kelly [23] suggest that RT-PCR assay in alveolar RMS may identify a group of patients who are at a high risk despite having histologically negative bone marrows.

The identification of the translocation variants in alveolar RMS appears to be of prognostic significance [24]. The t(1;13) has been reported to occur in alveolar RMS affecting younger individuals, and the prognosis may be somewhat less unfavorable than that for patients with t(2;13) [24]. Our group of patients is too small to draw conclusions in this respect. However, the age of patients with t(1;13) was lower in the reported series of patients than that in patients with t(2;13). Of patients with t(1;13), one of five presented with metastatic disease at the time of diagnosis, whereas five of ten patients with t(2;13) were diagnosed with a generalized disease. A further follow up of the patients is under way.

In conclusion, the application of RT-PCR techniques in the classification of childhood RMS may help to resolve histological controversies in some cases by the use of criteria based on genetic differences between the alveolar and embryonal RMS. Alveolar histology may be focal within an embryonal tumor and, admittedly, may be missed by an incomplete sampling either by a surgeon or by a pathologist. From that reason, proper handling of the tumor specimens submitted for histopathological examination remains a high-priority task to avoid misinterpretations. When employing the RT-PCR analysis into the diagnostic support, we may detect fusion gene transcripts, and, therefore, chromosomal translocations specific for the alveolar type of RMS. Beside the histopathological classification, the RT-PCR has a significant impact on specification of diagnosis and on selecting an optimal therapeutic approach. RT-PCR techniques may have a role in staging, in monitoring the effects of therapy, in recognizing malignant cells at the tumor resection margins, in assessing the efficacy of purging protocols for autologous stem cell transplantation, and in post-therapy follow up.

Acknowledgements The study was supported by the Grant FN Motol IG 9746, the Research Project of the Ministry of Education, Youth, and Sports of the Czech Republic No. 0021620813 and by the Research Project of the Ministry of Health No. 00000064203. We thank Dr. E. Stejskalova, Department of Pediatric Oncology, for the cytogenetic evaluation of case number 3. The authors wish to thank William A. Newton, Jr., M.D., president of the International Consortium for Cure of Childhood Cancer in China, Columbus, OH, USA, and Stephen J. Qualman, M.D., Head of the Department of Pathology, Children's Hospital, Columbus, OH, USA, for valuable comments to the manuscript.

References

1. Afify A, Mark HF (1999) Trisomy 8 in embryonal rhabdomyosarcoma detected by fluorescence in situ hybridization. Cancer Genet Cytogenet 108:127–132
2. Anderson J, Gordon A, Pritchard-Jones K, Shipley J (1999) Genes, chromosomes, and rhabdomyosarcoma. Genes Chromosomes Cancer 26:275–285
3. Barr FG (1997) Molecular genetics and pathogenesis of rhabdomyosarcoma. J Pediatr Hematol Oncol 19(6):483–491
4. Barr FG (1999) The role of chimeric paired box transcription factors in the pathogenesis of pediatric rhabdomyosarcoma. Cancer Res 59(7 Suppl):1711–1715
5. Bober E, Franz T, Arnold HH, Gruss P, Tremblay P (1994) PAX3 is required for the development of limb muscles: a possible role for the migration of dermomyotomal muscle progenitor cells. Development 120:603–612
6. Cessna MH, Zhou H, Perkins SL, Tripp SR, Pickering D, Daines C, Coffin CM (2001) Are myogenin and MyoD1 expression specific for rhabdomyosarcoma? A study of 150 cases, with emphasis on spindle cell mimics. Am J Surg Pathol 25:1150–1157
7. Chen B, Dias P, Jenkins JJ III, Savell VH, Parham DM (1998) Methylation alterations of the MyoD1 upstream region are predictive of subclassification of human rhabdomyosarcomas. Am J Pathol 152(4):1071–1079
8. Coffin CM, Rulon J, Smith L, Bruggers C, White FV (1997) Pathologic features of rhabdomyosarcoma before and after treatment: a clinicopathologic and immunohistochemical analysis. Mod Pathol 10:1175–1187
9. d'Amore ES, Tollot M, Stracca-Pansa V, Menegon A, Meli S, Carli M, Ninfo V (1994) Therapy associated differentiation in rhabdomyosarcomas. Mod Pathol 7:69–75
10. Davis RJ, Barr FG (1997) Fusion genes resulting from alternative chromosomal translocations are overexpressed by gene-specific mechanisms in alveolar rhabdomyosarcoma. Proc Natl Acad Sci U S A 94:8047–8051

11. Davis RJ, D'Cruz CM, Lovell MA, Biegel JA, Barr FG (1994) Fusion of PAX7 to FKHR by the variant t(1;13)(p36;q14) translocation in alveolar rhabdomyosarcoma. Cancer Res 54 (11):2869–2872
12. Davis RL, Weintraub H, Lassar AB (1987) Expression of a single transfected cDNA converts fibroblasts to myoblasts. Cell 51(6):987–1000
13. Dias P, Chen B, Dilday B, Palmer H, Hosoi H, Singh S, Wu C, Li X, Thompson J, Parham D, Qualman S, Houghton P (2000) Strong immunostaining for myogenin in rhabdomyosarcoma is significantly associated with tumors of the alveolar subclass. Am J Pathol 2:399–408
14. Douglass EC, Valentine M, Etcubanas E, Paraham D, Webber BL, Houghton PJ, Houghton JA, Green AA (1987) A specific chromosomal abnormality in rhabdomyosarcoma. Cytogenet Cell Genet 45:148–155
15. Douglass EC, Rowe ST, Valentine M, Paraham DM, Berkow R, Bowman WP, Maurer HM (1991) Variant translocations of chromosome 13 in alveolar rhabdomyosarcoma. Genes Chromosomes Cancer 3(6):480–482
16. Douglass EC, Shapiro DN, Valentine M, Rowe ST, Carroll AJ, Raney RB, Ragab AH, Abella SM, Paraham DM (1993) Alveolar rhabdomyosarcoma with the t(2;13): cytogenetic findings and clinicopathologic correlations. Med Pediatr Oncol 21:83–87
17. Downing JR, Khandekar A, Shurtleff SA, Head DR, Paraham DM, Webber BL, Pappo AS, Hulshof MG, Conn WP, Shapiro DN (1995) Multiplex RT-PCR assay for the differential diagnosis of alveolar and Ewing's sarcoma. Am J Pathol 146 (3):626–634
18. Fletcher JA, Kozakewich HP, Hoffer FA (1991) Diagnostic relevance of clonal cytogenetic aberrations in malignant soft-tissue tumors. N Engl J Med 324:436–442
19. Frascella E, Toffolatti L, Rosolen A (1998) Detection of the MyoD1 transcript in rhabdomyosarcoma cell lines and tumor samples by reverse transcription polymerase chain reaction. Am J Pathol 152(2):577–582
20. Gabert J (1999) Detection of recurrent translocations using real time PCR; assessment of the technique for diagnosis and detection of minimal residual disease. Haematologica 84:107–109
21. Gattenloehner S, Dockhorn-Dworniczak B, Leuschner I, Vincent A, Muller-Hermelink HK, Marx A (1999) A comparison of MyoD1 and fetal acetylcholine receptor expression in childhood tumors and normal tissue. J Mol Diagn 1(1):23–31
22. Israeli RS, Miller WH, Su SL, Powell CT, Fair WR, Samadi SD, Huryk RF, DeBlasio A, Edwards ET, Wise GJ (1994) Sensitive nested reverse transcription polymerase chain reaction detection of circulating prostatic tumor cells. Comparison of prostate specific membrane antigen and prostate specific antigen-based assay. Cancer Res 54:6306–6310
23. Kelly KM (1996) Minimal disease detection in patients with alveolar rhabdomyosarcoma using a reverse transcription polymerase chain reaction method. Cancer 15:1320–1327
24. Kelly KM (1997) Common and variant gene fusions predict distinct clinical phenotypes in rhabdomyosarcoma. J Clin Oncol 15(5):1831–1836
25. Kodet R (1989) Rhabdomyosarcoma in childhood. An immunohistochemical analysis with myoglobin, desmin and vimentin. Pathol Res Pract 185:207–213
26. Kullendorff CM, Donner M, Mertens F, Mandahl N (1998) Chromosomal aberrations in a consecutive series of childhood rhabdomyosarcoma. Med Pediatr Oncol 30:156–159
27. Kumar S, Perlman E, Harris CA, Raffeld M, Tsokos M (2000) Myogenin is a specific marker for rhabdomyosarcoma: an immunohistochemical study in paraffin-embedded tissues. Mod Pathol 13:988–993
28. Kushner BH, LaQuaglia MP, Cheung NK, Kramer K, Hamelin AC, Gerald WL, Ladanyi M (1999) Clinically critical impact of molecular genetic studies in pediatric solid tumors. Med Pediatr Oncol 33:530–535
29. Leuschner I, Harms D, Mattke A, Koscieniak E, Treuner J (2001) Rhabdomyosarcoma of the urinary bladder and vagina: clinicopathologic study with emphasis on recurrent disease: a report from the Kiel Pediatric Tumor Registry and the German CWS Study. Am J Surg Pathol 25:856–864
30. Miettinen M, Rapola J (1989) Immunohistochemical spectrum of rhabdomyosarcoma and rhabdomyosarcoma-like tumors. Expression of cytokeratin and 68-kD neurofilament protein. Am J Surg Pathol 13:120–132
31. Miki H, Kobayashi S, Kushida Y, Sasaki M, Haba R, Hirakawa E, Ogura K, Ohmori M (1999) A case of infantile rhabdomyofibrosarcoma with immunohistochemical, electron microscopical, and genetic analyses. Hum Pathol 30(12):1519–1522
32. Mitterbauer G, Zimmer C, Pirc-Danoewinata H, Haas OA, Hojas S, Schwarzinger I, Greinix H, Jager U, Lechner K, Mannhalter C (2000) Monitoring of minimal residual disease in patients with MLL-AF6-positive acute myeloid leukaemia by reverse transcriptase polymerase chain reaction. Br J Haematol 109(3):622–628
33. Newton WA, Gehan EA, Webber BL, Marsden HB, van Unnik AJ, Hamoudi AB, Tsokos MG, Shimada H, Harms D, Schmidt D (1995) Classification of rhabdomyosarcomas and related sarcomas. Pathologic aspects and proposal for a new classification—an Intergroup Rhabdomyosarcoma Study. Cancer 75 (6):1073–1085
34. Parham DM (2001) Pathologic classification of rhabdomyosarcomas and correlation with molecular studies. Mod Pathol 14:506–514
35. Parham DM, Webber B, Holt H, Williams WK, Maurer H (1991) Immunohistochemistry of childhood rhabdomyosarcomas and related neoplasms. Results of an Intergroup Rhabdomyosarcoma Study project. Cancer 67:3072–3080
36. Qualman SJ, Bowen J, Parham DM, Brantom PA, Meyer WH (2003) Protocol for the examination of specimens from patients (children and young adults) with rhabdomyosarcoma. Arch Pathol Lab Med 127:1290–1297
37. Rowe D, Gerrard M, Gibbons B, Malpas JS (1987) Two further cases of t(2;13) in alveolar rhabdomyosarcoma indicating a review of the published chromosome breakpoints. Br J Cancer 56:379–380
38. Ruymann FB, Newton WA, Ragab AH, Donaldson HM, Foulkes M (1984) Bone marrow metastases at diagnosis in children and adolescents with rhabdomyosarcoma. Cancer 53:368–373
39. Scrable H, Witte D, Shimada H, Seemayer T, Sheng WW, Soukup S, Koufos A, Houghton P, Lampkin B, Cavenee W (1989) Molecular differential pathology of rhabdomyosarcoma. Genes Chromosomes Cancer 1(1):23–35
40. Stuart ET, Gruss P (1996) PAX: developmental control genes in cell growth and differentiation. Cell Growth Differ 7(3):405–412
41. Thomson B, Hawkins D, Felgenhauer J, Radich J (1999) RT-PCR evaluation of peripheral blood, bone marrow and peripheral blood stem cells in children and adolescents undergoing VACIME chemotherapy for Ewing's sarcoma and alveolar rhabdomyosarcoma. Bone Marrow Transplant 24(5):527–533
42. Tobar A, Avigad S, Zoldan M, Morc C, Goshen Y, Zaizov R (2000) Clinical relevance of molecular diagnosis in childhood rhabdomyosarcoma. Diagn Mol Pathol 9(1):9–13
43. Tobal K, Moore H, Macheta M, Yin JA (2001) Monitoring minimal residual disease and predicting relapse in APL by quantitating PML-RARalpha transcripts with a sensitive competitive RT-PCR method. Leukemia 15(7):1060–1065
44. Tsokos M (1994) The diagnosis and classification of childhood rhabdomyosarcoma. Semin Diagn Pathol 11:26–38
45. Turc-Carel C, Lizard-Nacol S, Justrabo E, Favrot M, Philip T, Tabone E (1986) Consistent chromosomal translocation in alveolar rhabdomyosarcoma. Cancer Genet Cytogenet 19:361–362

46. Wachtel M, Dettling M, Koscielnik E, Stegmaier S, Treuner J, Simon-Klingenstein K, Buhlmann P, Niggli FK, Schafer BW (2004) Gene expression signatures identify rhabdomyosarcoma subtypes and detect a novel t(2;2)(q35;p23) translocation fusing PAX3 to NCOA1. Cancer Res 64(16):5539–5545
47. Wang NP, Marx J, McNutt MA, Rutledge JC, Gown AM (1995) Expression of myogenic regulatory proteins (myogenin and MyoD1) in small blue round cell tumors of childhood. Am J Pathol 147(6):1799–1810
48. Weintraub H, Davis R, Tapscott S, Thayer M, Krause M, Benezra R, Blackwell TK, Turner D, Rupp R, Hollenberg S (1991) The myoD gene family: nodal point during specification of the muscle cell lineage. Science 251(4995):761–766 (Review)
49. Weitz J, Kienle P, Lacroix J, Willeke F, Benner A, Lehnert T, Herfarth C, von Knebel Doeberitz M (1998) Dissemination of tumor cells in patient undergoing surgery for colorectal cancer. Clin Cancer Res 4:343–348

Virchows Arch (2006) 448: 459–462
DOI 10.1007/s00428-005-0130-0

ORIGINAL ARTICLE

Torsten Hansen · Kathrin Katenkamp · Detlef Katenkamp

D2-40 staining in sinonasal-type hemangiopericytoma—further evidence of distinction from conventional hemangiopericytoma and solitary fibrous tumor

Received: 28 October 2005 / Accepted: 2 November 2005 / Published online: 16 December 2005

Abstract D2-40 is a monoclonal antibody, which reacts with a fixative-resistant epitope of lymphatic endothelium. Sinonasal-type hemangiopericytoma (SHP) and tumors of the (conventional) hemangiopericytoma/solitary fibrous tumor family (HP/SFT) are characterized by prominent vasculature. However, data concerning D2-40 labeling of these tumors are very sparse. In the present study, we investigated D2-40 staining in tissue specimens of 17 patients with SHP (male to female ratio of 2.4:1, median age of 63 years) and compared the immunolabeling with 20 cases of HP/SFT, including three SFT cases from nasal mucosa. D2-40 was detected in vascular channels of all SHP patients examined. By contrast, all cases of HP/SFT did not reveal any vascular channel being positive for D2-40, neither in the nasal cases nor in the remaining patients. This study presented for the first time data on D2-40 labeling in a series of SHP, HP/SFT, and supports the distinction of SHP from HP/SFT.

Keywords D2-40 · Sinonasal-type hemangiopericytoma · Conventional hemangiopericytoma · Solitary fibrous tumor

Introduction

D2-40 is a monoclonal antibody, which is directed against an oncofetal antigen called M2A antigen [6, 14]. This monomeric surface sialoglycoprotein (Mr=40,000) was found first in fetal germ cells and different germ cell neoplasias, mainly in seminoma [14]. Thereafter, it was shown to react with a fixation-resistant epitope on lymphatic endothelium. In several studies, D2-40 could label normal, reactive, and neoplastic lymphatics [6, 9, 10]. Thus, it is now considered to be the best commercially available antibody for the delineation of normal, reactive, and neoplastic lymphatic endothelial cells [10]. Among the vascular tumors tested for this marker, lymphangioma [6, 8, 9], Kaposi sarcoma [6, 9], kaposiform hemangioendothelioma [3], papillary intralymphatic angioendothelioma (so-called Dabska tumor) [6], hobnail hemangioma [5], and a subset of angiosarcomas were particularly positive [6, 9]. By contrast, hemangiomas, glomus tumors, vessels in angiolipomas, and nearly all epithelioid hemangioendotheliomas did not reveal immunoreactivity for this molecule [6, 9].

In the present study, we analyzed sinonasal-type hemangiopericytoma, another tumor type with a prominent vascular component, for D2-40 staining. For comparison, tissue specimens of patients with tumors of the conventional hemangiopericytoma/solitary fibrous tumor family (HP/SFT) were additionally examined.

T. Hansen (✉) · K. Katenkamp · D. Katenkamp
Institute of Pathology, Friedrich-Schiller-University of Jena,
Ziegelmühlenweg 1,
07743 Jena, Germany
e-mail: TorstenHansen@gmx.de
Tel.: +49-3641-934002
Fax: +49-3641-933111

Materials and methods

The records from the Soft Tissue Tumor Registry of the Institute of Pathology in Jena were searched for cases coded as sinonasal-type hemangiopericytoma (SHP) from 1995 to the present. We found 17 cases of SHP with a male to female ratio of 2.4:1 and a median age of 63 years ranging from 38 to 86 years. All tumors were localized in the nose and the paranasal sinuses, respectively. For comparison of D2-40 labeling, tissue specimens from each of the 20 patients suffering from HP/SFT were retrieved from the case files of the Soft Tissue Registry. SFT was separated from HPC by common histological findings (according to the World Health Organization classification [7]): tumors consistently showing branching vessels with a staghorn configuration and closely packed spindle-shaped to ovoid cells, were designated as HPC. Tumors having patternless architecture and areas of fibrosis were regarded as SFT. HP/SFT patients had a male to female ratio of about 0.9:1 and were 60.3 years old on average (ranging from 8 to 93 years). Nine HP/SFTs were localized in the trunk, six in the head & neck area, including three tumors affecting the nasal and

Table 1 Data on the primary antibodies used for this study

Marker		Dilution	Pretreatment
1[a]	Alpha 1-smooth-muscle actin (clone 1A4)	1:600	None
2[a]	BCL-2 (clone 124)	1:400	Microwave
3[b]	CD34 (clone QBEND 10)	1:200	None
4[a]	D2-40 (clone D2-40)	1:400	Microwave

[a]Manufactured by Dako (Hamburg, Germany)
[b]Manufactured by SIGNET (Dedham, MA, USA)

paranasal mucosa, each one in the orbita, the lung, the lower arm, and the small bowel, while the localization of one tumor was unknown. None of the HP/SFTs examined showed signs of malignancy, and neither recurrences nor metastases have been described for any of these studied cases.

Immunohistochemical staining was performed according to previous protocols [11] using antibodies against α-smooth-muscle actin (ASMA), BCL-2, CD34, and D2-40. The primary antibodies applied for the immunohistochemical analysis are summarized in Table 1. D2-40 labeling was semiquantitatively analyzed and scored as follows: no vessels positive, <20% of vessels positive, >20% and <50% of vessels positive, and >50% of vessels positive.

Results

All of the SHPs studied were localized in the submucosa. They were unencapsulated and revealed a diffuse growth pattern. The epithelium lining the tumors showed not infrequently squamous metaplasia. Tumor cells were spindle-shaped or ovoid and were arranged in various forms. Most common were fascicular, storiform, and whorled patterns. The nuclei showed blunt edges, cytoplasm was eosinophilic. Signs of atypia such as pleomorphism or significant mitotic rate were not found. Besides thin-walled and variable-sized vessels, hyalinized vascular spaces were occasionally detected (Fig. 1a,b).

Immunohistochemistry demonstrated expression of ASMA in all cases, occurring both in spindle-cells and vessel walls. CD34 was mainly expressed in the vessels, with the exception of four patients revealing faint labeling in the spindle-shaped cells as well. In contrast, BCL-2 was negative in all cases. D2-40 was detected in vascular channels of all SHP patients examined. This molecule revealed a strong membranous and cytoplasmic staining of the endothelial cells, while nuclei were not labeled. D2-40 positive vessels were observed at the periphery and in the center of the SHPs. Centrally located positive vessels were surrounded by numerous sheets of spindle-shaped cells. Semiquantitative analysis revealed eight SHPs with more than 50% of vessels being positive; six SHPs were found with more than 20% and less than 50% of vessels positive; the remaining 3 cases revealed only less than 20% of vessels with D2-40 positivity. D2-40 negative vessels sometimes showed hyalinized perivascular stroma (Fig. 1b). The spindle-shaped cells were completely negative for this antibody. Sometimes, positive staining was observed at the basal lining of epithelial cells in areas of squamous metaplasia (Fig. 1b).

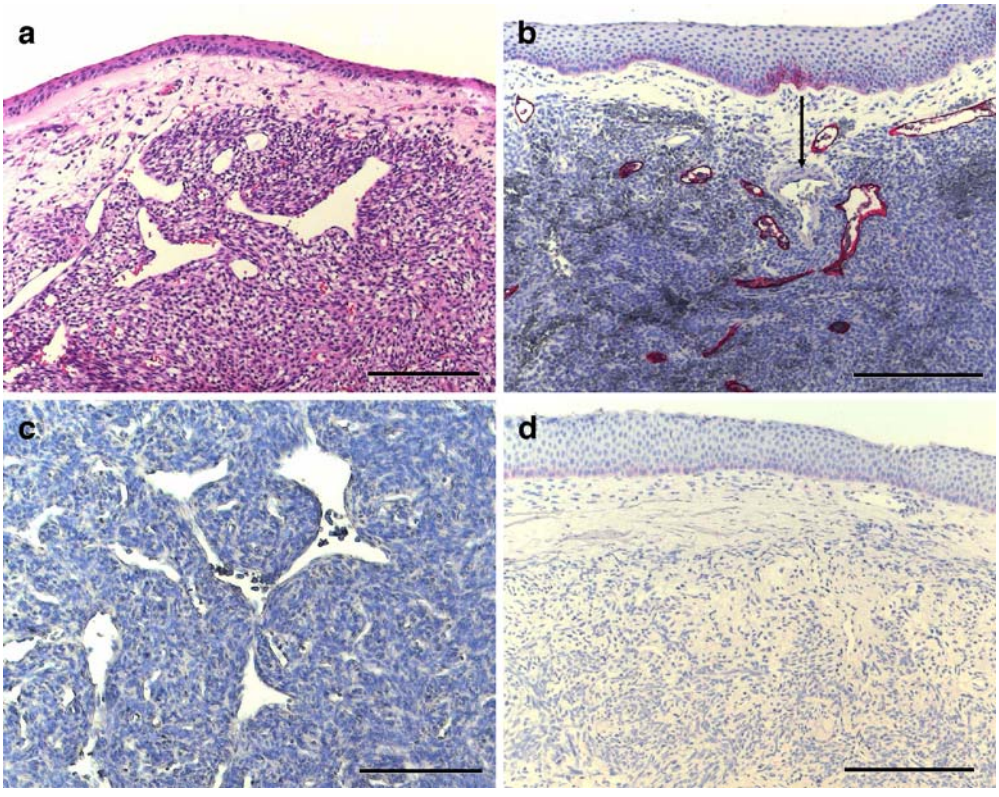

Fig. 1 **a** Overview of SHP shows squamous metaplasia of the nasal mucosa and a mesenchymal tumor with spindle-shaped and ovoid cells, which surround vessels in a concentric fashion (H&E ×100, bar=100 μm). **b** D2-40 labeling of SHP demonstrates numerous positive vessels (*red*) at the periphery and in the center of the tumor. Note a vessel with prominent perivascular hyalinization (*arrow*) being negative for D2-40. A few basal epithelial reveal staining for D2-40 (×100 bar=100 μm). **c** Conventional HP reveals numerous, sometimes staghorn-like vessel spaces, which are surrounded by numerous spindle cells. Note complete negativity for D2-40 (×200, bar=50 μm). **d** SFT of the nasal mucosa do not obtain D2-40 positive vessels. Note squamous metaplasia of the nasal mucosa with a few epithelia faintly stained for D2-40 (*red*; ×100; bar=100 μm)

By contrast, all cases of HP/SFT analyzed did not show any intratumoral vessel or vascular channel being positive for D2-40 (Fig. 1c). In the nasal and paranasal cases, D2-40 was completely absent in tumor areas (Fig. 1d). In the nasal mucosa lining the tumors, squamous metaplasia was also observed, and the basal epithelia showed some D2-40 positivity. D2-40 also stained some residual vessels with localization outside the tumors. On the other hand, all HP/SFT cases revealed a nearly thorough positivity for CD34 and bcl-2 with five cases also focally expressing ASMA.

Discussion

D2-40 is a monoclonal antibody, which has been demonstrated to react with a fixative-resistant epitope of lymphatic endothelium. Several vascular tumors have been tested for this marker [3, 5, 6, 8–10]. Sinonasal-type hemangiopericytoma, also called sinonasal hemangiopericytoma-like tumor, (conventional) hemangiopericytoma, and solitary fibrous tumor are characterized by a prominent vasculature [2, 7, 22]. However, data concerning D2-40 labeling of these tumors are very sparse. Kahn et al. [9] only reported on one case of HP, which did not show D2-40 staining. Therefore, we were prompted to analyze tissue specimens of patients with SHP, HP, and SFT for labeling with D2-40. Because it is now generally accepted that HP and SFT comprise different histological features of a single tumor entity [7], we included cases previously diagnosed as either HP or SFT in one group.

Most interestingly, D2-40 could be exclusively detected in vessels of SHP, while the HP/SFT group revealed a complete negativity. SHP is a rare tumor, which is now generally believed to be different from HP/SFT. SHP shows some differences from HP/SFT concerning the histological architecture and cellularity [20]. Furthermore, it has been shown that SHP can be separated from HP/SFT by means of immunohistochemistry. In contrast to HP/SFT, SHP commonly stains positive for ASMA [12, 17, 20]. While CD34 and BCL-2 are well-known markers for spindle-shaped tumor cells of both HP/SFT, they were only faintly or not detected in previous immunohistochemical studies on SHP [12, 20, 21]. This is in line with our results, which showed only a weak expression of CD34 in the minority of SHP cases and complete negativity for BCL-2.

It should be stressed out that the different immunolabeling of D2-40 in the vessels of SHP, as compared to HP/SFT, further supports the necessary discrimination between the entities. This is of special importance as it is known that SHP has a generally better prognosis than HP with a lower rate of recurrences and metastases [4, 12, 20]. Moreover, cases of HP/SFT family have been reported to occasionally occur in the nasal mucosa [15, 18, 23]. The clinical and macroscopic features may be similar to those of SHP. Thus, nasal HP/SFT represents a relevant differential diagnosis of SHP. One might contradict that D2-40 staining in SFT presented in this study was false negative. However, in the case of nasal SFT positivity of D2-40 could be observed not only in some residual lymphatics, but also in basal epithelial of the nasal mucosa. The latter finding has been previously described by Kaiserling [10] as well. These data strongly argue against a false negative labeling.

It is known that nasal mucosa typically contains large numbers of lymphatic vessels which play a crucial role in different complaints such as inflammatory diseases [19]. In our study, we found numerous lymphatics labeled by D2-40 in the periphery and in the center of SHP. Particularly in the latter, surrounding spindle-shaped tumor cells were observed. Therefore, it can be considered that D2-40 labeling in SHP is tumor-associated. Several molecules were described as important inductors of lymphangiogenesis and also have been found in lymphatic vascular tumors. Among them, vascular endothelial growth factor (VEGF) C and its receptor, VEGFR-3, seem to play a central role. The two molecules were detected in several lymphatic neoplasms including lymphangioma and hobnail hemangioma [13, 16]. Furthermore, Choi et al. [1] recently reported on significant correlation between VEGFC and D2-40 in breast carcinoma, which possibly could be due to an interaction of the two molecules. However, there is no report so far showing an induction or stimulation of D2-40 by any angiogenetic factor. Furthermore, the role of D2-40 in vascular tumors is not known. Thus, conclusions concerning the possible interrelationships and functions of D2-40 in the pathogenesis of these neoplasias (including SHP) remain speculative. Nevertheless, we suggest from our data that the D2-40 positive vessels found in SHP do not represent residual lymphatics only, but might be associated with the tumor development.

In summary, this study presented for the first time data on D2-40 labeling in a series of SHP and HP/SFT, and thus, contributes to the immunohistochemical mapping of D2-40 in (peri-)vascular tumors. Because D2-40 labeling was found exclusively in SHP but not in HP/SFT, including cases from the nasal mucosa, the following conclusions can be drawn: (1) D2-40 further contributes to the differentiation from HP/SFT, and (2) D2-40 stained vessels in SHP do not represent residual lymphatics of the nasal mucosa only, but might have a role in tumor development.

Acknowledgements We wish to thank Mrs. Bergholz, Mrs. Geier, and Mrs. Pelzer (Institute of Pathology, University of Jena) for their excellent technical assistance. We acknowledge the support of Mrs. Gröschel (Tumor Registry, Jena) for providing case data from the consultation files. Special thanks to Dr. Alexander Berndt, (Institute of Pathology, University of Jena) for technical assistance in preparing the figures.

We are very grateful to all pathologists who sent case material and clinical details from patients included in this study.

References

1. Choi WW, Lewis MM, Lawson D, Yin-Goen Q, Birdsong GG, Cotsonis GA, Cohen C, Young AN (2005) Angiogenic and lymphangiogenic microvessel density in breast carcinoma: correlation with clinicopathologic parameters and VEGF-family gene expression. Mod Pathol 18:143–152

2. Compagno J, Hyams VJ (1976) Hemangiopericytoma-like intranasal tumors. A clinicopathologic study of 23 cases. Am J Clin Pathol 66:672–683
3. Debelenko LV, Perez-Atayde AR, Mulliken JB, Liang MG, Archibald TH, Kozakevich HP (2005) D2-40 immunohistochemical analysis of pediatric vascular tumors reveals positivity in kaposiform hemangioendothelioma. Mod Pathol, (published online)
4. Eichhorn JH, Dickersin GR, Bhan AK, Goodman ML (1990) Sinonasal hemangiopericytoma. A reassessment with electron microscopy, immunohistochemistry, and long-term follow-up. Am J Surg Pathol 14:856–866
5. Franke FE, Steger K, Marks A, Kutzner H, Mentzel T (2004) Hobnail hemangiomas (targetoid hemosiderotic hemangiomas) are true lymphangiomas. J Cutan Pathol 31:362–367
6. Fukunaga M (2005) Expression of D2-40 in lymphatic endothelium of normal tissues and in vascular tumors. Histopathology 46:396–402
7. Guillou L, Fletcher JA, Fletcher CDM, Mandahl N (2002) Extrapleural solitary fibrous tumour and haemangiopericytoma. In: Fletcher CDM, Unii KK, Mertens F (eds) WHO Classification of tumours of soft tissue and bone. IARC, Lyon, pp 86–90
8. Hornick JL, Fletcher CDM (2005) Intraabdominal cystic lymphangiomas obscured by marked superimposed reactive changes: clinicopathological analysis of a series. Hum Pathol 36:426–432
9. Kahn HJ, Bailey D, Marks A (2002) Monoclonal antibody D2-40, a new marker of lymphatic endothelium, reacts with Kaposi's sarcoma and a subset of angiosarcomas. Mod Pathol 15:434–440
10. Kaiserling E (2004) Immunohistochemical identification of lymph vessels with D2-40 in diagnostic pathology. Pathologe 25:362–374
11. Katenkamp K, Katenkamp D (2005) Low-malignant peripheral nerve sheath tumors of nasal and sinonasal mucous membranes. Pathologe 26:90–95
12. Kuo FY, Lin HC, Eng HL, Huang CC (2004) Sinonasal hemangiopericytoma-like tumor with true pericytic myoid differentiation: a clinicopathologic and immunohistochemical study of five cases. Head Neck 27:124–129
13. Lymboussaki A, Partanen TA, Olofsson B, Thomas-Crusells J, Fletcher CDM, de Waal RMW, Kaipanen A, Alitalo K (1998) Expression of the vascular endothelial growth factor C receptor VEGFR-3 in lymphatic endothelium of the skin and in vascular tumors. Am J Pathol 153:395–403
14. Marks A, Sutherland DR, Bailey D, Iglesias J, Law J, Lei M, Yeger H, Banerjee D, Baumal R (1999) Characterization and distribution of an oncofetal antigen (M2A antigen) expressed on testicular germ cell tumors. Br J Cancer 80:569–578
15. Mentzel T, Bainbridge TC, Katenkamp D (1997) Solitary fibrous tumor: clinicopathological, immunohistochemical, and ultrastructural analysis of 12 cases arising in soft tissues, nasal cavity and nasopharynx, urinary bladder and prostate. Virchows Arch 430: 445–453
16. Mentzel T, Partanen TA, Kutzner H (1999) Hobnail hemangioma ("targetoid hemosiderotic hemangioma"): clinicopathologic and immunohistochemical analysis of 62 cases. J Cutan Pathol 26: 279–286
17. Miettinen M (ed) (2003) Diagnostic soft tissue pathology. Churchill Livingstone, Philadelphia, p 333
18. Munks S (2003) Solitary fibrous tumor (SFT) of the nasal mucosa. Laryngorhinootologie 82:655–658
19. Saaristo A, Partanen TA, Arola J, Jussila L, Hytönen M, Mäkitie A, Vento S, Kaipainen A, Malmberg H, Alitalo K (2000) Vascular endothelial growth factor-C and its receptor VEGFR-3 in the nasal mucosa and in nasopharyngeal tumors. Am J Pathol 157:7–14
20. Thompson LD, Miettinen M, Wenig BM (2003) Sinonasal-type hemangiopericytoma. A clinicopathologic and immunophenotypic analysis of 104 cases showing perivascular myoid differentiation. Am J Surg Pathol 27:737–749
21. Tse LLY, Chan JKC (2002) Sinonasal haemangiopericytoma-like tumor: a sinonasal glomus tumor or a haemangiopericytoma? Histopathology 40:510–517
22. Weiss SW, Goldblum JR (eds) (2001) Soft tissue tumors. 4th edn. Mosby, St. Louis, pp 1016–1019
23. Zuckerberg LR, Rosenberg AE, Randolph G, Pilch BZ, Goodman ML (1991) Solitary fibrous tumor of the nasal cavity and paranasal sinuses. Am J Surg Pathol 15:126–130

Virchows Arch (2006) 448: 463–471
DOI 10.1007/s00428-005-0142-9

ORIGINAL ARTICLE

Mami Kouchi · Kazuo Okimoto · Izumi Matsumoto
Kohji Tanaka · Masashi Yasuba · Okio Hino

Natural history of the Nihon (*Bhd* gene mutant) rat, a novel model for human Birt–Hogg–Dubé syndrome

Received: 1 November 2005 / Accepted: 25 November 2005 / Published online: 31 January 2006

Abstract In the Nihon rat, an established model of hereditary renal cell carcinoma (RCC), the propensity for tumor development, is inherited as an autosomal dominant trait due to a single germline nucleotide insertion mutation in the rat *Bhd* ortholog. The Birt–Hogg–Dubé (BHD) syndrome is a rare autosomal dominant disease characterized by fibrofolliculoma, pulmonary cysts, spontaneous pneumothorax, and renal neoplasm. The renal lesions of the Nihon rat are characterized, and extrarenal lesions are also described in this work. The earliest lesion of the RCC was identified as an altered tubule at as early as 3 weeks of age and rapidly progressed through adenoma to carcinoma with the primary cell type being clear/acidophilic where some similarities were evident to RCCs in BHD syndrome. The Nihon rats demonstrate a heterotopic ossification within RCCs and three extrarenal lesions, clear cell hyperplasia/adenoma of the endometrium, clear cell change of the epithelium of striated portions of salivary glands, and cardiac rhabdomyomatosis. This rat model of hereditary RCC provides a useful tool for analyzing the series of events leading to renal tumorigenesis and for studying *BHD* gene functions.

Keywords Birt–Hogg–Dubé syndrome · Nihon rat · Eker rat · Renal cell carcinoma · Extrarenal lesion

M. Kouchi (✉) · K. Okimoto · I. Matsumoto · K. Tanaka · M. Yasuba
Toxicology Group, Safety Research Laboratories,
Dainippon Sumitomo Pharma Co., Ltd.,
33-94, Enoki-cho,
Suita, Osaka 564-0053, Japan
e-mail: mami-kochi@ds-pharma.co.jp
Tel.: +81-6-63375923
Fax: +81-6-63377053

O. Hino
Department of Pathology,
Juntendo University School of Medicine,
2-1-1, Hongo, Bunkyo-ku,
Tokyo 113-8421, Japan

Introduction

In the United States, renal cell carcinoma (RCC) affects more than 35,000 people annually and causes approximately 12,000 cancer-related deaths [14]. There are several histologic variants, but the most common form is the conventional (clear cell) RCC (about 75%) and next in frequency is the papillary RCC (about 10%). Chromophobic RCC and oncocytoma are more rare (about 5%, each) [18, 35]. The vast majority of RCCs are sporadic, but there are several hereditary syndromes associated with RCCs, including Von Hippel–Lindau disease, hereditary papillary renal carcinoma, hereditary leiomyomatosis and renal cell carcinoma (HLRCC), familial renal oncocytoma, tuberous sclerosis, and Birt–Hogg–Dubé (BHD) syndrome, that have been identified [4, 13, 21, 25, 30, 40, 42, 43].

The Eker rat was the first animal model to be established for such hereditary RCCs—featuring an autosomal dominant trait due to a germline defect in the tuberous sclerosis 2 (*Tsc2*) tumor suppressor gene [7, 8, 16]. The animal shows a spectrum from early preneoplastic lesions in the age of 2 months to frank neoplasms in virtually all heterozygotes by the age of 1 year [9–11]. We have established a novel hereditary RCC model from a colony of Sprague–Dawley rats and named it the "Nihon rat" [26]. RCC development is again inherited as an autosomal dominant trait [26]. The heterozygote of the Nihon rat, unlike the Eker rat, begins to manifest preneoplastic lesions for RCC at 3 weeks of age and develops adenomas predominantly consisting of clear cells by the age of 8 weeks [17]. The homozygous mutant condition is lethal at an early stage of fetal life [26]. A germline mutation has been identified in the rat *Bhd* gene where insertion of a single nucleotide results in a frameshift at codon 17 and production of a stop codon 26 amino acids (aa) downstream [12, 27]. A high frequency of loss of heterozygosity (LOH) in primary RCC at the *Bhd* locus and the finding of a point mutation (nonsense) in one LOH-negative case indicate that tumorigenesis is initiated by "Knudson's two-hit" in the Nihon rat [12, 27].

BHD is a rare autosomal dominant disease characterized by the development of fibrofolliculoma, trichodiscoma, or acrochordon, first described in 1977 [4]. BHD families also have other phenotypic features, including RCC development, pulmonary cysts, and/or spontaneous pneumothorax [4, 25, 29, 41, 44]. Several histopathological variants of RCC, including chromophobe RCC (34%), hybrid of oncocytic neoplasms consisting of chromophobe RCC, and oncocytoma (50%), as well as conventional (clear cell) RCC (9%), have been described in the BHD, whereas RCC in Von Hippel–Lindau disease are always composed of clear cells [21, 29]. The *BHD* gene has been mapped to chromosome 17p11.2, identified, and is known to encode mRNA for a novel protein called folliculin [25]. A canine model for BHD has also been described in German Shepherd dogs where hereditary multifocal renal cystadenocarcinomas, nodular dermatofibrosis, and uterine leiomyoma are naturally occurring [22]. The renal tumors in the dogs are primarily chromophobic and oncocytoma types and histologically similar to RCCs in human BHD cases [22].

In the Nihon rat, the histologic variant of RCC still remains to be investigated, and extrarenal lesions have hitherto not been described. The present work was conducted to characterize RCC and extrarenal lesions of the Nihon rat and to compare the phenotypes with those in the human BHD syndrome.

Materials and methods

Rats

All procedures involving rats were performed in accordance with institutional animal care guidelines established following the Association for Assessment and Accreditation of Laboratory Animal Care International.

Offsprings were obtained by brother–sister mating of male and female heterozygous rats or of male heterozygous and female wild-type rats. Phenotypic expression was determined for these rats by gross or histologic examinations of the kidney since genotypic expression has been assured to be consistent with phenotypic expression when the kidneys were grossly or histologically examined [12]. Among the offsprings, 179 rats (39 and 27 wild-type male and female rats, respectively, and 53 and 60 heterozygous male and female rats, respectively) were used at 55 weeks of age for assessment of histological and biological features of preneoplastic lesions and RCCs of the kidneys and extrarenal lesions (group I). As for cardiac lesions, another 188 offsprings obtained during weeks 9–68 of age (25 and 38 wild-type male and female rats, respectively, and 64 and 61 heterozygous male and female rats, respectively) were subjected for evaluation (group II).

Clinical features

For group I, body weights were measured once in 2 months, and the blood and plasma were evaluated for hematological and biochemical findings, respectively, at necropsy at week 55 using a THMS H.1 (Bayer Medical Ltd.) and a 7170 automatic analyzer (Hitachi, Ltd.), respectively.

Necropsy

All rats in groups I and II were anesthetized with sodium pentobarbital (50 mg/kg body weight, i.p.), exsanguinated, and necropsied. Kidney weights were measured at week 55 of age in group I.

Histopathology

All organs in group I and the hearts in group II were fixed in 10% buffered formalin, and slices were embedded in paraffin. Histological sections were cut at 3 μm and stained with hematoxylin and eosin (H & E). The periodic acid–Schiff (PAS) reaction, Hale's colloidal iron, and immunohistochemical stainings were also applied for the kidneys and the PAS reaction and Hale's colloidal iron staining for the uterus, salivary gland, and heart. Immunohistochemical staining was performed according to standard procedures using mouse monoclonal anti-human cytokeratin (clone: AE1 + AE3, DakoCytomation, Japan) and mouse monoclonal anti-swine vimentin (DakoCytomation) primary antibodies. The renal lesions were grouped into four stages: altered tubule, atypical hyperplasia, adenoma, and carcinoma. The cell types of the renal lesions were classified as clear/acidophilic, acidophilic, basophilic, chromophobic, and oncocytic following the nomenclature of Bannasch [3].

Electron microscopy

Small cubes of the RCCs were fixed in buffered 2.5% glutaraldehyde, postfixed in 1% osmium tetroxide, and embedded in Epon. Ultrathin sections were cut, contrasted with uranyl acetate and lead citrate, and examined using a Hitachi 7600 transmission electron microscope (Hitachi High-Technologies Co.).

Statistical analysis

Data are presented as mean±SD, with statistical analysis by the Student's t test at $P<0.05$ for body weights, hematology, blood chemistry, and kidney weights.

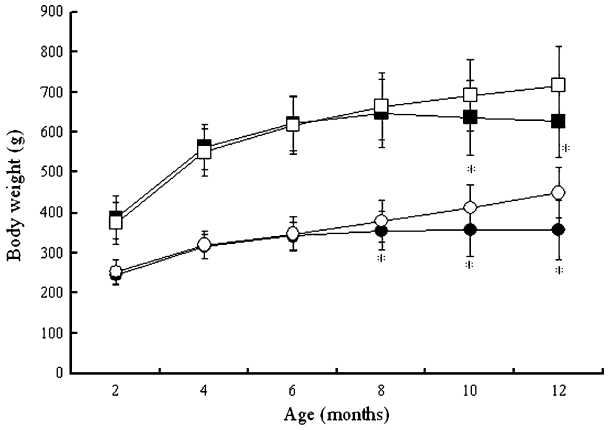

Fig. 1 Body weight curves for normal (rats without RCCs) and heterozygous (rats with RCCs) rats. Mean body weights are expressed as mean±SD as compared to age-matched normal rats (*, P<0.05). Open square (□), solid square (■), open circle (○) and solid circle (●) indicate normal males, heterozygous males, normal females and heterozygous females, respectively

Results

Clinical feature

In group I, 14 of 53 and 10 of 60 heterozygous male and female rats, respectively, were found dead or euthanized in extremis during weeks 42–53 of age. For these rats, primary signs included emaciation, anemia, and hematuria, and body weight gain declined from 8 months of age (Fig. 1). Decreased erythrocyte counts and increased leukocyte and platelet counts (Fig. 2a–c) and elevated urea nitrogen and creatinine (Fig. 2d,e) were the findings of hematology and blood chemistry, respectively.

Gross findings

In both groups I and II, heterozygous rats had bilaterally multiple cysts and white nodules on the surface of kidneys. The normal renal parenchyma was replaced in some heterozygous rats by large nodules or cysts filled with sero-

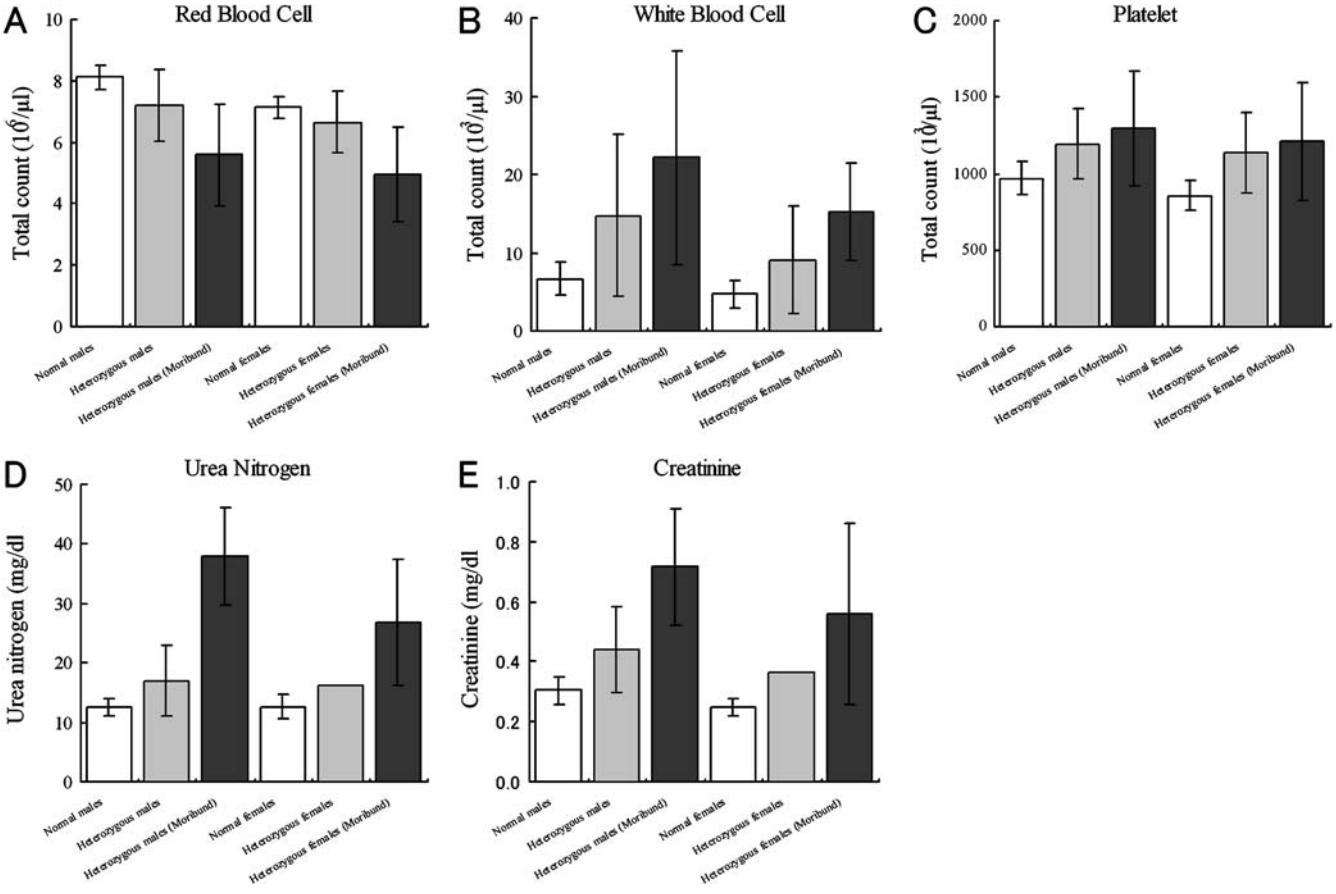

Fig. 2 Hematology and blood chemistry data for normal (rats without RCCs) and heterozygous (rats with RCCs) rats. The total red blood cell count (**a**), total white blood cell count (**b**), total platelet count (**c**), plasma urea nitrogen (**d**), plasma creatinine (**e**) from normal (open bars) and heterozygous (semi-solid bars) rats, as well as heterozygous rats euthanized in extremis (solid bars) are expressed as mean±SD values (*, P<0.05)

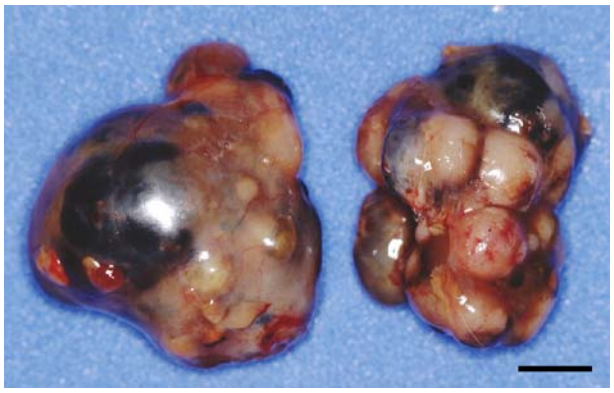

Fig. 3 Gross appearance of kidney in a Nihon rat (rat with RCCs). A 55-week-old heterozygous rat. Multiple large white to tan nodules and cysts filled with blood have replaced the normal kidney parenchyma. Scale bar: 1 cm

sanguinous fluid (Fig. 3). In group I, the kidney weights of the wild-type male and female rats were 3.4±0.4 and 2.3±0.3 g, respectively, and those of the heterozygous male and female rats reached 19.3±16.3 g (3.3–59.4 g, $P<0.05$) and 8.7±7.2 g (2.1–35.4 g, $P<0.05$). Large RCCs occasionally adhered to surrounding organs, but no metastatic lesions were evident in any of the rats.

Histopathology

RCC

In group I, RCCs had developed in 63 of 93 (68%) offsprings derived from mating of male and female heterozygous rats and in 50 of 86 (58%) offsprings derived from mating of male heterozygous rats and wild-type female rats. These incidences were those expected in Nihon rats according to Mendelian inheritance. Altered tubule, atypical hyperplasia, adenoma, and carcinoma, the findings being peculiar to Nihon rats, were observed in the kidneys of heterozygous rats (Fig. 4a–d). These lesions developed at the multiple sites and were scattered throughout the renal cortex and outer medulla in both the kidneys. The growth manners of the adenomas and carcinomas were variable, with tubular, solid, cystic, or cystic–papillary patterns observed.

Altered tubules, considered to be the initial stage of development of RCCs, were defined as a single or clusters of tubules lined by hypertrophic clear or acidophilic epithelium, the former being characterized by unstained cytoplasm and eccentrically located hyperchromatic small nuclei and the latter by centrally located nuclei, distinct cell membranes, and granular and/or vesicular cytoplasm. The altered tubules of clear cell type were often continuous with the collecting duct (Fig. 4a).

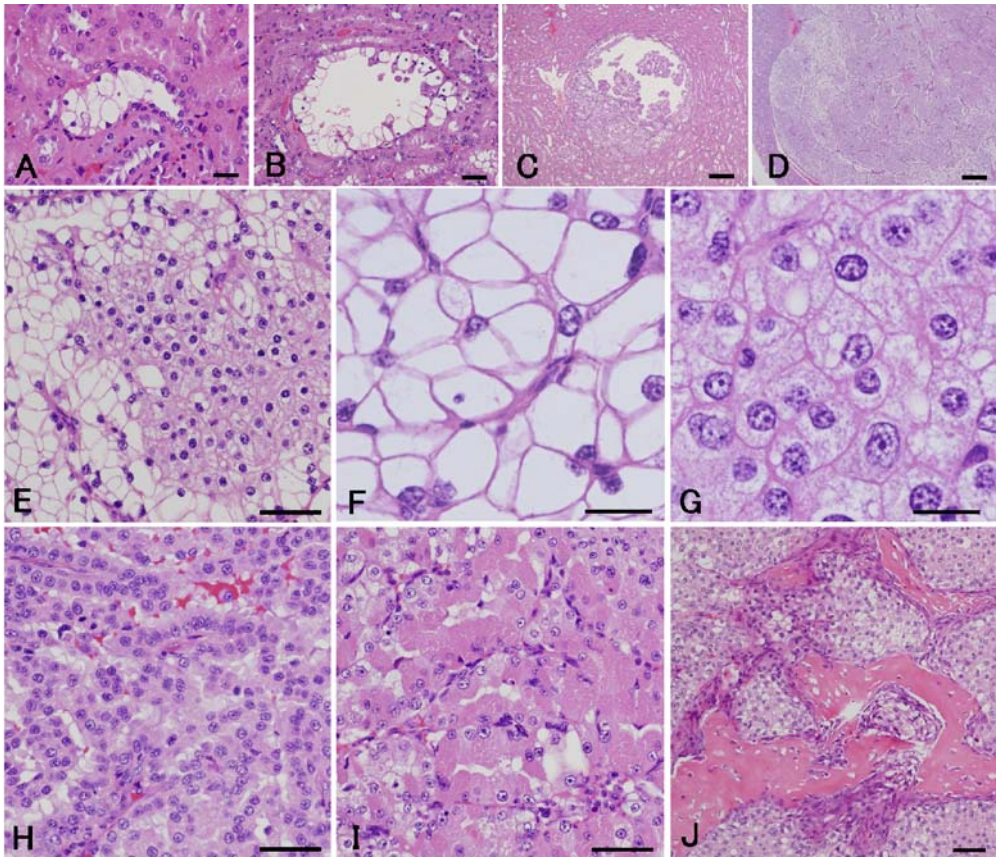

Fig. 4 Renal histopathology in Nihon rats (rats with RCCs). **a**: An altered tubule composed of clear cells continuous with a collecting duct (H.E.; Scale bar, 20 μm). **b**: An atypical hyperplasia composed of clear cells and acidophilic cells (H.E.; Scale bar, 50 μm). **c**: An adenoma showing papillary growth composed of acidophilic cells (H.E.; Scale bar, 200 μm). **d**: A carcinoma showing a large nodule (H.E.; Scale bar, 400 μm). **e**: A carcinoma composed of mixed population of clear and acidophilic cells (H.E.; Scale bar, 50 μm). **f**: High magnification of clear cells with abundant clear cytoplasm and small eccentric nuclei (H.E.; Scale bar, 20 μm). **g**: High magnification of acidophilic cells with acidophilic granular cytoplasm (H.E.; Scale bar, 20 μm). **h**: Basophilic cells with basophilic cytoplasm in a papillary lesion. **i**: Oncocytic cells with abundant acidophilic granular cytoplasm (H.E.; Scale bar, 50 μm). **j**: Heterotopic ossification with mature bone in a clear/acidophilic RCC (H.E.; Scale bar, 50 μm)

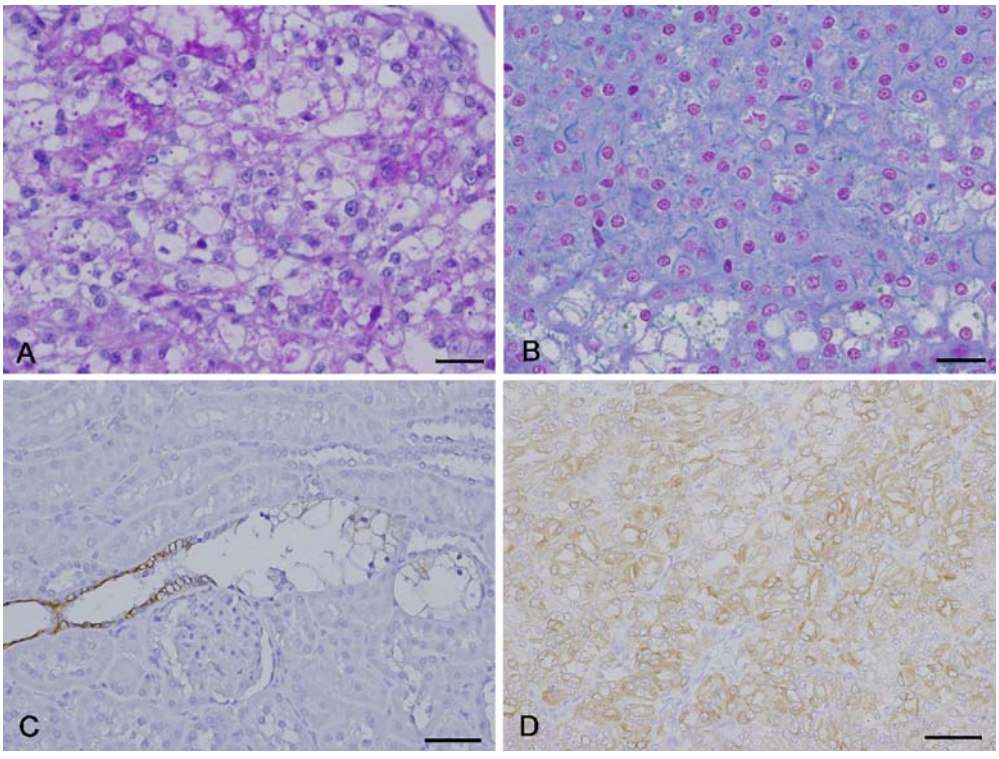

Fig. 5 Special stainings and immunohistochemistry of RCCs in Nihon rats. **a**: Clear cells are partially positive for PAS reaction (Scale bar, 20 μm). **b**: Acidophilic cells are positive for Hale's colloidal iron staining (Scale bar, 20 μm). **c**: Clear cells and epithelial cells of a collecting duct are immunoreactive for cytokeratin (Scale bar, 50 μm). **d**: Neoplastic cells in a RCC are immunoreactive for cytokeratin (Scale bar, 50 μm)

These tinctrial features of the altered tubules were maintained across the development through RCCs. It appeared, however, in most lesions that monomorphic population of clear or acidophilic cell type found in the altered tubules shifted to mixed population of these cell types along with the development of RCCs. It was often noted that clear cells were arranged along the periphery of the lesions, and acidophilic cells occupied the center of the lesions (Fig. 4e–g). RCCs composed exclusively either of clear or acidophilic cell type were uncommon. There were also lesions consisting of basophilic cells or oncocytic cells at a low incidence. The basophilic cell types were only occasionally noted in focal areas of RCCs in the papillary form (Fig. 4h), and oncocytic cells were few in any form of RCCs (Fig. 4i).

PAS reaction revealed the cytoplasm of clear cells to be partially positive (Fig. 5a) and that of acidophilic cells to be positive for Hale's colloidal iron staining (Fig. 5b). The RCCs were immunoreactive for cytokeratin (Fig. 5c,d), irrespective of cell types or growth manner, whereas they were uniformly non-immunoreactive for vimentin (data not shown).

In addition to the renal component, heterotopic ossification was evident within 37 of 113 RCCs found at 55 weeks of age. This change was limited to the clear/acidophilic RCCs with a solid form (Fig. 4j) and showed the whole spectrum of osteogenesis, including the presence of osteoblasts, deposition of osteoid, mature bone formation with bone marrow, and remodeling by osteoclasts.

Vascular lesions

Heterozygous rats had vascular lesions in various organs. Although the total incidence reached 21 of 113 heterozygous rats, 14 among these 21 rats were found dead or euthanized in extremis. Primary lesions consisted of thickening of the arteriolar wall in the kidney, mesentery, testis, spleen, and heart, often accompanied by advanced vascular lesions, consistent with periarteritis nodosa in the four former organs (data not shown).

Table 1 Incidence data for extrarenal lesions: uterus and salivary gland

	Male		Female		Total	
	Normal	Heterozygote	Normal	Heterozygote	Normal	Heterozygote
Uterus						
Clear cell hyperplasia/adenoma	NA	NA	0/27 (0%)	18/60 (30%)	0/27 (0%)	18/60 (30%)
Salivary gland						
Clear cell change	0/39 (0%)	3/53 (6%)	0/27 (0%)	12/60 (20%)	0/27 (0%)	15/113 (13%)

Number of rats with the lesion per total number of rats
NA Not applicable

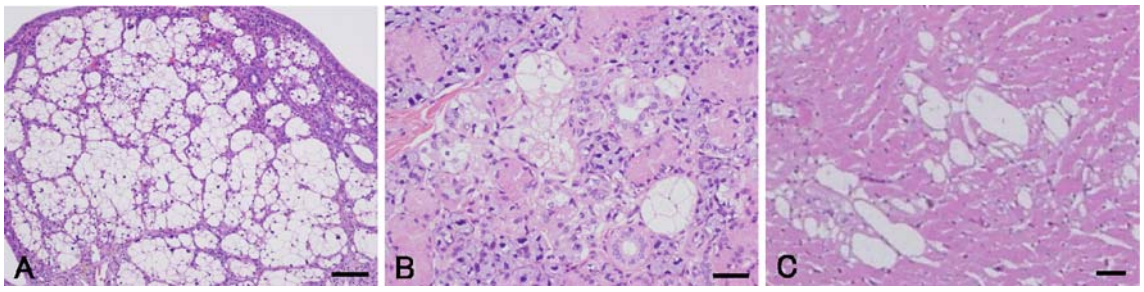

Fig. 6 Histopathology of extrarenal lesions in Nihon rats. **a**: A clear cell adenoma of the endometrium of the uterus (H.E.; Scale bar, 100 μm). **b**: Clear cell changes of the epithelium of the striated portion in the salivary gland (H.E.; Scale bar, 50 μm). **c**: Cardiac rhabdomyomatosis (H.E.; Scale bar, 50 μm)

Extrarenal lesions

Upon detailed microscopic examinations of all the organs and tissues, three distinctive extrarenal lesions besides RCCs were found in heterozygous rats: (a) clear cell hyperplasia/adenoma of the endometrium; (b) clear cell change of the striated portion of the salivary gland; and (c) cardiac rhabdomyomatosis, all the findings being absent in normal rats.

(a) Clear cell hyperplasia/adenoma of the endometrium of the uterus
The lesion was observed in 18 of 60 heterozygous females (Table 1). Histologically, the initial lesion consisted of the endometrial gland with irregularly arranged clear cells that had PAS-reactive and Hale's colloidal iron staining negative clear cytoplasm and eccentrically located hyperchromatic nuclei, features resembling clear cells in RCCs. These lesions extended across the endometrium to form large nests of clear cells with occasional nodular projections into the glandular and uterine lumen, consistent with adenoma development (Fig. 6a). No mitotic figures were found in any of the lesions.

(b) Clear cell change of the striated portion of the salivary gland
The epithelium of the striated portion of the salivary gland also demonstrated cluster of clear cells with PAS-reactive and Hale's colloidal iron staining negative cytoplasm and eccentrically located hyperchromatic nuclei, at an incidence of 15 of 113 heterozygous rats (Table 1). The lesion was usually multifocal; however, it never became morphologically neoplastic (Fig. 6b).

(c) Cardiac rhabdomyomatosis
Cardiac rhabdomyomatosis was found in 15 of 125 heterozygous rats (Table 2). Young heterozygous rats were more predisposed to the lesions; the incidence for rats in the age ranges of 9–13, 14–26, 27–52, and 53–68 weeks were 9/26, 4/50, 2/15, and 0/34, respectively (Table 2). Lesions were found in the right and left ventricular walls and/or septum and were histologically characterized by multifocal clusters of clear cells with PAS-reactive and Hale's colloidal iron staining negative cytoplasm and eccentrically located hyperchromatic nuclei (Fig. 6c). The spider cells described for human cardiac rhabdomyoma were occasionally present within the lesions. There was no evidence of neoplasia, and no mitotic figures were apparent.

Electron microscopy

Common architectural findings among all the clear, acidophilic, and basophilic cell types of renal lesion included intermediate junctions, interdigitations, and microvilli at the luminal cell surface (Fig. 7c, d). In addition, the cytoplasm of the clear cells was occupied in large part by monoparticulate glycogen that accounted for the clear appearance in paraffin-embedded sections (Fig. 7a). Also noted in the clear cells were a few mitochondria, lysosomes, and lipid droplets in the rim of remaining cytoplasm (Fig. 7a). The acidophilic cells had similar organelles and characteristic lamellar bodies in various proportions, the monoparticulate glycogen being less predominant (Fig. 7b). In the some acidophilic cells, intracytoplasmic lumina with several microvilli were also observed (Fig. 7c). Large

Table 2 Incidence data for cardiac rhabdomyomatosis

Age (weeks)	Male		Female		Total	
	Normal	Heterozygote	Normal	Heterozygote	Normal	Heterozygote
9–13	0/8 (0%)	7/19 (37%)	0/11 (0%)	2/7 (29%)	0/19 (0%)	9/26 (35%)
14–26	0/6 (0%)	2/23 (9%)	0/11 (0%)	2/27 (7%)	0/17 (0%)	4/50 (8%)
27–52	0/2 (0%)	0/7 (0%)	0/6 (0%)	2/8 (25%)	0/8 (0%)	2/15 (13%)
53–68	0/9 (0%)	0/15 (0%)	0/10 (0%)	0/19 (0%)	0/19 (0%)	0/34 (0%)

Number of rats with the lesion per total number of rats

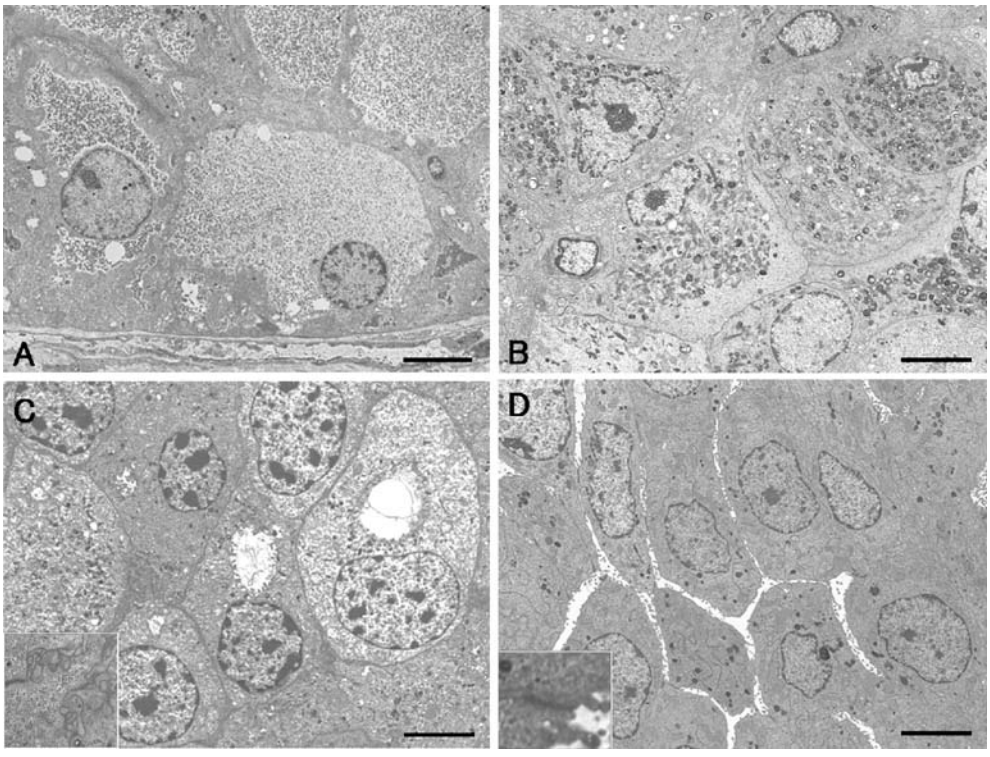

Fig. 7 Electronmicroscopy of RCCs in Nihon rats. **a**: Clear cells have abundant monoparticulate glycogen, a few mitochondria, lysosomes and lipid droplet in the cytoplasm. **b** and **c**: Acidophilic cells have various numbers of mitochondria, concentric lamella structures and intracytoplasmic lumen lined with microvilli. The inset in C shows interdigitations. **d**: Basophilic cells have abundant rough endplasmic reticulum, free and membrane-bound ribosomes, and scattered mitochondria and lysosomes. Microvilli are observed at the surface of the cytoplasm. The inset in D shows a intermediate junction. Scale bars: 5μm

amount of rough endoplasmic reticulum and free and membrane-bound ribosomes were features of the basophilic cells (Fig. 7d).

Discussion

In the Nihon rat, the initial stage of RCCs represented by altered tubules was found to appear at as early as 3 weeks of age and rapidly progressed to frank neoplasms by 8 weeks of age with high penetrance [17]. The onset of these lesions clearly distinguishes the Nihon from the Eker rat where preneoplastic lesions first occur at 2 months and adenomas at 1 year of age [9–11]. Genotypic analysis also demonstrated a difference between the two rat RCC models. The *Tsc2* tumor suppressor gene has been shown to be responsible for development of RCCs in the Eker rat, whereas the *Bhd* gene is involved in the Nihon rat [16, 27]. These distinct features warrant consideration of this latter animal as a novel model of hereditary RCC.

The Nihon rat model and human BHD exhibit similarities in various aspects, the most notable being the causative gene mutation. The predisposing gene for the human BHD is reported to be located on chromosome 17p11.2 in the germline of patients [25]. The susceptibility gene of the RCC in the Nihon rat has been mapped to distal rat chromosome 10, syntenic with several human chromosome segments including chromosome 17p11.2, and a germline single nucleotide insertion has been identified in the rat *Bhd* ortholog [12, 16, 27].

The second similarity involves phenotypic expression during RCC development. However, there are dissimilarities as well as similarities in the cytologic features between RCCs in human and the Nihon rat. One of the predominant types of RCC in the BHD syndrome is chromophobic, which is further subclassified into granular (type I cells), eosinophilic granular with perinuclear halos (type II cells), and clear cytoplasm (type III cells) [2, 29, 41]. Chromophobic RCCs, unlike conventional RCCs, contain abundant mucopolysaccharides that react positively with Hale's colloidal iron [5, 36, 38]. Although they are immunoreactive for cytokeratin, they are negative for vimentin [5, 6, 15, 20, 23]. Ultrastructurally, the RCCs are characterized by numerous cytoplasmic microvesicles, which are thought to arise from outpouchings of the mitochondria [19, 37, 39]. In the Nihon rat, morphologic findings for RCCs are in many aspects consistent with human counterparts of chromophobic type. They include unstained clear cytoplasm under H & E-stained sections, reactivity to Hale's colloidal iron, immunoreactivity for cytokeratin, and non-immunoreactivity for vimentin. However, at the electron microscope level, intracytoplasmic microvesicles are only present in human RCCs and abundant monoparticulate glycogen only in the Nihon rats.

The cytogenetic origin of RCCs is also most likely to be common in both human and Nihon rat kidneys. One of the characteristic features of RCCs in the Nihon rat is that altered tubules often merge into normal cortical or medullary collecting duct, strongly suggesting an origin from the epithelium of the collecting duct system. This notion is

further strengthened by the fact that RCCs were immunoreactive to cytokeratin and not vimentin, consistent with normal collecting duct. It has also been reported that chromophobic RCCs and oncocytomas common in BHD originate from intercalated cells of renal collecting tubules and distal tubules, respectively [1, 33, 34].

In contrast to these similarities, the skin and lung were within normal limit in the Nihon rat unlike in BHD syndrome where fibrofolliculoma and pulmonary cysts or pneumothorax, respectively, are reported to occur.

It is of interest to note additional distinctive lesions in the Nihon rat. Heterotropic ossification was associated with RCCs at approximately 30%, the finding and incidence being unexpected. Ossification also occurs within RCCs in humans though only at a low incidence [32]. The extrarenal lesions including clear cell hyperplasia/adenoma of the endometrium of the uterus, clear cell change of the epithelium of striated portion in the salivary gland, and cardiac rhabdomyomatosis are of types rarely found as spontaneous change in rats. All three lesions as well as RCCs share the finding of clear cell alteration despite occurring in different organ system. Another phenotypic similarity between Nihon rats and human BHD syndrome is present in the salivary gland where salivary (parotid) oncocytoma of clear cell variant has been reported in human [28]. Although the *BHD* gene product, folliculin, has no known function at present, it may play a role in clear cell alteration in the Nihon rat [25].

Approximately 20% of the Nihon rats were found dead or needed to be euthanized in extremis before the age of 1 year, with severe anemia or renal dysfunction as the most likely responsible causes, reflecting hemorrhage from hematomas within RCCs and the replacement of the normal renal parenchyma, respectively. These observations suggest malignant biologic behavior of the renal cell tumor of the Nihon rat, even though no metastasis have so far been observed, unlike the human RCC case where metastasis is reported to occur in nearly 30% [24]. In addition, the vascular lesions noted in the Nihon rat found dead or euthanized in extremis strongly indicated a hypertensive status. Hypertension is subdivided into essential and secondary types [31]. The former has no known cause, while the latter has an identifiable cause such as renal artery stenosis and renal parenchymal disease [31]. Thus, it is likely that large nodules or cysts of RCCs lead to the secondary hypertension in the Nihon rat, resulting ultimately in death.

In conclusion, we have established the Nihon rat model of hereditary RCC and, in this communication, document characterization of phenotypic and genotypic aspects in comparison with human BHD syndrome. The Nihon rat will provide a useful tool for analyzing the series of events that lead to renal tumorigenesis and for studying *BHD* gene function.

Acknowledgements We thank Drs. Toshiyuki Kobayashi and Kazuyasu Kijima for their help. This work was supported by a Grant-in-Aid for Cancer Research and Grant-in-Aid for Scientific Research from the Ministry of Education, Culture, Sports, and Science and Technology of Japan and the Ministry of Health, Labour, and Welfare of Japan.

References

1. Aizawa S, Kikuchi Y, Suzuki M, Furusato M (1987) Renal cell carcinoma of lower nephron origin. Acta Pathol Jpn 37: 567–574
2. Akhtar M, Kardar H, Linjawi T, McClintock J, Ali MA (1995) Chromophobe cell carcinoma of the kidney. A clinicopathologic study of 21 cases. Am J Surg Pathol 19:1245–1256
3. Bannash P, Zerban H (1968) Renal cell adenoma and carcinoma, rat. In: Jones TC, Mohr U, Hunt RD (eds) Monographs on pathology of laboratory animals. Springer, Berlin Heidelberg New York, pp 112–139
4. Birt AR, Hogg GR, Dube WJ (1977) Hereditary multiple fibrofolliculomas with trichodiscomas and acrochordons. Arch Dermatol 113:1674–1677
5. Cochand-Priollet B, Molinie V, Bougaran J, Bouvier R, Dauge-Geffroy MC, Deslignieres S, Fournet JC, Gros P, Lesourd A, Saint-Andre JP, Toublanc M, Vieillefond A, Wassef M, Fontaine A, Groleau L (1997) Renal chromophobe cell carcinoma and oncocytoma. A comparative morphologic, histochemical, and immunohistochemical study of 124 cases. Arch Pathol Lab Med 121:1081–1086
6. Cohen C, McCue PA, Derose PB (1988) Histogenesis of renal cell carcinoma and renal oncocytoma. An immunohistochemical study. Cancer 62:1946–1951
7. Eker R (1954) Familial renal adenomas in Wistar rats; a preliminary report. Acta Pathol Microbiol Scand 34:554–562
8. Eker R (1961) A dominant gene for renal adenomas in the rat. Nature 189:858–859
9. Everitt JI, Goldsworthy TL, Wolf DC, Walker CL (1992) Hereditary renal cell carcinoma in the Eker rat: a rodent familial cancer syndrome. J Urol 148:1932–1936
10. Hino O, Klein-Szanto AJ, Freed JJ, Testa JR, Brown DQ, Vilensky M, Yeung RS, Tartof KD, Knudson AG (1993) Spontaneous and radiation-induced renal tumors in the Eker rat model of dominantly inherited cancer. Proc Natl Acad Sci U S A 90:327–331
11. Hino O, Fukuda T, Satake N, Kobayashi T, Honda S, Orimoto K, Yamashita Y, Kikuchi Y (1999) TSC2 gene mutant (Eker) rat model of a Mendelian dominantly inherited cancer. Prog Exp Tumor Res 35:95–108
12. Hino O, Okimoto K, Kouchi M, Sakurai J (2001) A novel renal carcinoma predisposing gene of the Nihon rat maps on chromosome 10. Jpn J Cancer Res 92:1147–1149
13. The European Chromosome 16 Tuberous Sclerosis Consortium (1993) Identification and characterization of the tuberous sclerosis gene on chromosome 16. Cell 75:1305–1315
14. Jemal A, Tiwari RC, Murray T, Ghafoor A, Samuels A, Ward E, Feuer EJ, Thun MJ (2004) American Cancer Society. Cancer statistics, 2004. CA Cancer J Clin 54:8–29
15. Kim MK, Kim S (2002) Immunohistochemical profile of common epithelial neoplasms arising in the kidney. Appl Immunohistochem Mol Morphol 10:332–338
16. Kobayashi T, Hirayama Y, Kobayashi E, Kubo Y, Hino O (1995) A germline insertion in the tuberous sclerosis (Tsc2) gene gives rise to the Eker rat model of dominantly inherited cancer. Nat Genet 9:70–74

17. Kouchi M, Okimoto K, Kikawa E, Toyosawa K, Koujitani T, Kuroki K, Tanaka K, Matsuoka N, Hino O (2001) "Nihon rat", a novel rat model for renal cell carcinoma. Proc Jpn Animal Models Human Dis 17:16–19
18. Kovacs G, Akhtar M, Beckwith BJ, Bugert P, Cooper CS, Delahunt B, Eble JN, Fleming S, Ljungberg B, Medeiros LJ, Moch H, Reuter VE, Ritz E, Roos G, Schmidt D, Srigley JR, Storkel S, van den Berg E, Zbar B (1997) The Heidelberg classification of renal cell tumours. J Pathol 183:131–133
19. Krishnan B, Truong LD (2002) Renal epithelial neoplasms. The diagnostic implications of electron microscopic study in 55 cases. Hum Pathol 33:68–79
20. Langner C, Wegscheider BJ, Ratschek M, Schips L, Zigeuner R (2004) Keratin immunohistochemistry in renal cell carcinoma subtypes and renal oncocytomas: a systematic analysis of 233 tumors. Virchows Arch 444:127–134
21. Latif F, Tory K, Gnarra J, Yao M, Duh FM, Orcutt ML, Stackhouse T, Kuzmin I, Modi W, Geil L, Schmidt L, Zhou FW, Li H, Wei MH, Chen F, Glenn G, Choyke P, Walther MM, Weng YK, Duan DSR, Dean M, Glavac D, Richards FM, Crossey PA, Ferguson-Smith MA, Lepaslier D, Chumakov I, Cohen D, Chinault AC, Maher ER, Linehan WM, Zbar B, lErman MI (1993) Identification of the von Hippel–Lindau disease tumor suppressor gene. Science 260:1317–1320
22. Lingaas F, Comstock KE, Kirkness EF, Sorensen A, Aarskaug T, Hitte C, Nickerson ML, Moe L, Schmidt LS, Thomas R, Breen M, Galibert F, Zbar B, Ostrander EA (2003) A mutation in the canine BHD gene is associated with hereditary multifocal renal cystadenocarcinoma and nodular dermatofibrosis in the German Shepherd dog. Hum Mol Genet 12:3043–3053
23. Martignoni G, Pea M, Brunelli M, Chilosi M, Zamo A, Bertaso M, Cossu-Rocca P, Eble JN, Mikuz G, Puppa G, Badoual C, Ficarra V, Novella G, Bonetti F (2004) CD10 is expressed in a subset of chromophobe renal cell carcinomas. Mod Pathol 17:1455–1463
24. Motzer RJ, Bander NH, Nanus DM (1996) Renal-cell carcinoma. N Engl J Med 335:865–875
25. Nickerson ML, Warren MB, Toro JR, Matrosova V, Glenn G, Turner ML, Duray P, Merino M, Choyke P, Pavlovich CP, Sharma N, Walther M, Munroe D, Hill R, Maher E, Greenberg C, Lerman MI, Linehan WM, Zbar B, Schmidt LS (2002) Mutations in a novel gene lead to kidney tumors, lung wall defects, and benign tumors of the hair follicle in patients with the Birt–Hogg–Dubé syndrome. Cancer Cell 2:157–164
26. Okimoto K, Kouchi M, Kikawa E, Toyosawa K, Koujitani T, Tanaka K, Matsuoka N, Sakurai J, Hino O (2000) A novel "Nihon" rat model of a Mendelian dominantly inherited renal cell carcinoma. Jpn J Cancer Res 91:1096–1099
27. Okimoto K, Sakurai J, Kobayashi T, Mitani H, Hirayama Y, Nickerson ML, Warren MB, Zbar B, Schmidt LS, Hino O (2004) A germ-line insertion in the Birt–Hogg–Dubé (BHD) gene gives rise to the Nihon rat model of inherited renal cancer. Proc Natl Acad Sci U S A 101:2023–2027
28. Liu V, Kwan T, Page EH (2000) Parotid oncocytoma in the Birt–Hogg–Dube syndrome. J Am Acad Dermatol 43: 1120–1122
29. Pavlovich CP, Walther MM, Eyler RA, Hewitt SM, Zbar B, Linehan WM, Merino MJ (2002) Renal tumors in the Birt–Hogg–Dubé syndrome. Am J Surg Pathol 26:1542–1552
30. Schmidt L, Duh FM, Chen F, Kishida T, Glenn G, Choyke P, Scherer SW, Zhuang Z, Lubensky I, Dean M, Allikmets R, Chidambaram A, Bergerheim UR, Feltis JT, Casadevall C, Zamarron A, Bernues M, Richard S, Lips CJ, Walther MM, Tsui LC, Geil L, Orcutt ML, Stackhouse T, Zbar B (1997) Germline and somatic mutations in the tyrosine kinase domain of the MET proto-oncogene in papillary renal carcinomas. Nat Genet 16:68–73
31. Schoen RJ, Cotran RS (1999) Blood vessels. In: Cotran RS, Kumar V, Collins T (eds) Robbins pathologic basis of disease. Saunders, Philadelphia, pp 493–542
32. Sostre G, Johnson JF III, Cho M (1998) Ossifying renal cell carcinoma. Pediatr Radiol 28:458–460
33. Storkel S, Pannen B, Thoenes W, Steart PV, Wagner S, Drenckhahn D (1988) Intercalated cells as a probable source for the development of renal oncocytoma. Virchows Arch B Cell Pathol Incl Mol Pathol 56:185–189
34. Storkel S, Steart PV, Drenckhahn D, Thoenes W (1989) The human chromophobe cell renal carcinoma: its probable relation to intercalated cells of the collecting duct. Virchows Arch B Cell Pathol Incl Mol Pathol 56:237–245
35. Storkel S, Eble JN, Adlakha K, Amin M, Blute ML, Bostwick DG, Darson M, Delahunt B, Iczkowski K (1997) Classification of renal cell carcinoma: Workgroup No. 1. Union Internationale Contre le Cancer (UICC) and the American Joint Committee on Cancer (AJCC). Cancer 80:987–989
36. Thoenes W, Storkel S, Rumpelt HJ (1985) Human chromophobe cell renal carcinoma. Virchows Arch B Cell Pathol Incl Mol Pathol 48:207–217
37. Thoenes W, Storkel S, Rumpelt HJ, Moll R, Baum HP, Werner S (1988) Chromophobe cell renal carcinoma and its variants—a report on 32 cases. J Pathol 155:277–287
38. Tickoo SK, Amin MB, Zarbo RJ (1998) Colloidal iron staining in renal epithelial neoplasms, including chromophobe renal cell carcinoma: emphasis on technique and patterns of staining. Am J Surg Pathol 22:419–424
39. Tickoo SK, Lee MW, Eble JN, Amin M, Christopherson T, Zarbo RJ, Amin MB (2000) Ultrastructural observations on mitochondria and microvesicles in renal oncocytoma, chromophobe renal cell carcinoma, and eosinophilic variant of conventional (clear cell) renal cell carcinoma. Am J Surg Pathol 24:1247–1256
40. Tomlinson IP, Alam NA, Rowan AJ, Barclay E, Jaeger EE, Kelsell D, Leigh I, Gorman P, Lamlum H, Rahman S, Roylance RR, Olpin S, Bevan S, Barker K, Hearle N, Houlston RS, Kiuru M, Lehtonen R, Karhu A, Vilkki S, Laiho P, Eklund C, Vierimaa O, Aittomaki K, Hietala M, Sistonen P, Paetau A, Salovaara R, Herva R, Launonen V, Aaltonen LA (2002) Germline mutations in FH predispose to dominantly inherited uterine fibroids, skin leiomyomata and papillary renal cell cancer. Nat Genet 30:406–410
41. Toro JR, Glenn G, Duray P, Darling T, Weirich G, Zbar B, Linehan M, Turner ML (1999) Birt–Hogg–Dubé syndrome: a novel marker of kidney neoplasia. Arch Dermatol 135: 1195–1202
42. van Slegtenhorst M, de Hoogt R, Hermans C, Nellist M, Janssen B, Verhoef S, Lindhout D, van den Ouweland A, Halley D, Young J, Burley M, Jeremiah S, Woodward K, Nahmias J, Fox M, Ekong R, Osborne J, Wolfe J, Povey S, Snell RG, Cheadle JP, Jones AC, Tachataki M, Ravine D, Shampson JR, Reeve MP, Richardson P, Wilmer F, Munro C, Hawkins TL, Stepp T, Ali JBM, Ward S, Green AJ, Yates JRW, Kwiatkowska J, Henske EP, Short MP, Haines JH, Jozwiak S, Kwiatkowski DJ (1997) Identification of the tuberous sclerosis gene TSC1 on chromosome 9q34. Science 277:805–808
43. Weirich G, Glenn G, Junker K, Merino M, Storkel S, Lubensky I, Choyke P, Pack S, Amin M, Walther MM, Linehan WM, Zbar B (1998) Familial renal oncocytoma: clinicopathological study of 5 families. J Urol 160:335–340
44. Zbar B, Alvord WG, Glenn G, Turner M, Pavlovich CP, Schmidt L, Walther M, Choyke P, Weirich G, Hewitt SM, Duray P, Gabril F, Greenberg C, Merino MJ, Toro J, Linehan WM (2002) Risk of renal and colonic neoplasms and spontaneous pneumothorax in the Birt–Hogg–Dubé syndrome. Cancer Epidemiol Biomarkers Prev 11:393–400

Virchows Arch (2006) 448: 472–479
DOI 10.1007/s00428-005-0140-y

ORIGINAL ARTICLE

Luana Anjos-Ramos · Marcela S. Carneiro-Ramos · Gabriela P. Diniz · Joelcimar Martins-Silva · Maria Luiza Morais Barreto-Chaves

Early cardiac hypertrophy induced by thyroxine is accompanied by an increase in VEGF-A expression but not by an increase in capillary density

Received: 1 November 2005 / Accepted: 30 December 2005 / Published online: 27 January 2006

Abstract Cardiac hypertrophy in response to hyperthyroidism is well known. However, the effects on cardiac microcirculation are still controversial in this model. The present study evaluated the effects of acute administration of two different thyroxine (T4) dose levels on the angiogenic response in the myocardium. Capillary density (CD), the CD to fiber density (FD) ratio (CD/FD), and intercapillary distance (ICD) were assessed, as was ventricle weight (VW) to body weight (BW) ratio (VW/BW). Collagen I and III messenger ribonucleic acid (mRNA) expression and VEGF-A expression were also determined by reverse transcriptase polymerase chain reaction (RT-PCR). Immunohistochemical detection of proliferating cell nuclear antigen (PCNA) expression in endothelial cell nuclei was also carried out. We simulated an acute hyperthyroidism situation in male Wistar rats by daily intraperitoneal injection of T4 (0.025 or 0.1 mg kg^{-1} day^{-1}) for 7 days. Hemodynamic parameters showed that T4 did not alter systolic blood pressure (SBP) but significantly increased heart rate (HR). Both T4 doses significantly increased VW. Morphologically, the higher T4 dose resulted in a 33% greater myocardial mass, which was not accompanied by alterations in collagen I and III mRNA expression. The CD and CD/FD parameters were significantly lower in the hyperthyroid rats treated with the higher dose than in the control animals, and PCNA-labeling analysis indicated total absence of marked capillary growth. However, although the acute treatment with T4 did not induce any alteration in capillary number and endothelial cell proliferation, the vascular endothelial growth factor (VEGF)-A mRNA and protein expression were significantly increased with the higher T4 dose. These data indicate that the cardiac hypertrophy induced by acute treatment with thyroid hormone precedes the angiogenic process, which probably occurs later.

Keywords Hyperthyroidism · Cardiac microcirculation · Angiogenesis · Capillary growth · VEGF · Hypertrophy

L. Anjos-Ramos · G. P. Diniz · J. Martins-Silva · M. L. M. Barreto-Chaves (✉)
Laboratory of Cell Biology and Functional Anatomy, Department of Anatomy, Biomedical Sciences Institute, University of São Paulo,
Av. Prof. Lineu Prestes 2415,
Cidade Universitária, São Paulo, SP 05508-900, Brazil
e-mail: mchaves@usp.br
Tel.: +55-11-38159695
Fax: +55-11-30917366

M. S. Carneiro-Ramos
Department of Cell and Developmental Biology, Biomedical Sciences Institute, University of São Paulo,
Av. Prof. Lineu Prestes 2415,
Cidade Universitária, São Paulo, SP 05508-900, Brazil

Introduction

Adaptive growth of the heart in response to hypertrophic stimuli involves functional and morphological changes that are predictable depending upon the stimulus and its duration. In recent years, some studies have described the thyroid-hormone-induced cardiac hypertrophy and the characteristics that separate it from other hypertrophic models. However, the effect that thyroid-hormone-induced cardiac hypertrophy has on myocardial capillarization has not always been consistent [4, 7, 12]. Furthermore, considering that hyperthyroidism increases cardiac load, which leads to cardiac hypertrophy in many species, it is not clear in these studies if the thyroid-hormone-induced coronary vessel alteration is due to direct hormonal effects or is secondary to the hemodynamic effects, such as increasing the blood pressure. In a previous study conducted in our laboratory, we confirmed that acute hyperthyroidism is able to promote cardiac hypertrophy [14]. In this study, there was no difference in systolic blood pressure (SBP) between thyroxine (T4)-treated animals and control animals, indicating that the cardiac hypertrophy was not due to elevated hemodynamic parameters. In addition, using the same experimental model, we have recently showed that this cardiac hypertrophy is notably characterized by disorganization of intercellular junctions, suggesting damage for effective cardiac contraction [15].

In general, most models of cardiac hypertrophy are accompanied by an increase in the formation of new capillaries (angiogenesis) and this adaptative process is dependent and secondary to a net balance between molecules that have positive and negative regulatory activity [22]. Numerous inducers of angiogenesis have been identified, including members of the fibroblast growth factor (FGF) family, vascular endothelial growth factor (VEGF), platelet-derived growth factor, and others [25]. The modification of the expression or activity of one of the vascular growth factors will result in a functional dysbalance within the vessel wall, leading to vascular dysfunction [31]. Of these, VEGF-A, one functionally relevant growth factor, has been most carefully studied for its crucial role in vascular development, angiogenesis, collateral growth, and enhancement of collateral perfusion [1, 20]. In vivo, myocardial expression of VEGF-A is significantly augmented by ischemia or hypoxia and stretch [23]. Once VEGF-A increased, this factor is beneficial to the ischemic region as a therapeutic agent promoting collateral formation, indicating that VEGF-A exerts a potent effect on angiogenic response in cardiovascular disease [27]. Although the VEGF has been related to some hypertrophic processes [26], nothing is known about VEGF in hyperthyroidism-induced hypertrophy.

Because most types of cardiac hypertrophy are accompanied by an increase in vascularization and as hyperthyroidism promotes a rapid increase in cardiac mass, the present study was designed to assess the effects of two different acute dose levels of T4—0.025 and 0.1 mg/kg body weight (BW), for 7 days—on capillary density (CD) and also to evaluate the potential involvement of VEGF-A in this cardiac hypertrophy model.

Materials and methods

Animals

Male Wistar rats, weighing 200–260 g, were obtained from the Instituto de Ciências Biomédicas, University of São Paulo. All of the animals were cared for and handled according to National Institutes of Health guidelines.

The rats were housed in Plexiglas cages on a 12-h light/dark cycle and received a rat pellet diet and water ad libitum before and during the experiment. L-Thyroxine was purchased from Sigma (St. Louis, MO, USA). Rats were randomized into two hyperthyroid groups, T4-25 and T4-100. Hyperthyroidism was simulated in T4-25 and T4-100 rats by daily intraperitoneal injections of T4 (0.025 and 0.1 mg kg BW^{-1} day^{-1}, respectively) for 7 days. These doses have been described previously as sufficient to cause a significant augment in the circulating thyroxine levels [17]. Animals from the control group received daily intraperitoneal injections of saline. All rats were killed 24 h after their treatments. All surgical procedures and protocols were performed in accordance with the Ethical Principles in Animal Research set forth by the Brazilian College of Animal Experimentation and were approved by the Biomedical Sciences Institute/USP Ethics Committee for Animal Research.

Hemodynamic parameters

In all rats, SBP and heart rate (HR) were measured every 2 days at the same time of day by tail–cuff plethysmography (Kent Scientific, Litchfield, CT, USA). The rats were familiarized with the apparatus for 7 days before the taking of measurements. In addition, BW was measured daily. The final SBP and BW measurements were taken immediately before the rats were killed.

Heart preparation

After 1 week, the animals were deeply anesthetized with sodium pentobarbital (3.3 ml/kg, intraperitoneal) and the thorax was opened. The animals were then submitted to transcardiac perfusion with saline solution. Cardiac arrest in diastole was induced by perfusion of potassium chloride (14 mM), followed by a fixative solution of 10% paraformaldehyde. The perfusion pressure was maintained within the same range as that of the conscious animals. The heart was then quickly excised, all surrounding fat and connective tissue were removed, and the heart (minus the atrium) was weighed. The left ventricle (LV) was isolated from the right ventricle (RV) free wall, leaving the septum and LV intact. Both RV and LV were weighed separately. However, only the LV free wall was used for histological and quantitative analysis.

Ventricle hypertrophy was assessed by measurement of wet ventricle weight (VW), and the ratio of VW in milligrams to animal BW in grams (VW/BW, mg/g) was determined. Cardiac hypertrophy was confirmed by analyzing VW as dry weight (data not shown).

Microscopic studies

The LV was transversely sectioned at the midpoint between apex and base. A cross-sectional slice was fixed in 10% paraformaldehyde at room temperature for 12–24 h. The slice was dehydrated in a graded alcohol series (70, 80, 95, and 100%) and embedded in paraffin. The samples were sectioned at 5 μm, and nine nonconsecutive sections were collected and stained with toluidine blue for morphometric analysis.

Following the method described by Amaral et al. [1], four microscopy fields per slice were analyzed from each of the nine slices. Only fields where the fibers were transversally sectioned were used because in the myocardium the fibers run in multiple directions. The fields were randomly chosen from different areas of the transverse sections. The morphometric analysis was made in transversal tissue sections using a light microscope (Nikon E1000) coupled to an analysis system (Cool-Snap-Prom, Image ProPlus) to determine the CD, fiber density (FD), and CD/

FD ratio. A magnification of ×40 was used for the morphometric analysis. All measurements were made under blind conditions. Capillaries were defined as small vessels lined by a single layer of endothelial cells. To avoid possible confusion with lymphatic capillaries, vessels with irregular profiles were excluded from the counts. Values for CD and FD (always obtained in a 0.0203-mm^2 field) were expressed as number per square millimeter. The number of capillaries and muscle fibers was counted using the correction-of-edge effect. These counts were used to calculate the CD/FD ratio for hearts in each group, expressed as CD/FD. The intercapillary distance (ICD) was estimated assuming a hexagonal array of capillaries by the formula ICD (μm)=1.076 √DC, according to the method described previously by Olivetti et al. [21].

Finally, the immunohistochemical detection of proliferating cell nuclear antigen (PCNA) protein in combination with haematoxylin and eosin staining was used.

Immunohistochemistry for PCNA

This method enables the identification of the different myocardial cell types that are within the synthesis phase of the cardiac cycle identifying the expression of proliferating cells. PCNA data were used to corroborate morphometric data [13].

Cross-sections (3 μm) from control or T4-treated hearts obtained from paraffin-embedded tissue were dew axed and mounted using conventional techniques. Sections were then subjected to microwave irradiation in citrate buffer to enhance antigen retrieval. The cardiac tissue was incubated with 1:200 primary mouse anti-PCNA antibody (Zymed). After rinsing in PBS, a secondary biotinylated antimouse IgG peroxidase-conjugated antibody (Vector, CA, USA) was applied to sections. Sections were then incubated with 3′-diaminobenzidine solution (DAB, Sigma, St. Louis, MO, USA), stained with haematoxylin and eosin and held with a coverslip. PCNA-positive nuclei were identified in cross-sections by their brown color. The same conditions, but in the absence of antibody, were used as negative control for the PCNA immunohistochemistry. Sections obtained from rat testicle tissue were used as a positive control. In general, only cells found on the margin of testicular tissue are in proliferation phase. The labeling for PCNA was analyzed using the magnification of ×20.

RT-PCR analysis

Total ribonucleic acid (RNA) was obtained from control or T4-treated hearts using Trizol LS reagent (Life Technologies) in accordance with the manufacturer's instructions. The complementary dioxyribonucleic acid (cDNA) species were synthesized with SuperScript II (Life Technologies) from 2 μg of total RNA in a total volume of 20 μl with an oligo (dT) primer in accordance with the manufacturer's instructions. cDNA reactions were performed for 1 h at 42°C and stopped by boiling for 5 min. cDNA was used as a template for polymerase chain reaction (PCR) with specific primers for VEGF-A. A 210-base-pairs sequence of the β-actin messenger ribonucleic acid (mRNA) was chosen as an internal standard RNA for PCR. β-Actin was selected as an internal RNA standard because its expression was not affected by either thyroid hormone [6] or myocardial hypertrophy [18]. To better characterize this cardiac hypertrophy model, collagen I and III mRNA expressions were also analyzed. To find the ideal conditions for the PCR, a curve of the number of cycles performed for each gene studied and another temperature curve were initially constructed and then points that were always localized in the linear phase were chosen.

The PCR cycling conditions were as follows: for VEGF-A (product 256 bp), 1 min at 94°C, 1 min at 66°C, and 1 min at 72°C, using 26 cycles; for collagen I (product 221 bp) and for collagen III (product 266 bp) 1 min at 94°C, 1 min at 60.4°C, and 1 min at 72°C, using 30 cycles; for β-actin (product 210 bp) 1 min at 94°C, 1 min at 59.8°C, and 1 min at 72°C, using 34 cycles and a ×20 diluted primer concentration. An initial denaturation step (3 min at 94°C) and a final extension (10 min at 72°C) were included in all PCRs. Ten microliters of the PCR were analyzed on 1.5% agarose gel. The following set of primers were used for VEGF-A: 5′ ACT GGA CCC TGG CTT TAC TC 3′ and 5′ACG CAC TCC AGG GCT TCA TC 3′; for collagen I: 5′ CTT CGT GTA AAC TCC CTC C 3′ and 5′ CAC TTT TGG TTT TTG GTC AC 3′; for collagen III: 5′ GCG GCT TTT CAC CAT ATT AG 3′ and 5′ GCA TGT TTC TCC GGT TTC 3′; and for β-actin: 5′ TAT GCC AAC ACA GTG CTG TCT GG 3′ and 5′ TAC TCC TGC TTC CTG ATC CAC AT 3′. All oligonucleotides were obtained from Invitrogen, Brazil. Ten microliters of the PCR were analyzed on 1.5% agarose gel. Using an Image Analysis System, the densitometric intensity related to VEGF-A, collagen (I and III), and β-actin bands were converted to numeric values. The mRNA expression was expressed as mRNA of the gene of interest and mRNA β-actin ratio in arbitrary units (densitometric intensity).

Western blot analysis

Samples from the left ventricle of rat were homogenized in an extraction buffer (90 mM KCl, 10 mM Hepes, 3 mM $MgCl^{2+}$, 5 mM EDTA, 1% glycerol, 1 mM DTT, 0.04% SDS, pH 7.4). Protein concentrations were determined by Bradford method and 150 μg of protein were then separated by electrophoresis on a 15% SDS-polyacrylamide gel, and then transferred to nitrocellulose membrane (Bio-Rad). The membrane was stained with Ponceau solution to demonstrate that the protein concentration was similar in the different lanes and, after that, the membrane was washed with Tris-buffered saline Tween-20 (TBST) (50 mM Tris, 150 mM NaCl, pH 7.5, and 2% Tween-20) for 10 min at room temperature. The membrane was then incubated at 37°C for 1 h and 30 min with a primary polyclonal antibody against VEGF, which recognizes the 165-, 189-, and 121-amino acid splice variants of VEGF (sc507,

Table 1 Hemodynamic parameters in rats before killing

Groups	Samples (*n*)	Systolic blood pressure (mmHg)	Heart rate (bpm)
Control	5	121.3±6.1	377.5±14.99
T4-25	5	128.6±7.1	400.9±11.55*
T4-100	5	131.4±7.5	408.6±11.25**

Values are expressed as means±SD
n Number of rats, *T4-25* animals treated with 0.025 mg kg^{-1} day^{-1} of thyroxine, *T4-100* treated with 0.1 mg kg^{-1} day^{-1} of thyroxine
*$p<0.05$ vs control; **$p<0.01$ vs control

Santa Cruz Biotechnology, Santa Cruz, CA, USA) at 1:500 dilution in TBST. The three isoforms of VEGF-A can be visualized at the same protein weight, once they all have similar weights. Washed blots were then incubated for 1 h at room temperature with a secondary goat antirabbit IgG antibody conjugated with peroxidase (Amersham Biosciences) at a 1:1,000 dilution in TBST. Washed blots were subjected to the ECL Western blotting detection reagent kit (Amersham Biosciences), which allowed the production of a signal by a chemiluminescence reaction that was detected by exposure to X-ray film. The protein bands, related to the three isoforms of VEGF-A, were quantified by densitometry and then the band densities were calculated. Molecular weight markers were commonly used to determine the relative molecular weight of the labeled bands and an immunoreactive band was regularly detected at ~45 kDa.

Statistical analysis

The data are expressed as means±SD. In the capillary density calculation, *n* was considered as the number of animals used in each group. Statistical analysis was performed using ANOVA, and *p* values <0.05 were accepted as statistically significant. Tukey's post hoc test was used to make individual comparisons between groups when a significant change was observed with ANOVA.

Results

The parameters of SBP and HR after T4 administration are summarized in Table 1. Both dose levels of thyroid hormone significantly increased HR but did not affect SBP, compared to control animals. The changes in HR and the BW gain during treatment served as an index of thyroid hormone activity.

The BW at the beginning of the experiment was the same in all groups of rats. Although BW after treatment with T4 had not been significantly different among all experimental groups, in hyperthyroid rats, BW gain during the 7 days of treatment was different to that of control animals (Table 2). In the hyperthyroid groups (T4-25 and T4-100), VW was significantly greater (19.4 and 37.5%, respectively) than in the control group (Table 2). However, VW/BW was significantly increased only in the T4-100 group ($p<0.01$, Table 2).

Wet-to-dry weight ratios did not differ significantly among the groups (data not shown). This indicates that the hormone-induced changes were due to changes in cardiac muscle mass and not to changes in myocardial water content.

Although the increase in cardiac muscle mass is mainly due to a significant increase in transverse diameter of cardiomyocytes [14], the levels of collagen I and III mRNA expression in the hypertrophic myocardium were analyzed (Fig. 1). The concentric hypertrophy obtained in the T4-100 group (Fig. 1a) was not accompanied by any alteration in collagen I or III mRNA levels (Fig. 1b), apparently indicating that at this early stage of hyperthyroidism, the increase in cardiac mass is just the result of myocyte growth and is not accompanied by a fibrosis process.

Figure 2 shows a representative transverse section of cardiac muscle obtained from a control animal and Fig. 3 presents the relationship between CD and CD/FD in the various groups studied. Treatment with different doses of T4 promoted a significant decrease in CD compared with the control group. However, there were no significant differences in the CD among both hyperthyroid groups (T4-25 and T4-100). Although the mean values for FD tended to be lower in all T4 groups than in the control group, it was significantly (17%) lower only in the T4-100 group (1,246±126 for T4-100 vs 1,507±134 for control, $p<0.05$). In fact, this lower FD in the T4-100 group was reflected by an accentuated decrease in the CD/FD (approximately 25% lower than in the controls), which was significantly lower only in this group ($p<0.01$). Furthermore, the average center-to-center ICD increased only in the T4-100 group as the result of myocyte size being greater than in the control group (39.6±2.1 vs

Table 2 BW gain (ΔBW), ventricular weight (VW), VW/ BW (g), and VW/BW (%) in the experimental groups

Groups	Samples (*n*)	ΔBW (BW_{final}–$BW_{initial}$), (g)	Ventricular weight (VW), (g)	VW/BW (g)	VW/BW (%)
Control	7	+11.8±4.46	0.72±0.02	3.06±0.21	
T4-25	5	−6.1±2.80*	0.86±0.08*	3.46±0.43	13.07
T4-100	6	−4.9±3.0*	0.99±0.06**	4.07±0.39*	33

Values are expressed as means±SD
n Number of rats, *T4-25* treated with 0.025 mg kg^{-1} day^{-1} of thyroxine, *T4-100* treated with 0.1 mg kg^{-1} day^{-1} of thyroxine
*$p<0.01$ vs control; **$p<0.001$ vs control

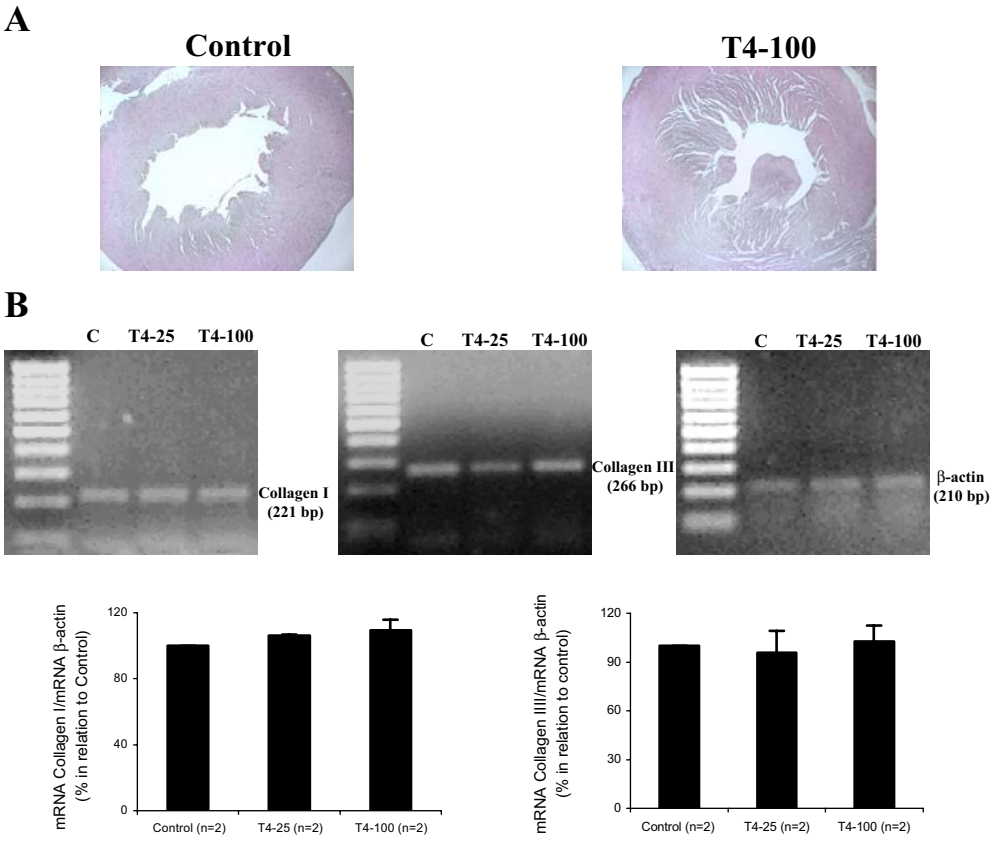

Fig. 1 **a** Representative photomicrography from a transverse section of the left ventricle showing the development of cardiac hypertrophy (*concentric*) in the rat heart treated with T4 (*on the right*) in relation to the control (*on the left*). Staining by eosin–hematoxylin, 2× magnification. **b** Analysis of collagen I and III mRNA expression levels in animals submitted to hyperthyroidism (T4-25 and T4-100 groups; 0.025 and 0.1 mg kg^{-1} day^{-1}, respectively) for 7 days. Values are expressed as means±SD

32.8±0.6, respectively) because no significant difference in capillary diameter was observed (3.15±0.30 μm in controls vs 3.35±0.80 μm in the T4-100 group).

With regard to the ability of thyroid hormone to decrease the CD in the myocardium, the effect of hormone on VEGF-A levels, a potent angiogenic factor in cardiovascular disease, was also evaluated. A representative electrophoresis gel obtained by reverse transcriptase polymerase chain reaction (RT-PCR) analysis is shown in Fig. 4a. The VEGF-A mRNA expression levels were not altered in the T4-25 group, but they were significantly higher in the T4-100 group than in the control group. The increased VEGF-A mRNA expression was accompanied by a significant elevation in VEGF-A protein levels, as shown in Fig. 4b.

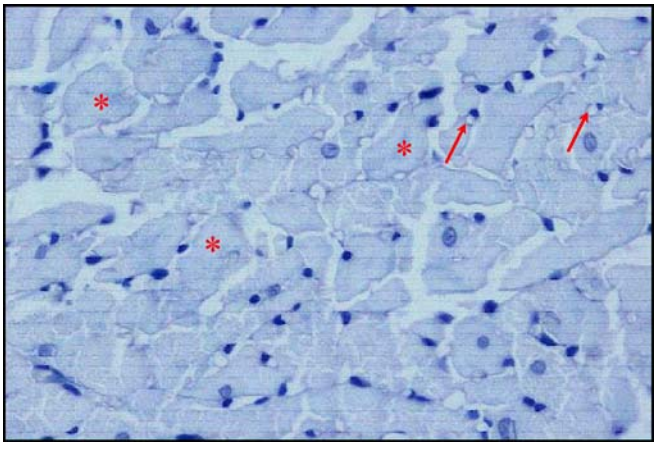

Fig. 2 Representative photomicrography from a transverse section showing the lateral wall of the left ventricle from a control myocardium containing capillaries. Staining by toluidine blue. The *asterisks* show the muscle fibers and the *arrows* show the capillaries. ×40 magnification

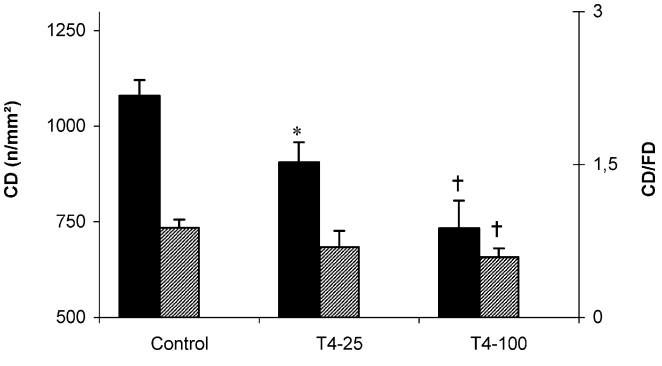

Fig. 3 Capillary density given as the number of capillaries to 2 mm^2 (*black bars*) and capillary density to fiber density ratio (CD/FD) (*hatched bars*) from animals submitted to hyperthyroidism by daily intraperitoneal injection of T4 (0.025 or 0.1 mg kg^{-1} day^{-1}) for 7 days. Values are expressed as means±SD. *p<0.05 vs control; †p<0.01 vs control

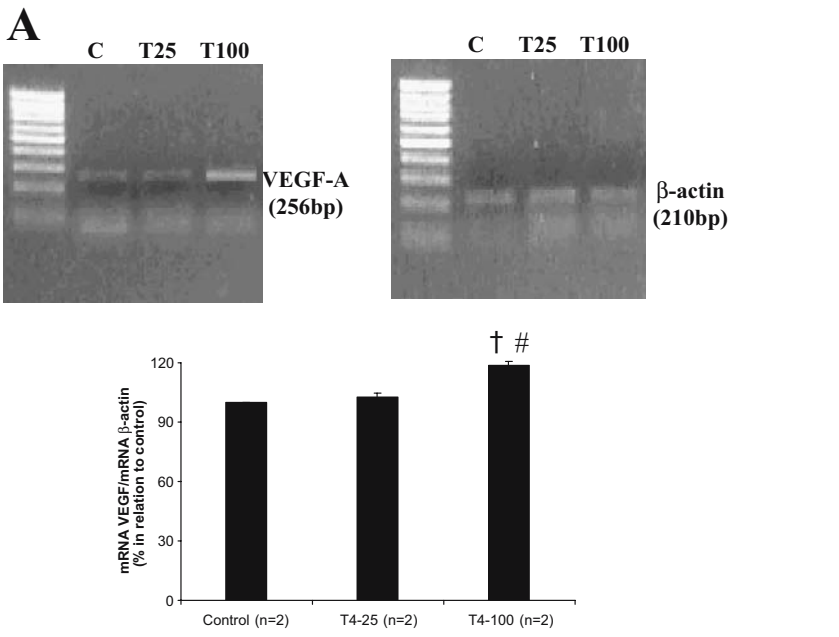

Fig. 4 **a** Analysis of VEGF-A mRNA expression in animals submitted to hyperthyroidism (T4-25 and T4-100 groups; 0.025 and 0.1 mg kg^{-1} day^{-1}, respectively) for 7 days. The mRNA expression was evaluated by semiquantitative RT-PCR, expressed as the VEGF-A to β-actin mRNA ratio. **b** VEGF-A protein levels in animals submitted to hyperthyroidism (T4-100 group). The protein expression was evaluated by Western blot and a 45-kDa band was densitometrically quantified. Values are expressed as means±SD. *p<0.05 vs control; †p<0.01 vs control; $^{\#}p$<0.01 vs T4-25

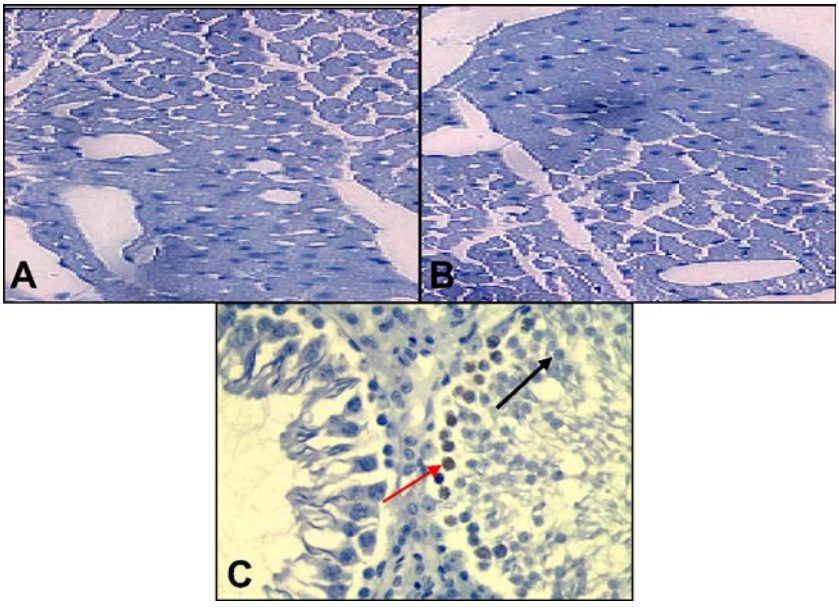

Fig. 5 **a** Immunohistochemistry for PCNA in a transverse section of the left ventricle from the control group and **b** group submitted to hyperthyroidism by daily intraperitoneal injection of T4 (0.1 mg kg^{-1} day^{-1}) for 7 days. **c** A section from rat testicle used as a positive standard for PCNA. The *red arrow* indicates a positive label for PCNA in the nucleus of a proliferating cell and the *black arrow* indicates absence of staining for PCNA in a cell localized out of the proliferative region. 20× magnification

However, despite the augmented VEGF-A levels, the lack of PCNA-positive endothelial nuclei in the control and T4-100 groups indicated an absence of endothelial cell proliferation, possibly reflecting a lack of capillary growth (Fig. 5a,b). Furthermore, no difference in PCNA-labeling in myocytes between control and T4-100 groups was detected; this absence agrees with the idea that myocyte proliferation is rare in adult animals and that this phenomenon is not changed by hyperthyroidism.

Discussion

The thyroid hormones play an important role in maintaining an optimal level of cardiac function and tissue oxygen consumption. Nevertheless, in hyperthyroidism, the increases in cardiac load and tissue metabolism usually result in a concomitant increase in tissue oxygen consumption and myocardial mass. In adults, in whom the angiogenic capacity is known to be diminished, excess thyroid hormone induces myocardial hypertrophy. Cardiac hypertrophy was produced in adult rats with excess thyroxine and the increase in cardiac mass observed in this study was in accordance with our own previous findings and with those of other authors [4, 14]. The increase in ventricular mass observed in both hyperthyroid groups was due to an increase in the myocyte component and not to an increase in myocardial water content or collagen expression. The physiological data show that the hearts of T4-treated animals are functioning under an increased cardiac rate, a condition that characterizes this model. In addition, a dissociation between elevated arterial pressure and increased myocardial mass was observed in this acute model of cardiac hypertrophy. This dissociation suggests the existence of stimuli, other than blood pressure, that are responsible for the development of intense cardiac hypertrophy [19]. Thus, the indirect effects of thyroid hormone seem to be mediated mainly by up- or down-regulation of alpha- and beta-adrenergic receptors [3], while the direct effects of the hormone result from its binding to nuclear receptors, which function as transcription factors [5, 30]. Furthermore, a series of studies have recently shown important nongenomic effects of thyroid hormone, inducing different cytosolic signaling cascades, which can directly affect gene expression [2, 9, 16].

The coronary microvasculature changes that occur in response to hypertrophy, as well as the increased oxygen demand, are potentially important factors in maintaining adequate oxygen supply to the myocardium. In this study, CD and CD/FD ratios were significantly lower after treatment with the hormone, despite the presence of myocardial hypertrophy. The CD, provided that it is expressed per square millimeter of muscle fiber, and the CD/FD ratio are valid and common indexes used in a wide range of animal models [10]. Although some studies that use a longer administration of thyroxine have previously demonstrated a potent angiogenic effect for thyroid hormone [4, 7, 28], the absence of labeled nuclei by PCNA immunohistochemistry in this acute study corroborates the fact that there was no endothelial proliferation. Thus, the cardiac hypertrophy induced by T4 in the early phase is a different model, which presents peculiar characteristics when compared to other models that are induced by overload pressure [24, 29]. In part, our results are in agreement with those from other previous studies involving the same model but evaluating the CD in different cardiac regions. Weiss and Grover [32] observed, in rabbits, that after 16 days of T4 administration, there was a significant decrease in the average number of capillaries per square millimeter in the subendocardium and subepicardium regions. Gerdes et al. [12] also observed a decrease in CD (endocardium, 12%; epicardium, 17%) during hyperthyroidism. The decrease in CD observed by these authors, however, was accompanied by approximately 69% hypertrophy, suggesting that, although there was severe ventricular hypertrophy in the hyperthyroid group, there was some degree of active capillary angiogenesis because the decrease in CD was less severe than the increase in ventricular mass. In contrast, the results obtained in this study show that the decrease of approximately 32% in CD observed after treatment with the higher T4 dose was similar to ventricular hypertrophy in this group (33%), suggesting that the capillary supply in the heart was not altered during treatment with thyroxine.

On the basis of the predictions made by Weiss and Grover [32], one might expect to find anoxic foci in the thyroid-treated animals of our study because we found no difference in the capillary diameter between the hyperthyroid (T4-100) and control groups (data not shown). On the other hand, Weiss and Grover [32] showed that an important compensation for the reduced size of the microvascular bed is a significant increase in the proportion of the bed that is perfused. It is possible that, in this model, the greater number of perfused capillaries (despite the lower CD) observed by the authors represents an attempt to maintain at least the minimum physiological conditions. It may be speculated that there is no immediate increase in capillary area in the early phase of T4-induced cardiac hypertrophy (the phase studied in our model). Therefore, this phenomenon may account for the ischemia and significant increase in mitochondrial volume that characterizes the myocardial hypertrophy seen under certain conditions in this model [8, 15].

Although we found no angiogenic effect for thyroid hormone in this study, the increased VEGF-A mRNA and protein levels suggest that the capillary proliferation may be observed after a longer treatment, as VEGF, a functionally relevant vascular growth factor [11], plays a crucial role in vascular development, angiogenesis, and collateral growth. Furthermore, because ischemia or hypoxia is a potent factor in inducing the expression of VEGF-A [23] and T4 promotes an increase in ICD as observed in the present study, this relationship appears to be understandable.

According to our data, we postulate that the increase in VEGF-A mRNA levels corresponds to the initial event that deflagrates the angiogenic process. As such, the observation of the formation of new microvessels may require a longer period of treatment with the hormone. Thus, our data indicate that cardiac hypertrophy installation precedes the formation of new microvessels.

In conclusion, our findings show, for the first time, a relationship between the development of cardiac hypertrophy, induced by acute hyperthyroidism and elevated VEGF-A levels (an important angiogenic growth factor) in the myocardium. This increase, however, was not accompanied by parallel endothelial cell proliferation or by any increase in the number of capillaries, at least during the early stage of myocardial hypertrophy, as represented by this study. It may be speculated that, perhaps in the later phase of thyroxine-induced cardiac hypertrophy, development of new microvessels occurs, possibly caused by the increased levels of VEGF-A observed herein.

References

1. Amaral SL, Zorn TMT, Michelini LC (2000) Exercise training normalizes wall-to-lumen ratio of the gracilis muscle arterioles and reduces pressure in spontaneously hypertensive rats. Hypertension 18:1563–1572
2. Bassett JH, Harvey CB, Williams GR (2003) Mechanisms of thyroid hormone receptor-specific nuclear and extra nuclear actions. Mol Cell Endocrinol 31:1–11
3. Bilezikian JP, Loeb JN (1983) The influence of hyperthyroidism and hypothyroidism on α- and β-adrenergic receptor systems and adrenergic responsiveness. Endocr Rev 414:378–387
4. Breisch AE, White FC, Hammond HK, Flynn S, Bloor CM (1989) Myocardial characteristics of thyroxine stimulated hypertrophy. A structural and functional study. Basic Res Cardiol 84:345–358
5. Brent GA, Moore DD, Larsen PR (1991) Thyroid hormone regulation of gene expression. Annu Rev Physiol 53:17–35
6. Carneiro-Ramos MS, Silva VB, Coutinho-Junior MB, Battastini AMO, Sarkis JJF, Barreto-Chaves MLM (2004) Thyroid hormone stimulates 5′-ecto-nucleotidase of neonatal rat ventricular myocytes. Mol Cell Biochem 265:195–201
7. Chilian WM, Wangler RD, Peters KG, Tomanek RJ, Marcus ML (1985) Thyroxine-induced left ventricular hypertrophy in the rat. Anatomical and physiological evidence for angiogenesis. Circ Res 57:591–598
8. Craft-Cormney C, Hansen JT (1980) Early ultrastructural changes in the myocardium following thyroxine-induced hypertrophy. Virchows Arch B Cell Pathol 33:267–273
9. Davis PJ, Davis FB (2002) Nongenomic actions of thyroid hormone on the heart. Thyroid 12:459–66
10. Egginton S and Turek Z (1990) Comparative distributions of numerical and areal indices of tissue capillarity. Adv Exp Med Biol 277:161–169
11. Ferrara N (2004) Vascular endothelial growth factor: basic science and clinical progress. Endocr Rev 25:581–611
12. Gerdes AM, Callas G, Kasten FH (1979) Differences in regional capillary distribution and myocytes size in normal and hypertrophic rat heart. Am J Anat 156:523–532
13. Heron MI, Rakusan K (1995) Proliferating cell nuclear antigen (PCNA) detection of cellular proliferation in hypothyroid and hyperthyroid rats hearts. J Mol Cell Cardiol 27(7):1393–1403
14. Hu LW, Benvenuti LA, Liberti EA, Carneiro-Ramos MS, Barreto-Chaves ML (2003) Thyroxine-induced cardiac hypertrophy: influence of adrenergic nervous system versus renin-angiotensin system on myocyte remodeling. Am J Physiol Regul Integr Comp Physiol 285(6):R1473–R1480
15. Hu LW, Liberti EA, Barreto-Chaves ML (2005) Myocardial ultrastructure in cardiac hypertrophy induced by thyroid hormone-an acute study in rats. Virchows Arch 446:265–269
16. Kavok NS, Krasilnikova OA, Babenko NA (2001) Thyroxine signal transduction in liver cells involves phospholipase C and phospholipase D activation. Genomic independent action of thyroid hormone. BMC Cell Biol 2:5
17. Kobori H, Ichihara A, Miyashita Y, Hayashi M, Saruta T (1999) Local renin–angiotensin system contributes to hyperthyroidism-induced cardiac hypertrophy. J Endocrinol 160:43–47
18. Lindpaintner K, Lu W, Neidermajer N, Schicffer B, Just H, Ganten D, Drexler H (1993) Selective activation of cardiac angiotensinogen gene expression in post-infarction ventricular remodeling in the rat. J Mol Cell Cardiol 25:133–143
19. Morgan HE, Kenneth M, Baker MD (1991) Cardiac hypertrophy: mechanical, neural, and endocrine dependence. Circulation 83:13–24
20. Nagy JA, Dvorak AM, Dvorak HF (2003) VEGF-A$^{164/165}$ and PlGF. Roles in angiogenesis and arteriogenesis. TCM 13(5): 169–175
21. Olivetti G, Anversa P, Loud AV (1980) Morphometric study of early postnatal development in the left and right ventricular myocardium of the rat. II. Tissue composition capillary growth, and sarcoplasmic alterations. Circ Res 46:503–512
22. Pepper MS (1997) Manipulating angiogenesis: from basic science to the bedside. Arterioscler Thromb Vasc Biol 17: 605–619
23. Pugh CW, Ratcliffe PJ (2003) Regulation of angiogenesis by hypoxia: role of the HIF system. Nat Med 9:677–84
24. Rakusan K, Cicutti N, Flanagan MF (1994) Changes in the microvascular network during cardiac growth, development and aging. Cell Mol Biol Res 40(2):117–22
25. Ribatti D (2004) The crucial role of vascular permeability factor/vascular endothelial growth factor in angiogenesis: a historical review. Br J Haematol 128:303–309
26. Shiojima I, Sato K, Izumiya Y, Schiekofer S, Ito M, Liao R, Colucci WS, Walsh K (2005) Disruption of coordinated cardiac hypertrophy and angiogenesis contributes to the transition to heart failure. J Clin Invest 115:2108–2118
27. Tanaka E, Hattan N, Ando K, Ueno H, Sugio Y, Mohammed MU, Voltchikhina SA, Mori H (2000) Amelioration of microvascular myocardial ischemia by gene transfer of vascular endothelial growth factor in rabbits. J Thorac Cardiovasc Surg 120(4):720–728
28. Tomanek RJ, Connell PM, Butters CA, Torry RJ (1995) Compensated coronary microvascular growth in senescent rats with thyroxine-induced cardiac hypertrophy. Am J Physiol 268: H419–H425
29. Tomanek RJ, Searls JC, Lachenbruch PA (1982) Quantitative changes in the capillary bed during developing peak and stabilized hypertrophy in a spontaneously hypertensive rat. Circ Res 51:295–304
30. Tsai MJ, O'Malley BW (1994) Molecular mechanisms of action of steroid/thyroid receptor superfamily members. Ann Rev Biochem 63:451–486
31. Waltenberger J (2005) Growth factor signal transduction defects in the cardiovascular system. Cardiovasc Res 65:574–580
32. Weiss HR, Grover GJ (1987) T4-induced cardiac hypertrophy and the perfused and total microvasculature of the heart. Can J Physiol Pharmacol 65:1848–1855

Virchows Arch (2006) 448: 480–484
DOI 10.1007/s00428-006-0165-x

ORIGINAL ARTICLE

Burkhard Helpap

The significance of the P504S expression pattern of high-grade prostatic intraepithelial neoplasia (HGPIN) with and without adenocarcinoma of the prostate in biopsy and radical prostatectomy specimens

Received: 10 November 2005 / Accepted: 25 January 2006 / Published online: 28 February 2006

Abstract Diagnosis of prostatic adenocarcinoma is usually not difficult in biopsy specimens. Problems may occur in biopsy specimens, containing only a few suspicious lesions. Recently, P504S has been tested as a new marker for prostatic carcinoma. When over-expressed in atypical glands without basal cells, it establishes the diagnosis of prostatic carcinoma. We analysed the staining intensity of P504S in 208 biopsy specimens from prostates (1) with adenocarcinoma (n=132), (2) with high-grade prostatic intraepithelial neoplasia (HGPIN) with adenocarcinoma (n=36), (3) with HGPIN alone (n=40) and in radical prostatectomy specimens with HGPIN adjacent to (n=54) or distant from adenocarcinoma (n=64). P504S expression was negative to weakly positive in biopsy specimens showing HGPIN without carcinoma and weakly positive in radical prostatectomy specimens revealing HGPIN distant from adenocarcinoma. In biopsy specimens with a combination of HGPIN and adenocarcinoma and in radical prostatectomy specimens with HGPIN adjacent to adenocarcinoma, P504S was strongly expressed. The same findings were made in radical prostatectomy specimens containing adenocarcinoma and HGPIN adjacent to or distant from adenocarcinoma and in preoperative biopsies revealing adenocarcinoma and HGPIN. These results suggest that moderate to strong P504S expression in HGPIN of biopsy specimens is indicative of an associated adenocarcinoma and may be helpful in the choice of therapy.

Keywords Prostatic adenocarcinoma · Prostatic intraepithelial neoplasia · P504S

B. Helpap (✉)
Department of Pathology,
Hegau-Bodensee-Hochrhein General Hospital Singen,
P.O. Box 720, 78207 Singen, Germany
e-mail: pathologie@hbh-kliniken.de
Tel.: +49-773-1892100
Fax: +49-773-1892105

Introduction

High-grade prostatic intraepithelial neoplasia (HGPIN) is the most likely precursor of prostate adenocarcinoma [2, 3]. The frequency of HGPIN in biopsy specimens that do not show any invasive prostate carcinoma ranges between 8 and 16% [2, 5]. When in these cases repeat biopsies were performed, they revealed adenocarcinoma in up to 15–30% of the cases [2, 3, 5, 8–10, 19, 20]. However, in 70–85% of the cases, the diagnosis remained HGPIN even after four and more repeat biopsies [5, 10]. This is a very problematic situation for the patient and the urologist, especially when the prostate-specific antigen level rises from year to year. In these circumstances, it would be helpful to have an immunohistochemical marker that is indicative of the presence of an adenocarcinoma of the prostate. Recently, the new tumour marker P504S (alpha-methylacyl-CoA racemase, AMACR) was used in the evaluation of diagnostic needle biopsy specimens from the prostate. P504S (AMACR) has been shown to be over-expressed in carcinoma of the prostate [1, 6, 11–16, 18].

In a preliminary study, we analysed the neoplastic potential of atypical small glandular lesions seen in biopsy specimens of the prostate by imunohistochemical screening for the expression of P504S and the basal cell markers P63 and 34ßE12. In 35.8% of the suspicious cases, an adenocarcinoma of the prostate was found [6]. In this study, we analysed the relationship between high-grade PIN and adenocarcinoma of the prostate in preoperative biopsy specimens and radical prostatectomy specimens by means of P504S immunostaining.

Materials and methods

Patients

For this study, core needle biopsy specimens and radical prostatectomy specimens were examined. Of the core needle biopsy specimens, 132 were from patients diagnosed as having prostatic adenocarcinoma, 36 HGPIN and

adenocarcinoma, and 40 HGPIN without adenocarcinoma. Radical prostatectomy specimens were available from 118 patients with HGPIN and adenocarcinoma. These were analysed by means of classic histology and immunohistochemistry. In addition, we studied 67 radical prostatectomy specimens, which had been diagnosed in our laboratory as prostatic adenocarcinoma on preoperative biopsy specimens from both lobes. Forty-two of the 67 cases showed HGPIN (62.7%).

Immunohistochemistry

Formalin-fixed, paraffin-embedded tissue blocks were cut into 4 μm sections and stained with hematoxylin and eosin. The sections were treated with Tris EDTA citrate buffer (pH 7.8) in an 800-W microwave oven for 30 min for antigen retrieval before immunostaining. The slides were stained on a Ventana–Nexes automated immunostainer (Ventana Medical System, Strasbourg, France) using an avidin–biotin complex staining procedure. The sections were incubated with a rabbit polyclonal antibody against AMACR (P504S) undiluted, or with a mouse monoclonal antibody against p63 protein (dilution of 1:50). Parallel to p63 immunostaining, the sections were incubated with a mouse monoclonal antibody against a high molecular weight cytokeratin clone 34ßE12 at a dilution of 1:20 for 32 min at 37°C followed by brief buffer washes. All sections were then incubated with I VIEW DAB (Ventana) for 30 min in a Ventana immunostainer. The sections were counter-stained with hematoxylin.

The P504S staining intensity in average of 100 carcinoma cells or HGPIN lesions was graded as negative, weak (focal apical granular staining), moderate (diffuse weak cytoplasmic staining), or strong (diffuse cytoplasmic staining) [20]. CK 34ßE12 or p63 immunohistochemical staining was recorded as positive or negative [17].

All 118 radical prostatectomy specimens showed high-grade prostatic carcinoma (Gleason >3+4=7) and clusters of HGPIN. In 64 cases, there were clusters of HGPIN at a distance of more than 5 mm from the adenocarcinoma. In 54 cases with HGPIN and carcinoma, the distance between the carcinoma and HGPIN lesions was less than 5 mm. In each of these cases, the P504S staining intensity was analysed in a mean of 50 foci of HGPIN distant from or adjacent to the carcinoma. The same procedure was used on the 42 preoperative biopsy cases and radical prostatectomy specimens with HGPIN and high-grade prostatic adenocarcinoma.

When we started immunohistochemical staining for P504S, we noticed, like other authors did previously [4, 6, 16], similar staining intensities in normal glands, PIN glands and carcinomatous glands. We overcome these difficulties by standardizing the fixation and staining procedure, as described in the "Materials and methods" section. After standardisation, we performed the analysis on archival material. On each slide, a control sample of moderately to strongly stained adenocarcinoma and one of nonstaining normal prostate tissues had been mounted for comparison with the test sample. The staining intensity in the test sample was only evaluated if the benign glands of the prostate tissue were negative. All sections were evaluated blindly by three independent pathologists (Ch.F., U.O. and B.H.), who reached a concordance rate of 95%.

For the statistical analysis, the Fisher's exact test was used.

Results

Biopsy specimens

In 132 biopsy specimens from the prostate, adenocarcinoma was diagnosed. Seventy percent had a Gleason score of 3+4=7, 25% a Gleason score of 6 and 5% Gleason scores of 8 and 9. P504S was expressed in all areas of the carcinomas. Moderate staining intensity was found in 42.2% and strong intensity in 57.8% (Fig. 1; Table 1).

In 40 of the biopsy specimens, we found HGPIN without adenocarcinoma of the prostate. In these specimens, the basal cell layer was moderately to strongly fragmented. The distinctly enlarged nuclei in this flat atypical epithelial layer showed prominent nucleoli like in a carcinoma in situ. The p63 staining revealed some positive nuclei. In these cases without adenocarcinoma, the P504S expression was mostly weak with focal apical granular staining (75%) but sometimes negative (25%) (Figs. 2, 3; Table 1).

In 36 biopsy specimens, we found HGPIN combined with adenocarcinoma of Gleason grade 6 or 7 (Fig. 4).The carcinomas did not express the basal marker p63 and the basal cell layer of HGPIN lesions was fragmented (Fig. 5). P504S was expressed in all foci of the adenocarcinoma and HGPIN. In 55.6% of the HGPIN lesions, the staining intensity was moderate and in 44.4% strong. This percent distribution of the staining intensity of HGPIN with adenocarcinoma was not significantly different from the staining intensity of the carcinomas but significantly different from the staining intensity of HGPIN without adenocarcinoma (p>0.0001) (Figs. 1, 6; Table 1).

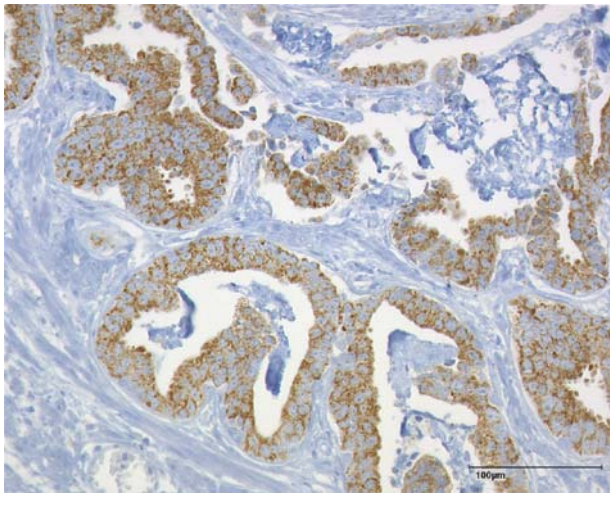

Fig. 1 Prostate biopsy: adenocarcinoma with strong, diffuse P504S expression. ABC method

Table 1 Intensity of P504S (AMACR) expression in high-grade PIN and adenocarcinoma of the prostate (*n*/%)

P504S (AMACR) staining intensity					
Diagnosis	*n*	Negative	Weak	Moderate	Strong
Carcinoma[1]	132	–	–	56 (42.2%)	76 (57.8%)
HGPIN with carcinoma[1§]	36	–	–	16 (44.4%)	20 (55.6%)
HGPIN without carcinoma[1§]	40	10 (25%)	30 (75%)	–	–
HGPIN adjacent To Pca[2§]	54	–	16 (29.6%)	26 (48.2%)	12 (22.2%)
HGPIN distant from PCa[2§]	64	8 (12.5%)	42 (65.6%)	14 (21.9%)	–

[1]In prostatic biopsy specimens
[2]In radical prostatectomy specimens
[§]$p>0.0001$
PCa Prostatic adenocarcinoma

Radical prostatectomy specimens

Also examined were 118 radical prostatectomy specimens, 54 with HGPIN adjacent to the adenocarcinoma (distance less than 5 mm) and 64 farther away from the adenocarcinoma (distance more than 5 mm).In 48.2% of the HGPIN lesions adjacent to adenocarcinoma, P504S staining was moderate and in 22.2% strong. In 29.6%, the staining intensity was weak. HGPIN lesions (12.5%) distant from prostate adenocarcinoma were negative for P504S. The

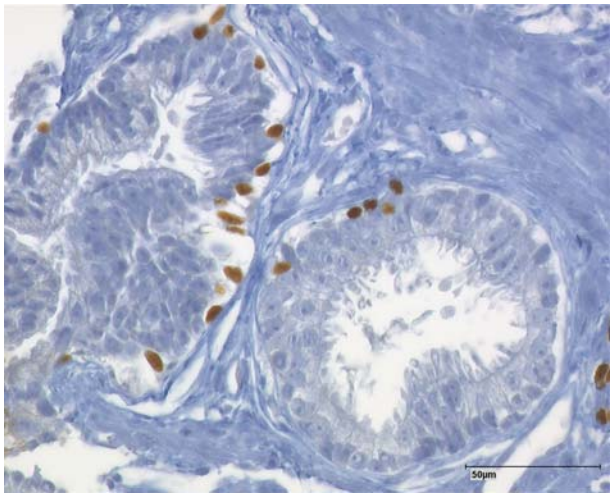

Fig. 2 Prostate biopsy: HGPIN but without adenocarcinoma and with fragmented basal cell layer. P63 staining, ABC method

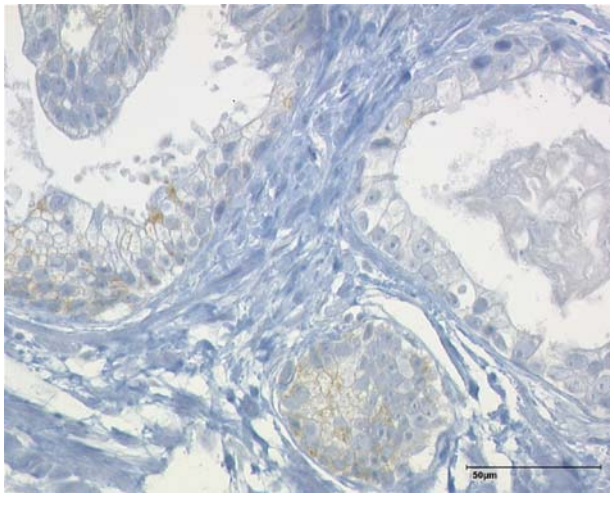

Fig. 3 Prostate biopsy: HGPIN without adenocarcinoma and with weak P504S expression. ABC method

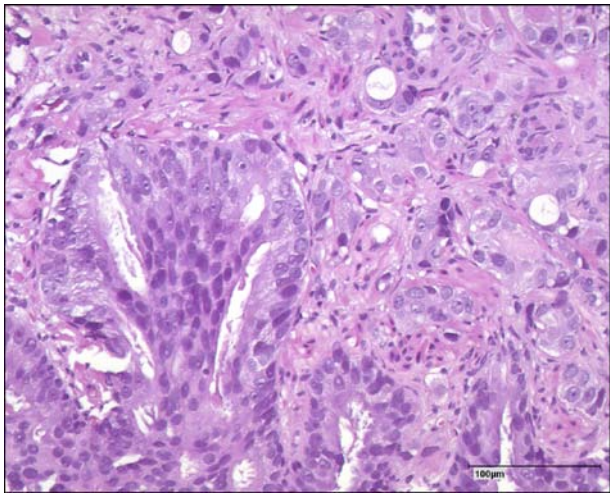

Fig. 4 Prostate biopsy: HGPIN and adenocarcinoma. H&E

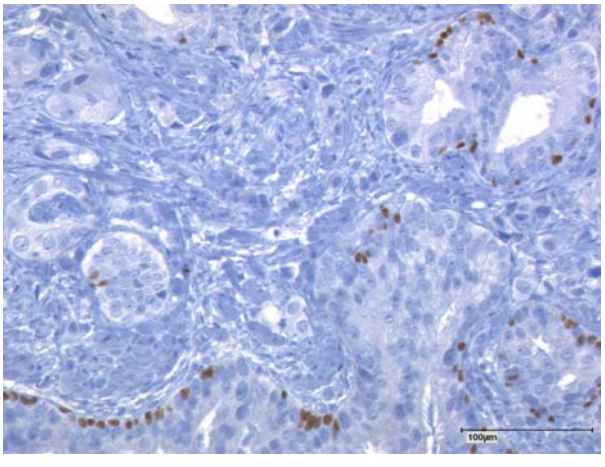

Fig. 5 Prostate biopsy: HGPIN with fragmented basal layer and adenocarcinoma with loss of basal cells. P63 IHC, ABC method

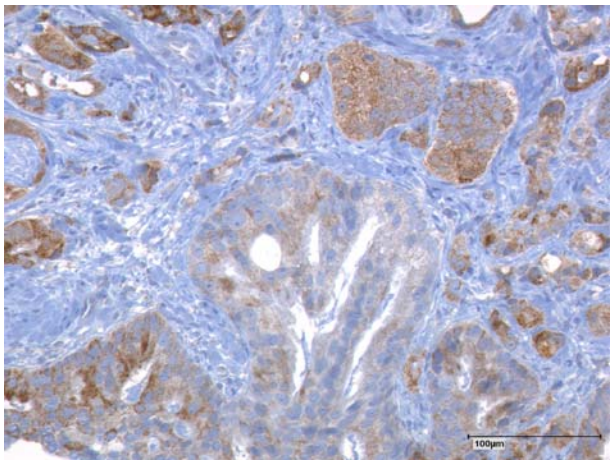

Fig. 6 Prostate biopsy: HGPIN with moderate to strong P504S expression. Strong P504S staining intensity in cells of the adjacent adenocarcinoma. ABC method

65.6% stained weakly, and 21.9% showed moderate staining intensity. No HGPIN lesions distant from adenocarcinoma showed strong P504S expression (Table 1). The differences in staining intensity between HGPIN lesions adjacent to and distant from adenocarcinoma were highly significant $p>0.0001$.

Comparison of preoperative biopsy specimens and radical prostatectomy specimens

We additionally investigated 67 patients in whom we had diagnosed adenocarcinoma in needle biopsy specimens before they underwent radical prostatectomy. Forty-two of the biopsy specimens additionally showed HGPIN lesions (62.7%). In 32 of the 42 cases (76.2%), the HGPIN lesions were adjacent to the adenocarcinomas (less than 5 mm distance). Ten cases of HGPIN were analysed by means of immunohistochemistry. They showed moderate to strong P504S expression (Table 2). This morphological and immunohistochemical pattern corresponded to the pattern seen in HGPIN and adenocarcinomas in the radical prostatectomy specimens from the same lobe. Ten of the preoperative biopsy specimens (23.8%) showed HGPIN lesions distant from the carcinomatous glands (more than 5 mm distance). Five of these cases were analysed immunohistochemically. They showed weak or negative P504S expression in the same lobe of the prostate (Table 2).

The difference in the staining intensity of HGPIN adjacent to or distant from adenocarcinoma in biopsy specimens was also significant ($p=0.0110$).

Discussion

P504S is an AMACR. P504S (AMACR) is a mitochondrial and peroxysomal enzyme involved in the metabolism of branched chain fatty acid and bile acid intermediates [1, 6, 11–22]. P504S has been found to be expressed in variants of prostatic adenocarcinoma, in cases treated with brachytherapy or hormones and in cases of HGPIN [1, 20, 21, 23]. In all these latter conditions, the staining intensity is weakly positive (granular and apical) [15]. However, the conventional adenocarcinoma of the prostate shows strong, diffuse cytoplasmic staining.

We studied the significance of P504S expression in two groups of patients. In the first study group, we detected strong diffuse P504S staining in core needle specimens from the prostate showing adenocarcinoma of Gleason score 6 or 7 and in core needle specimens showing HGPIN adjacent to adenocarcinoma of the prostate. Only in biopsy specimens revealing HGPIN without adenocarcinoma was the intensity of P504S staining negative to weakly positive.

In the second study group, P504S expression in HGPIN was determined in 118 radical prostatectomy specimens. HGPIN foci adjacent to adenocarcinoma (less than 5 mm) had a significantly higher P504S positivity rate than HGPIN foci at a distance of more than 5 mm from the adenocarcinoma. These results are in agreement with the study by Wu et al. [20].

To confirm these findings, we analysed 67 radical prostatectomy specimens of patients in whom preoperative biopsy specimens were available. In 76.2% of the biopsy specimens, the HGPIN lesions were adjacent to the adenocarcinomas in one or both lobes and showed moderate to strong P504S expression similar to the adenocarcinoma in the same lobe of the radical prostatectomy specimens. The remaining 23.8% of the biopsy cases in which the HGPIN lesions were distant from foci of adenocarcinoma were negative for P504S or stained only weakly. In the corresponding lobe of the radical prostatectomy specimens, the distance between HGPIN foci and the adenocarcinoma was more than 5 mm and in most cases, the foci of adenocarcinoma were very small.

Table 2 Intensity of P504S (AMACR) expression in high-grade PIN and adenocarcinoma of the prostate (*n*/%) in preoperative biopsy specimens and subsequent radical prostatectomy

P504S (AMACR) staining intensity					
Diagnosis	*n*	Negative	Weak	Moderate	Strong
HGPIN adjacent to PCa[1,2§]	10/15	–	–	6/15	4/15
HGPIN distant from PCa[1,2§]	5/15	2/15	2/15	1/15	–

[1]Prostatic biopsy specimens
[2]Radical prostatectomy specimens
[§]$p=0.0110$

Therefore, we agree with the conclusion of Wu et al. [20] that HGPIN showing strong P504S positivity in HGPIN is more closely associated with carcinoma than HGPIN distant from adenocarcinoma that is negative or weakly positive for P504S. This immunohistochemical reaction in biopsy specimens may be helpful in the discussion of further diagnostic steps, e.g. control biopsies at very short intervals or surgery. In such a case, we diagnosed an invasive adenocarcinoma in radical prostatectomy specimens after repeated preoperative core needle biopsies had revealed HGPIN without invasive adenocarcinoma [7].

Acknowledgement The author would like to thank Dr. G. Klöppel for the critical reading of the manuscript.

References

1. Beach R, Gown AM, de Peralta-Venturina MN, Folpe AL, Yaziji H, Salles PG, Grignon DJ, Fanger GR, Amin MB (2002) P504S immunohistochemical detection in 405 prostatic specimens including 376 18-gauge needle biopsies. Am J Surg Pathol 26:1588–1596
2. Bishara T, Ramnani DM, Epstein JI (2004) High-grade prostatic intraepithelial neoplasia on needle biopsy. Risk of cancer on repeat biopsy related to number of involved cores and morphologic pattern. Am J Surg Pathol 28:629–633
3. Bostwick DG (1995) High grade prostatic intraepithelial neoplasia. The most likely precursor of prostate cancer. Cancer 75:1823–1836
4. Gologan A, Bastacky S, McHale T, Yu J, Cai C, Monzon-Bordonaba F, Dhir R (2005) Age-associated changes in alpha-methyl CoA racemase (AMACR) expression in nonneoplastic prostatic tissues. Am J Surg Pathol 29:1435–1441
5. Helpap B (1998) Differential diagnosis of glandular proliferations in the prostate. A conventional and immunohistochemical approach.Virchows Arch 433:397–405
6. Helpap B (2004) Prostatic adenocarcinoma—still a diagnostic problem. Verh Dtsch Ges Pathol 88:152–157
7. Helpap B (2005) Radical prostatectomy without preoperative diagnosis of invasive carcinoma. Is it justified? A case report. In: Egevad L, Algaba F (eds) The most challenging cases of the year in uropathology. 20th European congress of pathology, Paris (in press)
8. Helpap B, Köllermann J (1999) Atypical acinar proliferations of the prostate. Pathol Res Pract 195:795–799
9. Helpap B, Köllermann J, Oehler U (2001) Limiting the diagnosis of atypical small glandular proliferations in needle biopsies of the prostate by the use of immunohistochemistry. J Pathol 193:350–353
10. Helpap B, Sinicina I (2002) Diagnostische Maßnahmen zur Therapieplanung des Prostatakarzinoms. Informationsaustausch zwischen Patienten-Urologen-Pathologen. Urologe B 42:121–127
11. Jiang Z, Woda BA, Rock KL, Xu Y, Savas L, Khan A, Pihan G, Cai F, Babcook JS, Rathanaswami P, Reed SG, Xu J, Fanger GR (2001) P504S: a new molecular marker for the detection of prostate carcinoma. Am J Surg Pathol 25:1397–1404
12. Jiang Z, Wu C-L, Woda BA, Dresser K, Xu J, Fanger GR, Yang XJ (2002) P504S/alpha-methylacyl-CoA racemase. A useful marker for diagnosis of small foci of prostatic carcinoma on needle biopsy. Am J Surg Pathol 26:1169–1174
13. Jiang Z, Fanger GR, Woda BA, Banner BF, Algate P, Dresser K, Xu J, Chu FG (2003) Expression of alpha-methylacyl-CoA racemase (P504S) in various malignant neoplasms and normal tissues: a study of 761 cases. Hum Pathol 34:792–796
14. Jiang Z, Wu CL,Woda BA, Iczkowski KA, Chu PG, Tretiakova MS, Young RH, Weiss LM, Blute RD, Brendler CB, Krausz T, Xu JC, Rock KL, Amin MB, Yang XJ (2004) Alpha-methylacyl-CoA racemase: a multi-institutional study of a new prostate cancer marker. Histopathology 45:218–225
15. Lou J, Zha S, Gage WR (2002) Alpha-methylacyl-CoA racemase: a new molecular marker for prostate cancer. Cancer Res 62:2220–2226
16. Magi-Galluzzi C, Luo J, Isaacs WB, Hicks JL, De Marzo AM, Epstein JI (2003) Alpha-methylacyl-CoA racemase. A variably sensitive immunohistochemical marker for the diagnosis of small prostate cancer foci on needle biopsy. Am J Surg Pathol 27:1128–1133
17. Molinie V, Herve JM, Lugagne PM, Baglin AC (2004) P63 and P504S cocktail is useful in ambiguous lesions of the prostate. Histopathology 44:403–404
18. Rubin MA, Zhou M, Dhanasekaran SM (2002) Alpha-methylacyl coenzyme. A racemase as a tissue biomarker for prostate cancer. JAMA 287:1662–1670
19. Varma M, Jasani B (2005) Diagnostic utility of immunohistochemistry in morphologically difficult prostate cancer: review of current literature. Histopathology 47:1–16
20. Wu C-L, Yang XJ, Tretiakova M, Patton KT, Halpern EF, Woda BA, Young RH, Jiang Z (2004) Analysis of alpha-methylacyl-CoA racemase (P504S) expression in high grade prostatic intraepithelial neoplasia. Hum Pathol 35:1008–1013
21. Zhou M, Chinnaiyan AM, Kleer CG, Lucas PC, Rubin MA (2002) Alpha-methylacyl-CoA racemase. A novel tumor marker over-expressed in several human cancers and their precursor lesions. Am J Surg Pathol 26:926–931
22. Zhou M, Jiang Z, Epstein JI (2003) Expression and diagnostic utility of alpha-methylacyl-CoA-racemase (P504S) in foamy gland and pseudohyperplastic prostate cancer. Am J Surg Pathol 27:772–778
23. Zhou M, Aydin H, Kanane H, Epsein JI (2004) How often does alpha-methylacyl-CoA racemase contribute to resolving an atypical diagnosis on prostate needle biopsy beyond that provided by basal cell markers. Am J Surg Pathol 28:239–243

Virchows Arch (2006) 448: 485–492
DOI 10.1007/s00428-005-0134-9

ORIGINAL ARTICLE

Jun Zou · Eishin Yaoita · Yusuke Watanabe · Yutaka Yoshida · Masaaki Nameta · Huiping Li · Zhenyun Qu · Tadashi Yamamoto

Upregulation of nestin, vimentin, and desmin in rat podocytes in response to injury

Received: 20 July 2005 / Accepted: 15 November 2005 / Published online: 18 January 2006

Abstract Podocytes in the renal glomerulus express unusual intermediate filament (IF) proteins for epithelial cells. To gain insight into the role of IF proteins in podocytes, we investigated the expression of nestin, vimentin, and desmin in puromycin aminonucleoside (PAN) nephrosis. A Western blot analysis for nestin, vimentin, and desmin demonstrated their exclusive expression in glomeruli and showed their increase in expression in nephrotic glomeruli. Immunolocalization studies showed nestin and vimentin to be located predominantly in the podocytes in both normal and nephrotic glomeruli and that enhancement of desmin staining only occurred in podocytes. A ribonuclease protection assay showed high levels of vimentin and nestin expression in normal glomeruli and an upregulation of all three IF transcripts in nephrotic glomeruli. One day after the PAN injection, however, the vimentin transcripts were found to already have significantly increased, whereas those of nestin or desmin showed no such increase. These findings indicate that podocytes express three IF proteins, namely, vimentin, desmin, and nestin, which are differentially regulated in response to injury. An upregulation of IF proteins may increase the mechanical stability of cells, thus enabling podocytes to undergo morphological changes on the tensile glomerular capillary wall.

Keywords Kidney · Intermediate filament · Nestin · Vimentin · Injury

J. Zou · E. Yaoita (✉) · Y. Yoshida · H. Li · Z. Qu · T. Yamamoto
Department of Structural Pathology, Institute of Nephrology, Niigata University Graduate School of Medical and Dental Sciences,
1-757 Asahimachi-dori,
Niigata 951-8510, Japan
e-mail: ren-path@med.niigata-u.ac.jp
Tel.: +81-25-2272152
Fax: +81-25-2270768

Y. Watanabe
Department of Nephrology, Saitama Medical College, Saitama, Japan

M. Nameta
Cooperative Laboratory of Electron Microscopy, Niigata University, Niigata, Japan

Introduction

Visceral epithelial cells of renal glomeruli, referred to as podocytes, are located on the glomerular basement membrane (GBM) as the terminal element in the filtration barrier. They have adapted themselves to facilitating the bulk flow of the glomerular filtrate through the intercellular spaces or filtration slits. Such adaptation has made podocytes a unique epithelium regarding their morphology, especially their cytoskeleton. Podocytes consist of a cell body, several primary processes, and numerous foot processes. In their cell body and primary processes, microtubules and intermediate filaments (IFs) dominate, whereas microfilaments are densely accumulated in the foot processes. Among the known cytoskeletal proteins, IF proteins are the most characteristic of podocytes. IF proteins are characterized by a considerable divergence, which derives from a variety of gene products employed in a fashion that is specific to both the cell type and stage of differentiation. Cytokeratins are typically found in epithelia, vimentin in mesenchyme, desmin in muscle, glial fibrillary acidic protein (GFAP) in astrocytes, and nestin in neuroepithelial stem cells [4, 29]. Although podocytes can be considered epithelial cells according to the classic definition [2], IFs of podocytes do not contain cytokeratins, but instead, react strongly to immunostaining for vimentin [1, 10, 16, 25, 30].

IFs form a continuous structural network extending from the nuclear surface to the cell periphery. In addition to their significant contribution to the mechanical integrity of cells and tissues, IFs play a crucial role in a variety of cellular functions, which range from the determination of cell shape and motility to cell cycle control and signal transduction [4, 29]. Tissue injury is often accompanied by changes in the IF

gene expression [5]. Podocytes have also been reported to alter their IF expression in response to injury. Enhanced desmin staining in podocytes is observed in a variety of experimental rat models of podocyte injury including puromycin aminonucleoside (PAN) nephrosis, Masugi nephritis, Heymann nephritis, diabetic nephropathy, and age-related glomerulosclerosis [11, 12, 17, 37]. Regarding vimentin, a main IF protein of podocytes, whether its expression changes in podocyte injury has yet to be elucidated. In addition, GFAP has been reported to be stained in podocytes [3]. A predominant nestin expression has been shown in the glomerulus using a DNA microarray [15]. As a result, the IF proteins expressed in podocytes and their response to cell injury still remain to be clarified. In the present study, we examined the IF protein expression in podocytes at the protein and transcript levels during PAN nephrosis, and thereby showed podocytes to express at least three IF proteins, which are differentially regulated in response to injury.

Materials and methods

Animals and antibodies

Female Wistar–Kyoto and Wistar rats, from 8 to 12 weeks of age, were purchased from Charles River Japan (Atsugi, Japan) and were used in these experiments. The following murine monoclonal antibodies were used: anti-vimentin antibody (clone V9, Sigma, Saint Louis, MO, USA), anti-nestin antibody (clone 25, BD Bioscience Pharmingen, San Diego, CA, USA), anti-desmin antibody (clone D-33, DakoCytomation, Glostrup, Denmark).

Induction of PAN nephrosis

A total of 91 rats were used in this experiment. PAN nephrosis was induced in 60 rats by a single intravenous injection of PAN (Sigma) at a dose of 5 mg/100 g of body weight in phosphate-buffered saline (PBS). In addition, 31 same-aged, normal rats were used as controls. The rats were housed in individual metabolic cages, and their 24-h urine specimens were collected before the injection of PAN 2, 4, 6, and 10 days after the injection. To examine IF proteins by Western blot analysis, the rats were killed under diethyl ether anesthesia, on days 2 (3 rats), 4 (3 rats), 6 (3 rats), and 10 (16 rats) in the PAN nephrosis group and in the control group (16 rats). To perform immunolocalization studies, rats from the PAN nephrosis group (2 rats) and from the control group (2 rats) were killed at day 10. To examine the transcript levels by a ribonuclease protection assay, the rats from the PAN nephrosis group were killed on days 1 (10 rats), 3 (10 rats), and 10 (13 rats) and from the controls (13 rats). The glomeruli isolated from four or six kidneys were pooled and used as one sample of glomerular protein or RNA. The procedures for the present study were approved by the Animal Committee at Niigata University School of Medicine, and all animals were treated according to the guidelines for animal experimentation of Niigata University.

Western blotting

The glomeruli were homogenized in lysis buffer (8 M urea, 1 mM dithiothreitol, 1 mM EDTA, 50 mM Tris–HCl, pH 8.0) with a sonicator on ice. The protein in the samples was quantified by Lowry's method after precipitation by trichloroacetate with sodium deoxycholate [32]. Western blotting was performed as described previously [26, 39]. In brief, a 10-μg sample of each protein was loaded onto 10% sodium dodecyl sulfate–polyacrylamide gel and the bands were transferred to a polyvinylidine difluoride membrane. The membranes were preincubated with 5% nonfat milk in PBS containing 0.05% Tween 20 for 1 h, incubated with 1:1,000 diluted anti-nestin, vimentin, or desmin antibody overnight, and then were washed in PBS containing 0.05% Tween 20. Next, they were incubated with a 1:2,000 diluted goat anti-mouse immunoglobulin-conjugated peroxidase-labeled dextran polymer (EnVision, DakoCytomation), and the immunoreactivity was visualized by use of an ECL plus Western blotting detection system (Amersham Biosciences, Buckinghamshire, UK). A densitometric analysis was performed with the NIH image software package (version 1.62).

Immunofluorescence microscopy

The indirect immunofluorescence technique was applied to frozen kidney sections [39]. In brief, the adult and neonatal rat kidneys were snap-frozen at −70°C, sectioned at a thickness of 3 μm in a cryostat, fixed in 2% paraformaldehyde in PBS for 10 min, and processed for double-label immunostaining. Murine monoclonal antibodies against vimentin (1:40 dilution), desmin (1:40 dilution), or nestin (1:100 dilution) in combination with rabbit anti-laminin antibody were applied as primary antibodies for double-labeling. After washing with PBS, the specimens were stained with fluorescein isothiocyanate (FITC)-conjugated goat anti-mouse IgG, rewashed with PBS, and subsequently reacted with tetramethylrhodamine isothiocyanate (TRITC)-conjugated goat anti-rabbit IgG. PBS, normal rabbit serum, or murine IgG1 monoclonal antibody (against rotavirus), which has been shown not to react with rat glomeruli, were used as negative controls for the primary antibodies. Immunofluorescence of the sections and cultured cells were observed with an Olympus microscope (BX50) equipped with epi-illumination optics and appropriate filters.

Immunoelectron microscopy

Immunoelectron microscopic observations of kidneys from rats with PAN nephrosis and from control rats were carried

out with a few modifications, as reported previously [19, 20]. In brief, 1-mm^3 tissue blocks from paraformaldehyde–lysine–periodate (PLP)-perfused kidneys were placed in the PLP fixative for 4 h at 4°C, hydrated, and then embedded in hydrophilic methacrylate resin. The ultrathin sections collected on nickel grids were stained with an immunogold technique. The sections were incubated with 5% normal goat serum for 1 h, transferred to the first antibody against nestin (1:200 dilution), and then incubated for 1 h at room temperature followed by 5 nm colloidal gold-AffiniPure goat anti-mouse IgG + IgM (H + L) (1:100 dilution; Seikagaku Corporation, Tokyo, Japan) for 2 h. The gold particles bound to IF proteins were then enhanced using an IntenSE M silver staining kit (Janssen Life Sciences, Beerse, Belgium) for 10 min. After washing in PBS and fixing with 2.5% glutaraldehyde, the sections were contrasted with uranyl acetate and lead citrate, and then were viewed with a Hitachi H-600A electron microscope.

Ribonuclease protection assay

A ribonuclease protection assay was performed as described previously [26, 39]. Isolated glomeruli, cortices, and medullae were homogenized in TRIzol (Life Technologies, Inc., Grand Island, NY, USA) with a sonicator, and total cellular RNA was extracted from these samples. Plasmids containing the cDNA corresponding to 4,534 to 4,797 (263 bp) of rat nestin (AF538924), 1,030 to 1,294 (264 bp) of rat vimentin (NM031140), and 759 to 1,054 (295 bp) of rat desmin (X73524) were prepared by cDNA amplified in a polymerase chain reaction, inserted in a pGEM-T Easy vector (Promega, Madison, WI, USA), and then were cloned and sequenced by DNA sequencer (ABI PRISM 310, Applied Biosystems Japan, Tokyo, Japan). The detection and analysis of bands were performed by phosphor-imaging techniques by use of the Molecular Imager FX (Bio-Rad Laboratories, Hercules, CA, USA). The results of the ribonuclease protection assay were

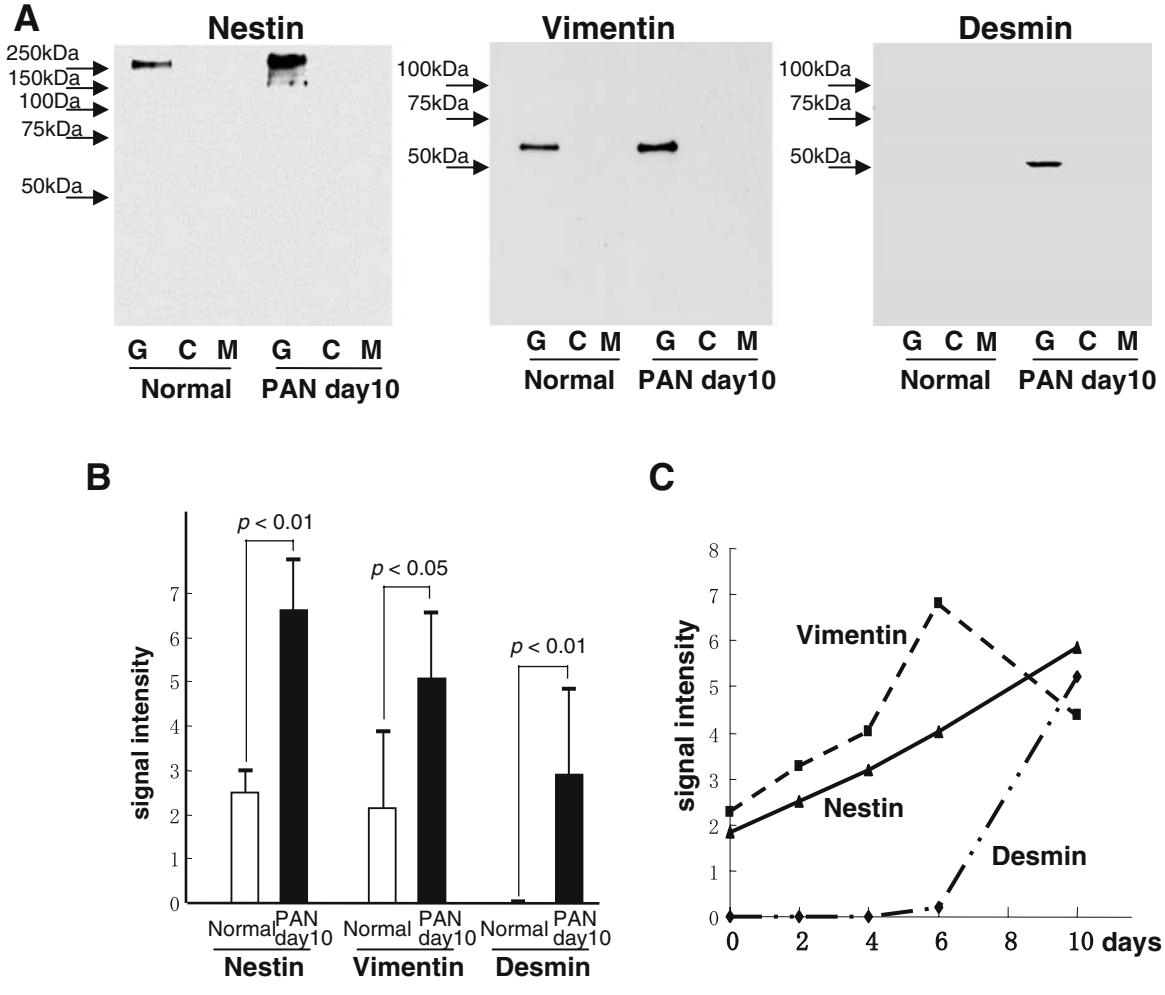

Fig. 1 A Western blot analysis of nestin, vimentin, and desmin in lysates from glomeruli (*G*), cortices (*C*), and medullae (*M*) in the normal and PAN-treated kidney. **a** Bands specific to each of the IF proteins are seen exclusively in the glomeruli. **b** A quantitative analysis of Western blotting using glomerular samples reveals significant increases of nestin, vimentin, and desmin at day 10 after PAN injection. All data from five samples are presented as means± SD. **c** In the time course of PAN nephrosis, each of the IF proteins in the glomeruli shows different increasing pattern

represented as the ratio of IFs to glyceraldehyde-3-phosphate dehydrogenase (*GADPH*), a housekeeping gene.

Statistics

All data were presented as means±SD. A statistical assessment of the significance between control animals and PAN-treated animals was made using Student's *t* test. Differences were considered statistically significant at $p<0.05$.

Results

Urinary protein in PAN nephrosis

The measurement of the 24-h urinary protein levels revealed that a single intravenous injection of PAN induced massive proteinuria on day 6 (129.9±69.2 mg/day) and day 10 (190.6±71.0 mg/day) after the injection. Either no increase in urinary protein or only a slight increase was detected at 2 or 4 days in comparison with control rats (1.4±0.5 mg/day).

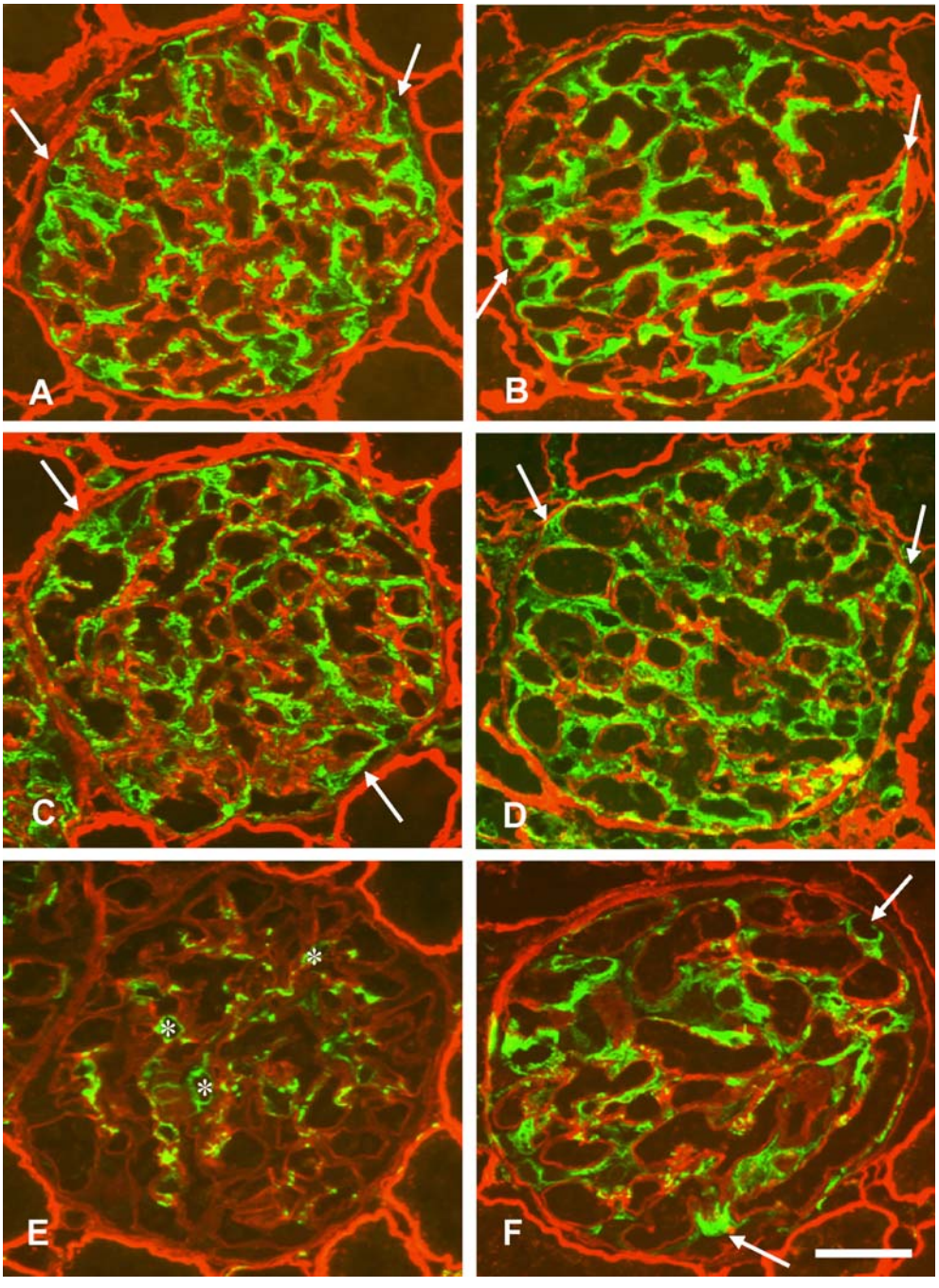

Fig. 2 Double-label immunofluorescence micrographs of frozen sections of rat kidneys incubated with murine monoclonal antibodies against nestin (**a**, **b**), vimentin (**c**, **d**), or desmin (**e**, **f**) in combination with rabbit anti-laminin antibody. Murine monoclonal antibodies were detected with FITC-conjugated goat anti-mouse IgG; rabbit anti-laminin antibody was detected with TRITC-conjugated goat anti-rabbit IgG. **a**, **c**, and **e** show a glomerulus of a normal kidney. **b**, **d**, and **f** are glomeruli of PAN-treated rats on day 10. **a**–**d** In both normal and PAN-treated glomeruli, the signals for nestin and vimentin are located predominantly at podocytes (*arrows*) outside the glomerular capillary wall stained with anti-laminin antibody. **e**, **f** Desmin staining is found in the mesangium (*asterisks*) in a normal glomerulus and in podocytes (*arrows*) in a PAN-treated glomerulus. Bar: 25 μm

IF proteins in the glomerulus in PAN nephrosis

A Western blot analysis was performed to confirm the specificity of the antibodies used in this study and to compare the levels of IF proteins in samples of glomeruli, cortices, and medullae from rats at day 10 in PAN nephrosis with those from normal rats. Each of the antibodies against nestin, vimentin, and desmin revealed a specific band with an apparent molecular mass of 260, 57, and 53 kDa, respectively (Fig. 1a). In both normal and PAN nephrotic kidneys, all IF proteins were detected exclusively in the glomeruli, although no signals for desmin or extremely faint ones were observed in the normal glomeruli (Fig. 1a). No signals were found in the cortices or medullae.

Because the signals in the glomeruli looked more intense in the nephrotic kidney, a densitometric analysis was done by increasing the sample number (n=5) (Fig 1b). Consequently, it was demonstrated that PAN nephrotic glomeruli showed significant increases in the protein levels of nestin, vimentin, and desmin in comparison to normal glomeruli.

To examine how the glomerular IF proteins increased in PAN nephrosis, glomerular samples were analyzed by Western blotting at 2, 4, 6, and 10 days after PAN injection (Fig. 1c). The pattern of increase was different among the IF proteins. Nestin and vimentin tended to increase before the onset of massive proteinuria, whereas desmin started to increase on day 6 after the onset of proteinuria. On day 10, vimentin started to decrease, whereas nestin continued to increase.

Immunolocalization of IF proteins in the glomerulus

The location of IF proteins in the normal and PAN nephrotic glomeruli was examined by double-label immunofluorescence microcopy using murine monoclonal antibodies against IF proteins in combination with rabbit anti-laminin antibody (Fig. 2). In the normal glomerulus, immunostaining for nestin was restricted to the podocytes located on the GBM facing Bowman's space (Fig. 2a). The GBM was outlined by laminin staining. In PAN nephrosis, nestin was also only observed in the podocytes (Fig. 2b). No parietal epithelial cells of Bowman's capsule showed any nestin staining. Vimentin staining in the normal glomerulus was observed predominantly in the podocytes and weakly in mesangial cells (Fig. 2c). The podocyte predominance of vimentin was the same in PAN nephrosis (Fig. 2d). In the normal kidney, anti-desmin antibody mainly reacted with the mesangial cells and vascular smooth muscle cells, and very weak staining was observed in the podocytes (Fig. 2e). In PAN nephrosis, conspicuously enhanced staining for desmin was seen in the podocytes, whereas no change in desmin staining was detected in the mesangium as shown in our previous study [37] (Fig. 2f). No significant staining for GFAP was observed in the glomerulus (data not shown).

The precise localization of nestin in the podocytes was examined by immunoelectron microscopy. Intensified immunogold particles for nestin were localized in the cell body and primary processes, but not the foot processes in both normal and PAN nephrotic glomeruli (Fig. 3a,b). No significant accumulation of nestin immunogold particles was detected in the endothelial cells, mesangial cells, or parietal epithelial cells of Bowman's capsule.

IF mRNA in the normal and PAN nephrotic kidney

The transcript levels of nestin, vimentin, and desmin were examined in the normal kidney by a ribonuclease protection assay. In parallel with the findings of a Western blot analysis, glomeruli predominated in the IF expression in the kidney (Fig. 4a). Significant signals for nestin and desmin were detected only in the glomeruli, but not in the cortices

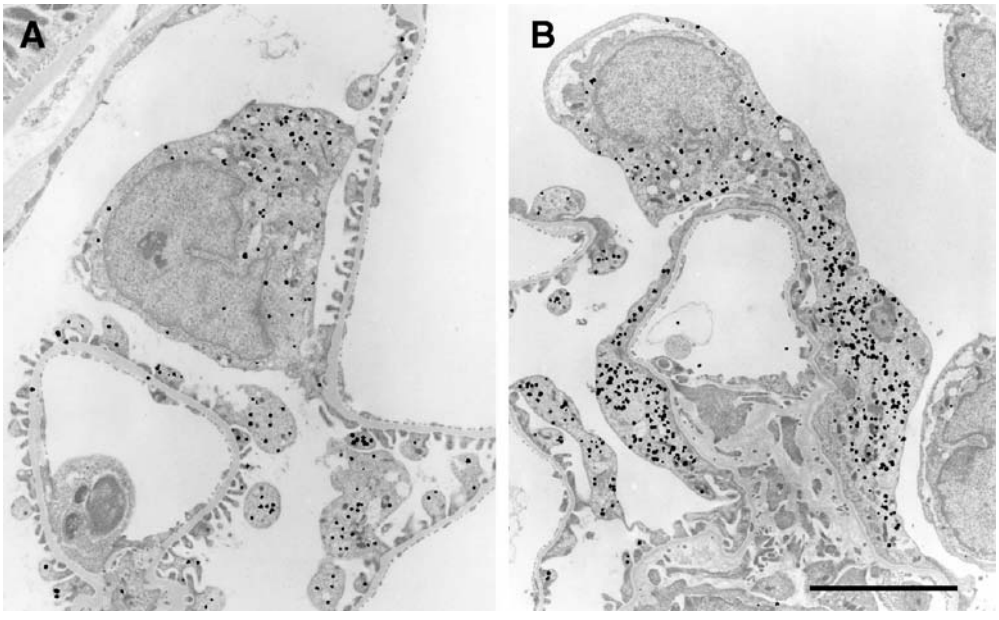

Fig. 3 Immunogold localization of nestin in the podocytes in a normal rat (**a**) and a PAN-treated rat at day 10 (**b**). Intensified immunogold particles for nestin are observed in the cell bodies and primary processes, but not in the foot processes in podocytes. Bar: 5 μm

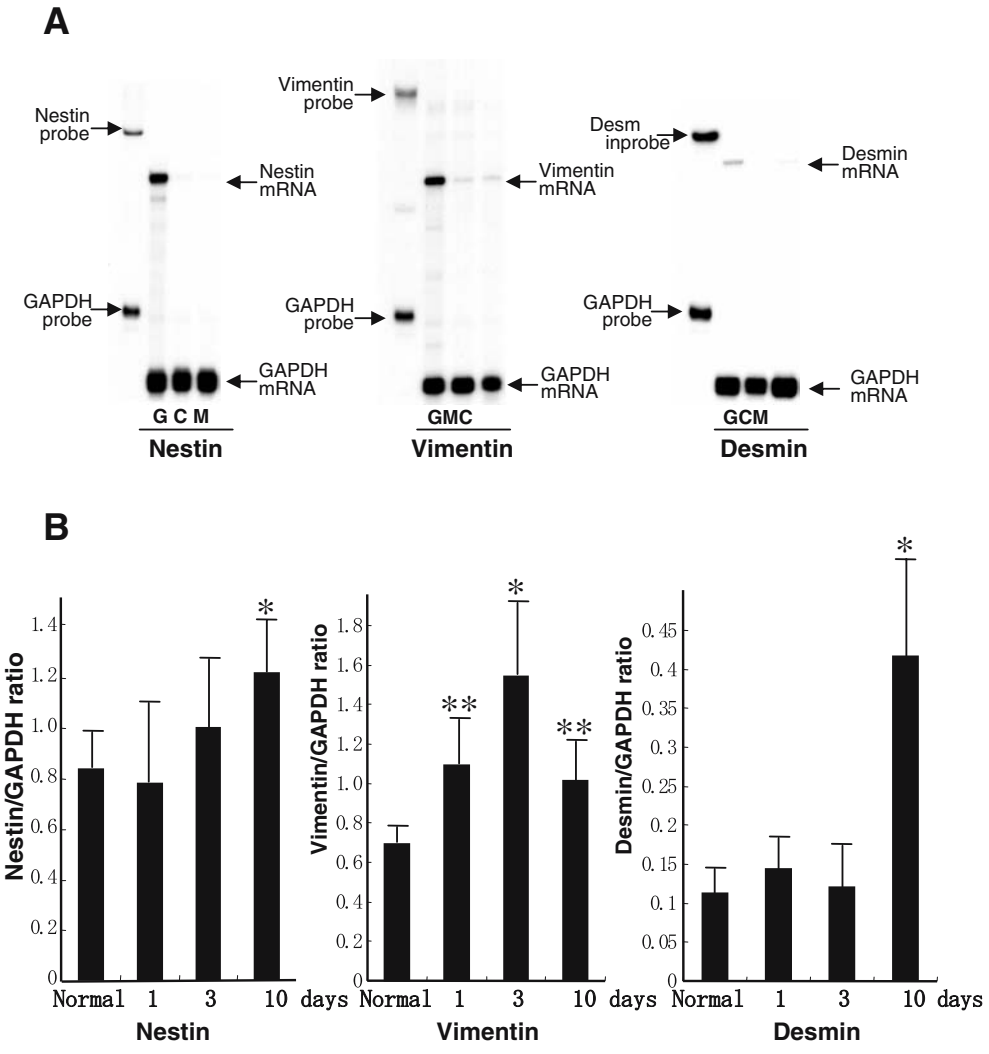

Fig. 4 A ribonuclease protection assay for nestin, vimentin, and desmin in RNA samples from the glomeruli (*G*), cortices (*C*), and medullae (*M*) in the normal kidney and PAN nephrosis. **a** In the normal kidney, nestin, vimentin, and desmin are expressed predominantly in the glomeruli. **b** A quantitative analysis of ribonuclease protection assay using glomerular samples reveals significant increases of nestin, vimentin, and desmin after PAN injection. All data from five samples are presented as means±SD. *$p<0.01$, **$p<0.05$ vs normal glomeruli

or the medullae, although the expression levels in the glomeruli were high in nestin and low in desmin. Vimentin signals were intensely found in the glomeruli, but they were weakly found in the cortices and medullae.

To examine the changes in the IF transcript levels after the PAN injection, IF mRNA were quantified on days 1, 3, and 10 by a molecular imaging analysis. As a result, significant increases in the IF transcripts were observed in the mRNA from the glomeruli in PAN nephrosis (Fig. 4b). It is interesting that the timing for the upregulation in PAN nephrosis was different among the IF transcripts. One day and 3 days after the PAN injection, vimentin was found to already be upregulated, but nestin and desmin did not show any significant increase. At day 10 of PAN nephrosis, the expression of all three IF proteins were significantly upregulated.

Discussion

In the present study, the distribution and expression of IF proteins was examined in the rat kidney with PAN nephrosis. Several relevant observations resulted from this analysis. First, nestin, vimentin, and desmin were expressed exclusively in the glomerulus, especially in the podocytes. Second, these IF proteins were upregulated in the nephrotic stage in PAN nephrosis. Third, the timing for the upregulation in PAN nephrosis was different among the three IF proteins.

The Western blot analysis and ribonuclease protection assay in this study detected distinct signals for nestin in the glomeruli at both protein transcript levels, and the immunolocalization study showed a nestin expression restricted to podocytes. These findings demonstrated that podocytes in adult rats express nestin at a significant level, thus indicating that podocytes contain three different IF proteins, i.e., nestin, vimentin, and desmin. GFAP expression was not detected by immunoblots and immunofluorescence, although the antibodies against GFAP worked on rat brain tissue (data not shown). Nestin, which was initially identified as a marker of neural stem and neural progenitor cells [23], is abundant in migrating and proliferating cells during the early stages of development in the peripheral and central nervous systems and in myogenic and other tissues. In general, nestin becomes downregulated on differentiation, and it is replaced by tissue-specific IF proteins. An excep-

tional expression in the adult brain is observed in the subventricular zone and dentate gyrus, where cell proliferation can continue throughout life [7, 14]. Podocytes do not conform to this case. In spite of the distinct expression of nestin, podocytes in the adult rarely undergo cell division even after a subtotal nephrectomy [13, 31, 33]. In addition, nestin is upregulated during podocyte differentiation: nestin weak staining in presumptive podocytes at the S-shaped body stage and enhanced staining at the capillary loop stage (data not shown). As a result, the mechanism controlling the nestin expression in podocytes is very unique.

Immunoelectron microscopy in this study revealed that nestin is localized in the cell bodies and primary processes of podocytes, but not in the foot processes, which show the same distribution as that of vimentin and desmin [8, 37]. Nestin is unable to form filaments on its own, and can readily form copolymer IFs when combined with type III IF proteins such as vimentin [24] or desmin [35]. Considering that vimentin and desmin can form heterodimers and heterotetramers, it is likely that nestin, vimentin, and desmin co-assemble together into mixed polymers in podocytes.

The present study revealed that nestin, vimentin, and desmin were upregulated in the podocytes in the nephrotic stage of PAN nephrosis. PAN nephrosis is widely used as a model of nephrotic syndrome progressing to focal segmental glomerulosclerosis [6]. A striking morphological feature in PAN nephrosis is the focal detachment of podocytes from the GBM coinciding with the onset of massive proteinuria [34]. Kim et al. [21] reported that PAN injection caused a marked decrease in the podocyte number and an increase in the glomerular size. Because of the lack of cell proliferation, podocytes adapt to the decrease in cell number and glomerular growth by cell hypertrophy [13, 27]. Extreme podocyte hypertrophy has also been observed in a primary culture [38]. The cultured cells exhibit intense immunostaining for desmin in addition to vimentin and nestin (data not shown) [38]. As desmin staining in podocytes is either not detected in vivo under physiological conditions or is only weakly detected, the intense signals for desmin indicate the upregulation of desmin in cultured podocytes [37, 38]. These findings thus suggest the existence of an intimate relationship between IF protein upregulation and podocyte hypertrophy. The idea of the relation between IFs and cell hypertrophy is corroborated by a study using reactive astrocytes lacking IFs [36]. Absence of IF proteins prevented hypertrophy of astrocytic processes. Podocytes are generally attached to several capillaries by way of their foot and primary processes. Therefore, cell hypertrophy on enlarged glomeruli itself increases the mechanical stress to the entire cytoskeleton. The function of IFs is primarily to increase the mechanical resistance of cells [29]. It is therefore tempting to speculate that the upregulation of IF proteins allow podocytes to progress to cell hypertrophy, which is suitable for glomerular growth.

Unexpectedly, the timing for the upregulation in PAN nephrosis differed among nestin, vimentin, and desmin, although it is likely that the three IF proteins co-assemble together into mixed polymers. The transcriptional levels of vimentin already increased 1 and 3 days after the PAN injection, but the nestin and desmin transcripts did not, although all three IF proteins showed a significant upregulation on day 10 in PAN nephrosis. In preliminary experiments, no significant glomerular hypertrophy could be detected until day 4 in spite of a 1.2-fold increase in the diameter of the glomeruli on day 10 (data not shown). Although the biological significance of vimentin upregulation remains obscure, studies on vimentin-deficient fibroblasts provide some interesting data. Eckes et al. [9] reported that not only mechanical stability but also mobility and contractile capacity were impaired in vimentin-deficient fibroblasts, thus revealing the significant contribution of IFs to cell functions dependent upon the dynamics of an actin microfilament system. The early morphological changes of podocytes in PAN nephrosis are mainly related with the foot processes, which are equipped with a complete microfilament-based contractile apparatus [8, 18]. The loss or retraction of the foot process structure is noticeable by day 2 of PAN nephrosis [34]. A significant alteration in the width of the foot processes has been found as early as 24 h following PAN injection [28]. It has been proposed that the foot processes have considerable tension to counteract the expanding forces exerted on the glomerular capillary wall by the pressure gradient across the filtration barrier [22]. Vimentin upregulation in the early phase of PAN nephrosis may enable the foot processes to retract on the tensile capillary wall by increasing the mechanical stability of the cytoskeletal network.

In conclusion, the present study has showed that podocytes express three IF proteins, namely nestin, vimentin, and desmin, all of which are upregulated in PAN nephrosis. The upregulation of IF proteins may thus play a critical role in the morphological changes of podocytes in response to injury.

Acknowledgement This work was supported in part by a Grant-in-Aid for Scientific Research (C) from the Japanese Ministry for Education, Culture, Sports, Science and Technology (No. 17590822).

References

1. Bachmann S, Kriz W, Kuhn C, Franke WW (1983) Differentiation of cell types in the mammalian kidney by immunofluorescence microscopy using antibodies to intermediate filament proteins and desmoplakins. Histochemistry 77:365–394
2. Bloom W, Fawcett DW (1975) A textbook of histology, 10th edn. Sanders, Philadelphia
3. Buniatian G, Traub P, Albinus M, Beckers G, Buchmann A, Gebhardt R, Osswald H (1998) The immunoreactivity of glial fibrillary acidic protein in mesangial cells and podocytes of the glomeruli of rat kidney in vivo and in culture. Biol Cell 90:53–61
4. Chang L, Goldman RD (2004) Intermediate filaments mediate cytoskeletal crosstalk. Nat Rev Mol Cell Biol 5:601–613
5. DePianto D, Coulombe PA (2004) Intermediate filaments and tissue repair. Exp Cell Res 301:68–76
6. Diamond JR, Karnovsky MJ (1986) Focal and segmental glomerulosclerosis following a single intravenous dose of puromycin aminonucleoside. Am J Pathol 122:481–487
7. Doetsch F, Caille I, Lim DA, Garcia-Verdugo JM, Alvarez-Buylla A (1999) Subventricular zone astrocytes are neural stem cells in the adult mammalian brain. Cell 97:703–716

8. Drenckhahn D, Franke RP (1988) Ultrastructural organization of contractile and cytoskeletal proteins in glomerular podocytes of chicken, rat, and man. Lab Invest 59:673–682
9. Eckes B, Dogic D, Colucci-Guyon E, Wang N, Maniotis A, Ingber D, Merckling A, Langa F, Aumailley M, Delouvee A, Koteliansky V, Babinet C, Krieg T (1998) Impaired mechanical stability, migration and contractile capacity in vimentin-deficient fibroblasts. J Cell Sci 111:1897–1907
10. Fleming S, Symes CE (1987) The distribution of cytokeratin antigens in the kidney and in renal tumours. Histopathology 11: 157–170
11. Floege J, Alpers CE, Sage EH, Pritzl P, Gordon K, Johnson RJ, Couser WG (1992) Markers of complement-dependent and complement-independent glomerular visceral epithelial cell injury in vivo. Lab Invest 67:486–497
12. Floege J, Hackmann B, Kliem V, Kriz W, Alpers CE, Johnson RJ, Kuhn KW, Koch KM, Brunkhorst R (1997) Age-related glomerulosclerosis and interstitial fibrosis in Milan normotensive rats: a podocyte disease. Kidney Int 51:230–243
13. Fries JW, Sandstrom DJ, Meyer TW, Rennke HG (1989) Glomerular hypertrophy and epithelial cell injury modulate progressive glomerulosclerosis in the rat. Lab Invest 60:205–218
14. Fukuda S, Kato F, Tozuka Y, Yamaguchi M, Miyamoto Y, Hisatsune T (2003) Two distinct subpopulations of nestin-positive cells in adult mouse dentate gyrus. J Neurosci 23: 9357–9366
15. Higgins JP, Wang L, Kambham N, Montgomery K, Mason V, Vogelmann SU, Lemley KV, Brown PO, Brooks JD, van de Rijn M (2004) Gene expression in the normal adult human kidney assessed by complementary DNA microarray. Mol Biol Cell 15:649–656
16. Holthöfer H, Miettinen A, Lehto VP, Lehtonen E, Virtanen I (1984) Expression of vimentin and cytokeratin types of intermediate filament proteins in developing and adult human kidneys. Lab Invest 50:552–559
17. Hoshi S, Shu Y, Yoshida F, Inagaki T, Sonoda J, Watanabe T, Nomoto K, Nagata M (2002) Podocyte injury promotes progressive nephropathy in zucker diabetic fatty rats. Lab Invest 82:25–35
18. Ichimura K, Kurihara H, Sakai T (2003) Actin filament organization of foot processes in rat podocytes. J Histochem Cytochem 51:1589–1600
19. Kamiie J, Nameta M, Ma M, Takata T, Fujinaka H, Yoshida Y, Yaoita E, Yamamoto T (2002) Localization and expression of the aquaporin-1 water channel in mesangial cells in the human glomerulus. Arch Histol Cytol 65:83–90
20. Kihara I, Yaoita E, Kawasaki K, Yamamoto T (1995) Limitation of podocyte adaptation for glomerular injury in puromycin aminonucleoside nephrosis. Pathol Int 45:625–634
21. Kim YH, Goyal M, Kurnit D, Wharram B, Wiggins J, Holzman L, Kershaw D, Wiggins R (2001) Podocyte depletion and glomerulosclerosis have a direct relationship in the PAN-treated rat. Kidney Int 60:957–968
22. Kriz W, Elger M, Mundel P, Lemley KV (1995) Structure-stabilizing forces in the glomerular tuft. J Am Soc Nephrol 5:1731–1739
23. Lendahl U, Zimmerman LB, McKay RD (1990) CNS stem cells express a new class of intermediate filament protein. Cell 60:585–595
24. Marvin MJ, Dahlstrand J, Lendahl U, McKay RD (1998) A rod end deletion in the intermediate filament protein nestin alters its subcellular localization in neuroepithelial cells of transgenic mice. J Cell Sci 111:1951–1961
25. Moll R, Hage C, Thoenes W (1991) Expression of intermediate filament proteins in fetal and adult human kidney: modulations of intermediate filament patterns during development and in damaged tissue. Lab Invest 65:74–86
26. Nagai M, Yaoita E, Yoshida Y, Kuwano R, Nameta M, Ohshiro K, Isome M, Fujinaka H, Suzuki S, Suzuki J, Suzuki H, Yamamoto T (2003) Coxsackievirus and adenovirus receptor, a tight junction membrane protein, is expressed in glomerular podocytes in the kidney. Lab Invest 83:901–911
27. Nagata M, Kriz W (1992) Glomerular damage after uninephrectomy in young rats. II. Mechanical stress on podocytes as a pathway to sclerosis. Kidney Int 42:148–160
28. Nevins TE, Gaston T, Basgen JM (1984) Quantitative indexes of aminonucleoside-induced nephrotic syndrome. Am J Pathol 117:30–36
29. Omary MB, Coulombe PA, McLean WH (2004) Intermediate filament proteins and their associated diseases. N Engl J Med 351:2087–2100
30. Oosterwijk E, Van Muijen GN, Oosterwijk-Wakka JC, Warnaar SO (1990) Expression of intermediate-sized filaments in developing and adult human kidney and in renal cell carcinoma. J Histochem Cytochem 38:385–392
31. Pabst R, Sterzel RB (1983) Cell renewal of glomerular cell types in normal rats: an autoradiographic analysis. Kidney Int 24:626–631
32. Peterson GL (1977) A simplification of the protein assay method of Lowry et al. which is more generally applicable. Anal Biochem 83:346–356
33. Rasch R, Nørgaard JOR (1983) Renal enlargement: comparative autographic studies of [^{3}H]thymidine uptake in diabetic and uninephrectomized rats. Diabetologia 25:280–287
34. Ryan GB, Karnovsky MJ (1975) An ultrastructural study of the mechanisms of proteinuria in aminonucleoside nephrosis. Kidney Int 8:219–232
35. Sjöberg G, Jiang WQ, Ringertz NR, Lendahl U, Sejersen T (1994) Colocalization of nestin and vimentin/desmin in skeletal muscle cells demonstrated by three-dimensional fluorescence digital imaging microscopy. Exp Cell Res 214:447–458
36. Wilhelmsson U, Li L, Pekna M, Berthold CH, Blom S, Eliasson C, Renner O, Bushong E, Ellisman M, Morgan TE, Pekny M (2004) Absence of glial fibrillary acidic protein and vimentin prevents hypertrophy of astrocytic processes and improves post-traumatic regeneration. J Neurosci 24:5016–5021
37. Yaoita E, Kawasaki K, Yamamoto T, Kihara I (1990) Variable expression of desmin in rat glomerular epithelial cells. Am J Pathol 136:899–908
38. Yaoita E, Yamamoto T, Takashima N, Kawasaki K, Kawachi H, Shimizu F, Kihara I (1995) Visceral epithelial cells in rat glomerular cell culture. Eur J Cell Biol 67:136–144
39. Yaoita E, Yao J, Yoshida Y, Morioka T, Nameta M, Takata T, Kamiie J, Fujinaka H, Oite T, Yamamoto T (2002) Up-regulation of connexin43 in glomerular podocytes in response to injury. Am J Pathol 161:1597–1606

Virchows Arch (2006) 448: 493–499
DOI 10.1007/s00428-005-0133-x

ORIGINAL ARTICLE

Junji Shibahara · Takeshi Kashima · Yoshinao Kikuchi · Akiko Kunita · Masashi Fukayama

Podoplanin is expressed in subsets of tumors of the central nervous system

Received: 10 September 2005 / Accepted: 7 November 2005 / Published online: 13 January 2006

Abstract Immunohistochemical analyses with the monoclonal antibody D2-40 were performed to ascertain the expression of podoplanin (a.k.a. T1-alpha, gp36, or aggrus) in tumors of the central nervous system (CNS) and to determine the diagnostic utility of the antibody. The analyses were performed on 325 tumors of various histologic types. The chief finding was almost constant immunoreactivity in ependymal tumors (37/40, 92.5%), choroid plexus papillomas (8/8, 100%), and meningiomas (100/100, 100%). The reactivity was considered "tissue-specific," as the corresponding normal tissue of each tumor was also found to express podoplanin. In addition, expression, not committed to the lineages, was found in many other tumor types, including astrocytic tumors, medulloblastomas, and hemangioblastomas, with variable frequency and intensity. The way of expression was not fully understood, but the expression in astrocytic tumors seemed to be associated with pronounced fibrous properties or malignant phenotype, as was shown by high-frequent expression in pilocytic astrocytomas (12/12, 100%) and glioblastomas (29/35, 82.9%). The present study has shown that podoplanin is expressed in several types of CNS tumors with variable frequency and intensity. Given the widespread expression of podoplanin, the antibody D2-40 is of little use in diagnostic practice for CNS tumors.

Keywords Podoplanin · D2-40 · Central nervous system · Tumor · Immunohistochemistry

J. Shibahara (✉) · T. Kashima · Y. Kikuchi · M. Fukayama
Department of Pathology, Graduate School of Medicine,
University of Tokyo,
7-3-1 Hongo, Bunkyo-ku,
113-0033 Tokyo, Japan
e-mail: jshiba-tky@umin.ac.jp
Tel.: +81-3-38155411
Fax: +81-3-58008785

A. Kunita
Institute of Molecular and Cellular Biosciences,
University of Tokyo,
Tokyo, Japan

Introduction

Podoplanin—otherwise known as T1-alpha [10], gp36 [17], or aggrus [7]—is a mucin-type transmembrane glycoprotein which was first identified in the rat glomerular epithelial cells (podocytes) [1]. Podoplanin is now established as a specific marker of the lymphatic endothelium [2]. D2-40, a monoclonal antibody originally raised against an unidentified M2A protein derived from germ cell tumors [11], has been shown to recognize podoplanin specifically [15]. Immunohistochemical analysis using D2-40 has detected the expression of podoplanin in many organs and tissues, including the lymphatic endothelium, mesothelial cells, osteocytes, glandular myoepithelial cells, and stromal reticular cells and follicular dendritic cells of lymphoid organs [15]. Expression of podoplanin, or positive immunoreactivity to D2-40, has also been confirmed in lymphangiomas, Kaposi's sarcomas, germ cell tumors, squamous cell carcinomas, mesotheliomas, and a subset of angiosarcomas [2, 4–6, 9, 15]. Lacking detailed knowledge on podoplanin expression in tumors of the central nervous system (CNS), we decided to perform immunohistochemical analyses on various CNS tumors with the antibody D2-40 to determine the distribution of podoplanin in the tumors and the diagnostic utility of the antibody.

Materials and methods

Tumor specimens

All the tumor specimens were retrieved from the archives of University of Tokyo Hospital. Most of the specimens had initially been selected for construction of tissue microarrays (TMAs) for use in future research. Selection was based on the availability of paraffin blocks and whether the tissues in the paraffin blocks were adequately thick. We prepared several unstained sections from each selected block before constructing the TMAs, then used these slides for the present study. We also added several

more cases to the study to increase the range of tumor types and the number of cases examined. Autopsy specimens and nonneoplastic regions of the tumor specimens were used to examine the nonneoplastic brain.

The histology of each tumor sample was reevaluated according to the World Health Organization (WHO) classification for tumors of the CNS (2000). In total, we examined 83 astrocytic tumors, including 12 pilocytic astrocytomas (WHO grade I), 19 diffuse astrocytomas (WHO grade II), 17 anaplastic astrocytomas (WHO grade III), and 35 glioblastomas (WHO grade IV); 19 oligodendroglial tumors, including 12 oligodendrogliomas (WHO grade II) and 7 anaplastic oligodendrogliomas (WHO grade III); 9 mixed gliomas, including 5 oligoastrocytomas (WHO grade II) and 4 anaplastic oligoastrocytomas (WHO grade III); 40 ependymal tumors, including 1 subependymoma (WHO grade I), 2 myxopapillary ependymomas (WHO grade I), 29 ependymomas (WHO grade II), 7 anaplastic ependymomas (WHO grade III), and 1 chordoid glioma of the third ventricle (a tumor now considered a specific type of ependymoma of subcommisural organ origin [3, 13]; WHO grade II); 16 neuronal and mixed neuronal–glial tumors, including 2 dysembryoplastic neuroepithelial tumors (WHO grade I), 12 central neurocytomas (WHO grade II), and 2 gangliogliomas (WHO grade II); 22 embryonal tumors, all of which were medulloblastomas (WHO grade IV); 110 meningeal tumors, including 100 meningiomas (WHO grade I) and 10 hemangiopericytomas/solitary fibrous tumors (WHO grade I; included together due to difficulty in clearly discriminating between them); 8 choroid plexus papillomas (WHO grade I); and 18 hemangioblastomas (WHO grade I). We also added a craniopharyngioma and a cavernous hemangioma to evaluate reactive piloid gliosis around the lesions.

Immunohistochemistry

The mouse monoclonal antibody D2-40 (Signet, Dedham, MA) was used in all cases. In some cases, expression of glial fibrillary acidic protein (GFAP) was also examined by a monoclonal antibody (Dako Corporation, Santa Barbara, CA) to ascertain the state of the reactive gliosis, a condition which often manifested positive D2-40 labeling. Immunohistochemical staining was performed by the avidin-biotinylated immunoperoxidase method. Briefly, 5-μm sections were deparaffinized and rehydrated. Antigen retrieval was performed by autoclave in a 10-mM citrate buffer (pH 6.0) for 5 min at 120°C. All the tissue was then exposed to 3% hydrogen peroxidase for 5 min (to block endogenous biotin reactivity), primary antibody for 25 min, biotinylated secondary antibody for 25 min, diaminobenzidine as a chromogen for 5 min, and hematoxylin counterstain for 5 min. All immunohistochemical staining was performed by an automatic stainer (Kyowa Hakko, Tokyo, Japan). The stained slides were then coverslipped using the Tissue-Tek.SCA automatic coverslipper (Sakura Finetek, Tokyo, Japan) and evaluated by two investigators (JS and YK). The validity of the D2-40 staining was confirmed by positive control (mesothelial cells) and internal negative control (blood vessels in the specimens). Leptomeningeal immunoreactivity was frequently used as internal positive control, as the staining was appreciated not only on the brain surface but also on the limiting membrane of perivascular space (Virchow–Robin space) due to the pial coat. Staining intensity of the normal leptomeninges (not infiltrated by tumor cells) was used as a standard for the following semiquantitative evaluation. It could also be applied to cases lacking the normal leptomeninges in the specimens, as the automatic stainer made little difference concerning the staining results of the normal leptomeninges. The staining intensity was evaluated as weak (lower intensity than the normal leptomeningeal staining), moderate (intensity almost equivalent to the normal leptomeningeal staining), or strong (intensity apparently stronger than the normal leptomeningeal staining). Immunohistochemical expression was graded as follows: 0, ≤5% of cells stained; 1+, 6–25% cells stained with weak intensity; 2+, >25% cells stained with weak intensity or 6–25% cells stained with variable intensity; +3, >25% cells stained with variable intensity; +4, ≥50% of cells stained with strong intensity. “Variable intensity” was meant to indicate any staining intensity except for entirely weak one (i.e., moderate or strong intensity was found somewhere).

Results

Podoplanin expression in normal structures and reactive states of the CNS

In the nonneoplastic brains, reactivity to D2-40 was observed in the ependyma, choroid plexus epithelium, and leptomeninges (pia and arachnoid mater; Fig. 1a–c). Reactivity to the ependymal cells and choroid plexus epithelium was noted on the surface aspect of the cell membrane. Leptomeningeal staining also labeled the cluster of arachnoid cells (arachnoid granulation). The cerebral parenchyma was almost nonreactive except for the subpial and paraventricular regions, where laminar immunoreactivity to D2-40 was frequently observed. Besides, the whiter matter, especially that of the aged patients, exhibited very low intensity of immunoreactivity. The molecular layer of the cerebellar cortex was also immunoreactive, and the radiating manner of staining denoted the labeling of the fibrillary processes of Bergmann glias (Fig. 1d). The staining on the cell surfaces of the Purkinje cells was problematic, as it was difficult to determine whether the staining was against the cell membrane or derived from glial processes towards the cell membrane. The granular layer and the white matter of the cerebellum exhibited much lower intensity of immunoreactivity.

Reactive gliosis, especially fibrous gliosis of the piloid type, was immunoreactive to D2-40, as was typically observed in piloid gliosis accompanying craniopharyngioma and cavernous hemangioma. In the analyses of the neuroepithelial tumors, peritumoral regions of relatively well-demarcated, slow-growing tumors such as epen-

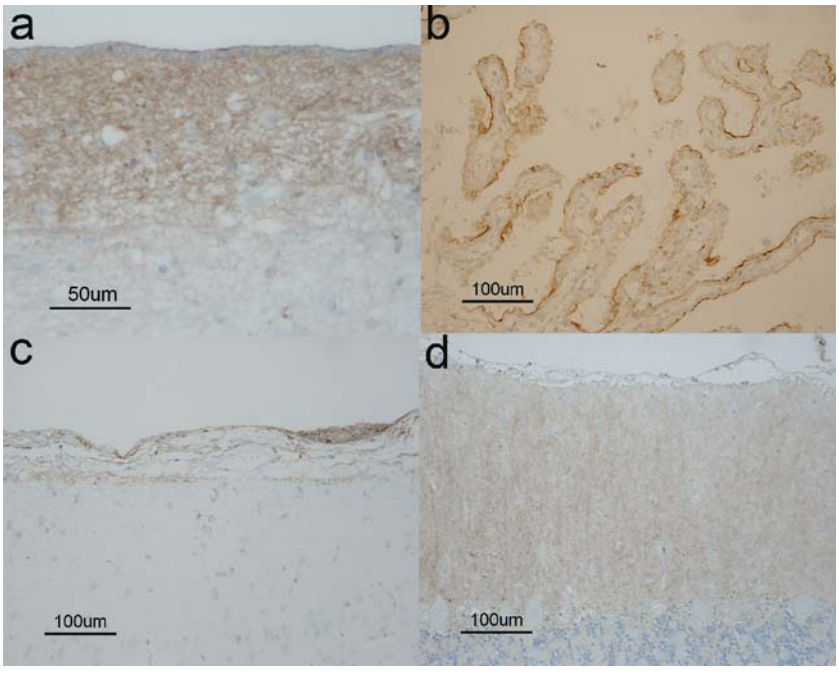

Fig. 1 Podoplanin expression in normal structures of the central nervous system (CNS). Expression was determined by the monoclonal antibody D2-40. **a** The ependyma showed immunoreactivity on the apical surface. The paraventricular parenchyma was also immunoreactive. **b** The choroid plexus epithelium demonstrated immunoreactivity on the surface aspect of the cell membrane. **c** Immunoreactivity was observed in the pia and arachnoid maters. The cluster of the arachnoids cells was also immunoreactive. **d** The cerebellar cortex was also immunoreactive. The radiating pattern of staining indicates expression in Bergmann glias

dymomas were accompanied by fibrillary gliosis immunoreactive to D2-40. Diffusely infiltrated tumors such as diffuse astrocytomas and oligodendrogliomas usually did not induce immunoreactive fibrillary gliosis. The exceptions were subpial and paraventricular regions of the involved sites, where D2-40 labeling was found to be fairly frequent. Moreover, reactive fibrillary gilosis commonly appeared in variable tumor types in the brain stem, spinal cord, and cerebellum (both cortex and white matter). Pilocytic astrocytomas, ependymomas, gangliogliomas, medulloblastomas, and hemangioblastomas were all frequently observed in these anatomic locations. We forewent evaluation at the tumor periphery, as this would have led to possible misinterpretation of the reactive gliosis. No other histologic types involving these locations were included in the study.

Expression of podoplanin in various CNS tumors

Podoplanin expression was observed in a number of tumor types with variable levels of intensity and frequency, as summarized in Table 1.

Astrocytic tumor

Among astrocytic tumors, constant immunoreactivity to D2-40 was confirmed in pilocytic astrocytomas (12/12, 100%). The immunoreactivity in this biphasic tumor was more intense in densely fibrous areas than that in loose, myxoid areas (Fig. 2a). Diffuse astrocytomas, including protoplasmic, fibrillary, and gemistocytic types, usually showed little to no reactivity (Fig. 2b), and only 3 of 19 cases (15.8%) were considered positive. One case exhibiting a relatively strong degree of immunoreactivity (3+) had been treated by preoperative irradiation. Anaplastic astrocytomas were immunoreactive to D2-40 more frequently (8/17, 47.1%) and exhibited variable degrees of staining. Most glioblastomas exhibited positive immunoreactivity (29/35, 82.9%), with membranous, cytoplasmic or diffuse (glial) staining of a generally strong intensity (Fig. 2c). Intense immunoreactivity was constantly observed adjacent to necroses.

Oligodendroglial tumor

Oligodendrogliomas were generally not shown to be positive for D2-40 (0/12, 0.0%; Fig. 2d). As an exception, small numbers of cells with "astrocytic" features, i.e., gliofibrillary astrocytes or minigemistocytes, showed weak cytoplasmic immunoreactivity. Two of seven anaplastic oligodendrogliomas (28.5%) showed positive reactivity. The reactivity was preferentially noted in gliofibrillary astrocytes or minigemistocytes.

Mixed glioma

Four of five oligoastrocytomas (80.0%) and two of four anaplastic oligoastrocytomas (50.0%) showed positive reactivity. Reactivity was noted in the astrocytic component rather than in the oligodendroglial component, and the staining was usually somewhat weak.

Ependymal tumor

Twenty-eight of 29 ependymomas (96.6%) and 6 of 7 anaplastic ependymomas (85.7%) showed positive reactivity with generally strong staining. The immunostained

Table 1 Podoplanin expression in central nervous system tumors

	Total case	Positive case (%)	Grade of reactivity					Average grade
			4+	3+	2+	1+	0	
Astrocytic tumor								
Pilocytic astrocytoma	12	12 (100%)	2	10	0	0	0	3.17
Diffuse astrocytoma	19	3 (15.8%)	0	1	0	2	16	0.26
Anaplastic astrocytoma	17	8 (47.1%)	1	2	3	2	9	1.06
Glioblastoma	35	29 (82.9%)	13	12	3	1	6	2.71
Oligodendroglial tumor								
Oligodendroglioma	12	0 (0.0%)	0	0	0	0	12	0.00
Anaplastic oligodendroglioma	7	2 (28.5%)	0	2	0	0	5	0.86
Mixed glioma								
Oligoastrocytoma	5	4 (80.0%)	0	1	0	3	1	1.50
Anaplastic oligoastrocytoma	4	2 (25.0%)	0	1	0	1	2	1.00
Ependymal tumor								
Subependymoma	1	1 (100%)	0	0	1	0	0	2.00
Myxopapillary ependymoma	2	1 (50.0%)	0	0	0	1	1	0.50
Ependymoma	29	28 (96.6%)	9	12	7	0	1	2.97
Chordoid glioma of the third ventricle	1	1 (100%)	0	1	0	0	0	3.00
Anaplastic ependymoma	7	6 (85.7%)	1	5	0	0	1	2.71
Neuronal and mixed neuronal–glial tumor								
Dysembryoplastic neuroepithelial tumor	2	0 (0.0%)	0	0	0	0	2	0.00
Central neurocytoma	12	1 (8.3%)	0	0	0	1	11	0.08
Ganglioglioma	2	2 (100%)	0	1	0	1	0	2.00
Embryonal tumor								
Medulloblastoma	22	6 (27.3%)	1	3	2	0	16	0.77
Meningeal tumor								
Meningioma	100	100 (100%)	22	63	14	1	0	3.06
Hemangiopericytoma/solitary fibrous tumor	10	7 (70.0%)	0	0	3	4	3	1.00
Others								
Choroid plexus papilloma	8	8 (100%)	0	8	0	0	0	3.00
Hemangioblastoma	18	9 (50.0%)	0	7	2	0	9	1.39

areas contrasted well with the surrounding brain parenchyma in some cases, whereas the peritumoral reactive gliosis showed more intense immunoreactivity than the tumor itself in others. Membranous, cytoplasmic, diffuse (glial), and dot- or ring-like patterns of staining were noted (Fig. 2e,f). Unlike the normal ependyma, membranous staining was not restricted to the luminal surfaces of the ependymal canals or tubes. Diffuse glial staining was prominent at the perivascular areas, highlighting perivascular pseudorosettes. Dot- and ring-like patterns of staining, presumed to be staining against microlumens formed by tumor cells, were characteristic to ependymomas. One subependymoma exhibited diffuse immunoreactivity, whereas myxopapillary ependymomas showed little to no reactivity. One chordoid glioma of the third ventricle exhibited membranous and cytoplasmic staining.

Neuronal and mixed neuronal–glial tumor

Immunoreactivity was absent in two dysembryoplastic neuroepithelial tumors (0.0%). One of 12 central neurocytomas (8.3%) exhibited focal immunoreactivity, while all of the others were almost entirely nonreactive (Fig. 2g). The single positive case was a "liponeurocytoma," an unusual neurocytoma with prominent lipidized tumor cells. The D2-40 reactivity in the tumor was against considerable numbers of GFAP-positive astrocytic tumor cells admixed in the tumor. The reactivity in the other cases was identified in limited areas where immunostaining for GFAP concurrently revealed increased numbers of astrocytic cells, presumably reactive ones. In addition, the tumor periphery was often labeled with D2-40 due to reactive gliosis against the tumor. Both gangliogliomas analyzed in this study showed positive reactivity (100%; Fig. 2h). The glial component was apparently reactive, whereas it was difficult to determine whether the staining on the ganglion cells was against the cell membrane or the surrounding glias.

Embryonal tumor

Six of 22 medulloblastomas exhibited positive immunoreactivity (27.3%) in the form of membranous and cytoplas-

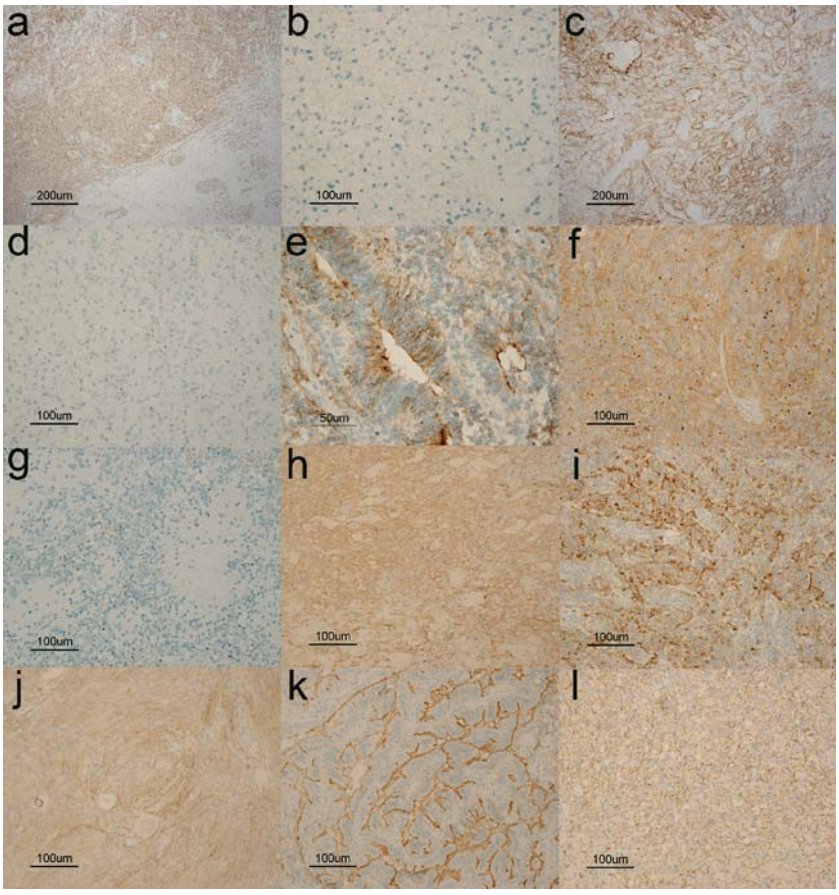

Fig. 2 Podoplanin expression in various tumors of the CNS. Expression was determined by the monoclonal antibody D2-40. **a** Pilocytic astrocytomas were strongly immunoreactive, especially in the fibrous areas. **b** Diffuse astrocytomas usually showed little to no immunoreactivity. **c** Glioblastomas frequently showed strong immunoreactivity. **d** Oligodendrogliomas were not reactive. **e**, **f** Ependymomas exhibited membranous (**e**), diffuse and, dot- and ring-like patterns (**f**) of immunoreactivity. **g** Most central neurocytomas contained a few reactive cells, if any. **h** Reactivity was apparent in the glial component of gangliogliomas. **i** Some of the medulloblastomas exhibited strong cytoplasmic and membranous staining. **j** All meningiomas showed positive immunoreactivity. **k** Choroid plexus papillomas showed membranous immunoreactivity. **l** Some hemangioblastomas were immunoreactive. However, it was difficult to determine whether the staining was against the cell membrane or interstitium in most of the positive cases

mic staining (Fig. 2i). Many other cases also showed partial positive reactivity with an interstitial pattern of staining. These cases were not considered positive, however, as concurrent interstitial immunoreactivity to GFAP in the positive areas indicated that this reactivity was largely against preexisting glias or reactive gliosis. D2-40-reactive cells also exhibited intense cytoplasmic immunoreactivity to GFAP, a finding indicative of glial phenotype, in some of the positive cases. Reactivity to GFAP was hardly discernible in the D2-40-reactive cells in the other positive cases.

Meningeal tumor

All of the meningiomas (100/100, 100%) were immunoreactive to D2-40 with a generally high degree of staining, irrespective of their histologic subtypes (Fig. 2j). Seven of 10 hemangiopericytomas/solitary fibrous tumors were also immunoreactive for D2-40, albeit with a generally lower degree of staining than most meningiomas.

Others

All cases of choroid plexus papilloma (8/8, 100%) were reactive to D2-40 (Fig. 2k). The staining was membranous and always diffuse. Nine of 18 hemangioblastomas (50%) were positive for D2-40 (Fig. 2l). It was difficult to determine whether the staining was against the cell membranes of the stromal cells or the interstitium, however, as diffuse interstitial staining of GFAP was noted in most of the positive cases.

Discussion

Immunohistochemical analysis using the antibody D2-40 has confirmed the expression of podoplanin in various types of CNS tumors.

The podoplanin expressions observed in the ependymomas of all grades, the choroid plexus papillomas and the meningiomas, were “tissue-specific” and could be predicted from the staining results of the normal structures corresponding to the tumors (ependyma, choroid plexus epithelium, and leptomeninges). Schacht et al. [15] and Roy et al. [14] have confirmed podoplanin expression or immunoreactivity to D2-40 in these normal structures of the mouse and human brains, respectively. Coarse dot- and ring-like patterns of staining observed in ependymomas were presumed to highlight microlumens formed by tumor cells. Similar patterns have been described in immunohistochemical staining of epithelial membrane antigen (EMA) [8]. One case of chordoid glioma of the third ventricle

showed membranous and cytoplasmic staining. This result is consistent with the presumed tumor origin from the specific ependyma of the subcommisural organ [3, 13]. All meningiomas expressed podoplanin, and most did so strongly. The hemangiopericytomas/solitary fibrous tumors, on the other hand, exhibited relatively weak to no immunoreactivity. The result supports the theory that the latter tumors are not of meningeal cell origin, as podoplanin expression seems to be an inherent trait of the leptomeninges.

Expression in astrocytic tumors was not committed to the lineage, but reflected certain phenotypic manifestations. Podoplanin cannot be a lineage-specific marker of astrocytes, given that the native astrocytes in the cerebrum and most of the diffuse astrocytomas were negative for D2-40. However, the pronounced fibrous property of both neoplastic and reactive conditions has been shown to lead to podoplanin expression, as typically manifested in the pilocytic astrocytomas and piloid gliosis around the craniopharyngioma and the cavernous hemangioma. Reactivity in the molecular layer of the cerebellar cortex also seems to result from the fibrillary nature of Bergmann glias. The diffuse (glial) expression pattern, prominent at the perivascular areas, of ependymomas might reflect a similar feature in the cell processes. Podoplanin expression was also associated with the malignant phenotype: expression was observed in the diffuse astrocytomas, the anaplastic astrocytomas, and the glioblastomas, in ascending order of frequency.

Podoplanin expression was usually absent in oligodendroglial tumors and neuronal tumors such as oligodendrogliomas and central neurocytomas, respectively. Immunoreactivity to D2-40 was almost exclusively confined to cells with astrocytic features (minigemistocytes or gliofibrillary astrocytes) in the oligodendroglial tumors and the astrocytic components of the mixed tumors. One central neurocytoma manifesting a histology of "liponeurocytoma" was focally immunoreactive to D2-40, but the positive areas were also labeled with GFAP, a finding indicative of the glial (astrocytic) phenotype. Several of the medulloblastomas, an embryonal tumor that typically manifests a neuronal immunophenotype, also exhibited concurrent immunoreactivity to D2-40 and GFAP in some parts of the stained tissue. The staining was cytoplasmic and membranous and could be differentiated from the reactivity of the native or reactive condition of cerebellum. Immunoreactivity to D2-40 in medulloblastomas, however, did not always result from the glial phenotype, as D2-40-positive tumor cells were not reactive to GFAP in the other cases.

Among the other tumor types, half of the hemangioblastomas exhibited positive immunoreactivity. This conflicted with the result by Roy et al. [14], who found constant immunoreactivity in the stromal cells of hemangioblastomas. Moreover, the positive finding was less than certain, as it was difficult to determine whether the staining was against the cell membranes of the stromal cells or the interstitium. We should note here that reactive astrocytes are sometimes numerous within the substance of hemangioblastomas [12]. Most of the positive cases in our study were diffusely immunoreactive to GFAP. While some of the stromal cells may have been reactive, these findings tell us that the reactivity was chiefly against the intervening astrocytes. The angioblastic nature of the stromal cells [16] also seems inconsistent with podoplanin expression.

This study also sought to elucidate the diagnostic utility of D2-40. We initially expected that podoplanin expression would be limited to "tissue-specific" ones, noted in ependymomas, choroid plexus papillomas, and meningiomas. Given the widespread expression in various CNS tumors and reactive condition, however, we found that the antibody is of little use in diagnosis of CNS tumors. Combinations with other makers will be required for diagnostic practices.

References

1. Breiteneder-Geleff S, Matsui K, Soleiman A, Meraner P, Poczewski H, Kalt R, Schaffner G, Kerjaschki D (1997) Podoplanin, novel 43-kd membrane protein of glomerular epithelial cells, is down-regulated in puromycin nephrosis. Am J Pathol 151:1141–1152
2. Breiteneder-Geleff S, Soleiman A, Kowalski H, Horvat R, Amann G, Kriehuber E, Diem K, Weninger W, Tschachler E, Alitalo K, Kerjaschki D (1999) Angiosarcomas express mixed endothelial phenotypes of blood and lymphatic capillaries: podoplanin as a specific marker for lymphatic endothelium. Am J Pathol 154:385–394
3. Cenacchi G, Roncaroli F, Cerasoli S, Ficarra G, Merli GA, Giangaspero F (2001) Chordoid glioma of the third ventricle: an ultrastructural study of three cases with a histogenetic hypothesis. Am J Surg Pathol 25:401–405
4. Chu AY, Litzky LA, Pasha TL, Acs G, Zhang PJ (2005) Utility of D2-40, a novel mesothelial marker, in the diagnosis of malignant mesothelioma. Mod Path 18:105–110
5. Dumoff KL, Chu C, Xu X, Pasha T, Zhang PJ, Acs G (2005) Low D2-40 immunoreactivity correlates with lymphatic invasion and nodal metastasis in early-stage squamous cell carcinoma of the uterine cervix. Mod Path 18:97–104
6. Kahn HJ, Bailey D, Marks A (2002) Monoclonal antibody D2-40, a new marker of lymphatic endothelium, reacts with Kaposi's sarcoma and a subset of angiosarcomas. Mod Path 15:434–440
7. Kato Y, Sasagawa I, Kaneko M, Osawa M, Fujita N, Tsuruo T (2004) Aggrus: a diagnostic marker that distinguishes seminoma from embryonal carcinoma in testicular germ cell tumors. Oncogene 23:8552–8556
8. Kawano N, Yasui Y, Utsuki S, Oka H, Fujii K, Yamashina S (2004) Light microscopic demonstration of the microlumen of ependymoma: a study of the usefulness of antigen retrieval for Epithelial Membrane Antigen (EMA) immunostaining. Brain Tumor Pathol 21:17–21
9. Kimura N, Kimura I (2005) Podoplanin as a marker for mesothelioma. Pathol Int 55:83–86
10. Ma T, Yang B, Matthay MA, Verkman AS (1998) Evidence against a role of mouse, rat, and two cloned human T1-alpha isoforms as a water channel or a regulator of aquaporin-type water channels. Am J Respir Cell Mol Biol 19:143–149
11. Marks A, Sutherland DR, Bailey D, Iglesias J, Law J, Lei M, Yeger H, Banerjee D, Baumal R (1999) Characterization and distribution of an oncofetal antigen (M2A antigen) expressed on testicular germ cell tumours. Br J Cancer 80:569–578
12. McComb RD, Eastman PJ, Hahn FJ, Bennett DR (1987) Cerebellar hemangioblastoma with prominent stromal astrocytosis: diagnostic and histogenetic considerations. Clin Neuropathol 6:149–154

13. Pasquier B, Peoc'h M, Morrison AL, Gay E, Pasquier D, Grand S, Sindou M, Kopp N (2002) Chordoid glioma of the third ventricle: a report of two new cases, with further evidence supporting an ependymal differentiation, and review of the literature. Am J Surg Pathol 26:1330–1342
14. Roy S, Chu A, Trojanowski JQ, Zhang PJ (2005) D2-40, a novel monoclonal antibody against the M2A antigen as a marker to distinguish hemangioblastomas from renal cell carcinomas. Acta Neuropathol (Berl) 109:497–502
15. Schacht V, Dadras SS, Johnson LA, Jackson DG, Hong YK, Detmar M (2005) Up-regulation of the lymphatic marker podoplanin, a mucin-type transmembrane glycoprotein, in human squamous cell carcinomas and germ cell tumors. Am J Pathol 166:913–921
16. Vortmeyer AO, Frank S, Jeong SY, Yuan K, Ikejiri B, Lee YS, Bhowmick D, Lonser RR, Smith R, Rodgers G, Oldfield EH, Zhuang Z (2003) Developmental arrest of angioblastic lineage initiates tumorigenesis in von Hippel–Lindau disease. Cancer Res 63:7051–7055
17. Zimmer G, Oeffner F, Von Messling V, Tschernig T, Groness HJ, Klenk HD, Herrler G (1999) Cloning and characterization of gp36, a human mucin-type glycoprotein preferentially expressed in vascular endothelium. Biochem J 341:277–284

Virchows Arch (2006) 448: 500–505
DOI 10.1007/s00428-005-0096-y

ORIGINAL ARTICLE

Hajime Kuroda · Jun-ichi Tamaru · Ikuya Takeuchi · Kiyoshi Ohnisi · Goi Sakamoto · Akiko Adachi · Kou Kaneko · Shinji Itoyama

Expression of E-cadherin, α-catenin, and β-catenin in tubulolobular carcinoma of the breast

Received: 18 June 2005 / Accepted: 8 September 2005 / Published online: 15 March 2006

Abstract Tubulolobular carcinoma (TLC) of the breast is a rare subtype of breast carcinoma categorized by Fisher et al. (Hum Pathol 8:679–683, 1977) as a tubular variant of lobular carcinoma. E-cadherin is a transmembrane glycoprotein, and complete loss of E-cadherin expression has been observed in invasive lobular carcinoma. Ductal carcinoma retains at least some expression of E-cadherin. Moreover, the adhesive function of E-cadherin is dependent on the integrity of the catenin components, which link E-cadherin to the actin filaments. In order to achieve improved categorization of TLC, we decided to investigate both E-cadherin and the catenins in TLCs and invasive lobular carcinomas. We reviewed all 1,430 cases of primary breast carcinoma that were surgically resected at Saitama Medical Center, Saitama Medical School, and at Saitama Red Cross Hospital between 1990 and 2005. Among these, 16 cases of TLC were reported retrospectively. The results were compared with those of 20 cases of invasive lobular carcinomas that were included as controls. Tumor tissue was immunostained for E-cadherin, α-catenin, and β-catenin. The presence of immunoreactivity in the TLC was seen in 12 (75%) cases for E-cadherin, in 8 (50%) cases for α-catenin, and in 10 (62.5%) cases for β-catenin. However, plasma-membrane-associated staining for E-cadherin, α-catenin, and β-catenin was completely absent in invasive lobular carcinomas. These results suggest the possibility that TLCs are not a variant of lobular carcinoma, but rather ductal carcinomas with a lobular growth pattern.

Keywords Breast cancer · Tubulolobular carcinoma · E-cadherin · α-catenin · β-catenin

H. Kuroda (✉) · J.-i. Tamaru · S. Itoyama
Department of Pathology,
Saitama Medical Center,
Saitama Medical School,
Saitama, Japan
e-mail: hajime@saitama-med.ac.jp
Tel.: +81-49-2251677
Fax: +81-49-2251677

I. Takeuchi · K. Ohnisi
Department of Surgery,
Saitama Medical Center,
Saitama Medical School,
Saitama, Japan

G. Sakamoto
Department of Breast Pathology,
Cancer Institute and Hospital,
Japanese Foundation for Cancer Research,
Tokyo, Japan

A. Adachi · K. Kaneko
Department of Pathology,
Saitama Red Cross Hospital,
Saitama, Japan

H. Kuroda
Saitama Medical Center,
Saitama Medical School,
1981 Tsujido, Kamoda, Kawagoe,
Saitama 350-8550, Japan

Introduction

In 1977, Fisher et al. described their experience of a rare type of tumor of the breast that shares histologic features of both tubular and lobular carcinoma of the breast [7]. They described the first series of this tumor, which they called "tubulolobular carcinoma" (TLC), as a tubular variant of lobular carcinoma. The characteristic histological features of this tumor are composed of intermixed, round to angulated tubules and single-file cell cords. Both the tubular and cell cord components demonstrate a diffuse and targetoid pattern as in classical lobular carcinoma. However, this histological subtype of breast carcinoma has still remained unclear due to the rarity of cases. Many questions exist about the clinicopathological significance of this subtype, especially regarding differential diagnosis [9, 28].

E-cadherin is a transmembrane glycoprotein that functions as an epithelium-specific cell-to-cell adhesion molecule [10, 19, 25, 26]. Previous studies have described the differential expression of E-cadherin in lobular and ductal mammary carcinomas [1, 5, 15, 22, 23, 28]. The expression of E-cadherin is significantly reduced in invasive lobular

carcinoma compared with invasive ductal carcinoma. Moreover, the cytoplasmic domain of E-cadherin interacts with groups of cytoplasmic proteins called catenins (α and β) [2, 11, 14, 18, 27]. These cytoplasmic proteins are necessary for cadherin function in cell–cell contact and organizing the cytoskeleton. Deletion of the intracellular catenin-binding domain of E-cadherin or alterations in the functionally active catenins result in the loss of E-cadherin's ability to promote cell adhesion [12, 16, 21]. α-Catenin binds E-cadherin to the cytoskeleton through β-catenin. β-Catenin links E-cadherin and α-catenin by interacting directly with the cytoplasmic domain of cadherin [4, 8, 17, 20, 29]. Furthermore, in several previous studies, the expression of catenins was examined in a series of human breast carcinomas [4, 13, 29]. Although these evaluations were based on a small number of cases, catenin expression was found to be reduced or lost, like E-cadherin expression, in invasive lobular carcinoma compared with invasive ductal carcinoma.

The recent development of immunohistochemical markers has provided another diagnostic tool that may be useful in addition to conventional histological criteria for differential diagnosis. In order to achieve improved categorization of TLC, we decided to investigate the clinicopathological features and morphological findings and the expression of both E-cadherin and the catenins in TLCs.

Patients and methods

The subjects were 1,430 patients with primary breast carcinomas that were examined at Saitama Medical Center, Saitama Medical School, and at Saitama Red Cross Hospital between 1990 and 2005. Sixteen of these cases were identified as TLC cases. The case histories were reviewed for age, stage, and tumor size. Clinical data were obtained from hospital records and contact with physicians. Follow-up examinations were performed either at our institute or at the patient's local hospital. Patients were followed until 2005, and the diagnosis of recurrent disease was based on clinical and radiological examinations and was confirmed by pathological findings.

The resected specimens were reviewed histologically to detect TLC. Classification was performed according to the histologic criteria previously described by Fisher et al. [7]. Paraffin-embedded slides stained with hematoxylin and eosin were used for the histological analysis. All histological slides were reviewed independently by two pathologists.

The expression of E-cadherin, α-catenin, and β-catenin was studied in 16 cases of invasive breast carcinoma. Twenty cases of classic lobular carcinoma were also stained for E-cadherin, α-catenin, and β-catenin for comparison. The primary antibodies and dilutions used are summarized in Table 1.

Immunohistochemical staining was performed according to the following protocol. Consecutive sections from formalin-fixed, paraffin-embedded tissue blocks were cut at 5-μm thickness, deparaffinized, and dehydrated with xylene and graded alcohol. Pressure cooker pretreatment (one cycle of 1 min) was performed at pH 6.0 for E-cadherin and α-catenin and at pH 8.0 for β-catenin. Endogenous peroxidase activity was quenched with 3% hydrogen peroxide at room temperature for 30 min. Sections were blocked with 10% goat serum for 60 min and then incubated with the primary antibody for 1 h at room temperature.

Table 1 Monoclonal antibodies used in the study

Antibody	Clone	Source	Dilution
E-cadherin	NCH-38	DAKOCytomation	X50
α-catenin	25B1	Novocastra	X50
β-catenin	17C2	Novocastra	X50

Evaluation of immunohistochemical staining was made according to the following criteria. The number of immunopositive cells was semiquantitatively estimated: grade + corresponded to 10–50% positive cells, and grade ++ to more than 50% positive cells (Fig. 4). Only tumor cells with clear membrane staining were scored as positive, and tumors were scored negative when less than 10% of the cells showed staining. Normal ductal epithelial cells were used as an internal control. Statistical analyses were performed by the Mann–Whitney *U* test. Differences in all statistical tests were considered significant at the $p<0.05$ level.

Results

All of the patients were women, and their ages ranged from 32 to 74 years (mean 51.5). The mean tumor size was 3.19 cm in maximum diameter. Six patients (37.5%) presented with stage I disease, six patients (37.5%) with stage II, four (25.0%) with stage III, and no patient with stage IV disease. Axial lymph node metastases were present in seven of 16 cases (43.7%). The treatments applied to operable patients included radical mastectomies in 13 cases and focal resections in three cases. Fourteen patients received postoperative radiation therapy. Follow-up data were available for 12 of the 16 patients diagnosed with TLC for 6 to 72 months. Of these 12 patients, no patient died of the disease following the initial diagnosis of the primary lesion.

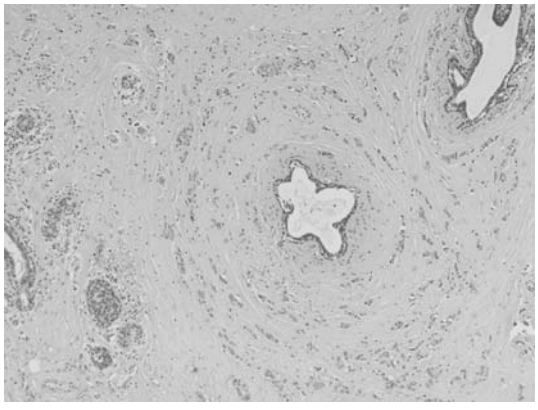

Fig. 1 The tumor demonstrates a diffuse and targetoid growth pattern at low magnification (hematoxylin and eosin stain)

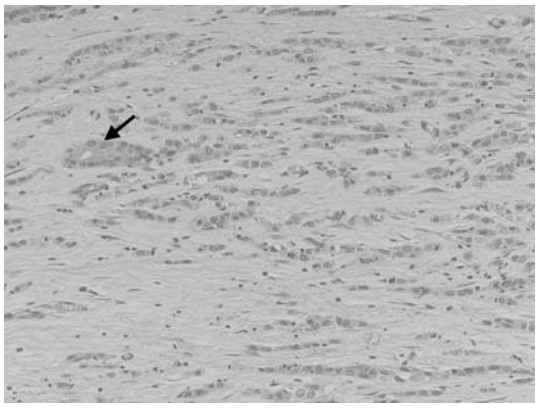

Fig. 2 The tumor is seen to be composed of single-cell file cords at high-power magnification (hematoxylin and eosin stain). Notice that traces of gland formation are evident (*arrow*)

Only two patients had local recurrence, and there was no systemic recurrence. Ten patients were alive and well with no evidence of disease.

Pathologic examination showed a diffuse and targetoid growth pattern at low magnification (Fig. 1). The tumors demonstrated a lobular pattern of infiltration comprising a mixture of single-cell file cords and small, round to angulated tubules on high power (Fig. 2). As most of these tumors showed a heterogeneous pattern with respect to the proportion of the TLC component (Fig. 3), we contend that TLC of the breast should be defined as a carcinoma that has a predominantly tubulolobular pattern.

Grading of the tumors was based on the recommendations made by Elston and Ellis [6]. The tumors were Elston and Ellis modified Bloom–Richardson grade I in 14 cases (87.5%) and grade II in two cases (12.5%). An in situ component was present in 12 of 16 cases: it was lobular in 5 of 12 cases, ductal in 3 of 12 cases, and contained separate ductal and lobular foci in 4 of 12 cases.

Table 2 Immunohistochemical staining for E-cadherin and catenins in mammary carcinoma

Carcinoma type	Staining intensity	E-cadherin (P=0.0001)	Catenins	
			α (P=0.0109)	β (P=0.0013)
TLC (16 cases)	+	10	5	8
	+	2	3	2
	−	4	8	6
Usual lobular carcinoma (20 cases)	+	0	0	0
	+	0	0	0
	−	20	20	20

All statistical analyses were performed by the Mann–Whitney U test

The results of the immunohistochemical analysis of immunophenotype are summarized in Table 2. In TLC, marked plasma-membrane-associated staining for E-cadherin was observed in 12 (75%) cases (indicated as +/++, Table 2). The staining pattern of TLC was predominantly characterized by plasma-membrane-associated staining of tumor cells at the cell–cell boundaries (Fig. 4). In most tumors, some areas also showed membranous E-cadherin staining at the epithelial–stromal boundary. Only four cases showed no significant staining.

However, in invasive lobular carcinomas, plasma-membrane-associated staining for E-cadherin was completely absent in 19 of 20 cases. Very weak cytoplasmic staining was seen in only 1 of the 20 lobular carcinomas without membranous E-cadherin expression. However, we could not classify this case as +/++.

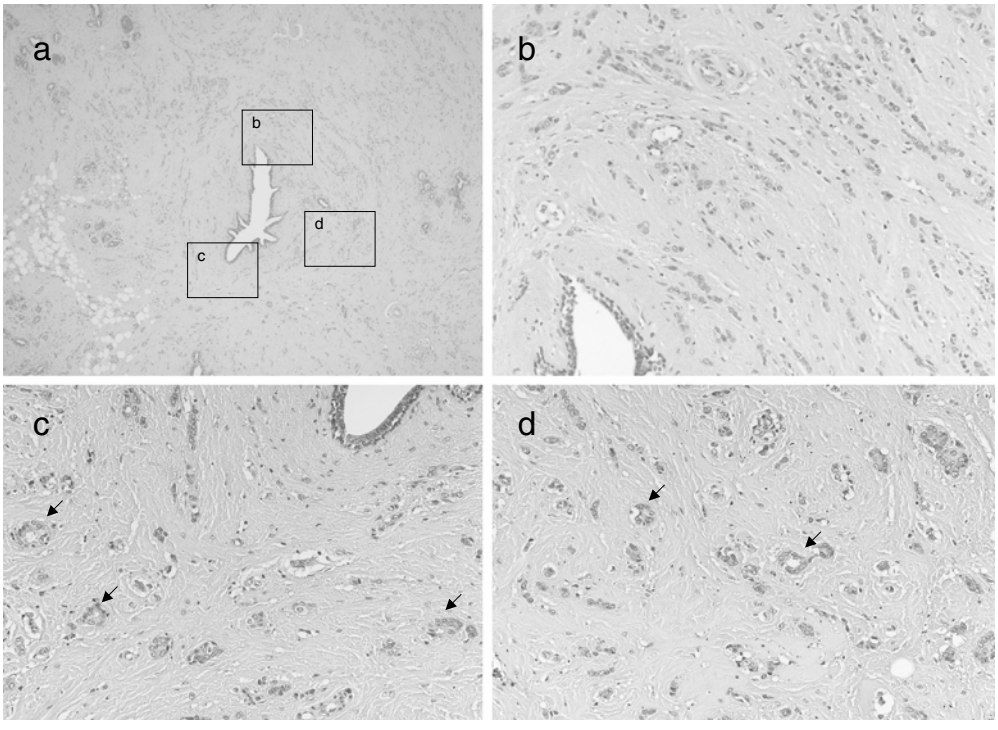

Fig. 3 Another area with targetoid growth pattern in the tumor is seen to be composed of single-cell file cords (**b**) and small tubules (*arrows*) (**c**, **d**) at high-power magnification (hematoxylin and eosin stain)

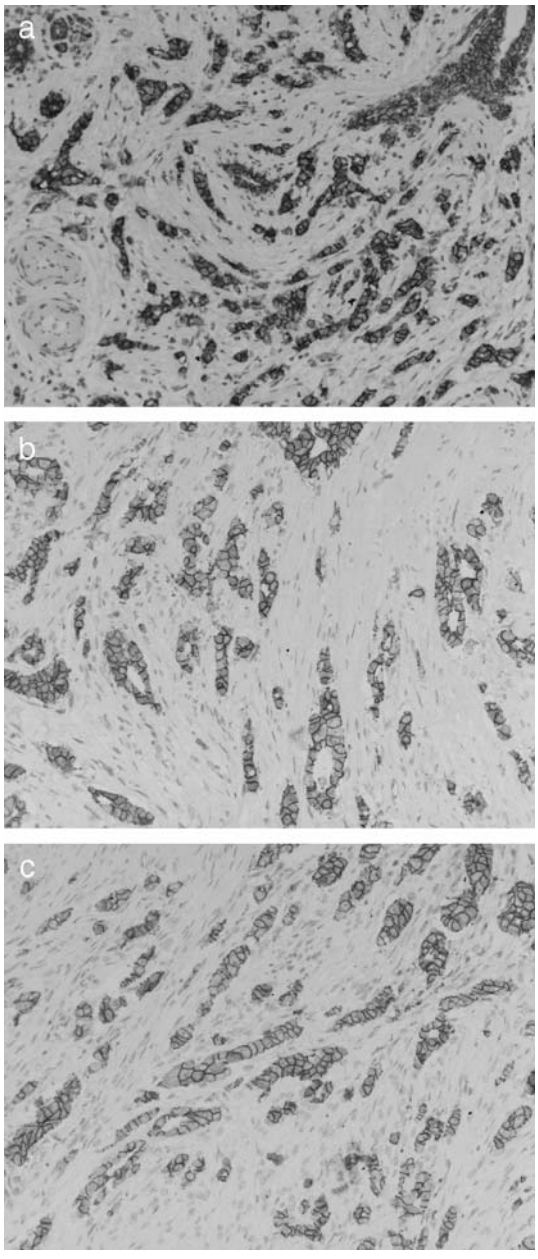

Fig. 4 TLC showing strong immunoreactivity for E-cadherin (**a**), α-catenin (**b**), and β-catenin (**c**) in both the cell cord and the tubular component

Expression of α-catenin and β-catenin was also investigated in the cases of TLC. In the cases of TLC, we observed marked plasma-membrane-associated staining for the two catenins. α-Catenin and β-catenin were observed in 8 (50%) and 10 (62.5%) cases of TLC (indicated as +/++, Table 2). Immunoreactivity for α-catenin and β-catenin was located at the cell–cell boundaries in most tumor cells. One case positive for α-catenin and two cases positive for β-catenin showed no significant staining of E-cadherin. In most of the cases of invasive lobular carcinoma, plasma-membrane-associated staining of catenins was completely absent. Weak cytoplasmic staining of β-catenin was seen in only 1 of 20 lobular carcinomas without membranous expression. However, we could not classify this case as +/++.

No plasma membrane staining of E-cadherin or the two catenins was observed in in situ lobular carcinoma around the TLC. On the other hand, the ductal in situ component around the TLC had plasma membrane staining in all seven cases that expressed E-cadherin. Five of seven cases of ductal carcinoma in situ showed expression of α-catenin, while six cases showed expression of β-catenin.

When the protein expression of E-cadherin, α-catenin, and β-catenin was compared in TLC vs classical lobular carcinoma, a significant association was found between expression of these proteins and TLC ($p<0.05$).

Discussion

The immunohistochemical data presented in this study showed that, in addition to the expression of E-cadherin, the expression of catenins was positive in a high percentage of tubulolobular carcinoma (TLC) compared with lobular carcinoma. Thus, TLC seemed to be a tumor of ductal origin rather than a variant of lobular carcinoma. Immunohistochemical detection of the expression of E-cadherin and catenins can be useful as a diagnostic tool for differentiation between tubulolobular carcinoma and classical lobular carcinoma.

Previous studies have described the differential expression of E-cadherin in ductal carcinoma and lobular carcinomas [1, 5, 15, 22, 23, 28]. Despite the lobular-like growth of TLCs, most of our cases demonstrated E-cadherin expression in both the tubular and single cell cord components. This result was in contrast to our control group of 20 classic lobular carcinomas, in which E-cadherin expression was reduced or lost. These results are in accord with a previous study that demonstrated a higher incidence of E-cadherin expression in TLC than in invasive lobular carcinomas. Wheeler et al. reported that E-cadherin was present in all 27 cases of TLC and E-cadherin expression was uniformly lost in all five control cases of lobular carcinoma [28]. They contended that the high incidence of expression of E-cadherin in TLC supports the ductal differentiation of these tumors.

In addition, we found that the reduction or loss of the catenins was more obvious in lobular carcinoma than in TLC. Investigations of α-catenin and β-catenin expression have been performed in ductal and lobular carcinoma in the breast in other studies. The expression of E-cadherin, α-catenin, and β-catenin was studied in 48 cases of invasive ductal breast carcinoma and 38 cases of lobular breast carcinoma by De Leeuw et al. [5]. They reported marked plasma-membrane-associated staining for α-catenin and β-catenin in ductal carcinoma, except in one case that was negative for α-catenin. Invasive lobular carcinomas that were negative for E-cadherin were also negative for α-catenin and β-catenin. Of 38 invasive lobular carcinomas, 32 showed complete loss of α-catenin and β-catenin, which is in agreement with our results and those of others.

From these results, it seems that TLC is of a ductal origin rather than a variant of lobular carcinoma.

As mentioned above, there have been suggestions in several reports that the protein expression of E-cadherin and catenins is higher in ductal carcinoma and lower in lobular carcinoma. However, Fisher et al. originally described TLCs as a tubular variant of lobular carcinoma based not only on their lobular growth pattern, but also their biological behavior [7]. They defined treatment failure as local recurrence, metastasis, or death and reported that the failure rate of TLC over a 32-month follow-up period was closer to that of pure lobular carcinoma than pure tubular carcinoma. However, in our study, no patients died of the disease and only two patients had local recurrence following the initial diagnosis of the primary lesion in the 12 patients available for follow-up. Probably due to the small number of cases followed up, the biological behavior could not be characterized in our study.

Furthermore, as in a previous study, we found many foci of in situ lobular carcinoma around TLCs, and this also seems to conflict with an explanation of TLC as being of ductal carcinoma origin [28]. The mechanism accounting for this result is still unclear. However, an interesting hypothesis that could explain this phenomenon was proposed in several reports. Buerger et al. reported based on a study of comparative genomic hybridization that a "high degree of genetic homology" was observed between lobular carcinoma in situ and well-differentiated intraductal carcinoma, an observation that led them to speculate that the two lesions might be "different phenotypic forms of a common genotype" [3]. Such a phenomenon is supported not only by the existence of the hybrid tubulolobular carcinoma phenotype, but also by the frequent coexistence of ductal proliferation with lobular carcinoma in situ and tubular carcinoma [24].

In addition, Wheeler et al. reported high-molecular-weight cytokeratin antibody 34β E12 to be a helpful marker for invasive lobular carcinoma, and in 25 of 27 of their TLC cases, dual immunostaining for both 34β E12 and E-cadherin was positive. From this result, they hypothesized that TLC may be a hybrid invasive tumor of the breast. However, of the 14 of 27 cases of TLC with immunostaining available for the in situ component, only two cases demonstrated hybrid staining for both 34β E12 and E-cadherin. Furthermore, they found the same hybrid immunophenotype in all five cases of pure tubular carcinoma in their comparison group, of which none of the cases was associated with a hybrid carcinoma. These findings finally led them to speculate that TLC as a ductal origin and hybrid immunophenotype may not be specific for tumors with dual ductal and lobular histology. In our results, there were some cases of TLCs that failed to stain for E-cadherin and catenins. This result might also reinforce the notion that TLC has hybrid histologic feature. However, there were only a small number of negative cases for E-cadherin and catenins, and the meaning of these results could not be determined in our study. Further studies will be needed with large numbers of E-cadherin-negative and catenin-negative TLCs.

In summary, this report describes the clinical and pathologic features and expression of E-cadherin, α-catenin, and β-catenin in 16 cases of TLC. Our findings show that TLC of the breast undoubtedly does not have the usual immunohistochemical features of invasive lobular carcinomas, and a ductal origin of TLC is suggested. E-cadherin, α-catenin, and β-catenin may be useful as markers for distinguishing TLC from lobular carcinoma in the majority of cases. Further studies will be necessary to elucidate the mechanism of this unique pattern of invasive carcinoma.

Acknowledgements We sincerely thank I. Miura, M.D.; Y. Toyozumi, M.D.; S. Momose, M.D.; T. Ougida, C.T.; M. Abe, C. T.; T. Masuda, C.T.; K. Hanami, C.T.; K. Kiuchi, C.T.; K. Oosawa, C. T.; K. Matuno, C.T.; and Y. Oono, C.T. for technical assistance and advice.

References

1. Berg J, Hutter R (1995) Breast cancer. Cancer 75:257–269
2. Boller K, Vestweber D, Kemler R (1985) Cell-adhesion molecule uvomorulin is localized in the intermediate junctions of adult intestinal epithelial cells. J Cell Biol 100:327–332
3. Buerger H, Simon R, Schafer KL, Diallo R, Littmann R, Poremba C, van Diest PJ, Dockhorn-Dworniczak B, Bocker W (2000) Genetic relation of lobular carcinoma in situ, ductal carcinoma in situ, and associated invasive carcinoma of the breast. Mol Pathol 53:118–121
4. Bukholm IK, Nesland JM, Karesen R, Jacobsen U, Borresen-Dale AL (1998) E-cadherin and alpha-, beta-, and gamma-catenin protein expression in relation to metastasis in human breast carcinoma. J Pathol 433:223–228
5. De Leeuw WJ, Berx G, Vos CB, Peterse JL, Van de Vijver MJ, Litvinov S, Van Roy F, Cornelisse CJ, Cleton-Jansen AM (1997) Simultaneous loss of E-cadherin and catenins in invasive lobular breast cancer and lobular carcinoma in situ. J Pathol 183:404–411
6. Elston CW, Ellis IO (1991) Pathological prognostic factors in breast cancer. I. The value of histological grade in breast cancer: experience from a large study with long-term follow-up. Histopathology 19:403–410
7. Fisher ER, Gregorio RM, Redmond C, Fisher B (1977) Tubulolobular invasive breast cancer: a variant of lobular invasive cancer. Hum Pathol 8:679–683
8. Gamallo C, Palacios J, Suarez A, Pizarro A, Navarro P, Quintanilla M, Cano A (1993) Correlation of E-cadherin expression with differentiation grade and histological type in breast carcinoma. Am J Pathol 142:987–993
9. Green I, McCormick B, Cranor M, Rosen PP (1997) A comparative study of pure tubular and tubulolobular carcinoma of the breast. Am J Surg Pathol 21:653–657
10. Gumbiner B (1996) Cell adhesion: the molecular basis of tissue architecture and morphogenesis. Cell 84:345–357
11. Herrenknecht K, Ozawa M, Eckerskorn C, Lottspeich F, Lenter M, Kemler R (1991) The uvomorulin-anchorage protein alpha catenin is a vinculin homologue. Proc Natl Acad Sci U S A 88:9156–9160
12. Hulsken J, Birchmeier W, Behrens J (1994) E-cadherin and APC compete for the interaction with beta-catenin and the cytoskeleton. J Cell Biol 127:2061–2069
13. Karayiannakis AJ, Nakopoulou L, Gakiopoulou H, Keramopoulos A, Davaris PS, Pignatelli M (2001) Expression patterns of beta-catenin in in situ and invasive breast cancer. Eur J Surg Oncol 27:31–36
14. McCrea PD, Turck CW, Gumbiner B (1991) A homolog of the armadillo protein in Drosophilia (plakoglobin) associated with E-cadherin. Science 254:1359–1361

15. Moll R, Mitze M, Frixen U, Birchmeier W (1993) Differential loss of E-cadherin expression in infiltrating ductal and lobular breast carcinomas. Am J Pathol 143:1731–1742
16. Nagafuchi A, Takeichi M (1988) Cell binding function of E-cadherin is regulated by the cytoplasmic domain. EMBO J 7:3679–3684
17. Nagafuchi A, Takeichi M (1989) Transmembrane control of cadherin-mediated cell adhesion: a 94 kDa protein functionally associated with a specific region of the cytoplasmic domain of E-cadherin. Cell 1:37–44
18. Nagafuchi A, Takeuchi M, Tsukita S (1991) The 102 kD cadherin-associated protein: similarity to vinculin and post-transcriptional regulation of expression. Cell 65:849–857
19. Nelson W (1994) Regulation of cell adhesion and development of epithelial cell surface polarity. Curr Top Membr 41:123–142
20. Ozawa M, Kelmer R (1992) Molecular organization of the uvomorulin-catenin complex. J Cell Biol 116:989–996
21. Ozawa M, Baribault H, Kemler R (1989) The cytoplasmic domain of the cell adhesion molecule ??unvomorulin associates with three independent proteins structurally related in different species. EMBO J 8:1711–1717
22. Rasbridge S, Gillett C, Sampson S, Walsh F, Millis R (1993) Epithelial (E-) and placental (P-) cadherin cell adhesion molecule expression in breast carcinoma. J Pathol 169:245–250
23. Rimm D, Sinard J, Morrow J (1995) Reduced alpha-catenin and E-cadherin expression in breast cancer. Lab Invest 72:506–512
24. Rosen PP (1999) Columnar cell hyperplasia is associated with lobular carcinoma in situ and tubular carcinoma. Am J Surg Pathol 23:1561
25. Takeichi M (1991) Cadherin cell adhesion receptors as a morphogenetic regulator. Science 251:1451–1455
26. Takeichi M (1995) Morphogenetic roles of classic cadherins. Curr Opin Cell Biol 7:619–627
27. Vestweber D, Kemler R (1984) Some structural and functional aspects of the cell adhesion molecule uvomorulin. Cell differ 15:269–273
28. Wheeler DT, Tai LH, Bratthauer GL, Waldner DL, Tavassoli FA (2004) Tubulolobular carcinoma of the breast. An analysis of 27 cases of a tumor with a hybrid morphology and immunoprofile. Am J Surg Pathol 28:1587–1593
29. Zschiesche W, Schonborn I, Behrens J, Herrenknecht K, Hartveit F, Lilleng P, Birchmeier W (1997) Expression of E-cadherin and catenins in invasive mammary carcinomas. Anticancer Res 17:561–567

Virchows Arch (2006) 448: 506–516
DOI 10.1007/s00428-005-0122-0

ORIGINAL ARTICLE

Frédéric Charlotte · Kamal Doghmi · Nathalie Cassoux · Hongtao Ye · Ming-Qing Du · Michèle Kujas · Annette Lesot · George Mansour · Phuc Lehoang · Nicole Vignot · Frédérique Capron · Véronique Leblond

Ocular adnexal marginal zone B cell lymphoma: a clinical and pathologic study of 23 cases

Received: 11 September 2005 / Accepted: 22 September 2005 / Published online: 2 December 2005

Abstract To better characterize ocular adnexal marginal zone lymphoma of mucosa-associated lymphoid tissue (MZL-MALT), we analyzed the clinical and pathologic features of 23 patients (11 men, 12 women, median age 66 years). The tumor was confined to one ocular structure in 18 cases (conjunctiva, *n*=8; orbit, *n*=8; or lacrimal gland, *n*=2). Concurrent extraorbital disease was detected by the staging procedure in five patients, and preferentially involved other MALT sites. Histogenetic B cell marker studies, available in 13 cases, showed an early post-germinal center (GC) phenotype (BCL-6$^-$/IRF4$^+$/CD138$^-$) (*n*=5) or a late post-GC phenotype (BCL-6$^-$/IRF4$^+$/CD138$^+$) (*n*=8), which could be helpful for discrimination from other types of small-B cell lymphoma. BCL10 was positive in 12 of 13 patients tested, with nuclear (*n*=4) or cytoplasmic (*n*=8) immunoreactivity. These staining patterns ruled out t(1;14)(p22;q32) translocation. T(11;18)(q21;q21), another MZL-MALT-specific translocation, was detected by reverse transcriptase polymerase chain reaction in four of 15 patients tested. Clinical outcome was excellent but the overall relapse rate was 26.1% with a median follow-up of 39 months (range 6–132 months). Regardless of the disease stage at diagnosis, combined chemotherapy and radiotherapy seemed to be more effective than chemotherapy alone in ocular adnexal MZL-MALT, as persistent complete remission was achieved in nine patients receiving combination therapy, while six of 14 patients treated with chemotherapy alone relapsed.

Keywords MALT · Lymphoma

F. Charlotte (✉) · M. Kujas · A. Lesot · G. Mansour · N. Vignot · F. Capron
Department of Pathology,
Service d'Anatomie Pathologique (Pr F. Capron),
Hôpital Pitié-Salpêtrière,
Boulevard de l'hôpital 75013 Paris, France
e-mail: frederic.charlotte@psl.ap-hop-paris.fr
Tel.: +33-1-42177772
Fax: +33-1-42177777

N. Cassoux · P. Lehoang
Department of Ophthalmology,
Pitié-Salpêtrière Hospital, AP-HP,
Paris, France

K. Doghmi · V. Leblond
Department of Hematology,
Pitié-Salpêtrière Hospital, AP-HP,
Paris, France

H. Ye · M.-Q. Du
Department of Histopathology,
University College of London,
London, UK

Introduction

Ocular adnexal lymphomas, which may involve the conjunctiva, orbital connective tissue and/or lacrimal glands, account for 8% of all extranodal non-Hodgkin lymphomas [18]. Most cases are classified as extranodal marginal zone B cell lymphomas of mucosa-associated lymphoid tissue (MZL-MALT) according to the World Health Organization (WHO) classification of lymphomas [5, 12, 22, 37, 43]. The diagnosis of MZL-MALT in the ocular adnexa can be difficult. MZL-MALT can consist of small lymphocytes without cytologic atypia, mimicking benign lymphoid hyperplasia. Immunohistochemical and molecular methods are powerful discriminatory tools. Differential diagnosis is also difficult between MZL-MALT and other low-grade B cell lymphomas such as mantle cell and follicular lymphoma (which can also involve the ocular adnexa), because of the lack of specific immunophenotypic markers of the marginal zone [21]. Furthermore, the pathologist cannot rely on the presence of lymphoepithelial lesions characteristic of MZL-MALT, owing to the absence of epithelial structures in intraorbital extrabulbar connective tissues. The study of histogenetic marker expression, such as BCL-6, MUM1/IRF4 (for multiple myeloma-1/interferon regulatory factor-4), and CD138/syndecan-1 (syn-1), could help to better characterize ocular adnexal MZL-MALT, thereby facilitating its discrimination from other subtypes of low-grade B cell lymphomas. BCL-6 is a POZ/zinc finger transcriptional repressor, mainly expressed by B cells of the germinal

center (GC) [10]. The transcription factor MUM1/IRF4 is expressed at the final step of B cell differentiation within the GC (late centrocyte) and during subsequent steps in plasma cell differentiation [17]. CD138/syn-1 is a marker of the later stage of B cell differentiation (post-GC cells) [8].

Two chromosomal translocations have been described in gastric and lung MZL-MALT but data on ocular adnexal lymphomas are lacking [1, 4, 24, 27, 35, 36, 39, 41]. The first translocation is t(11;18)(q21;q21) which fuses the amino-terminal end of the *API2* gene to the carboxy terminal end of the *MALT1* gene and generates a chimeric fusion product [14] that activates NF-κB [31, 42]. The second nonrandom cytogenetic alteration associated with MZL-MALT is t(1;14)(p22;q32), which deregulates BCL10 [44], a factor that binds to its normal partner MALT1 and affects the NF-κB signaling pathway, resulting in NF-κB activation [40]. A high level of BCL10 expression in both the nucleus and cytoplasm of neoplastic cells is highly predictive of t(1;14)(p22;q32) [47].

Many reports on ocular adnexal lymphomas [3, 16, 23, 25, 34, 37, 43, 46] were published before the advent of the revised European–American lymphoma classification in 1994 [20] and the WHO classification in 2001 [22]. A few studies specifically focused on ocular adnexal MZL-MALT, or provided detailed clinicopathologic data on a large series of patients [11, 26, 32, 33]. This prompted us to examine the clinicopathologic characteristics and outcome of 23 patients with ocular adnexal MZL-MALT treated in the same institution, with special emphasis on the expression of B cell histogenetic markers and the occurrence of two chromosomal translocations: t(11;18)(q21;q21) assessed by reverse transcriptase polymerase chain reaction (RT-PCR), and t(1;14)(p22;q32) evaluated indirectly by BCL10 immunostaining.

Patients, materials and methods

Case selection

Thirty-eight cases of lymphoma involving the ocular adnexae were identified in the files of the Pathology Department, Pitié-Salpêtrière, France, between January 1990 and December 2001. They were classified according to the WHO classification of tumors of hematopoietic and lymphoid tissues [22]. The 38 cases comprised 29 MZL-MALT, two follicular lymphomas, six large-cell lymphomas, and one T/NK cell lymphoma. Six of the 29 MZL-MALT cases were excluded because tissue samples or clinical data were lacking. The same pathologist (Frédéric Charlotte), who was unaware of clinical data, reviewed each case.

Clinical evaluation

The following clinical data were recorded in each case: the medical history (with special emphasis on autoimmune diseases, age, sex, and anatomical location of the tumor, disease stage at diagnosis according to the Ann Arbor staging modified for extranodal disease) [9]; the type and extent of therapy; the disease course; and the last follow-up data. Patients with bilateral ocular adnexal involvement without extraorbital extension were considered to have stage IE disease. The staging evaluation included physical examination, full blood count, serum lactate dehydrogenase (LDH) and β2-microglobulin assay, serum electrophoresis and immunoelectrophoresis, bone marrow biopsy, chest radiography, computerized tomography (CT) and/or magnetic resonance imaging of the orbit, CT scan of the thorax and abdomen, and gastroscopy.

Light microscopy

All tissue samples were obtained by surgical biopsy. They were fixed in 10% formalin and embedded in paraffin. Four-micrometer thick tissue sections were stained with hematoxylin and eosin, and also with the Giemsa and Gordon-Sweet methods.

Immunohistochemistry

The immunostaining procedure was performed on formalin-fixed, deparaffinated 4-μm thick tissue sections by using a commercial kit (LSAB, DakoCytomation, Glostrup, Denmark,) or the EnVision+DAB system (DakoCytomation), and an automated immunostainer (DakoCytomation) according to the manufacturer's instructions. The primary antibodies used in this study are listed in Table 1. The sections were heated in a water bath at 98°C for 30 min in citrate buffer pH 6.1 (DakoCytomation Target Retrieval solution), before incubation with antibodies against CD20, kappa and lambda light-chain immunoglobulin; or in DakoCytomation Target Retrieval solution High pH before incubation with antibodies against CD3, CD5, CD10, cyclin D1, BCL-6, IRF4/MUM1, CD138/syn-1 and BCL10. The immunostaining reaction was visualized using 0.05% 3.3'-diaminobenzidine in Tris–HCl buffer containing 0.01% hydrogen peroxide, pH 7.6. The sections were lightly counterstained with hematoxylin. BCL-6, IRF4 and CD138 immunostaining was quantified as follows: negative if<5% of cells positive; 1 if more than 5% and less than one-third of cells are positive; 2 if one-third to two-third of cells are positive; and 3 if more than two-third of cells are positive.

Detection of t(11;18)(q21;q21) by reverse transcriptase polymerase chain reaction

The results of t(11;18)(q21;q21) detection by RT-PCR in 15 patients with sufficient material have been reported elsewhere [48]. Total RNA was extracted from formalin-fixed and paraffin-embedded tissues by using the Ambion RNA isolation kit (AMS Biotechnology, Oxon, UK) as previously described [28]. Five to ten 5-μm paraffin sections were deparaffinated in xylene, digested with proteinase K

Table 1 Immunohistochemical panel

Antibody	Type	Dilution	Source[a]
CD20	L26	1:250	DakoCytomation
CD3	F7.2.38	1:100	DakoCytomation
CD5	4C7	1:25	DakoCytomation
CD10	56C6	1:40	Novocastra
Cyclin D1	SP4	1:50	Lab Vision
Kappa	Polyclonal	1:4	Oxoid
Lambda	Polyclonal	1:8	Oxoid
BCL-6	PG-B6	1:10	DakoCytomation
IRF4/MUM1	ICSAT/M17	1:400	SC
CD138/Syn-1	B-B4	1:200	Serotec
BCL10	Clone 151	1:60	Dr MQ Du (London, UK)

[a]DakoCytomation, Glostrup, Denmark; Lab Vision, Fremont CA; Novocastra, Newcastle-upon-Tyne, UK; Oxoid, Dardilly, France; SC, Santa Cruz Biotechnology, Santa Cruz, CA; Serotec, Oxford, UK

1 mg/ml for 2 h at 45°C, and solubilized in guanidinium-based buffer. RNA was extracted with acid phenol: chloroform and precipitated in isopropanol. Precipitated RNA was washed in 75% ethanol and redissolved in 20 µl of RNA Storage Solution. The complementary DNA was synthesized using the SuperScript Preamplification System (Invitrogen, Paisley, UK) with a mixture of gene-specific primers (including a primer for *G6PD*), specially designed for use with formalin-fixed paraffin-embedded tissues [28]. Three sets of PCR primers, with a common sense primer covering 93% of the known breakpoints on the *API2* gene (p-S: 5'-GGAAGAGGAGAGAGAAAGAGCA) and three antisense primers (p-AS1: 5'-CCAAGACTGCCTTTGACT CT, p-AS2: 5'-GGATTCAGAGACGCCATCAA, and p-AS3: 5'-CAAAGGCTGGTCAGTTGTTT) targeting all four breakpoints on the *MALT1* gene were used for PCR of the *API2-MALT1* fusion transcript, as previously described [28]. *G6PD* was amplified in parallel as a control. PCR was performed separately with each primer set, in duplicate. PCR products were analyzed by electrophoresis on 10% polyacrylamide gels.

Results

Clinical findings

The main clinical features of the 23 patients are listed in Table 2. The patients consisted of 12 women and 11 men aged 32 to 95 years at presentation (median, 66 years). In 18 cases (78.3%), the tumor was confined to one anatomical ocular site as follows: conjunctiva (eight cases, 34.7%), orbit (eight cases, 34.7%), and lacrimal gland (two cases, 8.7%). In five cases (21.8%), more than one anatomical ocular site was involved. Five patients (21.8%) had bilateral involvement of the ocular adnexa. None of the patients had a history of autoimmune disease. The staging procedure revealed extraorbital involvement (stomach, lung, parotid, thyroid, liver, spleen, lymph node, or bone marrow) in five patients (21.8%). No B symptoms (fever, weight loss or night sweats) were present. The serum LDH level was normal in 20 patients (87%) and elevated in three (13%). The serum β2-microglobulin level was always normal. Four patients (17.3%) had a serum M-component consisting of monoclonal IgM (patients 1, 15, 19, and 21).

Histologic findings

The histologic features of the 23 patients are listed in Table 3. The lymphoid proliferation was located in a fibro-adipose tissue without epithelial structures in 18 patients, and in the lamina propria of a conjunctival mucosa in five cases. No lymphoepithelial lesions were observed in the latter five patients. The lymphoid infiltration was diffused in 19 cases, with vague nodular areas in four cases. These nodular areas corresponded to reactive GCs with (patient 10) or without follicular colonization (patients 6, 19, and 22). The cytologic aspect was lymphocytic in seven cases, lymphocytic with monocytoid cells in one case, and centrocyte-like in 15 cases, with and without monocytoid cells in 11 and 4 cases, respectively (Fig. 1). Areas of plasmacytic differentiation were noted in seven cases.

Immunophenotypic findings and t(11;18)(q21;q21) reverse transcriptase polymerase chain reaction results

All the patients exhibited immunophenotypic features of MZL-MALT, as the neoplastic cells expressed CD20 and were always negative for CD5 and CD10. All the cases with centrocytic-like cells tested for cyclin D1 were negative. A few T lymphocytes intermingled with tumor cells were revealed by CD3 and CD5 immunostaining. Four of the seven cases with areas of plasmacytic differentiation expressed a monotypic kappa light-chain, and three expressed a monotypic lambda light-chain (Table 3).

Because of a lack of paraffin-embedded tissue, only 13 patients could be evaluated for B cell histogenetic markers and BCL10 (Table 3). None of these 13 cases expressed BCL-6. Residual GCs not colonized by tumor cells were positive for BCL-6 in three cases (patients 6, 19, and 22). MUM1/IRF4, expressed in the nucleus, was consistently positive with weak expression by tumor cells in five cases, moderate expression in seven cases and strong expression in one case. CD138/syn-1, expressed by the cytoplasmic membrane, was positive in eight cases, with weak expression by tumor cells in six cases and moderate in two cases. According to the expression profile of the histogenetic markers, BCL-6, MUM1/IRF4 and CD138, the 13 cases fell into two groups, namely five cases with an early post-GC B cell

Table 2 Clinical features, therapy and outcome of patients with ocular adnexal MZL-MALT

Case no.	Age (year)/ sex	Ocular site	Laterality	Extraorbital site	Stage	LDH (>ULN)	Therapy	Response	Follow-up (months)	Relapse (months)	Ocular adverse effects	Outcome
1	59/M	LG	Bilateral	Stomach, parotid, lymph node, spleen, and bone marrow	IV	Normal	ChOP	RC	56	local (43)	None	Alive, 2nd CR
2	50/M	Orbit	Right	None	IE	Normal	ChOP+ RT (40 Gy)	RC	84	None	None	Alive, CR
3	70/F	Orbit	Left	None	IE	Normal	CBL+ CS	RC	36	None	None	Died of gastric carcino-ma
4	66/M	Orbit	Left	None	IE	Normal	ChOP+ RT (30 Gy)	RC	36	None	None	Alive, CR
5	76/F	Orbit	Left	None	IE	Normal	CBL+ CS+ RT (30 Gy)	RC	43	None	conjunctivitis, cataract	Alive, CR
6	74/F	Conj	Left	None	IE	Normal	CBL+ CS	RC	74	Local (34)	None	Alive, 2nd CR
7	80/F	Conj/ orbit	Right	None	IE	Normal	CBL+ CS	RC	48	None	None	Alive, CR
8	72/M	Orbit	Right	None	IE	Normal	ChOP+ RT (40 Gy)	RC	74	None	Eye dryness	Alive, CR
9	58/F	Conj/ orbit	Right	None	IE	High	ChOP+ RT (30 Gy)	RC	35	None	conjunctivitis, cataract	Alive, CR
10	90/F	Conj	Right	None	IE	High	CBL+ CS	RC	39	None	None	Alive, CR
11	43/M	Orbit	Right	None	IE	Normal	ChOP+ RT (30 Gy)	RC	36	None	Eye dryness, cataract	Alive, CR
12	71/F	Conj	Left	Bone marrow	IV	Normal	CBL+ CS	RC	30	Local (8)	None	Alive, 2nd CR
13	40/M	Conj	Bilateral	None	IE	Normal	ChOP+ RT (30 Gy)	RC	12	None	None	Alive, CR
14	54/F	Conj/ sclera/ LG/ orbit	Left	None	IE	Normal	CBL+ CS	RC	36	None	None	Alive, CR
15	60/M	LG	Bilateral	Stomach, lung, parotid, thyroid and bone marrow	IV	Normal	ChOP	RC	25	None	None	Alive, CR

Table 2 (continued)

Case no.	Age (year)/ sex	Ocular site	Laterality	Extraorbital site	Stage	LDH (>ULN)	Therapy	Response	Follow-up (months)	Relapse (months)	Ocular adverse effects	Outcome
16	89/F	Conj	Right	None	IE	Normal	CBL+ CS	RC	40	local (22)	None	Alive, 2nd CR
17	32/M	Conj	Left	Lung, liver, parotid, lymph node and spleen	IV	High	ChOP	RC	13	systemic (10)	None	Alive, 2nd CR
18	62/F	Conj	Right	Stomach	IV	Normal	CBL+ CS	RC	30	None	None	Alive, CR
19	71/F	Conj	Left	None	IE	Normal	CBL+ CS	RC	6	None	None	Alive, CR
20	95/M	Conj/ LG	Left	None	IE	Normal	CBL+ CS	RC	69	None	None	Alive, CR
21	52/F	Orbit	Left	None	IE	Normal	ChOP+ RT (33 Gy)	RC	44	None	None	Alive, CR
22	75/M	Conj/ LG	Bilateral	None	IE	Normal	CBL+ CS	RC	84	local (22)	None	Alive, 2nd CR
23	59/M	Orbit	Bilateral	None	IE	Normal	ChOP+ RT (45 Gy)	RC	132	None	Radiation retinopathy	Alive, CR

M Male; *F* female; *ChOP* cyclophosphamide, doxorubicin at low dose (25 mg/m^2) vincristine, and prednisone; *CBL* chlorambucil; *Conj* conjunctiva; *CR* complete remission; *CS* corticosteroids; *RT* local radiotherapy; *LG* lacrimal gland

Table 3 Pathologic findings in ocular adnexal MZL-MALT

Case no.	Architecture	Lymphocytic	Monocytoid	CCL	Plasmacytic differentiation	Ig light chain restriction	CD138	IRF4	BCL-6	BCL-10	RT-PCR for t(11;18) (q21;q21)
1	D	0	1	1	0	0	NA	NA	NA	NA	NA
2	D	1	0	0	1	κ	1	1	0	+, cyt	−
3	D	0	1	1	0	0	1	2	0	++, nu	−
4	D	0	1	1	0	0	NA	NA	NA	NA	NA
5	D	0	0	1	0	0	1	3	0	++, nu	+
6	D&N	0	1	1	1	λ	0	2	0/CG	+, cyt	−
7	D	0	1	1	0	0	NA	NA	NA	NA	NA
8	D	1	0	0	0	0	1	1	0	+, cyt	−
9	D	0	1	1	0	0	NA	NA	NA	NA	NA
10	D&N	0	0	1	0	0	0	1	0	+, cyt	−
11	D	1	1	0	1	κ	1	2	0	+, cyt	−
12	D	0	1	1	0	0	0	1	0	+, cyt	−
13	D	1	0	0	0	0	NA	NA	NA	NA	+
14	D	0	0	1	0	0	NA	NA	NA	NA	−
15	D	1	0	0	1	λ	2	2	0	++, nu	+
16	D	0	1	1	1	κ	NA	NA	NA	NA	NA
17	D	1	0	0	1	κ	NA	NA	NA	NA	NA
18	D	1	0	0	0	0	NA	NA	NA	NA	NA
19	D&N	0	1	1	1	λ	0	2	0/CG	+, nu	+
20	D	0	1	1	0	0	1	2	0	+, cyt	−
21	D	0	0	1	0	0	0	1	0	+, cyt	−
22	D&N	0	1	1	0	0	2	2	0/CG	−	−
23	D	1	0	0	0	0	NA	NA	NA	NA	NA

D Diffuse, *N* nodular, *NA* not available, *nu* nuclear, *cyt* cytoplasmic

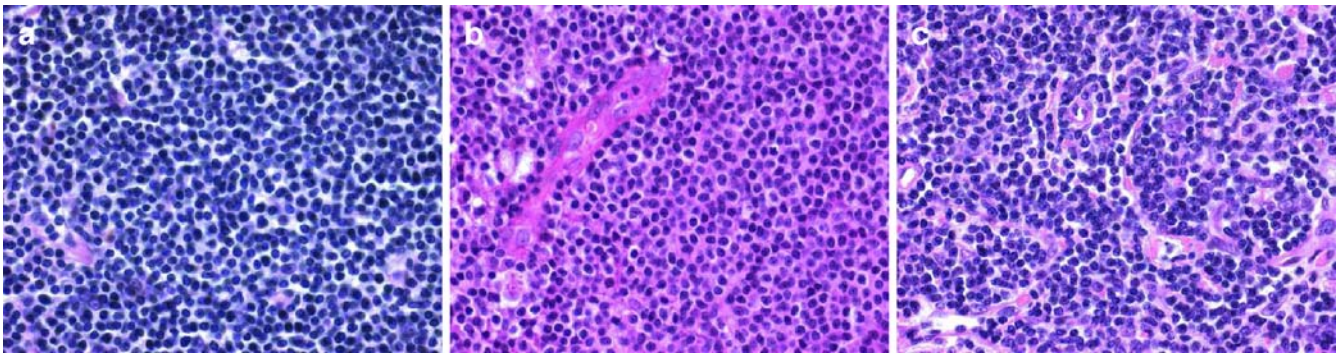

Fig. 1 Cytologic aspects of ocular adnexal MZL-MALT. Lymphocytic (**a**), monocytoid (**b**), and centrocyte-like (**c**) areas, in case number 2, 19, and 10, respectively

phenotype (BCL-6$^-$/IRF4$^+$/CD138$^-$) and eight cases with a late post-GC B cell phenotype (BCL-6$^-$/IRF4$^+$/CD138$^+$) (Fig. 2).

BCL10, which was positive in 12 of 13 tested cases, exhibited weak nuclear expression in one case, moderate nuclear expression in three cases, and cytoplasmic expression in the other eight cases (Fig. 2). The pattern of BCL10 expression did not suggest the presence of t(1;14)(p22;q32) in any of these cases.

Four (26.7%) of the 15 cases tested were positive for t(11;18)(q21;q21) by RT-PCR. Three of these cases, in which material was available for immunostaining, showed nuclear expression of BCL10 (Table 3). It should be mentioned that the 11 cases without detectable t(11;18) by RT-PCR were truly negative because all of them demonstrated *G6PD* amplification as an internal control.

Treatment and clinical outcome (Table 2)

Eleven patients were given anthracycline-containing regimens (ChOP), i.e., cyclophosphamide, vincristine and prednisone, and doxorubicin at low dose, i.e., 25 mg/m^2 [19]. Eight of these patients also had orbital radiotherapy. Twelve patients received an alkylating agent, chlorambucil combined with corticosteroids. One of these patients was also treated with orbital radiotherapy.

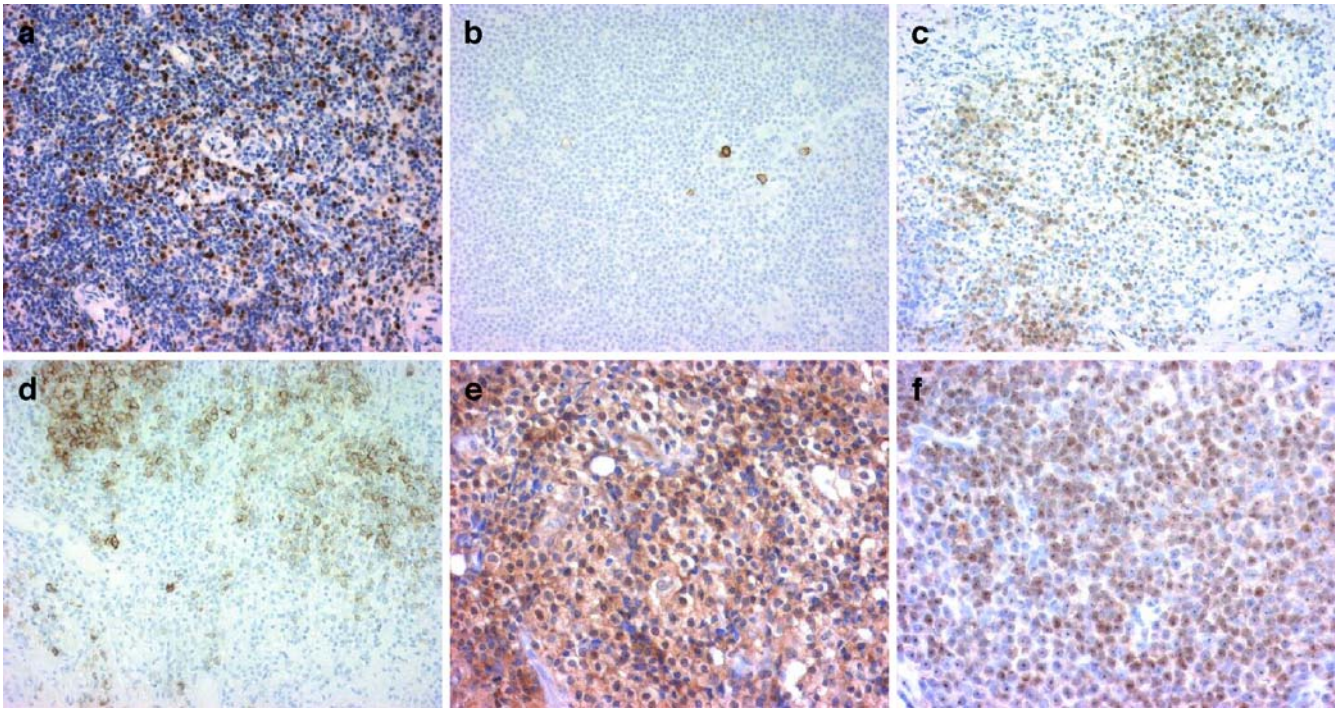

Fig. 2 B cell histogenetic markers and BCL10 immunostaining in ocular adnexal MZL-MALT. A case of early post-GC case (no. 6) with moderate IRF4 (nuclear) (**a**), and negative CD138 (membranous) expression (**b**). One late post-GC case (no. 15) with moderate IRF4 (nuclear) (**c**), and CD138 (membranous) expression (**d**). BCL10 immunoreactivity was cytoplasmic in case no. 6 (**e**) and nuclear in case no. 15 (**f**)

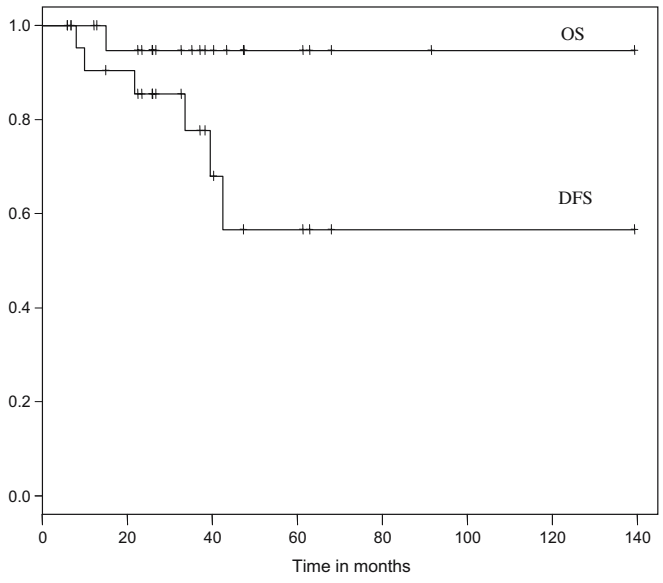

Fig. 3 Overall survival (OS) and disease-free survival (DFS) for 23 patients with ocular adnexal MZL-MALT

The follow-up lasted for 6 to 132 months, with a median of 39 months. The overall survival- and disease-free survival were not reached (Fig. 3). Six patients (26.1%) relapsed, but at the last follow-up, no evidence of lymphoma was detected in the 22 patients who lived and in another patient who died of gastric carcinoma after 36 months.

Complete remission was achieved and persisted throughout follow-up (median 43 months, range 12–132 months) in the nine patients who received both chemotherapy and radiotherapy. By contrast, after a median follow-up of 37.5 months (range 6–84 months), six of the 14 patients treated with ChOP or chlorambucil alone had local (n=5) or extraorbital (n=1) relapses 8 to 42 months after initial diagnosis. A second complete remission was obtained in all the relapsed patients, with systemic chemotherapy (patients 6, 12, 16, 17, and 22) or anti-CD20 monoclonal antibody (patient 1).

The orbital radiotherapy dose ranged from 30 to 45 Gy, with a median of 30 Gy (Table 2). Four patients experienced side effects such as dry eye, conjunctivitis and cataract. One patient, who received a dose of 45 Gy, developed blindness due to radiation-induced retinopathy.

Discussion

The clinicopathologic features of ocular adnexal MZL-MALT have previously been described in a few detailed reports (Table 4) [1, 5, 7, 11, 13, 26, 32, 33, 43], but only four studies specifically focused on this lymphoma subtype with detailed clinical and biological data from a large series [11, 26, 32, 33]. We found that MZL-MALT accounted for 76.4% of all lymphomas involving the ocular adnexa, compared to 50 to 86% in previous series [5, 7, 32, 33, 43].

Our patients' median age was 66 years, a value similar to that in previous studies (44 to 66 years) (Table 4) [1, 5, 7, 11, 13, 26, 32, 33, 43]. Orbit connective tissue and the conjunctiva are the most involved anatomical sites (Table 4). One particular characteristic of ocular adnexal MZL-MALT in our study is the high rate of bilateral tumors (21.8% of patients) and the frequent involvement of several intraorbital sites (21.8% of patients).

The diagnosis of ocular adnexal MZL-MALT can be difficult when the neoplastic infiltrate is composed of small lymphoid cells, mimicking a reactive lymphoid hyperplasia. This difficulty is compounded by the fact that lymphoepithelial lesions, which are helpful for MZL-MALT diagnosis, are rare in ocular adnexal localizations as no case was observed in our series. Nevertheless, the pathologist can rely on the monomorphic aspect of the infiltrate and the predominance of centrocyte-like or monocytoid cells to establish the diagnosis of malignancy [34]. By applying these histologic criteria to our series, we had difficulty making the diagnosis in four cases (patients 8, 13, 18, and 23), in which the infiltrate was purely lymphocytic and the immunoglobulin light chain restriction could not be demonstrated on paraffin-embedded material. However, the immunohistochemical study revealed that these cases were lymphoma as the infiltrating cells expressed CD20 antigen almost exclusively without lymphoid follicles, whereas reactive diffuse lymphoid hyperplasia is mainly composed of T lymphocytes.

Because no specific marker of the marginal zone is available, it can also be difficult to distinguish MZL-MALT from follicular or mantle cell lymphomas. The phenotypic profile of MZL-MALT is characterized by the absence of CD5 and CD10 antigen expression, but it has been reported that mantle cell lymphomas and follicular lymphomas may also lack CD5 and CD10, respectively [6, 29, 45]. The use of cyclin D1 immunostaining is particularly helpful in the diagnosis of CD5-negative mantle cell lymphomas, a form that appears to be frequent in the orbit [30]. Using the histogenetic B cell markers BCL-6, MUM1/IRF4 and CD138/syn-1, we found that our cases had an early post-GC B cell phenotype (BCL-6$^-$/IRF4$^+$/CD138$^-$) or a late post-GC B cell phenotype (BCL-6$^-$/IRF4$^+$/CD138$^+$). These markers, together with CD5, CD10, and cyclin D1, could be helpful for distinguishing between MZL-MALT and B cell lymphomas originating from the germinal center or mantle zone.

Seven of our patients had ocular adnexal MZL-MALT with plasmacytic differentiation, illustrating the problem of distinguishing MZL-MALT from lymphoplasmacytic lymphoma/Waldenström macroglobulinemia (WM). In two of these cases (patients 15 and 19), the possibility of ocular adnexal involvement by WM was supported by the presence of a serum monoclonal IgM. However, neither patient met the WHO criteria for WM [22]. One patient (patient 19) exhibited monocytoid differentiation, which is not observed in WM [2]. The other patient (patient 15) presented with involvement of several extranodal MALT sites, including the stomach, lung, parotid, and thyroid without spleen enlargement, which does not match the anatomical distribution of WM [15]. The MALT origin was confirmed in both cases by the nuclear localization of BCL10 immunostaining, which is specific for MZL-MALT. This demon-

Table 4 Ocular adnexal MZL-MALT: comparison of clinical features, treatment, and outcome in this study and other published series

	White et al. (1995) [43]	Baldini et al. (1998) [5]	Cahill et al. (1999) [7]	McKlevie et al. (2001) [33]	Mannami et al. (2001) [32]	Cho et al. (2003) [11]	Adachi et al. (2004) [1]	Coupland et al. (2005) [12]	Lee et al. (2005) [26]	Current study
No. patients	15	11	10	44	37	61	51	136	37	23
Age at diagnosis range (median)	44–89 (61)	27–75 (54)	35–73 (52)	19–87 (65)	23–86 (61)	24–86 (45)	26–83 (66)	19–91 (64)	21–80 (44)	32–95 (66)
Sex (no. male)	6 (40%)	1 (9%)	nd	16 (36%)	21 (57%)	25 (41%)	26 (51%)	36 (26%)	22 (59%)	11 (48%)
Anatomical localization										
Orbit	Nd	2 (18%)	5 (50%)	21 (48%)	17 (46%)	15 (25%)	19 (37%)	54 (40%)	9 (24%)	8 (34.7)
Conjunctiva	Nd	9 (82%)	5 (50%)	15 (34%)	14 (38%)	42 (68%)	25 (49%)	73 (53%)	24 (65%)	8 (34.7)
LG	Nd	0	0	8 (18%)	6 (16%)	4 (7%)	7(14%)	10 (7%)	4(11%)	2 (8.7%)
>1 ocular site	Nd	0	0	0	0	Nd	Nd	Nd	Nd	5 (21.8)
Bilaterality	Nd	0	0	Nd	6 (16%)	6 (10%)	8 (16%)	16 (12%)	7 (19%)	5 (21.8)
Relapse										
Local	0	2 (18%)	1 (10%)	2 (5%)	0	5 (6.5%)	14 (27%)	27 (23%)	3 (8%)	5 (21.8)
Time to relapse (months) range (median)		54–62 (58)	24	24–138 (52)		15–80 (Nd)	5–114 (13)	(20)	19–28 (24)	8–43 (22)
Extraorbital	3 (20%)	1 (9%)	1 (10%)	7 (17%)	2 (5%)	3 (4.3%)	3 (6%)	38 (32%)	1 (3%)	1 (4.3%)
Time to spread (months) Range (median)	10–141	62	36	24–76 (36)	4–24 (14)	Nd	15–60 (40)	2–125 (5)	3	10
Death	2 (13%)	1 (9%)	1 (10%)	3 (7%)	0	2 (3%)	1 (2%)	32 (27%)	1 (3%)	1 (4%)
Lymphoma-related	0	0	0	1 (2%)	0	1 (2%)	1 (2%)	18 (15%)	1 (3%)	0
Time to death (months) range (median)	24, 30	72	Nd	37		49	60	Nd	3	36
Follow-up period (months) range (median)	6–201 (36)	24–141 (76)	12–96 (42)	4–150 (50)	5–120 (27)	0–108 (32)	0–114 (Nd)	2–239 (49)	(21)	6–132 (39)
Treatment										
None	0	0	0	0	12	0	Nd	Nd	3	0
Surgery	2	2	4	7	0	4	Nd	Nd	2	0
Surgery+RT	0	0	6	0	0	44	Nd	Nd	0	0
RT	11	8	0	12	22	0	Nd	89	29	0
Chlorambucil	2	1	0	21	0	0	Nd	Nd	0	11
Systemic CT	0	0	0	2	0	1	Nd	Nd	3	3
CT+RT	0	0	0	0	1	11	Nd	Nd	0	9
CS	0	0	0	1	0	0	Nd	Nd	0	0

Nd None described, *RT* radiotherapy, *CT* chemotherapy

strates the utility of BCL10 for distinguishing MZL-MALT from ocular adnexal involvement by WM.

T(11;18)(q21;q21), which is exclusively found in MZL-MALT, occurs in 35–50% of gastric and 55–75% of pulmonary involvement by this lymphoma subtype but is rarely found in other locations such as the thyroid and salivary glands [27, 28]. The incidence of t(11;18)(q21;q21) in ocular adnexal lymphomas has previously been investigated in a few small series [4, 24, 27, 35, 36, 39]. In the present study, t(11;18)(q21;q21) was detected by RT-PCR in 26.7% of the 15 patients tested. Recently, two larger series were reported with contradictory results: Takada et al. [41] found that 3 of 23 (13%) ocular adnexal lymphomas harbored t(11;18), whereas Adachi et al. [1] could not detect this translocation in a series of 69 cases. Further studies are needed to clarify this point but all these data suggest that similar mechanisms of carcinogenesis may be implicated in gastric MZL-MALT and at least a subset of ocular adnexal MZL-MALT. As previously described in gastric MZL-MALT,in which t(11;18) is preferentially found in the most advanced stages [27], two of our four cases harboring this translocation had bilateral orbital involvement or were at an advanced stage of the disease. It has been reported that another specific chromosomal translocation, t(1;14)(p22;q32), found in only 5% of MZL-MALT [44], is associated with strong immunohistochemical BCL10 expression in the nucleus and cytoplasm of lymphoma cells [47]. It is highly unlikely that any of our cases harbored t(1;14)(p22;q32) as none displayed this pattern of BCL10 immunostaining.

As in previous reports [1, 5, 7, 11, 26, 32, 33, 43], 75% of our patients presented with localized stage IE ocular adnexal MZL-MALT. This study underlines the interest of the staging procedure in cases presenting with ocular adnexal MZL-MALT because five of our patients (1, 12, 15, 17, and 18) had concurrent extraorbital disease at diagnosis involving the lymph nodes, spleen, and bone marrow and also other MALT sites such as the stomach, lung, parotid, thyroid, and liver. Three of these patients (1, 12, and 17) relapsed after treatment, suggesting that extraorbital involvement might be a factor of poor prognosis. Our results confirm that the search for neoplastic involvement of other MALT sites should be routinely included in the lymphoma staging procedure [38].

Chlorambucil or low-dose anthracycline-based regimens (ChOP), with or without local radiotherapy, yielded complete remission in every case. However, relapses were frequent (26.1% of patients) as in previous reports. In contrast to previous series [5, 7, 11, 26, 32, 33, 43], a high proportion of our patients received a combination of chemotherapy and local radiotherapy, and none received local radiotherapy alone (Table 4). Combination therapy appeared more effective than chemotherapy alone in preventing recurrences, even in patients with localized stages. Indeed, persistent complete remission was achieved in all the patients who received a combination therapy (median follow-up 43 months), whereas 43% of patients relapsed after treatment with ChOP or chlorambucil alone (median follow-up 37.5 months). Local radiotherapy alone offers excellent local control but appears inadequate to prevent systemic relapses, as previous studies with sufficient follow-up data (Table 4) showed a higher rate of systemic recurrence (5–32%) than that observed among our patients (4.3%). The choice of chemotherapy in our series was based on the results reported by Raderer et al. [38] who performed an extensive staging in patients with MZL-MALT and showed that apparently localized MZL-MALT lymphoma occurred in fact simultaneously at different MALT sites in nearly a quarter of patients at diagnosis with a higher frequency of multi-organ involvement in case of extra-gastrointestinal MZL-MALT. It is worth noting that in this study, these lymphomatous sites were clinically occult and were proved by biopsy. This suggests that chemotherapy may prevent systemic relapses by controlling early and occult dissemination of the disease. It should be mentioned that the inclusion of anti-CD20 therapy in first-line treatment could also be a future possibility for reducing the rate of systemic relapses.

Although combined with chemotherapy, orbital radiotherapy (total dose 30–40 Gy) was relatively well tolerated (Table 2). Only one severe adverse effect occurred (blindness due to radiation-related retinopathy) in a patient (patient 23) who received 45 Gy. In keeping with most published data [1, 5, 7, 11, 26, 32, 33, 43], death was rarely related to MZL-MALT: Twenty-two of our 23 patients were alive at the cut-off date for this analysis. The only death was due to gastric carcinoma in a patient with no evidence of lymphoma. This was partly due to the efficacy of second-line treatment, consisting of systemic chemotherapy or anti-CD20 monoclonal antibody.

In conclusion, MZL-MALT is the most frequent type of lymphoma involving the ocular adnexa. Its diagnosis is challenging, but immunohistochemistry helps to distinguish MZL-MALT from lymphoid hyperplasia and other types of small B cell lymphoma. T(11;18)(q21;q21), which is specific to MZL-MALT, was present in 27% of our patients, while the BCL10 immunostaining pattern ruled out t(1;14)(p22;q32) in every cases. The clinical outcome of ocular adnexal MZL-MALT is excellent, despite a relapse rate of 26.1% in our series. Combined chemotherapy and radiotherapy seems to be more effective in preventing recurrences, but prospective studies are needed to confirm these retrospective data.

References

1. Adachi A, Tamaru JI, Kaneko K, Kuroda H, Miura I, Kojima T, Hoshino S, Ishinohasama R, Itoyama S (2004) No evidence of a correlation between BCL10 expression and API2-MALT1 gene rearrangement in ocular adnexal MALT lymphoma. Pathol Int 54:16–25
2. Andriko JA, Swerdlow SH, Aguilera NI, Abbondanzo SL (2001) Is lymphoplasmacytic lymphoma/immunocytoma a distinct entity? A clinicopathologic study of 20 cases. Am J Surg Pathol 25:742–751
3. Auw-Haedrich C, Coupland SE, Kapp A, Schmitt-Graff A, Buchen R, Witschel H (2001) Long term outcome of ocular adnexal lymphoma subtyped according to the REAL classification. Revised European and American Lymphoma. Br J Ophthalmol 85:63–69

4. Baens M, Maes B, Steyls A, Geboes K, Marynen P, De Wolf-Peeters C (2000) The product of the t(11;18), an API2-MLT fusion, marks nearly half of gastric MALT type lymphomas without large cell proliferation. Am J Pathol 156:1433–1439
5. Baldini L, Blini M, Guffanti A, Fossati V, Colombi M, La Targia ML, Bertoni F, Alietti A, Neri A, Bertoni G (1998) Treatment and prognosis in a series of primary extranodal lymphomas of the ocular adnexa. Ann Oncol 9:779–781
6. Barcus ME, Karageorge LS, Veloso YL, Kornstein MJ (2000) CD10 expression in follicular lymphoma versus reactive follicular hyperplasia: evaluation in paraffin-embedded tissues. Appl Immunohistochem Mol Morphol 8:263–266
7. Cahill M, Barnes C, Moriarty P, Daly P, Kennedy S (1999) Ocular adnexal lymphoma-comparison of MALT lymphoma with other histological types. Br J Ophthalmol 83:742–747
8. Carbone A, Gloghini A, Gaidano G, Franceschi S, Capello D, Drexler HG, Falini B, Dalla-Favera R (1998) Expression status of BCL-6 and syndecan-1 identifies distinct histogenetic subtypes of Hodgkin's disease. Blood 92:2220–2228
9. Carbone PP, Kaplan HS, Musshoff K, Smithers DW, Tubiana M (1971) Report of the nomenclature committee on Hodgkin's disease staging. Cancer 31:1860–1861
10. Cattoretti G, Chang CC, Cechova K, Zhang J, Ye BH, Falini B, Louie DC, Offit K, Chaganti RS, Dalla-Favera R (1995) BCL-6 protein is expressed in germinal center B cells. Blood 86:45–53
11. Cho EY, Han JJ, Ree HJ, Ko YH, Kang YK, Ahn HS, Ahn SD, Park CJ, Huh J (2003) Clinicopathologic analysis of ocular adnexal lymphomas: extranodal marginal zone B cell lymphoma constitutes the vast majority of ocular lymphomas among Koreans and affects younger patients. Am J Hematol 73:87–96
12. Coupland SE, Krause L, Delecluse HJ, Anagnostopoulos I, Foss HD, Hummel M, Bornfeld N, Lee WR, Stein H (1998) Lymphoproliferative lesions of the ocular adnexa. Analysis of 112 cases. Ophthalmology 105:1430–1441
13. Coupland SE, Hellmich M, Auw-Haedrich C, Lee WR, Anagnostopoulos I, Stein H (2005) Plasmacellular differentiation in extranodal marginal zone B cell lymphomas of the ocular adnexa: an analysis of the neoplastic plasma cell phenotype and its prognostic significance in 136 cases. Br J Ophthalmol 89:352–359
14. Dierlamm J, Baens M, Wlodarska I, Stefanova-Ouzounova M, Hernandez JM, Hossfeld DK, De Wolf-Peeters C, Hagemeijer A, Van den Berghe H, Marynen P (1999) The apoptosis inhibitor gene API2 and a novel 18q gene, MLT, are recurrently rearranged in the t(11;18)(q21;q21) associated with mucosa-associated lymphoid tissue lymphomas. Blood 93:3601–3609
15. Dimopoulos MA, Panayiotidis P, Moulopoulos LA, Sfikakis P, Dalakas M (2000) Waldenström's macroglobulinemia: clinical features, complications and management. J Clin Oncol 18:214–226
16. Ellis JH, Banks PM, Campbell RJ, Liesegang TJ (1985) Lymphoid tumors of the ocular adnexa. Clinical correlation with the Working Formulation classification and immunoperoxidase staining of paraffin sections. Ophthalmology 92:1311–1324
17. Falini B, Fizzotti M, Pucciarini A, Bigerna B, Marafioti T, Gambacorta M, Pacini R, Alunni C, Natali-Tanci L, Ugolini B, Sebastiani C, Cattoretti G, Pileri S, Dalla-Favera R, Stein H (2000) A monoclonal antibody (MUM1p) detects expression of the MUM1/IRF4 protein in a subset of germinal center B cells, plasma cells and activated T cells. Blood 95:2084–2092
18. Freeman C, Berg JW, Cutler SJ (1972) Occurrence and prognosis of extranodal lymphomas. Cancer 29:252–260
19. French Cooperative Group on CLL (1986) Effectiveness of CHOP regimen in advanced untreated chronic lymphocytic leukemia. Lancet 1:1346–1349
20. Harris NL, Jaffe ES, Stein H, Banks PM, Chan JK, Cleary ML, Delsol G, De Wolf-Peeters C, Falini B, Gatter KC, Grogan TM, Isaacson PG, Knowles DM, Mason DY, Muller-Hermelink HK, Pileri SA, Piris MA, Ralfkiaer E, Warnke RA (1994) A revised European-American classification of lymphoma neoplasms: a proposal from the International Lymphoma Study Group. Blood 84:1361–1392
21. Isaacson PG (1990) Lymphomas of the mucosa-associated tissue (MALT). Histopathology 16:617–619
22. Jaffe ES, Harris NL, Stein H, Wardiman JW (ed) (2001). World Health Organization classification of tumors: pathology and genetics of tumors of hematopoietic and lymphoid tissues. International Agency for Research on Cancer Press, Lyon, France
23. Jakobiec FA, Iwamoto T, Patell M, Knowles DM (1986) Ocular adnexal monoclonal lymphoid tumors with a favorable prognosis. Ophthalmology 93:1547–1557
24. Kalla J, Stilgenbauer S, Schaffner C, Wolf S, Ott G, Greiner A, Rosenwald A, Dohner H, Muller-Hermelink HK, Lichter P (2000) Heterogeneity of the API2-MALT1 gene rearrangement in MALT-type lymphoma. Leukemia 14:1967–1974
25. Knowles DM, Jakobiec FA, McNally L, Burke JS (1990) Lymphoid hyperplasia and malignant lymphoma occurring in the ocular adnexa (orbit, conjunctiva, and eyelids): a prospective multiparametric analysis of 108 cases during 1977 to 1987. Hum Pathol 21:959–973
26. Lee JL, Kim MK, Lee KH, Hyun MS, Chung HS, Kim DS, Shin SO, Cho HS, Bae SH, Ryoo HM (2005) Extranodal marginal zone B cell lymphomas of mucosa-associated lymphoid tissue-type of the orbit and ocular adnexal. Ann Hematol 84:13–18
27. Liu H, Ye H, Dogan A, Ranaldi R, Hamoudi RA, Bearzi I, Isaacson PG, Du MQ (2001) T(11;18)(q21;q21) is associated with advanced mucosa-associated lymphoid tissue lymphoma that expresses nuclear BCL10. Blood 98:1182–1187
28. Liu H, Ye H, Ruskone-Fourmestraux A, De Jong D, Pileri S, Thiede C, Lavergne A, Boot H, Caletti G, Wundisch T, Molina T, Taal BG, Elena S, Thomas T, Zinzani PL, Neubauer A, Stolte M, Hamoudi RA, Dogan A, Isaacson PG, Du MQ (2002) T(11;18) is a marker for all stage gastric MALT lymphomas that will not respond to H. pylori eradication. Gastroenterology 122:1286–1294
29. Liu Z, Dong HY, Gordzya W, Tsang P, Cohen P, Stephenson CF, Berger CS, Wu CD, Weisberger J (2002) CD5- mantle cell lymphoma. Am J Clin Pathol 118:216–224
30. Looi A, Gascoygne RD, Chhanabhai M, Connors JM, Rootman J, White VA (2005) Mantle cell lymphoma in the ocular adnexal region. Ophthalmology 112:114–119
31. Lucas PC, Yonezumi M, Inohara N, McAllister-Lucas LM, Abazeed ME, Chen FF, Yamaoka S, Seto M, Nunez G (2001) Bcl10 and MALT1, independent targets of chromosomal translocation in malt lymphoma, cooperate in a novel NF-kappa B signaling pathway. J Biol Chem 276:19012–19019
32. Mannami T, Yoshino T, Oshima K, Takase S, Kondo E, Ohara N, Nakagawa H, Ohtsuki H, Harada M, Akagi T (2001) Clinical, histopathological, and immunogenetic analysis of ocular adnexal lymphoproliferative disorders: characterization of MALT lymphoma and reactive lymphoid hyperplasia. Mod Pathol 14:641–649
33. McKelvie PA, McNab A, Francis IC, Fox R, O'Day J (2001) Ocular adnexal lymphoproliferative disease: a series of 73 cases. Clin Experiment Ophthalmol 29:387–393
34. Medeiros LJ, Harris NL (1989) Lymphoid infiltrates of the orbit and conjunctiva. A morphologic and immunophenotypic study of 99 cases. Am J Surg Pathol 13:459–471
35. Motegi M, Yonezumi M, Suzuki H, Suzuki R, Hosokawa Y, Hosaka S, Kodera Y, Morishima Y, Nakamura S, Seto M (2000) API2-MALT1 chimeric transcripts involved in mucosa-associated lymphoid tissue type lymphoma predict heterogeneous products. Am J Pathol 156:807–812
36. Nakamura T, Nakamura S, Yonezumi M, Suzuki T, Matsuura A, Yatabe Y, Yokoi T, Ohashi K, Seto M (2000) Helicobacter pylori and the t(11;18)(q21;q21) translocation in gastric low-grade B cell lymphoma of mucosa-associated lymphoid tissue type. Jpn J Cancer Res 91:301–309
37. Nakata M, Matsuno Y, Katsumata N, Takenaka T, Kobayashi Y, Narabayashi M, Kagami Y, Ikeda H, Kaneko A, Tobinai K (1999) Histology according to the Revised European-American Lymphoma Classification significantly predicts the prognosis of ocular adnexal lymphoma. Leuk Lymphoma 32:533–543

38. Raderer M, Vorbeck F, Formanek M, Osterreicher C, Valencak J, Penz M, Kornek G, Hamilton G, Dragosics B, Chott A (2000) Importance of extensive staging in patients with mucosa-associated lymphoid tissue (MALT)-type lymphoma. Br J Cancer 83:454–457
39. Remstein ED, James CD, Kurtin PJ (2000) Incidence and subtype specificity of API2-MALT1 fusion translocations in extranodal, nodal, and splenic marginal zone lymphomas. Am J Pathol 156: 1183–1188
40. Ruland J, Duncan GS, Elia A, del Barco Barrantes I, Nguyen L, Plyte S, Millar DG, Bouchard D, Wakeham A, Ohashi PS, Mak TW (2001) Bcl10 is a positive regulator of antigen receptor-induced activation of NF-kappaB and neural tube closure. Cell 104:33–42
41. Takada S, Yoshino T, Tanikawi M, Nakamura N, Nakamine H, Oshima K, Sadahira Y, Inagaki H, Oshima K, Tadaastu A (2003) Involvement of the chromosomal translocation t(11–18) in some mucosa-associated lymphoid tissue lymphomas and diffuse large cell lymphomas of the ocular adnexa: evidence from multiplex reverse transcriptase-polymerase chain reaction and fluorescence in situ hybridization on using formalin fixed, paraffin-embeded specimens. Mod Pathol 16:445–452
42. Uren AG, O'Rourke K, Aravind LA, Pisabarro MT, Seshagiri S, Koonin EV, Dixit VM (2000) Identification of paracaspases and metacaspases: two ancient families of caspase-like proteins, one of which plays a key role in MALT lymphoma. Mol Cell 6:961–967
43. White WL, Ferry JA, Harris NL, Grove AS Jr (1995) Ocular adnexal lymphoma. A clinicopathologic study with identification of lymphomas of mucosa-associated lymphoid tissue type. Ophthalmology 102:1994–2006
44. Willis TG, Jadayel DM, Du MQ, Peng H, Perry AR, Abdul-Rauf M, Price H, Karran L, Majekodunmi O, Wlodarska I, Pan L, Crook T, Hamoudi R, Isaacson PG, Dyer MJ (1999) Bcl10 is involved in t(1;14)(p22;q32) of MALT B cell lymphoma and mutated in multiple tumor types. Cell 96:35–45
45. Wohlschlaeger Ch, Lange K, Merz H, Feller AC (2003) Aberrant phenotype in mantle cell lymphoma. Leuk Lymphoma 44:269–273
46. Wotherspoon AC, Diss TC, Pan LX, Schmid C, Kerr-Muir MG, Lea SH, Isaacson PG (1993) Primary low-grade B cell lymphoma of the conjunctiva: a mucosa-associated lymphoid tissue type lymphoma. Histopathology 23:417–424
47. Ye H, Dogan A, Karran L, Willis TG, Chen L, Wlodarska I, Dyer MJ, Isaacson PG, Du MQ (2000) BCL10 expression in normal and neoplastic lymphoid tissue: nuclear localization in MALT lymphoma. Am J Pathol 157:1147–1154
48. Ye H, Liu H, Attygalle A, Wotherspoon AC, Nicholson AG, Charlotte F, Leblond V, Speight P, Goodlad J, Lavergne-Slove A, Martin-Subero JI, Siebert R, Dogan A, Isaacson PG, Du MQ (2003) Variable frequencies of t(11;18)(q21;q21) in MALT lymphomas of different sites: significant association with CagA strains of H pylori in gastric MALT lymphoma. Blood 102:1012–1018

Virchows Arch (2006) 448: 517–520
DOI 10.1007/s00428-006-0151-3

CASE REPORT

Martino Bosco · Elena Allia · Jean-Michel Coindre · Chiara Odasso · Alberto Pagani · Donatella Pacchioni

α-fetoprotein expression in a dedifferentiated liposarcoma

Received: 14 December 2005 / Revised: 21 December 2005 / Accepted: 21 December 2005 / Published online: 18 February 2006

Abstract Extremely rare cases of paraneoplastic syndromes or ectopic production of proteins associated with liposarcoma are reported in literature. We describe a unique case of relapsing retroperitoneal dedifferentiated liposarcoma with biochemical, immunohistochemical, and molecular evidence of alpha-fetoprotein (AFP) ectopic production. The lesion was associated to elevated AFP plasma levels that subsided after tumor removal. Immunohistochemical studies showed AFP production by a minority of tumor cells and reverse transcriptase polymerase chain reaction confirmed AFP mRNA expression. Finding of MDM2 and CDK4 iperexpression by immunohistochemistry confirmed the diagnosis of dedifferentiated liposarcoma.

Keywords Dedifferentiated liposarcoma · Alpha-fetoprotein · Ectopic production

M. Bosco · E. Allia · D. Pacchioni (✉)
Department of Biomedical Sciences and Human Oncology,
University of Turin, Italy,
Via Santena 7,
Turin 10126, Italy
e-mail: dpacchioni@molinette.piemonte.it
Tel.: +39-116334274
Fax: +39-116635267

J.-M. Coindre
Department of Pathology, Institut Bergonié,
rue de Saint-Genes 5,
Bordeaux 33076, France

C. Odasso
Department of General Surgery, University of Turin,
C.so Dogliotti 3,
Turin 10126, Italy

A. Pagani
Department of Pathology, Ospedale Civile di Pinerolo,
via Brigata Cagliari 34,
Pinerolo 10064, Italy

Introduction

Liposarcoma is the most common soft tissue sarcoma in adults and occurs in four main forms: atypical lipomatous tumor/well differentiated, myxoid/round cell, dedifferentiated, and pleomorphic liposarcoma. Dedifferentiated liposarcoma is defined as a malignant adipocytic neoplasm showing transition from atypical lipomatous tumor/well-differentiated liposarcoma to high-grade nonlipogenic sarcoma. The neoplasia most frequently involves the retroperitoneum, while other anatomic sites are less frequently involved [6].

Sporadic cases of paraneoplastic syndromes associated with liposarcomas, including paraneoplastic pemphigus, leucocytosis, and granulocyte colony-stimulating factors ectopic production, are reported in literature [7, 9, 13].

In this study, we report a case of dedifferentiated liposarcoma arising from retroperitoneum producing α-fetoprotein (AFP) at the time of relapse.

Case report

In September 2004, a 72-year-old male patient came to medical attention for intestinal subocclusion. A nephrectomy with surgical removal of a perirenal retroperitoneal well-differentiated liposarcoma had been performed 7 years previously. Abdominal tomography and ultrasound examinations disclosed a large mass infiltrating the retroperitoneal spaces. Hematochemical analysis showed normal values for gastrointestinal cancer-associated antigen, carcinoembryonic antigen, and prostate-specific antigen and elevated α-fetoprotein (AFP) levels (705 ng/ml, normal range in adult <30 ng/ml). The patient was human immunodeficiency virus and hepatitis C virus-negative and anti-HbcAg-positive. Serum levels of alanine transaminase, aspartate transaminase, alkaline phosphatase, gamma-GT were in the normal range and image studies showed no focal or diffuse lesions in liver. The patient underwent surgical removal of the retroperitoneal lesion. After surgery, levels of AFP decreased to 20 ng/ml.

Two months after the surgical resection the patient had clinical evidences of relapse with progressive increase of AFP serum concentration (up to 200 ng/ml) and died for septic shock. Autopsy was not performed.

Materials and methods

Immunohistochemistry

All specimens were fixed in 4% formalin and embedded in paraffin. For immunocytochemistry, the endogenous peroxidase in formalin-fixed, paraffin-embedded tissue was inhibited by incubating specimens with 3% H_2O_2 for 5 min before incubation with the primary monoclonal antibody or polyclonal rabbit serum. Immunohistochemical staining was performed using the streptavidin–biotin peroxidase method. Primary antibodies and working dilutions used are reported in Table 1. Heat-based antigen retrieval was performed for all immunohistochemical reactions in 10 mm citrate buffer, pH 6.

RT-PCR analysis for AFP mRNA

The presence of AFP mRNA was investigated in formalin-fixed, paraffin-embedded tissue by means of reverse transcriptase polymerase chain reaction (RT-PCR). A set of primers was designed which amplifies a 172-bp fragment between exon 4 and exon 5 of AFP gene: the sequence of the primers are 5′-TGTCACAAGCTGT GAAGCAT -3′ for the forward and 5′-GCTTTGCAG CAAGATGGAAT -3′ for the reverse oligonucleotide, respectively. Amplification reactions were carried out with 40 cycles made by three steps: denaturation at 94°C for 30 s, annealing at 60–50°C for 30 s, and extension at 72°C for 1 min; the initial annealing temperature of 60°C was reduced by 2°C after every two cycles to reach 50°C for the final 30 cycles.

Table 1 Primary antibodies and working dilutions used in this work

Antigen	Clone	Source	Dilution
AFP	ZSA06	Zymed	1:200
Cytokeratins	AE1/AE3	DAKO	1:50
hCG	Rabbit polyclonal	DAKO	1:200
S100	Rabbit polyclonal	DAKO	1:3,500
ki-67	Mib-1	DAKO	1:100
Desmin	D33	DAKO	1:100
Hepatocyte	OCH1E5	DAKO	1:50
CD30	Ber-H2	DAKO	1:50
Vimentin	V9	DAKO	1:50
MDM2	IF2	Zymed	1:100
CDK4	DCS-31	Biosource	1:200

Results

The tumor removed in 1997 originated from the retroperitoneal space and infiltrated left kidney and left psoas muscle. Grossly, the lesion was 12 cm in diameter and was represented by fat intermixed with small amount of compact, white tissue. Microscopically, it was mainly composed by small mature adipocytes and fibrous/myxoid areas with mostly tipical spindle cells. Moreover, cells with atypical, enlarged plurilobated nuclei with dense chromatin were found, particularly in myxoid areas (Fig. 1) but no multivacuolated lipoblast was found. A diagnosis of atypical lipomatous tumor/well-differentiated liposarcoma was made.

The lesion removed in 2004 was a large mass (30 cm in largest dimension), with irregular margins and a yellow–white cut surface with many necrotic and hemorragic areas. The lesion was localized in retroperitoneal space and infiltrated the body and the tail of pancreas.

Microscopically, it showed a heterogeneous cellular composition which included atypical spindle cells, small round cells, epithelioid elements, and focal areas composed by large, pleomorphic, occasionally multinucleated cells (Fig. 2a,b). The neoplastic population displayed a high proliferation rate, with mitotic figures per 10 high power fields and 68% of ki-67 positive cells. Unequivocal lipoblasts could not be found. The lesion was grade 3 according to Federation National des Centres de Lutte Contre le Cancer grading system [4]. Surgical margins were positive.

Immunohistochemical studies showed diffuse vimentin positivity, absence of cytocheratin expression, faint S100-protein positivity, focal positivity for desmin (mostly in areas morphologically suggestive of rhabdomyoblastic differentiation), focal positivity for MDM2 and CDK4 (Fig. 3a,b), intense, focal positivity for AFP (particularly in the most pleomorphic areas) (Fig. 3c,d), negative staining for antihepatocyte and antihuman chorionic gonadotropin (hCG), and faint, focal membrane expression of CD30 in

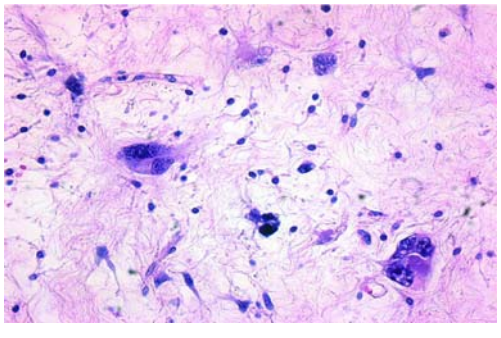

Fig. 1 Retroperitoneal mass removed in 1997. Large, atypical cells with hyperchromatic and plurilobated nuclei with prominent nucleoli scattered in myxoid stroma with prominent small vassells (×400)

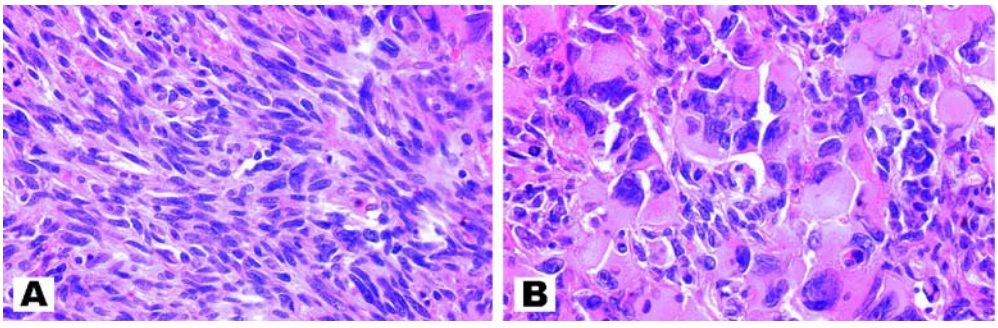

Fig. 2 Retroperitoneal mass removed in 2004. The lesion was largely composed by atypical spindle cells vaguely arranged in bundles (**a**), with sparse areas composed by epithelioid, pleomorphic cells with large eosinophilic cytoplasm (**b**) (×400)

few areas prevalently composed by small round elements. RT-PCR expression of AFP mRNA was detected in the tumor (Fig. 4).

Altogether, the morphological, immunohistochemical, and molecular features displayed by this lesion, together of a previous history of well-differentiated liposarcoma, suggested the diagnosis of dedifferentiated liposarcoma with ectopic production of AFP.

A retrospective immunohistochemical evaluation of AFP protein on sections from the lesion excised in 1997 was made and resulted completely negative.

Discussion

AFP is a single chain α-globulin with a molecular weight of ~70 KDa. In the developing fetus, AFP is produced by both yolk sac and fetal liver. AFP is thought to serve biochemical functions similar to that of albumin [12]. In addition to this function, many studies have established that AFP can act as a growth regulator during ontogenesis and tumor progression [14]. In the adult life, its expression is reactivated and its serum levels increase in chronic liver diseases and in malignances such as hepatocellular carcinoma, embrional carcinoma and yolk sac tumors [1]. Cases of AFP-producing adenocarcinoma, commonly exhibiting histological features of hepathoid differentiation, are reported in literature [8, 10, 11].

We describe a unique case of relapsing dedifferentiated liposarcoma with biochemical, immunohistochemical, and molecular evidence of AFP production. The morphological and immunohistochemical features of this lesion are not reminiscent of anyone of the usual causes of AFP production. In particular, absent expression of hepatocellular antigen (clone OCH1E5) and cytokeratin, together with morphological findings and clinical history, exclude an extrahepatic diffusion of a hepatocellular carcinoma. No histopathological evidence of a yolk sack tumor could be found in this lesion, except for focal CD30 expression. The focal expression of MDM2 and CDK4, which is strongly correlated to amplification status of their respective genes, also confirmed the diagnosis of dedifferentiated liposarcoma [3].

To our knowledge, no other case of AFP-producing sarcoma has been described so far, except for a report of a rhabdomyosarcoma of the urinary bladder [2]. However, rare paraneoplastic syndromes or ectopic productions associated to liposarcomas are described in literature [7,

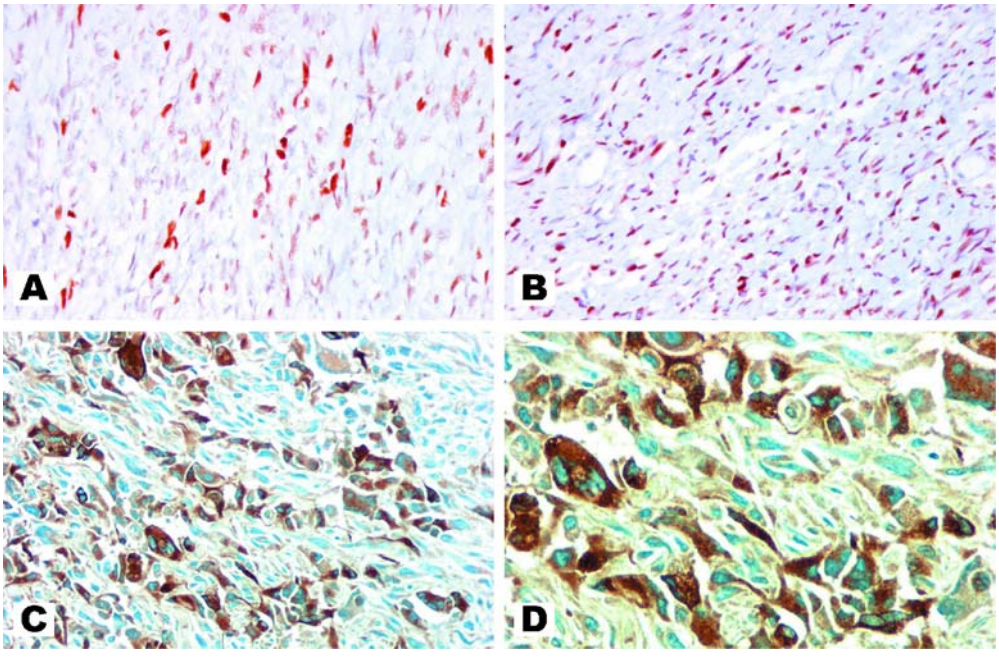

Fig. 3 The tumor showed focal expression of MDM2 (**a**) and CDK4 (**b**). Focal, intense reactivity with anti-AFP antibody was found in some areas with pleomorphic elements (**c**, **d**)

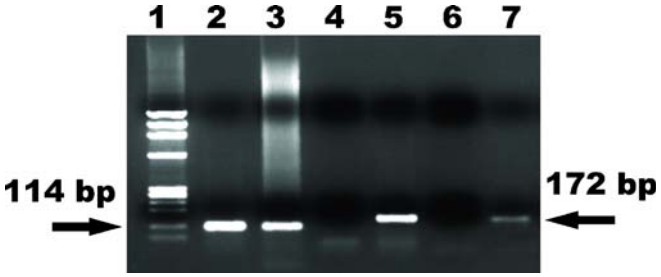

Fig. 4 Agarose gel of RT-PCR for AFP mRNA. Bands at 114 and 172 bp correspond to beta2-microglobulin and AFP amplification products, respectively. *Line 6* and *7* are sample from two different areas of the lesion, one of which showing presence of AFP mRNA. *Line 1* markers; *line 2* beta2-microglobulin, fetal liver; *line 3* beta2 microglobulin, sample; *line 4* no RNA; *line 5* AFP, fetal liver; *line 6*, *7* AFP, sample

9, 13]. One of them is a report of leucocytosis associated with liposarcoma recurrence [7].

Reactivation of AFP gene transcription in tumors is thought to be mediated by several mechanisms which include iperexpression of specific transcription factors [15] and loss of function of proteins involved in postnatal *AFP* gene silencing [5]. Some of these mechanisms could be involved in reactivation of *AFP* gene expression in this case of dedifferentiated liposarcoma.

This report adds dedifferentiated liposarcoma to the list of the unusual neoplastic causes of high AFP serum levels.

Acknowledgement This study was supported by grant from The Regione Piemonte (Turin, D.D. 173 30/10/2003).

References

1. Abelev GI (1971) α-fetoprotein in association with malignant tumors. Adv Cancer Res 14:295–357
2. Badve SS, Saxena R, Soman CS, Kiri VM, Raghuvanshi SR, Patoria NK (1992) α-fetoprotein production by rhabdomyosarcoma of the urinary bladder. Indian J Cancer 29:177–180
3. Binh MB, Sastre-Garau X, Guillou L, de Pinieux G, Terrier P, Lagace R, Aurias A, Hostein I, Coindre JM (2005) MDM2 and CDK4 immunostainings are useful adjuncts in diagnosing well-differentiated and dedifferentiated liposarcoma subtypes: a comparative analysis of 559 soft tissue neoplasms with genetic data. Am J Surg Pathol 29:1340–1347
4. Coindre JM, Terrier P, Bui NB, Bonichon F, Collin F, Le Doussal V, Mandard AM, Vilain MO, Jacquemier J, Duplay H, Sastre X, Barlier C, Henry-Amar M, Mace-Lesech J, Contesso G (1996) Prognostic factors in adult patients with locally controlled soft tissue sarcoma. A study of 546 patients from the French Federation of Cancer Centers Sarcoma Group. J Clin Oncol 14:869–877
5. Cui R, Nguyen TT, Taube JH, Stratton SA, Feuerman MH, Barton MC (2005) Family members p53 and p73 act together in chromatin modification and direct repression of alpha-fetoprotein transcript ion. J Biol Chem 280:39152–39160
6. Dei Tos AP, Pedeutour F (2002) Dedifferentiated liposarcoma. In: Fletcher CDM, Unni KK, Mertens F (eds) Tumours of Soft Tissue and Bone: Pathology and Genetics. World Health Organization Classification of Tumours, IARC, Lyon, pp 38–39
7. des Guetz G, Mariani P, Freneaux P, Pouillart P (2004) Paraneoplastic syndromes in cancer: Case 2. Leucocytosis associated with liposarcoma recurrence: original presentation of liposarcoma recurrence. J Clin Oncol 22:2242–2243
8. Hocking GR, Shembrey M, Hay D, Ostor AG (1995) α-fetoprotein-producing adenocarcinoma of the sigmoid colon with possible hepatoid differentiation. Pathology 27:277–279
9. Kaplan I, Hodak E, Ackerman L, Mimouni D, Anhalt GJ, Calderon S (2004) Neoplasms associated with paraneoplastic pemphigus: a review with emphasis on non-hematologic malignancy and oral mucosal manifestations. Oral Oncol 40:553–562
10. Kono K, Amemiya H, Sekikawa T, Iizuka H, Takahashi A, Fujii H, Matsumoto Y (2002) Clinicopathologic features of gastric cancers producing α-fetoprotein. Dig Surg 19:359–365
11. Maida Y, Kyo S, Takakura M, Kanaya T, Inoue M (1998) Ovarian endometrioid adenocarcinoma with ectopic production of alpha-fetoprotein. Gynecol Oncol 71:133–136
12. Mizejewski GJ (1985) New insights into AFP structure and function: potential biomedical applications. In: Mizejewski GJ and Porter IH (eds) α-fetoprotein and Congenital Disorders. Academic, Orlando, pp 5–34
13. Nakamura A, Tanaka S, Takayama H, Sakamoto M, Ishii H, Kusano M, Onizuka Y, Ota S, Mitamura K (1998) A mesenteric liposarcoma with production of granulocyte colony-stimulating factor. Intern Med 37:884–890
14. Wang XW and Xie H (1998) Stimulation of tumor cell growth by α-fetoprotein. Int J Cancer 75:596–599
15. Yano T, Kishimoto T, Tomaru U, Kawarada Y, Kato H, Yoshiki T, Ishikura H (2003) Further evidence of hepatic transdifferentiation in hepatoid adenocarcinomas of the stomach: quantitative analysis of mRNA for albumin and hepatocyte nuclear factor-4alpha. Pathology 35:75–78

Virchows Arch (2006) 448: 521–523
DOI 10.1007/s00428-005-0125-x

LETTER TO THE EDITOR

Saral S. Desai · Anita M. Borges

Melanin bearing myoepithelial cells in a pigmented salivary gland carcinoma: a new avatar of myoepithelial cell? A case report

Received: 12 September 2005 / Accepted: 21 September 2005 / Published online: 21 January 2006

Abstract Melanocytes can be found in the stroma of salivary glands and their tumors. However, the presence of melanin pigment in the tumor cells of salivary gland origin is exceedingly rare. A 42-year-old man presented with a nasal tumor that was black in color. The histology was that of a minor salivary gland carcinoma with foci resembling an adenoid cystic carcinoma. The myoepithelial cells of this tumor contained melanin pigment. The possible histogenesis of this lesion and an explanation for the occurrence of melanin pigment in a salivary gland tumor are discussed.

Introduction

The myoepithelial cells can take on a variety of different forms in neoplastic conditions. However, the presence of melanin pigment within the cells of a minor salivary gland carcinoma is exceedingly rare. We report here a case of a melanotic nasal tumor of minor salivary gland type in which the pigment-bearing cells expressed a myoepithelial phenotype.

Case report

A 42-year-old man presented with a mass in the nose. The mass was present on the lateral wall of the nasal cavity in relation with the nasal mucosa. The radiographs revealed a tumor invading the maxillary bone. An enlarged neck node was also identified. A medial maxillectomy was performed to excise the tumor together with ipsilateral dissection of the neck nodes.

S. S. Desai · A. M. Borges
Institute of Pathology, Tata Memorial Hospital,
Dr. Ernest Borges Road, Parel,
Mumbai 400 012, India

S. S. Desai (✉)
3-Bhagwat, 50 Vallabh Nagar Soc.,
NS Road No. 2, JVPD Scheme,
Mumbai 400 056, India
e-mail: saraldesai@hotmail.com
Tel.: +91-22-26123123

Pathological findings

The tumor mass measured 1.5 cm. It was solid, firm and black in color. The lymph nodes were enlarged and black-brown in color.

On histology, the nasal mass was a minor salivary gland tumor. The tumor was focally circumscribed, while at some places the tumor infiltrated into the bone (Fig. 1a). This tumor consisted of sheets and nests of cells, with focal areas showing glandular structures and squamous differentiation (Fig. 1b,c). Furthermore, the tumor showed cribriform and tubular pattern of an adenoid cystic carcinoma (Fig. 2).The tumor did not fit neatly into any particular World Health Organization (WHO) type, although it most resembled an adenoid cystic carcinoma. The tumor cells showed the presence of brown pigment akin to melanin in their cytoplasm (Fig. 3a). The pigment was also noted in the stroma. This pigment could be bleached with perioxidase and potassium permanganate, and it did not give a positive reaction with Prussian blue.

The lymph node showed tumor metastasis. Here too, the tumor cells had adenoid cystic pattern and showed the presence of brown–black pigment. There was no extracapsular spread of the tumor.

Immunohistochemistry

Immunohistochemical analysis was done using the avidin–biotin complex after bleaching the sections with potassium permanganate and confirming under the microscope that there was no residual pigment. All the antibodies were applied after the sections were bleached so as to negate the interference of melanin pigment in the evaluation of immunohistochemical reactivity. The tumor cells expressed myoepithelial markers, viz. cytokeratin (MNF 116), epithelial membrane antigen, S-100 protein, calponin, CD10, smooth muscle actin and p63. They also expressed HMB-45 (Fig. 3b), a marker for immature melanosomes. The stromal cells did not react with either S-100 protein or HMB-45, and thus, were not thought to be of melanocytic

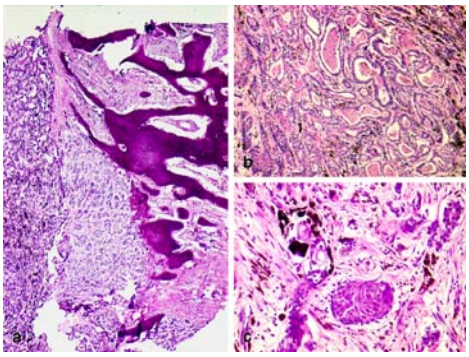

Fig. 1 **a** Tumor infiltrating the bone (H & E, ×4). **b** Parts of the tumor show glandular architecture (H & E, ×10). **c** In some places, the tumor formed a solid nest and showed squamous differentiation (H & E, ×10). Note the brown pigment in all the photomicrographs

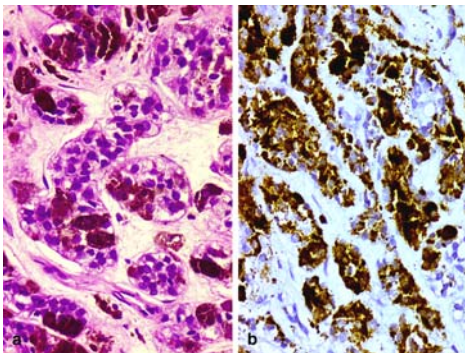

Fig. 3 **a** Nests of myoepithelial tumor cells with clear cytoplasm and containing brown pigment (H & E, ×40). **b** These cells exhibit strong immunoreactivity for HMB-45 antibody

origin, and were fibroblasts or histiocytes (some were CD68-positive).

Histological diagnosis

The tumor was labeled as a pigmented minor salivary gland carcinoma showing myoepithelial differentiation and resembling an adenoid cystic carcinoma.

Discussion

Melanin pigment has been previously described in rare salivary gland tumors, one being an adenoid cystic carcinoma where the melanin has essentially been found in the stromal cells [4]. The other cases were of mucoepidermoid tumors, where the pigment-producing cells were proved to be melanocytes [1–3, 8]. More recently, a case of pleomorphic adenoma with melanin pigment has been described [7].

The salivary gland carcinoma of the nose described in the present case report was so heavily pigmented that it clinically resembled a melanoma. The melanin pigment

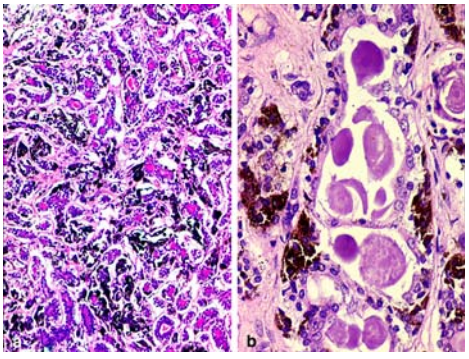

Fig. 2 Adenoid cystic carcinoma pattern. **a** Tubular and cribriform structures (H & E, ×10). **b** Photomicrograph from the lymph node metastasis showing tubular complex, with the central space containing hyaline eosinophilic material, and lined by an inner layer of cells with eosinophilic cytoplasm and an outer layer of basaloid cells. Some of the cells contain brown pigment (H & E, ×40)

was present within the clear myoepithelial cells. The nature of the pigment was discerned by HMB-45 immunoreactivity, bleaching with potassium permanganate, positive reaction with Fontana–Masson, and a negative Perls reaction. The panel of immunohistochemistry performed points toward myoepithelial differentiation of these cells.

Myoepithelial cells are known for their divergent phenotypes, viz clear, spindle, plasmacytoid, and epithelioid. In addition, they can also show keratinizing squamous and lipocytic differentiation. However, to the best of our knowledge, the presence of intracellular melanin pigment within these has not been described. The possibility of this being a collision of malignant melanoma and a salivary gland tumor can be excluded because there were no two distinct tumors. This tumor looked like a salivary gland tumor, and the only difference was that it had pigment in the tumor cells.

The question arises as to the origin of melanin in the present tumor. The melanin was undoubtedly in the cells that expressed the myoepithelial characteristics. Were the myoepithelial cells the source of the pigment or were these cells merely storing it? Melanin is normally produced by cells of neural crest origin, and the salivary glands do not belong to this lineage. However, melanocytes can be found in salivary glands [5, 6]. Stromal melanocytes are the source of abnormal melanin accumulation in the tumor cells of some adnexal tumors of the skin, viz. eccrine poroma and cylindromas, which are analogous to basal cell adenomas of the salivary glands. A case of mucoepidermoid carcinoma has been recently described, wherein the tumor was colonized by melanocytes, and the tumor cells phagocytosed the melanin pigment [2]. Could this be the explanation for the pigmentation in our case? Occasional stromal cells containing pigment were noted in the tumor. However, these did not have the histological appearance of the dendritic melanocytes nor were they S-100 protein or HMB-45-positive. Although we have no ultrastructural proof, the presence of heavy pigmentation present mainly in the myoepithelial cells, their strong reaction with HMB-45 and the lack of dendritic melanocytes in the stroma leads us to believe that the myoepithelial cell can, under unusual conditions, produce melanin. It is interesting

to note that adenoid cystic carcinoma, a tumor rich in myoepithelial cells, is one of the three salivary gland tumors in which pigment has previously been reported. Perhaps, melanin production should be added to the long list of phenotypic avatars that this most fascinating and plastic cell type assumes under conditions of neoplasia.

References

1. Aufdemorte TB, Van Sickels JE, Glass BJ (1985) Melanin pigmentation in a mucoepidermoid tumor of a minor salivary gland. J Oral Maxillofac Surg 43(11):876–879
2. Marucci G, Marchetti C, Betts CM, Foschinin MP (2005) Pigmented mucoepidermoid carcinoma of the oral cavity: a case report. Int J Surg Pathol 13:295–297
3. Sekine J, Anami M, Fujita S, Vieth M, Inokuchi T (2005) A case of mucoepidermoid carcinoma with melanin pigmentation manifested in the palate. Virchows Arch 446(4):460–462
4. Takeda Y (1996) Stromal melanocytosis of an adenoid cystic carcinoma arising from the palatal minor salivary gland. Pathol Int 46(6):467–470
5. Takeda Y (1997) Melanocytes in the human parotid gland. Pathol Int 47(8):581–583
6. Takeda Y (2000) Existence and distribution of melanocytes and HMB-45-positive cells in the human minor salivary glands. Pathol Int 50(1):15–19
7. Takeda Y, Masanobu S, Nakamura S (2004) Pigmented pleomorphic adenoma, a novel melanin-pigmented benign salivary gland tumor. Virchows Arch 445:199–202
8. Thomas KM, Hutt MSR, Borgstein J (1980) Salivary gland tumors in Malawi. Cancer 46:2328–2334

Virchows Arch (2006) 448: 524
DOI 10.1007/s00428-006-0178-5

ANNOUNCEMENTS

6 May 2006
Problems in Breast Pathology
Malta College of Pathologists
Malta

Course Director
Professor J.G. Azzopardi

Scientific Secretariat
J. De Gaetano and V. Eusebi

The congress fee is 30 ∈, that includes light lunch payable on the spot.

Scientific Organizer:
Dr. James De Gaetano
Pathology Department
St. Luke's Hospital
Gwardamangia
Malta
tel.n. xx356 25951117
e-mail james.degaetano@gov.mt

Venue and Hotel accomodation:
Hilton Hotel
Portomaso
St. Julians
Malta PTM01
Tel.n. XX 356 21383383
www.hilton.com.mt

1–3 June 2006
Technology Transfer in Diagnostic Pathology
1st Central European Regional Meeting: Liver & Pancreas Pathology
Eger, Hungary

The Hungarian Division of the International Academy of Pathology announces the ***Liver & Pancreas Pathology*** both for young and well-trained pathologists and clinicians.

The Meeting will focus on the practical clinicopathological aspects of liver and pancreatic diseases and conclude in a consensus. Among the highlights will be the differential diagnosis of hepatic and pancreatic tumors and premalignant alterations presented by *internationally renowned* experts, in active interaction with the attendants.

Plenary lectures will cover the themes of steatohepatitis, reversibility of cirrhosis, chronic hepatitis, classification and diagnosis of liver tumors, progenitor cells in the liver, pancreatitis, tumors of the pancreas.

Slide seminars will discuss autoimmune liver diseases (PBC, PSC, CAH), toxic liver injuries, benign and malignant liver tumors, tumor-like lesions of the liver, pancreatitis and pancreatic tumors.

Poster presentations will be reviewed and discussed individually by the participants.

For further information please contact

Scientific information:
Prof. Dr. Zsuzsa Schaff, Course Director,
schaff@korb2.sote.hu
Prof. Dr. Anna Kádár
kadann@korb2.sote.hu
Congress secretariat:
Ms. Katalin Mtray, K&M Congress Ltd.
Podmaniczky u. 75
H-1064 Budapest, Hungary
Phone: +36-1-3012000,
Fax: +36-1-3012001
e-mail: info@kmcongress.com
Website: www.kmcongress.com

15–16 June 2006
Thyroid Pathology for the Practicing Pathologist
15 rue de l'Ecole de Médecine, Paris,France

A 2-day course will take place in Paris again under the auspices of the French Division of the I.A.P.

This course will be given in English by Prof. M. Sobrinho-Simões (Porto) and Prof. R. Heimann (Brussels).

It will consist of lectures alternating with slide reviews and a slide seminar over a multihead microscope. The cases of this seminar will be sent (on CD) before the meeting.

The audience will be limited to 22 participants.
Course fees: 390 euros (320 euros for members of any I.A.P. division).
The fees include registration, hand-out, CD of the slide seminar and coffee breaks.

For further information please contact
Mrs. M. Fontaniére
Administrative Secretary
French Division of the I.A.P.
32 Cours Albert Thomas
69008, Lyon, France
Fax: 33 4 78754311
e-mail: academie.pathologie@wanadoo.fr

Virchows Arch (2006) 448: 525–531
DOI 10.1007/s00428-005-0095-z

REVIEW ARTICLE

P. Zagorianakou · N. Zagorianakou · D. Stefanou · G. Makrydimas · N. J. Agnantis

The enigmatic nature of apocrine breast lesions

Received: 27 March 2005 / Accepted: 12 September 2005 / Published online: 29 March 2006

Abstract Epithelial cells of fetal breast glandular structures, at the third trimester of pregnancy (28 weeks), produce GCDFP-15, in the absence of specific apocrine morphology. Apocrine epithelium of the breast may be a normal process of differentiation rather than a result of metaplasia, and it has been demonstrated that it is estrogen-receptor, progesterone-receptor and bcl-2 negative, but androgen-receptor (AR) positive. The significance of AR expression in apocrine epithelium is uncertain. Apocrine epithelium is seen in a wide spectrum of breast entities, ranging from benign lesions to invasive carcinoma. Breast cancer accounts 32% of all cancer cases among women and is the most common type of cancer in women. Little is known about breast carcinogenesis. Widely, it is accepted that breast cancer, like most other type of cancer, is being developed through the accumulation of genetic aberrations. Apocrine epithelium may reflect instability of the breast epithelium, creating an environment favouring further oncogenic alterations. In the last decade, several lines of evidence support the idea that some breast benign epithelial apocrine lesions are clonal lesions and may be considered as truly pre-malignant or precursors of breast carcinoma. Apocrine changes in many cases do not present any diagnostic difficulty; on the other hand, apocrine proliferations with cytologic atypia can be particularly difficult and challenging. The purpose of this study is to collect and highlight the areas of consensus in the literature as well as the controversial areas concerning the apocrine epithelium of the breast.

Keywords Breast · Apocrine epithelium · GCDFP-15 · Fibrocystic changes · Apocrine carcinoma · Molecular alterations

P. Zagorianakou · N. Zagorianakou · D. Stefanou · N. J. Agnantis (✉)
Department of Pathology, University of Ioannina, Medical School, University Campus, P.O. Box 1186, 45110 Ioannina, Greece
e-mail: nagnanti@cc.uo
Tel.: +30-26150-97792
Fax: +30-26510-97858

G. Makrydimas
Department Obstetrics and Gynaecology, Medical School, University of Ioannina, Ioannina, Greece

Introduction

The apocrine epithelium, from the Greek word από + έκκριση, is a normal constituent of apocrine glands of axillary, anogenital skin, eyelids (Moll), ears (ceruminous) and mammary gland, which consists of cells with eosinophilic cytoplasm that may contain lipid, iron, lipofuscin, PAS-positive diastase-resistant granules and a large nucleus located near the base of the cell (Fig. 1). Fragments of apical cytoplasm are found in the lumen of these glands. The apocrine glands develop as epithelial buds from the outer root sheath of the hair follicles in 5 to 6-month-old fetuses and continue into late embryonic life as long as new hair follicles develop [81, 67]. Nevertheless, morphologically and functionally, the apocrine epithelium is different from cutaneous, sebaceous and sweat glands [69]. A wide spectrum of benign and malignant breast lesions contains epithelial cells that are identical to those that consist the apocrine glands [37, 48]. Immunohistochemical studies of benign and malignant breast lesions, showing apocrine differentiation, report that cells stain positive for androgen receptors (AR) and lack estrogen receptor (ER), progesterone receptors (PR) and exhibiting bcl-2 negativity in normal breast epithelium. Morphological features of apocrine differentiation were valuable criteria, leading the Pathologists to a benign diagnosis. In a review paper of Love et al. [49] on fibrocystic disease, the authors are wondering whether it is reasonable to consider apocrine cells a pathological phenomenon inasmuch as about 90% of adult breasts show evidence of them. To date, with the advent of new technologies, there are compelling molecular data on these lesions that change the existing concept [40, 80].

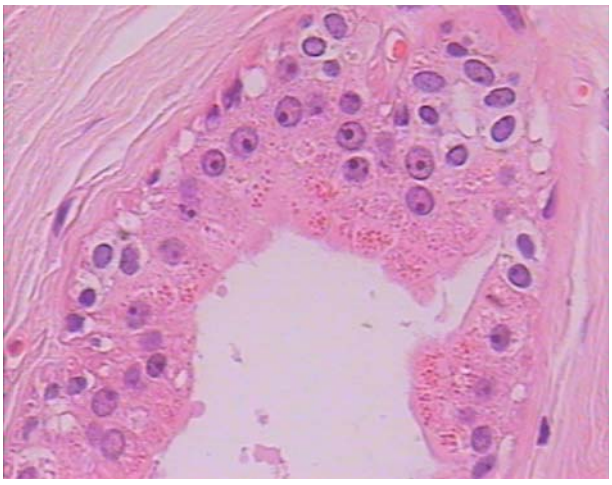

Fig. 1 High magnification of apocrine epithelium (H+E×400)

Apocrine markers

The glycoprotein GCDFP-15 (15 kDa), the major component of cyst fluid, represents an immunocytochemical marker of apocrine differentiation that is more reliable than morphology and the detection of prolactin inducible protein (PIP)/GCDFP-15 mRNA using in situ hybridization (Fig. 2) [27, 59, 48]. It is identical to the gene of the PIP described in the breast cancer cell line T-47D [77, 57, 33]. The gene is expressed in apocrine glands and in exocrine organs that have common phylogenetic features with apocrine glands, such as the bronchial epithelium, the sweat, salivary and lacrimal glands and the seminal vesicles. According to human genome sequencing data, the GCDFP/PIP is localized at 7q34 [45].

The GCDFP-15 had 95% specificity and 74% sensitivity as a marker for breast cancer [93, 94] and has been used to support breast origin in metastatic carcinoma of unknown primary origin (Figs. 3, 4 and 5). GCDFP-15 is present at a very low concentration in the plasma of physiological women and is 140,000 times higher in breast cyst fluid compared to plasma. The concentration in amniotic fluid of pregnant women is 7.200 ng/ml [34].

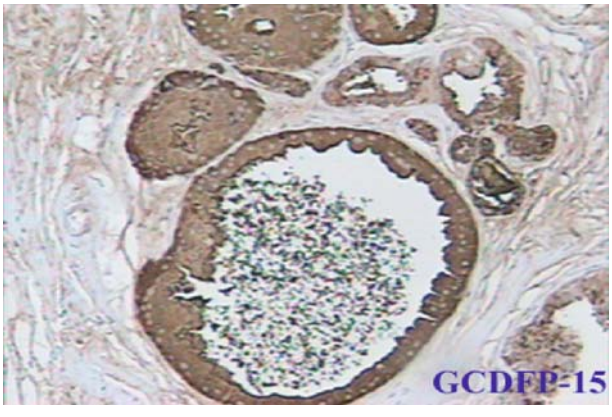

Fig. 2 GCDFP-15, immunostaining in apocrine cysts (DAB ×200)

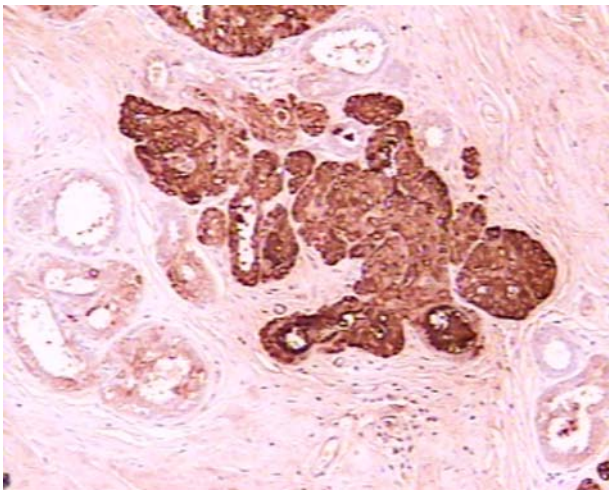

Fig. 3 Intense cytoplasmic immunostaining for GCDFP-15 in: in situ (Fig. 4), infiltrating (Fig. 5) and metastatic to a lymph node (Fig. 6) apocrine carcinoma

An appreciable discriminating feature between apocrine cells and normal luminal epithelial cells of the breast is that while the former expresses AR and lacks ER, PR and bcl-2, the latter is ER/PR positive and AR negative. The apocrine cells differ from normal cells not only morphologically but also biologically [72, 30].

Theories

The origin of apocrine cells has always been a contradictory issue. Several answers have been given for the presence of this enigmatic entity. The existence of apocrine cells in the breast has generally been regarded as a metaplastic process [86], but this issue has recently been debated [3, 14, 16, 84, 90]. Some authors believe that apocrine metaplasia, in general, is a terminally differentiated entity [10, 66], others considered that the apocrine epithelium is a degenerated epithelium [19, 92]; several authors suggested that these cells are normal element of the glandular structure of the breast [27] or a metabolic active epithelium [53]. These different opinions in the international literature make the

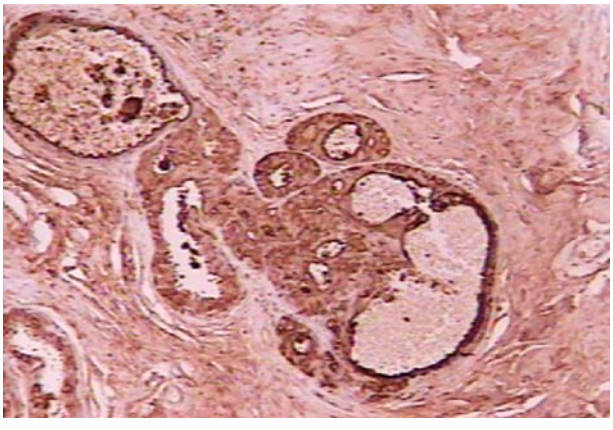

Fig. 4 Intense cytoplasmic immunostaining for GCDFP-15 in in situ apocrine carcinoma

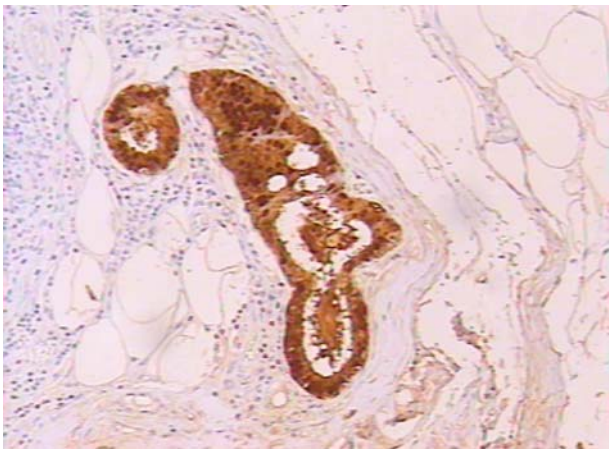

Fig. 5 Intense cytoplasmic immunostaining for GCDFP-15 in infiltrating apocrine carcinoma

subject of apocrine epithelium very controversial. Despite the fact that apocrine changes have been considered a metaplastic process in the mammary gland, usually associated with physiological changes in the hormonal milieu and ageing, there is a strong evidence to suggest that a part of apocrine changes show molecular alterations using the existing reliable technology. The molecular changes are more frequently observed in entities such as apocrine adenosis and apocrine hyperplasia. We would suggest that, nowadays, there is overwhelming molecular data that some of these apocrine changes in proliferative lesions maybe precursors of malignant transformation [40, 74–75, 90, 91]. It would be possible that those data are misleading, but nevertheless they should be considered mandatory for further investigation in interesting "hot area" of breast research.

Epithelial cells, in some very primitive structures with no particular distribution, produce CDFP-15 in normal fetal breast, where their overall number was increased with gestational age [89]. McKiernan et al. [51] studied the histology of breast development and reported the existence of lobular structures, dilated ducts and apocrine secretion. In the newborn breast, the epithelial cells have an eosinophilic cytoplasm with typical apocrine secretion [70]. It was mentioned in the infant under development that apocrine metaplasia was observed as part of the post neonatal involution [38]. Others suggest that apocrine epithelium belong to entrapped cutaneous apocrine glands in the area of mammary gland during the process of development [89].

Apocrine cell-epithelial lesions

Apocrine phenotype is observed in a spectrum of breast epithelial lesions spanning from benign metaplasia to apocrine carcinoma. Apocrine metaplastic epithelium (APM) is a frequent finding, occurring in approximately 40% of benign breast biopsies [25]. Apocrine cells in the breast appear frequently in benign breast lesions such as fibrocystic disease (Fig. 6) [17, 26–29, 56], papillomas [65], fibroadenomas [4, 25], sclerosing adenosis [13, 79] atypical apocrine proliferations, apocrine ductal carcinoma in situ (DCIS), invasive apocrine carcinoma [47, 1] and lobular carcinoma [26].

Fibrocystic changes (FCC) are a common finding, and it is clinically evident in about 50% of women of reproductive age. In the western countries, 7% of women develop palpable breast cysts [33]. Single or multiple cysts are the most prevalent lesion of the female breast [42]. Gross cystic changes, a common finding in premenopausal women, generally present as a single cyst. Cysts are thought to arise through obstruction of the ducts. There are two types of cysts. Type I cysts (apocrine or secretory) have high levels of potassium ions ($Na^+/K^{+\ ratio}<3$), large concentrations of steroid hormones, epidermal growth factor and gross cystic disease fluid protein, and it is thought to be under androgen regulation [36, 7, 52]. Apocrine changes are prevalent in flat to cuboidal cells lining type I cysts. Type II cysts with content $Na^+/K^{+\ ratio}>3$ are lined by flattened epithelium. The morphological presentations of hyperplastic changes include papillary or micropapillary lesions composed of apocrine cells.

However, several follow-up studies have suggested that apocrine epithelium may be a predictor of the subsequent development of malignancy [35, 60].

Several reports have assessed the relation between palpable breast cysts and breast carcinoma and suggested that there is an increased risk of breast carcinoma, which ranges from 1.7 to 7.5 times [68, 17, 8, 11, 6]. Haagensen et al. found a fivefold-increased incidence of carcinoma associated with papillary apocrine metaplasia in fibrocystic changes, although this fact has subsequently been questioned [12, 35]. Dixon, et al., has shown no significant association between cyst type and breast-cancer risk [20]. Dupont and Page [22], in their long-term follow-up study of women with benign breast lesions, found an increased relative risk only of 1.7 in cases without complications. A slightly elevated relative risk of 2.4 for subsequent development of malignancy has been noticed for those cases with complex papillary lesions [61].

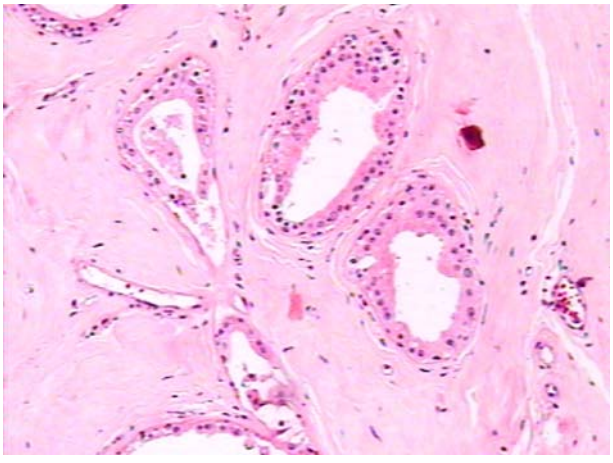

Fig. 6 Apocrine cysts in a breast with fibrocystic changes (H+E × 100)

The presence of focal apocrine metaplasia within epithelial breast proliferations is generally considered as an important indicator in the histopathologic diagnosis of benignity [78].

The definition of apocrine metaplasia is based on the following criteria: (a) eosinophilic cytoplasm with fine granularity, (b) large and moderately vesicular nuclei with an occasional prominent red nucleoli and (c) sporadic presence of apical snouts [83, 58].

Borderline apocrine lesions are classified into two categories: atypical apocrine adenosis and atypical ductal hyperplasia of apocrine type [46]. In 1963, Papanicolaou [63] used the descriptive term of "non-malignant atypia" for apocrine cells, "the individual cells or cellular clusters that show enlargement, metaplasia, engulfment and vacuolation, which is often extreme".

O'Malley et al. [58] used morphologic–cytologic criteria and extent criteria. Apocrine lesions that measured less than 8 mm were called benign. The human breast epithelium is a dynamic entity that is remodeled under the influence of sex hormones and growth factors. This dynamic ability of breast cells reflects instability of the breast epithelium, creating an environment susceptible to carcinogenesis. Breast lesions with APM epithelium appear to demonstrate abnormal oncoprotein and apoptosis-related protein expression associated with a high proliferation rate [74]. Increased cellular and architectural atypia may indicate an increased risk of developing apocrine carcinoma [97].

Apocrine adenosis (AA) is a rare breast lesion, which is characterized as sclerosing adenosis associated with marked apocrine metaplastic changes [79, 13]. Simpson et al. [79] identified in a retrospective study of 10,000 benign biopsies of 55 cases of apocrine adenosis.

AA has been misdiagnosed as carcinoma due to the cytologic atypia of the apocrine cells, and it is occasionally so florid that it gives rise to a distinct mass, which can be mistaken clinically for cancer [93, 76]. Wells et al. [93] have suggested that apocrine adenosis may be a precancerous lesion, mainly on the basis of the expression of c-erbB2 protein.

Apocrine adenoma is another rare breast neoplasm, composed exclusively of apocrine cells, which is sharply demarcated and shows back-to-back glands with papillary fronds projecting into the lumina. This rare lesion should be distinguished from well-differentiated apocrine carcinoma [10, 5].

Neoplastic transformation may occur in metaplastic epithelium. Cancer of the bladder, stomach, lung and cervix have their origin in these metaplastic areas. The metaplastic epithelium returns to the normal epithelium when the stimulus is removed. The stimuli leading to metaplasia could also lead to carcinogenesis of the metaplastic epithelium. The stimulus for apocrine metaplasia is unknown. Chemicals, vitamins, and growth factors play a significant role in metaplasia [18].

It is well known that some hyperplastic breast lesions might actually be clonal in origin. The detection of allelic imbalances in ductal hyperplasia and papillomas suggested that these lesions might be neoplastic (monoclonal) rather than hyperplastic (polyclonal) proliferations [44, 87].

The findings of molecular alterations in benign proliferative apocrine lesions such as APM, apocrine hyperplasia and apocrine adenosis support the idea that these lesions are clonal. Several authors using comparative genomic hybridization demonstrated loss of 1p, 2p, 10q, 16q, 17q and 22q and gain of 1p, 2q and 13q [40], and analyses of heterozygosity/allelic imbalance have demonstrated that the average number of genetic changes (overall gains and losses) at 1p, 11q, 13q, 16q and 17q is frequent event in APM, AA and apocrine hyperplasia [73, 75, 89, 90].

Two studies have shown aneuploidy in apocrine metaplastic cells [39, 88]. Abnormal oncogene expression has been discovered in apocrine metaplastic epithelium by Papamichalis et al. [62] using an antibody to c-myc oncoprotein. Agnantis et al. [2] studied 12 cases of apocrine breast carcinomas, 5 of these cases were associated with benign apocrine lesions, either adjacent to the tumor or distant, and demonstrated the expression of c-myc p62 and GCDFP-15 (Agnantis et al., unpublished data presented at 4th International Symposium and Workshop, Problèmes Actuels de Pathologie Mammaire, Paris December 5–8, 1988). Four years later, Agnantis et al. [2] reported that the great majority of complex cystic disease shows elevated expression of both c-myc p62 and ras p21, when associated with apocrine metaplastic papillary proliferations.

Apocrine DCIS-apocrine carcinoma

Apocrine lobular in situ neoplasias and apocrine ductal in situ carcinomas are well-defined entities [26, 83, 1]. The consensus conference on the classification of DCIS recognized apocrine DCIS as a special variant, which is characterized by remarkable proliferation of apocrine cells showing nuclear pleomorphism with enlarged nuclei, multiple prominent nucleoli and irregular nuclear membranes. The presence of necrosis is not mandatory for the diagnosis of DCIS [85]. On the other hand, based on the World Health Organization (WHO) histological classification of breast tumors of 2003, apocrine DCIS is not recognized as a distinct entity, but is incorporated in the morphological changes of DCIS [84]. Apocrine differentiation may be present in up to 50% of the cases of DCIS, although Eusebi et al. [27] consider it an infrequently recognized phenomenon. Simpson et al. [80] supported that the common assumption at Diagnostic Pathology that a proliferative lesion with the pattern of micropapillary DCIS is thought to be benign because it has abundant pink cytoplasm that may be erroneous. There are substantial molecular data that some of these lesions may be the precursors of high grade DCIS and invasive cancer.

The recognition of apocrine carcinoma as a special type of breast carcinoma continues to be a subject of debate, due to the lack of uniform criteria for reliable recognition by light microscopy. Apocrine carcinoma is an unusual variant of breast carcinoma, probably of ductal origin or sweat

gland duct [42, 28]. The incidence of apocrine carcinoma varies from 0.3 to 4% of all cases. Rosen [69] stated that the term should be used for neoplasms as composed entirely or predominantly of apocrine-type epithelium [4, 54].

On the other hand, scattered areas or focal apocrine cells were found in about 60% of carcinomas of no special type (ductal, NST) [35]. Eusebi and Azzopardi [25] suggested that the basic criteria for a diagnosis of apocrine carcinoma should include neoplastic cells with copious, variably granular eosinophilic cytoplasm and vesicular nuclei with prominent nucleoli. Three years later, Haagensen et al. [35] proposed the following criteria: large size of the neoplastic cells, acidophilia of the cytoplasm and cytoplasmic "snouts" projecting into the lumina of glands. The degree of atypia varies, and tumor cells may occasionally present with bizarre, multilobulated nuclei containing multiple nucleoli [29]. The nuclear chromatin is irregular and often condensed along the periphery of the nuclear membrane. Most apocrine carcinoma cells are recognized as grade 2 or 3 according to a modified Scarff–Bloom–Richardson grading [23]. Cytologic smears of apocrine carcinoma yield abundant, pleomorphic tumor cells. The cells occur singly and with syncytia in the background of numerous degenerated apocrine cells, and characteristic cell detritus are found. The cells have abundant basophilic to eosinophilic granular cytoplasm. The nuclei are enlarged and vesicular and are centrally or eccentrically located. The nuclei measure > or = 12 μm in diameter, when compared to benign apocrine metaplasia with atypia. The nucleoli are prominent and may be multiple [21, 32, 95, 96]. Apocrine carcinoma is a rare variant of breast carcinoma that occurs in advanced age, the peak incidence being the sixth and seventh decades of life [2]. Apocrine carcinoma occurs in both females and males and manifests as a solid or cystic mass ranging from 0.5 to 5 cm in diameter [9]. Mammographic presentation did not present differences from those of ductal carcinomas [31]. Apocrine carcinomas are mostly variants of ductal carcinomas, but areas of apocrine differentiation have been reported in pleomorphic lobular carcinoma [26, 41, 82] and papillary [64]. They are predominantly ER and PR negative, but AR positive [30, 71]. On the other hand, 35–91% of breast cancers are also reported to express AR [43, 55, 24, 15]. The prognosis of apocrine carcinoma is the same with other types of breast carcinoma. Matsuo et al. [50] have reported that the positive rate of p53, HER2 and BCL-2 in apocrine carcinoma was almost the same as that of non-apocrine carcinomas.

Conclusions

In conclusion, we propose the term apocrine precursor cells, for GCDFP-15 positive breast epithelium cells, without apocrine morphology. Based on the existing recent molecular data, we conclude that benign proliferative apocrine lesions showing molecular alterations could be considered as clonal and precursors of malignant transformation. We believe that more clinical follow up and molecular data are needed for a comprehensive knowledge of the natural history of these lesions.

References

1. Abati AD, Kimmel M, Rosen PP (1990) Apocrine mammary carcinoma. A clinicopathologic study of 72 cases. Am J Clin Pathol 94(4):371–377
2. Agnantis NJ, Mahera H, Maounis N, Spandidos DA (1992) Immunohistochemical study of ras and myc oncoproteins in apocrine breast lesions with and without papillomatosis. Eur J Gynaecol Oncol 13:309–331
3. Ahmed A (1975) Apocrine metaplasia in cystic hyperplastic mastopathy. Histochemical and ultrastructural observations. Pathol (Lond) 115:211–214
4. Azzopardi J (1979) Problems in breast pathology. Saunders, Philadelphia, pp 341–344
5. Baddoura FK, Judd RL (1990) Apocrine adenoma of the breast. Report of a case with investigation of lectin binding patterns in apocrine breast lesions. Mod Pathol 3:373–376
6. Belanger A, Caron S, Labrie F et al (1990) Levels of eighteen nonconjugated and conjugated steroids in human breast cysts fluid; relationship with cyst type. Eur J Cancer 26:277–281
7. Boccardo F, Valenti G, Zanardi S, Cerruti G, Fassio T, Bruzzi P, De Francis V, Barreca A, Del Monte P, Minuto F (1988) Epidermal growth factor in breast cyst fluid: relationship with intracystic cation and androgen conjugate content. Cancer Res 45:5860–5863
8. Bruzzi P, Dogliotti L, Naldoni C et al (1997) Cohort study of association risk of breast cancer. BMJ 314:925–928
9. Bryant J (1981) Male breast cancer: a case of apocrine carcinoma with psammoma bodies. Hum Pathol 12:751–753
10. Bussolati G, Sapino A, Gugliotta P, Marci L (1992) Cytological analysis of benign breast disease. Cancer Detect Prev 16:89–92
11. Bundred NJ, West RR, O'Dowd J, Mansel RE (1991) Is there an increased risk of breast cancer in women who have a breast cyst aspirated? Br J Cancer 64:953–955
12. Cancer Committee of the College of American Pathologists (1986) Is 'fibrocystic disease' of the breast precancerous? Arch Pathol Lab Med 110:171–173
13. Carter DJ, Rosen PP (1991) Atypical apocrine metaplasia in sclerosing lesions of the breast: a study of 51 patients. Mod Pathol 4:1–5
14. Castagnetta L, Granata OM, Brignone G, Blasi L, Arcuri F, Mesiti MD, Aquino A, Preitano W (1990) Steroid patterns of benign breast disease. Ann N Y Acad Sci 586:79–82
15. Collett K, Maehle BO, Skjarven R et al (1996) Prognostic role of oestrogen, progesterone and androgen receptor in relation to patient age in patient age in patients with breast cancer. Breast 5:123–126
16. Collette J, Hendrick JC, Jaspar JM, Franchimont P (1986) Presence of alpha-lactalbumin, epidermal growth factor, epithelial membrane antigen, and gross cystic disease fluid protein (15,000 Daltons) in breast cyst fluid. Cancer Res 46(7):3728–3733
17. Constantini M, Bucchi I, Dogliotti et al (1994) Cohort study of women with aspirated gross cysts of the breast: an update in recent developments in the study of benign breast disease. In: Mansel RE (ed) Recent developments in the study of benign breast disease. Parthenon Publishing Group, Manchester, pp 227–240
18. Cotran RS, Kumar V, Robbins SL (1994) Cellular growth and differentiation. In: Robbins SL (ed) Robbins pathologic basis of disease, 5th edn. WB Saunders, Philadelphia, pp 35–50
19. Dawson EK (1932) Sweat gland carcinoma of the breast. A morphohistological study. Edinb Med J 39:409–438
20. Dixon JM, McDonald, Elton RA, Miller WR (1999) Risk of breast cancer in women with palpable breast cysts: a prospective study. Edinburgh Breast Group. Lancet 353:1742–1745

21. Duggan MA, Young GK, Hwang WS (1998) Fine-needle aspiration of an apocrine breast carcinoma with multivacuolated lipid-rich giant cells. Diagn Cytopathol 4:62–66
22. Dupont WD, Page DL (1985) Risk factors for breast cancer in women with proliferative disease. N Engl J Med 312:146–151
23. Durham JR, Fechner RE (2000) The histologic spectrum of apocrine lesions of the breast. Am J Clin Pathol 113:3–18
24. Ellis LM, Wittliff L, Bryant MS et al (1989) Correlation of oestrogen, progesterone and androgen receptors in breast cancer. Am J Surg 157:577–581
25. Eusebi V, Azzopardi JG (1980) Lobular endocrine neoplasia in fibroadenoma of the breast. Histopathology 4:413–428
26. Eusebi V, Betts CM, Haagensen DE, Bussolati G, Azzopardi JG (1984) Apocrine differentiation in lobular carcinoma of the breast. Hum Pathol 15:134–140
27. Eusebi V, Damiani S, Losi L, Millis RR (1997) Apocrine differentiation in breast epithelium. Adv Anat Pathol 4:139–155
28. Frable WJ (1989) Needle aspiration biopsy: past, present, and future. Hum Pathol 20:504–517
29. Frable WJ, Kay S (1968) Carcinoma of the breast. Histologic and clinical features of apocrine tumors. Cancer 21:756–763
30. Gatalica Z (1997) Immunohistochemical analyses of apocrine breast lesions. Consistent over-expression of androgen receptor accompanied by the loss of estrogen and progesterone receptors in apocrine metaplasia and apocrine carcinoma in situ. Pathol Res Pract 193:753–758
31. Gilles R, Guinebretiere JM, Toussaint C et al (1994) Locally advanced breast cancer: contrast-enhanced subtraction MR imaging of response to preoperative chemotherapy. Radiology 191:633–638
32. Gupta RK, Wakefield SJ, Naran S, Dowle CC (1989) Immunocytochemical and ultra-structural diagnosis of a rare mixed apocrine-medullary carcinoma of the breast in a fine needle aspirate. Acta Cytol 33:104–108
33. Haagensen DE Jr, Mazoujian G (1996) In: Haagenson, CD (ed) Diseases of the breast, 3rd edn. WB Saunders, Philadelphia, pp 474–500
34. Haagensen DE Jr, Gall SA, Brazy JE, Giannola J, Wells SA Jr (1980) Analysis of amniotic fluid, maternal plasma, and cord blood for a human breast gross cystic disease fluid protein. Am J Obstet Gynecol 138(1):25–32
35. Haagensen CD, Bodian C, Haagensen DE Jr (1981) Apocrine epithelium. Breast carcinoma, WB Saunders, Philadelphia pp 83–105
36. Haagensen DE, Dilley WG, Mazoujian G et al (1990) Review of GCDFP-15: an apocrine marker protein. Ann N Y Acad Sci 586:161–173
37. Higginson JF, McDonald JR (1949) Apocrine tissue, chronic cystic mastitis and sweat gland carcinoma of the breast. Surg Gynecol Obstet 88:1–10
38. Howard BA, Gusterson BA (2000) Human breast development. J Mammary Gland Biol Neoplasia 5(2):119–137
39. Izuo M, Okagaki T, Richart R, Lattes R (1971) DNA content in 'apocrine metaplasia'of fibrocystic disease of the breast. Cancer 27:643–650
40. Jones C, Damiani S, Wells D, Chaggar R, Lakhani SR, Eusebi V (2001) Molecular cytogenetic comparison of apocrine hyperplasia and apocrine carcinoma of the breast. Am J Pathol 158:207–214
41. Kaya H, Aribal E, Yegen C (2002) Apocrine differentiation in invasive pleomorphic lobular carcinoma with in situ ductal and lobular apocrine carcinoma: case report. Pathol Oncol Res 8 (2):151–152
42. Kline TS (1988) Handbook of fine needle aspiration biopsy cytology. CV Mosby, St. Louis
43. Kuenen-Boumeester V, Van der Kwast TH, van Putten WL, Claasen C, van Ooijen B, Henzen-Longmans SC (1992) Immunohistochemical determination of androgen receptors in relation to oestrogen and progesterone receptors in female breast cancer. Int J Cancer 52:581–584
44. Lakhani SR, Slack DN, Hamoudi RAA, Collins N, Stratton MR, Sloane JP (1996) Detection of allelic imbalance indicates that a proportion of mammary hyperplasia of usual type is clonal, neoplastic proliferations. Lab Invest 74:129–135
45. Lander ES, Linton LM, Birren B, Nusbaum C, Zody MC, Baldwin J, Devon K, Dewar K, Doyle M, FitzHugh W, Funke R, Gage D et al (2001) Initial sequencing and analysis of the human genome. Nature 409:860–921
46. Lininger RA, Tavassoli FA (1997) Atypical intraductal hyperplasia of the breast. In: Silverstein MJ (ed) Ductal carcinoma in situ of the breast, Williams & Wilkins, Baltimore, pp 195–222
47. Lodato RF, Maguire HC Jr, Greene MI, Weiner DB, LiVolsi VA (1990) Immunohistochemical evaluation of c-erbB-2 oncogene expression in ductal carcinoma in situ and atypical ductal hyperplasia of the breast. Mod Pathol 3(4):449–454
48. Losi L, Lorenzini R, Eusebi V, Bussolati G (1995) Apocrine differentiation in invasive carcinoma of the breast. Comparison of monoclonal and polyclonal gross cystic disease fluid protein-15 antibodies with prolactin-inducible protein mRNA gene expression. Appl Immunohistochem 3:91–98
49. Love SM, Gelman RS, Silen W (1982 Oct 14) Sounding board. Fibrocystic Disease of the breast—a non disease? N Engl J Med 307(16):1010–1014
50. Matsuo K, Fukutomi T, Hasegawa T, Akashi-Tanaka S, Nanasawa T, Tsuda H (2002) Histological and immunohistochemical analysis of apocrine breast carcinoma. Breast Cancer 9:43–49
51. McKiernan O, Coyne J, Cahalane S (1988) Histology of breast development in early life. Arch Dis Child 63:136–139
52. Miller WR, Forrest APM (1983) Androgen conjugates in human breast secretions and cyst fluids. In: Angeli A, Bradlow HL, Dogliotti L (eds) Endocrinology of cystic disease. Raven Press, New York, pp 77–84
53. Moriya T, Sakamoto K, Sasano H, Kawanaka M, Sonoo H, Manabe T, Ito J (2000) Immunohistochemical analysis of Ki-67, p53, p21 and p27 in benign and malignant apocrine lesions of the breast: its correlation to histologic findings in 43 cases. Mod Pathol 13:13–18
54. Mossler JA, Barton TK, Brinkhous AD et al (2005) Apocrine differentiation in human mammary carcinoma. Cancer 46: 2463–2471
55. Moinfar F, Okcu M, Tsybrovskyy O et al (2003) Androgen receptors frequently are expressed in breast carcinomas: potential relevance to new therapeutic strategies. Cancer 9:335–336
56. Murad TM, von Hamm E (1968) The ultrastructure of fibrocystic disease of the breast. Cancer 22:587–600
57. Murphy LC, Lee-Wing M, Goldenberg GJ, Shiu RPC (1987) Cancer Res 47:4160–4164
58. O'Malley FP, Page DL, Nelson EH, Dupont WD (1994) Ductal carcinoma in situ of the breast with apocrine cytology: definition of a borderline category. Hum Pathol 25:164–168
59. Pagani A, Sapino A, Eusebi V, Bergnolo P, Bussolati G (1994) PIP/GCDFP-15 gene expression and apocrine differentiation in carcinomas of the breast. Virchows Arch 425:459–465
60. Page DL, Van der Zwaar R, Rogers LW, Williams LT, Walker WE, Hartmann WH (1978) Relation between component parts of fibrocystic disease complex and breast cancer. J Natl Cancer Inst 61:1055–1063
61. Page DL, Dupont WD, Jensen RA (1996) Papillary apocrine change of the breast: association with atypical hyperplasia and risk of breast cancer. Cancer Epidemiol Biomarkers Prev 5: 29–32
62. Papamichalis G, Francia K, Karachaliou FE, Anastasiades OT, Spandidos DA (1988) Expression of the c-myc oncoprotein in human metaplastic epithelial cells of fibrocystic disease. Anticancer Res 8:1217–1222
63. Papanicolaou GN (1963) Atlas of exfoliative cytology. Harvard University Press, Cambridge, p 55
64. Papotti M, Eusebi V, Gugliotta P et al (1983) Immunohistochemical analysis of benign and malignant papillary lesions of the breast. Am J Surg Pathol 7:451–461

65. Pier WJ, Garancis JC, Kuzma JF (1970) The ultrastructure of apocrine cells in intracystic papilloma and fibrocystic disease of the breast. Arch Pathol 89:446–452
66. Raju U, Zarbo RJ, Kubus J et al (1993) The histologic spectrum of apocrine breast proliferations: a comparative study of morphology and DNA content by image analysis. Hum Pathol 24:173–181
67. Rosai J (1996) Ackerman's surgical pathology, 8th edn. CV Mosby, St. Louis, pp1582–1583
68. Roberts MM, Jones V, Elton RA et al (1984) Risk of breast cancer in women with a history of benign disease of the breast. BMJ 288:275–278
69. Rosen PP (2001) Rosen's Breast Pathology, 2nd edn. Lippincott Williams & Wilkins, Philadelphia
70. Russo J, Russo IH (2004) Development of the human breast. Maturitas 24;49(1):2–15
71. Sapp M, Malik A, Hanna W (2003) Hormone receptor profile of apocrine lesions of the breast. Breast J 9:335–336
72. Selim AG, Wells CA (1999) Immunohistochemical localization of androgen receptor in apocrine metaplasia and apocrine adenosis of the breast: relation to oestrogen and progesterone receptors. J Clin Pathol 52:838–841
73. Selim AG, Ryan A, El-Ayat G, Wells CA (2001) Loss of heterozygosity and allelic imbalance in apocrine adenosis of the breast. Cancer Detect Prev 25:262–267
74. Selim AGA, El-Ayat, Wells CA (2002) Expression of c-erbB2, p53, Bcl-2, Bax, c-myc and Ki-67 in apocrine metaplasia and apocrine change within sclerosing adenosis of the breast. Virchows Arch 441:449–455
75. Selim AG, Ryan A, El-Ayat G, Wells CA (2002) Loss of heterozygosity and allelic imbalance in apocrine metaplasia of the breast: microdissection microsatellite analysis. J Pathol 196:287–291
76. Seidman JD, Ashton M, Lefkowitz M (1996) Atypical apocrine adenosis of the breast: a clinicopathologic study of 37 patients with 8.7-year follow up. Cancer 77:2529–2537
77. Shiu RPC, Iwasiow BM (1985) Prolactin inducible proteins in human breast cancer cells. J Biol Chem 260:11307–11313
78. Silverberg SG, Masood S (1997) The breast. In: Silverberg SG, Delellis RA, Frable WJ (eds) Principles and practice of surgical pathology and cytopathology, 3rd edn. Churchill Livingstone, New York, pp 575–674
79. Simpson JF, Page DL, Dupont WD (1990) Apocrine adenosis—a mimic of mammary carcinoma. Surg Pathol 3:289–299
80. Simpson PT, Reis-Fihlo JS, Gale T, Lakhani S (2005) Molecular evolution of breast cancer. J Pathol 205:248–254
81. Sternberg SS (1997) Histology for pathologists, 2nd edn. Lippincott-Raven, Philadelphia, p 26
82. Tashiro T, Hirokawa M, Iuchi K, Emoto K, Tanaka T, Monobe Y, Sano T (2003) Cytology of pleomorphic lobular carcinoma with apocrine cell differentiation of the breast. A case report. Acta Cytol 47(2):265–269
83. Tavassoli FA, Norris HJ (1994) Intraductal apocrine carcinoma: a clinicopathologic study of 37 cases. Mod Pathol 7:813–818
84. Tavassoli F, Devilee P (2003) Pathology and genetics of tumors of the breast and female genital organs. IARC Press, Lyon, p 10
85. The Consensus Conference Committee (1997) Consensus conference on the classification of ductal carcinoma in situ. Cancer 80:1798–1802
86. Tremblay G (1968) Histochemical studies of oxidative enzymes in apocrine like cells of the breast and in axillary apocrine glands. J Invest Dermatol 50:238–243
87. Tsuda H, Fukutomi T, Hirohashi S (1995) Pattern of gene alterations in intraductal breast neoplasms associated with histological type and grade. Clin Cancer Res 1:261–267
88. Vasiu R, Olinici CD (1990) DNA nuclear content of apocrine cells in fibrocystic mastopathy and breast cancer. Morphol Embryol 36:43–47
89. Viacava P, Naccarato AG, Bevilaqua G (1997) Apocrine epithelium of the breast: does it result from metaplasia? Virchows Arch 431:205–2090
90. Washington C, Dalbegue F, Abreo F, Taubenberger JK, Lichy JH (2000) Loss of heterozygosity in fibrocystic change of the breast: genetic relationship between benign proliferative lesions and associated carcinomas. Am J Pathol 157:323–329
91. Wellings SR, Alpers CE (1987) Apocrine cystic metaplasia: subgross pathology and prevalence in cancer-associated versus random autopsy breasts. Hum Pathol 18:381–386
92. Wellings SR, Jensen HM, Marcum RG (1975) An atlas of subgross pathology of the human breast with special reference to possible precancerous lesions. J Natl Cancer Inst 55:231–243
93. Wells CA, McGregor IL, Makunura CN, Yeomans P, Davies JD (1995) Apocrine adenosis: a precursor of aggressive breast cancer? J Clin Pathol 48:737–742
94. Wick MR, Lillemoe TJ, Copland GT, Swanson PE, Manivel JC, Kiang DT (1989) Gross cystic disease fluid protein-15 as a marker for breast cancer: immunohistochemical analysis of 690 human neoplasms and comparison with a-lactalbumin. Hum Pathol 20:281–287
95. Yoshida K, Inone M, Furuta S, Sakai R, Imai R, Hayakawa S, Fukatsu T, Nagasaka T, Nakashima N (1996) Apocrine carcinoma versus Apocrine metaplasia with atypia of the breast. Use of aspiration biopsy cytology. Acta Cytol 40(2):247–251
96. Zajdela A, Ghossein NA, Pilleran JP et al (1975) The experience of aspiration cytology in the diagnosis of breast cancer. Experience at the Fondation Curie. Cancer 35:499–506
97. Zoran G (1997) Immunohistochemical analysis of apocrine breast lesions: consistent overexpression of androgen receptor accompanied by the loss of estrogen and progesterone receptors in apocrine metaplasia and apocrine in situ. Pathol Res Pract 193:753–758

Virchows Arch (2006) 448: 532–538
DOI 10.1007/s00428-006-0168-7

ORIGINAL ARTICLE

Mario Sarbia

The histological appearance of oesophageal adenocarcinoma—an analysis based on 215 resection specimens

Received: 31 August 2005 / Accepted: 30 January 2006 / Published online: 24 February 2006

Abstract The current study was performed to determine whether the histopathological appearance of oesophageal adenocarcinoma (AC) differs significantly from that of cardiac or gastric AC. Therefore, HE-stained slides of 215 primarily resected oesophageal AC, 108 cardiac and 184 gastric AC were classified according to a variety of clinicopathologic parameters. According to Lauren's classification, oesophageal AC (1.4%) less frequently belonged to the diffuse type than cardiac (2.8%) and gastric AC (23.9%; $p<0.0001$). Tubular and papillary AC, as defined by the WHO classification, were more frequent among oesophageal (94.4%) than among cardiac (87.0%) and gastric AC (59.2%; $p<0.0001$). Solid carcinomas, according to Carneiro's classification, were less frequent among oesophageal (2.8%) than among cardiac (10.2%) and gastric AC (9.2%; $p<0.0001$). Oesophageal AC were graded more frequently G1/G2 (53.9%) than cardiac (30.6%) and gastric AC (27.7%; $p<0.0001$). Among oesophageal AC, Lauren's classification ($p=0.0067$), Carneiro's classification ($p=0.0170$), tumour grade ($p=0.0005$), lymphatic vessel invasion ($p<0.0001$) but not WHO classification were histological predictors of postoperative survival. In conclusion, oesophageal AC displays the same histological spectrum as cardiac and gastric AC. However, the relative proportion of differentiated, gland-forming carcinomas is significantly more frequent in the oesophagus than in the cardia and in the stomach.

Keywords Barrett's oesophagus · Histology · Adenocarcinoma · Gastric cancer · Cardiac cancer

M. Sarbia (✉)
Institute of Pathology,
Sana Klinikum Lichtenberg/Unfallkrankenhaus Berlin,
Fanningerstr. 32/Warenerstr. 7,
10365 Berlin, Germany
e-mail: m.sarbia@sana-kl.de
Tel.: +49-30-55182811
Fax: +49-30-55182899

Introduction

Barrett's oesophagus is the predisposing condition of the vast majority of oesophageal adenocarcinomas. Under the chronically damaging effect of gastrooesophageal reflux, the metaplastic Barrett's epithelium is promoted through a (low-grade/high-grade) intraepithelial neoplasia sequence towards invasive cancer [20]. Oesophageal (Barrett's) adenocarcinoma (AC) is an entity of increasing clinical importance due to a rapidly rising incidence during the previous decades [4].

In spite of the rapidly growing number of publications on oesophageal AC, systematic investigations on the histological appearance of this tumour type are sparse and based on small, probably non-representative series of cases. Thus, a Medline-based search revealed only five systematic investigations on the histological appearance of oesophageal AC between 1980 and 2004, comprising a total of 151 oesophageal AC [8, 9, 13, 18, 26]. Three of these investigations [8, 9, 26] included a morphologic comparison with the most related tumour entities, i.e., cardiac cancer [8, 9] and gastric cancer [8, 26]. Only one investigation [8] tested oesophageal AC on the basis of Lauren's classification but none on the basis of the current WHO classification. Nonetheless, the histologic spectrum of oesophageal AC is generally considered to be well defined. Thus, the current issue of the AFIP atlas of oesophageal and gastric tumours [11] states that oesophageal AC "shows a spectrum virtually identical to that found in the stomach" and a current gastrointestinal pathology textbook points out that "histologically, cancers arising in the setting of Barrett's oesophagus and those arising in the cardia are virtually identical" [6].

Given the obviously limited evidence of these statements, the current study compares the histological features of three large series of oesophageal, cardiac and gastric AC based on well-defined histological classifications and criteria.

Materials and methods

The current study is based on 215 primary AC of the oesophagus that underwent surgical resection (n=204) or endoscopic mucosal resection (EMR) (n=11) between 1 January 1987 and 31 January 2004. Of the surgically treated cases, 143 had been resected at the Department of Surgery at the Technical University, Munich; and 61 had been resected at the Department of Surgery at the University of Dusseldorf, Germany. The EMR specimens were obtained from various contributing hospitals of the Department of Pathology by the University of Dusseldorf. As control groups, 108 cardiac and 184 gastric AC were included that underwent surgical resection at the Department of Surgery at the University of Dusseldorf between 1 Janury 1984 and 31 December 2002. None of the tumours had been treated by preoperative radio- or chemotherapy. Differentiation between oesophageal and cardiac AC was based on a review of the original macroscopic pathologic descriptions of the operation specimens by the author. Therefore, standard criteria were applied [19]: tumours with their epicentres more than 1 cm above the gastro-oesophageal (GO) junction were regarded as oesophageal in origin and tumours with their epicentres between 1 cm above and 2 cm below the GE junction were regarded as cardiac in origin. The GO junction was defined as the oral end of the gastric folds and/or the border between the tubular oesophagus and the saccular stomach. In the forefront of the study, 20 AC at the GO junction could not be classified according to these criteria as oesophageal or cardiac because the macroscopic description did not allow localization of the tumour's epicentres in relation to the GO junction. These cases were, therefore, excluded from any analyses described in this manuscript. The pT and the pN category of the tumours were re-determined according to the current TNM classification [24]. Cardiac carcinomas were classified as tumours of the stomach.

Histological classification

All cases were histologically classified by the author on the basis of H&E stained tumour slides. Between one and 45 slides per tumour (median: 4) were available for histological review. As no generally accepted histological evaluation system exists for oesophageal AC, all tumours were typed according to histological classification systems originally defined for gastric cancer, i.e. the WHO classification [7], Lauren's classification [10] and Carneiro's classification [3]. Tumours with a proportion of more than 5% of the tumour mass with diffuse or gland-forming cancer cells were grouped into the mixed categories according to Lauren's classification and according to Carneiro's classification [3]. According to the WHO classification, beside tubular AC and papillary AC, the category of papillotubular AC was considered, which is described as an optional subcategory of papillary carcinomas that is characterized by tubular differentiation [7]. Carcinomas were categorized as papillotubular when they were composed of a mixture of tubular and papillary structures.

Tumour grading for all carcinomas was determined according to the WHO classification of gastric carcinomas [7]. In accordance with the WHO recommendations for colorectal carcinomas, mucinous carcinomas and tumours with diffuse or signet-ring cell component comprising more than 5% of the tumour mass were categorized as G3. Additionally, invasion of tumour cells into lymphatic vessels was determined as described previously [16].

Mucosal AC was separated from high-grade intraepithelial neoplasia either by the presence of neoplastic cells that had penetrated through the basement membrane and that were located in the lamina propria or in the muscularis mucosae. In addition, the presence of architecturally complex collections of neoplastic cells in the lamina that could not be explained by the presence of pre-existing Barrett's mucosa was considered as evidence of mucosal AC [12]. The patients' and tumours' characteristics are summarized in Table 1.

Statistical analyses

Correlation analysis between tumour types and clinicopathologic parameters were done using the chi-square test. Survival analyses were performed by means of the log-rank test and Cox regression analysis. P values smaller 0.05 were considered as statistically significant.

Table 1 Clinicopathological parameters in oesophageal (n=215), cardiac (n=108), and gastric adenocarcinomas (AC) (n=184) under investigation

	Oesophageal AC	Cardiac AC	Gastric AC
Age – median (range)	64 (33–83)	63 (29–83)	68 (30–90)
Gender			
Male	194 (90%)	89 (82%)	103 (56%)
Female	21 (10%)	19 (18%)	81 (44%)
pT category			
1 (mucosa)	50 (23%)	2 (2%)	20 (11%)
1 (submucosa)	50 (23%)	9 (8%)	17 (9%)
2	40 (19%)	55 (51%)	74 (40%)
3	75 (35%)	33 (31%)	59 (32%)
4	0	9 (8%)	14 (8%)
pN category			
0	118[1] (58%)	23 (21%)	58 (32%)
1–3	86 (42%)	85 (79%)	126 (68%)
Tumour size (mm) – median (range)	40 (4–160)	55 (14–135)	70 (6–220)

[1]In 11 oesophageal AC, nodal status could not be determined because they had been treated by endoscopic mucosal resection

Results

Clinico-pathological parameters

Preference of male sex was more pronounced in oesophageal (90%) and cardiac AC (82%) than in gastric AC (56%). Oesophageal AC belonged more frequently to early tumour stages (pT1 46%; pN0 58%) than cardiac AC (10%; 21%) and gastric (20%; 32%) AC. No differences between the three tumour entities became apparent by comparison according to patient's age and tumour size (Table 1).

Histological parameters

According to Lauren's classification, oesophageal AC (1.4%) less frequently belonged to the diffuse type than cardiac (2.8%) and gastric AC (23.9%). The difference was statistically significant when the three groups were compared as a whole ($p<0.0001$) and when oesophageal AC was compared with cardiac AC ($p=0.0010$) and with gastric AC ($p<0.0001$) separately. Tubular, papillotubular and papillary AC, as defined by the WHO classification, were more frequent among oesophageal (94.4%) than among cardiac (87.0%) and gastric AC (59.2%; $p<0.0001$; oesophageal vs cardiac AC: $p=0.0097$; oesophageal vs gastric AC: $p<0.0001$). In particular, the papillotubular growth pattern was more frequent in oesophageal (32.5%) than in cardiac (17.6%) and gastric (8.1%) AC (Fig. 1) Solid carcinomas, according to Carneiro's classification, were less frequent among oesophageal (2.8%) than among cardiac (10.2%) and gastric AC (9.2%; $p<0.0001$; oesophageal vs cardiac AC: $p<0.0001$; oesophageal vs gastric AC: $p<0.0001$). Oesophageal ACs were graded G1/G2 more frequently (53.9%) than cardiac (30.6%) and gastric AC (27.7%; $p<0.0001$; oesophageal vs cardiac AC: $p=0.0003$; oesophageal vs gastric AC: $p<0.0001$) (Table 2).

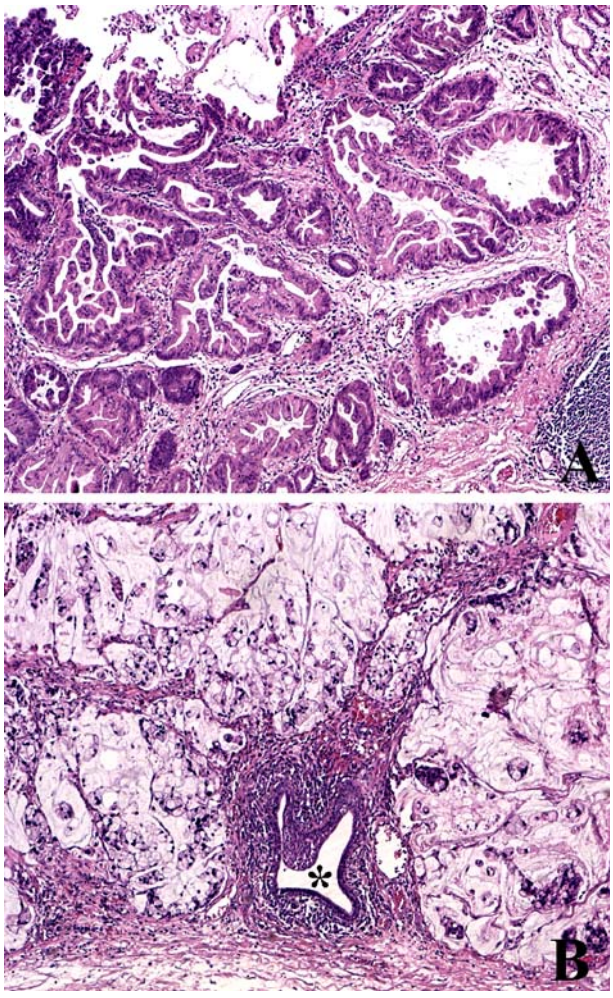

Fig. 1 **a** Oesophageal adenocarcinoma of the papillotubular subtype according to the WHO classification (original magnification: ×50; H&E). **b** Oesophageal adenocarcinoma of the mucinous subtype (original magnification: ×50; H&E). Squamous epithelium-lined duct, indicating intraoesophageal location of the tumour (*asterisk*)

Subgroup analysis of histological parameters according to depth of infiltration (pT category)

As oesophageal AC belonged to early tumour stages more frequently than cardiac and gastric AC, a subgroup analysis according to pT category was performed. This was done to exclude that the above-described histological differences were caused by differences in stage distribution only.

Among locally advanced carcinomas (pT2–pT4), the above-described differences in histological growth patterns remained significant for Lauren's classification (oesophageal vs cardiac AC: $p=0.0275$; oesophageal vs gastric AC: $p<0.0001$) and Carneiro's classification (oesophageal vs cardiac AC: $p=0.0233$; oesophageal vs gastric AC: $p<0.0001$). Concerning WHO classification, oesophageal ACs were significantly different from gastric AC ($p<0.0001$) but not from cardiac AC. The distribution of tumour grades was not significantly different among advanced oesophageal, cardiac and gastric AC (Table 3).

Furthermore, a subgroup analysis of oesophageal and gastric AC confined to the mucosa was performed. Cardiac ACs were excluded from this analysis due to the low number of cardiac pT1m tumours ($n=2$). According to this analysis, oesophageal AC ($n=50$), again significantly more often, belonged to the intestinal type, according to Lauren ($p<0.0001$), to the tubular and papillotubular type, according to the WHO ($p<0.0001$) and to the glandular type, according to Carneiro ($p<0.0001$) than gastric AC ($n=20$). Moreover, oesophageal AC, more frequently, were graded G1 or G2 than gastric AC ($p<0.0001$) (Table 4).

We, furthermore, determined whether the histological appearance of oesophageal AC confined to the mucosa differs from more advanced tumours (Table 5). In that analysis, it became apparent that mucosal carcinomas more frequently belonged to the intestinal type, according to Lauren ($p=0.0244$), and to the glandular type, according to Carneiro ($p=0.0143$), than advanced tumours. Moreover,

Table 2 Comparison of histological and clinical parameters in oesophageal (n=215), cardiac (n=108) and gastric adenocarcinomas (n=184)

	Oesophageal AC (OAC)	Cardiac AC (CAC)	Gastric AC (GAC)	OAC vs CAC vs GAC p value	OAC vs CAC p value	OAC vs GAC p value
Lauren's classification				<0.0001	0.0010	<0.0001
Intestinal type	193 (89.8%)	80 (74.1%)	95 (51.6%)			
Mixed type	19 (8.8%)	25 (23.1%)	45 (24.5%)			
Diffuse type	3 (1.4%)	3 (2.8%)	44 (23.9%)			
WHO classification				<0.0001	0.0097	<0.0001
Tubular type	130 (60.5%)	74 (68.5%)	94 (51.1%)			
Papillotubular type	70 (32.5%)	19 (17.6%)	15 (8.1%)			
Papillary type	3 (1.4%)	1 (0.9%)	0			
Mucinous type	3 (1.4%)	1 (0.9%)	9 (4.9%)			
Signet-ring cell type	9 (4.2%)	13 (12.1%)	66 (35.9%)			
Carneiro's classification				<0.0001	<0.0001	<0.0001
Glandular type	185 (86.0%)	69 (63.9%)	78 (42.4%)			
Solid type	6 (2.8%)	11 (10.2%)	17 (9.2%)			
Mixed type	21 (9.8%)	25 (23.1%)	45 (24.5%)			
Isolated-cell type	3 (1.4%)	3 (2.8%)	44 (23.9%)			
Grade				<0.0001	0.0003	<0.0001
G1	19 (8.8%)	2 (1.9%)	7 (3.8%)			
G2	97 (45.1%)	31 (28.7%)	44 (23.9%)			
G3	99 (46.1%)	75 (69.4%)	133 (72.3%)			
Sex				<0.0001	NS	<0.0001
Female	21 (9.8%)	19 (17.6%)	81 (44.0%)			
Male	194 (90.2%)	89 (82.4%)	103 (56.0%)			

Chi-square test

mucosal carcinomas more frequently were well differentiated (G1) than advanced tumours (p<0.0001).

Survival analyses

Follow-up data were available from 163 of the 215 oesophageal ACs under analysis. The follow-up ranged between 1 and 115 months (median: 17 months). Thirty-five cases were excluded from survival analyses because they either died within the first 30 days after resection or had tumour infiltrated resection margins (R1 resection) or had evidence of distant metastasis (M1). Of the 128 cases left for survival analyses, 47 were dead at the end of the follow-up.

According to Lauren's classification, the mean survival time of intestinal carcinomas was 67 months as compared to 16 months of mixed carcinomas (only two diffuse carcinomas; p=0.0067, log-rank test). According to Carneiro's classification, mean survival times were 68 months for glandular carcinomas, 17 months for mixed carcinomas and 19 months for solid carcinomas (only two isolated cell carcinomas; p=0.0170). According to the WHO classification, survival was best for tubular carcinomas (53 months) followed by papillotubular (37 months) and signet-ring cell carcinomas (29 months) (only two mucinous and two papillary carcinomas; not significant). Grading according to the WHO was associated with survival with G1 (49 months) and G2 (77 months) tumours showing better outcome than G3 tumours (33 months; p=0.0005). Calculation of mean survival time among G1 carcinomas was limited by short follow-up period in this group. Tumours with lymphatic vessel invasion (n=30) showed poorer outcome (20 months) than tumours without (n=98; 78 months; p<0.0001). Multivariate Cox regression analysis indicated that lymphatic vessel invasion (p<0.0001), but none of the other histological parameters, was an independent predictor of survival.

Discussion

The current study indicates that the currently held view that the histological appearance of oesophageal adenocarcino-

Table 3 Comparison of histological and clinical parameters in locally advanced (pT2–pT4) oesophageal (n=115), cardiac (n=97), and gastric adenocarcinomas (n=147)

	Oesophageal AC (OAC)	Cardiac AC (CAC)	Gastric AC (GAC)	OAC vs CAC vs GAC p value	OAC vs CAC p value	OAC vs GAC p value
Lauren's classification				<0.0001	0.0275	<0.0001
Intestinal type	99 (86.1%)	69 (71.1%)	78 (53.1%)			
Mixed type	14 (12.2%)	25 (25.8%)	31 (21.1%)			
Diffuse type	2 (1.7%)	3 (3.1%)	38 (25.8%)			
WHO classification				<0.0001	NS	<0.0001
Tubular type	71 (61.7%)	66 (68.1%)	77 (52.4%)			
Papillotubular type	34 (29.6%)	16 (16.5%)	11 (7.5%)			
Papillary type	3 (2.6%)	1 (1.0%)	0 (0%)			
Mucinous type	0 (0%)	1 (1.0%)	9 (6.1%)			
Signet-ring cell type	7 (6.1%)	13 (13.4%)	50 (34.0%)			
Carneiro's classification				<0.0001	0.0233	<0.0001
Glandular type	91 (79.2%)	58 (59.8%)	61 (41.5%)			
Solid type	6 (5.2%)	11 (11.3%)	17 (11.6%)			
Mixed type	16 (13.9%)	25 (25.8%)	31 (21.1%)			
Isolated-cell type	2 (1.7%)	3 (3.1%)	38 (25.8%)			
Grade				NS	NS	NS
G1	1 (0.9%)	2 (2.1%)	2 (1.3%)			
G2	47 (40.9%)	25 (25.8%)	37 (25.2%)			
G3	67 (58.2%)	70 (72.1%)	108 (73.5%)			
Sex				<0.0001	NS	<0.0001
Female	10 (8.7%)	17 (17.5%)	64 (43.5%)			
Male	105 (91.3%)	80 (82.5%)	83 (56.5%)			

Chi-square test

mas is virtual identical to that of cardiac and gastric AC is not correct. Based on the so-far largest histologically investigated series of oesophageal AC, we could show that the relative proportion of differentiated, gland-forming carcinomas is significantly more frequent in the oesophagus than in the cardia and in the stomach. On the other hand, we can corroborate the findings of others that nearly all histological variants of adenocarcinoma found in the stomach can also develop in the oesophagus. This is true also for rare histological variants, including mucinous and solid carcinomas, and also for signet-ring cell carcinomas.

Until now, only three studies systematically compared the histological appearance of oesophageal AC with AC of the cardia [8, 9] and the stomach [8, 26]. The studies of Kalish et al. [9] and Wang et al. [26] did not find distinguishing features between the three tumour entities. In contrast, Heidl et al. [8] reported significant differences in the histological appearance of oesophageal and gastric AC, but not between oesophageal and cardiac AC. However, all three studies have methodological disadvantages, i.e. the small number of oesophageal AC included and poor definition of histological features under analysis. The results of Heidl et al. [8] and those of the current investigation are partially congruent; however, the former study does not allow definitive conclusions, as it included a mixture of oesophageal AC diagnosed on resection specimens (n=36) or on biopsy specimens (n=30), and it did not provide reproducible definitions of the histopathological categories used.

As shown in the current study, loss of tumour differentiation with increasing depth of infiltration is a characteristic histological feature of oesophageal AC. Similar observations have already been published by others [13, 25]. Again, this is a discriminating feature from mucosal gastric AC where poor differentiation and signet-ring cell-growth pattern is found in a substantial number of cases. The high prevalence of well or moderately differentiated, gland-forming mucosal AC in the oesophagus has important therapeutic implications. Thus, oesophageal AC confined to the mucosa has obviously a very low risk of lymph node metastasis. In a recent literature review of 150 mucosal ACs of the oesophagus [2], lymph node metastases were documented only in three cases (2%). Similarly, in our own series of 39 mucosal AC that underwent oesophageal resection, neither lymph node metastasis nor lymphatic vessel invasion was present. The relatively benign behaviour of oesophageal AC confined to the mucosa opens the opportunity for limited treatment options such as endoscopic resection [14] and limited surgical resection [21].

Table 4 Comparison of histological and clinical parameters in oesophageal (n=50) and gastric adenocarcinomas (n=20) restricted to the mucosa (pT1m)

	Oesophageal AC	Gastric AC	p value
Lauren's classification			<0.0001
Intestinal type	50 (100%)	9 (45%)	
Mixed type	0	8 (40%)	
Diffuse type	0	3 (15%)	
WHO classification			<0.0001
Tubular type	33 (66%)	8 (40%)	
Papillotubular type	17 (34%)	3 (15%)	
Papillary type	0	0	
Mucinous type	0	0	
Signet-ring cell type	0	9 (45%)	
Carneiro's classification			<0.0001
Glandular type	50 (100%)	9 (45%)	
Solid type	0	0	
Mixed type	0	8 (40%)	
Isolated-cell type	0	3 (15%)	
Grade			<0.0001
G1	17 (34%)	3 (15%)	
G2	28 (56%)	3 (15%)	
G3	5 (10%)	14 (70%)	
Sex			<0.0001
Female	1 (2%)	10 (50%)	
Male	49 (98%)	10 (50%)	

Chi-square test

Determination of a tumour's origin is considered problematic when the tumour infiltrates the gastrooesophageal junction (GOJ), which means that parts of the tumour are located in the oesophagus and parts in the stomach. In the classification proposed by Siewert and Stein [19], adenocarcinomas of the GOJ are defined as tumours having their epicentre within 5 cm proximal and distal of the anatomical cardia. Among these tumours, three different subtypes are considered, i.e. adenocarcinoma of the distal oesophagus (type I tumour), true carcinoma of the cardia (type II tumour) and subcardial gastric carcinoma (type III tumour). In this classification system as well as in the recommendations by the Association of Directors of Anatomic and Surgical Pathology [1], the anatomic location of the epicentre or predominant tumour mass is used to determine whether the tumour is oesophageal, cardiac or gastric in origin. In contrast, the recent WHO classification has lumped together all tumours that cross the GOJ as carcinomas of the gastrooesophageal junction, regardless of the localization of the tumour centre [7].

We confirm that separation between oesophageal and cardiac AC may be impossible in some cases, i.e. due to distortion of anatomic landmarks by tumour growth or hiatal hernia. However, based on our histological findings, we believe that lumping together of oesophageal AC (involving the GOJ) and cardiac AC into one category—as proposed by the WHO—may blur obvious differences between the two entities. Thus, we could clearly show that in terms of histological appearance, cardiac AC takes an intermediate position between oesophageal and gastric AC. This point of view is also supported by immunohistological [23] and molecular pathologic [17, 22] studies as well as by a study that investigated patterns of lymph node metastases [5] where significant differences between oesophageal and cardiac AC have been demonstrated. Therefore, the need of separation between (distal) oesophageal and cardiac AC is increasingly considered [15].

In conclusion, our data provide evidence that oesophageal, cardiac and gastric AC are distinct pathologic entities. Oesophageal AC is characterized by a relatively high proportion of differentiated, gland-forming tumours.

Table 5 Comparison of histological and clinical parameters in mucosal (n=50) and more advanced (n=165) adenocarcinomas of the oesophagus

	pT1m	pT1sm – pT4	p value
Lauren's classification			0.0244
Intestinal type	50 (100%)	143 (86.7%)	
Mixed type	0	19 (11.5%)	
Diffuse type	0	3 (1.8%)	
WHO classification			NS
Tubular type	33 (66.0%)	97 (58.8%)	
Papillotubular type	17 (34.0%)	53 (32.1%)	
Papillary type	0	3 (1.8%)	
Mucinous type	0	3 (1.8%)	
Signet-ring cell type	0	9 (5.5%)	
Carneiro's classification			0.0143
Glandular type	50 (100%)	135 (81.8%)	
Solid type	0	6 (3.7%)	
Mixed type	0	21 (12.7%)	
Isolated-cell type	0	3 (1.8%)	
Grade			<0.0001
G1	17 (34.0%)	2 (1.2%)	
G2	28 (56.0%)	69 (41.8%)	
G3	5 (10.0%)	94 (57.0%)	
Sex			0.0347
Female	1 (2.0%)	20 (12.1%)	
Male	49 (98.0%)	145 (87.9%)	

Chi-square test

Acknowledgements The author appreciates the help of Prof. H. Stein and Dr. M. Feith who allocated information about the outcome of oesophageal AC patients. Dr. R. Willers supported the statistical analysis of data and Mrs. H. Huβ provided expert technical assistance. This study was supported by Deutsche Krebshilfe, Grant Nr. 70-2789.

References

1. Association of Directors of Anatomic and Surgical Pathology (2000) Recommendations for the reporting of resected oesophageal carcinomas. Virchows Arch 437:348–350
2. Buskens CJ, Westerterp M, Lagarde SM, Appelman HD (2004) Prediction of appropriateness of local endoscopic treatment for high-grade dysplasia and early adenocarcinoma by EUS and histopathologic features. Gastrointest Endosc 60:703–710
3. Carneiro F, Seixas M, Sobrinho-Simoes M (1995) New elements for an updated classification of the carcinomas of the stomach. Pathol Res Pract 191:571–584
4. Devesa SS, Blot WJ, Fraumeni JF (1998) Changing patterns in the incidence of oesophageal and gastric carcinoma in the United States. Cancer 83:2049–2053
5. Dresner SM, Lamb PJ, Bennett MK, Hayes N, Griffin SM (2001) The pattern of metastatic lymph node dissemination from adenocarcinoma of the esophagogastric junction. Surgery 129:103–109
6. Fenoglio-Preiser C, Stemmermann GN, Lantz PE, Listrom MB, Rilke FO (1999) Gastrointestinal pathology, 2nd edn. Lippincott-Raven, Philadelphia, p 119
7. Hamilton SR, Aaltonen LA (eds) (2000) World Health Organisation. Classification of tumours. Pathology and genetics of tumours of the digestive system. IARC, Lyon
8. Heidl G, Langhans P, Mellin W, Bunte H, Grundmann E (1993) Adenocarcinomas of oesophagus and cardia in comparison with gastric carcinoma. J Cancer Res Clin Oncol 120:95–99
9. Kalish RJ, Clancy PE, Orringer MB, Appelman HD (1984) Clinical, epidemiologic, and morphologic comparison between adenocarcinomas arising in Barrett's oesophageal mucosa and in the gastric cardia. Gastroenterology 86:461–467
10. Lauren P (1965) The two histological main types of gastric carcinoma: diffuse and so-called intestinal-type carcinoma. Acta Pathol Microbiol Immunol Scand 64:31–49
11. Lewin KJ, Appelman HD (1996) Atlas of tumour pathology: tumours of the oesophagus and stomach. Armed Forces Institute of Pathology, Washington, District of Columbia, p 127
12. Ormsby AH, Petras RE, Henricks WH, Rice TW, Rybicki LA, Richter JE, Goldblum JR (2002) Observer variation in the diagnosis of superficial oesophageal adenocarcinoma. Gut 51:671–676
13. Paraf F, Flejou JF, Pignon JP, Fekete F, Potet F (1995) Surgical pathology of adenocarcinoma arising in Barrett's oesophagus. Analysis of 67 cases. Am J Surg Pathol 19:183–191
14. Pech O, May A, Gossner L, Ell C (2003) Barrett's oesophagus: endoscopic resection. Gastrointest Endosc Clin N Am 13: 505–512
15. Rusch VW (2004) Are cancers of the oesophagus, gastro-esophageal junction, and cardia one disease, two, or several? Semin Oncol 31:444–449
16. Sarbia M, Porschen R, Borchard F, Horstmann O, Willers R, Gabbert HE (1995) Incidence and prognostic significance of vascular and neural invasion in squamous cell carcinomas of the oesophagus. Int J Cancer 61:333–336
17. Sarbia M, Geddert H, Klump B, Kiel S, Iskender E, Gabbert HE (2004) Hypermethylation of tumour suppressor genes ($p16^{INK4A}$, $p14^{ARF}$, APC) in adenocarcinomas of the upper gastrointestinal tract. Int J Cancer 111:224–228
18. Saubier EC, Gouillat C, Samaniego C, Guillaud M, Moulinier B (1985) Adenocarcinoma in columnar-lined Barrett's oesophagus. Analysis of 13 esophagectomies. Am J Surg 150:365–369
19. Siewert JR, Stein H (1998) Classification of adenocarcinoma of the esophago-gastric junction. Br J Cancer 85:1457–1459
20. Spechler SJ (2002) Clinical practice. Barrett's Esophagus. N Engl J Med 46:836–842
21. Stein HJ, Feith M, von Rahden BH, Siewert JR (2003) Approach to early Barrett's cancer. World J Surg 27:1040–1046
22. Taniere P, Martel-Planche G, Maurici D, Lombard-Bohas C, Scoazec JY, Montesano R, Berger F, Hainaut P (2001) Molecular and clinical differences between adenocarcinomas of the oesophagus and of the gastric cardia. Am J Pathol 158:33–40
23. Taniere P, Borghi-Scoazec G, Saurin JC, Lombard-Bohas C, Boulez J, Berger F, Hainaut P (2002) Cytokeratin expression in adenocarcinomas of the esophagogastric junction: a comparative study of adenocarcinomas of the distal oesophagus and of the proximal stomach. Am J Surg Path 26:1213–1221
24. UICC, Sobin LH, Wittekind Ch (eds) (2002) TNM classification of malignant tumours, 6th edn. Wiley, New York
25. van Sandick JW, van Lanschot JJ, ten Kate FJ, Offerhaus GJ, Fockens P, Tytgat GN, Obertop H (2000) Pathology of early invasive adenocarcinoma of the oesophagus or esophagogastric junction: implications for therapeutic decision making. Cancer 88:2429–2437
26. Wang HH, Antonioli DA, Goldman H (1986) Comparative features of oesophageal and gastric adenocarcinomas: recent changes in type and frequency. Hum Pathol 17:482–487

Virchows Arch (2006) 448: 539–544
DOI 10.1007/s00428-005-0146-5

ORIGINAL ARTICLE

Serena Bonin · Davide Brunetti · Elena Benedetti · Nader Gorji · Giorgio Stanta

Expression of cyclin-dependent kinases and CDC25a phosphatase is related with recurrences and survival in women with peri- and post-menopausal breast cancer

Received: 6 December 2005 / Accepted: 8 December 2005 / Published online: 27 January 2006

Abstract Progression through the mammalian cell cycle is regulated by cyclin—cyclin-dependent kinase (CDKs) complexes that are activated throughout the cell cycle. Alteration in cell cycle control could lead to proliferation and tumourogenesis. This study was designed to analyse, at messenger RNA (mRNA) level, cyclins and CDKs involved in the retinoblastoma pathway, as well as cell division cycle 25a phosphatase (CDC25a), which activates some of the CDKs that were analysed. The aim of the study was to determine the possible prognostic relevance of these molecules in 73 women with peri- and post-menopausal breast cancer. Cyclins A, D1 and E; CDKs 2, 4 and 6 and phosphatase CDC25a expression status were analysed in primary tumours at mRNA level, by reverse transcriptase polymerase chain reaction analysis in paraffin-embedded primary breast cancers. High expression levels of CDK2, CDK4 and CDC25a were related to tumour recurrence. Over-expression of CDK2 and CDC25a was also associated with reduced overall survival; moreover, the CDK2 expression level was able to define a short-living cohort of patients with tumour-positive lymph nodes. CDK2, CDK4 and CDC25a can be used as reliable biomarkers to predict prognosis in women with peri- and post-menopausal breast cancer.

Keywords Breast cancer · Survival · Quantitative RT-PCR · Formalin-fixed and paraffin-embedded tissues · CDK2 · CDK4 · CDC25a

S. Bonin · G. Stanta
Department of Clinical, Morphological and Technological Sciences, University of Trieste,
Trieste, Italy

S. Bonin · G. Stanta (✉)
International Centre for Genetic Engineering and Biotechnology,
Trieste, Italy
e-mail: stanta@icgeb.org
Tel.: +39-40-3757351
Fax: +39-40-226555

D. Brunetti
Friuli-Venezia Giulia Cancer Registry,
Udine, Italy

E. Benedetti
International Centre for Genetic Engineering and Biotechnology,
Trieste, Italy

N. Gorji
Surgical Pathology Unit, S. Andrea Hospital,
La Spezia, Italy

Introduction

Breast cancer is the most common internal malignancy in women [12]. Treatment response and overall outcome can differ among women with breast cancers characterised by the same histological features and the same stage at diagnosis. New tools such as complementary DNA expression profiles [20, 21] and proteomics [22] are not able to give uniform, simple and reliable predictions of the patient's clinical outcome. The aim of the present study is to quantify the expression of seven cell-cycle-regulating molecules involved in the retinoblastoma (RB) pathway and G2/M checkpoint at the messenger RNA (mRNA) level, and to investigate the relationship between their expression and breast cancer prognosis.

The RB pathway plays a critical role in eukaryotic cell cycle progression. It acts as a crucial negative regulator of cellular proliferation when cells exit G0 or G1 phases and enter S phase [14]. The loss of the G1/S checkpoint during cell cycle progression is a common paradigm in the oncogenic transformation of human cells. Alterations in at least one of the components of the RB pathway were found in the majority of sporadic human cancers [15]. Like most human solid neoplasms, breast cancer harbours frequent alterations in the RB pathway, including over-expression of cyclins and the silencing of p16 and RB [15]. The phosphatase cell division cycle 25a (CDC25a) also seems to play an important role in cell cycle progression and in malignant transformations in breast cancer. This enzyme removes inhibitory phosphates from serine and threonine

Table 1 Oligonucleotides sequences

GENES	PRIMER SEQUENCES
Cyclin A	up: 5′-CCA TTG GTC CCT CTT GAC-3′ sense dw: 5′-CAC TCA CTG GCT TTT CAT C-3′ antisense probe: 5′-GTA TGT GGT GAC TCA AAA CTA CCA TCC A-3′ sense
Cyclin D1	up: 5′-AGC TGT GCA TCT ACA CCG-3′ sense dw: 5′-GGT TCC ACT TGA GCT TGT T-3′ antisense probe: 5′-AGG AGC TGC TGC AAA TGG AGC TGC T-3′ sense
Cyclin E	up: 5′-GTG CTC ACC CGG CCC GGT-3′ sense dw: 5′-GCC GCC GTC CTC CTT CAT-3′ antisense probe: 5′-ACC CGG GTC CAC AGG GAT GCG AAG GA-3′ sense
CDK 2	up: 5′-CCC TGG ATG AAG ATG GAC-3′ sense dw: 5′-CTG GAA GAA AGG GTG AGC-3′ antisense probe: 5′-GTG CAG CAT TTG CGA TAA CAA GCT-3′ sense
CDK 4	up: 5′-GAG GTG GCT TTA CTG AGG-3′ sense dw: 5′-TAC CTT GAT CTC CCG GTC-3′ antisense probe: 5′-GCA TCC CAA TGT TGT CCG GCT GAT-3′ sense
CDK 6	up: 5′-CGT GGA AGT TCA GAT GTT G-3′ sense dw: 5′-TGG GAA GGG CAA CAT CTC-3′ antisense probe: 5′-GCA TCC CAA TGT TGT CCG GCT GAT-3′ sense
CDC25a	up: 5′-AGC CCC AAA GAG TCA ACT AA-3′ sense dw: 5′-GTC CAA AAT GTT CTC AAT GG-3′ antisense probe: 5′-AAG GCC CAT GAG ACT CTT CAT CAG T-3′ sense

Primers up and down (dw) were used in the PCR reaction, the probe was used in the hybridisation of the dot blots

Table 2 RT-PCR and hybridisation conditions

Marker	PCR Conditions			Hybridisation Conditions	
	Annealing temperature (°C)	RNA quantity (ng)	N° of PCR cycles	Temperature (°C)	Percentage of formamide
Cyclin A	55	500	50	45	7.5
Cyclin D1	53	100	45	52	2.0
Cyclin E1	55	125	45	50	0.0
CDK2	55	250	45	45	10.0
CDK4	53	125	50	52	7.5
CDK6	52	250	50	52	7.5
CDC25a	57	100	45	48	10.0

Table 3 Characteristics of the 73 breast carcinomas by stage, grading and patients age at diagnosis

Stage	Grading				Years of age at diagnosis	
	G1[a]	G2[b]	G3[c]	N° of cases	Mean	Range
I	10	15	4	29	64	49–79
IIA	7	13	4	24	65	45–87
IIB	1	4	1	6	56	48–63
IIIA	3	5	2	10	59	45–76
IIIC	0	3	1	4	70	47–90
All stages	21	40	12	73	64	45–90

[a]G1 Well differentiated
[b]G2 Moderately differentiated
[c]G3 Poorly differentiated

residues of cyclin-dependent kinases (CDKs), and it has also been found to be over-expressed in breast cancer [4]. Furthermore, it was reported that this over-expression is correlated with higher levels of CDK2 enzymatic activity in vivo [4].

We analysed cyclins, CDKs involved in the RB pathway and the G2/M checkpoint at the mRNA level, to obtain an insight into breast cancer progression.

Materials and methods

Seventy-three women permanently residing in the north-eastern Italian province of Trieste, and whose first primary cancers were unilateral invasive breast carcinomas, were selected from the database of the Surgical Pathology Department of the University of Trieste. Cancers were diagnosed at the age of 45 years or older between 1971 and 1989 and were only treated with Halsted radical mastectomy and complete axillary dissection. All the slides from the diagnosed tumours were reviewed by one of the authors (G.S.). Carcinomas were histologically graded according to Elston and Ellis [5] and grouped in stages according to the *TNM Classification of Malignant Tumours*, 6th edition [9].

The cohort of women was followed through the general population-based Cancer Registry of the Province of Trieste from the diagnosis of breast cancer until death or until 31 December 2001, whichever came first [11]. No patient was lost at follow-up. During the observation period, 60 women died and all of these underwent complete autopsies at the Surgical Pathology Department of Trieste University.

Formalin-fixed paraffin-embedded specimens from primary breast cancers were used to isolate and quantify the RNA, as described in detail elsewhere [2, 17, 18]. In brief, RNAs were extracted from 6-μm sections of paraffin-embedded tissues. Ten sections were cut for each specimen. Reverse transcriptase polymerase chain reaction (RT-PCR) was performed, as previously reported [16], by using the oligonucleotides described in Table 1 for Cyclin A, Cyclin D1, Cyclin E, CDK2, CDK4, CDK6 and CDC25a genes and the amount of total RNA and the amplification program shown in Table 2. We used paraffin

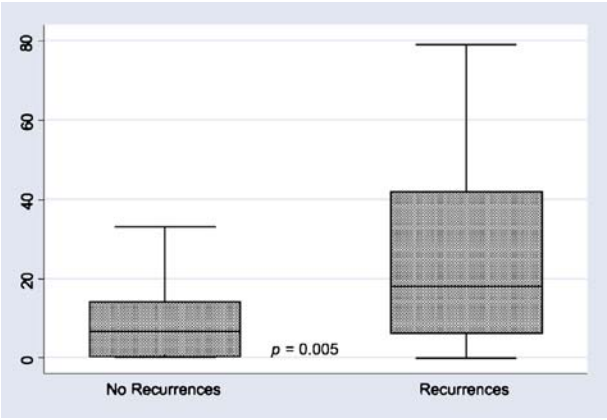

Fig. 1 Quantitative determination of CDK2 expression in the case study, according to the development of recurrences during the follow-up period. *Box plot* summarises the confidence interval (*lower* and *higher horizontal lines*), 25th–50th and 75th percentiles (*horizontal lines* of the *box*)

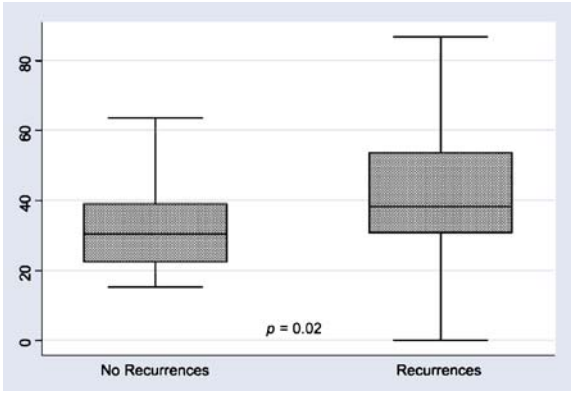

Fig. 3 Quantitative determination of CDC25a expression in the case study, according to the development of recurrences during the follow-up period. *Box plot* summarises the confidence interval (*lower* and *higher horizontal lines*), 25th–50th and 75th percentiles (*horizontal lines* of the *box*)

blocks without tissues as negative controls. The basal level of expression of the genes was quantified by analysing ten normal mammary glands. RNA extracted from breast cancer cell line (BT-549) was used as a positive control. To test the reproducibility of the method, for every gene analysed we randomly selected ten samples from the case study for resubmission for RT-PCR analyses. Amplification products were quantified by dot hybridisation as previously reported [16].

One-way analysis of variance was applied to compare the mean value of the expression of each gene in cells from normal mammary glands with that of cells from breast cancers which had not developed metastases in regional lymph nodes or in other sites, and with that of cells from breast cancers which had spread into regional nodes or into other organs. The Scheffé test was used to identify statistically significant differences between these groups.

The log-rank test [10] was used to check the dependence of the survival of the women with breast cancer on the seven molecular markers, the patients' age at diagnosis, the degree of differentiation [5] and the stage of the primary tumour [9], taken one at time. Subsequently, to estimate the joint effects of the above-mentioned covariates on patients' survival, the data were analysed by fitting the Cox proportional hazards regression model [10]. The proportional hazards assumption was evaluated according to Grambsch and Therneau [8]. In these analyses, tumours with expressions of molecular markers lower or higher than the mean value were classified as low or high status, respectively.

Statistical analyses were performed with the Stata/SE 8.0 package (Stata, College Station, TX, USA).

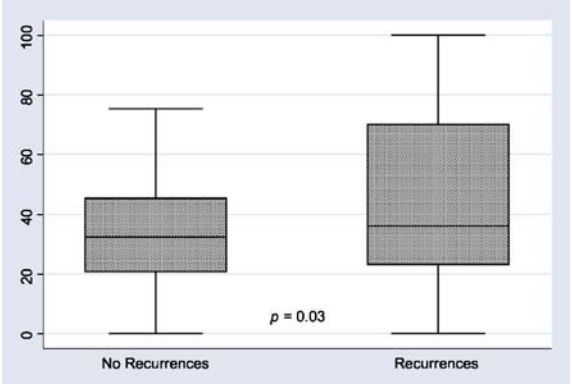

Fig. 2 Quantitative determination of CDK4 expression in the case study, according to the development of recurrences during the follow-up period. *Box plot* summarises the confidence interval (*lower* and *higher horizontal lines*), 25th–50th and 75th percentiles (*horizontal lines* of the *box*)

Results

The cohort of 73 women with breast cancer showed a median age at diagnosis of 63 years (25th–75th percentile=55–71). All of them were affected by infiltrating duct carcinoma of the breast, the diameter of which was not larger than 3.0 cm at pathological examination. The primary cancer was well differentiated in 21 women, moderately differ-

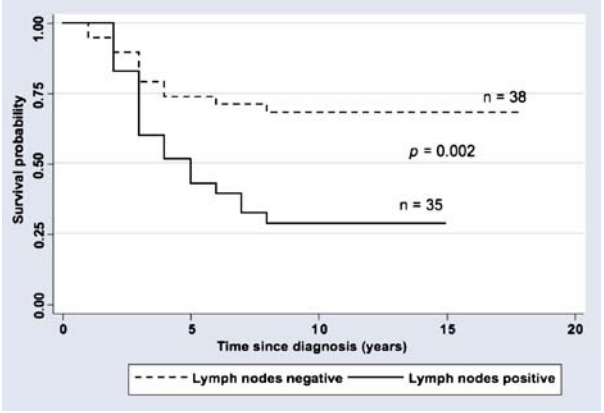

Fig. 4 Kaplan–Meier survival curves according to the presence of metastatic lymph nodes at the diagnosis

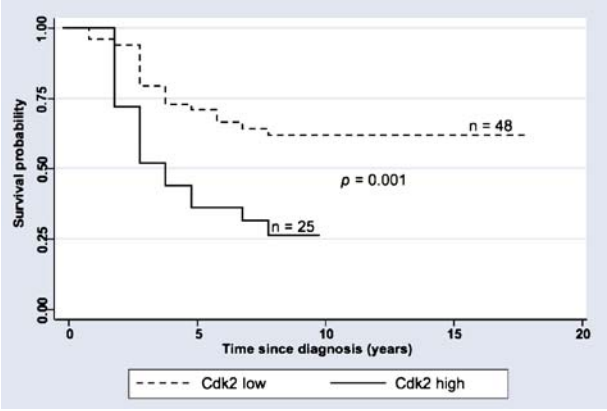

Fig. 5 Kaplan–Meier survival curves with respect to CDK2 expression level in the subgroups of low CDK2 (CDK2 expression lower than the mean value) or high CDK2 (CDK2 expression higher than the mean value)

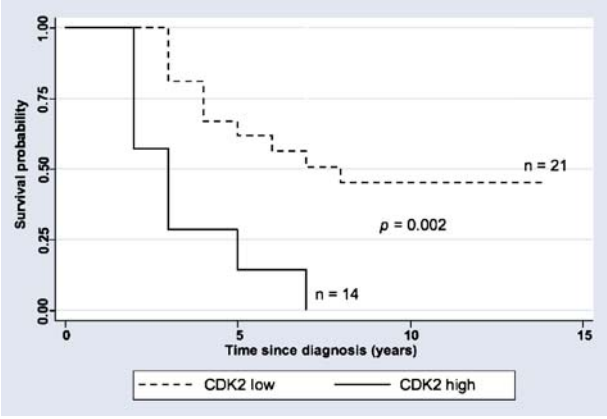

Fig. 7 Kaplan–Meier survival curves for patients with metastatic lymph nodes at diagnosis with respect to CDK2 expression level in the subgroups of low CDK2 (CDK2 expression lower than the mean value) or high CDK2 (CDK2 expression higher than the mean value)

entiated in 39 women and poorly differentiated in 14 women (Table 3). In 38 patients, the axillary lymph nodes were tumour-negative, while in 35 they were tumour-positive at the time of diagnosis of the breast cancer. The median number of tumour-positive nodes was three (range = 1–15). During the period of observation, 36 patients developed distant metastases. The median duration of follow-up was 7 years (25th–75th percentile = 3–8 years). Of the 60 patients who died during the follow-up period, 36 died from breast cancer metastases and 23 from non-neoplastic diseases.

For the cyclins genes, there were no significant differences between the group of patients who developed metastases and the patients who did not do so (Cyclin A, $p = 0.1$; Cyclin D1, $p = 0.1$; Cyclin E, $p = 0.5$). For CDKs CDK2 and CDK4 the level of expression was significantly higher in women with recurrences ($p = 0.005$ and $p = 0.03$, respectively) (Figs. 1 and 2), while CDK6 expression showed no significant differences ($p = 0.2$). A higher expression of phosphatase CDC25a was also found in patients with metastases ($p = 0.02$, Fig. 3). On the other hand, gene expression did not differ between women with lymph node involvement and those without node metastasis.

Women with lymph nodes positive for metastases showed a lower overall survival in comparison with those characterised by no metastasis ($p = 0.002$, Fig. 4). Patients characterised by high CDK2 status presented a decreased overall survival in comparison to those with low CDK2 ($p = 0.001$, Fig. 5). A similar result was found for CDC25a ($p = 0.01$, Fig. 6).

The prognostic contribution of CDK2 and CDC25a combined with lymph node status was investigated in more detail. Survival analysis revealed the worst prognosis in patients with high CDK2 or CDC25a status and tumour-positive lymph nodes ($p = 0.0002$, $p = 0.04$, respectively; Figs. 7 and 8). The same analysis restricted to tumour-negative lymph node patients was not statistically significant ($p = 0.31$ and $p = 0.491$). Cox regression analysis

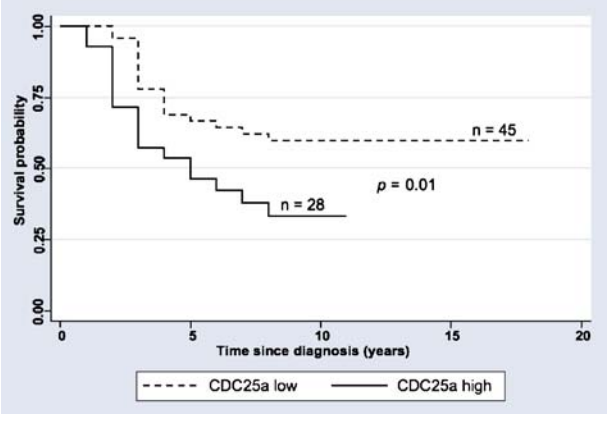

Fig. 6 Kaplan–Meier survival curves with respect to CDC25a expression level in the subgroups of low CDC25a (CDC25a expression lower than the mean value) or high CDC25a (CDC25a expression higher than the mean value)

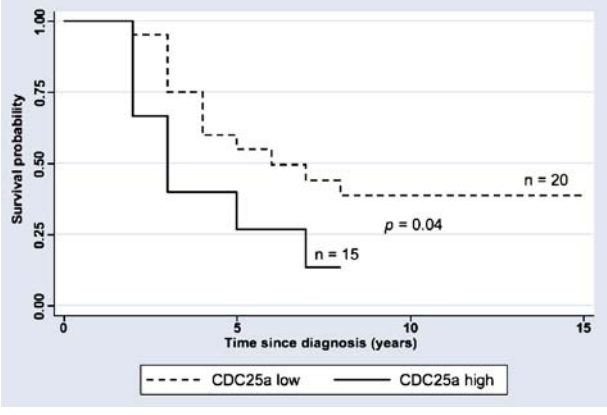

Fig. 8 Kaplan–Meier survival curves for patients with metastatic lymph nodes at diagnosis with respect to CDC25a expression level in the subgroups of low CDC25a (CDC25a expression lower than the mean value) or high CDC25a (CDC25a expression higher than the mean value)

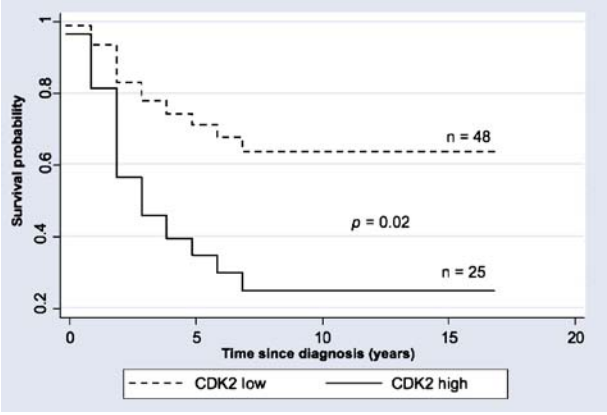

Fig. 9 Survival curves related to Cox proportional hazard regression with respect to CDK2 expression level in the subgroups of low CDK2 (CDK2 expression lower than the mean value) or high CDK2 (CDK2 expression higher than the mean value)

confirmed the results obtained with the log-rank test for CDC25a and CDK2. In particular, for CDK2 the hazard ratio was 3.1 (95% confidence interval, 1.25–7.69) (Fig. 9). In the multivariate analysis of prognostic factors on survival, tumour stage, as expected, showed an independent influence on cancer-specific death. Conversely, tumour grade, age of the patient at the diagnosis and the remaining molecular markers analysed did not have an effect on survival.

Discussion

Cyclins, CDKs and CDK inhibitors are frequently deregulated in cancer. In our study carried out on 73 women with peri- and post-menopausal infiltrating duct carcinoma of the breast, the expression level of cyclin A, E and D1 at the mRNA level was higher in tumours in comparison with normal mammary glands (data not shown). However, none of these cyclins presented differences in the expression level between carcinomas characterised by recurrences and those with no recurrences.

Despite the fact that previous studies have shown some correlation between cyclin A, D and E over-expression and breast cancer development and/or progression [3, 6, 7], and despite the fact that cyclin E has been shown to be the best prognostic marker for breast cancer to date [19], we have failed to find evidence that the expression of these cyclins influences the survival probability of women with breast cancer, at least in the present study. The exact cause of this discrepancy is difficult to explain, but it may be due to a different composition of patient groups, with regard to clinicopathological parameters, and also to the different techniques employed in the studies (Western blot or immunohistochemistry). With regard to cyclin E, the existence of low and high molecular weight isoforms of this enzyme could explain our results. It seems that high levels of low-molecular-weight isoforms are the true prognostic indicators because of their influence on cell proliferation and genetic instability [1].

In our study, over-expression of CDK2 and CDK4 seems to be related to breast cancer progression during the follow-up period; moreover, CDK2 over-expression also seems to have an influence on patients' survival. It is well known that progression through the G1/S phase and the initiation of DNA synthesis, or entry to S phase, are regulated by CDKs, which are sequentially regulated by cyclins D, E and A through the formation of cyclin–CDK complexes [13]. To our knowledge, this is the first report showing that CDK2 and CDK4 could influence breast cancer prognosis, although our results are derived from only 73 women with breast cancer.

A high expression level of phosphatase CDC25a was found in breast carcinomas with recurrences and was associated with poor survival. Our findings confirm those of Cangi et al. [4]. CDC25a is involved in cellular progression at the level of the G1/S checkpoint. It dephosphorylates CDK2 at serine and threonine residues with the activation of the kinase [4].

The results presented here suggest that high expression of CDK2, CDK4 and CDC25a could represent crucial factors in breast cancer progression and could be used as prognostic biomarkers especially in those patients with positive regional lymph nodes. Furthermore, specific inhibitors of both CDC25a, CDK2 and CDK4 could be developed as possible targeted drugs.

Acknowledgement The authors thank Dr. Georgine Faulkner for the English revision of the manuscript.

References

1. Akli S, Keyomarsi K (2003) Cyclin E and its low molecular weight forms in human cancer and as targets for cancer therapy. Cancer Biol Ther 2:S38–S47
2. Bonin S, Pascolo L, Croce LS, Stanta G, Tiribelli C (2002) Gene expression of ABC proteins in hepatocellular carcinoma, perineoplastic tissue, and liver diseases. Mol Med 8:318–325
3. Bukholm IR, Bukholm G, Nesland JM (2001) Over-expression of cyclin A is highly associated with early relapse and reduced survival in patients with primary breast carcinomas. Int J Cancer 93:283–287
4. Cangi MG, Cukor B, Soung P, Signoretti S, Moreira G Jr, Ranashinge M, Cady B, Pagano M, Loda M (2000) Role of the Cdc25A phosphatase in human breast cancer. J Clin Invest 106:753–761
5. Elston CW, Ellis IO (1991) Pathological prognostic factors in breast cancer. I. The value of histological grade in breast cancer: experience from a large study with long-term follow-up. Histopathology 19:403–410
6. Esteva FJ, Hortobagyi GN (2004) Prognostic molecular markers in early breast cancer. Breast Cancer Res 6:109–118
7. Gillett CE, Lee AH, Millis RR, Barnes DM (1998) Cyclin D1 and associated proteins in mammary ductal carcinoma in situ and atypical ductal hyperplasia. J Pathol 184:396–400
8. Grambsch PM, Therneau TM (1994) Proportional hazards test and diagnostic based on weighted residuals. Biometrika 81: 515–526
9. Greene FL, Page DL, Fleming ID, Fritz A, Balch MC, Haller DG, Morrow M (eds) (2002) AJCC cancer staging manual, 6th edn. Springer, Berlin Heidelberg New York
10. Kalbfleisch JD, Prentice RL (1980) The statistical analysis of failure time data. Wiley, New York

11. Parkin DM, Whelan SL, Ferlay J, Raymond L, Young J (1997) Cancer incidence in five continents—Vol VII, vol 153. IARC Scientific Publications, Lyon, pp 562–565
12. Parkin DM, Bray F, Ferlay J, Pisani P (2001) Estimating the world cancer burden: Globocan 2000. Int J Cancer 94:153–156
13. Sherr CJ (1996) Cancer cell cycles. Science 274:1672–1677
14. Sherr CJ, McCormick F (2002) The RB and p53 pathways in cancer. Cancer Cell 2:103–112
15. Simin K, Wu H, Lu L, Pinkel D, Albertson D, Cardiff RD, Dyke TV (2004) pRb Inactivation in mammary cells reveals common mechanisms for tumor initiation and progression in divergent epithelia. PLoS Biol 2:E22
16. Stanta G, Bonin S (1998) RNA quantitative analysis from fixed and paraffin-embedded tissues: membrane hybridization and capillary electrophoresis. Biotechniques 24:271–276
17. Stanta G, Schneider C (1991) RNA extracted from paraffin-embedded human tissues is amenable to analysis by PCR amplification. Biotechniques 11:304–308
18. Stanta G, Bonin S, Losi L, Eusebi V (1998) Molecular characterization of intraductal breast carcinomas. Virchows Arch 432:107–111
19. Sutherland RL, Musgrove EA (2002) Cyclin E and prognosis in patients with breast cancer. N Engl J Med 347:1546–1547
20. van' t Veer LJ, Dai H, van de Vijver MJ, He YD, Hart AA, Mao M, Peterse HL, van der Kooy K, Marton MJ, Witteveen AT, Schreiber GJ, Kerkhoven RM, Roberts C, Linsley PS, Bernards R, Friend SH (2002) Gene expression profiling predicts clinical outcome of breast cancer. Nature 415:530–536
21. van de Vijver MJ, He YD, van't Veer LJ, Dai H, Hart AA, Voskuil DW, Schreiber GJ, Peterse JL, Roberts C, Marton MJ, Parrish M, Atsma D, Witteveen A, Glas A, Delahaye L, van der Velde T, Bartelink H, Rodenhuis S, Rutgers ET, Friend SH, Bernards R (2002) A gene-expression signature as a predictor of survival in breast cancer. N Engl J Med 347:1999–2009
22. Yazidi-Belkoura IE, Adriaenssens E, Vercoutter-Edouart AS, Lemoine J, Nurcombe V, Hondermarck H (2002) Proteomics of breast cancer: outcomes and prospects. Technol Cancer Res Treat 1:287–296

Virchows Arch (2006) 448: 545–551
DOI 10.1007/s00428-006-0154-0

ORIGINAL ARTICLE

Marco Volante · Stefano La Rosa · Isabella Castellano · Giovanna Finzi · Carlo Capella · Gianni Bussolati

Clinico-pathological features of a series of 11 oncocytic endocrine tumours of the pancreas

Received: 20 October 2005 / Accepted: 29 December 2005 / Published online: 21 February 2006

Abstract Oncocytic changes may occur very infrequently in neuroendocrine tumours. To estimate the prevalence, pathological features and clinical behaviour of oncocytic endocrine tumours of the pancreas, we reviewed a series of 227 lesions from two institutions. Eleven cases with predominant oncocytic features were selected, representing 4.85% of the whole series. The morphological features and immunophenotype of such tumours did not differ from conventional endocrine pancreatic tumours, except for the presence of abundant eosinophilic and granular cytoplasm. Anti-mitochondrial antigen was positive in all cases tested, and by electron microscopy, numerous mitochondria were observed in the cytoplasm of tumour cells. The majority of cases were nonfunctioning, and in most cases, pathologic signs of malignancy, leading to a diagnosis of endocrine carcinoma, were observed. In addition, the three non-malignant cases matched the criteria of well-differentiated tumours of uncertain malignant potential. Nearly 50% of the cases were clinically aggressive, and lymph node and liver metastases were present at the time of diagnosis in a minority of cases. Therefore, oncocytic endocrine pancreatic tumours represent a peculiar morphological and clinical variant characterised by frequent hormonal inactivity and malignant behaviour, which should be considered in the differential diagnosis, especially when dealing with a metastatic lesion.

Keywords Oncocytic · Pancreas · Endocrine · Tumour · Malignant

M. Volante · I. Castellano · G. Bussolati (✉)
Department of Biomedical Sciences and Human Oncology,
University of Turin,Via Santena 7,
10126, Turin, Italy
e-mail: gianni.bussolati@unito.it
Tel.: +39-011-6334274
Fax: +39-011-6635267

S. La Rosa · G. Finzi · C. Capella
Department of Human Morphology, University of Insubria,
Varese, Italy

S. La Rosa · G. Finzi · C. Capella
Department of Pathology, Ospedale di Circolo,
Varese, Italy

Introduction

Oncocytic cells are traditionally defined by the presence of an abundant granular acidophylic cytoplasm. Such cells, also called oxyphilic or—in the thyroid gland—Hürthle cells, are rich in mitochondria, as revealed by special cytochemical stainings and ultrastructural studies [27, 39]. Non-neoplastic lesions formed of oncocytes are described in the thyroid, parathyroid, salivary and respiratory mucosal glands, whereas oncocytic tumours are more widely distributed and can be observed in all the above tissues as well as in several other organs such as the kidney and pituitary. Neuroendocrine tumours with oncocytic features are very rare, and few case reports have been published of tumours in the thyroid [16], lung [14, 21], larynx [41], stomach [5, 6] and thymus [24].

In the pancreas, although no oncocytic cells have been described in the normal endocrine component, single cases of oncocytic neuroendocrine tumours have been reported [8, 15, 28, 33, 36, 37]. In a recent report, a biphasic tumour with typical endocrine cells and oncocytes was associated with Von Hippel–Lindau disease [10]. Among these, accounting to a total of eight cases so far reported in the literature to our knowledge, all cases but one were malignant, and the majority was nonfunctioning. The functioning tumours were two insulinomas [33, 37], whereas one other reported case [36] was associated with the glucagonoma syndrome with insulin-dependent diabetes mellitus and chronic diarrhea and focal immunohistochemical positivity for insulin, glucagon and somatostatin. It is interesting that in the case reported by Chetty and co-workers [10], the oncocytic component showed widespread vascular invasion and lymph node involvement. In the recent WHO classification of tumours of endocrine organs [11], oncocytic features in endocrine pancreatic tumours are mentioned as occasional findings but not defined as a specific morphological or clinico-pathological variant.

The occurrence of pancreatic tumours composed of oncocytes is not strictly related to the neuroendocrine phenotype and may represent a pitfall in the differential diagnosis of such lesions. In fact, cases of oncocytic tumours of the pancreas lacking neuroendocrine marker expression have been described [4, 19, 32, 38, 42]. Moreover, oncocytic

changes have been described in mucinous exocrine pancreatic tumours [3], in pancreatic intraepithelial neoplasia [1] and in intraductal papillary neoplasms [20, 31]. In addition, when diagnosed as metastatic deposits in the liver, differential diagnosis with primary hepatocellular carcinoma or with metastases from oncocytic tumours from other sites should also be considered.

To determine the prevalence of pancreatic endocrine tumours with oncocytic features, we reviewed a series of 227 cases from our two institutions. The clinico-pathological features of the 11 selected cases are reported.

Materials and methods

Case selection

Two hundred and twenty-seven cases from the files of the Department of pathology at the University of Torino and the University of Varese were collected. Two to ten histological slides, stained in haematoxylin and eosin, were available for review. For most cases, representative paraffin blocks were also available for further histology or immunohistochemical reactions. Eleven cases showing prominent oncocytic changes were selected. Two cases (cases 7 and 8, see Table 1) have been previously reported [33]. In one case (case 7, Table 1), only cytological material from a liver fine-needle aspiration biopsy was available. In two other cases (cases 9 and 11, Table 1), cytological material was available in adjunct to the surgical specimen. All cases were classified according to the recent WHO classification of tumours of endocrine organs [11].

Clinico-pathological data for the selected cases were collected, and follow-up information were available in all cases.

Immunohistochemistry

To confirm the endocrine nature of the tumours, serial sections coated on Superfrost (Ventana Medical Systems, Illkirch, France) slides from all 11 selected cases were stained for pan-endocrine marker chromogranin A (monoclonal, LK2H10, diluted 1:500; Biogenex, San Ramon, CA, USA) and synaptophysin (monoclonal, SP11, diluted 1:100; NeoMarker, Fremont, CA, USA), and for pancreatic (insulin: monoclonal, HB125, diluted 1:400, Biogenex; glucagon: polyclonal, pre-diluted, Biogenex; somatostatin: polyclonal, diluted 1:400, DakoCytomation, Glostrup, Denmark; and PP polyclonal, diluted 1:2,000, Dako) and ectopic (gastrin: polyclonal, pre-diluted, Ventana; calcitonin: monoclonal, undiluted, Ortho Diagnostic System, Raritan, NJ, USA) hormones in an automated immunostainer (Ventana Benchmark XT). Four cases were also stained for chromogranin B (monoclonal, B11, diluted 1:4,000, Dr. Siccardi, University of Milan, Italy).

To confirm their oncocytic morphology, all cases but one were stained with anti-mitochondrial antigen (monoclonal, 113-1, diluted 1:75, Biogenex) [34]. Proliferation index was evaluated by means of Ki-67 immunostaining (monoclonal, MIB-1, diluted 1:50, Dako) and counted as the percentage of positive cells/1,000 tumour cells, in the most positive areas.

Endogenous biotin blocking procedure before primary antibodies incubation was performed to prevent unspecific background [7].

Electron microscopy

Electron microscopy was performed in four cases. In case 17, tumour samples were directly fixed in Karnovsky fixative (2% paraformaldehyde and 2% glutaraldehyde in 0.05 M, pH 7.3 cacodylate buffer), while in the other three cases (9, 11 and 14), formalin-fixed wet tissues were fixed in Karnovsky fixative, post-fixed in osmium tetroxide and embedded in epoxy resin. Thin sections were stained with uranyl acetate and lead citrate and subsequently examined using a Philips Morgagni electron microscope.

Results

The main clinico-pathological features of our series of 11 oncocytic endocrine tumours of the pancreas are summarised in Table 1.

Among our series of 227 endocrine pancreatic tumours, the 11 oncocytic lesions represented 4.85%. The mean age was 49 years (range 30 to 70 years), and the male to female ratio was 3:8. The mean tumour diameter was 8 cm (range 1.8 to 20 cm), and most tumours were located in the body or tail of the pancreas (9 of 11). Most cases clinically presented with nonspecific symptoms such as abdominal pain or asthenia. In two cases, jaundice occurred as a sign of a mass in the head of the pancreas (cases 12 and 14, Table 1). Hypoglycemia was the main symptom in the insulin-producing tumour (case 8, Table 1). Two and five cases presented lymph node and liver metastases at diagnosis, respectively. Vascular invasion (Fig. 1) was evident in all but one case (case 13, Table 1). The mean mitotic index (×10 high power fields) was 2 (limits<1–7), and the proliferation status as evaluated by Ki-67 immunostaining was 4.2% (range 0.2 to 15%). Six patients were alive and well, three were alive with disease at the time of follow-up and the two remaining died of the disease (mean survival 68 months). As compared to the complete series, 9 of 11 (81%) were nonfunctioning (as compared to 112 of 227, 49%), and 8 of 11 (73%) were malignant (as compared to 87 of 227, 38%; X^2 test, $p<0.05$). In accordance with the recent WHO classification of pancreatic endocrine tumours [11], the three non-metastatic cases matched the criteria of well-differentiated tumours of uncertain malignant potential, for the size larger than 2 cm, a mitotic rate greater than 2 and the presence of vascular invasion, either alone or in combination.

The morphological features of the 11 oncocytic tumours did not differ from those of conventional endocrine pancreatic tumours, except for the presence of abundant eosinophilic and granular cytoplasm, mild pleomorphism and large

Table 1 Clinico-pathological features of 17 cases of oncocytic endocrine tumours of the pancreas (from the literature and the present series)

Number	Diagnosis	Hormonal syndrome	Sex/ age	Location/ size (cm)	Clinical presentation	Extension/ metastases	Vascular invasion	Mitoses/ Ki-67 LI	IHC positive findings	Follow-up (months)	Reference
1	WDEC	Glucagon	F/58	Head/5	Diabetes mellitus, chronic diarrhea	Lymph node mts	Yes	<1/na	Insulin, glucagon, somatostatin	AWD 5	[36]
2	UBET	NF	M/40	Tail /8	Polyarteritis nodosa	–	No	<1/na	NSE	NED 60	[15]
3	WDEC	NF	F/53	Head/4	Pancreatic exocrine insufficiency	Lymph node mts	Yes	<1/na	Serotonin	DOD 13	[8]
4	WDEC	Insulin	F/54	Head/3	Hypoglycemia	Lymph node mts	Yes	<1/na	NSE, insulin, glucagon, VIP	NED 36	[37]
5	WDEC	NF	M/60	Body/3	Abdominal pain, anorexia	Lymph node and liver mts	Yes	<1/na	Cga	DOD 6	[28]
6	WDEC^	NF	F/41	Head, body, tail/2.5	VHL; jaundice	Lymph node mts	Yes	na/na	CgA, syn, CD56, VIP (focal)	NED (?)	[10]
7	WDEC	NF	M/36	Body/8	Abdominal pain	Multiple liver mts	Yes	<1/na	CgA, CgB, MT	AWD 7 (CT only)	Present series and [33]
8	WDEC	Insulin	F/57	Tail/13	Abdominal pain; hypo-glycemia	Extrapancreatic extension	Yes	1/3	CgA, insulin, MT	NED 9	Present series and [33]
9	WDEC	Glucagon	M/57	Tail/8	Abdominal pain; mild diabetes	Extrapancreatic (spleen) growth; multiple liver mts	Yes	7/15	CgA, glucagon, MT, syn	AWD 8	Present series
10	UBET^	NF	F/40	Body–tail/11	Abdominal pain	–	Yes	2/3	CgA, syn	NED 36	Present series
11	WDEC	NF	F/70	Body–tail/6	Asthenia, abdominal pain	Lymph node and multiple liver mts	Yes	1/5	CgA; MT, syn	AWD 2	Present series
12	WDEC	NF	M/34	Head/na	Jaundice	Liver mts	Yes	3/2.5	CgA, MT	DOD 16	Present series
13	UBET	NF	F/65	Body/1.9	Occasional finding	–	No	3/0.8	CgA, CgB, MT	NED 66	Present series
14	WDEC	NF	F/62	Head/4	Jaundice	Lymph node mts	Yes	1/1.7	CgA, MT	NED 84	Present series
15	WDEC	NF	F/30	Body–tail/20	Asthenia, weight loss	Spleen, stomach, colon invasion	Yes	2/3	Calcitonin, MT	NED 108	Present series
16	UBET	NF	F/55	Body/1.8	Occasional finding	–	Yes	<1/0.2	CgA, CgB, PP, MT	NED 102	Present series
17	WDEC^	NF	F/37	Tail/6	Abdominal pain	Liver mts	Yes	1/7	CgA, CgB, somatostatin, MT	DOD 120	Present series

WDEC Well-differentiated endocrine carcinoma; *UBET* well-differentiated endocrine tumour, uncertain behaviour; ^ zonal oncocytic changes; *FNAB* fine-needle aspiration biopsy; *mts* metastasis; *NF* nonfunctioning; *na* not available; *LI* labeling index (%); *IHC* immunohistochemistry; *NSE* neuron specific enolase; *Cg* chromogranin; *Syn* synaptophysin; *MT* anti-mitochondrial antigen; *PP* pancreatic polypeptide; *AWD* alive with disease; *NED* no evidence of disease; *DOD* died of disease

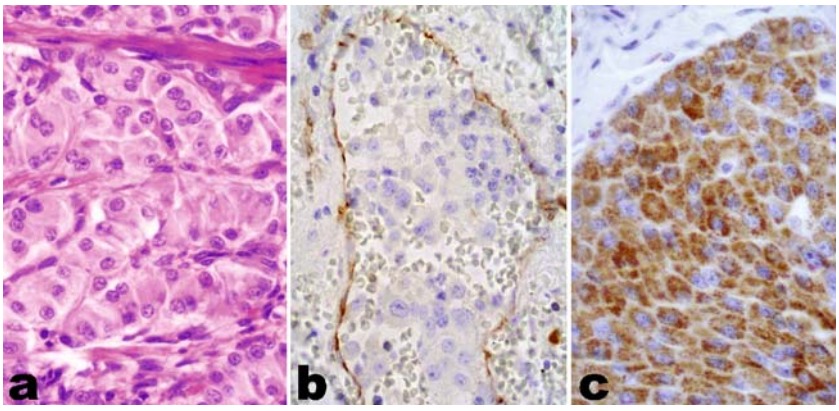

Fig. 1 Case 16 (see Table 1). Histological aspect of the oncocytic tumour which is composed of monomorphic cells with mild nuclear atypia and abundant eosinophilic cytoplasm (**a**). At the periphery of tumour, neoplastic thrombi within vascular vessels lined by CD31-positive endothelial cells were found (**b**). Most tumour cells were positive for mitochondrial antigen (**c**)

ground-glass nuclei (Figs. 1 and 2); prominent nucleoli were observed in about half of the cases, being either diffusely present within the tumour or in focal areas. Predominant trabecular and pseudocanalicular growth patterns were observed, with occasional rosette-like and glandular formations. Oncocytic features were extensive in all but two cases (cases 10 and 17, Table 1), where they represented patch-like changes (covering more than one third of the tumour) in otherwise conventional endocrine tumours. By immunohistochemistry, chromogranins A and B, synaptophysin and mitochondrial antigen were positive in all cases tested. The latter antibody showed in all tumours tested the typical granular cytoplasmic pattern of staining, in the majority of tumour cells. Chromogranin A staining showed a strong and diffuse cytoplasmic positivity in one third of the cases (including the two functioning tumours), whereas a more patchy immunoreactivity was observed in the remaining cases. Synaptophysin presented a diffuse, moderate to strong cytoplasmic immunostaining in all tumours. By contrast, chromogranin B was mainly focal in the four cases tested. Concerning pancreatic hormones, insulin and glucagon were positive in the majority of tumour cells in the two functioning tumours (cases 8 and case 9, respectively; Table 1), while a focal positivity for calcitonin, pancreatic polypeptide and somatostatin was observed in case 15, 16 and 17, respectively (Table 1). Whenever available from surgical excision, lymph node and liver metastases presented the same morphological and immunocytochemical features as the corresponding primary tumour. In the three cases in which pre-operative fine-needle aspiration material from liver metastasis was available, the cytological features of tumour cells were comparable to those of the corresponding surgical samples (Fig. 2).

In the four cases examined, electron microscopy demonstrated the presence of numerous tumour cells with the cytoplasm densely packed with innumerable round or oval, sometimes distorted, mitochondria (Fig. 3). The mitochondrial structure was often abnormal, as the pattern of the cristae, forming circles, clubs, arcades, and three-dimensional tubular networks, was disturbed. Moreover, the intermembrane spaces were often distended. Occasional intramitochondrial dense inclusions could be found, especially in case 11. Secretory granules with dense cores were rare in the typical oncocytic cells. A few densely granulated non-oncocytic cells containing small D1-type secretory granules or targetoid glucagon-type granules were found in case 11 and in cases 14 and 17, respectively.

Discussion

Tumours composed entirely or partially of oncocytic cells may occur in a variety of tissues, including endocrine and neuroendocrine ones. Most typical examples in neuroendocrine tissues are represented by oncocytic adenomas [2] and carcinomas [12] of the parathyroid and adenomas of the pituitary, where a more aggressive behaviour has been postulated by some authors [29] but not confirmed by others [30].

Neuroendocrine tumours in other organs containing dispersed neuroendocrine cells have been occasionally reported [5, 6, 14, 16, 21, 23, 41]. In the pancreas, endocrine tumours composed of oncocytic cells have been described also, either sporadic [8, 15, 28, 33, 36, 37] or associated to inherited multiple endocrine tumour syndromes such as Von Hippel–Lindau disease [10].

Although in the endocrine and neuroendocrine organs where oncocytic tumours most frequently occur (namely, thyroid, parathyroid and pituitary) no evidence exists of a peculiar clinical behaviour as compared to the non-oncocytic counterpart, most of the above-mentioned reported cases, especially those described in the pancreas, clinically showed a malignant behaviour. Therefore, we aimed to review a large consecutive series of endocrine pancreatic tumours, searching for oncocytic morphological changes, and to determine peculiar clinico-pathological features of oncocytic lesions. Of the 11 oncocytic cases selected in a series of 227 endocrine pancreatic tumours (representing 4.85%), eight cases were classified as carcinomas, presenting lymph node, liver or visceral metastases at the time of diagnoses, and five cases had an aggressive clinical behaviour, such that the patients are either alive with disease or had died of the disease at time of follow-up.

Mostly investigated in the thyroid gland, oncocytic changes are driven by several molecular defects in mitochondrial DNA, and alterations in mitochondrial metabolism have been detected in oncocytic cells and related tumours, including over-expression of regulatory proteins [13], mutations and/or deletions of mitochondrial DNA and

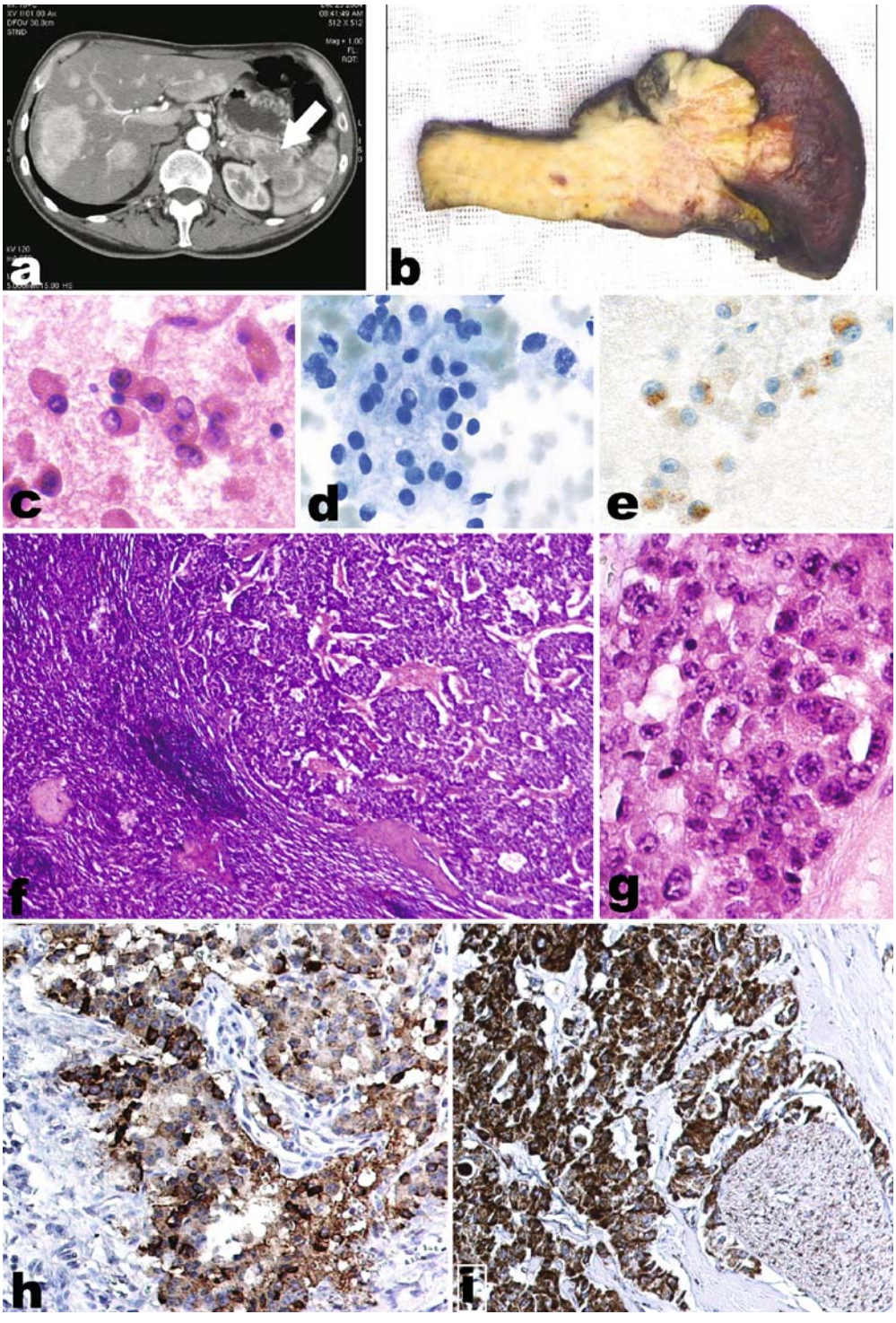

Fig. 2 Case 9 (see Table 1). CT scan (**a**) revealed a mass in the tail of the pancreas (*arrow*) infiltrating the spleen, with multiple liver metastases; an ill-defined, whitish, dys-homogeneous lesion was observed at macroscopic examination (**b**), with focal areas of haemorrage and necrosis. Cytological sample of a liver metastasis by fine needle aspiration showed the presence of neoplastic cells with abundant cytoplasm (**c** and **d**), positive for Chromogranin A by immunohistochemistry (**e**). In the surgical sample, the lesion infiltrated the spleen parenchyma (**f**) and was composed of atypical tumour cells similar to those in the cytological sample, in a solid/trabecular growth pattern (**g**). Tumour cells were strongly reactive by immunohistochemistry for glucagon (**h**) and anti-mitochondrial antigen (**i**)

cytochrome C oxidase deficiency [22, 25, 26]. Very recently, mutations in the GRIM-19 gene, a member of the interferon-beta and retinoic-acid-induced pathway of cell death, have been detected in oncocytic thyroid tumours [23]. In different organs, where tumours bearing oncocytic features have been described (namely, kidney and salivary gland), such features are constantly associated with a more benign behaviour, a phenomenon which was interpreted as related to the slow proliferation rate and to the long time required for the process of cytoplasmic accumulation of mitochondria, necessary for acquiring the oncocytic phenotype [40]. The prevailing aggressiveness associated to the occurrence of oncocytic features in endocrine tumours of the pancreas (overall 13 of the 17 cases, including the present series and those reported in the literature) is, therefore, surprising and still unexplained.

It should be noted that, probably as a consequence of late diagnosis due to the absence of specific symptoms of

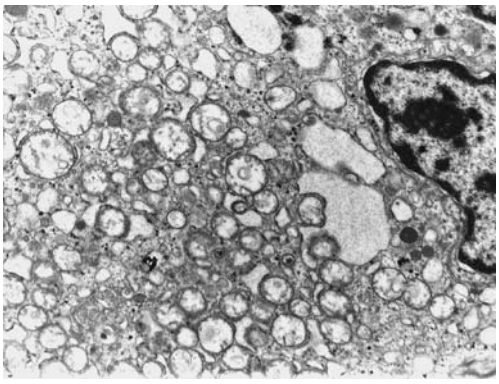

Fig. 3 Ultrastructural feature of an oncocytic cell (case 17) showing numerous packed mitochondria in the cytoplasm (original magnification ×14,000)

hormonal secretion, most of the lesions here reported presented with a large tumour size which, in endocrine pancreatic tumours, is related to a more aggressive behaviour. Moreover, it is interesting that both small tumours of our series did not relapse. Therefore, the possibility that the malignant phenotype in oncocytic endocrine pancreatic tumours could be related to the late diagnosis and advanced stage in most tumours cannot be excluded.

Another interesting observation concerns the hormonal profile of such tumours. In agreement with the majority of previously published cases, all but two cases of our series were clinically nonfunctioning, thus explaining the delay in their clinical and nonspecific onset and the large mean tumour size (8 cm). The metabolic alterations, particularly in the energetic machinery, that characterise oncocytic cells may be responsible for the deficiency in hormone production of such lesions, but functional data in vivo would be needed to clarify this aspect.

No other peculiar clinical or morphological features were observed, being both the location and the histological growth patterns comparable to conventional non-oncocytic pancreatic endocrine tumours.

In the pancreas, oncocytic changes are not restricted to neuroendocrine tumours. In most instances, tumours with oncocytic features are well-defined entities, such as mucinous exocrine pancreatic tumours [3], pancreatic intraepithelial neoplasia [1], intraductal papillary neoplasms [20, 31], thus, not representing difficulties in their differential diagnosis. However, oncocytic carcinomas, lacking neuroendocrine markers of differentiation or neurosecretory granules by electron microscopy, with predominant solid growth patterns and tumour cells with abundant eosinophilic cytoplasm have been observed and may represent a diagnostic problem [4, 19, 32, 38, 42]. These neoplasms must be distinguished from oncocytic endocrine tumours because of their more aggressive behaviour. Another possible pitfall in the differential diagnosis with oncocytic endocrine tumours is represented by pancreatic acinar cell carcinoma, composed of tumour cells with abundant eosinophilic cytoplasm arranged in a solid-trabecular, pseudo-glandular growth. By electron microscopy, the granularity of the cytoplasm is due to abundance of zymogen-like granules rather than mitochondria, but the occurrence of focal expression of neuroendocrine markers in about one third of the cases of acinar cell carcinoma [17] may lead to misdiagnoses. The presence of atypical large nuclei with prominent nucleoli, periodic acid–Schiff-positive cyoplasmic granules and immunoreactivity for trypsin and lipase all favour the diagnosis of acinar cell carcinoma. Conversely, a diffuse immunoreactivity for general endocrine markers, including synaptophysin and chromogranins and/or specific pancreatic hormones, combined with less atypical nuclear features, points to a diagnosis of an endocrine neoplasm. A further pancreatic primary tumour which may show prominent oncocytic features and enter in the differential diagnosis with oncocytic endocrine tumours is pancreatoblastoma, where an endocrine component is recognisable in a high percentage of cases [18]. Age is one of the major helpful criterion to differentiate pancreatoblastoma from endocrine tumours because the latter are very rare in the first decade of life. In addition, the presence of squamoid nests, acinar structures and the reactivity for α-fetoprotein support the diagnosis of pancreatoblastoma. Finally, the recently described pancreatic endocrine tumours with "rhabdoid" features [9] may mimic oncocytic endocrine tumours because of the abundance of eosinophilic cytoplasm of their cells, due to the presence of characteristic inclusion formed by aggregates of intermediate filaments. Immunohistochemistry can help in differentiating "rhabdoid" tumours from oncocytic endocrine neoplasms, as the former show a typical paranuclear dot-like or globular immunoreactivity for cytokeratin AE1/3. Moreover, ultrastructurally, rhabdoid tumours are characterised by juxtanuclear deposition of aggregates of intermediate filaments, corresponding to the globular cytokeratin immunoreactivity, while oncocytic tumours are characterised by the presence of abundant mitochondria.

In three of our cases, a preoperative diagnosis was made on a liver fine-needle aspiration biopsy. In such cases, additional differential diagnoses should be taken into account, from primary hepatocellular carcinomas (namely, the fibrolamellar variant) to other oncocytic neoplasms metastatic to the liver (among them gastrointestinal hepatoid carcinomas, oncocytic carcinomas from various sites or even soft tissue tumours or melanomas with prominent eosinophilic features) [35].

In conclusion, oncocytic endocrine pancreatic tumours represent a peculiar morphological and clinical variant of endocrine pancreatic tumours, characterised by oncocytic features comparable to those of oncocytic tumours from other sites, by frequent hormonal inactivity and malignant behaviour. When looking at a metastatic oncocytic tumour and looking for the possible organ of primary origin, the pancreas should be considered among the alternatives.

Acknowledgements The experiments included in the present paper comply with the current laws of the country in which they were performed. The authors wish to thank Dr. R. Coda (Ospedale Gradenigo, Torino), P. Chiodera and S. Squillaci (Ospedale di Esine, Brescia) and B. Frigerio (Ospedale di Saronno, Varese) for their help in providing tissue specimens and clinical data. This work was supported by grants from Ministry for Universities, Instruction and Research (MIUR) (ex 60% to MV and GB), Rome, and the Compagnia di San Paolo/FIRMS, Torino, Italy.

References

1. Albores-Saavedra J, Wu J, Crook T, Amirkhan RH, Jones L, Hruban RH (2005) Intestinal and oncocytic variants of pancreatic intraepithelial neoplasia. A morphological and immunohistochemical study. Ann Diagn Pathol 9:69–76
2. Baloch ZW, LiVolsi VA (1999) Oncocytic lesions of the neuroendocrine system. Semin Diagn Pathol 16:190–199
3. Bartlett AS, Deo S, Oosthuysen W, Krishna G (2004) Oncocytic mucinous cystadenoma of the pancreas. Pathology 36:286–288
4. Bondeson L, Bondeson AG, Grimelius L, Kjellstrom U (1990) Oncocytic tumour of the pancreas. Report of a case with aspiration cytology. Acta Cytol 34:425–428
5. Bordi C, Yu JY, Baggi MT, Davoli C, Pilato FP, Baruzzi G, Gardini G, Zamboni G, Franzin G, Papotti M et al (1991) Gastric carcinoids and their precursor lesions. A histologic and immunohistochemical study of 23 cases. Cancer 67:663–672
6. Bordi C, Falchetti A, Azzoni C, D'Adda T, Canavese G, Guariglia A, Santini D, Tomassetti P, Brandi ML (1997) Aggressive forms of gastric neuroendocrine tumors in multiple endocrine neoplasia type I. Am J Surg Pathol 21:1075–1082
7. Bussolati G, Gugliotta P, Volante M, Pace M, Papotti M (1997) Retrieved endogenous biotin: a novel marker and a potential pitfall in diagnostic immunohistochemistry. Histopathology 31:400–407
8. Carstens PH, Cressman FK Jr (1989) Malignant oncocytic carcinoid of the pancreas. Ultrastruct Pathol 13:69–75
9. Chetty R, Asa SL (2004) Pancreatic endocrine tumour with cytoplasmic keratin whorls. Is the term rhabdoid appropriate? J Clin Pathol 57:1106–1110
10. Chetty R, Kennedy M, Ezzat S, Asa SL (2004) Pancreatic endocrine pathology in von Hippel–Lindau disease: an expanding spectrum of lesions. Endocr Pathol 15:141–148
11. DeLellis RA, Lloyd RV, Heitz PU (eds) (2004) WHO classification of tumours. Pathology and genetics, tumours of endocrine organs, chapter 4. IARC, Lyon
12. Erickson LA, Jin L, Papotti M, Lloyd RV (2002) Oxyphil parathyroid carcinomas: a clinicopathologic and immunohistochemical study of 10 cases. Am J Surg Pathol 26:344–349
13. Faure-Vigny H, Heddi A, Giraud S, Chautard D, Stepien G (1996) Expression of oxidative phosphorylation genes in renal tumours and tumoral cell lines. Mol Carcinog 16:165–172
14. Ghadially FN, Block HJ (1985) Oncocytic carcinoid of the lung. J Submicrosc Cytol 17:435–442
15. Gotchall J, Traweek ST, Stenzel P (1987) Benign oncocytic endocrine tumour of the pancreas in a patient with polyarteritis nodosa. Hum Pathol 18:967–969
16. Harach HR, Bergholm U (1988) Medullary (C cell) carcinoma of the thyroid with features of follicular oxyphilic cell tumours. Histopathology 13:645–656
17. Hoorens A, Gebhard F, Kraft K, Lemoine NR, Kloppel G (1994) Pancreatoblastoma in an adult: its separation from acinar cell carcinoma. Virchows Arch 424:485–490
18. Hua C, Shu XK, Lei C (1996) Pancreatoblastoma: a histochemical and immunohistochemical analysis. J Clin Pathol 49:952–954
19. Huntrakoon M (1983) Oncocytic carcinoma of the pancreas. Cancer 51:332–336
20. Jyotheeswaran S, Zotalis G, Penmetsa P, Levea CM, Schoeniger LO, Shah AN (1998) A newly recognized entity: intraductal "oncocytic" papillary neoplasm of the pancreas. Am J Gastroenterol 93:2539–2543
21. Kuwahara T, Maruyama K, Mochizuki S, Seki Y, Sawada K (1984) Oncocytic carcinoid of the lung. An ultrastructural observation. Acta Pathol Jpn 34:355–359
22. Maximo V, Soares P, Rocha AS, Sobrinho-Simoes M (1998) The common deletion of mitochondrial DNA is found in goitres and thyroid tumours with and without oxyphil cell changes. Ultrastruct Pathol 22:271–273
23. Maximo V, Botelho T, Capela J, Soares P, Lima J, Taveira A, Amaro T, Barbosa AP, Preto A, Harach HR, Williams D, Sobrinho-Simoes M (2005) Somatic and germline mutation in GRIM-19, a dual function gene involved in mitochondrial metabolism and cell death, is linked to mitochondrion-rich (Hurthle cell) tumours of the thyroid. Br J Cancer 92:1817–1818
24. Moran CA, Suster S (2000) Primary neuroendocrine carcinoma (thymic carcinoid) of the thymus with prominent oncocytic features: a clinicopathologic study of 22 cases. Mod Pathol 13:489–494
25. Muller-Hocker J (1992) Random cytochrome-*c*-oxidase deficiency of oxyphil cell nodules in the parathyroid gland. A mitochondrial cytopathy related to cell ageing? Pathol Res Pract 188:701–706
26. Muller-Hocker J, Jacob U, Seibel P (1998) Hashimoto thyroiditis is associated with defects of cytochrome-*c*-oxidase in oxyphil Ashkanazy cells and with the common deletion (4,977) of mitochondrial DNA. Ultrastruct Pathol 22:91–100
27. Nesland JM, Sobrinho-Simoes M, Holm R, Sambade MC, Johannessen JV (1985) Hürthle-cell lesions of the thyroid: a combined study using transmission electron microscopy, scanning electron microscopy, and immunocytochemistry. Ultrastruct Pathol 8:269–290
28. Nguyen-Ho P, Nguyen GK, Jewell LD (1994) Oncocytic neuroendocrine carcinoma of the pancreas. Report of a case with needle aspiration cytology, immunocytochemistry and electron microscopy. Acta Cytol 38:611–613
29. Nishioka H, Ito H, Hirano A (1999) Immunohistochemical demonstration of oncocytes in nongonadotrophic pituitary adenomas. Virchows Arch 435:428–433
30. Niveiro M, Aranda FI, Paya A, Boix E, Peiro G, Pico A (2004) Oncocytic transformation in pituitary adenomas: immunohistochemical analyses of 65 cases. Arch Pathol Lab Med 128:776–780
31. Noji T, Kondo S, Hirano S, Ambo Y, Tanaka E, Katoh C, Tsukamoto E, Tamaki N, Katoh H (2002) Intraductal oncocytic papillary neoplasm of the pancreas shows strong positivity on FDG-PET. Int J Gastrointest Cancer 32:43–46
32. Nozawa Y, Abe M, Sakuma H, Ogata M, Haga J, Sakuma H, Wakasa H (1990) A case of pancreatic oncocytic tumour. Acta Pathol Jpn 40:367–370
33. Pacchioni D, Papotti M, Macri L, Forte G, Bussolati G (1996) Pancreatic oncocytic endocrine tumors. Cytologic features of two cases. Acta Cytol 40:742–746
34. Papotti M, Gugliotta P, Forte G, Bussolati G (1994) Immunocytochemical identification of oxyphilic mitochondrion-rich cells. Appl Immunohistochem 2:261–267
35. Papotti M, Cassoni P, Taraglio S, Bussolati G (1999) Oncocytic and oncocytoid tumours of the exocrine pancreas, liver, and gastrointestinal tract. Semin Diagn Pathol 16:126–134
36. Radi MJ, Fenoglio-Preiser CM, Chiffelle T (1985) Functioning oncocytic islet-cell carcinoma. Report of a case with electron-microscopic and immunohistochemical confirmation. Am J Surg Pathol 9:517–524
37. Sadoul JL, Saint-Paul MC, Hoffman P, Plazza M, Birtwisle Y, Freychet P, Loubiere R (1992) Malignant pancreatic oncocytoma. An unusual cause of organic hypoglycemia. J Endocrinol Invest 15:211–217
38. Sironi M (1993) Oncocytic tumour of the pancreas. Acta Cytol 37:113
39. Sobrinho-Simoes M, Nesland JM, Holm R, Sambade MC, Johannessen JV (1985) Hürthle cell and mitochondrion-rich papillary carcinomas of the thyroid gland: an ultrastructural and immunocytochemical study. Ultrastruct Pathol 8:131–142
40. Sobrinho-Simoes M, Maximo V, Castro IV, Fonseca E, Soares P, Garcia-Rostan G, Oliveira MC (2005) Hürthle (oncocytic) cell tumours of thyroid: etiopathogenesis, diagnosis and clinical significance. Int J Surg Pathol 13:29–35
41. Stanley RJ, DeSanto LW, Weiland LH (1986) Oncocytic and oncocytoid carcinoid tumours (well-differentiated neuroendocrine carcinomas) of the larynx. Arch Otolaryngol Head Neck Surg 112:529–535
42. Zerbi A, De Nardi P, Braga M, Radice F, Sironi M, Di Carlo V (1993) An oncocytic carcinoma of the pancreas with pulmonary and subcutaneous metastases. Pancreas 8:116–119

Virchows Arch (2006) 448: 552–560
DOI 10.1007/s00428-006-0157-x

ORIGINAL ARTICLE

Hiroki Mizukami · Nobuhisa Yajima
Ryuichi Wada · Kazuhito Matsumoto
Motohiro Kojima · Günter Klöppel
Soroku Yagihashi

Pancreatic malignant fibrous histiocytoma, inflammatory myofibroblastic tumor, and inflammatory pseudotumor related to autoimmune pancreatitis: characterization and differential diagnosis

Received: 24 November 2005 / Accepted: 10 January 2006 / Published online: 15 March 2006

Abstract Malignant fibrous histiocytoma (MFH) and inflammatory myofibroblastic tumor (IMT) are uncommon primary non-epithelial cell tumors of the pancreas. In addition, there are inflammatory pseudotumors (IPT) that may arise in the course of autoimmune pancreatitis (AIP). In the English language literature, only 24 cases of IMT and nine cases of MFH in the pancreas have been reported to date. We investigated three individual spindle cell tumors of the pancreas that were identified as MFH, IMT, and IPT, respectively, using immunohistochemical and molecular analysis. Both the MFH and the IMT, but not the IPT, showed nuclear p53 expression and mutations of the *p53* gene. The MFH and the IMT also had higher mitotic and Ki-67 (MIB-1) indexes than the IPT. The IPT was found to be a tumor-like case of AIP. Many IgG4-positive plasma cells, which are considered to be a feature of AIP, were found in all three tumors. It is concluded that in this series of spindle cell tumors of the pancreas, apart from immunohistochemical features, the demonstration of *p53* mutations may be helpful in distinguishing true neoplastic tumors from pseudotumors such as IPTs arising in the context of AIP.

H. Mizukami · N. Yajima · R. Wada · S. Yagihashi (✉)
Department of Pathology,
Hirosaki University School of Medicine,
Hirosaki 036-8562, Japan
e-mail: yagihashi@cc.hirosaki-u.ac.jp
Tel.: +81-172-395025
Fax: +81-172-395026

K. Matsumoto
Division of Surgical Pathology, National Hirosaki Hospital,
5 Zaifu-cho,Hirosaki 036-8562, Japan

M. Kojima · G. Klöppel
Department of Pathology, University of Kiel,
Kiel, Germany

Keywords Pancreatic tumor · Malignant fibrous histiocytoma · Inflammatory myofibroblastic tumor · Autoimmune pancreatitis · *p53* mutation

Introduction

Malignant tumors of the pancreas are mostly of epithelial origin, predominantly ductal adenocarcinomas. Non-epithelial malignant tumors of mesenchymal origin are extremely rare and account for only 0.6% of the cases [4, 25]. The most common among the latter are leiomyosarcomas, liposarcomas, neurogenic sarcomas (schwannomas or peripheral neuroectodermal tumors), and malignant lymphomas [25, 43]. These tumors may cause difficulties in the differential diagnosis, even after extensive immunohistochemical analysis [25, 43]. In particular, in tumors with a spindle cell pattern, it may be difficult to distinguish malignant fibrous histocytomas (MFH) (now often called myxofibrosarcomas [11]) from inflammatory myofibroblastic tumors (IMT) or inflammatory pseudotumors (IPT), but this distinction is crucial for predicting the prognosis and selecting the proper treatment [7, 11, 43].

In the pancreas, so far, only nine cases of MFH [1, 3, 12, 14, 23, 26, 27, 33, 46] and 24 cases of IMT [2, 8, 10, 17, 20, 24, 28, 31, 32, 34–36, 39, 41, 42, 44, 47, 48, 50, 52] have been reported in the English language literature. Furthermore, IPT and IMT have often been used synonymously [10, 48, 50], though they can differ in their pathogenesis [29, 30]. We recently encountered representative cases of primary MFH, IMT, and IPT. On these cases, we conducted immunohistochemical and gene mutational analyses which, we believe, provide valuable clues for the characterization of these tumors and important information for the differential diagnosis. We will also discuss the relation of IPT to autoimmune pancreatitis (AIP).

Patients' histories

Case 1

A 44-year-old woman was admitted to the hospital in May 2003 with a mass in the left upper abdomen and epigastralgia. She had a history of uterine cervical cancer (early stage) that had been successfully operated on 4 years earlier. Blood tests revealed mild anemia and slightly elevated levels of the tumor marker immune-suppressor acid protein (IAP) (521 μg/ml, normal <500 μg/ml). C-reactive protein (1.1, <0.3 mg/dl) was elevated, but immunoglobulins were not examined. Liver function tests and pancreatic enzymes were normal and there was no elevation in markers of cholestasis (alkaline phosphatase, bilirubin, etc). Ultrasonography (US), computed tomography (CT), and magnetic resonance imaging (MRI) revealed a tumor mass in the dorsal area of the stomach and enlarged peripancreatic and para-aortic lymph nodes. The latter lymph nodes appeared to obstruct the left ureter, causing hydronephrosis. Angiography results revealed that the tumor originated from the pancreas. A creatinine clearance test for 24 h showed dysfunction of the kidney. Administration of Ga-diethylenetriamine pentaacetic acid (DTPA) did not result in enhancement of the mass. A malignant pancreatic tumor with lymph node metastasis was diagnosed and the tumor and a lymph node were resected. However, as the tumor adhered firmly, radical resection was not achieved. After the operation, the patient received extensive chemotherapy. During a follow-up period of 20 months, there was no recurrence.

Case 2

A 64-year-old male was admitted to the hospital in October 1995 for left lower thoracic pain at inspiration and an abdominal mass in the left upper abdomen. His past history was not informative. A blood test revealed mild anemia and elevated serum amylase (269, 50~228 IU/l), elastase (470, 100–400 ng/dl), and IAP (739, <500 mg/ml). Liver function tests were normal, and there was no sign of bile duct stenosis. Immunoglobulin was not examined. US, CT, and MRI results revealed a well-circumscribed homogeneous mass originating in the pancreas body. After administration of Ga-DTPA, the area surrounding the mass was enhanced. Endoscopic retrograde pancreatography showed an irregular stricture of the pancreatic duct in the body. A pancreatic carcinoma was suspected and a resection of the tail and body of the pancreas was performed. No metastasis was found during operation. Five years after the operation, the patient is disease-free.

Case 3

A 40-year-old male was admitted to the hospital with epigastric pain and fever. He had been free of disease until this event. He had noticed thirst, polydipsia, and weight loss for the last 6 months and was found to have diabetes and acute hepatitis. Two months later, he developed jaundice, general fatigue, epigastric pain, and restlessness. He was referred to our hospital and diagnosed as having a pancreatic mass and acute obstructive cholangitis. Laboratory data revealed marked anemia, leukocytosis, elevated levels of bilirubin, bile tract markers, CA19-9 (41.3, <37 IU/ml), and serum ferritin (941, 25–280 ng/ml). Immunoglobulin was not examined. Abdominal ultrasound and CT results disclosed a large low-density mass in the head of the pancreas with diffuse swelling of the body. A diagnosis of pancreatic carcinoma was made clinically and a Whipple procedure was performed.

After the operation, the patient suffered from diabetes, which was controlled by insulin injection. However, 8 months after the operation, his general condition worsened and he died. An autopsy was not performed.

Materials and methods

Tissues

Specimens from the pancreatic tumors were fixed in 10% formalin and processed to obtain 4-μm paraffin sections that were stained with hematoxylin and eosin, Azan, silver, elastica van Gieson, periodic acid–Schiff , and alcian blue.

Immunohistochemistry

For immunohistochemistry, the standard streptavidin–biotin technique was applied. The list of antibodies used and their sources as well as staining conditions are summarized in Table 1. Negative control stains were performed by omitting the primary antibodies or substituting nonimmune rabbit or swine sera. The number of cells showing nuclear staining for p53 and Ki-67 (MIB-1) was determined in areas with high cellularity and recorded as the number of positive cells per 100 tumor cells.

Genetic analysis

For the detection of *p53* and *K-ras* mutations, genomic DNA was extracted from sections cut from paraffin-embedded tissue blocks. Briefly, the sections were depar-

Table 1 Antibody data and immunohistochemical results

Antibody	Source	Dilution	Case 1	Case 2	Case 3
Cytokeratin	DAKO	1:100[a]	(−)	(−)	(−)
EMA	DAKO	1:100	(−)	(−)	(−)
CD68	DAKO	1:100[a]	(−)	(−)	(−)
LCA	VENTANA	Kit	(−)	(−)	(−)
Vimentin	DAKO	1:100[a]	(+)	(+)	(+)
α-SMA	VENTANA	Kit	(−)	(+)	(+)
H-caldesmon	DAKO	1:100[a]	(−)	(−)	(−)
HHF35	DAKO	1:100	(−)	(−)	(+)
Desmin	DAKO	1:100	(−)	(−)	(−)
S100	VENTANA	Kit	(−)	(−)	(−)
CD34	VENTANA	Kit	(−)	(−)	(−)
C-kit	DAKO	1:50	(−)	(−)	(−)
CD23	Novocastra	1:40[a]	(−)	(−)	(−)
CD35	DAKO	1:200	(−)	(−)	(−)
CD30	DAKO	1:40[a]	(−)	(−)	(−)
ALK	DAKO	1:50[a]	(−)	(−)	(−)
p53	DAKO	1:100[a]	25%	9%	0%
MIB-1 index	Immunotech	1:200[a]	19%	7%	1%
IgG4	Bindingsite	1:1000[a]	(+)	(+)	(±)

[a]Antibody pretreatment by either microwave pretreatment for 3×5 min, autoclave pretreatment 120 °C for 5 min, or 0.05% pronase for 15 min

affinized with xylene, washed with 100% ethanol, and subsequently dried. Tumor tissue was scratched off the slides with a fine needle. DNA was extracted and purified with DNAeasy extraction kits (QIAGEN, Valencia, CA, USA). Polymerase chain reaction (PCR) was performed as previously described [37]. PCR Amplicon was ligated to the vector with a TOPO cloning kit (Invitrogen, Carlsbad, CA, USA). After blue–white selection, purified vector was digested with *Eco*RI. An about 100-bp insert clone was loaded onto a 3% agarose gel. The positive clone was amplified using a VIC dye sequence kit (Applied Biosystems, Foster City, CA, USA) and a purified Qiagen kit. Direct sequencing was carried out with a Perkin Elmer ABI Prism 310 sequence analyzer (Applied Biosystems).

Results

Pathological findings

Case 1

The left-sided pancreatectomy specimen contained a well-encapsulated, light yellowish firm mass measuring 8.3×5.6×6.0 cm (Fig. 1a). Microscopic spindle- to oval-shaped tumor cells mixed with variable numbers of polymorphic or multinucleated giant cells were arranged in a storiform pattern (Fig. 2a). There were some areas with high cellularity, and atypical mitoses were also seen. Lymphocytes, plasma cells, and eosinophils infiltrated within the tumor area (Fig. 2b). There were areas of stromal myxoid changes, but no necrosis or hemorrhage was found. The resected lymph node revealed a metastasis of the pancreatic tumor.

Case 2

The left-sided pancreatectomy specimen contained a light yellowish firm mass in the pancreatic body measuring 10.0×9.0×8.5 cm (Fig. 1b). The tumor consisted of mainly

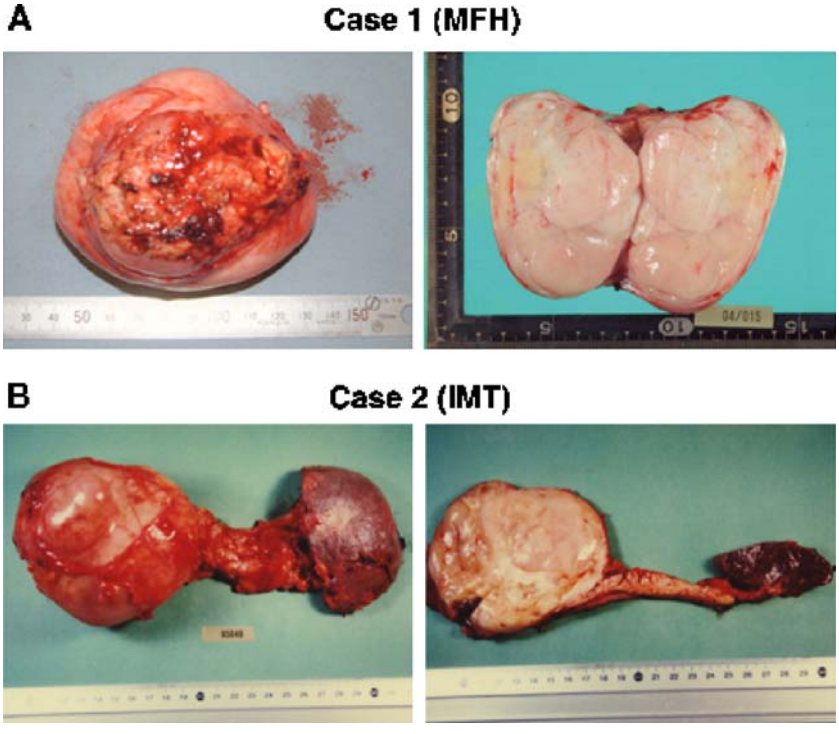

Fig. 1 Macroscopic appearances of pancreatic MFH (case 1) (**a**) and IMT (case 2) (**b**). Both tumors show large expansive masses with a fibrous capsule. On cut surface, they are multinodular and whitish with some yellow areas

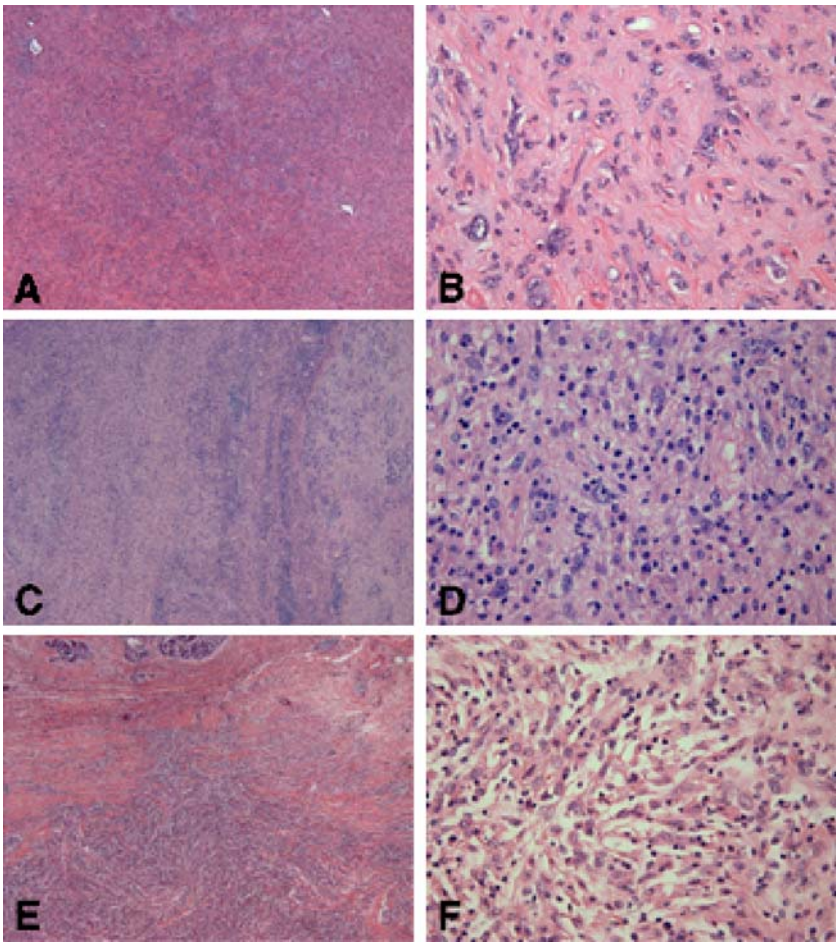

Fig. 2 Light microscopic appearances of pancreatic MFH (case 1), IMT (case 2), and IPT (case 3). Case 1: the low power view shows a diffuse eosinophilic fibrous area mixed with sporadic lymphoid aggregates (**a**). The high power view shows haphazardly oriented large pleomorphic cells with a typical storiform-like growth pattern (**b**). Case 2: the low power view shows conspicuous inflammatory changes occupying a large area (**c**). Some atrophic exocrine tissues are visible. The high power view reveals spindle cells admixed with eosinophilic and lymphoid cells (**d**). Case 3: the low power view shows a large inflammatory area with marked proliferation of spindle cells adjacent to atrophic exocrine tissues (**e**). In the high power view, spindle cells show nuclear enlargement and pleomorphism growing with a typical storiform pattern mixed with inflammatory cells (**f**)

microscopic spindle- to oval-shaped cells arranged in a storiform pattern. There were scattered polymorphic or multinucleated cells (Fig. 2c,d), but nuclear polymorphism was less than in case 1. Mitoses were not found. The stroma was rich in collagen, and there was extensive lymphoplasmacytic infiltration.

Case 3

The Whipple resection specimen contained a mass 7.5×3.6×2.0 cm in size in the head of the pancreas. The tumor had a hard consistency and its cut surface was solid, lobulated, and relatively well circumscribed. The normal pancreatic tissue was replaced by a meshwork of microscopic spindle-shaped fibroblastic cells arranged in a storiform pattern and some foamy histiocytes (Fig. 2e). The spindle cells showed nuclear enlargement and hyperchromatism (Fig. 2f). Mitoses were not found. Detailed examinations of the tumor and its surrounding pancreatic tissue revealed features of autoimmune pancreatitis, such as periductal lymphoplasmacytic infiltration or venulitis. The lymphoplasmacytic infiltration extended into the pancreatic parenchyma, replacing most of the acinar cells

Table 2 Clinicopathological features of the three tumors

	Case 1	Case 2	Case 3
Size (cm)	8.3×5.6×6.0	10.0×9.0×8.5	7.5×3.6×2.0
Location	Body~tail	Body	Head~body
Metastasis	Para-aortic lymph nodes	No evidence	No evidence
Complication	lt. hydronephrosis	Mass and abdominal pain	Jaundice
Inflammation	± (background) (plasma cells, lymphocytes, eosinophils, etc.)	++ (diffuse) (plasma cells, lymphocytes, eosinophils, etc.)	+++ (widespread) (plasma cells, lymphocytes, eosinophils, etc.) venulitis
Major histological pattern	Pleomorphic, storiform	Pleomorphic, storiform	Storiform
Mitotic index	26/50HPF	0/50HPF	0/50HPF

lt left, *HPF* high power field

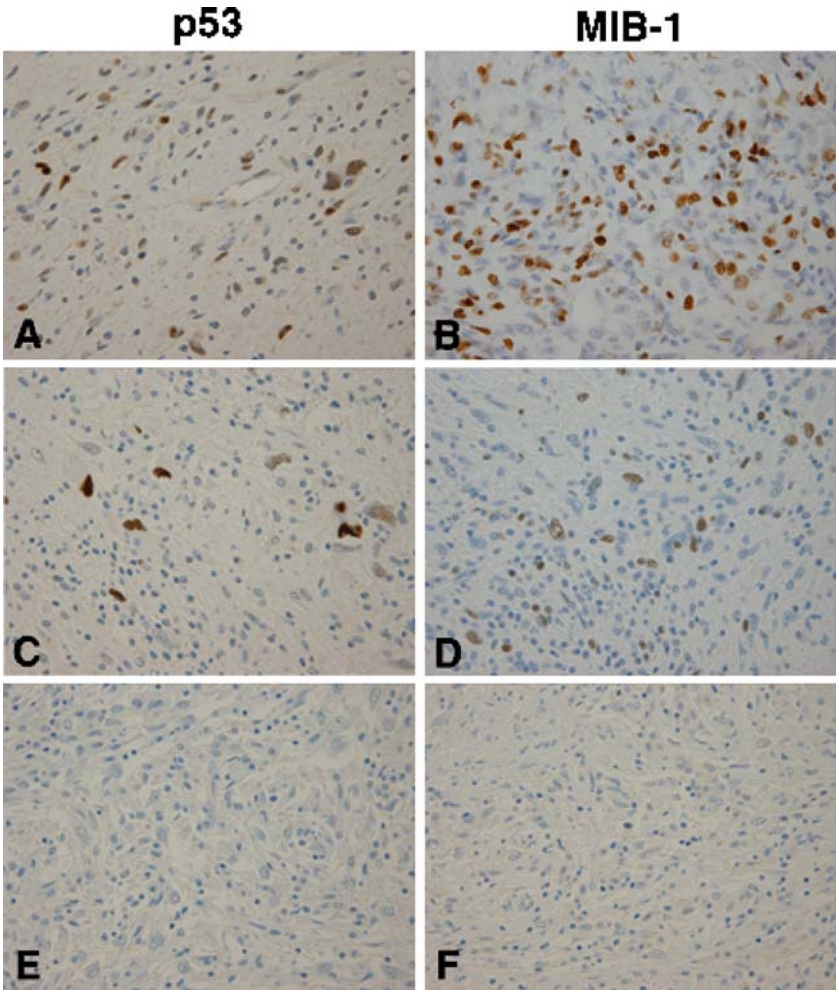

Fig. 3 p53 and MIB-1 expression in pancreatic MFH (case 1), IMT (case 2), and IPT (case 3). Case 1: large pleomorphic tumor cells show positive reactions to p53 at a level of 25% (**a**). They also show a high level (19%) of MIB-1 expression (**b**). Case 2: similar to Case 1, the tumor cells show strong p53 positivity in some areas reaching 9% (**c**). They also show high MIB-1 index up to 7% level, but the reaction is less intense compared to case 1 (**d**). Case 3: in contrast to the above cases, p53 is negative (**e**). The MIB-1 index is also very low (<1%) (**f**)

and encasing medium-sized ducts. Mild inflammatory changes were also seen in the bile duct wall, the gallbladder, and the ampulla of Vater.

All clinicopathological features are summarized in Table 2.

Immunohistochemistry

Table 1 summarizes the immunohistochemical results. In case 1, spindle cells and pleomorphic cells showing a storiform pattern were positive for vimentin but negative for epithelial, muscle, neural, adipocytic, or lymphoma markers as well as anaplastic lymphoma kinase (ALK) and

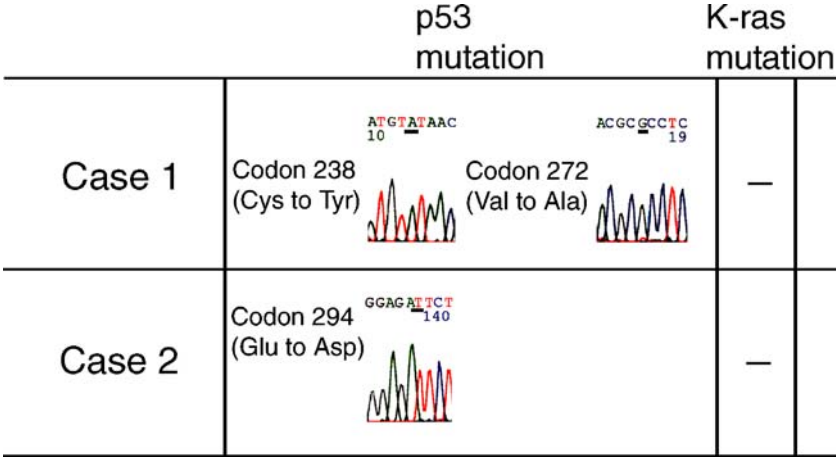

Fig. 4 Direct sequencing of the *p53* gene. In case 1, there are two point mutations at codon 238 and 272. In case 2, a point mutation at codon 294 is detected

Table 3 Cases of pancreatic malignant fibrous histiocytoma reported in the English literature[a]

	Author	Year	Age/sex	Location	Size (cm)	Major histology	Metastasis	Outcome
1	Margules et al.	1976	22/F	Head	10	Myxoid	Duodenum	Alive for 17 months
2	Suster et al.	1989	71/M	Head	5	Giant cell		ND
3	Pascal et al.	1989	39/F	Head	9×8×6	SP		Dead after 1 month
4	Garvey et al.	1989	77/M	Head	12.5×10×6	SP		Alive for 4 years
5	Allen et al.	1990	46/M	Body–tail	15×9×6	Pleomorphic	Liver	Dead after 5 months
6	Haba et al.	1996	70/M	Head	9×7×6.5	Myxoid and SP	None	NED for 22 months
7	Liu et al.	1999	27/F	Body–tail	8×10	Myxoid		NED for 6 months
8	Bastian et al.	1999	67/M	Body	5.2×6.0×5.5	Storiform	Lymph node	NED for 34 months
9	Mai G et al.	2003	71/F	Body	6×5×5	Giant cell		Dead after 24 months
10	Mizukami et al.	2005	44/F	Body–tail	8.3×5.6×6.0	SP	Lymph node	Alive for 20 months

SP Storiform–pleomorphic, *ND* not described, *NED* no evidence of death
[a]Cases accompanied with mucinous cystic tumors are excluded

CD34. Between the tumor cells, there were CD68 positive macrophages. The tumor cells showed frequently positive for p53 to an extent of 25% level (Fig. 3a). The MIB-1 index of the tumor cells was 19% of the cells (Fig. 3b). In case 2, the spindle cells were also positive for vimentin and negative for epithelial, neural, and lymphoma markers, including ALK and follicular dendritic cell markers. Single spindle cells were positive for smooth muscle actin (SMA) and HHF35 but negative for CD34. They were positive for p53 at a level of 9% and the MIB-1 index was 7% of the cells (Fig. 3c,d). CD68 positive macrophages were present. In case 3, the spindle cells were positive for vimentin but negative for CD34, cytokeratin, EMA, S-100, myoglobin, or desmin. P53 was negative (Fig. 3e). The MIB-1 index was less than 1% (Fig. 3f).

Scattered IgG4-positive plasma cells were consistently detected in all three cases but most conspicuous in case 3.

Genetic analysis

Because nuclear p53 expression was found in cases 1 and 2, direct DNA sequencing for *p53* exon 5–8 was carried out (Fig. 4). In case 1, two point mutations were detected: G-to-A transversion at codon 238, resulting in an amino acid change from cysteine to tyrosine, and T-to-C transversion at codon 272, resulting in an amino acid change from valine to alanine. In case 2, one point mutation was found, G-to-T transversion at codon 294, resulting in an amino acid change from glutamate to asparatate. On the other hand, the tumors in both cases 1 and 2 carried a wild-type *K-ras* oncogene.

Discussion

In this study, we analyzed the immunohistochemical and molecular features of three pancreatic tumors that shared a microscopic spindle-cell pattern with abundant collagen production admixed with inflammatory cells. This analysis revealed that individual features of the three tumors allowed them to be typed as MFH, IMT, and AIP-associated IPT.

The first step in the investigation of these tumors was to distinguish them from undifferentiated carcinomas, which may show a sarcomatoid pattern [16, 43]. As our tumors were negative for cytokeratin, this possibility could be easily excluded. The next tumor to be ruled out was a sarcomatous nodule in association with a mucinous cystic neoplasm [49, 53]. We, therefore, examined multiple sections but failed to find any evidence of a cystic lesion. The diagnoses we finally considered were MFH, IMT, and IPT.

The diagnosis of MFH, which was made in the first patient, was based on the tumor's microscopic features (i.e., anaplastic spindle cells arranged in a storiform pattern), its sole positivity for vimentin, and the immunohistochemical exclusion of any other tumor, such as malignant peripheral nerve sheath tumor, by the negativity for the respective tumor markers. So far, only nine cases of MFH of pancreatic origin have been reported [1, 3, 12, 14, 23, 26, 27, 33, 46] (Table 3). A review of these cases revealed that their features compare well with those of our case. In addition, we detected nuclear p53 expression and a *p53* mutation. This finding is in accordance with the 35% positivity rate for nuclear p53 expression recently reported in MFHs of various origins [9]. In our case, the demonstration of a *p53* mutation clearly established the neoplastic nature of the tumor and distinguished it from any non-neoplastic pseudotumor.

In the second patient, we diagnosed an IMT. This is a low-grade tumor composed of fibroblasts and myofibroblasts in association with inflammatory cells, whose molecular pathogenesis was partially elucidated recently. In approximately 50% of IMTs, various gene aberrations including the anaplastic lymphoma kinase gene at chromosome 2p23 have been identified [13, 15, 32, 38, 45]. In our case, no ALK gene abnormality was found. However,

Table 4 Cases of pancreatic IPT or IMT reported in the English literature

Author, year	Age/ sex	Size (cm)	Location	Outcome	Major symptom	Features suggesting IMT or AIP
Haith et al. 1964	6/M	3	Head	2 M	Jaundice	
Johnson et al. 1983	29/F	10	Head	1 Y, recurrence (+)	Abdominal pain	
Abrebanel et al. 1984	12/F	12×10×6	Body	2 Y	Abdominal mass, pain	Phlebitis
Scott et al. 1988	2.5/F	13×10×7	Body	6 M<	Fever, abdominal mass	
Stringer et al. 1992	5/F	7×4×4	Head	9 M	Fever, abdominal pain	
Dudiak et al. 1993	45/M	No mass	Body–tail	NA	Abdominal pain	
Palazzo et al. 1993	52/F	3×4	Tail	6 M	Fever, abdominal pain	Arthritis
Uzoaru et al. 1993	8/F	No mass	Head	1 Y	Jaundice	
Purdy et al. 1994	23/F	1.5×6.0	Head	NA	NA	
Eckstein et al. 1995	65/F	No mass	Head	4 Y	Chest and back pain	Sjögren's syndrome, elevated gamma globulin
Kroft et al. 1995	42/F	7×6×4	Body	6 M	Back pain	
Dine et al. 1997	29/M	11×5	Tail	5 M	Abdominal mass	
Morris-Stift et al. 1998	11/M	10×10×7	Body–tail	3 Y	Lethargy	IgG elevation
Petter et al. 1998	64/M	5.0×4.0×3.5	Head	4 Y	Jaundice	Periductal lymphoplasmacytic infiltrate
Shankar et al. 1998	8/F	10.7×9.9×9.4	Body–tail	2 Y	Abdominal mass, pain	
Walsh et al. 1998	35/M	5×4×3	Head	8 Y	Jaundice, abdominal pain	Phlebitis, vasculitis, chronic sialadenitis
McClain et al. 2000	11/F	3.2×1.6×3.4	Head	NA	Jaundice, abdominal pain	
Liu et al. 2000	54/F	5.0×4.5×2.5	Head	2 Y	Abdominal pain	
Slavotinek et al. 2000	4/F	3×3	Head	4 Y	Jaundice, malaise	
Wresman et al. 2001	62/M	3	Head	6 Y	Jaundice	Phlebitis
Wresman et al. 2001	56/M	NA	Head	5 Y	Jaundice, diabetes	Phlebitis
Wresman et al. 2001	50/M	5	Head	4 Y	Jaundice, pain	Phlebitis
Wresman et al. 2001	57/F	NA	Head	3 Y	Jaundice	Phlebitis
Wresman et al. 2001	45/M	No mass	Head	10 Y	Jaundice, diabetes	Phlebitis
Wresman et al. 2001	32 / F	2.5	Head	12 Y	Abdominal pain	Phlebitis
Yamamoto et al. 2002	55/M	1.5	Head	28 M	Abdominal mass, diabetes	
Esposito et al. 2004	69/M	NA	Body–tail	7 M, died of sepsis	Abdominal pain	Phlebitis, arteritis, elevated IgG, periductal fibrosis
Pungpapong et al. 2004	70/M	3.8	Tail	10 M	Abdominal pain	
Nakamura et al. 2005	29/F	6×5	Head	1 Y	Abdominal mass, diabetes	
Mizukami et al.	64/M	10×9×8.5	Body	5 Y	Abdominal mass, pain	IgG4(+) cells
Mizukami et al.	40/M	7.5×3.6×2.0	Head	8 M, dead	Abdominal pain, jaundice	Phlebitis, IgG4(+) cells

IPT Inflammatory pseudotumor, *IMT* inflammatory myofibroblastic tumor, *AIP* autoimmune pancreatitis, *NA* not available, (sex) *F* female, *M* male, (follow-up) *M* months, *Y* years

an ALK gene abnormality is more often seen in children or young adults than in elderly people. This may explain why we did not detect an ALK gene abnormality in our case [6, 22]. The diagnosis of an IMT was, therefore, based on the microscopic diagnostic criteria such as fasciitis-like, fascicular, and sclerosing areas with a prominent chronic inflammatory infiltrate. In addition, we found nuclear p53

expression and a *p53* mutation, findings that have also been reported in IMTs [51].

In the third patient, the tumor expressed neither SMA, S100 and CD34 nor nuclear p53. Together with its histological features, we concluded that the tumor represented an IPT. IPTs that arise in the course of AIP must be clearly distinguished from MFHs or IMTs, considering their different pathogenesis and therapy (i.e., its treatment with steroids). However, many previous reports of IMTs in the pancreas did not give any consideration to IPTs arising in the course of AIP (Table 4). Judging from the published illustrations and the descriptions, we believe that many previous cases of IMTs and IPTs arose in the setting of AIP [2, 8, 10, 17, 19, 20, 24, 28, 31, 32, 34–36, 39, 41, 42, 44, 47, 48, 50, 52] (see Table 4).

IMTs and IPTs associated with AIP have many clinicopathological features in common. First, both are mass-forming lesions which commonly focus on the pancreas head and cause obstructive jaundice. Therefore, such patients are often suspected to suffer from pancreatic ductal adenocarcinoma [18, 19]. Second, involvement of the distal bile duct, as reported in many IMTs, is a common finding in patients with AIP [18, 19]. Third, a lymphoplasmacytic infiltrate and myofibroblasts arranged in a storiform pattern are seen in both lesions [10, 26, 48, 50].

It has been reported that IgG4-positive plasma cells are abundant in AIP which help to establish its diagnosis [18, 54]. In this study, the demonstration of IgG4-positive plasma cells was not useful for the differential diagnosis as these cells were also found in both the MFH and the IMT. Nevertheless, constant presence of IgG4 cells in these tumors might indicate non-incidental occurrence of mesenchymal tumors with background of AIP.

In summary, we report three cases of tumorous spindle cell lesions of the pancreas, two of which were found to be neoplasms and the other an inflammatory process. p53 expression and gene mutation provided an important clue for distinguishing the two true neoplasms from the pseudotumor.

References

1. Allen KB, Skandalakis LJ, Brown BC, Gray SW, Skandalakis JE (1990) Malignant fibrous histiocytoma of the pancreas. Am Surg 56:364–368
2. Abrebanel P, Sarfaty S, Gal R, Chaimoff C, Kessler E (1984) Plasma cell granuloma of the pancreas. Arch Pathol Lab Med 108:531–532
3. Bastian D, Ramaswamy A, Barth PJ, Gerdes B, Ernst M, Bartsch D (1999) Malignant fibrous histiocytoma of the pancreas: a case report with genetic analysis. Cancer 85:2352–2358
4. Baylor SM, Berg JW (1973) Cross-classification and survival. Characteristics of 5,000 cases of cancer of the pancreas. J Surg Oncol 5:335–358
5. Chutaputti A, Burrell NI, Boyer J (1995) Pseudotumor of the pancreas associated with retroperitoneal fibrosis: a dramatic response to corticosteroid therapy. Am J Gastroenterol 90:1155–1158
6. Coffin CM, Patel A, Perkins S, Elenitoba-Johnson KS, Perlman E, Griffin CA (2001) ALK1 and p80 expression and chromosomal rearrangements involving 2p23 in inflammatory myofibroblastic tumor. Mod Pathol 14:569–576
7. Dehner LP (2004) Inflammatory myofibroblastic tumor. The continued definition of one type of so-called inflammatory pseudotumor. Am J Surg Pathol 28:1652–1654
8. Dudiak KM (1993) Inflammatory pseudotumor of the pancreas. Am J Roentgenol 160:1324–1325
9. Engellau J, Persson A, Bendahl PO, Akerman M, Domanski HA, Bjerkehagen B,Lilleng P, Weide J, Rydholm A, Alvegard TA, Nilbert M (2004) Expression profiling using tissue microarray in 211 malignant fibrous histiocytomas confirms the prognostic value of Ki-67. Virchows Arch 445:224–230
10. Esposito I, Bergmann F, Penzel R, di Mola FF, Shrikhande S, Büchler MW, Friess H, Otto HF (2004) Oligoclonal T-cell populations in an inflammatory pseudotumor of the pancreas possibly related to autoimmune pancreatitis: an immunohistochemical and molecule analysis. Virchows Arch 444:119–126
11. Fletcher CD (1992) Pleomorphic malignant fibrous histiocytoma: fact or fiction? A critical reappraisal based on 159 tumors diagnosed as pleomorphic sarcoma. Am J Surg Pathol 16: 213–228
12. Garvey JF, Ng A, England JF, Sheldon DM (1989) Malignant fibrous histiocytoma of the pancreas. HPB Surg 1:233–237
13. Griffin CA, Hawkins AL, Dvorak C, Henkle C, Ellingham T, Perlman EJ (1999) Recurrent involvement of 2p23 in inflammatory myofibroblastic tumors. Cancer Res 59:2776–2780
14. Haba R, Kobayashi S, Hirakawa E, Miki H, Okino T, Kurokawa T, Yamamoto S (1996) Malignant fibrous histiocytoma of the pancreas. Pathol Int 46:515–519
15. Hojo H, Newton Jr WA, Hamoudi AB, Qualman SJ, Wakasa H, Suzuki S, Jaynes F (1995) Pseudosarcomatous myofibroblastic tumor of the urinary bladder in children: a study of 11 cases with review of the literature. An Intergroup Rhabdomyosarcoma Study. Am J Surg Pathol 19:1224–1236
16. Hoorens A, Prenzel K, Lemoine NR, Klöppel G (1998) Undifferentiated carcinoma of the pancreas: analysis of intermediate filament profile and K-ras mutations provides evidence of a ductal origin. J Pathol 185:53–60
17. Johnson RL, Page DL, Dean RH (1983) Pseudotumor of the pancreas. South Med J 76:647–649
18. Kamisawa T, Funata N, Hayashi Y, Eishi Y, Koike M, Tsuruta K, Okamoto A, Egawa N, Nakajima H (2003) A new clinicopathological entity of IgG4-related autoimmune disease. J Gastroenterol 38:982–984
19. Klöppel G, Lüttges J, Löhr M, Zamboni G, Longnecker D (2003) Autoimmune pancreatitis: pathological, clinical, and immunological features. Pancreas 27:14–19
20. Kroft SH, Stryker SJ, Winter JN, Ergun G, Rao MS (1995) Inflammatory pseudotumor of the pancreas. Int J Pancreatol 18:277–283
21. Kutok JL, Pinkus GS, Dorfman DM, Fletcher CD (2001) Inflammatory pseudotumor of lymph node and spleen: an entity biologically distinct from inflammatory myofibroblastic tumor. Hum Pathol 32:1382–1387
22. Lawrence B, Perez-Atayde A, Hibbard MK, Rubin BP, Dal Cin P, Pinkus JL, Pinkus GS, Xiao S, Yi ES, Fletcher CD, Fletcher JA (2000) TPM3-ALK and TPM4-ALK oncogenes in inflammatory myofibroblastic tumors. Am J Pathol 157:377–384
23. Liu DM, Jeffrey RB, Mindelzun RE (1999) Malignant fibrous histiocytoma presenting as cystic pancreatic mass. Abdom Imaging 24:299–300
24. Liu TH, Consorti ET (2000) Inflammatory pseudotumor presenting as a cystic tumor of the pancreas. Am Surg 66:993–997
25. Lüttges J, Pierre E, Zamboni G, Weh G, Lietz H, Kussmann J, Klöppel G (1997) Malignant non-epithelial tumors of the pancreas. Pathologe 18:233–237
26. Mai G, Baer HU, Mittler M, Uhl W, Buchler MW, Rodriguez RU, Ruchti C (2002) Malignant fibrous histiocytoma of the pancreas. Pancreas 25:320–324

27. Margules RM, Allen RE, Dunphy JE (1976) Pancreatic tumor of mesenchymal origin presenting as obstructive jaundice. Am J Surg 131:357–359
28. McClain MB, Burton EM, Day DS (2000) Pancreatic pseudotumor in an 11-year-old child: imaging findings. Pediatr Radiol 30:610–613
29. Meis-Kindblom JM, Kjellstrom C, Kindblom LG (1998) Inflammatory fibrosarcoma: update, reappraisal, and perspective on its place in the spectrum of inflammatory myofibroblastic tumors. Semin Diagn Pathol 15:133–143
30. Meis JM, Enzinger FM (1991) Inflammatory fibrosarcoma of the mesentery and retroperitoneum. A tumor closely simulating inflammatory pseudotumor. Am J Surg Pathol 15:1146–1156
31. Morris-Stiff G, Vujanic GM, Al-Wafi A, Lari J (1998) Pancreatic inflammatory pseudotumour: an uncommon childhood lesion mimicking a malignant tumor. Pediatr Surg Int 13:52–54
32. Palazzo JP, Chang CD (1993) Inflammatory pseudotumor of the pancreas. Histopathology 23:475–477
33. Pascal RR, Sullivan L, Hauser L, Ferzli G (1989) Primary malignant fibrous histiocytoma of the pancreas. Hum Pathol 20:1215–1217
34. Petter LM, Martin JK Jr, Menke DM (1998) Localized lymphoplasmacellular pancreatitis forming a pancreatic inflammatory pseudotumor. Mayo Clin Proc 73:447–450
35. Pungpapong S, Geiger XJ, Raimondo M (2004) Inflammatory myofibroblastic tumor presenting as a pancreatic mass: a case. JOP 5:360–367
36. Qanadli SD, d'Anthouard F, Cugnec JP, Frija G (1997) Plasma cell granuloma of the pancreas: CT finding. J Comput Assist Tomogr 21:735–736
37. Scarpa A, Capelli P, Mukai K, Zamboni G, Oda T, Iacono C, Hirohashi S (1993) Pancreatic adenocarcinomas frequently show *p53* gene mutations. Am J Pathol 142:1534–1543
38. Sciot R, Dal Cin P, Fletcher CD, Hernandez JM, Garcia JL, Samson I, Ramos L, Brys P, Van Damme B, Van den Berghe H (1997) Inflammatory myofibroblastic tumor of bone: report of two cases with evidenceof clonal chromosomal changes. Am J Surg Pathol 21:1166–1172
39. Scott L, Blair G, Taylor G, Dimmick J, Fraser G (1988) Inflammatory pseudotumors in children. J Pediatr Surg 23: 755–758
40. Scully RE, Mark EJ, McNeely BU (1982) Weekly clinicopathological exercises. Case 6-1982. N Engl J Med 306: 349–358
41. Shankar KR, Losty PD, Khine MM, Lamont GL, McDowell HP (1998) Pancreatic inflammatory tumour: a rare entity in childhood. J R Coll Surg Edinb 43:422–423
42. Slavotinek JP, Bourne AJ, Sage MR, Freeman JK (2000) Inflammatory pseudotumour of the pancreas in a child. Pediatr Radiol 30:801–803
43. Solcia E, Capella C, Klöppel G (1997) Atlas of tumor pathology. Tumors of pancreas. AFIP series #20, Washington, DC, pp 211–213
44. Stringer MD, Ramani P, Yeung CK, Capps SN, Kiely EM, Spitz L (1992) Abdominal inflammatory myofibroblastic tumours in children. Br J Surg 79:1357–1360
45. Su LD, Atayde-Perez A, Sheldon S, Fletcher JA, Weiss SW (1998) Inflammatory myofibroblastic tumor: cytogenetic evidence supporting clonal origin. Mod Pathol 11:364–368
46. Suster S, Philipps M, Robinson MJ (1989) Malignant fibrous histiocytoma (giant cell type) of the pancreas. Cancer 64: 2303–2308
47. Uzoaru I, Chou P, Reyes-Mugica M, Shen-Schwarz S, Gonzalez-Crussi F (1993) Inflammatory myofibroblastic tumor of the pancreas. Surg Pathol 5:181–188
48. Walsh SV, Evangelista F, Khettry U (1998) Inflammatory myofibroblastic tumor of the pancreaticobiliary region: morphologic and immunocytochemical study of three cases. Am J Surg Pathol 22:412–418
49. Wilentz RE, Albores-Saavedra J, Hruban RH (2000) Mucinous cystic neoplasms of the pancreas. Semin Diagn Pathol 17: 31–42
50. Wreesmann V, van Eijck CH, Naus DC, van Velthuysen ML, Jeekel J, Mooi WJ (2001) Inflammatory pseudotumour (inflammatory myofibroblastic tumour) of the pancreas: a report of six cases associated with obliterative phlebitis. Histopathology 38:105–110
51. Yamamoto H, Oda Y, Saito T, Sakamoto A, Miyajima K, Tamiya S, Tsuneyoshi M (2003) p53 mutation and MDM2 amplification in inflammatory myofibroblastic tumours. Histopathology 42:431–439
52. Yamamoto H, Watanabe K, Nagata M, Tasaki K, Honda I, Watanabe S, Soda H, Takenouti T (2002) Inflammatory myofibroblastic tumor (IMT) of the pancreas. J Hepatobiliary Pancreat Surg 9:116–119
53. Zamboni G, Scarpa A, Bogina G, Iacono C, Bassi C, Talamini G, Sessa F, Capella C, Solcia E, Rickaert F, Mariuzzi GM, Klöppel G (1999) Mucinous cystic tumors of the pancreas: clinicopathological features, prognosis, and relationship to other mucinous cystic tumors. Am J Surg Pathol 23:410–422
54. Zen Y, Harada K, Sasaki M, Sato Y, Tsuneyama K, Haratake J, Kurumaya H, Katayanagi K, Masuda S, Niwa H, Morimoto H, Miwa A, Uchiyama A, Portmann BC, Nakanuma Y (2004) IgG4-related sclerosing cholangitis with and without hepatic inflammatory–pseudotumor, and sclerosing pancreatitis-associated sclerosing cholangitis: do they belong to a spectrum of sclerosing pancreatitis? Am J Surg Pathol 28:1193–1203

Virchows Arch (2006) 448: 561–569
DOI 10.1007/s00428-006-0174-9

ORIGINAL ARTICLE

Yu Takahashi · Nobuyoshi Hiraoka · Kaoru Onozato · Tatsuhiro Shibata · Tomoo Kosuge · Yuji Nimura · Yae Kanai · Setsuo Hirohashi

Solid–pseudopapillary neoplasms of the pancreas in men and women: do they differ?

Received: 9 January 2006 / Accepted: 6 February 2006 / Published online: 8 March 2006

Abstract Solid–pseudopapillary neoplasms (SPNs) of the pancreas are uncommon and occur preferentially in young women. The question whether the features of SPNs occurring in men differ from those in women has not yet been studied. For a better understanding of the clinicopathological features of SPNs of both sexes, we studied a series of 14 tumors surgically resected at a Japanese hospital within a period of 14 years. This series was composed of seven men and seven women. All these SPNs demonstrated nuclear and cytoplasmic accumulation of β-catenin protein in immunohistochemistry and 86% of them had activating mutations of β-catenin gene. No pancreatic neuroendocrine tumors showed such immunohistochemical findings and genetic alterations. In our series, most SPNs in women showed encapsulation by thick fibrous tissue and massive degenerative changes. Most SPNs in men exhibited solid components without prominent degenerative changes, even though they were of a similar size to those in women. These findings suggest that SPNs in men tend to be a solid mass with slower progression of degenerative changes during their growth compared to that in women. Nuclear accumulation of β-catenin appears to be a useful marker of SPN, which allows male SPNs to be correctly diagnosed despite their less typical features.

Y. Takahashi · N. Hiraoka · K. Onozato · T. Shibata · Y. Kanai · S. Hirohashi (✉)
Pathology Division, National Cancer Center Research Institute,
5-1-1 Tsukiji, Chuo-ku, Tokyo 104-0045, Japan
e-mail: shirohas@ncc.go.jp
Tel.: +81-3-35422511
Fax: +81-3-32482463

T. Kosuge
Division of Hepato-Biliary and Pancreatic Surgery,
National Cancer Center Hospital,
Tokyo, Japan

Y. Takahashi · Y. Nimura
Division of Surgical Oncology, Department of Surgery,
Nagoya University Graduate School of Medicine,
Nagoya, Japan

Keywords Solid–pseudopapillary neoplasm of the pancreas · β-Catenin · Sex distribution

Introduction

Solid–pseudopapillary neoplasm (SPN) of the pancreas is a distinctive but uncommon neoplasm which is classified as a tumor of the exocrine pancreas according to the World Health Organization (WHO) tumor classification system [12]. It is known to occur preferentially in young women and has a favorable prognosis [9, 10, 23]. The clinicopathological characteristics of SPN have been well described in recent years [9, 23], although it remains uncertain if the features of SPNs occurring in men differ from those in women.

It can be difficult to differentiate between SPN and other pancreatic neoplasms especially pancreatic neuroendocrine tumor (PET) as these two can share morphological features, such as solid monomorphous growth and rosette-like structures. In addition, a SPN often expresses neuroendocrine markers, such as synaptophysin, neuron-specific enolase (NSE), and CD56 [3, 9, 13, 16, 23]. In fact, there are many reported cases of SPN being initially misdiagnosed as PET [2, 4, 8, 16]. However, an accurate distinction between SPN and PET is important because SPN is generally curable, even though it may present as a huge, locally invasive tumor with or without multiple metastases.

β-Catenin is a submembranous component of the cadherin-mediated cell adhesion system and is a downstream transcriptional activator in the Wnt signaling pathway. Mutations of β-catenin have been reported in various tumors [21]; these are thought to cause stabilization of β-catenin leading to constitutive activation of TCF/LEF-1-dependent transcription [7, 20]. Genetic studies have recently shown that neither ductal adenocarcinomas nor PETs are associated with mutations in the β-catenin gene [5], whereas Tanaka et al. [25, 26] and Abraham et al. [1] demonstrated that aberrrant accumulation of β-catenin protein in the tumor cell nuclei and activating β-catenin

oncogene mutations occurred in almost all of the SPNs they tested. They concluded that almost all SPNs show alterations in the adenomatous polyposis coli (APC)/β-catenin pathway, even though K-ras, DPC4, and P-53 do not play a major role in the neoplastic progression of SPN [1].

To understand the clinicopathological characters of SPNs between the genders, we re-evaluated all pancreatic tumors (except ductal adenocarcinomas) that had been surgically resected at a single institution using immunohistochemical and genetic analyses for β-catenin alterations in addition to conventional histopathological examination. There were 14 SPNs identified from seven women and seven men and we investigated their clinicopathological features.

Materials and methods

Case selection

This study was approved by the Ethics Committee of the National Cancer Center, Japan. The study population consisted of 14 Japanese patients with pancreatic SPN who underwent surgical resection at the National Cancer Center Hospital, Tokyo, Japan between 1991 and 2004. Information on age, sex, the location of the tumor within the pancreas, and the presence or absence of distant metastases was retrieved from the patients' medical records. The patients' tumor samples, which had been fixed in 10% buffered formalin and embedded in paraffin, were retrieved from the archive. For histopathological examinations of the tumor tissues, 4-μm sections were prepared and stained with hematoxylin and eosin (HE). In addition to conventional histopathological observations, the following pathological factors were carefully examined: encapsulation of the tumor, presence or absence of calcification or ossification in the tumor, and counts of mitotic figures in tumor cells per ten high-power fields (HPFs) on microscopy.

As controls, clinical data and archive samples for 15 patients with PET were also retrieved. All 15 had undergone curative resection at the same hospital over the same time period. The PET patients were aged 18 to 81 years (median, 58 years) and none had hormonal symptoms. Their tumors comprised three benign, well-differentiated endocrine tumors, five well-differentiated endocrine tumors of uncertain biological behavior, and seven well-differentiated endocrine carcinomas according to WHO classification criteria [22]. Tumor size ranged from 1 to 8 cm in diameter (median, 3.6 cm).

Immunohistochemistry

Immunohistochemical staining was performed on the formalin-fixed, paraffin-embedded tissues using the avidin–biotin complex method. In brief, 4-μm-thick sections of representative blocks were deparaffinized and rehydrated using an alcohol gradient. After blocking endogenous peroxidase with methanol containing 0.3% H_2O_2, the sections were autoclaved at 121°C for 10 min in citrate buffer (10 mM sodium citrate, pH 6.0) for antigen retrieval. After blocking with normal goat serum, the sections were reacted overnight with appropriately diluted primary antibodies (listed in Table 1). The sections were then sequentially reacted with biotin-conjugated anti-mouse or anti-rabbit immunoglobulin G antibodies (Vector Laboratories, Burlingame, CA, USA) and Vectastain Elite ABC regent (Vector Laboratories). Diaminobenzidine was used as the chromogen, and the nuclei were counterstained with hematoxylin.

Semiquantitative assessments of the immunohistochemical results (except for Ki-67) were obtained by calculating the histoscore (multiplying the percentage of positive cells by their staining intensity) [6]. Scores for the percentages of positive cells were evaluated as follows: 0, <5% labeled cells; 1, 5–30% labeled cells; 2, 31–70% labeled cells; and 3, >71% labeled cells. Islet cells were used as an internal positive control; the intensity of immunolabeling of the tumor cells was compared to that of the islet cells in an adjacent nontumor area, and the labeling intensity of the tumor cells was evaluated as follows: 0, negative; 1, weaker than the intensity of islet cells; 2, equal intensity to that of islet cells; and 3, stronger intensity than that of islet cells. Multiplying the score for the percentage of positive cells by the score for the intensity of immunolabeling then gave overall staining scores as follows: −, 0; 1+, 1 or 2; 2+, 3 or 4; and 3+, 6 to 9. The Ki-67 labeling index (LI) was determined by counting a minimum of 1,000 nuclei in the most densely positively stained areas [19]. Three different counts were performed for each sample, and the highest score was taken as the index value.

Table 1 Primary antibodies used in the immunohistochemical study

Antigens (clone names)	Host species	Working dilution	Source
Chromogranin A (poly)	Rabbit	1:400	DAKO (Glostrup, Denmark)
Synaptophysin (poly)	Rabbit	1:50	DAKO (Glostrup, Denmark)
Neuron-specific enolase (BBS/NC/VI-H14)	Mouse	1:400	DAKO (Glostrup, Denmark)
CD56 (NCC-Lu-243)	Mouse	1:200	Nippon Kayaku (Tokyo, Japan)
Vimentin (V9)	Mouse	1:50	DAKO (Glostrup, Denmark)
Ki-67 (MIB-1)	Mouse	1:50	DAKO (Glostrup, Denmark)
Estrogen receptor (ER88)	Mouse	1:4	Biogenex (San Ramon, CA, USA)
Progesterone receptor (PR88)	Mouse	1:1	Biogenex (San Ramon, CA, USA)
β-Catenin (14)	Mouse	1:100	Transduction Laboratories (Lexington, KY, USA)

DNA extraction, polymerase chain reaction, and sequencing analysis of the β-catenin gene

Mutation analysis of the β-catenin gene was performed as previously described [21]. The samples were fixed with 10% (*v*/*v*) formalin and embedded in paraffin. Four-micrometer-thick sections from each specimen were stained briefly with HE, and DNA was extracted as follows. The tumor areas were microdissected separately using a sterile toothpick under a microscope. Adjacent non-tumor tissue was dissected separately as a control. Three PETs were also dissected in the same way. The dissected samples were incubated in 200 μl DNA extraction buffer [50 mM Tris–HCl, pH 8.0, 1 mM ethylenediaminetetraacetic acid (EDTA), 0.5% (*v*/*v*) Tween-20 and 200 μg/ml proteinase K (Roche Diagnostics, Mannheim, Germany)] at 56°C overnight, then the proteinase K was inactivated by heating at 100°C for 10 min. The extracted genomic DNA was purified by phenol extraction, dissolved in 20 μl TE buffer (10 mM Tris–HCl, pH 8.0, and 1 mM EDTA), and subjected to polymerase chain reaction (PCR) with a pair of primers that encompassed codons 22–63 of exon 3 of the β-catenin gene. This region includes the glycogen synthase kinase-3β (GSK-3β)-phosphorylation sites. The structures of the forward and reverse primers were CT-S-F (5′ ATGGAACCAGACAGAAAAGCG-3′) and CT-S-R (5′ CAGGATTGCCTTTACCACTCA-3′), respectively [21]. PCR was performed under the following conditions: 3 min at 94°C for initial denaturing, followed by 35 cycles at 94°C for 30 s, 55°C for 30 s, and 72°C for 30 s, and a final extension at 72°C for 3 min. The PCR products were checked by agarose gel electrophoresis and purified using a QIAquick PCR Purification Kit (QIAGEN, Hilden, Germany). The isolated PCR products were directly sequenced with the CT-S-F primer using the ABI Prism 3100 Genetic Analyzer system (Applied Biosystems, Foster City, CA, USA) according to the manufacturer's instructions. Mutated sequences were sometimes not clearly detected, in which case we subcloned the PCR products into a TA vector (TOPO TA Cloning Kit, Invitrogen, Carlsbad, CA, USA) and sequenced the PCR products from their subcloned plasmids, extracted from at least 30 different clones. Each experiment, including DNA extraction, was performed at least twice.

Results

We tested the usefulness of β-catenin immunohistochemistry in differentiating between SPN and PET. We initially identified ten patients (seven women and three men) with SPNs from our pathology files (Table 2, patients 1–7, 8, 9, and 13). Preliminary immunohistochemical studies revealed nuclear accumulation of β-catenin protein in the tumor cells in all ten of these SPNs, whereas it was not observed in the 15 PET controls. We then re-evaluated all pancreatic tumors (except ductal adenocarcinomas) that had been surgically resected at the National Cancer Center Hospital, Tokyo, Japan between 1991 and 2004 (a total of 514 pancreatic tumors when ductal adenocarcinomas were counted). At first, we evaluated them by conventional histopathological examination and identified 14 SPNs which included ten cases previously diagnosed as SPNs and four suspected cases. It was easy to differentiate these ten SPNs from PETs by their characteristic cellular and structural findings. Four tumors being suspected SPN, which had initially been diagnosed as PETs, in four male patients revealed solid proliferation of the uniform polygonal cells with round to oval and indented nuclei arranged in sheets with an abundant microvasculature, though there were no prominent degenerative changes including cystic degeneration and pseudopapillary structure. These findings were consistent with the features of SPN, whereas these tumors did not have any apparent features of PETs such as characteristic trabecular or gyriform growth pattern that was usually seen as minor

Table 2 Clinicopathological findings in 14 patients with SPNs

Patient	Sex	Age (years)	Location in pancreas	Diameter (cm)	Ratio of solid and cystic components	Encapsulation	Calcification	Metastasis	Mitosis/10 HPFs	Follow-up (months)
1	F	65	Head	8.5	10:90	C	++ (OS)		1	AFD (45)
2	F	35	Tail	8	20:80	C	+++ (OS)	Liver	1	AFD (126)
3	F	42	Tail	7.5	20:80	P	+++ (OS)		0	AFD (94)
4	F	43	Body	5	10:90	C	++ (OS)		0	AFD (28)
5	F	24	Body	4.6	20:80	C	–		0	AFD (154)
6	F	70	Tail	3.5	5:95	C	++ (OS)		0	AFD (37)
7	F	40	Head	1.5	95:5	–	–		0	AFD (61)
8	M	36	Head	7.5	80:20	C	+		3	AFD (4)
9	M	45	Body	6.4	95:5	–	–		0	AFD (66)
10	M	47	Body	5	30:70	–	+		1	AFD (101)
11	M	35	Head	3.1	80:20	–	–		0	AFD (123)
12	M	36	Body	2	90:10	–	–		1	AFD (135)
13	M	55	Body	1.6	95:5	–	+		1	AFD (52)
14	M	61	Body	0.8	95:5	–	–		0	AFD (118)

C Completely encapsulated, *P* partially encapsulated, *OS* with ossification, *AFD* alive free of disease, +++ high, ++ medium, + low, – none

component even if the tumor showed predominantly solid or glandular growth pattern. The tumor cells in these four tumors also showed the expression of vimentin diffusely and no expression of chromogranin A in immunohistochemical examination that were consistent with SPN than PET as described later. After these careful reviewing, we considered these four tumors as SPNs. Then, we examined the nuclear accumulation of β-catenin protein in the tumor cells by immunohistochemistry and these four tumors revealed nuclear and cytoplasmic β-catenin accumulation. We also searched for mutations in the β-catenin gene and these tumors were also confirmed to have β-catenin gene mutations, as described below. Thus, a total of 14 SPNs was identified (seven in women and seven in men).

Clinicopathological features of SPNs in women

The mean age of the female SPN patients was 45.5 years (range, 24–70 years). Their SPNs were distributed throughout the pancreas without a particular site of predilection (Table 2). The average size of these SPNs was 5.1 cm (range, 1.5–8.5 cm) in diameter. All the female patients showed characteristic clinicopathological features of SPN as described previously. Only one (patient 2) presented with simultaneous multiple metastases in the liver and underwent resection of both the primary lesion and the liver metastases. All the SPNs in the female patients were globular or oval-shaped and well demarcated. Most of them (in patients 1, 2, and 4–6) were completely encapsulated by thick fibrous tissue; only one (in patient 3) was incompletely encapsulated. There were macroscopic cystic changes with extensive hemorrhages and necrodegenerative changes (Fig. 1a,b). A small proportion of each tumor was histologically occupied by solid proliferations of fairly uniform, small-to-medium-sized, polygonal epithelial cells with prominent nuclear grooves. These were arranged in a sheet or so-called patternless arrangement and had a rich microvasculature. The majority of each tumor showed cystic or degenerative changes. Extensive calcification, often with ossification, was observed in these areas (Fig. 1c). In areas of relatively mild degeneration, the tumor cells were arranged around delicate fibrovascular stalks displaying pseudopapillary and pseudoglandular formations (Fig. 1d,e). No cellular mitosis was observed in the majority of the samples, but mitosis was seen in one of ten HPFs in two patients, including patient 2, who had coexisting liver metastases and vascular invasion. All of the patients were followed-up and remain alive without any disease recurrence (Table 2).

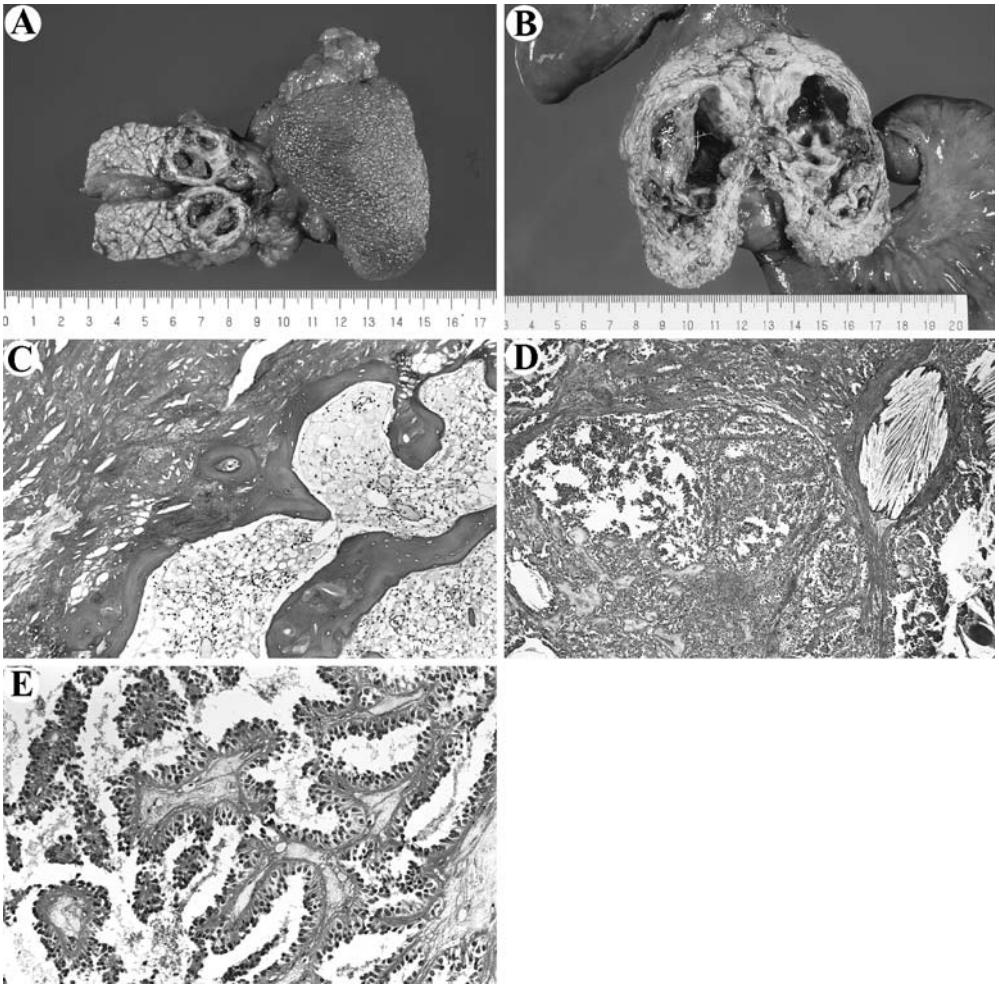

Fig. 1 Pathological features of SPNs in female patients. **a**,**b** The cut surfaces of the SPNs show extensive degeneration surrounded by a thick fibrous capsule with calcification and ossification. These massive degenerative changes are apparent even in the relatively small tumor shown in **a** (**a**, patient 6; **b**, patient 1). **c** Ossification is present in extensively calcified areas (HE, ×50). **d** Gradual degenerative changes comprising pseudoglandular and pseudopapillary formations can be seen (HE, ×20). A cholesterol crystal deposit can be seen on the *right*. **e** The pseudopapillary and pseudoglandular formations are formed by the tumor cells around microvasculature left from collapsing by the degeneration. (HE, ×100)

Clinicopathological features of SPNs in men

The group comprised three patients originally diagnosed as having SPN (patients 8, 9, and 13) and four rediagnosed after originally being diagnosed as having PET (patients 10–12 and 14) (Table 2). The mean age of the male group was 45.0 years (range, 35–61 years). The average size of the SPNs was 3.8 cm (range, 0.8–7.5 cm) in diameter, which was smaller than that in cases among women. Regarding their gross appearance, most of the tumors had a predominant solid area with few prominent cystic changes, except in one case (patient 10) (Fig. 2a,b). They were generally circumscribed but not encapsulated; only one tumor (patient 8) had a thin fibrous capsule, but this did not resemble the thick fibrous capsules seen around the female patients' tumors. The majority of the tumor area was histologically occupied by a solid proliferation of tumor cells. A few cystic changes were located in the center of the tumor in some patients, while others showed microcysts scattered within the solid areas. The basic tumor histology of the solid area in the male tumors was indistinguishable from that in the female ones (Fig. 2e,f). The tumors did not have capsules but infiltrated directly into the adjacent pancreatic parenchyma without any inflammatory cell reaction or fibrous proliferation. The pancreatic parenchyma just seemed to be replaced with tumor nests (Fig. 2c,d). Isolated, small, non-neoplastic parenchymal cells were often left among the tumor cells. Degenerative changes were present in only small areas of the tumors and three patients (patients 8, 10, and 13) showed a small amount of calcification without ossification. One patient (patient 8) showed partial nuclear pleomorphism, in which the mitotic rate was slightly increased (three mitoses per ten HPFs). Neither perineural invasion nor regional lymph node metastasis was observed in the male patients, and all patients were alive and disease-free after a mean follow-up period of 81.7 months (range 4–154 months). The smallest tumor (in patient 14) was initially found by his health check-up.

Immunohistochemistry

The details of the immunohistochemical results are summarized in Table 3. SPN cells showed strong nuclear and cytoplasmic accumulation of β-catenin protein. Positive cells were distributed diffusely throughout every SPN (Fig. 3a). Patient 2 exhibited a similar amount of staining in both her primary and metastatic tumors. In the adjacent non-tumorous pancreatic tissue, the ductal epithelial cells, acinar cells, and some islet cells expressed β-catenin

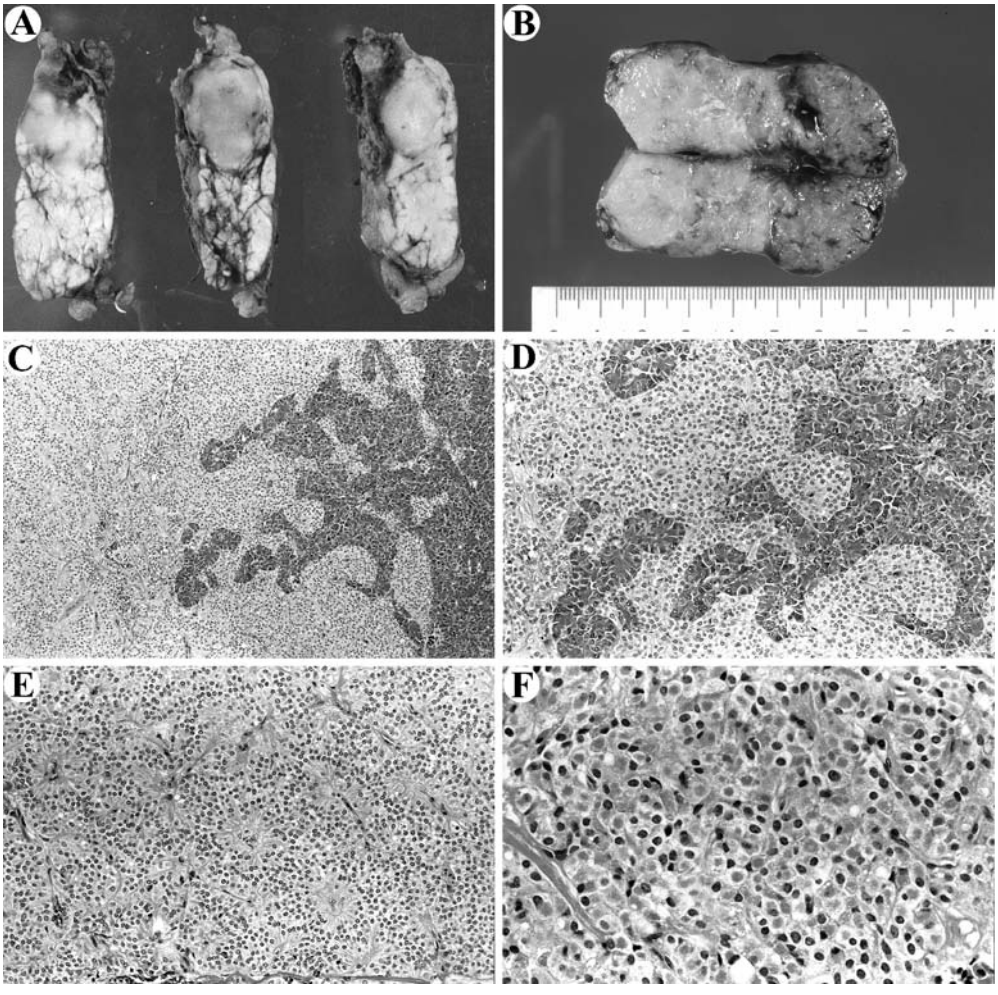

Fig. 2 Pathological features of SPNs in male patients. **a**,**b** The cut surfaces of the SPNs show well-demarcated, whitish, solid masses with minimal cystic changes and hemorrhages and no fibrous capsule, even in the large tumor shown in **b** (**a**, patient 12; **b**, patient 9). **c**,**d** In the solid area, uniform polygonal epithelial cells with a rich microvasculature are arranged in a sheet. At the periphery of the tumor, the tumor cells infiltrate directly into the adjacent pancreatic parenchyma without any stromal reaction (HE, **c** ×50, **d** ×100). **e** In the solid area, the pale cytoplasmic tumor cells are arranged around the abundant microvasculature with their nuclei lined up along the vessels. This formation appears as a rosette-like structure in cross-section (HE, ×100). **f** Eosinophilic inclusion bodies can sometimes be seen in the tumor cells. (HE, ×200)

protein in their membrane, especially in the cell borders (data not shown). In contrast, all 15 PETs showed membranous and rarely cytoplasmic (i.e., no nuclear) immunoreactivity for anti-β-catenin antibody (Fig. 3b).

Neuroendocrine cell markers were almost always expressed in both SPN and PET (Table 3). Staining for chromogranin A was absent in SPNs, except in two samples which showed weak focal reactivity, whereas PETs were strongly and diffusely stained. Intense, diffuse vimentin expression was observed in every SPN, whereas only infrequent focal expression was seen in PETs. All SPNs were negative for estrogen receptors; however, they were almost all positive for progesterone receptors, even in men. No overt differences in the sex distribution were observed for the four neuroendocrine markers, vimentin, or the two sex hormone receptors.

With regard to the Ki-67 LI in SPNs, positive cells were scattered throughout the tumor area and indices tended to be higher in the larger tumors. The LI appeared to reflect a low proliferation capacity and showed no definite correlation with biological malignancy.

Table 4 Mutations of the β-catenin gene (exon-3) in SPNs

Patient	Mutated codon	Base change/ deletion	Amino acid substitution
1	32	GAC→TAC	Asp→Tyr
2	32	GAC→AAC	Asp→Asn
3	37	TCT→TGT	Ser→Cys
4	32	GAC→GAG	Asp→Glu
5	37	TCT→TTT	Ser→Phe
6	–		–
7	34	GGA→CGA	Gly→Arg
8	37	TCT→TGT	Ser→Cys
9	32	GAC→TAC	Asp→Tyr
10	–		–
11[a]	28	CAG→CAC	Gln→His
	29–32	Deletion[a]	
12	34	GGA→CGA	Gly→Arg
13	37	TCT→TGT	Ser→Cys
14	32	GAC→GGC	Asp→Gly

[a]Compared with the corresponding wild-type sequence (g, tct, tac, ctg, ga), (cag, tct, tac, ctg, gac) was deleted, thus codon 28 was mutated from cag to cac and codons 29–32 were deleted

Mutations in the β-catenin gene

β-Catenin gene mutations were detected in most of the SPNs (12 of 14, 85.7%), which occurred in exon 3 encoding the amino acids corresponding to the GSK-3β phosphorylation sites and their flanking regions (Table 4). Eleven patients showed 1-bp missense mutations in the region between codons 32 and 37 as follows: codon 32 (five patients), codon 34 (two patients), and codon 37 (four patients). These codons are known mutation 'hot spots', as reported previously [1, 25]. In one patient (patient 11), there was a 12-bp deletion (g tct tac ctg ga) corresponding to codons 28 to 32. Because of this deletion, the amino acid at codon 28 was changed from Gln to His and the four amino acids corresponding to codons 29 to 32 were deleted, but no frame-shift occurred. This mutation has not previously been reported in pancreatic tumors. No muta-

Table 3 Results of immunohistochemical analyses in 14 patients with SPNs compared with those in PETs

Patients with SPNs	β-Catenin[a]	CRM	SYN	NSE	CD56	VIM	ER	PR	Ki-67 LI[b] (%)
1	3+	–	1+	2+	3+	3+	–	1+	5
2	3+	–	2+	3+	2+	3+	–	1+	1
3	3+	1+	1+	3+	3+	3+	–	3+	2
4	3+	–	1+	3+	2+	3+	–	1+	2
5	3+	–	1+	2+	1+	3+	–	1+	0
6	3+	–	–	3+	1+	3+	–	3+	0
7	3+	–	1+	3+	2+	3+	–	3+	0
8	3+	–	3+	2+	3+	3+	–	1+	5
9	3+	–	1+	2+	3+	3+	–	1+	5
10	3+	–	1+	2+	–	3+	–	–	0
11	3+	–	1+	2+	3+	3+	–	2+	2
12	3+	–	1+	2+	3+	3+	–	2+	2
13	3+	1+	1+	2+	3+	3+	–	1+	1
14	3+	–	3+	2+	3+	3+	–	1+	0
PETs[c]	–[d]	3+	3+	2+	2+	–[e]	–	2+	

CRM chromogranin A, *SYN* synaptophysin, *NSE* neuron-specific enolase, *VIM* vimentin
ER estrogen receptor, *PR* progesterone receptor
[a]Antigen expressed in both nucleus and cytoplasm
[b]Ki-67 labelling index (%) as described in "Materials and methods"
[c]Summary of the immunohistochemical results from 15 PETs
[d]No nuclear immunocreativity was found
[e]Infrequent focal expression was sometimes observed

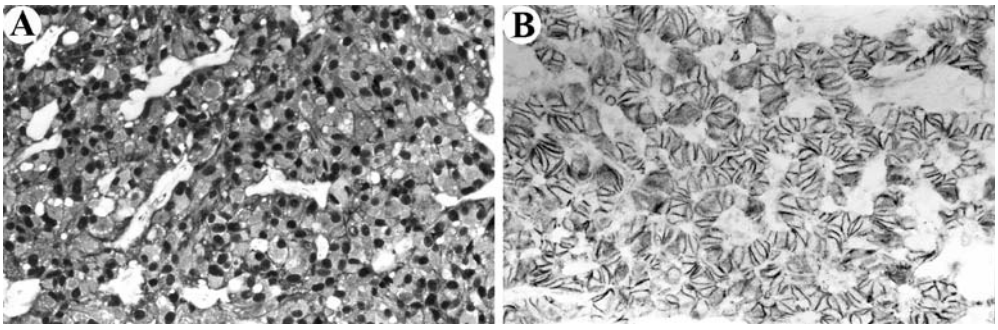

Fig. 3 Immunohistochemical appearance of β-catenin protein in SPN and other pancreatic tumors. **a** β-Catenin protein is extensively accumulated in both the nuclei and the cytoplasm of SPN cells (×200). β-Catenin-positive tumor cells are diffusely distributed. **b** Membranous staining for β-catenin is observed in PET (×200)

tions were detected in any of the corresponding non-tumor tissues or the tumor tissues of the three PET controls.

Discussion

Most SPNs have recently been reported to contain somatic mutations in the β-catenin gene. Alterations in the APC/β-catenin pathway have also been observed, and these appear to be associated with the neoplastic progression of SPN [1, 25]. Immunohistochemical detection of aberrant β-catenin protein accumulation in SPN cell nuclei is suggestive of these mutations, as mutations in the β-catenin gene always occur at GSK-3β phosphorylation sites or in their flanking regions. These impair normal phosphorylation by GSK-3β and subsequent ubiquitin-mediated degradation of β-catenin protein. Indeed, we (this study) and other groups [1, 25, 26] have demonstrated strong accumulation of β-catenin protein in the nuclei and cytoplasm of the tumor cells in SPN. In this study, 100% (14 of 14) of the SPNs showed intense, widespread nuclear and cytoplasmic accumulation of β-catenin protein (Table 3) and 86% (12 of 14) contained β-catenin gene mutations caused by exchange or deletion of the amino acids at GSK-3β phosphorylation sites or in their flanking region (Table 4). Other groups have also demonstrated nuclear and cytoplasmic accumulation of β-catenin protein in the majority of tumor cells in all SPNs tested [1, 25, 26], while 83% (15/18) [25] to 90% (18/20) [1] of these SPNs had mutations in the β-catenin gene at GSK-3β phosphorylation sites or in their flanking region. Constitutive production of cyclin D1, one of the intranuclear targets of the β-catenin complex, was also frequently apparent in these SPNs [1, 16]. We (this study) and others [5, 26] have conversely demonstrated the absence of nuclear accumulation of β-catenin protein and mutations in exon 3 of the β-catenin gene in PETs, even though membranous localization (and rarely cytoplasmic accumulation) of β-catenin protein was observed.

The initial clinical appearance of SPN and PET is often similar. It can sometimes be quite difficult to differentiate between SPN and PET, especially for SPT showing solid monomorphous growth without characteristic degenerative changes including massive cystic degeneration or pseudopapillary feature. Expression of neuroendocrine markers by SPN can also cause confusion in the pathological differential diagnosis. From this study combined with previous reports [2, 3, 5–7], chromogranin A and vimentin seem to be relatively good markers for differentiating between SPN and PET, although even a combination of markers including vimentin and the four neuroendocrine antigens could not distinguish SPN from PET completely. In contrast, nuclear accumulation of β-catenin protein appeared to be a useful marker of SPN, which allowed it to be differentiated from PET. We, therefore, believe that pathological investigations on a combination of vimentin, neuroendocrine markers, and β-catenin would make the differential diagnosis of SPN more accurate.

SPN has been reported to occur preferentially in young women and fewer than 10% of SPNs arise in male patients. In contrast, we found that the male-to-female ratio of SPNs at a single institution was 7:7. The proliferating tumor cells in the male and female SPNs were basically similar with regard to both histological and immunohistochemical analyses. No apparent differences of β-catenin gene mutations and expressions of sex hormone receptors between genders were also found in this study. However, solid components that lacked prominent pseudopapillary or pseudoglandular formations occupied the majority of the tumor area in almost all the specimens from men. In contrast, SPN samples from women showed the typical features of SPN, i.e., nearly complete cystic degeneration, encapsulation by thick fibrous tissue, and extensive calcification with ossification (Table 2). Smaller tumors generally consist mainly of solid components while larger ones show cystic and/or hemorrhagic and marked degenerative changes [9, 15]. The SPNs in our male patients tended to be predominantly solid tumors without massive degenerative changes, even when they were large.

A detailed information on SPNs in male patients is available from nine previously published case reports [11, 15, 17, 18, 24, 27, 28]. Except in one case [27], all of these tumors were surrounded by a fibrous capsule and contained large cystic areas filled with hemorrhagic and necrotic material. Most of them were larger (median diameter, 9 cm; range, 4.5–13 cm) than those described here and had classical morphological features; thus, they were relatively easy to diagnose as SPNs, even though they occurred in men. However, SPNs with no cystic formations and few pseudopapillary structures, such as in the case reported by Tomioka et al. [27], might be confused with PETs. These published findings combined with the results of this study suggest that, compared to SPNs in women, SPNs in men are more likely to occur as a solid mass and to degenerate

less frequently and more slowly during their growth. There is currently no good explanation to this phenomenon. In addition to this, Lam et al. [14] conducted a review of the literature on SPN. They identified a total of 452 cases, of which 189 occurred in Asian and 59 in Black populations. The highest number of cases occurred in Japan. In these Japanese cases, SPNs tended to be found in older patients and were more frequent among men than usual. It is possible that there are regional or ethnic differences in the frequency of SPN in male patients.

In summary, we have demonstrated that nuclear accumulation of β-catenin protein is a useful pathological hallmark of SPN which allows it to be differentiated from PET. We carried out clinicopathological investigations on 14 SPNs (seven from men and seven from women) surgically resected at a Japanese institution, and all of the SPNs had β-catenin alterations. Marked degenerative changes which could have occurred earlier in tumor growth were the features of SPNs in women, whereas those in men tended to be a solid mass with slower progression of degenerative changes. These less typical features of SPNs in male patients can make them difficult to diagnose with conventional methods. In this situation, male SPNs are diagnosed correctly by immunohistochemical detection of nuclear β-catenin accumulation combined with immunohistochemical findings for vimentin and neuroendocrine markers.

Acknowledgements The authors wish to thank Dr. Kazuaki Shimada, Dr. Tsuyoshi Sano, Dr. Yoshihiro Sakamoto, Dr. Hidenori Ojima, and Dr. Yuri A. Fukasawa for useful discussions and Dr. Yukihiro Yoshida and Mr. Taizo Masuda for their technical advice. This work was supported by a Grant-in-Aid for Third Term Comprehensive 10-year Strategy for Cancer Control from the Ministry of Health, Labor, and Welfare of Japan.

References

1. Abraham SC, Klimstra DS, Wilentz RE, Yeo CJ, Conlon K, Brennan M, Cameron JL, Wu TT, Hruban RH (2002) Solid–pseudopapillary tumors of the pancreas are genetically distinct from pancreatic ductal adenocarcinomas and almost always harbor β-catenin mutations. Am J Pathol 160:1361–1369
2. Buetow PC, Buck JL, Pantongrag-Brown L, Beck KG, Ros RR, Adair CF (1996) Solid and papillary epithelial neoplasm of the pancreas: imaging-pathologic correlation in 56 cases. Radiology 199:707–711
3. Choi YL, Oh YL, Kim SH, Park CK, Ahn G (2002) Comparative study of non-functional islet tumors and pancreatic solid and papillary neoplasms: biological behavior and immunohistochemistry. Pathol Int 52:358–366
4. de la Roza G, Cleary KR, Ordonez NG, El-Naggar A, Mackay B (1997) Solid and papillary tumor of the pancreas: ultrastructural observation on two contrasting cases. Ultrastruct Pathol 21:439–447
5. Gerdes B, Ramaswamy A, Simon B, Pietsch T, Bastian D, Kersting M, Moll R, Bartsch D (1999) Analysis of β-catenin gene mutations in pancreatic tumors. Digestion 60:544–548
6. Hansel DE, Rahman A, Hermans J, de Krijger RR, Ashfaq R, Yeo CJ, Cameron JL, Maitra A (2003) Liver metastases arising from well-differentiated pancreatic endocrine neoplasms demonstrate increased VEGF-C expression. Mod Pathol 16:652–659
7. Hirohashi S, Kanai (2003) Cell adhesion system and human cancer morphogenesis. Cancer Sci 94:575–581
8. Horisawa M, Niinomi N, Sato T, Yokoi S, Oda K, Ichikawa M, Hayakawa S (1995) Frantz's tumor (solid and cystic tumor of the pancreas) with liver metastasis: successful treatment and long-term follow-up. J Pediatr Surg 30:724–726
9. Klimstra DS, Wenig BM, Heffess CS (2000) Solid–pseudopapillary tumor of the pancreas: a typically cystic carcinoma of low malignant potential. Semin Diagn Pathol 17:66–80
10. Klöppel G, Morohoshi T, John HD, Oehmichen W, Opitz K, Angelkort A, Lietz H, Ruckert K (1981) Solid and cystic acinar cell tumour of the pancreas. A tumour in young women with favourable prognosis. Virchows Arch 392:171–183
11. Klöppel G, Maurer R, Hofmann E, Luthold K, Oscarson J, Forsby N, Ihse I, Ljungberg O, Heitz PU (1991) Solid–cystic (papillary–cystic) tumours within and outside the pancreas in men: report of two patients. Virchows Arch A Pathol Anat Histopathol 418:179–183
12. Klöppel G, Solcia E, Longnecker DS, Capella C, Sobin LH (1996) Histological typing of tumors of the exocrine pancreas. WHO international histological classification of tumors, 2nd edn. Springer, Berlin Heidelberg New York
13. Kosmahl M, Seada LS, Jänig U, Harms D, Klöppel G (2000) Solid–pseudopapillary tumor of the pancreas: its origin revisited. Virchows Arch 436:473–480
14. Lam KY, Lo CY, Fan ST (1999) Pancreatic solid–cystic–papillary tumor: clinicopathologic findings in eight patients from Hong Kong and review of the literature. World J Surg 23:1045–1050
15. Mancini GJ, Dudrick PS, Grindstaff AD, Bell JL (2004) Solid–pseudopapillary tumor of the pancreas: two cases in male patients. Am Surg 70:29–31
16. Notohara K, Hamazaki S, Tsukayama C, Nakamoto S, Kawabata K, Mizobuchi K, Sakamoto K, Okada S (2000) Solid–pseudopapillary tumor of the pancreas. Immunohistochemical localization of neuroendocrine markers and CD10. Am J Surg Pathol 24:1361–1371
17. Ohashi K, Nakajima Y, Hisanaga M, Nakano H, Tsutsumi M, Kondoh S, Konishi Y (1993) A solid and papillary (solid–cystic) tumor of the pancreas occurring in a 36-year-old man: report of a case. Surg Today 23:551–555
18. Ohiwa K, Igarashi M, Nagasue N, Nagasaki M, Harada T (1997) Solid and cystic tumor (SCT) of the pancreas in an adult man. HBP Surg 10:315–321
19. Pelosi G, Bresaola E, Bogina G, Pasini F, Rodella S, Castelli P, Iacono C, Serio G, Zamboni G (1996) Endocrine tumors of the pancreas: Ki-67 immunoreactivity on paraffin sections is an independent predictor for malignancy: a comparative study with proliferating-cell nuclear antigen and progesterone receptor protein immunostaining, mitotic index, and other clinicopathologic variables. Hum Pathol 27:1124–1134
20. Polakis P (2000) Wnt signaling and cancer. Genes Dev 14:1837–1851
21. Sekine S, Shibata T, Matsuno Y, Maeshima A, Ishii G, Sakamoto M, Hirohashi S (2003) β-Catenin mutations in pulmonary blastomas: association with morule formation. J Pathol 200:214–221
22. Solcia E, Klöppel G, Sobin LH (1996) Histologic typing of endocrine tumors. WHO international histological classification of tumors, 2nd edn. Springer, Berlin Heidelberg New York
23. Solcia E, Capella C, Klöppel G (1997) Tumors of the pancreas. Atlas of tumor pathology, 3rd series, fascicle 20. Armed Forces Institute of Pathology, Washington, DC

24. Takahashi H, Hashimoto K, Hayakawa H, Kusakawa M, Okamura K, Kosaka A, Mizumoto R, Katsuta K (1999) Solid cystic tumor of the pancreas in elderly men: report of a case. Surg Today 29: 1264–1267
25. Tanaka Y, Kato K, Notohara K, Hojo H, Ijiri R, Miyake T, Nagahara N, Sasaki F, Kitagawa N, Nakatani Y, Kobayashi Y (2001) Frequent β-catenin mutations and cytoplasmic/nuclear accumulation in pancreatic solid–pseudopapillary neoplasm. Cancer Res 61:8401–8404
26. Tanaka Y, Notohara K, Kato K, Ijiri R, Nishimata S, Miyake T, Fukunaga M, Horisawa M, Nakatani Y (2002) Usefulness of beta-catenin immunostaining for differential diagnosis of solid–pseudopapillary neoplasm of the pancreas. Am J Surg Pathol 26:818–820
27. Tomioka T, Inoue K, Yamamoto T, Motojima K, Tsunoda T, Kanematsu T (1993) Solid and cystic tumor of the pancreas occurring without cyst formation in adult male. Int J Pancreatol 14:195–200
28. Tsunoda T, Eto T, Tsurifune T, Tokunaga S, Ishii T, Motojima K, Matsumoto T, Segawa T, Ura K, Fukui H (1991) Solid and cystic tumor of the pancreas in an adult male. Acta Pathol Jpn 41:763–770

Virchows Arch (2006) 448: 570–575
DOI 10.1007/s00428-006-0166-9

ORIGINAL ARTICLE

Pin Liang · Jian-Wei Hong · Hideyuki Ubukata · Huan-Ran Liu · Yoshinori Watanabe · Motonobu Katano · Gyo Motohashi · Teruhiko Kasuga · Ichiro Nakada · Takafumi Tabuchi

Increased density and diameter of lymphatic microvessels correlate with lymph node metastasis in early stage invasive colorectal carcinoma

Received: 18 September 2005 / Accepted: 25 January 2006 / Published online: 22 February 2006

Abstract To determine whether lymphangiogenesis was associated with the development of colorectal carcinoma and whether the mean maximal diameter of lymphatic microvessels (LMMMD) or lymphatic microvessel density (LMVD) is associated with lymph node metastasis in early stage invasive colorectal carcinoma (T1 carcinoma), we used immunohistochemical staining with podoplanin to measure LMMMD and LMVD in intratumoral (LMMMDit, LMVDit) and peritumoral areas (LMMMDpt, LMVDpt) of T1 carcinomas (n=87). By comparing the LMMMD and LMVD in normal large intestine (n=10), adenoma (n=15), and Tis carcinoma (n=15), we found out that the LMVDpt in T1 carcinoma with lymphatic vessel invasion (LVI) was significantly high (P<0.001), and there was a significant decrease in LMMMDpt in T1 carcinoma (P=0.031). Both LMMMDpt and LMVDpt were significantly increased in the T1 carcinomas, with LVI compared with the T1 carcinomas without LVI (P=0.018, P=0.003). Multivariate analysis revealed that LVI and combined greater LMMMDpt and greater LMVDpt were associated with lymph node metastases (P=0.005, P=0.036). These results indicate that lymphangiogenesis might be induced in the surrounding tumor areas of the T1 colorectal carcinoma with LVI; thus, evaluation of the diameter and density of lymphatic microvessels is important in T1 colorectal carcinoma to predict lymph node metastases.

Keywords Lymphatic · Microvessel · Density · Podoplanin · Diameter of lymphatic microvessels · Early-stage colorectal carcinoma · Lymph node metastasis

P. Liang (✉) · H. Ubukata · H.-R. Liu · Y. Watanabe · M. Katano · G. Motohashi · T. Kasuga · I. Nakada · T. Tabuchi
Fourth Department of Surgery, Tokyo Medical University, Kasumigaura Hospital,
3-20-1 Chuo, Ami, Inashiki,
Ibaraki, 300-0395, Japan
e-mail: lp212003@yahoo.com
Tel.: +81-29-8871161
Fax: +81-29-8402089

J.-W. Hong
Department of Pathology, Tokyo Medical University, Kasumigaura Hospital,
Ibaraki, 300-0395, Japan

Introduction

Early carcinoma of the colon and rectum is defined as carcinoma that is limited to the mucosa (Tis carcinoma) or that infiltrated into the submucosa (T1 carcinoma). One reasonable treatment method of these colorectal carcinomas would be endoscopic mucosal resection (EMR). However, lymph node metastasis is one of the main reasons for recurrence of T1 carcinoma after EMR [10, 17]. In such cases, a radical excision after the EMR would be necessary, as in advanced colorectal carcinomas. Thus, it is very important to accurately assess the risk of lymph node metastasis after EMR for T1 carcinoma. Recent evidence suggests that cancer cells frequently spread quickly to regional lymph nodes via lymphatic vessels [24]. Tumor lymphangiogenesis promotes lymphatic metastasis [14, 20]. However, the absence of specific markers for lymphatic microvessels has made the identification of tumor lymphatic microvessels difficult. Recently, podoplanin, a specific lymphatic microvessel marker, has enabled us to investigate lymphatic microvessels in paraffin-embedded sections [4, 26]. However the mean maximal diameter of lymphatic microvessels (LMMMD) expressed by podoplanin has not been reported before, and the significance of lymphatic microvessel density (LMVD) in colorectal carcinoma remains unclear. We therefore used immunohistochemical staining with podoplanin to measure LMMMD and LMVD in a retrospective series of T1 colorectal carcinomas and correlated the findings with the

expression of desmoplastic response, lymphatic endothelium proliferation (Ki67), and clinicopathologic data.

Materials and methods

Patients and tissues We studied 87 patients with T1 carcinoma, who underwent resection from 1985 to April 2005 in our department. The 59 men and 28 women had a mean age of 67.9 years old (range 39~83). Of these, 67 tumors were in the colon and 20 in the rectum. Depth of tumor invasion and lymph node status were classified according to the tumor–node–metastasis classification. The depth of submucosal invasion in T1 carcinoma was divided into three classes according to the method of Kudo [9]: (1) SM1, carcinoma invading into the upper one-third of the submucosa, thus showing minimal submucosal invasion; (2) SM2, carcinoma invading into the middle part of the submucosa; and (3) SM3, carcinoma invading into the lower layer of the submucosa. Among 87 patients, 8 (9.2%) patients had lymph node metastasis. As controls, we randomly selected normal large intestine tissues (NLI, n=10) from the proximal or distal margins of resection (at least 10 cm away from the edge of primary carcinoma), adenomas (n=15), and Tis carcinomas (n=15).

Immunohistochemistry Immunostaining procedures for podoplanin and Ki67 were performed using the Envision+/HRP method with heat-induced antigen retrieval. Two representative blocks of each tumor were selected for immunostaining analysis of podoplanin, Ki67, and serial 3-μm paraffin sections containing the tumor margin were dewaxed in xylene, then rehydrated in alcohol. For podoplanin staining, the sections were heated to 95°C in an oven (650 Watts) for 45 min to reactivate the antigen. The endogenous peroxidase activity was suppressed by a solution of 3% hydrogen peroxide in methanol for 20 min. After being rinsed three times in phosphate-buffered saline (PBS), sections were incubated for 90 min at room temperature with monoclonal antibody against podoplanin (11-003, AngioBio, Del Mar, CA, USA) and monoclonal antibody against Ki67 (MIB-1, DakoCytomation, Glostrup, Denmark). After washing in PBS, the sections were treated with goat anti-mouse immunoglobulins conjugated to peroxidase-labeled dextran polymer (Dako, Carpinteria, CA, USA) for 1 h at room temperature. The sections were then washed in PBS and developed in 0.05 M Tris–HCl buffer (pH 7.5), containing 0.6 mg/ml 3,3′-diaminobenzidine tetrahydrochloride, for 6 min for Ki67 staining and 10 min for podoplanin staining at room temperature. After washing in water, the nuclei were counterstained with Mayer's hematoxylin. Negative control sections were stained by omitting the primary antibody.

Desmoplastic response was diagnosed by the hematoxylin and eosin specimen [6]. Determination of desmoplastic response was performed according to the method of Nakada et al. [15]. No or mild response was considered negative, and moderate or severe response was considered positive.

Determination of LMVD was performed according to the method of Straume et al. and Weidner et al. [25, 27]. Briefly, the sections were scanned at low magnifications (×40 and ×100) to identify the areas of the tumors with the highest amount of lymphatic vessels ("hot spots"). Within these areas, five fields at ×200 magnification [high power field (HPF), 0.708 mm^2/field] were examined, and the mean values of these fields were calculated. Vessels more than one-half HPF (×200) away from the invasive margin were not counted. Any endothelial cell or cell cluster, highlighted by podoplanin reactivity and clearly separated from adjacent vessels, tumor cells, and connective tissue elements, was regarded as a distinct countable vessel [13]. The calculation of LMVD in intratumoral (LMVDit) and in peritumoral areas (LMVDpt) was established for each case, and the result given as vessels per millimeter squared.

The calculation of LMMMD in intratumoral (LMMMDit) and in peritumoral areas (LMMMDpt) was also recorded. The smallest diameter of the largest lymphatic vessel in each hot spot field was recorded as the diameter at ×400 magnification and the mean value of five diameter was calculated. For LMMMDit, all lymphatic microvessels with less than five lymphatic microvessels within all tumor areas were selected. Five of the largest axis lymphatic vessels in the mucosa and in the submucosa near the tumor in adenoma and Tis carcinoma were selected for calculation.

Lymphatic vessel invasion (LVI) in a given tumor was considered to be present if tumor cells could be seen within any one podoplanin positive profile in the entire field [13, 18]. Sections were scored by two independent investigators who had no clinical knowledge of the patients.

Statistics

The Kruskal–Wallis test, Mann–Whitney test, and logistic regression analysis were used. For all tests, a value of 0.05 or less was considered to indicate a statistically significant difference.

Results

Lymphatic microvessel density and mean maximal diameter of lymphatic microvessels in different tissues

Lymphatic microvessels were more prominent in submucosal loose connective tissue than in mucosa of the colon and rectum. There were no differences in the lymphatic densities and diameter among normal large intestine, adenomas, and Tis carcinomas groups, either in the mucosa or in the submucosa (Table 1).

In T1 carcinomas, most lymphatic vessels were located in the peritumoral areas, near the margin of invasive tumors, as reported previously [13]. Intratumoral lymphatic vessels were extremely rare and were observed only in narrow or collapsed lymphatic spaces. The LMVD and LMMMD in peritumoral areas was significantly greater

Table 1 LMVD (mean±SD, mm^{-2}) and LMMMD (mean±SD, μm) in normal large intestine, adenomas, and Tis carcinomas

	LMVD		LMMMD	
	Mucosa	Submucosa	Mucosa	Submucosa
Normal large intestine	4.2±1.9	5.1±2.5	17.9±8.8	26.1±14.2
Adenoma	4.4±2.3	5.7±3.1	19.4±10.5	26.7±15.3
Tis carcinoma	3.9±1.1	5.2±2.7	18.6±8.6	24.5±11.8

No significant difference was found between any groups (all $P>0.05$, Kruskal–Wallis test)

than in intratumoral areas (both $P<0.001$, Table 2). Neither LMVD nor LMMMD in intratumoral areas was associated with any clinical parameters.

LMVD, LMMMD, and lymphatic vessel invasion (Figs. 1 and 2)

The LMMMD and LMVD in peritumoral areas (Figs. 1 and 2) were significantly increased in the T1 carcinomas with LVI than in the T1 carcinomas without LVI ($P=0.0033$, $P=0.0182$, respectively; see Table 2). By comparing LMMMD and LMVD among different groups (Fig. 3a,b), we found out through the Kruskal–Wallis test that the LMMMA in peritumoral areas of T1 carcinoma was significantly smaller and the LMVD in peritumoral areas in the T1 with LVI was significantly greater than the LMVD in the submucosa of normal large intestine, adenoma, and Tis carcinoma.

LMVD, LMMMD, and lymph node metastases

For logistic regression analysis, the median values of LMVDpt (≤7.4 vs >7.4 lymphatic microvessels/mm^{-2}) and LMMMDpt (≤1.8 vs >1.8 μm) were used as cut-off values defining groups with low and high LMVDpt or LMMMDpt, respectively. Univariate analysis showed that the tumors with high LMVDpt or LMMMDpt tended to have high rate of lymph node metastasis. Among the significant correlations with lymph node metastases indicated by univariate analysis, multivariate analysis indicated that the LVI and combined high LMVDpt and high LMMMDpt, but not high LMVDpt or LMMMDpt only, were independent factors associated with lymph node metastases (Table 3). Only one LVI within a tumor area was found in eight cases with lymph node metastases, while LVI in surrounding tumor areas were found in all eight cases ($P=0.008$, Mann–Whitney test).

Table 2 LMVD (mean±SD, mm^{-2}) and LMMMD (mean±SD, μm) in T1 carcinomas

	Number of patients	LMMMDpt	LMMMDit	LMVDpt	LMVDit
Total	87	18.4±10.3*	9.5±6.4*	7.4±4.2**	2.1±1.7**
Size[a]					
≥21 mm^2	61	18.9±9.9	9.76±6.2	7.6±4.1	2.2±1.8
<21 mm^2	26	17.3±10.7	8.9±7.1	6.9±3.8	1.9±1.4
Macroscopic type[b]					
Elevated	58	19.6±9.8	9.9±6.3	7.8±4.2	2.2±1.8
Depressed	26	16.9±9.6	8.8±5.9	6.5±3.3	1.9±1.4
Flat	3	12.5±11	8.2±7.0	6.9±5.2	2.8±2.3
Tumor differentiation[a]					
Well-differentiated	45	17.9±9.5	9.8±6.5	6.7±3.4	2.1±1.7
Moderately differentiated	42	18.9±10.1	9.2±6.1	8.1±4.5	2.2±1.9
Depth of invasion [b]					
SM1	30	18.3±9.7	9.1±6.2	6.8±3.1	2.1±1.6
SM2	22	17.1±8.8	9.8±7.1	6.6±3.9	1.9±1.7
SM3	35	19.1±11.1	9.7±6.1	7.9±4.6	2.3±2.0
LVI [a]					
Positive	28	23.5±11.2****	10.5±6.8	9.7±4.8***	2.0±1.5
Negative	59	16.0±7.9****	9.0±5.9	6.3±2.9***	2.2±1.8
Lymph node metastasis[a]					
Positive	8	22.4±10.5	10.9±9.4	8.9±4.7	2.2±1.9
Negative	79	18.0±9.1	9.3±6.2	7.2±3.8	2.1±1.6
Desmoplastic response[a]					
Positive	32	20.1±10.6	8.6±5.1	8.2±4.9	2.3±2.0
Negative	55	17.3±9.8	10.0±6.8	6.9±3.3	2.0±1.5

*;**;***$P<0.01$,****$P<0.05$
[a] Mann–Whitney test
[b] Kruskal–Wallis test

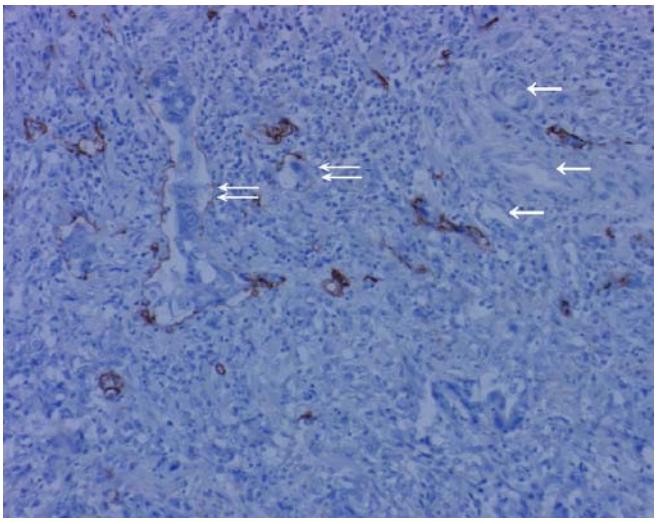

Fig. 1 High LMVD and increased LMMMD in peritumoral areas, assessed by anti-podoplanin immunostaining. Unstained blood vessels (*arrows*). Lymphatic vessel invaded by tumor cells (*double arrows*). Original magnification 200×

LMMMD, LMVD, and desmoplastic response

The desmoplastic response was not related to the LMMMA or LMVD in these specimens (Table 2).

Lymphatic endothelial proliferation and expression of Ki67

In all samples, serial sections were taken and stained for proliferating lymphatic endothelial cells using successive podoplanin and Ki67 staining. No Ki67 positive staining was seen in any lymphatic microvessel. There was no clear evidence supporting the presence of proliferating lymphatic endothelial cells either within or near the early-stage colorectal carcinomas, regardless of whether the tumor cells were clearly stained with Ki67.

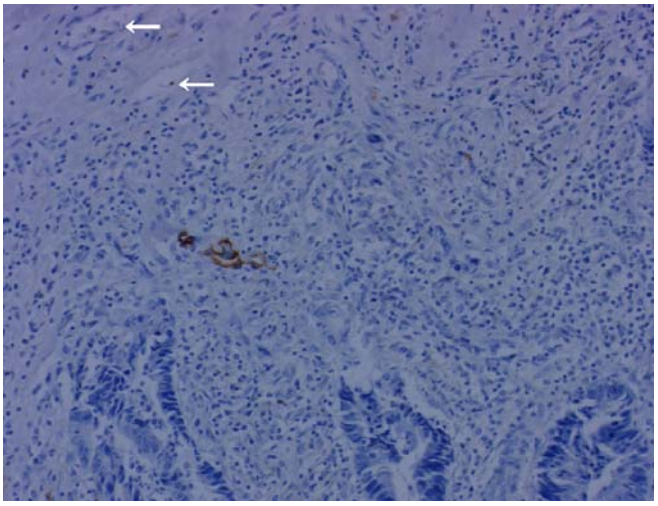

Fig. 2 Low LMVD and decreased LMMMD in peritumoral areas, assessed by anti-podoplanin immunostaining. Unstained blood vessels (*arrows*). Original magnification 200×

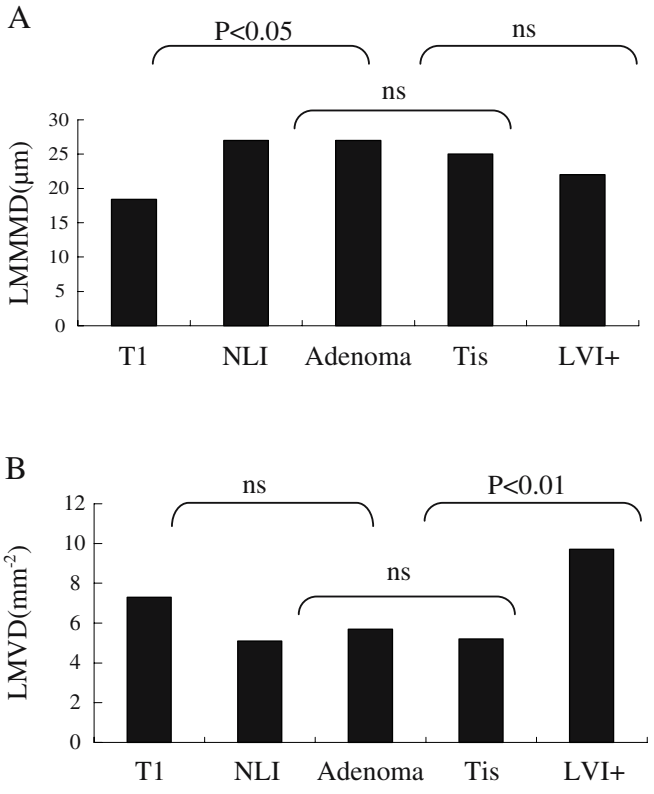

Fig. 3 a, **b** Comparison of LMMMD or LMVD among different groups: the peritumoral LMVD or LMMMD in the T1 carcinoma (T1), the submucosal LMMMD or LMVD of normal large intestine (NLI), adenoma, Tis carcinoma (Tis) and the peritumoral LMVD or LMMMA in the T1 carcinoma with LVI (LVI+). *ns* No significant difference

Discussion

Although lymphangiogenesis has been proven in some human carcinomas [1, 20, 26], information on the organization of lymphatic network in human colorectal cancer is limited. Little is known about density and diameter of

Table 3 Logistic regression analysis in relation to lymph node metastasis

Factor	Univariate *P*	Multivariate	
		Odds ratio	*P*
LVI positive	<0.0001	7.801	0.0052
Wall invasion SM1& SMm2 vsSM3	0.0047	2.370	0.3057
LMVDpt >7.3 vs ≤7.3	0.0120	0.194	0.1642
LMMMDpt >1.8 vs ≤1.8	0.0208	0.458	0.4987
LMVDpt >7.3 with LMMMDpt >1.8	0.0008	4.382	0.0363

lymphatic vessels in early-stage colorectal cancer. According to the adenoma–carcinoma sequence theory, most colorectal carcinomas arise from adenomas, which gradually increase in size and dysplastic grade. In this study, we present data about lymphatic microvessels in normal large intestine, adenomas, Tis carcinomas, and T1 carcinoma tissues using immunohistochemistry staining with antibodies to human podoplanin.

The peritumoral LMVD in the T1 carcinomas with LVI was greater than the submucosal LMVD of normal large intestine, adenoma, and Tis carcinoma; thus, the increased LMVD could be speculated to be caused by the tumor compacting the peritumoral areas, with overgrowing tumor cells (therefore increasing LMVD), or due to lymphangiogenesis. However, there was no significant difference among four groups, the peritumoral LMVD in the T1 carcinomas, LMVD in the submucosa of normal large intestine, adenoma, and Tis carcinoma, which supports the concept that lymphangiogenesis might be induced in the surrounding tumor areas of the T1 colorectal carcinoma with LVI. Similar results were also found in human breast cancer and malignant melanoma [20, 21]. Recent studies indicated that increased tumor expression of endothelial growth factors such as vascular endothelial growth factor C and VEGF-D could increase lymphangiogenesis around the primary tumor, and increase the number of tumor lymphatic vessels [22, 23].

Lymphatic vessels were almost exclusively found at the invasion margin of tumor, not within the tumor, a finding that agrees with recent studies [12, 13, 16, 20]. Unlike cardiovascular microvessels, which possess smooth muscle cells, lymphatic microvessels are highly sensitive to interstitial pressure [5, 11]. The increased interstitial pressure within the tumor, generated by overgrowing tumor cells, collapses lymphatic vessels, rendering them nonfunctional [12, 16]. The fact that we found rare lymphatic vessels with small LMMMD within tumor and that both main lymphatic vessels and most LVI were located in peritumoral areas also supports this theory. This fact also provides evidence that the lymphatic vessels, which are in areas surrounding the tumor, but not within tumor, are functional lymphatic vessels, which play a role in lymphatic metastases in T1 colorectal carcinoma.

It has been speculated that different type of extracellular matrices may cause difference in interstitial pressure [2]. Desmoplastic response, a kind of extracellular matrix change with highly fibrous stroma around invasive carcinomas [15], was not associated with LMMMD either within or surrounding tumor in these specimens. We speculated that the difference of LMMMD between peritumoral area of T1 carcinoma and in the submucosa of normal large intestine, adenoma, and Tis carcinoma might be related to tumor cells or combined tumor cells and stroma but not by stroma only.

The positive association between both LMVD and LMMMA in the peritumoral areas and LVI in T1 carcinoma could be explained through a lymphangiogenesis-induced increase of the "lymphatic window" or an increase of "lymphatic window areas" providing tumor cells with more opportunities to enter into lymphatic vessels. However, multivariate analysis indicated that high LMVDpt or LMMMDpt were not independent factors for lymph node metastases. Therefore, it is easy to speculate that high density or large diameter of lymphatic vessels is a prerequisite for lymphovascular invasion by tumor cells, but one has also to keep in mind that multiple factors, steps, and molecular participants are probably involved in the process of metastases from primary tumor cells to lymph nodes through the lymphatic system [2, 3, 7, 8, 14, 19].

In this study, there was no evidence of lymphatic endothelium proliferation at the time of excision. Therefore, active lymphangiogenesis could not be detected immunohistochemically. This neither confirms nor denies that lymphangiogenesis has occurred, as the increase in LMVD could have occurred while the tumor was growing before excision, and the newly formed, tumor-stimulated lymphatic microvessels may be in a mature state rather than in a proliferative state.

Our results also indicate that analysis of LMMMD and LMVD surrounding tumor before operation or after EMR could thus be useful for predicting lymph node metastasis and could contribute to the correct selection of treatment (EMR or radical excision) in patients with T1 carcinoma.

In conclusion, our results showed that the increased LMVDpt of T1 carcinoma in cases with LVI might be brought about by lymphangiogenesis; thus, evaluation of diameter and density of lymphatic vessels is important and is a good predictor of lymph node metastases in T1 colorectal carcinoma.

Acknowledgements The authors thank Mr. Tsutomu Kohda for technical assistance and Prof. J. Patrick Barron of the International Medical Communications Center of Tokyo Medical University for his review of this manuscript. This work was supported by the Tokyo Medical University Cancer Foundation (200409).

References

1. Birner P, Obermair A, Schindl M, Kowalski H, Breitenecker G, Oberhuber G (2001) Selective immunohistochemical staining of blood and lymphatic vessels reveal independent prognostic influence of blood and lymphatic vessel invasion in early-stage cervical cancer. Clin Cancer Res 7:93–97
2. Boardman KC, Swartz MA (2003) Interstitial flow as a guide for lymphangiogenesis. Circ Res 92:801–808
3. Bonfil RD, Bustuoabad OD, Ruggiero RA, Meiss RP, Pasqualini CD (1988) Tumor necrosis can facilitate the appearance of metastases. Clin Exp Metastasis 6:121–129
4. Breiteneder-Geleff S, Soleiman A, Kowalski H et al (1999) Angiosarcomas express mixed endothelial phenotypes of blood and lymphatic capillaries: podoplanin as a specific marker for lymphatic endothelium. Am J Pathol 154:385–394
5. Gerli R, Ibba L, Fruscheli C (1991) Ultrastructural cytochemistry of anchoring filaments of human lymphatic capillaries and their relation to elastic fibers. Lymphology 24:105–112
6. Hewitt RE, Powe DG, Carter GI, Turner DR (1993) Desmoplasia and its relevance to colorectal tumor invasion. Int J Cancer 53:62–69
7. He YL, Karpanen T, Alitalo K (2004) Role of lymphangiogenic factors in tumor metastasis. Biochim Biophys Acta 1654:3–12

8. Kozaki K, Koshikawa K, Tatematsu Y et al (2001) Multifaceted analyses of a highly metastatic human lung cancer cell line NCI-H460-LNM35 suggest mimicry of inflammatory cells in metastasis. Oncogene 20:4228–4234
9. Kudo S (1993) Endoscopic mucosal resection of flat and depressed type of early colorectal cancer. Endoscopy 25: 455–461
10. Kudo S, Tamegai Y, Yamano H, Imai Y, Kogure E, Kashida H (2001) Endoscopic mucosal resection of the colon: the Japanese technique. Gastrointest Endosc Clin N Am 11:519–535
11. Leak LV, Burke JF (1968) Electron microscopic study of lymphatic capillaries in the removal of connective tissue fluids and particulate substances. Lymphology 1:39–52
12. Leu AJ, Berk DA, Lymboussaki A, Alitalo K, Jain RK (2000) Absence of functional lymphatics within a murine sarcoma: a molecular and functional evaluation. Cancer Res 60:4324–4327
13. Liang P, Hong JW, Ubukata H et al (2005) Myofibroblasts correlates with lymphatic microvessel density and lymph node metastasis in early-stage invasive colorectal carcinoma. Anticancer Res 25:2705–2712
14. Mandriota SJ, Jussila L, Jeltsch M et al (2001) Vascular endothelial growth factor-C-mediated lymphangiogenesis promotes tumour metastasis. EMBO J 20:672–682
15. Nakada I, Tasaki T, Ubukata H et al (1998) Desmoplastic response in biopsy specimens of early colorectal carcinoma is predictive of deep submucosal invasion. Dis Colon Rectum 41:896–900
16. Padera TP, Kadambi A, Tomaso E et al (2002) Lymphatic metastasis in the absence of functional intratumor lymphatics. Science 296:1883–1886
17. Repici A, Tricerri R (2004) Endoscopic polypectomy: techniques, complications and follow-up. Tech Coloproctol 8: 283–290
18. Roche WD, Norris HJ (1975) Microinvasive carcinoma of the cervix. The significance of lymphatic invasion and confluent patterns of stromal growth. Cancer 36:180–186
19. Schoppmann SF, Schindl M, Breiteneder-Geleff S et al (2001) Inflammatory stromal reaction correlates with lymphatic microvessel density in early-stage cervical cancer. Anticancer Res 21:3419–3423
20. Schoppmann SF, Bayer G, Aumayr K, Taucher S, Geleff S, Ruda (2004) Prognostic value of lymphangiogenesis and lymphovascular invasion in invasive breast cancer. Ann Surg 240:306–312
21. Shields JD, Borsetti M, Rigby H et al (2004) Lymphatic density and metastatic spread in human malignant melanoma. Br J Cancer 90(3):693–700 (Feb 9)
22. Skobe M, Hawighorst T, Jackson DG et al (2001) Induction of tumor lymphangiogenesis by VEGF-C promotes breast cancer metastasis. Nat Med 7(2):192–198
23. Stacker SA, Caesar C, Baldwin ME et al (2001) VEGF-D promotes the metastatic spread of tumor cells via the lymphatics. Nat Med 7:186–191
24. Stacker SA, Baldwin ME, Achen MG (2002) The role of tumor lymphangiogenesis in metastatic spread. FASEB J 16:922–934
25. Straume O, Jackson DG, Akslen LA (2003) Independent prognostic impact of lymphatic vessel density and presence of low-grade lymphangiogenesis in cutaneous melanoma. Clin Cancer Res 9:250–256
26. Valencak J, Heere-Ress E, Kopp T, Schoppmann SF, Kittler H, Pehamberger H (2004) Selective immunohistochemical staining shows significant prognostic influence of lymphatic and blood vessels in patients with malignant melanoma. Eur J Cancer 40:358–364
27. Weidner N, Semple JP, Welch WR, Folkman J (1991) Tumor angiogenesis and metastasis-correlation in invasive breast carcinoma. N Engl J Med 324:1–8

Virchows Arch (2006) 448: 576–583
DOI 10.1007/s00428-006-0163-z

ORIGINAL ARTICLE

T. De Brito · L. F. Menezes · Dirce M. C. Lima · Silvia Lourenço · Ana Maria G. Silva · V. A. F. Alves

Immunohistochemical and in situ hybridization studies of the liver and kidney in human leptospirosis

Received: 22 August 2005 / Accepted: 18 January 2006 / Published online: 16 March 2006

Abstract An in situ hybridization (ISH) assay for the detection of leptospiral DNA in tissues was described and its diagnostic and pathogenetic usefulness in combination with immunohistochemistry (IHC) was evaluated in formalin-fixed, paraffin-embedded liver and kidney samples from human fatal cases of leptospirosis. IHC assays with anti-E-cadherin antibodies assessed the liver-plate disarray frequently observed in leptospirosis. Immunohistochemistry detected leptospiral antigen (LAg) in macrophages, both in human liver and kidney. In guinea pigs, in addition to these findings, staining on cell membranes of hepatocytes and, occasionally, in apical membrane of kidney tubular cells was demonstrated. Positive ISH signal was observed chiefly in the nuclei of human hepatocytes and in the cytoplasm and nuclei of liver cells of experimentally infected guinea pigs. Loss of E-cadherin membrane expression is associated with liver-plate disarray. These findings were discussed in the contention that, in leptospirosis, cell membrane damage might be important for the pathogenesis of the disease. Finally, it was suggested that both IHC and/or ISH might be used for both diagnostic and research purposes.

T. De Brito (✉) · L. F. Menezes · D. M. C. Lima · S. Lourenço · A. M. G. Silva · V. A. F. Alves
Institute of Tropical Medicine,
University of Sao Paulo Medical School,
Sao Paulo, SP, Brazil
e-mail: thalesbr@usp.br
Tel.: +55-11-30667066
Fax: +55-11-30645132

T. De Brito · L. F. Menezes · D. M. C. Lima · S. Lourenço · A. M. G. Silva · V. A. F. Alves
Department of Pathology,
University of Sao Paulo Medical School,
Sao Paulo, SP, Brazil

V. A. F. Alves
Adolpho Lutz Institute, Sao Paulo Health Service,
Sao Paulo, Brazil

Keywords Leptospirosis · Liver and kidney pathology · Antigen detection · E-cadherin immunohistochemistry · In situ hybridization

Introduction

Leptospirosis is an acute septicemic febrile illness, caused by *Leptospira interrogans*, which affects humans or animals in all parts of the world. In humans, it is a zoonosis and its reservoirs are chronically infected carrier animals. There is a worldwide strong occupational association and a universal risk from rodent-carrier-mediated infection, especially prevalent in tropical countries where it occurs in endemic and epidemic bouts, chiefly during the rainy season [7, 14].

Leptospirosis has a biphasic clinical presentation, beginning with a septicemic phase followed by an immune phase with antibody production and urinary excretion of leptospire. In severe cases, leptospirosis is a multisystemic febrile illness, chiefly with hepatic, renal, and pulmonary involvement. The most severe form of leptospirosis is known as Weil's syndrome and can lead to fatality in a short time [18].

Microscopic agglutination test remains an excellent serological assay and yields information on the presumptive infecting serogroup. In fatal human cases [1] and in farm animals [13], diagnosis by immunohistochemistry (IHC) is specific and also offers clues to the understanding of the pathogenesis of the disease.

Morphology and antigenic structure as well as the genetic composition and organization of ribosomes and nucleic acids of leptospires were recently reviewed [14]. rRNA genes are very conserved throughout the bacterial kingdom and partial sequences have been analyzed in terms of oligonucleotide signatures. Mérien et al. [19] reported the development of a sensitive assay for leptospires DNA based upon amplification of oligonucleotide sequences of the *Leptospira* rrs (16S) gene [15]. Recently, the complete genomic sequence of a representative virulent serovar type (*Lai*) of *L. interrogans* was obtained by the

Chinese National Human Genome Center at Shanghai [28]. The genomic sequence of *L. interrogans*, serovar *Copenhageni*, was established by a Brazilian group [21, 22].

In the light of these results, this paper describes an in situ hybridization assay (ISH) for the detection of leptospire DNA in tissues. Liver and kidney lesions were chosen for analysis because, with vascular lesions, they form an important part of the systemic manifestations of leptospirosis. The diagnostic and chiefly the pathogenetic usefulness of this technique were evaluated and compared to immunohistochemistry in formalin-fixed, paraffin-embedded liver and kidney samples from human fatal cases of leptospirosis. In addition, E-cadherin expression was used as a marker of cell–cell junction integrity to assess the specificity and potential pathogenetic role of liver-plate disarray, a common histological finding in leptospirosis.

Materials and methods

Human samples

Ten patients, eight males and two females, ranging from 20- to 68 years old, were autopsied with a diagnosis of Weil's syndrome. Major clinical and laboratory findings are shown in Table 1. In brief, illness duration ranged from 3 to 15 days (average of 7.8 days) and all patients commenced suddenly with headache, malaise, muscle pains and, except for one, high fever. All of them developed marked jaundice, palpable enlarged liver, acute renal failure, and, with one exception, pulmonary and digestive tract hemorrhage with conjunctival suffusions. Epidemiological data showed that most patients had had contact with contaminated water, mainly from floods and sewage cleaning. Serology was performed in five patients. One of them had enzyme-linked immunosorbent assay (ELISA) IgM+seroagglutination 1/3,200 for *L. interrogans*, serovar, and serogroup *Cynopteri.* In three other patients, with 5 days of illness, serological tests were negative. In another patient, also with 5 days of illness, blood culture was positive for *L.interrogans* serovar *Butembo*, serogroup *Autumnalis*.

Kidney and liver samples were obtained from autopsies performed after 6 to 12 h of death (average 9 h). The tissues were fixed in formalin, embedded in paraffin, and routinely stained with hematoxylin eosin. The kidney and liver samples of eight non-leptospirotic patients were obtained from autopsies performed within the same post-mortem interval; three normal liver biopsies obtained from liver

Table 1 Leptospirosis: clinical and laboratory data

Case no./ sex/age (years)	Clinical and epidemiological information	Illness duration (days)	Laboratory data related to leptospirosis
1/f/54	Contact with contaminated water (floods); fever, headache, conjunctival suffusion, muscular pain, acute renal failure, hemorrhagic sputum, jaundice, dehydration	11	ELISA IgM+, seroagglutination 1/3,200 (*L. interrogans* serovar and serogroup *Cynopteri*)
2/m/58	Contact with contaminated water (floods); fever, jaundice, muscular pain, acute renal failure, dehydration, pulmonary hemorrhage	5	Serological tests for leptospirosis, negative
3/m/59	Contact with contaminated water (fall into a well); muscular pain, acute renal failure, jaundice, dehydration	3	Blood culture positive for *L. interrogans* serovar *Butembo*, serogroup *Autumnalis*
4/m/53	Contact with contaminated water (floods); fever, jaundice, muscular pain, acute renal failure, dehydration, hemorrhagic syndrome (pulmonary and digestive tract)	15	None available
5/m/46	Contact with contaminated water (floods); fever, jaundice, muscular pain, dyspnea and hemorrhagic sputum	5	None available
6/m/68	Fever for the last 5 days, muscular pain, jaundice, acute renal failure	7	Seroagglutination negative, ELISA IgM positive
7/m/27	Contact with sewage and rats; fever for the last 5 days, jaundice, muscular pain, acute renal failure, hemorrhagic syndrome (pulmonary and digestive tract)	5	Seroagglutination negative, ELISA IgM positive
8/m/51	Fever for the last 7 days, marked jaundice and muscular pain for the last two days, anemia, leukocytosis, thrombocytopenia and renal failure; patient was HIV+	7	None available
9/m/20	Fever, muscular pain for the last 5 days, jaundice for the last 4 days, bipalpebral edema and acute renal failure, pulmonary hemorrhage, abdominal pain and vomits, low platelets count	5	None available
10/f/67	Contact with rats and contaminated water; fever and muscular pain for the last 8 days, jaundice for the last 6 days and conjunctival hemorrhage, dyspnea and hemorrhagic sputum, acute renal failure	8	None available

transplant donors were used as negative controls. The samples were processed as described above.

Guinea pig samples

Fifteen guinea pigs were infected with a virulent culture of *L. interrogans*, serovar *Copenhageni*. The animals developed the disease 5 days after inoculation. Liver and kidney samples were obtained and processed as described above. The tissues were compared to the human samples and used as positive controls. Liver and kidney samples of nine non-infected guinea pigs were used as negative controls.

Immunohistochemistry assay

IHC studies were performed to assess the presence of leptospiral antigen/s (LAg) and abnormalities in cell–cell junctions. Two primary sera were used for the detection of LAg. One serum was obtained by hyper-immunizing the sheep with sequential intravenous doses of 1, 2, 3, and 4 ml of *L. interrogans*, serogroup *Icterohaemorrhagiae*. The leptospires were obtained from 7 to 10 days of cultures grown at 28°C in Ellinghausen–McCullough–Johnson–Harris medium (DIFCO). Seven days after the last inoculation, an 80-ml blood sample was drawn. IgG was obtained by octanoic acid fractionation, purified, and used in a 1:30,000 concentration in 1% bovine serum albumin (BSA) in phosphate-buffered saline (PBS). The second immune serum was raised in rabbits according to a previously described standard procedure [12].

Anti-E-cadherin monoclonal antibody was employed to assess cell–cell attachment status in liver. These studies were restricted to five leptospirotic and five non-leptospirotic patient autopsies and three liver transplant donor biopsies. All autopsies were performed within 6 h post-mortem and showed well-preserved histopathological structures.

Kidney and liver 3-μm sections were analyzed using EnVision (Dako, USA)-based immunohistochemistry methods. Antigen retrieval protocol, primary antibodies clones, sources, and concentrations are summarized in Table 2. Staining was completed with the chromogen 3,3′ diaminobenzidin. All specimens were then lightly counterstained with hematoxylin.

The presence of nonspecific staining with the LAg sheep antibody was assessed in experiments with pre-cleared sera. In brief, 1-ml aliquots of anti- *L. interrogans* antibody was absorbed at 4°C, overnight, with 100 mg of normal human liver and 30 mg of normal human kidney powder, and used for immunohistochemistry in tissues not subjected to antigen retrieval. In this procedure, the primary sheep antibody was diluted at 1:40,000 in 1% BSA in PBS. Reactions in which primary antibody was replaced with saline or normal human serum were also performed as negative controls.

In situ hybridization

Two oligonucleotide probes were synthesized to detect leptospiral nucleic acids. Probe one (5′-CAA GTC AAG CGG AGT AGC AAT ACT CAG CGG CGA ACG GGT G-3′, Eurogentec S/A) is a sense fluorescein-labeled probe complementary to sequences A and C used for polymerase chain reaction (PCR) assays described by Mérien et al. [19].

Probe two (5′-GAT CTG AAC TTT ATA GAT TGA TTT CTA AAA TGT-3′, Invitrogen, USA) was designed based on the published genomic sequence of *L. interrogans*, serovar *Lai*, serogroup *Icterohaemorrhagiae*. Genes coding for small proteins of unknown function, conserved in *Leptospira* but with low identity levels in vertebrates, were chosen as candidates for probe generation. Thirty to thirty-three base sense cDNA probes were designed using PRIMER3 [25] with default conditions. The probes thus obtained were tested for nonspecific human complementary sequences using short-sequence nucleotide–nucleotide Blast (http://www.nebi.nlm.nih.gov/BLAST); those with least similarity were also checked against hepatitis B virus genome to minimize the chances of cross-reaction. Using this approach, a sequence also present in *L. interrogans*, serovar *Copenhageni*, was chosen from the sequence AEO11585.1:119–250 and used for fluorescein-labeled cDNA synthesis. Both probes recognize sequences conserved in several species of leptospires, both pathogenic and saprophites. Probe one has 45% identity (a sequence of 18 nucleotides) and probe two 57% (sequence of 19 nucleotides) with the human genome.

A negative control probe (scrambled probe 5′-CAG AAC GCG AGA CGT TAG ACC TCA ATG ACG GAG GGC AGG T-3′, Invitrogen) was obtained from probe one using a scrambling algorithm developed by T. Schubert (http://www.personal.uni-jena.de/~sth/scramble.html). To reduce the possibility of cross-reactions with other genes, the scrambled probe was compared to genomic banks of

Table 2 Immunohistochemical protocols

Primary serum	Clone	Source	Antigen retrieval	Primary serum titer	Secondary antibody
L intrrogans (sheep polyclonal)	–	See text	Steamer in citrate, pH 6.0	1:30,000	EnVision peroxidase (DAKO code K1490)
L interrogans (rabbit polyclonal)	–	[12]	Steamer in citrate, pH 6.0	1:5,000	EnVision peroxidase (DAKO code K1490)
E-cadherin (mouse monoclonal)	Clone 36B5	Novocastra Lab, Newcastle, UK	Steamer in in TRS (DAKO code S1699)	1:25 (autopsies) 1:50 (liver biopsies)	EnVision peroxidase (DAKO code K4001)

various organisms using the BLAST program (http://www.ncbi.nih.gov/BLAST) showing no significant similarities.

For ISH, 3-μm sections were deparaffinized, rehydrated through a graded series of ethanol, and washed with water treated with 0.1% diethylpyrocarbonate (DEPC) for 5 min. The sections were incubated with 25 μg/ml of Proteinase K (Sigma, St Louis, MO, USA) in PBS for 10 min at 37°C and then permeabilized with 2% Triton in Tris–HCl, 10 mM, at room temperature. The sections were rinsed with DEPC water for 10 min and incubated at 95°C for 7 min in hybridization buffer (50% dextran sulphate, 20× SSC, 50× Denhart's, 10 mg/ml of salmon sperm DNA, 10 mg/ml of yeast tRNA, 1 mg/ml of Poly A–Poly C, 100 mg/ml of inorganic pyrophosphate in 1 M Tris buffer, pH 7.4, deionized formamide, and DEPC). The sections were then incubated overnight at 55°C, with the corresponding probe, at a concentration of 0.340 μg/μl in hybridization buffer. After incubation, the sections were washed in Tris–HCl, pH 7.4, at 37°C for 10 min and further washed with water, five times for 5 min.The slides containing the tissue sections were finally air dried and mounted with Vecta-Shield and the reactions were visualized under epi-fluorescence microscope.

As an alternative, after proteinase K 12.5 mg/ml during 10 min at 37°C, the probes were incubated overnight at 42°C in a different hybridization buffer (50% deionized formamide, 10% dextran sulphate, 2× SSC, and 0.4 mg/ml salmon sperm DNA).

Results

The clinico-epidemiological data of the selected patients were highly suggestive of leptospirosis. The illness was usually of short duration and this, associated with delayed clinical diagnosis, contributed to the lack of some important confirmatory laboratory tests. Autopsies showed classical findings described in patients dying of Weil's syndrome [5, 8, 24], including acute myositis with hyalin change of necrotic muscular fibers affecting chiefly calf musculature; pulmonary and/or digestive hemorrhage; focal myocarditis; and liver pathology manifested chiefly by cholestatic hepatitis with complete or partial liver-plate

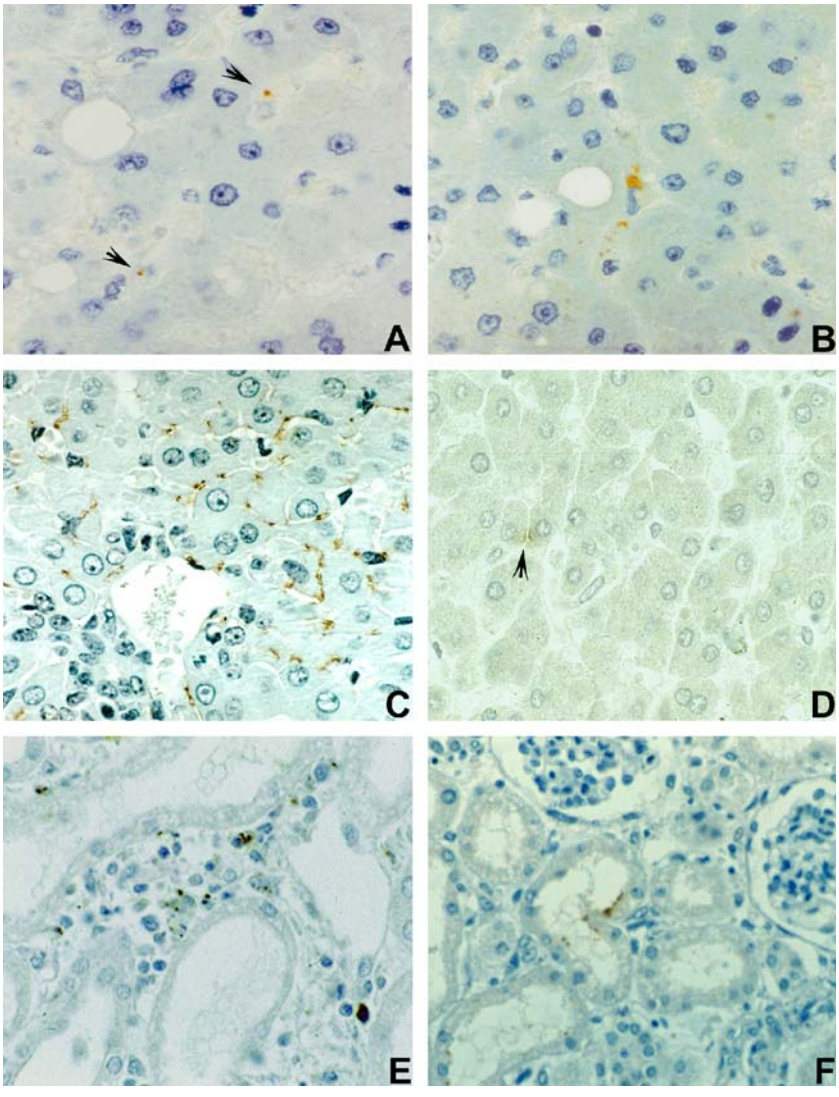

Fig. 1 **a** Liver in human fatal leptospirosis. LAg deposits visualized as small dots in the cytoplasm of Kupffer cells (*arrows*). There are isolated hepatocytes showing fatty change. IHC and light hematoxylin counterstain, ×400. **b** Liver in human fatal leptospirosis. LAg deposit in the cytoplasm of a Kupffer cell. Focal fatty change is also present. IHC and hematoxylin, ×400. **c** Experimental leptospirosis of the guinea pig. LAg detected on the liver cell membrane. IHC and hematoxylin, ×400. **d** Human fatal leptospirosis. Faint LAg deposit on the cell membrane of two adjacent liver cells (*arrow*). There is liver-plate disarray. IHC and hematoxylin, ×400. **e** Kidney in human fatal leptospirosis. LAg is present in the cytoplasm of monocytes of the kidney mixed interstitial inflammatory infiltrate. Tubules dilated with flat epithelial lining (acute tubular necrosis), ×400. **f** Kidney in human fatal leptospirosis. Focal LAg deposit on the luminal side of proximal tubule cells. Reactive nonspecific mesangioproliferative glomerulitis is also present. IHC and hematoxylin, ×300

disarray, occasional mitotic figures, and binucleation of hepatocytes; portal spaces' edema with acute and chronic inflammation; and proliferation of Kupffer cells along the sinusoidal lining [5]. Renal pathology showed focal interstitial nephritis, with lymphocytes, macrophages, plasma cells, and occasionally few eosinophils. Interstitial edema was observed in areas of tubular necrosis. In all cases, mild focal nonspecific reactive mesangio-proliferative glomerulonephritis was seen.

IHC analysis showed similar results with both immune sera. In addition, the experiments with pre-cleared sera confirmed the staining pattern. In nine of the ten patients, LAg was detected usually as dots, rarely as deposits in the cytoplasm of isolated macrophages which are part of the mixed portal inflammatory infiltrate, and more frequently in the cytoplasm of macrophages along the sinusoidal lining (Kupffer cells and circulating macrophages) (Fig. 1a,b). LAg expression was not observed on hepatocytes' membrane, except for one case in which a faint focal LAg deposit was detected on the cell membrane of two adjacent hepatocytes (Fig. 1d). In the kidney, LAg deposits were observed also in the cytoplasm of macrophages associated with the focal interstitial infiltrate (Fig. 1e). LAg deposits were seldom seen on the luminal side of tubular cells (Fig. 1f).

Diseased guinea pigs showed areas of liver-plate disarray and linear deposits of LAg on the hepatocyte membrane (Fig. 1c) as well as granular deposits in macrophages detected in portal spaces and Kupffer cells. In the kidney, the LAg deposits were observed in macrophages of the interstitial infiltrate. Linear deposits of LAg were occasionally seen on the luminal side of tubular cells.

Expression of E-cadherin was prominent on the cell membrane of hepatocytes both in liver transplant donor biopsies and in autopsy control specimens (Fig. 2a). In leptospirotic patients, expression of E-cadherin in liver cells was irregular. In areas of liver-plate disarray, hepatocytes without any expression of E-cadherin were present adjacent to hepatocytes with partial presence of E-cadherin on the cell membrane (Fig. 2b). In hepatic areas without disarray, the E-cadherin expression was similar to the control livers.

In situ hybridization staining revealed similar results with both probes and protocols. In nine patients, signal was observed in a few hepatocytes as an apple-green round or ring-like structure in the nuclei of liver cells (Fig. 2c). Only one patient (Table 1, case 9), in whom frequent mitotic figures could be detected in the liver, showed both cytoplasmic and nuclear signal (Fig. 2d). No convincing signal was seen in cells of the portal inflammatory infiltrate. Definite nuclear ISH signal was not observed in kidney tubular cells and was absent in macrophages of the interstitial focal inflammatory infiltrate.

The liver of 8 of 15 infected guinea pigs exhibited nuclear signal similar to that seen in human cases. In two of the eight guinea pigs, a small round cytoplasmic signal was also detected in the liver cells. No convincing signal was observed in the kidney. Human and guinea pig negative controls displayed no leptospiral ISH signals.

Discussion

Leptospirosis is an acute septicemic disease involving several organs. The demonstration by immunohistochemistry of LAg in cells of the inflammatory infiltrate both in human liver and kidney is expected as a response to circulating antigen/s. In the experimental model, LAg is

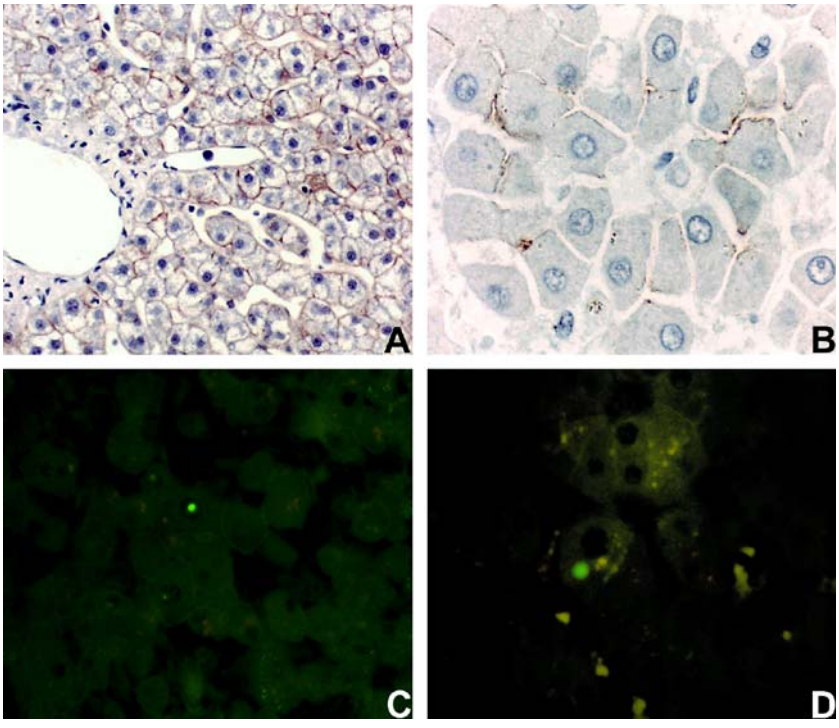

Fig. 2 **a** Control (non-leptospirotic) human liver showing normal E-cadherin expression over the cell membrane. IHC and hematoxylin, ×200. **b** Human fatal leptospirosis. Liver shows liver-plate disarray and irregular expression of E-cadherin. There are hepatocytes with no E-cadherin expression adjacent with others showing partial membrane E-cadherin expression. IHC and hematoxylin, ×400. **c** Human fatal leptospirosis. In situ hybridization (*ISH*). Hepatocyte showing nuclear signal. Fluorescent in situ hybridization (*FISH*), ×300. **d** Human fatal leptospirosis. Cytoplasmic signal close to the nucleus of a hepatocyte. FISH, ×400

demonstrated not only phagocytized by macrophages but also adhering to hepatocyte membrane, particularly at the zone III of the liver lobule where liver-plate disarray is usually more pronounced [2, 3, 20]. Adhesion of leptospires and/or their degradation products to cell and even to basement membranes and extracellular matrix has been described [2, 3, 14]. In our previous studies, immunoelectron microscopy in the guinea pig model of leptospirosis had revealed gold-labeled LAg close to cell membranes of hepatocytes, kidney tubular cells, and endothelial cells of the interstitial capillaries. The antigen/s were afterward internalized by hepatocytes and renal tubular cells and eventually found in lysosomes within damaged cells [12]. The affinity of leptospires for cell and basal membranes is directly related to its virulence. It is interesting that a fibronectin-binding protein expressed on the surface of virulent *L. interrogans*, serovar *Icterohaemorrhagiae*, is believed to be important for adhesion and invasion of leptospires [6].

In humans, LAg deposits are usually not found on the membrane of hepatocytes and can seldom be detected at the luminal side of renal tubular cells. The difference in expression pattern between the human disease and the guinea pig model may be attributed to several reasons: (1) in the experimental model, the number of injected leptospires could be much larger than in average human infection, leading to higher detection rate in the animals; (2) as mentioned earlier, LAg is initially localized to the cell membranes but is later found in lysosomes and is finally degraded; therefore, it is conceivable that different phases in the disease progression might account for differences in staining patterns; (3) the disease process might be different between both species; and (4) finally, post-mortem alterations might be responsible for decreased signal intensity in human samples.

Cadherins are members of a family of adhesion molecules involved in calcium-dependent homotypic cell–cell interactions [4]. E-cadherin is a 120-kDa glycoprotein that is highly expressed during development and is the predominant cadherin of the liver epithelium. It is concentrated in the adherens junction, where it interacts with actin filaments. In the absence of E-cadherin, epithelial cells are not capable of a stable intercellular adhesion.

Our results suggest an irregular expression of E-cadherin in liver cells in human leptospirosis. This alteration might be primarily related to cell membrane lesion or secondary to other hepatocyte injuries. In either case, the persistence, at least partially, of E-cadherin expression might be a marker for restoration of a normal liver cell membrane function in cases of recovery from the disease and merits attention as a potential prognostic marker and/or factor.

Liver cell-plate disarray, when present at autopsy, is a major histopathologic marker of liver involvement in leptospirosis [5, 8, 24]. However, it was not observed in biopsy studies [1, 10, 11] and its absence raised the hypothesis that this aspect might appear only at a more acute phase of the disease or during the agonal period. The proponents of this idea argued that human biopsies could only be performed when the hemorrhagic phase had subsided and the patients, therefore, were in an early recovery phase of the disease. Furthermore, experimental work on a sequential daily basis validated the liver-plate disarray [3, 20]. Taken together, these results suggest that, even if agonal and post-mortem changes can worsen the liver pattern, the lesion is genuine and regresses rapidly, which justifies its absence in biopsy studies.

Deposits on the host cell membrane of LAg and loss of E-cadherin membrane expression in leptospirotic patients might corroborate previous suggestions that cell membrane damage is the primary lesion in leptospirosis, mediated by a glycolipoprotein (GLP) [12, 26, 27] or lipoproteins transported to the leptospiral surface and/or secreted [22]. In agreement with these suggestions is the demonstration that GLP in the experimental model has also an intense affinity for hepatocyte cell membranes and is detected by IHC only at the late phase of the disease as granules both in the cytoplasm of macrophages and on the cell membranes, suggesting that its presence is the result of partial leptospiral degradation secondary to phagocytosis [2, 3, 23]. Vinh et al. [27] suggested that such adherence of leptospires and/or their products might lead subsequently to the microorganism fatty acids to be intercalated into the cell membrane. It is worth remembering, however, that leptospires have, as the major carbon and energy sources, long-chain fatty acids from which energy is derived mainly by beta-oxidation [14]. Therefore, as an alternative to Vinh's [27] suggestion, we might speculate that the microorganism's adherence to cell is necessary to supply its energy requests which would be provided by cell membrane fatty acids.

ISH detected sequences of leptospires chiefly in the nuclei of liver cells in human cases. The relevance of this finding, if any, is unknown at the moment. However, when we take into account the occasional human and experimental ISH findings showing also a cytoplasmic signal together with the immunoelectron findings of the experimental disease [12], it is possible to suppose that leptospiral nucleotide sequences, initially localized on the cell membrane and subsequently internalized by the endocytic lysosomic pathway, might migrate to the nucleus. Supporting this hypothesis, Darji et al. [9], working with an attenuated strain of *Salmonella typhimurium*, observed a similar nuclear staining pattern and suggested that lysis of bacteria in the phagolysosome compartment and escape to the cytosol of the host cell should precede the plasmid DNA transfer into the nucleus. Moreover, Holmgren et al. [17] demonstrated that cultivation of apoptotic bodies derived from Epstein–Barr virus (EBV)-carrying cell lines with either fibroblasts, monocytes, or endothelial cells resulted in the uptake of DNA and expression of EBV-specific markers in the recipient cells. Therefore, it is conceivable that specific nuclear staining could be visualized in leptospirotic patients. The weaker signal observed with ISH when compared to IHC might have several explanations: (1) IHC reactions were performed using amplification-based protocols, which usually increase the signal by several folds and (2) the LAg sera were obtained from whole *Leptospira*, and it is expected to recognize several

different epitopes, which would result in stronger signal when compared to the single-sequence-based small ISH probes.

The characteristics mentioned above might render the IHC reactions prone to nonspecific results. Our results, however, confirm that the available antibodies are specific and might be used, as previously reported [16, 29], for diagnostic purposes in situations in which leptospirosis is suspected and/or to study disease process in leptospirosis animal models [1–3, 20]. ISH and IHC apparently can detect leptospirosis with the same sensibility. The unique ISH staining pattern, however, suggests that this technique might be more useful in human and experimental pathogenetic assays.

In conclusion, this study brings further support to the idea that cell membrane lesion might play an important role in leptospirosis pathogenesis. Furthermore, we show herein that the loss of E-cadherin membrane expression is associated with liver-plate disarray, stressing that this feature is a genuine lesion in leptospirosis and suggesting that this finding might have prognostic relevance. Finally, we suggest that IHC and ISH might be used for both diagnostic and research purposes.

Acknowledgements This work was supported by grants of the CNPq (300857 / 94-2 -NV) and LIM 06 FMUSP. Dr.Bruce Kline, from the Mayo Clinic, Rochester, MN, USA, and Dr.Glaucia Paranhos, from Inserm, France, advised on probe one design.

References

1. Alves VAF, Vianna MR, Yasuda PH, De Brito T (1987) Detection of leptospiral antigen in the human liver and kidney using an immunoperoxidase staining procedure. J Pathol 15:125–131
2. Alves VAF, Gayotto LCC, Yasuda PH, Wakamatsu A, Kanamura CT, De Brito T (1991) Leptospiral antigens (*L. interrogans* serogroup *Ictero-haemorrhagiae*) in the kidney of experimentally infected guinea pigs and their relation to the pathogenesis of the renal injury. Exp Toxicol Pathol 42:81–93
3. Alves VAF, Gayotto LCC, De Brito T, Santos RTM, Wakamatsu A, Vianna MR, Sakata EE (1992) Leptospiral antigens in the liver of experimentally infected guinea pigs and their relation to the morphogenesis of liver damage. Exp Toxicol Pathol 44:425–434
4. Andreoli TE (1999) Cell adhesion molecules and human disease. Am J Med 106:466–476
5. Arean V (1962) The pathologic anatomy and pathogenesis of fatal human leptospirosis (Weil's disease). Am J Pathol 40:393–423
6. Barnett JK, Barnett D, Bolin C, Summers TA, Wagar EA, Cheville NF, Hartskeerl RA, Haake DA (1999) Expression and distribution of leptospiral outer membrane components during renal infection of hamsters. Infect Immun 67:853–861
7. Barthi AR, Nally JR, Ricaldi JN, Matthias MA, Diaz MM, Lovett MA, Levett PN, Gilman MR, Willig MR, Gotuzzo E, Vinetz JM (2003) Review leptospirosis: a zoonotic disease of global importance. Lancet Infect Dis 3:757–771
8. Beitzke H (1916) Ueber die pathologische Anatomie der ansteckenden Gelbsucht (Weilsche Krankheit). Klin Wochenschr 53:188–191
9. Darji A, Guzmán CA, Gerstel B, Wachholz P, Timms KN, Wehland J, Chakraborty T, Weiss S (1997) Oral somatic transgene vaccination using attenuated *S. typhimurium*. Cell 91:765–775
10. De Brito T, Marcondes Machado M, Montans SD, Hoshino S, Freymuller E (1967) Liver biopsy in human leptospirosis: a light and electron microscopy study. Virchows Arch Path Anat 342:61–69
11. De Brito T, Penna DO, Hoshino S, Pereira VC, Caldas ACPG, Rothstein W (1970) Cholestasis in human leptospirosis: a clinical, histochemical, biochemical and electron microscopy study based on liver biopsies. Beitr Path Anat 140:345–361
12. De Brito T, Prado MJBA, Negreiros VAC, Nicastri AL, Sakata EE, Yasuda PH, Santos RT, Alves VAF (1992) Detection of leptospiral antigen (*L. interrogans* serovar *Copenhageni* serogroup *Icterohaemorrhagiae*) by immunoelectron microscopy in the liver and kidney of experimentally infected guinea pigs. Int J Exp Pathol 73:633–642
13. Ellis TM, Robertson GM, Hustas L, Kirby M (1983) Detection of leptospires in tissue using an immunoperoxidase staining procedure. Aust Vet J 60:364–367
14. Faine S, Adler B, Bolin C, Perolat P (eds) (1999) Leptospira and leptospirosis, 2nd edn. MediSci, Melbourne, Australia
15. Fukunaga M, Horie I, Okuzako N, Mifuchi I (1990) Nucleotide sequence of a 16S rRNA gene for *Leptospira interrogans* serovar canicola strain Moulton. Nucleic Acids Res 18:366
16. Guarner I, Wun Ju S, Morgan J, Bragg SL, Bajani MD, Tappero JW, Zaki S (2001) Leptospirosis mimicking acute cholecystitis among athletes participating in a thriathlon. Hum Pathol 32:750–752
17. Holmgren L, Szeles A, RajnavölgyI E, Folkman J, Klein G, Ernberg I, Falk KI (1999) Horizontal transfer of DNA by the uptake of apoptotic bodies. Blood 93:3956–3963
18. Levett PN (2001) Leptospirosis. Clin Microbiol Rev 14:296–326
19. Mérien F, Amouriaux P, Perolat P, Baranton G, Saint Girons I (1992) Polymerase chain reaction for detection of *Leptospira* spp in clinical samples. J Clin Microbiol 30:2219–2224
20. Nally JE, Chantranuwat C, Wu XY, Fishbein MC, Pereira MM, Silva JJP, Blanco DR, Lovett MA (2004) Animal model: alveolar septal deposition of immunoglobulin and complement parallels pulmonary hemorrhage in a guinea pig model of severe pulmonary leptospirosis. Am J Pathol 163(4):1115–1127
21. Nascimento ALT, Ko AI, Martins EAL, Monteiro-Vitorello CB, Ho PL, Haake DA, Verjovski Almeida S, Hartskeerl RA, Marques MV, Oliveira MC, Menck CFM, Leite LCC, Carrer H, Coutinho LL, Degrave WM, Dellagostin OA, El-dorry H, Ferro ES, Ferro MIT, Furlan LR, Gamberini M, Giglioti EA, Góes Neto A, Goldman GH, Goldman MHS, Harakava R, Jerônimo SMB, Junqueira-de-Azevedo ILM, Kimura ET, Kuramae EE, Lemos EGM, Lemos MVF, Marino CL, Nunes LR, de Oliveira RC, Pereira GG, Reis MS, Schriefer A, Siqueira WJ, Sommer P, Tsai SM, Simpson AJG, Ferro JÁ, Camargo LEA, Kitajima JP, Setubal JC, Van Sluys MA (2004) Comparative genomics of two *Leptospira interrogans* serovars reveals novel insights into physiology and pathogenesis. J Bacteriol 186:2164–2172
22. Nascimento ALT, Verjovski Almeida S, Van Sluys MA, Monteiro Vitorello CB, Camargo LEA, Digiampitri LA, Harstkeerl RA, Ho PL, Marques MV, Oliveira MC, Setubal JC, Haake DA, Martins EAL (2004) Genome features of *Leptospira interrogans* serovar *Copenhageni*. Braz J Med Biol Res 37:459–478

23. Pereira MM, Andrade J, Lacerda MD, Batoreu NM, Marchevisky RS, Ribeiro dos Santos R (1997) Demonstration of leptospiral antigens on tissues using monoclonal antibodies and avidin–biotin–peroxidase staining. Exp Toxicol Pathol 49:505–511
24. Pick L (1917) Zur pathologischen Anatomie des infektiösen Ikterus. Klin Wochenschr 54:451–455
25. Rozen S, Skaletsky HJ (2000) Primer on the WWW for general users and for biologist programmers. In: Krawetz S, Misener S (eds) Bioinformatics methods and protocols—methods in molecular biology. Humana, Totowa, NJ, pp 365–386 (Code available at http://www-genome.wi.mit.edu/genome-software/other/primer3.html)
26. Vinh T, Adler B, Faine S (1986) Ultrastructure and chemical composition of lipopolysaccharide extracted from *Leptospira interrogans* serovar *Copenhageni*. J Gen Microbiol 132:103–109
27. Vinh T, Adler B, Faine S (1986) Glycoprotein cytotoxin from *Leptospira interrogans* serovar *Copenhageni*. J Gen Microbiol 132:111–123
28. Xi Ren S, Fu G, Jiang XG, Zeng R, Miao YG, Xu H, Zhang YX, Xiong H, Lu G, Lu LF, Jiang HQ, Jia J, Tu YF, Jiang JX, Gu WY, Zhang YQ, Cal Z, Sheng HH, Yin HF, Zhang Y, Zhu GF, Wan M, Huang HL, Qian Z, Wang SY, Ma W, Yao ZJ, Shen Y, Qiang BQ, Xia QC, Guo XK, Danchin A, Saint Girons I, Somerville RL, Wen YM, Shi MH, Chen Z, Xu JG, Zhao GP (2003) Unique physiological and pathogenic features of *Leptospira interrogans* revealed by whole-genome sequencing. Nature 422:888–893
29. Zaki SR, Shieh WJ, Epidemic Working Group (1996) Leptospirosis associated with outbreak of acute febrile illness and pulmonary haemorrhage, Nicaragua, 1995. Lancet 347:535–536

Virchows Arch (2006) 448: 584–590
DOI 10.1007/s00428-006-0160-2

ORIGINAL ARTICLE

Alina Romanenko · Luisa Morell-Quadreny · David Ramos · Valentin Nepomnyaschiy · Alexander Vozianov · Antonio Llombart-Bosch

Extracellular matrix alterations in conventional renal cell carcinomas by tissue microarray profiling influenced by the persistent, long-term, low-dose ionizing radiation exposure in humans

Received: 7 June 2005 / Accepted: 27 December 2005 / Published online: 9 March 2006

Abstract The present study was carried out in order to examine molecular alterations of extracellular matrix (ECM), associated with cell–cell communication in conventional (clear-cell) renal cell carcinomas (cRCCs) influenced by persistent long-term, low-dose ionizing radiation (IR) exposure to patients living more than 19 years after the Chernobyl accident in Cesium 137 (^{137}Cs)-contaminated areas of Ukraine. The ECM major components such as fibronectin, laminin, E-cadherin/β-catenin complexes and p53 tumor suppressor gene protein, and transforming growth factor beta 1 (TGF-β1) were immunohistochemically (IHC) evaluated in cRCCs from 59 Ukrainian patients, which represented 18 patients living in non-contaminated areas and 41 patients from ^{137}Cs-contaminated areas. In contrast, a control group of 19 Spanish patients with analogue tumors were also investigated. For IHC evaluation, a tissue microarray technique was used. Decrease or loss and abnormal distribution of fibronectin, laminin, E-cadherin/β-catenin complexes accompanied by elevated levels of p53 and TGF-β1 were detected in the Ukrainian cRCCs from ^{137}Cs-contaminated areas with statistically significant differences. Thus, our study suggests that chronic long-term, low-dose IR exposure might result in global remodeling of ECM components of the cRCCs with disruption in peri-epithelial stroma and epithelial basement membranes.

Keywords Conventional renal cell carcinoma · Extracellular matrix · Ionizing radiation

Abbreviations cRCCs: Conventional renal cell carcinomas · BM: Basement membrane · ECM: Extracellular matrix · ^{137}Cs: Cesium-137 · IR: Ionizing radiation · TGF-β1: Transforming growth factor-β1 · IHC: Immunohistochemistry · TMA: Tissue microarray

Introduction

The biologic effects of chronic low doses of ionizing radiation (IR) and its relationship with carcinogenesis have received a great deal of attention in the last few years [6]. Redox homeostatic processes in the microenvironment, involving interaction between cell–cell and cell–extracellular matrix (ECM), could be targets for chronic low-dose IR. The accident at the Chernobyl power plant in Ukraine on April 1986, introduced for the first time the problem of chronic persistent long-term human low-dose exposure to IR. Recent studies by our group showed increases in morbidity, aggressivity, and proliferative activity of Conventional renal cell carcinomas (RCCs) in patients living permanently in Cesium 137 (^{137}Cs)-contaminated areas of the Ukraine. We have previously documented for the first time that chronic persistent long-term low-dose IR exposure leads to the development of a previously unknown "radiation sclerosing proliferative atypical nephropathy" in peritumoral kidney tissue and which demonstrated a good correlation with the duration of radiation exposure [21, 22].

Microenvironment composition is a critical determinant of cancer suppression or promotion. Nonmutagenic effects of IR can have persistent effects that perturb the multicellular system in a manner that clearly promotes, and may

A. Romanenko · V. Nepomnyaschiy
Department of Pathology, Institute of Urology,
Academy of Medical Sciences of Ukraine,
9a, Yu. Kotzubinsky Street,
04053, Kiev, Ukraine

L. Morell-Quadreny · D. Ramos · A. Llombart-Bosch (✉)
Department of Pathology,
Medical School of Valencia University,
Avda Blasco Ibañez 17,
46010, Valencia, Spain
e-mail: antonio.llombart@uv.es
Fax: +34-96-3864173

A. Vozianov
Department of Urology, Institute of Urology,
Academy of Medical Sciences of Ukraine,
9a, Yu. Kotzubinsky Street,
04053, Kiev, Ukraine

initiate, the neoplastic processes [1]. The mediators of cellular responses to DNA damage caused by radiation are very well characterized, and the *p53* tumor suppressor gene is considered to be the major cellular sensor and signal of DNA damage. Whereas intracellular mediators of *p53* stability after radiation exposure have been the subject of intense study, little is known about the extracellular factors that affect the *p53* response to IR. An early and persistent event in irradiated tissues is the activation of the pluripotent cytokine, transforming growth factor beta 1 (TGF-β1). TGF-β is produced as a latent complex that is secreted and requires extracellular activation that permits TGF-β1 to bind to ubiquitous receptors and to function as a specific link between cell stress response to damage (IR) and the signaling mediated through the microenvironment [1].

It has been pointed out that laminin is also present in the basement membrane (BM) of invasive RCCs [10], and it has even been suggested that laminins accompany cancer cells and may play a significant role in the initial phase of cancer invasion [18].

The migration of RCC cells is stimulated in a different manner by various components of the ECM, whereby, fibronectin is the most stimulating factor. Fibronectin is an extracellular glycoprotein that binds to and signals through heterodimeric cell surface receptors known as integrins [4, 13]. This molecule is known to be regulated by the von Hippel–Lindau (VHL) gene, and VHL inactivation results in defective fibronectin extracellular matrix assembly. Furthermore, fibronectin gene expression has been correlated with increased tumor cell growth and invasiveness of VHL-defective RCCs [4, 13].

Adhesion of tumor cells to the endothelium and invasion into the ECM is mediated by cell adhesion and membrane-bound surface molecules from various molecular families, including among others, cadherins [5, 15]. The cadherin gene superfamily contains more than 40 members that encode for transmembrane proteins regulating calcium-dependent cell–cell adhesion [3]. Epithelial (E)-cadherin is a crucial epithelial adhesion molecule that links cells via a homophilic extracellular domain and is anchored intracellularly to the cytoskeleton via dynamic interactions with the catenins [12].

β-catenin is a key regulator located within the Wingless signal transduction (Wnt) cascade, involved in the control of cell adhesion and cell polarity [16]. Several studies have shown that loss or reduction of either E-cadherin or catenin expression is linked to a decrease in cellular and tissue differentiation and increased histological grade of different epithelial neoplasms and with increased risk for the development of metastases in human tumors [14, 26]. It has previously been suggested that immunohistochemical cytoplasmic E-cadherin staining could be associated with poorly-differentiated clear-cell renal carcinomas and demonstrated that the loss of E-cadherin resulted as a poor prognostic marker for RCCs [17].

The present study was, thus, designed to compare ECM molecular alterations in cRCCs of three groups of patients: group 1 from Valencia University Hospital (Spain), group 2 from the so-called "clean" (no radioactive contamination) areas of the Ukraine, and group 3 from radio-contaminated areas of the Ukraine. TGF-β1, laminin, fibronectin, and components of the E-cadherin/β-catenin complex were evaluated in cRCCs, in an attempt to detect molecular lesions of ECM with a possible role in renal carcinogenesis in patients chronically exposed to low-dose IR after the Chernobyl accident in Ukraine.

Materials and methods

Case selection

Paraffin-embedded specimens from 78 patients (47 men and 31 women; male/female ratio 1.5:1) were selected for the present study. Patients with 19 primary cRCCs who underwent surgery between 1993–2003 in the University Clinic Hospital of Valencia (Spain), represented control group 1, in comparison with 59 analogue patients with cRCCs, who underwent surgery between 1999 and 2005 in the Institute of Urology, Academy of Medical Sciences of Ukraine in Kiev (Ukraine). The Ukrainian patients were selected as group 2 (18 patients from "clean" areas, with no indicated radio-contamination), and group 3 (41 patients from radio-contaminated areas, including Kiev city). These patients resided in the same areas during the pre- and post-Chernobyl accident periods. All specimens were reevaluated with regard to pathological tumor (pT) stage, grade and histologic subtype. The pT stage was adjusted according to the International Union Against Cancer tumor, nodes, metastasis (TNM) system [8, 27]. Histologic nuclear grading was determined according to the method of Fuhrman et al. [11]. Moreover, we evaluated the presence and percentage of sarcomatoid changes, plus the presence and intensity of inflammatory response and the presence of necrotic areas.

Immunohistochemistry

For immunohistochemical (IHC) evaluation, a tissue microarray (TMA) technique was used. It allows the staining of a large number of specimens in only one slide. Two different TMAs were constructed containing cRRCs from groups 1–3 and normal kidney for the histologic control. A manual tissue arraying instrument (Beecher Instr, Sun Prairie, WI) was used. With respect to the known histologic heterogeneity of cRCCs, at least two different cylinders of tissue (1.5 mm in diameter), were taken from different sites of each tumor and arrayed in a recipient paraffin TMA block. Initial sections were stained with hematoxylin–eosin (H&E) to verify the histopathological findings. Sections (3 μm) from TMA blocks were mounted on ChemMate capillary gap microscope (Dako Cytomation, Denmark slides for IHC analysis.

The slides were baked overnight in a 56°C oven. Sections were deparaffinized in xylene for 20 min, rehydrated through a graded ethanol series and washed with PBS. Antigen retrieval was achieved by a 2-min heat

treatment in autoclave at 1.5 atm and using citrate buffer ph 6.5 (10 mmol/l sodium citrate buffer, Dako, Denmark). Endogenous peroxidase activity was *inhibited* with 1.5% hydrogen peroxide in methanol for 10 min. IHC staining was performed on these sections using the primary antibodies against p53 (1:50, Dako-Cytomation); fibronectin (1:200, Dako-Cytomation); laminin (1:50, Dako-Cytomation); E-cadherin (1:20, Novocastra); β-catenin (1:50, S. Cruz Technology); TGF-β1(1:50, S. Cruz Technology). Immunodetection was performed with the LSAB visualization system (Dako) using 3,3-diaminobenzidine chromogen as substrate. As controls, known positive tissue sections were used, and for negative controls, exposure to the primary antibody was omitted. The IHC analysis was performed independently by at least two pathologists in a blind fashion without knowledge of the patient group.

Quantitative analysis

The IHC score was evaluated according to the extent, intensity, and distribution patterns. Intensity of staining was scored using the following criteria: no detectable staining, low, moderate, and strong staining. The extent of staining was scored as 0—no detectable staining; 1—low (less than 10% scattered cells); 2—moderate (more than 10 but less than 50% stained cells); 3—strong homogenous staining (more than 50% stained cells). Immunoreactivity scoring was determined by the average positivity of all core biopsies.

Statistical analysis

For analysis of variables, each had a qualitative or quantitative connotation, depending upon their possibility for evaluation. Ages of patients and tumor size had a quantitative connotation, and the others (clinical, histological, and immunohistological) had qualitative ones. Statistical analysis was performed to determine whether pathological and IHC data were related to each other, and to the different groups of patients. We applied a χ^2 test for statistical analysis between qualitative variables. ANOVA and mean difference tests were used to assess the relationships between qualitative and quantitative variables.

Results

Histopathology

Characteristics of all patients associated with TNM stage, grade, and pathological features of cRCCs in the different groups are summarized in Table 1. The Ukrainian patients were significantly younger than the Spanish ones, and TNM stage was significantly more localized in both Ukrainian groups, in comparison with the Spanish control group (χ^2=22.52; p=0.004). Comparative analysis between all Ukrainian and Spanish groups showed significantly more frequent incidences of high grade conventional RCCs in Ukrainian patients, particularly, in group 3 patients.

Sarcomatoid transformation was present in less than 10% of the total tumor volume in 14 (18%) cases and predominantly showed the perivascular extent and was detected only in tumors from Ukrainian patients. Intratumoral inflammatory response was more frequently associated with the Spanish control group 1 tumors with significant differences between groups. The reverse correlations demonstrate the incidence of tumoral necrosis, which was more frequent in groups 2 and 3 with significant differences.

Immunohistopathology

IHC results for p53, fibronectin, laminin, β-catenin, E-cadherin, and TGF-β1 in cRCCs in groups 1, 2, and 3 are shown in Table 2. Immunohistochemical findings in cRCCs from the Ukrainian patients inhabiting in radiocontaminated areas (group 3) are illustrated in Fig. 1.

The nuclear p53 protein overexpression was detected in nine tumors from Ukrainian patients, which were predominantly high grade, with sarcomatoid transformation, and from patients living in radiocontaminated areas. P53 expression was negative in the Spanish group of tumors.

Fibronectin was positive in 100 and 85% of cases from Spanish and Ukranian cRCCs, respectively. In the majority of cases, the nests of positive tumor cells were surrounded

Table 1 Patient characteristics. Epidemiological and pathological features

	Group 1	Group 2	Group 3
Males	13	7	27
Females	6	11	14
Mean age (range)	65 (49–80)	54 (40–73)	54 (18–80)
Year surgery	1995–1999	1999–2005	1999–2005
[1]Contamination level in soil (Ci/km^2)	[2]NC	NC	0.5–30
Mean size (range) cm	7.42 (3–12)	5.38 (3–12)	7.78 (2–12)
Tumor stage			
pT1a	2	8	5
pT1b	2	7	13
pT2	6	3	15
pT3	9	–	8
Grade**			
1	10	6	5
2	9	11	15
3	–	1	16
4	–	–	5
Sarcomatoid changes *	–	4 (22%)	10 (24%)
Inflammatory changes	15 (78%)	6 (33%)	10 (24%)
Necrosis	5 (26%)	7 (38%)	29 (70%)

[1]Contamination data are from Raes et al. (1991)
[2]*NC Non-contaminated area*
*p<0.05
**p<0.01

Table 2 Immunohistochemical results in relationship with groups and tumor grade

	Groups				Tumor Grade			
	1	2	3	Significance	1	2	3+4	Significance
p53				ns				$\chi 2$=16.009; p=0.06
Negative	19	16	34		21	32	16	
<10%	–	2	2		–	2	2	
>10%	–	–	5		–	1	4	
Fibronectin				$\chi 2$=9.18; p=0.05				$\chi 2$=13.9; p=0.03
Negative	–	1	8		–	4	5	
<50%	9	10	24		14	16	13	
>50%	10	7	9		7	15	4	
Laminin				$\chi 2$=17.51; p=0.008				ns
Negative	6	10	28		13	14	17	
<50%	4	4	4		4	6	2	
>50%	9	4	9		4	15	3	
β-catenin				$\chi 2$=16.37; p=0.003				ns
Negative	6	7	21		10	14	10	
<50%	4	10	16		8	14	8	
>50%	9	1	4		3	7	4	
E-cadherin				ns				ns
Negative	7	7	21		9	13	13	
<50%	6	7	10		9	10	4	
>50%	6	4	10		3	12	5	
TGF-β1				$\chi 2$=12.03; p=0.01				ns
Negative	13	8	10		12	11	8	
<50%	6	7	23		9	18	9	
>50%	–	3	8		–	6	5	

by extracellular stroma that had weak or negative fibronectin staining in both Spanish and Ukrainian cRCCs, with predominant disappearance of cytoplasmic fibronectin in group 3 cRCCs (Fig. 1f). In comparison, the Spanish group 1 cRCCs demonstrated a high percentage and strong intensity of staining in ECM and tumor cells in 100% of cRCCs. Moreover, high grade (3 and 4) tumors revealed a loss of IHC staining against fibronectin compared to low grade (1 and 2) cRCCs with significant differences (χ^2=13.9; p=0.03).

Overall, laminin was positive in 44% of 78 cRCCs. The laminin-positive staining in cRCCs of groups 2 and 3 was predominantly membranous with frequent fragmentation of basement membranes (Fig. 1e). Remarkably, the homogeneous laminin staining in tumor cell cytoplasm was detected in 24% of group 3 cRCCs associated with weak or even loss of the membranous staining in the same tumors. Statistically significant differences were obtained for laminin between groups. The indicative tendency to lose laminin immunoreactivity was shown in high grade (grades 3 and 4) compared with low grade (grades 1 and 2) tumors; however, there were no significant differences. Within p53 positive Ukrainian cRCCs, 77% were laminin-negative. There was no significant correlation between laminin-immunoreactivity and TNM or with other clinicopathological features of cRCCs.

Additionally, β-catenin and E-cadherin were positive in 56 and 55% of 78 cRCCs, respectively. There was a relationship between groups with β-catenin and E-cadherin positive tumors, with a decrease of intensity and of the percentage of stained cells in the Ukrainian group 3 RRCs. It is important to note that both β-catenin and E-cadherin had accumulated in cytoplasm (Fig. 1c,d) in 29 and 24% of the Ukrainian cRCCs, respectively, in comparison with 15 and 10% of the Spanish group 1 tumors, where β-catenin and E-cadherin showed predominantly membranous staining. Interestingly, the intensity of the granular or homogeneous cytoplasmic β-catenin and E-cadherin immunoreactivity was inversely related with the intensity of the membranous staining in the same tumors. Moreover, the inverse relation was obtained between p53 overexpression and decreased levels of predominantly cytoplasmic β-catenin in six of nine p53 positive Ukrainian cRCCs. There were no statistical associations between β-catenin and E-cadherin with TNM stage, grade and other morphologic features.

In total, TGF-β1 was positive in 60% of 78 cRCCs. All group 1 TGF-β1 positive tumors showed only membranous staining. Furthermore, both cytoplasmic (Fig. 1b) and cytoplasmic and membranous TGF-β1 staining were represented in 38 and 44% of cRCCs from Ukrainian groups 2 and 3 with significant differences (χ^2=16.45; p=0.012). Strong cytoplasmic TGF-β1 staining was also

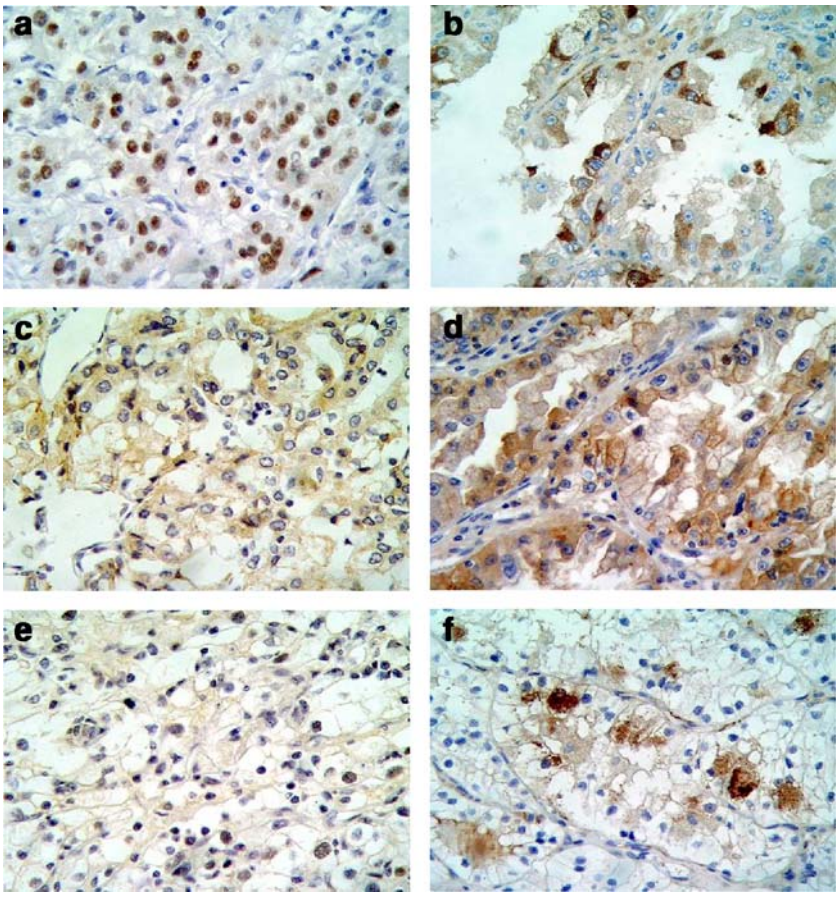

Fig. 1 Immunohistochemical findings for conventional renal-cell carcinomas from radio-contaminated areas. **a** p53 expression. **b** Granular cytoplasmic TGF-β1 expression in tumor and endothelial cells. **c** Predominant cytoplasmic β-catenin expression. **d** Membranous and cytoplasmic E-cadherin expression. **e** Expression of laminin is lost or shows discontinuity of basement membranes in tumor. **f** Atypical cytoplasmic granular fibronectin immunostaining in tumor cells. Magnification ×400

noted in the stromal endothelial cells and fibroblasts of the Ukrainian group 3 cRCCs (Fig. 1b). Moreover, moderate and high levels in percentage of stained cells were detected in both Ukrainian groups (55 and 75% of cRCCs in groups 2 and 3, respectively), with significant differences between them. On the other hand, only six (31%) in Spanish group 1 cRCCs were positive, with less than 50% of stained cells. Interestingly, we can see a strong membranous and cytoplasmic overexpression in 89% of the p53 positive Ukrainian group 3 cRCCs. Moreover, high grade Ukrainian cRCCs showed a tendency for increased TGF-β1 staining, without significant differences. No relationships were found between TGF-β1 expression, TNM stage and other histological features.

Discussion

This is the first study attempting to characterize the local expression of the three major components of the extracellular matrix: fibronectin, laminin, E-cadherin/β-catenin complexes and to examine their association with the TGF-β1 signaling pathway and with p53 tumor-suppressor gene protein overexpression in cRCCs from the Ukrainian patients chronically exposed to long-term, low-dose rate IR, in comparison with the non-exposed Spanish patients.

We found disruption of all the above mentioned ECM components associated with strongly activated TGF-β1 in cRCCs of patients who have lived longer than 19 years in ^{137}Cs-contaminated areas of Ukraine, and therefore, these alterations might, in our opinion, be a result of chronic long-term low-dose IR exposure. This suggestion is supported by our recent study [23], which showed that the analogue RCCs patients living in the ^{137}Cs-contaminated areas of Ukraine demonstrate the highest levels of urinary ^{137}Cs excretion which is known to constitute roughly 90% of internal radioactivity and is concentrated and eliminated through the kidneys [19]. However, it is necessary to note that there were no significant correlations between the above mentioned IHC markers of ECM and TNM stage, nor with other histopathological features of cRCCS.

In our study, IHC staining of the basement membrane for laminin demonstrated significant differences in the incidences, intensity and distribution of laminin expression between three groups of tumors. Predominantly, membranous and less disrupted laminin immunoreactivity was observed in Spanish cRCCs. Although the majority of the Ukrainian cRCCs from patients living in radio-contaminated areas were laminin-negative, 17% of cRCCs demonstrated the cytoplasmic staining for laminin associated with a weak discontinuous membranous staining. Subsequently, fragmentation and disruption of basement membrane continuity in RCCs with reduced local presence of laminin has been associated with the process of tumoral invasion [17]. Moreover, it has been pointed out that

laminin is often also present in the cytoplasm of cancer cells, indicating a high invasive potential of the tumor and possibly related to distant metastasis and poor prognosis [22, 28, 29].

Adhesion of tumor cells to the endothelium and the invasion into ECM is known to be mediated by cell adhesion molecules with E-cadherin/β-catenin complexes among them. Our findings indicate that alterations of E-cadherin/β-catenin are frequent in the Ukrainian cRCCs, especially of people living in radio-contaminated areas. Interestingly, increased protein levels and abnormal intracellular location of β-catenin, in our study, was associated with p53 protein overexpression in six (67%) of nine p53 positive cRCCs of Ukrainian patients. Recent studies showed that aberrant activation of β-catenin signaling is common in cancers of different origins and results from mutations that induce the accumulation of p53 [25]. This elevation in p53 is achieved, at least in part, by induction of the ARF gene promoter [7]. The pivotal role of the p14ARF promoter hypermethylation in the pathogenesis of the Ukrainian RCCs from patients living in radio-contaminated areas was recently documented by our group [23]. The possibly mutated oncogenic β-catenin expression in analogue Ukrainian cRCCs might activate the p53 response which, in turn, can enhance the degradation of β-catenin by a negative feedback loop during increased tumor progression [24]. The loss of β-catenin in our group 3 tumors was accompanied by a reduction in E-cadherin associated with abnormal cytoplasmic location which might be related to the metastatic process and to poorly differentiated forms of these tumors [17, 25].

Evidence has accumulated that nonmutagenic effects of IR, however, can have persistent effects that result in interactions with the microenvironment: stromal–epithelial, cell–cell and cell–extracellular matrix [1]. While excess reactive oxygen species production generated by IR clearly damages DNA, persistent low levels of IR might affect cell-signaling, particularly, redox modulation. TGF-β1 is a major extracellular signaling sensor of damage as it mediates redox homeostasis in cells and contributes to cell–cell communication [2]. TGF-β1 is also known as a mediator of tissue response to IR, pointing to a role in orchestrating changes due to oxidative stress [9]. The present results indicate the significantly high levels and alteration of TGF-β1 expression in the cRCCs of the Ukrainian patients living in the radio-contaminated areas, as compared to both Spanish and Ukrainian controls. Furthermore, TGF-β1 immunostaining was found to be most pronounced as stromal, membranous and infrequently even as tumor cell cytoplasmic expression. Remarkably, TGF-β1-positive stromal endothelial cells and fibroblasts were also detected. Therefore, our data support the idea that the irradiated stroma dramatically increases the ability of the tumor progression [1].

Our results showed that the presence of TGF-β1 was associated with a loss of E-cadherin immunoreactivity in 24% of the Ukrainian cRCCs. Moreover, 89% of the Ukrainian p53-positive cRCCs showed strongly enhanced levels of TGF-β1. A variety of studies have linked p53 status and TGF-β1 responsiveness in cancer cells [20, 30]. A number of striking similarities exists between p53 and TGF-β: both are induced by a variety of damaging factors, specifically by IR, both exhibit redox modulation of protein activity, both are very rapidly activated and so on. However, p53 is accumulated intracellularly and mediates individual cell fate, while TGF-β1 is extracellular and orchestrates diverse multicellular fates. The functional intersection of TGF-β1 and p53 supports the hypothesis that genomic stability can be significantly affected by the character and activity of the microenvironment [1].

Thus, there is mounting evidence that IR exposure can promote malignant tumor progression by pathways other than gene mutation. Our study suggests that chronic, long-term, low-dose IR exposure might result in global remodeling of ECM components with changes in peri-epithelial stroma and epithelial basement membranes (including fibronectin, laminin, E-cadherin/β-catenin complexes alterations). We found that cRCCs from the Ukrainian patients chronically exposed to long-term, low-dose IR are characterized by significantly disrupted ECM with a lack of orchestrated communication between cells and between cells and ECM, that leads to loss of cellular differentiation. These factors may also become relevant targets for novel therapeutic strategies.

Acknowledgements The authors are grateful to Alejo Sempere for his technical assistance. Source of support: GV04 B208 from the Generalitat Valenciana, Spain.

References

1. Barcellos-Hoff MH (2005) Integrative radiation carcinogenesis: interactions between cell and tissue responses to DNA damage. Semin Cancer Biol 15:138–148
2. Barceloss-Hoff MH, Brooks AL (2001) Extracellular signaling through the microenvironment: a hypothesis relating carcinogenesis, bystander effect and genomic instability. Radiat Res 156:618–627
3. Bindels EM, Vermey M, De Both NJ, van der Kwast TH (2001) Influence of the microenvironment of invasiveness of human bladder carcinoma cell lines. Virchows Arch 439:522–529
4. Bluyssen HAR, Lolkema MPJK, van Beest M, Holstege FCP, Giles RH, Voest EE (2004) Fibronectin is a hypoxia-independent target of the tumor suppressor VHL. FEBS Lett 556:137–142
5. Brenner W, Langer P, Oesch F, Edgel C-JS, Wieser RJ (1995) Tumor cell—endothelium adhesion in an artificial venule. Anal Biochem 225:213–219
6. Clarke RH (2001) Control of low-level radiation exposure: what is the problem and how can it be solved? Health Phys 80:391–396
7. Damalas A, Kahan, S, Shtutman M, Ben-Ze'ev A, Oren M (2001) Deregulated β-catenin induces a p53- and ARF-dependent growth arrest and cooperates with Ras in transformation. EMBO J 20:4912–4922
8. Eble JN, Sauter G, Epstein JI, Sesterhenn IA (eds) (2004) Pathology and genetics of tumours of the urinary system and male genetic organs. World Health Organization Classification of Tumours. IARC, Lyon
9. Ehrhart EJ, Segarini P, Tsang ML, Carrol AG, Barceloss-Hoff MH (1997) Latent transforming growth factor-beta1 activation in situ: quantitative and functional evidence after low-dose gamma-irradiation. FASEB J 11:991–1002

10. Flug M, Korf-Maier P (1995) The basement membrane and its involvement in carcinoma cell invasion. Acta Anat 152:69–84
11. Fuhrman SA, Lesky LC, Limas C (1982) Prognosis significance of morphologic parameters in renal cell carcinoma. Am J Surg Pathol 6:655–663
12. Gumbiner BM (2000) Regulation of cadherin adhesive activity. J Cell Biol 148:399–404
13. He Z, Liu S, Guo M, Mao J, Hughson MD (2004) Expression of fibronectin and HIF-1 alpha in renal cell carcinomas: relationship to von Hippel–Lindau gene inactivation. Cancer Genet Cytogenet 152:89–94
14. Heimann R, Lan F, McBride R, Hellman S (2000) Separating favorable from unfavorable prognostic markers in breast cancer: the role of E-cadherin. Cancer Res 60:298–304
15. Liotta LA (1992) Cancer cell invasion and metastasis. Sci Am 2:34–41
16. Moon RT, Bowerman B, Boutros M, Perrimon N (2002) The promise and perils of the Wnt signaling through beta-catenin. Science 296:1644–1646
17. Morell-Quadreny L, Rubio J, Lopez-Querrero JA, Casanova J, Ramos D, Iborra I, Solsona E, Llombart-Bosch A (2003) Disruption of basement membrane, extracellular matrix metalloproteinases and E-cadherin in renal-cell carcinoma. Anticancer Res 23:5005–5010
18. Pyke C, Salo S, Ralfker E, Romer J, Dano K, Tryggvason K (1995) Laminin-5 is a marker of invading cancer cells in some human carcinomas and is coexpressed with receptor for urokinase plasminogen activator in budding cancer cells in colon adenocarcinomas. Cancer Res 53:4132–4139
19. Raes F, De Cort M, Graziani G (1991) Multi-factoral nature of radioactivity deposition on soil after the Chernobyl accident. Health Phys 61:271
20. Reiss M, Vellucci VF, Zhou, ZL (1993) Mutant *p53* tumor suppressor gene causes resistance to transforming growth factor-beta1 in murine keratinocytes. Cancer Res 53:899–904
21. Romanenko A, Morell-Quadreny L, Nepomnyaschy V, Vozianov A, Llombart-Bosch A (2000) Pathology and proliferative activity of renal-cell carcinomas (RCCs) and renal oncocytomas in patients with different radiation exposure after the Chernobyl accident in Ukraine. Int J Cancer 87:880–883
22. Romanenko A, Morell-Quadreny L, Nepomnyaschy V, Vozianov A, Llombart-Bosch A (2001) Radiation sclerosing proliferative atypical nephropathy of peritumoral tissue of renal-cell carcinomas after the Chernobyl accident in Ukraine. Virchows Arch 438:146–153
23. Romanenko A, Morell-Quadreny L, Lopez-Guerrero JA, Pellin A, Nepomnyaschy V, Vozianov A, Llombart-Bosch A (2004) The INK4a/ARF-locus: role in cell cycle control for renal cell epithelial tumor growth after the Chernobyl accident. Virchows Arch 445:298–304
24. Sadot E, Geiger B, Oren M, Ben-Ze'ev A (2001) Down-regulation of β-catenin by activated p53. Mol Cell Biol 21:6768–6781
25. Shtutman M, Zhusinsky J, Oren M, Levina E, Ben-Ze'ev A (2002) PML is a target gene of β-catenin and plakoglobin and coactivates β-catenin mediated transcription. Cancer Res 62:5947–5954
26. Slaton JW, Inoue K, Perrotte P, El-Naggar AK, Swanson DA, Fidler IJ, Dinney CPN (2001) Expression levels of genes that regulate metastasis and angiogenesis correlate with advanced pathological stage of renal cell carcinoma. Am J Pathol 158:735–743
27. Sobin LH, Wittekind C (eds) (2002) TNM Classification of Malignant Tumors, 6th ed. Wiley-Liss, New York
28. Takahashi S, Hasebe T, Oda T, Sasaki S, Kinoshita T, Konishi M, Ochiai T, Ochiai A (2002) Cytoplasmic expression of laminin gamma 2 chain correlates with postoperative hepatic metastasis and poor prognosis in patients with pancreatic ductal adenocarcinoma. Cancer 94:1894–1901
29. Tani T, Lehto V-P, Virtanen I (1999) Expression of laminins 1 and 10 in carcinoma cells and comparison of their roles in cell adhesion. Exp Cell Res 248:115–121
30. Wyllie FS, Dawson T, Bond JA, Goretzki P, Game S, Prime S (1991) Correlated abnormalities of transforming growth factor-beta1 response and p53 expression in thyroid epithelial cell transformation. Mol Cell Endocrinol 76:13–21

Virchows Arch (2006) 448: 591–596
DOI 10.1007/s00428-006-0152-2

ORIGINAL ARTICLE

Diclehan Orhan · Gülsev Kale · Melda Çağlar · Safiye Göğüş · Ergun Karaağaoğlu

Histone mRNA in situ hybridization and Ki 67 immunohistochemistry in pediatric adrenocortical tumors

Received: 26 October 2005 / Revised: 9 December 2005 / Accepted: 22 December 2005 / Published online: 18 February 2006

Abstract Adrenocortical tumors in the pediatric population are rare. Classification of these tumors as adenomas or carcinomas using histological criteria is often difficult. Immunohistochemical expressions of proliferative markers are currently under investigation for utilization in the differential diagnosis and prediction of clinical outcomes. The value of histone proteins as prognostic markers in adrenocortical tumors has not yet been elucidated. We evaluated the histological features, immunohistochemical staining of Ki 67, and in situ hybridization for histone mRNA in 30 pediatric adrenocortical tumors. We investigated the relationship between these parameters and the prognosis. Using the classification proposed by Weiss, 19 tumors were classified as carcinomas and 11 as adenomas. Ki 67 and histone mRNA labeling indices (LIs, the percentage of Ki 67-positive and histone mRNA-positive tumor cells, respectively) were significantly higher in carcinomas than in adenomas (Ki 67 LI was 14.62±5.79 in adenomas and 20.35±6.23 in carcinomas, p=0.02. Histone mRNA LI was 1.73±1.71 in adenomas and 6.62±2.28 in carcinomas, p=0.00). The proliferative activity assessed by histone mRNA was lower than that assessed by Ki 67 in both diagnostic groups. The cut off point for the diagnosis of malignancy was found to be 14.55 for Ki 67 LI and 5.75 for histone mRNA LI. A correlation was found between a histone mRNA LI ≥5 and poor prognosis (recurrence, metastasis, or death). We concluded that the proliferative activity of the tumor assessed by Ki 67 and histone mRNA may assist in differentiating adrenocortical adenomas and carcinomas. In addition, our results suggest that the most reliable parameter to predict prognosis in pediatric adrenocortical tumors is the histone mRNA LI.

Keywords Adrenocortical tumors · Pediatric · Ki 67 · Histone mRNA · Prognosis · In situ hybridization

D. Orhan (✉) · G. Kale · M. Çağlar · S. Göğüş
Division of Pediatric Pathology,
Hacettepe University Faculty of Medicine,
İhsan Doğramacı Children's Hospital,
06100 Sıhhiye/Ankara, Turkey
e-mail: diclehan@hacettepe.edu.tr
Tel.: +90-312-3051304
Fax: +90-312-3118226

E. Karaağaoğlu
Department of Biostatistics,
Hacettepe University Faculty of Medicine,
Ankara, Turkey

Introduction

Adrenocortical tumors are rare in children with an incidence of 0.3 cases per 1,000,000 children per year, and these tumors represent 0.2% of all childhood tumors [17]. The distinction between benign and malignant adrenocortical tumors is difficult [6, 17]. Despite histological criteria by which such a distinction may be possible, the behavior of adrenocortical tumors in childhood is usually unpredictable, and distinction based only on histological classification is difficult. Many reports conclude that the adrenocortical tumors in children and adolescents differ from those occurring in adults, both clinically and histologically [3, 17, 19, 25]. Due to the low incidence of these tumors in childhood, there is paucity of data on the histological and molecular markers that could help in differential diagnosis or in predicting clinical outcomes. In recent studies, the proliferative activity of tumor cells is being investigated to assess their role in differentiating benign and malignant tumors. For this purpose, immunohistochemical expressions of Ki 67 and PCNA were evaluated in many human tumors. The diagnostic and prognostic value of the immunohistochemical Ki 67 expression in adrenocortical tumors remains unclear [11, 17]. A recent method for the identification of proliferating cells in tissue sections is the use of in situ hybridization for the localization of histone mRNA. Nonisotopic histone mRNA in situ hybridization allows the detection of cells in the S phase of the cell cycle in paraffin-embedded tissues [5, 15]. There have been studies evaluating the in situ hybridization of histone mRNA in cerebral astrocytomas, head and neck tumors, and benign tissues [2, 5, 16]. To our knowledge, in situ hybridization

of histone mRNA in adrenocortical neoplasms has not undergone investigation as a diagnostic tool and a prognostic marker.

The aim of this study was to evaluate the relevance of the immunohistochemical staining with Ki 67 and non isotopic in situ hybridization of histone mRNA in the differential diagnosis and clinical course of pediatric adrenocortical tumors.

Materials and methods

Pathological examination

Thirty pediatric adrenocortical tumors diagnosed in Hacettepe University, Faculty of Medicine, Children's Hospital, Division of Pediatric Pathology, were included in the study group. All patients had undergone a minimum of 4 years of clinical follow-up. All cases were reviewed (DO) and classified as either adenoma or carcinoma using the histopathological criteria according to the methods of Weiss [26]. Hematoxylin and eosin-stained histological sections of each case were evaluated for nine histopathological features. The nuclear grade was assessed using the criteria of Fuhrman et al. [8]. Mitosis was evaluated by counting at random 50 high power fields (hpf; magnification at ×40 with a ×10 objective lens using an Olympus BX51 microscope) in the area of the greatest number of mitotic figures. Presence of atypical mitosis was also noted. The percentage of clear cells resembling the normal zona fasciculata was evaluated. Architecture was defined as diffuse if more than one-third of the tumor formed sheets of cells with no pattern. Necrosis was considered to be positive when it involved confluent nests of cells. Invasion of sinusoids (endothelium-lined vessels with no smooth muscle in the wall) and veins (vessels with smooth muscle in the wall) was recorded. Capsular invasion was scored as present when nests or cords of tumor extended into or through the capsule.

A tumor with two or fewer of the criteria below was classified as an adenoma; tumors with three or more criteria were considered carcinomas:

1. High nuclear grade (III or IV) assessed using the criteria of Fuhrman et al
2. Mitotic rate >5/50 hpf
3. Presence of a typical mitosis
4. Clear tumor cell cytoplasm (<25% of the tumor cells)
5. Diffuse architecture
6. Necrosis
7. Venous invasion
8. Sinusoidal invasion
9. Capsular invasion

Immunohistochemistry

Immunohistochemical staining was performed using the primary antibody against Ki 67 (Neomarkers, CA, USA; clone: MIB-1, dilution:1/100) with streptavidin–biotin peroxidase method (Dako LSAB 2 System, Peroxidase, CA, USA). Pretreatment in citrate buffer was performed for antigen retrieval by heating in a microwave oven. For negative control, primary antibody was replaced with normal mouse serum. Sections of tonsils were used as positive control. All tumor cell nuclei with dark brown staining, even those with vague speckling patterns, were considered to be Ki 67-positive. Ki 67 counts were performed according to these staining criteria. The count of Ki 67-positively stained nuclei was performed in areas of greatest labeling density within each tumor. About 1,000 tumor cells were counted at a magnification of ×400. Ki 67 labeling index (LI) was defined as the number of Ki 67-positive tumor cell nuclei per 100 tumor cells.

Nonisotopic in situ hybridization assay

For the nonisotopic in situ hybridization, 10-μm sections were obtained from paraffin-embedded tissue blocks and placed on 3-aminopropyltriethoxy-sialine slides (Novocastra Laboratories, New Castle upon Tyne, UK). A commercial fluorescein-labeled oligonucleotide cocktail was used for the detection of histone H2B, H3, and H4 mRNA sequences (Novocastra Laboratories). The nonisotopic in situ hybridization protocol was the same as that recommended by the manufacturer. Tissue sections were deparaffinized in xylene, rehydrated through ethanol series and immersed in distilled water. The sections were then treated with proteinase K (Novocastra Laboratories) (20 μg/ml in 5 mM Tris–HCl buffer, pH 7.6) for 30 min at 37°C. After washing in distilled water and dehydrating through 95% and 99% ethanol, the sections were air dried and hybridization with fluorescein isothiocyanate (FITC)-labeled cocktail was performed in the supplied buffer overnight at 37°C. The Novocastra histone probe ISH kit (Novocastra Laboratories), which included alkaline phosphatase conjugated rabbit Fab anti-FITC, enzyme substrate (5-bromo-4-chloro-3-indolyl-phosphate and nitro blu tetrazolium), and an inhibitor (levamisole), was used for the detection of histone mRNA-positive cells. All solutions and equipment used for the stages up to the hybridization were treated with H_2O_2 and diethyl pyrocarbonate to remove ribonuclease, and all procedures were carried out while wearing gloves.

Histone mRNA-expressing tumor cells were counted by light microscope at ×400 magnification. The total number of cells counted was 1,000. Histone mRNA LI was defined as the number of histone mRNA-positive tumor cells per 100 tumor cells.

Statistics

All statistical analyses were performed with the Statistical Package of Social Sciences for Windows 12.0. A p value <0.05 was considered statistically significant. An independent t test was used to determine whether Ki 67 LI and histone mRNA LI differed significantly between adenoma–carcinoma groups and prognostic groups.

Table 1 Histological features of 30 pediatric adrenocortical tumors

	Nuclear grade III, IV	Mitosis (>5/50 hpf)	Abnormal mitosis	Clear cells (<25%)	Diffuse architecture	Necrosis	Capsular invasion	Venous invasion	Sinusoidal invasion
Carcinoma (n=19)	17	11	10	16	15	17	17	11	12
Adenoma (n=11)	9	4	0	2	1	2	0	0	0

Receiver operating characteristics (ROC) curve analyses were used to determine how well Ki 67 LI and histone mRNA LI discriminate between adenoma and carcinoma patients. The prognostic value of Ki 67 LI and histone mRNA LI was also analyzed by ROC curve analysis. Comparison of Ki 67 LI and histone mRNA LI was made using the area under the ROC curves. The best cut off points for both diagnostic and prognostic groups were found at the points where the sum of false positive and false negative rates was at the minimum value.

Results

Based on the histopathological classification proposed by Weiss, 19 tumors were classified as adrenocortical carcinomas and 11 as adenomas. Microscopic findings of the tumors are summarized in Table 1. All adenomas had two or fewer Weiss criteria. No single histological criterion could be used to distinguish a carcinoma from an adenoma. However, none of the adenomas showed abnormal mitosis, capsular, venous, or sinusoidal invasion.

Among the patients with adenoma, one had local recurrence during follow-up. Three of the patients that had carcinomas were alive with no evidence of disease, and the others showed poor prognoses (recurrence, metastasis, or death).

The staining of nonisotopic histone mRNA in situ hybridization was localized to the cytoplasm and nuclear membrane (Fig. 1). Immunohistochemical expression of Ki 67 was observed as nuclear immunostaining (Fig. 2). There was a statistically significant difference of Ki 67 LI between adenoma (mean 14.62±5.79) and carcinoma (20.35±6.23) groups (p=0.02). Histone mRNA LI also differed significantly between adenoma (1.73±1.71) and carcinoma (6.62±2.28) groups (p=0.00) (Table 2). Individual results of Ki 67 and histone mRNA labeling are shown in Table 3.

To evaluate the discriminatory power of histone mRNA and Ki 67, the area under the ROC curves was evaluated. The area under the ROC curve for Ki 67 LI was 0.78 (p=0.012), and for histone mRNA LI, the area was 0.957 (p=0.00), indicating that there is a statistically significant difference between the two parameters (p=0.049) (Table 4).

The best cut off point for the diagnosis of malignancy was found to be 14.55 for Ki 67 LI and 5.75 for histone mRNA LI. Considering these cut off points, the sensitivity and the specificity of Ki 67 LI were 94.7% and 63.6%, respectively. A histone mRNA LI ≥5.75 was significant for the diagnosis of malignancy with 84.2% sensitivity and 100% specificity (Fig. 3).

Both Ki 67 and histone mRNA LIs were significantly higher in tumors with poor prognosis. Mean Ki 67 LI and histone mRNA LI with standard deviations for good and poor prognostic groups are shown in Table 5. The cut off point for poor prognosis was also determined for both Ki 67 and histone mRNA LIs. Tumors with a Ki 67 LI ≥12.65 showed poor prognosis with 100% sensitivity and 38.5% specificity. As a prognostic marker, the best cut off point for histone mRNA LI was 5. Ki 67 turned out to be almost significant when the area under the ROC curve was considered. Histone mRNA appeared to be a gold standard

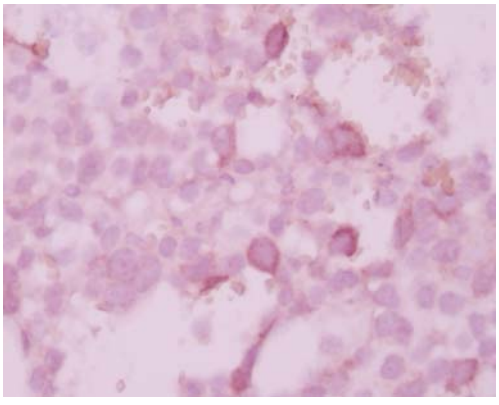

Fig. 1 Brown cytoplasmic and nuclear staining of nonisotopic histone mRNA in situ hybridization in adrenocortical carcinoma (×100)

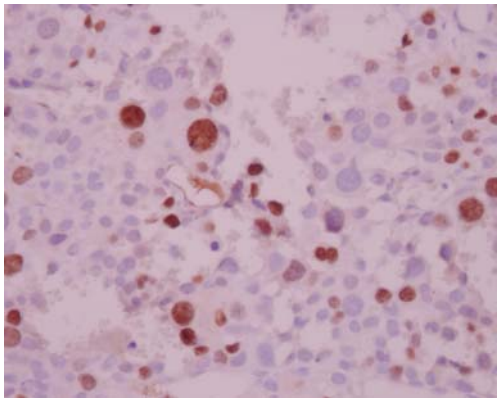

Fig. 2 Immunohistochemical expression of Ki 67 in an adrenocortical carcinoma (×100)

Table 2 Ki 67 and histone mRNA LIs in adrenocortical adenomas and carcinomas

	Diagnosis	*n*	Mean	Standard deviation	
Ki 67 LI	Adenoma	11	14.62	5.79	t=2.49, p=0.02
	Carcinoma	19	20.35	6.23	
Histone mRNA LI	Adenoma	11	1.73	1.71	t=6.14, p=0.00
	Carcinoma	19	6.62	2.28	

test for prediction of prognosis (Fig. 4). The difference between the discriminatory power of the two parameters was also statistically significant (p=0.00) (Table 6).

Three patients with carcinoma who showed good prognoses had Ki 67 LIs (18.8, 19.6, and 16.4) greater than the cut off point for Ki 67 LI, but the histone mRNA LIs of these tumors were all lower than the cut off point for mRNA LI (1.4, 1.2, and 4.6). An adenoma with local recurrence had a Ki 67 LI of 13.1 and a histone mRNA LI of 5.4 (higher than the cut off point for poor prognosis for histone mRNA LI).

Table 3 Ki 67 and histone mRNA LIs of individual patients

Patient no	Diagnosis	Ki 67 LI	Histone LI
1	Carcinoma	15.2	7.3
2	Carcinoma	23.6	8.4
3	Carcinoma	24.1	6.2
4	Carcinoma	15.8	9.3
5	Carcinoma	18.8	1.4
6	Carcinoma	19.6	1.2
7	Carcinoma	19.9	6.3
8	Carcinoma	19.3	7.6
9	Carcinoma	38.0	10.2
10	Carcinoma	14.9	6.1
11	Carcinoma	29.7	8.7
12	Carcinoma	15.3	6.1
13	Carcinoma	19.8	7.3
14	Carcinoma	17.1	6.4
15	Carcinoma	17.3	7.1
16	Carcinoma	29.2	8.1
17	Carcinoma	13.0	6.2
18	Carcinoma	19.8	7.4
19	Carcinoma	16.4	4.6
20	Adenoma	11.2	0.1
21	Adenoma	8.4	0.3
22	Adenoma	9.7	1.1
23	Adenoma	13.1	5.4
24	Adenoma	18.3	2.4
25	Adenoma	16.5	3.2
26	Adenoma	26.2	3.7
27	Adenoma	22.6	0.2
28	Adenoma	14.2	1.1
29	Adenoma	12.3	0.7
30	Adenoma	8.4	0.9

Discussion

Despite the presence of well-established histological criteria in the differential diagnosis of adrenocortical tumors in adults, it may be extremely difficult to distinguish between benign and malignant tumors [7, 14]. Weiss, Hough et al. and Van Slooten et al. proposed a variety of parameters to differentiate these tumors [11, 23, 26]. Aubert et al. confirmed the value of the Weiss system [1]. Because of the lack of histological criteria for the discrimination of adrenocortical adenomas and carcinomas in the pediatric population, the current classifications of adrenocortical tumors based on adult criteria are used in pediatric patient studies [17, 18, 24]. We too applied the Weiss criteria to classify the tumors in our study group as adenomas or carcinomas. Pediatric adrenocortical tumors are histologically different from those in adults [4, 12, 17, 19]. Although Weieneke et al. found only 31% of histologically malignant pediatric tumors behaving badly, Sawin and colleagues reported the long-term survival rate of children with adrenocortical carcinomas to be between 10 and 46%. Complete resection was associated with an improved survival rate (67%) despite a 38% local recurrence rate. Mortality, recurrence, and metastasis rates of the current series are within the limits mentioned in literature.

Weiss et al. reported that in pediatric patients, adrenocortical adenomas showed mitotic activity, broad fibrous bands, and nuclear pleomorphism more frequently than in adult adenomas [26, 27]. Supporting this knowledge, in our series, 4 of 11 adenomas had mitosis >5/50 hpf and 2 had necrosis. Similar to the results of the study by Weieneke and colleagues, there was no adenoma with capsular or vascular invasion in our series. As reported previously, we found no single histologic feature that reliably identified malignancy, either. All adenomas but one in our study diagnosed according to the Weiss criteria had a good clinical outcome. One patient with adenoma showed local recurrence during follow-up. Three patients with diagnosis of adrenocortical carcinoma were alive with no evidence of disease, and the others had poor prognoses. These results suggest that the Weiss criteria were not very valid in all pediatric adrenocortical tumors and that other parameters are also needed to predict the clinical outcomes of these tumors.

Table 4 Area under the ROC curve for diagnosis

	Area	Standard error	*p*
Ki 67 LI	0.78	0.098	0.012
Histone mRNA LI	0.95	0.033	0.000

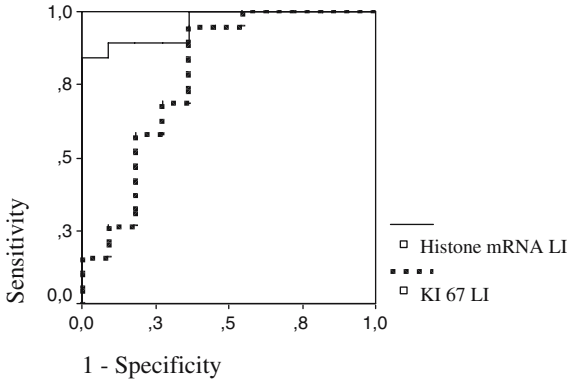

Fig. 3 Comparison of ROC curves of Ki 67 and histone mRNA for the diagnosis of malignancy

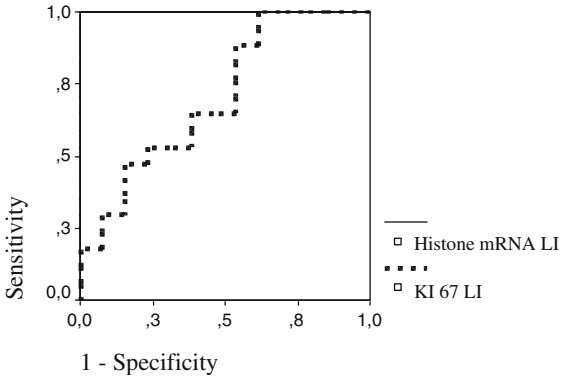

Fig. 4 Comparison of ROC curves of Ki 67 and histone mRNA for prognosis

Reports on the role of molecular markers, such as cellular DNA content and proliferative activity of tumor cells, in the differential diagnosis and prognoses of adrenocortical tumors are seen in literature. There are several studies suggesting flow cytometric DNA analysis to be a reliable prognostic factor in adrenocortical tumors [3, 21]. Some other studies, however, indicate that ploidy is not a significant indicator of histological diagnosis or prognosis in these tumors [6, 14].

Another approach to make differential diagnosis and to find reliable prognostic factors for adrenocortical tumors involves the use of immunohistochemical proliferation markers such as Ki 67. Ki 67 is a nuclear protein expressed by proliferating cells in G_1, G_2, S, and M phases of the cell cycle. Ki 67 expression can be observed immunohistochemically in paraffin-embedded material by using the primary antibody MIB 1 [7, 9, 13, 16, 19, 20, 24]. Goldblumet et al. and Vargas et al. found a strong correlation between Ki 67 expression and the malignancy of adrenocortical tumors in adults [9, 22]. Vargas et al. showed that the tumor's proliferative activity, determined by the percentage of Ki 67-positive tumor cells, was 1.49% in adenomas, 20.8% in carcinomas, and 16.1% in recurrent and metastatic tumors [22]. Aubert and colleagues also observed a statistically significant difference in Ki 67 labeling between adenomas (2.4±1.3%) and carcinomas (21.2±18.44%) [1]. Weieneke et al. and Sbragia and colleagues have investigated Ki 67 expression in pediatric adrenocortical tumors, and they have reported that Ki 67 immunostaining did not have a value in predicting clinical outcomes [19, 25]. In our series, we found that Ki 67 expression was significantly higher in carcinomas than adenomas, and a Ki 67 LI ≥14.55 was found to be an indicator of malignancy for pediatric adrenocortical neoplasms. The assessment of cells in the S phase of the cell cycle is an alternative method for evaluating proliferating cells [2, 5, 10]. In situ hybridization of histone H3 and/or H4 mRNA is an assay used to detect S-phase cells in archival paraffin-embedded material [15, 16]. Histones are a class of nuclear proteins that play an essential role in the packing and expression of the eukaryotic genome. Synthesis of histone protein is restricted to the S phase. During the S phase of the cell cycle, the level of histone mRNA increases over 50-fold and rapidly disappears at the start of G_2. The rapid degradation of the histone mRNA after the S phase provides an opportunity to distinguish the proliferating cells in S phase by in situ hybridization for histone mRNA [2, 10, 15]. Rauttiainen et al. reported that nonisotopic histone mRNA in situ hybridization is a reproducible method for measuring the proliferative activity of tumor cells and an independent prognostic factor in astrocytomas [16]. In our study, we found that all carcinomas had a higher histone mRNA LI than adenomas, and that a histone mRNA LI ≥5.75 was significant for malignancy with 84.2% sensitivity and 100% specificity. Both Ki 67 and histone mRNA LIs exhibited a striking difference between adenomas and carcinomas. In our series, the number of Ki67-positive cells was greater than histone mRNA-bearing cells both in adenomas and carcinomas. This may be because Ki 67 is expressed not only in the S phase of the cell cycle, but also in G_1, G_2, and M phases. In contrast, histone mRNA in situ hybridization labels the cells only in the S phase [16]. Ki 67 LI did not demonstrate a sensitivity or specificity of 100% in the differential diagnosis. However, histone mRNA showed 100% specificity for both differential diagnosis and clinical outcome.

Table 5 Ki 67 and histone mRNA LIs of 30 pediatric adrenocortical tumors according to the prognostic groups

	Prognosis	*n*	Mean	Standard deviation	
Ki 67 LI	Good	13	15.58	5.53	t=2.04, p=0.05
	Poor	17	20.30	6.76	
Histone mRNA LI	Good	13	1.60	1.42	t=11.38, p=0.00
	Poor	17	7.30	1.30	

Table 6 Area under the ROC curve for prognosis

	Area	Standard error	*p*
Ki 67 LI	0.706	0.098	0.057
Histone mRNA LI	1.000	0.000	0.000

A single patient with an adenoma diagnosed according to the histological criteria showed local recurrence, and this patient's tumor had a histone mRNA LI >5. All other adenomas had histone mRNA LIs lower than 5. Three patients having carcinomas with histone mRNA LIs of less than 5 had disease-free survivals of at least 4 years. All these carcinoma patients had Ki 67 LIs higher than the cut off point for Ki 67 LI for poor prognosis. These data could indicate that children with adrenocortical tumors with histone mRNA LIs of less than 5 may have good prognoses. Statistical analysis showed that nonisotopic in situ hybridization of histone mRNA was a better predictor of prognosis in pediatric adrenocortical tumors than immunohistochemical Ki 67 expression.

The results of this study indicate that the assessment of Ki 67 and histone mRNA LIs complements histological criteria in the diagnosis of malignancy in adrenocortical tumors. In addition, histone mRNA LI may also prove to be a valuable marker in predicting the clinical outcomes of pediatric patients with adrenocortical neoplasms.

Acknowledgements This study was supported by the Scientific research Project of Hacettepe University (02G013). The authors are grateful to Ayşe Yüzbaşıoğlu and Köksal Özgül for their technical assistance.

References

1. Aubert S, Wacreiner A, Leroy X, Devos P, Bruno C, Proye C, Wemeau JL, Lecomte-Houcke M, Leteurtre E (2002) Weiss system revisited. A clinicopathological and immunohistochemical study of 49 adrenocortical tumors. Am J Surg Pathol 26:1612–1619
2. Bosch FX, Udvarhelyi N, Venter E, Herold-Mende C, Schuhmann A, Maier H, Weidauer H, Born AI (1993) Expression of the histone H3 gene in benign semi-malignant lesions of the head and neck: a reliable proliferation marker. Eur J Cancer 29A:1454–1461
3. Bowlby LS, Bebault LE, Abraham SR (1986) Flow cytometric analysis of adrenal cortical tumor DNA: relationship between cellular DNA and histopathologic classification. Cancer 58:1499–1505
4. Cagle PT, Hough AJ, Pysher TJ, Johnson EH, Kirkland RT, Holcombe JH, Hawkins EP (1986) Comparison of adrenal cortical tumors in children and adults. Cancer 57:2235–2237
5. Chou MY, Chang ALC, McBride J, Donoff B, Gallagher GT, Wong DTW (1990) A rapid method to determine proliferation patterns of normal and malignant tissues by H3 mRNA in situ hybridization. Am J Pathol 136:729–733
6. Cibas ES, Medeiros LJ, Weinberg DS, Gelb AB, Weiss LM (1990) Cellular DNA profiles of benign and malignant adrenocortical tumors. Am J Surg Pathol 14(10):948–955
7. DeLellis RA, Mangray S (2004) The adrenal glands. In: Mills SE, Carter D, Greenson JK, Oberman HA, Reuter V, Stoler MH (ed) Sternberg's diagnostic surgical pathology. Lippincott Williams & Wilkins, Philadelphia, pp 622–677
8. Fuhrman SA, Lasky LC, Limas C (1982) Prognostic significance of morphologic parameters in renal cell carcinoma. Am J Surg Pathol 6:655–663
9. Goldblum JR, Shannon R, Kaldjian EP, Thiny M, Davenport R, Thompson N, Lloyd LV (1993) Immunohistochemical assessment of proliferative activity in adrenocortical neoplasms. Mod Pathol 6:663–668
10. Hayama M, Ota H, Toki T, Ishii K, Honda T, Momose M, Nakata R (2002) Cell kinetic study of the endometrium by nonisotopic in situ hybridization for histone H3 messenger RNA and immunohistochemistry for Ki-67 and for estrogen and progesterone receptors. Anat Rec 266:234–240
11. Hough AJ, Hollifield JW, Page DL, Hartmann WH (1979) Prognostic factors in adrenal cortical tumors. A mathematical analysis of clinical and morphologic data. Am J Clin Pathol 72:390–399
12. Liou LS, Kay R (2000) Adrenocortical carcinoma in children: review and recent innovations. Urol Clin North Am 27: 403–421
13. Martins ACP, Cologna AJ, Tucci S, Suaid HJ, Falconi RAR (2005) Clinical features and immunoexpression of p53, MIB-1 and Proliferating Cell Nuclear Antigen in adrenal neoplasms. J Urol 173:2138–2142
14. Medeiros LJ, Weiss LM (1992) New developments in the pathologic diagnosis of adrenal cortical neoplasms: a review. 97:73–83
15. Millar MR, Sharpe RM, Maguire SM, Saunders PT (1993) Cellular localisation of messenger RNAs in rat testis: application of digoxigenin-labelled ribonucleotide probes to embedded tissue. Cell Tissue Res 273:269–277
16. Rautiainen E, Haapasssalo H, Sallinen I, Helen P, Helin H (1998) Histone mRNA in-situ hybridization in astrocytomas: a comparison with PCNA, MIB 1 and mitosis in paraffin-embedded material. Histopathology 32:43–50
17. Ribeiro RC, Figueiredo B (2004) Childhood adrenocortical tumors. Eur J Cancer 40:1117–1126
18. Sawin RS (1997) Functioning adrenal neoplasms. Semin Pediatr Surg 6:156–163
19. Sbragia L, Oliveira-Filho AG, Vassallo J, Pinto GA, Guerra-Junior G, Bustorff-Silva J (2005) Adrenocortical tumors in Brazilian children: immunohistochemical markers and prognostic factors. Arch Pathol Lab Med 129:1127–1131
20. Stojadinovic A, Brennan MF, Hoos A, Omeroglu A, Leung DH, Dudas ME, Nissan A, Cordon-Cardo C, Ghossein RA (2003) Adrenocortical adenoma and carcinoma: histopathological and molecular comparative analysis. Mod Pathol 16:742–751
21. Taylor SR, Roederer M, Murphy RF (1987) Flow cytometric DNA analysis of adrenocortical tumors in children. Cancer 59:2059–2063
22. Vargas MP, Vargas HI, Kleiner De, Merino MJ (1997) Adrenocortical neoplasms: role of prognostic factors MIB-1, p53 and RB. Am J Surg Pathol 21:556–562
23. Von Slooten H, Schaberg A, Smeenk D, Moolenaar AJ (1985) Morphological characteristics of benign and malignant adrenal cortical tumors. Cancer 55:766–773
24. Wachenfeld C, Beuschlein F, Zwermann O, Mora P, Fassnacht M, Allolio B, Reincke M (2001) Discerning malignancy in adrenocortical tumors: are molecular markers useful? Eur J Endocrinol 145:335–341
25. Weieneke JA, Thompson LD, Heffess CS (2003) Adrenal cortical neoplasms in the pediatric population: a clinicopathologic and immunophenotypic analysis of 83 patients. Am J Surg Pathol 27:867–881
26. Weiss LM (1984) Comparative histologic study of 43 metastasizing and nonmetastasizing adrenocortical tumors. Am J Surg Pathol 8:163–169
27. Weiss LM, Medeiros LJ, Vickery AL Jr (1989) Pathologic features of prognostic significance in adrenocortical carcinoma. Am J Surg Pathol 13:202–206

Virchows Arch (2006) 448: 597–603
DOI 10.1007/s00428-005-0141-x

ORIGINAL ARTICLE

Nabiha Missaoui · Sihem Hmissa · Lucien Frappart · Amel Trabelsi · Atef Ben Abdelkader · Cheick Traore · Moncef Mokni · Mohamed Tahar Yaacoubi · Sadok Korbi

$p16^{INK4A}$ overexpression and HPV infection in uterine cervix adenocarcinoma

Received: 29 September 2005 / Accepted: 23 November 2005 / Published online: 22 February 2006

Abstract Human papillomaviruses (HPVs) are causally involved in the genesis of cervical carcinomas and their precursors, and there is a strong relationship between the cyclin-dependant kinase inhibitor $p16^{INK4A}$ and HPV infection. This study was carried out to assess the correlations between $p16^{INK4A}$ expression as an early biomarker of the endocervical adenocarcinoma and HPV infection. $p16^{INK4A}$ expression and HPV typing were performed on 46 samples including 5 normal endocervix, 9 benign lesions of the endocervix, 25 endocervical adenocarcinomas, and 7 endometrioid adenocarcinomas of the uterine corpus. A semiquantification of the $p16^{INK4A}$ immunostaining was realized (using both the staining intensity and the percentage of positive cells) and was graded from 0 to 15. All of the 25 endocervical adenocarcinomas overexpressed $p16^{INK4A}$; the adjacent epithelium and the connective tissue were strictly negative. No $p16^{INK4A}$ was detected in nine benign endocervical lesions and in five normal endocervix. Few endometrioid adenocarcinomas of the uterine corpus that infiltrate the endocervix exhibited a low immunoreactivity (score 0/15 or 1/15). This pattern of expression is significantly associated with HPV infection ($p<10^{-3}$), mainly high-risk HPV types ($p=0.02$). Our results suggest that $p16^{INK4A}$ is a putative molecular biomarker that consistently discriminates uterine cervix adenocarcinomas from benign lesions and from endometrioid adenocarcinomas of the uterine corpus.

Keywords Uterine cervix · Adenocarcinoma · $p16^{INK4A}$ · HPV

N. Missaoui (✉) · L. Frappart · C. Traore
Anatomie Pathologique, Bat 10, Hôpital Edouard Herriot,
69437 Lyon, Cedex 03, France
e-mail: missaouinabiha@mail2world.com

S. Hmissa · A. Trabelsi · A. B. Abdelkader ·
M. Mokni · M. T. Yaacoubi · S. Korbi
Anatomie Pathologique, CHU Farhet Hached,
rue du Docteur Moreau,
BP176, 4000 Sousse, Tunisie

Introduction

Worldwide, uterine cervix carcinoma is one of the most prevalent cancers and is a major cause of cancer-related mortality in women [25]. The majority of these tumors are squamous cell carcinomas, whereas adenocarcinomas are relatively rare [44]. Although the incidence of squamous cell carcinomas has decreased during the last decade due to screening programs, uterine cervix adenocarcinomas are diagnosed more frequently [44]. The early detection of precursors of invasive uterine cervix cancer still represents a major challenge in screening programs. In fact, the cytological screening of invasive adenocarcinoma and its precursors is affected by a high rate of false negative reports as a result of sampling errors and interpretation problems, which especially influence the diagnosis sensitivity of Pap smears [15]. Colposcopy is also ineffective in recognizing endocervical lesions [36]. Therefore, well-differentiated adenocarcinomas are also difficult to identify in histopathology, and precursors may be interpreted as reactive changes [16]. Moreover, these lesions are reported to progress faster than squamous intraepithelial lesions [28]. An improvement of the diagnostic capabilities may be reached using new tools and new specific markers of uterine cervix cancerogenesis.

Numerous epidemiologic and molecular studies have demonstrated that high risk types of human papillomavirus (HPV) are the agents of the overwhelming majority of cases of invasive cervix squamous cell carcinoma and of the great majority of endocervical carcinomas and precursors [47, 48]. HPV infection has been detected in almost all precancerous and cancerous lesions of the cervix [29, 48]. Malignant transformation of the cervical epithelial cells is associated with persistent high-risk HPV infections, such as HPV 16 and 18 [48, 49]. HPVs encode E6 and E7 oncoproteins, multifunctional immortalizing and growth-promoting proteins, that bind to and inactivate the tumor suppressor proteins p53 and the retinoblastoma family of tumor suppressor, respectively [43, 48]. E7 contributes to cellular transformation by interfering with the $p16^{INK4A}$/CDK4/Cyclin D1/pRb cell cycle regulatory

pathway and by directing the catabolism of tumor-suppressor protein pRb [10]. The inactivation of these tumor suppressor genes through high-risk HPVs results in uncontrolled cellular proliferation of the host cell [22].

The CDKN2A gene product, p16 protein (p16), is a tumor suppressor protein that inhibits CDK4 and CDK6 which phosphorylate pRb [5, 31]. $p16^{INK4A}$, a member of the INK4A family of cell cycle regulatory proteins, specifically inhibits the formation of cyclin D/CDK4, 6 complexes by interacting with CDK4 and 6 which in turn counteract the activity of pRb by phosphorylation. The retinoblastoma tumor-suppressor protein, pRb, regulates the cell cycle at the G1/S restriction point by complexing with and inhibiting the activity of E2F, which serves as a transcription-dependent promoter of cell cycle progression. The E2F–pRb complex dissociates activating E2F, which in turn initiates the transcription of genes required for DNA replication [5, 12].

Overexpression of $p16^{INK4A}$ protein has been demonstrated in squamous cell carcinoma and precursors associated with high-risk HPV types [1, 11, 13, 14]. Klaes et al. [13, 14] reported that $p16^{INK4A}$ immunostaining may be a powerful tool to identify squamous cell carcinomas and their precursors with prognostic implications.

This study was carried out to assess the correlations between $p16^{INK4A}$ expression and the HPV infection and to ascertain the role of $p16^{INK4A}$ immunostaining as an early biomarker of uterine cervix adenocarcinoma.

Material and methods

Tissue samples

Forty-six specimens were retrieved from the surgical pathology files of the Department of Pathology, Farhet Hached University Hospital, Sousse, Tunisia, and the Department of Pathology, Edouard Herriot University Hospital, Lyon, France.

The cases studied were distributed into the following groups, according to the World Health Organization (WHO) Classification of Tumors of the Breast and Female Genital Organs, 2003 [40]: normal endocervix (n=5), benign lesions of uterine cervix including florid immature squamous metaplasia, microglandular hyperplasia, papillary hyperplasia, and decidual reaction (n=9), primary uterine cervix adenocarcinomas (n=25), and endometrioid adenocarcinomas with infiltration of the uterine cervix (n=7). The five cases of normal endocervix were selected mainly among women in their reproductive years who scheduled for hysterectomy due to benign gynecological abnormalities. These cases were selected randomly, and the slides were reviewed by two pathologists. All tissues had been routinely fixed in 4% buffered formalin and paraffin embedded.

HPV detection and typing using PCR

DNA extraction was realized on sections fixed in formaldehyde and included in paraffin using DNA Master Pure Technique (Tebu, France). Fetal liver was used as negative control and β-globine (268 bp) gene amplification as quality control of DNA extraction.

HPV detection and typing were performed by polymerase chain reaction (PCR) using general primers GP5/GP6 which amplify a 140-bp fragment in the L1 region common to numerous HPV as described before [38], and type specific primers for E6/E7 sequence region of HPV 6/11 (product size: 302 bp), as described by Soler et al [39], and for E6 and E7 sequence region of HPV 16 (465–292 bp), HPV 18 (419–266 bp), HPV 31 (434–270 bp), and HPV 33 (429–292 bp).

Thereafter, PCR products indicating infection with HPV 6/11, 16, 18, 31, or 33 were identified on agarose gels with ethidium bromide and reading under an ultraviolet lamp.

Immunohistochemistry for $p16^{INK4A}$ protein

The immunostaining procedure was then carried out as already described for other issues [13, 14]. Briefly, one or two paraffin blocks containing representative portions of the tumors were selected for each case, and 4-μm-thick serial sections were obtained and mounted on silanized slides. Sections were incubated for 30 min with primary monoclonal antibodies against anti-p16 antibody (Dako Cytomation, K5334, clone E6H4, dilution 1:50). The remaining part of the procedure was performed as previously published [8, 18]. One uterine cervix squamous cell carcinoma with known diffuse and strong immunoreactivity with p16 antibody was used as a positive control. Negative controls, using monoclonal mouse immunoglobulin G (IgG2a) antibody at a comparable concentration, were included.

Quantification of $p16^{INK4A}$ immunostaining

Immunoreactivity was evaluated as described previously [20, 35, 46]. Briefly, two independent pathologists carried out a semiquantification of the $p16^{INK4A}$ immunostaining with both the staining intensity (0, no staining; 1, weak staining intensity; 2, intermediate; and 3, strong staining intensity) and the percentage of positively stained tumor cells (0, no positive cells; 1, <25%; 2, 26–50%; 3, 51–75%; 4, 76–99%; 5, 100% positive tumor cells). After multiplication of both values, the immunostaining results were graded from 0 (no reactivity in tumor cells) to 15 (100% positive tumor cells with strong staining intensity).

Statistical analysis

The data were examined by Chi-square statistics using the Epi Info 2002 software as previously described [9, 46]. Probability values of 0.05 or less were considered statistically significant.

Results

HPV Detection and Typing in uterine cervix adenocarcinoma

HPV typing was carried out on 25 endocervical adenocarcinomas, 7 endometrioid adenocarcinomas of the uterine corpus with infiltration of the endocervix, and 9 benign lesions of the uterine endocervix. HPV results were considered contributory in 23 cases (56.1%); of these, 12 were GP5/GP6-positive (52.2%) (Table 1). All HPV-positive cases were endocervical adenocarcinomas. Among 12 HPV-positive uterine cervix adenocarcinomas, eight cases were positive for HPV 16 (66.7%), two cases were positive for HPV 31 (16.7%), one case was positive for HPV 18 (8.3%), and only one patient had an unknown HPV type. HPV DNA were detected in none of the endocervical benign lesions and the endometrioid adenocarcinomas that infiltrate the endocervix, and they were therefore regarded as HPV-negative. In this study, no positive case for low-risk HPV 6/11 was observed.

Immunostaining for $p16^{INK4A}$

Immunohistochemical analysis for $p16^{INK4A}$ was performed in all 46 specimens investigated with E6H4 clone, and the results are summarized in Table 1. $p16^{INK4A}$ immunoreactivity was not detected in the normal glandular epithelium or connective tissue cells of five control cases. However, $p16^{INK4A}$ was expressed in all uterine cervix adenocarcinomas investigated: 22 cases were scored 15, with strong and diffuse $p16^{INK4A}$ immunostaining uniformly observed in both the nuclei and the cytoplasm of 100% of the tumor cells. The three remaining uterine cervix adenocarcinomas were scored 12, with strong and diffuse $p16^{INK4A}$ immunoreactivity observed in 76–99% of tumor cells. The in situ component observed at the border of the invasive uterine adenocarcinoma is always highly positive (Fig. 1c,d). Endocervical neoplastic lesions were always clearly distinguishable from the adjacent normal or reactive epithelia and connective tissue cells (Fig. 1e,f). In nine benign endocervical lesions, no $p16^{INK4A}$ immunoreactivity (score 0) was detected (Fig. 1a,b). In endometrioid adenocarcinoma that infiltrated the endocervix, there was a focal and very low immunostaining with $p16^{INK4A}$ involving less than 25% of tumor cells (score 1) for four cases; three endometrioid adenocarcinomas were scored 0 (Fig. 1g,h).

Relationship between $p16^{INK4A}$ immunoreactivity and HPV subtype

In our study, data of HPV infection were contributory for only 12 uterine cervix adenocarcinomas. All 12 HPV-positive uterine cervix adenocarcinoma cases showed strong and diffuse $p16^{INK4A}$ overexpression in 100% of cancer cells (score 15). $p16^{INK4A}$ overexpression was significantly associated with HPV infection ($p<10^{-3}$), mainly high-risk HPV types including HPV 16, 18, and 31 ($p=0.02$) and HPV 16 ($p=0.02$).

Table 1 HPV typing and $p16^{INK4A}$ expression in benign endocervical lesions, endocervical and endometrioid adenocarcinomas

Histopathology	*N*	β-Globine	HPV detection and typing						$p16^{INK4A}$ immunostaining score				
			GP5/GP6[a]	HPV6/11	HPV16[b]	HPV18	HPV31	HPV33	0	1	2–9	12	15
Benign endocervical lesions	9	6	–	–	–	–	–	–	9 (100%)	–	–	–	–
Endocervical adenocarcinomas	25	12	12	–	8 (66.7%)	1 (8.3%)	2 (16.7%)	–	–	–	–	3 (12%)	22 (88%)
Endometrioid adenocarcinomas	7	5	–	–	–	–		–	3 (42.8%)	4 (57.2%)	–	–	–

[a]Correlations between HPV infection and $p16^{INK4A}$ expression, $p<10^{-3}$
[b]Correlations between HPV 16 infection and $p16^{INK4A}$ expression, $p=0.02$

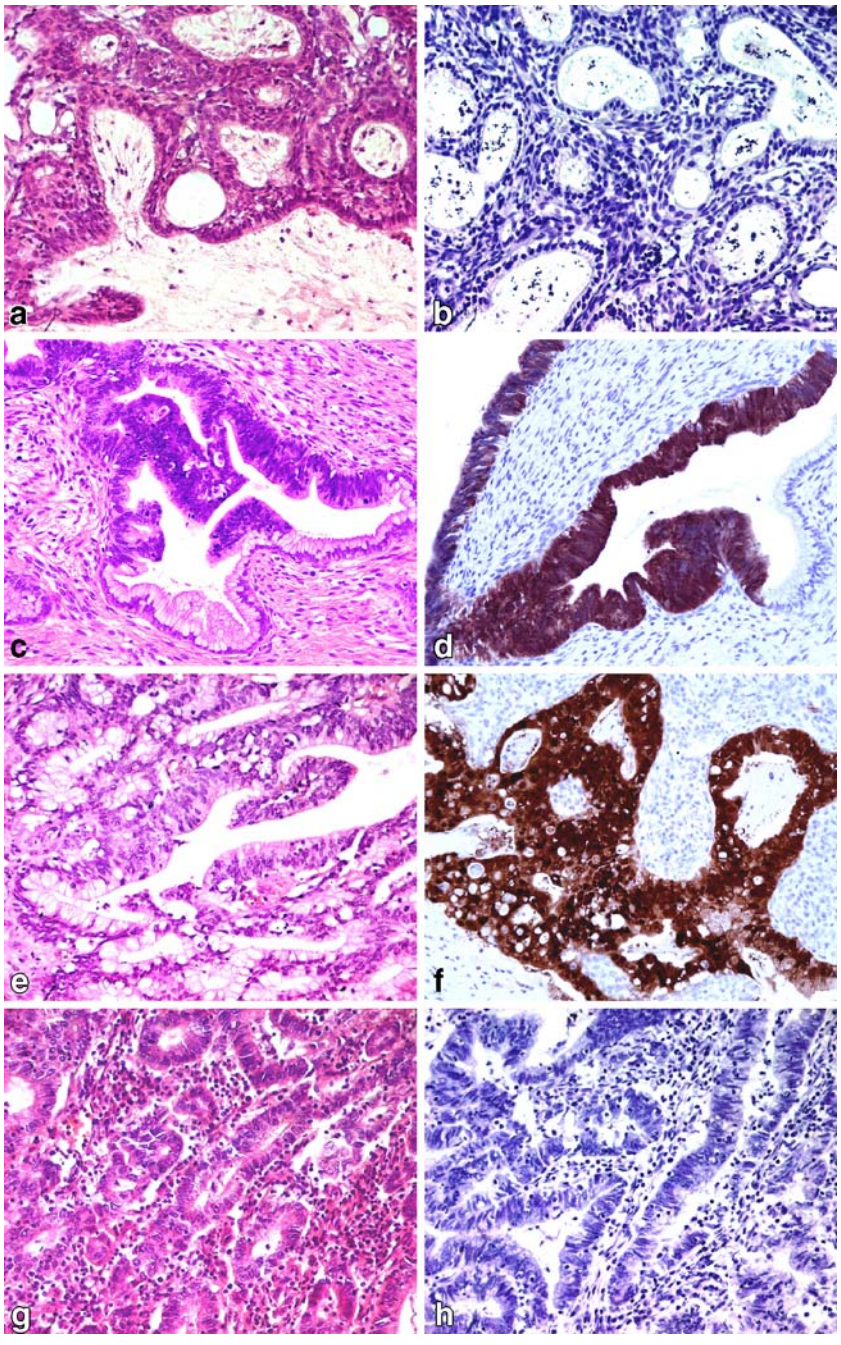

Fig. 1 **a** Microglandular endocervical hyperplasia: tightly packed, varying-sized glandular or tubular units with flattened to cuboidal cells and subcolumnar reserve cell hyperplasia (HPS, M ×200). **b** Microglandular endocervical hyperplasia, no p16 immunoreactivity (M ×200). **c** Adenocarcinoma in situ component of an invasive uterine cervix adenocarcinoma. The normal endocervical epithelium is partly replaced by cytologically malignant epithelium with pseudostratification, coarse chromatin and mitoses (HPS, M ×200). **d** Adenocarcinoma in situ component of an invasive uterine cervix adenocarcinoma-p16 immunolabeling : heavy staining of the glandular epithelium, nuclei, and sometimes the cytoplasm of the malignant cell (M ×200). **e** Moderately differentiated invasive adenocarcinoma of the endocervix (HPS, M ×200). **f** Moderately differentiated invasive adenocarcinoma of the endocervix-P16 immunolabeling of the nuclei of the malignant cell (M ×200). **g** Well-differentiated endometrioid adenocarcinoma (HPS, M ×200). **h** Well-differentiated endometrioid adenocarcinoma: no p16 immunoreactivity (M ×200).

Discussion

The carcinogenesis of glandular epithelium has not been fully elucidated, and there is no clear agreement concerning the association with HPVs [2, 17, 44]. In contrast to cervical squamous cell carcinoma, the overall HPV DNA prevalence in uterine cervix adenocarcinoma varies between 32 and 84% in different studies, depending on the method chosen [3, 41]. The method must be highly sensitive because of a lower viral load, fewer episomal viral particles, and loss of portions of the viral genome during integration in glandular cells [6, 32]. In our study, using PCR, 12 cervical adenocarcinomas investigated were HPV DNA-positive, with 75% (9/12) with the high-risk types (HPV 16 and 18) and 66.7% (8/12) with the HPV 16 type. Anderson et al. [2] reported PCR-detected HPV DNA in 71% of cervical adenocarcinoma. In different histological subtypes of cervical adenocarcinoma and related tumors analyzed using broad-spectrum HPV DNA amplification and genotyping performed with the SPF10 primer set and line probe assay, Pirog et al. [27] detected a high prevalence of HPV DNA (91%) among mucinous adenocarcinomas and adenosquamous carcinomas of the cervix similar to that reported for cervical squamous cell carci-

noma. Thus, they considered that only rare histological variants of cervical adenocarcinomas seem unrelated to HPV infection. This is more in line with the findings of Zielinski et al. [46] that reported high-risk HPV-positive adenocarcinoma prevalence (94%) identical to that found in squamous cell carcinoma, with HPV 18 being the most common type in adenocarcinoma.

Several recent reports describe the value of $p16^{INK4A}$ as a specific antibody for the detection of cervical neoplasia [1, 9, 11, 13, 14, 24, 30]. A strong overexpression of $p16^{INK4A}$ in cervical squamous cell carcinomas has been associated with HPV infection [11] and occurs when pRb is inactivated by HPV E7 or by mutation [23, 26]. Interestingly, we found that all 25 cases of cervical adenocarcinoma exhibited $p16^{INK4A}$ overexpression, and among them, 22 were very strongly and diffusely stained with the antibody (100% of tumor cells); however, this $p16^{INK4A}$ immunoreactivity was absent in all nine benign lesions of the endocervix as well as in adjacent normal endocervical glands. Therefore, $p16^{INK4A}$ immunostaining appears to be a useful tool to distinguish cervical adenocarcinomas from benign conditions and glandular atypia which may be associated with inflammation or irradiation.

Recently, Tringler et al. [42] found a strong, uniform, $p16^{INK4A}$ expression in all cases of endocervical glandular dysplasia, in situ and invasive adenocarcinoma studied. They observed also a weaker or focal expression in benign ciliated columnar cells of normal endocervical glands, tubal metaplasia, reserve cells, and Nabothian cysts. They suggested that $p16^{INK4A}$ immunostaining would be used, with caution, as an objective marker to increase the diagnostic reproducibility for both glandular dysplasia and in situ adenocarcinoma.

In our study, the lack of $p16^{INK4A}$ immunoreactivity in all normal glandular cells and benign lesions does not necessarily imply loss of $p16^{INK4A}$ expression with gene inactivation, but may represent a physiological normal state in nonneoplastic or nonproliferative cells [7]. Interestingly, in most normal cells, $p16^{INK4A}$ expression is known to be low at both the mRNA and protein levels [7].

These immunohistochemical results clearly evidenced that $p16^{INK4A}$ is a putative molecular biomarker that consistently discriminates cervical adenocarcinomas from benign lesions of the endocervix, endometrial carcinoma, and its precursors [34]. These findings are in agreement with those reported by Negri et al. [24]: using E6H4 clone, all eight in situ adenocarcinomas and 17 (94%) of 18 invasive cervical adenocarcinomas exhibited diffuse positive $p16^{INK4A}$ overexpression. However, in endocervical glandular atypia, only focal expression was observed, and no $p16^{INK4A}$ immunoreactivity was found in atypia of repair [24]. In 95 cases, including benign endocervical controls, a strong, diffuse $p16^{INK4A}$ positivity occurred exclusively within adenocarcinoma in situ [30]. However, in other studies with different $p16^{INK4A}$ antibodies and conditions, detectable expression has been described in 58 to 86% of cervical adenocarcinoma [9, 21].

In this study, we demonstrated a significant correlation between a diffuse and strong $p16^{INK4A}$ immunoreactivity, the presence of high risk HPVs (HPV 16 and 18) and a malignant lesion of the endocervix ($p<0.05$). These results confirmed the study of Sano et al. [33]. Strong $p16^{INK4A}$ overexpression indicates that the suppressor function of cyclin–CDK complexes may be overcome in the presence of viral oncogenes (E6 and E7 oncoproteins) and malignant transformation can still occur [35].

However, all endometrial adenocarcinomas were HPV-negative, showing that in these tumors, an HPV-independent pathway of carcinogenesis would be postulated. Two main types have been described: type I, in which hyperestrogenism seems to be causally related to the development of endometrioid carcinomas, and type II, with an independent estrogen pathway of endometrial carcinogenesis in which p53 mutation plays a central role [37]. The histological distinction between primary endometrial, especially endometrioid and endocervical adenocarcinomas, may be problematic particularly in small biopsies and when a tumor is present in both endometrial and endocervical specimens [19]. Moreover, ascertaining the exact origin of an adenocarcinoma may be difficult or even impossible when the tumor involves the lower uterine segment or uterine isthmus and upper endocervix. This origin distinction is important, because it governs primary surgical modalities and even adjuvant treatments [19, 45]. Several recent studies have investigated the interest of different antibodies, such as carcinoembryonic antigen, estrogen receptor, and vimentin, to distinguish between primary endometrial and endocervical adenocarcinoma with some success [20]. However, there is an immunohistochemical overlapping in some cases, suggesting the limits of these antibodies to distinguish definitively the origin of an adenocarcinoma [4]. Interestingly, in our study, we found diffuse and strong positivity with $p16^{INK4A}$ involving 100% of cells in 22 primary uterine cervix adenocarcinomas (including the in situ component) and more than 75% of tumor cells in three cases. However, four endometrioid adenocarcinomas that infiltrate the endocervix exhibit just a focal staining involving less than 25% of tumor cells. Thus, we believe that $p16^{INK4A}$ may be of value to distinguish an endometrioid from an endocervical adenocarcinoma. These results confirm the study of McCluggage and Jenkins [19], who proposed that $p16^{INK4A}$ immunoreactivity would assist in the distinction between endometrial and endocervical adenocarcinoma. Moreover, Schorge et al. [35] postulated that $p16^{INK4A}$ would be a biomarker with a potential clinical utility as an adjunct to current screening methods.

In summary, we have found that $p16^{INK4A}$ overexpression is common in uterine cervix adenocarcinoma; this pattern of overexpression is significantly associated with HPV infection (mainly high-risk HPV types). We propose that $p16^{INK4A}$ immunoreactivity is of value to differentiate an adenocarcinoma from endocervical or endometrial origin. $p16^{INK4A}$ overexpression may be a clue in the elucidation of the carcinogenesis of cervical adenocarcinoma.

Acknowledgements We thank Mrs. Intissar Klibi-Toumi and Catherine Gadois for her technical assistance and Dr. Bernard Fontanière and Mrs. Evelyn Bayle for reviewing the manuscript.

Nabiha Missaoui is a recipient of a fellowship from l'Agence Universitaire de la Francophonie (AUF). This work was supported bye the Ligue contre le Cancer, Comité de la Loire.

References

1. Agoff SN, Lin P, Morihara J, Mao C, Kiviat NB, Koutsky LA (2003) p16(INK4a) expression correlates with degree of cervical neoplasia: a comparison with Ki-67 expression and detection of high-risk HPV types. Mod Pathol 16:665–673
2. Andersson S, Rylander E, Larsson B, Strand A, Silfversvard C, Wilander E (2001) The role of human papillomavirus in cervical adenocarcinoma carcinogenesis. Eur J Cancer 37:246–250
3. Bjersing L, Rogo K, Evander M, Gerdes U, Stendahl U, Wadell G (1991) HPV 18 and cervical adenocarcinomas. Anticancer Res 11:123–127
4. Castrillon DH, Lee KR, Nucci MR (2002) Distinction between endometrial and endocervical adenocarcinoma: an immunohistochemical study. Int J Gynecol Pathol 21:4–10
5. Cho NH, Kim YT, Kim JW (2002) Alteration of cell cycle in cervical tumor associated with human papillomavirus: cyclin-dependent kinase inhibitors. Yonsei Med J 43:722–728
6. Choo KB, Lee HH, Pan CC, Wu SM, Liew LN, Cheung WF, Han SH (1988) Sequence duplication and internal deletion in the integrated human papillomavirus type 16 genome cloned from a cervical carcinoma. J Virol 62:1659–1666
7. Dublin EA, Patel NK, Gillett CE, Smith P, Peters G, Barnes DM (1998) Retinoblastoma and p16 proteins in mammary carcinoma: their relationship to cyclin D1 and histopathological parameters. Int J Cancer 79:71–75
8. Ghabreau L, Roux JP, Frappart PO, Mathevet P, Patricot LM, Mokni M, Korbi S, Wang ZQ, Tong WM, Frappart L (2004) Poly(ADP-ribose) polymerase-1, a novel partner of progesterone receptors in endometrial cancer and its precursors. Int J Cancer 109:317–321
9. Ishikawa M, Fujii T, Masumoto N, Saito M, Mukai M, Nindl I, Ridder R, Fukuchi T, Kubushiro K, Tsukazaki K, Nozawa S (2003) Correlation of p16INK4A overexpression with human papillomavirus infection in cervical adenocarcinomas. Int J Gynecol Pathol 22:378–385
10. Jones CJ, Shaw JJ, Wyllie FS, Gaillard N, Schlumberger M, Wynford-Thomas D (1996) High frequency deletion of the tumour suppressor gene P16INK4a (MTS1) in human thyroid cancer cell lines. Mol Cell Endocrinol 116:115–119
11. Keating JT, Cviko A, Riethdorf S, Riethdorf L, Quade BJ, Sun D, Duensing S, Sheets EE, Munger K, Crum CP (2001) Ki-67, cyclin E, and p16INK4 are complimentary surrogate biomarkers for human papilloma virus-related cervical neoplasia. Am J Surg Pathol 25:884–891
12. Khleif SN, DeGregori J, Yee CL, Otterson GA, Kaye FJ, Nevins JR, Howley PM (1996) Inhibition of cyclin D-CDK4/CDK6 activity is associated with an E2F-mediated induction of cyclin kinase inhibitor activity. Proc Natl Acad Sci USA 93:4350–4354
13. Klaes R, Friedrich T, Spitkovsky D, Ridder R, Rudy W, Petry U, Dallenbach-Hellweg G, Schmidt D, von Knebel Doeberitz M (2001) Overexpression of p16(INK4A) as a specific marker for dysplastic and neoplastic epithelial cells of the cervix uteri. Int J Cancer 92:276–284
14. Klaes R, Benner A, Friedrich T, Ridder R, Herrington S, Jenkins D, Kurman RJ, Schmidt D, Stoler M, von Knebel Doeberitz M (2002) p16INK4a immunohistochemistry improves interobserver agreement in the diagnosis of cervical intraepithelial neoplasia. Am J Surg Pathol 26:1389–1399
15. Krane JF, Granter SR, Trask CE, Hogan CL, Lee KR (2001) Papanicolaou smear sensitivity for the detection of adenocarcinoma of the cervix: a study of 49 cases. Cancer 93:8–15
16. Kurman, Norris HJ, Wilkinson E (1992) Tumors of the cervix. Glandular lesions. In: Rosai J, Sbin LH (eds) Tumors of the cervix, vagina and vulva, vol 4. Armed Forces Institute of Pathology, Washington, DC, pp 77–95
17. Lee MF, Chang MC, Wu CH (1998) Detection of human papillomavirus types in cervical adenocarcinoma by the polymerase chain reaction. Int J Gynaecol Obstet 63:265–270
18. Magdinier F, Billard LM, Wittmann G, Frappart L, Benchaib M, Lenoir GM, Guerin JF, Dante R (2000) Regional methylation of the 5′ end CpG island of BRCA1 is associated with reduced gene expression in human somatic cells. FASEB J 14:1585–1594
19. McCluggage WG, Jenkins D (2003) p16 immunoreactivity may assist in the distinction between endometrial and endocervical adenocarcinoma. Int J Gynecol Pathol 22:231–235
20. McCluggage WG, Sumathi VP, McBride HA, Patterson A (2002) A panel of immunohistochemical stains, including carcinoembryonic antigen, vimentin, and estrogen receptor, aids the distinction between primary endometrial and endocervical adenocarcinomas. Int J Gynecol Pathol 21:11–15
21. Milde-Langosch K, Riethdorf S, Kraus-Poppinghaus A, Riethdorf L, Loning T (2001) Expression of cyclin-dependent kinase inhibitors p16MTS1, p21WAF1, and p27KIP1 in HPV-positive and HPV-negative cervical adenocarcinomas. Virchows Arch 439:55–61
22. Munger K, Howley PM (2002) Human papillomavirus immortalization and transformation functions. Virus Res 89:213–228
23. Nakao Y, Yang X, Yokoyama M, Ferenczy A, Tang SC, Pater MM, Pater A (1997) Induction of p16 during immortalization by HPV 16 and 18 and not during malignant transformation. Br J Cancer 75:1410–1416
24. Negri G, Egarter-Vigl E, Kasal A, Romano F, Haitel A, Mian C (2003) p16INK4a is a useful marker for the diagnosis of adenocarcinoma of the cervix uteri and its precursors: an immunohistochemical study with immunocytochemical correlations. Am J Surg Pathol 27:187–193
25. Parkin DM, Pisani P, Ferlay J (1999) Estimates of the worldwide incidence of 25 major cancers in 1990. Int J Cancer 80:827–841
26. Parry D, Bates S, Mann DJ, Peters G (1995) Lack of cyclin D-Cdk complexes in Rb-negative cells correlates with high levels of p16INK4/MTS1 tumour suppressor gene product. EMBO J 14:503–511
27. Pirog EC, Kleter B, Olgac S, Bobkiewicz P, Lindeman J, Quint WG, Richart RM, Isacson C (2000) Prevalence of human papillomavirus DNA in different histological subtypes of cervical adenocarcinoma. Am J Pathol 157:1055–1062
28. Plaxe SC, Saltzstein SL (1999) Estimation of the duration of the preclinical phase of cervical adenocarcinoma suggests that there is ample opportunity for screening. Gynecol Oncol 75:55–61
29. Richart RM (1973) Cervical intraepithelial neoplasia. Pathol Annu 8:301–328
30. Riethdorf L, Riethdorf S, Lee KR, Cviko A, Loning T, Crum CP (2002) Human papillomaviruses, expression of p16, and early endocervical glandular neoplasia. Hum Pathol 33:899–904
31. Rocco JW, Sidransky D (2001) p16(MTS-1/CDKN2/INK4a) in cancer progression. Exp Cell Res 264:42–55
32. Sano T, Sakurai S, Fukuda T, Nakajima T (1995) Unsuccessful effort to detect human papillomavirus DNA in urinary bladder cancers by the polymerase chain reaction and in situ hybridization. Pathol Int 45:506–512
33. Sano T, Oyama T, Kashiwabara K, Fukuda T, Nakajima T (1998) Expression status of p16 protein is associated with human papillomavirus oncogenic potential in cervical and genital lesions. Am J Pathol 153:1741–1748
34. Schmitz MJ, Hendricks DT, Farley J, Taylor RR, Geradts J, Rose GS, Birrer MJ (2000) p27 and cyclin D1 abnormalities in uterine papillary serous carcinoma. Gynecol Oncol 77:439–445
35. Schorge JO, Lea JS, Elias KJ, Rajanbabu R, Coleman RL, Miller DS, Ashfaq R (2004) P16 as a molecular biomarker of cervical adenocarcinoma. Am J Obstet Gynecol 190:668–673

36. Sellors JW, Sankaranarayanan R (2003) Colposcopy and treatment of cervical intraepithelial neoplasia: a beginner's manual. IARC, Lyon
37. Sherman ME, Kurman RJ (1998) Evolving concepts in endometrial carcinogenesis: importance of DNA repair and deregulated growth. Hum Pathol 29:1035–1038
38. Snijders PJ, Schulten EA, Mullink H, ten Kate RW, Jiwa M, van der Waal I, Meijer CJ, Walboomers JM (1990) Detection of human papillomavirus and Epstein–Barr virus DNA sequences in oral mucosa of HIV-infected patients by the polymerase chain reaction. Am J Pathol 137:659–666
39. Soler C, Allibert P, Chardonnet Y, Cros P, Mandrand B, Thivolet J (1991) Detection of human papillomavirus types 6, 11, 16 and 18 in mucosal and cutaneous lesions by the multiplex polymerase chain reaction. J Virol Methods 35:143–157
40. Tavassoli FA, Devilee P (eds) (2003) Tumours of the breast and female genital organs. IARC, Lyon
41. Tenti P, Romagnoli S, Silini E, Zappatore R, Spinillo A, Giunta P, Cappellini A, Vesentini N, Zara C, Carnevali L (1996) Human papillomavirus types 16 and 18 infection in infiltrating adenocarcinoma of the cervix: PCR analysis of 138 cases and correlation with histologic type and grade. Am J Clin Pathol 106:52–56
42. Tringler B, Gup CJ, Singh M, Groshong S, Shroyer AL, Heinz DE, Shroyer KR (2004) Evaluation of $p16^{INK4A}$ and pRb expression in cervical squamous and glandular neoplasia. Hum Pathol 35(6):689–696
43. Van Tine BA, Kappes JC, Banerjee NS, Knops J, Lai L, Steenbergen RD, Meijer CL, Snijders PJ, Chatis P, Broker TR, Moen PT Jr, Chow LT (2004) Clonal selection for transcriptionally active viral oncogenes during progression to cancer. J Virol 78:11172–11186
44. Vizcaino AP, Moreno V, Bosch FX, Munoz N, Barros-Dios XM, Parkin DM (1998) International trends in the incidence of cervical cancer: I. Adenocarcinoma and adenosquamous cell carcinomas. Int J Cancer 75:536–545
45. Zaino RJ (2002) The fruits of our labors: distinguishing endometrial from endocervical adenocarcinoma. Int J Gynecol Pathol 21:1–3
46. Zielinski GD, Snijders PJ, Rozendaal L, Daalmeijer NF, Risse EK, Voorhorst FJ, Jiwa NM, van der Linden HC, de Schipper FA, Runsink AP, Meijer CJ (2003) The presence of high-risk HPV combined with specific p53 and p16INK4a expression patterns points to high-risk HPV as the main causative agent for adenocarcinoma in situ and adenocarcinoma of the cervix. J Pathol 201:535–543
47. zur Hausen H (1996) Papillomavirus infections—a major cause of human cancers. Biochim Biophys Acta 1288:F55–F78
48. zur Hausen H (2002) Papillomavirus and cancer: from basic studies to clinical appplication. Nat Rev Cancer 2: 342-50
49. zur Hausen H, de Villiers EM (1994) Human papillomaviruses. Annu Rev Microbiol 48:427–447

Virchows Arch (2006) 448: 604–611
DOI 10.1007/s00428-006-0150-4

ORIGINAL ARTICLE

C. Langner · G. Hutterer · T. Chromecki · P. Rehak · R. Zigeuner

Patterns of invasion and histological growth as prognostic indicators in urothelial carcinoma of the upper urinary tract

Received: 21 November 2005 / Revised: 22 December 2005 / Accepted: 22 December 2005 / Published online: 9 March 2006

Abstract The biological significance of squamous and glandular differentiation and different patterns of invasion in upper urinary tract urothelial carcinoma is unclear. We reviewed 268 cases of consecutive upper urinary tract carcinomas with respect to the presence of squamous and/or glandular differentiation and different patterns of invasion (nodular, trabecular, and infiltrative) and correlated data with patient outcome. Squamous or glandular differentiation occurred in 47/268 (18%) tumors and its presence correlated with high tumor stage ($P<0.001$) and grade ($P<0.001$). Invasive patterns were nodular in 49/227 (22%), trabecular in 95/227 (42%), and infiltrative in 83/227 (37%) tumors. The nodular pattern prevailed in low stage ($P<0.001$) and low-grade ($P<0.001$) tumors, whereas the infiltrative pattern prevailed in high stage ($P<0.001$) and high-grade ($P<0.001$) tumors. Multivariate analysis proved that tumor stage ($P<0.001$) and the infiltrative pattern ($P<0.001$) are independent predictors of metastasis-free survival, whereas tumor grade and squamous and glandular differentiation lacked independent influence on patient outcome. In conclusion, the infiltrative pattern of invasion significantly correlated with advanced disease and poor patient outcome. In contrast, the presence of squamous and/or glandular invasion did not prove independent influence on patient outcome. The pattern of invasion should be commented upon separately in the pathology report.

Keywords Urothelial carcinoma · Squamous differentiation · Glandular differentiation · Pattern of invasion · Prognosis

C. Langner (✉)
Institute of Pathology, Medical University Graz,
Auenbruggerplatz 25,
Graz 8036, Austria
e-mail: cord.langner@meduni-graz.at
Tel.: +43-316-38583665
Fax: +43-316-384329

G. Hutterer · T. Chromecki · R. Zigeuner
Department of Urology, Medical University Graz,
Auenbruggerplatz 7,
Graz 8036, Austria

P. Rehak
Department of Surgery, Research Unit for Biomedical Engineering & Computing, Medical University Graz,
Auenbruggerplatz 29,
Graz 8036, Austria

Introduction

Upper urinary tract urothelial carcinoma (UC) is relatively uncommon, accounting for approximately 5% of all epithelial tumors of the urinary tract with most tumors occurring in the bladder [10]. Standard treatment for localized upper tract UC is radical nephroureterectomy with bladder cuff resection [18]. Although numerous investigations showed that stage is the most important predictor of outcome [3, 5–8, 12–15, 19, 24, 31, 32, 34, 35], the clinicopathologic features predictive of metastatic disease are not well defined and the assessment of tumor grade shows considerable variation due to observer subjectivity [2, 44]. Thus, the identification of other prognostic variables that can easily be determined in routinely hematoxylin and eosin (H&E)-stained sections is required to select candidates for adjuvant therapy.

The majority of primary epithelial neoplasms of the urinary tract display conventional urothelial morphology but some tumors may additionally show aberrant differentiation thought to arise from metaplastic change [22, 39]. These areas are most frequently squamous or glandular in nature and their frequency was shown to increase with tumor grade and stage [1, 11, 42, 43, 45]. Thus, most urological oncologists share the view that mixed histology implies more aggressive disease, which may be less susceptible to radio- or chemotherapy [16, 25, 29]. However, there is only one study analyzing the prognostic impact of squamous and/or glandular differentiation in a series of 70 bladder carcinomas [30], whereas a systematical investigation analyzing the clinical significance of squamous and/or glandular differentiation in upper urinary tract cancer,

including both univariate and multivariate statistical analysis, is currently lacking.

Recently, Jiminez et al. [17] described three different patters of invasion (nodular, trabecular, and infiltrative) in a series of 93 muscle-invasive bladder cancers. According to their data, the infiltrative growth pattern may be associated with unfavorable patient outcome despite lack of significance in multivariate analysis. In a subsequent study by Krüger et al. [20] involving 153 muscle-invasive bladder cancers, the infiltrative pattern proved to be an independent predictor of poor disease-related survival. The authors concluded that the classification by Jiminez et al. [17] may serve as an additional tool to predict the prognosis of patients undergoing radical cystectomy for bladder cancer.

In the present study, we aimed to evaluate the potential prognostic significance of squamous and/or glandular differentiation in a large consecutive series of upper urinary tumors. Moreover, our study is the first to apply the classification introduced by Jiminez et al. [17] to this type of urothelial cancer and to assess its role in predicting metastasis-free survival. By performing a multivariate analysis, we analyzed the potential of the different histological variables to serve as independent predictors of patient outcome.

Materials and methods

Case selection

Two hundred sixty-eight consecutive upper urinary tract UCs (169 pelvic and 99 ureteral tumors) from 239 consecutive patients (108 women and 131 men) undergoing surgery between January 1984 and December 2004 were retrieved from the files of our institute. The mean and median ages of patients were 70 and 71 years (range 39–89), respectively. Seventeen out of 239 (7%) patients presented with local lymph node metastases at the time of their primary operation. All tumor specimens were examined by the same protocol including multiple sections obtained from the tumor itself, the kidney, and the pelvic wall adjacent to and distant from the tumor, along with the ureter and lymph nodes, if present.

For the correlation of histopathological data with metastasis-free survival, all noninvasive cancers (41 tumors from 33 patients) and all tumors from patients with multiple invasive cancers (37 tumors from 16 patients) were excluded resulting in a final sample of 190 UCs (134 pelvic and 56 ureteral tumors) from 190 patients (77 women and 113 men). Standard treatment included nephroureterectomy with bladder-cuff resection (n=130), alternatively, nephrectomy alone (n=40) or distal ureteral resection with reimplantation (n=20) were performed. Patients did not receive adjuvant therapy. Follow-up regimen included abdominal ultrasound and cystoscopy every 3 months for the first 3 years, every 6 months for the subsequent 2 years, and yearly thereafter and chest X-ray and computerized tomography every 6 months for the first 3 years and yearly thereafter. All procedures were in accord with the ethical standards established by our institution. Informed consent is not required for retrospective analyses dealing with archival material obtained during routine medical treatment.

Histopathology

H&E-stained slides from routinely formalin-fixed and paraffin-embedded material were systematically reevaluated by one pathologist (C. L.) who was blinded to regional lymph node status and the subsequent disease course. pT-stages were adjusted according to the International Union Against Cancer 2002 issue of the Tumor, Nodes, Metastasis system [41]. Grading was performed according to the recently published two-tiered WHO grading system following the WHO/International Society of Urological Pathology consensus classification [27]. During the process of reviewing the slides, special attention was drawn toward the presence of aberrant histological differentiation. According to the WHO criteria for the diagnosis of histological variants of urothelial cancer [27], squamous differentiation was defined as the presence of intercellular bridges or keratinization. Glandular differentiation was defined as the presence of true glandular spaces and gland-like lumina within tumor cell nests; special care was taken to differentiate these glandular structures from pseudoglandular spaces caused by drop-out of necrotic cells or artifact. A significant proportion of tumors displayed both squamous and glandular differentiation. In these cases both patterns were recorded. Three main architectural patterns of tumor invasion were recognized following the definition by Jiminez at al. [17]: The nodular pattern was composed of well-delineated round nests of tumor cells. These nests varied in diameter but a tendency of roundness was maintained throughout (Fig. 1a). Desmoplasia was usually not prominent and necrosis was not observed. The trabecular pattern consisted of infiltrating broad trabeculae that usually anastomosed with each other and were sometimes associated with extensive necrosis and a desmoplastic stroma (Fig. 1b). The trabeculae were at lest three cells thick. The infiltrative pattern showed infiltrating narrow cords or single tumor cells (Fig. 1c). Desmoplasia and necrosis were common. Cells were usually highly pleomorphic or small and undifferentiated. Tumor heterogeneity represents a well-known phenomenon in urothelial cancers and different subclones with different phenotypes are known to coexist within the same tumor, among which, those bearing the most aggressive biological potential eventually determine patient outcome [4]. Accordingly, in cases showing two or more patterns of invasion, only the most aggressive type of tumor growth (infiltrative > trabecular > nodular) was recorded.

Statistical analyses

Associations between patterns of invasion or histological differentiation and tumor stage as well as tumor grade were

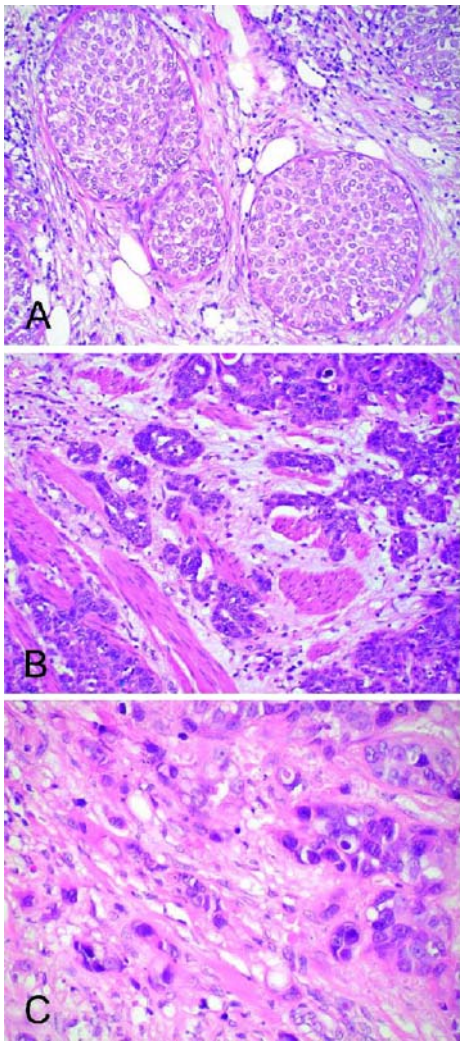

Fig. 1 Urothelial carcinoma of the upper urinary tract with nodular (**a** H&E), trabecular (**b** H&E), and infiltrative (**c** H&E) pattern of invasion according to the definition by Jiminez et al. [17]

analyzed using the Fisher's exact test. Patient outcome was investigated using the Kaplan–Meier method and compared by the log-rank test. Disease progression was defined as the occurrence of nodal and/or distant metastases. Metastasis-free survival was calculated from definitive treatment of upper tract disease (e.g., nephroureterectomy) to the occurrence of metastatic disease or the last follow-up in patients with no evidence of disease progression. For multivariate testing, a Cox's proportional hazards regression model was performed. All reported *P* values were two-sided with significance at $P<0.05$.

Results

Overall, stage pTa was present in 41 (15%), pT1 in 102 (38%), pT2 in 37 (14%), pT3 in 80 (30%), and pT4 in eight (3%) cases. One hundred forty-one (53%) tumors were of low tumor grade and 127 (47%) were of high tumor grade. Pelvic and ureteral tumors showed a comparable distribution regarding the different categories. High tumor grade was associated with high tumor stage [53/139 (38%) pT1/pT2 vs 74/88 (84%) pT3/pT4, $P<0.001$]; no high-grade tumors were detected among noninvasive cancers.

Squamous differentiation occurred in 47/268 (18%) tumors. The majority of them showed small interspersed islands of squamous epithelium with mild to moderate atypia in otherwise typical urothelial carcinoma (Fig. 2a). In some cases, however, poorly differentiated tumor cells showing squamous differentiation (with or without keratinization) gradually merged with the surrounding urothelial tumor cells, ultimately representing the predominant histological growth pattern (Fig. 2b). Squamous differentiation prevailed in high stage [15/180 (8%) pTa-pT2 vs 32/88 (36%) pT3/pT4, $P<0.001$] and high grade [8/141 (6%) low grade vs 39/127 (31%) high grade, $P<0.001$] cancers (Table 1).

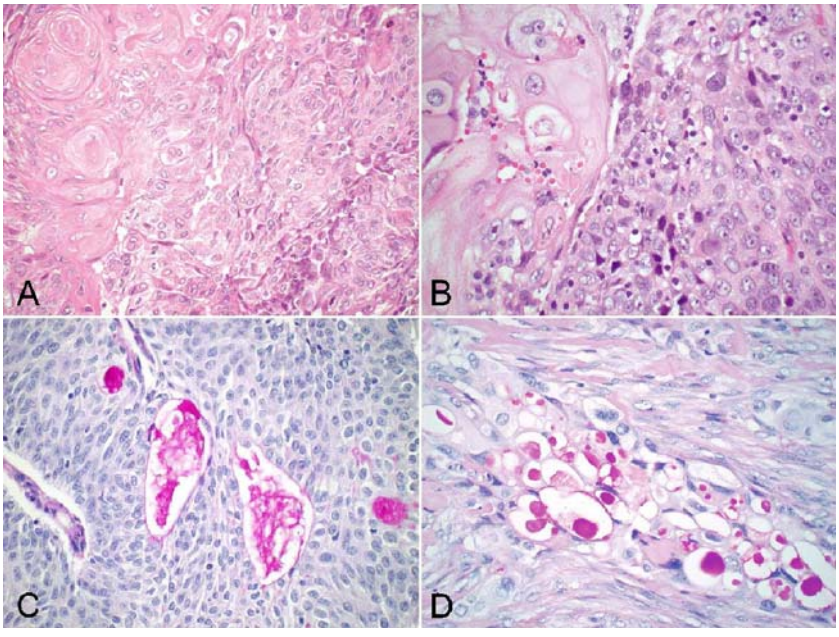

Fig. 2 Urothelial carcinoma of the upper urinary tract with squamous (**a**–**b** H&E) and glandular differentiation (**c**–**d** PAS) as demonstrated in low-grade (**a** and **c**) and high-grade (**b** and **d**) tumors

Table 1 Squamous differentiation in upper urinary tract urothelial carcinomas related to tumor stage (pT1a–pT4) and tumor grade [low grade (LG) and high grade (HG)]

	All tumors		Pelvic tumors		Ureteral tumors	
	Samples	%	Samples	%	Samples	%
pTa	1/41	2	1/19	5	0/22	0
pT1	8/102	8	6/60	10	2/24	5
pT2	6/37	16	3/20	15	3/17	18
pT3	29/80	36	21/62	34	8/18	44
pT4	3/8	38	3/8	38	–	–
LG	8/141	6	4/48	5	4/57	7
HG	39/127	31	30/85	35	9/42	21
Total	47/268	18	34/169	20	13/99	13

Glandular structures were observed in 47/268 (18%) tumors. The amount of glandular differentiation was variable with the majority of cases showing only focal glands bordered by a single layer of cuboidal or columnar cells or gland-like lumina scattered among nests of otherwise typical urothelial carcinoma (Fig. 2c). In some cases, however, the glandular differentiation represented the predominating histological growth pattern (Fig. 2d). Glandular differentiation prevailed in high stage [22/180 (12%) pTa-pT2 vs 25/88 (28%) pT3/pT4, P=0.002] and high grade [17/141 (12%) low grade vs 30/127 (24%) high grade, P=0.02] cancers (Table 2). Occasionally, the glands underwent cystic dilatation, resulting in a microcystic appearance. One case displayed a colloid-mucinous pattern characterized by nests of cells "floating" in extracellular mucin. It is interesting to note that the glandular growth pattern was associated with the presence of squamous differentiation. Thus, 20/47 (43%) tumors with glandular lumina simultaneously showed foci of squamous differentiation compared with 27/221 (12%) tumors without glandular differentiation (P<0.001).

According to Jiminez et al. [17], patterns of invasion were nodular in 49/227 (22%), trabecular in 95/227 (42%), and infiltrative in 83/227 (37%) tumors. The nodular pattern prevailed in low stage [45/139 (32%) pT1/pT2 vs 4/88 (5%) pT3/pT4, P<0.001] and low grade [44/100 (44%) low grade vs 5/127 (4%) high grade, P<0.001] cancers, whereas the infiltrative pattern prevailed in high stage [20/139 (14%) pT1/pT2 vs 63/88 (72%) pT3/pT4, P<0.001] and high grade [0/100 (0%) low grade vs 83/127 (65%) high grade, P<0.001] cancers (Table 3).

Follow-up data were available from 186/190 (98%) patients. After a mean and median follow-up of 46 and 31 months, respectively, progressive disease was observed in 74/186 (40%) patients including 60 patients who died from cancer and 14 patients who are currently alive with metastatic disease. Mean time to progression was 19 months (median 8.3, range 0–110). Twenty-five patients died from causes not related to cancer. Actuarial overall and metastasis-free survival rates were 63 and 56% at 5 years and 52 and 45% at 10 years.

The development of distant metastases was associated with the presence of squamous and/or glandular differentiation. Thus, 25/43 (58%) UCs with squamous differentiation developed disease progression compared with 49/143 (34%) UCs without squamous differentiation (P=0.001; Fig. 3). Actuarial 5-year metastasis-free survival rates for patients with UCs with and without squamous differentiation were 33 and 63%, respectively. Similarly, 19/36 (53%) UCs with glandular differentiation developed disease progression, compared with 55/150 (37%) UCs without glandular differentiation (P=0.04; Fig. 4). Actuarial 5-year metastasis-free survival rates for patients with UCs with and without glandular differentiation were 45

Table 2 Glandular differentiation in upper urinary tract urothelial carcinomas related to tumor stage (pT1a–pT4) and tumor grade [low grade (LG) and high grade (HG)]

	All tumors		Pelvic tumors		Ureteral tumors	
	Samples	%	Samples	%	Samples	%
pTa	6/41	15	3/19	16	3/22	14
pT1	10/102	10	5/60	8	5/42	12
pT2	6/37	16	5/20	25	1/17	6
pT3	23/80	29	19/62	31	4/18	22
pT4	2/8	25	2/8	25	–	–
LG	17/141	12	12/84	14	5/57	9
HG	30/127	24	22/85	26	8/42	19
Total	47/268	18	34/169	20	13/99	13

Table 3 Patterns of invasion in upper urinary tract urothelial carcinomas related to tumor stage (pT1–pT4), tumor grade [low grade (LG) and high grade (HG), and tumor location (pelvic and ureteral)]

	Nodular		Trabecular		Infiltrative	
	Samples	%	Samples	%	Samples	%
pT1 (*n*=102)	39	38	52	51	11	11
pT2 (*n*=37)	6	16	22	59	9	24
pT3 (*n*=80)	4	5	20	25	56	70
pT4 (*n*=8)	–	–	1	13	7	88
LG (*n*=100)	44	44	56	56	–	–
HG (*n*=127)	5	4	39	31	83	65
Pelvic (*n*=150)	34	23	61	41	55	37
Ureteral (*n*=77)	15	19	34	44	28	36
Total (*n*=227)	49	22	95	42	83	37

and 59%, respectively. In addition, disease progression was associated with the pattern of invasion. Thus, only 3/41 (7%) UCs with a nodular pattern developed disease progression compared with 18/78 (23%) UCs with a trabecular pattern and 53/67 (79%) UCs with an infiltrative pattern (P<0.002; Fig. 5). Actuarial 5-year metastasis-free survival rates for UCs with nodular, trabecular, and infiltrative pattern of invasion were 94, 74, and 12%, respectively (Table 4). No significant prognostic influence was observed for tumor location, patient age, and gender.

In a Cox's proportional hazards regression model including age, gender, tumor stage, grade, and location (pelvis vs ureter), squamous and glandular differentiation, as well as the different patterns of invasion, pT-stage >1 [P<0.001, risk ratio (RR)=4.02, 95% confidence interval (CI)=1.82–8.84] and the infiltrative pattern of invasion (P<0.001, RR=3.88, 95% CI=1.87–8.05) proved to be independent predictors of metastatic disease. Patients with UCs showing a nodular pattern of invasion were less likely to develop disease progression but this difference was not statistically significant (P=0.16, RR=0.39, 95% CI=0.11–1.43). Tumor grade and location and presence of squamous and/or glandular differentiation lacked independent influence on patient outcome.

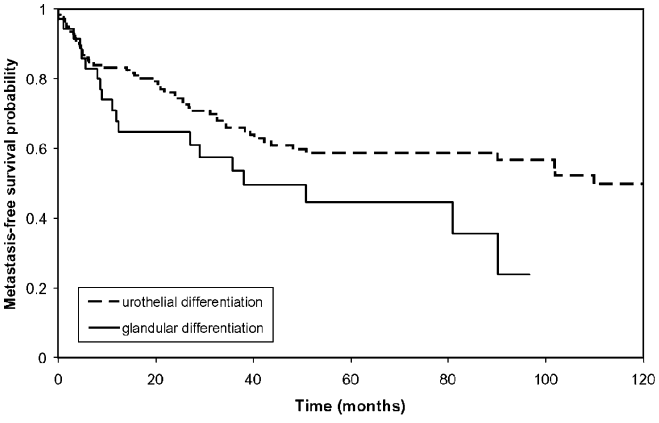

Fig. 4 Metastasis-free survival (months) in patients with upper urinary tract urothelial cell carcinomas related to the presence of glandular differentiation (P=0.04, log-rank test)

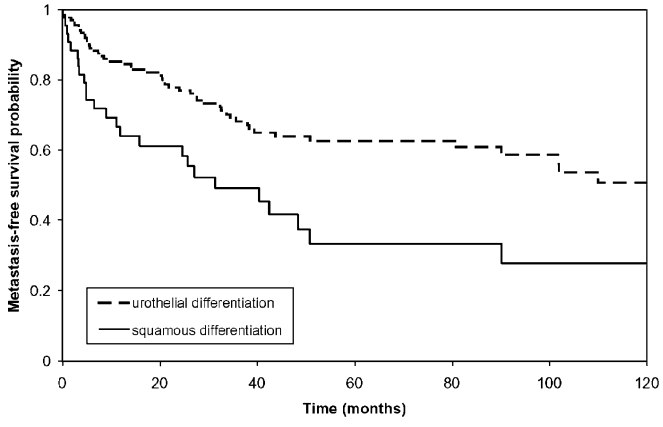

Fig. 3 Metastasis-free survival (months) in patients with upper urinary tract urothelial cell carcinomas related to the presence of squamous differentiation (P=0.001, log-rank test)

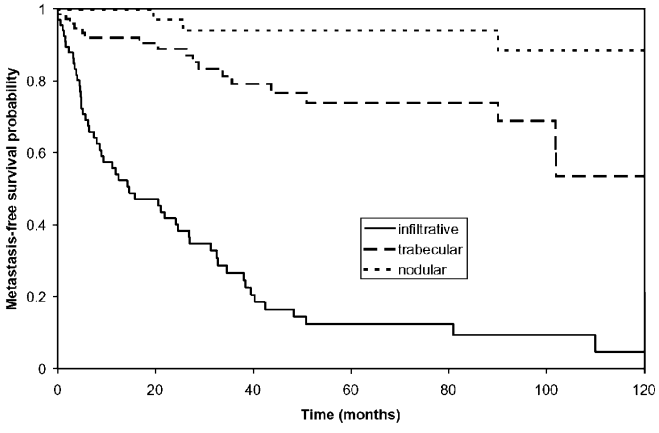

Fig. 5 Metastasis-free survival (months) in patients with upper urinary tract urothelial cell carcinomas related to different patterns of invasion (P<0.001, log-rank test)

Table 4 Disease progression in upper urinary tract urothelial carcinomas related patterns of invasion (nodular, trabecular, and infiltrative) and histological differentiation (pure urothelial, squamous, and glandular)

	All tumors		Pelvic tumors		Ureteral tumors	
	Samples	%	Samples	%	Samples	%
Overall disease progression	74/186	40	57/131	44	17/55	31
Nodular pattern	3/41	7	2/30	7	1/11	9
Trabecular pattern	18/78	23	15/54	28	3/24	13
Infiltrative pattern	53/67	79	40/47	85	13/20	65
Urothelial differentiation	41/126	33	30/87	34	11/39	28
Squamous differentiation	25/43	58	21/32	66	4/11	36
Glandular differentiation	19/36	53	16/28	57	3/8	38

The follow-up data available are from 186 patients

Discussion

According to literature, metastatic disease occurs in 19–54% of upper tract urothelial cancers and a significant proportion of patients eventually die due to tumor dissemination [6, 8, 13–15, 31, 32, 34, 35, 37]. Thus, the identification of independent prognostic factors is an essential step for the evaluation of affected patients not only to predict disease evolution, thus aiding surveillance strategies, but also to identify subgroups that might benefit from adjuvant cancer therapy.

Primary squamous cell carcinoma and adenocarcinoma of the renal pelvis and ureter, defined as tumors showing pure squamous or pure glandular phenotype, are highly uncommon, representing less than 1% of all primary tumors of the upper urinary tract [36]. Their pathogenesis was related to urothelial metaplasia due to long-standing chronic irritation and/or inflammation leading to dysplasia (intraepithelial neoplasia) and ultimately to squamous cell carcinoma or adenocarcinoma [28]. Thus, medical history of affected patients commonly discloses information regarding chronic pyelonephritis and/or nephrolithiasis. Patients often present at an advanced stage of the disease and the outcome is generally poor [23, 33, 38, 40].

In contrast, aberrant squamous and/or glandular differentiation in otherwise typical urothelial cancers is by far more common, occurring in 7–60% of bladder [1, 9, 22, 26, 29, 30, 42, 45] and 10–15% of upper urinary tract UCs [7, 11]. In our series, squamous or glandular differentiation occurred in 74/268 (28%) upper urinary tract tumors, its presence being significantly correlated with high tumor stage and grade. Both squamous and glandular differentiation indicated poor prognosis in univariate analysis. However, multivariate analysis revealed that neither squamous nor glandular differentiation possessed independent influence on patient outcome. Our data are in line with a previous study investigating bladder cancer by Mazzucchelli et al. [30] who reported a significant correlation between squamous differentiation and prognosis in univariate analysis (P=0.05), but not in multivariate analysis.

The high frequency of squamous and/or glandular differentiation in otherwise typical urothelial cancers is not easy to understand because the urinary tract is normally exclusively lined by urothelial cells. To bring light in this topic, Kunze and Francksen [21, 22] systematically investigated carcinoma tissues from human and rat urinary bladder. The authors were able to show that the underlying histogenetic principle is based on the pluripotent metaplastic potential of normal and neoplastic urothelium to undergo several pathways of cellular and architectural differentiation. By demonstrating a direct conversion of typical urothelial carcinoma cells into squamous and/or glandular cells, they concluded that squamous and glandular differentiation develop by a metaplastic process within preexisting conventional UC. This process occurs during tumor progression and dedifferentiation, most probably owing to the embryologic origin of the urinary tract from pluripotent tissues of the cloacal endoderm and the mesodermal Wolffian ducts.

The infiltrative pattern according to Jiminez et al. [17] was significantly associated with the development of metastatic disease and proved to be a new independent prognostic marker that can be determined in routinely H&E-stained sections and is thus easily applicable worldwide. The original analysis by Jiminez et al. [17] and a subsequent study by Krüger et al. [20], which were both restricted to bladder tumors, revealed comparable results. The infiltrative pattern serves as an independent histological prognosticator with a relative risk comparable to that of tumor stage, emphasizing the necessity for pathologists to comment specifically on its presence (or absence).

Tumor heterogeneity represents a well-known phenomenon in urothelial cancers and a significant proportion of tumors in our study and in the previous reports on bladder cancer displayed two or more patterns of invasion. For this reason, a major and a minor pattern was recorded for each patient in both previous reports [17, 20]. However, because both previous studies clearly showed that the presence alone of a minor infiltrative component had the same impact on patient outcome as the presence of a major infiltrative component, we recorded only the most aggressive type of tumor invasion (infiltrative > trabecular > nodular) to improve practicability of the system in daily routine work. In contrast to Krüger et al. [20] who suggested an abbreviated two-tiered classification of invasion

(infiltrative vs noninfiltrative), we retained the original three-tiered system because analogous to the negative prognostic effect of the infiltrative pattern, the nodular pattern indicated a tendency toward a more favorable outcome.

In summary, tumor stage and the infiltrative pattern of invasion significantly correlated with advanced disease and enhanced local and distant metastatic spread, clearly indicating that the pattern of invasion is a reliable prognostic factor for patients with upper urinary tract cancer. In contrast, the presence of squamous and/or glandular invasion did not prove independent influence on patient outcome. The pattern of invasion should be commented upon separately in the pathology report.

Acknowledgements The authors thank Mr. R. Christof and Ms. A. Kaps for photographic expertise and excellent technical support.

References

1. Billis A, Schenka AA, Ramos CC, Carneiro LT, Araujo V (2001) Squamous and/or glandular differentiation in urothelial carcinoma: prevalence and significance intransurethral resections of the bladder. Int Urol Nephrol 33:631–633
2. Bol MG, Baak JP, Buhr-Wildhagen S, Kruse AJ, Kjellevold KH, Janssen EA, Mestad O, Ogreid P (2003) Reproducibility and prognostic variability of grade and lamina propria invasion in stages Ta, T1 urothelial carcinoma of the bladder. J Urol 169:1291–1294
3. Charbit L, Gendreau MC, Mee S, Cukier J (1991) Tumors of the upper urinary tract: 10 years of experience. J Urol 146: 1243–1246
4. Cheng L, Neumann RM, Nehra A, Spotts BE, Weaver AL, Bostwick DG (2000) Cancer heterogeneity and its biologic implications in the grading of urothelial carcinoma. Cancer 88:1663–1770
5. Corrado F, Ferri C, Mannini D, Corrado G, Bertoni F, Bacchini P, Lelli G, Lieber MM, Song JM (1991) Transitional cell carcinoma of the upper urinary tract: evaluation of prognostic factors by histopathology and flow cytometric analysis. J Urol 145:1159–1163
6. Cozad SC, Smalley SR, Austenfeld M, Noble M, Jennings S, Raymond R (1995) Transitional cell carcinoma of the renal pelvis or ureter: patterns of failure. Urology 46:796–800
7. Das AK, Carson CC, Bolick D, Paulson DF (1990) Primary carcinoma of the upper urinary tract. Effect of primary and secondary therapy on survival. Cancer 66:1919–1923
8. Fiori E, Cavallaro G, Paparelli C, Decesare A, Bononi M, Galati G, Tiziano G, Cavallaro A, Cangemi V (2004) Significance of T stadium and grading as prognostic factors in transitional cell carcinoma of the ureter. Anticancer Res 24: 1921–1924
9. Fung CY, Shipley WU, Young RH, Griffin PP, Convery KM, Kaufman DS, Althausen AF, Heney NM, Prout GR Jr (1991) Prognostic factors in invasive bladder carcinoma in a prospective trial of preoperative adjuvant chemotherapy and radiotherapy. J Clin Oncol 9:1533–1542
10. Genega EM, Porter CR (2002) Urothelial neoplasms of the kidney and ureter. An epidemiologic, pathologic, and clinical review. Am J Clin Pathol 117(Suppl):S36–S48
11. Genega EM, Kapali M, Torres-Quinones M, Huang WC, Knauss JS, Wang LP, Raghunath PN, Kozlowski C, Malkowicz SB, Tomaszewski JE (2005) Impact of the 1998 World Health Organization/International Society of Urological Pathology classification system for urothelial neoplasms of the kidney. Mod Pathol 18:11–18
12. Guinan P, Vogelzang NJ, Randazzo R, Sener S, Chmiel J, Fremgen A, Sylvester J (1992) Renal pelvic cancer: a review of 611 patients treated in Illinois 1975–1985. Cancer incidence and end results committee. Urology 40:393–399
13. Hall MC, Womack S, Sagalowsky AI, Carmody T, Erickstad MD, Roehrborn CG (1998) Prognostic factors, recurrence, and survival in transitional cell carcinoma of the upper urinary tract: a 30-year experience in 252 patients. Urology 52:594–601
14. Huben RP, Mounzer AM, Murphy GP (1988) Tumor grade and stage as prognostic variables in upper urinary tract urothelial tumors. Cancer 62:2016–2020
15. Inoue K, Kamada M, Slaton JW, Fukata S, Yoshikawa C, Tamboli P, Dinney CP, Shuin T (2002) The prognostic value of angiogenesis and metastasis-related genes for progression of transitional cell carcinoma of the renal pelvis and ureter. Clin Cancer Res 8:1863–1870
16. Jenkins BJ, Martin JE, Baithun SI, Zuk RJ, Oliver RT, Blandy JP (1990) Prediction of response to radiotherapy in invasive bladder cancer. Br J Urol 65:345–348
17. Jimenez RE, Gheiler E, Oskanian P, Tiguert R, Sakr W, Wood DP Jr, Pontes JE, Grignon DJ (2000) Grading the invasive component of urothelial carcinoma of the bladder and its relationship with progression-free survival. Am J Surg Pathol 24:980–987
18. Kirkali Z, Tuzel E (2003) Transitional cell carcinoma of the ureter and renal pelvis. Crit Rev Oncol Hematol 47:155–169
19. Krogh J, Kvist E, Rye B (1991) Transitional cell carcinoma of the upper urinary tract: prognostic variables and post-operative recurrences. Br J Urol 67:23–36
20. Krüger S, Noack F, Bohle A, Feller AC (2004) Histologic tumor growth pattern is significantly associated with disease-related survival in muscle-invasive transitional cell carcinoma of the urinary bladder. Oncol Rep 12:609–613
21. Kunze E (1998) Histogenesis of nonurothelial carcinomas in the human and rat urinary bladder. Exp Toxicol Pathol 50: 341–355
22. Kunze E, Francksen B (2002) Histogenesis of nonurothelial carcinomas of the urinary bladder from pre-existent transitional cell carcinomas. A histopathological and immunohistochemical study. Urol Res 30:66–78
23. Lauritzen AF, Kvist E, Bredesen J, Luke M (1987) Primary carcinoma of the upper urinary tract. Acta Pathol Microbiol Immunol Scand [A] 95:7–10
24. Lee SH, Lin JS, Tzai TS, Chow NH, Tong YC, Yang WH, Chang CC, Cheng HL (1996) Prognostic factors of primary transitional cell carcinoma of the upper urinary tract. Eur Urol 29:266–270
25. Logothetis CJ, Dexeus FH, Chong C, Sella A, Ayala AG, Ro JY, Pilat S (1989) Cisplatin, cyclophosphamide and doxorubicin chemotherapy for unresectable urothelial tumors: the M. D. Anderson experience. J Urol 141:33–37
26. Lopez-Beltran A, Martin J, Garcia J, Toro M (1988) Squamous and glandular differentiation in urothelial bladder carcinomas. Histopathology, histochemistry and immunohistochemical expression of carcinoembryonic antigen. Histol Histopathol 3: 63–68
27. Lopez-Beltran A, Sauter G, Gasser T, Hartmann A, Schmitz-Dräger BJ, Helpap B, Ayala AG, Tamboli P, Knowles MA, Sidransky D, Cordon-Cardo C, Jones PA, Cairns P, Simon R, Amin MB, Tyczynski JE (2004) Tumours of the urinary system. Infiltrating urothelial carcinoma. In: Eble JN, Sauter G, Epstein JI, Sesterhenn IA (eds) World Health Organization classification of tumours. Pathology and genetics. Tumours of the urinary system and male genital organs. IARC, Lyon, pp 93–109
28. Manunta A, Vincendeau S, Kiriakou G, Lobel B, Guille F (2005) Non-transitional cell bladder carcinomas. BJU Int 95: 497–502
29. Martin JE, Jenkins BJ, Zuk RJ, Blandy JP, Baithun SI (1989) Clinical importance of squamous metaplasia in invasive transitional cell carcinoma of the bladder. J Clin Pathol 42:250–253

30. Mazzucchelli L, Bacchi M, Studer UE, Markwalder R, Sonntag RW, Kraft R (1994) Invasion depth is the most important prognostic factor for transitional-cell carcinoma in a prospective trial of radical cystectomy and adjuvant chemotherapy. Int J Cancer 57:15–20
31. Miyake H, Hara I, Gohji K, Arakawa S, Kamidono S (1998) The significance of lymphadenectomy in transitional cell carcinoma of the upper urinary tract. Br J Urol 82:494–498
32. Mullerad M, Russo P, Golijanin D, Chen HN, Tsai HH, Donat SM, Bochner BH, Herr HW, Sheinfeld J, Sogani PC, Kattan MW, Dalbagni G (2004) Bladder cancer as a prognostic factor for upper tract transitional cell carcinoma. J Urol 172: 2177–2181
33. Nativ O, Reiman HM, Lieber MM, Zincke H (1991) Treatment of primary squamous cell carcinoma of the upper urinary tract. Cancer 68:2575–2578
34. Olgac S, Mazumdar M, Dalbagni G, Reuter VE (2004) Urothelial carcinoma of the renal pelvis. A clinicopathologic study of 130 cases. Am J Surg Pathol 28:1545–1552
35. Ozsahin M, Zouhair A, Villa S, Storme G, Chauvet B, Taussky D, Gouders D, Ries G, Bontemps P, Coucke PA, Mirimanoff RO (1999) Prognostic factors in urothelial renal pelvis and ureter tumours: a multicentre Rare Cancer Network study. Eur J Cancer 35:738–743
36. Papadopoulos I, Wirth B, Weichert-Jacobsen K, Loch T, Wacker HH (1996) Primary squamous cell carcinoma of the ureter and squamous adenocarcinoma of the renal pelvis: 2 case reports. J Urol 155:288–289
37. Racioppi M, D'Addessi A, Alcini A, Destito A, Alcini E (1997) Clinical review of 100 consecutive surgically treated patients with upper urinary tract transitional tumours. Br J Urol 80: 707–711
38. Raghavendran M, Rastogi A, Dubey D, Chaudhary H, Kumar A, Srivastava A, Mandhani A, Krishnani N, Kapoor R (2003) Stones associated renal pelvic malignancies. Indian J Cancer 40:108–112
39. Sakamoto N, Tsuneyoshi M, Enjoji M (1992) Urinary bladder carcinoma with a neoplastic squamous component: a mapping study of 31 cases. Histopathology 21:135–141
40. Sivaramakrishna B, Aron M, Ansari MS, Seth A, Goel R, Mundada OP, Balchander (2004) Squamous cell carcinoma of the renal pelvis manifesting after percutaneous nephrolithotomy for long standing calculus. Int Urol Nephrol 36:149–151
41. Sobin LH, Wittekind C (eds) (2002) TNM classification of malignant tumors, 6th edn. Wiley-Liss, New York
42. Starklint H, Kjaergaard J, Jensen NK (1976) Types of metaplasia in forty urothelial bladder carcinomas. A systematic histological investigation. Acta Pathol Microbiol Scand [A] 84:137–142
43. Strobel SL, Jasper WS, Gogate SA, Sharma HM (1984) Primary carcinoma of the renal pelvis and ureter. Evaluation of clinical and pathologic features. Arch Pathol Lab Med 108:697–700
44. Tosoni I, Wagner U, Sauter G, Egloff M, Knonagel H, Alund G, Bannwart F, Mihatsch MJ, Gasser TC, Maurer R (2000) Clinical significance of interobserver differences in the staging and grading of superficial bladder cancer. BJU Int 85:48–53
45. Young RH, Eble JN (1991) Unusual forms of carcinoma of the urinary bladder. Hum Pathol 22:948–965

Virchows Arch (2006) 448: 612–622
DOI 10.1007/s00428-006-0155-z

ORGINAL ARTICLE

Michal Michal · Tomas Vanecek · Radek Sima · Petr Mukensnabl · Ondrej Hes · Dmitry V. Kazakov · Jozef Matoska · Anna Zuntova · Vladimir Dvorak · Alexander Talerman

Mixed germ cell sex cord–stromal tumors of the testis and ovary. Morphological, immunohistochemical, and molecular genetic study of seven cases

Received: 7 October 2005 / Accepted: 2 January 2006 / Published online: 15 March 2006

Abstract We present the morphological, immunohistochemical, and molecular genetic features of three cases of testicular and four cases of ovarian mixed germ cell sex cord–stromal tumors (MGSCT). The germ cells in the testicular MGSCTs morphologically differed from those in classical seminomas by lacking the typical "square off" quality of the nuclei. In contrast to the nuclei in classical seminomas, their size in testicular MGSCTs was smaller and nucleoli were inconspicuous and the cytoplasm was Periodic Acid-Schiff (PAS) negative. Quite on the contrary, the variability in the size of the nuclei of the germ cells in the testicular MGSCTs was more similar to that seen in the germ cells of spermatocytic seminomas. Immunohistochemically, the germ cells of MGSCTs in one case reacted positively with antibody to AE1–AE3 by paranuclear dot-like or rodlike positivity. All three testicular MGSCTs had a negative reaction with the rest of antibodies, including placental alkaline phosphatase (PLAP), OCT4, and c-kit protein. Ovarian MGSCT in our series differed from the testicular lesions in both the germ cell component and the sex cord component. The germ cells in all four ovarian cases had cytomorphological and immunohistochemical features identical to those in classical seminomas/dysgerminomas. They possessed the typical "square off" quality of the nuclei, which were much more blastic, with more mitoses compared with the testicular tumors in our series, and they were PLAP (4/4), OCT4 (4/4) and c-kit protein (3/4) positive immunohistochemically. The cytoplasm of the germ cells in ovarian neoplasms contained PAS positive glycogen. Germ cells in one ovarian MGSCTs showed amplification of 12p. All other germ cells were negative for amplification of 12p. All five successfully analyzed cases showed no mutation in all studied exons and exon–intron junctions in c-kit and PDFGRA genes.

Keywords Unclassified mixed germ cell sex cord–stromal tumor · Testis · Ovary

M. Michal · T. Vanecek · R. Sima · P. Mukensnabl · O. Hes · D. V. Kazakov
Sikl's Department of Pathology,
Charles University Hospital,
Pilsen, Czech Republic

J. Matoska
Department of Pathology,
St. Elizabeth Oncology Institute,
Bratislava, Slovakia

A. Zuntova
Department of Pathology and Molecular Medicine,
2nd Medical Faculty,
Charles University,
Prague, Czech Republic

V. Dvorak
Ob/gyn Clinic,
Brno, Czech Republic

A. Talerman
Department of Surgical Pathology,
Thomas Jefferson University Hospital,
Philadelphia, PA, USA

M. Michal (✉)
Sikl's Department of Pathology,
Laboratore Spec. Diagnostiky, Medical Faculty Hospital,
Alej Svobody 80,
304 60 PILSEN, Czech Republic
Tel.: +420-603886633
Fax: +420-37-7104650
e-mail: michal@medima.cz

Introduction

A distinctive gonadal neoplasm composed of germ cells associated with sex cord stroma derivatives has been described and designated as "Pflügerome" [5, 21] or mixed germ cell sex cord–stromal tumor (MGSCT) [33, 34]. Most cases of MGSCT were described in the ovaries [1, 14, 19, 27, 32, 33, 35, 37, 38, 41, 47]; however, there were also a few cases of MGSCT reported in the testis [3, 8, 28]. Yet the existence of these tumors in the testis had recently been

questioned by a group of authors, who considered these lesions to represent sex cord–stromal tumors with entrapped germ cells rather than genuine MGSCT [43, 46]. We present morphological features, as well as immunohistochemical and molecular genetic findings in three testicular and four ovarian cases of MGSCT. One case of testicular MGSCT [23] and two cases of ovarian MGSCT [1, 47] included in our series have been published previously.

Materials and methods

Tissues from three cases of testicular and four cases of ovarian MGSCT were available. In one testicular case, only a limited amount of unstained reserve slides was available. In one testicular case, practically the entire tumor was sampled and its tissue was histologically processed. Two cases were seen in consultation by one of the authors (AT), two cases were seen in consultation by another author (MM), two cases were contributed by two other authors of the study (JM and AZ), and tissue from one case was contributed by generosity of Dr. J. Arroyo. Tissues were fixed in 4% formaldehyde and embedded in paraffin using routine procedures. Five-micrometer thick sections were cut from the tissue blocks and stained with routine staining methods.

Immunohistochemistry

For immunohistochemical investigations, the following primary antibodies were used: MIB1 (MIB1, 1:1,000, NeoMarkers, Fremont, CA, USA), c-kit protein (polyclonal, 1:100, DakoCytomation, Glostrup, Denmark), CD30 (Ber-H2: DakoCytomation), Inhibin (R1, Serotec, Düsseldorf, Germany), cytokeratins (AE1/AE3, 1:1,000, Boehringer), low molecular weight cytokeratin (CAM 5.2, 1:50, Becton Dickinson, San Jose, CA, USA), placental alkaline phosphatase (polyclonal: DakoCytomation), α-smooth muscle actin (1A4; DakoCytomation), neuron specific enolase (polyclonal; DakoCytomation), and EMA (E29, DakoCytomation). A polyclonal primary goat- anti-OCT4 antibody (Santa Cruz, CA, USA) raised against the –COOH terminus of the protein was used.

Microwave pretreatment of the tissue sections was used before applying of the primary antibodies. The primary antibodies were visualized using the anti-goat antibody labeled with peroxidase (Santa Cruz, CA) for the anti-OCT4 antibody and supersensitive streptavidin–biotin–peroxidase complex (BioGenex, San Ramon, CA, USA) for all the rest of the primary antibodies. Appropriate positive and negative control slides were employed.

Molecular genetics and cytogenetics

DNA extraction

DNA was extracted from formalin-fixed, paraffin-embedded tissues. Several 5-μm thick sections were placed on the slides. Hematoxylin eosin stained slides were examined for determination of area of tumor tissue. Then, tumor tissue from unstained slides was scraped, and DNA was isolated by the DNeasy Tissue Kit (QIAgen, Hilden, Germany) according to the manufacturer's protocol. In several cases where quality or amount of extracted DNA was low, concentration with Microcon 100 (Millipore, Billerica, MA, USA) according to the manufacturer's protocol was carried out.

Mutation status of the exons 9, 11, 13, and 17 of the c-kit gene (accession number U63834) and exons 12 and 18 of PDGFRA gene (accession number D50017) by PCR and direct sequencing

PCR was carried out using primers shown in Table 1. The reaction conditions were as follows: 12.5 μl of HotStart Taq PCR Master Mix (QIAgen), 10 pmol of each primer, 100 ng of template DNA and distilled water up to 25 μl. The amplification program consisted of denaturation at 95°C for 15 min and then 40 cycles of denaturation at 95°C for 1 min, annealing at 54°C for 1 min, and an extension at 72°C for 1.5 min for all amplicons. The program was finished by 72°C incubation for 7 min.

Successfully amplified PCR products were purified with a QIAquick spin PCR purification kit (QIAgen), side sequenced using a Big Dye Terminator Sequencing kit (PE/Applied Biosystems, Foster City, CA, USA) and run on an automated sequencer ABI Prism 310 (PE/Applied Biosystems) at a constant voltage of 11.3 kV for 20 min.

Tissue pretreatment and fluorescence in situ hybridization using CEP 12 and 12p probes

From each specimen, 4-μm thick sections were placed onto positively charged slide. Hematoxylin and eosin stained slides were examined for determination of areas for cell counting. The unstained slides were routinely deparaffinized and treated by a 30% sodium bisulfite for 30 min at 42°C. Then, the slides were washed twice in 2× sodium salt citrate (2×SSC) and immersed into digestion solution consisting of 2×SSC/proteinase K (0.25 mg/ml) for 30 to 60 min at 42°C. The slides were then placed into distilled water for 2 min, dehydrated in a series of ethanol solution, and air-dried. Probes for 12p Spectrum Green, CEP 12 Spectrum Orange (factory premixed) and LSI/WCP hybridization buffer (VYSIS/Abbott, IL, USA) were mixed in

Table 1 PCR primers used in the study

Gene/exons	Name	Primers
c-kit exon 9a[a]	c-kit e9aNF	GAGTAAGCCAGGGCTTTTGTT
	c-kit e9aNR	CGTGCCATTGTGCTTGAAT
c-kit exon 9b[b]	c-kit e9bNF	CCGTTTGGAAAGCTAGTGGT
	c-kit e9bNR	CAGAGCCTAAACATCCCCTTA
c-kit exon 11	c-kit e11F	CTATTTTTCCCTTTCTCCCC
	c-kit e11R	TACCCAAAAAGGTGACATGG
c-kit exon 13	c-kit e13F	CATGCGCTTGACATCAGTTT
	c-kit e13R	CAATAAAAGGCAGCTTGGACA
c-kit exon 17	c-kit e17F	GGTTTTCTTTTCTCCTCCAACC
	c-kit e17R	TGCAGGACTGTCAAGCAGAG
PDGFRA exon 12	PDG e12F	CTCTGGTGCACTGGGACTTT
	PDG E12R	GGAGGTTACCCCATGGAACT
PDGFRA exon 18	PDG e18F	GCTACAGATGGCTTGATCCTG
	PDG e18R	GACCAGTGAGGGAAGTGAGG

[a] 5′ end of exon 9
[b] 3′ end of exon 9

a 1:2:7 ratio. An amount of 10 μl of probe mix was applied on specimens and co-denatured simultaneously at 85°C for 10 min. After hybridization overnight in a humidified chamber at 37°C, the slides were washed for 2 min in washing buffer consisting of 0.4×SSC/0.3% NP-40 at 73°C and then in buffer consisting of 2×SSC/0.1% NP-40 at room temperature. The slides were air-dried in the dark, counterstained with 4′,6-diamidino-2-phenylindole·2HCl (DAPI) in an antifade medium, and immediately examined.

FISH interpretation

The sections were examined with an Olympus BX60 fluorescence microscope using a 100× objective and filter sets Triple Band Pass [DAPI/fluorescein isothiocyanate (FITC)/Texas Red) and Dual Band Pass (FITC/Texas Red). Scoring of amplification was performed by counting the ratio of the number of both fluorescent signals (12p: CEP12) in 60 randomly selected nonoverlapping tumor cell nuclei. Each slide was independently enumerated by two observers (TV and RS). Tumors with a ratio of signals <1.5 as a mean per nucleus were interpreted as non-amplified, whereas cases exhibiting a ratio of signals ≥1.5 as a mean were classified as amplified ones [17]. In all cases, counting of germ cell nuclei population was performed.

Results

Case histories

Case 1

A 35-year-old phenotypically normal man with karyotype 46XY presented with a gradually enlarging, asymptomatic left testicular mass that had been present for 25 years. Otherwise, the affected testis was elastic and painless, and the contralateral testis had normal size and consistency; both testes were normally descended. No enlarged lymph nodes or metastases were revealed by ultrasonography and computed tomography. Serum levels of α-fetoprotein, β-human chorionic gonadotropin (HCG), and carcinoembryonic antigen were within the normal range. A left orchiectomy was performed. Grossly, the parenchyma of involved testis was replaced by a uniform whitish soft tissue; no involvement of testicular adnexa and tunica albuginea was noted. The tumor was round-shaped, well-circumscribed, white in color, and measured 4×5×5 cm. The unaffected testicular tissue was compressed by the tumor. No adjuvant chemotherapy and radiotherapy was given or administered. The patient is free of disease 11 years after the surgical excision.

Case 2

A normally developed 41-year-old man consulted an urologist because of urinary frequency that was attributed to the cystitis. He also noticed a slowly progressive, painless enlargement of the right testis during the last 4 years, which was unrelated to his current complaint. The urologic examination disclosed a right-sided testicular tumor that was solid and firm. The left testis was normal. Both testes were normally descended. Relevant laboratory and radiological investigations, including serum α-fetoprotein and HCG determinations, showed no abnormalities. Two years after the right radical orchiectomy, the patient was well without any evidence of recurrence or metastases.

Case 3

A 27-year-old man presented with complaints of pain in the right scrotum. Clinical examination revealed a testicular mass. Orchiectomy was performed. The affected testis measured 7×4 cm and was replaced by a well-circumscribed tumor, two-thirds of which exhibited a cystic change. There were no signs of necrosis or hemorrhage. The follow-up of the patient is not available.

Case 4

The patient, a 30-year-old woman, nullipara and nulligravida with normal karyotype (46XX) was admitted for treatment because of a persistent pelvic pain. Examination revealed a right adnexal mass 7×4-cm in size. There was no evidence of residual tumor in the pelvis at operation. The postoperative recovery was uneventful. Sixty-seven months later, a large, palpable pelvic mass was found above the uterine fundus. At laparotomy, a 7-cm tumor adherent to the serosa of the uterus was identified and surgically removed. Postoperatively, the patient was further treated with chemotherapy (bleomycin, cisplatin, and etoposide) with an excellent response. She was clinically free of disease 10 months later.

Case 5

A 4-year-old girl presented with symptoms of precocious isosexual pseudopuberty, including mammary enlargement. The gynecological examination revealed an infantile uterus and a left adnexal mass. The vulva was slightly swollen and no pubic hair could be demonstrated. The vaginal cytology revealed estrogenic stimulation. The serum levels of somatotropin, luteinizing hormone, α-fetoprotein, prolactin, and β-HCG were within normal limits. The karyotype of the patient was 46XX and her sex chromatin was normal. She was treated with a right oophorectomy. A bosselated, irregular, 8×4×4-cm mass was found in the right ovary. The patient subsequently received radiotherapy (total dose 40 Gy applied during 4 weeks) and chemotherapy (5-fluorouracil, actinomycin D, and cyclophosphamide). After surgery, the vaginal cytology returned to normal in 2 months. Her breast enlargement regressed slowly to the normal size 1 year after the operation. Thirteen years after the oophorectomy, the patient achieved normal puberty and there was no evidence of recurrence or metastasis.

Case 6

A 39-year-old woman presented with a round-shaped tumor mass in the left ovary measuring 9 cm in diameter. The patient suffered from ascites. She underwent a bilateral ovariectomy. The contralateral ovary proved to be normal both grossly and histologically. The karyotype of the patient was 46XX. Seven years after the ovariectomy, the patient is well and free of disease.

Case 7

An 11-year-old girl was noted to have precocious pseudopuberty and was found to have an ovarian tumor affecting the right ovary and measuring 6×4×3 cm. The left ovary was normal. The karyotype of the patient was 46XX. After the operation there was regression of the pseudopuberty symptoms. She achieved normal puberty and was followed for 6 years without any evidence of recurrent disease.

Histology

Histologically, all seven cases of MGSCT revealed two components: germ cells and sex cord stromal component (SCC). No evidence of other type of germ cell tumors such as seminoma/dysgerminoma, embryonal carcinoma, yolk sac tumor, or teratoma [37, 44] and no sarcomatous differentiation, as described in spermatocytic seminomas [8, 11, 24, 42], were seen in our cases of MGSCT. Neither HCG secreting multinucleated cells, as seen in 5% of dysgerminomas and in seminomas, nor calcifications were present in our cases. Because histology of the germ cells, stromal SCC, and immunohistochemical findings of testicular and ovarian tumors differed they will be described separately.

Testicular tumors All three testicular MGSCTs had a similar histological appearance. The tumors showed germ cells arranged in groups or as solitary units within the background of dense, diffuse proliferations of spindle-shaped sex cord stromal cells. Within a tumor, there were areas where the SCC predominated (Fig. 1), as well as areas where the dominant cells were the germ cells (Fig. 2). The germ cells were characterized by an abundant clear cytoplasm and a variably blastic nucleus with a fine chromatin, having one to several inconspicuous nucleoli. No areas, in which the germ cells resembled entrapped cells within testicular tubules or within a sex cord stromal tumor were observed in any of the reviewed slides. At low magnification, it was apparent that the germ cells formed an integral part of the neoplasm (Fig. 3). The germ cells often demonstrated variation in the size of their nuclei, and these ranged from small, deeply basophilic to large blastic ones (Fig. 2). In Cases 1 and 3, they revealed mitoses including atypical ones (Fig. 4). A copious amount of the cytoplasm and relatively smaller nuclei of the germ cell often rendered the germ cell a targetoid appearance (Fig. 5). The germ cells in the testicular MGSCTs morphologically differed from those in classical seminomas by lacking the typical “square off” quality of the nuclei. In contrast to the nuclei in classical seminomas, their size in testicular MGSCTs was smaller and nucleoli were inconspicuous. In addition, Periodic Acid-Schiff

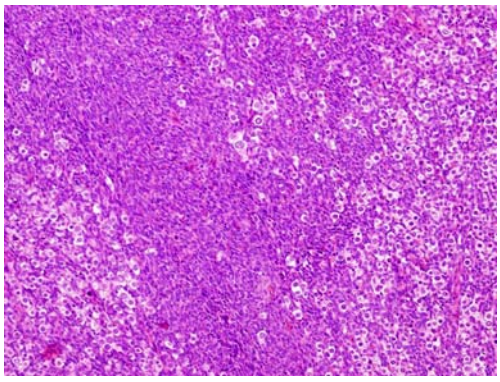

Fig. 1 Testicular MGSCT showing predominance of spindle cell stromal component in some areas. Hematoxylin and eosin staining

(PAS) revealed no glycogen in the cytoplasm of MGSCTs. SCC was composed of spindle cells with nuclei having longitudinal clefts and inconspicuous nucleoli (Fig. 5). Focally, SCC formed peripheral palisading. In many areas, the tumor cells were intermixed with dense collagen (Fig. 6). Rarely, the collagenous extracellular matrix formed Call-Exner-like bodies. Leydig-like and lutein cells and concentric calcifications typical of gonadoblastoma were lacking. Immunohistochemically, the germ cells of MGSCTs in Case 1 reacted positively with antibody to AE1–AE3 (Boehringer: Mannheim) by paranuclear dot-like or rod-like positivity (Fig. 7). The germ cells in the other two cases of testicular MGSCTs were AE1–AE3 negative. All three testicular MGSCTs were negative with the rest of antibodies, including placental alkaline phosphatase (PLAP), OCT4, and c-kit protein. MIB1 antibody stained almost exclusively the germ cell component, and in Case 1, as many as 40% of all germ cells stained with the MIB1 antibody (Fig. 8), while the SCC revealed only very rare MIB1 positive cells (less than 1%). Inhibin stained the cells of SCC (Fig. 9). Actin antibody stained only capillary pericytes (Table 2).

Ovarian tumors Ovarian tumors in our series differed from the testicular lesions in both the germ cell component and the SCC. The germ cells in all four ovarian cases had

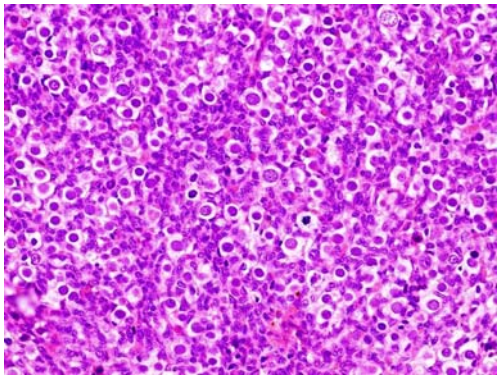

Fig. 2 Testicular MGSCT showing that the germ cells often varied in size, ranging from small deeply basophilic cells to large blastic cells. Hematoxylin and eosin staining

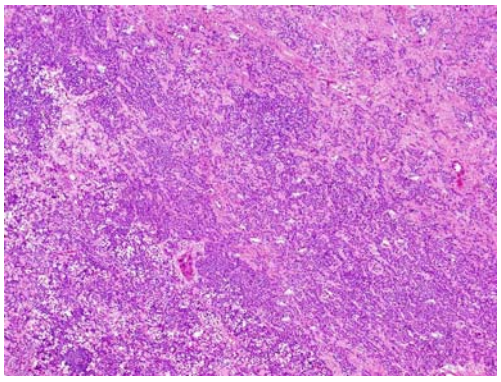

Fig. 3 Testicular MGSCT showing at low magnification that the germ cells form an integral part of the neoplasm and that they do not represent entrapped nonneoplastic germ cells in testicular tubules. Hematoxylin and eosin staining

cytomorphological features identical to those present in classical seminomas/dysgerminomas. They possessed the typical "square off" quality of the nuclei (Fig. 10), which were much more blastic with more mitoses compared with the testicular tumors in our series. The cytoplasm of the germ cells in ovarian neoplasms contained PAS positive glycogen. SCC differed from case to case. In Case 4, it formed lobules composed of cells with clear to eosinophilic cytoplasm forming either hollow microfollicles inside the lobules or microfollicles filled with collagen. These features, along with a peripheral palisading of the lobules (Fig. 11), imparted to the tumors an appearance somewhat similar to the sex cord tumors with annular tubules [45] (Fig. 12). In Cases 6 and 7, the SCC formed less well-defined lobules with greater amount of fibrous septa dividing them. In Case 6, the sex cord stromal cells focally differentiated into a columnar glandular epithelium with a ciliated brush border (Fig. 13). The SCC in Case 5 differed from the other three ovarian cases in that it formed trabeculae with stromal cells lying perpendicular to the long axis of the trabeculae (Fig. 14). The germ cells and SCC formed sharply circumscribed lobules (Fig. 15). In no case in our series did the germ cells grow outside the confines bordered by the SCC. There were no Leydig-like cells, lutein cells, or concentric calcifications typical of gonadoblastoma whatsoever.

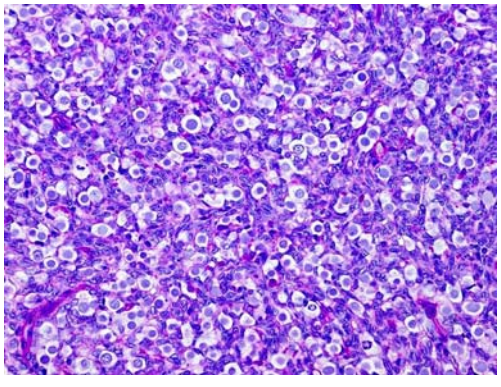

Fig. 4 Testicular MGSCT. Atypical mitoses were found in the germ cells. Giemsa staining

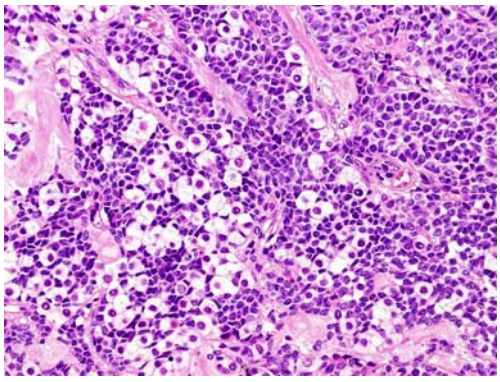

Fig. 5 Testicular MGSCT. A copious amount of cytoplasm and relatively smaller nuclei of the germ cell rendered them a targetoid appearance. The SCC was composed of spindle cells with nuclei having longitudinal clefts and inconspicuous nucleoli. Hematoxylin and eosin staining

Immunohistochemically, the germ cells in all four ovarian tumors stained positively with the antibodies to neuron specific enolase (NSE), PLAP (Fig. 15), OCT4 and, with the exception of Case 7, they reacted positively for the c-kit protein antibody. Rare germ cells in Case 5 stained positively with the antibody to cytokeratins AE1–AE3; otherwise, the germ cells in all cases were negative with all the rest of the antibodies. SCC was immunohistochemically positive with inhibin antibody in all four cases (in Case 5 only focally) and with cytokeratin AE1–AE3 antibody in three out of four cases. It was negative with the rest of the antibodies. The MIB1 antibody reacted in 20–30% of the germ cells, and only very rare cells of the SCC (less than 1% in all four cases) were positive with this antibody (Table 2).

Molecular genetic findings

Of the seven cases studied, mutation status of c-kit and PDGFRA genes was successfully analyzed in five cases (Cases 1, 2, 4, 5, and 7). In Case 6, no amplifiable DNA was presented probably due to wrong fixation. In Case 3, no tissue was at hand for molecular genetic study. All successfully analyzed cases showed no mutation in all studied exons and exon–intron junctions.

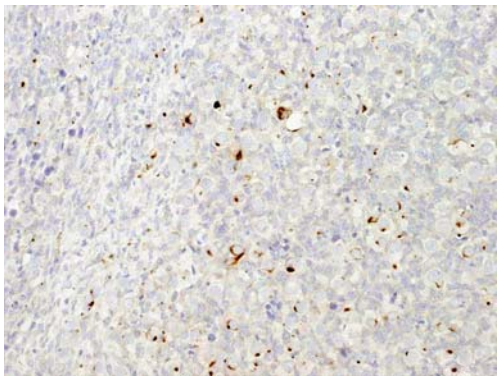

Fig. 7 Testicular MGSCT. Many germ cells reacted positively with the antibody to AE1–AE3 revealing a paranuclear dot- or rod-like signal

Molecular cytogenetics finding

Of the seven studied cases, FISH was successfully performed in four cases (1, 4, 5, and 7). In Cases 2 and 6, no signals of 12p and CEP 12 probe were visible after repeated FISH analysis. In Case 3, no tissue was at hand for molecular cytogenetic study. Of all successfully analyzed cases, only Case 7 showed amplification of 12p (Fig. 16). All others were negative for amplification of 12p. Results of FISH are summarized in Table 3.

Discussion

MGSCTs occur in the gonads of phenotypically and genetically normal subjects. They were first described by Masson as a Pflügerome in 1912 [21] and later as "epitheliomas pflugeriens" in 1923 [22]. Later, there were several cases published in the ovaries [1, 14, 19, 27, 32, 33, 35, 37, 38, 41, 47] and occasional cases in the testes [3, 28, 36, 37]. However, the existence of these

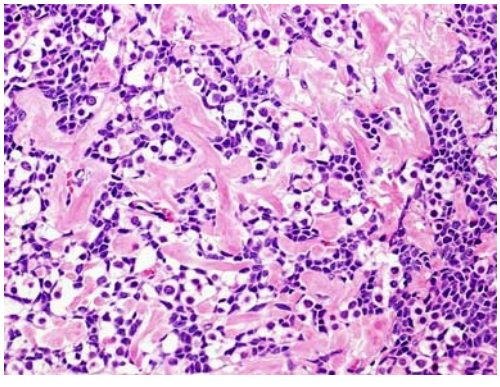

Fig. 6 Testicular MGSCT. In many areas, the tumor cells were intermixed with dense collagen. Hematoxylin and eosin staining

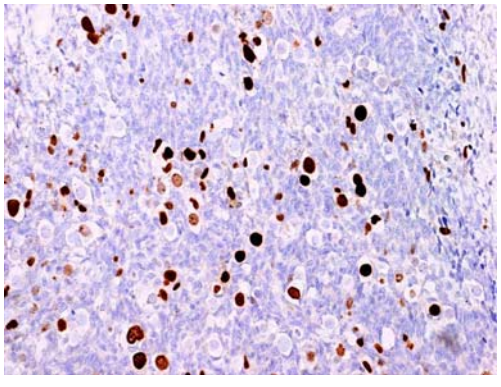

Fig. 8 Testicular MGSCT. In Case 1 as many as 40% of all germ cells stained with the MIB1 antibody

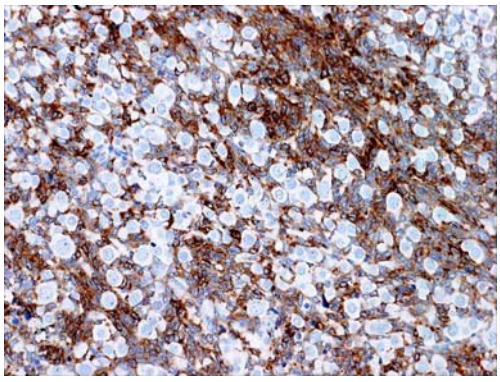

Fig. 9 Testicular MGSCT. Inhibin stained the sex cord stromal cells

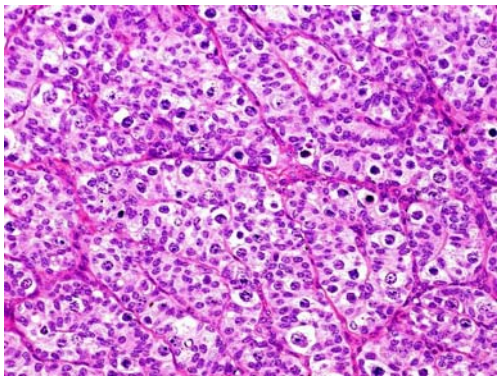

Fig. 10 The germ cells in all four ovarian cases had cytomorphological features identical to those seen in the classical seminomas/dysgerminomas. The cells possessed the typical "square off" quality of the nuclei. Hematoxylin and eosin staining

tumors in the testis has recently been questioned by a group of authors who reviewed nine testicular sex cord–stromal tumors containing germ cells, which closely mimicked MGSCT but differed from the latter, in that the germ cells were entrapped and nonneoplastic rather than neoplastic [43, 46]. They thought that these tumors closely resembled MGSCT, but represented sex cord stromal tumors with entrapped germ cells, which they considered were nonneoplastic. The evidence presented to support this view was that the germ cells were distributed peripherally and were associated with entrapped seminiferous tubules. They were also said to occur in clusters with vaguely tubular shapes, consistent with preexisting seminiferous tubules. Although some of these cases may have represented sex cord–stromal tumors with entrapped germ cells, germ cells seemed not to have any relation to preexistent seminiferous tubules in some of them and were scattered haphazardly forming true predominant part of the lesion, while in other parts of the sex cord elements predominated. The germ cells showed variable appearances. In one of those cases, inhibin stain showed an association of the germ cells with nonneoplastic Sertoli cells. The germ cells in their cases lacked large, vesicular nuclei with prominent nucleoli, closely resembling type A spermatogonia [43].

Our testicular cases differed from the cases of Ulbright et al. [43]. Our tumors were composed of germ cells with vesicular nuclei and spindle-shaped sex cord–stromal cells. No association whatsoever was found, even on intentional search, between the germ cells and preexisting seminiferous tubules in any of the 20 sampled blocks of Case 1, nor was this feature observed in multiple sections in Cases 2 and 3. Furthermore, in most of the slides, the germ cells formed a predominant part of the microscopic fields. In addition, the size of the germ cells varied, ranging from cells with small hyperchromatic nuclei to large blastic cells with vesicular nuclei. In that respect, the nuclear variations in the germ cell component in our case had some similarities to nuclear variations seen in spermatocytic seminomas [30]. Atypical mitoses in germ cells present in two of the three testicular cases are another argument supporting their neoplastic nature. Immunonegativity with the antibodies to PLAP, NSE, c-kit protein, and OCT4 [6, 12] and the absence of cytoplasmic glycogen within the germ cells in our testicular cases do not necessarily preclude their nonneoplastic nature, because germ cells in spermatocytic seminomas, in our experience, lack cytoplasmic glycogen and they are consistently negative with

Table 2 Immunohistochemical results

Case antibodies	Case 1 (testicular)	Case 2 (testicular)	Case 3 (testicular)	Case 4 (ovarian)	Case 5 (ovarian)	Case 6 (ovarian)	Case 7 (ovarian)
NSE	Neg	Neg	Neg	GC+ SCC−	GC+ SCC−	GC+ SCC−	GC+ SCC−
PLAP	Neg	Neg	Neg	GC+ SCC−	GC+ SCC−	GC+ SCC−	GC+ SCC−
OCT4	Neg	Neg	Neg	GC+ SCC−	GC+ SCC−	GC+ SCC−	GC+ SCC−
c-kit protein	Neg	Neg	Neg	GC+ SCC−	GC+ SCC−	GC+ SCC−	Neg
AE1–AE3	GC+ SCC−	Neg	Neg	SCC+ GC−	GC+ SCC−	SCC+ GC−	SCC+ GC−
CAM 5.2	Neg	Neg	Neg	Neg	Neg	Neg	Neg
EMA	Neg	Neg	Neg	Neg	Neg	Neg	Neg
CD30	Neg	Neg	Neg	Neg	Neg	Neg	Neg
Inhibin	SCC+ GC−	SCC+ GC−	Neg	SCC+ GC−	SCC+ GC−	SCC+ GC−	SCC+ GC−
ASMA	Neg	Neg	Neg	Neg	Neg	Neg	Neg

Neg Negative, *ASMA* α-smooth muscle actin, *PLAP* placental alkaline phosphatase, *EMA* epithelial membrane antigen, *GC* germ cells, *SCC* sex cord stromal component

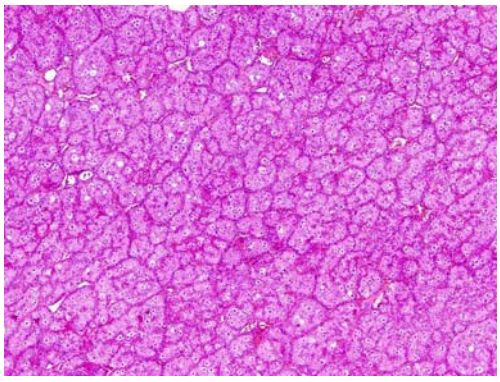

Fig. 11 Ovarian MGSCT. These neoplasms formed a lobular pattern. Sex cord stromal cells formed a peripheral palisading. Hematoxylin and eosin staining

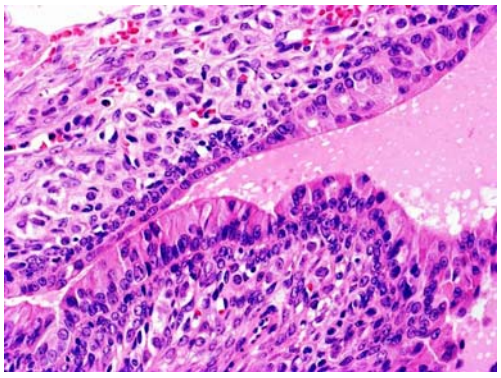

Fig. 13 Ovarian MGSCT. In one case (Case 6), the sex cord stromal cells differentiated into a columnar glandular epithelium with a ciliated brush border. Hematoxylin and eosin staining

all these antibodies as well. Positivity with the anti-cytokeratin antibody AE1–AE3 in one testicular and one ovarian MGSCT is an interesting and hitherto unreported feature of MGSCT. Cytokeratin immunoreactivity, including AE1–AE3, has been repeatedly described in classical seminomas [7, 10]. Cheville et al. [7] for example showed that 36% of classical seminomas reacted with this antibody. Occasional cytokeratin positivity in spermatocytic seminomas was described as well [8]. However, no such cytokeratin immunoreactivity can be seen in germ cells of the normal testes.

When judging the figures of other published cases of testicular MGSCT [3, 28], it seems that they were morphologically very similar to our cases. Typical for testicular MGSCTs in our series and those in the literature [3, 28] is the SCC composed of spindle-shaped cells incorporating clusters of germ cells with a copious cytoplasm rendering them a targetoid appearance. In contrast, the SCC and germ cells of the ovarian MGSCTs differed from testicular MGSCTs. The SCC either formed trabeculae with perpendicularly arranged sex cord stromal cells or it formed lobules or tubules with peripheral palisading. A clear to eosinophilic and homogeneous cytoplasm of these sex cord stromal cells imparted a vague similarity of sex cord tumor with annular tubules to one ovarian MGSCT in our series [45]. Besides the patterns of SCC seen in our cases, several other patterns were described in the literature in the ovaries including a retiform tubular pattern [41], a pattern forming hollow tubules [19], and others [14, 37]. Moreover, germ cells in ovarian MGSCTs had a "square off" appearance [44] of classical seminomas/dysgerminomas. They contained PAS positive diastase sensitive glycogen in their cytoplasm and further they lacked the targetoid appearance of germ cells in the testicular MGSCTs. Immunohistochemistry revealed additional differences between the germ cells in the testicular and ovarian MGSCTs, inferring their different nature. The ovarian MGSCTs were PLAP, OCT4, and NSE positive, while no positivity with these markers was found in the testicular neoplasms. All four ovarian tumors were immunohistochemically c-kit protein positive. All these markers are typically positive in classical seminomas/dysgerminomas [2, 40].

KIT protein is expressed in most cases of classical seminomas/dysgerminomas, both in gonadal [40] and extragonadal location [25], while it is negative in nonseminomatous germ cell tumors. We have not found KIT protein expression in any of the 14 cases of spermatocytic seminomas in our files. To date there have

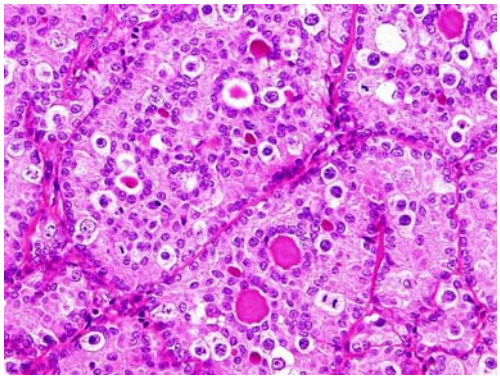

Fig. 12 Ovarian MGSCT. One ovarian tumor showed a vague similarity to sex cord tumor with annular tubules. Hematoxylin and eosin staining

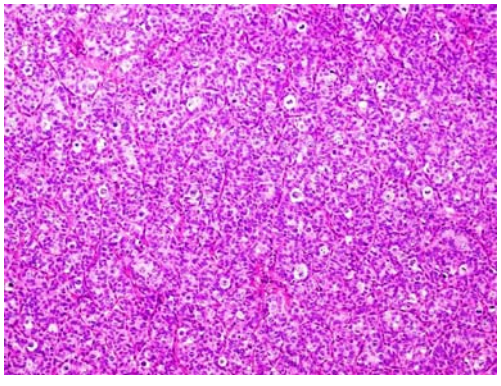

Fig. 14 Ovarian MGSCT. The SCC in Case 5 differed from the other three ovarian cases in that it formed trabeculae with sex cord stromal cells lying perpendicular to the long axis of the trabeculae. Hematoxylin and eosin staining

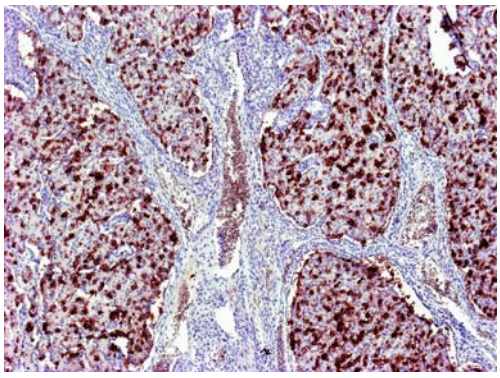

Fig. 15 Ovarian MGSCT. The germ cells and SCC formed sharply circumscribed lobules. In no case in our series did the germ cells grow outside borders of these lobules. The germ cells in this Case 5 stained strongly with the antibody to placental alkaline phosphatase

been several reports of Kit mutations found in exon 17 in germ cell tumors. Tian et al. found c-kit exon 17 mutations in 2/23 cases of the gonadal [39] seminomas/dysgerminomas. Przygodzki et al. [26] found it in 3/17 cases of mediastinal seminomas with mutations and Kemmer et al. [16] found exon 17 of *c-kit* gene mutations in 14/54 cases

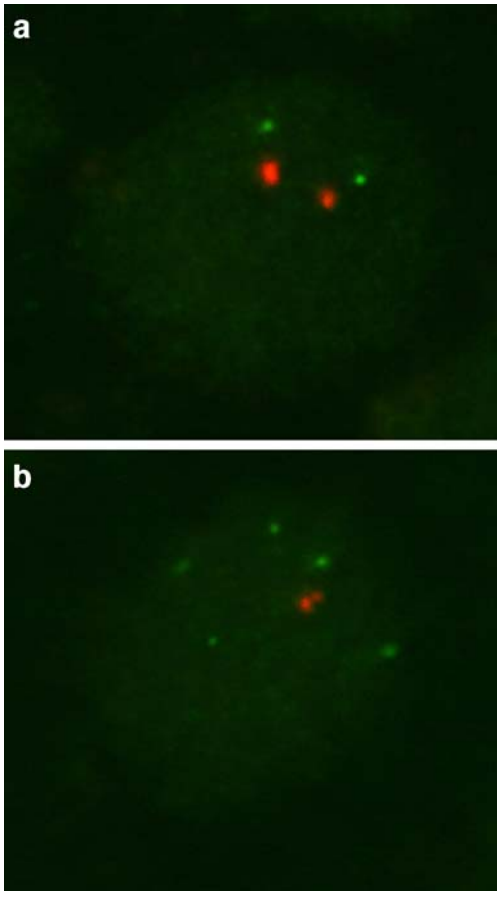

Fig. 16 Ovarian MGSCT. FISH analysis using 12p (Spectrum Green) and CEP 12 (Spectrum Orange) probe. Visualization under Dual Band Pass filter. **a** Case 5—non-amplified two green (12p) and two red (CEP 12) signals are presented in the nuclei. **b** Case 7—amplified five green (12p) and two red (CEP 12) signals are presented in the nuclei

Table 3 Molecular cytogenetics results

Case number	12p:CEP 12 ratio	Result
1	1.15	–
2	AF	AF
3	NA	NA
4	1.14	–
5	1.15	–
6	AF	AF
7	1.59	+

AF Analysis failed, *NA* not available, (+) amplified, (–) not amplified

of gonadal seminomas/dysgerminomas. Pauls et al. [25] described a case of primary retroperitoneal seminoma with a point mutation in codon 557 of exon 11 of *c-kit* gene. No mutations were found in this case in exon 17. We searched for activation mutations in exon 9, 11, 13, and 17 of *c-kit* gene and exon 12 and 18 of the PDGFRA gene, which are mutations often found in gastrointestinal stromal tumors [9]. While 75% of ovarian cases expressed KIT protein at immunohistochemical level, we found no activating mutations on any exons of c-kit and PDGFRA genes in any of MGSCTs in our series.

Another point supporting the similarity of germ cells in the ovarian MGSCTs to germ cells in dysgerminomas is the fact that several cases of ovarian MGSCTs progressed into invasive dysgerminoma [13, 18, 19, 37]. In four children, there is a described malignant overgrowth by other malignant germ cell elements, including choriocarcinoma and yolk sac tumor [18]. In three of these patients, the tumor metastasized and resulted in the deaths of the patients [18]. No such events have ever been described in testicular MGSCTs.

The finding of excess genetic material of the short arm of chromosome 12 in one of our two ovarian MGSCTs is of great interest. This genetic abnormality occurs in all primary sites and histologic types of all human germ cells tumors [4, 17, 20] with the exception of spermatocytic seminomas and prepubertal teratomas of the testis. Data suggest that the consistent gain of genetic material from chromosome 12 may be crucial for the development of an invasive germ cell tumor [29]. Overrepresentation of 12p renders the tumor cells independent from the supporting Sertoli cells. Cells of intratubular germ cell neoplasia therefore lack overrepresentation of 12p [20]. The presence of gain in the short arm of chromosome 12 in our case 7 is in accordance with the well-documented ability of ovarian MGSCTs to produce invasive dysgerminoma and other neoplastic germ cell components [13, 18, 19, 37]. The longer follow-up and more cases would be necessary to find out whether this genetic event in ovarian MGSCTs has a prognostic significance in relation to development of an invasive component.

In contrast to the ovarian MGSCTs, germ cells in all three cases of testicular MGSCTs in our series lacked cytoplasmic glycogen and immunohistochemical positivity with PLAP, OCT4, and c-kit protein. Interestingly, in our

experience and that of others [8], all these markers, including OCT4 [15, 44] are absent in spermatocytic seminomas. MIB1 immunoreactivity revealed that the germ cells are a quickly proliferating component of the neoplasms, while the sex cord stromal cells represent a relatively slowly proliferating part of the tumors. This militates against the suggestion that germ cells in the testicular MGSCTs represent nonneoplastic, possibly entrapped germ cells [43, 46].

Another interesting feature of the tumors was the relation of the sex cord stromal cells and the germ cells. In no case in our series did the germ cells grow outside the confines bordered by the SCC. It looked as though the sex cord stromal cells of the tumors possessed a homing phenomenon to the germ cells. In the differential diagnosis, MGSCT should be distinguished especially from gonadoblastoma [31]. In contrast to our cases, all of which had normal karyotype, the gonadoblastomas nearly always occur in patients with pure or mixed gonadal dysgenesis with an altered karyotype or, in men, pseudohermaphrodites in streak gonad or testis. Leydig-like and lutein cells and concentric calcifications typical of gonadoblastoma were uniformly lacking in our cases. In contrast to gonadoblastomas, there is no evidence of virilization in MGSCTs and, if there are signs of abnormal endocrine activity in MGSCTs, they manifest themselves as feminization. MGSCTs show also proliferative activity in the sex cord–stromal component, while in gonadoblastoma, proliferative activity is seen in only the germ cells.

The widespread presence of germ cells distinguishes MGSCTs from Sertoli–Leydig cell tumors, especially from those neoplasms showing a retiform component.

In summary, we presented three cases of testicular and four cases of ovarian MGSCTs. The morphology and immunohistochemical profile of testicular and ovarian MGSCTs differed. The immunoprofile of the germ cells in testicular MGSCTs was similar to that observed in spermatocytic seminoma, and the immunoprofile of the germ cells in ovarian lesions was similar to that seen in classical seminoma/dysgerminoma. However, the number of published testicular examples of MGSCTs is too small to generalize that all of them differ from ovarian MGSCTs. It cannot be excluded that, in addition to the testicular MGSCTs in which the germ cells have immunohistochemical properties of the spermatocytic seminomas as in our series, there might exist MGSCTs with immunohistochemical properties of classical seminoma/dysgerminoma indistinguishable from the ovarian examples of MGSCTs.

Acknowledgement We would like to thank to Dr. J. Arroyo for allowing us to use a tissue from his case [1] for the study.

References

1. Arroyo JG, Harris W, Laden A (1998) Recurrent mixed germ cell–sex cord stromal tumor of the ovary in an adult. Int J Gynecol Pathol 17:281–283
2. Baker PM, Oliva E (2005) Immunohistochemistry as a tool in the differential diagnosis of ovarian tumors: An update. Int J Gynecol Pathol 24:39–55
3. Bolen JW (1981) Mixed germ cell–sex cord stromal tumor. A gonadal tumor distinct from gonadoblastoma. Am J Clin Pathol 75:565–573
4. Bosl GJ, Ilson DH, Rodriguez E, Motzer RJ, Reuter VE, Chaganti RS (1994) Clinical relevance of the i(12p) marker chromosome in germ cell tumors. J Natl Cancer Inst 86:349–355
5. Cabanne F (1971) Gonadoblastomes et tumeurs de l'ebauche gonadique. Ann Anat Pathol (Paris) 16:387–404
6. Cheng L (2004) Establishing a germ cell origin for metastatic tumors using OCT4 immunohistochemistry. Cancer 101:2006–2010
7. Cheville JC, Rao S, Iczkowski KA, Lohse CM, Pankratz VS (2000) Cytokeratin expression in seminoma of the human testis. Am J Clin Pathol 113:583–588
8. Cummings OW, Ulbright TM, Eble JN, Roth LM (1994) Spermatocytic seminoma: An immunohistochemical study. Hum Pathol 25:54–59
9. Daum O, Klecka J, Ferda J, Treska V, Vanecek T, Sima R, Mukensnabl P, Michal M (2005) Gastrointestinal stromal tumor of the pancreas: case report with documentation of kit gene mutation. Virchows Arch 446:470–472
10. Denk H, Moll R, Weybora W, Lackinger E, Vennigerholz F, Beham A, Franke WW (1987) Intermediate filaments and desmosomal plaque proteins in testicular seminomas and non-seminomatous germ cell tumours as revealed by immunohistochemistry. Virchows Arch A Pathol Anat Histopathol 410:295–307
11. Floyd C, Ayala AG, Logothesis CJ, Silva EG (1988) Spermatocytic seminoma with associated sarcoma of the testis. Cancer 61:409–414
12. Hattab EM, Pang-Hsien T, Wilson DJ, Cheng L (2005) OCT4 immunohistochemistry is superior to placental alkaline phosphatase (PLAP) in the diagnosis of central nervous system germinoma. Am J Surg Pathol 29:368–371
13. Hughesdon PE, Kumarasamy T (1970) Mixed germ cell tumours (gonadoblastomas) in normal and dysgenetic gonads. Case reports and review. Virchows Arch A Pathol Pathol Anat 349:258–280
14. Jacobsen GK, Braendstrup O, Talerman A (1991) Bilateral mixed germ cell sex–cord stroma tumour in a young adult woman. APMIS 23:132–137
15. Jones TD, Ulbright TM, Eble JN, Baldridge LA, Cheng L (2004) OCT4 staining in testicular tumors: a sensitive and specific marker for seminoma and embryonal carcinoma. Am J Surg Pathol 28:935–940
16. Kemmer K, Corless CL, Fletcher JA, McGreevey L, Haley A, Griffith D, Cummings OW, Wait C, Town A, Heinrich M (2004) KIT mutation common in testicular seminomas. Am J Pathol 164:305–313
17. Kernek KM, Brunelli M, Ulbright TM, Eble JN, Martignoni G, Zhang S, Michael H, Cummings OW, Cheng L (2004) Fluorescence in situ hybridization analysis of chromosome 12p in paraffin-embedded tissue is useful for establishing germ cell origin of metastatic tumors. Mod Pathol 17:1309–1313
18. Kurman RJ (2002) In: Talerman A (ed) Germ cell tumors of the ovary. Blaustain's Pathology of the Female Genital Tract, 5th edn. Springer, Berlin Heidelberg New York
19. Lacson AG, Gillis DA, Shawwa A (1988) Malignant mixed germ cell sex cord stromal tumors of the ovary associated with isosexual precocious puberty. Cancer 61:2122–2133
20. Looijenga LHJ, Zafarana G, Grygalewicz B, Summersgill B, Debiec-Rychter M, Veltman J, Schoenmakers EFPM, Rodriguez S, Jafer O, Clark J, van Kessel ADG, Shipley J, van Gurp RJHLM, Gillis AJM, Oosterhuis JW (2003) Role of gain of 12p in germ cell tumour development. APMIS 111:161–173
21. Masson P (1912) Pflügerome. Bull Soc Anat Paris 14:403–404

22. Masson P (1923) Les tumeurs. Epitheliomas pflugeriens. In: Diagnostics de Laboratoire. Maloine Editions, Paris, pp 477–478
23. Matoska J, Talerman A (1989) Mixed germ cell–sex cord stroma tumor of the testis. A report with ultrastructural findings. Cancer 64:2146–2153
24. Matoska J, Talerman A (1990) Spermatocytic seminoma associated with rhabdomyosarcoma. Am J Clin Pathol 94:89–95
25. Pauls K, Wardelmann E, Franke FE, Heukamp L, Büttner R, Mey U, Zhou H (2005) Primary extragonadal germ cell tumour: unusual localization of a c-kit mutated retroperitoneal seminoma in the gastric wall. Histopathology 47:11–113
26. Przygodzki RM, Hubbs AE, Zhao FQ, O'Leary TJ (2002) Primary mediastinal seminomas: evidence of single and multiple KIT mutations. Lab Invest 82:1369–1375
27. Reeves G, Elias E, Sarancone S, Albertengo A (2001) Lesiones mixtas de células germinales, cordones sexuales y estroma del ovaria. Patologia 39:116–126
28. Rames RA, Richardson M, Swiger F, Kaczmarek A (1995) Mixed germ cell–sex cord stromal tumor of the testis: the incidental finding of a rare testicular neoplasm. J Urol 154:1479
29. Reuter VE (2005) Origins and molecular biology of testicular germ cell tumors. Mod Pathol 18:S51–S60
30. Rosai J, Silber I, Khodadoust K (1969) Spermatocytic seminoma. I. Clinicopathologic study of six cases and review of the literature. Cancer 24:92–116
31. Scully RE (1970) Gonadoblastoma: a review of 74 cases. Cancer 25:1340–1356
32. Speleman F, Dermaut B, De Potter CR, van Gele M, van Roy N, De Paepe A, Laureys G (1997) Monosomy 22 in a mixed germ cell sex cord–stromal tumor of the ovary. Genes Chromosomes Cancer 19:192–194
33. Talerman A (1972) A mixed germ cell–sex cord stroma tumor of the ovary in a normal female infant. Obstet Gynecol 40:473–478
34. Talerman A (1972) A distinctive gonadal neoplasm related to gonadoblastoma. Cancer 30:1219–1294
35. Talerman A, van der Harten JJ (1977) Mixed germ cell–sex cord stromal tumor of the ovary associated with isosexual precocious puberty in a normal girl. Cancer 40:889–894
36. Talerman A (1979) Gonadal tumours composed of germ cells and sex cord stroma derivatives. Patol Pol 30:221–228
37. Talerman A (1980) The pathology of gonadal neoplasms composed of germ cells and sex cord stroma derivatives. Pathol Res Pract 170:24–38
38. Tavassoli FA (1983) A combined germ cell–gonadal stromal–epithelial tumor of the ovary. Am J Surg Pathol 7:73–84
39. Tian Q, Frierson HF, Krystal DW, Moskaluk CA (1999) Activating c-kit gene mutations in human germ cell tumors. Am J Pathol 154:1643–1647
40. Tickoo SK, Hutchinson B, Bacik J, Mazumdar M, Motzer RJ, Bajorin DF, Bosl GJ, Reuter VE (2002) Testicular seminoma: A clinicopathologic and immunohistochemical study of 105 cases with special reference to seminomas with atypical features. Int J Surg Pathol 10:23–32
41. Tokuoka S, Aoki Y, Hayashi Y, Yokoyama T, Ishii T (1985) A mixed germ cell sex cord stromal tumor of the ovary with retiform tubular structure: a case report. Int J Gynecol Pathol 4:161–170
42. True LD, Otis CN, Delprado W, Scully RE, Rosai J (1988) Spermatocytic seminoma of testis with sarcomatous transformation. A report of five cases. Am J Surg Pathol 12:75–82
43. Ulbright TM, Srigley JR, Reuter VE, Wojno K, Roth LM, Young RH (2000) Sex cord stromal tumor of the testis with entrapped germ cells. A lesion mimicking unclassified mixed germ cell-sex cord stromal tumor. Am J Surg Pathol 24:535–542
44. Ulbright TM (2005) Germ cell tumors of the gonads: a selective review emphasizing problems in differential diagnosis, newly appreciated, and controversial issues. Mod Pathol 18(Suppl 2): S61–S79
45. Young RH, Dickersin GR, Scully RE (1983) A distinctive ovarian sex cord stromal tumor causing sexual precocity in the Peutz Jeghers syndrome. Am J Surg Pathol 7:233–243
46. Young RH (2005) Sex cord–stromal tumors of the ovary and testis: their similarities and differences with consideration of selected problems. Mod Pathol 18:S81–S98
47. Zuntova A, Motlik K, Horejsi J, Eckschlager T (1992) Mixed germ cell–sex cord stromal tumor with heterologous structures. Int J Gynecol Pathol 11:227–233

Virchows Arch (2006) 448: 623–629
DOI 10.1007/s00428-005-0085-1

ORIGINAL ARTICLE

Kiyoshi Takahashi · Yuriko Nishikawa · Hiaki Sato · Takashi Oka · Tadashi Yoshino · Katsuya Miyatani

Dendritic cells interacting mainly with B cells in the lymphoepithelial symbiosis of the human palatine tonsil

Received: 23 May 2005 / Accepted: 31 August 2005 / Published online: 8 March 2006

Abstract The lymphoepithelial symbiosis (LES) of the human palatine tonsil is composed of spindle- or star-shaped epithelial cells forming a loose meshwork, containing numerous lymphocytes and dendritic cells (DCs). In the present study, we immunohistochemically characterized DCs in the LES (LES-DCs). LES-DCs were phenotypically immature DCs that were S100β+, fascin−, HLA-DR+, CD1a−, CD80−, CD83−, CD86−, and CD123−. The most characteristic feature of LES-DCs was that they contacted many B cells, which were mostly IgM+ IgD+ resting naive B cells. Langerhans cells (LCs) located in the nonsymbiotic squamous epithelium were immature DCs that were S100β+, fascin−, and CD1a+ and did not contact lymphocytes. In contrast to LES-DCs, interdigitating dendritic cells (IDCs) in the T zone were mature DCs that were HLA-DR+, CD1a−, fascin+, CD80+, CD83+, and CD86+ and contacted numerous CD4+ T cells. Two subsets of IDC, S100β+ fascin+ IDC (IDC-1) and S100β− fascin+ IDC (IDC-2), were identified, and the majority of IDCs are IDC-2. In contrast to IDCs, which were distributed in the T-cell area in groups, LES-DCs were distributed along the crypt as if forming a barrier. These findings suggest that LES-DCs are a novel type of DC playing an important role in the induction of humoral immune response against incoming air- or food-borne pathogenic antigens.

K. Takahashi (✉) · Y. Nishikawa · H. Sato
Faculty of Health Science,
Okayama University Medical School,
2-5-1, Shikata-cho,
Okayama City, 700-8558, Japan
e-mail: dend@md.okayama-u.ac.jp
Tel.: +81-86-2356896
Fax: +81-86-2356896

T. Oka · T. Yoshino
Department of Pathology,
Okayama University Graduate School
of Medicine and Dentistry,
Okayama, Japan

K. Miyatani
Department of Pathology,
Mitoyo General Hospital,
Kagawa, Japan

Introduction

It is well established that dendritic cells (DCs) have a unique ability to stimulate resting naive T cells to proliferate in an antigen (Ag)-specific manner [3], but it has long been believed that DCs are not directly involved in the regulation of B-cell-mediated immunity. To become activated, Ag-specific resting naive B cells require simultaneous exposure to native Ag and Ag-specific CD4+ T cells [14]. However, the question of how rare resting naive B cells can encounter native Ag and simultaneously and efficiently interact with rare Ag-specific CD4+ T cells remains to be answered. It has been suggested that DCs act as a matrix upon which Ag-specific T and B cells interact efficiently and that DCs can deliver native Ags to Ag-specific resting naive B cells [13, 15, 31]. Thus, DCs may play an important role in the induction of the humoral immune response.

Several recent investigations have demonstrated that DCs are directly involved in regulating T-cell-mediated humoral immune responses [7, 5]. Bjork et al. reported evidence indicating that naive B cells actually interact with DCs in human tonsils [5]. We also previously demonstrated that interdigitating dendritic cells (IDCs) sometimes interact with resting naive B cells directly in the T-cell area of the lymph node [29]. However, because such B cells are usually detected infrequently and in small numbers, we search for such types of DCs that usually interact with the large number of resting naive B cells.

In the present study, we demonstrated the presence of a special type of DCs in the lymphoepithelial symbiosis (LES) of the human palatine tonsil. We showed that these DCs in the LES (LES-DCs) are phenotypically different from Langerhans cells (LCs) and IDCs and usually contact many resting naive B cells. The present study suggests that LES-DCs are involved in the induction of the humoral

immune response against incoming air- or food-borne pathogenic Ags.

Materials and methods

Antibodies

Mouse monoclonal antibodies (mabs) to HLA-DR (LN-3; Nichirei, Tokyo, Japan), CD1a (O10; Immunotech, Marseille, France), CD3 (Novocastra, Newcastle, UK), CD4 (Ventana, Yokohama, Japan), CD8 (Nichirei), CD20 (L26; Nichirei), CD79α (Nichirei), human cytokeratin (CK) AE1/AE3 (DAKO, Glostrup, Denmark), and human fascin (Research Diagnostics Inc., Flanders, NJ, USA) were purchased. These mabs can detect Ag in paraffin-embedded tissues. Rabbit polyclonal antibody (pab) to S100β subunit had been prepared previously [29]. Rabbit pab to human IgG, IgM, IgD, or IgA were purchased from DAKO. In addition, mabs to CD11a, CD11b, CD11c, CD13, CD14, CD16 (FcγRIII), CD32a (FcγRII), CD33, CD34, CD35, CD64 (FcγRI), CD68, CD80, CD83, and CD86 were purchased from DAKO; the mab to CD123 was supplied by Pharmingen (Tokyo, Japan).

Tissue preparation

Human palatine tonsils without inflammation were obtained at the time of surgery from two adult patients with benign squamous papilloma of the tonsil. Prior consent was obtained from both patients. Tissues were routinely fixed in formalin and embedded in paraffin. Sections (3-μm-thick) were cut from the paraffin blocks and examined immunohistochemically. Unfixed tissues were snap-frozen in Tissue-Tek OCT compound (Salura Finetek, Torrance, CA, USA). Frozen sections (6-μm-thick) were cut, mounted on glass slides, fixed in acetone for 10 min at 4°C, air-dried, and examined immunohistochemically.

Immunohistochemistry

Dewaxed paraffin sections were immersed in citrate buffer (0.01 mol/l citrate, pH 6.0), microwaved for 15 min at 600 W, and then cooled at room temperature for 20 min. Paraffin sections were rinsed with phosphate buffered saline (PBS) and examined immunohistochemically.

Immunoperoxidase methods

Some sections were stained by immunoperoxidase methods using DAKO Envision System Peroxidase (Carpinteria, USA) according to manufacturer's instructions. After washing, sections were counterstained with hematoxylin.

Immunofluorescent staining

Paraffin or frozen sections were examined by two-color immunofluorescence methods using a combination of rabbit pab and mouse mab. Rabbit pab was detected by fluorescein isothiocyanate (FITC)-conjugated anti-rabbit IgG (DAKO), and mouse mab was detected by phycoerythrin (PE)-conjugated anti-mouse IgG (DAKO). Preparations, which included dewaxed paraffin sections and frozen sections, were immersed in PBS containing 10% normal goat serum (DAKO) for 30 min. After rinsing with PBS, sections were simultaneously incubated for 12 h at 4°C with rabbit pab (at a dilution of 20 μg/ml of anti-S100β subunit or at a dilution of 1:500 of antibody to each class of human immunoglobulin heavy chains) and each of the mabs. Sections were then washed with PBS and further treated for 30 min at room temperature with a combination of FITC-conjugated goat anti-rabbit IgG (DAKO) at a dilution of 1:50 and PE-conjugated goat anti-mouse IgG at a dilution of 1:50. After washing with PBS, sections were immersed in fluorescent mounting medium (DAKO) and examined with an LSM 510 confocal laser scanning microscope (Carl Zeiss, Tokyo, Japan).

Results

Enzyme immunohistochemistry

The human palatine tonsil is covered by squamous epithelia, which form many deep crevices called tonsillar crypt, and numerous secondary lymphoid follicules are located along the crypt (Fig. 1). The LES is the specific region of the squamous epithelia covering these follicules. Immunoperoxidase staining for CK AE1/AE3 indicated that the epithelial cells of the LES, which were positive for CK AE1/AE3, were spindle- or star-shaped cells forming a loose meshwork, containing numerous leukocytes (Fig. 2a,b).

In order to elucidate the distribution of DCs in the human palatine tonsil, we performed enzyme immunohistochemistry for S100β and fascin. Immunoperoxidase staining for S100β or fascin indicated that the distribution of S100β+ DCs was quite different from that of fascin+ DCs. Specifically, S100β+ DCs were densely distributed along the crypt as if forming a barrier (Fig. 2c), whereas fascin+ DCs were distributed in the T-cell area (Fig. 2d).

Immunofluorescent analysis of tonsillar tissue

DCs and lymphocytes in the LES were examined by two-color immunofluorescent microscopy using a confocal laser scanning microscope. Analysis of frozen sections by two-color immunostaining for immunoglobulin heavy chains (FITC) and CK AE1/AE3 (PE) showed that the vast majority of lymphocytes in the LES were IgM+ IgD+ resting naive B cells (Fig. 3a,b). IgA+ B cells were also

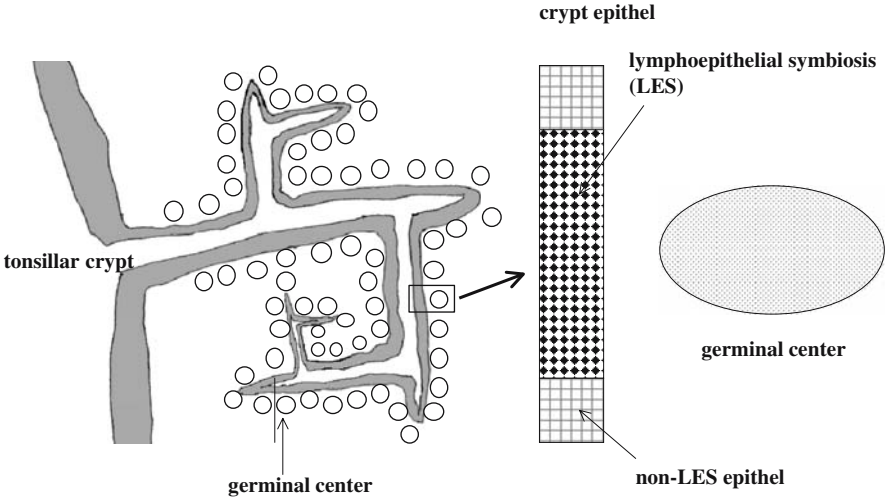

Fig. 1 A general view of the human palatine tonsil and lymphoepithelial symbiosis (*LES*)

detected in small numbers, but no IgG+ B cells (data not shown).

S100β subunit cannot be detected in frozen sections because of its extremely water-soluble nature. We therefore used formalin-fixed, paraffin-embedded tissue sections to detect S100β+ DCs. Two-color immunofluorescent analysis for S100β (FITC) and CK AE1/AE3 (PE) demonstrated a considerable number of S100β+ CK-DCs (green) among the S100β-CK+ epithelial cells (red) in the LES (Fig. 3c,d). Two-color analysis for S100β (FITC) and each of the antigens HLA-DR, CD79α, CD20, CD3, and CD4 (PE) indicated that S100β+ LES-DCs were weakly positive for HLA-DR and that they attached to many B cells, which were HLA-DR+ (Fig. 3e), CD79α+ (Fig. 3f), and CD20+ (Fig. 3g). LES-DCs also attached to a small number of CD3+ CD4+ T cells (Fig. 3h,i). CD8+ T cells were rare in the LES (data not shown). When 100 LES-DCs were analyzed, one LES-DC contacted a mean of 4.0±0.7 B cells and 0.6±0.21 T cells ($p<0.001$). These findings indicated that LES-DCs interact mainly with B cells and also with a small number of CD4+ T cells. Taken together with the finding that lymphocytes in LES were mostly IgM+ IgD+ resting naive B cells, we concluded that S100β+ LES-DCs interact mainly with resting naive B cells.

The vast majority of S100β+ LES-DCs were negative for CD1a, although a small number of them were found to be positive for CD1a (Fig. 3j). To further confirm that LES-DCs are negative for CD1a, two-color immunofluorescent analysis using frozen sections was performed since immunohistochemical detection of CD1a in paraffin sections is

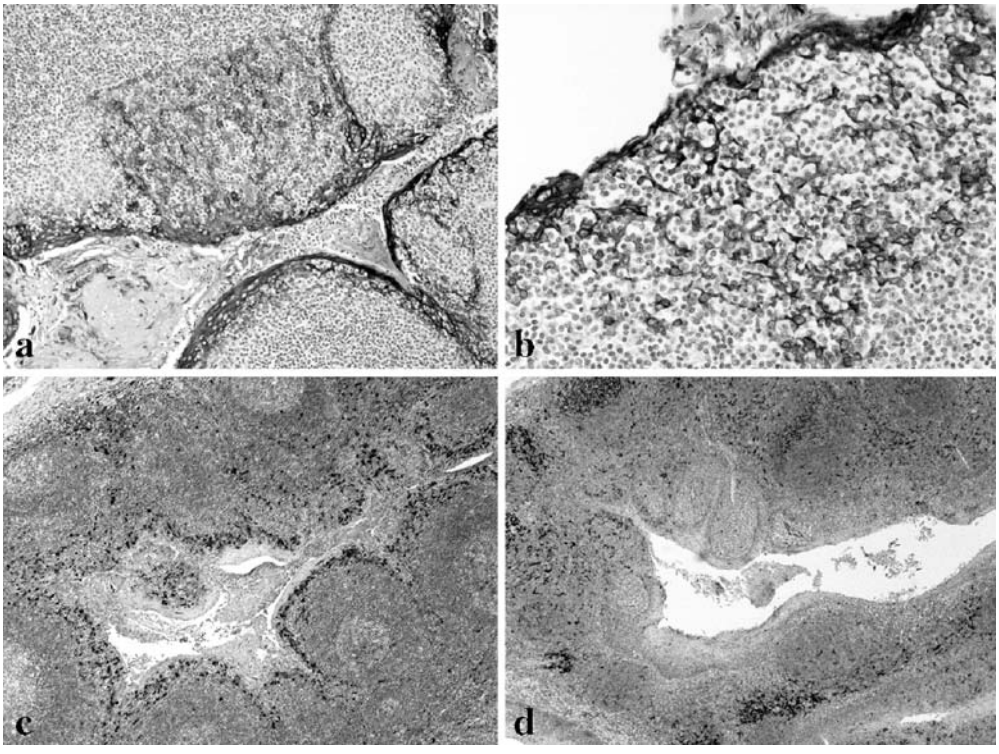

Fig. 2 **a**, **b** Immunoperoxidase staining for CK AE1/AE3 counterstained with hematoxylin. Note that CK AE1/AE3+ epithelial cells covering the follicules form a mesh configuration. **a** Magnification, ×80; **b** magnification, ×540. **c** Immunoperoxidase staining for S100β counterstained with hematoxylin. Note the S100β+ DCs distributed along the crypt. Magnification, ×40. **d** Immunoperoxidase staining for fascin counterstained with hematoxylin. Note that fascin+ DCs are distributed mainly in the T-cell area. Magnification, ×40

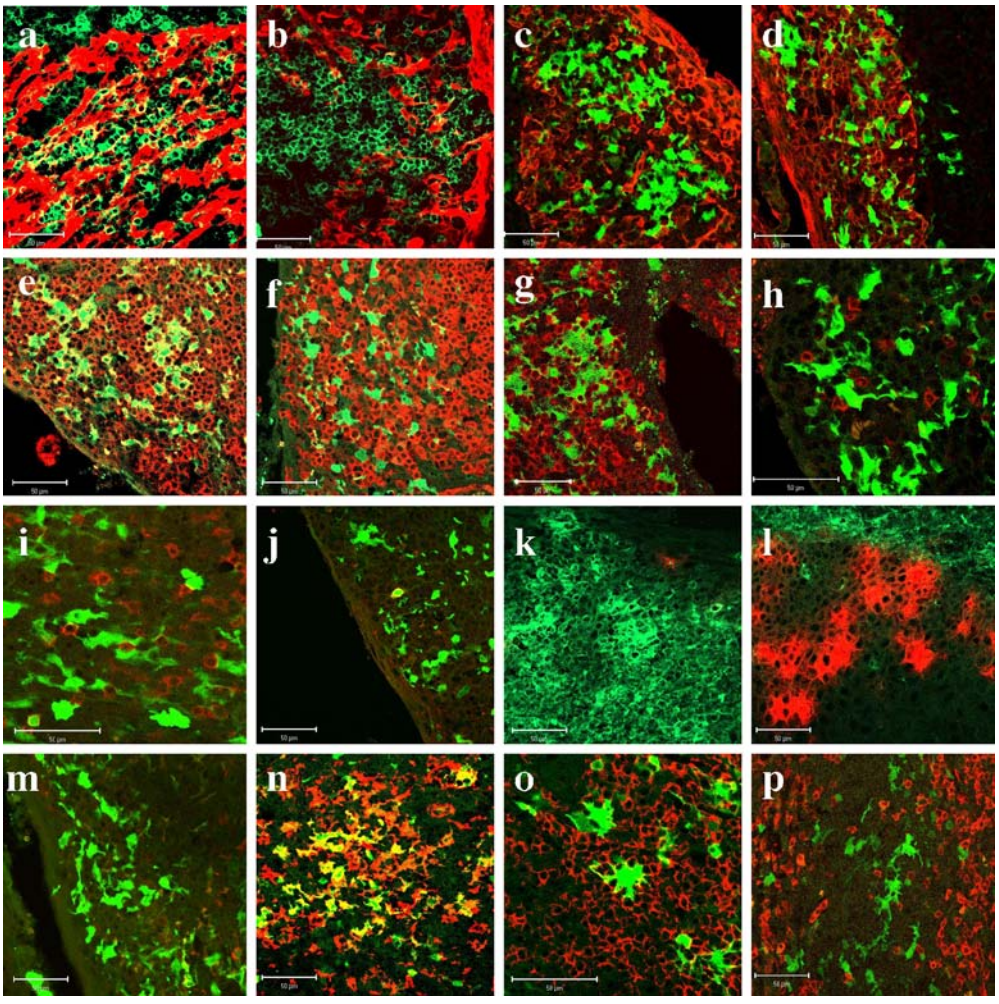

Fig. 3 Two-color immunofluorescent microscopy of tonsillar frozen and paraffin sections. *Horizontal bars* indicate 50 μm. **a**, **b** Frozen sections: immunofluoresent staining of the LES for IgM (FITC) (**a**) or IgD (FITC) (**b**) and CK AE1/AE3 (PE) (**a** and **b**). Note numerous IgM+ IgD+ resting naive B cells in the LES. **c**, **d** Paraffin sections: immunofluoresent staining of the LES for S100β (FITC) and CK AE1/AE3 (PE). Note numerous S100β+ DCs in the LES. **e**: Paraffin sections: immunofluoresent staining of the LES for S100β (FITC) and HLA-DR (PE). Note numbers of S100β+ HLA-DR+ LES-DCs surrounded by numerous HLA-DR+ B cells. **f**, **g** Paraffin sections: immunofluoresent staining of the LES for S100β (FITC) (**f** and **g**) and CD79α (PE) (**f**) or CD20 (PE) (**g**). Note numerous CD79α+ CD20+ B cells attaching to S100β+ LES-DCs. **h**, **i** Paraffin sections: immunofluoresent staining of the LES for S100β (FITC) and CD3 (PE) (**h**) or CD4 (PE) (**i**). Note that few CD3+ CD4+ T cells are attaching to S100β+ LES-DCs. **j** Paraffin section: immunofluoresent staining of the LES for S100β (FITC) and CD1a (PE). Note that the vast majority of LES-DCs are negative for CD1a. **k** Frozen section: immunofluoresent staining of the LES for HLA-DR (FITC) and CD1a (PE) applied on a frozen section. Note that HLA-DR+ LES-DCs surrounded by HLA-DR+ B cells are negative for CD1a. **l** Paraffin section: immunofluoresent staining of the LES for IgM (FITC) and CD1a (PE). Note that LCs in non-LES epithelia are strongly positive for CD1a and do not attach to IgM+ resting naive B cells. **m** Paraffin section: immunofluoresent staining of the LES for S100β (FITC) and fascin (PE). Note that S100β+ LES-DCs are completely negative for fascin. **n** Paraffin section: immunofluorescent staining of the T-cell area for S100β (FITC) and fascin (PE). Note that IDCs are either S100β− fascin+ or S100β+ frascin+. **o** Paraffin section: immunofluoresent staining of the T-cell area for S100β (FITC) and CD4 (PE). Note numerous CD4+ T cells contacting S100β+ IDCs. **p** Paraffin section: immunofluoresent staining of the T-cell area for S100β (FITC) and CD79α (PE). Note only a small number of CD79α+ B cells contacting S100β+ IDCs

sometimes unsuccessful. Because S100β cannot be detected in frozen sections, we used HLA-DR as a marker for LES-DCs. Two-color analysis for HLA-DR (FITC) and CD1a (PE) indicated that the vast majority of HLA-DR+ LES-DCs, which contacted to HLA-DR+ B cells, were negative for CD1a (Fig. 3k). In contrast, two-color analysis for IgM (FITC) and CD1a (PE) indicated that $CD1a^{bright}$ LCs in non-LES epithelia did not contact IgM+ naive B cells (Fig. 3l).

Two-color immunofluorescent analysis for S100β (FITC) and fascin (PE) indicated that S100β+ LES-DCs were completely negative for fascin (Fig. 3m). The LES did not contain fascin+ DCs, although epithelial cells in the LES were sometimes dimly positive for fascin (data not shown).

Furthermore, LES-DCs were negative for mature-DC markers including CD80, CD83, and CD86; macrophage markers including CD68; IgG-Fc receptors including

Table 1 Results of the immunohistochemical analysis are summarized in the table

Antigens	LES-DC	LC	IDC	Specificity, property	Positive cells
HLA-DR	+	+	+	MHC-class II	DCs and macrophage
S100β	+	+	−/+	S100β-subunit	LC, IDC
Fascin	−	−	+	Actin-bundling protein	IDC
CD1a	−	+	−	T6-antigen	LC, thymic T cells
CD3	−	−	−	CD3 complex	T cells
CD4	−	−	−	Th-marker	Helper/inducer T cells
CD8	−	−	−	Ts-marker	Cytotoxic T cells
CD11a	−	−	+	LFA-1	Monocyte, granulocyte, NK cell
CD11b	−	−	+	CR 3	Monocyte/macrophage
CD11c	−	−	−	CR4/integrin α-X	Monocyte/macrophage
CD13	−	−	+	GP-150	Granulocyte, myeloid precursors
CD14	−	−	−	LPS-R	Monocyte/macrophage
CD16	−	−	−	FcγRIII	Monocyte/myeloid cells
CD20	−	−	−	Bp35	B cell
CD32a	−	−	−	FcγRII	B cell, macrophage
CD33	−	−	−	gp67 (sialoadhesion)	Myeloid cells
CD34	−	−	−	CD62 ligand	Hematopoietic precursors
CD35	−	−	−	CR1	FDC, B cell
CD64	−	−	−	FcγRI	Monocyte/macrophage
CD68	−	−	−	gp110	Macrophage
CD79α	−	−	−	BCR-α chain	B cells
CD80	−	−	+	B7	B cell, IDC
CD83	−	−	+	HB15	IDC
CD86	−	−	+	B70	IDC
CD123	−	−	−	IL3R	Plasmacytoid DC
CK AE1/AE3	−	−	−	Pan-cytokeratin	Epithelial cell

CD16, CD32, and CD64; and complement C3-receptors including CD11b, CD11c, and CD35 (Table 1).

IDCs in the T-cell area were also examined by immunofluorescent microscopy. Two-color immunostaining for S100β (FITC) and fascin (PE) indicated that IDCs, which were morphologically identified as large dendriform cells, were divided into two subsets, S100β+ fascin+ IDC (IDC-1) and S100β- fascin+ IDC (IDC-2). The majority of IDCs were IDC-2 (Fig. 3n).

Two-color immunofluorescent analysis for S100β and T-cell antigens including CD3, CD4, and CD8 indicated that IDCs contacted numerous CD4+ T cells (Fig. 3o), but that they rarely contacted CD79α+ B cells (Fig. 3p). IDCs were positive for mature-DC markers including CD80, CD83, and CD86 (Table 1).

A few S100β+ fascin- small lymphoid cells were also detected in the T-cell area. They were mostly T cells expressing CD3 and CD8 (data not shown).

Discussion

In our previous study, we demonstrated that IDCs in the T-cell area of the lymph nodes contact resting naive B cells [29]. However, B cells contacting IDCs are usually detected infrequently and in small numbers. In contrast, as shown in this study, LES-DCs usually contact many B cells, mostly IgM+ IgD+ resting naive B cells. DCs that habitually interact with so many B cells have not previously been identified outside the germinal centers of lymphoid tissues. LES-DCs have been regarded as IDCs because they are positive for IDC markers such as HLA-DR and S100β, a member of the S100 protein family present in human IDCs and LCs [6, 27], and are mostly negative for CD1a, a specific marker for LCs [10, 16]. However, as shown in this study, LES-DCs are completely negative for fascin, a 55-kDa, actin-bundling protein highly specific for mature DCs [1, 9, 21–23], whereas IDCs in the T-cell area are strongly positive for fascin. Taken together with the present findings that LES-DCs do not express mature DC markers that are expressed on IDCs (e.g., CD80, CD83, and CD86) [4, 20, 25], it is clear that LES-DCs are immature DCs distinct from IDCs.

Immature DCs, such as LCs, have been demonstrated to be negative for fascin [18, 21]. LCs are strongly positive for CD1a and usually present in nonsymbiotic squamous epithelium, where LCs do not contact any type of lymphocytes. It is therefore clear that LES-DCs differ from LCs and IDCs in distribution, phenotype, and association with neighboring cells. Germinal center DCs, which were recently identified in germinal centers of the palatine tonsil [8], are reported to be strongly positive for fascin [24]. Follicular dendritic cells (FDCs) in germinal centers are

also positive for fascin [12] and express CD35 on their surfaces [2, 30], but LES-DCs are negative for CD35.

LES-DCs are also negative for CD123, a marker expressed on plasmacytoid DCs, a type of DC distributed around the high endothelial venule in the T-cell area of lymphoid tissues including the palatine tonsil [11, 26]. Hence, LES-DCs are phenotypically different from these known DCs in the human palatine tonsil.

The present finding that LES-DCs interact with many resting naive B cells suggests that they are involved in the Ag-specific stimulation of resting naive B cells. It has been well established that both the native form of Ag and Ag-specific CD4+ T cells are necessary for the stimulation of resting naive B cells. The present findings that LES-DCs contacted a small number of CD4+ T cells is consistent with the view that LES-DCs act as a matrix upon which resting naive B cells efficiently interact with Ag-specific CD4+ T cells. Judging from the present findings that LES-DCs are phenotypically immature DCs lacking the expression of costimulatory factors such as CD80 and CD86, it seems likely that the role of LES-DCs is to stimulate resting naive B cells but not resting naive T cells. If this is the case, then the question arises as to how LES-DCs deliver Ag in the native form to resting naive B cells, which is essential for their stimulation. As shown in this study, LES-DCs do not express FcγRs recognized by mabs CD16, CD32, and CD64, or C3R recognized by mab CD35 on their surface. These proteins might allow LES-DCs to retain Ags within cell surface immune complexes [17, 19]. It has been shown that DCs have the ability to retain Ag in the native form for a long time and to deliver it to resting naive B cells to stimulate antibody synthesis [15]. We speculate that LES-DCs are a special type of DC, in which this ability is particularly strong, and that these cells devote themselves to the Ag-specific stimulation of resting naive B cells. The palatine tonsil is one of the first barriers against numerous pathogenic air- or food-borne Ags. The present study suggests that LES-DCs play an important role in the induction of the humoral immune response against such Ags. The origin of LES-DCs and their ontogenic relationship with LCs and IDCs also remain to be determined.

Finally, it is noteworthy that S100β+ fascin- small lymphoid cells are present in the T-cell area of peripheral lymphoid tissues including the palatine tonsil. These are CD3+ CD8+ T cells rather than IDCs and should not be mistaken as IDCs [28]. Their biological significance and association with DCs also remain to be established.

References

1. Al-Alwan MM, Rowden G, Lee TD, West KA (2001) Fascin is involved in the antigen presentation activity of mature dendritic cells. J Immunol 166:338–345
2. Bagdi E, Krenacs L, Krenacs T, Miller K, Isaacson PG (2001) Follicular dendritic cells in reactive and neoplastic lymphoid tissues: a reevaluation of staining patterns of CD21, CD23, and CD35 antibodies in paraffin sections after wet heat-induced epitope retrieval. Appl Immunohistochem Mol Morphol 9:117–1124
3. Banchereau J, Steinman RM (1988) Dendritic cells and the control of immunity. Nature 392:245–252
4. Berchtold S, Muhl-Zurbes P, Heufler C, Winklehner P, Schuler G, Steinkasserer A (1999) Cloning, recombinant expression and biochemical characterization of the murine CD83 molecule which is specifically upregulated during dendritic cell maturation. FEBS Lett 461:211–216
5. Bjorck P, Flores-Romo L, Liu YJ (1997) Human interdigitating dendritic cells directly stimulate CD40-activated naive B-cells. Eur J Immunol 27:1266–1274
6. Cocchia D, Michetti F, Donato R (1981) Immunochemical and immunocytochemical localization of S100 antigen in normal human skin. Nature 294:85–87
7. Feyette J, Dubois B, Vandenabeele S, Bridon JM, Vanbervliet B, Durand I, Banchereau J, Caux C, Briere F (1997) Human dendritic cells skew switching of CD40-activated naive B-cells towards IgA1 and IgA2. J Exp Med 185:1909–1918
8. Grouard G, Durand I, Filgueira L, Banchereau J, Liu YJ (1996) Dendritic cells capable of stimulating T-cells in germinal centres. Nature 384:364–367
9. Hiroi M, Kuroda N, Toi M, Hayashi Y, Miyazaki E, Naruse K, Enzan H (2004) Fascin-positive dendritic cells and fibroblastic reticulum cells build a framework of T-cell areas in lymph nodes. Virchows Arch 444:158–163
10. Hunger RE, Sieling PA, Ochoa MT, Sugaya M, Burdick AE, Rea TH, Brennan PJ, Belisle JT, Blauvelt A, Porcelli SA, Modlin RL (2004) Langerhans cells utilize CD1a and langerin to efficiently present nonpeptide antigens to T-cells. J Clin Invest 113:701–708
11. Jahnsen FL, Lund-Johansen F, Dunne JF, Farkas L, Haye R, Brandtzaeg P (2000) Experimentally induced recruitment of plasmacytoid (CD123high) dendritic cells in human nasal allergy. J Immunol 165:4062–4068
12. Kazakov DV, Palmedo G, Mukensnabl P, Hes O, Kempf W, Michal M (2004) Follicular lymphoma of the skin and superficial soft tissues associated with a prominent follicular dendritic cell proliferation: an unusual pattern which may represent a diagnostic pitfall. Pathol Res Pract 200:557–565
13. Kushnir N, Liu L, MacPharson G (1998) Dendritic cells and resting B-cells form clusters in vitro and in vivo: T cell independence, partial LFA-1 dependence, and regulation by cross-linking surface molecules. J Immunol 160:1774–1781
14. Liu YJ, Arpin C (1997) Germinal center development. Immunol Rev 156:111–126
15. MacPherson G, Kushnir N, Wykes M (1999) Dendritic cells, B-cells and the regulation of antibody synthesis. Immunol Rev 172:325–334
16. Murphy GF, Bhan AK, Sato S, Mihm MC, Harrist JT (1981) A new immunologic marker for human Langerhans cells. N Engl J Med 304:791–792
17. Petrasch S, Brittinger G, Wacker HH, Schmitz J, Kosco-Vilbois M (1994) Follicular dendritic cells in non-Hodgkin's lymphomas. Leuk Lymphoma 15:33–43
18. Pinkus GS, Lones MA, Matsumura F, Yamashiro S, Said JW, Pinkus JL (2002) Langerhans cell histiocytosis immunohistorchemical expression of fascin, a dendritic cell marker. Am J Clin Pathol 118:335–343
19. Qin D, Wu J, Vora KA, Ravetch JV, Szakal AK, Manser T, Tew JG (2000) Fc gamma receptor IIB on follicular dendritic cells regulates the B cell recall response. J Immunol 164:6268–6275
20. Radvanyi LG, Banerjee A, Weir M, Messner H (1999) Low levels of interferon-alpha induce CD86 (B7.2) expression and accelerates dendritic cell maturation from human peripheral blood mononuclear cells. Scand J Immunol 50:499–509
21. Ross R, Ross XL, Schwing J, Langin T, Reske-Kunz AB (1998) The actin-bundling protein fascin is involved in the formation of dendritic processes in maturing epidermal Langerhans cells. J Immunol 160:3776–3782

22. Ross R, Jonuleit H, Bros M, Ross XL, Yamashiro S, Matsumura F, Enk AH, Knop J, Reske-Kunz AB (2000) Expression of the actin-bundling protein fascin in cultured human dendritic cells correlates with dendritic morphology and cell differentiation. J Invest Dermatol 115:658–663
23. Said JW, Pinkus JL, Yamashita J, Mishalani S, Matsumura F, Yamashiro S, Pinkus GS (1997) The role of follicular and interdigitating dendritic cells in HIV-related lymphoid hyperplasia: localization of fascin. Mod Pathol 10:421–427
24. Said JW, Pinkus JL, Shintaku IP, deVos S, Matsumura F, Yamashiro S, Pinkus GS (1998) Alterations in fascin-expressing germinal center dendritic cells in neoplastic follicles of B-cell lymphomas. Mod Pathol 11:1–5
25. Saunders D, Lucas K, Ismaili J, Wu L, Maraskovsky E, Dunn A, Shortman K (1996) Dendritic cell development in culture from thymic precursor cells in the absence of granulocyte/macrophage colony-stimulating factor. J Exp Med 184:2185–2196
26. Summers KL, Hock BD, McKenzie JL, Hart DN (2001) Phenotypic characterization of five dendritic cell subsets in human tonsils. Am J Pathol 159:285–295
27. Takahashi K, Isobe T, Ohtsuki U, Sonobe H, Takeda I, Akagi T (1984) Immunohistochemical localization and distribution of S100 proteins in the human lymphoreticular system. Am J Pathol 116:497–503
28. Takahashi K, Yoshino T, Hyashi K, Sonobe H, Ohtsuki Y (1987) S100β positive human T lymphocytes: their characteristics and behavior under normal and pathologic conditions. Blood 70:214–220
29. Takahashi K, Asagoe K, Teramoto N, Kondo E, Oka T, Hayashi K, Yoshino T, Akagi T (2001) Morphological interaction of interdigitating dendritic cells with B and T-cells in human mesenteric lymph nodes. Am J Pathol 159:131–138
30. Tsunoda R, Nakayama M, Onozaki K, Heinen E, Cormann N, Kinet-Denoel C, Kojima M (1990) Isolation and long-term cultivation of human tonsil follicular dendritic cells. Virchows Arch B Cell Pathol Incl Mol Pathol 59:95–105
31. Wykes M, Pombo A, Jenkins C, MacPherson GG (1998) Dendritic cells interact directly with naive B lymphocytes to transfer antigen and initiate class switching in a primary T-dependent response. J Immunol 161:1313–1319

Virchows Arch (2006) 448: 630–638
DOI 10.1007/s00428-005-0071-7

ORIGINAL ARTICLE

Susanne Korff · Nora Riechert · Frank Schoensiegel · Dieter Weichenhan · Frank Autschbach · Hugo Albert Katus · Boris Tomislav Ivandic

Calcification of myocardial necrosis is common in mice

Received: 24 April 2005 / Accepted: 19 August 2005 / Published online: 7 October 2005

Abstract Independent of the severity, phenotypes and clinical outcomes of myocardial infarction may vary considerably in patients, suggesting a strong genetic influence on healing and adaptive processes. Since little is known about these genetic determinants, we examined the tissue response to myocardial injury in seven inbred mouse strains, including those employed for gene targeting or transgenic overexpression. Myocardial necrosis was produced by non-ischemic, trans-diaphragmal freeze–thaw injury in strains C57BL/6, C3H/He, DBA/2, BALB/c, 129S1, FVB/n and A/J. Two days after injury, necrotic cardiomyocytes calcified in C3H/He, DBA/2, BALB/c and 129S1, a phenotype known as dystrophic cardiac calcinosis (DCC). The susceptibility to DCC of 129S1 was determined by *Dyscalc1*, a locus on chromosome 7, which was identified previously in C3H/He and DBA/2. DCC was also observed in C3H/He following ischemic injury by permanent coronary artery ligation, indicating that DCC was independent of the mode of injury. In contrast, strains C57BL/6, FVB and A/J were resistant to DCC, showing formation of a fibrous scar without calcification. The development of DCC was studied in detail in C3H/He and C57BL/6. In both strains, no calcium deposition and only little structural disintegration were noted in necrotic myocardium 24 h after injury upon calcium-sensitive fluorescence staining. Ultrastructural examination revealed calcified mitochondria in C3H/He that may have served later as a nidus for rapid intracellular calcification of cardiomyocytes. We concluded that the susceptibility to calcification of myocardial necrosis may be common among inbred strains and should be recognised as a strong genetic modifier of experimental myocardial injury.

Keywords Myocardial infarction · Necrosis · Healing · Tissue calcification · Response to injury · Dystrophic cardiac calcinosis · Dyscalc

S. Korff · N. Riechert · F. Schoensiegel · D. Weichenhan · H. A. Katus · B. T. Ivandic
Department of Medicine III, Division of Cardiology,
University of Heidelberg,
Im Neuenheimer Feld 410,
69120 Heidelberg, Germany

F. Autschbach
Institute of Pathology, University of Heidelberg,
Im Neuenheimer Feld 220,
69120 Heidelberg, Germany

B. T. Ivandic (✉)
Medizinische Klinik III,
Im Neuenheimer Feld 410,
69120 Heidelberg, Germany
e-mail: Boris.Ivandic@med.uni-heidelberg.de
Tel.: +49-6221-5639119
Fax: +49-6221-56-4866

Introduction

Myocardial necrosis may result from irreversible cell injury of various aetiologies, most often caused by thromboembolic occlusion of a coronary artery as a consequence of atherosclerotic plaque rupture. The subsequent response of tissue involves inflammation and removal of necrotic tissue and usually results in scarring and thinning of the affected myocardial wall. Interestingly, up to 7.6% of the survivors of acute myocardial infarctions may also exhibit calcified myocardial necrosis [2].

Myocardial calcification was also observed in certain inbred mouse strains, such as C3H and DBA [8]. This form of soft tissue calcification was independent of calcium and phosphate plasma concentrations and was referred to as dystrophic cardiac calcinosis (DCC). Frequency and severity of DCC were influenced by age, sex, hormones, diet and infectious agents [9–11, 13]. Employing trans-diaphragmal freeze–thaw injury of the myocardium, Brunnert and Altman [4] presented the first evidence that myocardial calcifications developed in genetically predisposed strains only after cardiomyocyte death had occurred. A strain-dependent susceptibility to DCC may also explain calcification of severely dystrophic myocardium in some gene-targeted mouse models of cardiomyopathy [12, 16, 17, 22].

Employing non-ischemic freeze–thaw injury, we investigated the phenotypes of myocardial necrosis in seven

frequently studied inbred mouse strains, including those relevant for gene targeting (strain 129S1) or transgenic overexpression (strain FVB). We found calcifying cardiomyocyte necrosis in C3H/He, DBA/2, BALB/c and 129S1 but not in C57BL/6, FVB/n and A/J. Strains C3H/He and C57BL/6 were examined by fluorescence and electron microscopy at several time points to describe the reaction of tissue to necrosis in greater detail and to determine the time and location of first calcium deposits. The susceptibility of some, but not all inbred strains, clearly indicated that DCC depended on strain background and was therefore genetically determined. Our data and the ancestral relationships among the studied strains may facilitate *in silico* mapping of the genetic causes of DCC in the future.

Material and methods

Animals

Mouse inbred strains C3H/HeNCrlBR (C3H/He), C57BL/6NCrlBR (C57BL/6), BALB/cAnNCrlBR (BALB/c), DBA/2NCrlBR (DBA/2), FVB/NCrlBR (FVB) and 129S1/SvImJ (129S1) were purchased from Charles River (Sulzbach-Rosenberg, Germany). A/J mice were obtained from the Jackson Laboratory (Bar Harbor, ME, USA). All mice were housed in groups of up to five animals in a climate- and pathogen-controlled environment (room temperature 22±2°C, relative humidity 55±10%, 15 air changes per hour) with a 12 h light/dark cycle. Mice had free access to standard rodent chow and tap water. Experimental procedures were conducted in concordance with the German Animal Welfare Act and were done on virgin females of 6–8 weeks of age. Ischemic myocardial injury was produced by permanent coronary ligation as reported by others [18]. Non-ischemic myocardial freeze–thaw injury was performed as described previously [1, 3]. Since mortality of freeze–thaw injury was below 5%, we employed this procedure to determine the susceptibility to DCC in all strains. All mice were killed by cervical dislocation 3 days after myocardial freeze–thaw injury or 5 days after coronary ligation. Whole hearts were removed quickly, rinsed in phosphate-buffered saline (PBS; pH 7.4) and stored in 4% paraformaldehyde for paraffin embedding or in tissue-freeze medium (Leica Instruments, Nussloch, Germany) until histological processing.

Histology

Serial 6- to 8-μm cryostat sections or 2-μm paraffin sections were prepared throughout the ventricles, and 40–60 sections per heart were collected on poly(D-lysine)-coated slides. Paraffin sections were stained with haematoxylin and eosin (H & E) according to standard protocols using Mayer's haematoxylin (Sigma, Taufkirchen, Germany) and 0.5% eosin Y aqueous (Shandon, Germany). For calcium staining, a 1% solution of alizarin red S (Sigma) was prepared and adjusted to pH 6.4 by adding drops of 0.1% NH_4OH [6]. Cryostat sections were stained for 2 min, rinsed twice with distilled water, dehydrated and then mounted with a xylene-compatible medium. For more sensitive, fluorescent calcium staining, cryostat sections were immersed in 0.1 mM calcein/50 mM Tris–buffer (pH 9.0; Sigma) for 30 min. After rinsing twice with PBS (pH 7.4), slides were incubated for 1 min in 2 μg/ml 4′,6-diamidino-2-phenylindole-dihydrochloride (DAPI; Molecular Probes, Leiden, the Netherlands) to visualize cell nuclei. After rinsing with PBS, slides were mounted using anti-fade medium (EMD Biosciences, Darmstadt, Germany). Specimens were examined using a green fluorescence setting (excitation 488 nm) for calcein and a blue fluorescence setting (excitation 358 nm) for DAPI on a fluorescence microscope (Leica, Bensheim, Germany). Photomicrographs were obtained separately for each fluorescence channel using a Leica 500 digital camera set-up. Grey-scale pictures displaying calcein and DAPI fluorescence were artificially coloured, using separate colour look-up tables, and were then fused into one picture, using Photoshop 6.0 (Adobe Systems, USA).

Electron microscopy

Myocardial specimens (approximately 1 mm^3) of C3H/He and C57BL/6 were fixed in PBS-buffered 3% glutaraldehyde (pH 7.4), treated with 1% osmium tetroxide, dehydrated and embedded in epoxy resin following standard protocols. Semi-thin toluidine-blue-stained sections (1 μm) were examined to select blocks for ultrathin sectioning and mounting on grids. Grids were analysed with a Philips EM 400 electron microscope after contrasting with uranyl acetate and lead citrate.

Genetic analysis

Genetic linkage of DCC to the *Dyscalc1* locus was tested by analysis of DCC and a genomic marker in 130 female (129S1×C57BL/6)×129S1 backcross progeny. At 6–8 weeks of age, all mice were phenotyped 3 days after freeze–thaw injury as outlined above. DNA was isolated from tail biopsies employing standard protocols. A simple sequence length polymorphism (SSLP), D7Mit229, was genotyped by PCR amplification and subsequent agarose gel electrophoresis as described previously [14, 15]. This genomic marker is located very close to *Dyscalc1* on proximal chromosome 7 and allowed to assess indirectly the segregation of the *Dyscalc1* alleles in the backcross [14].

Results

Common laboratory strains are susceptible to DCC

We examined three to five female mice of each strain C3H/He, C57BL/6, A/J, BALB/c, DBA/2, FVB, 129S1 to determine the histological phenotypes of myocardial necrosis

at the indicated time points. Lesions were detectable by gross inspection as early as 2 days after freeze–thaw injury (data not shown). Transmural necrosis was located in the right ventricular wall and extended into the interventricular septum (Fig. 1). Necrotic tissue was delineated sharply from surrounding vital myocardium. Strains C57BL/6 and FVB exhibited a necrotic lesion without any trace of calcification (Fig. 1a,c). Only a few single-cell calcifications were found in the necrotic lesions of A/J mice (Fig. 1e). Therefore, this strain was also considered resistant to DCC. In contrast, all DBA/2 mice showed very severe calcification comprising the entire necrotic lesion (Fig. 1d). The degree of calcification was similar in all C3H/He (Fig. 1b) and 129S1 (Fig. 1f) and was almost as severe as seen in DBA/2. In comparison to C3H/He, DCC exhibited less severity and a larger variance among BALB/c mice: only one animal showed extensive calcifications (Fig. 1g), while focal calcifications of few myofibers only were found in the remaining three mice (data not shown).

Dyscalc1 determined the susceptibility to DCC of strain 129S1

The locus *Dyscalc1* was identified previously as the major genetic determinant of the recessively inherited susceptibility to DCC in strains C3H/He and DBA/2 [5, 14, 15]. The susceptibility to DCC of 129S1 was a novel finding

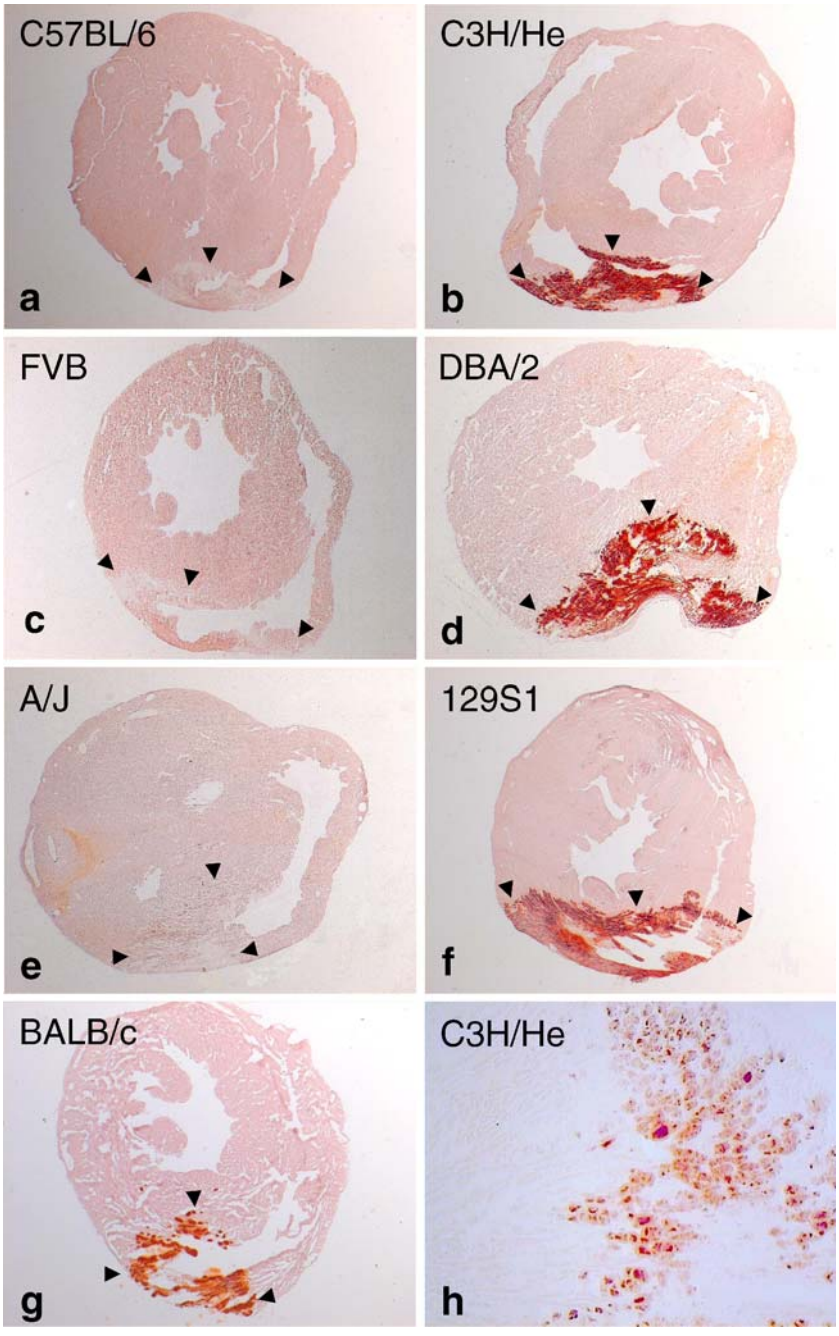

Fig. 1 Myocardial necrosis 3 days after freeze–thaw injury in strains C57BL/6, C3H/He, FVB, DBA/2, A/J, 129S1 and BALB/c (**a**–**g**, ×12.5). DCC in C3H/He 5 days after permanent ligation of the left anterior descending artery (**h**, ×100). Lesion perimeters are delineated by *arrowheads*. Calcifications stained bright *red* with alizarin red S

prompting us to test whether *Dyscalc1* determined DCC in 129S1 as well. Since the *Dyscalc1* gene is still unknown, the *Dyscalc1* alleles had to be assessed indirectly by genotyping the alleles of the SSLP D7Mit229, a genomic marker closely linked to *Dyscalc1*. We produced a (129S1×C57BL/6)×129S1 backcross and screened 130 female progeny for DCC 3 days after freeze–thaw injury. Confirmed by calcium-specific alizarin red S staining, 59 mice (45%) exhibited myocardial calcification whereas 71 mice (55%) were resistant to DCC. All 59 susceptible mice exhibited predisposing homozygous 129S1 alleles at the locus of D7Mit229, while 70 resistant mice were heterozygous (129S1×C57BL/6) at this locus. One animal was apparently resistant to DCC despite a predisposing homozygous 129S1 genotype. Since homozygous 129S1 alleles at D7 Mit229 were almost exclusively associated with DCC, *Dyscalc1* must be the major genetic determinant of DCC in 129S1.

Ischemic injury also leads to DCC

The mechanisms involved in ischemic damage or reperfusion injury may differ from those involved in non-ischemic freeze–thaw injury. Therefore, we tested in C3H/He, as an example of a DCC-susceptible strain, whether the mode of injury may be critical for the development of DCC. Permanent ligation of the left anterior descending artery resulted in necrotic calcifications throughout the apical anterior ventricular wall (Fig. 1h). Compared to the myocardial calcifications seen after freeze–thaw injury (Fig. 1b, d,f,g), these calcifications exhibited a more focal pattern of distribution, suggesting that potentially incomplete ischemia may have caused necrosis of single myocytes or some myofiber bundles only. Further attempts to produce large infarctions were not made, because this evidence confirmed that DCC is not dependent on the mode of injury.

Intracellular calcification of necrotic cardiomyocytes

Histological composition of myocardial necrosis in the lesion perimeter was studied in greater detail 3 days after injury. Cellular infiltrates included fibroblasts, lymphocytes and macrophages (Fig. 2). No major differences in cellular composition were noted among the strains upon standard H & E staining. Vital cardiomyocytes displayed strong eosinophilic staining and large, oval, faint blue nuclei with several nucleoli. In strains C57BL/6, FVB and A/J, necrotic cardiomyocytes disintegrated into small

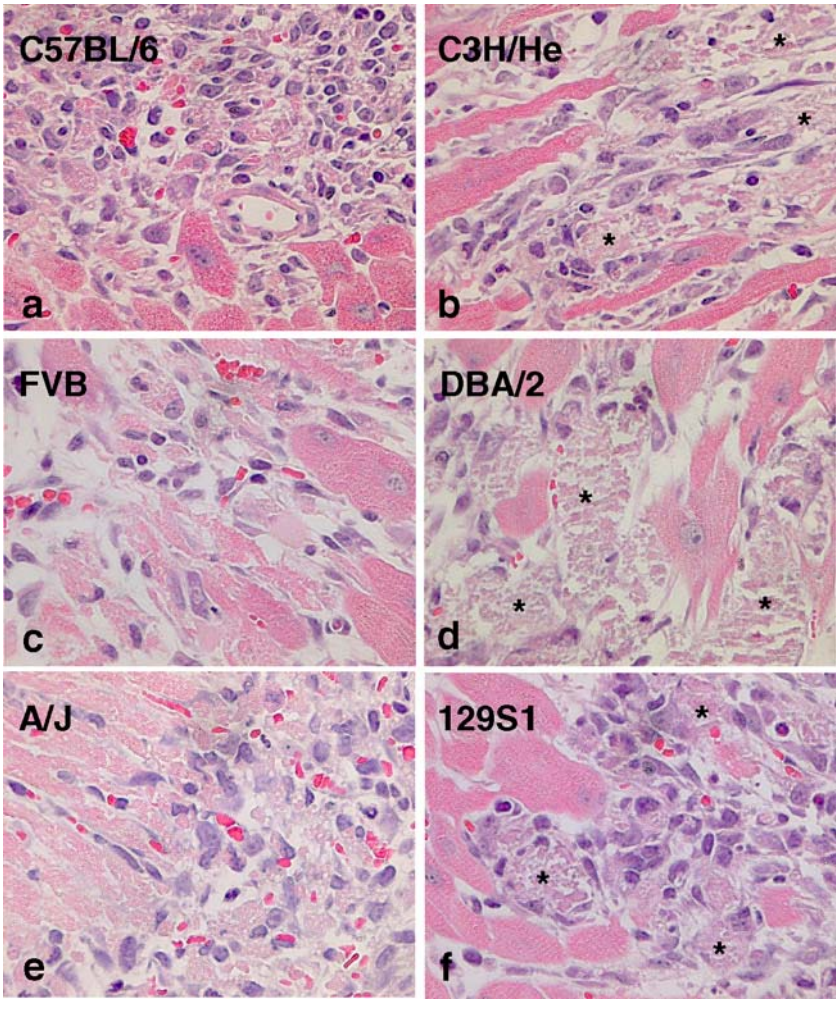

Fig. 2 Necrosis and calcification in the perimeter of myocardial lesions 3 days after trans-diaphragmal freeze–thaw injury in strains C57BL/6, C3H/He, FVB, DBA/2, A/J and 129S1 (**a**–**f**, H & E, ×1,000). Calcified necrotic cardiomyocytes (*asterisks*) stained *purple-greyish*. Vital cardiomyocytes and their non-calcified remnants were coloured *reddish* and *pale pink*. Erythrocytes appeared bright *red*

pieces with residual eosinophilic staining, which were removed by phagocytosis (Fig. 2a,c,e). In the lesions of DBA/2, C3H/He, 129S1 (Fig. 2b,d,f, respectively) and DCC-positive BALB/c (data not shown), the outlines of calcified necrotic myocytes remained intact and disintegrated only slowly, although calcified myocytes were surrounded by macrophages. Limited by intercalating discs and basal laminae, myocyte calcification was confined strictly to the intracellular compartment. Three days after injury, we were unable to quantify the proportion of necrotic myocytes that entered calcification, because non-calcified myocyte remnants were either completely removed by phagocytosis or, in the process of decay, could not be distinguished reliably from extracellular wound matrix. In the perimeter of the lesions, vital cardiomyocytes and calcified remnants coexisted side by side, giving rise to a gritty pattern of calcification upon gross examination (data not shown). Calcified myocytes attracted macrophage-like cells excluding major defects of chemotaxis and adhesion. Removal of calcified remnants by phagocytosis was delayed and still ongoing in DBA/2, C3H/He, 129S1 and DCC-positive BALB/c 3 days after injury, whereas debridement and formation of a fibrotic scar were much more advanced in C57BL/6, FVB and A/J. Histological characteristics of bone formation were not observed.

Calcification of cardiomyocytes occurs later than 24 h after injury

We examined DCC-resistant C57BL/6 and susceptible C3H/He mice 24 h after freeze–thaw injury by employing highly sensitive, fluorescent calcein staining to determine the time of first appearance and the localization of myocardial calcifications. Both C3H/He (Fig. 3a) and C57BL/6 (data not shown) exhibited lesions with remarkably preserved morphology of myofibers, edema and little inflammatory cell infiltration. Injured myocardium displayed a fainter calcein fluorescence than non-injured myocardium (Fig. 3a). At higher magnification, calcein fluorescence showed a cross-striation pattern consistent with myofilament-bound calcium. In necrotic tissue, the banding pattern appeared patchy and displayed interruptions consistent with a condensation and breakup of necrotic cardiomyocytes (Fig. 3b). Notably, larger circumscribed calcium deposits were absent during the first 24 h after freeze–thaw injury.

Calcified cardiomyocytes were subject to phagocytosis

Phagocyte activity was assessed indirectly by tracking calcein fluorescence of cardiomyocyte remnants in lysosomes of macrophages. These remnants were evident as accumulations of small, green-fluorescent bodies co-localized with the blue-fluorescent, DAPI-stained nuclei of macrophages. DCC-resistant C57BL/6 (Fig. 3c) and susceptible strain C3H/He (Fig. 3d) were compared 3 days after injury. In lesions of C57BL/6, cardiomyocyte remnants disintegrated into small particles exhibiting only very faint calcein fluorescence (the photographic illustration of these cellular remnants was digitally enhanced in Fig. 3c to allow their visualization). These cellular remnants were removed by phagocytosis of macrophages, which were distributed evenly throughout the lesion (Fig. 3c). In C3H/He, the majority of the macrophages appeared to attach to calcified cardiomyocyte remnants, which emitted strong calcein fluorescence (Fig. 3d). We noticed also large macrophages

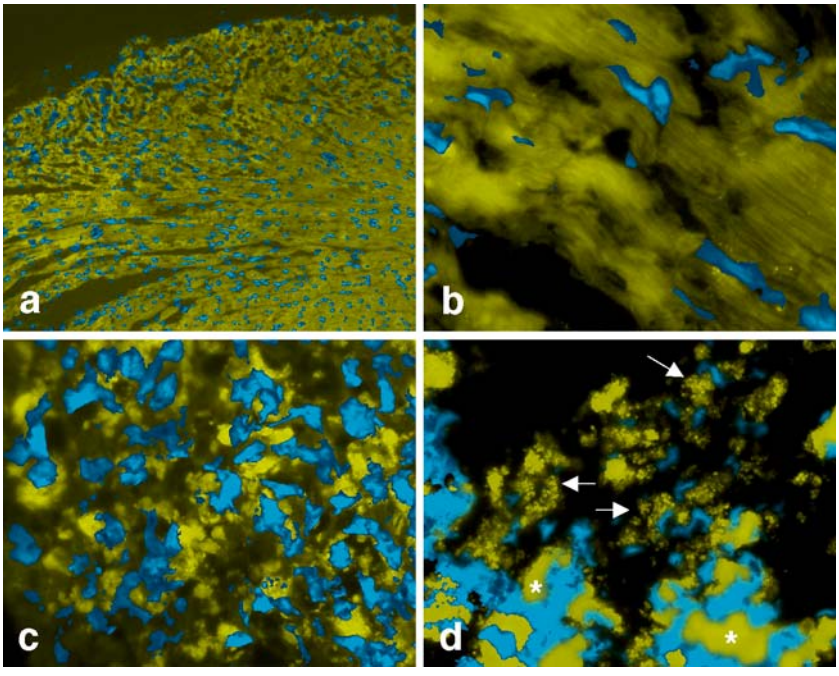

Fig. 3 Morphological changes in C3H/He myocardium 24 h after freeze–thaw injury (**a**, ×100 and **b**, ×1,000). Calcium stained *green-yellow* with calcein, while nucleic acids stained *blue* with DAPI. Activity of phagocytosis 3 days after injury in the lesion perimeter in C57BL/6 (**c** ×1,000) and C3H/He (**d**, ×1,000). Calcified cardiomyocyte remnants (*asterisks*) were surrounded by macrophages (identified indirectly by their blue nuclei), which contained multiple, calcium-positive cell remnants in their lysosomes (*arrows*)

containing multiple vesicles filled with calcein-positive material. Electron microscopy confirmed that this fluorescent material was consistent with calcified cardiomyocyte remnants engulfed by phagocytosis (data not shown). There was no evidence of primary calcium deposition in the extracellular matrix of the lesions.

Mitochondrial calcification precedes calcification of cardiomyocytes

In C57BL/6 and C3H/He, we examined ultrastructural changes occurring 2 to 9 days after freeze–thaw injury to identify the potential initiator of calcification of necrotic

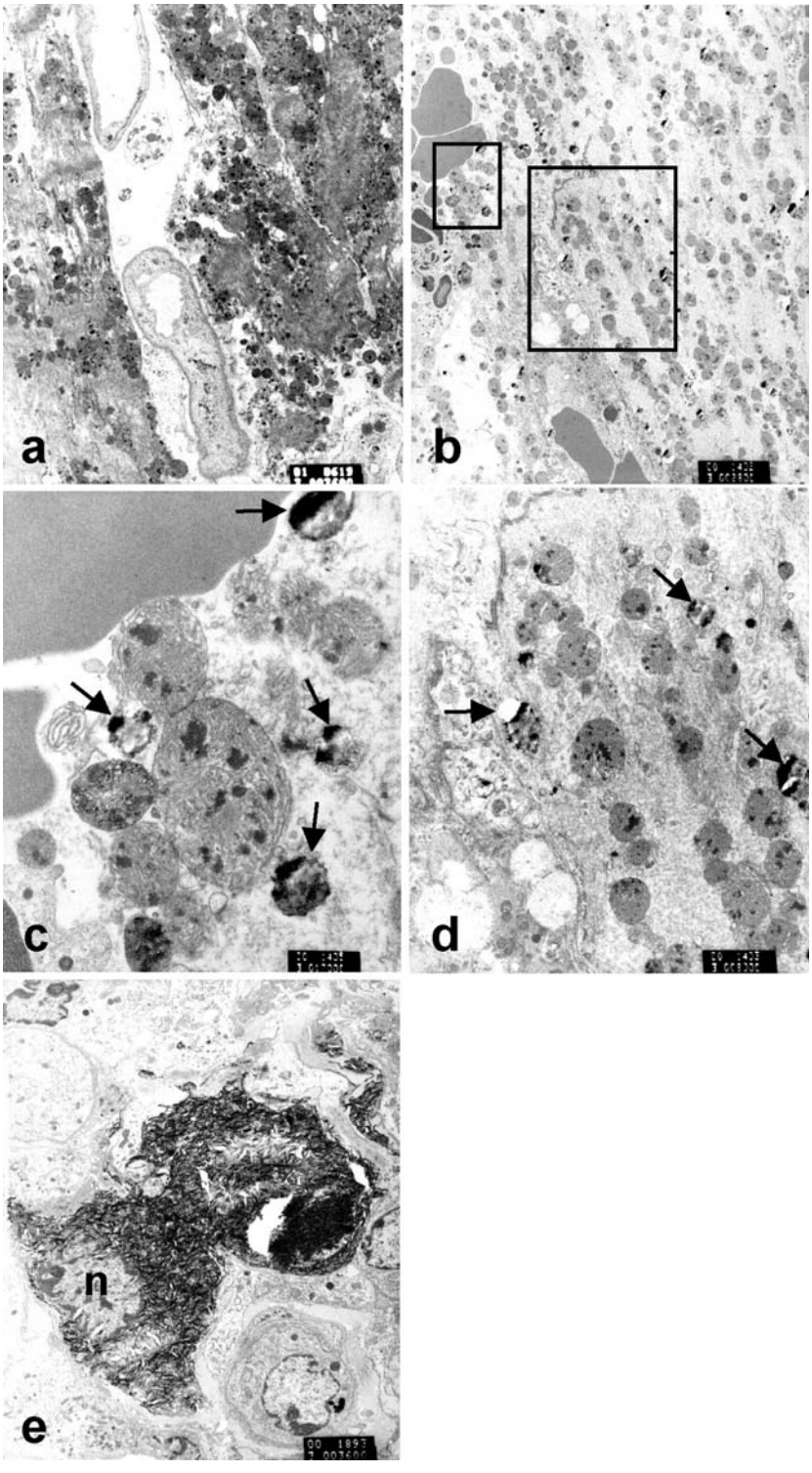

Fig. 4 Ultrastructure of myocardial necrosis in C57BL/6 (**a**, ×8,280) and C3H/He (**b**–**e**) 2 and 7 days after freeze–thaw injury (**a**–**d** and **e**, respectively). Illustrations **c** (×39,100) and **d** (×18,400) are magnifications of areas delineated by *rectangles* in **b** (×6,440). Condensed mitochondria with amorphous calcium phosphate deposits are marked by *arrows* (**c**, **d**). "*n*" labels the nucleus of a cardiomyocyte, which exhibited complete intracellular calcification consistent with the formation of hydroxyapatite crystals (**e**, ×8,280)

cardiomyocytes. Two days after injury, both strains showed cardiomyocyte necrosis with disintegration of myofilaments and other cytoplasmic contents as well as mitochondrial swelling and aggregation. Mitochondria exhibited various sizes and loss of cristae by fragmentation or extrusion (Fig. 4a–d). Multiple amorphous matrix densities were observed in swollen mitochondria of both DCC-resistant C57BL/6 and susceptible C3H/He mice. Closer examination, however, revealed a subset of mitochondria with a different phenotype observed only in strain C3H/He. These mitochondria were small and condensed and exhibited electron-dense granular bodies consistent with amorphous precipitations of calcium phosphate near one of their poles (Fig. 4c,d). Later stages of DCC revealed the formation of hydroxyapatite crystals comprising the entire necrotic sarcoplasm (Fig. 4e). Calcified cardiomyocytes were subject to phagocytosis by macrophages, which exhibited typical lysosomal bodies (data not shown). Polynuclear osteoclasts were not seen.

Discussion

We investigated the response to myocardial necrosis in common laboratory mouse strains to identify strain backgrounds that account for a calcifying phenotype of myocardial infarction or cardiomyopathy in a mouse model. Thus, we focused on the identification of inbred mouse strains susceptible to DCC, rather than presenting a detailed quantitative analysis of wound healing in a single mouse strain. Many experimenters use genetically manipulated mouse models with various mixed genetic backgrounds that may drastically influence the phenotype under study [19]. Such a phenotype is the healing of myocardial infarction, which may involve necrotic calcification in mice with a susceptible background. In this regard, our analysis of various laboratory strains contributed knowledge on inbred mouse strains as experimental models of myocardial diseases. A strain-related, genetically determined susceptibility to DCC was first proposed by Dipaolo et al. [8], who demonstrated spontaneous myopericardial calcification in strains DBA, Swiss ICR and C as well as strains derived from the latter, including C3H, CHI and CBA. DCC was noticed in BALB/c in studies of viral myopericarditis [13] and in NMRI as a result of dietary magnesium and phosphorous imbalances [24]. Even direct freeze–thaw injury of the myocardium may lead to necrotic calcification [4]. Thus, accumulated evidence suggested that DCC required myocyte death irrespective of the nature of the preceding irreversible injury. In contrast, strain C57BL/6 was reported to be resistant to DCC in several studies, because it exhibited a fibrotic lesion devoid of calcific deposits in response to injury.

Including strains used for gene targeting (strain 129S1) or transgenic overexpression studies (strain FVB), several novel findings in this study were presented: (a) We identified the susceptibility to DCC of strain 129S1 and confirmed *Dyscalc1* as the major genetic determinant of DCC in this strain. Interestingly, 129S1 was found previously to exhibit some genetic contamination with C3H that might involve the *Dyscalc1* locus as well [21, 23]. (b) FVB exhibited a resistant phenotype similar to C57BL/6. Consistent with this, there are, to our knowledge, no transgenic mouse models on a FVB background exhibiting necrotic myocardial calcifications. (c) We demonstrated that A/J was almost resistant to DCC. (d) We added chronic ischemic injury by coronary ligation to the list of aetiologies leading to necrotic calcifications in susceptible C3H/He.

DCC is a common response of myocardium to injury in mice

Our results suggested that DCC may be rather common in mice, because four of seven different inbred strains exhibited DCC [21, 23]. The classical laboratory strains have a common *Mus musculus* ancestor, which gave rise to at least six groups or major branches of more closely related strains [28]. One major branch of this mouse family tree included DBA and C3H exhibiting a high penetrance of DCC, while BALB/c and A/J [in which we found a low (one of four mice) and a very low penetrance of DCC, respectively] belonged to a more distally related side branch of the same major branch. The different degrees of penetrance suggested that the genetic basis of DCC is complex and may have arisen early in the history of laboratory mouse breeding [8]. Although most strains were inbred independently, they may share some additional genomic homology due to early interstrain contaminations. Recently, analysis of single nucleotide polymorphisms (SNP) revealed that the genome of substrain 129S1 contained a single, large piece of chromosome 7 (approximately 60 Mb) from DCC-susceptible C3HeB/FeJ [20]. This chromosomal piece includes *Dyscalc1* and may therefore explain the susceptibility to DCC of 129S1. This hypothesis remains to be confirmed in other potentially DCC-resistant substrains of 129 which have not been contaminated. Therefore, the determination of susceptibility to DCC in many different strains may provide the opportunity to locate and identify the causative genes by ancestral haplotype mapping [7, 27]. The availability of increasingly dense SNP maps will greatly facilitate *in silico* mapping of quantitative trait loci in the future.

The development of DCC

To understand the mechanisms leading to DCC, we employed several histological techniques to determine time and location of the initial calcification. Our results compared well to data reported previously [3]. Within the first 24 h after freeze–thaw injury, lesions exhibited little cell infiltration. Although cardiomyocytes remained mostly intact in peripheral lesion areas, sensitive, fluorescent calcium staining revealed the beginning of disintegration of myofilaments. Necrotic and vital cardiomyocytes were distributed heterogeneously in this lesion area. Even on the cellular level, necrotic cardiomyocytes exhibited various

stages of disintegration of their cytoplasmic content. Swollen mitochondria contained matrix densities and formed intracellular aggregates. In C3H/He, however, some mitochondria exhibited also electron-dense calcific deposits and complete mineralization 2 days after injury. After ≥3 days, mineralization has proceeded to comprise the entire cardiomyocyte, which was still delineated by basal lamina [25, 26]. The process of calcium deposition may have occurred very rapidly, because we did not observe partial sarcoplasmic calcification as seen by others [3]. It is possible that calcified mitochondria may have served as a nidus for further calcium precipitation once the local calcium × phosphate solubility product was exceeded. Mitochondrial mineralization was implicated previously as the initial event in the development of DCC [3]. Mitochondria sequester calcium, protecting the cell against toxic intracellular calcium concentrations following injury. Pathways of apoptosis and calcium homeostasis as well as mitochondrial channel and matrix proteins may be involved in the initial events of necrotic calcification. In this regard, our study is limited, since we have not examined specific candidate genes. Further studies of apoptosis should include the examination of B-cell-activated X-protein, Bax, which is a major pro-apoptotic switch. *Bax* is an interesting candidate gene, because its locus is closely linked to the *Dyscalc1* locus.

The tissue response to cardiomyocyte calcification included removal by phagocytosis and "neutralisation" by fibrosis. At day 3 after injury, macrophage-like cells adhered to calcified necrotic tissue presumably attracted and immobilized by the calcium-binding, chemotactic protein osteopontin that is expressed strongly in calcified myocardial lesions [1]. Although we have seen large macrophages containing calcified cell remnants, debridement appeared delayed in DCC-susceptible compared to resistant strains. Based on our morphological evidence, we consider this difference a consequence of the calcification of the necrotic cardiomyocytes. Presumably, more effective phagocytosis of calcified necrosis may have required osteoclasts, a highly specialized macrophage population, which was absent in the lesions. A week after injury, fibroblasts surrounded calcified cardiomyocyte remnants. At this point, increasing fibrosis may have insulated myocardial calcifications from phagocytes, preserving them for many weeks [14]. Further investigations are needed to clarify whether phagocytosis was impaired by a malfunction, an exhausted capacity (relative insufficiency), or by excessive fibrosis, and to what extent such an abnormality may have contributed to DCC.

Acknowledgements We thank Mrs. Scheurer for assistance in histological sectioning and staining. We are very thankful to Prof. E. Schramm, who carried out electron microscopy, and to Dr. Klinger and Dr. Berger for discussions of the ultrastructural data. We are indebted to Dr. Aherrahrou and Mr. Kaczmarek for assistance in work related to the model of ischemic injury and other mouse work. This work was supported by grants Iv10/3-1 and Iv10/3-2 of the Deutsche Forschungsgemeinschaft DFG.

References

1. Aherrahrou Z, Axtner SB, Kaczmarek PM, Jurat A, Korff S, Doehring LC, Weichenhan D, Katus HA, Ivandic BT (2004) A locus on chromosome 7 determines dramatic up-regulation of osteopontin in dystrophic cardiac calcification in mice. Am J Pathol 164:1379–1387
2. Brean HP, Marks JH, Sosman MC, Schlesinger MJ (1950) Massive calcification in infarcted myocardium. Radiology 54:33–42
3. Brunnert SR (1997) Morphologic response of myocardium to freeze–thaw injury in mouse strains with dystrophic cardiac calcification. Lab Anim Sci 47:11–18
4. Brunnert SR, Altman NH (1990) Dystrophic cardiac calcinosis in mice: abnormal myocardial response to freeze–thaw injury. Lab Anim Sci 40:616–619
5. Brunnert SR, Shi S, Chang B (1999) Chromosomal localization of the loci responsible for dystrophic cardiac calcinosis in DBA/2 mice. Genomics 59:105–107
6. Dahl LK (1952) A simple and sensitive histochemical method for calcium. Proc Soc Exp Biol Med 80:474–479
7. Darvasi A (2001) In silico mapping of mouse quantitative trait loci. Science 294:2423
8. Dipaolo JA, Strong LC, Moore GE (1964) Calcareous pericarditis in mice of several genetically related strains. Proc Soc Exp Biol Med 115:496–497
9. Eaton GJ, Custer RP, Johnson FN, Stabenow KT (1978) Dystrophic cardiac calcinosis in mice: genetic, hormonal, and dietary influences. Am J Pathol 90:173–186
10. Everitt JI, Olson LM, Mangum JB, Visek WJ (1988) High mortality with severe dystrophic cardiac calcinosis in C3H/OUJ mice fed high fat purified diets. Vet Pathol 25:113–118
11. Everitt JI, Ross PW, Neptun DA, Mangum JB (1988) Effect of a purified diet on dystrophic cardiac calcinosis in mice. Lab Anim Sci 38:426–429
12. Fatkin D, Christe ME, Aristizabal O, McConnell BK, Srinivasan S, Schoen FJ, Seidman CE, Turnbull DH, Seidman JG (1999) Neonatal cardiomyopathy in mice homozygous for the Arg403Gln mutation in the alpha cardiac myosin heavy chain gene. J Clin Invest 103:147–153
13. Gang DL, Barrett LV, Wilson EJ, Rubin RH, Medearis DN (1986) Myopericarditis and enhanced dystrophic cardiac calcification in murine cytomegalovirus infection. Am J Pathol 124:207–215
14. Ivandic BT, Qiao JH, Machleder D, Liao F, Drake TA, Lusis AJ (1996) A locus on chromosome 7 determines myocardial cell necrosis and calcification (dystrophic cardiac calcinosis) in mice. Proc Natl Acad Sci U S A 93:5483–5488
15. Ivandic BT, Utz HF, Kaczmarek PM, Aherrahrou Z, Axtner SB, Klepsch C, Lusis AJ, Katus HA (2001) New Dyscalc loci for myocardial cell necrosis and calcification (dystrophic cardiac calcinosis) in mice. Physiol Genomics 6:137–144
16. Mavroidis M, Capetanaki Y (2002) Extensive induction of important mediators of fibrosis and dystrophic calcification in desmin-deficient cardiomyopathy. Am J Pathol 160:943–952
17. McConnell BK, Jones KA, Fatkin D, Arroyo LH, Lee RT, Aristizabal O, Turnbull DH, Georgakopoulos D, Kass D, Bond M, Niimura H, Schoen FJ, Conner D, Fischman DA, Seidman CE, Seidman JG, Fischman DH (1999) Dilated cardiomyopathy in homozygous myosin-binding protein-C mutant mice. J Clin Invest 104:1235–1244
18. Michael LH, Entman ML, Hartley CJ, Youker KA, Zhu J, Hall SR, Hawkins HK, Berens K, Ballantyne CM (1995) Myocardial ischemia and reperfusion: a murine model. Am J Physiol 269:H2147–H2154
19. Montagutelli X (2000) Effect of the genetic background on the phenotype of mouse mutations. J Am Soc Nephrol 11:S101–S105

20. Petkov PM, Ding Y, Cassell MA, Zhang W, Wagner G, Sargent EE, Asquith S, Crew V, Johnson KA, Robinson P, Scott VE, Wiles MV (2004) An efficient SNP system for mouse genome scanning and elucidating strain relationships. Genome Res 14:1806–1811
21. Simpson EM, Linder CC, Sargent EE, Davisson MT, Mobraaten LE, Sharp JJ (1997) Genetic variation among 129 substrains and its importance for targeted mutagenesis in mice. Nat Genet 16:19–27
22. Thornell L, Carlsson L, Li Z, Mericskay M, Paulin D (1997) Null mutation in the desmin gene gives rise to a cardiomyopathy. J Mol Cell Cardiol 29:2107–2124
23. Threadgill DW, Yee D, Matin A, Nadeau JH, Magnuson T (1997) Genealogy of the 129 inbred strains: 129/SvJ is a contaminated inbred strain. Mamm Genome 8:390–393
24. van den Broek FA, Beynen AC (1998) The influence of dietary phosphorus and magnesium concentrations on the calcium content of heart and kidneys of DBA/2 and NMRI mice. Lab Anim 32:483–491
25. Vracko R, Cunningham D, Frederickson RG, Thorning D (1988) Basal lamina of rat myocardium. Its fate after death of cardiac myocytes. Lab Invest 58:77–87
26. Vracko R, Thorning D, Frederickson RG, Cunningham D (1988) Myocyte reactions at the borders of injured and healing rat myocardium. Lab Invest 59:104–114
27. Wade CM, Kulbokas EJ III, Kirby AW, Zody MC, Mullikin JC, Lander ES, Lindblad-Toh K, Daly MJ (2002) The mosaic structure of variation in the laboratory mouse genome. Nature 420:574–578
28. Witmer PD, Doheny KF, Adams MK, Boehm CD, Dizon JS, Goldstein JL, Templeton TM, Wheaton AM, Dong PN, Pugh EW, Nussbaum RL, Hunter K, Kelmenson JA, Rowe LB, Brownstein MJ (2003) The development of a highly informative mouse simple sequence length polymorphism (SSLP) marker set and construction of a mouse family tree using parsimony analysis. Genome Res 13:485–491

Virchows Arch (2006) 448: 639–643
DOI 10.1007/s00428-006-0158-9

CASE REPORT

Alberto Zamò · Roberta Zanotti · Maurizio Lestani · German Ott · Tiemo Katzenberger · Aldo Scarpa · Giovanni Pizzolo · Fabio Menestrina · Marco Chilosi

Molecular characterization of composite mantle cell and follicular lymphoma

Received: 3 October 2005 / Accepted: 8 January 2006 / Published online: 21 February 2006

Abstract Composite lymphomas are rare associations of two distinct lymphoma types at the same anatomical site. Reporting of such cases is important because they pose major biologic, diagnostic, and therapeutic dilemmas. In this study, we describe the third reported case of mantle cell and follicular lymphoma. We performed accurate immunohistochemical and molecular studies to define the mono- vs biclonal nature of this neoplasm. We used both manual and LASER-capture microdissection combined to multiple molecular approaches for clonality determination, including detection of heavy and light chain recombination, as well as presence of κ/Kde recombination and sequence analysis. By immunohistochemistry and FISH, we confirmed the presence of two distinct lymphoma types characterized by specific translocations [namely, t(11;14) and t(14;18)], while we demonstrated two distinct and not clonally related cell populations by molecular techniques. The light chain approach, and particularly the kappa and κ/Kde recombination detection, proved very useful for solving the clonality issue.

Keywords Composite lymphoma · Mantle cell lymphoma · Follicular lymphoma · Laser-capture microdissection · Clonality

A. Zamò (✉) · M. Lestani · A. Scarpa · F. Menestrina · M. Chilosi
Department of Pathology, University of Verona, Strada Le Grazie, 8, 37134 Verona, Italy
e-mail: alberto.zamo@univr.it
Tel.: +39-045-8027693
Fax: +39-045-8027136

R. Zanotti · G. Pizzolo
Department of Clinical and Experimental Medicine, Section of Hematology, University of Verona, Verona, Italy

G. Ott · T. Katzenberger
Department of Pathology, University of Würzburg, Würzburg, Germany

Introduction

Only two cases of composite mantle cell (MCL) and follicular (FL) lymphoma have been described from two different groups [7, 11]. In this study, we describe a third case of composite MCL and FL, which showed a particular clinical course that distinguishes it from the two previously reported. This case has been extensively immunophenotyped, characterized using fluorescence in situ hybridization (FISH) probes, and then studied at the molecular level using multiple PCR-based approaches, manual and LASER-assisted microdissection, and sequence analysis. These techniques allowed us to verify the diagnosis and to clarify that the two entities are not clonally related.

Materials and methods

Case history A 65-year-old man presented with persistent left inguinal adenopathy in May 2001. Laboratory tests showed a mild lymphocytosis (6.7×10^9/l). A lymph node biopsy, bone marrow biopsy, and immunophenotypical study of peripheral blood were performed. In October 2003, the patient underwent splenectomy. At the last follow-up in November 2005, the patient was in a good condition despite the stable condition of his disease, with a WBC count of 36.9×10^9/l (neutrophils 8.0×10^9/l, lymphocytes 20.1×10^9/L).

Immunohistochemistry Antibodies used were CD3 (SP7, Labvision), CD5 (4C7, Novocastra), CD10 (56C6, Novocastra), CD20 (L26, Dako), CD23 (1B12, Novocastra), CD79a (JCB117, Dako), Bcl-2 (124, Dako), Cyclin D1 (SP4, Neomarkers), and p27 (SX5348, Dako). Immunostaining was performed using a semiautomated cell-staining system (GenoMx i6000, Biogenex, San Ramon, CA, USA). For a more precise characterisation, $p27^{KIP1}$ staining was used in addition to the standard panel of markers [5]. For cyclin D1 staining, a newly available rabbit monoclonal antibody with superior performance was used [4].

Western blotting for cyclin D1 Immunoblot analysis for cyclin D1 (Cyclin D1 H295 rabbit polyclonal antibody, Santa Cruz Biotechnology, Santa Cruz, CA, USA) was performed by standard procedures on the peripheral blood (PB) cells, alongside with positive (Granta-519 MCL cell line, obtained from DSMZ, Braunschweig, Germany) and negative (a case of FL) controls.

Extraction of DNA from peripheral blood and spleen samples DNA was obtained from 10^7cells (peripheral blood) or 3 mg of frozen tissue (spleen) by standard proteinase K digestion and phenol–chloroform extraction.

Microdissection All microdissection experiments were performed on formalin-fixed and paraffin-embedded tissue sections of the lymph node sample. Manual microdissection was performed using a sterile 25-gauge needle. Laser-capture microdissection (LCM) was performed on a PixCell II instrument (Arcturus, Mountain View, CA, USA). Neoplastic follicles, perifollicular areas, and the diffuse component were discriminated morphologically on hematoxylin and eosin stained slides. The center of three or four follicles and corresponding perifollicular areas, as well as about 300 cells from the diffuse component, were microdissected in three independent sessions. For immuno-LCM (I-LCM), slides were first stained for CD10 or cyclin D1 before LCM. Microdissected tissue was digested in 50 μl lysis buffer. The presence of amplifiable DNA was tested by PCR amplification of *c-KIT* exon 8 (protocol details available from the authors upon request).

Detection of t(14;18) by PCR BCL-2 translocation was detected by PCR as previously described [3], with some modifications.

Clonality detection Detection of rearranged *Ig* genes was performed using the FR1, FR2, and FR3A approach for heavy chain (IgH) as previously described [2, 9], and the FR3 approach was used for light chains [6]. For the Vκ/kappa-deleting element (Kde) approach, we used the same Vκ primers combined with one Kde primer. We used a primer designed with DNAsis Max software (Hitachi software, Hamburg, Germany) using GenBank X05286 sequence. Primer sequence is TGC TCG CCT AGT CCT CAT CT. Amplification products were either run on 6% acrylamide gels or on an Agilent 2100 bioanalyzer (Agilent Technologies, Waldbronn, Germany). For heteroduplex analysis, samples were denatured at 95°C for 5′ and then cooled at 4°C for 1 h. Purified products were either directly sequenced or after cloning using the pSTBlue-1 Giga kit (Novagen, Madison, WI, USA). Sequences were compared using DNAsis Max software (Hitachi software); gene usage was analyzed using IgBLAST database [1].

FISH FISH studies for the t(11;14) and t(14;18) were performed by standard procedures (details available upon request) on paraffin sections of the lymph node sample, using commercially available probes (LSI IGH/CCND1 and LSI IgH/BCL2, Abbott GmbH) according to manufacturer's instructions.

Sequence analysis Sequence analysis was performed using BigDye 3.1 chemistry and ABI 310 automated sequencer (details available upon request).

Results

Histology and immunophenotype The lymph node presented an effaced architecture, with an evident follicular pattern of infiltration; the neoplastic follicles lacked polarity and tingible body macrophages and were composed of small cells with centrocytic morphology. Few nonneoplastic follicles were present, mostly at the periphery. On one side, a band-like nodular and diffuse area was present; this rim was separated from the follicular component by a thin fibrous band (Fig. 1). The follicular component showed a classic FL phenotype (CD20+, CD79a+, CD10+, BCL-2+, CD5−, CD23−, cyclin D1−, p27+), while the peripheral nodules showed MCL markers (CD20+, CD79a+, CD5+, CD10−, CD23−, cyclin D1+, p27−) (Fig. 2). Interfollicular areas were mostly CD5+ and showed a distinct cyclin D1 staining on many cells, especially at the periphery of neoplastic follicles (mantle zone pattern) (Fig. 2). Proliferative activity, ascertained by Ki-67 staining, was almost absent in the follicles and low in the perifollicular area and peripheral nodules.

The bone marrow trephine showed an interstitial and nodular infiltration by small intermediate cells. Cells were CD20+, CD5+, and p27 negative.

The spleen showed a marked nodular infiltration by cells of variable size; these elements were present also in the portal tracts of the liver biopsy. The immunophenotype was typical for MCL, including cyclin D1 expression.

The PB immunophenotype by flow cytometry was CD20+, CD5+, CD23−, λ+, CD79a+, CD10−. Western blotting was positive for cyclin D1.

Fish FISH analysis was performed on the lymph node and showed that in the MCL area 36% of cells harbored the t(11;14)(q13;q32), while a minority showed the t(14;18)(q32;q21). In the FL area, 42% of cells had evidence of the t(14;18)(q32;q21) and 35% of the cells harbored the t(11;14)(q13;q32) (Fig. 3).

PCR detection of t(14;18) BCL-2 translocation was evident by PCR on the follicular component of the manually microdissected sample but absent from all the MCL components (lymph node, spleen, and peripheral blood).

Microdissection and clonality detection of the lymph node A first round of analyses, including FR1, FR2, and FR3A VH approaches performed on DNA obtained from whole sections or manually microdissected samples and on the peripheral blood DNA, showed a single amplifiable clonal band. A second round of experiments, including only

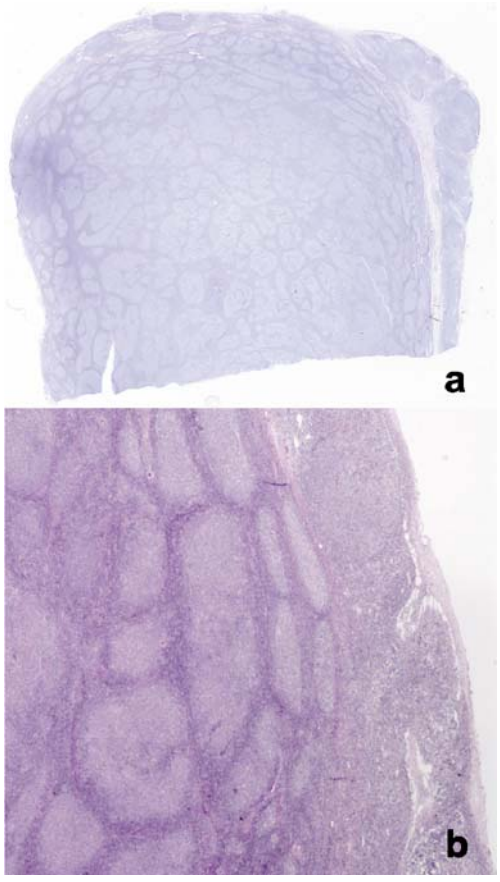

Fig. 1 Histology. **a** Low power view (1×, PAS stain) shows the larger follicular area and the rim containing broad nodules. **b** Medium power view (100×, H&E stain) at the border between the follicular area and the peripheral rim containing the broad coalescent nodules

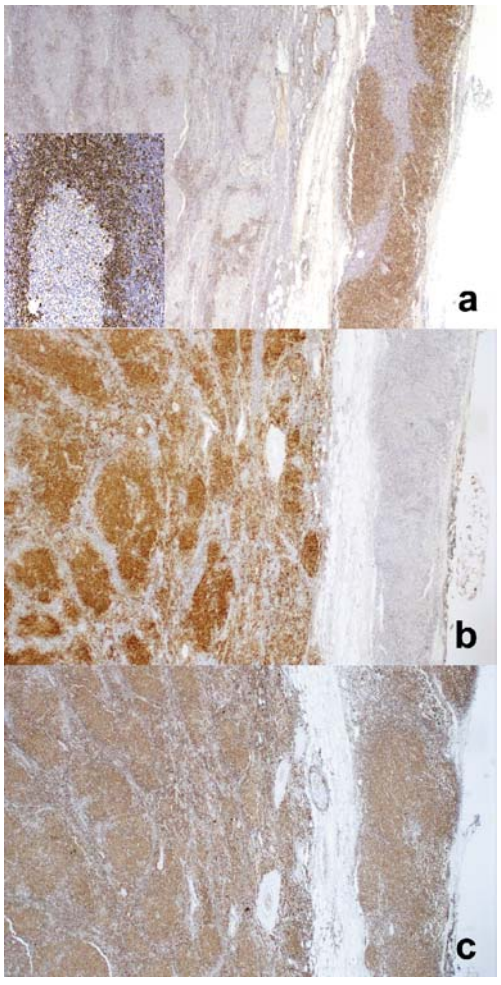

Fig. 2 Immunohistochemistry. **a** Cyclin D1 is positive both in the broad nodules and in the perifollicular areas (also depicted in the *inset*) (100×, inset 200×). **b** CD10 is positive in the follicles and negative in the MCL area. **c** Bcl-2 is positive in the follicles and also in the MCL area; one residual reactive follicle is negative

FR3A, kappa and lambda rearrangements with careful cell selection by immuno-LASER-capture microdissection, showed that despite the presence of amplifiable DNA, no FR3A product in the FL component was obtained (Fig. 4a). Using the light chain approach, a clonal band for kappa was visible only in the FL samples (Fig. 4b). On the contrary, all the MCL components (peripheral nodules and perifollicular areas in the lymph node, neoplastic nodules in the spleen, and DNA from peripheral blood) were kappa-negative and positive for the lambda and kappa/Kde rearrangement. Sequence analysis showed that the rearranged κ gene in the FL component was A23, while the κ gene rearranged to the Kde region in the MCL component was L14. Further sequence analysis of the FR1 products of the MCL component showed the VH4-34/D2-15, with a 3% somatic mutation rate.

Discussion

Based on reported frequencies, composite MCL and FL is extremely rare, this report representing the third recognized case [7, 11]. In accordance to previous reports, our case followed an indolent course. FL and MCL were present simultaneously, but progression was due to the MCL component exclusively, with progressive increase of spleen size, mild lymphocytosis, and thrombocytopenia. However, 1 year after splenectomy, the condition of the disease remains stable and relatively controlled, with mild lymphocytosis.

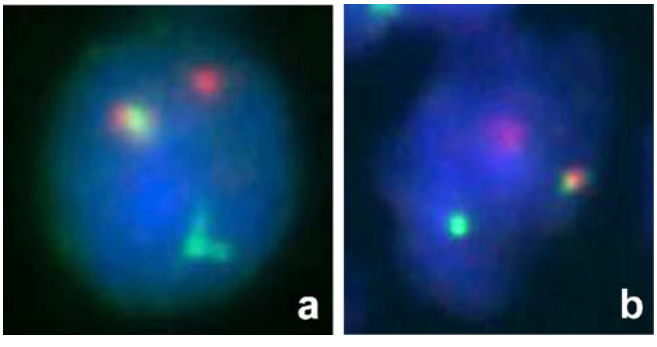

Fig. 3 FISH. **a** t(11;14), **b** t (14;18)

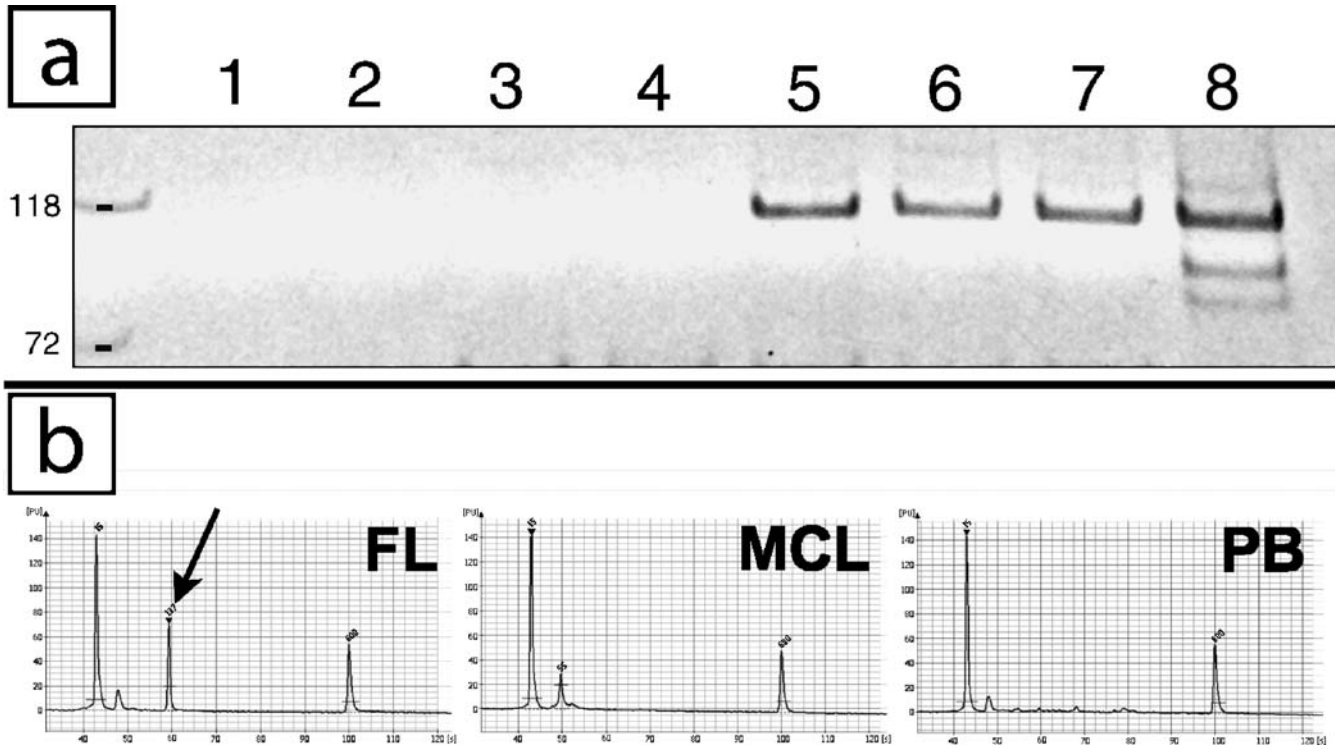

Fig. 4 Most relevant molecular biology data. **a** FR3 amplification of rearranged immunoglobulin heavy chain genes shows a product only in peripheral blood (*lane 8*) and MCL areas, both peripheral (*lane 5*) and perifollicular (*lanes 6* and *7*). FL areas (*lanes 1* to *4*) do not show any product, despite the presence of amplifiable DNA (not shown). (PCR products run on polyacrylamide gel) **b** Light chain FR3 amplification shows that kappa rearrangement is present only in the FL component (*arrow*), while it is absent in the MCL component, both in tissue and peripheral blood. (PCR products run on Agilent 2100 bioanalyzer; first and last peaks: size markers, 15 and 600 bp, respectively; small peaks after 15 bp peak: primers)

Histologically, all the cases reported share the common pattern of MCL cells surrounding neoplastic FL follicles, in addition to more diffuse areas. In our case, the MCL cells also formed a separate rim at the node periphery, reminiscent of a "node in node." The cytology of our case and that of other cases was classical, with no evidence for blastoid transformation.

Immunohistochemically, all cases are quite typical, except for the lack of demonstrable cyclin D1 protein expression in the cases reported by the other groups. Tsang and colleagues, however, demonstrated presence of the t(11;14) by Southern blot. Our case is more straightforward, as the expression of cyclin D1 was readily demonstrated by immunohistochemistry on both lymph node and spleen specimens, and by Western blotting on the PB sample. These data were further supported by the unequivocal demonstration of the t(11;14) and t(14;18) by FISH in the two neoplastic components.

The issue of clonality is a very intriguing one, and as expected, it is a matter of debate [8]. The group of Tsang et al. brought evidence favoring the hypothesis of monoclonality, while the group of Fend et al. stated that unless a very careful microdissection is performed, a minor clonal component might be missed. In fact, as clearly shown by cyclin D1 staining, neoplastic follicles can be surrounded and often partially infiltrated by MCL cells, whose DNA is readily amplifiable and can thus take over on the poorly primed (due to somatic hypermutations) FL DNA. We therefore used multiple microdissection techniques, and only when we carefully captured CD10+ and cyclin D1+ cells by immuno-LASER-capture microdissection did we not obtain a PCR product for rearranged VH genes in the FL component, despite the presence of amplifiable DNA. However, the strongest proof in favor of a biclonal origin was provided by the use of the light chain FR3 and κ/Kde PCR. Using these techniques, we were able to demonstrate a rearranged κ chain only in the FL component. We also demonstrated that the MCL component deleted the κ allele by juxtaposing the Kde to a V κ gene, a rearrangement that would render the rearrangement nonamplifiable by standard techniques [10]. Indeed, the κ V segment juxtaposed to the Kde (L14) in the MCL component is different from the one that appears to be rearranged in the FL component (A23), thus providing the final proof of the true biclonality of this unusual composite neoplasm.

The usefulness of the κ and κ/Kde approach has been stated by a multicenter study, although using different primers [12]. The aforementioned study on the light chain FR3 approach [6] does not suppose the use of a Kde primer. We actually combined the two approaches, optimizing conditions to work with the kappa FR3 primers. This might provide a simple solution to the issue of clonality detection in composite lymphomas, even without the use of high-cost LASER-capture microdissection.

Acknowledgements Sources of support: Supported in part by Associazione Italiana Ricerca sul Cancro (AIRC, Milan) and Fondazione Cariverona. All the experiments done for this work comply with the laws of the country in which they were performed.

References

1. IgBLAST, NCBI: Bethesda, MD. p. database online
2. Achille A, Scarpa A, Montresor M, Scardoni M, Zamboni G, Chilosi M, Capelli P, Franzin G, Menestrina F (1995) Routine application of polymerase chain reaction in the diagnosis of monoclonality of B cell lymphoid proliferations. Diagn Mol Pathol 4:14–24
3. Albinger-Hegyi A, Hochreutener B, Abdou MT, Hegyi I, Dours-Zimmermann MT, Kurrer MO, Heitz PU, Zimmermann DR (2002) High frequency of t(14;18)-translocation breakpoints outside of major breakpoint and minor cluster regions in follicular lymphomas: improved polymerase chain reaction protocols for their detection. Am J Pathol 160:823–832
4. Cheuk W, Wong KO, Wong CS, Chan JK (2004) Consistent immunostaining for cyclin D1 can be achieved on a routine basis using a newly available rabbit monoclonal antibody. Am J Surg Pathol 28:801–807
5. Chiarle R, Budel LM, Skolnik J, Frizzera G, Chilosi M, Corato A, Pizzolo G, Magidson J, Montagnoli A, Pagano M, Maes B, De Wolf-Peeters C, Inghirami G (2000) Increased proteasome degradation of cyclin-dependent kinase inhibitor p27 is associated with a decreased overall survival in mantle cell lymphoma. Blood 95:619–626
6. Diss TC, Liu HX, Du MQ, Isaacson PG (2002) Improvements to B cell clonality analysis using PCR amplification of immunoglobulin light chain genes. Mol Pathol 55:98–101
7. Fend F, Quintanilla-Martinez L, Kumar S, Beaty MW, Blum L, Sorbara L, Jaffe ES, Raffeld M (1999) Composite low grade B cell lymphomas with two immunophenotypically distinct cell populations are true biclonal lymphomas. A molecular analysis using laser capture microdissection. Am J Pathol 154: 1857–1866
8. Fend F, Quintanilla-Martinez L, Raffeld M (2000) Composite lymphoma. Hum Pathol 31:626–627
9. Kuppers R, Zhao M, Hansmann ML, Rajewsky K (1993) Tracing B cell development in human germinal centres by molecular analysis of single cells picked from histological sections. EMBO J 12:4955–4967
10. Perfetti V, Vignarelli MC, Palladini G, Navazza V, Giachino C, Merlini G (2004) Insights into the regulation of immunoglobulin light chain gene rearrangements via analysis of the kappa light chain locus in lambda myeloma. Immunology 112:420–427
11. Tsang P, Pan L, Cesarman E, Tepler J, Knowles DM (1999) A distinctive composite lymphoma consisting of clonally related mantle cell lymphoma and follicle center cell lymphoma. Hum Pathol 30:988–992
12. van Dongen JJ, Langerak AW, Bruggemann M, Evans PA, Hummel M, Lavender FL, Delabesse E, Davi F, Schuuring E, Garcia-Sanz R, van Krieken JH, Droese J, Gonzalez D, Bastard C, White HE, Spaargaren M, Gonzalez M, Parreira A, Smith JL, Morgan GJ, Kneba M, Macintyre EA (2003) Design and standardization of PCR primers and protocols for detection of clonal immunoglobulin and T cell receptor gene recombinations in suspect lymphoproliferations: report of the BIOMED-2 Concerted Action BMH4-CT98-3936. Leukemia 17:2257–2317

Virchows Arch (2006) 448: 644–647
DOI 10.1007/s00428-006-0169-6

CASE REPORT

A. Makino · S. Serra · R. Chetty

Composite adenocarcinoma and large cell neuroendocrine carcinoma of the rectum

Received: 30 November 2005 / Accepted: 30 January 2006 / Published online: 1 March 2006

Abstract Composite glandular-endocrine tumors of the gastrointestinal tract are rare neoplasms. Even more uncommon are the so-called amphicrine tumors, lesions in which dual epithelial and endocrine differentiation occurs in the same cell. We describe a patient who complained of rectal pain and bleeding with a mixed or composite adenocarcinoma and neuroendocrine carcinoma of the rectum. Histological examination revealed a distinct adenocarcinoma of conventional type with glandular structures admixed intimately with a neuroendocrine carcinoma. The latter component was deeply infiltrative, while the adenocarcinoma occupied the more superficial aspect of the tumor. What was interesting was the immunophenotype of the lesion: cytokeratin (CK) 20 expression was very focal in the adenocarcinoma component and negative in the neuroendocrine carcinoma, while CK 7 was expressed strongly in the adenocarcinoma and only focally in the neuroendocrine component. This cytokeratin profile suggests a possible origin from the anal transitional zone.

Keywords Rectum · Adenocarcinoma · Neuroendocrine carcinoma · Combined carcinoma · Cytokeratin

Introduction

Tumors composed of both glandular and endocrine components are rare and were given a somewhat confusing and misleading collection of terminologies. Basically, these dual-natured tumors can be divided into three subtypes as proposed by Lewin [10] in 1987: composite (mixed) tumors, collision tumors, and amphicrine tumors. The term mixed or composite tumor applies to those neoplasms that contain intimately mixed glandular and endocrine components in near equal proportions. The term "collision" applies when glandular and endocrine components are closely juxtaposed but the individual cell types are not mixed. Lastly, Lewin [10] emphasized that the term "amphicrine" should be used only when dual differentiation was present within the same cell.

Cases of amphicrine tumors in the rectum are not yet encountered, although there are a few isolated reports describing the presence of such tumors in other sites of the gastrointestinal (GI) tract [10, 14–17, 19]. Composite carcinomas, on the other hand, are usually a mixture of adenocarcinoma with carcinoid or an atypical carcinoid [1, 8, 9, 11, 13, 16]. We report a case of a composite carcinoma of the rectum consisting of conventional adenocarcinoma and large cell neuroendocrine carcinoma and review the literature on these uncommon neoplasms.

A. Makino · S. Serra · R. Chetty (✉)
Department of Pathology, University Health Network,
Princess Margaret Hospital,
610 University Avenue, Fourth Floor, Suite 302, Room 312,
Toronto, ON M5G 2M9, Canada
e-mail: runjan.chetty@uhn.on.ca
Fax: +1-416-9466579

A. Makino · S. Serra · R. Chetty
Toronto Medical Laboratories, University of Toronto,
Toronto, Canada

Clinical features

A 94-year-old Caucasian woman presented with rectal bleeding and pain of a few weeks duration. Colonoscopy revealed hemorrhoids and a large ulcerative lesion 1.5 cm from the anal verge that was biopsied. Subsequently, an abdominoperineal resection (the anal verge was not included in the resection specimen) was performed from which the patient made an uneventful recovery. In view of the patient's age, no further treatment was offered.

Materials and methods

The specimen was fixed in 10% formal saline, routinely processed, and hematoxylin and eosin stain sections were evaluated. Immunohistochemistry was performed on paraffin embedded, formalin fixed tissue for the following antibodies: cytokeratin (CK) 7 (monoclonal, OV-TL 12/30,

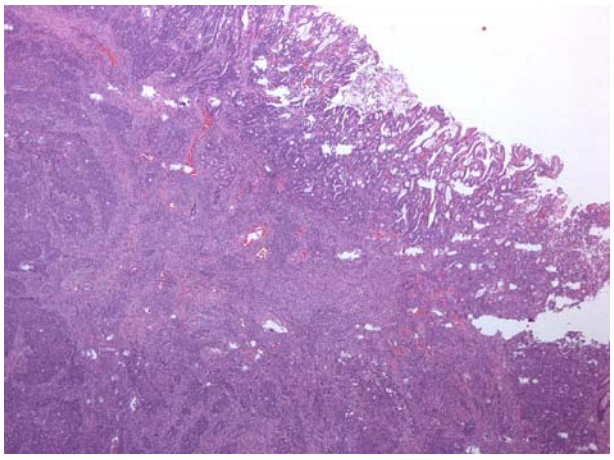

Fig. 1 Low power illustrating the conventional adenocarcinoma occupying the superficial aspects of the tumor while the more solid, sheet-like component is present in the deep aspects of the lesion (H&E×50)

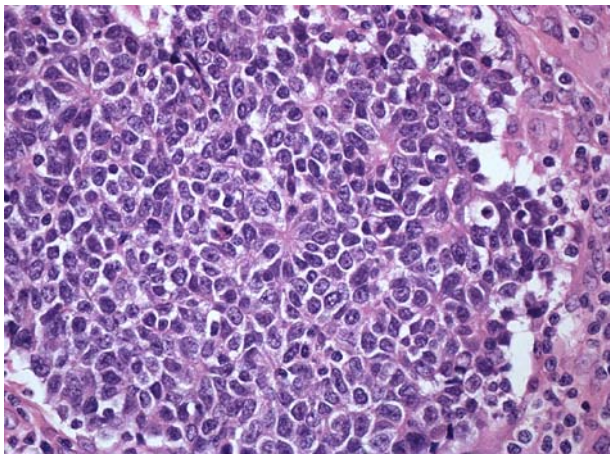

Fig. 3 The large cell neuroendocrine component consisted of large polygonal to round cells with focal rosette formation (H&E×400)

Dakocytomation, Ontario, Canada, dilution 1 in 2,000), CK 20 (Dakocytomation, KS 208 1/100), chromogranin (monoclonal, LK2H10, Biomeda, Foster City, CA, USA, 1/400), synaptophysin (polyclonal, 27G12, Dakocytomation, 1/10), CD56 (monoclonal, 123C3, Zymed, San Francisco, CA, USA, 1/100), and carcinoembryonic antigen (CEA) (monoclonal, Biomeda, 1/5,000).

Tissue from the formalin-fixed paraffin wax block was taken for electron microscopic examination.

Pathology

The resection specimen consisted of a 20-cm segment of the bowel including the rectum. On opening the specimen, a slightly elevated tumor measuring 6.0×3.0×1.5 cm was present. The lesion was very clear of both proximal and distal resection margins.

Histological examination showed a tumor composed of two elements (Fig. 1). Approximately 60% of the tumor was composed of an adenocarcinoma in which glandular structures were easily identified (Fig. 2). Surface epithelium displayed foci of both high-grade and low-grade dysplasia. At the base of the tumor, intimately admixed with the adenocarcinomatous component, were nests and sheets of large tumor cells (Fig. 3). This second component consisted of large round to polygonal cells with salt and pepper nuclear chromatin, occasional prominent nucleoli, and a moderate amount of eosinophilic cytoplasm. The mitotic rate was in excess of 10 mitoses per 10 high power fields. Foci of single cell necrosis or apoptosis and more confluent areas of coagulative tumor necrosis were also identified. Focally, rosette formation was noted (Fig. 3). A small cell component was not present. The morphological features of the second component conformed to that of a large cell neuroendocrine carcinoma.

Both components extended through the rectal wall into the serosal fat. Metastatic tumor was found in three of 18

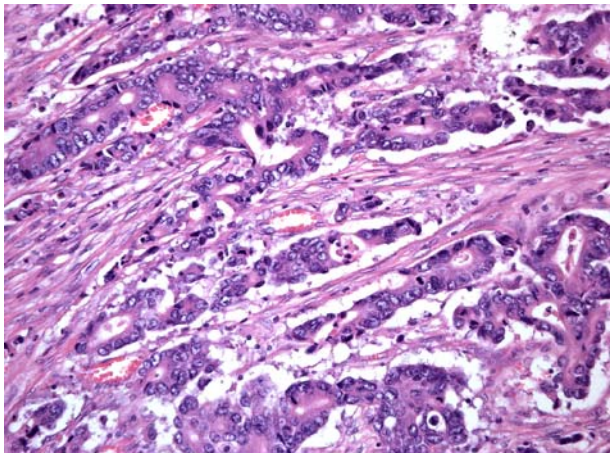

Fig. 2 The infiltrating adenocarcinoma was of conventional type with well-formed glandular structures permeating muscularis propria (H&E×400)

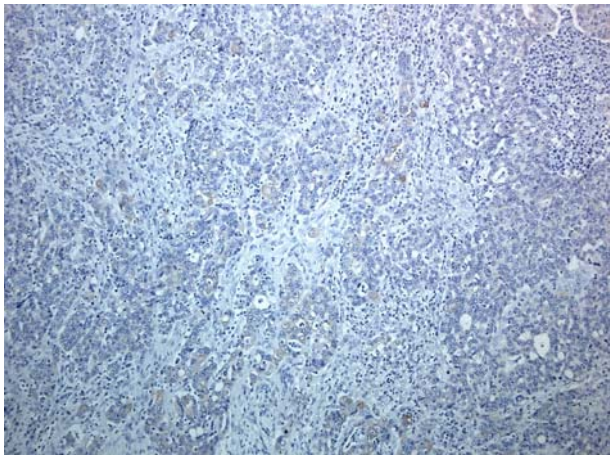

Fig. 4 CK20 staining in the adenocarcinomatous component was patchy and focal in distribution. Even well-formed glandular structures were not well decorated (CK20×400)

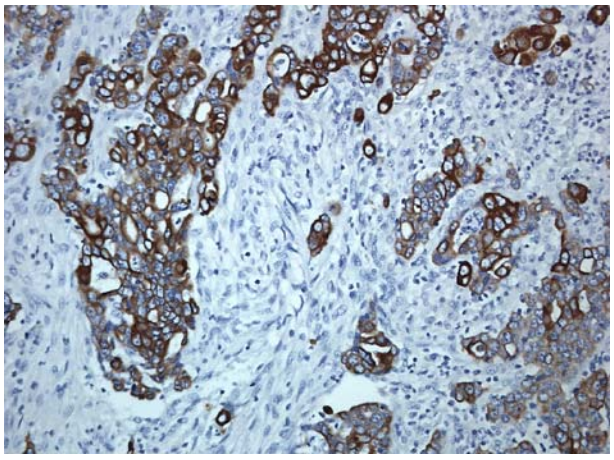

Fig. 5 CK7 staining, in contrast to CK20, was strong and diffuse in the adenocarcinoma (CK7×400)

regional lymph nodes. It is interesting to note that two of the lymph nodes consisted only of metastatic conventional adenocarcinoma while the third lymph node showed both adenocarcinoma and large cell neuroendocrine carcinoma.

Immunohistochemistry showed the adenocarcinoma to exhibit focal CK 20 positivity (Fig. 4) but strong and diffuse CK 7 expression (Fig. 5). CEA was also positive in the adenocarcinomatous component. The adenocarcinoma was negative for chromogranin, synaptophysin, and CD56. The large cell neuroendocrine component was positive for chromogranin, synaptophysin and, CD56 (Fig. 6); focally positive for CK 7; and negative for CK 20.

Electron microscopy showed poor preservation of cells, however, occasional membrane-bound neurosecretory granules were seen.

Taking the morphological and immunohistochemical features into account, this is a composite tumor of the rectum composed of conventional adenocarcinoma and coexistent large cell neuroendocrine carcinoma.

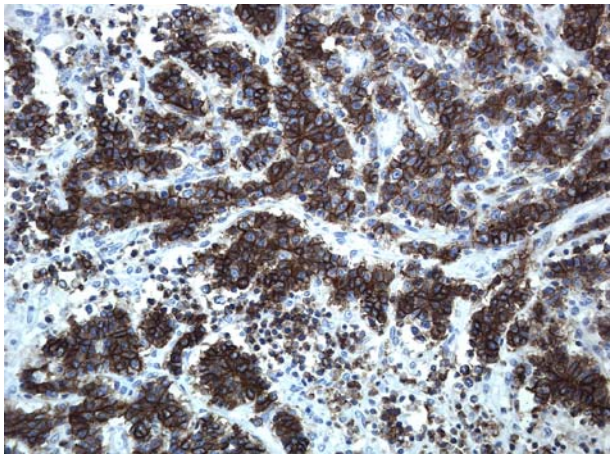

Fig. 6 The large cell neuroendocrine carcinoma displayed strong and diffuse immunopositivity with CD56 (CD56×400)

Discussion

There were several isolated reports describing composite colorectal tumors, most of which describe mixed carcinoid and adenocarcinoma [3, 10, 17] and mixed carcinoid with adenoma [10, 17]. Small cell carcinoma of the rectum occurring on its own was described [4, 12]. In addition, large cell neuroendocrine carcinoma of the rectum was also documented [2]. This is a rare tumor that accounts for less than 1% of all colorectal cancers [2]. In the latter publication, cases of neuroendocrine carcinoma coexisting with foci of adenocarcinoma within the colon and rectum was mentioned [2]. It is assumed that some of these cases containing both components are similar to the case reported herein. However, there is no description of the relationship between the large cell neuroendocrine carcinoma focus and the adenocarcinoma [2]. The criteria employed in making the diagnosis of large cell neuroendocrine carcinoma of the rectum is identical to their lung counterparts [2]. There is a predilection for large cell neuroendocrine carcinoma to occur in the cecum and rectum [2]. In general, neuroendocrine carcinomas have an aggressive course and the prognosis is poor. Prognosis of composite tumors is a matter of debate. It was suggested that a mixed endocrine tumor and adenocarcinoma leads to a more aggressive form of malignancy [3]. It is generally accepted that composite appendiceal tumors, namely, goblet-cell carcinoids, carry an intermediate prognosis between that of a classical carcinoid and adenocarcinoma [19]. Initially, it was believed that composite tumors of the colon had a better prognosis than ordinary adenocarcinomas; however, recent evidence shows that composite tumors of the colon may carry a poorer prognosis [10]. A recent study of colorectal adenocarcinomas, neuroendocrine cells within the conventional adenocarcinoma, was seen in 20–50% of cases and these tumors were associated with a poor prognosis [5]. It should be remembered that these are cases of conventional adenocarcinoma harboring a significant proportion of neuroendocrine cells and not two separate tumors. Because very few, if any, combined large cell neuroendocrine carcinoma and conventional adenocarcinoma cases were documented, very little information is available regarding behavior of this specific entity. It is safe to assume that the neuroendocrine component would confer an adverse prognosis compared to cases with only conventional adenocarcinoma of similar stage.

The histogenesis of tumors containing both glandular and endocrine components has aroused much interest although it was not fully elucidated. There are two main views: (1) simultaneous and coincidental malignant change in mature cells of different cell lines and (2) monoclonal origin of the two components that arise from multipotential stem cells that show biphenotypic differentiation after carcinogenesis is initiated. Histological and molecular studies suggest that both the glandular and endocrine components of a mixed tumor share a multipotential stem cell origin. Two different studies of mixed tumors of the GI tract found a strong genetic relationship between the two tumor components regardless of the combination of tumor

types, grade, or primary site [6, 18]. It was further suggested that amphicrine tumors originate from pluripotential cells with dual differentiation abilities [10]. It is tempting to speculate that this case, although within the rectum, arose from the anal transitional zone. Multidifferentiation is a well-recognized phenomenon in the anal transitional zone and would account for the two components encountered in this tumor. In addition, the cytokeratin immunoprofile of the tumor described in this paper most closely resembles that of the anal transitional zone. The normal anal transitional zone is usually CK 7 positive and CK 20 negative. It is noteworthy that the adenocarcinoma component showed only focal positivity for CK 20. Neuroendocrine carcinomas on the other hand, are typically negative for CK 20. A single case of CK 20 positive large cell neuroendocrine carcinoma of the colon was described [7]. Based on this immunohistochemical finding together with CK 7 negativity, the authors suggested a link between neuroendocrine carcinoma and conventional adenocarcinoma [7].

Composite tumors of the rectum are rare, especially those composed of an admixture of conventional adenocarcinoma and large cell neuroendocrine carcinoma. In the case described herein, the cytokeratin immunoprofile fits in with origin from the anal transitional zone. Not only is this case unusual in terms of it being a composite tumor of the rectum, but the focal CK 20 positivity in the adenocarcinoma component is also somewhat unusual. Given the usual cytokeratin expression pattern of the anal transitional zone and its propensity for divergent differentiation, we feel that the composite rectal tumor encountered in this case is most likely of anal transitional zone origin.

References

1. Anagnostopoulos GK, Arvanitidis D, Sakorafas G, Pavlakis G, Kolilekas L, Arkoumani E, Stefanou D (2004) Combined carcinoid-adenocarcinoma tumour of the anal canal. Scand J Gastroenterol 39:198–200
2. Bernick PE, Klimstra DS, Shia J, Minsky B, Saltz L, Shi W, Thaler H, Guillem J, Paty P, Cohen AM, Wong WD (2004) Neuroendocrine carcinomas of the colon and rectum. Dis Colon Rectum 47:163–169
3. Capella C, La Rosa S, Uccella S, Billo P, Cornaggia M (2000) Mixed endocrine-exocrine tumors of the gastrointestinal tract. Sem Diagn Pathol 17:91–103
4. Cebrian J, Larach SW, Ferra A, Williamson PR, Trevisani MF, Lujan HJ, Kassir A (1999) Small-cell carcinoma of the rectum: report of two cases. Dis Colon Rectum 42:274–277
5. De Bruine AP, Wiggers T, Beck C (1993) Endocrine cells in colorectal adenocarcinomas: incidence, hormone profile and prognostic relevance. Int J Cancer 4:765–771
6. Furlan D, Cerutti R, Genasetti A, Pelosi G, Uccella S, La Rosa S, Capella C (2003) Microallelotyping defines the monoclonal or the polyclonal origin of mixed and collision endocrine-exocrine tumors of the gut. Lab Invest 83:963–971
7. Kato T, Terashima T, Tomida S, Yamaguchi T, Kawamura H, Kimura N, Ohtani H (2005) Cytokeratin 20-positive large cell neuroendocrine carcinoma of the colon. Pathol Int 55:524–529
8. Knight BK, Hayes MM (1987) Mixed adenocarcinoma and carcinoid tumour of the colon. A report of 4 cases with postulates on histogenesis. S Afr Med J 72:708–710
9. Levendoglu H, Cox CA, Nadimpalli V (1990) Composite (adenocarcinoid) tumors of the gastrointestinal tract. Dig Dis Sci 35:519–525
10. Lewin K (1987) Carcinoid tumors and the mixed (composite) glandular-endocrine cell carcinomas. Am J Surg Pathol 11:71–86
11. Lyda MH, Fenoglio-Preiser CM (1998) Adenoma-carcinoid tumors of the colon. Arch Pathol Lab Med 122:262–265
12. Mills SE, Allen MS, Cohen AR (1983) Small-cell undifferentiated carcinoma of the colon. Am J Surg Pathol 7:643–651
13. Moyana TN, Qizilbash AH, Murphy F (1988) Composite glandular-carcinoid tumors of the colon and rectum. Report of two cases. Am J Surg Pathol 12:607–611
14. Pasquinelli G, Santini D, Preda P, Cariani G, Bonora G, Martinelli GN (1993) Composite gastric carcinoma and precursor lesions with amphicrine features in chronic atrophic gastritis. Ultrastruct Pathol 17:9–24
15. Reis-Filho JS, Schmitt FC (2001) Amphicrine gastric carcinoma. Arch Pathol Lab Med 125:1513–1514
16. Saclarides TJ, Szeluga D, Staren ED (1994) Neuroendocrine cancers of the colon and rectum. Dis Colon Rectum 37:635–642
17. Seretis E, Gavrill A, Agnantis N, Golematis V, Voloudakis-Baltatzis IE (2001) Comparative study of serotonin and bombesin in adenocarcinomas and neuroendocrine tumours of the colon. Ultrastruct Pathol 25:445–454
18. Vortmeyer AO, Lubensky IA, Merino JA, Wang CY, Pham T, Furth EE, Zhuang Z (1997) Concordance of genetic alterations in poorly differentiated colorectal neuroendocrine carcinomas and associated adenocarcinomas. J Natl Cancer Inst 89:1448–1453
19. Yang GC, Rotterdam H (1991) Mixed (composite) glandular-endocrine cell carcinoma of the stomach: report of a case and review of literature. Am J Surg Pathol 15:592–598

Virchows Arch (2006) 448: 648–654
DOI 10.1007/s00428-005-0109-x

CASE REPORT

Hermann Herbst · Gerald Niedobitek

Sporadic EBV-associated lymphoepithelial salivary gland carcinoma with EBV-positive low-grade myoepithelial component

Received: 11 July 2005 / Accepted: 29 September 2005 / Published online: 1 March 2006

Abstract Salivary gland lymphoepithelial carcinomas (LECs) are associated with Epstein–Barr virus (EBV) in endemic areas, whereas sporadic cases are usually EBV negative. We have studied two EBV-associated LECs from Caucasian patients for their EBV gene expression profile and their immunophenotype. Tumour cells of case 1 showed expression of EBNA1 only, corresponding to an EBV latency type I. Tumour cells of this case expressed various basal and glandular cytokeratins. In case 2, the LEC was accompanied by a low-grade spindle cell lesion with an immunophenotype of myoepithelial cells, whereas the high-grade tumour expressed cytokeratin (Ck) 8 only. In case 2, the high-grade tumour showed an EBV lantency II pattern with expression of EBNA1, LMP1 and LMP2A (latency II). The spindle cell lesion of this case was also EBV-infected and showed low levels of EBNA1 and LMP1 expression, while LMP2A was not detectable. The detection of EBV in both components of case 2 together with immunophenotypic evidence of transition between both components supports the notion that at least some LECs arise through a low-grade myoepithelial intermediate. Expression of LMP2A may be of therapeutic interest because it may make such cases amenable to immunotherapy with EBV-specific cytotoxic T cells.

H. Herbst
Institute of Pathology,
University Hospital Münster,
Münster, Germany

H. Herbst (✉)
Fachbereich Pathologie,
Vivantes Klinikum Neukölln,
Rudower Str. 48,
12351 Berlin, Germany
e-mail: Hermann.Herbst@vivantes.de
Tel.: +49-030-60042680
Fax: +49-030-60043030

G. Niedobitek
Institute of Pathology,
Friedrich-Alexander-University,
Erlangen, Germany

Keywords Salivary gland · Carcinoma · Myoepithelial lesions · Epstein–Barr virus

Introduction

Lymphoepithelial carcinomas (LECs) were originally described in their two major histological patterns by Schmincke [28] and Regaud et al. [25] as distinct neoplasms of the nasopharynx characterized by undifferentiated epithelial tumour cells associated with an abundant lymphoid stroma. Subsequently, morphologically similar tumours were described at various primary sites such as lacrimal and salivary glands, tonsil, thymus, lung, breast, uterus, stomach, urinary bladder and skin [9]. For some of these tumours, peculiar geographic patterns of distribution were observed. LEC of the nasopharynx, generally a rare tumour, occurs at high incidence rates in Southeast Asia, particularly in Hong Kong, and in the Arctic regions [9]. Similarly, salivary gland LECs display a high incidence in native populations of Greenland and Alaska and also occur more frequently in Southeast Asia [4, 13, 16, 19, 27].

In the nasopharynx, both endemic and sporadic LECs are invariably associated with Epstein–Barr virus (EBV) infection [9]. By contrast, LECs of the uterine cervix, urinary bladder and skin have been reported to be EBV negative [9]. LECs occurring at other sites show more complex patterns of EBV association. Approximately 80% of gastric LECs harbour the virus regardless of the geographical origin [20]. The association of salivary gland and thymic LECs with the virus is largely restricted to areas where nasopharyngeal LEC is endemic, whereas morphologically indistinguishable tumours arising in Caucasians are mostly EBV negative [1, 6, 10, 12, 14, 16, 26, 29, 30].

Except for limited periods of replicative infection, EBV infection is latent and then characterized by the variable expression of a limited set of so-called latent gene products, including two small non-polyadenylated nuclear RNAs (EBER1, EBER2), six nuclear antigens (EBNA1–6) and three latent membrane proteins, LMP1, LMP2A and LMP2B [9]. Nasopharyngeal carcinoma displays expres-

sion of the EBERs, EBNA1, LMP1 and LMP2A (latency type II) [7, 9]. A more restricted pattern of EBV latent gene expression, characterized by the presence of only the EBERs and EBNA1 (latency type I), is found in Burkitt lymphoma [9].

In virtually all cases of EBV-associated undifferentiated carcinoma, the cell of origin is not known because of the absence of dysplastic changes and EBV from normal epithelial cells adjacent to the tumour. Salivary gland LECs may be informative in this respect because, in a proportion of cases, the LECs are accompanied by so-called benign lymphoepithelial lesions (BLEL), the relationship of which to the neighbouring LECs is a matter of debate. Some authors postulated that LECs represent the malignant counterpart of BLEL and thus proposed the term "malignant lymphoepithelial lesion" for these tumours [3, 11, 13, 24]. Other authors explicitly rejected the idea of such a relationship [17, 27], particularly in view of the absence of EBV infection from BLEL.

Here, we report two cases of sporadic EBV-associated LECs, one of which was accompanied by an EBV-positive low-grade spindle cell proliferation. We have determined the EBV gene expression profile and the immunophenotype of tumour cells and tumour infiltrating lymphocytes. Controls comprised four cases of typical BLEL in Sjögren syndrome and five marginal zone B-cell lymphomas (MZBCL). The findings may be relevant for the understanding of the pathogenesis, the histopathologic diagnosis and immunotherapy of salivary gland LECs.

Materials and methods

Patients

Case 1 A female Caucasian patient, 45 years of age, showed a left parotid gland enlargement. The firm whitish tissue measured up to 65 mm. Frozen section and paraffin diagnosis revealed an undifferentiated carcinoma with lymphoid stroma. No additional manifestations were found in the neck dissection specimen. Tumour extension and spread were classified as pT2pN0.

Case 2 A 64-year-old Caucasian man was admitted with a right cervical tumour. After excision, histology revealed the metastasis of a LEC. The search for the primary tumour with emphasis on the nasopharynx revealed no pathological findings except for an enlarged right submandibular gland. Upon ectomy, sectioning of the gland showed a firm, white nodule of 20 mm diameter with a rim of regularly lobulated gland parenchyma. At the periphery of the node, several small cystic spaces up to 2 mm were noted. The tumour extension and spread were classified as pT1pN1.

Parotid gland tissues from four cases of so-called myoepithelial sialadenitis (MESA), clinically characterized as Sjögren's disease, five cases of MZBCL as well as five tonsils served as controls.

Immunohistology

Four-micrometer sections of paraffin-embedded tissue blocks were stained with antibodies directed at EBV proteins EBNA1 (clone 1H4, kindly provided by E. Kremmer, Munich, Germany), LMP1 (clones CS1–4, DakoCytomation, Hamburg, Germany) and LMP2A (clone 15F9, kindly provided by E. Kremmer) as well as cytokeratins (Ck) 5/6 (clone D5/16B4; Zymed, San Francisco, CA, USA), Ck7 (OV-TL-12/30, DakoCytomation), Ck8/18 (clone 5D3; Dianova, Hamburg, Germany), Ck13 (clone DE-K13, DakoCytomation), Ck14 (LI002, Dianova), Ck19 (RCK 108, DakoCytomation), Ck20 (Ks20.8, DakoCytomation), vimentin (clone V9; DakoCytomation), smooth muscle α-actin (SMA, clone 1A4; Sigma-Aldrich, St. Louis, MO, USA), S-100 protein (rabbit polyclonal; DakoCytomation), epithelial membrane antigen (EMA, clone E29, DakoCytomation) and the proliferation-associated Ki-67 nuclear antigen (clone MIB-1, DakoCytomation) using the peroxidase–anti-peroxidase method with diaminobenzedine (DAB) as a chromogen or employing streptavidin–biotinylated alkaline phosphatase complex in conjunction with Fast Red (Sigma) as described [7, 18]. For the detection of LMP2A and EBNA1, a tyramide signal amplification system was used as described [7].

In situ hybridization

Transcription and labelling of EBER RNA probes were performed as outlined recently [18]. The procedure, including pre-hybridization, hybridization, removal of non-specifically bound probe by RNase A digestion and further washing procedures, was carried out as described [18].

Results

Morphology

Case 1 displayed a high-grade tumour in a Regaud-type pattern comprising solid cords of undifferentiated neoplastic epithelium embedded in a lymphoid stroma with numerous germinal centres.

The high-grade component of case 2 showed the classical Schmincke-type pattern with syncytial clusters of undifferentiated tumour cells intermingled with lymphoid cells (Fig. 1a). In this case, the high-grade component was associated with a low-grade spindle cell proliferation with microcyst formation at the periphery of the high-grade neoplasm (Fig. 1b). In addition to its different cell morphology and cytological grade, this component was characterized by a comparative scarcity of infiltrating lymphoid cells (Fig. 1a,b).

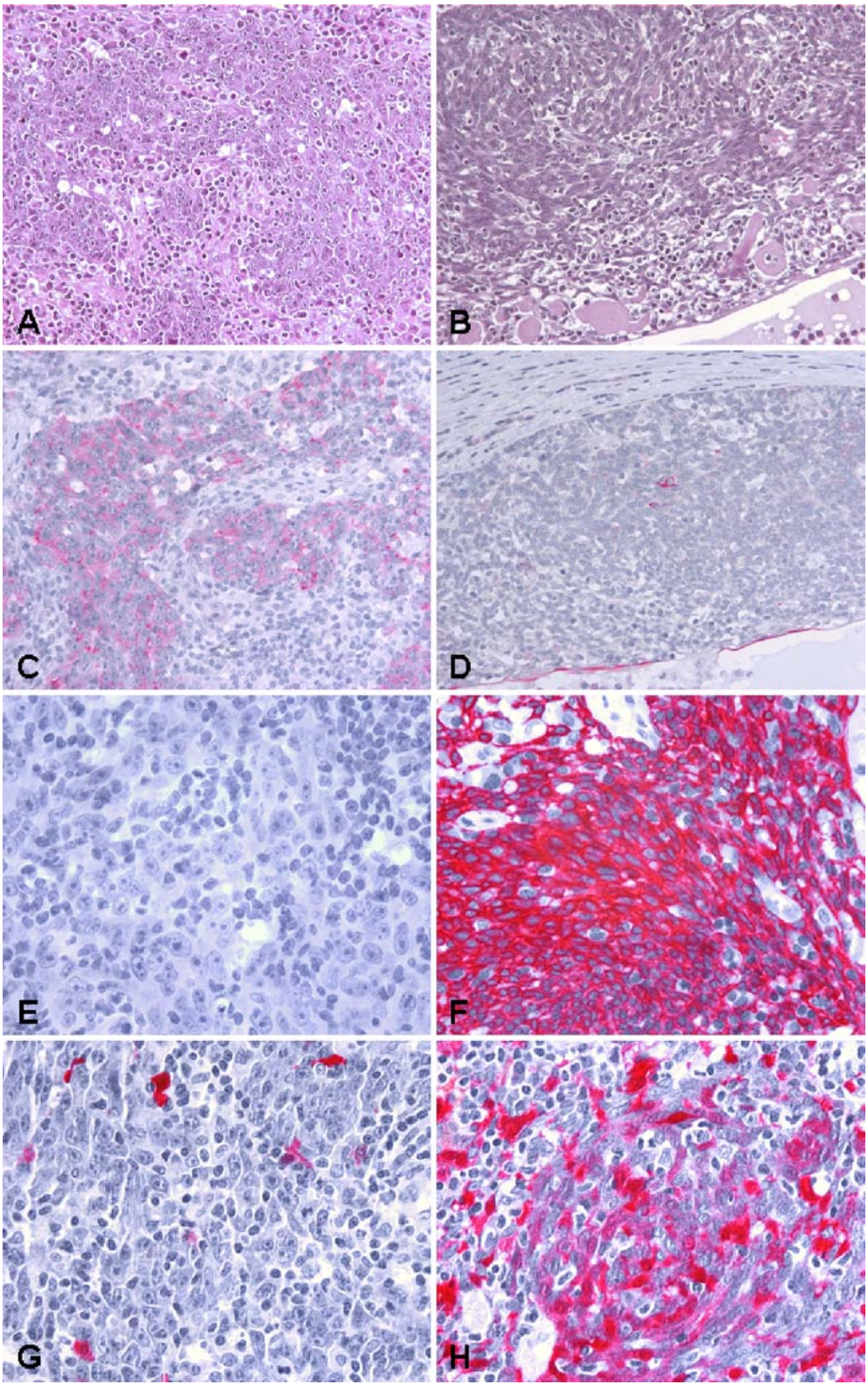

Fig. 1 Histological examination of case 2 shows an undifferentiated lymphoepithelial carcinoma (LEC, **a**) accompanied by a low-grade spindle cell component (**b**). Immunohistochemistry shows expression of cytokeratin (Ck) 8 in the undifferentiated LEC (**c**), while only rare cells of the accompanying spindle cell proliferation express Ck8 (**d**). By contrast, immunostaining for basal cytokeratins Ck5/6 (**e**, **f**) and S-100 protein (**g**, **h**) yields negative results in the LEC (**e**, **g**) and is strongly positive in the spindle cell lesion (**f**, **h**)

EBV gene expression

Virtually all tumour cells of both cases harboured EBV as shown by strong nuclear in situ hybridization signals when probed for EBER1 and EBER2 (Fig. 2a; Table 1). Interestingly, the spindle cell component of case 2 was also EBER positive (Fig. 2b). Strong nuclear immunostaining for EBNA1 was observed in both high-grade tumours (Fig. 2c), whereas the nuclei of the spindle cell lesion of case 2 were only weakly labelled (Fig. 2d). LMP1

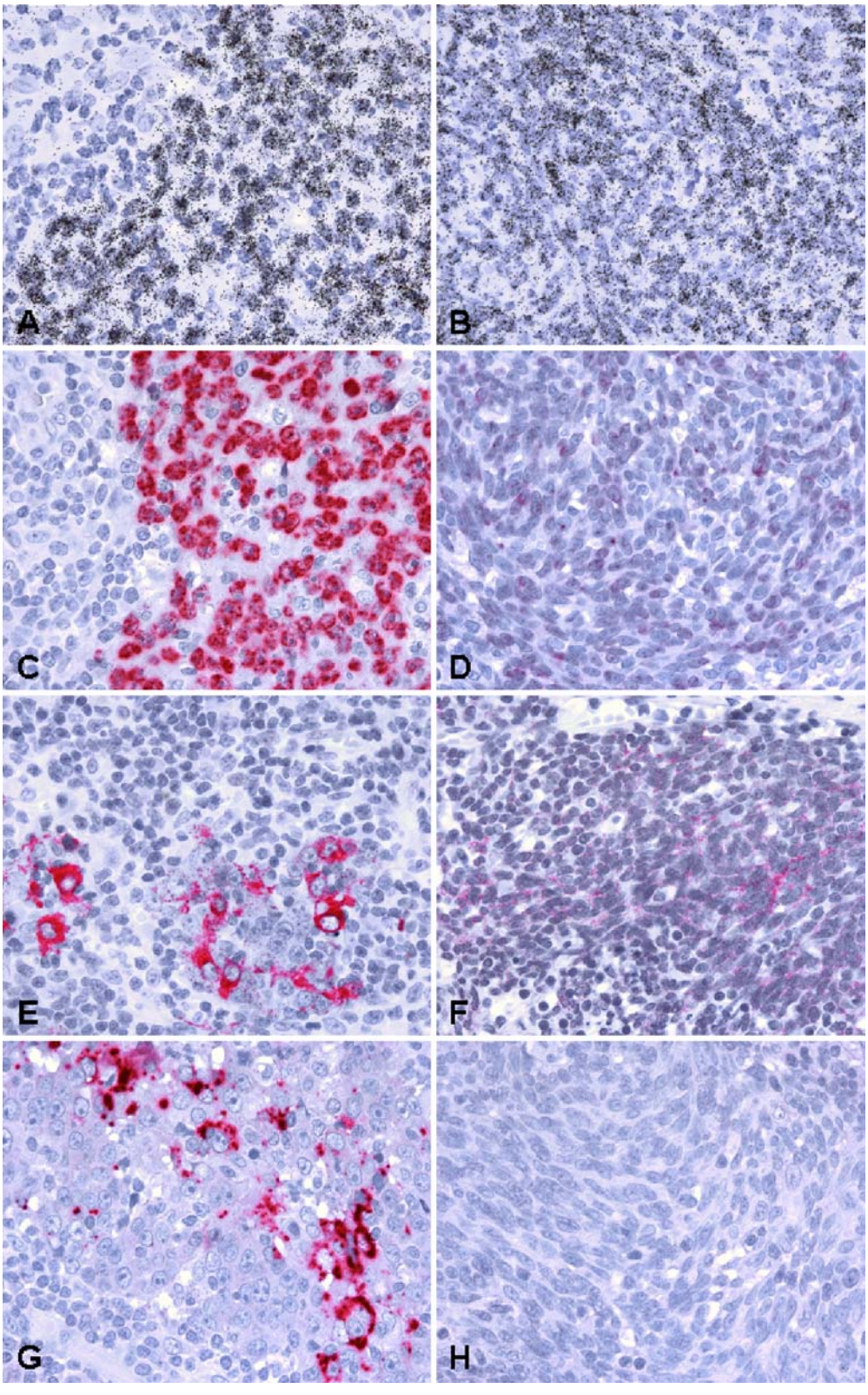

Fig. 2 By in situ hybridization with ^{35}S-labelled probes and subsequent autoradiography, expression of EBER transcripts is detected in the LEC (**a**) and the spindle cell (**b**) components of case 2. Similarly, EBNA1 (**c**, **d**) and LMP1 (**e**, **f**) are detectable, although labelling is weaker in the spindle cell component (**d**, **f**). Expression of LMP2A is detectable only in the LEC (**g**) but not in the accompanying spindle cell lesion (**h**)

and LMP2A were absent from case 1 but were strongly expressed in a proportion of the high-grade tumour cells of case 2 with a patchy membranous and cytoplasmic staining (Fig. 2e,g). The spindle cell component of case 2 showed weak expression of LMP1 and no detectable expression of LMP2A (Fig. 2f,h). All BLEL were EBV negative as assessed by EBER-specific in situ hybridization.

Table 1 Summary of immunohistology and in situ hybridization results

Gene product	LEC case 1	LEC case 2	MEL case 2
EBER1/2	++	+++	++
EBNA1	+	++	(+)
LMP1	−	++	(+)
LMP2A	−	++	−
Ck5/6	+	−	+
Ck7	−	−	−
Ck8	+	+	−
Ck10	−	−	−
Ck13	+	−	−
Ck14	−	−	+
Ck18	+	−	−
Ck19	−	−	−
Ck20	−	−	−
EMA	+	+	(+)
S-100 protein	−	−	++
SMA	−	−	(+)
Vimentin	−	(+)	(+)
Growth fraction (Ki-67)	60%	80%	<4%

LEC lymphoepithelial carcinoma, *Ck* cytokeratin, *EMA* epithelial membrane antigen, *SMA* smooth muscle α-actin, *MEL* myoepithelial lesion

+++: strong, ++: moderate, +: weak, (+): faint, and −: absent reactivity

Immunophenotype

The undifferentiated carcinoma cells of case 1 expressed various cxtokeratin types as well as EMA, whereas cytokeratin expression in the high-grade component of case 2 was restricted to Ck8 (Table 1; Fig. 1c). The spindle cell component of case 2 lacked Ck8 expression and displayed an immunophenotype reminiscent of myoepithelial cells with expression of basal cytokeratins Ck5/6 and Ck14 as well as of vimentin, S-100 protein and, weakly, SMA (Table 1; Fig. 1f,h). Ck5/6, Ck14 and S-100 protein were absent from the undifferentiated carcinoma component of case 2 (Table 1; Fig. 2e,g). Both high-grade tumours showed a growth fraction of more than 60% as determined by immunostaining with antibody MIB-1, while the spindle cell lesion displayed a small growth fraction of less than 4% (Table 1). The epithelial cells of BLEL in so-called MESA, MZBCL and tonsillar crypts expressed Ck5/6 and Ck14 in the absence of S-100 protein, vimentin and SMA (not shown).

Discussion

Salivary gland LECs occur as endemic tumours in Arctic and Southeast Asian populations but are exceedingly rare among Caucasians [4, 13, 16, 19, 27]. In high incidence areas, virtually all cases of salivary gland LECs are associated with EBV infection [1, 14, 16, 26, 29, 30]. By contrast, the association of sporadic salivary gland LECs with EBV appears to be variable with only one well-documented EBV-positive case in the literature [6, 10, 12].

We report two cases of sporadic salivary gland LECs in Caucasian patients. Both cases were EBV positive as demonstrated by in situ hybridization. Thus, it appears that association with EBV is not restricted to cases occurring in high incidence areas. Further immunohistological characterization revealed an EBV latency type II in case 2 (EBNA1 and LMP1/LMP2A positive) as characteristically seen in nasopharyngeal LEC. This is in agreement with a previous reverse transcription-polymerase chain reaction (RT-PCR) study of salivary gland carcinoma [23]. The expression of LMP2A is of particular interest because it might make EBV-associated salivary gland LECs amenable to immunotherapeutic approaches based on the application of EBV-specific cytotoxic T cells [15]. Case 1 revealed expression of EBNA1, but both LMPs were not detectable by immunohistology. Thus, similar to nasopharyngeal LEC, viral gene expression patterns in salivary gland LECs as detected by immunohistochemistry are heterogeneous. As a consequence, exclusion of EBV as a cofactor in salivary gland LECs requires the application of EBER in situ hybridization and cannot solely rely on LMP1 immunohistochemistry.

Case 2 was unusual because, in addition to the undifferentiated high-grade carcinoma component, it showed a focal proliferation of spindle cells displaying only minor cytological atypia and microcyst formation. Morphologically, this spindle cell component was reminiscent of the "dysplastic BLEL" described by Nagao et al. [17] which, however, were EBV negative, and of the EBV-positive spindle cell LECs reported by Christiansen et al. [2]. It has previously been established that BLEL, as typically found in so-called myoepithelial sialadenitis (MESA), in lymphoepithelial cysts and in MZBCL, do not display a myoepithelial phenotype [8]. Rather, the phenotype corresponds to basal epithelium similar to the lining of crypts in oropharynegeal lymphatic tissue [8]. In contrast, the EBER-positive spindle cell lesion of case 2 displayed staining for vimentin, S-100 protein, SMA, Ck5/6 and Ck14, the combination of which is an attribute of myoepithelial cells. It is possible that the previously described spindle cell BLEL accompanying salivary gland LECs as well as the EBV-positive spindle cell LECs were also proliferations of true myoepithelial cells [2, 17]. Our case 2 is also reminiscent of a case reported by Piana et al. [21]. In that case, an EBV-positive LEC was accompanied by a low-grade tumour classified as epi-myoepithelial carcinoma which was also EBV-associated [21].

To assess the relationship between low- and high-grade tumour components in case 2, we determined the immunophenotype with emphasis on expression of cytokeratins and myoepithelial markers. Whereas the high-grade component of case 1 displayed no significant expression of cytokeratins except for Ck8 and of EMA, the spindle cell proliferation expressed Ck5/6 and Ck14 in the absence of the other specific cytokeratin types tested. However, small complexes

of larger cells at the periphery of the spindle cell component expressed Ck5/6, EMA, and vimentin, suggesting areas of transition between these otherwise distinct tumour components. The fact that both components were associated with EBV infection also suggests that these morphologically distinct cell populations formed part of the same neoplastic process since EBV has been shown to be absent from salivary gland tumours other than LECs [1, 22].

Like its high-grade component, the entire spindle cell proliferation of case 2 was characterized by EBV latency type II. However, expression levels of EBNA1 and LMP1 were, by comparison, modest, and there was no detectable expression of LMP2 in these cells. This correlates well with the smaller growth fraction in the spindle cell component because EBNA1 is required for the maintenance of viral episomes in proliferating cells [32]. The smaller proportion of infiltrating lymphocytes in the spindle cell component is also in support of this interpretation. Thus, our observation of EBV infection of both components and areas of phenotypic transition lends support to the notion that a true myoepithelial lesion may be an immediate precursor of LEC in this case. Tumour cells of case 2 expressed Ck5/6, Ck8, Ck13 and Ck18, indicating immunophenotypic heterogeneity among salivary gland LECs.

The mode of infection of myoepithelial cells by EBV is not clear. Some authors postulated that EBV persisted in the parotid gland [31]. However, this has not been confirmed by others [5]. Other parotid gland tumours have been reported to be EBV negative, suggesting that EBV infection in salivary gland neoplasms is restricted to LECs [1, 22].

In conclusion, the detection of EBV in both components of case 2 supports the notion that at least some LECs arise through a low-grade myoepithelial lesion. This idea is also supported by a similar case reported previously [21]. The mode of viral infection of these myoepithelial cells remains undisclosed. The detection of a low-grade component accompanying a salivary gland LEC is indeed an argument to consider the tumour primary to the gland and makes a metastatic tumour unlikely. The proportion of EBV-associated LECs in Caucasians may be larger than previously anticipated. EBV-associated LECs may differ in their latency form, so that assignment of EBV infection should always rest on detection of EBER transcripts. LMP expression, in particular LMP2A, may be of therapeutic interest because it may make such cases amenable to immunotherapy with EBV-specific cytotoxic T cells.

Acknowledgements This research was supported by grants from the Medical Faculty, University Münster (IMF HU120115), and from the Wilhelm Sander Foundation (to GN).

References

1. Chan JKC, Yip TTC, Tsang WYW, Poon YF, Wong CSC (1994) Specific association of Epstein–Barr virus with lymphoepithelial carcinoma among tumors and tumorlike lesions of the salivary gland. Arch Pathol Lab Med 118:994–997
2. Christiansen MS, Mourad WA, Hales ML, Oldring DJ (1995) Spindle cell malignant lymphoepithelial lesion of the parotid gland: clinical, light microscopic, ultrastructural, and in situ hybridization findings in one case. Mod Pathol 8:711–715
3. Cleary KR, Batsakis JG (1990) Undifferentiated carcinoma with lymphoid stroma of the major salivary glands. Ann Otol Rhinol Laryngol 99:236–238
4. Fibiger J (1923) Über das Vorkommen von Krebs und Geschwülsten in Grönland: Ergebnisse der vom dänischen Cancerkomitee bewerkstelligten Untersuchungen. Z Krebsforsch 20:148–187
5. Frangou P, Buettner M, Niedobitek G (2005) Epstein–Barr virus (EBV) infection in epithelial cells in vivo: rare detection of EBV replication in tongue mucosa but not in salivary glands. J Infect Dis 191:238–242
6. Hamilton-Dutoit SJ, Hamilton-Therkildsen M, Nielsen NH, Jensen H, Hensen JPH, Pallesen G (1991) Undifferentiated carcinoma of the salivary gland in Greenland Eskimos: demonstration of Epstein–Barr virus DNA by in situ hybridization. Hum Pathol 22:811–815
7. Heussinger N, Buttner M, Ott G, Brachtel E, Pilch BZ, Kremmer E, Niedobitek G (2004) Expression of the Epstein–Barr virus (EBV)-encoded latent membrane protein 2A (LMP2A) in EBV-associated nasopharyngeal carcinoma. J Pathol 203:696–699
8. Ihrler S, Zietz C, Sendelhofert A, Riederer A, Lohrs U (1999) Lymphoepithelial duct lesions in Sjogren-type sialadenitis. Virchows Arch 434:315–323
9. International Agency for Research on Cancer (1997) Epstein–Barr virus and Kaposi's Sarcoma herpesvirus/human herpesvirus 8. In: IARC monographs on the evaluation of carcinogenic risks to humans, vol 70. WHO, Lyon, France
10. Kotsianti A, Costopoulos J, Morgello S, Papadimitriou C (1996) Undifferentiated carcinoma of the parotid gland in a white patient: detection of Epstein–Barr virus by in situ hybridization. Hum Pathol 27:87–90
11. Kott ET, Goepfert H, Ayala AG, Ordonez NG (1984) Lymphoepithelial carcinoma (malignant lymphoepithelial lesion) of the salivary glands. Arch Otolaryngol 110:50–53
12. Kountakis SE, SooHoo W, Maillard A (1995) Lymphoepithelial carcinoma of the parotid gland. Head Neck 17:445–450
13. Krishnamurthy S, Lanier AP, Dohan P, Lanier JF, Henle W (1987) Salivary gland cancer in Alaskan natives, 1966–1980. Hum Pathol 18:986–996
14. Lanier AP, Clift SE, Bornkamm G, Henle W, Goepfert H, Raab-Traub N (1991) Epstein–Barr virus and malignant lymphoepithelial lesions of the salivary gland. Arct Med Res 50:55–61
15. Lee SP, Chan AT, Cheung ST, Thomas WA, Croom-Carter D, Dawson CW, Tsai CH, Leung SF, Johnson PJ, Huang DP (2000) CTL control of EBV in nasopharyngeal carcinoma (NPC): EBV-specific CTL responses in the blood and tumors of NPC patients and the antigen-processing function of the tumor cells. J Immunol 165:573–582
16. Leung SY, Chung LP, Yuen ST, Ho CM, Wong MP, Chan SY (1995) Lymphoepithelial carcinoma of the salivary gland: in situ detection of Epstein–Barr virus. J Clin Pathol 48:1022–1027
17. Nagao T, Ishida Y, Sugano I, Tajima Y, Matsuzaki O, Hino T, Konno A, Kondo Y, Nagao K (1996) Epstein–Barr virus-associated undifferentiated carcinoma with lymphoid stroma of the salivary gland in Japanese patients. Comparison with benign lymphoepithelial lesion. Cancer 78:695–703
18. Niedobitek G, Herbst H (2001) In situ detection of Epstein–Barr virus DNA and of viral gene products. In: Wilson JB, May GHW (eds) Epstein–Barr virus protocols. Humana, Totowa, NJ, pp 79–91
19. Nielsen NH, Mikkelsen F, Hansen JPH (1978) Incidence of salivary gland neoplasms in Greenland with special reference to an anaplastic carcinoma. Acta Pathol Microbiol Scand [A] 86:185–193

20. Osato T, Imai S (1996) Epstein–Barr virus and gastric carcinoma. Semin Cancer Biol 7:175–182
21. Piana S, Damiani S, Asioli S, Magrini E, Barbieri W, Cavazza A (2004) Epstein–Barr-positive lymphoepithelial carcinoma and epi-myoepithelial cell carcinoma of the parotid gland: a hitherto unreported example of hybrid tumour. Virchows Arch 445:425–428
22. Pollock AM, Toner M, McMenamin M, Walker J, Timon CI (1999) Absence of Epstein–Barr virus encoded RNA and latent membrane protein (LMP1) in salivary gland neoplasms. J Laryngol Otol 113:906–908
23. Raab-Traub N, Rajadurai P, Flynn K, Lanier AP (1991) Epstein–Barr virus infection in carcinoma of the salivary gland. J Virol 65:7032–7036
24. Redondo C, Garcia A, Vazquez F (1981) Malignant lympho-epithelial lesion of the parotid gland: poorly differentiated squamous cell carcinoma with lymphoid stroma. Cancer 48:289–292
25. Regaud C, Reverchon L (1921) Sur un cas d'epithelioma epidermoide developpe dans le massif maxillaire superieur. Rev Laryngol Otol Rhinol (Bord) 42:369–378
26. Saemundsen AK, Albeck H, Hansen JPH, Nielsen NH, Anvret M, Henle W, Henle G, Thomsen KA, Kristensen HK, Klein G (1982) Epstein–Barr virus in nasopharyngeal and salivary gland carcinomas of Greenland Eskimoes. Br J Cancer 46:721–728
27. Saw D, Lau WH, Ho JHC, Chan JKC, Ng CS (1986) Malignant lymphoepithelial lesion of salivary gland. Hum Pathol 17:914–923
28. Schmincke A (1921) Über lympho-epitheliale Geschwülste. Beitr Pathol Anat Allg Pathol 68:161–170
29. Sheen TS, Tsai CC, Ko JY, Chang YL, Hsu MM (1997) Undifferentiated carcinoma of the major salivary gland. Cancer 80:357–363
30. Tsai CC, Chen CL, Hsu HC (1996) Expression of Epstein–Barr virus in carcinomas of major salivary glands: a strong association with lymphoepithelioma-like carcinoma. Hum Pathol 27:258–262
31. Wolf H, Haus M, Wilmes E (1984) Persistence of Epstein–Barr virus in the parotid gland. J Virol 51:795–798
32. Yates J, Waren N, Reisman D, Sugden B (1984) A *cis*-acting element from the Epstein–Barr virus genome that permits stable replication of recombinant plasmids in latently infected cells. Proc Natl Acad Sci U S A 81:3806–3810

Virchows Arch (2006) 448: 655–658
DOI 10.1007/s00428-006-0175-8

CASE REPORT

Ines Gütgemann · Jens Standop · Hans-Peter Fischer

Primary intrahepatic malignant mesothelioma of epithelioid type

Received: 22 November 2005 / Accepted: 12 February 2006 / Published online: 16 March 2006

Abstract A case of epithelioid mesothelioma presenting as a primary intrahepatic tumor is described. The patient was a 62-year-old man with a 5.8-cm intrahepatic mass on an incidental intra-abdominal CT scan. Thorough clinical and radiographic examination did not reveal any evidence of tumor elsewhere. Macroscopic and microscopic examination demonstrated an intrahepatic tumor consisting of tubular and papillary proliferations of large epithelioid cells, surrounded by a densely mixed inflammatory infiltrate. The tumor cells were strongly positive for pancytokeratin, CK7, CA-12.5, and calretinin, as well as D2-40, and were faintly positive for thrombomodulin and vimentin. The proliferative rate was focally increased up to 20% by Ki-67 staining and the tumor expressed focally p53. Ultrastructurally, numerous microvilli on the cell surface, and abundant desmosomal plaques, characteristic of mesothelial cells, were found. To date, this is the third reported case of a primary intrahepatic mesothelioma.

Keywords Liver · Epithelioid mesothelioma

Introduction

Primary malignant nonepithelial neoplasms in the liver are rare and encompass angiosarcomas, fibrosarcomas, and leiomyosarcomas in descending order. Mesothelioma occurring primarily inside the liver has been reported exceedingly rarely in the world literature [7, 10]. Malignant mesotheliomas are observed in the pleural cavity (70%) and less often, in the peritoneum (20–25%; see p. 25 of [1]). In up to 70% of patients, mesotheliomas are associated with prior asbestos exposure [12]. They most often present with diffuse spread and advanced clinical stage. Less commonly they occur as solitary, localized lesions, as benign multicystic mesotheliomas [4], or benign papillary mesotheliomas [2]. Mesotheliomas locally occurring in the liver are exceedingly rare; more often, they occur as peritoneal tumors that involve the liver secondarily [11]. Previously designated "localized fibrous mesotheliomas" [8, 9], in retrospect, should better be classified as solitary fibrous tumors, if CD34-positive [13].

We report a case of a primary intrahepatic epithelioid mesothelioma in a 62-year-old patient who presented with nonspecific complaints of upper abdominal discomfort. This is the third reported instance of this type of lesion in this particular location. The clinicopathologic features and differential diagnosis of this tumor are described.

Clinical history

The patient was a 62-year-old accountant with no significant history of asbestos exposure, who presented with minor upper abdominal discomfort.

By ultrasound and computer tomography, a mass with cystic areas in the right liver lobe near the right adrenal gland was found. NMR studies revealed an encapsulated mass within the liver, most likely benign. The patient underwent radiographically guided biopsies that demonstrated mesothelial cell proliferations; a malignancy could not be excluded. Thorough clinical and radiographical intra- and extra-abdominal examination showed no other mass lesion. Subsequently, he underwent hepatic segmentectomy. Abdominal laparotomy showed no extrahepatic lesions. Five months after surgery, metastatic mesothelioma was detected within three periaortic lymph nodes.

I. Gütgemann (✉) · H.-P. Fischer
Institute of Pathology, University of Bonn (UKB),
Sigmund-Freud-Str. 25,
53105 Bonn, Germany
e-mail: ines.guetgemann@ukb.uni-bonn.de
Tel.: +49-228-2876968
Fax: +49-228-2875030

J. Standop
Department of Surgery, University of Bonn,
Bonn, Germany

Materials and methods

The tissues were fixed in neutral buffered formalin and embedded in paraffin for histologic processing. Tissue sections were stained with hematoxylin and eosin (H&E) and periodic acid-Schiff stain for conventional histology. Representative paraffin-fixed tissue blocks were cut and processed for immunohistochemical studies. The antibodies tested included the following: pancytokeratin MNF 116 (DAKO), calretinin (Chemicon), calretinin (DAKO), cytokeratin 7 (DAKO), D2-40 (Signet), WT-1 (DCS), thrombomodulin (DAKO), desmin (DAKO), CA 12-5 (DAKO), vimentin (DAKO), Ki-67 (DAKO), cytokeratin 5/6 (DAKO), cytokeratin 20 (DAKO), BerEp4 (DAKO), CA 19-9 (DAKO), prostate specific antigen /PSA (DAKO), prostate secretory protein /PSP (DAKO), thyroid transcription factor 1/TTF1(DAKO), HepPar-1 (DAKO), alpha-feto-protein/AFP (DAKO), CD31 (DAKO), CD34 (DAKO), carcinoembryonic antigen/CEA (DAKO), and p53 (DAKO). Immunohistochemical stains were performed on an immunostainer (Techmate 500; DAKO) and detected by means of the avidin–biotin complex (ABC method) using AEC (3-amino-9-ethylcarbayol) as chromogen.

For electron microscopy, formalin-fixed tissue in paraplast was dewaxed and diced into 1-mm^3 cubes, postfixed in 3% glutaraldehyde, and embedded in EPON. Ultrathin sections were stained with uranyl acetate and lead citrate and viewed in a Philips electron microscope CM10.

Results

The liver specimen showed a subcapsular, intrahepatic tan-white mass that measured 5.8 × 3.3 × 5.3 cm. The tumor was sharply demarcated against the surrounding normally appearing liver, but not encapsulated. The cut surface showed gray-white glossy tissue containing foci of recent hemorrhage (Fig. 1).

On scanning magnification of cytological and histological preparations, the tumor consisted of numerous epithelioid tumor cells arranged in cords, solid and papillary patterns (Fig. 2a–c). On higher magnification (Fig. 2b) and on cytologic preparations (Fig. 2c), the tumor contained islands and cords composed of round to polygonal cells with abundant pale eosinophilic cytoplasm. Other areas showed a more solid proliferation of epithelioid cells containing large atypical nuclei with prominent central or slightly eccentric nucleoli. Few mitotic figures were found and nuclear pleomorphism was noted. The tumor background consisted of rich inflammatory infiltrate composed of histiocytes, lymphocytes, and plasma cells (Fig. 2b). The tumor grew with blunt borders towards the surrounding liver tissue. Furthermore, the overlying liver capsule showed a dense inflammatory and fibrosing reaction with clefts lined by reactive mesothelial cells. Tumor cells did not reach the peritoneal cavity.

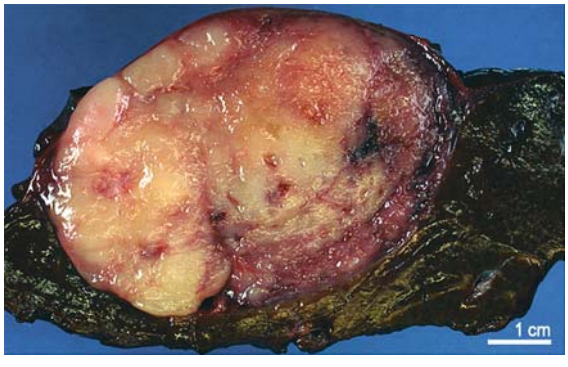

Fig. 1 Intrahepatic gray-white tumor, confined to the liver

The tumor cells were strongly positive for pancytokeratin, cytokeratin 7, D2-40, WT-1, CA 12-5, calretinin; focally and faintly positive for thrombomodulin (Fig. 2d–h); and weakly positive for vimentin. Focally, the tumor stained intensely positive for p53 in a nuclear pattern (Fig. 2i). Interestingly, similar focal expression was observed for the proliferation marker Ki-67 in up to 20% of tumor cells. Stains for cytokeratin 5/6, cytokeratin 20, BerEp4, CA 19-9, PSA, PSP, TTF1, HepPar-1, alpha-fetoprotein, CD31, CD34, and carcinoembryonic antigen were negative in the tumor cells.

Ultrastructural examination revealed flattened to polygonal tumor cells closely apposed to each other and delimited by a well-developed basal lamina (Fig. 3a). The cell surfaces abundantly contained long and slender microvilli (Fig. 3b). The tumor cells were connected to each other by well-formed desmosomes with attached tonofilaments (Fig. 3b). The nuclei were oval to round with occasional indentation of the nuclear envelope and they contained a single, prominent nucleolus (Fig. 3a). The cytoplasm contained scattered mitochondria, short strands of rough endoplasmic reticulum, polysomes, and abundant intermediate filaments. No secretory or mucin granules or any other specific organelles could be identified in the tumor cells.

Discussion

Localized malignant mesothelioma of the peritoneal cavity is rare. Even more uncommon are cases of mesotheliomas occurring primarily in the liver; therefore, they represent an important pitfall in pathologic practice. They are currently not listed in the World Health Organizaton classification of hepatic tumors [6]. Review of the literature only disclosed two previously reported instance of this rare occurrence [7, 10]. Interestingly, these mesotheliomas also were of epithelioid type.

Histomorphologically, mesotheliomas can be separated into localized and diffuse types. They are further subdivided into predominantly epithelioid, sarcomatoid, and biphasic types. Within the epithelioid category, morphologic variations such as tubulopapillary and solid can be distinguished [1]. In some cases, extensive leukocytic infiltrations can be observed adjacent to the tumor cells. The diffuse dense infiltration by leukocytes has been previously described as “mesothelioma with leukocytic

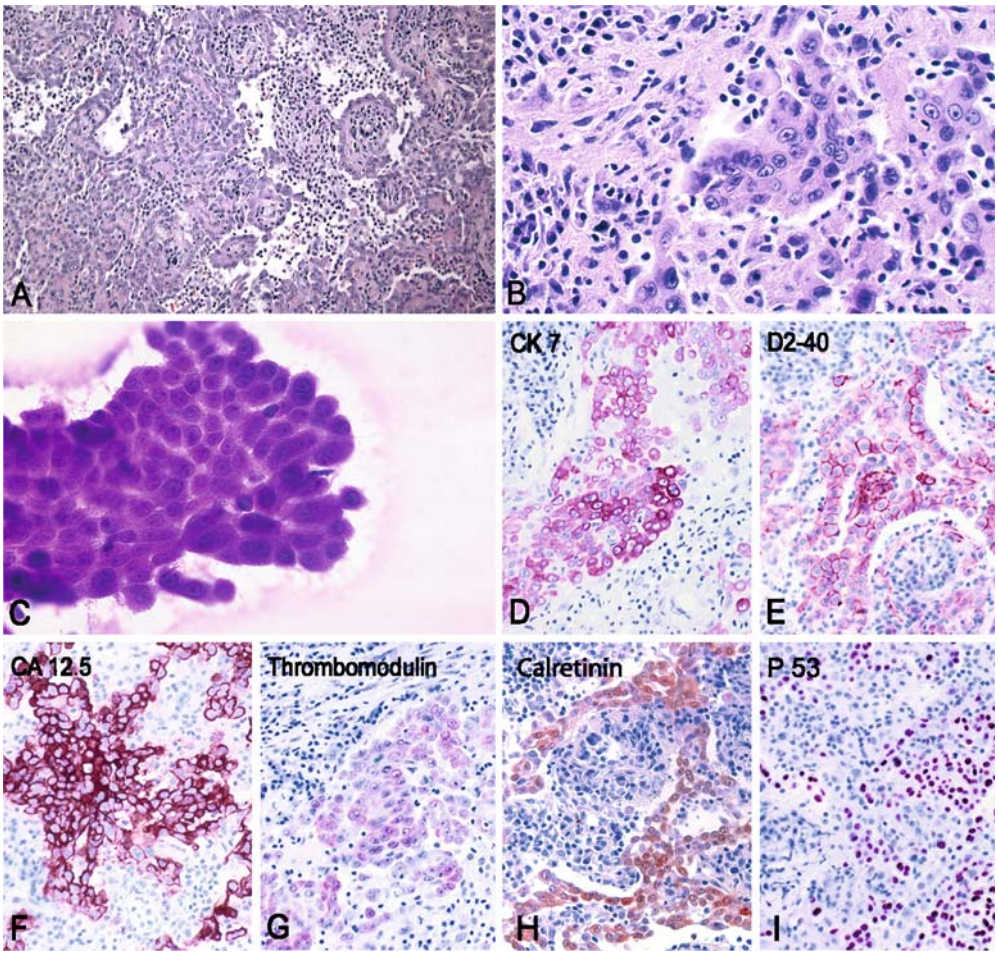

Fig. 2 Intrahepatic epithelioid mesothelioma, with **a** tubular and papillary patterns and clefts surrounded by an extensive mixed inflammatory infiltrate (H&E, 200×), **b** epithelioid tumor cells with atypical nuclei and prominent nucleoli (H&E, 400×), **c** papillary fronds in cytologic scrape preparation (H&E, 400×). Tumor cells express **d** CK7, **e** D2-40, **f** CA 12-5, **g** thrombomodulin, and **h** calretinin, and they are focally stained with **i** anti-p53 (DAB, 200×)

infiltrate" [5]. The case presented here showed an extensive, tumor-associated leukocytic infiltration, which was in contrast to the bland surrounding liver tissue.

With the extensive inflammatory background, it sometimes becomes exceedingly difficult to distinguish malignant mesothelial cells from their benign reactive counterpart. However, the intrahepatic localization of this tumor, the histomorphological features with monomorphic tumor cells, and highly atypical nuclei argue against reactive mesothelial cells. Furthermore, negative desmin stain on most tumor cells and positive focal p53 and Ki-67 positive nuclei support the diagnosis of a malignant epithelioid mesothelioma [3, 14]. In contrast, the intrahepatic mesothelioma observed by Imura et al. [7] showed a diffuse p53 staining pattern and a proliferative rate of 25%.

Based on clinical grounds primary liver tumors as well as a metastasis from a distant site enter the differential diagnosis. Cholangiocarcinoma, although CK7-positive, can be ruled out due to expression of mesothelial markers such as calretinin, thrombomodulin, and D2-40, as well strong expression of CA-12-5. The negative staining for HepPar-1 and the aforementioned positive mesothelial markers rule out a hepatocellular carcinoma. In terms of a metastasis, helpful findings are a lack of BerEp4, CA19-9, PSA, PSP, and TTF1.

The further differential diagnosis includes adenomatoid tumors, that can have an identical immunohistochemical

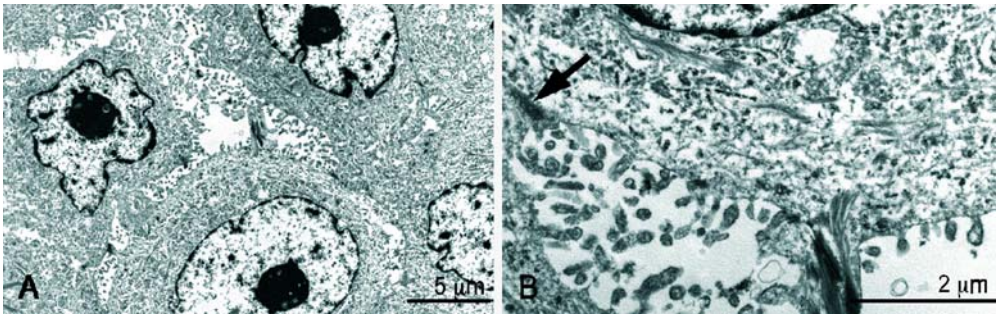

Fig. 3 Electron microscopically, epithelioid tumor cells show **a** atypical nuclei with prominent nucleoli and nuclear notches and **b** prominent microvilli and desmosomes (*arrowhead*)

staining pattern due to their similar histogenesis. The occurrence of these tumors in extragenital locations is however distinctively rare. In our tumor, the morphologic appearance of large polygonal cells, which are clearly malignant and morphologically consistent with the diagnosis of mesothelioma, and the observation of a dense leukocytic infiltrate support our interpretation.

It remains to be shown in more cases whether the prognosis of primary intrahepatic mesotheliomas is similar to peritoneal mesotheliomas and whether epithelioid morphology and circumscription is a common feature of these rare tumors.

Acknowledgements We thank J. Bedorf for electron microscopic analysis. Fundings and grants: I. Gütgemann by Deutsche Krebshilfe (#70-3238).

References

1. Battifora H EMW (1994) Tumors of the serosal membranes. Armed Forces Institute of Pathology, Washington, DC, pp 1–128
2. Burrig KF, Pfitzer P, Hort W (1990) Well-differentiated papillary mesothelioma of the peritoneum: a borderline mesothelioma. Report of two cases and review of literature. Virchows Arch A Pathol Anat Histopathol 417:443–447
3. Cagle PT, Truong LD, Roggli VL, Greenberg SD (1989) Immunohistochemical differentiation of sarcomatoid mesotheliomas from other spindle cell neoplasms. Am J Clin Pathol 92:566–571
4. Di Blasi A, Boscaino A, De Dominicis G, Marsilia GM, D'Antonio A, Nappi O (2004) Multicystic mesothelioma of the liver with secondary involvement of peritoneum and inguinal region. Int J Surg Pathol 12:87–91
5. Dorfmuller P, Krismann M, Muller KM (2004) Mesotheliomas with leucocytic infiltration. Pathologe 25:349–355
6. Hamilton SR, Aaltonen LA (eds) (2000) Pathology and genetics. Tumours of the digestive system. WHO classification of tumours. IARC, Lyon
7. Imura J, Ichikawa K, Takeda J, Iwasaki Y, Tomita S, Kubota K, Fujimori T (2002) Localized malignant mesothelioma of the epithelial type occurring as a primary hepatic neoplasm: a case report with review of the literature. APMIS 110:789–794
8. Kim H, Damjanov I (1983) Localized fibrous mesothelioma of the liver. Report of a giant tumor studied by light and electron microscopy. Cancer 52:1662–1665
9. Kottke-Marchant K, Hart WR, Broughan T (1989) Localized fibrous tumor (localized fibrous mesothelioma) of the liver. Cancer 64:1096–1102
10. Leonardou P, Semelka RC, Kanematsu M, Braga L, Woosley JT (2003) Primary malignant mesothelioma of the liver: MR imaging findings. Magn Reson Imaging 21:1091–1093
11. Marubayashi S, Ohdan H, Asahara T, Ikeda M, Hinoi T, Fukuma K, Maeda T, Oshiro Y, Shimamoto F, Dohi K (1998) Malignant mesothelioma originating in the hepatic falciform ligament: report of a case. Surg Today 28:929–931
12. McDonald JC, McDonald AD (1990) Asbestos and carcinogenicity. Science 249:844
13. Moran CA, Ishak KG, Goodman ZD (1998) Solitary fibrous tumor of the liver: a clinicopathologic and immunohistochemical study of nine cases. Ann Diagn Pathol 2:19–24
14. Zoppi JA, Pellicer EM, Sundblad AS (1995) Diagnostic value of p53 protein in the study of serous effusions. Acta Cytol 39:721–724

Virchows Arch (2006) 448: 659–660
DOI 10.1007/s00428-005-0013-4

LETTER TO THE EDITOR

Hans-Ulrich Schildhaus · Frank Dombrowski

Undifferentiated (sarcomatous) carcinoma of the liver with osteoclast-like giant cells presenting as tumor thrombus in the inferior vena cava

Received: 3 March 2005 / Accepted: 28 April 2005 / Published online: 13 September 2005

Dear Editor:
Hepatic tumors containing osteoclast-like giant cells (OGC) are very rare, and only few cases have been published since they were first reported by Munoz and co-workers in 1980 [4]. The nature of these tumors and the histogenetic origin of the giant cells have remained obscure for a long time. However, the association of hepatocellular carcinoma with highly pleomorphic tumor areas containing OGC has been recently described [3], a finding that was also confirmed by other authors. On the other hand, hepatic sarcomatous cholangiocarcinomas are also very uncommon, with only 17 cases published to date [2], and only one single cholangiocarcinoma with OGC has been reported [1].

We describe an extraordinary case of a cytokeratin 19-positive undifferentiated carcinoma with OGC and predominantly intravasal tumor growth into the heart, a manifestation of tumor spread resembling leiomyosarcomas of the inferior vena cava.

The patient, a 77-year-old Caucasian woman suffering from diabetes and liver cirrhosis, suddenly died of thrombotic occlusion of the inferior vena cava. The thrombus extended from the main branch of the right liver vein (Fig. 1a, arrow) to the ostium of the vena cava inferior in the right atrium (Fig. 1b). Metastases were noted in hilar lymph nodes and in the myocardium of the left ventricle, as well as in the thyroid. The tumor thrombus consisted of sarcomatoid anaplastic tumor cells (Fig. 1c) without mucus formation, intermingled with osteoclast-like giant cells (Fig. 1d). Neither chemotherapy nor chemoembolization of the tumor was performed. The tumor cells were strongly immunopositive for cytokeratins (Fig. 1e, antibody AE1/AE3), cytokeratin 19 (Fig. 1f), and vimentin. Cytokeratin 7 was weakly positive, whereas CD68 was exclusively detectable in giant cells and macrophages within the tumor thrombus. Tumor cells were immunonegative for hepatocyte antigen (HepPar1), alpha-fetoprotein, carcinoembryonic antigen, carbohydrate antigen 19-9, actin, smooth muscle-specific actin, desmin, CD31, CD34, S100, Melan A, HMB45, cytokeratins 5/6 and 20, thyroid transcription factor 1, thyreoglobulin, and CD117. After extensive examination, we noted a small invasive tumor area beneath the right liver vein (Fig. 1g), which was considered the primary hepatic tumor. Having assessed a total of over 30 tumor and liver tissue blocks, neoplastic glandular formations, atypia of intrahepatic bile ducts, and tumor areas resembling hepatocellular carcinoma were not detected. The lesion described here originated in a complete liver cirrhosis, with no morphologic or anamnestic clue as to its cause. A primary tumor of extrahepatic origin was excluded by autopsy.

Considering the results of our immunohistochemical examinations, we excluded several differential diagnoses, i.e. carcinosarcoma, nonhepatocytic malignant mixed tumor, epithelioid haemangioendothelioma, leiomyosarcoma, and other mesenchymal tumors. The strong expression of cytokeratins, including cytokeratins 19 and 7, supports our diagnosis of an undifferentiated (sarcomatous) carcinoma of the liver with cholangiocellular rather than hepatocellular differentiation.

Among the hepatic carcinomas, tumor expansion within the vena cava is more typical for hepatocellular carcinomas, as cases reaching the right atrium are known. However, caval invasion does not seem to be an exclusive feature of this carcinoma type, because even the first hepatic tumor with OGC, reported by Munoz et al. [4], invaded the hepatic vein. Interestingly, they considered the latter tumor an osteoclastoma-like giant cell tumor of Kupffer cell origin; however, later studies have clarified the reactive histiocytic nature of the osteoclast-like giant cells against the background of carcinoma cells in these tumors [3, 5]. Also, in our case, the benign-appearing, non-neoplastic giant cells were immunopositive for CD68 but not for epithelial markers.

H.-U. Schildhaus · F. Dombrowski (✉)
Department of Pathology, Otto von Guericke University,
Leipziger Strasse 44,
39120 Magdeburg, Germany
e-mail: Frank.Dombrowski@medizin.uni-magdeburg.de
Tel.: +49-391-6717869
Fax: +49-391-6717952

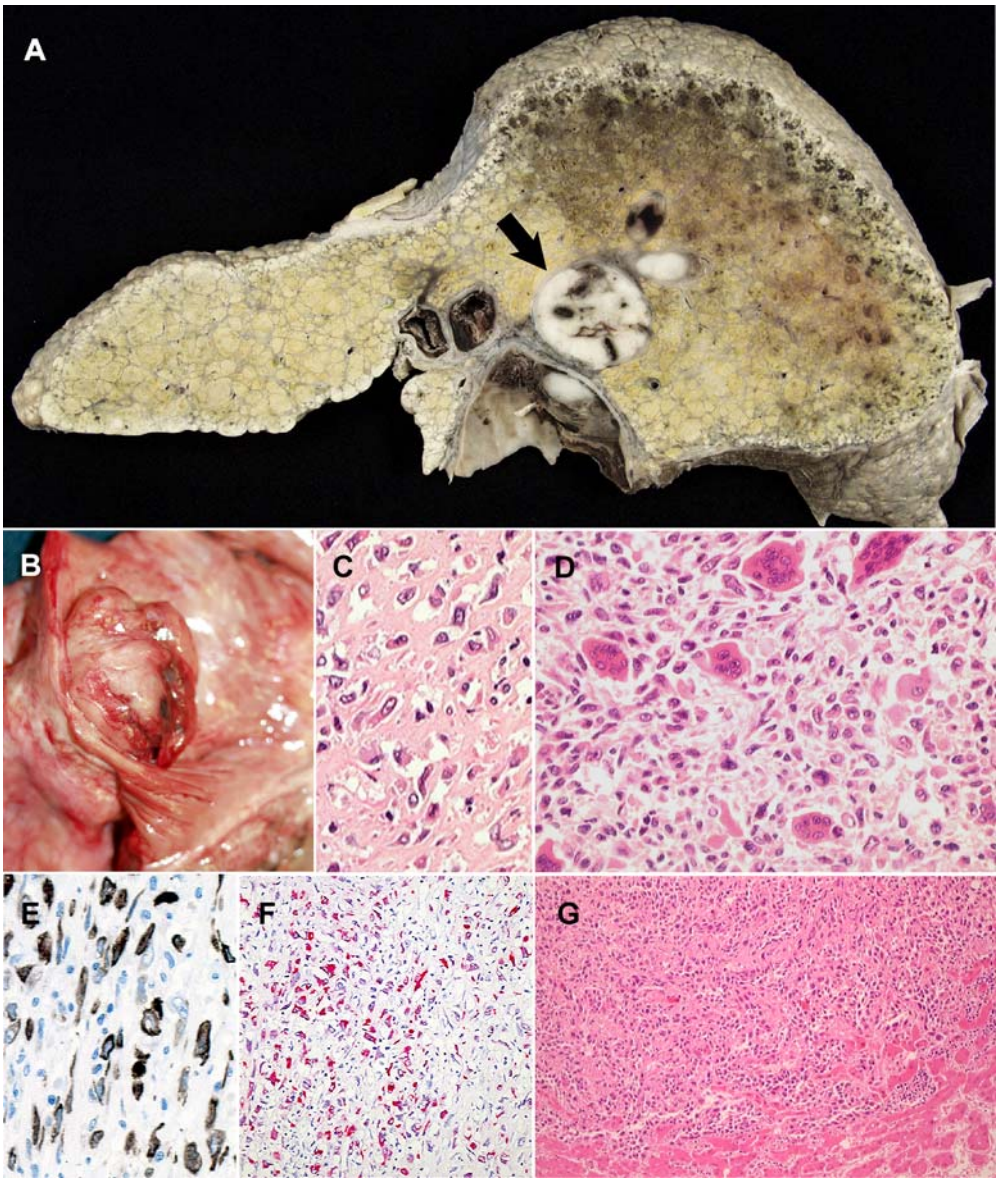

Fig. 1 **a** Within a completely cirrhotic liver, a white firm tumor thrombus was found in the right liver vein (*arrow*). **b** The thrombus extended to right atrium via the inferior caval vein. **c**, **d** The thrombus consisted of anaplastic sarcomatoid tumor cells and osteoclast-like giant cells (H&E). The tumor cell were immunopositive for cytokeratins (**e** AE1/AE3) and cytokeratin 19 (**f**). **g** Beneath the right liver vein, an invasive tumor focus was found in the liver parenchyma (H&E). *Lower edge* of the figure represents **c** 155 μm, **d** 540 μm, **e** 143 μm, **f** 610 μm and **g** 1,080 μm

Therefore, we prefer the term undifferentiated carcinoma with osteoclast-like giant cells for these rare hepatic tumors.

References

1. Haratake J, Yamada H, Horie A, Inokuma T (1992) Giant cell tumor-like cholangiocarcinoma associated with systemic cholelithiasis. Cancer 69:2444–2448
2. Kaibori M, Kawaguchi Y, Yokoigawa N, Yanagida H, Takai S, Kwon AH, Uemura Y, Kamiyama Y (2003) Intrahepatic sarcomatoid cholangiocarcinoma. J Gastroenterol 38:1097–1101
3. Kuwano H, Sonoda T, Hashimoto H, Enjoji M (1984) Hepatocellular carcinoma with osteoclast-like giant cells. Cancer 54: 837–842
4. Munoz PA, Rao MS, Reddy JK (1980) Osteoclastoma-like giant tumor of the liver. Cancer 46:771–779
5. Westra WH, Sturm P, Drillenburg P, Choti MA, Klimstra DS, Albores-Saavedra J, Montag A, Offerhaus GJ, Hruban RH (1998) K-*ras* oncogen mutations in osteoclast-like giant cell tumors of the pancreas and liver. Genetic evidence to support origin from duct epithelium. Am J Surg Pathol 22:1247–1254

Virchows Arch (2006) 448: 661–663
DOI 10.1007/s00428-006-0159-8

LETTER TO THE EDITOR

Suhail Al-Salam · Moueid Al Ashari

Ectopic pancreatic tissue in the anterior mediastinum

Received: 28 December 2005 / Accepted: 3 January 2006 / Published online: 1 March 2006

Dear Sir:

Heterotopia of pancreatic tissue is a common developmental anomaly reported in about 2% of all autopsies. Ectopic pancreatic tissue is most frequently found in the stomach (25–35%), duodenum (30%), jejunum (15–20%) and ileum (5%) [2]. In contrast, pancreatic tissue within the thoracic cavity and mediastinum is distinctly uncommon and is generally seen as a component of gastroenteric duplication cyst, intralobar pulmonary sequestration, or mature teratoma [4, 8]. Even rarer are benign mediastinal cysts with pancreatic tissue as their sole component. To our knowledge, the literature reports only five earlier examples of this lesion [2, 3, 7, 9, 10]. We report this case because of its rarity and the differences in the clinical presentation as well as part of the histological pattern from other reports.

A 40-year-old man presented with high fever, neck swelling, and difficulty in breathing for a few days. On examination, his body temperature was 39.4°C and his blood pressure 144/74 mmHg. The chest was clear and the abdomen was soft. Magnetic resonance imaging (MRI) revealed an anterior mediastinal cystic mass measuring 8×6×6 cm, with no evidence of any pulmonary lesion or pleural effusion (Fig. 1). The complete blood picture showed leukocytosis with a white blood cell count of 12,700/mm^3 and a high erythrocyte sedimentation rate of 81 mm/h. All biochemical tests including blood sugar and urine analysis were normal. A diagnosis of anterior mediastinal abscess was suggested. A drainage tube inserted under general anesthesia to drain the cyst, yielded 100 ml of turbid fluid, which was sent for cytological and microbiological examination, all of which were negative. After 1 week of antibiotic administration had failed to produce any clinical or radiological improvement, the decision was made to remove the lesion surgically under general anesthesia and the specimen was submitted for histopathologic examination.

Histologically, the cyst wall, which was in continuity with the thymic tissue, was lined by cuboidal to columnar epithelium with focal areas of pseudostratified ciliated columnar epithelium. The cyst wall itself was fibrotic and contained a disorganized mixture of ducts, acini, and islets of cells with typical appearance of pancreatic tissue. The ducts were variable in size and resembled interlobular and intralobular ducts. The ductal epithelium was simply columnar and mucinous. The exocrine acini were formed by polygonal cells with prominent eosinophilic apical cytoplasm with the characteristic appearance of zymogen granules (Fig. 2). These acini ranged in size from small, irregular aggregates of three to four cells to large lobules containing intralobular ducts and islet cells. The endocrine component was also variable in size and appearance; the islets ranged from small cellular aggregates to hyperplastic islets with irregular contour intermixed with exocrine acini. In numerous areas, the endocrine cells were connected directly to ducts and formed ductuloinsular complexes (Fig. 3). The distribution of the exocrine and endocrine components was highly variable within the cyst wall, but areas with large exocrine components tended to have few islets just as those with predominantly endocrine appearance had very few acini. In addition, areas of fibrosis were seen between islets and acini, which are not seen in normal pancreatic tissue (Fig. 3).

The cells of the examined tissue were phenotyped immunohistochemically by the streptavidin–biotin method using antibodies (DAKO), all diluted to 1:50. The neuroendocrine elements "neuron-specific enolase, chromogranin, PGP 9.5 and synaptophysin" were uniformly positive throughout the islets (data not shown), while immunoreactivity to insulin was seen in the majority of islet cells and

S. Al-Salam (✉)
Department of Pathology,
Faculty of Medicine and Health Sciences,
United Arab Emirates University,
Al Ain, UAE
e-mail: suhsalam@yahoo.com
Tel.: +971-37672000
Fax: +971-37671966

M. Al Ashari
Department of Pathology, Tawam Hospital,
Al Ain, UAE
e-mail: alrosi_2000@yahoo.com
Tel.: +971-37072411

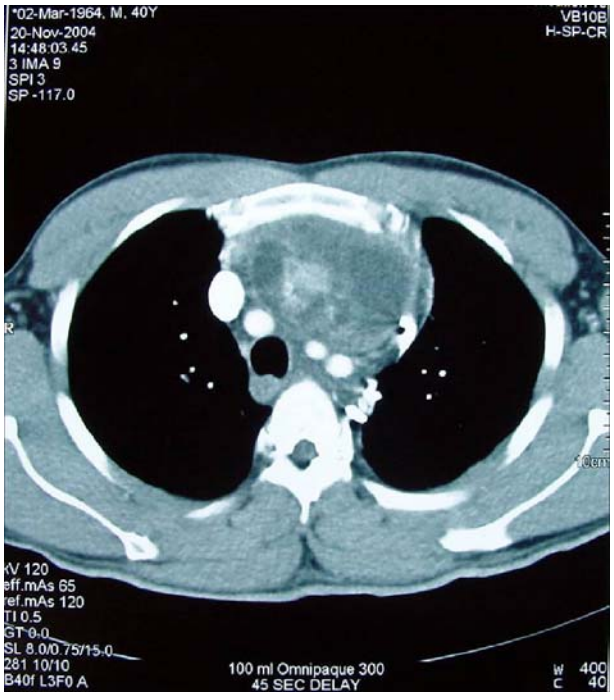

Fig. 1 MRI showing anterior mediastinal cyst

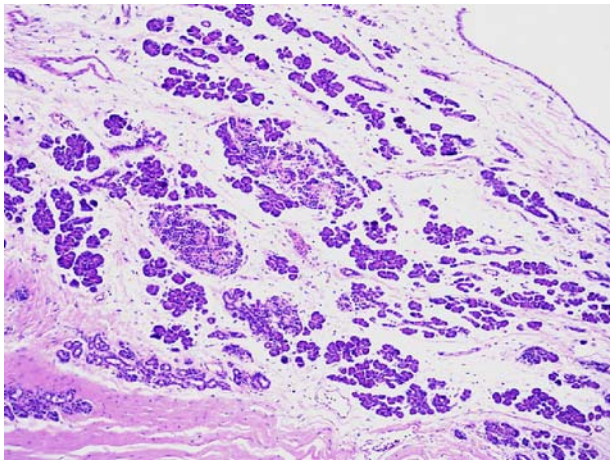

Fig. 2 Showing the cyst wall which is lined by low columnar epithlium and containing a mixture of a predominantly exocrine component with a few foci of endocrine component.H&EX50

in ductuloinsular complexes (data not shown). Glucagon and pancreatic polypeptide were discernible in a few cells in the periphery of the islets of Langerhans. In addition, pancreatic polypeptide was detectable in ductuloinsular complexes (data not shown). The immunoreactivity for somatostatin was seen in many more islet cells and in a few cells in ductuloinsular complexes (data not shown). Immunoreactivity to gastrin was seen in a large number of islet cells and in cells within exocrine ducts (Fig. 4). A diffuse staining for cytokeratin was also observable among the exocrine ducts, acini, and the lining of the cyst (data not shown).

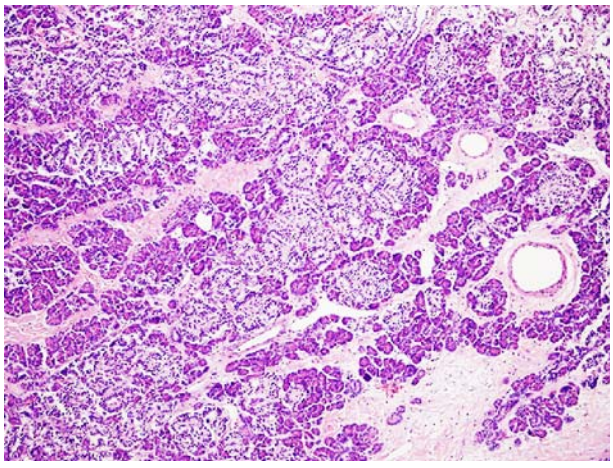

Fig. 3 A predominantly endocrine component of the ectopic pancreatic tissue showing the ductuloinsular complex.H&E, X50

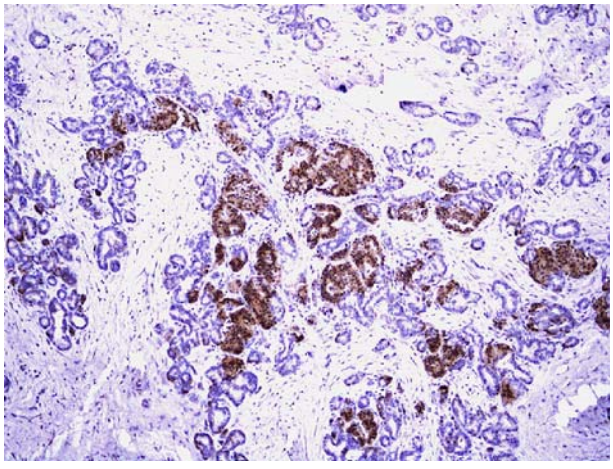

Fig. 4 Gastrin immunostaining, showing position staining of a large number of islet cell as well as scattered intraductal cell of the exocrine pancreatic component. Immunoperoxidase, X50

Mediastinal cysts formed only by pancreatic tissue are extremely rare, with only five cases being previously reported in the literature. In the report by Carr et al. [3], the exocrine component was described as predominant, whereas, Shilltoe and Wilson [9], both reported that islets were the more abundant tissue. In the reports by Perez et al. [7] , Cagirici et al. [2], and Tamura Y et al. [10], the distribution and architecture of acini and islets were irregular and haphazard as in the present case. It is noteworthy, however, that there were identifiable areas showing predominance of either acini or islets. In addition, there were hyperplastic islets and ductuloinsular complexes reminiscent of the microscopic appearance of diffuse nesidioblastosis [6].

Immunohistochemical staining confirmed the presence of the endocrine and exocrine pancreatic constituents of the cyst wall. This demonstrated a predominance of insulin-secreting cells in islets and ductuloinsular complexes. The similarity between the lesion and the fetal pancreas is

further supported by the increase in the number of gastrin-containing islet cells [5]. Gastrin-producing cells are present in a large number in fetal pancreas but are rarely, if ever, seen in adult pancreas and seem to play an important role as a trophic factor during intrauterine pancreatic development [5].

The presence of isolated neuroendocrine cells within ductal epithelium supports the hypothesis of a common duct epithelial stem-cell origin for ductal, acinar, and endocrine cells [6]. Our patient had no symptoms suggestive of hyperinsulinism or hypoglycemia, similar to other reports of mediastinal cysts and extragonadal teratomas [2, 3, 6, 8]. It has been suggested that the lack of clinical symptoms in these patients is due to the relatively small amount of functional neuroendocrine tissue present in these lesions and to its responsiveness to homeostatic mechanisms [1].

The pancreas and the lower respiratory tract share a common embryologic origin, the primitive foregut [7]. Therefore, we think that this lesion might represent a derivative of the ventral wall of the primitive foregut. Alternatively, it might have arisen as a result of unidirectional differentiation of primordial germ cells, which are frequently the source of anterior mediastinal teratomas. It is also probable that the lesion in our patient represents a developmental anomaly of undifferentiated endodermal epithelium, which, under unknown influences, differentiated into ventral fetal pancreatic tissue instead of into lower respiratory tract tissue [1]. This is supported by the presence of foci of pseudostratified ciliated columnar epithelium as a component of the lining epithelium of the cyst. Reports of pancreatic tissue within intralobar pulmonary sequestration provide evidence of the capacity of primitive foregut to differentiate along these seemingly dissimilar pathways [4]. The significance of gastrin in the histogenesis of this lesion is unclear; it is likely, however, that it plays a significant part in the growth and differentiation of this lesion, given its role as a growth factor in the neonatal pancreas [5]. In conclusion, the histogenesis of the lesion is unclear. We think that this lesion represents a derivative of the ventral wall of primitive foregut, but unidirectional differentiation of a benign cystic teratoma cannot be excluded. Anatomic location of the lesion and associated clinical observation may be important factors in establishing the final diagnosis.

Acknowledgements The authors would like to acknowledge Prof. Jean-François Fléjou in the Pathology department, St-Antoine Hospital, Paris, France as well as Prof. Ernest Adeghate in the Anatomy department and Dr. Samir Attoub in the Pharmacology department, in the Faculty of Medicine and Health Sciences, United Arab Emirates University, Al Ain, UAE, for their support during this work.

References

1. Bordi C, De Vita O, Pollice L (1985) Full pancreatic endocrine differentiation in a mediastinal teratoma. Human Pathol 16:961–965
2. Cagirici U, Ozbaran M, Veral A, Posacioglu H (2001) Ectopic mediastinal pancreas. Eur J Cardiothoracic Surg 19:514–517
3. Carr MJT, Deiraniya AK, Judd PA (1977) Mediastinal cyst containing mural pancreatic tissue. Thorax 32:512–516
4. Corrin B, Danel C, Allway A, Warner J, Lenney W (1985) Intralobar pulmonary sequestration of ectopic pancreatic tissue with gastropancreatic duplication. Thorax 40:637–638
5. Gittes GK, Rutter WJ, Debas HT (1993) Initiation of gastrin expression during the development of the mouse pancreas. Am J Surg 165:23–25
6. Hara M, Tsutsum Y (1986) Immunohistochemical studies of endocrine cells in heterotopic pancreas. Virchows Arch A Pathol Anat Histopathol 408:385–394
7. Perez-Ordonez B, Wesson DE, Smith CR, Asa SL (1996) A pancreatic cyst of the anterior mediastinum. Mod Path 9: 210–214
8. Qazi FM, Geisinger KR, Nelson JB, Moran JR, Hopkins MB (1990) Symptomatic congenital gastroenteric duplication cyst of the esophagus containing exocrine and endocrine pancreatic tissues. Am J Gastroenterol 85:65–67
9. Shilltoe AJ, Wilson J (1957) Enterogenous cyst of thorax with pancreatic tissue as a constituent. J Thorac Surg 34:810–813
10. Tamura Y, Takahama M, Kushibe K, Taniguchi S (2005) Ectopic pancreas in the anterior mediastinum.T Jpn J Thorac Cardiovasc Surg 53:498–501

Virchows Arch (2006) 448: 664
DOI 10.1007/s00428-006-0203-8

ANNOUNCEMENTS

1–3 June 2006
Technology Transfer in Diagnostic Pathology
1st Central European Regional Meeting: Liver & Pancreas Pathology
Eger, Hungary

The Hungarian Division of the International Academy of Pathology announces the ***Liver & Pancreas Pathology*** both for young and well-trained pathologists and clinicians.

The Meeting will focus on the practical clinicopathological aspects of liver and pancreatic diseases and conclude in a consensus. Among the highlights will be the differential diagnosis of hepatic and pancreatic tumors and premalignant alterations presented by *internationally renowned* experts, in active interaction with the attendants.

Plenary lectures will cover the themes of steatohepatitis, reversibility of cirrhosis, chronic hepatitis, classification and diagnosis of liver tumors, progenitor cells in the liver, pancreatitis, tumors of the pancreas.

Slide seminars will discuss autoimmune liver diseases (PBC, PSC, CAH), toxic liver injuries, benign and malignant liver tumors, tumor-like lesions of the liver, pancreatitis and pancreatic tumors.

Poster presentations will be reviewed and discussed individually by the participants.

For further information please contact

Scientific information:
Prof. Dr. Zsuzsa Schaff, Course Director,
schaff@korb2.sote.hu
Prof. Dr. Anna Kádár
kadann@korb2.sote.hu

Congress secretariat:
Ms. Katalin Mátray, K&M Congress Ltd.
Podmaniczky u. 75
H-1064 Budapest, Hungary
Phone: +36-1-3012000,
Fax: +36-1-3012001
e-mail: info@kmcongress.com
Website: www.kmcongress.com

15–16 June 2006
Thyroid Pathology for the Practicing Pathologist
15 rue de l'Ecole de Medecine, Paris, France

A 2-day course will take place in Paris again under the auspices of the French Division of the I.A.P.

This course will be given in English by Prof. M. Sobrinho-Simoes (Porto) and Prof. R. Heimann (Brussels).

It will consist of lectures alternating with slide reviews and slide seminar over a multuhead microscope. The cases of this seminar will be sent (on CD) before the meeting.

The audince will be limited to 22 participants.
Course fees: 390 euros (320 euros for members of any I.A.P. division).
The fees include registration, hand-out, CD of the slide seminar and coffee breaks.

For further information please contact
Mrs. M. Fontaniere
Administrative Secretary
French Division of the I.A.P.
32 Cours Albert Thomas
69008, Lyon, France
Fax: +33-4-18754311
e-mail: academic.pathologie@wanadoo.fr

Virchows Arch (2006) 448: 665–737
DOI 10.1007/s00428-006-0204-7

2ND INTER-CONGRESS OF THE EUROPEAN SOCIETY OF PATHOLOGY

SESSION A

DISPLAYED ON THURSDAY, MAY 25TH, 08.30-14.00

SESSION B

DISPLAYED ON THURSDAY, MAY 25TH, 15.00-20.00

SESSION C

DISPLAYED ON FRIDAY, MAY 26TH, 08.30-14.00

SESSION D

DISPLAYED ON FRIDAY, MAY 26TH, 15.00-20.00

P001

Paget's disease of bone in young man

Psarelis Savvas[1], Gazi Sousana[1], Trovas Georgios[2], Syrou Alexantra[3], Mahera Helen[3], Lyritis Georgios[2].
[1]Department of Rheumatology, [2]Laboratory for the Research of Musculoskeletal System, [3]Department of Pathology General Hospital of Attica "KAT", Athens Greece

Background: Paget disease of bone is an idiopathic metabolic disease of bone which is characterized by abnormal bone remodeling. Most often remains asymptomatic and usually occurs after age 40 years.
Objectives: We present a case of twenty years old young man who was referred to our department because of a high level of alkaline phospatase (ALP)in a routine blood test.
Case presentation: A complete clinical, laboratory, imaging investigation and bone biopsy from fourth lumpar vertebra was performed. Laboratory findings: ESR , CRP were within normal levels , BUN=36, Cr=1 , Cholesterol=262, HDL=56, LDL=148,8, VLDL=83, triglyceride=286, uric acid=6,2, SGOT=20, SGPT=36, bilirubin=0,8, albumin electrophoresis α1=2,7, α2=9,5, β=13,1 γ=12,6, Bence-Jones (-), CEA<0,8, AFP=1,35, CA19-9=0,1, PSA=0,53, HBsAg(-), Anti HCV(-), Anti HIV(-), TSH=1,843, T3= 1,03, T4=8,63Ca^{++}=10,1, P=3,6, ALP=149 (<128), Bone ALP=133 (<41,3), CTX serum=0,878(0-0,58), NTX serum=53,9 (5,4-24,2), Pyrilinks-D=7 (2,3-5,4), NTX urine=81 (20-50)LH=4,37, FSH=4,48, PRL=300,5, 25(OH) D3=32, PTH=23,5, Testosterone=4,38, Ca^{++}/Cr=0,054, P/Cr=0,62 Imaging findings:
a) The plain radiographs of lumbar spine (F/P) raised a suspicion of sclerosis of L_4 vertebra,
b) The bone scan with Tc99 revealed increased radionuclide uptake at L_4 vertebra, at right sacroiliac joint and at the caput of right femur
c) The Computer Tomography (CT) of lumbar spine showed mixed lytic and blastic lesions of L_4 vertebra.
d) The MRI of lumbar spine revealed collapse of the superior part of the body of L_4 vertebra with disturbance of bone architecture
e) Bone biopsy: Histologically, trabecular plates with abundant cement lines are recognized, which give rise to a "mosaic"pattern. Small pieces of fibrous tissue are intermingled between and bone tissue and only few osteoclasts are included. Moreover, the trabeculae have an osteoblastic rimming .After exclusion of others bone diseases the diagnosis of Paget's disease was made and the patient was treaded with pamidronate120 mg intravenously.The patient's blood test for ALP, every three months, was within normal limits and one year later a new MRI of lumbar spine showed the same lesions of bone but reduced bone oedema.
Conclusion: The Paget's disease of the bone rarely occurs at ages under 40 years old. In these cases the diagnosis is based on a detailed clinical, laboratory and imagine study to exclude other bone diseases but bone biopsy is always necessary to confirm the diagnosis.

P002

Acral skeletal metastases

J. Sopta*, M. Atanackovic*, A.Djordjevic**
*Institute of Pathology, School of Medicine , Belgrade, Serbia
**Institute for orthopedic surgery "Banjica", Belgrade, Serbia

Metastatic bone tumors are 25 times frequent than prime bone tumors, but skeletal metastases in distal bones than elbow and knee, are very rare. Phalanges of finger is extremely rare localization for metastases and occurred less than 1% from all localizations.
During the last 10 years (1996-2005) in the Register of bone biopsy, Institute of Pathology, School of Medicine, Belgrade is registered 624-bone metastases and just 3 cases of metastic carcinoma in phalanges witch present 0,48% of all metastases. All patients were mails (47, 55 and 77 years old, middle edge 59). Clinically all of them had swelling and pain of finger. Radiological all lesions were osteolytic, but without cortical destruction and no fracture. The clinical diagnosis was (in all cases) cystic lesion of phalanges, suspect enchondroma. After biopsy 2 cases were diagnosed as metastases of adenocarcinoma (we suggested lung or digestive tract as a primary localization) and one case as metastatic renal cell carcinoma. Patient with metastases of renal cell carcinoma had a diagnosis of prime tumor and nephrectomi was performed one year before. Patients with adenocarcinoma had no anamnesis of malignant disease and first clinical sign was swelling and pain of hand finger. On bronchoscope bronchial carcinoma was confirmed as a prime malignant tumor in both cases.
Acral skeletal metastases are very rare but they confirmed that haemathogenic dissemination of carcinoma is unpredictable. Unfortunately presence of acral bone metastases is sign of progressive malignant disease and poor prognostic factor.

P003

Malignant transformation of chronic fibroblastic periostal lesions

J. Sopta*, M. Atanackovic*, A.Djordjevic**
*Institute of Pathology, School of Medicine , Belgrade, Serbia
**Institute for orthopedic surgery "Banjica", Belgrade, Serbia

On the Register of bone biopsy, Institute of Pathology, Belgrade was registered 2 cases of malignant transformation of chronic proliferate fibroblastic periostal lesions. In our opinion this lesions should be analyzed as separate entities in bone tumors pathology. Both patients were males. First patient, 24 years old BM had a slow growing tumor in proximal part of tibia with 5 years long anamnesis. After the first biopsy lesion was described as a proliferate, posttraumatic fibroblastic lesion of periost. Patient had 6 relapses durind the 13 years until the final diagnosis- osteosarcoma. Second patient, ST was 34 years old when was performed the first biopsy of femoral lesion after trauma. In the period of 9 years he had 3 relapses and repeted byopsis. The final diagnosis was again osteosarcoma (low grade superficial). Proliferate potential of this lesions was investigated by Ki67. Expression of Ki67 were les intensiv This cases have in common a few elements: sex of patients, long evolution of lesions (13, and 9 years), trauma in anamnesis, many relapses (6 and 3), primary diagnosis of proliferate periostal lesions and finally, lesions were firstly clinically manifested when patients were young adults (period of life when osteosarcoma is the most frequent). Radiography, CT scan, MR, scintigraphy and histopathology characteristics of lesions firstly pointed to fibroblastic periostal proliferate lesions with expressive osteoid production up to mature bone. After many relapses and repeated biopsies with identical morphological findings- no malignancy but intensive proliferation of periostal fiber tissue and production of mature bone arise transformation and lesions become low grade malignant tumors (low grade malignant e in first biopsy and it become intensive in relapses, finale it was the most intensive in the last biopsy when was made diagnosis osteosarcoma. We conclude that increase of expression's intensity of Ki 67 prove to malignant transformations of posttraumatic proliferate fibroblastic periostal lesions.

P004

Fibrocartilaginous dysplasia. A very rare bone-tumor

Syrou Alexandra, Apostolou George, Staikidou Ioanna,
Babis George, Mahera Helen
General Hospital of Attikis "KAT", Department of Pathology

Fibrocartilaginous dysplasia is an extremely rare, mainly monostotic lesion, involving the femur, which is considered as fibrous dysplasia with massive cartilaginous differentiation. We present this case, concerning a 46-year old woman who visited our hospital complaining about a pain in her right knee which appeared 2 years ago, because of its rarity and bifocal appearance. On x-rays, an

osteolytic tumor at the distal metaphysis of the right femur was discovered. The tumor was eccentric originating from the bone cortex of the condylus lateralis, with a sclerotic rim and stippled calcifications, measuring 4×3cm. Subsequent CT and MRI imaging revealed the presence of fat in the central region of the lesion. There was another osteolytic eccentric lesion at the condylus medialis measuring approximately 1cm in diameter. It did not show any calcifications or fat. The lesions showed homogeneously high signal intensity on T2W images.The removed lesions was fixed in 10% buffered formalin and routinely processed for microscopic examination. The paraffin-embedded tissues were investigated by means of histopathology using hematoxylin and eosin stain and immunohistochemistry. Histologically, the first tumor consisted of a fibro-osseous lesion, characteristic of fibrous dysplasia, in juxtaposition to a large amount of hyaline cartilage, creating islands or nodules sharply demarcated from the surrounding fibro-osseous tissue. Enchondral ossification was focally seen as well as an infiltration of foamy histiocytes, which was visible between larger areas of predominantly fibrous tissue. Bone trabeculae around the cartilage islands were surrounded by osteoblasts. Immature osteoid formation was barely present. The second lesion, on the lateral condylus, also had the characteristic feature of fibrocartilaginous dysplasia.

P005

Uncommon site of chondrosarcoma development in a young adult

Alexandra Syrou, Patroklos Katafygiotis, Pikoulas Konstantios, George A. Apostolou, Christos Eliadis, Helen Mahera
Department of Pathology ,General Hospital of Attikis "KAT"',
2 Nikis St., Kifisia, Greece

Chondrosarcoma is a rare malignant bone neoplasm, which usually develops in the proximal extremities and the ribs and the majority of patients are older than 50 years. Chondrosarcomas in people younger than 45 years are rare and only individual cases are reported in very young patients. Our case concerns a 25-year-old woman who visited our hospital due to pain in the mean of her left tibia, with a 2-year duration, which occurred during touch, strike, or humidity. Radiologically, in the diaphysis of the left tibia an osteolytic region 10 cm in vertical dimension is found with explicit limits, that causes bone expansion and thick periosteal reaction. In the CT, linear calcifications are demonstrated in the superior and inferior department of the lesion. The removed lesion was fixed in 10% buffered formalin and routinely processed for microscopic examination. The paraffinembedded tissues were investigated by means of histopathology using hematoxylin and eosin stain. Histologically, features of a well-differentiated chondroblastic neoplasm are seen. The combination of the histological features, clinical and radiological data leads to the diagnosis of a well-differentiated chondrosarcoma, Grade I.

P006

Dedifferentiated chordoma – a case report

Vogiatzis P.[1], Kaltsa R.[1], Kritselis A.[2], Lekka I.[1]
[1]Pathology Department, [2]1st Department of Surgery,
METAXA Cancer Hospital, Piraeus, Greece

Chordoma is a rare malignant bone tumor of adult age that is restricted to the axial skeleton.The most common location is the sacrum (50%),followed by the skull base (35%) and the mobile spine (15%). Dedifferentiated chordoma is an even more rare subtype of chordoma which contains areas of high grade sarcoma in an otherwise conventional or chondroid chordoma. A 53 years old man with a clinical history of neurologic symptoms of radiculopathy at the lower extremities was admitted to the hospital with dramatically increasing pain, bladder and bowel dysfunction.Computed tomography of the pelvis showed a 15x13x10cm uncircumscribed mass, centered in the upper portion of the sacrum, extending caudally and involving the sacrum and the small pelvis.The surgical speciment biopsy showed the presence of conventional chordoma.Radiation therapy for two months was performed with no sign of improvement followed by a wide surgical operation.The histologic examination reported the presence of focies of dedifferentiated chordoma,with high grade sarcomatous features.Forty two months later,radical pelvic resection was performed due to reccurence.Chordoma with diffuse necrosis was found. According to the literature dedifferentiated chordoma has a worse biologic behavior than conventional/ chondroid chordoma due to its high metastatic potential.Because of this fact,all chordomas and particularly recurrent lesions,should be sectioned carefully,in order to exclude the possibility of a high grade sarcomatous component.

P007

Chondrosarcoma of the spine with an unusual presentation

Panelos J.D.[1], Batistatou A.[1], Voulgaris S.[2],
Michos E.[2], Agnantis N.J.[1]
Departments of [1]Pathology and [2]Neurosurgery,
University of Ioannina Medical School, Greece

Chondrosarcoma is the third most common primary malignancy of bone affecting primarily the bones of pelvis and being extremely rare in the spine. Herein, we present a case of a 65-year-old woman who presented with a persistent dry cough. Radiographic examination revealed the presence of a solitary nodule of the lung, with morphologic features most consistent with metastasis. Magnetic resonance imaging (MRI) and CT-scan revealed an ill-defined osteolytic lesion of the L5 vertebra with extension to the surrounding soft tissues. The patient underwent surgery and the mass was excised. The histopathologic examination revealed a moderately cellular multilobular neoplasm, with chondroid and myxoid matrix and focal necrosis. Under high power view multicellular lacunae of chondrocytes with moderate nuclear pleomorphism and hyperchromasia were observed. Mitotic figures were conspicuous. The tumor was diagnosed as chondrosarcoma, grade II. The patient underwent radiotherapy and is alive 6 months later. This is the first case of the rare chondrosarcoma of the spine presenting initially with symptomatology from the lung metastasis.

P008

Condensing osteitis of the clavicle (OCC). Report of two cases in males.

K. Revelos[1,2], M. Kalfa[2], A. Ntinis[2], Th. Filippidis[1,2].
[1]Pathology Department, 251 Hellenic Air Force General Hospital, Athens, Greece. [2]Micromedica Histopathology Laboratories, Athens, Greece.

Condensing osteitis of the clavicle is a rare, benign, variably painful condition affecting the medial end of the clavicle and it is characterised by sclerosis, expansion of the clavicular head and increased radiodensity. It is most commonly seen in middle-aged women. Reports of cases affecting males are few in the literature. Histologic examination reveals mature lamellar bone with thickened and irregularly broadened trabeculae and with slightly irregular cement lines. The trabeculae are focally lined by a single rim of osteoblasts. The intervening marrow is slightly fibrotic. A thickening of the cartilage, periosteal hyperplasia and fibrosis were recognised. We are adding two new histologically proved cases of the above entity occuring in men. The exact etiology of OCC still remains obscure but it has been postulated as a response to abnormal mechanical stress at the sternoclavicular joint (athletic stress, repeated episodes of heavy lifting, direct or repetitive trauma). Our first patient did not mention any previous trauma but the histological

findings were strongly suggestive of such a history and the second one used to exercise himself regularly. Further investigation and explanation of the discrepancy in the number of reported cases of OCC in men versus women is needed.

P009

Implication of the IL-6 – STAT3 signal transduction pathway and VEGF in the pathogenesis and progression of human chondrosarcomas

Dionysios J. Papachristou*, Odysseas A. Papaefthymiou*, Michael Doukas, Dimitrios Strefanou, Anna Batistatou and Niki J. Agnantis (*)
Equal contribution to the study
Department of Pathology, University Hospital of Ioannina, Greece

The molecular mechanisms that underlie chondrosarcoma (CS) pathogenesis are unclear. The STAT family of proteins is pivotal in mediating cytokine signaling. STAT3 is frequently activated in human malignancies and transformed cell lines, primarily via up-regulation of the IL-6/IL-6 Receptor – JAK1 signaling axis. In vitro and in vivo data suggest that IL-6 and the JAK1-STAT3 pathway induce up-regulation of the major angiogenetic factor, VEGF. In the present study we evaluated by immunohistochemistry the expression levels of IL-6, JAK1, its substrate STAT3 and VEGF, in 45 conventional CS, 21 enchondromas (EC) and in normal cartilage. Positive immunostaining for the examined proteins was observed in the majority of the CS, but in a small fraction of EC. The expression levels of all proteins were significantly and positively correlated to each other. These levels were substantially augmented in high-grade compared to low-grade CS and to EC. Our findings provide novel evidence that the IL-6 - STAT3 pathway is implicated in CS development and progression, either independently or through coordinated up-regulation of VEGF. Furthermore, our results reveal that VEGF can qualify as reliable molecular marker for the prediction of high-grade CS.

P010

Modecular Detection of Ewing Sarcoma Translocation T(11;22) by RT-PCR

Dabić M.M.[1], Meljanac K. [1], Bonevski A.[2], Seiwerth S.[1].
[1]Laboratory of Molecular Pathology, Institute of Pathology, Medical Faculty, [2] Department of Oncology,
Children Hospital Center Klaićeva, Zagreb, Croatia

Objectives: The Ewing sarcoma (ES) family of tumors appears as a bone or soft tissue lesion in a child or young adult and it is characterized with EWS-FLI1 t(11;22)(q24;q12) translocation. Our aim was to follow-up patients with detected translocations in parrafin blocks/fresh tissue, peripheral blood and/or bone marrow.
Patients and Methods: From October 2003 until January 2006 we received tumor samples paired with blood samples of eleven patients diagnosed with Ewing sarcoma during the treatment according to EURO EWING 99 protocol and also, we received six blood samples and six bone marrow samples collected from patients who finished the treatment. Total RNA was isolated and the EWS-FLI1 fusion transcripts were detected by RT-PCR using primers EWS22.2 Bam and FLI1C that specifically amplify both 125 pb type 1 fusion and 191 pb type 2 variant.
Results: Nine paraffin samples were positive for type I EWS-FLI1 fusion of which two didn't survive, and two for type II. Two blood samples were positive, one for type I, and another one for type II fusion in patients who finished the treatment. Conclusion: This specific RT-PCR assay is essential for Ewing sarcoma diagnosis and monitoring minimal residual disease, especially in EWS-FLI1 positive patients who have finished the treatment protocol.

P011

Mast cell sarcoma of tibia

Brčić L., Batelja, Vuletić L., [1]Stepan J.,
[1]Bonevski A., [1]Jakovljević G., Seiwerth S.
Institute of Pathology, Medical Faculty University of Zagreb, Croatia; [1]Oncology Department, Children's Hospital Zagreb, Croatia

Mastocytosis is a rare and mainly sporadic disease. Its main feature is an abnormal proliferation and tissue accumulation of mast cells. Mast cell sarcoma is a very rare disease, with 3 well-documented cases described in literature. It is characterized by local proliferation of atypical mast cells, destructive growth and very poor prognosis. A 4-year-old boy, presented with painful edema and deformation of his right lower leg. X-rays and CT revealed destructive tumorous mass. Histopathology showed tumour very rich with large, atypical cells, with hyperchromatic oval and polygonal nuclei. Cytoplasm around them was eosinophilic with many PAS-positive and Toluidine-Blue-positive granules. Immunohistochemically mast cells were positive for CD68, vimentin, CD 117 and CD 45. Soon rush developed with elevated serum tryptase level. One month after biopsy, disease progressed to mast cell leukemia. Follow-up computed tomography showed oval masses in both lower limbs. Targeted biopsy of the right tibia showed same pathohistological findings as the first one. Despite intensive chemotherapy patient died 8 months after first symptoms. Based on pathological findings, histochemistry and immunohisto-chemistry, we diagnosed for the first time a mast cell sarcoma of a bone, leading to leukemic transformation and death.

P012

Solitary plasmacytoma of the rib: analysis of a case

Bonitsis NG, Androulaki M, Raptis L, Gossios K*, Stefanaki S**, Kakadellis I***, Soutopoulos A, Mastora M, Akritidis N
Departments of Internal Medicine, Radiology*, Pathology** and Thoracosurgery Clinic***, Hatzikosta G. H. of loannina, Greece

Objectives: Solitary plasmacytomas occur mainly at male patients ≥ 50 years old and they reflect the 3-5% of all the plasmacytoma lesions.
Methods: Herein, we describe the clinical, histopathologic and immunohistochemical features of a case of a solitary plasmacytoma in a 45 - year-old man.
Results: The patient complained of chest pain and a mass parasternal at the right anterior chest wall. A chest X-ray showed a tumor shadow in the 8th right rib. Thoracic CT revealed a well-circumscribed mass measuring 11×7×6 cm infiltrating the anterior border of the 8th rib and extending into the 7th and 9th rib. The patient had no fever or fatigue. Laboratory findings were as following: Hct: 38%, ESR: 29 mm/h. IgA: 1875, IgE: 1150, IgM: 205. Serum sample: kappa chains: 1040, lamda chains : 365, TPR: 8.5mg/dl. Urinalysis was normal. Serum electrophoresis showed a low band monoclonal gammopathy. Bone marrow biopsy revealed 10% plasmacytosis. Histopathologic and immunohistochemical findings were compatible with k-mono-clonal mature plasma cell myeloma. The mass had been excised completely and the patient remains asymptomatic and the M-proteins were disappeared.

Conclusions: Solitary plasmacytoma is a rare thoracic tumor, whose complete surgical excision appears to be curative.

P013

Primary osseous classical Hodgkin's lymphoma: a rare entity.
Ipatia Doussis-Anagnostopoulou[1], Efthymia Giannitsioti[2], Fani Pliarchopoulou[2], Vassiliki Pappa[3], Kostantinos Soultanis[4], Christos Kittas[1].
[1]Laboratory of Histology and Embryology, National and Kapodistrian University, Athens Medical School, [24]th and [32]nd Department of Internal Medicine and [41]st Orthopedic Department, University of Athens, Attikon University Hospital, Chaidari, Athens, Greece

Classical Hodgkin's lymphoma (CHL) can involve extranodal sites, with bone being one of them. However, primary osseous CHL is a rarity. We present here a case of CHL localized in the pelvis in a 34 year old female, who presented with pelvic pain and fever. An x-ray and CT scan revealed a lytic lesion in the right pelvis and a first biopsy was reported as inflammatory pseudotumor. A second surgical biopsy that followed fifteen days latter revealed typical Hodgkin Reed-Sternberg cells surrounded by a reactive cell population, infiltrating intertrabecular areas and the surrounding soft tissues. The neoplastic cells were CD30+, CD15, LCA-, L26-, CD3-, EMA- and a diagnosis of CHL, mixed cellularity type was made. Clinical and laboratory investigation excluded systematic localisation of the disease. The patient received full chemotherapy (ABVD) for stage IV CHL. Last circle of chemotherapy was induced in November 2005. Since then, no relapse of the disease was noticed, while bone lesions have been partly restored. Primary osseous CHL should be differentiated from secondary infiltration of bone in nodal CHL and from osseous metastasis in advanced disease, as it carries a better prognosis.

P014

Constitutional Disorders of Bone of the Fetus and Infant: the Pathologist's Contribution
A.E. Konstantinidou[1], G. Agrogiannis[1], M. Petersen[2], H. Karadimas[2], E. Patsouris[1], G. Adamopoulos[3].
[1]Dept. Pathology, Medical Faculty, National Kapodistrian University of Athens, Greece, [2]Dept. Genetics, Institute of Child Health, Agia Sofia Children's Hospital, Athens, Greece,
[3]6th Orthopaedic Clinics, Asklepieion Hospital, Voula, Athens, Greece

Constitutional bone disorders (CBDs) are a large group of genetic disorders, comprising skeletal dysplasias (osteochondrodysplasias) and dysostoses. Skeletal dysplasias are a group of disorders with a disturbance in the development of cartilage and bone, resulting in growth defects of the skeleton. Dysostoses are defined as localized skeletal malformations occurring singly or in combination. Skeletal disorders may be prenatally detected by ultrasonography or result in intrauterine or early postnatal death. In this study, we present radiological, histopathological and molecular data of 21 CBDs diagnosed among 1322 fetal and perinatal autopsies over an 8-year period. The overall frequency of CBDs was 1:63 autopsies. Osteogenesis Imperfecta types IIa and IIb, Thanatophoric Dysplasia type I and the group of Short Rib with or without Polydactyly were the more frequently encountered disorders. Osteochondrodysplasias were diagnostically approached by prenatal ultrasound in 76% of cases, with a correct typing of the disorder achieved only in 19%. Dysostoses were represented only by Spondylocostal Dysplasia autosomal recessive type (Jarcho-Levin syndrome) and evaded prenatal ultrasonographic detection. The pathologist at autopsy is responsible of the correct interpretation of the radiographical, gross and histological findings, in order to accurately classify particular CBDs and enable genetic counseling.

P015

Eosinophilic fasciitis. A case report
Psarelis Savvas[1], Gazi Sousana [1], Mouflouzeli Helen[1], Nirakis Konstantinos[1], Tsatsani Panagiota[1], Mahera Helen[2].
[1]Department of Rheumatology, [2]Department of Pathology General Hospital of Attica "KAT", Athens Greece

Background: Eosinophilic fasciitis (EF) is an idiopathic, fibrotic disorder with the histopathologic hallmark of fascial fibrosis. The presentation is acute with painful, swollen extremities progressing to disabling cutaneous fibrosis.
Objectives: We present a woman sixty four years old who referred to our department because of diffuse sclerosis of extremities and upper part of the body.
Case presentation: The symptoms began one year ago and she hospitalised in internal medicine clinic with possible diagnosis of sclerodermia. The laboratory and imagine study were normal. The skin biopsy was compatible with her age. The patient was treated with D-Penicillamine 500mg/day and Prednizolone 10mg/day.
One year later she referred to our department complained for progressiveness of skin induration despite the therapy.
Physical examination revealed a diffuse, erythematous tenderness of the upper extremities and upper torso and cutaneous induration with a finely dimpled appearance (peau d'orange) of the extremities with normal skin of the hands.
Laboratory: WBC=6970, NEUT=65%, LYMPH=25%, EOS= 3,4%, HGB=12,2, HCT=38,2, PLT=156000, Glu=96, Cr=O,9, Bun=29, LDH=417, SGOT=19, SGPT=14, G-GT=16, ALP=172, ESR=20, CRP=11,8 ANA= 1/160, ds-DNA=(-), ENA=(-), SCL-70= (-),CA125=7,9, CA19-9=2, AFP=4,1, AFP=4,1, CEA=4.
Imagine: Plain radiographs of chest, Ultrasound of abdomen, U/s of heart, Computer Tomography of Chest were normal. A full-thickness incisional biopsy specimen obtained including skin, fat, fascia, and superficial muscle in continuity.
Histologic Findings: The epidermis was normal. Inflammatory infiltrate, including lymphoid follicles, involves the lower dermis, the septae, the fascia, and the muscle. The inflammatory infiltrate is mild to moderate and consists of lymphocytes, histiocytes and plasma cells. Eosinophils were not found. The findings were suggestive for the diagnosis of Eosinophilic fasciitis. Because of the EF diagnosis the patient was treated with Methotrexate 25mg/week subcouteneously and Prednizolone 20mg/day per os with good response.
Conclusion: The Eosinophilic fasciitis is a rare autoimmune disease and there is a debate whether EF represents a variant of scleroderma or it is a different disease. It is essential to put precise diagnosis because EF is not a systemic disease with better prognosis. For this reason biopsy is always necessary and the specimen must include skin, fat, fascia, and muscle in continuity.

P016

Angiomatoid fibrous histiocytoma containing cystic epithelial inclusions
T. Koletsa, D. Televantou, P. Hytiroglou, N. Fakhouri, G. Karkavelas.
Department of Pathology, Aristotle University, Medical School, Thessaloniki, Greece

We present two cases of angiomatoid fibrous histiocytoma (AFH) containing cystic epithelium-lined spaces. The tumors occurred in young women and were located in the subcutis of the lower extremities. On microscopic examination, they were moderately cellular and consisted of relatively uniform spindle or ovoid cells that

were arranged diffusely. A number of blood-filled cystic spaces were present. Hemosiderin deposits were observed. On immunohistochemical stains, the neoplastic cells were positive for vimentin and CD68, whereas stains for SMA, desmin, CD34, CD31, factor VIII-RA, S-100, EMA and various cytokeratins (CKs) were negative. In addition, the first tumor contained several cystic spaces of sweat duct origin, lined by a double cell layer with focal squamous metaplasia. On immunohistochemical stains, the inner layer of cells showed positivity for EMA and CKs cam5.2, AE1/AE3 and 17, while the outer layer was positive for SMA, and CKs cam5.2 and 17. The second tumor also contained a cystic structure, lined by keratinizing stratified squamous epithelium. To our knowledge, these are the first reported cases of AFH containing cystic epithelial inclusions of adnexal origin. These cases illustrate a mechanism of adnexal dilatation, which may be operative in neoplasms involving the dermis and subcutis, resulting in formation of tumors with unusual histologic features.

P017

Expression of Vascular Endothelial Growth Factor and its receptor, KDR/Flk-1, in Soft Tissue Sarcomas

Ann C. Goussia[1], Emilios E. Pakos[2], Pericles G. Tsekeris[3], Ioannis Nesseris[1], Evangeli S. Lampri[1], Dionysios J. Papachristou[1], Dimitrios Stefanou[1], Theodore Xenakis[2], Niki J. Agnantis[1]
Departments of Pathology[1], Orthopaedics[2] and Radiation Therapy[3], Medical School, University of Ioannina, 45110 Ioannina, Greece

Vascular endothelial growth factor (VEGF) is a protein that acts as a mitogen for endothelial cells and induces angiogenesis and changes in vascular permeability, both involved in tumor vascularization and growth. The aim of the study was to evaluate the association of VEGF and its receptor, KDR/Flk-1, with tumor grade, microvessel density (MVD) and clinical outcome in patients with soft tissue sarcomas (STSs). Tissue specimens of 28 patients with STSs were analyzed immunohistochemically using specific monoclonal antibodies Tissue specimens were obtained prior to treatment. Half of the STSs exhibited strong expression of VEGF that was associated statistically significantly with high tumor grade (p=0.006). Strong expression of KDR/Flk-1 was detected in only 2 sarcomas. No association was demonstrated between VEGF and KDR/Flk-1 expression. MVD was significantly associated with tumor grade (p=0.035) and was higher in sarcomas with strong VEGF expression. Limited data on clinical outcome precluded solid analyses for an association with disease progression. This study provides further evidence on the role of VEGF and MVD in tumor aggressiveness in STSs.

P018

Sclerosing rhabdomyosarcoma in a young adult

S. Barbanis, E. Kostopoulou, M. Ioannou, M. Nakou, D. Kourtis, G. Koukoulis.
Department of Pathology, University Hospital, Larissa, Greece.

Rhabdomyosarcoma (RMS) is rare in adults, represented primarily by its pleomorphic subtype. Recent reports present a novel variant of adult rhabdomyosarcoma, characterized by hyalinizing, matrix-rich stroma and designated as “sclerosing RMS”. Sclerosing RMS is rare in children, with 14 cases reported. Only eight cases of sclerosing RMS have been reported in adults. We present a case of a 26 year old man with a thigh tumor rapidly growing in the soft tissues and invading the femoral bone. The tumor and portion of the femoral bone were resected. The neoplasm showed moderate cellularity with short spindle cells embedded in a peculiar hyalinized matrix, reminiscent of primitive osteoid. No calcifications were present. Areas of necrosis were found. Many neoplastic cells showed strong nuclear immunoreactivity for MyoD1 but not for myogenin, an immunophenotype closer to embryonal RMS. One year later, the patient developed metastasis in his right arm with similar histological and immunohistochemical features and died 10 months later, despite aggressive treatment.
Sclerosing RMS is a rare variant which can be easily mistaken for other sarcomas such as osteosarcoma, sclerosing epithelioid fibrosarcoma and chondrosarcoma. Recognition of this rare variant is important in order to avoid a diagnostic pitfall and in order to clarify if this morphologic variation reflects genetic or biologic/prognostic differences.

P019

Epithelioid MPNST: Report of two cases.

Gerasimidou D, Manthou M-E, Kontopoulos A, Hytiroglou P, Karkavelas G.
Department of Pathology, Aristotle University Medical School, Thessaloniki, Greece.

Five percent or less of malignant peripheral nerve sheath tumors exhibit epithelioid features (EMPNST), which can raise difficult issues of differential diagnosis. We present two cases of EMPNST, encountered in women (both 43 years of age), one of whom had a history of NF1. This patient developed a lobulated neck mass, measuring 8.2 cm. The second patient had a relapsing tumor occupying the left cerebellopontine angle and measuring 3 cm. On microscopic examination, both cases consisted of diffusely arranged spindle or oval neoplastic cells with clear or eosinophilic cytoplasm. The cells had round or ovoid nuclei, some containing prominent nucleoli. In the first case, the epithelioid cells formed fascicles and whorls, sometimes surrounding vessels. A large peripheral nerve was seen in the fibrous pseudocapsule surrounding the tumor. Both cases exhibited large areas of necrosis. Immunophenotype: Case 1: (+) for vimentin, S-100, Leu7, CD117; focally (+) for NSE, GFAP, SMA, cam 5.2, CD34, (mild), NF (rare cells); and (-) for desmin, AE1/AE3, EMA, HMB-45. Case 2: (+) for vimentin, NSE; focally (+) for S-100, Leu7, GFAP, NF, cam 5.2, AE1/AE3; and (-) for SMA, desmin, EMA, CD117, CD34, HMB-45. Our findings emphasize the importance of immunohistochemistry in making the diagnosis of EMPNST. History of NF1 and origin from a peripheral nerve, as seen in our first case, are strongly suggestive of this diagnosis.

P020

Elastofibroma: Immunohistochemical Study of 5 Cases

Banu D. Gun*, Burak Bahadir*, Kemal Behzatoglu**, Mustafa O. Gun***, Sukru O. Ozdamar*
Departments of Pathology; Zonguldak Karaelmas University School of Medicine *, Istanbul Training and Research Hospital**, Zonguldak Ataturk State Hospital***, Turkey

Elastofibroma is a rare fibrous lesion characterized by accumulated abnormal elastic fibers and its etiology remains largely unknown. In this study, we analyzed five cases of elastofibroma to further explore the characteristics of its cellular composition and to learn more about their histogenesis. Immunohistochemistry was performed for mast cell tryptase, S-100, vimentin, CD34, smooth muscle actin (SMA) and collagen IV. Histochemical staining for Gomori’s trichrome and Verhoeff elastica-von Gieson, were also evaluated. Histopathologically a haphazard array of collagen, eosinophilic amorphous fibers, and globules in a fibrous tissue was seen. The elastic nature of the fibers was confirmed by elastic stain and with trichrome, collagen fibers were also demonstrated. The interspersed spindle or stellate cells were almost consistently positive for vimentin and frequently

positive for CD34. Mast cell triptase positive cells were present in three of the cases; collagen IV immunoreactivity was seen in two. No staining was observed with SMA and S-100. In conclusion, these findings suggest that CD34-positive mesenchymal cells are an integral component of elastofibroma and the presence of mast cells may play a role in the production of abnormal elastic fibers as a constant of subclinical trauma and repair.

P021

Soft tissue malignant tumors with epithelioid pattern - study of 15 cases.

Violeta Comanescu[1], Corina Gruia[1], Camelia Foarfa[2], Mirela Ghilusi[1], Iancu Emil Plesea[2], Bogdan Zaharia[2]
Departments of Pathology, [1]Emergency Universitary Hospital, [2]University of Medicine and Pharmacy, Craiova, Romania

Introduction, Aims: The study established the histogenetic type of soft tissue epthelioid malignant tumors using an immunohistochemical algorithm.
Materials and methods: 15 cases with epithelioid pattern were selected from a group of 135 soft tissue malignant tumors. Serial sections were stained with H-E and a wide pannel of antibodies.
Results: 4 of the cases arised in males and 11 in women. Most of them were in the 5th and in the 7th decades of life. The most frecvent sites of occurrence were the trunck and the lower limbs. In 1st step, 5 tumors were PCK. + and labeled as malignant synoviomas. In the 2nd step, the rest of 10 cases were all Vimentin + thus excluding neuroendocrin origin or other anaplastic tumors. In the 3d step, 3 cases were SMA +. and labeled as leyomiosarcomas. In the next step, 4 tumors were anti-S100 + and additionally, anti-HMB45 –, being thus considered malignant peripheric nervous sheet tumors. From the 3 cases S100 –, one case was CD31 CD34 + being considered angiosarcoma; one case, considered hemangioendothelioma, was CD31 + CD34 –; one was CD31 CD34 – and additionally anti-CD68+ being considered malignant fibrous histiocytoma.
Conclusion : The use of a guided multistep IHC algorithm resulted in establishing the correct histogenetic type in all studied cases.

P022

Expression of bone morphogenetic proteins and their receptors in neural tumors

Cheva A, Hytiroglou P, Kotoula V, Papadimitriou C, Karkavelas G.
Department of Pathology, Aristotle University Medical School, Thessaloniki, Greece

Bone morphogenetic proteins (BMPs) belong to the transforming growth factor β superfamily of proteins and play important roles in the regulation of cell survival, proliferation, differentiation and apoptosis. A variety of normal and neoplastic cell types have been found to express BMPs and BMP receptors. We investigated the expression of BMP-2, BMP-4, BMP-6, BMP-7, BMP receptor Ia and BMP receptor Ib in 12 paragangliomas, 5 pheochromocytomas and 7 glioblastomas multiforme by immunohistochemistry. Paragangliomas were characterized by moderate to strong, often extensive staining for BMP-6, while pheochromocytomas showed moderate to strong staining in significant numbers of tumor cells for all four BMPs assessed. Glioblastomas also showed moderate to strong positivity for all four BMPs, but the number of positive cells was usually small (<10%). All three tumor types were found to express BMP receptor Ia and BMP receptor Ib. These findings suggest that BMP signaling is involved in the development of these tumors. Despite their morphological similarities, paragangliomas and pheochromocytomas may have different mechanism of development.

P023

Axonal regeneration stimulated by erythropoietin after end-to-side nerve repair

Lykissas MG[1], Sakelariou A[1], Batistatou A[2], Korompilias AV[1], Mitsionis GI[1], Agnantis NJ[2], Beris AE[1].
[1]Department of Orthopaedics, University Hospital of Ioannina, Greece, [2]Department of Pathology, University Hospital of Ioannina, Greece

Aim of this study is to evaluate the effects of erythropoietin (Epo) in an end-to-side (e-t-s) nerve repair model. Forty-five male Wistar rats were evaluated in four groups: (A) e-t-s neurorrhaphy, (B) e-t-s neurorrhaphy and Epo administration for 20 days, (C) end-to-end neurorrhaphy, and (D) nerve stumps buried into neighboring muscles. Evaluation included functional and histologic examination, and wet weights of the tibialis anterior muscle. Quantitative evaluation included axonal counting and calculation of percent neural tissue (100 x neural area/intrafascicular area). During the first three weeks after surgery, the comparison between the four groups showed that there was significant difference between groups A, C, D and group B, with group B having clearly better results ($P<0.001$). However, there was rapid deterioration in the functional recovery when Epo's administration was discontinued. As a consequence, at the end of this study, erythropoietin failed to maintain its initial stimulating effect in axonal regeneration. Epo appears to facilitate peripheral nerve regeneration at the initial phase of its administration. Further investigation will be necessary to optimise the conditions (dose, mode of administration) in order to maintain its effects.

P024

Can end-to side neurorrhaphy bridge large defects?

Lykissas MG[1], Sakelariou A[1], Batistatou A[2], Vekris MD[1], Mitsionis GI[1], Agnantis NJ[2], Beris AE[1].
[1]Department of Orthopaedics, University Hospital of Ioannina, Greece,
[2] Department of Pathology, University Hospital of Ioannina, Greece.

This study was undertaken to evaluate collateral sprouting capability in an end-to-side repair model with long regenerative distance. Forty-five male Wistar rats were divided into four groups: (A) end-to-side neurorrhaphy with regenerative distance of 0.6 cm, (B) end-to-side neurorrhaphy with regenerative distance of 1.2 cm, (C) end-to-end neurorrhaphy, and (D) nerve stumps buried into neighboring muscles. Evaluation 150 days after surgery included peroneal and tibial nerve histologic and morphometric examination, and wet weights of the tibialis anterior muscle. Quantitative evaluation included axonal counting and calculation of percent neural tissue (100 × neural area/intrafascicular area). Functional evaluation using Peroneal Function Index demonstrated that there was no statistically significant difference between groups A and B, neither between groups B and C ($P>0.01$). Statistically, the differences in muscle weight of the reinnervated tibialis anterior between groups A, B, and C were insignificant ($P>0.01$). Furthermore, preliminary data on axonal counting did not reveal significant difference between groups A, B, and C. Our data support that a collateral sprouting mechanism can effectively bridge 1.2 cm nerve gaps. Thus end-to-side neurorrhaphy may be useful for the repair of divided human nerves with long gaps.

P025

Elastofibroma: Immunohistochemical Study of 5 Cases

Banu D. Gun*, Burak Bahadir*, Kemal Behzatoglu**, Mustafa O. Gun***, Sukru O. Ozdamar*
Departments of Pathology; Zonguldak Karaelmas University School of Medicine *, Istanbul Training and Research Hospital**, Zonguldak Ataturk State Hospital***, Turkey

Elastofibroma is a rare fibrous lesion characterized by accumulated abnormal elastic fibers and its etiology remains largely unknown. In this study, we analyzed five cases of elastofibroma to further explore the characteristics of its cellular composition and to learn more about their histogenesis. Immunohistochemistry was performed for mast cell tryptase, S-100, vimentin, CD34, smooth muscle actin (SMA) and collagen IV. Histochemical staining for Gomori's trichrome and Verhoeff elastica-von Gieson, were also evaluated. Histopathologically a haphazard array of collagen, eosinophilic amorphous fibers, and globules in a fibrous tissue was seen. The elastic nature of the fibers was confirmed by elastic stain and with trichrome, collagen fibers were also demonstrated. The interspersed spindle or stellate cells were almost consistently positive for vimentin and frequently positive for CD34. Mast cell triptase positive cells were present in three of the cases; collagen IV immunoreactivity was seen in two. No staining was observed with SMA and S-100. In conclusion, these findings suggest that CD34-positive mesenchymal cells are an integral component of elastofibroma and the presence of mast cells may play a role in the production of abnormal elastic fibers as a constant of subclinical trauma and repair.

P026

Parachordoma or Myoepithelioma: Case Report

Kemal Behzatoglu*, Burak Bahadir**, Banu D. Gun**, Sule Canberk*, Erol R. Bozkurt*, Sukru O. Ozdamar**.
Departments of Pathology; Istanbul Training and Research Hospital*, Zonguldak Karaelmas University School of Medicine **, Turkey

Parachordoma is a rare soft tissue tumor with characteristic histologic appearance similar to chordoma. However, immunohistochemically they express different staining patterns; both chordoma and parachordoma express S100 protein, unlike chordoma parachordoma also expresses cytokeratins. Having significant differences in therapy and prognosis, the distinction between these two entities are clinically important. Histogenesis of parachordoma has remained uncertain. In the recent WHO classification, myoepithelioma and parachordoma were included in the same category. Studies suggesting that they should be regarded as separate entities also exist. The current case represents a 65-year-old woman with a slowly growing, immobile and deeply located mass on her left popliteal region. Microscopically, the tumor was composed of multinodular nests of epithelioid cells many with vacuolated cytoplasm resembling physaliferous cells typically found in chordomas. Immunohistochemically, the cells were reactive with GFAP, LMW cytokeratin, vimentin, S-100, SMA and calponin. In summary, histologic findings of the current case were typical of parachordoma; nevertheless immunohistochemistry supported a myoepithelial origin. Parachordoma needs to be studied more to uncover its nature.

P027

Myxoid liposarcoma in a child. A comparative morphological and immunohistochemical study with benign pediatric adipose tumours

C. Kaprilian[1], A.M. Athanassiadou[1], K. Stefanaki[1], C. Van Vliet, Konstantinidou[1], E. Dimitriadis[2], A. Patereli[1], N. Pandis[2], O. Karentzou[1].
Dept of Pathology[1], Aghia Sofia Children's Hospital, Dept of Genetics, [2]Agios Savvas Anticancer Hospital, Athens Greece

Adipose lesions account for only 6% of pediatric soft tissue neoplasms, while liposarcoma comprises less than 1% of pediatric sarcomas. Prompted by the diagnosis of a myxoid liposarcoma in the thigh of a 11 year old girl, we have reviewed our archives for 7 years and investigated the features of adipose lesions. Our material comprised 29 lipomas, 9 lipoblastomas, 3 lipofibromatoses and 1 myxoid liposarcoma. The Steptavidin Biotin method was performed for the detection of Smooth muscle actin, Desmin, CD34, S-100, bcl-2, Ki-67, p53, p75/NGFR, c-kit. Three lipoblastomas were diffuse and 6 circumscribed, while the myxoid liposarcoma did not invade the adjacent skeletal muscle. Six lipoblastomas demonstrated a variable proportion of cellular and myxoid areas. S-100 and CD34 were detected in variable stellate cells in all lipoblastomas and the myxoid liposarcoma, while bcl-2, p75 and p-53 were detected in 2 lipoblastomas. Ki-67 was detected in 1-15% of the nuclei in lipoblastomas and in 5-15% of the liposarcoma. The diagnosis of myxoid liposarcoma was confirmed by the detection of the FUS/CHOP fusion gene by long PCR. Morphology and genetics play the major role in the differential diagnosis of pediatric myxoid liposarcoma from lipoblastomas.

P028

Extra-abdominal desmoid tumor. Case report and literature review

Ch. Tsobanidou[1], Th. Jivannakis[2], A. Kapraki[2], N. Papadopoulos[3], A. Eleftheriadis[4]
[1]Department of Pathology, Theagenio Anticancer Institute, Greece, [2]Department of Pathology, General Hospital of Drama, Greece, [3]Dep. Histopathology-Embryology, Democritus University of Thrace, Greece, [4]Medical Center of Alexandria, Greece

Objectives: Desmoid tumor (aggressive fibromatosis) is an aggressive fibroblastic proliferation of well circumscribed, locally invasive, differentiated fibrous tissue. Is a rare tumor with a high potential for recurrence.
Case Report: We report a case of 59 years old woman with a slowly growing tumor on the buttock, which was completely surgically removed. Grossly the tumor was firm and whitish with ill-defined outline and with a diameter 4,5 cm. Microscopically composed of proliferating cells with features of fibroblast and smooth muscle cells without cytologic atypia or mitotic activity. These cells infiltrate the adjacent muscle bunds. Between the proliferated cells there are small amount of collagen. The diagnosis of desmoid tumor was done. The patient remains asymptomatic 43 months after surgery.
Conclusions: Desmoid tumor is a rare lesion having intermediate biological behavior between benign fibrous lesion and fibrosarcoma. Genetic, endocrine and physical factors have been implicated as causative agents. The diagnosis is made histologically. Reactive fibromatosis and fibrosarcoma must be eliminated in differential diagnosis. A high incidence of recurrence was seen. The rarity of cases in even anticancer centers has traditionally limited the ability to study this disease. The treatment of choice is a prompt radical excision including a wide margin of involved tissue. Adjuvant therapy, such as x-ray treatment, chemo-and hormone therapy, are indicated when the tumor is inoperable or too extensive for surgery.

P029

Desmoplastic small round cell tumor

Ch. Tsobanidou[1], N. Vladika[1], A. Dimasis[2], D. Paikos[3], P. Xirou[1], Th. Toliou[1]
[1]Pathology Department, Theagenio Anticancer Institute, Thessaloniki, Greece, [2]Surgery Department, Theagenio Anticancer Institute, Thessaloniki, Greece, [3]Gastroenterology Department, Theagenio Anticancer Institute, Thessaloniki, Greece

Objectives: Demoplastic small round cell tumor (DSRCT) is a rare, highly aggressive neoplasm with characteristic age incidence, anatomic location, histologic appearance, immunohistochemic profile and molecular genetic features. This tumor characterized by nests of small undifferentiated cells that show immunohistochemical evidence of epithelial mesenchymal and neural differentiation.
We report the morphologic and immunohistochemical features of a case of DSRCT
Material and Methods: A 29-year-old man presented to the hospital with a short history of severe hypogastric pain. Computed Tomography (CT) revealed an ovoid solid mass located within the mesentery, which attached to large bowel. Evaluation of metastatic disease yielded no evidence of metastasis. Laboratory values for human chorionic gonadotropin, alpha-fetoprotein and carcinoembryonic antigen were within normal limits.
Results: Macroscopically, the mass consisted of a well circumscribed, non encapsulated, ovoid, nodular tumor, measuring 8,5×8×5,5 cm. A segment of unremarkable large bowel was attached to the superior surface of the tumor. The surrounding omentum was studded with numerous variably sized but overall small tumor nodules.
Microscopically, the tumor and tumor nodules composed of compact nests of round and oval cells separated by desmoplastic stroma. The tumor cells were relatively uniform with round-to-oval hyperchromatic nuclei and inconspicuous nucleoli. The cytoplasm was scarce and the cell borders were indistinct. Mitosis were frequent. Immunohistochemically, the tumor cells showed strongly positivity for NSE, Neurofilament, Myoglobulin, SMA, Vimentin, CEA, EMA, Ker 8/18, focal positivity for S-100, Ker AE1/AE3 and they were negative for Cromogranin, Calretinin, PLAP, TTF-1, CD-99, CD117, CerbB2, Synaptophysin, Desmin, Ker7, KerHMW.
The patient was treated with chemotherapy and was alive 14 months after the operation.
Conclusions: Tumors with divergent differentiation often posed problems of diagnosis particularly with regard to distinction from a number of small cell tumors. The immunohistochemical evidence is particularly useful to confirm the diagnosis of these rare tumors.

P030

Mechanisms of tumor progression in Kaposi's sarcoma.
MT Femández-Figueras, L Puig**, E Musulen,
RM Penín, C Ferrándiz*, G Sirera, I Bielsa*, A Ariza.
Depts. of Pathology and Dermatology*, Hospital Universitari Germans Trias i Pujol, Badalona, Spain, and Dermatology**, Hospital de la Santa Creu i Sant Pau, Barcelona, Spain

The most common clinical presentations of Kaposi's sarcoma (KS) in our environment are classic KS (C-KS), and AIDS-associated KS (AIDS-KS).
Objectives: Tissue arrays representative of 79 biopsy specimens of KS (51 AIDS-KS: 16 plaques, 16 tumors, 12 extracutaneous lesions and 7 regressive lesions, and 28 C-KS: 15 plaques and 13 tumors) were studied in order to compare mechanisms of tumor progression in both forms of KS.
Methods: We evaluated the immunohistochemical expression of molecules involved in cell cycle acceleration, apoptosis inhibition, angiogenesis and local invasion: p53, Skp2, p38, c-kit, Bcl-2, survivin, NFkappa, VEGFR2, VEGFR3, beta-catenin, CD44H, CD44v3, CD44v6, metalloproteinases (MMPs) 3,7,10,14,15,16 and 23, and tissue inhibitors of metalloproteinases (TIMPs) 1,2, 3 and 4. We also evaluated the intensity of HHV8 expression, proliferation index (Ki68), and presence of iron deposits.
Results: We found statistically significant differences between C-KS andAIDS-KS as regards the expression of survivin, VEGFR2 and MMP10 and, differences in the expression of HHV8, beta-catenin, p53, Skp2, Bcl-2, p38, VEGFR2, MMP10, TIMP3 and TIMP4 in relation to stage.

Acknowledgement: Work financed by Grant FIS PI020514 of the Spanish Ministerio de Sanidad y Consumo.

P031

Soft tissue malignant tumors with small round cells - study of 21 cases
Camelia Foarfa[1], Serenada Bala[2], Stelian Danut Enache[2], Iancu Emil Plesea[1], Mirela Ghilusi[2], Bogdan Zaharia[1]
Departments of Pathology, [1]University of Medicine and Pharmacy; [2]Emergency Universitary Hospital, Craiova, Romania

Introduction, Aims: The study established the histogenetic type of soft tissue small round cells (SRC) malignant tumors using an immunohistochemical algorithm.
Material and Methods: 21 cases with SRC pattern were selected from a group of 135 soft tissue malignant tumors. Serial sections were stained with H-E and a wide pannel of antibodies.
Results: 9 of the cases arised in males and 12 in women. 1/3 of them were in the 7th decade of life. The most frecvent sites of occurrence were the trunck and the lower limbs. In 1st step, all tumors were PCK. – excluding SRC carcinoma and polyphenotipic tumor. In the 2nd step, all cases were Vimentin, + suggesting the use of myogenic markers. In the 3d step, 11 cases were Desmin and Myoglobin + SMA – and labeled as rhabdomyosarcomas. In the next step, the remaining 10 tumors – to myogenic markers, were stained simultaneously for neuroendocrine markers and S100-protein. 5 cases were synaptophysine (Sy), chromogranin (Ch) and S100+ and considered as Ewing sarcomas. 4 cases were Sy and Ch – and S100 +, being considered as lyposarcomas. The case Sy, Ch and S100 – and also CD31 CD34 –, CD68 – and collagen IV – was considered fibrosarcoma.
Conclusions: The use of a guided multistep IHC algorithm resulted in establishing the correct histogenetic type in all studied cases.

P032

Intraspinal Melanocytoma (A Case Report)
Banu D. Gun*, Burak Bahadir*, Mustafa O. Gun**,
Sukru O. Ozdamar*, Gamze M. Kuzey***.
Departments of Pathology; Zonguldak Karaelmas University School of Medicine*, Zonguldak Ataturk State Hospital**, Hacettepe University School of Medicine***, Turkey

Melanocytoma is a primary melanocytic neoplasms of the central nerve system and accounts for %0.06–0.1 of all brain tumors. These tumors are biologically benign and originate most frequently from the melanocytes of the leptomeninges that are derived from the neural crest. Here a rare case of melanocytoma in the spinal cord of a 49 year-old woman is presented. Histopathologically the tumor cells were arranged in tight nests, sheets and fascicles with a variable amount of pigment. Mitotic rates ranged from zero to one per 10 high-power fields and no necrosis was seen. Immunohistochemically positivity with S100 and HMB 45 favored melanocytic origin, but there were no reaction with GFAP, vimentin and EMA. It has been expressed that melanocytoma must be distinguished from other pigmented CNS lesions and especially from malign melanoma, that has a different biological behavior.

P033

Primary central nervous system lymphoma. A case report
Vasilakaki Th, Petrakopoulou N, Nikolaidou ME,
Katsamagkou E, Zizi – Serbetzoglou A
Department of Pathology, Tzaneion General Hospital of Piraeus, Piraeus, Greece

Primary central nervous system lymphoma is an uncommon form of non Hodgkin's lymphoma that has been increasing in incidence over the past three decades. It is seen in immunocompetent and immunodeficient population, the later group associated with the Epstein-Barr virus. The causative factors accounting for this increase in the number of cases are unknown. Primary central nervous system lymphoma can affect the brain, leptomeninges, spinal cord or eyes. PCNSL shows a male preponderance with a peak incidence in the 5th-7th decade (3rd-4th in AIDS). The initial symptoms are specific neurologic deficits, mental status changes , seizures and symptoms and signs of increased intracranial pressure (headache, naesea, vomiting). We report a case of a 72-year-old woman who came to our hospital with headache and neurological deficits for the last 2 months. CT scan image have shown a mass in the right bregmatic region. The diagnosis was based on the histological study of the specimen obtained through a stereotactic biopsy. The surgical specimen was histologically high malignant non Hodgkin Lymphoma of the diffuse large B cell type. Immunohistochemically the tumor cells were positive for LCA and L26 but were negative for EMA, cytokeratins, vimentin, GFAP, BerH2 and S-100 protein. After additional clinical and laboratory screening there was no other evidence of lymphatic disease. The patient was submitted to the anticancer hospital for further treatment. The majority of primary central nervous system lymphomas are large B cell variants of high grade malignancy. Low grade subtypes and T cell lymphomas are rare. The treatment is based on a combination of methotrexate based chemotherapy followed by whole brain radiotherapy. Unfortunately, treatment related neurotoxicity is common, especially in the elderly. Treatment of recurrence also remains controversial and the mortality rate is still high.

P034

Vascular endothelial growth factor immunohistochemical expression in meningiomas

Zagorianakou P[1], Voulgaris S[2], Zagorianakou N[1], Zissi A[2], Pachatouridis D[2], Polyzoidis K[2], Stefanou D[1], Agnantis NJ[1].
Departments of Surgical Pathology[1], Neurosurgery[2],
University Hospital of Ioannina, Medical School of Ioannina, Greece

Background: In human meningiomas, histological evaluation alone does not always predict the clinical outcome and behavior. Monoclonal antibody to Ki-67 (MIB1), a nuclear protein related to cell proliferation has therefore, become a potential tool in the histopathological grading of these tumors. Meningiomas are hypervascular tumors and require neovascularization for growth. Vascular endothelial growth factor (VEGF) is a key factor in vasculogenesis. Morphologically tumor vasculogenesis is assessed by measuring microvessel density (MVD). The purpose of this study was to investigate the MVD in 55 cases with primary diagnosis of meningioma, and the possible correlations with VEGF and ki-67 immunohistochemical expression, peritumoral edema and disease progression.
Methods: A total of 55 intracranial meningiomas, classified as benign (51cases), atypical (3 cases), and anaplastic (1 case) were analyzed. VEGF expression and microvessel density (MVD) were immunohistochemically investigated; the expression of CD34 was examined by immunohistochemistry so as to calculate the microvessel density (MVD).
Results: Six of the cases presented with recurrence during the period of observation (7.5 years). The histological type of primary tumor did not change in recurrences; with the exception of one case where classical initial tumor became atypical in recurrences. Cases with large peritumoral edema had elevated expression of VEGF. A statistical significant correlation was found between MVD and VEGF ($p<0.001$). A statistical significant correlation was found between VEGF and MIB-1 ($p<0.001$). No significant statistical correlation was found between VEGF and Ki-67 ($p<0.001$).
Conclusions: VEGF inhibition can be an attractive therapeutic strategy because it is highly specific and may be less toxic than cytotoxic therapy and best suited for long-term therapy.Antioangiogenic therapy in meningiomas may require additional studies and larger group of patients.

P035

The expression of tissue and serum VEGF in patients with brain tumours. The prognostic value

Miliaras G[1,2], Goussia A[3], Kostoula A[4], Katsaraki A[5], Mitlianga P[2], Tachmazoglou F[2], Panelos J.D[3], Kyritsis A[1,6], Stefanou D[3], Levidiotou S[4], Polyzoidis K[1,2].
[1] Neurosurgical Institute of University of Ioannina. Departments of Neurosurgery [2] Pathology [3] Microbiology [4] Statistics [5] Neurology [6] of University Hospital of Ioannina, Greece

Brain tumours from sixty six patients were studied immunohistochemically for VEGF, flk-1 (the main of receptor of VEGF), CD34 (a microvascular density index), thrombospondin-1 (TSP-1) and MIB-1 expression. From preoperative blood samples full blood count was assessed in all patients, and using ELISA, VEGF was measured in the serum Serum VEGF was also measured in eight healty controls. VEGF expression was statistically correlated to flk-1 expression and CD34 ($P<0,001$). Moreover, MIB-1 (a strong prognostic factor) expression was correlated with VEGF, flk-1, and CD34 ($P<0,001$). Serum VEGF was elevated only in patients with metastatic brain tumours compared to healthy controls ($P<0,05$). The number of platelets in the peripheral blood was elevated according to the levels of serum VEGF ($P<0,05$). In conclusion, like MIB-1, tissue VEGF, flk-1, and CD34 seem to have a prognostic value in patients with a brain tumour. VEGF in the serum can help differentiate patients with primary and secondary brain neoplasms. The platelets seem to intervene in VEGF circulation.

P036

Expression of EGFR, VEGF-R3 AND MDM-2 in human gliomas

Diamantopoulou K., Leodara V., Chranioti S., Thoma-Tsangli E.
Pathology Dep., Gen. Hospital Asklepieio Voula, Athens, Greece.

Epidermal growth factor receptor (EGFR) is considered to play a major role in the control of cell proliferation and contribute to the evolution of human gliomas. Vascular endothelial growth factor (VEGF) and its receptors (VEGF-R) are involved in tumor angiogenesis and are variably detected in human low and high grade gliomas. MDM-2 protein, related to the pathway of tumor suppressor gene p53, may be involved in progression of gliomas and play an important role as a prognostic marker. The expression of EGFR, VEGF-R3, MDM-2 and Ki-67 (MIB-1) was analyzed by immunohistochemistry in 15 human gliomas, 12 (80%) of which were high grade (gr III & IV) and 3 (20%) were low grade (gr II). The expression of EGFR was different in intensity and distribution in 88,89% of high grade gliomas, with no expression in low grade gliomas. VEGF-R3 was expressed in 85,71% of gliomas (glioblastomas, astrocytic gliomas gr II & III, and oligodendrogliomas). MDM-2 was mainly expressed in high grade gliomas (75%). Low grade gliomas did not express MDM-2. MIB-1 (Ki-67) indices showed a highly significant increase from low grade gliomas (mean 1,33%)to high grade gliomas (mean 12,67%). The importance of EGFR, VEGF-R3 and MDM-2 expression is correlated to therapy. Especially, the treatment of glioblastoma multiforme, except for the

conventional surgical resection and radiotherapy, may include new therapies like anti-angiogenic agents and EGFR-inhibitors. MDM-2 expression is correlated to drug chemoresistance.

P037

Profound Hypothermic Circulatory Arrest is Associated with Increased Bcl-2 Immunoreactivity in Selectively Vulnerable Brain Regions

Bibou AN[1], Ananiadou OG [2], Charchanti A[1], Drossos GE[2], Bai M[3], and Johnson EO[1].
[1]Department of Anatomy-Histology-Embryology, [2]Department of Cardiac Surgery, and [3]Department of Pathology, University of Ioannina, Medical School, Ioannina, Greece

Profound cooling to 10 C compared to traditional 18 C was found to significantly reduce neurological injury during HCA as assessed by the Tunel assay. The present study assesses the effects of HCA at both 18 C and 10o C on Bcl-2 expression in the porcine brain. 12 piglets underwent 75 minutes of HCA after cardiopulmonary bypass at 18 C (n=6) and 10 C (n=6), and 4 were normal controls. After 80 minutes of gradual rewarming and reperfusion, brains were collected. H/E histology was used as counterstaining. Bcl-2 positive cells were scored on a scale of 0 to 3 (0: negative; 1: weakly positive; 2: positive; 3: moderately positive) and were compared using the Mann Whitney-U test. Positive bcl-2 immunostaining was observed in the neocortex and hippocampus. The cerebellum, medulla and thalamus were negative for Bcl-2. Profound cooling to 10oC resulted in a significant increase in bcl-2 immunostaining in the neocortex as compared to 18o C ($P<0.05$). These findings support the activation of anti-apoptotic mechanisms and mechanisms of cell survival during profound hypothermia.

P038

Caspase-3 immunohistochemical expression correlates with ssDNA expression and predicts early recurrence of patients with intracranial meningiomas

Konstantinidou A.E.[1], Givalos N.[1], Gakiopoulou H.[1], Korkolopoulou P.[1], Agrogiannis G.[1], Kotsiakis X.[2], Boviatsis E.[3], Mahera H.[4], Patsouris E.[1].
[1]Department of Pathology, Medical Faculty, National Kapodistrian University of Athens, 75 Mikras Asias, 11527, Athens, Greece, [2]Department of Neurosurgery, General Hospital of Hania, Creta, Greece, [3]Department of Neurosurgery, "Evangelismos" Hospital, Athens, Greece, [4]Laboratory of Pathology, "KAT" General Hospital, Athens, Greece

Caspase-3 is the ultimate executioner caspase that is essential for the nuclear changes associated with apoptosis. In this study, we investigated caspase-3 immunohistochemical expression (CPP32) in 56 primary nonmalignant intracranial meningiomas in relation to baseline apoptosis - as illustrated by the expression of anti-single stranded DNA (ss-DNA), the antiapoptotic protein bcl-2, proliferation indices (Ki-67, PCNA, topoisomerase IIa, mitosin C), hormonal status (estrogen, progesterone, androgen receptors), standard clinicopathological parameters and patients' disease-free survival. Immunostaining for caspase-3 was observed in 60.7% of cases and its labeling index (LI) was significantly correlated with ss-DNA LI ($p=0.038$), as expected. Caspase-3 LI positively correlated with the mitotic index ($p=0.001$) and PCNA LI ($p=0.004$). Grade II meningiomas demonstrated a significantly increased caspase-3 labeling index ($p<0.0001$), as related to grade I tumors. In univariate and multivariate survival analyses caspase-3 predicted meningioma recurrence, independently affecting disease-free survival ($p=0.011$ and $p=0.047$ respectively). The apoptotic index and mitosin LI were additional prognosticators of shorter disease-free survival. Our findings confirm previously published observations on the prognostic implication of apoptotic markers in meningioma recurrence. Caspase-3 may prove to be a useful predictor of early recurrence in this group of neoplasms characterized by the frequent discordance between histology and clinical behavior.

P039

Malignant Solitary Fibrous Tumor of the Tongue

Parasi A, Pantoula P, Mennonna R, Sotiriou E, Karayannis M, Karakosta A, Moschovakis E*.
Pathology and Otolaryngology* Department, General Hospital of Nikaia-Piraeus «Agios Panteleimon», Greece

A case of malignant solitary fibrous tumor of the tongue is reported. The patient, a 25 year old man, presented with a nodular lesion, infiltrating the lingual muscle, measured 1cm in maximum diameter. Microscopically, areas of the tumor had a patternless spindle cell appearance with collagenized stroma and thin-walled branching vessels. A transition to a more cellular area, consisting of round epithelioid cells with prominent nucleoli and high mitotic activity (6 mitoses per 10 HPF) was found. Immunohistochemically, the tumor cells stained for Vimentin, CD34 and CD99, while pan-keratin, EMA and S-100 protein were negative. The patient underwent a broader excision and is now free of disease within a follow up period of 21 months. The diagnostic difficulties in the recognition of this neoplasm in unusual sites and the differential diagnosis of CD34-positive mesenchymal neoplasms are discussed. Solitary fibrous tumors of the tongue are extremely rare and this is the second reported malignant case in literature.

P040

VEGF in inverted sinonasal papillomas

Ćorić M., Bilić M., [1]Nagy P., Brčić L., Batelja Vuletić L., Bura M., Seiwerth S.
Institute of Pathology and ENT Clinic Medical Faculty University of Zagreb, Croatia; [1]National Medical Center Budapest, Hungary

Although for inverted papillomas (IP) local aggressiveness and marked tendency to recur have been known for decades, association with squamous cell carcinoma (SCC) is still a subject of investigation since neither histologic feature nor local aggressiveness can be used as prognostic marker. According to our previous results and to results of other p53 and Ki67 immunohistochemistry have some diagnostic but little prognostic potential. We analyzed 50 cases of IP including 6 cases of synchronous SCC. The patients had diagnosed IP in the period from 1982 to 2005 at the Departments of Pathology, University in Zagreb, University of Osijek and the National Medical Center Budapest, Hungary. Immunohistochemistry for VEGF was performed according to manufacturers' specification (Santa Cruz, USA). A PC based image analysis system (ISSA/SFORM, Vamstec, Zagreb) was used to determine the rate and intensity of nuclear staining. The histological pattern and intratumoral distribution of immunoreactivity was accessed together with the immunoreactivity of neighboring normal epithelium. Although the normal sinonasal epithelium shows VEGF immunoreactivity, the epithelium of both benign and malignant inverted papillomas demonstrated stronger reactivity following the histological pattern.

P041

Expression of annexin, and decorin in the corneas of cats with mucoplysaccharidosis VI

C Mura , O Villa, M Haskins, J Alroy. New England Medical Center, Tufts University Schools of Medicine and Veterinary Medicine, Boston, MA; University of Pennsylvania, School of Veterinary Medicine, Philadelphia, PA

Background: Lysosomal storage diseases are a group of over 45 distinct inherited disorders. Lysosomes are a recycling center they catabolize cellular and extracellular macromolecules and provide substrate for resynthesis of cellular and extracellular molecules. A common biochemical feature of lysosomal storage diseases is the intra-lysosmal accumulation of undegraded or partially degraded substrate leading to cell dysfunction. One of the phenotypic characteristic of human and animals affected with mucopolysaccharidosis (MPS)-I, (Hurler disease) and MPS-VI (Maroteaus-Lamy disease) is cloudy cornea. MPS-I there is deficient activity of α-L-iduronidase, and storage of dermatan sulfate and heparan sulfate. In MPS-VI there is deficient activity of arylsulfatase B and storage of dermatan sulfate. Currently morphologic explanations for this clinical manifestation include the presence of enlarged secondary lysosomes packed with storage material and the disorganization of collagen in the corneal matrix; however, the molecular basis remains unknown.
Results: Using differential display proteomic analysis we previously showed expression of α, β and γ crystallins in corneas of cats with MPS-I and MPS-VI. Subsequent analysis also indicated changes of expression of decorin and annexin. To confirm these results we have used Western blot analysis and specific antibodies against decorin and annexin. To determine the levels of expression of these two genes they were normalized against β-actin as housekeeping gene. Preliminary results indicate upregulation of decorin between normal cat corneas and MPS-VI cats corneas. In contrast, annexin expression appears down regulated when normal cat corneas are compared with corneas of MPS-VI cats.
Conclusions: In the current study we demonstrate that interruption of recycling of dermatan sulfate caused by deficient enzyme activity in MPS-VI leads also to an accumulation of decorin, which is the protein component of proteoglycan to which the dermatan sulfate is attach. Although the accumulation of decorin resulted in upregulation of α, β and β crystallins, there is down regulation of annexin. The α, β and β crystallins have a chaperone-like activity that is needed to degrade the accumulated decorin

P042

Mesectodermal leiomyoma of the ciliary body

T. Koletsa, G. Karayannopoulou, P. Hytiroglou, C. Papadimitriou.
Department of Pathology, Aristotle University Medical School, Thessaloniki, Greece

We present a case of mesectodermal leiomyoma of the ciliary body emphasizing the immunohistochemical features of this rare tumor and the differential diagnosis from malignant melanoma. A 53 year-old woman presented because of decrease in visual acuity. On examination, a ciliary body tumor was found in the right eye. A malignant melanoma was highly suspected due to her age and the growth rate, and the globe was enucleated. A well-defined ciliary body tumor was found on macroscopic examination, measuring 12×9×7mm. The lesion was moderately cellular and consisted of spindle and ovoid cells with normochromatic, mostly roundish nuclei. There was no appreciable mitotic activity. Immunohistochemical stains revealed positivity of the tumor cells to vimentin, smooth muscle actin, caldesmon, CD56 and NSE. Stains for desmin, cytokeratins AE1/AE3, chromogranin, synaptophysin, NF, Leu-7, S-100, peripherin, GFAP, CD34, CD117, CD105, calcitonin, EGFR and fascin were negative. On Ki-67/mib-1 stain less than 1% of tumor cell nuclei were positive. Mesectodermal leiomyoma is considered to originate from the ciliary body smooth muscle, which is a neural crest derivative. In a review of the literature we found only 15 cases of this tumor. Pathologists should be aware of this rare entity that often masquerades as malignant melanoma on clinical examination.

P043

Primary ameloblastoma of the maxilla diagnosed by FNA. cytological and immunocytochemical features

Bobos M[1], Mandrali A[1], Koletsa T[1], Teliousi S[1],
Asimaki A[2], Kommata A[3], Ioannou-Banava O[1]
Departments of Cytopathology[1], Pathology[2] and Oral and Maxillofacial Surgery[3] General Hospital "G. Papanicolaou", Thessaloniki, Greece

Ameloblastomas (ABL) are extremely rare tumors and represent the most frequent primary epithelial odontogenic neoplasms. We present a case of a 60 years-old male patient with a painless cystic non-tender mass in the right maxilla. FNA was performed and the material was processed using Thin-Prep method. The material showed a moderate cellularity. The predominant population was composed of small round cells, arranged in clusters or nests with vague peripheral palisading, little cytoplasm and hyperchromatic nuclei. The cytologic pleomorphism was minimal. The specimen also contained small number of squamous epithelial cells, singly or in small nests, foamy macrophages and neutrophils. On immunocytochemical investigation the neoplastic cells were positive for cytokeratins 5 and AE1/AE3 and negative for cytokeratin CAM5.2. Based on cytomorphology and immunocytology the case was diagnosed as ameloblastoma. Following complete excision of the mass, the histopathological examination was consistent with follicular ameloblastoma. Cytologic features of ameloblastoma are unique and well defined, suggesting that FNA is a valuable tool in the initial diagnosis.

P044

Caspase-3 expression in head and neck squamous cell carcinoma

Maky Hafidh, Andrew Jones, Tim Helliwell.
Departments of Pathology and Surgery,
University of Liverpool, Liverpool, U.K.

Caspase-3 is a key protease involved in the initiation of apoptosis. Expression has been linked to apoptosis in several human malignancies but there is little information on its role in head and neck carcinomas. The objective of this study was to evaluate the patterns of expression of caspase-3 in head and neck squamous carcinomas and to examine the association with other apoptosis-related markers and prognosis. A tissue microarray was created from archived wax blocks of 200 primary squamous carcinomas (83 larynx, 72 pharynx and 45 oral cavity). 75 cases had tissue from nodal metastases available for study. Immunocytochemical labelling was performed for caspase-3, p53, mdm2, bcl-2 and bax proteins. Caspase-3 labelling is seen in both the nucleus and cytoplasm of a small proportion of malignant cells, and in apoptotic nuclear debris. Nuclear labelling is present in a mean of 3.79% cells in laryngeal carcinomas, 2.53% cells in pharyngeal carcinomas and 2.09% cells in oral carcinomas. A similar extent of expression occurs in primary carcinomas and their nodal metastases. The % cells showing nuclear caspase-3 expression correlates with poorly-differentiated carcinomas and with nodal metastasis. Cytoplasmic caspase-3 expression does not show similar correlations. Nuclear caspase-3 expression is positively correlated with the expression of mdm-2, bax and survivin, and negatively correlated with involucrin expression. We conclude that nuclear caspase-3 expression may be a useful measure of apoptotic activity in head and neck squamous carcinoma.

P045

Nerve growth factor p75 receptor, cytokeratin 18 neoantigen expression and TUNEL data in human normal salivary gland and pleomorphic adenoma

Groma V.[1], Kazanceva A.[2], Kornevs E.[2].
[1]Institute of Anatomy and Anthropology and [2]Department of Oral Maxilla Facial Surgery, Riga Stradins University, Riga, Latvia

It has been generally appreciated that pleomorphic adenoma shows a great degree of pathohistological variability, which, in turn, reflects peculiarities of the epithelial component differentiation and growth pattern as well as the stromal component morphological diversity. Modulations of cell proliferation and biological behaviour of this tumour are common, and reflect the action of some genetic, environmental and other factors. A mechanism which regulates the balance of proliferative activity and apoptosis in this tumour is not completely understood. The aim of this study was to evaluate the occurrence and extent of apoptosis based on appearance of nerve growth factor p75 receptor (p75), cytokeratin 18 neoantigen expression, and terminal deoxynucleotidyl transferase-mediated deoxyuridine triphosphate nick-end labeling method (TUNEL) in human normal salivary gland and pleomorphic adenoma. The estimation of morphological details of cell death events was assessed by immunohistochemistry applying the anti-p75 antibody and M30 antibody for evaluation of the cytokeratin 18 cleavage, as well as by use of TUNEL kit. The salivary gland tissue (N=7) was obtained during parotidectomy and fixed according to standard light microscopy procedure in 10% formalin, embedded in paraffin. Immunohistochemistry was performed using ABC peroxidase kit according to the manufacturer s instructions. Identification of positive nuclei for DNA fragmentation was performed after application of TUNEL kit. The results of the pleomorphic adenoma analysis were compared with those obtained from the residual normal nontumorous gland parenchyma and, additionally, with gland parenchyma obtained during surgery for the removal of the entire gland because of sialolithiasis and sialadenitis. P75 consistently displayed membrane reactivity in myoepithelial cells arranged as a continuous layer around normal ducts and acinar parenchyma units, vascular adventitia and nerve bundles. This myoepithelial expression became stronger in case of sialolithiasis with prominent atrophy (N=2) revealing the presence of immunostaining around the remnants of the lobular units. In pleomorphic adenoma p75 expression was detected on the myoepithelial cells outlining ductal structures, and in some solid proliferate zones composed by myoepithelial-like cells. Positive M30 reaction products were found in the cytoplasm of acinar cells in the restricted lobules of nontumorous gland parenchyma and parenchyma obtained due to sialolithiasis and sialadenitis, as well as in the luminal contents of duct-like structures in pleomorphic adenomas. In the normal salivary gland cells with different pattern of cytoplasmic positivity, from weak to very strong, were found. The cytokeratin cleavage product localization was restricted to the lobular parenchyma, but not the chondroid and osseous (N=2) stroma. Identification of apoptotic nuclei DNA fragmentation in human normal salivary gland and parenchyma removed due to sialolithiasis revealed some TUNEL-positive cells nuclei within lobular acinar units. The TUNEL-positive cells nuclei were also present in the inflammatory parenchyma areas in case of sialadenitis, the occasional reactivity was restricted to these areas lymphocytes. In pleomorphic adenoma apoptosis was suppressed – TUNEL reaction was negative. These results suggest that suppression of apoptosis takes a place in case of pleomorphic adenoma comparing with normal salivary gland. Suppression of death events in particular epithelial and/or stromal cells may cause changes that are thought to be linked to the growth of tumour. The values of different cell death markers – cell surface, cytoplasmic as well as DNA fragmentation applied in this study require a further elucidation and explanation. Detection of DNA fragmentation by TUNEL method seems to be sensitive; identification of cytoskeleton cleavage along apoptosis process can be additionally used for evaluation of extent of apoptosis; the varying degree of staining may reflect the stage of process.

P046

STRUCTURAL MARKERS OF THE GUM TISSUES REMODELLING AT PATIENTS WITH CHRONIC PERIODONTITIS

Valentina M Mudra, Olga S. Reshetnikova, Sergiy A. Morozov.
Department of Pathologic Anatomy, Lugansk State Medical University, 1, kv. 50-let Oborony Luganska, 91045, Lugansk, Ukraine

Numerous data suggested that periodontal diseases have high incidence rate worldwide Treatment plans involving tooth replacement, often used for sites diagnosed with chronic periodontitis (CP). Thus, there is a problem of finding pathogenically based methods of structural changes correction in gum in case of CP. Morphological study was undertaken to help further evaluate gum tissues remodelling with and without pre-implantation treatment of CP. Methods. 10 gums biopsies were taken from volunteers without CP symptoms (group of comparison), 10- from patients with CP undergoing surgical operation without therapy (group 1) and 10- from CP patients with pre-implantation treatment by glutarginum and vector-therapy (group 2). Histological slides were studied stereologically. Collagen I and III types were stained with specific antibodies. The results have shown that the increase of volume fractions of inflammatory infiltrates, vessels, foci of periodontal connective tissue dystrophy and necrosis are determined in group I. Immunohistochemical analyses showed that both expression and distribution of the I type collagen was diminished here too. Unlike this, the III type collagen was registered here more often with increased intensity of expression. In group 2 the resulting data clearly demonstrate a reduction of hyperemia, vessels number, inflammatory infiltrates and areas of connecting tissue dystrophy. Type I collagen dominated over the III type collagen expression. These findings suggested the CP without adequate treatment stimulates the forming of immature connective tissue and persistent inflammation in the gum of patients. There is braking of repair processes, which can unfavorably affect implant osteointegration. The use of glutarginum, possessing antioxidant and membranes protective properties, in conjunction with the mechanical debridement by vector-therapy, allows normalizing gum tissue's metabolism, to recover the normal parameters of collagen stromal components. These seem to be effective in maintaining structure and function of the gums and periodontal tissues at pre-implantation period of patient's treatment.

P047

The Value of CDX2 and P63 in diagnosis of Primary Intestinal-Type Sinonasal Adenocarcinomas

Parasi A, Pantoula P, Karayannis M,
Sotiriou E, Mennonna R, Karakosta A
Department of Pathology, General Hospital of Nikaia-Piraeus «Agios Panteleimon» Greece

Objectives: Non Salivary Sinonasal Adenocarcinomas are rare, interesting tumors, divided into intestinal (SN ITACs) and non-intestinal type of low and high-grade differentiation. SN ITACs are morphologically similar to intestinal type GI adenocarcinomas, especially colonic adenocarcinomas and share the same immunohistochemical features, with the exception of the variability in CK7 and CK20 expression. Cdx2, the highly specific for intestinal type adenocarcinomas marker, has recently been demonstrated in ITACs, allowing their distinction from the non-intestinal type. P63, on the other hand, is consistently expressed in SN Non Keratinizing

Squamous cell Carcinomas (NKSCCs). The possibility of p63 expression in SN ITACs, due to their common origin from Schneiderian epithelium, has not, to our knowledge, been examined.
Methods: Antibodies to Cdx2, p63, CK7 and CK20 were used to examine 8 (biopsy and surgical material of 4 patients) primary SN adenocarcinomas of moderate to low differentiation with intestinal_type morphology. The expression of cdx2 and p63 was also examined in 5 colonic and 5 intestinal type gastric adenocarcinomas and in 5 NKSCCs.
Results: All specimens of SN adenocarcinomas (100%) were diffusely positive for Cdx2, even the isolated tumor cells in cases with almost necrotic biopsy material. All intestinal type GI adenocarcinomas were also diffusely positive and, as expected, all NKSCCs were negative. In 3 out of 4 patients (75%), a focal (5% 25%) p63 nuclear positivity was found, especially in cells with oval or elongated nuclei in more solid areas of the tumors. The NKSCCs were diffusely p63 positive and the GI adenocarcinomas were negative. CK7 and CK20 expression in ITACs was variable: 2 cases were CK20-positive and CK7-negative (colonic type immunophenotype), 1 case was CK7-CK20-positive and 1 case was CK7-CK20 negative.
Conclusion: Cdx2 appears to be a sensitive marker for the diagnosis of SN ITACs, even in small biopsies and in lower-differentiated tumors. P63 expression, although only focally found, could be a useful complementary marker for the recognition of SN ITACs and the exclusion of a metastatic intestinal type GI adenocarcinoma in the Head and Neck region. The specific value of this marker needs to be evaluated in additional studies.

P048

Molecular detection of Epstein – Barr virus (EBV) in nasopharyngeal carcinoma

Ceausu Mihai, Iosif Cristina, Butur Georgeta,
Georgescu Alina G.M., Florea Gramada Zenaida,
Ardeleanu Carmen
"Victor Babes" National Institute of Pathology,
Splaiul Independentei, 99-101, sector 5, 050096, Bucharest,
Romania

EBV is the etiological agent of infectious mononucleosis, but it can determine also, various types of cancer: nasopharyngeal undifferentiated carcinoma, Burkitt lymphoma, esophageal or gastric carcinomas. The study was carried out on 9 formalin fixed paraffin embedded samples of nasopharyngeal type undifferentiated carcinoma (with different locations: ethmoidal sinus and maxillar sinus), using the indirect tristadial ABC method for IHC detection of EBNA2 nuclear antigen and latent membrane protein of Epstein-Barr virus (LMP-EBV), as well as in situ hybridization (ISH) for the Epstein-Barr RNA transcripts EBER 1. A positive reaction for LMP-EBV or EBNA 2 was founded in 4 cases (44%). The IHC reaction showed positivity in cytoplasm for LMP-EBV and nuclear for EBNA 2. These tumors had a high proliferating index demonstrated by PCNA stain, in correlation with IHC stain for EBV antigens in tumor cells. ISH for EBV RNA transcript EBER1 confirmed infection in all 4 cases with positive IHC reaction. IHC expression of LMP-EBV may be one stage in the diagnosis of undifferentiated nasopharyngeal carcinoma, Epstein-Barr virus infection being closely associated with the development of this type of tumor. Also, the etiological identification of EBV can be completed by molecular techniques such as ISH for EBV RNA transcript EBER1.

P049

Initial diagnosis of T cell lymphoblastic lymphoma in parotidectomy for warthin tumor. A rare colision tumor.

K. Giaslakiotis[1], K. Kokkori[1], P. Alexandrou[1],
E. Bariami[2], P. Korkolopoulou[3], A. Androulaki[1]
[1]Department of Pathology, [2]First Department of Internal Medicine,
[3]Pathology Laboratory, University of Athens Medical School,
Laiko General Hospital, Mikras Asias 75, 115 27 Athens, Greece

Warthin tumor (WT) is a benign neoplasm of the salivary gland epithelium composed of varying proportions of bilayered columnar and basaloid oncocytic epithelium associated with lymphoid stroma. The latter, uncommonly, may give rise to or be involved by malignant lymphoma. We report a case of T-cell lymphoblastic lymphoma (TdT +, CD99+, CD3 +, CD5 +, CD 43 +, CD4 +, CD8-,) initially diagnosed in the WT diagnostic specimen. Staging procedures immediately after diagnosis demonstrated disseminated disease (stage IVA). The patient received combination chemotherapy treatment. 6 months after remission he is free of relapse. To best of our knowledge this is the first report in the English literature of a collision tumor composed of T-cell lymphoblastic lymphoma and Warthin tumor. Our report indicates that the lymphoid stroma of WT, as part of the systemic lymphoid tissue, is likely to be involved in disseminated lymphoma. The association of a T-cell lymphoblastic lymphoma with Warthin tumour does exist, although extremely rare.

P050

Salivary gland carcinomas express c-erbB2 oncoprotein according to different subtypes.

Kiziridou A., Moysidis I., Andreadis Ch., Maganaris A. Toliou T.
Pathology Department, "Theagenion" Anticancer Hospital,
Thessaloniki, Greece.

Objective: Salivary gland carcinomas (SGC) are rare neoplasms (less than 1% of all cancers) thus there are limited data about the biological behaviour and the appropriate therapeutical management. This study will attempt to evaluate the use and incidence of immunohistochemical marker c-erbB2 in SGC.
Materials and Methods: We studied 32 samples from salivary gland carcinomas (8 mucoepidermoid, 10 adenoid cystic and 14 adenocarcinomas)using the monoclonal antibody p185/Her2 for immunohistochemical detection of the oncoprotein. Expression was positive if more than 10% of the neoplastic cells expressed strong (3+) or moderate(2+) membrane staining.
Results: 1/8 mucoepidermoid carcinomas and 10/12 adenocarcinomas expressed moderate and strong immunoreactivity with the antibody. None of the adenoid cystic carcinomas was positively expressed.
Conclusions: The c-erbB family gene products are expressed in salivary gland carcinomas. The overexpression is frequently associated with high grade tumors and poor prognosis. Given the suboptimal response rate and toxicity of chemotherapy, a complete understanding of the biology of these tumors may allow a better prognosis and an improved treatment strategy. With the emergence of molecular targeted therapy they become an optimal candidate for trials of new drugs.

P051

Kaposi's sarcoma of the nasal mucosa

Venizelos I[1], Andreadis H[2], Tatsiou Z[1], Chatzitolios A[1], Moulla A[1]
[1]Department of Pathology, Hippokratio General Hospital,
[2]Department of Internal Medicine, Theagenio Hospital,
Thessaloniki, Greece

Kaposi's sarcoma (KS) is an unusual vascular tumor characterized by multiple reddish blue nodules, which usually present on the skin of the lower and upper extremities. KS may also involve mucosal sites, lymph nodes and visceral organs. During the last two decades, with the large increase in the incidence of this tumor associated with the acquired immune deficiency syndrome (AIDS), there has been increasing number of cases with KS presenting on the skin or mucosa of the head and neck. A review of the literature

revealed that only one case of KS of the nasal cavity has been reported.We report the case of a 59-year-old woman who presented 4 years ago with a tumor in her left nasal vestibule, associated with nasal obstruction and rhinorrea. Physical examination revealed the presence of a fleshy tumor arising from the nasal septum, which was excised. Histological examination of the tumor showed morfological and immunohistocemical features of Kaposi's sarcoma. The tumor was excised within free surgical margins. A complete physical and laboratory examination revealed no other pathological findings. The patient received no further treatment and 4 years later she is in a good condition.In the present study we report a very rare case where the primary manifestation of the KS was in the nasal mucosa in a patient with an adequate immune system.

P053

Acute growth hormone administration enhances angiogenesis in a porcine model of myocardial infarction

K Hatzistergos, A Mitsi[1], L Pappa, D Niokou[2], GG Baltogiannis[1], A Papalois[3], T Kolettis[1], V Malamou-Mitsi.
Departments of Pathology, [1]Cardiology, [2]Anaesthesiology, University of Ioannina, Ioannina Greece, [3]ELPEN Research Laboratory Athens Greece.

We examined the angiogenic effects of a single, high dose of Growth Hormone (GH), administered acutely after myocardial infarction (MI) in pigs. MI was generated in 35 pigs while 5 were sham operated. Ten minutes after reperfusion, pigs were randomised (2:1) to GH (1 IU/kg) or normal saline (NS) and sacrificed 4 weeks later. Immunohistochemistry against a-smooth muscle actin (Biogenex) was performed in a)infarcted myocardium (IZ) and subendocardium (SIZ), b)remote noninfarcted myocardium (NIZ) and subendocardium (SNIZ) c)border zone (BZ). Positive stained vessels with obvious lumen and diameter <20μm, (neovessels) were counted by three independent observers, blinded to treatment assignment. Microvascular densities (MVD, number of neovessels per high power field) were compared using oneway ANOVA, followed by Tukey's multiple comparisons test. Results are shown in table 1. Intracoronary GH administration enhanced angiogenesis in the IZ, the BZ and the NIZ.

Table 1 Microvascular densities

	IZ	SIZ	BZ	NIZ	SNIZ
NS	66, 2±27,5	64, 6±46,8	68, 9±56,5	78, 1±86,1	33, 9±12,9
GH	91, 5±23,1*	178, 3±59,8*	129, 8±48,8*	196, 8±70,9*	172, 8±69,9*
SHAM				53, 8±18,3	48, 2±9,9

*p<0.05 compared to either NS or sham (where applicable)

P054

Batista's partial left ventriculectomy: histomorphometric semiquantitative assessment one-year later

Jovan D. Vasiljević, Petar Otašević, Siniša Gradinac, Sofija Glumac, Zoran V. Popović, Aleksandar Nešković
Institute of Pathology, Belgrade University School of Medicine, Serbia and Montenegro Dedinje Cardiovascular Institute, Belgrade, Serbia and Montenegro

Objectives: Left ventricular contractility may be improved by partial left ventriculectomy (PLV) in patients with severe heart failure. Histological assessment by using semiquantitative morphometric parameters of the left ventricle after surgery, and endomyocardial biopsies (EMB) one-year postoperatively.
Method: The study group consisted of 15 consecutive PLV survivors, predominantly male (13/15), aged 45+12 years. Surgical specimens were taken from the inferior- and/or lateral wall of the LV, processed routinely, and stained with Masson-trichrome. Postoperative EMB, 3 to 5 per patient, were taken 12 months later and processed in the same manner. The following morphometric parameters were assessed: (1) degree of hypertrophy and attenuation (fibre diameter); (2) nuclear evidence of hypertrophy (diameter); (3) myofibrilar volume fraction; (4) degree of degenerative, vacuolar changes, and (5) fibrosis volume fraction. These parameters were graded in the usual fashion (0-none, 1-mild, 2-moderate, 3-severe).
Results : Both NYHA functional class and EF improved 12 months following operation as compared to preoperative values (2.40+0.69 vs. 3.33+0.49, p<0.001, and 33.21+12.05% vs. 20.21+9.07%, p<0.001, respectively). Semiquantitative morphometric analysis demonstrated postoperative decrease in the degree of attenuation as compared to preoperative values (1.40+0.51 vs. 2.47+0.64, p<0.01), as well as decrease in fibrosis volume fraction (2.07+0.80 vs. 2.67+0.49, p<0.001) and nuclear hypertrophy (1.27+0.46 vs. 1.67+0.62, p<0.05). There was postoperative increase in myofibrilar volume fraction (1.87+0.61 vs. 1.40+0.61, p<0.01). There was no difference in post- and preoperative degree of myofibrilar hypertrophy and degenerative changes.
Conclusion: One-year postoperatively, PLV had favourable effects on myocardial morphology that parallels improvement in patient's functional status and LV systolic function.

P055

Autopsy findings in corrected transposition of the great arteries

Sofija Glumac, Zoran Popovic, Sanja Radojevic-Skodric, Zorica Stojsic, Darko Babic, Jovan D. Vasiljevic
Institute of Pathology, Medical School, University of Belgrade, Serbia and Montenegro; Department of Pathology, Bezanijska Kosa Hospital, New Belgrade, Serbia and Montenegro

Objectives: Congenitally corrected transposition of the great arteries (C-TGA) represents the combination of atrio-ventricular and ventriculo-arterial discordance, with completely normal circulation. The aim of this study was to analyze the cases of C-TGA (sex, age and causes of death, atrial situs), and presence of associated cardiac and/or extra-cardiac anomalies.
Method: During the period from 1926-2006, a total number of 1.444 cases of congenital heart diseases (CHD) were diagnosed at the Institute of Pathology, Medical School, University of Belgrade.All autopsies were performed using standard or modified Rokitansky technique and accepted segmental approach. C-TGA was found in 31 cases (2.15 % of all CHD).
Results: There were 20 males (64.52%) and 11 females (35.48%); in 25 cases the heart was in situs solitus (80.65%) and in 6 in situs inversus (19.35%). The viscera was always in situs solitus. Majority of the patients had 2 or more associated cardiac anomalies (25 ASD, 11 VSD, 3 AVSD, 7 PDA), and only 1 case had no communications between heart chambers; in 11 cases we found 1 communication, in 17 cases 2, and in 1 case 3. In addition, pulmonary atresia was present in 7 cases (22.58 %), and pulmonary stenosis in 4 (13%). Anomalous connection of pulmonary veins was found in 5 cases (16.13%), and anomalies of the coronary arteries too (hypoplasia in 3 and single coronary artery in 2). Most of patients died within the first month of life (20 or 64.52%), 6 within the first year (19.35%), 2 in the second year (6.45%), 1 in the third year (3.23%), and 2 lived over 20 years (6.45%). Extra-cardiac causes of death were predominant within the first year of life: bronchopneumonia (14 or 45.16%), athelectasis (7 or 22.58%), cerebral hemorrhage (3 or 9.68%), acute heart failure (3 or 9.68%), and myocarditis/endocarditis (2 or 6.45%).
Conclusion: Our results show higher incidence of C-TGA among CHD, male and situs solitus predominance, and the most frequent cause of death due to extra-cardiac complications.
Majority of patients in our series died within the first year of life, and

the most often associated cardiac anomalies were: ASD, VSD, pulmonary atresia or stenosis, and AVSD.

P057

Morphological characteristics of unstable atherosclerotic plaques of the carotid arteries

Fedorina T.A., Bugaeva L.N.
Samara State Medical University, Samara, Russia

Research to understand the role and importance of atherosclerotic damage of the carotids is essential for effective surgical correction of blood flow in arteries of the head and neck aiming to decrease the risk of acute cerebro-vascular events (ACVE). **The aim** of this study was to determine early signs of unstable or prone-to-damage plaques in the carotids in patients with increased risk of ACVE. **The study material** consisted of tissues samples of the carotids removed during endoscopic surgery for blood flow restoration performed on the arteries. In total we examined 102 fragments of the carotids received from 86 patients aged 42-67 years; the majority were males.
Methods: the fragments were examined microscopically and morphologically. Histological preparations (of 8 um thickness, stained with hematoxylin -eosine, by histochemical methods and using p-53 and Ki-63 immunohistochemical markers) of 134 atherosclerosis plaques were examined. Separate smooth muscles cells of the median arterial membrane were examined using alkaline dissociation methods. A set of morphometric techniques was applied. Study material was divided into 2 groups: 65 samples of damaged atherosclerotic plaques and 69 samples of plaques without signs of damage that included 44 stable plaques and 25 unstable plaques.
Results: damaged atherosclerotic plaques had macro- and microscopic signs of hemorrhage, destruction of fibrotic cover and thrombosis formation and were easy to diagnose. Differential diagnosis between stable and unstable plaques without signs of damage is of a greater importance. Stable atherosclerotic plaques had a compact lipid nucleus, insignificant destruction of elastic fibers and poorly developed capsule fibrosis. Unstable atherosclerotic plaques had the following characteristics: increased volume of the lipid nucleus and fibrotic and smooth muscular tissues, substantial destruction of elastic fibers and presence of glycosamine sulfate in their walls. The parenchymal cellular density index in stable atherosclerosis plaques was 2.7 while it was 6.4 in the group of unstable plaques. Morphologically these cells belonged to macrophages, lymphocytes, smooth muscles cells. Examination of separate smooth muscles cells demonstrated their high proliferative activity in unstable atherosclerosis plaques. A high level of expression to apoptotic factors was detected in this group of unstable plaques and may be a cause of their destruction and disruption resulting in manifestation of clinical symptoms of atherosclerosis. The thickness of stable atherosclerosis plaques cover was 1.14 0.03 um and 0.67 0.04 um in unstable plaques.
Conclusions: the results of our study demonstrate that susceptibility to damage of atherosclerosis plaque as a form of atherosclerotic progression in the carotids plays a significant role in realization of ACVE. Morphological characteristics of unstable atherosclerotic plaques shows discorrelation between the process of lipoidisation, cellular density of proliferating smooth muscular cells and degree of death of cellular elements in the arterial wall.

P059

Different type of cardiac mast cells in rats acutely poisoning by T-2 toxin: a morphometric classification

Vesna Jacevic, Iivica Milosavljevic, Dubravko Bokonjic, Lidija Zolotarevski, Katarina Jelic, Milos P. Stojiljkovic
National Poison Control Centre, Military Medical Academy, Belgrade, Serbia and Montenegro

We evaluated basic classes of cardiac MCs according to the following quantitative morphometric parameters: perimeter (P), area (A) and roundness (R) using commercial morphometric software (Camia, 2005). Wistar rats were treated by T-2 toxin (1 LD50 0.23 mg/kg sc) and sacrificed on day 1, 3, 5, 7, 14, 21 and 28 after treatment, as well as control ones. In the control groups the majority of MCs were tiny (P ά 7.99 μm), hypogranular (H0-MCs) (A ά 14.3 μm2) and ovoid (R ά 0.65 μm). MCs with discreet granules, hypergranular (H1-MCs), had quantitative values of the parameters (P ά 14.9 μm; A ά 20.0 μm2; R ά 0.38 μm). Minority of MCs were determinate as degranular (D-MCs) had large (P > 15.0 μm), irregular shapes (A > 20.0 μm2) and showed degranulation (R < 0.3 μm). In the heart of T-2 toxin-treated rats the quantitative parametars values of H0-MCs and H1-MCs were similar to the control group. D-MCs showed significantly increase in perimeter and area ($p < 0.05$), while their roundness were decreased ($p < 0.05$). We concluded that chosen quantitative morphometric parameters of cardiac DMCs are useful for evaluation of a functional state of the heart both under normal and pathological conditions, such as during the acute T-2 poisoning.

P060

Immunohistochemical investigation of calretinin, VEGF-C and CD34 in distinction between cardiac myxomas and mural myxomatous thrombi

Bobos Mattheos, Pappas Dimitrios, Hatzibougias Dimitrios, Tzioufa Valentini, Nenopoulou Eleni Department of Pathology, Aristotle University Medical School, Thessaloniki, Greece

Objective: Cardiac myxoma is the most common primary cardiac tumor in adults. The histogenesis is still controversial, as well as the differential diagnosis from a myxomatous mural thrombus. The aim of our study was to investigate the usefulness of specific immunohistochemical markers in order to dinstinct myxomas from mural myxomatous thrombi.
Methods: Formalin-fixed paraffin-embedded tissues from 10 cardiac myxomas >2cm in greatest diameter and 5 mural myxomatous thrombi were analyzed immunohistochemically for the expression of calretinin, VEGF-C and CD34 using the LSAB visualization system.
Results: All cardiac myxomas showed diffuse and moderate to strong positivity for calretinin with predominantly cytoplasmic staining pattern. VEGF-C detected virtually in all stromal and endothelial cells with strong cytoplasmic staining. CD34 antigen was positive in endothelial and scattered stromal cells, as well as in a variable number of neoplastic cells. Mural myxomatous thrombi were not reactive for calretinin whereas VEGF-C was strongly and diffusely positive. CD34 was expressed in endothelial and in a small number of stromal cells.
Conclusion: Calretinin can be important diagnostic marker for cardiac myxoma and useful marker in differential diagnosis from myxomatous mural thrombus.

P061

The Pathology of Diastolic Heart Failure

Patrick J Gallagher and Ruth Mathers
Department of Pathology, Southampton University Hospitals, Southampton SO16 6YD UK

Traditionally heart failure has been viewed as a disorder of ventricular function produced by ischaemic heart disease, valvular disorders or hypertension. Although survival is improved with modern therapy heart failure remains a disorder with a poor long term outcome and a substantial risk of sudden death. Echocardiography is the most reliable method of confirming the diagnosis. Cardiologists now recognise that a proportion of patients with typical signs and symptoms of heart failure appear to have

preserved ventricular function with a normal or near normal ejection fraction (≥ 50%). This is generally termed diastolic heart failure. We have studied the macroscopic changes at post mortem in 116 patients who died suddenly of cardiac disease. Our intention was to identify patients who might have fulfilled criteria for the clinical diagnosis of diastolic heart failure. Features of established heart failure such as oedema and hepatic congestion were recorded and graded and wherever possible the cause of cardiac failure was identified. Mitral valve circumference, left ventricular thickness and the distance from the valve ring to apex were recorded. We classified the shape of the left ventricular cavity as globular (31), normal conical (27), cylindrical (36) and pencil shaped (22). 89 of the 116 sudden deaths had clear evidence of cardiac disease. 53 of these had obvious ischaemic or valvular disease. Of the remaining 36 patients 6 had no evidence of chronic heart failure and 15 had dilated ventricles. Of the remaining 15 patients 8 had evidence of cardiac hypertrophy. We believe that the macroscopic changes in these patients meet the requirements for the diagnosis of diastolic heart failure. All had died of cardiac disease but had no clear evidence of ischaemic or valvular disease. In each case the ventricular cavity had a non globular shape. Whilst we must accept that diastolic heart failure is a significant clinical problem it is not a common entity at post mortem (8 out of 116 cases). We may have underestimated the number of cases by excluding patients with ischaemic heart disease. We also suspect that patients who initially develop so called diastolic heart failure progress to a more typical pathological form of disease by the time of their death.

P062

P53 and bcl-2 expression in dilated carciomyopathy

A. Tsipis, N. Kavantzas, A.-M. Athanassiadou, P. Athanassiadou, I. Giannopoulou, G. Agrogiannis, E. Patsouris
Department of Pathology, Medical School,
University of Athens, Greece.

Dilated cardiomyopathy (DCM), a disease of unknown etiology and pathogenesis, is associated with heart failure and compensatory hypertrophy. Apoptosis has been attributed an essential role in DCM. In order to investigate the pathogenesis of DCM we examined the expression of bcl-2 and p53 oncoproteins in tissues from patients with DCM. Twenty five cardiac tissue postmortem specimens (20 with DCM and 5 control subjects) included in this study. An immunohistochemical method was performed with the use of anti-p53 and anti-bcl-2 antibodies. Samples from the DCM patients stained more intensely with anti-p53 antibody than those from control group ($p<0.05$). The tissues showed little expression for bcl-2. Our results suggest that p53 and bcl-2 expression and apoptosis may play some role in the pathogenesis of DCM.

P063

Isolated eisinophilic coronary periarteristis: A post – mortem diagnosis case of unusual churg – strauss syndrome presentation

Agapitos E, Glava C, Agrogiannis G
Department of Pathology, National and Kapodistrian
University of Athens, Athens, Greece

Introduction: Eosinophil coronary arteritis is rare and occurs principally as a manifestation of cardiac involvement in Churg – Strauss syndrome.
Case Report: A 33-year-old woman was found dead of ventricular fibrillation in her bath in June 2005. The woman was autopsied. Macroscopically, lungs showed passive congestive pulmonary edema. Her heart weighed 340g and all measurements corresponded to maximum physiological limits (thickness of right wall 0,5cm, thickness of left wall 1,3cm, thickness of interventricular septum 1,2cm). Configuration of the valves was normal. Coronary arteries did not show significant alterations, except for a left anterior descending artery tract where, on cross section, transmural thickening, greyish white colour and elastic hard consistence were observed. Histological examination was accomplished on sections of heart, lungs, liver and kidney. Microscopic examination of heart sections revealed the presence of old infracted areas and dense eosinophil infiltration of the coronary adventitia. Some eosinophils invaded the media and the intima, which additionally presented type Va arterosclerotic lesions and stenosis up to 50%. On the ventral inferior wall an extensive old infracted area of the myocardium was observed. Microscopic examination to the other sections evidenced grey sclerosis of the lung and passive hyperaemia of liver and kidney.
Discussion: Pericoronaric eosinophilic infiltration is mainly associated with advanced stages of Churg – Strauss syndrome. In the present case, this microscopic finding was not accompanied by eosinophilic infiltration of the lung and this renders the expression of the syndrome unusual. Additionally, in the present case no myocarditis and no extravascular granulomas or extravascular eosinophilic infiltration were detected. In bibliography, three other similar cases are reported. In 1989, Kajihara et al reported the sudden death of a 40-year-old man of instable angina. Microscopic examination revealed inflammatory infiltration, mostly eosinophilic, localized in adventitia of coronary arteries located in the subepicardial region. In 2005, Taira et al reported the sudden cardiac death of a 52-year-old man. The only finding the eosinophilic infiltration of the coronary adventitia. In 2005 as well, Lepper et al described the case of a 43-year-old woman who died after spontaneous dissection of all three coronary arteries. Microscopic examination of coronary vessels showed severe eosinophilic infiltrates, whereas all extracardiac arteries were intact and free of inflammatory cells. There have been described several limited forms of presentation of Churg – Strauss syndrome. However, to the best of our knowledge, this is the fourth reported case of sudden cardiac death whose only finding was isolated eosinophilic coronary periarteritis.
Conclusion: Clinical and histological expression of the Churg – Strauss syndrome is various. In bibliography, several uncommon forms are reported. Coronary eosinophilic periarteritis may constitute part of the expression of the Churg – Strauss syndrome. The absence in the present case of lung involvement, extravascular granulomas or extravascular tissue eosinophilic infiltration renders this expression unusual. In fact, to the best of our knowledge, this is the fourth case reported.

P064

Apoptosis profile of normal human thymus

Michael Doukas[1], Alexandra Papoudou-Bai[1], Evangeli Lampri[2], Sevasti Kamina[2], Antonia Charchanti[1], Dimitra Rontogianni[3], Niki J. Agnantis[2], Panagiotis Kanavaros[1], Maria Bai[2].
Departments of Anatomy[1] and Pathology[2] University of Ioannina, Ioannina 45110, Greece, Department of Pathology,
Evangelismos Hospital of Athens[3], Greece

We analysed the immunotopographical distribution of the apoptosis associated proteins bcl2, bcl-xl, mcl1, bim, bak, bax, bid, FLIPs/l and the apoptotic cells (TUNEL and active caspase3 positive) in twenty normal human thymuses. Bcl-xl was mainly found in the cortical thymocytes, while Bcl2, mcl1 and bim were mainly detected in the medullary thymocytes. Bax and bid were strongly expressed in all thymocytes, whereas Bak was undetectable in thymocytes and was mainly expressed in Hassal bodies. Expression of FLIPs/l, Fas and FasL were found only in the thymic epithelial cells (TECs). Fas expression was higher in medullary TECs and in Hassal bodies. FLIPs/l was observed in all TEC types except subcapsular epithelial cells. Apoptotic cells (TUNEL and active caspase3 positive) were mainly found in the cortex and the corticomedullary junction. Our study suggests that bcl2 and mcl1 expression may reflect the surviving medullary, while bcl-xl

expression may reflect the surviving cortical thymocytes. Bax and bid may be involved in thymocyte apoptosis, whereas bak does not seem to play major role in thymocyte apoptosis.

P065

Primary cutaneous T-cell rich B-cell lymphoma

Venizelos I[1], Tatsiou Z[1], Chatzitolios A[1], Moulla A[1], Mandala E[2].
[1]Department of Pathology, [2]Department of Internal Medicine, Hippokratio General Hospital, Thessaloniki, Greece

T-cell rich B-cell lymphoma (TRBL) is a lately recognized B-cell lymphoma variant, characterized by a minor population of neoplastic B-cells existing in a background of predominant reactive T-lymphocytes.It is a rare entity, accounting for approximately 1-2% of all non–Hodgkin's lymphomas. It has both nodal and extranodal presentation. Primary cytaneous TRBL is an extremely rare lymphoma and only 17 cases have been documented thus far in the medical literature. We report the case of a 46-year-old man who presented in our hospital due to a slowly growing, painless skin nodule on the left temporofrontal region of the scalp .A complete surgical excision was performed and histological examination revealed morphological and immunohistochemical features of cutaneous TRBL. On physical examination there was no hepatosplenomegaly, peripheral lymphadenopathy or other skin abnormalities. Hematological examination was within normal ranges. A metastatic work-up, including chest X-ray, CT-scan of the abdomen, bone scan and bone marrow aspirate and biopsy revealed no evidence of disease. The patient received 6 courses of systemic chemotherapy with Mabthera and CHOP and 2 years later he is in good condition, without evidence of local recurrence or metastatic disease.In this study we report a very rare case of TRBL presented primarily in the skin. Although rare, it is important to make the correct diagnosis using the appropriate immunohistochemical stains.

P066

Morphological criteria and molecular markers as possible prognostic factors in Hodgkin's lymphoma

Kovrigina A., Probatova N.
Department of Pathology, N.N. Blokhin Cancer Research Center, Kashirskoye shosse 24, 115478 Moscow, Russia

Objective: In spite of using clinical prognostic factors for dividing pts with Hodgkin's lymphoma (HL) into 3 groups: early, intermediate and advanced stage there are about 10% of early and late relapse in each groups of pts. Besides the late toxicity is well known complication of modern chemotherapy (such as BEACOPP and escalated BEACOPP). So the majority of patients should not be exposed superfluous treatment. The aim of our study is revealing of morphological and molecular factors of poor prognosis in primary patients with HL.
Material and methods: We examined lymph node's biopsies of 2 groups of patients with HL before treatment. The groups of pts were formed using the results of standard chemotherapy+RT (1987-2001). 1-st group included 71 pts with favorable prognosis, mediana-25,5 years, I stage-9, II-42 pts, III-11pts, IY-9 pts. 2nd group was generated by results of treatment with presence failure of complete remission, early and late relapses - 70 pts, mediana-25,5 years, I stage-7 pts, II-35 pts, III-8 pts, IY-20 pts. NS and mixed cellularity variants were predominated in both groups: 1st group – NS I 34,3%, NS II 15,7%, mixed cellularity 34,3%; 2nd group- NS I 35,2%, NS II 31.0%, mixed cellularity 28,2%. We used morphological codification with semiquantitative estimation of neoplastic cells, reactive cellular background, character of growth (separately neoplastic cells and tumor in lymph node), fibrosis, necrosis. Expression of p53, p27, BCL-2 was also evaluated in 2 groups of pts .Multifactor dispersive analysis, discriminant and factor analyses were performed.
Results: Expression of BCL-2 was independent factor of poor prognosis in I-IY stages ($p<0.001$). Following morphological criteria had significant difference: I stage- amount of neoplastic cells, lymphocytes, eosinophils , neutrophils, character of neoplastic cell's growth; II stage- neoplastic cells, necrosis ($p<0,01$). III and IY stages hadn't significant difference by morphological analysis. Eosinophils were significant higher in 2nd group in NS ($p<0,01$).
Conclusion: Morphological features may be used as prognostic factors in I-II stages in pts with HL. Clinical prognostic factors (such as tumour masses, expansion of neoplastic process) have conducting value in advanced stages.

P067

Diagnostics of "grey zone" large lymphomas

Kovrigina A.
Department of Pathology, N.N. Blokhin Cancer Research Center, Kashirskoye shosse 24, 115478 Moscow, Russia

Objective: Grey zone is complicated for the account of TCRBCL, anaplastic variant of DBCL, primary mediastinal B-cell large lymphoma (PMBL), anaplastic large-cell lymphoma (ALCL). We analyzed a group of large cell lymphomas (prospective consultative material 2002-2004) and revealed cases which had morphological difficulties of differential diagnostics between Hodgkin's lymphoma(HL) (classical HL and nodular lymphoid predominance NLPHL).
Materials and methods: We investigated morphological picture and immunophenotype of paraffin embedded lymph node specimens 159 large cell lymphomas using wide panel of antibodies CD3, CD4, CD8, CD10, CD15, CD20, CD21, CD23, CD30, CD43, CD45, CD57, Granzyme B, ALK, EMA, BCL-2, BCL-6, PAX 5, MuM.1
Results: We diagnosed 22 cases of TCRBCL (m:f 0,8:1,0; mediana 47,5 years, range 21-67). In 20 cases of TCRBCL diffuse growth was marked and in 2 cases- nodular growth. Concerning peculiarities of cytomorphology of neoplastic cells and histological picture differential diagnostic between TCKBCL and HL (NLPHL and mixed cellularity) was fulfilled in 31,8% cases TCRBCL. 59 cases with large mediastinal masses in debut of disease(m:f 1,0:3,5; mediana 31,5 years, range 16-62).) were diagnosed as PMBL. 16,9% cases of PMBL were differentiated with NSII. 2 cases of PMBL (using morphological features) were characterized by "chimeric phenotype": CD45+,CD15+, CD20+, CD23+, CD30+, MuM.1+. Neoplastic cells were 23-positive in 60,8% cases. Anaplastic variant of DBCL was detected in 2 cases which were characterized by monomorphic expression CD20, CD30 and markers of postfollicular origin MuM.1+, CD138+. ALCL was diagnosed in 76 cases (m:f 1,1:1.0; mediana 22 years, range 2,5-79). Expression of ALK was detected in 53,9% cases. 70,8% cases of ALK-negative had characterized by marked polymorphism and multinuclear cells like R-S cells among abundant reactive background. These cases of ALCL have been needed to differentiation with HL (NS II, lymphocyte depletion). The cytotoxic molecules (Granzyme B was positive in 93,7% cases) and B-transcriptional factors (PAX 5 together with MuM.1) must be included in immunohistochemical differential panel between ALCL, ALK-negative and HL as decision of differential diagnostic problem.

Conclusion: Detail comparison of morphological and immunohistochemical features allow us to suggest 2-step diagnostic algorithm of "grey zone" large lymphomas.

P068

The prognostic significance of the percentage and pattern of bone marrow infiltration in patients with multiple myeloma

Hadjileontis C[1], Zervas K[2], Papadimitriou C[1], Kaloutsi V[1].
[1]Pathology Dept, Medical School, Aristotle University of Thessaloniki, Greece. [2]Haematology Clinic, Theagenion Cancer Hospital of Thessaloniki, Greece.

Within the frame of drawing new strategies for the confrontation of multiple myeloma (MM), the reevaluation of parameters that are considered to be prognostic for the disease, is inevitably included. We investigated the percentage and pattern of bone marrow (BM) infiltration in BM biopsies from 100 patients with newly diagnosed MM. These parameters were reevaluated after the treatment of the patients with conventional chemotherapy. In order to determine the prognostic significance of the above parameters, our results were statistically correlated with the survival of the patients during the years 1994-2004 (Spearman's and Kruskal-Walis's tests). Statistical analysis brought up a significant correlation between the alterations of the percentage of BM infiltration before and after treatment and the patients' survival ($R=0,51$ και $p<0,05$), exhibiting therefore the importance of the percentage of BM as an independent prognostic marker for the disease. The comparison of the pattern of BM infiltration with the patient's survival on the other hand, did not reveal a statistically significant correlation.

P069

Investigation of the prognostic significance of multiple myeloma differentiation and type of paraproteinaemia, through a retrospective study of 100 cases

Hadjileontis C[1], Zervas K[2], Papaioannou M[2],
Papadimitriou C[1], Kaloutsi V[1].
[1]Pathology Dept, Medical School, Aristotle University of Thessaloniki, Greece. [2]Haematology Clinic, Theagenion Cancer Hospital of Thessaloniki, Greece.

The degree of multiple myeloma (MM) differentiation as well as the type of paraproteinaemia (TP) are thought to be parameters of independent prognostic value for the disease. We studied MM differentiation and the TP in bone marrow (BM) biopsies of 100 patients with newly diagnosed MM. The study was performed at first diagnosis and after treating the above patients with conventional chemotherapy. The TP was determined both immunohistochemically in BM biopsies, as well as by electrophoresis of the patients' urine and serum. The prognostic significance of these parameters was evaluated as the degree of the statistical correlation they showed with the survival of the patients during the years 1994-2004 (Spearman's and Kruskal-Walis's tests). Our results oppose the authors suggesting the prognostic significance of these two parameters, since no statistically significant correlations between either the degree of MM differentiation (with or without plasmablasts) or the TP detected and the patients' survival were found.

P070

Primary CD 30 + T-Lymphoproliferative disorders of the skin in childhood. Report of 3 cases

C. Michail-Strantzia[1], I. Bonou[1], P. Giamarelou[1],
L. Dimitriou[2], H. Kosmidis[3]
Pathology[1], Surgical[2] and Oncology[3] Department of Children's Hospital of Athens, P. & A. Kyriakou

The diagnosis and classification of cutaneous lymphomas remain one of the most challenging areas in dermatopathology. The primary cutaneous CD30 + T-lymphoproliferative disorders are linked by the common histological feature of large atypical lymphoid cells expressing CD30 and include Anaplastic Large Cell Lymphoma T/null cell primary cutaneous type, LyP, and borderline cases of the EORTC classification with overlapping features of the other two conditions. We present the clinicopathologic findings in 3 female children with primary cutaneous CD30 + T-lymphoproliferative disorders, presented with a rapidly enlarging and ulcerating mass involving the skin and subcutaneous tissue. The patients' age ranges from 9 to 10 years. The histologic and immunohistochemical investigation evaluated sheets of large atypical lymphoid CD45 positive cells, that were strongly CD30 positive in all cases. Cells were of T-cell phenotype and in 1 case there was a large sharing of CD1a positive cells. Staining for anaplastic lymphoma kinase was negative in 2 cases. No evidence of systemic involvement was noted. The primary cutaneous CD30 + T-LPD are rare in childhood and have different behavior, prognosis and treatment requirements to nodal lymphomas.

P071

Development of intrinsic innervation in human lymphoid organs

Valsamo Anagnostou, Ipatia Anagnostopoulou, Dina Tiniakos,
Despina Karandrea, Emmanouil Agapitos*, Christos Kittas
Laboratories of Histology-Embryology and *Pathology,
Medical School, National and Kapodistrian University of Athens, Greece

The aim of the study was to assess the distribution of parenchymal nerves in human fetal thymus and spleen. Our material consisted of tissue sections from 23 human fetuses (18-39 gestational weeks). We used the biotin-streptavidin immunohistochemical technique with antibodies specific to NSE, NF, PGP9.5, S100 and TH. In thymus, NSE-, NF-, S100-, PGP9.5- and TH- positive nerves were identified associated with the vasculature from 18 gw, increasing in density during development. Their branches penetrated the septal areas at 20 gw, reaching the cortex at 23 gw. Few nerve fibers were seen close to medullary epithelial thymic cells, at 20 gw. In human fetal spleen, NSE-, NF-, S100-, PGP9.5- and TH - positive nerve fibers were seen surrounding the splenic artery at 18 gw. Perivascular nerve fibers were seen extending into the white pulp in association with the central artery. Scattered nerve fibers were localised in the red pulp from 18 gw. TH- positive cells were observed in the white pulp during the third trimester. Human fetal thymus appears richly innervated in contrast to fetal spleen. The predominant perivascular distribution of most intraparenchymal nerves implies that the intrinsic innervation of lymphoid organs plays an important functional role during intrauterine life.

P072

CD27 and DBA44 expression in splenic marginal zone lymphomas

Theodore Argyrakos[1], Ipatia Doussis-Anagnostopoulou[2],
Dimitra Rontogianni[3], Paraskevi Oikonomou, Themis Karmiris[4],
Ioannis Dervenoulas[5], Christos Kittas[2]
[1]Pathology Department, "G. Gennimatas" General National Hospital, [2]Laboratory of Histology and Embryology,
National and Kapodistrian University, Athens Medical School,
[3,4]Evangelismos General Hospital, Athens and Attikon University Hospital, Chaidari, Athens, Greece

CD27 is an activation antigen that characterizes memory lymphocytes (B and T), while DBA44 is an antigen expressed in hairy cell leukemia and naïve mantle B cells. In order to investigate the cell of origin of splenic marginal zone lymphomas (SMZLs),

we studied the expression of DBA44 and CD27 in SMZLs. Twenty four (24) cases of CD20+, CD5-, CD23-, bcl-6-, Cyclin D1-SMZLs were immunohistochemically examined with the monoclonal antibodies CD27 (NOVOCASTRA) and DBA44 (DAKO), using the microwave antigen retrieval method and the Envision polymer method. 13/24(54.1%) cases were DBA44 negative, whereas 11/24(45.9%) cases exhibited partial positivity, either in the neoplastic white pulp (2/24, 8,33%) or in the red pulp (9/24, 37.5%. On the latter the positivity was observed either in a few scattered cells (5/24, 20.83%) or in many neoplastic cells infiltrating the red pulp (4/24, 16%). 20/24 (83.3%) SMZLs exhibited CD27 positive nodules and partial positivity in the neoplastic cells of the white pulp, while 4/24(16.6%) showed negative nodules with few scattered positive cells in the red and white pulp. In conclusion, SMZLs are in their majority CD27 positive in the neoplastic nodules, while DBA44 negative in the nodules and positive in the red pulp. CD27 expression rather supports the theory of memory B cell origin of SMZLs, while DBA44 positivity in the red pulp could correlate with the pattern of infiltration.

P073

Localized castleman's diasease associated with systematic AA amyloidosis. Regression of amyloid deposits after tumor removal.

K. Giaslakiotis[1], K. Kokkori[1], G. Liapis[1], P. Alexandrou[1], X. Giakoumi[2], P. Korkolopoulou[3], A. Androulaki[1].
[1]Department of Pathology, [2]First Department of Internal Medicine, [3]Pathology Laboratory, University of Athens Medical School, Laiko General Hospital, Mikras Asias 75, 115 27 Athens, Greece.

Castleman's disease is a rare B-cell lymphoproliferative disorder, comprising anatomically unicentric and multicentric forms and histologically vascular and plasma cell variants. We report a case of systemic AA amyloidosis complicating Castleman's disease – unicentric, retroperitoneal, plasma cell variant - in a 49 year old white woman, in whom the underlying primary diagnosis was made after years of illness. The patient underwent tumor resection and a rapid clinical and laboratory resolution was achieved. She remains free of disease two years post-operatively. Castleman's disease may be complicated by acquired AA systemic amyloidosis and can be cured surgically even in advanced cases.

P074

The variant form of hairy cell leukaemia. Report of a rare case through retrospective bibliographic study

Alexopoulou E, Lafioniatis S*, Fericean A, Hadjileontis C.
Pathology Department and Unit of Thalassaemia*
"Achillopouleion" General Hospital, Volos, Hellas

Hairy cell leukaemia (HCL) accounts for about 2% of all cases of leukaemia, while its variant form represents less than 10% of these cases. This rare form affects elderly or middle age patients, usually males, exhibiting cytopenia with lymphocytosis and splenomegaly. We present the case of a 56 year-old male patient who presented with anaemia and splenomegaly. Bone marrow biopsy revealed infiltration of the marrow spaces by small to medium sized lymphoid cells, counting up to 40% of the marrow population. The lymphoid cells demonstrated specifically round or ovoid nuclei with prominent nucleoli and abundant irregular cytoplasm with or without hairy projections. Cells of similar morphology that proved to be B-lymphocytes by flow cytometry, were also found in the bone marrow aspirate as well as the peripheral blood of the patient measuring up to 2.7% and 0.6 % of the circulating cells respectively. The immunophenotype of these cells was CD20+, CD11C+, CD22+, CD103+, CD25- and CD123- with monoclonal expression of κ light chains. Immunohistochemistry showed positivity of the bone marrow lymphoid cells for CD45, CD20, CD22 and DBA44. The above findings were indicative of the variant form of HCL, the patient underwent splenectomy without chemotherapy and two years later he is in good general condition with no signs of relapse.

P075

Pathophysiology of the spleen in the thalassemic HBB^{TH-3} mouse model; Administration of G-CSF ± hydrea (HU) provokes dramatic alterations in spleen size and histology.

Evangelia Athanasiou, Evangelia Yannaki, Garyfallia Karponi, Aglaia Antoniou, Fani Zervou, Angeliki Xagorari, Athanasios Fassas, Achilles Anagnostopoulos
Gene and Cell Therapy Center, Hematology Department-Bone Marrow Transplantation Unit, George Papanikolaou Hospital, Thessaloniki, Greece

Spleen in thalassemic patients can become excessively enlarged, due to extamedulary hematopoiesis and the trapping of damaged red blood cells within splenic sinuses. The collection of autologous hematopoietic stem cells (HSCs) for genetic modification from these patients is a previously unexplored issue as gene therapy only recently has become a realistic potential for thalassemia.
The cytokine G-CSF (Granulocyte Colony Stimulating Factor) is the most widely used inducer of peripheral blood stem cell (PBSC) mobilization in normal donors and in patients with hematologic malignancies. Currently, G-CSF- mobilized PBSC is the preferable source of HSCs for transplantation due to higher yield of stem/progenitor cells compared to bone marrow harvest. A G-CSF-related splenic enlargement has been documented which very rarely may result in splenic rupture. **The aim** of the study was to investigate the G-CSF influence in a condition of splenomegaly as in the thalassemic mouse model, any potential increased risk for rupture as well as the histopathological changes of splenic parenchyma. A possible beneficial effect of HU, which has been shown to reduce extramedullary hemopoiesis, in preventing splenic rupture was also explored.
Material and methods: We used heterozygous knockout thalassemic HBBth-3 mice, which clinically resemble the human thalassemia intermedia. Untreated, wild type (wt) C57Bl6 mice were also included in the experiments. In three independent experiments, 8-10 weeks-old mice, were randomly classified in four groups. Group A and B (n=4+4) included untreated wt and thalassemic mice, Group C (n=10) G-CSF (200μgr/kgX8days, intraperitoneally)-treated thal mice and Group D (n=11) thal mice treated with HU (60mg/kgX30days, via gavage)+G-CSF. Animals were sacrificed the last day of G-CSF administration. Spleen weight was determined as a ratio to total body weight. Immunohistochemistry was performed for lineage markers with MPO, Glycophorin, CD61, CD45RO, CD45RA, CD20 and histochemistry with Gomori stain.
Results: In Group B, spleens were enlarged due to extramedullary hematopoiesis with no clear distinction between red and white pulp. Red pulp in was almost replaced by erythroid hyperplasia in contrast to Group A, where spleens were smaller in size with a well-organized white pulp and limited red pulp. In Group C, there was a dramatic enlargement in spleen weight (p=0,02) and extreme hypercellularity. Splenic parenchyma was replaced almost entirely of red pulp with predominance of granulocytic hyperplasia and foci of neutrophils homing around splenic cords. Erythoid and megakaryocytic lineages were also hyperplastic. Splenic cords and fibrous septae were ill-defined, discontinued or collapsed. Infarcts and/or capsular micro-ruptures were detected in 5/10 mice although there was no clinically observed splenic rupture in G-CSF-treated (0/21) animals. In Group D, fibrous septae were basically incessant and extramedullary hematopoiesis was still evident however, in lower levels than in Group C . These findings correlated with a reduced rate in splenic infracts (3/11) and decreased splenic enlargement as compared to Group C.

Conclusions: G-CSF provokes enormous extramedullary hematopoiesis with predominance of granulocytic hyperplasia in the spleen of thalassemic mice leading to further enlargement of the spleen size. The extreme hypercellularity of splenic parenchyma destroys the splenic cords and leads to infarcts and/or capsular microruptures. However, these findings were self-limited resulting in no clinically detected splenic rupture. Pretreatment with HU may prevent these complications potentially increasing the safety of mobilization in thalassemia.

P076

Method concordance for the assessment of ALK abnormalities in anaplastic large cell lymphomas (ALCL) in pathology practice.

Bobos M, Kostopoulos I, Kotoula V, Karayannopoulou G, Kaloutsi V, Papadimitriou CS
Department of Pathology Aristotle University Medical School, Thessaloniki, Greece

Objective: Translocations involving the ALK gene, such as NPM-ALK (t[2;5][p23;q35]), have become the hallmark genetic alterations in ALCL as conferring a better prognosis to these rare tumors. The most common method currently used in pathology practice for the detection of ALK abnormalities is immuno-histochemistry (IHC) for ALK protein. The aim of this study was to evaluate the specificity of molecular methods in comparison to IHC for the assessment of ALK abnormalities in ALCL.
Methods: Forty four ALCL cases were assessed for the presence of ALK abnormalities with IHC (MoAb ALK1), with RT-PCR on material extracted from paraffin sections and dual color FISH with the LSI ALK break-apart probe.
Results: 17 cases were ALK+ and 27 ALK-. NPM-ALK fusion transcripts were detected in 14/44 (32%) cases and ALK rearrangements by FISH in 12/41 (29%) cases. NPM-ALK transcripts were found in 10/17 ALK1+ (59%) and in 4/27 ALK- (15%) cases (P=0,006), including 9/9 cases with nuclear/cytoplasmic ALK1 staining and 1/8 cases with cytoplasmic staining only (P<0,001). ALK gene rearrangements were observed in 8/11 (73%) of ALK+ cases and in 4/30 (13%) of ALK- cases (P=0,001). FISH and RT-PCR results were highly concordant (P<0,001). Combined, FISH and RT-PCR demonstrated ALK abnormalities in 12/16 (75%) ALK+, but also in 5/26 (19%) ALK- cases (P=0,001).
Conclusions: Our results show that the combination of FISH and RT-PCR is more specific than IHC in revealing ALK genetic alterations. These methods may be particularly useful in cases where the production of ALK chimeric proteins is inhibited.

P077

Microvessel density and expression of angiogenic proteins VEGF, VEGFR1, VEGFR2 and HIF1a in Hodgkin and Reed-Stenberg cell (HRS) of classical Hodgkin lymphoma (cHL)

Evangeli Lampri[1], Evangelos Briasoulis[2], Lazaros Nikiforidis[2], Michael Doukas, Anna Goussia[1], Asimina Demou[4], Nikolaos Pavlidis, Niki J Agnantis[1], Panagiotis Kanavaros[3], Maria Bai[1]
Department of Pathology[1], Oncology[2] and Anatomy-Histology-Embryology[3], Medical School, University of Ioannina. Department of Pathology of General Hospital of Ioannina, "G. Hatzikosta"[4]

Few studies have focused on angiogenesis in cHL. Therefore in the present study we analysed the immunohistochemical expression of the VEGF, VEGFR1, VEGFR2 and HIF1a proteins in 95 cases of cHL. Moreover, microvessel density (MVD) was estimated after immunostaining for CD34(MVD-CD34) and CD105(MVD-CD105). Expression (at least 10% positive HRS cells) of VEGF, VEGFR1, VEGFR2 and HIF1a proteins was found in 78/90(86.7%), 32/95(33.7%), 18/89(20.2%) and 46/81(56.8%) cases, respectively. The MVD-CD34 and the MVD-CD105 were 61(±28.7) and 12 (±7.65), respectively. Significant positive correlations were found between VEGF/VEGFR2 and VEGF/MVD-CD34 (p=0.003 and p=0.02, respectively). Furthermore, a reverse correlation was found between VEGFR2 and clinical stage of the disease (p=0.02, r=-0.505). The present study shows that the angiogenic proteins VEGF, VEGFR1, VEGFR2 and HIF1a are expressed in HRS cells of cHL. VEGF produced by HRS cells may act in a paracrine and autocrine fashion in cHL and possibly implicated in the pathogenesis of the disease.

P078

Thymic tumor with partial neuroendocrine differentiation – a case report

Jelena Stojsic, Dragan Subotic, Jelena Radojicic
Institute for Lung Diseases and Tuberculosis, Clinical Centre of Serbia, Belgrade, Serbia

Predominance of neuroendocrine elements in thymic tumor differs it from the thymic tumors containing scattered group of neuroendocrine cells. The epithelial neuroendocrine cells of the thymus compose typical or atypical carcinoid and are demonstrated by neuroendocrine monoclonal antibodies. We present a case of thymic tumor with predominant neuroendocrine differentiation. The patient was a male, age of 61. Tumor was detected on chest x-ray examination performed before operation of inguinal hernia. There was no any paraneoplastic or compressive symptoms. Tumor was localised in anterior mediastinum, without infiltration of surrounding mediastinal stuctures measured 110mm. Solid, shiny and fleshy tumor node was separated by a distinct fibrous septa. One part, measured 70x50x50mm, was focaly osteocartilaginously changed. Trabecular structures and "rosettes" with a dense fibrovascular stroma were performed. Mitoses and necrosis were absent. There was infiltration of tumor capsula. Neuron-specific enolase and synaptophisin were positive. Beside carcinoid tumor, node was rich of lymphocytes which expressed CD3 and terminal deoxynucleotid transferase. The conclusion was that it was predominant neuroendocrine tumor in B1 thymoma with focal infiltration of capsula. There is not recurrence of the tumor and local and distant metastases until today. It was noted that 75 thymic tumors were diagnosed in a period of ten years. It was the first one with predominant neuroendocrine differention.

P079

Immunotopographical distribution of cells expressing neuroendocrine markers in normal human thymus.

Alexandra Papoudou-Bai[1] Michael Doukas[1], George Karatzias[1], Ann Goussia[2], Sevasti Kamina[1], Kalliopi Stefanaki[3], Niki J. Agnantis[2], Maria Bai[2], Panagiotis Kanavaros[1]
Departments of Anatomy[1] and Pathology[2], University of Ioannina, Department of Pathology[3], Agia Sophia Hospital of Athens, Greece.

Neuroimmune interactions are thought to play key roles in the thymic biology and pathology. We analyzed by immunohistochemistry the distribution of cells expressing neuroendocrine markers in twenty normal thymuses. In subcapsular cortical epithelial cells low expression of NSE, PGP 9.5, TrkA and beta-tubulin II and high expression of beta-tubulin IV were found. In cortical epithelial cells low expression of synaptophysin and beta-tubulin II, intermediate expression of NSE, PGP 9.5 and TrkA and high expression of beta-tubulin IV were observed. In medullary epithelial cells low

expression of chromogranin, synaptophysin, tyrosine hydroxylase and NF 68kDa, intermediate expression of NSE and beta-tubulin IV and high expression of beta-tubulin II were detected. In Hassall's corpuscles low expression of chromogranin, synaptophysin, NF 140-160, NF 200 and p75 and high expression of NSE, NF68, beta-tubulin II and beta-tubulin IV were noticed. All these proteins were undetectable in thymocytes. The diversity of the immunotopographical distibution and the expression levels of neuroendocrine markers in the subtypes of thymic epithelial cells may reflect the diversity of their biological functions and/or their different stages of differentiation. Moreover, the above results may be helpful for the further understanding of the histogenesis of the neuroendocrine thymic tumors.

P080

The expression of p27, PTEN, Cks1 and Skp2 in thymomas.

Vassiliki Zolota[1], Vassiliki Tzelepi[1], Chaido Sirinian[1], Stavroula Salakou[2], Demetrios Kardamakis[3] and Demetrios Dougenis[4]
Departments of Pathology[1], Neurology[2], Radiotherapy[3] and Cardiosurgery[4], University of Patras, Medical School, Greece

Loss of one of the major cell-cycle inhibitory proteins, p27Kip1, is the result of increased proteasome-dependent degradation, mediated by its specific ubiquitin ligase subunits: Skp2 and Cks1. PTEN is a tumor suppressor gene which upregulates, indirectly, p27Kip1. A total of 20 thymomas (classified according WHO and TNM) were immunostained for p27, PTEN, Cks1 and Skp2 antibodies. Staining evaluation was made according to the percentage of positive tumor (epithelial) cells as follows: <10%: -/+, 10-25%: 1+, 26-50%: 2+ and >50%: 3+. P27 expression was lost in 20% of the cases, whereas 25%, 10% and 45% of the cases showed 1+, 2+ and 3+ respectively. 10% of the cases showed low PTEN expression levels (1+), 20% showed 2+ and 70% showed 3+. Cks1 and Skp2 showed comparative levels of expression as follows: -/+ 35%, 1+ 25%, 2+30%, 3+ 10% for cks1 and -/+ 35%, 1+45%, 2+20% for skp2. Histological type or staging were not associated with the expression of any of the markers studied. These results suggest a) loss of PTEN expression is uncommon in thymomas, b) loss of p27 expression is not associated with ominous histologic type or stage, c) skp2 and cks1 are expressed in low or moderate levels in the majority of the cases and do not seem to play a significant role in p27 loss in thymomas.

P081

Concomitant alterations of the p53, Rb and p27 pathways in diffuse large B-cell lymphomas (DLBCL)

Elena Tsanou[1], Angelos Skyrlas[1], Ioannis Sainis[1], John D. Panelos[1], Anna Batistatou[1], Vasiliki Malamou-Mitsi[1], Maria Bai[1], Panagiotis Kanavaros[2]
Departments of Pathology[1] and Anatomy[2], Medical Faculty, University of Ioannina, Ioannina 45110, Greece

The expression of p14, p21, Hdm2 and cyclin D2 proteins were studied by immunohistochemistry in DLBCL. The results were correlated with other cell cycle proteins. Expression of p14, p21, Hdm2 and cyclin D2 proteins was observed in 39/71, 22/76, 43/74 and 11/77 cases, respectively. Alterations of the p53 [p53-Hdm2-p21-p14], Rb [Rb-p16-cyclin D (D2 or D3)] and p27 [p27-cyclin E] tumor suppressor pathways were found in 50/76, 43/79 and 30/79 cases, respectively. Alterations of at least one of the pathways were found in 60/79 cases. Two or three concomitant alterations of the pathways were found in 40/79 cases. The analysis of the combined alterations of the pathways with respect to the expression levels of Ki67, cyclin A and cyclin B1 showed that 1) alterations of either p53 or Rb or p27 pathways were not significantly correlated with the expression levels of Ki67, cyclin A or cyclin B1 and 2) two or three concomitant alterations of p53, Rb and p27 pathways were significantly correlated with high expression levels of cyclin A ($p=0.032$). The present results indicate that concomitant alterations of the p53, Rb and p27 pathways in DLBCL exert a cooperative effect resulting in enhanced tumor cell proliferation.

P082

Expression of bcl2 family proteins and active caspase-3 in Hodgkin and Reed-Sternberg (HRS) cells of classical Hodgkin lymphomas (cHL)

Nikolaos Horianopoulos[1], Alexandra Papoudou-Bai[2], Elena Tsanou[1], Nafsika Simou[1], Anna Goussia[1], Niki[1] J. Agnantis[1], Panagiotis Kanavaros[2], Maria Bai[1]
Departments of Pathology[1] and Anatomy[2], Medical Faculty, University of Ioannina, Ioannina 45110, Greece

The expression of the proteins bad, bid, bim, bcl2, bcl-xl, mcl1, bax, bak and activated caspase-3 and the TUNEL index were assessed in order to gain further insight in the apoptosis profile of cHL. In addition, the relations between the apoptosis profile and the proliferation profile were analysed. High expression of bcl2, bcl-xl, mcl1, bax, bak, bad, bid and bim was found in 27/101, 95/101, 27/97, 73/95, 37/102, 85/94, 19/109 and 43/91 cases, respectively. Active caspase-3 and TUNEL positive HRS cells were detected in 47/70 cases (range 0-12%) and 60/71 cases (range 0-19.39%), respectively. Significant positive correlations were found between bax/bcl2, bad/bcl2, bad/bcl-xl, bim/mcl1, active caspase-3/bax, active caspase-3/TUNEL index, bax/cyclin D2, bcl2/cyclin B, mcl1/cyclin A and mcl1/cyclin B (all $p<0.05$). The results suggest that the proteins bcl-xl, bax and bad may play a predominant role in the regulation of apoptosis in HRS cells. Moreover, the proapoptotic activity of bax, bad and bim may be counteracted by the antiapoptotic activity of the bcl2, bcl-xl and mcl1 in HRS cells.

P083

Is fine needle aspiration cytology is a useful method in the dignosis of cervical tularemia lymphadenitis?

Banu D. Gun*, Burak Bahadir*, Guven Celebi**, Gamze Numanoglu*, Sukru O. Ozdamar*, Gamze M. Kuzey***
Zonguldak Karaelmas University, School of Medicine, Department of Pathology*, Department of Clinical Microbiology and Infectious Diseases**, Turkey
***Hacettepe University, School of Medicine, Department of Pathology, Turkey

Francisella Tularensis is a gram-negative coccobacilus that causes zoonotic disease tularemia. The clinical features of the disease depend on the route of inoculation and symptoms are nonspecific. Histopathological examination of lymph node biopsy in tularemia reveals suppurative granulomatous inflammation and caseous necrosis may be accompanied. Diagnosis is mainly made on the evidence of elevated agglutinating antibodies to F. Tularensis. In this study, the results of fine needle aspiration cytology (FNAC) of nine cervical lymphadenopaties, that had known tularemia diagnosis clinically and serologically, were evaluated and the cytomorphological features were described. All of the cases revealed suppurative inflammation and some caseous necrosis; in four epithelioid histiocytes and multinuclear giant cells were observed additionally. The differential diagnosis of tularemia principally with tuberculosis and with the other bacterial lymphadenitis was made and the utility of FNAC in tularemia cases were evaluated.

P084

Cytokine effects on Fas-mediated apoptosis in A549 lung carcinoma cells

Vassiliki Galani[1], George Vartholomatos[2], Eufemia Balasi[1]
George Chondrogiannis[1], Michalis Kastamoulas[1],
Elizabeth Markatzinou[1], Evangelia Voti[1], Maria Bai[3],
George Nakos[4], Marilena Lekka[5], Panagiotis Kanavaros[1]
Department of Anatomy[1]; Laboratory of Hematology[2];
Departments of Pathology[3] and Intensive Care[4];
Department of Biochemistry[5]; University of Ioannina,
Ioannina 45110, Greece

A549 cells were treated with TNFα, IFNγ, IL1β, IL13 and Fas (clone CH11) and analyzed by flow cytometry. The results were: 1) IFNγ induces time- and dose-dependent apoptosis, 2) the combinations IFNγ-IL13, CH11-IFNγ-IL13, CH11-TNFa-IL13, CH11-IFNγ-TNFa and CH11-IFNγ-TNFa-IL13 increased apoptosis, 3) in the combination CH11-TNFa, 100 ng/ml of TNFa showed antiapoptotic effects on A549 cells whereas 50 ng/ml of TNFa did not attenuate the proapoptotic effects of CH11. Pretreatment of A549 cells by 50 ng/ml of TNFa for 24 h showed antiapoptotic effects on CH11-treated cells and 4) IFNγ pretreatment (24 h) increased CH11-induced apoptosis whereas IL1β or IL13 pretreatment (24 h) decreased CH11-induced apoptosis in 48 h. TNFa has dose-dependent antiapoptotic effects on Fas-induced apoptosis of A549 cells; especially when A549 cells are pretreated by TNFa. IFNγ promotes whereas IL1β and IL13 prevent Fas-mediated apoptosis.

P085

Association of Pleuropulmonary Blastoma (PPB) with Cystic Nephroma and Small Bowel Polyp: Case Report and Data from the International PPB Registry

K. Stefanaki[1], F. Boman[2], A. Stassinopoulou[3], G. M. Williams[4,5],
J. C. Fournet[6], D. Bouron - Dal Soglio[6], A. Chauvenet[7], A. Hill[8],
Y. Messinger[4,5], J. R. Priest[5]
Department of [1]Pathology, Children's Hospital Aghia Sophia,
Athens, Greece; [2]Pathology, University Hospital of Lille, France;
[3]Oncology, Athens Pediatric Center, Athens, Greece; [4]Hematology/
Oncology, [5]International PPB Registry, Children's Hospitals
and Clinics of Minnesota, St. Paul, USA; [6]Pathology, Hôpital
Sainte-Justine, Montréal, Québec, Canada; [7]Pediatrics,
Wake Forest University Medical Center, Winston-Salem, USA;
[8]Lauren V. Ackerman Laboratory of Surgical Pathology,
Barnes-Jewish and St. Louis Children's Hospitals,
Washington University Medical Center, St. Louis, USA.

Pleuropulmonary blastoma (PPB) is a rare malignant mesenchymal tumor of lung in young children. Cystic nephroma (CN) represents one of the most common neoplasms associated with PPB. We report here an infant girl with unilateral Type I PPB; multiple, bilateral, progressive CN; and intussusception due to ileal 3.2 cm juvenile-like polyp. The child had multiple surgeries, and has been receiving chemotherapy according to the recommendations of the International PPB Registry for Type I (purely cystic) PPB. Eighteen patients with PPB from the Registry, and literature, were noted to have renal neoplasia, most often CN, in themselves (11) or close family members, but only two had the association of PPB, CN and intestinal polyps. In the other case we know of, an infant girl presented with Type I and Type II (solid and cystic) bilateral PPB, bilateral CN, intussusception and multiple small bowel juvenile-like polyps; she received chemotherapy but died at 14 months of age. The association of PPB, CN, and small bowel polyps might be a subset of the familial PPB/CN association that represents a new tumor predisposition syndrome.

P086

Comparative characteristics of morphological changes in rat lungs exposed to different regimens of mainstream smoke

Genova S, Damjanov Iv, Popov D, Bojadgiev N,
Schterev Ph, Yvancheva R, Jankova Zl
Department of Pathology – Medical University - Plovdiv
Department of Physiology – Medical University Plovdiv
Department of Pulmology –University Hospital 'St. George'

Emphysema and chronic bronchiolitis are major components of chronic obstructive pulmonary disease in smokers.Our aim is to estimate the quantitative and qualitative pulmonary parametes in short-term mainstream smoke exposition (30 days) in lungs of rats, with high concentration of mainstream smoke (MS), applying two different regimens of exposition. Three groups of male Wistar rats (4 months old 30 in total) were studied: Ist group – 10 rats daily exposed to cigarette smoke (20 cigarettes per day). IInd group – 10 rats with 5 days mainstream smoke exposition, followed by 2 days rest. IIIrd group – 10 control rats. All the experimental animals exposed to smoke developed emphysema with different level of emphysematous change. Due to different regimen conditions, we achieved the following results: average – 60%/I group versus 41%/II group developed emphysema in their lungs, centro-acinar type. Hyperplasia of goblet cells is seen in 9 animals from the Ist group versus 2 animals from the IInd group. Epithelial atipia is expressed in 1 animal from the Ist group, squamos metaplasia in 1 from the IInd group. 8 rats from the Ist group developed intersticial pneumonitis versus 1 rat from the IInd group. All experimental animals showed peribronchial lymphoid hyperplasia and increased intraalveolar macrophages. The application of short-term mainstream smoke exposition led to development of different with respect to degree changes in pulmonary parenchyma depending on the specific regimen. More expressed were emphysema, bronchiolar metaplasia into secretory type and inflammatory reaction in long-term exposition.

P087

Immunocytochemical panel for distinguishing between reactive mesothelial cells and adenocarcinoma in pleural effusions

Teliousi S, Koletsa T, Bobos M, Mandrali A, Ioannou-Banava O
Department of Cytopathology, General Hospital
"G. Papanikolaou", Thessaloniki, Greece

In pleural effusion cytology the distinction of reactive mesothelial cells (RMC) from metastatic adenocarcinoma (MAC) may be a diagnostic challenge. The aim of this study is to investigate whether a panel of four antibodies can potentially be utilized for facilitating this distinction. Fifty-two Thin Prep cytologic specimens of pleural effusions were selected retrospectively, which included 30 cases of RMC and 22 of MAC. Immunocytology was performed using calretinin, HBME-1, CA 125 and cytokeratins 8/18/19 antibodies. Calretinin was detected in 30 (100%) reactive cases while none of the adenocarcinomas was positive for this marker. HBME-1 was detected in 29/30 (96,7%) of RMC cases and in 14/22 (63,6%) of MAC. CA 125 expression was observed in 19/30 (63,3%) of reactive specimens and in 11/22 (50%) cases of MAC. Cytokeratins 8/18/19 was observed in a slightly higher percentage of RMC (29/30-96,7%) than in MAC (21/22-95,4%) cases. Our results demonstrate calretinin the most specific marker for mesothelial cells, whereas CA125 and HBME-1 do not label mesothelial cells with sufficient specificity. However, suspicious cells negative for HBME-1, it is unlikely to be reactive mesothelial cells. Conclusively, calretinin, HBME-1 and cytokeratins 8/18/19 antibodies appears to be a useful panel for differentiating metastatic carcinomas from reactive mesothelial cells.

P088

Correlation of hyperamylasaemia to histologic type in lung cancer

M.Mastora, E. Tsiami, L. Liappis, E. Kitsiou*, A. Katsanou, G. Dimos, S.Stefanaki*, I.Kakadellis**, N. Akritidis
Department of Internal Medicine, Department of Pathology*, Department of Thoracic Surgery**, General Hospital "G. Hatzikosta" Ioannina, Greece

Raised serum amylase in lung cancer due to ectopic amylase production in carcinoma of the lung has been reported in the literature.
Aim of the study: To correlate the raised serum amylase to histological type in neoplasms of the lung.
Material and methods: 65 patients, who diagnosed and treated during 1 year period, were studied retrospectively (57 male and 8 female). Age ranged from 46 – 88 years. We searched for serum and urine amylase and in patient with abnormaly raised levels we correlated to histologic type of cancer.
Results: From the 67 patients, raised amylase levels were found in 13 patients(20%). Levels of the amylase in serum ranged from 152-4114 IU/L (normal valius=100). Amylase in urine was also raised. Histologic confirmation was possible for 11 patients (males, 46 – 78 years of age). These were 7 adenocarcinomas, 3 squamous cell carcinomas and 1 small cell carcinomas and the majority of them were poorly differentiated.
Conclusion: Adenocarcinoma appears to relate closely to hyper-amylasaemia.This finding agrees to the data from the literature.

P089

Lymphoepithelial-like carcinoma of the lung: report of two cases

Valavanis C.[1,2]., Tzaida O.[1], Konstantoudakis S.[1], Gavresea Th.[1], Vecchini G.[1], Hatzimichalis A.[3], Arapantoni-Dadioti P.[1]
[1]Dept. of Pathology, [2]Molecular Pathology Unit,
[3]Dept. of Thoracic Surgery, METAXA Cancer Hospital, Piraeus, Greece

Two cases of lymphoepithelial-like carcinoma of the lung, a rare malignant epithelial neoplasm, are presented. This tumor is considered as a subtype of undifferentiated large-cell carcinoma with abundant lymphocytic infiltration.
It has morphologic features similar to lymphoepithelial carcinomas arising in the nasopharynx (most cases) and in others anatomic sites (salivary gland, thymus, skin, cervix, stomach, urinary bladder, esophagus). LELC of the lung is strongly associated with Epstein-Barr virus (EBV) mainly in Asians and less commonly in Caucasians. This neoplasm is thought to have a highly variable biologic behavior and to be more chemosensitive than other lung tumors.
The patients, one female 72 years old and one male 66 years old, presented a slowly growing mass located at the right middle lobe and the left upper lobe of the lung, measuring 3 and 6.5 cm, respectively. The microscopical examination of the two specimens after lobectomy revealed malignant epithelial tumors. The neoplasms consisted of irregular shaped islands of large, anaplastic, eosinophilic, epitheliod cells within a mature type lymphocytic–rich stroma. The immunohistochemical study confirmed the epithelial nature of the neoplasms and the concomittant benign lymphocytic infiltration. Immunohistochemical detection of LMP1 expression and in situ hybridization of Epstein-Barr virus DNA were negative revealing no association with EBV infection.
Differential diagnosis to other pulmonary tumors, possible aetiology/pathogenesis and terminology as well are discussed.

P090

Clinicopathological differential diagnostic approach of BOOP/COP

R. Tringidou MD[1], K. Malagari MD[2], C. Lambrakis MD[1], I. Scotis MD[1], M.A. Dimadi MD[1]
Pathology Dept. – 1st and 2nd Pulmonary Depts and 1st Surgical Thoracic Dept of Athens Chest Hospital "SOTIRIA", Dept of Radiology – University of Athens - Greece

Background: Bronchiolitis obliterans with organizing pneumonia (BOOP) is a clinicopathological entity described in 1985 by Epler. In the recent ATS-ERS classification of Inerstitial Lung Diseases / ILD (2002) was used the term COP (cryptogenic organizing pneumonia) to describe cases of organizing pneumonia of unknown etiology.
Aim: The correlation of clinical, radiological and histological findings, for the correct diagnosis, in difficult cases especially those with clinical suspicion of malignancies or other interstitial diseases.
Methods: We studied four (4) years (2000-2004) archival material from Pathology, 1st-2nd Pneumonology Depts of Athens Chest Hospital, concerning cases diagnosed as BOOP or COP, based on recent criteria proposed by ATS-ERS classification.
Results: From the retrospective study we select a number of fifteen (15) cases, 9 males and 6 females, with known clinical history in eight (8) cases and unknown etiology in the rest seven (7) cases. Three (3) of the seven (7) cases represent radio logically as "solid intrapulmonary lesion" and have differential diagnostic "dilemma" with malignancy and four (4) cases of unknown etiology have "atypical" clinical and CT findings. We categorized the 15 cases in 3 groups.**Group 1:** Eight (8) cases as secondary BOOP, **Group 2:** Four (4) cases as COP and **Group 3:** Three (3) cases as "solid BOOP".
Conclusions: 1. "Focally organizing pneumonia" may be the final diagnosis in a small proportion of surgical removed cases with "intrapulmonary solid lesion" and clinical suspicion of malignancy. 2. In every case diagnosed as BOOP or COP, the correlation with clinical and CT findings for the final diagnosis must be take in mind. 3. The diagnosis of BOOP/COP is a diagnosis of exclusion, because similar histological changes can be observed in other interstitial diseases/ILD (EAA, H.P., UIP, DAD).

P091

Intrapulmonary Castleman disease in male with allergic rhinitis

Jelena Stojsic, Tatjana Eminovic, Dragan Subotic, Svetlana Krstic
Department of Molecular Genetic Bases of Production Processes, Institute for Lung Diseases and Tuberculosis, Clinical Centre of Serbia, Belgrade, Serbia

Localized Castleman disease (CD) is often reported in mediastinum. CD localised in intrapulmonary lymphnodes is rare. We present a male, aged 25, who went under thoracotomy because of tumorous node in middle lobe of right lung. Tumorous mass was detected on chest x-ray and CT scan examinations, made because of coughing. Patient suffered from allergic rhinitis on Ambrosia (Ambrosia artemisiifolia, Ambrosia elatior) and was treated by steroids. There was not any immune dysregulation before the thoracotomy: level of immunoglobulins and proteins were regular on routine blood tests. Patient was HIV seronegative. The middle right lobe with tumorectomy was performed. CD of hyalino-vascular type was diagnosed on well circumscribed, solid tumor node, measured approximatively 30mm in the largest diameter. Numerous lymphoid follicles of concetric layers of small, inactive lymphocytes without mitoses and interfollicular vascular hyperplasia was found. Post-operatively there was not found recurrence of tumor. He still sufferes from allergic rhinitis. CD is of still unknown etiology and remains a question whether CD is a response of organism for

allergic condition. Hyalino-vascular type of CD is most frequently diagnosed in young males, as mediastinal mass according to the Ioachim's checklist. Intrapulmonary localistion of CD is rare. CD could be developed in every organ where lymphoid tissue normaly persists.

P092

Prognostic impact of lymphangiogenesis and lymphatic invasion (CD105 expression) in small cell lung carcinomas

Hardavella G[2], Arkoumani E[1], Nesseris I[1],
Constantopoulos S[2] and Stefanou D[1]
[1]Department of Pathology and [2]Department of Pneumology,
University of Ioannina, Medical School, Greece

Lymphangiogenesis is an essential process in the metastasis of malignant tumors that has not been thoroughly studied. The aim of this study is to evaluate the prognostic impact of tumor lymphangiogenesis and lymphatic invasion in SCLCs. 49 patients were retrospectively reviewed. Intratumoral lymphatic microvessel density (ILMVD) and lymphatic invasion were determined with an anti-CD105 monoclonal antibody (Menarini Hellas).Tumor specimens exhibiting ILMVD<50 and lymphatic invasion corresponded to a mean survival of 8,75 months being opposed to 11,37 months for patients without lymphatic invasion. ILMVD≥50 with lymphatic invasion corresponded to a mean survival of 7,5 months, while the absence of lymphatic invasion increased the mean survival to 12,67 months. There is a direct correlation between ILMVD and the mean survival in SCLC patients. Increased ILMVD and lymphatic invasion are related with poor patient outcome, therefore constituting a prognostic role on SCLC.

P093

In situ protein expression profiling of lung cancer tumor progression using tissue microarrays, virtual sections and a new software

Krenács T1, Pápay J[1], Molnár B[2], Moldvay J[3], Ficsór L[4],
Varga VS[4], Stelkovics É[5], Furák J[6] & Kopper L[1]
[1]1st Department of Pathology and Experimental Cancer Research &
[2]2nd Department of Internal Medicine, Semmelweis University,
Budapest; [3]County Hospital of Pulmonology, Törökbálint;
[4]3DHISTECH Ltd, Budapest; [5]Laboratory of Tumor Pathology and
Molecular Diagnostics, Bay Zoltán Foundation for Applied
Research, Szeged; [5]Department of Surgery, University of Szeged;
Hungary

This study aimed at the prognostic immunomorphological profiling of nonsmall cell lung cancer (NSCLC) tumor progression using tissue microarrays (TMA). Donor blocks were form 87 patients, including 33 non-metastatic primary NSCLC (18 SCC, 13 ADC, 1 LCC and 1 APC), 26 metastatic primary NSCLC (14 SCC, 10 ADC, 2 LCC) and the brain metastases of the latter group. TMA sections immunostained for molecules of cell adhesion, cell growth, cell cycle and apoptosis regulation were digitalized and the Mirax TMA software was used for validated scoring and linking image and patients data for analyses. Prominent expression of collagen XVII, CD44v6 and caspase-9, and the reduced production of β-catenin and cellular apoptosis susceptibility (CAS) protein were significantly associated with the brain metastatic primary NSCLC. Survival analyses revealed a highly significant negative correlation with the brain-metastatic NSCLC group, a positive correlation with β-catenin expression and an almost significant inverse link with cyclinD3 or p16 expression. 2/3rd of the brain-metastatic cases (16/26) formed a cluster of 24 cases out of 85, based on cyclinD1, -D3, Ki67, p16, p53, β-catenin and collagen XVII expression (correlation: 0.74). Members of the in-cluster group showed significantly poorer survival then those set outside the cluster. The metastatic capacity of NSCLC into the brain may be predicted from the concurrent demonstration of cell cycle activation (cyclinD1, -D3, Ki67), the up-regulation of p16 and Collagen XVII, and the down-regulation of β-catenin. The software highly facilitated this study.

P094

Retrospective study on 838 cases of renal tumors diagnosed and operated in the Center for Surgical Urology, Dialysis and Renal Transplant - Fundeni Clinical Institute, Bucharest-Romania between 01.01. 2000-01.01.2006

Monica Hortopan, V. Herlea, M. Mihai, E. Stoica, C. Pecheanu,
Liana Marzan, S. Voinea, M. Harza, M. Manu, B. Serbanescu,
I. Sinescu
Department of Pathology, Fundeni Clinical Institute; Center for
Surgical Urology, Dialysis and Renal Transplant, Fundeni Clinical
Institute, Bucharest; GRHD Foundation, Bucharest.

From 838 parenchymatous renal tumours treated by radical nephrectomy in our Center we recorded clinical and instrumental data which concluded to the diagnosis of parenchymatous renal tumor. All the cases experienced an anterior transperitoneal radical nephrectomy together with regional lymph nodes dissection. For each kidney sagittaly sectioned, pelvis, ureteral stump and renal vein opened, we evaluated the weight, the size and the tumor's features; presence/absence of the invasive aspects and the aspect of residual renal parenchyma. Microscopic exam was performed for 3-5 tumor fragments, 1-2 adjacent parenchyma, 1-2 pelvis fragments, elements with pedicle and lymph nodes identified. Four-micrometer tissue sections were stained with H&E, special stains (vanGieson, Masson trichromic, PAS) and examined by two pathologists. In 20 cases immunohistochemical stains were performed. The histology type and tumor staging respect the Classification of the Renal Parenchymatous tumors. Postoperative follow-up was done by imagistic exam every 3-6 months.

P095

The relationship between COX-2 expression, microvessel density and various clinicopathologic parameters in clear cell type renal cell carcinoma

Hasan Gucer, Elife Sahan, Aysenur A. IGDEM , Alpay Cetin,
Umit S. TETIKKURT, Nusret Erdogan
Department of Pathology, Taksim Training and Research Hospital,
34433 Istanbul, Turkey

Overexpression of cyclooxygenase-2 (COX-2) and its association with angiogenesis is shown in various carcinomas. In this study, we investigated COX-2 expression in the clear cell type renal cell carcinoma (CRCC) and its association with microvessel density (MVD) and clinicopathologic parameters.
Fifty cases of CRCC were included in this study. COX-2 expression was examined immunohistochemically. MVD was estimated using the video-microscope system described. We evaluated the correlation between COX-2 expression, MVD and clinicopathologic findings.
COX-2 was expressed in 76% of cases. There was no association with COX-2 expression and MVD, age, sex, tumor size, nuclear grade, stage and cytoplasmic eosinophilia (p=0.616, p=0.844, p=0.920, p=0.631, p=0.251, p=0.385 ve p=0.874). Only there was an association with MVD and cytoplasmic eosinophilia (p=0.003).
Most of CRCC expressed COX-2, but there was no relationship between COX-2 and various clinicopathologic parameters.

P096

Prenatal Diagnosis of Joubert Syndrome with Medullary Cystic Kidneys

Diclehan Orhan*, Şafak Güçer*, Özgür Özyüncü**, Lütfü Önderoğlu**, Gülsev Kale*
Hacettepe University Faculty of Medicine, İhsan Doğramacı Children's Hospital, Division of Pediatric Pathology, Ankara, Turkey, ** Hacettepe University Faculty of Medicine, Department of Obstetrics and Gynecology, Ankara, Turkey

We present the autopsy findings of a fetus with Joubert syndrome with medullary cystic kidneys diagnosed prenatally. Twenty-eight years old patient at 19 weeks gestation was admitted to our hospital with gravidity 3, parity 0. Her obstetric history was remarkable. Her first pregnancy was terminated at the 17th week of gestation as the prenatal scan revealed isolated encephalocele. Necropsy was not available. Her second pregnancy was an anembryonic pregnancy and dilatation and curettage was performed at the 6th week of gestation. Prenatal scan at the 19 weeks of this gestation revealed a cyst at the posterior fossa and encephalocele with an occipital bone defect. Elective termination was performed at the 19th week of gestation that revealed a 220 grams female fetus. An autopsy was performed. Examination of the central nervous system at autopsy revaled agenesis of the cerebellar vermis, occipital meningocele, Dandy-Walker malformation and agenesis of the corpus callosum. Extracerebral malformations were medullary cystic kidneys and congenital hepatic fibrosis. This case had bilateral medulary cystic kidneys which has not been previously described in this syndrome.

P097

Morphometric and immunohistochemical study of the fibrosis in the interstitial compartment of kidneys with primary glomerulopathies

Slavica Kostadinova - Kunovska[1], Gordana Petrusevska[1], Rubens Jovanovic[1], Ladislava Grcevska[2], Momir Polenakovic[2]
[1]Insitute of Pathology, Faculty of Medicine, Skopje, Macedonia
[2]Department of Nephrology, Clinical Center, Skopje, Macedonia

The mechanisms of the interstitial damage in all glomerular diseases are almost the same, resulting in interstitial fibrosis. The interstitial inflammatory cells influence the tubular epithelial cells which undergo the process of epithelial-mesenchymal transdifferentiation, expressing de novo mesenchymal proteins. We made a morphometric and immunohistochemical study on 10 renal biopsies, previously diagnosed as IgA nephropathy or membranoproliferative glomerulonephritis. We found fibrosis occupying more than 10% of the tubulointerstitial surface in all 10 patients and 6 of them had moderate level of fibrosis, occupying more that 20% of the tubulointerstitial space. The inflammatory infiltrate was more prominent in the areas with fibrosis, with a slight predominance of the CD43 positive T-lymphocytes. In these areas the tubules showed marked injury and atrophy. The epithelial cells in the atrophic tubules showed positivity for HLA-DR, vimentin and SMA, acquiring mesenchymal phenotype. These results are consistent with the present understanding of the processes in the interstium of kidneys with primary glomerular diseases and encourage further investigations in that field.

P098

The prognostic value of several immunohistochemical markers in renal cell carcinoma

M. Strataki, C. Petraki, C. Magkou, A. Rigas, G. Kanellis, K. Demosthenous, S. Stefanakis, M. Koutsilieris.
Department of Pathology, Evangelismos Hospital, Athens, Greece

To evaluate the prognostic value of the immunohistochemical markers ck7, ker34βε12, ck19, ck8-18, rcc, vimentin, ema, cd9, cd10 and e-cadherin, as well as of the hale's iron stain in localized renal cell carcinoma (rcc). the study comprised 94 patients who underwent radical nephrectomy (median follow-up period: 37 months, range: 2-156 months). the streptavidin-biotin-peroxidase method of immunostaining was performed. of 94 rcc cases, 67 (71.3%) were of clear cell type, 3 (3.2%) of chromophobe type, 5 (5.3%) of papillary type i, 5 (5.3%) of papillary type ii, 9 (9.6%) unclassified oncocytic and 5 (5.3%) unclassified pleomorphic. in univariate analysis, type i papillary, chromophobe and unclassified oncocytic rccs had better prognosis than type ii papillary, clear cell and unclassified pleomorphic rccs (p=0.0010). nuclear grade, pt stage, mitotic index and vimentin immunoexpression were inversely correlated with disease specific survival (p<0.0001, p<0.0001, p<0.0001 and p=0.0030, respectively). however, in mulitivariate analysis, only pt stage, vimentin and cd10 immunoexpression were proved to be independent prognostic factors (p<0.001, p=0.010 and p=0.036, respectively). we conclude that vimentin and cd10 immunoexpression in combination with pt stage may predict a poor disease outcome in localized rcc.

P099

The diagnostic utility of several immunohistochemical markers in the subtyping of renal cell carcinoma.

C. Magkou, C. Petraki, M. Strataki, A. Rigas, I. Evangelou, P. Argyriou, D. Malovrouvas, M. Koutsilieris
Department of Pathology, Evangelismos Hospital, Athens, Greece

To evaluate the diagnostic value of the immunohistochemical markers CK7, Ker34βE12, CK19, CK8-18, RCC, vimentin, EMA, CD9, CD10 and E-cadherin, as well as of the Hale's iron stain in localized renal cell carcinoma (RCC). The study comprised 94 patients who underwent radical nephrectomy for RCC (median follow-up period: 37 months, range: 2-156 months). The streptavidin-biotin-peroxidase method of immunostaining was performed for all antibodies assessed. The relationships between markers'expression and the histological type were evaluated by Pearson's 2 test. Three major phenotypes were recognized: i. CK7(-), E-cadherin(-) and Hale's(-) phenotype (in 78% of clear cell RCCs), ii. RCC(-), Vimentin(-), CK7(+), E-cadherin(+) and Hale's(+) phenotype (in 100% of chromophobe RCCs) and iii. CK7(+) and CK19(+) immunophenotype (in 90% of papillary RCCs, type I and II). According to these phenotypes, we attempted to classify the so-called unclassified cases. Of the unclassified oncocytic RCCs, 7/9 were of clear cell type, 1 case was of chromophobe type and 1 case of oncocytic type. Of the unclassified pleomorphic RCCs, 4/5 were of clear cell type and 1 case was of papillary type. We conlude that CK7, CK19, E-cadherin, vimentin and Hale's iron stain are useful markers in the subtyping of RCC.

P100

Inflammatory pseudotumor of the renal pelvis associated with tuberculosis

Alexandrou Paraskevi, Liapis George, Kokkori Katerina, Kyriakou Vassiliki, Androulaki Athina
Department of Pathology, LAIKO General Hospital

Inflammatory pseudotumor is an uncommon manifestation of mycobacterial infection predominantly affecting immunosuppressed individuals. Urogenital tuberculosis is still frequent but the pseudotumoral manifestation is a rare entity that has only recently been described in one case. We report a case of 40-year-old male who presented with fever, painless gross haematuria and tenderness in the right lumbar region. The radiological and CT scan findings were suggestive of a pelvic tumor and a radical right nephrectomy was

performed. Macroscopy revealed a white tan tumor (9,2 x 6 x 4,5 cm) hard in consistency, involving the peripelvic fat and protruding into the pelvic system. Microscopic examination exhibited a hypocellular spindle cell lesion with a collagenous fibrous stroma admixed with variable lymphoplasmacytic and neutrophilic infiltrates admixed with isolated Langhans' giant cells. Scattered epithelioid granulomas with foci of caseous necrosis were found at the periphery of the lesion on serial sections. Although Ziehl-Nielsen did not show any acid-fast bacilli, PCR subsequently confirmed the suspicion of mucobacterial inflammatory pseudotumor. By recognizing this entity which may have a misleading clinical presentation the pathologist does not only avoid misinterpretation but also provides an accurate diagnosis of infection that can be treated immediately and specifically.

P101

Solitary fibrous tumor of the kidney

Liapis George, Alexandrou Paraskevi, Giaslakiotis Konstantinos, kyriakou Vassiliki
Department of Pathology, LAIKO General Hospital, Athens

Solitary fibrous tumor is encountered in many organs while its occurrence in the kidney seems to be a rarity since only fifteen cases have been reported in the reviewed literature. We present a rare case of solitary fibrous tumor of the kidney which was found incidentally in a 26-year old man after a car accident. CT scan revealed a large tumor which occupied the upper pole and the middle portion of the right kidney compressing the pelvis. A right nephrectomy was performed. The tumor measured 7x5,6x4,4 cm, was solid and firm with a whitish cut surface. Microscopically, a spindle cell neoplasm with altrnating hyper- and hypocellular areas, hemangiopericytomatous pattern and dense keloid-type collagen deposition was found. Immunohistochemically, the tumor cells were consistent positive for CD34, CD99 and bcl- 2 while they were negative to HMB-45 and desmin antibodies. A diagnosis of solitary fibrous tumor was established. Differential diagnosis includes high and low grade sarcomas such as synovial sarcoma and low grade myxoid fibrosarcoma as well as neoplasms with a totally benign behavior such as mixed epithelial stromal tumor and angiomyolipoma. As far as histogenesis is concerned, most of the published cases favor a capsular or peripelvic origin.

P102

Fetal kidneys stroma remodelling in cases of IUGR

Olexander P. Sysoenko, Olga S. Reshetnikova, Sergiy A. Morozov
Department of Pathologic Anatomy, Lugansk State Medical University, 1, kv. 50-let Oborony Luganska, 91045, Lugansk, Ukraine

It is suggested that fetal intrauterine growth retardation (IUGR) may lead to hypertension in adults. Alteration of kidneys tissue maturation may play an important role in the pathogenesis of a hypertension too. The aim of present study was to determine the distribution of the III type collagen in forming of connecting tissue of the fetal kidneys in cases of IUGR. Methods: 20 pairs of fetal kidneys (including 10 pairs of kidneys in cases of IUGR) from the late medical abortions because of psychotherapeutic reasons at 20-22 weeks of gestation were weighted, studied macroscopically and microscopically, and then the distribution of the III type collagen with the help of antibodies was investigated. Results have shown that kidneys in IUGR group have macroscopic and histological signs of both organ and tissue growth restriction. The intensity of the III type collagen expression and the area of its distribution increased, mainly in the perivascular connective tissue, kidneys cortex and medulla's stroma. Conclusion: Fetal IUGR is accompanied with the lesion of renal tissue formation. The intensified synthesis of collagen III may be a marker of tissue remodeling when connective tissue formation and sclerosis outrun the parenchyma elements growth and maturation.

P103

Lynphangioma of the kidney: case report

Papanikolaou A[1], Chatzitolios A[1], Amplianitis I[1], Tougiaris C[2], Tatsiou Z[1], Salpigidis G[2]
[1]Department of Pathology, Hippokratio Hospital of Thessaloniki, Greece, [2]Department of Urology, Hippokratio Hospital of Thessaloniki, Greece

Renal lymphangioma is an exceedingly rare tumor, with only 36 cases reported Worldwide, so far. Our case is about a 32 year old man who was admitted to hospital after a syncopic episode.During the patient's examination an abdominal CT scan was performed which sawn a 4,5x3,8 cm. multiloculated cystic mass in the mid-portion of the right kidney.The followed needle biopsy sawn benign neoplasm of the kidney probably multicystic nephroma.Therefore enulceation of the tumor was performed.Pathological evaluation of the specimen diagnosed lymphagioma arising from the kidney.The patient is free of disease after an 1 month follow-up period.The purpose of this paper is to describe the clinicopathological characteristics of the disease,stressing on the differential diagnosis between the renal lymphangioma and the multicystic nephroma.

P104

Paraganglioma of urinary bladder

GHAINI M.Hossein, SAKI Soheil, FROOTAN Kazem,
Presetining auther: SAKI Soheil
Student of medicine, Faculty of medicine, Tehran
University of Medical scineces, Iran

"Urinary bladder is a rare site of paraganglioma. Wedescribe a paraganglioma of the urinary bladder in a 51-year-old female who presented with painless gross hematuria. Abdominal ultrasonography revealed a protruding well-defined mass, about 3Cm. in diameter over the left lateral wall of the urinary bladder. The tumor was not completely resected by transurethral resection of bladder tumor (TURBT) due to involvement of the bladder wall. Histologic examination of the tumor indicated clustersof polygonal chromaffin cells, arranged in nests (zellballen). Although there was marked pleomorphism and atypia in nuclei, no evidence of recuurence or metastasis has seen since about 1year. There is no reliable method for predicting their clinical behavior, so long-term follow-up is required. We also provide a brief review of the literature for comparison."

P105

Primary signet-ring cell carcinoma of urinary bladder: A case report

Papanikolaou A.[1], Tatsiou Z.[1], Moulla A.[1], Chatzitolios A.[1], Xiromeritis M.[2], Brouskelis N.[2], Athanasiou E[1]
Department of Pathology[1] and Urology[2],
Hippokratio General Hospital, Thessaloniki, Greece

Primary signet-ring cell carcinoma (SRC) of urinary bladder is a rare tumour, accounting for less than 1% of all bladder malignancies. In this study we report a case of a 60-year old man who consulted for complaints of painless gross hematuria. The bladder biopsy showed signet-ring cell carcinoma. The exploration of gastrointestinal tract and prostate did not reveal any other tumour localizations. A total cystoprostatectomy was performed. Macroscopically a large bladder intrawall tumor revealed resembling linitis plastica of the stomach. Microscopically, the tumour consisted entirely of signet ring cells which infiltrated the entire bladder wall and the peribladder lipoid

tissue. The immunohistochemical profile of neoplastic cells was: cytokeratin 7+, cytokeratin 20+, PSA-, PSAP-. The patient died 1 year after the cystoprostatectomy. The aim of this study is to describe the clinicopathological characteristics of this rare and very aggressive tumour.

P106

Fascin expression in urothelial carcinomas

F. Karasavvidoua, S. Barbanisa, D. Pappaa, E. Tziastoudi, G. Kalodimosa, M. Ioannoua, V. Tzortzisb, M. Melekosb, A. Soumelidisa, G. Koukoulisa.
Departments of Pathologya and Urologyb, University Hospital, Larissa, Greece

Fascin is an actin-bundling protein with a role in increased motility of various transformed cells. There is only one report concerning its expression in urothelial carcinomas.
We examined by immunohistochemistry the expression of fascin in 98 samples of urothelial carcinomas, of 98 patients, 84 men and 14 women. Fifty eight cases were of low grade and stage (pTa) and 40 were of high grade, 9 stage pTa, 14 pT1 and 17 pT2.
The intensity of immunoreactivity was semiquantitatively graded by comparing it to the average staining intensity of endothelial cells: "*weak*", "*moderate*" and "*intense*". None of the low grade/pTa tumors showed "*intense*" staining, with more than 70% of these tumors showing only weak immunoreaction. "*Intense*" staining was seen exclusively in invasive carcinomas, frequently (more than half of them), and not restricted to the invasive component. pTa carcinomas of low or high grade showed comparable fascin expression. Notably, in 15% of high grade carcinomas, most of them invasive, fascin expression was not detectable immunohistochemically.
Our results show an association between strong intensity of fascin immunostaining and high grade invasive urothelial carcinomas, suggesting that fascin expression may be an indicator of biologic aggressiveness of these neoplasms.

P107

CDX2 expression in urothelial transitional carcinoma

S. Barbanis, F. Karasavvidou, M. Ioannou, G. Kalodimos, R. Papamichali, E. Tziastoudi, G. Koukoulis.
Department of Pathology, University Hospital, Larissa, Greece.

CDX2 (caudal-related homeobox gene 2) is a recently cloned gene that encodes an intestine specific transcription factor, which is important for the establishment and maintenance of intestinal cells. CDX2 is a sensitive marker of intestinal metaplasia and is also expressed in neoplasms of intestinal origin and some neoplasms with intestinal differentiation. Very few reports have investigated CDX2 expression in a small number of urinary bladder metaplasias and neoplasms. It is usually absent in primary adenocarcinomas and totally absent in transitional carcinomas of the urinary bladder. We present a case of urinary bladder carcinoma with CDX2 expression. This was a case of a 59 year old man with a high grade, widely invasive urothelial carcinoma showing areas with glandular differentiation. The glandular component showed strong CDX2 nuclear immunopositivity, in addition to cytokeratins 7 and 20 immunostaining. Interestingly, CDX2 positivity was also seen in foci of conventional urothelial transitional carcinoma without morphologic glandular differentiation. We investigated 10 additional cases of urothelial transitional carcinomas without glandular differentiation, all of which were negative for CDX2. This aberrant expression of CDX2 is reported for the first time in urothelial transitional carcinoma. It may be used as an early marker of glandular/intestinal differentiation of neoplastic or reactive/metaplastic urothelium, similarly to its proposed application in Barrett's esophagus.

P108

The presence and nature of lipoblast-like cells in urothelial carcinomas.

Dimitris Hatzianastassiou[1], Elias Drakos[2], Konstantinos Giaslakiotis[2], Nikolaos Goutas[3], Sofia Havaki[1], Evangelos Marinos[1], Johanna Delladetsima[2].
[1]Laboratory of Histology–Embryology, Medical School, University of Athens, [2]Department of Pathology, Laiko General Hospital, [3]Laboratory of Forensic Medicine and Toxicology, Medical School, University of Athens, 75 Mikras Asias, 115 27 Athens, Greece.

Lipoblasts-like cells (LBLCs) in urothelial cell carcinomas (UCCs) are rare and their presence defines the lipid-cell UCC variant. 450 cases of urothelial carcinomas, diagnosed in our department over a period of three years, were screened for LBLCs and the selected three cases were stained for mucins and immunohistochemically for cytokeratin 7, low molecular weight keratins, S-100 and vimentin. In one case, paraffin embedded tissue was processed for electron microscopy. The diagnosis of UCC, lipid-cell variant was justified in one case, while the other two cases showed focal presence of LBLCs. All three cases were high grade urothelial carcinomas. LBLCs were negative for mucin, S-100 and vimentin; cytokeratins were strongly positive. EM findings were consistent with intracellular lipid accumulation showing various-sized, predominantly free, and in a lesser number, membrane-bound lipid droplets. LBLCs in the setting of UCC, either as a constituent of lipid cell variant, or as a focal phenomenon, are rarely encountered. EM findings provide evidence of true intracellular lipid accumulation.

P109

The prognostic value of CK20, 34betaE12, p53, bcl2, c-erbB-2, Ki-67, CD44 and PSMA immunohistochemical expression (IHCE) in patients with primary low-stage (pTa/T1) urothelial urinary bladder carcinoma (UUBC).

K. Revelos[1], C. Magkou[2], I. Kouda[2], F. Michalopoulou[2], E. Theophanous[2], M. Strataki[2], A. Takou[2], S. Stefanakis[3], D. Malovrouvas[3], C. Petraki[2].
[1]Pathology Dept., 251 Hellenic Air Force Hospital and [2]Pathology and [3]Urology Depts., Evangelismos Hospital, Athens, Greece.

The prognostic value of the IHCE of CK 20, 34βE12 antigen, p53, bcl2 & c-erbB-2 oncoproteins, the cell proliferation marker Ki-67, the cell adhesion molecule CD44 and the prostate- specific membrane antigen (PSMA), in predicting tumor relapse in patients (pts) with primary low-stage (pTa/T1) UUBC was investigated. Included in the study were 174 consecutive pts, who underwent transurethral resection (TUR) and 132 of them (76%) had a low-stage disease (pTa: 36 , T1: 96 pts). Median follow-up period was 11.5 (3-20) months and 46 (35%) pts recurred. CK20, p53, c-erbB-2, Ki-67, CD44 and PSMA showed a statistically significant positive relation with histological grade (HG) and pathological stage and bcl2 only with HG. The recurrence rate of the pTa/T1 subgroup was positively related with HG, pathological substaging, CK20, bcl2 and Ki-67. HG, pathological substaging, CK20, bcl2, c-erbB-2 and Ki-67 had a positive statistically significant relation with the recurrence-free interval. HG, Ki-67 and PSMA were independent unfavourable predictors for recurrence and may be useful markers for decision management in this group of patients.

P110

Correlation between grade and EGFR overexpression in TCC of bladder

M.R. Jalali Nadoushan, F. Zaeri, H. Ahmadi.
Shahed University, Tehran, Iran

Introduction: TCC of the urinary bladder is second common cancer of genitourinary tract several parameters such as clinical, pathological and molecular factor have effect on determination of prognosis and type of treatment. In this study we show that grade in TCC has a direct relationship with EGFR.
Methods: This cross-sectional study was performed in paraffin embedded tissue from 75 patient with TCC of urinary bladder 3micron section were provided from each one in all section grade of tumor was determined an ordering to WHO/ISUP criteria The present of EGFR positive cell were counted from microscopic observation in each section.
Findings: in this study 14 case were LMP (18.7%) that 10 case among them had negative cells about EGFR (71.4%) and 4 case had positive cells (28.6%) 35 case were low grade (46.7%) that 18 case among them had negative cells about EGFR (51.4%) and 17 case had positive cells (48.6%) 26 case were high grade(34.7%) that 9 case among them had negative cells about EGFR (34.6%) and 17 case had positive cells (65.4%).
Conclusion: Over expression of EGFR has direct relationship with tumor grade that some of previous studies had these results too other studies with more case and check over expression of EGFR could be used as prognostic in TCC of urinary bladder.

P111

Evaluation of the role of Vascular Endothelial Growth Factor (VEGF)-C in the urothelial carcinomas of the bladder.

[1]Gorandonakis G, [1]Magkou C, [1]Nomikos A, [3]Zarogiannos A, [2]Giannopoulou I, [1]Zoumbouli C, [3]Zervas A,1[2]Nakopoulou L.
[1]Second Pathology Department, Attikon Hospital, [2]First Pathology Department, Medical School, [3]Department of Urology,
Laikon Hospital.

Vascular endothelial growth factor-C (VEGF-C) is significantly associated with angiogenesis and lymphangiogenesis in cancer. The aim of the present study was to examine VEGF-C expression along with classical clinicopathological parameters and patient survival, and to investigate its possible antiapoptotic and proliferative role in BUC. Immunohistochemistry was applied on 123 paraffin-embedded specimens of BUC for the detection of the VEGF-C, Ki-67 and bax proteins. VEGF-C was mainly expressed in tumor cell cytoplasm. Of 123 BUCs, 27 (22.0%) were VEGF-C positive. VEGF-C was inversely correlated with tumor pathological stage (p=0.007) and negatively associated with bax immunoexpression (p=0.032). VEGF-C expression was related neither to classic prognosticators i.e. tumor grade nor to Ki-67. Patients with VEGF-C positive tumors tended to have better prognosis. The present study implies that VEGF-C may be an early event in the carcinogenesis and might have an antiapoptotic role. However, its potential prognostic significance remains to be clarified.

P112

Primary non-Hodgkin lymphoma of urinary bladder with eight years later renal involvement and absence of systemic lymphoma. A case report.

[1]Tatjana Terzic, [1]Sanja Radojevic, [2]Vesna Cemerikic,
[1]Gordana Basta-Jovanovic, [1]Sanja Citlucanin, [1]Dragan Mitrovic,
[1]Jasmina Markovic-Lipkovski
[1]Institute of Pathology, School of Medicine University of Belgrade,
[2]Histolab, Belgrade, Serbia and Montenegro

Primary bladder non-Hodgkin lymphoma (PBNHL) is very rare, especially as extranodal B-small lymphocytic lymphoma (B-SLL). Also, late isolated renal manifestation of PBNHL is extremely unusual. The diagnosis was based on morphology and immunostaining. Imunohistochemical analysis was performed on 10% formalin-fixed paraffin embedded sections using streptavidin-peroxidase technique. A case report: A-56-year-old women was presented with a solitary tumor situated outside at the left lateral bladder wall. A transvaginal needle biopsy of the tumor was performed. A diagnosis of primary extranodal B-SLL was made in the absence of lymph node, bone marrow or blood involvement. She was treated with LOP protocol until achievement of complete remission. Eight years later, she developed nephrotic syndrome. The renal biopsy revealed parenchymal involvement by the NHL cells with the same imunophenotype like in bladder wall eight years ago (B-SLL). Restaging procedure showed no evidence of disease elsewhere. Chemotherapy was recently performed and she will be carefully followed up. To our knowledge, it is the first case of very rare primary extranodal bladder B-SLL associated with late renal involvement, but without any evidence of disease elsewhere.

P113

Uncommon Neoplasms of the Urinary Bladder: 4 Case Reports

Kemal Behzatoglu*, Burak Bahadir**, Nilsen Y. Erdogan*,
Sule Canberk*, Gulben E. Huq*, Banu D. Gun**,
Sukru O. Ozdamar**
Departments of Pathology; Istanbul Training and
Research Hospital*, Zonguldak Karaelmas University
School of Medicine**, Turkey

We present four cases of uncommon malignant neoplasms of the urinary bladder with more aggressive clinical courses requiring different treatment modalities; two adenocarcinoma in situ, one lymphoepithelioma-like carcinoma, and an additional neoplasm with features resembling yolk sac tumor. Microscopically, the yolk sac-like tumor was hypercellular and composed of undifferentiated cells with high mitotic index. Microcysts lined by flattened cells with luminal eosinophilic material were also observed. No hepatoid appearance was noted histologically. By immunohistochemistry, tumor cells were positive for AFP, β-HCG, and vimentin and focally expressed cytokeratins. CEA, EMA and PLAP were negative. The histologic examination of the second case, previously diagnosed as urothelial carcinoma revealed undifferentiated cells associated with prominent lymphocytic infiltrate consistent with lymphoepithelioma-like carcinoma. Cases diagnosed as in situ adenocarcinoma showed flat columnar surface epithelium without papillary projections fulfilling morphologic criteria of in situ carcinoma. Considering urothelial carcinomas may contain areas differentiating toward other cell origins, pathologists should be aware of these uncommon tumors with pure patterns.

P114

Multiple urogenital neoplasia: a case of a triple carcinoma

Ioannis EFSTRATIOU, Irina ZINOVIEVA Institute of Pathology, Papageorgiou General Hospital, Thessaloniki, Greece

We report a rare case of a patient with three synchronous carcinomas originating from the urinary bladder, the kidney and the prostate gland. A 65-year-old man underwent a transurethral resection of a urinary bladder tumor. The histological diagnosis was transitional cell carcinoma with infiltration of the muscular wall. Meanwhile a CT showed a tumor in the left kidney. A subsequent cystoprostatectomy, pelvine lymphadenectomy and nephrectomy were performed. The histology of the resected specimens revealed: 1) a residual high grade bladder tumor invading the deep muscle (pT3apN0, Grade III), 2) a 0,8cm in diameter adenocarcinoma of

the prostate gland (Gleason score: 3+3=6) and 3) a well differentiated papillary (chromophil) renal cell carcinoma 2,7cm in diameter. Multiple primary neoplasia increases with age and, although rare, it is nowadays more frequent due to the increasing life expectancy and more accurate diagnostic procedures. A combination of bladder and prostate carcinoma is not infrequent. In our case the rare event is a third malignancy also located in the urogenital tract. There are specific predisposing factors for each of the three malignant tumors. Our patient was a heavy smoker. Chromophil renal cell carcinoma has a characteristic pattern of cytogenetic abnormalities. Clinicians should always investigate the possibility of a synchronous or metachronous tumor in patients suffering from cancer.

P115

Prognostic value of EGFR, MIB-1 and P 53 in urothelial bladder carcinoma

Zizi-Serbetzoglou A, Grammatoglou X, Glava C, Vasilakaki Th. Department of Pathology, Tzaneion General Hospital of Piraeus, Piraeus, Greece

Bladder cancer is a common malignancy with highly varied growth patterns. EGFR has been associated with the genesis of bladder tumors. The aim of this study was to investigate the expression of EGFR, MIB-1 cell proliferation and p53 and examine their prognostic value in the progression of bladder cancer.
Material and methods: We examined the immunohistohemical expression of EGFR, MIB-1 and p53 in formalin-fixed paraffin tissue samples from 89 cases of urothelial carcinoma (TUR) , 42 low grade and 47 high grade urothelial carcinomas, corresponding in 69 superficial tumors (40pTa,19pT1a,10pT1b) and 20 infiltrative tumors (pT2). EGFR expression was stronger in invasive tumors ($p<0,0001$) and in high grade tumors ($p<0,0001$). Median nuclear over-expression of MIB-1 and p53 index were 58% and 12% respectively.
Conclusion: MIB-1 antigen and p53 index correlated significantly with the clinical outcome. There is a link between EGFR expression, cell proliferation and high tumor stage/grade and also between EGFR/MIB-1 expression and poor outcome of bladder. The staining pattern of EGFR and its widespread expression in bladder cancer makes it a good target for antigrowth factor or gene therapy.

P116

Frameshift mutations in target genes of the microsatellite instability pathway in urothelial carcinomas of the bladder

Maria S. Karlou, Angelica A. Saetta, Penelope A. Korkolopoulou, Elias A. El-Habr, Irene Thymara, Euphemia Thomas-Tsagli, Efstratios S. Patsouris Department of Pathology, Medical School, National and Kapodistrian University of Athens, Greece

Microsatellite instability (MSI) is an indicator of deficiency in the DNA mismatch repair system. We searched for mutations at target genes of the MSI pathway in correlation with the expression of MMR genes, hMLH1 and hMSH2, in urothelial carcinomas (UCs) of the urinary bladder and evaluated their possible prognostic significance. Seventy-two tumour samples from patients with primary UC were examined for mutations at repetitive sequences of hMSH3 (A)8, hMSH6 (C)8, Bax (G)8, TGF-bRII (A)10, IGFIIR (G)8 and caspase-5 (A)10 genes and immunohistochemical expression of hMLH1 and hMSH2 in correlation with MSI. Bax gene was altered in one case and TGF-βRII in 11 cases. Microsatellite alterations at hMSH3, hMSH6, IGFIIR and caspase-5 were not observed. Frameshift mutations at mononucleotide repeats in target genes of the MSI pathway in urothelial carcinomas of the bladder are rarely observed in urinary bladder carcinogenesis, in which the MSI pathway is rather uncommon. Nevertheless, hMLH1 protein expression is an important indicator for disease recurrence.

P117

Combined small cell and urothelial carcinoma of the urinary bladder

Tzelepi V[1], Gkermpesi M[1], Zisis FI[2], Chionis H[2], Bonikos DS[1]
Departments of [1]Pathology and [2]Urology, University Hospital, Rio-Patras, Greece.

Small cell carcinoma of the urinary bladder is rare accounting for <1% of urinary bladder carcinomas. In 50% of the cases coexists another carcinoma component, usually urothelial carcinoma. In the vast majority of the cases urothelial component comprises a small percentage of the total tumor. A 58 year old male patient presented to the Urology Department with intermittent hematuria. Cysteoscopic evaluation revealed a protruding ulcerated mass in the right lateral wall of the bladder. Preoperative clinical examination and imaging studies showed no evidence of metastatic disease. Radical cystectomy and bilateral iliac lymphectomy was carried out. The pathology report was infiltrating combined small cell carcinoma and high grade (WHO 2004) urothelial carcinoma of the urinary bladder. There was a gradual transition of one component to the other. Each component comprised about half of the tumor mass. No lymph node metastases were found. Cytokeratin profile of the tumor cells of the two components was the same, although the extent of immunostaining was different. The patient received no other treatment and is alive and well, with no evidence of disease 6 months after the initial diagnosis. Gradual transition of the tumor cells of one component to the other and similar cytokeratin expression profile favor a common origin of small cell and urothelial carcinoma of the urinary bladder.

P118

Correlation between transurethral resection of prostate (TURP) and prostate-specific antigen (PSA) screening

Silvia Lacramioara Roznovan[1], Doinita Radulescu[1], Simona Stolnicu[2]
[1] Department of Pathology, University of Medicine, Iasi, Romania
[2] Department of Pathology, University of Medicine, Targu Mures, Romania

Prostate-specific antigen (PSA)screening had increased the detection of prostate adenocarcinoma in stage T1c. The aim of our study was to compare the frequency of incidental prostatic adenocarcinoma found in transurethral resection of prostate (TURP) specimens for a two years period before and two years after PSA screening. TURP specimens were routinely processed and evaluated in order to identify incidental prostatic adenocarcinoma, prostatic intraepithelial neiplasia and atypical adenomatous hyperplasia. We collected 217 and 206 TURP specimens respectively. The comparison revealed a significant decrease in prevalence of T1b prostate carcinomas from 9,21% to 5,33%, with the introduction of PSA screening, representing an improvement in prostate carcinoma staging, with no influence on the incidence of T1a stage, prostatic intraepithelial neoplasia or atypical adenomatous hyperplasia in TUPR specimens.

P119

Prognostic factors in patients with bone metastasis prostate cancer

Doinita Radulescu[1], Silvia Lacramioara Roznovan[1], Simona Stolnicu[2]
[1] Department of Pathology, University of Medicine, Iasi, Romania
[2] Department of Pathology, University of Medicine, Targu Mures, Romania

Although the prognosis of patients with prostate carcinomas metastatic to the bone is poor, several studies have demonstrated that survival is dependent on the extent of metastatic spread within

the skeletal system at presentation. The aim of our study was to examine the clinical and pathologic features in patients who underwent surgery for metastatic prostate carcinoma, in order to identify prognostic markers. Seven patients with underwent surgery for the stabilization of pathological fractures of the femoral neck were diagnosed with metastatic prostate carcinomas. Serum prostate specific antigen (PSA) and bone scintigraphy were performed. Pathologic characteristics examined included Gleason score and immunohistochemical stains for ki-67 and Cytokeratin 7. Features that were found to be statistically significant with poor prognosis were: the interval between the diagnosis of metastasis and the surgery for metastasis, the number of metastatic sites and the Gleason score. The particularity of these cases was that bone metastases permitted the identification of primary prostate carcinomas and that cancer-specific survival may be assessed by tumour differentiation of the metastasis.

P120

Relationship between p16 promoter hypermethlation and protein expression in different hystologic parts of heterogenic prostate tumor tissue

Popova O.P., Kekeeva T.V., Kouznetzova A.V.,
Danilova T.I. and Ivanov A.A.
Research Institute of Molecular Medicine at Sechenov's Moscow Medical Academy, Moscow, Russia.

Purpose of the study: The p16 tumor repressor gene has been found to be inactivated by promoter region hypermethylation in many tumor types including prostate cancer. Relationship between p16 promoter, protein expression and other clinicopathological features can be controversial. The aim of the study is to determine the correspondence between promoter hypermethylation and p16 protein expression in malignant acini, preneoplastic (PIN) and benign hyperplastic glands and adjacent stroma of highly heterogenic prostate tumor tissue.
Materials and methods: Formalin-fixed, paraffin embedded tissues from 80 patients with prostate adenocarcinoma of wide range of histological grade (Gleason score) were stained for p 16 by standard immunohistochemistry. After microscopic analysis and laser micro-dissection it was investigated the methylation status of morphologically different zones of the tumors by methylation sensitive PCR using HpaII and HhaI restrictases.
Results: Hypermethylation of p16 was found in 44% cases directly within the focuses of adenocarcinoma highly to moderately differentiated (score 2-7), despite the fact that majority of them were immunopositive for p16 protein. In PIN areas immediately adjacent to adenocarcinoma the methylation status and protein immunoreactivity were the same as in associated malignancy with few exceptions. The malignant glands of poorly differentiated tumors (score 8-10) were not immunoreactive for p16 in 87% but no methylation was found. According to our results we could suggest that p16 methylation is not the main pathway of that gene inactivation in the most advanced cases. No significant correlation between p16 promoter hypermethylation and immunohistocemical detection of p 16 was observed in nearest benign glands, although not methylated glands were more frequently p16 positive than those with hypermethylation. Cells of surrounding connective tissue in all cases displayed the same frequency of hypermethylation as in adjacent altered epithelium.
Conclusions: Immunohistochemical detection of p 16 is unrelated to promoter methylation status, being strongerly related to morphologic tumor characteristics of poor prognosis. Other genetic alterations of p16 rather than promoter methylation status could serve as prognostic marker of disease in prostate cancer. The same percentages of methylation in altered glands and surrounding connective tissue may be the evidence for the influence of displastic or malignant epithelium to adjacent paraneoplastic stroma.

P121

Invasive cystic hypersecretory carcinoma of the breast. A 2 case report.

Apostolikas N, Papaevangelou M., Psichoyiou H.,
Patereli A., Koniaris T.
Dept. of Pathology of the Hellenic Anticancer Institute,
'St.Savvas' Hospital, Athens, Greece.

The Invasive Cystic Hypersecretory Carcinoma (I. C. H. C.), first described by Posen in 1984, is a very rare entity of a breast adenocarcinoma. We present the clinical and pathological features of 2 cases of I.C.H.C. and review the literature. The patients were females aged 54 and 52 years. Both tumors were located in the left breast. The presenting symptom was a palpable mass. U/S, FNA and mammography were positive for malignancy in both cases. Gross pathology: the tumors measured 2.5cm and 5.5cm respectively, and were distinct from the surrounding parenchyma. The interesting gross feature was the presence of numerous cysts surrounding the main bulk of both tumors but also within the main lesion itself in the second case. The cysts measured up to 0.4cm and the secretion was mucinous or gelatinous. Microscopy: the invasive part of the tumors was a high grade Non Otherwise Specified ductal carcinoma, surrounded by an widely spread intraductal componment, which had all the typical characteristics of a cystic hypersecretory carcinoma (CHC). Especially in the second case the background of the invasive carcinoma showed a wide spectrum of pathologic lesions ranging from cystic hypersecretory hyperplasia (CHH) to atypical CHH and CHC. The first patient was treated with lumpectomy and excision of 12 auxiliary lymph nodes which had no metastases. The second patient had a modified radical mastectomy and 7/27 positive lymph nodes. The expressions of estrogen and progesterone receptors, c-erb-B2, p53, ki-67, CEA, SMA and PAS-Alcian blue are discussed. Only 13 cases have been reported so far in the literature. We add two more cases in order to contribute to the correct diagnosis of a poorly recognized histological entity. More over it seems that the accurate recognition of a CHC may prevent and avoid the development of an ICHC.

P122

Immunohistochemical expression of tissue markers in patients with surgically treated localized prostate cancer and their prognostic value for biochemical failure prediction.

K. Revelos[1], C. Petraki[2], P. Konstantinou[1], A. Rellaki[1],
C. Meristoudis[2], A. Savvani[2], S. Stefanakis[3],
D. Malovrouvas[3] and M. Koutsilieris[4].
[1]Department of Pathology, 251 Hellenic Air Force General Hospital, Athens, Greece, [2]Departments of Pathology and [3]Urology, Evangelismos Hospital, Athens, Greece, [4]Department of Experimental Physiology, Medical School, University of Athens, Greece.

Objectives: To estimate the prognostic value of the immunohistochemical expression (IHCE) of the cyclin-dependent kinase inhibitor p27, the cell proliferation marker Ki67, bcl2 & p53 oncoproteins , the preapoptotic protein Par-4 , androgen receptors (AR) status, neuroendocrine differentiation (NED) assessed by chromogranin A (Chr) & microvessel density (MVD) assessed by CD34.
Patients & methods: Included in the study were 130 consecutive patients (pts) who underwent radical prostatectomy (RP) for localized prostate cancer (PC). Follow-up information was available for 94 pts. The median follow-up period was 28 (1-97) months. A cut-off value of 0.2 ng/ml of serum PSA was established as a biochemical failure (BF) threshold. The immunohistochemical method of streptavidin-biotin-peroxidase was performed. Results: High expression of NED & MVD were significantly correlated with advanced Gleason score (GS) (P=0.003 & 0.021 respectively), high bcl2 with the absence of PIN (P=0.001), low p27, high p53, NED &

MVD with increased tumour volume (P=0.025, 0.027, 0.00 & 0.003 respectively) & reduced p27 expression with high preoperative serum PSA values (P=0.002). Positive surgical margins were predicted by AR status & increased NED (P=0.021 & 0.048 respectively), periprostatic tissue infiltration (PTI) by high p53, NED & MVD (P=0.010, 0.00 & 0.005 respectively), seminal vesicles invasion (SVI) by low p27, AR status, high NED & MVD (P=0.009, 0.016, 0.00 & 0.012 respectively), & finally pelvic lymph nodes metastasis (PLNM) by high Ki67, Par-4 & NED (P=0.006, 0.036 & 0.004 respectively). BF was observed in 35/94 (37%) pts. Kaplan-Meier survival curves showed that significant predictors of BF were low p27and high Ki67, bcl2, p53, NED, MVD (P=0.0005, 0.004, 0.0101, 0.0429, 0.0006 & 0.00 respectively), as well as the synchronous low p27 & high Ki67 IHCE, high bcl2 & p53 IHCE & high NED & MVD (P=0.0011, 0.0450 & 0.0003 respectively). Gleason score(GS), periprostatic tissue infiltration (PTI), seminal vesicles invasion (SVI) and pelvic lymph nodes metastasis (PLNM) were significant predictors for BF (P=0.040, 0.0012, 0.0003 & 0.0038 respectively). However, in the multivariate analysis (Cox Regression) MVD & bcl2 IHCE were the only independent prognostic factors for BF.
Conclusions: Microvessel density & bcl2 immunoexpression may be useful markers for biochemical failure prediction and selection of high-risk patients with clinically localized prostate cancer after radical prostatectomy as candidates for adjuvant therapies.

P123

Immunohistochemical detection of Epidermal Growth Factor receptor as a prognostic indicator in prostate cancer

Amelia Petrescu[1], Florin Andrei[2], Liviu Niculescu[3]
[1]"Prof. Dr. Th. Burghele "Hospital, Bucharest, Romania,
[2]"Victor Babes "Institute of Pathology, Bucharest, Romania,
[3]University of Medicine and Pharmacy "Carol Davila", Bucharest, Romania.

The aim of this study was to evaluate the immunohistochemical expression of epidermal growth factor receptor (EGF-R) in a series of 47 prostate cancer (10 radical prostatectomies, 37 transurethral resection), 10 cases of benign prostate hyperplasia (BPH) and its utility as a prognostic indicator.
Material and methods: A hematoxylin-eosin stained slide from a representative block of each case was examined and Gleason scores were assigned in each case of prostate adenocarcinoma. Additional paraffin sections from the lame blok were stained immunohisto-chemically for EGF-R using EGFR clone 29.1 (Sigma , St Louis, USA) dilution 1:1000.
Results: Three of 4 well-differentiated tumors (Gleason score 2-4), twelve of 33 moderate differentiated (Gleason score 5-7) and eight of 10 poorly differentiated tumors (Gleason score over 8) expressed EGFR. Overall 40,5% of well and moderate and 80% of poorly differentiated tumors expressed this marker. Only two of 10 benign cases were positive. . An interesting observation was that EGFR source Sigma St. Louis stained vessels in 25% of cases.
Conclusions: We consider EGFR expression correlate with high Gleason score, high tumor proliferation and metastatic rate. For low differentiated cases should be considered a prognostic factor.

P124

Comparative study of correlatios between the amount of intratumoral stromal fibrillary components and grading markers in prostate and breast carcinomas

Carmen Popescu[1], Iancu Emil Plesea[2], Stelian Danut Enache[1], Mihaela Tenovici[3], Claudia Valentina Georgescu[1]
Departments of Pathology, [1]Emergency County Universitary Hospital; [2]University of Medicine and Pharmacy,
[3]National Railways System Universitary Hospital, Craiova, Romania

Objectives: This study compared the relationship between the the the amount of stromal fibrillary components (SFC) and the grading factors in prostatic carcinoma (PC) and ductal invasive breast carcinoma (DIBC).
Material and Methods: 20 cases with DIBC and 34 with PC were selected. Stromal fibrillary components were stained with Gömöri technique. Grading factors considered were: degree of tubular formation (T) and nuclear pleomorphism (P) for DIBC and Gleason patterns (dominant and secondary), for PC. 100 fields in DIBC group and 340 fields in PC group were selected randomly using x10 and x20 objectives respectively and subdivided in 3 T subgroups and 3 P subgroups and in Gleason patterns subgroups (G1 - G5) respectively.
Results: The most numerous subgroups were 3-T and 2-P in DIBC and G3 and G4, in PC. In DIBC, SFC ranged between 27,6% and 30% in T subgroups, with and between 25,85% and 34,9% in P subgroups. In PC, there is significant difference between G3 and G4 and betweem G5 an all the other patterns.
Conclusions: In DIBC, SFC showed no significant variations related with T but seems to correlate with nuclear atypia. In PC, SFC tends to increase both in G3 and G5 areas, with a lower value in G4.

P125

Comparative study of correlatios between vascular density and grading markers in prostate and breast carcinomas

Stelian Danut Enache[1], Maria Comanescu[2], Iancu Emil Plesea[2], Carmen Popescu[1], Claudia Valentina Georgescu[1]
Departments of Pathology, [1]Emergency County Universitary Hospital; [2]University of Medicine and Pharmacy; Craiova, Romania

Objectives: This study compared the relationship between the the intratumoral capillaries density (Cd) and the grading factors in prostatic carcinoma (PC) and ductal invasive breast carcinoma (DIBC).
Material and Methods: 20 cases with DIBC and 34 with PC were selected. Intratumoral capillaries were marked for CD34. Grading factors considered were: degree of tubular formation (T) and nuclear pleomorphism (P) for DIBC and Gleason patterns (dominant and secondary), for PC. 100 fields in DIBC group and 340 fields in PC group were selected randomly using x10 and x20 objectives respectively and subdivided in 3 T subgroups and 3 P subgroups and in Gleason patterns subgroups (G1 - G5) respectively.
Results: The most numerous subgroups were 3-T and 2-P in DIBC and G3 and G4, in PC. In DIBC, Cd ranged between 39/mm2 and 43/mm2 in T subgroups and was higher in II- P and III- P groups. In PC, there is high significant difference between Cd in G2 and all the other patterns. G5 presented significant differences compared with G3 and G4.
Conclusions: In DIBC, Cd showed no significant variations related to T and P. In turn, in PC, Cd tends to increase from well differentiated areas to poorely differentiaded ones, with the highest values in G4 solid areas.

P126

Complete androgen insensitivity syndrome with bilateral testicular hamartomata and paratesticular leiomyoma and cystadenoma

A. Papanikolaou[1], D.G. Goulis[2], E. Athanasiou[3], D. Hatzibougias[3], M. Bobos[3], I. Papadimas[2]
Department of Pathology[1], Ippokratio General Hospital, Thessaloniki, Greece
First Department of Obstetrics & Gynecology[2] and Department of Pathology[3], Aristotle University of Thessaloniki, Greece.

Complete androgen insensitivity syndrome (CAIS) is the most common form of male pseudohermaphroditism. It is caused in the majority of the cases by a mutation of the androgen receptor gene.

Patients with CAIS have classically a normal female phenotype with well developed external sexual organs and 46,XY karyotype. We report the case of a 18 year-old girl with CAIS presented as primary amenorhea. After confirmation of CAIS, bilateral orchidectomy was performed. The testis were immature. Multiple hamartomata were found on the testis and two paratesticular tumors (one cystic and one leiomyomatus) on the left. The cystic tumor was a cystadenoma. Benign tumors are developed in 86% of cases of CAIS, being usually hamartomatous nodules of testis. Association of paratesticular cystadenoma to synchronous hamartomata and leiomyomatus tumor is a very rare finding.

P127

An application of web based virtual microscopy as teaching aid in oral pathology

Janusz Szymas[1], Mikael Lundin[2]
[1]Dept. Pathology. Univ. Med. Sciences. 60-355 Poznan, Poland
[2]Biomed. Inform. Res. Group, Univ. of Helsinki, Helsinki, Finland

Recent advances in microcomputers, high resolution digital cameras and robotized microscopes provide pathologists the opportunity to develop virtual slides. With the use of a microcomputer-based workstation these slides can be viewed in a web browser in a manner that closely simulates examination of glass slides with a real microscope. Aims of our study were to develop an educationally useful aid for teaching and evaluation of student competence in oral pathology. By using a robotic microscope and adopted and modified commercially software, a virtual microscopy system was developed that allows fully automated slide scanning and image distribution system. More than 250 slides were scanned and archived on an image server residing within a high speed university network. Students can view entire specimen at any magnification within a standard web browser. The virtual slides are supplemented with concise textual descriptions. Virtual slides can also be viewed for self assessment or examination. Both students and teaching staff enthusiastically adapted to the use of virtual microscopy. Questionnaire feedback from students strongly indicated that virtual slides solved a number of problems in their learning, while providing excellent image quality. Allocation of two students per workstation promoted collaboration and helped to maintain interest in both oral pathology and digital microscopy. We do believe that the use of web based microscopy can guarantee that microscopic examination of tissues remains both important to the dental curriculum (http://ampat.amu.edu.pl).

P128

Virtual slides for second opinion in breast cancer. A comparative study on 81 consecutive needle core biopsies with 5 pathologists from 3 countries.

Marius Nap[1], Paul Theunissen[1], Janina Kulka[2], Rob Teunissen[1], Nathalie Vandevijver[1] and Anna Batistatou[3]
[1]Institute of Pathology Atrium Medical Center Heerlen NL
[2]2nd Dept of Pathology, Semmelweis University Budapest, Hungary.
[3]Dept of Pathology Univ of Ioannina, Greece.

Virtual slides may come to replace real glass slides in second opinions. From 81 breast needle core biopsies, virtual slides were produced using the MIRAX scanning microscope equipped with a 20x objective. No selection was made. The files ranged from 80MB to 500MB. The images were distributed on disc, together with the MIRAX viewer software, for evaluation by 5 pathologists. All reviewers were instructed to use the following scores: 0= no diagnosis possible; 1= normal breast; 2= certainly benign disorder; 3= uncertain benign; 4= uncertain malignant and 5= certainly malignant. Kappa scores with respect to the glass slides were above 80% for 4/5 pathologists. Kappa values between the 5 pathologists ranged from 70% to 80%. If scores 0 to3 and scores 4 and 5 were grouped together these values varied from 94% to 99% for the glass slides and among the pathologists a kappa was found between 91% and 97%. The discrimination between benign and malignant appears to be achieved on virtual slides with a high interobserver agreement, making this approach a valuable additional tool in second opinion procedures.

P129

Ploidometry reasons for the law of the stepped staging in cancerogenesis

Avtandilov G.G.
Russian Medical Academy for Postgraduate Education, Moscow.

Background: The problem of unification of tumours and tumour-like lesions diagnosis has gained a special significance in the modern oncology. The aim. Is to use the ploidometry research in epithelial cells clones study in the prostate, mammary glands, uterus and cervix uteri, thyroid glands, and kidneys for substantiation of different stages in cancerogenesis.
The methods: The computer test was carried out for 56000 epithelial cell nuclei in biopsies at different stages of cancerogenesis. Nuclei ploidy was defined by means of the computer image analyzer “Images-CH” (“Avtan-San” software version).
Results: It was established that the ploidy index for normal epithelial cells averages 2.4 c; the ploidy indices for cells in the conditions of hyperplasia, mild and moderate dysplasia, and benign tumours are within the limits of 2.5 ρ to 3.4 ρ (benign tumours). The increasing quantity nuclei with ploidy indices in the range 3.5 c - 4.4 ρ gives evidence for diagnostics of severe displasia and cancer "in situ" (*border neoplasm condition*).
Malignant tumours (the first degree of infiltrative carcinoma) are determined by the average ploidy indices within the limits of 4.5 ρ to 5.4 ρ. The following nuclei choice shows the cell clones with the average ploidy indices from 5.5 ρ to 6.4 ρ (the second degree of carcinoma) and the average ploidy indices from 6.5 ρ to 7.4 ρ (the third degree of carcinoma). The higher ploidy indices (above 7.5 c) - give evidence for non-differentiated forms of malignant tumours. Revealed principles of cancerogenesis are described mathematically by the linear dependence between the stage (time of development) and the quantitative indication - average indices of ploidity of nuclei cells on the certain stage of cancerogenesis: $\sigma = N + xc$, where σ - average of tumour nuclei ploidity; N – average of normal nuclei ploidtiy index; ρ - ploidy unit; x - ordinal number of cancerogenesis stage -«the code of malignansy»: 1,2, 3-6 [$x = (y-N)/c$].
The presented mathematical model provides some evidence for the stepped staging of neoplasm development owing to predominance of cells with increasing nuclei ploidity. The change to the consequent stage of cancerogenesis arises from prevalence of the new clone cells (70%) with maintenance of preceding clones al the levels of 20% and 10% (Avtandilov G.G., 1984, 2004).
The conclusion: The results of tumor cells computer ploidometry give proof for the law of stepped staging benign, border and malignant tumours development, due to initialor following DNA mass increase in nuclei per one unit of ploidity.

P130

Problems during Tissue Microarrays process

Stephanos Milias, Mattheos Bobos, Ioannis Kostopoulos
Department of Pathology, Aristotle University of Thessaloniki, Greece

Objectives: Tissue microarray (TMA) is a procedure which reduces the cost of immunohistochemical or molecular methods of archival tissue blocks.Protocols have been described elsewhere, but problems often occur during the procedure.

Methods and results: The quality and the temperature of the paraffin were substantial for the success of the process. Covering the back side of the cassette with paraffin,induced its strength. Not recently prepared,and not properly stored blocks,were sensitive. The recipient blocks constructed,contained about 120 to 250 cores each,at least five cores per case. Clefts and "actiniformed" paraffin breakings were observed,leading sometimes to block destruction.Setting the cores of the same type of tissue in the same line, according to the hardness of each tissue was also helpful. A "multi-zoned" core was constructed when thin tissue block was punched, constituting of multiple small cores of the tissue.Before sectioning,incubation of the recipient blocks was done, for 50 minutes in 37oC and in three sessions, to flatten the surface. A thin layer of wet paraffin covered the surface of the recipient block, after sectioning,so it could be stored and re-used for a long period ,preventing the oxidation of the tissues and DNA destruction.
Discussion: TMA is a useful and a cost-effective procedure which contributes to the development of a Pathology Laboratory. New technologies and ideas can improve it

Stephanos Milias M.D.
1, P. Kakani Str,
54248, Thessaloniki, Greece
Tel. (+30) 2310459764
e-mail: smilias@yahoo.com

P131

Computer-supported quality control in DNA flowcytometry analysis

Nick van Rodijnen[1,2], Erik Postma[2], Sjack Hoop and Marius Nap[1]
[1]Atrium medical center Heerlen, [2]IKAT, University of Maastricht, The Netherlands

Automation of the ploidy analysis of DNA histograms may contribute to the reliability of the final classification. We present an algorithm that models a flowcytometry dataset and maps all individual DNA histograms onto a standardised neutral interpretation axis (NIX), after a linearity check and diploid G0/G1 peak analysis. The NIX mapping corrects for drifting. A number of pre-defined classification characteristics are counted to arrive at a ploidy classification. We applied the algorithm to 833 manually labelled DNA histograms, which may contain errors due to inconsistent labelling. The algorithm rejected 4% (33 cases) of the DNA histograms because of non-linearity, in 0,4% (3 cases) of the histograms the diploid G0/G1 peak was detected incorrectly. 11% (94 cases) with a skewed diploid G0/G1 peak could not be analysed. In 701 cases an automatic classification could be given, with on-screen inspection for acceptance or rejection. In 635 / 701 cases two evaluators accepted the automatic label suggestion. The kappa value of the two evaluators with the automated classification label is resp. 0.9186 and 0.9458. NIX mapping allows for automated quality control of the manual ploidy labelling.

P132

Thymidine Phosphorylase expression in breast cancer: The prognostic significance, its association with angiogenesis, extracellular matrix components, and clinicopathological features

Antigony Mitselou[1], Elli Ioachim[2], Constantina Damala2, Elena Tsanou[2], Michael Doukas[2], Theodore Vougiouklakis[1], Niki Agnantis[2].
Departments of [1]Forensic Pathology, [2]Pathology, Medical School, University of Ioannina, Greece.

Thymidine Phosphorylase (TP), also known as platelet-derived endothelial cell growth factor (PD-ECGF), is an enzyme that catalyzes the reversible dephosphorylation of thymidine, deoxyuridine and their analogs. TP also promotes angiogenesis. We examined the TP expression using immunohistochemistry in paraffin-embedded formalin-fixed tissue of 91 invasive breast carcinomas. The cytoplasmic thymidine phosphorylase, nuclear and stroma was estimated semi-quantitatively. Cytoplasmic high TP expression was found in 33 cases (36.3%) of carcinomas, high nuclear expression was seen in 2 cases (2.2%) and 22 cases (24.2%) expressed strongly immunostaining in stroma. A statistical significant relationship between TP cytoplasmic and TP nuclear expression was found ($p=0.03$), as well as between TP stroma expression and TP nuclear expression ($p<0.0001$). No correlation was found between TP cytoplasmic expression and grade of the tumor, type of tumor, size, lymph node involvement and hormonal (PR and GR) status. Statistical correlation between TP stroma expression and MIB-1 ($p=0.014$) and PCNA ($p=0.044$) was found. Regarding the correlation between TP and extracellular components we found association between TP tumor expression with tenascin ($p=0.002$). A statistical significant relationship between overall survival (OS) and TP tumor expression was found ($p=0.018$). In conclusion, our findings suggest that TP has little effect on tumor angiogenesis of breast carcinoma.

P133

Immunohistochemical detection of mismatch repair proteins hMLH1, hMLS2 and hMSH6 in familial breast cancer and correlation with clinicopathological parameters.

Arkoumani E[1], Stefanou D[1], Batistatou A[1], Briasoulis E[1], Kontostolis E[3] and Agnantis NJ[1].
[1]Department of Pathology, [2]Department of Medical Oncology, [3]Department of Obstetrics and Gynaecology, University of Ioannina, Medical School, Greece.

Defects in mismatch repair genes are associated with a variety of cancers. However, it is not yet understood whether clinical parameters influence the MMR status. In the present study 30 cases of familial breast cancer were examined for the expression of hMLH1, hMLS2 and hMSH6 using the monoclonal antibodies MLH1, MSH2 and MSH6 (BIOCARE MED-Menarini Diagnostics). We found loss of expression of MLH1 in 8/30 (26%), of MSH2 in 4/30 (13%) and of MSH6 in 13/30 (43,3%) of the cases examined. Three carcinomas (10%) were negative for both MLH1 and MSH2 and seven (23,3%) were negative for both MLH1 and MSH6, showing a strong correlation between the expression of these proteins. Statistical analysis revealed that there is a positive correlation between reduced expression of these proteins, tumor size and estrogen status , but no correlation with lymph node status. Our data suggest that the impaired expression of MMR proteins can be used as a prognostic factor.

P134

EGFR and phosphorylated EGFR expression in HER-2 overexpressing breast carcinomas

Batistatou A., Stefanou D., Arkoumani E, Simou N., Agnantis N.J.
Department of Pathology, University of Ioannina Medical School, Greece

Her-2/neu overexpression is an important prognostic parameter in breast cancer patients and a determinant of targeted therapy. Interactions between Her-2/neu and other members of the EGFR family have been implicated in trastuzumab resistance. In the present study we have analyzed the immunohistochemical expression of EGFR and phosphorylated EGFR (monoclonal antibodies anti-EGFr, 31G7 and anti-phospho-EGFr, Y1086, ZYMED Labs) in 51 HER-2/neu overexpressing breast tumors (score2+ and 3+, Herceptest, DAKO) and investigated potential correlations with clinicopathological parameters and hormone receptor status. Fourteen and 16 out of

51 cases were positive for EGFR and phosphorylated EGFR (27.5% and 31.4% respectively). EFGR expression was inversely correlated with estrogen and progesterone receptor status and positively correlated with phosphorylated EGFR expression. Our data contribute to the further characterization of the EGF receptor tyrosine kinase family and identification of its role in breast carcinogenesis.

P135

The missing kiss of life: Analysis of mutation and protein expression of the metastasis-suppressor gene KISS1 in early breast cancer.

L. Kostadima[1], G. Pentheroudakis[1], L. Dova[2], I. Georgiou[3], V. Malamou-Mitsi[4], G. Vartholomatos[2], G. Fountzilas[6], N. Kolaitis[2], M. Ntemou[5], N. Pavlidis[1].
[1]Dept. of Medical Oncology, [2]Lab of Hematology-Molecular Biology Unit, [3]Dept. of Obstetrics and Gynaecology-Genetics Unit, [4]Dept. of Pathology, Ioannina University Hospital, [5]Dept. of Pathology, Ioannina General Hospital, [6]Medical School, Aristotle University of Thessaloniki, Greece

Metastasis-suppressor genes have emerged as molecular hallmarks for clonal evolution of malignancies towards systemic dissemination. We studied tissue expression of KISS1 protein by immunohistochemistry and screened the relevant gene for mutations in 50 women with stage II/III early breast cancer. DNA was extracted for PCR of exons III, IVa, IVb of KISS1 gene, mutation screening with Single Strand Conformational Polymorphism (SSCP) and sequencing of aberrant bands. SSCP was also performed in peripheral blood lymphocyte DNA of 50 healthy controls. An aberrant exon IVa SSCP band was found in 30 patients, but none of 50 controls. The band was sequenced and found to harbor the 242 C to G base substitution, resulting in a proline to arginine switch at codon 81 (P81R) and alteration of the KISS1 tertiary structure. Immunoexpression of KISS1 protein was weak to moderate in the majority of tumours. The observation of a loss-of-function KISS1 gene mutation in more than half of patients with high-risk early breast cancer may shed light in the complex pathway of metastatic dissemination and pave the way for development of new targeted therapeutic approaches.

P136

VEGF and BCL-2 in serum at breast cancer in comparison with CEA and CA15-3. Which factor can detect the recurrence earlier?

R. Iosifiduo, G. Galaktiduo, F. Patakiouta, A. Bousoulegas
Aanticancer Hospital, Theagenio, Thessalokini

The purpose of our study is to examine if the expression of VEGF and bcl-2 in serum can detect the recurrence much earlier of CEA and CA15-3 in women with breast cancer. 200 patients with breast cancer stage I and II are enrolled in this study. The age of the patients was 59,65±11,65 years. 102 patients had mastectomy with axillary node desection and 98 had quadrectomy and axillary node desection. All had supplementary therapy. 14 patients had recurrence of the disease 18 months after the surgical therapy. Serum VEGF and bcl-2 was measured pre-operative, post-operative one and two years after the surgical treatment with ELISA and CEA and CA15-3 every 4 months until the two years with RIA. The results were analysed with statistical methods (ROC curves and Pearson). ROC curves shows that bcl-2 can detect the recurrence pre-operative (p=0,066), post-operative (p-0,037) and the second year (p=0,029) and VEGF post-operative (p=0,003). CEA and CA15-3 can detect the recurrence 20 (p=0,098) and 8 months (p=0,045) after the surgical treatment. There is no statistical relation between these factors with the size of the tumor, the histological type and the lymph node status (Pearson). The tumor markers VEGF and bcl-2 can detect the recurrence of the disease much earlier of CEA ana CA15-3 and the clinical appearance and so they can be used in the follow-up of the patients. Bcl-2 marker is the most significant as can detect the recurrence in the most measurements.

P137

Deregulation of annexin I expression in invasive brest carcinomas

Tsanou E[1], Damala K[1], Peschos D[2], Stefanou D[1] and Agnantis N.J[1].
Department of Pathology-Cytology[1] and Forensic Medicine[2], Medical School, University of Ioannina, 45110 Greece

Annexins are calcium-dependent binding proteins, implicated in regulation of membrane trafficking, cellular adhesion and metastatic cascade.
Aims: To demonstrate immunohistochemically the patterns of annexin I expression in breast cancer and to establish any relationship with clinicopathological features and proteins correlated with the prognosis of breast cancer, especially anti-oxidant proteins (MnSOD) and growth factors (VEGF).
Material-Method: Annexin I immunohistochemical expression was studied in 86 cases of breast cancer. We estimated both the percentage of positive cancer cells and the intensity of immunostaining. Staining of >10% of tumor cells was considered to be positive for the expression of annexin I.
Results: 49 cases (57%) showed increased Annexin I expression compared to normal ductal structures. Annexin I expression was correlated to tumor size (p=0.05), strong immunopositivity for VEGF (p=0.049) and MnSOD (p=0.03). Patients with positive lymph nodes exhibited strong intensity for annexin I (p=0.039).
Conclusions: Up-regulation of annexin I is correlated with advanced T stage, while close association was observed between annexin I and VEGF and MnSOD. We can postulate based on the correlation with the above mentioned proteins the implication of annexin I in early phase carcinogenesis in breast cancer.

P138

Clinicopathologic and prognostic significance of the blood and lymphatic microvessel density in invasive breast carcinoma

[1]Nomikos A, [2]Mylona E, [2]Giannopoulou I, [1]Athanassiadou S, [3]Markaki S, [3]Keramopoulos A, [1]Nakopoulou L.
Pathology Departments of [1]Attikon Hospital, [2]Medical School and [3]Alexandra Hospital

Our aim was to investigate the blood and lymphatic vascular density (BVD and LVD, respectively) in invasive breast carcinomas. Immunohistochemistry was applied on paraffin-embedded sections from 146 patients with invasive breast carcinomas to detect blood and lymphatic vessels. Vessel density was evaluated by image analysis. Both BVD and LVD correlated positively with histological grade (p=0.066 and p=0.056 respectively) and inversely with ER (p=0.031 and p=0.056 respectively) and bcl-2 (p=0.013 and p=0.031 respectively). Moreover, BVD correlated positively with topoIIa and LVD with c-erbB2 (p=0.031 and p=0.058). Neither BVD nor LVD correlated with any of the VEGFs. BVD exerted unfavorable impact on both overall and disease-free survival of the patients (p=0.018 and p=0.040 respectively) and specifically of patients with tumor size 2-5cm (p=0,0002 and p=0,0049 respectively). Moreover, intratumoral BVD was recognized to be an independent, unfavorable predictor of overall survival (p=0.051). In the present study BVD and LVD were related to tumors of aggressive phenotype. High BVD may be an unfavorable prognostic indicator for long-term survival in breast cancer.

P139

The effect of the different matrix metalloproteinase (MMP)-9 protein localizations and intensity of expression on the tumor phenotype and prognosis of the patients with invasive breast carcinomas.

[1]Magkou C, [1]Nomikos A, [2]Mylona E, [2]Alexandrou P,
[2]Liapis G, [1]Nakopoulou L.
Pathology Departments of [1]Attikon Hospital and [2]Medical School

We Immunohistochemically investigated the expression of MMP-9 and its clinicopathological and prognostic value in 174 invasive breast carcinomas. MMP-9 was detected in the cytoplasm of the malignant cells and the peritumoral fibroblasts. Moderate cytoplasmic expression of MMP-9 was inversely associated with Ki67 and topoIIa (p=0.034 and p=0.004 respectively), whereas intensively stained cases were found to demonstrate shorter overall and disease-free survival in ER-positive (p=0,022 and p=0,066), c-erbB-2 negative (p=0,0031 and p=0,0005 respectively) and LN-negative (p=0,0106 and p=0,0146 respectively) patients. Fibroblastic MMP-9 was more frequently observed in c-erbB-2 positive samples (p=0,043) and in tumors of higher histological grade (p=0.07), exerting unfavorable impact on both overall (p=0,0203) and disease-free survival (p=0,0274) of the patients. Concluding, moderate cytoplasmic expression of MMP-9 was related to tumors of low proliferative potential, while the high expression exerted unfavorable impact on the prognosis of ER(+), c-erbB2(-) and LN(-) patients. Stromal MMP-9 was associated with tumors of aggressive phenotype, affecting negatively both overall and disease-free survival of the patients.

P140

Immunohistochemical profile of papillary breast tumors using cytokeratins

KIZIRIDOU A., ANESTAKIS D., LAMBROPOULOU M.,
DESTOUNI C., BOUSOULEGAS A., TOLIOU T.
Pathology and Surgery Department, Theagenion Anticancer Hospital, Thessaloniki

Objective: Papillary tumors of the breast often cause differential diagnosis problems despite the well-described histological features. Sometimes there are difficulties in diagnosing a papilloma(PL) versus a papillary ductal carcinoma in situ (DCIS).This study examine the cytokeratin (CK) profile of these tumors, that may contribute to the correct diagnosis.
Materias and methods: We studied archival tissue of 30 papillary lesions of the breast (15 papillomas and 15 papillary ductal carcinomas in situ) using immunohistochemical method(Biotin-Streptavidin/HRP)by an automated staining machine. We used three monoclonal antibodies against cytokeratins [High molecular weight CK-CK1,5,10,14(DAKO-Dilution 1:600) (clone 34βE12) , CK-14 (Novocastra-Dilution 1:20) and CK5/ CK6(DAKO, Dilution 1:100). Staining intensity was graded 1+(weak) to 3+++(strong) and was evaluated in luminal and myoepithelial cells.
Results: As far as CK5/6, 8/15 papillomas expressed strong reactivity, 2/15 moderate and 5/15 weak intensity. DCIS 10/15 were negative and 5/15 showed weak positivity. CK14 was expressed in 10/15 papillomas with strong, 4/15 with moderate and 1/15 weak reaction. DCIS was 8/15 negative, 4/15 weak to moderate and 3/15 weak reaction respectively. CK34βE12 was expressed in 8/15 papillomas with strong, 6/15 with moderate and 1/15 with weak reaction. DCIS was 10/15 weak, 2/15 moderate and 2/15 weak reaction, 1/15 was negative.
Conclusions: 1)The CKs could help besides to morphology, in differential diagnosis of papillary breast tumors. 2)It seems that CK 14 is more specific for papillomas especially when combined with CK 5/6. 3) CK 34βE12 is less useful, because of the lower detection rate in papillomas.

P141

Adenomyoepithelioma: an unusual neoplasm of the breast

Sibel Bektas, Burak Bahadir, Banu D. Gun,
Sacide Colak, Sukru O. Ozdamar
Zonguldak Karaelmas University, School of Medicine,
Department of Pathology, Turkey

Adenomyoepithelioma is characterized by proliferation of both epithelial and myoepithelial cells. The consultation material of total mastectomy and axillary lymph node dissection from a 34-year-old female were evaluated. Microscopic examination of the 6,5 cm well-circumscribed tumor revealed rounded tubules lined by both epithelial and myoepithelial cells in a myxomatous stroma. More prominent myoepithelial hyperplasia caused obliteration of some of the tubular lumens. Obvious smooth muscle differentiation was also noted. Immunohistochemically, myoepithelial cells and cells with smooth muscle differentiation exhibited vimentin and smooth muscle actin; myoepithelial cells were also reactive for S-100 protein and epithelial membrane antigen. Luminal epithelial cells revealed positive reaction for epithelial membrane antigen and pan-cytokeratin (AE1/AE3), but displayed only focal staining with carcinoembryonic antigen. Differential diagnosis of adenomyoepithelioma from its malignant counterpart and usual mammary carcinoma may occasionally be challenging. Moreover, although considered an indolent neoplasm but with a potential risk for recurrence and sometimes metastasis, adenomyoepithelioma of the breast requires long-term follow-up.

P142

Metaplastic breast carcinomas: report of 16 cases with emphasis on histopathological findings, hormone status and c-erb-B2 expression.

Kiziridou[1] A., Dimitriadis[1] I., Valeri R., Patakiouta F[1]., Toliou1 T.
Pathology[1] Department, “Theagenion” Anticancer Hospital,
Thessaloniki, Greece.

Objective: Metaplastic breast carcinomas is a rare cancer, consisting of a heterogeneous group of neoplasms, accounting for less than 1 % of all invasive mammary carcinomas. These tumors can subclassified into different types, each of them usually causes problems in the differential diagnosis of breast neoplasms. The aim of this study is to refer 16 new cases of metaplastic carcinomas, emphasising to histopathological findings, oestrogen (ER) and progesterone (PR) receptors and cerb-B2 oncoprotein expression.
Materials and Methods: The slides of 16 metaplastic breast carcinomas from the files of our Department, (2001 to 2005) were revised and classified according to WHO classification.
Results: The frequency of different subtypes was: 7 of sqamous type, 6 of spindle cell type, 2 of matrix producing type and 1 with choriocarcinomatous elements. Immunohistochemically the epithelial cells expressed Cytokeratins antibodies (CK7 or CK AE1/AE3) and occasionally EMA or CEA. The metaplastic elements expressed different antibodies as S-100, Vimentin, SMA.
Conclusions: 1) Metaplastic carcinomas, assume a broad spectrum of phenotypes. 2) Immunohistochemistry is a useful tool in differential diagnosis. 3) They usually don't express oestrogen and progesterone receptors. 4) Sometimes they express cerb-B2 oncoprotein.

P143

Immunohistochemical and FISH study of EGFR protein expression and gene amplification in 153 invasive breast carcinomas.

T. Koletsa, I. Kostopoulos, V. Kotoula,
E. Nenopoulou, C. Papadimitriou.
Department of Pathology, Aristotle University Medical School, Thessaloniki, Greece

EGFR gene amplification, mutations at the genomic level and protein over-expression are among the parameters that are currently tested as potentially predictive markers for EGFR inhibitors. However, it is still not clear whether EGFR gene amplification leads to over-expression of the EGFR protein, such as the case with HER2. In this study we evaluated EGFR gene and protein status in breast cancer. A total of 153 breast carcinomas were examined. Immunohistochemical (IHC) analysis with two different antibodies (EGFR-PharmDX and EGFR-31G7) and Fluorescence In Situ Hybridization (FISH) for EGFR was performed on tissue arrays. Immunopositivity with EGFR PharmDX was observed in 18/153 (11,76%) and in 26/153 (16,99%) cases with EGFR-31G7 (p = ns). Lobular carcinomas and grade I tumors were negative for EGFR IHC. Amplification of the EGFR gene was not observed, while 23/128 cases (17,96%) exhibited polysomy of chromosome 7. Only 4 out of these 23 cases were positive with EGFR IHC. Thus, in line with recent reports in other tumor systems, EGFR protein (over) expression does not seem to be related to EGFR gene copy numbers in breast carcinomas, and can not be predicted by assessing this parameter.

P144

Herstatin is associated with the status of HER expression and activation in breast cancer.

T. Koletsa, A. Boutis*, I. Kostopoulos, B. Christoforidou*,
Th. Toliou*, C.S. Papadimitriou, V. Kotoula.
Department of Pathology, Aristotle University Medical School, and *Theageneion Cancer Hospital, Thessaloniki, Greece

Herstatin (HST) is a truncated protein produced by alternative splicing from the HER2 gene and serves as a natural endogenous inhibitor of HER receptor dimers. In this study, we investigated HST expression along with HER related parameters in 70 infiltrative breast carcinomas and matched non-cancerous tissues (MNTCs). HST immunopositivity was demonstrated in 27/70 (39%) tumor and 11/70 (16%) MNTCs. Relative expression of HST mRNA positively correlated with relative HER2 ($p<0.001$) and HER3 ($p=0.018$) expression, tended to be higher in tumors than MNTCs ($p=0.022$), but did not correlate with HST protein presence. The latter was associated with cytoplasmic localization of pHER2-Y1248 ($p=0.006$), non-membranous HER3 ($p=0.003$) and nuclear localization of pAKT/PKB-S473 ($p=0.045$). EGFR phosphorylation correlated positively with HER2 immunostaining in HST negative tumors ($p<0.001$) but not in HST positive ones. Patients with HER2 3+ / HST positive tumors responded better to trastuzumab ($p=0.010$). In conclusion, HST is expressed in a subset of breast carcinomas in association with HER2. This protein may affect the activation of HER2/EGFR dependent pathways by interfering with the expression of HER3. HST may prove useful as an adjuvant marker for the prediction of response to HER2 targeting treatments.

P145

Image analysis of digitized mammograms and correlation with histopathology

G. Giannakopoulou[1], S. Golemati[2], D. Koulocheri[1], A. Tsakiri[1], J. Stoitsis[2], A. Nonni[1] , F. Zagouri[1], K. S. Nikita[2], G. C. Zografos[1], and J. Bramis[1]
[1]Breast Unit of Hippokration General Hospital of Athens (1st Propaedeutic Surgery Clinic of Medical School, University of Athens, Radiology Department, Pathology Department of Medical School, University of Athens, Greece) [2]Department of Electrical and Computer Engineering, National Technical University of Athens, Greece

Purpose: To correlate breast tissue histology with image texture features, in an attempt to investigate the validity of texture analysis techniques and their potential application in clinical practice.
Materials and methods: 33 patients with non-palpable breast lesions, including masses and microcalcifications, underwent stereotactic directional vacuum-assisted breast biopsies. Tissue samples were subsequently sent for histological examination. Regions of interest (ROIs), corresponding to suspect lesions, were defined and outlined by a radiologist on the digitized mammograms. Texture analysis of the selected ROIs was performed using first-order mathematical descriptors estimated from the normalized gray-level histograms of the image ROIs. These included minimal, maximal, median, and mean gray-levels, standard deviation of gray levels, coefficient of variation, and gray-level skewness, kurtosis, entropy, and energy. The fractal dimension was also estimated.
Results: Compared to the 21 benign cases, the histograms of the 12 malignant cases had a significantly (Student's t-test, $p<0.05$) higher gray-level skewness and kurtosis. Gray-level skewness characterizes the deviation of the distribution from a symmetrical reference one. Benign lesions had negative values for skewness (-0.05 ± 0.33) corresponding to a left-skew distribution, whereas malignant lesions had positive values (9.81 ± 13.80) corresponding to skewness to the right. Kurtosis is related to the steepness of the distribution and its values were -0.67 ± 0.86 for benign and 34.09 ± 56.52 for malignant cases.
Discussion/Conclusion: Estimation of mathematical descriptors of digitized mammograms provides a quantitative operator-independent assessment of breast lesion type and may be helpful as an additional parameter in differential diagnosis of breast lesions.

P146

Invasive cystic hypersecretory carcinoma of the breast. A 2 case report.

Apostolikas N., Papaevangelou M., Psichoyiou H.,
Patereli A., Koniaris E.
Dept. of Pathology of the Hellenic Anticancer Institute, 'St.Savvas' Hospital, Athens, Greece.

The Invasive Cystic Hypersecretory Carcinoma (I. C. H. C.), first described by Rosen in 1984, is a very rare entity of a breast adenocarcinoma. We present the clinical and pathological features of 2 cases of I.C.H.C. and review the literature. The patients were females aged 54 and 52 years. Both tumors were located in the left breast. The presenting symptom was a palpable mass. U/S, FNA and mammography were positive for malignancy in both cases. Gross pathology: the tumors measured 2.5cm and 5.5cm respectively, and were distinct from the surrounding parenchyma. The interesting gross feature was the presence of numerous cysts surrounding the main bulk of both tumors but also within the main lesion itself in the

second case. The cysts measured up to 0.4cm and the secretion was mucinous or gelatinous. Microscopy: the invasive part of the tumors was a high grade Non Otherwise Specified ductal carcinoma, surrounded by an widely spread intraductal component, which had all the typical characteristics of a cystic hypersecretory carcinoma (CHC). Especially in the second case the background of the invasive carcinoma showed a wide spectrum of pathologic lesions ranging from cystic hypersecretory hyperplasia (CHH) to atypical CHH and CHC. The first patient was treated with lumpectomy and excision of 12 auxiliary lymph nodes which had no metastases. The second patient had a modified radical mastectomy and 7/27 positive lymph nodes. The expressions of estrogen and progesterone receptors, c-erb-B2, p53, ki-67, CEA, SMA and PAS-Alcian blue are discussed. Only 13 cases have been reported so far in the literature. We add two more cases in order to contribute to the correct diagnosis of a poorly recognized histological entity. More over it seems that the accurate recognition of a CHC may prevent and avoid the development of an ICHC.

P147

The Immunohistological Expression of Estrogen Receptors -a and –b in lobular neoplasia.

A. Nonni[1], G. Zografos[2], F. Zagouri[2], A. Lazaris[1], G. Giannakopoulou[2], P. Antonakis[2], E. Nika[2], M. Fotou[2], K. Papadimitriou[2], E. Patsouris[1], J. Bramis[2]
[1]Department of Pathology, Medical School of Athens, Greece
[2]Breast Unit, 1st Surgical Dep., Medical School of Athens, Greece

The designation lobular neoplasia(LN) includes atypical lobular hyperplasia and lobular carcinoma in situ. Even if these lesions have no prognostic significance, they constitute a precursor lesion of subsequent invasive breast carcinoma(BC). Estrogen(ER) play a significant role in promoting the development and progression of BCs. We evaluated the ER-a, and ER-b status in patients with LN. Tissue specimens were taken from 30 patients with LN. Adjacent normal breast tissues were estimated serving as controls. A standard immunohistochemical procedure, using monoclonal antibodies to ER-a, and ER-b was applied. Both the estrogen receptors were expressed in all the samples. There was no statistically significant difference in the percentage of ER-a expression between LN (Med65%,SD0,18) and normal tissue samples(Med60%,SD 0,18, Mann Whitney U test, p=0.438). Interestingly, ER-b expression was significantly decreased in LN samples (Med70%,SD0,17) in comparison to normal tissue samples (Med85%,SD0,09, Mann Whitney U test, $p<0.01$). Our results and especially the decrease of ER-b receptors in LN may have a potential role in the determination of women, predisposition for breast carcinoma development.

P148

Vacuum-assisted breast biopsy of microcalcifications: Correlation between mammographic images and histological findings.

D. Koulocheri, G. Giannakopoulou, A. Tsakiri, A. Nonni, F. Zagouri, G. Philippakis, N. Pararas, G.C. Zografos, J. Bramis
Breast Unit, 1st Surgical Depart., Medical School of Athens, Greece

The purpose of our study is to correlate between the histological findings of microcalcifications in breast tissue using the vacuum-assisted 11G biopsy (MammotomeR) device and the mammographic estimation according to the BI-RADS of the American College of Radiology. 190 mammograms of patients with microcalcifications were diagnosed by two independent radiologists and classified using the BI-RADS categories. The patients were biopsed using the MammotomeR device in combination with the stereotactic Fischer's table. Histological examinations were performed and their findings were classified in 3 categories; benign lesions, atypia (ADH, ALH) and malignancies (in situ and invasive carcinoma). 61/190 mammographic images were classified as BI-RADS 3 and 129/190 as BI-RADS 4. We statistically evaluated the histological findings to the BI-RADS classification and our results are: for BI-RADS 3 , 49/61 cases were benign lesions (80,32%), 11/61 were atypia (18,03%) and 1/61 were malignant lesions(1,64%). For BI-RADS 4, 93/129 cases were benign lesions (72,10%), 12/129 were atypia (9,30%) and 24/129 were malignant lesions (18,60%). According to our results, the radiological estimation was successfully made for microcalcifications in conformity with the BI-RADS categories and their histopathology.

P149

Breast Metastasis from Uterine Leiomyosarcoma Diagnosed by Fine Needle Aspiration (FNA). *A Case Report*

Lina Pappa[1], Nektaria Zagorianakou[1], Evangelia Kitsiou[2], Maria Bafa[1], Evdoxia Sintou-Mantela[1] and Vassiliki Malamou-Mitsi[1].
Department of Cytology[1], University Hospital of Ioannina, Greece
Department of Pathology[2], General Hospital "G. Hatzikosta", Ioannina, Greece.

Background: Leiomyosarcomas of the breast are a rare subgroup of primary breast sarcomas. Even more rare is breast metastasis of an extra-mammary leiomyosarcoma. Only four cases have been published up to now in the literature.
Case: We report a case of breast metastatic leiomyosarcoma occurred in a 58-year-old woman with a prior history of uterine leiomyosarcoma, resected 18 months earlier. The breast mass was palpable and a fine needle aspiration performed by a Cytologist. The microscopic examination showed cellular smears composed of loosely structured clusters and tissue fragments of spindle-shaped and polygonal or rounded malignant cells in disorderly arrangement. The tumor cells were medium or large-sized with basophilic cytoplasm and enlarged, irregular, hyperchromatic nuclei with nucleoli. Tumor giant cells and multinucleation were also present. The morphological features along with immunocytochemical positivity for desmin, muscle-specific actin and vimentin put the diagnosis of a metastatic leiomyosarcoma.
Conclusion: FNA cytology can be a reliable method for the diagnosis of a leiomyosarcoma. The morphologic criteria in combination with the clinical history and the immunocytochemical findings can put a definitive diagnosis and avoid additional painful and time consuming diagnostic procedures for the appropriate patient's further clinical management.

P150

The assessment of sensitivity, specificity and positive predictive value of the mammographic evaluation of non-palpable lesions of the breast using the breast imaging reporting & data system (BI-RADS) in an anticancer institute

H. Trihia[1], H. Kajanis[2], O. Tzaida[1], D. Kondylis[3], P. Arapantoni-Dadiotis[1].
[1]Departments of Pathology, [2]Radiology and [3]Surgery,
Metaxa Cancer Hospital, Piraeus, Greece

Objective: The purpose of the study was to assess the usefulness of the BI-RADS application in the evaluation of the mammographic findings of non-palpable lesions of the breast in our hospital.
Material and Methods: We retrospectively evaluated 165 non-palpable mammographically detected lesions, on which surgical biopsy was performed. Each lesion was classified according to BI-RADS descriptors for masses (margins and shape) and calcifications (morphology and distribution) and was categorized by the BI-RADS

final assessment categories as category 2 ('benign'), category 3 ('probably benign'), category 4 ('suspicious') and category 5 ('highly suggestive of malignancy'). Mammographic and pathologic findings were reviewed.
Results: Carcinoma was present in 58 of the 165 lesions (35.7%). 38 of them presented as stellate lesions, with- or without calcifications and 19 as pure calcifications. A single case which was categorized mammographically as BIRADS 3 lesion, presented as a relatively well defined lesion. For the 165 lesions subject to biopsy, BI-RADS final assessment categories were 'category 2' in 22 lesions (13.3%), 'category 3' in 63 lesions (38.1%), 'category 4' in 50 (30.3%) lesions and 'category 5' in 30 lesions (18.1%). Carcinoma was present in all 30 'category 5' lesions (100%) compared with 27 of 50 'category 4' lesions (54%) and in one of the 63 'category 3' lesions (1.58%). Of the carcinomatous lesions, 51 (87.9%) were infiltrative of which 9 microinvasive (15.3%) and 7 (12%) were in situ. Of the infiltrative carcinomas, four were of low grade and six multicentric. Precancerous lesions, in the form of atypical ductal hyperplasia were present in 9 (5.45%) of the 165 lesions, six in 'category 3' lesions and three in 'category 4' lesions. Foci of LN/LCIS (incidental finding) were present in 6 cases, four in 'category 3' lesions and two in 'category 4' lesions. The sensitivity of the mammographic evaluation was 98.3% and specificity 82.3%. Positive predictive value for 'category 5' was 100%, 'category 4' 64% and 'category 3' 98.4%. The false positive rate was 31% and false negative rate 1.72%.
Conclusion: The standardized terminology of the BI-RADS lexicon allows quantification of the likelihood of carcinoma in non-palpable breast lesions. By providing a common language, BI-RADS facilitates communication between radiologists, referring clinicians and women undergoing mammography. In our study BI-RADS categories '4' and '5' were useful predictors of the relative likelihood of malignancy and confirms that spiculated margins, irregular shape and pleomorphic calcifications have a higher propability of malignancy.

P151

Occult breast carcinoma presenting with axillary lymph node metastases- three cases report.
Tzaida O, Trihia H, Simoulis A, Kondylis D* , Arapantoni-Dadioti P.
Pathology Department, METAXA Cancer Hospital, Piraeus, Greece
*Surgery Department, METAXA Cancer Hospital, Piraeus, Greece

Background: Breast carcinoma presenting with axillary metastases and no apparent primary tumor in the breast is an uncommon form of Stage II disease. Fewer than 1% of patients diagnosed with breast cancer initially present with axillary lymphadenopathy as the only clinical manifestation of their disease. We present three such cases of occult Ca and we discuss the issues of evaluation and management of patients.
Material and Methods: Three postmenopausal female patients presenting with a palpable axillary mass and normal findings at physical examination, mammography and ultrasound of both breasts, were reported to our hospital between 1979 and 2001. Lymph node mass biopsy revealed a metastatic adenocarcinoma of presumed primary breast origin based on histological tumor phenotype. One patient underwent total mastectomy and in the two others breast conserving surgery combined with lymph node dissection was performed. All patients received hormone therapy and breast radiation as well as adjuvant systemic therapy.
Results: In the patient subjected to total mastectomy and in one of the two cases with partial mastectomy, despite a thorough pathologic examination, no primary tumor was found. These two patients were free of disease at 18 and 7 years follow-up, respectively. In the third patient microscopic examination revealed the presence of in situ Ca, comedo type, without an infiltrating component. The histological and immunohistochemical characteristics of the breast tumor were entirely compatible with the ipsilateral axillary metastasis. Immunohistochemical study also revealed a tumor phenotype indicative of an aggressive biologic course. Despite receiving several types of systemic therapy, plus radiation, plus total excision of the rest of the breast this patient presented inflammatory breast disease, two local recurrences, cervical lymphadenopathy and lung metastases at 3, 10 and 30 months follow-up.
Conclusions: Despite a careful and extensive pathologic examination, in some cases of occult breast Ca, a primary tumor remains undetected. The examination of lymph node metastasis is sufficient and reliable to confirm the tumor origin, to suspect the biologic potential of the disease and to plan the most appropriate patient management.

P152

Analysis of known and novel TP53 gene mutations in breast cancer patients from the region of Epirus, Greece
Chr. Zachariou, V.D. Malamou-Mitsi and N.J. Agnantis
Department of Pathology, Molecular Pathology Unit,
University of Ioannina, Ioannina, Greece

Alterations of p53 gene are probably the most common genetic abnormalities in human malignancies. In breast cancer, the majority of mutations is located in the conserved DNA-binding domain of p53 (exons 5-8) and has been reported to be associated with more aggressive disease and worse overall survival. As direct sequencing of the entire gene is a time-consuming and laborious procedure, several pre-screening methods have been developed. Among them, Denaturing Gradient Gel Electrophoresis (DGGE) appears to be more sensitive, nearly 100%. We used a PCR and GC-clamped DGGE assay, followed by sequencing, to investigate the presence of point mutations within exons 5-8 of p53 gene, in DNA samples from 60 breast cancer patients, from the region of Epirus, Greece. Out of the 60 cases analyzed, 12 (20%) seemed to be carriers of a p53 alteration [7 in exon 6, 2 in exon 7, 2 in exon 8 and 1 in exon 5]. Samples that produced a variant DGGE-pattern were sequenced and carefully examined. In all but one (inadequate sample) cases, sequence alterations were identified by sequencing. Base changes were searched for and validated in the IARC TP53 Mutation Database. Of these, two point mutations [g.13418T>A (p.Y220N) and g.13270delG] and one silent polymorphism [g.13399A>G (p.R213R)] have not been previously reported in breast cancer. Our data indicate that PCR-DGGE assay is an efficient and highly sensitive prescreening approach for p53 mutation detection in DNA samples of breast cancer patients.

P153

Trophoblast expression of EGFR in preeclampsia - a tissue micro-array study
Staribratova D*, Bruder Elizabeth**
*Department of Pathology, Plovdiv Medical University, Bulgaria,
**Institute of Pathology, Kantonspital Basel, Switzerland

Placental pathology in preeclampsia and in pregnancies with intrauterine growth retardation are associated with changes of EGFR expression of the villous trophoblast. The present study is aiming at establishing the EGFR expression of the trophoblast in preeclampsia and intrauterine growth retardation in comparison with normal pregnancies. Tissue micro-array study including 30 placentas from preeclamptic cases, 30 - with intrauterine growth retarded fetuses и 30 normal control placentas are semi-quantitatively examined for EGFR expression of the trophoblast. Positive immuno-expression of EGFR is established in the cytoplasm on the membranes of syncitiotrophoblast, as well as in cytotrophoblast. Comparing the immunopositivity of EGFR in the trophoblast from normal pregnancies, the groups with preeclampsia and retarded fetuses exhibit statistically significant lower expression of EGFR ($P < 0.05$). There is no correlation between the expression of the growth factor and clinical data such as fetal weight and Apgar score ($P >$

0.01). The established lower expression of EGFR in the trophoblast from pregnancies complicated with preeclampsia and intrauterine growth retardation can be discussed in the context of the pathologic 'switch' in normal placental development.

P154

Structural Patterns of the placenta remodelling in cases of IUGR

Olga S. Reshetnikova, Olga V. Kononenko, Inna M. Goryanikova, Sergiy A. Morozov
Department of Pathologic Anatomy, Lugansk State Medical University, 1, kv 50-let Oborony Luganska, 91045, Lugansk, Ukraine, State Medical University of Lugansk, Ukraine

Placental insufficiency is an important factor of the fetal intrauterine growth restriction (IUGR). To confirm the relation between placental morphology changes and fetal IUGR 20 placentas from the late medical abortions because of psychotherapeutic reasons in cases of IUGR at 20-25 weeks of gestation (wg) were compared with 20 placentas at the same wg but without fetal IUGR. All material was divided into four groups, including 10 placentas at 20-22wg and 10 - at 23-25wg both in cases of IUGR, which were studied with corresponding 10 (20-22wg) and 10 (23-25wg) controls. Volume fractions (vf) of the major placental components were determined from 5mmk paraffin sections. The results have shown that both placental and fetal weights in IUGR groups were smaller than in controls. The poor vascularisation and immaturity of the villous tree were found in many cases of IUGR. The thickness of placental membrane increased from 10.74±0.09 at 20-22wg and 10.92±0.09 at 23-25wg in controls to 11.62±0.1 and 11.87±0.12mmk, $p<0.05$ correspondingly. The tendency of the decrease of fetal vessels vf and increase of the interstitium vf in cases of IUGR at 20-22wg has reached the significant level at 23-25 wg: correspondingly - 9.38± 1.31 and 58.56±1.98 vs 14.38±2.48 and 52.07±2.75%, $p<0.05$ in controls. Conclusions: the histopahological changes in placentas and the increased thickness of placental membrane might represent an important factor in the pathogenesis.

P155

Ultrastructural peculiarities of the villouse membrane under hypoxia conditions

Olga S. Reshetnikova, Ganna E. Mylovydova, Inna M. Goryanikova, Sergiy A. Morozov.
Department of Pathologic Anatomy, Lugansk State Medical University, 1, kv 50-let Oborony Luganska, 91045, Lugansk, Ukraine, Laboratory of Pathomorphology, Institute of General and Urgent Surgery of Academy of Medical Sciences of Ukraine, 1,vyizd Balakireva, Kharkiv, 61018, Ukraine

The electron microscopic investigation of placenta under hypoxia condition caused by maternal iron-deficiency anaemia and EPH-gestosis was carried. Electronograms from 30 placentas, including 10 cases of EPH-gestosis, 10-maternal anaemia and 10-uncomplicated pregnancy (controls) were studied stereometrically by point count method at magnification X 5600. Pathological ultrastructure's alterations of a placental barrier, including a damage of microvilli, thickening of basal membranes both of epithelium and endothelium, a stromal fibrosis were found. Compensatory proliferations of cytotrophoblast in cases of EPH-gestosis and in anaemia group; as well as hyperaemia of foetal vessels in EPH-gestosis group were seen too. The increase of the syncytiotrophoblast volume fraction (VF) in anaemia group (35,71±0,66 vs. 32,19± 0,26 % in controls), as well as cytotrophoblast, epithelium and endothelium basal membranes VF's both in anaemia (A) and gestosis(G) groups had registered (correspondingly: A- 2,76± 0,04; 3,52±0,02; 0,57±0,06; G- 1,05± 0,03; 4,76±0,03; 0,74±0,04 vs. 0,76±0,04; 3,04±0,01; 0,38±0,12% in controls, $P<0,05$). The capillary lumen increased to 14,70±0,26% in gestosis group (13,5±0,21% VF in controls, $P<0,05$).Pathological changes of a placental barrier could be a structural basis of a placental insufficiency. It was suggested that the process of ultrastructural remodelling of the placental membrane may compensate for different pathologies at the terminal parts of the villous chorion, which is essential base of the morphological correction of a placental insufficiency.

P156

Exaggerated placental site lesion of the cervix

Simona Stolnicu[1], Francisco Nogales[2],
Irina Timar[1], Lucian Puscasiu[3]
[1]Department of Pathology, University of Medicine, Targu Mures, Romania, [2]University of Granada Medical School, Spain,
[3]Department of Obstetrics and Gynaecology 1,
University of Medicine, Targu Mures, Romania

Exaggerated placental site is a nonmolar miscellaneous trophoblastic lesion included by World Health Organization in the classification of the gestational trophoblastic disease. Its location is exceptional in the cervix.We report the case of a 55 year old non-menopausal patient admitted for vaginal bleeding and irregular menses for two months. Menarche occurred at 14, she was gesta 6, para 4, aborta 2 and the last normal pregnancy occurred 15 years ago. She did not receive any hormonal therapy in the last two months. Because of massive methrorrhagia, an emergency simple total hysterectomy was performed. Macroscopy revealed a 20 mm red, ill-defined plaque lesion in the ectocervix, extended to the outer cervical stroma. Microscopically, the superficial cervical stroma at the squamocolumnar junction was infiltrated by cords and small sheets of intermediate (extravillous) mono/and multinucleated trophoblastic cells. These cells were large, polygonal or spindle shaped, had abundant eosinophilic cytoplasm and atypical, hyperchromatic nuclei and were located mainly perivascular- or intravascularly. Mitotic activity was absent. Immunohistochemically, they were invariably positive for Cytokeratin 18, CD10, hPL, but were only focally positive for hCG and Placental Alkaline Phosphatase. Ki-67 and Inhibin were negative. There was a massive hemorrhagic infiltration of the stroma, but no necrosis. The neighbouring endocervical glands showed a focal Arias-Stella phenomenon. No chorionic villi were found. In the corpus uteri, endometrial glands of the spongiosa layer were voluminous with epithelial and intraluminal secretion and were associated with dense decidualized compacta, stromal oedema and a well-developed spiral arterial system. Exaggerated placental site nodules must be differentiated from placental site trophoblastic tumor, and other trophoblastic lesions, invasive nonkeratinizing high grade squamous carcinoma, cervical blue nevi, atypical mesenchymal cells of the type associated with vaginal polyps and other mesenchymal lesions. This is a normal physiological process that can occur many years after a normal pregnancy and that does not require any specific treatment. Serum β-hCG analysis 2 month after the surgery was negative. This case is particularly relevant because of the age of the patient (who still had at 55 years old regular menses) and the most unusual cervical localization of the lesion.

P157

Vaginal non-DES related clear cell adenocarcinoma in a 77 years-old woman. Cytological and histopathological findings.

Makri S., Athanasiou E., Papanikolaou A.,
Hadzibougias J., Konstandoulas M.
Department of Midwifery, School of Health and Medical Care, Technological Educational Institution of Thessaloniki.

A 77-old woman visited a physician for vaginal bleeding. Vaginal examination showed a small-sized bleeding tumor protruding from the vaginal wall. Vaginal smear sampling revealed malignant

cells resemble those of an adenocarcinoma with ball and glandular like growth patterns. Then, followed excision of the tumor and the histological diagnosis was clear cell adenocarcinoma of the vagina. Grossly, the tumor was mostly exophytic, approximately 1cm in size and superficially invasive. Microscopically, the tumor was composed of microcysts, solid areas and papillary formations. The predominant cell type was honail-shaped cells and scattered cells with Müllerian differentiation and moderate nuclear atypia. There was no data of prenatal exposure to DES or related nonsteroid estrogens. The age distribution of all patients with CCAC showed two distinct peaks: at mean age of 23 and 71 years respectively including cases in which DES exposure had been excluded. The bimodal age distribution suggests a carcinogenesis-promoting role of menarche and menopause and/or the existence of a subpopulation with genetic risk factors or exogenous risk factors other than exposure to DES. Despite that cytologic examinations are informative in 65% of CCAC, in our case was diagnostic.

P158

EGFR (HER-1), c-erbB2 and c-Kit expression of uterine sarcomas.

Kiziridou A., Dimitriadis I., Fotiou Ch., Kartsiounis Ch., Toliou T.
Pathology Department, "Theagenion" Anticancer Hospital, Thessaloniki, Greece.

Objective: Uterine sarcomas are rare tumors characterized by their resistance to traditional treatment. The tyrosine kinase receptors family has been recognized of particular importance in many human malignancies. The role of c-kit oncoprotein in gastrointestinal tumors is also encouraging the use of these data in other tumors.
Methods: Formalin-fixed, paraffin embedded archival tissues from 8 carcinosarcomas and 5 endometrial stromal sarcomas from 13 patients surgically resected or biopsy specimens were examined immunohistochemically using EGFR(HER-1), c-erb-B2(HER-2) and c-kit(CD117).
Results: EGFR(HER-1) was positive in 3 of the 5 (60%) endometrial stromal sarcomas, but only in stromal elements of 2/8(25%) carcinosarcomas. HER-2 was negative in all mesenchymal elements of the tumors. C-kit(CD117) immunoexpression was positively expressed in 4/5(80%) of stromal sarcomas and in 3/8(37,5%) of carcinosarcomas.
Conclusion: Our findings suggest the possible role of new therapeutic approachment using monoclonal antibodies in uterine sarcomas treatment. Further studies with greater number of cases and clinical studies are needed to investigate this prospect.

P159

Tubular dysgerminoma of the ovary – a case report.

Jolanta Kupryjańczyk
Department of Molecular Pathology, Institute of Oncology and Department of Pathology, Brσdnowski Hospital and II-nd Faculty of Medicine, Medical University,Warsaw, Poland.

A 27 y.o. female was diagnosed in 1988 with ovarian tumor. She underwent left salpingo-oophorectomy and a hysterectomy. A primary diagnosis of juvenile granulosa cell tumor was changed to androblastoma. Because of the diagnosis and FIGO IA disease the patient was left for observation. One year later the patient appeared with massive and disseminated recurrence and she died 15 months after the primary surgery. The ovarian tumor measured 27 cm in the largest diameter; it was solid and cystic, with haemorrhagic necrosis. Microscopically, it presented with sharply demarcated islands and nests of cells, similar to those observed in insular carcinoids. Peripheral palisading was seen. Uni- and multilayered cysts were a marked component of the tumor. There were also tubules of varying sizes, either hollow ones lined by a single layer of cells or solid. Lymphocytic infiltrate was sparse. Cytologically, the majority of cells - either infiltrating singly or in nests or forming cysts and tubules were compatible with cells in dysgerminoma. The germ cell nature of the cells was confirmed by diffuse positive nuclear staining for OCT4 antibody. This is the first report of tubular dygerminoma of the ovary (consultation by Dr Robert E.Scully is gratefully acknowledged).

P160

Benign Brenner tumor of the ovary with unusual large size. A case report with immunohistochemical analysis.

F. Karasavvidou, G. Kalodimos, D. Pappa, E. Tziastoudi, Ch. Galani, E. Kostopoulou, G. Koukoulis.
Department of Pathology, University Hospital, Larissa, Greece.

We report a case of benign Brenner tumor of the left ovary that occurred in a 59-year-old woman. The patient presented with uterine bleeding. Clinically an abdominal mass was palpable. A CT scan displayed a left solid adnexal mass. Surgical excision of the mass and total hysterectomy was performed. Grossly, the tumor was 18 cm in maximal dimension with lobulated outline and solid, firm, gray-white, fibromatous cut surface. Microscopically, the tumor was characterized by sharply demarcated nests of epithelial cells within an abundant fibrous stroma. Immunohistochemical examination showed: the epithelial nests were positive for the cytokeratin 7 and p63 and negative for cytokeratin 20 and thrombomoduline. The stromal cells were positive for progesterone and negative for estrogen receptors. On the basis of the histological findings the diagnoses of benign Brenner tumor was made. This represents a case of unusually large Brenner tumor, which can be considered one of the largest ever documented in the literature.

P161

***CHFR* gene analysis in ovarian carcinomas.**

Agnieszka H. Ludwig[1], Mateusz Bujko[2], Jolanta Kupryjanczyk[1]
[1]Department of Molecular Pathology, [2]Department of Molecular Biology, The Maria Sklodowska-Cuire Memorial Cancer Center, Insitute of Oncology, ul. Roentgena 5, Warsaw 02-781, Poland.

CHFR is a mitotic checkpoint protein that under mitotic stress (caused also by taxanes) delays progression into mitosis. The cells with defective CHFR gene would be more vulnerable to taxane treatment. We looked for CHFR gene (605209) alterations and its promoter hypermethylation in 48 ovarian carcinomas either sensitive or resistant to taxane treatment. We used single-strand conformation polymorphism analysis, sequencing and methylation specific polymerase chain reaction. Neither mutations in the CHFR gene nor hypermethylation of its promoter region were found. A novel single nucleotide polymorphism (Val154Val) was identified in exon 5 of alternatively spliced transcript. Our results indicate that CHFR gene status cannot serve as a molecular predictor of ovarian cancer sensitivity to taxanes. (supported by the KBN grant 601/PO5/2004/27).

P162

Predictive factors in ovarian carcinomas from patients treated with taxanes

J. Kupryjanczyk[1,5], I. Ziolkowska-Seta[2], T. Szymanska[1], R. Mądry[4], A. Timorek[6], E. Kraszewska[3], A. Rembiszewska[1], J. Markowska[4], J. Stelmachow[6], M. Bidzinski[2]
[1]Dpt Mol Pathol, [2]Dpt Gynecol Oncol, [3]Dpt Biostatistics, Inst Oncol, Warsaw; [4]Chair Oncol,Med Uni, Poznań; [5]Dpt Pathol, [6]Dpt Gynecol Oncol, Brσdnowski Hospt, II-nd Faculty of Med, Med Uni, Warsaw; Poland

We aimed to evaluate clinical significance of TP53, BCL-2 and BAX expression in ovarian cancer patients uniformly treated with taxanes and platinum compounds. Immunohistochemical analysis was performed on archival samples from 196 ovarian carcinomas FIGO stage IIB-IV; the results were analyzed by the Cox and logistic regression models. Statistical analyses were performed in the whole tumor group, and separately in the TP53-negative and T53-positive group. Similarly to the results previously obtained for patients treated with platinum-based regimens (Br J Cancer 2003), complete remission was negatively influenced by high BAX expression in all patients group (OR 0.5; p=0.05; 95% CI for OR [0.25, 1.02]) and by BCL2 expression in the TP53(-) group only (OR 0.27;p=0.05; 95% CI for OR [0.07, 1.04]). Our results confirm that binomial TP53 status divides ovarian carcinomas into two biologically distinct groups. BCL-2 and BAX expressions have predictive value in ovarian cancer patients treated with taxanes and platinum-compounds (supported by the KBN grant 601/PO5/2004/27).

P163

RCAS1 expression in endometrial cancer: correlation with clinicopathological variables

Zannis Voulgaris[1], Stamatios Theocharis[2], Alexandros Rodolakis[1], Sonia Markaki[3], Theocharis Papageorgiou[1], Georgios Vlachos[1], Emmanuel Diakomanolis[1], Aristidis Antsaklis[1].
First Department of Obstetrics and Gynecology[1], Department of Forensic Medicine and Toxicology[2], University of Athens; Department of Pathology[3], Alexandra Hospital, Athens, Greece

The tumor associated antigen “receptor-binding cancer antigen expressed on SiSo cells” (RCAS1) inhibits the growth of receptor expressing cells and induces apoptosis. RCAS1 protein expression was examined immunohistochemically in paraffin embedded tissue sections of 48 endometrial cancer cases and was correlated with clinico-pathological parameters. RCAS1 positivity, overexpression (positivity in more than 50% of tumor cells), and intensity of staining (mild, moderate, intense) were correlated with the clinicopathological variables: patients’ age, FIGO stage, tumor histological type, grade, and proliferative capacity (Ki-67 labeling index). RCAS1 protein positivity was noted in all of the examined cases, while it was overexpressed in 33 out of 48 cases (71%). RCAS1 protein overexpression was statistically significantly correlated with tumor histological grade (p=0,003) and FIGO stage (p=0,022), but not with patients’ age, tumor histological type and proliferative capacity. The intensity of staining for RCAS1 protein was not correlated with any of the examined clinico-pathological variables. RCAS1 protein is widely expressed in endo-metrial cancer cases and its overexpression is correlated with important clinicopathological variables for patients’ management. Further mole-cular and clinical studies are required in order to delineate the significance of RCAS1 protein participation in endometrial neoplasia.

P164

pKDR expression in endometrial cancer cells related to HIF1a/VEGF factors.

A. Giatromanolaki[1], Ch. Charalampidis[1], M.I. Koukourakis[2], E.Sivridis[1].
[1]Department of Pathology, [2]Department of Radiotherapy / Oncology, Democritus University of Thrace Medical School, Alexandroupolis - Greece

Vascular endothelial growth factor (VEGF) is a potent angiogenic factor for many malignant neoplasms exerting its function through activation of specific membrane receptors, i.e. KDR/flk-1, residing in endothelial cells. Using a novel monoclonal antibody, recognizing the activated (phosphorylated) form of the KDR receptor (pKDR), we assessed the expression of pKDR in normal and malignant endometrium. A strong and consistent cytoplasmic and nuclear pKDR expression was noted in the normally cycling endometrium, including epithelial, stromal and endothelial cells, suggesting a role in the normal menstrual cycle. Approximately one third of the 70 endometrioid adenocarcinomas analyzed exhibited an intense cytoplasmic and nuclear pKDR expression in both cancer cells and peritumoral vessels. It was noted that such pKDR reactivity in cancer cells was related directly to VEGF, VEGF/KDR complexes and HIF1a (hypoxia inducible factor 1a) expression. Furthermore, pKDR expression was significantly associated with poor prognosis. It is concluded that the VEGF/KDR pathway is activated in both normally cycling and malignant endometrium, suggestive of an important role in the biology of this tissue.

P165

Loss of FOXP1 is a common event in early endometrial cancer: relationship with estrogen receptors and HIF1α expression.

A. Giatromanolaki[1], Ch. Charalampidis[1], M.I. Koukourakis[2], E. Sivridis[1].
[1]Department of Pathology, [2]Department of Rathiotherapy / Oncology, Democritus Univercity of Thrace Medical School, Alexandroupolis - Greece

The FOXP1 gene has an important role in cellular transformation, differentiation and proliferation. We studied the expression of FOXP1 in normal and malignant endometrial phases. Normal endometrial cycle showed a predominantly nuclear FOXP1 expression during the proliferate phase, and during the secretory phase of the cycle. Loss of nuclear expression was the most striking event in endometrial adenocarcinomas. Tumors with an exclusively weak cytoplasmic expression of FOXP1 were linked with deep myometrial invasion and hypoxia - inducible factors 1a (HIF-1a) expression. On the other hand, the presence of nuclear FOXP1 expression was significantly linked with ER-α reactivity. Survival analysis did not reveal significant differences among patients grouped by FOXP1 expression, presumably due to the high curability of stage I disease. This study provides evidence on pathways to be investigated to elucidate the interplay between FOXP1, ER-a and HIF-1a in hormone dependent cancers.

P166

Rare primary neoplasms of the female pelvic cavity: report of two cases of transitional cell carcinoma

Kamina S., Zioga C., Batistatou A., Doukas M., Balasi E., Tzioras S., Agnantis N.J.
Department of Pathology, University of Ioannina Medical School, Ioannina, Greece

Transitional cell carcinoma is rare in the female genital tract. Extremely rare is also the primary peritoneal transitional cell carcinoma. Herein, we describe the clinical, histopathologic and immunohistochemical features of two such cases of transitional cell carcinoma. The first case refers to a 53-year-old woman with transitional cell carcinoma of the endometrial cavity, invading more than half of the myometrium. The second case refers to a 75-year-old woman with multiple tumor nodules in the peritoneal cavity. Microscopically, they had the appearance of transitional cell carcinoma, grade 2. Neoplastic cells were noted invading the surface and the cortical stroma of the right ovary, which contained a large mature cystic teratoma. In both cases upon immunohistochemical examination, the neoplastic cells were Ca125 and cytokeratin 7

positive, cytokeratin 13 and 20 negative. In addition, in both women cysteoscopy revealed no abnormalities. Based on the morphologic and immunohistochemical features the diagnosis of primary transitional cell carcinoma of the endometrium and the peritoneal cavity, respectively, was made. Transitional cell carcinoma is a rare, distinct subtype of gynaecological malignancy, which has morphologic features of urothelial differentiation, but retains a müllerian immunoprofile.

P167

Prognostic value of cell proliferation, growth and differentiation regulatory proteins in early stage cervical carcinoma

Neli Basheska, Genghis Yashar, Katerina Kubelka-Sabit, Irina Prodanova
Department of Histopathology and Clinical Cytology, Institute of Radiotherapy and Oncology, Medical Faculty, Skopje, Republic of Macedonia

Objectives: The aim of this study was to evaluate the immunohistochemical histochemical expression of cell proliferation, growth, and differentiation regulatory proteins in early stage cervical carcinoma and to assess their prognostic value by exploring their relationships to various clinicopathological characteristics (age, lymph node involvement, tumor diameter, depth of invasion, thickness of uninvolved cervical stroma, histotype, grade, lymphvascular space invasion, inflammatory infiltrate), human papillomavirus (HPV) status and influence on disease-free survival.
Methods: This retrospective study comprised 83 patients, all subjected to radical hysterectomy with bilateral pelvic lymphadenectomy for early stage cervical carcinoma and postoperative irradiation therapy. Expression of Ki-67, c-erbB-2, EGFR protein, as well as estrogen and progesterone receptors was evaluated by immunohistochemistry using avidinbiotin-peroxidase complex method. The results were assessed semiquantitatively in the surface area, center and invasive front of each tumor as the percentage of the immunostained cells and/or intensity of immunostaining for each protein. The presence of HPV was assessed by conventional in situ hybridization (ISH) technique and catalyzed reporter deposition signal amplification ISH using mixed biotinylated probes to identify types 6/11, 16/18 and 31/33 or 31/33/51. RESULTS: In our case series, 73 (88%) patients had a tumor limited to the uterine cervix less than 4 cm in diameter (pT1b1), while 10 (12%) patients had larger neoplasms belonging to pT1b2 category. Pelvic lymph node involvement was found in 20 (24%) patients. During the follow-up period (range, 65-181, mean, 121 months) recurrences were observed in 9 patients. The 5-, 10- and 15-year disease-free survival rate was 92.7%, 90.8% and 86.6%, respectively. Important predictive indicators of recurrence in the univariate analysis were pelvic lymph node involvement (P=0.0008), tumor diameter (P=0.035), depth of stromal invasion (P=0.029), histological type (P=0.0009), grade of differentiation (P=0.056), HPV DNA presence (P=0.056), HPV type (P=0.043), as well as Ki-67 (P=0.031), and EGFR protein (P=0.0066) expression in the tumor's invasive front. Among these variables, however, the histological type, HPV DNA presence, Ki-67 and EGFR protein expression were identified as independent significant prognostic factors for disease-free survival in multivariate analysis using Cox regression model.
Conclusions: The invasive front of carcinomas proved to be the most important area for the evaluation of prognostic significance of the expression of cell proliferation, growth, and differentiation regulatory proteins. In addition to the detection of HPV presence and morphological parameters, the evaluation of Ki-67 and EGFR protein expression may provide additional prognostic information in patients with early stage cervical carcinomas.

P168

CD57 is a reliable marker for monitoring natural killer cells in pregnancy. A morphologic and immunohistochemical study in endometrial and decidual paraffin embedded tissues of 88 women with recurrent miscarriage: Correlation with immunotheraphy results

Athanasiou E., Danihel L.[1], Bobos M.[2], Papanikolaou A.[3], Hatzibugias D[2], Hainoglou D., Kiriazaki A., Hatzibugias I.
Department of Midwifery, School of Health and Medical Care, Technological Educational Institution of Thessaloniki
[1]Department of Pathology, Komenius University of Bratislava, [2]Department of Pathology, Aristotle University of Thessaloniki, [3]Department of Pathology, Hippokratio General Hospital of Thessaloniki

The role of NK cells in early pregnancy is still unknown and controversial. At the time of implantation the endometrium is populated by lymphocytes expressing antigens characteristic of Large Granular Lymphocytes which correspond to a minor population of NK cells and is due to contact with fetal antigens. In anembyonic and recurrent spontaneous abortions NK cytotoxicity was increased. Women with recurrent miscarriage represent a heterogeneous group and no single pathology can underlie all cases.The aim of our study was to investigate the presence, distribution and immunohistochemical profile of lymphocytic population and NK cells in endometrium and deciduas of 88 women with recurrent abortions. Furthermore we try to correlate the presence of NK cells with the immunotherapy results.
Material and methods: Endometrial and decidual paraffin embedded tissues were collected from 88 women with recurrent miscarriage (number of miscarriages n=1-4) in first trimester and of 10 women with elective termination of first-trimester pregnancy. The monoclonal antibodies CD19, CD20, CD45RO, CD4, CD8, CD57and CD16 were performed by an immunohistochemical method in order to investigate the immunological lymphocytic profile of endometium and deciduas. The immunotherapy included prezolone, aspirin, flaxyparin, anti-lympocytic serum and vaccinate from the futher(male) serum.
Results: The predominal lymphocytic population expressed in all cases of recurrent abortions was CD56+, CD16-cells. The number of these cells was slightly increased in recurrent abortions than in cases of elective termination of first-trimester pregnancy. CD56+ cells infiltrated the deciduas and the endometrium and invaded the endometrial glands. More lymphocytes were CD4+ than CD8+ and few cells expressed B-cell antigens (CD19, CD20). A subpopulation expressed CD57 positivity (26/88) and infiltrated the endometrium and invaded the endometrial glands, such as CD56+ cells done Fourteen women tried a new pregnancy, 6 were positive for CD57 cells and 5 of theme received immunotherapy resulting in live birth except one woman who aborted again. One woman did not received immunotherapy and aborted too. The rest 8 women did not expressed CD57 cells and gained live birth in all cases without any treatment.
Conclusions: NK lymphocytes that express CD56 and especially CD57antigen seem to play a crucial role in pathogenesis of recurrent miscarriage as they are not found in increased numbers in normal pregnancies. Women with recurrent miscarriage who expressed CD56 and CD57 in deciduas and endometrium seemed to benefit by immunotherapy and lead in successful pregnancies. This evidence indicate that CD57 revealed a subpopulation of NK cells responsible for a subset of miscarriages and could be a specific marker for this group. Farther studies including larger number of cases and more markers needed to investigate the pathogenesis of recurrent miscarriages and find new therapeutics goals.

P169

Pallister-Killian syndrome: A chromosomal abnormality with great variability of the fetal phenotype

P.Ctena-Agapitou, E.Agapitos, P.Dimou, C.Tsarpalis, E.Patsouris
Department of Pathology, Medical School, University of Athens

The first prenatal diagnosis of Pallister-Killian syndrome (PKS) was reported by Gilgenkrantz et al in 1985. This report was referring to about 60 prenatal cases, but both sonographic and cytogenetic diagnosis were difficult. Although ultrasound anomalies such as congenital diaphragmatic hernia, polyhydramnios and rhizomelic micromelia in association with fetal overgrowth are very suggestive of the syndrome, they are inconstant and they may even be absent. The mosaic distribution of the supernumerary isochromosome 12p greatly increases these difficulties. No prenatal cytogenetic technique is sensitive enough to ensure prenatal diagnosis and false-negative results have been described on fetal blood, chorionic villi and amniocentesis. In this study we report a prenatal case of PKS which illustrates great variability of the fetal phenotype. A pregnant woman of 25 years old was referred to our hospital at the 22 week of gestation with the symptoms of polyhydramnios and suspected rhizomelic micromelia in routine ultrasound examination. Fetal chromosome analysis was performed using fibroblasts obtained by amniocentesis and mosaicism of 47XY and isochromosome of 12p were diagnosed . The mother vaginally delivered a male fetus who died just after the delivery. Autopsy findings included rhizomelic micromelia, narrow and angulated palate and skin fibroblastic polyp at the left small finger of 0.5 cm in diameter. Micrognathia, flattened nose and low-set ears were also noted. Pallister-Killian syndrome is a clinically recognized syndrome, usually due to a tissue-limited mosaicism for a supernumerary 12p isochromosome (i12p). Premeiotic mitotic error may be the most likely mechanism for i(12p) formation which is maternally inherited. A quite wide spectrum of associated congenital malformations including diaphragmatic hernia, rhizomelic micromelia, mental retardation, cleft palate, pigmentary skin changes and physiognomy alterations have been reported in Pallister-Killian syndrome. Since diaphragmatic hernia and acral hypoplasia can be also found in Fryns syndrome, the differential diagnosis between the two conditions depends on the demonstration of the 12p isochromosome by FISH. Our case did not appear diaphragmatic hernia which is the most common skeletal malformation. Instead of cleft palate, our patient had narrow and angulated palate with minor facial signs and there was an additional minor feature: a skin fibroblastic polyp of the left small finger. Primary cultures of skin fibroblasts obtained by amniocentesis revealed an extra metacentric chromosome i(12p). In reviewing the 63 reported cases of PKS, Doray et al attempt to determine ultrasound indicators of the syndrome and to define a cytogenetic strategy. In cases where ultrasound indicators are present, they proposed first to perform chorionic villus of placental sampling and then amniocentesis when the first cytogenetic result is normal. Fetal blood sampling is the least indicated method because of the low frequency of the isochromosome in lymphocytes. In this cytogenetic strategy fluorescent in situ hybridization (FISH) and especially interphase FISH on non-cultured cells increases the propability of identifying the isochromosome. The analysis of cord blood lymphocytes revealed only 0.5% incidence of tetrasomy of 12p. The incidence of tetrasomy was 8.0% for the placental chorionic villi, 48.0% for the fibroblasts obtained from the umbilical cord and 70.0% for the skin fibroblasts. Thus the diagnosis of PKS is confirmed by mosaicism of i(12p) with the abnormal karyotype expression limited in lymphocytes but marked in skin fibroblasts.

P170

Immunohistochemical expression and prognostic signifficance of the biological markers bcl-2, p53, mdm-2 and Ki-67 in early stages of invasive cervical carcinomas

Irina Prodanova, Katerina Kubelka-Sabit,
Genghis Yashar, Neli Basheska
Department of Histopathology and Clinical Cytology,
Institute of Radiotherapy and Oncology, Medical Faculty, Skopje,
Republic of Macedonia

Objectives: The objectives of this study were the evaluation of the immunohistochemical expression of apoptosis regulating proteins (bcl-2, mdm-2 and p53 protein) in correlation with proliferation (Ki-67), human papillomavirus (HPV) infection and other histopathological and clinical parameters in early stage cervical carcinomas and estimation of their prognostic significance.
Methods: The subject of this study was a series of 83 surgically treated patients with cervical carcinoma confined to the uterine cervix, who subsequently received complete radiotherapy. The presence of HPV DNA in the neoplasm was determined by the conventional method of in situ hybridization (ISH) and catalyzed reporter deposition signal amplification ISH using mixed biotinylated probes to identify types 6/11, 16/18 and 31/33 or 31/33/51. The immunohistochemical expression of the biological markers was semiquantitatively evaluated as the percentage of immunostained cells in the three compartments of the neoplasm: the surface, the middle layer and the invasive front.
Results: 73 patients had a tumor confined to the uterine cervix less than 4 cm in diameter (pT1b1) and the other 10 had larger neoplasms that belong to the pT1b2 category. Regional lymph node involvement was found in 20 (24%) of the patients. During the clinical followup (mean, 120.7, range 4.4-181 months) a relapse was diagnosed in 9 (10.8%) patients, 6 of which (7.2%) died of the disease. The expected 5-, 10- and 15- year overall survival was 94.4%, 92.7% and 92.7%, and disease-free survival was 92.7%, 90.8% and 86.6%, respectively. The results of the univariate analysis indicate that significant predictive indicators for recurrence are: lymphonodal status, maximal tumor diameter, depth of stromal invasion, histological type, HPV DNA presence and type, and the immunohistochemical expression of bcl-2, mdm-2 and Ki-67 in the invasive front of the neoplasm. In the multivariate analysis, histological type, HPV DNA presence and the expression of Ki-67 in the invasive front have been selected as the most significant independent prognostic parameters (P=0.0024). The value of the prognostic index (PI), calculated using the Cox regression model, provided the basis on which the patients were classified into two distinct risk groups with significantly different disease-free survival period (P=0.0009).
Conclusions: The results indicate that the invasive front of the neoplasms proved to be the most important area for the evaluation of immunohistochemical expression of biological markers. The prognostic index as an indicator of the patient's place in the prognostic spectrum enables the identification of the risk group of patients in whom, due to a higher risk of relapse, better results are to be expected with the application of more aggressive therapy.

P171

Female genital actinomycosis: a review of 24 cases

Katerina Kubelka-Sabit, Irina Prodanova,
Genghis Yashar, Gjorgji Zografski, Neli Basheska
Department of Histopathology and Clinical Cytology,
Institute of Radiotherapy and Oncology, Medical Faculty, Skopje,
Republic of Macedonia

Objectives: The aim of this retrospective study was to present the clinical characteristics of the patients with female genital actinomycosis in correlation with the histopathological findings. Actinomycosis is a relatively rare chronic granulomatous inflammatory disease caused by the bacteria Actinomyces israelii, a normal comensal of the gastrointestinal and genital tract. The abdominal form of the disease is rare, however the incidence of the female genital and pelvic actinomycosis is rising, especially among the intrauterine device (IUD) users (8-20%).

Methods: According to the computer database at our department, 965 cases of endometritis, 6,313 cases of cervicitis and 584 cases of pelvic inflammatory disease (PID) were diagnosed in a 15 year period (1991-2005). However, only 21 (2.2%) cases of endometrial, 1 (0.02%) cervical actinomycosis and 2 (0.3%) cases of pelvic actinomycosis were identified in this period. Explorative curettage was performed in 21 patients due to prolonged uterine bleeding and extirpation of an IUD was done in 19 of them. One patient had a biopsy taken for a suspicion of cervical neoplasm, consecutively diagnosed as endometrial adenocarcoma. In the PID group, one patient with a previous history of tubal pregnancy underwent a transabdominal biopsy for a paravesical tumor, two weeks after extirpation of an IUD. The last patient had no IUD and was surgically treated with hysterectomy and bilateral adnexectomy for a suspicion of malignant ovarian tumor. The biopsy, curettage and operative materials were formalin fixed, routinely processed and paraffin embedded. 4_ thin sections were cut and slides were stained using standard hematoxyllin–eosin staining procedure.
Results: The mean age of the patients was 52.3 ranging from 41 to 68. Macroscopically visible sulfur granules were not identified in any of the cases of disease confined to the uterus. However microscopically, in all the 22 biopsy and curettage materials, elements of chronic granulomatous endometritis and/or cervicitis were seen, together with branching filaments of Actinomyces. In the paravesical tumor, abscesses filled with necrotic debris and scattered Actinomyces colonies were found. Macroscopically visible sulfur granules were identified only in the operative material, where a rough necrotic grayish-yellow area was seen on the serosal surface on the left side and posterior wall of the uterine corpus, measuring 4 × 3 cm. A left tubo-ovarian abscess measuring 4 × 3 × 3 cm was also found. On sectioning, several small and large abscesses filled with puss were present. The histological examination confirmed multiple actinomycotic abscesses in the ovary, paraovarian region and the external third of the left lateral uterine wall.
Conclusions: Female genital actinomycosis is a rare and obscure granulomatous disease. It is most prevalent in IUD carriers and easily diagnosed when confined to the uterus. However, the pelvic actinomycosis is often misdiagnosed, simulating malignant pelvic or ovarian tumor. Therefore, unnecessary surgical interventions can be avoided with a careful examination of these patients and a timely identification of the disease.

P172

Synchronous endometrioid carcinoma of the uterine corpus and ovary: A case report

Vasilakaki Th, Grammatoglou X, Glava C, Katsamagkou E, Zizi-Serbetzoglou A
Department of Pathology, Tzaneion General Hospital of Piraeus, Piraeus, Greece

Synchronous endometrioid carcinoma of the uterine corpus and ovary is an uncommon but well recognized event. Diagnosis as either separate independent primary or as metastatic tumors requires careful consideration of a number of gross and histological features. These features illustrate the criteria helpful in distinguishing independent primaries from metastatic carcinomas which have a different therapeutic implication. The possible link between fertility drugs and carcinogenesis still remains controversial. We report a case of a 52 year old woman who came to our hospital with cystic left ovarian mass (8cm). Hysterectomy and bilateral salpingo-oophorectomy were carried out. Histological examination showed well differentiated endometrioid endometrial cancer. Endometrial tumor was intra-mucosal without myometrial or vascular invasion and was associated with atypical complex hyperplasia. The woman had not been previously treated with ovulation induction drugs. She was free of recurrence 20 months after surgery. Patients with synchronous endometrioid tumors of the endometrium and ovary are generally younger than reported for either endometrial adenocarcinomas or ovarian epithelial adenocarcinomas. They tend to be low grade and early stage and are frequently associated with endometriosis. The prognosis of endometrioid type carcinomas is better than other histological types of carcinoma.

P173

Clinicopathological study of Bcl-2 immunohistochemical expression in endometrioid adenocarcinoma

Bobos M[1], Kalogiannidis I[2], Papanikolaou A[2], Makedos A[2], Makedos G[2], Nenopoulou E[1]
[1]Departments of Pathology, and [2]Obstetrics and Gynecology, Aristotle University Medical School, Thessaloniki, Greece

Objective: The Bcl-2, an anti-apoptotic protein, plays a central role in apoptosis, acting as an inhibitor of the apoptotic process. The aim of our study was to evaluate the expression of Bcl-2 in endometrioid adenocarcinoma and its clinocopathological significance.
Methods: 78 patients with endometrioid adenocarcinoma were included in the study. The median follow-up time was 43 months. Immunohistochemical analysis for Bcl-2 antigen was performed on formalin-fixed, paraffin embedded tissues of 74 patients.
Results: The median age of the women was 65 years. The cancer related survival was significant correlated with advanced FIGO stage (P=0.0025) and metastatic disease (P=0.0005). Disease free survival was closely associated with tumor diameter (P=0.04), risk factor (P=0.035) and tumor depth (P<0.013), while the most important correlations were associated with metastatic status (P=0.007), FIGO stage (P<0.001) and tumor differentiation (P<0.001). Bcl-2 immunoreactivity was detected in 24/74 (32%) cases of histologic grade 1 and 2, P=0.028. Lack of Bcl-2 expression was directly correlated with high risk patients (9/38), P=0.001.
Conclusions: Bcl-2 is an early event in endometrioid adenocarcinoma. The anti-apoptotic effect of the Bcl-2 is limited in advance stage carcinomas as well in high risk patients.

P174

P53 overexpression and prognostic impact in endometrial carcinoma of endometrioid subtype

Kalogiannidis I[1], Papanikolaou A[1], Bobos M[2], Nenopoulou E[2], Aplianitis I[3], Makedos G[1].
[1]Department of Obstetrics and Gynecology and [2]Pathology, Aristotle University Medical School, Thessaloniki, Greece, [3]Department of Pathology, Hippokration Hospital, Thessaloniki, Greece

Objective: Overexpression of p53 in endometrial carcinoma has been reported to correlate with the unfavourable clinicopathologic features and poor prognosis. The aim of the study was to investigate the p53 overexpression and its prognostic significance in patients with endometrial cancer.
Methods: Immunohistochemistry for p53 expression was performed on paraffin embedded material of 71 surgically treated patients with endometrial carcinoma of endometrioid histologic subtype. The evaluation of staining was performed using a relative rank scale from 0 to 2. The 2+ was considered as overexpression. The median follow-up time was 43 months.
Results: The median age of the women was 65 years (range 35-80). Thirty seven of the 71 cases (52%) stained positive for p53, while overexpression of p53 was detected in 20/71 cases (28%). p53 overexpression was significant correlated with unfavourable tumor differentiation (P=0.028) and positive nodal status (P=0.032), while with the overall survival and disease free survival was insignificant (P=NS).

Conclusion: According to our data p53 overexpression is more commonly found in low differentiated tumors and retroperitoneal disease.

P175

Uterine sarcomas and carcinosarcomas: Immunohistochemical study with docus on potential theraputic targents

Sotiropoulou M, Papaspyrou I, Theocharidou D,
Klapsinou I, Markoulis P, Sdrenia P, Markaki S.
Histopathology Department, Alexandra General Hospital,
Athens, Greece

Background: Carcinosarcomas and pure high grade sarcomas of the uterus are highly aggressive tumors and therapeutic tools are of limited value. The aim of this study was to determine the expession of proteins Her-1 (EGFR) and Her2/neu (cerbB-2), known to be targeted by therapeutic agents, in these neoplasms.
Material and methods: Parafin-embedded archival tissue from 16 carcinosarcomas, 21 leiomyosarcomas, 10 stromal sarcomas and 1 mixed heterologous sarcoma was used for immunohistochemical analysis. All hematoxylin-eosin stained sections were reviewed to confirm the pathologic diagnosis. Sections were stained with monoclonal antibodies against EGFR (clone 31G7, Zymed)and Her-2 (clone CB11, BioGenex). Unequivocal staining of at least 5% tumor cells was considered positive.
Results: EGFR stained in mesenchymal component of 12/16 (75%) and in epithelial component of 6/16 (37,5%) of carcinosarcomas and in 17/32 (53%) of pure sarcomas. Her-2 displayed strong positive membrane staining (+++) in the epithelial component of 2/16 of the carcinosarcomas while stromal component was negative (- or +) in each case. The 30/32 of pure sarcomas were negative in Her-2 (- or +) while 2 of them were, focally, mild positive (++).
Conclusions: Since optimal treatment of carcinosarcomas and high grade uterine sarcomas remains unknown, novel therapeutic approaches need to be investigated. The expression of EGFR in high percentage of pure uterine sarcomas could be used for target treatment. The different expression between epithelial and mesenchymal components in carcinosarcomas must be examined with caution since only one of the tumor's components expresses this marker. Her-2 is a poor thepareutic target for sarcomas and carcinosarcomas because only a small proportion of epithelial component expresses the protein.

P176

Vaginal non-DES related clear cell adenocarcinoma in a 77 years-old woman. Cytological and histopathological findings.

Makri S., Athanasiou E., Papanikolaou A.,
Hadzibougias J., Konstandoulas M.
Department of Midwifery, School of Health and Medical Care,
Technological Educational Institution of Thessaloniki.

A 77-old woman visited a physician for vaginal bleeding. Vaginal examination showed a small-sized bleeding tumor protruding from the vaginal wall. Vaginal smear sampling revealed malignant cells resemble those of an adenocarcinoma with ball and glandular like growth patterns. Then, followed excision of the tumor and the histological diagnosis was clear cell adenocarcinoma of the vagina. Grossly, the tumor was mostly exophytic, approximately 1cm in size and superficially invasive. Microscopically, the tumor was composed of microcysts, solid areas and papillary formations. The predominant cell type was honail-shaped cells and scattered cells with Müllerian differentiation and moderate nuclear atypia. There was no data of prenatal exposure to DES or related nonsteroid estrogens. The age distribution of all patients with CCAC showed two distinct peaks: at mean age of 23 and 71 years respectively including cases in which DES exposure had been excluded. The bimodal age distribution suggests a carcinogenesis-promoting role of menarche and menopause and/or the existence of a subpopulation with genetic risk factors or exogenous risk factors other than exposure to DES. Despite that cytologic examinations are informative in 65% of CCAC, in our case was diagnostic.

P176B

Histologic findings in 619 laparoscopically removed ovarian cysts

Vassiliki Tziortzioti, Leonidas Papadopoulos,
Dimitrios Mathiopoulos, George J. Vlahos, Dimitrios Mavrelos,
Dimitrios Tziortziotis LITO Maternity Hospital, Athens

The frequency of laparoscopic removal of ovarian cysts is continuously rising over the recent years. We have registered the histologic findings in 619 laparoscopically removed ovarian cysts over the three-year period 2003-2005. Patient age ranged from 15 to 71 years. The cysts measured from 2 to 22 cm in greatest diameter. Frozen section was performed when judged necessary by the clinician.
The vast majority (427/69%) were identified as endometriotic cysts. Moreover, we had a case (0.1%) of atypical endometriosis, a case (0.1%) of atypical proliferative endometrioid tumor developing in an endometriotic cyst, a case (0.1%) of endometrioid adenocarcinoma developing in an endometriotic cyst, and a case (0.1%) of clear cell adenocarcinoma developing in an endometriotic cyst.
The benign non neoplastic diseases observed were 17 (3%) parovarian cysts, 9 (1.5%) hemorrhagic corpus luteum cysts, 3 (0.5%) follicle cysts, and one (0.1%) massive ovarian edema.
The benign neoplasms observed were 65 (10.5%) benign cystic teratomas (dermoid cysts), 50 (8%) serous cystadenomas, and 17 (3%) mucinous cystadenomas.
The atypical proliferative and malignant tumors observed, besides those associated with endometriosis mentioned above, were 20 (3.2%) atypical proliferative serous tumors, 3 (0.5%) atypical proliferative mucinous tumors endocervical – like, one (0.1%) atypical proliferative mucinous tumor gastrointestinal type, one (0.1%) atypical proliferative serous tumor with microinvasion, and one (0.1%) atypical proliferative mucinous tumor endocervical – like with foci of non invasive micropapillary serous carcinoma.

P177

Papillary carcinoma of the thyroid associated with systemic sarcoidosis

Moroz EA, Rotin DL, Pavlovskaya AI, Ermilova VD
Department of the Human Pathology of NN Blokhin Cancer
Research Center, Kashirskoye Shosse 24, 115478 Moscow, Russia

Introduction: Sarcoidosis is a systemic chronic granulomatous disease of unknown etiology most commonly affecting young females. The disease was described by Beck in 1899. Thyroid involvement is extremely rare in systemic sarcoidosis and was originally described in 1938. Papillary carcinoma of the thyroid gland also occurs more frequently in female. We described a case of coincidence of both those diseases in male patient.
Objective: (Case report): A 53-year-old male presented with dyspnoea, weight loss and cough. Clinically, no data of tuberculosis and multiple lung metastases were obtained. Transbronchial biopsy of lung lesions was performed in order to exclude the possibility of unknown co-existent disease. FNA of the nodule in thyroid suspected papillary carcinoma.
Methods: The paraffin blocks obtained after the lung biopsy and thyroidectomy were routinely processed, sliced and stained with HE, PAS and van Gieson.

Results: Histologically in thyroid specimens were observed the sarcoid granulomas and papillary adenocarcinoma. Similar granulomas were also found in lung biopsy. The finding of granulomas in the thyroid and lung allowed us to interpret the clinical manifestations of our patient leading to the diagnosis of sarcoidosis.
Conclusions: The thyroid cancer co-incidence in systemic sarcoidosis is supposed to be secondary to immunological abnormalities associated with the latter disease.

P178B

Papillary thyroid carcinoma (PTC) in an 11-years old female child. Cytological and histopathological findings
Makri S., Athanasiou E., Hadzibougias J.
Department of Midwifery, School of Health and Medical Care, Technological Educational Institution of Thessaloniki.

We presented a rare case of PTC in an 11-years old female child who was diagnosed on FNAC. The child presented with a well-defined nodule, measuring about 2cm in diameter, in the right lobe. FNAC of the thyroid nodule revealed clusters of malignant cells and papillary fronds with scanty thick colloid in the background. The thyroid hormonal profile was within normal limits. The child was subjected to total thyroidectomy with regional lymphadenectomy. The diagnosis of PTC was confirmed on histological examination of right lobe nodule but scattered neoplasti foci were found in the left lobe too. Metastases were found in all regional lymph nodes. The child is on regular follow up with hormonal supplementation of thyroxine and no evidence of any comlication till date after 6 years of surgery. PTC is a very rare neoplasm in childhood but seems to have an excellent prognosis.

P179

Immunohistochemical investigation of angiogenic factorsin parathyroid proliferative lesions
Theodore Brousalis, Sofia Tseleni-Balafouta, Thomas G. Papathomas, Aphrodite Nonni, Georgia E. Thomopoulou, Andreas C. Lazaris, George Agrogiannis, Efstratios S. Patsouris
1st Department of Pathology, Medical School, National and Kapodistrian University of Athens, Mikras Asias 75, 11527 Athens, Greece

Endoglin (CD105) is a proliferation-associated and hypoxiainducible protein abundantly expressed in angiogenic endothelial cells. VEGF induces angiogenesis and VEGF-R2 is a tyrosine kinase receptor expressed early in development by endothelial cell precursors. The aim of the present study was to examine whether immunohistochemical expression of CD105, VEGF and VEGF-R2 may be useful in distinguishing between parathyroid hyperplasia and neoplasia as well as to elucidate, to some extent, the mechanism of neovascularization in proliferative lesions of the parathyroid gland. Tissue specimens were taken from 38 patients with primary hyperparathyroidism (HPT) (17 adenomas and 21 primary hyperplasias) and from 30 patients with secondary HPT. Ten parathyroid glands served as normal controls. In a standard immunohistochemical procedure, monoclonal antibodies to endoglin, VEGF and VEGF-R2 were applied to detect angiogenic endothelial cells. Immunostaining was estimated by image analysis and statistical analysis was subsequently performed. Positive CD105 immunoreaction was significantly increased in parathyroid adenomas by comparison with primary hyperplasias (p=0.033) and with secondary hyperplasias (p=0.033). When parathyroid adenomas, primary hyperplasia and secondary hyperplasia specimens were comparatively evaluated, VEGF immunoreaction was much more common in adenomas (p=0.018). In addition, no significant association emerged between VEGF expression and CD105 immunostaining. In samples with secondary hyperplasia, VEGF-R2 immunoreactivity was positively linked with VEGF expression (p=0.038). This study shows increased angiogenesis in parathyroid adenomas compared with parathyroid hyperplastic lesions. The positive correlation seen between VEGF expression and VEGF-R2 suggests that both may have an important influence on the course of secondary hyperplasias, while the lack of correlation between CD105 and VEGF expression suggests that VEGF, on its own, is not likely to be the primary proangiogenic factor in parathyroid tissue.

P180

Hyalinizing trabecular adenoma.
Gerasimidou D, Karayannopoulou G, Hytiroglou P, Gamvros O, Papadimitriou CS.
Department of Pathology, Aristotle University Medical School, Thessaloniki, Greece.

Hyalinizing trabecular adenoma (HTA) of the thyroid gland is an uncommon benign follicular neoplasm, which shares some of the histopathologic features of papillary carcinoma; therefore, the true nature of HTA has been a subject of controversy. We present two cases of HTA, which occurred in women of 23 and 51 years of age, respectively. Both tumors were composed of polygonal or cylindrical neoplastic cells, arranged in trabeculae, compact clusters and follicles. The cells contained oval or round nuclei, which in some areas exhibited intranuclear pseudoinclusions and grooves, as well as nuclear overlapping. Hyalinizing septa of fibroconnective tissue were present among the trabeculae. Both tumors contained calcifications, which in the first one had the appearance of psammoma bodies. Both tumors were surrounded by a fibrous capsule. No invasion of the capsule or vessels was observed. Immunohistochemical stains showed both tumors to be positive for thyroglobulin, and negative for calcitonin and chromogranin. Immunopositivity for cyto 19 was present in many cells of the first case, and only rare cells of the second case. Staining for Ki-67/mib-1 showed strong membranous positivity only in the second case. Our findings suggest that HTA may show heterogeneity in the expression of various immunohistochemical markers. Results from large series of cases will be necessary to appreciate the full spectrum of these tumors.

P181

Relative expression of EGFR and its auto-inhibitor p55 mRNAs in thyroid carcinomas.
E. Charalambous[1], G. Karayannopoulou[1], T. Koletsa[1], C. Mitsiades[3], N. Mitsiades[3], S. Tseleni-Balafouta[2], C.S. Papadimitriou[1], V. Kotoula[1]
[1]Dept. of Pathology, Aristotle University Medical School, Thessaloniki, and [2]Dept. of Pathology, University of Athens, Athens, Greece; [3]Dept. of Medical Oncology, Dana-Farber Cancer Institute, Harvard Medical School, Boston, MA, USA.

EGFR-p55, a truncated EGFR protein, is an endogenous EGFR inhibitor that is derived from an alternatively spliced EGFR mRNA (variant 3 [v3]). The aim of this study was to investigate the expression of EGFRv3 in carcinomas with established EGFR pathway activation. Relative quantification for non-spliced EGFR (EGFRns) and for EGFRv3 mRNA targets was applied in samples from 6 anaplastic (ATC) and 12 papillary (PTC) thyroid carcinomas, 12 matched non-cancerous tissues (MNCT), and 11 thyroid carcinoma cell lines (TCL) that were tested to be resistant to targeted EGFR inhibition. In comparison to MNCTs, the expression of EGFRns mRNA was not higher in TCLs, PTCs and ATCs. EGFRv3 transcripts were identified in 42/43 (97%) samples. Relative expression of EGFRv3 vs EGFRns was at least 1 log order higher in TCLs and carcinomas (p=.003),

especially in PTCs (p=.005), than in MNCTs. In conclusion, while EGFR is not overexpressed, production of its endogenous auto-inhibitor EGFRv3 seems to be upregulated in thyroid cancer in comparison to MNCTs.

P182

EGFR phosphorylation and downstream effector activation in thyroid carcinomas.

G. Karayannopoulou[1], T. Koletsa[1], I. Pliakos[1], C. Mitsiades[3], N. Mitsiades[3], S. Tseleni-Balafouta[2], C.S. Papadimitriou[1], V. Kotoula[1]
[1]Dept. of Pathology, Aristotle University Medical School, Thessaloniki, and [2]Dept. of Pathology, University of Athens, Athens, Greece; [3]Dept. of Medical Oncology, Dana-Farber Cancer Institute, Harvard Medical School, Boston, MA, USA.

The aim of this study was to investigate the expression and activation status of the EGFR pathway and its downstream effector pAKT/PKB-S473 in thyroid carcinomas in comparison to matched non-cancerous tissues (MNCTs). Immunohisto-chemistry for EGFR membranous localization, pEGFR-Y992, pEGFR-Y1068, pEGFR-Y1173, pAkt-S473 and pAsk1-S83 (pAkt dependent) was performed on 104 thyroid carcinomas and 92 MNCTs. EGFR scores 2+/3+, and positivity for pEGFR-Y992, pEGFR-Y1068 were similar in tumors and MNCTs. Strong positivity for pEGFR-Y1173, cytoplasmic pAkt and pAsk1 were significantly more frequent in tumors than in MNCTs (p=.001, p=.001 and p<.0001, respectively). However, none of these parameters correlated with tumor aggressiveness or clinical outcome. These data show that EGFR activation is present in MNCTs and carcinomas. Specific patterns of EGFR phosphorylation and differences in the activation of EGFR downstream effectors are encountered in carcinomas, which, however, are not associated with disease aggressiveness.

P183

Relationship between: thrombospondin-1, angiogenic factor (VEGF), microvessel density (CD31), tumor suppressor gene (p53), proliferation marker (Ki-67), and anti-apoptotic marker (bcl-2) in thyroid pathologies.

Antigony Mitselou[1], Dimitrios Peschos[1], Pavlos Dallas[1], Niki Agnantis[2], Theodore Vougiouklakis[1].
[1]Department of Forensic Pathology [2]Department of Pathology, Medical School, University of Ioannina, Greece .

Thrombospondin (TSP) is a multifunctional extracellular matrix protein that affects tumor growth, modulation and angiogenesis. TSP is expressed in various cell types under physiological and pathological states including wound healing, angiogenesis and neoplasia. Vascular endothelial growth factor (VEGF) is an angiogenic factor which paly crucial role in neovascularization and CD31 is a marker to determine the microvascular density of the tumors. The tumor suppressor gene p53 is involved in the regulation of angiogenesis and the antiapoptotic marker bcl-2 seems to provide the necessary signal to increase the state of VEGF.
Tissue specimens were obtained from the archives of the Department of Forensic Pathology, University Hospital of Ioannina. The cases consisted of 50 carcinomas, 30 adenomas and 40 hyperplastic disorders of thyroid gland. Immunohistochemistry was performed in paraffin-embedded formalin-fixed tissue, with streptavidin-biotin method, using antibodies against TPS-1, VEGF, CD31, p53, Ki-67, and bcl-2. Statistical analysis was performing using the SPSS for windows (version 6.0) statistical package.
Results: Normal thyroid tissues showed immunostaining for TSP-1 confined to the interfollicular stroma, and to the vasculature endothelium. A similar degree of reactivity was found in hyperplastic lesions and adenomas. TSP-1 was strongly expressed in papillary carcinomas with a desmoplastic stroma, but weak to moderate in cancer epithelium. VEGF was observed intensively in epithelial cells of the tumors, a statistically significant correlation between TSP-1 and VEGF (p=0.022) was found. No statistical significant correlation between TSP-1 expression and p53 protein and Ki-67 proliferating marker was found. Statistical inverse correlation between bcl-2 and TSP-1 (p=0.044) was found.
In conclusion, these results suggest that in papillary carcinomas, the expression of TSP-1 restricted to the stroma, might be act as protective effects against tumor progression. In addition, TSP-1 expression could be plays an important role in cancer cell growth.

P184

The expression of E-cadherin is preferentially reduced compared with that of syndecan-1 in thyroid pathologies.

Antigony Mitselou[1], Dimitrios Peschos[1], Elli Ioachim[2], Konstantinos Charalabopoulos[3], Theodore Vougiouklakis[1], Niki Agnantis[2]
Departments of [1]Forensic Pathology, [2]Pathology, [3]Clinical and Experimental Physiology, Medical School, University of Ioannina, Greece.

Cadherins and syndecans are transmembrane glycoproteins implicated in cell-cell and cell-matrix adhesion. Impairment of E-cadherin and syndecan-1 play an important role in the acquisition of invasive and metastatic propierties by neoplastic epithelial cells. The purpose of this study was to elucidate the role and alterations of syndecan-1 expression in comparison with those of E-cadherin in normal and pathological thyroid glands. A total of 55 carcinomas, 40 adenomas, 40 cases of hyperplastic disorders and 20 cases of normal thyroid gland tissue, retrieved from our archives. The staining, intensity and distribution of syndecan-1 and E-cadherin in sequential sections were examined and semiquantified. Immunostaining of syndecan-1 and E-cadherin was strong in normal follicular cells. No significant changes were observed in either molecule in hyperplastic disorders compared with adenomas. A significant reduction in expression of both proteins was seen in well-differentiated carcinomas as compared with normal epithelium (p=0.0001 and p=0.032, respectively). Similarly, there was significant reduction of syndecan-1 and E-cadherin in poorly differentiated and anaplastic carcinomas compared with the well-differentiated carcinomas (syndecan-1, p=0.0037; E-cadherin p=0.075). In conclusion, decreased syndecan-1 and E-cadherin expression with decreasing cellular differentiation may be involved in the complex mechanism of thyroid lesions.

P185

Cell cycle associated markers (cyclins A, B1, D1, E) expression in papillary carcinomas and microcarcinomas of the thyroid gland

Antigony Mitselou[1], Dimitrios Peschos[1], Pavlos Dallas[1], Theodore Vougiouklakis[1], Niki Agnantis[2].
Departments of [1]Forensic Pathology and [2]Pathology Medical School, University of Ioannina- Greece.

The aim of this study was to determine the cell-cycle cyclins by immunohistochemistry in papillary carcinomas (PCs) and papillary microcarcinomas (PMCs) of thyroid gland.Tissue specimens were obtained from our archives. The cases consisted of 14 primary conventional PCs, 42 PMCs, 5 cases of normal thyroid gland, and 5 cases of hyperplastic lesions. Immunohistochemistry was performed in paraffin-embedded, formalin-fixed tissue, using antibodies against cyclin A, B1, D1, E, and proliferation marker KI-67. Statistical analysis was performed using the SPSS for windows (version 6.0) statistical package. Cyclin E expression was found in 89.7% of PCs and 30.95% of PMCs. Cyclin D1 was evident in the nuclei of cancer cells of 92.85% PCs, and 42.85% in PMCs. No statistical correlation

between these groups was found. Cyclin A expression was seen in 49.98% of PC and 21.42% of PMCs. Cyclin B1 was found in 35.74% cases of PCs and 11.90% of PMCs. Statistical analysis revealed that cyclin D1 and cyclin E significantly higher in PMCs >5mm than PMCs <5mm ($p<0.00024$). There was no significant difference between cyclin A and B1 in PCs and PMCs. In conclusion these results suggest that cyclin D1 and cyclin E, rather than cyclin A and cyclin B1 might be contribute significantly to aggressive character of thyroid microcarcinomas. Further studies will be necessary to clarify the role of these cell-cycle regulators in growth and aggressiveness of papillary carcinomas and microcarcinomas.

P186

HBME-1, cytokeratin 19, high molecular weight keratin 34BE12 and MIB-1 in thyroid lesions

H.P. Kourea, A. Liava, C.E. Vagianos[1], C.D. Scopa
Departments of Pathology and [1]Surgery,
University of Patras Medical School, Patras, Greece

Incompletely developed nuclear features of papillary thyroid carcinoma (PTC) can be observed in nodular goiter (NG), follicular adenoma (FA) and follicular carcinoma (FC). Tumors have also been classified as well differentiated tumors of uncertain malignant potential (WDT-UMP) and well differentiated carcinomas not otherwise specified (WDCa,NOS). To distinguish the above tumors, the use of immunohistochemistry for HBME-1, CK19, 34BE12 and MIB-1 was studied in paraffin sections of 107 thyroid lesions (48 PTC, 26 FA, 13 FC, 3 WDT-UMP, 1 WDCa, NOS) and 16 NG. The immunoreactivity was interpreted as 0, 1+ & 2+ if observed in 0, <20% or ≥20% of the cells, respectively. HBME-1 and CK19 2+ expression was noted in 88% (42/48) & 90%(43/48) PTC, 100%(3/3) & 67%(2/3) WDT-UMP, 100%(1/1) WDCa, 6%(1/16) & 38%(6/16) NG, 27%(7/26) & 15% (4/26) FA, 31%(4/13) & 38%(5/13) FC, respectively. Foci of CK19 highlighted even minor nuclear enlargement or clearing. 34BE12 was negative in most lesions of all types while MIB-1 was noted in <1% of cells in all lesions studied. HBME-1 is useful in differentiating PTC from questionable FA and FC and highlights the proximity of PTC with WDT-UMP and WDCa. CK19 is less specific. 34BE12 and MIB-1 do not exhibit diagnostic value.

P187

FNA application in cytological examination of the thyroid goiter.

Sopta J.*, Havelka M.*, Tatic S.*, Markovic LJ.**, Mijucic V.***, Radojevic S.*, Glumac S.*
* Institute of Pathology, School of Medicine, Belgrade
** Institute of Pathophysiology, School of Medicine, Belgrade
***National cancer centar, Belgrade

Introduction: FNA is very useful method in cytological diagnosing of different lesion in the thyroid gland, among them is benign goiter.
Material and methods: In the period of 2 years citologically was analyzed 600 aspirates from the thyroid lesions. We analyzed: sex distribution, age distribution, correlation between clinical and cytological diagnoses and goiter classification in accordance with cytological characteristics.
Results: From 600 analyzed aspirates 414 cases (69%) were diagnosed as goiter. This lesion was five times frequent in females then males (348 women, 66 men). X^2 test confirmed high significance for arising goiter ($X^2=192,08$; $p<0,005$) in females. In our examination the most patients were old between 41 and 50 years. The least patients (6) were younger then 20. The youngest patient was 13, and the oldest 78 years old. Statistically was confirmed high significance for arising goiter ($X^2=494,30$; $p<0,005$) according to the ages of life. From 414 cytological confirmed goiters 222 had clinical diagnosis "nodular goiter", 127 "diffuse goiter", Our conclusions are: 84% of cytological diagnosed goiters had the some clinical diagnosis, in only 1,5% of all patients clinically tumor was suspected. We confirmed high correlation between clinical and cytological diagnosis.
Conclusion: FNA permits a substantial reduction or even elimination of other diagnostic procedure, such as imaging, with consequent saving in time and money. Furthermore, benign cystic lesion may be cured by FNA (a diagnostic and unexpected therapeutic value of FNA).

P188

Fine needle aspiration diagnosis of hyperplastic and neoplastic follicular nodules of thyroid. A computerized nuclear morphometric study.

Zaxou K, Nenopoulou E, Zaraboukas T, Vrettou E,
Karkavelas G, Papadimitriou CS
Department of Pathology, Aristotle University Medical School,
Thessaloniki, Greece

Objective: Fine needle aspiration of the thyroid is limited in differentiating hyperplastic nodular goiters from follicular neoplasms and in separating follicular adenomas from follicular carcinomas. To determine the value of computerized interactive morphometry in the preoperative prediction of malignancy in fine needle aspirates of follicular lesions of thyroid, we studied the morphometric parameters of nuclear area, perimeter, diameter, short axis, long axis, axis ratio, form Ar, form Pe, Form NCI, contour ratio, and nucleαr roundness.
Study design: We measured samples from FNA aspirates obtained from 22 hyperplastic nodules, 22 follicular adenomas and 22 follicular carcinomas and follicular variant of papillary carcinomas, all of which where subsequently confirmed by histological examination.
Results: The mean values of nuclear area, perimeter, diameter, short axis and long axis were significantly different (p less then 0,009) between the adenoma and carcinoma cases as well as between adenomas and hyperplastic nodules. No differences were found for the axis ratio, form Ar, form Pe, form NCI, Contour and nuclear roundness.
Conclusion: Computerized nuclear morphometry can be considered a helpful ancillary tool for the preoperative differential diagnosis of follicular lesions of the thyroid.

P189

Adrenocortical tumors with the neuroendocrine IHC and EM features

Rotin DL, Smirnova EA, Moroz EA
Department of Human Pathology, NN Blokhin Cancer Research Center, Kashirskoye Shosse 24, 115478 Moscow, Russia

Introduction: Medullary features in adrenocortical tumor cells were originally described by Eranko и Hanninen in 1960. These features include immunohistochemical and EM neuroendocrine appearance. Sometimes it could lead pathologist away from the correct diagnosis.
Objective: We investigated and evaluated different "medullary" immunohistochemical and ultrastructural features in group of adrenocortical tumors clinically mimicking pheochromocytoma and compared these proprieties with control group of pheochromocytomas.
Methods: We investigated expression of Melan A, Chromogranin A, Synaptophysin, CD 56, NSE, Vimentin and Citokeratins in "simulating a pheochromocytoma" 10 adrenal cortical tumors (5-adenomas and 5 – carcinomas) and in 5 pheochromocytomas. EM was performed in all 15 cases.
Results: All adrenocortical tumors – both adenomas and carcinomas, were Melan A - positive and Chromogranin A - negative. The features of the neuroendocrine differentiation, including expression of other neuroendocrine IHC markers (NSE,

CD 56 and Synaptophysin) and ultrastructurely - defined adrenalin-type neurosecretory granules were seen in different degree and variable combinations in all cases of this group. All pheochromocytomas were positive to all neuroendocrine markers and negative to Melan A.
Conclusion: Positive expression of Melan A and negative reaction with chromogranin A are supposed to be most reliable markers in differential diagnosis between medullary and cortical origination of the tumor. Any other features of the neuroendocrine differentiation (including IHC and EM) are not occurred to play an useful role in the differential diagnosis.

P190

Galectin-3 expression in functioning and silent corticotroph adenomas of the pituitary gland

Theodore Argyrakos, Eleni Thodou, George Kontogeorgos
Department of Pathology, G. Gennimatas General
Hospital of Athens, Hellas

Galectin-3 (Gal-3) belongs to the family of carbohydrate-binding proteins with high affinity for β-galactoside and it is involved in many biological processes including cell growth, cell adhesion, apoptosis and metastasis. We have recently studied immunohistochemically the expression of Gal-3 in 30 corticotroph pituitary adenomas (19 functioning and 11 silent). Antigen retrieval was achieved by 3-minute pressure boiling in citrate buffer solution. The independent variables t-test was used for comparing the mean percentages of Gal-3 in the two different subgroups. Eighteen of the functioning corticotroph adenomas (94.73%) expressed Gal-3 with a cytoplasmic and focally membranous distribution. The mean percentage of Gal-3 positive adenoma cells was 77%. Among the silent corticotroph adenomas 9 (81.81%) were negative for Gal-3, while two of the remaining adenomas expressed Gal-3 in 15% and 80% of their tumour cells respectively (mean percentage: 8.72%). The statistical differences between functioning and silent adenomas were highly significant (p=0.001). Gal-3 is expressed in the substantial majority of functioning corticotroph adenomas of the pituitary gland, whereas the majority of silent adenomas are negative or express focally Gal-3. We conclude that these observations can be proved helpful in distinguishing silent corticotroph adenomas of the pituitary gland.

P191

Bilateral adrenal and extra-adrenal pheochromocytomas: Related or look-alikes?

[1]Esther Korpershoek, [1]Bart-Jeroen Petri, [1]Francien H. van Nederveen, [1]Winand N.M. Dinjens, [2]Albert A. Verhofstad, [3]Wouter W. de Herder, [4]Sonja Schmid, [4]Aurel Perren, [4]Paul Komminoth, [1]Ronald R. de Krijger
[1]Department of Pathology, Josephine Nefkens Insitute, Erasmus MC, University Medical Center Rotterdam, Rotterdam, The Netherlands [2]Department of Pathology, [3]Departments of Pathology,
Radboud University Nijmegen Medical Center, Nijmegen,
The Netherlands [3]Department of Internal Medicine, Erasmus MC, University Medical Center Rotterdam, Rotterdam, The Netherlands
[4]Department of Pathology, University Hospital Zurich, Zurich, Switzerland

Pheochromocytomas (PCC) are rare tumors that arise from chromaffin tissue in the adrenal medulla, but can also occur in the abdomen outside the adrenals and are then called extra-adrenal PCC. Up to 25% of adrenal and extra-adrenal PCC are caused by germline mutations in RET, VHL, SDHB, or SDHD, but little is known about the contribution of these genes in bilateral and extra-adrenal PCC.
We have performed mutation analysis on tumor DNA of 32 patients with bilateral PCC and 27 patients with extra-adrenal PCC for RET (exon 10, 11 and 16) and the entire coding region of VHL, SDHB, and SDHD. When alterations were found, sequence analysis was performed to identify the mutation.
Eighteen RET and two VHL germline mutations were found in the patients with bilateral adrenal PCC. In extra-adrenal PCC one novel SDHB germline and one novel somatic SDHB mutation were observed. In addition, two SDHD germline mutations were found in extra-adrenal PCC.
Because only RET and VHL mutations were found in patients with bilateral PCC, and SDHB and SDHD mutations were only seen in patients with extra-adrenal PCC, we conclude that different mechanisms are involved in the pathogenesis of these groups of tumors. Therefore, it should be considered that patients with bilateral adrenal PCC will be tested first for RET or VHL mutations, and patients with extra-adrenal PCC should be examined first for SDHB or SDHD mutations.

P192

Array CGH Analysis in sporadic benign pheochromocytomas

Francien H. van Nederveen[1], Esther Korpershoek[1],
Ronald J. deLeeuw[2], Wan L. Lam[2], Winand N.M. Dinjens[1]
and Ronald R. de Krijger[1]
[1]Department of Pathology, Josephine Nefkens Insitute, Erasmus MC, University Medical Centre Rotterdam, Rotterdam, The Netherlands,
[2]Department of Cancer Genetics and Developmental Biology,
British Colombia Cancer Research Centre, Vancouver, Canada

Pheochromocytomas (PCC) are neuro-endocrine tumours usually arising in the adrenal medulla. There are 4 important candidate genes that are involved in PCC tumorigenesis: RET causing multiple endocrine neoplasia type 2; VHL causing Von Hippel-Lindau disease; and SDHB/SDHD, causing the so-called pheochromocytoma-paraganglioma syndrome. Together, germ line mutations in one of these four genes account for up to 25% of PCC patients, but the pathogenesis of the remaining 75%, truly sporadic, PCC is still largely unknown. We selected a group of 42 benign PCC, with a negative family history for PCC or relevant cancer syndromes, and isolated DNA from fresh frozen tumour tissue. Benign PCC were defined as those tumours that did not show evidence of metastasis within an average follow-up period of 4 years. 17 patients were lost to follow-up. Tiling high-resolution comparative genomic hybridisation (CGH) micro-arrays were used for genome-wide analysis. The most striking loss concerned the short arm of chromosome 1, in 65% of all PCC analysed. We could not detect a smallest region of minimal loss of 1p, in contrast to our earlier studies on a different group of tumours, and in contrast to previously published studies of others. The second most frequent loss was found on the long arm of chromosome 3, comprising 40% of all PCC. Additional losses were detected at high frequency on the short arm of chromosome 17 (43%), and the long arms of chromosome 21 (35%) and 22 (48%). Interestingly, we could separate a subgroup of 7 PCC that did not have loss of 1p, but instead showed distinct partial losses of chromosomes 3 and 11. This pattern has previously been reported to be associated with VHL-disease related PCC. From these results we conclude that: 1) truly sporadic benign PCC can be separated into 2 distinct groups, based on their genomic aberrations, one group displaying loss of 1p, 3q, 17p, 21q, 22q, and another group characterized by a so-called “VHL-pattern” of chromosomes 3 and 11 loss; 2) in addition to previously described chromosomal regions

(1p, 3q, 17p) further analysis for their role in PCC tumorigenesis of 21q and 22q appears warranted.

P193

Human pheochromocytoma with prominent piecemeal degranulation of endocrine granules

The aim of the study was the evaluation of pheochromocytoma patients using different morphological techniques and correlation of those results with clinical presentation of the disease. We studied 18 cases (6 women and 12 men) of adrenal pheochromocytoma. The patients age ranged from 37 to 62 yrs (mean 48 yrs). All patients had typical clinical syndromes related to pheochromocytoma with paroxysmal hypertension without response to pharmacological treatment. The hypertensive crises continue from several minutes up to one hour, and breaks between attacks were longer than 7 days. The raises in blood pressure were accompanied by sweating, skin as well as abdominal manifestations. All other neuroendocrine tumors as well as other causes of hypertension were excluded in those patients. In all cases before surgery the diagnosis was confirmed by total urinary free catecholamines level (in all patients over 1000 nmol/24hrs). In all cases adrenal tumors were surgically removed and tissue samples were processed for routine histology, immunohistochemistry and routine transmission electron microscopy (TEM). In all cases histo-pathological studies confirmed diagnosis of pheochromocytoma. Moreover using tissue specimens the immunohistochemical studies for p53, Ki67 and PCNA were done. Ultrastructural studies in TEM revealed well maturated cells with typical features of cytoplasm arrangement. In TEM we focused on studies on activity of nuclei, secretory activity as well as interaction between pheochromocytoma cells infiltrating adrenal cortex with normal cortical cells. There were found differences in the ultrastructure of nuclei between cases. In two cases, the vast majority of cells in tumor mass had enlarged nuclei with enlarged nucleoli. And the nuclear membrane had irregular shape. In some of such cell nuclei expressions of p53 and PCNA as well as Ki67 were observed. Moreover, in all patients using TEM technique we evaluated interaction between tumor cells and the normal adrenal gland, as well as relation of tumor tissue to the vasculature. There were found areas of insertion of tumor cells into vascular lumen, and some of those cells were expelling their content directly to the blood stream. In studied material we found a direct release of neuroendocrine granules into blood vessels or indirectly through the endothelial calls. Sporadically, the tumor cells were also degranulating directly into extracellular space, especially in the areas of adrenal cortex invasion. In such area in cells of zona fasciculata we observed high number of tubulo-vesicular mitochondria characteristic for cell producing cortisol. In this studies we confirmed piecemeal degranulation of pheochromocytoma cells into tumor capillaries. It could be responsible for uncontrolled high elevations of blood pressure in our patients. Second important finding of this study was that adrenal cortex cells that had a contact with tumor cells contained numerous tubulo-vesicular mitochondria. It verify their high activity for cortisol synthesis.

P194

Mutational analysis of the *BRAF* gene in human adrenocortical carcinomas

S. Tseleni-Balafouta[1], E. Sozopoulos[1], H. Litsiou[1], G. Voutsinas[2], G. Fanourakis[1], N. Mitsiades[3], K. Mitsiades[3], E. Patsouris[1]
[1]Department of Pathology, Medical School, University of Athens, [2]Laboratory of Enviromental Mutagenesis and Carcinogenesis, Institute of Biology, NCSR ´Demokritos´, Athens, Greece,
[3]Dana Farber Cancer Institute, Harvard Medical School, Boston, MA, USA

Activating mutations in the *BRAF* gene are present in several types of human malignancies. It has been proposed that ‚Braf is important for cAMP-mediated signaling pathways regulating proliferation, in response to cell-specific trophic hormones that activate adenylate cyclase. Angiotensin II and ACTH activate adenylate cyclase in adrenocortical cells, so the latter could be targets for *BRAF* mutations that would lead to tumorigenesis (adrenocortical carcinoma). We thus evaluated the presence of *BRAF*, *KRAS* and *NRAS* mutations in adrenal carcinomas (30 tumor specimens and 2 cell lines) by DNA sequencing. 5 mutations were found in 4 of 30 tumor specimens: Two BRAF substitutions (G463E, V600E), a KRAS substitution (G12C), and two NRAS substitutions (V8A and L16N). No mutations were found in the 2 adrenocortical cell lines. These data suggest that activating *BRAF* mutations occur in a small subset of human adrenocortical carcinomas supporting a role for Ras/Raf-mediated signaling, and suggest that inhibitors of this pathway may provide clinical benefit for some patients with this malignancy.

P195

Histologic and immunohistochemical findings in hyperinsulinemic hypoglycemia in pediatric patients

Diclehan Orhan*, Saniye Ekinci**, Zuhal Akçören*, Arbay Çiftçi**, Gülsev Kale*
Hacettepe University Faculty of Medicine, İhsan Doğramacı Children's Hospital, Division of Pediatric Pathology, Ankara, Turkey, ** Hacettepe University Faculty of Medicine, Department of Pediatric Surgery, Ankara, Turkey

Pancreas from 8 children with idiopathic hyperinsulinemic hypoglcsemia was evaluated histopathologically using immunohistochemical staining. The patients ranged from newborn to 3 years in age. Hematoxylin and eosin stained sections were evaluated for the presence or absence of islet cell displasia and the distribution of islet cells. Immunohistochemical staining for insulin, glucagons, somatostatin, pancreatic polypeptide and neuron specific enolase was performed. In 2 cases, intraoperative frozen sections were examined. All patients were diagnosed as nesidiodysplasia. Islet cell dysplasia was observed in every case. Immunohistochemical staining revealed the the extent of islet cell proliferation. Scattered insulin-positive islet cells were seen easily with immunostaining. As islet cell dysplasia was observed in all cases, performing intraoperative frozen section evaluation was found to be beneficial to direct the extent of pancreatectomy as was the case in our 2 patients. We conclude that immunohistochemical analysis is useful to identify the small intralobular islet cell aggregates and scattered islet cells.

AA/018

Carcinoid tumors of the jejunum and ileum

Doinita Radulescu[1], Simona Stolnicu[2]
[1]Department of Pathology, University of Medicine, Iasi, Romania
[2]Department of Pathology, University of Medicine, Targu Mures, Romania

The purpose of this study was to describe the clinical, pathological and immunohistochemical characteristics of jejunoileal carcinoid tumors and to evaluate the predicting factors of behaviour and prognosis. Ten cases of ileal and two cases of jejunal carcinoids were retrospectively studied with emphasis on clinical, pathologic, immunohistochemical and prognostic features. Our cases involved 10 men and 2 women, with mean ages of 52 years old. Only one patient presented a carcinoid syndrome. In 2 cases, tumours were multiple, in 10 were transmurally invasive and in 3 cases presented regional lymph node metastases. Tumoral cells were disposed in solid nests, in rosette type and glandular-like structures. Most tumor

cells were intensely argyrophilic-, Chromogranin- and Serotonin-positive. Survival was negatively correlated with distant metastases at the time of surgery, tumour multiplicity, mitotic rate and depth of invasion. Jejunoileal carcinoid tumors have generally a relatively high rate of transmural invasion and aggressive clinical behaviour, differing from those occurring in other sites of the gut in that they are often at an advanced stage at the time of presentation, as we also observed in the reported cases. Other pathologic characteristics are that they are usually insular and argentafin, with a high rate of Chromogranin and Serotonin positivity and these features differentiated the presented jejunoileal carcinoids from other gastrointestinal carcinoids.

P197

Primary Clear cell Sarcoma of the Small Intestine: The Diagnostic Difficulties of a visceral case

Parasi A, Karakosta A, Sotiriou E, Mennonna R, Karayannis M, Pantoula P
Department of Pathology General Hospital of Nikaia-Piraeus «Agios Panteleimon» Greece

A rare case of clear cell sarcoma, arising primarily in the small intestine of a 48 year old man is described. Microscopically, a circumferential tumor, focally ulcerated, diffusely infiltrating the intestinal wall and the mesenterium without lymph node metastases was found. The neoplasm consisted of nests and fascicles of ovoid to spindle-shaped cells with slightly eosinophilic and rarely clear cytoplasm, vesicular uniform nuclei with prominent nucleoli and marked mitotic activity. Immunohistochemically, the tumor cells stained only for Vimentin and S-100 protein. HMB-45, MELAN-A, MART-1 were negative, as well as Keratins, EMA, CD117, CD34, CD1a, CD99, Synaptophysin, Chromogranin, Neurofilaments, SMA, Desmin and Myogenin. Five years later, a liver metastasis with similar histological features was found. Clear cell sarcoma and Malignant Melanoma are immunohistochemically indistinguishable, but the cytologic uniformity and the distinctive infiltrative growth pattern of our tumor, in combination with the localized for several years disease, allowed the exclusion of a metastatic melanoma. Primary clear cell sarcomas arising in the GI tract, although very rare, are increasingly recognized and show an aggressive behavior. They are rarely negative to Melanoma antigens, demonstrating only the characteristic (12;22) translocation, which confirms the diagnosis.

P198

EGFR profiling in cancer of unknown primary (CUP): Gene mutation, amplification, regulation and tissue protein expression in fifty cases.

L. Dova[1], G. Pentheroudakis[2], I. Georgiou[3], V. Malamou-Mitsi[4], G. Vartholomatos[1], G. Fountzilas[5], N. Kolaitis[1], E. Kitsiou[6], N. Pavlidis[2].
[1]Hematological Laboratory-Molecular Biology Unit, [2]Dept. of Medical Oncology, [3]Dept. of Obstetrics and Gynaecology-Genetics Unit, [4]Dept. of Pathology, Ioannina University Hospital, [5]Medical School, Aristotle University of Thessaloniki, [6]Dept. of Pathology, Ioannina General Hospital, Greece.

EGFR signaling contributes to malignant tranformation and survival. We studied known markers of EGFR activation in 50 patients with CUP. Tumor sections were stained for EGFR protein by IHC. PCR amplification, SSCP and direct sequencing were used to study EGFR intron 1 (CA) repeat length as well as exon 18,19,21 activating mutations and amplification. 37 tumors (74%) expressed EGFR protein but only 6 (12%) strongly. In intron 1, we detected five alleles with 16 to 20 CA repeats, allele 16 being the most common. All samples were heterozygous, the commonest genotype being 16/18 dinucleotides. Five samples had three intron-1 alleles and were associated with EGFR overexpression in 40% of cases. When a 16-CA allele was present, the length of the other allele was inversely correlated to EGFR expression (p=0.04). There was no evidence of exon 18,19,21 amplification. Two mutations were detected: Exon 21 [2508C>T, a silent polymorphism (R836R)] and exon 19 [G>A (IVS19+24G>A) resulting in aberrant mRNA splicing]. Neither EGFR expression nor CA repeats length were prognostic factors. Our data provide evidence for lack of contribution of EGFR in the development of CUP and lack of benefit from EGFR modulation.

P199

Serous cystadenoma of the pancreas in a child

Liviu Niculescu[1], Rafira Catu[1], Amelia Petrescu[2]
[1]"Grigore Alexandrescu" Children Hospital, Bucharest, Romania, [2]"Prof. Dr. Th. Burghele" Hospital, Bucharest, Romania

Pancreatic tumors and cyst are very rare in children. When encountered they can present a diagnostic and therapeutic challenge to the pediatric surgeon. The **aim** of this work is to report a new case of 12 years old girl with a short history of epigastric pain, vomiting and local discomfort. Sonography and computed tomography showed a pancreatic head mass. The surgeons decided to remove the tumour. Macroscopically examination carried out the removed tumour showed a 3,8 /1,2/ 2,5 cm multiloculated mass, small cystic cavities filled with a serous "clear" and haemorrhagic fluid.
Material and methods: Fragments of the tumour were fixed in formaldehyde 10 %, included in paraffin and the sections were stained with H.E, V.G. and immunohistochemically: EMA, Muc 1, low molecular weight keratin.
Results: The histological examination revealed multiple small cysts lined by cuboidal cells; myoepithelial cells were also present beneath this epithelium surrounded by prominent vascularized conective tissue. Immunohistochemically: EMA, low molecular weight keratin, Muc 1 positive reaction.
Conclusions: These findings plead for the diagnosis of serous cystadenoma of the pancreas.

P200

Inflammatory Myofibroblastic tumor arising in hyperplastic polyp of the stomach

Orlowska J[1], Zakrzewska K[2], Albinski J[3]
Histopathology Laboratory of the Department of Gastroenterology, Medical Center for Postgraduate Education[1],
Department of Pathology[2], Department of Surgery of the Upper Gastrointestinal Tract[3], Oncology Center, WARSAW, POLAND

Inflammatory Myofibroblastic Tumor (IMT) is a lesion reported mainly in lungs, mesentery and omentum. Only 50 stomach IMTs were described in a period of 1970 - 2006. The following case is, to our knowledge, the first one in which the stomach IMT has grown on the ground of gastric Hyperplastic Polyp.
A 67-year-old man was admitted to the Dept. of Gastroenterology with one year history of fatigue and postprandial abdominal pain. Low hematocrit (26%) and RBC (3,82), and highly increased ESR (144) were disclosed. Gastroscopy revealed a large polypoid tumor of the stomach. In biopsy specimens only fragments of hyperplastic polyp were found. However, a total gastrectomy with regional lymphadenectomy D2 was performed. An ulcerated, fragile, polycyclic tumor measuring 6,5x 5,0x 2,5cm localized in the body and antrum was found. Microscopically it was mostly composed of interlacing fascicles of elongated spindle-shaped fibroblasts / myofibroblasts weekly positive for desmin and SMA, and strongly positive for vimentin; CD117, CD34, S-100 and CKAE1/3 were negative. They were localized inside the structures typical for hyperplastic polyp. The diagnosis of IMF inside hyperplastic polyp

was established. The surgical margins and all lymph nodes were free from the tumor. Long term follow-up is recommended because of the risk of IMT local recurrence.

P201

Immunohistochemical expression and prognostic signifficance of DCC (deleted in colon cancer), p53 protein and proliferative marker Ki-67 in colorectal cancer patients

Genghis Yashar[1], Neli Basheska[1], Irina Prodanova[1], Katerina Kubelka-Sabit[1], Aleksandar Dimovski[2], Ana-Marija Stefanovska[2], George Zografski[1]
[1]Department of Histopathology and Clinical Cytology, Institute of Radiotherapy and Oncology, Medical Faculty, Skopje, Republic of Macedonia, [2]Center for Genetic Engineering and New Technologies, Macedonian Academy of Sciences and Arts, Skopje, Republic of Macedonia.

Objectives: The objective of this study was to evaluate the immunohistochemical expression of Deleted in colon cancer (DCC), p53 protein and proliferating index Ki-67 in correlation with various clinico-pathological (age, sex, tumor status, lymph node involvement, localization, tumor diameter, grade of differentiation, histological type) and biomolecular parameters (loss of heterozygosity of the long arm of chromosome 18 and microsatellite instability) in colorectal cancer patients. In addition, the prognostic significance of their influence on overall survival (OS) was also estimated.
Methods: A retrospective analysis of 100 patients with colorectal cancer who underwent large bowel resection with regional lymphadenectomy was conducted in the period between 1995 and 2000. All the patients were in stage II and stage III of the disease according to the postoperative TNM classification of UICC (1997) guidelines. The immunohistochemical expression of protein products of the DCC, p53 tumor suppressor genes and Ki-67 proliferating index were semi-quantitatively evaluated. Biomolecular analyses for the loss of heterozygosity of the chromosome 18q and microsatellite instability were performed with the Polymerase chain reaction (PCR) technique.
Results: In our case series, 57 (57%) patients were in stage II, and the remaining 43 (43%) patients in stage III of the disease. During the follow-up period (mean 53, range 5-97 months), 41(41%) patients died of the disease. The expected 5-year OS rate was 58.6%. In the univariate analysis, tumor status, lymph node involvement, sex, age, tumor grade, p53 protein expression and Ki-67 proliferating index were parameters with prognostic significance related to OS ($p<0.05$). Among these variables, in the multivariate analysis the tumor status and Ki-67 proliferating index were selected as independent and significant prognostic factors related to OS ($p=0.0019$). According to the value of the prognostic index (PI) defined by Cox regression model, the patients were categorized in two distinct risk groups. The 5-year OS rate of the low- and high-risk group patients was 65.0% vs. 29.4% ($p=0.001$). The 5-year OS for stage II was 71.1% vs. 40.0% ($p=0.05$) and for stage III of the disease it was 54.8% vs. 25.0% ($p=0.03$), respectively.
Conclusions: These data indicate that defining prognostic groups in each stage of the disease allow an exact and objective selection of colorectal cancer patients with different death risk. Therefore, the prognostic index (PI) as an indicator of the patient's place in the prognostic spectrum could be a sound basis for an appropriate planning.

P202

Pseudomyxoma Peritonei

Papaevangelou Maria MD, Koniaris E. MD, Gazalidou Maria MD, Papathanasaki Antigoni MD, Biteli Maria MD, Apostolikas N. MD
Dept. of pathology, Hellenic Anticancer Institute, 'St. Savvas' Hospital, Athens Greece

Pseudomyxoma peritonei is a rare condition which is referred to a widespread mucin accumulation within the peritoneal cavity. Microscopically it is composed of extracellular mucin accumulation and well-differentiated tumor cells, fibrosis, hyperemia, and mesothelial reaction. It usually affects the ovaries, their involvement is usually bilateral and represents secondary deposits from appendiceal neoplasms. However synchronous, similar tumors to the ovary, adenocarcinomas, are not rare and the pathologist confronts a difficult differential diagnosis. We present such a case and we review the literature.
Keywords: pseudomyxoma peritonei, secondary deposits, adenocarcinoma of the ovary.

P203

Signet ring cell adenocarcinoma of the colon or primary linitis plastica of the colon. A case report.

Apostolikas N., Koniaris E., Papaevangelou M.
Dept. of Pathology, Hellenic Anticancer Institute, 'St. Savvas' Hospital, 171 Alexandras Av., 11522, Athens Greece.

Our aim is to report a rare case of signet ring cell adenocarcinoma of the colon (SRCA) or primary linitis plastica of the colon and review the literature. SRCA is an uncommon type of colorectal cancer with an incidence rate varying from 0.1% to 2.6% of all large bowel cancers. A 73 year old patient who had been operated on an adenocarcinoma of the kidney, admitted to the hospital again two months later, because of a mild constipation and weight loss. After colonoscopy and biopsy an adenocarcinoma of the left colon was diagnosed. The patient underwent a left colectomy. The received specimen had 10.6cm length and a narrowed lumen up to 1.3cm with a widespread neoplastic thickening of the intestinal wall (maximum diameter 8.4cm) was found. Histological examination revealed a tumor which grew in a diffuse fashion without any glandular formation, consisted of sheets or files of typical signet–ring cells. The tumor infiltrated diffusely under the mucosa, disseminating into the pericolic fat as well. No metastases developed in the five excised lymph nodes and no peritoneal dissemination was found (stage B2 Astler and Coller) The immunohistochemistry showed that the tumor was mainly negative in CK7 and positive in CK20. Metastases from stomach were excluded. Only 15 cases have been reported in the literature during the last ten years.

P204

Immunohistochemical evaluation of the EGFR expression in advanced metastatic colorectal cancer using two commercially available antibodies.

Arapantoni-Dadioti P.[1], Valavanis C.[1,2], Karampola M.[1], Vecchini G.[1], Iakovidou J.[1].
Technical assistance: Kontogianni H., Charalabidou A.
[1]Dept. of Pathology – [2]Molecular Pathology Unit, METAXA Cancer Hospital, Piraeus, Greece

Background and objective: Colorectal carcinoma is one of the most common malignancies worldwide and manifests a high mortality, especially at late stages of the disease. Currently available therapeutic strategies have a modest effect on overall survival of patients with advanced and/or metastatic disease. Recently, targeted therapy drugs, such as EGFR inhibitors, are in use for the management of advanced-stage colorectal cancer. It is well known that the dysregulation of the epidermal growth factor receptor (EGFR) signal transduction pathway is involved in colon cancer development and progression, and overexpression of the receptor confers a poor prognosis. Thus targeting the EGFR has become a rational approach for the treatment of colorectal carcinoma. In this context we investigated the expression of

EGFR in advanced/metastatic colorectal cancer using two different antibodies against EGFR and compared the incidence, the cellular distribution and the intensity of its expression as given by the two antibodies.
Methods: In this study, 121 archival specimens of metastatic colorectal cancer were analysed immunohistochemically, using two different antibodies against EGFR, the mouse monoclonal anti-human EGFR clone 2-18C9 of the EGFR pharmDx kit (DAKO) and clone 31G7 (Zymed). Immunostaining was evaluated as membranous, and the intensity of the immunostaining was graded 0 (negative), 1+ (weak), 2+ (moderate) and 3+ (strong).
Results and conclusions: Overall, 34.7 % of the adenocarcinoma cases had membranous EGFR reactivity; 9.1 % of the tumors had 3+ reactivity in 3-30% of the neoplastic cells, 17.4% of them displayed 2+ reactivity and 8.3% exhibited 1+ in the same tumor cell percentage. EGFR expression in colorectal carcinomas seems to correlate with differentiation grade. However, there were no associations with Dukes' stage, site, patient age or gender.
There was high concordance (92%) in evaluating EGFR expression between the two antibodies used in this study, with no differences in the incidence, the cellular distribution and the intensity of EGFR expression.

P205

Liver cell proliferation in renal transplant and immunocompotent patients with HCV infection.
K. Giaslakiotis[1], P. Aleksandrou[1], M. Psichogiou[2], G. Nikolopoulos[2], J. Boletis[3], J. Delladetsima[1].
[1]Dept of Pathology, Laiko Hospital, [2]Dept of Hygiene and Epidemiology, Athens University, [3]Transplantation Center, Laiko Hospital, 75 Mikras Asias, 115 27 Athens, Greece.

Liver cell proliferation in HCV infection is still unclear and available data are controversial. In the present study hepatocellular proliferation was assessed in liver biopsies of HCV infected renal transplant (RT) and immunocompotent (IC) patients (pts) and was correlated with hepatitis grade and stage, viremia, genotype and age. Liver biopsies from 58 RT recipients and 46 from ICpts were examined histologically. Hepatocyte proliferation was assessed by immunohistochemical detection of Ki67, while the proliferation activity index (PAI) was defined by the mean number of positive hepatocellular nuclei per 10 high power fields. Serum HCV RNA levels and HCV genotype were also determined. In ICpts PAI was 14.7 in minimal (6 cases), 25.6 in mild (32 cases) and 52.7 in moderate (8 cases) hepatitis. In RTpts PAI was 9.9 in minimal (42 cases), 19.7 in mild (14 cases) and 84 in moderate (2 cases) hepatitis. In ICpts, PAI correlated with lobular activity ($p<0.01$). Mean PAI was significantly higher in ICpts (mean 28.9IC vs 14.8RT, $|z|= 0$), especially in the mild hepatitis group ($p<0.01$) and in all three grades of lobular activity (minimal, $p<0.01$), mild, $p<0.05$) moderate, $p<0.05$). No correlation was observed between PAI and hepatitis stage, HCV genotype, serum HCV RNA and age. Hepatocellular proliferation in HCV infected ICpts is closely related to necroinflammatory activity. The deficient proliferation in RTpts may be related to immunosupresive therapy.

P206

Hereditary non-polyposis colorectal cancer (Lynch syndrome) - A case report.
Tzaida O.[1], Valavanis C.[1,2], Britsou M.[1], Vogiatzis P.[1], Akrivos T.[3], Arapantoni-Dadioti P.[1]
[1]Pathology Department, [2]Molecular Pathology Unit, [3]Department of Gynecology, METAXA Cancer Hospital, Piraeus, Greece.

Background: Hereditary non-polyposis colorectal cancer (HNPCC, Lynch syndrome) is a an autosomal dominant disorder, characterized by the development of colorectal carcinoma, endometrial carcinoma and a range of other mlignancies including neoplasms of renal pelvis/ureter, stomach, small bowel, ovary, brain, hepatobiliary tract and sebaceous glands. The proposed revised criteria by International Collaborative Group on HNPCC, referred as Amsterdam Criteria II (ACII), concern a set of clinical, pathological and genetic features appropriate to diagnose HNPCC syndrome. Germline mutations in the DNA mismatch repair (MMR) genes particularly MLH1, MSH2 and MSH6 underline this disorder. A characteristic such case of HNPCC is presented.
Case description: A female patient 65 years old with a family cancer history of her first degree relatives (mother and sister with endometrial cancer) was admitted to our hospital complaining for vaginal bleeding during last year. A preoperative diagnostic endometrial biopsy was performed. The thorough clinical and laboratory patient investigation, including CT and colonoscopic studies, revealed a bulky tumor located in the sigmoid as well as two smaller polypoid growths of the trasverse colon. The patient underwent a total hysterectomy as well as a resection of the sigmoid with excision of the colonic polyps.
Pathologic findings: The histological examination of the surgical specimens revealed: villous adenomas of the transverse colon, a moderately differentiated adenocarcinoma of the sigmoid with a mucinous component and adenomatous remnants at the tumor margin, classified as Dukes C, T2N2 Ca, a moderately differentiated endometrial adenocarcinoma of the endometriod type invading the endometrium, as well as two occult, microscopical foci of sex cord-stromal ovarian neoplasms (Sertoli type). An immunohistochemical analysis of the MMR gene products was performed.
Results: Based on the former, accumulated pathologic- immunohistochemical features and on the family history, the patient was considered to fulfill ACII criteria as a HNPCC case, and was advised to further genetic counseling and mutation investigation.

P207

Immunohistochemical expression of syndecan-1 protein in gastric cancer
Antonia Charchanti[1], Ann C. Goussia[2], Eufemia Balasi[2], Catherine Zioga[2], George Fountzilas[3], Panagiotis Kanavaros[1], Niki J. Agnantis[2], Maria Bai[2]
Departments of [1]Anatomy-Histology-Embryology and [2]Pathology, Medical School, University of Ioannina, 45110, Ioannina, Greece
Department of [3]Medical Oncology, Medical School, Aristotle's University of Thessaloniki, Thessaloniki, Greece

Syndecan-1 (SDC-1) is a transmembrane heparan sulfate proteoglycan, that binds to various extracellular matrix components, mitogenic and growth factors via its heparan sulfate chains. In the present study, we analyzed the immunohistochemical expression of SDC-1 in 103 cases of gastric adenocarcinomas. SDC-1 expression was observed in both neoplastic and stromal cells. Strong neoplastic and stromal staining (>50% of cells) was found in 16.3% and 4.8% of the cases respectively, moderate (10-50% of cells) in 24% and 21.2% of the cases, respectively and weak (<10% of cells) in 59.6% and 74% of the cases, respectively. SDC-1 expression in neoplastic cells lower in more invasive cases (mucosa/submucosa vs muscularis propria/serosa/perigastric fat, $p=0.034$) and in cases with lymph vessel invasion ($p=0.035$). Low stromal SDC-1 expression was correlated with histologic type (intestinal vs diffuse/mixed, $p= 0.04$), histologic grade (I vs II/III, $p= 0.04$) and with greater tumor size ($p=0.026$). It is concluded that low epithelial and stromal SDC-1 expression are associated with unfavorable histopathological parameters in gastric carcinomas.

P208

The potential role of activated stellate cells in liver biopsies with hepatitis C compared with hepatitis C/diabetes mellitus.

AC Tsamandas, V Zolota, A Liava, D Dimitropoulou, C Gogos, CD Scopa. University of Patras Medical School, Patras, Greece

Hepatitis C virus (HCV) infection is a major cause of chronic liver disease. Steatosis is a common finding both in HCV and diabetes mellitus (DM). Activated liver stellate cells (ASC-αSMA+ cells) are a major factor responsible for fibrosis and progression to chronic liver disease. This study investigates the presence of ASC in liver biopsies from patients with HCV alone and in patients with HCV/DM. Fifty liver biopsies (HCV-35 and HCV/DM-15) were immunostained with the anti-aSMA antibody. Results were expressed as %(+) cells and correlated with degree of steatosis, inflammation and fibrosis. The mean±SD value, in HCV/DM and HCV patients was: for steatosis 1.1 ±0.4 and 0.5±0.2 (p=0.01), for inflammation 1.9±0.3 and 1.5±0.2 (p=0.03), for fibrosis 2.8±0.2 and 1.6±0.1 (p<0.0001). The mean % ASC for all zones was 1.3 for HCV/DM and 1.2 for HCV (p=0.39). However, when both diagnostic groups were combined, a significant % of ASC was observed in periportal areas and portal tracts for fibrosis stages >2 vs stages ≤2 (p<0.0001). In addition, a statistically significant increase in %ASC was observed in zone 1 for HCV/DM group (mean 1.5) compared to HCV group (mean 1.2) regardless of fibrosis stage (p=0.02). This study suggests that in patients with HCV or HCV/DM, activated stellate cells are predominantly located in periportal areas and correlate with advanced fibrosis stages (>2). Periportal stellate cell activation is significantly increased in the HCV/DM group compared to HCV group.

P209

Report of two rare cases of hepatoid adenocarcinoma with gastric and gallbladder localization.

Gakiopoulou H., Liapis G., Givalos N.,
Agrogiannis G., Patsouris E, Delladetsima I.
Department of Pathology, Medical Faculty, National Kapodistrian University of Athens & Department of Pathology, Laikon Hospital, 75 Mikras Asias, 11527, Athens, Greece

Hepatoid adenocarcinoma (HAC) is a rare variant of adenocarcinoma associated with hepatic differentiation in both morphological and functional terms. Although it was first described as a specific type of primary gastric cancer, HAC has recently been reported in various anatomic locations. We present two rare cases of HAC observed the first in the stomach and the second in the gallbladder. The later constitutes a very rare localization since a thorough research of the literature has revealed only six previously reported cases.
Histologically, within a conventional gallbladder adenocarcinoma and a gastric adenocarcinoma with enteroblastic features, areas of hepatoid differentiation were observed composed of eosinophilic or clear cells arranged in a trabecular, nested or rosettoid pattern. Bile plugs were additionally noticed in the gallbladder HAC. Immunohistochemistry in the hepatoid areas demonstrated HepPar 1 reactivity (strong and diffuse in the gallbladder and focal in the gastric HAC), polyclonal CEA positivity with a canalicular pattern of expression and AFP immunoreactivity (strong and diffuse in the gastric but faint and focal in the gallbladder HAC). Based on the histological and immunohistochemical findings, these cases were diagnosed as adenocarcinomas with hepatoid differentiation. Knowledge of this rare histologic variant is important in the differential diagnosis from metastatic hepatocellular carcinoma.

P210

Prognostic and therapeutic implications of Replication Protein A (RPA) immunohistochemical expression for colon cancer patients

Givalos N[2], Agrogiannis G[1], Gakiopoulou H[1], Konstantinidou AE[1], Skliri M[1], Lelouda M[1], Kouraklis G[2], Karatzas G[2], Patsouris E[1]
[1]Department of Pathology & [2]Department of Surgery,
Medical Faculty, National Kapodistrian University of Athens,
75 Mikras Asias, 11527, Athens, Greece

Replication protein A (RPA), a component of the origin recognition complex, is required for stabilization of single stranded DNA at early and later stages of DNA replication being thus critical for eukaryotic DNA replication. Moreover, RPA is involved in DNA recombination and repair. This protein is present in cells as a heterotrimeric complex consisting of three subunits which, in order of decreasing size, have been designated as RPA1 (70kDa), RPA2 (32kDa), and RPA3(14kDa). The aim of the present study was to investigate for the first time the value of RPA1 and RPA2 proteins, as prognostic indicators and possible therapeutic targets in colon cancer patients. RPA1 and RPA2 protein expression was analyzed in a series of 130 colon cancer resection specimens in relation to conventional clinicopathological parameters and patients' survival. Immunohistochemistry (ABC-HRP method) was performed using monoclonal antibodies (Oncogene, NA13 and NA 18, respectively). For statistical analysis the following tests were used: Spearman's rho, Kruskal Wallis, Mann-Whitney U, Wilcoxon Signed Ranks. Survival analysis was univariate (Log-Rank test) and multivariate (Cox regression model).
Statistical significant positive associations emerged between: a) RPA1 and RPA2 protein expressions (p=0.0001), b) RPA1 and RPA2 labeling indices (LIs) and advanced stage of the disease (p=0.001 and p=0.003 respectively), c) RPA1 and RPA2 LIs and the presence of lymph node metastasis (p=0.002 and p=0.004 respectively), d) RPA1 LI and the number of infiltrated lymph nodes (p=0.021), e) RPA2 LI and histological grade of carcinomas (p=0.05). Moreover, a statistical significant higher RPA1 LI was observed in the metastatic sites compared to the original ones (p=0.012). RPA1 and RPA2 protein expression associated with adverse patients' outcome in both univariate (Log Rank test: p<0.00001 and p<0.00001 respectively) and multivariate (Cox model: p=0.092 and p=0.0001 respectively) statistical analysis. Statistical significant differences according to the expression of RPA1 and RPA2 proteins were also noticed in the survival of stage B (p<0.00001 and p=0.0016 respectively) and stage C (p=0.0029 and p=0.0079 respectively) patients. In conclusion, RPA1 and RPA2 proteins appear to be useful prognostic indicators in colon cancer patients and attractive targets for regulation by tumor supressors or other proteins involved in the control of cell proliferation.

P211

Hepatocellular adenoma with telangiectatic changes, focal hemorrhagic necrosis and heavy lipofuscin - like pigment deposition in a 45 year old male.

K. Giaslakiotis, D. Hatzianastasiou, G. Liapis,
K. Kokkori, J.K. Delladetsima
Department of Pathology, Laiko General Hospital, 75 Mikras Asias, 115 27 Athens, Greece.

Heavily pigmented hepatocellular adenoma in men without a history of streroid use in very rare, while a pigmented subtype with telangiectatic changes has not been reported. A 49-year-old man, with no previous steroid use, presented with a hepatic mass, discovered incidentally. A limited hepatic resection was performed. On macroscopic examination, the lesion measured 9cm in diameter with a well limited contour, congestive areas and focal hemorrhagic necroses. Histologically the lesion consisted of hepatocytes arranged in one to two cell thick plates, mildly pleomorphic, densely loaded with coarse granules of iron negative brown pigment. No mistoses were indentified, while the reticulin network was preserved. Of note were extensive areas with peliod changes. Dissecting fibrous septa thick walled arterial branches and dilated

veins were also present, but the absence of reactive bile ductules excluded focal nodular hyperlasia. CD34 immunohistochemical staining was focally positive. Based on the histopathologic findings, the changes were in keeping with a hepatocellular adenoma. Two years after resection the patient is free of relapse.

P212

Heterotopic mesenteric ossification

Chatzigianni E., Katafyghiotis P., Bouza E., Kyratzis G, Mahera H.
Department of Pathology & B'Surgical Department,
General Hospital of Attikis "KAT" Greece

We present a case of a 42 year old male patient who was admitted to our Hospital with bowel obstruction apparently due to symphysis from a previous colectomy for a malignancy. The specimen, we received in the Pathology Department consisted of two pieces of bowel specimen joined firmly with lots of symphysis, while in the surrounding fatty tissue there were several whitish-yellowish hard, firm areas ill defined, resembling fat necrosis. The histologic findings showed that these areas contained foci of bone while the rest there were foci of fat necrosis, fibrosis, hemorrhagic and inflammatory changes. Subsequently the patient had a normal recovery, but six months later re- admitted, for recurrent bowel obstruction with the same lesion as previously mentioned. Our diagnosis was heterotopic mesenteric ossification which is a rare entity occurring mainly in young or middle aged males up to the age of 72. The size of the tumor ranges between 3,5cm up to 20cm.It occurs mostly in association with trauma, infection, or chemotherapy while the main aetiologic factors have not yet been clarified.

P213

Immunohistochemical expression of syndecan-1 protein in gastric cancer

Antonia Charchanti[1], Ann C. Goussia[2], Eufemia Balasi[2], Catherine Zioga[2], George Fountzilas[3], Panagiotis Kanavaros[1], Niki J. Agnantis[2], Maria Bai[2]
Departments of [1]Anatomy-Histology-Embryology and [2]Pathology, Medical School, University of Ioannina, 45110, Ioannina, Greece Department of [3]Medical Oncology, Medical School, Aristotle's University of Thessaloniki, Thessaloniki, Greece

Syndecan-1 (SDC-1) is a transmembrane heparan sulfate proteoglycan, that binds to various extracellular matrix components, mitogenic and growth factors via its heparan sulfate chains. In the present study, we analyzed the immunohistochemical expression of SDC-1 in 103 cases of gastric adenocarcinomas. SDC-1 expression was observed in both neoplastic and stromal cells. Strong neoplastic and stromal staining (>50% of cells) was found in 16.3% and 4.8% of the cases respectively, moderate (10-50% of cells) in 24% and 21.2% of the cases, respectively and weak (<10% of cells) in 59.6% and 74% of the cases, respectively. SDC-1 expression in neoplastic cells lower in more invasive cases (mucosa/submucosa vs muscularis propria/ serosa/perigastric fat, p=0.034) and in cases with lymph vessel invasion (p=0.035). Low stromal SDC-1 expression was correlated with histologic type (intestinal vs diffuse/mixed, p= 0.04), histologic grade (I vs II/III, p= 0.04) and with greater tumor size (p=0.026). It is concluded that low epithelial and stromal SDC-1 expression are associated with unfavorable histopathological parameters in gastric carcinomas.

P214

Heat Shock Protein (HSP)-27, -70 and -90 expression in gastric cancer: correlation with clinicopathological variables

Costantinos Giaginis[1], Stella Daskalopoulou[1,2], Olga Nousia[1], Ioannis Sfiniadakis[1,3], Gregorios Kouraklis[2], Stamatios Theocharis[1]
Depts of Forensic Medicine-Toxicology[1] and Propaedeutic Surgery[2], University of Athens; Dept of Pathology[3], Naval Hospital; Athens, Greece

Heat Shock Proteins (HSPs) are crucial for the maintenance of cell integrity in normal and malignant cell growth. In the present study HSP-27, -70 and -90 expression was examined immunohistochemically on paraffin embedded gastric cancer tissue sections obtained from 56 patients. HSP-27, -70 and -90 positivity, overexpression (positivity in more than the mean percentage value) and intensity of staining (mild, moderate, intense) were correlated with patients'age, gender and TNM stage, tumor histological type, grade and proliferative capacity (Ki-67 labeling index). HSPs were abundantly expressed in gastric cancer cases examined. HSP-27 overexpression was statistically significantly correlated with tumor size (T, p=0,008) and the presence of nodular metastasis (N, p=0,049). HSP-90 intensity of staining was statistically significantly correlated with tumor histological type (p=0,004). No correlation was noted between either HSP-70 protein positivity, or overexpression, or intensity of staining and the clinicopathological variables examined. Our findings verify that HSPs are widely expressed in gastric cancer suggesting participation of these proteins in gastric carcinogenesis.

P215

Granular cell tumors of the sigmoid and rectum.

Papaevangelou M.[1], Koniaris E.[1], Papathanasaki A.[1], Gazalidou M.[1], Biteli M.[1], Tsamakidis K.[2]
[1]Dept. of Pathology of the Hellenic Anticancer Institute, 'St. Savvas' Hospital, Athens, Greece.
[2]Dept. of Gastroenterology of the Hellenic Anticancer Institute, 'St. Savvas' Hospital, Athens, Greece.

Granular cell (Abrikossoff's) tumors are uncommon in the gastrointestinal tract and are quit rare in the colon and the rectum. To date 64 cases of granular cell tumors of the colon have been reported in the literature. We present a 56-year old patient admitted to our hospital for further evaluation because of blood in his stool. The endoscopic examination revealed a spherical non-pedunculated polyp with smooth surface, measured 2x2cm, located in the sigmoid (50cm from the anal sphincter). Another polyp with similar endoscopic features, measured 0.8x0.8cm, was also found 5cm from the anal sphincter and both tumors were resected by endoscopic loop. Endoscopic examination of the entire colon up to the caecum did not reveal any other lesions. The histological examination disclosed two submucosal tumors consisted of large tumor cells with abundant granular cytoplasm and small round nuclei. The tumors cells expressed S-100 protein, Neuron Specific Enolase, Period Acid Schiff and Vinmentin but were negative for Smooth Muscle Actin, Desmin and CD117.
Granular cell tumors are rare in the gastrointestinal tract and the pathologist must be aware of this. They can be misinterpreted to indicate a possible malignancy on a biopsy. The theraupeutic approach, since granular cell tumors are usually benign must be conservative and in multiple tumors a strict endoscopic follow-up is suggested.

P216

B-raf mutations and Microsatellite Instability analysis in sporadic Basal Cell Carcinomas.

Angeliki I. Stamatelli, Angelica A. Saetta, Kiriaki G. Aroni, Fanie L. Gigelou, Efstratios S. Patsouris
Department of Pathology, Medical School, National and Kapodistrian University of Athens, Greece

Alterations of BRAF have been linked with colorectal cancers exhibiting microsatellite instability (MSI). Our aim was to investigate the role of BRAF in basal cell carcinomas (BCC) in correlation with the presence of MSI. 75 BCCs were screened for mutations in the kinase domain of BRAF gene by single-strand conformation polymorphism (SSCP) analysis followed by DNA sequencing. The presence of MSI was based on the analysis of two mononucleotide markers: BAT25, BAT26. Four additional markers were analysed in cases where matched normal tissue was available: BAT40, D2S123, D5S346 and D17S250. The repetitive sequences within the known target genes, TGF-β receptor type II (TGF-βRII), hMSH3 and hMSH6 were also analysed. A mutation in BRAF gene exon 15 was detected in one case, which was classified as microsatellite stable. MSI was found in 8% of the tumours investigated. TGF-βRII frameshift mutations were identified in four cases. Four BCCs carried hMSH3 mutations, one of which was scored as microsatellite unstable. There were no alterations in hMSH6. According to our results the investigated BRAF gene does not appear to be a significant target for mutations in BCCs. The implication of the MAP kinase ERK signalling pathway in the pathogenesis of BCC mandates further evaluation.

P217

A low cost strategy for detection of hereditaty nonpolyposis colorectal cancer (HNPCC)

H. Bouzourene, L. Taminelli, C Monnerat, W. Seelentag, D. Sandmeier, S Andrejevic, M Matter, F Bosman, J Benhattar
Institute of Pathology, Lausanne, Switzerland

The detection of microsatellite instability (MSI) in colorectal cancer (CRC) allows to detect HNPCC but it also appears that MSI cancers respond differently to chemotherapy than cancers with chromosomal instability. The purpose of this study was to develop a strategy for HNPCC detection with the highest sensitivity and the lowest cost. In 148 CRC, expression of MLH1, MSH2, MSH6 protein was analyzed, MSI was tested by PCR and methylation of MLH1 promoter was examined. MSI-H was detected in 14.2 % CRC. MSI-H tumors were right located, were of mucinous typer or have a high number of tumor infiltrating lymphocytes. Twenty of 21 MSI-H cancers showed loss of expression of MLH1, MSH2, or MSH6 genes. Out of 15 tumors immunohistochemically MLH1 silent, 3 tumors did not present methylation of the MLH1 promoter. We propose the following algorithm for HNPCC cases detection: 1/ selection of MSI searching would be based on CRC morphology and immunohistochemical analysis might represent the first step in MSI detection. 2/ in cases of abnormal expression of MLH1 protein, MLH1 methylation detection should be required and represent the second step. 3/ in non methylated MLH1 cases and in MSH2, MSH6 immunohistochemically negative cases further molecular analysis should be performed for the detection of HNPCC.

P218

Hepatocellular carcinoma in patients who underwent partial hepatectomy: prognostic factors and therapeutic implications

AC Tsamandas, V Zolota, N Pagoni, A Liava, T Petsas, C Karatza, CD Scopa. University of Patras Medical School, Patras Greece.

In this study the gross and pathologic features of 76 hepatocellular carcinomas (HCC), were investigated and correlated with features of invasive growth and disease-free survival. The study included 76 HCCs removed, by partial hepatectomy, from equal number of patients. In these tumors, several gross and microscopic features were assessed, graded and correlated with disease-free survival. HCCs begin as small, well-differentiated tumors that have an increased proliferation rate and neoangiogenesis. Vascular invasion, is the strongest predictor of disease recurrence, (95%CI: 1.42-16-p<0.001) and is significantly correlated with the number of tumor nodules (included in the specimen), major diameter of the tumors, worst grade and apoptosis/mitosis (A/M) ratio. In the absence of vascular invasion, the size of the largest tumor nodule (p=0.006), the A/M (p=0.03) and the number of neoplastic nodules (p=0.04) were independent predictors of disease-free survival. Tumors with A/M ratio >3 displayed higher disease-free survival compared to those with A/M ratio <3 (p<0.01). From the 8 cases with A/M ratio >6, none developed recurrence 5 years after hepatectomy. In conclusion, this study showed that, in humans, the prognosis of HCC depends on several biological factors. Aggressive biological behavior (vascular invasion and recurrence) correlated significantly with: a) alterations in the apoptosis/mitosis ratio and b) architectural and cellular alterations.

P219

Characteristics of colorectal cancers with or without DNA polymerase epsilon mutations.

Collan Y, Zhou Q, Elzagheid A, Sundstrom J, Talvinen K, Pospiech H, Syvaoja J
Department of Pathology, University of Turku, Kiinamyllynkatu 10, FI-20520 Turku, and Departments of Biochemistry, Universities of Oulu, and Joensuu, Finland

In an earlier study Zavrides et al. (Pol J Pathol, 56, 4, 179-185, 2005) demonstrated that bcl-2 positivity in colorectal cancer was associated with stage of the disease, and improved prognosis. They also showed that bcl-2 expression and Ki-67 index showed an association. We decided to compare our material of 16 colorectal cancers with (N=5) or without (N=11) DNA polymerase epsilon mutations with their findings. The mutations were associated with the second largest subunit of the DNA polymerase epsilon. 3 changes consisted of AATT deletions in intron 18, and 2 of cases showing several single nucleotide transitions in different locations of the gene, and suggesting an amino acid change (tyrosine – histidine) in the protein product of exon 17.
In our material significant or nearly significant associations were found between Ki-67 index, and the location of neoplasms (right side/ left side), bcl-2 index, and Her-2 index. Higher p53 positivity was associated with more advanced stage, Her-2 staining index, but also with higher bcl-2 index. The tumors with mutations had higher Ki-67 index than the nonmutated tumors. Especially the two cases showing point mutations had high Ki-67 indices.
The study suggests that DNA polymerase epsilon mutations have a potential to influence the biological behavior of colorectal cancer. The mutations found may be a reflection of general genomic instability in the studied neoplasms.

P220

Malakoplakia of the colon associated with colonic adenocarcinoma, diagnosed in colonic biopsies.

F. Karasavvidou[a], SP. Potamianos[b], S. Barbanis[a], E. Stathakisa, E. Tziastoudi[a], AN. Kapsoritakis[b], G. Koukoulis[a]
Departments of Pathology[a] and Gastroenterology[b], University Hospital, Larissa, Greece.

Malakoplakia is an uncommon form of chronic inflammation caused by chronic infections and characterized by accumulation of distinct macrophages. Malakoplakia typically involves the urinary tract. It has also been found in various sites such as the gastrointestinal tract, pancreas, liver, lymph nodes, skin, respiratory tract, adrenal gland, vagina and brain.
We present a case of a 64 year old man who referred to our hospital with cachexia and radiologic evidence of metastatic tumor in the liver. Colonoscopy revealed a large malignant-appearing polypoid mass of the ascending colon and multiple distinct polyps throughout the rest of the colon.
Biopsies of the ascending colon mass confirmed the diagnosis of adenocarcinoma. Histological examination of one of the other polyps revealed malakoplakia characterized by aggregates of granular histiocytes with Michaelis – Gutmann bodies, confirmed histochemically with periodic acid-Schiff and von Kossa stains.
This is one of few cases diagnosed on endoscopic sample. Most of the reported cases were found in surgical speciments.
In addition the endoscopic appereance is unusual. There are no reports of malakoplakia mimicking multiple colonic polyposis.

P221

The relationship between expression of c-erbB-2 protein and clinicopathological factors in gastric carcinomas and prognostic significance of c-erbB-2 overexpression

Hakan H. Ozgur, Aysenur A Igdem, Elife Sahan, Nusret Erdogan
Taksim Training and Research Hospital, Pathology Department, 34433, Istanbul, Turkiye.

The c-erbB-2 or HER-2/neu oncogene is a member of the tyrosine kinase oncogene family, and encodes a transmembrane glycoprotein of 185 kDa. It is expressed in a variety of human adenocarcinomas. Expression of c-erbB-2 protein in breast cancer has been reported to be associated with poor prognosis. The overexpression of c-erbB-2 protein has been reported to take place in gastric carcinomas. We wanted to investigate the freqency and clinical significance of c-erbB-2 protein expression in gastric carcinoma. In this retrospective study formaline-fixed, paraffin-embedded tissue sections were prepared from gastrectomy specimens from 61 patients with gastric carcinoma. We investigated the relationships between expression of c-erbB-2 oncoprotein and clinicopathologic characteristics of tumours In this study, correlations of c-erbB-2 protein expression with prognostic outcomes in 46 of 61 gastric adenocarcinomas was evaluated. There was a correlation between the immunohistochemycall score for c-erbB-2 protein and the degree of histological differantiation of gastric carcinoma (p=0.006). Kaplan-Meier analysis (log-rank statistics) revealed a significant association of increasing positive expression of c-erbB-2 with shorter disease-free survival (p=0,042). We concluded that positivity with c-erbB-2 in gastric carcinomas, especially intestinal type carcinomas was specific. We have reported that 9 of the 61 gastric carcinomas showed expression of c-erbB-2 protein and we evaluated that c-erbB-2 protein is a useful prognostic indicator in gastric carcinoma.

P222

Promoter Hypermethylation of RassF1A, DAP kinase, E-cadherin and hMLH1 genes in sporadic colon carcinomas

F.L. Gigelou, A.A. Saetta, P.I. Papanastasiou, M.S. Karlou,
A. I. Stamatelli, E.A. El-Habr, N.V. Michalopoulos,
N. Kavantzas, P.A. Korkolopoulou, E. S. Patsouris
Department of Pathology, Medical School,
The National and Kapodistrian University of Athens, Greece

The aberrant methylation of promoter CpG islands is considered as an important mechanism of inactivation of tumor-related genes. In order to investigate its clinicopathological significance in colon tumorigenesis, we examined the methylation status of DAP kinase, RassF1A, E-cadherin and hMLH1 genes in 86 tumor specimens from Greek patients with sporadic colon cancer. We performed Methylation Specific - PCR and sequencing. The MSI status of these tumor specimens was also evaluated. Hypermethylation of the promoters of RassF1A, DAP kinase, E-cadherin and hMLH1 genes was detected in 22%, 17%, 16% and 8% of the examined cases, respectively. In 11 out of 86 tumors simultaneous promoter hypermethylation of at least 2 genes was found. 13% of the hypermethylated samples were classified as MSI positive. No RassF1A promoter hypermethylation was observed in MSI positive tumors. Abnormal patterns of methylation are commonly observed in various genes during tumorigenesis. The examined genes seem to contribute to colon carcinogenesis even though they exhibited moderate levels of epigenetic aberration.

P223

Expression of Bax protein in gastric carcinomas. A clinicopathological and immunohistochemical study.

Anagnostopoulos G, Stefanou D, Arkoumani E,
Chalkley L, Tsianos E, Agnantis NJ.
Department of Pathology and Gastroenterology,
University of Ioannina, Medical School, Greece.

Bax plays a key role in apoptosis by accelerating cell death. Bax protein suppression is an early event in gastric tumorigenesis. In the present study we immunohistochemically analyzed Bax protein expression in 47 cases of gastric cancer and correlated its expression with clinicopathological parameters.Positive staining for Bax protein was found in 20 (42.4%) of the 47 adenocarcinomas examined. Negative Bax protein expression was correlated with lymph node metastasis and degree of differentiation. Multivariate analysis showed that the only variable with an impact on survival was Bax protein expression ($p<0.05$). Kaplan-Meier curves showed that the 5-year survival was 36.8% in cases with positive Bax protein expression compared with 16 % in negative cases. Negative Bax expression in gastric cancer is associated with de-differentiation, lymph node metastases, and poor clinical prognosis. Therefore, Bax protein expression might play an important role in the development and phenotypic differentiation of gastric carcinomas and tumor progression.

P224

Expression of a-SMA, MMP-2, MMP-9, TIMP-1, TIMP-2 and TGFβ in chronic viral liver diseases.

Patsiaoura K[1], Vrettou E[2], Tzioufa V[2], Hytiroglou P[2],
Koufogiannis D[3]
[1]Department of Pathology "Hippokration" General Hospital,
[2]Department of Pathology and [3]Laboratory of Medical Informatics,
both of Medical School, Aristotle University of Thessaloniki, Greece

Liver fibrosis is a common result of chronic hepatic injury of diverse causes. It is a complex biophysical phenomenon, with reversible and irreversible stage. In order for the liver fibrosis to be developed, an imbalance between fibrogenesis and fibrolysis is necessery to exist, which is characterized by the deposition of extracellular matrix from fibrogenic cells. The aim of our study was to compare the expression of a-SMA, MMP-2, MMP-9, TIMP-1, TIMP-2 and TGFβ in chronic hepatitis B and hepatitis C and the probable correlation with the progression of the disease. We studied 82 cases of chronic hepatitis of different stages histologically and immunohistochemically, using monoclonal antibodies for the above factors. Our results showed: 1)

Statistically significant correlation of the fibrosis stage to the expression percentage of a) a-SMA (R=0.82, P<0.001), b) TIMP-1 (R=0.54, P<0.001) and c) TGFβ (R=0.55, P<0.001). 2) Statistically significant correlation of the expression percentage of a-SMA to the expression percentage of a) TIMP-1 (R=0.46, P<0.001) and b) TGFβ (R=0.57, P<0.001). Our findings suggest that immunohistochemical stains for a-SMA, TIMP-1 and TGFβ may be helpful in assessing the progress of liver fibrosis in chronic hepatitis.

P225

Alternative mediators of apoptosis in toxic induced liver injury

Eleonora Codorean, C. Tanase, C. Iosif, E. Raducan,
D. Popescu, V. Barca
National Institute of Pathology "Victor Babes" Bucharest, Romania

TNF-α is a key cytokine triggering apoptosis of liver cells and may mediate it through alternative pathway involving cathepsin B, an apoptotic noncaspase mediator acting as a dominant execution protease in a mitochondrial pathway.Aim of the study is to evaluate the potential modulation of the toxic liver injury by cathepsin B specific inhibitors. Wistar rats were intoxicated with alcohol, with or without pretreatment of a cathepsin B inhibitor. After dosing fragments of the liver were routinely prepared for histological/ imunohistochemical analysis (TNF-α receptor) and to evaluate DNA fragmentation by puls field gel electrophoresis. The incidence of TNF-α positive cells was higher compared to cells undergoing apoptosis in liver of the rat receiving cathepsin B inhibitor. The feature were associated with lower liver morphological changes – reduced area with hepatocyte injury, minimal necrotic area and absence of fibrotic area. DNA fragmentation level, a sensitive indicator of apoptosis were also decreased in synergic action of alcohol and cathepsin B inhibitor compared to alcohol intoxication. Conclusion: the results may indicate that the alcoholic liver injury was reduced in presence of cathepsin B inhibitor. This lysosomal enzyme may play a pivotal role in TNF-α induced apoptosis and might be a potential new pharmacological target in therapy of ethanol induced liver diseases.

Background: In a wide variety of inflammatory liver diseases, TNF-α has been implicated as a key cytokine triggering apoptosis through TNF-α receptor expressed by liver cells. The start point of the study was the recent observation that TNF-α might mediate apoptosis through alternative pathway involving cathepsin B, a lysosomal cysteine protease, representing an apoptotic noncaspase mediator acting as a dominant execution protease in programed cell death by an alternative mitochondrial pathway.

Aims of the study is to evaluate the potential modulation of the liver toxic injury by cathepsin B specific inhibitors.

Material and methods: Male Wistar rats were intoxicated with alcohol, with or without pretreatment of a cathepsin B inhibitor. After 2 - 4h the rats were sacrificed and fragments of the liver routinely prepared for histological/ imunohistochemical analysis and to evaluate DNA fragmentation by puls field gel electrophoresis.

Results: TNF-α expressing cells and incidence of apoptosis were compared in intoxicated liver with or without cathepsin B inhibitor and in control lot. The incidence of TNF-α positive cells was higher than the cells undergoing apoptosis in liver of the rat receiving cathepsin B inhibitor, associated with lower morphological changes – reduced area with hepatocyte injury, minimal necrotic area and absence of fibrotic area. DNA fragmentation values, a sensitive indicator of apoptosis were also decreased in synergic action of alcohol and cathepsin B inhibitor compared to alcohol intoxication.

Conclusion: Our preliminary results indicate that the alcoholic liver injury was reduced in presence of cat B inhibitor suggesting that a cat B may play a pivotal role in TNF-α induced hepatocyte apoptosis and might be a potential new pharmacological target for inhibiting TNF-α mediated toxic liver injury.

P226

Gastrointestinal dialysis related amyloidosis: Severe complications in two patients under long term hemodialysis.

K. Giaslakiotis[1], D. Stamatiadis[2], J. Bokos[3],
J.N. Boletis[4], J.K. Delladetsima[1]
[1]Department of Pathology, [2]Department of Nephrology, [3]Department of Surgery, [4]Renal Transplantation Unit, Laikon General Hospital, Mikras asias 75, 115 27 Athens, Greece.

Dialysis related amyloidosis (DRA) is a disabling complication of end stage renal failure, associated with beta-2-microglobulin amyloid deposition principally in the osteoarticualr system, while complications related to gastrointestinal involvement are rarely reported. We report two cases of gastrointestinal DRA with fatal outcome presented with ileus and acute colonic perforation respectively. Patients' age was 64 and 57 years; time from iniatiation of hemodialysis was 19 and 20 years respectively; the former patient presented with intestinal pseudoobstruction and the latter with acute abdomen. Clinical evidence of preexistent osteoarticular involvement was present only in the latter. In both patients amyloid depositions were found predominantly in the outer muscular layer and blood vessels. Both patients died of sepsis after sigmoid colon resection. Intermittent ileus, as well as spontaneous bowel perforation, even in the absence of osteoarticular manifestations, should raise suspicion of underlying gastrointestinal amyloidosis in long term hemodialysis patients.

P227

Chemoradiation In Scc Of Esophagous.

B. Mofid, H.R. Mirzaei
Shahid Beheshti University of Medical Sciences-Tehran-Iran.

Purpose: Esophageal cancer ranks among the ten most common cancers worldwide, with high prevalence in Iran. Previously surgery or radiotherapy alone was choice of treatment but they were not effective. Today number of patients receiving definitive chemo radiation has been increasing worldwide. Therefore it is important for evaluate response rate and tolerance patients to chemo radiation.

Material and method: This study is Quasi experimental clinical trial. Patients were evaluated with S.c.c of the esophageal and treated with chemo radiation without metastases, with P.S between 0-2 and adequate organ function (Kidney, liver, bone arrow). Patients were treated with two protocols: a) Cisplatin 40 mg/m weekly plus 50-60 Gyb) Cisplatin 75mg/m day 1 and 5-Fu 1000mg/m day 1-4 in weeks 1, 5,9,13 and concomitant RT 50 GY.

Results: There were 39 patients who received definitive chemo radiation during the period: 1377-1382 in radiation oncology department of Shohada Tajrish hospital. 30 patients matched the recruitment Criteria. The characteristics of the 30 patient were: 23 male and 7 female, median age 65 years(range, 35-75 years). One patient suffered neutropenic fever and there were two treatment related death including sepsis in one patient and uncertain causes on death in another. Of 30 patients, 23(76.6%) achieved complete response.

Conclusion: Chemo radiation has low complication and high efficacy. Other studies for confirmation of these results are recommended.

P228

Colorectal carcinoma incidence in patients under age 30

Simona Stolnicu[1], Doinița Rădulescu[2]
[1]Department of Pathology, University of Medicine Targu Mures
[2]Department of Pathology, University of Medicine, Iasi

The aim of the study is to find colorectal carcinoma incidence in patients under age 30 and to describe the distributions depending on localization, histological type and stage, comparing to older patients. The study was performed between January 1995 and December 2005, on 257 patients with invasive adenocarcinoma. We found 7 patients under age 30, representing 2,72 % of all invasive cancer. The youngest patient was 21 years old. There were no reliable differences between older and younger patients considering localization, histological type and stage of the disease. The 5-years survival is the same in both categories of patients. strategy of the therapeutical approach. Its application is helpful in the identification of patients with unfavorable prognostic characteristics who require a modified and more aggressive therapy.

P230

Immune – effective reactance in Helicobacter pylori infected children, teenagers and young people

Kakabadze Yulia, Kakabadze Sergei
Republic Pathologoanatomic Bureau, Vladikavkas, Russia

Immune-effective reactance was estimated on biopsies from 294 patients with Helicobacter pylori (HP) gastritis according to Sydney system. Within the limits of age group hyporeactions is represented by the variants with prevalence of immune reactance with equality immune and effective reactance and with absence of effective reactance at significant prevalence of the latter. Adequate reactance is represent with variants with low, average and high degree in decreasing frequency. Hyperreactance is represented mainly with variants with equality of immune and effective reactance and with prevalence of immune reactance. In an age of observations group among variants of immune – effective hyporeactance the share of variants with prevalence of immune reactance gradually accrues. Such dynamics is characteristic also for variants with immune – effective hyperreactance. Among variants with adequate immune – effective reactance the share of variants with an average and high degree also gradually accrues. On the generalized data of hyporeactance and hyperreactance, triple prevalence of active follicles above inactive is characteristic and at adequate reactance – double. The received results on differentiated immune – effective reactance at HP – gastritis allow to estimate anti-HP resistance more objectively and show the positive tendency of its increase from children to youth.

P231

VEGF Polymorphisms and VEGF gene expression status and angiogenic activity in Gastric Cancer Development, Prognosis and Survival

N. Tzanakis[1], M. Gazouli[2], Ch. Gakiopoulou[3],
V. Atsaves[3], Z. Christoni[4], A.C. Lazaris[3], P. Karakitsos[4],
E. Patsouris[3], N. Nikiteas[5]
[1]4th Surgical Department, "Attikon" Hospital, University of Athens; [2]Department of Biology, School of Medicine, University of Athens; [3]1st Department of Pathology, School of Medicine, University of Athens; [4]Department of Histology-Embryology, School of Medicine, University of Athens; 52nd Surgical Department, "Laiko" Hospital, University of Athens, Athens, Greece

Angiogenesis plays an important role in growth, progression and metastasis of tumors. VEGF overexpression has been associated with advanced stage and poor survival in several cancers. In the present study, we evaluated the association of functional single nucleotide polymorphisms (SNPs) of VEGF gene as well as VEGF expression status and angiogenic activity, with gastric cancer development, prognosis, and survival in a case-control study of 100 gastric cancer Greek patients. Included in the study were four SNPs (-2578C/A, -1154G/A, -634G/C, and +936C/T) in the VEGF gene. The genotyping was performed with PCR-RFLP techniques. The VEGF expression status was evaluated with immunohistochemistry. Tumor vasculature was highlighted using the anti-CD105 MoAb technique. Our results revealed a marginally significant association of the 634CC genotype (p=0.042) with increased risk for gastric cancer development. None of the rest of the examined polymorphisms or haplotypes conferred any gastric cancer susceptibility. A strong association between the -2578AA (p=0.025), -634CC (p=0.013), +936CT (p=0.028), +936TT (p=0.0001) genotypes and a larger tumor size was observed, while the 2578AA and -634CC genotypes were strongly correlated to poor differentiation (p=0.01) and advanced stage of disease (p=0.039), respectively. In addition, our results indicated that metastatic disease frequency was more accentuated among the +936TT carriers (p=0.0035). Interestingly, carrying the -634CC genotype was associated with decreased overall survival rates (46.67%). VEGF overexpression was observed in 36% cases and was accompanied with high vascularization. No significant association was observed between VEGF protein production and VEGF gene polymorphisms. However, a strong correlation between the VEGF overexpression and lymph node metastasis was observed (p=0.028). Furthermore, overexpression of VEGF was related with poor survival. The present study suggests that VEGF polymorphisms may contribute to gastric tumor characteristics and confirms the association between VEGF overexpression and poor survival in gastric cancer. These observations, however, require further confirmation in a larger multi-ethnic study.

P232

The potential role of activated stellate cells in liver biopsies with hepatitis C compared with hepatitis C/diabetes mellitus.

AC Tsamandas, V Zolota, A Liava, D Dimitropoulou, C Gogos, CD Scopa. University of Patras Medical School, Patras, Greece

Hepatitis C virus (HCV) infection is a major cause of chronic liver disease. Steatosis is a common finding both in HCV and diabetes mellitus (DM). Activated liver stellate cells (ASC-αSMA+ cells) are a major factor responsible for fibrosis and progression to chronic liver disease. This study investigates the presence of ASC in liver biopsies from patients with HCV alone and in patients with HCV/DM. Fifty liver biopsies (HCV-35 and HCV/DM-15) were immunostained with the anti-aSMA antibody. Results were expressed as % (+) cells and correlated with degree of steatosis, inflammation and fibrosis. The mean±SD value, in HCV/DM and HCV patients was: for steatosis 1.1±0.4 and 0.5±0.2 (p=0.01), for inflammation 1.9±0.3 and 1.5±0.2 (p=0.03), for fibrosis 2.8±0.2 and 1.6±0.1 (p<0.0001). The mean %ASC for all zones was 1.3 for HCV/DM and 1.2 for HCV (p=0.39). However, when both diagnostic groups were combined, a significant % of ASC was observed in periportal areas and portal tracts for fibrosis stages >2 vs stages ≤2 (p<.0001). In addition, a statistically significant increase in %ASC was observed in zone 1 for HCV/DM group (mean 1.5) compared to HCV group (mean 1.2) regardless of fibrosis stage (p=0.02). This study suggests that in patients with HCV or HCV/DM, activated stellate cells are predominantly located in periportal areas and correlate with advanced fibrosis stages (>2). Periportal stellate cell activation is significantly increased in the HCV/DM group compared to HCV group.

P233

Eosinophilic esophagitis: Report of 3 cases

Bobos M[1], Televantou D[1], Akriviadis E[2],
Mavropoulou S, Leontidis C, Hytiroglou P[1].
Departments of Pathology[1] and Internal Medicine[2],
Aristotle University Medical School, Thessaloniki, Greece

Eosinophilic esophagitis (EE) is a chronic inflammatory disorder of the esophagus with a growing incidence over the recent years. The characteristic histologic finding is the increased number of mucosal eosinophils (>20) per high power field (eos/hpf). We present 3 cases of EE in young men. The first patient presented with acute dysphagia. On endoscopy, there was vertical furrowing of the lower two thirds of the esophageal mucosa and granularity of the upper third. Biopsies revealed many eosinophils (mean eos/hpf: 30) in the esophageal squamous epithelium. The second patient complained for heartburn, retrosternal discomfort and dysphagia. Endoscopic examination showed vertical furrows and rings in the proximal esophageal mucosa. Biopsies revealed a dense eosinophilic infiltration of the epithelium (mean eos/hpf: 114) with several eosinophilic micro-abscesses. The third patient presented with food impaction and occasional gastroesophageal reflux. Endoscopy showed whitish color of the mucosa, furrows and rings. On histologic examination, there were numerous intramucosal eosinophils (mean eos/hpf: 57). After appropriate treatment, the patients were asymptomatic without sings of recurrence. Both clinicians and pathologists should be aware of the typical features of EE, in order to be able to recognize this entity in the appropriate setting.

P234

An unusual multifocal leiomyosarcoma of the small and the large intestine

Vasilakaki Th, Glava C, Petrakopoulou N, Grammatoglou X, Zizi-Serbetzoglou A
Department of Pathology, Tzaneion General Hospital of Piraeus, Piraeus, Greece

Malignant tumors of the small bowel are rare and account for less than 2% of the total gastrointestinal malignancy. Leiomyosarcoma accounts for less than 15% of the cases with diverse presentation and high incidence of metastasis. In this case we report an unusual presentation of multifocal leiomyosarcoma in the large intestine (descending part of the duodenum). A 71-year-old man came to our hospital complaining about intense pain in the right hypochondrium. Clinical examination showed hepatomegaly. Ultrasound imaging of the superior abdomen showed multiple nodules in the liver with mixed echogenity. Abdominal computed tomography revealed a small bowel mass in close proximity to the head of the pancreas expanding towards the liver. There was para-aortic lymph nodes enlargement and thrombosis of the inferior cava vein. Gastroscopy performed showed a diffusely reddish region, an edema in the descending tract of the duodenum in close proximity to the Vater's ampulla and biopsies were taken. Also colonoscopy was performed and two lumps one in correspondence to the caecum and the other in the descending colon were observed and biopsied. Histological examination of the specimens showed a spindle cell tumor with morphologic and immunohistochemical features (the tumor was positive for alpha-smooth muscle actin and desmin but negative for CD34, CD117, S-100 protein and cytokeratins) compatible with leiomyosarcoma. Neoplastic cells demonstrated prominent cellular atypia, a mitotic rate >10 mitoses/10 high power fields and high expression of the cell proliferation marker Ki67. The majority of leiomyosarcomas grow extraluminally but infrequently tumor can grow both extra and intaluminally. Tumor size varies from 1 to 20 cm and in more than 3/4th of patients tumor is >5 cm. The most common route of metastasis is hematogenous and common sites are liver and lungs. The most frequent site of leiomyosarcoma in the small bowel is jejunum, followed by ileum and duodenum. Surgical resection is the mainstay of treatment in these tumors. Unfortunately leiomyosarcomas are notoriously radioresistant and attempts at using adjunctive radiotherapy and chemotherapy have failed

P235

Expression of syndecan-1 in colorectal carcinomas: its association with angiogenesis, extracellular matrix components, clinicopathological features, and prognostic significance

Antigony Mitselou[1], Elli Ioachim[2], Melli Machera[2], Ioannis Nesseris[2], Eufemia Balassi[2], Michael Doukas[2], Theodore Vougiouklakis[1], Niki Agnantis[2]
[1]Department of Forensic Pathology, [2]Department of Pathology, Medical School, University of Ioannina, Greece

Syndecan-1 is a transmembrane heparan sulphate proteoglycan, which regulates cell-to-cell or cell-to-extracellular interactions and may influence malignant cell behavior.
Tumor development in the large bowel is associated with loss of normal epithelial adhesion and altered patterns of expression of cell adhesion molecules, possibly including syndecan-1. To evaluate changes in syndecan-1 we studied 97 colorectal carcinomas by immunohistochemistry. The staining intensity and distribution was examined, semi-quantified and compared with vascular endothelial growth factor (VEGF), tenascin, fibronectin, collagen IV, laminin, and clinicopathological features.
Strong staining of syndecan-1 was observed in 52 cases (74.2%), moderate in 20 cases (20.6%), and weak in 5 cases (52.2%) of colorectal carcinomas. The expression of syndecan-1 was positively correlated with VEGF of the tumor (p=0.001) and VEGF of the vessels (p=0.007).
The relationship between syndecan-1 expression, clinicopathological parameters, and extracellular matrix components, collagen IV, fibronectin, laminin was not significant. A borderline statistical significance between syndecan-1 expression and tenascin was observed (p=0.053).
In conclusion, our results indicate that disruption of cell-matrix adhesion is critical in colorectal cancinogenesis, and angiogenesis might be plays a significant role in the tumor –stromal microenvironment in cancer. Further studies with a large number of patients are needed to clarify the influence of syndecan-1 in colorectal carcinomas.

P236

Unusual presentation of choriocarcinoma. A case report

Eufemia Balassi[1], Elli Ioachim[1], Antigony Mitselou[2], Vasilios Nousias[3], Costas Nikolaides[4], Nicholas Pavlidis[4], Angelos Kappas[3], Vasiliki Malamou-Mitsi[1]
Departments of [1]Pathology, [2]Forensic Pathology, [3]Surgery, [4]Internal Medicine - University Hospital of Ioannina. Greece.

We report a case of primary choriocarcinoma of the ascendant colon in a 60-year-old woman. The patient consulted a physician because of fever and abdominal pain. On admission at hospital, ultrasonography (US) showed an obscure mass in the right lower quadrant of the abdomen measuring 9x5x7 cm with neovascularisation. The patient underwent resection of about 26 cm of ileum and 22 cm of colon with an end-to-end anastomosis, part of bowel mesentery. A mass was found proximal to ileocaecal valve, in the large bowel. The tumour was 6.5x3.5x3.5 cm in size. Microscopic examination, revealed a proliferation of tumour cells that was composed of two distinctive elements, poor differentiated adenocarcinoma and cytotrophoblasts having eosinophilic cytoplasm and round vesicular nuclear. Numerous mitoses are present as well giant multinucleated cells. Immunohistochemical staining revealed that the tumour cells were positive for EMA, CEA, cytoker 19, cytoker 20 (in some cells), CA19-9, strongly positively for human chorionic gonodotrophin (β-hCG), and negative for cytoker 7. This case of mixed tumor in gastrointestinal tract, suggest that unexpected trophoblastic differ-

entiation may result from aberrant differentiation of locally proliferating cells, so called retrodifferentiation from adenocarcinoma cells, rather than originating in ectopic germ cells or in foci of embryonic totipotent cells.

P237

Expression of syndecan-1 in colorectal carcinomas: its association with angiogenesis, extracellular matrix components, clinicopathological features, and prognostic significance

Antigony Mitselou[1], Elli Ioachim[2], Melli Machera[2], Ioannis Nesseris[2], Eufemia Balassi[2], Michael Doukas[2], Theodore Vougiouklakis[1], Niki Agnantis[2]
[1]Department of Forensic Pathology, [2]Department of Pathology, Medical School, University of Ioannina, Greece

Syndecan-1 is a transmembrane heparan sulphate proteoglycan, which regulates cell-to-cell or cell-to-extracellular interactions and may influence malignant cell behavior.
Tumor development in the large bowel is associated with loss of normal epithelial adhesion and altered patterns of expression of cell adhesion molecules, possibly including syndecan-1. To evaluate changes in syndecan-1 we studied 97 colorectal carcinomas by immunohistochemistry. The staining intensity and distribution was examined, semi-quantified and compared with vascular endothelial growth factor (VEGF), tenascin, fibronectin, collagen IV, laminin, and clinicopathological features.
Strong staining of syndecan-1 was observed in 52 cases (74.2%), moderate in 20 cases (20.6%), and weak in 5 cases (52.2%) of colorectal carcinomas. The expression of syndecan-1 was positively correlated with VEGF of the tumor (p=0.001) and VEGF of the vessels (p=0.007).
The relationship between syndecan-1 expression, clinicopathological parameters, and extracellular matrix components, collagen IV, fibronectin, laminin was not significant. A borderline statistical significance between syndecan-1 expression and tenascin was observed (p=0.053).
In conclusion, our results indicate that disruption of cell-matrix adhesion is critical in colorectal cancinogenesis, and angiogenesis might be plays a significant role in the tumor –stromal microenvironment in cancer. Further studies with a large number of patients are needed to clarify the influence of syndecan-1 in colorectal carcinomas.

P238

Expression of the anti-angiogenic factor Thrombospondin-1 in colorectal carcinomas: its association with angiogenesis, extracellular matrix components, clinicopathological features and prognostic significance.

Antigony Mitselou[1], Elli Ioachim[2], Melli Machera[2], Ioannis Pamelos[2], Nafsika Simou[2] Evangeli Lampri[2], Theodore Vougiouklakis[1], Niki Agnantis[2]
[1]Department of Forensic Pathology, [2]Department of Pathology, Medical School, University of Ioannina, Greece.

Thrombospondin-1 (TSP-1) is a multifunctional platelet and extracellular matrix protein that is envolved in angiogenesis. Under certain pathological conditions, e.g. malignant tumors, high concentrations of TSP-1 work as an angiogenic agonist. Angiogenesis, the process leading to the formation of new blood vessels from a preexisting vascular network, is necessary from tumor growth, invasion, and metastasis.
Surgical specimens of primary colorectal carcinomas (n=87) were selected from the archives of the Department of Pathology at University Hospital of Ioannina. The specimens were fixed in 10% neutral buffered formaldhehyde and embedded in paraffin. Immunohistochemical staining was performed by the streptavidin-biotin method. The antibodies used are anti VEGF, anti CD34, anti p53, anti tenascin, anti fibronectin, anti collagen IV.
To extrapolate the correlation of TSP-1 with tumor neovascularization we examined the relationship of TSP-1 with microvessel density (CD34) and with angiogenesis (VEGF). The tumor TPS-1, the stroma TPS-1 and the vessel TPS-1 were estimated semi-quantitatively. Strong cytoplasmic expression of TSP-1 protein was detected in 14 cases (16.1%) of tumor cells, strong expression in stroma was observed in 24 cases (27.6%), and 18 cases (20.7%) expressed strongly in vessels. Positive relationship between TSP-1 cytoplasmic and TSP-1 stroma (p=0.0001) was found, as well as between TSP-1 stroma and Tsp-1 vessels (p<0.0001). The level of TSP-1 stroma expression increased in histological grade (p=0.041) and histological type (p=0.001) of the tumor. The relationship of TSP-1 vessel and VEGF vessel of the tumor was statistically significant (p=0.06). Positive relationship between TSP-1 stroma with tenascin and fibronectin (p=0.053 and p=0.063, respectively) was observed.
In conclusion, as a modulator of angiogenesis, TSP-1 is expressed in colorectal carcinomas and is likely to contribute to the extensive neovascularization and spread of these tumors.

P239

Expression patterns of cyclins D1, E, cyclin dependent kinase inhibitors p21 Waf1/Cip1, p27 Kip1, in colorectal carcinoma. Correlation with other cell cycle regulators (pRb, p53, Ki-67 and PCNA), and clinicopathological parameters.

Antigony Mitselou[1], Elli Ioachim[2], Melli Machera[2], Pamelos Ioannis[2], Nafsika Simou[2], Evangeli Lampri[2], Theodore Vougiouklakis[1], Niki Agnantis[2]
[1]Department of Forensic Pathology, [2]Department of Pathology, Medical School, University of Ioannina, Greece.

Aberrations in the cell cycle regulators are common features of many tumors and several have been shown to have prognostic significance in colorectal cancer. The expression patterns of cyclins D1 and E, as well as cyclin dependent kinase inhibitors p21, p27 and their relationship with other cell cycle checkpoint proteins (p53, pRb, Ki-67 and PCNA) were investigated in colorectal cancer in order to ascertain co-regulation and influence on tumor behavior or survival.
The molecular markers were analyzed immunohistochemically using the monoclonal antibodies against cyclin D1, cyclin E, p21, p27, p53, pRb, MIB-1 and PC10, in colorectal cancer tissue from 97 patients. Data were analyzed statistically using the SPSS software program.
Overexpression of cyclin D1, E, and p21 was seen in 5.9%, 30%, and 7.2% of the cases respectively. We observed increased levels of cyclin D1 (p=0.0001), and p21 protein (p=0.03) in tumors with mucous differentiation. Overexpression of cyclin D1 was correlated with tumor stage (p=0.03), the lymph node involvement (p=0.02) and p21 protein expression (p<0.0001).
Cyclin E was found positively correlated with p21 protein expression (p=0.014), as well as with cell proliferation labeling index as measured by PCNA (p=0.011) and Ki-67 score (p=0.07). The prognostic significance of cyclin D1, E, p21, p27 in determining the risk of recurrence and overall survival with both univariate and multivariate methods of analysis showed no statistically significant differences.
In conclusion, these findings suggests that, the levels of cell cycle regulators studied, do not seems to have a prognostic value, in terms of predicting the risk of early recurrence and overall survival in patients with colorectal carcinoma.

P240

Expression of PTEN, MVD and Caspase-3 and their clinicopathological significance in primary gastric cancer

Zizi-Serbetzoglou A, Glava C, Grammatoglou X, Petrakopoulou N, Katsamagou E, Vasilakaki Th.
Department of Pathology, Tzaneion General Hospital of Piraeus, Piraeus, Greece

Introduction: Gastric cancer is one of the commonest malignancies in the world. In patients with gastric cancer the natural disease process consists of carcinogenesis, metastasis and eventual death. The aim of this study was to detect the relation of PTEN, MVD and Caspase-3 and metastasis of gastric cancer.
Materials and methods: We examined the immunohistochemical expression of PTEN, MVD and Caspase-3 protein, in formalin-fixed paraffin embedded tissue sections, taken from 75 cases of total or subtotal gastrectomy for gastric cancer, in primary gastric cancer and adjacent non- tumor mucosa.
Results: PTEN was positively expressed in the nuclei of adjacent epithelial cells and neoplastic cells of gastric cancer in 79,5% and 52,9% of tumor respectively ($p<0,05$). There was no correlation between PTEN and microvessel density (MVD). There was a significant association between PTEN expression and invasive depth, metastasis, growth pattern and Lauren's classification ($p<0,05$). Neoplasmatic cells showed less frequent immunoreactivity to Caspase-3 than epithelial cells of adjacent gastric mucosa (30%, 60,4% $p<0,05$). Furthermore, Caspase-3 expression was dependent of PTEN expression in primary gastric cancer ($p<0,05$).
Conclusion: The down-regulated expression of PTEN and Caspase-3 played an important role in tumorigenesis of the gastric cancer.

P241

Glomus tumor of the stomach. A case report

Vasilakaki Th[1], Zizi – Serbetzoglou A[1], Zisis D[2], Grammatoglou X[1], Nikolaidou ME[1]
[1]Department of Pathology, [2]Department of Gastroenterology, Tzaneion General Hospital of Piraeus, Piraeus, Greece

Glomus tumors are usually benign neoplasms that arise from modified smooth muscle cells of the glomus body. They usually occur in the dermis or subcutis of the extremities. Rare cases have been reported in the visceral location, most often in the stomach. Since glomus tumors are essentially benign and are amenable to conservative excision, it is important to separate them preoperatively from more aggressive gastric neoplasms. We report a case of a 75-year-old man who came to our hospital with gastrointestinal bleeding and epigastric pain. Endoscopic examination revealed an ulcer (1cm) at the lesser curvature, near the antrum, that was biopsied and the diagnosis of glomus tumor was made. The patient underwent an operation and under the ulcer a submucosal tumor 2x1,8cm was observed which was extending to the serosa. Histologically, the tumor was composed of typical glomus cells arranged in a predominantly solid pattern with low mitotic activity. There was no indication of atypia in these cells. Immunohistochemically, the tumor cells were positive for alpha-smooth-muscle Actin and Vimentin, but were negative for CD34, CD117, L26, B, T, Chromogranin, Desmin and S-100 protein. The expression of the cell proliferation marker Ki67 was low. Gastric glomus tumors are rare, benign and normally solitary lesions in the antrum of pyloric region and they have a good overall prognosis, but a small unpredictable potential for malignant behaviour exists. Although rare, glomus tumor should be in the differential diagnosis among other gastric lesions, such as carcinoid tumor, epithelioid GIST, lymphoma and adenocarcinoma. Treatment is local excision.

P242

Cavernous Hemangioma of the Thyroid: a case report with review of the literature

Valavanis C.[1,2], Gavresea Th.[1], Konstantoudakis S.[1], Petridis N.[3], Vecchini G.[1]
[1]Dept. of Pathology – [2]Molecular Pathology Unit, [3]Dept. of Otorhinolaryncology, METAXA Cancer Hospital, Piraeus, Greece

Cavernous hemangioma of the thyroid gland is an extremely rare pathologic entity. It is considered a developmental malformation resulting from the inability of angioblastic mesenchyma to form complete blood vessels. We report a case of cavernous hemangioma of the thyroid gland in a euthyroid 74 year old woman with caughing episodes for 3 months The scan revealed a cold nodule in the middle portion of the right lobe of the thyroid gland and the organ was removed for histopathological examination. The microscopical examination showed lesions of nodule goiter associated with chronic non specific thyroiditis. Focally, a small cavernous hemangioma measuring 0.6 x 0.5 cm was recognized. The lesion was poorly circumscribed and composed of dilated thin-walled blood vessels. The vessels were lined by flattened CD34 positive endothelial cells and were congested with blood.Secondary hemangioma of the thyroid after fine needle aspiration was excluded according to the clinical history of the patient. A review of the relevant literature is presented.

P243

Type 1 neurofibromatosis (von Recklinghausen's disease) associated with multiple GISTs of the small bowel and a rectal adenocarcinoma. A case report and review of the literature.

I. Evangelou, N. Alevizopoulos, G. Kanellis, K. Dimosthenous, C. Meristoudis, C. Petraki
Department of Pathology, Evangelismos Hospital, Athens, Greece.

Type 1 neurofibromatosis, (NF-1) or von Recklinghausen's disease is an autosomal dominant disorder, presenting with multiple neurofibromas throughout the body. Gastrointestinal stromal tumours (GISTs) and endocrine tumours are other rare gastrointestinal manifestations of NF-1. Furthermore, the association of NF-1 with several non-endocrine tumours of different organs has been also reported. We present a 70 years old man with multiple cutaneous tumours of the upper extremities and the trunk and an established diagnosis of rectal cancer post a six month history of rectal blood loss. A rectosigmoid resection was performed and during the surgery multiple solid tumours were found in the small intestinal wall. Two of them, as well as two of the cutaneous solid tumours were resected. The histological and immunohistochemical study revealed: i) a moderately differentiated, p T3N2 rectal adenocarcinoma, ii) GISTs of low malignant potential of the small bowel and iii) cutaneous neurofibromas. The imaging tests revealed no colon cancer metastatic disease. The patient underwent adjuvant chemotherapy and is still alive, with no evidence of disease relapse, one year post surgery. Reviewing the relevant literature thoroughly, we did not find a match of our case that combined NF-1, multiple GISTs of the small bowel and rectal adenocarcinoma.

P244

Comparative Analysis of Small Bowel Biopsies and Serological Markers in the Diagnosis of Celiac Disease

Maria Sajin, M. Craiu, M. Iordachescu, Alina Stanescu
IOMC - "Alfred Russescu" Hospital, Bucharest, Romania

This study is focused on the morphological and serological aspect of the intestinal mucosa in patients sensitive to gluten, hospitalized in the last 7 years.

Methods: Intestinal biopsies, in children aged between 1,3 - 8 years. 117 cases were analyzed serological (positive IgA anti-endomysial antibodies), morphologically (HE, histochemical coloring) and IHC (L B, LT with possible subtypes).
Results: The lesions counted according to the Marsh score were: • 47 Marsh I infiltrating lesions but positive coeliac serology is only for 41 patients; • 18 Marsh II infiltrating lesions with enlarged crypts and infiltrated with lymphocytes, with positive coeliac serology; • 15 Marsh IIIa destructive lesions with partial villi atrophy (VA) and hyperplasic crypts / HPC but positive coeliac serology is only for 12 patients; • 19 Marsh IIIb destructive lesions with subtotal VA, widened HPC containing immature epithelial cells with a higher growth rate and influx of inflammatory cells but positive coeliac serology is only for 16 patients; • 28 Marsh IIIc hyperplasic lesions but positive coeliac serology is only for 27 patients. The IHC tests have indicated the prevalence of T lymphocytes (CD3, CD4, CD8, γδ) This study is presented in order to illustrate the absence of concordance between serology and the intestinal microscopically aspects of the coeliac disease.

P245

Nuclear Morphometric Analysis in Gastrointestinal Stromal Tumors: A Preliminary Study.
Sukru O. Ozdamar*, Sibel Bektas*, Sevim E. Ozdamar**, Gokhan Gedikoglu***, Banu D. Gun*, Burak Bahadir*
Departments of Pathology; Zonguldak Karaelmas University School of Medicine*, Hacettepe University School of Medicine***, Department of Neurology, Hacettepe University School of Medicine**, Turkey

Gastrointestinal stromal tumors (GISTs) are considered a specialized group of mesenchymal neoplasm. In this study, the histomorphologic and immunohistochemical features of GISTs are compared with nuclear morphometric results. Morphometric nuclear parameters such as mean area, mean roundness factor, mean formellipse, mean length and mean perimeter were evaluated in a total of 22 GISTs, 9 benign and 13 with malignant potential. Results were compared with tumor behavior and size, the presence of necrosis, mitotic index, and immunohistochemical expressions of p53 and proliferating cell nuclear antigen (PCNA). No correlation has been found between morphometric features and GISTs' behavior, tumor size, index of PCNA and p53 expressions ($p>0.05$). However we found that tumor necrosis were correlated with mean nuclear roundness factor, mean nuclear formellipse, mean nuclear length and mean nuclear perimeter ($p<0.05$). Mitotic index were also correlated with mean nuclear roundness factor and mean nuclear formellipse ($p<0.05$). The relative concordance of the results and general histomorphologic and clinical data exhibited the importance of nuclear morphometric analysis.

P246

Alternative mediators of apoptosis in toxic induced liver injury
Eleonora Codorean, C. Tanase, C. Iosif, E. Raducan,
D. Popescu, V. Barca
National Institute of Pathology "Victor Babes" Bucharest, Romania

TNF-α is a key cytokine triggering apoptosis of liver cells and may mediate it through alternative pathway involving cathepsin B, an apoptotic noncaspase mediator acting as a dominant execution protease in a mitochondrial pathway. **Aim** of the study is to evaluate the potential modulation of the toxic liver injury by cathepsin B specific inhibitors. Wistar rats were intoxicated with alcohol, with or without pretreatment of a cathepsin B inhibitor. After dosing fragments of the liver were routinely prepared for histological/ imunohistochemical analysis (TNF-α receptor) and to evaluate DNA fragmentation by puls field gel electrophoresis. The incidence of TNF-α positive cells was higher compared to cells undergoing apoptosis in liver of the rat receiving cathepsin B inhibitor. The feature were associated with lower liver morphological changes – reduced area with hepatocyte injury, minimal necrotic area and absence of fibrotic area. DNA fragmentation level, a sensitive indicator of apoptosis were also decreased in synergic action of alcohol and cathepsin B inhibitor compared to alcohol intoxication.
Conclusion: the results may indicate that the alcoholic liver injury was reduced in presence of cathepsin B inhibitor. This lysosomal enzyme may play a pivotal role in TNF-α induced apoptosis and might be a potential new pharmacological target in therapy of ethanol induced liver diseases.
Background: In a wide variety of inflammatory liver diseases, TNF-α has been implicated as a key cytokine triggering apoptosis through TNF-α receptor expressed by liver cells. The start point of the study was the recent observation that TNF-α might mediate apoptosis through alternative pathway involving cathepsin B, a lysosomal cysteine protease, representing an apoptotic noncaspase mediator acting as a dominant execution protease in programed cell death by an alternative mitochondrial pathway.
Aims of the study is to evaluate the potential modulation of the liver toxic injury by cathepsin B specific inhibitors.
Material and methods: Male Wistar rats were intoxicated with alcohol, with or without pretreatment of a cathepsin B inhibitor. After 2 - 4h the rats were sacrificed and fragments of the liver routinely prepared for histological/ imunohistochemical analysis and to evaluate DNA fragmentation by puls field gel electrophoresis.
Results: TNF-α expressing cells and incidence of apoptosis were compared in intoxicated liver with or without cathepsin B inhibitor and in control lot. The incidence of TNF-α positive cells was higher than the cells undergoing apoptosis in liver of the rat receiving cathepsin B inhibitor, associated with lower morphological changes – reduced area with hepatocyte injury, minimal necrotic area and absence of fibrotic area. DNA fragmentation values, a sensitive indicator of apoptosis were also decreased in synergic action of alcohol and cathepsin B inhibitor compared to alcohol intoxication.
Conclusion: Our preliminary results indicate that the alcoholic liver injury was reduced in presence of cat B inhibitor suggesting that a cat B may play a pivotal role in TNF-α induced hepatocyte apoptosis and might be a potential new pharmacological target for inhibiting TNF-α mediated toxic liver injury.

P246B

Neonatal menetrier disease
Identification of a novel age-related subtype
A.E. Konstantinidou, A. Nonni, G. Morphopoulos,
E. Tsekoura, I. Thymara, E. Patsouris
Dept. Pathology, Medical Faculty, National University of Athens
B'Neonatal Intensity Care Unit, Agia Sofia Children's Hospital, Athens, Greece

Menetrier disease (MD), a rare hypertrophic gastropathy, has been described in adult and pediatric patients. Both pediatric and adult types of the disease share similar histological and clinical features, while a specific pattern of transforming growth factor-α (TGF-α) overexpression has been described in both adults and children with MD. Despite these similarities, pediatric MD is a transient condition, frequently associated with cytomegalovirus gastric infection, whereas adult MD is more chronic and may require gastrectomy. In early infancy, MD has only rarely been reported. In this article, on the occasion of two new neonatal cases, we describe the clinical, laboratory and pathological data available for all the reported cases in early infancy. In addition, we describe an abnormal pattern of TGF-α and EGFR immunohistochemical localization and expression in the gastric mucosa of 4 infants with MD diagnosed in our department. From the comparative examination of the total of neonatal cases (n=9), we are led to presume that neonatal MD may represent a

separate subtype of the disease with a fatal clinical outcome. We also suggest that MD should not be considered a specific disease, but rather a reaction of the gastric mucosa to various insults, mediated by TGF-α and EGFR activation.

P246C

Potential involvement of PTEN expression in resistance to anti-HER2 targeted therapies in pancreatic ductal adenocarcinoma: A combined chromogenic in situ hybridization and immunohistochemistry analysis based on tissue microarrays

E Tsiambas[1], A Karameris[1], D Tiniakou[2], P Karakitsos[2], Ch Kittas[2]
[1]Department of Pathology, 417 VA (NIMTS) Hospital, Athens, Greece, [2]Lab of Histology & Embryology, Medical School, National and Kapodestrian University of Athens, Greece.

Background: Although HER2/neu overexpression is observed in different proportions in pancreatic ductal adenocarcinomas (PDAC), the specific mechanisms of gene deregulation and chemo resistance to novel targeted therapeutic agents remain under investigation. Our aim was to identify HER2/neu gene alterations in PDAC correlating them to its protein levels and also to PTEN suppressor gene expression, which normally opposes the activation of PI3K-Akt-m TOR signaling pathway.
Materials and Methods: Using tissue microarray technology, fifty (n=50) paraffin embedded tissue samples of histologically confirmed primary PDACs were cored at a diameter of 2mm and re embedded into the final recipient block. Ten (n=10) samples of normal epithelia, adjacent to cancerous tissue were used as normal control group. Immunohistochemistry was performed by the use of anti-HER2/neu monoclonal antibody (TAB 250) and anti-PTEN polyclonal antibody. Chromogenic in situ hybridization was applied based on the use of HER2/neu gene and 17 centromeric probes, respectively. Protein expression levels were evaluated using an image analysis system. SPSS (chi square test and interrater kappa) was performed for statistical analysis.
Results: HER2/neu protein over expression was observed in 10/50 (20%) correlated only to grade (p=0.019). Low levels or loss of PTEN protein expression were observed in 17/50 (34%) cases associated to grade and stage (p=0.044 and p=0.02, respectively) Gene analysis identified 8/50 (16%) HER2/neu low-level gene amplified cases. Chromosome 17 analysis detected aneuploidy in 19/50 (38%) cases. Simultaneous HER2/neu overexpression and reduced PTEN expression was observed in 7 cases, whereas six of them demonstrated HER2/neu gene amplification (overall 95% CI kappa=0.12). Concerning control group, HER2/neu protein overexpression was identified in one case, whereas two cases demonstrated low-level PTEN protein expression.
Conclusions: Our results indicate that a subset of PDAC is characterized by simultaneous HER2/neu over- and PTEN reduced expression including sporadic cases of HER2/neu gene amplification. Because, on binding to the HER2/neu receptor, monoclonal antibodies, such as trastuzumab, stabilize and activate PTEN, frequently loss of its expression in PDAC maybe influence the efficacy of targeted therapeutic strategies, especially in the cases of gene amplification, which are associated to response to those agents, earning survival benefit regarding breast cancer.

P247

The value of agnors index in the typing of basal cell carcinomas and prediction of recurrence

Doinita Radulescu[1], Simona Stolnicu[2], Claudia Costea[1]
[1] Department of Pathology, University of Medicine, Iasi, Romania
[2] Department of Pathology, University of Medicine, Targu Mures, Romania

Basal cell carcinoma (BCC) is the most common cutaneous cancer in humans and its incidence increases with age and exposure to ultraviolet rays. Although generally presents a relatively benign course, in classic form of BCC (BCC1), some cases show aggressive behaviour (BCC2). In order to identify reliable prognostic indicators that correlate with outcome, we investigated Nucleolar Organizer Regions (AgNORs) and their correlation with tumor aggressiveness. We selected 35 cases of BCC2 from a total 149 cases of BCCs using the following criteria: nuclear pleomorphism, high mitotic index, absence of cellular peripheral palisading, hyaline fibrosing stroma and irregular spiky pattern of invasion. BCC2 samples showed statistically significant higher counts of AgNORs than did BCC1, a finding that in many other malignancies is linked to a more activated state of neoplastic cells. Our results suggest that the increase of proliferative activity, evaluated by AgNOR index may represent an important step in the acquisition of the aggressive phenotype in human BCCs. Evaluation of AgNOR in BCC may be helpful in selecting patients with high risk for recurrence (BCC2), who could benefit from additional therapies and closer follow-up, in order to improve the quality of life and to prolong the overall survival.

P248

Spindle and epithelioid cell nevus (Spitz Nevus)

Doinita Radulescu, S. Dumitriu
Department of Pathology,
University of Medicine and Pharmacy, Iassy, Romania.

12 cases with spindle and epithelioid cell nevus occurred in children were analyzed clinically and morphologically. The results indicate that Spitz nevus is composed of cells resembling those of a malignant melanoma. There are some morphological aspects such as: discontinuous junctional proliferation, the sparse mitotic activity, the process of maturation of the cells with increasing depth, considered as valuable marks for the benign character of this type of tumor.

P249

Histological control of excised tissue edges in the operative treatment of basal cell carcinomas of the eyelid

Claudia Costea[1], Doinita Radulescu[2], Simona Stolnicu[3], L. Popa[2]
[1]"Sf.Treime" Hospital, Iasi, Romania, [2]Department of Pathology, University of Medicine, Iasi, Romania, [3] Department of Pathology, University of Medicine, Tg.Mures, Romania

Surgical treatment of Basal Cell Carcinoma generally aims at primary and radical excision of the lesion. The curability of Basal Cell Carcinoma is particularly good, because the risk of metastasis is extremely low. There is a relation between the clinical diameter of the tumor and a safe margin that can guarantee long-term radical excision. The edges of 250 basal-cell carcinoma specimens were evaluated histologically to assess subclinical extension and to ensure radical excision. This procedure is considerably simpler and faster than the standard method of microscopically controlled surgery. Since this procedure is simple, it can be routinely used for all primary basal cell carcinoma and thus eliminates recurrence, which usually results in considerably longer defects. With this method, no recurrences of lesions, excised were observed, during a 4 ½ year observation.

P250

Clinical and histopathologic aspects in anorectal malignant melanoma

Simona Stolnicu[1], Doinița Rădulescu[2], Simona Mocan[1]
[1]Department of Pathology, University of Medicine Targu Mures
[2]Department of Pathology, University of Medicine, Iasi

We present 3 cases of anorectal malignant melanoma developed in the inferior portion of rectum. In two cases, endoscopic examination relived a large exophitic, brown tumor mass. In one case, the gross appearance was of a small polipoid lesion, 1 centimetre in diameter, with the head of the polyp pigmented. Microscopic examination showed sheets of atypical spindle cells, with granular material in the cytoplasm, positive with Masson Fontana staining. All 3 tumors present an in situ component identified both in the squamous and cilindrical epithelium, covering the tumors. The spindle cells expressed HMB-45. Anorectal malignant melanoma is a very rare tumor, with a long term evolution, discovered late because frequently is asymptomatic.

P251

E-cadherin/catenin complex and dysadherin expression in benign and malignant melanocytic lesions.

Panelos J.D.[1], Batistatou A.[1], Zioga C.[1], Nakanishi Y.[2], Hirohashi S.[2], Charalabopoulos K.[3], Agnantis N.J.[1]
Departments of [1]Pathology and [3]Physiology, Clinical Unit, University of Ioannina Medical School, Greece, [2]Pathology Division, National Cancer Center Research Institute, Tokyo, Japan.

Adhesion molecules are believed to play an important role in melanocytic tumor progression. To gain detailed insight in this allocated role we examined the immunohistochemical expression of E-cadherin, the associated proteins α- and β-catenin, and the recently discovered dysadherin, in compound and dermal nevi, Spitz nevi, blue nevi and cutaneous melanomas. We noted changes in E-cadherin expression in the majority of benign and malignant melanocytic lesions. These alterations were more pronounced in melanomas and were correlated with reduction of β-catenin expression. Interestingly, in benign melanocytic lesions preserved expression of β-catenin was demonstrated. α-catenin immunostaining was not detected in our material. Increased dysadherin expression was noted primarily in melanomas, but there was no significant inverse correlation with E-cadherin expression. Our findings indicate that changes in the expression of E-cadherin, β-catenin and dysadherin occur in melanocytic lesions, probably reflecting the various stages of their progression.

P252

The effect of polarized-infrared light on secondary skin wound healing. An experimental study.

Koniaris E.[1], Papaevangelou M.[1], Athanasiou A.[2], Iordanou P.[3]
[1]Dept. of Pathology, Helenic Anticancer Institute, 'St. Savvas' Hospital, 171 Alexandras Av., 11522, Athens, Greece, [2]Dept. of Plastic Surgery, Hellenic Anticancer Institute, 'St. Savvas' Hospital, 171 Alexandras Av., 11522, Athens, Greece, [3]Assistant Professor, Nursing TEI of Athens, Greece.

The purpose of our experiment is to investigate the association between the polarized infrared light and the secondary skin wound healing. For this purpose 40 Wistar mice were used. All of them had the same skin wound and they were divided into two groups. The first one was named experiment group and all those mice were treated with polarized infrared light (480-3400nm for 5 min) while the others, named control group, were not. Samples from the skin of the mice that were sacrificed on the 5th, 10th, 15thand 20th day were taken. Those preparations were formalin embedded, paraffin treated, and then stained for Haematoxylin-Eosin (HE), Vascular Endothelial Growth Factor antibody (VEGF), Smooth Muscle Actin-α (SMA-α) and Vimentin (Vim). Our histological findings support the evidence that the polarized infrared light promotes, especially in the initial phase, the process of secondary wound healing. In fact the experiment group mice were found to have a quicker response to the healing process, as it was demonstrated that they developed much faster granulation tissue, and early maturation of the newly formed capillary network from the first days. Moreover the transformation of myofibroblasts, forming collagen bundles parallel to the surface, and the re-epithelialization of the surface of the wound were faster in the experiment group mice.

P253

Aggressive Digital Papillary Adenocarcinoma. Report of two cases.

K. Revelos[3], P. Kitsanta[1], E. Keramidas[2], G. Miller[2], S.K. Suvarna[1]
Departments of [1]Histopathology and [2]Plastic Surgery, Sheffield Teaching Hospitals, NHS Trust, Sheffield, U.K and [3]Pathology Department, 251 Hellenic Air Force General Hospital, Athens, Greece.

Aggressive Digital Papillary Adenocarcinoma (ADPAca) and aggressive digital papillary adenoma (ADPA) are rare sweat gland tumours. There are only 75 published cases in the literature. The tumours typically involved the dermis and subcutaneous tissue of fingers, toes, and/or the adjacent skin of the palms and soles. They presented as a solitary, asymptomatic, gradually enlarging area of swelling or cystic mass. Histologically, the tumours were not well circumscribed, were composed of nodules of tubuloalveolar and ductular structures with areas of papillary projections into cystic spaces separated by fibrocollagenous stroma. Focally, the glandular spaces contained eosinoplilic, amorphous material. Single or double layers of cuboidal or columnar cells lined the glands and cystic lumens. The mitotic rate was low. ADPAca was previously differentiated from ADPA by its glandular differentiation, necrosis, mitotic rate, cytologic atypia and invasion of soft tissue, bone and blood vessels but now all lesions are regarded as malignant. They are locally aggressive with 50% of local recurrence and can give metastasis in 14% of cases. The treatment is wide excision or amputation at the appropriate level. We report two cases of this rare neoplasm.

P254

Malignant eccrine spiradenoma; an exceedingly rare tumor. Report of a case and comparison with a benign eccrine spiradenoma.

George Apostolou, Ismini Vassilaki, Syrou Alexandra, Helen Mahera
General Hospital of Attikis "KAT", Departmnt of Pathology

Malignant eccrine spiradenoma (MES) is an exeedingly rare tumor of the skin appendages, that apparently arises (malignant transformation) within a long-standing solitary lesion of benign eccrine spiradenoma (BES) .We report a case of MES that occured in a 46-year-old woman on the skin of the left antebrachium, four years ago. The removed part of the skin and soft tissue was fixed in 10% buffered formalin and routinely processed for microscopic examination.The paraffin-embedded tissues were investigated by means of histopathology using hematoxylin and eosin stain and immunohistochemistry. The tumor consisted of two circumscribed nodules. Two distinct components were seen: typical benign eccrine spiradenoma and carcinoma, with areas of transitions. Tumor cells were atypical with a high mitotic rate and penetration through the capsule into the adjacent stroma.The epithelial nature of the tumor cells was demostrated by positivity for epithelial membrane antigen (EMA) and CAM5,2. To confirm the clinicopathological entity of MES, it is important to compare MES and BES.

P255

Kaposi's sarcoma(NON AIDS)as unique skin lesion

M. Mastora, D. Petrakis, A. Ntemou*, F. Koutsouka, E. Nanos, H. Papathanasiou, H. Liapis, S. Stefanaki*, N Akritidis
Department of Internal Medicine, Department of Pathology*, General Hospital,"G. Hatzikosta" Ioannina, Greece.

Aim of this study is to signalize the existence of the relation between NON AIDS Kaposi's sarcoma and other malignancy, but mainly to signalize the difficult diagnostically problem that primary disease, without biopsy, represents.
Material and methods: Our material is composed by 6 patients, 5 men and 1 woman, between 67 and 90 years. All of them were admitted to our institution, because of skin lesions, for examination and treatment. Complete clinical, laboratory controls and biopsy of skin lesion were accomplished.
Results: The specimen of the skin lesion confirmed the diagnosis of Kaposi's sarcoma to all the cases. The clinical and laboratory findings were compatible with malignant haematological disease in 3 of the patients. In these, skin lesion was extended. In the other 3 patients (3 men), Kaposi's sarcoma was primary, manifested with located, at the limbs, skin lesion.
The ablation of the skin lesion and the histological examination has shown vascular slits and structures mixed with fascicles of spindle cells, extravasated erythrocytes and PAS positive globules.
Conclusion: The NON AIDS Kaposi's sarcoma is present also in our country. Skin biopsy is imposed in unique skin lesions. The sensitivity about this disease contributes to precocious diagnosis and treatment.

P256

Causes and histopathological findings of leukocytoclastic vasculitis. A retrospective study of 12 cases.
Raptis L[1], Stefanaki S[2], Mastora M[1], Gizas N[1], Gousis C[1], Demou A[2], Kitsiou E[2], Akritidis N[1]
[1]Internal Medicine Clinic and [2]Pathology Department of General Hospital 'G Hatzikosta', Ioannina, Greece.

Introduction: Leukocytoclastic vasculitis (LCV) is a histopathologic term commonly used to denote a small-vessel vasculitis. LCV could be a manifestation of many diseases such as collagen vascular disease, HIV, Hepatitis C.
Aim: The scope of this study to present the causes of leukocytoclastic vasculitis in a five-year retrospective study and their histopathological findings.
Material and methods: A total of 12 patients (F/M 7/5) with a mean age 57,5 years participated in a retrospective study during the years 2003-2005. All patients had palpable purpura of the body and extremities, with lesions 1-3 mm in diameter. Skin biopsy was performed in all patients.
Results: There was a positive exposure to drugs such as antibiotics (beta-lactam) (60%), cumarin treatment (10%) and viral infections (30%). A skin biopsy sample revealed the presence of perivascular infiltration of polymorphonuclear leukocytes with formation of nuclear dust (leukocytoclasis), extravasation of erythrocytes, and fibrinoid necrosis of the vessel walls.
Conclusion: In our study, drugs especially antibiotics caused leukocytoclastic vasculitis in 60%. The second most frequent causes were viral infections in 30%.

P257

Malignant eccrine spiradenoma of the breast: a case report
Eufemia Balassi[1], Catherine Zioga[1], Ann C. Goussia[1], Sevasti Kamina[1], Emmanuel Kontostolis[2], Dimitrios Stefanou[1]
Departments of Pathology[1] and Obstetrics-Gynaecology[2], Medical School, University of Ioannina, 45110 Ioannina, Greece

Eccrine spiradenoma is a generally benign skin appentage neoplasm. Malignant cases are very rare. We describe a case of malignant eccrine spiradenoma that occurred in the breast of a 71-year-old woman. The patient presented with a breast mass and was scheduled for surgical excision of the lesion and intraoperative frozen section. The surgical specimen was consisted of breast tissue covered by a piece of skin. Sectioning revealed a cutaneous encapsulated tumor 4 cm of maximal diameter and several small satellite nodules. Histology of the frozen section from the main lesion showed an almost solid proliferation of epithelioid cells with nuclear pleomorphism and occasional mitotic figures. At the permanent sections of the main and satellite lesions, lobules of monomorphic large cells with oval, pleomorphic nuclei and numerous mitoses surrounded by a delicate reticulin network were observed. Ductular structures as well as areas with small, dark basaloid cells were rarely identified. Histology of the axillary lymph nodes showed an extensive metastatic involvement. Immunohistochemically, pancytokeratin, keratin 8 and ER were expressed in most neoplastic cells. Focal reactivity of CEA was observed in ductal luminal cells. A diagnosis of a malignant eccrine spiradenoma was performed. The patient underwent radiotherapy and chemotherapy with tamoxifen.

P258

Perianal paget's disease
Pazarli E., Katsiki E., Dermitzogloy A., Kakoylidis D., Kafanas. A.
Department of Pathology & Dermatology, General Hospital of Serres, Serres, Greece.

Aim: Extramammary Paget's disease (EMPD) with perianal region localization presents a very rare condition with variable clinical appearance and difficulties in differential diagnosis. We report two cases of extramammary Paget's disease (EMPD) both involving the perianal region with successful surgical treatment.
It may be associated with an underlying carcinoma of the rectum, which may exist simultaneously with the diagnosis of Paget's disease or may appear later.
Due to the rarity of EMPD we review the medical literature.
Material-Method-Results: 1st case: A 37 year old man presented with an erythematous, scaly and prurigitous exanthema in the perianal region. In a period of two years, the exanthema became an ulcerated white plaque with irregular margins about 7cm in diameter. Topical treatment was performed without success. The following step taken was a skin biopsy for histology. The results of the histological examination were typical findings of Paget's disease. After this, the patient was screened for an underlying malignancy. The colonoscopy and the gastroscopy were negative. A broad surgical excision of the affected skin was performed. The patient has been well until now and is in follow up every 6 months.
2nd case: A 68 year-old man has been complaining for pruritus in the perianal region for the last 5 years. At the first examination, the exanthema was erythematous, scaly, with irregular borders and ulcerated. It was located in and around the anus (3cm). The lesion did not respond to topical treatment. So, skin biopsy was taken and histological examination showed typical findings of Paget's disease.
Conclusions: Patients with persistent chronic prurigitous and eczematous lesion in the perianal region that weren't treated with various topical medications for some time, have to be biopsied for histological examination.
In cases of perianal Paget disease it is necessary to evaluate the rectum and anus to determine if the lesion is a manifestation of underlying rectal or anal adenocarcinoma.
The wide local surgical excision is the primary treatment and a long term follow-up is necessary because of the frequent recurrences and the possibility of development of malignancy in the future.

P259

Gallbladder metastatic melanoma mimicking acute cholecystitis.

Koletsa T[1], Dokmetzioglou G[2], Pappas D[1], Pliakos G[2], Maganaris A[3], Bobos M[1], Nenopoulou [1]
[1]Department of Pathology, [2]3rd Department of Surgery, Medical School, Aristotle University, [3]Department of Otolaryngology, Theageneion Hospital, Thessaloniki, Greece

Both primary and metastatic melanoma of the gallbladder are rare. Although it is known that metastatic malignant melanoma can occur in every organ of the body, gallbladder involvement in the absence of disseminated disease is rare. We present a case of metastatic melanoma of the gallbladder that mimicking acute cholecystitis. A 84-year-old woman presented clinically with obstructive cholecystitis and cholecystectomy was performed. When the specimen sectioned a polypoid mass was found to be attached to the mucosa. Morphological and immunohistochemical findings confirmed the diagnosis of malignant melanoma. Medical history of the patient revealed a skin lesion that was locally excised 6 years ago and was proved to be malignant melanoma. So, this case was considered as a solitary metastasis. The patient was re-examined a year after the cholecystectomy and was found to be free of any reccurence. Surgical excision remains the treatment of choice for isolated metastasis of malignant melanoma. Complementary chemotherapy and immunotherapy is still being examined in such cases.

P260

Mucosal melanomas

Zioga C., Kamina S., Dimou S., Goussia A., Simou N., Agnantis N.J.
Department of Pathology, University Hospital of Ioannina, Greece

Primary mucosal melanoma arising from the melanocytes located in the epithelia or the dispersed regional melanocytes are extremely rare. They develop in areas that have no sun exposure and definitive risk factors have not been identified. Due to their rarity, mucosal melanomas have not been adequately characterized and significant questions have been raised regarding their pathogenesis and behavior patterns, rendering further studies necessary. During the last decade we have diagnosed six mucosal melanomas: two located at the nasal diaphragm, one at the outer urethral canal, two at the vagina and one at the colon. All six cases occurred in relatively old patients (>70 yrs old), four women and two men. Herein, we describe the macroscopic and microscopic features (gross appearance, size, presence of ulceration, cell morphology, number of mitoses, presence of neoplastic emboli, immunophenotype of cells) of these neoplasms, as well as provide evidence for a rich vascular network (immunohistochemical study). All the above data are correlated with the therapeutic efforts and patient prognosis.

Virchows Arch (2006) 448: 739–743
DOI 10.1007/s00428-006-0164-y

EDITORIAL

Gianni Bussolati

Dissecting the pathologist's brain: mental processes that lead to pathological diagnoses

Received: 19 January 2006 / Accepted: 19 January 2006 / Published online: 21 March 2006

On the interest of morphology

The specificity of the discipline of pathological anatomy is the study of seats and causes of diseases through morphological interpretation at a macroscopical and microscopical level. Such interpretation and categorization of visible features are being effected through mental processes, which are still poorly understood, despite their interest.

First of all their study might allow to reach a more sound, objective and motivated selection of residents and applicants to the discipline. We know very little about the characteristics which will make a good pathologist, but tests devised for assessing visual memory [17] might help in the selection. We do not even know, for instance, if gender makes any difference and if women are better fit for this speciality than men or vice versa. Indeed, recent evidence shows that women perform better in some forms of memory [14], and this might have to be taken in consideration. In addition, again for the recruitment, we might find ways to better motivate students and applicants.

The second reason why this study is important is to improve reproducibility in pathological classifications and diagnoses because we might thus be able to select and focus our attention on those specific steps of the mental process that are more prone to affect reproducibility.

Other medicine specialists involved in morphological interpretation such as radiologist have already been pursuing an analysis of the process leading to interpretation of images. Following the percourse of perception and decision making during morphological interpretation, they concluded that long decision times work against performance [18]. It is worth mentioning that this might apply as well to cytological reading of pap smears.

The third reason, which makes an analysis worthwhile, is that we might find a way to improve the image of pathology. Morphology is presently regarded as being too subjective, not being based on numbers, and we have to acknowledge that its ranking among scientific disciplines is not high despite the legacy of morphological sciences to medicine and their great impact on the process of medical evolution.

Sources

The feasibility of such study is presently linked to indirect information because no studies were so far specifically addressed to clarify the process leading pathologists to formulate diagnoses. As a result, we have to derive suggestions and information from various alternative sources.

One source is philosophy and psychology. Since Aristotle, from the very beginning of philosophy, human beings have been trying to understand how form is interpreted. In the nineteenth century, mainly German psychologists and philosophers worked on the "Gesthalt theorie," the theory of the form, and they have been trying to establish laws whereby people can understand the forms [23]. For instance, Wertheimer's seventh law establishes the principle that the past experience addresses to the correct interpretation [24]. A clarifying example comes from Kanizsa's figure (Fig. 1), indicating that our mind does not only consider what is present but what is missing as well [7]. This applies so well to the interpretation of histopathological slides: what you do not see has to be taken into consideration, and what is missing is sometimes more important than what you actually see in the microscopic figure.

A considerable source of information are art critics, which have been trying to understand how people look at pictures and perceive art. What are the mental mechanisms that make us appreciate a masterpiece? Martin Kemp has

Lecture presented at the XXth Congress of the European Society of Pathology held in Paris on September 4, 2005.

G. Bussolati (✉)
Department of Biomedical Sciences and Human Oncology,
University of Turin,
Via Santena, 7,
10126 Turin, Italy
e-mail: gianni.bussolati@unito.it
Tel.: +39-011-6334274
Fax: +39-011-6635267

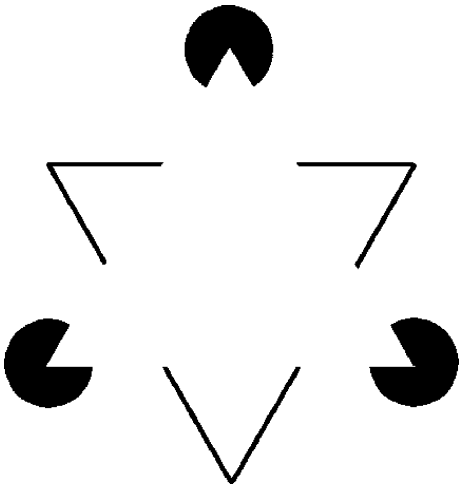

Fig. 1 Kanizsa's triangle

been publishing about this subject [9], and in recent times, Semir Zeki, a neurophysiologist, has been trying to explore the relationship between art and the brain from a neurophysiological point of view [25]. He came out with a very interesting theory which might apply as well to the interpretation of histological slides or of pathological lesions in general: the theory of multistage integration of visual consciousness. Visual brain does not process images as a whole, but through several multistage processing systems. Each system is specialized in a given attribute such as colour or motion or form and so on, working either in parallel or in sequence, finally leading to the interpretation (diagnosis). Support to this theory comes from neurophysiological investigations, which, in recent times, have been providing very important information, especially through functional magnetic resonance images (fMRIs) showing for instance that in right-handed people observing faces rather than objects, it is the medial temporal lobe which is involved and activated [8].

Category-specific breakdowns provide some information: already in the past, it was known that ischaemic infarcts in the medial temporal region of the right hemisphere cause a failure in the rapid recognition of familiar faces [13], and that patients with bilateral insult to the medial temporal lobe cannot transform present experience into future conscious recollection. Radiologist have been trying to understand how [4] expert radiologist process X-ray images, and it appears that they process such images in the way that we all process faces: by quickly devoting processing resources to features that distinguish one stimulus from another [16]. Such process is likely to apply as well to the morphological interpretation of histological slides.

Analysis of the mental process

When trying to analyse the mental processes leading to interpretation of images in pathology, we have to select and analyse different and sequential steps. Four steps can be identified in sequence: (1) to look, (2) to see, (3) to recognize and (4) to understand.

The first step, that of looking, is easily understood because of course, the stimulus goes from the eye to the calcarine sulcus in the occipital lobe.

Thereafter, the stimulus is transferred to other areas devoted to the interpretation of colour, form and faces, mainly located in the fusiform area and in the medial temporal lobe [25].

The second step, that of seeing, is deeply intermingled with the understanding process.

The art critic Martin Kemp observed that "content and recognition are inextricably involved in all our visual acts, since in no occasion you have seeing without meaning, without recollecting" [9]. So let us consider the step of seeing together with that of recognizing. A good example is the following. In 1609, a British astronomer, Thomas Harriot, looked at the moon with his telescope. What he saw and what he described was a sphere, dark and bright areas being separated by an irregular line. He gave no other information or interpretation. A few weeks later Galileo Galilei looked at the moon with his telescope, and what he saw and described in his book *Sidereus Nuncius* (Star Announcement) were mountains and valleys and seas and craters and so on. He saw an irregular line and he could interpret it. Why? Most probably because Galileo had been growing in the atmosphere of Italian Renaissance at the time when the laws of perspective has been discovered and applied to paintings, so he could understand what the irregularities meant and he could interpret them [10].

The process of seeing and that of recognition are strictly linked to the fusiform gyrus, as shown by fMRI, and confirmative evidence comes from the observation that such nucleus is selectively activated by faces [8].

Specifically, if we analyse the diagnostic process of pathological interpretation, we can subdivide different sequences: first of all, a visual search of the image, then interpretation of the perceived information and finally, a combination of the collected information. Such process has been analysed and experimentally investigated by Tiersma and coworkers [22]. The experiment was carried out using a helmet endowed with a beam that could follow the direction of the eye and the gazing in different points so that such a scan eye tracking system was enabling the visualisation of the eye points of gaze of a subject and thus provided the possibilities to create computerised graphic representations of scanning patterns.

This study indicates that the well-known (almost obvious) fact that experienced pathologists reach diagnoses (i.e. categorization of the lesions) in a shorter time is related to their focusing on the most significant areas. Moreover, these processes (searching, focusing and moving) constitute the unconscious phase, to be followed and completed by the final, conscious stage of diagnosis. We have to conclude that the diagnostic process is not just a sequence of three steps (search, interpretation and association), but such steps have to be repeated several times back and forth, again and again, till the process reaches the conscious state. We have to conclude that while making a pathological

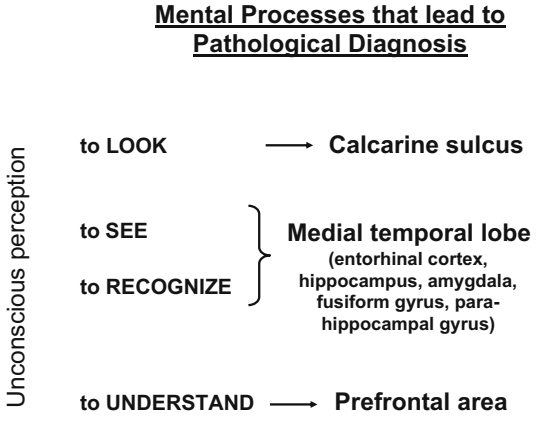

Fig. 2 Mental processes that lead to pathological diagnosis

diagnosis, we experience first an unconscious stage and then a conscious state. The unconscious stage is fast and laborious: in a few seconds, the eye goes here and there, interpreting the different areas and images. Thereafter, the process reaches consciousness, and the diagnosis is made. Such sequence had already been investigated by radiologist who described the steps of visual scanning, pattern recognition and decision making as the sequence of events taking place during pulmonary nodule detection [11]. They also concluded on the influence of expertise on X-ray image processing [16].

Following the analysis of the unconscious steps of looking, seeing and recognizing, we have to take into consideration the last step, the conscious one, that of understanding. This stage is most probably linked to the pre-frontal area, as shown by the recent observation by fMRI that when people look at an image, at a painting for instance, and then reach the conclusion that they like it, the pre-frontal area is selectively activated [2]. We have to conclude that the process of looking is linked to the calcarine sulcus, that of seeing and recognizing to the medial temporal lobe, to hippocampus and amygdala, fusiform gyrus and parahippocampus gyrus, and that finally, when pathologists reach the diagnosis, it is the pre-frontal area that is selectively involved (Fig. 2).

On the complexity of pathology

We have to acknowledge that the analytical processes leading to the interpretation of pathological images are not comprehensive of the whole complexity of pathology. The processes relate to pattern recognition, which represents a basic part of pathology, but not the whole of it. Let us now consider the factors that seem essential for forming a good pathologist. Good sight is important, but "we see what we know" [5], so culture is important. Knowledge of previous discoveries and observations is fundamental in our discipline, but knowledge is to remember [19]. Memory and experience are extremely important in pathology. Now, what exactly is memory? The study of memory and of its different forms was conducted by several philosophers and psychologists, but mainly, I'm referring to a philosopher, Henry Bergson, whose main contribution was related to the unravelling of the different types of memory. He lived and worked in Paris, at the beginning of the twentieth century, in the same town and at the same time when Marcel Proust, who was a relative of Bergson, was engaged in the *Recherche du Temp Perdu*. According to Bergson, we can subdivide a memory by repetition, and that of recollection/recording via intensity, via affection [1]. This represents a common experience for pathologists, who can remember cases they observed years before, because they were so impressed and interested so that every single particular is vividly remembered.

From a neurophysiological point of view, during the memorizing process, by repetition, the area of hippocampus is directly stimulated, while in the process, via intensity, the hippocampus is indirectly stimulated through the area of the amygdala [21].

However, not everything is known about memory and its mechanism. A recent study shows that if you give a stimulus, its performance deteriorates during the day, but if you have a short nap, then the performance improves, and after a good sleep, it improves again and again till it reaches a plateau [15]. Our experience as pathologists teaches us something else. Sometimes, not only memory is consoli-

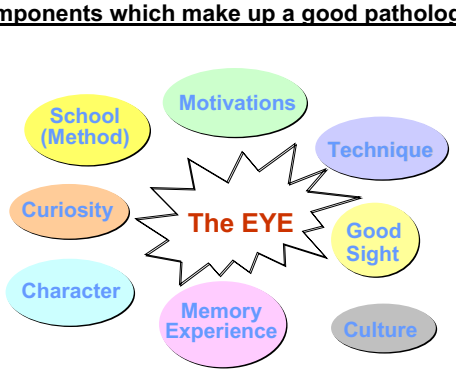

Fig. 3 Components which make up a good pathologist

Fig. 4 Freude an der Morphologie

dated, but even recollection is enhanced by sleep. We look at a peculiar case and we cannot give a proper interpretation, then we go back home, and the day after, the solution immediately is obvious. Moreover, a recent observation indicates that some neurones in the medial temporal lobe are selectively activated by strikingly different pictures of given objects, and it cannot be excluded that single neurones are dedicated to a given face or image [20]. Such observations indicate that we are far from having a complete and well-assessed knowledge of the extremely complex and fascinating process of memory, a process of fundamental importance in the process of diagnosis of pathological lesions.

Besides good sight, culture, memory and experience, of course, technique is important for pathologists, and of course, a school which gives a method, a system.

But a list of the different components of the characteristics which make up a good pathologist would not be complete without taking into consideration a special and dedicated ability, a gift or a knack, what John Azzopardi used to call "oculus patologicus," the pathological eye, the ability to select and recognize morphological subtleties (Fig. 3). This was also the opinion of a German-Swiss pathologist, Paul Ernst, who subdivided his students into three groups: the great majority unable to see what is shown, then a relatively small, but valuable group, able to see and understand what is shown, and then a minute minority, who can even see what is not shown [3].

On the essence of pathology

The priming factor, the most important component for making up a good pathologist, is still failing to our search, but we should agree that among the different factors, three characteristics are really essential for forming a good pathologist: the "eye," the experience and finally, the school. These are clearly the pillars that make up a good pathologist. When I presented these three alternatives to colleagues collected at the *Meeting along the way to Santiago* (May 2004) and asked the colleagues' opinion, the audience divided into three groups. Some people said that the school is the most important factor, somebody else said that the eye, sort of an inborn ability, is the most valuable one and then, of course, experience is fundamental.

The only dissenting opinion was expressed by Francisco Gonzalez-Crussi, a prominent pathologist, author of several scientific papers and a successful writer of rather hectic books such as *On the nature of things erotic* [6]. He came out with the observation that "Love," love for pathology is the priming factor. This opinion has merits and reasons because in fact, memory is stimulated, motivated by interest, by affection, by love. What is the eye, if not a total dedication to morphology, faith in morphology. Finally, the school, in its ultimate essence, is nothing but the transfer of an interest, the transfer of a passion, the transfer through generations of a small flame, the tantalizing but vital flame of curiosity. However, while searching for a proper term to indicate dedicated interest and passion, the English term "love" seems inappropriate, being perhaps too abused and uncommitted. A better term is the one proposed by Karl Lennert [12]: he used the term "freude an der morphologie," enjoyment for morphology. Such inspiring German expression is inextricably linked to Schiller's *Hymn to Joy* and of course, to the music from Beethoven's *9th Symphony*.

So let us conclude that by dissecting a pathologist's brain, ultimately, what you find is a dedicated heart (Fig. 4).

Acknowledgements My sincere thanks go to all curious and inspiring friends and colleagues who have been sharing my interests, furnished suggestions and helped to enlighten this multifaceted search.

References

1. Bergson H (1990) Matter and memory, The MIT Press, Cambridge
2. Cela-Conde CJ, Marty G, Maestu F, Ortiz T, Munar E, Fernandez A, Roca M, Rossello J, Quesney F (2004) Activation of the prefrontal cortex in the human visual aesthetic perception. Proc Natl Acad Sci U S A 101:6321–6325
3. Ernst P, cited in Lennert K (1984) Eröffnungsrede des Vorsitzenden. In: Hübner K (ed) Verhandlungen der Deutschen Gesellschaft fur Pathologie 68. Tagung Metastasen. Fischer, Stuttgart
4. Fried I, MacDonald KA, Wilson CL (1997) Single neuron activity in human hippocampus and amygdala during recognition of faces and objects. Neuron 18:753–765
5. Goethe JW (1999) Elective affinities. Oxford University Press, Oxford
6. Gonzalez Crussi F (1989) On the nature of things erotic. Vintage, London
7. Kanizsa G (1980) Grammatica del Vedere. Il Mulino, Bologna
8. Kanwisher N, McDermott J, Chun MM (1997) The fusiform face area: a module in human extrastriate cortex specialized for face perception. J Neurosci 17:4302–4311
9. Kemp M (2002) Seen and unseen: art from a different perspective. Perseus, New York
10. Kemp M (1992) The science of art. Optical themes in western art from Brunelleschi to Seurat. Yale University Press, London
11. Kundel HL, Nodine CF, Carmody D (1978) Visual scanning, pattern recognition and decision-making in pulmonary nodule detection. Invest Radiol 13:175–181
12. Lennert K (1984) Eröffnungsrede des Vorsitzenden. In: Hübner K (ed) Verhandlungen der Deutschen Gesellschaft fur Pathologie 68. Tagung Metastasen. Fischer, Stuttgart
13. Logothetis NK, Sheinberg DL (1996) Visual object recognition. Annu Rev Neurosci 19:577–621
14. Maitland SB, Herlitz A, Nyberg L, Backman L, Nilsson LG (2004) Selective sex differences in declarative memory. Mem Cognit 32:1160–1169
15. Maquet P, Peigneux P, Laureys S, Smith C (2002) Be caught napping: you're doing more than resting your eyes. Nat Neurosci 5:618–619
16. Myles-Worsley M, Johnston WA (1998) The influence of expertise on x-ray image processing. J Exp Psychol 14:553–557

17. Ninio J (2004) Testing sequence effects in visual memory: clues for a structural model, Acta Psychol (Amst) 116:263–283
18. Nodine CF, Mello-Thoms C, Kundel HL, Weinstein SP (2002) Time course of perception and decision making during mammographic interpretation. Am J Roentgenol 179:917–923
19. Plato (1999) Menon. In: Great dialogues. Signet, New York
20. Quiroga RQ, Reddy L, Kreiman G, Koch C, Fried I (2005) Invariant visual representation by single neurons in the human brain. Nature 435:1102–1107
21. Tadié JY, Tadié M (1999) Le sens de la memoire. Gallimard, Paris
22. Tiersma ES, Peters AA, Mooij HA, Fleuren GJ (2003) Visualising scanning patterns of pathologists in the grading of cervical intraepithelial neoplasia. J Clin Pathol 56:677–680
23. von Helmholtz H (1896) Handbuch der Physiologischen Optik. Voss, Hamburg
24. Wertheimer M (1922) Untersuchungen zur Lehre von der Gestalt, I. Psychol Forsch 1:47–58
25. Zeki S (1999) Inner vision. An exploration of art and the brain. Oxford University Press, Oxford

Virchows Arch (2006) 448: 744–755
DOI 10.1007/s00428-006-0189-2

REVIEW ARTICLE

Manfred Dietel · Christine Sers

Personalized medicine and development of targeted therapies: the upcoming challenge for diagnostic molecular pathology. A review

Received: 4 July 2005 / Accepted: 20 September 2005 / Published online: 22 April 2006

Abstract Due to continuous technical developments and new insights into the high complexity of many diseases, molecular pathology is a rapidly growing field gaining center stage in the clinical management of tumors as well as in the pharmaceutical development of new anti-cancer drugs. The application of novel compounds in clinical trials has revealed promising results; however, the current diagnostic procedures available for determining which patients will primarily benefit from rational tumor therapy are insufficient. To read a patient's tissue as "deeply" as possible, in the future, gaining information on the morphology and on genetic, proteomic, and epigenetic alterations will be the upcoming task of surgical pathologists experienced in molecular diagnostics to provide the clinicians with information relevant for an individualized medicine. Among the different high-throughput technologies, DNA microarrays are now the first array approach close to enter routine diagnostics. Technically advanced and well-established microarray platforms can nowadays be evaluated by distinct bioinformatic tools capable of identifying both novel genes associated with disease development and clusters of genes predicting clinical outcome of an individual tumor. The automatic, highly parallel analysis of proteins and complex proteins lysates for early detection of cancers such as breast, prostate and ovary as proteomic patterns in the serum also appears at the horizon. In addition, an improved analysis of tumor samples via antibody or reverse-phase protein arrays is likely to provide the pathologist in the future with information about activated oncogenic signaling pathways and other cell functions, such as drug response or the potential to metastasize. While expression microarrays and proteomic analysis rely on relatively unstable material incompatible with paraffin-embedded tissue samples, an investigation of DNA methylation using specialized high-throughput platforms has revealed the potential of being used in future diagnostics. Each of these approaches on its own might not suffice to extract all information required for an efficient individualized diagnostics. Therefore, a "multiplex approach" combining the different biological levels DNA, RNA, and protein, may be necessary to functionally classify malignant tumors. This appears to become a major challenge for diagnostic pathologists.

Keywords Review · Molecular pathology · Targeted therapy

M. Dietel · C. Sers
Institute of Pathology, Charité,
University Hospital Berlin,
Humboldt-University,
Schumannstr. 20-21,
10117 Berlin, Germany

M. Dietel (✉)
Oligene GmbH,
Berlin, Germany
e-mail: manfred.dietel@charite.de
Tel.: +49-30-450536002
Fax: +49-30-450536900

Introduction

Standard diagnostic procedures for human tumors are currently based on a combination of histopathology and immunohistology closely connected with clinical data. This strategy, in most cases, provides precise information on dignity, tissue origin, tumor type, stage, and grade as well as information on the completeness of surgical tumor removal. Up to now, these data comprise the most relevant information on a patient's prognosis and are a rational basis for therapy design. As the diversity of alterations in tumor cells is not completely mirrored by tumor cell morphology, pathologists and clinicians often observe that two patients harboring the "same" type of tumor in a seemingly "identical" stage show different clinical outcome with respect to survival and, in particular, with respect to therapy response. To improve this unsatisfactory situation, a patient-specific disease prediction based on tissue examination by pathologists would be extremely helpful.

During recent years, many molecular markers and marker patterns ("signatures") have been disclosed which, at least, partially predict prognosis and therapeutic

effectiveness. Considering the fact that cell function is controlled by a complex network of functionally active signaling pathways, it is unlikely that expression analysis of a single or a small number of proteins will precisely predict the clinical outcome of an individual tumor. Hanahan and Weinberg (2000) have described six essential alterations in cancer cells that are common to most human tumors: self-sufficiency in growth signals, insensitivity to growth-inhibitory signals, evasion of apoptosis, limitless replicative potential, sustained angiogenesis, and tissue invasion and metastasis. However, each of these alterations is achieved by different modifications in signal transduction, gene or protein expression, protein modification, and localization. Thus, a different and improved characterization of malignant tumors as compared to current standard diagnostics is required to reflect the multitude of genetic, proteomic, and metabolomic alterations typical for malignant cells. Several newly developed high-throughput technologies, such as DNA microarrays, protein and antibody arrays, proteome technologies such as mass spectroscopy MALDI-TOF, metabolomic analyses, methylation arrays, reverse-phase protein microarrays (RPAs), etc., provide the technical platforms for this approach and will gain more interest in the future. By integrating these technologies into standard diagnostic procedures, future molecular pathology will be able to dramatically increase the relevance of tissue-based examinations. Pathology will play a crucial role in therapy design and, by providing molecular diagnostic approaches, also in therapy adjustment and selection of effective drugs.

In this review, we will describe genomic, proteomic, and epigenomic approaches which have been shown recently to improve diagnostics and prognosis. We will focus on DNA microarrays as the most advanced technology in this field and suggest the development of an integrated approach for future diagnostic molecular pathology.

Genomics—DNA microarrays

Technology

The generation of gene expression profiles from cultured cells and tissue samples is nowadays a well-established method. In the majority of experiments, DNA fragments specific for individual genes on activated glass surfaces are used [13, 62]. RNA is prepared from the biological material to be analyzed, reverse transcribed into cDNA, labeled with fluorescent dyes, and hybridized to the array. The hybridization signals are detected by a laser scanner, the images are normalized in various ways, and the relative expression levels obtained for individual genes are further clustered into groups of genes with similar or identical expression patterns.

DNA microarrays consist of thousands of DNA elements (10,000–80,000 or even more) robotically tethered to a solid surface, e.g., coated glass slide, silicon, or nylon. The DNA sequences are either oligonucleotides or cDNA and represent different genes of interest. Each gene is usually represented by more than one feature to increase the specificity of the analysis. The cDNA clones are often selected from public databases, amplified from cDNA libraries, and purified before spotting. Oligonucleotides (20–80 bp) are alternatively chemically synthesized and spotted or may be directly synthesized on the array surface. In addition to sequences representing known genes, sequences representing expressed sequence tags (EST) coding for genes of unknown function can also be spotted on the solid surface, offering the potential of investigating new marker genes.

The target DNA usually is a cDNA derived from tumor cell mRNA which is amplified and simultaneously labeled by reverse transcriptase-polymerase chain reaction (PCR). The RNA is prepared from rapidly processed cell cultures or fresh frozen tissue. Novel fixation techniques and preparation methods are currently tested which might also allow in the future the use of RNA prepared from paraffin-embedded tissues to be utilized in diverse microarray experiments [28, 30, 54]. Target DNA, of course, can also be prepared from genomic DNA fragments. For labeling, fluorescent dyes are used nowadays. The expression intensity of each gene is determined after hybridization of the target DNA to the immobilized array DNA.

The hybridization signal generated on each spot reflects the expression of the corresponding gene. The quantification of the signals is performed using special software which allows to correct for spot integrity and for technical deviations during array production and hybridization and to interpret the signal intensity. For this purpose, cDNA of normal tissue or any other reference cDNA has to be introduced. The final results provide a genetic expression profile indicating overexpression, underexpression, no change, or complete absence for each gene in the tissue samples to be compared to each other (for review, see [52]).

Bioinformatics

The enormous amount of data obtained not only from each high-throughput experiment but also from data documentation, data processing, and data interpretation is a unique challenge requiring close cooperation between pathologists and bioinformatic specialists. Therefore, methods and bioinformatic tools have been developed for the extraction of complex information, the evaluation via statistical methods, and the translation of molecular information into clinically relevant data. cDNA microarrays today have been used for a variety of different objectives. To choose the method of statistical analysis that is appropriate for each study, it is helpful to distinguish different types of array analysis. Simon et al. [72] have distinguished three different types of study objectives: “class discovery” (find a new class), “class comparison” (find differences between two predefined classes), and “class prediction” (find a predictive gene set for a certain predefined class). For each type of study, different statistical strategies for evaluation should be used. According to Simon et al., using methods incompatible with the goal and the design of the

study is one of the most common errors in the analysis of microarray data.

Several methods for data analysis and interpretation have been developed, which can be separated into two classes: supervised and unsupervised methods [11]. A supervised approach means that some external information such as tumor grading or patients' survival define the relevant classes before the analysis; this method is used for "class prediction" and "class comparison" studies.

In contrast, for "class discovery" studies, an unsupervised approach is used, which defines different groups of tumors exclusively according to their gene expression profiles without using external information. An unsupervised classification detects similarities in gene expression profiles. For this purpose, the hierarchical clustering [24] combined with a graphic presentation is an excellent tool (Fig. 1). K-means or self-organizing maps are further examples of unsupervised methods frequently used in microarray analyses [79, 82]. It is important to note that cluster analysis should not be used for class prediction and class comparison studies.

Especially for "class prediction" studies, supervised approaches should be applied. The supervised algorithm establishes a model on the training set of samples, which assigns gene sets with a defined expression profile to predefined groups of tumor samples. After the class prediction algorithm has been trained, it can be used to predict the class of new samples. To assess the error rate (e.g., percentage of incorrectly classified tumors), a crossvalidation approach is often used. In this approach, the available data sets are split repeatedly into a training set and a test set. The algorithm is then trained on the training set and applied to the test set, and correct and false predictions are counted. A special type of cross-validation is the leave-one-out strategy, where just one sample is omitted from the training set (training on $n-1$). This one sample is then used as the test set. This procedure is repeated n times, each time using another sample as a test set. This approach achieves maximal efficiency of training yet requires high computational resources.

Such sample classification can be helpful to identify the set of genes that discriminates between predefined groups of patients with good or poor survival, e.g., estrogen receptor (ER) positivity or ER negativity. This approach has been described to discriminate, e.g., between tumor entities like different solid tumors [78], subgroups of acute myeloid leukemia and acute lymphocytic leukaemia [31], diffuse large B-cell lymphomas, between early- and late-stage ovarian carcinomas [52], and breast carcinomas with or without the potency to metastasize [85].

In a critical commentary, Simon, Radmacher, Dobbin, and McShane [72] already worried that "many investigators are not experienced in the analytical steps needed to convert thousands of noisy data points into reliable and

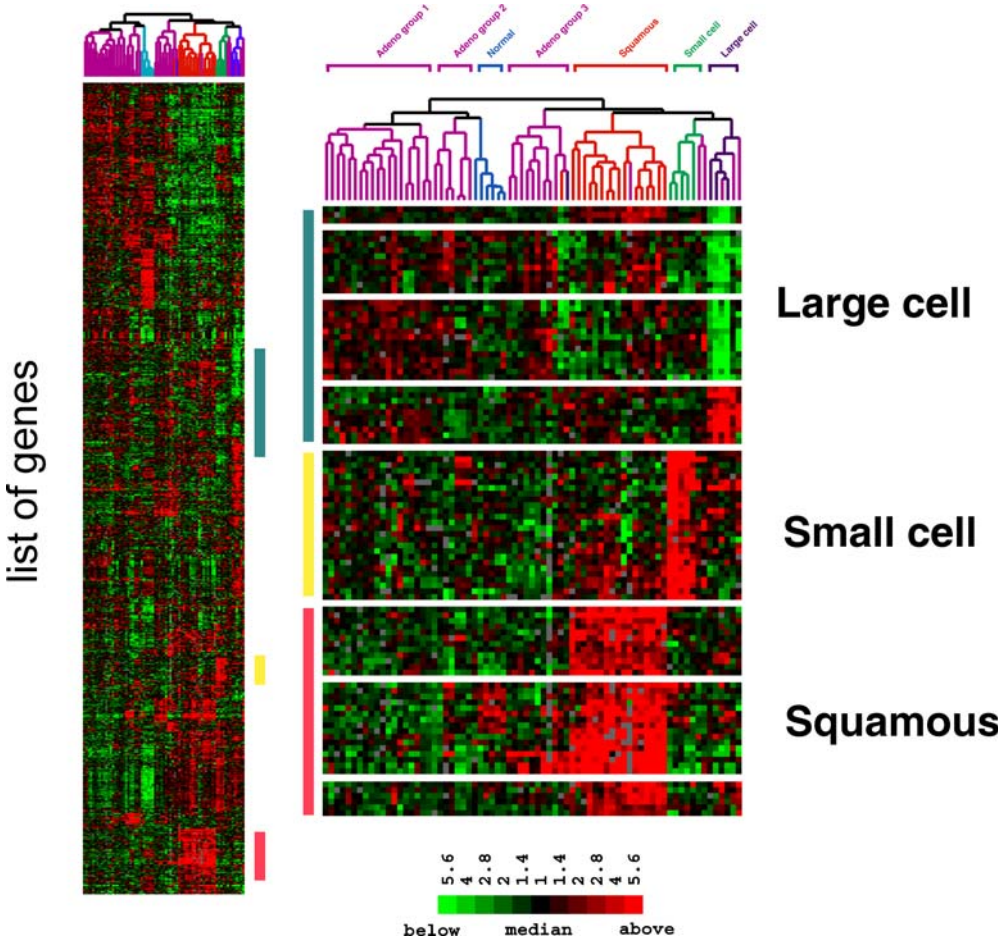

Fig. 1 Hierarchical clustering analysis exemplified for Topotecan-resistant (*R*) and Topotecan-sensitive (*S*) cell lines. All cell lines resistant to Topotecan (*left panel*) and all cell lines sensitive to Topotecan (*right panel*) express a unique set of genes. Each *row* in the cluster indicates the expression profile of a specific gene across all 19 cell lines. Each *column* indicates the individual cell line in which the gene is expressed. *Red*, *green*, and *black squares* indicate that expression of the gene is greater than, less than, or equal to the median level of expression across all cell lines, respectively. The *scale bar* reflects the fold increase (*red*) or decrease (*green*) for any given gene relative to the median level of expression across all samples

interpretable biological information". Furthermore, the molecular profiles are often relatively unstable due to tumour heterogeneity and platform specificity. The authors listed a number of prerequisites necessary to avoid misinterpretation of the data. In particular, the issue of class prediction is discussed as it includes derivation of classifiers, which predict prognosis, response to therapy, potential to metastasize, and many more. In a very recent publication by Michiels et al. [53], several of the most prominent classifiers were doubted. The authors concluded that the list of genes included in a molecular signature largely depends on the constitution and size of the training sets used and even claimed that a majority of the published classifiers are not significant. A comprehensive overview is also given by Scharpf et al. [67], suggesting several methodological approaches and illustrating the associated software to generate interpretable, robust, and less platform-dependent results.

A relatively new unsupervised approach to analyze array data is provided by linear independent component analysis (ICA) [37, 48, 49]. In contrast to cluster analysis methods, which assume that each gene belongs to just one cluster, ICA is based on the idea of a combinatorial control which is more realistic from a biological point of view. Gene expression levels are described as linear functions of common hidden variables which are (in the ideal case) related to distinct biological causes of variation such as transcriptional regulators or responses to treatments. Thus, ICA-based results show increased biological relevance and might describe new biological links previously undetected by clustering methods. An interesting study was conducted on endometrial carcinomas and benign endometrial samples [66]. The authors compared the power of ICA to other established methods and thereby detected (a) an improved separation of benign and malignant groups, (b) a characteristic expression pattern corresponding to the histological classification, and (c) a novel pattern of coregulated genes related to fatty acid metabolism which are clinically associated with endometrial carcinoma. Thus, a careful examination of histopathologically well-characterized tumor material via high-throughput methods and sophisticated bioinformatic approaches might even unravel novel disease mechanisms during such advanced diagnostic schemes.

Application of DNA microarrays

The application of high-throughput cDNA and oligonucleotide array technologies and the establishment of gene expression profiles has already revolutionized experimental tumor diagnostics in the last couple of years. With the use of these tools, otherwise indistinguishable tumor subgroups have been identified [2]. In addition, the development of gene signatures enabled prognostic conclusions which could not be drawn using standard histopathological and immunohistochemical methods [35, 84, 85], opening the door for a more comprehensive tumor analysis by diagnostic pathology. In the following, some examples of microarray applications will be described to demonstrate the wide range of applications where this technique could support and even improve the predictive power of histopathological diagnostics.

Molecular classification and prognosis

Based on hundreds of international studies including thousands of patients, an international classification system for malignant tumors based on conventional histopathology supported by immunohistochemistry has been established, the UICC–TNM system [73]. In general, the TNM system helps to estimate the prognosis of groups of tumors. However, this classical approach with conventional histopathology, analyzing morphological parameters, is not completely sufficient when the prognosis of an individual case shall be predicted. Therefore, the DNA microarray technique is currently under investigation to improve the current classification system by correlating array results with histomorphology and clinical behavior of tumors.

The first step towards a molecular classification was done by Khan et al. [39] who defined expression signatures from cancer cell lines which were indicative for the organ type of origin. A landmark study including gene expression profiling with DNA microarrays as an extension of histopathological classification has shown the possibility to differentiate between AML and ALL and to improve the precision of prognosis prediction [31].

Tumors with similar histological appearance but with different clinical behavior, such as small blue round tumors of childhood, are difficult to classify on a routine microscopical basis. Genetic profiling proved to correctly identify the four subgroups neuroblastoma, rhabdomyosarcoma, Ewings sarcoma, and special types of non-Hodgkin's lymphoma [40] and, thus, can be a valuable help in tumor classification.

The WHO grading system of oligodendrogliomas is somewhat limited due to subjectivity of histopathological evaluation. Gene expression profiling now unraveled two molecularly distinct subgroups which correspond to the morphological grading and, thus, can be applied to provide a more objective tool for grading and prediction of prognosis [89]. This approach may be extended towards other brain tumors where reproducible histological assessment is often difficult, if not impossible.

In a group of 55 breast cancer patients with balanced clinicopathological features, three subclasses of tumors with different 5-year survival could be identified by analyzing mRNA expression of only ≈1,000 candidate genes [7, 8]. In a population-based study, Sotiriou et al. [75] were able to suggest distinct aspects of breast cancer classification and prognosis based on gene signatures. The molecular analysis of pre-invasive vs invasive breast tumors revealed extensive similarities of the genetic alterations [51], suggesting that, in the early stage, the potential for invasive growth is already almost fully developed—an insight which might change the current strategy of early breast cancer treatment.

Further genetic subclassifications of tumor entities with distinct clinical features have been described for breast cancer [60, 74], cutaneous malignant melanoma [10, 86], large B-cell lymphoma [2], and B-cell lymphoma [14], pediatric ALL [92] and acute leukemia with MLL translocation [3], and adenocarcinoma of the lung [9, 26], ovary [57, 69], colon [25], and prostate [21].

Metastatic potential

Up to now, it is impossible to determine precisely whether a tumor which has not developed clinically detectable metastases at the time of diagnosis will metastasize during the following years. This information, however, would be of utmost importance to decide, e.g., whether an adjuvant therapy is necessary or not. The first steps to elucidate the metastasizing potency of an individual tumor have been published by van't Veer et al. [85]. In breast carcinomas with T1/T2, NO at time of diagnosis, the authors defined 70 "predictor genes" whose signature predicts with approximately 80% sensitivity and specificity the chance to set lymph node metastases. A recent study by Wang et al. [88] confirmed these data. This provides a rational to treat patients with adjuvant therapy or not.

Tissue assignment, primary and occult metastases

In clinical practice, it may happen that a metastasis is found while the primary tumor is unknown or it is unclear whether a certain metastasis is derived from a known primary tumor. Most often, histopathology, in addition to morphological immunophenotyping, can disclose the tissue origin. Nonetheless, gene expression profiling may be of additional help to classify cancer cells according to their tissue of origin [29, 39, 63, 78]. It was shown that the molecular signature of the primary tumor is preserved in its metastases and, thus, allows a clear assignment which gives the necessary information for an adequate treatment. Furthermore, it could be shown that DNA arrays are able to distinguish between lung adenocarcinomas and metastases of extrapulmonary origin [9]. The origin of cancer of unknown primary can be derived from characteristic expression patterns as the tumors often harbor distinct gene expression profiles characteristic for the organ type of origin [83].

Therapy response and drug resistance

Drug resistance remains a major problem during therapy for systemic cancer disease. Due to the high potency to adapt to therapeutical intervention, malignant tumor cells frequently develop escape mechanisms in response to radiation or cytostatic drugs. Although many attempts have been made [45, 46], up to now, reliable and practically applicable techniques to predict a tumor's reaction to drugs or radiation do not exist. The reason for this are multiple cellular mechanisms such as increased DNA repair, elevated levels of drug transporters, overexpression of detoxifying enzymes, and decreased rates of apoptosis which are often involved in the development of drug resistance. To monitor multiple alterations occurring in tumors being drug insensitive, highly parallel analyses, such as the DNA microarray technique and also proteomic analysis, are required. This opportunity opens new dimensions to predict therapy resistance and sensitivity.

A recent National Institutes of Health study [68] investigated 60 tumor cell lines (NCI60) which have been treated independently with more than 70,000 different agents, one at a time. Among other results, the study linked bioinformatics and chemoinformatics by correlating cellular drug response with transcriptomic information derived from DNA microarrays. The aim was to associate clusters of related drugs with clusters of gene alterations and, thereby, to define drug–gene relationships. This approach may contribute to the establishment of a defined expression database on which an individualized molecular pharmacology of tumor drug response can be established.

By comparing wild-type cell lines with derivatives resistant for thymidilate synthase (TS) inhibitors, Wang et al. [87] were able to identify certain patterns of genetic alterations correlating with TS resistance. The associated gene expression profile was partly tissue dependent, e.g., *YES1* was overexpressed in the epithelial cell lines while it was not upregulated in a lymphoblast cell line. Cisplatinum (cDDP) resistance was shown by microarray analysis to be accompanied with altered expression of genes coding for membrane proteins and a glycoprotein hormone subunit [33] not previously known to play any role in cDDP resistance.

In an excellent study by Zembutsu et al. [94], 85 human cancer xenografts were tested with regard to characteristic expression profiles in response to nine anticancer drugs often used in clinical therapy. More than 1,500 genes were identified whose expression profile has correlated in some way with chemosensitivity. The authors identified sets of genes which could partly be associated with chemosensitivity of particular tumor types (colon, breast, non-small cell lung cancer, etc.) to the different drugs applied. To predict the efficacy of adjuvant therapy in esophageal tumors, the DNA microarray technique was applied to 20 cancer specimens with clinically known responses [41]. There were 52 genes identified which were likely to correlate with patients' outcome and possibly with chemosensitivity and chemoresistance. This approach shows some potential to determine drug response in advance. In addition, bone marrow samples from 19 patients with acute lymphoblastic leukemia were investigated with regard to resistance to an ABL tyrosine kinase inhibitor [34]. On the basis of 95 differentially expressed genes, it appeared to be possible to distinguish responder from non-responder. Raponi et al. [65] showed the possibility to detect the pathways modulated by inhibitory drugs in AML elucidating the mechanisms of drug action. Thus, gene expression profiling can be helpful for the pretreatment assessment of anti-cancer therapy. Although a

vast number of experiments still have to be conducted, it might become possible to predict chemoresistance (Fig. 2) and to avoid non-effective drugs and unnecessary side effects for the patients. The discrimination between responders and non-responders before therapy will further stimulate the development of an individualized therapeutic strategy with a personalized combination of drugs.

Pitfalls of DNA microarray analyses

Numerous studies have shown characteristic expression patterns related to certain aspects of tumor biology. Dozens of genes were associated with prognosis, drug resistance, potential to metastasize, etc.; however, the clinical confirmation of the results is so far only on the way. The clinical application of DNA microarrays will require a high level of reproducibility and reliability of technology, of sample processing, and of analysis. A major obstacle is the still low inter-laboratory and inter-platform reproducibility of microarray data. Several of the reasons underlying this problem were described in 2003 by Tan et al. [80]. A comparison of the three most widely used commercially available platforms revealed significant discordance, which could in part be attributed not only to differences between the types of array but also to the different algorithms used for data evaluation. In 2001, the MIAME standard was already suggested, which includes a predefined set of information for a certain microarray experiment which allows for an independent evaluation of the results and for a conclusion to be drawn [12]. In a more recent publication by the Toxicogenomics Research Consortium, the impact of array type, data handling, image analysis, and experimental protocol onto the reproducibility of microarray analysis between different laboratories was investigated [5]. This study revealed that, like in the earlier reports, the type of microarray used has by far the largest influence onto the comparability of microarray data. More importantly, the authors conclude that, upon application of a common, commercial microarray platform, standardized experimental image analysis and data processing approaches correlation coefficients up to 0.9 can be achieved between experiments performed in different laboratories.

Thus, careful experimental design and a strict standardization of the whole procedure will be of utmost importance in the future for the reproducibility of microarray experiments. Furthermore, one should keep in mind the fundamental challenges, which have frequently obstructed cancer research during the last decades. These include inter- and intratumor heterogeneity, specimens either extracted, stored, or diagnosed inappropriately, and unexpected changes of cell line properties. These complications are still relevant and may be even accelerated by high-throughput techniques.

Proteomics

The rapid development of proteome technology has lifted tumor diagnostics to a new level. Despite the high relevance of DNA- and RNA-based information discussed above, nucleic acids are several layers of abstraction away from the physiological events that determine disease characteristics. Proteins govern metabolic processes, protein interaction, and posttranslational modifications and are, therefore, the major targets to be included in future molecular pathological approaches (see also review by Hanash [32]). Three fields of application are beginning to emerge: (a) highly sensitive mass spectroscopy coupled to an array-based separation of complex protein lysates (surface enhanced laser desorption time-of-flight, SELDI-TOF) or microdissected tumor samples are used for early

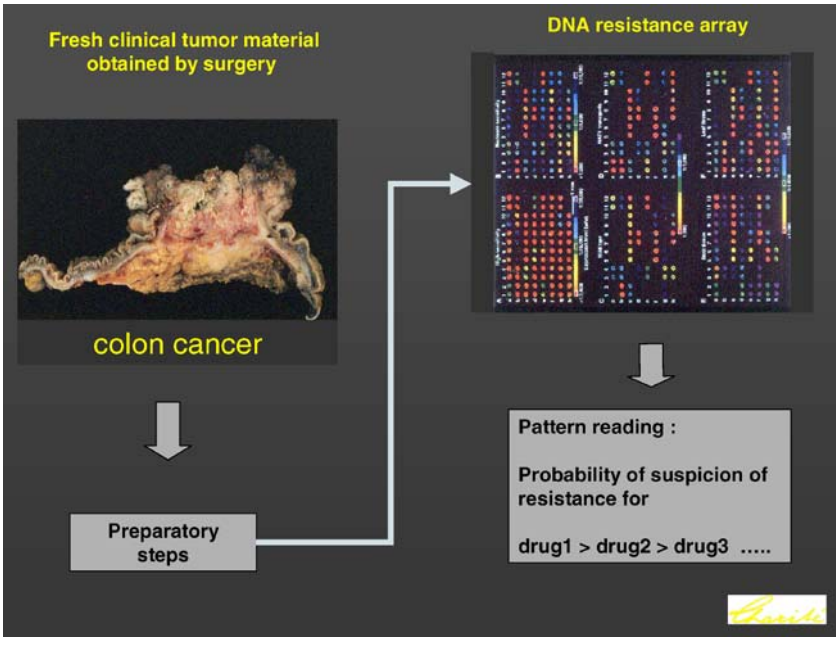

Fig. 2 A possible approach to predict chemosensitivity and/or chemoresistance of clinically relevant tumor samples. The low-density DNA arrays are specially designed to indicate the altered expression profile of sensitivity/resistance associated genes or EST. Different patterns appear to be correlated with sensitivity or resistance of malignant tumors for certain cytostatic drugs

detection and identification of new biomarkers for human tumors [59, 61], (b) a direct mass spectroscopic analysis and the establishment of protein profiles of tumor and normal tissue [14, 76, 91], and (c) the application of protein and antibody arrays for the specific identification of certain proteins and their activated forms in tumors [50, 55, 77].

Although technically advanced screening methods have improved early cancer detection, in some cancer types, such as ovarian carcinoma, new methods which allow easy and routine screening are urgently needed to ameliorate the currently frustrating clinical outcomes. For this purpose, the highly sensitive SELDI-TOF approach appeared as the most promising technological development during recent years. Petricoin et al. [61] reported the identification of serum proteomic patterns using SELDI-TOF and developed a bioinformatic tool to distinguish neoplastic ovarian disease from the normal status. By applying the serum spectra from 50 healthy women and 50 ovarian carcinoma patients as training sets, they proposed a proteomic signature which segregated cancer from non-cancer with a sensitivity of 100% and a specificity of 95%. Yet, these results were severely criticized and the expectations were smoothened in recent publications [4, 17, 96]. Furthermore, this provoked an intense debate about future processes of establishing and proving the reliability of novel technologies [22, 23, 64]. Thus, despite being an exciting new approach, K. Coombes et al. [17] recently stated that the "current state of the art in serum proteome profiling allows considerable room for improvement".

While serum proteomic analysis is currently tested in the identification of new and early cancer markers, SELDI-TOF has been successfully applied to the characterization of distinct tumor areas carefully dissected by the help of laser capture microdissection. This approach was used to identify markers differentially expressed in prostate cancer cells as compared to prostatic prostate intraepithelial neoplasms (PIN) lesions and normal prostate epithelium [16, 97]. Similar experimental schemes were also developed for a proteomic evaluation of bladder carcinoma [43], colon carcinoma [47], and breast carcinoma [19].

In addition to the direct identification of proteins using mass spectroscopy, antibody arrays and so-called reverse phase protein array approaches have also been developed and applied for the identification of tumor-associated proteins and also their activated phosphorylated derivatives. Nowadays still in a developmental stage, both types

Table 1 Examples of targeted therapy approaches

Drug	Tumor type	Target	Known action	Detection method	Remarks
Trastuzumab	Metastatic breast cancer	HER-2/neu	Rc blocking	IH, FISH, ISH	1
Cetuximab + Irinotecan	Metastatic colorectal cancer	EGFR	Rc blocking/immunologic response	IH, FISH	1
Imatinib Mesylate (Gleevec)	CML, GIST with activated c-kit receptor tyrosine kinase, other sarcomas	Bcr/abl, c-Kit, PDGF-R	Tyrosine kinase inhibitor	IH	1
Bevacizumab (Avastin) (+5FU)	Colorectal cancer	VEGF	Rc blocking	IH	2
G3139 (Genta, Berkley)	Hematologic malignancies and malignant melanoma	Antiapoptotic gene *bcl*-2 in	Bcl-2 antisense oligonucleotidecreasing Bcl-2 mRNA	Immunophenotyping by IH	2
Bortezomib, Epoxomicin	Multiple myeloma	Proteasome	Proteasome inhibitor		
Gefitinib (Iressa)	Non-small cell lung cancer	Mutated EGFR	Kinase inhibitor	Mutational analyses, immunoblotting	4
Erlotinib (Tarceva)	Non-small cell lung cancer	Mutated EGFR	Kinase inhibitor	Mutational analyses, immunoblotting	4
Rituximab (+ CHOP), Y90-Ibritumomab, I131-Tositumomab	Non-Hodgkin lymphoma	CD20	Lympholytic	Immunophenotyping IH	3
Gemtuzumab-Ozogamicin (calicheamycin)	AML (>60 years)	CD33	Anti-CD33 guided cytotoxic antibiotic, reduction of P-glycoprotein	Immunophenotyping by IH	3
Alemtuzumab (Campath)	B-CLL, T-NHL, osteogenic tumors[a]	CD52	Lympholytic	Immunophenotyping by IH	3
Rapamycin RAD001	Breast, prostate, renal cancer	TOR	Kinase inhibitor		4
BMS 354825	GIST	Kit	Tyrosine kinase inhibitor	IH	4
BAY43-9006	Melanoma	RAF kinase	Kinase inibitor		4

1 FDA-approved drugs requiring a pretherapeutic diagnostic eligibility test, *2* FDA-approved drugs targeting a specific pathway—no tests available, *3* FDA-approved antibody-targeted therapies for hematologic maliognancies guided by immunophenotyping, *4* under development, *Rc* receptor, *IH* immunohistochemistry, *ISH* in situ hybridization, *FISH* fluorescence in situ hybridization

[a]Patent no. EP:03029464.9, V. Krenn, Institute of Pathology (submitted)

of arrays might become valuable alternatives to cDNA or oligoarrays and also for immunohistochemical analyses during daily pathological routine. A major obstacle, among others, for these applications is the broad range of antibody specificity and affinity which complicates detection of defined antibody–antigen interactions [44]. Several studies which used antibody arrays to profile protein patterns in tumor samples derived from heptocellular carcinomas [81] or breast carcinomas [36, 42] applied verification strategies such as standard immunohistochemistry on tissue microarrays to demonstrate specificity of their platform. An interesting derivative of antibody microarrays are the RPAs. In this case, instead of antibodies, whole protein lysates are spotted onto glass surfaces and distinct proteins are detected via antibodies [58]. This procedure can be combined with laser capture microdissection and each patient set can be applied in miniature dilution curves to improve quantification accuracy and to enlarge the dynamic range. RPAs are generated from frozen tissue samples and, therefore, allow the use of detection antibodies specific for phospho-proteins. This technology was consequently described to compare survival pathway activation as measured by phosporylated Akt and Erk in normal prostate epithelium, in PIN, and in invasive prostate cancer [58]. In addition, it has been used in pathology for the investigation of the relative expression levels of Bcl-2 and Akt family members in follicular lymphomas [95]. One can anticipate the future implication of these methods in the elucidation of intracellular signaling networks downstream of tyrosine kinase receptors such as HER2 and also emerging from intracellular oncogenes such as RAS during cancer therapy. Many of the substances in the new generation of cancer drugs are designed to interfere with specific molecular targets, which are believed to have a critical role in tumor growth by regulating key signaling pathways (Table 1; Fig. 3). Yet, this requires the development of optimized protocols and superior detection techniques [27] and the use of reference standards as described recently by Sheehan et al. [70].

Epigenomics

Epigenetic modification of DNA by the addition of a methyl group to cytosine residues in CpG dinucleotides is one of the most important mechanisms of tumor suppressor gene inactivation known today [6, 38]. A DNA-based methylation analysis has several advantages when compared to the RNA-based gene expression analysis. The preparation of DNA suitable for such experiments can be successfully obtained from both frozen and paraffin-embedded tissues. Furthermore, according to current knowledge, methylation of genes is a rather stable modification not prone to produce as many artifacts due to RNA decay as in mRNA expression analysis. Methylation arrays are now consequently designed for the high-throughput analysis of DNA methylation at distinct CpG positions. Furthermore, a real-time PCR-based assay for gene- and methylation-specific detection has recently been developed [18]. For methylation arrays, genomic DNA from the tissue under investigation is treated with sodium bisulphite, resulting in the conversion of unmethylated cytosine residues into uracil [56]. Following this procedure, specific fragments from the regulatory, CpG-containing regions of genes are PCR-amplified using fluorescent-labeled primers. The uracil residues (UpG) are replaced by tyrosine residues (TpG) during PCR amplification. These fragments are then hybridized to their complementary oligonucleotides spotted onto a microarray, which are specific for the originally non-methylated CpG dinucleotide.

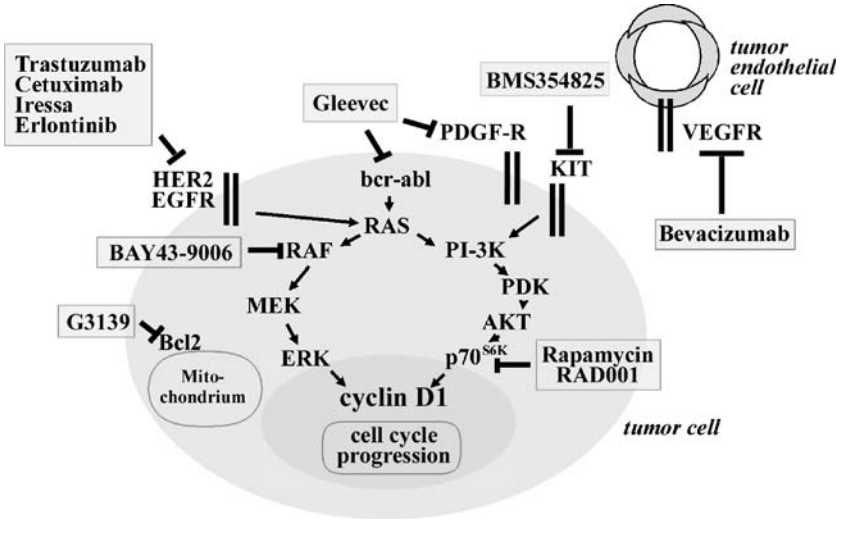

Fig. 3 Novel cancer drugs targeting signaling pathways. Several growth-stimulatory signaling pathways are activated in tumors due to tyrosine kinase receptor overexpression (*HER2* and *EGFR*) and mutation (*EGFR* and *KIT*). Inhibition of tumor cell proliferation is expected to occur via inhibition of receptor tyrosine kinases on tumor cells or on endothelial cells (*VEGFR*). Furthermore, intracellular protein kinases such as bcr/abl and RAF and phosphatidylinositol-related kinases such as mTOR can be targeted by specific inhibitors. Proteins like the antiapoptotic Bcl-2 can also be inhibited to support chemotherapy

The hybridization conditions are designed in a such way that a single mismatch between TpG and CpG variants yields a specific detection signal. Such applications have been used for the identification of CpG island methylation correlated with tumor progression [1] and to evaluate a potential significance for disease-free survival in ovarian carcinoma patients after chemotherapy [90]. In addition, sophisticated technologies (methylation target array) have enabled the detection of CpG island methylation of known tumor suppressor genes such as *WT1*, *BRCA1*, *p16INK4A*, and others in hundreds of tumor samples at the same time [15]. An interesting further development is the combined use of expression and methylation arrays, even in conjunction with an analysis of histone acetylation [71] using the same tissue samples. Such an approach allows the correlation of methylation data with expression data and the identification of functionally relevant genes harboring hypermethylated CpG islands with a higher accuracy [93]. Although a multitude of publications on high-throughput analysis of DNA methylation in tumor tissues already exist, it is evident that this technology has to be further developed to enter routine clinical diagnostic procedures. Nevertheless, it becomes clear that, in the future, a combination of transcriptomic, proteomic, and epigenomic analysis is required to identify the tumor-specific alterations with the highest relevance for prognosis and therapy.

Outlook—an integrated approach in future diagnostics

In recent years, the efforts devoted to unraveling the connection between activated receptor tyrosine kinases, intracellular oncogenes, and distinct intracellular signaling pathways and their role in growth control have uncovered a large number of potential therapeutic target structures. Herceptin and Gleevec targeting the *HER2/neu*, and *BCR/ABL*, *c-KIT*, and *PDGF-R oncoproteins*, respectively, are the first designer drugs which are already used with considerable success in the clinic. In the meantime, other drugs which act more or less specifically against a broad range of receptors and signaling components have entered clinical trials (Table 1) [20]. This development is intimately connected with the expectation that tumor therapy can be dramatically improved in the near future. To date, the percentage of patients responding to the new inhibitors is often below 30%. This indicates that the current portfolio of diagnostic methods based on immunohistochemical or DNA analysis (e.g., fluorescence insitu hybridization) of single target molecules is still insufficient. For the identification of those patients who will benefit from novel therapies, special methods capable of detecting the entire spectrum of rate-limiting oncogenic pathways in tumors before and during therapy have to be developed and adapted to routine diagnostic pathology. This will clearly play an increasing role in the future tasks of pathological institutes.

Before transmission and establishment of such an integrated approach into daily routine can occur, extensive research has to be performed to allow a firm prediction on the activation of a certain pathway in clinical material. In this case, a strategy consisting of a parallel analysis of gene expression and methylation combined with a proteomic analysis of activated signaling pathways and overexpressed proteins will be the method of choice.

The implementation of bioinformatic procedures, which will undergo further standardization together with highly parallel tissue analyses, opens the door for a broad profiling of human cancer tissue, thus improving the possibility to predict the biological behavior of single tumors. Such a "multiplex approach" may help to functionally classify malignant tumors, provided that a "diagnostic algorithm", beginning with conventional histopathology in combination with immunohistochemistry, provides the basis. This basic evaluation will then be supplemented by specialized disease-specific analyses such as different kinds of micorarrays to predict tumor-associated features including tumor progression, drug response, and metastatic potential, which will have an important impact on tumor prognosis and adequate individual therapy.

The recent technical developments also indicate changing demands for routine pathological diagnostics within the next years. Only a consequent integration of the methods described within this review into pathological diagnostics will guarantee that, in the future, pathology is also the discipline holding the main body of knowledge about disease etiology and disease mechanisms.

However, the demonstration that there exists a real benefit for the patients with, e.g., longer survival times or better response to therapy is still open. Only when well-designed clinical studies prove the progress an implementation of molecular tumor profiling with individualized therapeutic strategies will become accepted to be routinely integrated in diagnosis and treatment of cancer. One major prerequisite for an advantageous way is the interdisciplinary cooperation of basis scientists, clinically oriented physicians, diagnostic pathologists, and clinicians which all must speak the same "language". They must have an understanding of their partners. The "translation" between different groups of researchers will be one of the most challenging tasks in modern experimental and diagnostic pathology.

Acknowledgements The comments on the manuscript by Nils Bluethgen, Institute for Theoretical Biology, Humboldt University, Berlin are gratefully acknowledged. We appreciate the help of Balacz Gyorffy and we are especially grateful for the secretarial work of Mrs. von Bogen. This work was supported by Oligene GmbH, Berlin.

References

1. Adorjan P, Distler J, Lipscher E, Model F, Muller J, Pelet C, Braun A, Florl AR, Gutig D, Grabs G, Howe A, Kursar M, Lesche R, Leu E, Lewin A, Maier S, Muller V, Otto T, Scholz C, Schulz WA, Seifert HH, Schwope I, Ziebarth H, Berlin K, Piepenbrock C, Olek A (2002) Tumour class prediction and discovery by microarray-based DNA methylation analysis. Nucleic Acids Res 30:e21

2. Alizadeh AA, Eisen MB, Davis RE, Ma C, Lossos IS, Rosenwald A, Boldrick JC, Sabet H, Tran T, Yu X, Powell JI, Yang L, Marti GE, Moore T, Hudson J Jr, Lu L, Lewis DB, Tibshirani R, Sherlock G, Chan WC, Greiner TC, Weisenburger DD, Armitage JO, Warnke R, Levy R, Wilson W, Grever MR, Byrd JC, Botstein D, Brown PO, Staudt LM (2000) Distinct types of diffuse large B-cell lymphoma identified by gene expression profiling. Nature 403:503–511
3. Armstrong SA, Staunton JE, Silverman LB, Pieters R, den Boer ML, Minden MD, Sallan SE, Lander ES, Golub TR, Korsmeyer SJ (2002) MLL translocations specify a distinct gene expression profile that distinguishes a unique leukemia. Nat Genet 30:41–47
4. Baggerly KA, Morris JS, Edmonson SR, Coombes KR (2005) Signal in noise: evaluating reported reproducibility of serum proteomic tests for ovarian cancer. J Natl Cancer Inst 97: 307–309
5. Bammler T, Beyer RP, Bhattacharya S, Boorman GA, Boyles A, Bradford BU, Bumgarner RE, Bushel PR, Chaturvedi K, Choi D, Cunningham ML, Deng S, Dressman HK, Fannin RD, Farin FM, Freedman JH, Fry RC, Harper A, Humble MC, Hurban P, Kavanagh TJ, Kaufmann WK, Kerr KF, Jing L, Lapidus JA, Lasarev MR, Li J, Li YJ, Lobenhofer EK, Lu X, Malek RL, Milton S, Nagalla SR, O'malley JP, Palmer VS, Pattee P, Paules RS, Perou CM, Phillips K, Qin LX, Qiu Y, Quigley SD, Rodland M, Rusyn I, Samson LD, Schwartz DA, Shi Y, Shin JL, Sieber SO, Slifer S, Speer MC, Spencer PS, Sproles DI, Swenberg JA, Suk WA, Sullivan RC, Tian R, Tennant RW, Todd SA, Tucker CJ, Van Houten B, Weis BK, Xuan S, Zarbl H (2005) Standardizing global gene expression analysis between laboratories and across platforms. Nature Methods 2:351–356
6. Baylin SB, Esteller M, Rountree MR, Bachman KE, Schuebel K, Herman JG (2001) Aberrant patterns of DNA methylation, chromatin formation and gene expression in cancer. Hum Mol Genet 10:687–692
7. Bertucci F, Nasser V, Granjeaud S, Eisinger F, Adelaide J, Tagett R, Loriod B, Giaconia A, Benziane A, Devilard E, Jacquemier J, Viens P, Nguyen C, Birnbaum D, Houlgatte R (2002) Gene expression profiles of poor-prognosis primary breast cancer correlate with survival. Hum Mol Genet 11: 863–872
8. Bertucci F, Viens P, Hingamp P, Nasser V, Houlgatte R, Birnbaum D (2003) Breast cancer revisited using DNA array-based gene expression profiling. Int J Cancer 103:565–571
9. Bhattacharjee A, Richards WG, Staunton J, Li C, Monti S, Vasa P, Ladd C, Beheshti J, Bueno R, Gillette M, Loda M, Weber G, Mark EJ, Lander ES, Wong W, Johnson BE, Golub TR, Sugarbaker DJ, Meyerson M (2001) Classification of human lung carcinomas by mRNA expression profiling reveals distinct adenocarcinoma subclasses. Proc Natl Acad Sci USA 98:13790–13795
10. Bittner M, Meltzer P, Chen Y, Jiang Y, Seftor E, Hendrix M, Radmacher M, Simon R, Yakhini Z, Ben Dor A, Sampas N, Dougherty E, Wang E, Marincola F, Gooden C, Lueders J, Glatfelter A, Pollock P, Carpten J, Gillanders E, Leja D, Dietrich K, Beaudry C, Berens M, Alberts D, Sondak V (2000) Molecular classification of cutaneous malignant melanoma by gene expression profiling. Nature 406:536–540
11. Brazma A, Vilo J (2000) Gene expression data analysis. FEBS Lett 480:17–24
12. Brazma A, Hingamp P, Quackenbush J, Sherlock G, Spellman P, Stoeckert C, Aach J, Ansorge W, Ball CA, Causton HC, Gaasterland T, Glenisson P, Holstege FC, Kim IF, Markowitz V, Matese JC, Parkinson H, Robinson A, Sarkans U, Schulze-Kremer S, Stewart J, Taylor R, Vilo J, Vingron M (2001) Minimum information about a microarray experiment (MIAME)—toward standards for microarray data. Nat Genet 29:365–371
13. Brown PO, Botstein D (1999) Exploring the new world of the genome with DNA microarrays. Nat Genet 21:33–37
14. Celis JE, Kruhoffer M, Gromova I, Frederiksen C, Ostergaard M, Thykjaer T, Gromov P, Yu J, Palsdottir H, Magnusson N, Orntoft TF (2000) Gene expression profiling: monitoring transcription and translation products using DNA microarrays and proteomics. FEBS Lett 480:2–16
15. Chen CM, Chen HL, Hsiau TH, Hsiau AH, Shi H, Brock GJ, Wei SH, Caldwell CW, Yan PS, Huang TH (2003) Methylation target array for rapid analysis of CpG island hypermethylation in multiple tissue genomes. Am J Pathol 163:37–45
16. Cheung PK, Woolcock B, Adomat H, Sutcliffe M, Bainbridge TC, Jones EC, Webber D, Kinahan T, Sadar M, Gleave ME, Vielkind J (2004) Protein profiling of microdissected prostate tissue links growth differentiation factor 15 to prostate carcinogenesis. Cancer Res 64:5929–5933
17. Coombes KR, Morris JS, Hu J, Edmonson SR, Baggerly KA (2005) Serum proteomics profiling—a young technology begins to mature. Nat Biotechnol 23:291–292
18. Cottrell SE, Distler J, Goodman NS, Mooney SH, Kluth A, Olek A, Schwope I, Tetzner R, Ziebarth H, Berlin K (2004) A real-time PCR assay for DNA-methylation using methylation-specific blockers. Nucleic Acids Res 32:e10
19. Cowherd SM, Espina VA, Petricoin EF III, Liotta LA (2004) Proteomic analysis of human breast cancer tissue with laser-capture microdissection and reverse-phase protein microarrays. Clin Breast Cancer 5:385–392
20. Dancey J, Sausville EA (2003) Issues and progress with protein kinase inhibitors for cancer treatment. Nat Rev Drug Discov 2:296–313
21. Dhanasekaran SM, Barrette TR, Ghosh D, Shah R, Varambally S, Kurachi K, Pienta KJ, Rubin MA, Chinnaiyan AM (2001) Delineation of prognostic biomarkers in prostate cancer. Nature 412:822–826
22. Diamandis EP (2004) Analysis of serum proteomic patterns for early cancer diagnosis: drawing attention to potential problems. J Natl Cancer Inst 96:353–356
23. Diamandis EP, van der Merwe DE (2005) Plasma protein profiling by mass spectrometry for cancer diagnosis: opportunities and limitations. Clin Cancer Res 11:963–965
24. Eisen MB, Spellman PT, Brown PO, Botstein D (1998) Cluster analysis and display of genome-wide expression patterns. Proc Natl Acad Sci USA 95:14863–14868
25. Eschrich S, Yang I, Bloom G, Kwong KY, Boulware D, Cantor A, Coppola D, Kruhoffer M, Aaltonen L, Orntoft TF, Quackenbush J, Yeatman TJ (2005) Molecular staging for survival prediction of colorectal cancer patients. J Clin Oncol 23:3526–3535
26. Garber ME, Troyanskaya OG, Schluens K, Petersen S, Thaesler Z, Pacyna-Gengelbach M, van de Rijn RM, Rosen GD, Perou CM, Whyte RI, Altman RB, Brown PO, Botstein D, Petersen I (2001) Diversity of gene expression in adenocarcinoma of the lung. Proc Natl Acad Sci USA 98:13784–13789
27. Geho D, Lahar N, Gurnani P, Huebschman M, Herrmann P, Espina V, Shi A, Wulfkuhle J, Garner H, Petricoin E III, Liotta LA, Rosenblatt KP (2005) Pegylated, steptavidin-conjugated quantum dots are effective detection elements for reverse-phase protein microarrays. Bioconjug Chem 16:559–566
28. Gianni L, Zambetti M, Clark K, Baker J, Cronin M, Wu J, Mariani G, Rodriguez J, Carcangiu M, Watson D, Valagussa P, Rouzier R, Symmans WF, Ross JS, Hortobagyi GN, Pusztai L, Shak S (2005) Gene expression profiles in paraffin-embedded core biopsy tissue predict response to chemotherapy in women with locally advanced breast cancer. J Clin Oncol 23(29): 7265–7277
29. Giordano TJ, Shedden KA, Schwartz DR, Kuick R, Taylor JM, Lee N, Misek DE, Greenson JK, Kardia SL, Beer DG, Rennert G, Cho KR, Gruber SB, Fearon ER, Hanash S (2001) Organ-specific molecular classification of primary lung, colon, and ovarian adenocarcinomas using gene expression profiles. Am J Pathol 159:1231–1238

30. Goldmann T, Flohr AM, Murua EH, Gerstmayer B, Janssen U, Bosio A, Loeschke S, Vollmer E, Bullerdiek J (2004) The HOPE-technique permits Northern blot and microarray analyses in paraffin-embedded tissues. Pathol Res Pract 200: 511–515
31. Golub TR, Slonim DK, Tamayo P, Huard C, Gaasenbeek M, Mesirov JP, Coller H, Loh ML, Downing JR, Caligiuri MA, Bloomfield CD, Lander ES (1999) Molecular classification of cancer: class discovery and class prediction by gene expression monitoring. Science 286:531–537
32. Hanash S (2003) Disease proteomics. Nature 422:226–232
33. Higuchi E, Oridate N, Furuta Y, Suzuki S, Hatakeyama H, Sawa H, Sunayashiki-Kusuzaki K, Yamazaki K, Inuyama Y, Fukuda S (2003) Differentially expressed genes associated with CIS-diamminedichloroplatinum (II) resistance in head and neck cancer using differential display and CDNA microarray. Head Neck 25:187–193
34. Hofmann WK, de Vos S, Elashoff D, Gschaidmeier H, Hoelzer D, Koeffler HP, Ottmann OG (2002) Relation between resistance of Philadelphia-chromosome-positive acute lymphoblastic leukaemia to the tyrosine kinase inhibitor STI571 and geneexpression profiles: a gene-expression study. Lancet 359:481–486
35. Huang E, Cheng SH, Dressman H, Pittman J, Tsou MH, Horng CF, Bild A, Iversen ES, Liao M, Chen CM, West M, Nevins JR, Huang AT (2003) Gene expression predictors of breast cancer outcomes. Lancet 361:1590–1596
36. Hudelist G, Pacher-Zavisin M, Singer CF, Holper T, Kubista E, Schreiber M, Manavi M, Bilban M, Czerwenka K (2004) Use of high-throughput protein array for profiling of differentially expressed proteins in normal and malignant breast tissue. Breast Cancer Res Treat 86:281–291
37. Hyvärinen A, Karhunen J, Oja E (2001) Independent component analysis. Wiley, New York
38. Jones PA, Baylin SB (2002) The fundamental role of epigenetic events in cancer. Nat Rev Genet 3:415–428
39. Khan J, Simon R, Bittner M, Chen Y, Leighton SB, Pohida T, Smith PD, Jiang Y, Gooden GC, Trent JM, Meltzer PS (1998) Gene expression profiling of alveolar rhabdomyosarcoma with cDNA microarrays. Cancer Res 58:5009–5013
40. Khan J, Wei JS, Ringner M, Saal LH, Ladanyi M, Westermann F, Berthold F, Schwab M, Antonescu CR, Peterson C, Meltzer PS (2001) Classification and diagnostic prediction of cancers using gene expression profiling and artificial neural networks. Nat Med 7:673–679
41. Kihara C, Tsunoda T, Tanaka T, Yamana H, Furukawa Y, Ono K, Kitahara O, Zembutsu H, Yanagawa R, Hirata K, Takagi T, Nakamura Y (2001) Prediction of sensitivity of esophageal tumors to adjuvant chemotherapy by cDNA microarray analysis of gene-expression profiles. Cancer Res 61:6474–6479
42. Knezevic V, Leethanakul C, Bichsel VE, Worth JM, Prabhu VV, Gutkind JS, Liotta LA, Munson PJ, Petricoin EF III, Krizman DB (2001) Proteomic profiling of the cancer microenvironment by antibody arrays. Proteomics 1:1271–1278
43. Krieg RC, Gaisa NT, Paweletz CP, Knuechel R (2005) Proteomic analysis of human bladder tissue using SELDI approach following microdissection techniques. Methods Mol Biol 293:255–267
44. Kusnezow W, Jacob A, Walijew A, Diehl F, Hoheisel JD (2003) Antibody microarrays: an evaluation of production parameters. Proteomics 3:254–264
45. Lage H, Dietel M (2000) Effect of the breast-cancer resistance protein on atypical multidrug resistance. Lancet Oncol 1: 169–175
46. Lage H, Dietel M (2002) Multiple mechanisms confer different drug-resistant phenotypes in pancreatic carcinoma cells. J Cancer Res Clin Oncol 128:349–357
47. Lawrie LC, Curran S (2005) Laser capture microdissection and colorectal cancer proteomics. Methods Mol Biol 293:245–253
48. Lee SI, Batzoglou S (2003) Application of independent component analysis to microarrays. Genome Biol 4:R76
49. Liebermeister W (2002) Linear modes of gene expression determined by independent component analysis. Bioinformatics 18:51–60
50. Liotta LA, Espina V, Mehta AI, Calvert V, Rosenblatt K, Geho D, Munson PJ, Young L, Wulfkuhle J, Petricoin EF III (2003) Protein microarrays: meeting analytical challenges for clinical applications. Cancer Cell 3:317–325
51. Ma XJ, Salunga R, Tuggle JT, Gaudet J, Enright E, McQuary P, Payette T, Pistone M, Stecker K, Zhang BM, Zhou YX, Varnholt H, Smith B, Gadd M, Chatfield E, Kessler J, Baer TM, Erlander MG, Sgroi DC (2003) Gene expression profiles of human breast cancer progression. Proc Natl Acad Sci USA 100:5974–5979
52. Macgregor PF, Squire JA (2002) Application of microarrays to the analysis of gene expression in cancer. Clin Chem 48: 1170–1177
53. Michiels S, Koscielny S, Hill C (2005) Prediction of cancer outcome with microarrays: a multiple random validation strategy. Lancet 365:488–492
54. Nessling M, Richter K, Schwaenen C, Roerig P, Wrobel G, Wessendorf S, Fritz B, Bentz M, Sinn HP, Radlwimmer B, Lichter P (2005) Candidate genes in breast cancer revealed by microarray-based comparative genomic hybridization of archived tissue. Cancer Res 65:439–447
55. Nielsen UB, Cardone MH, Sinskey AJ, MacBeath G, Sorger PK (2003) Profiling receptor tyrosine kinase activation by using Ab microarrays. Proc Natl Acad Sci USA 100:9330–9335
56. Olek A, Oswald J, Walter J (1996) A modified and improved method for bisulphite based cytosine methylation analysis. Nucleic Acids Res 24:5064–5066
57. Ono K, Tanaka T, Tsunoda T, Kitahara O, Kihara C, Okamoto A, Ochiai K, Takagi T, Nakamura Y (2000) Identification by cDNA microarray of genes involved in ovarian carcinogenesis. Cancer Res 60:5007–5011
58. Paweletz CP, Charboneau L, Bichsel VE, Simone NL, Chen T, Gillespie JW, Emmert-Buck MR, Roth MJ, Petricoin EF III, Liotta LA (2001) Reverse phase protein microarrays which capture disease progression show activation of pro-survival pathways at the cancer invasion front. Oncogene 20:1981–1989
59. Paweletz CP, Trock B, Pennanen M, Tsangaris T, Magnant C, Liotta LA, Petricoin EF III (2001) Proteomic patterns of nipple aspirate fluids obtained by SELDI-TOF: potential for new biomarkers to aid in the diagnosis of breast cancer. Dis Markers 17:301–307
60. Perou CM, Sorlie T, Eisen MB, van de Rijn RM, Jeffrey SS, Rees CA, Pollack JR, Ross DT, Johnsen H, Akslen LA, Fluge O, Pergamenschikov A, Williams C, Zhu SX, Lonning PE, Borresen-Dale AL, Brown PO, Botstein D (2000) Molecular portraits of human breast tumours. Nature 406:747–752
61. Petricoin EF, Ardekani AM, Hitt BA, Levine PJ, Fusaro VA, Steinberg SM, Mills GB, Simone C, Fishman DA, Kohn EC, Liotta LA (2002) Use of proteomic patterns in serum to identify ovarian cancer. Lancet 359:572–577
62. Pollack JR, van de Rijn RM, Botstein D (2002) Challenges in developing a molecular characterization of cancer. Semin Oncol 29:280–285
63. Ramaswamy S, Tamayo P, Rifkin R, Mukherjee S, Yeang CH, Angelo M, Ladd C, Reich M, Latulippe E, Mesirov JP, Poggio T, Gerald W, Loda M, Lander ES, Golub TR (2001) Multiclass cancer diagnosis using tumor gene expression signatures. Proc Natl Acad Sci USA 98:15149–15154
64. Ransohoff DF (2005) Lessons from controversy: ovarian cancer screening and serum proteomics. J Natl Cancer Inst 97:315–319
65. Raponi M, Belly RT, Karp JE, Lancet JE, Atkins D, Wang Y (2004) Microarray analysis reveals genetic pathways modulated by tipifarnib in acute myeloid leukemia. BMC Cancer 4:56
66. Saidi SA, Holland CM, Kreil DP, MacKay DJ, Charnock-Jones DS, Print CG, Smith SK (2004) Independent component analysis of microarray data in the study of endometrial cancer. Oncogene 23:6677–6683

67. Scharpf R, Garrett ES, Hu J, Parmigiani G (2003) Statistical modeling and visualization of molecular profiles in cancer. Biotechniques 34:S22–S29
68. Scherf U, Ross DT, Waltham M, Smith LH, Lee JK, Tanabe L, Kohn KW, Reinhold WC, Myers TG, Andrews DT, Scudiero DA, Eisen MB, Sausville EA, Pommier Y, Botstein D, Brown PO, Weinstein JN (2000) A gene expression database for the molecular pharmacology of cancer. Nat Genet 24:236–244
69. Schwartz DR, Kardia SL, Shedden KA, Kuick R, Michailidis G, Taylor JM, Misek DE, Wu R, Zhai Y, Darrah DM, Reed H, Ellenson LH, Giordano TJ, Fearon ER, Hanash SM, Cho KR (2002) Gene expression in ovarian cancer reflects both morphology and biological behavior, distinguishing clear cell from other poor-prognosis ovarian carcinomas. Cancer Res 62:4722–4729
70. Sheehan KM, Calvert VS, Kay EW, Lu Y, Fishman D, Espina V, Aquino J, Speer R, Araujo R, Mills GB, Liotta LA, Petricoin EF III, Wulfkuhle JD (2005) Use of reverse phase protein microarrays and reference standard development for molecular network analysis of metastatic ovarian carcinoma. Mol Cell Proteomics 4:346–355
71. Shi H, Wei SH, Leu YW, Rahmatpanah F, Liu JC, Yan PS, Nephew KP, Huang TH (2003) Triple analysis of the cancer epigenome: an integrated microarray system for assessing gene expression, DNA methylation, and histone acetylation. Cancer Res 63:2164–2171
72. Simon R, Radmacher MD, Dobbin K, McShane LM (2003) Pitfalls in the use of DNA microarray data for diagnostic and prognostic classification. J Natl Cancer Inst 95:14–18
73. Sobin LH, Wittekind Ch (eds) (2002) TNM classification of malignant tumors, UICC, 6th edn. Wiley, New York
74. Sorlie T, Perou CM, Tibshirani R, Aas T, Geisler S, Johnsen H, Hastie T, Eisen MB, van de Rijn RM, Jeffrey SS, Thorsen T, Quist H, Matese JC, Brown PO, Botstein D, Eystein LP, Borresen-Dale AL (2001) Gene expression patterns of breast carcinomas distinguish tumor subclasses with clinical implications. Proc Natl Acad Sci USA 98:10869–10874
75. Sotiriou C, Neo SY, McShane LM, Korn EL, Long PM, Jazaeri A, Martiat P, Fox SB, Harris AL, Liu ET (2003) Breast cancer classification and prognosis based on gene expression profiles from a population-based study. Proc Natl Acad Sci USA 100:10393–10398
76. Souchelnytskyi S (2002) Proteomics in studies of signal transduction in epithelial cells. J Mammary Gland Biol Neoplasia 7:359–371
77. Sreekumar A, Nyati MK, Varambally S, Barrette TR, Ghosh D, Lawrence TS, Chinnaiyan AM (2001) Profiling of cancer cells using protein microarrays: discovery of novel radiation-regulated proteins. Cancer Res 61:7585–7593
78. Su AI, Welsh JB, Sapinoso LM, Kern SG, Dimitrov P, Lapp H, Schultz PG, Powell SM, Moskaluk CA, Frierson HF Jr, Hampton GM (2001) Molecular classification of human carcinomas by use of gene expression signatures. Cancer Res 61:7388–7393
79. Tamayo P, Slonim D, Mesirov J, Zhu Q, Kitareewan S, Dmitrovsky E, Lander ES, Golub TR (1999) Interpreting patterns of gene expression with self-organizing maps: methods and application to hematopoietic differentiation. Proc Natl Acad Sci USA 96:2907–2912
80. Tan PK, Downey TJ, Spitznagel EL Jr, Xu P, Fu D, Dimitrov DS, Lempicki RA, Raaka BM, Cam MC (2003) Evaluation of gene expression measurements from commercial microarray platforms. Nucleic Acids Res 31:5676–5684
81. Tannapfel A, Anhalt K, Hausermann P, Sommerer F, Benicke M, Uhlmann D, Witzigmann H, Hauss J, Wittekind C (2003) Identification of novel proteins associated with hepatocellular carcinomas using protein microarrays. J Pathol 201:238–249
82. Tavazoie S, Hughes JD, Campbell MJ, Cho RJ, Church GM (1999) Systematic determination of genetic network architecture. Nat Genet 22:281–285
83. Tothill RW, Kowalczyk A, Rischin D, Bousioutas A, Haviv I, van Laar RK, Waring PM, Zalcberg J, Ward R, Biankin AV, Sutherland RL, Henshall SM, Fong K, Pollack JR, Bowtell DD, Holloway AJ (2005) An expression-based site of origin diagnostic method designed for clinical application to cancer of unknown origin. Cancer Res 65:4031–4040
84. van de Vijver MJ, He YD, van't Veer LJ, Dai H, Hart AA, Voskuil DW, Schreiber GJ, Peterse JL, Roberts C, Marton MJ, Parrish M, Atsma D, Witteveen A, Glas A, Delahaye L, van der Velde T, Bartelink H, Rodenhuis S, Rutgers ET, Friend SH, Bernards R (2002) A gene-expression signature as a predictor of survival in breast cancer. N Engl J Med 347:1999–2009
85. van't Veer LJ, Dai H, van de Vijver MJ, He YD, Hart AA, Bernards R, Friend SH (2003) Expression profiling predicts outcome in breast cancer. Breast Cancer Res 5:57–58
86. Vihinen PP, Pyrhonen SO, Kahari VM (2003) New prognostic factors and developing therapy of cutaneous melanoma. Ann Med 35:66–78
87. Wang W, Marsh S, Cassidy J, McLeod HL (2001) Pharmacogenomic dissection of resistance to thymidylate synthase inhibitors. Cancer Res 61:5505–5510
88. Wang Y, Klijn JG, Zhang Y, Sieuwerts AM, Look MP, Yang F, Talantov D, Timmermans M, Meijer-van Gelder ME, Yu J, Jatkoe T, Berns EM, Atkins D, Foekens JA (2005) Gene-expression profiles to predict distant metastasis of lymph-node-negative primary breast cancer. Lancet 365:671–679
89. Watson MA, Perry A, Budhjara V, Hicks C, Shannon WD, Rich KM (2001) Gene expression profiling with oligonucleotide microarrays distinguishes World Health Organization grade of oligodendrogliomas. Cancer Res 61:1825–1829
90. Wei SH, Chen CM, Strathdee G, Harnsomburana J, Shyu CR, Rahmatpanah F, Shi H, Ng SW, Yan PS, Nephew KP, Brown R, Huang TH (2002) Methylation microarray analysis of late-stage ovarian carcinomas distinguishes progression-free survival in patients and identifies candidate epigenetic markers. Clin Cancer Res 8:2246–2252
91. Wulfkuhle JD, Sgroi DC, Krutzsch H, McLean K, McGarvey K, Knowlton M, Chen S, Shu H, Sahin A, Kurek R, Wallwiener D, Merino MJ, Petricoin EF III, Zhao Y, Steeg PS (2002) Proteomics of human breast ductal carcinoma in situ. Cancer Res 62:6740–6749
92. Yeoh EJ, Ross ME, Shurtleff SA, Williams WK, Patel D, Mahfouz R, Behm FG, Raimondi SC, Relling MV, Patel A, Cheng C, Campana D, Wilkins D, Zhou X, Li J, Liu H, Pui CH, Evans WE, Naeve C, Wong L, Downing JR (2002) Classification, subtype discovery, and prediction of outcome in pediatric acute lymphoblastic leukemia by gene expression profiling. Cancer Cell 1:133–143
93. Yu YP, Paranjpe S, Nelson J, Finkelstein S, Ren B, Kokkinakis D, Michalopoulos G, Luo JH (2005) High throughput screening of methylation status of genes in prostate cancer using an oligonucleotide methylation array. Carcinogenesis 26:471–479
94. Zembutsu H, Ohnishi Y, Tsunoda T, Furukawa Y, Katagiri T, Ueyama Y, Tamaoki N, Nomura T, Kitahara O, Yanagawa R, Hirata K, Nakamura Y (2002) Genome-wide cDNA microarray screening to correlate gene expression profiles with sensitivity of 85 human cancer xenografts to anticancer drugs. Cancer Res 62:518–527
95. Zha H, Raffeld M, Charboneau L, Pittaluga S, Kwak LW, Petricoin E III, Liotta LA, Jaffe ES (2004) Similarities of prosurvival signals in Bcl-2-positive and Bcl-2-negative follicular lymphomas identified by reverse phase protein microarray. Lab Invest 84:235–244
96. Zhang Z, Bast RC Jr, Yu Y, Li J, Sokoll LJ, Rai AJ, Rosenzweig JM, Cameron B, Wang YY, Meng XY, Berchuck A, Haaften-Day C, Hacker NF, de Bruijn HW, van der Zee AG, Jacobs IJ, Fung ET, Chan DW (2004) Three biomarkers identified from serum proteomic analysis for the detection of early stage ovarian cancer. Cancer Res 64:5882–5890
97. Zheng Y, Xu Y, Ye B, Lei J, Weinstein MH, O'Leary MP, Richie JP, Mok SC, Liu BC (2003) Prostate carcinoma tissue proteomics for biomarker discovery. Cancer 98:2576–2582

Virchows Arch (2006) 448: 756–762
DOI 10.1007/s00428-006-0188-3

ORIGINAL ARTICLE

Natsuko Tatsumi · Ryoji Kushima · Michael Vieth · Ken-ichi Mukaisho · Rie Kakinoki · Hidetoshi Okabe · Franz Borchard · Manfred Stolte · Takeshi Okanoue · Takanori Hattori

Cytokeratin 7/20 and mucin core protein expression in ulcerative colitis-associated colorectal neoplasms

Received: 10 August 2005 / Accepted: 6 March 2006 / Published online: 12 April 2006

Abstract Different histogenetic pathways have been suggested between ulcerative colitis (UC)-associated neoplasia and sporadic colorectal neoplasia. Little is known about the cytokeratin (CK) and mucin expression in UC-associated neoplasms. To clarify the characteristics of UC-associated colorectal carcinogenesis, we examined the immunohistochemical expression of CK7, CK20, MUC2, MUC5AC and MUC6 in 90 colorectal neoplasms, including 22 UC-associated adenocarcinomas (colitic cancer; CC), ten high-grade dysplasias (HGD) in UC, nine low-grade dysplasias (LGD) in UC, 24 sporadic tubular adenomas (TA) and 25 adenocarcinomas (AC). CK7 was positive in most of UC-associated neoplasms: 59% of CC cases, 80% of HGD and 89% of LGD, respectively, whereas, in non-UC associated neoplasia, 21% of TA and 12% of AC. The frequency of MUC6 expression in UC-associated neoplasia was 32% in CC, 30% in HGD and 44% in LGD, respectively, whereas, in non-UC associated neoplasia, 4.2% in TA and 0% in AC. MUC5AC expression in UC-associated neoplasia was detectable in 73% of CC, 90% of HGD and 89% of LGD, respectively; in non-UC associated neoplasia 67% in AC and 20% in TA. There were obvious differences in the expression of CK7 and MUC6 between UC-associated neoplasms and sporadic tumors. The incidence of MUC5AC expression in UC-associated neoplasms was also higher than sporadic tumors. *These results suggest that gastric-type mucins play an important role in the initial step of CC-tumorigenesis*, and CK7 and gastric-type mucins may be useful in the differential diagnosis between UC-associated neoplasms and sporadic ones.

Keywords Ulcerative colitis · Dysplasia · Colon carcinoma · Cytokeratin · Mucin

N. Tatsumi · T. Okanoue
Molecular Gastroenterology and Hepatology, Kyoto Prefectural University of Medicine, Graduate School of Medical Science, Kamigyo-ku,
602-8566 Kyoto, Japan

R. Kushima (✉) · R. Kakinoki · H. Okabe
Division of Diagnostic Pathology,
Shiga University of Medical Science,
Otsu,
520-2192 Shiga, Japan
e-mail: kushima@belle.shiga-med.ac.jp
Tel.: +81-77-5482621
Fax: +81-77-5482407

M. Vieth · M. Stolte
Klinikum Bayreuth, Institute of Pathology,
95445 Bayreuth, Germany

K. Mukaisho · T. Hattori
Department of Pathology, Shiga University of Medical Science,
Otsu,
520-2192 Shiga, Japan

F. Borchard
Klinikum Aschaffenburg, Institute of Pathology,
63739 Aschaffenburg, Germany

Introduction

Ulcerative colitis (UC) is a chronic relapsing inflammatory bowel disease of still unclear etiology. The initial case report of colorectal cancer emerging from UC was first published by Crohn and Rosenberg in 1925 [6]. Since then, it has been well established that long-standing UC predisposes to development of colorectal carcinoma [12]. To date, these cancers are thought to have a distinct histogenetic pathway from that of sporadic colorectal cancers involving precursor stages of low- and high-grade dysplasia (LGD and HGD), respectively. There are some reports of differential gene abnormalities between sporadic colonic and ulcerative colitis (UC) associated neoplasia [1, 2, 9, 18]. Although *p53* alteration occurs rather often with loss of heterozygosity (LOH), a low prevalence of *APC* and *ras* mutations in UC-associated tumors has been described, along with a high LOH frequency of chromosomes 3 and 18 and *p16*, compared to sporadic colorectal cancers [31].

Cytokeratins (CKs) are cytoplasmic structural proteins in normal epithelial cells, and a variable expression has been demonstrated depending on the cellular differentiation [19, 21]. CK20 has been widely applied as a useful

Table 1 Summary of cytokeratin (CK) and mucin expressions in ulcerative colitis-associated neoplasms and sporadic adenoma–carcinoma group

	CK7	MUC6	MUC5AC	MUC2	CK20
Ulcerative colitis-associated neoplasm	29/41(71%)[a]	14/41(34%)[a]	33/41(80%)	37/41(90%)	36/41(88%)
Sporadic adenoma–carcinoma group	8/49(16%)[b]	1/49(2.0%)[b]	21/49(43%)	37/49(76%)	45/49(92%)

a vs b, $p<0.01$

marker of colon adenocarcinomas. CK7 is found in the normal epithelium of the lung, cervix, breast, bile ducts and bladder transitional cell epithelium. However, CK7 is essentially absent in the normal gastrointestinal epithelium [22]. CK7 has also been reported to be a possible marker of transient dedifferentiation in the sequence between gastritis, metaplasia, dysplasia and cancer of the stomach [14]. Most recently, we reported the high incidence of CK7-expression in hyperplastic polyps and serrated adenomas of the colon [26]. These colon lesions have been considered to progress through the pathway which is different from the so-called adenoma–carcinoma sequence. There have been many studies about CK7/CK20 expression in sporadic colorectal and other carcinomas; however, the expression in UC-associated colorectal neoplasms has not extensively been evaluated.

On the other hand, initial histochemical studies showed typically changes in the biochemical characteristics of mucin occurring in intestinal disorders [10, 11]. It has been reported that quantity and quality of mucin secretion are affected in inflammatory bowel disease (IBD) [8]. Additionally, the recent identification of several mucin genes [7] and the production of monoclonal antibodies to mucin protein cores has led to the immunohistochemical localization of several mucin species. More than ten genes encoding distinct mucin proteins have recently been identified by molecular cloning. Among them, MUC5AC, MUC6 and MUC2 are specifically expressed in gastric surface mucous cells, pyloric gland cells and intestinal goblet cells of the mature gastrointestinal tract, respectively [23, 28]. There have been some reports about expression of MUC2 in UC-associated neoplasms, but the results were controversial [13, 24, 29, 30]. Little is known about the expression of the gastric-type mucins in UC-associated intraepithelial neoplasms.

In the present study, we targeted the expression of CK7, CK20, MUC2, MUC5AC and MUC6 in UC-associated colorectal neoplasms as compared to sporadic colon carcinoma, to further investigate colitic cancer carcinogenesis.

Materials and methods

Tissue specimens

The material consisted of 90 paraffin-embedded tissue sections of colorectal neoplasms from 77 patients. The material consisted of 41 UC-associated neoplasms, 24

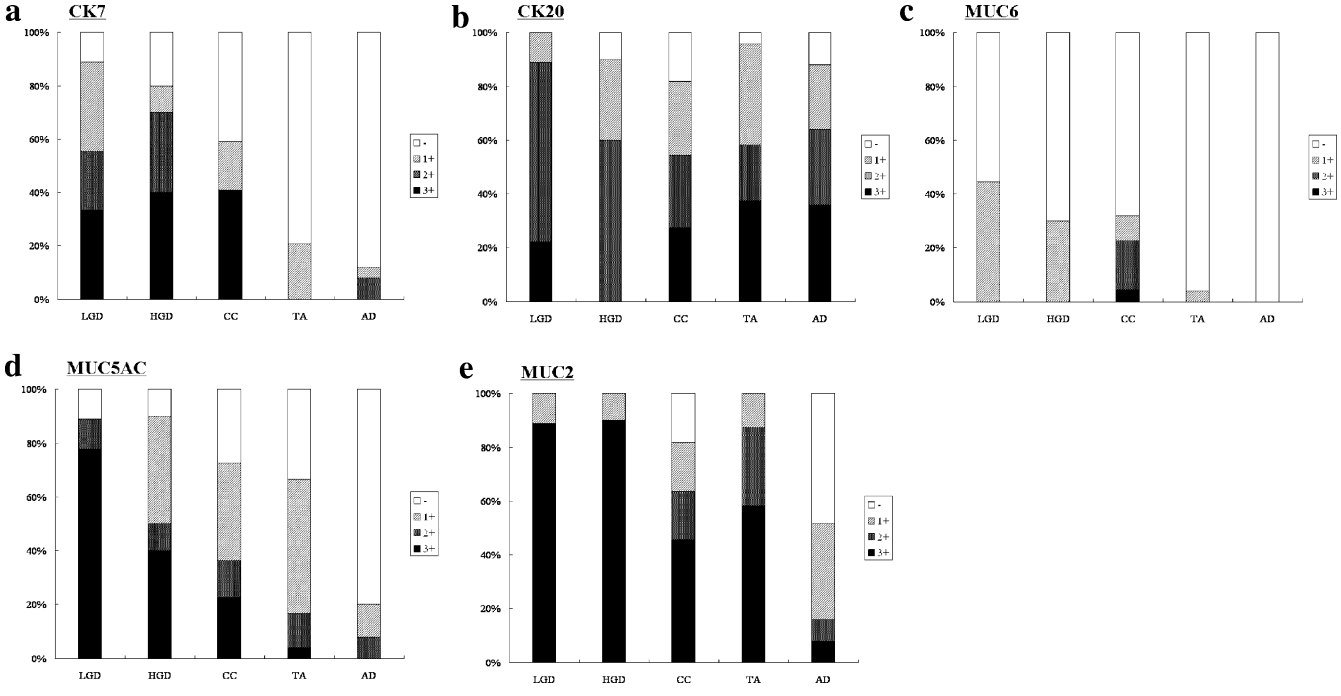

Fig. 1 Schematic presentation of scoring results of each neoplasm for cytokeratin (*CK*) and mucin. **a** CK7; **b** CK20; **c** MUC6; **d** MUC5AC; **e** MUC2. *LGD* Low-grade dysplasia, *HGD* high-grade dysplasia, *CC* colitis cancer, *TA* tubular adenoma, *AD* adenocarcinoma

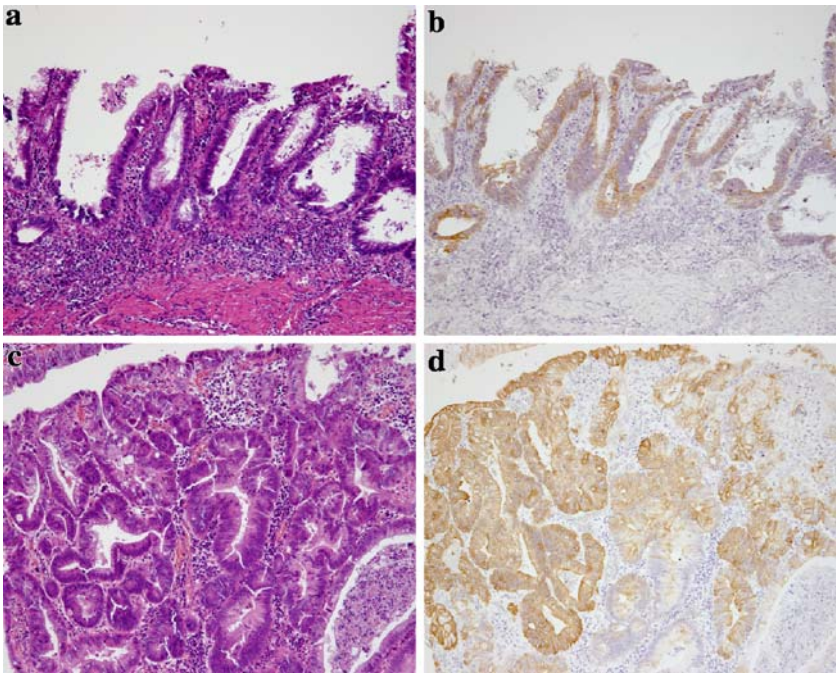

Fig 2 Histological and immunohistochemical (CK7) findings of *LGD* (**a**,**b**) and *HGD* (**c**,**d**) in ulcerative colitis. Positivity for CK7 is diffuse and cytoplasmic

sporadic adenomas and 25 adenocarcinomas. Of the UC-associated neoplasms, nine were low-grade dysplasia (LGD), ten were high grade dysplasia (HGD), and 22 were colitic cancer (CC). Specimen collection procedures were approved by the ethics committee of our university, and informed consent was obtained from all patients.

Mucin histochemical and immunohistochemical studies

Immunohistochemical staining was carried out with the following monoclonal antibodies (MAbs): CK7 (OV-TL 12/30, 1:50, NovoCastra, UK), CK20 (Ks20.8, 1:50, NovoCastra, UK), MUC2(Ccp58; 1:100, NovoCastra, UK); MUC5AC (CLH2, 1:100, NovoCastra, UK) and MUC6 (CLH5, 1:100, NovoCastra, UK). The standard streptavidin–biotin method of detection was used. Peroxidase binding sites

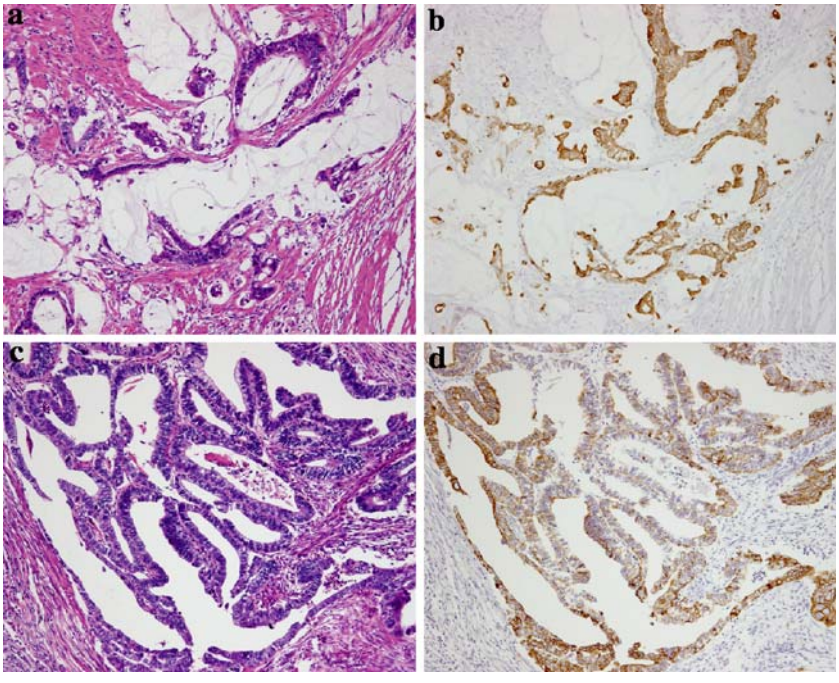

Fig. 3 Histological and immunohistochemical (CK7) findings of *CC*. Examples of mucinous adenocarcinoma (**a**,**b**) and papillary adenocarcinoma (**c**,**d**) are displayed. Positivity for CK7 is diffuse and cytoplasmic

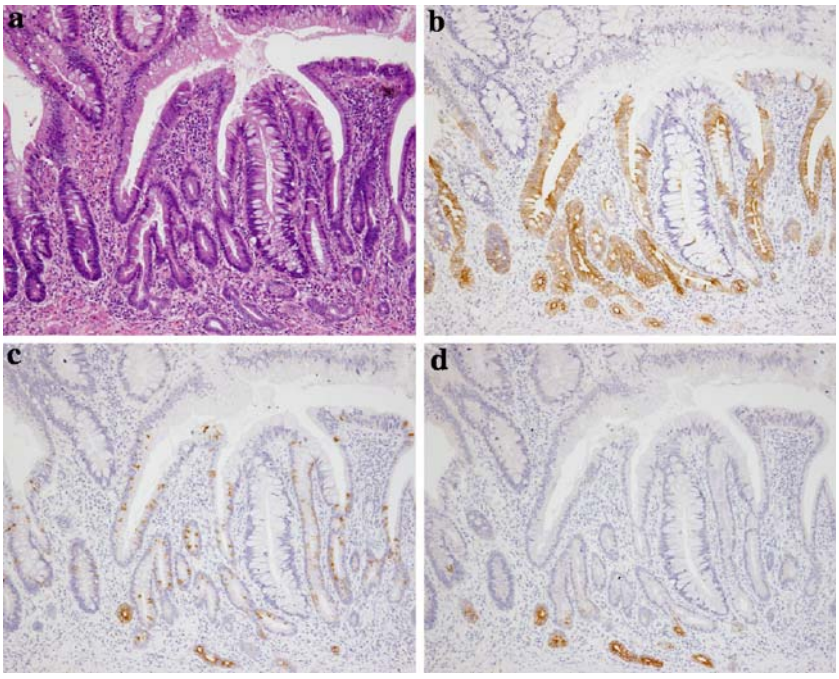

Fig. 4 Comparative demonstration of histology (**a**), CK7- (**b**), MUC5AC- (**c**), and MUC6-expression (**d**) of *LGD* in ulcerative colitis. MUC6-positivity is confined to the bottom of crypts

were visualized by diaminobenzidine method, and the sections were slightly counterstained with hematoxylin.

The following controls were performed: negative controls: (1) slides run without the primary antibody; (2) careful examination of non-epithelial structures (vessels, muscles and connective tissue); positive controls; inclusion of normal tissues known to express CK7 (bile duct), CK20 and MUC2 (small intestine), MUC5AC (gastric foveolar cells), and MUC6 (pyloric gland cells), respectively.

Scoring of immunostaining and statistical analysis

The extent of positivity for CK7, CK20, MUC2, MUC5AC and MUC6 was scored according to the percentage of neoplastic cells stained: −, no positive cells or essentially none (<5%); 1+, some positive cells (5–30%); 2+, diffuse areas of positive cells (30–60%); 3+, extensive areas of positive cells (>60%). The chi-square test with Yates correction was used for statistical analysis. Differences were considered to be significant at $p<0.05$. Fisher's test was applied whenever appropriate.

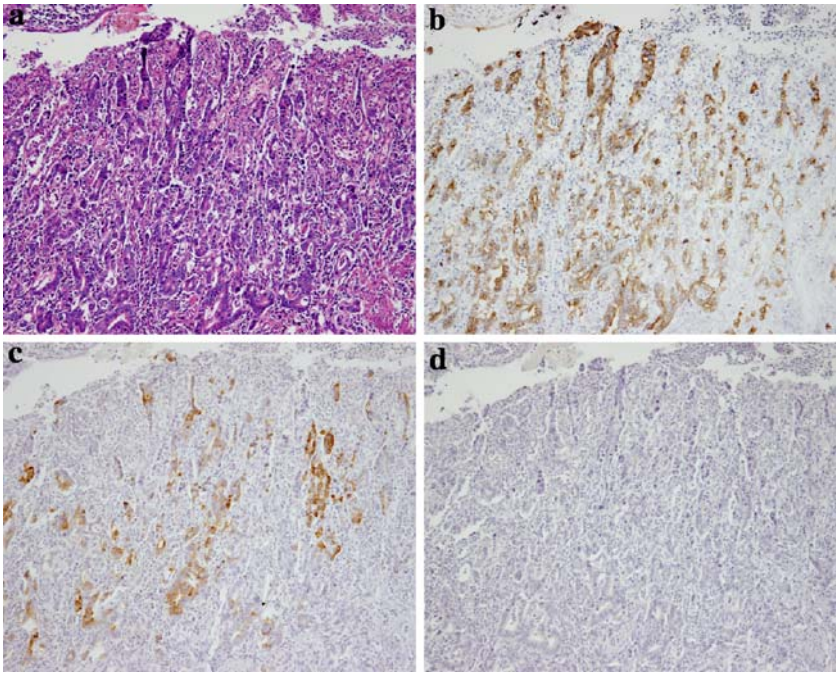

Fig. 5 Comparative demonstration of histology (**a**), CK7- (**b**), MUC5AC- (**c**), and MUC6-expression (**d**) of *CC*. In this case of poorly differentiated adenocarcinoma, MUC6 is not expressed

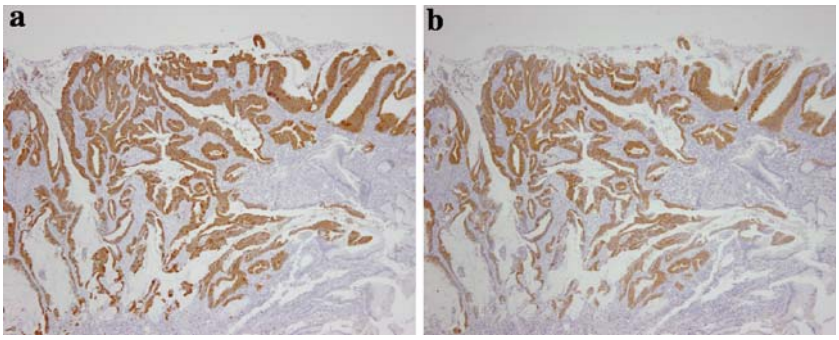

Fig. 6 An example of CC (papillary adenocarcinoma) strongly showing both gastric-type mucins (**a** MUC5AC; **b** MUC6)

Results

The immunohistochemical results with comparison of the UC-associated neoplasms and the sporadic adenoma–carcinoma group (CA and AD) are summarized in Table 1, and the scoring results of each neoplasm are shown in Fig. 1.

CK7 and CK20 expression

CK7 Typical staining patterns of the various neoplasms are shown in Figs. 2, 3, 4 and 5. CK7 was not expressed in normal colorectal epithelium; however, the hyperplastic epithelium near the colorectal carcinoma occasionally expressed CK7. In CK7 positive colorectal neoplasms, the positivity was generally diffuse and cytoplasmic, and it was expressed without preference within the glandular epithelium of the crypts. There was a significant difference in CK7 expression between the UC-associated neoplasms and the sporadic adenoma–carcinoma group (CA and AD) (Table 1). The vast majority of cases with UC-associated neoplasms were positive for CK7; whereas, a small percentage of cases with sporadic adenomas and adenocarcinomas were CK7-positive (71 vs 16%, $p<0.01$). CK7 expression was detected in 88% (eight of nine) of LGD and 80% (eight of ten) of HGD and 59% (13 of 22) of CC, while only 21% (five of 24) of sporadic adenomas and 12% (three of 25) of adenocarcinomas were CK7-positive. None of sporadic adenoma–carcinoma group showed 3+, whereas, 39% (16 of 41) of UC-associated neoplasms expressed 3+ (Fig. 1a).

CK20 CK20 was expressed in normal colorectal surface epithelium. The most cases of UC-associated and UC-nonassociated neoplasms were positive for CK20 which are as follows: in 100% (nine of nine) of LGD and 90% (nine of ten) of HGD and 82% (18 of 22) of CC, while 96% (23 of 24) of TA and 88% (22 of 25) of AD, respectively (Fig. 1b). There was no significance in the positive rate of CK20 expression between UC-associated and sporadic adenoma–carcinoma group. However, carcinomas (CC and AD) showed a lower expression than intraepithelial neoplasia (LGD and HGD) and adenomas (TA).

MUC6, MUC5AC and MUC2 expression

MUC6 UC-associated neoplasms showed a significantly increased expression than cases of the sporadic adenoma–carcinoma group (34 vs 2.0%, $p<0.01$; Table 1). The positive rate of MUC6 in UC-associated neoplasms was in 32% of cases with CC, 30% of HGD and 44% of LGD, respectively (Fig. 1c). In non-UC-associated neoplasms the frequencies were: 4.2% in TA and 0% in AC. Only one case of TA showed a 1+ expression, whereas, all AD cases were negative for MUC6 expression. For the most in UC-associated neoplasms, MUC6 expression was restricted to the bottom of crypts (Fig. 4).

MUC5AC UC-associated neoplasms showed high positive rates of MUC5AC; LGD: 89%, HGD: 90%, CC: 73%. The positive rate of CA was relatively high (67%), but the positive rate of AD was lower (20%) (Fig. 1d). In UC-associated neoplasms, the percentage of neoplastic cells positive for MUC5AC tended to decrease with the severity of dysplasia. However, CC showed higher positivity than sporadic adenocarcinoma (73 vs 20%, $p<0.01$). The expression pattern of gastric mucins (MUC5AC detected in the upper portion of glands and MUC6 in the bottom of glands) was detected especially in LGD but not detected in CC (Figs. 4, 5 and 6).

MUC2 There was no significant difference in MUC2 expression among all categories, but carcinomas (CC and AD) showed a tendency for lesser expression than compared to cases with dysplasias and adenomas. All cases of LGD, HGD and CA showed MUC2 expression, while the frequency of MUC2 expression was 82% in CC and 52% in AD, respectively (Fig. 1e).

Discussion

Our results showed that CK7 and MUC6 expression was significantly higher in UC-associated neoplasms than sporadic ones. MUC5AC was also detected at a higher level in UC-associated neoplasms.

Expressions of CKs 7 and 20 have been commonly investigated to determine the primary site of the metastatic lesion. Colorectal adenocarcinomas typically express CK20 but not CK7, and this CK7−/CK20+ profile has been used to distinguish colonic adenocarcinoma from

metastatic carcinomas of other origin [15, 17, 20, 27]. Although CK7 is negative in the normal stomach and most gastric carcinomas, it is expressed in fetal stomach and intestinal metaplasia and dysplasia [25]. Kirchner et al. [14] suggested that metaplastic and neoplastic changes in the gastritis-cancer sequence are associated to dedifferentiated epithelial cells which are defined by CK7 expression and those cells exhibited a low proliferation and beta-catenin accumulation similar to stem cells. Most recently, we demonstrated the high incidence of CK7-expression in hyperplastic polyps and serrated adenomas of the colon [26]. In this respect, hyperplastic polyps/serrated adenomas and UC-associated neoplasms show a similar phenotypic expression.

It is well-known that preneoplastic and neoplastic tissues can express fetal-like morphological and phenotypic characteristics. MUC5AC is expressed in embryonic intestine during a limited period with close relation to development of intestinal differentiation [4]. Recently, aberrant expression of gastric-type mucin such as MUC5AC and MUC6 is suggested to play an important role in regeneration of intestinal epithelium [3]. Our group and others suggested that gastric-type mucins play an important role in epithelial regeneration and healing after prior mucosal injury in Crohn's disease in addition to mucosal protection [5, 16]. In studies of expressions of MUC2, MUC5AC and gastric trefoil factor (TFF1) in Crohn's disease and UC, Shaoul et al. have suggested that gastric-type mucins may play an important role in epithelial wound healing after mucosal injury in IBD [24]. Therefore, our results suggested that gastric-type mucins play an important role in the initial step of CC tumorigenesis in the regenerative process against the chronic persistent and relapsing inflammation.

In conclusion, these findings enable us to consider the possibility that gastric differentiation contributes to the development of UC-associated neoplasms. CK7 and gastric-type mucins may be useful in the differential diagnosis between UC-associated neoplasms and sporadic tubular adenomas and adenocarcinomas.

References

1. Aust DE, Terdiman JP, Willenbucher RF, Chang CG, Molinaro-Clark A, Baretton GB, Loehrs U, Waldman FM (2002) The APC/beta-catenin pathway in ulcerative colitis-related colorectal carcinomas: a mutational analysis. Cancer 94:1421–1427
2. Aust DE, Haase M, Dobryden L, Markwarth A, Lohrs U, Wittekind C, Baretton GB, Tannapfel A (2005) Mutations of the *BRAF* gene in ulcerative colitis-related colorectal carcinoma. Int J Cancer 115:673–677
3. Bartman AE, Sanderson SJ, Ewing SL, Niehans GA, Wiehr CL, Evans MK, Ho SB (1999) Aberrant expression of MUC5AC and MUC6 gastric mucin genes in colorectal polyps. Int J Cancer 80:210–218
4. Buisine MP, Devisme L, Savidge TC, Gespach C, Gosselin B, Porchet N, Aubert JP (1998) Mucin gene expression in human embryonic and fetal intestine. Gut 43: 519–524
5. Buisine MP, Desreumaux P, Leteurtre E, Copin MC, Colombel JF, Porchet N, Aubert JP (2001) Mucin gene expression in intestinal epithelial cells in Crohn's disease. Gut 49:544–551
6. Crohn BB, Rosenberg H (1925) The sigmoidoscopic picture of chronic ulcerative colitis (non-specific). Am J Med Sci 170:220–228
7. Devine PL, McKenzie IF (1992) Mucins: structure, function, and associations with malignancy. Bioessays 14:619–625
8. Ehsanullah M, Filipe MI, Gazzard B (1982) Mucin secretion in inflammatory bowel disease: correlation with disease activity and dysplasia. Gut 23:485–489
9. Ezaki T, Watanabe M, Inoue N, Kanai T, Ogata H, Iwao Y, Ishii H, Hibi T (2003) A specific genetic alteration on chromosome 6 in ulcerative colitis-associated colorectal cancers. Cancer Res 63:3747–3749
10. Filipe MI (1979) Mucins in the human gastrointestinal epithelium: a review. Invest Cell Pathol 2:195–216
11. Filipe MI, Fenger C (1979) Histochemical characteristics of mucins in the small intestine. A comparative study of normal mucosa, benign epithelial tumours and carcinoma. Histochem J 11:277–287
12. Harpaz N, Talbot IC (1996) Colorectal cancer in idiopathic inflammatory bowel disease. Semin Diagn Pathol 13:339–357
13. Hinoda Y, Akashi H, Suwa T, Itoh F, Adachi M, Endo T, Satoh M, Xing PX, Imai K (1998) Immunohistochemical detection of MUC2 mucin core protein in ulcerative colitis. J Clin Lab Anal 12:150–153
14. Kirchner T, Muller S, Hattori T, Mukaisyo K (2001) Metaplasia, intraepithelial neoplasia and early cancer of the stomach are related to dedifferentiated epithelial cells defined by cytokeratin-7 expression in gastritis. Virchows Arch 439:512–522
15. Kummar S, Fogarasi M, Canova A, Mota A, Ciesielski T (2002) Cytokeratin 7 and 20 staining for the diagnosis of lung and colorectal adenocarcinoma. Br J Cancer 86:1884–1887
16. Kushima R, Borchard F, Hattori T (1997) A new aspect of gastric metaplasia in Crohn's disease: bidirectional (foveolar and pyloric) differentiation in so-called 'pyloric metaplasia' in the ileum. Pathol Int 47:416–419
17. Lee MJ, Lee HS, Kim WH, Choi Y, Yang M (2003) Expression of mucins and cytokeratins in primary carcinomas of the digestive system. Mod Pathol 16:403–410
18. Matsumoto N, Yoshida T, Okayasu I (2003) High epithelial and stromal genetic instability of chromosome 17 in ulcerative colitis-associated carcinogenesis. Cancer Res 63:6158–6161
19. Moll R, Schiller DL, Franke WW (1990) Identification of protein IT of the intestinal cytoskeleton as a novel type I cytokeratin with unusual properties and expression patterns. J Cell Biol 111:567–580
20. Park SY, Kim HS, Hong EK, Kim WH (2002) Expression of cytokeratins 7 and 20 in primary carcinomas of the stomach and colorectum and their value in the differential diagnosis of metastatic carcinomas to the ovary. Hum Pathol 33:1078–1085
21. Quinlan RA, Schiller DL, Hatzfeld M, Achtstatter T, Moll R, Jorcano JL, Magin TM, Franke WW (1985) Patterns of expression and organization of cytokeratin intermediate filaments. Ann N Y Acad Sci 455:282–306
22. Ramaekers F, van Niekerk C, Poels L, Schaafsma E, Huijsmans A, Robben H, Schaart G, Vooijs P (1990) Use of monoclonal antibodies to keratin 7 in the differential diagnosis of adenocarcinomas. Am J Pathol 136:641–655
23. Reis CA, David L, Nielsen PA, Clausen H, Mirgorodskaya K, Roepstorff P, Sobrinho-Simoes M (1999) Intestinal metaplasia of human stomach displays distinct patterns of mucin (MUC1, MUC2, MUC5AC, and MUC6) expression. Cancer Res 59:1003–1007
24. Shaoul R, Okada Y, Cutz E, Marcon MA (2004) Colonic expression of MUC2, MUC5AC, and TFF1 in inflammatory bowel disease in children. J Pediatr Gastroenterol Nutr 38: 488–493
25. Stosiek P, Brautigam E, Kasper M (1991) Expression of cytokeratin 7 in human glandular epithelium of fetal stomach. Acta Histochem 91:21–23

26. Tatsumi N, Mukaisho K, Mitsufuji S, Tatsumi Y, Sugihara H, Okanoue T, Hattori T (2005) Expression of cytokeratin 7 and 20 in serrated adenoma and related diseases. Dig Dis Sci 50 (9):1741–1746
27. Tot T (2002) Cytokeratins 20 and 7 as biomarkers: usefulness in discriminating primary from metastatic adenocarcinoma. Eur J Cancer 38:758–763
28. Tsukashita S, Kushima R, Bamba M, Sugihara H, Hattori T (2001) MUC gene expression and histogenesis of adenocarcinoma of the stomach. Int J Cancer 94:166–170
29. Tytgat KM, Opdam FJ, Einerhand AW, Buller HA, Dekker J (1996) MUC2 is the prominent colonic mucin expressed in ulcerative colitis. Gut 38:554–563
30. Weiss AA, Babyatsky MW, Ogata S, Chen A, Itzkowitz SH (1996) Expression of MUC2 and MUC3 mRNA in human normal, malignant, and inflammatory intestinal tissues. J Histochem Cytochem 44:1161–1166
31. Yamashita K, Yasuda S, Kuba T, Otani Y, Fujiwara M, Okayasu I (2004) Unique characteristics of rectal carcinoma cell lines derived from invasive carcinomas in ulcerative colitis patients. Cancer Sci 95:211–217

Virchows Arch (2006) 448: 763–767
DOI 10.1007/s00428-006-0183-8

ORIGINAL ARTICLE

Anna Batistatou · Alexander K. Charalabopoulos · Chrisoula D. Scopa · Yukihiro Nakanishi · Angelos Kappas · Setsuo Hirohashi · Niki J. Agnantis · Konstantinos Charalabopoulos

Expression patterns of dysadherin and E-cadherin in lymph node metastases of colorectal carcinoma

Received: 27 November 2005 / Accepted: 3 March 2006 / Published online: 29 March 2006

Abstract Reduction/loss of E-cadherin is associated with the development and progression of many epithelial tumors, while in a limited number of neoplasms, E-cadherin is re-expressed in metastases. Dysadherin, recently characterized by members of our research team, has an anti-cell–cell adhesion function and downregulates E-cadherin in a posttranscriptional manner. Colorectal cancer (CRC) is one of the most common tumors in the developed world, and lymph node metastases are harbingers of aggressive behavior. The aim of the present study was to examine the dysadherin and E-cadherin expression patterns in lymph node metastases vs primary CRC. Dysadherin and E-cadherin expression was examined immunohistochemically in 78 patients with CRC, Dukes' stage C in the primary tumor and in one lymph node metastasis. Dysadherin was expressed in 42% while E-cadherin immunoreactivity was reduced in 45% of primary tumors. In lymph nodes, 33 and 81% of metastatic tumors were positive for dysadherin and E-cadherin, respectively. Dysadherin expression was not correlated with E-cadherin expression in the primary tumor with a reverse correlation evident in the lymph node metastases. Our results suggest that different mechanisms govern E-cadherin expression in the primary tumor and the corresponding lymph node metastases.

Keywords Dysadherin · E-cadherin · Colon · Adenocarcinoma · Metastases · Lymph nodes

A. Batistatou (✉) · N. J. Agnantis
Department of Pathology,
University of Ioannina Medical School,
University Campus,
P.O. Box 1186, 451 10 Ioannina, Greece
e-mail: abatista@cc.uoi.gr
Tel.: +30-26510-97574
Fax: +30-26510-97850

A. K. Charalabopoulos
Department of Surgery, Peterborough and Stamford Hospitals,
Cambridgeshire, UK

A. K. Charalabopoulos · A. Kappas
Department of Surgery, University of Ioannina Medical School,
Ioannina, Greece

C. D. Scopa
Department of Pathology, University of Patras Medical School,
Patras, Greece

Y. Nakanishi · S. Hirohashi
Pathology Division, National Cancer Center Research Institute,
Tokyo, Japan

K. Charalabopoulos
Department of Physiology,
Clinical Unit, University of Ioannina Medical School,
Ioannina, Greece

Introduction

Colorectal cancer (CRC) is one of the most common tumors in the developed world and the second leading cause of death following lung cancer in the United States [29]. The tumor develops in the mucosa, extends locally, invading through the bowel wall into adjacent tissues, and metastasizes through the lymphatics and blood vessels to regional lymph nodes and distant organs. Primary tumor resection with/without postoperative chemotherapy is the standard therapeutic approach of CRC. If the neoplasm has extended through the bowel wall but has not given lymph node metastases (Dukes' stage B), then, the 5-year survival rates for patients is 70–80% [26]. Lymph node metastases or distant metastases through blood vessels (i.e. liver, lung, ovaries) have been shown to be the most significant prognostic factors for patients with CRC. In particular, when the tumor has spread to the lymph nodes (Dukes' stage C), the survival rate drops sharply (5-year survival, 25–50%) [29]. The usual malignant tumor of the large bowel is a well to moderately differentiated adenocarcinoma. Based on histopathological observations, it has been shown that lymph node metastases are most common in tumors with poorly differentiated areas and a highly infiltrative pattern of growth [28]. The cellular and molecular steps required for metastases of neoplastic cells are starting to be elucidated. The metastatic cascade

starts with a downregulation of the epithelial bonds which enables tumor cells to leave epithelial structures, to invade the stroma, to enter the blood stream or the lymphatics, to extravasate, and to colonize the target organs. Interestingly, invasive growth and metastases often recapitulate embryonic development and are greatly influenced by the stromal microenvironment [15]. Thus, carcinoma cells interact bidirectionally with neighboring fibroblasts, endothelial cells, and lymphocytes through growth factors, chemokines, cell adhesion molecules, and extracellular matrix proteases.

The cadherin family is a group of Ca^{2+}-dependent cell–cell adhesion molecules, which are essential for the induction and maintenance of tissue structures. E-cadherin is present in most epithelial cells and plays a crucial role in the architecture of the epithelial junctions [24]. Reduction/loss of E-cadherin has been associated with the development and progression of many epithelial tumors, by contributing to carcinogenesis, tumor invasion, and metastases [7, 8, 15]. Aberrant E-cadherin expression (heterogeneous, cytoplasmic, or absent) has been detected immunohistochemically in a variety of poorly differentiated, invasive, and metastatic carcinomas, including head and neck carcinoma, gastric adenocarcinoma, lobular breast carcinoma, lung cancer, CRC, prostate adenocarcinoma, pancreatic, and bladder cancer [8, 9, 15, 23, 37, 38]. In CRC, downregulation of E-cadherin has been associated with loss of differentiation, increased likelihood of metastases, and poor prognosis [1, 10–12, 14]. Furthermore, there are less than a handful of studies showing reexpression of E-cadherin in the metastatic lymph nodes [11, 10, 16]. Recently, we have reported the cloning and characterization of dysadherin (HSPCii3, IWU-1, KCT1, PIC), a cell membrane glycoprotein which has an anti-cell–cell adhesion function and downregulates E-cadherin in a posttranscriptional manner [18, 35]. So far, there are only a few reports on the function and expression of dysadherin in human malignancies. This novel cancer-associated protein has been detected in head and neck, gastric, testis, pancreatic, esophageal, thyroid, tongue, and cervical carcinomas and in malignant melanoma and is associated with tumor aggressiveness [2, 21, 24, 25, 27, 30–34, 36]. Recently, Aoki et al. reported that in advanced CRC, dysadherin expression has prognostic significance [1]. The aim of the present study was to examine the dysadherin and E-cadherin expression patterns in lymph node metastases vs primary CRC.

Materials and methods

Seventy-eight formalin-fixed, paraffin-embedded archival tissue blocks of CRC and an equal number of blocks from corresponding lymph node metastases (from the same patients) were included in the current study. They represented an equal number of patients (mean age: 64 years, range: 39–82). Forty-five were male and 33 were female. The patients had no family history of CRC. They had not received chemotherapy or radiation treatment before surgery. The histopathological stage of tumors in all patients was Dukes C. All tumors were moderately differentiated adenocarcinomas. The middle part and the advancing edge of the tumor were always included in the blocks from the primary tumor.

Immunohistochemistry

We performed immunostaining on formalin-fixed, paraffin-embedded tissue sections using the EnVision System (DAKO) and the monoclonal antibodies: NCC-M53 against dysadherin [1] and E-cadherin (CM170B, Biocare Medical). Briefly, 4-ìm thick tissue sections were deparaffinized in xylene; rehydrated through graded concentrations of alcohol and heated in a microwave oven for two cycles of 15 min each at 300 W, in citrate buffer, for antigen retrieval. Endogenous peroxidase activity was blocked with H_2O_2 solution in methanol (0.01 M), for 30 min. After washing with phosphate buffered saline (PBS) for 5 min, the primary antibodies, NCC-M53 (dilution 1:1,000) and CM170B (dilution 1:50), were applied for incubation (30 min at room temperature and overnight at 4°C, respectively). Then, the slides were washed for 10 min with PBS and were visualized with the EnVision system using diaminobezidine tetrahydrochloride as a chromogen. Finally, all sections were counterstained with hematoxylin. Positive staining of endothelial cells and lymphocytes was used as an internal positive control for dysadherin. As an internal positive control for E-cadherin, positive staining of normal colorectal epithelial cells was used. As a negative control, the first antibody was substituted with normal mouse immunoglobulin of the same class.

Evaluation of the staining

Two pathologists (AB and CDS) performed independently semiquantitative evaluation of the staining. When disagreement arose, slides were reviewed together and a consensus view was obtained. For each sample, at least 1,000 neoplastic cells were counted, and the percentage of the cancer cells with positive membranous immunostaining and the staining intensity were recorded. For the purposes of statistical analysis, as described previously, when more than 50% of tumor cells were stained for dysadherin, the tumor was evaluated as “positive dysadherin expression (Dys(+))” [1]. When less than 50% of tumor cells were stained for dysadherin, the tumor was evaluated as “negative dysadherin expression (Dys(−)).” Regarding E-cadherin, when more than 80% of tumor cells showed complete membranous staining, the tumor was evaluated as “preserved E-cadherin expression (E-cad(+)),” while when less than 80% of tumor cells were positive, the tumor was evaluated as “reduced E-cadherin expression (E-cad(−))” [1].

Statistical analysis

Analyses were conducted in SPSS software version 11.0 (SPSS, Chicago, IL). For comparisons between antibodies' expression with clinicopathological variables, we used the chi-square (χ^2) test. All differences were considered statistically significant if $p<0.05$. p values are two-tailed.

Results

Dysadherin expression

Dysadherin expression was not detected in non-neoplastic colorectal epithelial cells. Dysadherin immunostaining was mostly observed in the membranes of the neoplastic cells and it was heterogeneous throughout the neoplasm (Fig. 1a,b). In particular, as described, preferential expression in the infiltrative border of tumors in the primary site was detected in some cases [1]. Overall, "positive dysadherin expression" was found in 42% (33 out of 78) of primary tumors. In lymph node metastases, the staining was more homogeneous but was noted in less cases, as only 26 out of 78 (33%) metastatic tumors were "dysadherin positive." In all the positive metastatic cases, primary tumors were positive for dysadherin as well (Table 1).

E-cadherin expression

Expression of E-cadherin was evident at the cell–cell borders of epithelial cells in normal colorectal mucosa. In CRC, the expression patterns varied; i.e., tumors with preserved, homogeneous, heterogeneous, and aberrant/cytoplasmic expression were observed. E-cadherin immunoreactivity was reduced in 45% of cases (35 out of 78) (Fig. 1c). Interestingly, the majority of lymph node metastases (81%, 63 out of 78) showed preserved expression of E-cadherin (Fig. 1d). All primary tumors with preserved E-cadherin expression retained this expression in the lymph node metastasis. Furthermore, the immunostaining was homogeneous regardless of the E-cadherin staining pattern of the primary tumor.

Dysadherin expression was not correlated with E-cadherin expression in the primary tumor ($p>0.05$). However, a reverse correlation between dysadherin and E-cadherin expression was evident in the lymph node metastases ($p<0.05$) (Table 1).

Discussion

In patients with CRC, lymph node metastases are harbingers of aggressive behavior, leading to a sharp drop of 5-year survival rates; thus, the search for new molecules, possibly involved in the metastatic pathway, is of high importance [26, 29]. To metastasize, neoplastic cells must dissociate from the primary tumor, invade the surrounding stroma, enter into the circulation, and extravasate in the target organs where they must grow again into tumors. There is growing evidence that adhesion molecules, in particular, E-cadherin, play pivotal role in this process not only by being downregulated at the primary site and but also by being reexpressed at the metastatic foci [10–12, 14]. Such observations have been made, so far, in invasive ductal and lobular carcinomas, in esophageal and lung carcinomas, and in gastric adenocarcinomas that progress to develop lymph node metastases [4, 5, 20, 22]. Regarding CRC, there are only three published studies, all showing downregulation of E-cadherin expression in the primary tumors simultaneous with upregulation of the same protein in the metastatic foci, although the percentages vary considerably [11, 16, 19].

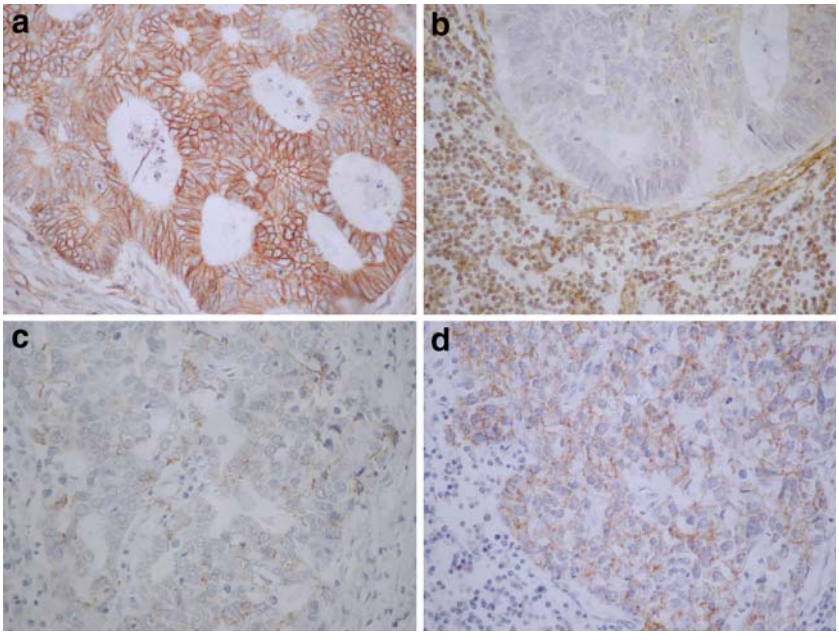

Fig. 1 **a** Positive dysadherin expression in colon adenocarcinoma (DABX400). **b** Loss of dysadherin expression in the lymph node metastasis of the same tumor. Adjacent lymphocytes serve as internal positive control (DABX400). **c** Reduced E-cadherin expression in colon adenocarcinoma (DABX400). **d** Reexpression of E-cadherin in the lymph node metastasis of the same tumor (DABX400)

Table 1 Results of immunostaining, classified by dysadherin and E-cadherin expression

E-cadherin expression	Dysadherin expression		
	<50%	>50%	*p*-value
Primary tumor			
Preserved	28	15	$p>0.05$
Reduced	17	18	
Lymph node metastasis			
Preserved	47	16	$p<0.05$
Reduced	5	10	

In the present study, we have also observed the same phenomenon, with 55% of primary tumors and 81% of lymph node metastases retaining E-cadherin expression. The significance and pathogenetic mechanisms of this phenomenon are issues under investigation. It has been shown that neoplastic cells with reduced/aberrant E-cadherin expression are far more likely to detach from the tumor mass in response to low shear forces such as those found in the lymphatic vessels or venules. The reexpression of E-cadherin in lymph nodes with *metastases* may play an important role in the growth of the cancer cells in the metastatic foci, offering them a survival advantage [6, 13]. In most studied tumors, loss of E-cadherin expression in the primary site is usually due to epigenetic mechanisms rather than mutations. Thus, it is conceivable that the observed reexpression of E-cadherin could be due to loss of epigenetic inhibition. An alternative hypothesis is that metastases arise from tumor cells that have never lost E-cadherin expression and constitute the focal E-cadherin positive component in an otherwise E-cadherin negative tumor. However, it is evident that metastases can occur irrespective of E-cadherin expression levels; thus, it is conceivable that E-cadherin plays a role in metastases by more than one mechanism [3, 17].

In vitro studies shave shown that dysadherin expression facilitates cell motility and metastatic potential of human pancreatic cancer cells [34]. In vivo, dysadherin expression has been studied in colorectal, pancreatic, gastric, esophageal, tongue, and thyroid carcinomas, and in cervical squamous cell carcinomas, testicular neoplasms including lymphomas and cutaneous malignant melanomas [1, 2, 21, 25, 27, 30–34, 36]. In all these cancer types, a general phenomenon is that dysadherin expression seems to reflect tumor aggressiveness, being furthermore, a marker of poor prognosis when considered alone or/and in combination with downregulation of E-cadherin. In most tumors examined, increased dysadherin expression was correlated with reduced/aberrant E-cadherin expression. This does not appear to be the case in CRC where the data presented, herein, and the one in accordance with a previously published report show that there is no correlation between dysadherin and E-cadherin expression in the primary tumors [1]. This finding suggests that other *mechanisms* apart from dysadherin regulation, are implicated in E-cadherin expression/activity both at transcriptional and posttranscriptional level in the primary site. Dysadherin may only partly suppress/regulate the activity of E-cadherin. Many other factors may also be involved, such as methylation of the promoter region, gene mutation, involvement of snail, sip-1, and slug transcription factors, *ubiquitination* of E-cadherin, tyrosine phosphorylation of β-catenin, and catenin abnormalities, such as absence of α-catenin. In contrast, we report that in metastatic neoplastic deposits, there is a negative association between dysadherin and E-cadherin expression resulting from the decrease of the former and increase of the latter. This observation leads to the hypothesis that different mechanisms *govern E-cadherin expression in the primary tumor and the corresponding lymph node metastasis*. If this is the case, then it is plausible that the increased expression of E-cadherin in the metastatic foci is truly a reexpression, possibly associated with dysadherin downregulation and loss of epigenetic inhibition and does not represent neoplastic clones that have never lost E-cadherin expression.

In conclusion, this is the first report on *dysadherin and E-cadherin expression* in lymph node metastases of CRC. Expression patterns were described and their possible involvement in the metastatic cascade have been discussed. As it is regarded that although the molecular pathways of tumorigenesis may vary among different tumors and the cascade of events required for metastases are similar for all neoplastic cells, it is conceivable that our observations hold true for other metastatic cancers as well. Larger prospective studies, fulfilling many clinicopathological parameters are needed to clarify the important issue of metastatic carcinoma.

References

1. Aoki S, Shimamura T, Shibata T, Nakanishi Y, Moriya Y, Sato Y, Kitajima M, Sakamoto M, Hirohashi S (2003) Prognostic significance of dysadherin expression in advanced colorectal carcinoma. Br J Cancer 88:726–732
2. Batistatou A, Scopa CD, Ravazoula P. Nakanishi Y, Peschos D, Agnantis NJ, Hirohashi S, Charalabopoulos KA (2005) Involvement of dysadherin and E-cadherin in the development of testicular tumors. Br J Cancer 93:1382–1387
3. Bogenrieder T, Herlyn M (2003) Axis of evil. Oncogene 29:6524–6536
4. Bongiorno PF, al-Kasspooles M, Lee SW, Rachwal WJ, Moore JH, Whyte RI, Orringer MB, Beer DJ (1995) E-cadherin expression in primary and metastatic thoracic neoplasms and in Barrett's oesophagus. Br J Cancer 71:166–172

5. Buckholm IK, Nesland JM, Boerresen-Dale A-L (2000) Re-expression of E-cadherin, α-catenin and β-catenin, but not of γ-catenin, in metastatic tissue from breast cancer patients. J Pathol 190:15–19
6. Byers SW, Sommers CL, Hoxter B, Mercurio Am, Torezen A (1995) Role of E-cadherin in the response of tumor cell aggregates to lymphatic, venous and arterial flow: measurement of cell–cell adhesion strength. J Cell Sci 108:2053–2064
7. Chang HW, Chow V, Lam KY, Wei WI, Yuen A (2002) Loss of E-cadherin expression resulting from promoter hypermethylation in oral tongue carcinoma and its prognostic significance. Cancer 94:386–392
8. Charalabopoulos K, Binolis J, Karkabounas S (2002) Adhesion molecules in carcinogenesis. Exp Oncol 24:249–257
9. Charalabopoulos K, Gogali A, Kostoula OK, Constantopoulos H (2004) Cadherin superfamily of adhesion molecules in primary lung cancer. Exp Oncol 16:256–260
10. Dorudi S, Hanby AM, Poulsom R, Northover J, Hart IR (1995) Level of expression of E-cadherin mRNA in colorectal cancer correlates with clinical outcome. Br J Cancer 71:614–616
11. Ghadimi BM, Behrens J, Hoffmann I, Haench W, Birchmeier W, Schlag PM (1999) Immunohistochemical analysis of E-cadherin, alpha-, beta- and gamma-catenin expression in colorectal cancer: implications for cell adhesion and signaling. Eur J Cancer 35:60–65
12. Gofuku J, Shiozaki H, Tsujinaka T, Inoue M, Tamura S, Doki Y, Matsui S, Tsukita S, Kikkawa N, Monden M (1999) Expression of E-cadherin and alpha-catenin in patients with colorectal carcinoma. Correlation with cancer invasion and metastasis. Am J Clin Pathol 111:29–37
13. Gupta A, Deshpande CG, Badve S (2003) Role of E-cadherins in development of lymphatic tumor emboli. Cancer 97:2341–2347
14. Hirohashi S (1998) Inactivation of E-cadherin-mediated cell adhesion system in human cancers. Am J Pathol 153:333–339
15. Hirohashi S, Kanai Y (2003) Cell adhesion system and human cancer morphogenesis. Cancer Sci 94:575–581
16. Ikeguchi M, Makino M, Kaibara N (2001) Clinical significance of E-cadherin–Catenin complex expression in metastatic foci of colorectal carcinoma. J Surg Oncol 77:201–207
17. Ilyas M (2000) Adhesion molecule expression in breast cancer: the phoenix in tumor metastasis? J Pathol 190:3–5
18. Ino Y, Gotoh M, Sakamoto M, Tsukagoshi K, Hirohashi S (2002) Dysadherin, a cancer-associated cell membrane glycoprotein, down-regulates E-cadherin and promotes metastasis. Proc Natl Acad Sci USA 99:365–370
19. Kanazawa N, Oda T, Gunji N, Nozue M, Kawamoto T, Todoroki T, Fukao K (2002) E-cadherin expression in the primary tumors and metastatic lymph nodes of poorly differentiated types of rectal cancer. Surg Today 32:123–128
20. Kowalski PJ, Rubin MA, Kleer CG (2003) E-cadherin expression in primary carcinomas of the breast and its distant metastases. Breast Cancer Res 5:R217–R222
21. Kyzas PA, Stefanou D, Batistatou A, Nakanishi Y, Hirohashi S, Agnantis NJ, Charalabopoulos K (2006) Dysadherin expression in head and neck squamous cell carcinoma: Association with lymphangiogenesis and prognostic significance. Am J Surg Pathol 30:185–193
22. Liu J, Ikeguchi M, Nakamura S, Kaibara T (2002) Re-expression of the cadherin–catenin complex in lymph nodes with metastasis in advanced gastric cancer: the relationship with patient survival. J Exp Clin Cancer Res 21:65–71
23. Massarelli E, Brown E, Tran NK, Liu DD, Izzo JG, Lee JJ, El-Naggar AK, Hong WK, Papadimitrakopoulou VA (2005) Loss of E-cadherin and p27 expression is associated with head and neck squamous tumorigenesis. Cancer 103:952–959
24. Nagar B, Overduin M, Ikura M, Rini JM (1996) Structural basis of calcium-induced E-cadherin rigidification and dimerization. Nature 380:360–364
25. Nakanishi Y, Akimoto S, Sato Y, Kanai Y, Sakamoto M, Hirohashi S (2004) Prognostic significance of dysadherin expression in tongue cancer: immunohistochemical analysis of 91 cases. Appl Immunohistochem Mol Morphol 12:323–328
26. Newland RC, Dent OF, Chapuis PH, Bokey L (1995) Survival after curative resection of lymph node negative colorectal carcinoma. A prospective study of 910 patients. Cancer 76:564–571
27. Nishizawa A, Nakanishi Y, Yoshimura K, Sasajima Y, Yamazaki N, Yamamoto A, Hanada K, Kanai Y, Hirohashi S (2005) Clinicopathologic significance of dysadherin expression in cutaneous malignant melanoma. Cancer 103:1693–1700
28. Rosai J (2004) Rosai and Ackerman's Surgical Pathology, 9th edn. Mosby-Elsevier, New York
29. Rosen M, Chan L, Beart RW Jr, Vukasin P, Anthone G (1998) Follow-up of colorectal cancer. A meta-analysis. Dis Colon Rectum 41:1116–1126
30. Sato H, Ino Y, Miura A, Abe Y, Sakai H, Ito K, Hirohashi S (2003) Dysadherin: expression and clinical significance in thyroid carcinoma. J Clin Endocrinol Metab 88:4407–4412
31. Shimada Y, Hashimoto Y, Kan T, Kawamura J, Okumura T, Soma T, Taratani N, Waranabe G, Ino Y, Sakamoto M, Hirohashi S, Imamura M (2004) Prognostic significance of dysadherin expression in esophageal squamous cell carcinoma. Oncology 67:73–80
32. Shimada Y, Yamasaki S, Hashimoto Y, Ito T, Kawamura J, Soma T, Ino Y, Nakanishi Y, Sakamoto M, Hirohashi S, Imamura M (2004) Clinical significance of dysadherin expression in gastric cancer patients. Clin Cancer Res 10:2818–2823
33. Shimamura T, Sakamoto M, Ino Y, Sato Y, Shimada K, Kosuge T, Sekihara H, Hirohashi S (2003) Dysadherin overexpression in pancreatic ductal adenocarcinoma reflects tumor aggressiveness: relationship to E-cadherin expression. J Clin Oncol 21:267–659
34. Shimamura T, Yasuda J, Ino Y, Gotoh M, Tsuchiya A, Nakajima A, Sakamoto M, Kanai Y, Hirohashi S (2004) Dysadherin expression facilitates cell motility and metastatic potential of human pancreatic cancer cells. Cancer Res 64:6989–6995
35. Tsuiji H, Takasaki S, Sakamoto M, Irimura T, Hirohashi S (2003) Aberrant O-glycosylation inhibits stable expression of dysadherin, a carcinoma-associated antigen, and facilitates cell–cell adhesion. Glycobiology 13:521–527
36. Wu D, Qiao Y, Kristensen GB, Li S, Troen G, Holm R, Nesland JM, Suo Z (2004) Prognostic significance of dysadherin expression in cervical squamous cell carcinoma. Pathol Oncol Res 10:12–218
37. Yantis R, Bosenberg M, Antonioli D, Odze R (2002) Utility of MMP-1, p53, E-cadherin and Collagen IV immunohistochemical stains in the differential diagnosis of adenomas with misplaced epithelium versus adenomas with invasive adenocarcinoma. Am J Surg Pathol 26:206–215
38. Zhang HK, Zhang QM, Zhao TH, Li YY, Yi YF (2004) Expression of mucins and E-cadherin in gastric carcinoma and their clinical significance. World J Gastroenterol 10:3044–3047

Virchows Arch (2006) 448: 768–775
DOI 10.1007/s00428-006-0195-4

ORIGINAL ARTICLE

Panayiotis A. Kyzas · Niki J. Agnantis · Dimitrios Stefanou

Endoglin (CD105) as a prognostic factor in head and neck squamous cell carcinoma

Received: 12 January 2006 / Accepted: 28 February 2006 / Published online: 13 April 2006

Abstract Endoglin (CD105) is a proliferation-associated protein abundantly expressed in angiogenic endothelial cells. Recent studies revealed that CD105 is intensively expressed in tumor vasculature, whereas intratumoral microvessel density (MVD) determined with the use of antibodies to CD105 has been found to be an important prognostic indicator for the outcome in a number of malignancies. In the current study, we investigated endoglin expression and evaluated MVD in 108 patients with head and neck squamous cell carcinoma. Endoglin was intensively expressed in intratumoral blood vessels, whilst lymphatics were rarely positive for CD105. High microvessel density was associated with a more aggressive tumor phenotype, including advanced clinical stage (p=0.008) and the presence of lymph node metastasis at the time of diagnosis (p=0.02). When microvessel counts were assessed for their prognostic values (high vs low MVD), there was a statistically significant difference in the overall survival among patients with tumors of the oral cavity and larynx (p<0.001) and in the disease-free survival among patients with tumors of the lower lip (p=0.01). The prognostic impact of microvessel density was not dependent on clinical stage or lymph node status. The results of the current study suggest that CD105 is a promising target for tumor imaging and prognosis.

Keywords CD105 · Endoglin · D2-40 · Angiogenesis · Head and neck cancer · Oral cancer

Introduction

Angiogenesis is the propelling force for tumor growth and metastatic dissemination in solid neoplasms [9, 11]. This process is tightly controlled by numerous positive and negative angiogenic factors and their receptors, the interaction of which regulates the cascades enabled in tumor neovascularization [8, 34]. However, the mechanisms underlying this procedure are not yet fully elucidated.

Endoglin (CD105) is a 180-kDa homodimeric transmembrane glycoprotein [8, 13]. It is a receptor for transforming growth factor-β (TGF-β) and modulates TGF-β signaling by interacting with TGF-β receptors I and III [12]. TGF-β acts as a negative regulator for tumor angiogenesis via inhibition of proliferation and migration of endothelial cells and, thus, interrupting the formation of microvessels, whereas CD105 counteracts these actions [8, 12]. A possible explanation for this paradox is the presentation of TGF-β signaling in a non-functional way by this receptor [12, 13]. Endoglin is strongly expressed in blood vessels of tumors, whilst it is absent or weakly expressed in blood vessels of normal tissues [13, 14]. Endoglin is induced by hypoxia [12] and associated with increased endothelial cell proliferation [12, 13] and decreased apoptosis [8]. It is also suggested that endoglin might have a role in tumor lymphangiogenesis [16]; however, its expression on lymphatic vessels has never been examined, so far, in tumor settings.

Intratumoral microvessel density (MVD) determined by antibodies against CD105 was correlated with decreased survival and increased tumor aggressiveness in a number of malignancies, such as breast cancer [7, 18], cutaneous melanoma [29], colon cancer [26, 36, 45], lung cancer [3, 30, 40], gynecological malignancies [4, 35, 38], and renal cancer [6, 44]. It was suggested that CD105 might be the optimal antibody for microvessel's highlight to preclude disturbances caused by the low accuracy of the pan-endothelial markers (CD31, CD34, and von Willebrand factor) used so far [12–14, 36].

Up to date, the prognostic impact of CD105 in tumor angiogenesis for head and neck cancer was examined by a limited number of studies [5, 27, 28, 31]. Thus, we performed immunohistochemical evaluation of CD105 expression in a cohort of patients with head and neck squamous cell carcinoma (HNSCC). Our aim was to

P. A. Kyzas (✉) · N. J. Agnantis · D. Stefanou
Department of Pathology,
University of Ioannina Medical School,
45110 Ioannina, Greece
e-mail: md03791@cc.uoi.gr
Tel.: +30-26510-94681
Fax: +30-26510-97898

examine the expression pattern of CD105 on tumor blood and lymphatic vessels, to assess the correlation of CD105-determined MVD with tumor aggressiveness and clinical outcome (if any), and to find possible explanations for the role of this molecule in the angiogenic procedure.

Materials and methods

Tissues and clinical parameters

One hundred and eight formalin-fixed, paraffin-embedded archival tissue blocks of head and neck squamous cell carcinoma specimens were included in the current study. There were 81 of the included samples that originated from complete resection material, and 27 were biopsy specimens. We reviewed all hematoxylin slides and selected the best section from each block showing central and peripheral areas of the tumor, avoiding areas with necrosis. Patients' records were reviewed, and clinicopathological characteristics and follow-up data were noted. Staging was established by IUCC system, and grading was performed according to WHO.

Immunohistochemistry

CD105 monostaining

We performed immunostaining on formalin-fixed, paraffin-embedded tissue sections using the EnVision System (DAKO) as described previously [19, 22]. In brief, one 4-μm-thick section from each paraffin-embedded block was cut. The sections were deparaffinized in xylene and rehydrated through graded concentrations of alcohol. Sections were incubated with Proteinase-K (DAKO) in a humid chamber for 25 min for antigen retrieval. The endogenous peroxidase's activity was blocked with H_2O_2 solution in methanol (0.01 M) for 30 min. After washing with phosphate-buffered saline (PBS) for 5 min, the primary antibody (mouse monoclonal antibody to CD105, clone SN6h, Diagnostic Biosystems, Netherlands, in a dilution 1:20) was incubated overnight at 4°C. Then, the slides were washed for 10 min with PBS. EnVision system (DAKO) was used for visualization of the expression of the antibody. Diaminobezidinetetrahydrochloride (DAB) was used as a chromogen. All sections were then counterstained with hematoxylin.

Double staining (CD105/D2-40)

The expression of endoglin in lymphatic vessels has never been evaluated in HNSCC [9]. Therefore, we contacted double immunostaining with CD105 and the specific lymphatic endothelium marker D2-40 (SIG-730, Signet Laboratories) [10] to investigate the presence of co-localization of the two antibodies [20]. Twenty randomly selected blocks were used as a convenient sample. In brief, the antibody against CD105 was applied as described above. After the visualization of the expression of endoglin with DAB, sections were washed in PBS for 5 min. Serum block was applied for 5 min and, afterwards, D2-40 (dilution 1:40) was applied for 30 min in a humid chamber at room temperature. Secondary antibody (Multilink, Biogenex, USA) was applied for 20 min, followed by 10 min washing with buffer. Alkaline-phosphatase link was applied for 20 min, and the expression of D2-40 was visualized with Fast-Red (Biogenex, USA) diluted in napthol phosphate. One drop of levimazole was added to reduce unspecific background staining. All sections were then counterstained with hematoxylin.

Antibody expression

Two observers (PK and DS) without knowledge of the clinical data performed evaluation of the staining. Quantitative analysis of the intratumoral microvessel density was performed as described previously [7, 19, 29, 42]. Three fields with the highest vascular density (hot spots) were identified in each sample using an Olympus BX-51 microscope at ×40 magnification, and vessels were counted using a ×200 magnification. Microvessel density was defined as the number of CD105-positive vessels per optical field (an optical field corresponds to an examination area of 0.7386 mm^2). For statistical analyses, the median value of the above measurements was used as a cut-off to separate tumors with high vs low microvessel density, as previously described [2].

Survival and recurrence analysis

The cohort of our patients was divided into two groups regarding the location of the primary tumor. It is well known that squamous cell carcinoma (SCC) of the lower lip is more curable than those of the oral cavity or the larynx [17, 33], and the major problem with this malignancy is local recurrence after surgical removal of the primary tumor. On the other hand, SCC of the oral cavity and larynx are more aggressive. Thus, we performed survival analysis in the subgroup of patients with oral–larynx SCC and recurrence analysis in the subgroup of patients with SCC of the lower lip.

Survival analysis was also stratified over clinical stage, lymph node status, and location. In a sensitivity analysis, we examined whether the influence of MVD on survival differed between complete resections and biopsy samples.

Statistical analysis

Analyses were conducted in SPSS software version 11.0 (SPSS, Chicago, IL, USA). For comparison between MVD with clinicopathological variables, we used chi-square (χ^2) test and Mann–Whitney U test, as appropriate [2]. Analyses for survival and recurrence were done using the

Kaplan–Meier method and different subgroups were compared using the log-rank test. Cox regression model was used to determine the importance of different factors. All differences were considered positive if $p<0.05$. p-values are two-tailed.

Results

Clinicopathologic data

The clinicopathologic characteristics of the patients enrolled in the study are listed in Table 1. The median age of the patients was 64.5 (range 33–98). There were 88 (81%) of the patients who were male and 20 (19%) were female. Twenty-eight patients (26%) presented with lymph node metastasis at the time of diagnosis. A total of 76 of the patients (70%) had cancer classified as initial (I and II) and of 32 (30%) as advanced (III and IV) clinical stage. There were 30 patients (38%) who had histologically high-grade tumors, 39 (36%) who had tumors with moderate differentiation, and with 39 (36%) of the tumors well differentiated (Table 1). A total of 23 (21%) of the tumors was located in the oral cavity, 35 (33%) were located in the larynx, and 50 (46%) were located at the lower lip.

The patients were treated in the Ear Nose Throat (ENT) Department of Ioannina University Hospital from 1998 to 2003. Available follow-up data existed for 93 of the patients. These were followed-up until death or recurrence, respectively, or for at least 24 months. There were 27 of the 58 patients with oral–larynx SCC who were dead at the end of the follow-up period, and 12 of the 35 patients with lip SCC had experienced local recurrence.

Treatment decision-making was based on clinical stage and on the presence or not of lymph node metastasis at the time of diagnosis [33]. All of the patients with squamous cell carcinoma of the lower lip underwent surgical resection of the tumor, and adjuvant radiotherapy was administrated only to two (4%) patients. All patients who presented with lymph node metastasis at diagnosis received neck dissection operation, simultaneously to the primary tumor removal (29). There were 14 (25%) of the patients with oral–larynx squamous cell carcinoma who were given only surgical treatment; 10 (17%) patients with lower-stage (I or II) laryngeal squamous cell carcinoma received only radiotherapy in an attempt of organ preservation (29); 20 (33%) patients underwent surgical treatment and received adjuvant radiotherapy; and, finally, 14 (25%) patients were treated with surgery plus combined adjuvant radiotherapy and chemotherapy.

Table 1 Correlation of clinicopathological characteristics of the patients included in the study with microvessel density

	N patients (%)	Microvessel density		*p*-value
		High	Low	
Histological grade				
Poorly	30 (28%)	15	15	NS
Moderate	39 (36%)	20	19	
Well	39 (36%)	18	21	
Stage				
I	53 (49%)	18	35	p=0.008
II	23 (21%)	13	10	
III	15 (14%)	9	6	
IV	17 (16%)	13	4	
N status				
N negative (N0, N*x*)	80 (74%)	34	46	p=0.02
N positive (N1, N2, N3)	28 (26%)	19	9	
Location				
Oral	23 (21%)	11	12	NS
Lower lip	50 (46%)	24	26	
Larynx	35 (33%)	18	17	
Material				
Complete resection	81 (75%)	41	40	NS
Biopsy	27 (25%)	12	15	

CD105 expression

Monostaining

It is interesting that CD105 stained intensively intratumoral vessels (Fig. 1a–f); vessels at the adjacent normal mucosa were only rarely expressing endoglin (Fig. 1d), and staining was faint and weak. Neoplastic, inflammatory, mesechymal, and hematopoietic cells were negative for endoglin.

Double staining (CD105/D2-40)

We observed a distinct expression pattern between CD105 and D2-40. The vast majority of the CD105-positive vessels were negative for D2-40 (Fig. 2a,b). D2-40-positive lymphatics were generally negative for endoglin immunostaining (Fig. 2a,b). Nevertheless, we observed co-localization of both markers in a limited number of small intratumoral vessels (Fig. 2b–d). However, this was a very rare phenomenon across the examined samples.

Evaluation of MVD

Microvessel density varied among tissue samples from 14 to 265 (median 49). Using the median MVD as a cut-off, 53 (49%) tumors were classified in the “high MVD” group and the rest, 55 (51%) tumors, consisted the “low MVD” group.

The correlation of the microvessel density with clinicopathologic parameters is summarized in Table 1. Higher microvessel density was correlated with a more aggressive tumor phenotype, including advanced clinical stage ($\chi^2 p$=0.008, Mann–Whitney $p<0.001$), and the presence of lymph node metastasis at the time of diagnosis ($\chi^2 p$=0.02, Mann–Whitney $p<0.001$). We did not observe

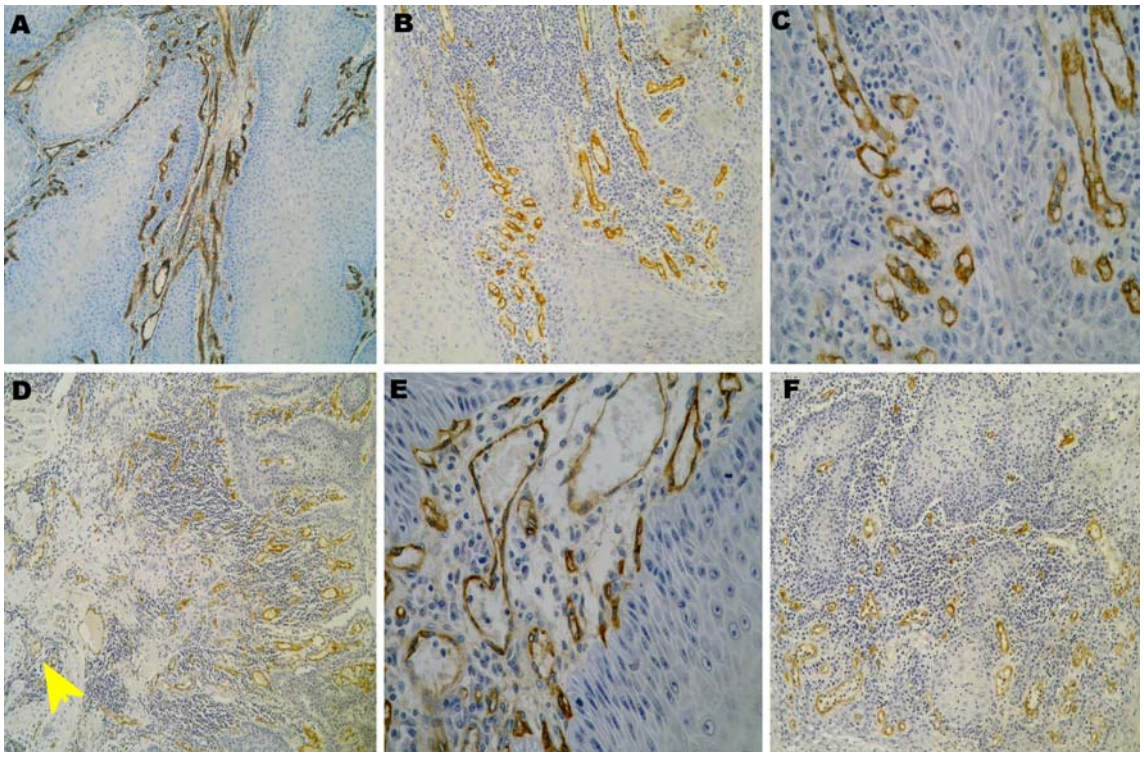

Fig. 1 Microvessels within hot spot areas, in the invasive front of a squamous cell carcinoma of the lower lip (**a**, **e**), larynx (**b**, **d**), and tongue (**c**, **f**). Endothelial cells of intratumoral vessels are intensively stained with CD105 (**b**, **d**, and **f**, magnification ×200; **a**, **c**, and **e**, magnification ×400). Notice the weak vessel staining in the normal mucosa adjacent to the neoplasm (**d**, *yellow arrow*)

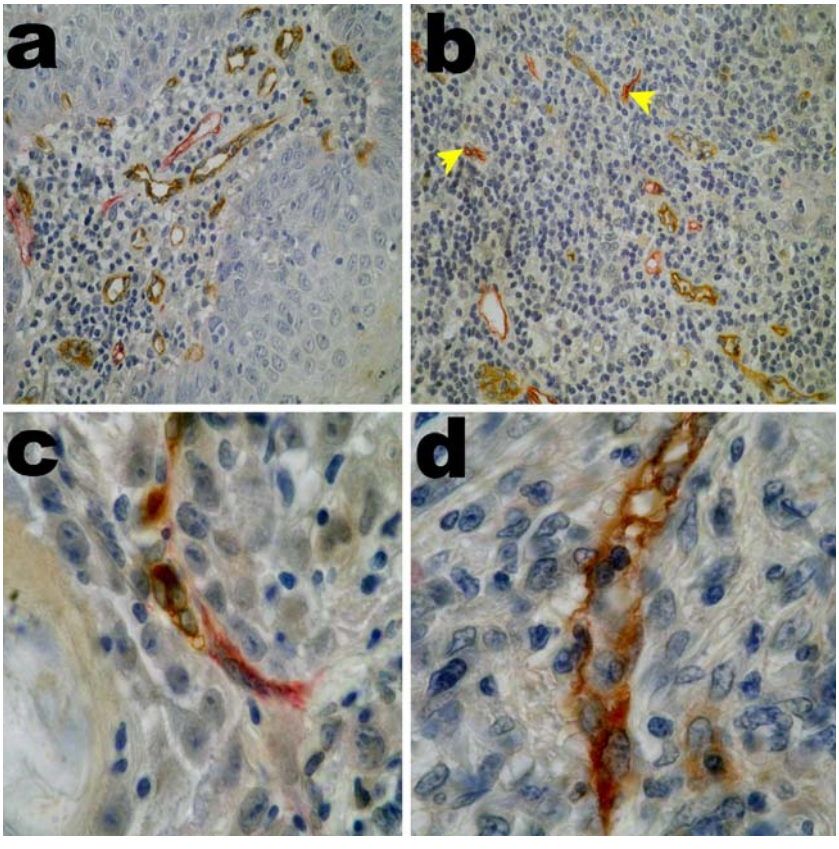

Fig. 2 Double immunostaining with CD105 and the specific lymphatic endothelium marker D2-40. The vast majority of the endoglin-positive microvessels are negative for D2-40 (**a**, **b**). D2-40 positive lymphatic vessels are generally negative for CD105 (**a**, **b**). Few intratumoral vessels exhibit co-localization of both markers (**b**, *yellow arrow*; **c**, **d**) (magnification ×400 for **a**, **b** and ×1,000 for **c**, **d**)

any significant association of MVD with age, sex, or differentiation grade. MVD did not depend on the primary tumor's location, did not correlate with treatment modality, and did not differ between biopsy samples and complete resections.

Survival and recurrence analysis

Advanced (III and IV) clinical stage, the presence of lymph node metastasis at the time of diagnosis, and high MVD associated with worse overall survival in patients with oral–larynx squamous cell carcinoma (in all cases, log-rank $p<0.001$, Fig. 3a–c). The impact of MVD on survival remained significant when the patients were further separated in oral cancer group (log-rank $p=0.02$) and larynx cancer group (log-rank $p=0.01$). Stratification over clinical stage and lymph node status revealed that the prognostic significance of MVD was not dependent on these factors (Fig. 3e–h). This last observation was confirmed when stage, lymph node status, and MVD were entered in a multivariate Cox model: all three prognostic factors remained significant (Table 2). Mortality was 2.7-fold higher in patients with high MVD (Cox $p=0.04$). The significant influence of high MVD on poor outcome was similar between patients with biopsy samples and complete resections.

High MVD was also associated with worse disease-free survival in patients with squamous cell carcinoma of the lower lip (Fig. 3d). The incidence of recurrence in the group of patients with high MVD was significantly higher than the group with low MVD (log-rank $p=0.02$).

Discussion

The results of the current study suggest a significant association of intratumoral microvessel density (determined with CD105) with poor prognosis in patients with head and neck squamous cell carcinoma. High MVD was an independent predictor of mortality in the subgroup of patients with squamous cell carcinoma of the oral cavity and larynx, with almost the same impact as lymph node status which is, up to date, the most reliable prognostic factor for these patients [33]. We also observed significantly lower disease-free survival in patients with highly vascular lower lip tumors. Our observations support previous findings for the prognostic significance of CD105 in HNSCC [5, 27, 28, 31].

There have been a number of studies evaluating the prognostic significance of microvessel density in head and neck squamous cell carcinoma [1, 15, 23, 24, 32, 37] with conflicting and contradictory results. In all of these reports, investigators used pan-endothelial markers, namely, CD34, CD31, and von Willebrand factor, to highlight microvessels. However, the accuracy of MVD assessment with these markers may not be the best possible, as their sensitivity and specificity are not optimal. All these markers are not always expressed in all intratumoral vessels (low sensitivity) [36, 43]. Von Willebrand factor can also stain lymphatic vessels [43]; CD31 has been observed in many hematopoietic cells, besides vascular endothelium; and CD34 is additionally expressed by a variety of mesechymal cells [36, 43]. All these aspects reflect the low specificity of these markers. It must be also mentioned that these pan-endothelial markers stain vessels in tumor and normal tissue with equal intensity. On the other hand, as we observed in the current study, endoglin stained intensively intratumoral vessels with high sensitivity, whereas vessels in non-neoplastic tissue were not or were weakly expressing CD105. This confirms previous observations that endoglin reacts specifically with angiogenic endothelial cells and that its expression declines as we move away from the invasive front of the tumor [39]. Neoplastic, inflammatory, mesechymal, and hematopoietic cells were not stained with endoglin. These observations have been also reported previously for other solid malignancies [4, 7, 26, 29, 30, 35, 44]. In addition, in our samples, lymphatic vessels were generally negative for endoglin, as confirmed with double staining with the specific lymphatic endothelium marker D2-40. However, we observed a small number of intratumoral vessels that were expressing both of the markers simultaneously. This was not reported previously. Hence, a possible role of endoglin in lymphangiogenesis cannot be excluded, as interactions between angiogenesis and lymphangiogenesis are common in tumors [16].

An increasing amount of studies evaluating MVD with CD105, in various neoplasms, is being published [4, 7, 26, 29, 30, 35, 44]. So far, with no exceptions, in all of these studies, a significant association of high MVD with poor prognosis was observed, and investigators agree that assessment of microvessel counts with endoglin seems to be better than the use of any other pan-endothelial marker. Thus, the use of CD105 offers a feasible solution to one of the major problems in studying angiogenesis in cancer samples: the selection of the optimal endothelial marker [41]. However, we must keep in mind that there are other equally important difficulties. Measuring microvessel density by examining small sections of archival tissue at a single point in time does not necessarily represent the angiogenic status of the tumor. There is also significant inter-observer variability for the identification and selection of the "hot spots". The selection of an unbiased cut-off for separation of tumors with high vs low microvessel density can also be problematic [21, 41]. Therefore, more studies, preferentially prospectively drifted, are needed to confirm the importance of MVD (determined with CD105) as a prognostic factor before it can be incorporated into clinical practice.

Although the importance of CD105 for microvessel staining is adequately supported by enough observational data, little is known about the direct implication of this molecule in the angiogenic procedure. Research is currently focusing on the discovery of the intracellular partners and molecules interacting with endoglin [12]. It was reported that CD105 gene promoter is predominantly active in proliferating endothelial cells, and its activity is induced by hypoxia [12–14, 25]. These aspects suggest that

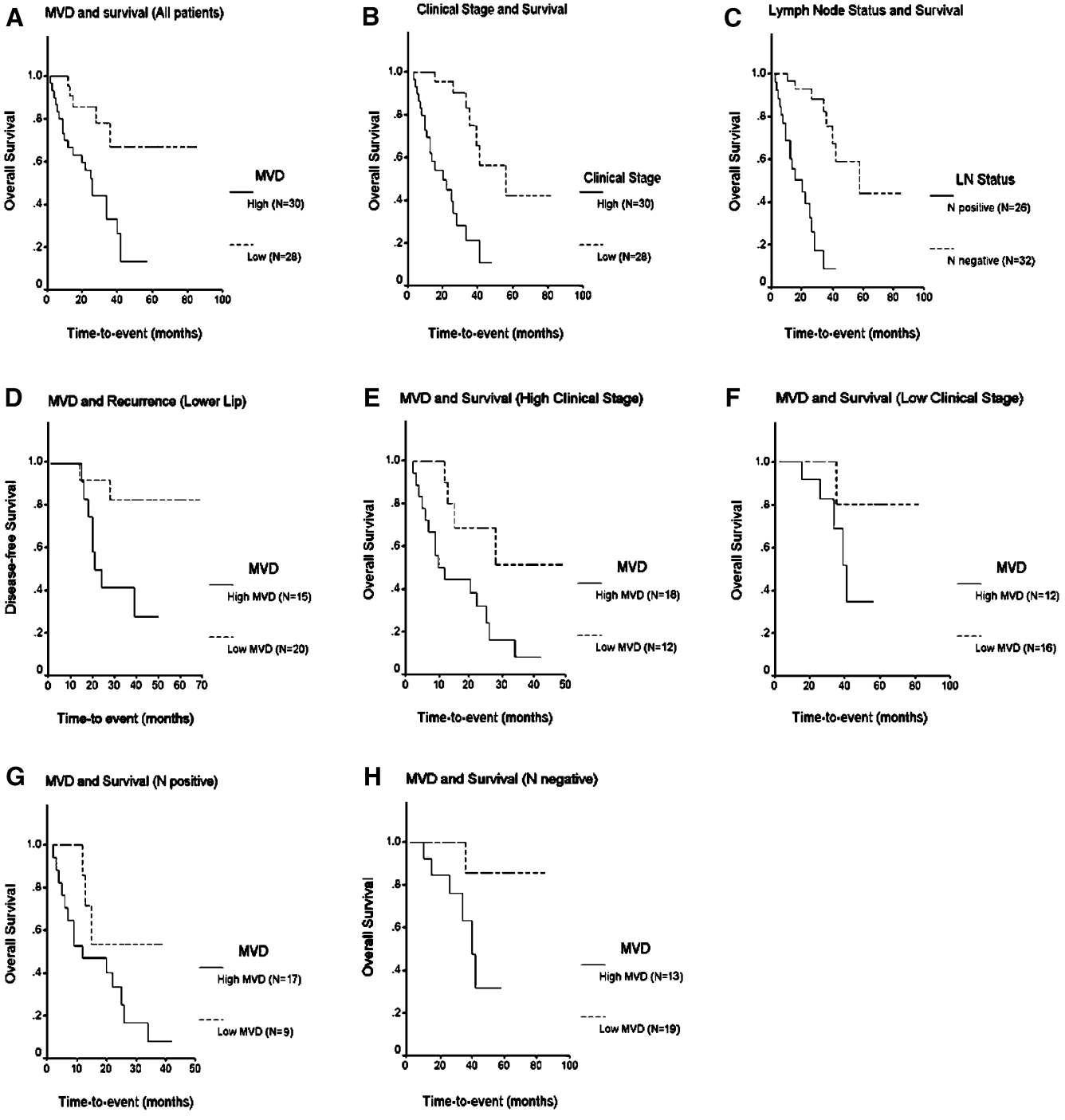

Fig. 3 **a** Kaplan–Meier curve for the overall survival of the patients with squamous cell carcinoma of the oral cavity and larynx, according to the CD105-determined microvessel density (high MVD vs low MVD). The two curves are significantly different (log-rank $p<0.001$). **b** Kaplan–Meier curve for the overall survival of the patients with squamous cell carcinoma of the oral cavity and larynx, according to clinical stage (IV + III vs I + II). The two curves are significantly different (log-rank $p<0.001$). **c** Kaplan–Meier curve for the overall survival of the patients with squamous cell carcinoma of the oral cavity and larynx, according to the lymph node status (N positive vs N negative). The two curves are significantly different (log-rank $p<0.001$). **d** Kaplan–Meier curve for the disease-free survival of the patients with squamous cell carcinoma of the lower lip, according to the CD105-determined microvessel density (high MVD vs low MVD). The two curves are significantly different (log-rank $p=0.02$). **e**–**h** Kaplan–Meier curves for the overall survival of the patients with squamous cell carcinoma of the oral cavity and larynx, according to the CD105-determined microvessel density (high MVD vs low MVD), stratified over clinical stage (**e**, **f**) and lymph node status (**g**, **h**). The prognostic significance of MVD on survival remains unchanged after stratification

Table 2 Multivariate survival analysis for patients with squamous cell carcinoma of the oral cavity and larynx

	Multivariate Cox		
	Hazard ratio	95% confidence intervals	*p*-value
Clinical stage (III + IV vs I + II)	2.4	1.3–4.5	p=0.003
Lymph node status (N+ vs N−)	2.9	1.1–8.7	p=0.04
MVD (high vs low)	2.7	1.1–7.5	p=0.04

CD105 gene could be an objective for targeted gene delivery in therapies directed to malignant neoplasms; but these observations must be further confirmed [12].

In conclusion, this study suggests that MVD evaluation with CD105 is a promising prognostic factor for outcome of patients with head and neck squamous cell carcinoma. We suggest that endoglin is a more sensitive and specific marker for microvessel highlight than the pan-endothelial markers currently in use and may represent a novel target for prognostic purposes and for novel therapeutic approaches. Our observations for the prognostic significance of endoglin should be confirmed in larger series of squamous cell carcinoma from the same anatomic location and suspected to the same treatment modalities before the incorporation of CD105 into clinical practice.

References

1. Aebersold DM, Beer KT, Laissue J, Hug S, Kollar A, Greiner RH, Djonov V (2000) Intratumoral microvessel density predicts local treatment failure of radically irradiated squamous cell cancer of the oropharynx. Int J Radiat Oncol Biol Phys 48:17–25
2. Altman DG, Lausen B, Sauerbrei W, Schumacher M (1994) Dangers of using "optimal" cutpoints in the evaluation of prognostic factors. J Natl Cancer Inst 86:829–835
3. Brattstrom D, Bergqvist M, Wester K, Hesselius P, Ren ZP, Scheibenpflug L, Wagenius G, Brodin O (2004) Endothelial markers and circulating angiogenic factors and p53 may be potential markers for recurrence in surgically resected non-small cell lung cancer patients. Med Sci Monit 10:331–338
4. Brewer CA, Setterdahl JJ, Li MJ, Johnston JM, Mann JL, McAsey ME (2000) Endoglin expression as a measure of microvessel density in cervical cancer. Obstet Gynecol 96:224–228
5. Chien CY, Su CY, Hwang CF, Chuang HC, Hsiao YC, Wu SL, Huang CC (2005) Clinicopathologic significance of CD105 expression in squamous cell carcinoma of the hypopharynx. Head Neck 2005 (In press)
6. Costello B, Li C, Duff S, Butterworth D, Khan A, Perkins M, Owens S, Al-Mowallad AF, O'Dwyer S, Kumar S (2004) Perfusion of 99Tcm-labeled CD105 Mab into kidneys from patients with renal carcinoma suggests that CD105 is a promising vascular target. Int J Cancer 109:436–441
7. Dales JP, Garcia S, Carpentier S, Andrac L, Ramuz O, Lavaut MN, Allasia C, Bonnier P, Charpin C (2004) Long-term prognostic significance of neoangiogenesis in breast carcinomas: comparison of Tie-2/Tek, CD105, and CD31 immunocytochemical expression. Hum Pathol 35:176–183
8. Duff SE, Li C, Garland JM, Kumar S (2003) CD105 is important for angiogenesis: evidence and potential applications. FASEB J 17:984–992
9. Ellis LM, Liu W, Fan F, Reinmuth N, Shaheen RM, Jung YD, Ahmad S (2001) Role of angiogenesis inhibitors in cancer treatment. Oncology (Huntingt) 15:39–46
10. Evangelou E, Kyzas PA, Trikalinos TA (2005) Comparison of the diagnostic accuracy of lymphatic endothelium markers: Bayesian approach. Mod Pathol 18:1490–1497
11. Folkman J (1990) What is the evidence that tumors are angiogenesis dependent? J Natl Cancer Inst 82:4–6
12. Fonsatti E, Del Vecchio L, Altomonte M, Sigalotti L, Nicotra MR, Coral S, Natali PG, Maio M (2001) Endoglin: an accessory component of the TGF-beta-binding receptor-complex with diagnostic, prognostic, and bioimmunotherapeutic potential in human malignancies. J Cell Physiol 1888:1–7
13. Fonsatti E, Altomonte M, Nicotra MR, Natali PG, Maio M (2003) Endoglin (CD105): a powerful therapeutic target on tumor-associated angiogenetic blood vessels. Oncogene 22: 6557–6563
14. Fonsatti E, Maio M (2004) Highlights on endoglin (CD105): from basic findings towards clinical applications in human cancer. J Transl Med 2:18–25
15. Gallo O, Masini E, Bianchi B, Bruschini L, Paglierani M, Franchi A (2002) Prognostic significance of cyclooxygenase-2 pathway and angiogenesis in head and neck squamous cell carcinoma. Hum Pathol 33:708–714
16. Hirakawa S, Hong YK, Harvey N, Schacht V, Matsuda K, Libermann T, Detmar M (2003) Identification of vascular lineage-specific genes by transcriptional profiling of isolated blood vascular and lymphatic endothelial cells. Am J Pathol 162:575–586
17. Hong WK, Lippman SM, Itri LM, Karp DD, Lee JS, Byers RM, Schantz SP, Kramer AM, Lotan R, Peters LJ (1990) Prevention of second primary tumors with isotretinoin in squamous-cell carcinoma of the head and neck. N Engl J Med 323:795–801
18. Kumar S, Ghellal A, Li C, Byrne G, Haboubi N, Wang JM, Bundred N (1999) Breast carcinoma: vascular density determined using CD105 antibody correlates with tumor prognosis. Cancer Res 59:856–861
19. Kyzas PA, Stefanou D, Agnantis NJ (2004) Immunohistochemical expression of vascular endothelial growth factor correlates with positive surgical margins and recurrence in T1 and T2 squamous cell carcinoma (SCC) of the lower lip. Oral Oncol 40:941–947
20. Kyzas PA, Geleff S, Batistatou A, Agnantis NJ, Stefanou D (2005) Evidence for lymphangiogenesis and its prognostic implications in head and neck squamous cell carcinoma. J Pathol 206:170–177
21. Kyzas PA, Loizou KT, Ioannidis JP (2005) Selective reporting biases in cancer prognostic factor studies. J Natl Cancer Inst 97:1043–1055
22. Kyzas PA, Stefanou D, Agnantis NJ (2005) COX-2 expression correlates with VEGF-C and lymph node metastases in patients with head and neck squamous cell carcinoma. Mod Pathol 18:153–160
23. Kyzas PA, Stefanou D, Batistatou A, Agnantis NJ (2005) Prognostic significance of VEGF immunohistochemical expression and tumor angiogenesis in head and neck squamous cell carcinoma. J Cancer Res Clin Oncol 131:624–630
24. Kyzas PA, Cunha IW, Ioannidis JP (2005) Prognostic significance of vascular endothelial growth factor immunohistochemical expression in head and neck squamous cell carcinoma: a meta-analysis. Clin Cancer Res 11:1434–1440
25. Kyzas PA, Stefanou D, Batistatou A, Agnantis NJ (2005) Hypoxia-induced tumor angiogenic pathway in head and neck cancer: an in vivo study. Cancer Lett 225:297–304
26. Li C, Gardy R, Seon BK, Duff SE, Abdalla S, Renehan A, O'Dwyer ST, Haboubi N, Kumar S (2003) Both high intratumoral microvessel density determined using CD105 antibody and elevated plasma levels of CD105 in colorectal cancer patients correlate with poor prognosis. Br J Cancer 88:1424–1431

27. Marioni G, Gaio E, Giacomelli L, Marchese-Ragona R, Staffieri C, Staffieri A, Marino F (2005) Endoglin (CD105) expression in head and neck basaloid squamous cell carcinoma. Acta Otolaryngol 125:307–311
28. Martone T, Rosso P, Albera R, Migliaretti G, Fraire F, Pignataro L, Pruneri G, Bellone G, Cortesina G (2005) Prognostic relevance of CD105+ microvessel density in HNSCC patient outcome. Oral Oncol 41:147–155
29. Massi D, Franchi A, Paglierani M, Ketabchi S, Borgognoni L, Reali UM, Santucci M (2004) Vasculogenic mimicry has no prognostic significance in pT3 and pT4 cutaneous melanoma. Hum Pathol 35:496–502
30. Mineo TC, Ambrogi V, Baldi A, Rabitti C, Bollero P, Vincenzi B, Tonini G (2004) Prognostic impact of VEGF, CD31, CD34, and CD105 expression and tumour vessel invasion after radical surgery for IB-IIA non-small cell lung cancer. J Clin Pathol 57:5917
31. Nagatsuka H, Hibi K, Gunduz M, Tsujigiwa H, Tamamura R, Sugahara T, Sasaki A, Nagai N (2005) Various immunostaining patterns of CD31, CD34 and endoglin and their relationship with lymph node metastasis in oral squamous cell carcinomas. J Oral Pathol Med 34:70–76
32. Pazouki S, Chisholm DM, Adi MM, Carmichael G, Farquharson M, Ogden GR, Schor SL, Schor AM (1997) The association between tumour progression and vascularity in the oral mucosa. J Pathol 183:39–43
33. Pfister DG, Ang K, Brockstein B, Colevas AD, Ellenhorn J, Goepfert H, Hicks WL Jr, Hong WK, Kies MS, Lydiatt W, McCaffrey T, Mittal BB, Ridge JA, Schuller DE, Shah JP, Spencer S, Trotti A 3rd, Urba S, Weymuller EA Jr, Wheeler RH 3rd, Wolf GT; National Comprehensive Cancer Network (2000) NCCN practice guidelines for head and neck cancers. Oncology (Huntingt) 14:163–194
34. Reinmuth N, Parikh AA, Ahmad SA, Liu W, Stoeltzing O, Fan F, Takeda A, Akagi M, Ellis LM (2003) Biology of angiogenesis in tumors of the gastrointestinal tract. Microsc Res Tech 60:199–207
35. Saad RS, Jasnosz KM, Tung MY, Silverman JF (2003) Endoglin (CD105) expression in endometrial carcinoma. Int J Gynecol Pathol 22:248–253
36. Saad RS, Liu YL, Nathan G, Celebrezze J, Medich D, Silverman JF (2004) Endoglin (CD105) and vascular endothelial growth factor as prognostic markers in colorectal cancer. Mod Pathol 17:197–203
37. Salven P, Heikkila P, Anttonen A, Kajanti M, Joesuu H (1997) Vascular endothelial growth factor in squamous cell head and neck carcinoma: expression and prognostic significance. Mod Pathol 10:1128–1133
38. Salvesen HB, Gulluoglu MG, Stefansson I, Akslen LA (2003) Significance of CD 105 expression for tumour angiogenesis and prognosis in endometrial carcinomas. APMIS 111:1011–1018
39. Schimming R, Marme D (2002) Endoglin (CD105) expression in squamous cell carcinoma of the oral cavity. Head Neck 24:151–156
40. Tanaka F, Otake Y, Yanagihara K, Kawano Y, Miyahara R, Li M, Yamada T, Hanaoka N, Inui K, Wada H (2001) Evaluation of angiogenesis in non-small cell lung cancer: comparison between anti-CD34 antibody and anti-CD105 antibody. Clin Cancer Res 7:3410–3415
41. Vermeulen PB, Gasparini G, Fox SB, Colpaert C, Marson LP, Gion M, Belien JA, de Waal RM, Van Marck E, Magnani E, Weidner N, Harris AL, Dirix LY (2002) Second international consensus on the methodology and criteria of evaluation of angiogenesis quantification in solid human tumours. Eur J Cancer 38:1564–1579
42. Weidner N, Semple JP, Welch WR, Folkman J (1991) Tumor angiogenesis and metastasis–correlation in invasive breast carcinoma. N Engl J Med 324:1–8
43. Wang JM, Kumar S, Pye D, Haboubi N, al-Nakib L (1994) Breast carcinoma: comparative study of tumor vasculature using two endothelial cell markers. J Natl Cancer Inst 86:386–388
44. Yagasaki H, Kawata N, Takimoto Y, Nemoto N (2003) Histopathological analysis of angiogenic factors in renal cell carcinoma. Int J Urol 10:220–227
45. Yu JX, Zhang XT, Liao YQ, Zhang QY, Chen H, Lin M, Kumar S (2003) Relationship between expression of CD105 and growth factors in malignant tumors of gastrointestinal tract and its significance. World J Gastroenterol 9:2866–2869

Virchows Arch (2006) 448: 776–787
DOI 10.1007/s00428-006-0196-3

ORIGINAL ARTICLE

Matthias Evert · Hans-Ulrich Schildhaus · Regine Schneider-Stock · Frank Dombrowski

Cystic cholangiomas after transplantation of pancreatic islets into the livers of diabetic rats

Received: 18 January 2006 / Accepted: 21 February 2006 / Published online: 7 April 2006

Abstract Islet transplantation is increasingly used as a therapy for human type 1 diabetes mellitus. In our study, we investigated the effect of the transplantation of a low number (n=350) of pancreatic islets into the right liver part on the neighboring portal bile ducts. Male streptozotocin-diabetic Lewis or autoimmune-diabetic BB/Pfd rats (n=1065) were subdivided into 11 experimental groups. A few days after low-number islet transplantation, cholangiocytes adjacent to the grafts showed an increase in proliferative activity. During the next 12–24 months, many peri-insular ductules progressed via tumor-like cystic lesions to large cystic cholangiomas, accompanied by a translocation of the insulin receptor into the cytoplasm and an increase in expression of insulin-related signaling proteins (Insulin-receptor-substrate-1, Raf-1, Mek-1). After 24 months, 53% of rats with low-number transplantation exhibited at least one cholangioma >10 mm, significantly outnumbering tumor development in the transplant-free left liver part and in any control group. No cholangiocarcinomas emerged. A graft cell origin of the tumors was excluded by Y chromosome in situ hybridization in cross-gender transplantations. Conclusively, low-number intrahepatic islet transplantation, most likely acting by permanent local hyperinsulinism, leads to prolonged cholangiocellular proliferation in streptozotocin- and in autoimmune-diabetic rats, resulting in the development of benign cystic cholangiomas.

M. Evert · R. Schneider-Stock · F. Dombrowski (✉)
Institute for Pathology,
Otto-von-Guericke-University Magdeburg,
Leipziger Strasse 44,
39120 Magdeburg, Germany
e-mail: Frank.Dombrowski@medizin.uni-magdeburg.de
Tel.: +49-391-6717869
Fax: +49-391-6717952

H.-U. Schildhaus
Institute for Pathology,
Rheinische Friedrich-Wilhelm-University,
Sigmund-Freud-Strasse 25,
53105 Bonn, Germany

Keywords Insulin · Cholangioma · Islet transplantation

Introduction

Transplantation of islets of Langerhans into the liver is regarded as an ideal therapy for treating human type 1 diabetic patients but clinical success, i.e., achievement of insulin independence, has not been reached for a long time. Recent advances in immunosuppressive regimens, beginning with a glucocorticoid-free therapy established by the Edmonton Group in Canada [51] and improved islet preparation techniques have meanwhile substantially contributed to the excellent long-term metabolic control in transplanted patients [46–49]. More than 750 patients have been treated so far, and further improvement of the immunosuppression protocols to reduce the risk of complications is one of the major future challenges [46, 47].

As a result of the long-term vitality of the islet grafts, the influence of islet hormones on adjacent liver tissue, i.e., hepatocytes, cholangiocytes, and non-parenchymal liver cells, will become a focus of increasing attention in the future. Naturally, detailed long-term morphologic studies on human recipient livers are lacking and most results are obtained in animal models, but there is an increasing number of case studies reporting on alterations in the liver parenchyma surrounding the islet grafts, i.e., focal steatosis in most cases [7, 17, 49, 53]. Focal glycogenosis and steatosis are long known to be induced by islet transplantation in rat animal models [11, 27].

Low-number islet transplantation (n=450) is ideal to study the effect of local high insulin levels on the adjacent cells of the downstream liver acinus, as it does not completely compensate hyperglycemia and the persisting mild diabetes thus stimulates the islet grafts to maximally synthesize and secrete insulin. Several studies have shown that these conditions, i.e., combined hyperglycemia and hyperinsulinism, lead to distinct alterations in the metabolism and growth control of the hepatocytes, such as glycogen and lipid accumulation, an altered enzyme expression pattern and increased proliferation and apoptose

kinetics [11–13, 22]. The hyperinsulinism has induced a translocation of the insulin receptor into the cytoplasm of altered hepatocytes, leading to increased intracellular insulin signaling via the Ras–Raf–MAPKinase pathway as demonstrated by the overexpression of key proteins such as insulin receptor substrate (IRS)-1, Raf-1, and Mek-1 and has also altered signaling via the insulin like growth factor (IGF) 1 axis [21, 50]. This altered liver acinus corresponds, in nearly every aspect, to the preneoplastic clear-cell hepatocellular focus known from chemical hepatocarcinogenesis [4], and indeed, proved to be of preneoplastic nature, as it was shown to progress to advanced stages of preneoplasias and subsequently to hepatocellular adenomas and carcinomas after 6–24 months [13].

It is most likely that the cholangiocytes of the directly adjacent portal bile ducts are also exposed to high local concentrations of islet hormones, in particular, insulin. Cholangiocellular alterations in human islet recipients have not yet been reported, but some authors described cholangiocellular cystic lesions in the liver of streptozotocin (STZ)-diabetic rats that received islet transplants [24, 25, 34]. However, there was substantial disagreement whether islet transplantation or streptozotocin treatment was responsible for their development. On the one hand, besides growth factors such as nerve growth factor, transforming growth factor (TGF) α and hepatocyte growth factor [26, 28, 56], insulin has, indeed, been shown to stimulate cholangiocellular proliferation in vitro [10]. Moreover, there are clear indications that growth factors are also involved in cholangiocellular metabolism and growth control of normal and preneoplastic cholangiocytes in vivo [38, 42]. However, to the best of our knowledge, the influence of insulin on the proliferative activity of bile duct epithelia in vivo has not yet been investigated. On the other hand, streptozotocin that is widely used in islet transplantation studies in rats, to establish diabetes, is genotoxic and has carcinogenic potential [9, 39]. Therefore, it is still not clarified whether insulin after islet transplantation or streptozotocin was responsible for the development of cholangiocellular lesions.

The aim of this study was, thus, to examine in detail the long-term influence of islet transplantation on the neighboring bile duct epithelia in diabetic rats and to evaluate the influence of streptozotocin in this setting. Moreover, we investigated whether the insulin-related Ras–Raf–MAPKinase pathway and TGF-α action are involved in cholangiocellular proliferation in this model.

Materials and methods

Animals and diabetes induction

Altogether, 1,065 animals were examined in this experiment. We used two different inbred rat strains, i.e., Lewis rats (n=324) and a substrain of autoimmune diabetic BB (bio-breeding) rats, the so-called BB-Pfd rats (n=741). BB rats become diabetic by an autoimmunological mechanism and serve, similar to the non-obese diabetic (NOD) mouse, as an animal model for human type 1 diabetes [37]. The substrain of BB/Pfd rats is characterized by a high probability of spontaneous reestablishment of the lost self-tolerance to the β-cells [32, 36]. Thus, most of these animals tolerate the transplanted isologous islet grafts without immunosuppressive therapy, whereas, the remaining rats destroy the grafts via the same autoimmunological mechanism, as they have done with their own islets before, and become diabetic again.

With the exception of some female donor animals that were used for the cross-gender transplantation and in situ hybridization, all animals were male. Lewis rats (Harlan Winkelmann, Borchen, Germany) were subdivided into four experimental groups (L1–L4) and treated according to Table 1. L1–L3 were made diabetic by a single intravenous injection of streptozotocin (80 mg/kg body weight), whereas, L4 stayed normoglycemic as a control Lewis group. BB/Pfd rats that developed the autoimmune diabe-

Table 1 Experimental design, blood glucose, and body weight

		L1	L2	L3	L4	BB1	BB2	BB3	BB4	BB5	BB6	BB7
Number of animals		142	83	39	80	148	86	40	144	118	40	165
Strain		Lewis	Lewis	Lewis	Lewis	BB/Pfd	BB/Pfd	BB/Pfd	BB/Pfd	BB/Pfd	BB/Pfd	BB/Pfd
Type of diabetes induction [streptozotocin (STZ)/ autoimmune]		STZ	STZ	STZ	No diabetes	Auto immune	Auto immune	Auto immune	STZ	STZ	STZ	No diabetes
Transplantation procedure	350 islets	X				X			X			
	1,000 islets		X				X			X		
	350 latex particles			X								
Blood glucose (mg/dl)		231±4	88±2	410±11	78±2	209±12	85±3	368±14	195±11	76±2	321±11	90±2
Body Weight (g)		254±3	366±7	223±7	446±11	288±5	348±8	254±6	296±6	367±7	289±8	328±7

The Lewis rats were subdivided into four experimental groups (L1–L4). The BB/Pfd rats either developed autoimmune diabetes (BB1–BB3) or were made diabetic by streptozotocin administration (BB4–BB6), similar to the Lewis rats. L4 and BB7 served as untreated and normoglycemic control groups. Blood glucose and body weight are given as mean value±standard error of the mean and were measured by the time of sacrifice

tes were subdivided into three groups (BB1–BB3). BB/Pfd rats that did not develop autoimmune diabetes (approximately 90% of the primary population) served as islet donors and were made diabetic (BB4–BB6) by streptozotocin injection (65 mg/kg body weight) or stayed normoglycemic as a BB/Pfd control group (BB7). All animals were inspected daily. Blood glucose and body weight were measured monthly and also 1 and 3 days after transplantation, immediately before and 2 days after streptozotocin treatment, and immediately before killing. Animals showing a weight loss of more than one third of their individual maximal body weight *post transplantationem* were given a subcutaneous insulin implant (Linplant, Linshin Canada, Scarborough, Ontario, Canada) to prevent death by diabetes, a measure that was not necessary in diabetic Lewis rats but has to be done in virtually all diabetic BB/Pfd rats with increasing time to avoid death by diabetic complications. Nevertheless, these animals still stayed diabetic; the hyperglycemia was only ameliorated. Animal treatment was in line with the guidelines of the Society for Laboratory Animal Service (GV-SOLAS) and the strict German Animal Protection Law.

Transplantation procedure

Animals were anesthesized (100 mg/kg ketamin, 4 mg/kg xylazin), and islets of Langerhans, consisting of approximately 85% β cells, were isolated from 3 to 5 months old nondiabetic donors (littermates in case of the BB/Pfd rats), weighing 250–350 g, and transplanted into the liver via the portal vein, 3 weeks after STZ treatment or onset of the autoimmune-diabetes, as described in detail previously [11]. During infusion, the branch supplying the left part of the liver (i.e., left lobe and left part of the middle lobe) was clamped, making sure that the transplants were embolized only into the right part of the livers (i.e., right lobe, right part of the middle lobe, caudate lobe, anterior and posterior papillary processus); the left part served as an intra-individual control. Ischemia for the left part lasted only for about 1 min. L1, BB1, and BB4 received a low number (n=350) and L2, BB2, and BB5, a high number of islet grafts (n=1,000), respectively. L3 received 350 polystyrene (Latex) particles (Polysciences, Warrington, PA) of about 90–100 μm in size to exclude an influence of ischemia, and the remaining groups (L4, BB3, BB6, and BB7) were not transplanted (Table 1).

Animal killings and 5-bromo-2′-desoxyuridine (BrdU) application

Animals were killed and matched in time-groups between 6 and 24 months after transplantation (Table 2). Some animals of each experimental group received osmotic minipumps (Alzet model 2ML1, Alza, Palo Alto, CA,

Table 2 Development of cholangiocellular cystic lesions and tumors

Time (months)		L1		L2		L3		L4		BB1		BB2		BB3		BB4		BB5		BB6		BB7	
		R	*L*	*R*	*L*	*R*	*L*	*R*	*L*	*R*	*L*	*R*	*L*	*R*	*L*	*R*	*L*	*R*	*L*	*R*	*L*	*R*	*L*
0–6	**n**	**35**		**19**		**15**		**20**		**33**		**20**		**10**		**30**		**30**		**5**		**25**	
	>0.5 mm %	17[a]	0	0	0	0	0	0	0	3	0	0	0	0	0	13	0	0	0	0	0	0	0
	>2 mm %	0	0	0	0	0	0	0	0	0	0	0	0	0	0	0	0	0	0	0	0	0	0
	>10 mm %	0	0	0	0	0	0	0	0	0	0	0	0	0	0	0	0	0	0	0	0	0	0
6–12	**n**	**24**		**15**		**12**		**20**		**84**		**35**		**17**		**74**		**56**		**19**		**83**	
	>0.5 mm %	46[abcdh]	4	7	7	8	8	10	5	36[ahk]	4	23	9	12	12	20[aik]	7	5	5	16	16	2	2
	>2 mm %	29[abcdh]	0	0	7	0	0	0	0	14[ahk]	2	0	0	0	0	0	0	0	0	0	0	0	0
	>10 mm %	0	0	0	0	0	0	0	0	0	0	0	0	0	0	0	0	0	0	0	0	0	0
12–18	**n**	**47**		**28**		**12**		**20**		**31**		**31**		**13**		**40**		**32**		**16**		**57**	
	>0.5 mm %	81[abcde]	17	11	4	16	16	20	20	58[afgk]	6	29[ak]	3	23	23	68[aijk]	13	9	13	31[k]	31	5	5
	>2 mm %	70[abcdeh]	4	7	4	8	8	10	10	26[agk]	6	23[agk]	3	0	8	53[aeijk]	10	6	6	6	6	0	0
	>10 mm %	38[abcdeh]	2	0	0	0	0	0	0	10	0	0	0	0	0	20[aik]	3	0	0	0	0	0	0
18–24	**n**	**36**		**21**		**0**		**20**		**0**		**0**		**0**		**0**		**0**		**0**		**0**	
	>0.5 mm %	92[abd]	33	38	24			35	30														
	>2 mm %	78[abd]	14	29	14			20	15														
	>10 mm %	53[abd]	0	5	0			0	0														

At each time period, the number of investigated animals (n) of the experimental Lewis (L 1–L4) and BB/Pfd (BB1–BB7) groups is followed by the percentages of animals, bearing at least one cholangiocellular lesion larger than 0.5, 2, and 10 mm in diameter in their transplant-bearing right (R) or transplant-free left (L) liver part. Fisher's exact test, p>0.05

[a]Significantly more animals, bearing cholangiocellular cystic lesions/tumors in the right liver part than in the left liver part

Significantly more animals, bearing right-sided cholangiocellular lesions/tumors than in:[b]L2, [c]L3, [d]L4, [e]BB1, [f]BB2, [g]BB3, [h]BB4, [i]BB5, [j]BB6, [k]BB7

USA) filled with 40 mg 5-bromo-2′-desoxyuridine (BrdU; Sigma, Heidelberg, Germany) 7 days before killing. Perfusion fixation and anesthesia was done as described previously [11].

Tissue sampling and processing

After fixation, the livers were removed, cut into sections (about 0.5 mm), and examined with a stereomicroscope. All macroscopic liver lesions and at least ten additional liver slices were embedded in paraffin. Serial sections (2–3 μm) of the liver specimens were stained with hematoxylin and eosin (H&E) and with the periodic acid-Schiff (PAS) reaction. Additional sections were made for immunohistochemistry. Semithin sections were stained according to Richardson [45].

Morphometric analysis

In addition to all lesions larger than 2 mm, six slides of different liver parts were investigated per animal. Cholangiocellular lesions or tumors were only counted if they consisted of foci of proliferating ductules, measuring at least 0.5 mm in diameter and were then subdivided into three groups according to their size: small foci of proliferating ductules measuring 0.5–2 mm, tumor-like lesions and small tumors measuring 2–10 mm, and large (cystic) tumors measuring more than 10 mm in diameter.

Immunohistochemistry

Paraffin sections were incubated with the following primary polyclonal rabbit antibodies: anti-insulin, anti-glucagon, and anti-somatostatin (all Dako, Hamburg, Germany, dilution 1:200). The Anti-CK 7 (Clone OV-TL 12/30, Novocastra, Newcastle upon Tyne, UK, dilution 1:50) and anti-BrdU antibody (Dako, dilution 1:100) were monoclonal. CK 7-immunohistochemistry required protease pretreatment for 10 min. Furthermore, we used anti-insulin receptor (A1314, concentration of 0.5 mg/ml; provided kindly by Dr. J.W. Unger, Department of Anatomy, University of Munich, Germany), anti-IRS-1 (Upstate Biotechnology, New York, dilution: 1:50, polyclonal), anti-Raf-1 (Santa Cruz Biotechnology, Heidelberg, Germany, dilution 1:50, polyclonal), anti-Mek-1 (Santa Cruz Biotechnology, dilution 1:100, polyclonal), anti-TGF-α (Oncogen-Sciences, Cambridge, MA, final concentration, 10 μg/ml, monoclonal) and anti-epidermal growth factor receptor (EGF-R; Biogenex, San Ramon, USA, dilution 1:25, no pretreatment, polyclonal) antibodies. The immunohistochemical reactions of the proteins were assessed semiquantitatively by comparison with the extrafocal liver tissue, in particular, with cholangiocytes of normal portal bile ducts. Details of the staining procedures, including antigen retrieval methods, secondary antibodies, blocking of endogenous peroxidase, counterstaining, and mounting of the tissue sections were described previously [11, 13, 21].

In situ hybridization

The rat Y chromosome probe was received in the plasmid pUC18 as a kind gift from Dr. Barbara Hoebee [18]. The plasmid was cloned into DH5α *E. coli* and amplified. Plasmid containing colonies were picked for further sequencing. The sequence was confirmed by analyzing the plasmid on an ABI 310 sequencer (Applied Biosystems, Darmstadt, Germany). Injection time was 25 s, using Pop-4 dRhodamine Matrix standard ABI Prism (Perkin Elmer, Weiterstadt, Germany). BLASTN (version 2.2.4) analysis of a 339-bp DNA fragment revealed 95% (281/295) sequence identity to the original *Rattus norvegicus* 91ES8 DNA sequence (gene bank accession number: X80155.1.)

The whole plasmid was then labeled by nick translation with digoxigenin (Kit# 1745816, Roche Diagnostics, Mannheim, Germany) according to the manufacturer's instructions, resulting in a probe size of 100–500 bp at a concentration of ~0.5 μg/ml. The polyclonal rabbit anti-DIG antibody (Code P 5104) was purchased from Dako, Glostrup, Denmark. Deparaffinization, prehybridization, and hybridization was performed according to O'Leary and Blakemore [40]. The hybridization mix consisted of: 10% salmon testes DNA (10 mg/ml), 20% deionized formamide, 10% 50× Denhardt's solution, 10% 20× saline-sodium citrate (SSC), and 50% dextrane sulphate (all purchased from Sigma-Aldrich, Munich, Germany). After hybridization, slides were washed four times for 5 min each with 2× SSC (48°C), four times for 5 min in 0.1× SSC (48°C), then for 15 min in 1× SSC containing 50% deionized formamide at 48°C (high stringency) or room temperature (low stringency), and finally for 5 min in 2× SSC and counterstained with hemalaun. Female and male control liver sections were used in each run. The tumors were only evaluated (high stringency washing) when these control sections gave correct results.

Twenty-six tumors in 15 male recipients of L1 and BB1 were evaluated. The percentage of labeled nuclei in cholangiomas and in 100 surrounding hepatocytes was determined in six animals of BB1 and L1 and given as mean±standard deviation.

Statistical analysis

We determined the percentages of animals in the experimental groups that had developed at least one cholangiocellular lesion of the respective size and compared differences between their right (transplant-bearing) and left (transplant-free) part of the liver for evaluating the effect of the transplantation. The effect of high local intrahepatic insulin levels was additionally tested by comparing the low- and high-number transplantation groups with their respective control groups, i.e., L1 with

L2–L4; L2 with L3 and L4; BB1 with BB2, BB4 and BB7; BB2 with BB3 and BB7; and BB4 with BB5–BB7.

Strain differences and the influence of streptozotocin-induced vs autoimmune diabetes were examined by comparing the low number transplantation groups (L1, BB1, and BB4) and the nondiabetic control groups (L4 and BB7) among each other. The effect of streptozotocin treatment was tested by comparing L3 with L4 and BB6 with BB7. Other differences were not tested. Fisher's exact test was used, and $p<0.05$ was considered statistically significant.

Results

Body weight and blood glucose

Body weight and blood glucose were inversely correlated (Table 1). As intended by the experimental design, animals treated by streptozotocin administration or developing spontaneous auto-immune diabetes became hyperglycaemic; in addition, low-number islet transplantation lowered the hyperglycemia, but the animals remained in a mild diabetic state, whereas, high-number islet transplantation established normoglycemia.

Morphology and quantitative analysis

Islet transplants were vital and located within the portal tracts. Already a few days after islet transplantation, small ductular proliferations were noted in each of the low-number groups (Fig. 1a). Exceptionally, formation of single ductules was also observed after high-number transplantation, but most islet grafts in these groups (L2, BB2, BB5) were free of neoductuli (Fig. 1f). These ductules usually had close contact to the islet grafts. Most of the ductular proliferation occurred at the border between the islet graft and the connective tissue of the portal tracts, but there were examples in which the ductules were located

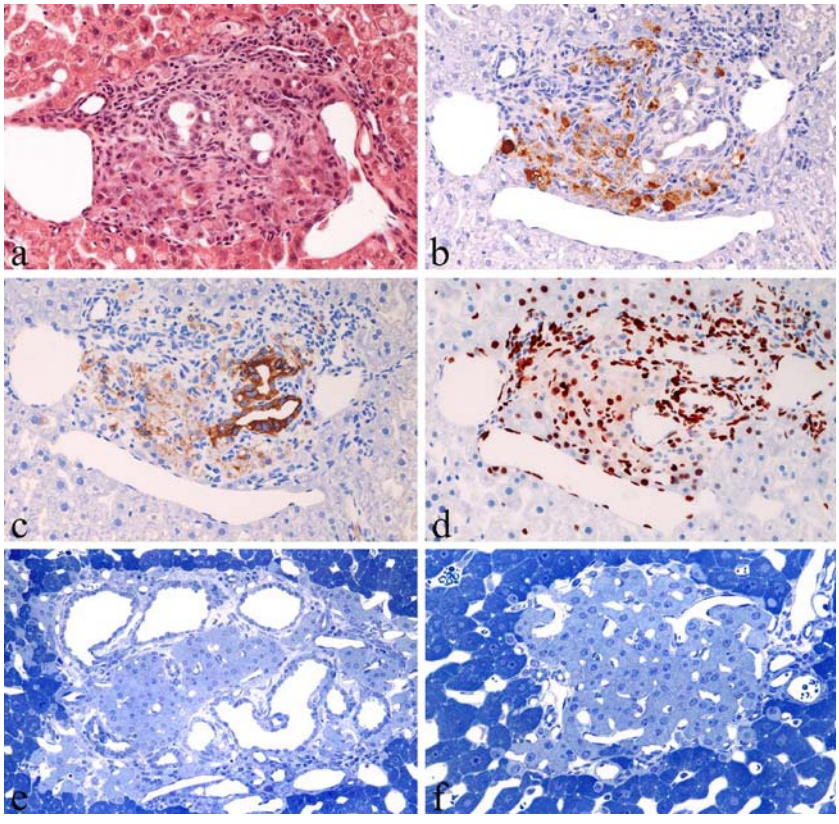

Fig. 1 **a**–**d** depict a transplanted islet graft and the surrounding tissue after low-number transplantation in a Lewis rat 7 days after transplantation. The islet is located in a portal tract infiltrated by some lymphocytes, and the adjacent hepatocytes show a clear cytoplasm owing to an increase in glycogen accumulation as a result of the local hyperinsulinism. The bile ducts are intermingled with islet cells, confirmed in insulin immunohistochemistry (**b**), in which is demonstrated that β-cells partly surround the bile ducts that show a strong immunohistochemical reaction for cytokeratin 7 (**c**). BrdU-labeling (**d**) demonstrates proliferative activity of the β-cells as a result of the systemic insulin deficiency and of the hepatocytes, endothelial cells, and the cholangiocytes. As a result of the increased cholangiocellular proliferation, new ductular structures develop that stay for a while in close contact to the islet grafts. This situation is maintained for weeks and months as shown 13 months after islet transplantation (L1, **e**). Rarely, similar neo-ductuli also develop after high-number transplantation, but normally, the islet grafts lie quiescent within the portal tracts, as these animals were normoglycemic and the β-cells were only weakly stimulated. As a result of the comparably lower local insulin concentration, no signs of cholangiocellular proliferation were then observed (**f**, L2, 13 months after transplantation). **a**–**d** Serial sections of the same islet graft stained with hematoxylin & eosin stain (**a**) or with insulin- (**b**), cytokeratin 7- (**c**), and BrdU-immunohistochemistry (**d**); semithin sections stained according to Richardson (**e** and **f**). The lower edge of the panels represent 480 μm (**a**–**d**), 530 μm (**e**), and 340 μm (**f**)

right within the islet grafts and were partly or completely surrounded by islet cells (Fig. 1a–d). In any case, the ductules were lined by a single layer of cuboidal to flat epithelial cells without any cytologic atypia (Fig. 1a,e). Positive CK 7-immunostaining proved the epithelial origin, thus, excluding vascular proliferations that must have also

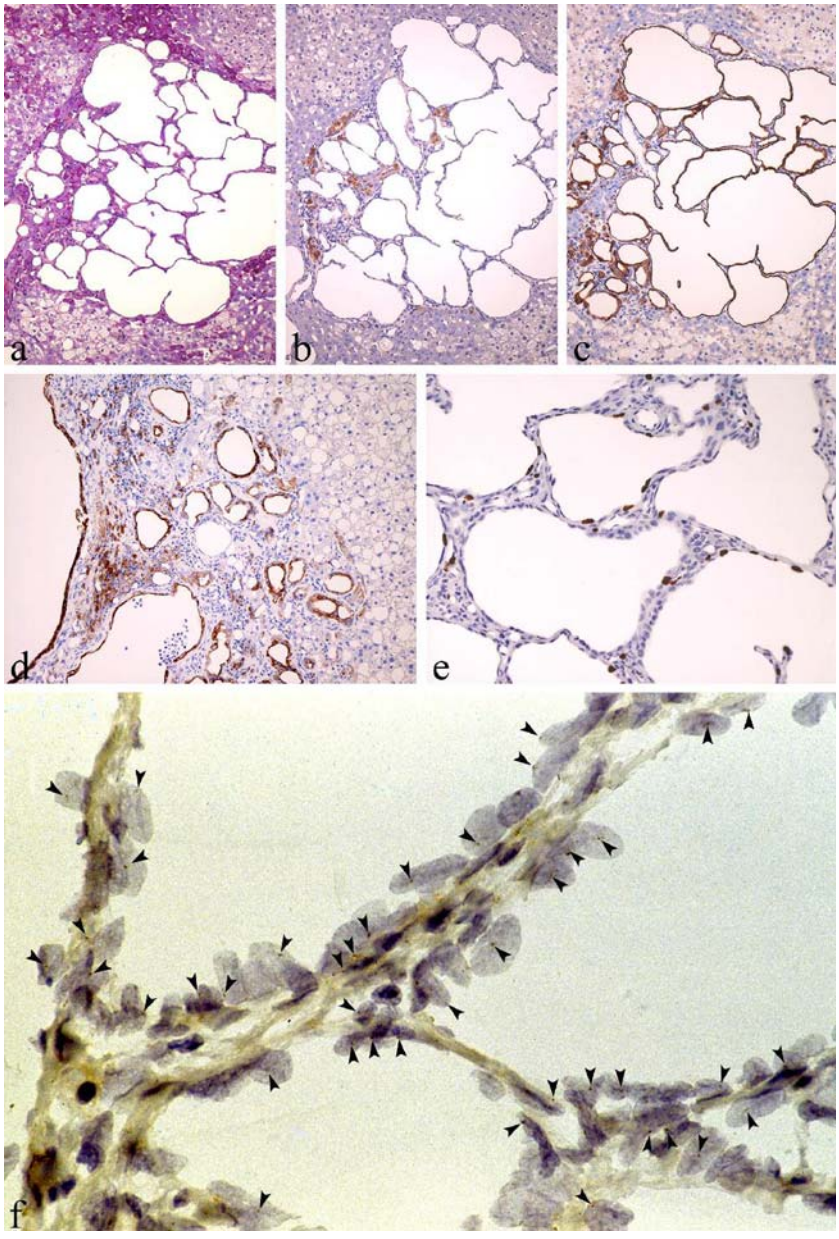

Fig. 2 Some of the ductules in the groups with low-number islet transplantation continued to proliferate and gave rise to cholangiomas measuring several millimeters. (**a**–**c**) depict a small cholangioma in serial sections that has developed after 14 months in a Lewis rat. The portal tract is located at the left margin. In the PAS reaction (**a**), the increase in glycogen in some hepatocytes of the surrounding preneoplastic focus is recognizable although most of the cells in this lesion are predominantly characterized by strong lipid accumulation. The close spatial relationship not only to the preneoplastic hepatocellular focus, but also to the islet, is demonstrated in insulin immunohistochemistry: the β-cells are dispersed and intermingled with the cholangioma (**b**). The epithelial lining is flat in larger cysts and cuboidal in smaller ducts, as highlighted at this low magnification by cytokeratine 7-immunohistochemistry (**c**). The development in the BB/Pfd rats was very similar. One minor difference was a stronger lymphocytic infiltration of the islet grafts owing to the disturbed immunological background in these animals (**d**). These lesions were also composed of smaller ductules and larger cysts (*left margin*). Note also the lipid accumulation in the preneoplastic hepatocytes in this animal. BrdU-labeling showed the proliferative activity of the epithelia lacking cytologic atypia throughout the entire experiment (**e**). In situ hybridization performed in liver tissue after cross-gender transplantation of female islet grafts into a male recipient always detected Y chromosomes (*arrowheads* in **f**) in the cells of all investigated tumors, ruling out an origin of transdifferentiated donor cells. PAS reaction (**a**), insulin- (**b**), cytokeratin 7- (**c** and **d**), and BrdU-immunohistochemistry (**e**). Y chromosome in situ hybridization (**f**). (**a**–**c**) L1, 14 months after islet transplantation. (**d**) BB1, 13 months after islet transplantation. (**e**) BB1, 14 months after transplantation. (**f**) L1, 13 months after islet transplantation. The lower edge of the panel represents: 800 μm (**a**–**c**), 960 μm (**d**), 480 μm (**e**), 150 μm (**f**)

been taken into account after rinsing the blood cells out of the vessels by the perfusion fixation. Some mitoses were seen, and several nuclei stained positive in BrdU-labeling, indicating proliferative activity (Fig. 1d). We did not notice a morphologically conspicuous transdifferentiation of islet cells or hepatocytes into duct-like cells or a proliferation of oval cells, which may have given rise to the ductular formation.

Concurrently, the liver acini of the hepatocytes that drain the hyperinsulinemic blood from the islet grafts in the low number transplantation groups developed into clear-cell foci of altered hepatocytes that often surrounded the ductular lesions which intermingled with the islet grafts (Figs. 2 and 3). All cholangiocellular and hepatocellular alterations did not occur in the left part of the liver and in the control groups that were not islet-transplanted.

In the first 6 months after transplantation, some of the lesions in the low-number transplantation groups (L1, BB1, and BB4) reached a diameter more than 0.5 mm (Table 2). These larger tumor-like lesions were always restricted to the right part of the liver. The lumina of the ductules often extended to small cysts that were still lined by a single layer of monomorphous epithelia. In some lesions, these cysts were separated by small amounts of connective tissue in which we often found islet cells, proven by immunohistochemical evidence of islet hormones within them (Figs. 1d and 2b).

Between 6 and 12 months *post transplantationem*, small lesions <2 mm were also noted in the livers of the control groups, but they were clearly exceeded by ductular proliferation in the low-number transplantation groups in which a considerable number of animals then already carried cystic tumors in their right liver half, measuring up

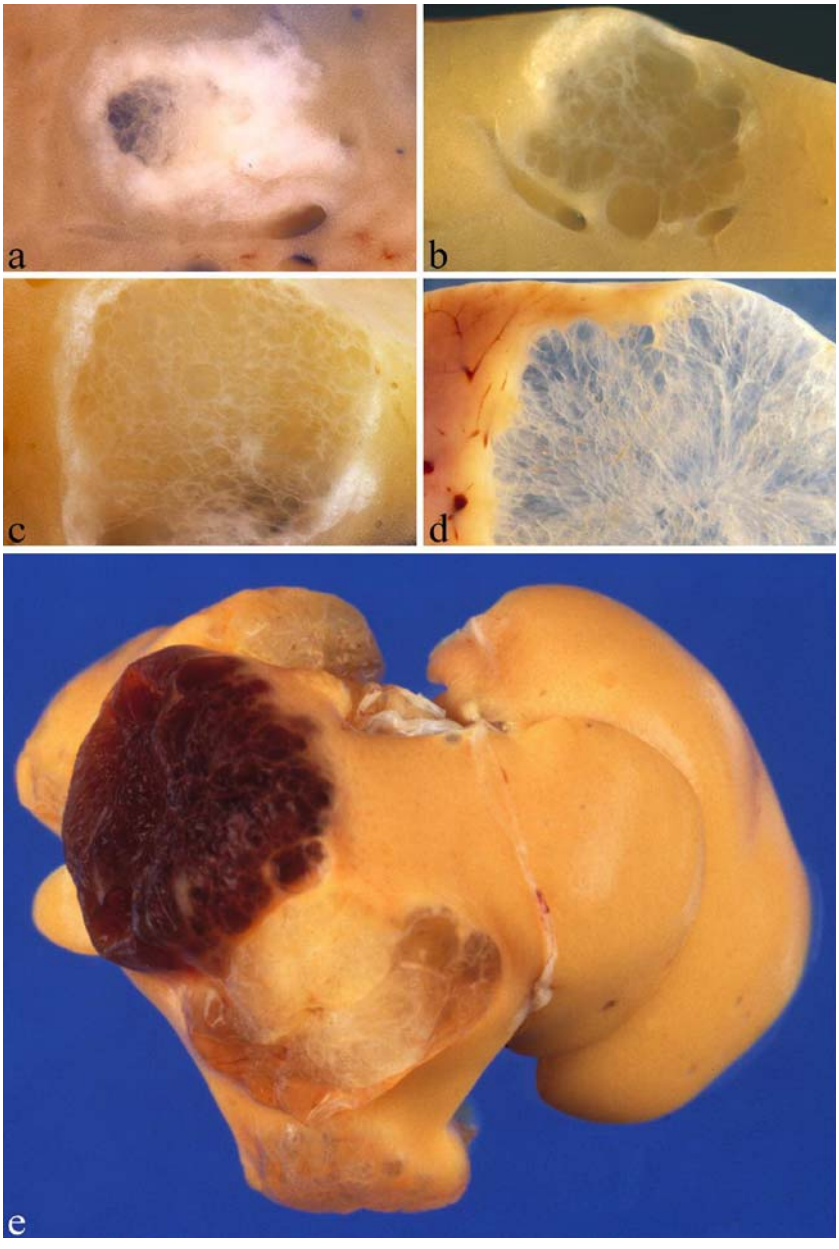

Fig. 3 After several months, some of the small lesions developed into large cystic tumors that were macroscopically recognizable. In the smaller lesions, the close spatial relationship between the preneoplastic hepatocellular focus and the cholangiocellular lesion was virtually always visible in stereomicroscopy (**a**–**c**). The cystic lesion depicted in this unstained liver slice after perfusion fixation (**a**) measures approximately 1.5 mm and is surrounded by white tissue corresponding to the preneoplastic hepatocellular focus (L1, 9 months after transplantation). **b** depicts a 3 mm large cystic lesion adjacent to white-colored preneoplastic hepatocellular tissue, 13 months after transplantation. **c** In this liver of a BB/Pfd rat 15 months after transplantation, a 4-mm cystic tumor still exhibits close topographical relation to the surrounding white preneoplastic hepatocellular lesion (BB1). **d** shows a 12-mm large cholangioma, 18 months after transplantation (L1). A surrounding hepatocellular preneoplasia is here not visible. In some animals, at the same time multiple large tumors developed occupying nearly the entire right liver part (**e**, whole liver, L1, 19 months after transplantation). Note that the left part of the liver, in which no islets have been transplanted, is also free of large cystic cholangiomas

to 10 mm in diameter (Table 2). In group L1, tumor formation was strongest: nearly half of the animals showed lesions <2 mm and nearly one-third of them carried cystic tumors measuring 2–10 mm. This was significantly more when compared not only to the left liver part and the other Lewis groups but also when compared with the streptozotocin-diabetic group BB4, which also received a low number of islet grafts. Autoimmune-diabetic BB1 animals showed also more lesions than streptozotocin-diabetic BB4 rats.

At 12–18 months after transplantation, the formation of cystic tumors progressed in all groups but still predominated in the low-number transplantation groups, of which L1 was again that with the strongest progression (Table 2). We also noticed the first tumors measuring more than 10 mm in diameter. These developed exclusively in the low-number transplantation groups (L1, BB1, BB4) (Fig. 3d,e). Some of these large tumors measured several centimeters, continued to grow so that they sometimes virtually occupied the whole liver, and caused death of some animals owing to rupture of the cysts or to compression of other organs. Histologically, even in these large tumors, the multicystic appearance and the benign cytology were preserved. We did not encounter any epithelial atypia or foci of invasion and even papillary epithelial projections were only focally seen. Positive BrdU-labeling still indicated proliferative activity, in particular, in areas with cuboidal and columnar epithelia or in the rare papillary areas (Fig. 2e). Bile accumulation was found in up to 30% of the larger tumors. Occasionally, we still recognized a close spatial relationship to islet graft remnants and hepatocellular foci of altered hepatocytes

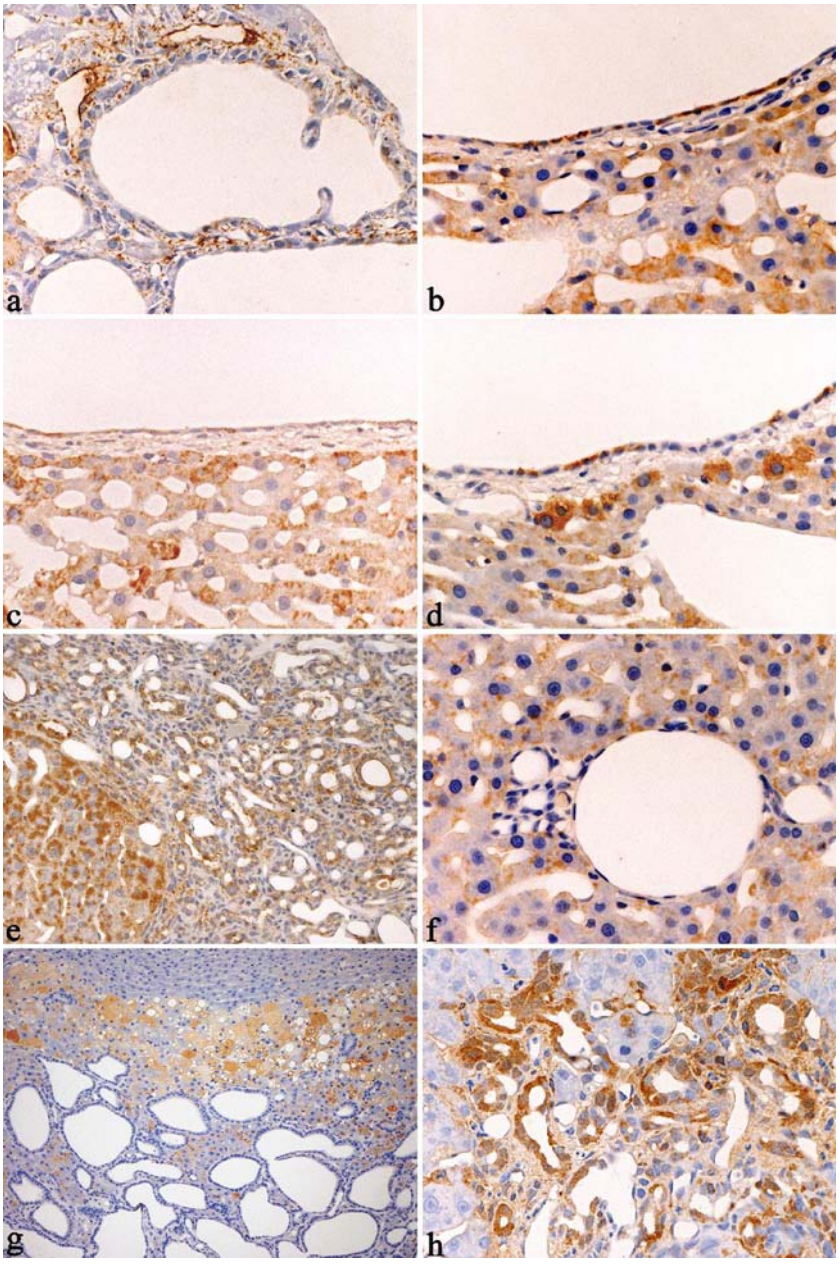

Fig. 4 Cholangiomas showed a translocation of the insulin receptor from the cell membrane into the cytoplasm, resulting in a granular reaction pattern (**a**). Proteins of the Ras–Raf–MAP-Kinase pathway, i.e., IRS-1 (**b**), Raf-1 (**c**), and Mek-1 (**d**) were moderately to strongly increased in cholangioma cells (*upper part of the panels*), although the pattern within one lesion was heterogenous and the signal intensity varied from cell to cell, including negative cells. There was no difference in Lewis rats (**a**–**d**) or BB rats (example of IRS-1 expression in **e**) and normal portal bile duct epithelia of extrafocal tissue were always negative (**f**). Cholangiomas (lower half in **g**) and extrafocal hepatocytes (upper edge in **g**) were transforming growth factor (TGF) α-negative but progressed hepatocellular preneoplasias that directly neighbor cholangiomas as depicted in (**g**), often showed strong TGF-α expression. As most cholangiomas expressed the receptor for TGF-α, i.e., the epidermal growth factor receptor (**h**), this may constitute an additional co-stimulatory paracrine stimulus for cholangioma proliferation during the course of the experiment. (**a**) L1, 13 months after transplantation. (**b**–**d**,**f**) L1, 13 months after transplantation (same animal; **b**–**d** serial sections). (**e**) BB1, 12 months after transplantation. (**g**) L1, 14 months after transplantation. (**h**) L1, 18 months after transplantation. *Lower edge of each panel* represents 203 μm except in (**e**) and (**g**) representing 406 and 810 μm, respectively

(FAH) or tumors (Fig. 3b,c). In this time period, the high-number transplantation group, BB2, which had developed autoimmune diabetes and was not treated with streptozotocin, also showed a significantly higher number of tumor-like lesions and tumors in their right liver part than in their left liver part and in the control groups BB3 and BB7 (Table 2). At this time-point, vice versa to 6–12 months, the number of small tumors, measuring 2–10 mm was higher in the streptozotocin-treated BB4 when compared with the autoimmune-diabetic BB1. It should also be noted that streptozotocin treatment increased the number of small lesions in BB6 when compared to BB7.

Lewis rats were examined for an additional 6 months to investigate whether some of the apparently benign tumors would transform into carcinomas. We found an increase in the number of lesions and tumors and in tumor size after 18–24 months (Table 2) but malignant transformation still did not occur.

Immunohistochemical expression of insulin-related signaling proteins (IR, IRS-1, Raf-1, Mek-1), TGF-α, and EGF-R

While cholangiocytes of normal portal bile ducts showed no expression or only barely detectable levels of the IR, IRS-1 (Fig. 4f), Raf-1, and Mek-1, the proliferating ducts of the majority of cholangiomas in the low-number transplantation groups L1, BB1, and BB4 revealed a moderate to strong expression of these proteins. The degree of intensity in the individual cell was comparable to the increased expression in hepatocytes of the surrounding preneoplastic hepatocellular focus, but it was more variable and pronounced in the periphery within cholangiocellular lesions. There was no difference between the streptozotocin-induced or spontaneously diabetic animals.

IR-immunohistochemistry revealed a granular cytoplasmic reaction pattern (Fig. 4a) in cholangioma cells suggesting the same translocation of the IR from the cell membrane into the cytoplasm after insulin binding that has formerly been shown for preneoplastic hepatocellular foci [21]. IRS-1, Raf-1, and Mek-1 were noted as an increased cytoplasmic expression in the cholangiomas (Fig. 4b–d), suggesting increased signaling via the insulin-related Ras–Raf–MAPKinase pathway in the cholangiocytes.

Cholangiomas also moderately to strongly expressed the EGF-R (Fig. 4h). TGF-α was not expressed in cholangiomas but in hepatocytes of adjacent preneoplastic hepatocellular lesions (Fig. 4g), suggesting that TGF-α if secreted in a paracrine manner by the hepatocytes may have co-stimulated proliferation of the cholangiomas, in particular, in large tumors that did no longer show insulin dependence.

In situ hybridization

In situ hybridization for the y chromosome in cross-gender transplantations (female islet donors, male recipients) was done to determine whether the tumors originated from recipient cholangiocytes or from graft cells that have undergone ductular transformation. The mean nuclear labelling index of hepatocytes was 84.8±8.7% (range, 72–93%) in the hepatocytes of the investigated male L1 and BB1 animals, whereas, female controls showed no hepatocellular nuclear signals. Owing to polyploid sets of chromosomes, some hepatocellular nuclei showed more than one (up to four) signals. If the y chromosome was not in the cut level, no nuclear signal was noted.

Nuclei of cholangiocellular tumor cells showed a mean labeling index of 58.2±14.9% (range, 35–72%). In cholangiomas, no more than one signal was noted per nucleus (Fig. 2f) which suggests that these cells were diploid and also explains the lower mean value of labeled nuclei when compared to hepatocytes. There was no single tumor that was devoid of y chromosome-containing cells; thus, each investigated tumor was derived from recipient cholangiocytes.

Additionally, two islet grafts were identified and showed no signals in islet cell nuclei, proving their female genetic background.

Discussion

This study indicates that after low-number transplantation of pancreatic islets into the livers of diabetic rats, local hyperinsulinism in combination with hyperglycemia leads to a prolonged proliferation of cholangiocytes that can progress into cystic cholangiomas within months. The important prerequisite was systemic diabetes, i.e., systemic hyperglycemia, which was not fully compensated by the low number of transplanted islets; thus, stimulating the β-cells in the grafts to maximally synthesize and secrete insulin. As a result, only liver acini located downstream of the islets were under the influence of combined hyperglycemia and hyperinsulinism, whereas, the remaining liver tissue (and the other organs) suffered from hypoinsulism. This particular metabolic situation leads to distinct alterations in the downstream hepatocytes that proved to be of preneoplastic character and developed within 6–24 months into hepatocellular adenomas and carcinomas in streptozotocin-diabetic [11–13, 20–22] and in autoimmune-diabetic rats [16], but not in non-parenchymal liver cells [19]. The hepatocellular alterations can be explained as initially adaptive changes to the local hyperinsulinism, including increased signaling via insulin-related intracellular signaling pathways, such as the activation of the Ras–Raf-MAPKinase pathway [21], which exert strong proliferative effects. It is obvious that cholangiocytes directly adjacent to the islet grafts had to be under the same metabolic condition as the hepatocytes but before this study, it was not known whether this exerted a relevant effect on cholangiocellular growth.

Interestingly, high-number islet transplantation in BB/Pfd rats (BB2) also led to a slight increase in the formation of small islet graft-induced cholangiocellular tumors in the left liver part, but large tumors did not develop. It can be assumed that in these normoglycemic animals, the meta-

bolic situation (comparably lower insulin, normal glucose) downstream of the islet grafts is not such a strong proliferative stimulus for the bile duct epithelia as is the combination of high insulin and high glucose levels after low-number transplantation. We encountered a similar situation regarding the hepatocytes, in which high-number transplantation alone did not suffice to induce tumors, but was a strong co-carcinogenic factor in chemical hepatocarcinogenesis [15].

The close topographical relationship between islets and tumors of any size and the absence of a similar tumor development in the transplant-free left liver part clearly indicates that high insulin levels after islet transplantation are the major cause for cholangiocellular tumorigenesis. This is confirmed by the immunohistochemical results, showing the same translocation of the insulin receptor and overexpression of insulin-related intracellular signaling proteins of the Ras–Raf–MAPKinase pathway as a result of increased insulin action and as it has previously been shown in preneoplastic hepatocellular foci [21]. Nevertheless, it is known that several rat strains have a certain susceptibility to spontaneously developing (usually small) cholangiocellular tumors, and streptozotocin treatment may also be of influence. Thus, we performed several control experiments to evaluate 1) the rate of spontaneous cholangioma development in normoglycemic and diabetic animals, 2) the influence of the rat strain, 3) an implication of the transplantation procedure/embolization per se and 4) most importantly, the influence of the modus of diabetes induction, i.e., streptozotocin treatment.

The absence of increased tumor formation after transplantation of polysterene particles in L3 excluded the embolization of the portal venule and ischemia as relevant factors, and strain differences have shown to have only a minor, if any, effect (L1 vs BB4, L2 vs BB5, and L4 vs BB7, respectively). Untreated (hypoinsulinemic) diabetes had also no significant influence (BB3 vs BB7).

As streptozotocin is a genotoxic compound of carcinogenic potential in rats [9, 39], it has to be excluded as a relevant contributor to tumor formation in this model. In the late 1970s, some research groups investigated a similar experimental setting of combined streptozotocin treatment or pancreatectomy and islet transplantation [24, 25, 34], but these studies lacked important control groups and investigated only very few animals (n=10–25). Thus, there was controversy about the question of whether the cholangiocellular tumors were a result of streptozotocin action as proposed by Feldman et al. [24] and Lorenz et al. [34], or of the islet transplantation as initially favored by Finch et al. [25] which could not be clarified. The present study shows that there is indeed a minor stimulatory influence of streptozotocin on cholangioma formation, as streptozotocin-administered but otherwise untreated rats (BB6) developed significantly more, albeit, only small cholangiocellular lesions than the corresponding completely untreated control animals (BB7) after 12–18 months. However, the very similar rate of cholangioma formation in BB/Pfd animals that became diabetic either spontaneously (BB1) or by streptozotocin administration (BB4) highlights hyperinsulinism after islet transplantation to be of much more importance than the minor streptozotocin effect.

The occasional intra-insular proliferation of small ductules in early stages as depicted in Fig. 1 and the high proliferative activity of islet cells which has previously been shown to potentially lead to islet hyperplasia and insulinomas in this model [14], raise the possibility that, at least, some of the cystic tumors may have originated from transplanted graft cells, i.e., periductular or intra-insular stem-like cells with a high capacity for differentiation even into liver cells. Such sort of ductular proliferation has been observed in several experimental settings [6, 29, 30, 33, 41, 43, 44], but this was excluded by in situ hybridization.

It is interesting that we neither noticed the development of cholangiocarcinomas, as they were induced by a variety of chemical carcinogens [3, 5, 8, 35, 54], nor the malignant transformation of primarily benign cystic tumors, as occasionally reported for human biliary cystadenocarcinoma [31, 57]. Bannasch and coworkers have shown that the administration of the nitrosamine *N*-nitrosomorpholine (NNM) leads to toxic necrosis of the liver parenchyma, followed by (reparative) oval cell proliferation and neoductular proliferation, which developed into mucous cholangiofibrosis [2, 3, 5]. Cholangiomas, morphologically identical to ours, originated from these cholangiofibrotic foci and represented a final benign end-stage of tumor development. Thus, our study is in line with Bannasch's results regarding the benign character of the lesions, but tumor development in our model did not involve oval cell proliferation or the formation of preneoplastic foci of mucous cholangiofibrosis. The existence of this way of tumor development has already been suggested by Bannasch [5] and is now convincingly demonstrated for the first time. Oval cell proliferation in the regenerating liver only takes place when the regenerating capacity of the primary cell population (hepatocytes, cholangiocytes, or both) is blocked or severe injury has occurred, whereas, differentiated cholangiocytes and hepatocytes otherwise undergo self-renewal [23, 52]. As no severe cell injury affected the liver cells in our model, it is plausible that cholangiocellular proliferation is the result of insulin-induced direct proliferation of differentiated bile duct epithelia but required oval cell proliferation in the *N*-nitrosomorpholine model. However, we noticed the development of cholangiocarcinomas originating from benign cholangiomas in a model of co-carcinogenesis, combining the tumorigenic effects of NNM-administration and islet transplantation (unpublished observations). This indicates that islet hormones in the present experimental context need a co-carcinogenic factor to induce malignant cholangiocellular tumors, something that we will investigate in detail in a future study.

Conclusively, we have shown that low-number islet transplantation into streptozotocin- and autoimmune-diabetic rats leads to the development of large cystic cholangiomas, most likely as a result of combined hyperglycemia and increased local insulin action on cholangiocytes of portal bile ducts. This study also

excluded streptozotocin as a relevant co-carcinogenic factor. Although our results were basic research investigating the effect of transplanted pancreatic islets on the cholangiocytes in an animal model, they may also be of interest for clinical islet transplantation. At present, similar findings have not been reported in large animal studies [1] or in human patients, including one study with a long-term follow-up after autologous islet transplantation [55]. Thus, it is possible that cholangioma formation as a consequence of low-number islet transplantation may be exclusive to the rat model. However, in particular, human studies naturally lack a detailed histopathologic examination of the recipient liver tissue, and most patients did not stay in a long-lasting mild diabetic state, which proved to be a prerequisite for tumor development but are either normoglycemic (insulin-independent) or became diabetic again and received exogenous insulin treatment, owing to graft rejection. The question if insulin has any similar substantial effect on the cholangiocytes in humans can, thus, only reliably be answered in a long-term follow-up including detailed histologic investigation of the livers (autopsy cases), in particular, in patients that did not reach normoglycemia by this procedure, and thus, would be prone to high local intrahepatic insulin levels downstream of the remaining islets.

Acknowledgements The authors wish to thank Gabriele Becker, Jörg Bedorf, Danuta Chrobok, Mariana Dombrowski, Mathilde Hau-Liersch, Kirsten Herrmanns, and Uta Schönborn for technical assistance, Yvonne Fischer and Kurt Rüdel for animal care, Thomas Jonczyk-Weber for photographic work, and Bernd Wüsthoff for editing the manuscript. We are indebted to Dr. Chantal Mathieu, University of Leuven, Belgium, for providing us with breeding pairs of the BB/Pfd rats.This work was supported by the Deutsche Forschungsgemeinschaft (grant numbers Do 622/1-3,1-4, and 1-5).

References

1. Alejandro R, Cutfield RG, Shienvold FL, Polonsky KS, Noel J, Olson L, Dillberger J, Miller J, Mintz DH (1986) Natural history of intrahepatic canine islet cell autografts. J Clin Invest 78:1339–1348
2. Bannasch P, Reiss W (1971) Histogenesis and cytogenesis of cholangiocellular tumors in nitrosomorpholine-intoxicated rats. A contribution to the morphogenesis of polycystic disease of the liver. Z Krebsforsch Klin Onkol Cancer Res Clin Oncol 76:193–215
3. Bannasch P, Massner B (1976) Histogenesis and cytogenesis of cholangiofibromas and cholangiocarcinomas in nitrosomorpholine-intoxicated rats. Z Krebsforsch Klin Onkol Cancer Res Clin Oncol 87:239–255
4. Bannasch P (1996) Pathogenesis of hepatocellular carcinoma: sequential cellular, molecular, and metabolic changes. Prog Liver Dis 14:161–197
5. Bannasch P, Schröder CH (2002) Tumours and tumour-like lesions of the liver and biliary tract: pathogenesis of primary liver tumours. In: MacSween RNM, Burt AD, Portmann BC, Ishak KG, Scheuer PJ, Anthony PP (eds) Pathology of the liver, 4th edn. Churchill Livingstone, London, pp 777–825
6. Bernard C, Berthault MF, Saulnier C, Ktorza A (1999) Neogenesis vs. apoptosis as main components of pancreatic β cell mass changes in glucose-infused normal and mildly diabetic adult rats. FASEB J 13:1195–1205
7. Bhargava R, Senior PA, Ackerman TE, Ryan EA, Paty BW, Lakey JRT Shapiro AM (2004) Prevalence of hepatic steatosis after islet transplantation and its relation to graft function. Diabetes 53:1311–1317
8. Bisgaard HC, Nagy P, Santoni-Rugiu E, Thorgeirsson SS (1996) Proliferation, apoptosis, and induction of hepatic transcription factors are characteristics of the early response of biliary epithelial (oval) cells to chemical carcinogens. Hepatology 23:62–70
9. Blasiak J, Sikora A, Wozniak K, Drzewoski J (2004) Genotoxicity of streptozotocin in normal and cancer cells and its modulation by free radical scavengers. Cell Biol Toxicol 20:83–96
10. de Groen PC, Vroman B, Laakso K, LaRusso NF (1998) Characterization and growth regulation of a rat intrahepatic bile duct epithelial cell line under hormonally defined, serum-free conditions. In Vitro Cell Dev Biol Anim 34:704–710
11. Dombrowski F, Lehringer-Polzin M, Pfeifer U (1994) Hyperproliferative liver acini after intraportal islet transplantation in streptozotocin-induced diabetic rats. Lab Invest 71:688–699
12. Dombrowski F, Filsinger E, Bannasch P, Pfeifer U (1996) Altered liver acini induced in diabetic rats by portal vein islet isografts resemble preneoplastic hepatic foci in their enzymic pattern. Am J Pathol 148:1249–1256
13. Dombrowski F, Bannasch P, Pfeifer U (1997) Hepatocellular neoplasms induced by low-number pancreatic islet transplants in streptozotocin diabetic rats. Am J Pathol 150:1071–1087
14. Dombrowski F, Klingmüller D, Pfeifer U (1998) Insulinomas derived from hyperplastic intra-hepatic islet transplants. Am J Pathol 152:1025–1038
15. Dombrowski F, Jost CM, Manekeller S, Evert M (2005) Co-carcinogenic effects of islet hormones and *N*-nitrosomorpholine in hepatocarcinogenesis after intra-hepatic transplantation of pancreatic islets in streptozotocin-diabetic rats. Cancer Res 65:7013–7022
16. Dombrowski F, Mathieu C, Evert M (2006) Hepatocellular neoplasms induced by low-number pancreatic islet transplants in autoimmune diabetic BB/Pfd rats. Cancer Res 66:1833–1843
17. Eckhard M, Lommel D, Hackstein N, Winter D, Ziegler A, Rau W, Choschzick M, Bretzel RG, Brendel MD (2004) Disseminated periportal fatty degeneration after allogeneic intraportal islet tranplantation in a patient with type 1 diabetes mellitus: A case report. Transplant Proc 6:1111–1116
18. Essers J, de Stoppelaar JM, Hoebee B (1995) A new rat repetitive DNA family shows preferential localization on chromosome 3, 12 and Y after fluorescence in situ hybridization and contains a subfamily which is Y chromosome specific. Cytogenet Cell Genet 69:246–252
19. Evert M, Dombrowski F, Schirmacher P, Pfeifer U (1998) Nonparenchymal cells in chronically hyperinsulinemic liver acini of diabetic rats, with special regard to hepatic stellate cells. J Hepatol 18:709–716
20. Evert M, Schneider-Stock R, Dombrowski F (2003) Apolipoprotein A-IV mRNA overexpression in early preneoplastic hepatic foci induced by low-number pancreatic islet transplants in streptozotocin-diabetic rats. Pathol Res Pract 199:373–379
21. Evert M, Sun JP, Pichler S, Slavova N, Schneider-Stock R, Dombrowski F (2004) Insulin receptor, insulin receptor substrate-1, Raf-1, and Mek-1 during hormonal hepatocarcinogenesis by intrahepatic pancreatic islet transplantation in diabetic rats. Cancer Res 64:8093–8100
22. Evert M, Schneider-Stock R, Dombrowski F (2005) Overexpression of fatty acid synthase in chemically and hormonally induced hepatocarcinogenesis of the rat. Lab Invest 85:99–108
23. Fausto N, Campbell JS (2003) The role of hepatocytes and oval cells in liver regeneration and repopulation. Mech Dev 120:117–130
24. Feldman S, Scharp D, Hirshberg G, Dodi G, Ballinger W, Lacy P (1977) Streptozotocin-induced liver tumors. Transplantation 24:152–154

25. Finch DR, Morris PJ, Vanhegan RI (1977) Cystic changes in the liver following experimental intraportal pancreatic islet transplantation. Transplantation 23:182–185
26. Gigliozzi A, Alpini G, Baroni GS, Marucci L, Metalli VD, Glaser SS, Francis H, Mancino MG, Ueno Y, Barbaro B, Benedetti A, Attili AF, Alvaro D (2004) Nerve growth factor modulates the proliferative capacity of the intrahepatic biliary epithelium in experimental cholestasis. Gastroenterology 127:1198–1209
27. Griffith RC, Scharp DW, Hartman BK, Ballinger WF, Lacy PE (1977) A morphologic study of intrahepatic portal-vein islet isografts. Diabetes 26:201–214
28. Joplin R, Hishida T, Tsubouchi H, Daikuhara Y, Ayres R, Neuberger JM, Strain AJ (1992) Human intrahepatic biliary epithelial cells proliferate in vitro in response to human hepatocyte growth factor. J Clin Invest 90:1284–1289
29. Kerr-Conte J, Pattou F, Lecomte-Houcke M, Xia Y, Boilly B, Proye C, Lefebvre J. Ductal cyst formation in collagen-embedded adult human islet preparations. A means to the reproduction of nesidioblastosis in vitro. Diabetes 45:1108–1114
30. Krakowski ML, Kritzik MR, Jones EM, Krahl T, Lee J, Arnush M, Gu D, Sarvetnick N (1999) Pancreatic expression of keratinocyte growth factor leads to differentiation of islet hepatocytes and proliferation of duct cells. Am J Pathol 154:683–691
31. Kubota E, Katsumi K, Iida M, Kishimoto A, Ban Y, Nakata K, Takahashi N, Kobayashi K, Andoh K, Takamatsu S, Joh T (2003) Biliary cystadenocarcinoma followed up as benign cystadenoma for 10 years. J Gastroenterol 38:278–282
32. Kuttler B, Mathieu C, Waer M, Hahn HJ, Bouillon R (1994) Lack of disease recurrence in diabetic BB/Pfd rats after syngeneic islet transplantation. Autoimmunity 15:107–112
33. Lardon J, De Breuck S, Rooman I, Van Lommel L, Kruhoffer M, Orntoft T, Schuit F, Bouwnens L (2004) Plasticity in the adult rat pancreas: transdifferentiation of exocrine to hepatocyte-like cells in primary culture. Hepatology 39:1499–1507
34. Lorenz D, Lippert H, Dorn A, Hahn HJ (1979) Absence of liver cysts after intraportal islet transplantation in pancreatectomized rats. Transplantation 27:71–73
35. Maronpot RR, Giles HD, Dykes DJ, Irwin RD (1991) Furan-induced hepatic cholangiocarcinomas in Fischer 344 rats. Toxicol Pathol 19:561–570
36. Mathieu C, Kuttler B, Waer M, Bouillon R, Hahn HJ (1994) Spontaneous reestablishment of self-tolerance in BB/Pfd rats. Transplantation 58:349–354
37. Mordes JP, Desemone J, Rossini AA (1987) The BB rat. Diabetes Metab 3:725–750
38. Nagy P, Bisgaard HC, Santoni-Rugiu E, Thorgeirsson SS (1996) In vivo infusion of growth factors enhances the mitogenic response of rat hepatic ductal (oval) cells after administration of 2-acetylaminofluorene. Hepatology 23:71–79
39. Okawa H, Doi K (1983) Neoplastic lesions in streptozotocin-treated rats. Jikken Dobutsu 32:77–84
40. O'Leary MT, Blakemore WF (1997) Use of a rat Y chromosome probe to determine the long-term survival of glial cells transplanted into areas of CNS demyelination. J Neurocytol 26:191–206
41. Pour PM, Weide L, Liu G, Kazakoff K, Scheetz M, Toshkov I (1997) Experimental evidence for the origin of ductal-type adenocarcinoma from the islets of Langerhans. Am J Pathol 150:2167–2180
42. Radaeva S, Ferreira-Gonzalez A, Sirica AE (1999) Overexpression of C-NEU and C-MET during rat liver cholangiocarcinogenesis: a link between biliary intestinal metaplasia and mucin-producing cholangiocarcinoma. Hepatology 29: 1453–1462
43. Rao MS, Dwivedi RS, Subbarao V, Usman MI, Scarpelli DG, Nemali MR (1988) Almost total conversion of pancreas to liver in the adult rat: a reliable model to study transdifferentiation. Biochem Biophys Res Commun 156:131–136
44. Rao MS, Dwivedi RS, Yeldandi AV, Subbarao V, Tan XD, Usman MI, Thangada S, Nemali MR, Kumar S, Scarpelli DG (1989) Role of periductal and ductular epithelial cells of the adult rat pancreas in pancreatic hepatocyte lineage. A change in the differentiation commitment. Am J Pathol 134:1069–1086
45. Richardson KC, Jarrett L, Finke EH (1960) Embedding in epoxy resins for ultrathin sectioning in electron microscopy. Stain Technol 35:313–325
46. Ricordi C, Strom TB (2004) Clinical islet transplantation: advances and immunological challenges. Nat Rev Immunol 4:259–268
47. Rother KI, Harlan DM (2004) Challenges facing islet transplantation for the treatment of type 1 diabetes mellitus. J Clin Invest 114:877–883
48. Ryan EA, Lakey JRT, Paty BW, Imes S, Korbutt GS, Kneteman NM, Bigam D, Rajotte RV, Shapiro AM (2002) Successful islet transplantation. Continued insulin reserve provides long-term glycemic control. Diabetes 51:2148–2157
49. Ryan EA, Lakey JRT, Rajotte RV, Korbutt GS, Kin T, Imes S, Rabinovitch A, Elliot JF, Bigam D, Kneteman NM, Warnock GL, Larsen I, Shapiro AM (2001) Clinical outcomes and insulin secretion after islet transplantation with the Edmonton protocol. Diabetes 50:710–719
50. Scharf JG, Ramadori G, Dombrowski F (2002) Analysis of the IGF axis in preneoplastic hepatic foci and hepatocellular neoplasms developing after low-number pancreatic islet transplantation into the livers of streptozotocin diabetic rats. Lab Invest 80:1399–1411
51. Shapiro AMJ, Lakey JR, Ryan EA, Korbutt GS, Toth E, Warnock GL, Kneteman NM, Rajotte RV (2000) Islet transplantation in seven patients with type 1 diabetes mellitus using a glucocorticoid-free immunosuppressive regimen. N Engl J Med 343:230–238
52. Shiojiri N, Lemire JM, Fausto N (2003) Cell lineages and oval cell progenitors in rat liver development. Cancer Res 51:2611–2620
53. Sohn J, Siegelman ES, Osiason AW (2001) Unusual patterns of hepatic steatosis caused by the local effect of insulin revealed on chemical shift MR imaging. Am J Roentgenol 176:471–474
54. Steinberg P, Hacker HJ, Dienes HP, Oesch F, Bannasch P (1991) Enzyme histochemical and immunohistochemical characterization of oval and parenchymal cells proliferating in livers of rats fed a choline-deficient/DL-ethionine-supplemented diet. Carcinogenesis 12:225–231
55. Wahoff DC, Papalois BE, Najarian JS, Kendall DM, Farney AC, Leone JP, Jessurun J, Dunn DL, Robertson RP, Sutherland DE (1995) Autologous islet transplantation to prevent diabetes after pancreatic resection. Ann Surg 222:562–575
56. Werneburg NW, Yoon JH, Higuchi H, Gores GJ (2003) Bile acids activate EGF receptor via a TGF-alpha-dependent mechanism in human cholangiocyte cell lines. Am J Physiol Gastrointest Liver Physiol 285:G31–G36
57. Woods GL (1991) Biliary cystadenocarcinoma. Case report of hepatic malignancy originating in benign cystadenoma. Cancer 47:2936–2940

Virchows Arch (2006) 448: 788–796
DOI 10.1007/s00428-006-0191-8

ORIGINAL ARTICLE

Heike Immervoll · Dag Hoem · Kalaiarasy Kugarajh · Solrun J. Steine · Anders Molven

Molecular analysis of the EGFR-RAS-RAF pathway in pancreatic ductal adenocarcinomas: lack of mutations in the *BRAF* and *EGFR* genes

Received: 24 August 2005 / Accepted: 28 November 2005 / Published online: 6 April 2006

Abstract The vast majority of tumors of the pancreas are ductal adenocarcinomas. This cancer type has an extremely poor prognosis and in many Western countries, it represents the fifth leading cause of cancer-related death. Pancreatic ductal adenocarcinomas exhibit the highest incidence of activating *KRAS* (Ki-Ras) mutations observed in any human cancer. It was therefore of interest to examine how this pattern would relate to mutations in the *BRAF* and *EGFR* genes, which are involved in the same signaling pathway as *KRAS*. We screened a series of 43 formalin-fixed, paraffin-embedded ductal adenocarcinomas of the pancreas. When DNA was extracted from whole tissue sections, *KRAS* codon 12 mutations were detected in 67% of the tumors. When cancerous ducts were isolated by laser-assisted microdissection, 91% were positive for *KRAS* mutations. Although it did not reach statistical significance, there was a trend in our material that survival after diagnosis varied according to *KRAS* mutation subtype, GTT-positive patients having the best prognosis. No alterations in *BRAF* exons 11 and 15 or in *EGFR* exons 18–21 were detected in *KRAS*-positive or *KRAS*-negative cases. We therefore conclude that the *BRAF* and *EGFR* mutations commonly seen in a variety of human cancers are generally absent from pancreatic ductal adenocarcinomas. Apparently, these tumors depend on no more than one genetic hit in the EGFR-RAS-RAF signaling pathway.

H. Immervoll · K. Kugarajh · S. J. Steine · A. Molven (✉)
Section for Pathology, The Gade Institute,
University of Bergen, Haukeland University Hospital,
Bergen N-5021, Norway
e-mail: anders.molven@gades.uib.no
Tel.: +47-55973169
Fax: +47-55973158

H. Immervoll · A. Molven
Department of Pathology, Haukeland University Hospital,
Bergen, Norway

D. Hoem
Department of Surgery, Haukeland University Hospital,
Bergen, Norway

Keywords Pancreatic cancer · Mutation analysis · *KRAS* · *BRAF* · *EGFR*

Introduction

Cancer of the exocrine pancreas is a highly aggressive tumor, which in Western countries—including Norway—represents the fifth leading cause of cancer death [8, 19]. The overall five-year survival rate is less than 5%. Even for the small group of resectable patients, the five-year survival rate remains low, around 20% [37, 46]. Most pancreatic tumors are ductal adenocarcinomas with a mortality rate almost equal to the incidence rate [9], reflecting the very dismal prognosis of the disease.

Some knowledge has been obtained about the etiological factors behind pancreatic cancer [23]. There is an uneven world distribution with five to seven times higher incidence rates in high-risk countries, implying that environmental factors (reaching an old age, smoking, and diet) and ethnicity play a role [26]. An inherited component is estimated to be responsible for up to 10% of the cases. At least seven different germline disorders are known to be associated with increased risk for cancer of the exocrine pancreas [28] and, in addition, familial pancreatic cancer is now recognized as an own entity [5].

As other cancers, pancreatic ductal adenocarcinomas (PDAC) accumulate genetic changes in oncogenes and tumor suppressor genes. Characteristic for these tumors is the activation of the *KRAS* (Ki-Ras) oncogene, a process that occurs by point mutations in codon 12. In fact, 70–100% of the ductal adenocarcinomas exhibit *KRAS*-mutations—the highest frequency of *RAS* alterations known in human neoplasms [16, 38, 44]. Among the tumor suppressor genes, *CDKN2A* (p16) is inactivated in around 95% of the PDACs [41]. High frequencies of inactivation are also observed for *TP53* (p53) and *SMAD4* (DPC4), which are affected in 40–75% and 50–55% of the cases, respectively (see [23]). The genetic changes are thought to follow a specific temporal order where a *KRAS* mutation arises early in pancreatic carcinogenesis. *KRAS*

activation is then succeeded by *CDKN2A* inactivation and subsequently by the loss of the activity of other tumor suppressor genes [15].

The RAS proteins are part of the mitogen-activated protein (MAP)-kinase pathway where the MAP-kinase ERK is activated via receptor tyrosine kinases, RAS, RAF, and MEK proteins. This signaling cascade mediates growth signals from the cell surface to the nucleus and results in complex changes in cell behavior, especially concerning growth and proliferation. Large screening projects have revealed that pathway members other than the *RAS* genes are also the subjects of frequent point mutations in human tumors. Davies et al. [11] reported cancer-related mutations in the *BRAF* gene in a majority of malignant melanomas (both primary tumors and cell lines) and lower but significant frequencies in other human cancers. More recently, Lynch et al. [29] and Paez et al. [34] demonstrated the presence of mutations in the epithelial growth factor receptor (*EGFR*) gene in a subset of sporadic, nonsmall-cell lung cancers.

Table 1 Clinicopathological characteristics and *KRAS* mutation status of 43 patients with pancreatic ductal adenocarcinoma

Case number	Age at diagnosis	Sex	Tumor size[a]	*T*	*N*	*M*	*R*[b]	Histologic grade	Survival[c]	*KRAS* mutation[d]
1	79	M	2.5	3	0	0	0	3	63	GAT
2	78	M	4	3	1	0	1	2/3	10	GAT
3	77	F	4	3	1	0	1	3	4	CGT
4	53	M	3	3	0	1	1	2	4	GAT
5	81	F	5.5	3	1	0	1	2/3	4	GTT
6	77	F	4.5	3	0	0	1	3	2	GAT
8	55	F	3.5	3	0	0	0	3	55	GAT
9	62	M	6	3	1	0	1	3	10	GCT
10	72	F	3	3	1	0	0	3	22	GTT
11	70	M	5	3	1	0	0	3	3	GTT
12	67	F	na	3	1	0	1	3	46	GAT
13	44	M	10	3	1	0	1	3	0	GAT
14	74	F	3.5	3	1	0	1	2	4	GAT
15	79	M	5	3	1	0	0	2	15	GAT
17	42	M	2.5	3	1	0	1	3	35	GAT
19	52	F	4	3	1	0	1	2	9	GAT
20	58	F	3	3	1	0	0	2/3	36	GTT
21	82	F	3	3	1	0	0	3	25	GTT
22	69	M	4	3	1	0	0	3	26	GAT
23	35	F	3	3	1	0	0	3	7	GAT
24[e]	77	M	3.5	na	1	0	nr	2	7	GAT
25[e]	76	M	4	3	na	0	nr	2	8	CGT
27	41	M	3	3	1	0	1	2	29	GAT/GTT
30[e]	45	F	6	3	1	0	nr	2	7	GAT
31[e]	80	M	6	4	na	0	nr	2	6	GAT/GTT
32[e]	53	M	4	3	na	0	nr	2	10	GAT
33	76	M	2	3	1	0	1	2/3	29	GTT
34	64	M	7	4	1	0	1	3	3	GTT
35	77	F	5	3	0	0	0	2	7	GAT
36	74	M	3	3	1	1	1	3	2	CGT
37	72	M	4	4	1	0	1	3	3	NM
38	79	F	1.5	1	0	0	0	3	15	GAT
39	54	M	6	3	1	0	0	3	7	CGT
40	77	F	6	2	0	0	0	2	28	GTT
41	58	F	3	3	1	0	0	2	37	CGT
42	45	M	2	3	0	0	0	2	71	GTT
44	75	F	3	3	0	0	0	2	27	CGT
45	76	F	2.5	3	1	0	1	3	8	NM
46	75	M	3	3	0	0	0	2	25	GAT
47	69	M	5	3	0	0	0	3	1	GAT
48	60	M	2	3	1	0	0	2	11	NM
50	72	M	6.5	3	1	0	1	3	8	NM
51	62	M	na	3	0	0	0	2	18	GTT

[a]Largest dimension in cm (*na* not available)
[b]Resection margin (*0* free, *1* not free, and *nr* no resection performed)
[c]Months after surgery
[d]Listed as the changed codon 12. The wild-type codon is GGT (*NM* no mutation detected)
[e]Needle biopsy obtained from unresectable tumor

The BRAF protein is a target of RAS. Moreover, overexpression of the receptor tyrosine kinase EGFR is generally observed in epithelial tumors including pancreatic ductal adenocarcinomas [21]. Thus, disturbances of the EGFR-RAS-RAF signaling system could be essential for the establishment and maintenance of pancreatic cancer cells. We therefore sought to undertake a careful mutational analysis of *KRAS*, *BRAF*, and *EGFR* in these tumors, using laser microdissection to isolate the cancerous ducts from the surrounding, nonneoplastic fibrous tissue. The *KRAS* mutation detection rate increased significantly in microdissected specimens compared to whole sections. However, *BRAF* or *EGFR* mutations were not observed, neither in the *KRAS*-positive nor in the *KRAS*-negative cases. We suggest that in this part of the MAP-kinase pathway, only one genetic hit is necessary for the development of the malignant phenotype of the highly aggressive PDAC tumors.

Materials and methods

Tissue specimens

Tissue blocks from 51 cases with adenocarcinomas of the pancreas, resected in the period 1996–2003, were obtained from the archives of the Department of Pathology, The Gade Institute, Haukeland University Hospital. All specimens were fixed in 10% buffered formalin and embedded in paraffin. The cases were revised by a pathologist (H. I.) to identify those tumors that were pancreatic ductal adenocarcinomas. The final diagnosis was based on an evaluation of hematoxylin–eosin (HE) and immunohistochemically stained sections and the patients' clinical records, including computerized tomography reports. Histological classification and staging were done according to the tumor, nodes, and metastasis stage classification system [2, 17]. The 43 cases of PDAC are listed in Table 1. Five specimens (#24, 25, 30, 31, and 32) represent intraoperative needle biopsies from unresectable patients, one specimen (#39) was a total pancreatectomy and the rest were surgical specimens from pancreas resections (classical Whipple procedure and modifications). The study was approved by the Regional Ethics Committee and performed according to the Helsinki declaration.

DNA extraction from whole sections

One representative, formalin-fixed and paraffin-embedded tissue block was selected from each case. Depending on the size of the tumor tissue, one or two 10-μm sections were cut. The sections were placed in 190 μl buffer G2 and 10 μl proteinase K solution of the MagAttract DNA mini M48 Kit (Qiagen GmbH, Hilden, Germany) and dissolved by shaking overnight at 56°C. DNA was then purified by using this kit in combination with a GenoM48 BioRobot system (Qiagen) in accordance with the manufacturer's instructions.

Laser microdissection and DNA extraction

Polyethylene naphthalate membrane-covered glass slides (P.A.L.M. Microlaser Technologies AG, Bernried, Germany) were treated for 30 min with 254 nm UV light. Tissue sections (7 μm) were placed on the slides and incubated at 70°C for 30 min. Deparaffination and HE staining were performed according to routine procedures but without xylene at the end of the dehydration process. The stained slides were dried at 60°C for at least 1 h. Cancerous ducts were then microdissected using a Zeiss Axiovert 200 inverted microscope equipped with a microlaser system (P.A.L.M. Microlaser Technologies). To achieve better morphology of the uncovered tissue sections, a 70% alcohol solution was dripped on the slides. Parallel, routinely processed HE-stained sections were used as guide for the selection of cancerous ducts.

Two separate samples with a total area of 150,000 to 300,000 μm^2 were microdissected from each section, catapulted, and captured in 15–30 μl digestion buffer (10 mM Tris–HCl, pH 8.3; 1 mM EDTA; 1% Tween 20) that had been placed in the lid of an Eppendorf tube. After spinning the material down into the tube, proteinase K was added to a final concentration of 0.5 μg/μl. The samples were then incubated for 16 h at 55°C, followed by proteinase K inactivation at 99°C for 10 min. One

Table 2 Primer sequences for the amplification of the *KRAS*, *BRAF*, and *EGFR* exons

Gene and exon	Forward primer	Reverse primer	Size of PCR product (bp)	Annealing temperature (°C)
KRAS exon 2	5′-AACCTTATGTGTGACATGTTCTAAT	5′-AATGGTCCTGCACCAGTAAT	221	55
BRAF exon 11	5′-TCCCTCTCAGGCATAAGGTAA	5′-CGAACAGTGAATATTTCCTTTGAT	313	59
BRAF exon 15	5′-TCATAATGCTTGCTCTGATAGGA	5′-GGCCAAAAATTTAATCAGTGGA	224	58
EGFR exon 18	5′-TTTCCAGCATGGTGAGGGCT	5′-TTGCAAGGACTCTGGGCTCC	258	55
Nested exon 18	5′-GGCTGAGGTGACCCTTGTC	5′-CTGCGGCCCAGCCCAGAG	202	58
EGFR exon 19	5′-AGCATGTGGCACCATCTCAC	5′-GAGAAAAGGTGGGCCTGAGG	218	58
EGFR exon 20	5′-ATGCGAAGCCACACTGACGT	5′-TGGCTCCTTATCTCCCCTCC	267	58
EGFR exon 21	5′-TCGGATGCAGAGCTTCTTCC	5′-AAGGCAGCCTGGTCCCTGG	277	55
Nested exon 21	5′-ATCTGTCCCTCACAGCAGG	5′-TCAGGAAAATGCTGGCTGA	229	58

microliter of this extract was used as template in the subsequent polymerase chain reactions (PCR).

PCR and DNA sequencing

KRAS (exon 1), *BRAF* (exons 11 and 15), and *EGFR* (exons 18–21) were PCR-amplified and screened for mutations by direct sequencing. Primer sequences are given in Table 2. For *EGFR* exons 18 and 21, a visible PCR product was often difficult to obtain after the initial amplification and nested PCR reactions were then performed with internal primer sets. In general, PCR reactions were run in a total volume of 25 μl with 0.3 μM of each primer using the AmpliTaq Gold PCR Master Mix (Applied Biosystems, Foster City, CA, USA). Samples were subjected to an initial denaturation at 95°C for 15 min, 40–45 cycles at 95°C for 50 s, annealing (see Table 2 for temperatures) for 50 s, and elongation at 72°C for 1 min, followed by a final elongation step at 72°C for 7 min. PCR products were column-purified by using the QIAquick PCR Purification Kit (Qiagen) or enzymatically treated with ExoSAP-IT (USB, Cleveland, OH, USA). The sequencing primers were identical to the PCR primers and all samples were sequenced in both directions employing the BigDye Terminator Cycle Sequencing Kit, version 1.1 (Applied Biosystems). The sequence reactions were analyzed on an ABI Prism 3100 Genetic Analyzer with Sequencing Analysis software, version 3.7 (Applied Biosystems). DNA extracted from cutaneous malignant melanomas and lung adenocarcinomas served as positive controls for *BRAF* and *EGFR* mutations, respectively.

KRAS and *BRAF* mutations were searched for in all 43 PDAC cases. *EGFR* mutations were screened in ten randomly selected *KRAS*-positive PDACs and in the four *KRAS*-negative cases. *KRAS* was examined in tumor DNA extracted from both whole tissue sections and laser-microdissected material, whereas *BRAF* and *EGFR* were sequenced only in laser-microdissected material.

Statistics

The statistical analyses were performed using the software package Statistica 4.1 (StatSoft, Tulsa, OK, USA). The Product-limit (Kaplan–Meier) Analysis Module was used for comparing the survival times between multiple groups. Survival times vs cumulative proportion surviving, according to breakdown by mutation groups, were plotted.

Results

Clinical material

Of the 51 collected adenocarcinomas from the pancreatic region, 43 cases were classified as PDACs after the reevaluation. The excluded cases were intraductal papillary mucinous neoplasms and ampullary, bile duct, and duodenal cancers. Clinicopathologic features of the 43 PDAC cases are shown in Table 1. The mean age of the patients was 66 years (range 35–82 years) and 42% were females. The tumor of case #31 had an anatomical location that involved the pancreatic body and tail, whereas cases #13, 39, and 50 involved the head and body. The remaining 39 tumors were confined to the pancreatic head. The median survival time after diagnosis was 10 months.

KRAS mutation analysis

We initially isolated DNA from whole tissue sections. *KRAS* mutation status was assessed by sequencing and 29 (67%) of the 43 cases were positive. However, PDACs are characterized by a varying and often very high ratio of desmoplastic stroma to tumor cell area. We therefore employed laser microdissection for isolating the cancerous ducts from the surrounding stromal component (Fig. 1). When *KRAS* sequencing was then repeated, 39 (91%) of the cases were positive. Figure 2a,b illustrates the improvement in sensitivity that was achieved from whole tissue sections to laser-microdissected material.

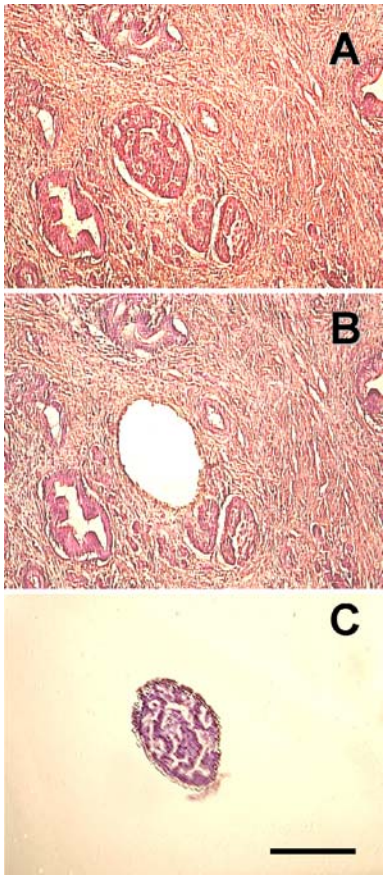

Fig. 1 Example of laser microdissection of a pancreatic ductal adenocarcinoma. A hematoxylin–eosin-stained section (7 mm) is shown before (**a**) and after (**b**) dissection. The isolated fragment with cancer cells in ductal arrangement is also shown (**c**). Scale bar: 200 μm

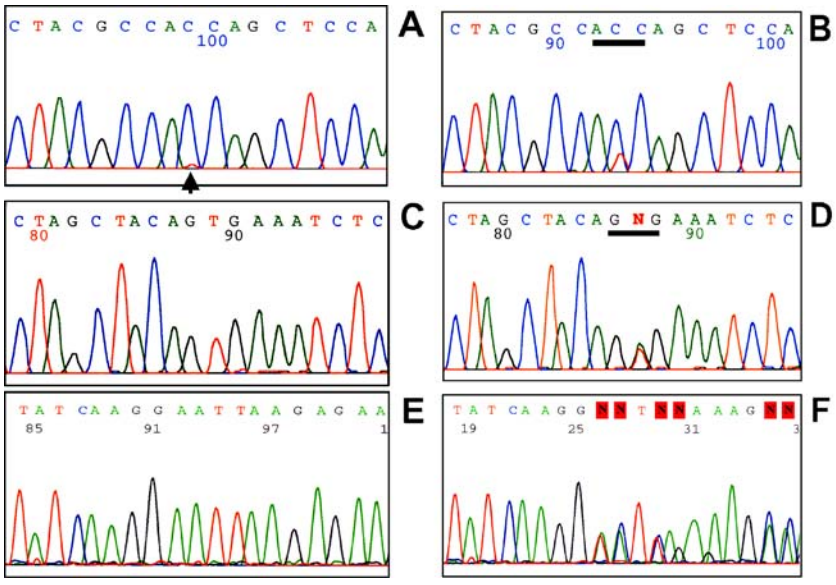

Fig. 2 Mutation analysis by direct DNA-sequencing of pancreatic ductal adenocarcinomas. **a**, **b** Part of the exon 1 sequence (*reverse direction*) of the *KRAS* gene. Codon 12 is *underlined*. For the sequence in subpanel **a**, DNA was extracted from a whole section of the pancreatic tumor. In subpanel **b**, DNA was extracted from laser-microdissected cancerous ducts of a parallel section. Note the improvement of the signal in **b** as compared to **a** (*arrowhead*). See also Fig. 1. **c**, **d** Example of sequence analysis of the *BRAF* gene. A part of exon 15 is shown (*forward direction*). All analyzed pancreatic tumors exhibited normal sequence as illustrated in subpanel **c**. Subpanel **d** shows a sample from a malignant melanoma, which contained the hot spot T1799A mutation of codon 600 (*underlined*) and served as positive control. **e**, **f** Example of sequence analysis of the *EGFR* gene. A part of exon 19 is shown (*forward direction*). All analyzed pancreatic tumors exhibited normal sequence as illustrated in subpanel **e**. Subpanel **f** shows a sample from a lung adenocarcinoma, which contained a deletion mutation in exon 19 and served as positive control

The distribution of different *KRAS* mutations in the material is shown in Fig. 3. The two most common alterations of the wild-type GGT (Gly) codon 12 was GAT (Asp) and GTT (Val), which were observed in 20 (47%) and ten (23%) of the cases, respectively. The mutations CGT (Arg) and GCT (Ala) were observed in six (14%) and one (2%) of the cases, respectively. No codon 13 mutation was detected. Two tumors contained different *KRAS* mutations in the two areas collected for laser microdissection (Table 1). In most tumors, the signal from the normal and mutated base was of comparable strength but in some cases, a complete change in the mutated base was observed, probably due to loss of the wild-type allele (data not shown).

KRAS mutations and patient survival

Data on survival after diagnosis were available for all cases. Univariate survival analyses demonstrated the expected correlation between negative lymph node status, tumor-free resection margin, and age less than 70 years with better prognosis (data not shown). We also examined whether *KRAS* mutation subtype correlated with survival. In our material, there was a trend where GTT-positive patients survived much longer (median 23.5 months) than GAT-positive patients (median 9.5 months), while the latter had a somewhat better prognosis than CGT-positive cases (median 7.5 months) (Fig. 4). The number of patients in each group is small and the differences did not reach statistical significance, but the tendency is the same as observed by Kawesha et al. [20].

BRAF and *EGFR* mutational analyses

Previously published tumor-associated mutations in these genes are restricted to exons 11 and 15 (*BRAF*) and exons 18–21 (*EGFR*) and we limited our analyses to these exons. No mutations were observed in *KRAS*-negative or *KRAS*-positive samples. DNA samples extracted from malignant

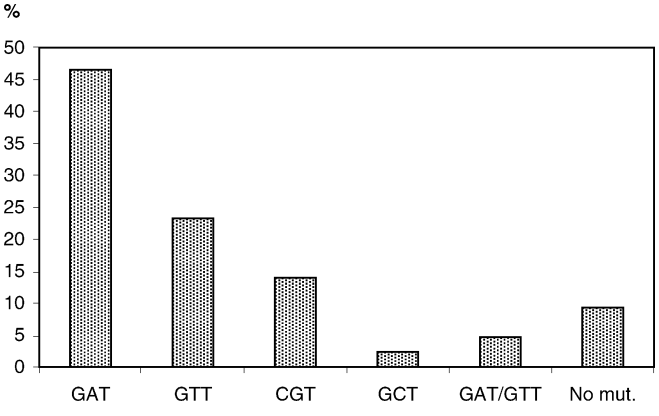

Fig. 3 Distribution of *KRAS* mutations in the material of 43 pancreatic ductal adenocarcinomas. Regions with tumor cells were isolated by laser microdissection and analyzed by direct DNA sequencing. Mutations were only seen in codon 12 (GGT) and are listed as the changed codon

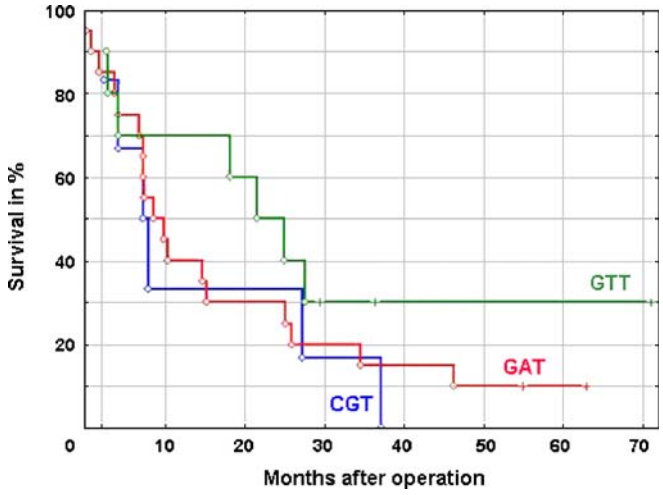

Fig. 4 Kaplan–Meier survival plot for 36 pancreatic adenocarcinomas according to breakdown by *KRAS* mutation subtype. Median survival time was 7.5, 9.5, and 23.5 months for the CGT, GAT, and GTT mutation groups, respectively. The observed survival times are indicated by *circles* (complete) or *crosses* (censored observations). The two cases with simultaneous GAT and GTT mutations were not included in the analysis

melanoma (*BRAF*) and nonsmall cell lung cancer (*EGFR*) were included as positive controls (Fig. 2c–f).

Discussion

The large-scale screening of cancer cell lines and primary tumors for somatic mutations has recently become the focus of several research efforts [47]. Enabled by the sequencing of the human genome, systematic analyses of gene families or signaling pathways have resulted in the identification of novel cancer-related mutations, often with a significant frequency in some malignancies. Examples include the discovery of *BRAF* alterations in melanomas and other cancers [11], *PIK3CA* alterations in colon and other cancers [40], and *EGFR* alterations in nonsmall cell lung cancer [29, 34]. These results are important because they extend our knowledge about the genetic changes necessary for cancers to arise, grow, and spread. Moreover, the presence of such mutations opens for molecular treatments tailor-made for the genetic damage that the tumors depend on. The latter concept is exemplified by the occurrence of *EGFR* mutations in adenocarcinomas of the lung and a positive response to gefitinib [29, 34], and by the possible effect of a RAF inhibitor against the most frequent *BRAF* mutation in malignant melanoma [48].

Pancreatic ductal adenocarcinomas are characterized by an extremely bad prognosis with a lack of treatment options for unresectable tumors. Thus, the identification of somatic mutations with a potentially therapeutic link would be an important finding even if the frequency turned out to be low in this cancer form. Ishimura et al. [18] were the first to report a screening for *BRAF* mutations in PDAC. They examined nine *KRAS*-negative and 19 *KRAS*-positive samples and found the common V599E (now denoted V600E) mutation of *BRAF* exon 15 in two cases. Both were *KRAS*-positive. Calhoun et al. [7] did not observe any *BRAF* mutations among 74 *KRAS*-positive tumors but detected the common exon 15 mutation in three out of nine *KRAS*-negative cases. The latter constituted a distinct subset of pancreatic cancer with a medullary morphology. Loukopoulos et al. [25] examined 22 cell lines and primary tumors without finding *BRAF* mutations. In the present work, we did not observe any *BRAF* mutations among 39 *KRAS*-positive and four *KRAS*-negative cases. Neither did we detect *EGFR* exon 18–21 mutations among the ten *KRAS*-positive and four *KRAS*-negative cases examined. Similarly, Lynch et al. [29] reported that *EGFR* exon 19 and 21 mutations were sought in 40 pancreatic tumors (classification not specified) without any positive findings.

Taken together, we conclude that *BRAF* and *EGFR* mutations are very infrequent in PDACs. This fits with a model where disturbances of several signaling cascades are necessary for cancer development, but where one genetic hit in each pathway is sufficient. In PDAC with its very high frequency of *KRAS* alterations, simultaneous accumulation of other mutations in the MAP-kinase pathway may not give the tumor a growth advantage and are therefore not selected for. That *RAS* and *BRAF* mutations generally are mutually exclusive is well documented by the majority of studies investigating both genes in tumors or tumor cell lines. Examples include malignant melanoma [1, 11], papillary thyroid carcinoma [13], hyperplasic polyps and serrated adenomas of the colon [10, 22], colorectal carcinomas [32, 35], small intestinal adenocarcinomas [6], Barrett's adenocarcinoma [43], and gallbladder carcinomas [39].

In colorectal cancer, *BRAF* and *KRAS* alterations associate with mismatch repair status [12, 35]. *BRAF* mutations are most frequent in mismatch-repair deficient (microsatellite instable) colorectal tumors, whereas *KRAS* mutations dominate when the mismatch-repair system is proficient. Pancreatic adenocarcinomas exhibiting DNA replication errors are rare and associated with wild-type *KRAS* and longer survival [14, 49]. They may have a ductal phenotype and may be linked to hereditary nonpolyposis colon cancer [30, 49] or their morphologic features may be consistent with medullary carcinoma [14]. Thus, the lack of *BRAF* mutations and very high frequency of *KRAS* mutations in pancreatic ductal adenocarcinomas could reflect the observation that mismatch repair deficiency seems to be of little importance in this tumor type [49]. Significantly shortened telomeres are detected in nearly all pancreatic intraepithelial neoplasias, the postulated precursor lesions for PDACs [45]. PDACs might therefore depend on the shortening of telomere length to disrupt chromosomal integrity, developing a mutator phenotype without impairment of mismatch repair.

Previous studies of *BRAF* [7, 18, 25] and *EGFR* [29] mutations in pancreatic ductal adenocarcinomas and this report all focus on those exons defined as mutational hotspots from initial, high-throughput screening efforts. Accordingly, one cannot exclude that genetic alterations outside exons 11 and 15 in *BRAF* and 18–21 in *EGFR* are

present in PDACs. Screening of the complete genes (and other genes of the MAP-kinase pathway), particularly in *KRAS*-negative tumors, might therefore be justified.

Methods employed in the screening of somatic cancer mutations include single-strand conformational polymorphism, denaturing gradient gel electrophoresis, and denaturing high-performance liquid chromatography. DNA sequencing is now commonly used for screening and serves as a gold standard for confirming and determining the identity of mutations revealed by other methods. However, the limited sensitivity of DNA sequencing is a pitfall because a mutation may remain undetected if normal or stromal cells outnumber the mutated cancer cells in a specimen [31, 33]. The sensitivity is of particular concern in PDAC where the cancerous ducts often constitute only a fraction of a tissue sample. This is illustrated by our results from the *KRAS* mutational analyses where we found 67% positive tumors when the DNA was isolated from whole sections, but 91% positive tumors after the cancerous ducts had been laser-microdissected. Only after an assurance that the analyzed material contains a significant fraction of tumor cells should direct DNA sequencing be recommended in the screening for somatic cancer mutations.

In various studies of PDAC, the number of *KRAS*-positive cases varies from 70 to 100% [4, 16, 36, 38, 44]. The lower estimates may reflect mutation detection techniques that were not sensitive enough and/or the presence of misclassified tumors in the material. In our collected archival material of 51 tumors originally classified as adenocarcinomas of the pancreas, eight cases (16%) were excluded because they had a morphology or site of origin not consistent with PDAC. Although some of the excluded cases also were *KRAS*-positive, the mutation frequency would have dropped from 91% to 82% if these cases had remained in the material (data not shown). We conclude that the true frequency of *KRAS* mutation in PDACs is at least 90%. A factor that may prevent this number from reaching 100% is that some PDACs arise because of germline mutations in tumor suppressor or DNA-repair genes and do not necessarily depend on *KRAS* activation [28, 49].

It is interesting to note that laser microdissection of two different samples from the same tumor led to the identification of different *KRAS* mutations in two cases (Table 1). *KRAS* mutations are likely to be an early event in pancreatic carcinogenesis as they are often seen in pancreatic intraepithelial neoplasia, increasing in frequency with cellular and architectural atypia [24, 27]. These mutations are also present in cancer-associated, morphologically normal duct epithelia, hyperplastic duct lesions, chronic pancreatitis, and in disease-free pancreas, especially at older ages. It is therefore not surprising that two different mutations may be detected in some cases of PDACs [44].

The distribution of *KRAS* mutation subtypes in our material of PDACs was similar to that observed in other series (see, for example, [16, 20]) with GAT (Asp) as the most commonly observed alteration of the wild type codon 12, followed by GTT (Val), and then CGT (Arg) (Fig. 3). A correlation between the presence and absence of *KRAS* mutation and survival is generally not observed [16, 20, 42]. However, the data of Kawesha et al. [20] suggested that mutation subtype could associate with survival because patients with GTT had a longer median survival than those with the GAT mutation, who again did better than those with CGT. We see the same trend in our material (Fig. 4) but these findings need verification in larger series. In this regard, we note that in advanced colorectal cancers, it is the GTT mutation that is associated with the most aggressive biological behavior and reduced survival [3].

In conclusion, *KRAS* remains the only oncogene for which somatic, activating mutations are known to be present at high frequency in PDACs. The absence of *BRAF* and *EGFR* mutations in these tumors supports a model where one mutational hit suffices to activate the MAP-kinase pathway. It is of fundamental importance to identify genetic alterations in pancreatic cancer with a therapeutic potential, but new candidates should preferentially be sought in other pathways.

Acknowledgements We thank Bendik Nordanger for expert technical assistance and Lars A. Akslen, Hanne Puntervoll, and Audny Hellebø for samples of positive control tissue. The study was supported by grants from the Meltzer Foundation, The Norwegian Cancer Society, and Helse Vest.

References

1. Akslen LA, Angelini S, Straume O, Bachmann IM, Molven A, Hemminki K, Kumar R (2005) BRAF and NRAS mutations are frequent in nodular melanoma but are not associated with tumor cell proliferation or patient survival. J Invest Dermatol 125:312–317
2. American Joint Committee on Cancer (1998) Cancer staging handbook, 5th edn. Lippincott Raven, Philadelphia
3. Andreyev HJ, Norman AR, Cunningham D, Oates J, Dix BR, Iacopetta BJ, Young J, Walsh T, Ward R, Hawkins N et al (2001) Kirsten ras mutations in patients with colorectal cancer: the 'RASCAL II' study. Br J Cancer 85:692–696
4. Banerjee SK, Makdisi WF, Weston AP, Campbell DR (1997) A two-step enriched-nested PCR technique enhances sensitivity for detection of codon 12 K-ras mutations in pancreatic adenocarcinoma. Pancreas 15:16–24
5. Bartsch DK (2003) Familial pancreatic cancer. Br J Surg 90:386–387
6. Blaker H, Helmchen B, Bonisch A, Aulmann S, Penzel R, Otto HF, Rieker RJ (2004) Mutational activation of the RAS-RAF-MAPK and the Wnt pathway in small intestinal adenocarcinomas. Scand J Gastroenterol 39:748–753
7. Calhoun ES, Jones JB, Ashfaq R, Adsay V, Baker SJ, Valentine V, Hempen PM, Hilgers W, Yeo CJ, Hruban RH et al (2003) BRAF and FBXW7 (CDC4, FBW7, AGO, SEL10) mutations in distinct subsets of pancreatic cancer: potential therapeutic targets. Am J Pathol 163:1255–1260
8. Cancer Registry of Norway (2005) Cancer in Norway 2002. Cancer Registry of Norway, Oslo
9. Carpelan-Holmstrom M, Nordling S, Pukkala E, Sankila R, Luttges J, Kloppel G, Haglund C (2005) Does anyone survive pancreatic ductal adenocarcinoma? A nationwide study re-evaluating the data of the Finnish Cancer Registry. Gut 54:385–387

10. Chan TL, Zhao W, Leung SY, Yuen ST (2003) BRAF and KRAS mutations in colorectal hyperplastic polyps and serrated adenomas. Cancer Res 63:4878–4881
11. Davies H, Bignell GR, Cox C, Stephens P, Edkins S, Clegg S, Teague J, Woffendin H, Garnett MJ, Bottomley W et al (2002) Mutations of the BRAF gene in human cancer. Nature 417:949–954
12. Domingo E, Espin E, Armengol M, Oliveira C, Pinto M, Duval A, Brennetot C, Seruca R, Hamelin R, Yamamoto H et al (2004) Activated BRAF targets proximal colon tumors with mismatch repair deficiency and MLH1 inactivation. Genes Chromosomes Cancer 39:138–142
13. Fukushima T, Suzuki S, Mashiko M, Ohtake T, Endo Y, Takebayashi Y, Sekikawa K, Hagiwara K, Takenoshita S (2003) BRAF mutations in papillary carcinomas of the thyroid. Oncogene 22:6455–6457
14. Goggins M, Offerhaus GJ, Hilgers W, Griffin CA, Shekher M, Tang D, Sohn TA, Yeo CJ, Kern SE, Hruban RH (1998) Pancreatic adenocarcinomas with DNA replication errors (RER+) are associated with wild-type K-ras and characteristic histopathology. Poor differentiation, a syncytial growth pattern, and pushing borders suggest RER+. Am J Pathol 152: 1501–1507
15. Hruban RH, van Mansfeld AD, Offerhaus GJ, van Weering DH, Allison DC, Goodman SN, Kensler TW, Bose KK, Cameron JL, Bos JL (1993) K-ras oncogene activation in adenocarcinoma of the human pancreas. A study of 82 carcinomas using a combination of mutant-enriched polymerase chain reaction analysis and allele-specific oligonucleotide hybridization. Am J Pathol 143:545–554
16. Hruban RH, Goggins M, Parsons J, Kern SE (2000) Progression model for pancreatic cancer. Clin Cancer Res 6:2969–2972
17. International Agency for Research on Cancer (2000) Tumours of the digestive system. In: Hamilton SR, Aaltonen LA (eds) WHO classification of tumours. IARC Press, Lyon
18. Ishimura N, Yamasawa K, Karim Rumi MA, Kadowaki Y, Ishihara S, Amano Y, Nio Y, Higami T, Kinoshita Y (2003) BRAF and K-ras gene mutations in human pancreatic cancers. Cancer Lett 199:169–173
19. Jemal A, Murray T, Samuels A, Ghafoor A, Ward E, Thun MJ (2003) Cancer statistics, 2003. CA Cancer J Clin 53:5–26
20. Kawesha A, Ghaneh P, Andren-Sandberg A, Ograeid D, Skar R, Dawiskiba S, Evans JD, Campbell F, Lemoine N, Neoptolemos JP (2000) K-ras oncogene subtype mutations are associated with survival but not expression of p53, p16 (INK4A), p21(WAF-1), cyclin D1, erbB-2 and erbB-3 in resected pancreatic ductal adenocarcinoma. Int J Cancer 89:469–474
21. Korc M, Chandrasekar B, Yamanaka Y, Friess H, Buchier M, Beger HG (1992) Overexpression of the epidermal growth factor receptor in human pancreatic cancer is associated with concomitant increases in the levels of epidermal growth factor and transforming growth factor alpha. J Clin Invest 90: 1352–1360
22. Lee EJ, Choi C, Park CK, Maeng L, Lee JQ, Lee A, Kim K-M (2005) Tracing origin of serrated adenomas with BRAF and KRAS mutations. Virchows Arch 447:597–602
23. Li D, Xie K, Wolff R, Abbruzzese JL (2004) Pancreatic cancer. Lancet 363:1049–1057
24. Lohr M, Kloppel G, Maisonneuve P, Lowenfels AB, Luttges J (2005) Frequency of K-ras mutations in pancreatic intraductal neoplasias associated with pancreatic ductal adenocarcinoma and chronic pancreatitis: a meta-analysis. Neoplasia 7:17–23
25. Loukopoulos P, Kanetaka K, Takamura M, Shibata T, Sakamoto M, Hirohashi S (2004) Orthotopic transplantation models of pancreatic adenocarcinoma derived from cell lines and primary tumors and displaying varying metastatic activity. Pancreas 29:193–203
26. Lowenfels AB, Maisonneuve P (2004) Epidemiology and prevention of pancreatic cancer. Jpn J Clin Oncol 34:238–244
27. Luttges J, Schlehe B, Menke MA, Vogel I, Henne-Bruns D, Kloppel G (1999) The K-ras mutation pattern in pancreatic ductal adenocarcinoma usually is identical to that in associated normal, hyperplastic, and metaplastic ductal epithelium. Cancer 85:1703–1710
28. Lynch HT, Shaw TG, Lynch JF (2004) Inherited predisposition to cancer: a historical overview. Am J Med Genet C Semin Med Genet 129:5–22
29. Lynch TJ, Bell DW, Sordella R, Gurubhagavatula S, Okimoto RA, Brannigan BW, Harris PL, Haserlat SM, Supko JG, Haluska FG et al (2004) Activating mutations in the epidermal growth factor receptor underlying responsiveness of non-small-cell lung cancer to gefitinib. N Engl J Med 350:2129–2139
30. Maple JT, Smyrk TC, Boardman LA, Johnson RA, Thibodeau SN, Chari ST (2005) Defective DNA mismatch repair in long-term (> or =3 years) survivors with pancreatic cancer. Pancreatology 5:220–227
31. Miller CJ, Cheung M, Sharma A, Clarke L, Helm K, Mauger D, Robertson GP (2004) Method of mutation analysis may contribute to discrepancies in reports of (V599E)BRAF mutation frequencies in melanocytic neoplasms. J Invest Dermatol 123:990–992
32. Nagasaka T, Sasamoto H, Notohara K, Cullings HM, Takeda M, Kimura K, Kambara T, MacPhee DG, Young J, Leggett BA et al (2004) Colorectal cancer with mutation in BRAF, KRAS, and wild-type with respect to both oncogenes showing different patterns of DNA methylation. J Clin Oncol 22:4584–4594
33. Ogino S, Kawasaki T, Brahmandam M, Yan L, Cantor M, Namgyal C, Mino-Kenudson M, Lauwers GY, Loda M, Fuchs CS (2005) Sensitive sequencing method for KRAS mutation detection by pyrosequencing. J Mol Diagn 7:413–421
34. Paez JG, Janne PA, Lee JC, Tracy S, Greulich H, Gabriel S, Herman P, Kaye FJ, Lindeman N, Boggon TJ et al (2004) EGFR mutations in lung cancer: correlation with clinical response to gefitinib therapy. Science 304:1497–1500
35. Rajagopalan H, Bardelli A, Lengauer C, Kinzler KW, Vogelstein B, Velculescu VE (2002) Tumorigenesis: RAF/RAS oncogenes and mismatch-repair status. Nature 418:934
36. Ren YX, Xu GM, Li ZS, Song YG (2004) Detection of point mutation in K-ras oncogene at codon 12 in pancreatic diseases. World J Gastroenterol 10:881–884
37. Richter A, Niedergethmann M, Sturm JW, Lorenz D, Post S, Trede M (2003) Long-term results of partial pancreaticoduodenectomy for ductal adenocarcinoma of the pancreatic head: 25-year experience. World J Surg 27:324–329
38. Rozenblum E, Schutte M, Goggins M, Hahn SA, Panzer S, Zahurak M, Goodman SN, Sohn TA, Hruban RH, Yeo CJ et al (1997) Tumor-suppressive pathways in pancreatic carcinoma. Cancer Res 57:1731–1734
39. Saetta AA, Papanastasiou P, Michalopoulos NV, Gigelou F, Korkolopoulou P, Bei T, Patsouris E (2004) Mutational analysis of BRAF in gallbladder carcinomas in association with K-ras and p53 mutations and microsatellite instability. Virchows Arch 445:179–182
40. Samuels Y, Wang Z, Bardelli A, Silliman N, Ptak J, Szabo S, Yan H, Gazdar A, Powell SM, Riggins GJ et al (2004) High frequency of mutations of the PIK3CA gene in human cancers. Science 304:554
41. Schutte M, Hruban RH, Geradts J, Maynard R, Hilgers W, Rabindran SK, Moskaluk CA, Hahn SA, Schwarte-Waldhoff I, Schmiegel W et al (1997) Abrogation of the Rb/p16 tumor-suppressive pathway in virtually all pancreatic carcinomas. Cancer Res 57:3126–3130
42. Sessa F, Bonato M, Bisoni D, Ranzani GN, Capella C (1998) Ki-ras and p53 gene mutations in pancreatic ductal carcinoma: a relationship with tumor phenotype and survival. Eur J Histochem 42(Spec Issue):67–76
43. Sommerer F, Vieth M, Markwarth A, Rohrich K, Vomschloss S, May A, Ell C, Stolte M, Hengge UR, Wittekind C et al (2004) Mutations of BRAF and KRAS2 in the development of Barrett's adenocarcinoma. Oncogene 23:554–558

44. Song MM, Nio Y, Dong M, Tamura K, Furuse K, Tian YL, He SG, Shen K (2000) Comparison of K-ras point mutations at codon 12 and p21 expression in pancreatic cancer between Japanese and Chinese patients. J Surg Oncol 75:176–185
45. van Heek NT, Meeker AK, Kern SE, Yeo CJ, Lillemoe KD, Cameron JL, Offerhaus GJ, Hicks JL, Wilentz RE, Goggins MG et al (2002) Telomere shortening is nearly universal in pancreatic intraepithelial neoplasia. Am J Pathol 161:1541–1547
46. Wagner M, Redaelli C, Lietz M, Seiler CA, Friess H, Buchler MW (2004) Curative resection is the single most important factor determining outcome in patients with pancreatic adenocarcinoma. Br J Surg 91:586–594
47. Weir B, Zhao X, Meyerson M (2004) Somatic alterations in the human cancer genome. Cancer Cell 6:433–438
48. Wilhelm SM, Carter C, Tang L, Wilkie D, McNabola A, Rong H, Chen C, Zhang X, Vincent P, McHugh M et al (2004) BAY 43-9006 exhibits broad spectrum oral antitumor activity and targets the RAF/MEK/ERK pathway and receptor tyrosine kinases involved in tumor progression and angiogenesis. Cancer Res 64:7099–7109
49. Yamamoto H, Itoh F, Nakamura H, Fukushima H, Sasaki S, Perucho M, Imai K (2001) Genetic and clinical features of human pancreatic ductal adenocarcinomas with widespread microsatellite instability. Cancer Res 61:3139–3144

Virchows Arch (2006) 448: 797–804
DOI 10.1007/s00428-006-0173-x

ORIGINAL ARTICLE

Paolo Piacentini · Massimo Donadelli · Chiara Costanzo · Patrick S. Moore · Marta Palmieri · Aldo Scarpa

Trichostatin A enhances the response of chemotherapeutic agents in inhibiting pancreatic cancer cell proliferation

Received: 11 January 2006 / Accepted: 8 February 2006 / Published online: 28 March 2006

Abstract Pancreatic cancer is an aggressive neoplasia, and standard chemotherapies are by and large ineffective. The purpose of this work was to get a comprehensive preclinical study on the ability of anticancer drug combinations that best inhibit growth of pancreatic adenocarcinoma cells. We evaluated the in vitro growth inhibition of ten pancreatic cancer cell lines to gemcitabine and 5-fluorouracil, newer generation cytotoxic agents (oxaliplatin, irinotecan), targeted therapy (gefitinib) and a histone deacetylase (HDAC) inhibitor (trichostatin A). Cells were treated with the single drug alone and all pairwise drug association. Our results demonstrate that TSA can effectively increase the drug sensitivity of all the cell lines studied. The association of TSA and irinotecan determines an increase in growth inhibition on the highest percentage of cell lines (80%). Our findings may represent an experimental basis for potential clinical application of HDAC inhibitors, in particular in association with drugs used in cancer clinical treatment, supporting the idea that HDAC inhibitors could act as sensitizers for chemotherapy.

Keywords Pancreatic adenocarcinoma · Trichostatin A · Cell proliferation

P. Piacentini · P. S. Moore · A. Scarpa
Department of Pathology, Section of Anatomic Pathology,
University of Verona,
Verona, Italy

M. Donadelli · C. Costanzo ·
M. Palmieri (✉)
Department of Neurological and Visual Sciences
Section of Biochemistry,
Strada Le Grazie 8,
37134 Verona, Italy
e-mail: marta.palmieri@univr.it
Tel.: +39-045-8027169
Fax: +39-045-8027170

Present address:
P. Piacentini
Medical Oncology, Ospedale di Arzignano,
ULSS n. 5 Ovest Vicentino,
Vicenza, Italy

Introduction

Pancreatic adenocarcinoma is one of the most aggressive human cancers. Its incidence nearly mirrors its mortality rate with a 5-year survival lower than 5% [16]; at diagnosis, less than 20% of patients are candidates for surgery with curative intent [21]. Standard treatments for advanced disease include radiotherapy and/or chemotherapy regimens. Radiotherapy has been shown to have some utility for regional confined cancers, but is often too toxic for tissues surrounding the neoplasia. Widely used chemotherapeutic regimes include 5-fluorouracil (5-FU) and gemcitabine, a novel nucleoside analogue of cytidine (2′,2′-difluorodeoxycytidine; dFdC) (GEM) [10]. However, even gemcitabine, which is now considered the gold standard, has a response rate of less than 20%, although it does provide an improvement in the quality of life [4]. A major cause of treatment failure in pancreatic cancer is believed to be resistance to chemotherapy, which seems to be related to the altered expression of genes such as those involved in the apoptotic pathway [28]. For instance, the *p53* gene, which shows a high rate of mutation in pancreatic cancer [12], has been shown to increase the sensitivity of pancreatic cancer cells to gemcitabine when reintroduced in these cells [5].

It is known that combination of drugs with different mechanisms of action can compensate the lack of functioning of crucial steps for the activity of a specific drug, thus overcoming mechanisms of resistance. Recent clinical studies have investigated the possibility that the association of different drugs may result in more efficient antitumoral action. For example, gemcitabine in combination with 5-fluorouracil, docetaxel, cisplatin, oxaliplatin, or irinotecan has been shown to give a response rate in phase II trials generally slightly higher than gemcitabine alone [10]. However, no randomized phase III trial has yet established a survival clinical benefit for combination therapy compared with gemcitabine alone. Thus, it is important to identify novel drug associations that are more effective than gemcitabine-based treatment for pancreatic cancer.

The new generation compounds oxaliplatin and irinotecan (CPT11) are among the most promising cytotoxic agents available for clinical cancer treatment. Oxaliplatin is a third generation platinum derivative that differs from cisplatin and carboplatin in that it contains a cyclic, bulky group that may confer greater resistance to DNA repair and efficiently prevent DNA replication once oxaliplatin-DNA adducts have been formed [25]. Oxaliplatin demonstrates mild toxicity and good clinical management [2, 6]. CPT11 is a derivate of camptothecin and acts by interfering with the activity of DNA topoisomerase I, which cuts and relegates single-strand DNA. This drug causes the conversion of single-strand DNA breaks into irreversible double-strand breaks, resulting in cell death [13].

Besides the interest into these new generation cytotoxic agents, intense study has recently focused on drugs directed against specific molecular targets. One of the most promising examples is gefitinib (iressa), which specifically inhibits activation of the EGFR. The drug is now in clinical use for lung cancer [23], although it is worth noting that EGF receptor family is overexpressed in pancreatic cancer as compared with normal pancreatic cells [30].

In the last few years, therapeutic interest on histone deacetylase (HDAC) inhibitors has been rapidly increasing and it has been demonstrated that these drugs, including trichostatin A (TSA), induce growth arrest, differentiation, and/or apoptosis in cancer cells [17]. Moreover, it has been recently demonstrated that TSA induces apoptosis and G2-phase cell cycle arrest in pancreatic cancer cell lines by a p53-independent mechanism [8]. Furthermore, HDAC inhibitors display selective toxicity to cancer cell lines [1], reduce growth of neoplastic cells in animal models at nontoxic doses [22, 29], and thus, may represent a new therapeutic approach for cancer treatment [21].

The aim of the present study was to evaluate the efficacy of growth inhibition of chemotherapeutic drugs used for treatment of pancreatic cancer in a panel of pancreatic adenocarcinoma cell lines. The drugs investigated include, in addition to 5-FU and GEM, cytotoxic agents of new generation (oxaliplatin, CPT11), a molecular targeted drug (iressa), and a HDAC inhibitor (TSA), alone and in pairwise combinations. Using this approach, we demonstrate that the association of TSA with GEM, oxaliplatin, iressa, or CPT11 determines a significantly higher growth inhibition compared to other drug combinations. Our findings provide an experimental basis for clinical application of therapies for pancreatic adenocarcinoma that include HDAC inhibitors.

Materials and methods

Cell lines and culture condition

Ten human pancreatic cancer cell lines were investigated, comprising seven cell lines derived from primary cancer (MiaPaca2, PaCa3, PaCa44, Panc1, PT45P1, PSN1, and PC) and three from metastatic cancers (HPAF II, CFPAC1, and T3M4) (for detailed descriptions of cell lines in terms of mutations commonly found in pancreatic cancer and origin, see [19]).

All cell lines were grown in RPMI 1640 supplemented with 20 mM glutamine, 10% FBS, and 50 μg/ml gentamicin sulfate (BioWhittaker, Italy), and were incubated at standard conditions (37°C with 5% CO_2). Cells were trypsinized, counted, and plated in 96-well cell culture plates (4×10^3 cells/well) and cultured for 24 h. Cells were treated for 48 h with drugs at the indicated concentration.

Chemicals

Six drugs were used and included: 5-fluorouracil (Fluorouracile, 5-FU; Teva Pharma), oxaliplatin (Eloxatin; Sanofi), and irinotecan (Campto, CPT11; Aventis); gemcitabine (2′,2′-difluorodeoxycytidine dFdC, Gemzar, GEM; Lilly) solutions prepared in sterile water and freshly diluted before each experiment; gefitinib (Iressa; Astra Zeneca) and trichostatin A (TSA; Sigma-Aldrich) were solubilized in DMSO and stored at −80°C until use.

Determination of IC_{50} values and cell proliferation assay

The IC_{50} value was defined as the drug concentration that causes 50% growth inhibition compared to controls. IC_{50} values of each drug in all cell lines were obtained using dose-dependent curves at 48 h. These concentration values were used to test the antiproliferative effect of the various treatments in all cell lines. The proliferation assay was determined by the Crystal Violet method: cells were stained with Crystal Violet (Sigma) and solubilized in 1% sodium dodecyl sulfate in phosphate-buffered saline. The cell proliferation rate was measured photometrically (A_{595}). Three independent experiments were performed for each assay condition.

Statistical analyses

The difference between the strongest single treatment against the combined treatment was evaluated using the Welch two-sample *t* test, considering a *P*-value <0.05 as significant.

Results

Determination of IC_{50} and inhibition of proliferation of pancreatic adenocarcinoma cell lines by single drugs

Ten pancreatic adenocarcinoma cell lines were treated with different concentrations of various individual drugs for 48 h, and the dose-dependent curves were determined (Fig. 1a,b). IC_{50} values are shown in Table 1. Examination

of dose-dependent curves and their relative IC_{50} values reveals that the differences in responsiveness among the ten cell lines is much greater after GEM, CPT11, and oxaliplatin treatments compared to 5-FU, iressa, and TSA. Moreover, treatment with GEM, 5-FU, or CPT11 did not lead to a complete inhibition of cell growth in contrast to oxaliplatin, TSA, and iressa, which resulted in near complete inhibition, suggesting the absence of a saturating effect. PSN1 was generally the most sensitive cell line to all drugs tested, while Panc1 was the most resistant. It is interesting to note that the IC_{50} mean value was significantly lower with GEM or CPT11 when metastatic cell lines were compared with primary cell lines ($p \leq 0.05$). No correlations were found between the sensitivity towards each single drug and the known, principal genetic aberrations in K-*ras*, *p53*, *p16*, and *DPC4* [19].

Inhibition of proliferation of pancreatic adenocarcinoma cell lines by pairwise combined drug treatment

To test whether pairwise combined treatments may increase the growth inhibitory activity of GEM, 5-FU, oxaliplatin, CPT11, iressa, or TSA on pancreatic adenocarcinoma cells, we analyzed cell proliferation using all possible drug combinations at a concentration corresponding to their respective IC_{50} (Fig. 2). Table 2 reports the increased percentage of cell growth inhibition by pairwise combination relative to that obtained with the single drug giving the higher growth inhibition. The percentages of the combined treatments that determined a significantly increased growth inhibition in each cell line are shown on the right side of the Table 2, while the percentages of cell lines that presented a significant cooperative effect on cell growth inhibition by the indicated combined treatments are reported at the

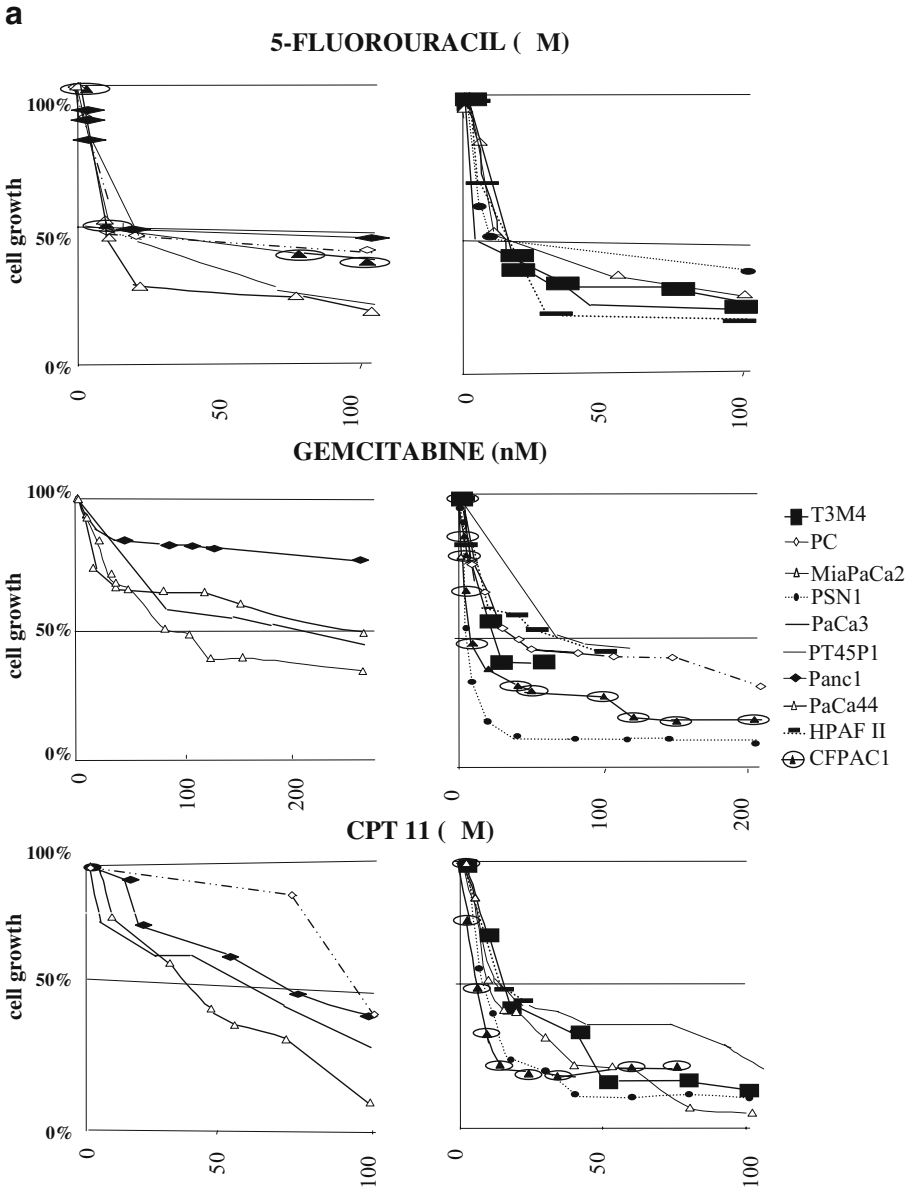

Fig. 1 **a** Growth inhibition curves of pancreatic adenocarcinoma cell lines. For each drug, cell lines are divided into two groups with higher and lower IC_{50} values. The *figure* shows a representative experiment. **b** Growth inhibition curves of pancreatic adenocarcinoma cell lines. For each drug, cell lines are divided into two groups with higher and lower IC_{50} values. The *figure* shows a representative experiment

Fig. 1 (continued)

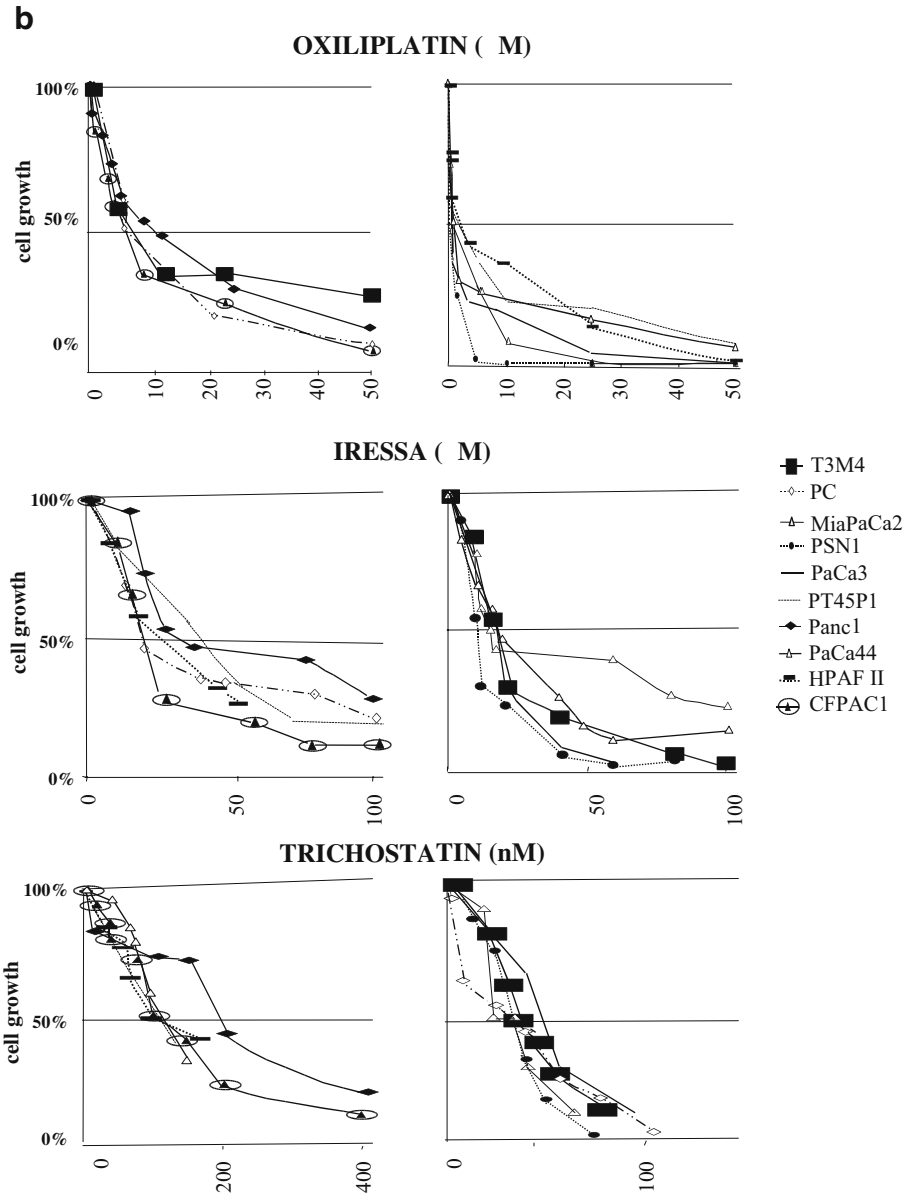

Table 1 IC_{50} values of single drug in pancreatic adenocarcinoma cell lines

Cell lines	Origin	5-FU (μM)	GEM (nM)	CPT11 (μM)	Oxaliplatin (μM)	Iressa (μM)	TSA (nM)
PSN1	Primary	4	8	8	0.4	11	50
MiaPaCa2	Primary	5	90	10	0.9	15	50
PC	Primary	8	30	100	5	20	60
PT45P1	Primary	8.8	50	20	1	35	98
PaCa3	Primary	3	220	60	0.6	17.5	65
PaCa44	Primary	8.1	250	45	1	17.5	105
Panc1	Primary	9.5	200*	87.5	9.8	28.5	200
CFPAC1	Metastasis (liver)	8	9.5	5	5	20	100
T3M4	Metastasis (node)	7	25	16	6.5	16	50
HPAFII	Metastasis (ascites)	5	40	20	1.75	27.5	95

*The lowest gemcitabine concentration determining maximal Panc1 cell growth inhibition (see Fig. 1)

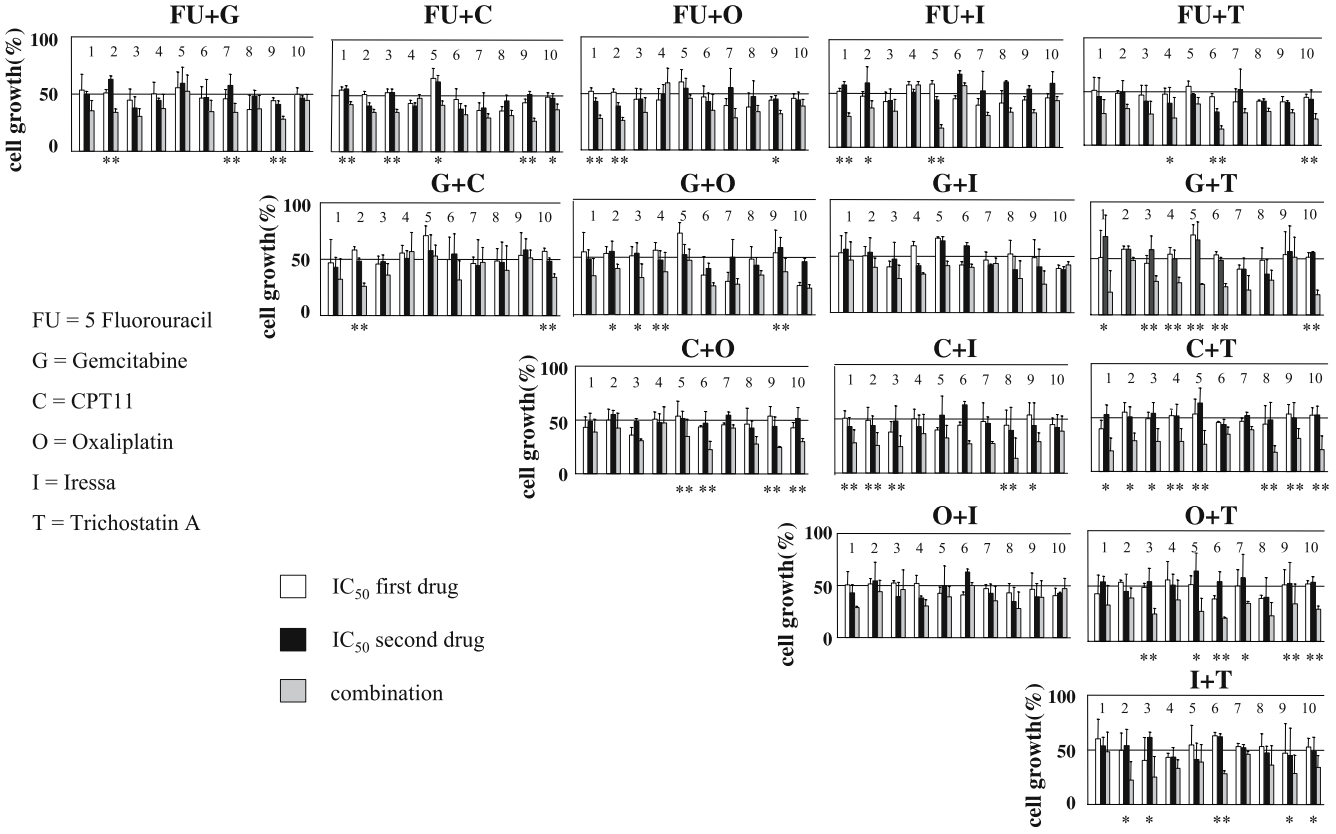

Fig. 2 Growth inhibition after single and pairwise drug combination treatments in pancreatic adenocarcinoma cell lines (*$p \leq 0.05$ and **$p \leq 0.01$ according to Welch two-sample *t* test). Cell lines are shown in the following order: *1* T3M4, *2* PaCa44, *3* PT45P1, *4* PC, *5* Panc1, *6* MiaPaCa2, *7* PSN1, *8* PaCa3, *9* HPAFII, *10* CFPAC1

Table 2 Effect of pairwise drug combination on pancreatic adenocarcinoma cell growth inhibition

	T + C	G + T	T + O	T + I	FU + C	C + I	C + O	G + O	FU + T	FU + G	FU + O	FU + I	G + C	G + I	O + I	Combined Treatment (%)
HPAFII	19**	3	14.6**	13*	17**	13*	19.5**	12.3**	7.5	16**	12*	12	7.3	12	1	60
CFPAC1	26**	33**	22.5**	13.7*	8.5*	5	13.3**	0	17**	3.5	6.5	4.2	14**	0	1	53
PaCa44	21.5*	10	3	14.2*	6	12**	7.3	12.3*	9.6	17**	14.3**	12*	22**	9	3.7	53
PT45P1	17.5*	13**	20.3**	16*	18**	13**	11	16.5*	9.7	7.3	7.3	8.3	8.2	8	0	47
Panc1	28**	36**	19.6*	2.5	17*	6	15.5**	2.3	8.5	3	7.7	26**	3	7	0	40
T3M4	20.7*	30.3*	10	3	13**	15**	6.25	6	16	12	14.3**	23**	6.2	3	9.3	40
MiaPaCa2	8	23**	17.5**	34**	6	7	18.3**	4.6	15**	10	11.3	0	10	0	0	33
PC	19**	17.5**	9.5	9.5	0	6	5	12**	10.6*	7	2.7	0	2	2	7.5	27
PaCa3	14.3**	2.6	10	12	1.3	15**	8.6	6	7.5	0	1.6	4.6	6.6	4	4	13
PSN1	8	9.6	17.3*	6	1	9	3	2.6	5	12**	7	4.3	0	1	0.6	13
Combined treatments (%)	80	60	60	50	50	50	40	40	30	30	30	30	20	0	0	

FU 5-Fluorouracil, *G* gemcitabine, *C* CPT11, *O* oxaliplatin, *I* iressa, *T* trichostatin A

The increases of growth inhibition for the indicated pair-wise combination relative to that obtained with the single drug giving the higher inhibition are shown (*$p \leq 0.05$ and **$p \leq 0.01$ according to Welch two-sample *t* test)

The percentages of the combined treatments that determined a significantly increased growth inhibition in each cell line are shown on the right side, while the percentages of cell lines that present a significant growth inhibitory effect by the indicated combined treatments are reported at the bottom

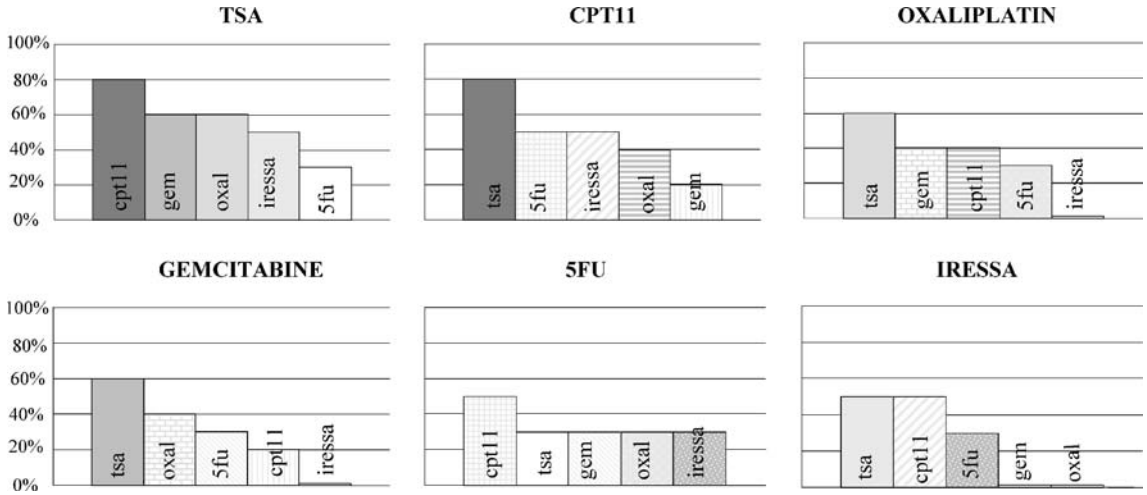

Fig. 3 Percentage of pancreatic adenocarcinoma cell lines showing increased effect on cell growth inhibition after the indicated combined treatment

bottom of the Table 2. Of particular interest, all drug combinations including TSA gave the highest value of cell growth inhibition. These results demonstrate that TSA is the best partner for all drugs with the exception of 5-FU; the combination of TSA and CPT11 determined the highest growth inhibition in the largest number of cell lines (Fig. 3).

Panc1, the most resistant cell line to single-drug treatments, showed a much stronger sensitivity in the combined treatments; while PSN1, the most sensitive cell line to single-drug treatments, becomes the most resistant cell line to all combined treatments. It is of interest to note that all pairwise combinations were less effective in PaCa3, which contains a functional *p53* gene.

Discussion

To date, few comprehensive preclinical studies have been performed on the ability of anticancer drug combinations to inhibit pancreatic adenocarcinoma cell growth [3, 9, 15, 18].

In this study, we present for the first time a comprehensive analysis on the growth inhibitory effect of five chemotherapeutic agents (GEM, 5-FU, oxaliplatin, iressa, and CPT11) in clinical use, with an inhibitor of HDACs (TSA) on pancreatic adenocarcinoma cell lines.

We are fully aware that our decision to use a wide panel of drugs and cell lines penalized the experimental plan which was necessarily simplified and was unable to answer the question whether the various drug combinations act in an additive or synergistic manner. However, our study presents the characterization of a panel of pancreatic cancer cell lines for their response to the most commonly used chemotherapeutic drugs either alone or in combination that will be useful for further work on the molecular mechanisms of drug action and interaction.

The most significant finding of our study is that TSA, together with GEM, oxaliplatin, iressa or, in particular, with CPT11, determines a significantly higher growth inhibition compared to the other pairwise drug combinations. Moreover, we also demonstrate that drug combinations including TSA determine the highest growth inhibition on the largest number of cell lines. These results demonstrate that TSA is the best partner for all drugs but 5-FU, and that TSA and CPT11 give rise to an optimal anticancer effect on 80% of cell lines studied, suggesting that it may be a promising treatment strategy for pancreatic adenocarcinoma.

Recently, we have shown that TSA induces growth arrest and apoptotic cell death on nine of the pancreatic adenocarcinoma cell lines described in this paper [8]. In addition, we and others previously demonstrated, by gene expression and proteomic profiling, that HDAC inhibition determined the variation of a relatively small number of genes involved in the regulation of proliferation (*p21*, *p19*, *p57*, and *cyclin A* and *B*), signal transduction (*TNF* and *TNFR* superfamily), and apoptosis (*BCL* superfamily) [7, 8, 11, 20, 27]. In particular, an increased ratio between the expression of proapoptotic (*Bim*) and antiapoptotic (*Bcl-xL* and *Bcl-w*) genes was observed [20]. These results suggested the possibility that an inhibitor of HDAC, such as TSA, may sensitize cells without a functional *p53* gene to the effect of current chemotherapeutic agents. Our data demonstrate that TSA can effectively increase the sensitivity of all pancreatic adenocarcinoma cell lines with a nonfunctional *p53* gene to other drugs. It is interesting to note that PaCa3 cells, which are wild type for the *p53* gene, were particularly resistant to all combined treatments, confirming the idea that the *p53* gene status is not relevant for cell sensitization by TSA.

In conclusion, combined treatments of anticancer drugs and the HDAC inhibitor TSA increase drug cytotoxicity in pancreatic adenocarcinoma cells and may open the way for combination therapy with HDAC inhibitors in pancreatic

cancer. In fact, inhibitors of HDAC are already in clinical use for other tumors and do not show apparent toxicity [14, 17, 24, 26].

Acknowledgements We thank Dr. E. Pinton and Dr. A. Sbarufatti (Aventis and Sanofi-Synthelabo) for providing irinotecan and oxaliplatin. This study was supported by Fondazione Cassa di Risparmio di Verona (Bando 2004); Fondazione Giorgio Zanotto, Verona, Italy; Associazione Italiana Ricerca sul Cancro, Milan, Italy; and the Italian Ministry of University and Research. Authors Paolo Piacentini and Massimo Donadelli have equally contributed to this paper.

References

1. Batova A, Shao LE, Diccianni MB, Yu AL, Tanaka T, Rephaeli A, Nudelman A, Yu J (2002) The histone deacetylase inhibitor AN-9 has selective toxicity to acute leukemia and drug-resistant primary leukemia and cancer cell lines. Blood 100:3319–3324
2. Becouarn Y, Agostini C, Trufflandier N, Boulanger V (2001) Oxaliplatin: available data in non-colorectal gastrointestinal malignancies. Crit Rev Oncol Hematol 40:265–272
3. Buchsbaum DJ, Bonner JA, Grizzle WE, Stackhouse MA, Carpenter M, Hicklin DJ, Bohlen P, Raisch KP (2002) Treatment of pancreatic cancer xenografts with Erbitux (IMC-C225) anti-EGFR antibody, gemcitabine, and radiation. Int J Radiat Oncol Biol Phys 54:1180–1193
4. Burris HA 3rd, Moore MJ, Andersen J, Green MR, Rothenberg ML, Modiano MR, Cripps MC, Portenoy RK, Storniolo AM, Tarassoff P, Nelson R, Dorr FA, Stephens CD, Von Hoff DD (1997) Improvements in survival and clinical benefit with gemcitabine as first-line therapy for patients with advanced pancreas cancer: a randomized trial. J Clin Oncol 15: 2403–2413
5. Cascallo M, Calbo J, Gelpi JL, Mazo A (2000) Modulation of drug cytotoxicity by reintroduction of wild-type p53 gene (Ad5CMV-p53) in human pancreatic cancer. Cancer Gene Ther 7:545–556
6. Cassidy J, Misset JL (2002) Oxaliplatin-related side effects: characteristics and management. Semin Oncol 29:11–20
7. Cecconi D, Scarpa A, Donadelli M, Palmieri M, Hamdan M, Astner H, Righetti PG (2003) Proteomic profiling of pancreatic ductal carcinoma cell lines treated with trichostatin-A. Electrophoresis 24:1871–1878
8. Donadelli M, Costanzo C, Faggioli L, Scupoli MT, Moore PS, Bassi C, Scarpa A, Palmieri M (2003) Trichostatin A, an inhibitor of histone deacetylases, strongly suppresses growth of pancreatic adenocarcinoma cells. Mol Carcinog 38:59–69
9. Giovannetti E, Mey V, Danesi R, Mosca I, Del Tacca M (2004) Synergistic cytotoxicity and pharmacogenetics of gemcitabine and pemetrexed combination in pancreatic cancer cell lines. Clin Cancer Res 10:2936–2943
10. Haller DG (2003) New perspectives in the management of pancreas cancer. Semin Oncol 30:3–10
11. Henderson C, Mizzau M, Paroni G, Maestro R, Schneider C, Brancolini C (2003) Role of caspases, Bid, and p53 in the apoptotic response triggered by histone deacetylase inhibitors trichostatin-A (TSA) and suberoylanilide hydroxamic acid (SAHA). J Biol Chem 278:12579–12589
12. Kalthoff H, Schmiegel W, Roeder C, Kasche D, Schmidt A, Lauer G, Thiele HG, Honold G, Pantel K, Riethmuller G et al (1993) p53 and K-RAS alterations in pancreatic epithelial cell lesions. Oncogene 8:289–298
13. Kawato Y, Aonuma M, Hirota Y, Kuga H, Sato K (1991) Intracellular roles of SN-38, a metabolite of the camptothecin derivative CPT-11, in the antitumor effect of CPT-11. Cancer Res 51:4187–4191
14. Kelly WK, Richon VM, O'Connor O, Curley T, MacGregor-Curtelli B, Tong W, Klang M, Schwartz L, Richardson S, Rosa E, Drobnjak M, Cordon-Cordo C, Chiao JH, Rifkind R, Marks PA, Scher H (2003) Phase I clinical trial of histone deacetylase inhibitor: suberoylanilide hydroxamic acid administered intravenously. Clin Cancer Res 9:3578–3588
15. Kornmann M, Butzer U, Blatter J, Beger HG, Link KH (2000) Pre-clinical evaluation of the activity of gemcitabine as a basis for regional chemotherapy of pancreatic and colorectal cancer. Eur J Surg Oncol 26:583–587
16. Li D, Xie K, Wolff R, Abbruzzese JL (2004) Pancreatic cancer. Lancet 363:1049–1057
17. Marshall JL, Rizvi N, Kauh J, Dahut W, Figuera M, Kang MH, Figg WD, Wainer I, Chaissang C, Li MZ, Hawkins MJ (2002) A phase I trial of depsipeptide (FR901228) in patients with advanced cancer. J Exp Ther Oncol 2:325–332
18. Monti P, Marchesi F, Reni M, Mercalli A, Sordi V, Zerbi A, Balzano G, Di Carlo V, Allavena P, Piemonti L (2004) A comprehensive in vitro characterization of pancreatic ductal carcinoma cell line biological behavior and its correlation with the structural and genetic profile. Virchows Arch 445:236–247
19. Moore PS, Sipos B, Orlandini S, Sorio C, Real FX, Lemoine NR, Gress T, Bassi C, Kloppel G, Kalthoff H, Ungefroren H, Lohr M, Scarpa A (2001) Genetic profile of 22 pancreatic carcinoma cell lines. Analysis of K-ras, p53, p16 and DPC4/Smad4. Virchows Arch 439:798–802
20. Moore PS, Barbi S, Donadelli M, Costanzo C, Bassi C, Palmieri M, Scarpa A (2004) Gene expression profiling after treatment with the histone deacetylase inhibitor trichostatin A reveals altered expression of both pro- and anti-apoptotic genes in pancreatic adenocarcinoma cells. Biochim Biophys Acta 1693:167–176
21. Neoptolemos JP, Cunningham D, Friess H, Bassi C, Stocken DD, Tait DM, Dunn JA, Dervenis C, Lacaine F, Hickey H, Raraty MG, Ghaneh P, Buchler MW (2003) Adjuvant therapy in pancreatic cancer: historical and current perspectives. Ann Oncol 14:675–692
22. Nervi C, Borello U, Fazi F, Buffa V, Pelicci PG, Cossu G (2001) Inhibition of histone deacetylase activity by trichostatin A modulates gene expression during mouse embryogenesis without apparent toxicity. Cancer Res 61:1247–1249
23. Paez JG, Janne PA, Lee JC, Tracy S, Greulich H, Gabriel S, Herman P, Kaye FJ, Lindeman N, Boggon TJ, Naoki K, Sasaki H, Fujii Y, Eck MJ, Sellers WR, Johnson BE, Meyerson M (2004) EGFR mutations in lung cancer: correlation with clinical response to gefitinib therapy. Science 304:1497–1500
24. Patnaik A, Rowinsky EK, Villalona MA, Hammond LA, Britten CD, Siu LL, Goetz A, Felton SA, Burton S, Valone FH, Eckhardt SG (2002) A phase I study of pivaloyloxymethyl butyrate, a prodrug of the differentiating agent butyric acid, in patients with advanced solid malignancies. Clin Cancer Res 8:2142–2148
25. Raymond E, Faivre S, Woynarowski JM, Chaney SG (1998) Oxaliplatin: mechanism of action and antineoplastic activity. Semin Oncol 25:4–12
26. Sandor V, Bakke S, Robey RW, Kang MH, Blagosklonny MV, Bender J, Brooks R, Piekarz RL, Tucker E, Figg WD, Chan KK, Goldspiel B, Fojo AT, Balcerzak SP, Bates SE (2002) Phase I trial of the histone deacetylase inhibitor, depsipeptide (FR901228, NSC 630176), in patients with refractory neoplasms. Clin Cancer Res 8:718–728

27. Sawa H, Murakami H, Ohshima Y, Sugino T, Nakajyo T, Kisanuki T, Tamura Y, Satone A, Ide W, Hashimoto I, Kamada H (2001) Histone deacetylase inhibitors such as sodium butyrate and trichostatin A induce apoptosis through an increase of the bcl-2-related protein Bad. Brain Tumor Pathol 18:109–114
28. Shi X, Liu S, Kleeff J, Friess H, Buchler MW (2002) Acquired resistance of pancreatic cancer cells towards 5-Fluorouracil and gemcitabine is associated with altered expression of apoptosis-regulating genes. Oncology 62:354–362
29. Vigushin DM, Ali S, Pace PE, Mirsaidi N, Ito K, Adcock I, Coombes RC (2001) Trichostatin A is a histone deacetylase inhibitor with potent antitumor activity against breast cancer in vivo. Clin Cancer Res 7:971–976
30. Yamanaka Y (1992) The immunohistochemical expressions of epidermal growth factors, epidermal growth factor receptors and c-erbB-2 oncoprotein in human pancreatic cancer. Nippon Ika Daigaku Zasshi 59:51–61

Virchows Arch (2006) 448: 805–810
DOI 10.1007/s00428-006-0180-y

ORIGINAL ARTICLE

Manrico Morroni · Angela Maria Cangiotti · Alfredo Guarino · Saverio Cinti

Unusual ultrastructural features in microvillous inclusion disease: a report of two cases

Received: 7 December 2005 / Accepted: 13 February 2006 / Published online: 12 April 2006

Abstract Microvillous Inclusion Disease (MID) is an inherited disorder characterized by intractable diarrhea in infancy. Ultrastructural detection of pathognomonic microvillous inclusions in the enterocytes is essential for diagnosis. The aim of this research is to contribute to the knowledge of MID studying enterocytes and goblet cells (gc). Samples of duodenal mucosa from two young infants with MID (aged 75 days and 3 months, respectively) were studied by light and electron microscopy. Detection in the intestinal villi of immature gc (with microvilli) in one of the cases led us to seek them in control samples. The total number of gc with microvilli (immature) and without microvilli (mature) were counted. In both MID specimens, light microscopy showed atrophy of villi and PAS-positive material in the enterocyte cytoplasm. The ultrastructure of villous enterocytes was characterized by brush-border abnormalities, microvillous inclusions, dense apical granules, and lysosomes. Intermediate structures between microvillous inclusions and lysosomes were also detected within a cell, as were rare microvilli on the lateral membrane of the enterocytes. In one MID specimen, immature gc were also identified in the absorptive compartment. Only mature gc were observed in the controls. The significance of the latter finding requires further studies.

Keywords Enterocytes · Goblet cells · Transmission electron microscopy · Microvillous inclusion disease · Chronic enteropathy

M. Morroni (✉) · A. Cangiotti · S. Cinti
Institute of Normal Human Morphology, Faculty of Medicine,
Polytechnic University of Marche,
Ancona, Italy
e-mail: m.morroni@univpm.it
Tel.: +39-071-2206085
Fax: +39-071-2206087

M. Morroni · A. Cangiotti · S. Cinti
Electron Microscopy Unit, University Hospital,
Ancona, Italy

A. Guarino
Department of Pediatrics, Federico II University,
Naples, Italy

M. Morroni
Istituto di Morfologia Umana Normale,
Facoltà di Medicina e Chirurgia,
Università Politecnica delle Marche,
Via Tronto 10/A,
60020 Ancona, Italy

Introduction

Microvillous inclusion disease (MID), or congenital microvillous atrophy [7], is a serious disorder within the syndrome of intractable diarrhea of infancy [8]. It appears to be transmitted as an autosomal recessive trait [7], although the relevant molecular abnormality has not been identified. A genetic cause is supported by cases described in siblings and by regional clusters of the disease reported in isolated populations [26]. There are two types of MID: congenital or early-onset MID arising in the first postnatal days with severe watery diarrhea accounts for the vast majority of cases; the less common late-onset MID develops after the neonatal period and carries a better prognosis [23]. Infants often die from severe hydroelectrolyte imbalance or from complications secondary to long-term total parenteral nutrition [7, 23]. Today, small bowel transplantation, alone or in combination with liver transplantation, seems to be the only effective treatment for MID and offers prospects of a good quality of life [29].

The main histological features of the disease include diffuse villous atrophy without inflammatory changes and accumulation of periodic acid-Schiff (PAS)-positive material within the apical cytoplasm of enterocytes [7, 8, 22, 23, 31]. The definitive diagnosis of MID rests on distinctive ultrastructural findings: microvillous inclusions (more frequently in villous enterocytes), increased electron-dense secretory granules (preferentially in crypt epithelial cells), and poorly developed brush-border microvilli on the intestinal surface epithelium [3, 7, 22, 23, 31, 33].

Cases with clinical features similar to MID exhibiting abnormal brush-border microvilli but without the charac-

teristic inclusions have been described as intestinal microvillous dystrophy [19, 27]. However, it is unclear whether the two diseases are related.

The pathogenesis of MID is unknown. The postulated cytoskeletal abnormalities involving actin, myosin, and vinculin [4, 5] cause a block in exocytosis, mainly of PAS-positive material related to the brush border. This mechanism correlates well with accumulation of PAS-positive secretory granules in the apical part of the enterocyte cytoplasm [24]. Recently, abnormalities in glycocalyx exocytosis were demonstrated in MID by Phillips et al. (2004) [25] using histochemical and immunohistochemical methods. The pathogenesis of secretory diarrhea seems to be related to abnormalities in the sodium transport system [18].

We describe the transmission electron microscopic features of two cases of MID to provide a further ultrastructural contribution to the knowledge of this rare disease, of which little more than 30 cases have been reported so far in world literature [15]. We investigated both the enterocytes and the goblet cells, which have poorly been studied in MID [3, 8]. The ultrastructural features of MID goblet cells were compared with those of controls.

Patients and methods

Patients

Small intestinal tissue fragments of per-oral mucosal biopsies from two MID patients, aged 75 days and 3 months, respectively, were available.

For the ultrastructural study of goblet cells, only case 1 could be compared with control tissue, as the specimen from case 2 was too small and was entirely needed for diagnostic purposes. Control tissue was represented by mucosal biopsy samples of the small intestine from seven different patients (ranging 3 up to 26 months in age), four of which were histologically normal and three abnormal, respectively. The clinical characteristics of MID patients and controls are summarized in Table 1. Histologically normal specimens were obtained from three infants with failure to thrive, who had no gastrointestinal cause identified (cases 3, 4, and 5) and from one with cystic fibrosis (case 6). The abnormal specimens came from an infant with chronic diarrhea and partial villous atrophy of the mucosa (case 7); one with celiac disease and villous atrophy (case 8); and one with milk protein intolerance with partial villous atrophy (case 9).

All biopsies were performed with fully informed parent consent as part of the routine investigation of patients with gastrointestinal disorders.

Table 1 Clinical details of patients

Case No.	Sex	Age at biopsy	Clinical data
Microvillous atrophy			
1 V.S.	M	75 days	MID (died)
2 G.A.	M	3 months	MID (died)
Normal histology			
3 T.L.	M	17 months	FTT
4 P.E.	F	26 months	FTT
5 B.D.	F	20 months	FTT
6 F.A.	M	9 months	Cystic fibrosis
Abnormal histology			
7 M.F.	F	13 months	Chronic diarrhoea
8 P. M.	M	12 months	Celiac disease
9 N. C.	M	3 months	Milk protein intolerance

MID microvillous inclusion disease, *FTT* failure to thrive

Light and transmission electron microscopy

Duodenal biopsy specimens were processed for light and electron microscopy. Specimens for light microscopy were fixed in 10% buffered formalin, processed according to standard protocols, and embedded in paraffin. Four-micron-thick sections were stained with haematoxylin and eosin (H&E) and PAS.

For electron microscopy, specimens were fixed in 2% glutaraldeyde/2% paraformaldehyde in 0.1 M phosphate buffer for 3 h at 4°C, postfixed in 1% osmium tetroxide in the same buffer solution, dehydrated in graded alcohols, and embedded in an Epon–Araldite mixture. Semi-thin sections (2 μm) were obtained with a MICROM HM 355 microtome (ZEISS, Oberkochen, Germany) and stained with toluidine blue. Thin sections were obtained with an MTX ultramicrotome (RMC, Tucson, AZ, USA), stained with lead citrate and examined with a CM10 transmission electron microscope (Philips, Eindhoven, The Netherlands).

As preliminary observation of the villi in the MID case 1 showed a well-developed microvillous apparatus in the apical part of some goblet cells, to exclude artefacts related to the plane of section, for the purpose of this study, an ultrastructural qualitative study was also performed. Thus, four grids, each containing about four 80-nm-thick serial sections for a total thickness of about 1.3 μm of tissue, were analyzed. Furthermore, as the goblet cells had microvilli in all examined sections, we investigated whether this unusual feature was also present in control specimens. The number of mature (without microvilli) and immature (with microvilli) goblet cells was, thus, counted in the MID case and in all control specimens as well. Only goblet cells with an intact apical cellular membrane (i.e. cells still containing mucous granules) on perfectly longitudinal sections were examined to better examine the ultrastructural details of the apical part of cytoplasm.

Results

Light microscopy

The duodenal biopsies taken at the age of 75 days in case 1 and at 3 months in case 2 showed partial and total villous

atrophy, respectively. PAS stain highlighted the neutral subgroup of mucins of goblet cells and showed abundant PAS-positive material in the apical part of the enterocyte cytoplasm (Fig. 1), likely corresponding to non-excreted material usually employed by the cell metabolic processes for the composition of the microvillous membrane–glycocalyx complex normally seen along the apical surface of the absorptive cells. In case 1, a diffuse lymphoplasmacytic infiltrate was also seen in the lamina propria.

Transmission electron microscopy

Enterocytes

The ultrastructural appearance of villous enterocytes was similar in both specimens. The microvilli were reduced in number and shortened. Large portions of epithelial cell surfaces were completely devoid of microvilli (Fig. 2). Many microvillous inclusions (MIs) of varying size and shape were detected in the apical part of the enterocyte cytoplasm (Fig. 2). They generally contained numerous and not well-oriented microvilli with well-represented filamentous core rootlets. Many voluminous apical lysosomal granules were also evident (Fig. 2). Transitional structures intermediate between MIs and lysosomes, i.e., granules containing few microvilli-like projections, were identified. These three distinct structures (MIs, lysosomes, and transitional granules) were simultaneously present in villous enterocytes whose apical surface was devoid of microvilli (Fig. 3). Small, membrane-bound dense granules (secretory granules) (Fig. 4) of variable shape and size (ranging from 100 to 300 nm), smaller than lysosomes, were also observed. In case 1, rare microvilli with filamentous core rootlet on the lateral membranes of the villous epithelium were also evident (Fig. 5). Crypt enterocytes had normal appearances and exhibited well-formed microvilli.

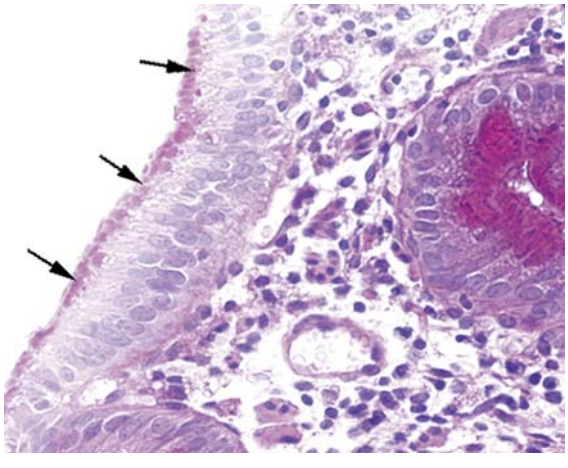

Fig. 1 Microvillous inclusion disease (case 1). PAS staining highlights abundant PAS-positive material (*arrows*) in the apical part of the enterocyte cytoplasm. PAS ×260

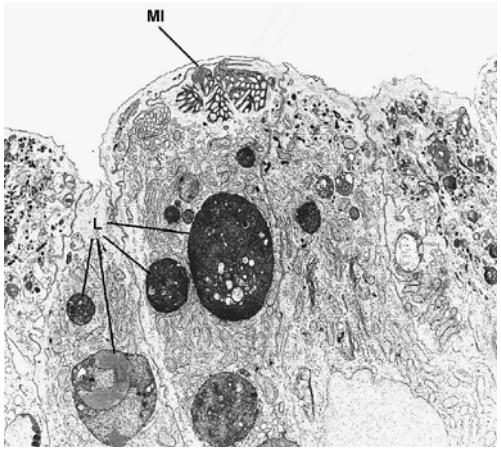

Fig. 2 Microvillous inclusion disease (case 1). The villous enterocytes lack brush-border microvilli, whereas, their apical cytoplasm contains a microvillous inclusion (*MI*) and numerous lysosomes (*L*). ×5.500

Goblet cells (case 1)

Goblet cells with an immature aspect were observed in the villi of MID case 1 (Table 2): they contained well-developed microvilli on the whole apical surface of the cell (Fig. 6a and inset of Fig. 6a). One of these cells, as further evidence of its immaturity, also contained few, non-confluent mucous granules and did not exhibit the characteristic goblet appearance (Fig. 6b and inset Fig. 6b). Some small (ranging from 20 to 80 nm in diameter) membrane-bound dense granules, likely a component of the external glycocalyx, were also present among microvilli (inset of Fig. 6a). Mature goblet cells (cells completely devoid of or with scanty peripheral microvilli) were never observed in this specimen (Table 2).

In the controls, we detected only goblet cells with a mature ultrastructural aspect (Table 2). They always showed the expected goblet appearances; their luminal surface was usually smooth and convex, and completely

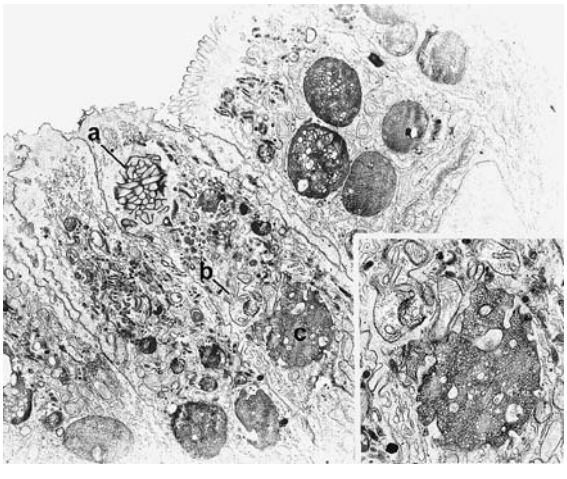

Fig. 3 Microvillous inclusion disease (case 1). From *top to bottom*: microvillous inclusion (**a**), a granule containing few microvilli (**b**), and a lysosome (**c**) detected in the same enterocyte. *Inset*: higher magnification of **b** and **c**. ×11.000, inset ×21.500

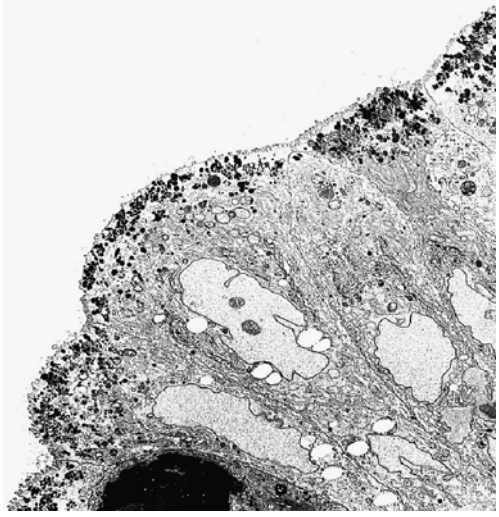

Fig. 4 Microvillous inclusion disease (case 2). The apical cytoplasm of villous epithelium shows an increased number of secretory granules associated with microvillous alterations. ×2.400

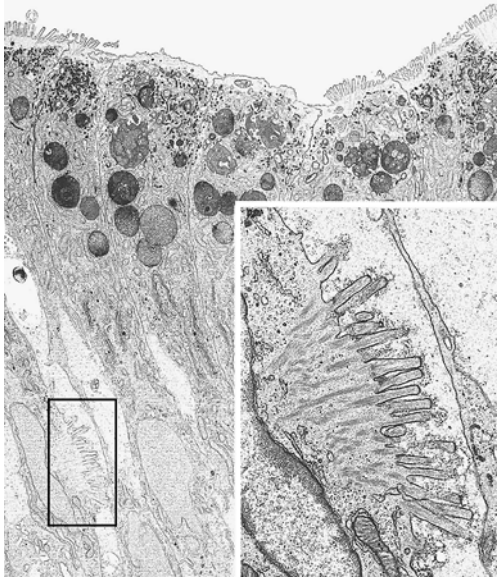

Fig. 5 Microvillous inclusion disease (case 1). Villous enterocytes: the *boxed area* shows microvilli on the lateral membrane. *Inset*: enlargement of the *boxed area*. ×6.200, *inset* ×22.500

lacked microvilli or exhibited few peripheral microvilli (Fig. 6c and inset of Fig. 6c).

Discussion

A few more than 30 cases of MID have been reported so far [15]. Two additional MID cases are herein described. Their submicroscopic features did not differ from previous descriptions: enterocytes with severe brush-border changes contained both secretory dense granules and microvillous inclusions. However, two additional ultrastructural features were detected in these cases, which have rarely been reported in MID enterocytes. In addition, an entirely novel finding is the presence of immature goblet cells.

Table 2 Quantification of the morphology of not secreting goblet cells in the villus

Case No.	No. of mature goblet cells	No. of immature goblet cells
Microvillous inclusion disease		
1	0	3
2	n.d.	n.d.
Normal histology		
3	2	0
4	4	0
5	2	0
6	4	0
Abnormal histology		
7	6	0
8	4	0
9	1	0

n.d. not done

The first uncommon feature that has been observed in (absorptive) villous enterocytes was the presence of transitional structures intermediate between microvillous inclusions and lysosomes in the apical part of cytoplasm. This finding is in line with a recent paper [28] demonstrating that the lysosomes accumulating into enterocytes derived from the transformation of microvillous inclusions (considered as early endosomes) via transformation into transitional structures (considered as late endosomes). In fact, microvillous inclusions stain with sucrase-isomaltase (SI) but are negative for lysosome specific markers, such as lysosome-associated membrane protein (LAMP), indicating their nature as early endosomes. Late endosomes express both LAMP and SI, whereas, lysosomes are strongly positive for LAMP and weak for SI. These data suggest that MID is caused by increased autophagocytosis of the apical membrane of enterocytes with formation of microvillous inclusion bodies [28].

The second observed feature was the presence of microvilli on the lateral membrane of villous enterocytes, which has previously been described [6, 23]. Lateral membrane microvilli have been also detected in rats after colchicine treatment [21]. According to Phillips and Schmitz (1992) [23], this ultrastructural finding may be ascribed to de novo synthesis of membrane, as the apical membrane is unlikely to migrate to a basolateral position. Recently, Ameen and Salas (2000) [2] hypothesized a role for ERM (ezrin, radixin, and moesin) proteins in this ultrastructural aspect: these proteins mediate the attachment of the actin/villin cores to the apical membrane to organize and stabilize the microvilli [32]. According to these authors, in MID the protein content decreases in the apical area and increases in the basolateral membrane. Croft et al. (2000) [6] reported a case of late-onset MID, where enterocytes were endowed with lateral membrane microvilli, and suggested that their presence may be related to a mild clinical phenotype. Phillips and Schmitz (1992)

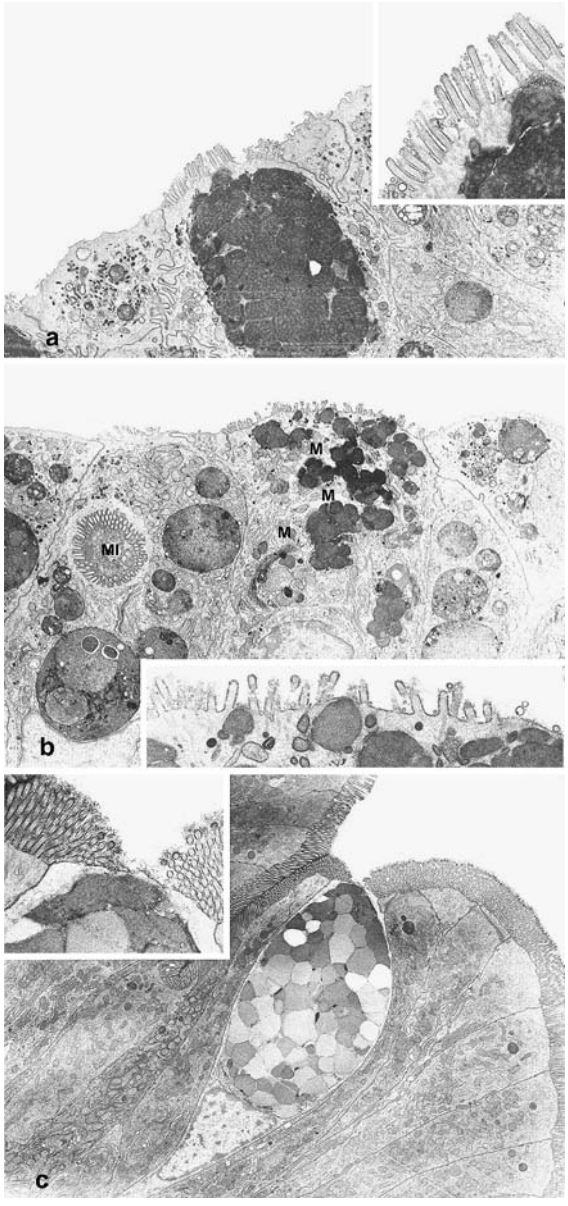

Fig. 6 Villous epithelial surface in microvillous inclusion disease (**a** and **b**, case 1) and in a control specimen (**c**). **a** Goblet cell with well-developed microvilli among enterocytes virtually devoid of microvilli. *Inset*: detail of the goblet cell surface; small dense likely glycocalyceal granules among microvilli are also evident. **b** Goblet cell with microvilli and scarce, non-confluent mucous granules (M). *Inset*: enlargement of goblet cell brush border. **c** Mature goblet cell with goblet aspect and confluent mucous granules among adjacent normal absorptive villous enterocytes. *Inset*: enlargement of goblet cell luminal surface. The microvilli are lacking in the central area and few at the periphery. *MI* microvillous inclusion. **a** ×6.250, *inset* ×18,000; **b** ×5.000, *inset* ×18.000; **c** ×3.400, *inset* ×12.500

[23] also observed a similar ultrastructural feature in early-onset cases and our finding supports this correlation.

The novel ultrastructural finding reported in this paper is the presence in case 1 of immature villous goblet cells characterized by both a well-developed apical brush border and the presence of scarce, non-confluent mucous granules: to our knowledge this finding has never been reported in MID.

The MID cytotype that has been most extensively investigated from an ultrastructural point of view is the enterocyte. Goblet cells have scarcely been studied and are described as cells with normal morphology and distribution [3, 8]. However, in a recent study Kučinskienė et al. (2004) [16] described a decreased number of goblet cells with low mucus secretion in a MID case. The mature goblet cell is characterized by an expanded apical cytoplasmic region containing confluent mucous granules. The luminal surface of the cell exhibits a few microvilli on the periphery of the cytoplasmic membrane, but it is usually smooth and convex over the secretory granules [11, 12, 30]. Similar goblet cells have been detected in villi from both normal and pathological controls, but immature goblet cells like those described in the villi of our MID case 1 have never been reported.

We can rule out that for technical reasons related to the plane of section the goblet cell microvilli observed in our MID case could be those normally localized at the periphery of the apical cell membrane. These cells were studied in serial sections by analysing a total thickness of about 1.3 μm of tissue (the microvilli measure 80–90 nm in diameter [11]) and were detected in all sections. Among the microvilli of immature goblet cells we observed some membrane-bound dense granules whose appearance corresponds with the glycocalyceal bodies found on the apical surface of normal and neoplastic epithelial cells of intestine [13, 17], respiratory tract [1, 9] and oesophagus [20]. Their function and nature are unknown [10, 14].

Even though the theory of a delayed differentiation of goblet cells needs to be confirmed in further MID cases, we hypothesize that the observed changes in these cells may be due to a mechanism of compensation in a severely disrupted absorptive compartment in this disease, as supported by the simultaneous presence in the same case of laterally sided microvilli.

In conclusion, we report the ultrastructural features of enterocytes in two MID cases and describe some morphological aspects of these cells that have been reported in very few of such cases. In addition, we describe for the first time immature goblet cells in MID villi, a finding that warrants further morpho-functional investigation.

Acknowledgements We are grateful to Drs. Mariella Marelli and Maria Cristina Zingaretti for their excellent technical assistance and to Dr. Michele Bisceglia for his critical reading and comments on the manuscript. This study was supported by a grant from the Polytechnic University of Marche (2005 FAR, formerly 60%) to M. M.

References

1. Afzelius BA (1984) Glycocalix and glycocalyceal bodies in the respiratory epithelium of nose and bronchi. Ultrastruct Pathol 7:1–8
2. Ameen NA, Salas PJI (2000) Microvillus inclusion disease: a genetic defect affecting apical membrane protein traffic in intestinal epithelium. Traffic 1:76–83

3. Bell SW, Kerner JA, Sibley RK (1991) Microvillous inclusion disease. The importance of electron microscopy for diagnosis. Am J Surg Pathol 15:1157–1164
4. Carruthers L, Dourmanshkin R, Phillips AD (1985) Disorders of the cytoskeleton of the enterocyte. Clin Gastroenterol 15:105–120
5. Carruthers L, Phillips AD, Dourmanshkin R, Walker-Smith JA (1986) Biochemical abnormality in brush border membrane protein of a patient with congenital microvillous atrophy. J Pediatr Gastroenterol Nutr 4:902–907
6. Croft NM, Howatson AG, Ling SC, Nairn L, Evans TJ, Weaver LT (2000) Microvillous inclusion disease: an evolving condition. J Pediatr Gastroenterol Nutr 31:185–189
7. Cutz E, Rhoads JM, Drumm B, Sherman PM, Durie PR, Forstner GG (1989) Microvillus inclusion disease: an inherited defect of brush-border assembly and differentiation. N Engl J Med 320:646–651
8. Davidson GP, Cutz E, Hamilton JR, Gall DG (1978) Familial enteropathy: a syndrome of protracted diarrhea from birth, failure to thrive and hypoplastic villus atrophy. Gastroenterology 75:783–790
9. Ellinger A, Gruber K, Stockinger L (1987) Glycocalyceal bodies—a marker for different epithelial cell types in human airways. J Submicrosc Cytol 19:311–320
10. Erlandson RA (ed) (1994) Intestinal-type microvilli. In: Diagnostic transmission electron microscopy of tumors. Raven, New York, pp 202–204
11. Fawcett DW (ed) (1994) Intestines. In: Bloom and Fawcett, A textbook of histology, 12th edn. Chapman & Hall, New York, pp 617–651
12. Freeman JA (1966) Goblet cell fine structure. Anat Rec 154:121–130
13. Ghadially FN (ed) (1985) Filamentous core rootlets and glycocalyceal bodies. In: Diagnostic electron microscopy of tumors, 2nd edn. Butterworths, London, pp 334–342
14. Ghadially FN (ed) (1997) Glycocalyceal bodies and filamentous core rootlets. In: Ultrastructural pathology of the cell and matrix, 4th edn. Butterworth-Heinemann, Boston, pp 1144–1151
15. Guandalini S, Nocerino A (2002) Congenital microvillus atrophy. Available at: URL http://www.emedicine.com/ped/topic461.htm. Last update May 25
16. Kučinskienė R, Jančiauskas D, Pužzs A, Adamonis K (2004) Microvillous inclusion disease. Medicina (Kaunas) 40:864–867
17. Marcus PB, Martin JH, Green RH, Krouse MA (1979) Glycocalyceal bodies and microvillous core rootlets. Arch Pathol Lab Med 103:89–92
18. Michail S, Collins JF, Xu H, Kaufman S, Vanderhoof J, Ghishan FK (1998) Abnormal expression of brush-border membrane transporters in the duodenal mucosa of two patients with microvillus inclusion disease. J Pediatr Gastroenterol Nutr 27:536–542
19. Mierau GW, Willis EJ, Wyatt-Ashmead J, Hoffenberg EJ, Cutz E (2001) Microvillous inclusion disease: report of a case with atypical features. Ultrastruct Pathol 25:517–521
20. Ozzello L, Savary M, Roethlisberger B (1977) Columnar mucosa of the distal esophagus in patients with gastroesophageal reflux. Pathol Annu 12:41–86
21. Pavelka MP, Gangl A (1983) Effects of colchicines on the intestinal transport of endogenous lipid. Gastroenterology 84:544–555
22. Phillips AD, Jenkins P, Raafat F, Walker-Smith JA (1985) Congenital microvillous atrophy: specific diagnostic features. Arch Dis Child 60:135–140
23. Phillips AD, Schmitz J (1992) Familial microvillous atrophy: a clinicopathological survey of 23 cases. J Pediatr Gastroenterol Nutr 14:380–396
24. Phillips AD, Szafranski M, Man L-Y, Wall WJ (2000) Periodic acid-Schiff staining abnormality in microvillous atrophy: photometric and ultrastructural studies. J Pediatr Gastroenterol Nutr 30:34–42
25. Phillips AD, Brown A, Swallow DM, Hicks S, Schüller S, Murch SH, Walker-Smith JA (2004) Acetylated sialic acid residues and blood group antigens localise within the epithelium in microvillous atrophy indicating internal accumulation of the glycocalyx. Gut 53:1764–1771
26. Pohl JF, Shub MD, Trevelline EE, Ingebo K, Silber G, Rayhorn N, Holve S, Hu D (1999) A cluster of microvillous inclusion disease in the Navajo population. J Pediatr 134:103–106
27. Raafat F, Green NJ, Nathavitharana KA, Booth IW (1994) Intestinal microvillous dystrophy: a variant of microvillous inclusion disease or a new entity? Hum Pathol 25:1243–1248
28. Reinshagen K, Naim HY, Zimmer KP (2002) Autophagocytosis of the apical membrane in microvillus inclusion disease. Gut 51:514–521
29. Ruemmele FM, Jan D, Lacaille F, Cézard J-P, Canioni D, Phillips AD, Peuchmaur M, Aigrain Y, Brousse N, Schmitz J, Revillon Y, Goulet O (2004) New perspectives for children with microvillous inclusion disease: early small bowel transplantation. Transplantation 77:1024–1028
30. Sandoz D, Nicolas G, Laine M-C (1985) Two mucous cell types revisited after quick-freezing. Biol Cell 54:79–99
31. Schofield DE, Agostini RM, Yunis EJ (1992) Gastrointestinal microvillus inclusion disease. Am J Clin Pathol 98:119–124
32. Shaw RJ, Henry M, Solomon F, Jacks T (1998) RhoA-dependent phosphorylation and relocalization of ERM proteins into apical membrane/actin protrusion in fibroblasts. Mol Biol Cell 9:403–419
33. Weeks DA, Zuppan CW, Malott RL, Mierau GW (2003) Microvillous inclusion disease with abundant vermiform, electron-lucent vesicles. Ultrastruct Pathol 27:337–340

Virchows Arch (2006) 448: 811–821
DOI 10.1007/s00428-006-0194-5

ORIGINAL ARTICLE

Masatoshi Akiyama · Haruo Ohtani · Eiichi Sato · Hiroshi Nagura · Koichi Tabayashi

Up-regulation of matrix metalloproteinase-2 and membrane-type 1-matrix metalloproteinase were coupled with that of type I procollagen in granulation tissue response after the onset of aortic dissection

Received: 28 February 2005 / Accepted: 18 November 2005 / Published online: 12 April 2006

Abstract The pathophysiological significance of matrix metalloproteinases (MMPs) in aortic dissection remains poorly understood. The purpose of the present study is to clarify the significance of MMPs in aortic dissection. The activities and distributions of MMP-2, membrane-type 1-MMP (MT1-MMP), and MMP-9 were evaluated by gelatin zymography, immunohistochemistry, and in situ hybridization in 29 patients and seven autopsy cases. To assess if these MMPs are related to a tissue remodeling process, we compared the expression of these MMPs with that of type I procollagen and platelet-derived growth factor receptor β chain (PDGF Rβ). Patients were divided into three groups based on histological findings: acute, intermediate, and healed groups. The most remarkable changes were observed in the intermediate group, in which MMP-2 activity peaked and tissue expression of mRNAs for MMP-2 and MT1-MMP were observed in spindle-shaped cells in the neointima, organizing thrombus, and the adventitia. These expression patterns were essentially coupled with those of type I procollagen mRNA and PDGF-Rβ protein. The association of MMP-2, MT1-MMP, type I procollagen, and PDGF-Rβ suggests that MMP-2 and MT1-MMP could be involved not only in the degradation of aortic tissue but also in tissue remodeling, which may be associated with the healing process.

Keywords Cardiovascular · Clin pathol · Extracell matrix · Immunohistochem · In situ hybrid

M. Akiyama (✉) · K. Tabayashi
Department of Cardiovascular Surgery,
Tohoku University Graduate School of Medicine,
1-1 Seiryo-machi, Aoba-ward,
Sendai 980-8574, Japan
e-mail: akiyamam@ccf.org
Tel.: +1-216-4453220
Fax: +1-216-4449198

M. Akiyama · H. Ohtani · E. Sato · H. Nagura
Department of Pathology,
Tohoku University Graduate School of Medicine,
1-1 Seiryo-machi, Aoba-ward,
Sendai 980-8574, Japan

H. Ohtani
Department of Pathology, Mito Medical Center,
280 Sakurano-sato, Ibaraki-machi, Higashi-Ibaraki-gun,
Ibaraki 311-3193, Japan

M. Akiyama
Department of Biomedical Engineering, Lerner Research Institute, The Cleveland Clinic Foundation,
9500 Euclid Avenue, ND-20,
Cleveland, OH 44195, USA

Introduction

Aortic dissection is a dynamic disease that may involve any portion of the aorta. Despite significant advances in diagnostic and therapeutic techniques, morbidity and mortality rates remain unsatisfactory. Conversely, the spontaneous closure of the false lumen has been documented in some patients and this event is a favorable prognostic factor [1, 25]. These clinical data suggest the significance of the healing and repair processes in dissections of the aorta.

Tissue remodeling is an essential part of all repair processes involving the degradation and synthesis of the extracellular matrix. Matrix metalloproteinases (MMPs) can degrade various components of the extracellular matrix. Most MMPs are secreted as zymogens that are most likely activated in the extracellular space by other proteases. Membrane-type 1-MMP (MT1-MMP) forms a complex with tissue inhibitor of metalloproteinase-2 (TIMP-2) serving as a cell surface receptor for pro-MMP-2 activation [22], and degrades collagen fibers [20]. Among the MMPs, MMP-2 and MMP-9 have been implicated in the pathogenesis of aortic aneurysms and atherosclerotic plaque [6, 14, 21]. MMP-1, MMP-2, and MMP-9 have been reported to play a role in the development and progression of aortic dissection [10, 12, 15, 23].

Considering the complex mechanisms involved with these matrix-degrading enzymes, we constructed the

present study to examine the gelatinolytic activities of MMP-2 and MMP-9, and in situ distributions of MMP-2, MMP-9, and MT1-MMP, and analyzed their role in aortic dissection. We also evaluated the tissue remodeling processes by examining in situ distributions of type I procollagen, a representative matrix protein, and platelet-derived growth factor receptor beta chain (PDGF-Rβ), a marker of activated fibroblasts/myofibroblasts [11]. The results reveal the complex significances of MMPs, and we propose that they are not only involved in tissue degradation but also in tissue remodeling after the onset of dissection.

Materials and methods

Patients

Twenty-nine patients with aortic dissection who underwent surgery at Tohoku University Hospital were analyzed in the present study (Tables 1, 2, and 3). To analyze the significance of MMPs after the onset of dissection, the patients were divided into three groups based on the histological findings [26]: acute, intermediate, and healed as described in the "Results" section. A full-thickness specimen oriented in cross-section was obtained from the dissected site adjacent to the entry site (within 3 cm) during surgery and processed for gelatin zymography, immunohistochemistry, and in situ hybridization. Aortic sample sites are listed in Tables 1, 2, and 3. Control specimens of the ascending aorta were obtained 1 to 3 h after death from seven autopsy cases without significant aortic disease (Table 4). To analyze the significance of MMPs at the onset of dissection, specimens from six patients just after the onset of dissection (<24 h, a subgroup of the acute group) were compared with specimens from seven normal individuals obtained during autopsy. A specimen from a macroscopically confirmed nondissected site was also obtained from the ascending aorta as "nondissected site (<24 h)" in five of six patients who received surgery within 24 h after the onset of a dissection.

The specimens were conventionally processed and stained with hematoxylin–eosin and elastica-Masson's staining for evaluation by light microscopy. Patients with Marfan's syndrome, a bicuspid aortic valve, or those undergoing reoperation were excluded from this study. Patients with a traumatic or iatrogenic aortic dissection were also excluded. This study was approved by the Ethical Committee of Tohoku University School of Medicine (#2000-119). Written informed consent was obtained from all patients.

Gelatin zymography

A fresh full-thickness specimen was snap-frozen in liquid nitrogen and stored at −80°C until use. The frozen tissue was homogenized in chilled 0.01 mol/l NaCl containing 0.01 mol/l $CaCl_2$, 0.05% Tween 20, 2 mmol/l PMSF, 0.02% NaN_3, 2% dimethylsulfoxide (DMSO), 2 mol/l urea, and 50 mol/l Tris–Cl at a pH of 7.5. The homogenate was centrifuged at 13,000 rpm for 15 min at 4°C. The supernatant was collected and applied to gelatin zymography. Gelatin zymography was performed as previously described, with minor modifications [13, 17]. Tissue extract containing 7.5 μg of protein was separated on a sodium dodecyl sulfate (SDS) polyacrylamide gel containing 0.8 mg/ml gelatin in a nonreducing condition. Purified MMP-2 and pro-MMP-9 (Yagai, Yamagata, Japan) were used as positive controls. After electrophoresis, the gel was washed three times for 15 min in a washing buffer containing 2.5% Tween 20, 10 mmol $CaCl_2$, 1 μmol $ZnCl_2$, and 50 mmol Tris–Cl (pH 7.5) to remove SDS. The gel was then incubated with an incubation buffer containing 1% Tween 20, 10 mmol $CaCl_2$, 1 μmol $ZnCl_2$, and 50 mmol Tris–Cl (pH 7.5) at 37°C for 18 h, and stained with

Table 1 Patient profiles (acute group)

Age and gender	Hypertension (Y/N)	Duration (days)	Stanford classification	FL (P/O)	Indications for surgery	Site of replacement	Sample site
52, M	Y	0	A	P	Shock, patent FL in Asc	Asc, Arch	Asc[a]
62, F	Y	0	A	P	Patent FL in Asc	Asc, Arch	Asc[a]
64, F	Y	0	A	P	Patent FL in Asc	Asc, Arch	Asc[a]
78, F	Y	0	A	P	Tamponade	Asc	Asc[a]
41, M	Y	0	A	P	Patent FL in Asc, AR	Root, Asc, Arch	Asc[a]
62, F	Y	0	A	P	Shock, Patent FL in Asc	Asc	Asc
65, F	Y	1	A	P	Patent FL in Asc	Asc	Asc
62, M	N	2	A	P	Patent FL in Asc	Asc	Asc
66, F	Y	3	A	P	Patent FL in Asc	Asc	Asc
77, F	Y	4	A	P	Patent FL in Asc	Asc	Asc
52, M	Y	4	A	P	Patent FL in Asc	Asc, Arch	Asc

[a]Specimens were obtained from the dissected and nondissected sites
FL false lumen, *P* patent, *O* occluded, *Asc* ascending aorta, *Arch* aortic arch, *AR* aortic regurgitation, *Root* aortic root

Table 2 Patient profiles (intermediate group)

Age and gender	Hypertension (Y/N)	Duration	Stanford classification	FL (P/O)	Indications for surgery (maximal aortic diameter)	Site of replacement	Sample site
81, F	Y	13 days	A	P	Impending rupture (60 mm)	Arch, Des	Des
67, M	N	14 days	A	O	Impending rupture (60 mm)	Asc, Arch	Asc
66, M	N	21 days	B	P	Impending rupture (55 mm)	Arch	Arch
50, F	Y	1 months	B	O	Redissection (53 mm)	Asc, Arch	Asc
76, F	N	2 months	A	O	Redissection (55 mm)	Asc	Asc
68, F	N	3 months	A	O	ULP (48 mm)	Asc, Arch	Asc
70, F	Y	3 months	B	O	Impending rupture (65 mm)	Arch	Arch
63, M	N	3 months	B	P	Impending rupture (55 mm)	Des	Des
65, M	Y	4 months	B	O	ULP (40 mm)	Des	Des

FL false lumen, *P* patent, *O* occluded, *Asc* ascending aorta, *Arch* aortic arch, *ULP* ulcer-like projection, *Des* thoracic descending aorta

Coomassie blue R250. The bands for total MMP-2, active MMP-2, and pro-MMP-9 were quantified by densitometry with Image Gauge (FUJI FILM, Tokyo, Japan). A reference sample in each gel was used to normalize scanned bands among the gels. All results are expressed as the average value obtained from repeating the analysis twice. The relative activities of MMPs were expressed in arbitrary units (AU). To determine if the gelatinolytic bands were derived from MMPs, an additional extraction was incubated with EDTA (20 mmol/l) added to the previously described buffer.

Immunohistochemistry

The methods employed during this study were described previously [2, 11]. We used frozen sections that were prefixed with periodate-lysine-4% paraformaldehyde for 16 h at 4°C. The primary antibodies employed were mouse monoclonal antibodies against human pro-MMP-2 (clone CA4001, IgG1, concentration 4.8 μg/ml) [9], TIMP-2 (67-4H11, IgG1k, 1.3 μg/ml, Fuji Chemical, Takaoka, Japan), pro-MMP-9 (GE213, 20 μg/ml) [16], PDGF-Rβ (61520.11, IgG1, 5 μg/ml, Genzyme, Cambridge, USA), and type I procollagen (PC-5-5, IgG1, 1.3 μg/ml, Takara, Kyoto, Japan). Frozen sections, 6 μm-thick, were incubated with these primary antibodies overnight and processed with a Nichirei Histofine Kit (Nichirei, Tokyo, Japan). Mouse monoclonal antibodies against human MT1-MMP (114-6G6 and 113-5B7, Fuji Chemical, Takaoka, Japan) were also employed. However, these antibodies were unsuccessful in detecting its respective antigen in frozen sections. As a negative control, the primary antibodies were replaced by isotype-matched control antibodies of the same concentration (DAKO, Grostrup, Denmark). All sections were then counterstained with hematoxylin.

Table 3 Patient profiles (healed group)

Age and gender	Hypertension (Y/N)	Duration (years)	Stanford classification	FL (P/O)	Indications for surgery (maximal aortic diameter)	Site of replacement	Sample site
55, M	Y	2	B	P	Impending rupture (59 mm)	Des	Des
56, F	Y	4	B	P	Aneurysm (48 mm)	Thoracoabd	Des
59, M	Y	4	B	P	Aneurysm (53 mm)	Des	Des
56, F	Y	5	B	P	Aneurysm (75 mm)	Thoracoabd	Des
78, F	Y	6	B	P	Impending rupture (50 mm)	Des	Des
72, M	Y	8	B	O	Aneurysm (63 mm)	Des	Des
75, M	Y	10	B	P	Aneurysm (70 mm)	Thoracoabd	Abd
72, M	Y	10	B	P	Aneurysm (63 mm)	Thoracoabd	Des
68, F	Y	12	B	P	Impending rupture (60 mm)	Des	Des

FL false lumen, *P* patent, *O* occluded, *Des* thoracic descending aorta, *Thoracoabd* thoraco–abdominal aorta, *Abd* abdominal aorta

Table 4 Patient profiles (autopsy group)

Age and gender	Hypertension (Y/N)	Diagnosis at autopsy	Sample site
53, M	N	Diastolic cardiomyopathy	Asc
55, M	Y	Gastric cancer	Asc
74, F	Y	Uterine cancer	Asc
81, M	Y	Gastric cancer	Asc
60, M	Y	Pulmonary embolism	Asc
63, F	Y	Colon cancer	Asc
60, M	Y	Pneumonia	Asc

All specimens were obtained from ascending aorta

In situ hybridization

The methods employed during this study were described previously [18]. We used the following cDNAs: (1) 2,654 bp *Hin*dIII-Xba I fragment of MMP-2 cDNA [9]; (2) 1,242 bp *Eco*R1–*Hin*dIII fragment of MT1-MMP cDNA [22]; (3) 1,098 bp *Eco*R1–*Eco*R1 fragment of type I procollagen cDNA [5]. Digoxigenin-labeled cRNAs were transcribed in vitro as described in the manufacturer's manual (DIG RNA Labeling Kit; Roche Diagnostics, Basel, Switzerland). For in situ hybridization, the specimen was fixed in 4% paraformaldehyde and 0.5% glutaraldehyde overnight, and then embedded in paraffin. The deparaffinized section was treated with 20 μg/ml proteinase-K for 30 min. The hybridization mixture containing 1 μg/ml antisense or sense probes was applied for 16 h at 50°C. After rinsing, alkaline-phosphatase-conjugated anti-digoxigenin antibody was added at a concentration of 1:500 overnight. The chromogen was nitroblue tetrachloride. All sections were then counterstained with methyl green.

Statistical methods

Statistical analysis for the results of gelatin zymography was performed with SPSS 11.5.1J (SPSS Japan, Tokyo, Japan). Differences among groups greater than three were analyzed by the Kruskal–Wallis rank test and Scheffe's *F* test. All tests were considered to be significant at $P<0.05$.

Two observers (MA and HO, with the latter being blind to the clinical data) independently performed semiquantitative analysis for immunohistochemistry and in situ hybridization. The expression of MMPs, PDGF-Rβ, and type I procollagen were semiquantified as follows: (+), abundant; (±), moderate; (−), minimal or absent. If the observers differed in their opinions, the two observers evaluated the microscopic fields and discuss the findings to reach a consensus.

Results

The clinical profiles of 29 patients and seven autopsy cases were shown in Tables 1, 2, 3, and 4. Twenty-nine patients were divided into three groups: acute ($n=11$, day 0–4, fibrin deposition, neutrophil infiltration, and minimal tissue response), intermediate ($n=9$, 13 days–4 months, abundant stromal cell-response and matrix synthesis), and healed ($n=9$, >2 years, sparse stromal cells and dense deposition of matrix) groups.

The mean age (year)±standard deviations of patients in acute, intermediate, and healed groups and that of autopsy cases were 61.9±9.7, 61.9±12.7, 65.7±9.2, and 63.7±10.2, respectively. There was no significant difference with regard to age among these four groups. As for five patients from whom the nondissected site (<24 h) was obtained, their mean age (year)±standard deviations were 56.2±9.7, which is also not different with that of autopsy cases.

Hypertension was present in 10 (91%), four (44%), and nine (100%) patients in the acute, intermediate, and healed groups, respectively. As for patients from whom the nondissected site (<24 h) was obtained, hypertension was present in all patients. Six of the autopsy cases (86%) had a history of hypertension.

Gelatin zymography

Figure 1 shows an example of gelatin zymography. First, we compared MMP levels among the three groups using all

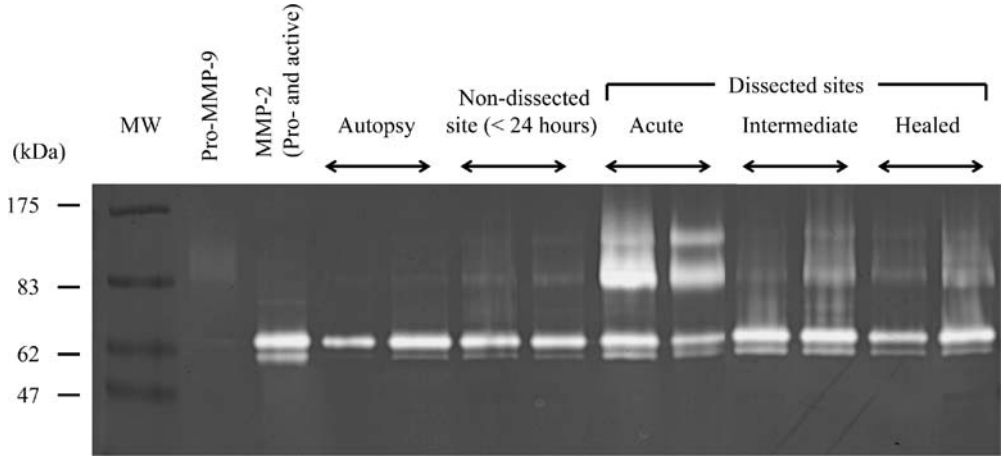

Fig. 1 An example of gelatin zymography. *Autopsy*, the cadaveric specimen from autopsy case; *nondissected site (<24 h)* the nondissected site just after the onset (<24 h); *acute* the dissected site in the acute group; *intermediate* the dissected site in the intermediate group; *healed* the dissected site in the healed group. The positions of molecular weight standards (MW) are indicated on the *left*. Purified pro-MMP-9 and MMP-2 commercially available were used as positive controls

cases. Active MMP-2 was most abundant in the intermediate group (Fig. 2a), while pro-MMP-9 was higher in the acute group (Fig. 2b). The total MMP-2 activity showed no significant differences among different groups. Next, we compared MMP levels between the dissected and non-dissected site just after the onset of dissection (<24 h; a subgroup of the acute group). As shown in Fig. 3a,b, the levels of active MMP-2 and pro-MMP-9 from the dissected sites were higher than the levels from the nondissected sites in those patients who received surgery within 24 h. The MMP levels in the nondissected sites (<24 h) did not differ from the levels found in the cadaveric specimens.

Immunohistochemistry and in situ hybridization

To clarify the in situ distribution, we performed immunohistochemistry and in situ hybridization to detect proteins and mRNAs, respectively. The semiquantitative results of these studies are shown in Table 5.

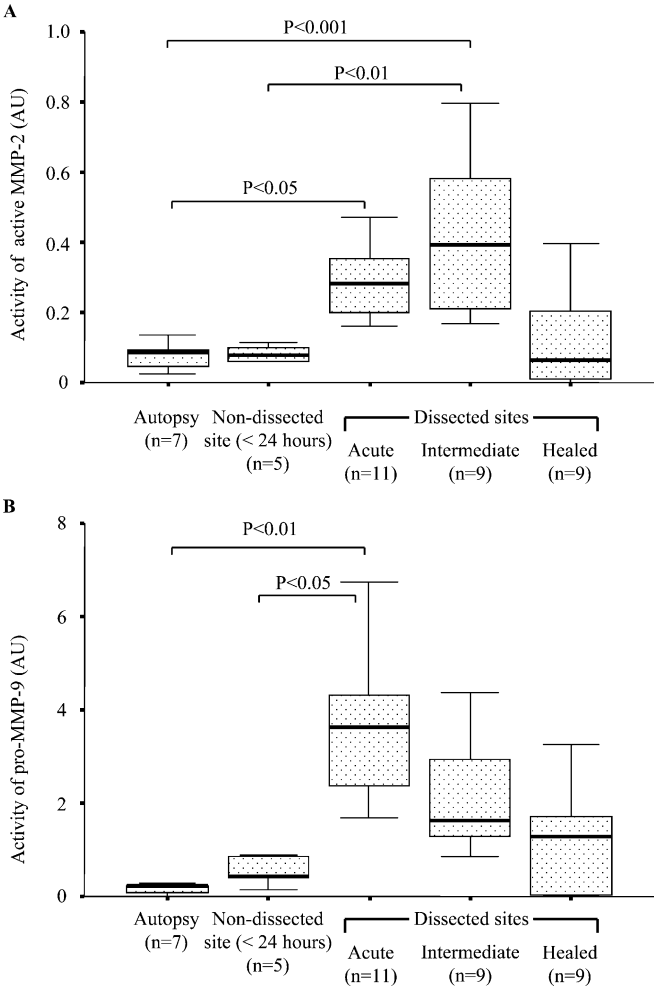

Fig. 2 Comparison of the activities of MMP-2 (**a**) and MMP-9 (**b**) from the dissected sites in different groups (acute, intermediate, and healed groups) by Box–Whisker plots. MMPs-2 and 9 peaked in the intermediate and the acute groups, respectively. The relative activities of MMPs were expressed in arbitrary units (AU)

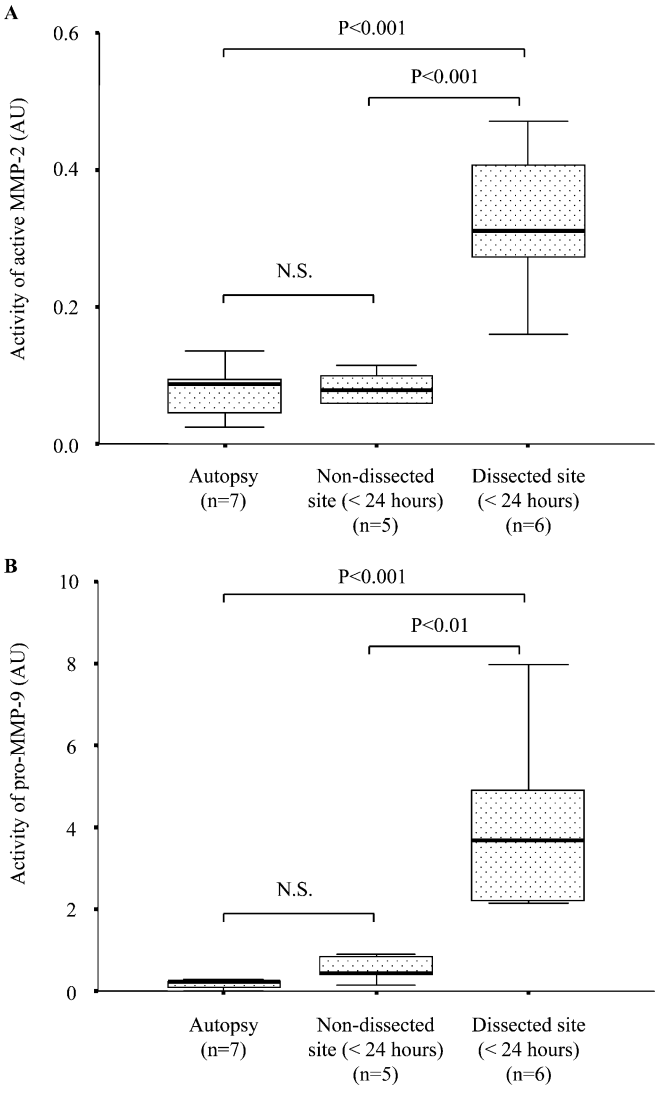

Fig. 3 Comparison of the activities of MMP-2 (**a**) and pro-MMP-9 (**b**) in the patients just after the onset (<24 h) and in the autopsy cases by Box–Whisker plots. The activities in the dissected sites were higher than those in the nondissected sites and in the cadaveric specimens. The relative activities of MMPs were expressed in arbitrary units (AU)

Dissected site in the acute group (>day 4, 11 patients)

As observed with light microscopy, a thin-layered thrombus was attached to the dissected surface (Fig. 4a), where it was infiltrated by neutrophils. These neutrophils abundantly expressed pro-MMP-9 protein (Fig. 4g). Neutrophils infiltrating in the adventitia also expressed pro-MMP-9. Medial spindle-shaped cells constitutively expressed pro-MMP-2 and TIMP-2 proteins (Fig. 4b,e) and moderately expressed mRNAs for MMP-2 and MT1-MMP (Fig. 4c,d). Type I procollagen mRNA was not observed (Fig. 4f).

In the nondissected site (<24 h, five patients), however, no case revealed expression of pro-MMP-9 protein or mRNAs for MMP-2, MT1-MMP, and type I procollagen. Medial spindle-shaped cells constitutively expressed pro-

Table 5 Summary for the results of immunohistochemistry and in situ hybridization

	Nondissected site, <24 h		Dissected site, acute		Dissected site, intermediate			Dissected site, healed		
	M	Ad	M	Ad	FL	M	Ad	FL	M	Ad
MMP-2 mRNA	−	−	±	±	+	−	+	−	−	−
MT1-MMP mRNA	−	−	±	±	+	−	+	−	−	−
Type I procollagen mRNA	−	−	−	−	+	−	+	−	−	−
Pro-MMP-2 protein	+	+	+	+	+	+	+	−	±	−
TIMP-2 protein	+	+	+	+	+	+	+	−	±	−
Type I procollagen protein	−	−	−	−	+	−	+	−	−	−
PDGF-Rβ protein	−	−	−	−	+	−	+	−	−	−
Pro-MMP-9 protein	−	−	+	+	+	−	±	−	−	−

M media, *Ad* adventitia, *FL* false lumen (neointima or organized thrombus), +, abundant; ±, moderate; −, minimal or absent

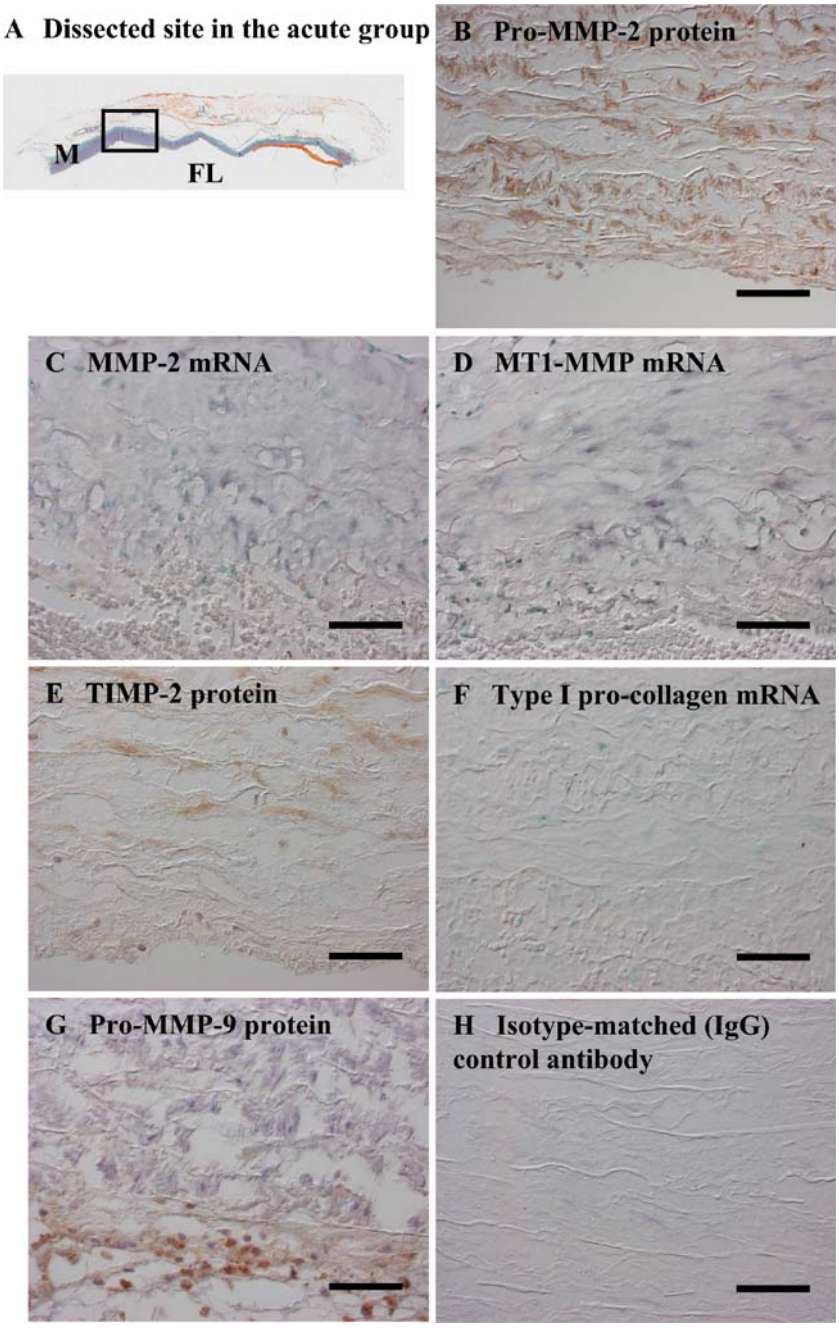

Fig. 4 Morphological results in the acute group (day 2). **a** A panoramic view. *FL* false lumen; *M* media. Higher magnifications of *boxed area* in **a**, showing the expression of pro-MMP-2 protein (**b**, *brown*, abundantly), MMP-2 mRNA (**c**, *dark blue*, moderately), MT1-MMP mRNA (**d**, *dark blue*, moderately), and TIMP-2 protein (**e**, *brown*, moderately) by the spindle-shaped cells in the media. Type I procollagen mRNA (**f**) was not detected. Pro-MMP-9 protein (**g**, *brown*) is abundantly positive in neutrophils. **h** Isotype-matched control antibody for pro-MMP-2 is not stained. Scale bar=50 μm

MMP-2 and TIMP-2 proteins as in dissected sites (data not shown). As shown in Fig. 4h, IgG isotype-matched control antibodies showed no specific stains in all patients, confirming the specificity of our results.

Dissected site in the intermediate group (day 13–4 months, nine patients)

The adventitia was markedly thickened (Fig. 5a). Neointima developed on the dissected surface in patients with patent false lumen. In patients with an occluded false lumen, the thrombus in the false lumen was partially organized, showing a proliferation of spindle-shaped cells and deposition of collagen fibers in the peripheral areas (Fig. 6a). Messenger RNAs for MMP-2 (Figs. 5b and 6b) and MT1-MMP (Figs. 5c and 6d), and pro-MMP-2 (Fig. 6c) and TIMP-2 (Figs. 5h and 6e) proteins were abundantly expressed by the spindle-shaped cells in the neointima, organizing thrombus, and adventitia, which were closely coupled with the expression of type I procollagen mRNA (Figs. 5d and 6f) and protein (Figs. 5i and 6g) in the same areas. The spindle-shaped cells in those areas further expressed PDGF-Rβ protein (Figs. 5j and 6h). The number of neutrophils expressing pro-MMP-9 protein decreased, and macrophages and multinucleated giant cells in the organizing thrombus were positive for pro-MMP-9 protein (Fig. 6i). As shown in Figs. 5e–g, the sense probes for mRNAs for MMP-2, MT1-MMP, and type I procollagen showed no specific signals in all patients, confirming the specificity of our results.

Dissected site in the healed group (>2 years, nine patients)

Spindle-shaped cells were sparse with dense deposition of collagen fibers in the neointima, organized false lumen, and adventitia (Fig. 7a). The number of cells positive for pro-MMP-2 (Fig. 7b), TIMP-2, type I procollagen (Fig. 7f), and PDGF-Rβ (Fig. 7g) proteins markedly decreased, and there were few cells expressing pro-MMP-9 protein (Fig. 7h). The cells positive for these substances were primarily localized around vasa vasorum in the adventitia. The number of cells positive for mRNAs for MMP-2 (Fig. 7c), MT1-MMP (Fig. 7d), and type I procollagen (Fig. 7e) also markedly decreased in those areas.

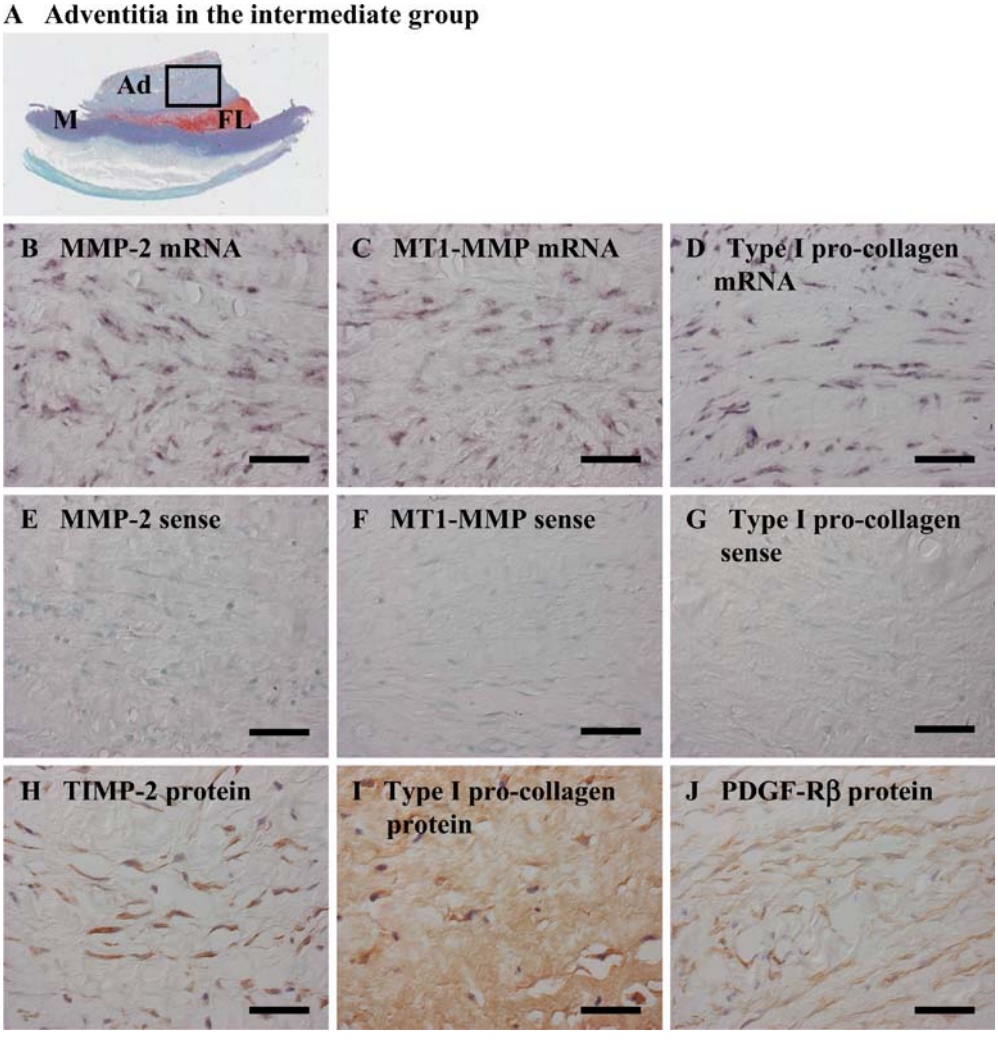

Fig. 5 Morphological results of the dissected site with a thickened adventitia from the intermediate group (day 14). **a** A panoramic view. *M* media; *FL* false lumen; *Ad* adventitia. Higher magnifications of *boxed area* in **a**, showing abundant expression of MMP-2 mRNA (**b**, *dark blue*), MT1-MMP mRNA (**c**, *dark blue*), and type I procollagen mRNA (**d**, *dark blue*) by the spindle-shaped cells in the adventitia. Note a clear similarity of the expression pattern of MMP-2, MT1-MMP, and type I procollagen mRNAs. Negative controls are shown in sense probe for MMP-2 mRNA (**e**), sense probe for MT1-MMP mRNA (**f**), and sense probe for type I procollagen mRNA (**g**). TIMP-2 protein (**h**, *brown*), type I procollagen protein (**i**, *brown*), and PDGF-Rβ protein (**j**, *brown*) are abundantly expressed by the spindle-shaped cells in the adventitia were shown. Scale bar=50 μm

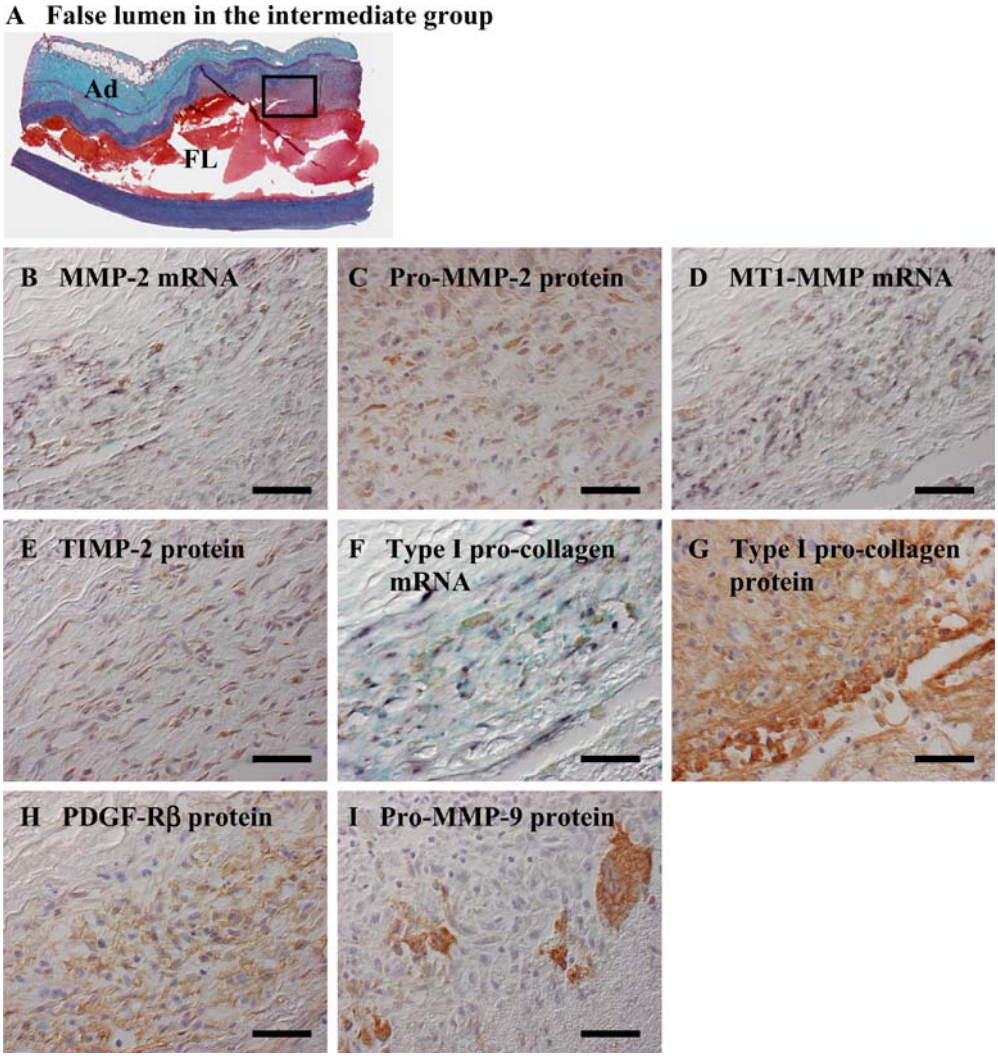

Fig. 6 Morphological results of the dissected site with organizing thrombus in the false lumen from the intermediate group (1 month). **a** A panoramic view. *FL* false lumen; *Ad* adventitia. Higher magnifications of *boxed area***a**, showing abundant expression of MMP-2 mRNA (**b**, *dark blue*), pro-MMP-2 protein (**c**, *brown*), MT1-MMP mRNA (**d**, *dark blue*), TIMP-2 protein (**e**, *brown*), type I procollagen mRNA (**f**, *dark blue*), type I procollagen protein (**g**, *brown*), and PDGF-Rβ protein (**h**, *brown*) by the spindle-shaped cells in the organizing thrombus. Pro-MMP-9 protein is detected in giant cells (**i**, *brown*). Scale bar=50 μm

Discussion

The present study was designed to clarify the significance of MMP-2, MT1-MMP, and MMP-9 in aortic dissection. We have revealed two types of distinctive up-regulation of MMPs: MMP-9 in the acute group, and MMP-2 in the intermediate group, the latter coupled with MT1-MMP, TIMP-2, type I procollagen, and PDGF-Rβ. The gelatinolytic activities and the in situ distribution of these MMPs in these groups were significantly higher than those in the nondissected aorta (<24 h) or the control aorta obtained from autopsy cases.

It is well known that immunohistochemistry for MMP-2 shows constitutive expression of its protein in smooth muscle cells irrespective of its production status [6, 14]. Therefore, in situ hybridization was performed to evaluate the in situ production of MMP-2 as reported previously [18, 19]. To consider the significance of MMPs in various stages after the onset of dissection, we have divided patients into three groups based on the histopathological changes [26] because these changes were related to the time course.

The most pronounced signal of MMP-2 mRNA was observed in the cytoplasm of spindle-shaped cells in the organizing thrombus, neointima, and thickened adventitia in the intermediate group, in which the gelatinolytic activity of MMP-2 was highest. The spindle-shaped cells in the same areas also abundantly expressed MT1-MMP mRNA and TIMP-2 protein in the same pattern. Moreover, such abundant expression of MMP-2, TIMP-2, and MT1-MMP were coupled with those of type I procollagen and PDGF-Rβ. These quite notable findings required us to consider tissue remodeling because matrix degradation is not only important for tissue degradation, but is also required for deposition of new collagen fibers in the injured vessels [24]. Morphologic findings showed the formation of granulation tissue on the surface of the false lumen in the intermediate group, which later became fibrosis (scar) in the equivalent areas in the healed group. The same findings were also observed in the thickened adventitia. Briefly, matrix synthesis is stimulated and matrix accumulation actually occurs in these areas where MMP-2, TIMP-2, and MT1-MMP are up-regulated. If we focused only on tissue degradation, it would have been difficult to explain these morphological findings. When the simultaneous up-regu-

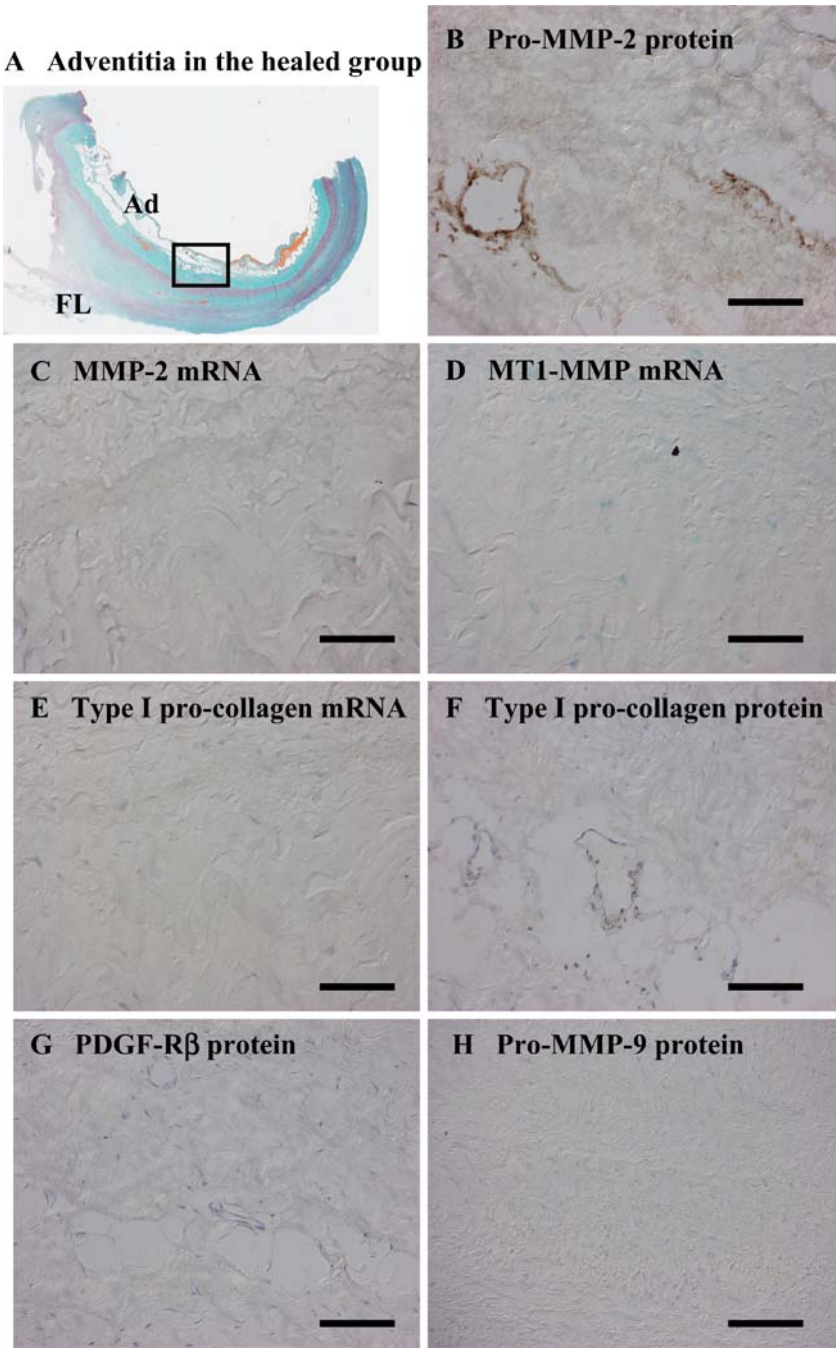

Fig. 7 Morphological results of the dissected site with scarring adventitia from the healed group (6 years). **a** A panoramic view. *FL* false lumen; *Ad* adventitia. Higher magnifications of *boxed area* in **a**, showing pro-MMP-2 protein (**b**, *brown*, scanty positive in spindle-shaped cells in vasa vasorum), MMP-2 mRNA (**c**, no signal), MT1-MMP mRNA (**d**, no signal), type I procollagen mRNA (**e**, no signal), type I procollagen protein (**f**, no staining), PDGF-Rβ protein (**g**, *brown*, no staining), and pro-MMP-9 protein (**h**, no staining). Scale bar=50 μm

lation of MMP-2, TIMP-2, MT1-MMP, type I procollagen, and PDGF-Rβ are compared with these morphologic changes described above, we have concluded that the up-regulation of these substances is most probably associated with the deposition of new collagen fibers. The spontaneous closure of false lumen is documented as a favorable prognostic factor [1, 25]. In this situation, the dissection may heal, obliterating the false lumen and leaving a linear scar in the outer media. Our data suggested that MMP-2, TIMP-2, and MT1-MMP in the intermediate group are related to the matrix regeneration process, which may be related to the healing process.

As for MMP-9, we observed its more pronounced expression in neutrophils in the acute group. Neutrophils play a role in tissue damage caused during the inflammatory process. The MMP-9 expressed by neutrophils is involved in the digestion of dead tissue that is a step in the tissue repair process [7]. We could consider two possibilities for this observation. First, from our data, it could be interpreted that MMP-9 may contribute to the degradation of the aortic wall in the early stage. This event may be one of the factors that worsen the prognosis of the disease. The other possibility is that MMP-9 activity may be significant in tissue remodeling. However, further study is required to elucidate the significance of MMP-9.

We compared the activities of MMP-2 and MMP-9 in the nondissected sites (<24 h), the dissected sites (<24 h), and the cadaveric specimens by gelatin zymography. The activities of these MMPs in the dissected sites (<24 h) were significantly higher than in the nondissected sites (<24 h) and in the cadaveric specimens. Our data suggested that the up-regulation of MMP-2 and MMP-9 have already been affected by the dissection itself, not indicating higher MMP-2 and MMP-9 before the dissection. Therefore, we have not obtained the data that supports the concept that MMP-2 and MMP-9 are involved in the onset of aortic dissection. However, the possibility remains that the actual MMP-2 and MMP-9 activities in the entry sites may be higher even before the aortic dissection because aortic dissection occurs at the points of presumed greatest hemodynamic stress [8], which can alter the MMPs activity [3, 4]. The present study revealed the distribution of mRNA and/or protein of MMP-2, MT1-MMP, TIMP-2, and type I procollagen. To evaluate the molecular events more precisely, we should explore in situ zymography or double/triple-labeling tissue staining in future studies. Also, our present study covered a rather limited number of patients, and therefore, future studies will require a larger patient cohort to more accurately compare MMP activities in various clinical conditions. In addition, the involvement of additional MMPs, such as MMP-1, MMP-8, and MMP-12 should be evaluated in the future studies.

In conclusion, the present study revealed the complex activities of MMPs and TIMPs, with a role not only in tissue degradation but also in tissue remodeling after the onset of an aortic dissection.

Acknowledgements We are grateful to Dr. Kazuhiko Igarashi (Department of Biomedical Chemistry, Hiroshima University School of Medicine) for his help with the molecular biological techniques, and to Dr. Shoko Miura and Dr. Isao Ohno (Department of Infectious and Respiratory Diseases, Tohoku University Graduate School of Medicine) for their technical guidance on gelatin zymography. Technical assistance from Ms. Fumiko Date is greatly appreciated. The present study was supported by the Japan Foundation of Cardiovascular Research from 2000 to 2002.

References

1. Akutsu K, Nejima J, Kiuchi K, Sasaki K, Ochi M, Tanaka K et al (2004) Effects of the patent false lumen on the long-term outcome of type B acute aortic dissection. Eur J Cardiothorac Surg 26:359–366
2. Arihiro S, Ohtani H, Hiwatashi N, Torii A, Sorsa T, Nagura H (2001) Vascular smooth muscle cells and pericytes express MMP-1, MMP-9, TIMP-1 and type I procollagen in inflammatory bowel disease. Histopathology 39:50–59
3. Bassiouny HS, Song RH, Hong XF, Singh A, Kocharyan H, Glagov S (1998) Flow regulation of 72-kD collagenase IV (MMP-2) after experimental arterial injury. Circulation 98: 157–163
4. Chesler NC, Ku DN, Galis ZS (1999) Transmural pressure induces matrix-degrading activity in porcine arteries ex vivo. Am J Physiol 277(5 Pt 2):H2002–H2009
5. Chu ML, Myers JC, Bernard MP, Ding JF, Ramirez F (1982) Cloning and characterization of five overlapping cDNAs specific for the human pro alpha 1(I) collagen chain. Nucleic Acids Res 10:5925–5934
6. Galis ZS, Sukhova GK, Lark MW, Libby P (1994) Increased expression of matrix metalloproteinases and matrix degrading activity in vulnerable regions of human atherosclerotic plaques. J Clin Invest 94:2493–2503
7. Heymans S, Luttun A, Nuyens D, Theilmeier G, Creemers E, Moons L et al (1999) Inhibition of plasminogen activators or matrix metalloproteinases prevents cardiac rupture but impairs therapeutic angiogenesis and causes cardiac failure. Nat Med 5:1135–1142
8. Hirst AE Jr, Johns VJ Jr, Kime SW Jr (1958) Dissecting aneurysm of the aorta: a review of 505 cases. Medicine (Baltimore) 37:217–279
9. Huhtala P, Eddy RL, Fan YS, Byers MG, Shows TB, Tryggvason K (1990) Completion of the primary structure of the human type IV collagenase preproenzyme and assignment of the gene (CLG4) to the q21 region of chromosome 16. Genomics 6:554–559
10. Ishii T, Asuwa N (2000) Collagen and elastin degradation by matrix metalloproteinases and tissue inhibitors of matrix metalloproteinase in aortic dissection. Hum Pathol 31:640–646
11. Katou F, Ohtani H, Nagura H, Motegi K (1998) Procollagen-positive fibroblasts predominantly express fibrogenic growth factors and their receptors in human encapsulation process against foreign body. J Pathol 186:201–208
12. Koullias GJ, Ravichandran P, Korkolis DP, Rimm DL, Elefteriades JA (2004) Increased tissue microarray matrix metalloproteinase expression favors proteolysis in thoracic aortic aneurysms and dissections. Ann Thorac Surg 78: 2106–2111
13. Kumagai K, Ohno I, Okada S, Ohkawara Y, Suzuki K, Shinya T et al (1999) Inhibition of matrix metalloproteinases prevents allergen-induced airway inflammation in a murine model of asthma. J Immunol 162:4212–4219
14. Li Z, Li L, Zielke HR, Cheng L, Xiao R, Crow MT et al (1996) Increased expression of 72-kd type IV collagenase (MMP-2) in human aortic atherosclerotic lesions. Am J Pathol 148:121–128
15. Manabe T, Imoto K, Uchida K, Doi C, Takanashi Y (2004) Decreased tissue inhibitor of metalloproteinase-2/matrix metalloproteinase ratio in the acute phase of aortic dissection. Surg Today 34:220–225
16. Margulies IM, Hoyhtya M, Evans C, Stracke ML, Liotta LA, Stetler-Stevenson WG (1992) Urinary type IV collagenase: elevated levels are associated with bladder transitional cell carcinoma. Cancer Epidemiol Biomarkers Prev 1:467–474
17. Miura S, Ohno I, Suzuki J, Suzuki K, Okada S, Okuyama A et al (2003) Inhibition of matrix metalloproteinases prevents cardiac hypertrophy induced by beta-adrenergic stimulation in rats. J Cardiovasc Pharmacol 42:174–181
18. Ohtani H, Motohashi H, Sato H, Seiki M, Nagura H (1996) Dual over-expression pattern of membrane-type metalloproteinase-1 in cancer and stromal cells in human gastrointestinal carcinoma revealed by in situ hybridization and immunoelectron microscopy. Int J Cancer 68:565–570
19. Ohtani H, Tabata N, Nagura H (1995) Immunoelectron microscopic localization of gelatinase A in human gastrointestinal and skin carcinomas: difference between cancer cells and fibroblasts. Jpn J Cancer Res 86:304–309
20. Ohuchi E, Imai K, Fujii Y, Sato H, Seiki M, Okada Y (1997) Membrane type 1 matrix metalloproteinase digests interstitial collagens and other extracellular matrix macromolecules. J Biol Chem 272:2446–2451
21. Sakalihasan N, Delvenne P, Nusgens BV, Limet R, Lapiere CM (1996) Activated forms of MMP2 and MMP9 in abdominal aortic aneurysms. J Vasc Surg 24:127–133
22. Sato H, Takino T, Okada Y, Cao J, Shinagawa A, Yamamoto E et al (1994) A matrix metalloproteinase expressed on the surface of invasive tumour cells. Nature 370:61–65

23. Schneiderman J, Bordin GM, Adar R, Smolinsky A, Seiffert D, Engelberg I et al (1998) Patterns of expression of fibrinolytic genes and matrix metalloproteinase-9 in dissecting aortic aneurysms. Am J Pathol 152:703–710
24. Strauss BH, Robinson R, Batchelor WB, Chisholm RJ, Ravi G, Natarajan MK et al (1996) In vivo collagen turnover following experimental balloon angioplasty injury and the role of matrix metalloproteinases. Circ Res 79:541–550
25. Sueyoshi E, Sakamoto I, Hayashi K, Yamaguchi T, Imada T (2004) Growth rate of aortic diameter in patients with type B aortic dissection during the chronic phase. Circulation 110(11 Suppl 1):II256–261
26. Virmani R, Burke AP (1991) Nonatherosclerotic diseases of the aorta and miscellaneous diseases of the main pulmonary arteries and large veins. In: Silver MD, Gotlieb AI, Schoen FJ (eds) Cardiovascular Pathology 3rd edn. Churchill Livingstone, New York, pp 107–137

Virchows Arch (2006) 448: 822–829
DOI 10.1007/s00428-006-0198-1

ORIGINAL ARTICLE

Yasuyoshi Miyata · Kojiro Ohba · Shigeru Kanda · Koichiro Nomata · Jiro Eguchi · Tomayoshi Hayashi · Hiroshi Kanetake

Pathological function of prostaglandin E2 receptors in transitional cell carcinoma of the upper urinary tract

Received: 9 September 2005 / Accepted: 11 December 2005 / Published online: 12 April 2006

Abstract The prostaglandin E2 receptor, EP4 receptor (EP4R), plays an important role in the development of transitional cell carcinoma of the upper urinary tract (TCC-UUT). However, the clinical significance of other EP receptors (EP1R–3R) is not clear. Furthermore, the pathological function of EP receptors in such patients is not understood. In the present study, we examined the expression of EP1R–3R in 101 TCC-UUT tissues by immunohistochemistry. Furthermore, we defined the relationship between cyclooxygenase (COX)-2 and EP receptor expression, proliferation index (PI), microvessel density (MVD), and expression of metalloproteinase-2 (MMP-2), urokinase-type plasminogen activator (uPA), and exon v6 containing CD44 isoform (CD44 v6) by multivariate analysis. The expression of EP1R, EP2R, and EP3R was positive in 20 (19.8%), 26 (25.7%), and 14 (13.9%) tumor samples, respectively. Expression of these receptors was not associated with pathological findings or survival. COX-2 and EP4R were independently associated with MVD and MMP-2, and uPA or PI and MMP-2, respectively. Other EP receptors were not influenced by any factors. Our results suggest that EP1R–3R play a minimal role in cancer progression in patients with TCC-UUT. On the other hand, EP4R regulates tumor progression via cancer cell proliferation and MMP-2, distinct from COX-2.

Keywords Protein expression · Transitional cell carcinoma · Upper urinary tract · Prognosis · Immunohistochemistry

This study was not funded by any commercial organization. It was supported in part by a Grant-in-Aid from the Japanese Society of the Promotion of Science.

Y. Miyata (✉) · K. Ohba · K. Nomata · J. Eguchi · H. Kanetake
Department of Urology,
Nagasaki University School of Medicine,
1-7-1 Sakamoto,
Nagasaki 852-8501, Japan
e-mail: int.doc.miya@m3.dion.ne.jp
Tel.: +81-95-8497340
Fax: +81-95-8497343

S. Kanda
Department of Molecular Microbiology and Immunology,
Nagasaki University Graduate School of Biomedical Science,
1-12-4 Sakamoto,
Nagasaki 852-8501, Japan

T. Hayashi
Department of Pathology, Nagasaki University Hospital,
1-7-1 Sakamoto,
Nagasaki 852-8501, Japan

Introduction

The clinical and pathological significance of cyclooxygenase (COX)-2 in cancer cells has become increasingly important due to mounting evidence demonstrating that COX-2 plays an important role in carcinogenesis, tumor development, and prognosis in several cancers including transitional cell carcinoma of the urinary bladder [9, 17, 24, 34, 37]. The main function of COX-2 is to convert arachidonic acid to prostaglandins (PGs); PGE2 is the most predominant and active end-product in this COX-2 pathway. PGE2 affects various physiological functions, including cell proliferation, angiogenesis, immune responsiveness, and apoptosis [4, 31, 32]. The role of PGE2 on these physiological activities has important implications for the malignant potential and aggressiveness of cancer cells. Therefore, much attention has focused on the pathological significance of PGE2, and enhanced synthesis of PGE2 and activation of malignant aggressiveness by PGE2 were observed in various cancers [18, 29, 36]. In addition to these cancers, PGE2 pathway was also reported to be associated with malignant aggressiveness in urothelial carcinomas of the bladder [10]. Furthermore, pharmacological and animal studies showed that the major antitumor action of nonsteroidal anti-inflammatory drugs (NSAIDs), which are COX-2 inhibitors, is mediated through the inhibition of PGE2 [11, 38]. The findings support the notion that PGE2 stimulates carcinogenesis and tumor development.

The biological activities of PGE2 can be attributed to their specific receptors (EP1 receptor to EP4 receptor; EP1R–EP4R) on target cells [6]. Therefore, one could hypothesize that one or any of the EP receptors may affect carcinogenesis and tumor progression. Indeed, EP receptors are reported to be associated with malignant potential, cancer cell development, and survival in several cancers [2, 5, 14, 15, 26, 30, 35]. In addition, we recently reported that the expression of COX-2 and EP4R was associated with high stage and poor prognosis in patients with transitional cell carcinoma of the upper urinary tract (TCC-UUT) [23]. However, there are no reports on the clinical significance and prognostic influence of EP1R–EP3R in patients with TCC-UUT.

COX-2 and PGE2 appear to influence tumor development and prognosis through a variety of mechanisms [7, 13, 19, 20–22, 27, 28]. For example, COX-2 and PGE2 regulate cancer cell proliferation, angiogenesis, matrix metalloproteinase (MMP)-2, urokinase-type plasminogen activator (uPA), and CD44 in various carcinomas [7, 19–21]. In patients with TCC-UUT, we previously reported that high proliferation index (PI), microvessel density (MVD), and MMP-2 expression were associated with high pT stage and poor prognosis [22], and several other investigators also showed similar trends and results [13, 28]. In contrast, Nakanishi et al. [27] reported that uPA expression was positively associated with tumor stage in patients with TCC-UUT. Furthermore, among CD44 proteins, exon v6 containing CD44 isoforms (CD44 v6) was associated with malignant potential and tumor invasion in TCC of the urinary tract [12]. Thus, PGE2 might regulate malignant aggressiveness and tumor development thorough a complex mechanism. However, the relationship between EP receptors and these COX-2/PGE2-related factors in TCC-UUT is not fully understood.

A number of investigators have assessed the potential usefulness of COX-2 inhibitors for the prevention of carcinogenesis and tumor development [1, 3, 25]. However, other investigators speculated that various EP receptor inhibitors can control carcinogenesis and cancer cell development [11, 15]. Therefore, detailed data regarding the independent action of COX-2 and each EP receptor will be required for planning prevention and treatment strategies.

The main objective of the present study was to clarify the clinical and prognostic significance of EP1-3 receptor in patients with TCC-UUT. A secondary objective was to elucidate the interaction between COX-2 or each EP receptor and PI, MVD, and MMP-2, uPA, and CD44 v6 by using multivariate analysis.

Materials and methods

Patients and tissue samples

One hundred and one consecutive patients who were diagnosed with nonmetastatic TCC of the renal pelvis and ureter were reviewed retrospectively. Our study included

Table 1 Relationships between expressions of EP1–3 receptors and clinicopathological features

	No. of patients	EP1R (%)		EP2R (%)		EP3R (%)	
		Negative	Positive	Negative	Positive	Negative	Positive
Total no.	101	81 (80.2)	20 (19.8)	75 (74.3)	26 (25.7)	87 (86.1)	14 (13.9)
Gender							
Male	74	57 (58.1)	17 (41.9)	55 (74.3)	19 (25.7)	63 (85.1)	11 (14.9)
Female	27	24 (44.4)	3 (55.6)	20 (74.1)	7 (25.9)	24 (44.4)	3 (55.6)
P value		0.186		0.980		0.629	
Multicentricity							
Absence	75	60 (80.0)	15 (20.0)	54 (72.0)	21 (28.0)	64 (85.3)	11 (14.7)
Presence	26	21 (80.8)	5 (19.2)	21 (80.8)	5 (19.2)	23 (88.5)	3 (11.5)
P value		0.932		0.378		0.932	
pT stage							
pTa	7	6 (85.7)	1 (14.3)	5 (71.4)	2 (28.6)	5 (71.4)	2 (18.6)
pT1	37	30 (81.1)	7 (18.9)	25 (67.6)	12 (32.4)	34 (91.9)	3 (8.1)
pT2	17	13 (76.5)	4 (23.5)	14 (82.4)	3 (17.6)	14 (82.4)	3 (17.6)
pT3	30	25 (83.3)	5 (16.7)	22 (73.3)	8 (26.7)	26 (86.7)	4 (13.3)
pT4	10	7 (70.0)	3 (30.0)	9 (90.0)	1 (30.0)	8 (80.0)	2 (70.0)
pTa + 1	44	36 (81.8)	8 (18.2)	30 (68.2)	14 (31.8)	39 (88.6)	5 (11.4)
pT2–4	57	45 (78.9)	12 (21.1)	45 (78.9)	12 (21.1)	48 (84.2)	9 (15.8)
P value		0.720		0.220		0.523	
Histologic grade							
Grade 1	18	15 (83.3)	3 (16.7)	10 (55.6)	8 (44.4)	16 (88.9)	2 (11.1)
Grade 2	39	30 (76.9)	9 (23.1)	32 (82.1)	7 (17.9)	33 (84.6)	6 (15.4)
Grade 3	44	36 (81.8)	8 (18.2)	33 (75.0)	11 (25.0)	38 (86.4)	6 (13.6)
P value		0.800		0.103		0.909	

72 men and 29 women, ranging in age from 39 to 87 years (median age, 67 years). The clinicopathological features of participating patients are summarized in Table 1. Patients who had received any preoperative therapy were excluded from the study. All histological diagnoses including tumor grade and pT stage were performed using formalin-fixed and paraffin-embedded specimens from radical surgery; staging and grading were assessed in accordance with the 1997 tumor–node–metastasis (TNM) classification. A single pathologist performed all of the pathological examinations. The median follow-up period was 44 months (range, 3–250 months).The study protocol was approved by the Human Ethics Review Committee of the Nagasaki University School of Medicine.

Immunohistochemistry

Sections (5 μm thick) were deparaffinized stepwise in xylene and rehydrated in graded solutions of ethanol. Antigen retrieval was performed at 95°C for 40 min in 0.01 M sodium citrate buffer (pH 6.0). All sections were then immersed in 3% hydrogen peroxide for 30 min to block endogenous peroxidase activity. Primary antibodies were obtained from Cayman Chemical Corporation (Ann Arbor, MI; antihuman EP1R, EP2R, EP3R, and EP4R antibody), American Diagnostica (Greenwich, CT; antihuman uPA antibody), and R&D systems, Inc. (Minneapolis, MN; antihuman CD44 v6 antibody). Sections were incubated with anti-EP1R–4R antibody (1:100), anti-uPA antibody (1:175), or anti-CD44 v6 antibody (1:1,200) at 4°C overnight. Excluding the EP4R, the sections were washed extensively prior to treatment with peroxidase using the labeled polymer method with DAKO EnVision+ Peroxidase (Dako Corporation, Carpinteria, CA) for 60 min after incubation with primary antibody. On the other hand, the sections were then incubated with biotinylated antirabbit IgG for anti-EP4R antibody, followed by incubation with horseradish-peroxidase-conjugated avidin. The peroxidase reaction was visualized with the liquid DAB substrate kit (Zymed Laboratories Inc., San Francisco, CA). Sections were counterstained with hematoxylin, dehydrated stepwise through graded alcohol series, and cleared in xylene before mounting. A consecutive section from each sample processed without the primary antibody was used as a negative control. Positive controls included normal kidney and breast cancer tissue samples stained for EP1R–4R and uPA, respectively. Immunohistochemical staining for Ki-67, CD31, and MMP-2 was performed as described previously [22].

Quantitative analysis and staining interpretation

All analyses of immunohistochemical staining were assessed by light microscopy within the tumor area. For evaluation of immunohistochemical staining for EP1R–3R, the staining intensity was graded as none, weak, moderate, or strong. Carcinoma cells that showed moderate or strong staining were considered positively stained. EP1R, EP2R, and EP3R expression was considered positive when at least 10.2, 61.2, and 33.1% of cancer cells were judged as positive cells, according to the ratio of positive cells in normal epithelium (this ratio is the upper limit of positive staining ratio in normal epithelium). Evaluation of EP4R expression was performed similar to a previously reported method [23]. Briefly, EP4R expression was considered positive when at least 20.0% of cancer cells were judged as positive cells. Expression of uPA was evaluated based on previously described criteria [27]. The staining intensity was scored from 0 to 3: none, weak, moderate, or strong staining. The extent of positive staining in the tumor area was scored from 0 to 3: none, focal (≤25%), regional (25–75%), or diffuse (>75%). These two scores were summed to yield the final score, ranging from 0 to 6. A score of at least 5 was considered positive. CD44 v6 expression was evaluated using the method described by Toma et al. [33]. In brief, tumors with positive staining rates greater than 50% were considered positive. Evaluation of immunohistochemical staining for Ki-67, CD31, and MMP-2 was performed as described previously [22]. For Ki-67 PI and MVD, the median value was considered as the higher group, and those with staining that does not exceed the median value were considered as the lower group for statistical evaluation. Slides were blindly evaluated twice at different times by two investigators who were blinded to the clinical characteristics and survival data.

Statistical analysis

Normality was evaluated by normal distribution and histograms for each variable, and the results were expressed as medians (interquartile range) unless otherwise stated. The Mann–Whitney U test was performed for continuous variables, and χ^2 test was used for categorical comparison of the data. The crude and adjusted effects on grade and immunohistochemical staining, as well as other risk factors, were estimated by logistic regression analysis and were described as odds ratios (OR) with 95% confidence intervals (95% CI), together with the P values. Variables that achieved statistical significance in univariate analysis were subsequently entered into a multivariate analysis model. Cause-specific survival rates were compared with Kaplan–Meier analysis and the log rank test. Variables that achieved statistical significance ($P<0.05$) in the univariate analysis were subsequently entered into a multivariate analysis using a Cox proportional hazards analysis. All statistical tests were two-sided and significance was defined as $P<0.05$. All statistical analyses were performed using the statistical package StatView (version 5.0).

Results

Expression and clinical significance of EP1–3 receptors

Representative examples of EP1R, EP2R, and EP3R in cancer cells are shown in Fig. 1a–c, respectively; staining was observed in the cancer cell membrane and cytoplasm. Representative examples of EP1R, EP2R, and EP3R in normal epithelial cells are shown in Fig. 1d–f, respectively. The median rates (range) of strongly or moderately stained normal epithelial cells of EP1R, EP2R, and EP3R were 5.3% (0.5–10.2%), 43.1% (3.8–61.2%), and 24.1% (5.1–33.1%), respectively. Finally, 20 (19.8%), 26 (25.7%), and 14 (13.9%) tumor sections were judged positive for EP1R, EP2R, and EP3R, respectively. This staining was specific for each EP receptor because it was performed when each antibody was preincubated with human recombinant protein (data not shown). Expression of EP1R, EP2R, and EP3R was not associated with COX-2 expression (P=0.578, 0.700, and 0.426, respectively). In addition, this expression was not associated with clinicopathological features including pT stage and grade (Table 1) and cause-specific survival (Fig. 2).

Correlation with cancer cell proliferation, angiogenesis, and expression of MMP-2, uPA, and CD44 v6

The PI and MVD in the tumor area were 17.2% (11.2–30.1%) and 43 per high-power field (HPF) (34–63/HPF), respectively. The PI in specimens negative for COX-2

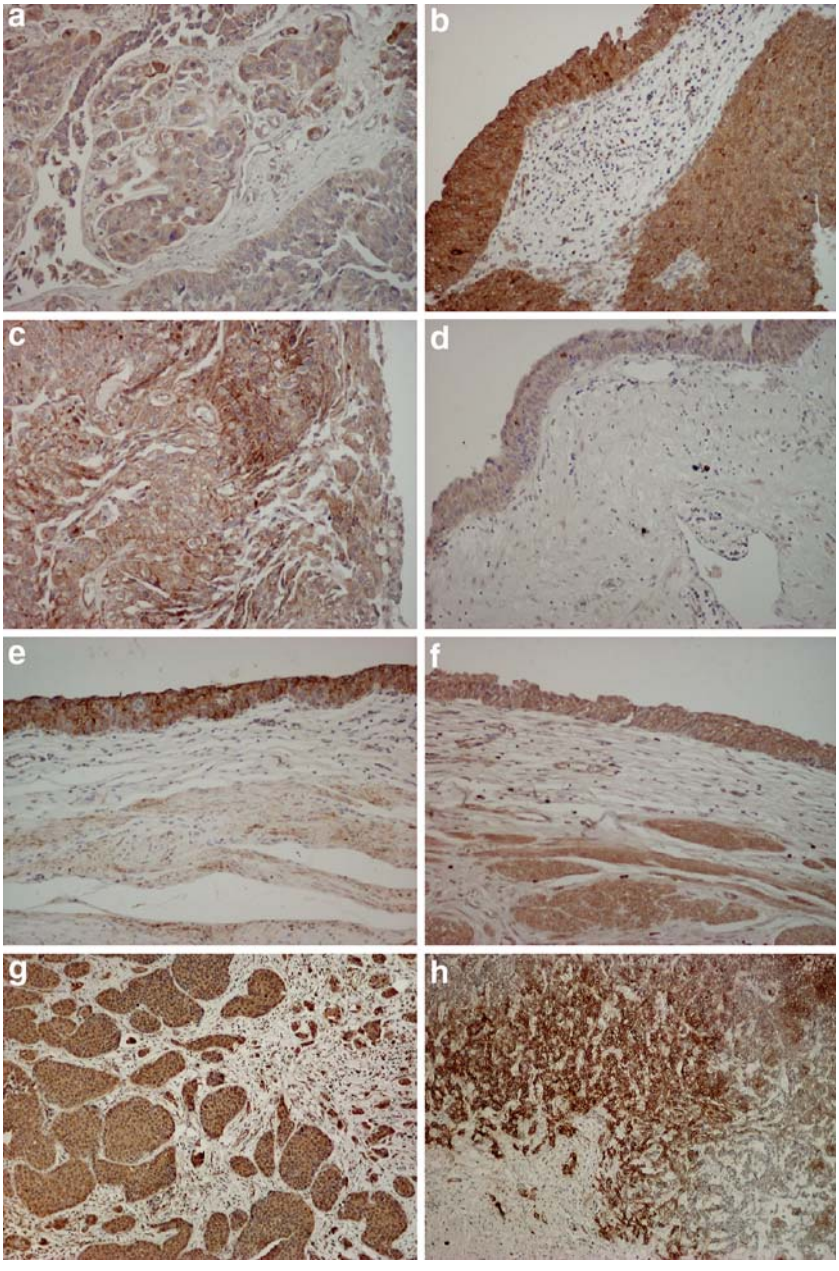

Fig. 1 Representative examples of expression of EP1 receptor (**a**), EP2 receptor (**b**), and EP3 receptor (**c**) in cancer cells, and expression of EP1 receptor (**d**), EP2 receptor (**e**), and EP3 receptor (**f**) in normal epithelium. Expression of all receptors was observed in the cytoplasm and cell membrane. Expression of uPA (**g**) and CD44 v6 (**h**) was detected in the cell cytoplasm and cell membrane, respectively (original magnification: ×200)

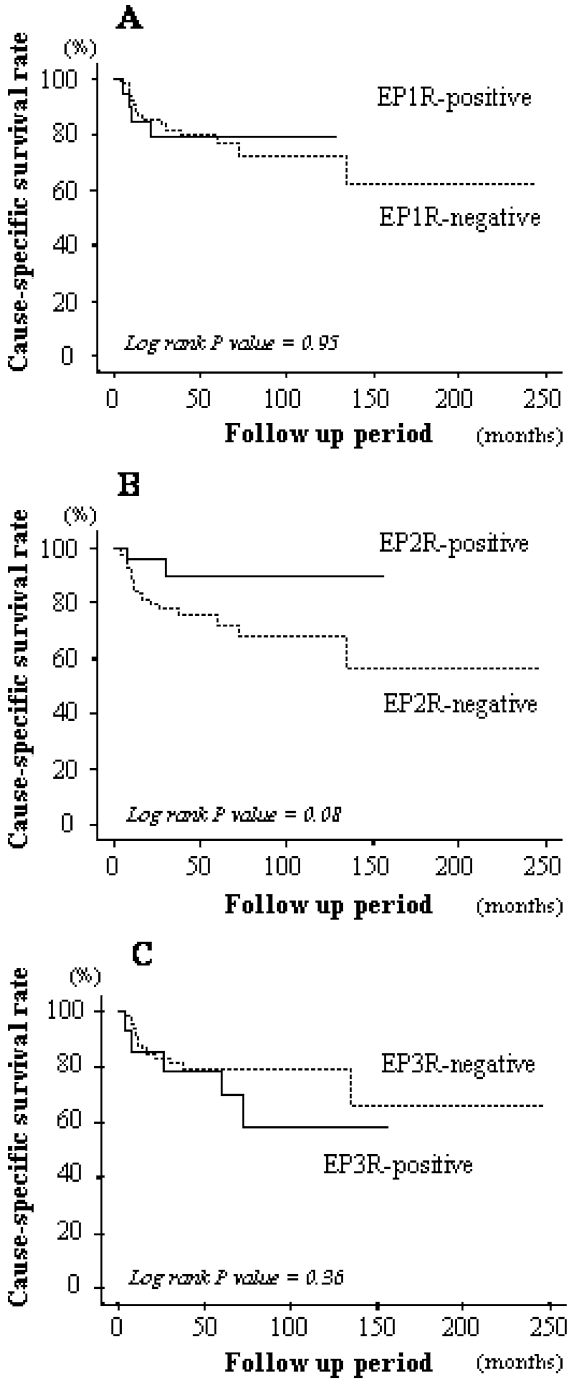

Fig. 2 Kaplan–Meier curves for cause-specific survival in patients with TCC-UUT according to EP1 receptor expression (**a**), EP2 receptor expression (**b**), and EP3 expression (**c**). Expression of these receptors was not prognostic for cause-specific survival

expression and those positive for COX-2 expression was 14.2% (10.8–25.1%) and 29.1% (15.2–34.7%), respectively, and there was a significant difference between the two groups ($P<0.001$). Likewise, the PI in tumors positive for EP4R expression (25.8%, 15.2–32.1%) was significantly higher ($P<0.001$) than that in tumors negative for EP4R (13.2%, 9.7–24.3%). In contrast, no such significant differences were found in EP1R, EP2R, and EP3R ($P=0.936$, 0.565, and 0.498, respectively).

The MVD in specimens negative for COX-2, positive for COX-2, negative for EP4R, and positive for EP4R expression was 41/HPF (34–51/HPF), 59/HPF (42–72/HPF), 41/HPF (34–51/HPF), and 55/HPF (39–70/HPF), respectively. The MVD in specimens positive for COX-2 or EP4R was significantly higher ($P<0.001$) than in specimens negative for COX-2 or EP4R. However, with regard to MVD, there were no significant differences in EP1R, EP2R, and EP3R ($P=0.946$, 0.664, and 0.170, respectively).

Representative expression of uPA and CD44 v6 is shown in Fig. 1g,h, respectively; uPA was stained mainly in the cell cytoplasm, and CD44 v6 was in the cell membrane. We then investigated the relationship between COX-2 expression or each EP receptor and expression of MMP-2, uPA, or CD44 v6 (Table 2) with the use of univariate analysis. There was a significant correlation between MMP-2 expression and COX-2 or EP4R expression ($P=0.003$ and <0.001, respectively). Likewise, positive staining for uPA was associated with positive expression of COX-2 ($P=0.014$) and EP4R ($P=0.023$). However, MMP-2 expression was not associated with EP1R ($P=0.400$), EP2R ($P=0.237$), and EP3R ($P=0.649$), and uPA expression was not associated with them ($P=0.298$, 0.608, and 0.087, respectively). In contrast, CD44 v6 expression was not associated with the expression of either COX-2 or EP receptors.

To investigate the independent roles of COX-2 or each EP receptor for high cancer cell proliferation, hypervascularity, and high expression of MMP-2, uPA, and CD44 v6, factors selected in the univariate analysis and high grade were included into a multivariate analysis model (Table 2). COX-2 expression was identified as an independent factor for high MVD and positive expression of MMP-2 and uPA (OR 2.84, 95% CI 1.18–6.82, $P=0.020$; OR 2.70, 95% CI 1.12–3.75, $P=0.028$; and OR 2.47, 95% CI 1.06–5.76, $P=0.036$). In contrast, EP4R expression was not an independent factor for high MVD ($P=0.402$) and uPA expression ($P=0.068$), but was independently associated with high PI (OR 3.16, 95% CI 1.25–7.98, $P=0.015$) and MMP-2 expression (OR 3.14, 95% CI 1.24–7.94, $P=0.016$).

Discussion

In the present study, our results did not demonstrate that EP1R-3R played a significant and important role in tumor development and survival in patients with TCC-UUT. To our knowledge, the clinical and pathological significance of EP1R–EP3R in these patients has not yet been clearly defined. However, we recently demonstrated that EP4R was positively associated with pT stage and grade, and was a useful predictive marker for cause-specific survival in patients with TCC-UUT [23]. Several investigators have assessed the pathological significance of EP1R–EP3R; for example, EP1 receptor may affect carcinogenesis and

Table 2 Regression analysis of expressions of COX-2 and each EP receptor with PI, MVD, and expressions of MMP-2, uPA, and CD44 v6

	Univariate analysis			Multivariate analysis[a]		
	OR	95% CI	*P* value	OR	95% CI	*P* value
PI (over median)						
COX-2-positive	3.28	1.45–7.44	0.004	2.40	0.97–5.90	0.057
EP1R-positive	0.80	0.30–2.13	0.653	–		
EP2R-positive	0.68	0.28–1.67	0.396	–		
EP3R-positive	1.02	0.33–3.16	0.968	–		
EP4R-positive	5.10	2.04–11.16	<0.001	3.16	1.25–7.98	0.015
MVD (over median)						
COX-positive	3.62	1.58–8.26	0.002	2.84	1.18–6.82	0.020
EP1R-positive	0.76	0.28–2.03	0.584	–		
EP2R-positive	0.79	0.32–1.94	0.608	–		
EP3R-positive	1.93	0.60–1.22	0.272	–		
EP4R-positive	2.75	1.89–6.15	<0.001	1.49	0.59–3.75	0.402
MMP-2 (positive)						
COX-2-positive	3.55	1.56–8.09	0.003	2.70	1.12–3.75	0.028
EP1R-positive	0.65	0.24–1.76	0.400	–		
EP2R-positive	0.58	0.23–1.43	0.237	–		
EP3R-positive	0.77	0.26–2.40	0.649	–		
EP4R-positive	4.67	2.02–10.81	<0.001	3.14	1.24–7.94	0.016
uPA (positive)						
COX-2-positive	2.76	1.23–6.20	0.014	2.47	1.06–5.76	0.036
EP1R-positive	1.70	0.63–4.59	0.298	–		
EP2R-positive	1.26	0.52–3.09	0.608	–		
EP3R-positive	2.94	0.86–10.09	0.087	–		
EP4R-positive	2.53	1.14–5.64	0.023	2.34	0.94–5.82	0.068
CD44 v6 (positive)						
COX-2-positive	0.94	0.43–2.06	0.871	–		
EP1R-positive	0.93	0.35–2.48	0.880	–		
EP2R-positive	1.83	0.74–4.52	0.189	–		
EP3R-positive	0.60	0.18–1.92	0.385	–		
EP4R-positive	0.55	0.25–1.21	0.138	–		

PI proliferation index, *COX* cyclooxygenase, *MVD* microvessel density, *MMP* matrix metalloproteinase, *uPA* urokinase-type plasminogen activator, CD44 v6 exon v6 containing CD44 isoform
[a]Adjusted for tumor grade

tumor development in colon cancer [11] and breast cancer [15]. Furthermore, EP2R and EP3R are also associated with malignant aggressiveness in endometrial adenocarcinoma [14] and prostate cancer [5] or lung cancer [35], respectively. From these reports, we hypothesized that, in addition to EP4R, one or some of the EP1R–3R also influence carcinogenesis, malignant aggressiveness, and survival in patients with TCC-UUT. However, contrary to our hypothesis, the expression of EP1R–3R was not significantly associated with clinicopathological features and survival. We speculate that the expression pattern and function of EP receptors may depend on the pathological type and origin of malignant cells. Finally, we speculate that among the EP receptors, only EP4R had clinical and prognostic significance in patients with TCC-UUT.

COX-2 and/or PGE2 affects the malignant potential of cancer cells through their capacity to regulate several factors [9, 37]. Among such factors, we paid attention to cancer cell proliferation, angiogenesis, and expression of MMP-2, uPA, and CD44 v6 because they are thought to be associated with malignant aggressiveness in TCC-UUT [12, 13, 22, 27, 28]. Our results demonstrated that COX-2 expression was positively associated with MVD, MMP-2 expression, and uPA expression. Based on these findings, we speculate that COX-2 influences cancer cell development and survival through tumor proliferation, angiogenesis, and MMP-2 in patients with TCC-UUT. Furthermore, our results also demonstrated that EP4R expression was positively associated with cancer cell proliferation and MMP-2 expression. Several factors are thought to be responsible for the pathological mechanism of EP4R in cancers. Asano et al. [2] reported that increased PGE2 influenced tumor growth and progression via EP4R in human gallbladder carcinoma. Chen and Hugh-Fulfold [5] also reported that PGE_2 modulated cell growth via EP4R in human prostate cancer cells (PC-3 cells). Furthermore, Dohadwala et al. [8] reported that signals via EP4R upregulated MMP-2 in non-small-cell lung cancer. In

agreement with our findings, Kinugasa et al. [16] reported that COX-2 inhibitors can prevent tumor invasion via downregulation of MMP-2 in oral cancer cell lines. The present study did not demonstrate a significant correlation between the expression of CD44 v6 and that of COX-2 and EP receptors. However, several investigators reported that CD44 was regulated by COX-2 or PGE2 in cancer cells [7, 8]. To our knowledge, there are no reports regarding the relationship between CD44 v6 and COX-2 or EP receptors in human cancer tissues. In addition, the relationship between COX-2 or EP receptors and standard or other variant isoforms of CD44 in TCC-UUT remains to be elucidated. We speculate that CD44 v6 is not associated with COX-2 or EP receptors in TCC-UUT. In addition, there was no significant correlation between EP1R–3R and these factors. These results support the findings that all EP1R–3R types were not associated with clinicopathological features and survival in patients with TCC-UUT.

The most interesting finding of the present study is that PI and MMP-2 expression was independently influenced by EP4R expression in a multivariate model that included COX-2 expression and grade. These findings suggest that inhibition of COX-2 activity cannot suppress cancer cell proliferation and MMP-2 activity under EP4R-positive conditions. We speculate that regulation of both COX-2 and EP4R can be more effective than that of COX-2 only for prevention of carcinogenesis or treatment in patients with TCC-UUT.

Our results demonstrated that EP1R–EP3R played a minimal role in tumor development and survival in patients with TCC-UUT. Univariate analysis showed that the expression of COX-2 and EP4R was positively associated with PI, MVD, MMP-2 expression, and uPA expression. Furthermore, COX-2 expression was also associated with MVD, MMP-2 expression, and uPA expression in a multivariate analysis model including grade. EP4R was independently associated with PI and MMP-2 expression in similar analysis. Considered collectively, our findings indicate that, in addition to COX-2, targeting EP4R could be therapeutically effective in the control of TCC-UUT progression.

Acknowledgements We thank Takumi Shimogama and Yoshikazu Tsuji for excellent assistance. This study was supported by in part by grant no. 17791080 from the Japanese Society of the Promotion of Science to Y. Miyata. This study did not receive any funding from any commercial source.

References

1. Arber N, Levin B (2005) Chemoprevention of colorectal cancer: ready for routine use? Recent Results Cancer Res 166:213–230
2. Asano T, Shoda J, Ueda T, Kawamoto T, Todoroki T, Shimonishi M, Tanabe T, Sugimoto Y, Ichikawa A, Mutoh M, Tanaka N, Miwa M (2002) Expression of cyclooxygenase-1 and prostaglandin E-receptors in carcinoma of the gallbladder: crucial role of arachidonate metabolism in tumor growth and progression. Clin Cancer Res 8:1157–1167
3. Braun JR, DuBois RN (2005) COX-2: a molecular target for colorectal cancer prevention. J Clin Oncol 23:2840–2855
4. Chang SH, Liu CH, Conway R, Han DK, Nithipatikom K, Trifan OC, Lane TF, Hla T (2004) Role of prostaglandin E2-dependent angiogenic switch in cyclooxygenase 2-induced breast cancer progression. Proc Natl Acad Sci USA 101:591–596
5. Chen Y, Hugh-Fulfold M (2000) Prostaglandin E2 and the protein kinase A pathway mediate arachidonic acid induction of c-fos in human prostate cancer. Br J Cancer 82:2000–2006
6. Coleman RA, Smith WL, Narumiya S (1994) International union of pharmacology classification of prostanoid receptors: properties, distribution, and structure of the receptors and their subtypes. Pharmacol Rev 46:205–229
7. Dohadwala M, Luo J, Zhu L, Lin Y, Dougherty GJ, Sharma S, Huang M, Pold M, Batra RK, Dubinett SM (2001) Non-small cell cancer cyclooxygenase-dependent invasion is mediated by CD44. J Biol Chem 276:20809–20812
8. Dohadwala M, Bartra RK, Luo J, Lin Y, Krysan K, Põld M, Sharma S, Dubinett SM (2002) Autocrine/paracrine PGE2 production by non-small cell lung cancer cells regulates MMP-2 and CD44 in COC-2 dependent invasion. J Biol Chem 52:50828–50833
9. Dubois RN, Abramson SB, Crofford L, Gupta RA, Simon LS, Van De Putte LB, Lipsky PE (1998) Cyclooxygenase in biology and disease. FASEB J 12:1063–1073
10. Eschwege P, Ferlicot S, Droupy S, Ba N, Conti M, Loric S, Coindard G, Denis I, Ferretti L, Cornelius A, Legrand A, Bedossa P, Benoit G, Jardin A, Scardiono P (2003) A histopathologic investigation of PGE(2) pathways as predictors of proliferation and invasion in urothelial carcinomas of the bladder. Eur Urol 44:435–441
11. Hansen-Petrik MB, McEntee MF, Jull B, Shi H, Zemel MB, Whelan J (2003) Prostaglandin E_2 protects intestinal tumors from nonsteroidal anti-inflammatory drug-induced regression in $APC^{min/+}$ mice. Cancer Res 62:403–408
12. Hong RL, Pu YS, Hsieh TS, Chu JS, Lee WJ (1996) Expressions of E-cadherin and exon v6-containing isoforms of CD44 and their prognostic values in human transitional cell carcinoma. J Urol 153:2025–2028
13. Inoue K, Kamada M, Salton JW, Fukata S, Yoshikawa C, Tamboli P, Dinney CF, Shuin T (2002) The prognostic value of angiogenesis and metastasis-related genes for progression of transitional cell carcinoma of the renal pelvis and ureter. Clin Cancer Res 8:1863–1870
14. Jabbour HN, Milne SA, Williams AR, Anderson RA, Boddy SC (2001) Expression of COX-2 and PGE synthase and synthesis of PGE(2) in endometrial adenocarcinoma: a possible autocrine/paracrine regulation of neoplastic cell function via EP2/EP4 receptors. Br J Cancer 85:1023–1031
15. Kawamori T, Uchiya N, Nakatsugi S, Watanabe K, Ohuchida S, Yamamoto H, Maruyama T, Kondo K, Sugimura T, Wakabayashi K (2002) Chemopreventive effects of ONO-8711, a selective prostaglandin E receptor EP1 antagonists, on breast cancer development. Carcinogenesis 22:2001–2004
16. Kinugasa Y, Hatori M, Ito H, Kurihara Y, Ito D, Nagumo M (2004) Inhibition of cyclooxygenase-2 suppresses invasiveness of oral squamous cell carcinoma cell lines via down-regulation of matrix metalloproteinase-2 and CD44. Clin Exp Metastasis 21:737–745
17. Kömhoff M, Guan Y, Shappell HW, Davis L, Jack G, Shyr Y, Koch MO, Shapper SB, Breyer MD (2000) Enhanced expression of cyclooxygenase-2 in high grade human transitional cell bladder carcinomas. Am J Pathol 157:29–35
18. Krysan K, Reckamp KL, Dalwadi H, Sharma S, Rozengurt E, Dohadwala M, Dubinett SM (2005) Prostaglandin E2 activates mitogen-activated protein kinase/Erk pathway signaling and cell proliferation in non-small cell lung cancer cells in an epidermal growth factor receptor-independent manner. Cancer Res 65:6275–6281
19. Li G, Yang T, Yan J (2002) Cyclooxygenase-2 increased the angiogenic and metastatic potential of tumor cells. Biochem Biophys Res Commun 299:886–890

20. Masferrer JL, Leahy KM, Koki AT, Zweifel BS, Settle SL, Woerner BM, Edwards DA, Flickinger AG, Moore RJ, Seibert K (2000) Antiangiogenic and antitumor activities of cyclooxygenase-2 inhibitors. Cancer Res 60:1306–1311
21. Miyata Y, Koga S, Kanda S, Nishikido M, Hayashi T, Kanetake H (2003) Expression of cyclooxygenase-2 in renal cell carcinoma: correlation with tumor cell proliferation, apoptosis, angiogenesis, expression of matrix metalloproteinase-2, and survival. Clin Cancer Res 9:1741–1749
22. Miyata Y, Shigeru K, Nomata K, Hayashida Y, Kanetake H (2004) Expression of metalloproteinase-2, -9, and tissue inhibitor of metalloproteinase-1 and -2 in transitional cells carcinoma of the upper urinary tract: correlation with tumor stage and survival. Urology 63:602–608
23. Miyata Y, Shigeru K, Nomata K, Eguchi J, Kanetake H (2005) Expression of cyclooxygenase-2 and EP4 receptor in transitional cell carcinoma of the upper urinary tract. J Urol 173:56–60
24. Mohammed SI, Knapp DW, Bostwick DG, Foster RS, Khan KNM, Masferrer JL, Woerner Snyder PW, Koki AT (1999) Expression of cyclooxygenase-2 (COX-2) in human invasive transitional cell carcinoma (TCC) of the urinary bladder. Cancer Res 59:987–990
25. Munkarah A, Ali-Fehmi R (2005) COX-2: a protein with an active role in gynecological cancers. Curr Opin Obstet Gynecol 17:49–53
26. Mutoh M, Watanabe K, Kitamura T, Shoji Y, Takahashi M, Kawamori T, Tani K, Kobayashi M, Maruyama T, Kobayashi K, Ohuchida S, Sugimoto Y, Narumiya S, Sugimura T, Wakabayshi K (2002) Involvement of prostaglandin E receptor subtype EP4 in colon carcinogenesis. Cancer Res 62:28–32
27. Nakanishi K, Kawai T, Torikata C, Aurues T, Ikeda T (1998) Urokinase-type plasminogen activator, its inhibitor, and its receptor in patients with upper urinary tract carcinoma. Cancer 82:724–732
28. Nakanishi K, Kawai T, Sato H, Aida S, Kasamatsu H, Aurues T, Ikeda T (2000) Expression of matrix metalloproteinase-2 (MMP-2) and of membrane-type-1matrix metalloproteinase (MT1-MMP) in transitional cell carcinoma of the upper urinary tract. Hum Pathol 31:193–200
29. Rigas B, Goldman IS, Levine L (1993) Altered eicosanoid levels in human colon cancer. J Lab Clin Med 122:518–523
30. Sales KJ, Katz AA, Davis M, Hinz S, Soeters RP, Hofmeyr MD, Millar RP, Jabbour HN (2001) Cyclooxygenase-2 expression and prostaglandin E2 synthesis are up-regulated in carcinomas of the cervix: a possible autocrine/paracrine regulation of neoplastic cell function via EP2/EP4 receptors. J Clin Endocrinol Metab 86:2243–2249
31. Sheng H, Shao J, Morrow JD, Beauchamp RD, Dubois RN (1998) Modulation of apoptosis and Bcl-2 expression by prostaglandin E_2 in human colon cancer cells. Cancer Res 58:326–362
32. Sheng H, Shao J, Washington MK, Dubois RN (2001) Prostaglandin E2 increases growth and motility of colorectal carcinoma cells. J Biol Chem 276:75–81
33. Toma V, Hauri D, Schmid U, Ackermann D, Maurer R, Alund G, Knönagel H, Rist M, Gasser TC, Sauter G, Roth J (1999) Focal loss of CD44 variant protein expression is related to recurrence in superficial bladder carcinoma. Am J Pathol 155:1427–1432
34. Wendum D, Masliah J, Trugnan G, Flejou JF (2004) Cyclooxygenase-2 and its role in colorectal cancer development. Virchows Arch 445:327–333
35. Yano T, Zissel G, Muller-Qernheim J, Shin SJ, Satoh H, Ichikawa T (2002) Prostaglandin E2 reinforces the activation of Ras signal pathway in lung adenocarcinoma cells via EP3. FEBS Lett 518:154–158
36. Yoshimatsu K, Golijanin D, Paty PB, Soslow RA, Jakobsson PJ, DeLellis RA, Subbaramaiah K, Dannenberg AJ (2001) Inducible microsomal prostaglandin E synthase is overexpressed in colorectal adenomas and cancer. Clin Cancer Res 7:3971–3976
37. Zha S, Yegnasubramanian V, Nelson WG, Isaacs WB, De Marzo AM (2004) Cyclooxygenases in cancer: progress and perspective. Cancer Lett 215:1–20
38. Zweifel BS, Davis TW, Ornberg RL, Masferrer JL (2002) Direct evidence for a role of cyclooxygenase 2-derived prostaglandin E_2 in human head and neck xenograft tumors. Cancer Res 62:6706–6711

Virchows Arch (2006) 448: 830–837
DOI 10.1007/s00428-006-0199-0

ORIGINAL ARTICLE

Tsuyoshi Ishihara · Tamotsu Takeuchi · Isao Nishimori · Yoshihiro Adachi · Tomoko Minakuchi · Jiro Fujita · Hiroshi Sonobe · Yuji Ohtsuki · Saburo Onishi

Carbonic anhydrase-related protein VIII increases invasiveness of non-small cell lung adenocarcinoma

Received: 17 October 2005 / Accepted: 28 February 2006 / Published online: 12 April 2006

Abstract Carbonic anhydrase-related protein VIII (CA-RP VIII) is believed to be an oncofetal antigen and is overexpressed in colorectal and non-small cell lung cancer. However, the pathobiological properties of CA-RP VIII in lung cancer remain unclear. In the present study, we examined ultrastructural changes caused by exogenous CA-RP VIII expression in a well-differentiated lung adenocarcinoma cell line, PC-9. Many vacuoles lined by cilia, sometimes large vacuoles pushing the nuclei to one side, were found in the cytoplasm of CA-RP VIII-expressing PC-9 cells, but not in control PC-9 cells. Moreover, signet-ring cells containing abundant intracytoplasmic mucin were often found among CA-RP VIII-expressing PC-9 cells, but rarely among control PC-9 cells. We subsequently examined CA-RP VIII expression in atypical adenomatous hyperplasia and early-stage lung adenocarcinoma (Stage Ia). Significant expression of CA-RP VIII was observed in invasive lung adenocarcinoma but not in noninvasive adenocarcinoma. Interestingly, CA-RP VIII was strongly expressed in signet-ring cell cancer and invasive mucinous adenocarcinoma components. CA-RP VIII also appeared to enhance the invasiveness of PC-9 cells in Matrigel invasion assay. The present findings suggest that CA-RP VIII expression in lung adenocarcinoma is related to cancer cell invasion.

Keywords Carbonic anhydrase-related protein · CA-RP VIII · Invasion · Lung cancer · Signet-ring cell

T. Ishihara · I. Nishimori · T. Minakuchi · S. Onishi
Department of Gastroenterology and Hepatology,
Kochi Medical School,
Nankoku, Kochi 783-8505, Japan

T. Takeuchi (✉) · Y. Adachi · Y. Ohtsuki
Department of Pathology, Kochi Medical School,
Nankoku, Kochi 783-8505, Japan
e-mail: takeutit@med.kochi-ms.ac.jp

J. Fujita
First Department of Internal Medicine, Faculty of Medicine,
University of the Ryukyus,
Senbaru, Nishihara, Okinawa 903-0213, Japan

H. Sonobe
Department of Laboratory Medicine and Pathology,
National Hospital Organization Fukuyama Medical Center,
Okinogami 4-14-17, Fukuyama, Hiroshima 720-8520, Japan

Introduction

The carbonic anhydrases (CA) (EC 4.2.1.1) constitute a family of zinc metalloenzymes that catalyze the reversible hydration of bicarbonate [10]. The human CA gene family includes 12 isozymes that characteristically exhibit carbonic anhydrase activity. In addition, three molecules that have a CA domain are considered CA isoforms and designated carbonic anhydrase-related proteins (CA-RPs) but lack CA activity because of the absence of one or more histidine residues required for binding to the zinc ion, which is critical for CO_2 hydration activity [4]. *CA8* refers to the carbonic anhydrase 8 gene including mRNA. In contrast, CA-RP VIII refers to the corresponding protein.

Although the biological properties of CA-RPs are still unclear, recent experiments including some from our laboratories have clearly indicated that CA-RP VIII without its enzymatic activity is one of oncofetal antigens and abundantly expressed in non-small cell lung cancers and colorectal cancers [1, 7, 8]. Almost all of the advanced adenocarcinomas of the lung express abundant CA-RP VIII, especially at the invasive front [1]. We, therefore, speculated that CA-RP VIII favors cancer invasion.

In the present study, we examined the pathobiological properties of CA-RP VIII in lung adenocarcinoma. Our findings suggest that CA-RP VIII might facilitate cancer cell invasion.

Materials and methods

Cell culture, plasmid, and transfection

Detailed procedures for maintaining PC-9, a well-differentiated adenocarcinoma cell line, and establishment of CA-RP VIII-expressing transfectants harboring pCI-neo (Promega, WI, USA) were previously described [1]. In the present study, we newly generated other CA-RP VIII-expressing transfectants with the use of a pEF1-His (Invitrogen, CA, USA) vector to achieve virus-promoter-free CA-RP VIII expression. Transfection using DOTAP transfection reagents (Boehringer Mannheim GmbH, Mannheim, Germany) and G418 selection were performed as previously described [14]. Cells were cultured in Dulbecco's modified Eagle's medium (Gibco Life Technologies, NY, USA) containing 10% heat-inactivated fetal bovine serum (FBS) and 50-μg/ml gentamycin (Gibco Life Technologies). In addition, DJM-1, a human skin cancer cell line, was also maintained in our laboratory and used as control experiments for several reverse transcriptase polymerase chain reaction (RT-PCR) experiments.

Reverse transcriptase polymerase chain reaction and real-time PCR

RT-PCR was performed as previously described [16]. Briefly, total cellular RNA was prepared from cell lysates using RNA-zol B (Biotex Laboratory, Houston, Texas). Serial fivefold dilutions were prepared from master lysates and used as a set in RT-PCR. Total RNA of human adult lung tissues was purchased from Chemicon International (Temecula, CA). cDNA synthesis from total RNA and subsequent PCR were performed using an RNA long and accurate (LA) PCR kit (Takara, Ohtsu, Japan). The procedure was performed according to the manufacturer's instructions. The primer sets used in this study were sense 5′-TCCTGATGCTAATGGGGAATACCAG-3′ and antisense 5′-CTAAGAGGCTGAGTGGGCCGAAAG-3′ for CA-RP VIII, sense 5′-CAGCCTGGGACTGCCCCCT GAT-3′ and antisense 5′-CAGGCCCCTCCGGGTCCTT CTC-3′ for matrix metalloproteinase (MMP)-2 [15], sense 5′-GCCATCGCGGAGATTGGGAACC-3′ and antisense 5′-CGGGGAACATCCGGTCCACCTC-3′ for MMP-9 [15], and sense 5′-TCCACCACCCTGTTGCTGTA-3′ and antisense 5′-ACCACAGTCCATGCCATCAC-3′ for glyceraldehyde-3-phosphate dehydrogenase (G3PDH). We also used primer sets MUC-1 sense primer, 5′-GTA CCA TCA ATG TCC ACG AC-3′, MUC-1 antisense primer 5′-CTA CGA TCG GTA CTG CTA GG, MUC-2 sense primer 5′-CCA TGC GTG CCT CTC TGC AA-3′ MUC-2 antisense primer 5′-GTG GGT TGG GTG ACA CAC TC-3′, MUC-4 sense primer 5′-GCT CTC CAA CAT CCT CCA CG-3′, MUC-4 antisense primer 5′-TCA CAC GAC CAC CAT TGA TG-3′, MUC-5AC sense primer 5′-TGA TGT GGA CTT TCC ATC CC-3′, MUC-5AC antisense primer 5′-TGG TTG TCC TGG ATT TCT GC, MUC-5B sense primer 5′-CTG CGA GAC CGA GGT CAA CAT C-3′, MUC5B antisense primer 5′-TGG GCA GCA GGA GCA CGG ERG-3′, MUC-7 sense primer 5′-CTT CTC GTT CAG TGA AGG TCG-3′, and MUC-7 antisense primer 5′-TGG AAG CTT AGG CCT ACA GC-3′.

The PCR-amplified products were electrophoretically separated on a 2% agarose gel. To assure reproducibility of results, the RT-PCR amplification was repeated three times using different clones.

Real-time PCR was also carried out by using representative PC-9 and transfectant clones according to the manufacturer's instructions (Applied Biosystem's (ABI) Prism 7000, Foster City, CA). Primer/probes: Set: Hs 00187850-ml (*CA8*) and Hs 99999905-ml *GAPDH* were purchased from ABI.

Electron microscopic examination

A fine structural study was performed using the methods described previously [13]. Briefly, cells were centrifuged and fixed in 3% glutaraldehyde and then 1% osmium tetroxide solutions. After dehydration in a graded series of ethanols, specimens were embedded in an epoxy resin (Luveak, Nakalai Tesque, Kyoto, Japan). Ultrathin sections were cut with a Porter-Blum MT2-B ultramicrotome (Sorvall, USA) equipped with a diamond knife (Diatome, Switzerland), doubly stained with uranyl acetate and lead citrate solutions, and observed with a Hitachi H-7100-type electron microscope.

Histochemical analysis of signet ring cells

Cultured cells were settled to remove large cell aggregates for 5 min at room temperature. The supernatant was then centrifuged at 1,000×*g* for 5 min. Sedimented cells in signet-ring cell-rich fractions were smeared on slide glasses, air-dried, fixed with 10% formaldehyde, and

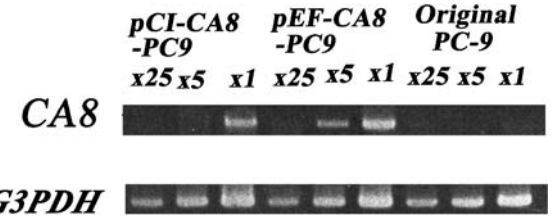

Fig. 1 *CA8* mRNA expression in cultured PC-9 cells and transfectants. A well-differentiated adenocarcinoma cell line, PC-9, was transfected with pEF-His- or pCIneo-based *CA8* expression vectors, designated pEF-CA8-PC9 and pCI-CA8-PC9, respectively. Semiquantitative *RT-PCR* using serially-diluted total RNA (indicated by ×1, ×5, and ×25) from each clone revealed that pEF-CA8-PC9 expressed much more *CA8* mRNA than pCI-CA8-PC9. Control PC-9 cells did not express *CA8* mRNA. G3PDH mRNA expression was monitored as a control. Results are taken from a single experiment representative of three yielding similar results. Notably, these results were reproducible in other pEF-CA8-PC9 and pCI-CA8-PC9 clones. Real-time *PCR* revealed that a pEF-CA-PC9 and pCI-CA8-PC9 transfectant clone, which was demonstrated in this figure, expressed *CA8* mRNA 10.5 and 5.5 times more than control PC9 cells, respectively

finally stained with hematoxylin and periodic acid-Schiff (PAS).

We also prepared the cell clot tissues of cultured cells and stained with PAS. We subsequently counted the percentage of signet-ring in an original PC-9 clot and three independent transfectant clones of pCI-CA8-PC9 or pEF-CA8-PC9 in five ×200 fields. The results were shown in mean and standard deviation of each clone.

Immunohistochemical staining

In the present study, archival tissues comprising atypical adenomatous hyperplasia (AAH) and stage Ia lung adenocarcinoma specimens were immunostained with a monoclonal antibody or control antibody using an automated immunostainer (Ventana, AZ, USA). According to the modified WHO lung tumor classification system, specimens were classified as 1) AAH, 2) bronchioloalveolar cancer (BAC), 3) mixed type adenocarcinoma (MX) with a predominantly bronchioloalveolar pattern, lepidic growth pattern, and invasive components, and 4) overt MX without bronchioloalveolar pattern. Procedures for preparation of a monoclonal antibody to human CA-RP VIII and immunohistochemical staining were described in detail previously [17]. As anti-CA-RP VIII antibody was of IgM class, we used isotype-matched monoclonal antibody to *Trichosporon beigelii,* a fungus [12]. Previous studies revealed that this control antibody did not react to human lung tissues tested. Based on the number of stained lung atypical epithelial or cancer cells, immunohistochemical staining was semiquantitatively scored as negative (less than 5%), weakly positive (5 to 20%), moderately positive (20 to 80%), or markedly positive (over 80%). The intensity of immunoreactivity of stained tumor cells was also scored, as follows: grade 1, positive but weaker than internal control (alveolar macrophages), grade 2, equal to immunoreactivity in the internal control, or grade 3, much stronger than internal control.

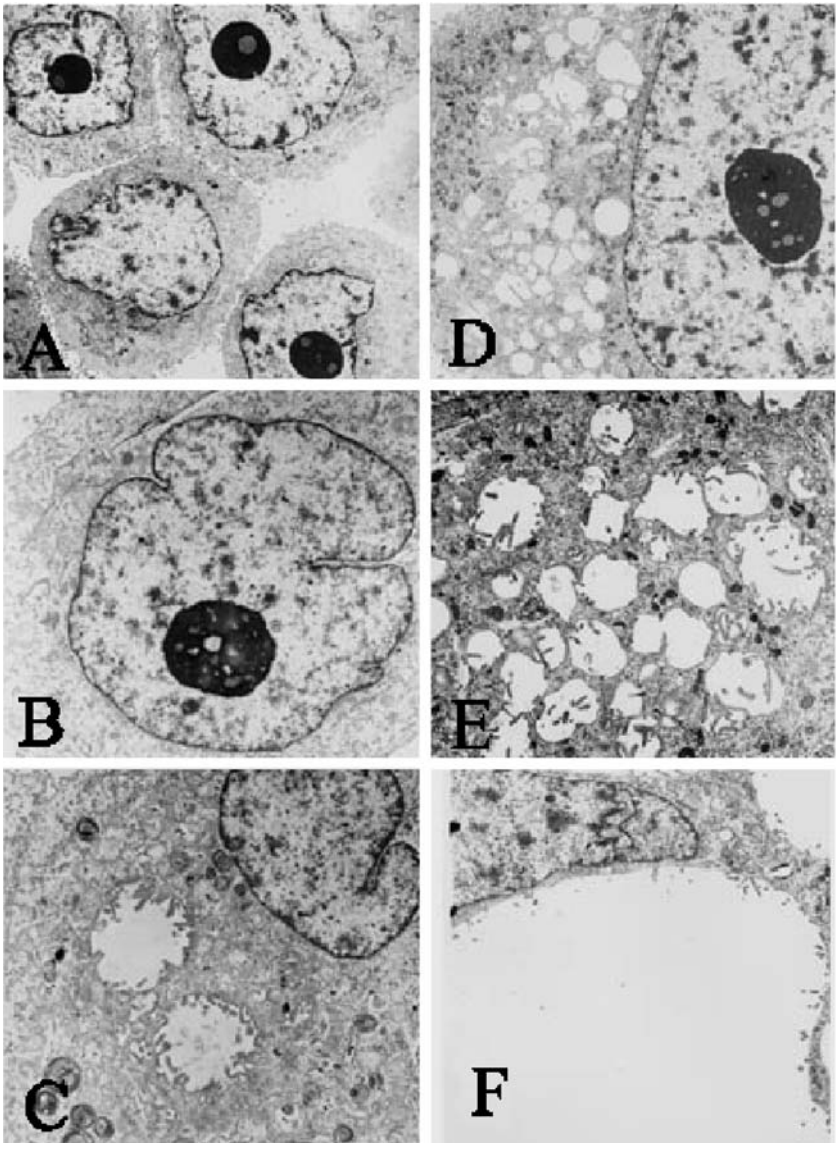

Fig. 2 General ultrastructural features of control PC-9 (**a** and **b**), CA-RP VIII-expressing PC-9 cells, pCI-CA8-PC-9 (**c**), and pEF-CA8-PC9 (**d**–**f**). Note the intracytoplasmic vacuoles in CA-RP VIII-expressing transfectants. Interestingly, pEF-CA8-PC-9 contained many more vacuoles than did pCI-CA8-PC-9. These vacuoles were lined on the surface with numerous microvilli and were, therefore, considered intracytoplasmic lumens. Few or no vacuoles were observed in control PC-9 cells. In several pEF-CA8-PC-9 cells, large vacuoles pushed the crescent-shaped nucleus to one side, as in 3signet-ring cancer cells (**f**, see also Fig. 3d)

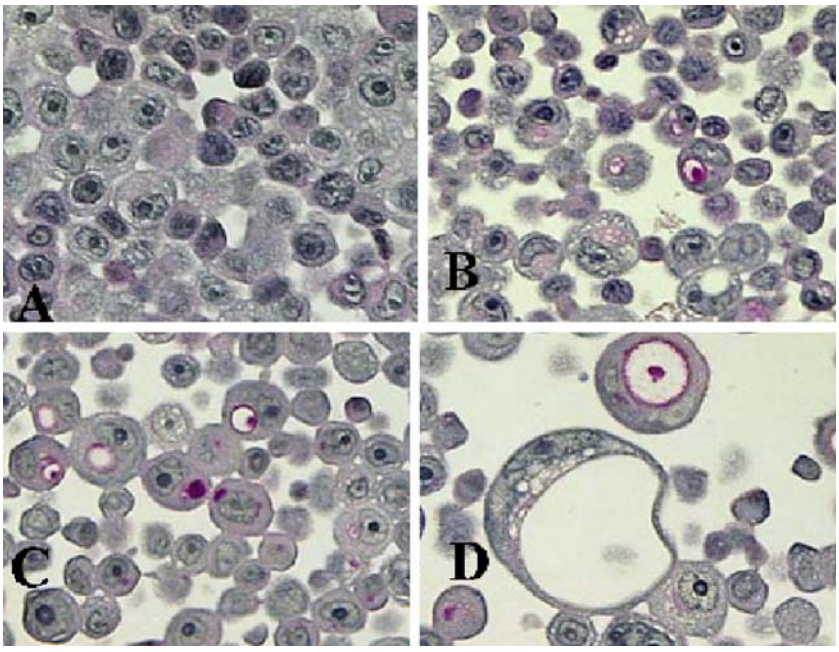

Fig. 3 Cytochemical staining of control PC-9 (**a**), CA-RP VIII-expressing PC-9 cells, pCI-CA8-PC-9 (**b**) and pEF-CA8-PC-9 (**c** and **d**) in formalin-fixed cell clots. Periodic acid-Schiff staining highlighted cytoplasmic mucin storage in pEF-CA-PC-9 (**c** and **d**), did so to a lesser extent in pCI-CA8-PC-9 (**b**), but did not in control PC-9 cells (**a**). The cells were also stained with hematoxylin to observe the nuclei. Original magnification: ×200 (**a**, **b**, and **c**), and ×400 (**d**)

Cell migration and invasion assay

Migration was defined as the ability of cells to penetrate the 8-μm pore nucleopore polycarbonate membrane insert of a 6.5-mm transwell according to the methods of Holting et al. [3]. Briefly, cells were seeded in the upper compartment of transwell insert at a concentration of 2×10^5 cells/ml serum-free Dulbecco's modified eagles medium (DMEM). Migration was induced by 10% fetal calf serum (FCS), which was added to the lower chamber beneath the insert membrane. After 24 h of incubation, the cell of the lower compartment was counted.

The invasiveness of cultured cells was determined using six-well BD BioCoat Matrigel Invasion Chamber Plates (BD Biosciences, CA) according to the manufacturer's protocol. Briefly, 1×10^5 cells were placed in the upper compartment of an invasion chamber. After 24 h of incubation with DMEM containing 10% (lower chamber) or 0% (upper chamber) FCS, the cells on the lower surface of the filter were counted.

Table 1 Immunohistochemical staining of atypical adenomatous hyperplasia and lung adenocarcinoma at stage Ia

A: Based on number of immunoreactive cells				
	Negative (<5%)	Weakly (5–20%)	Moderate (20–80%)	Marked (>80%)
AAH	3	0	0	0
BAC	8	2	1	0
MX with BAC pattern	3	4	4	0
Overt MX	0	1	3	4
B: Based on intensity of staining				
		Grade 1	Grade 2	Grade 3
AAH		2	0	0
BAC		7	2	0
MX with BAC pattern		2	5	3
Overt MX		0	2	6

Few or no immunoreactive neoplastic cells were found in specimens including one AAH, two BAC, and a MX with BAC pattern. These cases were not included in the Table. In contrast, when we observed positive neoplastic cells, even when they comprised fewer than 5% of cells, we determined the intensity of staining. When the tumor cells exhibited various intensities of staining in a specimen, grade was assigned based on the strongest intensity of staining

Results

Exogenous CA-RP VIII expression enhanced intracytoplasmic vacuole formation in PC-9 cells

We established three PC-9 transfectant clones in which CA-RP VIII was stably expressed under a human elongation factor 1á promoter. RT-PCR clearly demonstrated that these transfectants, designated pEF-CA8-PC9, expressed abundant *CA8* mRNA compared to the previously established cytomegalovirus promoter-dependent CA-RP VIII-expressing transfectants, designated as pCI-CA8-PC9 (Fig. 1).

Subsequent electron microscopic examination revealed that CA-RP VIII-expressing PC-9 cells contained many vacuoles of various sizes in the cytoplasm. Each vacuole appeared to be lined by numerous microvilli (Fig. 2c–f). Notably, large intracytoplasmic lumens sometimes pushed the nucleus to one side, as found in signet-ring cell cancer (Fig. 2f). Increased numbers of vacuoles were found in pEF-CA8-PC9 clones (Fig. 2d–f) compared with pCI-CA8-PC9 clones (Fig. 2c). In contrast, few or no vacuoles were found in control PC9 cells (Fig. 2a,b).

Signet-ring cells among CA-RP VIII-expressing PC-9 cells

In the process of establishing and maintaining the pEF-CA8-PC9 transfectants, we found that the transfectants loosely aggregated together and often grew sparsely as single cells.

As demonstrated in Fig. 3, scattered CA-RP VIII-expressing cells often exhibited signet-ring cell features, with abundant mucin stores pushing the nucleus to one side. Notably, signet-ring cells were more frequently found among pEF-CA8-PC9 cells (Fig. 3c,d) than among pCI-CA8-PC9 cells (Fig. 3b). The percentage of signet-ring cell in the cell clot of PC-9, pCI-CA8-PC9, and pEF-CA8-PC9 were 0.2, 1.7±0.9, and 3.7±0.08%.

Immunohistochemical staining

Previous studies revealed that almost all of advanced and invasive non-small lung cancer specimens exhibited strong CA-RP VIII expression, especially at cancer invasion front [1]. In the present study, we attempted to determine when CA-RP VIII was expressed in lung adenocarcinoma. We immunohistochemically examined CA-RP VIII expression in AAH, which is thought to be premalignant for adenocarcinoma and early-stage lung cancer specimens (stage Ia). The results of immunohistochemical staining using a specific antibody to CA-RP VIII are summarized in Table 1, and representative staining is demonstrated in Fig. 4. Alveolar macrophages were stained with monoclonal antibody to CA-RP VIII and were used as an internal control. As previously described [1], no significant staining was observed in alveolar epithelial cells. Little or no CA-RP VIII expression was observed in AAH specimens (Fig. 4a). CA-RP VIII immunoreactivity was barely observed in several BAC specimens (three of eleven; 27%) (Fig. 4b,g).

In contrast, CA-RP VIII expression was observed in eight of eleven (73%) and all of eight MX with BAC pattern and overt MX specimens, respectively (Fig. 4c–e). Notably, invasive lung cancer at an early stage expressed

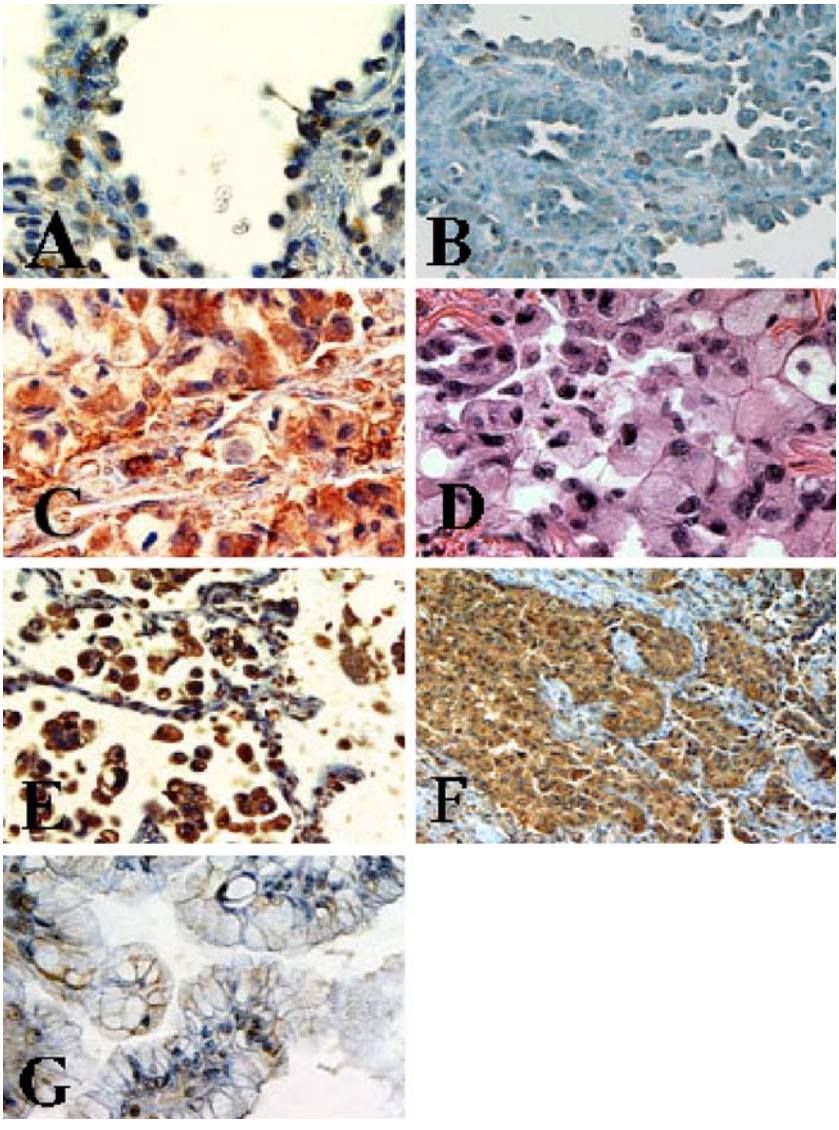

Fig. 4 Representative immunohistochemical staining of AAH and lung adenocarcinoma stage Ia specimens. CA-RP VIII was minimally expressed in AAH (**a**) and BAC (**b**). In contrast, intense staining was observed in lung adenocarcinoma with invasive foci (**c**, **e**, and **f**), especially in signet-ring cancer components (**c**: immunostaining, **d**: HE staining) and mucinous adenocarcinoma components (**e**). The signet-ring cancer cells in figure **e** exhibited immunoreactivity with anti-cytokeratin 7 and anti-TTF-1 antibodies, but not with anti-cytokeratin 20. This phenotype is consistent with that of signet-ring cell-type mucinous carcinoma [9]. The CA-RP VIII immunoreactivity was also observed in non-mucinous invasive adenocarcinoma (**f**). CA-RP VIII was minimally expressed in cancer cells with features of mucinous type BAC (**g**), whereas, infiltrating lymphocytes in alveolar septum strongly expressed CA-RP VIII. Original magnification: ×100 (**e**, and **f**), ×200 (**a**, **b**, and **g**), and ×400 (**c** and **d**)

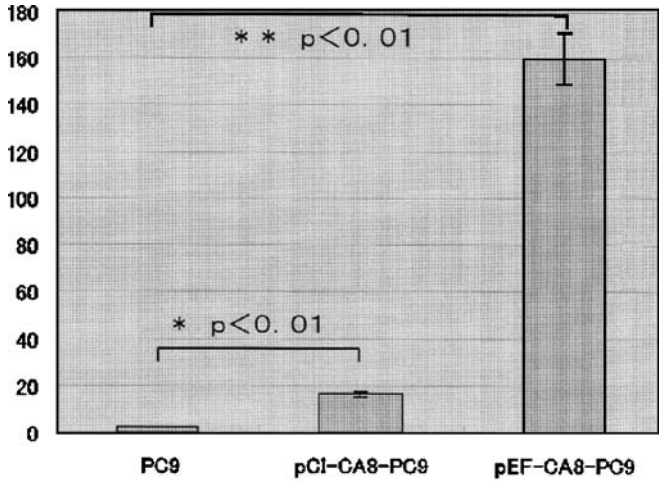

Fig. 5 Exogenously-expressed CA-RP VIII increased invasiveness of PC-9 cells. Representative result demonstrates that pEF-CA8-PC-9 cells (indicated by CA-RP VIII expression) had a significant activity compared to original PC-9 cells in Matrigel assay. Mean value and standard deviation (*SD*) of invasion pEF-CA8-PC-9 cells was 160 and 6.48 (n=4). By contrast, mean value and *SD* of invasion PC-9 cells were 4 and 1.71 (n=4). Notably, these results were reproducible in other pEF-CA8-PC-9 clones

CA-RP VIII in both the central portion of the tumor mass and at the invasive front. No significant staining was observed with isotype-matched control antibody.

Pure signet-ring cell adenocarcinoma of the lung is quite rare, but signet-ring features can occur in various types of pulmonary adenocarcinoma. In the present study, we also examined three lung adenocarcinoma specimens with signet-ring cell components. As shown in Fig. 4c, signet-ring cell cancer cells exhibited strong CA-RP VIII immunoreactivity in all three specimens. Notably, we also found abundant CA-RP VIII expression in invasive mucinous adenocarcinoma. (Fig. 4f). In contrast, BAC of mucinous type expressed little CA-RP VIII (Fig. 4g).

The present immunohistochemical staining suggested that CA-RP VIII expression was related to invasive activity.

Exogenous CA-RP VIII expression enhanced PC-9 adenocarcinoma cell invasion

To test whether exogenously CA-RP VIII-expressing PC-9 cells were more invasive than control PC-9 cells, we performed a Matrigel invasion assay. CA-RP VIII expressing PC-9 cells, but not control cells, exhibited significant invasiveness, as demonstrated in Fig. 5.

However, we did not observe any significant expression of *MMP-2* and *MMP-9* mRNA by RT-PCR (Fig. 6a). Moreover, exogenous CA-RP VIII expression did not alter the MUC expressions (Fig. 6b). Further, migration assay demonstrated no significant differences between PC-9 and transfectants (PC-9: 1,100±100 cells, pCI-CA8-PC9: 1,000±200 cells, pEF-CA8-PC9: 1,100±100 cells).

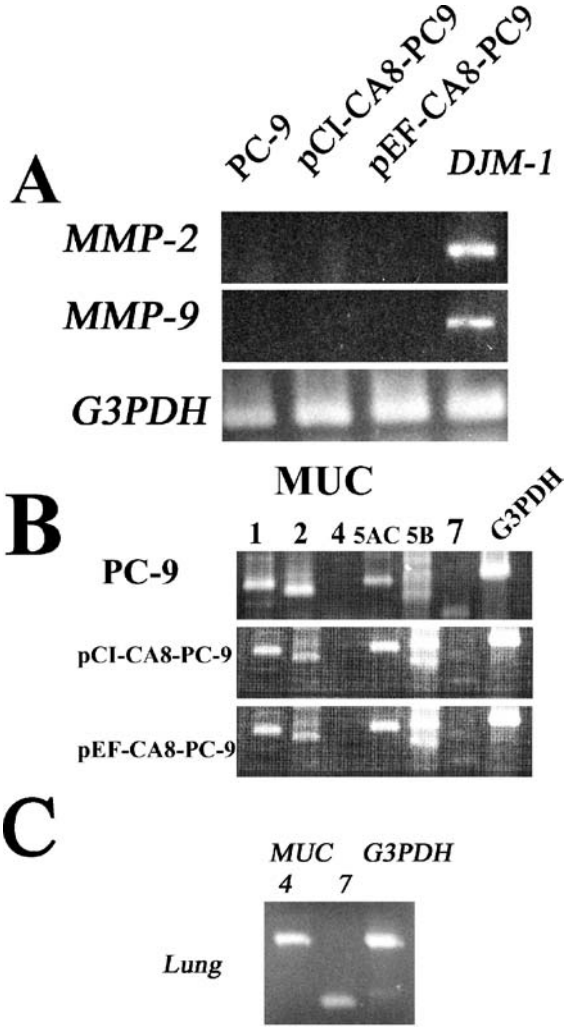

Fig. 6 Exogenously-expressed CA-RP VIII did not alter the *MMP-2*, *MMP-9, or MUCs* mRNA expression in PC-9 cells. **a** Representative result of RT-PCR by using independent transfectants was demonstrated. PC-9 and CA-RP VIII expressing PC-9 cells did not express detectable level of *MMP* mRNAs. The expected transcript size of *MMP-2*, *MMP-3*, and *G3PDH* is 300, 400, and 456 bp, respectively. The control transcript bands from a cultured human skin cancer cell, DJM-1, are also demonstrated. **b** There are no significant differences of *MUC* mRNAs expression between PC-9 and CA-RP VIII expressing PC-9 cells. The expected transcript size of *MUC 2*, *4*, *5AC*, *5B*, and *7* is 308, 443, 383, 415, and 178 bp, respectively. *MUC1 RT-PCR* band may represent carcinoma associated splicing form of MUC1, designated as Episialin [6], with 352 bp, whereas, expected size of *MUC1* transcript is 577 bp. **c** The control transcript bands of *MUC4* and *MUC7* from lung tissues were demonstrated

Discussion

In the present study, we demonstrated that exogenously expressed-CA-RP VIII enhanced invasion activity of PC-9 cells in vitro. Further, immunohistochemical staining indicated that CA-RP VIII expression was related to cancer invasiveness. We examined whether CA-RP VIII altered the expression of invasion-related molecules, including c-met, COX-2, and iNOS in PC-9 cells. However, evidence showing that CA-RP VIII directly altered the expression of

such molecules was not obtained; whereas, melanoma cell lines tested expressed these molecules (data not shown). It is well characterized that MMP-2 and -9 play an important role for lung cancer invasion. However, we could not detect any significant *MMP-2* and *-9* mRNA expressions in PC-9 and transfectants (Fig. 6). We cannot exclude the possibility that unexamined invasion-related molecules including uncharacterized ones might be responsible for the high degree of invasiveness of CA-RP VIII-expressing PC-9 cells. However, the present findings rather suggest that CA-RP VIII expression might directly facilitate lung cancer cell invasion. As no significant difference of migration activity was found between PC-9 and transfectants, we speculate that CA-RP VIII provide the suitable microenvironment for matrix-degradation in cancer foci. Following experiments to unravel the exact molecular mechanism, by which CA-RP VIII facilitate the cancer invasion, is now undergoing.

One interesting finding of the present study is that CA-RP VIII induced signet-ring cell formation among PC-9 cells. As demonstrated in Fig. 3, CA-RP VIII induced intracytoplasmic vacuole formation, possibly in a dose-dependent manner. Signet-ring cells are typically found in poorly differentiated and dedifferentiated adenocarcinomas and not only in gastric but in other cancers as well. We suspect that CA-RP VIII expression induced dedifferentiation of PC-9, a well-differentiated adenocarcinoma cell line and signet-ring cell formation. Signet-ring cell cancer, which can arise from various organs, is highly invasive. Tsuta et al. reported that primary lung cancer with signet-ring cell cancer exhibited significant tendency toward blood vessel invasion, lymph vessel invasion, and lymph node metastasis [18]. As demonstrated in Fig. 4c, signet-ring cell components exhibited strong staining with anti-CA-RP VIII antibody. Furthermore, mucinous adenocarcinoma with invasion foci expressed CA-RP VIII, while mucinous type BAC without foci of invasion expressed little CA-RP VIII. These findings indicated that CA-RP VIII was not directly related to mucinous cell differentiation but related to invasion. In fact, we examined expression of various members of the mucin family, including MUC1, 4, 5AC, 5B, and 7 but failed to detect any significant difference in expression of these molecules between CA-RP VIII-expressing and control PC-9 cells (Fig. 6b).

The histogenesis of signet-ring cell cancer of the lung remains unclear. It appears that factors other than CA-RP VIII are required for signet-ring cell formation among PC-9 cells as a large number of CA-RP VIII-expressing PC-9 cells remain as non-signet-ring cells. Concerning the histogenesis of signet-ring cell cancer, Kobayashi et al. also demonstrated that high Phosphatidylinositol (PI) 3-kinase activity can convert differentiated cells with polarity to less differentiated cells with signet-ring cell features [5]. More recently, Xu et al. reported that the PI 3-kinase-Rac-p38 MAP kinase pathway is involved in the formation of gastric signet-ring cell cancer [19]. Interestingly, Hirota et al. reported that carbonic anhydrase-related protein could bind inositol 1,4,5-trisphosphate receptor type 1 [2]. PI 3-kinase can enhance inositol 1,4,5-trisphosphate production [11]. These findings together suggest that CA-RP VIII might convert PC-9 cells to signet-ring cells by alternating the cross-talk of PI 3-kinase-Rac-p38 MAP kinase and inositol 1,4,5-trisphosphate signal pathway. A study to demonstrate the relationships between CA-RP VIII expression and these signet-ring cell formation-related molecules is now going on.

In conclusion, the present study demonstrated that 1) exogenously expressed CA-RP VIII altered morphology of PC-9 cells, formation of intracytoplasmic lumens and most notably, signet-ring cell formation. 2) CA-RP VIII expression increased the invasiveness of PC-9 cells in vitro without affecting migration activity. 3) CA-RP VIII was also expressed in invasive lung adenocarcinoma at an early stage but barely so in noninvasive adenocarcinoma and AAH specimens.

Acknowledgements We thank Mr. Yamaguchi, Takuya, Ms. Nakamura, Naoyo (Department of Pathology, Kochi Medical School), and Ms. Matumura, Rumi (Division of Molecular Biology, Kochi Medical School) for skillful technique. This study was supported by grants from the Japanese Ministry of Education, Science, and Culture (KAKEN 17590270, 17590654, 15590656) and the Medical Research Fund of Kochi Medical School.

References

1. Akisawa Y, Nishimori I, Taniuchi K, Okamoto N, Takeuchi T, Sonobe H, Ohtsuki Y, Onishi S (2003) Expression of carbonic anhydrase-related protein CA-RP VIII in non-small cell lung cancer. Virchows Arch 442:66–70
2. Hirota J, Ando H, Hamada K, Mikoshiba K (2003) Carbonic anhydrase-related protein is a novel binding protein for inositol 1,4,5-trisphosphate receptor type 1. Biochem J 372:435–441
3. Holting T, Zielke A, Siperstein AE, Clark OH, Duh QY (1994) Transforming growth factor-beta 1 is a negative regulator for differentiated thyroid cancer: studies of growth, migration, invasion, and adhesion of cultured follicular and papillary thyroid cancer cell lines. J Clin Endocrinol Metab 79:806–813
4. Kato K (1990) Sequence of a novel carbonic anhydrase-related polypeptide and its exclusive presence in the Purkinje cells. FEBS Lett 71:137–140
5. Kobayashi M, Nagata S, Iwasaki T, Yanagihara K, Saitoh I, Karouji Y, Ihara S, Fukui Y (1999) Dedifferentiation of adenocarcinomas by activation of phosphatidylinositol 3-kinase. Proc Natl Acad Sci USA 96:4874–4879
6. Ligtenberg MJ, Vos HL, Gennissen AM, Hilkens J (1990) Episialin, a carcinoma-associated mucin, is generated by a polymorphic gene encoding splice variants with alternative amino termini. J Biol Chem 265:5573–5578
7. Lu SH, Takeuchi T, Fujita J, Ishida T, Akisawa Y, Nishimori I, Kohsaki T, Onishi S, Sonobe H, Ohtsuki Y (2004) Effect of carbonic anhydrase-related protein VIII expression on lung adenocarcinoma cell growth. Lung Cancer 44:273–280
8. Miyaji E, Nishimori I, Taniuchi K, Takeuchi T, Ohtsuki Y, Onishi S (2003) Overexpression of carbonic anhydrase-related protein VIII in human colorectal cancer. J Pathol 201:37–45
9. Rossi G, Murer B, Cavazza A, Losi L, Natali P, Marchioni A, Migaldi M, Capitanio G, Brambilla E (2004) Primary mucinous (so-called colloid) carcinomas of the lung: a clinicopathologic and immunohistochemical study with special reference to CDX-2 homeobox gene and MUC2 expression. Am J Surg Pathol 28:442–452
10. Sly WS, Hu PY (1995) Human carbonic anhydrases and carbonic anhydrase deficiencies. Annu Rev Biochem 64:375–401

11. Smith AJ, Surviladze Z, Gaudet EA, Backer JM, Mitchell CA, Wilson BS (2001) p110β and p110δ phsophatidylinositol 3-kinases up-regulate FcεRI-activated Ca^{2+} influx by enhancing inositol 1, 4, 5-triphosphate production. J Biol Chem 276:17213–17220
12. Takeuchi T, Kobayashi M, Moriki T, Miyoshi I (1988) Application of a monoclonal antibody for the detection of *Trichosporon beigelii* in paraffin-embedded tissue sections. J Pathol 156:23–27
13. Takeuchi T, Furihata M, Heng HH, Sonobe H, Ohtsuki Y (1998) Chromosomal mapping and expression of the human B120 gene. Gene 213:189–193
14. Takeuchi T, Misaki A, Liang SB, Tachibana A, Hayashi N, Sonobe H, Ohtsuki Y (2000) Expression of T-cadherin (CDH13, H-Cadherin) in human brain and its characteristics as a negative growth regulator of epidermal growth factor in neuroblastoma cells. J Neurochem 74:1489–1497
15. Takeuchi T, Nicole S, Misaki A, Furihata M, Iwata J, Sonobe H, Ohtsuki Y (2001) Expression of SMARCF1, a truncated form of SWI1, in neuroblastoma. Am J Pathol 158:663–672
16. Taniuchi K, Nishimori I, Takeuchi T, Ohtsuki Y, Onishi S (2002) Developmental expression of carbonic anhydrase-related proteins VIII, X, and XI in the human brain. Neuroscience 112:93–99
17. Tsuboi H, Matsui Y, Hayashida K, Yamane S, Maeda-Tanimura M, Nampei A, Hashimoto J, Suzuki R, Yoshikawa H, Ochi T (2003) Tartrate resistant acid phosphatase (TRAP) positive cells in rheumatoid synovium may induce the destruction of articular cartilage. Ann Rheum Dis 62:196–203
18. Tsuta K, Ishii G, Yoh K, Nitadori J, Hasebe T, Nishiwaki Y, Endoh Y, Kodama T, Nagai K, Ochiai A (2004) Primary lung cancer with signet-ring cell cancer components: clinicopathological analysis of 39 cases. Am J Surg Pathol 28:868–874
19. Xu Q, Karouji Y, Kobayashi S, Ihara S, Konishi H, Fukui Y (2003) The PI3-kinase-Rac-p38 MAP kinase pathway is involved in the formation of signet-ring cell carcinoma. Oncogene 22:5537–5544

Virchows Arch (2006) 448: 838–842
DOI 10.1007/s00428-006-0186-5

ORIGINAL ARTICLE

Francesca Micci · Ioannis Panagopoulos · Bodil Bjerkehagen · Sverre Heim

Deregulation of *HMGA2* in an aggressive angiomyxoma with t(11;12)(q23;q15)

Received: 20 February 2006 / Accepted: 23 February 2006 / Published online: 28 March 2006

Abstract Aggressive angiomyxoma is a soft-tissue neoplasm with a predilection for the pelvic and perineal regions and a tendency to recur locally. Cytogenetic data on this tumor type are limited to five cases, three of which showed rearrangement of chromosomal bands 12q13–15. Molecular investigation of two of the tumors identified the *HMGA2* gene as the target of the 12q rearrangements. However, the two previously analyzed tumors were different at the molecular level: in one, the rearrangement of 12q13–15 resulted in a fusion product, whereas, in the second case, the breakpoint was telomeric (3′) to the *HMGA2*, leaving the gene intact although expressed in its entire length. To shed more light on the pathobiology of aggressive angiomyxoma and to investigate the molecular mechanisms behind the involvement of the *HMGA2* gene in this tumor type (fusion transcript vs deregulated expression), we investigated, cytogenetically and with molecular techniques, one such tumor which presented a t(11;12)(q23;q15) as the sole karyotypic aberration. FISH analyses demonstrated no structural alteration of *HMGA2* at the cytogenetic level; however, expression of the full-length gene was detected molecularly.

F. Micci (✉) · S. Heim
Department of Medical Genetics,
The Norwegian Radium Hospital,
0310 Oslo, Norway
e-mail: francesca.micci@labmed.uio.no
Tel.: +47-22934436
Fax: +47-22935477

I. Panagopoulos
Department of Clinical Genetics, University Hospital,
Lund, Sweden

B. Bjerkehagen
Department of Pathology, The Norwegian Radium Hospital,
Oslo, Norway

S. Heim
Faculty of Medicine, University of Oslo,
Oslo, Norway

Keywords Aggressive angiomyxoma · Cytogenetic *HMGA2*

Introduction

Aggressive angiomyxoma is an infiltrative mesenchymal tumor composed of fibroblasts, myofibroblasts, and numerous thick-walled blood vessels embedded in an abundant myxoid matrix. It occurs in adult women during reproductive years. In addition to its location in the external genitalia of women, cases have also been reported in men, where they occur in the perineal/perianal region [3, 8, 33]. Although the tumor is locally aggressive and prone to recur after surgical removal, metastases are exceedingly rare [10, 20, 23, 34].

Cytogenetic studies have revealed clonal chromosomal abnormalities in five aggressive angiomyxomas. Four tumors had abnormalities involving chromosome 12, including one case with monosomy 12 among other changes [12] and three cases with rearrangements of chromosomal bands 12q13–15 [4, 15, 24]. The fifth tumor showed monosomy of the X chromosome as the sole karyotypic aberration [17]. Molecular investigations of two cases with structural rearrangements of 12q13–15 have identified the high-mobility-group (HMG) protein gene, *HMGA2*, previously known as *HMGIC*, as the target gene [14, 24]. Its involvement differed between the two analyzed tumors, however. The 12q15 rearrangement in an aggressive angiomyxoma with the karyotype 46,XX,der(5)t(5;12)(q31;p11),der(12)inv(12)(p11q15)t(5;12)(q31;p11) resulted in a fusion product containing the first three exons of *HMGA2* followed by a novel 317 bp sequence mapping to 12p11 [14]. The second molecularly examined tumor, with the karyotype 46,XX,t(8;12)(p12;q15), had a breakpoint telomeric (3′) of *HMGA2*, leaving the gene intact but deregulated and expressed.

To shed more light on the pathobiology of aggressive angiomyxoma and, in particular, to investigate the molecular mechanisms behind the involvement of the *HMGA2* gene in this tumor type (fusion transcript vs deregulated

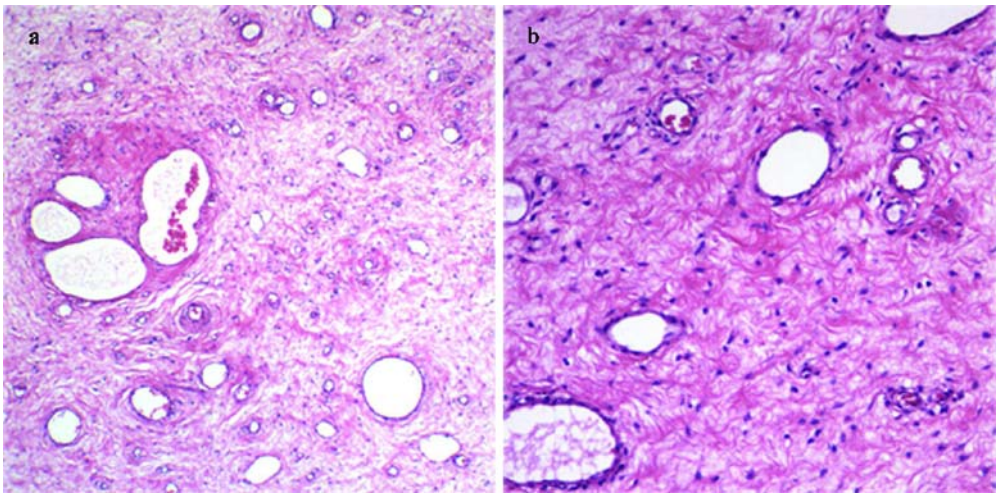

Fig. 1 Histological sections of the aggressive angiomyxoma showing a myxoid stroma with bundles of collagen (**a**) and vessels (**b**)

expression), we examined using molecular techniques another such tumor which presented a t(11;12)(q23;q15) as the sole karyotypic aberration.

Materials and methods

Tumor

A 44-year-old woman had an 11-cm large tumor in the right labium majus close to the bladder, the urethra, and the vagina. Histologic examination of the operation specimen showed a tumor consistent with the diagnosis aggressive angiomyxoma. The tumor consisted of an abundant amount of myxoid tissue in which were seen bland spindle cells with small round or oval nuclei. Cellularity was low. A vascular component consisting of small and medium-sized vessels was also present (Fig. 1) and, in small areas, microhemorrhages could be seen. Bundles of smooth muscles and variable amounts of collagen were present in the myxoid stroma, especially around vessels. There was an infiltrative growth pattern but no mitotic figures. Necrosis was absent. The resection margins were not microscopically free of tumor, but no recurrence or metastases have been seen after 5 years and 4 months of follow-up.

Cytogenetic investigation

The specimens intended for cytogenetic analysis were mechanically and enzymatically disaggregated and short-term-cultured according to Mandahl [19]. Chromosome preparations were made and G-banded using Wright stain. The subsequent cytogenetic analysis and karyotypic description followed the recommendations of the ISCN [13]. Because no metaphase spreads were available for fluorescence in situ hybridization (FISH) analysis, interphase nuclei were used to check for possible rearrangement of the *HMGA2* gene. A pool of cosmid clones spanning the *HMGA2* breakpoint region, 142H1, 245E8, and 154F9 containing exons 1–2 and 156A4 and 27E12 containing exons 4–5, was selected [30]. The clones were grown in selective media, and DNA was extracted according to standard methods [28]. DNA probes were directly labeled with Cy3-dCTP (Amersham, Buckinghamshire, UK) and indirectly with Biotin-dUTP (Molecular Probes, Invitrogen, Carlsbad, CA, USA) by nick-translation, and detected with streptavidin-diethylaminocoumarin (DEAC; Invitrogen). The subsequent hybridization conditions as well as the detection procedure were according to standard protocols [16]. The hybridization was analyzed using a CytoVision system (Applied Imaging, Newcastle, UK).

Molecular genetic investigations

Tumor tissue adjacent to that used for cytogenetic analysis and histologic examination had been frozen and stored at −80°C. *HMGA2* transcripts were detected by reverse-transcribed PCR (RT-PCR); the primers used for PCR amplification are listed in Table 1. Total RNA was extracted using Trizol reagent according to the manufacturer's instructions (Invitrogen).

Table 1 Primers used for PCRs of *HMGA2*

Designation	Sequence	Position	Accession number
HMG848F	5′-ACTTCAGCCCAGGGACAA	848–865	U28749
HMG846F	5′-CCACTTCAGCCCAGGGACAACC	846–867	U28749
HMG1021R	5′-GGCCGTTTTTCTCCAGTG	1021–1038	U28749
HMG1169R	5′-TCCCTTCAAAAGATCCAACTGCTGC	1169–1193	U28749

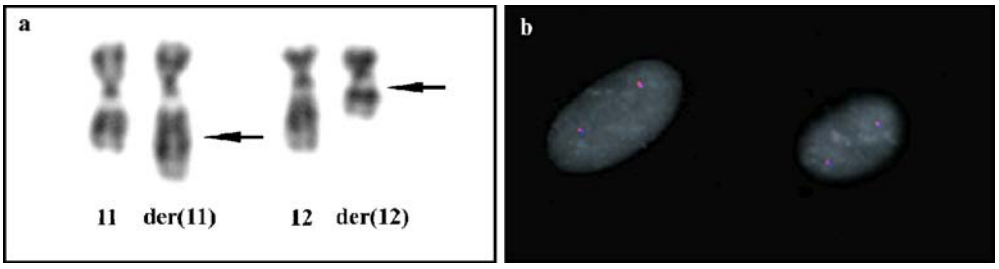

Fig. 2 Chromosome banding and FISH analyses of the aggressive angiomyxoma. **a** Partial G-band karyogram illustrating the (11;12)-translocation; normal chromosomes are included to facilitate comparison; *arrows* indicate breakpoint positions. **b** Image of interphase nuclei showing FISH co-localization of the differently labeled probes (clones 142H1, 245E8, and 154F9 containing exons 1–2 in *blue* color and clones 156A4 and 27E12 containing exons 4–5 in *red* color)

cDNA was synthesized using 5 μg of total RNA in 20 μl reaction mixture [50 mM Tris–HCl pH 8.3 (at 25°C), 75 mM KCl, 3 mM $MgCl_2$, 10 mM dithiothreitol (DTT), 1 mMol each dNTP, 20 U RNAse inhibitor (RNA guard, Amersham Biosciences, Piscataway, USA), 0.5 pM random hexamers, and 400 U M-MLV Reverse Transcriptase (Invitrogen)]. The reaction was carried out at 37°C for 60 min, heated for 5 min at 65°C, and then kept at 4°C until analysis. As an internal control, cDNA quality was checked using *ABL1*-specific primers [25].

The PCR amplification was performed using 1 μl of the cDNA as template in 50 μl reaction volume containing 20 mM Tris–HCl pH 8.4 (at 25°C), 50 KCl, 1.25 mM $MgCl_2$, 0.2 mM of each dNTP, 1 U Platinum *Taq* polymerase (Invitrogen), and 0.5 μM of each of the forward and reverse primers used. The *HMGA2* transcripts were amplified using an initial denaturation for 5 min at 95°C, followed by 35 cycles of 30 s at 95°C, 30 s at 59°C, and 1 min at 72°C and a final extension for 5 min at 72°C. The PCR products were analyzed by electrophoresis through 1.2% agarose gel stained with ethidium bromide.

Results

The G-banding karyotype of the aggressive angiomyxoma was 46,XX,t(11;12)(q23;q15)[16]/46,XX[4] (Fig. 2a). A total of 120 nuclei were analyzed by FISH but showed no rearrangement of the *HMGA2* gene, i.e., signals from the differentially labeled probes co-localized in all analyzed nuclei (Fig. 2b). The breakpoint, therefore, mapped either centromeric to cosmid 154F9 or telomeric to cosmid 154A4. RT-PCR products obtained with primer combinations for exons 1–3 and 1–5 of the *HMGA2* gene showed the presence of two transcripts of 200 and 350 bp, respectively (Fig. 3). The expression of full-length *HMGA2*, i.e., exons 1–5, was, therefore, demonstrated. Transcript of *HMGA2* exons 1–3 was detected using the HMG848F and HMG1021R primer combination, whereas, transcript of *HMGA2* exons 1–5 was detected with the HMG846F and HMG1169R primer combination.

Discussion

Based on the observation that chromosomal bands 12q13–15 are nonrandomly involved in structural abnormalities in aggressive angiomyxoma, they have been found rearranged in three out of five previously analyzed tumors, and that *HMGA2* was the target gene in the only two examined tumors having such rearrangements, we decided to assess the status of *HMGA2* in an aggressive angiomyxoma showing a t(11;12) as the sole karyotypic abnormality. FISH analyses detected no structural alteration of *HMGA2*, but PCR analysis of the gene using a specific primer combination for exons 1–3 and 1–5 revealed that it was expressed with an intact, full-length product. Expression of the entire *HMGA2* gene has been shown to be achieved through alterations affecting 5′ regulatory elements or the

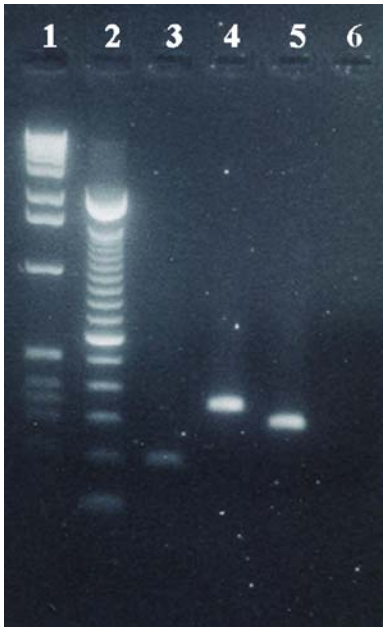

Fig. 3 Detection of the HMGA2 transcript. Total RNA was reversely transcribed and cDNA used as a template in PCR amplification with specific primer combinations; HMG848F and HMG1021R for exons 1–3, lane 3; HMG846F and HMG1169R for exons 1–5, lane 4; chimeric transcript for the *ABL* gene used as an internal control, lane 5; 1 kb DNA ladder, lane 1; 100 bp DNA ladder, lane 2; no RNA in the cDNA, lane 6

3′ untranslated region, leading to a stabilized mRNA in uterine leiomyomata and transfected HeLa cells [6, 26, 29].

As we only analyzed interphase nuclei by FISH, we could not determine the exact position of the breakpoint on 12q, whether it was 5′ or 3′ of the *HMGA2* gene, and, therefore, we could not identify which mechanism led to a stable *HMGA2* mRNA in our sample, i.e., alteration of the 5′ regulatory elements or disruption of the 3′ untranslated region. However, FISH data on the previously reported aggressive angiomyxoma showing a full-length *HMGA2* transcript placed the breakpoint 3′ (telomeric) to *HMGA2* [24]. An alternative activation mechanism for *HMGA2* was reported by Kazmierczak et al. [14] in an aggressive angiomyxoma with inv(12)(p11.2q15); in that tumor, the third exon of *HMGA2* was fused with a 317-bp ectopic sequence from 12p. Apparently, both main molecular mechanisms of *HMGA2* involvement, the generation of a fusion transcript and deregulation of expression, may be operative in aggressive angiomyxoma [14, 24].

This variability in how activation of *HMGA2* is achieved is similar to what has been found in other benign mesenchymal tumors showing involvement of this gene. Both in bone and soft tissue chondromas [9] and uterine leiomyomata [26], the transcriptional activation may occur via alternative mechanisms. It is also noteworthy that some tumors apparently express both full-length and truncated *HMGA2* transcript [9, 32]. In the aggressive angiomyxoma with a inv(12)(p11q15) resulting in a *HMGA2* fusion product reported by Kazmierczak et al. [14], the novel sequence was not homologous to any known gene or expressed-sequence tag, and theoretically contributed only seven amino acid residues before the in-frame stop codon, effectively resulting in a truncated HMGA2 protein containing just the three DNA-binding domains.

The *HMGA2* gene encodes a member of the high-mobility group A (HMGA) of small, non-histonic, chromatin-associated proteins. These proteins are believed to affect transcription as architectural elements by bending the DNA and by interacting with a large number of other proteins, mainly transcription factors, but also to influence chromatin changes during the cell cycle [27]. The *HMGA2* gene is highly expressed in embryonic tissues but has in adults only been found expressed in kidney, lung, and synovia [7, 11]. It has nevertheless been predicted to play a role in adult tissues as well [27]. Experiments on mice demonstrated the importance of the HMGA2 protein for embryonic cell growth [2, 35]. Recently, Ligon et al. [18] reported an 8-year-old boy with a constitutional de novo chromosomal inversion resulting in disruption of *HMGA2* and aberrant adiposity and somatic overgrowth. This phenotype, particularly with respect to overgrowth and lipogenesis, is strikingly similar to that of murine models expressing truncated *Hmga2* transcripts [2].

HMGA2 has been found rearranged in a variety of solid tumors including lipoma, uterine leiomyoma, chondroma, and pulmonary chondroid hamartoma [1, 9, 22, 26, 29]. It recombines with other chromosomal sites through translocations, insertions, and inversions. The involvement of *HMGA2* in different mesenchymal tumors and the promiscuous nature of the translocations involving this gene are reminiscent of that of another gene encoding a nuclear scaffold protein associated with neoplasia. The mixed lineage leukemia (*MLL*) gene is rearranged in numerous acute lymphoid and myeloid leukemias in humans and more than 40 different partner genes have been identified [21]. MLL contains three motifs located near its amino terminus that are highly homologous to the core AT hook DNA-binding domains of the HMGA2 protein; however, whether the HMGA proteins and MLL share any common mechanism of transformation remains to be shown.

Aggressive angiomyxomas are infiltrative tumors with a marked tendency to recur locally. Immunostaining and ultrastructural studies indicate that this neoplasm derives from a primitive mesenchymal cell normally found in the lower female genital tract and capable of myofibroblastic differentiation. Because the most common pattern of behavior of this tumor involves no metastasis, aggressive angiomyxoma has been considered invariably benign [10, 20, 23]. However, two cases of aggressive angiomyxoma with metastasis leading to the patients' death [5, 31] highlight the need to consider it an intermediate tumor with unpredictable and sometimes unfavorable behavior [5]. On the other hand, as *HMGA2* has hitherto only been found to be pathogenetically involved in benign mesenchymal tumors [1, 9, 22, 26, 29], the involvement of the same gene in aggressive angiomyxoma favors its classification as a benign neoplasm. In addition, as normal tissues adjacent to aggressive angiomyxomas are negative for *HMGA2* expression, inappropriate *HMGA2* expression may potentially be useful as a marker of microscopic residual disease using the immunoperoxidase technique with an anti-HMGA2 antibody [20, 23].

Acknowledgements This work was supported by grants from The Norwegian Cancer Society, COST Action B-19—Molecular cytogenetics of solid tumors—Short-term Scientific Mission programme, and The Gunnar Nilsson's Cancer Foundation.

References

1. Ashar HR, Fejzo MS, Tkachenko A, Zhou X, Fletcher JA, Weremowicz S, Morton CC, Chada K (1995) Disruption of the architectural factor HMGI-C: DNA-binding AT hook motifs fused in lipomas to distinct transcriptional regulatory domains. Cell 82:57–65
2. Battista S, Fidanza V, Fedele M, Klein-Szanto AJ, Outwater E, Brunner H, Santoro M, Croce CM, Fusco A (1999) The expression of a truncated HMGI-C gene induces gigantism associated with lipomatosis. Cancer Res 59:4793–4797
3. Begin LR, Clement PB, Kirk ME, Jothy S, McCaughey PB, Ferenczy A (1985) Aggressive angiomyxoma of pelvic soft parts: a clinicopathologic study of nine cases. Hum Pathol 16:621–628
4. Betz JL, Meloni AM, U'Ren LA, Moore GE, Sandberg AA (1995) Cytogenetic findings in a case of aggressive angiomyxoma of the vaginal wall. Cancer Genet Cytogenet 84:157
5. Blandamura S, Cruz J, Faure VL, Machado PI, Ninfo V (2003) Aggressive angiomyxoma: a second case of metastasis with patient's death. Hum Pathol 34:1072–1074

6. Borrmann L, Wilkening S, Bullerdiek J (2001) The expression of HMGA genes is regulated by their 3'UTR. Oncogene 20:4537–4541
7. Broberg K, Tallini G, Hoglund M, Lindstrand A, Toksvig-Larsen S, Mertens F (2001) The tumor-associated gene HMGIC is expressed in normal and osteoarthritis-affected synovia. Mod Pathol 14:311–317
8. Clatch RJ, Drake WK, Gonzales JG (1993) Aggressive angiomyxoma in men. Arch Pathol Lab Med 117:911–913
9. Dahlen A, Mertens F, Rydholm A, Brosjo O, Wejde J, Mandahl N, Panagopoulos I (2003) Fusion, disruption, and expression of HMGA2 in bone and soft tissue chondromas. Mod Pathol 16:1132–1140
10. Fetsch JF, Stenman G (2002) Tumors of uncertain differentiation. In: Fletcher CDM, Unni KK, Mertens F (eds) Tumours of soft tissue and bone: pathology & genetics. IARC, Lyon, pp 189–190
11. Gattas GJ, Quade BJ, Nowak RA, Morton CC (1999) HMGIC expression in human adult and fetal tissues and in uterine leiomyomata. Genes Chromosomes Cancer 25:316–322
12. Horsman DE, Berean KW, Salski CB, Clement PB (1991) Aggressive angiomyxoma of the pelvis: cytogenetics findings in a single case. Cancer Genet Cytogenet 56:130–131
13. Mitelman F (ed) (1995) ISCN: an international system for human cytogenetic nomenclature. S. Karger, Basel
14. Kazmierczak B, Dal Cin P, Wanschura S, Bartnitzke S, Van Den Berghe H, Bullerdiek J (1998) Cloning and molecular characterization of part of a new gene fused to HMGIC in mesenchymal tumors. Am J Pathol 152:431–435
15. Kazmierczak B, Wanschura S, Meyer-Bolte K, Caselitz J, Meister P, Bartnitzke S, Van de Ven W, Bullerdiek J (1995) Cytogenic and molecular analysis of an aggressive angiomyxoma. Am J Pathol 147:580–585
16. Kearny L, Hammomd DW (2001) Molecular cytogenetic technologies. In: Rooney DE (ed) Human cytogenetics—malignancy and acquired abnormalities. Oxford University Press, Oxford pp 129–163
17. Kenny-Moynihan MB, Hagen J, Richman B, McIntosh DG, Bridge JA (1996) Loss of an X chromosome in aggressive angiomyxoma of female soft parts: a case report. Cancer Genet Cytogenet 89:61–64
18. Ligon AH, Moore SD, Parisi MA, Mealiffe ME, Harris DJ, Ferguson HL, Quade BJ, Morton CC (2005) Constitutional rearrangement of the architectural factor HMGA2: a novel human phenotype including overgrowth and lipomas. Am J Hum Genet 76:340–348
19. Mandahl N (2001) Methods in solid tumors cytogenetics. In: Rooney DE (ed) Human cytogenetics—malignancy and acquired abnormalities. Oxford University Press, Oxford, pp 165–203
20. McCluggage WG (2005) A review and update of morphologically bland vulvovaginal mesenchymal lesions. Int J Gynecol Pathol 24:26–38
21. Mecucci C, Rosati R, Starza RL (2002) Genetic profile of acute myeloid leukemia. Rev Clin Exp Hematol 6:3–25
22. Nilsson M, Panagopoulos I, Mertens F, Mandahl N (2005) Fusion of the HMGA2 and NFIB genes in lipoma. Virchows Arch 447:855–858
23. Nucci MR, Fletcher CD (2000) Vulvovaginal soft tissue tumours: update and review. Histopathology 36:97–108
24. Nucci MR, Weremowicz S, Neskey DM, Sornberger K, Tallini G, Morton CC, Quade BJ (2001) Chromosomal translocation t(8;12) induces aberrant HMGIC expression in aggressive angiomyxoma of the vulva. Genes Chromosomes Cancer 32:172–176
25. Panagopoulos I, Mertens F, Domanski HA, Isaksson M, Brosjo O, Gustafson P, Mandahl N (2001) No EWS/FLI1 fusion transcripts in giant-cell tumors of bone. Int J Cancer 93:769–772
26. Quade BJ, Weremowicz S, Neskey DM, Vanni R, Ladd C, Dal Cin P, Morton CC (2003) Fusion transcripts involving HMGA2 are not a common molecular mechanism in uterine leiomyomata with rearrangements in 12q15. Cancer Res 63:1351–1358
27. Reeves R (2001) Molecular biology of HMGA proteins: hubs of nuclear function. Gene 277:63–81
28. Sambrook J, Fritsch EF, Maniatis T (1989) Molecular cloning: a laboratory manual. Cold Spring Harbor Laboratory, Cold Spring Harbor
29. Schoenberg FM, Ashar HR, Krauter KS, Powell WL, Rein MS, Weremowicz S, Yoon SJ, Kucherlapati RS, Chada K, Morton CC (1996) Translocation breakpoints upstream of the HMGIC gene in uterine leiomyomata suggest dysregulation of this gene by a mechanism different from that in lipomas. Genes Chromosomes Cancer 17:1–6
30. Schoenmakers EF, Wanschura S, Mols R, Bullerdiek J, Van Den Berghe H, Van de Ven WJ (1995) Recurrent rearrangements in the high mobility group protein gene, HMGI-C, in benign mesenchymal tumours. Nat Genet 10:436–444
31. Siassi RM, Papadopoulos T, Matzel KE (1999) Metastasizing aggressive angiomyxoma. N Engl J Med 341:1772
32. Tkachenko A, Ashar HR, Meloni AM, Sandberg AA, Chada KK (1997) Misexpression of disrupted HMGI architectural factors activates alternative pathways of tumorigenesis. Cancer Res 57:2276–2280
33. Tsang WY, Chan JK, Lee KC, Fisher C, Fletcher CD (1992) Aggressive angiomyxoma. A report of four cases occurring in men. Am J Surg Pathol 16:1059–1065
34. Wilkinson EJ (2002) Premalignant and malignant tumors of the vulva. In: Kurman RJ (ed) Blaustein's pathology of the female genital tract. Springer, Berlin Heidelberg New York, pp 132–133
35. Zhou X, Benson KF, Ashar HR, Chada K (1995) Mutation responsible for the mouse pygmy phenotype in the developmentally regulated factor HMGI-C. Nature 376:771–774

Virchows Arch (2006) 448: 843–846
DOI 10.1007/s00428-006-0177-6

CASE REPORT

Karen Deraedt · Vincent Vander Poorten · Chris Van Geet · Marleen Renard · Ivo De Wever · Raf Sciot

Multifocal kaposiform haemangioendothelioma

Received: 7 March 2005 / Accepted: 18 April 2005 / Published online: 5 April 2006

Abstract Kaposiform haemangioendothelioma (KHE) is a rare, locally aggressive vascular spindle cell proliferation, with resemblance to Kaposi's sarcoma. This tumour usually occurs in skin and retroperitoneum of infants and young children and is often complicated by the Kasabach–Merritt phenomenon (KMP). A 3-year-old boy presented with a right submandibular swelling due to lymphadenopathies, a violaceous skin lesion at the left commissure of the lips and an ill-defined lesion in the right thyroid lobe. There were some signs of KMP. Histological examination revealed a typical infiltrative multilobular spindle cell proliferation with slit-like vascular spaces in these three localisations. Immunohistochemical stains showed positivity for CD34 and CD31 and many alpha-smooth muscle actin-positive spindle cells around the vascular spaces. There was no Herpes virus type 8 expression. The presented case is unique in two ways. First, thyroid involvement of KHE has never been described in the literature until now. Secondly, and most remarkably, the multifocal presentation in three anatomically distinct and separated localisations is extremely unusual.

K. Deraedt · R. Sciot (✉)
Department of Pathology, University Hospital St. Rafaël,
Katholieke Universiteit Leuven,
Minderbroedersstraat 12,
3000 Leuven, Belgium
e-mail: raf.sciot@uz.kuleuven.ac.be
Tel.: +32-16336593
Fax: +32-16336548

V. Vander Poorten
Head and Neck Surgery, University Hospital,
Catholic University of Leuven,
Leuven, Belgium

C. Van Geet · M. Renard
Pediatrics, University Hospital, Catholic University of Leuven,
Leuven, Belgium

I. De Wever
Oncological Surgery, University Hospital,
Catholic University of Leuven,
Leuven, Belgium

Keywords Kaposiform haemangioendothelioma · Kasabach–Merritt phenomenon · Consumptive coagulopathy · Multifocal

Introduction

Kaposiform haemangioendothelioma (KHE) is defined as a locally aggressive vascular neoplasm, characterised by a predominantly Kaposi sarcoma-like fascicular spindle cell growth pattern [17]. The tumour usually occurs in the skin [3, 7, 8, 11, 18, 20] and retroperitoneum [1, 9, 11, 16, 20] of infants and young children, but some adult cases have been described [5, 10]. KHE is often complicated by Kasabach–Merritt phenomenon (KMP), a condition of severe thrombocytopenia and consumptive coagulopathy [1–3, 6, 7, 11, 14, 16, 18–20]. Some cases of KHE are associated with lymphangiomatosis [7, 20]. Unlike juvenile haemangioma, KHE shows no tendency for spontaneous regression [7, 8]. Regional lymph node metastasis is rare, but distant metastasis has not been reported yet [7]. Mortality is mostly due to KMP with life-threatening haemorrhage [7, 14]. We recently encountered a case of KHE with a multifocal presentation and infiltration into the thyroid gland, a hitherto undescribed phenomenon.

Clinical history

A 3-year-old boy presented with three episodes of fever and a right submandibular swelling of 3 cm in diameter, which was due to painless, but firm lymphadenopathies. Since there was no regression of the adenopathies, an excisional biopsy of a right neck lymph node was taken 4 months after the first consultation. Afterwards, the boy was referred to our center. He was in good general condition. Besides the submandibular lymphadenopathies, clinical examination also revealed a slightly elevated violaceous skin lesion as big as a rice-grain, situated left laterally of the mouth (Fig. 1a). There was no trombocytopenia, but still an elevation of the D-dimer level

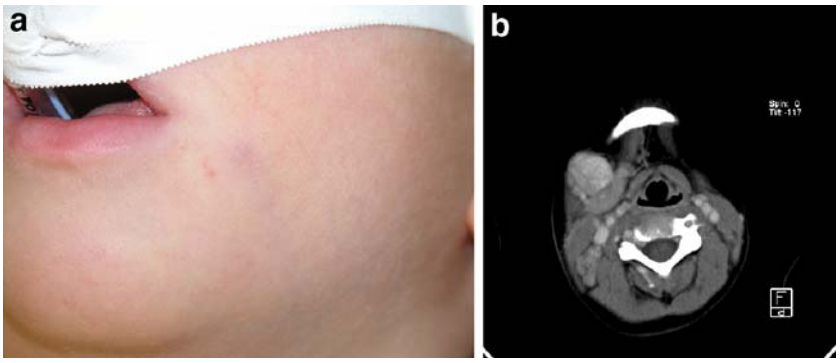

Fig. 1 **a** A violaceous skin lesion at the left commissure of the lips. **b** CT scan: a prominent submandibular lymph node group at the right side

(2,007 μg/l) (normal values 0–500 μg/l), thyroglobulin (43.5 μg/l) (normal values 0.0–25.0) and LDH (625 U/l) (normal values 240–480 U/l). Imaging revealed a prominent submandibular lymph node group and adenopathies along the right internal jugular vein (Fig. 1b). Furthermore, a lesion in the right thyroid lobe was seen, but could not further be specified on CT scan. Because of the presence of multiple lesions and the possibility of malignancy, a right hemithyroidectomy and a right lymph node dissection of levels I to IV was performed. Preoperatively, there was no connection between the thyroid lesion and the enlarged lymph nodes. During the same surgery, the skin lesion was excised. After the operation, there was a normalisation of the D-dimers (340 μg/l).

Materials and methods

The right thyroid lobe, the right neck dissection specimen and the skin lesion were received fresh. A small part of the lesion in the thyroid and the lymph nodes was snap-frozen in liquid-nitrogen-cooled isopentane. The rest of the specimens were fixed in 6% formalin and processed to paraffin. Five-micrometer thick tissue sections were subjected to haematoxylin and eosin. Immunohistochemical studies were performed on formalin-fixed, paraffin-embedded tissue, using a three-step indirect peroxidase complex method. The following antibodies were used: CD31 (1:50 dilution, monoclonal, Dako, Glostrup, Denmark), CD34 (1:10 dilution, monoclonal, Becton Dickinson, San Jose, USA), alfa-SMA (1:100 dilution, monoclonal, Dako, Glostrup, Denmark), HHV-8 (1:20 dilution, Novocastra, Newcastle, UK).

Pathological findings

The right thyroid lobe, measuring 2.2×1.5×1 cm, contained an ill-defined lesion of 1.3×0.9×1 cm. The right neck dissection specimen consisted of enlarged lymph nodes along the right jugular vein and next to the right submandibular gland, which was not infiltrated. The skin biopsy measured 0.5×0.5×0.7 cm.

Histopathological examination of the three resected specimens showed the same picture. The tumour was characterised by an infiltrative multilobular spindle cell proliferation. The infiltrative growth pattern caused destruction of the thyroid parenchyma (Fig. 2a) and the lymph node parenchyma (Fig. 2b). The skin biopsy showed that the tumour was situated in the deeper part of the dermis and in the upper part of the subcutis (Fig. 2c). The tumour consisted of nodules of compact spindle cell fascicles with hardly recognisable interspersed vascular spaces. Thin-walled dilated and probably lymphatic vessels were seen in-between and around the nodules (Fig. 3). The spindle cells did not show cytological atypia or nuclear pleomorphism. Mitotic activity was inconspicuous. Convincing microthrombi were very rare, as well as hyaline globules.

The tumour showed strong positivity for CD34 (Fig. 4) and CD31. Many SMA-positive spindle cells, presumably pericytes, were present around the vascular spaces. A HHV-8 stain was negative.

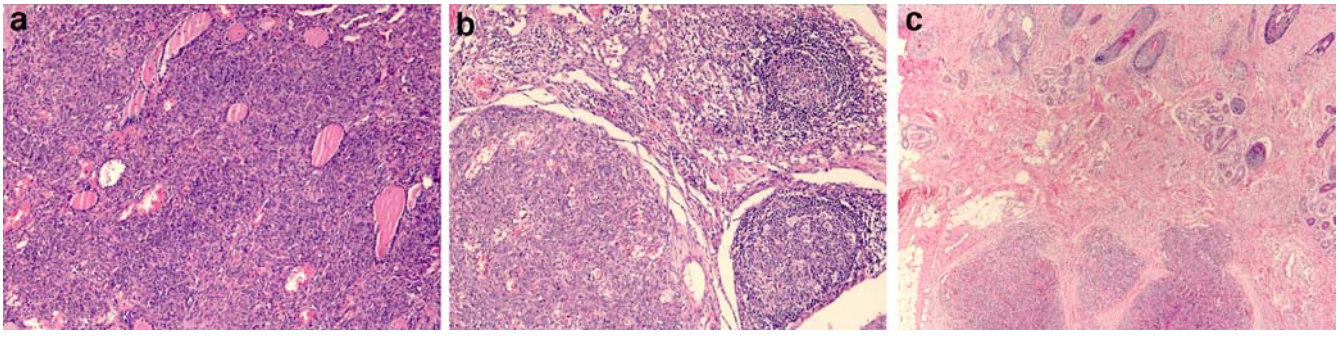

Fig. 2 **a** A spindle cell proliferation with destructive infiltration of the thyroid (hematoxylin-eosin stain ×100). **b** A vascular spindle cell proliferation involving a lymph node (hematoxylin-eosin stain ×100). **c** A multilobular spindle cell proliferation in dermis and subcutis (hematoxylin-eosin stain ×50)

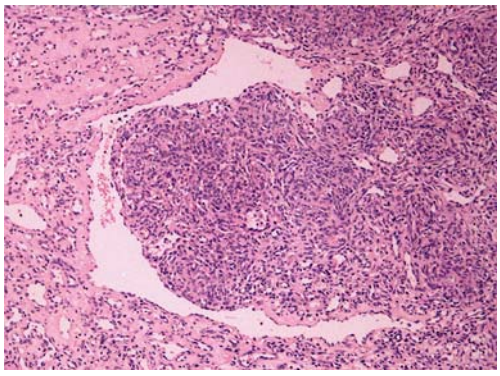

Fig. 3 Thyroid: a dilated thin-walled vessel encircling a tumour nodule (hematoxylin-eosin stain ×100)

Based on these morphological and immunohistochemical findings, a diagnosis of KHE was made.

Discussion

The term 'Kaposiform haemangioendothelioma' was introduced in 1993 by Zukerberg et al. Ever since, fewer than 100 cases have been reported in the literature [1–11, 14–16, 18–20].

KHE usually occurs in early childhood, and often in the first decade of life. KHE mostly involves the skin and the retroperitoneum. The tumour occurs less commonly in the head and neck region [2, 5–7, 15, 20] and in the deep soft tissue of the extremities and the trunk [7, 20]. Rare cases have been described in the mediastinum [7], thymus (one case) [19] and scrotum (one case) [7]. To our knowledge, we present in this paper the first case involving the thyroid.

KHE is often associated with KMP. In our case, there was an elevation of D-dimers, an important marker of consumptive coagulopathy. Therefore, it seems likely that this child showed some evidence of KMP, although platelet count was normal and fibrin thrombi were rare. Yet the recent study of Lyons et al. mentioned that the number of platelet thrombi does not correlate with the presence of KMP [7]. Moreover, normalisation of D-dimers after resection of the lesions proves that the trigger for consumptive coagulopathy has been removed. This trigger has been thought to be related to unique architectural features that favour turbulent blood flow and platelet activation [7]. Absence or presence of KMP is an important prognostic factor, since life-threatening haemorrhage can cause mortality.

Our case illustrates both the nodules of compressed vessels and the ectatic vascular component of KHE. This biphasic pattern has been described before in the literature [1, 7, 9, 11, 15, 20].

In contrast to juvenile haemangioma, KHE shows no tendency to involute. KHE is a locally aggressive tumour, and distant metastasis is not described to date. When reviewing the literature, we found one case of congenital cutaneous multifocal haemangioendothelioma [4]. This report mentions the case of a newborn having multiple cutaneous lesions with the histopathological picture of KHE. All these lesions were confined to the skin. In the present case, we describe KHE in three anatomically distinct and separate lesions. Moreover, we do not have evidence of congenital disease.

Theoretically, one could consider metastatic and aggressive disease because of the separate locations. However, in our case, just as in all earlier described KHEs, there were no histological features of malignancy. In addition, some benign vascular lesions, like the spindle cell haemangioma, can give rise to multiple lesions in the same general area [13]. Finally, another benign vascular tumor, the retiform haemangioendothelioma, occasionally metastasises to the lymph nodes without systemic spread and without aggressive behaviour [12]. In our case, multifocal presentation seems more likely than metastasis from the right thyroid lobe to contralateral lymph nodes only and not to ipsilateral lymph nodes. Obviously, the patient will be followed very closely and only a long-term follow-up will be to disclose the true biologic behaviour. At present, it seems that KHE can be added to the list of vascular tumours with an occasional multifocal presentation.

Acknowledgement We are grateful to Professor C. D. M. Fletcher, Harvard Medical School, Boston, for confirming the diagnosis.

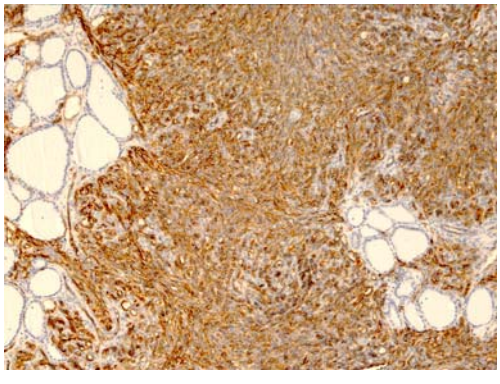

Fig. 4 Thyroid: an infiltrative CD34-positive proliferation between the thyroid follicles (×100)

References

1. Brasanac D, Janic D, Boricic I, Jovanovic N, Dokmanovic L (2003) Retroperitoneal kaposiform hemangioendothelioma with tufted angioma-like features in an infant with Kasabach–Merritt syndrome. Pathol Int 53:627–631
2. Chung MT, Chen CH, Chiu CH, Yang CP, Hsueh C, Jaing TH (2003) Successful nonoperative therapy for Kaposiform hemangioendothelioma involving the neck: report of 1 case. Otolaryngol Head Neck Surg 129:605–607
3. Fukunaga M, Ushigome S, Ishikawa E (1996) Kaposiform haemangioendothelioma associated with Kasabach–Merritt syndrome. Histopathology 28:281–284
4. Gianotti R, Gelmetti C, Alessi E (1999) Congenital cutaneous multifocal kaposiform hemangioendothelioma. Am J Dermatopathol 21:557–561

5. Hardisson D, Prim MP, De Diego JI, Patron M, Escribano A, Rabanal I (2002) Kaposiform hemangioendothelioma of the external auditory canal in an adult. Head Neck 24:614–617
6. Lalaji TA, Haller JO, Burgess RJ (2001) A case of head and neck kaposiform hemangioendothelioma simulating a malignancy on imaging. Pediatr Radiol 31:876–878
7. Lyons LL, North PE, Mac-Moune Lai F, Stoler MH, Folpe AL, Weiss SW (2004) Kaposiform hemangioendothelioma: a study of 33 cases emphasizing its pathologic, immunophenotypic, and biologic uniqueness from juvenile hemangioma. Am J Surg Pathol 28:559–568
8. Mac-Moune Lai F, To KF, Choi PC, Leung PC, Kumta SM, Yuen PP, Lam WY, Cheung AN, Allen PW (2001) Kaposiform hemangioendothelioma: five patients with cutaneous lesion and long follow-up. Mod Path 14:1087–1092
9. Martinez AE, Robinson MJ, Alexis JB (2004) Kaposiform hemangioendothelioma associated with nonimmune fetal hydrops. Arch Pathol Lab Med 128:678–681
10. Mentzel T, Mazzoleni G, Dei Tos AP, Fletcher CD (1997) Kaposiform hemangioendothelioma in adults. Clinicopathologic and immunohistochemical analysis of three cases. Am J Clin Pathol 108:450–455
11. Niedt GW, Greco MA, Wieczorek R, Blanc WA, Knowles DM (1989) Hemangioma with Kaposi's sarcoma-like features: report of two cases. Pediatr Pathol 9:567–575
12. O'Hara CD, Nascimento AG (2003) Endothelial lesions of soft tissues: a review of reactive and neoplastic entities with emphasis on low-grade malignant ("borderline") vascular tumors. Adv Anat Pathol 10:69–87
13. Perkins P, Weiss SW (1996) Spindle cell hemangioendothelioma: An analysis of 78 cases with reassessment of its pathogenesis and biologic behavior. Am J Surg Pathol 20:1196–1204
14. Sarkar M, Mulliken JB, Kozakewich HP, Robertson RL, Burrows PE (1997) Thrombocytopenic coagulopathy (Kasabach–Merritt phenomenon) is associated with Kaposiform hemangioendothelioma and not with common infantile hemangioma. Plast Reconstr Surg 100:1377–1386
15. Tello MA, Shields G, Gadre SA, Ryan M (2004) Pathology quiz case 2. Diagnosis: Kaposiform hemangioendothelioma (KHE). Arch Otolaryngol Head Neck Surg 130:991 Diag 993–994
16. Tsang WY, Chan JK (1991) Kaposi-like infantile hemangioendothelioma. A distinctive vascular neoplasm of the retroperitoneum. Am J Surg Pathol 15:982–989
17. Tsang WY (2002) Kaposiform haemangioendothelioma. In: Fletcher CDM, Unni KK, Mertens F (eds) World Health Organization classification of tumours. Pathology and genetics of tumours of soft tissue and bone. IARC, Lyon, pp 163–164
18. Vin-Christian K, McCalmont TH, Frieden IJ (1997) Kaposiform hemangioendothelioma. An aggressive, locally invasive vascular tumor that can mimic hemangioma of infancy. Arch Dermatol 133:1573–1578
19. Wilken JJ, Meier FA, Kornstein MJ (2000) Kaposiform hemangioendothelioma of the thymus. Arch Pathol Lab Med 124:1542–1544
20. Zukerberg LR, Nickoloff BJ, Weiss SW (1993) Kaposiform hemangioendothelioma of infancy and childhood. An aggressive neoplasm associated with Kasabach–Merritt syndrome and lymphangiomatosis. Am J Surg Pathol 17:321–328

Virchows Arch (2006) 448: 847–851
DOI 10.1007/s00428-006-0184-7

CASE REPORT

Florian Grabellus · Friederike von Winterfeld · Sien-Yi Sheu · Klaus A. Metz · Klaus Jahnke · Kurt W. Schmid

Unusual aggressive course of a giant cell tumor of soft tissue during immunosuppressive therapy

Received: 29 December 2005 / Accepted: 26 February 2006 / Published online: 5 April 2006

Abstract Giant cell tumor of soft tissue with low malignant potential (GCT-ST) is a low-grade, primary soft tissue sarcoma with histological and clinical features similar to giant cell tumor of the bone. The main tumor localizations are the extremities, but it may also occur in the head and neck region. GCT-ST shows a recurrence rate of approximately 15%, but it very rarely metastasizes. The risk of cancer development, especially of the skin, is up to fivefold increased in immunosuppressed patients after organ transplantation. The association of sarcomas and immunosuppressive therapy is best known for Kaposi sarcomas, whereas other types of sarcomas are rarely found. We report of a GCT-ST of low malignant potential, which developed under long-term immunosuppression in a patient 12 years after heart transplantation. The tumor presented with an unusual aggressive course and metastatic site: the parotid gland. Therefore, we suggest that in patients with immunosuppression, even low malignant cancerous lesions should be carefully observed, as their local behavior may be aggressive with development of metastasis.

Keywords Sarcomas · Soft tissue · Transplantation pathology

F. Grabellus (✉) · S.-Y. Sheu · K. A. Metz · K. W. Schmid
Institute of Pathology and Neuropathology,
University Hospital of Essen,
University Duisburg-Essen,
Hufelandstrasse 55,
45122 Essen, Germany
e-mail: florian.grabellus@medizin.uni-essen.de
Tel.: +49-201-7233324
Fax: +49-201-7235926

F. von Winterfeld · K. Jahnke
Department of Otorhinolaryngology,
University Hospital of Essen,
Essen, Germany

Introduction

The development of various types of malignancies, especially skin cancer, in patients receiving immunosuppression after organ transplantation is well-recognized. These patients have an up to fivefold increased risk of cancer compared with the general population [5, 13], which indicates that the development of de novo malignancies emerges as a serious long-term complication after organ transplantation [6]. The development of sarcomas under immunosuppressive therapy is unequivocally documented for human herpesvirus 8-associated Kaposi sarcomas [8], but the occurrence of other types of sarcomas seems to be rare.

Giant cell tumor of soft tissue with low malignant potential (GCT-ST) is a rare, low-grade soft tissue sarcoma. This tumor seems to be clinically and histologically similar to the giant cell tumor of the bone. GCT-ST can affect patients of all ages but is predominantly seen in middle-aged patients. The main tumor localizations are the extremities, but about 10% of the cases occur in the head and neck region. GCT-ST has a moderate local recurrence rate of approximately 15% and it rarely metastasizes [9].

The development of GCT-ST in association with the application of an immunosuppressive therapy has not been reported to date. We report a case of a GCT-ST with an unusual aggressive biologic behavior in a patient who underwent heart transplantation 12 years before the occurrence of a GCT-ST.

Clinical history

We describe a 73-year-old male patient who presented in 2004 with a palpable, round, solid mass of the subcutaneous tissue, measuring ~10 mm, of the left temporal forehead (Fig. 1). The mass was surgically resected and the histological examination was consistent with a GCT-ST. The patient suffered from various internal disorders and had received heart transplantation 12 years ago. Due to long-term medical treatment with a triple combination of

immunosuppressive drugs (FK-506, prednisone, and azathioprine), precancerous (actinic keratosis) and cancerous lesions (basal cell carcinoma and squamous cell carcinoma) of the skin developed at different sites of the face. An in situ squamous cell carcinoma of the skin was resected in the same region. Seven months later, a GCT-ST occurred in that region.

The patient had two tumor relapses of the GCT-ST after 6 and 11 months. Thirteen months after the first diagnosis of GCT-ST, the patient presented with a painless swelling of the left parotid gland. A contrast-enhanced cranial computed tomography (CT) image showed a 23.5-mm measuring tumor (Fig. 2a,b). Histological examination of the lumpectomy revealed a metastasis of GCT-ST in the parotid gland (Fig. 2c). A subsequently performed whole-body positron emission tomography/CT imaging for tumor staging could not detect any other suspect lesions.

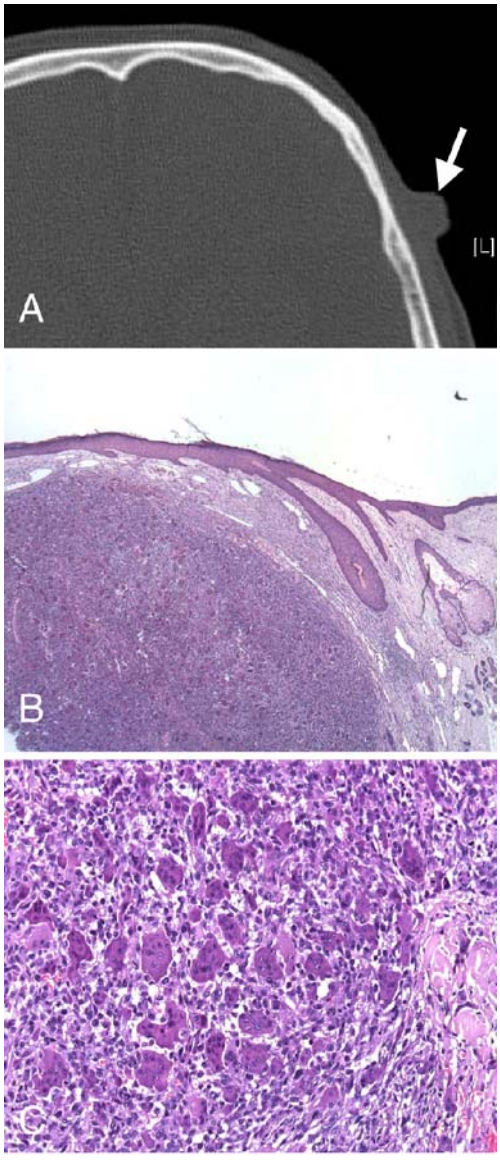

Fig. 1 **a** Cranial CT scan with subcutaneous GCT-ST of the left temporal region (*arrow*). **b** GCT-ST with overlying epidermis (H&E ×25). **c** Typical mixture of multinucleated osteoclast-like giant cells with mononuclear cells in GCT-ST (H&E ×200)

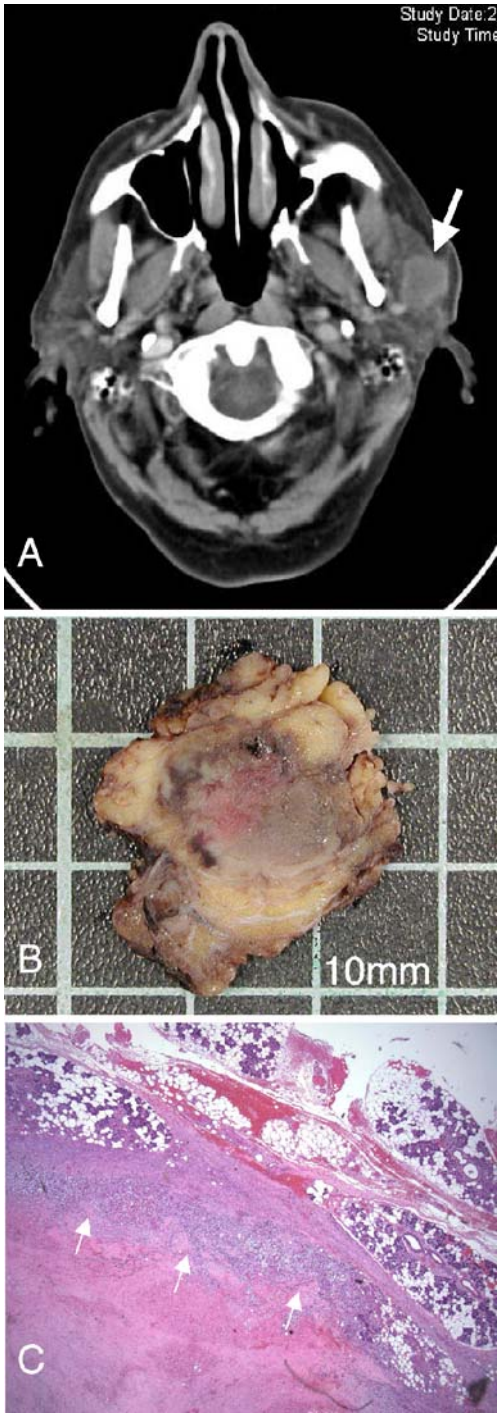

Fig. 2 **a** Cranial CT scan with a 23.5-mm GCT-ST metastasis of the left parotid gland (*arrow*). **b** Cut surface of the left parotid gland with a *grayishbrown* tumor. **c** Histopathologic investigation of the lumpectomy of the parotid gland showed a central necrotic GCT-ST (*arrows* show the rim of vital tumor tissue at the periphery, H&E ×25)

Materials and methods

Light microscopy and immunohistochemistry

Tumor specimens were reviewed by using hematoxylin and eosin-stained (H&E) slides.

For immunohistochemistry, 4-μm sections were cut from formalin-fixed (4% buffered formalin) and paraffin-embedded tissue blocks. Immunohistochemistry was performed using the DAKO EnVision+ System peroxidase method with antibodies against CD68 (DAKO, clone PG-M1, dilution 1:1,200), smooth muscle actin (DAKO, clone 1A4, dilution 1:500), Ki-67 (DCS, clone SP6, dilution 1:1,200), and HHV-8 (Novocastra, clone 13B10, dilution 1:50).

In situ hybridization

For the detection of a latent Epstein–Barr virus (EBV) infection by in situ hybridization, sections from paraffin-embedded GCT-ST tumor tissue (primarius) were analyzed.

In brief, slides were dewaxed, rehydrated, and dried at 45°C. Afterwards, they were pretreated with proteinase K for 25 min at 37°C. Two drops of EBV specific fluorescein isothiocyanate (FITC)-labeled RNA oligonucleotide probe [DAKO, Epstein–Barr virus (EBER) PNA Probe/Fluorescein, Code No. Y5200] were added to the tissue section, and slides were covered with coverslips. The hybridization was carried out for 90 min at 55°C. After washing the slides with diethylpyrocarbonate water, oligonucleotide binding was indirectly detected by an anti-FITC antibody conjugated to alkaline phosphatase (DAKO, PNA ISH detection kit, Code No. K5201).

Results

Pathological findings

Primary tumor

The 27×17×10-mm operation specimen grossly consisted of skin and subcutaneous fat tissue. On the cut surface, a 9-mm, brownish red, well-delineated tumor was seen in the subcutaneous tissue.

The histological investigation of the primary tumor specimen showed a multinodular growth pattern with conspicuous fibrous tissue septa in between the cell-rich tumor nodules. The tumor tissue contained a mixture between multinucleated, osteoclast-like giant cells and a mononuclear type of tumor cells (Fig. 1b,c). High mitotic activity was observed within all areas of the tumor (28 mitotic figures per 10 high-power fields). Atypical mitoses or obvious pleomorphism of the tumor cells was absent. The tumor showed a small area of necrosis, measuring less than 0.1 mm, and focally angiectatic spaces reminiscent of aneurysmal bone cyst changes could be detected.

The histopathological findings were consistent with the diagnosis of a marginal, completely resected GCT-ST.

Metastatic tumor

We received a 39×30×25-mm parotid gland resected specimen and six resection margin specimens. On the cut surface of the lumpectomy specimen from the parotid gland, a 17×16×14-mm, extensively necrotic brown to gray tumor was seen (Fig. 2b).

On histopathological investigation, the metastasis of the tumor had extensive central necrosis and hemorrhage. A small rim of vital tumor was seen at the periphery of the

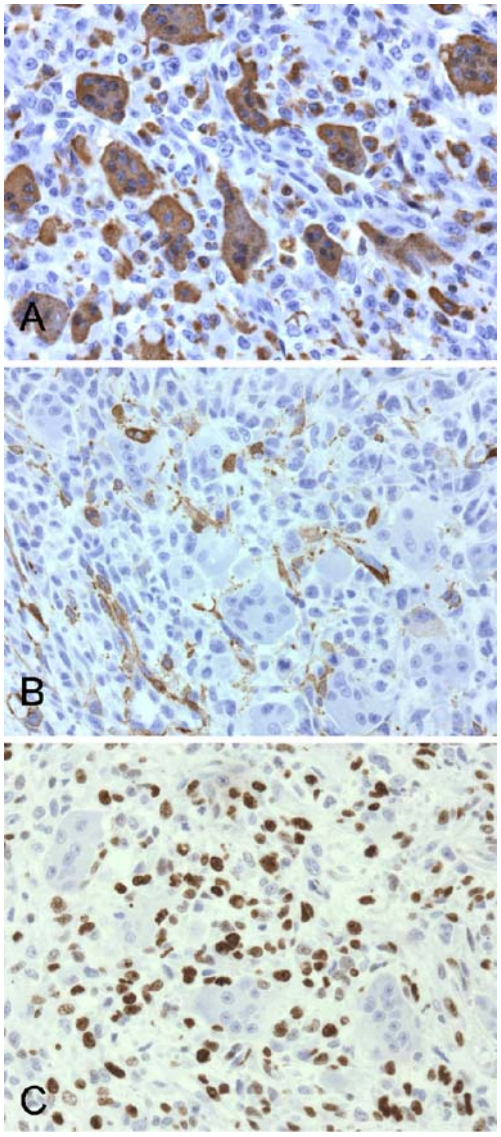

Fig. 3 **a** The immunohistochemical investigation using CD68 antibodies revealed a positive reaction of multinucleated osteoclast-like giant cells and a few mononuclear tumor cells (×400). **b** Staining with smooth muscle actin antibodies showed a positive reaction exclusively with a few mononuclear cells (×400). **c** A high proliferation of the GCT-ST was seen in Ki-67-immunohistochemistry (hot spot, ×400)

nodule (Fig. 2c). The histologic features of this tumor tissue were similar to those described for the primary tumor. The tumor was completely resected with clear margins.

Immunohistochemistry

Immunohistochemical analysis of the tumor tissue revealed that all giant cells and a smaller portion of the mononuclear cells (20%) reacted with antibodies against CD68 (Fig. 3a). A positive reaction with antibodies against smooth muscle actin (Fig. 3b) was exclusively detected in some mononuclear tumor cells. The Ki-67 labeling index was approximately 25% (Fig. 3c).

Tumor tissue was additionally stained with antibodies against human herpesvirus 8 (HHV-8) latent nuclear antigen 1 with a negative result.

RNA in situ hybridization

A latent EBV infection could not be detected in tumor specimens of the primary giant cell tumor by RNA in situ hybridization.

Discussion

Long-term complications of solid organ transplantation have assumed increasing importance as short-term patient and graft survival have improved. It is generally recognized that malignancies are more common after organ transplantation than in the overall population. Generally, this increased risk for developing cancer encompasses almost every type of cancer, but a subset of tumor entities bears an extraordinarily high risk to develop during immunosuppressive therapy [13]. Besides malignant melanoma, non-Hodgkin's lymphoma and carcinomas of the kidney, nonmelanotic skin cancers, particularly squamous cell carcinomas, remain the most common malignancies in solid organ transplant recipients. The incidence of skin cancer increases with survival time after transplantation, and it is noteworthy that the biological behavior of these tumors seems to be much more aggressive than in nonimmunosuppressed skin cancer patients [3, 15]. So it seems to be reasonable to assume that (low-) malignant mesenchymal neoplasms like GCT-ST may behave in a similarly more aggressive fashion under immunosuppressive treatment.

There are different mechanisms that may lead to cancer in patients with immunosuppression [12]. Firstly, immunosuppressive agents can directly cause damage to DNA or interfere with the proper function of DNA repair mechanisms. Secondly, a subset of cancer entities is known to be triggered by specific viral infections that are regularly found in patients with immunosuppression. Finally, immune surveillance, which ordinarily prevents the growth and development of malignancies, is impaired by immunosuppressive drug treatment.

In 1999, Folpe et al. [4] described a subset of malignant giant cells containing soft tissue tumors with low malignant potential. These tumors were termed as "giant cell tumor of low malignant potential." The authors suggested that the term "malignant giant cell tumor" should be restricted to histologically high-grade soft tissue sarcomas. This division was included in the current WHO Classification of Tumors of Soft Tissue and Bone (2002) [9], in which giant cell tumors of soft parts are represented by two entities. The low-malignant end is covered by GCT-ST (i.e., giant cell tumor of low malignant potential) and the high-grade spectrum by the diagnosis of undifferentiated pleomorphic sarcoma with giant cells (i.e., giant cell malignant fibrous histiocytoma or malignant giant cell tumor of soft parts).

The development of soft tissue sarcomas during long-term immunosuppressive therapy is uncommon with the exception of HHV8 associated Kaposi's sarcoma [2] and, to a much lesser extent, EBV-associated leiomyosarcoma [7]. Virus infection, as etiologic background for GCT-ST development, has not been reported to date. Moreover, according to the WHO classification (2002) [9], the etiology of GCT-ST remains completely unclear. EBV-mRNA or HHV8-antigens could not be detected in the tumor tissue of the present GCT-ST, suggesting a lack of association between GCT-ST development and EBV or HHV8-infection.

The metastatic potential of GCT-ST was shown to be very low. Almost 7 years after the definition of the tumor entity by Folpe et al. [4], approximately 70 cases of patients with GCT-ST have been published mainly in three large cohorts [4, 10, 11]. Follow-up data of 53 patients were available, and only three (including the present case) of these patients developed metastasizing disease. A singular distant metastasis of GCT-ST to the parotid gland has not been reported so far, and the spread of other soft tissue sarcomas to this site is extraordinarily rare and is reported sporadically only [1, 14]. Both previously reported patients with metastatic GCT-ST died of tumor after 12 and 13 months, respectively, with widespread pulmonary metastases.

We conclude that patients on chronic immunosuppression have a high risk to develop different (and rare) types of cancer. Even low malignant cancerous lesions should be observed carefully, as their local behavior may be much more aggressive and they might have an enhanced metastatic potential.

References

1. Aleman Lopez O, Carreno VM, Duran R, Garcia-Ortega F, Bonnin OJ, Malluguiza CR (1999) Parotid metastasis of liposarcoma of the lower limbs. Acta Otorrinolaringol Esp 50:667–670
2. Dantal J, Soulillou JP (2005) Immunosuppressive drugs and the risk of cancer after organ transplantation. N Engl J Med 352:1371–1373

3. Euvrard S, Kanitakis J, Claudy A (2003) Skin cancers after organ transplantation. N Engl J Med 348:1681–1691
4. Folpe AL, Morris RJ, Weiss SW (1999) Soft tissue giant cell tumor of low malignant potential: a proposal for the reclassification of malignant giant cell tumor of soft parts. Mod Pathol 12:894–902
5. Gourin CG, Terris DJ (2004) Head and neck cancer in transplant recipients. Curr Opin Otolaryngol Head Neck Surg 12:122–126
6. Hoshida Y, Aozasa K (2004) Malignancies in organ transplant recipients. Pathol Int 54:649–658
7. Lee ES, Locker J, Nalesnik M, Reyes J, Jaffe R, Alashari M, Nour B, Tzakis A, Dickman PS (1995) The association of Epstein–Barr virus with smooth-muscle tumors occurring after organ transplantation. N Engl J Med 332:19–25
8. Moosa MR (2005) Kaposi's sarcoma in kidney transplant recipients: a 23-year experience. QJM 98:205–214
9. Nascimento AG (2002) Giant cell tumor of soft tissue. In: Fletcher CDM, Unni KK, Mertens F (eds) World Health Organization classification of tumours. Pathology and genetics of tumours of soft tissue and bone. IARC Press, Lyon, pp 118–119
10. O'Connell JX, Wehrli BM, Nielsen GP, Rosenberg AE (2000) Giant cell tumors of soft tissue: a clinicopathologic study of 18 benign and malignant tumors. Am J Surg Pathol 24:386–395
11. Oliveira AM, Dei Tos AP, Fletcher CD, Nascimento AG (2000) Primary giant cell tumor of soft tissues: a study of 22 cases. Am J Surg Pathol 24:248–256
12. Penn I (1994) Depressed immunity and the development of cancer. Cancer Detect Prev 18:241–252
13. Penn I (2000) Post-transplant malignancy: the role of immunosuppression. Drug Saf 23:101–113
14. Saiz AD, Sachdev U, Brodman ML, Deligdisch L (1998) Metastatic uterine leiomyosarcoma presenting as a primary sarcoma of the parotid gland. Obstet Gynecol 92:667–668
15. Traywick C, O'Reilly FM (2005) Management of skin cancer in solid organ transplant recipients. Dermatol Ther 18:12–18

Virchows Arch (2006) 448: 852–856
DOI 10.1007/s00428-006-0181-x

CASE REPORT

Jun Nishio · John D. Gentry · James R. Neff · Marilu Nelson · Wayne Daniels · Deborah Perry · Zoran Gatalica · Julia A. Bridge

Monoallelic deletion of the *p53* gene through chromosomal translocation in a small cell osteosarcoma

Received: 11 January 2006 / Accepted: 21 February 2006 / Published online: 5 April 2006

Abstract Small cell osteosarcoma is a rare bone tumor of high-grade malignancy that most often arises in the metaphysis of long bones in the second decade of life. Cytogenetic and molecular genetic findings in small cell osteosarcoma are poorly defined. Conventional cytogenetic analysis of a small cell osteosarcoma arising in the proximal tibia of a 9-year-old male revealed a diploid chromosomal complement with complex structural rearrangements involving chromosomes 6, 16, and 17. Immunohistochemical assessment of p53 protein expression revealed nuclear p53 immunoreactivity in approximately 15% of the neoplastic cells. Subsequent fluorescence in situ hybridization (FISH) analyses confirmed loss of the *p53* gene locus on the derivative chromosome 17 homolog and were negative for amplification of the *MDM2*, *CDK4*, *c-MYC*, *HER-2/neu*, *CCND1*, and *COPS3* gene loci. To the best of our knowledge, this represents the first demonstration of monoallelic deletion of *p53* in small cell osteosarcoma, suggesting that *p53* alterations may play an important role in the development of small cell osteosarcoma as well as conventional osteosarcoma.

Keywords Small cell osteosarcoma · p53 · Cytogenetics · FISH

J. Nishio · J. D. Gentry · J. R. Neff · D. Perry · J. A. Bridge
Department of Pathology and Microbiology,
University of Nebraska Medical Center,
983135 Nebraska Medical Center,
Omaha, NE 68198-3135, USA

J. R. Neff · J. A. Bridge
Orthopaedic Surgery,
University of Nebraska Medical Center,
Omaha, NE, USA

M. Nelson · J. A. Bridge (✉)
Pediatrics, University of Nebraska Medical Center,
Omaha, NE, USA
e-mail: jbridge@unmc.edu
Tel.: +1-402-5597212
Fax: +1-402-5596018

D. Perry
Department of Pathology, Children's Hospital,
Omaha, NE, USA

W. Daniels · Z. Gatalica
Department of Pathology, Creighton University,
Omaha, NE, USA

Introduction

Osteosarcoma is the most common nonhematopoietic primary malignant tumor of bone in children and young adults. The most recent World Health Organization classification recognizes eight separate types: conventional, telangiectatic, small cell, low-grade central, secondary, parosteal, periosteal, and high-grade surface [8]. Small cell osteosarcoma, first described by Sim et al. [22] in 1979, is a rare, usually highly malignant bone tumor that comprises 1.5% of all osteosarcomas. Histologically, small cell osteosarcoma is composed of small cells with round to oval nuclei and finely dispersed chromatin. By definition, tumor osteoid is always present, although variable in amount, and has a fine, lace-like appearance [8, 16, 22]. There is no specific immunophenotype for this tumor. Clinical and radiographic features of small cell osteosarcoma are similar to those of conventional osteosarcoma. Survival data suggest a slightly worse prognosis when compared to conventional osteosarcoma [8]. Cytogenetically, only two cases of small cell osteosarcoma have been previously reported [18, 23]. No consistent chromosomal abnormality has been identified.

In this study, we present detailed cytogenetic and molecular cytogenetic findings of a small cell osteosarcoma. In contrast to most conventional osteosarcomas, the modal chromosome number was stable with a single abnormal clone. The aberrant complement featured complex translocations involving chromosomes 6, 16, and 17 that were further characterized by multiple fluorescence in situ hybridization (FISH) assays. The presence of p53 protein expression was identified immunohistochemically

and a hemizygous deletion of the *p53* gene locus was confirmed by FISH.

Clinical history

A previously healthy 9-year-old male presented with a 6-month history of a limp referable to his right lower extremity, accentuated while running. His mother later noticed a tender mass over the pes anserine region of his right proximal tibia. A plain film radiograph revealed a destructive process in the right proximal tibial metaphysis. MRI displayed a 12-cm intramedullary lesion centered in the metaphysis, with an extraosseous component crossing the growth plate to involve the epiphysis. The knee joint was not involved. An open biopsy was performed, followed by neoadjuvant chemotherapy. A radical local transarticular resection of the proximal tibia was performed and the limb was reconstructed using a tibial rotationplasty technique.

The highly cellular biopsy specimen was composed of small- to medium-sized cells arranged in sheets. Individual cells exhibited fine chromatin, small nucleoli, and scant cytoplasm. Mitoses, some of them atypical, were frequent (greater than 20 mitoses per 10 high-powered fields). Focal areas of necrosis were present as well. Neoplastic osteoid was sparse, in the form of fine eosinophilic material surrounding neoplastic cells, in some areas appearing lace-like (Fig. 1a).

Immunohistochemically, the neoplastic cells were immunoreactive for vimentin and bcl-2 and were negative for cytokeratins (AE1/AE3, CK7, and CK8/18), CD99, chromogranin, neuron-specific enolase, neurofilament, S-100 protein, synaptophysin, leukocyte common antigen, CD34, myogenin, myoglobin, and desmin. The Ki-67 (MIB-1) proliferation-related labeling index was approximately 40%. Based on a previously described classification: (−) no obvious staining; (+) 5% or less of tumor cells positive; (++) 5–50% of tumor cells positive; (+++) more than 50% of tumor cells positive [19], the extent of p53 immunoreactivity was graded as ++ (Fig. 1b). A diagnosis of small cell osteosarcoma was rendered (consultation and confirmation of diagnosis with Dr. K. Krishnan Unni, Mayo Clinic, Rochester, MN, USA).

The resection specimen contained residual tumor with a histology similar to that seen in the biopsy. Post-therapy tumor necrosis was extensive; approximately 10% of viable tumor remained.

Materials and methods

Culturing, harvesting, and slide preparation were performed as previously described [5]. Metaphase cells were banded with Giemsa trypsin and the karyotypes were expressed according to the International System for Human Cytogenetic Nomenclature (ISCN 2005) [12].

Dual-color FISH studies were performed on clonally abnormal metaphase cells in an effort to further characterize the complex anomalies detected by conventional cytogenetics utilizing the LSI p53 (17p13.1) Spectrum Orange-labeled probe with TelVysion 16p Spectrum Green-labeled probe (Vysis, Abbott Molecular, Des Plaines, IL, USA) and the Smith–Magenis (FITC Spectrum)/Miller-Dieker/ILS (Texas Red Spectrum) probe combination which is specific for 17p11.2 (*FLI*) and 17p13.3 (*LIS1*), respectively (Cytocell Technologies, Cambridge, UK). In addition, to determine the presence or absence of various gene amplifications familiar to conventional osteosarcoma, dual-color FISH assays were conducted on cytologic touch preparations of lesional tissue using the following DNA probe sets: PathVysion LSI HER-2 (Spectrum Orange)/Centromere (CEP)17 (Spectrum Green) for *HER-2/neu*, LSI C-MYC (Spectrum Orange)/CEP8 (Spectrum Green) for *c-MYC*, LSI Cyclin D1 (Spectrum Orange)/CEP11 (Spectrum Green) for *CCND1*, bacterial artificial chromosome (BAC) clone RP11-775J10/CEP12 (Spectrum Orange) for *MDM2*, BAC clone RP11-571M6/CEP12 (Spectrum Orange) for *CDK4*, and BAC clone RP11-45M22/CEP17 (Spectrum Orange) for *COPS3*. BAC-derived probes were directly labeled by nick translation with Spectrum Green-dUTP utilizing the manufacturer's protocol (Vysis). BAC clones were obtained from Research Genetics (Huntsville, AL, USA) and other probes were provided by Vysis.

After pretreatment of the slides, the cells and probes were codenatured at 75°C for 1 min and incubated at 37°C overnight using the HYBrite denaturation/hybridization system (Vysis). Posthybridization washing was performed

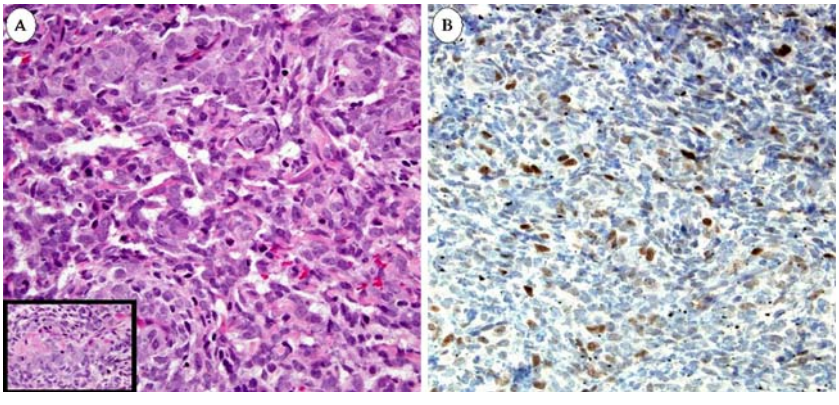

Fig. 1 **a** Histological appearance of small cell osteosarcoma with inconspicuous osteoid (400×, original); more defined focus of osteoid shown in *inset* (200×, original). **b** Approximately 15% of tumor cell nuclei are immunoreactive for p53 (200×, original)

in 0.4× SSC/0.3% NP-40 at 72°C for 2 min, followed by 2× SSC/0.1% NP-40 at room temperature for 1 min. The slides were air-dried in the dark and counterstained with 4′, 6-diamidino-2-phenylindole (DAPI II; Vysis). Hybridization signals were assessed in 100 interphase nuclei or in a minimum of five metaphase cells with strong and well-delineated signals. As a negative control, normal peripheral blood lymphocytes were simultaneously hybridized with these probes. An interphase cell specimen was interpreted as amplification if the ratio of oncogene signals to corresponding centromere signals was greater than 2. Images were acquired using the CytoVision Image Analysis System (Applied Imaging, Santa Clara, CA, USA).

Results

Traditional cytogenetic analysis of the open biopsy specimen revealed complex structural rearrangements involving chromosomes 6, 16, and 17 (Fig. 2). Examination of the resection specimen showed similar karyotypic abnormalities.

Metaphase FISH studies confirmed a translocation between the short arms of chromosomes 16 and 17 observed in GTG-banding analysis (Fig. 3a) and detected monoallelic deletion of the *p53* gene locus on the der(17) (Fig. 3b). The following nomenclature was assigned: 46,XY,der(6)t(6;17)(q27;q21.32),der(16)t(16;17)(p13.3;p13.1),der(17)del(17)(p13.1;p13.1)t(6;17)(q27;q21.32)t(16;17)(p13.3;p13.1) [31].ish der(16)(LIS1+,P53−),der(17)(16ptel+,P53−,FLI+). FISH analyses were negative for amplification of the *MDM2*, *CDK4*, *c-MYC*, *HER-2/neu*, *CCND1*, and *COPS3* genes.

Discussion

Small cell osteosarcoma is histologically characterized by a proliferation of small cells associated with osteoid production. Small cell osteosarcoma may be diagnostically confused with other small cell mesenchymal tumors such as Ewing's sarcoma and mesenchymal chondrosarcoma because of overlapping histological features and/or lack of specific immunohistochemical markers, particularly in small biopsy specimens. In the present case, a diagnosis of small cell osteosarcoma was established on the basis of the presence of lace-like osteoid.

The majority of conventional osteosarcomas are marked by complex chromosomal complements with abundant structural and numerical aberrations and variable modal chromosome numbers [3, 4, 21]. Common structural abnormalities involve 1p11–p13, 1q11–q12, 1q21–q22, 11p14–p15, 14p11–p13, 15p11–p13, 17p, and 19q13. Numerically, gain of chromosome 1 and loss of chromosomes 9, 10, 13, and 17 are frequent [21]. Of the cytogenetic abnormalities observed in the present case,

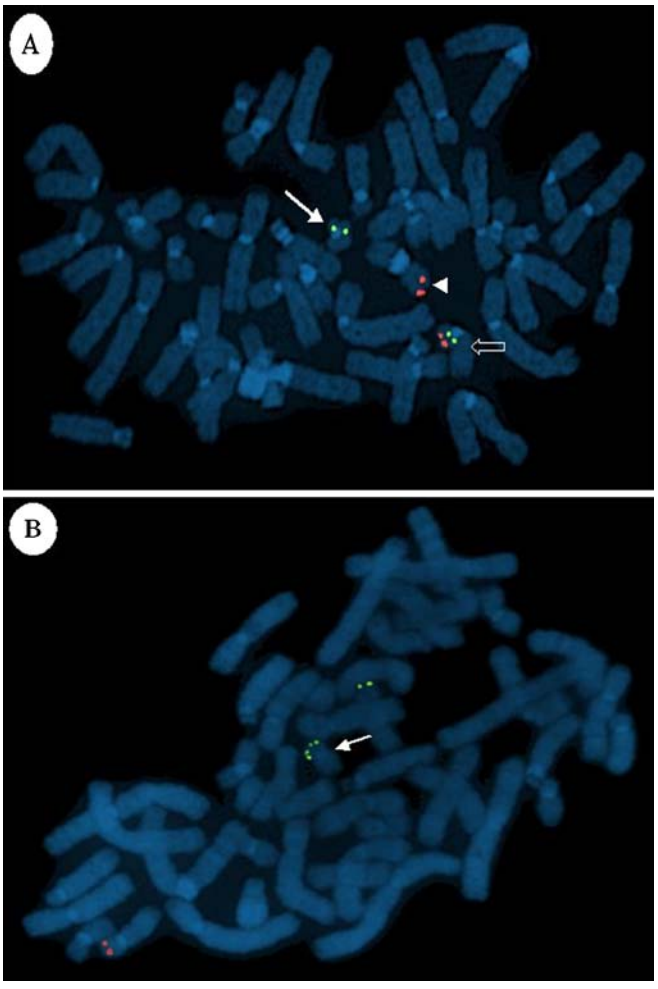

Fig. 3 **a** Dual-color FISH analysis with a Smith–Magenis probe (17p11.2; green) and a Miller–Dieker/ILS probe (17p13.3; red) confirms the translocation of distal chromosome 17 short arm material to the short arm of one chromosome 16 homolog (*arrowhead*). Only the proximal probe (*green signal*) remains on the derivative 17 (*arrow*) in contrast to normal chromosome 17 homolog (*adjacent green* and *red signals*, *openarrow*). **b** Dual-color FISH analysis with LSI p53 (17p13.1; orange) and TelVysion 16p (16pter; green) probes reveals loss of *one orange signal* on the derivative 17 (*arrow*) consistent with monoallelic deletion of the *p53* gene. Remaining chromosomes with *orange* and *green signals* represent the normal chromosome 17 and 16 homologs, respectively

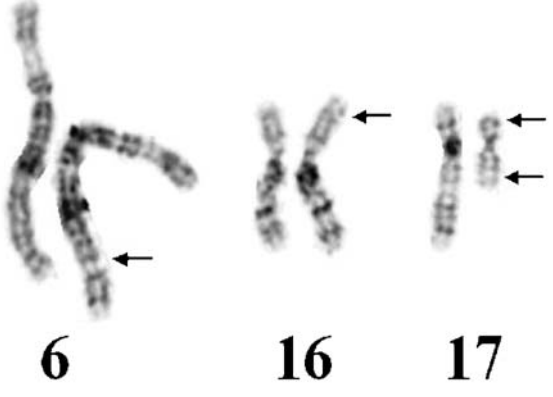

Fig. 2 Partial GTG-banded karyotype illustrating the complex rearrangement involving chromosomes 6, 16, and 17. *Arrows* indicate breakpoints

only one (a translocation involving 16p13.3) has been seen in two other reported cases [3, 4]. Unlike conventional osteosarcoma, cytogenetic abnormalities of small cell osteosarcoma are not well established. Including the present case, only three cases of small cell osteosarcoma have been subjected to cytogenetic analysis [18, 23]. No consistent anomaly has been identified. One small cell osteosarcoma case reportedly exhibited an 11;22 translocation identical to that of Ewing's sarcoma [18], but subsequent studies have failed to repeat this finding [2, 9, 21]. The 13;21 Robertsonian translocation described in two cases of mesenchymal chondrosarcoma [17] has not been seen in small cell osteosarcoma.

The chromosome band 17p13.1 harbors the tumor suppressor gene *p53*, which regulates cell growth, monitors DNA damage, and facilitates DNA repair. Mutations of *p53* are seen in approximately 35% of sporadic osteosarcomas [8]. Deletions of *p53* are common and are believed to be important in the development of osteosarcoma [6, 21]. Overexpression of the p53 protein is seen in at least one-fourth of osteosarcomas [15, 19]. Wild-type *p53* gene overexpression has been demonstrated to block osteosarcoma cell growth [7]. Shorter event-free survival has been documented in osteosarcomas with *p53* alterations [26]. In the current study, we found that monoallelic deletion of the *p53* gene can occur through chromosomal translocations in small cell osteosarcoma. To the best of our knowledge, this is the first case of osteosarcoma to demonstrate a *p53* monoallelic deletion through chromosomal translocation.

Numerous candidate genes related to tumorigenesis are sited in the breakpoint regions detected in this small cell osteosarcoma. For example, the *ETS* variant gene 4 (*ETV4*), cancer susceptibility candidate 3 (*CASC3*), and breast cancer 1 (*BRCA1*) are located at 17q21. The product of *ETV4* has sequence similarity in a region required for sequence-specific DNA binding by members of the *ETS* oncogene family and may be associated with tumor cell invasion and metastasis by activating promoters of matrix metalloproteinases [11]. The protein coded by *CASC3* is essential for nonsense-mediated mRNA decay, a surveillance mechanism that degrades mRNAs with premature translation termination codons. Expression of this product has been demonstrated in lymph nodes containing metastatic carcinomas of the breast but not in normal lymph nodes or fibroadenomas [25]. *BRCA1* is implicated in the transcriptional regulation of DNA damage-inducible genes that function in cell cycle arrest. It is interesting to note that loss of heterozygosity at the *BRCA1* gene locus has been demonstrated in 21% of sporadic osteosarcomas, suggesting that inactivation of *BRCA1* may play a role in the development and/or progression of sporadic osteosarcoma [24].

Chromosomal band 6q27 is the locus for the programmed cell death 2 (*PDCD2*) and myeloid/lymphoid or mixed lineage leukemia, translocated to, 4 (*MLLT4*) genes. The *PDCD2* gene is the human homolog of *Rp8*, a rat gene associated with programmed cell death in thymocytes. *BCL6*, a known transcriptional repressor, targets *PDCD2* and may regulate apoptosis via this mechanism [1]. *MLLT4* has been described as a "partner gene" to 11q23, a common locus involved in translocations seen in acute lymphoblastic and myeloid leukemias. Its product shares a motif present in many proteins involved in signal transduction at cell–cell junctions [20]. Whether these or other genes located on 6q27 are involved in the development of small cell osteosarcoma remains to be elucidated.

Gene amplification is an important mechanism for oncogene overexpression in human cancer. Gene amplification is frequent in osteosarcoma. Amplification of *MDM2*, *CDK4*, *GLI*, *CHOP*, *SAS*, *HMGI-C*, *OS-4*, *OS-9*, and *PRIM1* localized to 12q13–q15, amplification of *COPS3* and *PMP22* localized to 17p11.2, and amplification of *c-MYC*, *HER-2/neu*, and *CCND1* localized to 8q24, 17q21, and 11q13, respectively, have been described in osteosarcoma [10, 14, 21, 27, 28]. In addition, amplification has been observed in several chromosomal regions where the target gene has not been identified such as 1q21–q22, 6p12–p21, 8q21–q22, and 19q12–q13 [13, 21]. In the current study, interphase FISH analyses of *MDM2*, *CDK4*, *c-MYC*, *HER-2/neu*, *CCND1*, and *COPS3* were negative for amplification. In contrast, Sjogren et al. [23] described high-level amplification of the *MDM2*, *CDK4*, and *SAS* genes and low-level amplification of the *HMGI-C* gene in association with a giant marker chromosome in a small cell osteosarcoma with mesenchymal chondrosarcoma-like features.

In summary, genetic data are lacking for small cell osteosarcoma. The findings identified in the current case share some similarities with conventional osteosarcoma but are distinctive from those reported for Ewing's sarcoma and mesenchymal chondrosarcoma. Additional studies are needed to determine the frequency of *p53* alterations in small cell osteosarcoma and their possible prognostic significance.

Acknowledgements This work was supported in part by the Nebraska State Department of Health (LB595) and NIH (P30 CA36727). Jun Nishio was supported by the Gladys Pearson Fellowship in Pediatric Cancer and Genetics. This study was performed in compliance with Institutional Review Board (IRB) regulations.

References

1. Baron BW, Anastasi J, Thirman MJ, Furukawa Y, Fears S, Kim DC, Simone F, Birkenbach M, Montag A, Sadhu A, Zeleznik-Le N, McKeithan TW (2002) The human programmed cell death-2 (PDCD2) gene is a target of BCL6 repression: implications for a role of BCL6 in the down-regulation of apoptosis. Proc Natl Acad Sci U S A 99:2860–2865
2. Biegel JA, Wormer RB, Emanuel BS (1989) Complex karyotypes in a series of pediatric osteosarcomas. Cancer Genet Cytogenet 38:89–100
3. Boehm AK, Neff JR, Squire JA, Bayani J, Nelson M, Bridge JA (2000) Cytogenetic findings in 36 osteosarcoma specimens and a review of the literature. Pediatr Pathol Mol Med 19:359–376
4. Bridge JA, Nelson M, McComb E, McGuire MH, Rosenthal H, Vergara G, Maale GE, Spanier S, Neff JR (1997) Cytogenetic findings in 73 osteosarcoma specimens and a review of the literature. Cancer Genet Cytogenet 95:74–87

5. Bridge RS Jr, Bridge JA, Neff JR, Naumann S, Althof P, Bruch LA (2004) Recurrent chromosomal imbalances and structurally abnormal breakpoints within complex karyotypes of malignant peripheral nerve sheath tumour and malignant triton tumour: a cytogenetic and molecular cytogenetic study. J Clin Pathol 57:1172–1178
6. Chandar N, Billig B, McMaster J, Novak J (1992) Inactivation of p53 gene in human and murine osteosarcoma cells. Br J Cancer 65:208–214
7. Diller L, Kassel J, Nelson CE, Gryka MA, Litwak G, Gebhardt M, Bressac B, Ozturk M, Baker SJ, Vogelstein B, Friend SH (1990) p53 functions as a cell cycle control protein in osteosarcomas. Mol Cell Biol 10:5772–5781
8. Fletcher CDM, Unni KK, Mertens F (eds) (2002) World Health Organization classification of tumours. Pathology and genetics of tumours of soft tissue and bone. IARC Press, Lyon
9. Giovannini M, Selleri L, Biegel JA, Scotlandi K, Emanuel BS, Evans GA (1992) Interphase cytogenetics for the detection of the t(11;22)(q24;q12) in small round cell tumors. J Clin Invest 90:1911–1918
10. Henriksen J, Aagesen TH, Maelandsmo GM, Lothe RA, Myklebost O, Forus A (2003) Amplification and overexpression of COPS3 in osteosarcomas potentially target TP53 for proteasome-mediated degradation. Oncogene 22:5358–5361
11. Higashino F, Yoshida K, Noumi T, Seiki M, Fujinaga K (1995) Ets-related protein E1A-F can activate three different matrix metalloproteinase gene promoters. Oncogene 10:1461–1463
12. ISCN (2005) An international system for human cytogenetic nomenclature. In: Shaffer LG, Tommerup N (eds) Karger, Basel
13. Knuutila S, Bjorkqvist A-M, Autio K, Tarkkanen M, Wolf M, Monni O, Szymanska J, Larramendy ML, Tapper J, Pere H, El-Rifai W, Hemmer S, Wasenius V-M, Vidgren V, Zhu Y (1998) DNA copy number amplifications in human neoplasms: review of comparative genomic hybridization studies. Am J Pathol 152:1107–1123
14. Ladanyi M, Gorlick R (2000) Molecular pathology and molecular pharmacology of osteosarcoma. Pediatr Pathol Mol Med 19:391–413
15. Lonardo F, Ueda T, Huvos AG, Healy J, Ladanyi M (1997) p53 and MDM2 alterations in osteosarcoma: correlation with clinicopathologic features and proliferative rate. Cancer 79:1541–1547
16. Nakajima H, Sim FH, Bond J, Unni KK (1997) Small cell osteosarcoma of bone. Cancer 79:2095–2106
17. Naumann S, Krallman PA, Unni KK, Fidler ME, Neff JR, Bridge JA (2002) Translocation der(13;21)(q10;q10) in skeletal and extraskeletal mesenchymal chondrosarcoma. Mod Pathol 15:572–576
18. Noguera R, Navarro S, Triche TJ (1990) Translocation (11;22) in small cell osteosarcoma. Cancer Genet Cytogenet 45:121–124
19. Papai Z, Feja CN, Hanna EN, Sztan M, Olah E, Szendroi M (1997) P53 overexpression as an indicator of overall survival and response to treatment in osteosarcomas. Pathol Oncol Res 3:15–19
20. Prasad R, Gu Y, Alder H, Nakamura T, Canaani O, Saito H, Huebner K, Gale RP, Nowell PC, Kuriyama K (1993) Cloning of the ALL-1 fusion partner, the AF-6 gene, involved in acute myeloid leukemias with the t(6;11) chromosome translocation. Cancer Res 53:5624–5628
21. Sandberg AA, Bridge JA (2003) Updates on cytogenetics and molecular genetics of bone and soft tissue tumors: osteosarcoma and related tumors. Cancer Genet Cytogenet 145:1–30
22. Sim FH, Unni KK, Beabout JW, Dahlin DC (1979) Osteosarcoma with small cells simulating Ewing's tumor. J Bone Joint Surg Am 61:207–215
23. Sjogren H, Orndal C, Tingby O, Meis-Kindblom JM, Kindblom L-G, Stenma G (2004) Cytogenetic and spectral karyotype analyses of benign and malignant cartilage tumours. Int J Oncol 24:1385–1391
24. Sztan M, Papai Z, van der Looij M, Olah E (1997) Allelic losses from chromosome 17 in human osteosarcomas. Pathol Oncol Res 3:115–120
25. Tomasetto C, Regnier C, Moog-Lutz C, Mattei MG, Chenard MP, Lidereau R, Basset P, Rio MC (1995) Identification of four novel human genes amplified and overexpressed in breast carcinoma and localized to the q11–q21.3 region of chromosome 17. Genomics 28:367–376
26. Tsuchiya T, Sekine K, Hinohara S, Namiki T, Nobori T, Kaneko Y (2000) Analysis of the p16INK4, p14ARF, p15, TP53, and MDM2 genes and their prognostic implications in osteosarcoma and Ewing sarcoma. Cancer Genet Cytogenet 120:91–98
27. van Dartel M, Hulsebos TJM (2004) Amplification and overexpression of genes in 17p11.2–p12 in osteosarcoma. Cancer Genet Cytogenet 153:77–80
28. Yotov WV, Hamel H, Rivard G-E, Champagne MA, Russo PA, Leclerc J-M, Bernstein ML, Levy E (1999) Amplifications of DNA Primase 1 (PRIM1) in human osteosarcoma. Genes Chromosomes Cancer 26:62–69

Virchows Arch (2006) 448: 857–861
DOI 10.1007/s00428-006-0187-4

CASE REPORT

Angela Pucci · Monica Suppo · Giovanni Lucchesi · Angela Celeste · Laura Viberti · Riccardo Pellerito · Mauro Papotti

Papillary thyroid carcinoma presenting as a solitary soft tissue arm metastasis in an elderly hyperthyroid patient. Case report and review of the literature

Received: 8 December 2005 / Accepted: 6 March 2006 / Published online: 28 March 2006

Abstract A case of papillary thyroid carcinoma (PTC) presenting as a solitary metastasis in the right arm muscle is described in an elderly hyperthyroid male patient. A 2-cm nodule in the right bycipites muscle was found to be a papillary carcinoma of thyroid origin and a primary, 3.5-cm tumor was subsequently found in the left lobe of a hyperfunctioning gland due to toxic goiter. Both tumors were well differentiated PTC, follicular variant. No high grade features, nor extrathyroidal spread, nor regional lymph node metastases were found, but histology evidenced intrathyroidal vascular invasion. After radical surgery and radioiodine therapy, the patient is currently disease-free 4 years after diagnosis. This is the third reported case of PTC manifesting as a single soft tissue metastasis and the first associated with hyperthyroidism. Hematogenous spread of differentiated PTC is rare, although less unusual in PTC follicular variant. Histological vascular invasion, hypervascularity and increased blood flow in the hyperfunctioning thyroid gland might have facilitated the dissemination of malignant tumor cells through the bloodstream. Literature data indicate that PTC in elderly patients is increasing and is often clinically aggressive. Radical surgical and radiometabolic treatments are required also in this age group to improve clinical outcome.

Keywords Papillary thyroid carcinoma · Soft tissue metastasis · Hyperthyroidism

This work was partially supported by grants from the Italian Ministry of Education and University (ex 60% to MP).

A. Pucci · A. Celeste
Division of Pathology of Regina Margherita Hospital,
Torino, Italy

L. Viberti
Division of Pathology of Valdese Hospital,
Torino, Italy

M. Suppo
Division of Surgery of CTO Hospital,
Torino, Italy

G. Lucchesi
Division of Surgery of Valdese Hospital,
Torino, Italy

R. Pellerito
Department of Nuclear Medicine, Mauriziano Hospital,
Torino, Italy

M. Papotti
Department of Clinical and Biological Sciences,
University of Turin and San Luigi Hospital,
Torino, Italy

A. Pucci (✉)
Division of Pathology, Azienda Ospedaliera OIRM-S.Anna,
P.za Polonia,
94-10126 Torino, Italy
e-mail: angelapucci@libero.it
Tel.: +39-011-3135342
Fax: +39-011-3135412

Introduction

Differentiated thyroid carcinoma presenting as a solitary distant metastasis is exceptional. Distant metastases are an uncommon event in differentiated thyroid cancer and are generally associated with follicular carcinoma histological type, rather than papillary. In addition, they are generally detected in lung and bone, and, less commonly, in the brain or liver, other sites being exceptional [5, 9, 12, 18, 19]. To our knowledge, papillary thyroid carcinoma (PTC) presenting as an isolated distant metastasis has been previously described in only three reports, in the pleura [14], in the submandibular gland [17] and in the choroid [20].

The reported prevalence of thyroid malignancy in hyperthyroid patients is varying from 1 to 9% of cases [21]. Anyhow, it is a rare occurrence, generally restricted to multinodular thyroid gland with hyperfunctioning nodules, one of them having malignant features of the follicular (possibly oncocytic) carcinoma type [7]. Small (less than 1.5 cm) papillary carcinomas have also been reported as incidental findings in hyperfunctioning thyroid glands resected for untreatable hyperthyroidism [4, 6, 15].

PTC in the elder (>70 years) population is very rare (approximately 7.6%), the median age of patients with PTC being 40 years for females and 44 years for males, with a female to male ratio of 4:1, age >45 years in males representing an adverse prognostic factor [7, 23].

We, herein, report a case of PTC which is unique for its presentation. It manifested, in fact, as a solitary soft tissue metastasis in the right arm, in an elderly patient affected by hyperthyroidism. The combination of these features has not been reported yet in the English Literature.

Clinical history

A 77-year-old male patient underwent surgical biopsy of a solid nodule of approximately 2 cm in size in his right arm, located within the bycipites muscle. This was interpreted at ultrasound scan and magnetic resonance imaging as a suspected soft tissue tumor. Histologically, an epithelial tumor with the morphological features of PTC was found. As a consequence, the thyroid gland was investigated and a 3.5-cm nodule in the left lobe of a multinodular gland was discovered. In addition, the patient revealed that he was treated with tapazole for a toxic goiter that had caused hyperthyroidism of 2-year duration. A fine needle aspiration biopsy of the left thyroid nodule confirmed the suspicion of PTC. Total thyroidectomy with left cervical lymphoadenectomy and radical excision of muscle metastasis were performed. Postoperative radioiodine treatment was administered (total dose of 3.7 GBq). At follow-up, total body scintiscan did not reveal any abnormal uptake; at the last check-up, the patient was alive and disease-free 4 years after diagnosis.

Materials and methods

Surgical specimens from both the arm muscle nodule and total thyroidectomy were formalin fixed and paraffin embedded. Sections were stained with hematoxylin and eosin for conventional histology. Serial sections were collected onto poly-L-lysine-coated slides for immunohistochemistry, using a standard manual immunoperoxidase procedure. Heat-induced antigen retrieval procedure was carried out by three 5-min passages in citrate buffer solution in microwave oven at 650 W. The following monoclonal antibodies were tested in both the primary carcinoma and the metastatic nodule: anti-thyroglobulin monoclonal antibody (DakoCytomation, Glostrup, Denmark, diluted 1/3,000), Galectin-3 (clone 9C4, Novocastra Laboratories, Newcastle, UK, diluted 1/400), HBME-1 (DakoCytomation, diluted 1/500), Cytokeratin 19 (clone b170, Novocastra Laboratories, diluted 1/150), p27 (clone 1B4, Novocastra Laboratories, diluted 1/30) and Ki67 (clone MIB-1, DakoCytomation, diluted 1/100). The immunoreaction was revealed by incubation with an enzyme-labelled polymer pre-conjugated with anti-mouse secondary antibodies (a biotin-free detection system) (Envision System, DakoCytomation), then with 3′-3′-diaminobenzidine-tetrahydrochloride. The sections were counterstained with Mayer's hemalum and mounted.

Results

Muscle nodule The biopsy and excisional surgical specimens of the right arm nodule were whitish irregular samples of 2×0.5 and 5×2 cm, respectively, surrounded by skeletal muscle fibers irregularly dissected by dense fibrotic tissue admixed with the tumor tissue. The tumor nodule had a similar appearance in both specimens, consisting of small follicles and of irregular papillary formations having a thin fibrovascular stalk. The cells lining the follicles or papillae had medium size, eosinophilic cytoplasm, an enlarged, central nucleus with an irregular profile, indentations, longitudinal grooves and occasional cytoplasmic inclusions (Fig. 1).

Thyroid nodule The thyroidectomy specimen measured 6×4 cm in the left and 6×5 cm in the right lobe and had an irregular multinodular profile. On cut surface, the nodules were dark red with hemorrhagic areas. But the largest (3.5 cm diameter) nodule, located in the mid-portion of the left lobe, was roundish, gray-whitish, partially cystic with a smooth profile and a harder consistency of the solid area. Histologically, the multiple thyroid nodules (except for the largest one) were made of follicles of variable size, containing scalloped colloid and lined by cubic and columnar hyperplastic thyrocytes. The major, capsulated nodule showed focal classical papillary areas and pre-

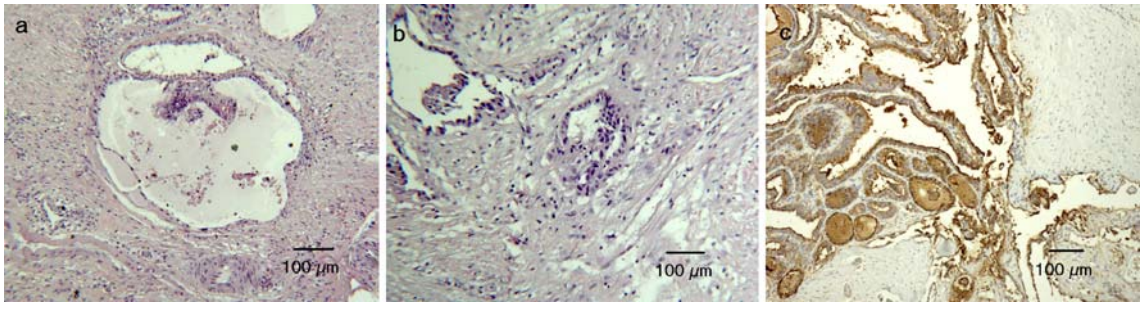

Fig. 1 **a**, **b** Right arm bycipites muscle metastasis of papillary thyroid carcinoma infiltrating muscle fibers and partially surrounded by fibrotic tissue (hematoxylin and eosin, original magnification: **a** ×25, **b** ×75. **c** Tumor cells diffusely express thyroglobulin (immunoperoxidase with hemalum nuclear counterstaining, original magnification ×100)

dominant follicular growth with small, and sometimes, large follicles in a fibrotic stroma. The follicles contained scant, dark colloid and were lined by large cuboidal cells with centrally located irregular, clear and ground-glass nuclei with numerous grooves and occasional cytoplasmic inclusions. Papillary formations lined by similar cells were focally seen. No areas of solid growth or of tall cell or columnar cell variant of PTC were seen in the primary, or in the metastatic tumor (Fig. 2a–d). Foci of intrathyroidal vein invasion were observed within the fibrous tissue surrounding the PTC nodule (Fig. 2e,f). The tumor had no extrathyroidal spreading and was staged pT2. No lymph node metastases were found in the lymphoadenectomy specimen which contained 15 small lymph nodes.

Both the primary tumor and the metastatic muscular nodule showed diffuse immunoreactivity for thyroglobulin. In addition, tumor cells expressed Galectin-3, HBME-1 and Cytokeratin 19 and had a down-regulation of p27, as reported in papillary carcinoma. Interestingly, this latter marker was uniformly expressed in hyperplastic, hyperfunctioning thyroid cells of toxic nodules surrounding the PTC nodule. The proliferative activity, evaluated by means of MIB-1 immunostaining in areas of highest labeling density was similar in primary and metastatic nodule, i.e. approximately 2%.

Discussion

We reported a case of PTC quite unique for three different reasons: a) the tumor manifested itself as a solitary muscular metastasis in the right arm; b) it affected an elder patient of 77 years; c) the patient suffered from hyperthyroidism due to toxic goiter. We will briefly comment on these issues.

Cancer and hyperthyroidism Scintigraphically highly uptaking follicular carcinomas, responsible for hyperthyroidism symptoms have been reported more commonly than PTC [7]. Occult (generally small) differentiated carcinomas can be encountered in glands resected for toxic multinodular goiter [22]. The present case was somewhat different because the PTC nodule measured 3.5 cm and was not really occult or an incidental finding, but it was considered part of the toxic multiple nodules responsible for the hyperthyroidism developed 2 years earlier. Morphologically, the primary thyroid tumor did not display any special features that could address to possible hyperfunction or to an aggressive behaviour (see below).

Elderly age PTC is classically affecting young adults and in some circumstances, young children heavily exposed to radiation (as that which occurred in the Chernobyl nuclear accident in 1986). It can, however, be diagnosed at any age. The recent study by Vini and coworkers shed new light on the current follow-up of elderly patients affected by differentiated thyroid carcinoma [23]. Between 2 and 12% of differentiated carcinomas occur in individuals older than 65, and the incidence in this age groups seems to be increasing. In such group, the prevalent histological type is PTC showing an unexpected more aggressive behaviour (with locally advanced disease in two-thirds of the cases and distant spread to bone and/or lung in 23% of patients at presentation) and requiring an aggressive therapeutic strategy (total thyroidectomy, lymph node dissection and early radioiodine treatment) [23]. The currently reported patient benefited from radioiodometabolic therapy immediately after radical surgery and is disease-free 4 years after diagnosis.

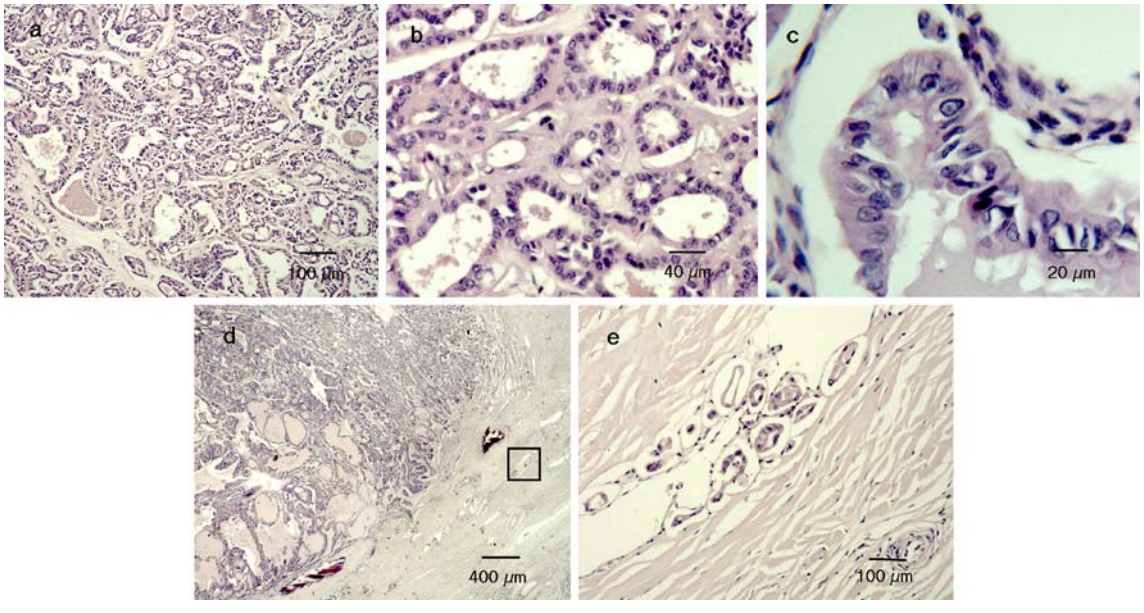

Fig. 2 **a** Primary thyroid papillary carcinoma showing a predominant follicular pattern of growth; **b**, **c** typical nuclear inclusions and grooves, **d**, **e** intrathyroidal vessel invasion, inset (e) is shown at a higher magnification (hematoxylin and eosin, original magnification: **a** ×25, **b** ×100, **c** ×400, **d** ×20, **e** ×100)

Type of presentation The present case presented with a single metastasis in the right arm bycipites muscle without any other synchronous (or metachronous after a 4-year follow-up) localization. Such presumable hematogenous spread occurred in a PTC entirely localized within the thyroid, without cervical lymph node metastases but with histologic evidence of intrathyroidal vascular invasion. Distant spread of differentiated thyroid carcinoma is relatively common for follicular carcinoma whose target organs are generally bone and/or lung and possibly liver or brain [7]. Other localizations of follicular carcinoma, including muscle and other soft tissues, are rare and become exceptional when this metastasis is the first and only clinical manifestation of the tumor, as reported in the pelvis, medial rectus muscle or mandible [3, 10, 13]. Another case was described to have soft tissue metastases of a follicular carcinoma, which were, however, synchronous with bony spread [16]. PTC is commonly associated with lymphatic spread to cervical lymph nodes [7, 8]. Distant (hematogenous) metastases (i.e. to lung, bone or liver) are rare, although they appear less exceptional in the follicular variant of PTC [1] that may share some genetic or molecular features with conventional follicular carcinoma of still unknown clinical significance [2]. Only three reports are on record on the exceptional hematogenous dissemination of differentiated PTC to pleura, submandibular gland and choroid at diagnosis [14, 17, 20]. Metachronous unusual metastasis of (differentiated) PTC have been reported in a few sites such as the mandible and choroids [5, 9].

In another anomalous case, during a 9-year follow-up, several metachronous metastases of a classical PTC were removed from unusual locations such as the thoracic wall, both groins and the thigh, the flow cytometry revealing many tetraploid metastatic tumor cells [11]. However, aggressive forms of PTC exist, including tall cell, columnar cell and solid variants [7]. In addition, cases of poorly differentiated thyroid carcinoma with residual PTC component have been described, causing distant metastatic spread and also a fatal outcome [24]. Such tumors are, however, solid patterned neoplasms, with high grade cytological features, necrosis and extrathyroid infiltration. All these features were absent in the presently reported case which was a partially cystic, follicular variant PTC, the only adverse sign being vascular invasion. The latter has recently been shown to correlate positively with hematogenous distant metastasis of PTC at initial diagnosis [8] and has been reported in 20.9% of cases of the follicular variant of PTC [8]. In the present case, the presence of hyperthyroidism may have further increased the vascularization of the thyroid gland and increased the blood flow, possibly facilitating the dissemination of malignant tumor cells through the bloodstream. Finally, in the present case, the immunophenotype, in terms of thyroglobulin production, expression of markers of malignant follicular-derived tumors, i.e. Galectin-3, HMBE- and Cytokeratin 19, p27 down-regulation and Ki 67 proliferative index were all in the expected profile of conventional PTC.

Conclusion

A case of PTC follicular variant unique for its presentation as solitary muscular metastasis in an elderly hyperthyroid patient was reported. The practical interest in this case is that differentiated thyroid carcinoma, although generally clinically indolent, may occasionally develop distant metastases and even manifest itself as a metastatic tumor. Fortunately, the morphological features of PTC are typical enough, even in metastatic deposits, to suggest a possible thyroid origin. Once the primary thyroid lesion has been identified, an aggressive surgical approach on primary and (hopefully) secondary tumors, immediately followed by radiometabolic therapy, is the treatment of choice, especially in elderly patients often affected by more aggressive thyroid tumors.

References

1. Carcangiou ML, Zampi G, Pupi A, Castagnoli A, Rosai J (1985) Papillary carcinoma of the thyroid. A clinicopathologic study of 241 cases treated at the University of Florence, Italy. Cancer 55:805–828
2. Castro P, Rebocho AP, Soares RJ, Magalhaes J, Roque L, Trovisco V, Vieira de Castro I, Cardoso-de-Oliveira M, Fonseca E, Soares P, Sobrinho-Simoes M (2006) PAX8-PPARgamma rearrangement is frequently detected in the follicular variant of papillary thyroid carcinoma. J Clin Endocrinol Metab 91: 213–220
3. Chaffanjon PCJ, Sturm N, Caravel JP, Chabre O, Brichon PY (2004) Métastase pelvienne intramusculaire d'un carcinome différencié de la thyroide. Ann Chir 129:100–102
4. Chao TC, Lin JD, Jeng LB, Chen MF (1999) Thyroid cancer with concurrent hyperthyroidism. Arch Surg 134:130–134
5. Colella G, Capone R, Cappabianca S (2003) Mandibular metastasis from papillary thyroid carcinoma: a case report. Tumori 89:452–454
6. Daou R (1998) Hyperthyroidism and cancer of the thyroid. Chir 123(6):604–608
7. De Lellis RA, Lloyd RV, Heitz PV, Eng C (2004). The WHO Classification of tumors of the endocrine organs. IARC, Lyon, pp 57–66
8. Falvo L, Catania A, D'Andrea V, Marzullo A, Giustiniani MC, De Antoni E (2005) Prognostic importance of histologic vascular invasion in papillary thyroid carcinoma. Ann Surg 241:640–646
9. Ferrer Garcia JC, Merino Torres JF, Ponce Marco JL, Pinon Selles F (2002) Unusual metastasis of differentiated thyroid carcinoma. An Med Interna 19:579–582
10. Friedman J, Karesh J, Rodrigues M, Sun CC (1990) Thyroid carcinoma metastatic to the medial rectus muscle. Ophthalmic Plastic Reconstr Surg 6:122–125
11. Johannessen JV, Sobrnones M, Lindmo T, Tangen KO, Kaalhus O, Brennhovd IO (1983) Anomalus papillary carcinoma of the thyroid. Cancer 51:1462–1467
12. Machens A, Holzhausen HJ, Lautenschläger C, Thanh PN, Dralle H (2003) Enhancement of lymph node metastasis and distant metastasis of thyroid carcinoma. A multivariate analysis of clinical risk factors. Cancer 98:712–719
13. Osguthorpe JD, Bratton JR (1982) Occult thyroid carcinoma appearing as a single mandibular metastasis. Otolaryngol Head Neck Surg 90:674–675
14. Perez Vega C, Lecube Torello A, Narvaez Garcia J, Vilaseca Momplet J (2003) Pleural metastasis as presenting form of papillary thyroid microcarcinoma: an exceptional case. Rev Clin Esp 203:217–218

15. Rios A, Rodriguez JM, Canteras M, Galindo PJ, Balsalobre MD, Parrilla P (2004) Risk factors for malignancy in multinodular goitres. Eur J Surg Oncol 30:58–62
16. Rodrigues G, Ghosh A (2003) Synchronous bony and soft tissue metastases from follicular carcinoma of the thyroid. J Korean Med Sci 18:914–916
17. Sarda AK, Pandey D, Bhalla SA, Goyal A (2004) Isolated submandibular gland metastasis from an occult papillary thyroid cancer. Indian J Cancer 41:89–91
18. Schlumberger M, Pacini F, Wiersinga WM, Toft A, Smit JW, Sanchez Franco F, Lind P, Limbert E, Jarzab B, Jamar F, Duntas L, Cohen O, Berg G (2004) Follow-up and management of differentiated thyroid carcinoma: a European perspective in clinical practice. Eur J Endocrinol 151:539–548
19. Shoup M, Stojadinovic A, Nissan A, Ghossein RA, Freedman S, Brennan MF, Shah JP, Shaha AR (2003). Prognostic indicators of outcomes in patients with distant metastases from differentiated thyroid carcinoma. J Am Coll Surg 197:191–197
20. Singh U, Kaushik S, Pandav SS, Dogra MR, Powari M, Das A, Hemachandra M (2003) Papillary carcinoma thyroid presenting as a choroidal metastasis. Report of a case and brief review of literature. Indian J Ophtalmol 51:81–83
21. Stocker DJ, Burch HB (2003) Thyroid cancer yield in patients with Graves' disease. Minerva Endocrinol 28:205–212
22. Vini L, Hyer S, Pratt B, Harmer C (1999) Good prognosis in thyroid cancer found incidentally at surgery for thyrotoxicosis. Postgrad Med J 75:169–170
23. Vini L, Hyer SL, Marshall J, A'Hern R, Harmer C (2003) Long-term results in elderly patients with differentiated thyroid carcinoma. Cancer 97:2736–2742
24. Volante M, Landolfi S, Chiusa L, Palestini N, Motta M, Codegone A, Torchio B, Papotti MG (2004) Poorly differentiated carcinomas of the thyroid with trabecular, insular, and solid patterns: a clinicopathologic study of 183 patients. Cancer 100:950–957

Virchows Arch (2006) 448: 862–866
DOI 10.1007/s00428-006-0185-6

CASE REPORT

Burkhard H. A. von Rahden · Björn L. D. M. Brücher · Mario Sarbia

Esophageal squamous cell carcinoma with entirely intramural growth pattern

Received: 12 January 2006 / Accepted: 3 March 2006 / Published online: 28 March 2006

Abstract Esophageal cancers are predominantly carcinomas, which are—due to their origin from the epithelial lining—visible by endoluminal view. We report in this study about the rare case of an esophageal squamous cell cancer with an unusual, entirely intramural growth pattern. The diagnosis could only be established postoperatively, because all preoperative biopsies had failed to demonstrate the tumor. The entirely intramural growth pattern of esophageal squamous cell cancer is an exceedingly rare variant, with only one previously reported case. Nevertheless, clinicians, radiologists, and pathologists should be aware of the potential existence of this condition, especially when clinical and imaging results suggest a malignant tumor that cannot be proven on biopsies. Surgical exploration must be considered under these circumstances.

Keywords Esophageal carcinoma · Intramural tumor growth · Intramural growth pattern

Introduction

Esophageal cancers are accounting for approximately 5% of the incidence and 10% of the deaths from cancers of the digestive system (US Cancer Statistics 2004 [4]). They are predominantly carcinomas, arising from the inner epithelial layer of the esophageal wall. Two histological tumor types are prevailing and are distinguished as different entities [10]: Squamous cell carcinomas, originating from the original squamous cell epithelium in any location (cervical, supracarinal, and infracarinal esophagus) and adenocarcinomas, arising almost exclusively in the distal third, within specialized intestinal metaplasia (Barrett's esophagus).

Advanced tumors of both carcinoma types are usually visible from endoluminal view (e.g., during endoscopic examination/examination of the resection specimen), typically showing polypous and/or ulcerative growth patterns [9]. These characteristics of esophageal cancers with epithelial origin are in contrast to esophageal sarcomas or melanomas, for which a growth pattern underneath an intact epithelium is typical [3]. The majority of esophageal tumors with mesenchymal origin are benign, mainly leiomyomas, and—due to their characteristic submucosal growth pattern—they are also addressed as submucosal tumors [8].

We present in this study a case of an esophageal squamous cell carcinoma arising in the cervical esophagus, exhibiting a very unusual intramural growth pattern. The indication for oncological treatment by means of surgical resection was made without earlier establishment of the diagnosis, which had failed due to repeatedly negative biopsies.

Clinical history

History and diagnostic work-up

A 58-year-old male patient suffering from repeated episodes of dysphagia was admitted to our University hospital in May 2004 with suspicion of malignant tumor growth in the supracarinal esophagus. The patient had a long-lasting history of tobacco (two packs per day for many years) and alcohol abuse (at least 2 l of beer/day). He had not experienced any weight loss, night sweat, or fatigue.

B. H. A. von Rahden
Department of Surgery, University Hospital Salzburg,
Paracelsus Medical University,
Salzburg, Austria

B. L. D. M. Brücher
Department of Surgery, Technical University Munich,
Munich, Germany

M. Sarbia (✉)
Institutes of Pathology,
Sana Klinikum Lichtenberg/Unfallkrankenhaus Berlin,
Fanningerstr. 32/Warenerstr. 7,
Berlin 10365, Germany
e-mail: m.sarbia@sana-kl.de
Tel.: +49-30-55182811
Fax: +49-30-55182899

Flexible endoscopy revealed a moderate stenosis of the cervical esophagus, which could be easily surmounted with the instrument. An area of 5 cm below the upper esophageal sphincter, measuring 3 cm in diameter, appeared suspicious for malignancy. However, there was no intraluminal tumor growth. Staining with Lugol's solution did not provide any additional information on potentially suspicious areas. Several biopsies were sampled using a standard biopsy forceps.

Endoscopic ultrasound (EUS) did not reveal unequivocal findings in favor of malignancy. The same was true for the computed tomography (multislice computed tomography, CT) which revealed moderate thickening of the esophageal wall and few enlarged adjacent lymph nodes (Fig. 1a). Furthermore, investigation by the ear, nose, and throat specialist, including laryngoscopy, as well as bronchoscopy (including cytologic evaluation of lavage) did not show any pathological findings.

Confirmation of esophageal neoplasm by means of biopsy failed: histopathologic evaluation of the biopsies revealed normal squamous cell epithelium. There were foci of mucosal hyperplasia, some fibrosis, and moderate infiltration with inflammatory cells, but no tumor cells or atypical or dysplastic cells could be detected in any of the biopsies (not shown).

The case was discussed in the interdisciplinary tumor conference and it was decided to reevaluate the findings after 1 month (June/July 2004): Endoscopy with sampling of biopsies was repeated and the findings were similar to the initial investigation: endoscopic evaluation still raised suspicion of malignant tumor growth in the supracarinal esophagus, but again no tumor cells were found on histopathologic examination. This situation remained unchanged when—after one more month—a second reevaluation was performed (August 2004). Again biopsies were negative.

In addition to endoscopy and EUS, a combined ^{18}FDG-PET/CT scan was performed, which also indicated a neoplastic lesion. A slightly increased ^{18}FGD uptake was found in projection on the thickened esophageal wall of the cervical and upper thoracic esophagus (see Fig. 1b). Now it was decided to establish the diagnosis by means of surgical exploration. Other methods (e.g., CT-guided biopsies) were not estimated suitable for tissue sampling in this localization.

Surgery: indication, findings, and procedure

The cervical esophagus was approached through a cervical incision. The aim was to establish the diagnosis intraoperatively by histopathologic examination of frozen sections. In case of confirmation of the cancer diagnosis, it was planned to proceed with limited cervical esophageal "sleeve" resection and reconstruction with interposition of a free jejunal graft. The latter is a procedure that is frequently employed as a limited surgical procedure for cervical esophageal carcinomas at our institution [1, 11].

Surgical exploration revealed tumor infiltration of the cervical esophagus (from close to the upper esophageal sphincter down to the level below the aortic arch). A frozen section was performed, and histopathologic examination established the diagnosis of a squamous cell carcinoma in the esophagus. Further exploration revealed that the extent of tumor growth did not permit a limited surgical procedure. A transhiatal esophagectomy was performed (blunt dissection of the esophagus through the diaphragmatic esophageal hiatus, without thoracotomy). The intestinal passage was restored with gastric pull-up through the anterior mediastinum (retrosternal) and cervical anastomosis.

Histopathologic examination of the surgical specimen

The operation specimen was opened longitudinally, pinned on a cork board, and fixed over night in 4% buffered formaldehyde. Macroscopic examination of the esophagectomy specimen (Fig. 2a) revealed an intact epithelium in the entire esophagus with only slight irregularities of the internal surface near the oral resection margin in an area of 4 cm length (Fig. 2b). The entire esophagus was then cut transversally into 5 mm-thick slices and embedded completely in paraffin blocks (40 slices of esophageal tissue in total). Histopathologic examination based on hematoxylin and eosin stained sections (Fig. 3a,b) revealed a poorly differentiated squamous cell carcinoma with infiltration of all layers of the esophageal wall from the lamina propria mucosae to the adventitia. No evidence of basaloid or adenoid differentiation was found in the tumor tissue. However, the esophageal squamous epithelium was

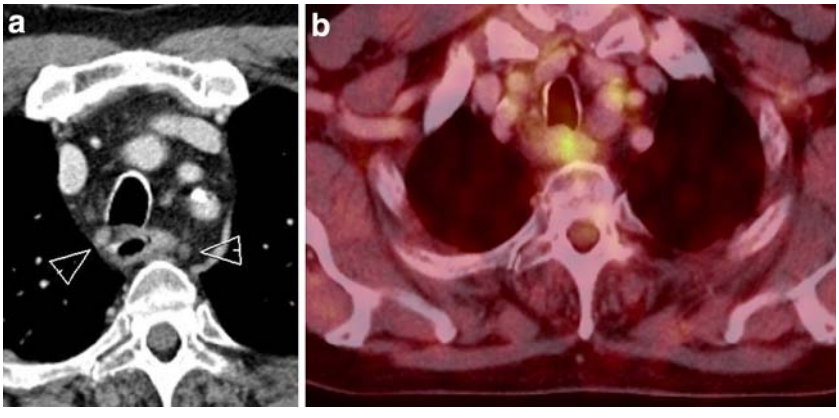

Fig. 1 Clinical findings in the 58-year-old patient with moderate dysphagia. The CT scan (**a**) as well as the combined PET/CT scan (**b**) were in favor of malignant tumor growth in the cervical/supracarinal esophagus, demonstrating a thickened esophageal wall and enlarged adjacent regional lymph nodes (**a**, *arrows*) and an increased ^{18}FDG uptake (**b**, *arrow*)

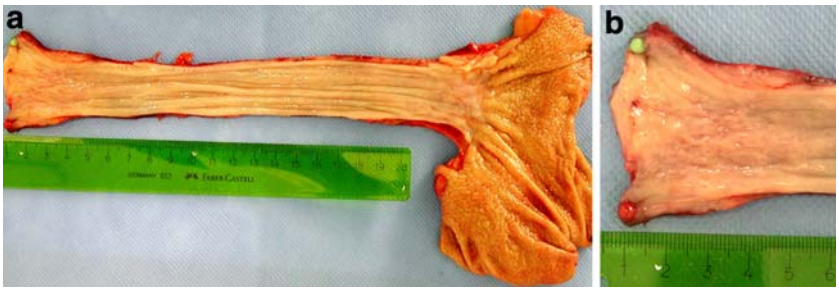

Fig. 2 Macroscopic evaluation of the surgical specimen shows intact squamous epithelium without obvious tumor growth (**a**). Higher magnification of the area near the oral resection margin, however, displays irregularities of the surface structure (**b**)

completely intact and no evidence of squamous intraepithelial neoplasia was found. The tumor was located near the oral resection margin. Reconstruction of the tumor size from the histologic slides revealed a maximum diameter of 5 cm. None of altogether eight dissected lymph nodes showed infiltration by tumor cells. No evidence of lymphovascular invasion or perineural invasion was found. The tumor stages according to UICC criteria [12] were pT3, pN0, and cM0. The resection of the tumor was incomplete at the circumferential margin (R1). Histological examination showed no evidence of esophageal diverticula or cysts.

Immunohistological investigations

One representative paraffin block containing squamous cell carcinoma and overlying esophageal squamous epithelium was selected. Serial sections were immunohistochemically stained using antibodies against p53 (DO-7; dilution 1:200; DAKO, Hamburg, Germany), Cyclin D1 (SP4; dilution 1:50; Dcs-diagnostics; Hamburg; Germany), EGFR (31 G7; dilution 1:60; Cytomed; Baden-Baden; Germany) Cytokeratin 5/6 (D5/16B4; dilution 1:100; DAKO, Hamburg, Germany), and Chromogranin A (DAK-A3; dilution 1:200; DAKO) using an automated stainer (Ventana Benchmark, Tuscon, Arizona, USA). Expression of p53 and EGFR was found in more than 90% of the tumor cells (Fig. 3c). In the overlying squamous epithelium only scattered cells were found to express p53, whereas expression of EGFR was found in all cells (weak staining intensity). Expression of Cyclin D1 was found only in a minority of cells, both in the cancer tissue as well as in the overlying squamous epithelium (less than 25% positive cells).

The light microscopic diagnosis of squamous cell carcinoma was supported by immunohistochemical inves-

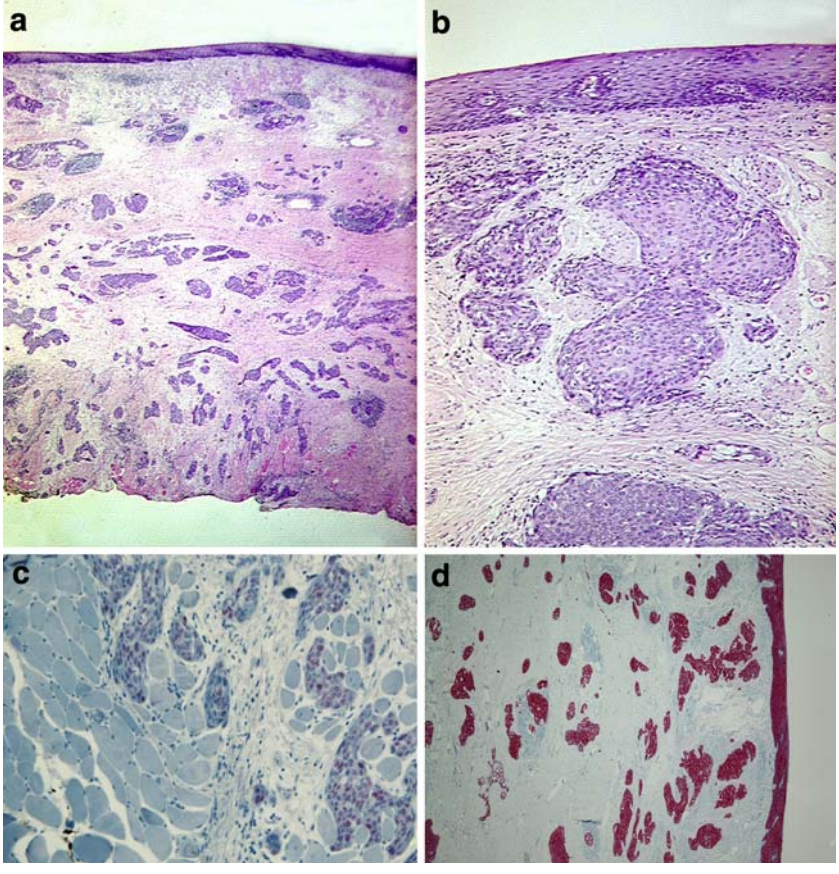

Fig. 3 Microscopic investigation of the esophagus. **a** At low power magnification a transmural infiltration of the esophageal wall by cancer nests is discernible. The overlying squamous epithelium is intact (H&E; ×16). **b** At higher magnification, cancer nests can be classified as poorly differentiated squamous cell carcinoma. The overlying squamous epithelium shows mild atrophy (H&E; ×100). Cancer cells invading muscle layer of the esophageal wall showing nuclear accumulation of the p53 protein (×200) (**c**). Strong expression of cytokeratin 5/6 in the cancer cells and in the overlying esophageal squamous epithelium (×40) (**d**)

tigations showing strong expression of cytokeratin 5/6 in all tumor cells (Fig. 3d). No evidence for neuroendocrine differentiation was found using immunostaining against chromogranin A.

Postoperative course and follow-up

The postoperative course was complicated with anastomotic leakage of the anastomosis, which was managed with temporary insertion of a T-tube. After healing of the anastomotic leak, the patient was discharged home 2 months postoperatively with a good swallowing function and in good general condition. Because of the incomplete resection at the circumferential resection margin it was proposed to perform additive radiochemotherapy (60 Gy + 5-FU). But the patient decided to receive this antineoplastic regimen only after a longer recovery period and depending on results of follow-up investigations. During the further course, the patient developed mild dysphagia, due to strictures of his cervical anastomosis. But neither endoscopic findings nor a recently (May 2005) performed CT scan provided clear evidence of tumor recurrence. The patient is in fine general condition, 13 months after surgical resection, and receives further surveillance with CT and endoscopy.

Discussion

The case presented in this study shows an unusual growth pattern of an esophageal squamous cell carcinoma with entirely intramural localization of the tumor cells. Only one similar case has been reported previously: In the paper by McGregor et al. [7], the tumor cells were also located exclusively intramurally and did not invade the overlying epithelium. Quite similar to the observations in our case, the tumor could not be confirmed by endoscopic investigation because of the intact and all in all nonsuspicious appearance of the mucosa. In contrast to our findings, an esophageal cyst was considered as the origin of the tumor in the publication by McGregor et al.

Another case report describes an esophageal squamous cell cancer with a predominantly submucosal growth pattern, however, preoperative diagnosis by means of endoscopic biopsy was feasible in this case [5].

Intramural growth of esophageal squamous cell carcinoma tissue has also been reported as metastasis to the stomach [2, 6]. In a series of 1,200 esophageal squamous cell cancers reported by Ebihara et al. [2], 13 intramural metastases in the stomach were described. Furthermore, the occurrence of intraesophageal metastases with intramural growth that originate from esophageal squamous cell carcinomas is well known [9]. As a consequence, whenever the diagnosis of a primary esophageal intramural squamous cell carcinoma is under consideration, metastatic origin has to be excluded. Furthermore, one must exclude continuous cancer invasion from the anatomical neighborhood. The most important tumors to be considered in this respect are nonsmall cell lung cancers with squamous differentiation, as well as squamous cell cancers of head and neck. In our case there was no evidence to suggest invasion of the esophageal wall by primary tumor tissue from any of these neighboring locations, as staging with ENT, bronchoscopy, and CT scan had been unremarkable in this respect.

Hypotheses regarding the pathogenesis

Regarding the pathogenesis of intramural squamous cell carcinoma of the esophagus, two different hypotheses may be proposed.

1. The tumor may have originated from squamous epithelium in an esophageal cyst or small diverticulum, like in the case reported by McGregor et al. [7]. Alternatively, squamous cell metaplasia in esophageal glands may be the origin of tumor growth. The fact that we have not been able to find such a lesion in association with the tumor does not rule out this possibility, as it is well known that advanced tumors may destroy preexisting anatomical structures.
2. Cells of a squamous intraepithelial neoplasia may have reached the submucosal layers by intraepithelial spread in a duct of submucosal glands. Subsequently, these cells may have gained capability of infiltrative growth and infiltration of the esophagus may have taken place under an intact epithelium.

Clinical importance

The clinical importance of esophageal cancer with exclusively intramural growth pattern of esophageal squamous cell cancer is demonstrated by the problems in pretherapeutic diagnosis we had experienced. Clinicians and pathologists have to keep this diagnosis in mind, when repeated biopsies remain negative, but clinical findings strongly suggest malignancy. Surgical exploration with excisional biopsy and/or resection must be considered when demonstration of the tumor by means of endoscopic biopsy fails.

References

1. Brücher BL, Stein HJ, Zimmermann F, Werner M, Sarbia M, Busch R, Dittler HJ, Molls M, Fink U, Siewert JR (2004) Responders benefit from neoadjuvant radiochemotherapy in esophageal squamous cell carcinoma: results of a prospective phase-II trial. Eur J Surg Oncol 30:963–971
2. Ebihara Y, Hosokawa M, Kondo S, Katoh H (2004) Thirteen cases with intramural metastasis to the stomach in 1259 patients with oesophageal squamous cell carcinoma. Eur J Cardiothorac Surg 26:1223–1225
3. Hamilton SR, Aaltonen LA (2000) Pathology and genetics of tumours of the digestive system. Tumours of small intestine. IARC, Lyon, pp 69–91

4. Jemal A, Tiwari RC, Murray T, Ghafoor A, Samuels A, Ward E, Feuer EJ, Thun MJ (2004) American Cancer Society. Cancer statistics, 2004. CA Cancer J Clin 54:8–29
5. Kishino T, Yamaguchi Y, Yamagishi T, Hashimoto T, Kyomasu Y, Mori H, Sugiyama M, Atomi Y, Saito S, Ishida H, Takahashi S (2000) Submucosal tumor (SMT)-like esophageal squamous cell carcinoma with gastric metastasis. Hepatogastroenterology 47:1581–1584
6. Koide N, Yazawa K, Koike S, Adachi W, Amano J, Ishii K (1998) Two cases of gastric involvement of esophageal cancer: intramural metastasis and intramural lymph node metastasis. Hepatogastroenterology 45:1619–1623
7. McGregor DH, Mills G, Boudet RA (1976) Intramural squamous cell carcinoma of the esophagus. Cancer 37: 1556–1561
8. von Rahden BHA, Stein HJ, Feussner H, Siewert JR (2004) Enucleation of submucosal tumors of the esophagus: minimally-invasive versus open approach. Surg Endosc 18:924–930
9. Sarbia M, Becker KF, Höfler H (2004) Pathology of upper gastrointestinal malignancies. Semin Oncol 31:465–475
10. Siewert JR, Stein HJ, Feith M, Brücher BLDM, Bartels H, Fink U (2001) Tumor cell type is an independent prognostic parameter in esophageal cancer: lessons learned from more than 1,000 consecutive resections at a single institution in the western world. Ann Surg 234:360–369
11. Siewert JR, Stein HJ, Sendler A, Molls M, Fink U (2002) Esophageal cancer: clinical management. In: Kelsen DA et al (eds) Gastrointestinal oncology: principles and practice. Williams & Wilkins, Philadelphia; pp 261–288
12. Sobin LH, Wittekind Ch (2002) UICC. TNM classification of malignant tumors (6th edition). Wiley, New York

Virchows Arch (2006) 448: 867–870
DOI 10.1007/s00428-006-0161-1

CASE REPORT

Hyun-Jung Kim · Sung-Jig Lim · Hoon Choi · Kyeongmee Park

Malignant clear-cell myomelanocytic tumor of broad ligament—a case report

Received: 13 October 2005 / Accepted: 19 December 2005 / Published online: 16 March 2006

Abstract Clear-cell myomelanocytic tumors (CCMT) of the perivascular epithelioid cell tumor (PEComa) family have been recently reported. We report a case involving a 12-year-old girl. The tumor (9 × 7.5 × 7 cm) was a firm, tan–gray mass with heavily dark pigmentation, massive hemorrhage, and necrosis, and was located in the right broad ligament attached to the right ovary. Histologically, the tumor was composed of polygonal cells exhibiting diffuse hemorrhage, multifocal necroses, and vascular invasion. Most of the tumor cells contained melanin pigments with Fontana–Masson positivity and ultrastructurally suspicious, membrane-bound premelanosomes. Immunohistochemical staining was positive against HMB-45 and focally positive for smooth muscle actin. The tumor recurred in the form of multiple conglomerated masses of the right iliac fossa, with the greatest measuring up to 3.8 cm in dimension, within 1 year. Most CCMT are believed to originate from falciform ligament/ligamentum teres. To the best of our knowledge, this case is the first report of CCMT in broad ligament and the second report of PECOMA, NOS in broad ligament. Further study for proper subclassification of the PECOMA family should be validated, not by anatomic site but by clinical behavior.

Keywords Clear-cell myomelanocytic tumor · Broad ligament · PEComa

H.-J. Kim · S.-J. Lim · K. Park (✉)
Department of Pathology,
Inje University Sanggye Paik Hospital,
761-1, Sanggye-7-dong, Nowon-gu,
Seoul, 139-707, Republic of Korea
e-mail: kmpark@sanggyepaik.ac.kr
Tel.: +850-82-29501263
Fax: +850-82-29516964

H. Choi
Department of Gynecology,
Inje University Sanggye Paik Hospital,
Seoul, Republic of Korea

Introduction

The "perivascular epithelioid cell (PEC)" was first described by Bonetti and colleagues in 1992 and was observed both in "sugar" tumors of the lung and in angiomyolipomas [3]. These PECs are characterized by an epithelioid shape, clear-to-faintly eosinophilic cytoplasm, perivascular location, and a unique coexpression of markers for smooth muscle actin and melanocytes. The PEComa family includes angimyolipomas; lymphangioleiomyomas; and clear-cell "sugar" tumors of the lung, pancreas, and uterus [2, 4, 8, 9]. Clear-cell myomelanocytic tumors (CCMT) of the PEComa family were first described by Folpe et al. in 2000 [7]. These tumors formed and exclusively developed at the falciform ligament or *ligamentum teres* of children or young adults. We encountered a case of CCMT presenting with a striking amount of melanin pigment, an unusual location, and histologically and clinically malignant features in a young girl.

Clinical history

A 12-year-old girl was admitted to the hospital reporting a right adnexal mass, which had been incidentally detected by abdominal sonogram at a local medical clinic. Physical examination revealed a hen-egg-sized, nontender, soft, movable mass at the right lower abdomen. Abdominal sonogram showed a low echogenic 7.6×6.9-cm mass of the right adnexa (Fig. 1). A pelviscopy-assisted right salpingo-oophorectmy was performed. A few newly developed masses with the same morphology were detected at the right iliac fossa within 1 year.

Pathologic findings

An ovoid, firm, gray mass, measuring 9 × 7.5 × 7 cm, was grossly attached to the right ovary and fallopian tube. The external surface was adhesive but unruptured. The cut

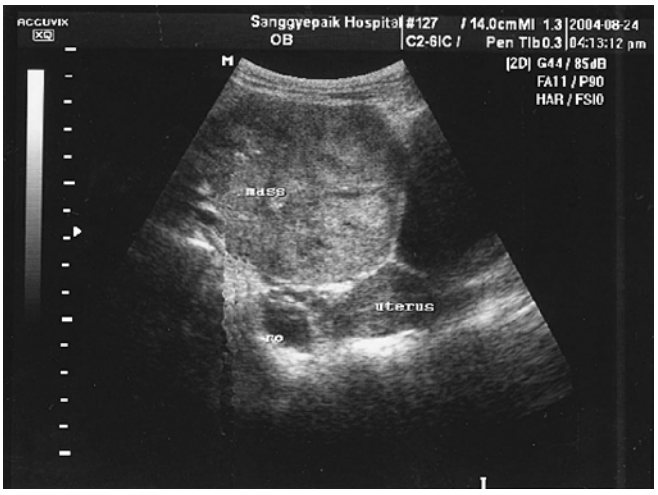

Fig. 1 Abdominal sonogram demonstrates a solid mass at the right broad ligament, which is anteriorly attached to the right ovary (*ro*)

surface was black-colored with diffuse hemorrhage (Fig. 2).

Microscopically, the tumor was circumscribed by a thick capsule, some portion of which was adhesive to the ovarian capsule and tubal serosa. The tumor showed striking vasculature and was composed of uniform, moderate-sized, epithelioid cells with an angiocentric arrangement. Large vessels, as well as small, arcing vessels, subdivided the lesions into coarse packets (Fig. 3a). The tumor cells were oval to elongated in shape, and each showed a single pleomorphic nucleus containing a small but distinct nucleolus. Mitotic figures were occasionally found (4/10 HPFs). The cytoplasm varied from clear to eosinophilic with abundant brownish pigments (Fig. 3b). Angioinvasion and coagulation necrosis were observed (Fig. 3c). Fontana–Masson staining revealed abundant melanin pigment in the tumor cell cytoplasm (Fig. 3d).

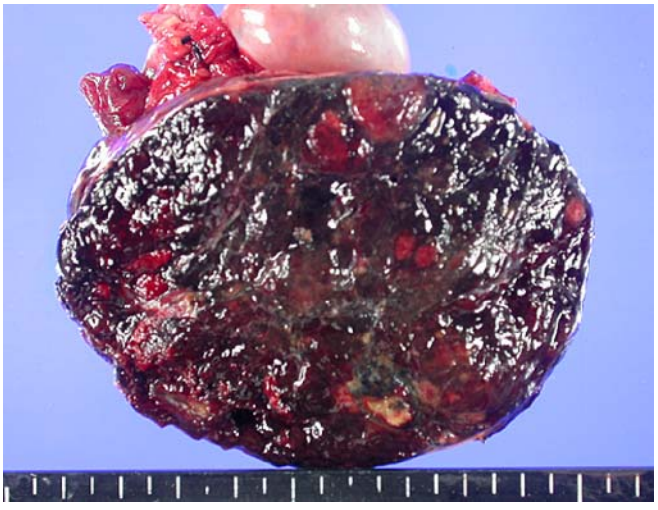

Fig. 2 Macroscopic findings reveal a solid mass attached to the ovary and fallopian tube. The cut surface of the mass is dark tan with diffuse hemorrhage

The immunohistochemical profile of the tumor was evaluated on 4-μm thick, formalin-fixed, deparaffinized sections based on the avidin–biotin–peroxidase complex. The tumor cells were strongly positive for HMB-45 (Immunotech, Marseille, Cedex, France), focally positive for smooth muscle actin (Dakocytomation, Carpinteria, CA, USA), and negative for S-100 protein (Dakocytomation) and pan-cytokeratin (Signet, Dedham, MA, USA) (Fig. 4a–d). The Ki-67 labeling index was low (less than 1%).

Ultrastructurally, the tumor cells had abundant premelanosomes with various stages (Fig. 5). A percutaneous needle biopsy specimen from recurred masses revealed morphology similar to the previous mass (Fig. 6).

Discussion

In this report, we describe a case of an unusual epithelioid tumor in the broad ligament, with pathologic and immunohistochemical features entirely compatible with those of a PEComa. PEComas are characterized by an epithelioid appearance, a clear-to-eosinophilic cytoplasm, and an intimate relationship with blood vessels. The cells are consistently immunoreactive to the melanocytic marker HMB-45, variably immunoreactive to smooth muscle actin, and negative for epithelial markers. Since the first description by Bonetti et al. [3], such tumors have been reported in several organs including the uterus, lungs, kidneys, liver, small and large bowel, and prostate.

The uterus is one of the most prevalent sites of involvement. However, so far, only 15 cases have been reported [9]. Uterine PEComa was subclassified into two groups by Vang et al. [10]. The tumors of one group are similar to low-grade endometrial stromal sarcomas with diffuse HMB-45 expression and focal smooth muscle markers. The tumors of the other group are composed of epithelioid cells with less prominent clear-cell features, smaller numbers of which are HMB-45-positive. The latter group exhibits on a morphologic spectrum similar to that of epithelioid smooth muscle tumors, based on the above classification. The predicted clinical course is of uncertain malignant potential.

"CCMT of the falciform ligament/*ligamentum teres*" are a recently recognized addition to the PEComa family, and possess unique histologic, immunohistochemical, and clinical features [2]. They appear to arise exclusively in the abdomens of young patients and show a predilection for the falciform ligament and *ligamentum teres* of the liver. CCMT are characterized by a fascicular and nested proliferation of uniform spindle cells with clear-to-lightly eosinophilic cytoplasm, vesicular nuclei, and small, prominent nucleoli. The gross and ultrastructural findings (numerous stage melanosomes) reported previously [7] revealed more melanocytic features rather than other PEComa groups. Unpublished data has shown the presence of microphthalmia transcription factor (MiTF) in seven cases of CCMT. MiTF is the product of the microphthalmia gene, which encodes a DNA-binding protein, essential for

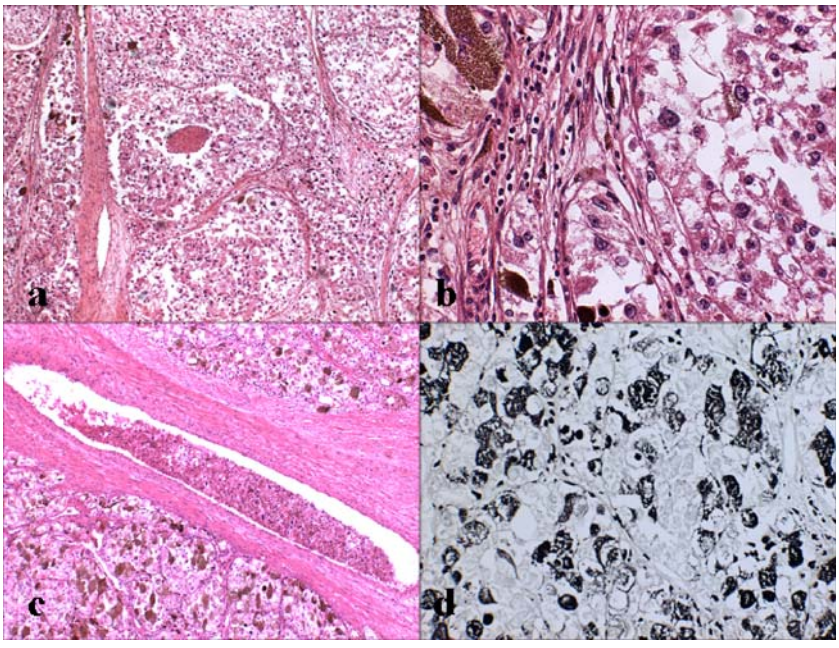

Fig. 3 **a** Low-power magnification shows a striking vasculature composed of uniform, moderate-sized epithelioid cells with an angiocentric and packet-like arrangement. **b** High-power magnification reveals oval-to-polygonal tumor cells with small but distinct nucleoli and clear cytoplasms, which contain abundant brownish pigment. **c** A conforming tumor embolus is found in a vascular structure. **d** Fontana–Masson special staining reveals abundant intracytoplasmic melanin pigment

melanocyte. These findings provide further evidence of melanocytic character in CCMT. The age predilection and location of CCMT suggest that these tumors arise from the umbilical vessels. The first differential diagnosis of CCMT is clear cell sarcoma (CCS) of tendons and aponeuroses, which can be supported by S-100 protein negativity. By cytogenetic study, CCMT had reported as a translocation between chromosome 3 and 10, but not the translocation (12; 22), of CCS.

A case of a heavily melanotic perivascular epithelioid clear cell tumor of the kidney was recently reported [1]. A large amount of cystoplasmic melanin was reported as a striking feature and the histochemical and immunohistochemical profiles support the extreme melanocytic differentiation. The reported case failed to demonstrate a myoid differentiation or spindle-shaped tumor cells.

The PEComa family is largely composed of an angimyolipoma (AML) and a non-AML group. The non-AML group has been subclassified based on anatomic sites (organ specificity). However, the pathologic classification did not provide any description of biologic behavior. The current and above reported cases are not compatible with the previously described PEComa group.

To the best of our knowledge, this is only the second report in literature of a PEComa arising in the broad ligament, the first being that of a 17-cm-sized pelvic mass in a 51-year-old woman [6]. Histologically, the mass was compatible with a high-grade sarcoma with extensive necrosis and hemorrhage.

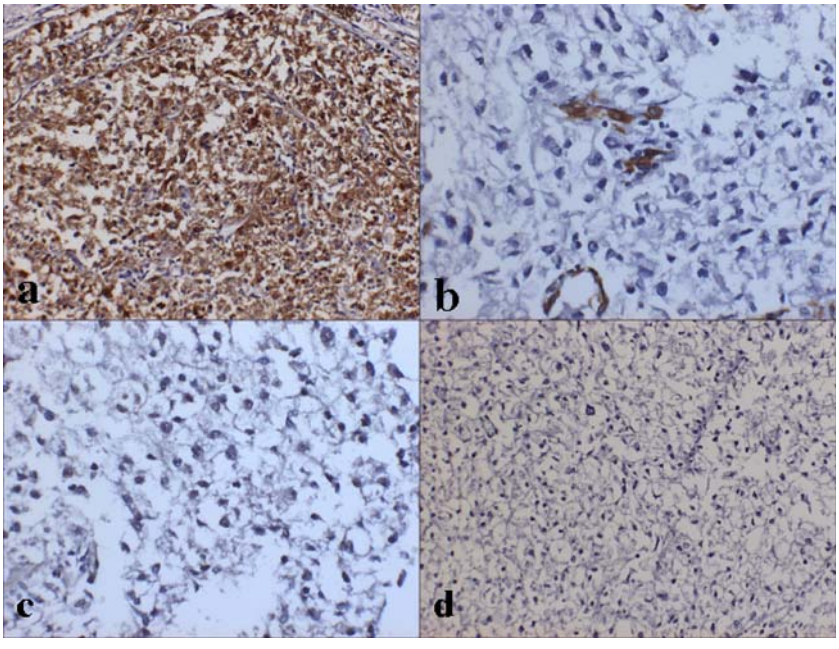

Fig. 4 The tumor cells are diffusely and strongly positive for HMB-45 (**a**), focally positive for smooth muscle actin (**b**), negative for S-100 protein (**c**), and negative for pan-cytokeratin (**d**)

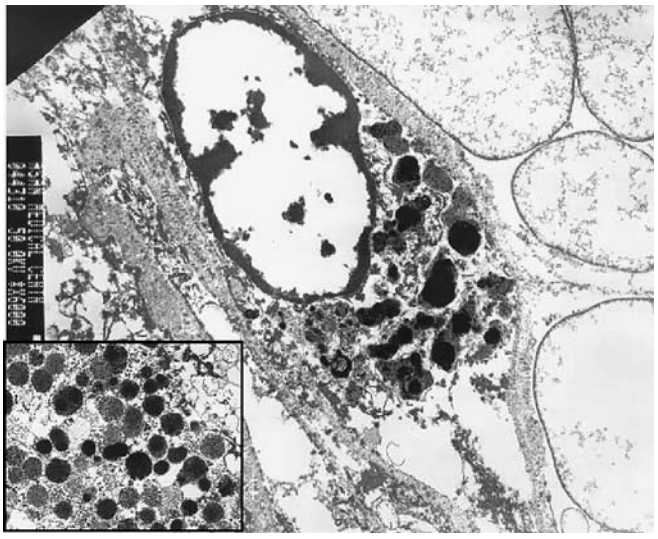

Fig. 5 Ultrastructurally, the tumor cells have abundant, membrane-bound premelanosomes (inset)

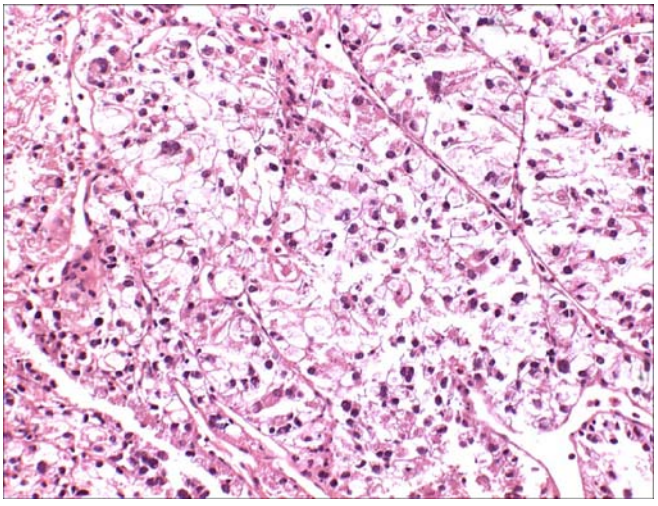

Fig. 6 The percutaneous needle biopsy from a recurred mass reveals similar morphology composed of polygonal cells with a clear cytoplasm and moderate nuclear atypia

A clinico-pathologic study with comparative genomic hybridization (CGH) analysis for PEComa, not otherwise specified, was done [5]. Five pathologic features of nonbenign cases and benign cases were significantly different; cytologic atypia, necrosis, lymphovascular invasion, size, and significant mitotic activity (more than six mitoses per 10 HPFs). The presenting case was histologically compatible with the nonbenign group. CGH and DNA ploidy analyses showed a balanced chromosomal profile. Further study for cytogenetic analyses of the PEComa group and definitive assessment for prognostic factors should be validated.

We present a case of a malignant clear-cell myomelanotic tumor of a broad ligament, which we classify as belonging to the PEComa group based on well-developed melanocytic differentiation and the young age of the patient.

References

1. Adachi S, Hanada M, Kobayashi Y, Tsutahara K, Fukuhara S, Mori N, Hara T, Mukai H, Shimasaku E, Kawai M, Kishikawa N, Yamaguchi S (2004) Heavily melanotic perivascular epithelioid clear cell tumor of the kidney. Pathol Int 54:261–265
2. Bonetti F, Martignoni G, Colato C, Manfrin E, Gambacorta M, Faleri M, Bacchi C, Sin VC, Wong NL, Coady M, Cahn JK (2001) Abdominopelvic sarcoma of perivascular epithelioid cells: report of four cases in young women, one with tuberous sclerosis. Mod Pathol 14:563–568
3. Bonetti F, Pea M, Martignoni G, Zamboni G (1992) PEC and sugar [Letter]. Am J Surg Pathol 16:307–308
4. Cibas ES, Goss GA, Kulke MH et al (2001) Malignant epithelioid angiomyolipoma ('sarcoma ex angiolipoma') of the kidney: a case report and review of the literature. Am J Surg Pathol 25:121–126
5. Fadare O, Parkash V, Yilmaz Y, Mariappan MR, Ma L, Hileeto D, Qumsiyeh MB, Hui P (2004) Perivascular epitelioid cell tumor (PEComa) of the uterine cervix associated with intraabdominal "PEComatosis": a clinicopathological study with comparative genomic hybridization analysis. World J Surg Onc 2:35–47
6. Fink D, Marsden DE, Edwards L, Camaris C, Hacker NF (2004) Malignant perivascular epithelioid cell tumor (PEComa) arising in the broad ligament. Int J Gynecol Cancer 14:1036–1039
7. Folpe AL, Goodman ZD, Ishak KG et al (2000) Clear cell myomelanocytic tumor of the falciform ligament/ligamentum teres: a novel member of perivascular epithelioid clear cell family of tumors with a predilection for children and young adults. Am J Surg Pathol 24:1239–1246
8. Ruco LP, Pilozzi E, Weddard BM et al (1998) Epithelioid lymphagioleiomyomatosis-like tumor of the uterus in a patient without tuberous sclerosis: a lesion mimicking epithelioid leiomyosarcoma. Histopathology 33:91–93
9. Pea M, Martignoni G, Zamboni G et al (1996) Peivascular epithelioid cell [Letter]. Am J Surg Pathol 20:185–188
10. Vang R, Kempson R (2002) Perivascular epithelioid cell tumor ('PEComa') of the uterus: a subset of HMB-45 positive epithelioid mesenchymal neoplasms with an uncertain relationship to pure smooth muscle tumors. Am J Surg Pathol 26:1–13

Virchows Arch (2006) 448: 871–872
DOI 10.1007/s00428-005-0131-z

LETTER TO THE EDITOR

M. Zamecnik · Z. Kinkor · A. Chlumska

CD10+ stromal cells in fibroadenomas and phyllodes tumors of the breast

Received: 26 September 2005 / Accepted: 2 November 2005 / Published online: 21 March 2006

Sir,

Mammary fibroadenoma (FA) and phyllodes tumor (PT) show a continuum of histologic features, and for this reason, the exact categorization of some lesions can be difficult [1, 5]. Therefore, we found recent reports of differences in CD10 expression between FA, benign PT, and malignant PT to be promising [3, 6]. In the breast pathology, CD10 has been known as a marker of myoepithelium [1], but recently, its expression was also found in stromal cells of fibroepithelial tumors [3, 4, 6]. In a large study of Tse et al. [6], the stroma of FAs was almost always CD10-negative, whereas the stromal cells of PTs, especially in malignant cases, were often CD10-positive. In our practice, we observed CD10 reactivity in several FAs, which is in contrast with previous results [3, 6]. Therefore, we decided to perform a study of CD10 expression in a small series of FA and PT to find out whether CD10 can help to decide the differential diagnosis between FA and PT, especially in core biopsy specimens offering only a limited amount of tissue.

We examined CD10 expression (56C6, Novocastra, Newcastle upon Tyne, UK) in 20 FAs and 6 PTs. In the FA series, the age of patients ranged from 23 to 57 years (average 39.3), whereas among PTs, the age range was 22–79 years (average 45.2). Five PTs were benign and one was of borderline malignancy [1, 5]. The tumor was considered CD10-positive if there was at least moderate staining in 20% or more stromal cells. CD10 positivity was seen in 12 FAs (60%) and in 4 PTs (67%; Fig. 1a–c). The borderline PT was CD10-negative (Fig. 1d). Subepithelial areas with higher cell density showed often more intense reactivity in both FA and PT.

Our results show that CD10 is frequently positive in both FA and PT (60 and 67%, respectively). Thus, we believe that this antibody cannot assist in the differential diagnosis between FA and PT. Our finding is in contrast with those of Tse et al. [6] and Mechtersheimer et al. [3], who found none or slight CD10 reactivity in FAs (for example, only 1 of 33 FAs was positive in the study of Tse et al.) and increasing positivity in PTs. We suppose that the discrepancy might be explained by different sensitivity of immunohistochemical techniques used in different laboratories. In both FA and PT, the positive cells were often more numerous in subepithelial areas where the cell density is higher, and this finding is similar to that seen in previous studies [3, 6].

In conclusion, our experience indicates that CD10 does not help in differentiation between FA and PT. Further investigations are needed to discover valuable markers that will help in this differential diagnosis.

M. Zamecnik
Laboratory of Surgical Pathology,
Pilsen, Czech Republic

M. Zamecnik (✉)
Biopticka Lab.,
Mikulasske nam. 4,
326 00 Pilsen, Czech Republic
e-mail: zamecnik@medima.cz
Fax: +420-37-7440539

Z. Kinkor · A. Chlumska
Sikl's Department of Pathology, Medical Faculty,
Charles University,
Pilsen, Czech Republic

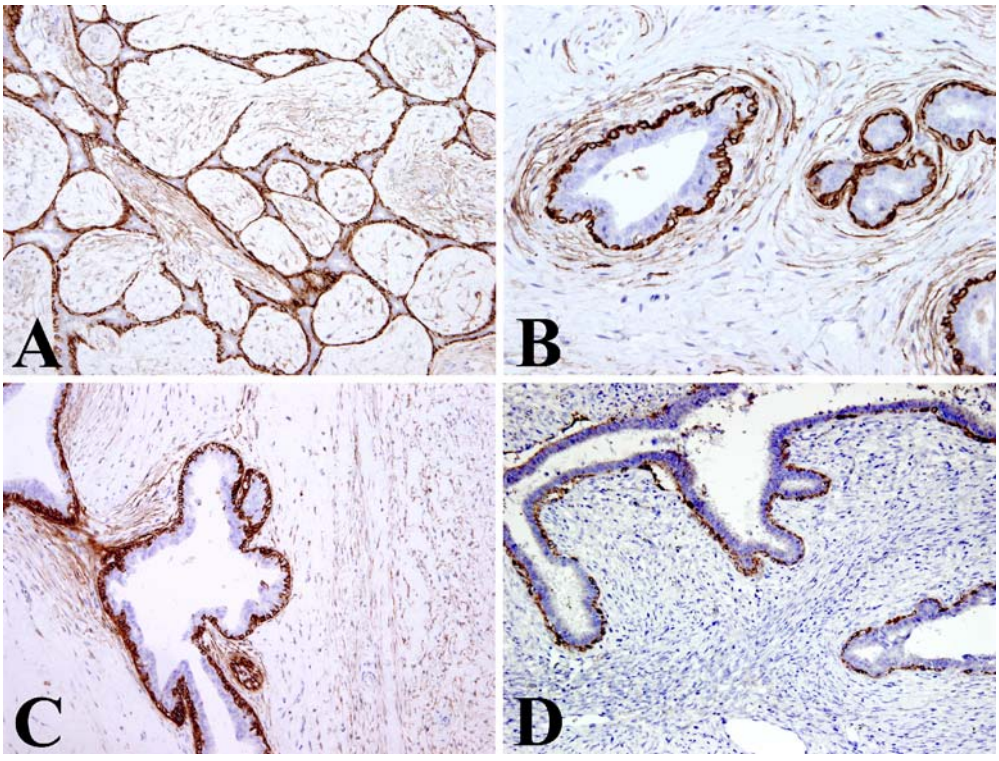

Fig. 1 CD10 expression in stromal cells of intracanalicular fibroadenoma (**a**), pericanalicular fibroadenoma (**b**), benign phyllodes tumor (**c**), and its lack in borderline phyllodes tumor (**d**). Positive myoepithelium serves as an internal control

References

1. Bellocq JP, Magro G (2003) Fibroepithelial tumours. In: Tavassoli FA, Devilee P (eds) WHO classification of tumours. Pathology and genetics of tumours of the breast and female genital organs. IARC, Lyon, pp 99–103
2. Gusterson BA, Monaghan P, Mahendran R, Ellis J, O'Hare MJ (1986) Identification of myoepithelial cells in human and rat breasts by anti-common acute lymphoblastic leukemia antigen antibody A12. J Natl Cancer Inst 77:343–349
3. Mechtersheimer G, Kruger KH, Born IA, Moller P (1990) Antigenic profile of mammary fibroadenoma and cystosarcoma phyllodes. A study using antibodies to estrogen- and progesterone receptors and to a panel of cell surface molecules. Pathol Res Pract 186:427–438
4. Mechtersheimer G, Moller P (1989) Expression of the common acute lymphoblastic leukemia antigen (CD10) in mesenchymal tumors. Am J Pathol 134:961–965
5. Rosen PP (2000) Fibroepithelial neoplasms. In: Breast pathology, 2nd ed. Lippincott-Raven, Philadelphia, PA, pp 176–197
6. Tse GM, Tsang AK, Putti TC, Scolyer RA, Lui PC, Law BK, Karim RZ, Lee CS (2005) Stromal CD10 expression in mammary fibroadenomas and phyllodes tumours. J Clin Pathol 58:185–189

Virchows Arch (2006) 448: 873
DOI 10.1007/s00428-006-0170-0

LETTER TO THE EDITOR

Juan Politei

Schiffmann R, Rapkiewicz A, Abu-Asab M, Ries M, Askari H, Tsokos M, Quezado M. Pathological findings in a patient with Fabry disease, who died after 2.5 years of enzyme replacement. Virchows Arch. 2005 Nov 29; 1–7

Received: 27 December 2005 / Accepted: 25 January 2006 / Published online: 8 March 2006

Dear Editor,
The patient was 47 years old, the diagnosis was made when he was 19, and symptoms began when he was 5. At the age of 37, the patient had a high serum creatinine level and also proteinuria. This makes us believe that there was an important deterioration in the glomerular filtration rate (GFR), because serum creatinine usually rises when GFR falls to at least 50%.

In the report of Schiffmann et al. [1], the age of the patient at the time of the beginning of the TRE is not specified. The autopsy showed acute myocardial infarction associated with coronary stenosis. At a renal level, there are isolated signs of mesangial sclerosis, which do not affect the vascular endothelial cells. The evaluation of the brain showed neuronal commitment, as well as the media and adventitia layers of the blood vessels, which again, did not affect the endothelial cells. In the report, it was suggested that the infused enzyme has limited access to nonvascular endothelial cells and that this may constitute a significant limitation of this therapeutic approach.

I personally believe that the main reason of the bad outcome of the patient is the extremely late beginning of the enzyme replacement therapy (ERT).

At the beginning of the treatment, the patient was close to a chronic renal insufficiency, which, as we well know nowadays, once the point of nonreturn is exceeded, the results of the ERT are not beneficial, as they would be at the early stages [2]. At the same time, we do not have a renal biopsy before the beginning of the ERT. Even though the vascular endothelial cells were clear from Gl3, we cannot know if the ERT reverted the lipid deposits in the interstitial and glomerular cells, which did not show existence of sclerosis.

It would be interesting to count with the latest results of serum creatinine and proteinuria, as the ones published have 10 years and perhaps the renal function was stabilized or could even demonstrate improvements. Although the vascular thrombosis would be accelerated in Fabry disease [3], this patient could have had a polymorphism in the genes of IL-6, eNOS, Factor V, or protein Z, which also adds another vascular risk factor. In conclusion, the ERT with Agalsidasa Beta (Fabrazyme) has clearly demonstrated the removal of Gl3 of endothelial and nonvascular cells [4]. In this report, due to the late beginning of the ERT, I do not believe it is possible to obtain a conclusion on the effectiveness of the enzyme used.

References

1. Schiffmann R, Rapkiewicz A, Abu-Asab M, Ries M, Askari H, Tsokos M, Quezado M (2005) Pathological findings in a patient with Fabry disease, who died after 2.5 years of enzyme replacement. Virchows Arch (in press)
2. Brenner BM, Grunfeld JP (2004) Renoprotection by enzyme replacement therapy. Curr Opin Nephrol Hypertens 13:231–241
3. Bodary PF, Shen Y, Vargas FB, Bi X, Ostenso KA, Gu S, Shayman JA, Eitzman DT (2005) Alpha-galactosidase A deficiency accelerates atherosclerosis in mice with apolipoprotein E deficiency. Circulation 111:629–632
4. Eng CM, Guffon N, Wilcox WR, Germain DP, Lee P, Waldek S, Caplan L, Linthorst GE, Desnick RJ, International Collaborative Fabry Disease Study Group (2001) Safety and efficacy of recombinant human it alpha-galactosidase A—replacement therapy in Fabry's disease. N Engl J Med 345 (1):9–16

J. Politei (✉)
Neurology Service, Fenandez Hospital,
Cerviño 3356,
Buenos Aires, 1426, Argentina
e-mail: jpolitei@hotmail.com
Tel.: +11-541-42245762
Fax: +11-541-48019349

Virchows Arch (2006) 448: 874–876
DOI 10.1007/s00428-005-0028-x

LETTER TO THE EDITOR

Tomoko Seguchi · Yuka Kyoraku · Kazuko Saita · Toshihiko Ihi · Miyuki Nagai · Yutaka Akiyama · Hiroshi Itoh · Hiroaki Kataoka

Human T-cell lymphotropic virus type I (HTLV-1) associated myelopathy and Sjögren's syndrome representing pulmonary nodular amyloidosis and multiple bullae: report of an autopsy case

Received: 20 February 2005 / Accepted: 10 June 2005 / Published online: 12 April 2006

Sir,

T-cell lymphotropic virus type I (HTLV-I), the first human retrovirus, is the causative agent for adult T-cell lymphoma/leukemia (ATL). It has also been reported that the same virus was implicated in the pathogenesis of HTLV-I associated myelopathy/tropical spastic paraparesis (HAM/TSP), HTLV-1 associated bronchopnumopathy (HAB), HTLV-I associated arthropathy, HTLV-I uveitis, and autoimmune diseases such as Sjögren's syndrome (SS) [2, 3]. Thus, HTLV-1 infection contributes to the development of various inflammatory disorders, and the pathogenesis of these inflammatory disorders, which was suspected to be related to the disruption of host immune system, appears to be different from that of ATL.

We experienced an autopsy case of a 59-year-old Japanese non-smoking woman who was found to have both HAM/TSP and SS representing pulmonary nodular amyloidosis and multiple bullae. She was in good health until the late 1980s, when she first noticed obstinate cough. In January 1994, she complained of progressive leg weakness, dysuria, and dyspnea, and she was hospitalized until death. The data of laboratory examination in 1994 was as follows: anti-ATL antibody, >64 titer (cerebrospinal fluid) and >4,096 titer (serum); serum antinuclear antibody (ANA), 80 titer; serum anti-SSA antibody, 16 titer; serum anti-SSB antibody, negative; and serum RA test, positive. The peripheral white blood cell counts were as follows: 7,100/μl in 1994; 3,900/μl in 1996; and 8,240/μl in 2002. In addition, no apparent ATL-like atypical lymphoid cells were seen. Neither apparent findings of ATL nor monoclonal gammopathy of undetermined significance (MGUS) was seen in the biopsy specimen of bone marrow in 1994. Serum α1-antitrypsin level was not examined. She noticed dryness of the conjunctiva and mouth, but neither sialography nor biopsy of the minor salivary gland was performed. Chest radiograph showed interstitial pneumonia pattern with some small bullae in both lung fields, but magnetic resonance imaging of the lumbar level was almost normal. These results clinically confirmed the diagnosis of HAM and SS. Conservative therapy was done; however, both neurological and lung functions gradually deteriorated, and chest radiograph and computed tomography revealed increased sizes of multiple cysts through both lungs and a small nodule in right lung (not shown). She finally died of respiratory failure on January 2003. An autopsy was performed 2 h after death. Various organs including both lungs, spinal cord, and submandibular glands were histologically examined in hematoxylin and eosin staining sections. Lung tissues suspected of amyloid deposition were also stained in Congo red with or without $KMnO_4$ treatment and immunostained with anti-amyloid-A antibody (DakoCytomation, Glostrup, Denmark) and anti-kappa and anti-lambda chains of immunoglobulin (DakoCytomation). Macroscopically, both lungs revealed varying sizes of bullae with some small nodules (Fig. 1), which were found to represent the amyloid deposition histologically. Microscopically, amyloid depositions were also found around the bullae and bronchioles (Fig. 2a), in addition to the nodular deposition with calcification and metaplastic bone formation (Fig. 2b). They were positive for Congo red stain, and the reaction disappeared after $KMnO_4$ treatment. They were also positive for kappa chain of immunoglobulin, but not for lambda chain nor amyloid-A (Fig. 2c,d), indicating the AL-amyloid. No amyloid deposition was identified in other organs. Organizing pneumonia probably associated with bronchopneumonia and

T. Seguchi · M. Nagai · Y. Akiyama · H. Itoh · H. Kataoka (✉)
Department of Pathology, Faculty of Medicine,
University of Miyazaki,
5200 Kihara, Kiyotake,
Miyazaki, 889-1692, Japan
e-mail: mejina@med.miyazaki-u.ac.jp
Tel.: +81-985-852809
Fax: +81-985-856003

Y. Kyoraku · K. Saita · T. Ihi
Division of Internal Medicine,
National Sanatorium Miyazaki-higashi Hospital,
4374-1 Tayoshi,
Miyazaki, 880-0911, Japan

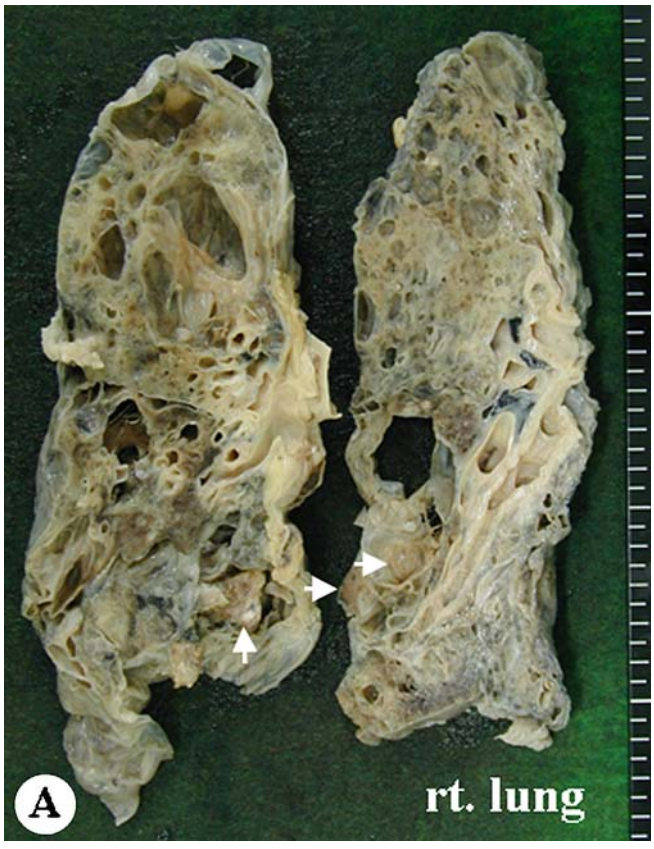

Fig. 1 Gross appearance of the right lung. The right lung showed multiple bullae formation and a few small nodules of amyloid deposition (*white arrows*). Same findings were also found in the left lung

severe interstitial lymphocytic and plasmacytic infiltration were also found in many portions of both lungs (not shown). Submandibular glands were atrophic with fat infiltration and showed destruction of the glands with lymphocytic infiltration (not shown), and these findings were compatible with SS. The atrophic middle and lower thoracic cords showed symmetric degenerative changes with demyelination accompanied by loss of axons (Fig. 2e). These changes were predominant in the lateral and anterior columns in luxol fast blue stain (inset of Fig. 2e). Mild thickening of the pia mater and sparse infiltration of T lymphocytes (CD8+ > CD4+) were also observed (Fig. 2e). These findings of the spinal cord appear to be compatible with those of HAM/TSP with a history of 8 years (inactive-chronic lesion).

This case represented HAM/TSP complicated by SS, nodular amyloidosis, and multiple emphysematous bullae. HAM/TSP has been reported to coexist with various disruptions of the immune system [2]. On the other hand, the pathogenesis of SS has been suspected to be an interaction of genetic, hormonal, and environmental factors. Several viruses, such as Epstein–Barr virus, HTLV-I, human immunodeficiency virus, and human herpesvirus-6, have been suggested as the causative infectious agents of SS and lymphoproliferative disorders [5, 6]. Considering the pathogenesis of the present case, HTLV-I infection was suspected to induce both HAM/TSP and SS. With regard to the lung lesions, the conditions reported in association with HTLV-I infection include HAB and SS [2, 5], and SS has been reported in association with lymphocytic interstitial

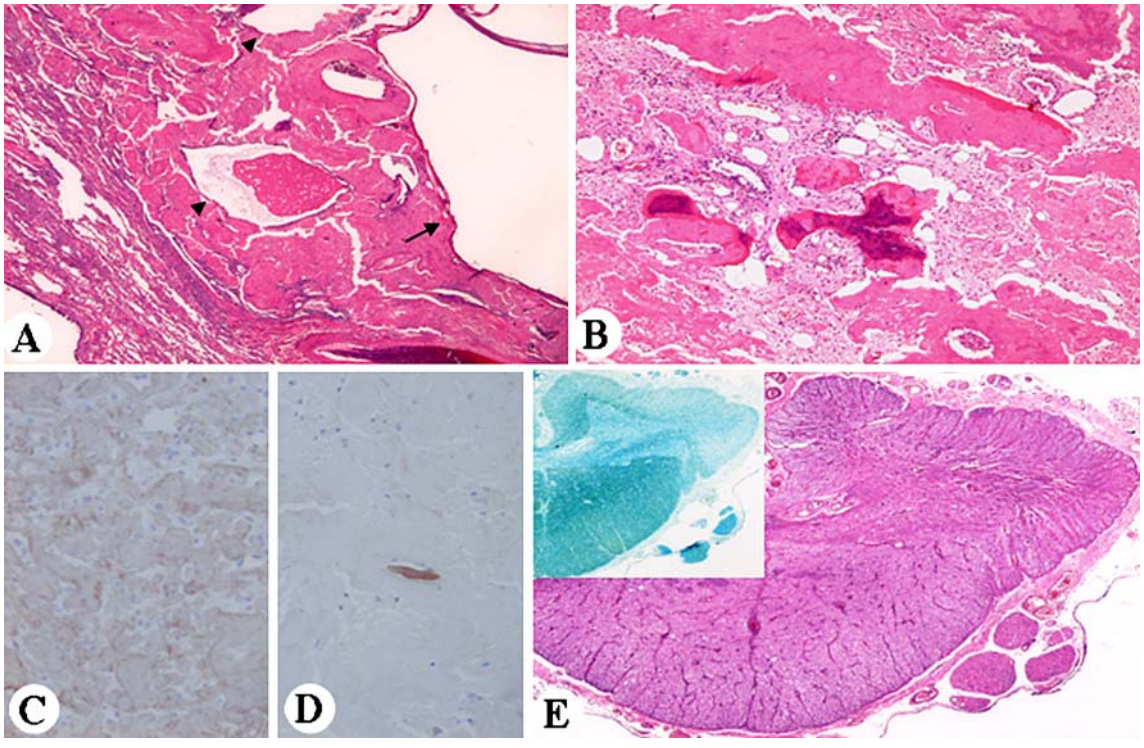

Fig. 2 Microscopic findings of the lung (**a**–**d**) and spinal cord (**e**). Amyloid depositions were found around the bullae (*arrow*) and bronchioles (*arrow heads*) (**a**), in addition to the nodular deposition with calcification and metaplastic bone (**b**); hematoxylin & eosin stain, original magnification ×40. Amyloid depositions were immunohistochemically positive for kappa chain of immunoglobulin (**c**) but not for amyloid-A protein (**d**); immunoperoxidase stain, original magnification ×100. Spinal cord (**e**) showed monotonous degeneration of the white matter [see also *inset* of (**e**), Luxol fast blue stain] and thickening of the pia mater. Inflammatory infiltrate is inconspicuous; hematoxylin & eosin stain, original magnification ×4

pneumonia and amyloidosis [4]. Therefore, it is possible to speculate that HTLV-I infection induced SS followed by amyloid deposition as a pulmonary manifestation of SS in the present case. Lymphoplasmacytic infiltration in lungs was most likely to be a lymphoproliferative process associated with SS, although the possible existence of HAB cannot be excluded totally. Amyloidosis is a well-recognized pulmonary complication of SS [4], and there has been one reported case of SS with multiple bullae and pulmonary nodular amyloidosis [1]. They speculated that the narrowing of the airway due to inflammatory cell infiltration and amyloid deposition to the bronchial wall acted as the check-valve mechanism and resulted in multiple bullae formation. The findings of the present case also supported this speculation. In addition, we assume that the destruction of alveolar walls by neutrophilic elastase and matrix metalloproteinases (MMPs) produced by neutrophils and macrophages at the sites of repeating extensive inflammation might also be associated with the formation of multiple bullae, although neutrophilic infiltration was considered to have already disappeared at the time of autopsy. To the best of our knowledge, a case representing HAM/TSP and SS with pulmonary nodular amyloidosis and multiple bullae has never been reported to date, and we believe this report is the first case.

Acknowledgements We thank Dr. M. Kawabata, Department of Pathology, Saitama Prefectural Cardiovascular and Respiratory Center, for valuable discussion in this case and Mr. T. Miyamoto and Mrs. Y. Nomura for their skillful technical assistance.

References

1. Kobayashi H, Matsuoka R, Kitamura S, Tsunoda N, Saito K (1988) Sjögren's syndrome with multiple bullae and pulmonary nodular amyloidosis. Chest 94:438–440
2. Kompoliti A, Gage B, Sharma L, Daniels JC (1996) Human T-cell lymphotropic virus type 1-associated myelopathy, Sjögren syndrome, and lymphocytic pneumonitis. Arch Neurol 53:940–942
3. Nakamura H, Kawakami A, Tominaga M, Hida A, Yamasaki S, Migita K, Kawabe Y, Nakamura T, Eguchi K (2000) Relationship between Sjögren's syndrome and human T-lymphotropic virus type I infection: follow-up study of 83 patients. J Lab Clin Med 135:139–144
4. Strimlan CV, Rosenow EC, Divertie MB, Harrison EG (1976) Pulmonary manifestations of Sjögren's syndrome. Chest 70: 354–361
5. Terada K, Katamine S, Eguchi K, Moriuchi R, Kita M, Shimada H, Yamashita I, Iwata K, Tsuji Y, Nagataki S, Miyamoto T (1994) Prevalence of serum and salivary antibodies to HTLV-1 in Sjögren's syndrome. Lancet 344:1116–1119
6. Travis WD, Fox CH, Devaney KO, Weiss LM, O'Leary TJ, Ognibene FP, Suffredini AF, Rosen MJ, Cohen MB, Shelhamer J (1992) Lymphoid pneumonitis in 50 adult patients infected with the human immunodeficiency virus: lymphocytic interstitial pneumonitis versus nonspecific interstitial pneumonitis. Human Pathol 23:529–541

Virchows Arch (2006) 448: 877–878
DOI 10.1007/s00428-005-0052-x

LETTER TO THE EDITOR

Manuel Sobrinho-Simões · Valdemar Máximo

Warthin's tumour

Received: 20 July 2005 / Accepted: 20 July 2005 / Published online: 12 April 2006

Dear Editor:
In a recent issue of *Virchows Archiv*, Teymoortash and Werner [8] review the pathogenesis of Warthin's tumour of the parotid gland and conclude that "... it may be classified in the group of tumour-like lesions".

We agree with the aforementioned conclusion, as well as with the assumption that Warthin's tumour may constitute a pathogenetically heterogeneous group of lesions characterized by the growth of oncocytes in a lymphoid stroma [8].

Teymoortash and Werner point out that the oncocytic transformation in Warthin's tumour and in the salivary glands of elderly individuals seems to be related with age-related metabolic deficiencies and may be secondary to damage to the mitochondrial deoxyribonucleic acid (mtDNA) induced by smoking [3]. Furthermore, they identify "oncocytic metaplasia and progressive proliferation of duct epithelium" as the early phase of Warthin's tumour development [8].

From what is known in other tumour and tumour-like models, we think that oncocytic transformation (or metaplasia) plays a pivotal role in the pathogenesis of Warthin's tumour.

M. Sobrinho-Simões · V. Máximo
Institute of Molecular Pathology and Immunology,
University of Porto (IPATIMUP),
Porto, Portugal

M. Sobrinho-Simões
Medical Faculty, University of Porto,
Porto, Portugal

M. Sobrinho-Simões
Hospital S. João,
Porto, Portugal

M. Sobrinho-Simões (✉)
IPATIMUP,
Rua Dr. Roberto Frias s/n,
4200-465 Porto, Portugal
e-mail: ssimoes@ipatimup.pt
Tel.: +351-22-5570700
Fax: +351-22-5570799

The accumulation of mitochondria in the cytoplasm of oncocytic cells may be due to a primary alteration of the mtDNA encoding for mitochondrial enzymes [5], or to mutations in the nuclear DNA encoding for mitochondrial proteins [4, 6]. The most typical mtDNA alteration in oncocytic cells is the presence of a large (about 5 kb) mtDNA deletion that has been detected in oncocytic cells of Hashimoto's thyroiditis and all sorts of oncocytic tumours of the thyroid, as well as in Warthin's tumour, as Teymoortash and Werner emphasize in their review [5–8]. The mitochondria containing deleted and/or mutated mtDNA proliferate more than the "normal" mitochondria, thus leading to a progressive increase in the percentage of abnormal mitochondria in the cells [5, 7].

The mitochondria can accumulate only in cells of tumours that are not actively dividing (i.e., in relatively slow-growing neoplasms); in rapidly growing neoplasms, the division of the cytoplasm of the neoplastic cells prevents the accumulation of the mitochondria. That is the reason why most oncocytic tumours are, like Warthin's tumour and renal oncocytoma, benign or low malignant neoplasms [6, 7].

The mechanism of tumour formation under these circumstances is not yet well understood [7]. It has been advanced that mitochondrial abnormalities block the apoptotic process, increasing the survival of the cells, and/or the deficient mitochondrial function is sensed as a hypoxic stimulus, leading to increased levels of the inducible form of the hypoxic-inducible factor, thus triggering angiogenesis (and proliferation) (for a review, see [1]).

A comparison of a malignant oncocytic tumour with its putative preneoplastic lesion (e.g., an oncocytic variant of PTC arising in the setting of an oncocytic multinodular goiter) discloses frequently the presence of oncogenic mutations in malignant tissues [e.g., in the oncocytic variant of papillary thyroid carcinoma (PTC), RET/PTC rearrangements or BRAF mutations have been detected] [4, 7, 9]. It would be very interesting to find out if the same holds true in rare oncocytic carcinomas arising in pre-existing Warthin's tumours [2].

References

1. Eng C, Kiuru M, Fernandez MJ, Aaltonen LA (2003) A role for mitochondrial enzymes in inherited neoplasia and beyond. Nat Rev Cancer 3:193–202
2. Foschini MP, Malvi D, Betts CM (2005) Oncocytic carcinoma arising in Warthin tumour. Virchows Arch 446:88–90
3. Lewis PD, Fradley SR, Griffiths AP, Baxter PW, Parry JM (2002) Mitochondrial DNA mutations in the parotid gland of cigarette smokers and non-smokers. Mutat Res 518:47–54
4. Máximo V, Botelho T, Capela J, Soares P, Lima J, Taveira A, Amaro T, Barbosa AP, Preto A, Harach HR, Williams D, Sobrinho-Simões M (2005) Somatic and germline mutation in GRIM-19, a dual function gene involved in mitochondrial metabolism and cell death, is linked to mitochondrion-rich (Hurthle cell) tumours of the thyroid. Br J Cancer 92:1892–1898
5. Máximo V, Soares P, Lima J, Cameselle-Teijeiro J, Sobrinho-Simões M (2002) Mitochondrial DNA somatic mutations (point mutations and large deletions) and mitochondrial DNA variants in human thyroid pathology. A study with emphasis on Hürthle cell tumors. Am J Pathol 160:1857–1865
6. Máximo V, Sobrinho-Simões M (2000) Hürthle cell tumours of the thyroid. A review with emphasis on mitochondrial abnormalities with clinical relevance. Virchows Arch 437:107–115
7. Sobrinho-Simoes M, Maximo V, Castro IV, Fonseca E, Soares P, Garcia-Rostan G, Oliveira MC (2005) Hurthle (oncocytic) cell tumors of thyroid: etiopathogenesis, diagnosis and clinical significance. Int J Surg Pathol 13:29–35
8. Teymoortash A, Werner JA (2005) Tissue that has lost its track: Warthin's tumour. Virchows Arch 446:585–588
9. Trovisco V, Soares P, Preto A, de Castro IV, Lima J, Castro P, Maximo V, Botelho T, Moreira S, Meireles AM, Magalhaes J, Abrosimov A, Cameselle-Teijeiro J, Sobrinho-Simoes M (2005) Type and prevalence of BRAF mutations are closely associated with papillary thyroid carcinoma histotype and patients' age but not with tumour aggressiveness. Virchows Arch 446:589–595

Virchows Arch (2006) 448: 879
DOI 10.1007/s00428-006-0229-y

ANNOUNCEMENTS

4–8 September 2006
Postgraduate Course
Diagnostic Breast Pathology
Department of Pathology
Medical University Graz, Austria

Course Director
Farid Moinfar, MD (Graz)

Guest faculty
Fattaneh A. Tavassoli, MD (New Haven, USA)

Course Objectives
This intensive course is designed for pathologists in training as well as practicing pathologists. During the course, the participants will review 100 cases dealing with a variety of benign and malignant breast neoplasms and tumor-like lesions. Several common diagnostic problems including papillary neoplasms, intraductal proliferative lesions, variants of ductal and lobular intraepithelial neoplasias, and infiltrating carcinomas are included.

On each day, 20 cases will be extensively discussed by an interactive approach. Particular attention will be paid to the diagnostic criteria with systematic analysis of differential diagnoses. Value and limitations of immunohistochemistry as a diagnostic adjunct will be demonstrated.

Course fee:
Euro 600,- Practicing pathologists
Euro 400,- Pathologists in training

For more information and registration please contact:
Edith Kleinferchner
Department of Pathology, Medical University Graz
Auenbruggerplatz 25
8036 Graz, Austria
Fax: 0043 (0) 316 385 3432
e-mail: edith.kleinferchner@meduni-graz.at
http://pathologie.meduni-graz.at/Pathologie/veranstaltungen.htm

11–13 October 2006
Postgraduate Course
Diagnostic Hepatopathology
Department of Pathology
Medical University Graz, Austria

Course Director
Carolin Lackner, MD (Graz)

Faculty
Helmut Denk, MD, FRCPath (Graz)

Guest faculty
Stefan G. Hübscher, MD (Birmingham)

Course Objectives
The differential diagnosis of chronic hepatitis is a problem frequently encountered in liver pathology. This three day course provides a comprehensive review of the histological features and differential diagnosis of chronic hepatitis in adults; i.e., viral hepatitis, autoimmune hepatitis, overlap syndromes, as well as recurrent chronic hepatitis in the transplanted liver. Liver injury due to drugs, toxins and metabolic disorders and steatohepatitis (ASH/NASH) will also be discussed.

Every day two key lectures, each dealing with a main diagnostic topic will be given. The course covers approx. 50 cases and per day approx. 15-20 cases will be discussed in an interactive approach. Additionally the participants will have ample opportunity for microscopic evaluation of each case.

Course fee:
Euro 400,- (Practicing pathologists)
Euro 280,- (Pathologists in training)

For more information and registration please contact:
Edith Kleinferchner
Department of Pathology, Medical University Graz
Auenbruggerplatz 25
8036 Graz, Austria
Fax: 0043 (0) 316 385 3432
e-mail: edith.kleinferchner@meduni-graz.at
http://pathologie.meduni-graz.at/Pathologie/veranstaltungen.htm

24–26 January 2007
Theorico-practical Course on Bone and Soft Tissue Tumors
Department of Pathology, Hospital del Mar, Barcelona, Spain

Faculty
Christopher Fletcher, M.D. (Brigham and Women's Hospital, Boston, USA)
Andrew Rosenberg, M.D. (Massachusetts General Hospital, Boston, USA)
Angelo Paolo Dei Tos, M.D. (Hospital of Treviso, Italy)
John Goldblum, M.D. (Cleveland Clinic, Cleveland, USA)
Paola Dal Cin, Ph.D. (Brigham and Women's Hospital, Boston, USA)

For further information please contact:
Francisco Alameda, M.D.
Department of Pathology
Hospital del Mar, Spain
E-mail: 86780@imas.imim.es
or
Esther Oliva, M.D.
Department of Pathology
Massachusetts General Hospital
55 Fruit Street, WRN-2
Boston, MA 02114, USA
E-mail: eoliva@partners.org